

# ORGANOMETALLICS

Volume 14, Number 11, November 1995

© Copyright 1995  
American Chemical Society

## Communications

### Hypercoordinate Carbon in Protonated Tetraauriomethane Molecules

H. Schmidbaur,\* F. P. Gabbaï, A. Schier, and J. Riede

Anorganisch-chemisches Institut der Technischen Universität München, Lichtenbergstrasse 4,  
D-85747 Garching, Germany

Received September 1, 1995<sup>®</sup>

**Summary:** The reaction of  $\{[(Ph_3P)Au]_3O\}^+BF_4^-$  with  $Me_3SiCHN_2$  gives dinitrogen and three crystalline products, two of which have been identified as  $\{Ph_3PCH[Au(PPh_3)]_2\}^+BF_4^-$  (**1**) and  $\{HC[Au(PPh_3)]_4\}^+BF_4^-$  (**2**). In crystals of  $2 \cdot 4CH_2Cl_2$ , the cation has a square pyramidal structure with an apical hydrogen atom at a central pentacoordinate carbon atom. The cations are associated to centrosymmetrical dimers with auriophilic contacts.

Hypercoordinate carbon with independent substituents is still a rare phenomenon in the structural chemistry of molecular species.<sup>1</sup> Protonated methane,  $CH_5^+$ , is an example: Although a plethora of data are available from quantum mechanical calculations, and detailed spectroscopic evidence has been accumulated, the structure is still unknown.<sup>2</sup> The same is true for protonated alkanes  $[CH_nR_{5-n}]^+$  or pentaalkylated carbocations  $CR_5^+$ .<sup>3</sup>

For this reason the discovery of related pentaaurated carbocations  $C(AuL)_5^+$ , with  $L = PR_3$ , has attracted considerable interest.<sup>4</sup> Salts of these cations were obtained in all attempts to generate neutral tetraauriomethane complexes  $C(AuL)_4$ , except for cases with very

bulky ligands  $L$ .<sup>5</sup> The experimental results indicated that the closed-shell (octet electron-precise at carbon)  $C(AuL)_4$  molecules (**A**) (Chart 1) exhibit surprisingly strong donor properties (!) toward  $LAu^+$  electrophiles. The cations were shown to have standard trigonal-bipyramidal structures (**B**, fluxional in solution) with pentacoordinate central carbon atoms.<sup>4</sup> A satisfactory picture of the bonding of these novel species is based on extensive quantum-chemical calculations using ab initio and density functional methods and including correlation and relativistic effects.<sup>6,7</sup>

We now report the isolation and structural characterization of a mixed species of the type  $HC(AuL)_4^+$ , **C**, in which both the proton and the (isolobal)<sup>8</sup>  $LAu^+$  cations are present simultaneously at a pentacoordinate carbon center. Formally, such species represent the products of a protonation of tetraauriomethane molecules (**A**), indicating beyond any doubt that species  $C(AuL)_4$  are indeed strong Lewis bases!

The reaction of (trimethylsilyl)diazomethane<sup>9</sup> with tris(triphenylphosphine)gold(I)oxonium tetrafluorobo-

(5) Schmidbaur, H.; Steigelmann, O. *Z. Naturforsch.* **1992**, *47b*, 1721–1724.

(6) (a) Görling, A.; Rösch, N.; Ellis, D. E.; Schmidbaur, H. *Inorg. Chem.* **1991**, *30*, 3986–3994. (b) Häberlen, O. D.; Schmidbaur, H.; Rösch, N. *J. Am. Chem. Soc.* **1994**, *116*, 8241–8248.

(7) (a) Pyykkö, P.; Zhao, Y.-F. *Chem. Phys. Lett.* **1991**, *177*, 103–106. (b) Li, J.; Pyykkö, P. *Inorg. Chem.* **1993**, *32*, 2630–2634. (c) Burdett, J. K.; Eisenstein, O.; Schweizer, W. B. *Inorg. Chem.* **1994**, *33*, 3261–3268. (d) Calhorda, M. J.; Veiros, L. F. *J. Organomet. Chem.* **1994**, *478*, 37–44.

(8) Hoffmann, R. *Angew. Chem., Int. Ed. Engl.* **1982**, *21*, 711–720.

(9) (a) Seyferth, D.; Dow, A. W.; Menzel, H.; Flood, T. C. *J. Am. Chem. Soc.* **1968**, *90*, 1080–1082. (b) Barton, T. J.; Hoekman, S. K. *Synth. React. Inorg. Metalorg. Chem.* **1979**, *9*, 297–300.

<sup>®</sup> Abstract published in *Advance ACS Abstracts*, October 15, 1995.

(1) Olah, G. A.; Prakash, G. K. S.; Williams, R. E.; Field, L. D.; Wade, K. *Hypercarbon Chemistry*; Wiley-Interscience: New York, 1987.

(2) (a) Olah, G. A. *Acc. Chem. Res.* **1987**, *20*, 422–428. (b) Raghavachari, K.; Whiteside, R. A.; Pople, J. A.; Schleyer, P. v. R. *J. Am. Chem. Soc.* **1981**, *103*, 5649–5657. (c) Schreiner, P. R.; Kim, S. J.; Schaeffer, H. F. *J. Chem. Phys.* **1993**, *99*, 3716–3720.

(3) Crabtree, R. H. *Chem. Rev.* **1995**, *95*, 987–1008.

(4) Scherbaum, F.; Grohmann, A.; Müller, G.; Schmidbaur, H. *Angew. Chem., Int. Ed. Engl.* **1989**, *28*, 463–465.

Chart 1

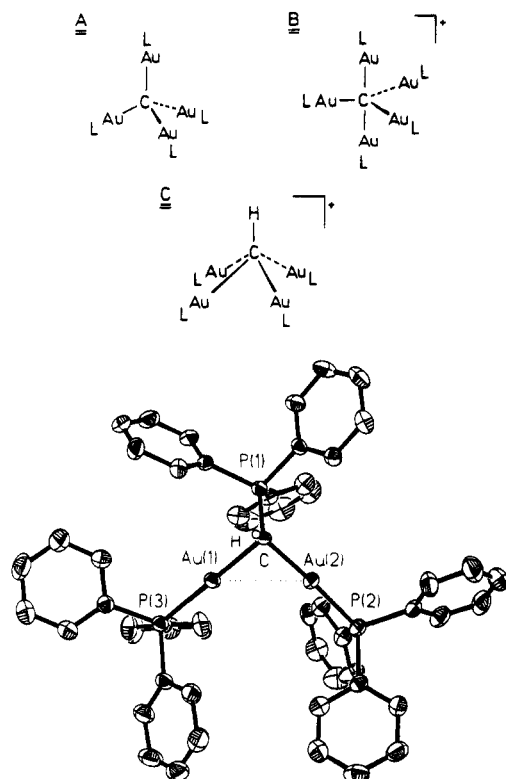
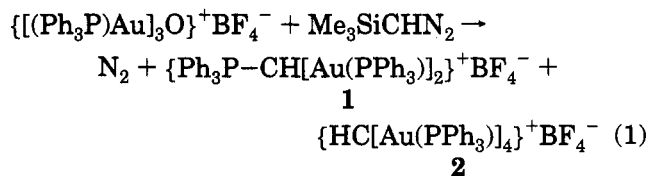


**Figure 1.** Molecular structure of the cation  $\text{Ph}_3\text{PCH}[\text{Au}(\text{PPh}_3)_2]^+$  in crystals of  $1 \cdot \text{CH}_2\text{Cl}_2$  (ORTEP, 50% probability ellipsoids, phenyl H atoms omitted for clarity).<sup>11</sup> Selected bond distances (Å) and angles (deg): P(1)–C 1.736(4), Au(1)–C 2.085(5), Au(2)–C 2.066(5), Au(1)–P(3) 2.269(1), Au(2)–P(2) 2.266(1), Au(1)···Au(2) 2.998(1); Au(1)–C–Au(2) 92.5(2), P(1)–C–Au(1) 109.3(2), P(1)–C–Au(2) 115.3(3), C–Au(1)–P(3) 179.3(1), C–Au(2)–P(2) 175.5(1).

rate<sup>10</sup> in a tetrahydrofuran/hexane mixed solvent (starting at  $-78^\circ\text{C}$  and reaching ambient temperature after 30 min) gives dinitrogen and a mixture of three products (1–3), which have been isolated as colorless to yellow crystalline solids by fractional crystallization in low yield (<10%). The compounds decompose slowly in air but can be handled in an inert atmosphere at ambient temperature.

Compound 1 has been identified by its analytical and spectroscopic data as {bis[(triphenylphosphine)aurio]-methyl}triphenylphosphonium tetrafluoroborate, and the structure of a solvate  $1 \cdot \text{CH}_2\text{Cl}_2$  was determined by single-crystal X-ray diffraction methods.<sup>11</sup> The result is shown in Figure 1. The cation has standard phosphonium geometry but features the expected small Au–C–Au angle at the methyl carbon atom typical of aurophilic bonding.<sup>12</sup> Product 1 probably was generated via loss of  $\text{N}_2$  and desilylation/auration of  $\text{Me}_3\text{SiCHN}_2$ , leaving a  $[\text{CH}(\text{AuL})_2]^+$  species, which was trapped by a triphenylphosphine ligand (eq 1).

Compound 2 has been shown to be tetrakis[(triphenylphosphine)gold(I)]methanium tetrafluoroborate.<sup>11,13</sup> Among the spectroscopic data, the 1:4:6:4:1 quintet couplings of the methyne hydrogen ( $J_{\text{P,H}} = 4.0$  Hz) and



carbon atoms ( $J_{\text{P,C}} = 65.0$  Hz) in the NMR spectra ( $\text{CDCl}_3$  solutions,  $25^\circ\text{C}$ ) are particularly diagnostic, as is the parent peak of the complete cation in the mass spectrum (FAB:  $m/z = 1849$ ). In particular, these spectra are important direct proof of the presence of a *methyne hydrogen atom*, which naturally is difficult to locate unambiguously in the single-crystal diffraction study.

The crystal structure of a tetrakis(dichloromethane) solvate  $2 \cdot 4\text{CH}_2\text{Cl}_2$  has been determined.<sup>11</sup> The individual cationic units feature a distorted *square-pyramidal* structure with a central carbon atom and with the hydrogen atom as the apical ligand and four gold atoms as the base ligands (Figure 2). The C–Au–P coordination at the gold atoms is close to linear. The Au–C–Au angles (for neighboring gold atoms) all are very small and virtually equal [ $82.2(2)$ – $82.8(2)^\circ$ ], associated with short Au···Au edge contacts [from 2.787(1) to 2.817(1) Å].

In the crystal, two of these  $\{\text{HC}[\text{Au}(\text{PPh}_3)_4]^+\text{BF}_4^-$  units are loosely associated into dimers through two interca-

(11) *Experimental details:* To a slurry of  $\{[(\text{Ph}_3\text{P})\text{Au}]_3\text{O}\}^+\text{BF}_4^-$  (500 mg, 0.34 mmol)<sup>10</sup> in THF (8 mL) cooled to  $-78^\circ\text{C}$  was added a 2 M solution of  $\text{Me}_3\text{SiCHN}_2$  (0.25 mL, 0.5 mmol).<sup>9</sup> The resulting mixture was allowed to reach  $25^\circ\text{C}$  over a period of 30 min (nitrogen evolution) and was stirred for another 3 h during which the solution turned brown in color. The THF solution was decanted, leaving a THF-insoluble precipitate. The solution was evaporated in a vacuum, and the residue was redissolved in dichloromethane (3 mL) and layered with hexane (3 mL) to give 24 mg (colorless, 4% yield) of 1, mp  $145^\circ\text{C}$  (dec, turns opaque) (satisfactory elemental analysis) MS (FAB):  $m/z$  1193  $[\text{Ph}_3\text{PCH}(\text{AuPPh}_3)_2]^+$ , 931  $[\text{CH}(\text{AuPPh}_3)_2]^+$ .  $^{31}\text{P}\{^1\text{H}\}$  NMR ( $\text{CDCl}_3$ ,  $25^\circ\text{C}$ ):  $\delta$  (ppm) 40.8 (d,  $J_{\text{P,P}} = 4.4$  Hz, PAu), 38.2 (t, PC).  $^{13}\text{C}\{^1\text{H}\}$  NMR ( $\text{CDCl}_3$ ):  $\delta$  ( $J_{\text{P,C}}$ ) 133.8 (13.8), 131.7, 129.2 (10.9), 129.9 (54.3) for PhPAu; 132.7(9.2), 129.2, 129.0 (11.0), 128.2 (50) for PhPC and *m*, *p*, *o*, and *ipso*, respectively; PCH not detected.  $^1\text{H}$  NMR ( $\text{CDCl}_3$ ): 7.15–7.90, m, Ph; CH not detected. *X-ray structure determinations:* Suitable crystals of 1 and 2 were mounted in glass capillaries and used for measurements of precise cell constants and intensity data collection. Diffraction intensities were corrected for decay [1,  $-1.5\%$ ; 2,  $-15.0\%$ ], Lp, and absorption effects [ $\psi$ -scans,  $T_{\text{min}}/T_{\text{max}} = 0.8295/0.9994$  (1),  $0.6337/0.9995$  (2)]. Crystal data of  $1 \cdot \text{CH}_2\text{Cl}_2 [2 \cdot 4\text{CH}_2\text{Cl}_2]$ :  $\{(\text{C}_6\text{H}_5)_3\text{PCH}[\text{AuP}(\text{C}_6\text{H}_5)_3]_2\}^+\text{BF}_4^- \cdot \text{CH}_2\text{Cl}_2$  [ $\{\text{CH}[\text{AuP}(\text{C}_6\text{H}_5)_3]_4\}^+\text{BF}_4^- \cdot 4\text{CH}_2\text{Cl}_2$ ],  $M_r = 1365.57$  [2276.60], triclinic, space group P1,  $a = 13.170(1)$  [14.337(1)] Å,  $b = 13.994(1)$  [16.438(2)] Å,  $c = 16.438(1)$  [18.774(2)] Å,  $\alpha = 114.67(1)$  [66.24(1)]°,  $\beta = 104.55(1)$  [78.75(1)]°,  $\gamma = 95.11(1)$  [87.59(1)]°,  $V = 2599.2$  [3968.3] Å<sup>3</sup>,  $Z = 2$ . With use of 11 248 [15 368] measured reflections (10 359 [14 214] unique, 8961 [12 278] "observed" with  $F_o \geq 4\sigma(F_o)$ ) collected at  $-62$  [ $-68$ ]°C with Mo K $\alpha$  radiation on an Enraf Nonius CAD4 diffractometer, the structures were solved by direct methods (SHELXTL-Plus<sup>17</sup>) and refined by full-matrix least-squares techniques (SHELXTL-Plus<sup>17</sup>) with anisotropic temperature factors for all non-hydrogen atoms except for the B, F, and solvent C and Cl atoms of compound 2. All hydrogen atoms were placed in idealized calculated positions and allowed to ride on their corresponding carbon atom with fixed isotropic contributions ( $U_{\text{iso}(\text{H})} = 0.08$  and  $0.05$  Å<sup>2</sup>, respectively), except for the Au–C–H in the cation of 2, which was located and included with fixed coordinates and isotropic contributions. Final  $R$  ( $R_w$ ) values: 0.0256 (0.0289) [0.0396 (0.0429)] for 613 [798] refined parameters.

(12) (a) Schmidbaur, H. *Gold Bull.* **1990**, 23, 11–21. (b) Scherbaum, F.; Grohmann, A.; Huber, B.; Krüger, C.; Schmidbaur, H. *Angew. Chem., Int. Ed. Engl.* **1988**, 27, 1544–1546.

(13) *Experimental details:* The THF-insoluble precipitate<sup>11</sup> was dissolved in dichloromethane (4 mL) and the solution layered with hexane (3 mL) to give a 60 mg crop of yellow crystals (6.5% yield), mp  $150^\circ\text{C}$  (dec, turns gray) (satisfactory elemental analysis). MS (FAB):  $m/z$  1849  $[\text{HC}(\text{AuPPh}_3)_4]^+$ , 1587  $[\text{HC}(\text{AuPPh}_3)_4] - \text{PPh}_3$ , 721  $[\text{Au}(\text{PPh}_3)_2]^+$ , 459  $[\text{AuPPh}_3]^+$ .  $^{31}\text{P}\{^1\text{H}\}$  NMR ( $\text{CDCl}_3$ ,  $25^\circ\text{C}$ ):  $\delta$  (ppm) 34.2, s.  $^{13}\text{C}\{^1\text{H}\}$  NMR ( $\text{CDCl}_3$ ):  $\delta$  ( $J_{\text{P,C}}$ ) 134.0 (d, 13.2, *m*), 131.3 (d, 51.5, *ipso*), 131.2 (s, *p*), 129 (br, *o*); 88.5 (quint, 65.0, Au<sub>4</sub>CH).  $^1\text{H}$  NMR ( $\text{CDCl}_3$ ): 7.0–7.5 (m, Ph); 4.85 (quint,  $J_{\text{P,H}} = 4.0$ , Au<sub>4</sub>CH). *Crystal structure:* see ref 11.

(10) Nesmeyanov, A. N.; Grandberg, K. I.; Dyadchenko, V. I.; Lemenovskii, D. A.; Perevalova, E. G. *Izv. Akad. Nauk SSSR, Ser. Khim.* **1974**, 740–750.



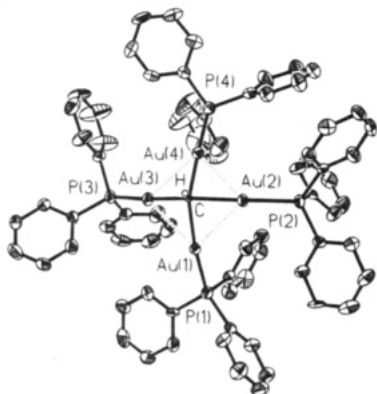


**Figure 2.** Molecular structure of the cation  $\text{HC}[\text{Au}(\text{PPh}_3)_4]^+$  in crystals of  $2 \cdot 4\text{CH}_2\text{Cl}_2$  (ORTEP, 50% probability ellipsoids, phenyl H atoms omitted for clarity).<sup>11</sup> Selected bond distances (Å) and angles (deg): Au(1)···Au(2) 2.817(1), Au(1)···Au(3) 2.812(1), Au(2)···Au(4) 2.796(1), Au(3)···Au(4) 2.787(1), Au(1)–C 2.13(1), Au(2)–C 2.132(7), Au(3)–C 2.126(7), Au(4)–C 2.112(8), Au(1)–P(1) 2.282(3), Au(2)–P(2) 2.275(2), Au(3)–P(3) 2.268(2), Au(4)–P(4) 2.275(2); Au(1)–C–Au(2) 82.8(3), Au(1)–C–Au(3) 82.8(3), Au(1)–C–Au(4) 129.0(4), Au(2)–C–Au(3) 145.0(4), Au(2)–C–Au(4) 82.4(3), Au(3)–C–Au(4) 82.2(2), C–Au(1)–P(1) 165.4(2), C–Au(2)–P(2) 175.0(2), C–Au(3)–P(3) 173.8(2), C–Au(4)–P(4) 175.2(3).

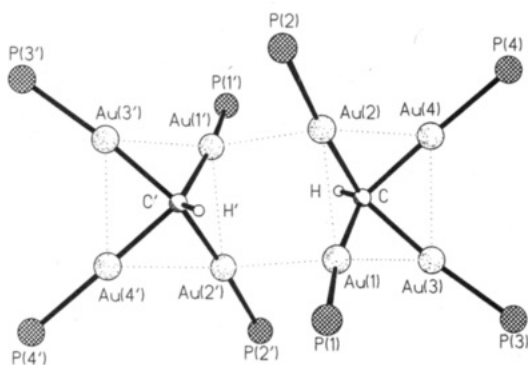


**Figure 3.** Association of the cations of compound **2** in crystals  $2 \cdot 4\text{CH}_2\text{Cl}_2$ . The components of the dimer are symmetry-related via a center of inversion. Intercationic contacts  $\text{Au}(1) \cdots \text{Au}(2)'/\text{Au}(1)' \cdots \text{Au}(2) = 3.367(1)$  Å. For other details see Figure 2.

tionic  $\text{Au} \cdots \text{Au}$  contacts [3.367(1) Å, equal by symmetry]. The monomers are related by a center of inversion (Figure 3). The mutual approach of the monomers clearly is the main reason for the distortion of the square pyramids, the fundamental structure of which is retained, however. The NMR data<sup>13</sup> (above) are in agree-

ment with a symmetrical species of 4-fold symmetry and thus suggest a dissociation of the dimers into their components in chloroform solution at ambient temperature.

It is plausible to assume that product **2** was also formed from the silyldiazomethane by loss of  $\text{N}_2$  and desilylation but with the CH unit ending up quadruply aurred. Compound **3** has not yet been identified, but from preliminary analytical and spectroscopic evidence it is expected to represent yet another methyne trapping product.

Compound **2** is a unique case in which a methyne unit is bridging four independent (closed-shell) metal atoms which are neither part of a metal–metal-bonded cluster system, tied together by polydentate ligands, nor fixed at the surface of a lattice. Most surprisingly, the system (**C**) is not a strong acid. Although the deprotonated species would be expected to be a stable molecule with tetracoordinate carbon (**A**), the cation remains intact even in the presence of a strong base like dimethylaniline.<sup>14</sup>

The new species (**C**) thus is another striking example in organogold chemistry of nonclassical structure and bonding which requires sophisticated new theoretical approaches. Structural parallels have previously been found with an analogous *alkylated* cation<sup>15</sup> of the type  $\{\text{MeC}[\text{Au}(\text{PPh}_3)]_4\}^+$  and with a tetraaurated arylphosphonium dication<sup>16</sup> of the type  $\{o\text{-TolP}[\text{Au}(\text{PPh}_3)]_4\}^{2+}$ , but only a preliminary description of their bonding has been advanced. Complementary experimental and computational studies therefore are in progress.

**Acknowledgment.** This work was supported by the Deutsche Forschungsgemeinschaft, by the Fonds der Chemischen Industrie, and—through the donation of chemicals—by Degussa AG and Heraeus GmbH. F.P.G. is grateful to the A. v. Humboldt Foundation for a research fellowship.

**Supporting Information Available:** Tables of crystallographic data, positional and thermal parameters, and interatomic distances and angles and ORTEP diagrams for **1** and **2** (15 pages). Ordering information is given on any current masthead page.

OM950687+

(14) Brachthäuser, B. Dissertation, Techn. Univ. Munich, 1992.

(15) Steigelmann, O.; Bissinger, P.; Schmidbaur, H. *Z. Naturforsch.* **1993**, *48b*, 72–78.

(16) Schmidbaur, H.; Zeller, E.; Weidenhiller, G.; Steigelmann, O.; Beruda, H. *Inorg. Chem.* **1992**, *31*, 2370–2376.

(17) Sheldrick, G. M. SHELXTL-PLUS, Release 4.0 for Siemens R3 Crystallographic Research System. Siemens Analytical Instruments, Inc., Madison, WI, 1989.

**(Arene)ruthenium(II) Complexes Containing the  
Monophosphine  $\text{RP}(\text{CH}_2\text{CO}_2\text{Me})_2$  or the Deprotonated  
Unsymmetrical Dianion  
 $[\text{RP}(\text{CHCO}_2\text{Me})(\text{CH}=\text{C}(\text{OMe})\text{O})]^{2-}$  as a Tripodal Chelating  
Ligand**

Jürgen Bank, Olaf Gevert, Werner Wolfsberger, and Helmut Werner\*

*Institut für Anorganische Chemie der Universität Würzburg,  
Am Hubland, D-97074 Würzburg, Germany*

Received July 11, 1995<sup>®</sup>

**Summary:** Reaction of the dichloro compounds  $[(\text{mes})\text{-RuCl}_2\{\eta^1(\text{P})\text{-RP}(\text{CH}_2\text{CO}_2\text{Me})_2\}]$  ( $\text{R} = i\text{Pr}$  (**3a**),  $t\text{Bu}$  (**3b**);  $\text{mes} = \text{mesitylene} = \text{C}_6\text{H}_3\text{Me}_3\text{-2,4,6}$ ) with 2 equiv of  $\text{AgPF}_6$  affords the dicationic  $\text{P},\text{O},\text{O}'$ -chelated complexes  $[(\text{mes})\text{Ru}\{\eta^3(\text{P},\text{O},\text{O}')\text{-RP}(\text{CH}_2\text{C}(\text{OMe})=\text{O})_2\}](\text{PF}_6)_2$  (**4a,b**) which in  $\text{CH}_2\text{Cl}_2$ , in the presence of water, undergo partial hydrolysis to give  $[(\text{mes})\text{Ru}\{\eta^2(\text{P},\text{O})\text{-RP}(\text{CH}_2\text{C}(\text{OMe})=\text{O})(\text{CH}_2\text{CO}_2\text{Me})\}\{\eta^1(\text{O})\text{-O}_2\text{PF}_2\}](\text{PF}_6)$  (**5a,b**). Compounds **4a,b** react with 2 equiv of  $\text{KOtBu}$  in  $t\text{BuOH}$  to yield the neutral complexes  $[(\text{mes})\text{Ru}\{\eta^3(\text{P},\text{C},\text{O})\text{-RP}(\text{C}(\text{HCO}_2\text{Me})(\text{CH}=\text{C}(\text{OMe})\text{O}))\}]$  (**6a,b**) containing both a five-membered phosphino enolate and a three-membered phosphinomethanide ring. A derivative, **7**, of the novel tripodal chelating system is formed by insertion of  $\text{PhNCO}$  into the  $\text{C}-\text{H}$  bond of the phosphino enolate unit of **6b**.

The chemistry of bifunctional phosphines of general composition  $\text{R}_2\text{P}(\text{CH}_2)_n\text{Y}$  and their transition-metal complexes has been an area of active research in recent years.<sup>1</sup> In particular for compounds where  $\text{Y}$  is  $\text{OMe}$ ,  $\text{C}(\text{=O})\text{R}'$ , or  $\text{C}(\text{=O})\text{OR}'$ , the oxygen donors temporarily are able to protect a vacant coordination site and thus allow the addition of better donor ligands to the metal center under fairly mild conditions. Moreover, with  $\beta$ -phosphino ketones or esters as starting materials, a number of O-metalated (phosphino enolate)metal compounds have been prepared and found to be useful starting materials for C-C coupling reactions with activated alkynes and isocyanates,<sup>2</sup> for the generation of metal acetylides from 1-alkynes,<sup>3</sup> and for reversibly binding carbon dioxide.<sup>4</sup>

In a continuation of our work on the reactivity of phosphino esters  $\text{R}_2\text{PCH}_2\text{CO}_2\text{R}'$  toward  $d^6$  and  $d^8$  metal centers,<sup>5</sup> we have recently developed a synthetic route to the trifunctional phosphines  $\text{RP}(\text{CH}_2\text{CO}_2\text{R}')_2$  and started to investigate their coordination capabilities.<sup>6</sup> Here we describe the synthesis of (mesitylene)ruthenium(II) complexes containing the potentially tridentate monophosphine  $\text{RP}(\text{CH}_2\text{CO}_2\text{Me})_2$  and the remarkable conversion of this molecule to a novel unsymmetrical

$\eta^3(\text{P},\text{C},\text{O})$ -bonded tripod-type ligand. A first example of isocyanate insertion into one of the  $\text{C}-\text{H}$  bonds of the dianionic ligand will also be reported.

The phosphines **2a,b**, which were prepared according to a recently published method by heating  $\text{RP}(\text{SiMe}_3)_2$  ( $\text{R} = i\text{Pr}, t\text{Bu}$ ) with 2 equiv of  $\text{ClCH}_2\text{CO}_2\text{Me}$  in benzene,<sup>7</sup> readily react with the dimeric starting material **1** in dichloromethane to afford the mononuclear air-stable dichlororuthenium(II) complexes **3a,b**.<sup>8</sup> Treatment of **3a,b** with 2 equiv of  $\text{AgPF}_6$  results in the abstraction of both chlorides to yield the dicationic derivatives **4a,b**, in which the intact phosphine behaves as a tridentate bis-chelating ligand.<sup>9</sup> The structural proposal shown in Scheme 1 is supported by the spectroscopic data as well as by conductivity measurements.<sup>9</sup> Since there is only one carbonyl stretching frequency at  $1621\text{ cm}^{-1}$  (**4a**) and  $1609\text{ cm}^{-1}$  (**4b**) which is lowered by about  $110\text{ cm}^{-1}$  compared with the frequency for the monodentate phosphine in **3a,b**, the IR spectra in particular leave no doubt that both ester units are linked to the metal center.

(5) (a)  $d^6$ ,  $\text{M} = \text{Ru}$ : Werner, H.; Stark, A.; Schulz, M.; Wolf, J. *Organometallics* **1992**, *11*, 1126-1130. Werner, H.; Stark, A.; Steinert, P.; Grünwald, C.; Wolf, J. *Chem. Ber.* **1995**, *128*, 49-62. Braun, T.; Steinert, P.; Werner, H. *J. Organomet. Chem.* **1995**, *488*, 169-176. (b)  $d^6$ ,  $\text{M} = \text{Os}$ : Werner, H.; Weber, B.; Nürnberg, O.; Wolf, J. *Angew. Chem.* **1992**, *104*, 1105-1107; *Angew. Chem., Int. Ed. Engl.* **1992**, *31*, 1025-1027. Weber, B.; Steinert, P.; Windmüller, B.; Wolf, J.; Werner, H. *J. Chem. Soc., Chem. Commun.* **1994**, 2595-2596. (c)  $d^8$ ,  $\text{M} = \text{Rh}$ : Wolfsberger, W.; Burkart, W.; Bauer, S.; Hampp, A.; Wolf, J.; Werner, H. *Z. Naturforsch., B: Anorg. Chem., Org. Chem.* **1994**, *49*, 1659-1673. (d)  $d^8$ ,  $\text{M} = \text{Ir}$ : Steinert, P.; Werner, H. *Organometallics* **1994**, *13*, 2677-2681.

(6) For other preparative methods to obtain the phosphino esters  $\text{RP}(\text{CH}_2\text{CO}_2\text{R}')_2$  see: (a) Proskurina, M. V.; Lutsenko, J. F.; Novikova, Z. S.; Voronova, N. P. *Otd. Obshch. Tekh. Khim.* **1967**, 8-10. (b) Bouaoud, S.-E.; Braunstein, P.; Grandjean, D.; Matt, D.; Nobel, D. *Inorg. Chem.* **1986**, *25*, 3765-3770. (c) Podlaha, J.; Jegerov, A.; Budesinsky, M.; Hanus, V. *Phosphorus Sulfur Relat. Elem.* **1988**, *37*, 87-93.

(7) Wolfsberger, W.; Bank, J.; Werner, H. *Z. Naturforsch., B: Anorg. Chem., Org. Chem.*, in press.

(8) (a) By the procedure described for  $[(\text{mes})\text{RuCl}_2(\text{PMe}_2\text{Ph})]$ ,<sup>5b</sup> compounds **3a,b** were isolated as red-brown air-stable solids in 90-95% yield. (b) Bennett, M. A.; Smith, A. K. *J. Chem. Soc., Dalton Trans.* **1974**, 233-241.

(9) The preparation of **4a** is as follows. A solution of **3a** (243 mg, 0.47 mmol) in 20 mL of  $\text{CH}_2\text{Cl}_2$  was treated with  $\text{AgPF}_6$  (240 mg, 0.95 mmol) and stirred for 30 min at room temperature. The solvent was removed, the residue was extracted with 20 mL of acetone, and the extract was brought to dryness in vacuo. An orange solid was obtained, which was repeatedly washed with small amounts of THF and dried: yield 271 mg (78%); mp  $157\text{ }^\circ\text{C}$  dec; conductivity (in  $\text{CH}_3\text{NO}_2$ )  $\Lambda = 108\text{ cm}^2\text{ }\Omega^{-1}\text{ mol}^{-1}$ . Anal. Calcd for  $\text{C}_{15}\text{H}_{25}\text{F}_{12}\text{O}_4\text{P}_3\text{Ru}$ : C, 29.56; H, 4.00. Found: C, 29.69; H, 4.25. Compound **4b** was prepared analogously: orange solid; yield 80%; mp  $167\text{ }^\circ\text{C}$  dec;  $\Lambda = 116\text{ cm}^2\text{ }\Omega^{-1}\text{ mol}^{-1}$ . Anal. Calcd for  $\text{C}_{15}\text{H}_{31}\text{F}_{12}\text{O}_4\text{P}_3\text{Ru}$ : C, 30.61; H, 4.19. Found: C, 30.49; H, 4.06.

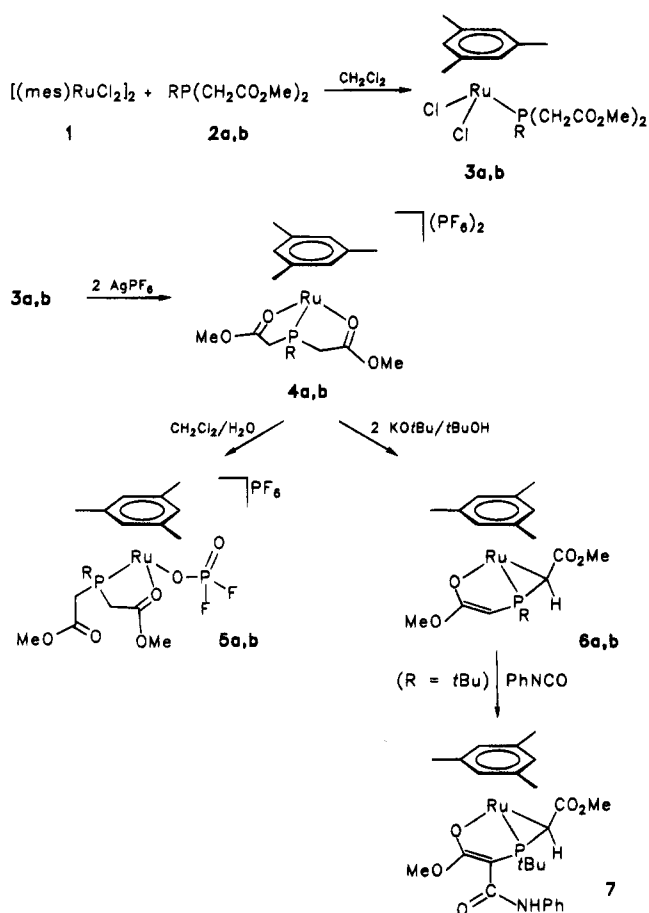
<sup>®</sup> Abstract published in *Advance ACS Abstracts*, October 1, 1995.

(1) Bader, A.; Lindner, E. *Coord. Chem. Rev.* **1991**, *108*, 27-110.

(2) (a) Bouaoud, S.-E.; Braunstein, P.; Grandjean, D.; Matt, D.; Nobel, D. *Inorg. Chem.* **1988**, *27*, 2279-2286. (b) Braunstein, P.; Gomes Carneiro, T. M.; Matt, D.; Balegroune, F.; Grandjean, D. *Organometallics* **1989**, *8*, 1737-1743. (c) Braunstein, P.; Nobel, D. *Chem. Rev.* **1989**, *89*, 1927-1945.

(3) Perera, S. D.; Shaw, B. L.; Thornton-Pett, M.; Vessey, J. D. *Inorg. Chim. Acta* **1992**, *198-200*, 149-158.

(4) (a) Braunstein, P.; Matt, D.; Dusausoy, Y.; Fischer, J.; Mitschler, A.; Ricard, L. *J. Am. Chem. Soc.* **1981**, *103*, 5115-5125. (b) Braunstein, P.; Matt, D.; Nobel, D. *Chem. Rev.* **1988**, *88*, 747-764.

Scheme 1<sup>a</sup>

In polar solvents such as dichloromethane, in the presence of small amounts of water, partial hydrolysis of the hexafluorophosphate anion of **4a,b** occurs leading to the monocationic (difluorophosphinato)ruthenium(II) complexes **5a,b** in almost quantitative yield.<sup>10</sup> Such a transition-metal-mediated conversion of  $\text{PF}_6^-$  to  $\text{PO}_2\text{F}_2^-$  is not without precedent<sup>11</sup> and with (arene)ruthenium compounds has been observed in the formation of  $[(\text{C}_6\text{Me}_6\text{Ru})_2(\mu\text{-O}_2\text{PF}_2)_3]\text{PF}_6$  from  $[(\text{C}_6\text{Me}_6\text{Ru}(\text{acetone}))_3](\text{PF}_6)_2$ .<sup>12</sup> The X-ray structural analysis of **5b** reveals<sup>13</sup> that the phosphino diester is bonded to ruthenium in a

(10) The preparation of **5a** was analogous to that described for **4a**, but the reaction mixture was stirred for 12 h at room temperature. Trace amounts of water were introduced from either  $\text{CH}_2\text{Cl}_2$  or the glass surface. After recrystallization from  $\text{CH}_2\text{Cl}_2/\text{OEt}_2$  (1:5), orange-red crystals were isolated: yield 90%; mp 168 °C dec;  $\Lambda = 84 \text{ cm}^2 \Omega^{-1} \text{ mol}^{-1}$ . Anal. Calcd for  $\text{C}_{18}\text{H}_{29}\text{F}_9\text{O}_6\text{P}_3\text{Ru}$ : C, 31.45; H, 4.25. Found: C, 31.37; H, 4.27. IR ( $\text{CH}_2\text{Cl}_2$ ):  $\nu(\text{C}=\text{O})_{\text{uncoord}} 1721$ ,  $\nu(\text{C}=\text{O})_{\text{coord}} 1609 \text{ cm}^{-1}$ . <sup>31</sup>P NMR (81.0 MHz,  $d_6$ -acetone):  $\delta$  50.0 (d,  $J(\text{PP}) = 4.4 \text{ Hz}$ ,  $i\text{PrP}(\text{CH}_2\text{CO}_2\text{Me})_2$ ), -12.7 (ddd,  $J(\text{PF}) = 970.7$  and  $957.6$ ,  $J(\text{PP}) = 4.4 \text{ Hz}$ ,  $\text{PO}_2\text{F}_2$ ), -142.7 (sept,  $J(\text{PF}) = 707.7 \text{ Hz}$ ,  $\text{PF}_6^-$ ). Compound **5b** was prepared analogously: orange-red solid; yield 91%; mp 166 °C dec;  $\Lambda = 82 \text{ cm}^2 \Omega^{-1} \text{ mol}^{-1}$ . Anal. Calcd for  $\text{C}_{19}\text{H}_{31}\text{F}_8\text{O}_6\text{P}_3\text{Ru}$ : C, 32.53; H, 4.45; Ru, 14.41. Found: C, 32.85; H, 4.46; Ru, 14.77. IR (KBr):  $\nu(\text{C}=\text{O})_{\text{uncoord}} 1722$ ,  $\nu(\text{C}=\text{O})_{\text{coord}} 1609 \text{ cm}^{-1}$ . <sup>31</sup>P NMR (81.0 MHz,  $d_6$ -acetone):  $\delta$  52.7 (d,  $J(\text{PP}) = 2.9 \text{ Hz}$ ,  $t\text{BuP}(\text{CH}_2\text{CO}_2\text{Me})_2$ ), -13.1 (ddd,  $J(\text{PF}) = 972.5$  and  $963.6$ ,  $J(\text{PP}) = 2.9 \text{ Hz}$ ,  $\text{PO}_2\text{F}_2$ ), -142.7 (sept,  $J(\text{PF}) = 707.7 \text{ Hz}$ ,  $\text{PF}_6^-$ ).

(11) (a) White, C.; Thompson, S. J.; Maitlis, P. M. *J. Organomet. Chem.* **1977**, *134*, 319–325. (b) Wimmer, F. L.; Snow, M. R. *Aust. J. Chem.* **1978**, *31*, 267–278. (c) Smith, G.; Cole-Hamilton, D. J.; Gregory, A. C.; Gooden, N. G. *Polyhedron* **1982**, *1*, 97–103. (d) Holland, P. R.; Howard, B.; Mawby, R. J. *J. Chem. Soc., Dalton Trans.* **1983**, 231–237. (e) Bauer, H.; Nagel, U.; Beck, W. *J. Organomet. Chem.* **1985**, *290*, 219–229. (f) Fernandez-Galan, R.; Manzano, B. R.; Otero, A.; Lanfranchi, M.; Pellinghelli, M. A. *Inorg. Chem.* **1994**, *33*, 2309–2312.

(12) Bennett, M. A.; Matheson, T. W.; Robertson, G. B.; Steffen, W. L.; Turney, T. W. *J. Chem. Soc., Chem. Commun.* **1979**, 32–33.

$\eta^2(\text{P},\text{O})$  mode, forming one five-membered chelate ring and leaving one  $\text{CH}_2\text{CO}_2\text{Me}$  group uncoordinated.

Compounds **4a,b** react with 2 equiv of  $\text{KOtBu}$  in 2-methyl-2-propanol to give the very moisture-sensitive neutral complexes **6a,b** in good yields.<sup>14</sup> Quite unexpectedly, the two  $\text{PCHCO}_2\text{Me}$  units in **6a,b** are not equally bonded to the metal center, which is illustrated by the IR and NMR spectroscopic data. While one chelating moiety forms a five-membered phosphino enolate ring resulting from O-metalation of one  $\text{PCHCO}_2\text{Me}$  unit, the other one constitutes a three-membered phosphinomethanide fragment which is the C-metalation product. We note that complexes with a  $\text{Ru}\{\eta^2(\text{P},\text{C})\text{-Me}_2\text{PCH}_2\}$  moiety but without an arene ligand are well-known<sup>15</sup> and have recently been used for the synthesis of monomeric hydroxo, phenolato, and amido ruthenium derivatives.<sup>16</sup>

The structure of **6a** has been confirmed by an X-ray crystal structure analysis (Figure 1).<sup>17</sup> The five-membered (phosphino enolate)metal unit is nearly planar, with the  $\text{OCH}_3$  substituent lying in the ring plane. The electron delocalization within the enolate ring is indicated by the short distances  $\text{P}-\text{C}_2$  and  $\text{C}_1-\text{C}_2$  and by the  $\text{C}_1-\text{O}_1$  bond length, which is between a  $\text{C}-\text{O}$  single and a  $\text{C}=\text{O}$  double bond. The interatomic bond distances and angles of the three-membered phosphinomethanide–ruthenium fragment are comparable

(13) Windmüller, B. Ph.D. Thesis, University of Würzburg, in preparation.

(14) The preparation of **6a** is as follows. A suspension of **4a** (216 mg, 0.30 mmol) in 15 mL of toluene/ $t\text{BuOH}$  (1:1) was treated with  $\text{KOtBu}$  (66 mg, 0.60 mmol) and irradiated for 15 min at room temperature in an ultrasonic bath. The solvent was removed, the residue was extracted with 15 mL of diethyl ether, and the extract was brought to dryness in vacuo. A yellow oily material was obtained, which was suspended in 20 mL of hexane and stirred for 12 h at room temperature. A yellow solid was formed, which was repeatedly washed with hexane and dried: yield 78 mg (60%); mp 93 °C dec; MS (70 eV)  $m/z$  439 ( $\text{M}^+$ ). Anal. Calcd for  $\text{C}_{18}\text{H}_{27}\text{O}_4\text{PRu}$ : C, 49.20; H, 6.19. Found: C, 49.23; H, 6.09. IR ( $\text{C}_6\text{H}_6$ ):  $\nu(\text{OCO})_{\text{ester}}$  and  $\nu(\text{OCO})_{\text{enolate}}$  1661  $\text{cm}^{-1}$  (br). Compound **6b** was prepared analogously: yellow solid; yield 65%; mp 99 °C dec; MS (70 eV)  $m/z$  453 ( $\text{M}^+$ ). Anal. Calcd for  $\text{C}_{19}\text{H}_{29}\text{O}_4\text{PRu}$ : C, 50.32; H, 6.45. Found: C, 49.99; H, 6.37. IR ( $\text{C}_6\text{H}_6$ ):  $\nu(\text{OCO})_{\text{ester}}$  1687,  $\nu(\text{OCO})_{\text{enolate}}$  1646  $\text{cm}^{-1}$ . Selected NMR spectroscopic data: **6a**, <sup>1</sup>H NMR (400 MHz,  $\text{C}_6\text{D}_6$ )  $\delta$  3.45 (d,  $J(\text{PH}) = 12.9 \text{ Hz}$ ,  $\text{CH}$  of phosphino enolate), 1.67 (s,  $\text{CH}$  of phosphinomethanide), <sup>13</sup>C NMR (100.6 MHz,  $\text{C}_6\text{D}_6$ )  $\delta$  44.61 (d,  $J(\text{PC}) = 74.6 \text{ Hz}$ ,  $\text{CH}$  of phosphino enolate), 4.90 (d,  $J(\text{PC}) = 9.8 \text{ Hz}$ ,  $\text{CH}$  of phosphinomethanide); **6b**, <sup>1</sup>H NMR (400 MHz,  $\text{C}_6\text{D}_6$ )  $\delta$  3.55 (d,  $J(\text{PH}) = 11.2 \text{ Hz}$ ,  $\text{CH}$  of phosphino enolate), 1.69 (d,  $J(\text{PH}) = 15.3 \text{ Hz}$ ,  $\text{CH}$  of phosphinomethanide), <sup>13</sup>C NMR (100.6 MHz,  $d_6$ -acetone)  $\delta$  43.98 (d,  $J(\text{PC}) = 72.8 \text{ Hz}$ ,  $\text{CH}$  of phosphino enolate), -8.72 (d,  $J(\text{PC}) = 3.3 \text{ Hz}$ ,  $\text{CH}$  of phosphinomethanide).

(15) (a) Werner, H.; Werner, R. *J. Organomet. Chem.* **1981**, *209*, C60–C64. (b) Gotzig, J.; Werner, R.; Werner, H. *J. Organomet. Chem.* **1985**, *285*, 99–114.

(16) (a) Hartwig, J. F.; Andersen, R. A.; Bergman, R. G. *Organometallics* **1991**, *10*, 1875–1887. (b) Burn, M. J.; Fickes, M. G.; Hartwig, J. F.; Hollander, F. J.; Bergman, R. G. *J. Am. Chem. Soc.* **1993**, *115*, 5875–5876.

(17) (a) Crystals were obtained from toluene. Crystal data (from 23 reflections,  $10^\circ < \theta < 16^\circ$ ): triclinic, space group  $\text{P}\bar{1}$  (No. 2),  $a = 7.913(8) \text{ \AA}$ ,  $b = 10.195(11) \text{ \AA}$ ,  $c = 13.48(2) \text{ \AA}$ ,  $\alpha = 99.47(7)^\circ$ ,  $\beta = 103.91(7)^\circ$ ,  $\gamma = 111.92(5)^\circ$ ,  $V = 939(2) \text{ \AA}^3$ ,  $Z = 2$ ,  $D_{\text{calcd}} = 1.554 \text{ g cm}^{-3}$ ,  $\mu(\text{Mo K}\alpha) = 9.25 \text{ cm}^{-1}$ ; crystal size  $0.15 \times 0.20 \times 0.30 \text{ mm}$ . Solution details: Enraf-Nonius CAD4 diffractometer, Mo K $\alpha$  radiation (0.709 30 Å), graphite monochromator, zirconium filter (factor 15.4),  $T = 293 \text{ K}$ ,  $\omega$  scan, maximum  $2\theta = 53^\circ$ , 3456 reflections measured, 3181 independent, 3181 used for refinement ( $2\theta > I > 2\sigma(I)$ ); intensity data corrected for Lorentz and polarization effects; structure solved by direct methods (SHELXS-86);<sup>17b</sup> atomic coordinates and anisotropic thermal parameters refined by full-matrix least squares on  $F_o^2$  (SHELXL-93);<sup>17c</sup> positions of the hydrogen atoms calculated according to ideal geometry and used only in structure factor calculation;  $R = 0.028$ ,  $R_w = 0.0681$  for 2784 reflections with  $I > 2\sigma(I)$ ,  $R = 0.041$ ,  $R_w = 0.077$  for all 3181 data reflections; reflection/parameter ratio 14.2; residual electron density  $+0.487/-0.562 \text{ e \AA}^{-3}$ . (b) Sheldrick, G. M. SHELXS-86; Universität Göttingen, Göttingen, Germany, 1986. (c) Sheldrick, G. M. SHELXL-93; Universität Göttingen, Göttingen, Germany, 1993.

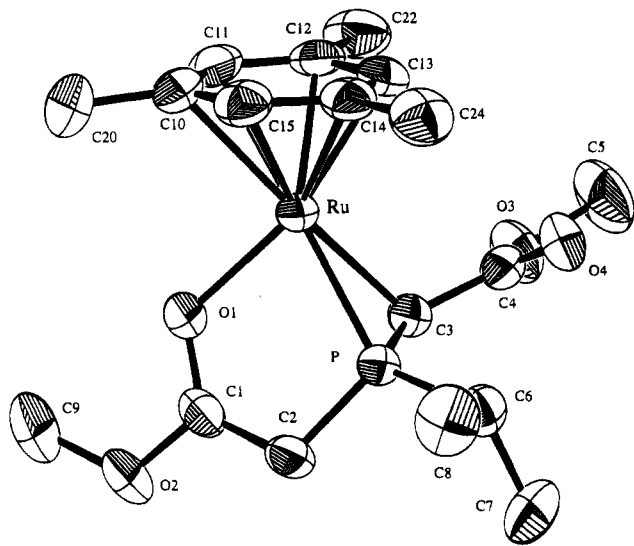


**Figure 1.** ORTEP diagram of compound **6a** (hydrogen atoms omitted for clarity). Selected bond distances (Å) and angles (deg): Ru–O1, 2.053(3); Ru–C3, 2.217(4); Ru–P, 2.301(2); O1–C1 1.295(5); C1–O2, 1.323(4); C1–C2, 1.394(5); P–C2, 1.671(4); P–C3, 1.727(4); P–C6, 1.884(4); C3–C4, 1.374(5); O1–Ru–C3, 88.03(14); O1–Ru–P, 80.65(11); C3–Ru–P, 44.91(11); Ru–O1–C1, 116.7(2); Ru–P–C2, 104.2(2); Ru–P–C3, 64.98(13); Ru–P–C6, 138.25(14); Ru–C3–C4, 111.3(3); Ru–C3–P, 70.11(13); O1–C1–C2, 127.7(3); O2–C1–C2, 118.0(3); O1–C1–O2, 114.2(3); C1–C2–P, 110.5(3); C2–P–C3, 106.1(2); C2–P–C6, 112.5(2); C3–P–C6, 119.8(2); P–C3–C4, 118.0(3).

to those found in  $[\text{Mn}(\text{CO})_4\{\eta^2(\text{P},\text{C})\text{-Ph}_2\text{PCH}_2\}]$ ,<sup>18a</sup>  $[\text{C}_5\text{H}_5\text{-Mo}(\text{CO})_2\{\eta^2(\text{P},\text{C})\text{-Ph}_2\text{PCH}_2\}]$ ,<sup>18b</sup> and  $[(\text{mes})\text{OsCl}\{\eta^2(\text{P},\text{C})\text{-}i\text{Pr}_2\text{PCHCO}_2\text{Me}\}]$ .<sup>18c</sup>

Preliminary studies on the reactivity of **6a,b** indicate that the novel P,C,O-coordinated tripodal ligand can be transformed into substituted derivatives. Thus, on treatment of **6b** with PhNCO, compound **7** is formed

by insertion of the isocyanate into the C–H bond of the phosphino enolate ring.<sup>19,20</sup> Even in the presence of excess PhNCO, no further insertion into the C–H bond of the phosphinomethanide unit and also no enlargement of the RuPC three-membered ring takes place. Work in progress is mainly aimed at further substituting the coordinated P,C,O-tripodal ligand and converting the dianionic unit of **6a,b** or **7** into a tri- or tetrafunctional chiral phosphine.

**Acknowledgment.** We gratefully acknowledge financial support from the Deutsche Forschungsgemeinschaft (Grant No. SFB 347), the Fonds der Chemischen Industrie, and Degussa AG. We are also grateful to Prof. P. Braunstein and Dipl. Chem. G. Henig for helpful discussions.

**Supporting Information Available:** Tables of crystallographic data, data collection, and solution and refinement details, positional and thermal parameters, and bond distances and angles for **6a** (6 pages). Ordering information is given on any current masthead page.

OM9505367

(18) (a) Lindner, E.; Starz, K. A.; Eberle, H.-J.; Hiller, W. *Chem. Ber.* **1983**, *116*, 1209–1218. (b) Lindner, E.; Küster, E. U.; Hiller, W.; Fawzi, R. *Chem. Ber.* **1984**, *117*, 127–141. (c) Henig, G.; Peters, K. Unpublished results.

(19) The preparation of **7** is as follows. A solution of **6b** (63 mg, 0.14 mmol) in 10 mL of toluene was treated with PhNCO (33 mg, 0.28 mmol) and stirred for 2 h at room temperature. The solvent was removed and the residue was repeatedly washed with hexane and dried: yield 56 mg (70%); mp 124 °C dec; MS (70 eV)  $m/z$  572 ( $M^+$ ). Anal. Calcd for  $\text{C}_{26}\text{H}_{34}\text{NO}_5\text{PRu}$ : C, 54.54; H, 5.99; N, 2.45. Found: C, 53.96; H, 5.77; N, 2.89. IR ( $\text{CH}_2\text{Cl}_2$ ):  $\nu(\text{NH})$  3380,  $\nu(\text{OCO})_{\text{ester}}$  1679,  $\nu(\text{OCO})_{\text{enolate}}$  1628  $\text{cm}^{-1}$ . Selected NMR spectroscopic data:  $^1\text{H}$  (400 MHz,  $\text{CDCl}_3$ )  $\delta$  9.10 (s, NH), 1.76 (d,  $J(\text{PH}) = 14.8$  Hz, CH of phosphinomethanide);  $^{13}\text{C}$  NMR (100.6 MHz,  $\text{C}_6\text{D}_6$ )  $\delta$  176.15 (d,  $J(\text{PC}) = 28.0$  Hz, OCOMe), 173.94 (s, C=O), 165.48 (d,  $J(\text{PC}) = 4.9$  Hz,  $\text{CO}_2\text{Me}$ ), 69.30 (d,  $J(\text{PC}) = 67.0$  Hz, PC=C), –3.52 (d,  $J(\text{PC}) = 2.8$  Hz, PCH).

(20) A few other examples of PhNCO insertion reactions into C–H bonds have been described by Braunstein et al.<sup>2a,c</sup>

## Selenoarsenation of Alkynes

Takahiro Kanda, Tadashi Koike, Susumu Kagohashi, Kazuaki Mizoguchi, Toshiaki Murai, and Shinzi Kato\*

Department of Chemistry, Faculty of Engineering, Gifu University,  
1-1 Yanagido, Gifu 501-11, JapanReceived September 1, 1995<sup>§</sup>

**Summary:** Carboxylic diphenylarsinous anhydroselenides were treated with phenylacetylene under reflux in benzene for 20 h to give the corresponding (*E*)-addition products in the range of 40–90% isolated yields with complete regio- and stereoselectivity.

During the course of our studies on selenic acid esters with a bond between selenium and a heavy heteroatom, we confirmed that selenic acid Se-arsanyl esters can be prepared and easily handled in air without appreciable decomposition.<sup>1–3</sup> This has prompted us to examine the reactivity of the Se–As bond toward C–C unsaturated bonds.<sup>4,5</sup> In this communication we describe the first example of selenoarsenation of alkynes with complete regio- and stereoselectivity (eq 1).

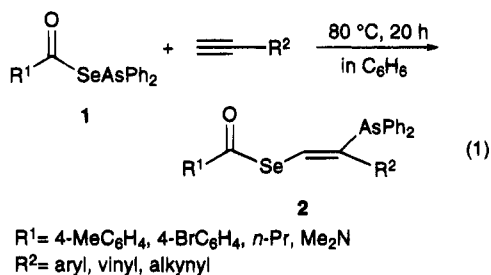


Table 1 summarizes our results on the selenoarsenation of conjugated alkynes. In one such reaction, an equimolar mixture of **1a** and phenylacetylene was stirred in benzene at reflux for 20 h. Removal of the

Table 1. Selenoarsenation of Alkynes<sup>a</sup>

entry	R <sup>1</sup>	R <sup>2</sup>	2, % <sup>b</sup>
1	4-MeC <sub>6</sub> H <sub>4</sub>	Ph	<b>2a</b> , 93, 63 <sup>c</sup>
2		4-MeC <sub>6</sub> H <sub>4</sub>	<b>2b</b> , 88
3		4-MeOC <sub>6</sub> H <sub>4</sub>	<b>2c</b> , 60, 32 <sup>c</sup>
4		4-ClC <sub>6</sub> H <sub>4</sub>	<b>2d</b> , 58, 35 <sup>c</sup>
5		Me	<b>2e</b> , 30
6			<b>2f</b> , 98, 89 <sup>c</sup>
7		PenC≡C- <sup>d</sup>	<b>2g</b> , 22
8	4-BrC <sub>6</sub> H <sub>4</sub>	Ph	<b>2h</b> , 50
9	<i>n</i> -Pr	Ph	<b>2i</b> , 40
10	Me <sub>2</sub> N	Ph	<b>2j</b> , 80, 60 <sup>c</sup>

<sup>a</sup>Conditions: **1** (0.5 mmol), alkyne (0.5 mmol), benzene (2 mL), reflux, 20 h. <sup>b</sup>Isolated yield. <sup>c</sup>Reaction was carried out at 20 °C. <sup>d</sup>Pen = *n*-pentyl.

solvent and subsequent recrystallization (hexane/CH<sub>2</sub>-Cl<sub>2</sub> = 1/1) gave the addition product **2a** in 93% isolated yield (entry 1).<sup>6</sup> <sup>1</sup>H and <sup>13</sup>C NMR studies showed that adduct **2a** was a single isomer (of four possible regio- and stereoisomers). In a difference NOE experiment, irradiation of the singlet at δ 7.18 corresponding to the vinylic proton gave 9% and 5% enhancement of only the aromatic protons at δ 7.45–7.61 (multiplet) and δ 7.67 (doublet), respectively (Figure 1).<sup>7</sup> This suggests that both the arsenic and selenium substituents are attached to the internal and terminal carbon atoms of the

(6) A typical procedure for selenoarsenation of alkynes (entry 1 in Table 1) follows: Into a dried, two-necked flask (10 mL) equipped with a reflux condenser were placed **1a** (0.5 mmol), phenylacetylene (0.5 mmol), benzene (2 mL), and a magnetic stirring bar. The mixture was heated under reflux for 20 h and concentrated in vacuo. The <sup>1</sup>H and <sup>13</sup>C NMR spectra (CDCl<sub>3</sub>) of the resulting crude product depicted the formation of a single isomer (*E*-addition product). By recrystallization with a mixed solvent [CH<sub>2</sub>Cl<sub>2</sub>/hexane = 1/1 (2 mL)], **2a** (0.47 mmol, 93%) was obtained pure as pale yellow needles.

(7) Spectral data for **2a** are as follows: pale yellow needles; mp 89–92 °C; IR (KBr) 1689 (C=O), 1654 (C=C) cm<sup>-1</sup>; <sup>1</sup>H NMR (CDCl<sub>3</sub>, 270 MHz) δ 2.33 (s, 3 H, CH<sub>3</sub>C<sub>6</sub>H<sub>4</sub>), 7.16 (d, *J* = 8.2 Hz, 2H, MeC<sub>6</sub>H<sub>4</sub>), 7.18 (s, 1 H, =CH), 7.21–7.29 (m, 5 H, Ph), 7.33–7.43 (m, 6 H, AsPh), 7.45–7.61 (m, 4 H, AsPh), 7.67 (d, *J* = 8.2 Hz, 2 H, MeC<sub>6</sub>H<sub>4</sub>); <sup>13</sup>C NMR (CDCl<sub>3</sub>, 68 MHz) δ 21.7, 126.7, 127.4, 127.5, 127.6, 128.4, 128.8, 129.5, 134.0, 136.0, 138.5, 142.3, 144.4, 144.9, 191.6; MS (CI, rel int, %) *m/e* 529 (<sup>80</sup>Se, M<sup>+</sup> + 1, 100). Anal. Calcd for C<sub>28</sub>H<sub>23</sub>AsOSe: C, 63.53; H, 4.38. Found: C, 63.56; H, 4.31.

(8) In order to grow larger crystals, a portion was dissolved in a small amount of ethyl acetate (0.5 mL), and to this hexane (1.5 mL) was carefully added to form a layer under an argon atmosphere. Crystals for X-ray structural analysis were obtained.

(9) Selected crystallographic data for **2a** (C<sub>28</sub>H<sub>23</sub>AsOSe; *M<sub>n</sub>* = 529.37): *I*<sub>4</sub><sup>1</sup>/*a* (No. 88, triclinic), *a* = 40.86(2) Å, *c* = 6.021(2) Å, *V* = 10052(19) Å<sup>3</sup>, *Z* = 16, ρ = 1.399 g cm<sup>-3</sup>, μ(Mo Kα) 28.18 cm<sup>-1</sup>, *R* (*R<sub>w</sub>*) = 0.056 (0.082). A total of 5285 reflections (2θ<sub>max</sub> = 55.0°) were collected on a Rigaku AFC7R diffractometer at 296 K using Mo Kα radiation (λ = 0.710 69 Å); an absorption correction using the program DIFABS was applied that resulted in transmission factors ranging from 0.58 to 1.19. The structure was solved by direct methods (SHELXS86) with the C, O, As, and Se atoms refined anisotropically.

<sup>§</sup> Abstract published in *Advance ACS Abstracts*, November 1, 1995.

(1) (a) Kageyama, H.; Kido, K.; Kato, S.; Murai, T. *J. Chem. Soc., Perkin Trans. 1* **1994**, 1083. (b) Kato, S.; Kageyama, H.; Kawahara, Y.; Murai, T.; Ishihara, H. *Chem. Ber.* **1992**, *125*, 417. (c) Kato, S.; Ibi, K.; Kageyama, H.; Ishihara, H.; Murai, T. *Z. Naturforsch.* **1992**, *47B*, 558.

(2) (a) Kanda, T.; Mizoguchi, K.; Koike, T.; Murai, T.; Kato, S. *Synthesis* **1994**, 282. (b) Kanda, T.; Mizoguchi, K.; Koike, T.; Murai, T.; Kato, S. *J. Chem. Soc., Chem. Commun.* **1993**, 1631.

(3) For reviews on organoarsenic selenium derivatives: (a) du Mont, W. W.; Hensel, R.; Kubiniok, S.; Lange, L. In *The Chemistry of Organic Selenium and Tellurium Compounds*; Patai, S., Rappoport, Z., Eds.; John Wiley & Sons: New York, 1987; Vol. 2, Chapter 15, pp 591–656. (b) Barton, D. H. R.; Dadoun, H.; Gourdon, A. *Nouv. J. Chim.* **1982**, *6*, 53. (c) Dehnert, P.; Grobe, J.; Hildebrandt, W.; Van, Duc le Z. *Naturforsch.* **1980**, *35B*, 149. (d) Chen, G. C.; Daniel, J. R.; Zingaro, R. A. *Carbohydr. Res.* **1976**, *50*, 53. (e) Chen, G. C.; Zingaro, R. A.; Thompson, C. R. *Carbohydr. Res.* **1975**, *39*, 61. (f) Anderson, J. W.; Drake, J. E.; Hemmings, R. T.; Nelson, D. L. *Inorg. Nucl. Chem. Lett.* **1975**, *11*, 233. (g) Sagan, L. S.; Zingaro, R. A.; Irgolic, K. J. *J. Organomet. Chem.* **1972**, *39*, 301.

(4) Heats of dissociation of the Se–As bond in AsSe and As<sub>2</sub>Se<sub>3</sub> are quite low (22.2 and 39.1 kcal/mol, respectively): Pelevin, O. V.; Mil'vidskii, M. G.; Belyaev, A. H.; Khotin, B. A. *Izv. Akad. Nauk. SSSR Neorg. Mater.* **1966**, *2*, 942; *Chem. Abstr.* **1966**, *65*, 4721d.

(5) To the best of our knowledge, no examples of additions of As–S, As–Se, and As–Te bonds to C–C unsaturated compounds have been reported. For examples of additions of As–Y bonds (Y: heteroelement) to olefins see the following. (a) Y = As: Cullen, W. R.; Dhaliwal, P. S.; Styan, G. E. *J. Organomet. Chem.* **1966**, *6*, 364. (b) Cullen, W. R.; Hota, N. K. *Can. J. Chem.* **1964**, *42*, 1123. For examples of addition to acetylenes see the following. (c) Y = As: Cullen, W. R.; Styan, G. E. *Can. J. Chem.* **1966**, *44*, 1225. (d) Y = Si: Cullen, W. R.; Dawson, D. S.; Styan, G. E. *Can. J. Chem.* **1965**, *43*, 3392.

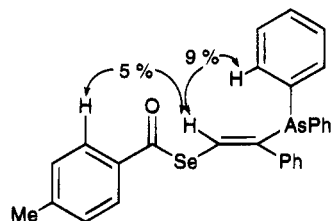


**Figure 1.** Enhancement of the peaks by irradiation of the vinylic proton of **2a** in  $^1\text{H}$  NMR.

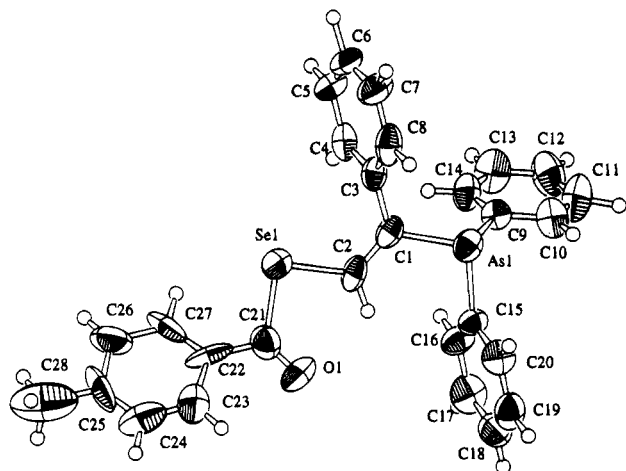


**Figure 2.** ORTEP drawing of the molecular structure of **2a**. Selected bond lengths (Å) and bond angles (deg): C1–C2 1.34(2), As1–C1 1.96(1), C1–C3 1.49(2), Se1–C2 1.89(1), As1–C15 1.95(1), As1–C9 1.96(1), O1–C21 1.15(2); As1–C1–C3 114(1), As1–C1–C2 122(1), Se1–C2–C1 124(1), C1–As1–C9 102.9(6), C9–As1–C15 96.9(5), C2–Se1–C21 93.2(7), Se1–C21–O1 123(1).

starting acetylene with *E*-stereochemistry. This structure was confirmed by an X-ray single-crystal diffraction analysis (Figure 2).<sup>8,9</sup> The X-ray structure reveals that the vinylic structure of **2a** is distorted because of steric repulsion between the substituents.<sup>10</sup>

The selenoarsenylation of aromatic acetylenes proceeded smoothly at reflux in benzene until the ester **1a**

was completely consumed, whereas similar reactions at 20 °C resulted in recoveries of **1a** (30–40%, entries 1, 3, 4). In the case of 1-ethynylcyclohexene, the addition went to completion even at 20 °C (entry 6). In the reactions with conjugated enynes and diynes, the corresponding dienes **2e,f** and enyne **2g** were obtained selectively, indicating that the olefinic and internal acetylenic functionalities remained intact, respectively (entries 5–7). 4-Bromobenzoyl (**1h**), butyroyl (**1i**), and carbamoyl derivatives (**1j**) were suitable reagents for the selenoarsenylation, affording the corresponding addition products **2h–j** in modest isolated yields (entries 8–10). The structures of products **2b–j** also were determined by NOE studies similar to that with **2a** (Supporting Information). Unfortunately, similar reactions of the esters **1** with olefins and terminal alkynes conjugated to electron-withdrawing groups such as carbonyl or nitrile hardly proceeded.

In summary, we have found that selenoic acid *Se*-arsanyl esters add to terminal alkynes conjugated with an olefinic, aromatic, or acetylenic substituent in refluxing benzene with complete regio- and stereoselectivity. The selenoarsenylation reaction is a useful addition to synthetic organoarsenic and organoselenium chemistry.

**Acknowledgment.** We thank Dr. Ebihara and Prof. Kawamura of Gifu University for helpful assistance with X-ray analysis. This work was supported by the Grant-in-Aid for Scientific Research (B) (No. 06453127) and partially by the Grant-in-Aid for Scientific Research on Priority Area of Reactive Organometallics (No. 07216228) from the Ministry of Education, Science, Sports and Culture of Japan.

**Supporting Information Available:** Text giving experimental details and characterization data for **1b–d** and **2b–j** and listings of crystallographic data (positional and thermal parameters and bond distances and angles) and a packing diagram for the addition product **2a** (13 pages). This material is contained in many libraries on microfiche, immediately follows this article in microfilm version of the journal, can be ordered from ACS, and can be downloaded from the Internet; see any current masthead page for ordering information and Internet access instructions.

(10) Such a distorted structure is readily confirmed by the torsion angles [Se1–C2–C1–As1 = 170.2°, O1–C21–Se1–C2 = 4(2)°].

## Diastereoselectivity and Regioselectivity in the Intramolecular Phosphine Attack on a Coordinated Alkyne Ligand in $\text{Co}_2(\text{CO})_4(\text{bmf})(\mu\text{-PhC}\equiv\text{C}\text{Ph})$ . Formation of the Chiral Hydrocarbyl Complex $\text{Co}_2(\text{CO})_4[\mu\text{-}\eta^2\text{-}\eta^2\text{-}\eta^1\text{-}\eta^1\text{-PhC:C(H)PPh}_2\text{C:C(PPh}_2\text{)C(O)OCH(OMe)}]$

Kaiyuan Yang, Simon G. Bott, and Michael G. Richmond

*Organometallics*, 1995, 14 (11), 4977-4979 • DOI: 10.1021/om00011a004 • Publication Date (Web): 01 May 2002

Downloaded from <http://pubs.acs.org> on March 9, 2009

### More About This Article

---

The permalink <http://dx.doi.org/10.1021/om00011a004> provides access to:

- Links to articles and content related to this article
- Copyright permission to reproduce figures and/or text from this article



ACS Publications  
High quality. High impact.



# Diastereoselectivity and Regioselectivity in the Intramolecular Phosphine Attack on a Coordinated Alkyne Ligand in $\text{Co}_2(\text{CO})_4(\text{bmf})(\mu\text{-PhC}\equiv\text{CH})$ . Formation of the Chiral Hydrocarbyl Complex



Kaiyuan Yang, Simon G. Bott,\* and Michael G. Richmond\*

Center for Organometallic Research and Education, Department of Chemistry,  
University of North Texas, Denton, Texas 76203

Received June 16, 1995<sup>®</sup>

**Summary:** The reaction between the alkyne-bridged compound  $\text{Co}_2(\text{CO})_6(\mu\text{-PhC}\equiv\text{CH})$  and the diphosphine ligand 3,4-bis(diphenylphosphino)-5-methoxy-2(5H)-furanone (bmf) affords the chelating diphosphine complex  $\text{Co}_2(\text{CO})_4(\text{bmf})(\mu\text{-PhC}\equiv\text{CH})$  (**1**), which exists as a mixture of four diastereomers. Thermolysis of **1** leads to the formation of a single diastereomer of the zwitterionic hydrocarbyl-bridged compound  $\text{Co}_2(\text{CO})_4[\mu\text{-}\eta^2,\eta^2,\eta^1,\eta^1\text{-PhC}=\text{C}(\text{H})\text{PPh}_2\text{C}=\text{C}(\text{PPh}_2)\text{C}(\text{O})\text{OCH}(\text{OMe})]$  (**3**) as a result of the diastereoselective and regioselective attack of the  $\text{PPh}_2$  moiety that is conjugated with the keto moiety of the bmf ligand.

The use of transition-metal-complexed alkynes for the regioselective and stereoselective construction of new C-X (where X = C, N, O) bonds in a variety of acyclic and cyclic compounds of natural products continues to attract strong interest in both the organometallic and organic communities.<sup>1</sup> Undoubtedly, the Pauson-Khand<sup>2</sup> and Nicholas<sup>3,4</sup> reactions represent the two best-known reactions involving the metal-mediated functionalization of alkynes. The former cyclization reaction leads to the coupling of an alkyne, alkene, and CO, with the synthesis of a larger, more complex molecule, often with impressive regiochemical and stereochemical control, while the latter reaction affords propargylium complexes capable of conversion to propargylated compounds without the troublesome complications that plague the traditional organic sequences.

The activation of a coordinated alkyne to give a  $\mu\text{-}\eta^2\text{:}\eta^1$ -hydrocarbyl moiety has only recently been demonstrated,<sup>5,6</sup> and examples of diastereoselectivity in the formation of a chiral  $\mu\text{-}\eta^2\text{:}\eta^1$ -hydrocarbyl moiety are, to

our knowledge, unknown. The novelty of a chiral hydrocarbyl moiety, coupled with its potential synthetic use, prompts us to report our results on the diastereoselectivity and regioselectivity associated with the formation of the title dicobalt compound.

Treatment of  $\text{Co}_2(\text{CO})_6(\mu\text{-PhC}\equiv\text{CH})$  with the oxidative decarbonylation reagent  $\text{Me}_3\text{NO}$  in the presence of the diphosphine ligand 3,4-bis(diphenylphosphino)-5-methoxy-2(5H)-furanone,<sup>7</sup> hereafter called bmf, affords the chelating diphosphine complex  $\text{Co}_2(\text{CO})_4(\text{bmf})(\mu\text{-PhC}\equiv\text{CH})$  (**1**). On the basis of the IR and <sup>31</sup>P NMR data, binuclear **1** exists as a mixture of four diastereomers, all of which contain a chelating bmf ligand.<sup>8</sup> Moreover, binuclear **1** displays spectral properties nearly identical with those of related 2,3-bis(diphenylphosphino)maleic anhydride (bma) substituted complexes already prepared in our laboratories.<sup>6,9</sup> While many different chelating diastereomers of **1** may be envisioned, the relative stereochemistries of the four most likely ones are<sup>10-12</sup>

(5) Takats, J.; Washington, J.; Santarsiero, B. D. *Organometallics* 1994, 13, 1078.

(6) (a) Yang, K.; Bott, S. G.; Richmond, M. G. *Organometallics* 1994, 13, 3767. (b) Submitted for publication in *J. Organomet. Chem.* 1995.

(7) Fenske, D.; Becher, H. J. *Chem. Ber.* 1975, 108, 2115.

(8) Synthesis and spectroscopic data for **1**: In a Schlenk tube containing 0.30 g (0.77 mmol) of  $\text{Co}_2(\text{CO})_6(\mu\text{-PhC}\equiv\text{CH})$  and 0.37 g (0.77 mmol) of the diphosphine ligand bmf in 50 mL of THF was added 0.12 g (1.61 mmol) of  $\text{Me}_3\text{NO}$ . The reaction mixture was stirred at room temperature for 1.5 h and then examined by TLC and IR analyses, which revealed the presence of the desired product. Solvent removal under vacuum, followed by chromatography over silica gel using  $\text{CH}_2\text{Cl}_2$ /petroleum ether (2:1), afforded the crude product. Recrystallization of **1** from  $\text{CH}_2\text{Cl}_2$ /heptane (8:2) at 0 °C gave 0.35 g (56% yield) of green-black **1**. IR ( $\text{CH}_2\text{Cl}_2$ , 24 °C):  $\nu$  2044 (s), 1985 (vs), 1770 (m, bmf C=O)  $\text{cm}^{-1}$ . <sup>1</sup>H NMR ( $\text{CDCl}_3$ , 24 °C):  $\delta$  3.25, 3.33, 3.38, 3.40 (MeO, all singlets), 4.94 (dd, =CH,  $J = 8.40$  and 3.25 Hz) 5.10 (s, broad, =CH), 5.14 (s, broad, =CH), 5.27 (dd, =CH,  $J = 10.2$  and 2.12 Hz), 5.52, 5.62, 5.64, 5.70 (H, furanone ring, all singlets), 6.60–8.00 (aromatic multiplet). <sup>31</sup>P{<sup>1</sup>H} NMR (THF, -97 °C):  $\delta$  44.05 and 49.50, 52.89 and 56.94, 61.21 and 61.89, 66.91 and 67.61. Anal. Calcd (found) for  $\text{C}_{41}\text{H}_{30}\text{Co}_2\text{O}_7\text{P}_2$ : C, 60.46 (60.38); H, 3.71 (4.04).

(9) Yang, K.; Bott, S. G.; Richmond, M. G. *Organometallics* 1994, 13, 3788.

(10) As is customary with this genre of alkyne compounds, we show phosphine coordination at the pseudo-axial and pseudo-equatorial sites in **1** (see ref 11 for terminology and related structures). These diastereomers minimize unfavorable intramolecular contacts between the Ph group of the alkyne and the bmf ligand. Moreover, preliminary X-ray diffraction data on a weak crystal of **1** have already confirmed the presence of the diastereomers labeled as C and D.

(11) (a) Thorn, D. L.; Hoffmann, R. *Inorg. Chem.* 1978, 17, 126. (b) Cunningham, R. G.; Hanton, L. R.; Jensen, S. D.; Robinson, B. H.; Simpson, J. *Organometallics* 1987, 6, 1470. (c) Sappa, E.; Predieri, G.; Marko, L. *Inorg. Chim. Acta* 1995, 228, 147.

(12) All compounds shown are racemic, with only one enantiomer shown for clarity.

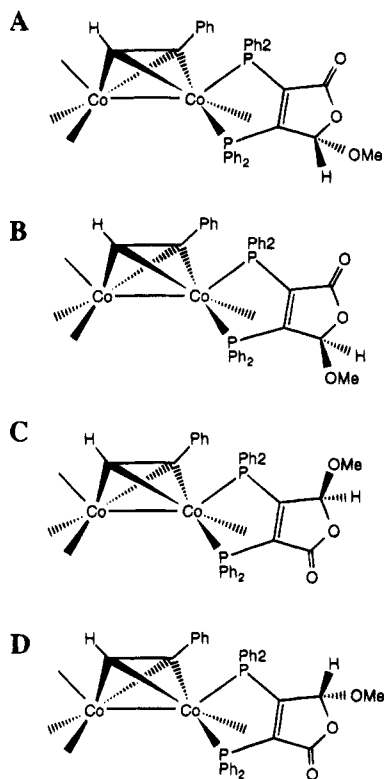
<sup>®</sup> Abstract published in *Advance ACS Abstracts*, October 1, 1995.

(1) (a) Harrington, P. J. *Transition Metals in Total Synthesis*; Wiley: New York, 1990. (b) Collman, J. P.; Hegedus, L. S.; Norton, J. R.; Finke, R. G. *Principles and Applications of Organotransition Metal Chemistry*; University Science Books: Mill Valley, CA, 1987.

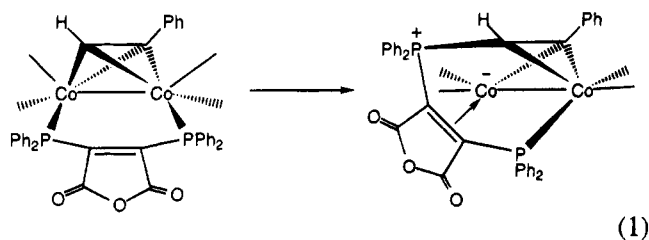
(2) (a) Pauson, P. L. *Tetrahedron* 1985, 41, 5855. (b) Krafft, M. E.; Juliano, C. A.; Scott, I. L.; Wright, C.; McEachin, M. D. *J. Am. Chem. Soc.* 1991, 113, 1693. (c) Krafft, M. A.; Scott, I. L.; Romero, R. H.; Feibelmann, S.; Van Pelt, C. E. *J. Am. Chem. Soc.* 1993, 115, 7199. (c) Jamison, T. F.; Shambayati, S.; Crowe, W. E.; Schreiber, S. L. *J. Am. Chem. Soc.* 1994, 116, 5505. (d) Jeong, N.; Hwang, S. H.; Lee, Y.; Chung, Y. K. *J. Am. Chem. Soc.* 1994, 116, 3159.

(3) (a) Nicholas, K. M. *Acc. Chem. Res.* 1987, 20, 207. (b) Bradley, D. H.; Khan, M. A.; Nicholas, K. M. *Organometallics* 1992, 11, 2598. (c) Caffyn, A. J. M.; Nicholas, K. M. *J. Am. Chem. Soc.* 1993, 115, 6438.

(4) (a) Schreiber, S. L.; Sammakia, T.; Crowe, W. E. *J. Am. Chem. Soc.* 1986, 108, 3128. (b) Schreiber, S. L.; Klimas, M. T.; Sammakia, T. *J. Am. Chem. Soc.* 1987, 109, 5749.



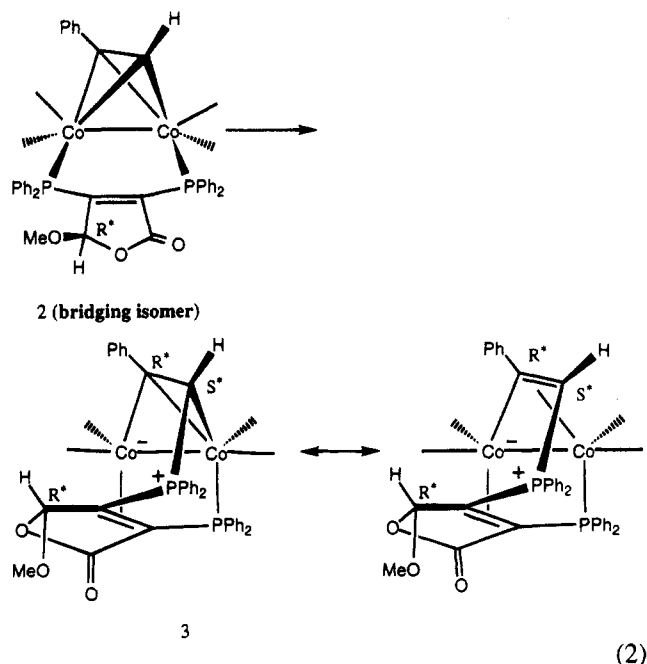
The thermolysis reactivity of **1** was next examined in 1,2-dichloroethane, because phosphine attack in the related complex  $\text{Co}_2(\text{CO})_4(\text{bma})(\mu\text{-PhC}\equiv\text{CH})$  has been shown to proceed by a chelate-to-bridge diphosphine conversion, followed by a rapid attack of the bridging diphosphine on the terminal carbon of the coordinated alkyne ligand to yield the corresponding zwitterionic hydrocarbyl-bridged complex (eq 1).<sup>6</sup>



Two key questions associated with the thermolysis reaction involving **1** need to be answered. First, would each chelating diastereomer react independently of the others in the P-C(alkyne) bond-forming step, and second, would any phosphine regiochemistry be observed, given the presence of inequivalent phosphines? *A priori*, we anticipated that the least basic  $\text{PPh}_2$  moiety (the one in conjugation with the keto group) should be more readily released and available for attack on the alkyne carbon.

A smooth transformation of **1** to the hydrocarbyl complex  $\text{Co}_2(\text{CO})_4[\mu\text{-}\eta^2\text{:}\eta^2\text{:}\eta^1\text{:}\eta^1\text{-}(Z)\text{-PhC}=\text{C}(\text{H})\text{PPh}_2\text{C}=\text{C}(\text{PPh}_2)\text{C}(\text{O})\text{OCH}(\text{OMe})]$  (**3**) was indeed observed, and to our surprise this reaction occurred with 100% diastereoselectivity and  $\text{PPh}_2$  regiochemistry. Added CO (100 psi) inhibits the conversion of **1** to **3**, which suggests that dissociative CO loss is a prerequisite for initiation of the required chelate-to-bridge bmf ligand reaction. Such an isomerization scheme has been shown to be

operative in the  $\text{PPh}_2$  attack on the alkyne ligand in  $\text{Co}_2(\text{CO})_4(\text{bma})(\mu\text{-PhC}\equiv\text{CH})$ <sup>6</sup> and P-C bond cleavage in  $\text{Co}_2(\text{CO})_4(\text{bma})(\mu\text{-PhC}\equiv\text{CPh})$ .<sup>9</sup> **3** was subsequently isolated and fully characterized in solution (IR and NMR) and by X-ray diffraction analysis.<sup>13</sup> The possibility of material loss and, hence, incomplete diastereomer characterization was addressed by repeating the thermolysis reaction of **1**  $\rightarrow$  **3** in  $\text{C}_6\text{D}_6$  in a sealed NMR tube containing *p*-(MeO)<sub>2</sub>C<sub>6</sub>H<sub>4</sub> as an internal standard. Here only one product was observed (>85%), which gave a <sup>1</sup>H NMR spectrum identical with that isolated from the preparative reaction. In analogy with the reaction conducted with the bma ligand, heating the diastereomeric mixture of **1** is also expected to give the transient bridging bmf isomer, followed by  $\text{PPh}_2$  attack on the terminal alkyne carbon (eq 2).<sup>14,15</sup>



The structure of **3** was unequivocally established by X-ray diffraction analysis.<sup>16</sup> Figure 1 shows the ORTEP diagram of **3** and confirms the regioselective migration of the least basic (i.e., weaker bound)  $\text{PPh}_2$  moiety associated with the bmf ligand to the terminal alkyne carbon of the coordinated phenylacetylene ligand. Moreover, the formation of the  $\mu\text{-}\eta^2\text{:}\eta^1\text{-hydrocarbyl}$  ligand is accompanied by 100% diastereoselectivity in this in-

(13) Synthesis and spectroscopic data for **3**: In a Schlenk tube containing 0.20 g (0.25 mmol) of the chelating isomer of **1** was added 20 mL of 1,2-dichloroethane, after which the solution was heated overnight at 75 °C. When the temperature was lowered, IR and TLC analyses revealed the presence of only the hydrocarbyl-bridged compound **3**. Purification by chromatography over silica gel using  $\text{CH}_2\text{Cl}_2$ /petroleum ether (3:1) as the eluant afforded the desired compound as a black solid. The analytical sample and single crystals suitable for X-ray diffraction analysis were grown from a  $\text{CH}_2\text{Cl}_2$  solution containing **3** that had been layered with hexane. Yield: 0.13 g (65%). IR ( $\text{CH}_2\text{Cl}_2$ , 24 °C):  $\nu(\text{CO})$  2023 (s), 1993 (vs), 1967 (s), 1955 (sh), 1735 (m, broad, C=O bmf)  $\text{cm}^{-1}$ . <sup>1</sup>H NMR ( $\text{CDCl}_3$ , 24 °C):  $\delta$  2.83 (MeO, s), 4.20 (dd, =CH,  $J = 38.16$  and  $7.23$  Hz), 4.31 (H, furanone ring, s), 7.00–8.10 (aromatic multiplet). <sup>31</sup>P{<sup>1</sup>H} NMR ( $\text{CDCl}_3$ , 24 °C):  $\delta$  4.58 (d,  $J = 85$  Hz, Co– $\text{PPh}_2$ ), 31.70 (d,  $J = 85$  Hz, HC–P). Anal. Calcd (found) for  $\text{C}_{41}\text{H}_{30}\text{Co}_2\text{O}_7\text{P}_2 \cdot 1/2\text{hexane} \cdot 1/2\text{THF}$ : C, 60.48 (61.04); H, 4.62 (4.26).

(14) The other enantiomer (*S,R,S*) observed in the unit cell of **3** is not shown.

(15) No mechanistic content is implied in the transformation given by eq 2. The possibility of this reaction proceeding by a coordinatively unsaturated species (i.e.,  $\text{Co}_2(\text{CO})_3(\text{bmf})(\mu\text{-PhC}\equiv\text{CH})$ ) is under investigation.

tramolecular P-ligand attack on the coordinated alkyne moiety. The zwitterionic nature of **3** requires a negative charge on Co(2) and a positive charge on P(2); the latter center is best described as a phosphonium center, given the tetrasubstituted nature of the P(2) atom. The maleic anhydride serves as a  $\eta^2$ -donor ligand in the product, which allows each cobalt center to achieve a coordinatively saturated state.

The presence of only one diastereomer of **3** suggests that the bmf ligand is equilibrated at some point prior to the P-C bond formation step, in a manner that is presently not clear. We believe that the stereochemistry of the methoxy group on the bmf ligand certainly assists in determining the outcome of the reaction depicted by eq 2. In the putative bridging isomer of **2** the methoxy group is situated away (exo) from the Co-Co vector and the ancillary carbonyl ligands. This particular conformation minimizes unfavorable van der Waals contacts between the methoxy group and the binuclear core of **2**. Transfer of the  $\text{PPh}_2$  to the terminal alkyne carbon, coupled with the breaking of the appropriate Co-C(alkyne) bond and coordination of the bmf alkene bond, completes this reaction.

In-depth studies on the equilibration of the bmf ligand at polynuclear centers are planned, and the functionalization and the reactivity of the hydrocarbonyl ligand in CO insertion reactions will be reported in due course.<sup>17</sup>

**Acknowledgment.** We wish to thank Prof. Roderick Bates for helpful discussions. Financial support from

(16) Crystal data for **3**:  $\text{C}_{41}\text{H}_{30}\text{Co}_2\text{O}_7\text{P}_2 \cdot \frac{1}{2}\text{hexane} \cdot \frac{1}{2}\text{THF}$ , MW = 892.64, monoclinic space group  $C2/c$ ,  $a = 23.913(4)$  Å,  $b = 20.844(2)$  Å,  $c = 16.907(3)$  Å,  $\beta = 102.51(1)^\circ$ ,  $V = 8227(2)$  Å<sup>3</sup>,  $Z = 8$ ,  $D_c = 1.441$  g/cm<sup>3</sup>,  $F(000) = 3680$ ,  $T = 24$  °C,  $\mu(\text{Mo K}\alpha) = 9.32$  cm<sup>-1</sup>. Diffraction data were collected in the  $\omega$ -scan mode ( $2^\circ < 2\theta < 44^\circ$ ); final  $R = 0.0598$  ( $R_w = 0.0660$ ) for 3042 unique reflections (with  $I > 3\sigma(I)$ ). The molecular structure was solved by SHELX-86, which revealed the positions of the Co and P atoms, and the final refinement employed MolEN and SHELXL-93. All remaining non-hydrogens were located with difference Fourier maps and full-matrix least-squares refinement. With the exception of the solvent and phenyl-ring carbons and hydrogens, all atoms were refined anisotropically.

(17) Facile insertion of CO into the  $\eta^1$  Co-C bond of  $\text{Co}_2(\text{CO})_4[\mu-\eta^2, \eta^2, \eta^1, \eta^1-(Z)\text{-PhC}=\text{C}(\text{H})\text{PPh}_2\text{C}=\text{C}(\text{PPh}_2)\text{C}(\text{O})\text{OC}(\text{O})]$  is promoted by addition of  $\text{PMe}_3$ : Unpublished results.

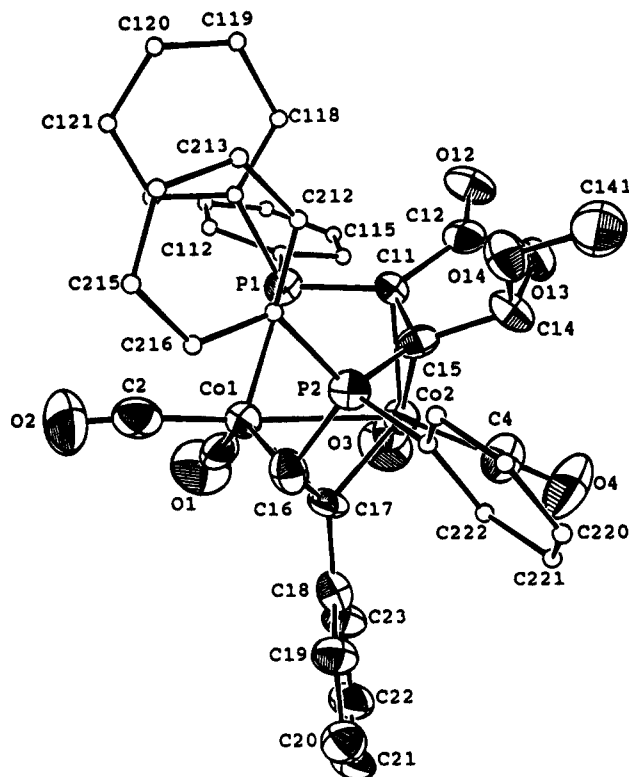


**Figure 1.** ORTEP drawing of **3**. Selected bond distances (Å) and angles (deg): Co(1)-Co(2) = 2.535(3), Co(1)-C(16) = 2.04(1), Co(1)-C(17) = 1.96(1), Co(2)-C(17) = 2.00(1), Co(1)-P(1) = 2.224(4), C(16)-P(2) = 1.76(1); Co(1)-C(16)-P(2) = 109.5(6), Co(1)-C(17)-Co(2) = 79.6(4).

the Robert A. Welch Foundation (Grant Nos. B-1202-SGB and B-1039-MGR) and the UNT Faculty Research Program is appreciated.

**Supporting Information Available:** Tables of crystal data, atomic positions, bond lengths, bond angles, and anisotropic thermal factors and a packing diagram for **3** (13 pages). Ordering information is given on any current masthead page.

OM9504617

## Synthesis of the Quatercyclopentadienyl Ligand and Its Half-Sandwich Tetratungsten Complexes

Cristina G. de Azevedo, Roland Boese, David A. Newman, and K. Peter C. Vollhardt

*Organometallics*, 1995, 14 (11), 4980-4982 • DOI: 10.1021/om00011a005 • Publication Date (Web): 01 May 2002

Downloaded from <http://pubs.acs.org> on March 9, 2009

### More About This Article

---

The permalink <http://dx.doi.org/10.1021/om00011a005> provides access to:

- Links to articles and content related to this article
- Copyright permission to reproduce figures and/or text from this article



# Synthesis of the Quatercyclopentadienyl Ligand and Its Half-Sandwich Tetratungsten Complexes

Cristina G. de Azevedo,<sup>1a</sup> Roland Boese,<sup>1b</sup> David A. Newman,<sup>1c</sup> and K. Peter C. Vollhardt<sup>\*,1c</sup>

Department of Chemistry, University of California at Berkeley,  
and Chemical Sciences Division, Lawrence Berkeley Laboratory, Berkeley, California 94720,  
and Institut für Anorganische Chemie der Universität-GH Essen, Universitätsstrasse 3-5,  
D-45117 Essen, Germany

Received August 23, 1995<sup>®</sup>

**Summary:** Double 3-oxocyclopentenylolation of the fulvalene dianion, followed by metalation, results in the four isomeric bis(enones) **1** which were elaborated via the bis(cyclopentadienes) **2** to the four regio- and stereoisomeric forms of (quatercyclopentadienyl)tetratungsten (connectivity 1,1',2',1'',3'',1''' (**3a,b** and **4a,b**) and 1,1',3',1'',3'',1''' (**3c,d** and **4c,d**)). The molecular structures of **1a** and **1b** have been determined by X-ray analysis. The tetramethyl complex **5** is obtained from **2d** by a metalation-methylation sequence involving deprotonation of the intermediate bis(tungsten hydride) with  $K^+(-OC(CH_3)_3)$ .

Half-sandwich oligocyclopentadienyl complexes can be viewed as cyclopentadienylmetal analogs of the corresponding fulvalene dimetals<sup>2</sup> and as such constitute attractive molecules with which to explore the basic chemical potential of rigidly held acyclic<sup>3</sup> metal arrays, in particular with respect to organic substrate activation, intrachain ligand migration, electron transfer, and ultimately, synergistic catalysis. The series contrasts topologically with that of the analogous and extensively investigated sandwich oligometalocenenes<sup>4</sup> and has up to now been extended only once, to the two isomers of

trimetalated tercyclopentadienyl.<sup>5</sup> We report now the synthesis of the next higher cyclopentadiene analog, quatercyclopentadienyl, complexed to four tungsten units. The free ligand can exist in three regioisomeric forms with connectivities designated as 1,1',2',1'',2'',1'''; 1,1',2',1'',3'',1'''; and 1,1',3',1'',3'',1''',<sup>6</sup> of which only the last two are described here. Transition-metal complexation renders the two center rings chiral and, depending on the presence and location of metal-metal (M-M) bonds, may give rise to a number of additional stereoisomers and (M-M) regioisomers, providing a unique opportunity to explore the influence of topology on the physical and chemical properties of these complexes.

Scheme 1 depicts the assembly of the target molecules patterned after the strategy used in the construction of (tercyclopentadienyl)trimetals.<sup>5</sup> Thus, double 3-oxocyclopentenylolation of the fulvalene dianion,<sup>7</sup> followed by metalation, gave the four purple isomers **1a-d**, separated initially by careful chromatography on silica ( $CH_2Cl_2$ -acetone gradient) into the two pairs of purple **1a,b** (1:1, 36.7%) and **1c,d** (1:1, 34%), which could be conveniently carried on as such through the scheme or separated further into the pure components by fractional crystallization. Complex **1d** was subjected to the sequence in Scheme 1 in pure form. The multiple organic and inorganic functionalities present in **1-4** render them extremely light, air, heat, acid, and base sensitive, sometimes to the detriment of isolated yields. Rigorous and self-consistent structural assignments were made primarily by <sup>1</sup>H NMR techniques, which readily corroborated the substitution patterns of the central rings (1,2 vs 1,3), symmetry (series **a,b** vs **c,d**), location of the tungsten-tungsten bond,<sup>8</sup> proximity of hydrogens (NOESY), and connectivity (TOCSY). Confirmation was obtained by the execution of X-ray crystal analyses on **1a** and **1b** (from  $CH_2Cl_2$ -hexane by vapor diffusion; Figures 1 and 2).<sup>9</sup>

The structures of **1a,b** can be viewed as being composed of  $FvW_2(CO)_6$  modified by cyclopentenone substitution. In **1a**, the planes defined by rings 1 (C7-C11) and 2 (C12-C16) form an angle of 25.9°, distortion from planarity occurring in the direction of the respective two attached metals W1 and W2. For **1b**, this angle is 22.3°. These values are similar to those observed for related compounds; in ( $\eta^5$ : $\eta^5$ : $\eta^5$ -1,1',3',1''-tercyclo-

<sup>®</sup> Abstract published in *Advance ACS Abstracts*, November 1, 1995.

(1) (a) Permanent address: Centro de Química Estrutural, Instituto Superior Técnico, Av. Rovisco Pais, 1096 Lisboa, Portugal. (b) Universität-GH Essen. (c) University of California at Berkeley.

(2) For leading references, see: (a) Tilset, M.; Vollhardt, K. P. C.; Boese, R. *Organometallics* **1994**, *13*, 3146. (b) McGovern, P. A.; Vollhardt, K. P. C. *Synlett* **1990**, 493.

(3) For recent work on "linear" oligometals, see, inter alia: (a) Herberhold, M.; Jin, G.-X.; Rheingold, A. L. *Angew. Chem., Int. Ed. Engl.* **1995**, *34*, 656. (b) Sundermeyer, J.; Runge, D. *Angew. Chem., Int. Ed. Engl.* **1994**, *33*, 1255. (c) Sundermeyer, J.; Runge, D.; Field, J. S. *Angew. Chem., Int. Ed. Engl.* **1994**, *33*, 678. (d) Laguna, A.; Laguna, M.; Jiménez, J.; Lahoz, F. J.; Olmos, E. *Organometallics* **1994**, *13*, 253. (e) Mashima, K.; Nakano, H.; Nakamura, A. *J. Am. Chem. Soc.* **1993**, *115*, 11632. (f) Yamamoto, Y.; Yamazaki, H. *Organometallics* **1993**, *12*, 933. (g) Herrmann, W. A.; Albach, R. W.; Behm, J. *J. Chem. Soc., Chem. Commun.* **1991**, 367. (h) Cazanoue, M.; Dahan, F.; Mathieu, R. *Inorg. Chem.* **1990**, *29*, 563. (i) Rardin, R. L.; Bino, A.; Poganiuch, P.; Tolman, W. B.; Liu, S.; Lippard, S. J. *Angew. Chem., Int. Ed. Engl.* **1990**, *29*, 812. (j) Firfiray, D. B.; Irving, A.; Moss, J. R. *J. Chem. Soc., Chem. Commun.* **1990**, 377. (k) Ferrer, M.; Perales, A.; Rossell, O.; Seco, M. *J. Chem. Soc., Chem. Commun.* **1990**, 1447. (l) Davies, S. J.; Howard, J. A. K.; Musgrove, R. J.; Stone, F. G. A. *Angew. Chem., Int. Ed. Engl.* **1989**, *28*, 624.

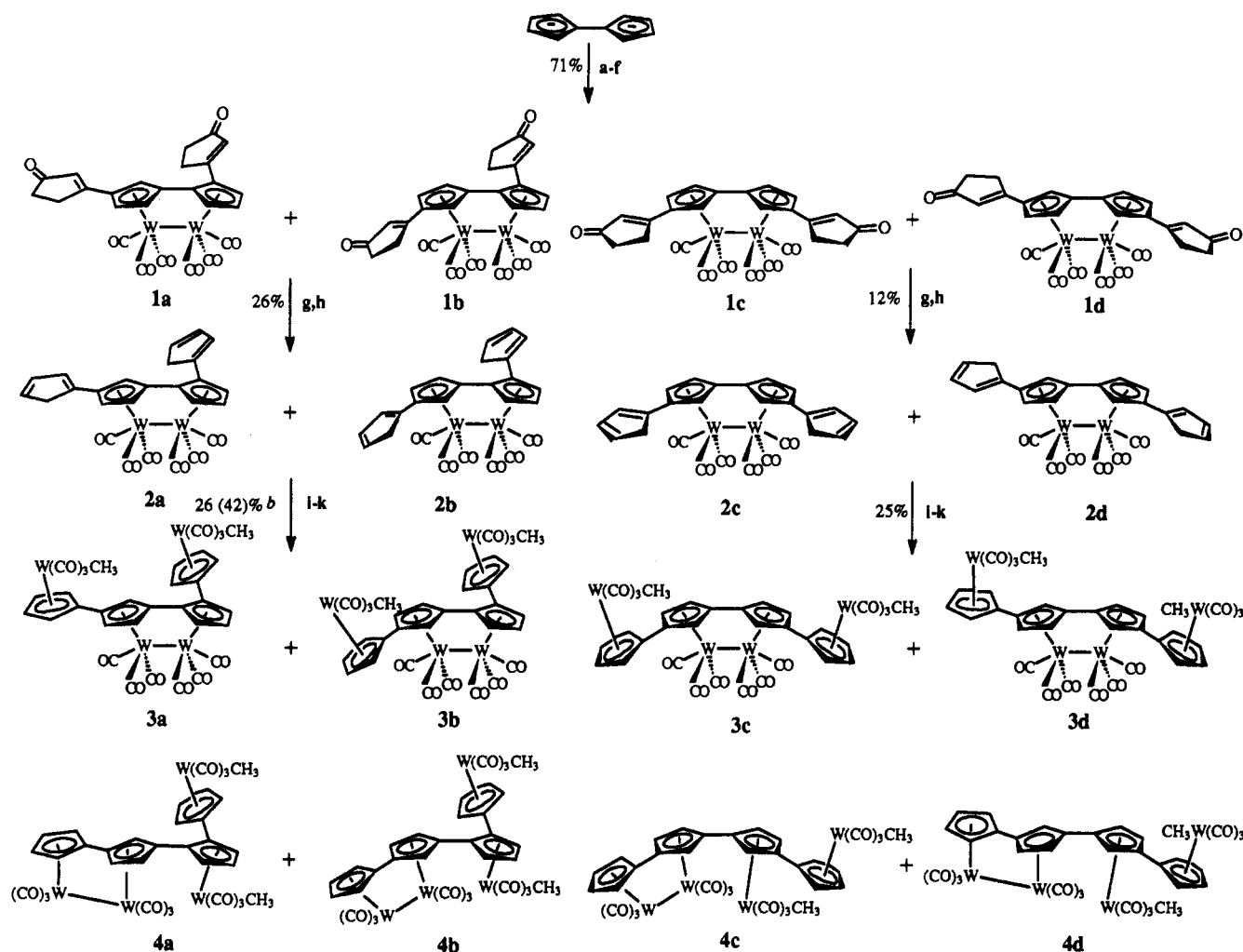
(4) For recent work, see, inter alia: (a) Dong, T.-Y.; Huang, C.-H.; Chang, C.-K.; Hsieh, H.-C.; Peng, S.-M.; Lee, G.-H. *Organometallics* **1995**, *14*, 1776. (b) Dong, T.-Y.; Lee, T.-Y.; Lee, S.-H.; Lee, G.-H.; Peng, S.-M. *Organometallics* **1994**, *13*, 2337. (c) Lai, L.-L.; Dong, T.-Y. *J. Chem. Soc., Chem. Commun.* **1994**, 2347. (d) Jaitner, P.; Schottenberger, H.; Gamper, S.; Obendorf, D. *J. Organomet. Chem.* **1994**, *475*, 113. (e) Foucher, D. A.; Honeyman, C. H.; Nelson, J. M.; Tang, B. Z.; Manners, I. *Angew. Chem., Int. Ed. Engl.* **1993**, *32*, 1709. (f) Oelckers, B.; Chávez, I.; Manriquez, J. M.; Román, E. *Organometallics* **1993**, *12*, 3396. (g) Dong, T.-Y.; Huang, C.-H.; Chang, C.-K.; Wen, Y.-S.; Lee, S.-L.; Chen, J.-A.; Yeh, W.-Y.; Yeh, A. *J. Am. Chem. Soc.* **1993**, *115*, 6357. (h) For early work, see: *Gmelin Handbook of Inorganic Chemistry*; Springer-Verlag: Berlin, 1977; Vol. 41, Pt. A, Ferrocene 6.

(5) Boese, R.; Myrabo, R.; Newman, D. A.; Vollhardt, K. P. C. *Angew. Chem., Int. Ed. Engl.* **1990**, *29*, 549.

(6) *IUPAC Nomenclature of Organic Chemistry*; Rigaudy, J., Klesney, S. P., Eds.; Pergamon Press: Oxford, U.K., 1979; Rules A-52, p 42; A-54, p 44; C-71, p 128.

(7) Smart, J. C.; Curtis, C. J. *Inorg. Chem.* **1977**, *16*, 1788.

(8) Meyerhoff, D. J.; Nunlist, R.; Tilset, M.; Vollhardt, K. P. C. *Magn. Reson. Chem.* **1986**, *24*, 709.

Scheme 1<sup>a</sup>

<sup>a</sup> Legend: (a) 3-chloro-2-cyclopentenone (1 equiv), 10 min,  $-78^{\circ}\text{C}$ , THF; (b) BuLi (2 equiv), 5 min,  $-78^{\circ}\text{C}$ ; (c) 3-chloro-2-cyclopentenone (2 equiv), 10 min,  $-78^{\circ}\text{C}$ ; (d) BuLi (1 equiv),  $-78^{\circ}\text{C}$  to room temperature; (e)  $\text{W}(\text{CO})_3(\text{NCET})_3$  (2 equiv), 5.5 h, room temperature; (f)  $\text{AgBF}_4$  (2 equiv),  $-78^{\circ}\text{C}$  to room temperature; (g)  $i\text{-Bu}_2\text{AlH}$ , 2 h,  $0^{\circ}\text{C}$ ,  $\text{CH}_2\text{Cl}_2$ ; (h) cat.  $4\text{-CH}_3\text{C}_6\text{H}_4\text{SO}_3\text{H}$ , 2 min,  $60^{\circ}\text{C}$ ,  $\text{C}_6\text{H}_6$ ; (i)  $\text{W}(\text{CO})_3(\text{NCET})_3$  (5 equiv), 3 days at room temperature, 3 h at  $50^{\circ}\text{C}$ , THF; (j)  $\text{LiN}(\text{TMS})_2$  (2.5 equiv), 7 min, room temperature; (k)  $\text{CH}_3\text{I}$  (10 equiv),  $-78^{\circ}\text{C}$  for 1 h, room temperature for 1 h; <sup>b</sup> Yield for the conversion of pure **2b** to **3b** and **4b**.

pentadienyl)[ $\text{W}(\text{CO})_3$ ][ $\text{W}(\text{CO})_3$ ][ $\text{W}(\text{CO})_3\text{CH}_3$ ]<sup>5</sup> the angle is  $22.5^{\circ}$ . The two rings are also somewhat twisted to avoid eclipsing strain associated with the carbonyl groups, which become approximately staggered by this distortion. For **1a**, the torsion angle is  $21.0^{\circ}$ , and for **1b** it is  $13.4^{\circ}$ . Cycles C7–C11 and C17–C21 are more nearly coplanar, with dihedral angles of  $9.3^{\circ}$  (**1a**) and  $9.1^{\circ}$  (**1b**), respectively. The fourth ring (C22–C26) is twisted with respect to the second, the dihedral angle between the planes C7–C11 and C22–C26 being  $46.0^{\circ}$  (**1a**) and  $33.4^{\circ}$  (**1b**). The twisting distortion observed for the  $\alpha$ -bonded cyclopentenone is not unexpected and can be ascribed to steric hindrance to achieving coplanarity. In contrast, in the  $\beta$ -bonded analog this effect is absent. Presumably, these distinctive structural

characteristics are present along the series 1–4 as exemplified by the crystal structures of  $(\eta^5\text{:}\eta^5\text{:}\eta^5\text{-}1,1',3',1''\text{-tercyclopentadienyl})[\text{W}(\text{CO})_3][\text{W}(\text{CO})_3][\text{W}(\text{CO})_3\text{CH}_3]$ <sup>5</sup> and  $(\eta^5\text{:}\eta^5\text{:}\eta^5\text{-}1,1',2',1''\text{-tercyclopentadienyl})[\text{Re}(\text{CO})_3][\text{Ru}(\text{CO})_2][\text{Ru}(\text{CO})_2]$ <sup>5</sup>. The shorter W1–W2 bond of  $3.252(2)$  Å for **1a**, compared with  $3.286(2)$  Å for **1b**, is in agreement with the higher torsion and bending angle for the former; the carbonyls in **1a** are perhaps more staggered, allowing for a shorter W–W distance. The W–W separations in **1a** and **1b** are closer to that in  $\text{Cp}_2\text{W}_2(\text{CO})_6$  ( $3.222(1)$  Å),<sup>10</sup> than to that in  $\text{FvW}_2(\text{CO})_6$  ( $3.347(1)$  Å),<sup>11</sup> again reflecting the eclipsed configuration of the carbonyls in the latter.

The enone functions in **1** (either as the pairs **1a,b** and **1c,d** or as pure **1d**) were elaborated initially by reduction to diastereomeric mixtures of the corresponding allylic alcohols and subsequently by acid-catalyzed dehydration to mixtures of the desired 1,3- and 1,4-cyclopentadiene isomers **2** (only the former are shown in Scheme 1). It was possible to separate **2a** from **2b** at this stage by chromatography (silica, ethyl acetate–

(9) (a) Crystallographic data for **1a**: triclinic,  $P\bar{1}$ ,  $Z = 2$ ,  $a = 8.955(1)$  Å,  $b = 9.434(1)$  Å,  $c = 14.271(1)$  Å,  $\alpha = 84.98(1)^{\circ}$ ,  $\beta = 80.82(1)^{\circ}$ ,  $\gamma = 86.76(1)^{\circ}$ ,  $V = 1184.3(2)$  Å<sup>3</sup>,  $\rho_{\text{calc}} = 1.801$  g/cm<sup>3</sup>; Nicolet R3m/V diffractometer, Mo K $\alpha$  radiation ( $\lambda = 0.71069$  Å); 6362 unique reflections, of which 4791 were observed ( $F_o \geq 4\sigma(F)$ );  $R = 0.0277$ ,  $R_w = 0.0273$ . (b) Crystallographic data for **1b**· $\text{CH}_2\text{Cl}_2$ : monoclinic,  $P2_1/c$ ,  $Z = 4$ ,  $a = 14.095(2)$  Å,  $b = 13.604(2)$  Å,  $c = 14.290(3)$  Å,  $\alpha = 90^{\circ}$ ,  $\beta = 96.20(1)^{\circ}$ ,  $\gamma = 90^{\circ}$ ,  $V = 2723.4(7)$  Å<sup>3</sup>,  $\rho_{\text{calc}} = 2.115$  g/cm<sup>3</sup>; Nicolet R3m/V diffractometer, Mo K $\alpha$  radiation ( $\lambda = 0.71069$  Å); 5011 unique reflections, of which 3513 were observed ( $F_o \geq 4\sigma(F)$ );  $R = 0.0594$ ,  $R_w = 0.0601$ .

(10) Adams, R. D.; Collins, D. M.; Cotton, F. A. *Inorg. Chem.* **1974**, *13*, 1086.

(11) Abrahamson, H. B.; Heeg, M. J. *Inorg. Chem.* **1984**, *23*, 2281.

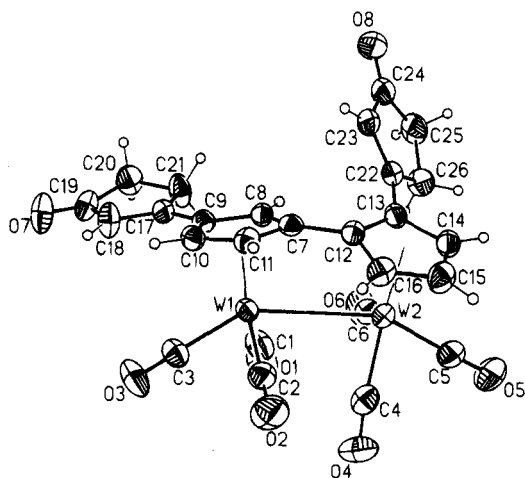


**Figure 1.** Molecular structure of **1a** in the crystal. Selected distances (Å): W1–W2, 3.252(2); W1–C1, 1.999(7); W1–C2, 1.969(7); W1–C3, 1.984(6); W2–C4, 1.978(7); W2–C5, 1.976(7); W2–C6, 1.983(5); C7–C12, 1.458(7); C9–C17, 1.468(7); C13–C22, 1.464(8).

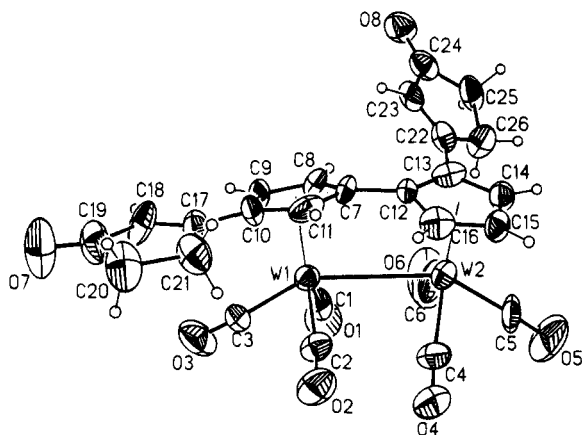
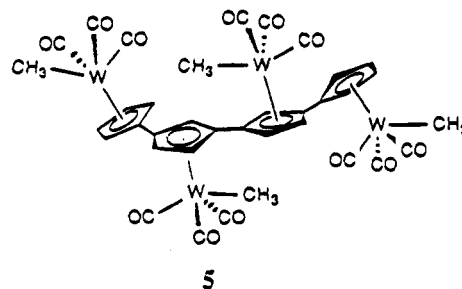


**Figure 2.** Molecular structure of **1b** in the crystal. Selected distances (Å): W1–W2, 3.286(2); W1–C1, 1.939(21); W1–C2, 2.004(18); W1–C3, 1.985(17); W2–C4, 1.995(19); W2–C5, 1.963(19); W2–C6, 1.970(24); C7–C12, 1.444(21); C10–C17, 1.489(26); C13–C22, 1.508(26).

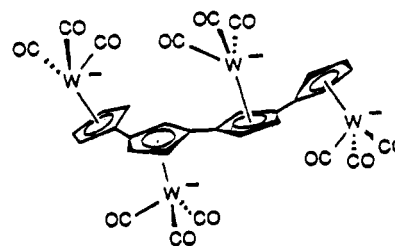
hexane, gradient), allowing for the later conversion of pure **2b** to **3b** and **4b**. Finally permatalation proceeded through the bis(tungsten hydrides) as intermediates (observed by  $^1\text{H}$  NMR from pure **2d**:  $\delta$  –6.91 (s,  $J_{183\text{W}-\text{H}} = 39.5$  Hz, 2H) ppm), which were deprotonated to the corresponding dianions and then methylated (with  $\text{CH}_3\text{I}$ ; in the case of pure **2b** with  $\text{CF}_3\text{SO}_3\text{CH}_3$ ) to give not only the purple (quatercyclopentadienyl)tungsten species **3** but also the rearranged purple complexes **4** (ratio **3b**:**4a,b** = 4:1; **3c,d**:**4c,d** = 3:1), separable by careful chromatography (silica, ethyl acetate–hexane, gradient). Migration of the W–W bond can be most readily envisioned to occur at the dianion stage by invoking attack of a charged metal center on the linked dinuclear core,<sup>12</sup> resulting in equilibration along a (tercyclopentadienyl)trimetal subunit. The regioselectivity of this process has topological origin, as the

(12) Corraine, M. S.; Atwood, J. D. *Organometallics* **1991**, *10*, 2315.

1,1',2',1''-connected portion of **3a,b** and **4a,b** is sterically prevented from achieving the required coplanarization of the three rings.<sup>5</sup> Interestingly, subjecting pure **2d** to the sequence **i–k** (Scheme 1) but using  $\text{K}^+(\text{OC}(\text{CH}_3)_3)$  as a base in **j** furnished none of the expected **3d** and **4d** but rather the yellow tetramethyltungsten derivative **5** (22%) as the sole isolable product.



5



6

Evidently, reduction of the W–W bond to produce **6** (or its functional equivalent) occurs under these conditions, perhaps by electron transfer–disproportionation before or during the methylation sequence. This explanation is plausible in light of the relatively facile electrochemical reduction of (fulvalene)ditungsten hexacarbonyl<sup>13</sup> and related literature reports.<sup>14</sup>

In summary, we have demonstrated that organometallic methodology can be applied to doubly extend the fulvalene nucleus to tetrametallic quatercyclopentadienyls. Application of the rich chemistry of the component subunits of these systems<sup>2,5</sup> to the whole should be a fruitful area of investigation, currently in progress.

**Acknowledgment.** This work was supported by the director, Office of Energy Research, Office of Basic Energy Sciences, Materials Science Division, of the U.S. Department of Energy under Contract DE-AC-03 76SF00098. C.G.A. is grateful to INVOTAN, FLAD, and the Fulbright Scholarship Program for financial support.

**Supporting Information Available:** Text and tables giving experimental details and spectral (including  $^1\text{H}$  NMR spectral assignments of **1a–d**, **3b–d**, and **4c,d**), analytical, and X-ray (for **1a,b**) data for new compounds (39 pages). Ordering information is given on any current masthead page.

OM950655M

(13) (a) Moulton, R.; Weidman, T. W.; Vollhardt, K. P. C.; Bard, A. *J. Inorg. Chem.* **1986**, *25*, 1846. (b) Kadish, K. M.; Lacombe, D. A.; Anderson, J. E. *Inorg. Chem.* **1986**, *25*, 2246.

(14) (a) Bergman, R. G.; Yang, G. K. *J. Am. Chem. Soc.* **1983**, *105*, 6045. (b) Schore, N. E.; Ilenda, C.; Bergman, R. G. *J. Am. Chem. Soc.* **1976**, *98*, 7436.



# Mono- and Binuclear Rhodium Complexes of a Chiral 1,1-Diphosphine. Syntheses and Crystal Structures

Angela Marinetti,\* Claude Le Menn, and Louis Ricard

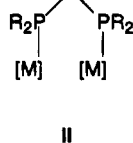
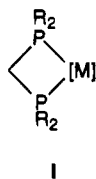
Laboratoire "Hétéroéléments et Coordination", URA CNRS 1499, DCPH, Ecole Polytechnique, 91128 Palaiseau Cedex, France

Received August 2, 1995<sup>®</sup>

**Summary:** The homochiral diphosphine **3**, bearing *PPh*<sub>2</sub> and menthylphosphetane moieties, has been prepared from the phosphetane oxide **1** through a stereoselective phosphorylation reaction. Monometallic and bimetallic "A-frame" rhodium complexes of **3** have been synthesized and characterized by X-ray diffraction.

Bis(diphenylphosphino)methane (dppm) and analogous 1,1-diphosphines hold a special place in organometallic chemistry, owing to their ability to assemble unusual mono- and bimetallic complexes.

The monometallic species **I** have a strained<sup>1</sup> four-membered-ring chelated structure. The abnormally small P-M-P bite angle and the concomitant anomalous structure of the valence orbitals confer an improved reactivity on the metal center in such complexes. Thus, 14-electron intermediates **I**, with [M] = Ni, Pd, Pt, RhCl, are high-energy fragments<sup>2</sup> displaying various intermolecular bond activation reactions as well as interesting catalytic properties.<sup>3</sup>

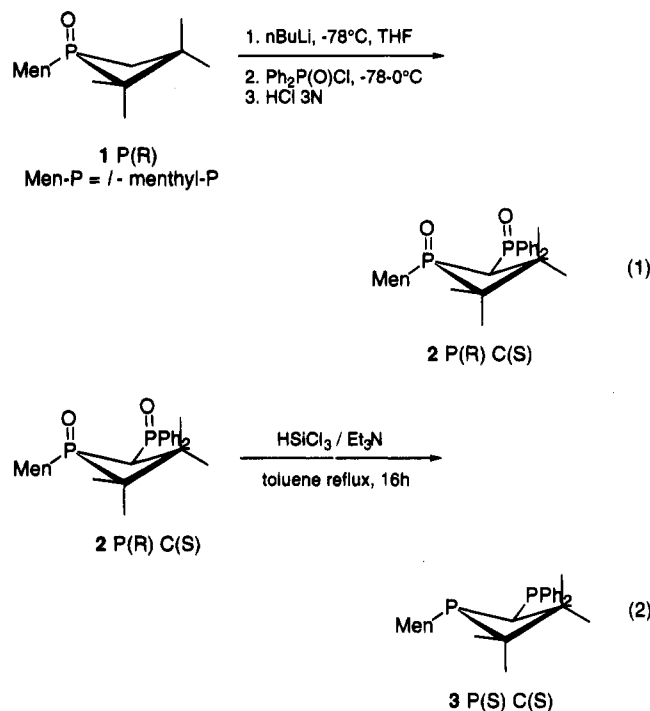


In the binuclear complexes<sup>4</sup> **II**, the two metals are kept in close proximity and are able to react cooperatively with substrate molecules in stoichiometric or catalytic systems.<sup>5a,b</sup> Remarkable results in hydroformylation reactions have been reported recently.<sup>5c</sup> Hundreds of papers on 1,1-diphosphine-transition-metal complexes have appeared over the last 20 years. Nevertheless, as far as we know, no chiral optically pure 1,1-diphosphines have been used as ligands for the synthesis of mononuclear or binuclear complexes.

We report here the synthesis of the new chiral 1,1-diphosphine **3** and the syntheses and X-ray structures of the two rhodium complexes **4** and **5**, in which **3** acts as a chelating and a bridging ligand, respectively.

The phosphine **3** has been prepared through a two-

step synthesis from the optically pure *P*-menthylphosphetane oxide **1**.<sup>6</sup>



Metalation of **1** with *n*BuLi, followed by treatment with 1 equiv of diphenylphosphinyl chloride, afforded the dioxide **2**<sup>7</sup> (eq 1) in about 50% yield after purification by column chromatography as a single isomer. On the basis of previous results concerning the  $\alpha$ -alkylation<sup>6,8</sup> of the same phosphetane oxide **1**, the *Ph*<sub>2</sub>*P*(*O*) substituent is expected to occupy an equatorial position, *anti* with respect to the menthyl group. The assumed stereochemistry for **2** has been confirmed by the X-ray

(6) Marinetti, A.; Ricard, L. *Tetrahedron* 1993, 49, 10291.

(7) *n*-Butyllithium (1.2 mL, 1.6 M solution in hexane) was added to a solution of phosphetane oxide **1** (500 mg, 1.8 mmol) in THF (25 mL) at -78 °C. After a few minutes, 1 equiv of *Ph*<sub>2</sub>*P*(*O*)Cl was added. The reaction mixture was warmed slowly to 0 °C and hydrolyzed with 3 N HCl (1 mL). After extraction with ether, the organic phase was chromatographed on a silica gel column with an ether-methanol gradient. The final product was eluted with ether-methanol (90:10): yield 0.4 g (48%); colorless solid. Selected data for **2** are as follows. Anal. Calcd for C<sub>25</sub>H<sub>43</sub>P<sub>2</sub>O<sub>2</sub>: C, 71.88; H, 8.74. Found: C, 70.55; H, 8.44. <sup>31</sup>P NMR (81 MHz, C<sub>6</sub>D<sub>6</sub>):  $\delta$  64.6 and 25.7 (<sup>2</sup>*J*<sub>P-P</sub> = 17.1 Hz). <sup>1</sup>H NMR (200 MHz, C<sub>6</sub>D<sub>6</sub>):  $\delta$  0.51 (d, <sup>3</sup>*J*<sub>H-H</sub> = 6.3 Hz, CHMe), 0.68 (d, <sup>3</sup>*J*<sub>H-H</sub> = 6.8 Hz, 3H, CHMe<sub>2</sub>), 0.84 (d, <sup>3</sup>*J*<sub>H-P</sub> = 19.1 Hz, 3H, PCMe<sub>2</sub>), 1.03 (d, <sup>3</sup>*J*<sub>H-H</sub> = 6.7 Hz, 3H, CHMe<sub>2</sub>), 1.13 (s, 3H, CMe<sub>2</sub>), 1.27 (s, 3H, CMe<sub>2</sub>), 1.34 (d, <sup>3</sup>*J*<sub>H-P</sub> = 16.9 Hz, 3H, PCMe<sub>2</sub>), 3.27 (dd, <sup>2</sup>*J*<sub>H-P</sub> = 15.9 Hz, <sup>2</sup>*J*<sub>H-P</sub> = 11.9 Hz, PCHP), 7.1, 8.0, and 8.6 (m, Ph). <sup>13</sup>C NMR (50 MHz, C<sub>6</sub>D<sub>6</sub>):  $\delta$  17.4 (Me), 18.4 (broad s, Me), 21.4 (Me), 22.0 (Me), 22.7 (Me), 23.3 (t, *J*<sub>C-P</sub> = 7.0 Hz, Me), 24.5 (d, *J*<sub>C-P</sub> = 11.5 Hz, CH<sub>2</sub>), 29.0 (dd, <sup>2</sup>*J*<sub>C-P</sub> = 9.2 Hz, *J*<sub>C-P</sub> = 2.9 Hz, Me), 30.6 (d, *J*<sub>C-P</sub> = 2.5 Hz, CH), 33.0 (d, *J*<sub>C-P</sub> = 12.4 Hz, CH), 32.8 (CH<sub>2</sub>), 34.6 (d, *J*<sub>C-P</sub> = 2.2 Hz, CH<sub>2</sub>), 41.5 (dd, <sup>2</sup>*J*<sub>C-P</sub> = 9.2 Hz, <sup>2</sup>*J*<sub>C-P</sub> = 4.6 Hz, CMe<sub>2</sub>), 41.7 (d, <sup>1</sup>*J*<sub>C-P</sub> = 43.8 Hz, PCH), 41.9 (CH), 51.2 (dd, <sup>1</sup>*J*<sub>C-P</sub> = 57.4 Hz, <sup>3</sup>*J*<sub>C-P</sub> = 10.4 Hz, PCMe<sub>2</sub>), 55.1 (dd, <sup>1</sup>*J*<sub>C-P</sub> = 60.5 Hz, <sup>1</sup>*J*<sub>C-P</sub> = 34.8 Hz, PCHP). MS(ET): *m/e* 484 (M, 50%), 201 (Ph<sub>2</sub>PO, 100%), [ $\alpha$ ]<sub>D</sub> = -141 (c = 1, CHCl<sub>3</sub>).

(8) Marinetti, A.; Ricard, L. *Organometallics* 1994, 13, 3956.

<sup>®</sup> Abstract published in *Advance ACS Abstracts*, October 15, 1995.

(1) Li, C.; Cucullu, M. E.; McIntyre, R. A.; Stevens, E. D.; Nolan, S. P. *Organometallics* 1994, 13, 3621.

(2) (a) Hofmann, P.; Perez-Moya, L. A.; Krause, M. E.; Kumberger, O.; Müller, G. Z. *Naturforsch., B* 1990, 45, 897. (b) Hofmann, P.; Heiss, H.; Müller, G. Z. *Naturforsch., B* 1987, 42, 395. (c) Hofmann, P.; Meier, C.; Englert, U.; Schmidt, M. U. *Chem. Ber.* 1992, 125, 353.

(3) See for example: (a) Hofmann, P.; Unfried, G. *Chem. Ber.* 1992, 125, 659. (b) Hofmann, P.; Meier, C.; Hiller, W.; Heckel, M.; Riede, J.; Schmidt, M. U. *J. Organomet. Chem.* 1995, 490, 51 and references therein.

(4) (a) Chaudret, B.; Delavaux, B.; Poilblanc, R. *Coord. Chem. Rev.* 1988, 86, 191. (b) Anderson, G. K. *Adv. Organomet. Chem.* 1993, 35, 1.

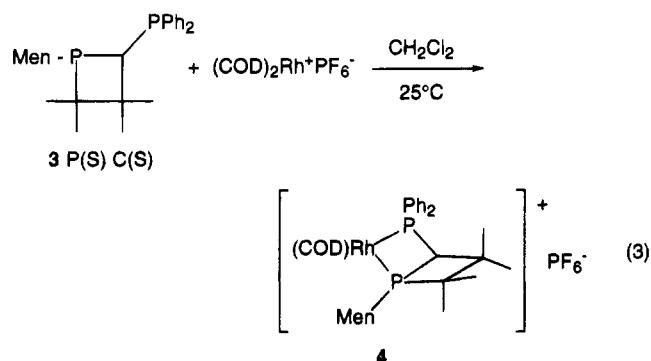
(5) (a) Kubiak, C. P.; Eisenberg, R. *J. Am. Chem. Soc.* 1980, 102, 3637. (b) Kubiak, C. P.; Woodcock, C.; Eisenberg, R. *Inorg. Chem.* 1982, 21, 2119. (c) Brüssard, M. E.; Juma, B.; Train, S. G.; Peng, W.-J.; Laneman, S. A.; Stanley, G. G. *Science* 1993, 260, 1784.

structure determinations reported hereafter. The *syn* orientation of the Ph<sub>2</sub>P(O) substituent with respect to the P=O bond, and hence the phosphetane phosphorus lone pair, is required to furnish a potential chelating diphosphine.

Reduction of **2** (eq 2) was performed with an excess (10 equiv) of HSiCl<sub>3</sub>/Et<sub>3</sub>N, in toluene at 110 °C in a sealed glass ampule. The conversion is quantitative according to <sup>31</sup>P NMR analysis of the reaction mixture. After hydrolysis with 20% NaOH, the final diphosphine **3**<sup>9</sup> was purified by filtration of the organic phase over an alumina column with hexane–ether (90:10) as eluent. The reduction proceeds with total retention of configuration of the phosphetane phosphorus atom. Diphosphine **3** is slightly air sensitive, and it must be handled under an inert atmosphere.

In the next step of our work, we examined the coordinating properties of **3** toward rhodium(I) derivatives, as an exploratory study preceding the use of this ligand in conventional asymmetric catalytic reactions. The synthesis of homochiral 1,1-diphosphines, as well as the catalytic properties of the corresponding transition-metal complexes, has been barely mentioned in the literature;<sup>10</sup> therefore, their potential has not been clearly established at present.

The diphosphine **3** reacts easily at room temperature with the cationic rhodium complex (COD)<sub>2</sub>Rh<sup>+</sup>PF<sub>6</sub><sup>-</sup> to afford the chelated complex **4**<sup>11</sup> as an orange solid (eq 3). Formation of the four-membered Rh–P–C–P ring



of **4** is shown by the <sup>31</sup>P NMR chemical shifts at high field with respect to the starting phosphine: δ (CDCl<sub>3</sub>) 4.2 (J<sub>P–Rh</sub> = 121 Hz) and –37.3 (J<sub>P–Rh</sub> = 126 Hz), J<sub>P–P</sub> = 62 Hz. The <sup>1</sup>H and <sup>13</sup>C NMR spectra of **4** are poorly resolved, due to the low solubility of **4** in CDCl<sub>3</sub> and the number of coupling constants to rhodium and phosphorus atoms; nevertheless, the signals of the COD (<sup>13</sup>C NMR: triplets at 89.0, 94.7, 95.2, and 97.7 ppm) and phosphetane ligands are observed.

Crystals of **4**, suitable for an X-ray structure determination,<sup>12</sup> could be grown from a CH<sub>2</sub>Cl<sub>2</sub> solution by slow addition of an ether–hexane mixture. The molec-

(9) Diphosphine **3** (240 mg, 85% yield) is obtained, as a colorless solid, from 300 mg of **2**. Selected data for **3** are as follows. <sup>31</sup>P NMR (C<sub>6</sub>D<sub>6</sub>): δ 24.4 and –18.6 (J<sub>P–P</sub> = 87.0 Hz). <sup>1</sup>H NMR (C<sub>6</sub>D<sub>6</sub>): δ –0.63 (qd, J = 13 Hz, J = 4.5 Hz, 1H, PCHCH<sub>2</sub>), 0.61 (d, J<sub>H–H</sub> = 6.4 Hz, CHMe), 0.71 (d, J<sub>H–H</sub> = 6.8 Hz, 3H, CHMe<sub>2</sub>), 0.86 (s, Me), 0.97 (d, J<sub>H–H</sub> = 6.8 Hz, 3H, CHMe<sub>2</sub>), 1.13 (d, J<sub>H–P</sub> = 17.1 Hz, 3H, PCMe<sub>2</sub>), 1.16 (d, J<sub>H–P</sub> = 4.0 Hz, 3H, PCMe<sub>2</sub>), 1.54 (d, J<sub>H–P</sub> = 2.5 Hz, 3H, CMe<sub>2</sub>), 2.24 (m, 1H, CHMe<sub>2</sub>), 3.15 (dd, J<sub>H–P</sub> = 5.1 Hz, J<sub>H–P</sub> = 2.6 Hz, PCHP), 7.0 and 7.6 (m, Ph). <sup>13</sup>C NMR (C<sub>6</sub>D<sub>6</sub>): tentative assignment δ 16.2 (Me), 22.4 (Me), 22.6 (d, J<sub>C–P</sub> = 4.5 Hz, Me), 22.7 (Me), 24.8 (dd, J<sub>C–P</sub> = 25.7, J<sub>C–P</sub> = 3.2 Hz, Me), 25.4 (d, J<sub>C–P</sub> = 9.3 Hz, CH<sub>2</sub>), 25.5 (dd, J<sub>C–P</sub> = 23.9, J<sub>C–P</sub> = 7.1 Hz, Me), 26.9 (d, J<sub>C–P</sub> = 4.4 Hz, Me), 29.1 (d, J<sub>C–P</sub> = 20.0 Hz, CH), 33.8 (d, J<sub>C–P</sub> = 3.0 Hz, CH), 34.7 (CH<sub>2</sub>), 34.8 (dd, J<sub>C–P</sub> = 36.5 Hz, J<sub>C–P</sub> = 2.9 Hz, PCH), 37.3 (dd, J<sub>C–P</sub> = 16.7, J<sub>C–P</sub> = 3.2 Hz, CMe<sub>2</sub>), 37.6 (CH<sub>2</sub>), 38.4 (dd, J<sub>C–P</sub> = 26.9, J<sub>C–P</sub> = 12.6 Hz, PCHP), 44.4 (dd, J<sub>C–P</sub> = 10.7, J<sub>C–P</sub> = 2.9 Hz, CMe<sub>2</sub>), 47.8 (d, J<sub>C–P</sub> = 24.5 Hz, CH). MS(EI): m/e 452 (M, 25%), 183 (Men PCH, 100%).

(10) Brunner, H.; Fürst, J. *Tetrahedron* **1994**, *50*, 4303.

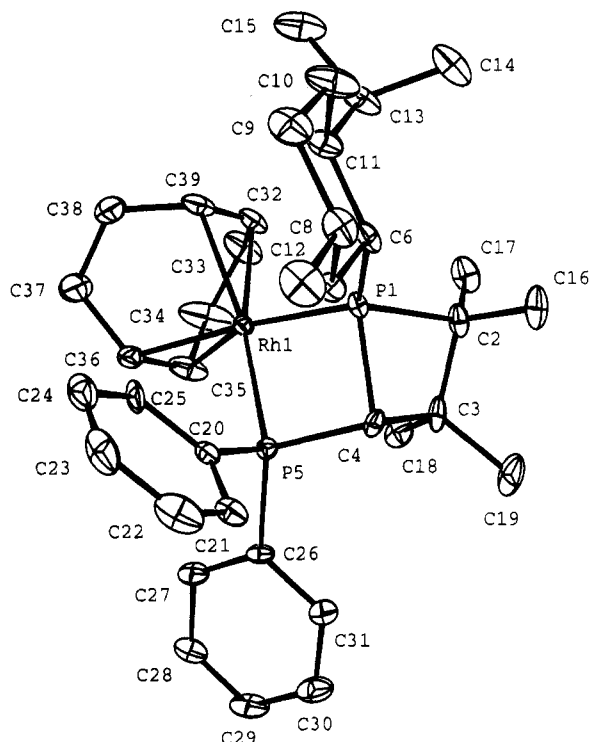


**Figure 1.** Crystal structure of complex **4**. Selected bond distances (Å) and angles (deg): Rh–P(1), 2.364(2); Rh–P(5), 2.309(2); P(5)–C(4), 1.827(7); P(1)–C(4), 1.873(8); P(1)–C(2), 1.898(7); C(2)–C(3), 1.56(1); C(4)–C(3), 1.60(1); Rh–C(39), 2.201(8); Rh–C(32), 2.225(8); Rh–C(35), 2.185(9); Rh–C(36), 2.194(8); P(1)–Rh–P(5), 70.99(6); Rh–P(1)–C(4), 92.2(2); P(1)–C(4)–P(5), 94.3(3); C(4)–P(5)–Rh, 95.2(2); C(2)–P(1)–C(4), 78.3(3); P(1)–C(4)–C(3), 87.7(5); C(4)–C(3)–C(2), 97.9(5); C(3)–C(2)–P(1), 88.1(4).

ular structure of **4** and the main bond distances and angles are given in Figure 1.

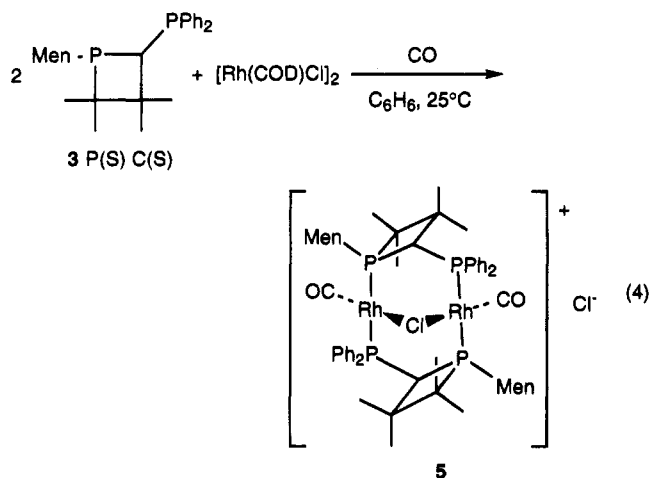
The most unique feature of complex **4** is the bicyclic structure formed by two fused four-membered rings, one of them containing the metal and the two phosphorus atoms. As a result, the ligand frame and its connection to the metal are conformationally fully fixed. A noteworthy structural parameter is the bond angle P(1)–Rh–P(5) of 70.99(6)°, which is significantly smaller than the corresponding P–M–P angles (ca. 75°)<sup>2c,3b</sup> in all other known 1,1-diphosphine complexes. As it appears that the P–M–P angle strain is responsible for the high reactivity of 14-electron metal fragments toward oxidative-addition processes,<sup>2</sup> we can expect an improved activity when 2-phosphinophosphetanes, such as **3**, are used as ligands in such complexes. The potential

(11) A 90 mg amount of phosphine **3** (0.2 mmol) was reacted with 0.2 mmol of (COD)<sub>2</sub>Rh<sup>+</sup>PF<sub>6</sub><sup>-</sup> in 2 mL of CH<sub>2</sub>Cl<sub>2</sub> at room temperature for a few minutes. The reaction was quantitative according to <sup>31</sup>P NMR analysis of the mixture. The solvent was partially removed. Orange crystals separated after addition of ether to the CH<sub>2</sub>Cl<sub>2</sub> solution. Cooling at –20 °C overnight afforded 95 mg of **4** (60%). Complex **4**: Anal. Calcd for C<sub>37</sub>H<sub>54</sub>F<sub>6</sub>P<sub>3</sub>Rh: C, 54.96; H, 6.73. Found: C, 54.38; H, 6.59. [α]<sub>D</sub> = –194 (c = 1, CHCl<sub>3</sub>).

(12) Crystal data for complex **4**: C<sub>37</sub>H<sub>54</sub>F<sub>6</sub>P<sub>3</sub>Rh·1/2CH<sub>2</sub>Cl<sub>2</sub>; space group P2<sub>1</sub>2<sub>1</sub>2<sub>1</sub> (No. 18); a = 25.475(2) Å, b = 27.952(1) Å, c = 11.318(2) Å, V = 8058.96 (1.04) Å<sup>3</sup>, Z = 8; d<sub>calcd</sub> = 1.403 g/cm<sup>3</sup>. Crystals contain two identical molecules in the asymmetric unit. Data were collected at –150 ± 0.5 °C on an Enraf-Nonius CAD4 diffractometer using Mo Kα radiation (λ = 0.710 73 Å) and a graphite monochromator. The crystal structure was solved and refined using the Enraf-Nonius MOLEN package. The SIR92 direct methods suite yielded a solution for all atoms. Anisotropic temperature factors were used for all non-hydrogen atoms in the final stages of least-squares refinement, and a non-Poisson weighting scheme was applied with a p factor equal to 0.08. The hydrogen atoms were included as fixed contributions in the final least-squares cycles: number of observed reflections 7496; final R = 0.048.

applicability of **3** to stoichiometric and catalytic reactions including an oxidative-addition step is thus suggested and open to investigation.

A second obvious use of the 1,1-diphosphine **3** is the building of new bimetallic complexes and the exploration of their reactivity. The chirality of the ligand provides a supplementary dimension with respect to previous studies. A bimetallic rhodium complex was synthesized, as shown in eq 4. The diphosphine **3** was



reacted with  $[(\text{COD})\text{RhCl}]_2$  in benzene; then, carbon monoxide was bubbled through the solution. Stirring under a CO atmosphere for about 2 h led to a yellow solution containing mainly the complex **5**,<sup>13</sup> which was purified by column chromatography (alumina, ether-methanol (90:10)) and obtained in 60% yield.

The <sup>31</sup>P NMR spectrum of **5** indicates the C<sub>2</sub> symmetry of the molecule with two equivalent phosphetane phosphorus atoms and two equivalent PPh<sub>2</sub> groups. <sup>31</sup>P NMR (CDCl<sub>3</sub>): δ 84.2, ddd, <sup>1</sup>J<sub>P-Rh</sub> = 110 Hz, <sup>2</sup>J<sub>P-P</sub> = 310 Hz (trans to Rh), <sup>2</sup>J<sub>P-P</sub> = 26 Hz; δ 16.5, ddd, <sup>1</sup>J<sub>P-Rh</sub> = 122 Hz.

The molecular structure of **5** was established by X-ray diffraction analysis.<sup>14</sup> Figure 2 shows the ORTEP diagram and lists the main bond distances and angles. In comparison to the corresponding dppm complex Rh<sub>2</sub>Cl<sub>2</sub>(CO)<sub>2</sub>(dppm)<sub>2</sub>,<sup>15</sup> complex **5** shows very different structural features. Whereas the dppm complex bears two terminal Cl ligands, one on each rhodium, in a *trans*

(13)  $[(\text{COD})\text{RhCl}]_2$  (50 mg) was added to a solution of **3** (90 mg, 0.2 mmol) in benzene (1 mL) at room temperature. After about 10 min, carbon monoxide was bubbled through the solution. The mixture was then stirred under the CO atmosphere for 2 h. The solution was directly chromatographed on a short alumina column, first with ether and then with ether-methanol (90:10) as eluent. The yellow band, eluted with the ether-methanol mixture, was collected. Removal of the solvent gave 75 mg (60%) of complex **5**. Selected data for complex **5** are as follows. Anal. Calcd for C<sub>60</sub>H<sub>84</sub>O<sub>2</sub>P<sub>4</sub>Cl<sub>2</sub>Rh<sub>2</sub>·2CH<sub>2</sub>Cl<sub>2</sub>: C, 52.90; H, 6.30. Found: C, 52.47; H, 6.48. IR: ν(CO) 1990 cm<sup>-1</sup>. <sup>13</sup>C NMR (CDCl<sub>3</sub>): δ 17.6 (Me), 21.9 (Me), 23.0 (2 Me), 24.0 (Me), 25.0 (d, J<sub>C-P</sub> = 12.2 Hz, CH<sub>2</sub>), 27.3 (dd, J<sub>C-P</sub> = 30.2, J<sub>C-P</sub> = 10.9 Hz, Me), 31.0 (d, J<sub>C-P</sub> = 5.5 Hz, Me), 32.8 (d, J<sub>C-P</sub> = 9.8 Hz, CH), 34.6 (CH<sub>2</sub>), 36.5 (CH<sub>2</sub>), 42.0 (CH), 45.4 (dd, J<sub>C-P</sub> = 16.8, J<sub>C-P</sub> = 10.7 Hz, PCHP), 46.7 (d, J<sub>C-P</sub> = 4.5 Hz, CMe<sub>2</sub>), 47.9 (dd, J<sub>C-P</sub> = 28.9, J<sub>C-P</sub> = 17.9 Hz, CMe<sub>2</sub>), 48.8 (d, J<sub>C-P</sub> = 7.5 Hz, CH).

(14) Crystal data for complex **5**: C<sub>60</sub>H<sub>84</sub>Cl<sub>2</sub>O<sub>2</sub>P<sub>4</sub>Rh<sub>2</sub>·2CH<sub>2</sub>Cl<sub>2</sub>; space group P2<sub>1</sub>2<sub>1</sub>2<sub>1</sub> (No. 19); a = 15.079(2) Å, b = 17.910(2) Å, c = 25.125(2) Å, V = 6785.4(2.2) Å<sup>3</sup>, Z = 4; d<sub>calc</sub> = 1.378 g/cm<sup>3</sup>. Data were collected at -150 ± 0.5 °C on an Enraf-Nonius CAD4 diffractometer using Mo Kα radiation (λ = 0.710 73 Å) and a graphite monochromator. The crystal structure was solved and refined using the Enraf-Nonius MOLEN package. The SIR92 direct methods suite yielded a solution for all atoms. Anisotropic temperature factors were used for all non-hydrogen atoms in the final stages of least-squares refinement, and a non-Poisson weighting scheme was applied with a p factor equal to 0.08: number of observed reflections 8046; final R = 0.054.

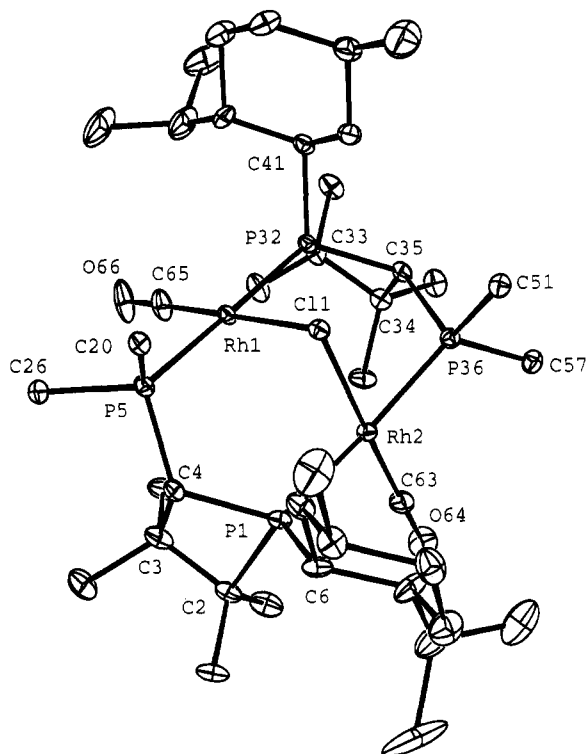


**Figure 2.** Crystal structure of complex **5**. For clarity, only the *ipso* carbon atoms of the phenyl rings are illustrated. Main bond lengths (Å) and angles (deg): Rh(1)–Cl(1), 2.390(1); Rh(2)–Cl(1), 2.372(1); Rh(1)–P(5), 2.354(1); Rh(1)–P(32), 2.324(1); Rh(2)–P(36), 2.352(1); Rh(2)–P(1), 2.336(1); Rh(1)–C(65), 1.796(6); P(5)–C(4), 1.839(5); C(4)–P(1), 1.879(5); P(1)–C(2), 1.881(5); C(2)–C(3), 1.564(9); C(3)–C(4), 1.585(7); Rh(1)–Cl(1)–Rh(2), 85.87(4); Rh(1)–P(5)–C(4), 110.9(2); P(5)–C(4)–P(1), 121.7(3); C(4)–P(1)–Rh(2), 120.2(2); C(4)–P(1)–C(2), 77.1(2); P(1)–C(2)–C(3), 89.8(3); C(2)–C(3)–C(4), 96.2(4); C(3)–C(4)–P(1), 89.3(3).

respective configuration, complex **5** shows a bridging chlorine atom, the second one acting as a counterion to the cationic complex. The structure of **5** is then much more similar to that of the cationic “A-frame” complex  $[\text{Rh}_2(\text{CO})_2\text{Cl}(\text{dppm})_2]^+\text{BF}_4^-$ .<sup>16</sup> The bridging chlorine atom lies on the C<sub>2</sub> symmetry axis of the molecule. Bonding angles and distances are in reasonable agreement with the above-cited structural determination, except for those directly affected by the phosphetane moiety.<sup>17</sup>

To our knowledge, complex **5** is the first bimetallic “A-frame” complex of a homochiral 1,1-diphosphine. Its easy accessibility encourages the development of the synthesis and reactivity of new homo- and heterobimetallic complexes of **3** and the exploration of their implications regarding bimetallic homogeneous asymmetric catalysis.

**Supporting Information Available:** For **4** and **5**, tables of X-ray crystal data and experimental details, positional and thermal parameters, and bond lengths and angles (18 pages). Ordering information is given on any current masthead page.

OM950601C

(15) (a) Cowie, M.; Dwight, S. K. *Inorg. Chem.* **1980**, *19*, 2500. (b) Mague, J. T. *Inorg. Chem.* **1969**, *8*, 119.

(16) Cowie, D.; Dwight, S. K. *Inorg. Chem.* **1979**, *18*, 2700.

(17) As an example, the Rh(2)–P(1)–C(4) and P(1)–C(4)–P(5) angles (120.2(2) and 121.7(3)°, respectively) are significantly larger than those previously observed in dppm complexes (112 and 115°, respectively).

# Highly Efficient Enantioselective Pauson-Khand Reactions<sup>†</sup>

Alistair M. Hay, William J. Kerr,\* George G. Kirk, and David Middlemiss<sup>‡</sup>

Department of Pure and Applied Chemistry, University of Strathclyde,  
Thomas Graham Building, Glasgow G1 1XL, Scotland, U.K.

Received September 1, 1995<sup>§</sup>

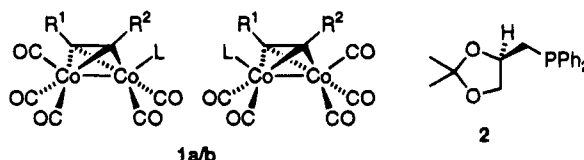
**Summary:** Diastereomeric (alkyne)pentacarbonyldicobalt complexes containing the chiral phosphine ligand (*R*)-(+)-Glyphos have been synthesized and separated chromatographically. The isolated, optically pure diastereomeric complexes have been employed in intermolecular Pauson-Khand reactions, using anhydrous *N*-methylmorpholine *N*-oxide as the reaction promoter under mild conditions, to give high yields of cyclopentenone products in good to excellent enantiomeric excesses.

The cobalt-mediated Pauson-Khand cyclization has been shown to be a powerful synthetic tool in organic synthesis.<sup>1</sup> More recently, this annulation has been improved by utilizing dry-state adsorption techniques<sup>2</sup> and tertiary amine *N*-oxides.<sup>3</sup> In particular, amine *N*-oxides have been used to accelerate the rate of cyclopentenone formation in both inter- and intramolecular examples at low temperatures (0–40 °C).

To date, examples of asymmetric versions of the Pauson-Khand reaction have been few in number and have been utilized with a limited range of substrates.<sup>4–6</sup> Diastereoselective approaches to intramolecular cyclizations using chiral auxiliaries are known<sup>4</sup> and have been extended to the intermolecular version of the cyclization.<sup>5</sup> However, these auxiliary-controlled examples are either restricted to the use of specific substrates or show poor stereocontrol and, in some cases, involve the use

of tediously prepared starting materials. In this communication we disclose the first series of efficient asymmetric intermolecular Pauson-Khand reactions which result in the formation of cyclopentenone products, containing no residual chiral auxiliary, in high yields and good to excellent enantiomeric excesses.

Alkyne complexes of the type **1** are chiral around the C<sub>2</sub>Co<sub>2</sub> cluster, provided R<sup>1</sup> ≠ R<sup>2</sup> and L ≠ CO. Examples where the ligand L is a phosphine such as triphenylphosphine and trimethyl phosphite are known,<sup>7</sup> and, if the optically active phosphine (*R*)-(+)-Glyphos (**2**) is used, the two diastereoisomers **1a** and **1b** are formed.<sup>8,9</sup> Previous studies on the phenylacetylene complex (**1a,b**: R<sup>1</sup> = Ph, R<sup>2</sup> = H, L = (*R*)-(+)-Glyphos (**2**)), by Pauson



and co-workers, have shown that after the separation of the diastereomeric complexes, by fractional recrystallization, reaction of one diastereoisomer with norbornene gave only a 31% yield of the Pauson-Khand product, but with excellent enantioselectivity.<sup>8</sup> Despite the high stereochemical control in this isolated example, the reaction yields were consistently poor. Furthermore, separation of the diastereoisomers was not trivial and the elevated temperatures required for reaction led to the interconversion of the two diastereomeric forms of the starting complex.

The initial aims of this study were to show that a range of homochiral complexes containing the Glyphos ligand were readily accessible and, in turn, that the diastereomeric mixtures could be more routinely separated. The chiral ligand (*R*)-(+)-Glyphos (**2**) was prepared in four steps from D-mannitol (**3**) by a modification of the known procedure.<sup>10</sup> The final step involved addition of potassium diphenylphosphide as a THF

<sup>†</sup> This paper is dedicated with warmth and the utmost respect to Professor Peter L. Pauson on the occasion of his 70th birthday.

<sup>‡</sup> Present address: Glaxo Wellcome, Medicines Research Centre, Gunnels Wood Road, Stevenage, Hertfordshire SG1 2NY, England, U.K.

<sup>§</sup> Abstract published in *Advance ACS Abstracts*, October 1, 1995.

(1) For reviews on the Pauson-Khand reaction see: Pauson, P. L.; Khand, I. U. *Ann. N.Y. Acad. Sci.* **1977**, *295*, 2. Pauson, P. L. *Tetrahedron* **1985**, *41*, 5855. Schore, N. E. *Org. React.* **1991**, *40*, 1. Schore, N. E. In *Comprehensive Organic Synthesis*; Trost, B. M., Ed.; Pergamon: Oxford, U.K., 1991; Vol. 5, pp 1037–1064.

(2) Smit, W. A.; Gybin, A. S.; Simonyan, S. O.; Shashkov, A. S.; Tarasov, V. A.; Ibragimov, I. I. *Izv. Akad. Nauk SSSR, Ser. Khim.* **1985**, *2650*. Smit, W. A.; Gybin, A. S.; Shashkov, A. S.; Strychkov, Y. T.; Kyz'mina, L. G.; Mikaelian, G. S.; Caple, R.; Swanson, E. D. *Tetrahedron Lett.* **1986**, *27*, 1241. Simonyan, S. O.; Smit, W. A.; Gybin, A. S.; Shashkov, A. S.; Mikaelian, G. S.; Tarasov, V. A.; Ibragimov, I. I.; Caple, R.; Froen, D. E. *Tetrahedron Lett.* **1986**, *27*, 1245. Smit, W. A.; Simonyan, S. O.; Tarasov, V. A.; Mikaelian, G. S.; Ibragimov, I. I.; Caple, R.; Froen, D. E.; Kragger, A. *Synthesis* **1989**, *472*. Smit, W. A.; Kireev, S. L.; Nefedov, O. M.; Tarasov, V. A. *Tetrahedron Lett.* **1989**, *30*, 4021.

(3) Shambayati, S.; Crowe, W. E.; Schreiber, S. L. *Tetrahedron Lett.* **1990**, *31*, 5289. Jeong, N.; Chung, Y. K.; Lee, B. Y.; Lee, S. H.; Yoo, S.-E. *Synlett* **1991**, 204. Chung, Y. K.; Lee, B. Y.; Jeong, N.; Hudeck, M.; Pauson, P. L. *Organometallics* **1993**, *12*, 220. Krafft, M. E.; Scott, I. L.; Romero, R. H.; Feibelmann, S.; Van Pelt, C. E. *J. Am. Chem. Soc.* **1993**, *115*, 7199.

(4) Castro, J.; Moyano, A.; Pericàs, M. A.; Riera, A.; Greene, A. E. *Tetrahedron: Asymmetry* **1994**, *5*, 307 and references cited therein.

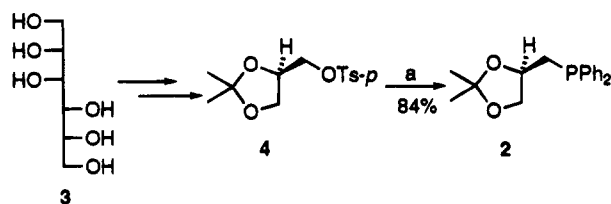
(5) Bernardes, V.; Verdager, X.; Kardos, N.; Riera, A.; Moyano, A.; Pericàs, M. A.; Greene, A. E. *Tetrahedron Lett.* **1994**, *35*, 575. Verdager, X.; Moyano, A.; Pericàs, M. A.; Riera, A. *J. Am. Chem. Soc.* **1994**, *116*, 2153. Fonquerna, S.; Moyano, A.; Pericàs, M. A.; Riera, A. *Tetrahedron* **1995**, *51*, 4239. Park, H. P.; Lee, B. Y.; Kang, Y. K.; Chung, Y. K. *Organometallics* **1995**, *14*, 3104.

(6) As well as the techniques described in the publications of refs 4 and 5, methods which simply involve complexation of homochiral enynes and their subsequent cyclizations (often with high degrees of stereoselectivity) have also been described: Magnus, P.; Becker, D. P. *J. Am. Chem. Soc.* **1987**, *109*, 7495. Roush, W. R.; Park, J. C. *Tetrahedron Lett.* **1991**, *32*, 6285. Takano, S.; Inomato, K.; Ogasawana, K. *J. Chem. Soc., Chem. Commun.* **1992**, 169. Takano, S.; Inomato, K.; Ogasawana, K. *Chem. Lett.* **1992**, 443. Stolle, A.; Becker, H.; Salaun, J.; de Meijere, A. *Tetrahedron Lett.* **1994**, *35*, 3517. Stolle, A.; Becker, H.; Salaun, J.; de Meijere, A. *Tetrahedron Lett.* **1994**, *35*, 3521.

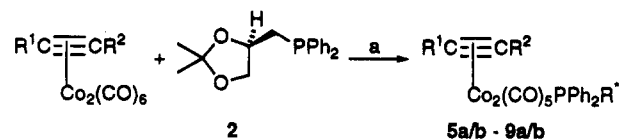
(7) Dunn, J. A.; Pauson, P. L. *J. Organomet. Chem.* **1991**, *419*, 383. D'Agostino, M. F.; Frampton, C. S.; McGlinchey, M. J. *Organometallics* **1990**, *9*, 2972.

(8) Bladon, P.; Pauson, P. L.; Brunner, H.; Eder, R. *J. Organomet. Chem.* **1988**, *355*, 449.

(9) Brunner, H.; Niederhuber, A. *Tetrahedron: Asymmetry* **1990**, *1*, 711.

Scheme 1<sup>a</sup>

<sup>a</sup> Conditions:  $\text{KPPH}_2/\text{THF}$ ; toluene; room temperature; 20 min.

Scheme 2<sup>a</sup>

a) Toluene, 60–70 °C, 3–4 h.

$\text{PPH}_2\text{R}^* = R\text{-}(+)\text{-Glyphos}$

<sup>a</sup> Conditions and definitions: toluene; 60–70 °C; 3–4 h;  $\text{PPH}_2\text{R}^* = R\text{-}(+)\text{-Glyphos}$ .

Table 1. Formation of Cobalt–Alkyne Complexes Containing  $R\text{-}(+)\text{-Glyphos}$ 

R <sup>1</sup>	R <sup>2</sup>	product	yield (%)
Ph	H	<b>5a,b</b>	78 <sup>a</sup>
$\text{CMe}_2\text{OH}$	H	<b>6a,b</b>	100
$\text{CH}_2\text{OH}$	H	<b>7a,b</b>	83 <sup>b</sup>
TMS	H	<b>8a,b</b>	68
TMS	$\text{CH}_3$	<b>9a,b</b>	57 <sup>c</sup>

<sup>a</sup> Bis- $R\text{-}(+)\text{-Glyphos}$  product also isolated in 13% yield. <sup>b</sup> Bis- $R\text{-}(+)\text{-Glyphos}$  product also isolated in 12% yield. <sup>c</sup> Yield based on recovered starting material.

solution<sup>11</sup> to the tosylate (**4**), giving an improved overall yield of 34% (Scheme 1). In turn, the diastereomeric complexes **5a,b-9a,b** were readily formed under thermal conditions in good to high yields (Scheme 2, Table 1). Furthermore, it was found that the diastereomeric mixtures of complexes **5a,b-7a,b** could be efficiently separated by preparative HPLC.<sup>12,13</sup>

With a range of optically pure complexes now readily available in good yields, our attention was turned to their use as substrates in cyclopentenone synthesis. The strained alkenes norbornene and norbornadiene are recognized as efficient olefins when used in the Pauson–Khand annulation. The first of these, norbornene, was used in the initial reactions with *diastereomeric mixtures* of our complexes. These studies showed that the complexes containing the chiral phosphine ligand reacted less readily than the parent hexacarbonyl complexes and generally gave lower yields and low enantiomeric excesses (ee; 0–13%) of cyclopentenone products. As an example, a 1:1 mixture of the diastereoisomers **5a** and **5b** gave a 52% yield of product **10a,b** in only 12% ee following reaction in toluene at 70 °C for 18 h, whereas reaction of the parent hexacarbonyl complex (1:  $\text{R}^1 = \text{Ph}$ ,  $\text{R}^2 = \text{H}$ ,  $\text{L} = \text{CO}$ ) gave a 75% yield of the same product after heating at the same temperature for

(10) Schmidt, U.; Talbiersky, J.; Bartkowiak, F.; Wild, J. *Angew. Chem., Int. Ed. Engl.* **1980**, *19*, 198. Baldwin, J. J.; Raab, A. W. Q.; Mensler, K.; Arison, B. H.; McLure, D. E. *J. Org. Chem.* **1978**, *43*, 4876. Brunner, H.; Leyerer, H. *J. Organomet. Chem.* **1987**, *334*, 369.

(11) Available commercially from Aldrich Chemical Co.

(12) Separation was achieved by use of a SPHERISORB™ Si-SB3-9961 HPLC column with varying percentages of *tert*-butyl methyl ether in heptane as the mobile phase.

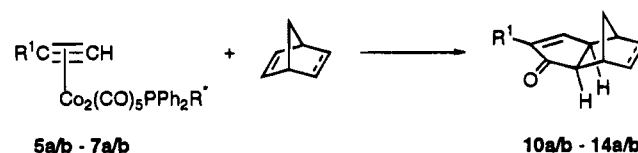
(13) Complexes **8a,b-9a,b** could not be separated on a preparative scale, although they could be separated on an analytical column.

Table 2. Enantioselective Pauson–Khand Reactions of Complexes **5-7a**

complex	R <sup>1</sup>	product	yield (%)	ee (%) <sup>c</sup>
Reactions with Norbornene <sup>b</sup>				
<b>5a</b>	Ph	<b>10a,b</b>	76	>99 of <b>10a</b>
<b>5b</b>	Ph	<b>10a,b</b>	79	>99 of <b>10b</b>
<b>6a</b>	$\text{CMe}_2\text{OH}$	<b>11a,b</b>	77	64 of <b>11a</b>
<b>6b</b>	$\text{CMe}_2\text{OH}$	<b>11a,b</b>	83	75 of <b>11b</b>
<b>6a</b>	$\text{CMe}_2\text{OH}$	<b>11a,b</b>	73 <sup>d</sup>	80 of <b>11a</b>
<b>6b</b>	$\text{CMe}_2\text{OH}$	<b>11a,b</b>	65 <sup>d</sup>	75 of <b>11b</b>
<b>7a</b>	$\text{CH}_2\text{OH}$	<b>12a,b</b>	90	93 of <b>12a</b>
<b>7b</b>	$\text{CH}_2\text{OH}$	<b>12a,b</b>	69	83 of <b>12b</b>
Reactions with Norbornadiene <sup>b</sup>				
<b>6a</b>	$\text{CMe}_2\text{OH}$	<b>13a,b</b>	77	75 of <b>13a</b>
<b>6b</b>	$\text{CMe}_2\text{OH}$	<b>13a,b</b>	75	74 of <b>13b</b>
<b>7a</b>	$\text{CH}_2\text{OH}$	<b>14a,b</b>	75	90 of <b>14a</b>
<b>7b</b>	$\text{CH}_2\text{OH}$	<b>14a,b</b>	77	84 of <b>14b</b>

<sup>a</sup> 6 equiv of anhydrous NMO added to a  $\text{CH}_2\text{Cl}_2$  solution of the complex and alkene (6–8 h). <sup>b</sup> 1.1 equiv of alkene was used in every reaction. <sup>c</sup> All enantiomeric excesses were calculated using a CHIRALCEL-OD-H HPLC column and 2% EtOH in heptane as the mobile phase. <sup>d</sup> Reaction temperature of 0 °C; reaction time of 18 h.

Scheme 3



only 4 h. Additionally, the complexes **7a,b** failed to give any cyclopentenone products under the same thermal conditions. Furthermore, even when the single diastereoisomers **6a** and **6b** were reacted with norbornene in toluene at 70 °C, enantiomeric excesses of only 14% and 21% were obtained. At the elevated temperatures employed in these reactions, we believe that interconversion of the diastereomeric complexes was occurring, leading to the low enantiomeric excesses achieved. Despite this and the lowered reactivity of the Glyphos complexes, we then endeavored to develop conditions which would provide cyclopentenones in enhanced rates and yields with good enantioselectivity.

As previously mentioned, amine *N*-oxides, as additive in the Pauson–Khand reaction, have been shown to readily promote annulations in a wide range of examples both in our laboratories<sup>14</sup> and elsewhere.<sup>3</sup> Following studies with suitable oxidants and careful optimization of conditions, anhydrous *N*-methylmorpholine *N*-oxide (NMO) was found to be the most efficient promoter in our reactions with the Glyphos-containing complexes. More specifically, when NMO is utilized in dichloromethane, reactions between single diastereomeric complexes **5a,b-7a,b** and norbornene or norbornadiene proceed relatively quickly (6–8 h) at room temperature (Scheme 3, Table 2).

More importantly, we have found that the reactions with both alkenes proceed to give only the *exo*-cyclopentenone products in good yields (65–90%) and, to our delight, in consistently high and, in some cases, excellent enantiomeric excesses (64–>99%). Additionally, reactions have also been shown to proceed at lower temperatures (0 °C), albeit over a longer period of 18 h, to give comparable yields and ee's (*e.g.*, Table 2, **6a,b**).

(14) Johnstone, C.; Kerr, W. J.; Lange, U. *J. Chem. Soc., Chem. Commun.* **1995**, 457.

It is also important to note that, despite the *R*-(+)-form of Glyphos having been used in every complex, each single diastereomeric complex yields one of the two possible enantiomeric forms of the cyclopentenone product in excess (*e.g.* **5a** → >99% ee of **10a**, and **5b** → >99% ee of **10b**).<sup>15</sup> This observation leads us to conclude that the enantioselection does *not* arise from the influence of the chiral Glyphos ligand but from the chiral C<sub>2</sub>Co<sub>2</sub> core. Therefore, the chiral *R*-(+)-Glyphos complexes, in principle, can provide routes to cyclopentenone products enriched with the enantiomer of choice.

In summary, we have shown that a range of cobalt-alkyne complexes containing the chiral ligand *R*-(+)-Glyphos can be readily synthesized and the diastereomers routinely separated by preparative HPLC. In turn, we have formulated enantioselective intermolecular Pauson-Khand cyclization techniques which are more flexible and applicable than the diastereoselective

processes previously reported. Using anhydrous *N*-methylmorpholine *N*-oxide under mild conditions, which prevent racemization of the cobalt compounds, techniques have been developed to give the cyclopentenone products in good to high yields and with powerful asymmetric control. Studies on a range of alkenes in this asymmetric version of the Pauson-Khand reaction are currently underway. The physical properties of the pure diastereomeric complexes, their diastereoselective formation, and a range of further reactions are currently being investigated in our laboratory and will be reported in due course.

**Acknowledgment.** We thank Glaxo Research and Development Ltd. for funding this research.

**Supporting Information Available:** Text giving all experimental procedures and relevant spectroscopic characterizations for the organometallic complexes and cyclopentenone products listed in Tables 1 and 2 (6 pages). This material is contained in many libraries on microfiche, immediately follows this article in the microfilm version of the journal, can be ordered from the ACS, and can be downloaded from the Internet; see any current masthead page for ordering information and Internet access instructions.

OM950689U

(15) At the present time the absolute configurations of the diastereomeric complexes or the enantiomeric products are unknown. However, these issues are currently being addressed by the combination of derivatization and crystallographic studies. It should also be stated that optical rotation studies show consistency in that one form of the starting complex gives predominantly the cyclopentenone product of the same sign; *e.g.*, at room temperature **6a** ( $[\alpha]_D^{20} = -168^\circ$ ) gives **11a,b** in 64% ee of **11a** ( $[\alpha]_D^{20} = -38.0^\circ$ ) and **6b** ( $[\alpha]_D^{20} = +172^\circ$ ) gives **11a,b** in 75% ee of **11b** ( $[\alpha]_D^{20} = +45.1^\circ$ ).

# Synthesis and Crystal Structure of a New Binuclear Organoiron Nonbridged Complex: Bis(*tert*-butoxycarbonyl)octacarbonyldiiron, [Fe(CO<sub>2</sub><sup>t</sup>Bu)(CO)<sub>4</sub>]<sub>2</sub>

Denis Luart,<sup>†</sup> Murielle Sellin,<sup>†</sup> Pascale Laurent,<sup>†</sup> Jean-Yves Salaün,<sup>†</sup>  
Roger Pichon,<sup>‡</sup> Loïc Toupet,<sup>§</sup> and Hervé des Abbayes<sup>\*,†</sup>

Laboratoire de Chimie, Electrochimie Moléculaires et Chimie Analytique, URA CNRS 322,  
and Laboratoire de Résonance Magnétique Nucléaire, Université de Bretagne Occidentale,  
UFR Sciences et Techniques, BP 809, 29285 Brest cedex, France, and Groupe Matière  
Condensée et Matériaux, URA CNRS 804, Université de Rennes 1, Campus de Beaulieu,  
35042 Rennes cedex, France

Received July 19, 1995<sup>®</sup>

**Summary:** The reaction of Na[Fe(CO<sub>2</sub><sup>t</sup>Bu)(CO)<sub>4</sub>] with 0.5 equiv of ClCOCOCl in tetrahydrofuran affords the new complex [Fe(CO<sub>2</sub><sup>t</sup>Bu)(CO)<sub>4</sub>]<sub>2</sub>, which is characterized by single-crystal X-ray diffraction analysis. Structural and spectroscopic observations show that it does not present any bridging ligands.

Binuclear complexes appear to afford an obvious link between the chemistry of mononuclear complexes, used extensively as homogeneous catalysts,<sup>1</sup> and those of polynuclear clusters, which may act as models for complex systems such as heterogeneous catalysts.<sup>2</sup>

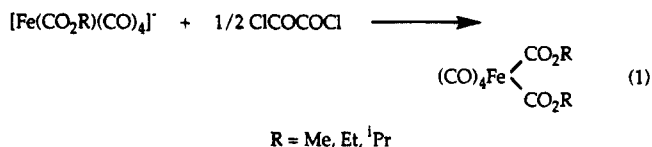
The nature of the chemical bonding in metal dimer compounds is of considerable interest, and among the numerous complexes with a direct metal–metal bond,<sup>3</sup> those that are stable without bridging ligands are more scarce.<sup>4</sup>

Homodinuclear complexes with a metal–metal single bond and an unsupported linkage are known in particular for metals in lower (–1, 0, 1) oxidation states. For example, compounds such as M<sub>2</sub>(CO)<sub>10</sub> (M = Mn, Tc, Re)<sup>5</sup> and cyclopentadienylmetal complexes M<sub>2</sub>-Cp<sub>2</sub>(CO)<sub>6</sub> (M = Cr, Mo, W)<sup>6</sup> are worthy of mention. Among the transition metals of the group 8, the non-bridged binuclear complexes Os<sub>2</sub>H<sub>2</sub>(CO)<sub>8</sub>,<sup>7</sup> Os<sub>2</sub>X<sub>2</sub>(CO)<sub>8</sub> (X = Cl, I),<sup>7,8</sup> Os<sub>2</sub>Me<sub>2</sub>(CO)<sub>8</sub>,<sup>9</sup> and Ru<sub>2</sub>(EMe<sub>3</sub>)<sub>2</sub>(CO)<sub>8</sub> (E =

Si, Ge, Sn)<sup>10</sup> have been characterized. Their homologue Fe<sub>2</sub>I<sub>2</sub>(CO)<sub>8</sub> has been spectroscopically described,<sup>11</sup> but compounds such as Fe<sub>2</sub>(R)(R')(CO)<sub>8</sub> with R, R' = alkyl, acyl, alkoxy-carbonyl, ..., are, to our knowledge, unknown.

We report herein the synthesis and the spectroscopic and the structural characterizations of the first non-bridged binuclear iron complex bearing alkoxy-carbonyl and carbonyl ligands.

We recently described the synthesis of *cis*-bis(alkoxy-carbonyl)tetracarbonyliron complexes, Fe(CO<sub>2</sub>R)<sub>2</sub>(CO)<sub>4</sub>, with R = Me, Et, <sup>i</sup>Pr by reaction of (alkoxy-carbonyl)-tetracarbonylferrates, [Fe(CO<sub>2</sub>R)(CO)<sub>4</sub>]<sup>–</sup>, with 1/2 equiv of oxalyl chloride (eq 1).<sup>12</sup>



Under the same conditions,<sup>13</sup> the reaction of (*tert*-butoxycarbonyl)tetracarbonylferrate, [Fe(CO<sub>2</sub><sup>t</sup>Bu)(CO)<sub>4</sub>]<sup>–</sup>, with oxalyl chloride does not lead to the corresponding *cis*-bis(*tert*-butoxycarbonyl)tetracarbonyliron complex. Indeed, the IR spectrum of the solution reveals the presence of the new neutral compound **1**. This complex is purified by low-temperature recrystallization from hexane to afford orange microcrystals. IR and NMR spectroscopic data<sup>15</sup> highlight the presence of both Fe(CO)<sub>4</sub> and CO<sub>2</sub><sup>t</sup>Bu groups. The NMR data show for **1** a symmetry that is confirmed by X-ray crystallography.<sup>16</sup> Its molecular structure is displayed in

(8) Bruce, M. I.; Cooke, M.; Green, M.; Westlake, D. J. *J. Chem. Soc. A* **1969**, 987.

(9) Motyl, K. M.; Norton, J. R.; Schauer, C. K.; Anderson, O. P. *J. Am. Chem. Soc.* **1982**, *104*, 7325.

(10) (a) Cotton, J. D.; Knox, S. A. R.; Stone, F. G. A. *Chem. Commun.* **1967**, 965. (b) Knox, S. A. R.; Stone, F. G. A. *J. Chem. Soc. A* **1969**, 2259. (c) Knox, S. A. R.; Stone, F. G. A. *J. Chem. Soc. A* **1971**, 2874.

(11) Cotton, F. A.; Johnson, B. F. G. *Inorg. Chem.* **1967**, *6*, 2113.

(12) Salaün, J.-Y.; Le Gall, G.; Laurent, P.; des Abbayes, H. *J. Organomet. Chem.* **1992**, *441*, 99.

(13) To a solution of KO<sup>t</sup>Bu (10 mmol, 1120 mg) in 20 mL of THF at 0 °C is added Fe(CO)<sub>5</sub> (15 mmol, 2 mL), according to the procedure used for the preparation of anions [Fe(CO<sub>2</sub>R)(CO)<sub>4</sub>]<sup>–</sup>.<sup>14</sup> After 0.5 h, the temperature is lowered to –20 °C and ClCOCOCl (5 mmol, 0.436 mL) is added. The solution instantly turns brown. The solvent is removed after 15 min of stirring, and the residue is extracted with hexane. After filtration, the solution is maintained overnight at –30 °C, yielding orange microcrystals (60% yield vs ClCOCOCl).

(14) McLean, J. L. *Ph.D. Thesis*, New York University, 1975.

<sup>†</sup> Laboratoire de Chimie, Electrochimie Moléculaires et Chimie Analytique, Université de Bretagne Occidentale.

<sup>‡</sup> Laboratoire de Résonance Magnétique Nucléaire, Université de Bretagne Occidentale.

<sup>§</sup> Université de Rennes 1.

<sup>®</sup> Abstract published in *Advance ACS Abstracts*, November 1, 1995.

(1) (a) Collman, J. P.; Hegedus, L. S.; Norton, J. R.; Finke, R. G. *Principles and Applications of Organotransition Metal Chemistry*, 2nd ed.; University Science Books: Mill Valley, CA, 1987. (b) Parshall, G. W. *Homogeneous Catalysis*; Wiley: New York, 1980. (c) Masters, C. *Homogeneous Transition Catalysts*; Chapman and Hall: London, 1981.

(2) (a) Muettterties, E. L.; Rhodin, P. N.; Brucker, C. F.; Pretzer, W. R. *Chem. Rev.* **1979**, *79*, 91. (b) *Transition Metal Clusters*; Johnson, B. F. G., Ed.; Wiley: New York, 1985. (c) *Metal Clusters*; Muskovits, M., Ed.; Wiley: New York, 1986.

(3) (a) Cotton, F. A.; Walton, R. A. *Multiple Bonds Between Metal Atoms*, 2nd ed., Oxford University Press: London, 1993. (b) Chisholm, M. H. *Acc. Chem. Res.* **1990**, *23*, 419.

(4) Herberhold, M.; Jin, G.-X. *Angew. Chem., Int. Ed. Engl.* **1994**, *33*, 964.

(5) (a) M = Mn: Almeningen, A.; Jacobsen, G. G.; Seip, H. M. *Acta Chem. Scand.* **1969**, *23*, 685. (b) M = Tc: Bailey, M. F.; Dahl, L. F. *Inorg. Chem.* **1965**, *4*, 1140. (c) M = Mn, Re: Churchill, M. R.; Amoh, K. N.; Wasserman, H. J. *Inorg. Chem.* **1981**, *20*, 1609.

(6) (a) M = Cr: Adams, R. D.; Collins, D. M.; Cotton, F. A. *J. Am. Chem. Soc.* **1974**, *96*, 749. (b) M = Mo, W: Adams, R. D.; Collins, D. M.; Cotton, F. A. *Inorg. Chem.* **1974**, *13*, 1086.

(7) Moss, J. R.; Graham, W. A. G. *Inorg. Chem.* **1977**, *16*, 75.



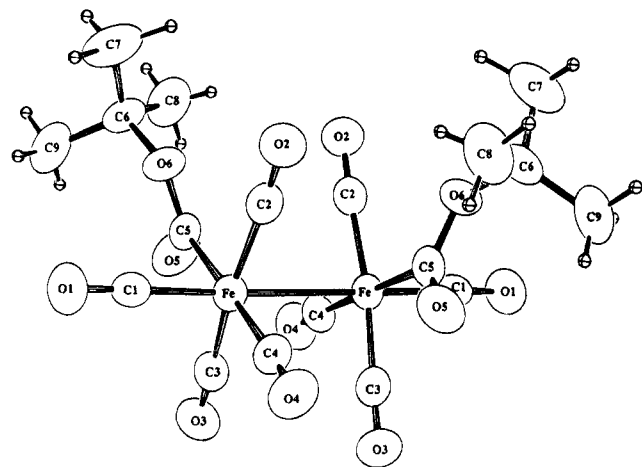


**Figure 1.** Molecular structure of **1**. Selected bond lengths (Å): Fe–Fe, 2.840(1); Fe–C(1), 1.819(5); Fe–C(2), 1.806(8); Fe–C(3), 1.816(8); Fe–C(4), 1.852(5); Fe–C(5), 2.024(4). Selected bond angles (deg): Fe–Fe–C(1), 174.2(2); Fe–Fe–C(2), 85.0(1); Fe–Fe–C(3), 83.5(2); Fe–Fe–C(4), 91.4(1); C(1)–Fe–C(2), 95.8(2); C(1)–Fe–C(3), 95.1(2); C(1)–Fe–C(4), 94.2(2); C(2)–Fe–C(3), 167.1(2).

Figure 1, together with the atom-numbering scheme and selected bond distances and angles.

Figure 1 reveals that complex **1** is a dimeric compound formed by two  $\text{Fe}(\text{CO}_2^t\text{Bu})(\text{CO})_4$  entities which presents no bridging ligand between the two metal centers. This absence of bridging carbonyl groups was already shown by IR and  $^{13}\text{C}$  NMR spectroscopy. The iron–iron bond (2.84 Å) is consistent with a single bond between the two metal centers, since the covalent radius of iron is estimated to be near 1.43 Å.<sup>17</sup> The coordination about each iron atom can be described as a distorted octahedron with the *tert*-butoxycarbonyl ligand in a position *cis* to the metal–metal bond. This is justified by a consideration of the angles defined by the ligands surrounding the central iron atom of  $\text{C}(1)\text{--Fe--C}(2) = 95.8^\circ$ ,  $\text{C}(1)\text{--Fe--C}(3) = 95.1^\circ$ ,  $\text{C}(1)\text{--Fe--C}(4) = 94.2^\circ$ ,  $\text{C}(1)\text{--Fe--C}(5) = 84.4^\circ$ , and  $\text{Fe--Fe--C}(1) = 174.2^\circ$ . Three of the four iron–carbonyl ( $\text{C}(1\text{--}3)$ ) bond distances (1.806–1.816 Å) are within the range of distances found for other carbonyliron complexes.<sup>17,18</sup>  $\text{Fe--C}(4)$  (1.852 Å) is significantly longer; this results from its position *trans* to the electron-withdrawing *tert*-butoxycarbonyl ligand, which decreases electrons available for back-donation. The distance between the metal and its *tert*-butoxycarbonyl ligand ( $\text{Fe--C}(5) = 2.024$  Å) and the lengths of the  $\text{C=O}$  bonds of this ligand ( $\text{C}(5)\text{--O}(5) = 1.197$  Å) are typical of other  $[\text{Fe}](\text{CO}_2^t\text{Bu})$  complexes.<sup>18</sup>

(15) **1**: IR (hexane)  $\nu_{\text{CO}}$ (terminal) 2114 (w), 2068 (vs), 2050 (vs, br), 2024 (vs) and  $\nu_{\text{C--O}}$  1667 (s, br)  $\text{cm}^{-1}$ ;  $^1\text{H}$  NMR (300 MHz;  $d_8$ -THF,  $-10^\circ\text{C}$ ) 1.39 (s) ppm;  $^{13}\text{C}\{^1\text{H}\}$  NMR (75.47 MHz;  $d_8$ -THF,  $-10^\circ\text{C}$ ) 212.0, 205.7, 207.7 (2:1:1) (CO), 194.1 ( $\text{CO}_2^t\text{Bu}$ ), 83.4 ( $\text{C}(\text{CH}_3)_3$ ), 28.6 ppm ( $\text{CH}_3$ ). Anal. Calcd for  $\text{Fe}_2\text{C}_{18}\text{H}_{18}\text{O}_{12}$ : C, 40.18; H, 3.37. Found: C, 40.24; H, 3.37.

(16) Crystal data:  $\text{Fe}_2\text{C}_{18}\text{H}_{18}\text{O}_{12}$ ,  $M_r = 538.04$ ; monoclinic, space group  $\text{C}2/c$ ;  $a = 19.302(4)$  Å,  $b = 10.151(3)$  Å,  $c = 12.099(2)$  Å,  $\beta = 97.66(2)^\circ$ ,  $V = 2349.4(9)$  Å<sup>3</sup>,  $Z = 4$ ,  $D_c = 1.521$  g  $\text{cm}^{-3}$ ;  $\mu(\text{Mo K}\alpha) = 12.88$   $\text{cm}^{-1}$ ,  $F(000) = 1096$ ,  $T = 294$  K. A parallelepiped of dimensions  $0.25 \times 0.35 \times 0.25$  mm was selected and studied on an Enraf-Nonius CAD 4 diffractometer, with graphite-monochromatized Mo K $\alpha$  radiation. The structure was solved by the Patterson method. A total of 1929 reflections were collected, of which 1226 ( $I \geq 2\sigma(I)$ ) were used to give  $R = 0.040$  and  $R_w = 0.038$ .

(17) Putnik, C. F.; Welter, J. J.; Stucky, G. D.; D'Aniello, M. J.; Sosinski, B. A.; Kirner, J. F.; Muetterties, E. L. *J. Am. Chem. Soc.* **1978**, *100*, 4107.

(18) Luart, D. Ph.D. Thesis, University of Brest, to be submitted for publication.

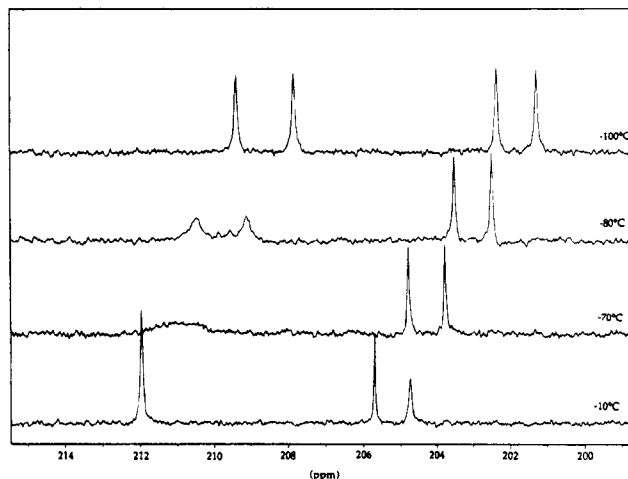


**Figure 2.** Temperature-dependent  $^{13}\text{C}$  NMR spectra of complex **1**.

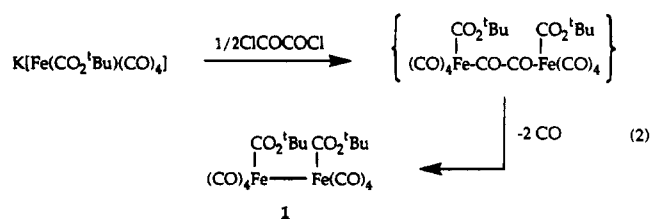
It is noteworthy that while in  $\text{Fe}_2\text{I}_2(\text{CO})_8$  the halide ligands are in positions *trans* to the iron–iron bond,<sup>11</sup> complex **1** possesses the same *cis* geometry as the dinuclear osmium homologues  $\text{Os}_2\text{Z}_2(\text{CO})_8$  ( $Z = \text{H}, \text{Cl}, \text{I}, \text{Me}$ ).<sup>7–9</sup>

To our knowledge, **1** is the first fully characterized nonbridged diiron complex bearing organic and carbonyl ligands.

The  $^{13}\text{C}$  NMR signals of the carbonyls of complex **1** are temperature-dependent, as shown in Figure 2.

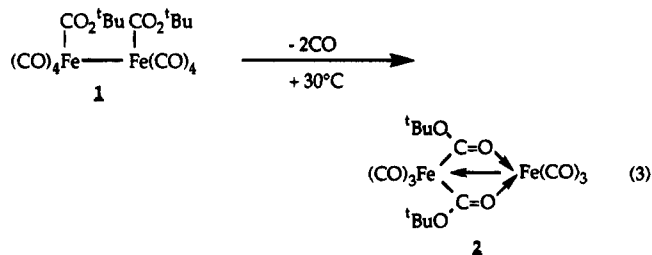
The limiting spectrum (at  $-100^\circ\text{C}$ ) exhibits all resonances for the four carbonyl ligands born by each equivalent iron atom at 213.5, 211.5, 206.5, and 205.4 ppm (1:1:1:1). The two first signals, ascribed to the  $\text{C}(2)\text{--O}(2)$  and  $\text{C}(3)\text{--O}(3)$  carbonyls, gradually coalesce so that, at  $-10^\circ\text{C}$ , the spectrum appears as three signals of intensities 2:1:1 at 212.0, 205.7, and 204.7 ppm. The nonequivalence at low temperature of these two carbonyl ligands probably results from a hindered rotation around the  $\text{Fe--CO}_2^t\text{Bu}$  or the  $\text{Fe--Fe}$  bond.

As proposed in reaction 2, the first step of the synthesis of **1** involves the formation of a bridged CO–CO compound (analogous intermediates have been detected during the synthesis of bis(alkoxycarbonyl)iron complexes<sup>12</sup>). Then a double decarbonylation would lead to complex **1** (eq 2).



Complex **1** is found to be stable in solution below  $15^\circ\text{C}$ . The thermal behavior of **1** has been studied by  $^{13}\text{C}$  NMR spectroscopy. When the temperature of the solution is raised up to  $30^\circ\text{C}$ , complex **1** disappears within 2 h together with carbon monoxide evolution and the formation of the new binuclear compound **2** (eq 3).<sup>19</sup>

(19) **2**:  $^{13}\text{C}\{^1\text{H}\}$  NMR ( $d_8$ -THF,  $25^\circ\text{C}$ ) 227.4 ( $\text{Fe}(\text{CO}_2^t\text{Bu})\text{Fe}$ ), 213.2, 207.4 ( $\text{Fe}(\text{CO})_3$ ), 86.5 ( $\text{C}(\text{CH}_3)_3$ ), 29.0 ppm ( $\text{CH}_3$ ), free CO is detected at 184 ppm;  $^1\text{H}$  NMR ( $d_8$ -THF,  $25^\circ\text{C}$ ) 1.38 ppm (s); IR (hexane)  $\nu_{\text{CO}}$  2084 (m), 2046 (s), 2024 (m), 2005 (s), 1515  $\text{cm}^{-1}$  (br, w).



Bis( $\mu$ - $\eta^2$ -acyl)hexacarbonyldiiron complexes, analogues of **2**, are rather well-known; they are obtained by oxidation with one-electron oxidizing agents of acyltetracarboxylferrates,  $[\text{Fe}(\text{COR})(\text{CO})_4]^-$ .<sup>20</sup> It is noteworthy that a similar reaction is observed with the (*tert*-butoxycarbonyl)tetracarboxylferrate. Indeed, the reaction of  $\text{K}[\text{Fe}(\text{CO}_2^t\text{Bu})(\text{CO})_4]$  with  $\text{Cu}(\text{SO}_3\text{CF}_3)_2$  leads to complex **2**.<sup>18</sup> This rules out the pathway involving an electron-transfer oxidation of the starting anionic compound followed by a dimerization for the synthesis of complex **1**. Furthermore, this last compound is found to be stable under these oxidation conditions.

(20) (a) Lindley, P. F.; Mills, O. S. *J. Chem. Soc. A* **1969**, 1279. (b) Fischer, E. O.; Kiener, V. *J. Organomet. Chem.* **1970**, *23*, 215. (c) Sundararajan, G.; San Filippo, J. *Organometallics* **1985**, *4*, 606. (d) Sundararajan, G. *Organometallics* **1991**, *10*, 1377.

The lability of the alkoxy group in  $[\text{M}](\text{CO}_2\text{R})$  complexes is well-known,<sup>21</sup> and in a previous study, we have illustrated this property by exchange experiments with alcohols for bis(alkoxycarbonyl)iron compounds  $\text{Fe}(\text{CO}_2\text{R})_2(\text{CO})_4$ .<sup>12</sup> Surprisingly, in the presence of methanol or ethanol, complex **1** is found to be unreactive and no exchange of its alkoxy group is observed.

Other reactions of this unique dimeric iron compound are currently under investigation. In addition, the synthesis of dialkyl or diacyl analogues of complex **1** is being studied. It is noteworthy that these compounds are not accessible by reaction of alkyl or acyl halide with the dianion  $[\text{Fe}(\text{CO})_8]^{2-}$ .<sup>22</sup> This new type of complex represents an interesting potential model for the study of dinuclear reductive elimination.

**Supporting Information Available:** Text giving details of the X-ray structure determination and tables of crystal data, bond distances and angles, and positional and thermal parameters for **1** (7 pages). Ordering information is given on any current masthead page.

OM950553W

(21) Cutler, A. R.; Hanna, P. K.; Vites, J. C. *Chem. Rev.* **1988**, *88*, 1363.

(22) Sumner, C. E.; Collier, J. A.; Pettit, R. *Organometallics* **1982**, *1*, 1350.

# From *trans*-Bis(alkylidene) to Nonsymmetric Bis(alkylidyne) Bridges. Synthesis of $(\text{Me}_3\text{P})_2\text{ClTa}(\mu\text{-CSiMe}_3)_2\text{TaCl}(\text{CH}_2\text{SiMe}_3)_2$ and Study of Its Axial-Equatorial Alkylidyne Ligand Exchange

Liting Li and Ziling Xue\*

Department of Chemistry, The University of Tennessee, Knoxville, Tennessee 37996-1600

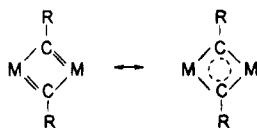
Glenn P. A. Yap and Arnold L. Rheingold

Department of Chemistry and Biochemistry, University of Delaware, Newark, Delaware 19716-2522

Received September 1, 1995<sup>®</sup>

**Summary:** The synthesis of a dimeric tantalum complex with two nonsymmetric alkylidyne bridging ligands, both of which coordinate with C=Ta double bonds to the same Ta atom (and with C-Ta single bonds to the other Ta atom), is reported. The two bridging alkylidyne ligands in **1**, which are coordinated to Ta(1) in the axial and equatorial positions, respectively, are involved in an unusual axial-equatorial ligand exchange.

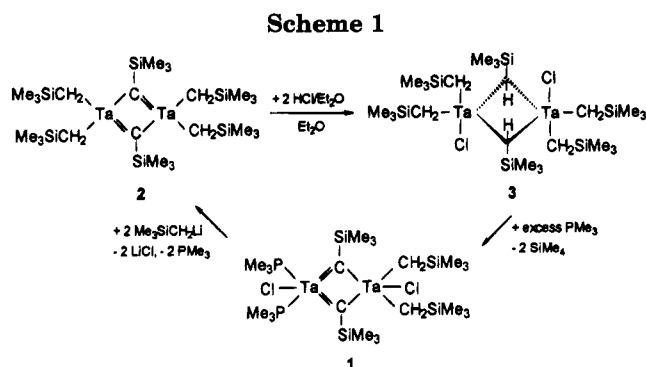
Bridging bis(alkylidyne) ligands are normally observed in coordinatively unsaturated complexes.<sup>1,2</sup> Such bridging ligands are usually bonded symmetrically to the two metal atoms:



We wish to report the synthesis and characterization of the dimeric tantalum complex  $(\text{Me}_3\text{P})_2\text{ClTa}(\mu\text{-CSiMe}_3)_2\text{TaCl}(\text{CH}_2\text{SiMe}_3)_2$  (**1**), which contains two rarely seen nonsymmetrically bonded alkylidyne bridging ligands (Scheme 1).

In our recent studies of  $(\text{Me}_3\text{SiCH}_2)_2\text{Ta}(\mu\text{-CSiMe}_3)_2\text{Ta}(\text{CH}_2\text{SiMe}_3)_2$  (**2**),<sup>1</sup> which is a byproduct in the preparation of the tantalum silyl complex  $(\text{Me}_3\text{SiCH}_2)_2\text{Ta}(\text{=CHSiMe}_3)\text{Si}(\text{SiMe}_3)_3$ ,<sup>3</sup> we discovered that addition of 2 equiv of HCl to **2** led to the formation of an unstable bridging bis(alkylidene) complex,  $(\text{Me}_3\text{SiCH}_2)_2\text{ClTa}(\mu\text{-CHSiMe}_3)_2\text{TaCl}(\text{CH}_2\text{SiMe}_3)_2$  (**3**).<sup>4</sup> The addition of an excess of  $\text{PMe}_3$  to the solution containing **3** converted it to the stable nonsymmetrically bonded bis(alkylidyne) complex **1** with the elimination of 2 equiv of  $\text{SiMe}_4$ .<sup>4</sup> The yellow crystalline complex **1** could be converted back to **2** by reaction with 2 equiv of  $\text{Me}_3\text{SiCH}_2\text{Li}$ . The reaction between **1** and  $\text{Me}_3\text{SiCH}_2\text{Li}$  involves an unusual alkyl migration between two tantalum atoms. The cycle of the transformations is summarized in Scheme 1.

The NMR spectra of thermally unstable **3** are consistent with a *trans* configuration (Scheme 1) of the two



bridging alkylidene ligands in the dimetallacyclobutane moiety.<sup>4,5</sup> The *trans* configuration with Cl ligands in the axial positions is perhaps sterically favored in the formation of **3**. The  $\alpha$ -hydrogen atoms in each of the two  $-\text{CH}_2\text{SiMe}_3$  ligands in **3** are thus diastereotopic, as seen in the  $^1\text{H}$  NMR spectrum.<sup>4</sup>

In the conversion of **3** to **1**, the two phosphine molecules were added to one Ta atom in **3**. This

(4) To a solution of **2** (2.0 g, 2.3 mmol) in diethyl ether (15 mL) at  $-78^\circ\text{C}$  was added slowly a 1.0 M solution of HCl in diethyl ether (4.54 mL, 4.54 mmol) via syringe. The color changed from red to yellow as **3** was formed. **3** decomposes above  $-50^\circ\text{C}$  and was identified by  $^1\text{H}$ ,  $^{13}\text{C}$ , and  $^1\text{H}-^{13}\text{C}$  HETCOR NMR spectroscopy. After the solution of **3** prepared *in situ* was stirred for 10 min,  $\text{PMe}_3$  (0.6 mL, 6 mmol) was added at  $-78^\circ\text{C}$ . A yellow precipitate of **3** was formed at once. The solution was warmed to  $23^\circ\text{C}$ , and the yellow precipitate dissolved. The solution was cooled to  $-20^\circ\text{C}$  to give 1.50 g of yellow crystals of **1** (total yield: 1.85 g, 88%). **3**:  $^1\text{H}$  NMR (toluene- $d_6$ , 400.1 MHz,  $-50^\circ\text{C}$ )  $\delta$  5.57 (s, 2H,  $\text{Me}_3\text{SiCH}_2$ ), 2.50 1.68 (d, 4H,  $\text{Me}_3\text{SiCH}_2\text{H}_b$ ,  $^2J_{\text{H-H}} = 12.4$  Hz), 2.04 1.68 (d, 4H,  $\text{Me}_3\text{SiCH}_2\text{H}_a$ ,  $^2J_{\text{H-H}} = 12.4$  Hz), 0.40 (s, 18H,  $\text{Me}_3\text{SiCH}_2$ ), 0.34 (s, 18H,  $\text{Me}_3\text{SiCH}_2$ ), 0.30 (s, 18H,  $\text{Me}_3\text{SiCH}_2$ );  $^{13}\text{C}$  NMR (toluene- $d_6$ , 100.6 MHz,  $-50^\circ\text{C}$ )  $\delta$  250.9 ( $\text{Me}_3\text{SiCH}_2$ ),  $^1J_{\text{C-H}} = 92.0$  Hz), 100.4 ( $\text{Me}_3\text{SiCH}_2$ ),  $^1J_{\text{C-H}} = 108.1$  Hz), 92.3 ( $\text{Me}_3\text{SiCH}_2$ ),  $^1J_{\text{C-H}} = 110.6$  Hz), 3.08 ( $\text{Me}_3\text{SiCH}_2$ ),  $^1J_{\text{C-H}} = 118.9$  Hz), 2.33 ( $\text{Me}_3\text{SiCH}_2$ ),  $^1J_{\text{C-H}} = 119.2$  Hz), 1.91 ( $\text{Me}_3\text{SiCH}_2$ ),  $^1J_{\text{C-H}} = 118.8$  Hz). **1**:  $^1\text{H}$  NMR (benzene- $d_6$ , 250.1 MHz,  $23^\circ\text{C}$ )  $\delta$  2.11, 0.82 (d, 4H,  $\text{Me}_3\text{SiCH}_2\text{H}_b$ ,  $^2J_{\text{H-H}} = 12.4$  Hz,  $^2J_{\text{Si-H}} = 8.3$  Hz), 1.39 (t, 18H,  $\text{PMe}_3$ ,  $^2J_{\text{P-H}} = 3.69$  Hz), 0.45 (s, 18H,  $\text{Me}_3\text{SiCH}_2\text{H}_b$ ,  $^2J_{\text{Si-H}} = 6.38$  Hz), 0.24 and 0.11 (s, 18H,  $\text{Me}_3\text{SiCH}_2\text{H}_a$ ,  $^2J_{\text{Si-H}} = 6.29$  Hz), 0.11 (s, 18H,  $\text{Me}_3\text{SiCH}_2\text{H}_a$ ,  $^2J_{\text{Si-H}} = 6.29$  Hz), 78.5 ( $\text{Me}_3\text{SiCH}_2$ ),  $^1J_{\text{C-H}} = 107.3$  Hz),  $^1J_{\text{Si-C}} = 42.0$  Hz), 16.4 ( $\text{PMe}_3$ ),  $^1J_{\text{C-H}} = 129.7$  Hz,  $^1J_{\text{P-C}} = 12.3$  Hz), 5.6 ( $\text{Me}_3\text{SiCH}_2$ ),  $^1J_{\text{C-H}} = 118.4$  Hz,  $^1J_{\text{Si-C}} = 44$  Hz). Anal. Calcd for  $\text{C}_{22}\text{H}_{58}\text{Cl}_2\text{P}_2\text{Si}_4\text{Ta}_2$  (**1**): C, 28.42; H, 6.29. Found: C, 28.60; H, 6.29.

(5) For other bridging alkylidene ligands, see: (a) Hartner, F. W., Jr.; Schwartz, J.; Clift, S. M. *J. Am. Chem. Soc.* **1983**, *105*, 640. (b) Hursthouse, M. B.; Jones, R. A.; Abdul Malik, K. M.; Wilkinson, G. *J. Am. Chem. Soc.* **1979**, *101*, 4128. Jones, R. A.; Wilkinson, G.; Galas, A. M. R.; Hursthouse, M. B.; Abdul Malik, K. M. *J. Chem. Soc., Dalton Trans.* **1980**, 1771. (c) Schrock, R. R.; Sharp, P. R. *J. Am. Chem. Soc.* **1978**, *100*, 2389. (d) Schmidt, G. F.; Muettterties, E. L.; Beno, M. A.; Williams, J. M. *Proc. Natl. Acad. Sci. U.S.A.* **1981**, *78*, 1318. (e) Müller, J.; Passon, B.; Pickardt, J. *J. Organomet. Chem.* **1982**, *228*, C51. (f) Isobe, K.; Okeya, S.; Meanwell, N. J.; Smith, A. J.; Adams, H.; Maitlis, P. M. *J. Chem. Soc., Dalton Trans.* **1984**, 1215.

<sup>®</sup> Abstract published in *Advance ACS Abstracts*, October 1, 1995.

(1) (a) Mowat, W.; Wilkinson, G. *J. Chem. Soc., Dalton Trans.* **1973**, 1120. (b) Hug, F.; Mowat, W.; Skapski, A. C.; Wilkinson, G. *Chem. Commun.* **1971**, 1477.

(2) See, e.g.: (a) Fanwick, P. E.; Ogilvy, A. E.; Rothwell, I. P. *Organometallics* **1987**, *6*, 73. (b) Chisholm, M. H.; Heppert, J. A.; Huffman, J. C. *J. Am. Chem. Soc.* **1984**, *106*, 1151 and references therein.

(3) Li, L.; Diminnie, J. D.; Xue, Z., manuscript in preparation.

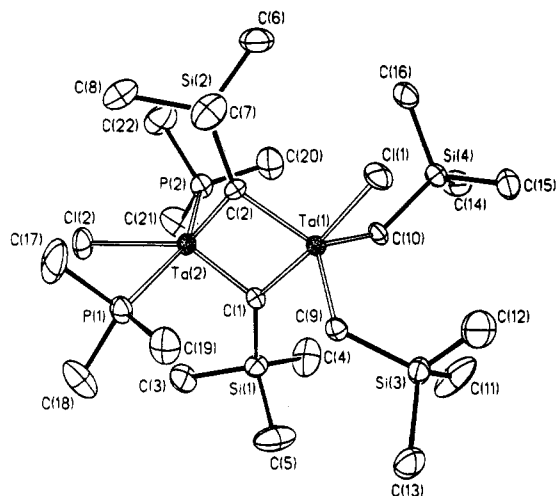


**Figure 1.** ORTEP drawing of **1**. Selected bond distances (Å): Ta(1)–Cl(1), 2.419(2); Ta(1)–C(1), 2.099(6); Ta(1)–C(2), 2.073(6); Ta(1)–C(9), 2.161(7); Ta(1)–C(10), 2.142(7); Ta(2)–Cl(2), 2.465(2); Ta(2)–P(1), 2.634(2); Ta(2)–P(2), 2.633(2); Ta(2)–C(1), 1.922(6); Ta(2)–C(2), 1.942(7). Selected bond angles (deg): Cl(1)–Ta(1)–C(1), 172.2(2); Cl(1)–Ta(1)–C(2), 92.2(2); C(1)–Ta(1)–C(2), 81.3(3); Cl(1)–Ta(1)–C(9), 88.1(2); C(1)–Ta(1)–C(9), 91.8(3); C(2)–Ta(1)–C(9), 122.5(3); Cl(1)–Ta(1)–C(10), 93.8(2); C(1)–Ta(1)–C(10), 93.3(3); C(2)–Ta(1)–C(10), 122.4(3); C(9)–Ta(1)–C(10), 114.9(3); Cl(2)–Ta(2)–P(1), 78.2(1); Cl(2)–Ta(2)–P(2), 79.0(1); P(1)–Ta(2)–P(2), 157.1(1); Cl(2)–Ta(2)–C(1), 135.1(2); P(1)–Ta(2)–C(1), 98.2(2); P(2)–Ta(2)–C(1), 97.9(2); Cl(2)–Ta(2)–C(2), 135.5(2); P(1)–Ta(2)–C(2), 97.9(2); P(2)–Ta(2)–C(2), 98.4(2); C(1)–Ta(2)–C(2), 89.4(3); Ta(1)–C(1)–Ta(2), 94.5(3); Ta(1)–C(1)–Si(1), 140.1(4); Ta(2)–C(1)–Si(1), 125.4(3); Ta(1)–C(2)–Ta(2), 94.8(3); Ta(1)–C(2)–Si(2), 139.3(4); Ta(2)–C(2)–Si(2), 125.9(3).

addition perhaps prompted the elimination of two SiMe<sub>3</sub> molecules through  $\alpha$ -hydrogen abstraction between the two Me<sub>3</sub>SiCH<sub>2</sub> ligands from the same Ta atom and the  $\alpha$ -hydrogen atoms of the two bridging alkylidene ligands. Surprisingly, the other half of the molecule in **3** remained intact in the conversion from **3** to **1**.

The crystal and molecular structure of **1** (Figure 1)<sup>6</sup> confirms the presence of nonsymmetric bridges involving the two alkylidyne ligands.<sup>7</sup> The bond distances between Ta(1) and C(1) and C(2) (2.099(6) and 2.073(6) Å, respectively) are significantly longer than those between Ta(2) and the bridging alkylidyne carbon atoms (1.922(6) and 1.942(6) Å, respectively). Cl(1), Ta(1), C(1), C(2), Ta(2), and Cl(2) are virtually coplanar (deviations from the least-squares plane  $\leq 0.07$  Å, mean 0.04 Å), thus making the two PMe<sub>3</sub> and two  $-\text{CH}_2\text{SiMe}_3$  ligands chemically equivalent, as seen in <sup>1</sup>H, <sup>13</sup>C, and <sup>31</sup>P NMR spectra. The ligands on Ta(1) are arranged in a slightly distorted trigonal-bipyramidal geometry with C(1) and C(2) at axial and equatorial positions, respectively. The two bridging alkylidyne ligands are involved in an axial–equatorial ligand exchange process, as seen from the Me<sub>3</sub>SiC $\equiv$  resonances in the variable-temperature <sup>1</sup>H NMR spectra of **1**. This exchange perhaps takes place through the conversion of the ground-state trigonal bipyramid into a square-

pyramidal transition state and back to a new trigonal-bipyramidal structure.<sup>8</sup> The activation enthalpy and entropy for the exchange are  $\Delta H^\ddagger = 13.6(0.4)$  kcal/mol and  $\Delta S^\ddagger = -5(2)$  eu.<sup>9</sup>

The reaction of **1** with 2 equiv of Me<sub>3</sub>SiCH<sub>2</sub>Li led to the replacement of the two chloride ligands and converted **1** back to the symmetric bis(alkylidyne) complex **2** (Scheme 1) with elimination of two PMe<sub>3</sub> ligands. An interesting alkyl migration from one Ta atom to another is involved in this conversion. Alkyl migrations from one metal center to another have been observed in early-transition-metal complexes that contain directly bonded metal centers.<sup>10–12</sup> Chisholm and co-workers reported an alkyl group transfer in the reaction between 1,2-Mo<sub>2</sub>-Br<sub>2</sub>R<sub>4</sub> and 2 equiv of *t*-BuOLi which led to the formation of 1,1-Mo<sub>2</sub>(O-*t*-Bu)<sub>2</sub>R<sub>4</sub>.<sup>10a</sup> Girolami and co-workers observed a terminal–terminal ligand exchange in the Cr(II) alkyl complex [Cr(CH<sub>2</sub>SiMe<sub>3</sub>)<sub>6</sub>]<sup>2-</sup>.<sup>10b</sup> Girolami and Anderson also studied the exchange between the *trans* and *gem* isomers of Mo<sub>2</sub>(O<sub>2</sub>CR')<sub>2</sub>R<sub>2</sub>L<sub>2</sub> (R = Me, CH<sub>2</sub>-SiMe<sub>3</sub>; R' = Me, CMe<sub>3</sub>; L = phosphine, phosphite).<sup>10c</sup> However, unlike the case in these complexes, the alkyl transfer in our compound **1** is between two metal atoms that are not directly bonded (the distance between the two Ta atoms is 2.956(1) Å in **1**). The migration of the Me<sub>3</sub>SiCH<sub>2</sub> ligand in the conversion of **1** to **2** (Scheme 1) nicely completes the reaction cycle that has started from **2**.

**Acknowledgment** is made to the National Science Foundation Young Investigator Award (NYI) program, Exxon Education Foundation, Du Pont Young Professor Award, the donors of the Petroleum Research Fund, administered by the American Chemical Society, and the University of Tennessee (Faculty Research Award) for support of this research (Z.X.). We also thank Professor G. S. Girolami for providing results before their publication.

**Supporting Information Available:** Temperature-dependent <sup>1</sup>H NMR spectra showing the axial–equatorial alkylidyne ligand exchange in **1**, a table of rate constants and Eyring plot of the axial–equatorial ligand exchange in **1**, and complete lists of the crystallographic data for **1** (14 pages). This material is contained in many libraries on microfiche, immediately follows this article in the microfilm version of the journal, can be ordered from the ACS, and can be downloaded from the Internet; see any current masthead page for ordering information and Internet access instructions.

OM9506882

(8) In the Berry pseudorotation, the two axial ligands and two of the three equatorial ligands are involved in an exchange: Huheey, J. E. *Inorganic Chemistry*, 3rd ed.; Harper & Row: New York, 1983; pp 247–249.

(9) Simulations of the dynamic NMR spectra were carried out with the use of the program DNMR. For its use and the error analysis, see: Morse, P. M.; Spencer, M. D.; Wilson, S. R.; Girolami, G. S. *Organometallics* **1994**, *13*, 1646.

(10) (a) Chisholm, M. H.; Foltz, K.; Hoffman, J. C.; Rothwell, I. P. *Organometallics* **1982**, *1*, 251. (b) Reference 9. (c) Girolami, G. S.; Mainz, V. V.; Andersen, R. A. Unpublished results.

(11) The following intramolecular alkyl transfers have been reported in complexes containing late-transition-metal atoms with direct metal–metal bonding: (a) Antwi-Nsiah, F.; Cowie, M. *Organometallics* **1992**, *11*, 3157. (b) Darensbourg, M. Y.; Ash, C. E.; Kao, S. C.; Silva, R.; Springs, J. *Pure Appl. Chem.* **1988**, *60*, 131. (c) Komiya, S.; Endo, I. *Chem. Lett.* **1988**, 1709. (d) Okeya, S.; Meanwell, N. J.; Taylor, B. F.; Isobe, K.; Vázquez de Miguel, A.; Maitlis, P. M. *J. Chem. Soc., Dalton Trans.* **1984**, 1453.

(12) Wolczanski and co-workers reported methyl exchange between Pt and Zr atoms in Cp\*(CD<sub>3</sub>)Zr( $\mu$ -OCH<sub>2</sub>Ph)<sub>2</sub>Pt(CH<sub>3</sub>)<sub>2</sub>; Baxter, S. M.; Ferguson, G. S.; Wolczanski, P. T. *J. Am. Chem. Soc.* **1988**, *110*, 4231.

(6) Crystal data for **1**: fw = 929.0, monoclinic, *P*2<sub>1</sub>/*c*, *a* = 10.668(2) Å, *b* = 17.481(2) Å, *c* = 20.962(3) Å,  $\beta$  = 94.98(1)°, *Z* = 4, *V* = 3894.3(10) Å<sup>3</sup>,  $\mu(\text{Mo K}\alpha)$  = 59.7 cm<sup>-1</sup>, *T* = 245 K, *R*(*F*) = 3.39%, *R*(w*F*) = 4.30%.

(7) A similar nonsymmetric bis(alkylidyne) complex, W<sub>2</sub>(Me<sub>3</sub>SiCH<sub>2</sub>)<sub>4</sub>( $\mu$ -CSiMe<sub>3</sub>)<sub>2</sub>( $\eta^2$ -PhC<sub>2</sub>Me), has been reported: Chisholm, M. H.; Huffman, J. C.; Heppert, J. A. *J. Am. Chem. Soc.* **1985**, *107*, 5116.

## (Hydroxyphenyl)oxazoline: a Novel and Remarkably Facile Entry into the Area of Chiral Cationic Alkylzirconium Complexes Which Serve as Polymerization Catalysts

Pier Giorgio Cozzi, Emma Gallo, Carlo Floriani, Angiola Chiesi-Villa, and Corrado Rizzoli

*Organometallics*, 1995, 14 (11), 4994-4996 • DOI: 10.1021/om00011a010 • Publication Date (Web): 01 May 2002

Downloaded from <http://pubs.acs.org> on March 9, 2009

### More About This Article

---

The permalink <http://dx.doi.org/10.1021/om00011a010> provides access to:

- Links to articles and content related to this article
- Copyright permission to reproduce figures and/or text from this article



ACS Publications  
High quality. High impact.

# (Hydroxyphenyl)oxazoline: A Novel and Remarkably Facile Entry into the Area of Chiral Cationic Alkylzirconium Complexes Which Serve as Polymerization Catalysts

Pier Giorgio Cozzi,<sup>†</sup> Emma Gallo, and Carlo Floriani\*

*Institut de Chimie Minérale et Analytique, BCH, Université de Lausanne, CH-1015 Lausanne, Switzerland*

Angiola Chiesi-Villa and Corrado Rizzoli

*Dipartimento di Chimica, Università di Parma, I-43100 Parma, Italy*

Received June 27, 1995<sup>®</sup>

**Summary:** How can the entry into the area of chiral cationic alkyl derivatives of group 4 metals be simplified? We succeeded in using readily available amino alcohols, which have been converted into chiral (hydroxyphenyl)-oxazolines. These compounds have been employed in the organometallic derivatization of early transition metals.

The widespread study of cationic zirconocene alkyl complexes,  $Cp_2Zr(R)^+$ , stems from the use of these electrophilic  $d^0$  species in both stoichiometric<sup>1</sup> and catalytic<sup>2</sup> reactions, especially  $\alpha$ -olefin polymerization.<sup>3</sup> The extensive range of modified Cp ligands all serve to force incoming substrate molecules toward a vacant coordination site *cis* to the M–R bond in the so-called equatorial binding plane. However, such ligands are rarely accessible via facile, large-scale syntheses.<sup>4</sup> Con-

sequently, there is a growing interest in the use of other non-Cp-based ligands as ancillary fragments for high-oxidation-state group 4 metals. Previously we have investigated the use of dibenzotetramethyltetraaza[14]-annulene, tmtaa, as just such an ancillary ligand,<sup>5</sup> and Jordan and co-workers have prepared the corresponding cationic alkyls,  $tmtaaZr(R)^+$ .<sup>6</sup> Although these complexes display a disappointingly low activity for the Ziegler-Natta polymerization of  $\alpha$ -olefins, they nevertheless exhibit interesting insertion chemistry and can promote intramolecular C–H activation.

We have since turned our attention toward the (hydroxyphenyl)oxazoline ligand and recently reported the synthesis and structures of dichlorobis((hydroxyphenyl)oxazolinato)titanium(IV) and -zirconium(IV),<sup>7</sup>  $[L_2MCl_2]$  ( $L =$  (hydroxyphenyl)oxazolinato anion). Herein, we communicate organometallic derivatives of  $[L_2MCl_2]$  ( $M = Zr, Hf$ ). These initial explorations have focused upon the achiral **1**<sup>8</sup> and the chiral **2**<sup>8</sup> and **3**<sup>8</sup> ligands, which are readily accessible on a large scale from commercially available amino alcohols.

Reaction of  $[L_2MCl_2]$  ( $L = 1-3$ ) with organolithium (MeLi) or organomagnesium (MeMgBr) reagents does not lead to the desired dialkyl complexes. However, direct alkane elimination arising from the reaction of **1-3** with  $M(CH_2Ph)_4$  gives the bis(benzyl) complexes **4-7** in good yields (typically 60–70%).<sup>9</sup>

In order to investigate the orientation and bonding mode of the benzyl ligands the crystal structure of **4** was determined.<sup>10</sup> Room-temperature <sup>1</sup>H NMR suggests that in solution **4** contains two  $\eta^1$ -CH<sub>2</sub>Ph ligands

\* To whom correspondence should be addressed.

<sup>†</sup> Present address: Istituto di Chimica "G. Ciamician", Università di Bologna, I-40216 Bologna, Italy.

<sup>®</sup> Abstract published in *Advance ACS Abstracts*, October 15, 1995.

(1) Collins, S.; Kuntz, B. A.; Collins, S. *J. Org. Chem.* **1989**, *54*, 4154. Jordan, R. F. *Adv. Organomet. Chem.* **1991**, *32*, 325. Grossman, R. B.; Davis, W. M.; Buchwald, S. L. *J. Am. Chem. Soc.* **1991**, *113*, 2321. Guram, A. S.; Swenson, D. C.; Jordan, R. F. *J. Am. Chem. Soc.* **1992**, *114*, 8991. Guram, A. S.; Guo, Z.; Jordan, R. F. *J. Am. Chem. Soc.* **1993**, *115*, 4902. Guram, A. S.; Jordan, R. F. *J. Org. Chem.* **1993**, *58*, 5595. Hong, Y.; Kuntz, B. A.; Collins, S. *Organometallics* **1993**, *12*, 964.

(2) Pino, P.; Cioni, P.; Wei, J. *J. Am. Chem. Soc.* **1987**, *109*, 6189. Waymouth, R. M.; Pino, P. *J. Am. Chem. Soc.* **1990**, *112*, 4911. Morken, J. P.; Didiuk, M. T.; Hoveyda, A. H. *J. Am. Chem. Soc.* **1993**, *115*, 6997. Rodewald, S.; Jordan, R. F. *J. Am. Chem. Soc.* **1994**, *116*, 4491 and references therein.

(3) Kaminsky, W.; Külper, K.; Brintzinger, H. H.; Wild, F. R. W. P. *Angew. Chem., Int. Ed. Engl.* **1985**, *24*, 507. Ewen, J. A.; Haspeslagh, L.; Atwood, J. L.; Zhang, H. *J. Am. Chem. Soc.* **1987**, *109*, 6544. Ewen, J. A.; Jones, R. L.; Razavi, A.; Ferrara, J. D. *J. Am. Chem. Soc.* **1988**, *110*, 6255. Hlatky, G. G.; Turner, H. W.; Eckman, R. R. *J. Am. Chem. Soc.* **1989**, *111*, 2728. Yang, X.; Stern, C. L.; Marks, T. J. *Am. Chem. Soc.* **1991**, *113*, 3623. Collins, S.; Gauthier, W. J.; Holden, D. A.; Kuntz, B. A.; Taylor, N. J.; Ward, D. G. *Organometallics* **1991**, *10*, 2061. Resconi, L.; Piemontesi, F.; Franciscano, L.; Abis, L.; Fiorani, T. *J. Am. Chem. Soc.* **1992**, *114*, 1025. Burger, P.; Diebold, J.; Gutmann, S.; Hund, H. U.; Brintzinger, H. H. *Organometallics* **1992**, *11*, 1319. Marks, T. *Acc. Chem. Res.* **1992**, *25*, 57. Coates, G. W.; Waymouth, R. M. *J. Am. Chem. Soc.* **1993**, *115*, 91. Erker, G.; Aulbach, M.; Knickmeier, M.; Wingbermhühle, D.; Krüger, C.; Nolte, M.; Werner, S. *J. Am. Chem. Soc.* **1993**, *115*, 4590. Guerra, G.; Cavallo, L.; Moscardi, G.; Vacatello, M.; Corradini, P. *J. Am. Chem. Soc.* **1994**, *116*, 2988. Yang, X.; Stern, C. L.; Marks, T. J. *J. Am. Chem. Soc.* **1994**, *116*, 10015.

(4) Hollis, K. T.; Rheingold, A. L.; Robinson, N. P.; Whelan, J.; Bosnich, B. *Organometallics* **1992**, *11*, 2812. Huttenloch, M.; Diebold, J.; Rief, U.; Brintzinger, H. H.; Gilbert, A. M.; Katz, T. J. *Organometallics* **1992**, *11*, 3600. Ellis, W. W.; Hollis, K. T.; Odenkirk, W.; Whelan, J.; Ostrander, R.; Rheingold, A. L.; Bosnich, B. *Organometallics* **1993**, *12*, 4391. Herrmann, W. A.; Anwender, R.; Riepl, H.; Scherer, W.; Whitaker, C. R. *Organometallics* **1993**, *12*, 4342. Rieger, B.; Jany, G.; Fawzi, R.; Steimann, M. *Organometallics* **1994**, *13*, 647.

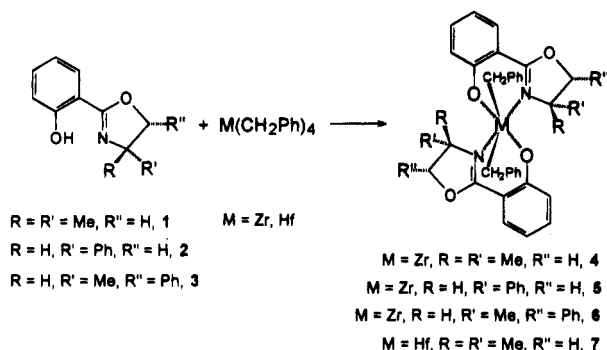
(5) (a) Ciurli, S.; Floriani, C.; Chiesi-Villa, A.; Guastini, C. *J. Chem. Soc., Chem. Commun.* **1986**, 1401. (b) Floriani, C.; Ciurli, S.; Chiesi-Villa, A.; Guastini, C. *Angew. Chem., Int. Ed. Engl.* **1987**, *26*, 70. (c) Floriani, C.; Mazzanti, M.; Ciurli, S.; Chiesi-Villa, A.; Guastini, C. *J. Chem. Soc., Dalton Trans.* **1988**, 1361. (d) Solari, E.; De Angelis, S.; Floriani, C.; Chiesi-Villa, A.; Rizzoli, C. *Inorg. Chem.* **1992**, *31*, 96. (e) De Angelis, S.; Solari, E.; Gallo, E.; Floriani, C.; Chiesi-Villa, A.; Rizzoli, C. *Inorg. Chem.* **1992**, *31*, 2520. (f) Giannini, L.; Solari, E.; Floriani, C.; Chiesi-Villa, A.; Rizzoli, C. *Angew. Chem., Int. Ed. Engl.* **1994**, *33*, 2204. (g) Goedken, V. L.; Ladd, J. A. *J. Chem. Soc., Chem. Commun.* **1981**, 910; **1982**, 142. (h) Housmekerides, C. E.; Pilato, R. S.; Geoffroy, G. L.; Rheingold, A. L. *J. Chem. Soc., Chem. Commun.* **1991**, 563. (i) Yang, C. H.; Ladd, J. A.; Goedken, V. L. *J. Coord. Chem.* **1988**, *18*, 317. (j) Floriani, C. *Polyhedron* **1989**, *8*, 1717.

(6) Uhrhammer, R.; Black, D. G.; Gardner, T. G.; Olsen, J. D.; Jordan, R. F. *J. Am. Chem. Soc.* **1993**, *115*, 8493.

(7) Cozzi, P. G.; Floriani, C.; Chiesi-Villa, A.; Rizzoli, C. *Inorg. Chem.* **1995**, *34*, 2921.

(8) Bolm, C.; Weickhardt, K.; Zehnder, M.; Ranff, T. *Chem. Ber.* **1991**, *124*, 1173.

Scheme 1



(indicated by the absence of the high-field shifts for the *ortho* protons and AB splitting pattern for the diastereotopic methylene protons), and such a proposal is confirmed by the X-ray study (Figure 1). The molecule possesses a crystallographic  $C_2$  symmetry. The two symmetry-related oxazolinato ligands, which are almost planar, are nearly mutually orthogonal (dihedral angles  $96.6(1)$  and  $102.4(1)^\circ$ ), resulting in a distorted-octahedral coordination around zirconium completed by the carbon atoms from two benzylic groups. The bond angles  $\text{Zr}-\text{C}18-\text{C}12$  ( $113.7(3)$  and  $113.4(3)^\circ$ ) are typical of the  $\eta^1$  coordination mode. This observation is initially surprising in view of the electron-deficient nature of the metal center. We assume that **5-7** adopt similar structures.

Complexes **8-10**<sup>11-13</sup> could be prepared from **4, 5**, and **7** via a protonolysis reaction with  $(\text{HNMe}_2\text{Ph})(\text{BPh}_4)$ ,

(9) To a stirred suspension of  $\text{M}(\text{CH}_2\text{Ph})_4$  ( $M = \text{Zr}, \text{Hf}$ ) (6–15 mmol) in  $\text{Et}_2\text{O}$  was added an  $\text{Et}_2\text{O}$  solution of the ligand (**1, 2**, or **3**) (12–30 mmol) in a dropwise fashion at  $-40^\circ\text{C}$ . The solution was then warmed to room temperature. For complexes **4, 5**, and **7**, the reaction mixture was partially concentrated and the yellow-orange solid was filtered and collected. Complex **6** was prepared with the same method except for the utilization of toluene instead of  $\text{Et}_2\text{O}$ . The solvent was removed, and pentane was added. The resulting orange oil was scraped with a spatula under nitrogen until a solid was obtained, which was quickly filtered. **4**:  $^1\text{H NMR}$  ( $\text{C}_6\text{D}_6$ , ppm)  $\delta$  7.85 (dd, 2 H,  $J = 1.41, 7.89$  Hz), 7.16 (dt, 2 H,  $J = 1.55, 8.67$  Hz), 7.06–6.95 (m, 22 H), 6.71 (dt, 2 H,  $J = 0.97, 8.05$  Hz), 3.24 (s, 4 H), 2.66 (AB, 4 H,  $J = 10.34$  Hz), 1.29 (s, 6 H), 0.52 (s, 6 H). IR: 1607, 1580, 1550  $\text{cm}^{-1}$ . Anal. Calcd for  $\text{C}_{36}\text{H}_{38}\text{N}_2\text{O}_4\text{Zr}$ : C, 66.13; H, 5.81; N, 4.28. Found: C, 66.14; H, 6.13; N, 4.39. Analytical and spectroscopic data for **5-7** are given in the Supporting Information.

(10) Crystal data for **4**:  $\text{C}_{36}\text{H}_{38}\text{N}_2\text{O}_4\text{Zr}$ , monoclinic, space group  $P2_1/c$ ;  $a = 22.254(1)$  Å,  $b = 9.199(1)$  Å,  $c = 16.842(2)$  Å,  $\beta = 110.34(1)^\circ$ ,  $V = 3232.8(6)$  Å<sup>3</sup>,  $Z = 4$ ,  $\rho_{\text{calcd}} = 1.344$  g  $\text{cm}^{-3}$ ; Cu  $K\alpha$  radiation ( $\lambda = 1.54178$  Å),  $\mu(\text{Cu } K\alpha) = 31.27$   $\text{cm}^{-1}$ ; crystal dimensions  $0.16 \times 0.31 \times 0.39$  mm. The structure was solved by the heavy-atom method and anisotropically refined for all the non-hydrogen atoms. The hydrogen atoms were located from a difference map and introduced as fixed contributors in the last stage of refinement ( $U_{\text{iso}} = 0.10$  Å<sup>2</sup>). For 4168 unique observed reflections ( $I > 2\sigma(I)$ ), collected at 295 K on a Rigaku AFC6S diffractometer ( $6 < 2\theta < 140^\circ$ ) and corrected for absorption, the final conventional  $R$  was 0.040 ( $wR2 = 0.103$ ). In the unit cell there are two crystallographically independent half-molecules (A and B, Figures 1 and S1 (Supporting Information)) related by a *pseudo* center of symmetry. Attempts to transform the starting unit cell to a higher symmetry one were unsuccessful. The data reported refer to molecule A. See the Supporting Information for more details.

(11) Preparation of **8**: to a solution of complex **4** (1.42 g, 2.173 mmol) in THF (60 mL) at  $-78^\circ\text{C}$ ,  $(\text{cp})_2\text{Fe}^+\text{BPh}_4^-$  in one portion, and the resulting slurry was warmed to room temperature. After a few minutes, the blue of the ferrocenium cation disappeared and a yellow compound started to precipitate. The mixture was stirred for 2 h at room temperature, and the orange-yellow compound was collected, washed with  $\text{Et}_2\text{O}$  (35 mL), and dried under vacuum. The cationic complex was recrystallized in a dichloroethane-THF mixture (46%).  $^1\text{H NMR}$  ( $\text{CD}_2\text{Cl}_2$ , ppm):  $\delta$  7.95 (dd, 2 H,  $J = 1.71, 7.89$  Hz), 7.72 (dt, 2 H,  $J = 2.06, 6.54$  Hz), 7.45–6.7 (m, 29 H), 4.13 (AB, 4 H,  $J = 8.91$  Hz,  $\text{OCH}_2$ ); 2.65 (AB, 2 H,  $J = 10.29$  Hz,  $\text{CH}_2\text{Ph}$ ), 3.78 (m, 6 H, THF,  $\text{CH}_2\text{C}(\text{CH}_2\text{Cl})$ ), 1.81 (m, 4 H, THF); 1.44 (s, 6 H, Me); 0.99 (s, 6 H, Me). IR: 1603, 1578, 1545  $\text{cm}^{-1}$ . Anal. Calcd for  $\text{C}_{55.5}\text{H}_{56}\text{BCl}_{0.5}\text{N}_2\text{O}_4.5\text{Zr}$ : C, 70.71; H, 5.94; N, 2.97. Found: C, 70.64; H, 6.64; N, 2.99.

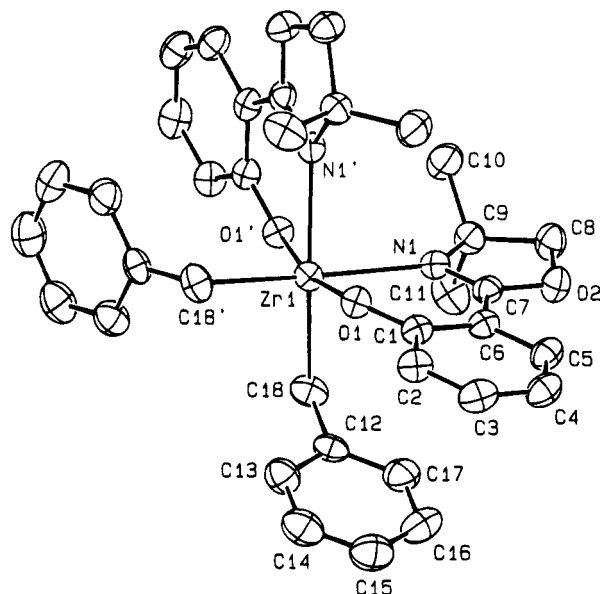


**Figure 1.** ORTEP drawing of molecule A in complex **4** (30% probability ellipsoids). Selected bond distances (Å) and angles (deg) (values in brackets refer to molecule B):  $\text{Zr}1-\text{O}1$ , 2.001(3) [2.007(4)];  $\text{Zr}1-\text{N}1$ , 2.398(4) [2.401(4)];  $\text{Zr}1-\text{C}18$ , 2.294(5) [2.280(5)];  $\text{O}1-\text{C}1$ , 1.333(4) [1.315(6)];  $\text{O}2-\text{C}7$ , 1.350(5) [1.340(6)];  $\text{O}2-\text{C}8$ , 1.450(6) [1.429(9)];  $\text{N}1-\text{C}7$ , 1.294(4) [1.290(7)];  $\text{N}1-\text{C}9$ , 1.513(6) [1.507(6)];  $\text{C}18-\text{Zr}1-\text{C}18'$ ,  $96.8(2)$  [ $94.1(2)$ ];  $\text{N}1-\text{Zr}1-\text{C}18'$ ,  $167.3(1)$  [ $167.0(1)$ ];  $\text{N}1-\text{Zr}1-\text{C}18$ ,  $89.7(1)$  [ $89.6(1)$ ];  $\text{O}1-\text{Zr}1-\text{C}18'$ ,  $91.3(1)$  [ $90.9(1)$ ];  $\text{O}1-\text{Zr}1-\text{C}18$ ,  $97.4(1)$  [ $99.9(2)$ ];  $\text{O}1-\text{Zr}1-\text{N}1'$ ,  $93.3(1)$  [ $92.5(1)$ ];  $\text{O}1-\text{Zr}1-\text{N}1$ ,  $77.0(1)$  [ $76.2(1)$ ];  $\text{O}1-\text{Zr}1-\text{O}1'$ ,  $166.9(1)$  [ $164.1(1)$ ];  $\text{Zr}-\text{O}1-\text{C}1$ ,  $141.8(3)$  [ $145.0(3)$ ];  $\text{Zr}1-\text{C}18-\text{C}12$ ,  $113.7(3)$  [ $113.4(3)$ ]. The prime denotes transformations of  $1-x, y, -0.5-z$  for molecule A and  $-x, y, 0.5-z$  for molecule B, respectively.

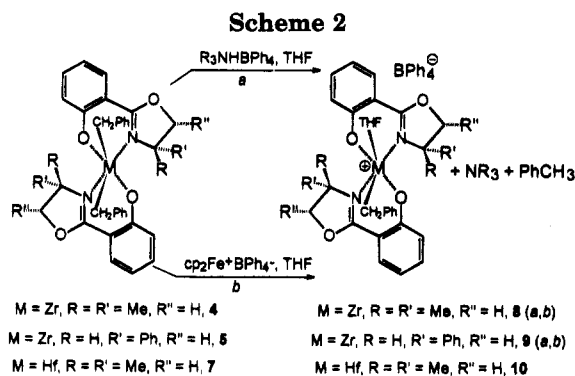
$(\text{HNEt}_3)(\text{BPh}_4)$ , or  $(\text{HNBu}_3)(\text{BPh}_4)$  or, more conveniently, in a number of cases by oxidative cleavage using  $\text{Cp}_2\text{FeBPh}_4$ .<sup>14</sup>

(12) Preparation of **9**: to a stirred solution of complex **5** (2.915 g, 3.74 mmol) in THF (80 mL) at  $-78^\circ\text{C}$  was added  $(\text{cp})_2\text{Fe}^+\text{BPh}_4^-$  (1.98 g, 3.74 mmol) was added in one portion. The blue solution was immediately warmed to room temperature. The solution turned orange, and it was stirred for 1 h at room temperature. The solvent was pumped off, and  $\text{Et}_2\text{O}$  (50 mL) was added to the remaining solid. The yellow suspension was stirred for 1 h at room temperature and filtered; the residue was washed with  $\text{Et}_2\text{O}$  (20 mL) and dried under vacuum (80%).  $^1\text{H NMR}$  ( $\text{CD}_2\text{Cl}_2$ , ppm):  $\delta$  8.1 (br, 2 H), 7.7 (t, 2 H,  $J = 6.5$  Hz), 7.4–6.8 (m, 41 H); 5.75 (br, 2 H), 4.5–4.0 (br, 4 H), 1.89 (br, 2 H), 0.8 (br, 6 H). IR: 1602.9, 1572.2, 1545.5  $\text{cm}^{-1}$ .  $[\alpha]_D^{23} = +34.3$  ( $c = 2.36$ ,  $\text{CH}_2\text{Cl}_2$ ). Anal. Calcd for  $\text{C}_{75}\text{H}_{85}\text{BN}_2\text{O}_7\text{Zr}$ : C, 73.34; H, 6.92; N, 2.28. Found: C, 73.06; H, 6.18; N, 2.3.

(13) Preparation of **10**: to a stirred solution of **7** (1.05 g, 1.42 mmol) in THF (70 mL) at  $-78^\circ\text{C}$  was added  $\text{HET}_3\text{N}^+\text{BPh}_4^-$  (0.58 g, 1.38 mmol) in one portion, and the mixture was warmed to room temperature. After a few minutes, the ammonium salt was dissolved and an orange-yellow solution was obtained. The solution was stirred for 2 h at room temperature; then the THF was pumped off.  $\text{Et}_2\text{O}$  was added (60 mL), and the mixture was stirred for 1 h at room temperature and then filtered. The collected solid was washed with  $\text{Et}_2\text{O}$  (20 mL) and dried under vacuum (75%).  $^1\text{H NMR}$  ( $\text{CD}_2\text{Cl}_2$ , room temperature, ppm):  $\delta$  7.98 (dd, 2 H,  $J = 2.06, 8.23$  Hz), 7.73 (dt, 2 H,  $J = 1.72, 7.24$  Hz), 7.4–6.6 (m, 29 H), 4.18 (br, 4 H,  $\text{OCH}_2$ ), 3.92 (br, 4 H, THF), 2.16 (s, 2 H,  $\text{CH}_2\text{Ph}$ ), 1.77 (m, 4 H, THF), 1.6 (br, 6 H, Me), 1.0 (br, 6 H, Me).  $^1\text{H NMR}$  ( $\text{CD}_2\text{Cl}_2$ , 213 K, ppm):  $\delta$  7.98 (dd, 2 H,  $J = 2.06, 8.23$  Hz), 7.73 (dt, 2 H,  $J = 1.72, 7.24$  Hz), 7.7–6.6 (m, 29 H), 4.34 (d, 1 H,  $J = 9$  Hz), 4.22 (d, 1 H,  $J = 9$  Hz), 4.18 (d, 1 H,  $J = 9$  Hz), 4.13 (d, 1 H,  $J = 9$  Hz), 3.99 (br, 2 H, THF), 3.85 (br, 2 H, THF), 2.18 (d, 1 H,  $J = 12$  Hz), 2.03 (d, 1 H,  $J = 12$  Hz), 1.76 (s, 3 H,  $\text{CH}_3$ ), 1.67 (br, 4 H, THF), 1.39 (s, 3 H,  $\text{CH}_3$ ), 0.95 (s, 3 H,  $\text{CH}_3$ ), 0.86 (s, 3 H,  $\text{CH}_3$ ). IR: 1604, 1576, 1533  $\text{cm}^{-1}$ . Anal. Calcd for  $\text{C}_{67}\text{H}_{55}\text{BHfN}_2\text{O}_5$ : C, 65.7; H, 5.67; N, 2.69. Found: C, 64.78; H, 5.91; N, 2.77.

(14) Jordan, R. F.; La Pointe, R. E.; Bradley, P. K.; Baenziger, N. C. *Organometallics* **1989**, *8*, 2892.





The characterization of **8–10** has been carried out by standard techniques, including an X-ray analysis of **10**·THF.<sup>15</sup> In this context we should mention that the <sup>1</sup>H NMR spectrum of **10** showed some nonsteroidicity of the complex, revealed by the broad resonances observed for the substituents of the oxazoline ring at 298 K, which sharpened on lowering the temperature to 213 K. Coordination around hafnium, shown in Figure 2, is distorted octahedral, closely resembling that of complex **4**, the two chelating oxazolinato ligands being mutually orthogonal (dihedral angle 90.0(3)°). Coordination is completed by a carbon atom from a  $\eta^1$ -benzylidene group and an oxygen atom from a THF group.<sup>16</sup> The best equatorial plane is defined by the O1, N2, O3, O5 atoms (maximum displacement 0.095(14) Å for O3), hafnium being displaced by 0.161(2) Å toward the C47 benzylidene carbon. There is no major structural difference between **4** and **10**. The structural parameters (*i.e.* M–O and M–N bond distances and associated angles) do not allow us to take into account a significant  $\pi$ -interaction of the zirconium with the donor atoms of the ligand, as a support for the rather low acidity shown by the reactivity of the cationic species. A nonsolvated form of **8–10** is expected to have a much higher reactivity. In fact, **8**, when generated in toluene solution (pathway *a*), does serve as an initiator for the polymerization of ethylene without the need for a cocatalyst, albeit of low activity.<sup>17</sup>

In conclusion, we have demonstrated that chiral, cationic d<sup>0</sup> species based on readily prepared and easily

(15) Crystal data for **10**: C<sub>33</sub>H<sub>39</sub>HfN<sub>2</sub>O<sub>5</sub>·C<sub>24</sub>H<sub>20</sub>B·C<sub>4</sub>H<sub>8</sub>O, monoclinic, space group *P2<sub>1</sub>/c*; *a* = 10.874(6) Å, *b* = 37.008(8) Å, *c* = 13.952(6) Å,  $\beta$  = 106.54(3)°, *V* = 5382(4) Å<sup>3</sup>, *Z* = 4,  $\rho_{\text{calc}}$  = 1.374 g cm<sup>-3</sup>; Cu K $\alpha$  radiation ( $\lambda$  = 1.54178 Å),  $\mu(\text{Cu K}\alpha)$  = 40.17 cm<sup>-1</sup>; crystal dimensions 0.18 × 0.23 × 0.31 mm. Solution of the structure was as for complex **4**. For 5308 unique observed reflections (*I* > 2 $\sigma$ (*I*)), collected at 295 K on a Rigaku AFC6S diffractometer (6 < 2 $\theta$  < 140°) and corrected for absorption, the final conventional *R* was 0.098 (wR2 = 0.236). The final difference map showed a residual peak of 2.7 e Å<sup>-3</sup> in a position inconsistent with the aromatic rings C21...C26 and C71...C76. A sound discussion concerning bond distances and angles within the complex is prevented due to the relatively low accuracy of the actual refinement. See the Supporting Information for more details.

(16) The <sup>1</sup>H NMR spectra of **9** and **10** show broad resonances for substituents of the oxazoline ring and the coordinated THF. Similarly, the <sup>13</sup>C spectra display a broad signal for the benzylic CH<sub>2</sub>. A complete low-temperature investigation will be presented in a forthcoming paper.

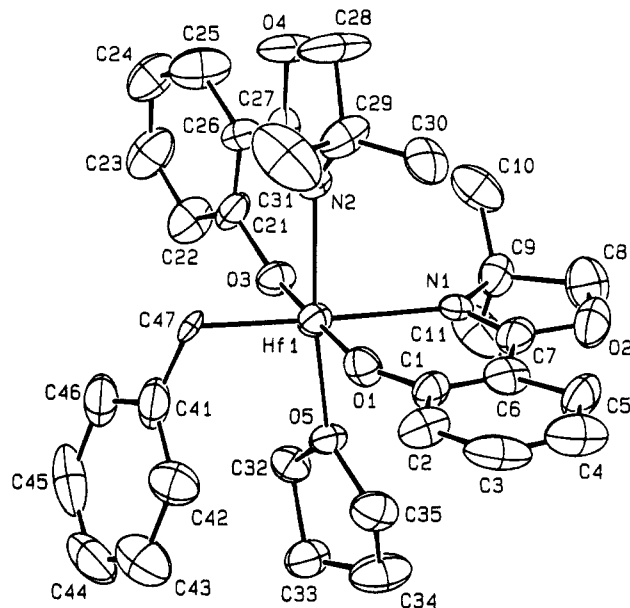


**Figure 2.** ORTEP drawing of complex **10** (30% probability ellipsoids). Selected bond distances (Å) and angles (deg): Hf1–O1, 2.005(14); Hf1–O3, 1.987(14); Hf1–O5, 2.177(10); Hf1–N1, 2.342(14); Hf1–N2, 2.234(12); Hf1–C47, 2.231(15); N1–Hf1–C47, 165.3(6); O5–Hf1–N2, 161.2(5); O3–Hf1–N2, 81.3(5); O3–Hf1–O5, 83.8(5); O1–Hf1–N2, 101.5(5); O1–Hf1–O5, 92.5(5); O1–Hf1–O3, 174.5(6); Hf1–O1–C1, 146.4(13); Hf1–O3–C21, 136.7(12).

modified (hydroxyphenyl)oxazoline ligands are accessible using methodologies developed for cationic metallocene derivatives. Future studies will concentrate on using such chiral d<sup>0</sup> complexes for promoting catalytic or stoichiometric reactions in organic synthesis.<sup>18</sup> Furthermore, we believe that the class of ligands we report herein may prove valuable in the development of stereoselective polymerization catalysts.

**Acknowledgment.** We would like to thank the “Fonds National Suisse de la Recherche Scientifique” (Grant No. 20-40268.94) and Ciba-Geigy Co. (Basel, Switzerland) for financial support.

**Supporting Information Available:** Tables giving experimental details associated with data collection, fractional atomic coordinates, thermal parameters, bond distances and angles, Figure S1 for complexes **4** and **10**, a figure showing molecule B of complex **4**, and text giving spectroscopic and analytical data for complexes **5–7** (15 pages). Ordering information is given on any current masthead page.

OM950503R

(17) Preparation of **8** in toluene solution: to a solution of **4** (1.56 g, 2.39 mmol) in toluene (50 mL) at –78 °C was added HNEt<sub>3</sub><sup>+</sup>BPh<sub>4</sub><sup>-</sup> (0.31 g, 0.71 mmol), and the yellow mixture was warmed to room temperature. Ethylene (1 atm) was added, and the solution was stirred for 1 day at room temperature. The mixture was quenched with MeOH/HCl (2 M), and the white-gray solid was collected, washed with MeOH, and filtered (7.0 g).

(18) We have synthesized Zr(Oxa)<sub>2</sub>OR<sup>+</sup>BPh<sub>4</sub><sup>-</sup> (R = diacetone- $\alpha$ -glucose), which shows low activity in the Mukaiyama aldol reaction: Cozzi, P. G.; Floriani, C. Unpublished results.

## Preparation and Characterization of $[(\eta\text{-indenyl})\text{Ni}(\text{PPh}_3)\text{Cl}]$

Trisha A. Huber, Francine Belanger-Gariepy, and Davit Zargarian

*Organometallics*, 1995, 14 (11), 4997-4999 • DOI: 10.1021/om00011a011 • Publication Date (Web): 01 May 2002

Downloaded from <http://pubs.acs.org> on March 9, 2009

### More About This Article

---

The permalink <http://dx.doi.org/10.1021/om00011a011> provides access to:

- Links to articles and content related to this article
- Copyright permission to reproduce figures and/or text from this article

# Preparation and Characterization of [( $\eta$ -indenyl)Ni(PPh<sub>3</sub>)Cl]<sup>†</sup>

Trisha A. Huber, Francine Bélanger-Gariépy, and Davit Zargarian\*

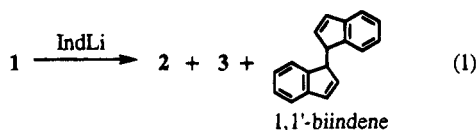
Département de chimie, Université de Montréal, Montréal (Québec), Canada H3C 3J7

Received July 21, 1995<sup>®</sup>

**Summary:** The complex [( $\eta$ -indenyl)Ni(PPh<sub>3</sub>)Cl] has been synthesized and characterized by single-crystal X-ray structural analysis and NMR (<sup>1</sup>H, <sup>13</sup>C, <sup>31</sup>P) spectroscopy. The energy barrier to indenyl ring rotation is ca. 16 kcal/mol.

Although  $\eta$ -Ind complexes (Ind = indenyl or its substituted derivatives) of many transition metals are known to display enhanced reactivities in various stoichiometric and catalytic reactions compared to their  $\eta$ -Cp analogues,<sup>1</sup> the chemistry of group 10 metal indenyl complexes remains virtually unexplored. We are studying this class of compounds and report herein the preparation and characterization of ( $\eta$ -Ind)Ni(PPh<sub>3</sub>)Cl, along with a discussion of the solution- and solid-state hapticity of the Ind ligand.

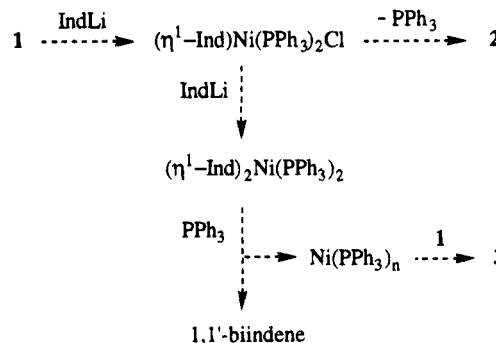
The reaction of IndLi with (PPh<sub>3</sub>)<sub>2</sub>NiCl<sub>2</sub> (**1**) results in a mixture of the title compound ( $\eta$ -Ind)Ni(PPh<sub>3</sub>)Cl (**2**), the Ni(I) species (PPh<sub>3</sub>)<sub>3</sub>NiCl (**3**), and 1,1'-biindenyl (eq 1). The relative proportions of these species in the



final reaction mixture vary with the reaction scale, temperature, solvent, concentration, and rate of addition of IndLi. Preliminary studies of the effects of these variables have allowed us to optimize the conditions for the formation of **2**, which can be prepared in 40–60% yield by the dropwise addition of a dilute Et<sub>2</sub>O solution of IndLi to a suspension of **1** in Et<sub>2</sub>O at room temperature. Even under these conditions, however, the byproducts **3** and 1,1'-biindenyl form in small amounts. We propose that **2**, **3**, and 1,1'-biindenyl originate from the common intermediate ( $\eta^1$ -Ind)Ni(PPh<sub>3</sub>)<sub>2</sub>Cl via two competing pathways (Scheme 1): loss of a PPh<sub>3</sub> and concomitant indenyl ring slippage gives **2**, whereas reaction with a second equivalent of IndLi, followed by reductive elimination, produces 1,1'-biindenyl and Ni(PPh<sub>3</sub>)<sub>n</sub>; the latter is known<sup>2</sup> to undergo a disproportionation reaction with **1** to give **3**.

Complex **3**<sup>3</sup> and 1,1'-biindenyl<sup>4</sup> are known species and were identified on the basis of comparisons to literature data; complex **2** is a new compound and has been fully

Scheme 1



characterized by X-ray crystallography<sup>5</sup> and NMR spectroscopy.<sup>6</sup> Inspection of C–C and Ni–C bond distances (Figure 1) reveals that (a) C1–C7a and C3–C3a > C1–C2 and C2–C3, (b) Ni–C3a,7a > Ni–C(1–3), and (c) Ni–C1 > Ni–C2 > Ni–C3 and Ni–C7a > Ni–C3a. Therefore, the hapticity of the Ind ligand is significantly distorted away from an idealized  $\eta^5$  mode toward an *unsymmetrical*  $\eta^3$  mode (*vide infra*). The main parameters for measuring the degree of hapticity distortions in  $\eta$ -Ind complexes are (a) hinge and fold angles (HA and FA) representing the bending of the Ind ligand at C1/C3 and C3a/C7a, respectively, and (b) the slip value represented by  $\Delta M-C = [M-C_{av}(\text{for C3a,7a})] - [M-C_{av}(\text{for C1,3})]$ .<sup>1</sup> In complex **2**, HA = 10.9°, FA = 11.7°, and  $\Delta M-C = 0.26$  Å. The only other structurally characterized  $\eta$ -Ind nickel complex is Ni(Ind)<sub>2</sub>, for which HA and FA are ca. 13–14° for both Ind ligands and  $\Delta M-C = 0.42$  Å.<sup>1</sup> Evidently, the slip-fold distortion toward an  $\eta^3$  mode is more pronounced in Ni(Ind)<sub>2</sub>, presumably because fully  $\eta^5$ -Ind ligands would lead to a 20-electron configuration in this complex but only an 18-electron configuration in complex **2**.

(5) Red crystals of **2** were grown from an Et<sub>2</sub>O/hexane solution at –20 °C. Crystallographic data for NiClPC<sub>27</sub>H<sub>22</sub> (*M* = 471.60): triclinic *P* $\bar{1}$ , *a* = 9.7128(10) Å, *b* = 10.046(2) Å, *c* = 13.098(2) Å,  $\alpha$  = 88.530(10)°,  $\beta$  = 85.420(10)°,  $\gamma$  = 66.010(10)°, *V* = 1099.2 Å<sup>3</sup>, *Z* = 2,  $\mu$ (Cu K $\alpha$ ) = 3.18 mm<sup>–1</sup>,  $\lambda$  = 1.540 56 Å,  $2\theta_{\text{max}}$  = 140.0°, *T* = 230 K, 8193 reflections measured using the  $\omega/2\theta$  scan mode ( $\Delta\omega = (0.80 + 0.14 \tan \theta)^\circ$ ); 4164 independent, 3753 observed, refinement by block-diagonal least squares gave *R*<sub>F</sub> = 0.0363 and *R*<sub>w</sub> = 0.0396. The ORTEP diagram is shown in Figure 1 along with pertinent bond distances.

(6) <sup>1</sup>H NMR ( $\delta$ ; toluene-*d*<sub>6</sub>): 294 K, 7.64 (m, PPh<sub>3</sub>), 7.33 (br, H4/H7), 7.0 (m, PPh<sub>3</sub> and H5/H6), 6.45 (t, *J*  $\approx$  3 Hz, H2), 6.15 (br, H4/H7), 5.9 (br, H1), 3.3 (br, H3); 380 K, 7.65 and 7.05 (br, PPh<sub>3</sub>), 6.86 (br, H5 and H6), 6.66 (br, H4 and H7), 6.48 (br, H2), 4.57 (br, H1 & H3); 220 K, 7.55 (m, PPh<sub>3</sub>), 7.41 (d, *J* = 7.8, H4/H7), 7.16 (t, *J*  $\approx$  7.6, H5/H6), 6.9 (br, PPh<sub>3</sub> and H5/H6), 6.44 (t, *J*  $\approx$  3, H2), 6.04 (d, *J* = 8.2, H4/H7), 5.94 (br, H1), 3.20 (br, H3); 183 K, 7.5 (br, PPh<sub>3</sub> and H4/H7), 7.22 and 6.95 (t, *J*  $\approx$  7.5, H5 and H6), 6.9 (br, PPh<sub>3</sub>), 6.44 (t, *J*  $\approx$  3, H2), 6.0 (br, H1 and H4/H7), 3.15 (br, H3). <sup>13</sup>C{<sup>1</sup>H} NMR ( $\delta$ ; toluene-*d*<sub>6</sub>, 233 K): 134.5 (d, *J* = 11.4, *o*-C of PPh<sub>3</sub>), 132.4 (d, *J* = 43.4, *i*-C of PPh<sub>3</sub>), 130.35 (d, *J* = 2, *p*-C of PPh<sub>3</sub>), 128.4 (d, *J* = 10, *m*-C of PPh<sub>3</sub>), 126.8 and 126.0 (C5/C6), 125.9 (C3a/C7a), 120.2 and 116.6 (C4/C7), 103.8 (C2), 90.2 (C1), 69.7 (C3); the missing resonance for C3a/C7a is obscured under the residual solvent resonances at ca. 129. <sup>31</sup>P{<sup>1</sup>H} NMR ( $\delta$ ; C<sub>6</sub>D<sub>6</sub>, 294 K): 28.2 (s).

<sup>†</sup> Dedicated to Prof. Stephen Hanessian on the occasion of his 60th birthday.

<sup>®</sup> Abstract published in *Advance ACS Abstracts*, October 1, 1995.

(1) Westcott, S. A.; Kakkar, A. K.; Stringer, G.; Taylor, N. J.; Marder, T. B. *J. Organomet. Chem.* **1990**, *394*, 777.

(2) D'Aniello, M. J.; Barefield, K. *J. Am. Chem. Soc.* **1978**, *100*, 1474.

(3) Mealli, C.; Dapporto, P.; Sriyonyongwat, V.; Albright, T. A. *Acta Crystallogr.* **1983**, *C39*, 995.

(4) Nicolet, P.; Sanchez, J.-Y.; Benaboura, A.; Abadie, M. J. M. *Synthesis* **1987**, 202.

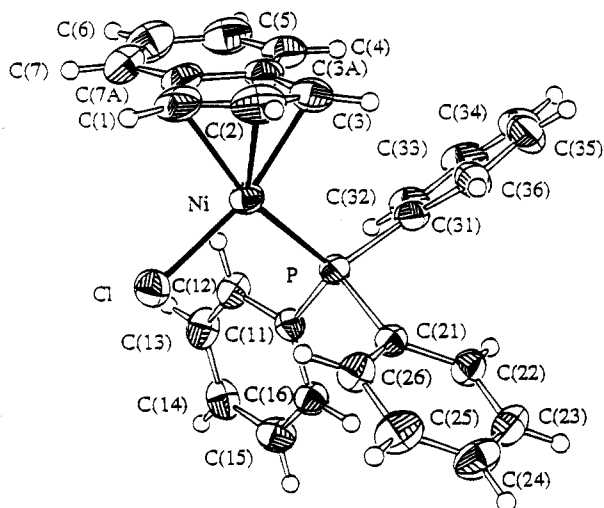


**Figure 1.** ORTEP view of complex **2**. Selected bond lengths (Å): Ni–P = 2.1835(7), Ni–Cl = 2.1822(7), Ni–C1 = 2.094(2), Ni–C2 = 2.061(2), Ni–C3 = 2.042(2), Ni–C3a = 2.318(2), Ni–C7a = 2.344(2), C1–C2 = 1.399(4), C2–C3 = 1.417(4), C3–C3a = 1.449(3), C3a–C7a = 1.422(3), C7a–C1 = 1.459(3), C3a–C4 = 1.394(3), C4–C5 = 1.382(4), C5–C6 = 1.381(5), C6–C7 = 1.385(4), C7–C7a = 1.398(4).

The ambient-temperature  $^1\text{H}$  and  $^{13}\text{C}\{^1\text{H}\}$  NMR spectra of complex **2** consist of both sharp and broad resonances which have been assigned by means of inverse gated decoupling and low-temperature heteronuclear correlation through multiple quantum coherence (HMQC) experiments.<sup>6</sup> NMR data are valuable in assessing indenyl hapticity; for instance, the difference in the  $^{13}\text{C}$  chemical shifts of the ring-junction carbons in  $\eta$ -Ind complexes and  $\text{NiInd}$  has been shown to correlate well with the  $\eta$ -Ind hapticity.<sup>7</sup> For complex **2** at 233 K,  $\Delta\delta_{\text{av}}(\text{C3a/C7a}) \approx -3$ , indicating<sup>7</sup> that the intermediate hapticity of the Ind ligand observed in the solid state is maintained in solution at *ca.*  $-40^\circ\text{C}$ . For comparison,  $\Delta\delta_{\text{av}}(\text{C3a/C7a})$  is  $-43.7$  for  $\text{Fe}(\eta^5\text{-Ind})_2$ ,<sup>1</sup>  $+3.6$  for  $\text{Ni}(\text{Ind})_2$ ,<sup>1</sup> and  $+25.7$  for  $(\eta^3\text{-Ind})\text{Ir}(\text{PMe}_2\text{Ph})_3$ .<sup>8</sup>

The variable-temperature  $^1\text{H}$  NMR spectra for complex **2**<sup>6</sup> show that gradually increasing the temperature causes the six broad resonances present in the ambient-temperature spectrum to disappear into the base line and reappear as three coalesced resonances; lowering the temperature sharpens the broad resonances and changes their chemical shifts. These results point to the hindered rotation of the Ind ligand as the cause of the resonance broadening observed in the ambient-temperature  $^1\text{H}$  and  $^{13}\text{C}\{^1\text{H}\}$  NMR spectra.<sup>9</sup> Using the Eyring equation for a two-site exchange process involving a molecular rotation,<sup>10</sup> an average  $\Delta G^\ddagger_{T_c}$  value of

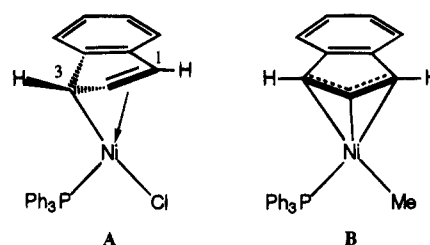
(7) Baker, R. T.; Tulip, T. H. *Organometallics* **1986**, *5*, 839–845. According to this procedure, when the average chemical shift of C3a/C7a in the  $\eta$ -Ind complex is significantly upfield or downfield of the corresponding shift in  $\text{NiInd}$ , the Ind ligand is thought to be coordinated in a  $\eta^5$  or  $\eta^3$  fashion, respectively; if, on the other hand, the two shifts are not very different, an intermediate hapticity is assumed.

(8) Merola, J. S.; Kacmarcik, R. T.; Van Engen, D. *J. Am. Chem. Soc.* **1986**, *108*, 329.

(9) The absence of a plane of symmetry in complex **2** means that rapid ring rotation is required in order for the halves of the Ind ligand (on either side of the plane containing C2 and the midpoints of C3a–C7a and C5–C6) to appear equivalent in solution NMR spectra. If this rotation is slow on the NMR time scale, some broadening might be expected below the coalescence temperature.

(10) Abraham, R. J.; Loftus, P. *Proton and Carbon-13 NMR Spectroscopy*; Wiley: New York, 1985; Chapter 7, pp 165–168, eq. 7.11.  $\Delta G^\ddagger/RT_c = 22.96 + \ln(T_c/\delta\nu)$ .

Chart 1



*ca.* 16 kcal/mol is obtained for the ring rotation process in complex **2**. To our knowledge, this value represents the largest energy barrier reported for indenyl ring rotation.

The hindrance of indenyl rotation is generally attributed to slip-fold distortions away from the  $\eta^5$  mode.<sup>11</sup> We propose that the large  $\Delta G^\ddagger_{T_c}$  value observed in complex **2** is due to the unsymmetrical character of the Ni–Ind bonding (Ni–C1 > Ni–C3; *vide supra*),<sup>12</sup> which is caused by a large difference between the ligand trans effects of  $\text{PPh}_3$  and  $\text{Cl}^-$ . Thus, the Ni–C3 interaction can be viewed as stronger and more  $\sigma$ -like, in contrast to a weaker,  $\pi$ -type interaction between Ni and C1–C2 (**A** in Chart 1). This picture of a partially localized bonding would require that C1 and C3 be quite different in terms of hybridization, which would explain the rather large chemical shift differences in the slow-exchange regime between C1 and C3 (>20 ppm) and H1 and H3 (>2.9 ppm).<sup>13</sup>

Relative ligand trans effects are known to influence the conformation of  $\eta$ -Ind complexes,<sup>14</sup> but their effect on the hapticity of the Ind ligand is unknown. If the large trans effect difference between  $\text{PPh}_3$  and  $\text{Cl}^-$  in **2** does distort the Ni–Ind bonding toward a localized  $\eta^1$ : $\eta^2$  mode, replacing the  $\text{Cl}^-$  ligand by a stronger trans effect ligand should reduce this distortion. We have prepared  $(\eta\text{-Ind})\text{Ni}(\text{PPh}_3)\text{Me}$ <sup>15</sup> and note that its *ambient-temperature*  $^1\text{H}$  NMR spectrum contains a single resonance for H1 and H3 at 4.76 ppm, very similar to the coalesced signal for H1/H3, which resonates at *ca.* 4.6 ppm in the *high-temperature* spectrum of complex **2**. Apparently, the smaller difference between the trans effects of  $\text{PPh}_3$  and  $\text{Me}^-$  leads to a more symmetrical, delocalized Ni–Ind bonding (**B** in Chart 1) and consequently a smaller rotational barrier in the Ni–Me derivative. These observations are consistent with our proposal that at low temperatures the Ind ligand in complex **2** coordinates in a partially localized fashion. This aspect of Ni–Ind bonding and the factors affecting

(11) (a) Barr, R. D.; Green, M.; Marder, T. B.; Stone, F. G. A. *J. Chem. Soc., Dalton Trans.* **1984**, 1261. (b) Marder, T. B.; Calabrese, J. C.; Roe, D. C.; Tulip, T. H. *Organometallics* **1987**, *6*, 2012.

(12) (a) A reviewer has suggested that the mechanism of the indenyl rotation might involve an ( $\eta^1$ : $\eta^2$ ) to  $\eta^1$  change of hapticity and, thus, the large energy barrier might imply that C1=C2 is strongly coordinated to Ni. We agree with this possibility and have in fact put forth a similar scenario in an earlier presentation,<sup>12b</sup> but no evidence exists in support of these ideas. (b) Huber, T. A.; Zargarian, D. Late Metal Indenyl/Amido Complexes. CIC 78th CSC Annual Conference, Guelph, Ontario, Canada, May 28–June 1 1995; Abstract 959.

(13) That these chemical shift differences are not due to the ring current effects of the  $\text{PPh}_3$  phenyl groups is supported by the observation that, in the  $\text{PMe}_3$  analogue of **2**, in which no ring current effect can be invoked, a similar difference is observed, *i.e.*  $\Delta\delta(\text{H1},\text{H3}) > 2.1$  ppm.

(14) (a) Faller, J. W.; Crabtree, R. H.; Habib, A. *Organometallics* **1985**, *4*, 929. (b) Husebo, T. L.; Jensen, C. M. *Organometallics* **1995**, *14*, 1087.

(15) Huber, T. A.; Dion, S.; Zargarian, D. Unpublished results.

it will be probed further by studying the hapticities of analogous ( $\eta$ -Ind)NiLX complexes.

**Acknowledgment.** We thank the NSERC (Canada), the FCAR (Québec), and the Université de Montréal for financial support, Professors M. J. McGlinchey and T. B. Marder for valuable discussions and constructive criticisms, and S. Dion, I. Dubuc, and A. Gagnon for contributions to our studies.

**Supporting Information Available:** Text giving procedures for the syntheses of complex **2** and its  $\text{PMe}_3$  and Me analogues, figures giving  $^1\text{H}$ ,  $^{13}\text{C}$ , and  $^{31}\text{P}$  NMR data for **2**, a table giving the elemental analysis of **2**, and complete details on the X-ray analysis of **2**, including tables of bond distances and angles, anisotropic thermal parameters, and atomic coordinates (39 pages). Ordering information is given on any current masthead page.

OM9505571

# A New Approach to Chiral Cyclopentadienylmetal Complexes

Lothar Schwink, Stephan Vettel, and Paul Knochel\*

Fachbereich Chemie der Philipps-Universität Marburg, Hans-Meerwein-Strasse,  
D-35032 Marburg, Germany

Received September 27, 1995<sup>®</sup>

**Summary:** A new enantioselective synthesis of chiral  $\alpha$ -oxygen-substituted cyclopentadienyl complexes of Fe and Ru is described. This method does not require a resolution procedure and involves a highly enantioselective preparation of chiral secondary cyclopentadienyl alcohols (89–98% ee).

Chiral transition-metal complexes have found numerous applications as catalysts in asymmetric reactions.<sup>1</sup> In particular, chiral cyclopentadienyl complexes have led to important advances in asymmetric catalysis.<sup>2,3</sup> Most of these complexes have been prepared by tedious resolution methods or by using precursors from the chiral pool.<sup>3</sup> Herein we report a new approach to complexes **1** by preparing chiral  $\alpha$ -oxygen-substituted cyclopentadiene derivatives of type **2** starting from the chiral allylic alcohols **3** (Scheme 1).

The alcohols **3** were obtained by the addition of various dialkylzincs<sup>4</sup> to cyclopentenecarboxaldehyde **4**<sup>5</sup> in the presence of catalytic amounts of (1*R*,2*R*)-bis-(trifluoromethanesulfonamido)cyclohexane<sup>6</sup> (5–8 mol %) and mixtures of titanium alkoxides (Ti(O-*i*-Pr)<sub>4</sub>/Ti(O-*t*-Bu)<sub>4</sub>, ca. 1:3)<sup>7</sup> in ether or toluene at –20 °C. Under these conditions, the allylic alcohols **3** are obtained with

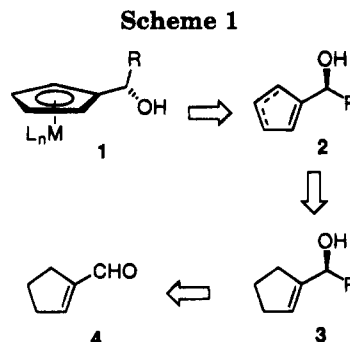
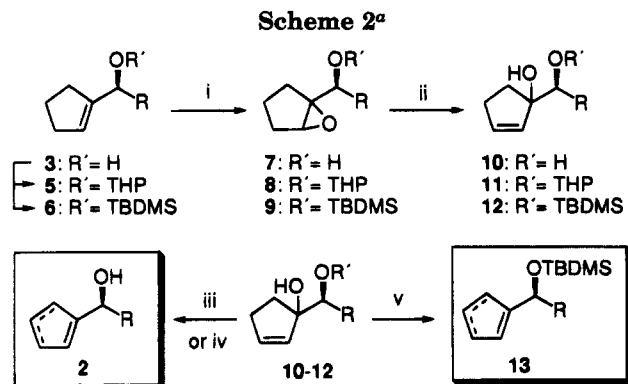


**Table 1.** Allylic Alcohols **3a–d** Obtained by the Catalytic Enantioselective Alkylation of **4**

entry no.	R	alcohol <b>3</b>	yield, %	ee, %
1	Me	<b>3a</b>	69	89
2	Et	<b>3b</b>	84	96
3	Pent	<b>3c</b>	89	97
4	(CH <sub>2</sub> ) <sub>3</sub> OPiv	<b>3d</b>	80	98



<sup>a</sup> Key: (i) MCPBA, 65–90%; (ii) (1) PhSeNa, (2) ROOH (R = H, cumyl), 64–88%; (iii) R' = THP, (1) TosOH (0.5–2 mol %), CH<sub>2</sub>Cl<sub>2</sub>, (2) TosOH (0.4 equiv), MeOH, 36–51%; (iv) R' = H, MgSO<sub>4</sub>, toluene, 100 °C, 45–57%; (v) R' = TBDMS, MgSO<sub>4</sub>, toluene, 100 °C, 67–76%.

good to excellent yields (69–89%) and high enantiomeric excess (89–98% ee; Table 1).<sup>8</sup>

The conversion of the unsaturated alcohols **3** to the previously unknown chiral dienic alcohols **2** has been achieved via three variations of a reaction sequence using intermediates **5–12** (Scheme 2). The alcohols **3** can be readily protected (THP, TBDMS) and converted to the corresponding epoxides **8** and **9**. Opening of the epoxides with sodium phenylselenide in ethanol followed by oxidation with hydrogen peroxide gives the allylic alcohols **11** and **12** (71–88% yield).<sup>9</sup> The elimination of water is achieved by treating alcohols **11** with TosOH

(8) The enantiomeric excess of alcohols **3** was determined by <sup>1</sup>H NMR analysis of the corresponding (S)-(+)-O-acetylmandelates: Parkers, D. J. *Chem. Soc., Perkin Trans. 2* **1983**, 83.

(9) Sharpless, K. B.; Lauer, R. F. *J. Am. Chem. Soc.* **1973**, *95*, 2697.

<sup>®</sup> Abstract published in *Advance ACS Abstracts*, November 1, 1995.

(1) (a) Noyori, R. *Asymmetric Catalysis in Organic Synthesis*; Wiley: New York, 1994. (b) Ojima, I., Ed. *Catalytic Asymmetric Synthesis*; VCH: New York, Weinheim, 1993. (c) Brunner, H. In *The Chemistry of the Metal-Carbon Bond*; Hartley, F. R., Ed. (Patai, S., Series Ed.); Wiley: New York, 1989; Vol. 5, p 109.

(2) (a) Hayashi, T.; Tajika, M.; Tamao, K.; Kumada, M. *J. Am. Chem. Soc.* **1976**, *98*, 3718. (b) Hayashi, T. *Pure Appl. Chem.* **1988**, *60*, 7. (c) Wild, F. R. W. P.; Zsolnai, L.; Huttner, G.; Brintzinger, H. H. *J. Organomet. Chem.* **1982**, *232*, 233. (d) Brintzinger, H. H.; Fischer, R.; Mühlaupt, R.; Rieger, B.; Waymouth, R. *Angew. Chem., Int. Ed. Engl.* **1995**, *34*, 1143. (e) Willoughby, C. A.; Buchwald, S. L. *J. Am. Chem. Soc.* **1992**, *114*, 7562. (f) Broene, R. D.; Buchwald, S. L. *J. Am. Chem. Soc.* **1993**, *115*, 12569. (g) Lee, N. E.; Buchwald, S. L. *J. Am. Chem. Soc.* **1994**, *116*, 5985. (h) Halterman, R. L.; Vollhardt, K. P. C. *Tetrahedron Lett.* **1986**, *27*, 1461. (i) Chen, Z.; Halterman, R. L. *Organometallics* **1994**, *13*, 3932. (j) Burk, M. J.; Gross, M. F. *Tetrahedron Lett.* **1994**, *35*, 9363. (k) Togni, A.; Breutel, C.; Schnyder, A.; Spindler, F.; Landert, H.; Tijani, A. *J. Am. Chem. Soc.* **1994**, *116*, 4062. (l) Abbenhuis, H. C. L.; Burekhardt, U.; Gramlich, V.; Togni, A.; Albinati, A.; Müller, B. *Organometallics* **1994**, *13*, 4481. (m) Schnyder, A.; Hintermann, L.; Togni, A. *Angew. Chem., Int. Ed. Engl.* **1995**, *34*, 931. (n) David, D. M.; Kane-Maguire, L. A. P.; Pyne, S. G. *J. Chem. Soc., Chem. Commun.* **1990**, 888.

(3) (a) Review: Halterman, R. L. *Chem. Rev.* **1992**, *965*. (b) Togni, A.; Hayashi, T., Eds. *Ferrocenes*; VCH: New York, Weinheim, 1995.

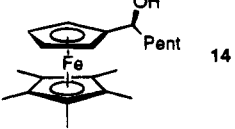
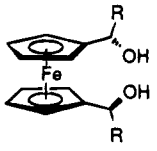
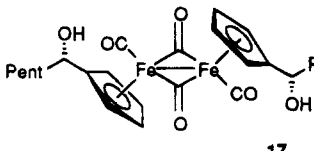
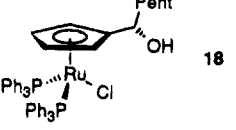
(4) (a) Rozema, M. J.; Sidduri, A.; Knochel, P. *J. Org. Chem.* **1992**, *57*, 1956. (b) Rozema, M. J.; Eisenberg, C.; Lütjens, H.; Ostwald, R.; Belyk, K.; Knochel, P. *Tetrahedron Lett.* **1993**, *34*, 3115. (c) Knochel, P. *Synlett* **1995**, 393.

(5) Brown, J. B.; Henbest, H. B.; Jones, E. R. H. *J. Chem. Soc.* **1950**, 3634.

(6) (a) Yoshioka, M.; Kawakita, T.; Ohno, M. *Tetrahedron Lett.* **1989**, *30*, 1657. (b) Takahashi, H.; Kawakita, T.; Ohno, M.; Yoshioka, M.; Kobayashi, S. *Tetrahedron* **1992**, *48*, 5691.

(7) The use of mixtures of Ti(O-*i*-Pr)<sub>4</sub> and Ti(O-*t*-Bu)<sub>4</sub> is mandatory for the addition of Me<sub>2</sub>Zn and improves the enantioselectivity for the addition of other dialkylzincs, especially in large-scale experiments (over 20 mmol): Nowotny, S.; Vettel, S.; Knochel, P. *Tetrahedron Lett.* **1994**, *35*, 4539.

**Table 2. Chiral (Hydroxyalkyl)cyclopentadienyl Fe and Ru Complexes 14–18 Obtained from the Cyclopentadienyl Alcohols 2 and 13**

Alcohol 2, 13	Product 14–18 <sup>a</sup>	Yield %	<i>dl</i> : <i>meso</i> <sup>b</sup> (% <i>ee</i> )
2c		74	(> 96) <sup>c</sup>
2a	15a R = Me	65	89:11 (99) <sup>d</sup>
2b	15b R = Et	74	
2c	15c R = Pent	70	
2d	15d R = (CH <sub>2</sub> ) <sub>3</sub> OPiv	43	
2c		65	89:11
13	16b R' = TBDMS	48	95:5 (99) <sup>e</sup>
2c		58	96:4
2c		48	(>96) <sup>c</sup>

<sup>a</sup> Reaction conditions are as follows. **14**: (1) *n*-BuLi (2.5 equiv), THF, -78 °C; (2) Cp\*Fe(acac), 0 °C. **15a–d**: (1) LDA (2.5 equiv), THF, -78 to 10 °C; (2) FeCl<sub>2</sub> (0.8 equiv), -10 °C to room temperature. **16a,b**: RuCl<sub>3</sub>, Zn, -40 °C. **17**: Fe<sub>2</sub>(CO)<sub>9</sub>, norbornene, *n*-octane, 130 °C, 4 h. **18**: Ru(PPh<sub>3</sub>)<sub>3</sub>Cl<sub>2</sub> toluene–EtOH. <sup>b</sup> Determined by NMR analysis. <sup>c</sup> Determined by <sup>1</sup>H NMR analysis in the presence of Eu(hfc)<sub>3</sub>. <sup>d</sup> Determined by HPLC analysis using a chiral column (Chiralcel OD). <sup>e</sup> Determined by HPLC analysis using a chiral column (Chiralcel OD-H) after deprotection with TBAF.

(0.5–2 mol %) in CH<sub>2</sub>Cl<sub>2</sub> (room temperature, 0.25 h). The THP group was removed by further addition of TosOH (0.4 equiv) and MeOH to afford the chiral cyclopentadienyl alcohols **2** in yields of 36–51% as a mixture of 1,5-H shift isomers. In the case of the TBDMS-protected diol **12** elimination with MgSO<sub>4</sub> proceeds smoothly (toluene, 100 °C, 1 h), leading cleanly to the TBDMS-protected alcohol **13** (R = Pent) in satisfactory yields (67–76%). The whole sequence can be performed without protecting the hydroxy group by a slight change of the reaction conditions. Thus, the use of aprotic conditions (cumene hydroperoxide, CH<sub>2</sub>-Cl<sub>2</sub>) was essential for the oxidation of the phenylselenide intermediate (**7** → **10**, Scheme 2). This variation shortens the procedure and improves the overall yield to 38% compared with 25–31% for the THP route (**3** → **2**).

Both alcohols **2** and **13** are well-suited for the formation of chiral cyclopentadienyl complexes (Table 2). Thus, treatment of **2c** with *n*-BuLi (2.5 equiv) or LDA (2.5 equiv) in THF at -78 °C affords a cyclopentadienyl

dianion which reacts with Cp\*Fe(acac)<sup>10</sup> (THF, 0 °C, 0.5 h), giving the heteroleptic ferrocene **14** in 74% yield (>96% ee). The C<sub>2</sub>-symmetrical ferrocenes<sup>11</sup> **15a–d**, which are highly interesting starting materials for catalyst synthesis, are readily obtained by the reaction of the lithium dianion of alcohols **2** with FeCl<sub>2</sub> (THF, -10 °C to room temperature, 14 h, 43–74% yield). A complete transfer of chirality from allylic alcohols **3** to the metallocenes **14** and **15** is observed. By treatment of the alcohol **2c** with RuCl<sub>3</sub>·3H<sub>2</sub>O and zinc<sup>12</sup> (EtOH, -40 °C, 1 h) the desired C<sub>2</sub>-symmetrical ruthenocene **16a** is obtained in good yield (65%) but with some racemization (*dl*:*meso* 89:11, starting with **2c** (97% ee)). In contrast, by using the silylated cyclopentadienyl alcohol **13** the ruthenocene **16b** is obtained containing less than 5% of the *meso* isomer (Table 2). Chiral dinuclear iron complexes such as **17** can be prepared by the reaction of **2c** with Fe<sub>2</sub>(CO)<sub>9</sub> in the presence of norbornene (octane, 130 °C, 4 h).<sup>13</sup> Complexes of type **17** have been shown to be precursors of synthetically interesting Fp anions (Fp = Cp\*Fe(CO)<sub>2</sub>).<sup>14</sup> Finally, the chiral half-sandwich ruthenium complex **18** has been prepared in >96% ee by treatment of **2c** with Ru(PPh<sub>3</sub>)<sub>3</sub>Cl<sub>2</sub> (toluene–EtOH, room temperature, 48 h; 48% yield).<sup>15</sup> The parent nonchiral ruthenium complex CpRu(PPh<sub>3</sub>)<sub>2</sub>Cl has found applications in catalytic carbon–carbon bond-forming reactions.<sup>16</sup>

In summary, we have developed a new efficient enantioselective preparation of transition-metal cyclopentadienyl complexes starting from chiral cyclopentadienyl alcohols of type **2**, which are readily available in high optical purity by a catalytic asymmetric addition of dialkylzincs to aldehyde **4** and a few transformations. The utility of some of the complexes **14–18** as catalysts for asymmetric reactions is currently being tested in our laboratories.

**Acknowledgment.** We thank the DFG (SFB 260) and the Fonds der Chemischen Industrie for generous financial support. We thank Witco AG, Chemetall, Sipsy, Bayer AG, and BASF AG for generous gifts of chemicals.

**Supporting Information Available:** Text giving experimental procedures and analytical data for the compounds **2**, **3**, and **6–18** (17 pages). This material is contained in many libraries on microfiche, immediately follows this article in the microfilm version of the journal, can be ordered from the ACS, and be downloaded from the Internet; see any current masthead page for ordering information and Internet access instructions.

OM950769Y

(10) Bunel, E. E.; Valle, L.; Manriquez, J. M. *Organometallics* **1985**, *4*, 1680.

(11) (a) Yamakawa, K.; Hisatome, M. *J. Organomet. Chem.* **1973**, *52*, 407. (b) Nefedova, M. N.; Mamedyarova, I. A.; Petrovski, P. P.; Sokolov, V. I. *J. Organomet. Chem.* **1992**, *425*, 125. (c) Lambusta, D.; Nicolosi, G.; Patti, A.; Piattelli, M. *Tetrahedron: Asymmetry* **1993**, *4*, 919. (d) Soai, K.; Hayase, T.; Takai, K.; Sugiyama, T. *J. Org. Chem.* **1994**, *59*, 7908.

(12) Pertici, P.; Vitulli, G.; Paci, M.; Porri, L. *J. Chem. Soc., Dalton Trans.* **1980**, 1961.

(13) Kochhar, R. K.; Pettit, R. *J. Organomet. Chem.* **1966**, *6*, 272.

(14) (a) Vargas, R. M.; Theys, R. D.; Hossain, M. M. *J. Am. Chem. Soc.* **1992**, *114*, 777. (b) Davies, S. G. *Pure Appl. Chem.* **1988**, *60*, 13.

(c) Marsi, M.; Rosenblum, M. *J. Am. Chem. Soc.* **1984**, *106*, 7264.

(15) Gilbert, J. D.; Wilkinson, G. *J. Chem. Soc. A* **1969**, 1749.

(16) (a) Trost, B. M.; Dyker, G.; Kulawiec, R. J. *J. Am. Chem. Soc.* **1990**, *112*, 7809. (b) Trost, B. M.; Kulawiec, R. J. *J. Am. Chem. Soc.* **1992**, *114*, 5579.



# Isolation of a Phosphenium Ion with a P–C $\sigma$ Bond

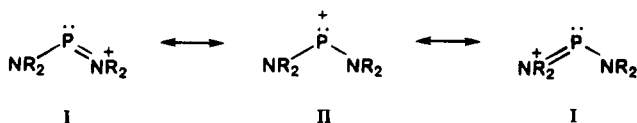
Robert W. Reed, Zuowei Xie, and Christopher A. Reed\*

Department of Chemistry, University of Southern California,  
Los Angeles, California 90089-0744

Received July 31, 1995\*

**Summary:** The first example of an X-ray crystallographically characterized two-coordinate phosphorus cation with a P–C single  $\sigma$  bond is described.  $[P(\text{mesityl})(N\text{-}i\text{-Pr}_2)][AlCl_4]$  was prepared by treatment of  $P(Cl)(\text{mesityl})(N\text{-}i\text{-Pr}_2)$  with  $Al_2Cl_6$  in dichloromethane. The phosphenium ion character of the cation is reflected in the large downfield  $^{31}P$  chemical shift (500 ppm) and can be compared to 313 ppm in the corresponding bis-(dialkylamido) cation  $[P(N\text{-}i\text{-Pr}_2)_2]^+$ .

Phosphenium ions,  $R_2P^+$ , isoelectronic with carbenes, are reactive species unless they are stabilized by the presence of strong  $\pi$ -donor substituents, classically two dialkylamino groups.<sup>1</sup> Iminium ion character (I) in these compounds compromises their phosphenium ion character (II). When less compromising substituents



are used, decreased stability has typically meant that these species have been characterized only on the basis of a downfield  $^{31}P$  chemical shift.<sup>2,3</sup> We now report the preparation and isolation of mesityl(diisopropylamino)-phosphenium tetrachloroaluminate, the first X-ray structurally characterized example of a phosphenium ion with a phosphorus–carbon single bond. Phosphorus–carbon  $\pi$  bonding is present in all other low-coordinate phosphorus cations that have been structurally characterized to date. These include the  $\eta^2$   $\pi$ -bonded species  $[(C_5Me_5)(NH\text{-}t\text{-Bu})P][AlCl_4]$ ,<sup>4</sup> the phosphalkene  $[Ph_3PC(H)=P(N\text{-}i\text{-Pr}_2)][BF_4]$ ,<sup>5</sup> a heterocyclic diazaphosphonium chloride,<sup>6</sup> and  $\eta^6$   $\pi$ -arene complexes of iminophosphenium cations.<sup>7</sup>

\* To whom correspondence should be addressed: Fax, (213) 740-0930; Tel, (213) 740-3337; email: careed@chem1.usc.edu.

† Abstract published in *Advance ACS Abstracts*, November 1, 1995.

(1) For reviews on phosphenium ions, see: Cowley, A. H.; Kemp, R. A. *Chem. Rev.* **1985**, *85*, 367. Sanchez, M.; Mazieres, M. R.; Lamande, L.; Wolf, R. In *Multiple Bonds and Low Coordination in Phosphorus Chemistry*; Regitz, M., Ed.; Thieme Verlag: Stuttgart, Germany, 1990; p 129.

(2) Cowley, A. H.; Lattman, M.; Wilburn, J. C. *Inorg. Chem.* **1981**, *20*, 2916.

(3) Attempts to generate phosphenium ions in the absence of at least one dialkylamino group have either failed ((a) Lambert, J. B.; So, Jeung-Ho, *J. Org. Chem.* **1991**, *56*, 5960) or led to Lewis acid–Lewis base adducts ((b) Burford, N.; Losier, P.; Sereda, S. V.; Cameron, T. S.; Wu, G. *J. Am. Chem. Soc.* **1994**, *116*, 6474). Even the most stable phosphenium ion, (*i*-Pr)<sub>2</sub>N<sub>2</sub>P<sup>+</sup>, reacts slowly with CH<sub>2</sub>Cl<sub>2</sub>: (c) Burford, N.; Losier, P.; Bakshi, P. K.; Cameron, S. T. *J. Chem. Soc., Dalton Trans.* **1993**, 201.

(4) Gudat, D.; Nieger, M.; Niecke, E. *J. Chem. Soc., Dalton Trans.* **1989**, 693.

(5) Gruetzmacher, H.; Pritzkow, H. *Angew. Chem., Int. Ed. Engl.* **1989**, *28*, 740.

(6) Friedrich, P.; Huttner, G.; Lubner, J.; Schmidpeter, A. *Chem. Ber.* **1978**, *111*, 1558.

(7) Burford, N.; Clyburne, J. A. C.; Bakshi, P. K.; Cameron, T. S. *Organometallics* **1995**, *14*, 1578.

In order to counter the electronic stabilization lost upon the replacement of a  $\pi$ -donor dialkylamino group at phosphorus, we chose a bulky mesityl substituent to provide kinetic stabilization close to the phosphorus center. As a starting material, chloro(diisopropylamino)mesitylphosphine (**1**) was prepared by the reaction of dichloromesitylphosphine with diisopropylamine.<sup>8</sup> In this phosphine the substituents are diastereotopic even at  $>60$  °C as demonstrated by the doubling of the  $^1H$  and  $^{13}C$  NMR methyl group signals arising from both the aryl and isopropyl moieties. Substitution of chloride for triflate by treatment of **1** ( $\delta(^{31}P)$  132 ppm) with silver trifluoromethanesulfonate affords the new phosphine **2**,  $P(OSO_2CF_3)(N\text{-}i\text{-Pr}_2)(\text{mesityl})$ , whose  $^{31}P$  resonance is shifted 53 ppm downfield to 185 ppm. This compound also shows diastereotopic *o*-methyl groups to  $>60$  °C for the mesityl substituent, but the diisopropylamino group is diastereotopic only below room temperature ( $\Delta G^\ddagger = 56$  kJ mol<sup>-1</sup>). Clearly, rotation about the P–N bond is more rapid than rotation about the P–C bond and is favored by the more labile anion. Related observations

(8) Synthesis adapted from: Schmidbauer, H.; Schnatterer, S. *Chem. Ber.* **1983**, *116*, 1947. The full synthetic procedures and identifying data for **1–3** are as follows. **1**: To a cold toluene solution (0 °C, 250 mL) of (mesityl)PCl<sub>2</sub> (6.20 g, 28.0 mmol) was slowly added *i*-Pr<sub>2</sub>NH (8.8 mL, 61 mmol). The mixture was then refluxed overnight. After it was cooled to 0 °C, the solution was filtered to remove *i*-Pr<sub>2</sub>NH<sub>2</sub><sup>+</sup>Cl<sup>-</sup>. Removal of the toluene *in vacuo* followed by recrystallization from dry acetonitrile (–30 °C) afforded large yellow blocks of **1**. Yield: 4.90 g, 17.1 mmol, 61%. Mp: 90–92 °C. Anal. Calcd: C, 63.04; H, 8.82; N, 4.90. Found: C, 62.87; H, 8.84; N, 4.93.  $^{31}P\{^1H\}$  NMR (145 MHz, CDCl<sub>3</sub>, 25 °C, 85% H<sub>3</sub>PO<sub>4</sub>):  $\delta$  132.  $^1H$  NMR (360 MHz (and 250 MHz), CDCl<sub>3</sub>, 25 °C, TMS):  $\delta$  6.70 (m, 2H), 3.46 (sept,  $^3J(HH) = 6.6$  Hz, 1H), 3.42 (sept,  $^3J(HH) = 6.6$  Hz, 1H), 2.68 (s, 3H; *o*-CH<sub>3</sub>), 2.67 (s, 3H; *o*-CH<sub>3</sub>), 2.04 (s, 3H; *p*-CH<sub>3</sub>), 1.32 (d,  $^3J(HH) = 6.6$  Hz, 6H), 0.88 (d,  $^3J(HH) = 6.6$  Hz, 6H).  $^{13}C\{^1H\}$  NMR (90 and 63 MHz, CDCl<sub>3</sub>, 25 °C, TMS):  $\delta$  142.7, 142.4, 139.8 (para), 131.0, 130.9, 130.3 (ipso), 49.5, 49.4, 23.7, 23.6, 23.5, 23.3 (2C), 23.1, 20.8. **2**: To a benzene solution of **1** (1.00 g, 3.5 mmol) was added Ag(CF<sub>3</sub>SO<sub>2</sub>) (0.91 g, 3.6 mmol), and the mixture was stirred overnight. The solution was filtered to remove AgCl and concentrated *in vacuo*. Pentane was added until the onset of turbidity, at which point the solution was gently warmed before cooling to –30 °C to afford **2** as a crystalline mass. Yield: 0.54 g, 1.4 mmol, 40%. Mp: 119–122 °C. Anal. Calcd: C, 48.12; H, 6.31; N, 3.51. Found: C, 47.86; H, 6.24; N, 3.42.  $^{31}P\{^1H\}$  NMR (109 MHz, C<sub>6</sub>D<sub>6</sub>, 25 °C, 85% H<sub>3</sub>PO<sub>4</sub>):  $\delta$  185.  $^1H$  NMR (360 MHz (and 250 MHz), CD<sub>2</sub>Cl<sub>2</sub>, –40 °C, TMS):  $\delta$  6.98 (m, 2H), 3.74 (m, 1H), 3.66 (m, 1H), 2.46 (s, 3H; *o*-CH<sub>3</sub>), 2.45 (s, 3H; *o*-CH<sub>3</sub>), 2.29 (s, 3H; *p*-CH<sub>3</sub>), 1.48 (d,  $^3J(HH) = 6.7$  Hz, 6H), 1.03 (d,  $^3J(HH) = 6.7$  Hz, 6H).  $^{13}C\{^1H\}$  NMR (90 MHz, C<sub>6</sub>D<sub>6</sub>, 25 °C, TMS):  $\delta$  141.5, 141.3, 141.0, 130.9, 130.8, 128.2, 119.5 (CF<sub>3</sub>,  $^1J(CF) = 319$  Hz), 50 (br), 23 (br), 22.2, 22.0, 20.5. **3**: To a cold (0 °C) stirred suspension of AlCl<sub>3</sub> (0.50 g, 3.8 mmol) in CH<sub>2</sub>Cl<sub>2</sub> was added a cold CH<sub>2</sub>Cl<sub>2</sub> solution of **1** (1.0 g, 3.5 mmol). The solution quickly developed an intense yellow color. Filtration through a fine frit, layering of the filtrate with toluene, and storage at –30 °C for 1 week produced large gemlike crystals of **3**. Yield: 1.12 g, 2.7 mmol, 76%. Mp: 133–135 °C. Anal. Calcd: C, 42.98; H, 6.01; N, 3.34. Found: C, 42.88; H, 6.02; N, 3.14.  $^{31}P\{^1H\}$  NMR (109 MHz, CD<sub>2</sub>Cl<sub>2</sub>, 25 °C, 85% H<sub>3</sub>PO<sub>4</sub>):  $\delta$  500 (t (1:1:1),  $^1J(P,N) = 65$  Hz).  $^{14}N\{^1H\}$  NMR (19 MHz, CD<sub>2</sub>Cl<sub>2</sub>, 25 °C, 85% CH<sub>3</sub>NO<sub>2</sub>):  $\delta$  –71.0 (d,  $^1J(P,N) = 65$  Hz).  $^{27}Al$  NMR (70 MHz, CD<sub>2</sub>Cl<sub>2</sub>, 25 °C, Al(H<sub>2</sub>O)<sub>6</sub><sup>3+</sup>):  $\delta$  –105 (s,  $w_{1/2} = 6$  Hz);  $^1H$  NMR (360 MHz (and 250 MHz), CD<sub>2</sub>Cl<sub>2</sub>, –40 °C, TMS):  $\delta$  7.09 (s, 2H), 4.67 (m, 2H), 2.36 (s, 3H), 2.31 (s, 6H), 1.83 (d, 6H,  $J = 6.25$  Hz), 1.38 (d, 6H,  $J = 6.44$  Hz).  $^{13}C\{^1H\}$  NMR (90 MHz, CD<sub>2</sub>Cl<sub>2</sub>, –40 °C, TMS):  $\delta$  146.7, 139.6, 139.5, 130.5, 127.3 ( $^1J(PC) = 47.5$  Hz), 64.5, 64.3, 58.2, 58.0, 29.4, 29.3, 21.46, 21.40, 21.35, 21.25, 21.23.

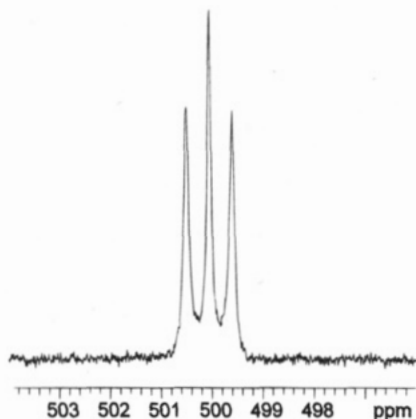


**Figure 1.** Proton-decoupled  $^{31}\text{P}$  NMR spectrum of the  $[(\text{mesityl})(i\text{-Pr}_2\text{N})\text{P}]^+$  cation in **3** (referenced vs  $\text{H}_3\text{PO}_4$ ).

on triflate lability have been made by Dahl<sup>9</sup> and by Niecke.<sup>4</sup> The triflate compound shows greatly increased sensitivity toward moisture. Abstraction of chloride from **1** with aluminum trichloride affords the new phosphonium ion mesityl(diisopropylamino)phosphonium tetrachloroaluminate (**3**). The  $^{31}\text{P}$  NMR resonance of **3** is now dramatically shifted downfield to 500 ppm (i.e. 368 ppm downfield from that of **1**). In addition, the signal has been transformed into a 1:1:1 triplet due to coupling to the quadrupolar  $^{14}\text{N}$  nucleus ( $J = 65$  Hz; see Figure 1). This is a very rare example of observable  $^{31}\text{P}$ - $^{14}\text{N}$  coupling.<sup>10</sup> The  $^{27}\text{Al}$  NMR spectrum in  $\text{CD}_2\text{-Cl}_2$  shows an extremely narrow singlet (width at half height 6 Hz,  $\delta$  105 ppm) comparable to that of free  $\text{AlCl}_4^-$  ions (8 Hz).<sup>11</sup> This indicates that **3** is ionic or is loosely ion-paired in solution. The methyl groups of the diisopropylamino substituent are diastereotopic below 50 °C, corresponding to a  $\Delta G^\ddagger$  for P-N bond rotation of 63 kJ mol<sup>-1</sup>. This barrier is the same as that in  $(\text{Me}_2\text{N})_2\text{P}^+$  (63 kJ mol<sup>-1</sup>)<sup>12</sup> but higher than that of  $(i\text{-Pr}_2\text{N})_2\text{P}^+$  (45 kJ mol<sup>-1</sup>).<sup>13</sup> The  $^{31}\text{P}$  chemical shift and the  $^{31}\text{P}$ - $^{14}\text{N}$  coupling constant of **3** are essentially unaffected by temperature. The *o*-methyl groups of the mesityl substituent are equivalent at all temperatures, indicating either unrestricted rotation about the P-C bond or, much more likely, orientation above and below a plane of symmetry. The large downfield chemical shift of **3** is matched only by  $\text{P}(\text{N}(\text{SiMe}_3)_2)_2^+$  (450 ppm) and  $\text{P}(t\text{-Bu})(\text{NMe}_2)^+$  (513 ppm).<sup>2</sup> Steric bulk in the former compound twists the  $\text{N}(\text{SiMe}_3)_2$  groups out of conjugation, whereas replacement of a P-N bond by a P-C  $\sigma$  bond in the latter must be the cause of the downfield shift. The effect of the mesityl group in **3** is similar to that of the *tert*-butyl group in  $\text{P}(t\text{-Bu})(\text{NMe}_2)^+$ , presumably because the aryl group is rotated out of conjugation (see the X-ray structure below).

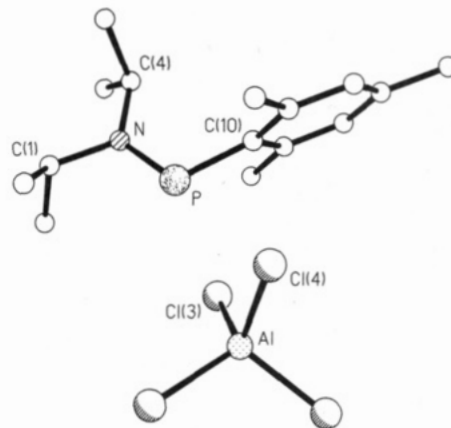


**Figure 2.** Perspective view of  $[(\text{mesityl})(i\text{-Pr}_2\text{N})\text{P}]^+[\text{AlCl}_4]^-$ .

Crystals of the phosphonium species **3** were obtained from dichloromethane/toluene. The X-ray structure<sup>15</sup> (Figure 2) reveals several notable features. Somewhat surprisingly, the P-N bond length of 1.617(5) Å is not significantly shorter than those found in  $[(i\text{-Pr}_2\text{N})_2\text{P}]^+[\text{AlCl}_4]^-$  (1.611(4) and 1.615(4) Å),<sup>13</sup>  $[(i\text{-Pr}_2\text{N})_2\text{P}]^+[\text{GaCl}_4]^-$  (1.587(12) and 1.601(13) Å),<sup>3c</sup> and  $[(\text{Me}_3\text{Si})_2\text{N}-\text{P}-\text{N}(\text{SiMe}_3)(\text{GaCl}_3)]$  (1.590(5) and 1.637(5) Å),<sup>14</sup> where PN double-bond character is distributed over two dialkylamido substituents. The P-C bond length of 1.787(6) Å is relatively short for phosphorus(III), presumably because of low coordination number and positive charge, but is nevertheless that of a single  $\sigma$  bond. Comparisons can be made to 1.848(5) Å for the same bond in the neutral chlorophosphine **1**<sup>16</sup> and 1.684(14) Å for the PC double bond in a cationic phosphalkene.<sup>5</sup> The mesityl group is rotated 69° out of the plane defined by the P, N, C(1), and C(4) atoms of the dialkylamido group, effectively preventing any conjugation of the mesityl  $\pi$  system with the empty 3p orbital on phosphorus. Of further interest, the C-P-N angle of 107.0(3)° is substantially smaller than the N-P-N angles in  $[(i\text{-Pr}_2\text{N})_2\text{P}]^+[\text{AlCl}_4]^-$  (114.8°)<sup>13</sup> and  $[(i\text{-Pr}_2\text{N})_2\text{P}]^+[\text{GaCl}_4]^-$  (117.0°),<sup>3c</sup> despite the closer proximity of the tetrachloroaluminate counterion. The shortest P...Cl contacts in **3** are 3.296(3) and 3.471(3) Å to Cl(3) and Cl(4), respectively, compared to 3.867(6) Å for the closest approach in  $[(i\text{-Pr}_2\text{N})_2\text{P}]^+[\text{GaCl}_4]^-$ .<sup>3c</sup> This suggests that a true phosphonium ion,  $\text{R}_2\text{P}^+$ , will have a more acute bond angle.

The closer approach to a true  $\text{R}_2\text{P}^+$  type phosphonium ion represented in the present work enhances the prospects of isolating and exploring the chemistry of even more reactive species. There will probably be a role in this chemistry for anions less reactive and less coordinating than  $\text{AlCl}_4^-$ . We note that at a certain threshold of leaving group basicity (Lewis), there is an abrupt switch from covalent/pyramidal to ionic/planar coordination. Thus, for *bis*(dialkylamino) species

(9) Dahl, O. *Tetrahedron Lett.* **1982**, 23, 1493.

(10) Gudat, D.; Schniffler, H. M.; Nieger, M.; Stalke, D.; Blake, A. J.; Grodey, H.; Niecke, E. *J. Am. Chem. Soc.* **1992**, 114, 8857. Niecke, E.; Gudat, D. In *Phosphorus-31 NMR Spectral Properties in Compound Characterization and Structural Analysis*; Quin, L. D., Verkade, J. G., Eds.; VCH: New York, 1994, p 159. The asymmetry of the triplet has its origin in differential relaxation rates: Harris, R. K. In *Nuclear Magnetic Resonance Spectroscopy*; Longman: Essex, U.K., 1986; p 139.

(11) Akit, J. W. *Annu. Rep. NMR Spectrosc.* **1972**, 5, 489.

(12) Thomas, M. G.; Schultz, C. W.; Parry, R. W. *Inorg. Chem.* **1977**, 16, 994.

(13) Cowley, A. H.; Cushner, M. C.; Szobota, J. S. *J. Am. Chem. Soc.* **1978**, 100, 7784.

(14) Oberdoerfer, R.; Nieger, M.; Niecke, E. *Chem. Ber.* **1994**, 127, 2397.

(15) Crystal data for **3**:  $M_r = 419.1$ , monoclinic,  $P2_1/c$ ,  $a = 8.175(1)$  Å,  $b = 16.015(1)$  Å,  $c = 16.501(1)$  Å,  $\beta = 95.78(1)^\circ$ ,  $V = 2149.4(3)$  Å<sup>3</sup>,  $Z = 4$ ,  $\rho_{\text{calc}} = 1.295$  Mg m<sup>-3</sup>. Data collection: Cu K $\alpha$ , 173 K,  $2\theta = 2.0$ – $105.0^\circ$ , 3205 measured reflections, 2318 independent reflections. Refinement: full-matrix least-squares refinement on  $|F^2|$  with 2106 reflections having  $F > 4\sigma(F)$ , direct methods (SHELXTL), 299 parameters, calculated H atom positions, Lorentzian polarization, absorption correction  $\mu = 6.066$  mm<sup>-1</sup>, max 0.9587, min 0.3991; residual electron density max 1.00, min  $-0.70$  e Å<sup>-3</sup>,  $R = 0.0594$ .

(16) Unpublished results.

of the  $\text{P}(\text{NR}_2)_2\text{X}$  type, the  $\text{X} = \text{Cl}^-$  compound is covalent but the  $\text{X} = \text{CF}_3\text{SO}_3^-$ ,  $\text{AlCl}_4^-$ , and  $\text{GaCl}_4^-$  compounds are ionic. However, for *mono*(dialkylamino) species of the  $\text{PAr}(\text{NR}_2)\text{X}$  type, the  $\text{X} = \text{Cl}^-$  and  $\text{CF}_3\text{SO}_3^-$  compounds are covalent and the  $\text{AlCl}_4^-$  species is ionic. This is in notable contrast to  $\text{R}_3\text{Si}^+$  type silylium ions, where there is an apparent continuum of cation/anion association and a gradual change from covalent to ionic.<sup>17</sup>

**Acknowledgment.** This work was supported by NSF Grant No. CHE 9407284.

**Supporting Information Available:** For **3**, tables giving a summary of X-ray collection and refinement data, atomic coordinates, bond lengths, bond angles, and anisotropic displacement factors and an atom-numbering diagram (9 pages). Ordering information is given on any current masthead page.

OM9505928

---

(17) Reed, C. A.; Xie, Z.; Bau, R.; Benesi, A. *Science* **1993**, *262*, 402.

# Intrinsic Ancillary Ligand Effects in Cationic Zirconium Polymerization Catalysts: Reactions of $[L_2ZrCH_3]^+$ Cations with $H_2$ and $C_2H_4$

N. George Alameddin,<sup>†</sup> Matthew F. Ryan,<sup>†</sup> John R. Eyler,<sup>†</sup> Allen R. Siedle,<sup>‡</sup> and David E. Richardson<sup>\*,†</sup>

Department of Chemistry, University of Florida, Gainesville, Florida, 32611-7200, and 3M Corporate Research Laboratories, St. Paul, Minnesota 55144

Received June 28, 1995<sup>®</sup>

**Summary:** Fourier transform ion cyclotron resonance mass spectrometry was used to study ion/molecule reactions of five cationic methyl metallocenes:  $[Cp_2ZrCH_3]^+$  (1; Cp = cyclopentadienyl),  $[(Ind)(Cp)ZrCH_3]^+$  (2; Ind =  $\eta^5$ -indenyl),  $[Ind_2ZrCH_3]^+$  (3),  $[(CH_3)_2Si(C_5H_4)_2ZrCH_3]^+$  (4), and  $[Flu_2ZrCH_3]^+$  (5; Flu =  $\eta^5$ -fluorenyl). The rate constants and products from reactions with  $H_2$  and  $C_2H_4$  are presented. From the kinetic data, the chelating ligand  $(CH_3)_2Si(C_5H_4)_2$  increases the intrinsic electrophilicity of the metal complex relative to Cp while substitution of Ind or Flu for Cp leads to a less electrophilic metal center.

Electrophilic  $d^0$  group 4 metallocenes, such as  $Cp_2Zr(CH_3)_2$  (Cp =  $\eta^5$ -cyclopentadienyl), are precursors of alkene polymerization catalysts.<sup>1,2</sup> The active species in these catalysts, now generally accepted to be  $[L_2ZrCH_3]^+$  (L = Cp or related ligands),<sup>2</sup> is formed via reaction of the neutral precursor with cocatalysts such as methalumoxane (MAO) and other strong Lewis acids.<sup>3</sup> In previous work, we reported gas-phase ion/molecule reactions of  $[Cp_2ZrCH_3]^+$  (1) with a number of substrates including dihydrogen, nitriles, and unsaturated hydrocarbons.<sup>4</sup> It was demonstrated that the intrinsic reactivity of these methylzirconium cations could be determined for critical reaction pathways such as  $\sigma$ -bond metathesis,  $\beta$ -H shift, and alkene insertion.

Improvements over the prototypical L = Cp polymerization catalyst have largely involved the modification of the Cp ligands to alter reactivity and stereoselectivity via combinations of electronic and steric effects.<sup>1</sup> In studies of polymerization activity as a function of the ancillary ligands, it has been shown that electron-rich ligands such as  $\eta^5$ -indenyl (Ind) and  $\eta^5$ -pentamethylcyclopentadienyl (Cp\*) often lead to increased activity relative to the Cp prototype catalyst. These observations seem counterintuitive because the electron density at the metal center would increase for L = Ind or Cp\* thereby reducing the electrophilic character of the metal and, presumably, the polymerization activity. In light of this contradiction and the widespread interest in

zirconocenes with modified ancillary ligands, we have expanded the scope of our original study to include reactions of  $H_2$  and  $C_2H_4$  with the following ions:  $[(Ind)(Cp)ZrCH_3]^+$  (2),  $[Ind_2ZrCH_3]^+$  (3),  $[(CH_3)_2Si(C_5H_4)_2ZrCH_3]^+$  (4), and  $[Flu_2ZrCH_3]^+$  (5; Flu =  $\eta^5$ -fluorenyl). It was expected that the rates of these reactions would correlate primarily with the intrinsic electronic effects of the ancillary ligands on the metal center (especially for the sterically undemanding reaction with  $H_2$ ). The kinetic influence of solvation and ion-pairing, which can significantly affect the reactivity of the cations in the condensed phase, will not be a factor in these experiments. In this way, we can isolate one critical feature of ancillary ligand effects and improve our understanding of these complex condensed-phase catalysts.

(5) (a) Richardson, D. E. In *Organometallic Ion Chemistry*; Freiser, B. S., Ed.; Kluwer Academic Publishers: Dordrecht, The Netherlands, 1995; in press. (b) Richardson, D. E.; Ryan, M. F.; Khan, Md. N. I.; Maxwell, K. A. *J. Am. Chem. Soc.* **1992**, *114*, 10482. (c) Ryan, M. F.; Eyler, J. R.; Richardson, D. E. *J. Am. Chem. Soc.* **1992**, *114*, 8611. (d) Ryan, M. F.; Richardson, D. E.; Lichtenberger, D. L.; Gruhn, N. *Organometallics* **1994**, *13*, 1190. (e) Ryan, M. F.; Siedle, A. R.; Burk, M. J.; Richardson, D. E. *Organometallics* **1992**, *11*, 4231. We proposed<sup>5e</sup> the  $\gamma$  parameter scale on the basis of gas-phase electron-transfer equilibria (ETE) measurements of the free energy of ionization for a series of substituted ruthenocenes and other metallocenes. The scale is anchored by assigning the arbitrary parameters  $\gamma_{Cp} = 0$  and  $\gamma_{Cp^*} = -1$  (Cp\* = pentamethylcyclopentadienyl). The parameter  $\gamma_L$  is a measure of the electronic influence of the substituted ligand on the metal relative to Cp (a ligand with a negative  $\gamma$  value is more electron-donating than Cp).

(6) The Fourier transform mass spectrometer used in this work has been described elsewhere (Sharpe, P.; Richardson, D. E. *Coord. Chem. Rev.* **1989**, *93*, 59). Substrate gases were introduced via precision leak valves to pressures of  $1 \times 10^{-6}$ – $5 \times 10^{-5}$  Torr, and the precursor dimethylzirconocene samples (Samuel, E.; Alt, H.; Hrnecir, D. C.; Rausch, M. D. *J. Organomet. Chem.* **1976**, *113*, 331. Samuel, E.; Rausch, M. D. *J. Am. Chem. Soc.* **1973**, *95*, 6263) were sublimed from a solids probe inserted so that the sample is  $\sim 50$  cm from the cell. The probe tip was heated to maintain a constant sample pressure on the order of  $3 \times 10^{-8}$ – $3 \times 10^{-7}$  Torr (for the dimethyl precursors of 1, 10–20 °C; 2, 60–70 °C; 3, 80–90 °C; 4, 50–60 °C; and 5, 100–120 °C). Electron impact on the dimethyl compounds by 10–12 eV electrons produces ions resulting from the loss of one and two methyl ligands, and monomethyl cations were isolated by resonantly ejecting all other ions formed during the beam event. The methyl cations 1–4 were allowed to thermalize via  $>50$  collisions with the background gas for 0.1–1.5 s (depending on total pressure) prior to obtaining kinetic data. In addition to the reaction with the substrate to produce the desired product ion, reaction of the methyl cation with background water ( $\sim 10^{-9}$  Torr) forms the metallocene hydroxide ion ( $[L_2ZrOH]^+$ ), and reaction of various cations with the neutral dimethyl parent compound produces dimer ions (i.e., binuclear Zr complex ions). These alternate pathways were incorporated into the full kinetic model used to fit the data. Details of the pressure corrections relevant to this experimental apparatus are discussed by Bruce and Eyler (Bruce, J. E.; Eyler, J. R. *J. Am. Soc. Mass Spectrom.* **1992**, *3*, 727). As an approximation, one can multiply the rate constants by the ion gauge sensitivity factor (0.4 for  $H_2$  and 2.3 for  $C_2H_4$ ) and divide by 2 to correct for the difference between the ion gauge and the cell. The errors on the rate constants in Table 1 represent experimental variance and are for comparison to ranges for other rate constants for the same reactant gas. Because of errors in pressure calibration, the absolute rate constants may have larger errors (up to  $\sim 50\%$ ).

<sup>†</sup> University of Florida.

<sup>‡</sup> 3M Laboratories.

<sup>®</sup> Abstract published in *Advance ACS Abstracts*, October 15, 1995.

(1) Mohring, P. C.; Coville, N. J. *J. Organomet. Chem.* **1994**, *479*, 1.

(2) Jordan, R. F. *Adv. Organomet. Chem.* **1991**, *32*, 325.

(3) (a) Yang, X.; Stern, C. L.; Marks, T. J. *J. Am. Chem. Soc.* **1994**, *116*, 10015 and references therein. (b) Marks, T. J. *Acc. Chem. Res.* **1992**, *25*, 57.

(4) (a) Christ, C. S.; Eyler, J. R.; Richardson, D. E. *J. Am. Chem. Soc.* **1988**, *110*, 4038. (b) Christ, C. S.; Eyler, J. R.; Richardson, D. E. *J. Am. Chem. Soc.* **1990**, *112*, 596. (c) Christ, C. S.; Eyler, J. R.; Richardson, D. E. *J. Am. Chem. Soc.* **1990**, *112*, 4778.

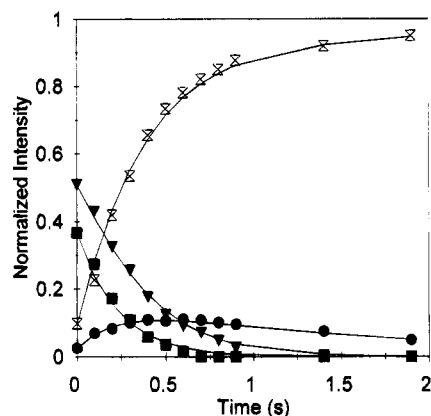


**Figure 1.** Plot of normalized ion intensity vs time for the reaction  $[(\text{CH}_3)_2\text{Si}(\text{C}_2\text{H}_4)_2\text{Zr}-\text{CH}_3]^+ + \text{C}_2\text{H}_4 \rightarrow \text{products}$ . Legend:  $\blacksquare$  = methyl cation,  $\blacktriangledown$  = hydroxide cation,  $\bullet$  =  $\eta^3$ -allyl complex ion, open stacked triangles = binuclear Zr complex ions. Solid lines represent the fit to the kinetic model used to describe the system, including the rate constant given in Table 1 for the reaction in eq 2.

**Table 1. Rate Constants for the Reaction of 1–4 with  $\text{H}_2$  ( $k_1$ ) and  $\text{C}_2\text{H}_4$  ( $k_2$ )**

cation	$\Sigma\gamma$	$k_1 (\text{M}^{-1} \text{s}^{-1})^{a,b}$	$k_2 (\text{M}^{-1} \text{s}^{-1})^{a,c}$
1	0.0 <sup>d</sup>	$(3.9 \pm 1.2) \times 10^{10}$	$(3.4 \pm 0.9) \times 10^{10}$
2	-0.41 <sup>d</sup>	$(2.6 \pm 0.7) \times 10^8$	$(2.1 \pm 1.4) \times 10^8$
3	-0.82 <sup>d</sup>	$(4.8 \pm 4.4) \times 10^7$	$(3.5 \pm 0.4) \times 10^8$
4	(0.16) <sup>e</sup>	$(6.9 \pm 0.3) \times 10^{10}$	$(9.6 \pm 1.8) \times 10^{10}$
5	-1.3 <sup>d</sup>	$\leq 10^7$	$\leq 10^7$

<sup>a</sup> Error limits on rate constants are quoted with  $\pm 1\sigma$  from multiple experiments. Relative errors among the rate constants for each substrate shown in this table are smaller than the absolute errors (up to  $\sim 50\%$ ) since relative rates do not depend on pressure calibration for the reactant gas. <sup>b</sup> Reaction with  $\text{H}_2$  (eq 1); product ion  $\text{L}_2\text{ZrH}^+$ . <sup>c</sup> Reaction with ethylene (eq 2); product ion  $\text{L}_2\text{ZrC}_3\text{H}_5^+$ . <sup>d</sup> Reference 5d. <sup>e</sup> Derived from kinetic data—see text.

We have also applied our previous parametrization of the electronic effects of Cp derivatives in metallocene ionization energetics ( $\gamma$  parameters<sup>5</sup>) to correlate the new kinetic data with the tendency of the Cp derivatives to act as electron-donating ( $\gamma < 0$ ) or electron-withdrawing ligands ( $\gamma > 0$ ) relative to Cp ( $\gamma = 0$ ) itself. This study represents the first application of these parameters to the prediction of intrinsic reactivity for electrophilic metallocenes.

The experimental methods for obtaining kinetic data by using Fourier transform ion cyclotron resonance mass spectrometry were similar to those described previously.<sup>4,6</sup> The observed ion/molecule reaction pathways were modeled as a series of pseudo-first-order elementary steps. The resulting set of coupled differential equations were solved to yield an analytical solution describing the time dependence of the intensity for each product ion and reactant ion, and the time dependence of ion intensities was fit to the model by optimizing the rate constants simultaneously. A typical nonlinear least squares fit is shown in Figure 1. Second-order rate constants are obtained from  $k_{\text{obs}}/P_{\text{sub}}$ , where  $P_{\text{sub}}$  is the pressure of the substrate. The rate constants for the  $\text{H}_2$  and  $\text{C}_2\text{H}_4$  reactions are collected in Table 1 and are plotted vs summed  $\gamma$  parameters in Figure 2. An effective value of  $\Sigma\gamma$  for 4 was chosen (+0.16) to give the best fit to the lines derived from fits to the Ind and Cp complexes.

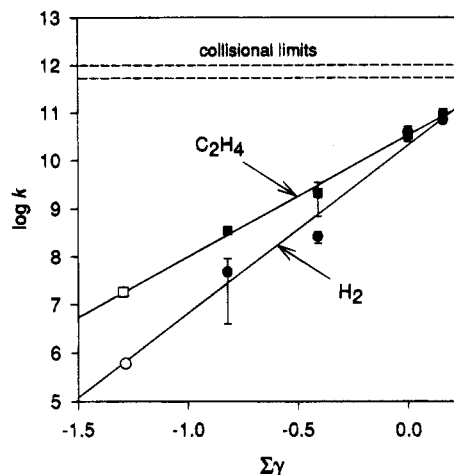
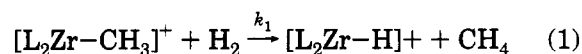


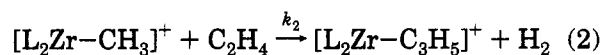
**Figure 2.** Plot of  $\log(k)$  vs  $\Sigma\gamma$  for  $k_1$  ( $\bullet$ ) and  $k_2$  ( $\blacksquare$ ). The solid lines represent the best fit to the available  $\gamma$  parameters. The dashed lines are the Langevin collisional limits for the second-order rate constants (upper line for  $\text{C}_2\text{H}_4$ , lower for  $\text{H}_2$ ). Open points are the predicted values of  $\log(k)$  for the reaction of 5 with  $\text{H}_2$  (lower) and  $\text{C}_2\text{H}_4$  (upper).

Reaction of  $\text{H}_2$  with 1–4 forms a hydride complex with loss of  $\text{CH}_4$  (eq 1). Sole loss of  $\text{CH}_3\text{D}$  in reactions with



$\text{D}_2$  is consistent with a four-center  $\sigma$ -bond metathesis transition state.<sup>4</sup> The rate of reaction 1 will be influenced by the energy of this transition state relative to the reactants, and decreased electron density at the metal would be expected to lower the energy of an activated complex that involves ligand binding.

In the reaction of  $\text{C}_2\text{H}_4$  with 1–4, the substrate inserts into the metal–methyl bond, and the resulting propyl complex dehydrogenates to give the final product, presumably an  $\eta^3$ -allyl complex (eq 2).<sup>4a,b</sup> The rate-



determining step for this reaction is not certain, but the energies of key intermediates and activated complexes will be affected by the electron deficiency at the metal center as in the simple hydrogenolysis reaction.

Attempts to study reactions of the  $[\text{Flu}_2\text{ZrCH}_3]^+$  (5) cation were unsuccessful due to the slow rates of reaction. Predicted values of the rates for  $\text{H}_2$  and  $\text{C}_2\text{H}_4$  from the  $\Sigma\gamma$  correlation for  $\text{L} = \text{Cp}$  and  $\text{Ind}$  (Figure 2) suggest that the rate constants are lower than the dynamic range of the experimental method (in favorable cases, 4–5 orders of magnitude below the collisional limited rate constants indicated by the dashed lines in Figure 2).

The rate constants for the reactions in eqs 1 and 2 decrease in the order  $4 > 1 > 2 > 3 > 5$ . The hydrogenolysis reaction (eq 1) has a stronger dependence on  $\Sigma\gamma$  than the insertion/dehydrogenation pathway, and both reactions are significantly retarded by increasing the electron-donating character of the ancillary ligands. We conclude that 4 is the most electrophilic ion of the group by a small margin and that replacement of Cp by Ind or Flu significantly reduces the electrophilicity of the metal center. Fluorenyl ( $\gamma_{\text{Flu}} = -0.65$ ) and indenyl ( $\gamma_{\text{Ind}} = -0.41$ ) ligands are strongly

electron-donating ligands<sup>5,7</sup> and are expected to decrease the electrophilicity of the zirconium(IV) center relative to the bis-Cp complex, as observed. X-ray photoelectron spectroscopy (XPS) studies of  $L_2ZrCl_2$   $3d_{5/2}$  binding energies (BE) confirm that Flu and Ind are electron-donating relative to Cp (relative to  $L = Cp$  at 182.2 eV,  $\Delta BE = -0.1$  eV for  $L = Ind$  (182.1 eV),  $\Delta BE = -0.3$  eV for  $L = Flu$  (181.9 eV)).

It has been argued<sup>8</sup> that the properties of the  $(CH_3)_3Si$  substituent would require that chelating  $(CH_3)_2Si(C_5H_4)_2$  be electron-donating in a zirconium(IV) complex relative to Cp. This conclusion was supported by XPS studies,<sup>8</sup> which showed that the  $(CH_3)_3SiC_5H_4$  ligand is electron-donating relative to Cp. ETE measurements on metallocenes have also confirmed the electron-donating character of  $(CH_3)_3SiC_5H_4$  ( $\gamma_{TMSCp} = -0.24$  based on ferrocene derivative data<sup>5a</sup>). However, other reports have suggested that  $(CH_3)_2Si(C_5H_4)_2$  is electron-withdrawing relative to Cp in zirconium(IV) chemistry. From density functional theory studies, Ziegler and co-workers<sup>9</sup> found a higher positive charge on the Zr in  $[(CH_3)_2Si(C_5H_4)_2ZrCH_3]^+$  compared to  $[Cp_2ZrR]^+$  (based on Mulliken population analyses). Electrochemical studies reported by Petersen and co-workers<sup>10</sup> show that the electrode potential for the  $[(CH_3)_2Si(C_5H_4)_2ZrCl_2]^{0/-}$  couple is  $\sim 200$  mV less negative than that of the  $[Cp_2ZrCl_2]^{0/-}$  couple. XPS studies by Siedle et al.<sup>11</sup> show a increased Zr  $3d_{5/2}$  binding energy in  $(CH_3)_2Si(C_5H_4)_2ZrCl_2$  (+2.4 eV) relative to  $Cp_2ZrCl_2$ , suggesting lower electron density at the metal center in the former case. Such physical measurements involving electrochemical reduction to Zr(III) and core ionization energies are

indirect predictors of the effect of the  $(CH_3)_2Si(C_5H_4)_2$  ancillary ligand on the reactivity of zirconium(IV) complexes for they do not directly address the question of relative electrophilicity of the  $[(CH_3)_2Si(C_5H_4)_2ZrR]^+$  ion, which is the critical form of the complex in catalytic systems.

Our results show that the effect of the  $(CH_3)_2Si(C_5H_4)_2$  ancillary ligand in the 14-electron methylzirconium cation is to increase the metal complex electrophilicity relative to the bis-Cp environment. XPS studies of dichloride complexes have also shown that the dimethylsilyl bridge leads to an increase in the Zr  $3d_{5/2}$  binding energy relative to unbridged  $Flu_2ZrCl_2$ ,<sup>12</sup> suggesting that the general effect of  $(CH_3)_2Si$  bridging in these zirconium(IV) metallocenes is to increase electrophilicity at the metal center by reducing the effective Lewis basicity of the carbocyclic ligands. The lower basicity of the dimethylsilyl-bridged ligands presumably results from structural distortion of the ligand positions away from their "preferred" binding angles and distances.<sup>10</sup>

The observed trends in the rate constants for Cp- and Ind-substituted complexes,  $1 > 2 > 3$ , are consistent with the strong electron-donating effect expected for Ind.<sup>5</sup> As noted above, the usual observation has been that the bis-indenyl substitution increases the polymerization activity in homogeneous zirconocene(IV) catalysts when compared to bis-Cp analogs.<sup>1</sup> The increased polymerization rates for these  $Ind_2ZrX_2$ -based catalysts are likely a consequence of decreased termination rates and/or increased initiation rates, because the lower electrophilicity resulting from replacement of Cp by Ind should *decrease* the propagation rate for monomer insertion.<sup>13</sup> Rates of termination by  $\beta$ -R elimination ( $R = H, alkyl$ ) and of initiation (by separation of an ion pair) could both be affected in the required direction by the increased steric bulk and higher electron-donating tendency of bis-indenyl ancillary ligands.

**Acknowledgment.** This work was supported in part by a grant from the National Science Foundation to D.E.R. and J.R.E. (CHE9311614). XPS studies were done by Dr. L. Zazzera (3M).

OM950505B

(7) Gassman, P. G.; Winter, C. H. *J. Am. Chem. Soc.* **1988**, *110*, 6130.

(8) Gassman, P. G.; Deck, P. A.; Winter, C. H.; Dobbs, D. A.; Cao, D. H. *Organometallics* **1992**, *11*, 959.

(9) Woo, T. K.; Fan, L.; Ziegler, T. *Organometallics* **1994**, *13*, 2252.

(10) Bajgur, C. S.; Tikkanen, W. R.; Petersen, J. L. *Inorg. Chem.* **1985**, *24*, 2539.

(11) Siedle, A. R.; Newmark, R. A.; Lamanna, W. M.; Schroepfer, J. N. *Polyhedron* **1990**, *9*, 301.

(12) Siedle, A. R. Unpublished work. The Zr( $3d_{5/2}$ ) binding energies of  $Flu_2ZrCl_2$  and  $(Me_2SiFlu_2)ZrCl_2$  are  $181.9 \pm 0.1$  and  $183.2 \pm 0.1$  eV, respectively (C(1s) = 285.0 eV).

(13) Richardson, D. E.; Alameddin, N. G.; Ryan, M. F.; Siedle, A. R. Manuscript in preparation.

# Reversible Insertion Reactions of a Platinum Germylene Complex

Kyle E. Litz,<sup>†</sup> Kenneth Henderson, Randall W. Gourley,<sup>‡</sup> and Mark M. Banaszak Holl<sup>\*,†</sup>

Department of Chemistry, Brown University, Providence, Rhode Island 02912

Received August 16, 1995<sup>®</sup>

**Summary:** Dihydrogen and carbon dioxide react reversibly with the three-coordinate complex  $(Et_3P)_2PtGe[N(SiMe_3)_2]_2$ . These reactions demonstrate the ability of germylenes to act as strong supporting ligands, while introducing new modes of reactivity via formal Ge(II)/Ge(IV) interconversion.

Despite the synthesis of many types of germylenes and metal–germylene complexes, the observed reactivity of metal germylene complexes has been dominated by irreversible insertion chemistry, resulting in the formal conversion of the germanium species from Ge(II) to Ge(IV).<sup>1</sup> The tendency of germylene ligands to undergo insertion has limited their use as supporting ligands or as internal Lewis acids capable of enhancing transition-metal reactivity. We now wish to report the synthesis and crystal structure of the platinum germylene complex  $(Et_3P)_2PtGe[N(SiMe_3)_2]_2$  (**1**) and the reversible reactions of **1** with dihydrogen and carbon dioxide, yielding *cis*- $(Et_3P)_2Pt(H)GeH[N(SiMe_3)_2]_2$  (**2**)

and *cis*- $(Et_3P)_2PtC(O)Ge[N(SiMe_3)_2]_2$  (**3**), respectively.

When a mixture of  $(Et_3P)_2Pt(C_2O_4)$  (1.13 g)<sup>2</sup> and  $Ge[N(SiMe_3)_2]_2$  (0.86 g)<sup>3</sup> was refluxed for 36 h in 50 mL of benzene under an argon atmosphere, the initially pale yellow solution turned a deep, intense yellow. All volatiles were removed *in vacuo*, and the resulting yellow powder was recrystallized from hexane, giving sparkling lemon yellow microcrystals of  $(Et_3P)_2PtGe[N(SiMe_3)_2]_2$  (**1**) (Scheme 1).<sup>4</sup> Integration of the <sup>1</sup>H NMR spectrum confirmed that the desired stoichiometry had been obtained, and an IR spectrum indicated that no oxalate fragments were present. Both <sup>31</sup>P and <sup>195</sup>Pt NMR supported the assignment of a three-coordinate monomer, since no <sup>3</sup>J<sub>Pt–P</sub> couplings indicative of a dimeric species were present. X-ray-quality crystals of **1** were obtained by slow evaporation of a 1:1 benzene/hexane solution. A single-crystal X-ray structure of **1** provided confirmation of the spectroscopic structure

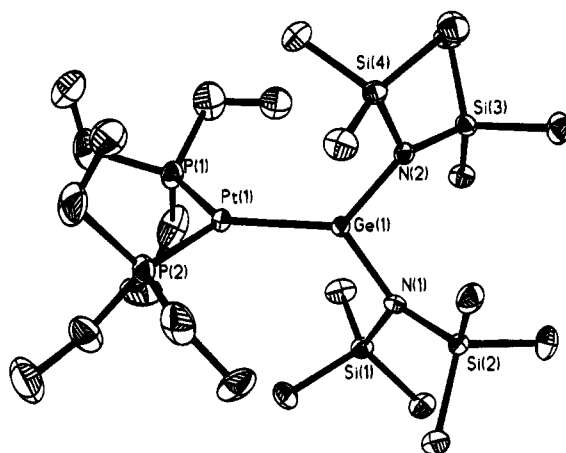
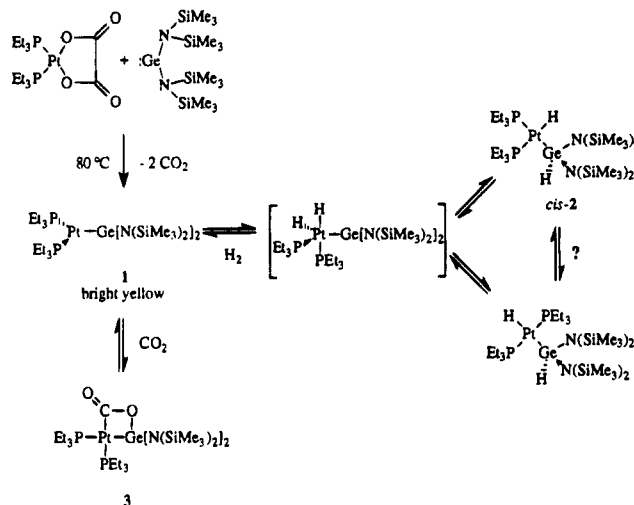


**Figure 1.** X-ray crystal structure of  $(Et_3P)_2PtGe[N(TMS)_2]_2$  (**1**).

## Scheme 1



assignment (Figure 1).<sup>5</sup> The geometry of the platinum and germanium atoms is trigonal planar with the P–Pt–P angle of 115.0(1)° somewhat smaller than the average P–Pt–Ge angle of 122.5(1)°, consistent with steric effects. The orientation of the germylene ligand aligns the Ge  $p_z$  orbital and the Pt  $d_{xy}$  orbital for a  $\pi$ -bonding interaction. The observed Pt–Ge distance is 0.12–0.17 Å shorter than the Pt–Ge bond length in the related complexes  $(Et_3P)_2Pt(GeClMe_2)_2$ ,<sup>6</sup>  $[(Pt\{\mu\text{-}Ge[N(SiMe_3)_2]_2\}(CO))_3]$ ,<sup>1c</sup> and  $(Et_3P)_2Pt(H)GeH[N(SiMe_3)_2]_2$  (**2**), indicating that some Pt–Ge multiple bonding may

(5) Crystal data for **1**:  $a = 10.955(2)$  Å,  $b = 21.634(4)$  Å,  $c = 16.319(4)$  Å,  $\beta = 91.88(2)^\circ$ ,  $V = 3865.5(14)$  Å<sup>3</sup>,  $Z = 4$ , space group  $P2_1/n$ , mol wt 824.77 for  $C_{24}H_{66}GeN_2P_2PtSi_4$ , density (calcd) 1.417 g/cm<sup>3</sup>,  $R = 0.051$ ,  $R_w = 0.115$ . Selected distances (Å) and angles (deg): Pt–Ge, 2.304(1); P(1)–Pt, 2.263(3); P(2)–Pt, 2.261(3); N(1)–Ge, 1.874(7); N(2)–Ge, 1.867(7); Si–N (av), 1.75(1); N(1)–Ge–N(2), 106.3(3); N(2)–Ge–Pt, 127.1(2); N(1)–Ge–Pt, 126.6(2); P(1)–Pt–P(2), 115.0(1); angle between P(1)–Pt–P(2) and N(1)–Ge–N(2) planes, 79.8(2).

\* To whom correspondence should be addressed. E-mail: mbanasza@umich.edu.

<sup>†</sup> Current address: Chemistry Department, University of Michigan, Ann Arbor, MI 48109-1055.

<sup>‡</sup> Current address: Fosroc, Inc., Georgetown, KY 40324.

<sup>®</sup> Abstract published in *Advance ACS Abstracts*, October 1, 1995.

(1) For recent reviews see: (a) Neumann, W. P. *Chem. Rev.* **1991**, *91*, 311–334. (b) Barrau, J.; Escudie, J.; Satgé, J. *Chem. Rev.* **1990**, *90*, 283–319. (c) Lappert, M. F.; Rowe, R. S. *Coord. Chem. Rev.* **1990**, *100*, 267–292. (d) Petz, W. *Chem. Rev.* **1986**, *86*, 1019–1047.

(2) Paonessa, R. S.; Prignano, A. L.; Trogler, W. C. *Organometallics* **1985**, *4*, 647–657.

(3) Gynane, M. J. S.; Harris, D. H.; Lappert, M. F.; Power, P. P.; Riviere, P.; Riviere-Baudet, M. *J. Chem. Soc., Dalton Trans.* **1977**, 2004–2009.

(4) Data for **1** are as follows: yield 64%; <sup>1</sup>H NMR ( $C_6D_6$ )  $\delta$  1.52 (q, 12H, <sup>3</sup>J<sub>H–H</sub> = 7.7 Hz,  $CH_3CH_2$ ), 1.00 (t, 18H, <sup>3</sup>J<sub>H–H</sub> = 7.7 Hz,  $CH_2CH_3$ ), 0.51 (s, 36H, N( $Si(CH_3)_2$ )), <sup>13</sup>C NMR ( $C_6D_6$ )  $\delta$  9.37 (pseudo-t, <sup>1</sup>J<sub>P–C</sub> = 10.4 Hz,  $CH_2CH_3$ ), 23.69 (m, <sup>1</sup>J<sub>P–C</sub> = 11.5 Hz,  $CH_2CH_3$ ), 5.90 (s, Si( $CH_3$ )), <sup>31</sup>P{<sup>1</sup>H} NMR  $\delta$  38.3 (s with Pt satellites, <sup>1</sup>J<sub>Pt–P</sub> = 4131 Hz); <sup>195</sup>Pt{<sup>1</sup>H} NMR  $\delta$  –4796 (t, <sup>1</sup>J<sub>Pt–P</sub> = 4130 Hz). The <sup>195</sup>Pt and <sup>31</sup>P shifts are reported vs  $K_2PtCl_6$  in  $D_2O$  and 85%  $H_3PO_4$  in  $D_2O$ , respectively. Anal. Calcd for  $C_{24}H_{66}GeN_2P_2PtSi_4$ : C, 34.95; H, 8.07; N, 3.40. Found: C, 34.71; H, 8.06; N, 3.34.



be occurring.<sup>7,8</sup> However, a similar decrease of about 0.1 Å in the Pt–P bond length also occurs, suggesting that the change in Pt–Ge bond length is related to the change from four- to three-coordination. Competition from the two nitrogen bases attached to germanium may minimize platinum  $d_{xy}$  donation into the germanium  $p_z$  orbital.<sup>9</sup> The observed orientation of the germylene ligand can be explained simply by steric effects.

Exposure of a stirred benzene solution (15 mL) of **1** (0.490 g) to 1 atm of  $H_2$  for 20 h at 20 °C results in a fading of the initially bright yellow solution to a light tan color and the formation of *cis*-( $Et_3P$ )<sub>2</sub>Pt(H)Ge(H)[N(SiMe<sub>3</sub>)<sub>2</sub>]<sub>2</sub> (*cis*-**2**; Scheme 1). Off-white microcrystals were isolated via recrystallization from pentane.<sup>10</sup> In principle, both platinum-centered oxidative addition followed by migratory insertion and 1,2-addition across the Pt–Ge bond are possible mechanisms for the formation of **2**. However, during the synthesis a secondary compound is transiently present. We have assigned this product as *trans*-**2**, an intermediate which appears most consistent with an oxidative-addition/migratory-insertion pathway.<sup>11</sup> Three other pieces of information are worth noting. First, when *cis*-**2** is heated for 12 h at 80 °C under 3 atm of  $D_2$ , complete conversion to *cis*-( $Et_3P$ )<sub>2</sub>Pt(D)Ge(D)[N(SiMe<sub>3</sub>)<sub>2</sub>]<sub>2</sub> (*d*<sup>2</sup>-*cis*-**2**) occurs. Second, no incorporation of deuterium occurs over a 20-h time span at 20 °C. Third, isomerization from *trans*-**2** to *cis*-**2** takes less than 20 h at 20 °C. From these observations we can conclude that  $H_2/D_2$  exchange is slower than *cis*–*trans* isomerization. Scheme 1 illustrates the observed interconversions and an intermediate which we deem to be most consistent with the experiments performed to date. A single crystal of **2** was grown from a saturated solution of a 1:1 benzene/hexane mixture, and

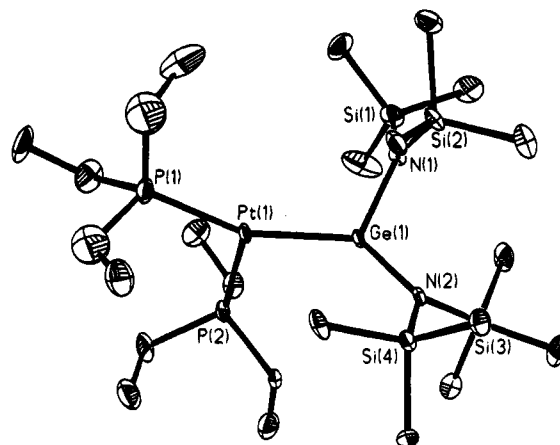


**Figure 2.** X-ray structure of *cis*-( $Et_3P$ )<sub>2</sub>Pt(H)Ge(H)[N(TMS)<sub>2</sub>]<sub>2</sub> (**2**).

an X-ray structure determination was performed to extend the understanding of Pt–Ge bond lengths.<sup>12</sup> Distances and angles were largely unremarkable, with the exception of the Pt–Ge bond length. Unlike the analogous alkyl complexes, the *cis* conformation is not enforced by a bidentate ligand,<sup>13</sup> although steric effects certainly favor a *cis* complex. It is also interesting that *cis*-**2** does not reductively eliminate upon heating, apparently preferring to follow an  $\alpha$ -elimination pathway.<sup>14,15</sup> The analogous complexes containing alkyls, *cis*-( $R_3P$ )<sub>2</sub>PtR(H), all undergo reductive elimination upon heating.<sup>13,16</sup> The difference in reactivity probably stems from the relative C–H and Ge–H bond strengths (about 100 vs 70 kcal/mol, respectively) and the apparent strength of the Pt–Ge dative bond of **1**. The observed reversibility allows the germylene ligand to function as a temporary “storage site” for a hydrogen atom.

Although investigation of the Pt–Ge moiety of **1** with small molecules was a major goal of the research, we had initially ignored  $CO_2$  as a potential substrate because 2 equiv of  $CO_2$  is produced in the reaction forming **1**. However, the reversible formation of **2** prompted us to pursue the reactivity of **1** with  $CO_2$  because the synthetic conditions employed could have prevented us from observing a reversibly formed complex. Exposure of a benzene solution of **1** to 1 equiv of  $CO_2$  at 20 °C for 6 h resulted in the formation of *cis*-

( $Et_3P$ )<sub>2</sub>PtC(O)OGe[N(SiMe<sub>3</sub>)<sub>2</sub>]<sub>2</sub> (**3**),<sup>17</sup> isolated as a white, air-stable, microcrystalline solid by filtration from pentane (Scheme 1). The formation of a four-membered

(12) Crystal data for **2**:  $a = 18.770(3)$  Å,  $b = 12.376(2)$  Å,  $c = 17.005(2)$  Å,  $\beta = 102.02(1)^\circ$ ,  $V = 3863.6(10)$  Å<sup>3</sup>,  $Z = 4$ , space group  $P2_1/c$ , mol wt 826.78 for  $C_{24}H_{68}GeN_2P_2PtSi_4$ , density (calcd) 1.421 g/cm<sup>3</sup>,  $R = 0.094$ ,  $R_w = 0.22$ . Selected distances (Å) and angles (deg): Pt–Ge, 2.422(2); P(1)–Pt, 2.285(4); P(2)–Pt, 2.300(4); N(1)–Ge, 1.91(1); N(2)–Ge, 1.91(1); Si–N (av), 1.73(1); N(1)–Ge–N(2), 106.9(4); N(2)–Ge–Pt, 122.1(3); N(1)–Ge–Pt, 112.0(3); P(1)–Pt–P(2), 106.8(1); P(1)–Pt–Ge, 159.0(1); P(2)–Pt–Ge, 92.7(1).

(13) Similar structurally characterized compounds containing bidentate phosphines include: (a) Hackett, M.; Ibers, J. A.; Jernakoff, P.; Whitesides, G. M. *J. Am. Chem. Soc.* **1986**, *108*, 8094–8095. (b) Hackett, M.; Ibers, J. A.; Whitesides, G. M. *J. Am. Chem. Soc.* **1988**, *110*, 1436–1448. (c) Mullica, D. F.; Sappenfield, E. L.; Hampden-Smith, M. J. *Polyhedron* **1991**, *10*, 867–872.

(14) We cannot rule out a 1,2-elimination of dihydrogen. Another example of a proposed  $\alpha$ -elimination: Yamashita, H.; Kobayashi, T.; Tanaka, M.; Samuels, J. A.; Streib, W. E. *Organometallics* **1992**, *11*, 2330–2333.

(15) 1,2-Eliminations have been reported for base-stabilized silylenes: Chauhan, B. P. S.; Corriu, R. J. P.; Lanneau, G. F.; Priou, C.; Auner, N.; Handwerker, H.; Herdtweck, E. *Organometallics* **1995**, *14*, 1657–1666.

(16) Hackett, M.; Whitesides, G. M. *J. Am. Chem. Soc.* **1988**, *110*, 1449–1462.

(6) Yamashita, H.; Kobayashi, T.; Tanaka, M.; Samuels, J. A.; Streib, W. E. *Organometallics* **1992**, *11*, 2330–2333.

(7) An analogous complex,  $(Ph_3P)_2Pt[Ge(N(TMS)_2)_2]$ , was previously described: Rowe, R. S. Ph.D. Thesis, University of Sussex, 1988.<sup>16</sup> To the best of our knowledge, a crystal structure has not been reported. Similar Pt(0) complexes have also been reported: (a) Hitchcock, P. B.; Lappert, M. L.; Misra, M. C. *J. Chem. Soc., Chem. Commun.* **1985**, 863–864. (b) Campbell, G. K.; Hitchcock, P. B.; Lappert, M. F.; Misra, M. C. *J. Organomet. Chem.* **1985**, *289*, C1–C4.

(8) Few cases of M=Ge double bonds have been reported; examples include (a) Gäde, W.; Weiss, E. *J. Organomet. Chem.* **1981**, *213*, 451–460. (b) Herrmann, W. A.; Kneuper, H.-J.; Herdtweck, E. *Chem. Ber.* **1989**, *122*, 433–436. For theoretical discussion of the issue see: (c) Kostic, N. M.; Fenske, R. F. *J. Organomet. Chem.* **1982**, *233*, 337–351.

(9) This has been observed in other systems, for example: (a) Herrmann, W. A.; Denk, M.; Behm, J.; Scherer, W.; Klingan, F.-R.; Bock, H.; Solouki, B.; Wagner, M. *Angew. Chem., Int. Ed. Engl.* **1992**, *31*, 1485–1488. (b) Grumbine, S. D.; Tilley, T. D.; Arnold, F. P.; Rheingold, A. L. *J. Am. Chem. Soc.* **1993**, *115*, 7884–7885.

(10) Data for *cis*-**2** are as follows: yield 60%; <sup>1</sup>H NMR ( $C_6D_6$ )  $\delta$  –4.54 (dd with Pt satellites, 1 H, <sup>1</sup>J<sub>Pt–H</sub> = 847 Hz, <sup>2</sup>J<sub>Pt–H</sub> = 22 Hz (trans), <sup>2</sup>J<sub>Pt–H</sub> = 16 Hz (cis), <sup>3</sup>J<sub>H–H</sub> = 3.4 Hz, H–Pt), 6.95 (dd with Pt satellites, 1 H, <sup>2</sup>J<sub>Pt–H</sub> = 167 Hz, <sup>3</sup>J<sub>Pt–H</sub> = 9.7 Hz, <sup>3</sup>J<sub>H–H</sub> = 3.4 Hz, H–Ge), 1.64 (s, 6H, CH<sub>2</sub>CH<sub>3</sub>), 1.46 (m, 6H, CH<sub>2</sub>CH<sub>3</sub>), 0.84 (m, 18H, CH<sub>2</sub>CH<sub>3</sub>), 0.59 (s, 6H, N(Si(CH<sub>3</sub>)<sub>3</sub>)<sub>2</sub>); <sup>13</sup>C NMR ( $C_6D_6$ )  $\delta$  8.51 (m, <sup>2</sup>J<sub>Pt–C</sub> = 3.3 Hz, <sup>3</sup>J<sub>Pt–C</sub> = 10.4 Hz, CH<sub>2</sub>CH<sub>3</sub>), 18.07 (m, <sup>1</sup>J<sub>Pt–C</sub> = 24.9 Hz, <sup>3</sup>J<sub>Pt–C</sub> = 3.0 Hz, <sup>2</sup>J<sub>Pt–C</sub> = 22.6 Hz, CH<sub>2</sub>CH<sub>3</sub>), 21.75 (m, <sup>1</sup>J<sub>Pt–C</sub> = 25.0 Hz, <sup>3</sup>J<sub>Pt–C</sub> = 2.9 Hz, <sup>2</sup>J<sub>Pt–C</sub> = 36.7 Hz, CH<sub>2</sub>CH<sub>3</sub>), 6.30 (s, Si(CH<sub>3</sub>)<sub>3</sub>); <sup>31</sup>P{<sup>1</sup>H} NMR  $\delta$  16.41 (d with Pt satellites, <sup>2</sup>J<sub>Pt–P</sub> = 14.98 Hz, <sup>1</sup>J<sub>Pt–P</sub> = 2129 Hz), 9.31 (<sup>2</sup>J<sub>Pt–P</sub> = 15.06 Hz, <sup>1</sup>J<sub>Pt–P</sub> = 2112 Hz); <sup>195</sup>Pt{<sup>1</sup>H} NMR  $\delta$  –5160 (pseudo-d, apparent <sup>1</sup>J<sub>Pt–P</sub> = 2124 Hz). IR (Nujol mull, cm<sup>–1</sup>): modes at 2115 (m) and 1949 (m), probably the Ge–H and Pt–H stretches, respectively, are observed to shift as expected upon deuterium labeling. We have not been able to unambiguously assign which stretch is associated with which moiety. Anal. Calcd for  $C_{24}H_{68}GeN_2P_2PtSi_4$ : C, 34.86; H, 8.29; N, 3.39. Found: C, 34.71; H, 8.20; N, 3.22.

(11) Data for *trans*-**2** are as follows: <sup>1</sup>H NMR ( $C_6D_{12}$ )  $\delta$  –8.00 (td with Pt satellites, 1 H, <sup>1</sup>J<sub>Pt–H</sub> = 796 Hz, <sup>2</sup>J<sub>Pt–H</sub> = 19 Hz (cis), <sup>3</sup>J<sub>H–H</sub> = 7.8 Hz, H–Pt), 7.21 (m with Pt satellites, 1 H, <sup>2</sup>J<sub>Pt–H</sub> = 159 Hz, H–Ge). The  $Et_3P$  and N(TMS)<sub>2</sub> groups overlap with the shifts for *cis*-**2**. Comparative shifts for *cis*-**2** in  $C_6D_{12}$  are  $\delta$  –4.53 and 6.67 for Pt–H and Ge–H, respectively. The Ge–H resonance for *trans*-**2** is partially obscured by solvent in  $C_6D_6$ .



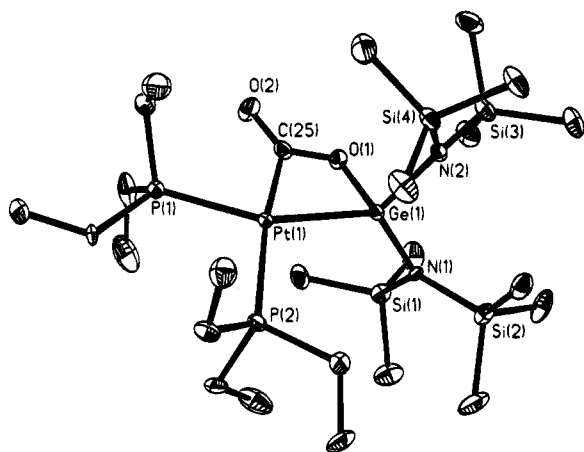


**Figure 3.** X-ray structure of *cis*-(Et<sub>3</sub>P)<sub>2</sub>PtC(O)OGe[N(TMS)<sub>2</sub>]<sub>2</sub> (**3**).

metallacycle was suggested by the observation of two new bands in the IR at 1622 and 1091 cm<sup>-1</sup>, <sup>1</sup>H, <sup>31</sup>P, and <sup>195</sup>Pt NMR spectra consistent with a square-planar complex, and the observation of the CO<sub>2</sub>-derived signal in the <sup>13</sup>C NMR spectrum at 171.35 ppm (<sup>1</sup>J<sub>Pt-C</sub> = 891 Hz). The IR and <sup>13</sup>C NMR data are consistent with the four previously characterized examples of CO<sub>2</sub> moieties side-bound to a metal and a heteroatom.<sup>18</sup> However, these previous examples were generated by alkoxide attack on bound CO ligands, not by direct reaction with free CO<sub>2</sub>. X-ray-quality crystals were grown by cooling a toluene solution under a CO<sub>2</sub> atmosphere, and the structure was determined to confirm the spectroscopic assignment.<sup>19</sup> As shown in Figure 3, complex **3** has a CO<sub>2</sub> molecule side-bound to the Pt-Ge moiety. The four-membered metallacycle is highly distorted as a consequence of the greatly differing Pt-Ge (2.420 Å) and C-O (1.33 Å) bond lengths. In addition, the ring is puckered such that the CO<sub>2</sub> fragment makes an angle of 15° with respect to the Pt-Ge bond vector. All previous examples of this binding mode exhibited planar rings.<sup>15</sup> Metallacycle distortion also affects the geometry about the nominally square-planar platinum center,

(17) Data for **3** are as follows: yield 70%; <sup>1</sup>H NMR (C<sub>6</sub>D<sub>6</sub>) δ 0.81 (m, 18 H, CH<sub>2</sub>CH<sub>3</sub>), 1.61 (m, 6 H, CH<sub>2</sub>CH<sub>3</sub>), 1.86 (m, 6 H, CH<sub>2</sub>CH<sub>3</sub>), 0.59 (s, 36 H, Si(CH<sub>3</sub>)<sub>3</sub>); <sup>13</sup>C NMR (C<sub>6</sub>D<sub>6</sub>) δ 8.41 (m, CH<sub>2</sub>CH<sub>3</sub>), 9.15 (m, CH<sub>2</sub>CH<sub>3</sub>), 15.99 (m, <sup>1</sup>J<sub>P-C</sub> = 27.2 Hz, CH<sub>2</sub>CH<sub>3</sub>), 21.01 (m, <sup>1</sup>J<sub>P-C</sub> = 24.4 Hz, CH<sub>2</sub>CH<sub>3</sub>), 7.06 (s, Si(CH<sub>3</sub>)<sub>3</sub>), 171.35 (dd with Pt satellites, <sup>2</sup>J<sub>P-C</sub> = 131 Hz (trans), <sup>2</sup>J<sub>P-C</sub> = 4 Hz (cis), <sup>1</sup>J<sub>Pt-C</sub> = 891 Hz); <sup>31</sup>P{<sup>1</sup>H} NMR δ 3.83 (d with Pt satellites, <sup>2</sup>J<sub>P-P</sub> = 11.5 Hz, <sup>1</sup>J<sub>Pt-P</sub> = 1758 Hz), 20.95 (d with Pt satellites, <sup>2</sup>J<sub>P-P</sub> = 11.5 Hz, <sup>1</sup>J<sub>Pt-P</sub> = 2380 Hz); <sup>195</sup>Pt{<sup>1</sup>H} NMR δ -4363 (dd, <sup>1</sup>J<sub>Pt-P</sub> = 1757 and 2387 Hz); IR (Nujol mull, cm<sup>-1</sup>) 1622 (C=O), 1091 (C-O). These bands shifted to 1585 and 1069 cm<sup>-1</sup>, respectively, upon <sup>13</sup>C labeling, consistent with the harmonic oscillator approximation. An excess of CO<sub>2</sub> is best for making **3** in quantity.

(18) (a) Wegner, P. A.; Guggenburger, L. J.; Muetterties, E. L. *J. Am. Chem. Soc.* **1970**, *92*, 3473-3474. (b) Vaughn, G. D.; Strouse, C. E.; Gladysz, J. A. *J. Am. Chem. Soc.* **1986**, *108*, 1462-1473. (c) Field, J. S.; Haines, R. J.; Sundermeyer, J.; Woollam, F. J. *Chem. Soc., Chem. Commun.* **1990**, 985-988. (d) Field, J. S.; Haines, R. J.; Sundermeyer, J.; Woollam, F. J. *Chem. Soc., Dalton Trans.* **1993**, 2735-2748. Other related complexes include: (e) Bennett, M. A.; Jin, H.; Willis, A. C. *J. Organomet. Chem.* **1993**, *451*, 249-256. (f) Szalda, D. J.; Chou, M. H.; Fujita, E.; Creutz, C. *Inorg. Chem.* **1992**, *31*, 4712-4714.

(19) Crystal data for **3**: *a* = 15.520(2) Å, *b* = 13.618(2) Å, *c* = 37.156(6) Å, *V* = 7853(2) Å<sup>3</sup>, *Z* = 8, space group *Pbca*, mol wt 868.78 for C<sub>25</sub>H<sub>66</sub>GeN<sub>2</sub>O<sub>2</sub>P<sub>2</sub>PtSi<sub>4</sub>, density (calcd) 1.470 g/cm<sup>3</sup>, *R* = 0.052, *R<sub>w</sub>* = 0.096. Selected distances (Å) and angles (deg): Pt-Ge, 2.4197(9); Pt-C(25), 2.086(9); C(25)-O(1), 1.333(10); C(25)-O(2), 1.214(10); P(1)-Pt, 2.309(2); P(2)-Pt, 2.346(2); N(1)-Ge, 1.864(6); N(2)-Ge, 1.882(7); Si-N (av), 1.748(1); P(1)-Pt-P(2), 98.97(8); P(2)-Pt-Ge, 105.92(6); P(1)-Pt-C(25), 89.1(2); C(25)-Pt-Ge, 65.8; P(1)-Pt-Ge, 154.87(6); P(2)-Pt-C(25), 167.0(3); Pt-C(25)-O(1), 110.5(6); C(25)-O(1)-Ge(1), 98.5(5); O(1)-Ge-Pt, 81.7(2); O(1)-C(25)-O(2), 119.9(9); O(2)-C(25)-Pt, 129.4(7); N(1)-Ge-O(1), 105.4(3); N(2)-Ge-O(1), 98.3; N(1)-Ge-N(2), 110.0(3); N(2)-Ge-Pt, 123.4(2); N(1)-Ge-Pt, 124.6(2).

reducing the C(25)-Pt-Ge angle to 65.8°. Despite or perhaps because of the considerable distortion of the metallacycle and the platinum center, all bond lengths fall within expected limits. Coordination about the germanium atom, also affected by the metallacycle-induced distortions, is best described as a distorted trigonal pyramid, the base formed by the platinum, germanium, and nitrogen atoms with O(1) forming the cap.<sup>20</sup> Previous examples of inserted germylene complexes have been better described as tetrahedral.<sup>21,22</sup>

As expected on the basis of the fact that we do not isolate **3** from the reaction used to form **1**, heating **3** to 80 °C causes the clear, colorless solution to turn yellow, regenerating **1** and producing CO<sub>2</sub>. In a sealed tube containing 1 equiv of CO<sub>2</sub>, the mixture can be cycled between **1** and **3** by heating to form **1** and cooling the tube, re-forming **3**. Although **3** is an air-stable compound, hydrocarbon solutions of **3** slowly decompose by giving off CO<sub>2</sub> and re-forming air-sensitive **1**, which is oxidized. The presence of the germylene ligand and the formation of a Ge-O bond is clearly crucial for the reaction of **1** with CO<sub>2</sub>, differentiating **1** from other three-coordinate Pt(0) complexes containing dative, two-electron donors. The similar three-coordinate complex Pt(PPh<sub>3</sub>)<sub>3</sub> does not react with CO<sub>2</sub>.<sup>23</sup> Despite the apparent analogy to metal carbene chemistry shown in the formation of metallacycle **3**, alkenes such as ethylene and norbornene do not react with **1** to form a metallacyclobutane.

In conclusion, the new germylene complexes *cis*-(Et<sub>3</sub>P)<sub>2</sub>Pt(H)Ge(H)[N(SiMe<sub>3</sub>)<sub>2</sub>]<sub>2</sub> (*cis*-**2**) and *cis*-(Et<sub>3</sub>P)<sub>2</sub>-PtC(O)OGe[N(SiMe<sub>3</sub>)<sub>2</sub>]<sub>2</sub> (**3**) have been synthesized from the common precursor (Et<sub>3</sub>P)<sub>2</sub>PtGe[N(SiMe<sub>3</sub>)<sub>2</sub>]<sub>2</sub> (**1**). The clean, reversible nature of the reactions observed is a unique observation in germylene insertion chemistry, which highlights the ability of germylenes to function as "supporting" ligands while also facilitating new types of reactivity.

**Acknowledgment.** The donors of the Petroleum Research Fund, administered by the ACS, are thanked for support of this research (Grant No. 26966-G3). The X-ray equipment was purchased with assistance from grants from the National Science Foundation (Grant No. CHE-8206423) and the National Institutes of Health (Grant No. RR-06462). D. A. Sweigart and P. T. Wolczanski are thanked for valuable discussions.

**Supporting Information Available:** Further details concerning the X-ray crystal structures of complexes **1-3**, including tables of crystal data and structure refinement details, positional and thermal parameters, and bond distances and angles (19 pages). This material is contained in many libraries on microfiche, immediately follows this article in the microfilm version of this journal, can be ordered from the ACS, and can be downloaded from the Internet; see any current masthead page for ordering information and Internet access instructions.

OM950649Q

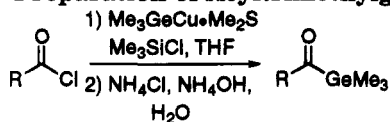
(20) The mean deviation from a plane for Pt, Ge, N(1), and N(2) is just 0.061 Å.

(21) Examples include: (a) Veith, M.; Stahl, L.; Huch, V. *Organometallics* **1993**, *12*, 1914-1920. (b) Hawkins, S. M.; Hitchcock, P. B.; Lappert, M. F.; Rai, A. K. *J. Chem. Soc., Chem. Commun.* **1986**, 1689-1690.

(22) Trigonal-pyramidal complexes of germanium are known: (a) Gurkova, S. N.; Gusev, A. I.; Alexeev, N. V.; Segelman, R. I.; Gar, T. K.; Khromova, N. Yu. *Zh. Strukt. Khim.* **1983**, *24*, 162. (b) Gurkova, S. N.; Gusev, A. I.; Alexeev, N. V.; Segelman, R. I.; Gar, T. K.; Khromova, N. Yu. *Zh. Strukt. Khim.* **1983**, *24*, 83-85.

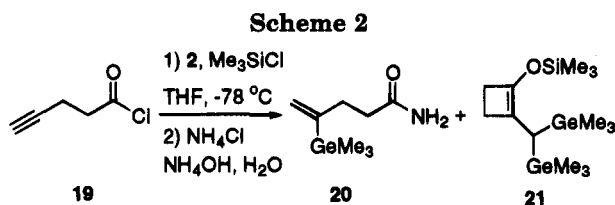
(23) Nyman, C. J.; Wymore, C. E.; Wilkinson, G. *J. Chem. Soc. A* **1968**, 561-563.



**Table 1. Preparation of Acyltrimethylgermanes**

entry no.	substrate	product	yield (%) <sup>a</sup>
1	3	11	92
2	4	12	88
3	5	13	90
4	6	14	88
5	7	15	89
6	8	16	82
7	9	17	92
8	10	18	82

<sup>a</sup> Yield of purified, distilled product.



The data given in Table 1 show that the method is compatible with the presence of a variety of functional groups, including a primary chloride (entry 3), a carbon-carbon double bond (entry 4), and benzyl ether functions (entries 5 and 6). Furthermore, the efficient conversion of adipoyl chloride **9** into the structurally novel diketone **17** is particularly noteworthy. In this transformation 3 equiv of reagent **2** and 2 equiv of  $\text{Me}_3\text{SiCl}$  were employed.

The experiment summarized in entry 8 of Table 1 requires additional comment. Since terminal alkynes are known to serve as good substrates for addition of organocopper(I) reagents, it was of interest to determine whether reagent **2** would react preferentially with an acyl chloride function or a terminal alkyne unit. Reaction of 4-pentynoyl chloride (**19**; Scheme 2) with **2** (1.05 equiv) and  $\text{Me}_3\text{SiCl}$  (1.05 equiv) in dry THF at  $-78^\circ\text{C}$ , followed by workup with aqueous  $\text{NH}_4\text{Cl-NH}_4\text{OH}$ , gave two products; the major product (42%) was shown to be the amide **20**. No acyltrimethylgermane corresponding to **19** was isolated. Clearly, reagent **2** had reacted preferentially with the alkyne function of **19** and the resultant intermediate was converted into **20** during the workup procedure.<sup>18</sup>

Interestingly, the chemoselectivity inherent in the reaction summarized in Scheme 2 was reversed when the terminal alkyne proton in **19** was replaced by a  $\text{Me}_3\text{-}$

(18) The minor product (13% yield) from this reaction, 1-(trimethylsilyloxy)-2-(bis(trimethylgermyl)methyl)cyclobutene (**21**; Scheme 2), was evidently also derived from initial chemoselective addition of **2** to the triple bond of **19**. The details of this transformation will be discussed in a full account of this study.

Si group. Reaction of substrate **10** with **2** under the normal reaction conditions provided the acyltrimethylgermane **18** in very good yield (Table 1, entry 8).

**Conclusion.** In summary, a practical procedure for preparing  $\text{Me}_3\text{GeLi}$  (**1**) from  $\text{Me}_3\text{GeH}$  has been developed and it has been shown that  $\text{Me}_3\text{GeCu}\cdot\text{Me}_2\text{S}$  (**2**) (easily prepared from **1**) is a valuable reagent for the preparation of acyltrimethylgermanes from readily accessible acyl chlorides. Investigations into the transformation of the acylgermanes into synthetically useful bifunctional reagents are underway.

**Experimental Section.** A typical experimental procedure, involving the conversion of **8** into **16**, is as follows. To a stirred solution of  $\text{Me}_3\text{GeH}$  (8.55 g, 72.0 mmol) in dry THF (25 mL) at  $-10^\circ\text{C}$  under an atmosphere of argon was added *t*-BuLi (33.9 mL, 1.77 M in pentane, 60.0 mmol) over a period of 3 min (*Warning!* gas evolution). After the light yellow solution had been stirred for 5 min, it was added *via* a cannula to a stirred suspension of  $\text{CuBr}\cdot\text{Me}_2\text{S}$  (12.34 g, 60.0 mmol) in THF (325 mL, argon atmosphere) at  $-78^\circ\text{C}$ . The resulting suspension was stirred at  $-78^\circ\text{C}$  for 1 h to afford a dark red solution.  $\text{Me}_3\text{SiCl}$  (4.35 g, 40.0 mmol) was added to the mixture, and stirring was continued for 5 min. A solution of ((4-methoxybenzyl)oxy)acetyl chloride (**8**; 8.59 g, 40.0 mmol) in dry THF (30 mL) was added *via* a cannula. The black reaction mixture was stirred at  $-78^\circ\text{C}$  for 1 h and at  $-30^\circ\text{C}$  for 2 h. The mixture was poured into aqueous  $\text{NH}_4\text{Cl-NH}_4\text{OH}$  (pH 8–9, 400 mL), and the resultant mixture was diluted with  $\text{Et}_2\text{O}$  (400 mL). The heterogeneous mixture was vigorously stirred until the aqueous phase was deep blue. The layers were separated, and the aqueous layer was extracted with  $\text{Et}_2\text{O}$  ( $3 \times 200$  mL). The combined organic solutions were washed (water, brine), dried ( $\text{MgSO}_4$ ), and concentrated. Subjection of the crude product to chromatography (silica gel), followed by bulb-to-bulb distillation ( $75\text{--}84^\circ\text{C}/0.005$  Torr) of the acquired liquid, afforded 9.76 g (82%) of **16** as a light yellow oil.  $^1\text{H NMR}$  (400 MHz,  $\text{CDCl}_3$ ):  $\delta$  7.25 (2 H, d,  $J = 8.7$  Hz), 6.87 (2 H, d,  $J = 8.7$  Hz), 4.50 (2 H, s), 3.99 (2 H, s), 3.79 (3 H, s), 0.33 (9 H, s).

**Acknowledgment.** We thank the NSERC of Canada for financial support, as well as the NSERC of Canada and Fonds FCAR (Québec) for Postgraduate Scholarships (to R.L.).

**Supporting Information Available:** Text giving spectral data for compounds **11–18**, **20**, and **21** (4 pages). This material is contained in many libraries on microfiche, immediately follows this article in the microfilm version of the journal, can be ordered from the ACS, and can be downloaded from the Internet; see any current masthead page for ordering information and Internet access instructions.

OM950636C

# The First Trifluorosilyl Hydrido Transition-Metal Compound: Metal Atom Synthesis and Structure of ( $\eta^6$ -Toluene)bis(trifluorosilyl)iron Dihydride

Zhengui Yao and Kenneth J. Klabunde\*

Department of Chemistry, Kansas State University, Manhattan, Kansas 66506

Received July 6, 1995\*

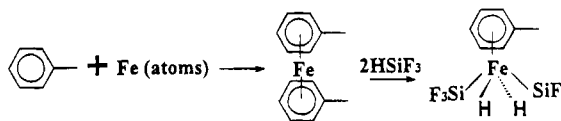
**Summary:** The compound ( $\eta^6$ -toluene)Fe(H)<sub>2</sub>(SiF<sub>3</sub>)<sub>2</sub> was synthesized from toluene-solvated iron atoms and tri-fluorosilane and characterized by <sup>1</sup>H NMR spectroscopy. The crystal and molecular structures of ( $\eta^6$ -toluene)Fe(H)<sub>2</sub>(SiF<sub>3</sub>)<sub>2</sub> were determined by X-ray crystallography.

There are very few well-characterized transition-metal compounds in which the SiF<sub>3</sub> ligand is bonded to a transition metal. The first metal trifluorosilyl compound, F<sub>3</sub>SiCo(CO)<sub>4</sub>, was prepared by the reaction of HSiF<sub>3</sub> with the dinuclear metal carbonyl Co<sub>2</sub>(CO)<sub>8</sub>.<sup>1</sup> Similar reactions at 160 °C with Mn<sub>2</sub>(CO)<sub>10</sub>, Re<sub>2</sub>(CO)<sub>10</sub>, and [( $\eta^5$ -C<sub>5</sub>H<sub>5</sub>)Fe(CO)]<sub>2</sub> yielded F<sub>3</sub>SiMn(CO)<sub>5</sub>, F<sub>3</sub>SiRe(CO)<sub>5</sub>, and ( $\eta^5$ -C<sub>5</sub>H<sub>5</sub>)Fe(SiF<sub>3</sub>)(CO)<sub>2</sub>.<sup>2</sup> A metal vapor/plasma technique has been used to prepare some main-group trifluorosilyl-substituted compounds, i.e., Te(SiF<sub>3</sub>)<sub>2</sub>, Bi(SiF<sub>3</sub>)<sub>2</sub>, Sb(SiF<sub>3</sub>)<sub>3</sub>, Cd(SiF<sub>3</sub>)<sub>2</sub>, Zn(SiF<sub>3</sub>)<sub>2</sub>, and Hg(SiF<sub>3</sub>)<sub>2</sub>.<sup>3</sup> Thus, metal vapors, generated by resistively heating a metal under a vacuum, were allowed to react with trifluorosilyl radicals, which were produced in a hexafluorodisilane plasma, at liquid-nitrogen temperature. Most of the compounds were not stable at room temperature, and additional stabilizing ligands were needed. In another example, a variety of methods were used to synthesize ( $\eta^6$ -toluene)Ni(SiF<sub>3</sub>)<sub>2</sub>, and the extreme lability of the arene allowed the synthesis of some substitution derivatives.<sup>4</sup>

Recently we reported the syntheses and studies of several novel  $\pi$ -arene Fe(IV) compounds, by reacting "arene-solvated iron atoms"<sup>5</sup> with HSiCl<sub>3</sub>.<sup>6</sup> Herein, we extend our studies to HSiF<sub>3</sub> and now report the synthesis and structure of the first trifluorosilyl hydrido transition-metal compound, ( $\eta^6$ -toluene)Fe(H)<sub>2</sub>(SiF<sub>3</sub>)<sub>2</sub>.

Trifluorosilane was prepared from the reaction of HSiCl<sub>3</sub> (10 mL, 0.1 mol), SbF<sub>3</sub> (53.7 g, 0.3 mol), and

SbCl<sub>5</sub> (5 mL, as catalyst) at room temperature for 3 h.<sup>4b,7</sup> The resultant products were distilled through a dry ice/acetone condenser into two traps. The first trap was at -93 °C with a toluene slush, while the second was at -196 °C with liquid nitrogen. The second trap contained HSiF<sub>3</sub>, which was distilled onto "toluene-solvated iron atoms"<sup>5</sup> formed by iron vapor (0.8 g) codeposited with excess toluene (90 g) at -196 °C. The matrix was warmed to -78 °C in a dry ice/2-propanol bath and held there for about 30 min followed by warming slowly to room temperature and stirring for 3 h. The reaction mixture was filtered through Celite under argon, volatiles were removed in vacuo, and the resultant yellow solid was recrystallized from a toluene/pentane mixture to yield light yellow crystals of ( $\eta^6$ -toluene)Fe(H)<sub>2</sub>(SiF<sub>3</sub>)<sub>2</sub> (1% yield based on iron evaporated).



The X-ray structure shows the expected piano-stool structure for ( $\eta^6$ -toluene)Fe(H)<sub>2</sub>(SiF<sub>3</sub>)<sub>2</sub> (Figure 1).<sup>8</sup> The two SiF<sub>3</sub> groups are *trans* to each other, but no hydride was located. The bond distance between Fe and the arene C atoms range from 1.95(2) to 2.11(2) Å, with the distance from the Fe to the ring (center) equal to 1.45 Å, significantly shorter than those in the SiCl<sub>3</sub> analogs (1.61 Å).<sup>6</sup> To our knowledge, this is the shortest distance between a transition metal and a coordinated arene. The toluene ligand is planar, with a maximum deviation of 0.017 Å and an average deviation of 0.011 Å, similar to the SiCl<sub>3</sub> analogs, but different from predictions by extended Hückel calculations.<sup>9</sup> The Si-F distances are between 1.56(1) and 1.64(1) Å, similar to those in (PMe<sub>3</sub>)<sub>3</sub>Ni(SiF<sub>3</sub>)<sub>2</sub> (1.580(8) and 1.596(9) Å).<sup>3a</sup>

The Fe-Si distances in ( $\eta^6$ -toluene)Fe(H)<sub>2</sub>(SiF<sub>3</sub>)<sub>2</sub> are between 2.251(5) and 2.261(5) Å, slightly longer than

(7) (a) Emeléus, H. J.; Maddock, A. G. *J. Chem. Soc.* **1944**, 293. (b) Booth, H. S.; Stillwell, W. D. *J. Am. Chem. Soc.* **1934**, 56, 1531.

(8) (a) Crystal data: single crystals of ( $\eta^6$ -toluene)Fe(H)<sub>2</sub>(SiF<sub>3</sub>)<sub>2</sub> at -160 °C are orthorhombic, space group Pna2<sub>1</sub> (No. 33), with *a* = 13.839(4) Å, *b* = 7.582(2) Å, *c* = 10.610(4) Å, *V* = 1113(1) Å<sup>3</sup>, and *Z* = 4 (*d*<sub>calcd</sub> = 1.898 g/cm<sup>3</sup>,  $\mu$ (Cu K $\alpha$ ) = 136.27 cm<sup>-1</sup>). A total of 886 reflections ( $2\theta_{\max}$  = 112.7°) were collected using  $2\theta/\omega$  scans with graphite-monochromated Cu K $\alpha$  radiation. The structure parameters have been refined to convergence; *R* = 0.055, *R*<sub>w</sub> = 0.073 (based on *F*) for reflections with *I* > 3 $\sigma$ (*I*). (b) Anal. Calcd for C<sub>7</sub>H<sub>10</sub>FeF<sub>6</sub>Si<sub>2</sub>: C, 26.16; H, 3.15; Fe, 17.44; Si, 17.55. Found: C, 24.79; H, 2.94; Fe, 19.83; Si, 16.39.

(9) Radonovich, L. J.; Koch, F. J.; Albright, T. A. *Inorg. Chem.* **1980**, 19, 3373.

\* Abstract published in *Advance ACS Abstracts*, November 1, 1995.

(1) (a) Hagen, A. P.; MacDiarmid, A. G. *Inorg. Chem.* **1967**, 6, 686. (b) Hagen, A. P.; MacDiarmid, A. G. *Inorg. Nucl. Chem. Lett.* **1970**, 6, 345.

(2) Schrieke, R. R.; West, B. O. *Inorg. Nucl. Chem. Lett.* **1969**, 5, 141.

(3) (a) Bierschenk, T. R.; Guerra, M. A.; Juhlke, T. J.; Larson, S. B.; Lagow, R. J. *J. Am. Chem. Soc.* **1987**, 109, 4855. (b) Guerra, M. A.; Bierschenk, T. R.; Lagow, R. J. *J. Am. Chem. Soc.* **1986**, 108, 4103. (c) Juhlke, T. J.; Braun, R. W.; Bierschenk, T. R.; Lagow, R. J. *J. Am. Chem. Soc.* **1979**, 101, 3229. (d) Bierschenk, T. R.; Juhlke, T. J.; Lagow, R. J. *J. Am. Chem. Soc.* **1981**, 103, 7340. (e) Guerra, M. A.; Bierschenk, T. R.; Lagow, R. J. *J. Chem. Soc., Chem. Commun.* **1985**, 1550.

(4) (a) Groshens, T. J.; Klabunde, K. J. *J. Organomet. Chem.* **1983**, 259, 337. (b) Lin, S. T.; Groshens, T. J.; Klabunde, K. J. *Inorg. Chem.* **1984**, 23, 1. (c) Lin, S. T.; Klabunde, K. J. *Organomet. Synth.* **1983**, 3, 156. (d) Choe, S. B.; Schneider, J. J.; Klabunde, K. J.; Radonovich, L. J.; Ballintin, T. A. *J. Organomet. Chem.* **1989**, 376, 419.

(5) (a) Klabunde, K. J.; Li, Y. X.; Tan, B. J. *Chem. Mater.* **1991**, 3, 30. (b) Zenneck, U. *Angew. Chem., Int. Ed. Engl.* **1990**, 29, 126. (c) Andrews, M. P.; Ozin, G. A. *Chem. Mater.* **1989**, 1, 174. (d) Klabunde, K. J.; Efner, H. F.; Murdock, T. O.; Ropple, R. J. *Am. Chem. Soc.* **1976**, 98, 1021.

(6) (a) Yao, Z.; Klabunde, K. J.; Asirvatham, V. S. *Inorg. Chem.* **1995**, 34, 5289. (b) Asirvatham, V. S.; Yao, Z.; Klabunde, K. J. *J. Am. Chem. Soc.* **1994**, 116, 5493.

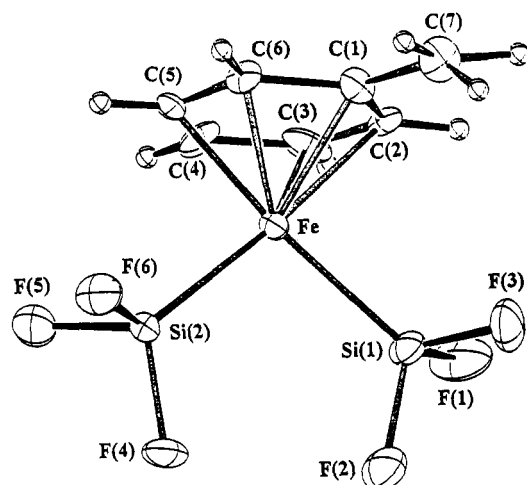


**Figure 1.** ORTEP drawing of  $(\eta^6\text{-toluene})\text{Fe}(\text{H})_2(\text{SiF}_3)_2$  with the atom-labeling scheme. No hydride was located. Selected bond distances (Å) and angles (deg): Fe–Si(1), 2.251(5); Fe–Si(2), 2.261(5); Fe–C(1), 2.11(2); Fe–C(2), 2.03(2); Fe–C(3), 1.99(2); Fe–C(4), 1.95(2); Fe–C(5), 1.97(2); Fe–C(6), 2.08(2); Si(1)–F(1), 1.56(1); Si(1)–F(2), 1.59(1); Si(1)–F(3), 1.60(1); Si(2)–F(4), 1.61(1); Si(2)–F(5), 1.64(1); Si(2)–F(6), 1.62(1); Si(1)–Fe–Si(2), 98.2(2).

those in  $(\eta^6\text{-toluene})\text{Fe}(\text{H})_2(\text{SiCl}_3)_2$  (2.222(2) and 2.218(2) Å). It is well-established that  $\pi$  back-bonding to phosphine and other third-row ligands involves hyperconjugative interactions between the transition metal and  $\text{PR}_3$   $\sigma^*$  orbitals.<sup>10,11</sup> Fluoride is an excellent  $\pi$ -donor and thus would be able to compete with iron to donate electrons to the silicon. Also, the Si–F  $\sigma^*$  orbitals are much higher in energy than Si–Cl  $\sigma^*$  orbitals and should be less accessible for  $\pi$  back-bonding. For these reasons,  $\text{SiF}_3$  should be a poorer  $\pi$ -acceptor than  $\text{SiCl}_3$ . The Ni–Si distances in four-coordinate  $\text{Ni}^{\text{II}}\text{--SiCl}_3$  complexes are quite short as well, 2.171(3) Å in  $[\text{Ni}(\text{SiCl}_3)_2\text{Cl}_2]^{2-}$ <sup>12</sup> and 2.202(1) Å in *cis*-(collidine)<sub>2</sub>Ni(SiCl<sub>3</sub>)<sub>2</sub>,<sup>4d</sup> presumably due to strong  $\pi$  back-bonding. However, the Ni–Si distance of 2.182(4) Å in  $(\text{PME}_3)_3\text{Ni}(\text{SiF}_3)_2$ <sup>3a</sup> is significantly shorter than that in a similar  $\text{SiCl}_3$  trigonal-bipyramidal compound,  $(\text{CO})_3\text{Ni}(\text{SiCl}_3)_2$  (2.286(3) Å).<sup>13</sup> This might be due to the presence of three strong  $\pi$ -acceptor CO groups, which would compete with  $\text{SiCl}_3$  for d electrons from Ni.

The <sup>1</sup>H NMR spectrum of  $(\eta^6\text{-toluene})\text{Fe}(\text{H})_2(\text{SiF}_3)_2$  in  $\text{C}_6\text{D}_6$  is shown in Figure 2. There are three sets of signals for the phenyl protons, a triplet at 4.93 ppm, a doublet at 4.87 ppm, and a triplet at 4.49 ppm. The peak for the methyl protons is a singlet at 1.40 ppm. The hydride peak is a septet at –19.00 ppm, with <sup>3</sup>J<sub>H–F</sub> = 9.2 Hz, nearly 2 ppm upfield relative to that in  $(\eta^6\text{-toluene})\text{Fe}(\text{H})_2(\text{SiCl}_3)_2$ . The IR spectrum showed  $\nu_{\text{Fe–H}}$  at 1962  $\text{cm}^{-1}$ .

A small amount of  $(\eta^6\text{-toluene})\text{Fe}(\text{H})_2(\text{SiF}_3)(\text{SiF}_2\text{Cl})$  was also observed in the <sup>1</sup>H NMR in some preparations.

(10) Wheeler, R. A.; Hoffmann, R.; Strähle, J. *J. Am. Chem. Soc.* **1986**, *108*, 5381.

(11) (a) Orpen, A. G.; Connelly, N. G. *J. Chem. Soc., Chem. Commun.* **1985**, 1310. (b) Marynick, D. S. *J. Am. Chem. Soc.* **1984**, *106*, 4064. (c) Xiao, S.-X.; Trogler, W. C.; Ellis, D. E.; Berkovitch-Yellin, Z. *J. Am. Chem. Soc.* **1983**, *105*, 7033.

(12) Brezinski, M. M.; Schneider, J. J.; Radonovich, L. J.; Klabunde, K. J. *Inorg. Chem.* **1989**, *28*, 2414.

(13) Janikowski, S. K.; Radonovich, L. J.; Groshens, T. J.; Klabunde, K. J. *Organometallics* **1985**, *4*, 396.

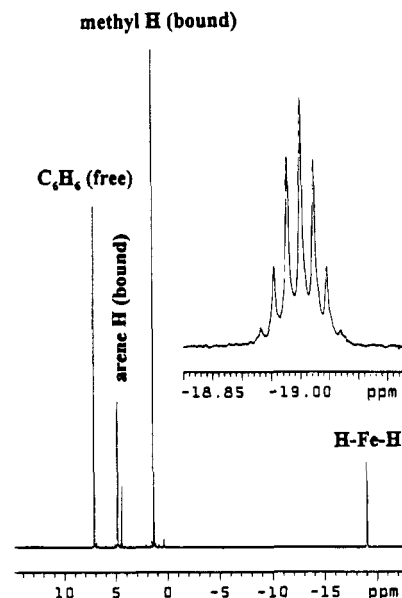


**Figure 2.** <sup>1</sup>H NMR spectrum of  $(\eta^6\text{-toluene})\text{Fe}(\text{H})_2(\text{SiF}_3)_2$  in  $\text{C}_6\text{D}_6$  at room temperature, with an insert of the hydride region.

The chemical shifts of the phenyl protons are 5.14 (t), 5.04 (d), and 4.73 (t) ppm, which are slightly upfield compared to those in  $(\eta^6\text{-toluene})\text{Fe}(\text{H})_2(\text{SiCl}_3)_2$  but downfield relative to those in  $(\eta^6\text{-toluene})\text{Fe}(\text{H})_2(\text{SiF}_3)_2$ . The methyl protons are at 1.46 (s) ppm, the same as those in  $(\eta^6\text{-toluene})\text{Fe}(\text{H})_2(\text{SiCl}_3)_2$ . A sextuplet for the hydride was observed at –18.71 ppm with <sup>3</sup>J<sub>H–F</sub> = 9.6 Hz, which lies between those in  $(\eta^6\text{-toluene})\text{Fe}(\text{H})_2(\text{SiCl}_3)_2$  and  $(\eta^6\text{-toluene})\text{Fe}(\text{H})_2(\text{SiF}_3)_2$ .

The mild fluorinating agent  $\text{AgBF}_4$  was successfully used to generate  $(\eta^6\text{-toluene})\text{Ni}(\text{SiF}_3)_2$  from  $(\eta^6\text{-toluene})\text{Ni}(\text{SiCl}_3)_2$ .<sup>4c,d</sup> When a toluene solution of  $(\eta^6\text{-toluene})\text{Fe}(\text{H})_2(\text{SiCl}_3)_2$  was treated with  $\text{AgBF}_4$ , only a black precipitate was formed; presumably  $\text{Ag}^+$  was reduced by the hydride.

The stability of this type of  $\pi$ -arene Fe(IV) compound apparently relies on the closed-shell 18-electron configuration, and probably the synergistic push–pull of electron density by the electron-rich arene and the electron-demanding  $\sigma$ -bound ligands. When the  $\text{SiF}_3$  group substitutes  $\text{SiCl}_3$ , the hydride peak moves close to 2 ppm upfield, and the chemical shifts of the phenyl protons also move upfield, due to further loss of aromaticity. This indicates that more electron density is shifting from toluene to iron, consistent with the very short distance between Fe and the arene (1.45 vs 1.61 Å).

**Acknowledgment.** Financial support from the National Science Foundation is acknowledged with gratitude. We thank Dr. Fusao Takusagawa for obtaining the crystal structure. We appreciate insightful suggestions from one of the reviewers.

**Supporting Information Available:** Tables of data collection information, atom coordinates, bond lengths, bond angles, and anisotropic thermal parameters for  $(\eta^6\text{-toluene})\text{Fe}(\text{H})_2(\text{SiF}_3)_2$  (4 pages). Ordering information is given on any current masthead page.

OM950518P

# Nickel-Catalyzed Tandem Coupling of Chlorotrimethylsilane, $\alpha,\beta$ -Enones, Alkynes, and Dimethylzinc

Shin-ichi Ikeda,\* Hiroaki Yamamoto, Kouji Kondo, and Yoshiro Sato\*

Faculty of Pharmaceutical Sciences, Nagoya City University, Tanabe-dori, Mizuho-ku, Nagoya 467, Japan

Received September 6, 1995<sup>©</sup>

**Summary:** A nickel and triphenylphosphine ( $PPh_3$ ) system catalyzed a new tandem coupling of chlorotrimethylsilane ((TMS)Cl),  $\alpha,\beta$ -enones **1**, alkynes, and dimethylzinc ( $Me_2Zn$ ) to furnish the coupling products **2**.

Tandem (or one-pot) reactions, which permit the construction of complex molecules in a few steps, are important topics in organic synthesis.<sup>1,2</sup> We recently reported that the nickel-catalyzed tandem coupling of  $\alpha,\beta$ -enones **1**, alkynes, alkynyltins, and chlorotrimethylsilane ((TMS)Cl) gave regio- and stereoselective conjugated enyne compounds in high yields.<sup>3</sup> This result led us to search for other organometallics which could be used instead of alkynyltins. We report here a new nickel-catalyzed tandem coupling of dimethylzinc ( $Me_2Zn$ ), **1**, alkynes, and (TMS)Cl to give coupling products **2** (reaction A in Scheme 1).

The results of the coupling are summarized in Table 1.<sup>4</sup> Typically, to a THF (5 mL) solution of  $Ni(acac)_2$  (5 mol %) and  $PPh_3$  (5 mol %) were added  $Me_2Zn$  (1.2 mmol), 1-octyne (1.1 mmol), 2-cyclopenten-1-one (**1a**) (1.0 mmol), and (TMS)Cl (1.2 mmol). The mixture was then stirred at 25 °C for 2 h. The coupling product **2** having the enol silyl ether function was converted into the corresponding carbonyl compound **3a** by treatment with aqueous acid,<sup>5</sup> and product **3a** was afforded in a yield of 89% by chromatography on a silica gel column (entry 1). The use of a Ni and  $PPh_3$  catalytic system was essential for this coupling. Although  $NiCl_2(PPh_3)_2$  (5 mol %) was also effective in this reaction (entry 2),  $Ni(acac)_2$  in the absence of  $PPh_3$  did not catalyze the reaction (entry 4). Other additives gave the following yields:  $P(o\text{-tolyl})_3$ , 56%;  $PBu_3$ , 11%; pyridine, 65%;  $Et_3N$ , 0%.

Although stereoisomers of the isolated products **3** were not detected by <sup>1</sup>H NMR or GC, the regioselectivity of **3** was dependent on the enones **1** and alkynes used. In the reaction with 1-octyne, a regioisomer of **3a** was detected as a minor product (entries 1–3). The reaction of **1a** with TMS-acetylene gave **3b** as the sole product, and it was assigned an *E* geometry by NOE (entry 5).

<sup>©</sup> Abstract published in *Advance ACS Abstracts*, October 15, 1995.

(1) Hall, N. *Science* **1994**, *266*, 32.

(2) (a) Ho, T.-L. *Tandem Organic Reactions*; Wiley: Interscience: New York, 1992. (b) Tietze, L. F.; Beifuss, U. *Angew. Chem., Int. Ed. Engl.* **1993**, *32*, 131. (c) Ho, T.-L. *Tactics of Organic Synthesis*; Wiley-Interscience: New York, 1994; p 79.

(3) (a) Ikeda, S.; Sato, Y. *J. Am. Chem. Soc.* **1994**, *116*, 5975. (b) Ikeda, S.; Cui, D.-M.; Sato, Y. *J. Org. Chem.* **1994**, *59*, 6877.

(4) All of the new compounds described herein gave spectral data and analytical results consistent with the assigned structures.

(5) The methylation at the enol silyl ether position of **2a** was not observed under the reaction conditions. See: Hayashi, T.; Katsuro, Y.; Kumada, M. *Tetrahedron Lett.* **1980**, *21*, 3951. Crouse, G. D.; Paquette, L. A. *J. Org. Chem.* **1981**, *46*, 4272.

Scheme 1

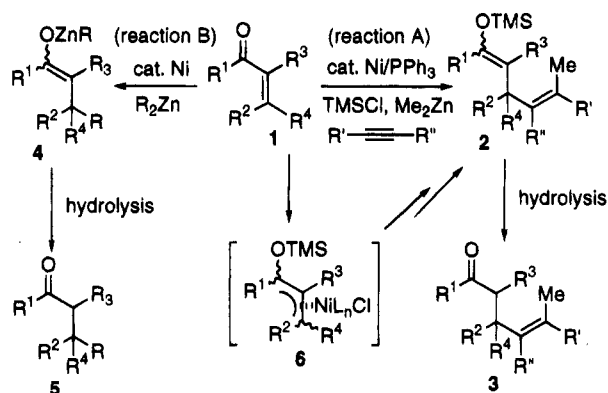


Table 1. Results of the Nickel-Catalyzed Tandem Coupling of **1**, Alkynes,  $Me_2Zn$ , and (TMS)Cl<sup>a</sup>

entry no.	enone <b>1</b>				alkyne		yield of <b>3</b> , <sup>b</sup> %
	R <sup>1</sup>	R <sup>2</sup>	R <sup>3</sup>	R <sup>4</sup>	R'	R''	
1	<b>1a</b>	-(CH <sub>2</sub> ) <sub>2</sub> -	H	H	hexyl	H	<b>3a</b> , 89 (89)
2	<b>1a</b>	-(CH <sub>2</sub> ) <sub>2</sub> -	H	H	hexyl	H	<b>3a</b> , 82 <sup>c</sup> (89)
3	<b>1a</b>	-(CH <sub>2</sub> ) <sub>2</sub> -	H	H	hexyl	H	<b>3a</b> , 76 <sup>d</sup> (89)
4	<b>1a</b>	-(CH <sub>2</sub> ) <sub>2</sub> -	H	H	hexyl	H	<b>3a</b> , 0 <sup>e</sup>
5	<b>1a</b>	-(CH <sub>2</sub> ) <sub>2</sub> -	H	H	TMS	H	<b>3b</b> , 69 (>98)
6	<b>1a</b>	-(CH <sub>2</sub> ) <sub>2</sub> -	H	H	Et	Et	<b>3c</b> , 70
7	<b>1b</b>	Me	H	H	hexyl	H	<b>3d</b> , trace
8	<b>1c</b>	H	H	Me	hexyl	H	<b>3e</b> , 60 (>98)
9	<b>1d</b>	Me	H	H	hexyl	H	<b>3f</b> , 61 (84)
10	<b>1e</b>	Me	Me	H	Bu	H	<b>3g</b> , trace
11	<b>1f</b>	Ph	H	H	Bu	H	<b>3h</b> , 58 <sup>d</sup> (48)

<sup>a</sup> Reaction conditions:  $Ni(acac)_2$  (0.05 mmol),  $PPh_3$  (0.05 mmol), **1** (1.0 mmol), alkyne (1.1 mmol),  $Me_2Zn$  (1.0 M in hexane, 1.2 mL), (TMS)Cl (1.2 mmol), and THF (5 mL) at 25 °C for 2 h under  $N_2$  and then hydrolysis by 10% HCl(aq) at 25 °C for 10 min. <sup>b</sup> Isolated yield; regioselectivity based on <sup>1</sup>H NMR is in parentheses. <sup>c</sup>  $PPh_3$  (0.2 mmol) was added. <sup>d</sup>  $NiCl_2(PPh_3)_2$  (0.05 mmol) was used instead of  $Ni(acac)_2$  and  $PPh_3$ . <sup>e</sup> Only  $Ni(acac)_2$  (0.05 mmol) was used.

While crotonaldehyde (**1c**) reacted with 1-octyne to give **3e** regioselectively (entry 8), the reaction with **1d** reduced the selectivity of the corresponding **3f** (entry 9). The product **3h** obtained from the reaction of **1f** with 1-hexyne did not show regioselectivity (entry 11). Reactions of both mesityl oxide (**1e**) (entry 10) and methyl vinyl ketone (**1b**) (entry 7), which was an effective substrate for coupling with alkynyltins,<sup>3a</sup> gave little of the corresponding coupling products under these reaction conditions.

It is well-known that the conjugate addition (Michael-type addition) of organozincs to **1** is accelerated in the presence of nickel catalyst to produce adducts **4** (or hydrolyzed products **5**) (reaction B in Scheme 1).<sup>6</sup> The addition of  $Me_2Zn$  to **1f** occurred in the presence of  $NiCl_2(PPh_3)_2$  at 25 °C over 20 h to give **5a** ( $R^1 = R^4 =$

Ph, R<sup>2</sup> = R<sup>3</sup> = H, R = Me) in 61% yield. However, the addition of (TMS)Cl to this reaction mixture resulted in a reduced yield of **5a** under the same reaction conditions (25% yield).<sup>7,8</sup> On the other hand, the coupling reaction of **1f**, 1-hexyne, and Me<sub>2</sub>Zn did not occur in the absence of (TMS)Cl. Moreover, the carbonylation of Me<sub>2</sub>Zn to 1-octyne followed by conjugated addition to **1a** did not proceed under these coupling conditions.<sup>9</sup> These results suggest that reaction parts A and B differ from each other. The tandem coupling

depicted in reaction A may proceed via the insertion of alkyne into **6**,<sup>10,11</sup> followed by the transmetalation of Me<sub>2</sub>Zn and reductive elimination to produce **2**.<sup>3</sup>

In summary, the present tandem coupling reaction can be used to efficiently construct carbon-carbon bonds and may provide a versatile method for synthesizing tri- or tetrasubstituted alkenes. Further detailed studies on the scope of this reaction are in progress.

**Supporting Information Available:** Text giving experimental details and spectral and analytical data for the obtained products (5 pages). This material is contained in many libraries on microfiche, immediately follows this article in the microfilm version of the journal, and can be ordered from the ACS; see any current masthead page for ordering information.

OM950709S

(6) Edrik, E. *Tetrahedron* **1992**, *44*, 9577.

(7) The conjugate addition of Me<sub>2</sub>Zn (1.2 mmol) to **1f** (1.0 mmol) in the presence of Ni(acac)<sub>2</sub> (0.05 mmol) at 25 °C for 1 h followed by hydrolysis gave **5a** in >99% GC yield.

(8) In contrast, it is well-known that the conjugate addition with organocopper reagents is accelerated in the presence of (TMS)Cl. See: (a) Corey, E. J.; Boaz, N. W. *Tetrahedron Lett.* **1985**, *26*, 6015. (b) Corey, E. J.; Boaz, N. W. *Tetrahedron Lett.* **1985**, *26*, 6019. (c) Alexakis, A.; Berlan, J.; Besace, Y. *Tetrahedron Lett.* **1986**, *27*, 1047. (d) Horiguchi, Y.; Matsuzawa, S.; Nakamura, E.; Kuwajima, I. *Tetrahedron Lett.* **1986**, *27*, 4025. (e) Nakamura, E.; Matsuzawa, S.; Horiguchi, Y.; Kuwajima, I. *Tetrahedron Lett.* **1986**, *27*, 4029.

(9) For allylzincation to alkynes, see: Negishi, E.; Miller, J. A. *J. Am. Chem. Soc.* **1983**, *105*, 6761.

(10) For preparation of complex **6**, see: Johnson, J. R.; Tully, P. S.; Mackenzie, P. B.; Sabat, M. *J. Am. Chem. Soc.* **1991**, *113*, 6172.

(11) The reaction did not give a product arising from insertion of the alkyne into the siloxy-substituted position of **6**.



# Tris(trimethylsilyl)germane as a Radical-Based Reducing Agent

C. Chatgililoglu\* and M. Ballestri

ICoCEA, Consiglio Nazionale delle Ricerche, Via P. Gobetti 101, 40129 Bologna, Italy

Received August 22, 1995<sup>®</sup>

**Summary:** Tris(trimethylsilyl)germane is an effective reducing agent for a variety of organic substrates. Among the group 14 hydrides, it has proven to be one of the most efficient H atom donors toward primary alkyl radicals.

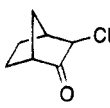
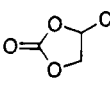
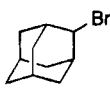
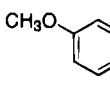
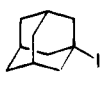
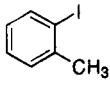
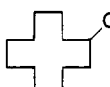
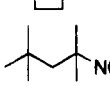
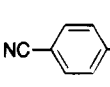
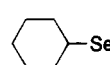
The majority of radical reactions of interest to synthetic chemists are chain processes under reducing conditions.<sup>1,2</sup> A feature associated with these reactions is hydrogen transfer from the reducing agent to a radical (eq 1). The resulting M<sup>•</sup> radical undergoes further



propagation step(s) to generate fresh R<sup>•</sup> radicals, thus completing the cycle of the chain reactions. Until a few years ago, the organometallic hydrides employed were limited to the R<sub>3</sub>SnH series.<sup>3</sup> The continuing demand for new tools for synthetic chemists prompted us and others to introduce a variety of group 14 hydrides and to invent new strategies.<sup>4,5</sup> For example, today (Me<sub>3</sub>Si)<sub>3</sub>SiH is, in most cases, an attractive alternative to the popular Bu<sub>3</sub>SnH. Herein we report our preliminary results on (Me<sub>3</sub>Si)<sub>3</sub>GeH as a reducing agent.<sup>6</sup>

The reduction of a variety of organic derivatives was carried out using (Me<sub>3</sub>Si)<sub>3</sub>GeH. A toluene solution (2.0–2.5 mL) containing the compound to be reduced (0.2 M), the germane (2 equiv), and α,α'-azoisobutyronitrile (AIBN; 10 mol %) was heated at 82 °C for 20–60 min. GC analysis using decane or undecane as internal standard showed the formation of the corresponding hydrocarbon in excellent yield (Table 1).<sup>7</sup> Reduction of chlorides, bromides, and iodides, deoxygenation of secondary alcohols *via* thiono esters (Barton–McCombie reaction), deamination of primary amines *via* isocya-

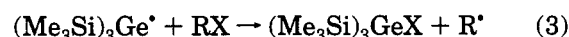
**Table 1.** Reaction of a Variety of Organic Compounds with (Me<sub>3</sub>Si)<sub>3</sub>GeH<sup>a</sup>

RX	yield of RH, <sup>b</sup> %
	99
	100
	99
	98
	98
	99
	99
	97
	96
	97

<sup>a</sup> Conditions: 0.2 M of RX, 0.4 M of (Me<sub>3</sub>Si)<sub>3</sub>GeH, and AIBN (10 mol %) in toluene were heated at 82 °C for 20–60 min. <sup>b</sup> Based on product formation in the crude reaction mixture; determined by GC analysis using decane or undecane as internal standard.

nides, removal of the PhSe group, and replacement of a tertiary nitro group by hydrogen were extremely effective.<sup>8</sup>

Evidence for a free radical chain mechanism (eqs 2 and 3) was provided by the observations (i) that in most cases the reactions started only in the presence of radical initiators such as AIBN and dibenzoyl peroxide and (ii) that the reactions were retarded by 2,6-di-*tert*-butyl-4-methylphenol and nitroxides such as TEMPO.



One of the intriguing aspects of reaction 1 is the ability of MH to donate hydrogen. In his review,

(8) For mechanistic details of these reactions with other reducing agents, see refs 1–4.

<sup>®</sup> Abstract published in *Advance ACS Abstracts*, October 1, 1995.

(1) For reviews, see: (a) Curran, D. P. *Synthesis* **1988**, 417, 489. (b) Jasperse, C. P.; Curran, D. P.; Fevig, T. L. *Chem. Rev.* **1991**, *91*, 1237. (c) Curran, D. P. In *Comprehensive Organic Synthesis*; Trost, B. M., Fleming, I., Eds.; Pergamon Press: Oxford, U.K., 1991; Vol. 4, pp 715–831. (d) Smadja, W. *Synlett* **1994**, 1.

(2) For books, see: (a) Giese, B. *Radicals in Organic Synthesis: Formation of Carbon-Carbon Bonds*; Pergamon Press: Oxford, U.K., 1986. (b) Motherwell, W. B.; Crich, D. *Free Radical Chain Reactions in Organic Synthesis*; Academic Press: London, 1992.

(3) Neumann, W. P. *Synthesis* **1987**, 665.

(4) For reviews, see: (a) Chatgililoglu, C. *Acc. Chem. Res.* **1992**, *25*, 188. (b) Chatgililoglu, C.; Ferreri, C. *Res. Chem. Intermed.* **1993**, *19*, 755. (c) Barton, D. H. R. *Tetrahedron* **1992**, *48*, 2529.

(5) For some more recent work, see: (a) Curran, D. P.; Xu, J.; Lazzarini, E. *J. Am. Chem. Soc.* **1995**, *117*, 6603. (b) Gimisis, T.; Ballestri, M.; Ferreri, C.; Chatgililoglu, C.; Boukherroub, R.; Manuel, G. *Tetrahedron Lett.* **1995**, *36*, 3897. (c) Clive, D. L. J.; Yang, W. *J. Org. Chem.* **1995**, *60*, 2607. (d) Rai, R.; Collum, D. B. *Tetrahedron Lett.* **1994**, *35*, 6221. (e) Oba, M.; Nishiyama, K. *J. Chem. Soc., Chem. Commun.* **1994**, 1703. (f) Barton, D. H. R.; Jang, D. O.; Jaszberenyi, J. Cs. *Tetrahedron* **1993**, *49*, 7193.

(6) Tris(trimethylsilyl)germane is commercially available from Aldrich. To our knowledge, the following two articles dealing with this compound exist only in the literature: (a) Brook, A. G.; Abdesaken, F.; Söllradl, H. *J. Organomet. Chem.* **1986**, *299*, 9. (b) Mallela, S. P.; Geanangel, R. A. *Inorg. Chem.* **1994**, *33*, 1115.

(7) The products of interest were identified by comparison of their retention times with those of authentic materials.



Newcomb discussed this topic regarding a number of carbon-centered radicals with the most common hydrogen atom transfer agents.<sup>9</sup> Furthermore, one of us reviewed this topic within the family of silicon hydrides.<sup>10</sup> In order to quantify the observed reactivity of  $(\text{Me}_3\text{Si})_3\text{GeH}$  and to provide a rate constant for H atom abstraction from this germane by primary alkyl radicals (eq 2), we utilized the 5-hexenyl cyclization as a free radical clock.<sup>9</sup> Under conditions in which the hydride concentration changed significantly during the experiments, the 5-hexenyl radical, which is formed as an intermediate in the reduction of the corresponding bromide, either abstracted H from the germane or cyclized prior to the hydrogen transfer. By measurement of the concentrations of 1-hexene and methylcyclopentane by GC analysis,<sup>11</sup> the mean value of  $k_{\text{GeH}}/k_c = 12.55 \text{ M}^{-1}$  was obtained from four independent experiments at 25 °C.<sup>12</sup> Taking  $k_c = 2.5 \times 10^5 \text{ s}^{-1}$ ,<sup>13a</sup> we calculate  $k_{\text{GeH}} = 3.1 \times 10^6 \text{ M}^{-1} \text{ s}^{-1}$  at 25 °C.

Figure 1 schematically illustrates the hydrogen donation abilities of the most representative group 14 hydrides.<sup>13</sup>  $(\text{Me}_3\text{Si})_3\text{GeH}$  is slightly more reactive than  $\text{Bu}_3\text{SnH}$ . It is worth mentioning that the replacement of *n*-butyl groups in  $\text{Bu}_3\text{GeH}$  by  $\text{Me}_3\text{Si}$  groups produces a 33-fold increase of the rate constant. On the basis of

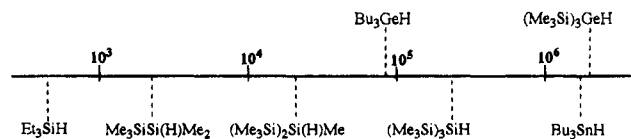


**Figure 1.** Rate constants for hydrogen abstraction ( $k_{\text{H}}$ ,  $\text{M}^{-1} \text{ s}^{-1}$ ) from a variety of group 14 reducing agents by primary alkyl radicals at 25 °C (taken from ref 13).

the experimental and theoretical studies of analogous silanes where this increase is ca. 600,<sup>10</sup> we suggest that the extra stability of the  $(\text{Me}_3\text{Si})_3\text{Ge}^{\cdot}$  radical is mainly due to a through-space (hyperconjugation) interaction between the bonding and/or antibonding Si–C  $\beta$ -bond.

In conclusion, we have shown that of the known group 14 hydrides  $(\text{Me}_3\text{Si})_3\text{GeH}$  is one of the most efficient H atom donors. It also rivals the effectiveness of the other group 14 hydrides in reduction processes. Further work on the kinetics and synthetic scope of these reactions is in progress.

**Acknowledgment.** We thank the Progetto Strategico "Tecnologie Chimiche Innovative" (CNR, Rome) for some financial support.

OM950656E

(9) Newcomb, M. *Tetrahedron* **1993**, *49*, 1151.

(10) Chatgililoglu, C. *Chem. Rev.* **1995**, *95*, 1229.

(11) The relative quantities of 1-hexene and methylcyclopentane varied in the expected manner as the concentration of germane changed. Minor quantities of cyclohexane (1.3%) were also formed.

(12) The  $k_{\text{GeH}}/k_c$  ratio was determined by using the equation  $[A]/[B] = 1/[B]\{[C] + k_c/k_{\text{GeH}}\}\{1 - e^{-k_{\text{GeH}}[B]/k_c}\} - 1$ , where [A], [B], and [C] are the concentrations of 1-hexene, methylcyclopentane and  $(\text{Me}_3\text{Si})_3\text{GeH}$  (initial), respectively.

(13) (a) For  $\text{Bu}_3\text{SnH}$ : Chatgililoglu, C.; Ingold, K. U.; Scaiano, J. C. *J. Am. Chem. Soc.* **1981**, *103*, 7739. (b) For  $\text{Bu}_3\text{GeH}$ : Luszyk, J.; Maillard, B.; Lindsay, D. A.; Ingold, K. U. *J. Am. Chem. Soc.* **1983**, *105*, 3578. (c) For  $\text{Et}_3\text{SiH}$ : Chatgililoglu, C.; Ferreri, C.; Lucarini, M. *J. Org. Chem.* **1993**, *58*, 249. (d) For  $\text{Me}_3\text{SiSi(H)Me}_2$ : Ballestri, M.; Chatgililoglu, C.; Guerra, M.; Guerrini, A.; Lucarini, M.; Seconi, G. *J. Chem. Soc., Perkin Trans. 2* **1993**, 421. (e) For  $(\text{Me}_3\text{Si})_2\text{Si(H)Me}$ : Chatgililoglu, C.; Guerrini, A.; Lucarini, M. *J. Org. Chem.* **1992**, *57*, 3405. (f) For  $(\text{Me}_3\text{Si})_3\text{SiH}$ : Chatgililoglu, C.; Dickhaut, J.; Giese, B. *J. Org. Chem.* **1991**, *56*, 6399.

# First Experimental Estimation of a Platinum–Silicon Bond Energy

Christopher J. Levy and Richard J. Puddephatt\*

Department of Chemistry, The University of Western Ontario,  
London, Ontario, Canada N6A 5B7

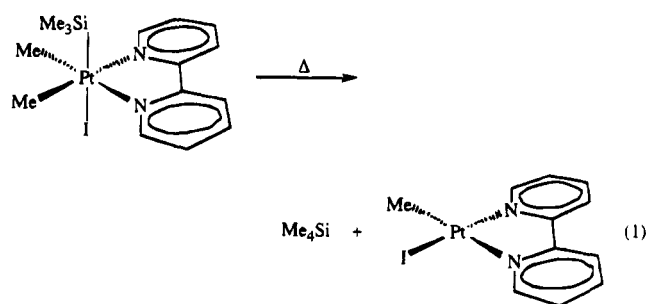
Received July 25, 1995<sup>Ⓢ</sup>

**Summary:** The platinum(IV) complex  $[\text{Pt}(\text{Me}_2\text{Si})(\text{Me}_3\text{Si})(\text{bpy})]$  ( $\text{bpy} = 2,2'$ -bipyridine) undergoes thermal decomposition (177–195 °C) to give  $\text{Me}_4\text{Si}$  and  $[\text{Pt}(\text{Me})(\text{bpy})]$ . Differential scanning calorimetry (DSC) shows the heat of reaction for this process to be  $-8 \pm 5 \text{ kJ mol}^{-1}$ . Using published bond energy data for Pt–Me and Si–Me, we obtain a  $D(\text{Pt}–\text{SiMe}_3)$  of  $233 \pm 14 \text{ kJ mol}^{-1}$ . This is the first experimental estimation of  $D(\text{Pt}–\text{SiMe}_3)$ . The Pt–Si bond is approximately  $100 \text{ kJ mol}^{-1}$  stronger than the Pt–CH<sub>3</sub> bond energy.

One problem in understanding organometallic reactivity, whether in stoichiometric or catalytic reactions, is that metal–ligand bond energies are difficult to obtain and are therefore not readily available. Silyl-platinum complexes are important in a number of catalytic cycles including hydrosilylation,<sup>1</sup> silane redistribution,<sup>2</sup> and silane oligomerization.<sup>3</sup> Platinum(0) and platinum(II) have also been reported to undergo oxidative additions of Si–Si and Si–X bonds<sup>4</sup> while the oxidative addition of the Si–Si  $\sigma$ -bond to palladium(0) is considered a key process in the palladium-catalyzed double silylation of olefin and acetylene.<sup>5</sup> The determination of values for  $D(\text{Pt}–\text{Si})$  is important for a better understanding of these catalytic processes and for the ability to predict reactivities. Sakaki and Ieki<sup>6</sup> have used *ab initio* calculations to estimate  $D(\text{Pt}–\text{SiH}_3)$  values for simple platinum(II)–phosphine complexes. These authors obtain values which range from 249 to 269  $\text{kJ mol}^{-1}$ , compared to 165 to 177  $\text{kJ mol}^{-1}$  for  $D(\text{Pt}–\text{Me})$  in analogous model complexes. The calculated Pt–Si bond lengths associated with these bond energies are in the range 2.366–2.399 Å, similar to the 2.337(3) Å found for  $[\text{Pt}(\text{Me}_2)(\text{Me}_3\text{Si})(\text{bpy})]$ .<sup>4a</sup> This article reports the estimation of  $D(\text{Pt}–\text{Si})$  for this complex; it

is the first experimentally estimated platinum–silicon bond energy.

Reactions which produce a single, nonreactive, volatile component are well suited to thermodynamic analysis by differential scanning calorimetry (DSC). Upon heating,  $[\text{Pt}(\text{Me}_2)(\text{Me}_3\text{Si})(\text{bpy})]$ <sup>4a,b</sup> is shown to give almost exclusively  $\text{Me}_4\text{Si}$  and  $[\text{Pt}(\text{Me})(\text{bpy})]$  (eq 1) as determined by <sup>1</sup>H NMR analysis of decomposition products<sup>7</sup> and thermogravimetric analysis (TGA), thus allowing estimation of the Pt–Si bond dissociation energy.



The enthalpy of a reaction can be approximated as the difference in dissociation energies between the bond formed and bonds broken. For the decomposition of  $[\text{Pt}(\text{Me}_2)(\text{Me}_3\text{Si})(\text{bpy})]$  this gives rise to eq 2 from which  $D(\text{Pt}–\text{SiMe}_3)$  can be determined.<sup>8</sup>

$$\Delta H_{\text{rxn}} = D(\text{Pt}–\text{CH}_3) + D(\text{Pt}–\text{SiMe}_3) - D(\text{Me}_3\text{Si}–\text{Me}) \quad (2)$$

Figure 1 shows the DSC result for the decomposition of  $[\text{Pt}(\text{Me}_2)(\text{Me}_3\text{Si})(\text{bpy})]$ .<sup>9</sup> Decomposition occurs over the range 177–195 °C, corresponding closely to the 172–194 °C range observed by TGA for the same process. The signal shows exothermic and endothermic regions.

(7) A sample of  $[\text{Pt}(\text{Me}_2)(\text{Me}_3\text{Si})(\text{bpy})]$  was heated in an oil bath at 155 °C. The solid darkened from yellow to brown-yellow. The tube was attached to a vacuum manifold, and the volatile components were distilled into a second NMR tube. Solvent was distilled into each tube by vacuum transfer. The <sup>1</sup>H NMR spectrum ( $\text{CD}_2\text{Cl}_2$ ) of the solid residue shows  $[\text{Pt}(\text{Me}_2)(\text{Me}_3\text{Si})(\text{bpy})]$  (not decomposed) as well as  $[\text{Pt}(\text{Me})(\text{bpy})]$  and  $[\text{Pt}(\text{Me}_2)(\text{bpy})]$ . The  $[\text{Pt}(\text{Me})(\text{bpy})]:[\text{Pt}(\text{Me}_2)(\text{bpy})]$  ratio was 97:3. Signals due to Me–Pt and Me–Si signals were as follows:  $[\text{Pt}(\text{Me}_2)(\text{Me}_3\text{Si})(\text{bpy})]$ ,  $\delta -0.33$  [s, 9H,  $^3J(\text{PtH}) = 19.0$  Hz, Me–Si], 1.45 [s, 6H,  $2J(\text{PtH}) = 64.3$  Hz, Me–Pt];  $[\text{Pt}(\text{Me})(\text{bpy})]$ ,  $\delta 1.15$  [s, 6H,  $^3J(\text{PtH}) = 75.8$  Hz, Me–Pt], 0.98 [s,  $2J(\text{PtH}) = 86.1$  Hz, Me–Pt]. The <sup>1</sup>H NMR spectrum of the volatiles ( $\text{C}_6\text{D}_6$ ) showed predominantly  $\text{Me}_4\text{Si}$  ( $\delta 0.00$ ) as well as a minor signal at 0.10 ppm (2% intensity compared to the  $\text{Me}_4\text{Si}$  resonance) which is not, as yet, assigned. The same products were obtained more rapidly at 175 °C.

(8) There are a number of approximations made in this type of treatment. The energies of bonds that are not directly involved in the reaction are assumed to remain constant, no account of the Pt(IV)–Pt(II) promotion energy is made, and the sublimation energies of platinum(IV) and platinum(II) complexes are assumed to be equal. As well, there are a number of difficulties associated with the practical aspects of DSC. For a discussion, see: MacKenzie, R. C. *Differential Thermal Analysis*; Academic Press: New York, 1970; Vol. 1.

\* Abstract published in *Advance ACS Abstracts*, November 1, 1995.

(1) (a) Cundy, C. S.; Kingston, B. M.; Lappert, M. F. *Adv. Organomet. Chem.* **1973**, *11*, 253. (b) Pawlenko, S. *Organosilicon Chemistry*; Walter de Gruyter: New York, 1986; p 36.

(2) (a) Baumford, W. R.; Lovie, J. C.; Watt, J. A. C. *J. Chem. Soc. C* **1966**, 1139. (b) Benkeser, R. A.; Beck, K. R. *J. Organomet. Chem.* **1984**, *264*, 239.

(3) (a) Yamamoto, K.; Okinoshima, H.; Kumada, M. *J. Organomet. Chem.* **1971**, *27*, C31. (b) Yamamoto, K.; Okinoshima, H.; Kumada, M. *J. Organomet. Chem.* **1970**, *23*, C7.

(4) (a) Levy, C. J.; Vittal, J. J.; Puddephatt, R. J. *Organometallics* **1994**, *13*, 1559. (b) Levy, C. J.; Vittal, J. J.; Puddephatt, R. J. *Organometallics*, submitted for publication. (c) Yamashita, H.; Kobayashi, T.; Hayashi, T.; Tanaka, M. *Chem. Lett.* **1990**, 1447. (d) Yamashita, H.; Hayashi, T.; Kobayashi, T.; Tanaka, M. *J. Am. Chem. Soc.* **1988**, *110*, 2330. (e) Yamashita, H.; Kobayashi, T.; Tanaka, M. *J. Am. Chem. Soc.* **1988**, *110*, 2330. (f) Yamashita, H.; Hayashi, T.; Tanaka, M. *Jpn. Pat. Appl.* **1988**, 88-254508. (g) Bentham, J. E.; Ebsworth, E. A. V. *Inorg. Nucl. Lett.* **1970**, *6*, 145. (h) Bentham, J. E.; Craddock, B. S.; Ebsworth, E. A. V. *J. Chem. Soc. A* **1971**, 587. (i) Ebsworth, E. A. V.; Henderson, S. G. D.; Rankin, D. W. H. *Inorg. Chim. Acta* **1981**, *48*, 159.

(5) (a) Ito, Y.; Matsuura, T.; Marakami, M. *J. Am. Chem. Soc.* **1988**, *110*, 3692. (b) Murakami, M.; Anderson, P. G.; Surinome, M.; Ito, Y. *J. Am. Chem. Soc.* **1991**, *113*, 3987.

(6) Sakaki, S.; Ieki, M. *J. Am. Chem. Soc.* **1993**, *115*, 2373.

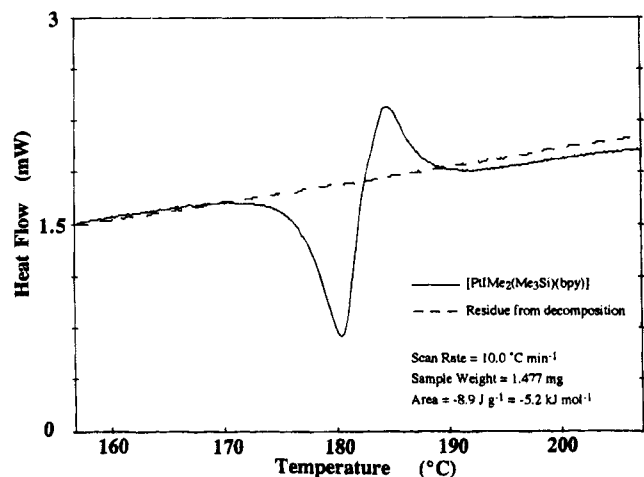


**Figure 1.** DSC signal for the reductive elimination of  $\text{Me}_4\text{Si}$  from  $[\text{PtIME}_2(\text{Me}_3\text{Si})(\text{bpy})]$ .

This can be accounted for in terms of an exothermic reaction which is accompanied by the endothermic volatilization of  $\text{Me}_4\text{Si}$ . The lag time between the formation and evolution of  $\text{Me}_4\text{Si}$  results in the bimodal nature of the signal. The heat of reaction was determined to be  $-8 \pm 5$  kJ/mol from eight experiments. In order to determine the Pt–Si bond energy, values for  $D(\text{Me}–\text{Pt})$  and  $D(\text{Me}–\text{Si})$  are required. The  $\text{Me}_3\text{Si}–\text{Me}$  bond energy has been derived by Walsh<sup>10</sup> to be  $376 \pm 8$  kJ mol<sup>-1</sup>. Several literature values are available for the

(9) DSC experiments were conducted using a Perkin-Elmer DSC7 with a TAC7/DX thermal analysis controller. Samples were weighed into empty aluminum pans, with the weight of each (0.5–3 mg) being determined using a microbalance (supplied with Perkin-Elmer TGA7). Pans were not sealed in order to allow for the escape of volatile products. The sample and reference compartments were purged with  $\text{N}_2$  during the experiments. A scan rate of  $20^\circ\text{C min}^{-1}$  was used.

(10) Walsh, R. *The Chemistry of Organic Silicon Compounds*; Patai, S., Rappaport, Z., Eds.; John Wiley & Sons: Toronto, 1989; pp 376–385.

$\text{Me}–\text{Pt}(\text{IV})$  bond dissociation energy. A value of  $134$  kJ mol<sup>-1</sup> is predicted by the generalized valence bond theory for  $[\text{PtCl}_2\text{Me}_2(\text{PH}_3)_2]$ ,<sup>11</sup> values of  $137$  and  $129$  kJ mol<sup>-1</sup> have been found for *cis*- $[\text{PtMe}_4\text{L}_2]$  ( $\text{L} = \text{MeCN}$ ,  $2,6\text{-Me}_2\text{C}_6\text{H}_3\text{NC}$ ),<sup>12</sup> and values of  $144$  and  $132$  kJ mol<sup>-1</sup> were found for  $[\text{PtIME}_3(\text{PMe}_2\text{Ph})_2]$  and  $[\text{PtIME}_3(\text{Ph}_2\text{PCH}_2\text{CH}_2\text{PPh}_2)]$ .<sup>13</sup> We will use an average of the experimentally determined bond dissociation energies of  $135 \pm 10$  kJ mol<sup>-1</sup>.<sup>14</sup> Using the literature bond dissociation energy data we obtain an estimated value for  $D(\text{Pt}–\text{SiMe}_3)$  in  $[\text{PtIME}_2(\text{Me}_3\text{Si})(\text{bpy})]$  of  $233 \pm 14$  kJ mol<sup>-1</sup>.<sup>14</sup> This is  $98$  kJ mol<sup>-1</sup> larger than the value of  $D(\text{Pt}–\text{Me})$  used in our calculations, clearly showing the stronger nature of the Pt–Si bond compared to Pt–Me. This result is consistent with the general stability trend  $\text{Pt}–\text{Si} > \text{Pt}–\text{C}$ .<sup>15</sup> The value of  $D(\text{Pt}–\text{Si})$  obtained for  $[\text{PtIME}_2(\text{Me}_3\text{Si})(\text{bpy})]$  ( $233$  kJ mol<sup>-1</sup>) agrees well with those obtained from the *ab initio* calculations,<sup>6</sup> and both studies indicate a Pt–Si bond which is approximately  $100$  kJ mol<sup>-1</sup> stronger than the Pt– $\text{CH}_3$  bond.

**Acknowledgment.** We thank the NSERC (Canada) for financial support.

OM9505773

(11) Low, J. J.; Goddard, W. A., III. *J. Am. Chem. Soc.* **1986**, *108*, 6115.

(12) Roy, S.; Puddephatt, R. J.; Scott, J. D. *J. Chem. Soc., Dalton Trans.* **1989**, 2121.

(13) (a) Brown, M. P.; Puddephatt, R. J.; Upton, J. *J. Chem. Soc., Dalton Trans.* **1974**, 2457. (b) Goldberg, K. I.; Yan, J.; Breitung, E. M. *J. Am. Chem. Soc.* **1995**, *117*, 6889.

(14) Error is estimated from the spread of the literature bond energy data and does not include errors arising from the approximations required by the DSC method (see footnote 8 and note that such errors are likely to cancel out when considering the difference between the Pt–Si and Pt–C bond energies). Data are corrected for thermal expansion of TMS.

(15) McKay, K. M.; Nicholson, B. K. *Comprehensive Organometallic Chemistry*; Wilkinson, G., Stone, F. G. A., Abel, E. W., Eds.; Pergamon: Oxford, U.K., 1982; Vol. 6, pp 1096–7.

# Reversible Yttrium Alkynide Coupling Supported by DAC (Deprotonated 4,13-Diaza-18-crown-6) Ligation

Lawrence Lee, David J. Berg,\* and Gordon W. Bushnell

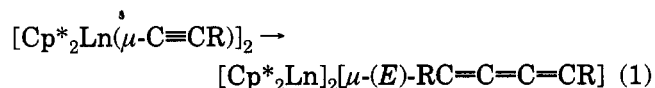
Department of Chemistry, University of Victoria, P.O. Box 3055 MS7152,  
Victoria, British Columbia, Canada V8W 3P6

Received August 4, 1995<sup>®</sup>

**Summary:** The reaction of  $Y(DAC)(CH_2SiMe_3)$  (**1**) with phenylacetylene produces an equilibrium mixture of the alkynide-coupled butatrienediyl complex  $[Y(\mu-DAC)]_2(\mu-(Z)-PhC=C=C=CPh)$  (**2**) and the uncoupled bridging alkynide dimer  $[(DAC)Y(\mu-C\equiv CPh)]_2$  (**3**). Unlike other butatrienediyl complexes of yttrium or the lanthanides, this unit adopts a Z conformation in complex **2**.

Recently, we reported the synthesis and thermal stability of a monomeric yttrium alkyl complex,  $(DAC)Y(CH_2SiMe_3)$  (**1**), containing the deprotonated macrocycle 4,13-diaza-18-crown-6 (DAC)<sup>1</sup> as the only ancillary ligand.<sup>2</sup> In our earlier studies, it became apparent that the DAC ligand is the approximate steric equivalent of two Cp\* units.<sup>3,4</sup> However, in terms of electronic properties, DAC differs substantially from two Cp\* ligands, since it can donate a variable number of electrons to the metal center. In addition, the coordination geometry provided by DAC is more flexible than that of the bis-Cp\* system. Currently, we are exploring the reactivity of **1** with small molecules in order to develop a better understanding of ancillary ligand effects in group 3 and f-element chemistry.<sup>5</sup>

Earlier work by Evans,<sup>6</sup> Teuben,<sup>7</sup> and Marks<sup>8</sup> revealed a fascinating reaction in which two bridging alkynide units couple to form a butatrienediyl complex, several examples of which have been characterized by X-ray crystallography (eq 1). Interestingly, this reaction



is not general but appears to be promoted by a high

degree of steric crowding.<sup>6b,c,7</sup> In one case, the coupling process is reversible and an equilibrium is established between the uncoupled bridging alkynide dimer and the butatrienediyl complex.<sup>7</sup> The evident sensitivity of this coupling reaction to steric and possibly electronic effects led us to investigate the reaction of **1** with terminal alkynes. In this contribution, we report the synthesis and properties of a bridging phenylacetylide and a 1,4-diphenylbutatrienediyl complex of yttrium supported by DAC ligation. To our knowledge, this is the first report of alkynide coupling in complexes containing ancillary ligands other than Cp\*.

The reaction of phenylacetylene (1 equiv) with  $(DAC)Y(CH_2SiMe_3)$  (**1**) in toluene produced a deep purple solution. The purple color is unusual for an  $Y^{3+}$  complex and suggests butatrienediyl formation.<sup>9</sup> Consistent with this, the  $^{13}C\{^1H\}$  NMR spectrum of the reaction mixture showed a doublet ( $^1J_{YC} = 38.4$  Hz) at 196.5 ppm characteristic of the butatrienediyl terminal carbon in  $[(DAC)Y]_2(\mu-(Z)-PhC=C=C=CPh)$  (**2**)<sup>10</sup> (cf. 208.6 ppm in  $(Cp^*_2La)_2(\mu-(E)-MeC=C=C=CMe)$ );<sup>7</sup> in addition, a further set of resonances was superimposed on those assigned to the coupled product, while hydrolysis produced phenylacetylene as well as a mixture of 1,4-diphenyl-1-buten-3-yne isomers.<sup>11</sup> These observations led us to conclude that formation of a second organoyttrium species, the uncoupled alkynide-bridged dimer  $[(DAC)Y(\mu-C\equiv CPh)]_2$  (**3**),<sup>10</sup> accompanied that of **2**. Crystalline samples of blue-purple **2** and white **3** were separately isolated from the reaction mixture. Dissolution of either crystalline **2** or **3** reproduced the NMR spectrum of the original reaction mixture (apart from

\* To whom correspondence should be addressed.

<sup>®</sup> Abstract published in *Advance ACS Abstracts*, October 1, 1995.

(1) Systematic name: 1,7,10,16-tetraoxa-4,13-diazacyclooctadecane.

(2) Lee, L.; Berg, D. J.; Bushnell, G. W. *Organometallics* **1995**, *14*, 8.

(3) Based on similar bond lengths in comparable complexes: Y-N(amide) bond lengths of  $Cp^*_2Y[N(SiMe_3)_2]^{4a}$  (molecule 1, 2.274(5) Å; molecule 2, 2.253(5) Å), and  $[DAC]Y[N(SiMe_3)_2]^{4b}$  (2.338(11) Å); Y-C(alkyl) bond lengths of  $Cp^*_2Y[CH(SiMe_3)_2]^{4a}$  (2.468(7) Å) and  $[DAC]Y[CH_2SiMe_3]^{4c}$  (2.45(2) Å).

(4) (a) den Haan, K. H.; de Boer, J. L.; Teuben, J. H.; Spek, A. L.; Kojić-Prodić, B.; Hays, G. R.; Huis, R. *Organometallics* **1986**, *5*, 1726. (b) Lee, L.; Berg, D. J.; Bushnell, G. W. *Inorg. Chem.* **1994**, *33*, 5302.

(5) The related dianionic porphyrin macrocycles also have been used as ancillary ligands in organolanthanide chemistry: (a) Schaverien, C. J. *J. Chem. Soc., Chem. Commun.* **1991**, 458. (b) Schaverien, C. J.; Orpen, A. G. *Inorg. Chem.* **1991**, *30*, 4968. (c) Arnold, J.; Hoffman, C. G.; Dawson, D. W.; Hollander, F. J. *Organometallics* **1993**, *12*, 3645. (d) Brand, H.; Arnold, J. *Organometallics* **1993**, *12*, 3655. (e) Brand, H.; Arnold, J. *Angew. Chem., Int. Ed. Engl.* **1994**, *33*, 95.

(6) (a) Evans, W. J.; Keyer, R. A.; Zhang, H.; Atwood, J. L. *J. Chem. Soc., Chem. Commun.* **1987**, 837. (b) Evans, W. J.; Keyer, R. A.; Ziller, J. W. *Organometallics* **1990**, *9*, 2628. (c) Evans, W. J.; Keyer, R. A.; Ziller, J. W. *Organometallics* **1993**, *12*, 2618.

(7) (a) Heeres, H. J.; Teuben, J. H. *Organometallics* **1991**, *10*, 1980. (b) Heeres, H. J.; Nijhoff, J.; Teuben, J. H.; Rogers, R. D. *Organometallics* **1993**, *12*, 2609.

(8) Forsyth, C. M.; Nolan, S. P.; Stern, C. L.; Marks, T. J.; Rheingold, A. L. *Organometallics* **1993**, *12*, 3618.

(9) Similarly,  $(Cp^*_2La)_2(\mu-(E)-MeC=C=C=CMe)$  is reported to be red, which also is an unusual color for a  $La^{3+}$  complex.<sup>7b</sup>

(10) Synthesis of **2** and **3**: All operations were carried out in an argon-filled glovebox. A solution of phenylacetylene (1.79 mL of a 0.513 M solution in benzene, 0.917 mmol) was added to a solution of  $Y(DAC)(CH_2SiMe_3)_2$  (0.40 g, 0.92 mmol) in 25 mL of benzene with stirring. Slow evaporation of the resulting purple solution gave blue-purple needles of **2** (0.280 g, 67.8%) as a benzene solvate (1.5 equiv). The above reaction was repeated, except that the reaction mixture was layered with hexane and allowed to stand at room temperature until white crystals of **3** slowly deposited (0.260 g, 63.4%). **2**:  $1.5C_6H_6$ ; mp: 90 °C dec; IR (Nujol, KBr) 1592, 1542  $cm^{-1}$  (m,  $\nu_{C-C}$ ). Anal. Calcd for  $C_{49}H_{67}N_4O_8Y_2$ : C, 57.82; H, 6.64; N, 5.50. Found: C, 57.75; H, 6.63; N, 5.36. Complex **3**: mp 120 °C dec; IR (Nujol, KBr) 2047  $cm^{-1}$  (m,  $\nu_{C-C}$ ). Anal. Calcd for  $C_{40}H_{58}N_4O_8Y_2$ : C, 53.34; H, 6.49; N, 6.22. Found: C, 53.61; H, 6.60; N, 5.62.  $^1H$  NMR ( $C_6D_6$ , 360 MHz, 302 K): **2**,  $\delta$  7.71 (d, o-aryl CH, 4H,  $J_{HH} = 7.5$  Hz), 7.29 (t, m-aryl CH, 4H,  $J_{HH} = 7.5$  Hz), 7.01 (t, p-aryl CH, 2H,  $J_{HH} = 8$  Hz, partially obscured); **3**,  $\delta$  7.63 (m, o-aryl CH, 4H), 7.11 (m, m-aryl CH, 4H), 6.99 (t, p-aryl CH, 2H,  $^3J_{HH} = 8$  Hz),  $^{13}C\{^1H\}$  NMR (90.56 MHz): **2**,  $\delta$  196.5 (d, C=CPh,  $^1J_{YC} = 38.4$  Hz), 169.5 (d, C=CPh,  $J_{YC} = 4.0$  Hz); **3**,  $\delta$  150.1 (C=CPh), PhC=C not observed. Complete NMR data are given in the supporting information.

(11) Hydrolysis gave the 1,4-diphenyl-1-buten-3-yne (*Z:E* ratio of 85:15 by GC) and not the expected 1,4-diphenylbutatriene. This has been explained by the rapid rearrangement of the initial, singly protonated butatrienyl species via a 1,3-metal shift, followed by the second protonation.<sup>7b</sup>

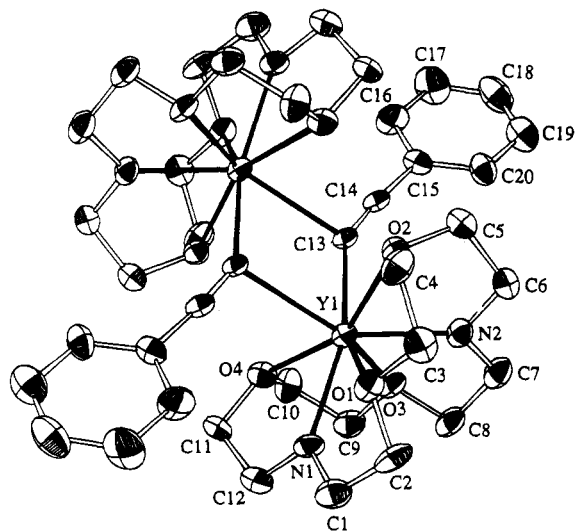


**Figure 1.** ORTEP<sup>14b</sup> drawing of **3**. Selected bond distances (Å) and angles (deg): Y(1)–N(1) = 2.279(8), Y(1)–N(2) = 2.275(8), Y(1)–O(1) = 2.637(6), Y(1)–O(2) = 2.536(7), Y(1)–O(3) = 2.509(6), Y(1)–O(4) = 2.500(7), Y(1)–C(13) = 2.601(9), Y(1)–C(13) = 2.627(12), C(13)–C(14) = 1.197(13); Y(1)–C(13)–Y(1') = 101.9(4), C(13)–Y(1)–C(13') = 78.1(4), Y(1)–C(13)–C(14) = 148.7(8), Y(1)–C(13)–C(14) = 104.0(9), C(13)–C(14)–C(15) = 173.5(10). Primed atoms are related by inversion symmetry.

SiMe<sub>4</sub> in the latter, formed by protonolysis of the CH<sub>2</sub>-SiMe<sub>3</sub> group), suggesting that these compounds exist in equilibrium (*vide infra*). Additionally, the IR spectrum of solid **3** contained a clear C≡C stretch at 2047 cm<sup>-1</sup> which was notably absent in **2**.<sup>12</sup>

The structure of **3** (Figure 1) reveals a centrosymmetric dimer with asymmetric bridging alkyne groups.<sup>13</sup> The asymmetry is particularly clear from the difference between the angles Y(1)–C(13)–C(14) and Y(1)–C(13)–C(14), 148.7(8) and 104.0(9)°, respectively ( $\Delta_{\text{ang}} = 44.7^\circ$ ). The Y(1)–C(13) and Y(1)–C(13) bridging distances of 2.603(13) and 2.627(12) Å, respectively, are not highly asymmetric ( $\Delta_{\text{dist}} = 0.024$  Å). The values for these parameters fall within the range observed for structurally characterized lanthanide dimers ([Cp<sub>2</sub>Er(μ-C≡C-*t*-Bu)]<sub>2</sub>,  $\Delta_{\text{ang}} = 34^\circ$ ,  $\Delta_{\text{dist}} = 0.05$  Å;<sup>15a</sup> [(C<sub>5</sub>H<sub>4</sub>-Me)<sub>2</sub>Sm(μ-C≡C-*t*-Bu)]<sub>2</sub>,  $\Delta_{\text{ang}} = 39^\circ$ ,  $\Delta_{\text{dist}} = 0$  Å;<sup>15b</sup> [(C<sub>5</sub>H<sub>4</sub>-

(12) While it has been pointed out previously<sup>8</sup> that the absence of ν<sub>C=C</sub> in the IR is not always good evidence for the absence of a ligand C≡C bond, the majority of alkyne complexes do indeed show such a stretch.<sup>15</sup>

(13) Crystal data for **3**: C<sub>40</sub>H<sub>58</sub>N<sub>4</sub>O<sub>8</sub>Y<sub>2</sub>, *M<sub>r</sub>* = 900.74, triclinic, space group P1 (No. 2), *a* = 10.032(3) Å, *b* = 11.7932(14) Å, *c* = 9.410(2) Å, α = 73.32(1)°, β = 88.28(2)°, γ = 85.74(2)°, *V* = 1063.5 Å<sup>3</sup>, *Z* = 2 (half of a dimer), *D<sub>c</sub>* = 1.406 g cm<sup>-3</sup>, μ(Cu Kα) = 41.32 cm<sup>-1</sup> (graphite monochromated), λ = 1.542 Å, *F*(000) = 467.95, 2θ range 2–100°. The data were collected on a Nonius CAD-4F diffractometer at ambient temperature (293 K) using the ω-θ scan mode. The data were corrected for Lorentz and polarization effects, and an empirical absorption correction (ψ scan) was carried out. The structure was solved using the Patterson method (SHELXS).<sup>14a</sup> A total of 1993 reflections with *I* > 2.5σ(*I*) from a total of 2169 unique reflections were used in the refinement. A total of 244 parameters were refined using SHELX76,<sup>14a</sup> and the structure converged satisfactorily (maximum shift/ead 0.055, *R* = 0.076; *R<sub>w</sub>* = 0.080).

(14) (a) Sheldrick, G. M. SHELX76, Programs for Crystal Structure Determination, University of Cambridge, Cambridge, U.K., 1976. (b) Johnson, C. K. ORTEP; Oak Ridge National Laboratory: Oak Ridge, TN, 1976.

(15) (a) Atwood, J. L.; Hunter, W. E.; Wayda, A. L.; Evans, W. J. *Inorg. Chem.* **1981**, *20*, 4115. (b) Evans, W. J.; Bloom, I.; Hunter, W. E.; Atwood, J. L. *Organometallics* **1983**, *2*, 709. (c) Shen, Q.; Zheng, D.; Lin, L.; Lin, Y. *J. Organomet. Chem.* **1990**, *391*, 307. (d) Duchateau, R.; van Wee, C. T.; Meetsma, A.; Teuben, J. H. *J. Am. Chem. Soc.* **1993**, *115*, 4931.

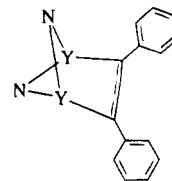
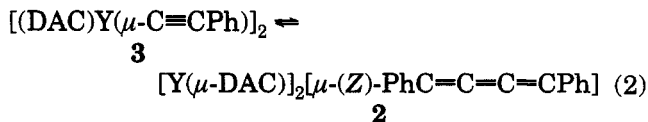


**Figure 2.** Sketch of the core geometry in **2** from preliminary X-ray studies.

*t*-Bu)<sub>2</sub>Sm(μ-C≡CPh)]<sub>2</sub>,  $\Delta_{\text{ang}} = 58.2^\circ$ ,  $\Delta_{\text{dist}} = 0.057$  Å;<sup>15c</sup> [(PhC(NSiMe<sub>3</sub>)<sub>2</sub>)<sub>2</sub>Y(μ-C≡CH)]<sub>2</sub>,  $\Delta_{\text{ang}} = 61.4^\circ$ ,  $\Delta_{\text{dist}} = 0.047$  Å<sup>15d</sup>). The β-C (C(14)) exhibits one short and one long contact with yttrium (C(14)–Y(1), 3.69(2); C(14)–Y(1'), 3.15(2) Å). However, the short C≡C bond length of 1.197(13) Å<sup>16</sup> suggests that any π interaction between the alkyne C≡C and yttrium is at best very weak. The Y–C(alkynide) distances in **3** are both considerably longer than the longest previously reported: for the other structurally characterized bridging alkyne complexes,<sup>15a–d</sup> bond lengths of this type span the range 2.44–2.556 Å, after correction for differences in metal ionic radii.<sup>17</sup> Thus, it is clear that **3** is highly crowded, a result which is consistent with earlier claims that steric crowding plays a major role in alkyne coupling.<sup>6–8</sup>

An X-ray crystallographic investigation of **2** was also carried out. Although disorder within the CH<sub>2</sub>CH<sub>2</sub> backbone of the DAC ligands prevented satisfactory refinement of the structure, connectivity within this molecule was established and two important differences from the Cp\* analogs were evident. First, the butatrienediyl fragment was clearly in a *Z* conformation, with both yttrium atoms on the same side of the C4 chain. Second, one N atom from each DAC ligand was in a bridging site between the two yttrium centers. A sketch of the core geometry is given in Figure 2. These structural conclusions are supported by the observation that the major hydrolysis product is the (*Z*)-enyne. Although isomerization during hydrolysis is possible,<sup>7b,11</sup> it is significant that (a) hydrolysis of [Cp\*<sub>2</sub>Ln]<sub>2</sub>(μ-*E*)-RC=C=C=CR) (R = Me, Ln = La, Ce; R = *t*-Bu, Ln = Ce) yielded primarily the (*E*)-enyne (*exclusively* for R = Me)<sup>7b</sup> and (b) isomerization of the (*Z*)-enyne to the *E* isomer is slow at room temperature. These data identify a structure which is unique among the known butatrienediyl complexes, and accordingly, attempts to complete a full structure determination are continuing.

The equilibrium between **2** and **3** (eq 2), which was established in seconds, was investigated by using variable-temperature <sup>1</sup>H NMR spectroscopy in the range 16–69 °C (Figure 3). The only related example of



equilibrium, that between [Cp\*<sub>2</sub>Ln(μ-C≡CR)]<sub>2</sub> and [Cp\*<sub>2</sub>Ln]<sub>2</sub>(μ-*E*)-RC=C=C=CR) (Ln = La, Ce; R = Me, *t*-Bu),<sup>7</sup> required 14 days for equilibrium to be established. A plot of ln *K<sub>eq</sub>* versus 1/*T* yields  $\Delta H^\circ = -67.0 \pm 2.0$  kJ mol<sup>-1</sup> and  $\Delta S^\circ = -228 \pm 8$  J mol<sup>-1</sup> K<sup>-1</sup> to give a *K<sub>eq</sub>*

(16) The reported C≡C bond length in free PhC≡CH is 1.208 Å, from microwave spectroscopy: Cox, P. A.; Ewart, I. C.; Stigliani, W. M. *J. Chem. Soc., Faraday Trans. 2* **1975**, 504.

(17) Using corrections of -0.124 (Ce), -0.060 (Sm), and +0.015 (Er) Å from: Shannon, R. D. *Acta Crystallogr.* **1976**, *A32*, 751.

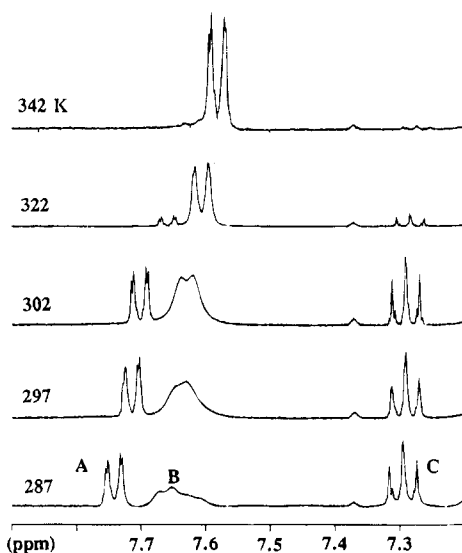


**Figure 3.** Variable-temperature  $^1\text{H}$  NMR ( $\text{C}_6\text{D}_6$ , 360 MHz) data for the downfield aryl region of the  $\mathbf{3} \rightleftharpoons \mathbf{2}$  equilibrium (A, *o*-aryl *H* of  $\mathbf{2}$ ; B, *o*-aryl *H* of  $\mathbf{3}$ ; C, *m*-aryl *H* of  $\mathbf{2}$ ).

value of 0.68 for  $\mathbf{3} \rightleftharpoons \mathbf{2}$  at 298 K. The position of the equilibrium is strongly temperature dependent due to the large negative entropy term. Thus, the purple solution containing  $\mathbf{2}$  and  $\mathbf{3}$  bleaches to colorless (conversion to  $\mathbf{3}$ ) when heated, but the purple color is regenerated on cooling.

The large negative entropy term further suggests that, although compound  $\mathbf{3}$  is dimeric in the crystal, it may be dissociated in solution. When the temperature is lowered, the resonances due to  $\mathbf{3}$  broaden noticeably (see Figure 3) and eventually split into two sets of resonances while those of  $\mathbf{2}$  remain sharp. This observation may be attributable to slow dissociation–reassociation between  $\mathbf{3}$  and the monomeric phenylacetylide  $\text{Y}[\text{DAC}](\text{C}\equiv\text{CPh})$ . Marks and co-workers reported NMR (temperature-dependent  $\text{Cp}^*$  shifts) and kinetic evidence for a similar alkyne monomer–dimer equilibrium in solutions of  $[\text{Cp}^*_2\text{La}(\text{C}\equiv\text{C}-t\text{-Bu})_2]_2$ ,<sup>8</sup> although the

present case appears to be the first where both species are directly observable. Dissociation would not be surprising, given the long Y–C(alkynide) bond lengths observed in the crystal structure of  $\mathbf{3}$ , and accordingly addition of THF leads to complete cleavage of the coupled product and formation of  $(\text{DAC})\text{Y}(\text{C}\equiv\text{CPh})\cdot(\text{THF})$  ( $\mathbf{4}$ ).<sup>18</sup>

In conclusion, the results described here show that alkyne coupling is not restricted to the  $\text{Cp}^*$  ligand system and support the idea that a congested metal center favors coupling. However, in contrast to the (*E*)-butatrienediyl unit found in the  $\text{Cp}^*$  system, the more flexible DAC ligand favors formation of the *Z* isomer. Since steric effects are finely balanced between the alkyne and butatrienediyl forms, the DAC system is ideal for investigation of the effect of changes in the electronic properties of the terminal alkyne on the position of the coupling equilibrium. This work and related reactivity studies with  $\mathbf{1}$  are currently in progress.

**Acknowledgment.** We thank Mrs. C. Greenwood for assistance in recording the NMR spectra and Dr. Becky Chak for help with the X-ray structural study. This research was supported by the NSERC (Canada) and a University of Victoria Internal Research Grant (to D.J.B.).

**Supporting Information Available:** Text giving complete NMR data for compounds  $\mathbf{2}$ – $\mathbf{4}$  and tables of atomic positional and equivalent isotropic displacement parameters, bond distances and angles, and anisotropic thermal parameters for  $\mathbf{3}$  (6 pages). Ordering information is given on any current masthead page.

OM9506476

(18) Complex  $\mathbf{4}$  was identified by NMR ( $d_8$ -THF):  $^1\text{H}$ ,  $\delta$  7.12 (d, 2H, *o*-aryl CH,  $^3J_{\text{HH}} = 7.1$  Hz), 7.01 (t, 2H, *m*-aryl CH,  $^3J_{\text{HH}} = 7.1$  Hz), 6.89 (t, 1H, *p*-aryl CH,  $^3J_{\text{HH}} = 7.3$  Hz), 4.20 (m, 4H, DAC-*H*), 4.10 (m, 4H, DAC-*H*), 3.86 (m, 4H, DAC-*H*), 3.78 (m, 4H, DAC-*H*), 3.40 (m, 4H, DAC-*H*), 2.92 (m, 4H, DAC-*H*);  $^{13}\text{C}\{^1\text{H}\}$ ,  $\delta$  149.1 (d, C=CPh,  $^1J_{\text{YC}} = 46.9$  Hz), 105.3 (C=CPh,  $^2J_{\text{YC}} = 9.6$  Hz). Complete NMR data are included in the supporting information.

## Articles

## Synthesis of ( $\mu$ -Bis(aminocarbene))dimetal Complexes of Chromium and Iron by the Reaction of Tertiary Diamides with $\text{Cr}(\text{CO})_5^{2-}$ or $\text{Fe}(\text{CO})_4^{2-}$ in the Presence of Chlorotrimethylsilane

Miroslav Havránek,<sup>†</sup> Michal Hušák,<sup>‡</sup> and Dalimil Dvořák<sup>\*,†</sup>

Departments of Organic and Solid State Chemistry, Prague Institute of Chemical Technology, Technická 5, 166 28 Prague 6, Czech Republic

Received April 11, 1995<sup>®</sup>

Reaction of an excess of  $\text{Cr}(\text{CO})_5^{2-}$  with  $N,N,N',N'$ -tetramethylisophthalamide (**1a**) or the  $N,N,N',N'$ -tetramethylamide of pyridine-2,6-dicarboxylic acid (**1c**) in the presence of chlorotrimethylsilane readily gives ( $\mu$ -bis(aminocarbene))dichromium complexes  $(\text{CO})_5\text{Cr}[\mu-1,3-(\text{C}(\text{NMe}_2))\text{C}_6\text{H}_4(\text{C}(\text{NMe}_2))]\text{Cr}(\text{CO})_5$  (**2a**) or  $(\text{CO})_5\text{Cr}[\mu-2,6-(\text{C}(\text{NMe}_2))(\text{C}_5\text{H}_3\text{N})(\text{C}(\text{NMe}_2))]\text{Cr}(\text{CO})_5$  (**2c**), respectively. Under the same conditions,  $N,N,N',N'$ -tetramethylphthalamide (**1b**), binaphthyl bis(amide) **1d**, and  $N,N,N',N'$ -tetramethylsuccinamide (**1e**) afford monocarbene complexes  $(\text{CO})_5\text{Cr}[\text{C}(\text{NMe}_2)(2-(\text{Me}_2\text{NCO})\text{C}_6\text{H}_4)]$  (**3b**), binaphthyl derivative **3c**, and  $(\text{CO})_5\text{Cr}[\text{C}(\text{NMe}_2)((\text{CH}_2)_2\text{CONMe}_2)]$  (**3d**) as the sole products.  $N,N,N',N'$ -Tetramethylglutaramide (**1f**) and  $N,N,N',N'$ -tetramethyladipamide (**1g**) form mixtures of both bis- and mono(carbene) complexes with the bis(carbene) complex strongly predominating. The reaction of  $\text{Fe}(\text{CO})_4^{2-}$  with diamide **1a** or **1c** under similar conditions produces the ( $\mu$ -bis(aminocarbene))diiron complexes  $(\text{CO})_4\text{Fe}[\mu-1,3-(\text{C}(\text{NMe}_2))\text{C}_6\text{H}_4(\text{C}(\text{NMe}_2))]\text{Fe}(\text{CO})_4$  (**2b**) or  $(\text{CO})_4\text{Fe}[\mu-2,6-(\text{C}(\text{NMe}_2))(\text{C}_5\text{H}_3\text{N})(\text{C}(\text{NMe}_2))]\text{Fe}(\text{CO})_4$  (**2d**), respectively. When a 1:1 molar ratio of **1a** and  $\text{Cr}(\text{CO})_5^{2-}$  is used, the monocarbene complex  $(\text{CO})_5\text{Cr}[\text{C}(\text{NMe}_2)(3-(\text{Me}_2\text{NCO})\text{C}_6\text{H}_4)]$  (**3a**) is formed in moderate yield along with **2a**. The monocarbene complex **3a** can be converted to the mixed chromium-iron  $\mu$ -bis(aminocarbene) complex  $(\text{CO})_5\text{Cr}[\mu-1,3-(\text{C}(\text{NMe}_2))\text{C}_6\text{H}_4(\text{C}(\text{NMe}_2))]\text{Fe}(\text{CO})_4$  (**4**) on reaction with  $\text{Fe}(\text{CO})_4^{2-}$  and chlorotrimethylsilane. This complex was fully characterized by X-ray diffraction study.

The chemistry of Fischer carbene complexes, in particular that of chromium, is well established and has found many applications in organic synthesis.<sup>1</sup> By contrast ( $\mu$ -bis(carbene))dimetal complexes of number of transition metals are rare<sup>2</sup> and their synthetic potential remains to be explored.<sup>3</sup> There are several methods reported for the preparation of Fischer ( $\mu$ -bis(carbene))-dimetal complexes of group 6 metals. The most useful methods for their preparation are based on the reaction of bis(lithio) or bis(Grignard) reagents with metal carbonyl followed by O-alkylation<sup>4</sup> and Michael type addition of  $\alpha$ -anions derived from group 6 carbene com-

plexes to  $\alpha,\beta$ -unsaturated carbene complexes of group 6 elements.<sup>2a-c</sup> Alkylation of  $\omega$ -diiodoalkanes by  $\alpha$ -anions derived from group 6 carbene complexes has also been described.<sup>5</sup>

A very efficient method for the preparation of chromium aminocarbene complexes is the reaction of  $\text{Cr}(\text{CO})_5^{2-}$  with tertiary amides in the presence of chlorotrimethylsilane.<sup>6</sup> We have recently shown that this methodology can also be utilized for the preparation of iron aminocarbene complexes lacking  $\alpha$ -hydrogens.<sup>7</sup> To the best of our knowledge, this method has never been used for the preparation of ( $\mu$ -bis(aminocarbene))-dimetal complexes. We have therefore studied the reaction of  $\text{Cr}(\text{CO})_5^{2-}$  and  $\text{Fe}(\text{CO})_4^{2-}$  with diamides,

(4) (a) Fischer, E. O.; Röhl, W.; Hoa Tran Huy, N.; Ackermann, K. *Chem. Ber.* **1982**, *115*, 2951. (b) Quy Dao, N.; Fevrier, H.; Jouan, M.; Fischer, E. O.; Röhl, W. *J. Organomet. Chem.* **1984**, *275*, 191. (c) Hoa Tran Huy, N.; Lefloch, P.; Robert, F.; Jeannin, Y. *J. Organomet. Chem.* **1987**, *327*, 211. (d) Anderson, D. M.; Bristow, G. S.; Hitchcock, P. B.; Jasim, H. A.; Lappert, M. F.; Skelton, B. W. *J. Chem. Soc., Dalton Trans.* **1987**, 2843. For recent example, see: Dumas, S.; Lastra, E.; Hegedus, L. S. *J. Am. Chem. Soc.* **1995**, *117*, 3368.

(5) Macomber, D. W.; Madhukar, P. *J. Organomet. Chem.* **1992**, *433*, 279.

(6) (a) Imwinkelried, R.; Hegedus, L. S. *Organometallics* **1988**, *7*, 702. (b) Schwindt, M. A.; Lejon, T.; Hegedus, L. S. *Organometallics* **1990**, *9*, 2814.

(7) Dvořák, D. *Organometallics* **1995**, *14*, 570.

<sup>†</sup> Department of Organic Chemistry.

<sup>‡</sup> Department of Solid State Chemistry.

<sup>®</sup> Abstract published in *Advance ACS Abstracts*, October 1, 1995.

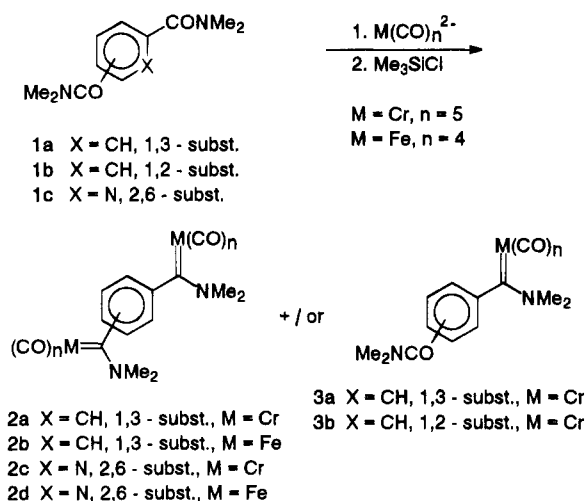
(1) For the most recent review on synthetic applications of transition metal carbene complexes, see: Hegedus, L. S. *Transition Metals in the Synthesis of Complex Organic Molecules*; University Science Books, Mill Valley, CA, 1994; pp 151-197.

(2) For references concerning ( $\mu$ -bis(carbene))homodimetal complexes of chromium, molybdenum, tungsten, manganese, rhenium, and iron see: (a) Macomber, D. W.; Hung, M.-H.; Madhukar, P.; Liang, M.; Rogers, R. D. *Organometallics* **1991**, *10*, 737 and references 5-8 cited therein. (b) Macomber, D. W.; Hung, M.-H.; Verma, A. G.; Rogers, R. D. *Organometallics* **1988**, *7*, 2072. (c) Macomber, D. W.; Hung, J. *Organomet. Chem.* **1989**, *366*, 147. (d) Macomber, D. W.; Madhukar, P.; Rogers, R. D. *Organometallics* **1991**, *10*, 2121. (e) Albrecht, T.; Sauer, J.; Nöth, H. *Tetrahedron Lett.* **1994**, *35*, 561.

(3) The only examples of the reactivity of ( $\mu$ -bis(carbene))dimetal complexes mentioned in the literature are in ref 2b and: Hoa Tran Huy, N.; Lefloch, P. *J. Organomet. Chem.* **1988**, *344*, 303.

**Table 1. Carbene Complexes Prepared by Reaction of  $\text{Cr}(\text{CO})_5^{2-}$  or  $\text{Fe}(\text{CO})_4^{2-}$  with Tertiary Diamides and Chlorotrimethylsilane**

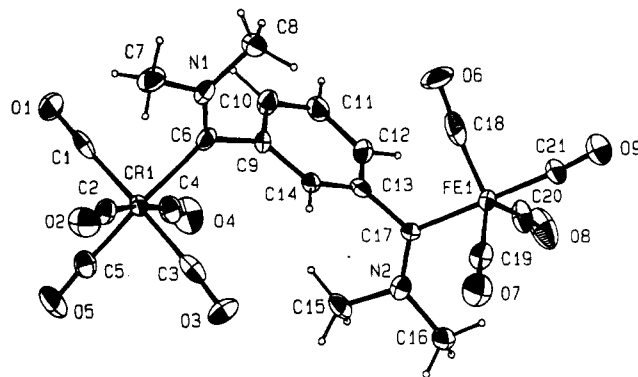
entry	amide	M	ratio $\text{M}(\text{CO})_n^{2-}/$ amide	product (isolated yield, %)
1	1a	Cr	4:1	2a (50.6)
2	1a	Fe	4:1	2b (55.7)
3	1a	Cr	1:1	2a (17.2) 3a (31.9)
4	1b	Cr	4:1	3b (29.7)
5	1c	Cr	4:1	2c (24.8)
6	1c	Fe	4:1	2d (46.5)
7	1d	Cr	4:1	3c (39.0)
8	1e	Cr	4:1	3d (55.1)
9	1f	Cr	4:1	2e (47.5) 3e (12.5)
10	1g	Cr	4:1	2f (16.5) 3f (8.3)
11	3a	Fe	4:1	4 (35.3)

**Scheme 1**

aiming at developing a new route for the preparation of  $(\mu\text{-bis(aminocarbene)})\text{dimetal}$  complexes of chromium and iron.

We chose  $N,N,N',N'$ -tetramethylisophthalamide (**1a**) as a model compound for the reaction of diamides with chromium and iron carbonylate anions in the presence of chlorotrimethylsilane. Aromatic amides have no  $\alpha$ -hydrogens, which is necessary for the successful preparation of the iron aminocarbene complexes.<sup>7</sup> Moreover the 1,3-disubstitution pattern causes no steric hindrance. By this choice we also hoped to avoid solubility problems, which are typical for the 1,4-disubstituted aromatics.

The reaction of diamide **1a** with excess of  $\text{Cr}(\text{CO})_5^{2-}$  in THF followed by addition of chlorotrimethylsilane (Scheme 1) readily afforded the desired  $(\mu\text{-bis(aminocarbene)})\text{dichromium}$  complex **2a** in 50% yield (Table 1, entry 1). Under the same conditions,<sup>8</sup>  $\text{Fe}(\text{CO})_4^{2-}$  gave the corresponding  $(\mu\text{-bis(aminocarbene)})\text{diiron}$  complex **2b** in 55% yield (Table 1, entry 2). When **1a** was treated with  $\text{Cr}(\text{CO})_5^{2-}$  in 1:1 molar ratio, besides the  $(\mu\text{-bis(aminocarbene)})\text{dichromium}$  complex **2a**, the aminocarbene **3a** was also isolated in a modest yield (Table 1, entry 3). Interestingly, the latter complex can easily

**Figure 1. Molecular structure of complex 4.****Table 2. Selected Bond Lengths (Å) and Bond Angles (deg) for Complex 4**

Cr(1)–C(1)	1.91(2)	Cr(1)–C(2)	1.87(1)
Cr(1)–C(3)	1.90(2)	Cr(1)–C(4)	1.87(1)
Cr(1)–C(5)	1.87(2)	Cr(1)–C(6)	2.15(1)
Fe(1)–C(17)	2.00(1)	Fe(1)–C(18)	1.78(2)
Fe(1)–C(19)	1.78(1)	Fe(1)–C(20)	1.76(1)
Fe(1)–C(21)	1.79(2)	O(1)–C(1)	1.16(2)
O(2)–C(2)	1.18(2)	O(3)–C(3)	1.17(2)
O(4)–C(4)	1.18(2)	O(5)–C(5)	1.15(2)
O(6)–C(18)	1.19(3)	O(7)–C(19)	1.11(2)
O(8)–C(20)	1.16(2)	O(9)–C(21)	1.13(2)
N(1)–C(6)	1.30(2)	N(1)–C(7)	1.47(2)
N(1)–C(8)	1.45(2)	N(2)–C(15)	1.50(2)
N(2)–C(16)	1.42(2)	N(2)–C(17)	1.32(2)
C(2)–Cr(1)–C(1)	91.0(6)	C(3)–Cr(1)–C(1)	177.4(5)
C(3)–Cr(1)–C(2)	87.1(5)	C(4)–Cr(1)–C(1)	92.1(6)
C(4)–Cr(1)–C(2)	173.2(7)	C(4)–Cr(1)–C(3)	89.7(5)
C(5)–Cr(1)–C(1)	89.6(5)	C(5)–Cr(1)–C(2)	88.8(6)
C(5)–Cr(1)–C(3)	88.5(6)	C(5)–Cr(1)–C(4)	85.2(6)
C(6)–Cr(1)–C(1)	90.4(5)	C(6)–Cr(1)–C(2)	97.0(5)
C(6)–Cr(1)–C(3)	91.6(5)	C(6)–Cr(1)–C(4)	89.1(5)
C(6)–Cr(1)–C(5)	174.2(5)	C(18)–Fe(1)–C(17)	93.3(5)
C(19)–Fe(1)–C(17)	89.2(5)	C(19)–Fe(1)–C(18)	115.5(6)
C(20)–Fe(1)–C(17)	87.0(5)	C(20)–Fe(1)–C(18)	123.7(7)
C(20)–Fe(1)–C(19)	120.8(7)	C(21)–Fe(1)–C(17)	177.7(5)
C(21)–Fe(1)–C(18)	86.6(6)	C(21)–Fe(1)–C(19)	92.9(6)
C(21)–Fe(1)–C(20)	91.0(6)	C(7)–N(1)–C(6)	122.6(12)
C(8)–N(1)–C(6)	124.9(11)	C(8)–N(1)–C(7)	112.4(10)
C(16)–N(2)–C(15)	112.7(10)	C(17)–N(2)–C(15)	120.9(10)
C(17)–N(2)–C(16)	126.4(11)	N(1)–C(6)–Cr(1)	130.8(9)
C(9)–C(6)–Cr(1)	113.8(8)	C(9)–C(6)–N(1)	115.1(11)
N(2)–C(17)–Fe(1)	125.9(8)	C(13)–C(17)–Fe(1)	117.2(8)
C(13)–C(17)–N(2)	116.8(10)		

be converted to the mixed chromium–iron  $\mu\text{-bis(aminocarbene)}$  complex **4** in 35% yield by the reaction with an excess of tetracarbonylferrate and chlorotrimethylsilane (Table 1, entry 11).

The reaction of *o*-phthalic diamide **1b** with  $\text{Cr}(\text{CO})_5^{2-}$  gave the monocarbene complex **3b** as the only product even when excess of the carbonylate anion was employed (Table 1, entry 4). The steric bulk of  $\text{Cr}(\text{CO})_5$  group apparently prevents reaction with the second amidic group.

The structure of the mixed  $\mu\text{-bis(aminocarbene)}$  complex **4** was confirmed by single-crystal X-ray crystallography. The molecular structure and atom-labeling scheme is presented in Figure 1, whereas selected bond distances and angles are summarized in Table 2. The complex **4** shows structural features typical for other aminocarbene complexes of chromium<sup>9</sup> and iron<sup>10</sup> with metal–carbene bonds perpendicular to the plane of the

(8) It is necessary to use  $\text{Fe}(\text{CO})_4^{2-}$ , prepared by reduction of  $\text{Fe}(\text{CO})_5$  with sodium naphthalenide in THF. The commercial product solvated by dioxane is insoluble in THF and therefore useless for this reaction (cf. ref 7).

(9) Schubert, U. *Coord. Chem. Rev.* **1984**, *55*, 261.

(10) Huttner, G.; Gartzke, W. *Chem. Ber.* **1972**, *105*, 2714.



benzene ring and with the bulky metallocarbonyl groups pointing to the opposite faces of the aromatic ring.

To establish the scope of the reaction we further turned our attention to binaphthyl-derived bis(amide) **1d**, *N,N,N',N'*-tetramethyl-2,6-pyridinedicarboxamide (**1c**), and amides of furane-2,5-dicarboxylic acid. The binaphthyl bis(amide) **1d** behaved similarly to the *o*-phthalic diamide **1b** in the reaction with  $\text{Cr}(\text{CO})_5^{2-}$  giving monocarbene complex **3c** as the only carbene product (Table 1, entry 7). On the contrary, no carbene complex was formed in the reaction of bis(amide) **1d** with  $\text{Fe}(\text{CO})_4^{2-}$ . Pyridine bis(amide) **1c** reacted readily with both  $\text{Cr}(\text{CO})_5^{2-}$  and  $\text{Fe}(\text{CO})_4^{2-}$  with formation of bis(carbene) complexes **2c** in low and **2d** in good yields (Table 1, entries 5 and 6). On the other hand, *N,N,N',N'*-tetramethyl-, *N,N,N',N'*-tetrabutyl-, and the bis(morpholine) amide of furane-2,5-dicarboxylic acid failed to give any carbene product in reaction with both  $\text{Fe}(\text{CO})_4^{2-}$  and  $\text{Cr}(\text{CO})_5^{2-}$ .<sup>11</sup>

The ( $\mu$ -bis(aminocarbene))dimetal complexes prepared from aromatic amides are yellow solids which decompose upon heating without melting. The <sup>1</sup>H-NMR spectra of these compounds show, as expected, two separate signals for the methyl groups of the *N,N*-dimethylamino substituent at  $\sigma \sim 3.1$  and 4.0 ppm, with the chemical shifts very similar for all the complexes prepared. For the aromatic region, a large upfield shift of the protons next to the carbene moiety is characteristic. This shift is 0.92 ppm for 4-H and 6-H and 1.37 ppm for the 2-H of the bis(chromium carbene) complex **2a**, which contrasts with the bis(amide) **1a**, whose aromatic protons form a singlet at 7.45 ppm. For the bis(iron aminocarbene) complex **2b**, these values are somewhat lower (0.79 and 1.13), and the corresponding upfield shifts for the mixed complex **4** fall between those for **2a** and **2b** (0.80 and 0.87 ppm for the 4-H and 6-H and 1.26 ppm for the 2-H). At the same time the chemical shift of the aromatic proton in 5-position remains practically unchanged as for the starting bis(amide) **1a** (7.42 ppm). Similar effects can be seen in the <sup>13</sup>C NMR spectra. Thus, for example, the aromatic carbons C-4 and C-6 in the bis(chromium carbene) complex **2a** have chemical shifts down at 11.17 ppm and the C-2 even at 16.01 ppm compared to the corresponding amide **1a**. At the same time, the change of chemical shift of C-5 is <1 ppm. Similar but less profound effects in the NMR spectra of the monocarbene complexes of chromium are known<sup>12</sup> and were attributed to the steric interactions of an aromatic ring with the rest of the molecule.<sup>13</sup>

Aliphatic diamides derived from oxalic<sup>14</sup> and malonic acids failed to give any isolable carbene product which,

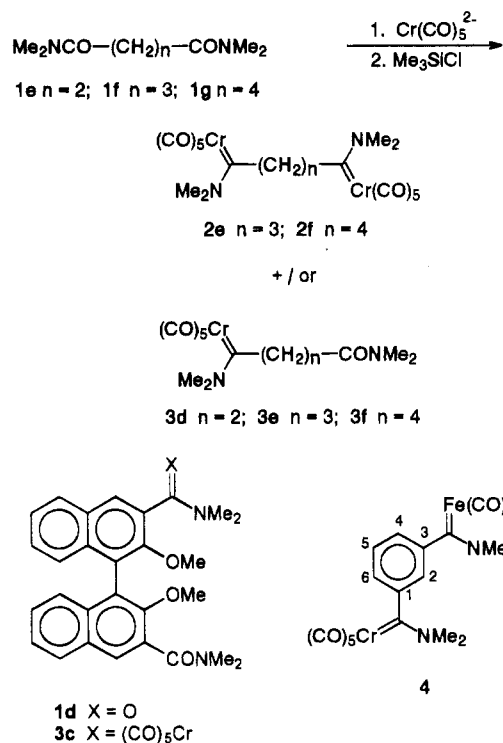
(11) In principle, this unreactivity might be a result of low solubility in the case of tetramethyl bis(amide) and steric hindrance in the case of tetrabutyl bis(amide) of furane-2,5-dicarboxylic acid. But the failure to react with the bis(morpholine) of 2,5-furandicarboxylic acid, which is reasonably soluble (approximately 2.5 g/100 mL THF), together with the fact that morpholine amides of monocarboxylic acids react smoothly with both  $\text{Cr}(\text{CO})_5^{2-}$  and  $\text{Fe}(\text{CO})_4^{2-}$  (refs 6a and 7), indicates that the reason for the observed behavior is the presence of disubstituted furane itself.

(12) Connor, J. A.; Jones, E. M.; Randall, E. W.; Rosenberg, E. J. *Chem. Soc., Dalton Trans.* **1972**, 2419.

(13) For further discussion of this phenomenon, see also note 29 in: Aoki, S.; Fujimura, T.; Nakamura, E. *J. Am. Chem. Soc.* **1992**, *114*, 2985.

(14) [ $\mu$ -1,2-bis(diethylamino)ethanediyldiene]bis(pentacarbonylchromium) is a known compound: Fischer, O. E.; Wittmann, D.; Himmelreich, D.; Neugebauer, D. *Angew. Chem., Int. Ed. Engl.* **1982**, *21*, 444.

## Scheme 2



in the latter case, may be due to deprotonation of the malonic acid diamide by the relatively strongly basic  $\text{Cr}(\text{CO})_5^{2-}$ . *N,N,N',N'*-Tetramethylsuccinamide (**1e**) reacted similarly to *N,N,N',N'*-tetramethylphthalamide (**1b**) to afford the monocarbene complex **3d** as the only product (Scheme 2), even if a large excess of  $\text{Cr}(\text{CO})_5^{2-}$  was used (Table 1, entry 8). This is rather surprising, because diamide **1e** is much more flexible than **1b** so that a smooth formation of the ( $\mu$ -bis(aminocarbene))-dichromium complex could be expected. *N,N,N',N'*-tetramethylglutaramide (**1f**) gave a mixture of both bis(aminocarbene)dichromium complex **2e** and monocarbene complex **3e** with former as the main product (Table 1, entry 9). *N,N,N',N'*-tetramethyladipamide (**1g**) behaved as expected, giving the ( $\mu$ -bis(aminocarbene))-dichromium complex **2f** in moderate yield. A small amount of monocarbene complex **3f** was also formed<sup>15</sup> (Table 1, entry 10). The structure of our aliphatic chromium carbene complexes thus obtained is confirmed by the <sup>1</sup>H-NMR and IR spectra.

In conclusion, the reaction of tertiary unhindered bis(amides) with  $\text{Cr}(\text{CO})_5^{2-}$  has been developed as a method for the preparation of ( $\mu$ -bis(aminocarbene))-dichromium complexes. Similarly,  $\text{Fe}(\text{CO})_4^{2-}$  can be used for the preparation of ( $\mu$ -bis(aminocarbene))-diiron complexes from aromatic diamides.

## Experimental Section

Melting points were determined on a Kofler block and are uncorrected. Unless otherwise noted, all <sup>1</sup>H NMR spectral

(15) To confirm the surprising outcome that succinamide **1e** gives exclusively monocarbene complex **3d** while the analogous reaction of the adipamide **1g** gives predominantly the bis(carbene) **2f**, a control experiment with an equimolar mixture of **1e** and **1g** and 4 equiv of  $\text{Cr}(\text{CO})_5^{2-}$  was done. Again no succinamide-derived bis(carbene) was formed. Interestingly, the yield of crude adipamide-derived bis(carbene) **2f** was higher (75%) compared to the nonmixed experiment in this case. This might be a result of the relatively higher amount of  $\text{Cr}(\text{CO})_5^{2-}$  in the reaction mixture (only 1 equiv of  $\text{Cr}(\text{CO})_5^{2-}$  reacts with **1e**).

**Table 3. Structure Determination Summary**

empirical formula	C <sub>21</sub> H <sub>16</sub> CrFeN <sub>2</sub> O <sub>9</sub>
fw	548.21
temp, K	293
diffractometer and radiation used	Enraf-Nonius CAD4, graphite monochromator, Cu K $\alpha$ ( $\lambda = 1.5418 \text{ \AA}$ )
scan technique	$\omega/2\theta$
cryst syst	orthorhombic
space group	$P2_12_12_1$
unit cell dimens, $\text{\AA}$	
<i>a</i>	6.464(2)
<i>b</i>	13.373(1)
<i>c</i>	27.27(8)
cell vol, $\text{\AA}^3$	2357(1)
<i>Z</i>	4
<i>d</i> (calcd), $\text{Mg/m}^3$	1.545
abs coef, $\text{mm}^{-1}$	9.29
abs corr	$\psi$ -scan
<i>F</i> (000)	1112
cryst dimens, mm	$0.8 \times 0.5 \times 0.2$
no. of reflcns used for cell determination	15
$\theta$ range for reflcns used for cell determination, deg	35–40
interval of std reflcns monitoring, min	120
intensity fluctuation	–1%
tot. no. of reflcns measd	3136
$2\theta$ range, deg	1–100
<i>h</i>	0 to 6
<i>k</i>	0 to 13
<i>l</i>	–27 to 27
no. of unique reflcns obsd	2888 (Friedel pairs not merged)
criterion for obsd reflcns	$I > 1.96\sigma(I)$
function minimized	$w( F_o  -  F_c )^2$
weighting scheme	Chebyshev series based on $F_o/F_c(\text{max})$ and $F_o - F_c$ , scheme 15 <sup>17</sup>
params refined	308
<i>R</i> , %	9.7
<i>R</i> <sub>w</sub> , %	11.5
<i>S</i>	1.13
max shift/esd	0.02
max and min heights in final $\Delta\rho$ map ( $\text{e}\cdot\text{\AA}^{-3}$ )	–0.92 to 0.72
programs used	SIR92, <sup>16</sup> CRYSTALS <sup>17</sup>

data were recorded in CDCl<sub>3</sub> at 300 MHz and chemical shifts are reported relative to TMS. <sup>13</sup>C NMR spectra were recorded at 75.46 MHz. Elemental analyses were performed by the analytical departments of UOCHB-AVČR and Prague Technical University. All experiments were carried out under argon. Tetrahydrofuran was distilled from benzophenone ketyl under the nitrogen atmosphere prior to use. Iron pentacarbonyl, chromium hexacarbonyl, and chlorotrimethylsilane were obtained from Aldrich and used without further purification. Neutral aluminum oxide (Brockman III grade) and silica were obtained from Lachema. Amides **1a–d** were prepared from acid chlorides and dimethylamine in ether. The yields are based on the starting amides.

**X-ray Data Collection, Structure Determination, and Refinement for Compound 4.** The single crystal suitable for the measurement was obtained by diffusion of pentane vapors into a toluene solution of **4** at room temperature. All pertinent data are summarized in Table 3. Data were corrected for Lorentz–polarization factors. Due to a high absorption caused by the wavelength used for the measurement, and the presence of Cr and Fe atoms in the molecule, it was necessary to use a correction of absorption based on a  $\psi$  scan of five reflections. The structure was solved by direct methods by the use of SIR92 program.<sup>16</sup> Because of the nonsymmetry of the  $P2_12_12_1$  space group the Cr and Fe atoms show high

**Table 4. Fractional and Thermal Parameters ( $\text{\AA}^2$ ) for Compound 4**

atom	<i>x/a</i>	<i>y/b</i>	<i>z/c</i>	<i>U</i> (iso)
Cr(1)	0.5257(3)	0.6381(1)	0.39444(7)	0.036(1)
Fe(1)	0.3586(3)	1.1933(1)	0.37119(6)	0.035(1)
O(1)	0.711(3)	0.4893(9)	0.3209(5)	0.070(7)
O(2)	0.130(2)	0.518(1)	0.4065(4)	0.073(6)
O(3)	0.340(2)	0.7745(8)	0.4735(4)	0.066(6)
O(4)	0.936(2)	0.749(1)	0.4041(6)	0.080(7)
O(5)	0.689(2)	0.5132(9)	0.4785(5)	0.068(6)
O(6)	0.305(2)	1.091(1)	0.2752(4)	0.067(7)
O(7)	0.028(2)	1.162(1)	0.4409(5)	0.080(7)
O(8)	0.716(3)	1.317(1)	0.3952(7)	0.088(9)
O(9)	0.152(3)	1.360(1)	0.3220(5)	0.079(7)
N(1)	0.314(2)	0.7178(7)	0.2978(4)	0.043(5)
N(2)	0.570(1)	1.0743(7)	0.4485(4)	0.039(5)
C(1)	0.639(3)	0.545(1)	0.3482(6)	0.048(8)
C(2)	0.281(2)	0.5639(9)	0.3983(5)	0.046(7)
C(3)	0.408(2)	0.725(1)	0.4420(6)	0.051(8)
C(4)	0.775(2)	0.709(1)	0.3984(5)	0.051(8)
C(5)	0.633(2)	0.5609(9)	0.4459(6)	0.049(7)
C(6)	0.431(2)	0.7347(9)	0.3357(4)	0.037(6)
C(7)	0.209(3)	0.622(1)	0.2898(5)	0.055(7)
C(8)	0.274(2)	0.7888(9)	0.2589(4)	0.048(6)
C(9)	0.533(2)	0.8322(8)	0.3362(4)	0.034(5)
C(10)	0.712(2)	0.8477(9)	0.3067(5)	0.041(6)
C(11)	0.818(2)	0.937(1)	0.3107(5)	0.049(7)
C(12)	0.760(2)	1.0105(8)	0.3413(4)	0.041(6)
C(13)	0.585(2)	0.9986(8)	0.3694(4)	0.038(6)
C(14)	0.470(2)	0.9092(7)	0.3662(4)	0.033(5)
C(15)	0.688(2)	0.986(1)	0.4672(5)	0.048(7)
C(16)	0.535(2)	1.1475(9)	0.4854(4)	0.044(6)
C(17)	0.515(2)	1.0803(7)	0.4021(4)	0.032(5)
C(18)	0.328(2)	1.129(1)	0.3143(7)	0.06(1)
C(19)	0.157(2)	1.1749(8)	0.4147(5)	0.032(6)
C(20)	0.572(2)	1.2694(9)	0.3851(6)	0.045(8)
C(21)	0.228(2)	1.296(1)	0.3427(5)	0.049(7)

anomalous dispersion and therefore the Friedel pairs were not merged. Refinement of parameters was achieved by the program CRYSTALS<sup>17</sup> (full-matrix refinement with hydrogen atoms fixed in positions found for geometry  $U(\text{iso}) = U(\text{eq})$  for the corresponding atom). The molecule **4** does not contain chiral centers, but the determination of the absolute configuration of the crystal should give the proper configuration of the molecules forming the studied crystal. However, the attempt to establish the absolute configuration by the refining of Flack's parameter was unsuccessful. The final value of Flack's parameter after refinement was 0.45(2). Final atomic coordinates are collected in Table 4.

***N,N,N,N'*-Tetramethylisophthalamide (1a):** <sup>1</sup>H NMR  $\delta$  2.96 (s, 6, CH<sub>3</sub>), 3.10 (s, 6, CH<sub>3</sub>), 7.45 (s, 4, ArH); <sup>13</sup>C NMR  $\delta$  35.88 (q, CH<sub>3</sub>), 40.10 (q, CH<sub>3</sub>), 126.16 (d, C-arom), 128.67 (d, C-arom); 129.11 (d, C-arom), 137.14 (s, C-arom), 171.26 (s, C=O).

**(CO)<sub>5</sub>Cr[ $\mu$ -1,3-(C(NMe<sub>2</sub>)<sub>2</sub>)<sub>2</sub>C<sub>6</sub>H<sub>4</sub>(C(NMe<sub>2</sub>)<sub>2</sub>)]Cr(CO)<sub>5</sub> (2a).** To a suspension of chromium hexacarbonyl (2.2 g, 10 mmol) in THF (10 mL) was added a 0.78 M THF solution of sodium naphthalenide (32 mL, 25 mmol) at –78 °C via canula, and the mixture was allowed to warm to 0 °C. After stirring at this temperature for 0.5 h, a solution of *N,N,N,N'*-tetramethylisophthalamide (0.55 g, 2.5 mmol) in THF (10 mL) was added, the reaction mixture was kept at 0 °C for another 0.5 h and then cooled to –78 °C, and then chlorotrimethylsilane (2 mL, 15.7 mmol) was added via syringe. The resulting mixture was stirred at –78 °C for 30 min and then allowed to warm slowly (1 h) to room temperature. Neutral alumina (8 g) was added, and the THF was evaporated. Chromatography on silica (130 g, hexane, then hexane–dichloromethane, 2:1) gave crude product (0.81 g). Crystallization (*n*-heptane–dichloromethane) afforded 0.724 g (50.6%) of a yellow solid: <sup>1</sup>H NMR  $\delta$  3.17 (s, 3, CH<sub>3</sub>), 4.00 (s, 3, CH<sub>3</sub>), 6.08 (s, 1, ArH), 6.53 (d, *J* = 7.2 Hz, 2, ArH), 7.42 (t, *J* = 7.5 Hz, 1, ArH); <sup>13</sup>C

(16) Altomare, A.; Burla, M. C.; Camalli, M.; Cascarano, G.; Giacovazzo, C.; Guagliardi, A.; Polidori, G. *J. Appl. Crystallogr.* **1994**, *27*, 435.

(17) Watkin, D. J. CRYSTALS, University of Oxford, 1990.

NMR  $\delta$  47.10 (q, CH<sub>3</sub>), 52.22 (q, CH<sub>3</sub>), 110.15 (d, C-arom), 117.50 (d, C-arom), 129.98 (d, C-arom), 153.88 (s, C-arom), 217.88 (s, *cis* CO), 224.15 (s, *trans* CO), 274.16 (s, C=Cr); IR (CCl<sub>4</sub>)  $\nu$  2053 (m), 1968 (m), 1936 (s), 1923 (s, sh) cm<sup>-1</sup>. Anal. Calcd for C<sub>22</sub>H<sub>16</sub>Cr<sub>2</sub>N<sub>2</sub>O<sub>10</sub>: C, 46.17; H, 2.82; N, 4.89. Found: C, 45.96; H, 2.84; N, 4.95.

(CO)<sub>4</sub>Fe[ $\mu$ -1,3-(C(NMe<sub>2</sub>)<sub>2</sub>)C<sub>6</sub>H<sub>4</sub>(C(NMe<sub>2</sub>)<sub>2</sub>)]Fe(CO)<sub>4</sub> (**2b**). The same procedure as for **2a** starting from Fe(CO)<sub>5</sub> (1.4 mL, 10 mmol), a 0.75 M THF solution of sodium naphthalene (32 mL, 24 mmol), and diamide **1a** (0.55 g, 2.5 mmol) gave after chromatography on neutral alumina (120 g) and crystallization from an *n*-heptane-dichloromethane mixture 0.73 g (55.7%) of pure **2b**: <sup>1</sup>H NMR  $\delta$  3.19 (s, 6, 2CH<sub>3</sub>), 4.02 (s, 6, 2CH<sub>3</sub>), 6.32 (s, 1, ArH), 6.67 (d, *J* = 7.7 Hz, 2, ArH), 7.41 (t, 1, *J* = 7.7 Hz, ArH); <sup>13</sup>C NMR  $\delta$  47.00 (q, CH<sub>3</sub>), 51.11 (q, CH<sub>3</sub>), 112.69 (d, C-arom), 118.94 (d, C-arom), 129.98 (d, C-arom), 154.13 (s, C-arom), 215.40 (s, CO), 258.54 (s, C=Fe); IR (CCl<sub>4</sub>)  $\nu$  2042 (m), 1970 (w), 1936 (s), 1927 (m, sh) cm<sup>-1</sup>. Anal. Calcd for C<sub>20</sub>H<sub>16</sub>Fe<sub>2</sub>N<sub>2</sub>O<sub>8</sub>: C, 45.84; H, 3.08, N, 5.35. Found: C, 46.06; H, 3.09; N, 5.32.

(CO)<sub>5</sub>Cr[C(NMe<sub>2</sub>)<sub>2</sub>(3-(Me<sub>2</sub>NCO)C<sub>6</sub>H<sub>4</sub>)] (**3a**). To a solution of Cr(CO)<sub>5</sub><sup>2-</sup>, prepared by reduction of chromium hexacarbonyl (2.2 g, 10 mmol) with a 0.75 M THF solution of sodium naphthalene (38 mL, 28.5 mmol) as described for **2a**, was added a solution of bis(amide) **1a** (2.2 g, 10 mmol) in THF (70 mL) at -78 °C. The mixture was allowed to warm to 0 °C, kept at this temperature for 0.5 h, and then again cooled to -78 °C, and chlorotrimethylsilane (4 mL, 31.5 mmol) was added via syringe. The reaction mixture was allowed to warm to 0 °C, alumina (16 g) was then added, and THF was evaporated. The residue was suspended in *n*-hexane (50 mL) and transferred to the top of a column filled with 65 g of silica. Naphthalene was washed out by hexane, then bis(carbene) **2a** (0.985 g, 17.2%) was eluted with *n*-heptane and dichloromethane (2:1), and finally **3a** (1.266 g, 31.9%) was washed out by dichloromethane-ethyl acetate (2:1) mixture. Carbene **3a** was a yellow oil, which solidified after several weeks in the refrigerator: mp 63-67 °C; <sup>1</sup>H NMR  $\delta$  2.98 (br s, 3, CH<sub>3</sub> amide), 3.08 (s, 6, CH<sub>3</sub> carbene), 3.11 (s, 3, CH<sub>3</sub> amide), 3.99 (s, 3, CH<sub>3</sub> carbene), 6.73 (s, 1, ArH), 6.78 (d, *J* = 7.7 Hz, 1, ArH), 7.21 (d, *J* = 7.7 Hz, 1, ArH), 7.44 (t, *J* = 7.7 Hz, 1, ArH); IR (CCl<sub>4</sub>)  $\nu$  2054 (s), 1970 (m), 1932 (vs), 1641 (s) cm<sup>-1</sup>. Anal. Calcd for C<sub>17</sub>H<sub>16</sub>CrN<sub>2</sub>O<sub>6</sub>: C, 51.51; H, 4.07; N, 7.07. Found: C, 51.53; H, 4.08; N, 7.36.

(CO)<sub>5</sub>Cr[C(NMe<sub>2</sub>)<sub>2</sub>(2-(Me<sub>2</sub>NCO)C<sub>6</sub>H<sub>4</sub>)] (**3b**). The same procedure as for **2a** starting from Cr(CO)<sub>5</sub> (2.2 g, 10 mmol), a 0.78 M THF solution of sodium naphthalene (30 mL, 23.4 mmol), and diamide **1b** (0.55 g, 2.5 mmol) furnished 0.816 g of crude product, which gave, after crystallization from an *n*-heptane-dichloromethane mixture, 0.294 g (29.7%) of **3b**: <sup>1</sup>H NMR  $\delta$  3.02 (s, 3, CH<sub>3</sub> amide), 3.15 (s, 3, CH<sub>3</sub> carbene), 3.16 (s, 3, CH<sub>3</sub> amide), 3.92 (s, 3, CH<sub>3</sub> carbene), 6.75 (d, *J* = 7.8 Hz, 1, ArH), 7.16 (t, *J* = 7.4 Hz, 1, ArH), 7.29 (d, *J* = 7.4 Hz, 1, ArH), 7.42 (t, *J* = 7.7 Hz, 1, ArH); IR  $\nu$  2053 (w), 1983 (w), 1966 (w), 1934 (s), 1919 (s), 1637 (w) cm<sup>-1</sup>. Anal. Calcd for C<sub>17</sub>H<sub>16</sub>CrN<sub>2</sub>O<sub>6</sub>: C, 51.51; H, 4.07; N, 7.07. Found: C, 51.81; H, 4.14; N, 6.87.

*N,N,N',N'*-Tetramethyl-2,6-pyridinedicarboxamide (**1c**): <sup>1</sup>H NMR  $\delta$  3.04 (s, 3, CH<sub>3</sub>), 3.13 (s, 3, CH<sub>3</sub>), 7.65 (d, *J* = 7.8 Hz, 2, PyH), 7.88 (t, *J* = 7.6 Hz, 1, PyH); <sup>13</sup>C NMR  $\delta$  36.33 (q, CH<sub>3</sub>), 39.64 (q, CH<sub>3</sub>), 124.62 (d, Py), 138.68 (d, Py), 153.80 (s, Py), 168.88 (s, C=O).

(CO)<sub>5</sub>Cr[ $\mu$ -2,6-(C(NMe<sub>2</sub>)<sub>2</sub>)C<sub>6</sub>H<sub>3</sub>N(C(NMe<sub>2</sub>)<sub>2</sub>)]Cr(CO)<sub>5</sub> (**2c**). The same procedure as for **2a** starting from Cr(CO)<sub>5</sub> (2.2 g, 10 mmol), a 0.78 M THF solution of sodium naphthalene (32 mL, 25 mmol), and diamide **1c** (0.553 g, 2.5 mmol) in 20 mL of THF gave after chromatography on silica (70 g, *n*-heptane, *n*-heptane-dichloromethane, 1:1 mixture) 0.380 g of crude product. Further purification by radial-layer chromatography (Chromatotron) under argon (heptane, ether, acetone, methanol, 50:30:17:3) afforded 0.355 g (24.8%) of pure **2c** as yellow crystals: <sup>1</sup>H NMR  $\delta$  3.21 (s, 3, CH<sub>3</sub>), 4.00 (s, 3, CH<sub>3</sub>), 6.62 (d,

*J* = 8 Hz, 2, PyH), 7.77 (t, *J* = 8 Hz, 1, PyH); <sup>13</sup>C NMR  $\delta$  47.73 (q, CH<sub>3</sub>), 51.97 (q, CH<sub>3</sub>), 113.69 (d, Py), 138.07 (d, Py), 161.23 (s, Py), 217.85 (s, *cis* CO), 224.20 (s, *trans* CO), 271.16 (s, C=Cr); IR (CHCl<sub>3</sub>)  $\nu$  2054 (m), 1974 (w), 1932 (s) cm<sup>-1</sup>. Anal. Calcd for C<sub>21</sub>H<sub>15</sub>Cr<sub>2</sub>N<sub>3</sub>O<sub>10</sub>: C, 43.99; H, 2.64; N, 7.33. Found: C, 43.88; H, 2.79; N, 7.25.

(CO)<sub>4</sub>Fe[ $\mu$ -2,6-(C(NMe<sub>2</sub>)<sub>2</sub>)C<sub>6</sub>H<sub>3</sub>N(C(NMe<sub>2</sub>)<sub>2</sub>)]Fe(CO)<sub>4</sub> (**2d**). Fe(CO)<sub>5</sub> (1.4 mL, 10 mmol) was added via syringe to a solution of sodium naphthalene prepared from sodium (0.60 g, 26 mmol) and naphthalene (3.5 g, 27 mmol) in THF (50 mL) at -60 °C. The mixture was allowed to warm to 0 °C. After being stirred at this temperature for 15 min, the solution was cooled to -78 °C, amide **1c** (0.553 g, 2.5 mmol) in 15 mL of THF was added, and the mixture was allowed to reach 0 °C and kept at this temperature for another 15 min. Then 20 mL of THF was added, the solution was cooled to -78 °C, and chlorotrimethylsilane (2.5 mL, 19.6 mmol) was added via syringe. The resulting mixture was allowed to warm to room temperature (1 h), neutral alumina (8 g) was added, and the THF was evaporated. Chromatography on alumina (150 g, *n*-heptane, *n*-heptane-dichloromethane, 2:1) gave 0.760 g of crude product. Crystallization from an *n*-heptane-dichloromethane mixture afforded 0.611 g (46.5%) of a yellow solid: <sup>1</sup>H NMR  $\delta$  3.22 (s, 3, CH<sub>3</sub>), 4.02 (s, 3, CH<sub>3</sub>), 6.90 (d, *J* = 7 Hz, 2, PyH), 7.81 (t, *J* = 7 Hz, 1, PyH); <sup>13</sup>C NMR  $\delta$  47.22 (q, CH<sub>3</sub>), 51.12 (q, CH<sub>3</sub>), 117.06 (d, C-Py), 138.32 (d, C-Py), 166.84 (s, C-Py), 215.18 (s, CO), 255.10 (s, C=Fe); IR (CHCl<sub>3</sub>)  $\nu$  2042 (s), 1968 (m), 1939 (vs) cm<sup>-1</sup>. Anal. Calcd for C<sub>19</sub>H<sub>15</sub>Fe<sub>2</sub>N<sub>3</sub>O<sub>8</sub>: C, 43.47; H, 2.88; N, 8.00. Found: C, 43.28; H, 3.02; N, 7.94.

**Bis(amide) 1d**: Mp 210 °C (EtOH-H<sub>2</sub>O); <sup>1</sup>H NMR  $\delta$  2.96 (s, 6, 2CH<sub>3</sub>), 3.20 (s, 6, CH<sub>3</sub>), 3.35 (bs, 3, CH<sub>3</sub>), 3.68 (bs, 3, CH<sub>3</sub>), 7.12-7.22 (m, 1, ArH), 7.24-7.32 (m, 3, ArH), 7.39-7.47 (m, 2, ArH), 7.87-8.01 (m, 4, ArH); <sup>13</sup>C NMR  $\delta$  35.55 (q, NCH<sub>3</sub>-amide), 38.97 (q, NCH<sub>3</sub>-amide), 62.09 (q, OCH<sub>3</sub>), 125.95 (d, Ar), 127.78 (d, Ar), 128.89 (d, Ar), 130.81 (s, Ar), 134.73 (s, Ar), 170.01 (s, CO); IR (CHCl<sub>3</sub>)  $\nu$  3010 (m), 2942 (w), 2878 (w), 1627 (vs), 1501 (m), 1459 (m), 1398 (m), 1354 (w) cm<sup>-1</sup>. Anal. Calcd for C<sub>28</sub>H<sub>28</sub>N<sub>2</sub>O<sub>4</sub>·H<sub>2</sub>O: C, 70.87; H, 6.37; N, 5.90. Found: C, 70.49; H, 6.50; N, 5.81.

**Carbene Complex 3c**. To the solution of Cr(CO)<sub>5</sub><sup>2-</sup>, prepared by reduction of chromium hexacarbonyl (0.88 g, 4 mmol) with a 0.80 M THF solution of sodium naphthalene (13 mL, 10.4 mmol) as described for **2a**, was added a solution of bis(amide) **1d** (0.456 g, 1 mmol) in THF at -78 °C. The mixture was allowed to warm to 0 °C, kept at this temperature for 0.5 h, and then again cooled to -78 °C, and chlorotrimethylsilane (0.8 mL, 6 mmol) was added via syringe. The reaction mixture was allowed to warm to 0 °C, alumina (4 g) was added, and THF was evaporated. Chromatography of the residue on silica (30 g) using gradually *n*-heptane, *n*-heptane-dichloromethane (2:1 and 1:1), and finally dichloromethane-ethyl acetate (1:1) mixtures gave crude **5**, which was further purified by chromatography on silica using an *n*-heptane-ether-acetone-methanol (50:30:17:3) mixture. By this way 0.27 g (39%) of carbene **5** was obtained as a clathrate with *n*-heptane in the form of yellow crystals: Mp 192-195 °C; <sup>1</sup>H NMR  $\delta$  0.88 (t, *J* = 7 Hz, 3, CH<sub>3</sub>-heptane), 1.27 (bs, 5, CH<sub>2</sub>-heptane), 2.94 (bs, 3, NCH<sub>3</sub>-amide), 3.19 (s, 3, CH<sub>3</sub>), 3.21 (s, 3, CH<sub>3</sub>), 3.22 (s, 3, CH<sub>3</sub>), 3.43 (bs, 3, NCH<sub>3</sub>-amide), 4.05 (s, 3, NCH<sub>3</sub>-carbene), 6.95-7.25 (m, 2, ArH), 7.3-7.5 (m, 4, ArH), 7.8-8.05 (m, 4, ArH); <sup>13</sup>C NMR (selected signals)  $\delta$  14.74 (q, CH<sub>3</sub>-heptane), 23.32 (t, CH<sub>2</sub>-heptane), 29.63 (t, CH<sub>2</sub>-heptane), 32.51 (t, CH<sub>2</sub>-heptane), 35.69 (q, NCH<sub>3</sub>-amide), 39.07 (q, NCH<sub>3</sub>-amide), 46.35 (q, NCH<sub>3</sub>-carbene), 51.82 (q, NCH<sub>3</sub>-carbene), 60.61 (q, OCH<sub>3</sub>), 62.08 (q, OCH<sub>3</sub>), 169.97 (s, CON(CH<sub>3</sub>)<sub>2</sub>), 218.22 (s, *cis* CO), 224.22 (s, *trans* CO), 271.84 (s, C=Cr); IR (CHCl<sub>3</sub>)  $\nu$  2053 (m), 1971 (w), 1928 (br s), 1627 (w) cm<sup>-1</sup>. Anal. Calcd for 2C<sub>33</sub>H<sub>28</sub>CrN<sub>2</sub>O<sub>8</sub>·C<sub>7</sub>H<sub>16</sub>: C, 64.22; H, 5.32; N, 4.10. Found: C, 64.07; H, 5.32; N, 4.09.

(CO)<sub>5</sub>Cr[C(NMe<sub>2</sub>)<sub>2</sub>((CH<sub>2</sub>)<sub>2</sub>CONMe<sub>2</sub>)] (**3d**). The same procedure as for **2a** was used, starting from Cr(CO)<sub>5</sub> (2.2 g, 10 mmol), a 0.78 M THF solution of sodium naphthalene (32

mL, 25 mmol), diamide **1e** (0.46 g, 2.5 mmol), chlorotrimethylsilane (2 mL, 15.7 mmol), and  $\text{Al}_2\text{O}_3$  (8 g). Elution with *n*-hexane followed by a dichloromethane–ethyl acetate mixture gave 0.48 g (55.1%) of **3d** as a yellow oil, which solidified to a yellow product: mp 65–69 °C dec;  $^1\text{H NMR}$   $\delta$  2.44 (br s, 2,  $\text{CH}_2$ ), 2.96 (s, 3,  $\text{CH}_3$  amide), 3.04 (s, 3,  $\text{CH}_3$  amide), 3.38 (s, 5,  $\text{CH}_3$  carbene +  $\text{CH}_2$ ), 3.85 (s, 3,  $\text{CH}_3$  carbene); IR ( $\text{CHCl}_3$ )  $\nu$  2054 (w), 1969 (w), 1924 (s), 1639 (m)  $\text{cm}^{-1}$ . Anal. Calcd for  $\text{C}_{13}\text{H}_{16}\text{CrN}_2\text{O}_6$ : C, 44.82; H, 4.64; N, 8.05. Found: C, 44.64; H, 4.82; N, 7.76.

$N,N,N',N'$ -Tetramethylglutaramide (**1f**):  $^1\text{H NMR}$   $\delta$  1.94 (quin,  $J = 7$  Hz, 2,  $\text{CH}_2$ ), 2.41 (t,  $J = 7$  Hz, 4,  $2\text{CH}_2$ ), 2.92 (s, 3,  $\text{CH}_3$ ), 3.01 (s, 3,  $\text{CH}_3$ ).

$(\text{CO})_5\text{Cr}[\mu\text{-C}(\text{NMe}_2)](\text{CH}_2)_3\text{C}(\text{NMe}_2)]\text{Cr}(\text{CO})_5$  (**2e**) and  $(\text{CO})_5\text{Cr}[\text{C}(\text{NMe}_2)(\text{CH}_2)_3\text{CONMe}_2]$  (**3e**). The same procedure as for the preparation of **2a** starting from  $\text{Cr}(\text{CO})_6$  (2.2 g, 10 mmol), a 0.78 M THF solution of sodium naphthalenide (32 mL, 25 mmol), diamide **1f** (0.46 g, 2.5 mmol), chlorotrimethylsilane (2 mL, 15.7 mmol), and  $\text{Al}_2\text{O}_3$  (8g) afforded upon chromatography on silica (70 g, *n*-heptane, *n*-heptane–dichloromethane, 2:1) 0.682 g of crude **2e**. Crystallization from an *n*-heptane–dichloromethane mixture gave 0.64 g (47.5%) of pure bis(carbene) complex **2e** as a yellow solid:  $^1\text{H NMR}$   $\delta$  1.49 (m, 2,  $\text{CH}_2$ ), 3.18 (m, 4,  $2\text{CH}_2$ ), 3.37 (s, 6,  $2\text{CH}_3$ ), 3.85 (s, 6,  $2\text{CH}_3$ ); IR ( $\text{CHCl}_3$ )  $\nu$  2052 (m), 1987 (w), 1921 (s)  $\text{cm}^{-1}$ . Anal. Calcd for  $\text{C}_{19}\text{H}_{18}\text{Cr}_2\text{N}_2\text{O}_{10}$ : C, 42.39; H, 3.37; N, 5.20. Found: C, 42.07; H, 3.42; N, 5.17. Crude monocarbene complex **3e** was obtained by further elution with a 1:1 dichloromethane–ethyl acetate mixture as a yellow oil, which was purified by radial-layer chromatography (Chromatotron) under argon (heptane, ether, acetone, methanol, 50:30:17:3). By this way 0.114 g (12.5%) of yellow oil was obtained:  $^1\text{H NMR}$   $\delta$  1.72 (m, 2,  $\text{CH}_2$ ), 2.44 (m, 2,  $\text{CH}_2$ ), 2.95 (s, 3,  $\text{CH}_3$ ), 3.02 (s, 3,  $\text{CH}_3$ ), 3.10 (m, 2,  $\text{CH}_2$ ), 3.50 (s, 3,  $\text{CH}_3$ ), 3.82 (s, 3,  $\text{CH}_3$ ); IR ( $\text{CHCl}_3$ )  $\nu$  2052 (m), 1966 (w), 1922 (s), 1638 (w)  $\text{cm}^{-1}$ . Anal. Calcd for  $\text{C}_{14}\text{H}_{18}\text{CrN}_2\text{O}_6$ : C, 46.41; H, 5.01; N, 7.73. Found: C, 46.55; H, 5.20; N, 7.58.

$(\text{CO})_5\text{Cr}[\mu\text{-C}(\text{NMe}_2)](\text{CH}_2)_4\text{C}(\text{NMe}_2)]\text{Cr}(\text{CO})_5$  (**2f**) and  $(\text{CO})_5\text{Cr}[\text{C}(\text{NMe}_2)(\text{CH}_2)_4\text{CONMe}_2]$  (**3f**). The preparation of **2a** used  $\text{Cr}(\text{CO})_6$  (2.2 g, 10 mmol), a 0.78 M THF solution of sodium naphthalenide (32 mL, 25 mmol), diamide **1g** (0.475 g, 2.5 mmol), chlorotrimethylsilane (2 mL, 15.7 mmol), and  $\text{Al}_2\text{O}_3$  (8 g) and afforded upon chromatography on silica (70 g, *n*-hexane, *n*-hexane–dichloromethane, 2:1) and crystallization (*n*-heptane, dichloromethane) 0.228 g (16.5%) of **2f**. Carbene **2f** was isolated as a light yellow solid:  $^1\text{H NMR}$   $\delta$  1.53 (s, 4,  $2\text{CH}_2$ ), 3.10 (s, 4,  $2\text{CH}_2$ ), 3.32 (s, 6,  $2\text{CH}_3$ ), 3.84 (s, 6,  $2\text{CH}_3$ ); IR ( $\text{CHCl}_3$ )  $\nu$  2057 (w), 1979 (w), 1927, 1885 (s), 1641 (w), 1543 (w)  $\text{cm}^{-1}$ . Anal. Calcd for  $\text{C}_{20}\text{H}_{20}\text{Cr}_2\text{N}_2\text{O}_{10}$ : C, 43.48; H, 3.65; N, 5.07. Found: C, 43.51; H, 3.82; N, 5.34. By further elution

with a 1:1 dichloromethane–ethyl acetate mixture and purification by radial-layer chromatography (Chromatotron) under argon (heptane, ether, acetone, methanol, 50:30:17:3) 0.078 g (8.3%) of a yellow oil containing according to the  $^1\text{H NMR}$  mainly monocarbene complex **3f** was obtained:  $^1\text{H NMR}$   $\delta$  1.47 (m, 2,  $\text{CH}_2$ ), 1.75 (m, 2,  $\text{CH}_2$ ), 2.37 (m, 2,  $\text{CH}_2$ ), 2.93 (s, 3,  $\text{CH}_3$ ), 3.00 (s, 3,  $\text{CH}_3$ ), 3.06 (m, 2,  $\text{CH}_2$ ), 3.33 (s, 3,  $\text{CH}_3$ ), 3.81 (s, 3,  $\text{CH}_3$ ).

$(\text{CO})_5\text{Cr}[\mu\text{-1,3-C}(\text{NMe}_2)]\text{C}_6\text{H}_4\text{C}(\text{NMe}_2)]\text{Fe}(\text{CO})_4$  (**4**). To a solution of  $\text{Fe}(\text{CO})_5$  (0.4 mL, 3 mmol) in THF (20 mL) was added a 0.78 M THF solution of sodium naphthalenide (9.5 mL, 7.4 mmol) at  $-78$  °C. The mixture was allowed to warm to 0 °C, kept at this temperature for 30 min, and then cooled to  $-78$  °C, and the carbene complex **3a** (0.6 g, 1.5 mmol) in THF (5 mL) was added. The reaction mixture was then allowed to warm to 0 °C, kept at this temperature for 30 min, and then cooled again to  $-78$  °C, and chlorotrimethylsilane (2 mL, 15.7 mmol) was added via syringe. The mixture was allowed to warm to 0 °C, alumina (4 g) was added, and the solvent was evaporated in vacuo. Chromatography on alumina (50 g, *n*-hexane, *n*-hexane–dichloromethane, 2:1) gave crude **4** (0.46 g, 55%). Crystallization from an *n*-heptane–dichloromethane mixture yielded pure **4** (0.295 g, 35.3%) as a yellow solid:  $^1\text{H NMR}$   $\delta$  3.16 (s, 3,  $\text{CH}_3$ ), 3.19 (s, 3,  $\text{CH}_3$ ), 4.01 (s, 6,  $2\text{CH}_3$ ), 6.19 (s, 1, ArH), 6.58 (d,  $J = 7.6$  Hz, 1, ArH), 6.65 (d,  $J = 6.2$  Hz, 1, ArH), 7.42 (m, 1, ArH);  $^{13}\text{C NMR}$   $\delta$  46.87 (q,  $\text{CH}_3$ ), 47.18 (q,  $\text{CH}_3$ ), 51.07 (q,  $\text{CH}_3$ ), 52.24 (q,  $\text{CH}_3$ ), 111.39 (d, C-arom), 118.14 (d, C-arom), 118.31 (d, C-arom), 129.95 (d, C-arom), 153.65 (s, C-arom), 154.20 (s, C-arom), 215.44 (s, C=O (Fe)), 218.00 (s, *cis* CO (Cr)), 224.04 (s, *trans* CO (Cr)), 258.86 (s, C=Fe), 273.86 (s, C=Cr); IR ( $\text{CCl}_4$ )  $\nu$  2054 (w), 2043 (w), 1970 (w), 1931 (s), 1925 (s, sh)  $\text{cm}^{-1}$ . Anal. Calcd for  $\text{C}_{21}\text{H}_{16}\text{CrFeN}_2\text{O}_9$ : C, 45.99; H, 2.94; N, 5.11. Found: C, 46.04; H, 3.00; N, 5.18.

**Acknowledgment.** Support of this research under Grant 203/95/0160 from the Czech Grant Agency is gratefully acknowledged. We also thank the Prague Institute of Chemical Technology and the Institute of Organic Chemistry and Biochemistry-AVČR for their support of our program.

**Supporting Information Available:** Tables of anisotropic thermal parameters, complete bond lengths and bond angles, and complete fractional and thermal parameters for compound **4** (8 pages). Ordering information is given on any current masthead page.

OM950258B

# Pentadienyl as a Stronger Binding but More Reactive Ligand Than Cyclopentadienyl: Syntheses, Reactions, and Molecular Orbital Studies of Half-Open Titanocenes

Isabella Hyla-Kryspin,<sup>1a</sup> Thomas E. Waldman,<sup>1b</sup> Enrique Meléndez,<sup>1b</sup>  
Wimonrat Trakarnpruk,<sup>1b</sup> Atta M. Arif,<sup>1b</sup> Manfred L. Ziegler,<sup>1a,c</sup>  
Richard D. Ernst,<sup>\*,1b</sup> and Rolf Gleiter<sup>\*,1a</sup>

Departments of Chemistry, University of Utah, Salt Lake City, Utah 84112, and Universität Heidelberg, 69120 Heidelberg, Germany

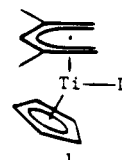
Received July 5, 1995<sup>®</sup>

The reactions of  $\text{Ti}(\text{C}_5\text{H}_5)\text{Cl}_2(\text{PR}_3)$  complexes ( $\text{R} = \text{Me}, \text{Et}$ ) with 2 equiv of a potassium pentadienide such as  $\text{KC}_5\text{H}_7$  or  $\text{K}(2,4\text{-C}_7\text{H}_{11})$  ( $\text{C}_7\text{H}_{11} = \text{dimethylpentadienyl}$ ) lead to the formation of diamagnetic 16 electron half-open titanocenes as monophosphine adducts. A single-crystal X-ray diffraction study of  $\text{Ti}(\text{C}_5\text{H}_5)(2,4\text{-C}_7\text{H}_{11})(\text{PEt}_3)$  revealed that the Ti–C bond lengths for the open dienyl ligand were much shorter than those for the  $\text{C}_5\text{H}_5$  ligand, 2.240(3) vs 2.346(4) Å, indicative of stronger Ti– $\text{C}_7\text{H}_{11}$  bonding. Reaction of this complex with  $\text{CH}_3\text{CN}$  leads to loss of the  $\text{PEt}_3$  ligand and coupling to the 2,4- $\text{C}_7\text{H}_{11}$  ligand. Thus, the  $\text{C}_7\text{H}_{11}$  ligand is not only more strongly bound than  $\text{C}_5\text{H}_5$ , it is also more reactive. A structural determination of this complex confirmed the mode of coupling and revealed that a dimeric species was formed. The phosphine ligands in the various complexes may readily be replaced by  $\text{P}(\text{OMe})_3$  or  $\text{P}(\text{OEt})_3$ . The  $\text{Ti}(\text{C}_5\text{H}_5)(2,4\text{-C}_7\text{H}_{11})(\text{PEt}_3)$  complex also reacts with CO, leading to a thermally unstable monocarbonyl and a thermally unstable dicarbonyl. While spectroscopic data revealed a symmetric structure for the monocarbonyl, the dicarbonyl complex is clearly unsymmetric. Molecular orbital calculations provide confirmation of stronger titanium–pentadienyl bonding and also the fact that the pentadienyl ligands serve as much better electron acceptors than cyclopentadienyl. To a large extent these may both be attributed to significant  $\delta$  bonding interactions between titanium  $d_{xy}$  and pentadienyl  $\pi_4^*$  orbitals.

Since the early reports on ferrocene,<sup>2</sup> the now ubiquitous cyclopentadienyl ligands have aroused great interest and may be regarded as the most important ligands in organometallic chemistry.<sup>3</sup> To a large extent, much of this interest may be attributed to the fact that cyclopentadienyl may be considered to be the most strongly binding of all the common organometallic ligands,<sup>3a</sup> leading to its great utilization as a “stabilizing ligand”. Metal pentadienyl compounds have more recently also attracted significant interest,<sup>4</sup> in large part due to the versatility and unique properties displayed by pentadienyl ligands. From various studies it has become clear that the pentadienyl ligands differ radi-

cally from their cyclic counterparts (e.g.,  $\text{C}_5\text{H}_5$ ,  $\text{C}_5\text{Me}_5$ , etc.). Thus, pentadienyl ligands have been shown to display a wide range of bonding modes (at least two types each of  $\eta^1$ ,  $\eta^3$ , and  $\eta^5$  coordination)<sup>4h,5</sup> and a variety of intriguing reaction chemistry.<sup>6</sup> Furthermore, they greatly favor bonding to metals in low oxidation states, exert greater steric demands than even  $\text{C}_5\text{Me}_5$ , tend to be much better back-bonding ligands, and bring about much greater metal–ligand orbital mixing.<sup>5</sup>

For the purposes of making comparisons between pentadienyl and cyclopentadienyl groups, the half-open metallocenes,  $\text{M}(\text{C}_5\text{H}_5)(\text{Pd})(\text{L})_n$  ( $\text{Pd} = \text{various pentadienyl ligands}$ ), have been of great importance, as the simultaneous presence of both ligands obviates complications that could arise from differences in symmetries, spin configurations, or steric environments.<sup>7</sup> The half-open titanocene  $\text{Ti}(\text{C}_5\text{H}_5)(2,4\text{-C}_7\text{H}_{11})(\text{PEt}_3)$  (1,  $\text{L} = \text{PEt}_3$ ,



$\text{C}_7\text{H}_{11} = \text{dimethylpentadienyl}$ ) actually provides some of the most interesting insights into the relationship between the open and closed dienyl ligands. In particular, one observes that not only does the open dienyl

<sup>®</sup> Abstract published in *Advance ACS Abstracts*, October 15, 1995.

(1) (a) Universität Heidelberg. (b) University of Utah. (c) Deceased, April 30, 1991.

(2) (a) Kealy, T. J.; Pauson, P. L. *Nature* **1951**, *168*, 1039. (b) Miller, S. A.; Tebboth, J. A.; Tremain, J. F. *J. Chem. Soc.* **1952**, 632.

(3) (a) Collman, J. P.; Hegedus, L. S.; Norton, J. R.; Finke, R. G. *Principles and Applications of Organotransition Metal Chemistry*; University Science Books: Mill Valley, CA, 1987; pp 164–165, 240. (b) Cotton, F. A.; Wilkinson, G. *Advanced Inorganic Chemistry*, 5th ed.; Wiley: New York, 1988; p 1171. (c) Shriver, D. F.; Atkins, P.; Langford, C. H. *Inorganic Chemistry*, 2nd ed.; Freeman: New York, 1994; pp 659–660, 687–693.

(4) (a) Powell, P. In *Advances in Organometallic Chemistry*; West, R., Stone, F. G. A., Eds.; Academic: New York, 1986; Vol. 26, p 125. (b) Kreiter, C. G. *Ibid.*, p 297. (c) Yasuda, H.; Nakamura, A. *J. Organomet. Chem.* **1985**, *285*, 15. (d) Villarreal, N. Z.; Paz-Sandoval, M. A.; Joseph-Nathan, P.; Esquivel, R. O. *Organometallics* **1991**, *10*, 2616. (e) Bleeker, J. R.; Haile, T.; New, P. R.; Chiang, M. Y. *Organometallics* **1993**, *12*, 517. (f) Lin, W.-J.; Lee, G.-H.; Peng, S.-M.; Liu, R. S. *Organometallics* **1991**, *10*, 2519. (g) Williams, G. M.; Rudisill, D. E. *Inorg. Chem.* **1989**, *28*, 797. (h) Bleeker, J. R.; Earl, P. L. *Organometallics* **1989**, *8*, 2735.

(5) Ernst, R. D. *Chem. Rev.* **1988**, *88*, 1255.

ligand give apparently stronger Ti–C interactions, as judged by the relative Ti–C bond lengths, but it also is more reactive, readily undergoing coupling reactions with a wide variety of unsaturated organic molecules.<sup>8</sup> Herein we present a complete report on, and rationale of, these aspects of metal–pentadienyl chemistry, including theoretical studies designed to address the question of the relative bonding favorabilities of the two dienyl ligands and the origin of the apparently enhanced Ti–pentadienyl interactions.

### Experimental Section

The compounds reported below are air-sensitive and were therefore prepared, handled, and stored under a nitrogen atmosphere. Hydrocarbon and ethereal solvents were distilled under nitrogen from benzophenone ketyl, while acetonitrile was dried according to a published procedure.<sup>9</sup> The various phosphines,<sup>10</sup> dienyl anions,<sup>11</sup>  $\text{Ti}(\text{C}_5\text{H}_5)(2,4\text{-C}_7\text{H}_{11})(\text{PET}_3)$ , and its acetonitrile coupling product were prepared as previously described,<sup>8</sup> while phosphites and  $\text{PBU}_3$  were purchased commercially. It is important to note that phosphine oxide impurities must be avoided in all the reactions below. Spectroscopic data were obtained as previously described.<sup>12</sup> <sup>13</sup>C NMR spectra were not integrated, but numbers of carbon atoms are indicated in accord with their assignments.

**(Triethylphosphine)(cyclopentadienyl)(pentadienyl)titanium,  $\text{Ti}(\text{C}_5\text{H}_5)(\text{C}_7\text{H}_7)(\text{PET}_3)$ .** To a magnetically stirred solution of 1.0 g (3.1 mmol) of  $\text{Ti}(\text{C}_5\text{H}_5)\text{Cl}_2 \cdot 2\text{THF}$  in 50 mL of THF under nitrogen at  $-78^\circ\text{C}$ , 0.45 mL (3.1 mmol) of  $\text{PET}_3$  was added, yielding a dark blue solution. To the resulting solution was added dropwise 0.66 g (6.2 mmol) of potassium pentadienide dissolved in 30 mL of THF, after which the mixture was allowed to stir for 2 h. The resulting brown solution was slowly warmed to room temperature, and a color change to green was observed after 4 h of additional stirring. The solvent was removed in vacuo and the crude product

(6) (a) Donaldson, W. A.; Bell, P. T.; Jin, M.-J. *J. Organomet. Chem.* **1992**, *441*, 449. (b) Bleeke, J. R.; Wittenbrink, R. J.; Clayton, T. W., Jr.; Chiang, M. Y. *J. Am. Chem. Soc.* **1990**, *112*, 6539. (c) Quiros-Guillou, C.; Lellouche, J.-P. *J. Org. Chem.* **1994**, *59*, 4693. (d) Roell, B. C., Jr.; McDaniel, K. F. *J. Am. Chem. Soc.* **1990**, *112*, 9004. (e) Seyferth, D.; Goldman, E. W. *J. Organomet. Chem.* **1981**, *208*, 189. (f) Lee T.-W.; Liu, R.-S. *Organometallics* **1988**, *7*, 878. (g) Yasuda, H.; Nakamura, A. *J. Organomet. Chem.* **1985**, *285*, 15. (h) Kralik, M. S.; Hutchinson, J. P.; Ernst, R. D. *J. Am. Chem. Soc.* **1985**, *107*, 8296. (i) Kralik, M. S.; Hutchinson, J. P.; Ernst, R. D. *Organometallics* **1987**, *6*, 2612.

(7) (a) Freeman, J. W.; Hallinan, N. C.; Arif, A. M.; Gedridge, R. W.; Ernst, R. D.; Basolo, F. *J. Am. Chem. Soc.* **1991**, *113*, 6509. (b) Elschenbroich, Ch.; Bilger, E.; Ernst, R. D.; Wilson, D. R.; Kralik, M. S. *Organometallics* **1985**, *4*, 2068. (c) Ernst, R. D.; Ma, H.; Sergeson, G.; Zahn, T.; Ziegler, M. L. *Organometallics* **1987**, *6*, 848. (d) Gleiter, R.; Hyla-Kryspin, I.; Ziegler, M. L.; Sergeson, G.; Green, J. C.; Stahl, L.; Ernst, R. D. *Organometallics* **1989**, *8*, 298. (e) Shen, J.-K.; Freeman, J. W.; Hallinan, N. C.; Rheingold, A. L.; Arif, A. M.; Ernst, R. D.; Basolo, F. *Organometallics* **1992**, *11*, 3215. (f) Gedridge, R. W.; Hutchinson, J. P.; Rheingold, A. L.; Ernst, R. D. *Organometallics* **1993**, *12*, 1553. (g) Trakarnpruk, W.; Arif, A. M.; Ernst, R. D. *Organometallics* **1994**, *13*, 2423.

(8) (a) Preliminary communication: Melendez, E.; Arif, A. M.; Ziegler, M. L.; Ernst, R. D. *Angew. Chem., Int. Ed. Engl.* **1988**, *27*, 1099. (b) Waldman, T. E.; Wilson, A. M.; Rheingold, A. L.; Melendez, E.; Ernst, R. D. *Organometallics* **1992**, *11*, 3201. (c) Wilson, A. M.; Waldman, T. E.; Rheingold, A. L.; Ernst, R. D. *J. Am. Chem. Soc.* **1992**, *114*, 6252.

(9) Jolly, W. L. *The Synthesis and Characterization of Inorganic Compounds*; Prentice-Hall: Englewood Cliffs, NJ, 1970; p 116.

(10) (a) Markham, R. T.; Dietz, E. A.; Martin, D. R. *Inorg. Synth.* **1976**, *16*, 153. (b) Wolfberger, W.; Schmidbauer, H. *Synth. React. Inorg. Met.-Org. Chem.* **1974**, *4*, 149. (c) Frajerman, C.; Meunier, B. *Inorg. Synth.* **1983**, *22*, 133.

(11) (a) Yasuda, H.; Yamauchi, M.; Ohnuma, Y.; Nakamura, A. *Bull. Chem. Soc. Jpn.* **1981**, *54*, 1481. (b) Wilson, D. R.; Stahl, L.; Ernst, R. D. In *Organometallic Synthesis*; King, R. B., Eisch, J. J., Eds.; Academic Press: New York, 1986; Vol. 3, p 136.

(12) Newbound, T. D.; Stahl, L.; Ziegler, M. L.; Ernst, R. D. *Organometallics* **1990**, *9*, 2962.

extracted with several portions of hexane and filtered through a coarse frit. Cooling the brown hexane solution to  $-78^\circ\text{C}$  afforded a light-brown crystalline compound in 65% yield (0.60 g, mp  $80^\circ\text{C}$ ). This compound is very air- and moisture-sensitive, but it can be stored under nitrogen.

<sup>1</sup>H NMR (benzene-*d*<sub>6</sub>, ambient):  $\delta$  6.08 (t, 1H, *J* = 11 Hz, H-3), 4.95 (d, 5H, *J* = 2 Hz, Cp), 4.51 (app q, 2H, *J* = 11 Hz, H-2,4), 2.05 (m, H-1,5 exo), 1.25 (m, 6H), 0.70 (m, 9H),  $-1.03$  (m, H-1,5 endo). <sup>13</sup>C NMR (benzene-*d*<sub>6</sub>, ambient):  $\delta$  112.7 (d, 1C, *J* = 158 Hz, C-3), 98.3 (d, 5C, *J* = 172 Hz, Cp), 93.1 (d, 2C, *J* = 159 Hz, C-2,4), 52.8 (t, 2C, *J* = 152 Hz, *J*<sub>C-P</sub> = 9 Hz, C-1,5), 18.8 (t, 3C, *J* = 129 Hz, *J*<sub>C-P</sub> = 11 Hz, PCH<sub>2</sub>), 7.9 (q, 3C, *J* = 128 Hz, CH<sub>3</sub>). <sup>31</sup>P{<sup>1</sup>H} NMR (benzene-*d*<sub>6</sub>, ambient):  $\delta$  41.7. IR (Nujol mull): 3170 (m), 1563 (m), 1304 (mw), 1262 (s), 1204 (m), 1170 (sh), 1149 (w), 977 (w), 898 (mw), 802 (s)  $\text{cm}^{-1}$ . Anal. Calcd for  $\text{C}_{16}\text{H}_{27}\text{PTi}$ : C, 64.43; H, 9.12. Found: C, 64.55; H, 9.12.

**(Trimethylphosphine)(cyclopentadienyl)(2,4-dimethylpentadienyl)titanium,  $\text{Ti}(\text{C}_5\text{H}_5)(2,4\text{-C}_7\text{H}_{11})(\text{PME}_3)$ .** A solution of 1.0 g (3.1 mmol) of  $\text{Ti}(\text{C}_5\text{H}_5)\text{Cl}_2 \cdot 2\text{THF}$  in 50 mL of THF was cooled with stirring to  $-78^\circ\text{C}$  under nitrogen, after which 0.30 mL (3.1 mmol) of  $\text{PME}_3$  was added, forming a blue solution. To this solution was slowly added 0.90 g (6.6 mmol) of (2,4-dimethylpentadienyl)potassium dissolved in 50 mL of THF, and the mixture was allowed to stir at  $-78^\circ\text{C}$  for 2 h. After slowly warming to room temperature, it was then stirred for about 4 h. The solvent was then removed in vacuo and the crude product extracted with several portions of pentane and filtered through a coarse frit. Cooling of the yellow-brown pentane solution to  $-25^\circ\text{C}$  for several days yielded a yellow-brown crystalline product. The product was isolated in 67% yield (0.59 g).

<sup>1</sup>H NMR (benzene-*d*<sub>6</sub>, ambient):  $\delta$  6.01 (s, 1H, H-3), 5.02 (d, 5H, *J* = 2.6 Hz, Cp), 1.81 (s, 6H, CH<sub>3</sub>), 1.69 (app quintet, 2H, *J* = 3.1 Hz, H-1,5 exo), 0.90 (d, 9H, *J* = 5.4 Hz,  $\text{PME}_3$ ),  $-0.91$  (m, H-1,5 endo). <sup>13</sup>C NMR (benzene-*d*<sub>6</sub>, ambient):  $\delta$  113.5 (d, 1C, *J* = 163 Hz, C-3), 101.7 (s, 2C, C-2,4), 100.9 (d, 5C, *J* = 170 Hz, Cp), 52.7 (d of t, 2C, *J* = 149 Hz, *J*<sub>C-P</sub> = 7 Hz, C-1,5), 31.4 (q, 2C, *J* = 119 Hz, CH<sub>3</sub>), 19.6 (q, 3C, *J* = 128 Hz, *J*<sub>C-P</sub> = 14 Hz,  $\text{PME}_3$ ). <sup>31</sup>P{<sup>1</sup>H} NMR (benzene-*d*<sub>6</sub>, ambient):  $\delta$  17.4. IR (Nujol mull): 3180 (m), 1564 (m), 1300 (w), 1281 (w), 1261 (m), 1170 (sh), 1155 (mw), 946 (s), 860 (w), 799 (s), 781 (s)  $\text{cm}^{-1}$ . Anal. Calcd for  $\text{C}_{15}\text{H}_{25}\text{PTi}$ : C, 63.40; H, 8.87. Found: C, 63.26; H, 8.74.

**(Tributylphosphine)(cyclopentadienyl)(2,4-dimethylpentadienyl)titanium,  $\text{Ti}(\text{C}_5\text{H}_5)(2,4\text{-C}_7\text{H}_{11})(\text{PBu}_3)$ .** This compound (mp  $47\text{--}47.5^\circ\text{C}$ ) was prepared as above, substituting  $\text{PBu}_3$  for  $\text{PME}_3$ . Isolation was accomplished by the same method, except that the much greater solubility of the  $\text{PBu}_3$  complex required substantial concentration of the pentane extracts, and generally greater time was required for crystallization to occur.

<sup>1</sup>H NMR (benzene-*d*<sub>6</sub>, ambient):  $\delta$  6.03 (s, 1H, H-3), 5.11 (s, 5H, Cp), 1.90 (br s, 2H, H-1,5 exo), 1.85 (s, 6H, CH<sub>3</sub>), 1.45–0.82 (br multiplets,  $\text{PBu}_3$ ),  $-0.70$  (br s, 2H, H-1,5 endo). <sup>31</sup>P{<sup>1</sup>H} NMR (benzene-*d*<sub>6</sub>, ambient):  $\delta$  36.5.

**(Trimethylphosphite)(cyclopentadienyl)(2,4-dimethylpentadienyl)titanium,  $\text{Ti}(\text{C}_5\text{H}_5)(2,4\text{-C}_7\text{H}_{11})[\text{P}(\text{OME})_3]$ .** To a light green solution of 0.40 g (1.2 mmol) of  $\text{Ti}(\text{C}_5\text{H}_5)(2,4\text{-C}_7\text{H}_{11})(\text{PET}_3)$  dissolved in 30 mL of hexane at room temperature was added 0.29 mL (2.4 mmol) of  $\text{P}(\text{OME})_3$ , leading immediately to a bright green solution. The reaction mixture was stirred for 20 min and then cooled to  $-78^\circ\text{C}$  for several days, yielding a bright-green air-sensitive product (mp  $64\text{--}65^\circ\text{C}$ ). Essentially complete conversion can be achieved through subsequent concentration and cooling of the supernatant.

<sup>1</sup>H NMR (benzene-*d*<sub>6</sub>, ambient):  $\delta$  6.15 (s, 1H, H-3), 5.12 (d, 5H, *J* = 2.1 Hz, Cp), 3.28 (d, 9H, *J* = 5.2 Hz, OCH<sub>3</sub>), 2.17 (app t, 2H, *J* = 6.3 Hz, H-1,5 exo), 1.78 (s, 6H, CH<sub>3</sub>),  $-0.46$  (app t, 2H, *J* = 7.1 Hz, H-1,5 endo). <sup>13</sup>C NMR (benzene-*d*<sub>6</sub>, ambient):  $\delta$  110.5 (d, 1C, *J* = 156 Hz, C-3), 102.1 (s, 2C, C-2,4),



100.7 (d, 5C,  $J = 172$  Hz, Cp), 54.4 (d of t, 2C,  $J = 151$  Hz,  $J_{C-P} = 12$  Hz, C-1,5), 50.5 (q, 3C,  $J = 145$  Hz, OCH<sub>3</sub>), 30.9 (q, 2C,  $J = 126$  Hz, CH<sub>3</sub>). <sup>31</sup>P{<sup>1</sup>H} NMR (benzene-*d*<sub>6</sub>, ambient):  $\delta$  212.8. IR (Nujol mull): 3170 (m), 1565 (m), 1304 (m), 1262 (mw), 1208 (w), 1169 (w), 1154 (mw), 973 (m), 891 (w), 847 (w), 802 (s), 769 (w) cm<sup>-1</sup>. Mass spectrum (EI, 17 eV) [ $m/z$  (relative intensity)]: 55 (27), 61 (61), 62 (100), 63 (12), 67 (12), 79 (30), 81 (64), 90 (100), 93 (96), 94 (44), 95 (40), 96 (50), 103 (11), 109 (60), 124 (67).

**(Triethylphosphite)(cyclopentadienyl)(2,4-dimethylpentadienyl)titanium, Ti(C<sub>5</sub>H<sub>5</sub>)(2,4-C<sub>7</sub>H<sub>11</sub>)[P(OEt)<sub>3</sub>].** To a light green solution of 0.40 g (1.2 mmol) of Ti(C<sub>5</sub>H<sub>5</sub>)(2,4-C<sub>7</sub>H<sub>11</sub>)(PEt<sub>3</sub>) in 25 mL of toluene at room temperature was added 0.38 mL (2.4 mmol) of P(OEt)<sub>3</sub>, leading immediately to a bright green solution. The reaction mixture was stirred for 30 min, and the solvent was removed in vacuo yielding a green oil. The green oil was extracted with hexane, filtered through a coarse frit, and concentrated to about 15 mL. Cooling of the solution to -78 °C for 48 h yielded an olive green crystalline solid. The yield is about 80% (0.36 g, mp 49–52 °C (d)) based on Ti(C<sub>5</sub>H<sub>5</sub>)(2,4-C<sub>7</sub>H<sub>11</sub>)(PEt<sub>3</sub>).

<sup>1</sup>H NMR (benzene-*d*<sub>6</sub>, ambient):  $\delta$  6.16 (s, 1H, H-3), 5.19 (d, 5H,  $J = 2.7$  Hz, Cp), 3.73 (app quintet, 6H,  $J = 7$  Hz, OCH<sub>2</sub>), 2.19 (app t, 2H,  $J = 2.6$  Hz, H-1,5 exo), 1.82 (s, 6H, CH<sub>3</sub>), 1.04 (t, 9H,  $J = 7.0$  Hz), -0.44 (app t, 2H,  $J = 4.2$  Hz, H-1,5 endo). <sup>13</sup>C NMR (benzene-*d*<sub>6</sub>, ambient):  $\delta$  110.7 (d, 1C,  $J = 155$  Hz, C-3), 102.0 (s, 2C, C-2,4), 100.8 (d, 5C,  $J = 171$  Hz, Cp), 60.6 (t, 3C,  $J = 144$  Hz, POC), 55.0 (d of t, 2C,  $J = 146$  Hz,  $J_{C-P} = 12$  Hz, C-1,5), 31.2 (q, 2C,  $J = 126$  Hz, CH<sub>3</sub>), 16.8 (d of q, 3C,  $J = 121$  Hz,  $J_{C-P} = 5$  Hz). <sup>31</sup>P{<sup>1</sup>H} NMR (benzene-*d*<sub>6</sub>, ambient):  $\delta$  205.2. IR (Nujol mull): 3180 (w), 1565 (m), 1304 (mw), 1261 (mw), 1159 (m), 1134 (w), 1097 (m), 928 (s), 854 (m), 838 (mw), 784 (s), 769 (w) cm<sup>-1</sup>. Mass spectrum (EI, 17 eV) [ $m/z$  (relative intensity)]: 65 (49), 81 (14), 82 (100), 83 (16), 111 (68), 113 (66), 121 (23), 139 (17), 166 (21), 204 (13), 206 (75), 207 (11). Anal. Calcd for C<sub>18</sub>H<sub>31</sub>PO<sub>3</sub>Ti: C, 57.75; H, 8.34. Found: C, 57.28; H, 8.30.

**Deuterioacetone Coupling Product with (Cyclopentadienyl)(2,4-dimethylpentadienyl)titanium, [Ti(C<sub>5</sub>H<sub>5</sub>)(C<sub>9</sub>H<sub>11</sub>D<sub>3</sub>N)]<sub>2</sub>.** This air-sensitive compound was prepared in an analogous manner as described for the CH<sub>3</sub>CN coupling product, substituting CD<sub>3</sub>CN for CH<sub>3</sub>CN.<sup>6</sup>

<sup>1</sup>H NMR (benzene-*d*<sub>6</sub>, ambient):  $\delta$  5.91 (s, 5H, Cp), 5.22 (t, 1H,  $J = 2$  Hz), 2.76 (d, 1H,  $J = 20.0$  Hz), 2.16 (d, 1H,  $J = 20.0$  Hz), 2.04 (s, 3H), 1.50 (d of d, 1H,  $J = 5.1$ , 2 Hz), 1.16 (s, 3H), 0.90 (d of d, 1H,  $J = 5.1$ , 2 Hz). No peak was observed at 1.31 ppm, demonstrating that that resonance in the CH<sub>3</sub>CN product was due to the former nitrile methyl group. <sup>13</sup>C{<sup>1</sup>H} NMR (benzene-*d*<sub>6</sub>, ambient):  $\delta$  174.1, 134.1, 122.3, 111.7, 76.5, 70.0, 60.6, 26.4, 22.0.

**(Dicarbonyl)(cyclopentadienyl)(2,4-dimethylpentadienyl)titanium, Ti(C<sub>5</sub>H<sub>5</sub>)(2,4-C<sub>7</sub>H<sub>11</sub>)(CO)<sub>2</sub>.** A solution of 1.00 g (3.06 mmol) of Ti(C<sub>5</sub>H<sub>5</sub>)(2,4-C<sub>7</sub>H<sub>11</sub>)[P(C<sub>2</sub>H<sub>5</sub>)<sub>3</sub>] in 50 mL of pentane was cooled to -78 °C and placed under an atmosphere of carbon monoxide; subsequent warming of the solution to ca. -25 °C resulted in a color change from orange to red and rapid uptake of carbon monoxide. The reaction temperature was maintained at -25 °C for 30 min, and then the solution was cooled to -78 °C, after which it was filtered through activated silica. A bright red filtrate was obtained from which red crystals (0.49 g, 61% yield) of the complex were obtained following evaporation of the solvent to ca. 10 mL under a CO stream and cooling to -80 °C for 2 days. The complex forms highly air-sensitive, platelike crystals that melt with decomposition at ca. 3–5 °C; however, the crystals may be stored for several months at -80 °C under a CO atmosphere.

<sup>1</sup>H NMR (toluene-*d*<sub>8</sub>, -89 °C):  $\delta$  4.58 (s, 1H, H-3), 4.36 (s, 5H, Cp), 2.37 (s, 1H, H-1,5 exo), 2.21 (s, 1H, H-1,5 exo), 2.11 (s, 3H, CH<sub>3</sub>), 1.34 (s, 3H, CH<sub>3</sub>), 1.01 (s, 1H, H-1,5 endo), 0.26 (s, 1H, H-1,5 endo). <sup>13</sup>C NMR (toluene-*d*<sub>8</sub>, -89 °C):  $\delta$  249.5 (s, 1C, CO), 235.3 (s, 1C, CO), 115.4 (s, 1C, C-2,4), 111.5 (s, 1C, C-2,4), 97.5 (d, 1C,  $J = 161$  Hz, C-3), 93.8 (d of quintets,

5C,  $J = 174$ , 7 Hz, Cp), 64.8 (t, 1C,  $J = 159$  Hz, C-1,5), 63.6 (t, 1C,  $J = 159$  Hz, C-1 or 5), 30.1 (q, 1C,  $J = 128$  Hz, CH<sub>3</sub>), 28.3 (q, 1C,  $J = 128$  Hz, CH<sub>3</sub>). IR (pentane solution,  $\nu_{CO}$ ): 1984 (vs, sh), 1932 (vs, sh) cm<sup>-1</sup>.

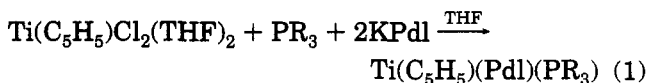
**(Carbonyl)(cyclopentadienyl)(2,4-dimethylpentadienyl)titanium, Ti(C<sub>5</sub>H<sub>5</sub>)(2,4-C<sub>7</sub>H<sub>11</sub>)CO.** The addition of 30 mL of precooled hexanes (0 °C) to 0.49 g of Ti(C<sub>5</sub>H<sub>5</sub>)(2,4-C<sub>7</sub>H<sub>11</sub>)(CO)<sub>2</sub> in a 100 mL 2-neck flask equipped with a nitrogen inlet and magnetic stirring bar resulted in a bright red solution. Rapid stirring was initiated, and a static vacuum was applied to the flask resulting in a slow (ca. 2 h) color change from red to orange. A solution IR spectrum of the reaction mixture displayed a single peak in the carbonyl region at 1959 cm<sup>-1</sup>. The solution was concentrated in vacuo to ca. 5 mL, and subsequent cooling at -80 °C for 12 h resulted in 0.43 g (97% yield) of orange-yellow platelets of Ti(C<sub>5</sub>H<sub>5</sub>)(2,4-C<sub>7</sub>H<sub>11</sub>)(CO). The complex is thermally unstable (mp 25–30 °C with decomposition); however, crystals may be stored for up to several weeks at -80 °C without decomposition.

<sup>1</sup>H NMR (toluene-*d*<sub>8</sub>, -89 °C):  $\delta$  5.83 (s, 1H, H-3), 4.86 (s, 5H, Cp), 2.23 (d,  $J = 6.0$  Hz, 2H, H-1,5 exo), 1.34 (s, 6H, CH<sub>3</sub>), 0.05 (d, 2H,  $J = 6.0$  Hz, H-1,5 endo). <sup>13</sup>C NMR (toluene-*d*<sub>8</sub>, -89 °C):  $\delta$  255.8 (s, 1C, CO), 109.2 (d, 1C,  $J = 155$  Hz, C-3), 107.9 (s, 2C, C-2,4), 101.3 (d of quintets, 5C,  $J = 174$ , 7 Hz, Cp), 58.8 (t, 2C,  $J = 157$  Hz, C-1,5), 29.5 (q, 2C,  $J = 125$  Hz, CH<sub>3</sub>). IR (pentane solution,  $\nu_{CO}$ ): 1959 (vs) cm<sup>-1</sup>.

**X-ray Structural Determinations.** Single crystals of Ti(C<sub>5</sub>H<sub>5</sub>)(2,4-C<sub>7</sub>H<sub>11</sub>)(PEt<sub>3</sub>) and its CH<sub>3</sub>CN-coupled complex were obtained by slowly cooling concentrated solutions in hexane or methylene chloride–hexane mixtures, respectively. The crystals were mounted and sealed in glass capillaries under nitrogen atmospheres and transferred to either a Nicolet-Siemens P1 or R3 diffractometer, respectively. In both cases nearly orthorhombic unit cells were found, but the departure of one angle in each case from 90°, along with the observation of 2/m Laue symmetry and systematic absences unique to space groups P2<sub>1</sub>/c and P2<sub>1</sub>/a, respectively, revealed that the unit cells were actually monoclinic. After the heavier atom locations were obtained the remaining non-hydrogen atom positions were obtained from a series of difference Fourier maps. Hydrogen atom positional parameters were refined for the phosphine adduct, while those for the dimeric product were idealized and allowed to ride with the carbon atom positions using the program HFIX. Pertinent data collection and refinement parameters are given in Table 1.

## Synthetic and Spectroscopic Results and Discussion

The synthesis of a half-open titanocene, Ti(C<sub>5</sub>H<sub>5</sub>)(2,4-C<sub>7</sub>H<sub>11</sub>)(PEt<sub>3</sub>) (**1**, C<sub>7</sub>H<sub>11</sub> = dimethylpentadienyl, L = PEt<sub>3</sub>), has been reported earlier, utilizing Ti(C<sub>5</sub>H<sub>5</sub>)(Cl)<sub>2</sub>(THF)<sub>2</sub> as the starting metal reagent.<sup>8</sup> This general route has now been expanded to include a variety of other related 16 electron species, which were prepared by the same general method (eq 1). The products are



PdI = 2,4-C<sub>7</sub>H<sub>11</sub>, R = Me, Et, *n*-Bu;

PdI = C<sub>5</sub>H<sub>7</sub>, R = Et

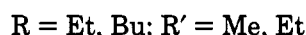
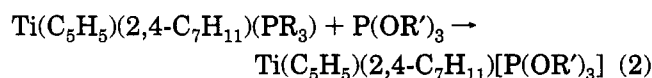
readily isolable by crystallization from hydrocarbon solutions and are air and water sensitive, in accord with the presence of Ti(II). As would be expected, their solubility in hydrocarbon solvents increases either upon addition of methyl groups to the dienyli skeleton or by the use of longer chain alkyl phosphines. As these

**Table 1. X-ray Data Parameters for  $\text{Ti}(\text{C}_5\text{H}_5)(2,4\text{-C}_7\text{H}_{11})(\text{PEt}_3)$  and  $[\text{Ti}(\text{C}_5\text{H}_5)(\text{C}_9\text{H}_{14}\text{N})_2]$**

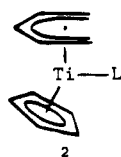
formula	$\text{TiC}_{18}\text{H}_{31}\text{P}$	$\text{Ti}_2\text{C}_{28}\text{H}_{38}\text{N}_2$
mol wt <sup>a</sup>	326.32	498.42
space group	$P2_1/c$	$P2_1/a$
lattice consts		
a (Å)	7.986(2)	14.377(7)
b (Å)	7.960(1)	10.440(8)
c (Å)	29.129(8)	16.920(10)
$\beta$ (deg)	90.18(2)	90.60(5)
V (Å <sup>3</sup> )	1851.8(8)	2539.5(20)
Z	4	4
radiation	Mo K $\alpha$	Mo K $\alpha$
cryst shape	bar, 0.1 × 0.25 × 0.7 mm	irregular, 0.3 × 0.3 × 0.4 mm
linear abs coeff (cm <sup>-1</sup> )	5.28	5.92
transm factors	0.71–1.00	0.74–1.00
scan type	$\theta$ – $2\theta$	$\theta$ – $2\theta$
scan speed (deg min <sup>-1</sup> )	2.0	2.5–29.5
bkgd/scan time	0.0 <sup>a</sup>	0.5
$2\theta$ limits (deg)	$3 \leq 2\theta \leq 48$	$3 \leq 2\theta \leq 60$
data colld	3383	ca. 7500
unique data with $I > 3\sigma(I)$	1852	3344
weighting	$1/\sigma^2(F)$	$1/\sigma^2(F)$
$R(F)$	0.066	0.050
$R_w(F)$	0.067	0.040
max diff Fourier peak (e/Å <sup>3</sup> )	0.9	0.16

<sup>a</sup> Backgrounds were estimated using the CARESS program: Packett, D. L.; Jensen, C. M.; Cowman, R. L.; Strouse, C. E.; Trogler, W. C. *Inorg. Chem.* **1985**, *24*, 3578.

complexes may find synthetic applications,<sup>8c</sup> the isolability of the  $\text{P}(n\text{-Bu})_3$  complex is notable, given that both the cost and air-sensitivity of this phosphine are significantly lower. Various phosphite complexes may readily be prepared by replacement of  $\text{PEt}_3$  or  $\text{P}(n\text{-Bu})_3$  from their complexes (eq 2).

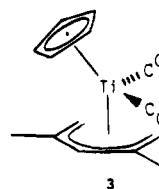


Analytical and spectroscopic data support the above formulations. The 16 electron complexes are diamagnetic, and <sup>1</sup>H and <sup>13</sup>C NMR spectroscopies reveal the presence of symmetry in the above complexes, consistent with structures 1 or 2. This is in accord with results from X-ray diffraction studies (*vide infra*).

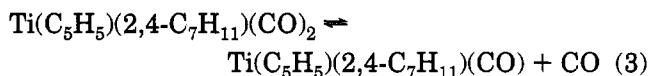


Exposure of a pentane solution of  $\text{Ti}(\text{C}_5\text{H}_5)(2,4\text{-C}_7\text{H}_{11})(\text{PEt}_3)$  to CO at  $-78^\circ\text{C}$  led to a rapid change in color from orange to blood-red. An infrared spectrum of the resulting solution displayed C–O stretching modes at 1932 and 1984  $\text{cm}^{-1}$ . After appropriate workup (see Experimental Section), the apparent dicarbonyl complex,  $\text{Ti}(\text{C}_5\text{H}_5)(2,4\text{-C}_7\text{H}_{11})(\text{CO})_2$ , could be isolated as dark red needles, which melted with decomposition around  $5^\circ\text{C}$ . As a result, characterization has necessarily relied upon spectroscopic methods. Both the low-temperature <sup>1</sup>H and <sup>13</sup>C NMR spectra reveal an unsymmetric pattern for the 2,4- $\text{C}_7\text{H}_{11}$  ligand, such that the two ligand ends are nonequivalent, as are the two carbonyl groups.

From the intensities of the C–O stretching frequencies observed in the infrared spectrum,<sup>13</sup> an OC–Ti–CO angle near  $84^\circ$  is indicated, consistent with the observed angles of 87.6(3) and 87.9(6) $^\circ$  in  $\text{Zr}(2,4\text{-C}_7\text{H}_{11})_2(\text{CO})_2$ <sup>14</sup> and  $\text{Ti}(\text{C}_5\text{H}_5)_2(\text{CO})_2$ ,<sup>15</sup> respectively. From these data, a structure such as 3 seems most reasonable.



As has been the case for other unsymmetrically oriented pentadienyl complexes,<sup>5,16</sup> higher temperatures lead to more symmetric NMR spectral patterns, which generally can be attributed to pentadienyl ligand oscillation or rotation. Indeed, above  $15^\circ\text{C}$ , the <sup>1</sup>H NMR spectrum possesses only four, instead of seven, resonances attributable to the pentadienyl ligand, at 5.18 (H-3), 2.16 (H-1,5 exo), 1.73 (CH<sub>3</sub>), and 0.49 (H-1,5 endo) ppm. The barrier ( $\Delta G^\ddagger$ ) for the site exchange process may be estimated as  $12.7 \pm 0.2$  kcal/mol.<sup>17</sup> However, several observations suggest that the exchange may possibly not be occurring via simple pentadienyl oscillation. First, the higher temperature spectrum reveals broadening not only of the resonances undergoing exchange but also of the H-3 and  $\text{C}_5\text{H}_5$  resonances. Furthermore, these two resonances experience significant downfield shifts (that for the  $\text{C}_5\text{H}_5$  ligand appearing at 4.62 ppm) which also would not be expected. This suggests the occurrence of an exchange process which does not require pentadienyl ligand oscillation. Notably, the H-3 and  $\text{C}_5\text{H}_5$  resonances for  $\text{Ti}(\text{C}_5\text{H}_5)(2,4\text{-C}_7\text{H}_{11})(\text{CO})$  (*vide infra*) are found significantly downfield from the corresponding resonances of its dicarbonyl analog, which thus provides the reason for their broadening under the conditions employed. Evidently, reversible CO dissociation from the dicarbonyl complex must be occurring, leading to the monocarbonyl, as in eq 3.



Thus, the observed signals at higher temperatures are averages of the positions for the two complexes, and this readily explains the downfield shifts as well as the broadening of the H-3 and  $\text{C}_5\text{H}_5$  resonances. While this process could by itself be responsible for the proton site exchange, the observed barrier is also not unreasonable for pentadienyl ligand oscillation.<sup>5,16</sup> It is quite possible

(13) (a) Lukehart, C. M. In *Fundamental Transition Metal Organometallic Chemistry*; Brooks/Cole: Monterey, CA, 1985; pp 78–79. (b) The absorbance ratio for the symmetric to asymmetric bands is ca. 0.81.

(14) Waldman, T. E.; Stahl, L.; Wilson, D. R.; Arif, A. M.; Hutchinson, J. P.; Ernst, R. D. *Organometallics* **1993**, *12*, 1543.

(15) Atwood, J. L.; Stone, K. E.; Alt, H. G.; Hrcncir, D. C.; Rausch, M. D. *J. Organomet. Chem.* **1977**, *132*, 367.

(16) Bleeker, J. R.; Wittenbrink, R. J.; Clayton, T. W., Jr.; Chiang, M. Y. *J. Am. Chem. Soc.* **1990**, *112*, 6539.

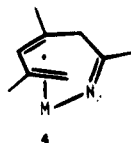
(17) (a) From low to high field, the frequency separations (Hz) and coalescence temperatures (K) are (48, 265), (234, 271), and (222, 273), corresponding to  $\Delta G^\ddagger$  values of 13.0, 12.5, and 12.6 kcal/mol ( $\pm 0.2$  kcal/mol each).<sup>17b</sup> (b) Gunther, H. In *NMR Spectroscopy*; Wiley: New York, 1980; p 243. (c) Kessler, H. *Angew. Chem.* **1970**, *9*, 219.



that both processes are reasonably competitive under the conditions employed.

As would be expected from the above observations, the dicarbonyl complex in solution is readily converted to a monocarbonyl species ( $\nu_{C-O} = 1959 \text{ cm}^{-1}$ ) under static vacuum at  $0^\circ\text{C}$ . Unfortunately, as for the dicarbonyl (and  $\text{Ti}(\text{C}_5\text{H}_5)_2(\text{CO})^{18}$ ), the complex is thermally unstable. Its  $^1\text{H}$  and  $^{13}\text{C}$  NMR spectra are relatively invariant with temperature and display patterns consistent with mirror plane symmetry for the molecule (i.e., **1**,  $L = \text{CO}$ ), in accord with structural results for vanadium analogs.<sup>7f</sup> As has been observed for a number of related complexes, infrared spectral data for the dicarbonyl complex indicate that the open dienyl ligands are better acceptors than  $\text{C}_5\text{H}_5$ .<sup>5,7f,19</sup> Thus, a replacement of  $\text{C}_5\text{H}_5$  by 2,4- $\text{C}_7\text{H}_{11}$  leads to higher C–O stretching frequencies:  $\text{Ti}(\text{C}_5\text{H}_5)_2(\text{CO})_2$ ,<sup>20</sup> 1897 and  $1975 \text{ cm}^{-1}$ , vs  $\text{Ti}(\text{C}_5\text{H}_5)(2,4\text{-C}_7\text{H}_{11})(\text{CO})_2$ , 1932 and  $1985 \text{ cm}^{-1}$ . For the monocarbonyls the data are more comparable, however:  $\text{Ti}(\text{C}_5\text{H}_5)(2,4\text{-C}_7\text{H}_{11})(\text{CO})$ ,  $1956 \text{ cm}^{-1}$  vs  $\text{Ti}(2,4\text{-C}_7\text{H}_{11})_2(\text{CO})$ ,<sup>19</sup>  $1952 \text{ cm}^{-1}$ . Of course, the greater number of methyl groups in the latter species may play a role in its decrease, but nonetheless it should be noted that in some other systems the  $\nu_{C-O}$  data for  $\text{C}_5\text{H}_5$  and pentadienyl ligands are fairly similar.<sup>21</sup> It is possible that steric interactions lead to extra M–CO weakening in more crowded systems, such as the dicarbonyls, and this would be consistent with their facile loss of CO.

The half-open titanocene  $\text{Ti}(\text{C}_5\text{H}_5)(2,4\text{-C}_7\text{H}_{11})(\text{PEt}_3)$  also reacts with acetonitrile, leading to a 1:1 formal replacement of the  $\text{PEt}_3$  ligand. On the basis of the precedent for butadiene complexes,<sup>22</sup> it was expected that the nitrile would couple to a terminal  $\text{CH}_2$  group of the 2,4- $\text{C}_7\text{H}_{11}$  ligand, leading to a fragment such as **4**. In fact, the proton-coupled  $^{13}\text{C}$  NMR spectrum



contains two  $\text{CH}_2$  resonances, one of which has a  $^1\text{H}$ – $^{13}\text{C}$  coupling constant of 125 Hz, typical of  $\text{sp}^3$  hybridization. The structural result (*vide infra*) did indeed confirm that coupling to one end has occurred, although some geometric differences were found relative to **4** (*vide infra*). The coupling process itself may be proposed to involve a nucleophilic attack on the appropriate carbon atom of a coordinated nitrile by the pentadienyl ligand, which formally is an anion with charge localized on the 1, 3, and 5 positions. This can then be regarded as being

(18) Liu, J.-Z.; Ernst, R. D. *J. Am. Chem. Soc.* **1982**, *104*, 3737.

(19) Newbound, T. D.; Rheingold, A. L.; Ernst, R. D. *Organometallics* **1992**, *11*, 1693.

(20) Calderazzo, F.; Salzmann, J. J.; Mosimann, P. *Inorg. Chim. Acta* **1967**, *1*, 65.

(21) (a) Paz-Sandoval, M. d. l. A.; Powell, P.; Drew, M. G. B.; Perutz, R. N. *Organometallics* **1984**, *3*, 1026. (b) Ma, H.; Weber, P.; Ziegler, M. L.; Ernst, R. D. *Organometallics* **1987**, *6*, 854. (c) These data may be less useful for comparative purposes since in the particular pentadienyl complexes there are nonequivalent sites for CO and  $\text{PR}_3$  binding. The CO ligands could then be preferentially occupying the best sites for back-bonding, thereby giving lower C–O stretching frequencies than would otherwise be found.

(22) (a) Yasuda, H.; Kajihara, Y.; Mashima, K.; Nagasuna, K. *Chem. Lett.* **1981**, 671. (b) López, L.; Berlekamp, M.; Kowalski, D.; Erker, G. *Angew. Chem., Int. Ed. Engl.* **1994**, *33*, 1114.

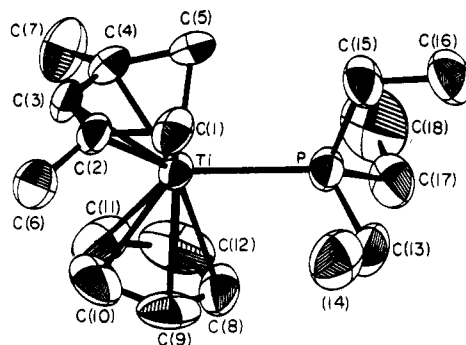
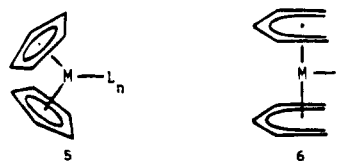


**Figure 1.** Perspective view and numbering scheme for  $\text{Ti}(\text{C}_5\text{H}_5)(2,4\text{-C}_7\text{H}_{11})(\text{PEt}_3)$ .

analogous to the reactions of Grignard reagents with ketones or nitriles. Conversion of the U conformation of the original pentadienyl fragment to a sickle geometry, followed by dimerization, would lead to the observed complex (*vide infra*). These steps almost certainly occur subsequent to the coupling step, given that the coupling reaction occurs at low temperatures.<sup>23</sup>

### Structural Results and Discussion

A perspective view of  $\text{Ti}(\text{C}_5\text{H}_5)(2,4\text{-C}_7\text{H}_{11})(\text{PEt}_3)$  is presented in Figure 1, while pertinent atomic coordinates and bonding parameters are given in Tables 2 and 3. In accord with spectral data (*vide supra*), and as found for related half-open vanadocene ligand adducts,<sup>7f</sup> the structure (**1**,  $L = \text{PEt}_3$ ) may be considered to be a hybrid between those for the ligand adducts of metallocenes (**5**)<sup>24</sup> and open metallocenes (**6**).<sup>14</sup> Thus, the



pentadienyl ligand plane is nearly parallel with the Ti–P vector, while there is a significant angle formed between the  $\text{C}_5\text{H}_5$  plane and the Ti–P vector.<sup>25</sup> The two 5 electron ligands are reasonably planar, with an angle of  $156.1^\circ$  between them. As is normal for pentadienyl ligands, the methyl groups are bent significantly out of the ligand plane toward the metal atom (average of  $0.23 \text{ \AA}$ ,  $8.6^\circ$ ),<sup>26</sup> which may be ascribed to an attempt to

(23) (a) An “envelope flip” process<sup>23b</sup> for the presumed initial coupled complex, having the original dienyl fragment still in the U conformation, would bring about its conversion to the observed structure having an S conformation for the original dienyl fragment. (b) Eaton, B.; King, J. A., Jr.; Vollhardt, K. P. C. *J. Am. Chem. Soc.* **1986**, *108*, 1359. (c) Interestingly,  $\eta^5$ -pentadienyl complexes could undergo an analogous flip through  $\eta^3$ -1,4,5 intermediates, having localized M–alkyl and M–olefin coordination, leading to formal racemization for unsymmetric dienyl ligands not having substituents on the terminal carbon atoms. Some observations suggest this may indeed occur for  $\eta^5$ -dienyl complexes.<sup>23d</sup> (d) Weng, W.-Q.; Ernst, R. D. Unpublished results.

(24) (a) Fieselmann, B. F.; Stucky, G. D. *J. Organomet. Chem.* **1977**, *137*, 43. (b) Lauher, J. W.; Hoffmann, R. *J. Am. Chem. Soc.* **1976**, *98*, 1729.

(25) The respective angles are  $5.7$  and  $18.2^\circ$ .

(26) (a) The sine of the tilt angle is defined by the deviation of a substituent from the plane, divided by the ligand C–substituent bond distance. (b) Ernst, R. D. *Struct. Bonding (Berlin)* **1984**, *57*, 1. (c) The C(2,4) positions actually deviate from the plane by  $0.025 \text{ \AA}$  toward the metal. Taking this into account, one can derive an average tilt angle of  $9.5^\circ$ .

**Table 2. Positional Parameters for the Non-Hydrogen Atoms of  $\text{Ti}(\text{C}_5\text{H}_5)(2,4\text{-C}_7\text{H}_{11})(\text{PEt}_3)$** 

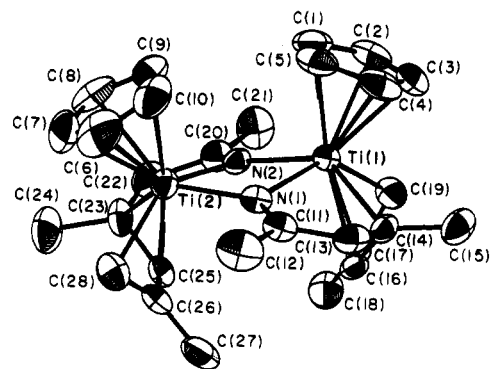
atom	x	y	z
Ti	0.64806(14)	0.04830(13)	0.64841(3)
P	0.71606(22)	0.24929(21)	0.58193(5)
C(1)	0.5513(16)	-0.1182(9)	0.5918(4)
C(2)	0.5377(8)	-0.2036(7)	0.6340(2)
C(3)	0.6632(9)	-0.2273(8)	0.6675(2)
C(4)	0.8229(10)	-0.1557(10)	0.6696(3)
C(5)	0.9007(9)	-0.0574(11)	0.6345(3)
C(6)	0.3633(10)	-0.2651(10)	0.6470(3)
C(7)	0.9192(14)	-0.1816(15)	0.7154(4)
C(8)	0.5612(17)	0.3142(10)	0.6773(3)
C(9)	0.4274(18)	0.2183(19)	0.6767(5)
C(10)	0.4608(22)	0.0865(13)	0.7078(5)
C(11)	0.6065(23)	0.1051(18)	0.7253(3)
C(12)	0.6704(17)	0.2462(27)	0.7083(7)
C(13)	0.5393(13)	0.3609(12)	0.5555(3)
C(14)	0.3959(14)	0.2580(15)	0.5361(4)
C(15)	0.8213(12)	0.1524(10)	0.5325(3)
C(16)	0.8565(16)	0.2613(14)	0.4917(3)
C(17)	0.8453(12)	0.4354(10)	0.5933(3)
C(18)	1.0075(20)	0.3954(17)	0.6157(6)

**Table 3. Pertinent Bond Distances (Å) and Angles (deg) for  $\text{Ti}(\text{C}_5\text{H}_5)(2,4\text{-C}_7\text{H}_{11})(\text{PEt}_3)$** 

Bond Distances			
Ti-C(1)	2.251(9)	C(8)-C(9)	1.313(16)
Ti-C(2)	2.230(6)	C(9)-C(10)	1.410(21)
Ti-C(3)	2.266(6)	C(10)-C(11)	1.278(17)
Ti-C(4)	2.227(7)	C(11)-C(12)	1.330(22)
Ti-C(5)	2.224(7)	C(8)-C(12)	1.364(23)
Ti-C(8)	2.382(8)	C(1)-C(2)	1.410(13)
Ti-C(9)	2.372(11)	C(2)-C(3)	1.408(9)
Ti-C(10)	2.310(9)	C(3)-C(4)	1.398(10)
Ti-C(11)	2.309(9)	C(4)-C(5)	1.430(10)
Ti-C(12)	2.356(12)	C(2)-C(6)	1.525(10)
Ti-P	2.571(2)	C(4)-C(7)	1.552(12)
P-C(13)	1.835(10)	C(13)-C(14)	1.516(15)
P-C(15)	1.840(7)	C(15)-C(16)	1.497(11)
P-C(17)	1.835(8)	C(17)-C(18)	1.483(17)
Bond Angles			
Ti-P-C(13)	116.9(3)	C(1)-C(2)-C(6)	116.4(8)
Ti-P-C(15)	115.3(3)	C(3)-C(2)-C(6)	115.7(6)
Ti-P-C(17)	119.1(3)	C(3)-C(4)-C(7)	115.7(6)
C(13)-P-C(15)	103.2(4)	C(5)-C(4)-C(7)	118.1(7)
C(13)-P-C(17)	96.7(5)	C(8)-C(9)-C(10)	105.8(12)
C(15)-P-C(17)	102.8(4)	C(9)-C(10)-C(11)	109.9(11)
C(1)-C(2)-C(3)	127.7(7)	C(10)-C(11)-C(12)	107.4(14)
C(2)-C(3)-C(4)	128.5(6)	C(11)-C(12)-C(8)	109.6(11)
C(3)-C(4)-C(5)	126.2(7)	C(12)-C(8)-C(9)	107.3(11)

improve metal-ligand orbital overlap.<sup>27</sup> This tilting is required for the pentadienyl ligand as a result of its greater width (at its open edge) and the resulting closer approach by the metal atom to its plane as compared to the  $\text{C}_5\text{H}_5$  plane (1.563 vs 2.049 Å).

Of primary interest are the Ti-C bond distances. Those for the cyclopentadienyl ligand range 2.309(9)–2.382(8) Å, averaging<sup>28</sup> 2.346(4) Å, while those for the pentadienyl ligand range 2.224(7)–2.266(6) Å, averaging 2.240(3) Å. Thus, the Ti-C pentadienyl bond lengths are 0.106(7) Å shorter. Similar trends, i.e., significantly shorter M-C bonds for pentadienyl relative to  $\text{C}_5\text{H}_5$  ligands, have been observed for related vanadium<sup>7f</sup> and chromium<sup>7a</sup> complexes and demonstrate that metal-pentadienyl bonding can be stronger than even the highly favorable metal-cyclopentadienyl bond-

**Figure 2.** Perspective view and numbering scheme for the dimeric acetonitrile coupling product with the  $\text{Ti}(\text{C}_5\text{H}_5)(2,4\text{-C}_7\text{H}_{11})$  moiety.

ing for at least the early transition metals, for which reasonable overlap with the large pentadienyl skeleton may be achieved. Together with the observation that reaction of this complex with  $\text{CH}_3\text{CN}$  leads to coupling with the pentadienyl ligand, this demonstrates that not only is the pentadienyl ligand more strongly bound than cyclopentadienyl, but it is also more reactive. While this may appear to be somewhat contradictory, a simple explanation exists, based upon the greater stabilization that can be achieved for the (aromatic) cyclopentadienyl ligand as a result of its greater  $\pi$  delocalization.<sup>26b,29</sup> The greater stabilization of the  $\text{C}_5\text{H}_5$  anion imparts to it a lower tendency to engage in additional bonding, as its stabilized filled orbitals render it a poorer donor, and its destabilized empty orbitals render it a poorer acceptor. However, in coupling reactions of these anionic ligands, the stabilization due to  $\pi$ -delocalization of the anions is lost, and such a loss is naturally much greater for the aromatic  $\text{C}_5\text{H}_5$  ligand, accounting for its lower tendency to engage in such reactions. An interesting analogy may be drawn with the work of Jonas, in which various anionic ligands have been demonstrated to displace the more resonance stabilized  $\text{C}_5\text{H}_5^-$  from its metal complexes.<sup>30</sup>

Within the 2,4- $\text{C}_7\text{H}_{11}$  ligand, the individual Ti-C bond lengths are reasonably similar,<sup>31</sup> although that for C-3 is slightly lengthened, which likely results from a slippage of the pentadienyl ligand away from the phosphine ligand. The carbon-carbon bond distances in the  $\text{C}_5\text{H}_5$  ligand appear to suffer from systematic shortening, brought about by thermal libration. This can readily be seen from the fairly large thermal parameters for these atoms. The delocalized C-C bonds for the pentadienyl ligand average 1.412(5) Å. The  $\text{PEt}_3$  ligand adopts a compact form that is common in crowded situations.<sup>32</sup> One arm of the phosphine ligand is situated between the two pentadienyl ligand ends and is bent back. The other two arms are therefore located closer to the  $\text{C}_5\text{H}_5$  ligand and bend to the sides, as is again often observed. Some degree of strain is apparently induced by this arrangement, which is reflected by the relatively small C(13)-P-C(17) angle of 96.7(5)°.

(29) Streitwieser, A. In *Molecular Orbital Theory for Organic Chemists*; Wiley: New York, 1967.

(30) Jonas, K. *Angew. Chem., Int. Ed. Engl.* **1985**, *24*, 295.

(31) The average Ti-C(1,5), Ti-C(2,4), and Ti-C(3) bond lengths are 2.237(6), 2.229(5), and 2.266(6) Å, respectively.

(32) (a) Bart, J. C.; Favini, G.; Todeschini, R. *Phosphorus Sulfur* **1983**, *17*, 205. (b) Stahl, L.; Ernst, R. D. *J. Am. Chem. Soc.* **1987**, *109*, 5673.

(27) (a) Elian, M.; Chen, M. M. L.; Mingos, D. M. P.; Hoffmann, R. *Inorg. Chem.* **1976**, *15*, 1148. (b) Haaland, A. *Acc. Chem. Res.* **1979**, *12*, 415.

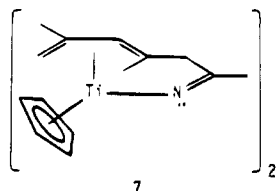
(28) The esd's given for average values are derived from esd's for the individual data and hence reflect the accuracy of the average but not the distribution of the data.

**Table 4. Positional Parameters for the Non-Hydrogen Atoms of [Ti(C<sub>5</sub>H<sub>5</sub>)(C<sub>9</sub>H<sub>14</sub>N)]<sub>2</sub>**

atom	x	y	z
Ti(1)	-0.14565(5)	0.10765(6)	0.65026(4)
Ti(2)	-0.22154(5)	-0.03217(7)	0.81958(4)
N(1)	-0.1936(2)	0.1502(3)	0.7697(2)
N(2)	-0.1472(2)	-0.0701(2)	0.7105(2)
C(1)	-0.2715(3)	0.0235(5)	0.5742(3)
C(2)	-0.2037(3)	0.0546(5)	0.5202(2)
C(3)	-0.1941(3)	0.1860(5)	0.5221(2)
C(4)	-0.2527(3)	0.2356(5)	0.5767(3)
C(5)	-0.3021(3)	0.1331(5)	0.6092(2)
C(6)	-0.3772(3)	-0.0138(6)	0.8703(3)
C(7)	-0.3517(4)	-0.1402(6)	0.8773(3)
C(8)	-0.3382(3)	-0.1929(5)	0.8054(3)
C(9)	-0.3578(3)	-0.0950(5)	0.7510(3)
C(10)	-0.3808(3)	0.0142(5)	0.7928(3)
C(11)	-0.1926(3)	0.2673(4)	0.7900(2)
C(12)	-0.2356(3)	0.3194(4)	0.8654(2)
C(13)	-0.1451(3)	0.3629(3)	0.7389(2)
C(14)	-0.0854(3)	0.2977(3)	0.6770(2)
C(15)	-0.0529(3)	0.3909(4)	0.6136(2)
C(16)	-0.0183(3)	0.2089(3)	0.7119(2)
C(17)	0.0200(2)	0.1103(4)	0.6700(2)
C(18)	0.0859(3)	0.0175(4)	0.7082(2)
C(19)	-0.0108(2)	0.0890(4)	0.5910(2)
C(20)	-0.1165(3)	-0.1824(3)	0.7013(2)
C(21)	-0.0798(3)	-0.2361(4)	0.6244(2)
C(22)	-0.1156(3)	-0.2711(4)	0.7720(2)
C(23)	-0.1338(3)	-0.1992(4)	0.8474(2)
C(24)	-0.1497(3)	-0.2939(4)	0.9156(2)
C(25)	-0.0713(3)	-0.0917(4)	0.8607(2)
C(26)	-0.0930(3)	0.0073(4)	0.9097(2)
C(27)	-0.0289(3)	0.1175(4)	0.9213(2)
C(28)	-0.1838(3)	0.0104(4)	0.9447(2)

Such an effect is also present in complexes such as Zr(2,4-C<sub>7</sub>H<sub>11</sub>)<sub>2</sub>(PEt<sub>3</sub>), for which the corresponding angle is 97.9(6)°, as compared to 101.8(4)° for the other two. The Ti-P bond distance, 2.571(2) Å, is rather long but similar to the distance of 2.550(2) Å observed in Ti(2,4-C<sub>7</sub>H<sub>11</sub>)<sub>2</sub>(PMe<sub>3</sub>).<sup>33</sup>

The structure of the acetonitrile coupling product is displayed in Figure 2, while positional and bonding parameters are contained in Tables 4 and 5. Most noticeable is the dimeric nature of the complex, which comes about as a result of the nitrogen centers adopting a bridging orientation between the two titanium centers. Additionally, one can see that the original dienyl fragments (e.g., C(13,14,16,17,19)) have rearranged to a sickle orientation, giving a ligand fragment as in 7,



rather than 4. As had been expected, the pentadienyl-nitrile coupling has converted the dienyl ligand to a diene and led to a formal negative charge on each nitrogen center.

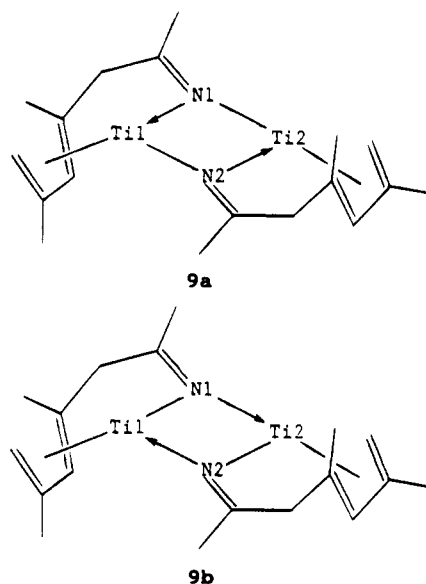
The two halves of the dimer are essentially equivalent. The Ti-C bond lengths for the two C<sub>5</sub>H<sub>5</sub> ligands average 2.388(2) Å, actually slightly longer than in Ti(C<sub>5</sub>H<sub>5</sub>)(2,4-C<sub>7</sub>H<sub>11</sub>)(PEt<sub>3</sub>). The four averaged Ti-C bond lengths for the diene fragments, beginning at the end CH<sub>2</sub> group, are 2.212(3), 2.410(3), 2.348(3), and

2.206(3) Å, while the corresponding C-C bond lengths are 1.430(4), 1.367(4), and 1.456(4) Å. The s-l-l-s and l-s-l patterns for the Ti-C and C-C bonds, respectively, implicate an enediyl bonding mode (8) for these fragments, thus leading to a Ti(IV) formulation. This is further supported by the J(<sup>13</sup>C-H) value of 136 Hz for the diene's terminal CH<sub>2</sub> group.<sup>34</sup>



A few noteworthy aspects of the diene methyl substituents can be mentioned. Just as in metal pentadienyl complexes,<sup>19,26</sup> the presence of a methyl group on an internal ligand carbon atom leads to a contraction of the atom's C-C-C bond angle, cf., an average of 118.7(3)° around C(17) and C(26) compared to 122.4(4)° for C(16) and C(25). The other two methyl substituents, C(15) and C(24), are bent significantly out of their diene planes, away from the titanium atoms, by 1.278 and 1.314 Å, respectively, corresponding to angles of 56.9 and 58.7°.

The key members of the Ti<sub>2</sub>N<sub>2</sub> portion of the molecule may be represented as in 9. The ring is nearly planar,



as can be seen from the respective average values of the N-Ti-N and Ti-N-Ti angles, 74.3(1) and 104.6(1)°. The Ti-N bonds alternate in magnitude, with the two shorter ones (Ti(1)-N(2), Ti(2)-N(1)) averaging 2.120(2) Å, compared to 2.183(2) Å for the other two. The asymmetry may readily be traced to the fact that the C-N vectors are each tilted toward different titanium centers, as a result of their being tied to, and restrained by, the coordinated diene fragments. Thus, two types of C-N-Ti angles are observed, one of which averages 138.8(3)°, and the other 116.5(2)°. As a result, the C(11)-N(1) vector tilts toward Ti(2), while the C(20)-N(2) vector tilts toward Ti(1), by an average of 11.2°. This would lead to greater nitrogen s orbital character in the Ti(1)-N(2) and Ti(2)-N(1) bonds, consistent with their shortening relative to the Ti(1)-N(1) and Ti(2)-

(33) Ernst, R. D.; Freeman, J. W.; Stahl, L.; Wilson, D. R.; Arif, A. M.; Nuber, B.; Ziegler, M. L. *J. Am. Chem. Soc.* **1995**, *117*, 5075.

(34) (a) Yasuda, H.; Tatsumi, K.; Nakamura, A. *Acc. Chem. Res.* **1985**, *18*, 120. (b) Newton, M. D.; Schulman, J. M.; Manus, M. M. *J. Am. Chem. Soc.* **1974**, *96*, 17.

Table 5. Pertinent Bond Distances (Å) and Angles (deg) for  $[\text{Ti}(\text{C}_5\text{H}_5)(\text{C}_9\text{H}_{14}\text{N})_2]$ 

Bond Distances							
Ti(1)–N(1)	2.187(3)	Ti(2)–N(1)	2.123(3)	Ti(1)–C(14)	2.210(4)	Ti(2)–C(23)	2.201(4)
Ti(1)–N(2)	2.117(3)	Ti(2)–N(2)	2.179(3)	Ti(1)–C(16)	2.348(4)	Ti(2)–C(25)	2.347(4)
Ti(1)–C(1)	2.378(4)	C(1)–C(2)	1.382(7)	Ti(1)–C(17)	2.402(4)	Ti(2)–C(26)	2.419(4)
Ti(1)–C(2)	2.410(4)	C(2)–C(3)	1.379(7)	Ti(1)–C(19)	2.200(4)	Ti(2)–C(28)	2.224(4)
Ti(1)–C(3)	2.414(4)	C(3)–C(4)	1.359(7)	C(11)–C(12)	1.524(5)	N(2)–C(20)	1.263(4)
Ti(1)–C(4)	2.379(4)	C(4)–C(5)	1.400(7)	C(11)–C(13)	1.491(6)	C(20)–C(21)	1.517(5)
Ti(1)–C(5)	2.362(4)	C(1)–C(5)	1.363(7)	C(13)–C(14)	1.521(5)	C(20)–C(22)	1.514(5)
Ti(2)–C(6)	2.413(5)	C(6)–C(7)	1.374(9)	C(14)–C(15)	1.525(5)	C(22)–C(23)	1.505(6)
Ti(2)–C(7)	2.401(5)	C(7)–C(8)	1.351(8)	C(14)–C(16)	1.458(5)	C(23)–C(24)	1.538(5)
Ti(2)–C(8)	2.383(5)	C(8)–C(9)	1.402(7)	C(16)–C(17)	1.369(5)	C(23)–C(25)	1.453(6)
Ti(2)–C(9)	2.359(4)	C(9)–C(10)	1.383(8)	C(17)–C(18)	1.497(5)	C(25)–C(26)	1.364(6)
Ti(2)–C(10)	2.379(5)	C(6)–C(10)	1.343(7)	C(17)–C(19)	1.421(5)	C(26)–C(27)	1.486(6)
				N(1)–C(11)	1.270(5)	C(26)–C(28)	1.439(6)

Bond Angles					
N(1)–Ti(1)–N(2)	74.3(1)	C(6)–C(7)–C(8)	110.8(6)	C(14)–C(16)–C(17)	122.5(5)
N(1)–Ti(2)–N(2)	74.3(1)	C(7)–C(8)–C(9)	105.3(5)	C(16)–C(17)–C(18)	121.3(4)
Ti(1)–N(1)–Ti(2)	104.4(1)	C(8)–C(9)–C(10)	108.2(5)	C(16)–C(17)–C(19)	118.7(4)
Ti(1)–N(2)–Ti(2)	104.9(1)	C(9)–C(10)–C(6)	108.2(5)	C(18)–C(17)–C(19)	119.7(4)
Ti(1)–N(1)–C(11)	116.3(3)	C(10)–C(6)–C(7)	107.5(5)	C(21)–C(20)–C(22)	116.8(4)
Ti(1)–N(2)–C(20)	138.5(4)	N(1)–C(11)–C(12)	124.5(4)	C(20)–C(22)–C(23)	111.4(4)
Ti(2)–N(1)–C(11)	139.2(5)	N(1)–C(11)–C(13)	119.4(4)	C(22)–C(23)–C(24)	110.1(4)
Ti(2)–N(2)–C(20)	116.7(3)	N(2)–C(20)–C(21)	125.1(4)	C(22)–C(23)–C(25)	113.8(4)
C(1)–C(2)–C(3)	106.9(5)	N(2)–C(20)–C(22)	118.0(4)	C(24)–C(23)–C(25)	118.5(4)
C(2)–C(3)–C(4)	109.4(5)	C(12)–C(11)–C(13)	116.0(4)	C(23)–C(25)–C(26)	122.3(5)
C(3)–C(4)–C(5)	107.3(5)	C(11)–C(13)–C(14)	111.5(4)	C(25)–C(26)–C(27)	121.4(5)
C(4)–C(5)–C(1)	107.7(5)	C(13)–C(14)–C(15)	112.2(4)	C(25)–C(26)–C(28)	118.8(5)
C(5)–C(1)–C(2)	108.9(5)	C(13)–C(14)–C(16)	112.4(4)	C(27)–C(26)–C(28)	119.5(5)
		C(15)–C(14)–C(16)	119.0(4)		

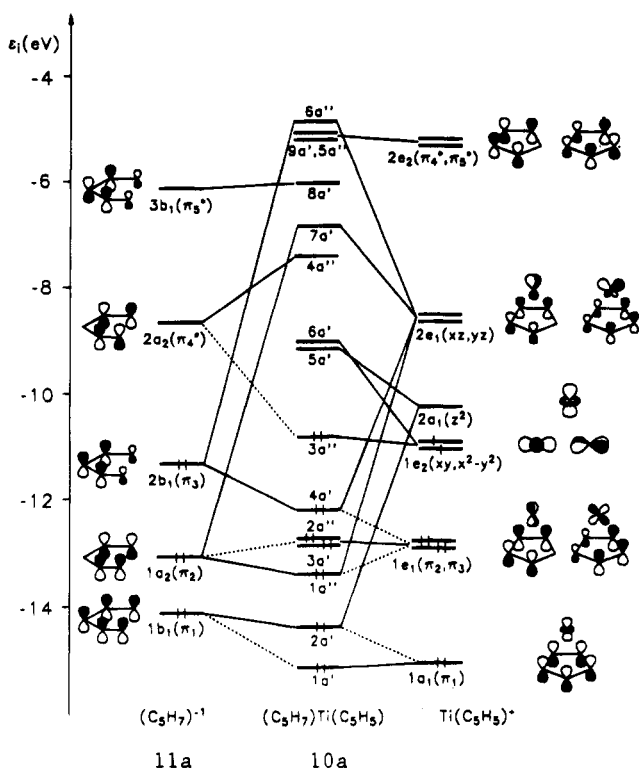
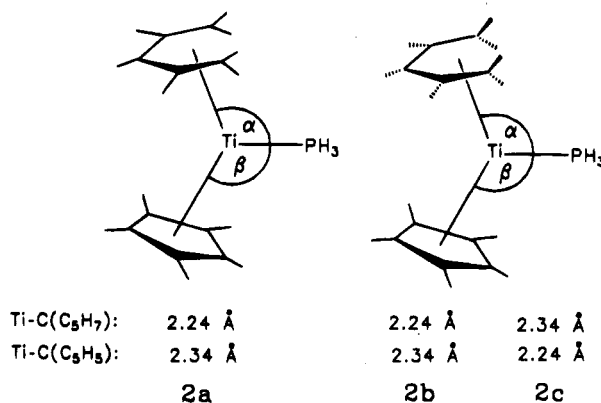


Figure 3. Simplified diagram for the interactions between the  $\text{Ti}(\text{C}_5\text{H}_5)^+$  unit and  $\text{C}_5\text{H}_7^-$  ligand **11a** to give **10a**.

$\text{N}(2)$  bonds. As a result, hybrid **9a** would seem slightly more important than **9b**. In either case, the nitrogen atoms would provide a total of three more electrons for each titanium center, leading to 16 electron configurations. The presence of C–N double bonds is indicated by their average distance, 1.266(3) Å.

The reorganization of the original dienyl fragment to a sickle orientation may be required in order to allow an outward extension of the nitrogen atoms, so that they may effectively bridge the two metal centers. Of course, it would be possible for the monomeric complex to have

Scheme 1



a 16 electron configuration, by virtue of a  $\pi$  N→Ti interaction, similar to what occurs in a monomeric bis-(ketone) coupling product,<sup>8b</sup> in which the U conformation of the original dienyl fragment is retained. However, in this case that would lead to cumulated double bonds about the nitrogen centers, and this may lead to both geometric (e.g., note  $\angle\text{C}–\text{N}–\text{Ti}$  above vs  $180^\circ$  expected for  $sp$  hybridization) and electronic destabilization. In support of this claim, it can be noted that we have observed the formation of monomeric coupling products from reactions involving 1 equiv of an imine.<sup>35</sup>

### Molecular Orbital Investigations

**Calculations.** To obtain some insight into the bonding properties of the ligands in complexes **1** and **2** as phosphine adducts, we have performed ab initio and extended-Hückel (EH) molecular orbital calculations for the model compounds **2a–c** (Scheme 1). For **2a–c** we have assumed  $C_s$  symmetry (mirror plane  $yz$ ) and we have replaced any alkyl substituents by hydrogen

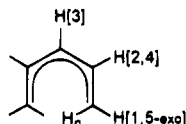
(35) Tomaszewski, R.; Rheingold, A. L.; Ernst, R. D. Unpublished results.

**Table 6. Extended-Hückel Parameters**

orbital	$H_{ii}$ (ev)	$\xi_1$	$\xi_2$	$C_1^a$	$C_2^a$	ref
H	1s	-13.60	1.30			39
C	2s	-21.40	1.625			39
	2p	-11.40	1.625			
P	3s	-18.60	1.75			40
	3p	-14.00	1.30			
Ti	4s	-8.97	1.075			
	4p	-5.44	0.675			
	3d	-10.81	4.55	1.40	0.4206	0.7839

<sup>a</sup> Contraction coefficients in the double- $\xi$  expansion. The optimized values of the angles  $\alpha$  and  $\beta$  are as follows: **2a**, 101.6°, 108.0°; **2b**, 95.9°, 112.9°; **2c**, 90.0°, 113.4°.

atoms. In **2a** the hydrogen atoms of the  $C_5H_7^-$  ligand lie in the C(1)–C(5) plane. For **2b,c**, more realistic positions were used, in which the hydrogen atom types H[1,5-exo], H[2,4], and H[3] have been bent out of the pentadienyl plane



toward the Ti atom by 20, 10, and 3°, respectively, consistent with structural data for **1** ( $L = PEt_3$ ) and related species.<sup>5</sup> The H[1,5-endo] atoms are bent in an opposite direction by 45°. With both calculation methods, constrained geometry optimizations have been performed for fixed bond distances, varying only the angles  $\alpha$  and  $\beta$  defined by the Ti–P vector and the normal to the C(1)–C(5) plane of both ligands (see Scheme 1).

In **2a,b** the bond distances were fixed at the experimental values found for complex **1** ( $L = PEt_3$ ). In the case of **2c** we have assumed 2.34 Å for the average Ti–C(pentadienyl) bond distance and 2.24 Å for the Ti–C(cyclopentadienyl) one. The parameters used in the EH calculations are given in Table 6. The ab initio calculations reported here were carried out with the Gaussian 92 program,<sup>36</sup> using Cartesian–Gaussian basis sets. For titanium and phosphorus, effective core potentials were used to replace the 1s, 2s, and 2p orbitals.<sup>37</sup> The valence orbitals of Ti and P were described by (8s, 5p, 5d)<sup>37a</sup> and (3s, 3p)<sup>37b</sup> basis sets, respectively, and contracted to a valence double- $\xi$  basis. The contraction scheme [341/311/41] at titanium and [21/21] at phosphorus has been employed. Respective basis sets of (10s, 5p) and (4s) were used for carbon and hydrogen and contracted to split valence.<sup>38</sup>

**Electronic Structure and Bonding.** The ab initio optimized values of the angles  $\alpha$  and  $\beta$  together with the relative energies and the results of Mulliken population analyses for the model compounds **2a–c** are collected in Table 7. Structure **2a**, with the angles  $\alpha$  and  $\beta$  equal to 99.3 and 103.6°, respectively, shows similarities to the bent metallocene ( $C_5H_5$ )<sub>2</sub>ML<sub>n</sub> mol-

ecules, **5**, for which in general the angles  $\alpha$  and  $\beta$  are equal and greater than 90°. The optimized values for  $\alpha$  (93.4°) and  $\beta$  (105.7°) for **2b** are in good agreement with the experimental values (95.7, 108.2°)<sup>25</sup> and support the conclusions from structural investigations that half-open metallocenes may be considered as hybrids between the ( $C_5H_5$ )<sub>2</sub>ML structures, **5**, and the open metallocene ( $C_5H_7$ )<sub>2</sub>ML structures, **6**. The model compound **2b** is more stable than **2a** by 37.5 kcal/mol.

To find out why **2b** is the preferred structure we examine first the bonding in corresponding PH<sub>3</sub>-free Ti( $C_5H_5$ )( $C_5H_7$ ) fragments, **10a,b**, making use of Hoffmann's fragment MO approach adapted to EH-calculations.<sup>39–43</sup> In Figure 3 we show the simplified interaction diagram for the bonding between the Ti( $C_5H_5$ )<sup>+</sup> unit and the planar  $C_5H_7^-$  ligand **11a** to give **10a**. The frontier orbitals of the M( $C_5H_5$ ) metal fragments are well-known.<sup>43</sup> For the d<sup>2</sup> case of Ti( $C_5H_5$ )<sup>+</sup> they are shown on the right side of Figure 3. On the left side of Figure 3 we show the frontier orbitals of the  $C_5H_7^-$  ligand **11a**. We notice that the MO shapes of **11a** are essentially the same as those for the well-known  $C_5H_5^-$  group,<sup>43</sup> however, their relative orbital energies are significantly different. According to the rules of perturbation theory, it is clear that with increasing distance between the carbon centers 1 and 5, the  $\pi$ -MO's of the  $C_5H_5^-$  ligand will be stabilized or destabilized, depending on the in-phase or out-of-phase relationships of the 2p $\pi$  AO's on the carbon atoms C(1) and C(5). Of course, breakage of the C(1)–C(5) bond, and its replacement by two C–H bonds, leads to more localization of negative charge and thereby destabilization of the dienyl anion. Thus, in contrast to the  $C_5H_5^-$  molecule, the  $C_5H_7^-$  ligand has a low-lying LUMO 2a<sub>2</sub> ( $\pi_4^*$ ) which should be able to engage in significant  $\delta$ -back-bonding interactions with metal electrons, whereas the higher energy of the LUMO of  $C_5H_5^-$  ligand (as well as the greater titanium– $C_5H_5$  ligand plane separation, 2.049 vs 1.563 Å, *vide supra*) greatly restricts such interactions. The bonding interactions present in **10a** are shown in the center of Figure 3. The 1b<sub>1</sub> MO ( $\pi_1$ ) of **11a** interacts with the 1a<sub>1</sub> ( $\pi_1$ ) and 2a<sub>1</sub> (d<sub>z<sup>2</sup></sub>) levels of Ti( $C_5H_5$ )<sup>+</sup> to give the 1a' and 2a' MO's and the LUMO 5a' of **10a**. The 1a<sub>2</sub> ( $\pi_2$ ) and 2b<sub>1</sub> ( $\pi_3$ ) MO's of **11a** interact with the 1e<sub>1</sub> ( $\pi_2$ ,  $\pi_3$ ) and 2e<sub>1</sub> (d<sub>xz</sub>, d<sub>yz</sub>) levels of Ti( $C_5H_5$ )<sup>+</sup> to give the occupied 1a'', 3a', 2a'', and 4a' MO's and the empty 7a' and 6a'' levels of **10a**. The degenerate 1e<sub>2</sub> (d<sub>xy</sub>, d<sub>x<sup>2</sup>-y<sup>2</sup></sub>) HOMO of the Ti( $C_5H_5$ )<sup>+</sup> unit becomes non-degenerate and is destabilized through interactions with occupied  $\sigma$  levels of **11a**. The resulting 3a'' and 6a' MO's of **10a** are split significantly in energy, due to the fact that the destabilizing interactions in the HOMO (3a'') are compensated for by a strong bonding admixture with the low-lying LUMO 2a<sub>2</sub> ( $\pi_4^*$ ) of **11a**, brought about by the closer energetic match between  $\pi_4^*$  of **11a** and the d<sub>xy</sub> orbital of titanium. This bonding admixture allows for an additional transfer of electron density from the metal center to the pentadienyl ligand, making the Ti–

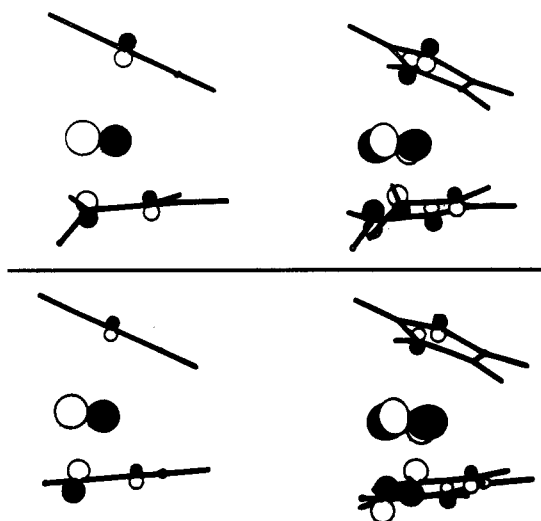
(39) Hoffmann, R. *J. Chem. Phys.* **1963**, *39*, 1397.(40) Summerville, R. H.; Hoffmann, R. *J. Am. Chem. Soc.* **1976**, *98*, 7240.(41) Lauher, J. W.; Hoffmann, R. *J. Am. Chem. Soc.* **1976**, *98*, 1729.(42) (a) Hoffmann, R.; Lipscomb, W. N. *J. Chem. Phys.* **1962**, *36*, 2179. (b) Anderson, A. B.; Hoffmann, R. *J. Chem. Phys.* **1974**, *60*, 4271. (c) Ammeter, J. H.; Bürgi, H.-B.; Thibeault, J. C.; Hoffmann, R. *J. Am. Chem. Soc.* **1978**, *100*, 3686.(43) Albright, T. A.; Burdett, J. K.; Whangbo, M.-H. In *Orbital Interactions in Chemistry*; Wiley: New York, 1985.

(36) Gaussian 92 (Revision A) was written by M. J. Frisch, G. W. Trucks, M. Head-Gordon, P. M. W. Gill, M. W. Wong, J. B. Foresman, B. G. Johnson, H. B. Schlegel, M. A. Robb, E. S. Replogle, R. Gomperts, J. L. Andres, K. Raghavachari, J. S. Binkley, C. Gonzales, R. L. Martin, D. J. Fox, D. J. Detrees, J. Baker, J. J. P. Stewart, and J. A. Pople; Gaussian, Inc., Pittsburgh PA, 1992.

(37) (a) Hay, J. P.; Wadt, W. R. *J. Chem. Phys.* **1985**, *82*, 299. (b) Wadt, W. R.; Hay, P. J. *J. Chem. Phys.* **1985**, *82*, 284.(38) Dunning, T. H.; Hay, P. J. In *Modern Theoretical Chemistry*; Plenum: New York, 1976; Chapter 1, pp 1–28.

**Table 7. Optimized Values of the Angles  $\alpha$  and  $\beta$ , Relative Energies, Charge Distributions, and Bond Overlap Populations (BOVP) for the Model Compounds 2a–c**

compd	$E_{\text{rel}}$ (kcal/mol)	$\alpha$ (deg)	$\beta$ (deg)	charge				BOVP		
				Ti	$\text{C}_5\text{H}_7$	$\text{C}_5\text{H}_5$	$\text{PH}_3$	Ti–C( $\text{C}_5\text{H}_7$ )	Ti–C( $\text{C}_5\text{H}_5$ )	Ti–P
2a	+37.5	99.3	103.6	+0.31	–0.27	–0.18	+0.14	0.23	0.12	0.08
2b	0.0	93.4	105.7	+0.43	–0.39	–0.18	+0.14	0.35	0.11	0.08
2c	+4.6	91.7	108.3	+0.40	–0.34	–0.19	+0.13	0.35	0.03	0.09

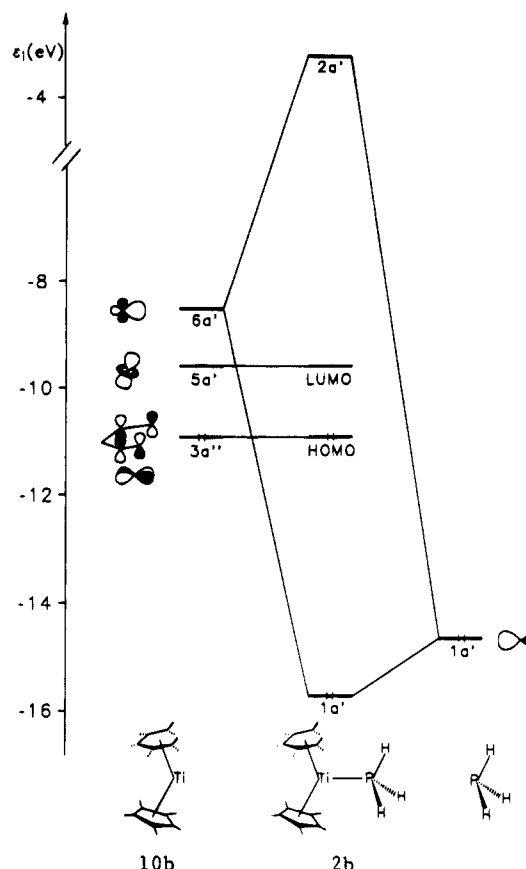
**Figure 4.** Spatial and computer-drawn HOMO ( $3a''$ ) of **10a** (top) and **10b** (bottom), perpendicular to the mirror plane.

C( $\text{C}_5\text{H}_7$ ) bonds stronger than even the Ti–C( $\text{C}_5\text{H}_5$ ) ones and provides an explanation for observations that indicate the open dienyl ligands to be much better acceptors than cyclopentadienyl.<sup>44</sup>

On going from **10a** to **10b**, one finds that the major feature of interest, the enhanced back-bonding by **11a**, remains. The predominant perturbation introduced by the bending of the hydrogen atoms of the pentadienyl ligand destabilizes the occupied  $\pi_1$ ,  $\pi_2$ , and  $\pi_3$  MO's and stabilizes the empty  $\pi_4^*$  and  $\pi_5^*$  levels, due to respective out-of-phase or in-phase admixtures of the hydrogen 1s orbitals with the  $\pi$ -levels. The stabilization of  $\pi_4^*$  is found to be ca. 0.3 eV, sufficiently large to lead to enhanced open dienyl back-bonding for **10b**. The bending of the hydrogen atoms has another consequence also. In Figure 4 we show the MO shapes of the HOMO ( $3a''$ ) in the metal fragments **10a,b**. We see that the bending of the hydrogen atoms changes the spatial direction of the  $p\pi$  components, leading to better bonding overlap in the case of **10b**, as well as **2b** (*vide infra*). We note that the HOMO ( $3a''$ ) in **10b** is more stable than that of **10a** by 0.4 eV. The coordination of the  $\text{PH}_3$  ligand to the 14 valence electron metal fragments **10a/10b** to give the 16 valence electron complexes **2a/2b** does not greatly influence the bonding between the Ti center and the  $\text{C}_5\text{H}_5^-$  or  $\text{C}_5\text{H}_7^-$  ligands. None of the occupied MO's of **10a/10b** has changed significantly in energy with respect to **2a/2b**.

The lone pair of the  $\text{PH}_3$  ligand has an appropriate shape to interact strongly with the LUMO + 1 ( $6a'$  MO

(44) (a) In addition to IR spectral data, structural data for  $\text{V}(\text{C}_5\text{H}_5)(\text{C}_5\text{H}_7)(\text{L})$  (L = CO,  $\text{PEt}_3$ ) complexes<sup>41</sup> show in each case shorter V–C distances for the open dienyl ligand; however, the difference is smaller in the CO complex, suggesting greater competition between CO and  $\text{C}_5\text{H}_7$  (rather than  $\text{C}_5\text{H}_5$ ) for back-bonding. (b) See also: Kowaleski, R. M.; Basolo, F.; Osborne, J. H.; Trogler, W. C. *Organometallics* **1988**, *7*, 1425.

**Figure 5.** Simplified diagram for the interactions between the  $\text{PH}_3$  ligand and the  $\text{Ti}(\text{C}_5\text{H}_5)(\text{C}_5\text{H}_7)$  metal fragment **10b** to give **2b**.

of the  $\text{Ti}(\text{C}_5\text{H}_5)(\text{C}_5\text{H}_7)$  fragment. The simplified interaction diagram in the case of **2b** is shown in Figure 5. The data collected in Table 7 support our qualitative analysis. The charge on the  $\text{C}_5\text{H}_5^-$  and  $\text{PH}_3$  ligands as well as the bond overlap populations Ti–C( $\text{C}_5\text{H}_5$ ) and Ti–P are essentially the same for complexes **2a,b**. Going from **2a** to **2b** the Ti center transfers an extra 0.12 e to the  $\text{C}_5\text{H}_7$  ligand and consequently the Ti–C( $\text{C}_5\text{H}_7$ ) bond overlap population is enhanced. It is clear that the bonding component to the bond overlap populations should follow the bond distances in the ground-state structure. We note that it is true for the repulsive component as well. In **2c** the Ti–C( $\text{C}_5\text{H}_7$ ) bond overlap population is the same as in **2b**, but for Ti–C( $\text{C}_5\text{H}_5$ ) it actually drops significantly, despite the shorter Ti–C( $\text{C}_5\text{H}_5$ ) distances, due to the fact that the additional repulsive interactions between the titanium center's 3(s,p) orbitals and the  $\sigma$ -orbitals of both  $\pi$ -ligands cannot be compensated for by enhanced Ti–cyclopentadienyl interactions, due to the large energy gap between the Ti  $d_{xy}$  MO and the  $\pi_4^*$  level of the  $\text{C}_5\text{H}_5^-$  ligand. Structure **2c** is thus less stable than **2b** by 4.6 kcal/mol.

### Conclusions

Half-open titanocenes of the general formula  $\text{Ti}(\text{C}_5\text{H}_5)(\text{Pd1})(\text{L})_n$  ( $\text{Pd1} = \text{C}_5\text{H}_7$ ,  $\text{L} = \text{PEt}_3$  for  $n = 1$ ;  $\text{Pd1} = 2,4\text{-C}_7\text{H}_{11}$ ,  $\text{L} = \text{PMe}_3$ ,  $\text{PEt}_3$ ,  $\text{PBu}_3$ ,  $\text{P}(\text{OMe})_3$ ,  $\text{P}(\text{OEt})_3$ ,  $\text{CO}$  for  $n = 1$  or  $\text{L} = \text{CO}$  for  $n = 2$ ) are readily accessible from  $\text{Ti}(\text{C}_5\text{H}_5)\text{Cl}_3$ . The pentadienyl ligands in such complexes readily undergo coupling reactions with acetonitrile (as well as many other unsaturated organic ligands), thus demonstrating that the pentadienyl ligands are more reactive than  $\text{C}_5\text{H}_5$ . On the other hand, a structural study of the  $\text{Ti}(\text{C}_5\text{H}_5)(2,4\text{-C}_7\text{H}_{11})(\text{PEt}_3)$  complex revealed much shorter Ti–C bond distances for the 2,4- $\text{C}_7\text{H}_{11}$  ligand compared to  $\text{C}_5\text{H}_5$ , indicating that the 2,4- $\text{C}_7\text{H}_{11}$  ligand is both more strongly bound and more reactive than  $\text{C}_5\text{H}_5$ . Molecular orbital studies confirm the enhanced bonding for the open dienyl ligands, which like their higher reactivity, may be traced to the nonaromatic nature of these ligands. Thus, the lower degree of  $\pi$  resonance delocalization experienced by the open ligands translates to higher energies for the filled  $\pi$  orbitals, and lower energies for the empty  $\pi^*$  orbitals, rendering the open ligands both better donors and acceptors than  $\text{C}_5\text{H}_5$ , thereby resulting in stronger metal–open dienyl bonding. At the same time, it must be recognized that, in coupling reactions, this resonance stabilization will be largely lost, and the aromatic cyclopentadienyl ligands have much more to lose in this

regard than the open dienyl ligands. Hence, the aromaticity of the “stabilizing”  $\text{C}_5\text{H}_5$  ligands leads both to their weaker bonding and lower chemical reactivity. Finally, the molecular orbital results reveal a particularly notable enhancement of the  $\text{M} \rightarrow$  open dienyl  $\delta$  back-bonding interactions, due to both energetic and spatial considerations, and whose counterparts in cyclopentadienyl chemistry are generally regarded as insignificant. These enhanced  $\delta$  back-bonding interactions nicely account for the previous spectroscopic indications that pentadienyl ligands serve as much stronger accepting ligands than  $\text{C}_5\text{H}_5$ ,<sup>44</sup> which may then also contribute both to the favorability exerted by pentadienyl ligands to bond to transition metal centers in low oxidation states and the inability of  $\text{N}_2$  to coordinate to even the 14 electron open titanocenes.

**Acknowledgment.** R.D.E. is grateful to the National Science Foundation for generous support of this work. R.G. and R.D.E. are also grateful to NATO for a travel grant.

**Supporting Information Available:** Tables of hydrogen atom parameters and anisotropic thermal parameters (4 pages). Ordering information is given on any current masthead page.

OM9505120



# Tandem Mass Spectrometry Study of the Zirconocenium Ion: Generation of Neutral Zirconocene in the Gas Phase

Dmitri V. Zagorevskii\* and John L. Holmes

Chemistry Department, University of Ottawa, Ottawa, Ontario K1N 6N5, Canada

Received June 13, 1995<sup>⊙</sup>

Tandem mass spectrometry methods were used to assign the structure of  $C_{10}H_{10}Zr^{+}$  ions produced by electron impact ionization of  $(C_5H_5)_2Zr(CH_3)_2$  and  $[(C_5H_5)_2ZrO]_2$ . The results were consistent with the formation of the zirconocenium radical-cation. The neutralization–reionization mass spectrum of this species showed a recovery signal, indicating that neutral monomeric zirconocene had been generated in the gas phase.

## Introduction

Bis(cyclopentadienyl) complexes,  $Cp_2M$ , of the second-row transition metals are usually very unstable species. Many of them have been observed only as reaction intermediates, and zirconocene is among these derivatives.<sup>1</sup> Attempts to produce this complex by the reduction of  $Cp_2ZrCl_2$ <sup>2,3</sup> resulted in products whose spectral characteristics indicated the presence of hydride and fulvalene ligands at the metal atom. The photolysis of  $Cp_2ZrMe_2$  resulted in a substance which was believed by the authors to be a “real” zirconocene because its IR spectrum showed no bands in the  $2000\text{ cm}^{-1}$  region which could be attributed to Zr–H bonds.<sup>4,5</sup> However, spectral characteristics provided in these and some other articles<sup>6</sup> did not unequivocally show the formation of pure zirconocene. It is obvious that so-called zirconocene is a highly reactive species;<sup>4,5</sup> produced *in situ*, it is widely used as a catalyst in organic synthesis.<sup>7</sup>

The aim of this work was to generate neutral, monomeric zirconocene in the gas phase using neutralization–reionization mass spectrometry (NRMS). This method has been previously applied to produce various neutral metal complexes,<sup>8</sup> including cyclopentadienyl complexes of transition metals.<sup>9–13</sup> Most of these species showed recovery signals in their NR mass spectra, indicating that the corresponding neutrals have been

generated as stable gas phase complexes. We have reported the “synthesis” of unstable metallocenes, such as the 19-electron rhodocene and its previously unknown monosubstituted derivatives, by NRMS.<sup>10</sup> A tandem mass spectrometry study has also been performed to generate titanocenium and neutral titanocene. The experimental result, however, showed that in the gas phase the latter species existed as hydride complexes rather than as the metallocenes.<sup>12</sup>

## Experimental Section

Electron impact, metastable ion (MI), collision-induced dissociation (CID), collision-induced dissociative ionization (CIDI), and neutralization–reionization (NR) mass spectra were recorded using a modified three-sector (BEE) VG ZAB-2F (VG Analytical Ltd., Manchester, U.K.) mass spectrometer. The ionizing electron energy was 70 eV; the ion source temperature was 120 °C. A heated inlet probe (120 °C) was used for the evaporation of organometallic compounds into the ion source.

In the CID experiments, helium and oxygen were used as collision gases; their pressure in the second collision cell (2CC) of the second field-free region (2FFR) was adjusted to give a main ion beam transmission of 85%. In the CIDI experiments, oxygen was used as collision gas at a pressure providing ca. 15% reduction of the main ion beam. In triple mass spectrometry experiments, ions of interest were produced in the 2FFR from mass-selected precursor ions; they were then energy selected by the first electric sector and collisionally activated (He or  $O_2$ ; 80% transmission) in the 3FFR. The resulting CID mass spectra were recorded by scanning the second electric sector voltage. In the NR experiments, He, Xe, and  $(CH_3)_2NH$  were used for neutralization. Their respective pressures in the first collision cells of the 2FFR or 3FFR were adjusted to provide 15%, 15%, and 50% reduction of the main ion beam. In all cases oxygen was used for reionization (80% transmission). In the NR experiments in the 2FFR and 3FFR the intercell distances were 10 and 2 cm, respectively. The best yield of survivor and other metal-containing ions was observed with the shorter intercell distance and using dimethylamine for neutralization.

## Results and Discussion

In this study, electron impact ionization of  $Cp_2ZrMe_2$  and its oxidation product,  $[Cp_2ZrO]_2$ , was used to

(12) Zagorevskii, D. V.; Holmes, J. L. *Org. Mass Spectrom.* **1993**, *28*, 49.

(13) Zagorevskii, D. V.; Nekrasov, Yu. S.; Holmes, J. L. *J. Am. Soc. Mass Spectrom.* **1993**, *4*, 216.

\* Author to whom correspondence should be addressed.  
<sup>⊙</sup> Abstract published in *Advance ACS Abstracts*, October 15, 1995.  
 (1) Cardin, D. J.; Lappert, M. F.; Raston, C. L.; Riley, P. I. In *Comprehensive Organometallic Chemistry*; Wilkinson, J., Ed.; Pergamon Press: Oxford, 1982; Vol. 3, Chapter 23.2, p 559. Pez, G. P.; Armor, J. N. *Adv. Organomet. Chem.* **1981**, *19*, 1. Geoffroy, G. L.; Wrighton, M. S. *Organometallic Photochemistry*; Academic Press: London, 1979; Chapter 6.  
 (2) Watt, G. W.; Drammond, F. O. *J. Am. Chem. Soc.* **1966**, *88*, 5926.  
 (3) Watt, G. W.; Drammond, F. O. *J. Am. Chem. Soc.* **1970**, *92*, 826.  
 (4) Alt, H. G.; Rausch, M. D. *J. Am. Chem. Soc.* **1974**, *96*, 5936.  
 (5) Gell, K. L.; Schwartz, J. *Inorg. Chem.* **1981**, *20*, 481.  
 (6) (a) Gell, K. L.; Schwartz, J. *J. Chem. Soc., Chem. Commun.* **1979**, 244. (b) Tyurin, Yu. M.; Panicheva, G. A.; Chetyrbok, L. N.; Flerov, V. N.; Buyanova, Z. A. *Nov. Polyarogr., Tezisy Dokl. Vses. Soveshch. Polyarogr.*, 6th **1975**, 244. (c) Hasari, S. K. S.; Sinha, A. *J. Bangladesh Acad. Sci.* **1988**, *12*, 135.  
 (7) See for example: Ito, H.; Taguchi, T.; Hanzawa, Y. *J. Org. Chem.* **1993**, *58*, 774.  
 (8) Zagorevskii, D. V.; Holmes, J. L. *Mass Spectrom. Rev.* **1994**, *13*, 133.  
 (9) Drewello, T.; Schwarz, H. *Int. J. Mass Spectrom. Ion Processes* **1989**, *93*, 177.  
 (10) Zagorevskii, D. V.; Holmes, J. L. *Organometallics* **1992**, *11*, 3224.  
 (11) Schröder, D.; Müller, J.; Schwarz, H. *Organometallics* **1993**, *12*, 1972.

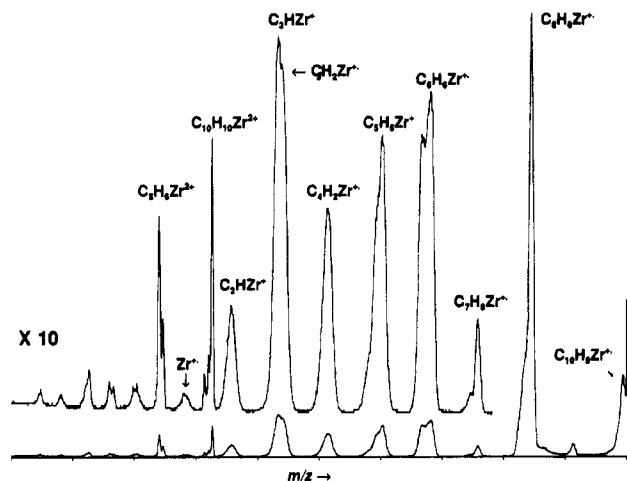


**Figure 1.** Collision-induced dissociation mass spectrum (He, 80% transmission) of  $(C_5H_5)_2Zr^{+}$  ions.

produce  $Cp_2Zr^{+}$  ions. In both cases the abundances of peaks corresponding to dehydrogenation of these ions were very small (<1% relative to  $C_{10}H_{10}Zr^{+}$ ), making insignificant any interference by lower mass isotope peaks in the mass selected  $C_{10}H_{10}^{90}Zr^{+}$  ions. Spectra of  $C_{10}H_{10}Zr^{+}$  ions containing the  $^{94}Zr$  isotope were also recorded to completely eliminate isotopic overlaps.

Before neutralization-reionization experiments, MI and CID mass spectra of  $C_{10}H_{10}Zr^{+}$  ions were recorded to obtain information about their structure. These spectra were independent of the origin of the ion.

The MI mass spectrum showed four peaks. They corresponded to  $H_2$ ,  $CH_4$ ,  $C_2H_2$ , and  $C_2H_2 + H_2$  losses with relative abundances of 14%, 2%, 79%, and 5%, respectively. The dominant formation of  $C_8H_8Zr^{+}$  ions most likely involved acetylene loss from one of the cyclopentadienyl rings. However, C and H atom mixing prior to decomposition cannot *a priori* be ruled out, because it has been observed in the molecular ions of some transition metal  $\pi$ -complexes ( $CpMC_7H_7^{+}$ , where  $M = Ti, V$ ,<sup>16</sup> methylferrocene,<sup>17</sup> etc.). To aid identification of the structure of the  $C_8H_8Zr^{+}$  ions (which relates to that of their precursors), species generated from metastable  $C_{10}H_{10}Zr^{+}$  ions in the 2FFR were mass selected and then collisionally activated in the 3FFR. The resulting CID mass spectrum showed peaks corresponding to metal-containing ions originating from various hydrocarbon losses. The  $CpZr^{+}$  ion was a particularly abundant species, implying that C and H atoms were lost from only one cyclopentadienyl ligand.

The CID mass spectrum of ion source generated  $C_{10}H_{10}Zr^{+}$  ions is shown in Figure 1. As with the MI spectrum of these ions, it contained abundant peaks due to dehydrogenation and acetylene loss. Loss of other hydrocarbon species was also observed. For example, the elimination of the second acetylene molecule followed by  $H_2$  loss resulted in  $C_6H_4Zr^{+}$  ions.

Collisional activation of  $C_{10}H_{10}Zr^{+}$  also produced  $C_5H_5Zr^{+}$  ions. They may originate from direct cleavage of the  $Cp-Zr$  bond in the  $Cp_2Zr^{+}$  ions or can be produced by stepwise reactions, for example, losses of  $C_2H_2 + C_3H_3$ . A CIDI mass spectrum of  $C_{10}H_{10}Zr^{+}$  was recorded in order to identify the lost neutral hydrocarbons by examining in turn the collision-induced dissociations of their molecular ions. A signal corresponding to  $C_5H_5^{+}$  ions was found in the CIDI mass spectrum, indicating that at least a portion of  $C_5H_5Zr^{+}$  species was formed by direct cyclopentadienyl loss from  $C_{10}H_{10}Zr^{+}$  precursors. However,  $C_5H_5^{+}$  ions were not as relatively abundant as in the CIDI (and NR) mass spectra of other metallocenium ions<sup>8,10,12,15</sup> and  $C_5H_5M^{+}$  species.<sup>9,10,12,13</sup> Thus, the successive losses of  $C_2H_2$  and  $C_3H_3$  should be entertained as a significant source of  $C_5H_5Zr^{+}$  ions.

Peaks at  $m/z$  115, 127, and 128 in the CID mass spectrum (Figure 1) may correspond to the metal-containing ions,  $ZrC_2H^{+}$ ,  $ZrC_3H^{+}$ , and  $ZrC_3H_2^{+}$ , respectively, or metal-free  $C_9H_7^{+}$ ,  $C_{10}H_7^{+}$ , and  $C_{10}H_8^{+}$ , ions, respectively. To identify the composition of these species, two kinds of experiment were carried out. In the first, ions with  $m/z$  115 and  $m/z$  127 were mass selected and collisionally excited in the 3 FFR. Their CID mass spectra clearly displayed Zr-containing singly and doubly charged ions and *did not* exhibit any hydrocarbon ions. This result is supported by the CID mass spectrum of  $C_{10}H_{10}^{94}Zr^{+}$  ions, in which all peaks above  $m/z$  89 underwent an upward shift by 4 amu, showing the presence of the metal atom.

Peaks for doubly charged zirconium-containing ions were observed in the CID mass spectrum of  $C_{10}H_{10}Zr^{+}$ . Their intensities relative to singly-charged ions increased substantially when oxygen was used as collision gas instead of helium. The most abundant species of this type were  $C_{10}H_8Zr^{2+}$ ,  $C_{10}H_6Zr^{2+}$ ,  $C_8H_8Zr^{2+}$ , and  $C_8H_6Zr^{2+}$  ions. Their formation is best explained by the rapid decomposition of energy rich  $C_{10}H_{10}Zr^{2+}$  ions produced by charge stripping of their singly charged precursors. This conclusion is based on a comparison of the CID mass spectrum of  $C_{10}H_{10}Zr^{+}$  ions and the MI mass spectrum of ion source generated  $C_{10}H_{10}Zr^{2+}$  ions. The spectra of both species exhibited the same doubly charged fragments.

To summarize the above experimental observations, the MI, CID, and CIDI mass spectra of  $C_{10}H_{10}Zr^{+}$  ions are consistent with the metallocene structure,  $Cp_2Zr^{+}$ . Formation of isomeric  $C_{10}H_{10}M^{+}$  species by hydrogen atom migration to the metal atom or cyclopentadienyl ligand coupling, which has been observed for the first-row transition element metallocenes,<sup>8,10,12,15</sup> did not take place in their zirconium-containing analogue or occurred only to a very small extent. The dissociation characteristics of  $C_{10}H_{10}Zr^{+}$  ions resembled those of metallocenium ions having heavy transition metals, such as Nb. The latter have been generated by ion molecule reactions of  $NbC_5H_6$  ions with cyclopentane or by metal-switching reactions in the  $Nb^{+}$ /ferrocene system and were characterized by their CID mass spectra.<sup>18</sup> Thus,  $C_{10}H_{10}Zr^{+}$  ions are a good source for neutral zirconocene.

The details of NR experiments were described in the Experimental Section, and the NR mass spectrum of  $Cp_2Zr^{+}$  ions is shown in Figure 2. It exhibited a

(14) Zagorevskii, D. V.; Nekrasov, Yu. S.; Chen, H.; Holmes, J. L.; Chizhevskii, I. T.; Rastova, N. I.; Kolobova, N. E. *Org. Mass Spectrom.* **1993**, *28*, 463.

(15) Zagorevskii, D. V.; Holmes, J. L. *J. Am. Soc. Mass Spectrom.* **1994**, *5*, 928.

(16) See for example: van Oven, H. O.; de Liefde Mejer, H. J. *J. Organomet. Chem.* **1970**, *23*, 159. Rettig, M. F.; Stout, C. D.; King, A.; Farnham, P. *J. Am. Chem. Soc.* **1970**, *92*, 5100.

(17) Zagorevskii, D. V.; Nekrasov, Yu. S.; Lemenovskii, D. A. *J. Organomet. Chem.* **1978**, *146*, 279.

(18) Buckner, S. W.; MacMahon, T. J.; Byrd, G. D.; Freiser, B. S. *Inorg. Chem.* **1989**, *28*, 3511.

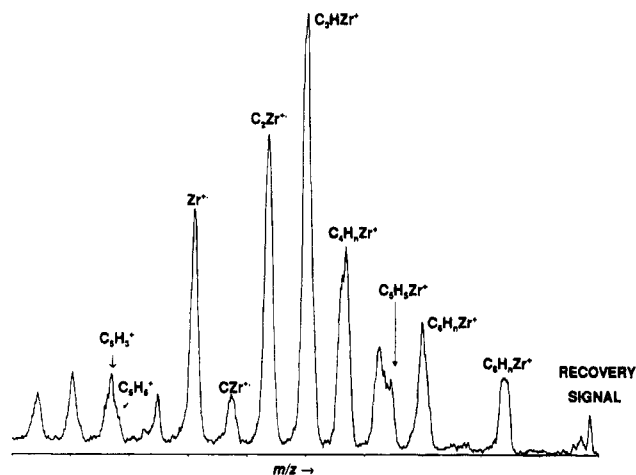


**Figure 2.** Neutralization-reionization mass spectrum ( $\text{Me}_2\text{NH}$ , 50% transmission;  $\text{O}_2$ , 80% transmission; intercell distance, 2 cm) of  $(\text{C}_5\text{H}_5)_2\text{Zr}^{++}$  ions.

recovery signal, unequivocally indicating that the corresponding neutral was generated. The abundance of survivor ions was affected by the neutralizing gas. Dimethylamine, which has previously been used in NR experiments with other metallocenes,<sup>8</sup> provided a high yield of reionized  $\text{Cp}_2\text{Zr}^{++}$  species. The observation of survivor ions in the experiment using a 10 cm intercell distance suggests that the lifetime of neutral  $\text{Cp}_2\text{Zr}$  is at least 1  $\mu\text{s}$ . The abundance of the recovery signal relative to other ions in the NR mass spectrum was roughly doubled when the experiments were carried out in the 3FFR with the two collision cells separated by 2 cm.

The NR mass spectrum of zirconocenium retains almost all the singly charged metal-containing ions that appeared in its CID mass spectrum. At the same time, enhanced abundances of ions having fewer carbon and hydrogen atoms were observed. For example, the most intense peaks in the NR mass spectrum corresponded to  $\text{ZrC}_3\text{H}^+$  and  $\text{ZrC}_2^+$  ions, while  $\text{ZrC}_6\text{H}_3^+$  and  $\text{ZrC}_8\text{H}_6^+$  ions were dominant species among  $\text{ZrC}_6\text{H}_n^+$  and  $\text{ZrC}_8\text{H}_n^+$  ions. The fragmentation of reionized zirconocene, rather than decomposition processes of neutral  $\text{Cp}_2\text{Zr}$ , is proposed to be the major source of the metal-containing

ions. The high abundances of dissociation products is simply accounted for by reionized  $\text{Cp}_2\text{Zr}^{++}$  having a higher internal energy than their ion source generated counterparts. The latter has been demonstrated in the results of an NRMS study of  $\text{W}(\text{CO})_6^{++}$  ions.<sup>19</sup>

The NR mass spectrum of  $\text{Cp}_2\text{Zr}^{++}$  ions containing the  $^{94}\text{Zr}$  isotope was recorded to separate metal-containing from metal-free ions. All peaks observed in the NR spectrum of  $\text{Cp}_2^{90}\text{Zr}^{++}$  ions at  $m/z \geq 90$  were found in the NR mass spectrum of  $\text{Cp}_2^{94}\text{Zr}^{++}$  ions but were shifted by 4 Da to higher mass. No peaks corresponding to  $\text{C}_{10}\text{H}_n^+$  ions were found, ruling out the coupling of two cyclopentadienyl ligands in the coordination sphere of the zirconium atom. Such hydrocarbon ions have been observed for other metallocenium ions, whose NR mass spectra have been published previously.<sup>8,10,12,15</sup> This lack of ligand coupling may be due to the larger  $\text{Zr}^+$  ion radius and a stronger M-C (M-Cp) bond relative to those of the first-row transition elements. No data are available on the  $\text{L}_n\text{Zr}^+-\text{Cp}$  bond dissociation energies, but it should be high, because no significant  $\text{CpZr}^{++}$  peaks were found in the mass spectrum of  $\text{Cp}_2\text{Zr}(\text{CH}_3)_2$ .

In conclusion, this tandem mass spectrometric study has shown that  $\text{C}_{10}\text{H}_{10}\text{Zr}^{++}$  ions produced in the gas phase from a variety of precursors indeed have the metallocene structure. Neutralization-reionization experiments with these ions showed the intermediate formation of neutral zirconocene and is the first reported observation of this molecule in its monomeric form. The results of the present work demonstrate again the great utility of neutralization-reionization mass spectrometry for the generation and characterization of gas phase neutral organometallic complexes, which are extremely labile in the condensed phase.

**Acknowledgment.** J.L.H. thanks the National Sciences and Engineering Research Council of Canada for continuing financial support. The authors thank N. George Alameddin (University of Florida, Gainesville, FL) for the samples of zirconium complexes.

OM950452Y

(19) Beranová, Š.; Wesdemiotis, C. *J. Am. Soc. Mass Spectrom.* **1994**, *5*, 1093.

# Theoretical Aspects of the Bonding in Organometallic Clusters Containing Exposed Dicarbon ( $C_2$ ) Entities. 1. Tetrametallic Systems

Gilles Frapper<sup>†</sup> and Jean-François Halet<sup>\*,†</sup>

Laboratoire de Chimie du Solide et Inorganique Moléculaire, URA CNRS 1495, Université de Rennes I, Avenue du Général Leclerc, 35042 Rennes Cedex, France

Received April 11, 1995<sup>®</sup>

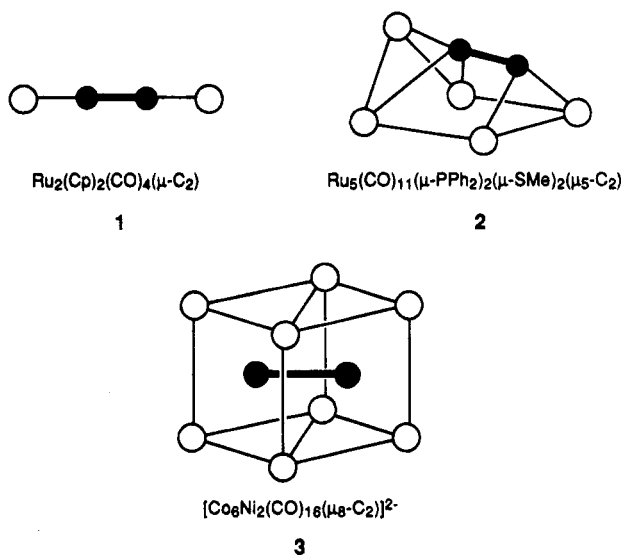
The electronic and geometrical structures of different tetrametallic- $C_2$  systems reported in the literature, such as  $Fe_2Ru_2(CO)_9(Cp)_2(C_2)$ ,  $Fe_2Ru_2(CO)_{10}(Cp^*)_2(C_2)$ , and  $Ru_4(CO)_{12}(\mu-PPh_2)_2(C_2)$ , are analyzed and compared by use of molecular orbital calculations. Various transformations between isomers, known and unknown, are discussed, and other arrangements not yet reported are proposed.

## Introduction

Diverse all-carbon ligands, such as  $C_n$  small linear carbon units ( $n = 3-18$ ),  $C_2$  dumbbells, or single carbon atoms, can now be stabilized in transition-metal complexes.<sup>1</sup> Such compounds are attractive not only as possible electronic and catalytic materials,<sup>1</sup> but also simply as molecular analogs of solid state carbide compounds.<sup>2</sup> In addition, complexes with a dicarbon ( $C_2$ ) unit are rapidly developing as models for elementary species on heterogeneous surfaces.<sup>3</sup>

Several coordination modes of the  $C_2$  entity, such as unsupported (end-on-bonded) (1),<sup>4</sup> supported (side-on-bonded) (2),<sup>5</sup> or fully encapsulated (3),<sup>6</sup> have been recognized in polymetallic- $C_2$  complexes.<sup>7,8</sup> As part of a general understanding of the bonding and reactivity of mono- and polycarbide ligands linked to polynuclear organometallic clusters,<sup>9-12</sup> we have undertaken a

theoretical analysis of the compounds listed in Table 1, containing supported (or *exposed*)  $C_2$  units. We report here our results obtained on the tetrametallic- $C_2$  systems. Calculations have been made using the extended Hückel method (see the Appendix).



## Geometric and Electron-Counting Considerations

Three different bonding modes of  $C_2$  have been established in the  $M_4C_2$  clusters listed in Table 1. The most common mode is that found in the complex  $[Fe_4(CO)_{11}(Cp)(C_2)]^-$ , 4, where the  $C_2$  ligand binds in a  $\mu_3-\eta^1(\sigma): \eta^2(\pi)(\perp)$  fashion<sup>26</sup> with a metallic triangle and

(12) Halet, J.-F. In *Topics in Physical Organometallic Chemistry*; Gielen, M., Ed.; Freund Publishing House: London, 1992; Vol. 4, p 221.

(13) Jensen, M. P.; Sabat, M.; Shriver, D. F. *J. Cluster Sci.* **1990**, *1*, 75.

(14) Akita, M. Unpublished results.

(15) Akita, M.; Terada, M.; Moro-oka, Y. *Organometallics* **1992**, *11*, 1825.

(16) Koutsantonis, G. A.; Selegue, J. P.; Wang, J.-G. *Organometallics* **1992**, *11*, 2704.

(17) Akita, M.; Sugimoto, S.; Tanaka, M.; Moro-oka, Y. *J. Am. Chem. Soc.* **1992**, *114*, 7581.

(18) Weidmann, T.; Weinrich, V.; Wagner, B.; Robl, C.; Beck, W. *Chem. Ber.* **1991**, *124*, 1363.

(19) Bruce, M. I.; Snow, M. R.; Tiekink, E. R.; Williams, M. L. *J. Chem. Soc., Chem. Commun.* **1987**, 701.

<sup>†</sup> e-mail address: gilles@univ-rennes1.fr and halet@univ-rennes1.fr

<sup>®</sup> Abstract published in *Advance ACS Abstracts*, October 1, 1995.

(1) See for example: (a) Chisholm, M. H. *Angew. Chem., Int. Ed. Engl.* **1991**, *30*, 673. (b) Diederich, F.; Rubin, Y. *Angew. Chem., Int. Ed. Engl.* **1992**, *31*, 1101. (c) Weng, W.; Ramsden, J. A.; Arif, A. M.; Gladysz, J. A. *J. Am. Chem. Soc.* **1993**, *115*, 3824 and references therein. (d) Lang, H. *Angew. Chem., Int. Ed. Engl.* **1994**, *33*, 547.

(2) See for example: (a) Simon, A. *Angew. Chem., Int. Ed. Engl.* **1988**, *27*, 159. (b) Li, J.; Hoffmann, R. *Chem. Mater.* **1989**, *1*, 83. (c) Adachi, G.-Y.; Imanaka, N.; Fuzhong, Z. In *Handbook on the Physics and Chemistry of Rare Earths*; Gschneider, K. A., Jr.; Eyring, L., Eds.; Elsevier: Amsterdam, 1991; vol. 15, p 62. (d) Pöttgen, R.; Jeitschko, W. *Z. Naturforsch.* **1992**, *47b*, 358. (e) Long, J. R.; Halet, J.-F.; Hoffmann, R.; Meyer, H.-J.; Saillard, J.-Y. *New J. Chem.* **1992**, *16*, 839. (f) Witkar, F.; Kahal, S.; Halet, J.-F.; Saillard, J.-Y.; Bauer, J.; Rogl, P. *J. Am. Chem. Soc.* **1994**, *116*, 251.

(3) (a) Sylvestre, J.; Hoffmann, R. *Langmuir* **1985**, *1*, 621. (b) Zheng, C.; Apeloig, Y.; Hoffmann, R. *J. Am. Chem. Soc.* **1988**, *110*, 749 and references therein.

(4) Koutsantonis, G. A.; Selegue, J. P. *J. Am. Chem. Soc.* **1991**, *113*, 2316. For a theoretical study see for example: (a) Heidrich, J.; Steimann, M.; Appel, M.; Beck, W.; Phillips, J. R.; Troger, W. C. *Organometallics* **1990**, *9*, 1296. (b) Frapper, G.; Kertesz, M. *Inorg. Chem.* **1993**, *32*, 732.

(5) Adams, C. J.; Bruce, M. I.; Skelton, B. W.; White, A. H. *J. Chem. Soc., Chem. Commun.* **1992**, 26.

(6) Arrigoni, A.; Ceriotti, A.; Della Pergola, R.; Manassero, M.; Masciocchi, N.; Sansoni, M. *Angew. Chem., Int. Ed. Engl.* **1984**, *23*, 322.

(7) Beck, W.; Niemer, B.; Wieser, M. *Angew. Chem., Int. Ed. Engl.* **1993**, *32*, 923.

(8) Akita, M.; Moro-oka, Y. *Bull. Chem. Soc. Jpn.* **1995**, *68*, 420.

(9) Halet, J.-F.; Saillard, J.-Y.; Lissillour, R.; McGlinchey, M. J.; Jaouen, G. *Organometallics* **1986**, *5*, 139.

(10) Halet, J.-F.; Mingos, D. M. P. *Organometallics* **1988**, *7*, 51.

(11) Halet, J.-F.; Evans, D. G.; Mingos, D. M. P. *J. Am. Chem. Soc.* **1988**, *110*, 87.

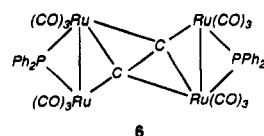
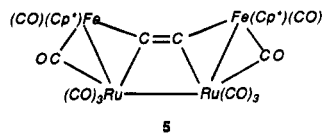
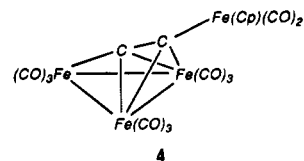
Table 1. X-ray Characterized Transition Metal Clusters Containing Exposed Dicarbon (C<sub>2</sub>) Units

compound	MVE <sup>a</sup>	bonding mode	$n(\text{C}_2^{2-})^c$	$d_{\text{C-C}}$ (Å)	ref
<i>M</i> <sub>4</sub> ( $\mu_4$ -C <sub>2</sub> )					
[Fe <sub>4</sub> (CO) <sub>11</sub> (Cp)(C <sub>2</sub> )]	66	A	8	1.288(5)	13
Fe <sub>4</sub> (CO) <sub>9</sub> (Cp* <sub>2</sub> (C <sub>2</sub> ))	66	A	8	1.292(9)	14
Fe <sub>3</sub> Co(Cp*)(CO) <sub>11</sub> (C <sub>2</sub> )	66	A	8	1.261(10)	14
Fe <sub>2</sub> Co <sub>2</sub> (Cp* <sub>2</sub> (CO) <sub>8</sub> (C <sub>2</sub> ))	66	A	8	1.34(3)	15
Fe <sub>2</sub> Ru <sub>2</sub> (CO) <sub>11</sub> (Cp)(H)(C <sub>2</sub> )	66	A	8	1.30(2)	14
[FeRu <sub>3</sub> (CO) <sub>11</sub> (Cp)(C <sub>2</sub> )]	66	A	8	1.271(9)	14
FeRu <sub>3</sub> (CO) <sub>11</sub> (Cp)(H)(C <sub>2</sub> )	66	A	8	1.33(2)	14
Fe <sub>2</sub> Ru <sub>2</sub> (CO) <sub>9</sub> (Cp) <sub>2</sub> (C <sub>2</sub> )	66	A	8	1.35(1)	16
Fe <sub>2</sub> Ru <sub>2</sub> (CO) <sub>10</sub> (Cp* <sub>2</sub> (C <sub>2</sub> ))	66	B	6	1.24(1)	17
Co <sub>2</sub> Re <sub>2</sub> (CO) <sub>14</sub> (C <sub>2</sub> )	66	A	8	1.282 (17)	18
Ru <sub>4</sub> (CO) <sub>12</sub> ( $\mu$ -PPh <sub>2</sub> ) <sub>2</sub> (C <sub>2</sub> )	68	C	8	1.275(11)	19
<i>M</i> <sub>5</sub> ( $\mu_5$ -C <sub>2</sub> )					
Fe <sub>2</sub> Ru <sub>5</sub> (CO) <sub>17</sub> Cp <sub>2</sub> (C <sub>2</sub> ) <sub>2</sub>	112	D	8	1.32(2)/1.34(2)	20
FeRu <sub>6</sub> (CO) <sub>16</sub> Cp( $\mu_5$ -C <sub>2</sub> H)(C <sub>2</sub> )	104	E	8	1.334(9)	20
Ru <sub>5</sub> (CO) <sub>11</sub> (py) <sub>2</sub> ( $\mu$ -PPh <sub>2</sub> ) <sub>2</sub> (C <sub>2</sub> )	78	F	8	1.301(5)	21
Ru <sub>5</sub> (CO) <sub>11</sub> ( $\mu$ -SMe) <sub>2</sub> ( $\mu$ -PPh <sub>2</sub> ) <sub>2</sub> (C <sub>2</sub> )	80	E	8	1.305(5)	5
Ru <sub>5</sub> (CO) <sub>12</sub> ( $\mu$ -SMe) <sub>2</sub> ( $\mu$ -PPh <sub>2</sub> ) <sub>2</sub> (C <sub>2</sub> )	82	E	8	1.26(2)/1.31(2)	5
<i>M</i> <sub>6</sub> ( $\mu_6$ -C <sub>2</sub> )					
[Fe <sub>3</sub> Co <sub>3</sub> (CO) <sub>18</sub> (C <sub>2</sub> )]	94	G	8	1.362(8)	22
Fe <sub>2</sub> Ru <sub>6</sub> (CO) <sub>17</sub> (Cp* <sub>2</sub> (C <sub>2</sub> ) <sub>2</sub> )	120	G	8	1.35(4)/1.37(3)	17
FeRu <sub>5</sub> (CO) <sub>14</sub> ( $\mu$ -SMe) <sub>2</sub> ( $\mu$ -PPh <sub>2</sub> ) <sub>2</sub> (C <sub>2</sub> )	94	H	8	1.355(9)	23
Co <sub>6</sub> (CO) <sub>18</sub> (C <sub>2</sub> )	96	G	8	1.426(9)	24
Co <sub>6</sub> (CO) <sub>14</sub> ( $\mu_4$ -S)(C <sub>2</sub> )	92	G	8	1.37(2)	25
<i>M</i> <sub>9</sub> ( $\mu_8$ -C <sub>2</sub> )					
[Co <sub>4</sub> Ru <sub>5</sub> (CO) <sub>18</sub> ( $\mu_3$ -SMe) <sub>2</sub> ( $\mu$ -PPh <sub>2</sub> ) <sub>2</sub> (C <sub>2</sub> )]	134	I	8	1.41(4)	23

<sup>a</sup> Abbreviations used: Me = CH<sub>3</sub>, Ph = C<sub>6</sub>H<sub>5</sub>, Cp = C<sub>5</sub>H<sub>5</sub>, Cp\* = C<sub>5</sub>Me<sub>5</sub>, Cp<sup>#</sup> = C<sub>5</sub>Me<sub>4</sub>Et, py = C<sub>5</sub>H<sub>5</sub>N. <sup>b</sup> Metallic Valence Electron Count. <sup>c</sup> Bonding mode: A =  $\mu_4$ - $\eta^2$ : $\eta^2$ : $\eta^1$ : $\eta^1$ , B =  $\mu_4$ - $\eta^1$ : $\eta^1$ : $\eta^1$ : $\eta^1$ , C =  $\mu_4$ - $\eta^2$ : $\eta^1$ : $\eta^2$ : $\eta^1$ , D =  $\mu_5$ - $\eta^1$ : $\eta^1$ : $\eta^1$ : $\eta^2$ : $\eta^1$ , E =  $\mu_5$ - $\eta^1$ : $\eta^1$ : $\eta^2$ : $\eta^2$ : $\eta^1$ , F =  $\mu_5$ - $\eta^1$ : $\eta^2$ : $\eta^1$ : $\eta^1$ , G =  $\mu_6$ - $\eta^1$ : $\eta^1$ : $\eta^1$ : $\eta^1$ : $\eta^1$ , H =  $\mu_6$ - $\eta^1$ : $\eta^1$ : $\eta^2$ : $\eta^2$ : $\eta^1$ : $\eta^1$ , I =  $\mu_8$ - $\eta^1$ : $\eta^1$ : $\eta^2$ : $\eta^2$ : $\eta^1$ : $\eta^1$ : $\eta^1$ . <sup>d</sup> Number of electrons of C<sub>2</sub><sup>2-</sup> given to the metallic framework.

in an  $\eta^1(\sigma)$  fashion with the remote iron center (bonding mode A). The former  $\mu_3(\perp)$  bonding mode is familiar in trimetallic-acetylide M<sub>3</sub>( $\mu_3(\perp)$ C<sub>2</sub>R) complexes.<sup>27</sup> The 66-metallic valence electron (MVE) M<sub>4</sub> compound **4** can be considered as an electron-precise molecule (i.e. with two-electron-two-center bonds) with the C<sub>2</sub><sup>2-</sup> entity<sup>28</sup> acting as an eight-electron donor. It can be viewed as an M<sub>4</sub> system comprising a 48-MVE trimetallic species linked to an 18-MVE mononuclear species via a C<sub>2</sub> bridge. Alternatively, it may be described as a closo-trigonal-bipyramidal Fe<sub>3</sub>C<sub>2</sub> structure with 52 cluster valence electrons (CVE) or six skeletal electron pairs (SEP) within the framework of the polyhedral skeletal electron pair (PSEP) theory.<sup>29</sup> In Fe<sub>2</sub>Ru<sub>2</sub>(CO)<sub>10</sub>(Cp\*<sub>2</sub>(C<sub>2</sub>)), **5**, the C<sub>2</sub> group is ensconced in the middle of a trapezoidal metallic framework in such a way that each carbon is

attached in a  $\sigma$  fashion to two metal atoms. To our knowledge such a bonding mode ( $\mu_4$ - $\eta^1$ : $\eta^1$ : $\eta^1$ : $\eta^1$ , mode B) is scarce and has been reported only in **5**. Despite the rather short C–C bond indicating that some triple-bond character might remain (see Table 1), compound **5** is an electron-precise system with 66 MVEs if the C<sub>2</sub><sup>2-</sup> ligand provides six electrons to the metallic framework. This leads Akita and co-workers to describe **5** as a permetalated ethene.<sup>17</sup> The third bonding mode ( $\mu_4$ - $\eta^2$ : $\eta^1$ : $\eta^2$ : $\eta^1$ , mode C) is exemplified by the cluster Ru<sub>4</sub>(CO)<sub>12</sub>( $\mu$ -PPh<sub>2</sub>)<sub>2</sub>(C<sub>2</sub>), **6**, where the C<sub>2</sub> unit asymmetrically bridges ( $\sigma + \pi$ ) two Ru<sub>2</sub> fragments.



(20) Akita, M.; Hirakawa, H.; Tanaka, M.; Moro-oka, Y. *J. Organomet. Chem.* **1995**, *485*, C14.

(21) Adams, C. J.; Bruce, M. I.; Skelton, B. W.; White, A. H. *J. Organomet. Chem.* **1992**, *423*, 97.

(22) Jensen, M. P.; Phillips, D. A.; Sabat, M.; Shriver, D. F. *Organometallics* **1992**, *11*, 1859.

(23) Adams, C. J.; Bruce, M. I.; Skelton, B. W.; White, A. H. *J. Chem. Soc., Chem. Commun.* **1993**, 446.

(24) (a) Brice, M. D.; Penfold, B. R. *Inorg. Chem.* **1972**, *11*, 1381. (b) Geiser, U.; Kini, A. M. *Acta Crystallogr.* **1993**, *C49*, 1322.

(25) Gervasio, G.; Rossetti, R.; Stanghellini, P. L.; Bor, G. *Inorg. Chem.* **1984**, *23*, 2073.

(26) Thomas, M. G.; Muettterties, E. L.; Day, R. O.; Day, V. W. *J. Am. Chem. Soc.* **1976**, *98*, 4645.

(27) See for example: (a) Sappa, E.; Tirripicchio, A.; Braunstein, P. *Chem. Rev.*, **1983**, *83*, 203. (b) Carty, A. J.; Taylor, N. J.; Sappa, E.; Tirripicchio, A.; Tirripicchio Camellini, M. *Organometallics* **1991**, *10*, 1907 and references therein.

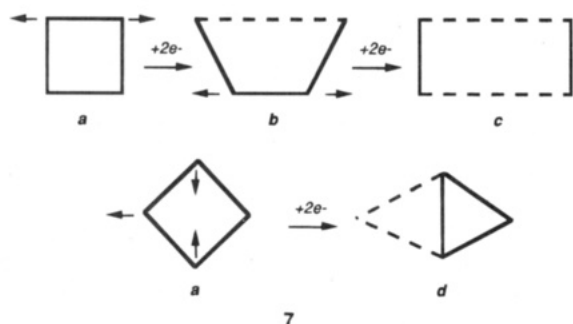
(28) There are different ways to formally count electrons of the dicarbon moiety. We choose here to consider C<sub>2</sub> as a dianionic species rather than a neutral species in order that it agrees with the octet rule. Note that the number of frontier molecular orbitals of C<sub>2</sub> which may participate to the M–C bonding is regardless of this electron-counting convention.

(29) Mingos, D. M. P.; Wales, D. J. *Introduction to Cluster Chemistry*, Prentice-Hall: Englewood Cliffs, NJ, 1990.

An electron-precise count of 68-MVE is achieved for **6** if the C<sub>2</sub><sup>2-</sup> bridge brings eight electrons to the metallic system.

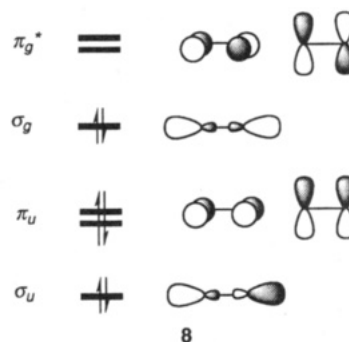
As illustrated in **7**, tetrametallic species **4–6** can in turn be derived from the 64-MVE square metal clus-

ters<sup>30</sup> upon formal addition of electrons. Adding two electrons to the square **7a** should result in the breaking of one edge leading to the trapezoidal structure **7b** analogous to that of the 66-MVE complex **5**. Further two-electron addition affords the rectangular **7c** framework with two M–M bonds as observed in the 68-MVE compound **6**. Structure **7d**, which is reported for the 66-MVE species **4**, can be obtained by cleavage of two bonds and formation of a new one. Consequently, with three M–M bonds models **7d** and **7b**, i.e. complexes **4** and **5**, can formally be regarded as skeletal M<sub>4</sub> isomers. However, such a description conceals the fact that the formal transformation of the “spiked” triangle present in **4** into the open square of **5** requires the addition of a two-electron ligand since C<sub>2</sub><sup>2-</sup> acts as an eight- and a six-electron donor ligand in **4** and **5**, respectively (compare also Fe<sub>2</sub>Ru<sub>2</sub>(CO)<sub>9</sub>(Cp)<sub>2</sub>(C<sub>2</sub>) and **5** in Table 1). This illustrates how the C<sub>2</sub> unit can also induce isomerism in these M<sub>4</sub>C<sub>2</sub> compounds. Both the number of metal-metal bonds and the coordination modes of C<sub>2</sub> must be considered for a full description of the tetrametallic-C<sub>2</sub> clusters.



Before describing the electronic structures of the different M<sub>4</sub>C<sub>2</sub> complexes, we may first need to consider the orbital and electronic characteristics of the C<sub>2</sub> ligand. The orbital pattern of a C<sub>2</sub><sup>2-</sup> species with a bond of ca. 1.34 Å, which is roughly the average C–C distance observed in the compounds reported in Table 1, is typical of that of homonuclear diatomic molecule.<sup>31,32</sup> The orbitals that may be involved in interaction with the metallic host are illustrated in 8. Of the ten valence electrons, eight occupy the σ<sub>u</sub>, π<sub>u</sub>, and σ<sub>g</sub> frontier molecular orbitals (FMO). Analogously to sulfur or chlorine, the C<sub>2</sub><sup>2-</sup> entity is a rather versatile ligand able to act as a formal donor of different numbers of electrons: 4, 6, or 8 (or 2, 4, and 6 if C<sub>2</sub> is counted as a neutral ligand<sup>28</sup>), depending on the electronic demands of the metallic fragment which it interacts with (see Table 1). It is also a rather strong π-acceptor through its vacant π<sub>g</sub>\* FMOs. Consequently, both forward and back donation to/from the metallic moiety leads to the anticipation of some bond lengthening compared to that of the “free” C<sub>2</sub> species.<sup>32</sup> In solid-state rare-earth or alkaline-earth metal carbide materials in which ionic bonding is generally important, the measured C–C bond lengths often constitute a gauge for evaluating the

formal charge of the C<sub>2</sub> units, i.e. (Ca<sup>2+</sup>)(C<sub>2</sub><sup>2-</sup>) (1.191 Å) or (Gd<sub>2</sub>Cl<sub>2</sub>)<sup>4+</sup>(C<sub>2</sub><sup>4-</sup>) (1.36 Å).<sup>33</sup> In contrast, the variation of the C–C distances in molecular organometallic-C<sub>2</sub> compounds, in which covalent bonding prevails, is not so straightforward and seems to depend on subtle electronic effects coming from the metallic environment (see Table 1).<sup>10</sup>



### The 66-Electron Model [Ru<sub>4</sub>(CO)<sub>11</sub>(Cp)(C<sub>2</sub>)]<sup>-</sup> and Its Experimental Analogues

We commence our study with the 66-electron complex [Ru<sub>4</sub>(CO)<sub>11</sub>(Cp)(C<sub>2</sub>)]<sup>-</sup>, **9**, of C<sub>s</sub> symmetry, used as a model system for compound **4** and analogues listed in Table 1 (see the Appendix). Using a fragment analysis, the formation of **9** can be envisaged as arising from interaction of the FMOs of the C<sub>2</sub><sup>2-</sup> ligand with those of the tetrametallic fragment [Ru<sub>4</sub>(CO)<sub>11</sub>(Cp)]<sup>+</sup>, as illustrated in Figure 1. The latter is comprised of an equilateral triangular Ru<sub>3</sub>(CO)<sub>9</sub> entity and a mononuclear Ru(Cp)(CO)<sub>2</sub> fragment. Consequently, above a nest of twelve nonbonding “t<sub>2g</sub>” metallic MOs (nine for Ru<sub>3</sub>(CO)<sub>9</sub> and three for Ru(CO)<sub>2</sub>(Cp)), we recognize the seven FMOs which characterize a metallic M<sub>3</sub>L<sub>9</sub> triangle (the in-

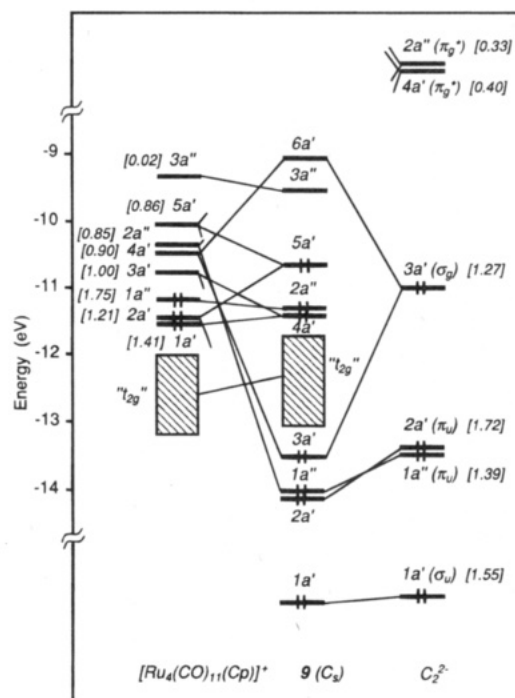


**Figure 1.** Molecular orbital diagram of the 66-MVE model **9**, [Ru<sub>4</sub>(CO)<sub>11</sub>(Cp)(C<sub>2</sub>)]<sup>-</sup>. The numbers in brackets indicate the electron occupation of FMOs after interaction.

(30) (a) Lauher, J. W. *J. Am. Chem. Soc.* **1978**, *100*, 5301. (b) Lauher, J. W. *Int. J. Quantum. Chem.* **1988**, *22*, 309.

(31) Albright, T. A.; Burdett, J. K.; Whangbo, M.-H. *Orbital Interactions in Chemistry*, Wiley: New York, 1985; pp 78–80.

(32) Bauschlicher, C. W., Jr.; Langhoff, S. R. *J. Chem. Phys.* **1987**, *87*, 2919.

(33) Miller, G.; Burdett, J. K.; Schwarz, C.; Simon, A. *Inorg. Chem.* **1986**, *25*, 4437.

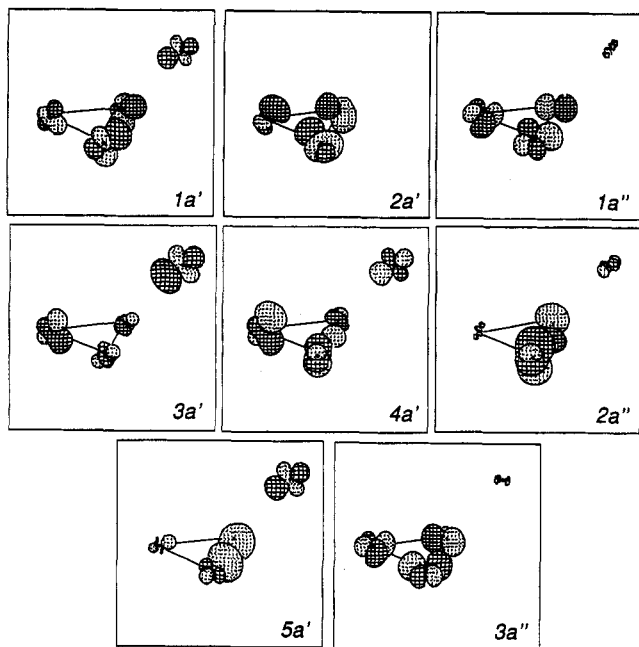
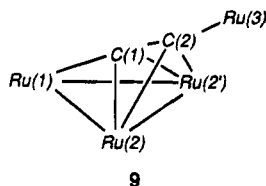


**Figure 2.** Frontier molecular orbitals of the metallic fragment  $[\text{Ru}_4(\text{CO})_{11}(\text{Cp})]^-$ .

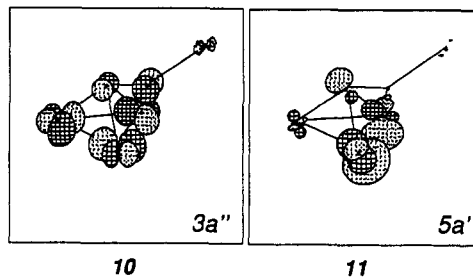
plane  $1a'$ ,  $1a''$ , and  $3a''$ , and the out-of-plane  $2a'$ ,  $4a'$ ,  $2a''$ , and  $5a'$  MOs),<sup>34</sup> together with  $3a'$  which corresponds to the  $\sigma$ -type FMO of the remote  $\text{ML}_5$  fragment.<sup>35</sup> They are sketched in Figure 2. Counting  $\text{C}_2$  as a dianion ligand, three metallic FMOs are formally occupied before interaction.



As expected, the out-of-plane FMOs of the trimetallic fragment interact strongly with the  $\text{C}_2$  FMOs. Both for overlap and energy reasons the main interaction occurs between the metallic  $4a'$  MO which is heavily weighted on Ru(1) and the  $\text{C}_2$   $3a'$  ( $\sigma_g$ ) FMO. This strongly bonding interaction formally corresponds to the Ru(1)–C(1)  $\sigma$ -bond. The  $\text{C}_2$   $3a'$  ( $\sigma_g$ ) FMO is also involved to a less extent in some  $\sigma$ -bonding with the in-plane metallic  $1a'$  FMO, which is localized on Ru(2) and Ru(2') (see Figure 2). The dicarbon unit is linked in a  $\pi$ -type fashion to Ru(2) and Ru(2') through strong forward electron donation from the  $\pi$  FMOs of  $\text{C}_2$  ( $2a'$  and  $1a''$ ) toward the acceptor metallic  $5a'$  and  $2a''$  FMOs, and a rather important back-donation from the metallic  $2a'$  and  $1a''$  FMOs into the  $\text{C}_2$   $\pi^*$   $4a'$  and  $2a''$  FMOs. In addition, a strong  $\sigma$ -type interaction occurs between the  $3a'$  metallic FMO which is localized on the remote metal center and the low-lying  $1a'$  ( $\sigma_u$ ) FMO of the dicarbon moiety. This interaction is responsible for the Ru(3)–C(2)  $\sigma$ -bond observed in model **9**. Note that despite the fact that **9** is an electron-precise molecule and that some MOs might formally correspond to two-electron-two-center bonds, the M–M and M–C bonding is rather delocalized overall.

The different orbital interactions between the metallic triangle and the  $\text{C}_2$  ligand described above lead to computed M–C overlap populations which reflect rather well the different M–C bond lengths measured in the experimental complexes analogous to model **9**.<sup>13–16,18</sup> The Ru(1)–C(1) and Ru(3)–C(2) overlap populations are large (0.54 and 0.51, respectively). They correspond to the shortest M–C contacts of  $\sigma$ -type.  $\pi$ -type M–C contacts are longer in agreement with the corresponding Ru(2)–C(1) and Ru(2)–C(2) overlap populations (0.20 and 0.24, respectively).

A rather large gap of ca. 1.2 eV separates the highest occupied molecular orbital (HOMO),  $5a'$ , from the lowest unoccupied molecular orbital (LUMO),  $3a''$ , ensuring the stability to model **9**. The LUMO, shown in **10**, consists mainly of the metallic  $3a''$  FMO. It is less than 6% carbon ( $\text{C}_2$ ) in character. The HOMO sketched in **11**, which derives mainly from the metallic  $2a'$  FMO mixed somewhat with the metallic  $5a'$  FMO, possesses less than 3% carbon character. Consequently, the reactivity with either nucleophilic or electrophilic incoming substrates should attack the metallic triangle rather than the dicarbon ligand if the reactions are orbital controlled. This statement needs, however, to be mitigated somewhat since the  $6a'$  MO which lies just above the  $3a''$  LUMO possesses significant carbon character, particularly on the most exposed C(1) atom (17%). This carbon atom should therefore be reactive vis-a-vis nucleophile reagents if this M–C antibonding MO plays a role.<sup>22</sup> Nevertheless, the occupied FMOs of the  $\text{C}_2^{2-}$  ligand being strongly involved in bonding with the metallic fragment, should render the  $\text{C}_2$  unit rather immune to electrophilic attack.



Calculations performed on the experimental clusters such as  $\text{Fe}_2\text{Ru}_2(\text{CO})_9(\text{Cp})_2(\text{C}_2)$  yield results comparable to those obtained for model **9**. We noted that C(2) was slightly more negatively charged than C(1), in agreement with the  $^{13}\text{C}$  NMR chemical shift values which indicate that the latter is generally more deshielded.<sup>13,15,22</sup>

From structural and physical property measurements, Akita and co-workers have suggested that a remote metallic fragment such as  $\text{Fe}(\text{Cp}^*)(\text{CO})_2$  in  $\text{Fe}_2\text{C}_2(\text{CO})_9(\text{Cp}^*)_2(\text{C}_2)$  behaves identically to an alkyl group.<sup>15</sup> Our calculations that we carried out on the acetylide model  $[\text{Ru}_3(\text{CO})_9(\text{C}_2\text{H})]^-$ , support these conclusions. HOMO–LUMO gaps, atomic net charges, electron transfers, and overlap populations are essentially the same as those computed for **9**.

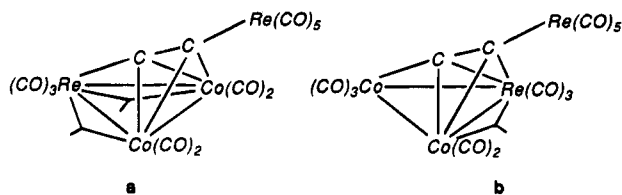
The reported mixed triangular transition metal  $\text{M}_m\text{M}'_{4-m}\text{L}_n(\text{C}_2)$  complexes (see Table 1) pose a question concerning the preference for M or M' to occupy the M(1) or the M(2) sites in the triangle (these sites are  $\sigma$ -bonded

(34) Schilling, B. E. R.; Hoffmann, R. *J. Am. Chem. Soc.* **1979**, *101*, 3456.

(35) Elian, M.; Hoffmann, R. *Inorg. Chem.* **1975**, *14*, 1058.



and  $\pi$ -bonded to the  $C_2$  ligand, respectively). For instance, two isomeric forms, **12a** and **12b**, could *a priori* exist for  $Co_2Re_2(CO)_{14}(C_2)$ , only the symmetrical skeletal isomer **12a** is found, at least in the solid state, in agreement with our calculations.<sup>18</sup> A very tiny energy difference (0.36 eV) is computed in favor of the symmetrical isomer **12a**. This is the case for all the heterometallic  $M_4C_2$  complexes listed in Table 1. Calculations on model **9** indicate that the Ru(1) site is almost neutral whereas the Ru(2) one is slightly negatively charged (-0.41). The Ru(3) site is slightly positive (+0.18) due to the presence of the electron-withdrawing Cp group. The less electronegative metal should occupy the M(1) site. According to the electronegativity scale (Ru < Re < Fe < Co),<sup>36</sup> this is the case for  $Fe_2Co_2(Cp^*)_2(CO)_8(C_2)$ <sup>15</sup> and  $Co_2Re_2(CO)_{14}(C_2)$ <sup>18</sup> but not for  $Fe_2Ru_2(CO)_{11}(Cp)(H)(C_2)$ <sup>14</sup> and  $Fe_2Ru_2(CO)_9(Cp)_2(C_2)$ .<sup>16</sup> The preference for only one skeletal isomer in the solid state has also been noticed and amply discussed in the literature for mixed transition-metal acetylide  $M_2M'L_n(\mu_3-C_2R)$  and acetylene  $M_2M'L_n(\mu_3-C_2R_2)$  clusters.<sup>37,38</sup> Both experimental and theoretical work on the latter have shown that the stabilities of the different possible isomers were rather similar and very sensitive to a range of parameters such as the nature of the ligand tethered to the metal centers, crystal packing forces, or weak coordination of solvent molecules.<sup>38</sup> These conclusions should also apply for the heterotetrametallic- $C_2$  complexes of Table 1.



12

### The 66-Electron Compound $Fe_2Ru_2(CO)_{10}(Cp^*)_2(C_2)$

The MO diagram shown in Figure 3 illustrates the pertinent interactions between the metallic fragment and the dicarbon unit in the model  $Ru_4(CO)_{10}(Cp)_2(C_2)$  of  $C_2$  symmetry, **13**, used to mimic the bonding mode B in the 66-MVE compound  $Fe_2Ru_2(CO)_{10}(Cp^*)_2(C_2)$ , **5**. Basically, the  $[Ru_4(CO)_8(\mu-CO)_2(Cp)_2]^{2+}$  metallic fragment of **13** consists of two  $d^6 ML_4L'$  and two  $d^6 ML_3L'$  entities with L being a terminal two-electron  $\sigma$ -donor and  $L'$  representing a two-electron  $\sigma$ -donor ligand equivalent to half a bridging carbonyl dianion.<sup>39</sup> A detective analysis reveals that the assemblage of these four units to form the open-square metallic fragment leads to five hybrid FMOs, separated from a band of low-lying, mainly d, orbitals. These metallic FMOs, 1a, 1b, 2a, 2b, and 3a, are drawn in Figure 4. Counting  $C_2$  as a dianion ligand, the two former FMOs are formally occupied before interaction.

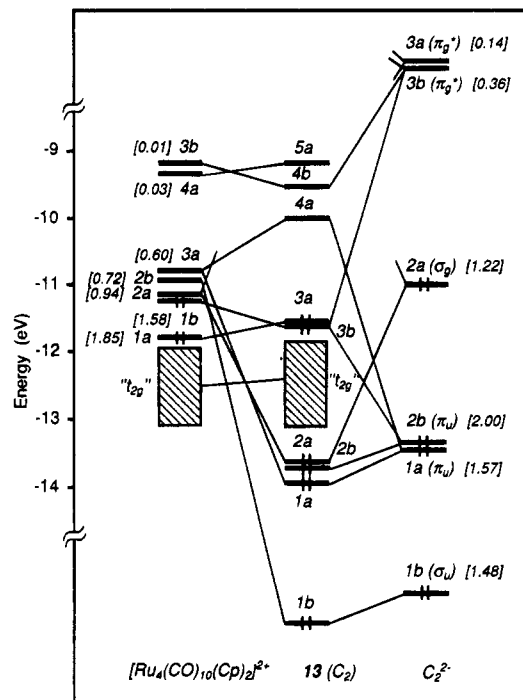


**Figure 3.** Molecular orbital diagram of the 66-MVE model **13**,  $Ru_4(CO)_{10}(Cp)_2(C_2)$ . The numbers in brackets indicate the electron occupation of FMOs after interaction.

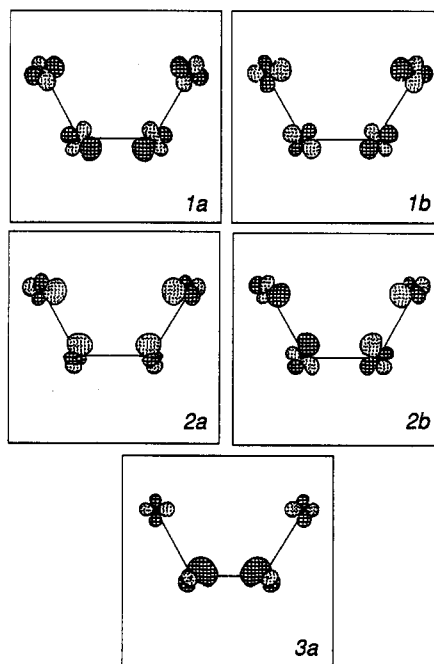
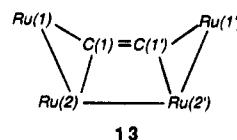


**Figure 4.** Frontier molecular orbitals of the metallic fragment  $[Ru_4(CO)_{10}(Cp)_2]^{2+}$ .



13

Among the five FMOs of the metallic framework, four interact rather strongly with those of the dicarbon moiety. The dominant interactions occur between the metallic 2a and 2b FMOs with the  $C_2$   $\sigma$ -type 2a and 1b orbitals, respectively. The metallic 3a FMO is pushed up in energy, interacting nicely with the low-lying  $\pi$ -in-

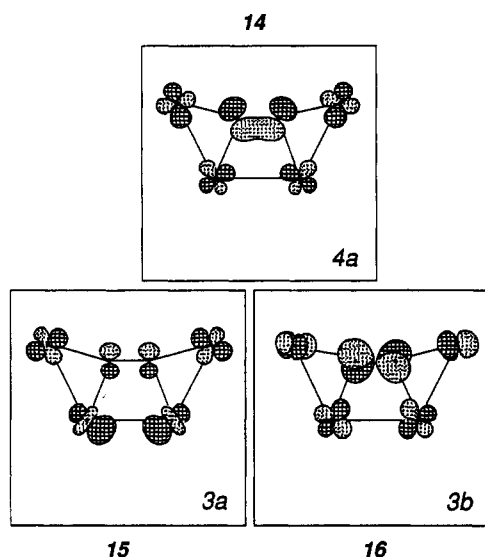
(36) See for example: Allred, A. L.; Rochow, E. G. *J. Inorg. Nucl. Chem.* **1958**, *5*, 264, 269.

(37) Carty, A. J.; Taylor, N. J.; Sappa, E.; Tiripicchio, A.; Tiripicchio Camellini, M. *Organometallics* **1991**, *10*, 1907 and references therein.

(38) Halet, J.-F. *Coord. Chem. Rev.*, in press and references therein.

(39) (a) Evans, D. G. *J. Chem. Soc., Chem. Commun.* **1983**, 675. (b) Lugan, N.; Fabre, P.-L.; de Montauzon, D.; Lavigne, G.; Bonnet, J.-J.; Saillard, J.-Y.; Halet, J.-F. *Inorg. Chem.* **1993**, *32*, 1363.

plane" 1a orbitals of C<sub>2</sub>. It becomes the 4a LUMO of model **13** (see **14**). The 3a HOMO of **13**, sketched in **15**, derives mainly from the metallic 1a FMO. In contrast to the LUMO which possesses a rather important carbon character (10%), a very tiny carbon character is noted in the HOMO (4%) due to a very weak participation of the low-lying C<sub>2</sub>  $\pi$ -type 1a orbital. However, the occupied 3b MO (**16**) is almost degenerate with the 3a HOMO. Resulting from the interaction of the metallic 1b FMO with the vacant high-lying  $\pi^*$ -“in-plane” 3b component and, to a lesser extent with the occupied low-lying  $\pi$ -“out-of-plane” 2b orbital of the dicarbon unit, this MO possesses a rather large carbon character (18%). Consequently, the C<sub>2</sub> ligand should be reactive toward both nucleophilic and electrophilic reagents if the reaction is orbital controlled.



Is **5** a permetalated ethene? At first sight, both the C–C bond (1.24 Å) and bond angles (M–C–C = 165° and 112°) are rather different from those observed in ethylene (1.34 Å and 120°, respectively) and militate against this assignment. Nevertheless, a comparison of the electronic structure of model **13** with that of C<sub>2</sub>H<sub>4</sub><sup>31</sup> indicates that compound **5** can be depicted as a permetalated ethene. As shown in Figure 3, in addition to the  $\sigma$ -type 1b and 2a FMOs, only one  $\pi$ - and one  $\pi^*$ -type component, the “in-plane” 1a and 3b FMOs of the dicarbon entity, are really involved in the M–C bonding. Their occupations are 1.57 and 0.36 electrons after interaction, respectively. The occupation of the “out-of-plane” 2b FMO is nearly two. Its slight destabilizing interaction with the filled metallic 1b FMO does not change its occupation after interaction. Consequently, this orbital plays a minor role in the M–C bonding. For comparison, the occupations in C<sub>2</sub>H<sub>4</sub> (the C–C bond distance was set at 1.275 Å, see Appendix) are 1.07 and 2.0, respectively. An overall picture of an “intact” C–C double bond and four M–C  $\sigma$ -bonds agrees with the structural results reported for complex **5**. Note also that **5** can be considered as a parallel-bonded “dinuclear” transition metal alkyne complex Ru<sub>2</sub>(CO)<sub>6</sub>(Fe(Cp)(CO)<sub>2</sub>C<sub>2</sub>-Fe(Cp)(CO)<sub>2</sub>).<sup>40</sup>

Why is the C–C bond so short in **5**? Starting from dianionic C<sub>2</sub><sup>2-</sup>, 1.73 electrons (0.52 from 1b ( $\sigma_u$ ), 0.43

from 1a ( $\pi_u$ ), and 0.78 from 2a ( $\sigma_g$ )) are donated to the metallic framework and 0.50 electrons are back-donated from the M<sub>4</sub> unit into the C<sub>2</sub>  $\pi^*$  FMOs. In ethylene, 2.4 electrons are given to the hydrogen atoms, of which 0.94 are from the  $\pi$  component, whereas 0.77 electrons are back-donated from the hydrogen atoms toward one of the C<sub>2</sub>  $\pi^*$  acceptor orbitals. A combination of reduced electron donation from the C<sub>2</sub> ligand to the rest of the molecule and reduced back-donation from the rest of the molecule into the C<sub>2</sub>  $\pi^*$  FMOs serve to shorten the C–C bond in complex **5**, compared to that of ethylene. The computed C–C overlap populations in models **9** and **13** (with a C–C bond length of 1.275 Å, see the Appendix) are 1.36 and 1.57, respectively, in accord with the experimental C–C bond distances of 1.35 and 1.24 Å measured in Fe<sub>2</sub>Ru<sub>2</sub>(CO)<sub>9</sub>(Cp)<sub>2</sub>(C<sub>2</sub>)<sup>16</sup> and Fe<sub>2</sub>Ru<sub>2</sub>(CO)<sub>10</sub>-(Cp\*)<sub>2</sub>(C<sub>2</sub>),<sup>17</sup> respectively. Both donation and back-donation are more important in model **9**. Therefore, despite the fact that the orbitals of the dicarbon unit are less involved in the bonding with the metallic framework in model **13** than in model **9**, the slight negative charges borne by the carbon atoms are roughly the same in both complexes.

### Two More Electrons: The 68-Electron Compound Ru<sub>4</sub>(CO)<sub>12</sub>( $\mu$ -PPh<sub>2</sub>)<sub>2</sub>(C<sub>2</sub>)

The third M<sub>4</sub>C<sub>2</sub> arrangement is that encountered in Bruce's 68-electron compound Ru<sub>4</sub>(CO)<sub>12</sub>( $\mu$ -PPh<sub>2</sub>)<sub>2</sub>(C<sub>2</sub>), **6** (bonding mode C), in which the C<sub>2</sub><sup>2-</sup> ligand formally donates eight electrons to the metallic fragment. Calculations were first performed on the planar Ru<sub>4</sub>(CO)<sub>12</sub>( $\mu$ -PH<sub>2</sub>)<sub>2</sub>(C<sub>2</sub>) system, **17**, of C<sub>i</sub> symmetry, used to model complex **6**. The metallic [Ru<sub>4</sub>(CO)<sub>12</sub>( $\mu$ -PH<sub>2</sub>)<sub>2</sub>]<sup>2+</sup> fragment can be considered as a composite of two “noninteracting” Ru<sub>2</sub>(CO)<sub>6</sub>( $\mu$ -PH<sub>2</sub>) units. As shown in Figure 5, the metallic [Ru<sub>4</sub>(CO)<sub>12</sub>( $\mu$ -PH<sub>2</sub>)<sub>2</sub>]<sup>2+</sup> fragment possesses a set of six hybrid FMOs above an array of twelve mainly d

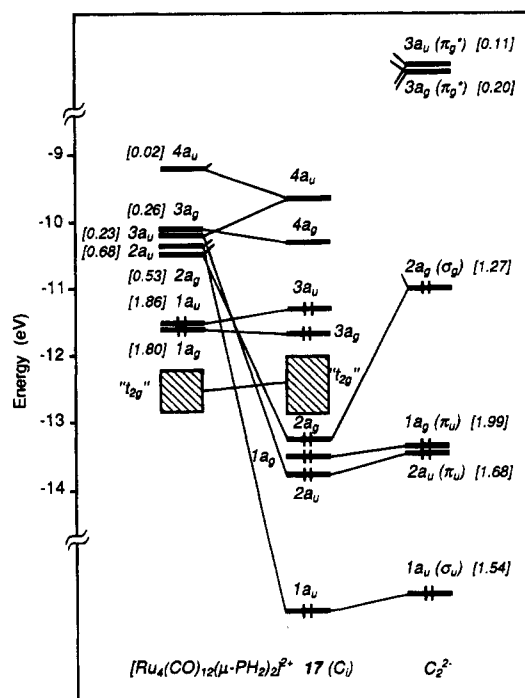


**Figure 5.** Molecular orbital diagram of the 68-MVE model **17**, Ru<sub>4</sub>(CO)<sub>12</sub>( $\mu$ -PH<sub>2</sub>)<sub>2</sub>(C<sub>2</sub>). The numbers in brackets indicate the electron occupation of FMOs after interaction.

(40) Hoffman, D. M.; Hoffmann, R.; Fisel, C. R. *J. Am. Chem. Soc.* **1982**, *104*, 3858.

orbitals. Indeed, these metallic FMOs,  $1a_g$ ,  $1a_u$ ,  $2a_g$ ,  $2a_u$ ,  $3a_u$  and  $3a_g$ , which are drawn in Figure 6, arise from the in-phase and out-of-phase combinations of the three frontier orbitals of the two  $Ru_2(CO)_6(\mu-PH_2)$  units. Considering  $C_2$  as a dianion ligand, the two former FMOs are occupied before interaction. They may be considered as corresponding to the Ru–Ru bonds.

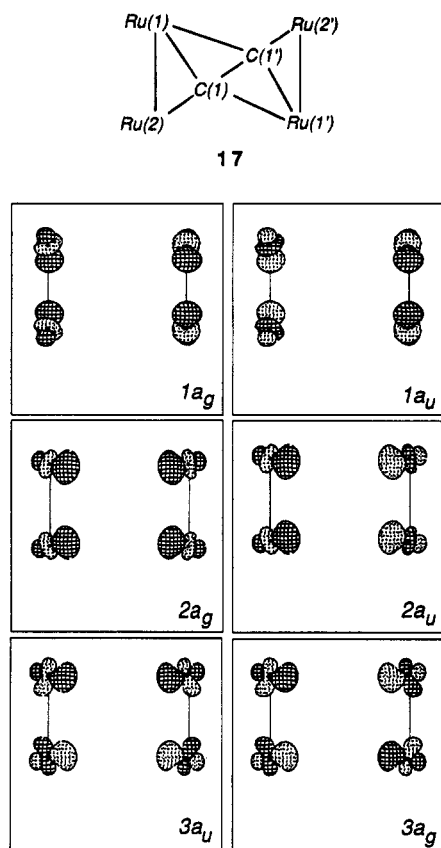
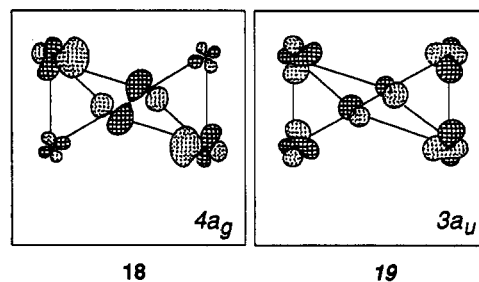


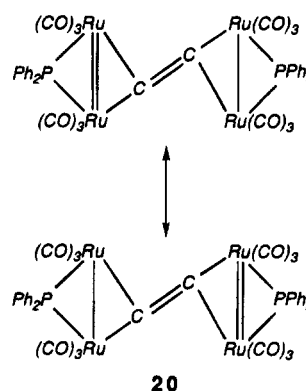
**Figure 6.** Frontier molecular orbitals of the metallic fragment  $[Ru_4(CO)_{12}(\mu-PH_2)_2]^{2+}$ .

The greatest bonding interaction between the metal and dicarbon fragments occurs between the metallic  $2a_g$  FMO and the  $C_2$   $\sigma$ -type  $2a_g$  orbital. Another large interaction occurs between the metallic  $2a_u$  and the low-lying  $C_2$   $\sigma$ -type  $1a_u$  orbitals. Additional bonding between the two fragments arises from some interaction between the metallic high-lying  $3a_u$  FMO and the  $\pi$ -type  $C_2$  "in-plane"  $2a_u$  component. Interaction of the metallic FMOs with the  $C_2$   $\pi$ -type acceptor  $3a_u$  and  $3a_g$  orbitals is rather weak. It involves mainly the metallic  $1a_g$  orbital with the  $C_2$   $3a_g$  FMO. The metallic  $3a_g$  FMO interacts poorly with the dicarbon unit and remains almost unperturbed after interaction. It constitutes the  $4a_g$  LUMO (92% metallic in character, see 18) which is positioned in the middle of a large gap between the vacant  $4a_u$  and the  $3a_u$  HOMO which derives principally from the metallic  $1a_u$  FMO (95% metallic in character, see 19). This  $4a_g$  MO is separated by 0.72 and 1.03 eVs from the  $4a_u$  and  $3a_u$  MOs, respectively. This is an unstable situation which should be improved if the  $4a_g$  MO could be destabilized.

Although electron counting requires that the dicarbon unit  $C_2^{2-}$  acts formally as an eight-electron donor to the metal framework, its  $\pi$  "out-of-plane"  $1a_g$  FMO hardly interacts with the metallic fragment. Its occupation is nearly two after interaction (see Figure 5). It turns out



that this is due to the particular nature of the FMOs of the tetrametallic fragment which lie mainly in the metallic plane. Therefore, the  $C_2^{2-}$  ligand contributes only three FMOs toward metal–carbon bonding, i.e. six electrons if the molecule is fully planar via its occupied  $1a_u$ ,  $2a_u$ , and  $2a_g$  FMOs. The metallic rectangle is then formally electron-deficient, and model 17 may be described by the Lewis resonance forms depicted in 20, with respect to the EAN formalism. Such resonance forms suppose that there is no bonding interaction between Ru(1) and C(1'), and Ru(1') and C(1). On the other hand, partial double Ru–Ru bond is expected. This description is in accord both with the calculations on 17 which indicate a Ru(1)–C(1') overlap population close to zero (0.02), and a C–C overlap population even larger than that computed for model 13 (1.66 vs 1.57). Indeed, the Ru(1)–C(1') separations measured in complex 6 are long (2.47 Å) and the Ru–Ru contacts are relatively short (2.75 Å). The C–C bond length (1.275 Å) is also short and comparable to that observed in compound 5 (1.24 Å) in which there is formally a C–C double bond.<sup>19</sup> Note that in effect, the planar model 17 and model 13 are isomeric species with the  $C_2^{2-}$  ligand acting as a six-electron donor. The two partial double Ru–Ru bonds (bond order of 1.5) present in 17 are replaced by three single Ru–Ru bonds in 13.<sup>49</sup>



A greater overlap with the  $\pi$ -type  $1a_g$  orbital of the  $C_2$  ligand, and consequently a stronger interaction, would occur if the two  $M_2$  fragments were perpendicular to each other. Indeed, a twist of  $42.5^\circ$  is noticed in Bruce's compound.<sup>19</sup> A larger twist is prevented by the carbonyls and the bulky phenyl groups on the bridging phosphido ligands.<sup>19</sup> Such a twist is rather far from  $90^\circ$ , the value for which the two  $M_2$  units would be perpendicular, but is sufficient to allow some interaction of the  $C_2$   $1a_g$  FMO and the metallic  $3a_g$  FMO. Calculations on the experimental structure of 6 indicate that the  $C_2$   $1a_g$  FMO is now involved somewhat in the M–C bonding. Its occupation is 1.89 electrons after interaction with the metal fragment. The occupation of its

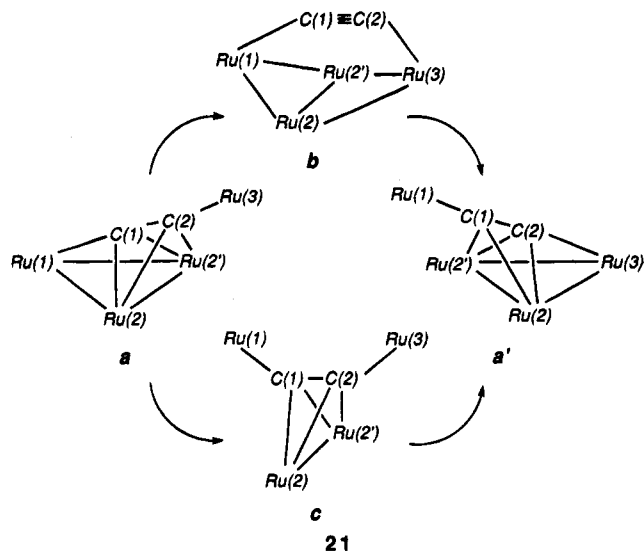
metallic counterpart FMO, the  $3a_g$  orbital, rises from 0.26 to 0.59 electron. The consequence of the interaction between these two FMOs, the metallic  $3a_g$  and the  $C_2$  "out-of-plane"  $1a_g$  orbitals, is the destabilization of the former above the  $4a_u$  MO and the stabilization of the latter. The HOMO–LUMO gap rises to 1.84 eV (vs 1.03 eV in model 17). A significant bonding energy is gained (0.30 eV) between the metal and  $C_2$  entities. Some bonding contact between M(1) and C(1') occurs (the calculated M(1)–C(1') overlap population is 0.12). The C–C overlap population drops slightly from 1.66 in 17 to 1.57, a value equal to that computed in model 13. Clearly, the twist of one  $M_2$  unit relative to the other allows the partial alleviation of the instability that we noted for the planar model 17. These results are in accordance with the robustness of **6** noted by Bruce and co-workers vis-a-vis thermal degradation or reaction with  $H_2$  or  $CO$ .<sup>19</sup>

### Isomerism and Fluxionality

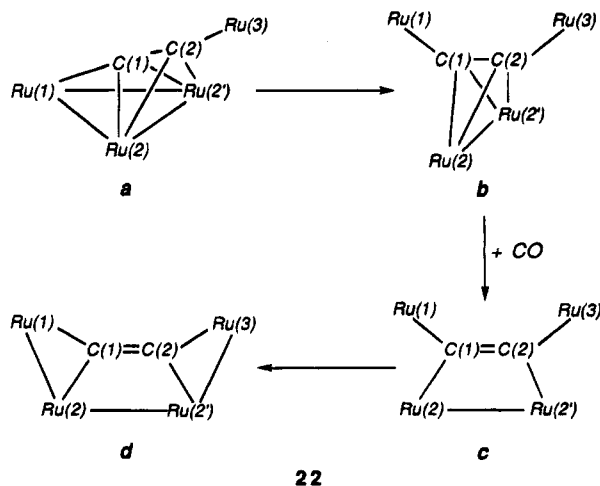
<sup>13</sup>C NMR spectroscopic measurements performed by Akita and co-workers at room temperature on  $Fe_2Co_2(Cp^*)_2(CO)_8(C_2)$ , an acetylide compound analogous to **4** (see Table 1), indicate an equivalence of the two  $Fe(Cp^*)$  units and an exchange between the carbonyls ligated to the remote iron center and those of  $FeCo_2$  metal triangle.<sup>15</sup> Analogous dynamic behavior has been noticed for the complex  $Fe_4(CO)_9(Cp^*)_2(C_2)$ .<sup>14</sup> The authors suggest that a dynamic process must be equilibrating the two iron centers in the molecule. They propose two possible mechanisms in which carbonyl scrambling and cluster skeletal rearrangement may be involved. These mechanisms, which consider that the rearrangements are intramolecular and without loss and/or capture of ligands, are schematized in **21** for  $Ru_4(CO)_9(Cp)_2(C_2)$ . In the first interconversion pathway, the remote Ru(3) center of the species **21a** moves toward the Ru(2)–Ru(2') edge of the  $Ru_3$  triangle to form an  $M_4$  butterfly array with the  $C_2$  ligand highly exposed and symmetrically bound to the two  $Ru(CO)_2(Cp)$  groups (intermediate **21b**). Scission of the Ru(2,2')–C bonds is then necessary in order that the Ru centers obey the 18-electron rule. Successive extrusion of the other Ru(1) atom via metal–metal bond cleavage then generates the species **21a'**, the topological stereoisomer of **21a**. In the second rearrangement, initial scission of Ru(1)–Ru(2-2') bonds proceeds to afford the coordinatively unsaturated intermediate **21c** (16-electron Ru(2-2') centers), which subsequently traps the other Ru(3) group to form model **21a'**.<sup>15</sup>

We did not fully explore the energy profile of these interconversion mechanisms in order to see for instance if one rearrangement is symmetry forbidden. Though comparison of extended Hückel total energies must be done with caution, calculations that we carried out on the two intermediates **21b** and **21c** indicate an energy preference of more than 2 eV for the latter. The bonding energy between the  $C_2^{2-}$  ligand and the  $[Ru_4]^{2+}$  fragment in **21c** (6.5 eV) is roughly the same as that of **21a**. On the other hand, it is less than 3 eV in **21b**. Noting also that the intermediate **21b** is rather sterically hindered, we propose that the interconversion between **21a** and **21a'** should occur through the intermediate **21c** rather than the **21b** one.

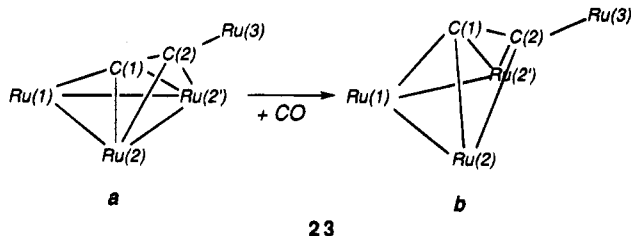
As mentioned previously, with three metal–metal bonds 66-electron models **9** and **13** may be considered



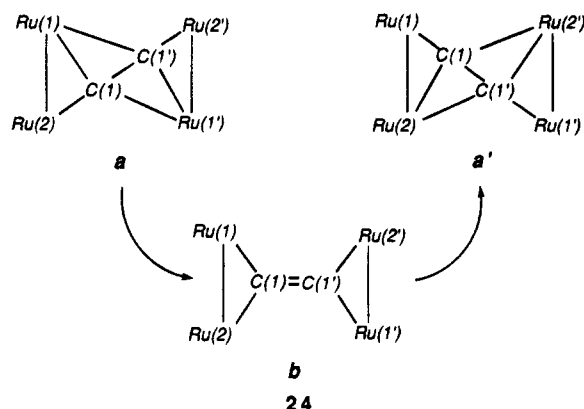
as "metallic" isomers (see **7**). Nevertheless, with the  $C_2^{2-}$  dicarbon unit acting as an eight-electron donor in the acetylide-type model **9** and as a six-electron donor in the ethene-type model **13**, the eventual transformation of the former into the latter requires the addition of a two-electron donor ligand to the metal framework. The simplest reaction pathway, between an acetylide-type cluster and an ethene-type cluster, that we could think of, is illustrated in **22** for  $Ru_4(CO)_9(Cp)_2(C_2)$ . The first step is a dissociative mechanism involving the rupture of metal–metal bonds and the formation of the unsaturated species **22b**, which is analogous to **21c**. In the second step, rotation of the dicarbon unit occurs accompanied with the capture of CO to generate the unsaturated intermediate **22c**. During this transformation the  $C_2^{2-}$  ligand changes from an eight-electron to a six-electron donor vis-a-vis the metallic moiety. Metal–metal bond formation in the final step leads to the ethene-type cluster  $Ru_4(CO)_{10}(Cp)_2(C_2)$ , **22d**. Note that the rearrangement of intermediate **22b** into intermediate **22c** is structurally reminiscent (but not electronically as there are two less electrons here) of the perpendicular-to-parallel conversion of bimetallic alkyne complexes that we know is costly in energy.<sup>40</sup> Model **22c** is computed to be only 1 eV less stable than the final compound **22d**, and the bonding energy between the metallic fragment and the dicarbon unit is roughly the same in the two models (ca. 6.5 eV).



Owing to the nature of the LUMO of the 66-MVE acetylide-type model **9** (vide supra), a competitive reaction which could be observed upon two-electron ligand addition is the breaking of the metal-metal bond spanned by the  $C_2$  unit leading to a 68-MVE species (see **23**). This would not affect the  $C_2^{2-}$  entity which would still contribute eight electrons to M-C bonding. Despite the fact that such a model seems to be rather sterically hindered, it is worth of mentioning the related compound  $Ru_3(CO)_9(\mu-SEt)(\mu_3-C_2Ph)$ , recently characterized by Jeannin and co-workers.<sup>41</sup>



Fluxional behavior can also be envisaged for the 68-electron compound **6**. As illustrated in **24**, a rotation of ca. 60° is sufficient to move from **24a** to its stereoisomer **24a'** via intermediate **24b**, in which the  $C_2$  ligand is end-on tethered to the metallic fragment. A barrier of less than 1 eV is computed for this symmetry-allowed

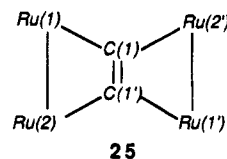


process with **24b** being the transition state. Calculations performed on this transition state indicate an unsaturated species. No HOMO-LUMO gap is computed. Indeed, **24b** is an electron-deficient species with 66 MVEs since the dicarbon unit  $C_2^{2-}$  acts as a six-electron donor, whereas it formally donates eight electrons in **24a**. A stable species with a rather large HOMO-LUMO gap (1.54 eV) would be obtained with two more electrons. Such a species would be achieved for instance if the  $C_2$  unit was replaced by an  $N_2$  ligand.

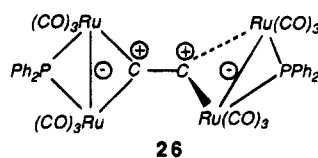
### $M_4C_2$ Geometries Not Yet Reported

$M_4C_2$  arrangements different from those already reported and which might be likely candidates for synthesis can be considered. We have seen in the previous section that the acetylide-type model **23b** was theoretically stable for 68 MVEs. There is also geometry **24b** for the count of 68 MVEs. An alternative arrangement for the same electron count is given in **25**, in which the dicarbon entity is side-on bound to the metallic "rectangle". These two species exhibit comparable M-C bonding, similar total energy and rather large HOMO-LUMO gaps (1.54 and 1.83 eV, respec-

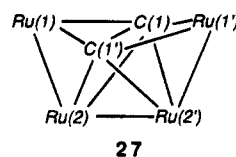
tively). With the  $C_2^{2-}$  unit acting formally as a six-electron-donor ligand, species **24b** and **25** are indeed permetalated ethene molecules. We are forced to conclude that such arrangements are possible. A two-electron reduction of the ethene-like molecule **5** would afford in principle a complex with an arrangement analogous to that of **23b** by cleavage of the Ru-Ru bond. Of relevance to this discussion are the end-on-bound vinylidene bimetallic compounds<sup>42</sup> such as  $Fe_2(CO)_5(\mu-PPh_2)(\mu-C_2(Ph)PPh_2PCH_2PPh_2)$  which has recently been synthesized and structurally characterized.<sup>43</sup>



The 68-electron " $D_{2d}$ " model **26**, reminiscent somewhat of the ethylene dication  $[C_2H_4]^{2+}$ ,<sup>44</sup> provides an example of an alternative geometry for compound **6**. Calculations indicate that this model is less stable than compound **6** and model **17** by 2.17 and 0.12 eV, respectively. A HOMO-LUMO gap of 1.18 eV is computed. Species **26** is unlikely since a localized bonding scheme requires a doubly "zwitterionic" nature with carbon cations violating the octet rule. This is in agreement with our calculations which show a  $C_2$  unit considerably poorer in electrons than in **6** or **17**.



A rotation of 90° of the  $C_2$  moiety in the ethene-like compound **5** with respect to the Ru-Ru bond can be envisaged leading to the 64-MVE  $M_4C_2$  arrangement shown in **27**, which can be described as the condensation of three  $M_2C_2$  tetrahedra with a dicarbon unit highly exposed. This rotation should be accompanied by a loss of two electrons, since the  $C_2^{2-}$  ligand acting as a six-electron donor in **5** acts as an eight-electron donor in **27**. Note that such a geometry has been reported with heavier elements for electron-rich compounds such as the 68-MVE species  $[Co_4(CO)_{11}(Sb_2)]^{2-}$ .<sup>45</sup> However, geometric constraints might preclude such an arrangement. Indeed, normal M-C bonding distances imply the closing of the nonbonding metal-metal vector with the loss of two electrons and a C-C bond penetrating the metallic square.<sup>46</sup>



**Acknowledgment.** Thanks are expressed to Pr. M. Akita, M. I. Bruce, R. L. Johnston, and J.-Y. Saillard for helpful comments and for sending results prior to publication. We acknowledge Dr. D. Proserpio for pro-

viding us with the CACAO program. G.F. is grateful to the Région Bretagne for financial support.

### Appendix

All calculations were carried out within the extended Hückel<sup>47</sup> formalism (using the weighted  $H_{ij}$  formula) with the CACAO program.<sup>48</sup> Ruthenium was chosen for all models in order to facilitate the comparison of their electronic structures. The exponents ( $\zeta$ ) and the valence shell ionization potentials ( $H_{ii}$  in eV) were respec-

tively: 1.3, -13.6 for H 1s; 1.625, -21.4 for C 2s; 1.625, -11.4 for C 2p; 2.275, -32.3 for O 2s; 2.275, -14.8 for O 2p; 1.6, -18.6 for P 3s; 1.6, -14.0 for P 3p; 1.9, -9.1 for Fe 4s; 1.9, -5.32 for Fe 4p; 2.078, -8.6 for Ru 5s; 2.043, -5.1 for Ru 5p.  $H_{ii}$  values for Fe 3d and Ru 4d were set equal to -12.6 and -12.2, respectively. A linear combination of two Slater-type orbitals of exponents  $\zeta_1 = 5.35$ ,  $\zeta_2 = 1.8$  and  $\zeta_1 = 5.378$ ,  $\zeta_2 = 2.303$  with the weighting coefficients  $c_1 = 0.5366$ ,  $c_2 = 0.6678$  and  $c_1 = 0.534$ ,  $c_2 = 0.6365$  was used to represent the 3d and 4d atomic orbitals of Fe and Ru, respectively. Unless specified in the text, the following distances (Å) and angles (deg) were used: Ru-Ru = 2.75; Ru-C = 2.065; Ru-C(O) = 1.9; Ru-C(Cp) = 2.241; Ru-P = 2.35; in  $C_2$ , C-C = 1.275; C-O = 1.15; C-C(Cp) = 1.399, C-H = 1.05; P-H = 1.41; Ru-C-O = 180; H-P-H = 109.47.

OM950256R

(42) Bruce, M. I. *Chem. Rev.* **1991**, *91*, 197. For a theoretical study see for example: Bursten, B. E.; Cayton, R. H. *J. Am. Chem. Soc.* **1986**, *108*, 8241.

(43) Cherkas, A. A.; Doherty, S.; Cleroux, M.; Hogarth, G.; Randall, L. H.; Breckenridge, S. M.; Taylor, N. J.; Carty, A. J. *Organometallics* **1992**, *11*, 1701.

(44) See for example: Lammertsma, K.; Barzaghi, M.; Olah, G. A.; Pople, J. A.; Kos, A. J.; Schleyer, P. v. R. *J. Am. Chem. Soc.* **1983**, *105*, 5252.

(45) See for example: Albright, T. A.; Yee, K. A.; Saillard, J.-Y.; Kahlal, S.; Halet, J.-F.; Leigh, J. S.; Whitmire, K. H. *Inorg. Chem.* **1991**, *30*, 1179.

(46) Kahlal, S.; Halet, J.-F.; Saillard, J.-Y. *Inorg. Chem.* **1991**, *30*, 2567.

(47) Hoffmann, R. *J. Chem. Phys.* **1963**, *39*, 1397.

(48) Mealli, C.; Proserpio, D. *J. Chem. Educ.* **1990**, *67*, 399.

(49) **Note Added in Proof.** Note that a  $Ru_4C_2$  arrangement close to that of **20** has been recently reported in the solid-state compound  $GdRuC_2$ : Hoffmann, R.-D.; Wachtmann, K. H.; Ebel, T.; Jeitschko, W. *J. Solid State Chem.* **1995**, *118*, 158.

# Enyne Metathesis Using Chromium Carbene Complexes. Synthesis of Heterocycles from Enynes Using Chromium Carbene Complexes

Susumu Watanuki and Miwako Mori\*

Faculty of Pharmaceutical Sciences, Hokkaido University, Sapporo 060, Japan

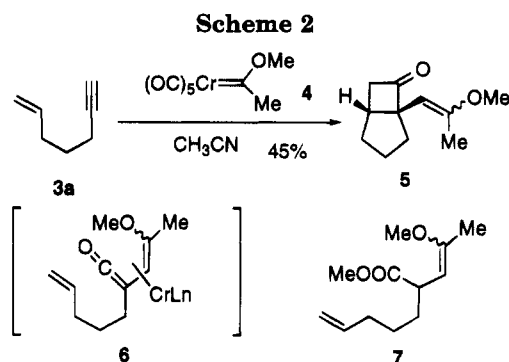
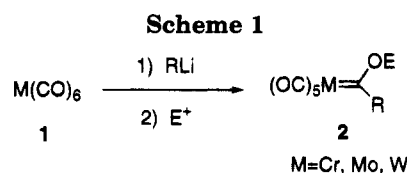
Received May 22, 1995<sup>®</sup>

A new synthesis of pyrrolidine and piperidine derivatives *via* a chromacyclobutane formed from a Fischer carbene complex and an enyne having nitrogen in a tether was developed. As the results of the substituent effects, the reaction of enynes having the electron-donating group on the alkene with a Fischer chromium carbene complex in CH<sub>3</sub>CN afforded preferentially metathesis products, and that of the enyne having the electron-withdrawing group gave the cyclized product fused with a cyclopropane ring.

The reactions of dienes, diynes, and enynes with transition metal complexes are very interesting and useful in synthetic organic chemistry. Recent studies of the reaction of enynes with Fischer carbene complexes **2**,<sup>1</sup> which are easily prepared from M(CO)<sub>6</sub> (**1**, M = Cr, Mo, and W) and alkyllithium followed by treatment with alkylating agent, have demonstrated a potential ring construction of bicyclic carbon skeletons (Scheme 1).

It was known that the chromium carbene complex did not react with unactivated alkene.<sup>2a</sup> However, Wulff reported that treatment of enyne **3a** with (methoxyethylidene)chromium (**4**) in CH<sub>3</sub>CN gave cyclobutanone **5** in 45% yield. When the reaction was carried out in CH<sub>3</sub>CN-MeOH, ester **7** was obtained in good yield. He described that the chromium carbene complex did not react with unactivated alkene and cyclobutanone was produced *via* the [2 + 2] cycloaddition of an alkene of **3a** and vinylketene **6** generated by the reaction of alkyne of **3a** with chromium carbene complex **4**.<sup>2,3</sup> (Scheme 2).

On the other hand, Hoyer reported that the reaction of enyne **3b** having an unactivated olefin with chromium carbene complex **4** afforded the cyclopropane derivative **8** in 69% yield.<sup>4</sup> It was very interesting that the reaction of enyne **3c** with **4** afforded metathesis product **9** although the yield was moderate.<sup>4</sup> The reaction of activated olefin **3d** with the Fischer carbene complex was reported by Harvey,<sup>5</sup> and he obtained cyclopropane derivative **8d** in good yield when molybdenum carbene complex **10a** was used. Katz reported that the reaction of enyne **3e** with tungsten carbene complex **12** afforded



metathesis product **9e** in 50% yield<sup>6a,b</sup> (Schemes 3 and 4).

These products were considered to be obtained from complex **III** or **IV**; namely, the reaction of the alkyne moiety of enyne **I** with the Fischer carbene complex affords vinylcarbene complex **II**. If vinylcarbene complex **II** converts into vinylketene complex **III**, the [2 + 2] cycloaddition occurs intramolecularly, and if vinylcarbene complex **II** reacts with the alkene part of the enyne intramolecularly, metallacyclobutane **IV** is formed. Now, we report the synthesis of heterocycles using the reaction of an enyne having nitrogen in a tether with a Fischer carbene complex. As a result, it was clear that the reaction course was controlled by the electronic factors of the substituent on the alkene<sup>7</sup> (Scheme 5).

## Results and Discussion

### Reaction of an Enyne with Pentacarbonyl-(ethoxyethylidene)chromium. Fischer chromium

(6) (a) Katz, T. J.; Sivavec, T. M. *J. Am. Chem. Soc.* **1985**, *107*, 737. (b) Sivavec, T. M.; Katz, T. J.; Chiang, M. Y.; Yang, G. Xu-Q. *Organometallics* **1989**, *8*, 1620. (c) Katz, T. J.; Yang, G. Xu-Q. *Tetrahedron Lett.* **1991**, *32*, 5895.

(7) Preliminary work: Mori, M.; Watanuki, S. *J. Chem. Soc., Chem. Commun.* **1992**, 1083. Watanuki, S.; Mori, M. *Heterocycles* **1993**, *35*, 679.

<sup>®</sup> Abstract published in *Advance ACS Abstracts*, September 15, 1995. (1) Fischer, E. O.; Maasböl, A. *Angew. Chem., Int. Ed. Engl.* **1964**, *3*, 590.

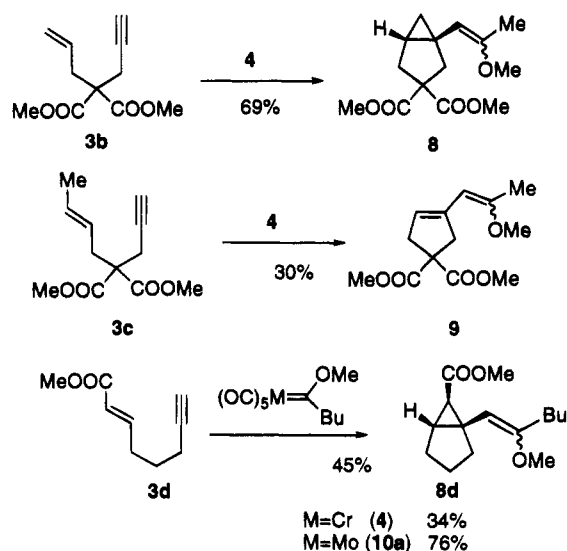
(2) (a) Wulff, W. D. In *Advances in Metal-Organic Chemistry*; Liebeskind, L. S., Ed.; JAI Press, Inc.; Greenwich, CN, 1989; Vol. 1. (b) Wulff, W. D.; Kaesler, R. W. *Organometallics* **1985**, *4*, 1461. (c) Kim, O. K.; Wulff, W. D.; Jiang, W. *J. Org. Chem.* **1993**, *58*, 5571.

(3) Hofmann, P.; Hammerle, M.; Unfried, G. *New. J. Chem.* **1991**, *15*, 769.

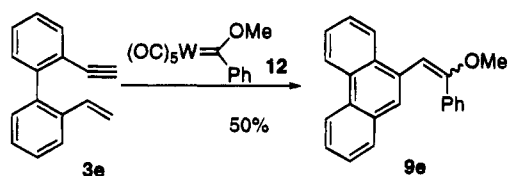
(4) (a) Hoyer, T. R.; Rehberg, G. M. *J. Am. Chem. Soc.* **1990**, *112*, 2841. (b) *Idem.* *Organometallics* **1989**, *8*, 2070. (c) Korkowski, P. F.; Hoyer, T. R.; Rydberg, D. B. R. *J. Am. Chem. Soc.* **1988**, *110*, 2676. (d) Hoyer, T. R.; Suriano, J. A. *Organometallics* **1992**, *11*, 2044.

(5) (a) Harvey, D. F.; Brown, M. F. *J. Am. Chem. Soc.* **1990**, *112*, 7806. (b) *Idem.* *Tetrahedron Lett.* **1990**, *31*, 2529. (c) Harvey, D. F.; Lund, K. P.; Neil, D. A. *Ibid.* **1991**, *32*, 6311. (d) Harvey, D. F.; Lund, K. P. *J. Am. Chem. Soc.* **1991**, *113*, 5066. (e) Harvey, D. F.; Lund, K. P.; Neil, D. A. *J. Am. Chem. Soc.* **1992**, *114*, 8424.

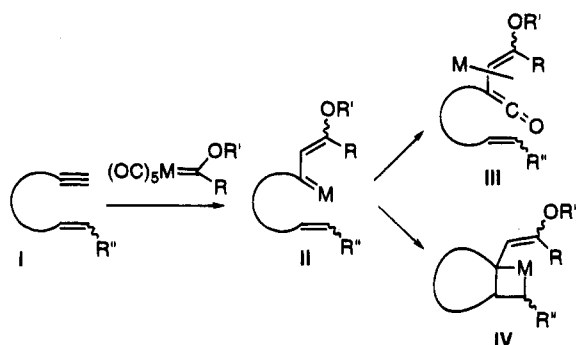
Scheme 3



Scheme 4



Scheme 5

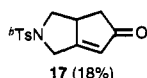


carbene complex **13a** was prepared from  $Cr(CO)_6$  and MeLi followed by treatment with the Meerwein reagent ( $Et_3O^+BF_4^-$ ). The starting enyne **14a** was prepared from *N*-(*p*-tolylsulfonyl)propargylamine and allyl bromide in the presence of NaH. When a  $CH_3CN$  solution of **14a** and pentacarbonyl(ethoxyethylidene)chromium (**13a**) was warmed at 70 °C for 4 h and then the solution was treated with  $[FeCl_4][FeCl_2(DMF)_3]^8$  (**15**), the cyclized product **16a** fused by a three-membered ring was obtained in 91% yield. Though the reaction was carried out under carbon monoxide (1 atm), the yield of **16a** was not affected (Table 1, run 2). Benzene and THF can be used as solvents for this reaction, but decreased yields of **16a** were shown (Table 1, runs 3 and 4). When THF was used as the solvent, the cyclopentenone derivative **17** was obtained in 18% yield along with **16a**. Though the reaction mechanism for the formation of compound **17** was not clear, it was considered that reductive cyclization by a low-valent chromium complex occurs. Thus, when **14a** was treated with  $Cr(CO)_6$  in THF, a small amount of **17** was produced. This means that the

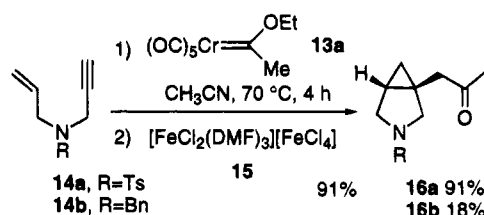
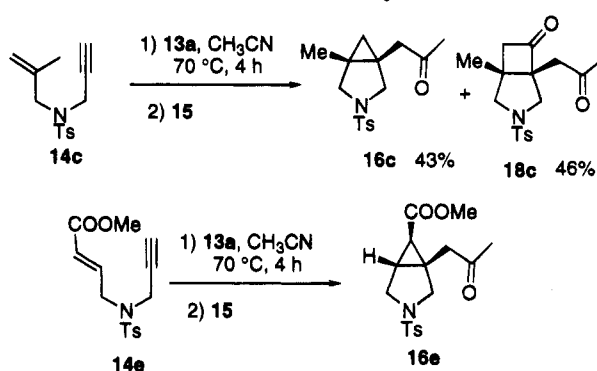
Table 1. Reaction of Enyne **14a** with Cr-Carbene Complex **13a**

run	solvent	yield of <b>16a</b> , %
1	$CH_3CN$	91
2 <sup>a</sup>	$CH_3CN$	84
3	PhH	55
4 <sup>b</sup>	THF	47

<sup>a</sup> Reaction was carried out under a CO atmosphere.



Scheme 6

Scheme 7. Reaction of Enynes with **13a**

reductive cyclization of enyne **14a** occurs by a low-valent chromium complex followed by the insertion of carbon monoxide to give **17**.<sup>3d,9</sup> On the other hand, when *N*-allylbenzylpropargylamine (**14b**) was treated with chromium carbene complex **13a** followed by treatment with 10% HCl, cyclopropane derivative **16b** was obtained in only 18% yield.<sup>10</sup> Presumably, the nitrogen of **14b** coordinates to the chromium carbene complex to give a complex mixture (Scheme 6).

The above results indicate that the reaction of enynes **14a,b** having an unactivated alkene with chromium carbene complex **13a** affords pyrrolidine derivatives **16a,b** fused by three-membered rings. Thus, the substituent effects on the alkenes of the enynes were examined. Reaction of enyne **14c** with chromium carbene complex **13a** afforded cyclopropane derivative **16c** and cyclobutanone derivative **18c** in 43% and 46% yields, respectively. However, the reaction of enyne **14e** having an activated alkene with **13a** gave cyclopropane derivative **16e** in 71% yield as the sole product (Scheme 7).

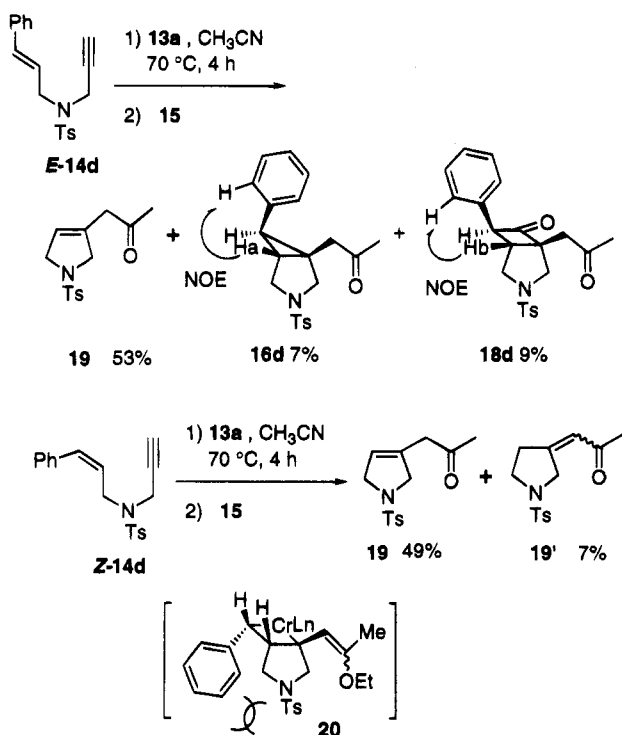
Subsequently, the reaction of enyne **E-14d** having a phenyl group on the alkene with **13a** was examined.

(9) Jordi, L.; Segundo, A.; Camps, F.; Ricart, S.; Moreto, J. M. *Organometallics* **1993**, *12*, 3795.

(10) Hoyer, T. R.; Suriano, J. A. *J. Am. Chem. Soc.* **1993**, *115*, 1154.

(11) Katz has reported that the reaction of the metal carbene complex with the enyne having nitrogen in a tether afforded the cyclopropane derivative. The carbene complex was made to absorb silica gel, and the reaction was carried out with no solvent.<sup>5c</sup>



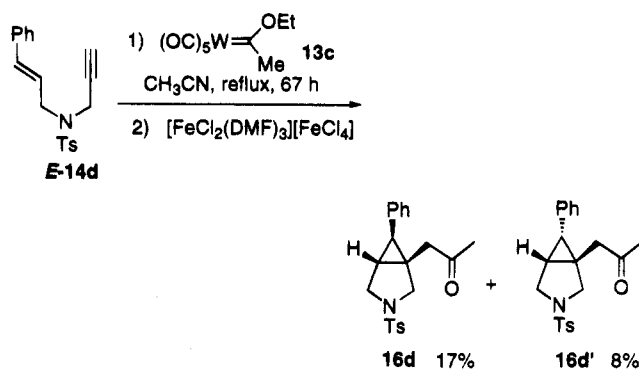
Scheme 8. Reaction of *E*- and *Z*-14d with 13a

Surprisingly, the metathesis product **19** was obtained in 53% yield as a main product along with cyclopropane derivative **16d** (7% yield) and cyclobutanone derivative **18d** (9% yield).<sup>12</sup> The NOE experiments of the ring junction proton Ha with the aromatic proton of compound **16d** or of the ring junction proton Hb with the aromatic proton of compound **18d** suggested that the reaction proceeded stereoselectively. On the other hand, the reaction of *Z*-14d with **13a** was carried out in a similar manner to give only metathesis products, **19** and **19'**, in 56% yield (**19/19'** = 7/1). Neither the cyclopropane derivative nor the cyclobutanone derivative was obtained in this case because of the steric repulsion between the phenyl group and the five-membered ring of **20** on the transition state for the formation of the three- or four-membered ring. When a CH<sub>3</sub>CN solution of *E*-14d with tungsten carbene complex **13c** was refluxed for 7 days, cyclopropane derivative **16d** was obtained in only 19% yield along with **16d'** in 17% yield. In this case, the reaction did not proceed with a stereoselective manner (Schemes 8 and 9).

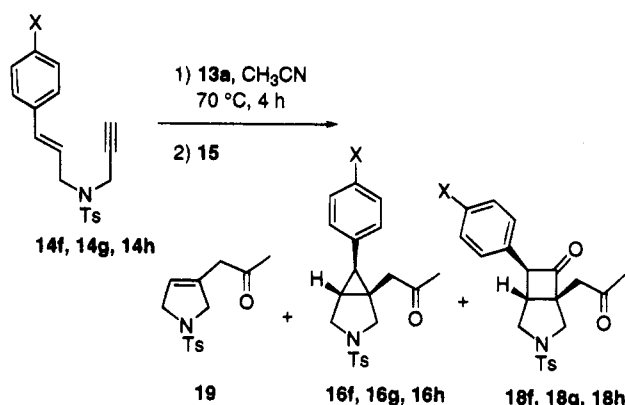
**Substituent Effects of the Aromatic Ring on the Alkene for the Reaction of an Enyne with a Chromium Carbene Complex.** It was very interesting that the enyne having an unsubstituted alkene afforded the cyclized product **16** fused by a three-membered ring and the metathesis products **19** were obtained from the enynes having a phenyl or methyl group<sup>3</sup> on the alkene.<sup>13</sup> If the formation of the metathesis product **19** or of the cyclopropane derivative **16** was controlled by the electronic factor of the substituent on the alkene, the substituent effect on the aromatic ring should be observed. The reactions of enynes **14f–h** with

(12) Though the reaction was carried out under carbon monoxide, the yield of **18d** was not increased and compounds **19**, **16d**, and **18d** were obtained in 26%, 5%, and 6% yield, respectively.

(13) A metathesis reaction using a chromium carbene complex and an electron-donating olefin is reported by Fischer: Fischer, E. O. *J. Organometal. Chem.* **1973**, *56*, 279.

Scheme 9. Reaction of *E*-14d with 13cTable 2. Reaction of Enyne **14** with Cr-Carbene Complexes

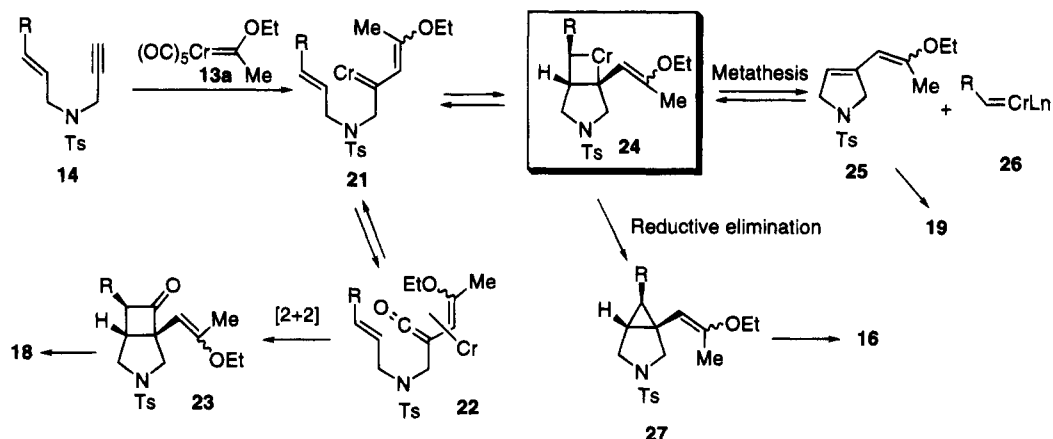
X	substrate	yield, %			
		19	16	18	19:16
NO <sub>2</sub>	14f	4	75	1:19	
Cl	14g	46	18	8	3:1
H	<i>E</i> -14d	53	7	9	7.7:1
Me	14h	62	6	1:0	

Scheme 10. Reaction of Enyne Having a *p*-Substituted Phenyl Group on the Alkene

chromium carbene complex **13a** were carried out in CH<sub>3</sub>CN upon heating, and the results were shown in Table 2. The reaction of compound **14g** having an electron-withdrawing group on the aromatic ring with **13a** increased the ratio of the cyclopropane derivative **16** to the metathesis product **19** (3:1). It was very interesting that compound **14f** having a *p*-nitrophenyl group on the alkene afforded the cyclopropane derivative **16f** as a main product. In the case of the reaction of **14h**, the metathesis product **19** was obtained as the main product and the cyclopropane derivative **16** was not produced. This means that the metathesis reaction is accelerated by the electron-donating group on the aromatic ring (Scheme 10).

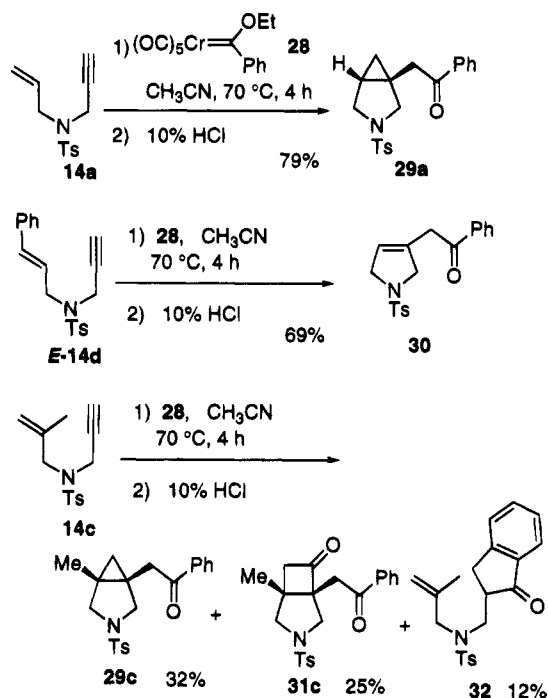
**Possible Reaction Course for the Reaction of Enynes with Chromium Carbene Complexes.** The mechanism for the reaction of enyne **14** with chromium carbene complex **13a** is not clear yet. However, the reaction course could be considered on the basis of the distribution of the products. The reaction of the alkyne part of enyne **14** with chromium carbene complex **13a** gave vinylcarbene complex **21**, which would form chromium ketene complex **22** or chromacyclobutane **24**. From the former pathway, the [2 + 2] cycloaddition of ketene and olefin would proceed, which affords cyclobutanone derivative **18** via **23**. On the other hand,

Scheme 11. Reaction Mechanism



cyclopropane derivative **27** and metathesis product **25** were obtained from chromacyclobutane **24**. If bond cleavage of chromacyclobutane occurs, alkylidene carbene **26** is formed along with metathesis product **25**. If the reductive elimination occurs from **24**, cyclopropane derivative **27** is formed. The unsubstituted alkene **14a** ( $R = H$ ) and the alkene **14f** having a *p*-nitrophenyl group on the alkene afforded the cyclopropane derivatives **16a,f**. In these cases, compounds **14a,f** afforded only the chromacyclobutanes **24a,f**. They afforded the cyclopropanes **16a,f** in good yields because corresponding (alkylidene)chromium carbene complexes **26a,f** were unstable. On the other hand, the electron-donating group on the alkene accelerated the metathesis reaction<sup>13</sup> because the alkylidene carbene complex **26** generated from chromacyclobutane **24** was stabilized by these groups. Thus enyne **14h** afforded only metathesis product **19**. Since the [2 + 2] cycloaddition reaction was controlled by a HOMO/LUMO interaction, it should be accelerated by the alkene having an electron-donating group. In the reaction of **14c** with **13a**, cyclobutanone derivative **18c** was obtained in 46% yield along with cyclopropane derivative **16c** (43% yield). However, cyclopropane derivative **16a** was a main product when compound **14a** was treated with chromium carbene complex **13a**. Since the higher HOMO energy of **14c** compared with that of **14a** favors the [2 + 2] cycloaddition of ketene and alkene, the formation of cyclobutanone derivative would be accelerated. It could be understood when compound **14e** was treated with **13a**, only cyclopropane derivative **16e** was obtained (Scheme 11).

**Reaction of Enynes with Pentacarbonyl(ethoxybenzylidene)chromium.** Subsequently, the reaction of enyne with pentacarbonyl(ethoxybenzylidene)chromium (**28**), which was prepared from  $\text{Cr}(\text{CO})_6$  and  $\text{PhLi}$  followed by treatment with  $\text{Et}_3\text{O}^+\text{BF}_4^-$ , was examined. A  $\text{CH}_3\text{CN}$  solution of **14a** with chromium carbene complex **28** was warmed at  $70^\circ\text{C}$  for 4 h followed by treatment with 10% HCl to give cyclopropane derivative **29a** in 79% yield. When *E*-**14d** was treated with **28** in  $\text{CH}_3\text{CN}$ , metathesis product **30** was obtained in 69% yield. The reaction of **14c** with **28** afforded cyclopropane derivative **29c**, cyclobutanone derivative **31c**, and indanone derivative **32**<sup>14</sup> in 32%, 25%, and 12% yields, respectively (Scheme 12).

Scheme 12. Reaction of Enynes with **28**

**Synthesis of Piperidine Derivatives Using Chromium Carbene Complexes.** Next, we attempted the synthesis of piperidine derivatives using the reaction of enynes with chromium carbene complexes. Recently, Harvey reported the synthesis of pyran derivative **34** from allyl ether **33** using molybdenum carbene complex **10a**.<sup>4</sup> However, homoallyl ether **35** did not afford the cyclized product. They claimed that the reason is due to the acidity at the carbon  $\alpha$  to the molybdenum carbene carbon of **36** (Scheme 13).

When propargylamine derivative **39a** was treated with chromium carbene complex **13a** in  $\text{CH}_3\text{CN}$  at  $70^\circ\text{C}$  for 4 h, piperidine derivative **40a** fused by a three-membered ring was obtained in 46% yield. In this reaction, the use of  $\text{CH}_3\text{CN}$  was found to be superior to THF and benzene (Table 3). In a similar manner, the reaction of enynes **39b,c** with **13a** afforded piperidine derivatives **40b,c** fused by three-membered rings in good yields, respectively. On the other hand, compound **39d** having a phenyl group on the alkene also afforded metathesis product **40d**, though the yield was low. The substituent effects for the synthesis of piperidine de-

(14) (a) Wulff, W. D.; Tang, P. C.; McCallum, K. S.; Yang, D. C.; Gilbertson, S. R. *Tetrahedron* **1985**, *41*, 5813. (b) Yamashita, A. *Tetrahedron Lett.* **1986**, *27*, 5915.

## Scheme 13. Formation of the Pyran Ring

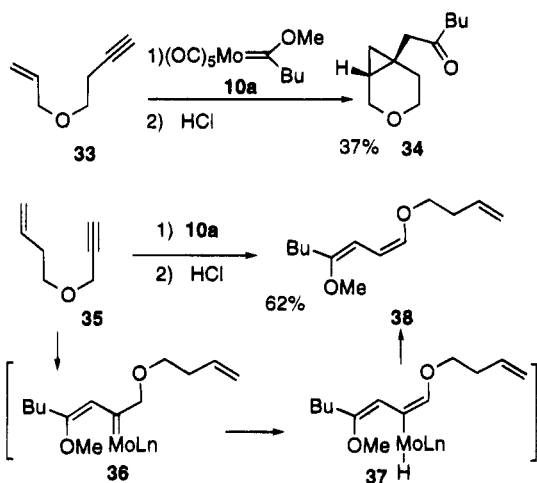
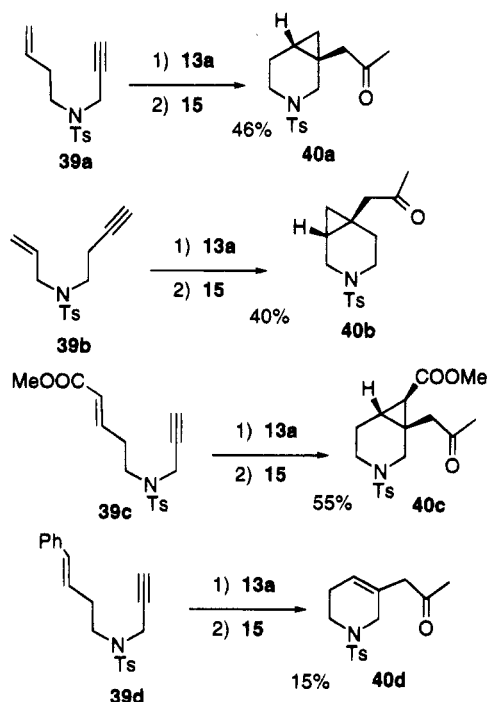


Table 3. Reaction of Enyne 39a with Cr-Carbene Complex 13a

run	conditions	yield of 40a, %
1	CH <sub>3</sub> CN, 70 °C, 4 h	46
2	THF, reflux, 4 h	36
3	PhH, 70 °C, 4 h	39

## Scheme 14. Synthesis of the Piperidine Ring



derivatives were the same as those for the synthesis of pyrrolidine derivatives (Scheme 14).

In conclusion, reactions of enynes with Fischer chromium carbene complexes gave the various pyrrolidine and piperidine derivatives. The reaction products were dramatically affected by the substituents on the alkene. The reaction of a compound having an electron-donating group on the alkene with a chromium carbene complex gave a metathesis product, and the electron-withdrawing group promotes the formation of a three-membered ring.

## Experimental Section

All manipulations were performed under an argon atmosphere using standard Schlenk techniques, and all the reaction

solutions were degassed through freeze-pump-thaw cycles. Solvents were distilled under an argon atmosphere from sodium benzophenone ketyl (THF) or CaH<sub>2</sub> (CH<sub>2</sub>Cl<sub>2</sub>). All other reagents and solvents were purified when necessary using standard procedures. Column chromatography was performed on silica gel 60 (70–230 mesh, 60 Å), and flash chromatography was performed on silica gel 60 (230–400 mesh, 60 Å) using the indicated solvent. Melting points are uncorrected. Preparations of enynes **14a–c** were already reported.<sup>14</sup>

**General Procedure for the Reaction of Fischer Carbene Complexes with Enynes.** An appropriate solution of Fischer carbene complex (1.2 equiv) and enyne (1 equiv) was degassed through a freeze-pump-thaw cycle, and the solution was stirred at an appropriate temperature. After cooling, a CH<sub>3</sub>CN solution of [FeCl<sub>2</sub>(DMF)<sub>3</sub>][FeCl<sub>4</sub>] (3.6 equiv) or 10% HCl was added and the solution was stirred overnight. Water was added, and the organic layer was extracted with ethyl acetate. The organic layer was washed with brine, dried over Na<sub>2</sub>SO<sub>4</sub>, and concentrated. The residue was purified by silica gel column chromatography.

**Reaction of Enyne 14a with 13a.** The crude product, which was prepared from **14a** (50.0 mg, 0.20 mmol) and **13a** (64 mg, 0.241 mmol) in CH<sub>3</sub>CN (1.5 mL) at 70 °C for 4 h followed by treatment with [FeCl<sub>2</sub>(DMF)<sub>3</sub>][FeCl<sub>4</sub>] (393 mg, 0.723 mmol), was purified by silica gel chromatography (ethyl acetate-hexane, 1:2) to give **16a**.

**rel-(1S,5S)-1-(2-Oxopropyl)-3-(p-tolylsulfonyl)-3-azabicyclo[3.1.0]hexane (16a):** 53.5 mg, 91%; IR (Nujol)  $\nu$  1715, 1597, 1341, 1161 cm<sup>-1</sup>; <sup>1</sup>H-NMR (CDCl<sub>3</sub>)  $\delta$  0.56 (dd, *J* = 5.9, 7.8 Hz, 1 H), 0.70 (dd, *J* = 4.4, 5.9 Hz, 1 H), 1.26 (ddd, *J* = 3.9, 4.4, 7.8 Hz, 1 H), 2.09 (s, 3 H), 2.44 (s, 3 H), 2.46 (d, *J* = 17.1 Hz, 1 H), 2.59 (d, *J* = 17.1 Hz, 1 H), 2.89 (d, *J* = 9.3 Hz, 1 H), 3.15 (dd, *J* = 3.9, 9.3 Hz, 1 H), 3.51 (d, *J* = 9.3 Hz, 1 H), 3.62 (d, *J* = 9.3 Hz, 1 H), 7.32 (d, *J* = 8.3 Hz, 2 H), 7.67 (d, *J* = 8.3 Hz, 2 H); <sup>13</sup>C-NMR (CDCl<sub>3</sub>)  $\delta$  206.5, 143.4, 133.7, 129.6, 127.5, 52.8, 49.7, 47.0, 30.0, 25.6, 21.5, 21.3, 13.7; MS *m/z* 293 (M<sup>+</sup>), 277, 250, 187, 155, 138, 91 (base peak); HRMS (*m/z*) calcd for C<sub>15</sub>H<sub>19</sub>NO<sub>3</sub>S 293.1073, found 293.1079. Anal. Calcd for C<sub>15</sub>H<sub>19</sub>NO<sub>3</sub>S: C, 61.41; H, 6.53; N, 4.77; S, 10.93. Found: C, 61.36; H, 6.54; N, 4.74; S, 10.92.

**7-Oxo-3-(p-tolylsulfonyl)-3-azabicyclo[3.3.0]oct-5-ene (17):** mp 139 °C; IR (Nujol)  $\nu$  1713, 1651, 1599, 1161 cm<sup>-1</sup>; <sup>1</sup>H-NMR (CDCl<sub>3</sub>)  $\delta$  2.06 (dd, *J* = 3.5, 18.1 Hz, 1 H), 2.44 (s, 3 H), 2.59 (dd, *J* = 6.3, 18.1 Hz, 1 H), 2.62 (dd, *J* = 9.3, 11.2 Hz, 1 H), 3.10–3.20 (m, 1 H), 4.01 (d, *J* = 9.3 Hz, 1 H), 4.03 (d, *J* = 16.6 Hz, 1 H), 4.34 (d, *J* = 16.6 Hz, 1 H), 5.99 (brs, 1 H), 7.35 (d, *J* = 8.3 Hz, 2 H), 7.73 (d, *J* = 8.3 Hz, 2 H); MS *m/z* 277 (M<sup>+</sup>), 155, 122, 94, 91 (base peak); HRMS (*m/z*) calcd for C<sub>14</sub>H<sub>15</sub>NO<sub>3</sub>S 277.0773, found 277.0784. Anal. Calcd for C<sub>14</sub>H<sub>15</sub>NO<sub>3</sub>S: C, 60.63; H, 5.45; N, 5.05; S, 11.56. Found: C, 60.45; H, 5.47; N, 4.87; S, 11.71.

**Reaction of Enyne 14b with 13a.** The crude product, which was prepared from **14b** (45.8 mg, 0.247 mmol) and **13a** (77.7 mg, 0.294 mmol) in CH<sub>3</sub>CN (2.5 mL) at 70 °C for 4 h followed by treatment with 10% HCl and then K<sub>2</sub>CO<sub>3</sub>, was purified by silica gel chromatography (ethyl acetate-hexane, 1:4–1:0) to give **14b**.

**rel-(1S,5S)-3-Benzyl-1-(2-oxopropyl)-3-azabicyclo[3.1.0]hexane (14b):** 10.4 mg, 18%; IR (neat)  $\nu$  1711 cm<sup>-1</sup>; <sup>1</sup>H-NMR (CDCl<sub>3</sub>)  $\delta$  0.46 (dd, *J* = 3.2, 7.2 Hz, 1 H), 1.19–1.28 (m, 2 H), 2.20 (s, 3 H), 2.26 (d, *J* = 8.5 Hz, 1 H), 2.47 (d, *J* = 15.8 Hz, 1 H), 2.48 (dd, *J* = 2.9, 8.6 Hz, 1 H), 2.70 (d, *J* = 15.8 Hz, 1 H), 2.98 (d, *J* = 8.6 Hz, 1 H), 3.04 (d, *J* = 8.5 Hz, 1 H), 3.64 (s, 2 H), 7.21–7.36 (m, 5 H); MS *m/z* 229 (M<sup>+</sup>), 186, 172, 152, 138, 91, 43 (base peak); HRMS (*m/z*) calcd for C<sub>15</sub>H<sub>19</sub>NO 229.1467, found 229.1480.

**Reaction of Enyne 14c with 13a.** The crude product, which was prepared from **14c** (52.4 mg, 0.20 mmol) and **13a** (62.9 mg, 0.238 mmol) in CH<sub>3</sub>CN (2.0 mL) at 70 °C for 4 h followed by treatment with [FeCl<sub>2</sub>(DMF)<sub>3</sub>][FeCl<sub>4</sub>] (390 mg, 0.717 mmol), was purified by silica gel chromatography (ethyl

acetate-hexane, 1:5-1:1) to give **14c** (26.1 mg, 43%) and **18c** (30.9 mg, 46%).

**rel-(1S,5S)-5-Methyl-1-(2-oxopropyl)-3-(p-tolylsulfonyl)-3-azabicyclo[3.1.0]hexane (14c)**: mp 104-5 °C; IR (Nujol)  $\nu$  1716, 1344, 1157  $\text{cm}^{-1}$ ;  $^1\text{H-NMR}$  ( $\text{CDCl}_3$ )  $\delta$  0.28 (d,  $J = 5.2$  Hz, 1 H), 0.87 (d,  $J = 5.2$  Hz, 1 H), 1.05 (s, 3 H), 2.12 (s, 3 H), 2.44 (s, 3 H), 2.89 (d,  $J = 9.1$  Hz, 2 H), 2.90 (d,  $J = 9.1$  Hz, 2 H), 3.54 (d,  $J = 9.0$  Hz, 1 H), 3.60 (d,  $J = 9.0$  Hz, 1 H), 7.32 (d,  $J = 8.1$  Hz, 2 H), 7.67 (d,  $J = 8.1$  Hz, 2 H); MS  $m/z$  307 ( $\text{M}^+$ ), 264, 152 (base peak), 108, 91, 43. Anal. Calcd for  $\text{C}_{16}\text{H}_{21}\text{NO}_3\text{S}$ : C, 62.51; H, 6.89; N, 4.56; S, 10.43. Found: C, 62.58; H, 6.85; N, 4.58; S, 10.49.

**rel-(1R,5S)-5-Methyl-7-oxo-1-(2-oxopropyl)-3-(p-tolylsulfonyl)-3-azabicyclo[3.2.0]heptane (18c)**: mp 143 °C; IR (Nujol)  $\nu$  1776, 1715, 1342, 1160  $\text{cm}^{-1}$ ;  $^1\text{H-NMR}$  ( $\text{CDCl}_3$ )  $\delta$  1.18 (s, 3 H), 2.10 (s, 3 H), 2.45 (s, 3 H), 2.63 (d,  $J = 9.8$  Hz, 1 H), 2.66 (d,  $J = 18.9$  Hz, 1 H), 2.70 (d,  $J = 9.8$  Hz, 1 H), 2.71 (d,  $J = 18.9$  Hz, 1 H), 3.08 (d,  $J = 18.1$  Hz, 1 H), 3.15 (d,  $J = 18.1$  Hz, 1 H), 3.64 (d,  $J = 9.8$  Hz, 1 H), 3.77 (d,  $J = 9.8$  Hz, 1 H), 7.34 (d,  $J = 8.3$  Hz, 2 H), 7.68 (d,  $J = 8.3$  Hz, 2 H); MS  $m/z$  335 ( $\text{M}^+$ ), 293, 250, 180, 155, 138, 91, 43 (base peak). Anal. Calcd for  $\text{C}_{17}\text{H}_{21}\text{NO}_4\text{S}$ : C, 60.88; H, 6.31; N, 4.18; S, 9.56. Found: C, 60.82; H, 6.29; N, 4.14; S, 9.58.

**Reaction of E-14d with 13a**. The crude product, which was prepared from **E-14d** (50.0 mg, 0.154 mmol) and **13a** (49.0 mg, 0.184 mmol) in  $\text{CH}_3\text{CN}$  (1.5 mL) at 70 °C for 4 h followed by treatment with  $[\text{FeCl}_2(\text{DMF})_3][\text{FeCl}_4]$  (300 mg, 0.552 mmol), was purified by silica gel chromatography (ethyl acetate-hexane, 1:5-1:1) to give **19** (22.8 mg, 53%), **16d** (4.1 mg, 7%), and **18d** (5.5 mg, 9%).

**3-(2-Oxopropyl)-1-(p-tolylsulfonyl)-2,5-dihydropyrrole (19)**: IR (neat)  $\nu$  1717, 1630, 1597, 1341, 1161  $\text{cm}^{-1}$ ;  $^1\text{H-NMR}$  ( $\text{CDCl}_3$ )  $\delta$  2.21 (s, 3 H), 2.43 (s, 3 H), 3.18 (s, 2 H), 4.09 (brs, 4 H), 5.48 (brs, 1 H), 7.32 (d,  $J = 8.3$  Hz, 2 H), 7.72 (d,  $J = 8.3$  Hz, 2 H);  $^{13}\text{C-NMR}$  ( $\text{CDCl}_3$ )  $\delta$  204.4, 142.5, 134.1, 132.2, 129.8, 127.4, 122.8, 56.4, 54.8, 43.3, 29.7, 21.5; MS  $m/z$  279 ( $\text{M}^+$ ), 236, 155, 91 (base peak), 82; HRMS ( $m/z$ ) calcd for  $\text{C}_{14}\text{H}_{17}\text{NO}_3\text{S}$  279.0929, found 279.0916. Anal. Calcd for  $\text{C}_{14}\text{H}_{17}\text{NO}_3\text{S}$ : C, 60.19; H, 6.13; N, 5.01; S, 11.48. Found: C, 60.33; H, 6.30; N, 4.93; S, 11.44.

**rel-(1R,5R,6R)-1-(2-Oxopropyl)-6-phenyl-3-(p-tolylsulfonyl)-3-azabicyclo[3.1.0]hexane (16d)**: IR (Nujol)  $\nu$  1715, 1599, 1345, 1163  $\text{cm}^{-1}$ ;  $^1\text{H-NMR}$  ( $\text{CDCl}_3$ )  $\delta$  1.76 (s, 3 H), 1.83 (dd,  $J = 3.9, 4.4$  Hz, 1 H), 2.20 (d,  $J = 4.4$  Hz, 1 H), 2.30 (d,  $J = 18.1$  Hz, 1 H), 2.36 (d,  $J = 18.1$  Hz, 1 H), 2.44 (s, 3 H), 3.04 (d,  $J = 9.3$  Hz, 1 H), 3.34 (dd,  $J = 4.4, 9.3$  Hz, 1 H), 3.70 (d,  $J = 9.3$  Hz, 1 H), 3.91 (d,  $J = 9.3$  Hz, 1 H), 7.00-7.04 (m, 2 H), 7.22-7.28 (m, 3 H), 7.32-7.36 (m, 2 H), 7.70-7.75 (m, 2 H);  $^{13}\text{C-NMR}$  ( $\text{CDCl}_3$ )  $\delta$  206.6, 143.5, 136.7, 133.8, 129.7, 128.6, 128.3, 127.5, 126.5, 54.1, 50.1, 42.1, 31.1, 30.0, 28.9, 25.6, 21.6; MS  $m/z$  369 ( $\text{M}^+$ ), 326, 278, 214, 156, 117 (base peak), 91; HRMS ( $m/z$ ) calcd for  $\text{C}_{21}\text{H}_{23}\text{NO}_3\text{S}$  369.1399, found 369.1373.

**rel-(1R,5R,6S)-7-Oxo-1-(2-oxopropyl)-6-phenyl-3-(p-tolylsulfonyl)-3-azabicyclo[3.2.0]heptane (18d)**: IR (Nujol)  $\nu$  1790, 1715, 1597, 1362, 1169  $\text{cm}^{-1}$ ;  $^1\text{H-NMR}$  ( $\text{CDCl}_3$ )  $\delta$  1.78 (s, 3 H), 2.24 (d,  $J = 18.6$  Hz, 1 H), 2.39 (d,  $J = 18.6$  Hz, 1 H), 2.48 (s, 3 H), 3.27 (brs, 1 H), 3.31 (ddd,  $J = 2.0, 3.4, 3.4$  Hz, 1 H), 3.79 (d,  $J = 10.7$  Hz, 1 H), 3.99 (dd,  $J = 3.4, 10.7$  Hz, 1 H), 4.06 (dd,  $J = 3.4, 10.7$  Hz, 1 H), 4.48 (d,  $J = 10.7$  Hz, 1 H), 6.95-6.99 (m, 2 H), 7.21-7.28 (m, 3 H), 7.40 (d,  $J = 7.8$  Hz, 2 H), 7.78 (d,  $J = 7.8$  Hz, 2 H);  $^{13}\text{C-NMR}$  ( $\text{CDCl}_3$ )  $\delta$  207.3, 204.8, 144.1, 137.1, 134.0, 130.0, 128.8, 127.5, 66.7, 58.3, 57.4, 53.3, 43.6, 40.3, 30.4, 21.6; MS  $m/z$  397 ( $\text{M}^+$ ), 354, 242, 155, 117 (base peak), 91; HRMS ( $m/z$ ) calcd for  $\text{C}_{22}\text{H}_{23}\text{NO}_4\text{S}$  397.1347, found 397.1331.

**Reaction of Z-14d with 13a**. The crude product, which was prepared from **Z-14d** (100 mg, 0.308 mmol) and **13a** (98.0 mg, 0.368 mmol) in  $\text{CH}_3\text{CN}$  (3.0 mL) at 70 °C for 4 h followed by treatment with  $[\text{FeCl}_2(\text{DMF})_3][\text{FeCl}_4]$  (600 mg, 1.10 mmol), was purified by silica gel chromatography (ethyl acetate-hexane, 1:4-1:2) to give **19** (42.2 mg, 49%) and **19'** (6 mg, 7%).

**3-(2-Oxopropyl)-1-(p-tolylsulfonyl)-3,3-didehydropyrrolidine (19')**: IR (neat)  $\nu$  1693, 1629, 1598, 1346, 1163  $\text{cm}^{-1}$ ;  $^1\text{H-NMR}$  ( $\text{CDCl}_3$ )  $\delta$  2.15-1.95 (m, 2 H), 2.17 (s, 3 H), 2.43 (s, 3 H), 4.40-3.10 (m, 4 H), 6.17 (brs, 1 H), 7.32 (d,  $J = 8.3$  Hz, 2 H), 7.83 (d,  $J = 8.3$  Hz, 2 H); MS  $m/z$  279 ( $\text{M}^+$ ), 236, 155, 91 (base peak), 82; HRMS ( $m/z$ ) calcd for  $\text{C}_{14}\text{H}_{17}\text{NO}_3\text{S}$  279.0929, found 279.0948.

**Reaction of E-14d with 13c**. The reaction procedure was same as that of the reaction of enyne with **13a**. A crude product, which was prepared from **Z-14d** (50.0 mg, 0.154 mmol) and **13c** (73.0 mg, 0.184 mmol) in  $\text{CH}_3\text{CN}$  (1.5 mL) under refluxing for 67 h followed by treatment with  $[\text{FeCl}_2(\text{DMF})_3][\text{FeCl}_4]$  (301 mg, 554 mmol), was purified by silica gel chromatography (ethyl acetate-hexane, 1:3) to give **16d** (9.7 mg, 17%) and **16d'** (4.6 mg, 8%).

**rel-(1R,5R,6R)-1-(2-Oxopropyl)-6-phenyl-3-(p-tolylsulfonyl)-3-azabicyclo[3.1.0]hexane (16d')**: IR (KBr)  $\nu$  1715, 1597, 1340, 1160  $\text{cm}^{-1}$ ;  $^1\text{H-NMR}$  ( $\text{CDCl}_3$ )  $\delta$  1.71 (dd,  $J = 4.8, 8.4$  Hz, 1 H), 2.08 (d,  $J = 8.4$  Hz, 1 H), 2.17 (s, 3 H), 2.38 (s, 3 H), 2.54 (d,  $J = 18.0$  Hz, 1 H), 3.02 (d,  $J = 18.0$  Hz, 1 H), 3.15 (d,  $J = 9.5$  Hz, 1 H), 3.40 (d,  $J = 9.5$  Hz, 1 H), 3.52 (dd,  $J = 4.8, 9.5$  Hz, 1 H), 3.56 (d,  $J = 9.5$  Hz, 1 H), 7.72-7.38 (m, 7 H), 7.76 (d,  $J = 8.4$  Hz, 2 H); MS  $m/z$  369 ( $\text{M}^+$ ), 326, 278, 214, 155, 117, 91 (base peak); HRMS ( $m/z$ ) calcd for  $\text{C}_{21}\text{H}_{23}\text{NO}_3\text{S}$  369.1399, found 369.1386.

**Reaction of 14e with 13a**. The crude product, which was prepared from **14e** (56.5 mg, 0.184 mmol) and **13a** (58.7 mg, 0.222 mmol) in  $\text{CH}_3\text{CN}$  (1.8 mL) at 70 °C for 4 h followed by treatment with  $[\text{FeCl}_2(\text{DMF})_3][\text{FeCl}_4]$  (360 mg, 662 mmol), was purified by silica gel chromatography (ethyl acetate-hexane, 1:2-1:3) to give **17e** (46 mg, 71%).

**rel-(1R,5R,6R)-6-(Methoxycarbonyl)-1-(2-oxopropyl)-3-(p-tolylsulfonyl)-3-azabicyclo[3.1.0]hexane (16e)**: mp 138 °C; IR (Nujol)  $\nu$  1726, 1719, 1348, 1161  $\text{cm}^{-1}$ ;  $^1\text{H-NMR}$  ( $\text{CDCl}_3$ )  $\delta$  1.88 (dd,  $J = 3.4, 3.9$  Hz, 1 H), 1.93 (d,  $J = 3.9$  Hz, 1 H), 2.06 (s, 3 H), 2.44 (s, 3 H), 2.78 (d,  $J = 18.4$  Hz, 1 H), 2.94 (d,  $J = 10.1$  Hz, 1 H), 3.05 (d,  $J = 18.4$  Hz, 1 H), 3.23 (dd,  $J = 3.4, 9.6$  Hz, 1 H), 3.62 (d,  $J = 10.1$  Hz, 1 H), 3.65 (s, 3 H), 3.73 (d,  $J = 9.6$  Hz, 1 H), 7.34 (d,  $J = 8.1$  Hz, 2 H), 7.67 (d,  $J = 8.1$  Hz, 2 H); MS  $m/z$  351 ( $\text{M}^+$ ), 320, 308, 196 (base peak), 155, 136, 91. Anal. Calcd for  $\text{C}_{17}\text{H}_{21}\text{NO}_5\text{S}$ : C, 58.10; H, 6.02; N, 3.99; S, 9.12. Found: C, 58.03; H, 6.03; N, 3.96; S, 9.14.

**Reaction of 14f with 13a**. The crude product, which was prepared from **14f** (50 mg, 0.135 mmol) and **13a** (43.0 mg, 0.162 mmol) in  $\text{CH}_3\text{CN}$  (1.4 mL) at 70 °C for 4 h followed by treatment with  $[\text{FeCl}_2(\text{DMF})_3][\text{FeCl}_4]$  (264 mg, 0.486 mmol), was purified by silica gel chromatography (ethyl acetate-hexane, 1:2-1:1) to give **19** (1.5 mg, 4%) and **16f** (42.2 mg, 75%).

**rel-(1R,5R,6R)-6-(4-Nitrophenyl)-1-(2-oxopropyl)-3-(p-tolylsulfonyl)-3-azabicyclo[3.1.0]hexane (16f)**: mp 153 °C; IR (Nujol)  $\nu$  1715, 1597, 1516, 1343, 1161  $\text{cm}^{-1}$ ;  $^1\text{H-NMR}$  ( $\text{CDCl}_3$ )  $\delta$  1.83 (s, 3 H), 1.92 (dd,  $J = 3.9, 4.4$  Hz, 1 H), 2.30 (d,  $J = 18.6$  Hz, 1 H), 2.36 (d,  $J = 4.4$  Hz, 1 H), 2.42 (d,  $J = 18.6$  Hz, 1 H), 2.45 (s, 3 H), 2.98 (d,  $J = 9.8$  Hz, 1 H), 3.33 (dd,  $J = 3.9, 9.3$  Hz, 1 H), 3.74 (d,  $J = 9.3$  Hz, 1 H), 3.96 (d,  $J = 9.8$  Hz, 1 H), 7.20 (d,  $J = 8.8$  Hz, 2 H), 7.36 (d,  $J = 8.3$  Hz, 2 H), 7.72 (d,  $J = 8.3$  Hz, 2 H), 8.12 (d,  $J = 8.8$  Hz, 2 H); MS  $m/z$  414 ( $\text{M}^+$ ), 371, 259, 116, 91, 43 (base peak); HRMS ( $m/z$ ) calcd for  $\text{C}_{21}\text{H}_{22}\text{N}_2\text{O}_6\text{S}$  414.1249, found 414.1259. Anal. Calcd for  $\text{C}_{21}\text{H}_{22}\text{N}_2\text{O}_6\text{S}$ : C, 60.86; H, 5.35; N, 6.76; S, 7.74. Found: C, 60.60; H, 5.30; N, 6.58; S, 7.63.

**Reaction of 14g with 13a**. The crude product, which was prepared from **14g** (50 mg, 0.139 mmol) and **13a** (44.0 mg, 0.167 mmol) in  $\text{CH}_3\text{CN}$  (1.4 mL) at 70 °C for 4 h followed by treatment with  $[\text{FeCl}_2(\text{DMF})_3][\text{FeCl}_4]$  (272 mg, 0.500 mmol), was purified by silica gel chromatography (ethyl acetate-hexane, 1:3-1:2) to give **19** (17.8 mg, 46%), **16g** (10.2 mg, 18%) and **18g** (5.0 mg, 8%).

**rel-(1R,5R,6R)-6-(4-Chlorophenyl)-1-(2-oxopropyl)-3-(p-tolylsulfonyl)-3-azabicyclo[3.1.0]hexane (16g)**: IR (Nujol)  $\nu$  1713, 1597, 1343, 1161  $\text{cm}^{-1}$ ;  $^1\text{H-NMR}$  ( $\text{CDCl}_3$ )  $\delta$  1.77

(dd,  $J = 3.9, 4.4$  Hz, 1 H), 1.81 (s, 3 H), 2.20 (d,  $J = 4.4$  Hz, 1 H), 2.29 (d,  $J = 18.6$  Hz, 1 H), 2.35 (d,  $J = 18.6$  Hz, 1 H), 2.44 (s, 3 H), 2.98 (d,  $J = 9.3$  Hz, 1 H), 3.31 (dd,  $J = 3.9, 9.3$  Hz, 1 H), 3.69 (d,  $J = 9.3$  Hz, 1 H), 3.91 (d,  $J = 9.3$  Hz, 1 H), 6.69 (d,  $J = 8.3$  Hz, 2 H), 7.22 (d,  $J = 8.3$  Hz, 2 H), 7.34 (d,  $J = 8.3$  Hz, 2 H), 7.71 (d,  $J = 8.3$  Hz, 2 H); MS  $m/z$  403 ( $M^+$ ), 306, 248, 155, 151, 91, 43 (base peak); HRMS ( $m/z$ ) calcd for  $C_{21}H_{22}NO_3S$  403.1009, found 403.1013.

**rel-(1R,5R,6S)-6-(4-Chlorophenyl)-7-oxo-1-(2-oxopropyl)-3-(p-tolylsulfonyl)-3-azabicyclo[3.2.0]heptane (18g):** IR (Nujol)  $\nu$  1786, 1717, 1597, 1354, 1165  $cm^{-1}$ ;  $^1H$ -NMR ( $CDCl_3$ )  $\delta$  1.84 (s, 3 H), 2.22 (d,  $J = 19.0$  Hz, 1 H), 2.45 (d,  $J = 19.0$  Hz, 1 H), 2.48 (s, 3 H), 3.28 (brs, 2 H), 3.76 (d,  $J = 10.7$  Hz, 1 H), 3.98 (dd,  $J = 2.9, 10.7$  Hz, 1 H), 4.05 (dd,  $J = 2.9, 10.7$  Hz, 1 H), 4.43 (d,  $J = 10.7$  Hz, 1 H), 6.92 (d,  $J = 8.3$  Hz, 2 H), 7.22 (d,  $J = 8.3$  Hz, 2 H), 7.40 (d,  $J = 8.3$  Hz, 2 H), 7.76 (d,  $J = 8.3$  Hz, 2 H); MS  $m/z$  433, 431 ( $M^+$ ), 388, 276, 151, 91, 43 (base peak); HRMS ( $m/z$ ) calcd for  $C_{22}H_{22}NO_4S$  433.0929, found 433.0944.

**Reaction of 14h with 13a.** The crude product, which was prepared from 14h (50 mg, 0.147 mmol) and 13a (47.0 mg, 0.177 mmol) in  $CH_3CN$  (1.5 mL) at 70 °C for 4 h followed by treatment with  $[FeCl_2(DMF)_3][FeCl_4]$  (289 mg, 0.531 mmol), was purified by silica gel chromatography (ethyl acetate–hexane, 1:3–1:2) to give 19 (25.6 mg, 62%) and 18h (3.5 mg, 6%).

**rel-(1R,5R,6S)-6-(4-Methylphenyl)-7-oxo-1-(2-oxopropyl)-3-(p-tolylsulfonyl)-3-azabicyclo[3.2.0]heptane (18h):** IR (Nujol)  $\nu$  1782, 1717, 1597, 1346, 1163  $cm^{-1}$ ;  $^1H$ -NMR ( $CDCl_3$ )  $\delta$  1.73 (s, 3 H), 2.17 (d,  $J = 18.6$  Hz, 1 H), 2.21 (s, 3 H), 2.32 (d,  $J = 18.6$  Hz, 1 H), 2.41 (s, 3 H), 3.16 (brs, 1 H), 3.21 (ddd,  $J = 1.0, 3.4, 3.4$  Hz, 1 H), 3.71 (d,  $J = 10.7$  Hz, 1 H), 3.90 (dd,  $J = 3.4, 10.7$  Hz, 1 H), 3.98 (dd,  $J = 3.4, 10.7$  Hz, 1 H), 4.38 (d,  $J = 10.7$  Hz, 1 H), 6.78 (d,  $J = 8.3$  Hz, 2 H), 6.98 (d,  $J = 7.8$  Hz, 2 H), 7.33 (d,  $J = 7.8$  Hz, 2 H), 7.70 (d,  $J = 8.3$  Hz, 2 H); MS  $m/z$  411 ( $M^+$ ), 368, 256, 131 (base peak), 91, 43; HRMS ( $m/z$ ) calcd for  $C_{23}H_{25}NO_4S$  411.1504, found 411.1485.

**Reaction of 14a with 28.** The crude product, which was prepared from 14a (149.6 mg, 0.6 mmol) and 28 (235.7 mg, 0.722 mmol) in  $CH_3CN$  (6.0 mL) at 70 °C for 4 h followed by treatment with 10% HCl, was purified by silica gel chromatography (ethyl acetate–hexane, 1:5–1:3) to give 29a (168.6 mg, 79%) as a colorless oil.

**rel-(1S,5S)-1-(2-Oxo-2-phenylethyl)-3-(p-tolylsulfonyl)-3-azabicyclo[3.1.0]hexane (29a):** IR (neat)  $\nu$  1685, 1600, 1340, 1160  $cm^{-1}$ ;  $^1H$ -NMR ( $CDCl_3$ )  $\delta$  0.58 (dd,  $J = 5.5, 7.7$  Hz, 1 H), 0.71 (dd,  $J = 4.0, 5.5$  Hz, 1 H), 1.33 (ddd,  $J = 3.7, 4.0, 7.7$  Hz, 1 H), 2.44 (s, 3 H), 3.00 (d,  $J = 9.2$  Hz, 1 H), 3.07 (d,  $J = 17.0$  Hz, 1 H), 3.14 (d,  $J = 17.0$  Hz, 1 H), 3.22 (dd,  $J = 3.7, 9.2$  Hz, 1 H), 3.53 (d,  $J = 9.2$  Hz, 1 H), 3.73 (d,  $J = 9.2$  Hz, 1 H), 7.32 (d,  $J = 8.2$  Hz, 2 H), 7.46 (d,  $J = 8.0$  Hz, 2 H), 7.52–7.59 (m, 1 H), 7.68 (d,  $J = 8.2$  Hz, 2 H), 7.85 (d,  $J = 8.0$  Hz, 2 H); MS  $m/z$  355 ( $M^+$ ), 250, 200, 155, 105 (base peak), 91. Anal. Calcd for  $C_{20}H_{21}NO_3S$ : C, 67.58; H, 5.95; N, 3.94; S, 9.02. Found: C, 67.45; H, 6.15; N, 3.78; S, 8.96.

**Reaction of 14c with 28.** The crude product, which was prepared from 14c (52.2 mg, 0.198 mmol) and 28 (77.7 mg, 0.238 mmol) in  $CH_3CN$  (2.0 mL) at 70 °C for 4 h followed by treatment with 10% HCl, was purified by silica gel chromatography (ethyl acetate–hexane, 1:6–1:3) to give 29c (23.7 mg, 32%), 30c (10.8 mg, 25%), and 31 (9.1 mg, 12%).

**rel-(1S,5S)-5-Methyl-1-(2-oxo-2-phenylethyl)-3-(p-tolylsulfonyl)-3-azabicyclo[3.1.0]hexane (29c):** IR (Nujol)  $\nu$  1686, 1598, 1344, 1164  $cm^{-1}$ ;  $^1H$ -NMR ( $CDCl_3$ )  $\delta$  0.31 (d,  $J = 5.3$  Hz, 1 H), 0.87 (d,  $J = 5.3$  Hz, 1 H), 1.11 (s, 3 H), 2.44 (s, 3 H), 2.93 (d,  $J = 17.6$  Hz, 1 H), 2.99 (d,  $J = 9.5$  Hz, 1 H), 3.03 (d,  $J = 9.5$  Hz, 1 H), 3.13 (d,  $J = 17.6$  Hz, 1 H), 3.57 (d,  $J = 8.9$  Hz, 1 H), 3.67 (d,  $J = 8.9$  Hz, 1 H), 7.32 (d,  $J = 8.3$  Hz, 2 H), 7.42–7.49 (m, 2 H), 7.53–7.60 (m, 1 H), 7.68 (d,  $J = 8.3$  Hz, 2 H), 7.88 (d,  $J = 8.7$  Hz, 2 H); MS  $m/z$  369 ( $M^+$ ), 264, 238, 214, 155, 105 (base peak), 91; HRMS ( $m/z$ ) calcd for  $C_{21}H_{23}NO_3S$  369.1399, found 369.1411.

**rel-(1R,5S)-5-Methyl-7-oxo-1-(2-oxo-2-phenylethyl)-3-(p-tolylsulfonyl)-3-azabicyclo[3.2.0]heptane (30c):** mp 165–6 °C; IR (Nujol)  $\nu$  1773, 1684, 1376, 1160  $cm^{-1}$ ;  $^1H$ -NMR ( $CDCl_3$ )  $\delta$  1.22 (s, 3 H), 2.47 (s, 3 H), 2.75 (d,  $J = 9.3$  Hz, 1 H), 2.81 (d,  $J = 9.3$  Hz, 1 H), 3.15 (d,  $J = 18.0$  Hz, 1 H), 3.24 (d,  $J = 18.9$  Hz, 1 H), 3.30 (d,  $J = 18.0$  Hz, 1 H), 3.32 (d,  $J = 18.9$  Hz, 1 H), 3.69 (d,  $J = 9.8$  Hz, 1 H), 3.85 (d,  $J = 9.8$  Hz, 1 H), 7.36 (d,  $J = 8.2$  Hz, 2 H), 7.40–7.48 (m, 2 H), 7.54–7.61 (m, 1 H), 7.71 (d,  $J = 8.2$  Hz, 2 H), 7.84 (d,  $J = 8.3$  Hz, 2 H); MS  $m/z$  397 ( $M^+$ ), 354, 250, 242, 200, 155, 105 (base peak), 91. Anal. Calcd for  $C_{22}H_{23}NO_4S$ : C, 66.48; H, 5.83; N, 3.52; S, 8.07. Found: C, 66.51; H, 5.77; N, 3.75; S, 7.79.

**3-[2-Aza-4-methyl-2-(p-tolylsulfonyl)-4-pentenyl]-indanone (31):** IR (neat)  $\nu$  1717, 1654, 1599, 1339, 1160  $cm^{-1}$ ;  $^1H$ -NMR ( $CDCl_3$ )  $\delta$  1.72 (s, 3 H), 2.43 (s, 3 H), 3.22 (dd,  $J = 3.3, 19.4$  Hz, 1 H), 2.79 (dd,  $J = 7.4, 19.4$  Hz, 1 H), 3.22 (dd,  $J = 11.2, 14.1$  Hz, 1 H), 3.38 (dd,  $J = 4.9, 14.1$  Hz, 1 H), 3.68 (d,  $J = 14.9$  Hz, 1 H), 3.72–3.82 (m, 1 H), 3.82 (d,  $J = 14.9$  Hz, 1 H), 4.90 (s, 3 H), 4.93 (s, 1 H), 7.32 (d,  $J = 8.2$  Hz, 2 H), 7.37–7.44 (m, 1 H), 7.50 (d,  $J = 7.2$  Hz, 2 H), 7.56–7.62 (m, 1 H), 7.70 (d,  $J = 8.2$  Hz, 2 H), 7.75 (d,  $J = 7.5$  Hz, 1 H); MS  $m/z$  369 ( $M^+$ ), 366, 238 (base peak), 155, 136, 91, 55; HRMS ( $m/z$ ) calcd for  $C_{12}H_{16}NO_2S$  238.0902, found 238.0904.

**Reaction of E-14d with 28.** The crude product, which was prepared from E-14d (200.8 mg, 0.617 mmol) and 28 (242.4 mg, 0.743 mmol) in  $CH_3CN$  (6.2 mL) at 70 °C for 4 h followed by treatment with 10% HCl, was purified by silica gel chromatography (ethyl acetate–hexane, 1:5–1:3) to give 30d (145 mg, 69%).

**3-(2-Oxo-2-phenylethyl)-1-(p-tolylsulfonyl)-2,5-dihydropyrrole (30d):** IR (neat)  $\nu$  1687, 1600, 1340, 1160  $cm^{-1}$ ;  $^1H$ -NMR ( $CDCl_3$ )  $\delta$  2.41 (s, 3 H), 3.70 (s, 2 H), 4.13 (brs, 4 H), 6.48 (brs, 1 H), 7.30 (d,  $J = 8.3$  Hz, 2 H), 7.32–7.64 (m, 3 H), 7.71 (d,  $J = 8.3$  Hz, 2 H), 7.88 (dd,  $J = 2.0, 7.9$  Hz, 2 H); MS  $m/z$  341 ( $M^+$ ), 236, 186, 155, 105 (base peak), 91. Anal. Calcd for  $C_{19}H_{19}NO_3S$ : C, 66.84; H, 5.61; N, 4.10; S, 9.39. Found: C, 66.75; H, 5.76; N, 3.99; S, 9.03.

**Reaction of 39a with 13a.** The crude product, which was prepared from 41a (30 mg, 0.114 mmol) and 13a (36 mg, 0.137 mmol) in  $CH_3CN$  (1.1 mL) at 70 °C for 4 h followed by treatment with  $[FeCl_2(DMF)_3][FeCl_4]$  (223 mg, 0.41 mmol), was purified by silica gel chromatography (ethyl acetate–hexane, 1:3–1:2) to give 40a (16.1 mg, 46%).

**rel-(1S,6R)-1-(2-Oxopropyl)-3-(p-tolylsulfonyl)-3-azabicyclo[4.1.0]heptane (40a):** IR (neat)  $\nu$  1715, 1599, 1339, 1165  $cm^{-1}$ ;  $^1H$ -NMR ( $CDCl_3$ )  $\delta$  0.55 (dd,  $J = 4.9, 9.3$  Hz, 1 H), 0.66 (dd,  $J = 4.9, 5.4$  Hz, 1 H), 0.85 (dddd,  $J = 1.6, 5.4, 8.0, 9.3$  Hz, 1 H), 1.84 (dddd,  $J = 1.6, 6.2, 9.8, 13.7$  Hz, 1 H), 2.06 (dddd,  $J = 4.0, 5.4, 8.0, 13.7$  Hz, 1 H), 2.09 (s, 3 H), 2.39 (s, 2 H), 2.42 (s, 3 H), 2.53 (ddd,  $J = 5.4, 9.8, 11.7$  Hz, 1 H), 2.75 (d,  $J = 11.7$  Hz, 1 H), 3.19 (ddd,  $J = 4.0, 6.2, 11.7$  Hz, 1 H), 3.53 (d,  $J = 11.7$  Hz, 1 H), 7.29 (d,  $J = 8.3$  Hz, 2 H), 7.59 (d,  $J = 8.3$  Hz, 2 H);  $^{13}C$ -NMR  $\delta$  207.1, 143.4, 139.9, 129.7, 127.5, 51.7, 48.4, 42.9, 30.2, 23.4, 21.5, 16.5, 16.2, 15.2; MS  $m/z$  307 ( $M^+$ ), 164, 155, 152 (base peak), 91. Anal. Calcd for  $C_{16}H_{21}NO_3S$ : C, 62.51; H, 6.89; N, 4.56; S, 10.43. Found: C, 62.39; H, 6.95; N, 4.45; S, 10.50.

**Reaction of 39b with 13a.** The crude product, which was prepared from 39b (30 mg, 0.114 mmol) and 13a (36 mg, 0.137 mmol) in  $CH_3CN$  (5.7 mL) at 70 °C for 4 h followed by treatment with  $[FeCl_2(DMF)_3][FeCl_4]$  (223 mg, 0.41 mmol), was purified by silica gel chromatography (ethyl acetate–hexane, 1:2–1:1) to give 40b (13.9 mg, 40%).

**rel-(1R,6R)-6-(2-Oxopropyl)-3-(p-tolylsulfonyl)-3-azabicyclo[4.1.0]heptane (40b):** IR (neat)  $\nu$  1715, 1598, 1340, 1160  $cm^{-1}$ ;  $^1H$ -NMR ( $CDCl_3$ )  $\delta$  0.47 (dd,  $J = 4.8, 8.8$  Hz, 1 H), 0.53 (dd,  $J = 4.8, 8.8$  Hz, 1 H), 0.79 (dddd,  $J = 1.8, 4.4, 4.8, 8.8$  Hz, 1 H), 1.63 (ddd,  $J = 4.4, 5.1, 13.9$  Hz, 1 H), 1.87 (ddd,  $J = 5.9, 10.3, 13.9$  Hz, 1 H), 2.01 (s, 3 H), 2.08 (d,  $J = 16.9$  Hz, 1 H), 2.36 (s, 3 H), 2.47 (ddd,  $J = 5.1, 10.3, 11.7$  Hz, 1 H), 2.49 (d,  $J = 16.9$  Hz, 1 H), 2.92 (dd,  $J = 4.4, 11.4$  Hz, 1 H), 3.14 (dddd,  $J = 1.8, 4.4, 5.9, 11.7$  Hz, 1 H), 3.51 (d,  $J = 11.4$  Hz, 1

H), 7.24 (d,  $J = 8.4$  Hz, 2 H), 7.55 (d,  $J = 8.4$  Hz, 2 H); MS  $m/z$  307 ( $M^+$ ), 264, 250, 155, 152, 91, 43 (base peak). Anal. Calcd for  $C_{16}H_{21}NO_3S$ : C, 62.51; H, 6.89; N, 4.56. Found: C, 62.40; H, 6.88; N, 4.43.

**Reaction of 39c with 13a.** The crude product, which was prepared from **39c** (40 mg, 0.124 mmol) and **13a** (39 mg, 0.149 mmol) in  $CH_3CN$  (1.2 mL) at 70 °C for 4 h followed by treatment with  $[FeCl_2(DMF)_3][FeCl_4]$  (243 mg, 0.446 mmol), was purified by silica gel chromatography (ethyl acetate–hexane, 1:2) to give **40c** (24.7 mg, 55%).

**rel-(1R,6R,7R)-7-(Methoxycarbonyl)-1-(2-oxopropyl)-3-(p-tolylsulfonyl)-3-azabicyclo[4.1.0]heptane (40c):** mp 138–9 °C; IR (KBr)  $\nu$  1715, 1595, 1340, 1160  $cm^{-1}$ ;  $^1H$ -NMR ( $CDCl_3$ )  $\delta$  1.54 (ddd,  $J = 1.0, 5.4, 8.3$  Hz, 1 H), 1.96 (dddd,  $J = 1.0, 6.8, 11.7, 14.2$  Hz, 1 H), 1.97 (d,  $J = 5.4$  Hz, 1 H), 2.08 (s, 3 H), 2.11 (dddd,  $J = 3.4, 5.4, 8.3, 14.2$  Hz, 1 H), 2.43 (s, 3 H), 2.50 (ddd,  $J = 5.4, 10.3, 11.7$  Hz, 1 H), 2.67 (d,  $J = 11.7$  Hz, 1 H), 2.78 (d,  $J = 18.6$  Hz, 1 H), 2.91 (d,  $J = 18.6$  Hz, 1 H), 3.29 (dddd,  $J = 1.5, 3.4, 6.8, 10.3$  Hz, 1 H), 3.65 (s, 3 H), 3.68 (dd,  $J = 1.5, 11.7$  Hz, 1 H), 7.30 (d,  $J = 8.3$  Hz, 2 H), 7.59 (d,  $J = 8.3$  Hz, 2 H); MS  $m/z$  365 ( $M^+$ ), 334, 332, 210, 155, 152, 91 (base peak), 43. Anal. Calcd for  $C_{18}H_{23}NO_5S$ : C, 59.16; H, 6.34; N, 3.83; S, 8.77. Found: C, 59.06; H, 6.37; N, 3.85; S, 8.68.

**Reaction of 39d with 13a.** The crude product, which was prepared from **39d** (30 mg, 0.088 mmol) and **13a** (28 mg, 0.106 mmol) in  $CH_3CN$  (4.4 mL) at 70 °C for 4 h followed by

treatment with  $[FeCl_2(DMF)_3][FeCl_4]$  (173 mg, 0.318 mmol), was purified by silica gel chromatography (ethyl acetate–hexane, 1:4–1:2) to give **40d** (3.9 mg, 15%).

**5-(2-Oxopropyl)-1-(p-tolylsulfonyl)-1,2,3,6-tetrahydropyridine (40d):** IR (neat)  $\nu$  1715, 1595, 1340, 1160  $cm^{-1}$ ;  $^1H$ -NMR ( $CDCl_3$ )  $\delta$  2.13 (s, 3 H), 2.18–2.28 (m, 2 H), 2.43 (s, 3 H), 3.08 (s, 2 H), 3.16 (t,  $J = 5.9$  Hz, 2 H), 3.50 (d,  $J = 2.0$  Hz, 2 H), 5.58 (brs, 1 H), 7.32 (d,  $J = 8.1$  Hz, 2 H), 7.67 (d,  $J = 8.1$  Hz, 2 H); MS  $m/z$  293 ( $M^+$ ), 277, 250 (base peak), 155, 138, 91, 43; HRMS ( $m/z$ ) calcd for  $C_{15}H_{19}NO_3S$  293.1086, found 293.1113.

**Acknowledgment.** This work was supported by the Grant-in-Aid for Scientific Research on Priority Area of Reactive Organometallics No. 05236106 from the Ministry of Education, Science, and Culture of Japan and the Asahi Glass Foundation.

**Supporting Information Available:** Text describing the preparation of the starting materials, **Z-14d-h** and **39a-d**, and Schemes 15 and 16 (14 pages). This material is contained in many libraries on microfiche, immediately follows this article in the microfilm version of the journal, and can be ordered from the ACS; see any current masthead page for ordering information.

OM950374E



# Chromium-Catalyzed Intramolecular Enyne Metathesis

Susumu Watanuki, Nagisa Ochifuji, and Miwako Mori\*

Faculty of Pharmaceutical Sciences, Hokkaido University, Sapporo 060, Japan

Received May 22, 1995\*

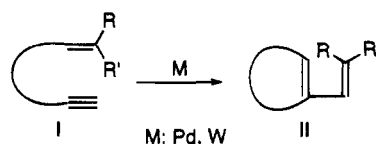
Intramolecular enyne metathesis is realized using a catalytic amount of Fischer chromium carbene complex. The reactions of the enynes **12**, which possess the same substituents on the alkene as those on the carbene carbon, with 10 mol % Fischer chromium carbene complexes **13** in MeOH proceeded smoothly to give the metathesis products in good to moderate yields.

Intramolecular enyne metathesis is quite interesting because the reaction involves formal [2 + 2] cycloaddition followed by ring opening of the resultant cyclobutane. As a result, one alkylidene group of the alkene migrates to the alkyne carbon. This process involves bond fission between alkene carbons and bond formation between the alkene carbon and the alkyne carbon (Scheme 1).

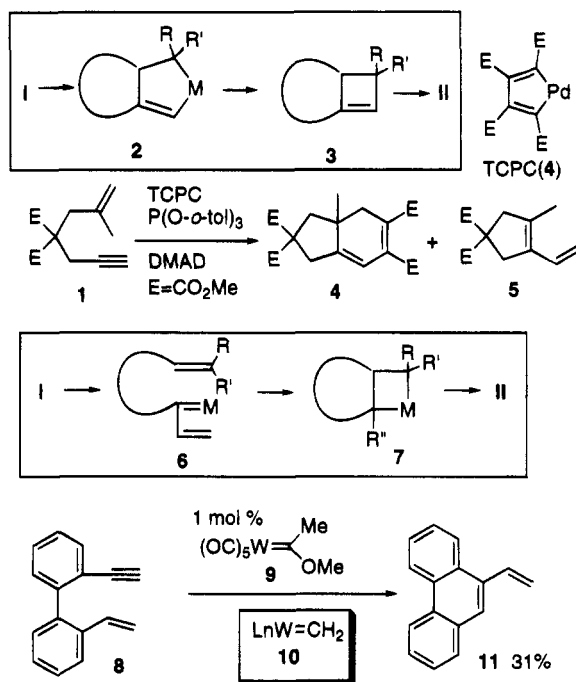
Until recently, two types of intramolecular enyne metathesis using transition metals have been known. One of them is the palladium-catalyzed [2 + 2] cycloaddition of the enyne reported by Trost,<sup>1</sup> and the other is the metal-catalyzed rearrangement of alkene-alkyne using the tungsten carbene complex reported by Katz.<sup>2</sup> In the former case, the reaction of enyne **1** with palladium catalyst (TCPC) in the presence of DMAD gave cyclized product **4** and **5** in good yield. In this case, highly strained cyclobutene **3** was formed from the five-membered metalacycles **2** by reductive elimination. Thus, the reaction seems like the formal [2 + 2] cycloaddition. On the other hand, in the latter case, the alkylidene carbene complex plays an important role and the reaction of alkyne of enyne with carbene complex gives metalcyclobutane **7**. This process was successfully demonstrated by Katz using a molecule with restricted bond rotations and a catalytic amount of the tungsten carbene complex **9** as an initiator. As a result, the (alkylidene)tungsten carbene complex **10**, which is not stabilized by a heteroatom, is formed and it acts as a real catalyst. On the other hand, ruthenium-catalyzed enyne metathesis was recently reported by three groups<sup>3</sup> (Scheme 2).

In a previous paper,<sup>4</sup> we reported enyne metathesis using a chromium carbene complex<sup>5</sup> and clarified the reaction course by substituent effects on the alkene. In

Scheme 1. Enyne Metathesis



Scheme 2



this reaction, the important intermediate is chromacyclobutane **14** generated from enyne **12** and a chromium carbene complex. If the electron-withdrawing groups are attached on the alkene of enyne **12**, three-membered ring formation is accelerated. And if the electron-donating groups are attached on the alkene, the metathesis reaction is accelerated because the (alkylidene)-chromium carbene complex **15** generated from **14** is stabilized by the substituents, R<sup>1</sup> and R<sup>2</sup>. In the metathesis reaction, if the substituents of the generated carbene **15**, R<sup>1</sup> and R<sup>2</sup>, are R and OEt, initial chromium carbene complex **13** would be regenerated. It means that chromium-catalyzed enyne metathesis would be realized.

In order to make the metathesis reaction proceed using a catalytic amount of the Fischer chromium carbene complex, the same substituents on the alkene

\* Abstract published in *Advance ACS Abstracts*, September 15, 1995.

(1) (a) Trost, B. M.; Yanai, M.; Hoogsteen, K. *J. Am. Chem. Soc.* **1993**, *115*, 5294. (b) Trost, B. M.; Hashmi, S. K., *Angew. Chem., Int. Ed. Engl.* **1993**, *32*, 1085. (c) For a review, see: Trost, B. M. *Acc. Chem. Res.* **1990**, *23*, 34. Trost, B. M.; Matsubara, S.; Caringi, J. J. *J. Am. Chem. Soc.* **1989**, *111*, 8745. Trost, B. M.; Chan, C.; Ruhter, G. *J. Am. Chem. Soc.* **1987**, *109*, 3486.

(2) (a) Katz, T. J.; Sivavec, T. M. *J. Am. Chem. Soc.* **1985**, *107*, 737. (b) Sivavec, T. M.; Katz, T. J. *Organometallics* **1989**, *8*, 1620.

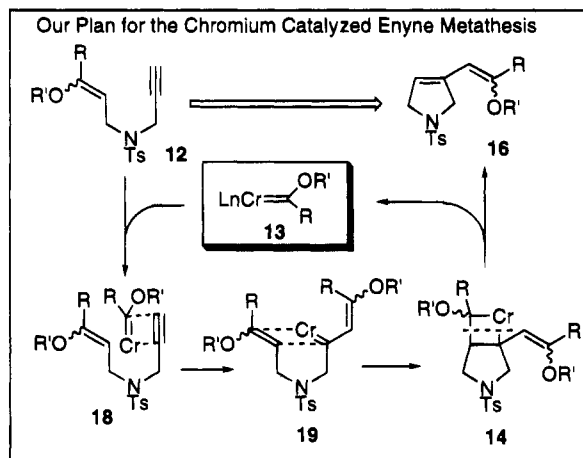
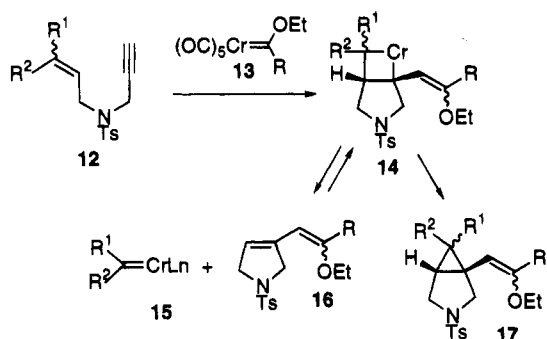
(3) (a) Chatani, N.; Morimoto, T.; Muto, T.; Murai, S. *J. Am. Chem. Soc.* **1994**, *116*, 6049. (b) Kim, S.-H.; Bowden, N.; Grubbs, R. H. *J. Am. Chem. Soc.* **1994**, *116*, 10801. (c) Kinoshita, A.; Mori, M. *Synlett* **1994**, 1020.

(4) (a) Mori, M.; Watanuki, S. *J. Chem. Soc., Chem. Comm.* **1992**, 1082. (b) Watanuki, S.; Mori, M. *Heterocycles* **1993**, *35*, 679. (c) Preliminary report for this work: Watanuki, S.; Ochifuji, N.; Mori, M. *Organometallics* **1994**, *13*, 4129.

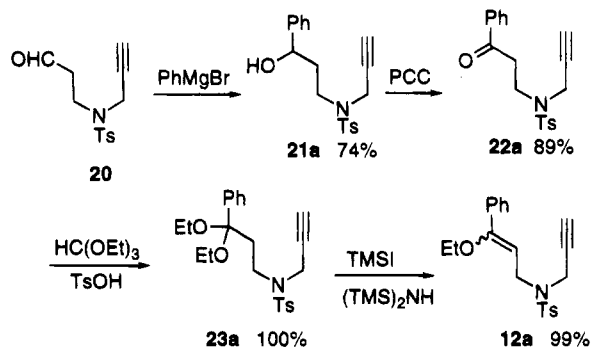
(5) Hoyo reported the metathesis reactions by a chromium carbene complex: Hoyo, T. R.; Suriano, J. A. *Organometallics* **1992**, *11*, 2044.



Scheme 3



Scheme 4. Preparation of the Substrate

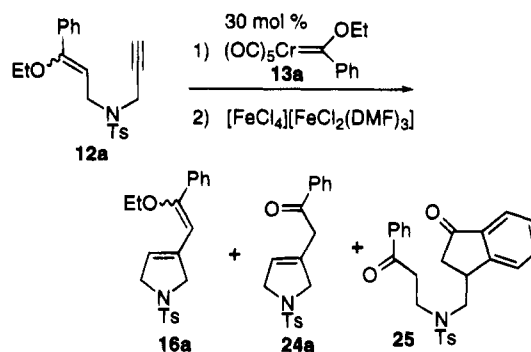


and on the carbene carbon are required. Our plan for the chromium-catalyzed intramolecular enyne metathesis reaction is shown in Scheme 3. If enyne **12** is treated with chromium carbene complex **13**, the chromacyclobutane **14** is produced *via* **18** and **19**. From **14**, initial chromium carbene complex **13** would be regenerated.

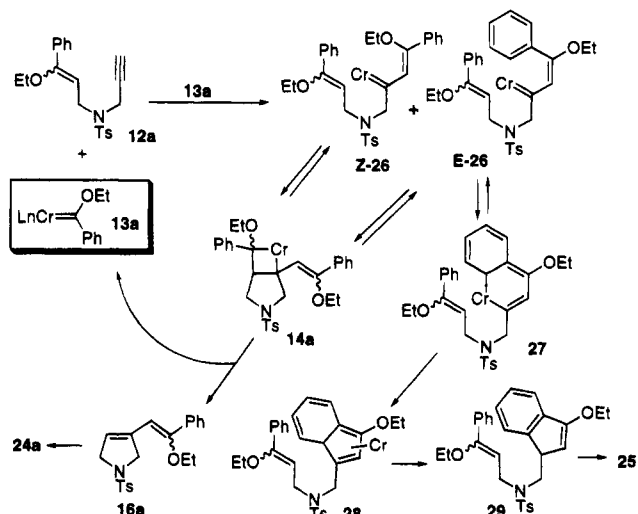
**Reaction of Enyne 12a with Fischer Chromium Carbene Complex 13a.** We chose compound **12a** as the starting enyne because the electron-donating group on the alkene would accelerate the metathesis reaction. The starting enyne **12a** was prepared from the aldehyde **20**. Treatment of the aldehyde **20** with PhMgBr followed by PCC oxidation afforded **22a** in high yield. Acetalization with ethyl orthoformate followed by treatment with TMSI in the presence of (TMS)<sub>2</sub>NH<sup>8</sup> gave enol ether **12a** in quantitative yield (Scheme 4).

When a CH<sub>3</sub>CN solution of enyne **12a** and chromium carbene complex **13a** (30 mol %) was refluxed for 18.5 h followed by treatment with [FeCl<sub>4</sub>][Fe(DMF)<sub>3</sub>Cl<sub>2</sub>],<sup>6</sup> the

Scheme 5. Reaction of 12a with 13a (30 mol %)



Scheme 6. Reaction Course for Enyne Metathesis



expected metathesis products, **16a** and **24a**, were obtained in 30% yields, along with the indanone **25** in 7% yield. The structures of these compounds were determined by the spectral data. The metathesis products **16a** and **24a** would be formed from **Z-26** and **E-26**. However, formation of indanone **25** would be derived from the carbene complex **E-26** generated from **12a** and **13a** as shown in Scheme 6. It is curious that the only benzannulation product was indanone **25** and not the naphthol. Presumably, the electron-rich enol ether functionality coordinates to chromium as a ligand and this would be expected to retard CO insertion. The chromium-catalyzed enyne metathesis is intercepted by formation of indanone **25** because a stoichiometric amount of the chromium carbene complex is consumed to produce the indanone **25**.<sup>7</sup> The reaction was carried out under various conditions (Table 1). Though the yields of metathesis products **16a** and **24a** using 30 mol % **13a** went up to 30% yield when EtOH, CH<sub>3</sub>CN, and THF were used as the solvents (runs 1–3), it is not clear whether the catalytic cycle is established or not. Various solvents can be used for this reaction, but the formation of **25** could not be suppressed in each case.

In order to confirm the regeneration of carbene complex **13a**, the reaction of enyne **12a** with the other carbene complex **13b** was tried. When a THF solution of **12a** and chromium carbene complex **13b** (30 mol %) was refluxed for 24 h followed by treatment with [FeCl<sub>4</sub>][Fe(DMF)<sub>3</sub>Cl<sub>2</sub>], the pyrrolidine derivatives **16a**

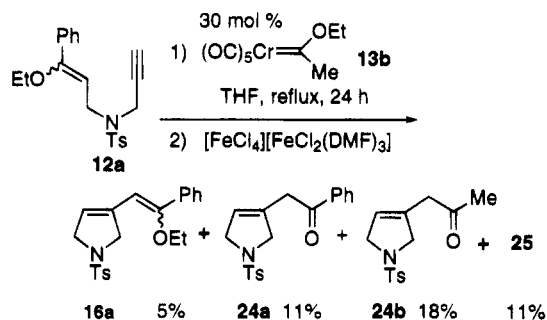
(7) Yamashita, A. *Tetrahedron Lett.* **1986**, 27, 5915.(8) Miller, R. D.; McKean, D. R. *Tetrahedron Lett.* **1982**, 23, 323.

**Table 1. Reaction of Enyne 12a with a Catalytic Amount of 13a<sup>a</sup>**

run	conditions	yield, %			
		16a + 24a	16a	24a	25
1	CH <sub>3</sub> CN, 70 °C, 18.5 h	30	16	14	7
2	THF, reflux, 17 h	31	9	22	22
3	EtOH, 70 °C, 24 h	35	14	21	21
4	CH <sub>2</sub> Cl <sub>2</sub> , reflux, 24 h	27		27	22
5	PhH, 70 °C, 12.5 h	24	5	19	18
6	PhMe, 70 °C, 24 h	17		17	27
7	DMF, 70 °C, 24 h	23	23		
8	i-PrOH, 70 °C, 24 h	25	12	13	20
9	acetone, 70 °C, 30 h	16	3	13	12
10	THF, reflux, 24 h <sup>b,c</sup>	20		20	20

<sup>a</sup> All reactions were carried out using 30 mol % of 13a.

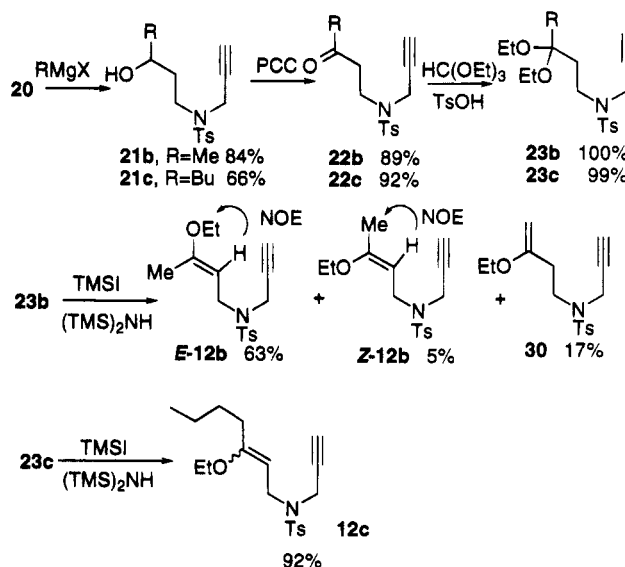
<sup>b</sup> Additive: PPh<sub>3</sub> (39 mol %). <sup>c</sup> 22a was recovered (30%).

**Scheme 7. Reaction of Enyne 12a with 13b**

and 24a,b were obtained in 5%, 11%, and 18% yields, respectively, along with 25 in 11% yield. Though metathesis product 24b was derived by the reaction of 12a with chromium carbene complex 13b, compounds 16a and 24a were formed by the reaction of 12a with 13a. These results indicate that the chromium carbene complex was regenerated in this reaction system (Scheme 7).

**Enyne Metathesis Using a Catalytic Amount of Fischer Chromium Carbene Complex.** For the chromium-catalyzed enyne metathesis, the use of chromium carbene complex 13a is not suitable because the formation of indanone is accompanied and it requires a stoichiometric amount of chromium carbene complex. Therefore, chromium carbene complex 13b was used for this reaction. In this case, the enyne 12b was required. The synthetic procedure of 12b was same as that of 12a as shown in Scheme 8. Treatment of acetal 23b with TMSI in the presence of (TMS)<sub>2</sub>NH gave a mixture of the *E*- and *Z*-isomers of 12b. Separation of *E*-12b and *Z*-12b was carried out by careful column chromatography on silica gel, and these isomers could be separated in 63% and 5% yields, respectively, along with 30 (17% yield). The stereochemistry of these compounds, *E*-12b or *Z*-12b, was determined by NOE experiments. Enyne 12c was prepared in a similar manner.

Refluxing a mixture of enyne *E*-12b and 10 mol % chromium carbene complex 13b in MeOH for 2 h followed by treatment with 10% HCl gave the metathesis product 24b in 70% yield. Even with the use of 5 mol % chromium catalyst, the desired product 24b was obtained in 39% yield (Table 2). Addition of PPh<sub>3</sub> as the ligand did not affect the yield of the desired product. As the solvent, THF (43%), toluene (50%), benzene (39%), EtOH (39%), and dichloroethane (31%) can be used for this reaction, but use of CH<sub>3</sub>CN (4%) or HMPA

**Scheme 8. Preparation of the Substrates****Table 2. Reaction of *E*-12b with a Catalytic Amount of 13b**

run	13b, mol %	additive	yield, %	
			24b	22b
1	10		70	
2	5		39	44
3	5	PPh <sub>3</sub> (5 mol %)	32	58

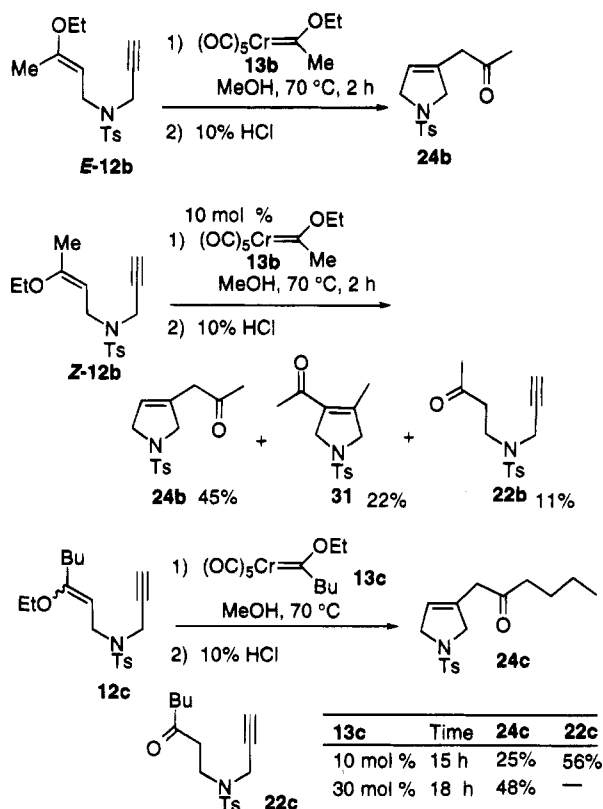
(0%) did not give good results. Treatment of *Z*-12b with 13b (10 mol %) in MeOH in a similar manner afforded the same metathesis product 24b in 45% yield. In this reaction, a fair amount of 31 (22%) was obtained. Presumably, 31 would be formed by the chromium-promoted oxidative cyclization of *Z*-12b. That is, the oxidative cyclization of *Z*-12b by the low-valent chromium complex afforded chromacyclopentene 32, which was converted into 33 by  $\beta$ -H elimination from the methyl group of 32. Then, reductive elimination from the chromium hydride complex occurs to give 31. The reason that 31 was obtained from only the *Z*-isomer of 12b is not clear yet. Moreover, compound 12c (*E/Z* = 2.7/1) was treated with chromium carbene complex 13c in MeOH followed by treatment with 10% HCl to give metathesis product 24c in 25% yield (22c was recovered in 56% yield). Use of 30 mol % 13c for this reaction afforded the desired product 24c in 48% yield. The chromium-promoted oxidative cyclization product was not produced in this case, though the starting material was a mixture of *E*- and *Z*-isomers [*E/Z* = 2.7/1]. Apparently,  $\beta$ -H elimination from the methylene group did not occur (Schemes 9 and 10).

The important characteristics for this reaction are as follows. The reaction proceeds with a catalytic amount of the Fischer chromium carbene complex. The chromium-catalyzed metathesis of the enyne having the same substituents on the alkene as on the carbene carbon of the chromium carbene complex means that the alkoxy-alkylidene carbon of the alkene formally migrates to the terminal alkyne of the enyne.

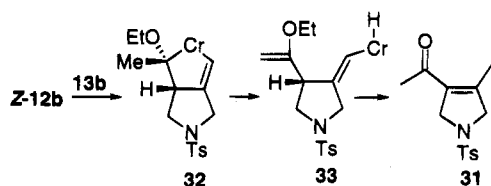
## Experimental Section

All manipulations were performed under an argon atmosphere using standard Schlenk techniques, and all the reaction solutions were degassed through freeze-pump-thaw cycles.

## Scheme 9. Chromium-Catalyzed Metathesis Reaction



## Scheme 10. Reaction Course for 31



Solvents were distilled under an argon atmosphere from sodium benzophenone (THF) or CaH<sub>2</sub> (CH<sub>2</sub>Cl<sub>2</sub>). All other reagents and solvents were purified when necessary using standard procedures. Column chromatography was performed on silica gel 60 (70–230 mesh, 60 Å), and flash chromatography was performed on silica gel 60 (230–400 mesh, 60 Å) using the indicated solvent. Melting points are uncorrected.

**General Procedure for the Synthesis of 21.** To a THF solution of **20** (1 equiv) was added RMgX (1.5 equiv) at –30 °C, and the solution was stirred at –10 °C for 2.5 h. Solvent was removed. To the residue was added saturated NH<sub>4</sub>Cl solution. The aqueous layer was extracted with ethyl acetate. The organic layer was dried over Na<sub>2</sub>SO<sub>4</sub> and concentrated. The residue was purified by column chromatography on silica gel to give **21**.

**4-Aza-1-phenyl-4-(p-tolylsulfonyl)-6-heptyn-1-ol (21a).** The crude product which was prepared from **20** (1.55 g, 5.84 mmol) in THF (14.0 mL) and PhMgBr (21 mmol) in THF (14 mL) was purified by column chromatography on silica gel (ethyl acetate–hexane, 2:5) to give **21a** as a colorless oil (1.48 g, 74%): IR (neat)  $\nu$  3524, 3287, 2119, 1345, 1159 cm<sup>-1</sup>; <sup>1</sup>H-NMR (CDCl<sub>3</sub>)  $\delta$  1.82–2.10 (m, 2 H), 2.05 (t,  $J$  = 2.4 Hz, 1 H), 2.43 (s, 3 H), 2.70 (d,  $J$  = 4.2 Hz, 1 H), 3.22 (dt,  $J$  = 14.2, 5.0 Hz, 1 H), 3.58 (dt,  $J$  = 14.2, 5.0 Hz, 1 H), 4.04 (dd,  $J$  = 2.4, 18.6 Hz, 1 H), 4.30 (dd,  $J$  = 2.4, 18.6 Hz, 1 H), 4.88 (dt,  $J$  = 4.2, 5.0 Hz, 1 H), 7.20–7.74 (m, 7 H), 7.75 (d,  $J$  = 8.3 Hz, 2 H); MS  $m/z$  343 (M<sup>+</sup>), 324, 222, 188, 155, 91, 68 (base peak). Anal. Calcd for C<sub>19</sub>H<sub>21</sub>NO<sub>3</sub>S: C, 66.45; H, 6.16; N, 4.08. Found: C, 66.18; H, 6.17; N, 3.99.

**5-Aza-5-(p-tolylsulfonyl)-7-octyne-2-ol (21b).** The crude product which was prepared from **20** (362 mg, 1.36 mmol) in THF (14.0 mL) and MeMgBr (1.92 mmol) in THF (14 mL) was purified by column chromatography on silica gel (ethyl acetate–hexane, 1:2) to give **21b** as a colorless oil (320 mg, 84%): IR (neat)  $\nu$  3500, 3280, 2110, 1595, 1340, 1160 cm<sup>-1</sup>; <sup>1</sup>H-NMR (CDCl<sub>3</sub>)  $\delta$  1.25 (d,  $J$  = 6.8 Hz, 3 H), 1.44–1.85 (m, 3 H), 2.05 (t,  $J$  = 2.3 Hz, 1 H), 2.44 (s, 3 H), 3.00–3.70 (m, 2 H), 3.80–4.23 (m, 3 H), 7.30 (d,  $J$  = 8.3 Hz, 2 H), 7.76 (d,  $J$  = 8.3 Hz, 2 H); MS  $m/z$  266, 222, 155, 126 (base peak), 91, 68. Anal. Calcd for C<sub>14</sub>H<sub>19</sub>NO<sub>3</sub>S: C, 59.76; H, 6.81; N, 4.98. Found: C, 59.68; H, 6.78; N, 4.87.

**8-Aza-8-(p-tolylsulfonyl)-10-undecyn-5-ol (21c).** The crude product prepared from **20** (1.14 g, 4.30 mmol) in THF (29 mL) to which was added BuMgBr (17.2 mmol) at rt (room temperature) was purified by column chromatography on silica gel (ethyl acetate–hexane, 1:3) to give **21c** as a colorless oil (922 mg, 66%): <sup>1</sup>H NMR (CDCl<sub>3</sub>, 270 MHz)  $\delta$  0.91 (t,  $J$  = 6.9 Hz, 3 H), 1.23–1.58 (m, 7 H), 1.71–1.83 (m, 1 H), 2.05 (dd,  $J$  = 2.5, 2.5 Hz, 1 H), 2.37 (d,  $J$  = 4.8 Hz, 1 H), 2.43 (s, 3 H), 3.18 (ddd,  $J$  = 4.1, 6.2, 14.4 Hz, 1 H), 3.52 (ddd,  $J$  = 6.1, 9.5, 14.4 Hz, 1 H), 3.74–3.83 (m, 1 H), 4.09 (dd,  $J$  = 2.5, 18.5 Hz, 1 H), 4.28 (dd,  $J$  = 2.5, 18.5 Hz, 1 H), 7.30 (d,  $J$  = 8.3 Hz, 2 H), 7.75 (d,  $J$  = 8.3 Hz, 2 H); IR (neat) 3532, 3286, 2118, 1598, 1344, 1160 cm<sup>-1</sup>; MS  $m/z$  323, 305, 221, 168, 155, 91. Anal. Calcd for C<sub>17</sub>H<sub>25</sub>NO<sub>3</sub>S: C, 63.12; H, 7.79; N, 4.33. Found: C, 63.03; H, 7.79; N, 4.40.

**General Procedure for the Synthesis of 22.** To a solution of **21** (1 equiv) and MS4A was added PCC (3 equiv) in CH<sub>2</sub>Cl<sub>2</sub> at 0 °C, and the solution was stirred at rt. Ether was added, the ether solution was chromatographed through a short column of Florisil, and the solution was concentrated. The residue was purified by column chromatography on silica gel to give **22**.

**4-Aza-1-phenyl-4-(p-tolylsulfonyl)-6-heptyn-1-one (22a).** The crude product which was prepared from **21a** (355 mg, 1.03 mmol), PCC (668 mg, 3.10 mmol), and MS4A (2.10 g) in CH<sub>2</sub>Cl<sub>2</sub> (20 mL) was purified by column chromatography on silica gel (ethyl acetate–hexane, 1:3) to give **22a** as a colorless oil (314 mg, 89%): IR (Nujol)  $\nu$  3289, 1674, 1595, 1348, 1161 cm<sup>-1</sup>; <sup>1</sup>H-NMR (CDCl<sub>3</sub>)  $\delta$  2.07 (t,  $J$  = 2.6 Hz, 1 H), 2.43 (s, 3 H), 3.42 (t,  $J$  = 6.9 Hz, 2 H), 3.62 (t,  $J$  = 6.9 Hz, 2 H), 4.21 (d,  $J$  = 2.6 Hz, 2 H), 7.30 (d,  $J$  = 8.4 Hz, 2 H), 7.43–7.52 (m, 2 H), 7.55–7.62 (m, 1 H), 7.75 (d,  $J$  = 8.4 Hz, 2 H), 7.92–7.99 (m, 2 H); MS  $m/z$  299, 222, 186 (base peak), 222, 155, 105, 91 (base peak); mp 102 °C. Anal. Calcd for C<sub>19</sub>H<sub>19</sub>NO<sub>3</sub>S: C, 66.84; H, 5.61; N, 4.10. Found: C, 66.96; H, 5.64; N, 4.06.

**5-Aza-5-phenyl-4-(p-tolylsulfonyl)-7-octyn-2-one (22b).** The crude product which was prepared from **21b** (95 mg, 0.338 mmol), PCC (218 mg, 1.01 mmol), and MS4A (665 mg) in CH<sub>2</sub>Cl<sub>2</sub> (6.8 mL) was purified by column chromatography on silica gel (ethyl acetate–hexane, 1:2) to give **22b** as a colorless oil (82.6 mg, 87%): IR (neat)  $\nu$  3260, 2110, 1715, 1595, 1340, 1160 cm<sup>-1</sup>; <sup>1</sup>H-NMR (CDCl<sub>3</sub>)  $\delta$  2.04 (t,  $J$  = 2.0 Hz, 1 H), 2.20 (s, 3 H), 2.43 (s, 3 H), 2.87 (t,  $J$  = 7.0 Hz, 2 H), 3.43 (t,  $J$  = 7.0 Hz, 2 H), 4.15 (d,  $J$  = 2.0 Hz, 2 H), 7.32 (d,  $J$  = 8.2 Hz, 2 H), 7.74 (d,  $J$  = 8.2 Hz, 2 H); MS  $m/z$  280 (M<sup>+</sup> + 1), 222, 155, 124 (base peak), 91. Anal. Calcd for C<sub>14</sub>H<sub>17</sub>NO<sub>3</sub>S: C, 60.19; H, 6.13; N, 5.01. Found: C, 60.17; H, 6.14; N, 5.00.

**8-Aza-8-(p-tolylsulfonyl)-10-undecyn-5-one (22c).** The crude product which was prepared from **21c** (49.8 mg, 0.154 mmol), PCC (98 mg, 0.454 mmol), and MS4A (307 mg) in CH<sub>2</sub>Cl<sub>2</sub> (3 mL) was purified by column chromatography on silica gel (ethyl acetate–hexane, 1:5) to give **22c** as a colorless oil (45.2 mg, 92%): IR (neat)  $\nu$  3288, 2118, 1712, 1596, 1338, 1160 cm<sup>-1</sup>; <sup>1</sup>H NMR (CDCl<sub>3</sub>, 270 MHz)  $\delta$  0.91 (t,  $J$  = 7.2 Hz, 3 H), 1.50–1.61 (m, 2 H), 1.23–1.38 (m, 2 H), 2.04 (t,  $J$  = 2.4 Hz, 1 H), 2.43 (t,  $J$  = 7.5 Hz, 2 H), 2.43 (s, 3 H), 2.83 (t,  $J$  = 6.9 Hz, 2 H), 3.43 (t,  $J$  = 6.9 Hz, 2 H), 4.14 (d,  $J$  = 2.4 Hz, 2 H), 7.30 (d,  $J$  = 8.3 Hz, 2 H), 7.73 (d,  $J$  = 8.3 Hz, 2 H); MS  $m/z$  321, 222, 166, 155, 91, 57. Anal. Calcd for C<sub>17</sub>H<sub>23</sub>NO<sub>3</sub>S: C, 63.52; H, 7.21; N, 4.36. Found: C, 63.43; H, 7.17; N, 4.37.

**General Procedure for the Synthesis of 23.** To a solution of **22** (1 equiv) and a catalytic amount of *p*-TsOH·H<sub>2</sub>O (1.5 mol %) in EtOH was added HC(OEt)<sub>3</sub> (3 equiv), and the solution was stirred at rt. To the solution was added saturated NaHCO<sub>3</sub> solution, and the aqueous layer was washed with ethyl acetate. The organic layer was washed with brine, dried over Na<sub>2</sub>SO<sub>4</sub>, and concentrated. The residue was purified by chromatography on silica gel to give **23**.

**4-Aza-7,7-diethoxy-7-phenyl-4-(*p*-tolylsulfonyl)heptyne (23a).** The crude product prepared from **22a** (1.15 g, 3.36 mmol), HC(OEt)<sub>3</sub> (1.7 mL, 10.1 mmol), and *p*-TsOH·H<sub>2</sub>O (10.0 mg) was purified by silica gel column chromatography (ethyl acetate–hexane, 1:9) to give **23a** as a colorless oil (1.39 g, 100%): IR (KBr)  $\nu$  3245, 2116, 1599, 1342, 1161 cm<sup>-1</sup>; <sup>1</sup>H NMR (CDCl<sub>3</sub>)  $\delta$  1.19 (t, *J* = 7.1 Hz, 6 H), 1.93 (t, *J* = 3.4 Hz, 1 H), 2.12–2.40 (m, 2 H), 2.39 (s, 3 H), 2.76–3.00 (m, 2 H), 3.31 (dt, *J* = 2.9, 7.1 Hz, 2 H), 3.45 (dt, *J* = 2.9, 7.1 Hz, 2 H), 3.98 (d, *J* = 3.4 Hz, 2 H), 7.22 (d, *J* = 8.3 Hz, 2 H), 7.20–7.52 (m, 5 H), 7.52 (d, *J* = 8.3 Hz, 2 H); MS *m/z* 370, 222, 214, 179 (base peak), 155, 91; mp 102 °C. Anal. Calcd for C<sub>23</sub>H<sub>29</sub>NO<sub>4</sub>S: C, 66.48; H, 7.03; N, 3.37. Found: C, 66.32; H, 7.09; N, 3.27.

**4-Aza-7,7-diethoxy-4-(*p*-tolylsulfonyl)octyne (23b).** The crude product prepared from **22b** (43.5 mg, 0.256 mmol), HC(OEt)<sub>3</sub> (0.4 mL, 0.299 mmol), and *p*-TsOH·H<sub>2</sub>O (1.5 mg) was purified by silica gel column chromatography (ethyl acetate–hexane, 1:5) in EtOH (1.2 mL) to give **23b** as a colorless oil (54.4 g, 99%): IR (KBr)  $\nu$  3250, 2110, 1595, 1340, 1160 cm<sup>-1</sup>; <sup>1</sup>H NMR (CDCl<sub>3</sub>, 270 MHz)  $\delta$  1.15 (t, *J* = 7.0 Hz, 6 H), 1.30 (s, 3 H), 1.76–2.05 (m, 2 H), 2.05 (t, *J* = 2.2 Hz, 1 H), 2.43 (s, 3 H), 3.12–3.40 (m, 2 H), 3.44 (q, *J* = 7.0 Hz, 4 H), 4.15 (d, *J* = 2.2 Hz, 2 H), 7.30 (d, *J* = 8.2 Hz, 2 H), 7.74 (d, *J* = 8.2 Hz, 2 H); MS *m/z* 338 (M<sup>+</sup> – Me), 308, 222, 155, 152 (base peak), 117, 91. Anal. Calcd for C<sub>18</sub>H<sub>27</sub>NO<sub>4</sub>S: C, 61.16; H, 7.70; N, 3.96. Found: C, 61.05; H, 7.68; N, 3.94.

**4-Aza-7,7-diethoxy-4-(*p*-tolylsulfonyl)undecyne (23c).** The crude product which was prepared from **22c** (32.4 mg, 0.101 mmol), HC(OEt)<sub>3</sub> (0.84 mL, 0.505 mmol), and *p*-TsOH·H<sub>2</sub>O (2 mg) in EtOH (0.5 mL) was purified by silica gel column chromatography (ethyl acetate–hexane, 1:5) to give **23c** as a colorless oil (40.3 mg, 100%): IR (neat)  $\nu$  3270, 2118, 1598, 1350, 1162 cm<sup>-1</sup>; <sup>1</sup>H NMR (CDCl<sub>3</sub>, 270 MHz)  $\delta$  0.90 (t, *J* = 6.6 Hz, 3 H), 1.15 (t, *J* = 7.1 Hz, 6 H), 1.21–1.35 (m, 4 H), 1.51–1.56 (m, 2 H), 1.91 (ddd, *J* = 5.0, 5.0, 8.3 Hz, 2 H), 2.07 (t, *J* = 2.5 Hz, 1 H), 2.42 (s, 3 H), 3.18 (ddd, *J* = 5.0, 5.0, 8.5 Hz, 2 H), 3.41 (q, *J* = 7.1 Hz, 2 H), 3.42 (q, *J* = 7.1 Hz, 2 H), 4.16 (d, *J* = 2.5 Hz, 2 H), 7.29 (d, *J* = 8.1 Hz, 2 H), 7.73 (d, *J* = 8.1 Hz, 2 H); MS *m/z* 349, 337, 221, 194, 155, 91. Anal. Calcd for C<sub>21</sub>H<sub>33</sub>NO<sub>4</sub>S: C, 63.76; H, 8.41; N, 3.54. Found: C, 63.46; H, 8.27; N, 3.61.

**General Procedure for the Synthesis of 12.** To a solution of **23** (1 equiv) and (TMS)<sub>2</sub>NH (3 equiv) in CH<sub>2</sub>Cl<sub>2</sub> was added TMSI (2 equiv), and the solution was stirred at rt overnight. To the solution was added aqueous saturated NaHCO<sub>3</sub> solution, and the aqueous layer was extracted with ethyl acetate. The organic layer was washed with brine, dried over Na<sub>2</sub>SO<sub>4</sub>, and concentrated. The residue was purified by chromatography on silica gel to give **12**.

**4-Aza-1-ethoxy-1-phenyl-4-(*p*-tolylsulfonyl)-1-hepten-6-yne (12a).** The crude product prepared from **23a** (371 mg, 0.895 mmol), (TMS)<sub>2</sub>NH (0.57 mL, 2.68 mmol), and TMSI (0.25 mL, 1.79 mmol) in CH<sub>2</sub>Cl<sub>2</sub> (5 mL) at rt for 15 h was purified by chromatography on silica gel (ethyl acetate–hexane, 1:10) to give enyne **12a** (328 mg, 99%): <sup>1</sup>H NMR (CDCl<sub>3</sub>, 400 MHz) (mixture of two isomers in a ratio of 2:1)  $\delta$  1.24 and 1.33 (t and t, *J* = 7.0 and 7.0 Hz, 3 H), 1.74 and 2.05 (t and t, *J* = 2.2 and 2.2 Hz, 1 H), 2.39 and 2.43 (s and s, 3 H), 3.69 and 3.81 (q and q, *J* = 7.0 and 7.0 Hz, 2 H), 3.89 and 4.12 (d and d, *J* = 7.3 and 7.3 Hz, 2 H), 4.05 and 4.15 (d and d, *J* = 2.2 and 2.2 Hz, 2 H), 4.65 and 5.16 (t and t, *J* = 7.3 and 7.3 Hz, 1 H), 7.20–7.43 (m, 7 H), 7.76 and 7.78 (d and d, *J* = 8.4 and 8.4 Hz, 2 H); IR (KBr) 3287, 2120, 1647, 1599, 1348, 1161 cm<sup>-1</sup>;

MS *m/z* 369 (M<sup>+</sup>), 368, 340, 324, 186 (base peak), 91, 77. Anal. Calcd for C<sub>21</sub>H<sub>23</sub>NO<sub>3</sub>S: C, 68.27; H, 6.27; N, 3.79. Found: C, 68.14; H, 6.26; N, 3.81.

**E- and Z-5-Aza-2-ethoxy-5-(*p*-tolylsulfonyl)-2-octen-7-yne (E- and Z-12b).** To a solution of **23b** (2.34 mg, 6.62 mmol) and (TMS)<sub>2</sub>NH (3.50 mL, 16.6 mmol) in CH<sub>2</sub>Cl<sub>2</sub> (40 mL) was added TMSI (1.40 mL, 9.84 mmol) under gentle reflux, and the solution was refluxed for 15 min. The crude product was purified by flash chromatography on silica gel (ethyl acetate–hexane, 1:10) to give **E-12a** (1.28 g, 63%), **Z-12b** (102 mg, 5%), and **30** (345 mg, 17%). **E-12b**: <sup>1</sup>H NMR (CDCl<sub>3</sub>, 270 MHz)  $\delta$  1.28 (t, *J* = 7.0 Hz, 3 H), 1.84 (s, 3 H), 1.99 (t, *J* = 2.4 Hz, 1 H), 2.44 (s, 3 H), 3.66 (q, *J* = 7.0 Hz, 2 H), 3.86 (d, *J* = 7.7 Hz, 2 H), 4.11 (t, *J* = 2.4 Hz, 2 H), 4.31 (t, *J* = 7.7 Hz, 1 H), 7.36 (d, *J* = 8.3 Hz, 2 H), 7.65 (d, *J* = 8.3 Hz, 2 H); <sup>13</sup>C NMR (CDCl<sub>3</sub>, 100 MHz)  $\delta$  158.17, 143.34, 136.28, 129.39, 127.78, 90.55, 77.18, 73.30, 62.33, 44.02, 34.88, 21.53, 16.48, 14.50; IR (neat) 3275, 2118, 1662, 1598, 1346, 1161 cm<sup>-1</sup>; MS *m/z* 308 (M<sup>+</sup> + 1), 222, 155, 152, 91 (base peak). Anal. Calcd for C<sub>16</sub>H<sub>21</sub>NO<sub>3</sub>S: C, 62.51; H, 6.89; N, 4.56; S, 10.43. Found: C, 62.51; H, 6.91; N, 4.51; S, 10.53. **Z-12b**: mp 64 °C; <sup>1</sup>H NMR (CDCl<sub>3</sub>, 270 MHz)  $\delta$  1.21 (t, *J* = 7.1 Hz, 3 H), 1.85 (s, 3 H), 1.99 (t, *J* = 2.4 Hz, 1 H), 2.43 (s, 3 H), 3.79 (q, *J* = 7.1 Hz, 2 H), 3.90 (d, *J* = 6.9 Hz, 2 H), 4.08 (t, *J* = 2.4 Hz, 2 H), 4.42 (t, *J* = 6.9 Hz, 1 H), 7.29 (d, *J* = 8.4 Hz, 2 H), 7.75 (d, *J* = 8.4 Hz, 2 H); <sup>13</sup>C NMR (CDCl<sub>3</sub>, 100 MHz)  $\delta$  155.16, 143.16, 136.56, 129.32, 127.76, 101.54, 77.58, 72.75, 63.20, 41.50, 35.68, 21.53, 17.76, 15.22; IR (neat) 3286, 1670, 1597, 1333, 1164 cm<sup>-1</sup>; MS (EI) *m/z* 307 (M<sup>+</sup>), 306 (M<sup>+</sup> – 1), 262, 222, 155, 152, 91, 71 (base peak). Anal. Calcd for C<sub>16</sub>H<sub>21</sub>NO<sub>3</sub>S: C, 62.51; H, 6.89; N, 4.56; S, 10.43. Found: C, 62.47; H, 7.07; N, 4.52; S, 10.38. **30**: <sup>1</sup>H NMR (CDCl<sub>3</sub>, 270 MHz)  $\delta$  1.30 (t, *J* = 7.0 Hz, 3 H), 2.05 (t, *J* = 2.4 Hz, 1 H), 2.38 (t, *J* = 7.3 Hz, 2 H), 2.44 (s, 3 H), 3.40 (t, *J* = 7.3 Hz, 2 H), 3.72 (q, *J* = 7.0 Hz, 2 H), 3.91 (d, *J* = 2.0 Hz, 1 H), 3.93 (d, *J* = 2.0 Hz, 1 H), 4.16 (d, *J* = 2.4 Hz, 2 H), 7.36 (d, *J* = 8.3 Hz, 2 H), 7.65 (d, *J* = 8.3 Hz, 2 H); <sup>13</sup>C NMR (CDCl<sub>3</sub>, 100 MHz) 159.67, 143.38, 136.21, 129.44, 127.71, 82.81, 76.92, 73.52, 62.86, 44.48, 36.72, 34.29, 21.54, 14.39; IR (neat) 3278, 2118, 1655, 1598, 1348, 1161 cm<sup>-1</sup>; MS (EI) *m/z* 307 (M<sup>+</sup>), 306 (M<sup>+</sup> – 1), 262, 222, 155, 152, 124, 91 (base peak). Anal. Calcd for C<sub>16</sub>H<sub>21</sub>NO<sub>3</sub>S: C, 62.51; H, 6.89; N, 4.56; S, 10.43. Found: C, 62.56; H, 6.76; N, 4.66; S, 10.36.

**E- and Z-8-Aza-5-ethoxy-8-(*p*-tolylsulfonyl)-5-undecen-10-yne (12c).** To a solution of **23c** (838 mg, 2.12 mmol) and (TMS)<sub>2</sub>NH (1.12 mL, 5.30 mmol) in CH<sub>2</sub>Cl<sub>2</sub> (21 mL) was added TMSI (0.45 mL, 3.16 mmol) with heating, and the solution was refluxed for 15 min. The crude product was purified by flash chromatography on silica gel (ethyl acetate–hexane, 1:30) to give **12c** (682 mg, 92%, *E:Z* = 2:1): <sup>1</sup>H NMR (CDCl<sub>3</sub>, 270 MHz) (mixture of two isomers in a ratio of 2.7:1)  $\delta$  0.89 (t, *J* = 7.1 Hz, 3 H), 1.22–1.54 (m, 7 H), 2.05 and 1.99 (t and t, *J* = 2.5 and 2.5 Hz, 1 H), 2.16 (t, *J* = 7.2 Hz, 2 H), 2.44 (s, 3 H), 3.64 (q, *J* = 7.1 Hz, 2 H), 3.36 and 3.86 (dd and d, *J* = 8.9, 8.9, and 7.8 Hz, 2 H), 4.11 and 4.17 (d and d, *J* = 2.5 and 2.5 Hz, 2 H), 4.27 and 4.42 (t and dd, *J* = 8.9, 8.9, and 7.8 Hz, 1 H), 7.31 (d, *J* = 8.4 Hz, 2 H), 7.76 (d, *J* = 8.4 Hz, 2 H); IR (neat) 3276, 2118, 1656, 1598, 1348, 1162 cm<sup>-1</sup>; MS *m/z* 349 (M<sup>+</sup>), 304, 222, 194, 155, 91 (base peak). Anal. Calcd for C<sub>19</sub>H<sub>27</sub>NO<sub>3</sub>S: C, 65.29; H, 7.79; N, 4.01; S, 9.17. Found: C, 64.97; H, 7.95; N, 3.99; S, 8.97.

**Typical Procedure for the Chromium-Catalyzed Metathesis Reaction.** To a solution of the enyne **E-12b** (50.0 mg, 163  $\mu$ mol) in MeOH (1.0 mL) under an argon atmosphere was added dropwise a solution of the carbene complex **13b** (4.3 mg, 0.016  $\mu$ mol) in MeOH (0.6 mL) at –78 °C. The solution was heated at 70 °C for 2 h and then quenched with 1.0 mL of 10% HCl. The aqueous layer was extracted with ethyl acetate, and the organic layer was washed with H<sub>2</sub>O and then brine, dried over Na<sub>2</sub>SO<sub>4</sub>, and concentrated. The residue was purified by chromatography on silica gel (hexane/ethyl acetate = 2/1) to give **24b** (32.1 mg, 70%): <sup>1</sup>H NMR (CDCl<sub>3</sub>, 270 MHz)  $\delta$  2.21 (s, 3 H), 2.43 (s, 3 H), 3.18 (s, 2 H), 4.02–4.15 (m, 4 H),

5.48 (brs, 1 H), 7.32 (d,  $J = 8.3$  Hz, 2 H), 7.72 (d,  $J = 8.3$  Hz, 2 H);  $^{13}\text{C}$  NMR ( $\text{CDCl}_3$ , 100 MHz)  $\delta$  204.35, 143.49, 134.09, 132.19, 129.75, 127.40, 122.77, 56.38, 54.85, 43.27, 29.68, 21.47; IR (neat) 1717, 1630, 1597, 1341, 1161  $\text{cm}^{-1}$ ; MS (EI)  $m/z$  279 ( $\text{M}^+$ ), 236, 155, 91 (base peak), 82; HRMS (EI) ( $m/z$ ) calcd for  $\text{C}_{14}\text{H}_{17}\text{NO}_3\text{S}$  279.0929; found 279.0916. Anal. Calcd for  $\text{C}_{14}\text{H}_{17}\text{NO}_3\text{S}$ : C, 60.19; H, 6.13; N, 5.01; S, 11.48. Found: C, 60.33; H, 6.30; N, 4.93; S, 11.44.

**Reaction of 12a with 13a.** According to the typical procedure, an EtOH (1.0 mL) solution of **12a** (35.8 mg, 0.153 mmol) and **13a** (9.5 mg, 0.029 mmol) was warmed at 70 °C for 24 h. After the usual workup, the residue was purified by column chromatography on silica gel (ethyl acetate–hexane, 1:6–1:3) to give **16a** (5.0 mg, 14%), **24a** (6.8 mg, 21%), and **25** (9.0 mg, 21%). **16a**:  $^1\text{H}$  NMR ( $\text{C}_6\text{D}_6$ , 270 MHz) (mixture of two isomers in a ratio of 1:1)  $\delta$  1.04 (t,  $J = 7.3$  Hz, 3 H), 1.89 and 1.92 (s and s, 3 H), 3.41 (q,  $J = 7.3$  Hz, 2 H), 3.77–3.83 and 4.01–4.08 (m and m, 2 H), 4.10–4.17 and 4.79–4.85 (m and m, 2 H), 4.92 and 5.11 (brs and brs, 1 H), 5.18 and 5.52 (s and s, 1 H), 6.79 and 6.82 (d and d,  $J = 8.4$  and 8.4 Hz, 2 H), 7.05–7.29 (m, 5 H), 7.71 and 7.90 (d and d,  $J = 8.4$  and 8.4 Hz, 2 H); IR (neat) 2777, 1643, 1596, 1345, 1164  $\text{cm}^{-1}$ ; MS (EI)  $m/z$  369 ( $\text{M}^+$ ), 367 ( $\text{M}^+ - 2$ ), 339, 234, 214, 186, 168, 105 (base peak). Anal. Calcd for  $\text{C}_{21}\text{H}_{23}\text{NO}_3\text{S}$ : C, 68.27; H, 6.27; N, 3.79; S, 8.68. Found: C, 68.12; H, 6.35; N, 3.67; S, 8.71. **24a**:  $^1\text{H}$  NMR ( $\text{CDCl}_3$ , 270 MHz)  $\delta$  2.41 (s, 3 H), 3.70 (s, 2 H), 4.08–4.12 (m, 4 H), 6.48 (brs, 1 H), 7.30 (d,  $J = 8.3$  Hz, 2 H), 7.45 (dd,  $J = 7.9$ , 8.2 Hz, 2 H), 7.50–7.60 (m, 1 H), 7.71 (d,  $J = 8.3$  Hz, 2 H), 7.88 (d,  $J = 7.9$  Hz, 2 H); IR (neat) 1687, 1595, 1340, 1160  $\text{cm}^{-1}$ ; MS (EI)  $m/z$  341 ( $\text{M}^+$ ), 236, 186, 155, 105 (bp), 91. Anal. Calcd for  $\text{C}_{19}\text{H}_{19}\text{NO}_3\text{S}$ : C, 66.84; H, 5.61; N, 4.10; S, 9.39. Found: C, 66.75; H, 5.76; N, 3.99; S, 9.03. **25**:  $^1\text{H}$  NMR ( $\text{CDCl}_3$ , 400 MHz)  $\delta$  2.43 (s, 3 H), 2.66 (dd,  $J = 3.4$ , 19.5 Hz, 1 H), 2.80 (dd,  $J = 7.8$ , 19.5 Hz, 1 H), 3.21 (dt,  $J = 18.1$ , 7.3 Hz, 1 H), 3.32 (dt,  $J = 18.1$ , 7.3 Hz, 1 H), 3.35 (dd,  $J = 9.3$ , 14.2 Hz, 1 H), 3.41 (dd,  $J = 5.9$ , 14.2 Hz, 1 H), 3.57 (t,  $J = 7.3$  Hz, 2 H), 3.74–3.82 (m, 1 H), 7.31 (d,  $J = 8.3$  Hz, 2 H), 7.38 (dd,  $J = 7.8$ , 7.8 Hz, 1 H), 7.46 (dd,  $J = 7.5$ , 8.8 Hz, 2 H), 7.56 (dd,  $J = 7.8$ , 7.8 Hz, 1 H), 7.55–7.61 (m, 2 H), 7.69 (d,  $J = 8.3$

Hz, 2 H), 7.75 (d,  $J = 7.8$  Hz, 1 H), 7.87 (d,  $J = 8.8$  Hz, 2 H); IR (KBr) 1712, 1682, 1595, 1340, 1160  $\text{cm}^{-1}$ ; MS (EI) 448 ( $\text{M}^+ + 1$ ), 316, 184, 155, 132, 91 (base peak). Anal. Calcd for  $\text{C}_{26}\text{H}_{25}\text{NO}_4\text{S}$ : C, 69.78; H, 5.63; N, 3.13; S, 7.16. Found: C, 69.60; H, 5.74; N, 3.15; S, 7.16.

**Reaction of Z-12b with 13b.** According to the typical procedure, a MeOH (1.5 mL) solution of **Z-12b** (47.0 mg, 0.153 mmol) and **13b** (4.0 mg, 0.015 mmol) was warmed at 70 °C for 2 h. After the usual workup, the residue was purified by column chromatography on silica gel (ethyl acetate–hexane, 1:2) to give **24b** (19.1 mg, 45%), **31** (9.2 mg, 22%), and **22b** (4.8 mg, 11%). **31**:  $^1\text{H}$  NMR ( $\text{CDCl}_3$ , 270 MHz)  $\delta$  2.02 (s, 3 H), 2.22 (s, 3 H), 2.44 (s, 3 H), 4.17–4.22 (m, 2 H), 4.30–4.38 (m, 2 H), 7.35 (d,  $J = 8.3$  Hz, 2 H), 7.73 (d,  $J = 8.3$  Hz, 2 H); IR (KBr) 1650, 1640, 1595, 1335, 1160  $\text{cm}^{-1}$ ; MS (EI)  $m/z$  279 ( $\text{M}^+$ ), 264, 236, 222, 155, 124, 91, 43 (base peak); HRMS (EI) ( $m/z$ ) calcd for  $\text{C}_{14}\text{H}_{17}\text{NO}_3\text{S}$  279.0930, found 279.0955.

**Reaction of 12c with 13c.** According to the typical procedure, a MeOH (1.5 mL) solution of **12c** (51.7 mg, 0.148 mmol) and **13c** (5.0 mg, 0.017 mmol) was warmed at 70 °C for 2 h. After the usual workup, the residue was purified by column chromatography on silica gel (ethyl acetate–hexane, 1:5) to give **24c** (12.0 mg, 25%) and **22c** (26.7 mg, 56%). **24c**:  $^1\text{H}$  NMR ( $\text{CDCl}_3$ , 270 MHz)  $\delta$  0.81 (t,  $J = 7.4$  Hz, 3 H), 1.19–1.35 (m, 2 H), 1.44–1.62 (m, 2 H), 2.30 (t,  $J = 7.4$  Hz, 2 H), 2.36 (s, 3 H), 3.13 (s, 2 H), 3.96–4.13 (m, 4 H), 5.44 (brs, 1 H), 7.31 (d,  $J = 8.3$  Hz, 2 H), 7.71 (d,  $J = 8.3$  Hz, 2 H); IR (neat) 1714, 1636, 1598, 1346, 1162  $\text{cm}^{-1}$ ; MS (EI)  $m/z$  321 ( $\text{M}^+$ ), 236 (base peak), 166, 155; HRMS (EI) ( $m/z$ ) calcd for  $\text{C}_{17}\text{H}_{23}\text{NO}_3\text{S}$  321.1399, found 321.1397;  $^{13}\text{C}$  NMR ( $\text{CDCl}_3$ , 100 MHz)  $\delta$  206.73, 143.47, 134.24, 132.41, 129.79, 127.47, 122.60, 56.49, 54.90, 42.50, 42.36, 25.73, 22.22, 21.53, 13.79.

**Acknowledgment.** This work was supported by the Grant-in-Aid for Scientific Research on Priority Area of Reactive Organometallics No. 05236106 from the Ministry of Education, Science, and Culture of Japan.

OM9503757

# Synthesis and Characterization of CO<sub>2</sub>-Bridged Bimetallic Compounds Derived from a Rhenium Metalloxyolate. Correlation of IR Spectral Data with Coordination Geometry and Bonding Type

Dorothy H. Gibson,\* Jaime O. Franco, Jayesh M. Mehta, Mark S. Mashuta, and John F. Richardson

Department of Chemistry and Center for Chemical Catalysis, University of Louisville, Louisville, Kentucky 40292

Received June 5, 1995<sup>⊗</sup>

The synthesis and characterization of CO<sub>2</sub>-bridged complexes, Cp\*Re(CO)(NO)(CO<sub>2</sub>)M (**3**, M = Re(CO)<sub>5</sub>; **5**, M = Mo(CO)<sub>2</sub>Cp; **7**, M = W(CO)<sub>3</sub>Cp; **8**, M = W(CO)<sub>2</sub>Cp) are described. Compound **5** has been structurally characterized. The geometry about the molybdenum atom in **5** is square-based pyramidal. All compounds have been characterized by DRIFTS IR spectral data. These data, together with DRIFTS and structural data from other symmetrical μ<sub>2</sub>-η<sup>3</sup>-CO<sub>2</sub> complexes characterized recently, show that the coordination geometry at the metal center which anchors the carboxyl oxygens determines the position of the ν<sub>asym</sub> band of the CO<sub>2</sub> ligand. The position of the ν<sub>sym</sub> band in these compounds varies only slightly and is determined by the metalloxyolate group.

## Introduction

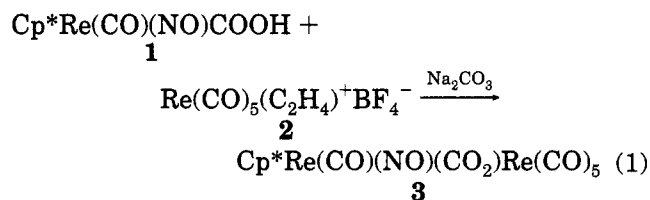
Complexes having CO<sub>2</sub> ligands bridged between two transition-metal centers provide homogeneous models for intermediates in the catalytic fixation of carbon dioxide.<sup>1</sup> Indeed, such bifunctional coordination has been suggested to be necessary for CO<sub>2</sub> activation.<sup>2</sup> Methods for the synthesis of the bridged complexes have generally involved displacement of a weakly coordinated ligand from one metal center by a nucleophilic metalloxyolate group. These methods might include the displacement of a weakly bound ethylene ligand from the coordination sphere of a metal cation. However, our

previous investigations, with an iron metalloxyolate, afforded carboxyethylene-bridged compounds as a result of nucleophilic additions to the ethylene ligands.<sup>3</sup>

We now report the reactions of two systems which readily lose coordinated ethylene to provide CO<sub>2</sub>-bridged compounds and the structural characterization of one of these products. Also, we provide further evidence, based on data from these and related new compounds, that the position of the IR ν<sub>asym</sub> bands in symmetrically bonded μ<sub>2</sub>-η<sup>3</sup>-CO<sub>2</sub> compounds is controlled by the coordination geometry at the metal center which binds the carboxyl oxygens.<sup>4</sup> Such data are expected to be useful in identifying active metal-bound CO<sub>2</sub>-containing species in catalytic processes.

## Results and Discussion

**Synthesis of CO<sub>2</sub>-Bridged Compounds.** We have used the reactions of the metalloxyolate Cp\*Re(CO)(NO)COOH (**1**; Cp\* = η<sup>5</sup>-C<sub>5</sub>Me<sub>5</sub>) with other metal complexes having weakly coordinated ligands to generate CO<sub>2</sub>-bridged complexes previously.<sup>1r,v,w</sup> Reaction of **1** with Re(CO)<sub>5</sub>(C<sub>2</sub>H<sub>4</sub>)<sup>+</sup>BF<sub>4</sub><sup>-</sup> (**2**)<sup>5</sup> in the presence of sodium carbonate afforded a product which has been formulated as the μ<sub>2</sub>-η<sup>2</sup>-CO<sub>2</sub> compound **3**, as illustrated in eq 1. The product has been characterized through



elemental analysis and spectral properties. The forma-

(3) Gibson, D. H.; Franco, J. O.; Harris, M. T.; Ong, T.-S. *Organometallics* **1992**, *11*, 1993.

(4) A preliminary account of some of this work was presented at the Third International Conference on Carbon Dioxide Utilization in Norman, OK, on May 1, 1995.

(5) Raab, K.; Olgemoeller, B.; Schloter, K.; Beck, W. *J. Organomet. Chem.* **1981**, *214*, 81.

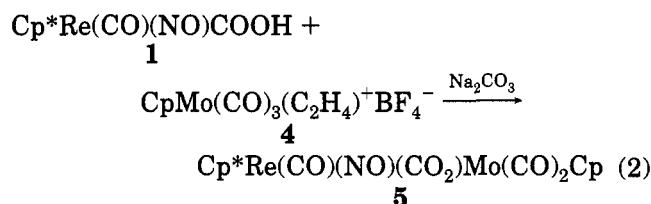
<sup>⊗</sup> Abstract published in *Advance ACS Abstracts*, October 1, 1995.

(1) (a) Audett, J. D.; Collins, T. J.; Santarsiero, B. D.; Spies, G. H. *J. Am. Chem. Soc.* **1982**, *104*, 7352. (b) Tso, C. T.; Cutler, A. R. *J. Am. Chem. Soc.* **1986**, *108*, 6069. (c) Gibson, D. H.; Ong, T.-S. *J. Am. Chem. Soc.* **1987**, *109*, 7191. (d) Senn, D. R.; Gladysz, J. A.; Emerson, K.; Larsen, R. D. *Inorg. Chem.* **1987**, *26*, 2737. (e) Bennett, M. A.; Robertson, G. B.; Rokicki, A.; Wickramasinghe, W. A. *J. Am. Chem. Soc.* **1988**, *110*, 7098. (f) Pilato, R. S.; Geoffroy, G. L.; Rheingold, A. L. *J. Chem. Soc., Chem. Commun.* **1989**, 1287. (g) Pilato, R. S.; Housmekerides, C. E.; Jernakoff, P.; Rubin, D.; Geoffroy, G. L.; Rheingold, A. L. *Organometallics* **1990**, *9*, 2333. (h) Field, J. S.; Haines, R. J.; Sundermeyer, J.; Woolam, S. F. *J. Chem. Soc., Chem. Commun.* **1990**, 985. (i) Gibson, D. H.; Richardson, J. F.; Ong, T.-S. *Acta Crystallogr.* **1991**, *C47*, 259. (j) Torreson, I.; Michelin, R. A.; Marsella, A.; Zanoardo, A.; Pinna, F.; Strukul, G. *Organometallics* **1991**, *10*, 623. (k) Vites, J. C.; Steffey, B. D.; Giuseppetti-Dery, M. E.; Cutler, A. R. *Organometallics* **1991**, *10*, 2827. (l) Gibson, D. H.; Ong, T.-S.; Ye, M. *Organometallics* **1991**, *10*, 1811. (m) Gibson, D. H.; Ye, M.; Richardson, J. F. *J. Am. Chem. Soc.* **1992**, *114*, 9716. (n) Szalda, D. J.; Chou, M. H.; Fujita, E.; Creutz, C. *Inorg. Chem.* **1992**, *31*, 4712. (o) Field, J. S.; Haines, R. J.; Sundermeyer, J.; Woolam, S. F. *J. Chem. Soc., Dalton Trans.* **1993**, 2735. (p) Gibson, D. H.; Richardson, J. F.; Mbadike, O. P.; *Acta Crystallogr.* **1993**, *B49*, 784. (q) Pinkes, J. R.; Cutler, A. R. *Inorg. Chem.* **1994**, *33*, 759. (r) Gibson, D. H.; Mehta, J. M.; Ye, M.; Richardson, J. F.; Mashuta, M. S. *Organometallics* **1994**, *13*, 1070. (s) Yang, Y.-L.; Chen, J.-D.; Liu, Y.-C.; Chen, M.-C.; Wang, Y. *J. Organomet. Chem.* **1994**, *467*, C8. (t) Pinkes, J. R.; Steffey, B. D.; Vites, J. C.; Cutler, A. R. *Organometallics* **1994**, *13*, 21. (u) Gibson, D. H.; Ye, M.; Richardson, J. F.; Mashuta, M. S. *Organometallics* **1994**, *13*, 4559. (v) Gibson, D. H.; Ye, M.; Sleadd, B. A.; Mehta, J. M.; Mbadike, O. P.; Richardson, J. F.; Mashuta, M. S. *Organometallics* **1995**, *14*, 1242. (w) Gibson, D. H.; Mehta, J. M.; Sleadd, B. A.; Mashuta, M. S.; Richardson, J. F. *Organometallics*, in press.

(2) (a) Fachinetti, G.; Floriani, C.; Zanazzi, P. F. *J. Am. Chem. Soc.* **1978**, *100*, 7405. (b) Gambarotta, S.; Arena, F.; Floriani, C.; Zanazzi, P. F. *J. Am. Chem. Soc.* **1982**, *104*, 5082.

tion of the  $\mu_2\text{-}\eta^2$  type of bridging CO<sub>2</sub> ligand in this case contrasts sharply with our previous results involving the reaction of **1** with *cis*-Re(CO)<sub>4</sub>(PPh<sub>3</sub>)(F-BF<sub>3</sub>), which led directly to the bridged complex with  $\mu_2\text{-}\eta^3$  bonding of the CO<sub>2</sub> ligand.<sup>1r</sup> Furthermore, **3** is not converted to the  $\mu_2\text{-}\eta^3$  type of product by solution thermolysis (3 h at room temperature in CD<sub>2</sub>Cl<sub>2</sub> or 45 min in toluene-*d*<sub>3</sub> at 57 °C) of the compound or by attempted thermolysis in the solid state (30 min at 105 °C); degradation results instead.

Reaction of **1** with CpMo(CO)<sub>3</sub>(C<sub>2</sub>H<sub>4</sub>)<sup>+</sup>BF<sub>4</sub><sup>-</sup> (**4**, Cp =  $\eta^5\text{-C}_5\text{H}_5$ ),<sup>6</sup> at room temperature and in the presence of sodium carbonate, afforded a product which has been identified as the CO<sub>2</sub>-bridged compound **5** with  $\mu_2\text{-}\eta^3$  bonding of the CO<sub>2</sub> ligand as illustrated in eq 2. Com-



ound **5** has been characterized by elemental analysis, spectral data, and an X-ray structure determination (see below). Conversion of the presumed intermediate  $\mu_2\text{-}\eta^2\text{-CO}_2$  compound to the  $\mu_2\text{-}\eta^3$  form occurs readily even under the mild conditions used for this reaction; we have not tried to probe for this intermediate under lower temperature conditions. The reasons CO<sub>2</sub>-bridged compounds **3** and **5** are formed instead of the carboxyethylene-bridged compounds are not understood at present. It is hoped that further investigations of the reactions will clarify these differences.

In order to be able to compare its spectral data with those for **5**, we decided to try to prepare the tungsten analog by the type of route we had used previously to prepare the dirhenium  $\mu_2\text{-}\eta^3\text{-CO}_2$  bridged complex:<sup>1r</sup> by reaction of the metal carbonyl complex CpW(CO)<sub>3</sub>(F-BF<sub>3</sub>) (**6**)<sup>7</sup> with the acid **1**. However, the properties of the resulting product were clearly in agreement with those expected for a  $\mu_2\text{-}\eta^2\text{-CO}_2$  complex instead (see the Experimental Section and discussion of spectral data below). This compound, **7**, afforded the desired  $\mu_2\text{-}\eta^3\text{-CO}_2$  complex (**8**) after mild thermolysis in the solid state. Compounds **7** and **8** were characterized by elemental analyses and spectral data.

**Structural Characterization of 5.** The solid-state structure of **5** was established by X-ray crystallography and shows the geometry about the molybdenum atom to be a distorted square-based pyramid with the cyclopentadienyl group at the apex; the geometry at this center is unique in comparison to the other symmetrical  $\mu_2\text{-}\eta^3\text{-CO}_2$  transition-metal complexes which we have characterized previously.<sup>1r,u,w</sup> The ORTEP diagram for **5** is shown in Figure 1. The crystallographic data for **5** are summarized in Table 1. Atomic positional parameters for **5** are shown in Table 2, and selected bond distances and angles are shown in Table 3. The structural data indicate highly symmetrical bonding about the bridging CO<sub>2</sub> ligand. The C-O bond lengths

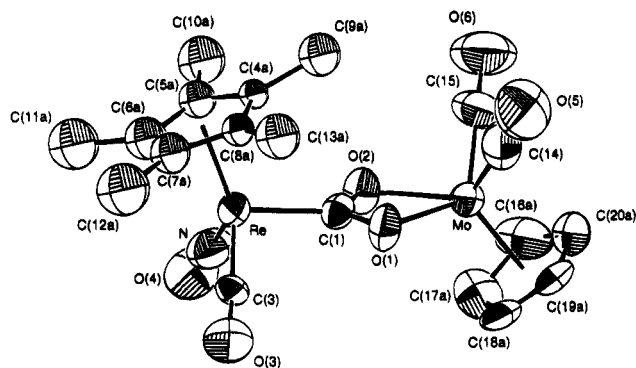


Figure 1. ORTEP drawing of **5** with thermal ellipsoids shown at the 50% probability level.

Table 1. Summary of Crystallographic Data for **5**

formula	C <sub>19</sub> H <sub>20</sub> MoNO <sub>6</sub> Re
cryst syst	monoclinic
space group	P2 <sub>1</sub> /c
a, Å	13.794(3)
b, Å	10.683(2)
c, Å	14.425(3)
β, deg	94.80(2)
V, Å <sup>3</sup>	2118.2(7)
Z	4
D <sub>c</sub> , g/cm <sup>3</sup>	2.008
cryst dimens, mm	0.43 × 0.33 × 0.15
cryst descriptn	magenta prism
μ(Mo Kα), cm <sup>-1</sup>	63.36
abs cor	ψ scans
transmission factors: min/max	0.58/1.00
radiation (λ, Å)	Mo Kα (0.710 73)
diffractometer	Enraf-Nonius CAD4
monochromator	graphite cryst
temp, °C	22(2)
scan range	0.80 + 0.35 tan θ
scan speed, deg/min	1-5
max 2θ, deg	46.0
no. of unique rflns collected	3126
no. of rflns included (I <sub>0</sub> > 3σ(I <sub>0</sub> ))	2151
no. of params	264
computer hardware	Silicon Graphics Iris Indigo
computer software	teXsan
ext coeff	9.23 × 10 <sup>-8</sup>
agreement factors <sup>a</sup>	
R	0.035
R <sub>w</sub>	0.035
function minimized	Σw( F <sub>o</sub> -  F <sub>c</sub>    <sup>2</sup> )
GOF	1.60
weighting scheme	[σ <sup>2</sup> (F <sub>o</sub> )] <sup>-1</sup>
high peak in final diff map, e	0.70

$$^a R = \sum |F_o| - |F_c| / \sum |F_o|; R_w = [\sum w(|F_o| - |F_c|)^2 / \sum w F_o^2]^{1/2}.$$

in **5** are 1.26(1) and 1.29(1) Å, and the O-Mo bond lengths are 2.149(7) and 2.158(7) Å.

**IR Spectral Data.** Over the past several years, we have developed a base of infrared data, collected by the DRIFTS technique<sup>8</sup> (diffuse reflectance infrared Fourier transform spectroscopy) which has been correlated with structural data on the CO<sub>2</sub>-bridged complexes.<sup>9</sup> All compounds of the  $\mu_2\text{-}\eta^2$  type show the  $\nu_{\text{asym}}$  and  $\nu_{\text{sym}}$  CO<sub>2</sub> bands near 1500 and 1140 cm<sup>-1</sup>, respectively. Thus, **3** shows these bands at 1514 and 1182 cm<sup>-1</sup> and **7** shows the bands at 1541 and 1100 cm<sup>-1</sup>. Compounds of the symmetrical  $\mu_2\text{-}\eta^3\text{-CO}_2$  type show the  $\nu_{\text{sym}}$  band in the region 1240-1290 cm<sup>-1</sup>. However, the higher frequency,  $\nu_{\text{asym}}$  band varies over a larger range. Data for nine compounds of this type, six of which have been structurally characterized, are summarized in Table 4.

(6) Cousins, M.; Green, M. L. H. *J. Chem. Soc.* **1963**, 889.

(7) Appel, M.; Schlöter, K.; Heidrich, J.; Beck, W. *J. Organomet. Chem.* **1987**, 322, 77.

(8) Griffiths, P. W.; de Haseth, J. A. *Fourier Transform Infrared Spectroscopy*; Wiley: New York, 1986; Chapter 5.

(9) A fuller discussion of these relationships is contained in ref 1v.



**Table 2. Atomic Positional Parameters for 5**

atom	x	y	z	$B_{\text{ewi}},^a \text{Å}^2$
Re	0.15409(4)	0.19796(4)	0.28365(3)	4.06(1)
Mo	0.37557(8)	-0.1160(1)	0.22682(7)	4.51(3)
O(1)	0.2290(5)	-0.0461(7)	0.2160(6)	5.1(2)
O(2)	0.3446(5)	0.0727(7)	0.2687(6)	5.0(2)
O(3)	0.0192(7)	0.1769(9)	0.1149(6)	7.5(3)
O(4)	0.2701(7)	0.4099(9)	0.2083(7)	7.9(3)
O(5)	0.2955(10)	-0.3399(10)	0.3318(8)	10.6(4)
O(6)	0.4983(9)	-0.135(1)	0.4112(8)	11.6(4)
N	0.2276(9)	0.325(1)	0.2368(7)	6.5(3)
C(1)	0.2537(8)	0.0619(10)	0.2505(8)	3.7(3)
C(3)	0.0749(7)	0.1838(10)	0.1787(7)	3.3(3)
C(4a)	0.178(2)	0.111(3)	0.431(2)	2.7(5)
C(4b)	0.149(3)	0.072(2)	0.417(2)	3.0(6)
C(5a)	0.186(3)	0.237(4)	0.440(2)	4.3(7)
C(5b)	0.204(2)	0.185(4)	0.441(2)	3.8(7)
C(6a)	0.099(3)	0.297(3)	0.405(2)	5.4(8)
C(6b)	0.139(2)	0.294(3)	0.427(2)	2.7(5)
C(7a)	0.034(2)	0.204(4)	0.380(2)	5.0(9)
C(7b)	0.046(2)	0.247(3)	0.390(2)	2.6(6)
C(8a)	0.080(3)	0.088(2)	0.390(2)	3.2(6)
C(8b)	0.047(2)	0.110(3)	0.383(2)	3.2(7)
C(9b)	0.194(2)	-0.054(2)	0.435(2)	4.8(6)
C(9a)	0.245(2)	0.006(2)	0.463(2)	5.5(6)
C(10b)	0.307(2)	0.197(3)	0.483(2)	6.3(6)
C(10a)	0.288(2)	0.285(3)	0.488(2)	6.9(7)
C(11b)	0.160(2)	0.428(2)	0.450(2)	4.8(6)
C(11a)	0.100(2)	0.447(3)	0.418(2)	7.7(8)
C(12a)	-0.074(2)	0.236(3)	0.348(2)	8.5(8)
C(12b)	-0.051(2)	0.316(2)	0.372(1)	3.7(5)
C(13a)	0.022(2)	-0.035(3)	0.372(2)	6.1(7)
C(13b)	-0.030(2)	0.018(2)	0.355(2)	4.9(6)
C(14)	0.325(1)	-0.255(1)	0.291(1)	6.8(4)
C(15)	0.453(1)	-0.126(1)	0.341(1)	7.1(5)
C(16a)	0.519(2)	-0.098(4)	0.156(2)	8.7(10)
C(16b)	0.486(7)	-0.09(1)	0.135(9)	5.7(10)
C(17b)	0.406(6)	-0.052(9)	0.089(6)	3(1)
C(17a)	0.450(3)	-0.028(3)	0.096(2)	8(1)
C(18a)	0.383(2)	-0.114(3)	0.063(1)	6.4(8)
C(18b)	0.339(5)	-0.167(7)	0.062(5)	4(1)
C(19b)	0.40(1)	-0.27(1)	0.119(9)	8.8(6)
C(19a)	0.401(4)	-0.231(3)	0.097(2)	8.0(10)
C(20a)	0.478(2)	-0.230(3)	0.149(2)	7.2(10)
C(20b)	0.516(5)	-0.206(9)	0.165(6)	4(1)

$B_{\text{eq}} = \frac{8}{3}\pi^2(U_{11}(aa^*)^2 + U_{22}(bb^*)^2 + U_{33}(cc^*)^2 + 2U_{12}aa^*bb^* \cos \gamma + 2U_{13}aa^*cc^* \cos \beta + 2U_{23}bb^*cc^* \cos \alpha)$ .

**Table 3. Selected Bond Distances (Å) and Bond Angles (deg) for 5**

Bond Distances			
C(1)–O(1)	1.29(1)	O(1)–Mo	2.149(7)
C(1)–O(2)	1.26(1)	O(2)–Mo	2.158(7)
Re–C(1)	2.08(1)		
Bond Angles			
O(1)–C(1)–O(2)	112.8(10)	O(1)–Mo–C(14)	85.9(5)
O(1)–Mo–O(2)	59.2(3)	O(2)–Mo–C(15)	85.3(5)
	C(14)–Mo–C(15)	74.7(7)	

The IR spectral bands have been assigned only after comparisons with numerous model compounds containing one or the other of the two metal fragments represented in the structure. Also, as noted previously,<sup>1w</sup> the bands for CO<sub>2</sub> in the zirconium complexes (entries 4–7 in Table 4) are analogous to those in Ti and Zr complexes characterized by Cutler,<sup>1k</sup> for which labeling experiments were used to assist in band assignments. The two characteristic bands for coordinated CO<sub>2</sub> are well defined in DRIFTS spectral data. For example, Figure 2 shows the spectral region from 1600 to 1000 cm<sup>-1</sup> for compounds **5**, **7**, and **8** and the related acid **1**. As expected, the  $\nu_{\text{asym}}$  and  $\nu_{\text{sym}}$  bands for **8** are closely similar to those for **5**. Six of the compounds shown in Table 4 are derived from the same rhenium metallo-

carboxylate; note that the position of the  $\nu_{\text{asym}}$  band varies by more than 100 cm<sup>-1</sup> while the  $\nu_{\text{sym}}$  band varies by only 10 cm<sup>-1</sup>. Interestingly, the latter band remains in nearly the same place even though the atomic weight of the metal center which anchors the carboxylate oxygens more than doubles in going from Zr to Re. However, comparisons of the  $\nu_{\text{asym}}$  bands show that there are clearly three groups of compounds represented in Table 4: (a) those which have an octahedral Re center bound to the carboxyl oxygens (entries 1–3), (b) those which have the carboxyl oxygens bound to an edge-capped tetrahedral Zr center (entries 4–7), and (c) those which have the oxygens bound to square-based pyramidal Mo or W centers (entries 8 and 9). It is apparent from the positions of the  $\nu_{\text{asym}}$  bands that the new Mo and W complexes **5** and **8** (entries 8 and 9 in the table) are unique. And, clearly, it is the coordination geometry at this center which controls the position of the  $\nu_{\text{asym}}$  band. Relationships between structure and reactivity of the coordinated CO<sub>2</sub> in these compounds are being probed.

## Experimental Section

**General Data.** Reactions and manipulations were carried out under an atmosphere of prepurified nitrogen in Schlenkware or in a Vacuum Atmospheres glovebox (with Dri-Train). All glassware was dried in the oven before use. Reagent grade dichloromethane was used as received. Benzene, toluene, and hexane were dried over concentrated sulfuric acid and fractionally distilled before use. Solvents used in the glovebox were distilled under nitrogen from P<sub>2</sub>O<sub>5</sub>: methylene chloride, acetone, pentane, hexane, benzene, and toluene. Acetone-*d*<sub>6</sub> and benzene-*d*<sub>6</sub> were obtained from Aldrich; dichloromethane-*d*<sub>2</sub> was obtained from Cambridge Isotope Laboratories or Aldrich. Cp\*Re(CO)(NO)COOH,<sup>1r</sup> Re(CO)<sub>5</sub>(C<sub>2</sub>H<sub>4</sub>)<sup>+</sup>BF<sub>4</sub><sup>-</sup>,<sup>5</sup> CpMo(CO)<sub>3</sub>(C<sub>2</sub>H<sub>4</sub>)<sup>+</sup>BF<sub>4</sub><sup>-</sup>,<sup>6</sup> CpW(CO)<sub>3</sub>CH<sub>3</sub>,<sup>10</sup> and CpW(CO)<sub>3</sub>(F–BF<sub>3</sub>)<sup>7</sup> were prepared as described previously. Spectral data were obtained on the following instruments: FT-NMR, Bruker AMX-500; FT-IR, Mattson Galaxy Series 5000. Diffuse-reflectance FT-IR data were obtained on the Mattson instrument with a DRIFTS accessory (Spectra Tech, Inc., Barnes Analytical Division) as KCl dispersions and at 1 cm<sup>-1</sup> resolution. <sup>1</sup>H and <sup>13</sup>C NMR chemical shifts were referenced to residual protons in the deuterated solvents. Melting points were obtained on a Thomas-Hoover capillary melting point apparatus and are uncorrected. Elemental analyses were performed by Midwest Microlab, Indianapolis, IN.

**Cp\*Re(CO)(NO)(CO)<sub>2</sub>Re(CO)<sub>5</sub> (3).** In a glovebox, (CO)<sub>5</sub>Re(CH<sub>2</sub>=CH<sub>2</sub>)<sup>+</sup>BF<sub>4</sub><sup>-</sup> (0.25 g, 0.57 mmol) was dissolved in 10 mL of acetone at 0 °C; to the solution was added solid Na<sub>2</sub>CO<sub>3</sub> (excess). Solid Cp\*Re(CO)(NO)COOH (0.25 g, 0.59 mmol) was then added, and the mixture was stirred at this temperature for 1 h. The mixture was filtered through Celite, and the filtrate was evaporated to dryness. The residue was extracted with ether (3 × 10 mL), and the combined extracts were filtered through Celite. The filtrate was evaporated to dryness, and the residue was dried under vacuum, giving an orange solid: 0.35 g (82% yield); mp 132 °C dec.

Anal. Calcd for C<sub>17</sub>H<sub>15</sub>NO<sub>9</sub>Re: C, 27.23; H, 2.02. Found: C, 27.56; H, 2.21. IR (CH<sub>2</sub>Cl<sub>2</sub>):  $\nu_{\text{CO}}$  2138 (w), 2028 (vs), 1970 (s, br) cm<sup>-1</sup>;  $\nu_{\text{NO}}$  1690 (m, br) cm<sup>-1</sup>. DRIFTS (KCl):  $\nu_{\text{CO}}$  1514 (w), 1182 (m) cm<sup>-1</sup>. <sup>1</sup>H NMR (CD<sub>2</sub>Cl<sub>2</sub>, -10 °C):  $\delta$  2.09 (s, CpMe<sub>5</sub>). <sup>13</sup>C NMR (CD<sub>2</sub>Cl<sub>2</sub>, -10 °C):  $\delta$  210.61 (s, CO), 192.72 (s, CO<sub>2</sub>), 183.49 (s, CO), 182.84 (s, CO), 104.46 (s, CpMe<sub>5</sub>), 10.48 (s, CpMe<sub>5</sub>).

**Cp\*Re(CO)(NO)(CO)<sub>2</sub>Mo(CO)<sub>2</sub>Cp (5).** Cp\*Re(CO)(NO)COOH (0.20 g, 0.47 mmol) was dissolved in 15 mL of acetone,

Table 4. Dependence of Carboxylate  $\nu_{\text{asym}}$  on Coordination Geometry

entry no.	symmetrical $\mu_2\text{-}\eta^3$ complex $\text{M}=\text{C} \begin{array}{c} \diagup \text{O} \diagdown \\ \diagdown \text{O} \diagup \end{array} \text{M}'$	IR (cm <sup>-1</sup> ) <sup>a</sup>		geometry at M'
		$\nu_{\text{asym}}$	$\nu_{\text{sym}}$	
1	CpFe(CO)(PPh <sub>3</sub> )(CO <sub>2</sub> )Re(CO) <sub>3</sub> [P(OEt) <sub>3</sub> ] <sup>b</sup>	1435	1252	octahedral
2	Cp*Re(CO)(NO)(CO <sub>2</sub> )Re(CO) <sub>3</sub> (PPh <sub>3</sub> ) <sup>c</sup>	1437	1282	octahedral
3	Cp*Re(CO)(NO)(CO <sub>2</sub> )Re(CO) <sub>2</sub> (PPh <sub>3</sub> ) <sub>2</sub> <sup>d</sup>	1435	1278	octahedral
4	Cp*Re(CO)(NO)(CO <sub>2</sub> )Zr(Cl)Cp <sub>2</sub> <sup>e</sup>	1348	1288	edge-capped tetrahedral
5	Cp*Re(CO)(NO)(CO <sub>2</sub> )Zr(CH <sub>3</sub> )Cp <sub>2</sub> <sup>e</sup>	1340	1288	not determined
6	Cp*Ru(CO) <sub>2</sub> (CO <sub>2</sub> )Zr(Cl)Cp <sub>2</sub> <sup>e</sup>	1339	1287	edge-capped tetrahedral
7	Cp*Ru(CO) <sub>2</sub> (CO <sub>2</sub> )Zr(CH <sub>3</sub> )Cp <sub>2</sub> <sup>e</sup>	1341	1285	not determined
8	Cp*Re(CO)(NO)(CO <sub>2</sub> )Mo(CO) <sub>2</sub> Cp <sup>f</sup>	1319	1285	square-based pyramidal
9	Cp*Re(CO)(NO)(CO <sub>2</sub> )W(CO) <sub>2</sub> Cp <sup>f</sup>	1321	1287	not determined

<sup>a</sup> DRIFTS data from KCl dispersions at 1 cm<sup>-1</sup> resolution. <sup>b</sup> Reference 1u. <sup>c</sup> Reference 1r. <sup>d</sup> Bardón, R. Unpublished results. <sup>e</sup> Reference 1w. <sup>f</sup> This work.

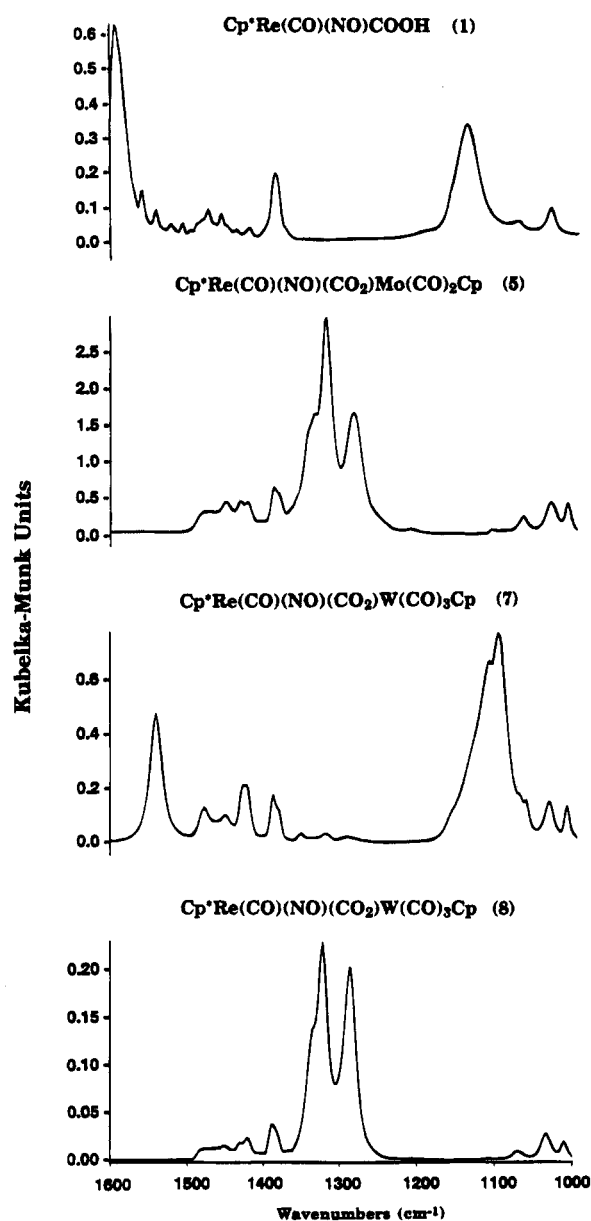


Figure 2. DRIFTS spectra of compounds 1, 5, 7, and 8 in the region 1600–1000 cm<sup>-1</sup>.

and to the yellow-orange solution was added solid Na<sub>2</sub>CO<sub>3</sub> (excess). CpMo(CO)<sub>3</sub>(CH<sub>2</sub>=CH<sub>2</sub>)<sup>+</sup>BF<sub>4</sub><sup>-</sup> (0.20 g, 0.56 mmol) was then added to the stirred mixture in portions. Stirring was continued for 30 min, during which time the color of the mixture became dark. The mixture was filtered through Celite, and the filtrate was evaporated to dryness. The residue was extracted several times with ether (30 mL total), and the combined extracts were filtered through Celite. After the

filtrate was evaporated to dryness, the dark purplish residue was dissolved in the minimum amount of toluene and the solution filtered into a Schlenk tube and layered with hexane. The sample was chilled to -30 °C overnight to give a dark purple solid (0.15 g, 50% yield); mp 136–137 °C.

Anal. Calcd for C<sub>19</sub>H<sub>20</sub>MoNO<sub>6</sub>Re: C, 35.63; H, 3.15. Found: C, 35.40; H, 3.18. IR (CH<sub>2</sub>Cl<sub>2</sub>):  $\nu_{\text{CO}}$  1975 (m, sh), 1955 (s), 1850 (m) cm<sup>-1</sup>;  $\nu_{\text{NO}}$  1705 (m) cm<sup>-1</sup>. DRIFTS (KCl):  $\nu_{\text{OCO}}$  1319 (m), 1285 (w) cm<sup>-1</sup>. <sup>1</sup>H NMR (acetone-*d*<sub>6</sub>):  $\delta$  5.86 (s, CpMo), 2.15 (s, CpMe<sub>5</sub>). <sup>13</sup>C NMR (acetone-*d*<sub>6</sub>):  $\delta$  267.76 (s, CO), 267.50 (s, CO), 217.80 (s, CO<sub>2</sub>), 208.34 (s, CO), 105.73 (s, CpMe<sub>5</sub>), 99.43 (s, CpMo), 10.35 (s, CpMe<sub>5</sub>).

Cp\*Re(CO)(NO)(CO<sub>2</sub>)W(CO)<sub>3</sub>Cp (7). CpW(CO)<sub>3</sub>CH<sub>3</sub> (0.24 g, 0.69 mmol) was dissolved in 10 mL of CH<sub>2</sub>Cl<sub>2</sub> and then allowed to react with 120  $\mu$ L of HBF<sub>4</sub> etherate. The yellow solution immediately turned purple, and after 15 min of stirring, the solvent was removed under vacuum. The residue was washed with hexane (2  $\times$  5 mL) and then pumped dry. It was then dissolved in 15 mL of acetone and solid Na<sub>2</sub>CO<sub>3</sub> (in excess) was added. To the mixture was added 0.24 g (0.57 mmol) of solid Cp\*Re(CO)(NO)COOH in portions. After it was stirred for 0.5 h, the mixture was filtered through Celite and the filtrate was evaporated to dryness. The residue was extracted with toluene (3  $\times$  5 mL), and the extracts were filtered through Celite. The filtrate was concentrated, and then hexane was added to give an orange-red precipitate which was collected by filtration and dried under vacuum (0.28 g, 65% yield). The solid was crystallized from benzene/pentane, giving orange-red crystals; mp 103 °C dec.

Anal. Calcd for C<sub>20</sub>H<sub>20</sub>NO<sub>7</sub>ReW: C, 31.75; H, 2.67. Found: C, 31.62; H, 2.63. IR (CH<sub>2</sub>Cl<sub>2</sub>):  $\nu_{\text{CO}}$  2025 (m), 1940 (vs, br) cm<sup>-1</sup>;  $\nu_{\text{NO}}$  1685 (m, br) cm<sup>-1</sup>. DRIFTS (KCl):  $\nu_{\text{OCO}}$  1541 (w), 1100 (m) cm<sup>-1</sup>. <sup>1</sup>H NMR (C<sub>6</sub>D<sub>6</sub>):  $\delta$  4.90 (s, CpW), 1.74 (s, CpMe<sub>5</sub>). <sup>13</sup>C NMR (C<sub>6</sub>D<sub>6</sub>):  $\delta$  239.06 (s, CO), 223.62 (s, CO), 223.54 (s, CO), 212.20 (s, CO), 190.33 (s, CO<sub>2</sub>), 104.21 (s, CpMe<sub>5</sub>), 93.78 (s, CpW), 10.14 (s, CpMe<sub>5</sub>).

Cp\*Re(CO)(NO)(CO<sub>2</sub>)W(CO)<sub>2</sub>Cp (8). A sample of Cp\*Re(CO)(NO)(CO<sub>2</sub>)W(CO)<sub>3</sub>Cp (0.11 g, 0.14 mmol) was placed in a glass tube and sealed under vacuum. The sample was heated to 105 °C for 1.5 h, during which time the dark red solid had turned almost black. The tube was opened in a glovebox, benzene was added, and the mixture was then filtered through a glass fiber pad. The filtrate was evaporated to dryness. The residue was triturated with pentane, and the remaining dark purplish solid was collected by filtration and dried (0.06 g, 57% yield). The solid was dissolved in benzene and the solution was layered with pentane and then chilled, affording dark purple crystals which decomposed at 128 °C without melting.

Anal. Calcd for C<sub>19</sub>H<sub>20</sub>NO<sub>6</sub>ReW: C, 31.32; H, 2.77. Found: C, 31.56; H, 2.83. IR (CH<sub>2</sub>Cl<sub>2</sub>):  $\nu_{\text{CO}}$  1980 (m), 1935 (s), 1825 (s) cm<sup>-1</sup>;  $\nu_{\text{NO}}$  1705 (m) cm<sup>-1</sup>. DRIFTS (KCl):  $\nu_{\text{OCO}}$  1321 (w), 1287 (w) cm<sup>-1</sup>. <sup>1</sup>H NMR (C<sub>6</sub>D<sub>6</sub>):  $\delta$  5.34 (s, CpW), 1.64 (s, CpMe<sub>5</sub>). <sup>13</sup>C NMR (C<sub>6</sub>D<sub>6</sub>):  $\delta$  261.68 (s, CO), 260.33 (s, CO), 217.17 (s, CO<sub>2</sub>), 207.70 (s, CO), 104.74 (s, CpMe<sub>5</sub>), 97.11 (s, CpW), 9.95 (s, CpMe<sub>5</sub>).

**X-ray Crystal Structure of 5.** A suitable crystal was grown by layering a benzene solution of **5** with hexane and then cooling the sample to 5 °C for 1 day followed by a second day at -10 °C. Data were collected on an Enraf-Nonius CAD4 diffractometer at 23 °C; the data are outlined in Table 1. Selected bond distances and bond angles are shown in Table 3. Of 3126 unique reflections, 2151 were considered observed ( $I > 3\sigma(I)$ ). The structure was solved using Patterson methods and refined with anisotropic thermal parameters for all non-hydrogen atoms not involved in the structural disorder. The pentamethylcyclopentadienyl ring was found to be disordered. It was satisfactorily modeled with two half-occupancy C<sub>10</sub> pentamethylcyclopentadienyl groups. Both groups, C4a-C13a and C4b-C13b, were refined with individual isotropic atoms. The cyclopentadienyl ring bonded to molybdenum was also found to be disordered. It was adequately modeled with one three-fourths occupancy set of atoms (C16a-C20a) refined anisotropically and one one-fourth set of atoms (C16b-C20b) refined isotropically. The calculated positions and thermal parameters for the hydrogen atoms were kept constant with temperature factors set to 1.2 times the temperature factors of the carbon atoms to which they are bonded. A final *R* index of 0.035 with  $R_w = 0.035$  was obtained for 264 variables. All

computations were performed using the teXsan package (Molecular Structure Corp.).

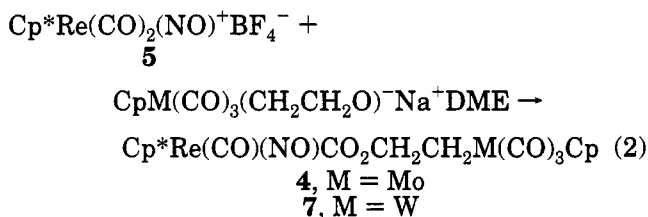
**Acknowledgment.** Support of this work by the United States Department of Energy, Division of Chemical Sciences (Office of Basic Energy Sciences), is gratefully acknowledged. The X-ray equipment was purchased with assistance from the National Science Foundation (Grant No. CHE-9016978). Support of the Molecular Structure Laboratory through the NSF/KY EPSCoR program (Grant No. EHR-9108764) is also gratefully acknowledged. We thank Dr. Michael T. Harris for preliminary work on compound **5**.

**Supporting Information Available:** Tables for anisotropic thermal parameters, H atom positional parameters, bond distances, bond angles, and torsional angles for **5** (15 pages). This material is contained in many libraries on microfiche, immediately follows this article in the microfilm version of the journal, and can be ordered from the ACS; ordering information is given on any current masthead page.

OM9504258

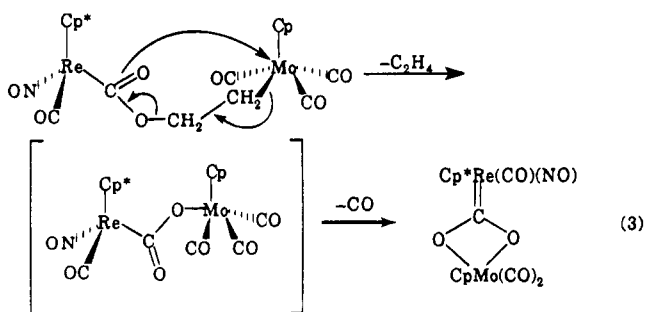


with  $\text{CpMo}(\text{CO})_3(\text{CH}_2\text{CH}_2\text{O})^-\text{Na}^+\text{DME}^{9a,11}$  in THF as shown in eq 2; this route provided **4** in 90% yield.



Compound **4** has been characterized by spectral data only because it degrades at a moderate rate upon standing even in the solid state; its properties are similar to those of the carboxyethylene-bridged iron complexes characterized previously and to its rhenium-tungsten analog which has been fully characterized (see below).

Thermolysis of **4** in the solid state, at 90 °C during 30 min, gives **3** as a major product (23%), but also gives several other products (see Experimental Section). The additional products are not formed from secondary decomposition of **3** since it is stable under the reaction conditions. Also, thermolysis of **4** in acetone is complete after 19 h at room temperature and gives **3** as the major product. Neither of these observations can account for the rapid formation of **3** in the reaction between **1** and **2** in this solvent. We have also examined the stability of cation **2** in acetone solution with, and without, sodium carbonate. Cation **2** is stable in acetone under these conditions, at least during the time needed for reaction with **1**. Thus, it appears that nucleophilic displacement of the coordinated ethylene in **2** occurs readily by the action of **1**. Also, it seems that the major pathway in the thermolysis of **4**, in solution or in the solid state, yields the  $\text{CO}_2$ -bridged complex **3**, presumably through initial loss of ethylene followed by loss of CO as shown in eq 3.



In contrast to the molybdenum cation,  $\text{CpW}(\text{CO})_3(\text{C}_2\text{H}_4)^+\text{BF}_4^-$  (**6**)<sup>9a</sup> reacted with **1** in THF and afforded the carboxyethylene-bridged compound (**7**; see eq 1) in 61% yield. Proton sponge was used as the base in this reaction; like  $\text{Na}_2\text{CO}_3$ , it does not deprotonate the acid **1**. Although the related  $\mu_2-\eta^2$  and  $\mu_2-\eta^3$   $\text{CO}_2$ -bridged complexes<sup>6</sup> are known to be stable under the reaction conditions, neither of them is observed as a product in the reaction between **1** and **6**. Compound **7** has been characterized by elemental analysis and by spectral data. The IR and <sup>1</sup>H NMR spectral data are quite similar to those for compound **4**; however, in the

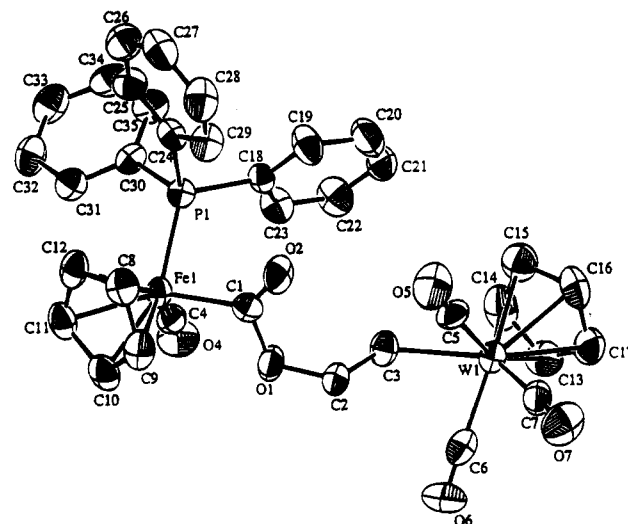


**Figure 1.** ORTEP drawing of **11** with thermal ellipsoids shown at the 50% probability level.

<sup>13</sup>C spectrum, the terminal carbonyls and the methylene carbon bound to tungsten in **7** are at higher field than those bound to molybdenum in **4**. Analogous to the alternate synthesis of **4**, a better yield (94%) of **7** was obtained by treating cation **5** directly with the ethyleneoxy anion,  $\text{CpW}(\text{CO})_3(\text{CH}_2\text{CH}_2\text{O})^-\text{Na}^+\text{DME}$ ,<sup>9a</sup> as indicated in eq 2. Compound **7** is much more stable than **4**; no decomposition to either of the known<sup>6</sup>  $\text{CO}_2$ -bridged complexes occurs during 3 days at room temperature in acetone.

A further example in which a stable carboxyethylene-bridged complex resulted from reaction of **1** is seen with the iron cation,  $\text{CpFe}(\text{CO})_2(\text{C}_2\text{H}_4)^+\text{BF}_4^-$  (**8**),<sup>12</sup> which gave the bridged compound,  $\text{CpRe}(\text{CO})(\text{NO})\text{CO}_2\text{CH}_2\text{CH}_2\text{Fe}(\text{CO})_2\text{Cp}$  (**9**; see eq 1), in 82% yield. This compound, also, has been characterized by elemental analysis and by spectral data which are consistent with the formulation.

Finally, an additional carboxyethylene-bridged product has been prepared by the reaction between the iron cation  $\text{CpFe}(\text{CO})_2(\text{PPh}_3)^+\text{I}^-$  (**10**)<sup>13</sup> and the tungsten ethyleneoxy anion. Although somewhat less stable than the analogous rhenium complex, the product,  $\text{CpFe}(\text{CO})(\text{PPh}_3)\text{CO}_2\text{CH}_2\text{CH}_2\text{W}(\text{CO})_3\text{Cp}$  (**11**), was isolated in 66% yield and has been fully characterized, including X-ray crystallographic analysis, which shows the expected carboxyethylene-bridged structure that is illustrated in the ORTEP diagram shown in Figure 1. This represents the first structural characterization of a compound with this type of bridging ligand. The crystallographic data for the compound are summarized in Table 1. Atomic positional parameters for **11** are shown in Table 2, and selected bond distances and bond angles are shown in Table 3. It is interesting to compare the characteristics of **11** with those of the  $\mu_2-\eta^2$   $\text{CO}_2$ -bridged complex derived from the same iron metalcarboxylate moiety which we reported several years ago.<sup>8a</sup> Compound **11** has a slightly shorter iron-carboxylate carbon bond: 1.946(8) Å in **11** and 1.994(3) Å in  $\text{CpFe}(\text{CO})(\text{PPh}_3)(\text{CO}_2)\text{Re}(\text{CO})_4(\text{PPh}_3)$ . The acyl C-O bond lengths are similar (1.224(10) Å in **11** and 1.226(3) Å in the

(11) Although most of the anion exists in the cyclic form as noted earlier,<sup>9a</sup> a small amount of the highly nucleophilic ethyleneoxy anion is present in equilibrium with the cyclic form.

(12) This compound was prepared by a modification of the method of Knoth;<sup>9a</sup> see Experimental Section.

(13) Treichel, P. M.; Shubkin, R. L.; Barnett, K. W.; Reichard, D. *Inorg. Chem.* **1966**, *5*, 1177.

**Table 1. Summary of Crystallographic Data for 11**

formula	C <sub>35</sub> H <sub>29</sub> FeO <sub>6</sub> PW
cryst syst	monoclinic
space group	P2 <sub>1</sub> /c
a, Å	8.057(3)
b, Å	33.556(13)
c, Å	11.616(3)
β, deg	100.34(2)
V, Å <sup>3</sup>	3089(1)
Z	4
D <sub>c</sub> , gm/cm <sup>3</sup>	1.76
cryst dimens, mm <sup>3</sup>	0.41 × 0.34 × 0.30
cryst color, habit	orange block
μ(Mo Kα) cm <sup>-1</sup>	42.91
abs corr	ψ scans
transm factors, min/max	0.79/1.00
radiation (λ, Å)	Mo Kα (0.710 73)
diffractometer	Enraf-Nonius CAD4
monochromator	graphite crystal
temp, °C	22(1)
scan range	0.80 + 0.35 tan θ
scan speed, deg/min	1–5
max 2θ, deg	50.0
no. of unique reflns colld	5553
no. of reflns included (I <sub>o</sub> > 3σ(I <sub>o</sub> ))	4201
no. of params	398
computer hardware	Silicon Graphics Iris Indigo
computer software	teXsan
ext coeff	1.60 × 10 <sup>-9</sup>
agreement factors <sup>a</sup>	
R	0.037
R <sub>w</sub>	0.049
function minimized	Σ <sub>w</sub> ( F <sub>o</sub>   -  F <sub>c</sub>  ) <sup>2</sup>
GOF	2.39
weighting scheme	[σ <sup>2</sup> (F <sub>o</sub> )] <sup>-1</sup>
high peak in final diff map, e	1.03

$$^a R = \sum ||F_o| - |F_c|| / \sum |F_o|; R_w = [\sum w(|F_o| - |F_c|)^2 / \sum w F_o^2]^{1/2}.$$

previous compound), but the second carboxyl C–O bond is longer in **11** (1.347(10) Å) than in the previous compound (1.298(3) Å). Finally, the carboxylate O–C–O angle is slightly smaller in **11** (120.5(8)°) than in the CO<sub>2</sub>-bridged complex (121.9(3)°).

Efforts to generate or observe Cp\*Re(CO)(NO)CO<sub>2</sub>-CH<sub>2</sub>CH<sub>2</sub>Re(CO)<sub>5</sub> from **1** and the requisite rhenium cation have not been successful and have resulted either in no reaction or generation of the μ<sub>2</sub>-η<sup>2</sup> CO<sub>2</sub>-bridged complex reported earlier.<sup>6</sup> We can conclude from these observations of the behavior of various ethylene cations toward **1** that it is the ease of nucleophilic displacement of ethylene, not the stability of an intermediate carboxyethylene-bridged compound, which determines the major reaction path. The results depend, in part, upon the solubility of the cation in the solvent medium, but other factors clearly influence the ease of ethylene displacement. Qualitatively, the ease of displacement of coordinated ethylene appears to be quite sensitive to the ligand environment present at the metal center. Where π-acceptor CO ligands are the only other ligands present (e.g., with Re(CO)<sub>5</sub>(C<sub>2</sub>H<sub>4</sub>)<sup>+</sup>BF<sub>4</sub><sup>-</sup>), back-bonding to the ethylene ligand is diminished<sup>14</sup> and the ligand is easily displaced. Even with one donor ligand present, molybdenum cation **2** (with three CO ligands) suffers loss of the ethylene ligand in reaction with **1** whereas iron cation **8** (with only two CO ligands) readily yields the carboxyethylene product. Also, the third-row element tungsten clearly binds ethylene more strongly

**Table 2. Atomic Positional Parameters for 11**

atom	x	y	z	B <sub>eq</sub> <sup>a</sup> (Å <sup>2</sup> )
W(1)	0.10915(5)	0.04634(1)	-0.22077(3)	3.161(9)
Fe(1)	0.3760(1)	0.11336(4)	0.36123(9)	2.73(3)
P(1)	0.2228(3)	0.16679(7)	0.3177(2)	2.71(5)
O(1)	0.3226(8)	0.0613(2)	0.1721(5)	4.0(2)
O(2)	0.3882(8)	0.1226(2)	0.1203(5)	4.4(2)
O(4)	0.0905(8)	0.0648(2)	0.3891(6)	4.8(2)
O(5)	0.390(1)	0.1114(2)	-0.1767(6)	6.3(2)
O(6)	0.238(1)	-0.0351(2)	-0.1122(7)	5.7(2)
O(7)	0.354(1)	0.0170(2)	-0.3830(6)	6.3(2)
C(1)	0.358(1)	0.1000(3)	0.1965(7)	3.1(2)
C(2)	0.318(1)	0.0492(3)	0.0491(7)	3.9(2)
C(3)	0.148(1)	0.0569(3)	-0.0220(7)	3.5(2)
C(4)	0.203(1)	0.0845(3)	0.3761(7)	3.1(2)
C(5)	0.289(1)	0.0863(3)	-0.1891(7)	3.9(2)
C(6)	0.193(1)	-0.0056(3)	-0.1515(8)	3.9(2)
C(7)	0.262(1)	0.0287(3)	-0.3244(7)	3.9(2)
C(8)	0.624(1)	0.1339(3)	0.3868(7)	3.9(2)
C(9)	0.624(1)	0.0928(3)	0.3714(7)	4.1(2)
C(10)	0.551(1)	0.0745(3)	0.4595(8)	4.3(2)
C(11)	0.514(1)	0.1065(3)	0.5334(7)	4.0(2)
C(12)	0.554(1)	0.1421(3)	0.4889(7)	3.9(2)
C(13)	-0.176(1)	0.0255(3)	-0.2696(9)	4.6(3)
C(14)	-0.171(1)	0.0598(4)	-0.2008(9)	5.5(3)
C(15)	-0.112(1)	0.0924(3)	-0.2610(9)	4.9(3)
C(16)	-0.079(1)	0.0768(4)	-0.3675(8)	4.9(3)
C(17)	-0.120(1)	0.0358(3)	-0.3714(9)	4.9(3)
C(18)	0.600(9)	0.1639(3)	0.1857(6)	2.8(2)
C(19)	0.063(1)	0.1845(3)	0.0840(8)	4.5(2)
C(20)	-0.061(1)	0.1798(3)	-0.0131(8)	5.2(3)
C(21)	-0.193(1)	0.1544(3)	-0.0090(8)	4.6(3)
C(22)	-0.200(1)	0.1334(3)	0.0917(9)	4.7(3)
C(23)	-0.072(1)	0.1376(3)	0.1870(7)	3.9(2)
C(24)	0.341(1)	0.2125(3)	0.2979(7)	3.0(2)
C(25)	0.336(1)	0.2464(3)	0.3661(8)	3.8(2)
C(26)	0.429(1)	0.2797(3)	0.3486(9)	4.9(3)
C(27)	0.525(1)	0.2800(3)	0.2622(9)	4.9(3)
C(28)	0.532(1)	0.2466(4)	0.1959(8)	5.1(3)
C(29)	0.444(1)	0.2130(3)	0.2132(7)	3.9(2)
C(30)	0.099(1)	0.1825(2)	0.4287(7)	2.8(2)
C(31)	0.152(1)	0.1711(3)	0.5434(7)	3.5(2)
C(32)	0.064(1)	0.1846(3)	0.6298(7)	4.4(3)
C(33)	-0.073(1)	0.2086(3)	0.6010(9)	4.8(3)
C(34)	-0.128(1)	0.2192(3)	0.4873(9)	4.7(3)
C(35)	-0.042(1)	0.2066(3)	0.4008(8)	4.1(2)

$$^a B_{eq} = \frac{8}{3}\pi^2[U_{11}(aa^*)^2 + U_{22}(bb^*)^2 + U_{33}(cc^*)^2 + 2U_{12}aa^*bb^* \cos \gamma + 2U_{13}aa^*cc^* \cos \beta + 2U_{23}bb^*cc^* \cos \alpha].$$

**Table 3. Selected Bond Distances (Å) and Bond Angles (deg) for 11**

Bond Distances			
C(1)–O(1)	1.347(10)	O(1)–C(2)	1.479(9)
C(1)–O(2)	1.224(10)	C(2)–C(3)	1.49(1)
Fe–C(1)	1.946(8)	W–C(3)	2.301(8)
Bond Angles			
O(1)–C(1)–O(2)	120.5(8)	C(1)–O(1)–C(2)	115.8(7)
Fe–C(1)–O(1)	113.9(6)	O(1)–C(2)–C(3)	110.4(7)
Fe–C(1)–O(2)	125.3(7)		

than molybdenum; reaction of cation **6** yields the carboxyethylene product whereas **2** yields the CO<sub>2</sub>-bridged product **3** as the major, or exclusive, product, depending on the reaction solvent. Independently, as the contrasting behavior of **4** and **7**, or **7** and **11**, makes clear, the stability of the carboxyethylene-bridged products is also controlled by the ligand environments at both metal centers and by metal–carbon bond strengths.

### Experimental Section

**General Data.** Reactions and manipulations were carried out under an atmosphere of prepurified nitrogen in Schlenkware or in a Vacuum Atmospheres glovebox (with Dri-train). All glassware was dried in the oven before use. Reagent grade

(14) For a general discussion of this effect, see: Collman, J. P.; Hegedus, L. S.; Norton, J. R.; Finke, R. G. In *Principles and Applications of Organotransition Metal Chemistry*; University Science Books: Mill Valley, CA, 1987; Chapter 3.

dichloromethane was used as received. Benzene, toluene, and hexane were dried over concentrated sulfuric acid and fractionally distilled before use. Solvents used in the glovebox were distilled under nitrogen from the following drying agents: sodium benzophenone ketyl for tetrahydrofuran (THF), dimethoxyethane (DME), and ether;  $P_2O_5$  for dichloromethane, pentane, hexane, acetone, benzene, and toluene.  $Mo(CO)_6$  and  $W(CO)_6$  were obtained from Strem Chemicals. Ethylene oxide was obtained from Fisher. Acetone- $d_6$ , benzene- $d_6$ , methylene chloride- $d_2$ , and toluene- $d_8$  were obtained from Cambridge Isotope Laboratories, and sodium cyclopentadienide and 1,8-bis(dimethylamino)naphthalene (proton sponge) were obtained from Aldrich.  $Cp^*Re(CO)(NO)COOH$ ,<sup>5</sup>  $Cp^*Re(CO)_2(NO)^+BF_4^-$ ,<sup>10</sup>  $CpFe(CO)_2(C_2H_4)^+BF_4^-$ ,<sup>12</sup>  $CpFe(CO)_2(PPh_3)^+I^-$ ,<sup>13</sup>  $CpMo(CO)_3(C_2H_4)^+BF_4^-$ ,<sup>9b</sup> and  $CpW(CO)_3(C_2H_4)^+BF_4^-$ <sup>9a</sup> were prepared as described previously. Spectral data were obtained on the following instruments: FT-NMR, Bruker AMX-500; FT-IR, Mattson Galaxy series 5000. Diffuse reflectance FT-IR data<sup>15</sup> were obtained on the Mattson instrument with a DRIFTS accessory (Spectra Tech, Inc., Barnes Analytical Division) as KCl dispersions and at 1  $cm^{-1}$  resolution.  $^1H$  and  $^{13}C$  NMR chemical shifts were referenced to residual protons in the deuterated solvents. Melting points were obtained on a Thomas-Hoover capillary melting point apparatus and are uncorrected. Elemental analyses were performed by Midwest Microlab, Indianapolis, IN.

**$CpMo(CO)_3(CH_2CH_2O)^-Na^+DME$ .**  $Mo(CO)_6$  (5.00 g, 18.9 mmol) and 1,2-dimethoxyethane (DME, 80 mL) were mixed in a flask under  $N_2$ . Sodium cyclopentadienide (12 mL, 24.0 mmol) was added, and the mixture was heated at reflux overnight. The orange mixture was filtered, and then ethylene oxide (15 mL) was added to the filtrate at 0 °C. The mixture was warmed to room temperature and stirred overnight. The reaction flask was sealed and transferred into a glovebox. The yellow solid that had precipitated was collected by filtration. Some additional solid was collected from the filtrate after further standing. The yellow solid was recrystallized from THF/DME to give the product (3.52 g, 8.76 mmol, 46% yield). The compound can be stored in a glovebox for short periods of time, but it decomposes slowly upon standing.  $^1H$  NMR ( $CD_3CN$ ):  $\delta$  5.12 (s, 5, Cp), 4.12 (m, 1,  $C_2H_4$ ), 3.01 (m, 1,  $C_2H_4$ ), 2.34 (m, 1,  $C_2H_4$ ), 1.47 (m, 1,  $C_2H_4$ ), 3.45 (s, 4,  $CH_2$ -DME), and 3.28 (s, 6,  $CH_3$ -DME).  $^{13}C$  NMR ( $CD_3CN$ ):  $\delta$  257.08 (CO), 253.67 (CO), 240.09 (CO), 93.20 (Cp), 93.20 (Cp), 71.08 ( $OCH_2$ ), 16.32 ( $Mo-CH_2$ ), 72.34 ( $CH_2$ -DME), and 58.87 ( $CH_3$ -DME).

**$CpW(CO)_3(CH_2CH_2O)^-Na^+DME$ .** This compound was prepared as indicated above for its Mo analog. Starting with  $W(CO)_6$  (5.00 g, 14.2 mmol), 4.08 g of  $CpW(CO)_3(CH_2CH_2O)^-Na^+DME$  (8.33 mmol, 59% yield) was isolated. The compound can be stored in a glovebox under nitrogen for several months without noticeable decomposition.  $^1H$  NMR ( $CD_3CN$ ):  $\delta$  5.21 (s, 5, Cp), 4.13 (m, 1,  $C_2H_4$ ), 3.16 (m, 1,  $C_2H_4$ ), 2.22 (m, 1,  $C_2H_4$ ), 1.51 (m, 1,  $C_2H_4$ ), 3.45 (s, 4,  $CH_2$ -DME), 3.28 (s, 6,  $CH_3$ -DME).  $^{13}C$  NMR ( $CD_3CN$ ):  $\delta$  251.16 (CO), 246.35 (CO), 246.35 (CO), 230.72 (CO), 91.95 (Cp), 72.89 ( $OCH_2$ ), 5.82 ( $W-CH_3$ ), 72.26 ( $CH_2$ -DME), 58.90 ( $CH_3$ -DME).

**$Cp^*Re(CO)(NO)CO_2CH_2CH_2MoCp(CO)_3$  (4).** **A.**  $CpMo(CO)_3CH_2CH_2O^-Na^+DME$  (0.24 g, 0.60 mmol) was dissolved in THF, and  $Cp^*Re(CO)_2(NO)^+BF_4^-$  (5; 0.30 g, 0.61 mmol) was added. The mixture was stirred for 20 min and then filtered through Celite, and the filtrate was evaporated to dryness. The residue was taken up in benzene, filtered through a glass pad, and then concentrated until almost dry. The sample was triturated with pentane to give an orange powder (0.38 g, 90%), mp 85 °C, decomp. The compound darkens upon standing for several hours (in vacuo) at room temperature. IR ( $CH_2Cl_2$ ):  $\nu_{CO}$  2020 (s), 1970 (m, br), 1925 (vs, br), 1605 (w)  $cm^{-1}$ ;  $\nu_{NO}$  1700 (m, br).  $^1H$  NMR ( $C_6D_6$ ):  $\delta$  4.61 (s, CpMo), 4.53 (m,  $OCH_2$ ), 1.90 (m,  $MoCH_2$ ), 1.73 (s, CpMe<sub>5</sub>).  $^{13}C$  NMR ( $C_6D_6$ ):  $\delta$

240.35 (s, CO), 227.78 (s, CO), 208.86 (s, CO), 188.15 (s,  $CO_2$ ), 104.24 (s, CpMe<sub>5</sub>), 92.34 (s, CpMo), 69.63 (s,  $OCH_2$ ), 9.84 (s, CpMe<sub>5</sub>), 0.41 (s,  $MoCH_2$ ).

**B.**  $Cp^*Re(CO)(NO)COOH$  (0.05 g, 0.12 mmol) was dissolved in THF, and  $Na_2CO_3$  (excess) was added. Solid  $CpMo(CO)_3(C_2H_4)^+BF_4^-$  (0.05 g, 0.14 mmol) was then added in portions. After being stirred at room temperature for 1 h, the mixture was filtered through a glass pad and the filtrate was evaporated to dryness. The residue was taken up in  $C_6D_6$ , ferrocene was added as an internal standard, and the  $^1H$  NMR spectrum taken showed a 45% yield of 4, 11% of 3, 6% of  $[CpMo(CO)_3CH_2CH_2]_2O$ ,<sup>9a</sup> and 3% of  $[CpMo(CO)_3]_2$  and other unidentified minor products.

**Thermolysis of 4.** In acetone: A 50 mg sample (0.07 mmol) of 4 was taken up in acetone- $d_6$ , transferred into an NMR tube, and sealed with a septum, and its  $^1H$  NMR spectrum was taken. The sample was allowed to stand for several hours, monitoring the changes every 2–3 h. After 19 h, when all of the starting material had disappeared, ferrocene was added as an internal standard. From its  $^1H$  NMR spectrum, the mixture showed 34% yield of 3 and 18% of  $[CpMo(CO)_3]_2$ . Also observed was a signal at  $\delta$  2.20 which corresponded to an unknown rhenium compound. A small amount of solid decomposition products was also present in the tube.

**B.** In the solid state: A 30 mg sample of 4 was sealed under vacuum in a glass tube and then heated at 90 °C for 30 min. The tube was cooled to room temperature and then cracked open in a glovebox, and the solid was taken up in  $C_6D_6$ , an internal standard (ferrocene) was added, and its  $^1H$  NMR spectrum was recorded. The mixture showed 23% of 3, 32% of  $[CpMo(CO)_3]_2$ , and an unidentified rhenium entity ( $\delta$  1.66). Also observed was 2% of the starting material.

**Attempted Thermolysis of 3.** A 30 mg sample of 3 was sealed in a tube, under vacuum, and heated at 95 °C for 1 h. The sample was taken up in  $C_6D_6$ , and its  $^1H$  NMR spectrum was recorded; it showed no sign of any decomposition of 3.

**$Cp^*Re(CO)(NO)CO_2CH_2CH_2WCp(CO)_3$  (7).**  $Cp^*Re(CO)(NO)COOH$  (1; 0.10 g, 0.23 mmol) was dissolved in THF, and to the solution was added 0.05 g (0.23 mmol) of proton sponge.  $CpW(CO)_3(C_2H_4)^+BF_4^-$  (6; 0.11 g, 0.25 mmol) was then added, and the sample was stirred for 0.5 h. After evaporating the solvent to dryness, the residue was extracted with ether, the extract was filtered and the filtrate evaporated to dryness. The residue was then triturated with pentane yielding the product as an orange powder which was collected by filtration and dried (0.11 g, 61% yield), mp 104 °C, decomp. Anal. Calcd for  $C_{22}H_{24}NO_7ReW$ : C, 33.68; H, 3.08. Found: C, 33.80; H, 3.15. IR ( $CH_2Cl_2$ ):  $\nu_{CO}$  2015 (s), 1975 (m, br), and 1915 (vs, br)  $cm^{-1}$ ;  $\nu_{NO}$  DRIFTS (KCl):  $cm^{-1}$ .  $\nu_{OCO}$  1614 (m) and 1020 (m)  $cm^{-1}$ .  $^1H$  NMR ( $C_6D_6$ ):  $\delta$  4.60 (s, CpW), 4.49 (m,  $OCH_2$ ), 1.97 (m,  $WCH_2$ ), 1.71 (s, CpMe<sub>5</sub>).  $^{13}C$  NMR ( $C_6D_6$ ):  $\delta$  229.59 (s, CO), 217.59 (s, CO), 208.89 (s, CO), 188.37 (s,  $CO_2$ ), 104.19 (s, CpMe<sub>5</sub>), 90.99 (s, CpW), 70.92 (s,  $OCH_2$ ), 9.85 (s, CpMe<sub>5</sub>), -11.54 (s,  $WCH_2$ ).

**B.** Cation 5 ( $Cp^*Re(CO)_2(NO)^+BF_4^-$ ; 0.40 g, 0.81 mmol) was dissolved in  $CH_2Cl_2$ , and the solution was cooled to -20 °C. Solid  $CpW(CO)_3(CH_2CH_2O)^-Na^+DME$  (0.40 g, 0.82 mmol) was added in portions, and the mixture was stirred for 0.5 h at this temperature and for another 0.5 h at 0 °C. The sample was filtered through Celite, and the filtrate was evaporated to dryness. The residue was extracted with ether (ca. 50 mL total), and the combined extracts were filtered through Celite and then evaporated to dryness to give a spectroscopically pure orange-red solid (0.60 g, 94% yield).

**Attempted Thermolysis of 7.** A sample of 7 (0.05 g) was dissolved in acetone- $d_6$ , and its  $^1H$  NMR spectrum was taken. The sample then stood at room temperature for 24 h, after which its  $^1H$  NMR spectrum was again recorded. No significant change in the sample had occurred during this time.

**Modified Procedure for the Preparation of  $CpFe(CO)_2(C_2H_4)^+BF_4^-$  (8).** A solution of  $[CpFe(CO)_2]_2$  (5.0 g, 14.0 mmol) in 30 mL of dry THF was added to an excess of Na/Hg

(15) Griffiths, P. W.; de Haseth, J. A. *Fourier Transform Infrared Spectroscopy*; Wiley: New York, 1986; Chapter 5.



under nitrogen in a three-necked round bottom flask at ambient temperature. The mixture was stirred for 3 h,  $\text{CH}_3\text{CH}_2\text{I}$  (4.37 g, 28.0 mmol) was added, and the mixture was stirred for an additional 30 min. The solution was decanted and filtered, and the THF was removed under vacuum. The crude product was taken up in 30 mL of dry  $\text{CH}_2\text{Cl}_2$  in a three-necked round bottom flask under nitrogen, and  $\text{Ph}_3\text{C}^+\text{BF}_4^-$  (9.24 g, 28.0 mmol) was added. The solution was stirred for 2 h at ambient temperature. The crude product was filtered off and then taken up in 10 mL of  $\text{CH}_3\text{CN}$ . Addition of anhydrous ether resulted in precipitation of 7.62 g (94%) of the orange product whose properties were identical with those reported previously.<sup>9a</sup>

**Cp\*Re(CO)(NO)CO<sub>2</sub>CH<sub>2</sub>CH<sub>2</sub>Fe(CO)<sub>2</sub>Cp (9).** In a glove-box under an atmosphere of dry nitrogen,  $\text{CpFe(CO)}_2(\text{C}_2\text{H}_4)^+\text{BF}_4^-$  (8; 0.11 g, 0.36 mmol) solid was added to a solution of proton sponge (0.04 g, 0.18 mmol) in  $\text{CH}_2\text{Cl}_2$  maintained at  $-5^\circ\text{C}$ .  $\text{Cp}^*\text{Re(CO)(NO)COOH}$  (1; 0.15 g, 0.35 mmol) was then slowly added over 5 h with stirring. The mixture was then filtered, and the solvent was removed under vacuum. The crude product was taken up in a mixture of toluene and hexane at a ratio of 1:9. The solution stood at  $-30^\circ\text{C}$  for 48 h to give 0.18 g (82%) of **9** as an orange powder, mp  $61-62^\circ\text{C}$ , decomp. Anal. Calcd for  $\text{C}_{21}\text{H}_{24}\text{FeNO}_6\text{Re}$ : C, 40.13; H, 3.85. Found: C, 39.99; H, 3.97. IR (Nujol):  $\nu_{\text{CO}}$  2000 (s), 1960 (s), 1940 (s), and 1620 (m)  $\text{cm}^{-1}$ ;  $\nu_{\text{NO}}$  1690  $\text{cm}^{-1}$ . DRIFTS (neat):  $\nu_{\text{CO}}$  1618 (m) and 1017 (m)  $\text{cm}^{-1}$ .  $^1\text{H NMR}$  ( $\text{CD}_2\text{Cl}_2$ ,  $-10^\circ\text{C}$ ):  $\delta$  4.85 (s), 4.00 (m), 2.09 (s), and 1.43 (m).  $^{13}\text{C NMR}$  ( $\text{CD}_2\text{Cl}_2$ ,  $-10^\circ\text{C}$ ):  $\delta$  217.46 (s), 208.57 (s), 188.97 (s), 104.59 (s), 85.30 (s), 70.07 (s), 10.05 (s), and 0.51 (s).

**CpFe(CO)(PPh<sub>3</sub>)CO<sub>2</sub>CH<sub>2</sub>CH<sub>2</sub>WCp(CO)<sub>3</sub> (11).** A 0.40 g sample of  $\text{CpFe(CO)(PPh}_3)^+\text{I}^-$  (10; 0.73 mmol) was dissolved in 20 mL  $\text{CH}_2\text{Cl}_2$ , and to the resulting yellow solution was added 0.40 g (0.82 mmol) of  $\text{CpW(CO)}_3(\text{CH}_2\text{CH}_2\text{O})^-\text{Na}^+\text{DME}$ . After the mixture had been stirred for 15 min, the sample was filtered and the filtrate was evaporated to dryness. The greenish-yellow residue was washed with ether ( $2 \times 5$  mL) to give a yellow solid and a green supernatant. The solid was collected by filtration and then dried under vacuum, affording 0.39 g (66% yield) of product, mp  $124^\circ\text{C}$ , decomp. Anal. Calcd for  $\text{C}_{35}\text{H}_{29}\text{FeO}_6\text{PW}$ : C, 51.49; H, 3.58. Found: C, 51.47; H, 3.47. IR ( $\text{CH}_2\text{Cl}_2$ ):  $\nu_{\text{CO}}$  2010 (s), 1935 (s, sh), and 1925 (vs)  $\text{cm}^{-1}$ . DRIFTS (KCl):  $\nu_{\text{CO}}$  1611 (m) and 990 (m)  $\text{cm}^{-1}$ .  $^1\text{H NMR}$  ( $\text{C}_6\text{D}_6$ ):  $\delta$  7.70 (m), 4.67 (s, CpW), 4.34 (d, CpFe,  $J_{\text{FH}} = 1.2$  Hz), 4.08 (m,  $\text{OCH}_2$ ), 1.54 (m,  $\text{WCH}_2$ ).  $^{13}\text{C NMR}$  ( $\text{C}_6\text{D}_6$ ):  $\delta$  229.53

(s, CO), 217.10 (s, CO), 220.18 (d,  $J_{\text{FC}} = 30$  Hz), 211.59 (d,  $J_{\text{FC}} = 34$  Hz), 90.71 (s, CpW), 84.73 (s, CpFe), 70.74 (s,  $\text{OCH}_2$ ),  $-11.93$  (s,  $\text{WCH}_2$ ).

**X-ray Crystal Structure of 11.** A suitable crystal was grown by layering a benzene/ether (50:50) solution of **11** with hexane and then allowing the sample to stand for 1 day at room temperature. Data were collected on an Enraf-Nonius CAD4 diffractometer at  $22^\circ\text{C}$ ; the data are outlined in Table 1. Selected bond distances and bond angles are shown in Table 3. Of 5553 unique reflections, 4201 were considered observed ( $I > 3\sigma(I)$ ). The structure was solved using Patterson methods and refined with anisotropic thermal parameters for all non-hydrogen atoms. The calculated positions and thermal parameters for the hydrogen atoms were kept constant with temperature factors set to 1.2 times the temperature factors of the carbon atoms to which they are bonded. A final  $R$  index of 0.037 with  $R_w = 0.049$  was obtained for 398 variables. All computations were performed using the teXsan package (Molecular Structure Corporation).<sup>16</sup>

**Acknowledgment.** Support of this work by the United States Department of Energy, Division of Chemical Sciences (Office of Basic Energy Sciences) is gratefully acknowledged. Partial support of this work through the NSF/EPSCoR program (Grant No. EHR-9108764) is also gratefully acknowledged. The X-ray equipment was purchased with assistance from the National Science Foundation (Grant No. CHE-9016978). Support of the Molecular Structure Laboratory through the NSF/KY EPSCoR program and support of M.T.H. through a traineeship from the DOE/KY EPSCoR program (Cooperative Agreement No. DE-FCO2-91ER-75661) are also gratefully acknowledged.

**Supporting Information Available:** Tables of anisotropic thermal parameters, H atom positional parameters, bond distances, bond angles and torsional angles for **11** (14 pages). This material is contained in many libraries on microfiche, immediately follows this article in the microfilm version of the journal, and can be ordered from the ACS; see any current masthead page for ordering information.

OM950508O

(16) teXsan: *Single Crystal Structure Analysis Software*, Version 1.6; Molecular Structure Corp.: The Woodlands, TX 77381, 1993.

# Electronic Interplay between Two Iron Centers across Polyaromatic Ligands: Syntheses, Redox Chemistry, and Electronic Structures of the Electron-Reservoir 36- to 38-Electron Complexes $[(\text{FeCp}^*)_2(\mu_2\text{-}\eta^{12}\text{-polyaromatic})]^{q+}$ ( $q = 0-2$ ) Including Mixed Valences and Biradicals

Hassan Rabaâ,<sup>†,‡</sup> Marc Lacoste,<sup>§</sup> Marie-Hélène Delville-Desbois,<sup>§</sup> Jaime Ruiz,<sup>§</sup>  
Bruno Gloaguen,<sup>§</sup> Nicole Ardoin,<sup>§</sup> Didier Astruc,<sup>\*,§</sup> Albert Le Beuze,<sup>†</sup>  
Jean-Yves Saillard,<sup>\*,†</sup> Jorge Linares,<sup>||</sup> François Varret,<sup>||</sup> Jean-Michel Dance,<sup>⊥</sup> and  
Emile Marquestaut<sup>⊥</sup>

*Laboratoire de Chimie Organique et Organométallique, URA CNRS No. 35, Université Bordeaux I, 351 cours de la Libération, 33405 Talence Cédex, France, Laboratoire de Chimie de Solide et Inorganique Moléculaire, URA CNRS No. 1495, Université Rennes I, Campus de Beaulieu, 35042 Rennes Cédex, France, Laboratoire de Chimie Théorique, Faculté des Sciences, Université Ibn Tofail, B.P. 133, Kénitra 14000, Morocco, Département de Recherches Physiques, URA CNRS No. 71, Université Pierre et Marie Curie, Case 136, 4 place Jussieu, 75252 Paris Cédex 05, France, and Laboratoire de Chimie du Solide, URP CNRS No. 8661, Université Bordeaux I, 351 cours de la Libération, 33405 Talence Cédex, France*

Received May 30, 1995<sup>⊗</sup>

A new series of diiron polyaromatic complexes,  $[(\text{Fe}^{\text{II}}\text{Cp}^*)_2(\mu_2\text{-}\eta^{12}\text{-polyaromatic})]^{2+}(\text{PF}_6^-)_2$  ( $\text{Cp}^* = \eta^5\text{-C}_5\text{Me}_5$ ; polyaromatic = dihydrophenanthrene, fluorene, diphenylmethane, fluorene, phenanthrene, triphenylmethane, pyrene, [2.2]paracyclophane), has been synthesized by reaction of  $[\text{FeCp}^*(\text{CO})_2\text{Br}]$  with  $\text{Al}_2\text{Cl}_6$  and  $\text{Al}_2\text{Cl}_3\text{Me}_3$ , avoiding hydrogenation of the polyaromatic ligand. One-electron and two-electron reductions have been achieved to investigate the electronic communication between the two iron atoms in the 37-electron (37e) mixed-valence complexes and in the 38e complexes. The  $\text{Cp}^*$  ( $\text{Cp}^* = \eta^5\text{-C}_5\text{Me}_5$ ) ligand stabilizes the 37e mixed-valence complexes which were synthesized by comproportionation between the 36e and 38e complexes. Mössbauer spectra show that these complexes are average valence on the Mössbauer time scale. The 38e complexes are thermally stable up to  $-20^\circ\text{C}$  and were studied by  $^1\text{H}$  NMR, ESR, and Mössbauer spectroscopy for phenanthrene, pyrene, and triphenylene. The absence of  $^1\text{H}$  NMR spectra in the diamagnetic region and the three  $g$  values around 2 in ESR are characteristic of 19e  $\text{Fe}^{\text{I}}$  complexes and indicate that these complexes do not undergo intramolecular chemical coupling (formation of the exocyclic double bond), in contrast to the dihydrophenanthrene and cyclophane complexes, which are shown by  $^1\text{H}$  NMR to be diamagnetic. The compared Mössbauer parameters of the 36e  $\text{Fe}^{\text{II}}\text{Fe}^{\text{II}}$ , 37e  $\text{Fe}^{\text{I}}\text{Fe}^{\text{II}}$ , and 38e  $\text{Fe}^{\text{I}}\text{Fe}^{\text{I}}$  polyaromatic complexes mentioned above are very similar, indicating that the 37th and 38th electrons are in mainly polyaromatic-based orbitals. The Mössbauer IS and QS values of the 38e complexes, however, are slightly higher than those of the 36e and 37e series, consistent with a slightly higher metal contribution. The cyclic voltammograms of the 36e polyaromatic complexes show a redox series of five oxidation states, contrasting with those of dihydrophenanthrene and [2.2]paracyclophane, which give only two waves because of intramolecular chemical coupling at the second reduction stage. Among the four one-electron waves, only the last one is chemically and electrochemically irreversible, showing the structural rearrangement in the course of the fourth reduction. SCF MS-X $\alpha$  calculations have been performed on the diiron pyrene species and were compared to similar calculations carried out on the related diphenyl system. The reduction of the 36e diphenyl complex leads to the occupation of its  $b_u$  LUMO, which is significantly  $\pi$ -bonding on the exocyclic bond, thus inducing chemical coupling. In the case of the 36e pyrene complex, the corresponding  $b_u$  vacant orbital is not the LUMO and has a poorer  $\pi$ -bonding character on the C-C bond susceptible to be involved in the chemical coupling. Therefore, this  $b_u$  level is not involved upon reduction. Instead, the  $a_u$  LUMO and the next  $a_g$  level are successively populated by the incoming electrons, the latter being more metal-centered than the former.

## Introduction

Binuclear transition-metal complexes containing an electronically delocalized bridging ligand are simple models of molecular conductors.<sup>1</sup> Addition or subtrac-

tion of a single electron in the diamagnetic precursors of such complexes allows the study of the electronic delocalization terms of trapped/detrapped mixed valences<sup>1-3</sup> as a function of the spectroscopic frequency. Addition or subtraction of two electrons leads to either



**Table 1. Syntheses of Diiron (II) Polyaromatic Complexes**

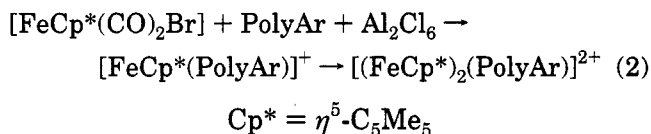
diiron polyaromatic (PF <sub>6</sub> <sup>-</sup> salt)	synthesis <sup>a</sup>	yield (%)
<b>4a</b> , [(FeCp*) <sub>2</sub> (dihydrophenanthrene)] <sup>2+</sup>	A	28
<b>8a</b> , [(FeCp*) <sub>2</sub> (phenanthrene)] <sup>2+</sup>	B (C)	40 (30)
<b>5a</b> , [(FeCp*) <sub>2</sub> (triphenylene)] <sup>2+</sup>	A	38
<b>9a</b> , [(FeCp*) <sub>2</sub> (pyrene)] <sup>2+</sup>	B	61
<b>10a</b> , [(FeCp*) <sub>2</sub> ([2.2]paracyclophane)] <sup>2+</sup>	B	55
<b>6a</b> , [(FeCp*) <sub>2</sub> (fluorene)] <sup>2+</sup>	A	36
<b>4b</b> , [(FeCp*) <sub>2</sub> (dihydrophenanthrene)] <sup>2+</sup>	D	32
<b>8b</b> , [(FeCp*) <sub>2</sub> (phenanthrene)] <sup>2+</sup>	D	20
<b>5b</b> , [(FeCp*) <sub>2</sub> (triphenylene)] <sup>2+</sup>	D	22
<b>6b</b> , [(FeCp*) <sub>2</sub> (fluorene)] <sup>2+</sup>	D	38

<sup>a</sup> (A) [FeCp\*(CO)<sub>2</sub>Br] and Al<sub>2</sub>Cl<sub>6</sub> in the melt; (B) [FeCp\*(CO)<sub>2</sub>Br] and Al<sub>2</sub>Cl<sub>3</sub>Me<sub>3</sub> + Al<sub>2</sub>Cl<sub>6</sub> in the melt; (C) Na/Hg reduction of **4a** to **11** followed by reaction with O<sub>2</sub> in the absence of Na<sup>+</sup>PF<sub>6</sub><sup>-</sup> and oxidation using [Fe<sup>III</sup>Cp<sub>2</sub>]<sup>+</sup>PF<sub>6</sub><sup>-</sup>; (D) FeCp<sub>2</sub> and Al<sub>2</sub>Cl<sub>6</sub> in the melt.

metal cluster chemistry.<sup>18,19</sup> We report here the first detailed study of the syntheses, electronic structures, and electron-transfer and radical chemistry of the 36e and 37e (mixed valence) and 38e complexes [(FeCp\*)<sub>2</sub>(PolyAr)]<sup>q+</sup> (*q* = 0–2) with PolyAr = phenanthrene, dihydrophenanthrene, [2.2]paracyclophane, triphenylene, and pyrene and compare the parent Cp series with the stabilized Cp\* series.<sup>22</sup> We show that the bireduced diiron complexes with ortho-condensed polyaromatics have a triplet ground state, unlike those of “nondelocalized polyaromatics”. These results are supported by SCF MS-Xα calculations on the pyrene complexes.

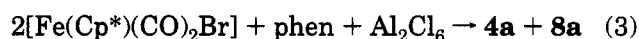
## Results and Discussion

**1. Synthesis of [(FeCp\*)<sub>2</sub>(μ<sub>2</sub>-η<sup>12</sup>-PolyAr)]<sup>2+</sup>.** The general method for complexation of polyaromatics using [FeCp\*(CO)<sub>2</sub>Br]<sup>20</sup> and Al<sub>2</sub>Cl<sub>6</sub> proceeds best in a melt.<sup>21</sup> This synthetic route is convenient when the polyaromatics cannot be hydrogenated in the course of the ligand exchange. This was the case for the dihydrophenanthrene, fluorene, and triphenylene complexes (eq 2 and Table 1).

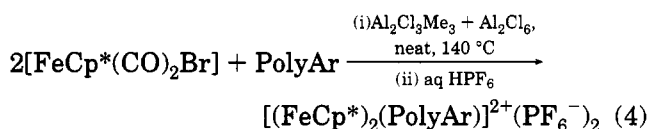


The known route<sup>21</sup> using Al<sub>2</sub>Cl<sub>6</sub>, however, does not work satisfactorily with more condensed polyaromatics (for instance phenanthrene) in the Cp\* series because

of partial hydrogenation (eq 3 and Scheme 1). The



dihydrophenanthrene and phenanthrene complexes obtained are tedious to separate. Thus, it is best to synthesize the diiron dihydrophenanthrene complex **4a** from dihydrophenanthrene. For the diiron phenanthrene complex, we decided to seek a synthetic route which would avoid this partial hydrogenation during the complexation reaction. The use of Al<sub>2</sub>Cl<sub>3</sub>Me<sub>3</sub><sup>23</sup> + Al<sub>2</sub>Cl<sub>6</sub> instead of Al<sub>2</sub>Cl<sub>6</sub> alone was successful in avoiding the hydrogenation. This indicates that H<sup>+</sup>AlCl<sub>4</sub><sup>-</sup> formed by contact of air (H<sub>2</sub>O) with Al<sub>2</sub>Cl<sub>6</sub> is responsible for hydrogenation of the polyaromatic ligand.<sup>24</sup> The Al–CH<sub>3</sub> bonds are very sensitive to protonation, yielding methane and consuming the protic impurities. It was thus possible in this way to synthesize the pure diiron complexes of phenanthrene, pyrene, and [2.2]paracyclophane (eq 4, Chart 1, Table 1).



With Al<sub>2</sub>Cl<sub>6</sub> alone, the synthesis of the cyclophane complex **10** gave a product which was found to be very impure by <sup>1</sup>H NMR because retro-Friedel–Crafts cleavage of the dimethylene bridges occurs.

The improved procedure using Al<sub>2</sub>Cl<sub>3</sub>Me<sub>3</sub> + Al<sub>2</sub>Cl<sub>6</sub> also enhances the facility of complexation. For instance, with pyrene, Al<sub>2</sub>Cl<sub>6</sub> alone is inefficient. Similarly, in the Cp series, no diiron pyrene complex can be made using Al<sub>2</sub>Cl<sub>6</sub>. In the cyclophane case, the complexation ability is so high with Al<sub>2</sub>Cl<sub>3</sub>Me<sub>3</sub> + Al<sub>2</sub>Cl<sub>6</sub> that no monometallic complex can be isolated even using the appropriate stoichiometry of reagents.

The difference in the abilities of the two dicationic phenanthrene complexes **8a** and **8b** to undergo the side-ring reduction to the dihydrophenanthrene complex has mechanistic significance. Since we now know that quenching H<sup>+</sup>AlCl<sub>4</sub><sup>-</sup> by Al<sub>2</sub>Cl<sub>3</sub>Me<sub>3</sub> inhibits the hydrogenation, it follows that protonation by H<sup>+</sup>AlCl<sub>4</sub><sup>-</sup> plays a major role. Protonation of the double bond in **8a** or **8b** in the first step is difficult because the complex is already a dication, but H<sup>+</sup>AlCl<sub>4</sub><sup>-</sup> is a very strong acid. Protonation is more difficult in the parent Cp complex **8b** than in the permethylated one **8a** because permethylation increases the low basicity of the double bond conjugated with the complexed ring. Presumably, the trication formed by protonation is very reactive and oxidizes phenanthrene before abstracting a H atom from the medium to give **4a** (Scheme 1).

In several cases, we have also reinvestigated the synthesis of the parent Cp compound, which has been found to be marred by hydrogenation during ligand exchange between the polyaromatic and ferrocene. For instance, the synthesis of the phenanthrene complex **8b** was reported to give mixtures resulting from partial hydrogenation.<sup>12</sup> In our hands, no hydrogenation was

(18) (a) Holm, R. H.; Ibers, J. A. In *Iron-Sulfur Proteins*; Lovenberg, W. Ed.; Academic Press: New York, 1976; Vol. 3, Chapter 7. (b) Dalh, L. F. *J. Am. Chem. Soc.* **1982**, *104*, 3409. (c) Kubas, G. J.; Vergamini, P. *Inorg. Chem.* **1981**, *20*, 2667.

(19) Sheldon, R. A.; Kochi, J. K. *Metal Catalyzed Oxidations of Organic Compounds*; Academic Press: New York, 1981; Chapter 8.

(20) (a) Hamon, J.-R.; Astruc, D.; Michaud, P. *J. Am. Chem. Soc.* **1981**, *103*, 758. (b) Astruc, D.; Hamon, J.-R.; Lacoste, M.; Desbois, M.-H.; Román, E. In *Organometallic Synthesis*; King, R. B., Ed.; Elsevier: Amsterdam, 1988; Vol. IV, p 172.

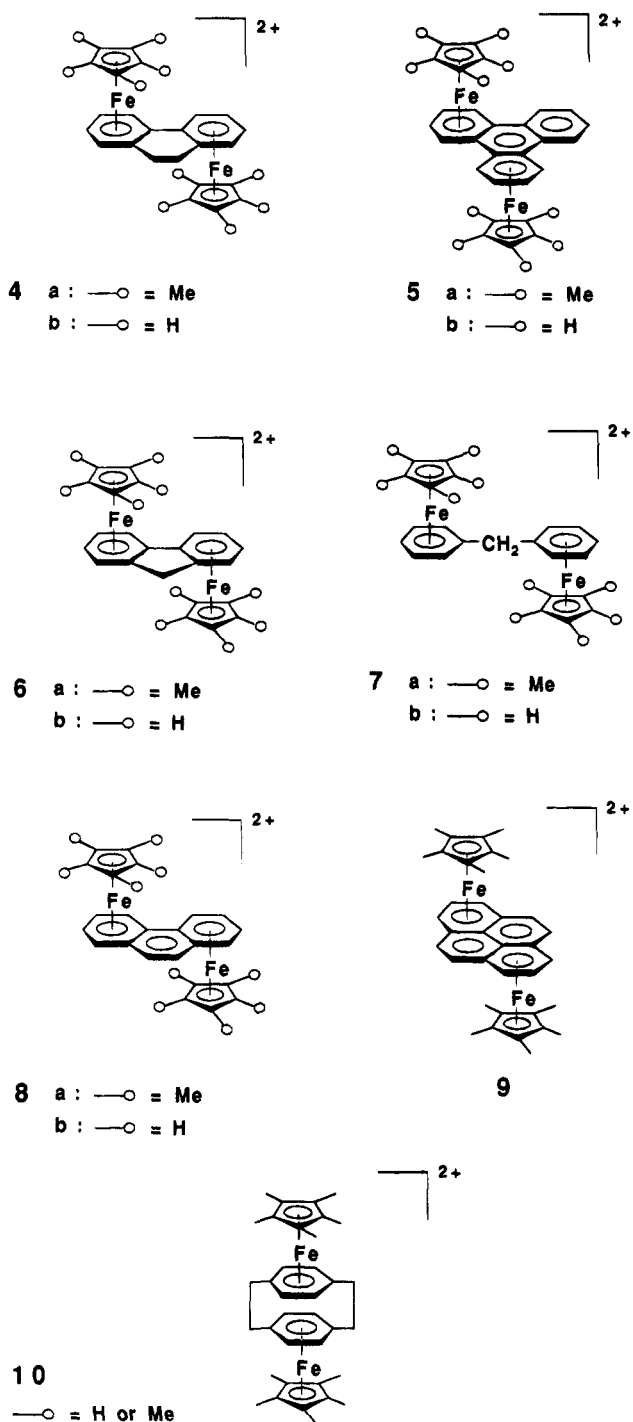
(21) (a) Lacoste, M.; Astruc, D. *J. Chem. Soc., Chem. Commun.* **1987**, 667. (b) Lacoste, M.; Rabaâ, H.; Astruc, D.; Le Beuze, A.; Saillard, J.-Y.; Précigoux, G.; Courseille, C.; Ardoin, N.; Bowyer, W. *Organometallics* **1989**, *8*, 2233.

(22) For preliminary communications see: Lacoste, M.; Varret, F.; Toupet, L.; Astruc, D. *J. Am. Chem. Soc.* **1987**, *109*, 6504. Astruc, D.; Ruiz, J.; Lacoste, M.; Gloaguen, B.; Ardoin, N.; Linares, J.; Varret, F. *J. Chem. Soc., Chem. Commun.* **1995**, 1565.

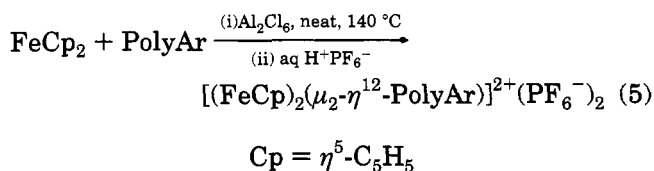
(23) Aluminum methyl sesquichloride Al<sub>2</sub>Me<sub>3</sub>Cl<sub>3</sub> has been reported to avoid the side reactions of cyclophanes: (a) Snider, B. B. *Acc. Chem. Res.* **1980**, *13*, 426. (b) Eltzinga, J.; Roseblaud, M. *Tetrahedron Lett.* **1982**, *23*, 1535.

(24) (a) Retro-Friedel–Crafts side reactions of AlCl<sub>3</sub> can also lead to π-C<sub>6</sub>Me<sub>5</sub>H complexes, starting from C<sub>6</sub>Me<sub>6</sub>.<sup>24b,c</sup> (b) Hamon, J.-R.; Saillard, J.-Y.; Toupet, L.; Astruc, D. *J. Chem. Soc., Chem. Commun.* **1989**, 1662. (c) Hamon, J.-R.; Astruc, D. *Organometallics* **1989**, *8*, 2243.

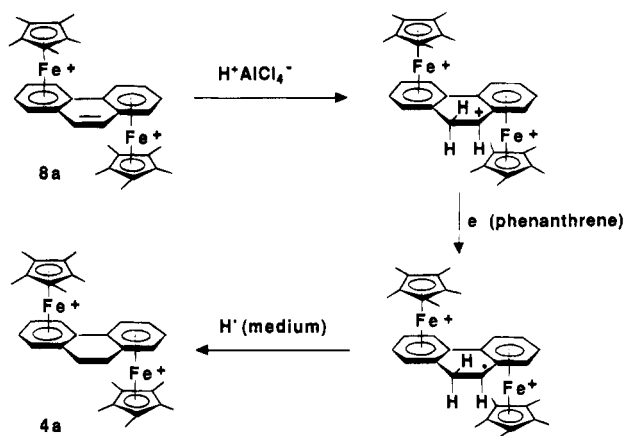
Chart 1



found, whatever the reaction conditions and the quality and quantity of  $\text{Al}_2\text{Cl}_6$  used: **8b** was the only complex obtained. An appreciable improvement occurred with the discovery that the cleanest reactions and best yields were obtained in the melt at  $140^\circ\text{C}$ . The new triphenylene complex **5b**, as well as the fluorene and dihydrophenanthrene complexes **6b** and **4b**, were also synthesized in this way (eq 5, Table 1).



Scheme 1



## 2. Electron-Transfer and Radical Chemistry of the Diiron Phenanthrene and Dihydrophenanthrene Complexes.

$\text{Na}/\text{Hg}$  reduction of the yellow diiron dihydrophenanthrene complex **4a** at  $20^\circ\text{C}$  gives the thermally stable, air-sensitive, dark blue complex **11**, which is ESR silent and shows the  $^1\text{H}$  and  $^{13}\text{C}$  NMR characteristics of a bicyclohexadienylidene ligand resulting from intramolecular chemical coupling between the two phenyl rings. For instance, the cyclohexadienyl protons are found around 5.7, 4, and 2.5 ppm. The typical cyclohexadienylidene peaks<sup>22</sup> are split in the  $^{13}\text{C}$  NMR spectrum because of the dissymmetry created by the dimethylene bridge, whereas the double-bond carbons are found at  $\delta$  103.9 ppm. The Mössbauer data for **11** are in agreement with a diamagnetic  $\text{Fe}^{\text{II}}$  complex, but the isomer shift is slightly higher (IS (78 K) =  $0.593 \text{ mm s}^{-1}$ ) than that of the parent bicyclohexadienylidene complex **3**.<sup>22</sup> We believe this effect is caused by steric constraints which lower the structural flexibility of the ligand required for the intramolecular chemical coupling.

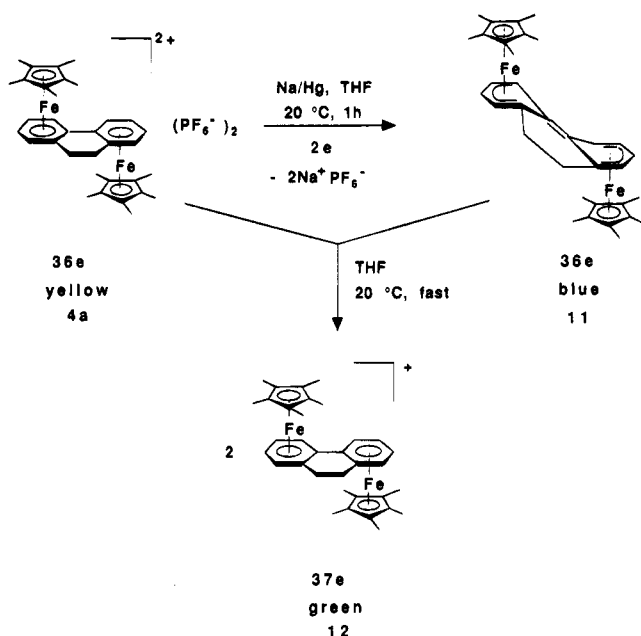
Mixing equimolar amounts of **4a** and **11** gave a 92% yield of the dark green complex **12**, which shows an ESR spectrum with three  $g$  values around 2 in THF at 77 K and a single quadrupole doublet on the Mössbauer time scale.<sup>25</sup> This electronic delocalization also indicates that the polyaromatic bridging ligand is planar, as in **2**, and thus that **12** is a 37e complex (Scheme 2).

The reaction of **11** with  $\text{O}_2$  at  $-20^\circ\text{C}$  in toluene or THF in the absence of  $\text{Na}^+\text{PF}_6^-$  gives double-H-atom abstraction at the two adjacent benzylic positions,<sup>27</sup> to yield the brown, neutral complex **13**, which is air-sensitive and thermally unstable above  $-15^\circ\text{C}$  (Scheme 3). Complex **13** does not exhibit NMR peaks in the diamagnetic region but shows an ESR spectrum in frozen solution at 77 K, with three  $g$  values around 2 characteristic of  $\text{Fe}^{\text{I}}$ . Complex **13** is identical (in color,

(25) (a) For previous Mössbauer studies of  $\text{Fe}^{\text{I}}$ <sup>25b</sup> and mixed-valence  $\text{Fe}^{\text{I}}\text{Fe}^{\text{II}}$  fulvalene<sup>25c,26</sup> complexes, see refs 6 and 25b,c. (b) Mariot, J.-P.; Michaud, P.; Lauer, S.; Astruc, D.; Trautwein, A. X.; Varret, F. *J. Phys. (Paris)* **1983**, *44*, 1377. (c) Guillin, J.; Desbois, M.-H.; Mariot, J.-P.; Lauer, S.; Trautwein, A. X.; Varret, F.; Astruc, D. *Hyperfine Interact.* **1986**, *28*, 761.

(26) For diiron fulvalene complexes see: (a) Desbois, M.-H.; Astruc, D.; Guillin, J.; Mariot, J.-P.; Varret, F. *J. Am. Chem. Soc.* **1985**, *107*, 52. (b) Desbois, M.-H.; Astruc, D.; Guillin, J.; Varret, F.; Trautwein, A. X.; Villeneuve, G. *J. Am. Chem. Soc.* **1989**, *111*, 5800. (c) Desbois, M.-H.; Guillin, J.; Mariot, J.-P.; Varret, F.; Astruc, D. *J. Chem. Soc., Chem. Commun.* **1985**, 447. (d) Desbois, M.-H.; Astruc, D.; Guillin, J.; Varret, F. *Organometallics* **1989**, *8*, 1848. (e) Desbois, M.-H.; Astruc, D. *Organometallics* **1989**, *8*, 1841.

Scheme 2



stability, ESR, and oxidation product) with that obtained by Na/Hg reduction of diiron phenanthrene complex **8a** at  $-35^\circ\text{C}$ . The molecular structure of **13** obtained by either route was confirmed by oxidation using 2 equiv of  $[\text{FeCp}_2]^+\text{PF}_6^-$ , which gave phenanthrene complex **8a** in 30% overall yield from **4a** after recrystallization from acetonitrile (compare Table 1). The orange complex **8a** obtained in this manner (method C) is also identical, by TLC and NMR, with that obtained by direct ligand exchange from phenanthrene using  $\text{Al}_2\text{Cl}_3\text{Me}_3$  (method B). The reaction of **11** with  $\text{O}_2$  in the presence of 2 equiv of  $\text{Na}^+\text{PF}_6^-$  in THF at  $-20^\circ\text{C}$  gives  $\text{Na}_2\text{O}_2$  and **4a** because  $\text{Na}^+\text{PF}_6^-$  inhibits the deprotonation of **12** by superoxide anion by disrupting the reactive ion pair containing  $\text{O}_2^{\cdot-}$ . Thus, simple back-ET is observed. Similarly, **13** reacts with  $\text{O}_2$  with  $\text{Na}^+\text{PF}_6^-$  in THF to give, as with  $[\text{FeCp}_2]^+\text{PF}_6^-$ , the ET product **8a**. From these results, we conclude that **13** is the  $\text{Fe}^{\text{I}}\text{Fe}^{\text{I}}$  complex of phenanthrene.

The reaction of 2 equiv of  $t\text{-BuOK}^{28}$  with **4a** at  $-20^\circ\text{C}$  also gives **13** by double deprotonation (although this route is not as useful as the two others because of the tedious filtration of  $\text{K}^+\text{PF}_6^-$  in the course of the toluene extraction). These routes from dihydrophenanthrene to phenanthrene complexes are the reverse of the hydrogenation of the phenanthrene complex in the presence of  $\text{H}^+\text{AlCl}_4^-$  during ligand exchange. A much easier hydrogenation of a phenanthrene complex involving

(27) (a) Reaction of  $\text{Fe}^{\text{I}}$  complex with  $\text{O}_2$  gives benzylic H-atom abstraction by an ET mechanism followed by deprotonation by  $\text{O}_2^{\cdot-}$  in the solvent cage.<sup>27b-d</sup> This cage deprotonation is inhibited by  $\text{Na}^+\text{PF}_6^-$  because of the double ion exchange between the two ion pairs disrupting the reactive cage.<sup>27d</sup> With Fe complexes having two extra valence electrons above the 18e count, two benzylic H atoms are abstracted.<sup>27e,f</sup> (b) Astruc, D.; Román, E.; Hamon, J.-R.; Batail, P. *J. Am. Chem. Soc.* **1979**, *101*, 2240. (c) Hamon, J.-R.; Astruc, D.; Román, E.; Batail, P.; Mayerle, J. J. *J. Am. Chem. Soc.* **1981**, *103*, 2431. (d) Hamon, J.-R.; Astruc, D. *Organometallics* **1988**, *7*, 1036. (e) Madonik, A.; Astruc, D. *J. Am. Chem. Soc.* **1984**, *106*, 2437. (f) Astruc, D.; Mandon, D.; Madonik, A. M.; Michaud, P.; Ardoin, N.; Varret, F. *Organometallics* **1990**, *9*, 2155.

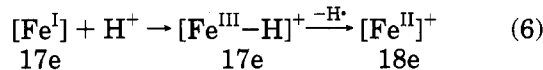
(28) In principle, deprotonation of  $[\text{Fe}^{\text{II}}\text{Cp}(\text{arene})]^+$  complexes by  $t\text{-BuOK}$  gives the same result as monoelectronic reduction of  $\text{Fe}^{\text{I}}$  followed by reaction with  $\text{O}_2$  in the absence of  $\text{Na}^+$  salt, but, in fact, the latter route is much cleaner and is usually preferred.<sup>27b</sup> See ref 14b-d and: Astruc, D. *Acc. Chem. Res.* **1986**, *19*, 377.

protonation is that carried out at the  $\text{Fe}^{\text{I}}\text{Fe}^{\text{I}}$  level (complex **13**) using  $\text{H}_2\text{O}$ .<sup>29</sup> Complex **13** reacts with  $\text{H}_2\text{O}$  at  $-20^\circ\text{C}$  to give **12** in THF (Scheme 3). Further oxidation to **4a** by  $\text{H}_2\text{O}$  alone does not occur at a significant rate. We believe that initial protonation of **13** at a metal center by  $\text{H}_2\text{O}$  is followed by hydride shift from Fe to the closest benzylic phenanthrene carbon. The intermediate radical is then expected to abstract a H atom from the medium. In **12**, the positive charge considerably reduces the basicity, compared to **11**, which precludes further protonation by a weak acid.

Finally, the unstable complex **13** thermally undergoes demetalation above  $-15^\circ\text{C}$  to give  $[\text{Fe}^{\text{I}}\text{Cp}^*(\eta^6\text{-dihydrophenanthrene})]$ ,<sup>21b</sup> characterized by its monoelectronic oxidation product, obtained using  $[\text{FeCp}_2]^+\text{PF}_6^-$  *in situ*. It is probable that the  $\text{Cp}^*\text{H}$  formed upon decomplexation protonates the monometallic  $\text{Fe}^{\text{I}}$  phenanthrene complex.

Since the voltammogram of **8a** shows a cascade of four one-electron waves, the first two being reversible at  $-30^\circ\text{C}$ , the 37e mixed-valence complex **14** is necessarily a discrete intermediate in the ET reactions between the 36e  $\text{Fe}^{\text{II}}\text{Fe}^{\text{II}}$  and 38e  $\text{Fe}^{\text{I}}\text{Fe}^{\text{I}}$  phenanthrene complexes **8a** and **13**: *i.e.*, interconversion does not proceed by a 2e transfer but involves stepwise monoelectronic transfers. A model complex of **14** is the mixed-valence triphenylene complex **22** (*vide infra*).

A partially decomplexed form of **13** (17e) might be responsible for the intermediate protonation of the  $\text{Fe}^{\text{I}}$  center by  $\text{H}_2\text{O}^{29c}$  in Scheme 3 (eq 6).



### 3. Intramolecular Coupling in the Cyclophane

**Complex 10a.** The Na/Hg reduction of the new cyclophane complex **10a**, in THF at  $20^\circ\text{C}$ , leads to formation of a slightly thermally unstable orange complex. We were surprised not to observe the intermediate intense purple color of the mixed-valence 37e complex **15b**, found for the parent Cp complex by Geiger's group.<sup>31</sup> Usually, the ferrocene-like  $[\text{Fe}^{\text{II}}\text{Cp}(\eta^5\text{-cyclohexadienyl})]$  complexes (without further conjugation of the ligands) are orange.<sup>32</sup> This is the case for the dimers  $[\text{Fe}^{\text{II}}(\text{C}_5\text{R}_5)(\eta^5\text{-C}_6\text{H}_6)]_2$  (**19**).<sup>32b,c</sup> We had hoped to stabilize the 37e mixed-valence complex by means of Cp permethylation to gain insight into plane-to-plane ET in **15**. Its  $^1\text{H}$  NMR spectrum shows the usual cyclohexadienyl signals around  $\delta$  3.4 and 5.2 ppm for the positions ortho and

(29) For some other examples of reactions of  $\text{H}_2\text{O}$  with 17e/19e transition-metal radicals see: (a) Ruiz, J.; Lacoste, M.; Astruc, D. *J. Am. Chem. Soc.* **1990**, *112*, 5471. (b) Desbois, M.-H.; Astruc, D. *Angew. Chem., Int. Ed. Engl.* **1989**, *28*, 460; *Angew. Chem.* **1989**, *101*, 459. (c) Lapinte, C.; Catheline, D.; Astruc, D. *Organometallics* **1984**, *3*, 817. (d) Gard, D. R.; Brown, T. L. *J. Am. Chem. Soc.* **1982**, *104*, 6340. (e) Koelle, U. In *Mechanisms and Processes in Molecular Chemistry*; Astruc, D., Ed.; Gauthier-Villars: Paris, 1992; New J. Chem. *16*, p 157.

(30) (a) Dihedral cyclohexadienyl angles in transition-metal complexes range between  $30$  and  $45^\circ$ <sup>30b</sup> but can be as small as  $11^\circ$  in deprotonated  $[\text{Fe}^{\text{II}}\text{Cp}(\text{fluorene})]$ .<sup>30c</sup> (b) Hoffmann, R.; Hofman, P. *J. Am. Chem. Soc.* **1976**, *98*, 598. (c) Johnson, J. W.; Treichel, P. M. *J. Chem. Soc., Chem. Commun.* **1976**, 688; *J. Am. Chem. Soc.* **1977**, *99*, 1427.

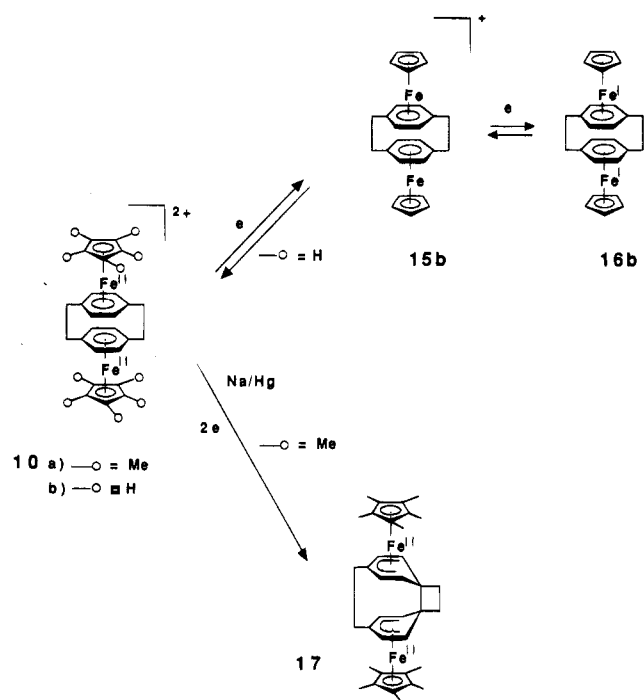
(31) Bowyer, W. J.; Geiger, W. E.; Boekelheide, V. *Organometallics* **1984**, *3*, 1979.

(32) (a) Khand, I. U.; Pauson, P. L.; Watts, W. E. *J. Chem. Soc.* **1968**, 2257; **1969**, 2024. (b) Nesmeyanov, A. N.; Vol'kenau, N. A.; Bolesova, A. N.; Petrakova, V. A. *Izv. Akad. Nauk SSSR, Ser. Khim.* **1974**, *9*, 2159. (c) See also refs 20 and 27d.

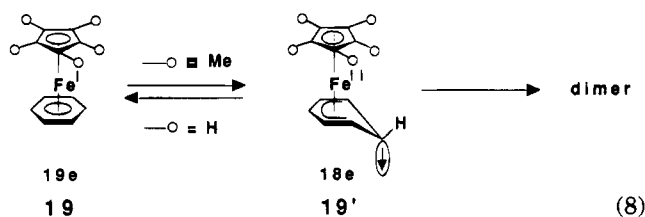




Scheme 4

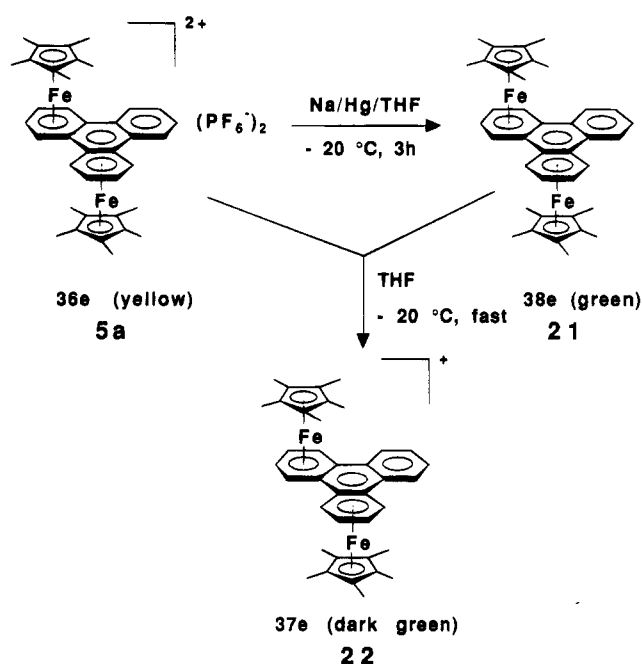


probably stabilizes the 18e form in 19 and 17 (eq 8).



**4. Syntheses and Spectroscopic Properties of the 37e and 38e Triphenylene, Phenanthrene, and Pyrene Complexes.** The Na/Hg reduction of the parent triphenylene complex 5b, in THF, rapidly leads to decomposition even when it is performed at  $-20^\circ\text{C}$ . On the other hand, Na/Hg reduction of 5a in THF at  $-35^\circ\text{C}$  gives a clear green color without decomposition and is complete in 3 h on a 0.5 mmol scale (Scheme 5). The very air-sensitive neutral green complex 21 could be extracted with—and crystallized from—toluene, and although it is thermally stable only up to  $-20^\circ\text{C}$  in the solid state, it could be analyzed by ESR and Mössbauer spectroscopy. Furthermore, it could be used stoichiometrically in ET chemistry. The absence of an NMR signal in the diamagnetic region and the ESR spectrum indicated that 21 is paramagnetic. The ESR spectrum in frozen THF at 7 K shows  $g$  values at  $g_x = 2.0691$ ,  $g_y = 2.0151$ , and  $g_z = 1.8279$ , characteristic of  $\text{Fe}^{\text{I}}$  complexes.<sup>35</sup> The Mössbauer spectra were informative, concerning the electronic structure and the thermal stability of 21. The spectra also indicated oxidized  $\text{Fe}^{\text{II}}$  and  $\text{Fe}^{\text{I}}\text{Fe}^{\text{II}}$  species, which could, however, be subtracted to provide clearer data (this oxidation results from some contact with air during the handling of the sample). The first spectra recorded at 77 K were found to contain  $67 \pm 3\%$  of  $\text{Fe}^{\text{I}}\text{Fe}^{\text{I}}$  complex 21. A previous, detailed study

Scheme 5



of the oxidation reactions of the solid-state  $\text{Fe}^{\text{I}}$  samples had shown that oxidation occurs at the surface of the samples, not in the bulk, and that the surface oxidation does not significantly perturb the examination of  $\text{Fe}^{\text{I}}$  electronic structures.<sup>27c</sup> It was also possible to record an increase of the oxidation impurities with time. The lines obtained for 21 were narrow and are interpreted in terms of an  $\text{Fe}^{\text{I}}\text{Fe}^{\text{I}}$  oxidation state. A characteristic, relatively weak temperature dependence of the quadrupole splitting (QS) around  $1.4 \text{ mm s}^{-1}$  was observed between 78 and 240 K, as expected for the Jahn–Teller-active  $\text{Fe}^{\text{I}}$  state with a HOMO–LUMO near-degeneracy.<sup>35</sup> The value of the isomer shift ( $\text{IS} = 0.63 \text{ mm s}^{-1}$  at 78 K) is too high for a chemically coupled  $\text{Fe}^{\text{II}}\text{Fe}^{\text{II}}$  state. However, it is sizably smaller than that of the reference complex  $[\text{Fe}^{\text{I}}\text{Cp}^*\text{Ar}]$  ( $0.73 \text{ mm s}^{-1}$  at 78 K), thus suggesting a considerable spin delocalization onto the polyaromatic ligand. The spectra in a magnetic field did not show a large magnetic interaction, indicating that antiferromagnetic coupling occurs and that there is considerable spin delocalization onto the polyaromatic ligand. This spin delocalization has been recorded in *mononuclear* polyaromatic complexes using electrochemistry, and checked using MO calculations.<sup>21b</sup> It is now enhanced in  $\text{Fe}^{\text{I}}\text{Fe}^{\text{I}}$  polyaromatic systems. The spectra under magnetic field showed a negligible magnetic contribution, indicating the onset of an antiferromagnetic coupling between moieties, in the frame of the  $\text{Fe}^{\text{I}}\text{Fe}^{\text{I}}$  state.

A green THF solution of 21 reacts with a stoichiometric amount of the precursor salt 5a at  $-20^\circ\text{C}$  to rapidly give a colorless solution and a precipitate of a dark green, thermally stable, air-sensitive derivative which gives a correct elemental analysis for the mixed-valence complex 22. An ESR spectrum characteristic of  $\text{Fe}^{\text{I}}\text{Fe}^{\text{II}}$ , with three  $g$  values close to 2, is found for 22 at 4.2 K ( $g_x = 2.0447$ ,  $g_y = 2.0005$ ,  $g_z = 1.8149$ ). Its Mössbauer spectrum shows a single doublet, indicating that the  $\text{Fe}^{\text{I}}\text{Fe}^{\text{II}}$  mixed valence is delocalized on the

(35) (a) Ammeter, J. H.; Swalen, J. H. *J. Chem. Phys.* **1972**, *57*, 678.  
(b) Rajasekharan, M. V.; Giezyński, S.; Ammeter, J. H.; Oswald, N.; Hamon, J.-R.; Michaud, P.; Astruc, D. *J. Am. Chem. Soc.* **1982**, *104*, 2400.

**Table 2. Mössbauer Data for the Dications (36e), Monocations (37e), and Neutral Complexes (38e)<sup>a</sup>**

compd	T (K)	IS (mm s <sup>-1</sup> )	QS (mm s <sup>-1</sup> )	Γ (mm s <sup>-1</sup> )
[(FeCp*)(dihydrophenanthrene)] <sup>2+</sup> ( <b>4a</b> )	78	0.549(1)	1.440(1)	0.290(2)
	290	0.476(2)	1.408(4)	0.282(6)
[(FeCp*) <sub>2</sub> (dihydrophenanthrene)] ( <b>11</b> )	298	0.511(1)	1.675(1)	0.236(2)
	78	0.592(1)	1.687(1)	0.256(2)
	4.2	0.599(2)	1.692(2)	
[(FeCp*) <sub>2</sub> (dihydrophenanthrene)] <sup>+</sup> ( <b>12</b> )	250	0.493(3)	1.437(6)	0.44(1)
	78	0.544(1)	1.466(3)	0.514(5)
	4.2	0.549(2)	1.470(5)	
[(FeCp*) <sub>2</sub> (triphenylene)] <sup>2+</sup> ( <b>5</b> )	77	0.537(1)	1.307(1)	0.258(3)
[(FeCp*) <sub>2</sub> (triphenylene)] ( <b>21</b> )	240	0.560(8)	1.34(1)	0.32(2)
	77	0.617(2)	1.437(4)	0.334(6)
	10	0.623(4)	1.426(6)	
[(FeCp*) <sub>2</sub> (triphenylene)] <sup>+</sup> ( <b>22</b> )	250	0.558(4)	1.148(4)	0.30*
	78	0.617(1)	1.186(2)	0.30*
[(FeCp*) <sub>2</sub> (phenanthrene)] <sup>2+</sup> ( <b>8a</b> )	77	0.546(1)	1.374(1)	0.23(2)
[(FeCp*) <sub>2</sub> (phenanthrene)] ( <b>13</b> )	78	0.603(2)	1.312(3)	0.43(1)
[(FeCp*) <sub>2</sub> (phenanthrene)] <sup>+</sup> ( <b>14</b> )	260	0.587(1)	1.252(5)	0.395(7)*
	77	0.587(1)	1.310(3)	0.395(7)*
	4.7	0.625(2)	1.404(3)	0.321(4)*
[(FeCp*) <sub>2</sub> (pyrene)] <sup>2+</sup> ( <b>9</b> )	77	0.568(1)	1.398(1)	0.231(2)
[(FeCp*) <sub>2</sub> (pyrene)] ( <b>23</b> )	200	0.623(3)	1.648(3)	0.30(1)
	140	0.646(2)	1.655(1)	0.30(1)
	78	0.660(1)	1.654(2)	0.30(1)
[(FeCp*) <sub>2</sub> (pyrene)] <sup>+</sup> ( <b>24</b> )	295	0.524(2)	1.393(2)	0.274(4)*
	160	0.597(2)	1.392(2)	0.276(3)*
	4.7	0.625(2)	1.404(2)	0.321(4)*

<sup>a</sup> IS values are reported versus Fe (303 K) as reference. Γ is the line width. An asterisk indicates an average value in the case of an unsymmetrical doublet.

**Table 3. Estimated Thermodynamic E° Values (±0.01 V) Calculated by Taking the Average between E<sub>pa</sub> and E<sub>pc</sub><sup>a</sup>**

	E° <sub>1</sub>	E° <sub>2</sub>	ΔE° <sub>12</sub>	E° <sub>3</sub>	E° <sub>4</sub>	ΔE° <sub>34</sub>
<b>20a</b> , [Fe <sub>2</sub> Fv(C <sub>6</sub> Me <sub>6</sub> ) <sub>2</sub> ] <sup>2+</sup>	-1.280	-1.760	0.480	-2.390	-2.740	0.350
<b>20b</b> , [Fe <sub>2</sub> Fv(C <sub>6</sub> H <sub>6</sub> ) <sub>2</sub> ] <sup>2+</sup>	-1.130	-1.460	0.330	-2.055	-2.330	0.275
<b>1a</b> , [(FeCp*) <sub>2</sub> (diphenyl)] <sup>2+</sup>	-1.300	-1.430	0.130			
<b>1b</b> , [(FeCp*) <sub>2</sub> (diphenyl)] <sup>2+</sup>	-1.120	-1.120	0.000			
<b>4a</b> , [(FeCp*) <sub>2</sub> (dihydrophenanthrene)] <sup>2+</sup>	-1.340	-1.500	0.160			
<b>4b</b> , [(FeCp*) <sub>2</sub> (dihydrophenanthrene)] <sup>2+</sup>	-1.130	-1.290	0.160			
<b>7</b> , [(FeCp*) <sub>2</sub> (diphenylmethane)] <sup>2+</sup>	-1.290	-1.350	0.090			
<b>10</b> , [(FeCp*) <sub>2</sub> ([2.2]paracyclophane)] <sup>2+</sup>	-1.500	-1.500	0.000			
<b>6a</b> , [(FeCp*) <sub>2</sub> (fluorene)] <sup>2+</sup>	-1.390	-1.690	0.300	-2.380	-2.380	0.000
<b>6b</b> , [(FeCp*) <sub>2</sub> (fluorene)] <sup>2+</sup>	-1.140	-1.320	0.180	-2.030	-2.030	0.000
<b>8a</b> , [(FeCp*) <sub>2</sub> (phenanthrene)] <sup>2+</sup>	-1.170	-1.440	0.270	-1.990	-2.190	0.200
<b>8b</b> , [(FeCp*) <sub>2</sub> (phenanthrene)] <sup>2+</sup>	-0.910	-1.090	0.180	-1.600	-1.880	0.280
<b>5a</b> , [(FeCp*) <sub>2</sub> (triphenylene)] <sup>2+</sup>	-1.220	-1.510	0.290	-2.000	-2.260	0.260
<b>5b</b> , [(FeCp*) <sub>2</sub> (triphenylene)] <sup>2+</sup>	-1.000	-1.190	0.190	-1.680	-1.850	0.170
<b>9</b> , [(FeCp*) <sub>2</sub> (pyrene)] <sup>2+</sup>	-1.000	-1.380	0.380	-2.040	-2.412	0.372

<sup>a</sup> Conditions: hanging Hg cathode, -35 °C, DMF, *n*-Bu<sub>4</sub>N<sup>+</sup>BF<sub>4</sub><sup>-</sup> 0.1 M, scan rate 300 mV s<sup>-1</sup>. E<sub>p</sub> values were recorded using [FeCp<sub>2</sub>]<sup>0/+</sup> as an internal reference. The one-electron waves are deduced by comparison with the height of the wave of [FeCp<sub>2</sub>]<sup>0/+</sup> (the diffusion coefficients are close: FeCp<sub>2</sub>, 1.6 × 10<sup>-6</sup> cm<sup>2</sup> s<sup>-1</sup>; **20a**, 2.8 × 10<sup>-6</sup> cm<sup>2</sup> s<sup>-1</sup>). The waves were checked as being diffusion controlled by verifying *i<sub>p</sub>*/*v*<sup>1/2</sup> is constant over a wide range of scan rates.<sup>40</sup> The E° values were independent of the electrode material (Hg, Pt). The *i<sub>a</sub>*/*i<sub>c</sub>* values are 1 ± 0.05 for the three first waves. The fourth wave shows 0 < *i<sub>a</sub>*/*i<sub>c</sub>* < 1; the ratio depends on scan rate and is difficult to measure accurately because of the overlap with the third wave. Nevertheless, *i<sub>a</sub>*/*i<sub>c</sub>* is ~0.8 ± 0.1 at 300 mV s<sup>-1</sup> for Cp complexes **5b** and **8b** and 0.2 ± 0.1 at 300 mV s<sup>-1</sup> for Cp\* complexes **5a** and **8a**.

Mössbauer time scale of 10<sup>-8</sup> s.<sup>36</sup> The IS and QS values are close to those of the other delocalized Fe<sup>I</sup>Fe<sup>II</sup> mixed-

(36) The mixed-valence ferrocene system has recently been subjected to a series of careful studies by Hendrickson's group showing that, although all the ferrocenium cationic derivatives are localized mixed valence on the infrared time scale, some of them are delocalized in the solid state on the Mössbauer time scale. This phenomenon was astutely proposed by Hendrickson to be a tunneling effect, whereas the trapped-valence compounds are due to some dissymmetry of the counterion in the lattice. (a) Hendrickson, D. N.; Oh, H. M.; Moore, M. F. *Comments Inorg. Chem.* **1985**, *4*, 329. (b) Dong, T. Y.; Hendrickson, D. N.; Pierpont, C. G.; Moore, M. F. *J. Am. Chem. Soc.* **1986**, *108*, 4423. (c) Dong, T. Y.; Hendrickson, D. N. *J. Am. Chem. Soc.*, **1986**, *108*, 963. (d) Webb, R. J.; Geib, S. J.; Staley, D. L.; Rheingold, A. L.; Moore, M. F. *J. Am. Chem. Soc.* **1990**, *112*, 5031.

valence complexes, **2** and **20**.<sup>16,25,26</sup> The IS value, however, is almost the same as that for Fe<sup>I</sup>Fe<sup>I</sup> complex **21**. This is consistent with delocalization of the second added electron almost exclusively onto the triphenylene ligand and corroborates the above Mössbauer observations concerning **21** (Table 2).

The chemistry and spectroscopy of the pyrene and phenanthrene complexes have the same characteristics as those of the triphenylene series. The data are gathered in Tables 2 and 3. The mixed-valence 37e pyrene and phenanthrene complexes **24** and **14** were stable at room temperature and were fully characterized

(including by elemental analysis). They are delocalized, average-valence complexes. The 38e complexes **23** and **13** are thermally unstable above  $-20\text{ }^{\circ}\text{C}$  and do not show any NMR signal in the diamagnetic region, which confirms the  $\text{Fe}^{\text{I}}\text{Fe}^{\text{I}}$  structure also inferred from the Mössbauer and electrochemical data.

In summary, the triphenylene, pyrene, and phenanthrene monoreduced and bireduced complexes show similar trends: the Mössbauer parameters of the 36e  $\text{Fe}^{\text{II}}\text{Fe}^{\text{II}}$  and 37e  $\text{Fe}^{\text{I}}\text{Fe}^{\text{II}}$  complexes are almost identical, which shows that the 37th electron is in a mainly polyaromatic orbital. The parameters of the 38e  $\text{Fe}^{\text{I}}\text{Fe}^{\text{I}}$  complexes are also close to those of the 36e and 37e complexes, but their increase is significant. The SCF-X $\alpha$  calculations (*vide infra*) indicate 33% metal character for the  $2a_u$  orbital of the 37th electron delocalized on two iron atoms. Thus, the metal character for each iron atom is 16%. This amount is very weak and is consistent with very little change in the Mössbauer parameters. On the other hand, the  $3a_g$  orbital of the 38th electron has 40% metal character. On average, the metal character is on the order of 33–40% for the 37th and 38th electrons. The contributions of these two orbitals (although they may be different from each other) to the IS and QS values are more significant. The ESR spectra of these 38e complexes indicate the characteristic behavior of  $\text{Fe}^{\text{I}}$  complexes with three  $g$  values around 2, whereas the  $[\text{Fe}_2(\text{fulvalene})(\text{C}_6\text{R}_6)_2]$  complexes ( $\text{R} = \text{H}, \text{Me}$ ) with a fully metal-based HOMO show only two  $g$  values.<sup>26b</sup> The triplet nature of these bireduced complexes contrasts with that of diphenyl and of dihydrophenanthrene, which are in a singlet state.

**5. Cyclic Voltammetry of the Diiron Polyaromatic Complexes.** Two types of behavior can be clearly distinguished by cyclic voltammetry (DMF,  $-35\text{ }^{\circ}\text{C}$ ,  $n\text{-Bu}_4\text{N}^+\text{BF}_4^-$ ).<sup>6,37,38</sup> The diiron complexes of diphenyl-type polyaromatics, such as dihydrophenanthrene complexes **4a** and **4b**, give only two close reversible waves. On the other hand, the diiron complexes of condensed polyaromatics, such as phenanthrene, triphenylene and pyrene, show a cascade of four cathodic waves: the two first waves are chemically and electrochemically reversible ( $i_a/i_c = 1$ ;  $E_{\text{pa}} - E_{\text{pc}} \approx 60\text{ mV}$ , no variation of  $E_{\text{pa}}$  and  $E_{\text{pc}}$  with scan rate), and the third wave is still chemically reversible but electrochemically irreversible (typically  $k_{\text{ET}} = 10^{-3}\text{ cm s}^{-1}$ ). The fourth wave is never chemically fully reversible ( $0 < i_a/i_c < 1$ , but accurate measurement is difficult) and also is electrochemically irreversible ( $k_{\text{ET}} \approx 10^{-4}\text{ cm s}^{-1}$ ; Figures 1 and 2). We have compared Cp\* and Cp complexes **4–10**, including the diphenylmethane complexes, which serve as references insofar as no electronic delocalization can occur between the two phenyl rings. The diphenyl complexes **4** give intramolecular coupling in their bireduced state in which the  $e^*_1$  orbital now lies at a much higher level than in the absence of intramolecular coupling (as with ferrocene,<sup>39</sup> a cathodic

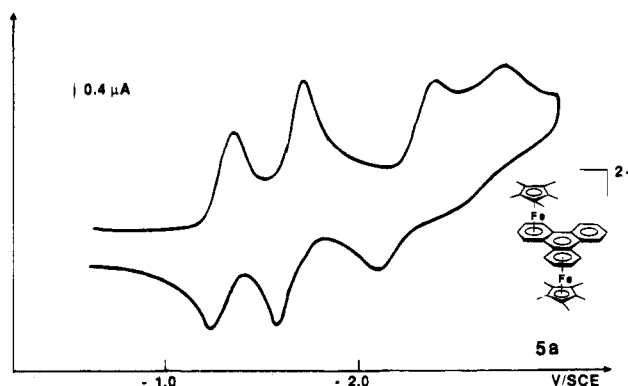


**Figure 1.** Cyclic voltammogram of a  $3 \times 10^{-5}\text{ M}$  DMF solution of  $[\text{Fe}_2\text{Cp}^*(\text{triphenylene})]^{2+}(\text{PF}_6^-)_2$  (0.1 M  $n\text{-Bu}_4\text{NBF}_4$  at an Hg cathode; scan rate  $300\text{ mV s}^{-1}$ ;  $-30\text{ }^{\circ}\text{C}$ ). See Table 3 for  $E^\circ$  values.

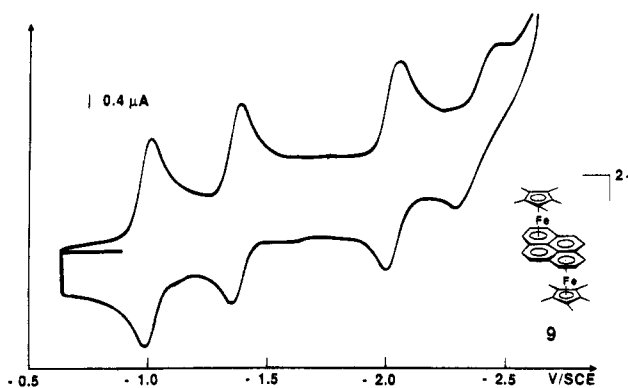


**Figure 2.** Cyclic voltammogram of a  $3 \times 10^{-5}\text{ M}$  DMF solution of  $[\text{Fe}_2\text{Cp}^*(\text{pyrene})]^{2+}(\text{PF}_6^-)_2$  (0.1 M  $n\text{-Bu}_4\text{NBF}_4$  at an Hg cathode; scan rate  $300\text{ mV s}^{-1}$ ;  $-30\text{ }^{\circ}\text{C}$ ). See Table 3 for  $E^\circ$  values.

potential more negative than  $-3.0\text{ V}$  vs SCE is required for further reduction). The second wave for these complexes (**1** and **4**) is also less separated from the first wave than in the polyaromatic and fulvalene complexes, which is another characteristic of the intramolecular coupling in the second ET. This is due to the energy gained in the structural transformation to bicyclohexadienylidene, which lowers the second reduction potential.<sup>21</sup> Thus, the difference between the two thermodynamic standard potentials,  $\Delta E^\circ = E^\circ_1 - E^\circ_2$ , gives an estimate of the coupling energy by comparison with  $\Delta E^\circ$  values of reference diiron compounds such as **20**, which do not couple in their bireduced state. In the reference compounds **20**,  $\Delta E^\circ$  is 0.33 V in the parent series **20b** and 0.48 V for **20a**, in which the ancillary ligand is permethylated.

It appears, in this polyaromatic series, that the bimethylene bridge in the dihydrophenanthrene complex brings about a steric constraint, reducing the structural flexibility required to couple *chemically*. Thus, the energy difference between the  $\text{Fe}^{\text{I}}\text{Fe}^{\text{I}}$  and coupled  $\text{Fe}^{\text{II}}\text{Fe}^{\text{II}}$  states is slightly weaker than in **1**. This ligand does couple, however (coupling energy about 0.11 V, *i.e.* 2.5 kcal mol $^{-1}$ ). In all the diiron complexes of condensed polyaromatics, the cascade of five redox states and the relatively large  $\Delta E^\circ$ , together with the

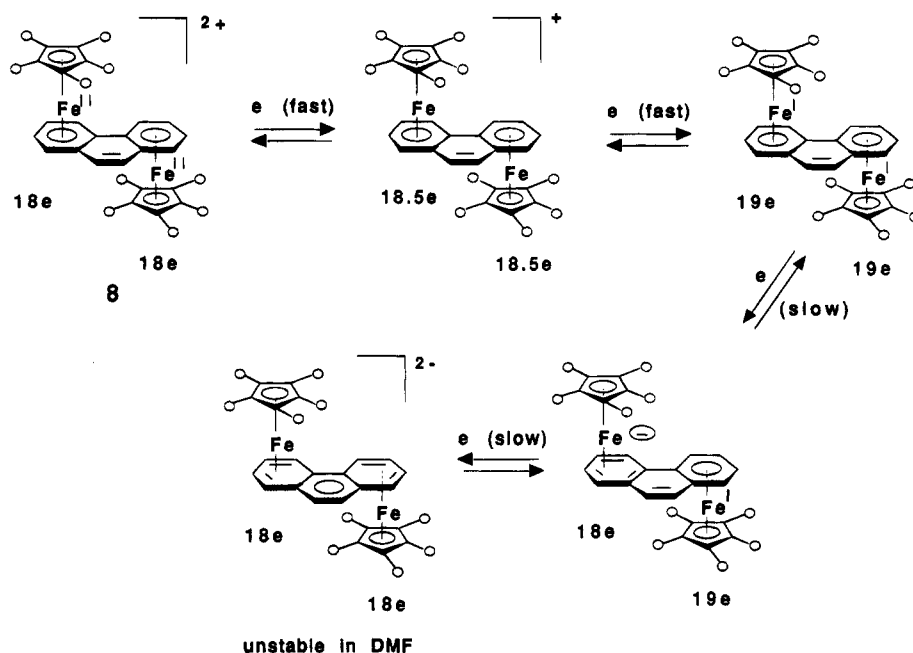
(37) For seminal work on the electrochemistry of  $[\text{FeCp}(\text{arene})]^+$  complexes, see: (a) Nesmeyanov, A. N.; Denisovitch, L. T.; Gubin, S. P.; Vol'kenau, N. A.; Sviotkina, F. I.; Bolesova, I. N. *J. Organomet. Chem.* **1969**, *20*, 169. (b) Dessy, R. E.; Stary, F. E.; King, R. B.; Waldrop, M. *J. Am. Chem. Soc.* **1966**, *88*, 471.

(38) For reviews on  $[\text{FeCp}(\text{arene})]^{+0}$ , see: (a) Connelly, N. G.; Geiger, W. E. *Adv. Organomet. Chem.* **1983**, *23*, 1. (b) Astruc, D. *Chem. Rev.* **1988**, *88*, 1189.

(39) Mugnier, Y.; Moise, C.; Tirouflet, J.; Laviron, E. *J. Organomet. Chem.* **1980**, *186*, C49.

(40) (a) Bard, A. J.; Faulkner, L. R. *Electrochemical Methods*; Wiley: New York, 1980; Chapter 6. (b) Geiger, W. E. *Prog. Inorg. Chem.* **1985**, *23*, 275.

**Scheme 6. Decoordination of Diiron Polyaromatic Complexes during the Third and Fourth Mono-electronic Reduction Steps of the Redox Cascade<sup>a</sup>**



<sup>a</sup> The example given is phenanthrene (O = H, Me). The triphenylene and pyrene diiron complexes show similar behaviors and reduced ET rates during the third and fourth ETs: a similar formulation can be drawn.

spectroscopic evidence for the paramagnetic  $Fe^I Fe^I$  state at the neutral level, are clear evidence of the absence of intramolecular *chemical* coupling. Thus, the border between the compounds that do and do not couple is just between the phenanthrene and dihydrophenanthrene complexes. Nevertheless, the  $\Delta E^\circ$  values for the diiron polyaromatic family is never as large as in **20**. Thus, *antiferromagnetic* coupling, which is weaker than *chemical* coupling, can be still reflected energetically in the  $\Delta E^\circ$  values, which is corroborated by the Mössbauer data of the  $Fe^I Fe^I$  complexes **14**, **21**, and **23**. There is, in fact, a *continuum* of situations between isolated and chemically coupled nuclei where the magnetic coupling is intermediate in this scale, as can be seen in Table 3.

The electrochemical irreversibility of the third and fourth ET shows that a structural reorganization probably takes place during these ET steps, due to oversaturation of the valence electron shell, e.g. the introduction of too many electrons into the antibonding orbitals. Indeed, one must envisage a reduced coordination of the polyaromatic to each iron center in order to keep the number of valence electrons closer to 18. This phenomenon has not yet occurred at the bireduced level, as discussed above, but must be operational at the tri- and tetra-reduced levels.<sup>41</sup> Thus, the most probable forms can be formulated as in Scheme 6. The cyclic voltammogram of the [2.2]paracyclophane complex **10a** at  $-35^\circ C$  in DMF on Hg shows only a broad wave at  $-1.5$  V vs SCE which is only partly chemically revers-

ible. In contrast, the parent Cp complex was shown by Geiger and Bowyer<sup>31</sup> to be a well-behaved complex, disclosing two mono-electronic reversible reductions. Thus, it appears from the in-depth study of Geiger's group that the parent complex does not dimerize in its bireduced state, whereas the Cp\* analogue undergoes intramolecular coupling to a thermally unstable  $Fe^{II} Fe^{II}$  complex in the course of the second ET. This intramolecular coupling is exergonic, as in the diphenyl-type complexes, and the second reduction potential is thus less negative and shifted toward the first one, which broadens the first CV wave. The instability of the coupled neutral complex precludes a better examination of the cathodic wave. In addition, the broadening is probably due to some demetalation, as is also observed in other polyaromatic complexes.

**6. MO Analysis of the Diiron Polyaromatic Complexes.** In a previous paper,<sup>16b</sup> we have shown using SCF MS-X $\alpha$  calculations that the chemical coupling which is undergone by the diiron diphenyl 36-electron species (**1**) upon reduction is principally due to the accessibility of a level of  $b_u$  symmetry which can be identified as derived from the LUMO of the free diphenyl ligand. This  $b_u$  level is  $\pi$ -antibonding on the phenyl rings but  $\pi$ -bonding between the rings. The occupation of this  $b_u$  level leads to the formation of a formal exocyclic double bond, corresponding to the formal reduction of the diphenyl ligand into a bicyclohexadienylidene ligand, which causes the  $Fe^{II}$  atom to shift toward the  $\eta^5$  coordination, in order to maintain its 18-electron configuration. In fact, in the diphenyl species the crucial level of  $b_u$  symmetry is not the  $3b_u$  LUMO of the 36-electron complexes but the higher  $4b_u$  level (see the left side of Figure 3). Indeed, the  $3b_u$  LUMO is of metal dominant character, while the  $4b_u$  MO is largely localized on the exocyclic bond. Because they have the same symmetry and are close in energy, the  $3b_u$  and  $4b_u$  MO's are allowed to mix somewhat. The

(41) For the electronic structure of monomeric late-transition-metal sandwiches, see for example: (a) Anderson, S. E.; Drago, R. S. *Inorg. Chem.* **1972**, *11*, 1564. (b) Anderson, S. E.; Rai, R. *Chem. Phys.* **1970**, *92*, 4851. (c) Warren, K. D. *Struct. Bonding* **1976**, *27*, 45. (d) Clack, D. W.; Warren, K. D. *Struct. Bonding*, **1980**, *39*, 1. (e) Ammeter, J. H. *J. Magn. Res.*, **1978**, *30*, 299. (f) Coutière, M.-M.; Demuyneck, J.; Veillard, A. *Theor. Chim. Acta* **1972**, *27*, 281. (g) Weber, J.; Geoffroy, M.; Penigault, A. *J. Am. Chem. Soc.* **1978**, *100*, 3395. (h) Weber, J.; Kundig, E. P.; Goursot, A.; Penigault, A. *Can. J. Chem.* **1985**, *63*, 1734. (i) Goursot, A.; Penigault, A.; Weber, J. *Nouv. J. Chim.* **1979**, *3*, 675. (j) Le Beuze, A.; Lissillour, R.; Weber, J. *Organometallics* **1993**, *12*, 47.

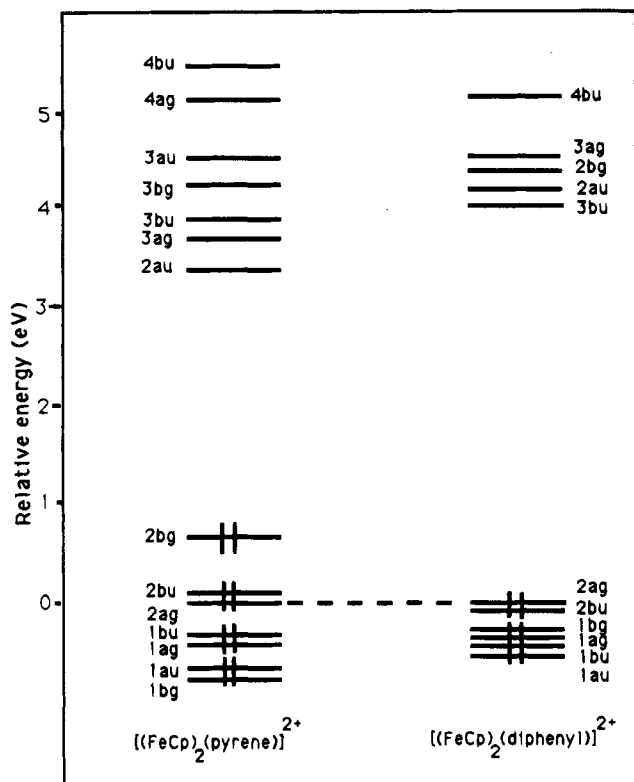


**Figure 3.** MO level diagrams of **9b** (left) and **1b** (right). The two diagrams have been rescaled by placing their  $3d_{z^2}$  nonbonding levels at the same energy.

mixing causes some stabilization of the lowest  $3b_u$  level. This mixing increases considerably when the distortion associated with the reduction is applied, in such a way that the energy of  $3b_u$  is considerably lowered, leading to a stable reduced species. In other words, an avoided crossing occurs between the two  $b_u$  levels during the chemical coupling, so that the resulting  $3b_u$  orbital, the HOMO of the diphenyl bireduced species, then resembles strongly the  $4b_u$  level of its dicationic parent, and vice versa.

We now turn the discussion to the possibility of chemical coupling upon reduction in 36-electron diiron complexes of larger polyaromatics such as phenanthrene, pyrene, and triphenylene, which contain the carbon skeleton of diphenyl as a fragment of their own skeleton, complexed in the same way as in **1**. If any, this chemical coupling should be weaker than for the diphenyl species, because of the greater rigidity of the fused-ring species (*i.e.* the corresponding distortion should weaken too many  $\sigma$  and  $\pi$  bonds). In these species, the crucial orbital susceptible to be responsible for the chemical coupling is the one derived from the  $b_u$  LUMO of their "diphenylic" fragment. When incorporated in a larger polyaromatic system, this  $b_u$  level interacts with orbitals of other fragments in such a way that it is shifted in energy and that it loses some localization on the exocyclic bond of the "diphenylic" fragment: this is delocalization at work. For example, simple extended Hückel calculations on free diphenyl give a 26% localization of the  $b_u$  LUMO on the exocyclic bond. Similar calculations on the free phenanthrene, pyrene, and triphenylene molecules indicate that the corresponding localization of the crucial level is significantly lower, suggesting a weaker potentiality for chemical coupling upon reduction of the 36-electron

**Table 4.** Energy and Percent Charge Distribution of the Highest Occupied and Lowest Unoccupied Orbitals of **9b**

	$E$ (eV)	Fe	Cp	pyrene	$i + o^a$
$4b_g$	-4.28	6	59	1	34
$4b_a$	-5.12	10	34	30	26
$4a_g$	-5.69	6	1	34	59
$3a_u$	-6.18	31	10	40	19
$3b_g$	-6.45	51	19	14	15
$3b_u$	-6.72	51	22	14	12
$3a_g$	-6.83	40	16	25	19
$2a_u$	-7.14	33	13	34	20
$2b_g$	-9.17	22	8	33	26
$2b_u$	-9.69	89	1	5	5
$2a_g$	-9.78	40	0	34	21
$1b_u$	-9.82	88	1	6	5
$1a_g$	-10.08	80	2	8	10
$1a_u$	-10.23	80	1	9	10
$1b_g$	-10.28	66	1	6	28

<sup>a</sup>  $i + o$  = inner and outer spheres.

diiron complexes: 19, 15, and 14%, respectively. In the case of phenanthrene and pyrene, the crucial level is destabilized by 0.16 and 0.53 eV, respectively. This destabilization renders the level somewhat less accessible than in the case of diphenyl. For triphenylene, however, this level is stabilized by 0.32 eV. In any case, it is clear that the fused-ring 36-electron complexes are much less susceptible to give stable chemically coupled reduced species. These qualitative considerations are fully corroborated by our calculations on  $[(\text{FeCp})_2(\text{pyrene})]^{2+}$  (**9b**) and some of its reduced states, with the same type of SCF MS-X $\alpha$  calculations as previously used for the related diphenyl and fulvalene complexes.<sup>16b,17d</sup> The computational details are given in the Experimental Section. The MO diagram of **9b**, corresponding to its highest occupied and lowest unoccupied levels, is shown on the left side of Figure 3. The energies and charge distributions of these orbitals are given in Table 4. Some of them are plotted in Figure 4. From the analysis of Figure 3, one can see that compounds **1b** and **9b** have HOMO's and LUMO's of different symmetries. This is the consequence of the different size of the polyaromatic ligands. Because of its larger size, pyrene has a larger number of  $\pi$  levels than diphenyl with a smaller HOMO/LUMO gap. As a consequence, the  $2b_g$  HOMO of **9b** is not one of the six " $t_{2g}$ "-type nonbonding metallic levels as in **1b** but derives principally from a  $\pi$ -type pyrene ligand, with some metal admixture due to its closeness to the " $t_{2g}$ " block (Table 4). A similar situation arises for the group of the lowest unoccupied levels of **9b**, which, compared to the case of **1b**, is augmented by two low-lying pyrene  $\pi$ -antibonding MO's, of  $a_u$  and  $a_g$  symmetry, derived from two low-lying vacant orbitals of pyrene and mixed significantly with metallic orbitals. This mixing is particularly large in the case of the  $2a_u$  LUMO of **9b** (Table 4). These results suggest that the redox behavior of 36-electron dinuclear complexes of diphenyl should be different from that of related complexes of larger polyaromatics. If experimentally possible, the one-electron oxidation of a diphenyl species will lead to the formation of a mixed-valence 17-electron/18-electron system, by the depopulation of a metallic " $t_{2g}$ " level. In the case of complexes of larger polyaromatics, there is a good chance that the HOMO is predominantly localized on the ligand, as in **9b**. Therefore, the removal of one electron would not change the formation 18-electron configuration of the metal

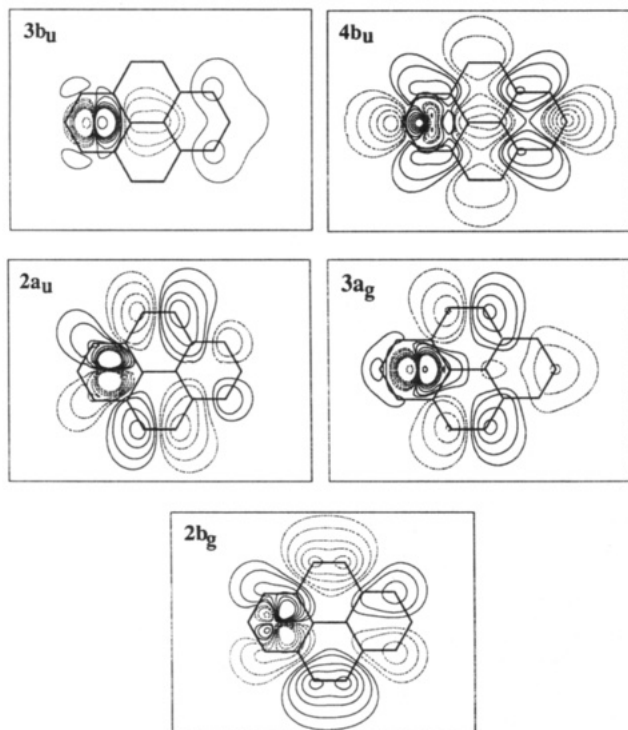


**Figure 4.** Contour plots of the HOMO and some lower unoccupied orbitals of **9b** in a plane parallel to the pyrene ligand and situated midway between this ligand and one Fe atom.

atoms but rather lead to the oxidation of the polyaromatic ligand. From the plot of the HOMO of **9b** (Figure 4), one can predict that the oxidation of 36-electron complexes of pyrene should lengthen six C–C bonds and shorten four others, without affecting the central one. One knows that the reduction of the 36-electron diphenyl species leads to a chemical coupling induced by the occupation of the  $3b_u$  LUMO, which is favored by the closeness in energy of the  $3b_u$  and  $4b_u$  levels (see above).<sup>16b,17d</sup> In the case of complexes of larger polyaromatics such as **9b**, the  $3b_u$  level is no longer the LUMO (Figure 3) and the energy difference between the  $3b_u$  and  $4b_u$  orbitals is larger. This situation disfavors the observation of chemical coupling upon reduction. Our calculations on the mono- and direduced states of **9b** are fully consistent with this suggestion. The 37-electron system is more stable, with the  $2a_u$  level being the singly occupied HOMO. When the single electron is placed in the  $3a_g$  or  $3b_u$  level, the energy raises by 0.43 or 0.54 eV, respectively. It is clear from the plots of Figure 4 that the occupation of  $2a_u$  or  $3a_g$  has no effect on the central C–C bond. Calculations on the 38-electron system give similar trends. The lowest triplet state is found to be  $2a_u^1 3a_g^1$ , suggesting that the second one-electron reduction of **5b** corresponds to the occupation of the  $3a_g$  level, which is more metal-localized than  $2a_u$ . This result is in full agreement with the Mössbauer data, which are consistent with the gain of metal character during the second electron transfer (vide supra). Clearly, the  $3b_u$  level is less accessible in **9b** than in **1b**. In **9b**, not only the accessibility of the  $b_u$  levels but also their ability to give rise to chemical coupling, *i.e.* their localization on the central C–C bond (see above), is weaker than in **1b**. In **9b**, the localization of  $3b_u$  and  $4b_u$  on this crucial bond is found to be 7 and 13%, respectively. The corresponding values obtained

for **1b** under the same computational conditions are 9 and 20%, respectively.<sup>16b</sup> Finally, it is worth noting that the  $3a_g$  LUMO of **9b** is equally distributed on the metal centers and the pyrene ligand. This is in agreement with the Mössbauer data for **23**, which indicate significant spin delocalization on the ligand.

### Concluding Remarks

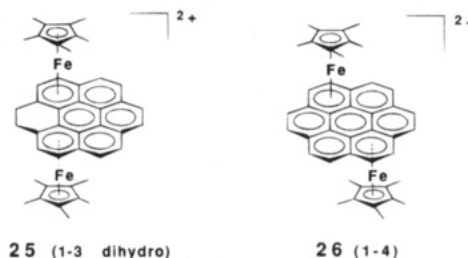
1. The first syntheses of complexes of the type  $[(\text{FeCp}^*)_2(\mu_2\text{-}\eta^{12}\text{-polyaromatic})]^{2+}$  have been achieved using both a classical ligand exchange procedure with  $[\text{FeCp}^*(\text{CO})_2\text{Br}]$  and an improved synthetic route using  $\text{Al}_2\text{Cl}_3\text{Me}_3 + \text{Al}_2\text{Cl}_6$ .<sup>42</sup> This second method proved very successful in avoiding side reactions, such as hydrogenation and retro-Friedel–Crafts C–C cleavage during the ligand exchange. In particular, the pure phenanthrene, pyrene, triphenylene and [2.2]paracyclophane complexes have been made in reasonable yields. Syntheses of parent Cp complexes have been improved by performing the reaction in the molten, neat reactants, allowing the preparation of, for instance, the diiron phenanthrene and triphenylene complexes.

2. A series of electron-transfer and H-atom-transfer reactions interconvert the complexes  $[(\text{FeCp}^*)_2(\text{phenanthrene})]^\ddagger$  and  $[(\text{FeCp}^*)_2(\text{dihydrophenanthrene})]^\ddagger$ , as in biological redox mediators. Hydrogenation also involves protonation of the ligand by the strong acid  $\text{H}^+\text{AlCl}_4^-$ , in the preparation of the dication **4a**, and by  $\text{H}_2\text{O}$ , in the preparation of the neutral form **13**. Complex **11** exhibits intramolecular chemical coupling to a bicyclohexadienylidene ligand structure in spite of the steric constraint of the dimethylene side chain, whose effect is shown by the higher  $\Delta G^\circ$  value ( $\sim 2.5$  kcal mol<sup>-1</sup>) estimated from the  $E^\circ_1 - E^\circ_2$  difference (0.16 V) in the CV of **4a** (compare to 0.27 V for **8a**). The delocalization in the 37e mixed-valence complex on the Mössbauer time scale of  $10^{-8}$  s is indicative of a nondistorted polyaromatic framework.

3. Unlike the parent Cp complex, the [2.2]paracyclophane complex undergoes direct two-electron transfer and intramolecular C–C coupling.

4. The mono- and bireduced polyaromatic complexes are the first cases of  $\text{Fe}^{\text{I}}\text{Fe}^{\text{II}}$  and  $\text{Fe}^{\text{I}}\text{Fe}^{\text{I}}$ , respectively) besides the fulvalene derivatives. The 37e  $\text{Fe}^{\text{I}}\text{Fe}^{\text{II}}$  polyaromatic complexes are relatively stable and are delocalized mixed-valence

(42) Attempts to apply the synthetic procedure to coronene gave only minuscule yields. Outer 1,3- and 1,4-coronene ring complexations give equal amounts of bimetallic isomers. However, under the ligand-exchange conditions allowing side-ring hydrogenation, the 1,3-isomer is easily hydrogenated, whereas the 1,4-isomer is not. The 1,3-dihydrogenated (**25**) and 1,4-non-hydrogenated complexes (**26**) could be synthesized on a milligram scale (along with the monometallic complex) and were identified by <sup>1</sup>H and <sup>13</sup>C NMR.



This attempt to complex a large polyaromatic may be compared to the lack of success *so far* to isolate an arene-type  $\pi$  complex with  $\text{C}_{60}$  (contrasting with the ease of formation of  $\eta^2$  complexes).



complexes (**2**, **12**, **22**, and **24**) on the Mössbauer time scale. The 37th electron has a large ligand character, and the second extra electron slightly increases the spin density on the iron atoms (small increase of the IS and QS between the first and second reductions). Thus, the diphenyl- and polyaromatic complexes all give rise to a common *average*-valence situation in the monoreduced 37e state, but these two types are clearly distinguished in the bireduced state: *chemical* coupling occurs in diphenyl-type complexes and *antiferromagnetic* coupling occurs in Fe<sup>I</sup>Fe<sup>I</sup> polyaromatic complexes, as indicated by Mössbauer spectroscopy of the thermally unstable 38e complexes.

5. This distinction between diphenyl and polyaromatic complexes is also clear in CV, where the diphenyl-type complexes **1a**, **4a**, and **4b** exhibit only two close reversible waves, whereas complexes **5**, **8**, and **9** of the condensed polyaromatics give a cascade of four successive one-electron waves. In this sense, these complexes resemble bioinorganic delocalized clusters, their synthetic models and C<sub>60</sub>, which also show redox *cascades* of single-electron transfers without large structural changes along the series.

6. Theoretical calculations on **9b** allow us to understand the different behavior upon reduction of the diphenyl complexes compared to the other polyaromatic complexes. The reduction of the diphenyl species corresponds formally to the occupation of the 4b<sub>u</sub> level, which lies at rather low energy and is dramatically stabilized upon chemical coupling, due to a significant bonding character on the C–C exocyclic bond. In the case of **9b**, the vacant orbitals of b<sub>u</sub> symmetry have a lower bonding character on the central C–C bond. Moreover, they are not the most accessible orbitals. Indeed, the LUMO is of a<sub>u</sub> symmetry and has no localization on the central C–C bond. These reasons, added to the intrinsic rigidity of the fused-ring ligand, forbid the stabilization by chemical coupling observed for the diphenyl species upon a two-electron reduction, favoring an antiferromagnetic behavior associated with a low thermal stability.

## Experimental Section

**1. General Data.** All manipulations of air-sensitive materials were conducted in a VAC argon Dri-Lab or under argon in Schlenk apparatus connected to a double manifold. Reagent grade tetrahydrofuran, pentane, and toluene were predried over Na foil and distilled from sodium benzophenone ketyl under argon. All other chemicals were used as received. <sup>1</sup>H NMR spectra were obtained with a Bruker AC 200 (200 MHz) or AC 250 (250 MHz) spectrometer, and <sup>13</sup>C NMR spectra were recorded with a Bruker AC 200 (50.3 MHz) or a Bruker AC 250 (67.9 MHz) spectrometer. NMR spectra were referenced to Me<sub>4</sub>Si (<sup>1</sup>H) or the appropriate deuterated solvent (<sup>13</sup>C). Cyclic voltammetry studies were performed with a Princeton Applied Research 273 potentiostat. Mössbauer spectra were recorded with a 25 mCi <sup>57</sup>Co source on Rh. The Mössbauer spectrometer operated in the constant-acceleration mode; typically, the reliability of the velocity scale is 0.2%. The instrumental line width is 0.215 mm s<sup>-1</sup>. For all the Mössbauer data, see Table 2. Elemental analyses were performed by the CNRS Center of Microanalyses at Lyon-Villeurbanne.

**2. Syntheses of the [(FeCp\*)<sub>2</sub>(μ<sub>2</sub>-η<sup>12</sup>-polyaromatic)]<sup>2+</sup>-(PF<sub>6</sub><sup>-</sup>)<sub>2</sub> Complexes. Method A.** The reactions were carried out in a 250 mL three-necked round-bottomed flask equipped with an argon inlet and a reflux condenser topped with a gas outlet. A mixture of [FeCp\*(CO)<sub>2</sub>Br] (9.8 g, 30 mmol), AlCl<sub>3</sub>

(27 g, 200 mmol), and the polyaromatic (5 mmol) were stirred for 5 min under argon. The neat mixture was melted and heated at 120 °C under argon with stirring, for 2 days. While still molten, the reaction mixture was hydrolyzed very slowly with 200 mL of degassed ice–water. Addition of concentrated aqueous NH<sub>4</sub>OH to pH 9 precipitated Al(OH)<sub>3</sub>. After filtration, a yellow solid was obtained by addition of aqueous HPF<sub>6</sub> (10 mmol). The precipitate was filtered, dissolved in 50 mL of acetonitrile, and dried for 1 h on MgSO<sub>4</sub>. After the yellow solution was filtered through a 2 cm layer of Al<sub>2</sub>O<sub>3</sub> and diluted with 20 mL of ethanol, slow evaporation of the acetonitrile under reduced pressure gave the crystalline yellow diiron complex.

**(a) [(FeCp\*)<sub>2</sub>(μ<sub>2</sub>-η<sup>12</sup>-dihydrophenanthrene)]<sup>2+</sup>-(PF<sub>6</sub><sup>-</sup>)<sub>2</sub> (**4a**(PF<sub>6</sub><sup>-</sup>)<sub>2</sub>).** Method A applied to 9,10-dihydrophenanthrene gave 1.2 g (28%) of **4a** as yellow microcrystals. Anal. Calcd for C<sub>34</sub>H<sub>42</sub>Fe<sub>2</sub>P<sub>2</sub>F<sub>12</sub>: C, 47.88; H, 4.93. Found: C, 47.40; H, 4.79. <sup>1</sup>H NMR (CD<sub>3</sub>CN, δ, ppm vs TMS): 6.4–6.2 (m, C<sub>6</sub>H<sub>4</sub>, 8H), 3.20 (s, CH<sub>2</sub>, 4H), 1.75 (s, C<sub>5</sub>Me<sub>5</sub>, 30H). <sup>13</sup>C NMR (CD<sub>3</sub>CN, δ, ppm): 105.1, 101.4 (C<sub>6</sub>H<sub>4</sub>), 93 (C<sub>5</sub>Me<sub>5</sub>), 91.6, 91.4, 90.0, 84.6 (CH), 24.2 (CH<sub>2</sub>), 9.9 (CH<sub>3</sub>). Cyclic voltammetry data (–30 °C, DMF, 0.1 M *n*-Bu<sub>4</sub>N<sup>+</sup>BF<sub>4</sub><sup>-</sup>, 0.2 V s<sup>-1</sup>): (Fe<sup>II</sup>Fe<sup>II</sup>)<sup>2+</sup>/(Fe<sup>II</sup>Fe<sup>I</sup>)<sup>+</sup>, E° = –1.34 V vs SCE (*i<sub>a</sub>/i<sub>c</sub>* ≈ 1, ΔE<sub>p</sub> = 45 mV, *n* = 1); (Fe<sup>II</sup>Fe<sup>I</sup>)<sup>+</sup>/(Fe<sup>I</sup>Fe<sup>I</sup>), E° = –1.50 V vs SCE (*i<sub>a</sub>/i<sub>c</sub>* ≈ 1, ΔE<sub>p</sub> = 90 mV, *n* = 1). See also the footnotes to Table 3.

**(b) [(FeCp\*)<sub>2</sub>(μ<sub>2</sub>-η<sup>12</sup>-fluorene)]<sup>2+</sup>-(PF<sub>6</sub><sup>-</sup>)<sub>2</sub> (**6a**(PF<sub>6</sub><sup>-</sup>)<sub>2</sub>).** Method A applied to fluorene gave 1.5 g (36%) of **6a** as yellow microcrystals. Anal. Calcd for C<sub>33</sub>H<sub>40</sub>Fe<sub>2</sub>P<sub>2</sub>F<sub>12</sub>: C, 47.25; H, 4.77. Found: C, 47.17; H, 4.80. <sup>1</sup>H NMR (CD<sub>3</sub>CN, δ, ppm vs TMS): 6.11 (m, aromatic CH, 8H), 3.73 (s, CH<sub>2</sub>, 2H), 1.5 (s, CH<sub>3</sub>, 30H). Cyclic voltammetry data (–30 °C, DMF, 0.1 M *n*-Bu<sub>4</sub>N<sup>+</sup>BF<sub>4</sub><sup>-</sup>, 0.2 V s<sup>-1</sup>): (Fe<sup>II</sup>Fe<sup>II</sup>)<sup>2+</sup>/(Fe<sup>II</sup>Fe<sup>I</sup>)<sup>+</sup>, E° = –1.39 V vs SCE (*i<sub>a</sub>/i<sub>c</sub>* ≈ 1, ΔE<sub>p</sub> = 45 mV, *n* = 1); (Fe<sup>II</sup>Fe<sup>I</sup>)<sup>+</sup>/(Fe<sup>I</sup>Fe<sup>I</sup>), E° = –1.69 V vs SCE (*i<sub>a</sub>/i<sub>c</sub>* ≈ 1, ΔE<sub>p</sub> = 55 mV, *n* = 1); third reduction, E° = –2.38 V vs SCE (*i<sub>a</sub>/i<sub>c</sub>* ≈ 0.7, ΔE<sub>p</sub> = 70 mV, *n* = 2).

**(c) [(FeCp\*)<sub>2</sub>(μ<sub>2</sub>-η<sup>12</sup>-triphenylene)]<sup>2+</sup>-(PF<sub>6</sub><sup>-</sup>)<sub>2</sub> (**5a**(PF<sub>6</sub><sup>-</sup>)<sub>2</sub>).** Method A applied to triphenylene gave 1.72 g (38%) of **5a** as yellow microcrystals. Anal. Calcd for C<sub>38</sub>H<sub>42</sub>Fe<sub>2</sub>P<sub>2</sub>F<sub>12</sub>: C, 50.66; H, 4.66. Found: C, 50.32; H, 4.72. <sup>1</sup>H NMR (C<sub>3</sub>D<sub>6</sub>O, δ, ppm vs TMS): 8.61, 7.80 (m, uncomplexed aromatic, 4H), 7.20, 6.40 (m, complexed aromatic, 8H), 1.40 (s, C<sub>5</sub>Me<sub>5</sub>, 30H). <sup>13</sup>C NMR (CD<sub>3</sub>CN, δ, ppm): 132.90, 127.70 (uncomplexed CH), 129.00 (uncomplexed C), 96.60, 90.80 (complexed C), 92.60, 92.84 (complexed CH), 93.30 (C of C<sub>5</sub>Me<sub>5</sub>), 9.30 (CH<sub>3</sub>). Cyclic voltammetry data (–30 °C, DMF, 0.1 M *n*-Bu<sub>4</sub>N<sup>+</sup>BF<sub>4</sub><sup>-</sup>, 0.2 V s<sup>-1</sup>): (Fe<sup>II</sup>Fe<sup>II</sup>)<sup>2+</sup>/(Fe<sup>II</sup>Fe<sup>I</sup>)<sup>+</sup>, E° = –1.22 V vs SCE (*i<sub>a</sub>/i<sub>c</sub>* ≈ 1, ΔE<sub>p</sub> = 40 mV, *n* = 1); (Fe<sup>II</sup>Fe<sup>I</sup>)<sup>+</sup>/(Fe<sup>I</sup>Fe<sup>I</sup>), E° = –1.51 V vs SCE (*i<sub>a</sub>/i<sub>c</sub>* ≈ 0.9, ΔE<sub>p</sub> = 52 mV, *n* = 1); (Fe<sup>I</sup>Fe<sup>I</sup>)/(Fe<sup>I</sup>Fe<sup>0</sup>), E° = –2.00 V vs SCE (*i<sub>a</sub>/i<sub>c</sub>* ≈ 0.8, ΔE<sub>p</sub> = 140 mV, *n* = 1); (Fe<sup>I</sup>Fe<sup>0</sup>)/(Fe<sup>0</sup>Fe<sup>0</sup>)<sup>2-</sup>, E° = –2.26 V vs SCE (ΔE<sub>p</sub> = 200 mV, *n* = 1).

**Method B. [(FeCp\*)<sub>2</sub>(μ<sub>2</sub>-η<sup>12</sup>-phenanthrene)]<sup>n+</sup>-(PF<sub>6</sub><sup>-</sup>)<sub>n</sub> (*n* = 0–2; **13**, **14**(PF<sub>6</sub><sup>-</sup>), **8a**(PF<sub>6</sub><sup>-</sup>)<sub>2</sub>).** Dication **4a** (0.2 g, 0.24 mmol) and 20 g (4 mmol) of Na/Hg were stirred for 1 h under argon in 50 mL of THF at 20 °C, in a Schlenk tube. The blue solution was then transferred into another Schlenk tube to separate the Na/Hg. After the THF was removed under vacuum, the dark residue was extracted with 10 mL of toluene and filtered by the Schlenk technique to remove the NaPF<sub>6</sub>. The toluene was removed under vacuum at 20 °C. Degassed THF was then added, and the solution was cooled to –20 °C; 8 mL of air (7.2 × 10<sup>-5</sup> mmol of O<sub>2</sub>) was added by a syringe. The blue solution instantaneously became brown (unisolated Fe<sup>I</sup>Fe<sup>I</sup> complex **13**). A suspension of 155.4 mg (0.5 mmol) of ferrocenium in 10 mL of cold (–10 °C) degassed THF was added. The solution rapidly became yellow. This new solution was kept at –40 °C for 16 h under argon. Filtration provided 0.062 g (31%) of **8a**, found to be pure by <sup>1</sup>H and <sup>13</sup>C NMR. If the reaction with ferrocenium was performed at 20 °C, it provided a 20/80 mixture of **8a** and **14**. **8a**: Anal. Calcd for C<sub>34</sub>H<sub>40</sub>Fe<sub>2</sub>P<sub>2</sub>F<sub>12</sub>: C, 48.00; H, 4.70. Found: C, 47.91; H, 4.72. <sup>1</sup>H NMR (CD<sub>3</sub>CN, δ, ppm vs TMS): 7.66, 7.80 (s, uncomplexed



aromatic CH, 2H), 7.10, 6.00 (m, complexed aromatic CH, 8H), 1.46 (s, CH<sub>3</sub>, 30H). <sup>13</sup>C NMR (CD<sub>3</sub>CN, δ, ppm): 131.80 (uncomplexed aromatic CH), 92.90, 91.90 (complexed aromatic C), 92.17, 91.50, 90.90, 90.46 (complexed aromatic CH), 92.67 (C<sub>5</sub>Me<sub>5</sub>), 9.50 (CH<sub>3</sub>). Cyclic voltammetry data (-30 °C, DMF, 0.1 M *n*-Bu<sub>4</sub>N<sup>+</sup>BF<sub>4</sub><sup>-</sup>, 0.2 V s<sup>-1</sup>): (Fe<sup>II</sup>Fe<sup>II</sup>)<sup>2+</sup>/(Fe<sup>II</sup>Fe<sup>I</sup>)<sup>+</sup>, E° = -1.17 V vs SCE (*i*<sub>a</sub>/*i*<sub>c</sub> ≈ 1, ΔE<sub>p</sub> = 56 mV, *n* = 1); (Fe<sup>II</sup>Fe<sup>I</sup>)<sup>+</sup>/(Fe<sup>I</sup>Fe<sup>I</sup>), E° = -1.44 V vs SCE (*i*<sub>a</sub>/*i*<sub>c</sub> ≈ 1, ΔE<sub>p</sub> = 70 mV, *n* = 1); (Fe<sup>I</sup>Fe<sup>I</sup>)/(Fe<sup>I</sup>Fe<sup>0</sup>)<sup>2-</sup>, E° = -1.99 V vs SCE (*i*<sub>a</sub>/*i*<sub>c</sub> ≈ 1, ΔE<sub>p</sub> = 200 mV, *n* = 1); (Fe<sup>I</sup>Fe<sup>0</sup>)<sup>2-</sup>/(Fe<sup>0</sup>Fe<sup>0</sup>)<sup>2-</sup>, E° = -2.22 V vs SCE (*i*<sub>a</sub>/*i*<sub>c</sub> ≈ 1, ΔE<sub>p</sub> = 250 mV, *n* = 1). **14**: <sup>1</sup>H NMR (CD<sub>3</sub>CN, δ, ppm vs TMS): 8.00, 7.00 (m, uncomplexed aromatic CH, 4H), 6.60–5.70 (m, complexed aromatic CH, 4H), 3.80–3.20 (m, CH<sub>2</sub>, 4H), 1.50 (s, CH<sub>3</sub>, 15 H).

**Method C. (a) [(FeCp\*)<sub>2</sub>(μ<sub>2</sub>-η<sup>12</sup>-[2.2]paracyclophane)]<sup>2+</sup>-(PF<sub>6</sub><sup>-</sup>)<sub>2</sub> (10a(PF<sub>6</sub><sup>-</sup>)<sub>2</sub>).** In a 500 mL three-necked round-bottomed flask equipped with an argon inlet and a reflux condenser topped with a gas outlet, 17.4 g (153.6 mmol) of Al<sub>2</sub>Cl<sub>6</sub> and 7.54 g (23 mmol) of [FeCp\*(CO)<sub>2</sub>Br] were introduced under argon. Degassed hexane (100 mL) was then introduced by a cannula, and 91 mL (153.6 mmol) of Al<sub>2</sub>Cl<sub>3</sub>Me<sub>3</sub> was quickly added by syringe. The mixture was refluxed for 30 min, and then 0.8 g (3.84 mmol) of [2.2]paracyclophane was added to the hot mixture as a solid in small portions. The reaction mixture was then refluxed for 2 days, during which time it progressively turned red and then was cooled to 0 °C. The mixture was quenched at 0 °C by slow addition of 20 mL of pure ethanol, and then 100 mL of degassed ice-water was added. The aqueous phase was decanted and washed twice with 100 mL of ether; Al(OH)<sub>3</sub> was precipitated by addition of concentrated aqueous NH<sub>4</sub>OH to pH 9 and was removed by filtration. An aqueous HPF<sub>6</sub> (10 mmol) solution was added to the aqueous solution, causing an orange solid to precipitate. The solid was dissolved in 100 mL of CH<sub>3</sub>CN, and the solution was dried over Na<sub>2</sub>SO<sub>4</sub>. The solution was passed through a short alumina column, and 20 mL of ethanol was added to the orange solution. Slow evaporation of acetonitrile under reduced pressure yielded 1.86 g (55%) of **10a** as orange microcrystals. Anal. Calcd for C<sub>36</sub>H<sub>46</sub>Fe<sub>2</sub>P<sub>2</sub>F<sub>12</sub>: C, 49.11; H, 5.27; Fe, 12.39. Found: C, 49.03; H, 5.07; Fe, 12.33. <sup>1</sup>H NMR (80 MHz, CD<sub>3</sub>CN, δ, ppm vs TMS): 5.16, 7.80 (s, C<sub>6</sub>H<sub>4</sub>, 8H), 2.97 (s, CH<sub>2</sub>, 8H), 1.70 (s, CH<sub>3</sub>, 30H). <sup>13</sup>C NMR (20.10 MHz, CD<sub>3</sub>CN, δ, ppm): 117.30 (quaternary C<sub>6</sub>H<sub>4</sub>), 86.90 (CH), 30.70, (CH<sub>2</sub>), 10.30 (CH<sub>3</sub>).

**(b) [(FeCp\*)<sub>2</sub>(μ<sub>2</sub>-η<sup>12</sup>-phenanthrene)]<sup>2+</sup>-(PF<sub>6</sub><sup>-</sup>)<sub>2</sub> (8a(PF<sub>6</sub><sup>-</sup>)<sub>2</sub>).** Method C applied to 0.5 g (2.81 mmol) of phenanthrene, 12.7 g (112.2 mmol) of Al<sub>2</sub>Cl<sub>6</sub>, 5.5 g (16.8 mmol) of [FeCp\*(CO)<sub>2</sub>Br], and 65.11 mL (112.2 mmol) of Al<sub>2</sub>Me<sub>3</sub>Cl<sub>3</sub> in 100 mL of hexane yielded 0.95 g (40%) of **8a** as orange microcrystals, characterized by NMR comparison with an authentic sample prepared according to method B.

**(c) [(FeCp\*)<sub>2</sub>(μ<sub>2</sub>-η<sup>12</sup>-pyrene)]<sup>2+</sup>-(PF<sub>6</sub><sup>-</sup>)<sub>2</sub> (9(PF<sub>6</sub><sup>-</sup>)<sub>2</sub>).** Method C applied to 0.7 g (3.43 mmol) of pyrene, 15.55 g (137.2 mmol) of Al<sub>2</sub>Cl<sub>6</sub>, 6.7 g (20.58 mmol) of [FeCp\*(CO)<sub>2</sub>Br], and 79 mL (137.2 mmol) of Al<sub>2</sub>Me<sub>3</sub>Cl<sub>3</sub> in 100 mL of hexane yielded 1.8 g (61%) of orange-red microcrystals of **9**. Anal. Calcd for C<sub>36</sub>H<sub>40</sub>Fe<sub>2</sub>P<sub>2</sub>F<sub>12</sub>: C, 49.42; H, 4.61; Fe, 12.80. Found: C, 49.34; H, 4.42; Fe, 12.51. Cyclic voltammetry data (-35 °C, DMF, 0.1 M *n*-Bu<sub>4</sub>N<sup>+</sup>BF<sub>4</sub><sup>-</sup>, 0.4 V s<sup>-1</sup>, Hg working electrode): (Fe<sup>II</sup>Fe<sup>II</sup>)<sup>2+</sup>/(Fe<sup>II</sup>Fe<sup>I</sup>)<sup>+</sup>, E° = -1.000 V vs SCE (*i*<sub>a</sub>/*i*<sub>c</sub> = 1, ΔE<sub>p</sub> = 50 mV, *n* = 1); (Fe<sup>II</sup>Fe<sup>I</sup>)<sup>+</sup>/(Fe<sup>I</sup>Fe<sup>I</sup>), E° = -1.380 V vs SCE (*i*<sub>a</sub>/*i*<sub>c</sub> = 1, ΔE<sub>p</sub> = 50 mV, *n* = 1); (Fe<sup>I</sup>Fe<sup>I</sup>)/(Fe<sup>I</sup>Fe<sup>0</sup>)<sup>-</sup>, E° = -2.040 V vs SCE (*i*<sub>a</sub>/*i*<sub>c</sub> = 1, ΔE<sub>p</sub> = 65 mV, *n* = 1); (Fe<sup>I</sup>Fe<sup>0</sup>)<sup>-</sup>/(Fe<sup>0</sup>Fe<sup>0</sup>)<sup>2-</sup>, E° = -2.412 V vs SCE (*i*<sub>a</sub>/*i*<sub>c</sub> = 0.7, ΔE<sub>p</sub> = 145 mV, *n* = 1). <sup>1</sup>H NMR (250 MHz, CD<sub>3</sub>CN, δ, ppm vs TMS): 8.05 (s, uncomplexed CH, 4H), 6.56, 6.23 (m, complexed CH, 6H), 1.33 (s, CH<sub>3</sub>, 30H). <sup>13</sup>C NMR (62.38 MHz, CD<sub>3</sub>CN, δ, ppm): 132.30 (uncomplexed C), 91.30, 89.20 (complexed C), 9.03 (CH<sub>3</sub>).

**(d) [(FeCp\*)<sub>2</sub>(dihydrocoronene)]<sup>2+</sup>-(PF<sub>6</sub><sup>-</sup>)<sub>2</sub> (25(PF<sub>6</sub><sup>-</sup>)<sub>2</sub>).** Method C applied to 0.7 g (3.43 mmol) of coronene, 15.55 g (137.2 mmol) of Al<sub>2</sub>Cl<sub>6</sub>, 6.7 g (20.58 mmol) of [FeCp\*(CO)<sub>2</sub>Br], and 39.75 mL (68.6 mmol) of Al<sub>2</sub>Me<sub>3</sub>Cl<sub>3</sub> in 100 mL of hexane

yielded 45 mg of red microcrystalline powder. Fractional crystallization from acetonitrile-ethanol gave a major fraction (39 mg) and a minor fraction (15 mg) from the liquor.

Major fraction: <sup>1</sup>H NMR (300 MHz, CD<sub>3</sub>CN, δ, ppm vs TMS): 7.20 (s, uncomplexed aromatic H's, 2H), 6.00 (AB system, uncomplexed aromatic H's, 4H), 6.00 (AA'BB' system, CH<sub>2</sub>, 4H), 1.80 (s, CH<sub>3</sub>, 30H). <sup>13</sup>C NMR (74.5 MHz, CD<sub>3</sub>CN, δ, ppm): 103.80, 103.20, 102.80 (quaternary uncomplexed aromatic C's), 97.40, 91.90 (C<sub>5</sub>Me<sub>5</sub>), 92.20, 91.30 (quaternary complexed aromatic C), 94.30, 89.90, 89.70, 97.40 (complexed aromatic C's), 35.5 (CH<sub>2</sub>), 10.00, 9.90 (CH<sub>3</sub> mixture).

The crude minor fraction (15 mg) mainly contained [(FeCp\*)-(η<sup>6</sup>-coronene)]<sup>+</sup>(PF<sub>6</sub><sup>-</sup>), from <sup>1</sup>H NMR (60 MHz, CD<sub>3</sub>CN, δ, ppm vs TMS): 8.20 (AB system, uncomplexed H, 4H), 8.10 (s, uncomplexed H, 2H), 7.8 (AB system, uncomplexed H, 8H), 1.90 (s, CH<sub>3</sub>, 15H).

**3. Syntheses of the Complexes [(FeCp)<sub>2</sub>(μ<sub>2</sub>-η<sup>12</sup>-polyaromatic)]<sup>2+</sup>-(PF<sub>6</sub><sup>-</sup>)<sub>2</sub>.** The reaction was carried out in a 250 mL three-necked round-bottomed flask equipped with an argon inlet and a reflux condenser topped with a gas outlet. A mixture of 18.6 g (100 mmol) of ferrocene, 13.3 g (100 mmol) of AlCl<sub>3</sub>, 0.54 g (20 mmol) of Al powder, and 10 mmol of polyaromatic was stirred for 5 min under argon. The mixture was heated neat at 120 °C under argon, with agitation for 16 h. The reaction mixture was hydrolyzed slowly with 100 mL of degassed ice-water. Addition of concentrated NH<sub>4</sub>OH to pH 9 precipitated Al(OH)<sub>3</sub>. After filtration, a yellow solid was obtained by addition of aqueous HPF<sub>6</sub> (10 mmol). The precipitate was filtered, dissolved in 50 mL of acetonitrile, and dried over 1 h over MgSO<sub>4</sub>. The solution was passed through a short-column 2 cm layer of Al<sub>2</sub>O<sub>3</sub>, and 20 mL of dry ethanol was added to the yellow solution. Slow evaporation of the acetonitrile gave yellow microcrystals.

**(a) [(FeCp)<sub>2</sub>(μ<sub>2</sub>-η<sup>12</sup>-triphenylene)]<sup>2+</sup>-(PF<sub>6</sub><sup>-</sup>)<sub>2</sub> (5b(PF<sub>6</sub><sup>-</sup>)<sub>2</sub>).** The procedure applied to 0.5 g (2.2 mmol) of triphenylene, 4 g (21 mmol) of ferrocene, 2.3 g (17 mmol) of AlCl<sub>3</sub>, and 0.1 g (3 mmol) of Al powder at 120 °C provided 0.8 g (48% yield) of yellow microcrystalline **5b**. Anal. Calcd for C<sub>28</sub>H<sub>22</sub>Fe<sub>2</sub>P<sub>2</sub>F<sub>12</sub>: C, 44.21; H, 2.89. Found: C, 43.80; H, 2.85. <sup>1</sup>H NMR (CD<sub>3</sub>CN, δ, ppm vs TMS): 8.40, 7.80 (m, uncomplexed aromatic, 4H), 7.33, 6.50 (m, complexed aromatic, 8H), 4.53 (s, C<sub>5</sub>H<sub>5</sub>, 10H). <sup>13</sup>C NMR (CD<sub>3</sub>CN, δ, ppm): 133.12, 127.19 (uncomplexed CH), 130.09 (uncomplexed C), 95.69, 92.77 (complexed C), 90.39, 89.52, 84.33, 83.54 (complexed CH), 80.00 (C<sub>5</sub>H<sub>5</sub>). Cyclic voltammetry data (-30 °C, DMF, 0.1 M *n*-Bu<sub>4</sub>N<sup>+</sup>BF<sub>4</sub><sup>-</sup>, 0.2 V s<sup>-1</sup>): (Fe<sup>II</sup>Fe<sup>II</sup>)<sup>2+</sup>/(Fe<sup>II</sup>Fe<sup>I</sup>)<sup>+</sup>, E° = -1.00 V vs SCE (*i*<sub>a</sub>/*i*<sub>c</sub> ≈ 1, ΔE<sub>p</sub> = 45 mV, *n* = 1); (Fe<sup>II</sup>Fe<sup>I</sup>)<sup>+</sup>/(Fe<sup>I</sup>Fe<sup>I</sup>), E° = -1.19 V vs SCE (*i*<sub>a</sub>/*i*<sub>c</sub> ≈ 0.9, ΔE<sub>p</sub> = 90 mV, *n* = 1); (Fe<sup>I</sup>Fe<sup>I</sup>)/(Fe<sup>I</sup>Fe<sup>0</sup>)<sup>-</sup>, E° = -1.68 V vs SCE (*i*<sub>a</sub>/*i*<sub>c</sub> ≈ 0.8, ΔE<sub>p</sub> = 55 mV, *n* = 1); (Fe<sup>I</sup>Fe<sup>0</sup>)<sup>-</sup>/(Fe<sup>0</sup>Fe<sup>0</sup>)<sup>2-</sup>, E° = -1.85 V vs SCE (ΔE<sub>p</sub> = 145 mV, *n* = 1).

(b) For other known polyaromatic compounds, this method gave pure complexes and improved yields indicated in Table 1, without hydrogenation of the side ring (phenanthrene and fluorene but not pyrene).

**4. Synthesis of [(FeCp\*)<sub>2</sub>(μ<sub>2</sub>-η<sup>10</sup>-dihydrophenanthrene)] (11).** A 0.72 g (0.8 mmol) sample of the dication **4a** and 50 g (10 mmol) of Na/Hg were stirred for 3 h under argon in 50 mL of THF at room temperature in a Schlenk tube. The resulting blue solution was transferred into another Schlenk tube to remove the Na/Hg. After removal of THF under vacuum, the dark residue was extracted with a minimum of toluene (10 mL) and filtered under argon. Pentane (100 mL) was added, and the solution was cooled to -90 °C, which provided, after rapid filtration, 0.3 g (64% yield) of dark blue microcrystalline powder. Complex **11** is very air sensitive and thermally stable at 20 °C. Anal. Calcd for C<sub>34</sub>H<sub>42</sub>Fe<sub>2</sub>: C, 75.59; H, 7.47. Found: C, 71.74; H, 7.49. <sup>1</sup>H NMR (C<sub>6</sub>D<sub>6</sub>, δ, ppm vs TMS): 6.00–5.40 (m, para CH, 2H), 4.20 (m, meta CH, 2H), 4.20–3.90 (m, meta' CH, 2H), 3.90 (m, CH<sub>2</sub>, 4H), 2.5 (m, ortho CH, 2H), 1.90 (s, CH<sub>3</sub>, 30H). <sup>13</sup>C NMR (C<sub>6</sub>D<sub>6</sub>, δ,

ppm): 103.90 (C=C), 84.20 (C of C<sub>5</sub>Me<sub>5</sub>), 81.30 (meta and meta' CH), 76.40 (para CH), 65.70 (ortho C), 54.00 (ortho CH), 10.70 (CH<sub>3</sub>).

**5. Synthesis of [(FeCp\*)<sub>2</sub>(μ<sub>2</sub>-η<sup>12</sup>-dihydrophenanthrene)]<sup>+</sup>(PF<sub>6</sub><sup>-</sup>) (12(PF<sub>6</sub><sup>-</sup>)).** A THF solution of 0.28 g (0.5 mmol) of the blue neutral complex **11** was added, under argon, to a suspension (0.430 g, 0.5 mmol) of the yellow dication complex **4a** in THF. After it was stirred for 30 min at room temperature, the solution became colorless and the mixture contained a suspension of a dark green powder. Filtration under argon gave 0.65 g (92% yield) of **12** as a dark green powder. Anal. Calcd for C<sub>34</sub>H<sub>42</sub>Fe<sub>2</sub>P<sub>2</sub>F<sub>12</sub>: C, 57.71; H, 5.94. Found: C, 57.31; H, 6.00.

**6. Synthesis of [(FeCp\*)<sub>2</sub>(μ<sub>2</sub>-η<sup>12</sup>-phenanthrene)] (13).** A 0.50 g (0.6 mmol) sample of the dication **8a** and 30 g (10 mmol) of Na/Hg were stirred for 3 h under argon in 20 mL of THF at -35 °C in a Schlenk tube. The solution became dark brown, and the THF was removed under vacuum. Extraction with 3 × 50 mL of degassed toluene at -35 °C provided, after evaporation of the solvent, 0.20 g (60% yield) of **13** as a very air sensitive brown powder, thermally stable up to -20 °C. ESR (77 K, THF matrix):  $g_x = 2.0617$ ,  $g_y = 2.0015$ ,  $g_z = 1.8566$ .

**7. Synthesis of [(FeCp\*)<sub>2</sub>(μ<sub>2</sub>-η<sup>12</sup>-phenanthrene)]<sup>+</sup>(PF<sub>6</sub><sup>-</sup>) (14(PF<sub>6</sub><sup>-</sup>)).** A THF solution of 0.130 g (0.23 mmol) of the purple-brown neutral complex **13** was prepared by reduction of **8a** at -35 °C as in procedure 6 and added under argon to a suspension (0.20 g, 0.23 mmol) of the orange dicationic complex **8a** in THF. After the mixture was stirred overnight at -20 °C and **8a** was completely consumed, the solution was filtered under argon, concentrated, and precipitated with pentane, yielding 0.260 g (80%) of a thermally stable, air-sensitive green powder, **14**.

**8. Synthesis of [(FeCp\*)<sub>2</sub>(μ<sub>2</sub>-η<sup>12</sup>-triphenylene)] (21).** A 0.46 g (0.5 mmol) sample of dication **5a** and 30 g (10 mmol) of Na/Hg were stirred for 3 h under argon in 20 mL of THF at -35 °C in a Schlenk tube. The solution became green, and the THF was removed under vacuum. Extraction with 3 × 50 mL of degassed toluene at -20 °C provided, after evaporation of the solvent, 0.210 g (66% yield) of **21** as a very air sensitive green powder, thermally stable up to -20 °C. ESR (11 K, frozen THF):  $g_x = 2.0691$ ,  $g_y = 2.0151$ ,  $g_z = 1.8279$ .

**9. Synthesis of [(FeCp\*)<sub>2</sub>(μ<sub>2</sub>-η<sup>12</sup>-triphenylene)]<sup>+</sup>(PF<sub>6</sub><sup>-</sup>) (22(PF<sub>6</sub><sup>-</sup>)).** A 0.2 g (0.22 mmol) sample of dication **5a** was reduced by procedure 6. The resulting green toluene solution of **21** was transferred very slowly by cannula into another Schlenk tube containing a 0.15 g (0.16 mmol) sample of **5a**. The solution immediately became colorless; addition of the neutral complex **21** was stopped when the green color persisted. Filtration under argon provided 250 mg (87% yield) of **22** as a very air sensitive, thermally stable, dark green powder. Anal. Calcd for C<sub>38</sub>H<sub>42</sub>Fe<sub>2</sub>PF<sub>6</sub>: C, 60.39; H, 5.56. Found: C, 60.82; H, 5.31. ESR (77 K, THF matrix):  $g_x = 2.0447$ ,  $g_y = 2.0005$ ,  $g_z = 1.8149$ .

**10. Synthesis of [(FeCp\*)<sub>2</sub>(μ<sub>2</sub>-η<sup>10</sup>-pyrene)] (23).** A 0.20 g (0.23 mmol) sample of dication **9** and 5 g (1 mmol) of Na/Hg were stirred overnight under argon in 20 mL of THF at -35 °C in a Schlenk tube. After the THF was removed under vacuum, the olive green solution was extracted with a minimum amount of toluene (10 mL) and filtered into another Schlenk tube to remove the Na/Hg. Pentane (100 mL) was added, and the solution was cooled to -80 °C, providing, after rapid filtration, 0.110 g (80% yield) of **23** as a very sensitive dark green microcrystalline powder thermally stable up to -20 °C. ESR (7 K, THF matrix):  $g_x = 2.0650$ ,  $g_y = 1.9550$ ,  $g_z = 1.8968$ .

**11. Synthesis of [(FeCp\*)<sub>2</sub>(μ<sub>2</sub>-η<sup>12</sup>-pyrene)]<sup>+</sup>(PF<sub>6</sub><sup>-</sup>) (24-(PF<sub>6</sub><sup>-</sup>)).** A THF solution of 0.314 g (0.23 mmol) of the dark green neutral complex **23** was prepared by reduction of **9** at

-35 °C in procedure **10** and added under argon to a suspension (0.2 g, 0.23 mmol) of the orange dicationic complex **9** in THF. After it was stirred overnight at -20 °C, the solution became colorless and the mixture contained a suspension of a dark brownish purple powder. Filtering under argon and washing with pentane gave 0.23 g (70% yield) of a thermally stable, air-sensitive purple-brown powder of **24**. Anal. Calcd for C<sub>36</sub>H<sub>40</sub>Fe<sub>2</sub>PF<sub>6</sub>: C, 59.28; H, 5.53. Found: C, 58.70; H, 6.12. ESR (20 K, solid-state sample):  $g_x = 2.0503$ ,  $g_y = 1.9968$ ,  $g_z = 1.8003$ .

**12. Synthesis of [(FeCp\*)<sub>2</sub>(μ<sub>2</sub>-η<sup>10</sup>-[2.2]paracyclophane)] (17).** A 0.187 g (0.212 mmol) sample of the dication **10** and 5 g (1 mmol) of Na/Hg were stirred for 3 h under argon in 50 mL of THF at room temperature in a Schlenk tube. The solution first took on a green color, which did not persist, and eventually turned orange. It was transferred into another Schlenk tube to remove the Na/Hg. After removal of the THF under vacuum, the orange residue was extracted with a minimum amount of toluene (10 mL), and this solution was filtered by the Schlenk technique. Pentane (100 mL) was added, and recrystallization gave 0.1 g (80% yield) of an orange microcrystalline powder of **17**, which was air sensitive but thermally stable at 0 °C. <sup>1</sup>H NMR (C<sub>6</sub>D<sub>6</sub>, δ, ppm vs TMS): 5.266, 5.246 (d, CH, 4H), 3.404, 3.383 (d, CH, 4H), 1.565 (m, CH<sub>2</sub>, 8H), 1.581 (s, CH<sub>3</sub>, 30H). <sup>13</sup>C NMR (C<sub>6</sub>D<sub>6</sub>, δ, ppm): 91.509 (C<sub>q</sub> of cyclophane), 82.471 (C<sub>q</sub> of C<sub>5</sub>Me<sub>5</sub>), 79.960, 55.792 (CH of cyclophane), 49.420 (C<sub>q</sub> of cyclophane), 39.520 (CH<sub>2</sub>), 10.635 (CH<sub>3</sub>).

**13. Computational Details.** All the calculations have been carried out within the standard version of the density functional SCF MS-Xα.<sup>43</sup> An idealized C<sub>2h</sub> geometry was assumed for **9b**, with both ligands planar and the same bond distances as those used previously for similar calculations on **1b** (Å);<sup>16b</sup> C-C = 1.40, C-H = 1.10, Fe-C<sub>5</sub>(centroid) = 1.68, Fe-C<sub>6</sub>(centroid) = 1.55. The radii of the muffin-tin spheres were chosen as follows: starting from geometry-induced touching spheres, obtained for metal and ligand atoms, the carbon radii were enlarged by 25% to provide a better description of the ring systems.<sup>44</sup> An additional empty sphere (E) was located in the center of each ligand ring. This procedure, which has been shown to give reliable results for similar complexes,<sup>41h-j</sup> leads to the following muffin-tin radii (au): Fe = 2.2795; C = 1.6535; H = 0.8758; E(C<sub>5</sub> ring) = 1.0843; E(C<sub>6</sub> ring) = 1.3226. A Watson sphere bearing the charge 2- and having the same radius as the outer sphere has been introduced in order to mimic the external stabilizing electrostatic field.<sup>45</sup> The exchange scaling parameters α were taken from Schwartz<sup>46</sup> for the heavy elements and from Slater<sup>47</sup> for hydrogen. The maximum *L* values in the partial wave expansion were *L* = 2 for the iron and outer spheres, *L* = 1 for the carbon spheres, and *L* = 0 for the hydrogen spheres. SCF calculations were converged to better than ±0.0001 Ry on each level.

**Acknowledgment.** We thank a reviewer for helpful comments, the CNRS, the Universities of Bordeaux I, Rennes I, Paris VI, and Kénitra, and the Région Aquitaine for financial support, and BASF for a gift of iron pentacarbonyl.

OM9504011

(43) (a) Slater, J. C. *Adv. Quantum Chem.* **1972**, *6*, 1. (b) Johnson, K. *Adv. Quantum Chem.* **1973**, *7*, 143.

(44) Herman, F.; Williams, A. R.; Johnson, K. H. *J. Chem. Phys.* **1974**, *61*, 3508.

(45) Watson, R. H. *Phys. Rev.* **1958**, *111*, 1108.

(46) (a) Schwartz, K. *Phys. Rev. B* **1972**, *5*, 2466. (b) Schwartz, K. *Theor. Chim. Acta* **1974**, *34*, 225.

(47) Slater, J. C. *Int. J. Quantum Chem.* **1973**, *7*, 533.

# Multistep CO<sub>2</sub> Reduction Catalyzed by [Ru(bpy)<sub>2</sub>(qu)(CO)]<sup>2+</sup> (bpy = 2,2'-Bipyridine, qu = Quinoline). Double Methylation of the Carbonyl Moiety Resulting from Reductive Disproportionation of CO<sub>2</sub>

Hiroshi Nakajima, Yoshinori Kushi, Hirotaka Nagao, and Koji Tanaka\*

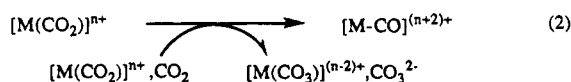
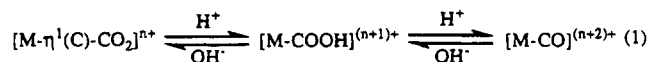
*Institute for Molecular Science, Department of Structural Molecular Science, The Graduate University for Advanced Studies, Myodaiji, Okazaki 444, Japan*

Received March 21, 1995\*

The title complexes catalyze the reductive disproportionation of CO<sub>2</sub> forming CO and CO<sub>3</sub><sup>2-</sup> in the electrochemical CO<sub>2</sub> reduction in CH<sub>3</sub>CN with LiBF<sub>4</sub>. The same reduction in the presence of Me<sub>4</sub>NBF<sub>4</sub> instead of LiBF<sub>4</sub> produces CH<sub>3</sub>C(O)CH<sub>3</sub> and CH<sub>3</sub>C(O)CH<sub>2</sub>COO<sup>-</sup> in addition to HCOO<sup>-</sup> and CO in CH<sub>3</sub>CN/DMSO (1:1, v/v). In this reaction Me<sub>4</sub>N<sup>+</sup> functions as the methylation agent of the carbonyl moiety resulting from the reductive disproportionation of CO<sub>2</sub>. The produced CH<sub>3</sub>C(O)CH<sub>3</sub> undergoes the abstraction of its α-proton and subsequent carboxylation to afford CH<sub>3</sub>C(O)CH<sub>2</sub>COO<sup>-</sup>.

## Introduction

A number of transition metal complexes have been shown to be active for generation of CO and/or HCOO<sup>-</sup> in electro-<sup>1</sup> and photochemical<sup>1n,2</sup> CO<sub>2</sub> reduction. The mechanistic studies on those reactions have been also examined,<sup>1k-m,3,7</sup> and some of them have suggested the participation of metal-carbonyl complexes ([M-CO]<sup>(n+2)+</sup>) in the CO<sub>2</sub> reduction.<sup>1l-m,7</sup> In protic media, [M-CO]<sup>(n+2)+</sup> may be formed through an acid-base equilibrium with [M-COOH]<sup>(n+1)+</sup> and [M-η<sup>1</sup>(C)-CO<sub>2</sub>]<sup>n+</sup> (eq 1),<sup>4</sup> while



oxide transfer reactions from [M(CO<sub>2</sub>)]<sup>n+</sup> to CO<sub>2</sub> or another [M(CO<sub>2</sub>)]<sup>n+</sup> become predominant pathways for

the metal-carbonyl formation in aprotic media (eq 2).<sup>5,25</sup> Recently we have reported the first multi-electron reduction of CO<sub>2</sub> affording HCHO, CH<sub>3</sub>OH, HOOCCHO, and HOOCCH<sub>2</sub>OH under homogeneous protic conditions,<sup>1m</sup> in which the smooth conversion from [Ru(bpy)(trpy)(η<sup>1</sup>(C)-CO<sub>2</sub>)] (bpy = 2,2'-bipyridine, trpy = 2,2':6,2''-terpyridine) to [Ru(bpy)(trpy)(CO)]<sup>2+</sup> (eq 1) serves the following reduction of the latter to [Ru(bpy)(trpy)(CHO)]<sup>+</sup> and [Ru(bpy)(trpy)(CH<sub>2</sub>OH)]<sup>+</sup>. From the viewpoint of CO<sub>2</sub> as a potential C1 source for organic compounds, using organic electrophiles instead of protons in multi-electron reduction of CO<sub>2</sub> may provide more versatile routes for the catalytic carbon-carbon bond formation.<sup>6</sup> The oxide transfer from [M(CO<sub>2</sub>)]<sup>n+</sup> to CO<sub>2</sub> in aprotic media (eq 2), therefore, is expected to be useful for multi-electron reduction of CO<sub>2</sub> in the presence of organic electrophiles.

A well-characterized [Ru(bpy)<sub>2</sub>(CO)(η<sup>1</sup>(C)-CO<sub>2</sub>)] is reversibly converted to [Ru(bpy)<sub>2</sub>(CO)<sub>2</sub>]<sup>2+</sup> via [Ru(bpy)<sub>2</sub>(CO)(COOH)]<sup>+</sup> (pK<sub>a</sub> = 9.5) in aqueous solutions (eq 1). No oxide transfer from [Ru(bpy)<sub>2</sub>(CO)(η<sup>1</sup>(C)-CO<sub>2</sub>)] to CO<sub>2</sub>, however, occurs in organic solvents.<sup>7</sup> Taking into

\* Abstract published in *Advance ACS Abstracts*, September 15, 1995.

(1) (a) Arana, C.; Keshavarz, M.; Potts, K. T.; Abruña, H. D. *Inorg. Chim. Acta* **1994**, *225*, 285. (b) Steffey, B. d.; Miedaner, A.; Maciejewski-Farmer, M. L.; Bernatis, P. R.; Herring, A. M.; Allured, V. S.; Carperos, V.; DuBois, D. L. *Organometallics* **1994**, *13*, 4844. (c) Szymaszek, A.; Pruchnik, F. *Rhodium Express* **1994**, *5*, 18. (d) Fujita, E.; Haff, J.; Sanzenbacher, R.; Elias, H. *Inorg. Chem.* **1994**, *33*, 4627. (e) Ogura, K.; Sugihara, H.; Yano, J.; Higasa, M. *J. Electrochem. Soc.* **1994**, *141*, 419. (f) Chardon-Noblat, S.; Collomb-Dunand-Sauthier, M.-N.; Deronzier, A.; Ziessel, R. *Inorg. Chem.* **1994**, *33*, 4410. (g) Christensen, P.; Hamnett, A.; Muir, A. V. G.; Timney, J. A.; Higgins, S. *J. Chem. Soc., Faraday Trans.* **1994**, *90*, 459. (h) Kimura, E.; Wada, S.; Shionoya, M.; Okazaki, Y. *Inorg. Chem.* **1994**, *33*, 770. (i) Kolodnick, K. J.; Schrier, P. W.; Walton, R. A. *Polyhedron* **1994**, *13*, 457. (j) Collomb-Dunand-Sauthier, M.-N.; Deronzier, A.; Ziessel, R. *J. Chem. Soc., Chem. Commun.* **1994**, 189. (k) Haines, R. J.; Wittig, R. E.; Kubiak, C. P. *Inorg. Chem.* **1994**, *33*, 4723. (l) Collomb-Dunand-Sauthier, M.-N.; Deronzier, A.; Ziessel, R. *Inorg. Chem.* **1994**, *33*, 2961. (m) Nagao, H.; Mizukawa, T.; Tanaka, K. *Inorg. Chem.* **1994**, *33*, 3415. (n) Halmann, M. M., Ed. *Chemical Fixation of Carbon Dioxide*; CRC Press: London, 1993. (o) Sullivan, B. P., Ed. *Electrochemical and Electrocatalytic Reduction of Carbon Dioxide*; Elsevier: Amsterdam, 1993; and references therein.

(2) (a) Ishitani, O.; George, M. W.; Ibusuki, T.; Johnson, F. P. A.; Koike, K.; Nozaki, K.; Pac, C.; Turner, J. J.; Westwell, J. R. *Inorg. Chem.* **1994**, *33*, 4712. (b) Matsuoka, S.; Yamamoto, K.; Ogata, T.; Kusaba, M.; Nakashima, N.; Fujita, E.; Yanagida, S. *J. Am. Chem. Soc.* **1993**, *115*, 601. (c) Calzaferri, G.; Hädener, K.; Li, J. *J. Photochem. Photobiol. A* **1992**, *64*, 259. (d) Kimura, E.; Bu, X.; Shinomiya, M.; Wada, S.; Maruyama, S. *Inorg. Chem.* **1992**, *31*, 4542 and references therein.

(3) (a) Ratliff, K. S.; Lentz, R. E.; Kubiak, C. P. *Organometallics* **1992**, *11*, 1986. (b) Jeget, C.; Fouassier, M.; Mascetti, J. *Inorg. Chem.* **1991**, *30*, 1521. (c) Jeget, C.; Fouassier, M.; Tranquille, M.; Mascetti, J. *Inorg. Chem.* **1991**, *30*, 1529. (d) Pugh, J. R.; Bruce, M. R. M.; Sullivan, B. P.; Meyer, T. J. *Inorg. Chem.* **1991**, *30*, 86. (e) Sullivan, B. P.; Meyer, T. J. *J. Chem. Soc., Chem. Commun.* **1984**, 1244.

(4) (a) Ishida, H.; Katsuyuki, F.; Ohba, T.; Ohkubo, K.; Tanaka, T.; Terada, T.; Tanaka, T. *J. Chem. Soc., Dalton Trans.* **1990**, 2155. (b) Ishida, H.; Tanaka, K.; Morimoto, M.; Tanaka, T. *Organometallics* **1986**, *5*, 724. (c) Tanaka, K.; Morimoto, M.; Tanaka, T. *Chem. Lett.* **1983**, 901. (d) Choudhury, D.; Cole-Hamilton, D. J. *J. Chem. Soc., Dalton Trans.* **1982**, 1885.

(5) (a) Lee, G. R.; Maher, J. M.; Cooper, N. J. *J. Am. Chem. Soc.* **1987**, *109*, 2956. (b) Maher, J. M.; Lee, G. R.; Cooper, N. J. *J. Am. Chem. Soc.* **1982**, *104*, 6792. (c) Maher, J. M.; Cooper, N. J. *J. Am. Chem. Soc.* **1980**, *102*, 7605. (d) Lee, G. R.; Cooper, N. J. *Organometallics* **1985**, *4*, 1467. (e) Guggenberger, L. J.; Herskovitz, T. *J. Am. Chem. Soc.* **1976**, *98*, 1615. (f) Belmore, K. A.; Vanderpool, R. A.; Tsai, J.-C.; Khan, M. A.; Nicholas, K. M. *J. Am. Chem. Soc.* **1988**, *110*, 2004.

(6) Another carbon-carbon bond formation has been achieved through electrocarboxylation of [RPd(PPh<sub>3</sub>)<sub>2</sub>]<sup>0</sup> and [RW(CO)<sub>5</sub>]<sup>-</sup> to afford RCOO<sup>-</sup> (R = methyl, aryl, and benzyl). See the following references: (a) Amatore, C.; Jutand, A.; Khalil, F.; Nielsen, M. F. *J. Am. Chem. Soc.* **1992**, *114*, 7076. (b) Amatore, C.; Jutand, A. *J. Am. Chem. Soc.* **1991**, *113*, 2819. (c) Fauvarque, J. F.; de Zelicourt, Y.; Amatore, C.; Jutand, A. *J. Appl. Electrochem.* **1990**, *20*, 338. (d) Torii, S.; Tanaka, H.; Hamatani, T.; Morisaki, K.; Jutand, A.; Pflüger, F.; Fauvarque, J.-F. *Chem. Lett.* **1986**, 169. (e) Kudarkoski, R.; Darenbourg, D. J. *J. Am. Chem. Soc.* **1984**, *106*, 3672.

account that the smooth conversion from anionic  $[\text{W}(\text{CO})_5(\eta^1(\text{C})\text{-CO}_2)]^{2-}$  and  $[\text{CpFe}(\text{CO})_2(\eta^1(\text{C})\text{-CO}_2)]^-$  to  $[\text{W}(\text{CO})_6]$  and  $[\text{CpFe}(\text{CO})_3]^+$  under  $\text{CO}_2$  atmosphere at low temperature,<sup>5a-c</sup> no reactivity of  $[\text{Ru}(\text{bpy})_2(\text{CO})(\eta^1(\text{C})\text{-CO}_2)]$  toward  $\text{CO}_2$  may be correlated with the weak basicity of  $[\text{Ru}(\text{bpy})_2(\text{CO})(\eta^1(\text{C})\text{-CO}_2)]$  compared with those anionic  $\eta^1(\text{C})\text{-CO}_2$  complexes. The basicity of  $\eta^1(\text{C})\text{-CO}_2$  complexes is reasonably estimated from the equilibrium constant ( $K_a$ ) of the hydroxycarbonyl complexes ( $[\text{M-COOH}]^{(n+1)+}$ ) in eq 1. The reported  $\text{p}K_a$  values of hydroxycarbonyl complexes range widely from ca. 14 to 2.5,<sup>4b,8</sup> which are quite different from those of organic carboxylic acids. On the basis of such a wide range of  $\text{p}K_a$  values, replacement of the carbonyl ligand in  $[\text{Ru}(\text{bpy})_2(\text{CO})(\eta^1(\text{C})\text{-CO}_2)]$  with an electron-donating group would greatly enhance the basicity of the  $\eta^1(\text{C})\text{-CO}_2$  moiety, which will be a promising gateway to the multi-electron reduction of  $\text{CO}_2$  in the presence of organic electrophiles in aprotic media.

This paper describes the first catalytic formation of acetone and acetoacetic acid in electrochemical  $\text{CO}_2$  reduction by  $[\text{Ru}(\text{bpy})_2(\text{qu})(\text{CO})]^{2+}$  (qu = quinoline) under aprotic conditions, which is composed of two key reactions. The first is the double methylation of  $[\text{Ru-CO}]^0$  to afford  $\text{CH}_3\text{C}(\text{O})\text{CH}_3$  where  $[\text{Ru-CO}]^{2+}$  is regenerated through the oxide transfer from  $[\text{Ru-}\eta^1(\text{C})\text{-CO}_2]^0$  to  $\text{CO}_2$  (eq 2). The second is the abstraction of the  $\alpha$ -proton from resulting  $\text{CH}_3\text{C}(\text{O})\text{CH}_3$  by  $[\text{Ru-}\eta^1(\text{C})\text{-CO}_2]$  to give  $[\text{Ru-COOH}]^+$  and  $\text{CH}_3\text{C}(\text{O})\text{CH}_2^-$ , the latter of which further undergoes carboxylation to produce  $\text{CH}_3\text{C}(\text{O})\text{CH}_2\text{COO}^-$ . A part of this study has been reported elsewhere.<sup>9</sup>

### Experimental Section

**Materials.** Tetramethylammonium tetrafluoroborate and lithium tetrafluoroborate were purchased and recrystallized from a methanol.  $\text{CH}_3\text{CN}$  and DMSO were distilled over  $\text{CaH}_2$  before use.<sup>10</sup> Tetrabutylammonium tetrafluoroborate for electrochemical use and all other chemicals were used as received.  $\text{Ru}(\text{bpy})_2\text{Cl}_2 \cdot 2\text{H}_2\text{O}$  was prepared according to the previously described method.<sup>11</sup>

**Preparation of  $[\text{Ru}(\text{bpy})_2(\text{qu})(\text{CH}_3\text{CN})](\text{PF}_6)_2$  (qu = Quinoline) (1).** An ethanol solution (30 mL) containing  $\text{Ru}(\text{bpy})_2\text{Cl}_2 \cdot 2\text{H}_2\text{O}$  (200 mg) and an excess amount of quinoline (1 mL) was refluxed for 4 h. The solution was concentrated to ca. 5 cm<sup>3</sup> under reduced pressure. An addition of 50 mL of aqueous  $\text{HPF}_6$  (12%) to the solution gave  $[\text{Ru}(\text{bpy})_2(\text{qu})\text{Cl}](\text{PF}_6)$  as a brown precipitate in a 70% yield. A 2-methoxyethanol solution (35 mL) containing  $[\text{Ru}(\text{bpy})_2(\text{qu})\text{Cl}](\text{PF}_6)$  (100 mg), equimolar  $\text{AgPF}_6$  (35 mg), and  $\text{CH}_3\text{CN}$  (0.5 mL) was heated at 70 °C for 1 h. Precipitated  $\text{AgCl}$  was removed by filtration with Celite, and the filtrate was evaporated under reduced pressure. An addition of excess  $\text{NH}_4\text{PF}_6$  to the aqueous solution of the product gave  $[\text{Ru}(\text{bpy})_2(\text{qu})(\text{CH}_3\text{CN})](\text{PF}_6)_2$  as an orange precipitate. Each product was purified by column chromatography on neutral alumina using a  $\text{C}_6\text{H}_6/\text{CH}_3\text{CN}$  (1:1, v/v) eluent, and the final product was further purified by recrystallization from an ethanol-acetone. Yield: ca. 60% (based on  $\text{Ru}(\text{bpy})_2\text{Cl}_2 \cdot 2\text{H}_2\text{O}$ ). Anal. Calcd for  $\text{C}_{31}\text{H}_{26}\text{N}_6\text{F}_{12}\text{P}_2$

Ru: C, 42.62; H, 3.01; N, 9.62. Found: C, 42.36; H, 3.20; N, 9.45. FAB-mass ( $m/z$ ): 729 (M -  $\text{PF}_6$ ).

**Preparation of  $[\text{Ru}(\text{bpy})_2(\text{qu})(\text{CO})](\text{PF}_6)_2$  (2).** A 2-methoxyethanol solution (35 mL) containing  $[\text{Ru}(\text{bpy})_2(\text{qu})\text{Cl}](\text{PF}_6)$  (100 mg) and equimolar  $\text{AgPF}_6$  (35 mg) was heated at 90 °C for 2 h with vigorous  $\text{CO}$  bubbling, during which time the solution changed from dark red to orange in color. Precipitated  $\text{AgCl}$  was removed by filtration with Celite, and the filtrate was evaporated under reduced pressure. An addition of excess  $\text{NH}_4\text{PF}_6$  to the aqueous solution of the product gave  $[\text{Ru}(\text{bpy})_2(\text{qu})(\text{CO})](\text{PF}_6)_2$  as a yellowish orange precipitate which was recrystallized from ethanol. Yield: ca. 60% (based on  $\text{Ru}(\text{bpy})_2\text{Cl}_2 \cdot 2\text{H}_2\text{O}$ ). IR (KBr):  $\nu(\text{C}=\text{O})$  1996 cm<sup>-1</sup>. Anal. Calcd for  $\text{C}_{30}\text{H}_{23}\text{ON}_5\text{F}_{12}\text{P}_2\text{Ru}$ : C, 41.86; H, 2.70; N, 8.13. Found: C, 41.82; H, 3.02; N, 8.32. FAB-mass ( $m/z$ ): 716 (M -  $\text{PF}_6$ ).

**Preparation of  $[\text{Ru}(\text{bpy})_2(i\text{-qu})(\text{CO})](\text{PF}_6)_2$  (i-qu = Isoquinoline).**  $[\text{Ru}(\text{bpy})_2(i\text{-qu})(\text{CO})](\text{PF}_6)_2$  was prepared in analogy with the method for **2** except that isoquinoline (1 mL) was used for the preparation of  $[\text{Ru}(\text{bpy})_2(i\text{-qu})\text{Cl}](\text{PF}_6)$ . Yield: ca. 50% (based on  $\text{Ru}(\text{bpy})_2\text{Cl}_2 \cdot 2\text{H}_2\text{O}$ ). IR (KBr):  $\nu(\text{C}=\text{O})$  1995 cm<sup>-1</sup>. Anal. Calcd for  $\text{C}_{30}\text{H}_{23}\text{ON}_5\text{F}_{12}\text{P}_2\text{Ru}$ : C, 41.86; H, 2.70; N, 8.13. Found: C, 41.48; H, 3.01; N, 8.29. FAB-mass ( $m/z$ ): 716 (M -  $\text{PF}_6$ ).

**Physical Measurements.** Cyclic voltammetric experiments were performed in  $\text{CH}_3\text{CN}$  containing  $\text{Me}_4\text{NBF}_4$  ( $5 \times 10^{-2}$  M) and the complexes ( $1 \times 10^{-3}$  M) with a Hokuto Denko HA-151 potentiostat/function generator and a Riken Denshi Co. F-35 X-Y recorder. One component cell using a glassy carbon working electrode (0.07 cm<sup>2</sup>), a platinum wire auxiliary electrode, and an  $\text{Ag}|\text{AgCl}$  reference electrode was employed. The working electrode was polished with an alumina paste and washed with distilled water before use. The  $E_{1/2}$  values reported here were determined from average of the oxidative and reductive peak potentials. IR spectra were obtained on a Shimadzu FTIR-8100 spectrophotometer. <sup>1</sup>H-NMR spectra were measured on a JEOL EX270 (270 MHz) spectrometer. FAB-mass and GC-mass spectra were obtained on Shimadzu/Kratos Concept 1S and Shimadzu GC-mass QP-1000EX, respectively. Elemental analyses were carried out at the Chemical Materials Center of the Institute for Molecular Science.

**IR Measurement under Electrolysis Condition.** The approximate cell constitution is depicted in Figure 1. The cell is constructed by plane KBr windows, spacers made of Novix files (purchased from Iwaki Co.), and a three-electrode system (an Au mesh for a working electrode, a Pt wire for an auxiliary electrode, and an  $\text{Ag}|\text{AgCl}$  reference electrode separated from the working electrode by a luggin capillary). The thickness of the cell is 0.3 mm, and the total cell volume is about 0.1 mL. The  $\text{CD}_3\text{CN}$  solution used for the measurement contains the complex ( $1 \times 10^{-2}$  M) and  $\text{LiBF}_4$  ( $5 \times 10^{-2}$  M) as an electrolyte. To prevent evaporation of the solution the cell was continually cooled by refrigerants and only exposed to an infrared lay on measuring.

**Electrochemical Reduction of  $\text{CO}_2$ .** Electrochemical reduction of  $\text{CO}_2$  was performed in  $\text{CO}_2$ -saturated  $\text{CH}_3\text{CN}$  or  $\text{CH}_3\text{CN}/\text{DMSO}$  (1:1, v/v) solutions containing the complex ( $1.0 \times 10^{-3}$  M) and an appropriate electrolyte ( $\text{Bu}_4\text{NBF}_4$  or  $\text{Me}_4\text{NBF}_4$ ,  $5 \times 10^{-2}$  M) under controlled potential electrolysis at a range of -1.50 to -1.60 V (vs  $\text{Ag}|\text{AgCl}$ ). The electrolysis cell consisted of three components, one for a glassy carbon working electrode, the second for a Pt plate auxiliary electrode which was separated from the working electrode cell by a Nafion membrane, and the third for an  $\text{Ag}|\text{AgCl}$  reference electrode. The first two were connected to volumetric flasks filled with  $\text{CO}_2$  gas with a stainless-steel tube. At an appropriate interval of coulombs consumed in the reduction, a 0.1 mL portion of gas was sampled from the gas phase of the working electrode component with a pressure-locked syringe. Characterization and quantification of gaseous products such as  $\text{CO}$  and  $\text{C}_2\text{H}_6$  were performed on a gas chromatograph. The analysis of the solution was carried out by sampling each 0.1 mL portion from the liquid phase of the working electrode component at an

(7) Ishida, H.; Tzeng, B.-C.; Nagao, H.; Peng, S.-M.; Tanaka, K. *Inorg. Chem.* **1993**, *32*, 1508.

(8) (a) Katz, N. E.; Szalda, D. J.; Chou, M. H.; Creutz, C.; Sutin, N. *J. Am. Chem. Soc.* **1989**, *111*, 6591. (b) Creutz, C.; Schwarz, H. A.; Wishart, J. F.; Fujita, E.; Sutin, N. *J. Am. Chem. Soc.* **1989**, *111*, 1153. (c) Sweet, J. R.; Graham, W. A. G. *Organometallics* **1982**, *1*, 982. (d) Bercaw, J. E.; Goh, L.-Y.; Halpen, J. *J. Am. Chem. Soc.* **1972**, *94*, 6534.

(9) Nakajima, H.; Mizukawa, T.; Nagao, H.; Tanaka, K. *Chem. Lett.*, in press.

(10) GC analysis revealed that DMSO and  $\text{CH}_3\text{CN}$  contained  $1.7 \times 10^{-2}$  and  $5.6 \times 10^{-3}$  M  $\text{H}_2\text{O}$ , respectively, even after the purification.

(11) Sullivan, B. P.; Salmon, D. J.; Meyer, T. J. *Inorg. Chem.* **1978**, *17*, 3334.

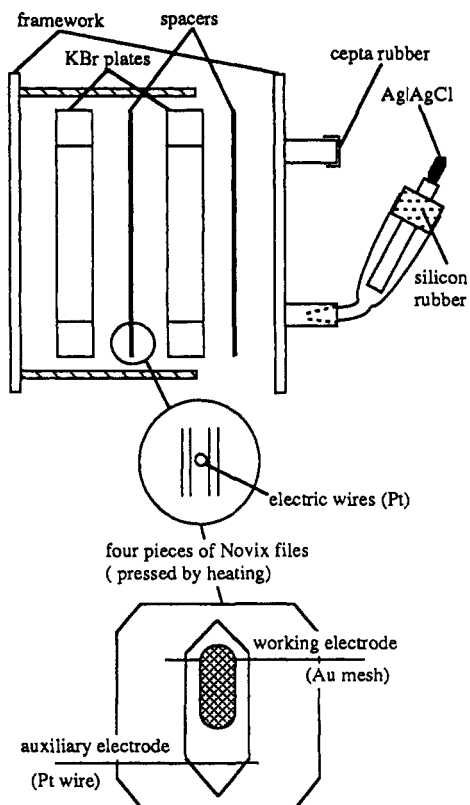


**Figure 1.** Approximate cell constitution employed for the IR measurements under the electrolysis condition.

appropriate interval of coulombs consumed. The amounts of the formic acid, acetone, and acetoacetic acid produced during the electrolysis were determined with an isotachopheretic analyzer, gas chromatograph, and HPLC, respectively.

## Results and Discussion

**Reaction of Two-Electron Reduced Form of [1]<sup>2+</sup> with CO<sub>2</sub>.** A cyclic voltammogram of [Ru(bpy)<sub>2</sub>(qu)(CH<sub>3</sub>CN)]<sup>2+</sup> ([1]<sup>2+</sup>) shows two successive one-electron redox waves at  $E_{1/2} = -1.37$  ([1]<sup>2+/1+</sup>) and  $-1.57$  V ([1]<sup>1+/0</sup>) (vs Ag|AgCl), while [Ru(bpy)<sub>2</sub>(qu)(CO)]<sup>2+</sup> ([2]<sup>2+</sup>) shows three reversible one-electron redox waves at  $-1.11$  ([2]<sup>2+/1+</sup>),  $-1.37$  ([2]<sup>1+/0</sup>), and  $-1.65$  V ([2]<sup>0/1-</sup>) (solid lines in Figure 2). Introduction of CO<sub>2</sub> into the CH<sub>3</sub>CN solutions of [1]<sup>2+</sup> and [2]<sup>2+</sup> by bubbling results in an appearance of strong cathodic currents at potentials more negative than the cathodic waves of the [1]<sup>2+/1+</sup> and [2]<sup>1+/0</sup> couples suggesting high reactivity of both reduced form of [1]<sup>2+</sup> and [2]<sup>2+</sup> with CO<sub>2</sub> (dotted lines in Figure 2). In fact, pouring a dark red CH<sub>3</sub>CN solution of [1]<sup>0</sup><sup>12</sup> upon dry ice<sup>13</sup> followed by warming the mixture to ambient temperature gave a small amount of a white precipitate of (Me<sub>4</sub>N)<sub>2</sub>CO<sub>3</sub> (characterized by comparison of the IR spectrum with an authentic sample). Moreover, the IR spectrum of the crude product obtained by evaporation of the solution under reduced pressure displayed a  $\nu$ -(C≡O) band at 1999 cm<sup>-1</sup> assignable to [2]<sup>2+</sup>. The identification of [2]<sup>2+</sup> and CO<sub>3</sub><sup>2-</sup> species in the reaction mixture suggests that the reaction of [1]<sup>0</sup> with CO<sub>2</sub> initially produces [Ru(bpy)<sub>2</sub>(qu)( $\eta^1$ (C)-CO<sub>2</sub>)]<sup>0</sup> (eq 3a), which then undergoes the oxide transfer by another CO<sub>2</sub> (eq 3b).

(12) Doubly reduced [1]<sup>2+</sup> ([1]<sup>0</sup>) was prepared by the controlled potential electrolysis of an orange solution of [1](PF<sub>6</sub>)<sub>2</sub> (2 × 10<sup>-2</sup> M) at  $-1.60$  V in the presence of Me<sub>4</sub>NBF<sub>4</sub> (5 × 10<sup>-2</sup> M) at 0 °C under N<sub>2</sub>.

(13) Dry ice used in this experiment was prepared by freezing a purified CO<sub>2</sub> gas with liquid N<sub>2</sub>.

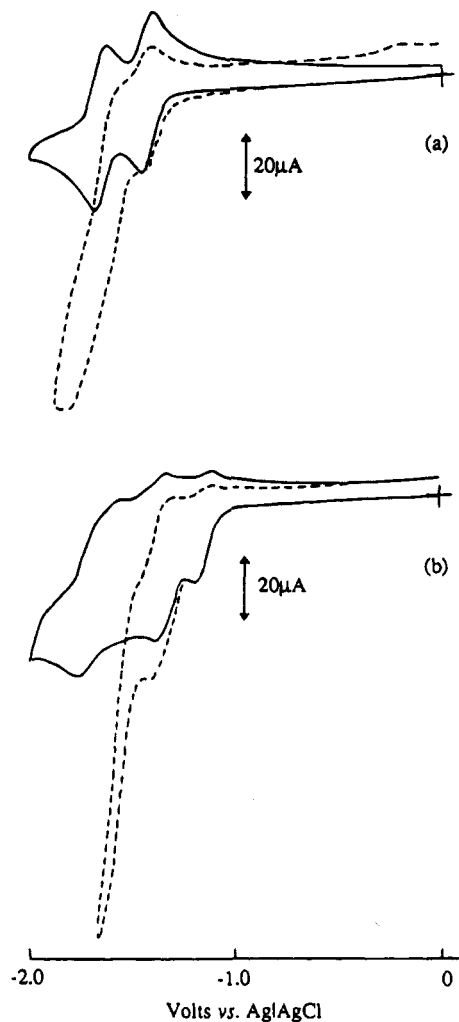
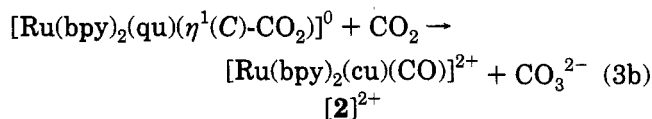
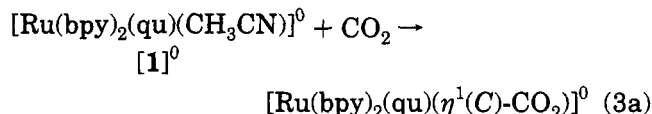
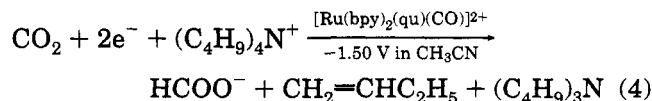


**Figure 2.** Cyclic voltammograms of CH<sub>3</sub>CN solutions containing Me<sub>4</sub>NBF<sub>4</sub> (5 × 10<sup>-2</sup> M) and [1](PF<sub>6</sub>)<sub>2</sub> (a) and [2](PF<sub>6</sub>)<sub>2</sub> (1 × 10<sup>-3</sup> M) (b). Solid and dotted lines are under N<sub>2</sub> and CO<sub>2</sub> atmospheres, respectively.  $dE/dt = 100$  mV/s.



**Electrochemical CO<sub>2</sub> Reduction by [2]<sup>2+</sup>.** As expected from Figure 2b, the two-electron reduced form of [2]<sup>2+</sup> ([2]<sup>0</sup>) also has an ability to catalyze CO<sub>2</sub> reduction. The controlled potential electrolysis of [2](PF<sub>6</sub>)<sub>2</sub> (1 × 10<sup>-3</sup> M) at  $-1.50$  V in CO<sub>2</sub>-saturated CH<sub>3</sub>CN using Bu<sub>4</sub>NBF<sub>4</sub> (5 × 10<sup>-2</sup> M) as an electrolyte predominantly produced HCOO<sup>-</sup> and CO with current efficiencies ( $\eta$ ) of 75 and 2%, respectively, after 70 C passed. Concomitant formation of CH<sub>2</sub>=CHC<sub>2</sub>H<sub>5</sub> and Bu<sub>3</sub>N without the generation of CO<sub>3</sub><sup>2-</sup> species in the electrolyte solution reveals the function of Bu<sub>4</sub>N<sup>+</sup> as a proton donor for HCOO<sup>-</sup> formation (eq 4).<sup>14</sup> On the



other hand, the similar electrochemical CO<sub>2</sub> reduction

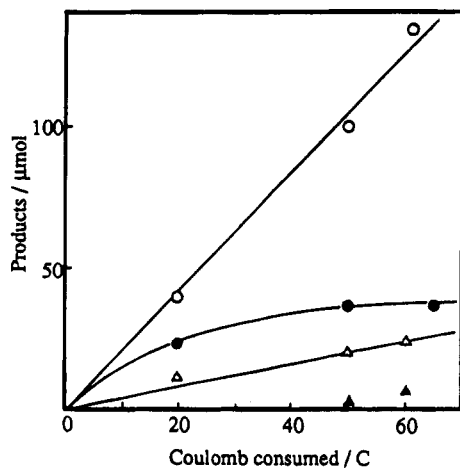
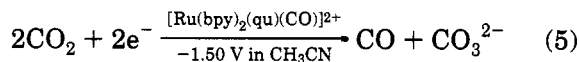


**Figure 3.** Plots of the amounts of CO (○),  $\text{CH}_3\text{C}(\text{O})\text{CH}_3$  (●),  $\text{HCOO}^-$  (Δ), and  $\text{CH}_3\text{C}(\text{O})\text{CH}_2\text{COO}^-$  (▲) against the electricity consumed in the  $\text{CO}_2$  reduction by  $[\mathbf{2}](\text{PF}_6)_2$  ( $1 \times 10^{-3}$  M) in  $\text{CH}_3\text{CN}/\text{DMSO}$  (1:1 v/v) with  $\text{Me}_4\text{NBF}_4$  ( $5 \times 10^{-2}$  M).

by  $[\mathbf{2}](\text{PF}_6)_2$  ( $1 \times 10^{-3}$  M) using  $\text{LiBF}_4$  ( $5 \times 10^{-2}$  M) instead of  $\text{Bu}^n_4\text{NBF}_4$  under otherwise the same conditions gave  $\text{Li}_2\text{CO}_3$  and CO ( $\eta = 78\%$  after 10 C passed),<sup>1k,15</sup> and  $\text{HCOO}^-$  was not detected (eq 5). Thus, the main product in the electrochemical  $\text{CO}_2$  reduction by  $[\mathbf{2}]^{2+}$  is changed from  $\text{HCOO}^-$  to CO (eqs 4 and 5) in the presence and the absence of the proton donor.



The reductive disproportionation of  $\text{CO}_2$  (eq 5) is of interest from the viewpoint of carbonyl generation as the starting material for organic synthesis in aprotic media. Deposition of  $\text{Li}_2\text{CO}_3$  on the glassy carbon electrode, however, gradually inhibited the progress of the  $\text{CO}_2$  reduction in  $\text{CH}_3\text{CN}$ . On the other hand, the electrochemical  $\text{CO}_2$  reduction by  $[\mathbf{2}](\text{PF}_6)_2$  ( $1 \times 10^{-3}$  M) using  $(\text{Me}_4\text{N})\text{BF}_4$  ( $5 \times 10^{-2}$  M) in  $\text{CH}_3\text{CN}/\text{DMSO}$  (1:1 v/v) smoothly proceeded without forming a  $(\text{Me}_4\text{N})_2\text{CO}_3$  layer on the electrode, and  $\text{CH}_3\text{C}(\text{O})\text{CH}_3$  and  $\text{CH}_3\text{C}(\text{O})\text{CH}_2\text{COO}^-$  ( $\eta = 16$  and 6%, respectively) were unexpectedly produced together with CO and  $\text{HCOO}^-$  ( $\eta = 42$  and 7%, respectively) after 60 C passed in the electrolysis (Figure 3). Furthermore,  $[\mathbf{1}]^{2+}$  was obtained in a relatively high yield (>70%) from the reaction residue (confirmed by NMR and IR spectra). The electrochemical  $\text{CO}_2$  reduction conducted in  $\text{CH}_3\text{CN}/\text{DMSO}-d_6$  under otherwise the same reaction conditions gave the same products, and neither  $\text{CD}_3\text{C}(\text{O})\text{CD}_3$  nor  $\text{CD}_3\text{C}(\text{O})\text{CH}_3$  was identified by GC-mass. This observation<sup>16</sup> clearly indicates that  $\text{CH}_3\text{C}(\text{O})\text{CH}_3$  is formed through double methylation of the carbonyl moiety resulting from the reductive disproportionation of  $\text{CO}_2$  by  $[\mathbf{2}]^{2+}$  (eq 5), in which  $\text{Me}_4\text{N}^+$  plays a role as the methylation agent (eq 6). It is worthy of note that  $[\mathbf{2}]^{2+}$

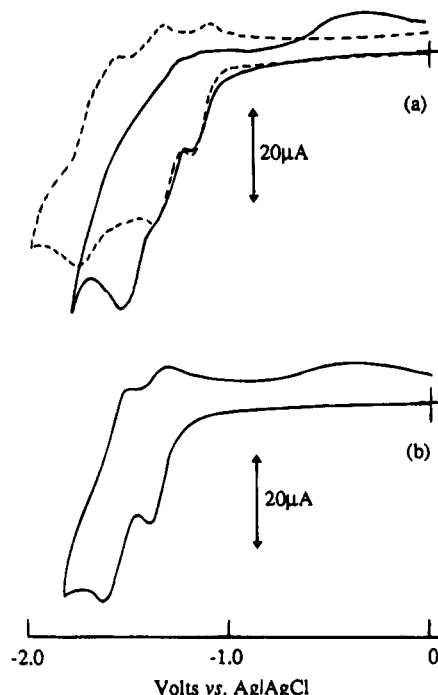
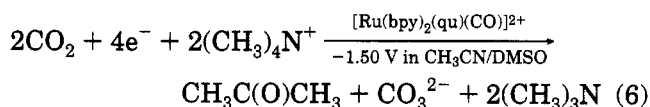
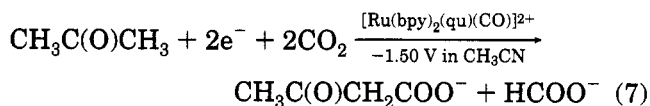


**Figure 4.** (a) Cyclic voltammograms of  $[\mathbf{2}](\text{PF}_6)_2$  ( $1 \times 10^{-3}$  M) in the  $\text{CH}_3\text{CN}$  solution with  $\text{Me}_4\text{NBF}_4$  ( $5 \times 10^{-2}$  M) under  $\text{N}_2$  in the presence (a solid line) and the absence (a dotted line) of  $\text{CH}_3\text{I}$  ( $1 \times 10^{-2}$  M). (b) Cyclic voltammogram of  $[\mathbf{1}](\text{PF}_6)_2$  ( $1 \times 10^{-3}$  M) in a  $\text{CH}_3\text{CN}$  solution under  $\text{N}_2$  containing  $\text{Me}_4\text{NBF}_4$  ( $5 \times 10^{-2}$  M) and  $\text{CH}_3\text{I}$  ( $1 \times 10^{-2}$  M).  $dE/dt = 100$  mV/s.



also catalyzes the carboxylation of the resulting  $\text{CH}_3\text{C}(\text{O})\text{CH}_3$  producing  $\text{CH}_3\text{C}(\text{O})\text{CH}_2\text{COO}^-$  and  $\text{HCOO}^-$  (eq 7) under the electrolysis conditions, since the electro-



chemical reduction of  $\text{CO}_2$  by  $[\mathbf{2}](\text{PF}_6)_2$  ( $1 \times 10^{-3}$  M) in the presence of  $\text{CH}_3\text{C}(\text{O})\text{CH}_3$  ( $1 \times 10^{-2}$  M) in  $\text{CH}_3\text{CN}/\text{DMSO}$  (1:1 v/v) predominantly produced those products.<sup>17</sup> Although electrochemical carboxylation of  $\text{PhC}(\text{O})\text{CH}_3$  affording  $\text{PhC}(\text{O})\text{CH}_2\text{COO}^-$  and  $\text{HCOO}^-$  by  $[\text{Fe}_4\text{S}_4(\text{SPh})_4]^{2-}$  and  $[\text{Ru}(\text{bpy})_2(\text{CO})_2]^{2+}$  in dry  $\text{CH}_3\text{CN}$  has been reported,<sup>18</sup> the present  $\text{CH}_3\text{C}(\text{O})\text{CH}_2\text{COO}^-$  is formed by the double methylation of the carbonyl ligand resulting from the reductive disproportionation of  $\text{CO}_2$  followed by the subsequent carboxylation, where three carbon-carbon bonds are newly formed.

**Reactivity of the Carbonyl Ligand on  $[\mathbf{2}]^0$ .** From the preceding discussion,  $[\mathbf{2}]^0$  possibly undergoes double methylation in the presence of  $\text{Me}_4\text{N}^+$  to afford  $\text{CH}_3\text{C}(\text{O})\text{CH}_3$  (eq 6). Although such unusual methylation of  $[\mathbf{2}]^0$  by  $\text{Me}_4\text{N}^+$  was not detected in the cyclic voltammogram of  $[\mathbf{2}](\text{PF}_6)_2$  in  $\text{CH}_3\text{CN}$  (a solid line of Figure 2b),  $[\mathbf{2}]^{2+}$  shows an additional cathodic wave at  $-1.53$  V in the presence of  $\text{CH}_3\text{I}$  ( $1 \times 10^{-2}$  M) (Figure 4a). On the other hand,  $\text{CH}_3\text{I}$  ( $1 \times 10^{-2}$  M) gave no significant effect

(17) In the absence of  $[\mathbf{2}]^{2+}$ , the carboxylation of  $\text{CH}_3\text{C}(\text{O})\text{CH}_3$  by  $(\text{CH}_3)_3\text{N}$  did not take place in  $\text{CO}_2$ -saturated  $\text{CH}_3\text{CN}/\text{DMSO}$  (1:1, v/v).

(14) (a) Bolinger, C. M.; Sullivan, B. P.; Conrad, D.; Gilbert, J. A.; Story, N.; Meyer, T. J. *J. Chem. Soc., Chem. Commun.* **1985**, 796. (b) Tezuka, M.; Yajima, T.; Tsuchiya, A.; Matsumoto, Y.; Uchida, Y.; Hidai, M. *J. Am. Chem. Soc.* **1982**, *104*, 6834.

(15) (a) Christensen, P.; Hamnett, A.; Muir, A. V. G.; Timney, J. A. *J. Chem. Soc., Dalton Trans.* **1992**, 1455. (b) Sullivan, B. P.; Bolinger, C. M.; Conrad, D.; Vining, W. J.; Meyer, T. J. *J. Chem. Soc., Chem. Commun.* **1985**, 1414.

(16) The similar electrolysis in  $\text{CH}_3\text{CN}/\text{DMSO}$  using  $\text{Et}_4\text{NBF}_4$  in the place of  $\text{Me}_4\text{NBF}_4$  afforded  $(\text{C}_2\text{H}_5)_2\text{C}(\text{O})(\text{C}_2\text{H}_5)$  without generation of  $\text{CH}_3\text{C}(\text{O})\text{CH}_3$  or  $\text{CH}_3\text{C}(\text{O})\text{C}_2\text{H}_5$ .



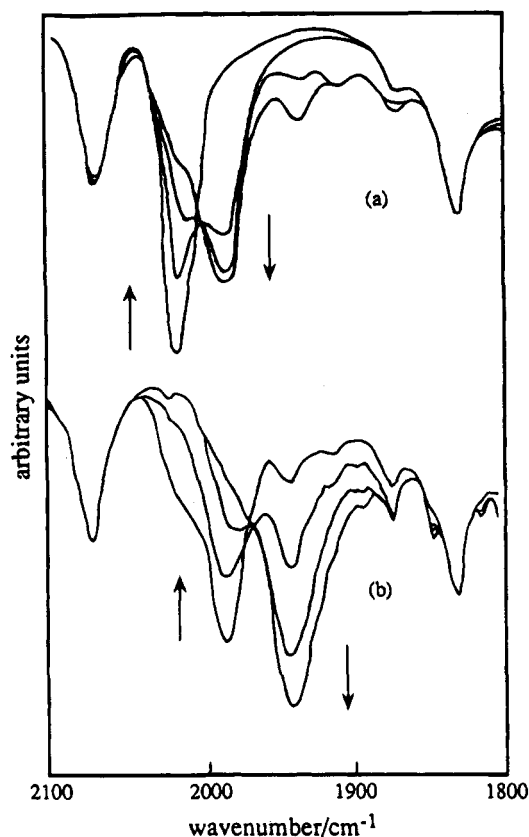
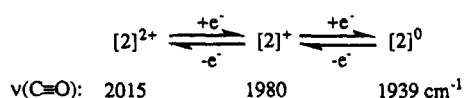


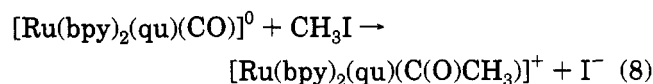
**Figure 5.** IR spectra of [2](PF<sub>6</sub>)<sub>2</sub> (1 × 10<sup>-2</sup> M) with the passage of time under constant potential electrolysis at -1.21 V (a) and subsequently at -1.50 V in a CD<sub>3</sub>CN solution with LiBF<sub>4</sub> (5 × 10<sup>-2</sup> M) under N<sub>2</sub> (b).

#### Scheme 1



on the cyclic voltammogram of [1](PF<sub>6</sub>)<sub>2</sub> (Figure 4b) up to -1.85 V. Thus, CH<sub>3</sub>I smoothly reacts with [2]<sup>0</sup> but not with [1]<sup>0</sup>, suggesting the formation of [Ru(bpy)<sub>2</sub>(qu)(C(O)CH<sub>3</sub>)]<sup>+</sup> rather than [Ru(bpy)<sub>2</sub>(qu)(CH<sub>3</sub>)]<sup>+</sup> (vide infra). The solution IR spectra of [2](PF<sub>6</sub>)<sub>2</sub> in CD<sub>3</sub>CN under controlled potential electrolysis conditions well afford the information for the induced reactivity of the carbonyl ligand. The strong ν(C=O) band of [2]<sup>2+</sup> at 2015 cm<sup>-1</sup><sup>19</sup> shifts to 1980 and 1939 cm<sup>-1</sup> upon the formation of [2]<sup>+</sup> and [2]<sup>0</sup> under electrolysis at -1.21 and -1.50 V, respectively (Figure 5).<sup>20</sup> Reoxidation of the resulting [2]<sup>+</sup> and [2]<sup>0</sup> solutions at 0 V essentially regenerated the original IR spectrum of [2]<sup>2+</sup> although the intensity of the ν(C=O) band of [2]<sup>2+</sup> decreased to some degree due to partial elimination of CO from [2]<sup>0</sup> (formally 20 electron complex) during the reduction-oxidation process. The red shift of the ν(C=O) band of [2]<sup>2+</sup> by about 40 cm<sup>-1</sup> per one electron reduction reflects the reactivity of the electrophilic attack of CH<sub>3</sub>I on the carbonyl ligand (Scheme 1). The ν(C=O) band at 1980 cm<sup>-1</sup> of [2]<sup>+</sup> prepared electrochemically in CH<sub>3</sub>CN was hardly affected by the presence of CH<sub>3</sub>I (even 5 times

molar concentration of the complex). While, similarly prepared [2]<sup>0</sup> reacted with CH<sub>3</sub>I (equimolar concentration of the complex) to bring about an appearance of a strong band at 1568 cm<sup>-1</sup> in the IR spectrum. In addition, the <sup>1</sup>H-NMR spectrum of the reaction mixture in DMSO-*d*<sub>6</sub> showed two singlet signals at δ = 1.71 and 1.67, and the prolonged reaction in the presence of three times excess of CH<sub>3</sub>I at 40 °C for 4 h resulted in disappearance of the latter signal with the generation of a singlet methyl signal of CH<sub>3</sub>C(O)CH<sub>3</sub> at δ = 2.01.<sup>21</sup> Accordingly, the 1568 cm<sup>-1</sup> band in the IR spectrum and the singlet signal at δ = 1.67 in the <sup>1</sup>H-NMR are reasonably assigned to the ν(C=O) band and the methyl signal<sup>22</sup> of [Ru(bpy)<sub>2</sub>(qu)(C(O)CH<sub>3</sub>)]<sup>+</sup> formed by the reaction of [2]<sup>0</sup> with CH<sub>3</sub>I (eq 8). Unfortunately, several attempts to separate the acyl complex from an unidentified product with a singlet signal at δ = 1.71 have been unsuccessful so far.



#### Electrochemical CO<sub>2</sub> Reduction in the Presence of CH<sub>3</sub>I.

The electrochemical CO<sub>2</sub> reduction by [2](PF<sub>6</sub>)<sub>2</sub> using Me<sub>4</sub>NBF<sub>4</sub> in CH<sub>3</sub>CN/DMSO affords CO, HCOO<sup>-</sup>, CH<sub>3</sub>C(O)CH<sub>3</sub>, and CH<sub>3</sub>C(O)CH<sub>2</sub>COO<sup>-</sup> as described above. The similar electrochemical CO<sub>2</sub> reduction in the presence of CH<sub>3</sub>I (3 × 10<sup>-2</sup> M) also gave the latter three products, but CO evolution was completely depressed.<sup>23</sup> Similarly, the electrochemical CO<sub>2</sub> reduction by [Ru(bpy)<sub>2</sub>(*i*-qu)(CO)](PF<sub>6</sub>)<sub>2</sub> (*i*-qu = isoquinoline) (1 × 10<sup>-3</sup> M) in the presence of CH<sub>3</sub>I (3 × 10<sup>-2</sup> M) and Me<sub>4</sub>NBF<sub>4</sub> (5 × 10<sup>-2</sup> M) also generated essentially same amounts of those products without CO evolution under otherwise the same electrolysis conditions. The depression of CO evolution in those reactions probably results from the smooth reaction of CH<sub>3</sub>I with [Ru(bpy)<sub>2</sub>(L)(CO)]<sup>0</sup> (L = qu and *i*-qu) forming [Ru(bpy)<sub>2</sub>(L)(C(O)CH<sub>3</sub>)]<sup>+</sup> (eq 8) as the precursor to CH<sub>3</sub>C(O)CH<sub>3</sub> prior to the Ru-CO bond cleavage (eq 5). Small amounts of ethane evolution, however, were observed in the CO<sub>2</sub> reduction catalyzed by [Ru(bpy)<sub>2</sub>(*i*-qu)(CO)]<sup>2+</sup> in contrast to the CO<sub>2</sub> reduction by [2]<sup>2+</sup> (Figure 6). In addition to the recovery of [Ru(bpy)<sub>2</sub>(L)(CH<sub>3</sub>CN)]<sup>2+</sup> (L = qu and *i*-qu) after the electrochemical CO<sub>2</sub> reduction in the presence of CH<sub>3</sub>I (in ca. 70% yield after 60 C passed on the basis of the NMR spectra), the C<sub>2</sub>H<sub>6</sub> formation depending on the substituent of [Ru(bpy)<sub>2</sub>(L)(CO)]<sup>2+</sup> may be related to the steric effects of those ligands and reasonably excludes the possibility of dissociation of the quinoline analogue ligands (L) and dechelation of the bpy ligands during the electrochemical CO<sub>2</sub> reduction. In the presence of CH<sub>3</sub>I, [Ru(bpy)<sub>2</sub>(L)(solvent)]<sup>0</sup> and/or [Ru(bpy)<sub>2</sub>(L)]<sup>0</sup> would be expected to undergo a competitive electrophilic attack of CH<sub>3</sub>I and CO<sub>2</sub> producing [Ru(bpy)<sub>2</sub>(L)(CH<sub>3</sub>)]<sup>+</sup> and [Ru(bpy)<sub>2</sub>(L)(η<sup>1</sup>(C)-CO<sub>2</sub>)]<sup>0</sup> (eq 3a), respectively. Assum-

(21) Silverstein, R. M.; Bassler, G. C.; Morrill, T. C., Eds. *Spectroscopic Identification of Organic Compounds*, 4th ed.; Wiley & Sons, Inc.: New York, 1981.

(22) (a) Reference 10, p 40. (b) Belt, S. T.; Ryba, D. W.; Ford, P. C. *J. Am. Chem. Soc.* **1991**, *113*, 9524. (c) Shafiq, F.; Kramarz, K. W.; Eisenberg, R. *Inorg. Chim. Acta* **1993**, *213*, 111. (d) Brumbaugh, J. S.; Whittle, R. R.; Parvez, M.; Sen, A. *Organometallics* **1990**, *9*, 1735.

(23) The current efficiencies for CO, HCOO<sup>-</sup>, CH<sub>3</sub>C(O)CH<sub>3</sub>, and CH<sub>3</sub>C(O)CH<sub>2</sub>COO<sup>-</sup> formation in the CO<sub>2</sub> reduction in the presence of CH<sub>3</sub>I are not so improved compared with those in the absence of CH<sub>3</sub>I because of large background currents of an I<sub>2</sub>/I<sup>-</sup> redox reaction on the working and auxiliary electrodes.

(18) (a) Tanaka, K.; Wakita, R.; Tanaka, T. *J. Am. Chem. Soc.* **1989**, *111*, 2428. (b) Tanaka, K.; Miyamoto, H.; Tanaka, T. *Chem. Lett.* **1988**, 2033.

(19) The CO stretching band of [2]<sup>2+</sup> observed at 1996 cm<sup>-1</sup> in a KBr pellet shifted to 2015 cm<sup>-1</sup> in CD<sub>3</sub>CN.

(20) Electrochemical reductions of [Re(bpy)(CO)<sub>3</sub>Cl] analogs have caused similar red shifts of ν(C=O) bands. See refs 1g and 15a.



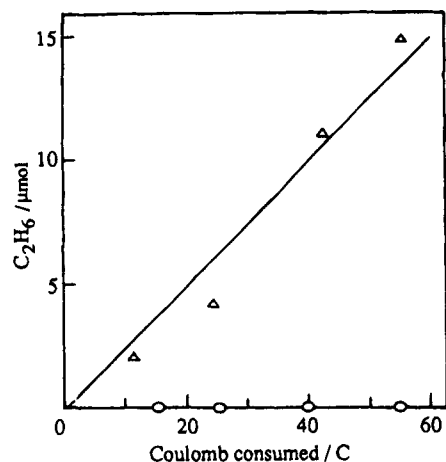


**Figure 6.** Plots of the amounts of  $C_2H_6$  evolved against the electricity consumed in the  $CO_2$  reduction by  $[Ru(bpy)_2(L)(CO)](PF_6)_2$  ( $L = qu$  (O);  $i-qu$  ( $\Delta$ )) ( $1 \times 10^{-3}$  M) in  $CH_3CN/DMSO$  (1:1 v/v) containing  $Me_4NBF_4$  ( $5 \times 10^{-2}$  M) and  $CH_3I$  ( $3 \times 10^{-2}$  M).

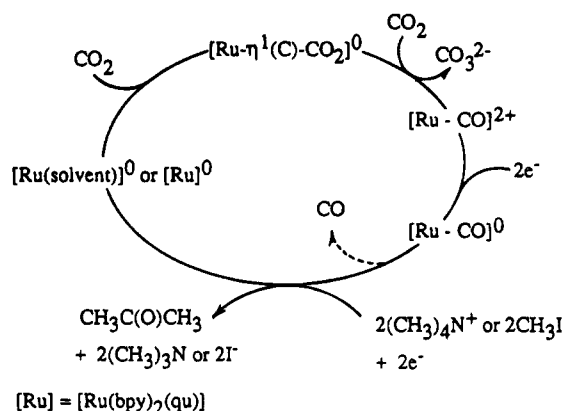
ing that the former is the precursor to  $C_2H_6$  no  $C_2H_6$  evolution in the  $CO_2$  reduction by  $[2]^{2+}$  (Figure 6) implies a large steric hindrance of the qu ligand against the electrophilic attack of bulky  $CH_3I$  on the metal center. Thus, the formation of  $C_2H_6$  (Figure 6) is reasonably explained by the position of the phenyl groups of the qu and  $i-qu$  ligands in those complexes.

**Mechanism.** The reaction of  $[1]^0$  with  $CO_2$  affording  $[2]^{2+}$  and  $CO_3^{2-}$  (eq 3) possibly proceeds via  $[Ru(bpy)_2(qu)(\eta^1(C)-CO_2)]$  and the subsequent oxide abstraction by  $CO_2$ . The reductive disproportionation of  $CO_2$  affording  $CO$  and  $CO_3^{2-}$  (eq 5) in the electrochemical  $CO_2$  reduction by  $[2]^{2+}$  in the presence of  $LiBF_4$  also could be ascribed to the participation of  $[1]^0$  and  $[Ru(bpy)_2(qu)(\eta^1(C)-CO_2)]$  in the catalytic cycle. It has been reported that two  $CO_2$  molecules react with  $Ir(C_8H_{14})Cl(PMe_3)_3$  and  $Mo(N_2)_2(PMe_3)_4$  to produce  $IrC(O)OC(O)O(Cl)(PMe_3)_3$  and  $Mo(\eta^2(O,O)-CO_3)(CO)(PMe_3)_4$ , respectively.<sup>24,25</sup> Although the condensation and disproportionation reactions of  $CO_2$  on those metal complexes are feasible models for the catalytic reductive disproportionation of  $CO_2$ , at least two coordination sites are required for the attack of  $CO_2$  on the metal centers in those reactions. Taking into account the rigidity of the ambient ligands on the hexacoordinated  $[Ru(bpy)_2(qu)(\eta^1(C)-CO_2)]$  and the strong basicity of the  $\eta^1(C)-CO_2$  moiety compared with that of  $[Ru(bpy)_2(CO)(\eta^1(C)-CO_2)]$ , the oxide transfer from  $[Ru(bpy)_2(qu)(\eta^1(C)-CO_2)]$  to another  $CO_2$  may not involve an expansion of the coordination number of the complex. In accordance with this,  $[W(CO)_6]$  formation in the reaction of  $Li_2[W(CO)_5(\eta^1(C)-CO_2)]$  with free  $CO_2$  is explained in terms of a direct oxide transfer through a  $W-C(O)O-CO_2Li$  intermediate.<sup>5a-c</sup> The formation of  $C_2H_5CH=CH_2$  and

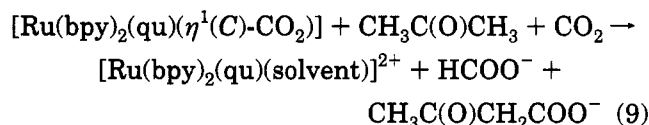
(24) Herschkovitz, T.; Guggenberger, L. *J. Am. Chem. Soc.* **1976**, *98*, 1615.

(25) Alvarez, R.; Atwood, J. L.; Carmona, E.; Pérez, P. J.; Poveda, M. L.; Rogers, R. D. *Inorg. Chem.* **1991**, *30*, 1493.

Scheme 2



$Bu_3N$  in the electrochemical  $CO_2$  reduction using  $Bu^u_4N^+$  (eq 4) also reflects the strong basicity of  $[Ru(bpy)_2(qu)(\eta^1(C)-CO_2)]$ , and  $[Ru(bpy)_2(qu)(C(O)OH)]^+$  may exist as the precursor for  $HCOO^-$  formation, since  $[Ru(bpy)_2(CO)(C(O)OH)]^+$  formed by the protonation of  $[Ru(bpy)_2(CO)(\eta^1(C)-CO_2)]$  is known as the precursor for the  $HCOO^-$  formation in photo- and electrochemical  $CO_2$  reductions.<sup>4a,26</sup> The oxide transfer from  $[Ru(bpy)_2(qu)(\eta^1(C)-CO_2)]$  to  $CO_2$  regenerates  $[2]^{2+}$  in the absence of a proton donor. The subsequent two-electron reduction of  $[2]^{2+}$  under the electrolysis conditions induces the double methylation of the carbonyl ligand with  $Me_4N^+$  and/or  $CH_3I$  to produce  $CH_3C(O)CH_3$  possibly via  $[Ru(bpy)_2(qu)(C(O)CH_3)]^+$  (Scheme 2). As similar to the case for  $Bu^u_4N^+$ , the resulting  $CH_3C(O)CH_3$  probably undergoes the abstraction of its  $\alpha$ -proton by  $[Ru(bpy)_2(qu)(\eta^1(C)-CO_2)]$ , and consequently both  $CH_3C(O)CH_2COO^-$  and  $HCOO^-$  would be formed under  $CO_2$  atmosphere (eq 9).<sup>27</sup>



The present work describes the first catalytic formation of  $CH_3C(O)CH_3$  and  $CH_3C(O)CH_2COO^-$  by the double methylation of the carbonyl moiety resulting from the reductive disproportionation of  $CO_2$  followed by the subsequent carboxylation in the electrochemical  $CO_2$  reduction, which demonstrates the feasibility of  $CO_2$  as a building block in organic synthesis.

**Acknowledgment.** This work is partially supported by JSPS Fellowships for Japanese Junior Scientists and a Grant-in-Aid for Scientific Research from the Ministry of Education of Japan.

OM950206M

(26) (a) Ishida, H.; Tanaka, K.; Tanaka, T. *Organometallics* **1987**, *6*, 181. (b) Ishida, H.; Terada, T.; Tanaka, T. *Inorg. Chem.* **1990**, *29*, 905.

(27) On the basis of the preferential  $HCOO^-$  formation in the electrochemical  $CO_2$  reduction by  $[2]^{2+}$  in the presence of  $Bu^u_4N^+$  (eq 4), the discrepancy in the amount of  $CH_3C(O)CH_2COO^-$  and  $HCOO^-$  in Figure 3 may result from the participation of  $H_2O$  involved in  $DMSO/CH_3CN$  (see ref 11) as well as the produced  $CH_3C(O)CH_3$  as proton sources for the formation of  $HCOO^-$  in the  $CO_2$  reduction.

# Comparison of Ru–C Bond Characters Involved in Successive Reduction of Ru–CO<sub>2</sub> to Ru–CH<sub>2</sub>OH

Kiyotsuna Toyohara, Kiyoshi Tsuge, and Koji Tanaka\*

*Institute for Molecular Science, Myodaiji, Okazaki 444, Japan*

Received June 22, 1995\*

Comparison of Raman spectra of a series of *cis*-[Ru(bpy)<sub>2</sub>(CO)X]<sup>n+</sup> complexes (X = CO, C(O)OH, C(O)OCH<sub>3</sub>, CO<sub>2</sub>, CHO, and CH<sub>2</sub>OH; n = 0–2) and their <sup>18</sup>O- or deuterium-substituted analogs permit reasonable assignments of ν(Ru–X) and ν(Ru–CO) bands around 500 and 470 cm<sup>-1</sup>. The validity of the assignments of those bands led to identification of two configurational isomers of *cis*-[Ru(bpy)<sub>2</sub>(CO)(CH<sub>2</sub>OH)]<sup>+</sup> with respect to the orientation of the CH<sub>2</sub>–OH bond. The ν(Ru–X) bands shift to higher wavenumbers as the Ru–X bond distances (*d*(Ru–X)) become longer. Such unusual dependence of ν(Ru–X) upon *d*(Ru–X) may be associated with multibond characters of the C≡O, C=O, and C–O bonds in the Ru–X moieties.

## Introduction

Conversion of CO<sub>2</sub> to highly reduced organic compounds has been attracting much attention from the viewpoint of utilization of CO<sub>2</sub> as a C1 resource. Taking into account that CO<sub>2</sub> reduction of Cu electrodes generates a variety of organic molecules such as CH<sub>4</sub>, C<sub>2</sub>H<sub>2</sub>, C<sub>2</sub>H<sub>5</sub>OH, and C<sub>3</sub>H<sub>7</sub>OH,<sup>1</sup> electrochemical CO<sub>2</sub> reduction by metal complexes may provide suitable models for the understanding of the multistep conversion of CO<sub>2</sub> to organic compounds on a metal surface. Although most CO<sub>2</sub> reductions using metal complexes give only CO and/or HCOOH,<sup>2–5</sup> multielectron reduction of CO<sub>2</sub> is more favorable than two-electron reduction in a thermody-

amic sense, because the *E*<sup>o</sup> values (25 °C, pH 0) for HCOOH, CO, HCHO, CH<sub>3</sub>OH, and CH<sub>4</sub> formation are –0.199, –0.103, –0.071, +0.030, and +0.169 V vs NHE, respectively. Recently, not only HCOOH and CO but also HCHO, CH<sub>3</sub>OH, HO(O)CCHO, and HO(O)CCH<sub>2</sub>OH have been obtained in electrochemical CO<sub>2</sub> reduction by [Ru(bpy)(trpy)(CO)]<sup>2+</sup> in EtOH/H<sub>2</sub>O at –20 °C,<sup>6</sup> in which Ru–CO<sub>2</sub>, Ru–C(O)OH, Ru–CO, Ru–CHO, and Ru–CH<sub>2</sub>OH species have been suggested to participate in the catalytic cycle. Such multistep conversion of CO<sub>2</sub> on Ru is inevitably accomplished by variation in the carbon orbital of the Ru–C bond (sp<sup>2</sup>, sp, and sp<sup>3</sup>), which would also have a crucial influence on the formation energy of HCOOH, CO, HCHO, CH<sub>3</sub>OH, and CH<sub>4</sub> in multielectron reduction of CO<sub>2</sub> by metal complexes. Vibrational spectroscopy may provide useful information about the Ru–C bond characters in the conversion from Ru–CO<sub>2</sub> to Ru–CH<sub>2</sub>OH.

Vibrational studies on organometallic compounds, including metal–CO<sub>2</sub> adducts, have been well documented and elucidated the presence of various couplings of metal–carbon stretching modes with many vibrational modes of other ligands.<sup>7</sup> We, therefore, have undertaken a Raman spectroscopic study of a series of *cis*-[Ru(bpy)<sub>2</sub>(CO)X]<sup>n+</sup> (X = CO<sub>2</sub>, C(O)OH, C(O)OCH<sub>3</sub>, CO, CHO, and CH<sub>2</sub>OH; n = 0–2) complexes and their <sup>18</sup>O- or deuterium-substituted analogs in order to assign ν(Ru–X) bands. Comparison of the Raman spectra among those homologous complexes would permit reasonable assignments of the ν(Ru–X) bands without serious variations in the extent of couplings with other vibrational modes.

\* Abstract published in *Advance ACS Abstracts*, October 1, 1995.

(1) Hori, Y.; Murata, A.; Takahashi, R.; Suzuki, S. *J. Chem. Soc., Chem. Commun.* **1988**, 17.

(2) Electrochemical CO<sub>2</sub> reduction and mechanisms: (a) Arana, C.; Keshavarz, M.; Potts, K. T.; Abruna, H. D. *Inorg. Chim. Acta* **1994**, *225*, 285. (b) Steffey, B. D.; Miedaner, A.; Maciejewski-Farmer, M. L.; Bernatis, P. R.; Herring, A. M.; Allured, V. S.; Carperos, V.; DuBois, D. L. *Organometallics* **1994**, *13*, 4844. (c) Szymaszek, A.; Pruchnik, F. *Rhodium Express* **1994**, *5*, 18. (d) Fujita, E.; Haff, J.; Sanzenbacher, R.; Elias, H. *Inorg. Chem.* **1994**, *33*, 4627. (e) Ogura, K.; Sugihara, H.; Yano, J.; Higasa, M. *J. Electrochem. Soc.* **1994**, *141*, 419. (f) Chardon-Noblat, S.; Collomb-Dunand-Sauthier, M.-N.; Deronzier, A.; Ziessel, R.; Zsoldos, D. *Inorg. Chem.* **1994**, *33*, 4410. (g) Christensen, P.; Hamnett, A.; Muir, A. V. G.; Timney, J. A.; Higgins, S. *J. Chem. Soc., Faraday Trans.* **1994**, *90*, 459. (h) Kimura, E.; Wada, S.; Shionoya, M.; Okazaki, Y. *Inorg. Chem.* **1994**, *33*, 770. (i) Kolodnick, K. J.; Schrier, P. W.; Walton, R. A. *Polyhedron* **1994**, *13*, 457. (j) Collomb-Dunand-Sauthier, M.-N.; Deronzier, A.; Ziessel, R. *J. Chem. Soc., Chem. Commun.* **1994**, 189. (k) Haines, R. J.; Wittig, R. E.; Kubiak, C. P. *Inorg. Chem.* **1994**, *33*, 4723. (l) Collomb-Dunand-Sauthier, M.-N.; Deronzier, A.; Ziessel, R. *Inorg. Chem.* **1994**, *33*, 2961. (m) Halmann, M. M., Ed. *Chemical Fixation of Carbon Dioxides*; CRC Press: London, 1993; p 67. (n) Bhugun, I.; Lexa, D.; Saveant, J.-M. *J. Am. Chem. Soc.* **1994**, *116*, 5015. (o) Sullivan, B. P., Ed. *Electrochemical and Electrocatalytic Reduction of Carbon Dioxide*; Elsevier: Amsterdam, 1993, and references therein.

(3) Photochemical reduction of CO<sub>2</sub>: (a) Ishitani, O.; George, M. W.; Ibusuki, T.; Johnson, F. P. A.; Koike, K.; Nozaki, K.; Pac, C.; Turner, J. J.; Westwell, J. R. *Inorg. Chem.* **1994**, *33*, 4712. (b) Matsuoka, S.; Yamamoto, K.; Ogata, T.; Kusaba, M.; Nakashima, N.; Fujita, E.; Yanagida, S. *J. Am. Chem. Soc.* **1993**, *115*, 601. (c) Calzaferri, G.; Haedener, K.; Li, J. *J. Photochem. Photobiol., A* **1992**, *64*, 259. (d) Kimura, E.; Bu, X.; Shinomiya, M.; Wada, S.; Maruyama, S. *Inorg. Chem.* **1992**, *31*, 4542 and references therein.

(4) Insertion of CO<sub>2</sub> into M–H. (a) Ratliff, K. S.; Lentz, R. E.; Kubiak, C. P. *Organometallics* **1992**, *11*, 1986. (b) Jegat, C.; Fouassier, M.; Mascetti, J. *Inorg. Chem.* **1991**, *30*, 1521. (c) Jegat, C.; Fouassier, M.; Tranquille, M.; Mascetti, J. *Inorg. Chem.* **1991**, *30*, 1529. (d) Pugh, J. R.; Bruce, M. R. M.; Sullivan, B. P.; Meyer, T. J. *Inorg. Chem.* **1991**, *30*, 86. (e) Sullivan, B. P.; Meyer, T. J. *J. Chem. Soc., Chem. Commun.* **1984**, 1244.

(5) CO formation in protic media: (a) Ishida, H.; Katsuyuki, F.; Ohba, T.; Ohkubo, K.; Tanaka, T.; Terada, T.; Tanaka, T. *J. Chem. Soc., Dalton Trans.* **1990**, 2155. (b) Ishida, H.; Tanaka, K.; Morimoto, M.; Tanaka, T. *Organometallics* **1986**, *5*, 724. (c) Tanaka, K.; Morimoto, M.; Tanaka, T. *Chem. Lett.* **1983**, 901. (d) Choudhury, D.; Cole-Hamilton, D. J. *J. Chem. Soc., Dalton Trans.* **1982**, 1885.

(6) (a) Nagao, H.; Mizukawa, T.; Tanaka, K. *Inorg. Chem.* **1994**, *33*, 3415. (b) Nagao, H.; Mizukawa, T.; Tanaka, K. *Chem. Lett.* **1993**, 955.

(7) (a) Caballol, R.; Sanchez, M. E.; Barthelat, J. C. *J. Phys. Chem.* **1987**, *91*, 1328. (b) Jegat, C.; Fouassier, M.; Tranquille, M.; Mascetti, J.; Tommasi, I.; Aresta, M.; Ingold, F.; Dedieu, A. *Inorg. Chem.* **1993**, *32*, 1279. (c) Jegat, C.; Fouassier, M.; Mascetti, J. *Inorg. Chem.* **1991**, *30*, 1521. (d) Jegat, C.; Fouassier, M.; Tranquille, M.; Mascetti, J. *Inorg. Chem.* **1991**, *30*, 1529.

## Experimental Section

**Materials.** Commercially available  $\text{H}_2^{18}\text{O}$  and  $\text{NaBD}_4$  were used without further purification. Preparation of  $\text{Cl}^-$  and  $\text{PF}_6^-$  salts of  $\text{cis-}[\text{Ru}(\text{bpy})_2(\text{CO})_2]^{2+}$  was described elsewhere.<sup>8</sup> The remaining complexes  $\text{cis-}[\text{Ru}(\text{bpy})_2(\text{CO})(\text{COOH})](\text{PF}_6)$ ,  $\text{cis-}[\text{Ru}(\text{bpy})_2(\text{CO})(\text{CO}_2)]$ , and  $\text{cis-}[\text{Ru}(\text{bpy})_2(\text{CO})(\text{CH}_2\text{OH})](\text{PF}_6)$  were prepared by reactions of  $\text{cis-}[\text{Ru}(\text{bpy})_2(\text{CO})_2](\text{PF}_6)_2$  with  $\text{Bu}_4\text{NOH}$  and  $\text{NaBH}_4$ , as reported previously.<sup>5b,6a,9</sup> Deuterium-substituted  $\text{cis-}[\text{Ru}(\text{bpy})_2(\text{CO})(\text{CD}_2\text{OH})]^+$  was prepared by the reaction of  $\text{cis-}[\text{Ru}(\text{bpy})_2(\text{CO})_2]^{2+}$  with  $\text{NaBD}_4$  in  $\text{CH}_3\text{CN}/\text{H}_2\text{O}$ .

**Synthesis of  $[\text{Ru}(\text{bpy})_2(\text{CO})(\text{CHO})](\text{PF}_6)$ .** An addition of a 1.5 molar excess of  $\text{NaBH}_4$  to a colorless  $\text{MeOH}/\text{H}_2\text{O}$  (2:1 v/v) solution of  $\text{cis-}[\text{Ru}(\text{bpy})_2(\text{CO})_2](\text{PF}_6)_2$  at  $-5^\circ\text{C}$  resulted in gradual precipitation of yellow  $\text{cis-}[\text{Ru}(\text{bpy})_2(\text{CO})(\text{CHO})](\text{PF}_6)$  (1), which was collected by filtration and washed with cold water; yield 75%. Anal. Calcd: C, 42.93; H, 2.76; N, 9.11. Found: C, 42.64; H, 2.85; N, 9.04. IR spectrum (KBr): 1608 ( $\nu(\text{C}=\text{O})$ ) and 1950  $\text{cm}^{-1}$  ( $\nu(\text{C}\equiv\text{O})$ ).  $^1\text{H}$  and  $^{13}\text{C}$  NMR:  $\delta$  13.9 and 265 ( $-\text{CHO}$ ). Similarly, deuterium-substituted  $\text{cis-}[\text{Ru}(\text{bpy})_2(\text{CO})(\text{CDO})]^+$  was prepared by a reaction of  $\text{cis-}[\text{Ru}(\text{bpy})_2(\text{CO})_2]^{2+}$  with  $\text{NaBD}_4$  in  $\text{CH}_3\text{OH}/\text{H}_2\text{O}$ .

**Raman Spectroscopy.** Raman spectra were measured on a Perkin-Elmer FT-Raman 2000 equipped with a Nd:YAG laser (laser power 500 mW at Rayleigh scattering 1064 nm, resolution 4  $\text{cm}^{-1}$ ) and an InGaAs detector. All measurements were carried out in KBr disks or solutions (ca. 50  $\text{mmol}/\text{dm}^3$ ) in 10 mm diameter glass tubes at room temperature.

**X-ray Analysis of  $[\text{Ru}(\text{bpy})_2(\text{CO})(\text{CH}_2\text{OH})](\text{PF}_6)$ .** Although we have reported the structure of the hydroxymethyl complex,<sup>6a</sup> detailed investigations of the IR and Raman spectra of  $\text{cis-}[\text{Ru}(\text{bpy})_2(\text{CO})(\text{CH}_2\text{OH})]^+$  suggested the existence of two isomers in the solid state. We carefully examined the final difference Fourier map again and found that the oxygen atom of the hydroxymethyl group was disordered over two sites, giving two isomers. The least-squares calculation including the disordered oxygen atom and the structure was successfully refined. All calculations were carried out on a Silicon Graphics IRIS Indigo computer system using TEXSAN.<sup>10</sup> The  $R$  and  $R_w$  values converged to 0.048 and 0.053 with the disordered oxygen atom, while they were 0.059 and 0.070 without the disordered atom. The bond lengths and angles are almost the same values as those in the previously determined structure, except for the hydroxymethyl group.

The crystallographic data, final atomic parameters, and bond lengths and angles have been deposited as supporting information.

## Results

Raman spectra have been widely employed to assess metal-carbon bond characters of organometallic complexes, and metal-carbon stretching modes usually emerge in the range 1000–200  $\text{cm}^{-1}$ .<sup>11</sup> To assign  $\nu(\text{Ru}-\text{CO})$  and  $\nu(\text{Ru}-\text{X})$  bands of  $\text{cis-}[\text{Ru}(\text{bpy})_2(\text{CO})\text{X}]^{n+}$  ( $\text{X} = \text{CO}_2$ ,  $\text{C}(\text{O})\text{OH}$ ,  $\text{C}(\text{O})\text{OCH}_3$ ,  $\text{CO}$ ,  $\text{CHO}$ , and  $\text{CH}_2\text{OH}$ ;  $n = 0-2$ ) in the Raman spectra, oxygen or hydrogen atoms in the substituent X were replaced by their isotopes because of the difficulty in synthesis of  $\text{cis-}[\text{Ru}(\text{bpy})_2(^{13}\text{CO})_2]^{2+}$  as the starting compound for the preparation of the series of complexes. Substitutions of the oxygen

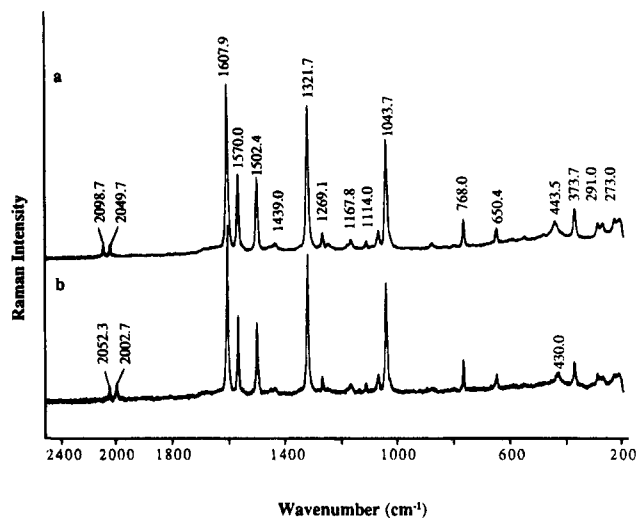
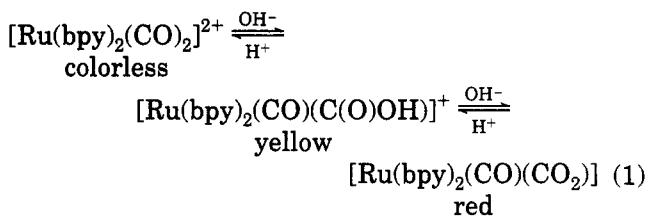


**Figure 1.** Raman spectra of (a)  $\text{cis-}[\text{Ru}(\text{bpy})_2(\text{C}^{16}\text{O})_2](\text{Cl})_2$  in  $\text{H}_2^{16}\text{O}$  and (b)  $\text{cis-}[\text{Ru}(\text{bpy})_2(\text{C}^{18}\text{O})_2](\text{Cl})_2$  in  $\text{H}_2^{18}\text{O}/\text{CH}_3\text{OH}$  (4/1 (v/v)).

atoms of  $\text{cis-}[\text{Ru}(\text{bpy})_2(\text{C}^{16}\text{O})_2]^{2+}$  and  $\text{cis-}[\text{Ru}(\text{bpy})_2(\text{CO})(\text{C}^{16}\text{O}_2)]$  by  $^{18}\text{O}$  were conducted by taking advantage of a facile equilibration reaction (eq 1) in  $\text{H}_2^{18}\text{O}$ .<sup>12</sup> The



assignments of the Ru-C stretching bands in the Raman spectra of  $\text{cis-}[\text{Ru}(\text{bpy})_2(\text{CO})_2]^{2+}$  and  $\text{cis-}[\text{Ru}(\text{bpy})_2(\text{CO})(\text{CO}_2)]$  were, therefore, based on the isomer shifts caused by the replacement of  $^{16}\text{O}$  by  $^{18}\text{O}$ . The conversion from  $\text{cis-}[\text{Ru}(\text{bpy})_2(\text{C}^{16}\text{O})_2]\text{Cl}_2$  to  $\text{cis-}[\text{Ru}(\text{bpy})_2(\text{C}^{18}\text{O})_2]\text{Cl}_2$  was easily monitored by the disappearance of the two  $\nu(\text{C}^{16}\text{O})$  bands at 2098.7 and 2052.3 ( $\text{m}$ )  $\text{cm}^{-1}$  of the former and appearance of the two  $\nu(\text{C}^{18}\text{O})$  bands at 2049.7 and 2002.7 ( $\text{m}$ )  $\text{cm}^{-1}$  of the latter in the Raman spectra in  $\text{H}_2^{18}\text{O}/\text{CH}_3\text{OH}$  (4:1 v/v) (Figure 1). Besides those  $\nu(\text{CO})$  bands, only one band at 443.6 ( $\text{m}$ )  $\text{cm}^{-1}$ , observed in  $\text{H}_2^{16}\text{O}/\text{CH}_3\text{OH}$ , shows an isotope shift to 430.0 ( $\text{m}$ )  $\text{cm}^{-1}$  in  $\text{H}_2^{18}\text{O}/\text{CH}_3\text{OH}$ . Not only the band positions but also the patterns of all other peaks detected in  $\text{H}_2^{16}\text{O}$  and  $\text{H}_2^{18}\text{O}$  are identical within  $\pm 1.0$   $\text{cm}^{-1}$ . The 443.6  $\text{cm}^{-1}$  band, therefore, is reasonably assigned to  $\nu_{\text{sym}}(\text{Ru}-\text{CO})$  of  $\text{cis-}[\text{Ru}(\text{bpy})_2(\text{CO})_2]^{2+}$ . The  $\nu_{\text{asym}}(\text{Ru}-\text{CO})$  band in the Raman spectrum of  $\text{cis-}[\text{Ru}(\text{bpy})_2(\text{CO})_2]\text{Cl}_2$  may be weakened by the local  $\text{C}_{2v}$  symmetry of  $\text{cis-}[\text{Ru}(\text{bpy})_2(\text{CO})_2]^{2+}$ .<sup>13</sup>

Similarly, the  $\nu(\text{CO})$  band at 1947.9 ( $\text{m}$ )  $\text{cm}^{-1}$  in  $\text{cis-}[\text{Ru}(\text{bpy})_2(\text{C}^{16}\text{O})(\text{C}^{16}\text{O}_2)]$  in  $\text{CH}_3\text{OH}/\text{H}_2^{16}\text{O}$  (4:1 v/v) moves to 1908.9 ( $\text{m}$ )  $\text{cm}^{-1}$  in  $\text{CH}_3\text{OH}/\text{H}_2^{18}\text{O}$  (4:1 v/v) (Figure 2). Furthermore, the shift of a band at 1242.3  $\text{cm}^{-1}$  in  $\text{CH}_3\text{OH}/\text{H}_2^{16}\text{O}$  to 1224.8  $\text{cm}^{-1}$  in  $\text{CH}_3\text{OH}/\text{H}_2^{18}\text{O}$  is associated with the  $\nu_{\text{sym}}(\text{CO}_2)$  band. On the basis of an assignment of the  $\nu_{\text{asym}}(\text{CO}_2)$  band at 1442.5  $\text{cm}^{-1}$  in the IR spectrum, the band may be obscured by the change

(8) Kelly, J. M.; O'Connell, C. M. *J. Chem. Soc., Dalton Trans.* **1986**, 253.

(9) (a) Tanaka, H.; Tzeng, B. C.; Nagao, H.; Peng, S. M.; Tanaka, K. *Organometallics* **1992**, *11*, 3171. (b) Tanaka, K.; Tzeng, B.-C.; Nagao, H.; Peng, S.-M.; Tanaka, K. *Inorg. Chem.* **1993**, *32*, 1508.

(10) TEXSAN: Single Crystal Structure Analysis Software, Version 1.6; Molecular Structure Corp., The Woodlands, TX 77381, 1993.

(11) (a) Hartley, F. R.; Patai, S., Eds. *The Chemistry of the Metal-Carbon Bond*; Wiley: Chichester, U.K., 1982; Vol. 1, references therein. (b) Nakamoto, K. *Infrared and Raman Spectra of Inorganic and Coordination Compounds*; Wiley-Interscience: New York, 1986, and references therein.

(12) Ishida, H.; Tanaka, K.; Tanaka, T. *Organometallics* **1987**, *6*, 181.

(13) Neither  $\nu_{\text{asym}}(\text{Ru}-\text{CO})$  nor  $\nu_{\text{sym}}(\text{Ru}-\text{CO})$  was detected in the IR spectrum due to strong bands of bpy ligands.

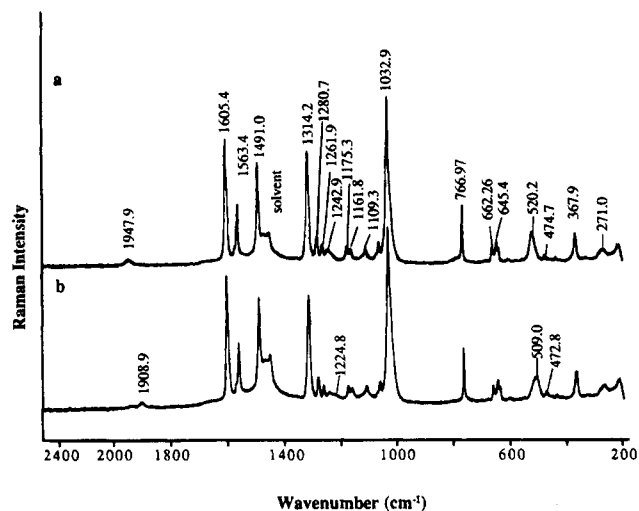


**Figure 2.** Raman spectra of (a) *cis*-[Ru(bpy)<sub>2</sub>(C<sup>16</sup>O)(C<sup>16</sup>O<sub>2</sub>)] in H<sub>2</sub><sup>16</sup>O/CH<sub>3</sub>OH and (b) *cis*-[Ru(bpy)<sub>2</sub>(C<sup>18</sup>O)(C<sup>18</sup>O<sub>2</sub>)](Cl)<sub>2</sub> in H<sub>2</sub><sup>18</sup>O/CH<sub>3</sub>OH (4/1 (v/v)).

in the optical intensity around 1450 cm<sup>-1</sup> in the Raman spectra. Besides the isotope shifts of the  $\nu(\text{CO})$  and  $\nu(\text{CO}_2)$  bands, two other bands undergo isotope shifts in the region 1000–200 cm<sup>-1</sup>; the bands at 520.2 (m) and 474.7 (w) cm<sup>-1</sup> in CH<sub>3</sub>OH/H<sub>2</sub><sup>16</sup>O shift to 509.1 (m) and 472.7 (s) cm<sup>-1</sup> in CH<sub>3</sub>OH/H<sub>2</sub><sup>18</sup>O (Figure 2). In accordance with this, an IR spectrum of a  $\eta^1$ -CO<sub>2</sub> titanium complex showed isotopic shifts of the bands of 1187 and 722 cm<sup>-1</sup> on <sup>18</sup>O substitution and a strong coupling of the Ti–C stretching mode with the O–C–O bending mode is suggested by normal coordination calculations.<sup>7d</sup> The replacement of oxygen atoms between *cis*-[Ru(bpy)<sub>2</sub>(C<sup>16</sup>O)(C<sup>16</sup>O<sub>2</sub>)] and *cis*-[Ru(bpy)<sub>2</sub>(C<sup>18</sup>O)(C<sup>18</sup>O<sub>2</sub>)] would have more serious effect on the  $\nu(\text{Ru–CO}_2)$  mode than on the  $\nu(\text{Ru–CO})$  mode. From the extent of the isotope shifts of two bands ( $\Delta\nu = 11.1$  and 2.0 cm<sup>-1</sup>) the main contributions to the 520.1 and 474.7 cm<sup>-1</sup> bands of *cis*-[Ru(bpy)<sub>2</sub>(C<sup>16</sup>O)(C<sup>16</sup>O<sub>2</sub>)], therefore, result from  $\nu(\text{Ru–CO}_2)$  and  $\nu(\text{Ru–CO})$  modes, respectively.

In the equilibrium reaction of eq 1, *cis*-[Ru(bpy)<sub>2</sub>(CO)-(C(O)OH)]<sup>+</sup> always exists as an equilibrium mixture with *cis*-[Ru(bpy)<sub>2</sub>(CO)<sub>2</sub>]<sup>2+</sup> and *cis*-[Ru(bpy)<sub>2</sub>(CO)(CO<sub>2</sub>)] or either of them, which hampered the measurement of the Raman spectra of *cis*-[Ru(bpy)<sub>2</sub>(CO)(C(O)OH)]<sup>+</sup> in aqueous solution. Accordingly, the assignment of  $\nu(\text{Ru–C(O)OH})$  and  $\nu(\text{Ru–CO})$  bands of *cis*-[Ru(bpy)<sub>2</sub>(CO)(C(O)OH)](PF<sub>6</sub>) was conducted by comparison of the Raman spectra of *cis*-[Ru(bpy)<sub>2</sub>(CO)(C(O)OCH<sub>3</sub>)](PF<sub>6</sub>) in KBr disks.<sup>14</sup> The  $\nu(\text{CO})$  bands of *cis*-[Ru(bpy)<sub>2</sub>(CO)-(C(O)OH)](PF<sub>6</sub>) and *cis*-[Ru(bpy)<sub>2</sub>(CO)(C(O)OCH<sub>3</sub>)](PF<sub>6</sub>) are observed at 1973.7 (m) and 1951.3 (m) cm<sup>-1</sup>, respectively. On the other hand, both Raman spectra are quite similar to each other in the region 1000–200 cm<sup>-1</sup> within  $\pm 1.0$  cm<sup>-1</sup>, except for two bands at 511.3 (m) and 473.1 (s) cm<sup>-1</sup> in *cis*-[Ru(bpy)<sub>2</sub>(CO)(C(O)OH)](PF<sub>6</sub>) and at 518.1 (m) and 471.7 cm<sup>-1</sup> (s) in *cis*-[Ru(bpy)<sub>2</sub>(CO)(C(O)OCH<sub>3</sub>)](PF<sub>6</sub>). The relative shifts of both bands between the two complexes ( $\Delta\nu = 6.8$  and 1.4 cm<sup>-1</sup>) indicate that the 511.3 and 473.1 cm<sup>-1</sup> bands of *cis*-[Ru(bpy)<sub>2</sub>(CO)(C(O)OH)](PF<sub>6</sub>) mainly reflect the  $\nu(\text{Ru–C(O)OH})$  and  $\nu(\text{Ru–CO})$  modes, respectively,

(14) No appreciable change was observed in the Raman spectra of [Ru(bpy)<sub>2</sub>(CO)(C(O)OH)](PF<sub>6</sub>) in CH<sub>3</sub>CN and in KBr disks.

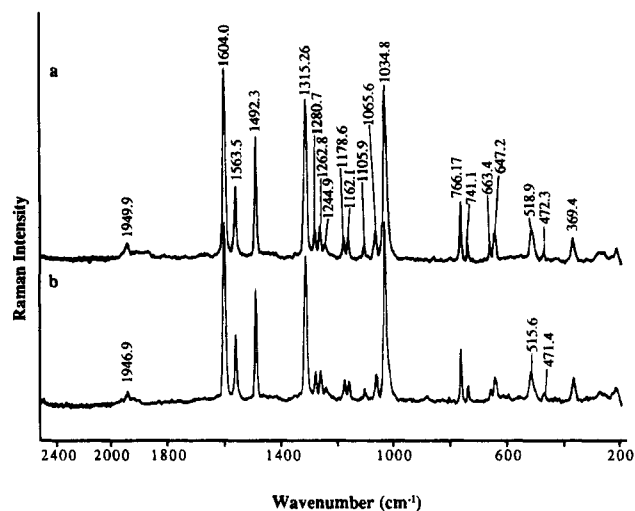


**Figure 3.** Raman spectra of (a) *cis*-[Ru(bpy)<sub>2</sub>(CO)(CHO)]-(PF<sub>6</sub>) and (b) *cis*-[Ru(bpy)<sub>2</sub>(CO)(CDO)](PF<sub>6</sub>) in KBr disks.

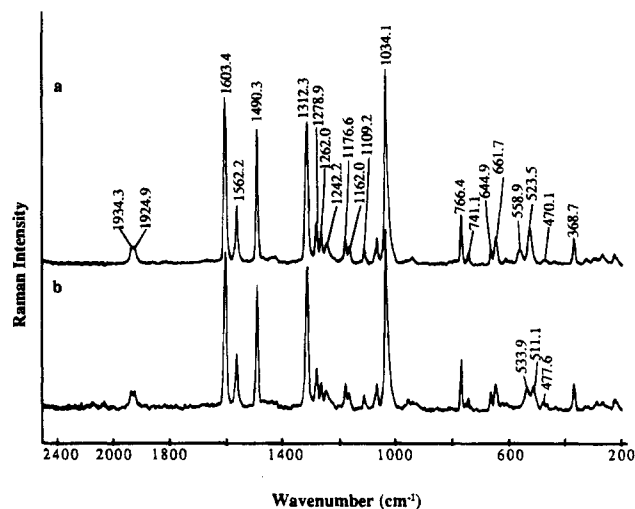


**Figure 4.** Raman spectra of (a) *cis*-[Ru(bpy)<sub>2</sub>(CO)(CH<sub>2</sub>OH)](PF<sub>6</sub>) and (b) *cis*-[Ru(bpy)<sub>2</sub>(CO)(CD<sub>2</sub>OH)](PF<sub>6</sub>) in KBr disks.

because the  $\nu(\text{Ru–C(O)OH})$  mode would undergo more pronounced perturbation than the  $\nu(\text{Ru–CO})$  mode by esterification of the C(O)OH moiety.

A yellow powder of *cis*-[Ru(bpy)<sub>2</sub>(CO)(CHO)](PF<sub>6</sub>) was quite stable in the solid state, but the formyl complex begins to decompose at  $-15$  °C in CH<sub>3</sub>CN solution. Therefore, the Raman spectrum of *cis*-[Ru(bpy)<sub>2</sub>(CO)-(CHO)](PF<sub>6</sub>) was measured in a KBr disk. The substitution of the CHO moiety of *cis*-[Ru(bpy)<sub>2</sub>(CO)(CHO)](PF<sub>6</sub>) by CDO causes a small shift of the  $\nu(\text{CO})$  band from 1950.0 to 1946.9 cm<sup>-1</sup>. Besides the shift of the  $\nu(\text{CO})$  band, a comparison of the spectra of *cis*-[Ru(bpy)<sub>2</sub>(CO)(CHO)](PF<sub>6</sub>) and *cis*-[Ru(bpy)<sub>2</sub>(CO)(CDO)](PF<sub>6</sub>) demonstrates the isotope shift of only two bands from 518.9 (m) and 472.3 (w) cm<sup>-1</sup> of the former to 515.6 (m) and 471.3 cm<sup>-1</sup> (w) of the latter (Figure 3). Such shifts also permit assignment of the 518.9 (m) and 472.3 cm<sup>-1</sup> (w) bands of *cis*-[Ru(bpy)<sub>2</sub>(CO)(CHO)]<sup>+</sup> to the  $\nu(\text{Ru–CHO})$  and  $\nu(\text{Ru–CO})$  modes, respectively.

The  $\nu(\text{CO})$  band of *cis*-[Ru(bpy)<sub>2</sub>(CO)(CH<sub>2</sub>OH)](PF<sub>6</sub>) is dependent on the medium. In the solid state, a small splitting of the  $\nu(\text{CO})$  band is observed at 1925 and 1934 cm<sup>-1</sup>, while two  $\nu(\text{CO})$  bands clearly appear at 1944.5 and 1986.9 cm<sup>-1</sup> in CH<sub>2</sub>Cl<sub>2</sub>. Similarly, *cis*-[Ru(bpy)<sub>2</sub>(CO)(CH<sub>2</sub>OH)](PF<sub>6</sub>)

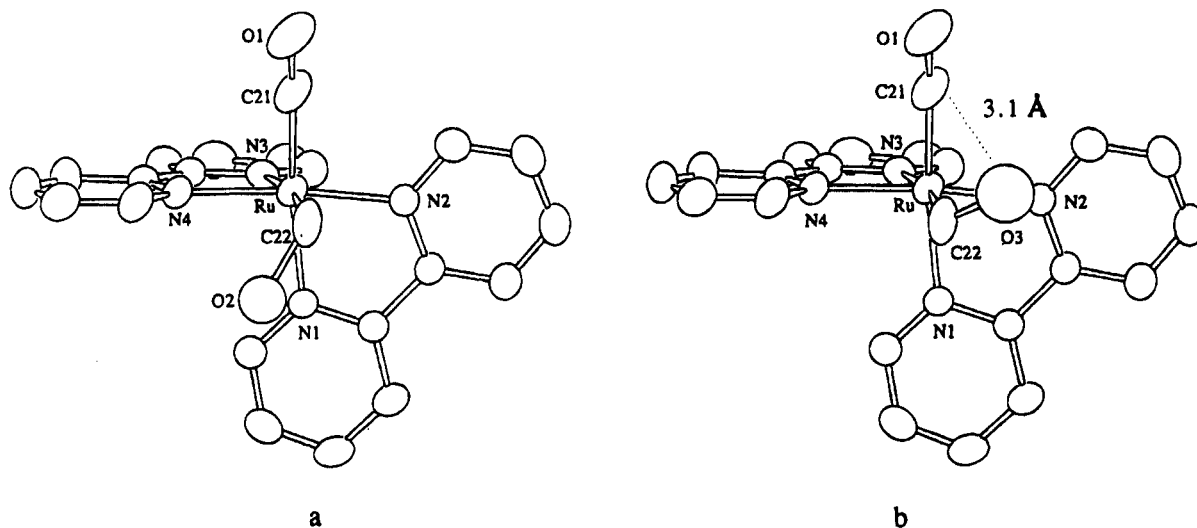


**Figure 5.** Molecular structures of two conformers of *cis*-[Ru(bpy)<sub>2</sub>(CO)(CH<sub>2</sub>OH)](PF<sub>6</sub>). The thermal ellipsoids are drawn at the 30% level.

**Table 1.** Relevant Raman Bands and Bond Parameters of [Ru(bpy)<sub>2</sub>(CO)X]<sup>n+</sup> (X = CO<sub>2</sub>, C(O)OH, C(O)OCH<sub>3</sub>, CO, CHO, CH<sub>2</sub>OH; n = 0–2)<sup>a</sup>

X (color)	$\nu(\text{Ru}-\text{X}), \text{cm}^{-1}$		$\nu(\text{Ru}-\text{CO}), \text{cm}^{-1}$		$\nu(\text{CO}), \text{cm}^{-1}$		$d(\text{Ru}-\text{CO}),$ Å	$d(\text{Ru}-\text{X}),$ Å	$\angle\text{X}-\text{Ru}-\text{CO},$ deg
	unlabeled	labeled	unlabeled	labeled	unlabeled	labeled			
CO <sub>2</sub> <sup>b</sup> (red)	520.2	509.1	474.4	472.7	1947.9	1908.9	1.81	2.06	88.5
C(O)OH (yellow)	511.3		473.1		1973.7				
C(O)OCH <sub>3</sub> (yellow)	518.1		471.7		1951.2		1.80	2.04	88.5
CO <sup>b</sup> (colorless)	443.6	430.0			2098.7	2049.7	1.87	1.87	88.8
					2052.3	2002.7	1.91	1.91	
CHO <sup>c</sup> (yellow)	518.9	515.6	472.3	471.3	1950.0	1946.9			
CH <sub>2</sub> OH <sup>c</sup> (orange)	558.9	534.6	477.7	475.7	1934.3	1934.9	1.85	2.19	90.9
	523.5	511.1	471.6	~470	1923.1	1923.7			

<sup>a</sup> The methods of isotope labeling are detailed in the text. <sup>b</sup> Labeled with <sup>18</sup>O. <sup>c</sup> Labeled with D.

(CO)(CD<sub>2</sub>OH)](PF<sub>6</sub>) shows the same splitting of  $\nu(\text{CO})$  in both the solid and solutions. Furthermore, four bands at 558.9 (m), 523.5 (m), 477.7 (w), and 471.6 (sh)  $\text{cm}^{-1}$  of *cis*-[Ru(bpy)<sub>2</sub>(CO)(CH<sub>2</sub>OH)](PF<sub>6</sub>) undergo isotope shifts to 534.6 (m), 511.1 (m), 475.7 (w), and ~470 (sh)  $\text{cm}^{-1}$ , respectively, in the Raman spectrum of *cis*-[Ru(bpy)<sub>2</sub>(CO)(CD<sub>2</sub>OH)](PF<sub>6</sub>) (Figure 4). The isotope shifts of the four bands in solid *cis*-[Ru(bpy)<sub>2</sub>(CO)(CH<sub>2</sub>OH)]<sup>+</sup> and *cis*-[Ru(bpy)<sub>2</sub>(CO)(CD<sub>2</sub>OH)]<sup>+</sup> were also detected in CH<sub>3</sub>CN at almost identical wavenumbers. This is in contrast to the pattern of the Raman spectra of *cis*-[Ru(bpy)<sub>2</sub>(CO)X]<sup>n+</sup> (X = CO<sub>2</sub>, C(O)OH, C(O)OCH<sub>3</sub>, CHO), showing one medium  $\nu(\text{Ru}-\text{X})$  band and a weak  $\nu(\text{Ru}-\text{CO})$  band around 530 and 470  $\text{cm}^{-1}$ , respectively. The appearance of two medium and two weak bands in the Raman spectra of *cis*-[Ru(bpy)<sub>2</sub>(CO)(CH<sub>2</sub>OH)]<sup>+</sup> in this region is not explained by the disorder between CO and CH<sub>2</sub>OH of *cis*-[Ru(bpy)<sub>2</sub>(CO)(CH<sub>2</sub>OH)](PF<sub>6</sub>), suggested in a previous X-ray crystal analysis.<sup>6a</sup> The discrepancy, therefore, motivated us to reexamine the crystal structure of *cis*-[Ru(bpy)<sub>2</sub>(CO)(CH<sub>2</sub>OH)](PF<sub>6</sub>) to confirm configurational isomers. Reinvestigation of the X-ray analysis of the crystal structure of [Ru(bpy)<sub>2</sub>(CO)(CH<sub>2</sub>OH)](PF<sub>6</sub>) clearly showed the presence of two isomers with respect to the orientation of the RuCH<sub>2</sub>-OH bond directed below and above the equatorial plane. The former is the same structure as the previously reported one with an Ru-C(22)-O(2) bond angle of 105° (Figure 5a). The latter has a Ru-C(23)-O(3) angle of 108°, and a weak interaction between O(3) and the carbonyl carbon, estimated from the relatively short distance (3.1 Å), would give two  $\nu(\text{Ru}-\text{X})$  and  $\nu(\text{Ru}-\text{CO})$  bands in the

Raman spectra. Thus, the four bands (558.9 (m), 523.5 (m), 477.7 (w), and 471.6 (w)  $\text{cm}^{-1}$ ) of *cis*-[Ru(bpy)<sub>2</sub>(CO)(CH<sub>2</sub>OH)](PF<sub>6</sub>) are concluded to result from the two isomers. From the relative intensities of these four bands, the 558.9 (m) and 477.7 (w)  $\text{cm}^{-1}$  pair and the 523.5 (m) and 471.6 (w)  $\text{cm}^{-1}$  pair are reasonably assigned to  $\nu(\text{Ru}-\text{CH}_2\text{OH})$  and  $\nu(\text{Ru}-\text{CO})$  modes, respectively, of the two isomers. The finding of two isomers of *cis*-[Ru(bpy)<sub>2</sub>(CO)(CH<sub>2</sub>OH)]<sup>+</sup> also results from the reasonable assignment of the  $\nu(\text{Ru}-\text{CH}_2\text{OH})$  bands and  $\nu(\text{Ru}-\text{CO})$  bands.

## Discussion

From the large isotope shift in the Raman spectra between *cis*-[Ru(bpy)<sub>2</sub>(C<sup>16</sup>O)<sub>2</sub>]<sup>2+</sup> and *cis*-[Ru(bpy)<sub>2</sub>(C<sup>18</sup>O)<sub>2</sub>]<sup>2+</sup>,  $\nu_{\text{sym}}(\text{Ru}-\text{C}^{16}\text{O})$  is straightforwardly assigned at 443  $\text{cm}^{-1}$ . A series of *cis*-[Ru(bpy)<sub>2</sub>(CO)X]<sup>n+</sup> complexes (X = CO<sub>2</sub>, C(O)OH, C(O)OCH<sub>3</sub>, CHO, and CH<sub>2</sub>OH; n = 0–2) shows one characteristic medium-intensity band in the range 558.9–511.3  $\text{cm}^{-1}$  and a weak band around 470  $\text{cm}^{-1}$ . The medium intensity band undergoes obvious isotope shifts compared to the weak one, and all the remaining bands in these complexes are almost invariant with the substituent X in the region from 1000 to 200  $\text{cm}^{-1}$ . The bands around 530 (m) and 470 (w)  $\text{cm}^{-1}$ , therefore, are reasonably associated with the Ru-X and Ru-CO stretching modes, respectively, and the coupling of  $\nu(\text{Ru}-\text{CO})$  and  $\nu(\text{Ru}-\text{X})$  modes would be very small due to a nearly perpendicular X-Ru-CO bond angle (Table 1). In addition, the deviation of the Raman spectrum of *cis*-

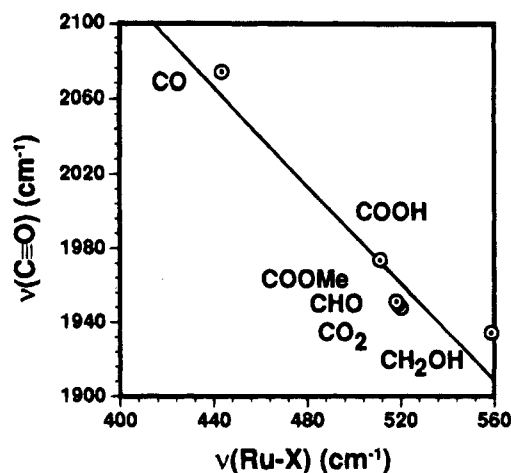


**Figure 6.** Plot of  $\nu(\text{C}\equiv\text{O})$  bands vs  $\nu(\text{Ru}-\text{X})$  bands of *cis*-[Ru(bpy)<sub>2</sub>(CO)X]<sup>n+</sup> ( $n = 0-2$ ; X = CO, C(O)OH, C(O)OCH<sub>3</sub>, CO<sub>2</sub>, CHO, CH<sub>2</sub>OH).

[Ru(bpy)<sub>2</sub>(CO)(CH<sub>2</sub>OH)]<sup>+</sup> from those of the other complexes has led to the confirmation of the two isomers. These facts suggest small or negligible contributions of other moieties to the  $\nu(\text{Ru}-\text{X})$  and  $\nu(\text{Ru}-\text{C})$  bands in the *cis*-[Ru(bpy)<sub>2</sub>(CO)X]<sup>n+</sup> series. The  $\nu(\text{Ru}-\text{X})$  and  $\nu(\text{Ru}-\text{CO})$  bands tentatively assigned are also collected in Table 1.

The  $\nu(\text{CO})$  and  $\nu(\text{Ru}-\text{X})$  bands in *cis*-[Ru(bpy)<sub>2</sub>(CO)X]<sup>n+</sup> are in the range 2098.9 (X = CO) to 1934.3 cm<sup>-1</sup> (X = CH<sub>2</sub>OH), and 558.9 (X = CH<sub>2</sub>OH) to 443.5 cm<sup>-1</sup> (X = CO), respectively, and the shift of  $\nu(\text{Ru}-\text{CO})$  is quite small compared with that of  $\nu(\text{Ru}-\text{X})$ . Although no clear correlation is observed between  $\nu(\text{Ru}-\text{X})$  and the mass of X (from CO to C(O)OCH<sub>3</sub>) or the charge of the complexes ( $n = 0-2$ ),  $\nu(\text{CO})$  bands move to lower wavenumbers as  $\nu(\text{Ru}-\text{X})$  bands shift to higher ones (Figure 6). The order of the shift of the  $\nu(\text{CO})$  bands to lower wavenumbers (X = CO < C(O)OH < CHO < CO<sub>2</sub> < CH<sub>2</sub>OH) correlates with the electron-donating ability of the substituent X. The correlation between  $\nu(\text{Ru}-\text{X})$  and  $\nu(\text{CO})$  in Figure 6, therefore, is explained by an enhancement of  $\sigma$ - and  $\pi$ -bonding characters of the Ru-X and Ru-CO bonds, respectively, with increasing electron-donating ability of X.

The crystal structures of most of these complexes, including the two isomers of *cis*-[Ru(bpy)<sub>2</sub>(CO)(CH<sub>2</sub>OH)]<sup>+</sup>, have been determined by X-ray analysis.<sup>6a</sup> The Ru-CO and Ru-X bond distances are also summarized in Table 1. There is no clear correlation between the Ru-CO bond distance and  $\nu(\text{Ru}-\text{X})$ . On the other

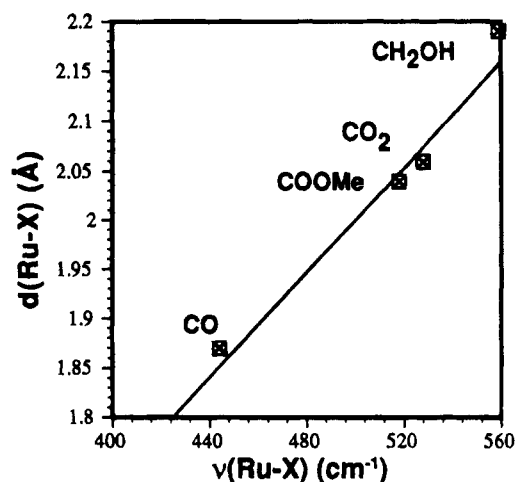


**Figure 7.** Relationship between Ru-X bond lengths ( $d(\text{Ru}-\text{X})$ ) and  $\nu(\text{Ru}-\text{X})$  bands of *cis*-[Ru(bpy)<sub>2</sub>(CO)X]<sup>n+</sup> ( $n = 0-2$ ; X = CO, C(O)OH, C(O)OCH<sub>3</sub>, CO<sub>2</sub>, CHO, CH<sub>2</sub>OH).

hand, a plot of the Ru-X bond distance ( $d(\text{Ru}-\text{X})$ ) against the  $\nu(\text{Ru}-\text{X})$  band gives a linear correlation (Figure 7). The gradual shortening of the Ru-X bond distances from Ru-CH<sub>2</sub>OH to Ru-CO<sub>2</sub> to Ru-C(O)-OCH<sub>3</sub> to Ru-CO is reasonably ascribed to the contraction of the radius of the carbon atom with the change of the hybridization from sp<sup>3</sup> to sp<sup>2</sup> to sp. The order of the shortening of Ru-X distances also reflects an increase in the  $d\pi-p\pi$  interactions between Ru and carbon. The order of the  $\pi$ -electron-acceptor ability is, therefore, inverse to that of  $\sigma$ -electron-donor ability of the substituents estimated from the shift of  $\nu(\text{CO})$  bands of *cis*-[Ru(bpy)<sub>2</sub>(CO)X]<sup>n+</sup> (CH<sub>2</sub>OH > CO<sub>2</sub> > CHO > C(O)OH > CO). The unusual relationship of  $\nu(\text{Ru}-\text{X})$  bands shifting to higher wavenumbers as the Ru-X distances are lengthened (Figure 7) may be explained by an assumption that the multiple-bond characters between carbon and oxygen (C≡O, C=O, and C-O) in the substituent X (CO, C(O)OH, C(O)OCH<sub>3</sub>, CO<sub>2</sub>, CHO, CH<sub>2</sub>OH) have more influence on the observed  $\nu(\text{Ru}-\text{X})$  band than do the Ru-C bond characters in these *cis*-[Ru(bpy)<sub>2</sub>(CO)X]<sup>n+</sup> complexes.

**Supporting Information Available:** Lists of crystallographic data, calculated positional parameters, anisotropic thermal parameters, and bond distances and angles for [Ru(bpy)<sub>2</sub>(CO)(CH<sub>2</sub>OH)](PF<sub>6</sub>) (11 pages). Ordering information is given on any current masthead page.

OM950483T

**Chemistry of C-Trimethylsilyl-Substituted  
Heterocarboranes. 18. Synthetic, Spectroscopic,  
Reactivity, and Bonding Studies on the Group 13  
Element Metallocarboranes: Crystal Structures of  
1-(CMe<sub>3</sub>)-1-Ga(2,2'-C<sub>10</sub>H<sub>8</sub>N<sub>2</sub>)-2,3-(SiMe<sub>3</sub>)<sub>2</sub>-2,3-C<sub>2</sub>B<sub>4</sub>H<sub>4</sub>,  
1-(CMe<sub>3</sub>)-1-Ga(L)-2,4-(SiMe<sub>3</sub>)<sub>2</sub>-2,4-C<sub>2</sub>B<sub>4</sub>H<sub>4</sub> [L = 2,2'-C<sub>10</sub>H<sub>8</sub>N<sub>2</sub>,  
2,2'-C<sub>8</sub>H<sub>6</sub>N<sub>4</sub>], *closo*-1-(Me<sub>2</sub>CH)-1-In-2,4-(SiMe<sub>3</sub>)<sub>2</sub>-2,4-C<sub>2</sub>B<sub>4</sub>H<sub>4</sub>,  
and 1-(Me<sub>2</sub>CH)-1-In(2,2'-C<sub>10</sub>H<sub>8</sub>N<sub>2</sub>)-2,4-(SiMe<sub>3</sub>)<sub>2</sub>-2,4-C<sub>2</sub>B<sub>4</sub>H<sub>4</sub>**

Narayan S. Hosmane,\* Anil K. Saxena, Kai-Juan Lu, John A. Maguire,  
Hongming Zhang, Ying Wang, Colacot J. Thomas, Dunming Zhu,  
Bobby R. Grover, Thomas G. Gray, and Jason F. Eintracht

*Department of Chemistry, Southern Methodist University, Dallas, Texas 75275*

Harold Isom and Alan H. Cowley

*Department of Chemistry and Biochemistry, University of Texas at Austin,  
Austin, Texas 78712*

*Received June 30, 1995\**

The reactions of the THF-solvated "carbons apart" dilithiacarboranes, *closo-exo*-5,6-[( $\mu$ -H)<sub>2</sub>Li(THF)]( $\mu$ -THF)-1-Li-2-(SiMe<sub>3</sub>)-4-(R)-2,4-C<sub>2</sub>B<sub>4</sub>H<sub>4</sub> [R = SiMe<sub>3</sub> (I), Me (II)], with freshly prepared [*t*-BuGaCl<sub>2</sub>]<sub>2</sub> or *i*-PrInI<sub>2</sub> in THF solution in molar ratios of 1:1 at 0 °C produced the corresponding *closo*-gallacarboranes, 1-(CMe<sub>3</sub>)-1-Ga-2-(SiMe<sub>3</sub>)-4-(R)-2,4-C<sub>2</sub>B<sub>4</sub>H<sub>4</sub> [R = SiMe<sub>3</sub> (III), Me (IV)], and *closo*-indacarboranes, 1-[(Me)<sub>2</sub>CH]-1-In-2-(SiMe<sub>3</sub>)-4-(R)-2,4-C<sub>2</sub>B<sub>4</sub>H<sub>4</sub> [R = SiMe<sub>3</sub> (X), Me (XI)], as colorless liquids or crystalline solids in 53, 59, 35, and 43% yields, respectively. These *closo*-metallocarboranes react with 2,2'-bipyridine, 2,2'-bipyrimidine, and 2,2':6',2''-terpyridine in benzene solution at room temperature to form the corresponding donor-acceptor complexes, 1-(CMe<sub>3</sub>)-1-Ga(2,2'-C<sub>10</sub>H<sub>8</sub>N<sub>2</sub>)-2-(SiMe<sub>3</sub>)-4-(R)-2,4-C<sub>2</sub>B<sub>4</sub>H<sub>4</sub> [R = SiMe<sub>3</sub> (VI), Me (VII)], 1-(CMe<sub>3</sub>)-1-Ga(2,2'-C<sub>8</sub>H<sub>6</sub>N<sub>4</sub>)-2,4-(SiMe<sub>3</sub>)<sub>2</sub>-2,4-C<sub>2</sub>B<sub>4</sub>H<sub>4</sub> (VIII), 1-(CMe<sub>3</sub>)-1-Ga(C<sub>15</sub>H<sub>11</sub>N<sub>3</sub>)-2,4-(SiMe<sub>3</sub>)<sub>2</sub>-2,4-C<sub>2</sub>B<sub>4</sub>H<sub>4</sub> (IX), 1-[(Me)<sub>2</sub>CH]-1-In(2,2'-C<sub>10</sub>H<sub>8</sub>N<sub>2</sub>)-2,4-(SiMe<sub>3</sub>)<sub>2</sub>-2,4-C<sub>2</sub>B<sub>4</sub>H<sub>4</sub> (XII), and 1-[(Me)<sub>2</sub>CH]-1-In(2,2'-C<sub>8</sub>H<sub>6</sub>N<sub>4</sub>)-2,4-(SiMe<sub>3</sub>)<sub>2</sub>-2,4-C<sub>2</sub>B<sub>4</sub>H<sub>4</sub> (XIII), in 40-90% yields. The compounds II-XIII were all characterized on the basis of <sup>1</sup>H, <sup>11</sup>B, and <sup>13</sup>C NMR spectra, IR spectra, and mass spectra. The compounds VI, VIII, X, and XII were also characterized by single-crystal X-ray analyses. For a comparative study, the 2,2'-bipyridine adduct of the "carbons adjacent" gallacarborane, 1-(CMe<sub>3</sub>)-1-Ga(2,2'-C<sub>10</sub>H<sub>8</sub>N<sub>2</sub>)-2,3-(SiMe<sub>3</sub>)<sub>2</sub>-2,3-C<sub>2</sub>B<sub>4</sub>H<sub>4</sub> (V), was synthesized and spectroscopically characterized, and its crystal structure was also determined. The crystal structures of V, VI, VIII, and XII show that each complex has a distorted pentagonal bipyramidal geometry, with the group 13 atom occupying the apical position and coordinating to the nitrogen atoms of the Lewis bases, whereas the crystal structure of the indacarborane (X) shows a dimer of two distorted *closo*-metallocarborane cages, similar to that found for the carbons adjacent isomer. The compounds V, VI, VIII, X, and XII crystallized in monoclinic or triclinic space groups *P*2<sub>1</sub>/*n*, *P*2<sub>1</sub>/*c*, *P*1̄, *C*2/*c*, and *P*1̄, respectively, with *a* = 9.778(2), 12.550(4), 9.611(4), 23.288(7), and 9.079(5) Å, *b* = 25.031(5), 15.885(5), 15.813(7), 9.169(7), and 16.127(6) Å, *c* = 11.376(2), 19.965(7), 19.808(7), 19.130(5), and 19.83(9) Å,  $\alpha$  = 90.00, 90.00, 69.40(3), 90.00, and 88.20(3)°,  $\beta$  = 96.47(2), 103.42(2), 93.81(3), 98.02(2), and 81.75(3)°,  $\gamma$  = 90.00, 90.00, 82.39(3), 90.00, and 79.21(3)°, *V* = 2766.6(9), 3871(2), 2784(2), 4045(2), and 2823(3) Å<sup>3</sup> and *Z* = 4, 4, 4, 4, and 4, respectively. The final refinements of V, VI, VIII, X, and XII converged at *R* = 0.0412, 0.0411, 0.056, 0.029, and 0.0495 and *R*<sub>w</sub> = 0.0488, 0.0517, 0.057, 0.039, and 0.0698, respectively.

### Introduction

There have been numerous reports of the syntheses, structures, and reactivities of the organometallic com-

pounds formed between main group metals and carborane ligands with the general form [R<sub>2</sub>C<sub>2</sub>B<sub>4</sub>H<sub>4</sub>]<sup>2-</sup> (R = hydrogen or a cage carbon substituent).<sup>1-4</sup> The carborane ligands bond to the metals with a set of  $\pi$ -type orbitals directed above the C<sub>2</sub>B<sub>3</sub> open face of the carborane and, in this regard, can be considered as cage

\* Abstract published in *Advance ACS Abstracts*, October 15, 1995.



analogues of  $(C_5R_5)^-$ .<sup>2b,4</sup> The carboranes can be divided into two main isomeric groups: the so-called "carbons adjacent", or 2,3- $C_2B_4$ , isomers in which the cage carbons are next to one another in the open pentagonal face and the "carbons apart", or 2,4- $C_2B_4$ , isomers where the carbons are separated by a boron atom. Although both ligands seem to bond equally well to metals, difficulties in the syntheses of the 2,4- $C_2B_4$  dianions have seriously limited their use as ligands; the bulk of the studies in the literature have been on the carbons adjacent system.

The first structure of a main group metallacarborane in the pentagonal bipyramidal system was that of 1-Ga( $CH_3$ )<sub>2</sub>-2,3- $C_2B_4H_6$ , reported in 1972 by Grimes and co-workers.<sup>5</sup> The complex was found to have a distorted pentagonal bipyramidal geometry in which the metal occupied the apical position above the open pentagonal face of the carborane. The metal was not symmetrically bound to the  $C_2B_3$  atoms, but was dislocated, or slipped, along the pseudo-mirror plane of the carborane, toward the unique boron atom. Subsequent structural studies of the trimethylsilyl-substituted metallacarboranes, 1-M-2-(SiMe<sub>3</sub>)<sub>2</sub>-3-(R)-2,3- $C_2B_4H_4$  [R = SiMe<sub>3</sub>, Me, or H; M = Sn,<sup>6,7</sup> Pb,<sup>8a</sup> (*t*-Bu)Ga,<sup>9,10</sup> on (*i*-Pr)In<sup>11,12</sup>], have confirmed that the gallacarborane structure is typical of all of the metallacarboranes in these systems. The capping metals have been found to be coordinatively unsaturated and to form complexes with monodentate,<sup>13</sup> bidentate,<sup>7,8b,9,10,12,14</sup> bis(bidentate),<sup>9,13a</sup> and tridentate bases.<sup>15</sup> The molecules of base are coordinated directly to the metal and are oriented opposite the cage carbons. Metal-base bonding invariably leads to an increase in the slip distortion of the metal toward the unique boron.

In contrast to the rather extensive structural information available on the carbons adjacent complexes, there is little information as yet on the analogous carbons apart complexes. As indicated earlier, the main reason for this imbalance has been the lack of a convenient preparative route to the carbons apart ligands. However, the recent high-yield synthesis of the

[2,4-(SiMe<sub>3</sub>)<sub>2</sub>-2,4- $C_2B_4H_4$ ]<sup>2-</sup> ligand offers the opportunity to extend the studies of the pentagonal bipyramidal metallacarboranes.<sup>16</sup> Recently, structural reports of 1-Sn(L)-2,4-(SiMe<sub>3</sub>)<sub>2</sub>-2,4- $C_2B_4H_4$  [L = 2,2'- $C_{10}H_8N_2$ , 2,2'- $C_8H_6H_4$ , and  $(\eta^5-C_5H_5)Fe(\eta^5-C_5H_4CH_2(Me)_2N)$ ] have appeared.<sup>4</sup> These base-stannacarborane adducts show that the capping tin is slipped away from the unique boron, which is opposite in direction from that found in their carbons adjacent analogues. Since the structure of the uncomplexed stannacarborane could not be obtained, it was not possible to ascertain the extent to which base coordination influenced this type of distortion. Semiempirical molecular orbital calculations indicated that the same factors that promoted slippage in the carbons adjacent stannacarboranes<sup>14b,17</sup> are also operable in the carbons apart complexes.<sup>4</sup>

The only structure of a group 13 metallacarborane in the 2,4- $C_2B_4$  ligand system is that of an unusual carborane-substituted digallane, *closo*-1-Ga[*σ-closo*-1-Ga-2,4-(SiMe<sub>3</sub>)<sub>2</sub>-2,4- $C_2B_4H_4$ ]-2,4-(SiMe<sub>3</sub>)<sub>2</sub>-2,4- $C_2B_4H_4$ , in which the apical galliums of two gallacarboranes are directly bonded to one another, resulting in formal +2 oxidation states for the metals.<sup>18</sup> The uniqueness of this digallane complex limits its use as a standard for comparing the structural consequences of permeating the facial atoms of the carboranes in the group 13 metallacarboranes. Therefore, we report herein the results of an investigation of the synthesis, characterization, and reactivity of several galla- and indacarboranes. To obtain more information on the effects of base coordination in these metallacarboranes, the X-ray crystal structures of 1-(CMe<sub>3</sub>)-1-Ga(2,2'- $C_{10}H_8N_2$ )-2,3-(SiMe<sub>3</sub>)<sub>2</sub>-2,3- $C_2B_4H_4$  (V), 1-(CMe<sub>3</sub>)-1-Ga(2,2'- $C_{10}H_8N_2$ )-2,4-(SiMe<sub>3</sub>)<sub>2</sub>-2,4- $C_2B_4H_4$  (VI), 1-(CMe<sub>3</sub>)-1-Ga(2,2'- $C_8H_6N_4$ )-2,4-(SiMe<sub>3</sub>)<sub>2</sub>-2,4- $C_2B_4H_4$  (VIII), *closo*-1-[(Me)<sub>2</sub>CH]-1-In-2,4-(SiMe<sub>3</sub>)<sub>2</sub>-2,4- $C_2B_4H_4$  (X) dimer, and 1-[(Me)<sub>2</sub>CH]-1-In(2,2'- $C_{10}H_8N_2$ )-2,4-(SiMe<sub>3</sub>)<sub>2</sub>-2,4- $C_2B_4H_4$  (XII) have also been determined.

## Experimental Section

**Materials.** 1,2-Bis(trimethylsilyl)-1,2-dicarba-*closo*-hexaborane(6) and 1-(trimethylsilyl)-2-(methyl)-1,2-dicarba-*closo*-hexaborane(6) were prepared by using literature methods<sup>16a,19</sup> and were converted to the corresponding tetrahydrofuran (THF)-solvated carbons apart dithiacarboranes, *closo-exo*-5,6-[(*μ*-H)<sub>2</sub>Li(THF)](*μ*-THF)-1-Li-2-(SiMe<sub>3</sub>)<sub>4</sub>-(R)-2,4- $C_2B_4H_4$  (R = SiMe<sub>3</sub>, Me), by reduction with Li/ $C_{10}H_8$ , as outlined previously.<sup>16a</sup> Before use, naphthalene (Aldrich), 2,2'-bipyridine (Aldrich), 2,2'-bipyrimidine (Lancaster Syntheses), 2,2':6',2''-terpyridine (Aldrich), and ferrocenylmethyl-*N,N*-dimethylamine (Strem Chemicals) were sublimed or distilled *in vacuo*, and their purity was checked by IR and NMR spectroscopy and melting point measurements. Lithium metal (Aldrich) was freshly cut in a drybox, and (*t*-BuGaCl<sub>2</sub>)<sub>2</sub> and *i*-PrInI<sub>2</sub> were prepared and

(1) Grimes, R. N. In *Comprehensive Organometallic Chemistry*; Wilkinson, G., Stone, F. G. A., Abel, E. W., Eds.; Pergamon: Oxford, U.K., 1982; Vol. 1, Chapter 5.5.

(2) (a) Saxena, A. K.; Maguire, J. A.; Banewicz, J. J.; Hosmane, N. S. *Main Group Chem. News* **1993**, *1*, 14. (b) Hosmane, N. S.; Maguire, J. A. *Adv. Organomet. Chem.* **1990**, *30*, 99.

(3) Hosmane, N. S.; Maguire, J. A. *J. Cluster Sci.* **1993**, *4*, 297.

(4) Hosmane, N. S.; Jia, L.; Zhang, H.; Maguire, J. A. *Organometallics* **1994**, *13*, 1411.

(5) Grimes, R. N.; Rademaker, W. J.; Denniston, M. L.; Bryan, R. F.; Greene, P. T. *J. Am. Chem. Soc.* **1972**, *94*, 1865.

(6) Cowley, A. H.; Galow, P.; Hosmane, N. S.; Jutzi, P.; Norman, N. C. *J. Chem. Soc., Chem. Commun.* **1984**, 1504.

(7) Hosmane, N. S.; de Meester, P.; Malder, N. N.; Potts, S. B.; Chu, S. S. C.; Herber, R. H. *Organometallics* **1985**, *5*, 772.

(8) (a) Hosmane, N. S.; Siriwardane, U.; Zhu, H.; Zhang, G.; Maguire, J. A. *Organometallics* **1989**, *8*, 566. (b) Hosmane, N. S.; Lu, K.-J.; Zhu, H.; Siriwardane, U.; Shet, M. S.; Maguire, J. A. *Organometallics* **1990**, *9*, 808.

(9) Hosmane, N. S.; Lu, K.-J.; Zhang, H.; Jia, L.; Cowley, A. H.; Mardones, M. A. *Organometallics* **1991**, *10*, 963.

(10) Hosmane, N. S.; Zhang, H.; Lu, K.-J.; Maguire, J. A.; Cowley, A. H.; Mardones, M. A. *Struct. Chem.* **1992**, *3*, 183.

(11) Hosmane, N. S.; Lu, K.-J.; Zhang, H.; Cowley, A. H.; Mardones, M. A. *Organometallics* **1991**, *10*, 392.

(12) Hosmane, N. S.; Lu, K.-J.; Saxena, A. K.; Zhang, H.; Maguire, J. A.; Cowley, A. H. *Organometallics* **1994**, *13*, 979.

(13) (a) Hosmane, N. S.; Fagner, J. S.; Zhu, H.; Siriwardane, U.; Maguire, J. A.; Zhang, G.; Pinkston, B. S. *Organometallics* **1989**, *8*, 1769. (b) Hosmane, N. S.; Lu, K.-J.; Zhang, H.; Maguire, J. A.; Barreto, R. D. *Organometallics* **1992**, *11*, 2458.

(14) (a) Siriwardane, U.; Hosmane, N. S.; Chu, S. S. C. *Acta Crystallogr., Sect. C* **1987**, *C43*, 1076. (b) Maguire, J. A.; Fagner, J. S.; Siriwardane, U.; Banewicz, J. J.; Hosmane, N. S. *Struct. Chem.* **1990**, *1*, 583.

(15) Siriwardane, U.; Maguire, J. A.; Banewicz, J. J.; Hosmane, N. S. *Organometallics* **1989**, *8*, 2792.

(16) (a) Zhang, H.; Wang, Y.; Saxena, A. K.; Oki, A. R.; Maguire, J. A.; Hosmane, N. S. *Organometallics* **1993**, *12*, 3933. (b) Hosmane, N. S.; Saxena, A. K.; Barreto, R. D.; Zhang, H.; Maguire, J. A.; Jia, L.; Wang, Y.; Oki, A. R.; Grover, K. V.; Whitten, S. J.; Dawson, K.; Tolle, M. A.; Siriwardane, U.; Demissie, T.; Fagner, J. S. *Organometallics* **1993**, *12*, 3001.

(17) (a) Barreto, R. D.; Fehlner, T. P.; Hosmane, N. S. *Inorg. Chem.* **1988**, *27*, 453. (b) Maguire, J. A.; Ford, G. P.; Hosmane, N. S. *Inorg. Chem.* **1988**, *27*, 3354.

(18) Saxena, A. K.; Zhang, H.; Maguire, J. A.; Hosmane, N. S.; Cowley, A. H. *Angew. Chem., Int. Ed. Engl.* **1995**, *34*, 332.

(19) (a) Hosmane, N. S.; Barreto, R. D.; Tolle, M. A.; Alexander, J. J.; Quintana, W.; Siriwardane, U.; Shore, S. G.; Williams, R. E. *Inorg. Chem.* **1990**, *29*, 2698. (b) Hosmane, N. S.; Jia, L.; Zhang, H.; Bausch, J. W.; Prakash, G. K. S.; Williams, R. E.; Onak, T. P. *Inorg. Chem.* **1991**, *30*, 3793. (c) Jia, L. M.S. Thesis, Southern Methodist University, Dallas, TX, 1992.

purified according to literature methods.<sup>20,21</sup> Benzene, THF, and *n*-hexane were dried over LiAlH<sub>4</sub> and doubly distilled; all other solvents were dried over 4–8 mesh molecular sieves (Aldrich) and either saturated with dry argon or degassed before use. 1-(CMe<sub>3</sub>)-1-Ga-2,3-(SiMe<sub>3</sub>)<sub>2</sub>-2,3-C<sub>2</sub>B<sub>4</sub>H<sub>4</sub> was prepared and characterized as previously described.<sup>9</sup>

**Spectroscopic and Analytical Procedures.** Proton, boron-11, and carbon-13 pulse Fourier transform NMR spectra, at 200, 64.2, and 50.3 MHz, respectively, were recorded on an IBM-WP200 SY multinuclear NMR spectrometer. Infrared spectra were recorded on a Perkin-Elmer Model 1600 FT-IR spectrophotometer and a Nicolet Magna 550 FT-IR spectrophotometer. Mass spectral determinations were performed at the Washington University Resource for Biomedical and Bioorganic Mass Spectrometry (St. Louis, MO). Elemental analyses were obtained from E+R Microanalytical Laboratory, Inc. (Corona, NY).

**Synthetic Procedures.** All experiments were carried out in Pyrex glass round bottom flasks of 250 mL capacity, containing magnetic stirring bars and fitted with high-vacuum Teflon valves. Nonvolatile substances were manipulated in either a drybox or evacuable glovebags under an atmosphere of dry nitrogen. All known compounds among the products were identified by comparing their IR and NMR spectra with those of authentic samples.

**Synthesis of *closo*-1-(CMe<sub>3</sub>)-1-Ga-2,4-(SiMe<sub>3</sub>)<sub>2</sub>-2,4-C<sub>2</sub>B<sub>4</sub>H<sub>4</sub> (III) and *closo*-1-(CMe<sub>3</sub>)-1-Ga-2-(SiMe<sub>3</sub>)-4-(Me)-2,4-C<sub>2</sub>B<sub>4</sub>H<sub>4</sub> (IV).** A 5.6 mmol (2.103 g) crystalline sample of *closo*-*exo*-5,6-[(*μ*-H)<sub>2</sub>Li(THF)](*μ*-THF)-1-Li-2,4-(SiMe<sub>3</sub>)<sub>2</sub>-2,4-C<sub>2</sub>B<sub>4</sub>H<sub>4</sub> (I) or a 6.95 mmol (2.20 g) crystalline sample of *closo*-*exo*-5,6-[(*μ*-H)<sub>2</sub>Li(THF)](*μ*-THF)-1-Li-2-(SiMe<sub>3</sub>)-4-(Me)-2,4-C<sub>2</sub>B<sub>4</sub>H<sub>4</sub> (II) was dissolved in 15 mL of anhydrous THF *in vacuo*. This solution was poured slowly, *in vacuo*, onto freshly prepared [*t*-BuGaCl<sub>2</sub>]<sub>2</sub> (1.107 g, 2.8 mmol, or 1.37 g, 3.47 mmol) at 0 °C, and the resulting brown heterogeneous mixture was stirred constantly at 0 °C for ~8 (for III) or 2 h (for IV), during which time the solution turned gray. The solvent, THF, was then removed at 0 °C *via* vacuum distillation over a period of 2 h. The reaction flask containing the gray residue was attached to a detachable U-trap that was immersed in an ice bath. After the residue in the flask was carefully heated to 130 °C using an oil bath, a colorless liquid, identified as *closo*-1-(CMe<sub>3</sub>)-1-Ga-2,4-(SiMe<sub>3</sub>)<sub>2</sub>-2,4-C<sub>2</sub>B<sub>4</sub>H<sub>4</sub> (III) (1.027 g, 2.98 mmol, 53% yield, bp 110 °C at 10<sup>-4</sup> Torr) or *closo*-1-(CMe<sub>3</sub>)-1-Ga-2-(SiMe<sub>3</sub>)-4-(Me)-2,4-C<sub>2</sub>B<sub>4</sub>H<sub>4</sub> (IV) (1.185 g, 4.13 mmol, 59% yield, bp 100 °C at 10<sup>-4</sup> Torr), was collected in the detachable U-trap at 0 °C. The side arms of both the reaction flask and the U-trap were maintained at ~100 °C with a heating tape during the distillation of the product. The remaining gray residue at the bottom of the reaction flask was insoluble in both polar and nonpolar organic solvents and was, therefore, discarded. Both III and IV were sensitive to air and moisture and were highly soluble in both polar and nonpolar organic solvents. Anal. Calcd for C<sub>12</sub>H<sub>31</sub>B<sub>4</sub>GaSi<sub>2</sub> (III): C, 41.85; H, 9.06; B, 12.55. Found: C, 42.07; H, 8.84; B, 12.28. Anal. Calcd for C<sub>10</sub>H<sub>25</sub>B<sub>4</sub>GaSi (IV): C, 41.94; H, 8.80. Found: C, 42.21; H, 8.84. Mass spectral analyses (HREI): theoretical mass for the parent ion grouping of III, <sup>12</sup>C<sub>12</sub><sup>1</sup>H<sub>31</sub><sup>11</sup>B<sub>4</sub><sup>28</sup>Si<sub>2</sub><sup>69</sup>Ga, <sup>12</sup>C<sub>12</sub><sup>1</sup>H<sub>31</sub><sup>11</sup>B<sub>3</sub><sup>10</sup>B<sub>1</sub><sup>28</sup>Si<sub>2</sub><sup>69</sup>Ga, and <sup>12</sup>C<sub>12</sub><sup>1</sup>H<sub>31</sub><sup>11</sup>B<sub>2</sub><sup>10</sup>B<sub>2</sub><sup>28</sup>Si<sub>2</sub><sup>69</sup>Ga *m/z* 344.1599, 343.1623, and 342.1669; measured mass *m/z* 344.1593, 343.1629, and 342.1665, respectively. The NMR and IR spectral data for III and IV are given in Tables 4 and 5.

**Synthesis of 1-(CMe<sub>3</sub>)-1-Ga(2,2'-C<sub>10</sub>H<sub>8</sub>N<sub>2</sub>)-2,3-(SiMe<sub>3</sub>)<sub>2</sub>-2,3-C<sub>2</sub>B<sub>4</sub>H<sub>4</sub> (V), 1-(CMe<sub>3</sub>)-1-Ga(2,2'-C<sub>10</sub>H<sub>8</sub>N<sub>2</sub>)-2,4-(SiMe<sub>3</sub>)<sub>2</sub>-2,4-C<sub>2</sub>B<sub>4</sub>H<sub>4</sub> (VI), and 1-(CMe<sub>3</sub>)-1-Ga(2,2'-C<sub>10</sub>H<sub>8</sub>N<sub>2</sub>)-2-(SiMe<sub>3</sub>)-4-(Me)-2,4-C<sub>2</sub>B<sub>4</sub>H<sub>4</sub> (VII).** A solution of 1-(CMe<sub>3</sub>)-1-Ga-2,3-(SiMe<sub>3</sub>)<sub>2</sub>-2,3-C<sub>2</sub>B<sub>4</sub>H<sub>4</sub> (0.483 g, 1.40 mmol), 1-(CMe<sub>3</sub>)-1-Ga-2,4-(SiMe<sub>3</sub>)<sub>2</sub>-2,4-C<sub>2</sub>B<sub>4</sub>H<sub>4</sub> (III) (0.526 g, 1.53 mmol), or 1-(CMe<sub>3</sub>)-1-Ga-2-(SiMe<sub>3</sub>)-4-(Me)-2,4-C<sub>2</sub>B<sub>4</sub>H<sub>4</sub> (IV) (0.30 g, 1.05 mmol) in

freshly distilled dry benzene (5 mL) was added to a flask containing a benzene solution (5 mL) of 2,2'-bipyridine (C<sub>10</sub>H<sub>8</sub>N<sub>2</sub>) (0.23 g, 1.40 mmol; 0.238 g, 1.5 mmol; or 0.163 g, 1.04 mmol, respectively) at 0 °C. The resulting homogeneous solution turned orange brown. This solution was stirred constantly for 24 h at room temperature, during which time it turned turbid. Benzene was then removed from the solution *in vacuo*, and the dark orange residue that remained in the flask was heated to 60 °C to collect unreacted 2,2'-bipyridine in a detachable U-trap at 0 °C. After complete removal of unreacted 2,2'-bipyridine, the flask containing the dark orange residue was attached to a new detachable U-trap that was immersed in an ice bath. Upon heating the flask to 150–160 °C *in vacuo*, a pale yellow crystalline solid identified as V (0.556 g, 1.11 mmol, 79% yield, mp 148 °C), VI as an orange crystalline solid (0.562 g, 1.12 mmol, 73% yield, mp 116 °C), or orange crystals of VII (0.199 g, 0.45 mmol, 43% yield, mp 112–115 °C) was collected on the inside walls of the U-trap at 0 °C. The side arms of both the reaction flask and the U-trap were maintained at ~100 °C with heating tape during the sublimation of the product. The remaining brown polymeric mass at the bottom of the reaction flask was insoluble in both polar and nonpolar organic solvents and was, therefore, discarded. At room temperature, V–VII are only slightly soluble in polar and nonpolar organic solvents. Anal. Calcd for C<sub>22</sub>H<sub>39</sub>N<sub>2</sub>B<sub>4</sub>Si<sub>2</sub>Ga (V): C, 52.77; H, 7.85. Found: C, 52.92; H, 7.73. Anal. Calcd for C<sub>22</sub>H<sub>39</sub>N<sub>2</sub>B<sub>4</sub>Si<sub>2</sub>Ga (VI): C, 52.77; H, 7.85; N, 5.59. Found: C, 52.63; H, 7.85; N, 5.43. Anal. Calcd for C<sub>20</sub>H<sub>33</sub>N<sub>2</sub>B<sub>4</sub>SiGa (VII): C, 54.28; H, 7.52; N, 6.33. Found: C, 54.08; H, 7.27; N, 6.14. The high-resolution electron impact (HREI) mass spectral analyses of V and VI do not exhibit the molecular ion. However, groupings with the major cutoffs at *m/z* 344.15, 329.13, and 156.06, corresponding to the fragments <sup>12</sup>C<sub>11</sub><sup>1</sup>H<sub>31</sub><sup>11</sup>B<sub>4</sub><sup>28</sup>Si<sub>2</sub><sup>69</sup>Ga, <sup>11</sup>C<sub>12</sub><sup>1</sup>H<sub>28</sub><sup>11</sup>B<sub>4</sub><sup>28</sup>Si<sub>2</sub><sup>69</sup>Ga, and <sup>12</sup>C<sub>10</sub>H<sub>8</sub><sup>14</sup>N<sub>2</sub><sup>+</sup>, respectively, were found. The NMR and IR spectral data of V–VII are given in Tables 4 and 5.

**Synthesis of 1-(CMe<sub>3</sub>)-1-Ga(2,2'-C<sub>8</sub>H<sub>6</sub>N<sub>4</sub>)-2,4-(SiMe<sub>3</sub>)<sub>2</sub>-2,4-C<sub>2</sub>B<sub>4</sub>H<sub>4</sub> (VIII).** In a procedure identical with that employed for the synthesis of the carbons adjacent isomer described elsewhere,<sup>9</sup> the *closo*-gallacarborane III (0.24 g, 0.69 mmol) was treated with freshly sublimed 2,2'-bipyrimidine (C<sub>8</sub>H<sub>6</sub>N<sub>4</sub>, 0.11 g, 0.69 mmol) in dry benzene (5 mL) at room temperature for 3 days. After the removal of benzene, the dark residue was heated to 80 °C to collect the unreacted 2,2'-bipyrimidine (not measured) in a detachable U-trap held at 0 °C. The resulting reddish brown residue was heated further to 160 °C to collect VIII (0.25 g, 0.50 mmol, 72% yield, mp 165 °C) as an orange crystalline product on the inside walls of the second U-trap held at 0 °C. The remaining dark polymeric mass at the bottom of the reaction flask was insoluble in both polar and nonpolar organic solvents and was discarded. Anal. Calcd for C<sub>20</sub>H<sub>37</sub>B<sub>4</sub>N<sub>4</sub>Si<sub>2</sub>Ga (VIII): C, 47.79; H, 7.42; N, 11.15. Found: C, 47.97; H, 7.22; N, 11.45. The NMR and IR spectral data for VIII are given in Tables 4 and 5.

**Synthesis of 1-(CMe<sub>3</sub>)-1-Ga(C<sub>15</sub>H<sub>11</sub>N<sub>3</sub>)-2,4-(SiMe<sub>3</sub>)<sub>2</sub>-2,4-C<sub>2</sub>B<sub>4</sub>H<sub>4</sub> (IX).** In a drybox, 0.59 g (1.7 mmol) of III was dissolved in 10 mL of benzene contained in a 250 mL vacuum flask equipped with a magnetic stirring bar. The flask was then transferred to a high-vacuum line, and a solution of 0.300 g (1.29 mmol) of freshly sublimed 2,2':6',2''-terpyridine (C<sub>15</sub>H<sub>11</sub>N<sub>3</sub>) in dry benzene (20 mL) was added, *in vacuo*, at ~5 °C. Addition of the terpyridine solution resulted in the immediate formation of a purple precipitate. The mixture was warmed slowly to room temperature and stirred for an additional 24 h. The solvent was then removed and the resulting purple violet solid was recrystallized from a warm THF/benzene (8 mL:12 mL) mixture to produce 0.93 g [1.6 mmol, 95% yield, mp 160 °C (dec)] of IX as needle-shaped crystals. Complex IX is slightly soluble in polar organic solvents. Anal. Calcd for C<sub>27</sub>H<sub>42</sub>B<sub>4</sub>N<sub>3</sub>Si<sub>2</sub>Ga (IX): C, 56.11; H, 7.32; N, 7.27. Found: C, 56.16; H, 7.13; N, 7.40. The NMR and IR spectral data for IX are given in Tables 4 and 5.

(20) Cleaver, W. M.; Barron, A. R. *Chemtronics* **1989**, 4, 146.

(21) Hoffman, G. G.; Faist, R. J. *J. Organomet. Chem.* **1990**, 391, 1.

**Synthesis of *closo*-1-(Me<sub>2</sub>CH)-1-In-2,4-(SiMe<sub>3</sub>)<sub>2</sub>-2,4-C<sub>2</sub>B<sub>4</sub>H<sub>4</sub> (X).** A 2.44 mmol (0.916 g) sample of **I** was dissolved in 10 mL of anhydrous THF *in vacuo*. This solution was poured slowly, *in vacuo*, onto freshly prepared *i*-PrInI<sub>2</sub> (1.004 g, 2.44 mmol) at 0 °C, and the resulting brown heterogeneous mixture was stirred constantly at this temperature for 2 h, during which time the solution turned gray. The solvent, THF, was then removed at 0 °C *via* vacuum distillation over a period of 2 h. The reaction flask containing the gray residue was then attached to a detachable U-trap that was immersed in an ice bath. After the gray residue was carefully heated in the flask to 130 °C using an oil bath, a colorless crystalline solid, identified as *closo*-1-(Me<sub>2</sub>CH)-1-In-2,4-(SiMe<sub>3</sub>)<sub>2</sub>-2,4-C<sub>2</sub>B<sub>4</sub>H<sub>4</sub> (**X**) (0.325 g, 0.86 mmol, 35% yield, mp 54–55 °C), was collected in the detachable U-trap held at 0 °C. The side arms of both the reaction flask and the U-trap were maintained at ~100 °C with a heating tape during the sublimation of the product. The remaining gray residue, at the bottom of the reaction flask, was insoluble in both polar and nonpolar organic solvents and was discarded. Compound **X** was sensitive to air and moisture and highly soluble in both polar and nonpolar organic solvents. Anal. Calcd for C<sub>11</sub>H<sub>29</sub>B<sub>4</sub>Si<sub>2</sub>In (**X**): C, 35.17; H, 7.80. Found: C, 35.35; H, 7.78. Mass spectral analyses (HREI and LR-FAB): theoretical mass for the ion groupings of **X**, <sup>12</sup>C<sub>11</sub><sup>1</sup>H<sub>29</sub><sup>11</sup>B<sub>4</sub><sup>28</sup>Si<sub>2</sub><sup>115</sup>In, <sup>12</sup>C<sub>10</sub><sup>13</sup>C<sup>1</sup>H<sub>28</sub><sup>11</sup>B<sub>3</sub><sup>10</sup>B<sub>1</sub><sup>28</sup>Si<sub>2</sub><sup>115</sup>In, and <sup>12</sup>C<sub>10</sub><sup>1</sup>H<sub>26</sub><sup>11</sup>B<sub>4</sub><sup>28</sup>Si<sub>2</sub><sup>115</sup>In *m/z* 376.1221, 375.1212, and 361.0986; measured mass *m/z* 376.1225, 375.1197, and 361.0998, respectively. The NMR and IR spectral data of **X** are given in Tables 4 and 5.

**Synthesis of *closo*-1-(Me<sub>2</sub>CH)-1-In-2-(SiMe<sub>3</sub>)<sub>4</sub>-(Me)-2,4-C<sub>2</sub>B<sub>4</sub>H<sub>4</sub> (XI).** A 1.124 g (3.54 mmol) sample of **II** was dissolved in 10 mL of anhydrous THF *in vacuo*. This solution was poured slowly, *in vacuo*, over 1.457 g (3.54 mmol) of freshly prepared *i*-PrInI<sub>2</sub> at 0 °C. The resulting heterogeneous mixture was stirred constantly at this temperature for 6 h, during which time the mixture turned gray. The solvent, THF, was then removed at this temperature *via* vacuum distillation over a period of 2 h. The reaction flask containing the gray residue was then attached to a detachable U-trap that was immersed in an ice bath. After the flask was carefully heated to 110–120 °C using an oil bath, a colorless liquid, identified as *closo*-1-(Me<sub>2</sub>CH)-1-In-2-(SiMe<sub>3</sub>)<sub>4</sub>-(Me)-2,4-C<sub>2</sub>B<sub>4</sub>H<sub>4</sub> (**XI**) (0.484 g, 1.523 mmol, 43% yield, bp 110–120 °C at 10<sup>-5</sup> Torr), was collected in the U-trap held at 0 °C. Compound **XI** is unstable and quite pyrophoric, bursting into flame even in a drybox. Because of this instability, a microanalysis of **XI** could not be obtained. The NMR and IR spectral data for this compound are given in Tables 4 and 5.

**Synthesis of 1-(Me<sub>2</sub>CH)-1-In(2,2'-C<sub>10</sub>H<sub>8</sub>N<sub>2</sub>)-2,4-(SiMe<sub>3</sub>)<sub>2</sub>-2,4-C<sub>2</sub>B<sub>4</sub>H<sub>4</sub> (XII).** A 5 mL benzene solution of 1-(Me<sub>2</sub>CH)-1-In-2,4-(SiMe<sub>3</sub>)<sub>2</sub>-2,4-C<sub>2</sub>B<sub>4</sub>H<sub>4</sub> (**X**) (0.78 g, 2.07 mmol) was added to a flask containing 2,2'-bipyridine (C<sub>10</sub>H<sub>8</sub>N<sub>2</sub>, 0.323 g, 2.07 mmol) in benzene (5 mL) at room temperature. The resulting homogeneous solution turned brown. This solution was stirred constantly for 24 h at room temperature, during which time it became turbid. Benzene was then removed from the solution *in vacuo*, and the resulting brown residue in the flask was washed seven times with dry hexane to collect an orange crystalline solid, identified as 1-(Me<sub>2</sub>CH)-1-In(2,2'-C<sub>10</sub>H<sub>8</sub>N<sub>2</sub>)-2,4-(SiMe<sub>3</sub>)<sub>2</sub>-2,4-C<sub>2</sub>B<sub>4</sub>H<sub>4</sub> (**XII**) (0.476 g, 0.89 mmol, 43% yield, mp 142–143 °C). At room temperature, **XII** is slightly soluble in polar organic solvents. Anal. Calcd for C<sub>21</sub>H<sub>37</sub>B<sub>4</sub>N<sub>2</sub>Si<sub>2</sub>In (**XII**): C, 47.43; H, 7.01; N, 5.27. Found: C, 47.35; H, 6.99; N, 5.31. The low-resolution electron impact (LREI) mass spectral analysis of **XII** does not exhibit the parent molecular ion. The NMR and IR spectral data for **XII** are given in Tables 4 and 5.

**Synthesis of 1-(Me<sub>2</sub>CH)-1-In(C<sub>8</sub>H<sub>6</sub>N<sub>4</sub>)-2,4-(SiMe<sub>3</sub>)<sub>2</sub>-2,4-C<sub>2</sub>B<sub>4</sub>H<sub>4</sub> (XIII).** In a procedure identical with that employed for the synthesis of the carbons adjacent isomer described elsewhere,<sup>12</sup> the *closo*-indacarborane **X** (0.287 g, 0.76 mmol) was treated with freshly sublimed 2,2'-bipyrimidine (C<sub>8</sub>H<sub>6</sub>N<sub>4</sub>, 0.121 g, 0.76 mmol) in dry benzene (10 mL) at room temper-

ature for 3 days, during which time the solution became turbid. Benzene was then removed *in vacuo* to yield a brown residue. This residue was recrystallized from a 4:1 dry hexane/benzene solvent mixture to produce orange needle-shaped crystals, identified as 1-(Me<sub>2</sub>CH)-1-In(C<sub>8</sub>H<sub>6</sub>N<sub>4</sub>)-2,4-(SiMe<sub>3</sub>)<sub>2</sub>-2,4-C<sub>2</sub>B<sub>4</sub>H<sub>4</sub> (**XIII**) (0.196 g, 0.38 mmol, 48% yield, mp 136–137 °C). Anal. Calcd for C<sub>19</sub>H<sub>35</sub>B<sub>4</sub>N<sub>4</sub>Si<sub>2</sub>In (**XIII**): C, 42.76; H, 6.61; N, 10.50. Found: C, 42.52; H, 6.40; N, 10.50. The NMR and IR spectral data for **XIII** are given in Tables 4 and 5.

**Attempted Syntheses of 1-(CMe<sub>3</sub>)-1-Ga[(η<sup>5</sup>-C<sub>5</sub>H<sub>5</sub>)Fe(η<sup>5</sup>-C<sub>5</sub>H<sub>4</sub>CH<sub>2</sub>(Me)<sub>2</sub>N)]-2,3-(SiMe<sub>3</sub>)<sub>2</sub>-2,3-C<sub>2</sub>B<sub>4</sub>H<sub>4</sub> and 1-(CMe<sub>3</sub>)-1-Ga[(η<sup>5</sup>-C<sub>5</sub>H<sub>5</sub>)Fe(η<sup>5</sup>-C<sub>5</sub>H<sub>4</sub>CH<sub>2</sub>(Me)<sub>2</sub>N)]-2,4-(SiMe<sub>3</sub>)<sub>2</sub>-2,4-C<sub>2</sub>B<sub>4</sub>H<sub>4</sub>.** A 5 mL benzene solution containing 0.350 g (1.01 mmol) of *closo*-1-(CMe<sub>3</sub>)-1-Ga-2,3-(SiMe<sub>3</sub>)<sub>2</sub>-2,3-C<sub>2</sub>B<sub>4</sub>H<sub>4</sub> or 0.100 g (0.29 mmol) of **III** was added to ferrocenylmethyl-*N,N*-dimethylamine (ferrocene amine, C<sub>13</sub>H<sub>17</sub>NFe, 0.380 g, 1.56 mmol, or 0.070 g, 0.29 mmol) in dry benzene (5 mL) at room temperature and stirred for 2 days. Attempts to remove the solvent by pumping *in vacuo* at 35 °C resulted in the complete transfer of all of the material in the reaction flask to a 0 °C trap. The <sup>11</sup>B, <sup>1</sup>H, and <sup>13</sup>C NMR spectra of the reaction mixture implied a combination of the spectra of the reactants and indicated that no complex was formed.

**X-ray Analyses of 1-(CMe<sub>3</sub>)-1-Ga(2,2'-C<sub>10</sub>H<sub>8</sub>N<sub>2</sub>)-2,3-(SiMe<sub>3</sub>)<sub>2</sub>-2,3-C<sub>2</sub>B<sub>4</sub>H<sub>4</sub> (V), 1-(CMe<sub>3</sub>)-1-Ga(2,2'-C<sub>10</sub>H<sub>8</sub>N<sub>2</sub>)-2,4-(SiMe<sub>3</sub>)<sub>2</sub>-2,4-C<sub>2</sub>B<sub>4</sub>H<sub>4</sub> (VI), 1-(CMe<sub>3</sub>)-1-Ga(2,2'-C<sub>8</sub>H<sub>6</sub>N<sub>4</sub>)-2,4-(SiMe<sub>3</sub>)<sub>2</sub>-2,4-C<sub>2</sub>B<sub>4</sub>H<sub>4</sub> (VIII), Dimeric *closo*-1-[(Me)<sub>2</sub>CH]-1-In-2,4-(SiMe<sub>3</sub>)<sub>2</sub>-2,4-C<sub>2</sub>B<sub>4</sub>H<sub>4</sub> (X), and 1-[(Me)<sub>2</sub>CH]-1-In(2,2'-C<sub>10</sub>H<sub>8</sub>N<sub>2</sub>)-2,4-(SiMe<sub>3</sub>)<sub>2</sub>-2,4-C<sub>2</sub>B<sub>4</sub>H<sub>4</sub> (XII).** Yellow crystals of **V**, red crystals of **VIII**, and colorless crystals of **X** were grown by vacuum sublimation onto glass surfaces in 8 mm tubes, whereas red crystals of **VI** and orange platelike crystals of **XII** were grown in benzene solutions. The crystals were all coated with an epoxy resin and mounted on a Siemens R3m/V diffractometer. Final unit cell parameters, given in Table 1, were obtained by least-squares fits of 24 accurately centered reflections, measured in the ranges 18 < 2θ < 29°, 19 < 2θ < 29°, 14 < 2θ < 26°, 20 < 2θ < 30°, and 19 < 2θ < 29°, and the intensity data were collected at 220–230 K in the ranges 3.5 ≤ 2θ ≤ 44.0°, 3.5 ≤ 2θ ≤ 46.0°, 3.5 ≤ 2θ ≤ 40.0°, 3.5 ≤ 2θ ≤ 42.0°, and 3.5 ≤ 2θ ≤ 42.0° for **V**, **VI**, **VIII**, **X**, and **XII**, respectively. Three standard reflections, monitored after every 150 reflections, did not show any significant change in intensity during the data collection. The data were corrected for Lorentz and polarization effects, and semiempirical absorption corrections (based on ψ scans) were applied with minimum and maximum transmission factors of 0.7435 and 0.9577, 0.6951 and 0.8252, 0.653 and 0.868, 0.510 and 0.644, and 0.644 and 0.817 for **V**, **VI**, **VIII**, **X**, and **XII**, respectively. The structures were solved by heavy atom methods using the *SHELXTL-Plus* package.<sup>22</sup> Full-matrix least-squares refinements were performed. All non-H atoms were refined anisotropically. The scattering factors, with anomalous dispersion corrections for heavy atoms, were taken from *International Tables for X-ray Crystallography*.<sup>23</sup> Carborane cage H atoms were located in difference Fourier maps, while the remaining H's were placed in idealized positions with fixed isotropic temperature factors (*U* = 0.08 Å<sup>2</sup>). The dimeric molecule of **X** possesses a center of symmetry that is located at the midpoint on the line between In and In(a) (1/2 - *x*, 1/2 - *y*, -*z*) (Figure 5). The final cycles of refinement converged at *R* = 0.0412, 0.0411, 0.056, 0.029, and 0.0495, *R<sub>w</sub>* = 0.0488, 0.0517, 0.057, 0.039, and 0.0698, and GOF = 1.37, 1.54, 1.35, 1.05, and 1.84 for **V**, **VI**, **VIII**, **X**, and **XII**, respectively. The final atomic coordinates are given in Table 2, and selected bond lengths and bond angles are presented in Table 3.

**Calculations.** Molecular orbital calculations on **VIII**A and **VIII**B, with the cage SiMe<sub>3</sub> groups replaced by H's, were

(22) Sheldrick, G. M. *Structure Determination Software Programs*; Siemens X-ray Analytical Instrument Corp.: Madison, WI, 1991.

(23) *International Tables for X-ray Crystallography*; Kynoch Press: Birmingham, U.K., 1974; Vol. IV.

Table 1. Crystallographic Data<sup>a</sup> for V, VI, VIII, X, and XII

	V	VI	VIII	X	XII
formula	C <sub>22</sub> H <sub>39</sub> N <sub>2</sub> B <sub>4</sub> Si <sub>2</sub> Ga	C <sub>22</sub> H <sub>39</sub> N <sub>2</sub> B <sub>4</sub> Si <sub>2</sub> Ga·2C <sub>6</sub> H <sub>6</sub>	C <sub>20</sub> H <sub>37</sub> N <sub>4</sub> B <sub>4</sub> Si <sub>2</sub> Ga	C <sub>22</sub> H <sub>58</sub> B <sub>8</sub> Si <sub>4</sub> In <sub>2</sub>	C <sub>21</sub> H <sub>37</sub> B <sub>4</sub> N <sub>2</sub> Si <sub>2</sub> In
fw	500.7	656.9	502.7	751.2	531.8
crystal system	monoclinic	monoclinic	triclinic	monoclinic	triclinic
space group	P2 <sub>1</sub> /n	P2 <sub>1</sub> /c	P1	C2/c	P1
a (Å)	9.778(2)	12.550(4)	9.611(4)	23.288(7)	9.079(5)
b (Å)	25.031(5)	15.885(5)	15.813(7)	9.169(7)	16.127(6)
c (Å)	11.376(2)	19.965(7)	19.808(7)	19.130(5)	19.83(9)
α (deg)			69.40(3)		88.20(3)
β (deg)	96.47(2)	103.42(2)	93.81(3)	98.02(2)	81.75(3)
γ (deg)			82.39(3)		79.21(3)
V (Å <sup>3</sup> )	2766.6(9)	3871(2)	2784(2)	4045(2)	2823(3)
Z	4	4	4	4	4
ρ <sub>calcd</sub> (g cm <sup>-3</sup> )	1.202	1.127	1.199	1.233	1.251
μ <sub>calcd</sub> (mm <sup>-1</sup> )	1.093	0.791	1.089	1.270	0.932
crystal dmns (mm)	0.20 × 0.30 × 0.15	0.25 × 0.35 × 0.20	0.30 × 0.15 × 0.10	0.05 × 0.30 × 0.15	0.35 × 0.30 × 0.20
scan type	θ-2θ	θ-2θ	θ-2θ	θ-2θ	θ-2θ
2θ range (deg)	3.5-44.0	3.5-46.0	3.5-40.0	3.5-42.0	3.5-42.0
T (K)	230	230	230	230	220
decay (%)	0	0	0	0	0
reflns collected	3840	5893	4630	2267	6207
obsd reflns, I > 3.0σ(I)	2340	3805	2263	1714	4612
params refined	280	388	419	163	545
Δρ (max,min) (e/Å <sup>3</sup> )	0.38, -0.38	0.38, -0.29	0.50, -0.36	0.42, -0.67	0.68, -0.78
GOF	1.37	1.54	1.35	1.05	1.84
R <sup>b</sup>	0.0412	0.0411	0.056	0.029	0.0495
R <sub>w</sub>	0.0488	0.0517	0.057	0.039	0.0698
g <sup>c</sup>	0.0005	0.0005	0.0005	0.0005	0.0010

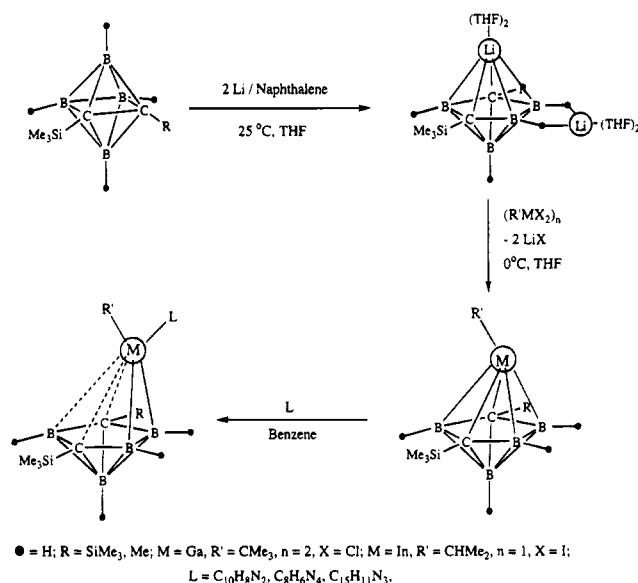
<sup>a</sup> Graphite-monochromatized Mo Kα radiation, λ = 0.710 73 Å. <sup>b</sup> R = Σ||F<sub>o</sub> - |F<sub>c</sub>||/Σ|F<sub>o</sub>| and R<sub>w</sub> = [Σw(F<sub>o</sub> - F<sub>c</sub>)<sup>2</sup>/Σw(F<sub>o</sub>)<sup>2</sup>]<sup>1/2</sup>. <sup>c</sup> w = 1/[σ<sup>2</sup>(F<sub>o</sub>) + g(F<sub>o</sub>)<sup>2</sup>].

carried out using the unparametrized Fenske-Hall method.<sup>24</sup> The basis functions used in the Fenske-Hall calculations were those generated by the numerical Xα atomic orbital program of Herman and Skillman,<sup>25</sup> used in conjunction with the Xα-to-Slater program of Bursten and Fenske.<sup>26</sup> The relative heavy atom positions were those in the crystal structures of the compounds, and the hydrogen positions were those used previously for the carbons apart base-stannacarborane complexes.<sup>4</sup> *Ab initio* molecular orbital calculations on the model compound, 1-(CMe<sub>3</sub>)-1-Ga-2,4-C<sub>2</sub>B<sub>4</sub>H<sub>6</sub>, were carried out using the SPARTAN package of programs.<sup>27</sup> The geometry of the model compound was optimized by assuming C<sub>1</sub> symmetry at the 3-21G(\*) level.

## Results and Discussion

**Synthesis.** The reactions of the carbons apart dilithiacarboranes *closo-exo-5,6*-[(μ-H)<sub>2</sub>Li(THF)](μ-THF)-1-Li-2-(SiMe<sub>3</sub>)-4-(R)-2,4-C<sub>2</sub>B<sub>4</sub>H<sub>4</sub> [R = SiMe<sub>3</sub> (I), Me (II)] with freshly prepared [t-BuGaCl<sub>2</sub>]<sub>2</sub> and *i*-PrInI<sub>2</sub> in THF solution in molar ratios of 1:1 at 0 °C produced the corresponding *closo*-metallacarboranes, *closo-1*-(CMe<sub>3</sub>)-Ga-2-(SiMe<sub>3</sub>)-4-(R)-2,4-C<sub>2</sub>B<sub>4</sub>H<sub>4</sub> [R = SiMe<sub>3</sub> (III), Me (IV)] and *closo-1*-[(Me)<sub>2</sub>CH]-1-In-2-(SiMe<sub>3</sub>)-4-(R)-2,4-C<sub>2</sub>B<sub>4</sub>H<sub>4</sub> [R = SiMe<sub>3</sub> (X), Me (XI)], in yields of 53, 59, 35, and 43%, respectively, as outlined in Scheme 1. These synthetic routes are similar to those employed for the preparation of the corresponding carbons adjacent metallacarboranes,<sup>9,12</sup> and the yields in the different carborane systems were similar, except for the fact that the yields of the gallacarboranes III and IV were somewhat lower than those reported for the respective carbons adjacent isomers. These results tend to support the conclusions obtained from the study of the stanna-

Scheme 1



carboranes, namely, that the carbons apart and carbons adjacent carborane dianions bond equally well to metals.<sup>4</sup>

The carbons apart *closo*-gallacarboranes and *closo*-indacarborane react readily with the bidentate, bis(bidentate), and tridentate Lewis bases 2,2'-bipyridine, 2,2'-bipyrimidine, and 2,2':6',2''-terpyridine to produce the 1:1 donor-acceptor complexes 1-(CMe<sub>3</sub>)-1-Ga(2,2'-C<sub>10</sub>H<sub>8</sub>N<sub>2</sub>)-2,4-(SiMe<sub>3</sub>)<sub>2</sub>-2,4-C<sub>2</sub>B<sub>4</sub>H<sub>4</sub> (VI), 1-(CMe<sub>3</sub>)-1-Ga(2,2'-C<sub>10</sub>H<sub>8</sub>N<sub>2</sub>)-2-(SiMe<sub>3</sub>)-4-(Me)-2,4-C<sub>2</sub>B<sub>4</sub>H<sub>4</sub> (VII), 1-(CMe<sub>3</sub>)-1-Ga(2,2'-C<sub>8</sub>H<sub>6</sub>N<sub>4</sub>)-2,4-(SiMe<sub>3</sub>)<sub>2</sub>-2,4-C<sub>2</sub>B<sub>4</sub>H<sub>4</sub> (VIII), 1-(CMe<sub>3</sub>)-1-Ga(C<sub>15</sub>H<sub>11</sub>N<sub>3</sub>)-2,4-(SiMe<sub>3</sub>)<sub>2</sub>-2,4-C<sub>2</sub>B<sub>4</sub>H<sub>4</sub> (IX), 1-[(Me)<sub>2</sub>CH]-1-In(2,2'-C<sub>10</sub>H<sub>8</sub>N<sub>2</sub>)-2,4-(SiMe<sub>3</sub>)<sub>2</sub>-2,4-C<sub>2</sub>B<sub>4</sub>H<sub>4</sub> (XII), and 1-[(Me)<sub>2</sub>CH]-1-In(2,2'-C<sub>8</sub>H<sub>6</sub>N<sub>4</sub>)-2,4-(SiMe<sub>3</sub>)<sub>2</sub>-2,4-C<sub>2</sub>B<sub>4</sub>H<sub>4</sub> (XIII) in 40-90% yields. For comparison, the carbons adjacent bipyridine-gallacarborane complex V was also prepared. The reaction of *closo*-gallacarborane III with 2,2'-bipyrimidine in a 2:1 molar

(24) Hall, M. B.; Fenske, R. F. *Inorg. Chem.* **1972**, *11*, 808.

(25) Herman, F.; Skillman, S. *Atomic Structure Calculations*; Prentice-Hall: Englewood, NJ, 1963.

(26) (a) Bursten, B. E.; Fenske, R. F. *J. Chem. Phys.* **1977**, *67*, 3138.

(b) Bursten, B. E.; Jensen, R. J.; Fenske, R. F. *J. Chem. Phys.* **1978**, *68*, 3320.

(27) SPARTAN, Version 3.1; Wavefunction Inc.: Irvine, CA, 1994.

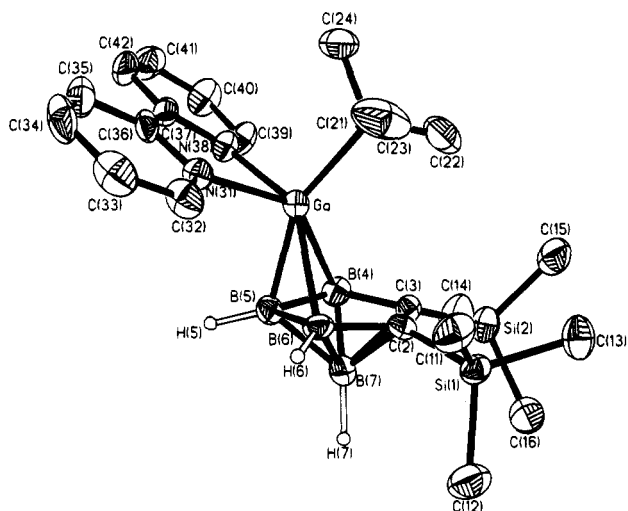


**Figure 1.** Perspective view of 1-(CMe<sub>3</sub>)-1-Ga(2,2'-C<sub>10</sub>H<sub>8</sub>N<sub>2</sub>)-2,3-(SiMe<sub>3</sub>)<sub>2</sub>-2,3-C<sub>2</sub>B<sub>4</sub>H<sub>4</sub> (V) showing the atom numbering scheme. The thermal ellipsoids are drawn at the 40% probability level. For clarity, all H's except on the carborane cage are removed.

ratio produced only the 1:1 adducts and not a bimetallic bridged compound, as found in the case of the corresponding carbons adjacent gallacarborane.<sup>9</sup> The monodentate base ferrocene amine did not form stable complexes with **III** or its carbons adjacent isomer. To date, the only ferrocene amine complexes reported have been those of the carbons adjacent group 14 metallacarboranes.<sup>13</sup>

**Characterization.** The *closo*-metallacarboranes, and their donor-acceptor complexes, were characterized by <sup>1</sup>H, <sup>11</sup>B, and <sup>13</sup>C pulse Fourier transform NMR (Table 4) and IR (Table 5) spectroscopy. Complexes **V**, **VI**, **VIII**, **X**, and **XII** were further characterized by single-crystal X-ray diffraction (Tables 1-3). The high-resolution electron impact mass spectra (HREI) and the isotope patterns of the *closo*-gallacarborane **III** and *closo*-indacarborane **X** are consistent with the respective molecular formulas. The high-resolution electron impact mass spectra of the donor-acceptor complexes did not exhibit peaks due to the parent ions, but did show peaks corresponding to fragment ions of their component metallacarboranes and Lewis bases.

**NMR and IR Spectra.** While the NMR and IR spectra of **I** have been described elsewhere,<sup>16a</sup> Tables 4 and 5, respectively, summarize the NMR (<sup>1</sup>H, <sup>11</sup>B, and <sup>13</sup>C) and IR spectral data for **II**-**XIII**. The resonances listed in Table 4 for the various nuclei are all consistent with the formulas listed in the Experimental Section and, in the cases of compounds **V**, **VI**, **VIII**, **X**, and **XII**, the results of X-ray structural determinations. The <sup>11</sup>B NMR spectra of pentagonal bipyramidal metallacarboranes, such as **III**-**XIII**, have been found to be quite sensitive to the nature of the capping metal group, and attempts have been made to interpret these spectra in terms of the strength of the metal-carborane interactions. As can be seen from Table 4, all complexes in this study show the same general pattern: an upfield resonance in the δ -38 to -50 range due to the apical boron [B(7) in Figures 1-3], while the resonances of the basal borons [those in the C<sub>2</sub>B<sub>3</sub> face, B(4)-B(6) in Figure 1, or B(3), B(5), and B(6) in Figures 2 and 3] were found in the δ 2-22 range. The <sup>11</sup>B NMR spectrum of *closo*-exo-5,6-[(μ-H)<sub>2</sub>Li(THF)](μ-THF)-1-Li-2,4-(SiMe<sub>3</sub>)<sub>2</sub>-2,4-C<sub>2</sub>B<sub>4</sub>H<sub>4</sub> shows resonances at δ 16.25, 13.94, and -42.28,

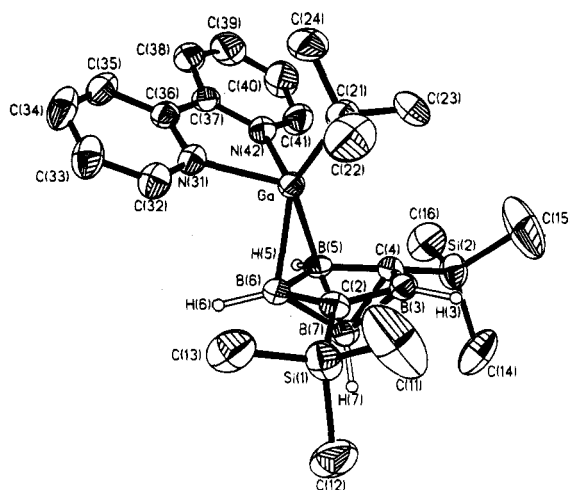


**Figure 2.** Perspective view of 1-(CMe<sub>3</sub>)-1-Ga(2,2'-C<sub>10</sub>H<sub>8</sub>N<sub>2</sub>)-2,4-(SiMe<sub>3</sub>)<sub>2</sub>-2,4-C<sub>2</sub>B<sub>4</sub>H<sub>4</sub> (VI) showing the atom numbering scheme. The thermal ellipsoids are drawn at the 40% probability level. For clarity, all H's except on the carborane cage are removed.

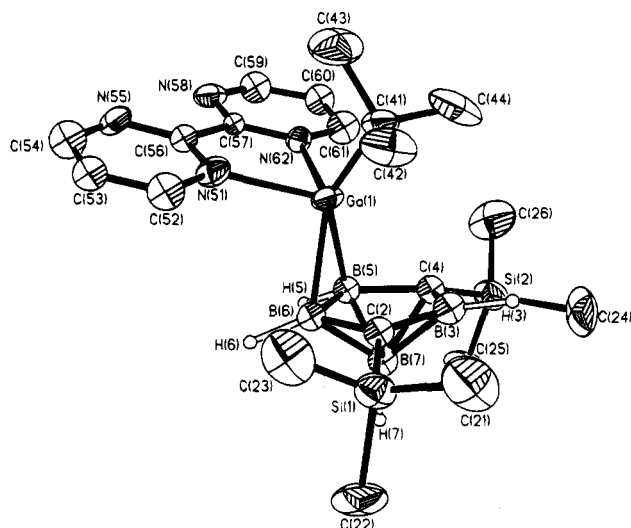


**Table 2. Atomic Coordinates ( $\times 10^4$ ) and Equivalent Isotropic Displacement Coefficients ( $\text{\AA}^2 \times 10^3$ )**

	<i>x</i>	<i>y</i>	<i>z</i>	<i>U</i> (eq) <sup>a</sup>		<i>x</i>	<i>y</i>	<i>z</i>	<i>U</i> (eq) <sup>a</sup>
<b>Structure V</b>									
Ga	1904(1)	6381(1)	4959(1)	29(1)	C(22)	2355(11)	5245(3)	5381(6)	121(5)
Si(1)	5453(2)	6157(1)	7873(1)	35(1)	C(23)	3893(7)	5653(3)	4148(8)	95(4)
Si(2)	1966(2)	5729(1)	8827(2)	46(1)	C(24)	1547(7)	5473(3)	3329(5)	65(3)
C(2)	3665(5)	6332(2)	7224(4)	30(2)	N(31)	2365(5)	6833(2)	3443(4)	37(2)
C(3)	2299(5)	6160(2)	7545(5)	30(2)	C(32)	3639(6)	7025(2)	3346(6)	49(2)
B(4)	1120(7)	6491(3)	6902(6)	39(2)	C(33)	3934(8)	7289(3)	2339(7)	61(3)
B(5)	1858(7)	6991(3)	6182(6)	36(2)	C(34)	2899(9)	7342(3)	1413(7)	63(3)
B(6)	3561(7)	6810(3)	6369(5)	33(2)	C(35)	1602(7)	7152(2)	1519(5)	51(3)
B(7)	2583(7)	6837(3)	7605(6)	38(2)	C(36)	1350(6)	6903(2)	2556(5)	36(2)
C(11)	6618(6)	6199(3)	6674(5)	53(3)	C(37)	-2(6)	6710(2)	2814(5)	35(2)
C(12)	6114(7)	6643(3)	9043(5)	66(3)	N(38)	-27(4)	6496(2)	3896(4)	34(2)
C(13)	5691(6)	5456(2)	8444(6)	55(3)	C(39)	-1207(5)	6320(2)	4232(5)	43(2)
C(14)	171(8)	5817(3)	9169(7)	100(4)	C(40)	-2418(6)	6345(3)	3480(6)	55(3)
C(15)	2156(7)	5008(2)	8514(5)	66(3)	C(41)	-2400(7)	6556(3)	2383(6)	59(3)
C(16)	3080(7)	5912(3)	10224(5)	61(3)	C(42)	-1194(7)	6743(2)	2037(5)	50(3)
C(21)	2395(6)	5644(2)	4451(5)	40(2)					
<b>Structure VI</b>									
Ga	2039(1)	923(1)	120(1)	40(1)	C(34)	2879(4)	-1970(3)	795(3)	73(2)
Si(1)	2023(1)	850(1)	-2090(1)	65(1)	C(35)	2546(3)	-1407(3)	1226(2)	59(2)
Si(2)	378(1)	3358(1)	-475(1)	61(1)	C(36)	2268(3)	-595(3)	992(2)	46(1)
C(2)	1620(3)	1246(2)	-1317(2)	44(1)	C(37)	1886(3)	60(3)	1398(2)	47(2)
B(3)	1675(4)	2178(3)	-1113(2)	44(2)	C(38)	1781(4)	-52(3)	2072(2)	64(2)
C(4)	911(3)	2313(2)	-618(2)	40(1)	C(39)	1426(5)	604(4)	2403(2)	80(2)
B(5)	452(3)	1459(3)	-408(2)	40(2)	C(4)	1151(5)	1357(3)	2070(3)	80(2)
B(6)	943(4)	712(3)	-897(2)	42(2)	C(41)	1256(4)	1430(3)	1402(2)	64(2)
B(7)	384(4)	1637(3)	-1272(2)	42(2)	N(42)	1632(3)	804(2)	1076(2)	48(1)
C(11)	3214(6)	1412(5)	-2254(4)	168(5)	C(51)	3892(9)	-2988(7)	-2017(4)	126(5)
C(12)	901(5)	1007(3)	-2879(2)	109(3)	C(52)	4130(6)	-3703(8)	-1709(5)	123(4)
C(13)	2303(5)	-288(3)	-2030(2)	88(2)	C(53)	3450(10)	-4060(4)	-1369(3)	115(4)
C(14)	-620(5)	3728(3)	-1254(3)	100(3)	C(54)	2504(10)	-3672(8)	-1346(4)	132(5)
C(15)	1484(5)	4133(3)	-278(4)	155(5)	C(55)	2253(8)	-2910(9)	-1690(6)	157(6)
C(16)	-373(5)	3353(3)	225(3)	93(3)	C(56)	3002(11)	-2601(5)	-2017(4)	134(5)
C(21)	3559(4)	1380(3)	416(3)	67(2)	C(61)	5531(5)	866(4)	3153(3)	94(3)
C(22)	4167(4)	1210(4)	-150(3)	114(3)	C(62)	6254(5)	550(3)	3699(3)	87(3)
C(23)	3534(4)	2318(3)	533(3)	107(3)	C(63)	6111(5)	683(3)	4343(3)	88(3)
C(24)	4200(4)	959(3)	1070(3)	102(3)	C(64)	5250(5)	1141(3)	4443(3)	88(3)
N(31)	2312(2)	-359(2)	350(2)	44(1)	C(65)	4525(5)	1469(3)	3889(4)	91(3)
C(32)	2614(3)	-928(3)	-61(2)	57(2)	C(66)	4667(5)	1330(4)	3252(3)	99(3)
C(33)	2893(3)	-1740(3)	137(3)	66(2)					
<b>Structure VIII</b>									
Ga(1)	9679(2)	7643(1)	2825(1)	40(1)	Ga(2)	798(2)	1959(1)	1792(1)	37(1)
Si(1)	12896(5)	8171(3)	1008(2)	55(2)	Si(3)	-2886(5)	4114(3)	1113(3)	57(2)
Si(2)	13241(5)	6141(3)	4063(3)	56(2)	Si(4)	-1692(4)	1547(3)	3958(2)	55(2)
C(2)	12253(14)	7805(9)	1971(7)	37(4)	C(12)	-1891(13)	3140(9)	1755(7)	33(4)
B(3)	12627(18)	6883(12)	2499(10)	46(5)	B(13)	-1746(17)	3038(11)	2548(9)	37(5)
C(4)	12328(13)	6913(9)	3280(7)	36(4)	C(14)	-1422(13)	2026(9)	2968(7)	31(4)
B(5)	11518(16)	7886(11)	3262(8)	33(5)	B(15)	-1155(17)	1473(11)	2469(9)	32(5)
B(6)	11461(17)	8454(11)	2342(9)	35(5)	B(16)	-1464(17)	2250(11)	1599(9)	38(5)
B(7)	12984(17)	7870(11)	2655(9)	42(5)	B(17)	-2614(19)	2201(12)	2369(10)	48(5)
C(21)	13444(19)	7209(11)	687(9)	111(12)	C(31)	-3179(22)	5104(11)	1417(11)	142(14)
C(22)	14454(15)	8851(11)	887(8)	87(10)	C(32)	-1922(16)	4477(11)	206(8)	92(10)
C(23)	11491(17)	8895(11)	429(8)	83(10)	C(33)	-4628(14)	3803(11)	996(9)	87(10)
C(24)	14375(18)	5207(10)	3818(9)	94(10)	C(34)	-1387(18)	270(10)	4288(8)	92(10)
C(25)	14428(15)	6777(10)	4355(8)	78(10)	C(35)	-471(15)	2002(12)	4382(8)	92(11)
C(26)	12036(16)	5595(12)	4854(8)	98(11)	C(36)	-3530(14)	1863(12)	4269(8)	86(11)
C(41)	8926(16)	6729(12)	2532(10)	53(9)	C(71)	2036(19)	1892(12)	953(8)	56(9)
C(42)	9339(17)	6844(11)	1760(9)	81(10)	C(72)	1930(18)	2788(11)	340(8)	86(10)
C(43)	7304(17)	6832(12)	2642(10)	103(13)	C(73)	1554(18)	1221(12)	668(8)	87(11)
C(44)	9411(19)	5781(12)	3020(9)	95(11)	C(74)	3596(16)	1582(12)	1086(9)	84(11)
N(51)	8120(11)	8788(8)	2537(7)	46(6)	N(81)	1528(12)	2958(7)	2068(6)	35(6)
C(52)	7999(16)	9391(10)	1848(9)	57(5)	C(82)	1276(14)	3853(10)	1730(8)	44(4)
C(53)	6987(15)	10111(10)	1746(8)	50(5)	C(83)	1776(15)	4462(11)	1973(8)	57(5)
C(54)	6168(17)	10233(12)	2317(9)	63(5)	C(84)	2494(16)	4105(12)	2566(9)	63(5)
N(55)	6256(12)	9646(9)	2989(8)	59(7)	N(85)	2773(12)	3228(9)	2928(6)	55(7)
C(56)	7252(17)	8948(10)	3078(8)	35(4)	C(86)	2258(14)	2677(10)	2639(8)	32(4)
C(57)	7487(15)	8286(9)	3788(7)	24(4)	C(87)	2549(14)	1715(10)	2979(8)	30(4)
N(58)	6693(11)	8408(8)	4361(7)	48(6)	N(88)	2001(11)	1198(7)	2677(5)	33(5)
C(59)	6982(16)	7774(11)	4997(9)	54(5)	C(89)	2238(14)	309(10)	2961(7)	37(4)
C(60)	7932(15)	7037(10)	5076(8)	51(5)	C(90)	2999(14)	-99(10)	3543(7)	40(4)
C(61)	8702(16)	6959(11)	4459(9)	55(5)	C(91)	3546(15)	452(11)	3821(8)	50(5)
N(62)	8435(11)	7603(8)	3812(6)	37(6)	N(92)	3299(12)	1353(8)	3554(6)	46(6)
<b>Structure X</b>									
In	1853(1)	1252(1)	167(1)	48(1)	C(11)	852(3)	1983(7)	-1796(3)	88(3)
Si(1)	512(1)	2917(9)	-1089(1)	55(1)	C(12)	343(2)	4832(6)	-1331(3)	77(2)
Si(2)	1434(12)	2748(2)	1983(1)	62(1)	C(13)	-169(3)	1977(8)	-960(3)	92(3)
C(2)	1043(2)	2842(5)	-274(2)	42(2)	C(14)	767(3)	1891(7)	2222(3)	78(2)
B(3)	909(2)	2274(6)	459(3)	43(2)	C(15)	1475(3)	4661(7)	2312(3)	97(3)
C(4)	1425(2)	2774(5)	1011(2)	44(2)	C(16)	2076(3)	1681(9)	2373(3)	139(4)
B(5)	1921(2)	3567(6)	661(3)	46(2)	C(21)	1933(2)	-1062(5)	115(3)	58(2)
B(6)	1662(2)	3622(6)	-219(3)	46(2)	C(23)	1487(3)	-1702(6)	-440(3)	92(3)
B(7)	1203(2)	4048(5)	398(3)	46(2)	C(22)	1909(3)	-1735(6)	837(3)	85(3)



Table 2 (Continued)

	x	y	z	U(eq) <sup>a</sup>		x	y	z	U(eq) <sup>a</sup>
Structure XII									
In(1)	4347(1)	3145(1)	3967(1)	65(1)	C(37)	5300(10)	-392(4)	7889(4)	77(3)
In(2)	1276(1)	1932(1)	8925(1)	62(1)	C(38)	4175(10)	931(6)	6879(4)	84(4)
Si(1)	1615(3)	3606(2)	2365(1)	74(1)	C(39)	7196(9)	947(6)	7398(4)	89(4)
Si(2)	1398(3)	1456(2)	4789(2)	101(1)	C(40)	1972(11)	4281(6)	9864(6)	121(5)
Si(3)	5209(3)	746(1)	7633(1)	63(1)	C(41)	5255(11)	3751(6)	9835(5)	110(5)
Si(4)	3737(3)	3831(1)	9303(1)	64(1)	C(42)	4025(14)	4569(5)	8570(5)	115(5)
C(2)	1969(8)	3262(4)	3234(3)	56(3)	N(51)	5544(7)	3210(4)	4938(3)	68(3)
B(3)	2079(10)	2344(5)	3474(4)	60(4)	C(52)	5488(10)	2644(6)	5437(5)	94(4)
C(4)	1915(8)	2352(5)	4264(4)	67(3)	C(53)	6267(13)	2609(7)	5968(6)	117(6)
B(5)	1881(10)	3267(7)	4542(5)	73(4)	C(54)	7136(12)	3200(8)	6010(5)	110(5)
B(6)	1929(10)	3885(6)	3844(5)	66(4)	C(55)	7247(10)	3796(6)	5502(4)	81(4)
B(7)	735(10)	3157(5)	3931(4)	59(3)	C(56)	6432(8)	3777(5)	4976(4)	58(3)
C(12)	4163(8)	1470(4)	8329(3)	53(3)	C(57)	6463(8)	4405(4)	4404(4)	60(3)
B(13)	4049(9)	2438(5)	8280(4)	54(3)	N(58)	5602(7)	4324(4)	3914(3)	62(2)
C(14)	3600(8)	2774(4)	9009(3)	51(3)	C(59)	5601(10)	4872(5)	3393(4)	77(4)
B(15)	3234(10)	2058(5)	9551(4)	55(3)	C(60)	6361(11)	5517(5)	3342(4)	87(4)
B(16)	3663(9)	1146(5)	9065(4)	54(3)	C(61)	7239(10)	5594(5)	3835(5)	83(4)
B(17)	4883(10)	1885(5)	8957(4)	53(3)	C(62)	7272(9)	5043(5)	4367(4)	75(3)
C(21)	6111(13)	2287(5)	3435(5)	118(6)	N(71)	-640(7)	1923(4)	9879(3)	63(2)
C(22)	-17(12)	2697(6)	8250(6)	113(5)	C(72)	-1003(10)	2526(5)	10357(5)	75(4)
C(23)	6324(11)	1452(6)	3573(5)	119(6)	C(73)	-2154(10)	2560(6)	10870(4)	81(4)
C(24)	6683(19)	2413(7)	2781(7)	237(11)	C(74)	-3020(10)	1959(6)	10903(4)	80(4)
C(25)	465(17)	2779(10)	7580(6)	319(16)	C(75)	-2704(9)	1319(5)	10426(4)	73(3)
C(26)	-869(22)	3432(10)	8492(7)	572(28)	C(76)	-1485(8)	1308(5)	9918(3)	56(3)
C(31)	3117(15)	4087(10)	1958(6)	211(11)	C(77)	-1034(8)	634(4)	9397(4)	57(3)
C(32)	1652(17)	2678(8)	1831(5)	166(8)	N(78)	144(7)	722(4)	8911(3)	63(3)
C(33)	-157(15)	4228(10)	2326(7)	197(10)	C(79)	578(8)	129(5)	8441(4)	73(3)
C(34)	-325(15)	1255(9)	4646(9)	273(14)	C(80)	-64(10)	-559(5)	8412(4)	75(4)
C(35)	1036(15)	1777(10)	5739(6)	191(9)	C(81)	-1238(10)	-645(5)	8893(5)	72(4)
C(36)	2957(14)	604(7)	4760(7)	173(8)	C(82)	-1748(9)	-50(5)	9395(4)	66(3)

<sup>a</sup> Equivalent isotropic  $U$  is defined as one-third of the trace of the orthogonalized  $U_{ij}$  tensor.

changes are quite different from those found in the stannacarborane system. The <sup>11</sup>B NMR spectrum of the stannacarborane analogue of **IX** shows resonances at  $\delta$  21.35, 19.45, and -9.03, with a 2:1:1 peak area ratio.<sup>4</sup> Coordination of the tin with a base, such as bipyridine, produces an upfield shift of the apical resonance, to  $\delta$  -11.5, with little change in the positions of the ring boron resonances. The relatively large deshielding of the cage borons, especially the apical boron, upon coordination with tin has been interpreted in terms of the withdrawal of electron density from the cage when it coordinates to the metal.<sup>14b,16a,17b</sup> The upfield shift that occurs upon base coordination was also rationalized by electron density change arguments.<sup>14b</sup> If the arguments are generally valid, the small deshielding of the cage borons upon forming the galla- and indacarboranes, shown in Table 4, could signify a more ionic (less covalent) interaction of the group 13 metals, compared to their group 14 analogues. However, the subsequent changes found upon base coordination are more difficult to rationalize, especially in light of the extreme cage distortions found in the group 13 metallacarborane-base complexes (see the following). It should be noted that changes in the boron paramagnetic shielding constants, which depend on factors other than gross electron density, have been shown to be important in determining the <sup>11</sup>B NMR chemical shifts in heterocarboranes.<sup>28</sup> It is most likely that changes in the paramagnetic shielding parameters are important in determining the shifts shown in Table 4 and that their importance complicates the interpretation of the spectral changes that accompany the formation and reactions of the carbons apart group 13 metallacarboranes.

Table 5 lists the infrared absorptions of compounds **II–XIII**. All show the expected B–H stretch absorptions in the 2500–2600 cm<sup>-1</sup> region. Other than that, there are no noteworthy facets to the spectra, and they are presented for the purpose of qualitative analysis.

**Crystal Structures of V, VI, VIII, X, and XII.** The solid state structures of **V**, **VI**, **VIII**, **X**, and **XII** were determined by single-crystal X-ray diffraction. Figures 1–6 show the structures of these complexes. Tables 1 and 2, respectively, give the pertinent crystallographic data and atomic coordinates of these compounds, while Table 3 lists some important bond distances and bond angles. A more extensive set of bond distances and bond angles, the anisotropic displacement parameters, and the H atom coordinates are available in Tables S-1–S-3, respectively, of the supporting information.

In compound **V**, the only carbons adjacent metallacarborane in this study, the gallium atom is located in the pseudo-mirror plane of the carborane,<sup>29</sup> but is slipped toward the unique boron [B(5) in Figure 1]. The dihedral angle between the plane of the bipyridine and the B(4)–C(3)–C(2)–B(6) plane is 30.6°.<sup>30</sup> This structure is very similar to that reported for the corresponding 2,2'-bipyrimidine complex, 1-(C<sub>5</sub>H<sub>6</sub>N<sub>4</sub>)Ga(CMe<sub>3</sub>)<sub>2</sub>-2,3-(CSiMe<sub>3</sub>)<sub>2</sub>B<sub>4</sub>H<sub>4</sub>.<sup>10</sup> The main differences between the two structures are that **V** has slightly shorter Ga–N bond distances (2.152 and 2.142 Å vs 2.174 and 2.178 Å), has a smaller base–C<sub>2</sub>B<sub>2</sub> dihedral angle (30.6 vs 37.5°), and exhibits a slightly greater slip distortion than does the bipyrimidine complex [the average Ga–C(2,3) distance in **V** is 2.956 ± 0.020 Å, compared to 2.88 ± 0.023 Å in

(29) In Figure 1, the plane containing B(5), B(7), and the C(2)–C(3) midpoint; in Figure 2, the plane containing B(3), B(7), and the B(5)–B(6) midpoint.

(30) The C<sub>2</sub>B<sub>2</sub> carborane faces are not planar, but are folded so that the unique borons are outside the planes of the other facial atoms.

(28) (a) Hermánek, S.; Hnyk, D.; Havlas, Z. *J. Chem. Soc., Chem. Commun.* **1989**, 1859. (b) Bühl, M.; Schleyer, P. v. R.; Havlas, Z.; Hnyk, D.; Hermánek, S. *Inorg. Chem.* **1991**, *30*, 3107. (c) Fehlner, T. P.; Czech, P. T.; Fenske, R. F. *Inorg. Chem.* **1990**, *29*, 3103.



**Table 3. Bond Lengths (Å) and Bond Angles (deg)**

Bond Lengths							
<b>Structure V</b>							
Ga-B(4)	2.436(7)	Ga-B(5)	2.069(7)	C(2)-B(7)	1.734(9)	C(3)-B(4)	1.537(8)
Ga-B(6)	2.401(6)	Ga-C(21)	2.008(6)	C(3)-B(7)	1.717(9)	B(4)-B(5)	1.699(10)
Ga-N(31)	2.152(5)	Ga-N(38)	2.143(4)	B(4)-B(7)	1.782(9)	B(5)-B(6)	1.715(9)
C(2)-C(3)	1.487(7)	C(2)-B(6)	1.537(8)	B(5)-B(7)	1.736(9)	B(6)-B(7)	1.788(10)
<b>Structure VI</b>							
Ga-B(5)	2.198(4)	Ga-B(6)	2.198(4)	B(3)-C(4)	1.544(6)	B(3)-B(7)	1.797(6)
Ga-C(21)	1.998(4)	Ga-N(31)	2.098(3)	C(4)-B(5)	1.569(6)	C(4)-B(7)	1.702(5)
Ga-N(42)	2.095(4)	C(2)-B(3)	1.532(6)	B(5)-B(6)	1.738(7)	B(5)-B(7)	1.731(6)
C(2)-B(6)	1.574(6)	C(2)-B(7)	1.692(6)	B(6)-B(7)	1.723(6)		
<b>Structure VIII</b>							
Ga(1)-B(5)	2.193(18)	Ga(1)-B(6)	2.194(16)	C(4)-B(7)	1.722(19)	B(5)-B(6)	1.729(21)
Ga(1)-C(41)	1.979(21)	Ga(1)-N(51)	2.148(11)	B(5)-B(7)	1.741(22)	B(6)-B(7)	1.685(22)
Ga(1)-N(62)	2.150(12)	Ga(2)-B(15)	2.226(15)	C(12)-B(13)	1.544(23)	C(12)-B(16)	1.538(24)
Ga(2)-B(16)	2.213(16)	Ga(2)-C(71)	1.951(17)	C(12)-B(17)	1.723(20)	B(13)-C(14)	1.531(19)
Ga(2)-N(81)	2.068(13)	Ga(2)-N(88)	2.121(10)	B(13)-B(17)	1.809(29)	C(14)-B(15)	1.514(25)
C(2)-B(3)	1.493(19)	C(2)-B(6)	1.537(24)	C(14)-B(17)	1.677(24)	B(15)-B(16)	1.763(20)
C(2)-B(7)	1.641(25)	B(3)-C(4)	1.555(24)	B(15)-B(17)	1.677(23)	B(16)-B(17)	1.756(24)
B(3)-B(7)	1.778(29)	C(4)-B(5)	1.621(21)				
<b>Structure X</b>							
In-Cnt(1)	1.989	In-C(2)	2.440(4)	B(3)-C(4)	1.555(6)	B(3)-B(7)	1.775(7)
In-B(3)	2.524(5)	In-C(4)	2.449(4)	C(4)-B(5)	1.590(7)	C(4)-B(7)	1.685(7)
In-B(5)	2.320(5)	In-B(6)	2.318(5)	B(5)-B(6)	1.708(8)	B(5)-B(7)	1.735(7)
In-C(21)	2.133(5)	C(2)-B(3)	1.567(7)	B(6)-B(7)	1.741(8)		
C(2)-B(6)	1.599(7)	C(2)-B(7)	1.696(7)				
<b>Structure XII</b>							
In(1)-C(2)	2.746(15)	In(1)-B(3)	2.918(16)	C(2)-B(7)	1.676(13)	B(3)-C(4)	1.553(14)
In(1)-C(4)	2.737(15)	In(1)-B(5)	2.338(14)	B(3)-B(7)	1.785(13)	C(4)-B(5)	1.584(15)
In(1)-B(6)	2.336(14)	In(1)-C(21)	2.091(13)	C(4)-B(7)	1.703(14)	B(5)-B(6)	1.682(16)
In(1)-N(51)	2.357(13)	In(1)-N(58)	2.386(13)	B(5)-B(7)	1.741(16)	B(6)-B(7)	1.731(16)
In(2)-C(12)	2.694(14)	In(2)-B(13)	2.901(16)	C(12)-B(13)	1.545(12)	C(12)-B(16)	1.567(13)
In(2)-C(14)	2.741(15)	In(2)-B(15)	2.352(14)	C(12)-B(17)	1.695(14)	B(13)-C(14)	1.532(12)
In(2)-B(16)	2.347(13)	In(2)-C(22)	2.119(14)	B(13)-B(17)	1.771(14)	C(14)-B(15)	1.601(13)
In(2)-N(71)	2.381(12)	In(2)-N(78)	2.372(13)	C(14)-B(17)	1.665(12)	B(15)-B(16)	1.736(14)
C(2)-B(3)	1.531(13)	C(2)-B(6)	1.589(14)	B(15)-B(17)	1.751(14)	B(16)-B(17)	1.762(15)
<b>Bond Angles</b>							
<b>Structure V</b>							
B(4)-Ga-C(21)	118.4(2)	B(5)-Ga-C(21)	153.5(2)	B(4)-B(5)-B(6)	101.8(5)	Ga-B(5)-B(7)	115.2(4)
B(6)-Ga-C(21)	116.0(2)	B(4)-Ga-N(31)	141.6(2)	B(4)-B(5)-B(7)	62.5(4)	B(6)-B(5)-B(7)	62.4(4)
B(5)-Ga-N(31)	100.0(2)	B(6)-Ga-N(31)	96.5(2)	Ga-B(6)-C(2)	93.8(3)	Ga-B(6)-B(5)	57.5(3)
C(21)-Ga-N(31)	100.0(2)	B(4)-Ga-N(38)	98.6(2)	C(2)-B(6)-B(5)	106.1(5)	Ga-B(6)-B(7)	99.3(3)
B(5)-Ga-N(38)	101.3(2)	B(6)-Ga-N(38)	143.3(2)	C(2)-B(6)-B(7)	62.3(4)	B(5)-B(6)-B(7)	59.3(4)
C(21)-Ga-N(38)	100.7(2)	N(31)-Ga-N(38)	74.2(2)	C(2)-B(7)-C(3)	51.1(3)	C(2)-B(7)-B(4)	90.9(4)
C(3)-C(2)-B(6)	112.6(4)	C(3)-C(2)-B(7)	63.9(4)	C(3)-B(7)-B(4)	52.1(3)	C(2)-B(7)-B(5)	97.2(4)
B(6)-C(2)-B(7)	66.0(4)	C(2)-C(3)-B(4)	111.9(5)	C(3)-B(7)-B(5)	97.7(4)	B(4)-B(7)-B(5)	57.7(4)
C(2)-C(3)-B(7)	65.0(4)	B(4)-C(3)-B(5)	66.2(4)	C(2)-B(7)-B(6)	51.7(3)	C(3)-B(7)-B(6)	91.7(4)
Ga-B(4)-C(3)	94.3(4)	Ga-B(4)-B(5)	56.7(3)	B(4)-B(7)-B(6)	95.9(4)	B(5)-B(7)-B(6)	58.2(4)
C(3)-B(4)-B(5)	106.8(5)	Ga-B(4)-B(7)	98.2(4)	Ga-N(31)-C(32)	122.1(4)	Ga-N(31)-C(36)	117.8(4)
C(3)-B(4)-B(7)	61.8(4)	B(5)-B(4)-B(7)	59.7(4)	Ga-N(38)-C(37)	117.7(4)	Ga-N(38)-C(39)	122.1(3)
Ga-B(5)-B(4)	79.9(3)	Ga-B(5)-B(6)	78.2(3)				
<b>Structure VI</b>							
B(5)-Ga-C(21)	134.3(2)	B(6)-Ga-C(21)	132.7(2)	C(4)-B(5)-B(7)	61.9(3)	B(6)-B(5)-B(7)	59.6(3)
B(5)-Ga-N(31)	124.4(1)	B(6)-Ga-N(31)	95.1(1)	Ga-B(6)-C(2)	96.3(2)	Ga-B(6)-B(5)	66.7(2)
C(21)-Ga-N(31)	101.0(2)	B(5)-Ga-N(42)	95.0(2)	C(2)-B(6)-B(5)	103.7(3)	Ga-B(6)-B(7)	112.1(2)
B(6)-Ga-N(42)	126.5(2)	C(21)-Ga-N(42)	100.5(2)	C(2)-B(6)-B(7)	61.5(3)	B(5)-B(6)-B(7)	60.0(3)
N(31)-Ga-N(42)	77.0(1)	B(3)-C(2)-B(6)	112.2(4)	C(2)-B(7)-B(3)	52.0(2)	C(2)-B(7)-C(4)	94.2(3)
B(3)-C(2)B(7)	67.5(3)	B(6)-C(2)-B(7)	63.6(3)	B(3)-B(7)-C(4)	52.3(2)	C(2)-B(7)-B(5)	99.2(3)
C(2)-B(3)-C(4)	107.9(4)	C(2)-B(3)-B(7)	60.5(3)	B(3)-B(7)-B(5)	93.9(3)	C(4)-B(7)-B(5)	54.4(2)
C(4)-B(3)-B(7)	60.7(3)	B(3)-C(4)-B(5)	111.9(3)	C(2)-B(7)-B(6)	54.9(3)	B(3)-B(7)-B(6)	94.1(3)
B(3)-C(4)-B(7)	67.0(3)	B(5)-C(4)-B(7)	63.8(3)	C(4)-B(7)-B(6)	99.1(3)	B(5)-B(7)-B(6)	60.4(3)
Ga-B(5)-C(4)	96.6(2)	Ga-B(5)-B(6)	66.7(2)	Ga-N(31)-C(32)	125.4(3)	Ga-N(31)-C(36)	115.9(3)
C(4)-B(5)-B(6)	103.9(3)	Ga-B(5)-B(7)	111.8(3)	Ga-N(42)-C(37)	115.7(3)	Ga-N(42)-C(41)	124.4(3)
<b>Structure VIII</b>							
B(5)-Ga(1)-C(41)	142.3(6)	B(6)-Ga(1)-C(41)	130.7(2)	C(2)-B(7)-B(5)	101.1(12)	B(3)-B(7)-B(5)	95.5(12)
B(5)-Ga(1)-N(51)	113.8(6)	B(6)-Ga(1)-N(51)	94.3(5)	C(4)-B(7)-B(5)	55.8(8)	C(2)-B(7)-B(6)	55.0(10)
C(41)-Ga(1)-N(51)	103.8(6)	B(5)-Ga(1)-N(62)	89.8(5)	B(3)-B(7)-B(6)	93.2(13)	C(4)-B(7)-B(6)	99.2(11)
B(6)-Ga(1)-N(62)	125.9(6)	C(41)-Ga(1)-N(62)	103.7(6)	B(5)-B(7)-B(6)	60.6(9)	Ga(1)-N(51)-C(52)	124.2(10)
N(51)-Ga(1)-N(62)	74.0(4)	B(15)-Ga(2)-C(71)	143.8(8)	Ga(1)-N(51)-C(56)	117.6(9)	Ga(1)-N(62)-C(57)	117.5(8)
B(16)-Ga(2)-C(71)	114.2(7)	B(15)-Ga(2)-N(81)	111.3(6)	Ga(1)-N(62)-C(61)	122.5(10)	B(13)-C(12)-B(16)	112.9(11)
B(16)-Ga(2)-N(81)	112.1(6)	C(71)-Ga(2)-N(81)	104.5(7)	B(13)-C(12)-B(17)	67.0(11)	B(16)-C(12)-B(17)	64.9(10)
B(15)-Ga(2)-N(88)	89.6(5)	B(16)-Ga(2)-N(88)	136.3(5)	C(12)-B(13)-C(14)	107.6(14)	C(12)-B(13)-B(17)	61.2(10)
C(71)-Ga(2)-N(88)	103.4(6)	N(81)-Ga(2)-N(88)	77.3(4)	C(14)-B(13)-B(17)	59.6(10)	B(13)-C(14)-B(15)	111.7(12)
B(3)-C(2)-B(6)	112.3(12)	B(3)-C(2)-B(7)	69.0(12)	B(13)-C(14)-B(17)	68.5(11)	B(15)-C(14)-B(17)	63.2(11)
B(6)-C(2)-B(7)	63.9(11)	C(2)-B(3)-C(4)	109.0(14)	Ga(2)-B(15)-C(14)	104.1(10)	Ga(2)-B(15)-B(16)	66.2(7)
C(2)-B(3)-B(7)	59.5(11)	C(4)-B(3)-B(7)	61.8(11)	C(14)-B(15)-B(16)	105.4(12)	Ga(2)-B(15)-B(17)	118.0(9)

Table 3 (Continued)

Bond Angles							
Structure VIII							
B(3)-C(4)-B(5)	110.2(11)	B(3)-C(4)-B(7)	65.5(11)	C(14)-B(15)-B(17)	63.2(11)	B(16)-B(15)-B(17)	61.3(9)
B(5)-C(4)-B(7)	62.7(9)	Ga(1)-B(5)-C(4)	91.9(10)	Ga(2)-B(16)-C(12)	103.4(11)	Ga(2)-B(16)-B(15)	67.0(7)
Ga(1)-B(5)-B(6)	66.8(8)	C(4)-B(5)-B(6)	101.5(12)	C(12)-B(16)-B(15)	101.8(13)	Ga(2)-B(16)-B(17)	115.0(11)
Ga(1)-B(5)-B(7)	108.7(11)	C(4)-B(5)-B(7)	61.5(9)	C(12)-B(16)-B(17)	62.7(10)	B(15)-B(16)-B(17)	56.9(9)
B(6)-B(5)-B(7)	58.1(9)	Ga(1)-B(6)-C(2)	96.1(10)	C(12)-B(17)-B(13)	51.8(9)	C(12)-B(17)-C(14)	93.7(12)
Ga(1)-B(6)-B(5)	66.7(7)	C(2)-B(6)-B(5)	106.1(11)	B(13)-B(17)-C(14)	51.9(9)	C(12)-B(17)-B(15)	98.0(11)
Ga(1)-B(6)-B(7)	110.9(9)	C(2)-B(6)-B(7)	61.0(10)	B(13)-B(17)-B(1)	92.5(12)	C(14)-B(17)-B(15)	53.7(10)
B(5)-B(6)-B(7)	61.3(9)	C(2)-B(7)-B(3)	51.6(9)	C(12)-B(17)-B(16)	52.5(9)	B(13)-B(17)-B(16)	92.1(12)
C(2)-B(7)-C(4)	95.1(12)	B(3)-B(7)-C(4)	52.7(9)	C(14)-B(17)-B(16)	99.1(11)	B(15)-B(17)-B(16)	61.8(9)
Structure X							
Cnt(1)-In-C(21)	150.3	Cnt(1)-In-H(5a)	127	C(2)-B(6)-B(7)	60.9(3)	B(5)-B(6)-B(7)	60.4(3)
Cnt(1)-In-H(6a)	126	B(3)-C(2)-B(6)	112.3(4)	C(2)-B(7)-B(3)	53.6(3)	C(2)-B(7)-C(4)	95.1(3)
B(3)-C(2)-B(7)	65.8(3)	B(6)-C(2)-B(7)	63.7(3)	B(3)-B(7)-C(4)	53.3(3)	C(2)-B(7)-B(5)	99.0(4)
C(2)-B(3)-C(4)	106.1(4)	C(2)-B(3)-B(7)	60.6(3)	B(3)-B(7)-B(5)	96.6(3)	C(4)-B(7)-B(5)	55.4(3)
C(4)-B(3)-B(7)	60.4(3)	B(3)-C(4)-B(5)	112.8(4)	C(2)-B(7)-B(6)	55.4(3)	B(3)-B(7)-B(6)	96.8(4)
B(3)-C(4)-B(7)	66.3(3)	B(5)-C(4)-B(7)	63.9(3)	C(4)-B(7)-B(6)	99.1(4)	B(5)-B(7)-B(6)	58.8(3)
C(4)-B(5)-B(6)	104.5(4)	C(4)-B(5)-B(7)	60.7(3)	In-C(21)-C(23)	111.5(3)	In-C(21)-C(22)	110.3(4)
B(6)-B(5)-B(7)	60.8(3)	C(2)-B(6)-B(5)	104.1(4)				
Structure XII							
B(5)-In(1)-C(21)	142.5(5)	B(6)-In(1)-C(21)	139.9(5)	C(4)-B(7)-B(5)	54.8(6)	C(2)-B(7)-B(6)	55.6(6)
B(5)-In(1)-N(51)	96.7(4)	B(6)-In(1)-N(51)	124.3(4)	B(3)-B(7)-B(6)	94.7(6)	C(4)-B(7)-B(6)	97.7(7)
C(21)-In(1)-N(51)	95.8(4)	B(5)-In(1)-N(58)	119.7(4)	B(50)-B(7)-B(6)	58.0(6)	C(12)-B(13)-C(14)	106.4(6)
B(6)-In(1)-N(58)	97.8(4)	C(21)-In(1)-N(58)	97.8(4)	C(2)-B(13)-B(17)	61.0(5)	C(14)-B(13)-B(17)	60.0(5)
N(51)-In(1)-N(58)	68.5(3)	B(15)-In(2)-C(22)	137.0(4)	B(13)-C(14)-B(15)	112.9(6)	B(13)-C(14)-B(17)	67.1(5)
B(16)-In(2)-C(22)	145.5(4)	B(15)-In(2)-N(71)	96.5(4)	B(15)-C(14)-B(17)	64.8(5)	In(2)-B(15)-C(14)	85.6(5)
B(16)-In(2)-N(71)	115.1(4)	C(22)-In(2)-N(71)	99.3(4)	In(2)-B(15)-B(16)	68.2(5)	C(14)-B(15)-B(16)	103.1(6)
B(15)-In(2)-N(78)	125.1(4)	B(16)-In(2)-N(78)	93.8(4)	In(2)-B(15)-B(17)	104.8(6)	C(14)-B(15)-B(17)	59.4(5)
C(22)-In(2)-N(78)	97.9(4)	N(71)-In(2)-N(78)	69.1(3)	B(16)-B(15)-B(17)	60.7(5)	In(2)-B(16)-C(12)	84.5(5)
B(3)-C(2)-B(6)	112.1(7)	B(3)-C(2)-B(7)	67.5(6)	In(2)-B(16)-B(15)	68.5(5)	C(12)-B(16)-B(15)	103.5(6)
B(6)-C(2)-B(7)	64.0(6)	C(2)-B(3)-C(4)	107.0(7)	In(2)-B(16)-B(17)	104.7(5)	C(12)-B(16)-B(17)	60.9(5)
C(2)-B(3)-B(7)	60.1(5)	C(4)-B(3)-B(7)	60.9(5)	B(15)-B(16)-B(17)	60.1(5)	C(12)-B(17)-B(13)	52.9(5)
B(3)-C(4)-B(5)	111.5(7)	B(3)-C(4)-B(7)	66.3(6)	C(12)-B(17)-C(14)	94.4(6)	B(13)-B(17)-C(14)	52.9(5)
B(5)-C(4)-B(7)	63.8(6)	In(1)-B(5)-C(4)	86.2(5)	C(12)-B(17)-B(15)	97.7(7)	B(13)-B(17)-B(15)	95.7(6)
In(1)-B(5)-B(6)	68.8(6)	C(4)-B(5)-B(6)	104.7(7)	C(14)-B(17)-B(15)	55.8(5)	C(12)-B(17)-B(16)	53.9(5)
In(1)-B(5)-B(7)	106.4(6)	C(4)-B(5)-B(7)	61.4(6)	B(13)-B(17)-B(16)	95.1(7)	C(14)-B(17)-B(16)	99.4(6)
B(6)-B(5)-B(7)	60.7(6)	In(1)-B(6)-C(2)	86.6(5)	B(15)-B(17)-B(16)	59.2(5)	In(1)-N(51)-C(52)	122.0(7)
In(1)-B(6)-B(5)	69.0(5)	C(2)-B(6)-B(5)	104.4(7)	In(1)-N(51)-C(56)	120.7(5)	In(1)-N(58)-C(57)	118.6(5)
In(1)-B(6)-B(7)	106.9(5)	C(2)-B(6)-B(7)	60.4(6)	In(1)-N(58)-C(59)	123.0(6)	In(2)-N(71)-C(72)	123.6(6)
B(5)-B(6)-B(7)	61.3(6)	C(2)-B(7)-B(3)	52.4(5)	In(2)-N(71)-C(76)	118.4(5)	In(2)-N(78)-C(77)	119.2(5)
C(2)-B(7)-C(4)	94.4(6)	B(3)-B(7)-C(4)	52.8(5)	In(2)-N(78)-C(79)	123.3(6)		
C(2)-B(7)-B(5)	98.3(7)	B(3)-B(7)-B(5)	94.7(6)				

the bipyrimidine complex].<sup>31</sup> The greater slip distortion and lower dihedral angle, as well as the shorter base-metal bond distances, all reflect the greater basicity of bipyridine compared to that of bipyrimidine.<sup>14b,17b</sup> Since the bonding interactions in **V** are essentially the same as those found in 1-(C<sub>8</sub>H<sub>6</sub>N<sub>4</sub>)Ga(CMe<sub>3</sub>)-2,3-(CSiMe<sub>3</sub>)<sub>2</sub>-B<sub>4</sub>H<sub>4</sub>, which has been considered in some detail elsewhere,<sup>10</sup> they need not be repeated here.

The structures of **VI** and **VIII** show some unique features. These complexes are slip-distorted to the extent that the carboranes can be considered to be η<sup>2</sup>-bonded to their respective metals through boron atoms B(5) and B(6). The unit cell of **VIII** contains two crystallographically independent molecules. In one, isomer **VIIIA**, the *tert*-butyl group is situated over the cage with the bipyrimidine molecule oriented opposite the unique boron, while in **VIIIB** the two groups are rotated almost 180°; these are shown in Figures 3 and 4, respectively. The central carbon of the *tert*-butyl group in **VIIIA** essentially lies in the pseudo-mirror plane of the carborane,<sup>29</sup> while in **VIIIB** the equivalent atom is well outside of that plane [the angle subtended by the Ga-C(Me<sub>3</sub>) bond and the carborane mirror plane is 8.5° in **VIIIA** and 28.9° in **VIIIB**]. The ligand orientations in **V**, **VI**, and **X** are similar to that of **VIIIA**

in that the alkyl group is centered above the carborane cage and the base occupies a more exo polyhedral position. With the exception of **X**, all structures show that the metals are severely slip-distorted (see Figures 1-6). The Ga-C(cage) and Ga-B(unique) distances are 2.790 ± 0.019 and 3.018 Å, respectively, in **VIIIA**, 2.980 ± 0.006 and 3.309 Å, respectively, in **VIIIB**, and 2.841 ± 0.001 and 3.118 Å, respectively, in **VI**. These are considerably longer than the Ga-C(cage) distances of 2.155 ± 0.009 Å and the Ga-B(unique) distance of 2.232 Å found in the carborane-substituted digallane, *closo*-1-Ga[σ-*closo*-1-Ga-2,4-(SiMe<sub>3</sub>)<sub>2</sub>-2,4-C<sub>2</sub>B<sub>4</sub>H<sub>4</sub>]-2,4-(SiMe<sub>3</sub>)<sub>2</sub>-2,4-C<sub>2</sub>B<sub>4</sub>H<sub>4</sub>.<sup>18</sup> For comparative purposes, the extent of the slip distortion can be measured by the parameter Δ, which is the lateral displacement, in angstroms, of the metal from an extension of the normal drawn from the apical boron to the C(2)-B(6)-B(5)-C(4) plane in **VI**, **VIII**, **X**, and **XII** or the B(4)-C(3)-C(2)-B(6) plane in **V**; a positive value of Δ indicates displacement toward the unique boron.<sup>32</sup> For reference, in the group 13 metallacarboranes the Δ's for the cage atoms are as follows: for the 2,4-C<sub>2</sub>B<sub>4</sub> cages, Δ[B(5,6)] = -1.05 ± 0.03 Å, Δ[C(2,4)] = 0.45 ± 0.01 Å, and Δ[B(3)] = 1.38 ± 0.02 Å (see Figures 2-6); for the 2,3-C<sub>2</sub>B<sub>4</sub> cages, Δ[C(2,3)] = -1.08 ± 0.03 Å, Δ[B(4,6)] = 0.36 ± 0.02 Å, and Δ[B(5)]

(31) Whenever average values of a measured parameter are quoted, the uncertainties listed are the average deviations. If no indeterminations are given, the input values were all equal.

(32) Δ gives the displacement of the metal compared to that of the apical boron; a value of Δ = 0 does not imply equivalent bonding of the metal to the C<sub>2</sub>B<sub>3</sub> facial atoms.

Table 4. FT NMR Spectral Data<sup>a</sup>

compd	$\delta$ splitting, assignment [ $^1J(^{11}\text{B}-^1\text{H})$ or $^1J(^{13}\text{C}-^1\text{H})$ , Hz]	relative area
200.13 MHz $^1\text{H}$ NMR Data <sup>b</sup>		
II	3.88, br, THF; 2.01, br, THF; 1.15, Me; 0.25, s, SiMe <sub>3</sub>	16:16:3:9
III	4.45, q(br), basal BH [ $^1J(^{11}\text{B}-^1\text{H})$ = unresolved]; 1.47, s, <i>t</i> -CMe <sub>3</sub> ; 0.63, s, SiMe <sub>3</sub>	1:3:6
IV	4.79, q(br), overlapping, basal H <sub>t</sub> [ $^1J(^{11}\text{B}-^1\text{H})$ = 140]; 4.62 q(br), overlapping, basal H <sub>t</sub> [ $^1J(^{11}\text{B}-^1\text{H})$ = 145]; 4.39, q(br), overlapping, basal H <sub>t</sub> [ $^1J(^{11}\text{B}-^1\text{H})$ = 151]; 3.43, q(br), apical H <sub>t</sub> [ $^1J(^{11}\text{B}-^1\text{H})$ = 164]; 2.27, s(br), CMe <sub>3</sub> ; 0.81, s, CMe <sub>3</sub> ; 0.27, s, SiMe <sub>3</sub>	1:1:1:1:3:9:9
V	8.71, s, bipy ring; 7.21, d, bipy ring [ $J(^{11}\text{B}-^1\text{H})$ = 5.7]; 7.16, t, bipy ring [ $^3J(^{11}\text{B}-^1\text{H})$ = 6.69]; 6.68, t, bipy ring [ $J(^{11}\text{B}-^1\text{H})$ = 4.78]; 5.10, q(br), overlapping, basal H <sub>t</sub> [ $^1J(^{11}\text{B}-^1\text{H})$ = unresolved]; 0.85, s, SiMe <sub>3</sub> ; 0.68, s, <i>t</i> -CMe <sub>3</sub>	2:2:2:2:3:18:9
VI	8.57, s, bipy ring; 8.24, d, bipy ring [ $J(^{11}\text{B}-^1\text{H})$ = 5.7]; 7.18, t, bipy ring [ $^3J(^{11}\text{B}-^1\text{H})$ = 6.69]; 6.69, t, bipy ring [ $J(^{11}\text{B}-^1\text{H})$ = 4.78]; 3.50, q(br), overlapping, basal H <sub>t</sub> [ $^1J(^{11}\text{B}-^1\text{H})$ = unresolved]; 0.83, s, <i>t</i> -CMe <sub>3</sub> ; 0.58, s, SiMe <sub>3</sub>	2:2:2:2:3:9:18
VII <sup>c</sup>	8.64, s, bipy ring; 7.46, d, bipy ring [ $J(^{11}\text{B}-^1\text{H})$ = 5.7]; 7.13, t, bipy ring [ $^3J(^{11}\text{B}-^1\text{H})$ = 8]; 6.69, t, bipy ring [ $J(^{11}\text{B}-^1\text{H})$ = 4.78]; 4.30, q(br), overlapping, basal H <sub>t</sub> [ $^1J(^{11}\text{B}-^1\text{H})$ = unresolved]; 2.61 (3.03), s, Me; 0.84 (0.79), s, <i>t</i> -CMe <sub>3</sub> ; 0.75 (0.65), s, SiMe <sub>3</sub>	2:2:2:2:3:3:9:9
VIII	8.47, d, bpmd ring [ $^3J(^{11}\text{B}-^1\text{H})$ = unresolved]; 6.50, t, bpmd ring [ $^3J(^{11}\text{B}-^1\text{H})$ = 5.34]; 4.37, q(br), overlapping, basal H <sub>t</sub> [ $^1J(^{11}\text{B}-^1\text{H})$ = 164.7]; 0.78, s, <i>t</i> -CMe <sub>3</sub> ; 0.35, s, SiMe <sub>3</sub>	4:2:3:9:18
IX	9.00, d, terpy ring; 7.58, d, terpy ring; 7.50, d, overlapping, terpy ring; 7.27, t, terpy ring; 7.19, t, terpy ring; 6.92, t, terpy ring; 4.40, q(br), basal H <sub>t</sub> [ $^1J(^{11}\text{B}-^1\text{H})$ = unresolved]; 0.91, s, <i>t</i> -CMe <sub>3</sub> ; 0.23, s, SiMe <sub>3</sub>	2:2:2:1:2:2:3:9:18
X	4.08, q(br), basal BH [ $^1J(^{11}\text{B}-^1\text{H})$ = 128.2]; 1.36, m, <i>i</i> -Pr CH; 0.99, d, <i>i</i> -Pr Me [ $^3J(^{11}\text{B}-^1\text{H})$ = 7.2]; 0.16, s, SiMe <sub>3</sub>	3:1:6:18
XI	2.30, s, CMe <sub>3</sub> ; 1.35, br, <i>i</i> -PrCH; 0.97, s, <i>i</i> -PrMe; 0.29, s, SiMe <sub>3</sub>	3:1:6:9
XII	8.69, s, bipy ring; 8.46, d, bipy ring [ $J(^{11}\text{B}-^1\text{H})$ = 5.7]; 7.45, t, bipy ring [ $^3J(^{11}\text{B}-^1\text{H})$ = 6.69]; 6.75, t, bipy ring [ $J(^{11}\text{B}-^1\text{H})$ = 4.78]; 3.10, q(br), overlapping, basal H <sub>t</sub> [ $^1J(^{11}\text{B}-^1\text{H})$ = unresolved]; 1.13, m, <i>i</i> -PrCH; 0.89, d, <i>i</i> -PrMe [ $^3J(^{11}\text{B}-^1\text{H})$ = 7.2]; 0.56, s, SiMe <sub>3</sub>	2:2:2:2:3:1:6:18
XIII	8.47, d, bpmd ring [ $^3J(^{11}\text{B}-^1\text{H})$ = unresolved]; 6.50, t, bpmd ring [ $^3J(^{11}\text{B}-^1\text{H})$ = 5.34]; 4.37, q(br), overlapping, basal H <sub>t</sub> [ $^1J(^{11}\text{B}-^1\text{H})$ = 164.7]; 0.99, m, <i>i</i> -PrCH; 0.86, d, <i>i</i> -PrMe [ $^3J(^{11}\text{B}-^1\text{H})$ = 7.68]; 0.35, s, SiMe <sub>3</sub>	4:2:3:1:6:18
64.21 MHz $^{11}\text{B}$ NMR Data <sup>d</sup>		
II	12.65, d, basal BH [unresolved]; 3.46, br, basal BH [unresolved]; -48.56, d, apical BH [153]	1:2:1
III	16.61, d, basal BH [164]; 11.28, d, basal BH [146]; -38.02, d, apical BH [174]	1:2:1
IV	12.95, d, basal BH [unresolved]; 9.54, d, basal BH [unresolved]; 5.56, d, basal BH [unresolved]; -38.67, apical BH [176]	1:1:1:1
V	16.84, d(br), basal BH [unresolved]; 1.33, d(br), basal BH [unresolved]; -47.67, d, apical BH [156]	2:1:1
VI	20.55, basal BH [unresolved]; 6.59, basal BH [unresolved]; -45.76, d, apical BH [162]	1:2:1
VII	19.8, v br, ill-defined peak, basal BH [unresolved]; 6.8, v br, basal BH [unresolved]; 4.7, v br, basal BH [unresolved]; -45.5, d, apical BH [164]	1:1:1:1
VIII	21.34, br, basal BH [unresolved]; 8.23, d, basal BH [unresolved]; -45.02, apical BH [179]	1:2:1
IX	11.81, d(br), ill-defined peak, basal BH [unresolved]; 1.54, d(br), basal BH [unresolved]; -38.95, d, basal BH [163.7]	1:2:1
X	17.39, d(br), basal BH [154]; 9.42, d, basal BH [131]; -41.41, d, apical BH [172]	1:2:1
XI	15.81, d(br), basal BH [115]; 10.24, d(br), basal BH [158]; 5.98, d(br), basal BH [146]; -40.07, d, apical BH [176]	1:1:1:1
XII	21.52, d(br), basal BH [unresolved]; 7.93, d, basal BH [unresolved]; -48.58, d, apical BH [152]	1:2:1
XIII	20.81, d(br), ill-defined peak, basal BH [unresolved]; 8.30, d, basal BH [unresolved]; -48.22, d, apical BH [165]	1:2:1
50.32 MHz $^{13}\text{C}$ NMR Data <sup>b,e</sup>		
II	97.62, cage C (SiCB); 81.34, cage C (CCB); 70.46, br, (THF); 28.29, br, (THF); 22.0, cage Me [126]; 0.89, SiMe <sub>3</sub> [119]	1:1:2:2:1:3
III	105.01, s(br), cage C; 30.62, q, Me [ $^1J(^{13}\text{C}-^1\text{H})$ = 121]; 29.68, s(br), CMe <sub>3</sub> ; 0.81, q, SiMe <sub>3</sub> [117]	2:3:1:6
IV	118.6, s(br), cage C (SiCB); 110.8, s(br), cage C (CCB); 30.18, q of m, CMe <sub>3</sub> [124]; 25.57, s(br), CMe <sub>3</sub> ; 21.6, q(br), cage Me [128.9]; 1.18, q(br), SiMe <sub>3</sub> [119.3]	1:1:3:1:1:3
V	148.22, s, bipy ring; 147.12, d, bipy ring [183]; 140.19, d, bipy ring [166]; 125.96, d, bipy ring [165]; 121.28, d, bipy ring [167]; 120.58, s(br), cage C (SiCB); 31.06, q of m, CMe <sub>3</sub> [123]; 25.99, s, CMe <sub>3</sub> ; 3.88, q, SiMe <sub>3</sub> [118]	2:2:2:2:2:2:3:1:6
VI	153.90, s, bipy ring; 148.84, d, dipy ring [176]; 137.68, d, bipy ring [162]; 126.71, s(br), cage C (SiCB); 124.31, d, bipy ring [163]; 121.11, d, d, bipy ring [160]; 30.33, q of m, CMe <sub>3</sub> [123]; 25.57, s, CMe <sub>3</sub> ; 2.18, q, SiMe <sub>3</sub> [118]	2:2:2:2:2:2:3:1:6
VII	150.02, s, bipy ring; 147.73, d, bipy ring [183]; 139.47, d, bipy ring [169]; 125.52, d, bipy ring [163]; 121.19, d, bipy ring [187]; 101.77 (118.51), s(br), cage C (SiCB); 93.91 (116.13), s(br), cage C (CCB); 30.54 (31.04), q of m, CMe <sub>3</sub> [123.8]; 24.03 (26.12), q, Me; 23.66 (21.24), s, CMe <sub>3</sub> ; 2.53 (2.19), q, SiMe <sub>3</sub> [118]	2:2:2:2:2:1:1:3:1:1:3
VIII	157.65, d, bpmd ring [187]; 156.97, s, bpmd ring; 122.63, d, bpmd ring [174]; 101.4, s, cage C; 30.60, q, CMe <sub>3</sub> [125.6]; 28.33, s, CMe <sub>3</sub> ; 1.28, q, SiMe <sub>3</sub> [118.6]	4:2:2:2:3:1:6
IX	150.79, s, terpy ring; 150.14, s, terpy ring; 138.34, d, terpy ring [178.2]; 124.83, d, terpy ring [162.6]; 121.59, d, terpy ring [162.8]; 121.26, d, terpy ring [164]; 120.96, d, terpy ring [164.7]; 118.72, d, terpy ring [164.3]; 115.02, s(br), cage C; 30.94, q, CMe <sub>3</sub> ; 30.19, s, CMe <sub>3</sub> ; 1.63, q, SiMe <sub>3</sub> [118.1]	2:2:2:1:2:2:2:2:2:6
X	105.48, s(br), cage C; 29.24, d, CHMe <sub>2</sub> [138.6]; 24.19, q, Me [127]; 1.30, q, SiMe <sub>3</sub> [117]	2:1:2:6
XI	109.5, s, cage C, SiCB; 100.4, s, cage CCB; 28.00, q, CHMe <sub>2</sub> [132.7]; 23.64, q, <i>i</i> -Pr Me [122.5]; 19.37, q, cage Me [126.8]; 0.89 q, SiMe <sub>3</sub> [118.2]	1:1:1:2:1:3
XII	151.05, s, bipy ring; 148.30, d, bipy ring [183.5]; 139.35, d, bipy ring [174]; 125.51, d, bipy ring [169]; 122.05, d, bipy ring [168]; 96.57, s(br), cage C; 30.12, d, CHMe <sub>2</sub> , [128]; 23.02, q, Me [131]; 2.35, q, SiMe <sub>3</sub> [119.4]	2:2:2:2:2:2:1:2:6
XIII	158.70, s, bpmd ring; 157.76, d, bpmd ring [187]; 122.76, d, bpmd ring [174]; 98.20, s, cage C; 26.83, d, CHMe <sub>2</sub> [127]; 23.34, q, Me [125.6]; 2.19, q, SiMe <sub>3</sub> [118.6]	2:4:2:2:1:2:6

<sup>a</sup> C<sub>6</sub>D<sub>6</sub> was used as solvent and an internal standard of  $\delta$  7.15 (in the  $^1\text{H}$  NMR spectra) with a positive sign indicating a downfield shift. Legend: s, singlet; d, doublet; t, triplet; q, quartet; v, very; br, broad. <sup>b</sup> Shifts relative to external Me<sub>4</sub>Si. <sup>c</sup> Values in parentheses are for the second isomer. <sup>d</sup> Shifts relative to external BF<sub>3</sub>·OEt<sub>2</sub>. <sup>e</sup> Since relaxation of a quaternary carbon is much slower than that of a CH unit, the relative areas of the substituted carbons of the cage, *tert*-butyl, bipyridine, bipyrimidine, and terpyridine moieties, could not be measured accurately.

= 1.41 ± 0.04 Å (see Figure 1). Table 6 lists the values of  $\Delta$  for some of the pentagonal bipyramidal galla-

indacarboranes. From this table it is also apparent that in VI and VIIIA the gallium atoms are almost directly

Table 5. Infrared Absorptions ( $\text{cm}^{-1}$ ;  $\text{C}_6\text{D}_6$  vs  $\text{C}_6\text{D}_6$ )<sup>a</sup>

compd	absorption
II	2947 (s), 2890 (s), 2854 (s) [ $\nu(\text{C}-\text{H})$ ], 2703.5 (ms), 2619 (ws), 2493 (m), 2407 (ss) [ $\nu(\text{B}-\text{H})$ ], 1466 (ms), 1387 (ms), 1321 (ms), 1242 (ss) [ $\delta(\text{CH})_{\text{sym}}$ ], 1170 (ss), 1064 (ss), 913 (ss), 841 (vs) [ $\rho(\text{CH})$ ], 762 (ss), 680 (ms), 615 (ms), 480 (vsbr)
III	2953 (vs), 2853 (ms) 2780 (w), 2564 (vs) [ $\nu(\text{B}-\text{H})$ ], 1467 (vs), 1247 (vs), 1152 (vs), 1028 (ms), 965 (ms), 854 (vvs), 780 (wbr), 689 (ws), 627 (ss), 553 (ms), 498 (ws)
IV	3234.8 (m), 2951.4 (m), 2930 (w), 2880 (sh), 2851 (vs), 2650 (sh), 2568 (m) [ $\nu(\text{B}-\text{H})$ ], 2280 (s), 1456 (m), 1332 (w), 1210 (w), 1070 (w), 1017 (w), 946 (w), 845 (m), 813 (vs), 680 (w), 480 (s)
V	3118 (sh), 3078 (sh), 2960 (vs), 2900 (ms), 2848 (s), 2710 (w), 2545 (w), 2486 (vs) [ $\nu(\text{B}-\text{H})$ ], 2361 (sh), 2242 (m), 1617 (s), 1571 (m), 1479 (w), 1446 (sh), 1425 (msh), 1367 (m), 1321 (m), 1255 (s), 1150 (vss), 1196 (m), 1018 (m), 913 (s), 847 (s), 726 (m), 729 (m), 663 (m), 435 (w)
VI	3157 (sh), 3091 (sh), 2960 (vs), 2900 (ms), 2710 (w), 2591 (vs) [ $\nu(\text{B}-\text{H})$ ], 2255 (m), 2098 (w), 1940 (w), 1880 (m), 1808 (sh), 1729 (w), 1466 (vs), 1255 (s), 1189 (s), 1046 (m), 920 (m), 840 (m), 720 (m), 650 (m), 544 (m), 445 (w)
VII	3236 (m), 2973 (s), 2854 (s), 2729 (m), 2571 (vs) [ $\nu(\text{B}-\text{H})$ ], 2387 (m), 2282 (s), 2104 (w), 2005 (w), 1874 (w), 1683 (w), 1617 (s), 1479 (s), 1466 (sh), 1334 (s), 1163 (sh), 1038 (m), 847 (m), 801 (w), 762 (w), 696 (m), 498 (m)
VIII	3164 (m), 3058 (m), 2960 (vs), 2927 (sh), 2868 (m), 2591 (m) [ $\nu(\text{B}-\text{H})$ ], 2381 (w), 2262 (s), 2236 (m), 1946 (w), 1795 (w), 1676 (w), 1630 (w), 1597 (w), 1558 (s), 1472 (s), 1406 (s), 1314 (w), 1262 (s), 1189 (m), 1097 (s), 1018 (sh), 1005 (sh), 906 (s), 854 (s), 729 (s), 656 (s), 590 (w), 500 (w)
IX	3160 (m), 3058 (m), 2946 (vs), 2852 (m), 2527 (m) [ $\nu(\text{B}-\text{H})$ ], 2270 (w), 2252 (sh), 1936 (w), 1715 (w), 1666 (w), 1620 (w), 1600 (sh), 1550 (s), 1462 (s), 1397 (s), 1310 (s), 1260 (s), 1180 (m), 1070 (s), 1052 (sh), 988 (sh), 916 (s), 844 (s), 719 (s), 666 (s), 600 (sh), 510 (w), 476 (w)
X	2953 (vs), 2853 (ms), 2780 (w), 2564 (vs) [ $\nu(\text{B}-\text{H})$ ], 1467 (vs), 1247 (vs), 1152 (vs), 1028 (ms), 965 (ms), 854 (vvs), 780 (wbr), 689 (ws), 627 (ss), 553 (ms), 498 (ws)
XI	3238 (m), 3056 (w), 2958 (vs), 2860 (m), 2742 (w), 2546 (vs) [ $\nu(\text{B}-\text{H})$ ], 2392 (ms), 2287 (vs), 1994 (w), 1938 (w), 1868 (w), 1805 (w), 1686 (w), 1623 (m), 1462 (s), 1330 (s), 1246 (m), 1141 (m), 1008 (m), 847 (m), 805 (w), 757 (m), 650 (sh), 610 (sh), 506 (s)
XII	3058 (m), 3012 (w), 2960 (s), 2927 (sh), 2854 (m), 2624 (w), 2525 (w) [ $\nu(\text{B}-\text{H})$ ], 2394 (w), 2282 (s), 1999 (w), 1874 (w), 1801 (w), 1696 (w), 1624 (s), 1591 (s), 1571 (m), 1466 (s), 1426 (s), 1341 (s), 1255 (m), 1174 (m), 1104 (w), 854 (s), 814 (s), 768 (s), 656 (w), 600 (w), 511 (s), 459 (sh)
XIII	3098 (s), 3039 (s), 2973 (m), 2894 (m), 2868 (m), 2512 (m) [ $\nu(\text{B}-\text{H})$ ], 2387 (w), 2321 (m), 2223 (w), 1966 (s), 1821 (s), 1755 (w), 1551 (m), 1492 (s), 1321 (w), 1268 (s), 1189 (m), 1104 (m), 1038 (s), 854 (s), 814 (s), 748 (s), 683 (s), 650 (s), 600 (sh), 540 (w), 460 (w)

<sup>a</sup> Legend: v, very; s, strong or sharp; m, medium; w, weak; sh, shoulder; br, broad.

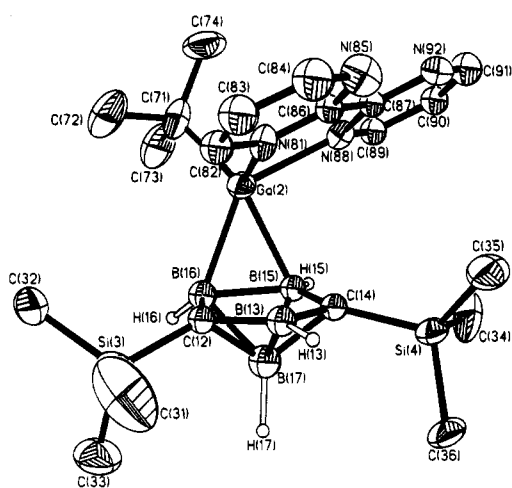


**Figure 4.** Perspective view of one molecule of 1-( $\text{CMe}_3$ )-1-Ga(2,2'- $\text{C}_8\text{H}_6\text{N}_4$ )-2,4-( $\text{SiMe}_3$ )<sub>2</sub>-2,4- $\text{C}_2\text{B}_4\text{H}_4$  (**VIII B**), with the *tert*-butyl group away from unique boron, showing the atom numbering scheme. The thermal ellipsoids are drawn at the 40% probability level. For clarity, all H's except on the carborane cage are removed.

over the B(5)–B(6) bond, while in **VIII B** the metal is well outside of the cage. On the other hand, while the indacarboranes **X** and **XII** both show slippage, the metals are well within the usual cage boundaries and can safely be considered to be endo polyhedral. Although the gallium in **VIII B** is exo polyhedral, there is no evidence that the metal participates in the M–H–B-bridged bonding that was observed by Hawthorne *et al.* in 1,2- $\text{C}_2\text{B}_9\text{H}_{12}\text{Ga}(\text{C}_2\text{H}_5)_2$ <sup>33</sup> and by Grimes *et al.* in  $\mu$ -[( $\text{CH}_3$ )<sub>2</sub>Ga] $\text{C}_2\text{B}_4\text{H}_7$ ,<sup>34</sup> these compounds can be de-

(33) Young, D. A. T.; Wiersema, R. J.; Hawthorne, M. F. *J. Am. Chem. Soc.* **1971**, *93*, 5687.

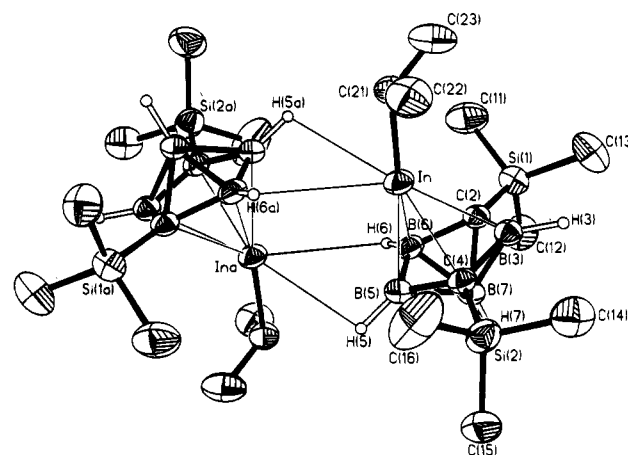


**Figure 5.** Perspective view of dimeric *closo*-1-[( $\text{Me}_2$ )CH]-1-In-2,4-( $\text{SiMe}_3$ )<sub>2</sub>-2,4- $\text{C}_2\text{B}_4\text{H}_4$  (**X**). The thermal ellipsoids are drawn at the 40% probability level. For clarity, all H's except on the carborane cage are removed.

scribed as carbons adjacent *nido*-carboranes in which the  $\text{C}_2\text{B}_3$  open faces contain both a bridging hydrogen and a bridging Ga(R)<sub>2</sub> group. In both *nido*-carboranes, the bridging metal M–H–B interactions gave rise to a splitting of the B–H stretching bands that appear in the 2500–2600  $\text{cm}^{-1}$  region of their infrared spectra. The infrared spectrum of **VIII**, summarized in Table 6, shows only a single band at 2527  $\text{cm}^{-1}$ . In addition, Figures 3 and 4 show that the terminal hydrogens on borons B(5) and B(6), which were located in difference Fourier maps, are oriented away from the gallium atoms.

(34) Magee, C. P.; Sneddon, L. G.; Beer, D. C.; Grimes, R. N. *J. Organomet. Chem.* **1975**, *86*, 159.

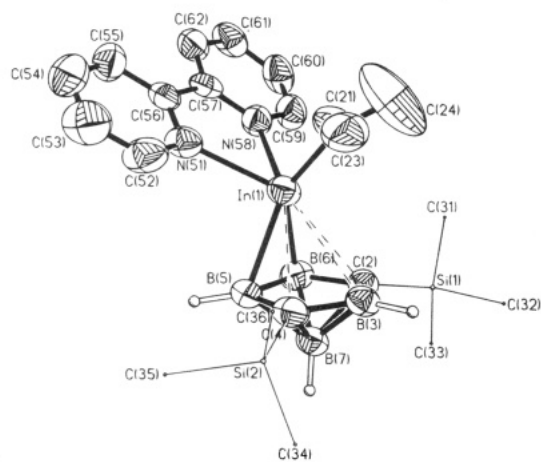


**Figure 6.** Perspective view of 1-[(Me<sub>2</sub>)CH]-1-In(2,2'-C<sub>10</sub>H<sub>8</sub>N<sub>2</sub>)-2,4-(SiMe<sub>3</sub>)<sub>2</sub>-2,4-C<sub>2</sub>B<sub>4</sub>H<sub>4</sub> (**XII**) showing the atom labeling. The thermal ellipsoids are drawn at the 40% probability level. For clarity, only the cage H's are shown, and the atoms of the silyl groups are drawn with circles of arbitrary radii.

**Table 6.** Slip Distortion and Cage Folding Parameters of Some Group 13 Pentagonal Bipyramidal Metallocarboranes

M	R	$\Delta^{b,c}$	folding angle <sup>d</sup>	ref
	1-M-2,4-(CR) <sub>2</sub> B <sub>4</sub> H <sub>4</sub> <sup>a</sup>			
LGa <sup>e</sup>	SiMe <sub>3</sub>	-0.09	1.22	18
Ga(CMe <sub>3</sub> )	H	-0.05	0.0	<i>f</i> (3-21G*)
(C <sub>10</sub> H <sub>8</sub> N <sub>2</sub> )Ga(CMe <sub>3</sub> )	SiMe <sub>3</sub>	-1.10	6.95	<i>f</i> ( <b>VI</b> )
(C <sub>8</sub> H <sub>6</sub> N <sub>4</sub> )Ga(CMe <sub>3</sub> )	SiMe <sub>3</sub>	-1.01	8.85	<i>f</i> ( <b>VIIIA</b> )
(C <sub>8</sub> H <sub>6</sub> N <sub>4</sub> )Ga(CMe <sub>3</sub> )	SiMe <sub>3</sub>	-1.36	7.70	<i>f</i> ( <b>VIIIB</b> )
In(CHMe <sub>2</sub> )	SiMe <sub>3</sub>	-0.25	3.64	<i>f</i> ( <b>X</b> )
(C <sub>10</sub> H <sub>8</sub> N <sub>2</sub> )In(CHMe <sub>2</sub> )	SiMe <sub>3</sub>	-0.75	6.87	<i>f</i> ( <b>XII</b> )
	1-M-2,3-(CR) <sub>2</sub> B <sub>4</sub> H <sub>4</sub> <sup>a</sup>			
Ga(Me)	H	0.20	-0.63	5
Ga(CMe <sub>3</sub> )	SiMe <sub>3</sub>	0.19	-2.68	9
(C <sub>8</sub> H <sub>6</sub> N <sub>4</sub> )Ga(CMe <sub>3</sub> )	SiMe <sub>3</sub>	1.01	-8.67	10
(C <sub>10</sub> H <sub>8</sub> N <sub>2</sub> )Ga(CMe <sub>3</sub> )	SiMe <sub>3</sub>	1.10	-8.49	<i>f</i> ( <b>V</b> )
In(CHMe <sub>2</sub> )	SiMe <sub>3</sub>	0.50	-4.42	12
(C <sub>10</sub> H <sub>8</sub> N <sub>2</sub> )In(CHMe <sub>2</sub> )	SiMe <sub>3</sub>	0.78	-5.34	12

<sup>a</sup> Atom numbering systems are given in Figures 1 and 2. <sup>b</sup> In angstroms; see text for definition. <sup>c</sup> For 1-M-2,4-(CR)<sub>2</sub>B<sub>4</sub>H<sub>4</sub>,  $\Delta[B(5,6)] = -1.05 \pm 0.03$  Å,  $\Delta[C(2,4)] = 0.46 \pm 0.01$  Å, and  $\Delta[B(3)] = 1.38 \pm 0.02$  Å. For 1-M-2,3-(CR)<sub>2</sub>B<sub>4</sub>H<sub>4</sub>,  $\Delta[C(2,3)] = -1.08 \pm 0.03$  Å,  $[B(4,6)] = 0.36 \pm 0.02$  Å and  $\Delta[B(5)] = 1.41 \pm 0.04$  Å. <sup>d</sup> The acute dihedral angle between the planes B(4)-C(3)-C(2)-B(6) and B(4)-B(5)-B(6) (Figure 1) or C(2)-B(6)-B(5)-C(4) and C(2)-B(3)-V(2) (Figure 2); a angle of 0 indicates a planar C<sub>2</sub>B<sub>3</sub> face, and a positive angle indicates ring folding toward the metal. <sup>e</sup> L = 1-Ga-2,4-(CSiMe<sub>3</sub>)<sub>2</sub>B<sub>4</sub>H<sub>4</sub>. <sup>f</sup> This work.

Several of the important aspects of the bonding and ligand orientations in the base-group 13 metallocarboranes can be better understood by reference to Figure 7, which shows the molecular orbital correlation diagram for **VIIIA** and **VIIIB**, with H's substituted for the SiMe<sub>3</sub> groups, in terms of their [C<sub>2</sub>B<sub>4</sub>H<sub>6</sub>]<sup>2-</sup> (CB) and [(C<sub>8</sub>H<sub>6</sub>N<sub>4</sub>)Ga(CMe<sub>3</sub>)<sup>2+</sup> (GF) fragments. Sketches of some of the important fragment orbitals, in terms of their input atomic orbitals, are also shown in Figure 7. As can be seen, gallium-carborane bonding is accomplished mainly through MO 61 formed by the interaction GB48, the LUMO of the gallium fragment, and CB14a', the HOMO of the carborane moiety. Fragment orbital CB14a' is heavily localized on the B(5,6) atoms [32.1% p<sub>π</sub> B(5) or B(6)], while GF48 is localized on the gallium atom (71%) and is polarized directly down from that fragment toward the carborane (see Figure 7). It is apparent that, for these highly slipped complexes, the interaction between these two fragment

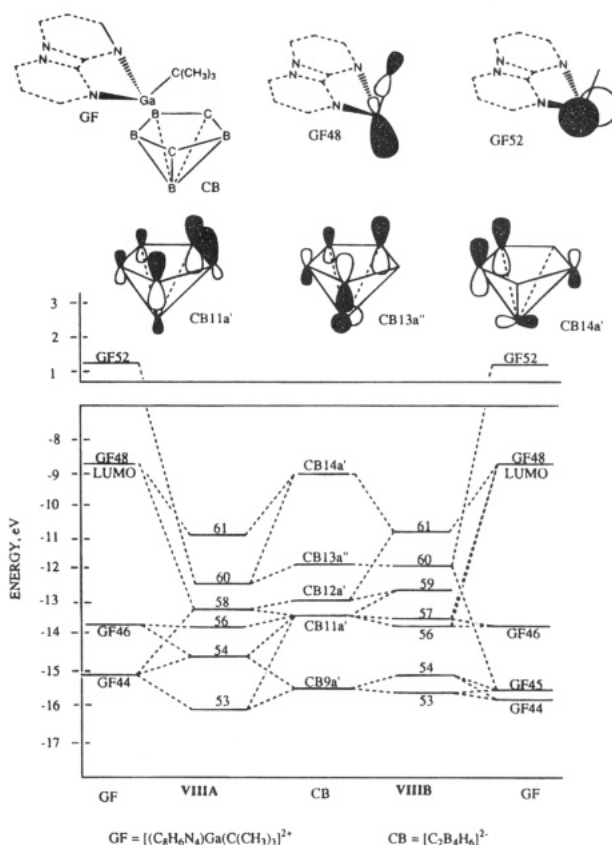


**Figure 7.** Molecular orbital correlation diagram for **VIIIA** and **VIIIB** in terms of their [(C<sub>8</sub>H<sub>6</sub>N<sub>4</sub>)Ga(CMe<sub>3</sub>)<sup>2+</sup> and [C<sub>2</sub>B<sub>4</sub>H<sub>6</sub>]<sup>2-</sup> fragments. Hydrogens have been substituted for the cage SiMe<sub>3</sub> groups.

orbitals should be the same irrespective of whether the bipyrimidine molecule is opposite the unique boron, as found in **VIIIA**, or is at some intermediate orientation, as found in **VIIIB**. There is a weaker interaction that is orientation dependent: that between GF52 and CB13a'' to give MO 60. Both of these orbitals are antisymmetric with respect to the pseudo-mirror plane that exists in **VIIIA**.<sup>29</sup> Since GF52 is a fairly high-energy orbital, and CB13a'' is polarized toward the more remote cage carbons [9% p<sub>π</sub> B(5) or B(6) vs 30% p<sub>π</sub> C(2) or C(4)], their interaction contributes little to the overall stability of the complexes. Indeed, in **VIIIB**, the energy of MO 60 is essentially that of its major component, CB13a'' (81%). An analysis of the bonding interactions in **VI** gives very similar results. That is, one would not expect a particular alignment of the metal ligands unless there were significant bonding interactions between the metal and a majority of the atoms in the C<sub>2</sub>B<sub>3</sub> face of the carborane.

The Ga-B(5,6) distances in **VI**, **VIIIA**, and **VIIIB** are all very similar, being 2.198, 2.194, and 2.220 ± 0.007 Å, respectively. The increase in the slip distortion parameter,  $\Delta$ , in going from **VI** (-1.10 Å) or **VIIIA** (-1.01 Å) to **VIIIB** (-1.36 Å) can be visualized as resulting from a rotation of the gallium fragment about the B(5)-B(6) bond. This would increase the Ga-C(cage) and Ga-B(unique) bond distances, while leaving the Ga-B(5,6) distances little changed. This phenomenon is even more apparent in the indacarboranes **X** and **XII**. In the uncomplexed indacarborane, **X**, the average In-B(5,6) distance is 2.319 ± 0.001 Å, compared to a value of 2.337 ± 0.001 Å in **XII** (see Table 3), while in going from **X** to **XII**, the In-C(cage) and



In-B(unique) distances increase by 0.3 and 0.4 Å, respectively. These variations in bond length differences stem from the competing changes that occur upon coordination of the capping metal with a base. In general there is a weakening of metal-carborane bonding upon coordination that tends to elongate all bonds and a slippage that tends to restore some bond distances and increase others. In the case of the M-B(5,6) distances in the group 13 carbons apart carboranes, these two changes tend to cancel one another, and there is little change in some of the bond lengths. In the carbons adjacent system these same changes take place, but the net result is an overall increase in most bond lengths. For example, in **V** the distances are Ga-B(4,6) = 2.418 ± 0.018 Å, Ga-C(2,3) = 2.956 ± 0.020 Å, and Ga-B(5) = 2.069 Å, compared to values of 2.185 ± 0.014, 2.286 ± 0.004, and 2.131 Å for the equivalent bond distances in the uncomplexed gallacarborane.<sup>9</sup> Unfortunately, since the structure of **III**, the *closo*-gallacarborane precursor for **VI** and **VIII**, could not be determined, an analogous comparison in the 2,4-C<sub>2</sub>B<sub>4</sub> system cannot be made. In order to obtain some idea of the extent of distortion in the uncomplexed gallacarboranes, the structure of the model compound, 1-(CMe<sub>3</sub>)-1-Ga-2,4-C<sub>2</sub>B<sub>4</sub>H<sub>6</sub>, was optimized using *ab initio* molecular orbital calculations at the 3-21G(\*) level. The optimized structure revealed that the Ga(CMe<sub>3</sub>) group resided in the mirror plane of the carborane and that the gallium was slipped slightly toward the equivalent of B(5,6) in Figure 2. By using the numbering system of Figure 2, the bond lengths of interest are Ga-B(5,6) = 2.178 Å, Ga-C(2,4) = 2.171 Å, and Ga-B(3) = 2.293 Å. The analogous distances in the carborane-substituted digallane, *closo*-1-Ga[*σ-closo*-1-Ga-2,4-(SiMe<sub>3</sub>)<sub>2</sub>-2,4-C<sub>2</sub>B<sub>4</sub>H<sub>4</sub>]-2,4-(SiMe<sub>3</sub>)<sub>2</sub>-2,4-C<sub>2</sub>B<sub>4</sub>H<sub>4</sub>, are Ga-B(5,6) = 2.136 ± 0.005 Å, Ga-C(2,4) = 2.160 ± 0.007 Å, and Ga-B(3) = 2.236 ± 0.004 Å.<sup>18</sup> Since the <sup>11</sup>B NMR spectrum of this digallane is identical with that of **III**, the two structures should not differ greatly in geometry. If the structure of **III** is similar to those of the model compound and the digallane, the complexation of the metal with a bidentate base does not materially change the Ga-B(5,6) bond distance, but greatly increases the other metal-carborane distances (see Table 3).

Another structural distortion found in the group 13 metallacarboranes that seems to be a function of the extent and direction of metal slippage is the nonplanarity of the C<sub>2</sub>B<sub>3</sub> faces of the carborane ligands. Table 6 lists the folding angles of some pentagonal bipyramidal group 13 metallacarboranes along with their values of Δ; the folding angle is the acute angle between the plane defined by the unique boron and its two nearest neighbor facial atoms [atoms B(4), B(5), and B(6) in Figure 1 or C(2), B(3), and C(4) in Figure 2] and the plane defined by all facial atoms except the unique boron [atoms B(4), C(3), C(2), and B(6) in Figure 1 or C(2), B(6), B(5), and C(4) in Figure 2]. A folding angle of zero signifies a planar C<sub>2</sub>B<sub>3</sub> face, while a positive angle denotes a displacement of the unique boron toward the metal group. The phenomenon of ring folding has long been recognized to be a structural consequence of the slip distortions of main group and transition metals, in both the pentagonal bipyramidal (MC<sub>2</sub>B<sub>4</sub>) and the icosahedral (MC<sub>2</sub>B<sub>9</sub>) cage systems.<sup>34-37</sup> However, most of the structural studies have been

conducted on the carbons adjacent cages where slippage is toward the unique boron, which results in negative folding angles. Table 6 shows that the carbons apart metallacarboranes exhibit slippages in the opposite direction, *i.e.*, away from the unique boron atom. Such slippages give rise to positive folding angles. It is also apparent from the table that there is, at least, a qualitative correlation between the magnitude of the folding angle and the extent of slippage.

There have been several other structural studies on carbons apart metallacarboranes. For example, Stone and co-workers have reported the structure of *closo*-1,1-(Et<sub>3</sub>P)<sub>2</sub>-1,2,4-PtC<sub>2</sub>B<sub>4</sub>H<sub>6</sub>;<sup>38</sup> other structures include the trimethylsilyl-substituted complexes of the type [*closo*-1-M-2,4-(SiMe<sub>3</sub>)<sub>2</sub>-2,4-C<sub>2</sub>B<sub>4</sub>H<sub>4</sub>]<sup>n</sup>, where n = 0, M = (C<sub>10</sub>H<sub>8</sub>N<sub>2</sub>)<sub>2</sub>Sn,<sup>4</sup> (C<sub>8</sub>H<sub>6</sub>N<sub>4</sub>)Sn,<sup>4</sup> [(η<sup>5</sup>-C<sub>5</sub>H<sub>5</sub>)Fe(η<sup>5</sup>-C<sub>5</sub>H<sub>4</sub>CH<sub>2</sub>(Me)<sub>2</sub>N)]Sn,<sup>4</sup> and (TMEDA)Ni,<sup>16a</sup> and n = -1, M = (TMEDA)Li.<sup>16a</sup> In most of these complexes the metal was either centered above the C<sub>2</sub>B<sub>3</sub> face or only slightly slip-distorted so that any ring folding that might have occurred was effectively masked. However, a reexamination of the structure of the bipyridine-stannacarborane complex [M = (C<sub>10</sub>H<sub>8</sub>N<sub>2</sub>)<sub>2</sub>Sn], which had the highest slip distortion (Δ = -0.41 Å), reveals a folding angle of 6.4°, which is consistent with the results summarized in Table 6. The effect of the position of the capping metal above the C<sub>2</sub>B<sub>3</sub> face on the overall geometry of the metal complexes 1-Sn-2,3-C<sub>2</sub>B<sub>4</sub>H<sub>6</sub> and 1-Sn-2,4-C<sub>2</sub>B<sub>4</sub>H<sub>6</sub> has been investigated theoretically by using MNDO semiempirical molecular orbital calculations.<sup>39</sup> The optimized cage geometries for a particular metal position showed the same general trends that are evident in Table 6, that is, planar C<sub>2</sub>B<sub>3</sub> faces (folding angles = 0) when the metal was centered, positive folding angles as the tin moved away from the unique boron, and negative angles as Δ became positive. Analysis of the different contributing energy terms indicated that an enhancement of metal-carborane bonding was the driving force for cage folding. The negative folding angle, caused by slippage toward the unique boron, promoted increased bonding between the metal and the two facial atoms directly bonded to the unique boron, while positive folding angles allowed stronger bonding of the tin with the unique boron.

It is an open question as to whether these arguments are generally applicable to other metallacarborane systems. It should be mentioned that the M-B(unique) interatomic distances in **VI**, **VIIIA**, **VIIIB**, and **XII** are large, being 3.118, 3.018, 3.309, and 2.920 Å, respectively. Given such separations, it would be surprising if the relatively large folding angles shown in Table 6 were solely due to the direct, through-space interactions of the metals and the unique borons. However, at present, there is no readily available alternative explanation for the structural distortions found in these group 13 metallacarboranes. It is apparent that a great deal of additional structural and theoretical information

(35) Mingos, D. M. P.; Forsyth, M. I.; Welch, A. J. *J. Chem. Soc., Dalton Trans.* **1976**, 363 (and references therein).

(36) (a) Colquhoun, H. M.; Greenough, T. J.; Wallbridge, M. G. H. *J. Chem. Soc., Dalton Trans.* **1985**, 761. (b) Colquhoun, H. M.; Greenough, T. J.; Wallbridge, M. G. H. *J. Chem. Soc., Chem. Commun.* **1976**, 1019.

(37) Jutzi, P.; Galow, P.; Abu-Orabi, S.; Arif, A. M.; Cowley, A. H.; Norman, N. C. *Organometallics* **1987**, *6*, 1024.

(38) Barker, G. K.; Green, M.; Stone, F. G. A.; Welch, A. J. *J. Chem. Soc., Dalton Trans.* **1980**, 1186.

(39) Maguire, J. A.; Hosmane, N. S.; Saxena, A. K.; Zhang, H.; Gray, T. G. *Phosphorus, Sulfur, Silicon* **1994**, *87*, 1299.

needs to be obtained on the carbons apart metallacarboranes before a general understanding of the forces dictating the geometries of these complexes can be attained.

**Acknowledgment.** This work was supported by grants from National Science Foundation (Grant No. CHE-9400672 to N.S.H. and Grant No. CHE-9108228 to A.H.C.), the Robert A. Welch Foundation (Grant No. N-1016 to N.S.H. and Grant No. F-135 to A.H.C.), and

the donors of the Petroleum Research Fund, administered by the American Chemical Society.

**Supporting Information Available:** Tables of selected bond lengths and bond angles (Table S-1), anisotropic displacement parameters (Table S-2), and H atom coordinates and isotropic displacement coefficients (Table S-3) for **V**, **VI**, **VIII**, **X**, and **XII** (19 pages). Ordering information is given on any current masthead page.

OM950509G



# Reactivity of (Pentadienyl)iron(1+) Cations: Nucleophilic Addition by Phosphines Is Reversible in Certain Cases

William A. Donaldson,\* Lewei Shang, Muthukumar Ramaswamy,  
Christine A. Droste, and Chunlin Tao

Department of Chemistry, Marquette University, P.O. Box 1881,  
Milwaukee, Wisconsin 53201-1881

Dennis W. Bennett

Department of Chemistry, University of Wisconsin—Milwaukee, Milwaukee, Wisconsin 53201

Received July 10, 1995<sup>®</sup>

The reaction of (pentadienyl)Fe(CO)<sub>3</sub><sup>+</sup> cations **1**, **5**, and **11** with phosphines was examined. At short reaction times, attack of PPh<sub>3</sub> on **1a** proceeds at both the unsubstituted and substituted pentadienyl termini to give **2a** and **3a**, respectively (2:1); however, over a period of ca. 21 h, the minor product **3a** isomerizes to the more thermodynamically stable **2a**. As the steric bulk of the 1-substituent is increased from methyl to ethyl (**1b**), kinetic attack by PPh<sub>3</sub> occurs exclusively at the unsubstituted pentadienyl terminus. The complex **2a** was characterized crystallographically, and the stereochemistry of PPh<sub>3</sub> attack was established to be opposite to Fe(CO)<sub>3</sub> by use of a stereoselectively labeled cation, *d*<sub>exo</sub>-**1a**. The reaction of PPh<sub>3</sub> with **11** initially gives *E,Z*-**12**, which isomerizes to *E,E*-**12** over a 22 h period. Reaction with **5** with ((*S*)-neomenthyl)diphenylphosphine gives two optically active diastereomers, **15a** and **15b** (3:2 ratio); fractional crystallization gives **15a** in greater than 80% mass recovery. In solution, pure **15a** isomerizes to a mixture of **15a** and **15b** (3:2). The interconversions of **3a** to **2a**, of *E,Z*-**12** to *E,E*-**12**, and of **15a** and **15b** are rationalized by reversible phosphine addition.

## Introduction

While ( $\eta^5$ -pentadienyl)iron(1+) cations (**1**) were first prepared more than 30 years ago,<sup>1</sup> the reactivity of these complexes is of renewed interest.<sup>2</sup> The addition of phosphines to **1** to generate dienylphosphonium salts **2** was initially examined by McArdle and Sherlock<sup>3</sup> and later extended by Salzer and Hafner.<sup>4</sup> Both groups reported that nucleophilic attack occurs at the less hindered pentadienyl terminus to give *E,Z*-diene complexes, which can subsequently isomerize in solution to the correspondingly more stable *E,E*-diene complex (Scheme 1). The structural assignment of **2** was based on NMR spectral data. The regiochemical assignment was further corroborated by X-ray crystal structure of the pentaene complex generated from **2a** via Wittig olefination.<sup>5</sup> More recently, Grée has reported the use of phosphonium salts of this type for the preparation of Fe(CO)<sub>3</sub>-complexed analogs of LTA<sub>4</sub>.<sup>6</sup> As part of our study of the applications of (pentadienyl)iron(1+) cations to organic synthesis, we have examined the reac-

tivity of 1,2- and 1,4-disubstituted (pentadienyl)iron(1+) cations with phosphine and other heteroatom nucleophiles.<sup>7</sup> We herein report on a detailed study of the title reaction, including an examination of the stereochemistry and reversibility of nucleophilic attack.<sup>8</sup>

## Results and Discussion<sup>9</sup>

The cations **1a–e** and **5** were prepared according to literature procedures.<sup>1,10</sup> Reaction of **1a** with PPh<sub>3</sub> (CH<sub>2</sub>Cl<sub>2</sub>, 21 h, 91%) gave the dienylphosphonium salt **2a**, as has been previously reported.<sup>3,4</sup> However, monitoring this reaction by <sup>1</sup>H NMR spectroscopy (CD<sub>3</sub>NO<sub>2</sub>) indicated the initial formation of a mixture of **2a** and **3a** (ca. 2:1). Over a period of 24–42 h, the signals for **3a** disappear, while the signals for **2a** increase in intensity with respect to the CD<sub>2</sub>HNO<sub>2</sub> signal. Likewise, precipitation of the reaction mixture of **1a** with PPh<sub>3</sub> (CH<sub>2</sub>Cl<sub>2</sub>, 1 h) gave a solid which was identified as a mixture of **2a** and **3a** by <sup>1</sup>H NMR spectroscopy. Upon dissolution of this mixture in acetone-*d*<sub>6</sub> or CDCl<sub>3</sub>, the slow (ca. 24 h) interconversion of **3a** into **2a** is again

<sup>®</sup> Abstract published in *Advance ACS Abstracts*, October 15, 1995.

(1) Mahler, J. E.; Gibson, D. H.; Pettit, R. *J. Am. Chem. Soc.* **1963**, *85*, 3959–3963.

(2) Quirosa-Guillou, C.; Lellouche, J.-P. *J. Org. Chem.* **1994**, *59*, 4693–4967. Roush, W. R.; Wada, C. K. *Tetrahedron Lett.* **1994**, *35*, 7347–7350. Takemoto, Y.; Yoshikawa, N.; Iwata, C. *J. Chem. Soc., Chem. Commun.* **1995**, 631–632.

(3) McArdle, P.; Sherlock, H. *J. Chem. Soc., Dalton Trans.* **1978**, 1678–1682.

(4) Salzer, A.; Hafner, A. *Helv. Chim. Acta* **1983**, *66*, 1774–1785.

(5) Hafner, A.; Bieri, J. H.; Prewo, R.; von Philipsborn, W.; Salzer, A. *Angew. Chem., Int. Ed. Engl.* **1983**, *22*, 713–715.

(6) Pinsard, P.; Lellouche, J.-P.; Beaucourt, J.-P.; Grée, R. *Tetrahedron Lett.* **1990**, *31*, 1141–1144.

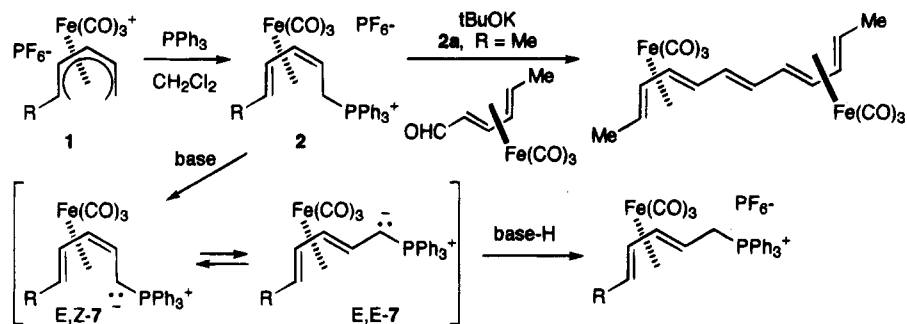
(7) (a) Donaldson, W. A.; Bell, P. T.; Jin, M.-J. *J. Organomet. Chem.* **1992**, *441*, 449–456. (b) Donaldson, W. A.; Jin, M.-J.; Bell, P. T. *Organometallics* **1993**, *12*, 1174–1179. (c) Donaldson, W. A.; Jin, M.-J. *Bull. Soc. Chim. Belg.* **1993**, *102*, 297–298.

(8) Preliminary communication: Donaldson, W. A.; Shang, L.; Rogers, R. D. *Organometallics* **1994**, *13*, 6–7.

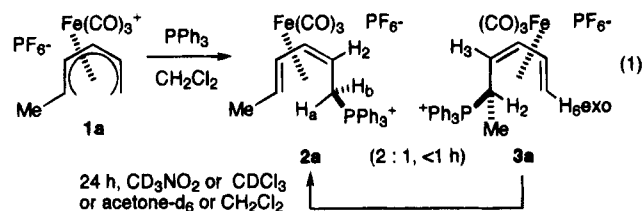
(9) All compounds are racemic mixtures of enantiomers, with the exception of **15a** and **15b**. Only one enantiomer has been pictured for clarity.

(10) (a) Donaldson, W. A.; Ramaswamy, M. *Synth. React. Inorg. Met.-Org. Chem.* **1987**, *17*, 49–56. (b) Ma, H.; Weber, P.; Ziegler, M. L.; Ernst, R. D. *Organometallics* **1986**, *5*, 2009–2013. (c) Pearson, A. J.; Ray, T. *Tetrahedron* **1985**, *41*, 5765–5770.

## Scheme 1



observed. Product **2a** was identified by comparison of its spectral data with the literature values.<sup>3,4</sup>



The assignment of **3a** as a ((3(*Z*),5-hexadien-2-yl)-triphenylphosphonium)Fe(CO)<sub>3</sub><sup>+</sup> salt is based upon its <sup>1</sup>H NMR spectral data. In particular, the three-proton doublet of doublets at δ 1.56 ppm, exhibiting a large <sup>31</sup>P–<sup>1</sup>H coupling (18.3 Hz), indicates that the PPh<sub>3</sub><sup>+</sup> functionality is attached next to the methyl substituent. In addition, the presence of signals at δ 2.38, 2.25, and 1.76 ppm (H<sub>3</sub>, H<sub>6</sub><sub>exo</sub>, and H<sub>6</sub><sub>endo</sub>, respectively) is characteristic of the (3(*Z*),5-hexadien-2-yl)Fe(CO)<sub>3</sub> group.

Our results indicate that there is little kinetic selectivity for nucleophilic attack of PPh<sub>3</sub> at either the unsubstituted or methyl-substituted pentadienyl termini of **1a** (ΔΔ*G*<sup>‡</sup> ≈ 0.4 kcal/mol) and that interconversion of **3a** to the more thermodynamically stable **2a** over an extended reaction time is responsible for the reported<sup>3,4,11</sup> isolation of **2a** as the sole product. In order to examine the mechanism of this process, the relative stereochemistry of attack by PPh<sub>3</sub> and of the interconversion was examined.

The reaction of (cyclohexadienyl)iron(1+) cation with PPh<sub>3</sub> has been shown unambiguously by X-ray crystallographic analysis to occur on the face opposite to the iron.<sup>12</sup> McArdle and Sherlock have previously noted<sup>3</sup> that the diastereotopic methylene protons H<sub>1a</sub> and H<sub>1b</sub> of **2a** appear well separated in its <sup>1</sup>H NMR spectrum (δ 3.4 and δ 4.1 ppm) and that these protons have conspicuously different coupling constants with H<sub>2</sub> (ca. 13 and 3.5 Hz, respectively). The difference in these coupling constants prompted an examination of the molecular structure of **2a**. The structure of **2a** was solved crystallographically. There are two, roughly mirror image, molecules per unit cell. The packing diagram is shown in Figure 1. The ORTEP II<sup>13</sup> perspective views of the two asymmetric molecules, with the crystallographic numbering schemes, are given in Figures 2 and 3. Both display the 2(*Z*),4(*E*) stereochem-

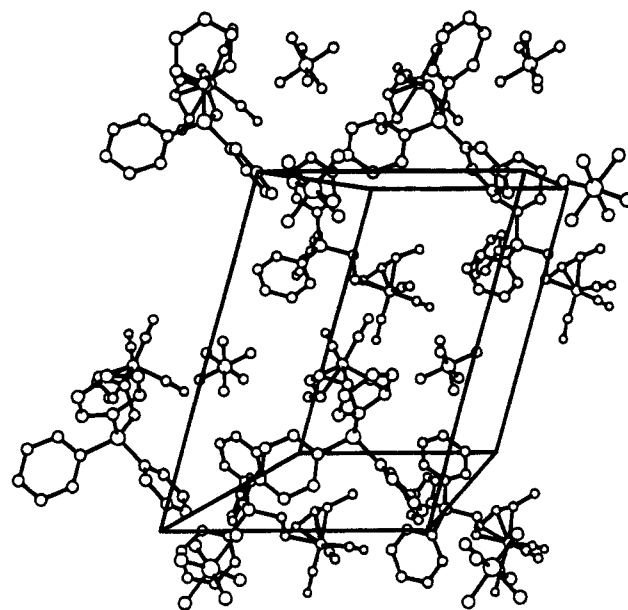


Figure 1. Crystal-packing diagram of **2a**.

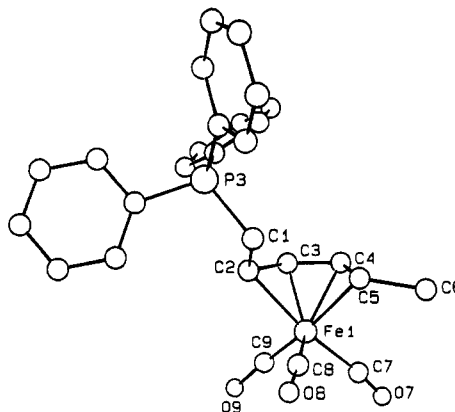


Figure 2. ORTEP II drawing of (η<sup>4</sup>-CH<sub>3</sub>CH=CH=CHCH<sub>2</sub>PPh<sub>3</sub><sup>+</sup>)Fe(CO)<sub>3</sub>PF<sub>6</sub><sup>-</sup> (**2a**, molecule I).

istry previously assigned<sup>3,4</sup> on the basis of <sup>1</sup>H NMR spectra data. Selected bond distances and bond angles are given in Table 1. The two mirror image molecules exhibit equivalent bond distances within error limits. The bond distances and angles of the (diene)Fe(CO)<sub>3</sub> fragment of **2a** are in good agreement with those for other complexes reported in the literature.<sup>14</sup> The torsional angles for H<sub>1a</sub>–C<sub>1</sub>–C<sub>2</sub>–H<sub>2</sub> and for H<sub>1b</sub>–C<sub>1</sub>–C<sub>2</sub>–H<sub>2</sub> are respectively 159 ± 6° (–140 ± 5°) and 38 ±

(11) The experimental sections of refs 3 and 4 do not indicate reaction times.

(12) Guy, J. J.; Reichert, B. E.; Sheldrick, G. M. *Acta Crystallogr., Sect. B* **1976**, *32B*, 2504–2506.

(13) Johnson, C. K. ORTEP II, Report ORNL-5138; Oak Ridge National Laboratory: Oak Ridge, TN, 1976.

(14) (a) Riley, P. E.; Davis, R. E. *Acta Crystallogr.* **1976**, *B32*, 381. (b) Donaldson, W. A.; Tao, C.; Bennett, D. W.; Grubisha, D. *J. Org. Chem.* **1991**, *56*, 4563–4566. (c) Maglio, G.; Musco, A.; Palumbo, R.; Sirigu, A. *J. Chem. Soc. D* **1971**, 100.

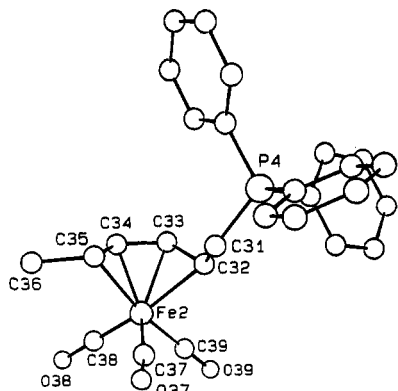


**Figure 3.** ORTEP II drawing of  $(\eta^4\text{-CH}_3\text{CH}=\text{CHCH}=\text{CHCH}_2\text{PPh}_3^+)\text{Fe}(\text{CO})_3\text{PF}_6^-$  (**2a**, molecule II).

**Table 1. Selected Bond Distances and Bond Angles for the Two Molecules in the Unit Cell of **2a**<sup>a</sup>**

molecule I		molecule II	
Bond Distances (Å)			
Fe1-C2	2.13(6)	Fe2-C32	2.12(4)
Fe1-C3	1.93(3)	Fe2-C33	2.00(6)
Fe1-C4	2.04(4)	Fe2-C34	1.88(7)
Fe1-C5	2.04(5)	Fe2-C35	2.09(6)
Fe1-C7	1.93(7)	Fe2-C38	1.67(3)
Fe1-C8	1.75(4)	Fe2-C37	1.82(6)
Fe1-C9	1.69(6)	Fe2-C39	1.77(7)
P3-C1	1.86(4)	P4-C31	1.77(4)
C1-C2	1.57(6)	C31-C32	1.50(5)
C2-C3	1.47(7)	C32-C33	1.46(7)
C3-C4	1.42(8)	C33-C34	1.31(6)
C4-C5	1.33(6)	C34-C35	1.31(7)
C5-C6	1.68(10)	C35-C36	1.55(6)
C7-O7	0.98(8)	C37-O37	1.13(7)
C8-O8	1.19(5)	C38-O38	1.22(4)
C9-O9	1.23(8)	C39-O39	1.12(8)
Bond Angles (deg)			
P3-C1-C2	107(3)	P4-C31-C32	119(3)
C1-C2-C3	120(4)	C31-C32-C33	126(4)
C2-C3-C4	122(4)	C32-C33-C34	120(5)
C3-C4-C5	117(5)	C33-C34-C35	123(5)
C4-C5-C6	111(5)	C34-C35-C36	114(4)
C1-C2-Fe1	115(4)	C31-C32-Fe2	121(3)
C6-C5-Fe1	123(3)	C36-C35-Fe2	118(4)
Fe1-C7-O7	173(5)	Fe2-C37-O37	173(5)
Fe1-C8-O8	175(4)	Fe2-C38-O38	176(3)
Fe1-C9-O9	174(4)	Fe2-C39-O39	179(6)
C7-Fe1-C8	101(2)	C37-Fe2-C38	103(2)
C7-Fe1-C9	87(3)	C37-Fe2-C39	98(3)
C8-Fe1-C9	103(2)	C38-Fe2-C39	88(2)

<sup>a</sup> Estimated standard deviations in this and all subsequent tables are given in parentheses.

$3^\circ$  ( $-23 \pm 3^\circ$ ) for molecule I (molecule II). Since rotation about the C1-C2 bond would bring the PPh<sub>3</sub> group into steric interaction with the remainder of the molecule, we propose that the solution structure of **2a** is relatively similar to that found in the solid state. On this basis, the upfield signal ( $\delta$  3.34) which exhibits a larger H1-H2 coupling ( $J = 12.9$  Hz) is assigned to the methylene proton which has the greater torsional angle with respect to H2 (i.e. H1<sub>a</sub>). The downfield signal ( $\delta$  4.07,  $J = 3.5$  Hz) is assigned to the methylene proton with the lesser torsional angle (H1<sub>b</sub>).

The molecular structure of **2a** has the PPh<sub>3</sub><sup>+</sup> oriented opposite to Fe(CO)<sub>3</sub> in the solid state. However, the relative positions of the PPh<sub>3</sub><sup>+</sup> and Fe(CO)<sub>3</sub> groups cannot be unambiguously interpreted to mean that nucleophilic attack occurs in an exo fashion, since endo

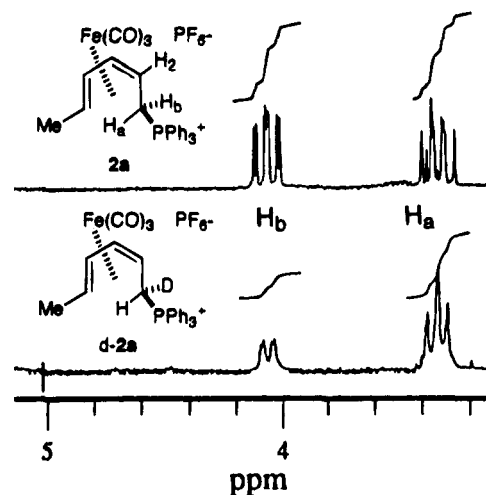
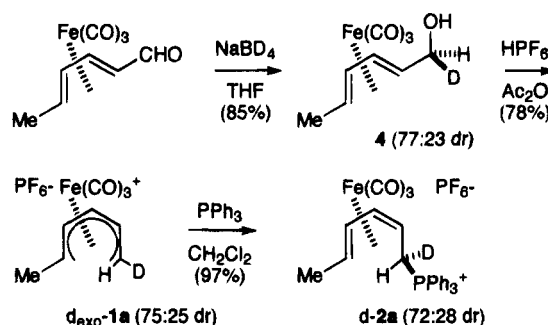


**Figure 4.** Partial <sup>1</sup>H NMR spectra of **2a** and **d-2a** (300 MHz, acetone-*d*<sub>6</sub>).

**Scheme 2**

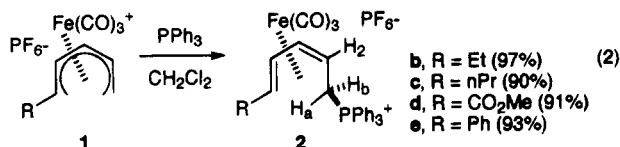


attack followed by rotation about the C1-C2 bond would produce the same structure. For this reason, a stereoselective isotopically labeled pentadienyl cation was prepared (Scheme 2). Reduction of (sorbalddehyde)Fe(CO)<sub>3</sub> with NaBD<sub>4</sub> in THF gave a mixture of isotopically labeled alcohols **4** in a 77:23 diastereomeric ratio (dr), as determined by integration of the diastereotopic methylene proton signals. It was not possible at this point to determine which was the major diastereomer. Treatment of the deuterium-labeled alcohols with HPF<sub>6</sub>/Ac<sub>2</sub>O gave the stereoselectively labeled pentadienyl cation *d*<sub>exo</sub>-**1a** (75:25 dr). Integration of the H1<sub>exo</sub> signal at  $\delta$  3.50 (d,  $J = 9$  Hz) and H1<sub>endo</sub> at  $\delta$  2.17 (d,  $J = 13$  Hz) established the ratio as well as the *d*<sub>exo</sub> stereochemistry of the major diastereomer.

Reaction of *d*<sub>exo</sub>-**1a** with PPh<sub>3</sub> (CH<sub>2</sub>Cl<sub>2</sub>, 21 h, 97%) gave the labeled phosphonium salt *d*-**2a** (Scheme 2). Notably, the diastereotopic signals at  $\delta$  4.07 and at  $\delta$  3.34 of *d*-**2a** lack the geminal coupling ( $J = 14.7$  Hz) (Figure 4) observed for the all-protio **2a**; thus, each molecule contains one and only one deuterium. Integration of these two signals indicates a 28:72 dr. Because this diastereomeric ratio is nearly equal to that of the cation of *d*<sub>exo</sub>-**1a**, it can be concluded that attack by PPh<sub>3</sub> occurs in a stereospecific fashion and, further, that the interconversion of **3a** to **2a** occurs in a stereospecific fashion with the same stereochemistry. Since we have previously assigned the signals at  $\delta$  3.34 and at  $\delta$  4.07 to H1<sub>a</sub> and H1<sub>b</sub>, respectively, then *d*-**2a** (major diastereomer) has the stereochemistry as indicated in Scheme 2. This establishes that attack by PPh<sub>3</sub> at the unsubstituted terminus of the acyclic pentadienyl ligand occurs on the face opposite to the Fe(CO)<sub>3</sub> group

(as had been previously demonstrated<sup>14</sup> for (cyclohexadienyl)Fe(CO)<sub>3</sub><sup>+</sup>). By analogy, we propose that attack by PPh<sub>3</sub> at the substituted terminus of **2** occurs on the face opposite to the Fe(CO)<sub>3</sub> group.

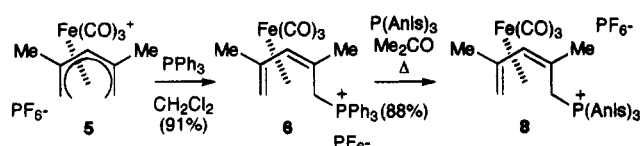
In comparison to **1a**, <sup>1</sup>H NMR spectral monitoring of the reaction of **1b** with PPh<sub>3</sub> (acetone-*d*<sub>6</sub>, 30 min) revealed only signals corresponding to **2b** (eq 2). This



phosphonium salt could be isolated in excellent yield using the standard protocol (CH<sub>2</sub>Cl<sub>2</sub> > 20 h). In general, the steric bulk of an ethyl substituent is not much greater than that of a methyl group. However, we have previously proposed that the methyl group of an ethyl substituent on the pentadienyl ligand is oriented away from the Fe(CO)<sub>3</sub> group, in order to minimize steric interactions. In this orientation, the ethyl group will present considerably greater steric hindrance to attack on the pentadienyl ligand on the face opposite to the metal. The reactions of **1c–e** with PPh<sub>3</sub> (CH<sub>2</sub>Cl<sub>2</sub>, 16–24 h) gave **2c–e** (eq 2). In each case, the product arises from nucleophilic attack at the unsubstituted pentadienyl terminus. It is of interest to note that nucleophilic attack by P(OMe)<sub>3</sub> on **1d** was previously reported to occur at both C5 and C2.<sup>15</sup> Complexes **2b–e** are assigned the 2(*Z*),4(*E*) stereochemistry by comparison of their <sup>1</sup>H NMR spectral data with those of **2a**. In particular, the signals for H3 appear as a broad triplet (*J* ca. 6.1), while signals for H4 appear as a doublet (*J* ca. 5.1, 9.0). The <sup>1</sup>H NMR spectra of **2b–e** exhibit chemical shifts and coupling constants for H1<sub>a</sub> and H1<sub>b</sub> which are similar to those of **2a**.

The reaction of **5** with PPh<sub>3</sub> gave the (*Z*)-dienylphosphonium salt **6** (91%, Scheme 3). The *Z* olefinic geom-

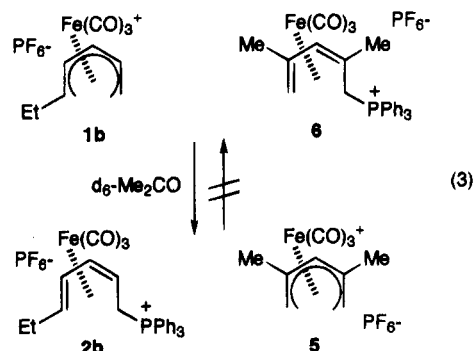
Scheme 3



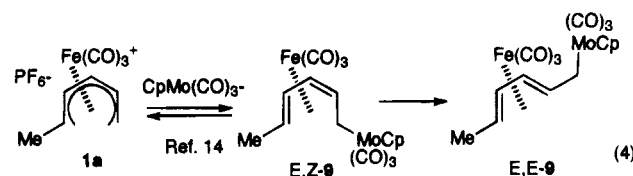
etry was assigned on the basis of its <sup>1</sup>H NMR spectral data. In particular, the signal at δ 1.40 ppm is consistent with a methyl group in the exo orientation at C2.

McArdle and Sherlock have reported slow isomerization of the complex *E,Z*-**2a** to the more thermodynamically stable *E,E* complex in CDCl<sub>3</sub> solution;<sup>3</sup> Salzer and Hafner reported *E,Z* to *E,E* isomerization only in CD<sub>3</sub>-OD/CD<sub>3</sub>ONa.<sup>4</sup> The latter authors have proposed that **2a** undergoes reversible deprotonation to generate the ylide *E,Z*-**7**. Isomerization of the ylide *E,Z*-**7** to *E,E*-**7** may be rationalized by delocalization of the ylide electron density onto the metal. Reprotonation of *E,E*-**7** gives the *E,E*-dienylphosphonium salt (Scheme 1). In our hands, the *E,Z* complexes **2a–d** were stable in acetone-*d*<sub>6</sub> at 23 °C for up to 6 h, as were **2e** and **6** in hot acetone-*d*<sub>6</sub> (60 °C, 24 h). In comparison, heating a

sample of **6** in the presence of tris(*p*-methoxyphenyl)-phosphine (P(Anis)<sub>3</sub>) gave the new phosphonium salt **8** (88%, Scheme 3). The spectral data for **8** are similar to those for **6**. Furthermore, monitoring of the reaction of **6** with **1b** by <sup>1</sup>H NMR spectroscopy (acetone-*d*<sub>6</sub>, 10 h) indicated the disappearance of signals for **6** and **1b** and the appearance of signals corresponding to **5** and **2b** (eq 2). In comparison, monitoring of the reaction of **5** and **2b** (acetone-*d*<sub>6</sub>, 25 h) showed no evidence for the formation of **6** or **1b** (eq 3).



The interconversion of **3a** to **2a**, the transformation of **6** to **8** in the presence of P(Anis)<sub>3</sub>, and phosphine exchange between **6** and **1b** may be rationalized by a single mechanism. We propose that nucleophilic attack of PPh<sub>3</sub> on (pentadienyl)Fe(CO)<sub>3</sub><sup>+</sup> cations is reversible, in certain cases. The situations where this attack is reversible are where there is steric hindrance between substituents present on the diene ligand and the triphenylphosphine group. Other instances of reversible nucleophilic addition to (pentadienyl)iron(1+) cations have been previously reported. For example, addition of CpMo(CO)<sub>3</sub><sup>-</sup> to **1a** at -78 °C has been reported to give the bimetallic diene complex *E,Z*-**9**.<sup>16</sup> This reaction has been shown to be reversible; equilibration of *E,Z*-**9** at room temperature leads to the bimetallic diene complex *E,E*-**9** (eq 4). Moreover, reaction of *E,Z*-**9** with PPh<sub>3</sub> leads to the formation of **2a**.



The 1,2,5-trisubstituted pentadienylFe(CO)<sub>3</sub> cation **11** (R = Me) was prepared by protonation<sup>17</sup> of the known triene complex **10**.<sup>18</sup> The reaction of **11** with PPh<sub>3</sub> was monitored by <sup>1</sup>H NMR spectroscopy (CD<sub>3</sub>NO<sub>2</sub>). At short reaction time (ca. 5 min) formation of *E,Z*-**12** was observed. Over a period of 22 h, the signals for *E,Z*-**12** slowly disappeared and were replaced by the signals for *E,E*-**12**. *E,E*-**12** could be isolated from the reaction of **11** with PPh<sub>3</sub> over an extended period (CH<sub>2</sub>Cl<sub>2</sub>, 21 h; Scheme 4). The structural assignments for both isomers of **12** are based on their <sup>1</sup>H NMR spectral data. In particular, the presence of only a single downfield

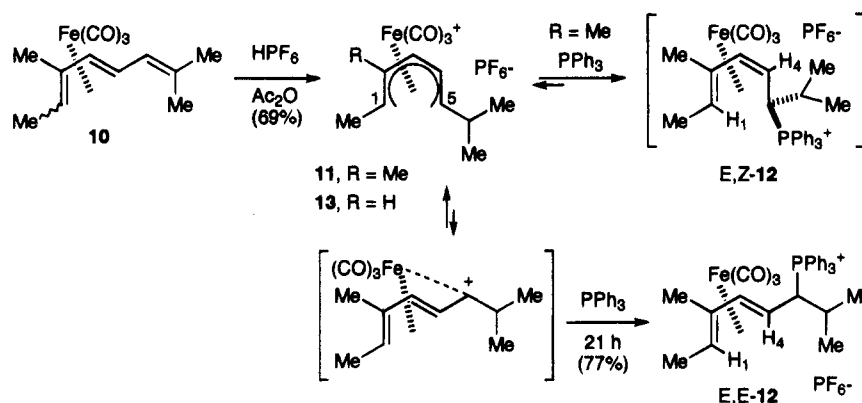
(16) Lehmann, R. E.; Kochi, J. K. *Organometallics* **1991**, *10*, 190–202.

(17) Johnson, B. F. G.; Lewis, J.; Parker, D. G.; Postle, S. R. *J. Chem. Soc., Dalton Trans.* **1977**, 794–797.

(18) Banthorpe, D. V.; Fitton, H.; Lewis, J. *J. Chem. Soc., Dalton Trans.* **1973**, 2051–2057.

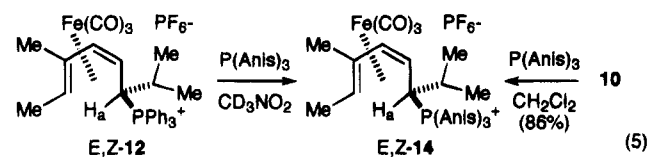
(15) Pinsard, P.; Lellouche, J.-P.; Beaucourt, J.-P.; Toupet, L.; Schio, L.; Grée, R. *J. Organomet. Chem.* **1989**, *371*, 219–312.

Scheme 4



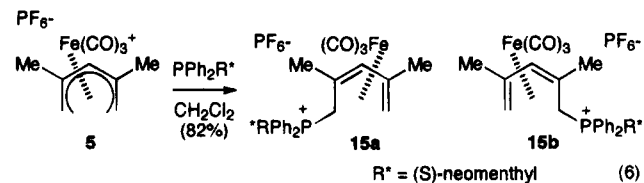
nonaryl doublet at ca.  $\delta$  4.7 and signals at ca.  $\delta$  1.8 (s, 3H) and 1.5 (d, 3H) are characteristic of the type of dienyl fragment present in structure 12.<sup>7b</sup> The signals for H4 and H1 of the initially formed isomer appear at  $\delta$  2.02 and 2.52, while those for H4 and H1 of the final isomer appear at  $\delta$  0.55 and 1.39, thus supporting the assignments as  $E,Z$ -12 and  $E,E$ -12, respectively.

Initial reaction of  $\text{PPh}_3$  with 11 must occur on the cisoid form of the cation, at the C5 (i.e. isopropyl-substituted) pentadienyl terminus. It should be noted that reaction of  $\text{PPh}_3$  with the structurally similar cation 13 (R = H) has been reported to occur at the C1 (methyl substituted) pentadienyl terminus.<sup>4</sup> Apparently the directing effect of the methyl group at C2 in 11 is sufficiently greater than that of the isopropyl substituent at the pentadienyl terminus. Since isomerization of  $E,Z$ -12 to  $E,E$ -12 occurs under neutral conditions, a mechanistic alternative to that of Salzer and Halfner is proposed. The isomerization involves reversible attack of  $\text{PPh}_3$  on cation 11, followed by slow isomerization of the cisoid form of 11 to the less stable transoid form (Scheme 4). Nucleophilic attack of  $\text{PPh}_3$  on the transoid form of 11 gives the thermodynamically more stable  $E,E$ -12. The reaction of freshly prepared  $E,Z$ -12 with tris(*p*-methoxyphenyl)phosphine was monitored by  $^1\text{H}$  NMR spectroscopy ( $\text{CD}_3\text{NO}_2$ ). Over a period of 6 h, the signals for  $E,Z$ -12 were replaced by signals for  $E,Z$ -14 (eq 5). The identity of the phosphonium salt  $E,Z$ -14 was



established by independent synthesis (reaction of 11 with  $\text{P}(\text{Ani})_3$ ). The rate of isomerization of  $E,Z$ -12 to  $E,E$ -12 is roughly comparable to the transformation of  $E,Z$ -12 into  $E,Z$ -14. This is consistent with an isomerization pathway which takes place via reversible phosphine attack.

The reaction of 5 with ((*S*)-neomenthyl)diphenylphosphine ( $\text{CH}_2\text{Cl}_2$ , 22 h) gave a mixture of two diastereomers, 15a and 15b (3:2, eq 6). Diastereomers 15a and 15b were identified as 2,4-dimethyl-2(*Z*),4-dienylphosphonium salts by comparison of their  $^1\text{H}$  NMR spectral data with those of 6. The signals for H3 of the two diastereomers are well separated, and the ratio 15a:15b was determined by integration of these signals. The ratio was not significantly affected by running this



reaction at 0 °C or at reflux. Slow, diffusion-controlled recrystallization of the mixture ( $\text{CH}_2\text{Cl}_2/\text{ether}$ ) over 6 days gave 15a (81% mass recovery), as indicated by  $^1\text{H}$  NMR spectroscopy. The structure of 15a, including its relative configuration, was solved crystallographically.<sup>8</sup> This optically pure dienylphosphonium salt gave a rotation of  $[\alpha]_{\text{D}} = +119.1$  ( $\text{CH}_3\text{CN}$ , after 15 min). Notably, if pure 15a is allowed to stand in  $\text{CD}_3\text{CN}$  (16 h), a mixture of 15a and 15b (3:2) is obtained, as indicated by  $^1\text{H}$  NMR spectroscopy. Over this same period, the optical rotation decreases to a constant value of  $[\alpha]_{\text{D}} = +41.7$  ( $\text{CH}_3\text{CN}$ ). This implies a calculated rotation for 15b of  $[\alpha]_{\text{D}} = \text{ca. } -74$  ( $\text{CH}_3\text{CN}$ ) (the rotations of 15a and 15b are not of equal magnitude, since they are diastereomers). The diastereoselectivity observed for addition of the chiral phosphine to 5 is the result of thermodynamic control. Isolation of greater than the equilibrium amount of 15a is rationalized on the basis of interconversion of 15a and 15b in solution and preferential crystallization of the major diastereomer, i.e. a second-order asymmetric transformation.<sup>19</sup> We attribute the interconversion of diastereomers 15a and 15b to reversible phosphine addition. The present results are in sharp contrast to the reaction of (cyclohexadienyl) $\text{Fe}(\text{CO})_3^+$  with ((*S*)-neomenthyl)diphenylphosphine.<sup>20</sup> For this latter reaction, the two possible diastereomers are found in an equimolar ratio, and while the diastereomers are separable by fractional crystallization, the individual diastereomers do not interconvert in solution. This provides yet another example of the differences in reactivity of acyclic (pentadienyl) $\text{Fe}(\text{CO})_3^+$  cations and (cyclohexadienyl) $\text{Fe}(\text{CO})_3^+$  cations.

In summary, for certain (pentadienyl) $\text{Fe}(\text{CO})_3^+$  cations addition of phosphine nucleophiles has been shown to be a reversible process. This appears to be the case where there may be significant steric interactions between the phosphine and other substituents present on the pentadienyl ligand (i.e. 2,4-disubstituted or

(19) Morrison, J. D.; Mosher, H. S. *Asymmetric Organic Reactions*; American Chemical Society: Washington, DC, 1976; p 24.

(20) Howell, J. A. S.; Thomas, M. J. *J. Chem. Soc., Dalton Trans.* 1983, 1401-1409.

attack at a substituted pentadienyl terminus). This reversible process may be responsible for the isomerization of dienylphosphonium salts (both regio- and stereoisomeric) under mild conditions, and the reversibility can be utilized for the generation of optically pure dienylphosphonium salts via desymmetrization.

### Experimental Section

**General Data.** For a description of general experimental conditions and instrumentation, see ref 7b. Tricarbonyl(pentadienyl)iron cations **1a–e** and **5** were prepared by literature methods.<sup>1,10</sup> Tricarbonyl((5-phenyl-2(*Z*),4-pentadien-1-yl)triphenylphosphonium)iron hexafluorophosphate (**2e**) was prepared by the literature procedure.<sup>7b</sup> The high-field <sup>1</sup>H NMR data are reported here. **2e**: <sup>1</sup>H NMR (300 MHz, *d*<sub>6</sub>-acetone) δ 8.0–7.7 (m, 15H), 7.4–7.1 (m, 5H), 6.29 (dd, *J* = 5.3, 10.2 Hz, 1H), 5.57 (br t, *J* = 5.6 Hz, 1H), 4.30 (ddd, *J* = 3.4, 14.4, 15.6 Hz, 1H), 3.86 (d, *J* = 10.3 Hz, 1H), 3.68 (ddd, *J* = 12.2, 13.8, 15.5, 1H) (signal for H2 obscured by H<sub>2</sub>O present in solvent).

**Reaction of 1a with PPh<sub>3</sub>.** To a solution of **1a** (20 mg, 0.055 mmol) in CD<sub>3</sub>NO<sub>2</sub> (0.4 mL) in a 5 mm NMR tube was added PPh<sub>3</sub> (20 mg, 0.076 mmol). The reaction mixture was monitored by <sup>1</sup>H NMR spectroscopy over a 42 h period (22 °C). Signals assigned to both **2a** and **3a** were initially observed (ca. 2:1 ratio). Over a period of 24–42 h, the signals for **3a** disappeared and the signals for **2a** increased in intensity.

On a preparative scale, to a solution of **1a** (0.69 g, 1.88 mmol) in CH<sub>2</sub>Cl<sub>2</sub> (50 mL) was added PPh<sub>3</sub> (0.49 g, 1.87 mmol), and the mixture was stirred for 1 h. The reaction mixture was concentrated and triturated with ether until cloudy. A crystalline solid was obtained which was identified as a mixture of **2a** and **3a** (2:1) by <sup>1</sup>H NMR spectroscopy. Over a period of 24 h in solution, the signals for **3a** disappeared and only the signals for **2a** remained. **3a** (obtained as a mixture with **2a**): mp 146–160 °C (mixture); <sup>1</sup>H NMR (300 MHz, CD<sub>3</sub>NO<sub>2</sub>) δ 5.46 (m, 1H), 5.18 (obscured by signal for **2a**), 3.12 (m, 1H), 2.38 (dt, *J* = 11.4, 9.3 Hz, 1H), 2.25 (dd, *J* = 3.6, 7.8 Hz, 1H), 1.76 (dd, *J* = 3.9, 9.9 Hz, 1H), 1.56 (dd, *J* = 6.6, 18.3 Hz, 3H). Anal. Calcd for C<sub>27</sub>H<sub>24</sub>O<sub>3</sub>FeP<sub>2</sub>F<sub>6</sub> (mixture of **2a** and **3a**): C, 51.62; H, 3.85. Found: C, 51.70; H, 4.00.

A pure sample of **2a** was prepared by stirring **1a** (1.00 g, 2.73 mmol) with PPh<sub>3</sub> (0.72 g, 2.75 mmol) in CH<sub>2</sub>Cl<sub>2</sub> (20 mL) for 21 h. The reaction mixture was added to a large excess of Et<sub>2</sub>O, and the resultant precipitate was collected by vacuum filtration and dried in vacuo to give **2a** as a yellow solid: 1.56 g, 91%. **2a**: mp 136–140 °C dec; IR (cm<sup>-1</sup>, CH<sub>2</sub>Cl<sub>2</sub>) 2051, 1977, 1464; <sup>1</sup>H NMR (300 MHz, *d*<sub>6</sub>-acetone) δ 8.0–7.7 (m, 15H), 5.40 (dd, *J* = 5.0, 9.3 Hz, 1H), 5.32 (br t, *J* = 6.1 Hz, 1H), 4.07 (dt, *J* = 3.4, 14.9 Hz, 1H), 3.34 (dt, *J* = 14.7, 12.9 Hz, 1H), 2.62 (ddt, *J* = 4.9, 7.7, 11.7, 1H), 1.44 (d, *J* = 6.1 Hz, 3H), signal for H5 obscured by H<sub>2</sub>O present in solvent; <sup>1</sup>H NMR (300 MHz, CD<sub>3</sub>NO<sub>2</sub>) δ 8.0–7.7 (m, 15H), 5.32 (dd, *J* = 5.4, 9.6 Hz, 1H), 5.18 (br t, *J* = 6 Hz, 1H), 3.69 (ddd, *J* = 3.3, 13.5, 15.6 Hz, 1H), 2.96 (ddd, *J* = 12.0, 13.5, 15.3 Hz, 1H), 2.67 (qd, *J* = 6.0, 9.6 Hz, 1H), 2.52 (m, 1H), 1.48 (d, *J* = 6.0 Hz, 3H); <sup>31</sup>P NMR (24 MHz, CDCl<sub>3</sub>) δ 23.7. Anal. Calcd for C<sub>27</sub>H<sub>24</sub>O<sub>3</sub>FeP<sub>2</sub>F<sub>6</sub>: C, 51.62; H, 3.85. Found: C, 51.18; H, 3.90.

**Tricarbonyl(1-deuterio-2,4-hexadienol)iron (4).** To a solution of tricarbonyl(2,4-hexadienyl)iron (3.40 g, 14.4 mmol) in dry THF (30 mL) was added NaBD<sub>4</sub> (96 atom % D, 0.84 g, 20 mmol). The reaction mixture was stirred at room temperature for 24 h and then diluted with ether (15 mL) and H<sub>2</sub>O (30 mL). After gas evolution ceased, the layers were separated and the aqueous layer was extracted with ether (2 × 15 mL). The combined ether layers were filtered through filter aid and dried (MgSO<sub>4</sub>), and the solvent was evaporated to give the product as a yellow oil: 2.93 g, 85%. The <sup>1</sup>H NMR spectrum of this product was similar to that of the known all-proton analog<sup>1a</sup> and indicated a 77:23 mixture of diastereomeric

deuterated alcohols. The ratio was determined from integration of the diastereotopic methylene protons at δ 3.60 and 3.70 ppm. Reduction of tricarbonyl(2,4-hexadienyl)iron with NaBD<sub>4</sub> in dioxane gave similar results (74:26 dr, 79%), while reduction with NaBD<sub>4</sub> in CH<sub>3</sub>OD gave considerably lower diastereoselectivity (58:42 dr, 89%).

**Tricarbonyl(1-*exo*-deuterio-2,4-hexadienyl)iron Hexafluorophosphate (*d*<sub>exo-1a</sub>).** To a solution of **3** (2.93 g, 12.3 mmol) in Ac<sub>2</sub>O (2 mL) at 0 °C was added dropwise an ice cold solution of HPF<sub>6</sub> (2.0 g) in Ac<sub>2</sub>O (2 mL), and the mixture was stirred for 15 min. Dropwise addition of the mixture to excess ether (200 mL) resulted in the formation of a yellow precipitate. The ether was decanted, and the precipitate was washed with ether (2 × 100 mL) and dried in vacuo to afford **3** as a yellow solid: 2.92 g, 78%. *d*<sub>exo-1a</sub>: <sup>1</sup>H NMR (60 MHz, CD<sub>3</sub>NO<sub>2</sub>) δ 6.93 (t, *J* = 6 Hz, 1H), 6.3–5.7 (complex m, 2H), 3.50 (br d, *J* = 9 Hz, 0.25 H), 3.25 (dq, *J* = 12, 6 Hz, 1H), 2.17 (d, *J* = 13 Hz, 0.75 H), 1.80 (d, *J* = 6 Hz, 3H).

**General Procedure for Preparation of Dienylphosphonium Salts.** To a solution of the tricarbonyl(pentadienyl)iron hexafluorophosphate in CH<sub>2</sub>Cl<sub>2</sub> (ca. 20 mL) was added an equimolar amount of solid PPh<sub>3</sub>. The reaction mixture was stirred for 16–24 h, the solvent was evaporated, the residue was dissolved in a minimal amount of CH<sub>2</sub>Cl<sub>2</sub> (ca. 5 mL), and this solution was added dropwise to excess Et<sub>2</sub>O (ca. 100–500 mL). The resultant precipitate was collected by vacuum filtration and dried in vacuo. The following dienylphosphonium salts were prepared in the above fashion.

**Tricarbonyl((1-deuterio-2(*Z*),4(*E*)-hexadien-1-yl)triphenylphosphonium)iron Hexafluorophosphate (*d*-**2a**).** The reaction of *d*<sub>exo-1a</sub> (0.50 g, 1.36 mmol) with PPh<sub>3</sub> gave the phosphonium salt *d*-**2a** as a yellow solid: 0.83 g, 97%; mp 166–168 °C (foams); IR (cm<sup>-1</sup>, KBr) 2365 w, 2334 w, 2056 s, 1976 s; <sup>1</sup>H NMR (300 MHz, *d*<sub>6</sub>-acetone) δ 8.0–7.7 (m, 15H), 5.40 (dd, *J* = 5.0, 9.3 Hz, 1H), 5.32 (br t, *J* = 6.1 Hz, 1H), 4.07 (dd, *J* = 3.4, 14.2 Hz, 0.28 H), 3.34 (br t, *J* = 12.6 Hz, 0.72H), 2.62 (m, 1H), 1.44 (d, *J* = 6.1 Hz, 3H), signal for H5 obscured by H<sub>2</sub>O present in solvent; <sup>31</sup>P NMR (24 MHz, CDCl<sub>3</sub>) δ 23.2. Anal. Calcd for C<sub>27</sub>H<sub>23</sub>DO<sub>3</sub>FeP<sub>2</sub>F<sub>6</sub>: C, 51.53; H, 4.00. Found: C, 51.56; H, 3.93.

**Tricarbonyl((2(*Z*),4(*E*)-heptadien-1-yl)triphenylphosphonium)iron Hexafluorophosphate (**2b**).** The reaction of **1b** (1.14 g, 3.00 mmol) with PPh<sub>3</sub> gave phosphonium salt **2b** as a yellow solid: 1.87 g, 97%; mp 159–160 °C dec; IR (cm<sup>-1</sup>, CH<sub>2</sub>Cl<sub>2</sub>) 2054, 1988; <sup>1</sup>H NMR (300 MHz, *d*<sub>6</sub>-acetone) δ 8.0–7.7 (m, 15H), 5.41 (dd, *J* = 5.0, 9.1 Hz, 1H), 5.35 (br t, *J* = 6.2 Hz, 1H), 4.10 (dt, *J* = 3.9, 14.9 Hz, 1H), 3.39 (dt, *J* = 14.9, 12.9 Hz, 1H), 2.79 (dt, *J* = 9.3, 6.8 Hz, 1H), 2.64 (m, 1H), 1.84 (m, 1H), 1.55 (ddq, *J* = 14.4, 7.2, 7.2 Hz, 1H), 1.06 (t, *J* = 7.3 Hz, 3H); <sup>13</sup>C NMR (75 MHz, *d*<sub>6</sub>-acetone) δ 135.8, 134.7 (*J*<sub>PC</sub> = 9.7 Hz), 131.0 (*J*<sub>PC</sub> = 12.1 Hz), 118.9 (*J*<sub>PC</sub> = 83.6 Hz), 95.6, 82.6, 69.5, 44.1 (*J*<sub>PC</sub> = 10.9 Hz), 25.0 (*J*<sub>PC</sub> = 40.0 Hz), 16.3; <sup>31</sup>P NMR (24 MHz, CDCl<sub>3</sub>) δ 23.0. Anal. Calcd for C<sub>28</sub>H<sub>26</sub>O<sub>3</sub>FeP<sub>2</sub>F<sub>6</sub>: C, 52.36; H, 4.08. Found: C, 52.39; H, 4.00.

**Tricarbonyl((2(*Z*),4(*E*)-octadien-1-yl)triphenylphosphonium)iron Hexafluorophosphate (**2c**).** The reaction of **1c** (200 mg, 0.508 mmol) with PPh<sub>3</sub> gave phosphonium salt **2c** as a yellow solid: 300 mg, 90%; mp 151–154 °C (foams); <sup>1</sup>H NMR (300 MHz, *d*<sub>6</sub>-acetone) δ 8.0–7.7 (m, 15H), 5.42 (dd, *J* = 5.1, 9.0 Hz, 1H), 5.35 (br t, *J* = 6.5 Hz, 1H), 4.11 (ddd, *J* = 3.8, 14.2, 15.6 Hz, 1H), 3.34 (ddd, *J* = 12.1, 13.1, 15.3 Hz, 1H), 2.78 (m, 1H), 2.64 (m, 1H), 1.64 (m, 2H), 1.47 (m, 2H), 0.90 (t, *J* = 7.3 Hz, 3H); <sup>13</sup>C NMR (15 MHz, CDCl<sub>3</sub>) δ 209.6, 135.5, 133.5 (*J*<sub>PC</sub> = 8 Hz), 130.6 (*J*<sub>PC</sub> = 11 Hz), 117.3 (*J*<sub>PC</sub> = 84 Hz), 95.3, 80.8 (*J*<sub>PC</sub> = 4 Hz), 67.2, 40.9 (*J*<sub>PC</sub> = 12 Hz), 37.6, 30.8, 25.0 (*J*<sub>PC</sub> = 43 Hz), 13.9; <sup>31</sup>P NMR (24 MHz, CDCl<sub>3</sub>) δ 23.4. Anal. Calcd for C<sub>28</sub>H<sub>28</sub>O<sub>3</sub>FeP<sub>2</sub>F<sub>6</sub>H<sub>2</sub>O: C, 51.65; H, 4.48. Found: C, 51.00; H, 4.32.

**Tricarbonyl((5-(methoxycarbonyl)-2(*Z*),4(*E*)-pentadien-1-yl)triphenylphosphonium)iron Hexafluorophosphate (**2d**).** The reaction of **1d** (500 mg, 1.22 mmol) with PPh<sub>3</sub> gave the phosphonium salt **2d** as a yellow solid: 750 mg, 91%; mp

167–169 °C;  $^1\text{H}$  NMR (300 MHz,  $d_6$ -acetone)  $\delta$  8.0–7.7 (m, 15H), 6.01 (dd,  $J = 5.2, 8.7$  Hz, 1H), 5.60 (br t,  $J = 5.4$  Hz, 1H), 4.24 (dt,  $J = 3.2, 15.1$  Hz, 1H), 3.64 (s, 3H), 3.40 (ddd,  $J = 12.1, 14.1, 15.3$ , 1H), 3.01 (m, partially obscured by  $\text{H}_2\text{O}$  present in solvent), 2.58 (dd,  $J = 1.0, 8.9$  Hz, 3H);  $^{13}\text{C}$  NMR (75 MHz,  $d_6$ -acetone)  $\delta$  174.2, 137.1, 135.9 ( $J_{\text{PC}} = 9.8$  Hz), 132.1 ( $J_{\text{PC}} = 12.2$  Hz), 119.9 ( $J_{\text{PC}} = 84.2$  Hz), 95.6, 87.5 ( $J_{\text{PC}} = 3.7$  Hz), 52.4, 48.1, 46.0 ( $J_{\text{PC}} = 9.8$  Hz), 25.4 ( $J_{\text{PC}} = 42.7$  Hz). Anal. Calcd for  $\text{C}_{28}\text{H}_{24}\text{O}_5\text{FeP}_2\text{F}_6$ : C, 50.02; H, 3.60. Found: C, 50.08; H, 3.57.

**Tricarbonyl((2,4-dimethyl-2(Z),4-pentadien-1-yl)triphenylphosphonium)iron Hexafluorophosphate (6).** The reaction of **5** (230 mg, 0.60 mmol) with  $\text{PPh}_3$  gave phosphonium salt **6** as a yellow solid: 350 mg, 91%; mp >185–187 °C;  $^1\text{H}$  NMR (300 MHz,  $\text{CD}_3\text{CN}$ )  $\delta$  7.9–7.6 (m, 15H), 4.95 (s), 4.07 (dd,  $J = 12.2, 15.5$  Hz), 2.86 (dd,  $J = 14.1, 15.5$  Hz), 1.87 (d,  $J = 3.9$  Hz), 1.72 (s, 3H), 1.40 (d,  $J = 2.1$  Hz, 3H), 1.19 (d,  $J = 4.5$  Hz);  $^{13}\text{C}$  NMR (75 MHz,  $\text{CD}_3\text{CN}$ )  $\delta$  211.4, 136.2 ( $J_{\text{PC}} = 3.6$  Hz), 134.9 ( $J_{\text{PC}} = 9.7$  Hz), 131.2 ( $J_{\text{PC}} = 12.2$  Hz), 119.3 ( $J_{\text{PC}} = 82.4$  Hz), 105.5, 93.1 ( $J_{\text{PC}} = 3.7$  Hz), 58.7 ( $J_{\text{PC}} = 13.3$  Hz), 46.3, 33.5, 31.4 ( $J_{\text{PC}} = 35.1$  Hz), 24.4. An analytically pure sample of **5** was prepared by precipitation from a concentrated  $\text{CH}_2\text{Cl}_2$  solution by slow addition of ether. Anal. Calcd for  $\text{C}_{28}\text{H}_{26}\text{O}_3\text{FeP}_2\text{F}_6$ : C, 52.24; H, 4.08. Found: C, 52.24; H, 3.98.

**Tricarbonyl((2,4-dimethyl-2(Z),4-pentadien-1-yl)tris(p-methoxyphenyl)phosphonium)iron Hexafluorophosphate (8).** To a solution of **6** (0.15 g, 0.23 mmol) in acetone (20 mL) was added tris(p-methoxyphenyl)phosphine (0.08 g, 0.23 mmol). The solution was heated at reflux for 5 h, cooled, and added dropwise to ether (300 mL). The resultant precipitate was collected by vacuum filtration and dried in vacuo to afford **8** as a yellow powder: 0.15 g, 88%; mp >174 °C dec;  $^1\text{H}$  NMR (300 MHz,  $\text{CD}_3\text{NO}_2$ )  $\delta$  7.71 (dd,  $J = 9.0, 11.7$  Hz), 7.27 (dd,  $J = 2.7, 8.9$  Hz), 5.08 (s), 3.96 (m), 3.96 (s, 9H), 2.88 (dd,  $J = 0.9, 15.0$  Hz), 2.12 (s, 3H), 1.96 (d,  $J = 4.5$  Hz), 1.87 (s, 3H), 1.52 (d,  $J = 2.1$  Hz), 1.24 (d,  $J = 4.2$  Hz);  $^{13}\text{C}$  NMR (75 MHz,  $\text{CD}_3\text{NO}_2$ )  $\delta$  212.1, 166.4 ( $J_{\text{PC}} = 2.5$  Hz), 137.2 ( $J_{\text{PC}} = 10.9$  Hz), 117.1 ( $J_{\text{PC}} = 13.4$  Hz), 110.4 ( $J_{\text{PC}} = 90.9$  Hz), 105.8, 94.0 ( $J_{\text{PC}} = 3.5$  Hz), 59.9 ( $J_{\text{PC}} = 12.2$  Hz), 56.9, 46.1, 33.8, 33.0 ( $J_{\text{PC}} = 38.8$  Hz), 24.7. Anal. Calcd for  $\text{C}_{31}\text{H}_{32}\text{O}_6\text{FeP}_2\text{F}_6$ : C, 50.82; H, 4.41. Found: C, 50.77; H, 4.41.

**Tricarbonyl((2-6- $\eta^6$ )-3,7-dimethyl-2,4-octadien-5-yl)iron Hexafluorophosphate (11).** The preparation of **11** utilized a modified procedure for the protonation of (triene)- $\text{Fe}(\text{CO})_3$  complexes<sup>17</sup> as follows. To tricarbonyl((2-5- $\eta^4$ )-3,7-dimethyl-2,4,6-octatriene)iron<sup>18</sup> (3.80 g, 13.8 mmol) was added a solution of  $\text{HPF}_6\text{-Ac}_2\text{O}$  (1:1, 10 mL). The mixture was allowed to stand for 1 h and was then added dropwise to excess ether (300 mL). The resultant precipitate was collected by vacuum filtration and dried in vacuo to afford **11** as a yellow solid: 4.04 g, 69%; mp >130 °C dec; IR ( $\text{cm}^{-1}$ ,  $\text{CH}_2\text{Cl}_2$ ) 2033, 1963;  $^1\text{H}$  NMR (300 MHz,  $\text{CD}_3\text{NO}_2$ )  $\delta$  6.73 (d,  $J = 7.5$  Hz, 1H), 5.78 (dd,  $J = 7.5, 12.6$  Hz, 1H), 3.58 (dd,  $J = 9.0, 12.6$ , 1H), 2.66 (q,  $J = 6.0$  Hz, 1H), 2.42 (s, 3H), 1.94 (m, 1H), 1.76 (d,  $J = 6.0$  Hz, 3H), 1.38 (d,  $J = 6.6$  Hz, 3H), 1.19 (d,  $J = 6.6$  Hz, 3H);  $^{13}\text{C}$  NMR (75 MHz,  $\text{CD}_3\text{NO}_2$ )  $\delta$  124.7, 103.0, 101.4, 93.1, 85.6, 37.8, 24.7, 24.0, 20.5, 17.2. This compound decomposes upon heating and did not give a satisfactory elemental analysis.

**Reaction of 11 with Triphenylphosphine.** To a solution of **11** (0.02 g, 0.05 mmol) in  $\text{CD}_3\text{NO}_2$  (1 mL) in an 5 mm NMR tube was added  $\text{PPh}_3$  (0.01 g, 0.05 mmol). The reaction mixture was monitored by  $^1\text{H}$  NMR spectroscopy over 20 h (22 °C). Signals assigned to the 4(Z),6(E)-dienylphosphonium salt (*E,Z*-**12**) were initially observed. *E,Z*-**12**:  $^1\text{H}$  NMR (300 MHz,  $\text{CD}_3\text{NO}_2$ )  $\delta$  8.0–7.7 (m, 15H), 4.82 (d,  $J = 7.5$  Hz, 1H), 3.27 (t,  $J = 13.5$  Hz, 1H), 2.52 (m, 2H), 2.02 (dt,  $J = 12.9, 8.1$  Hz, 1H), 1.80 (s, 3H), 1.53 (d,  $J = 6.3$  Hz, 3H), 1.50 (d,  $J = 6.3$  Hz, 3H), 0.47 (d,  $J = 6.9$  Hz, 3H). Over a period of 20 h, these signals were replaced by those assigned to the 4(E),6(E)-isomer (*E,E*-**12**). A sample of *E,E*-**12** was prepared by stirring **10** (0.15 g, 0.36 mmol) with  $\text{PPh}_3$  (0.11 g, 0.42 mmol) in  $\text{CH}_2\text{Cl}_2$  (12

Table 2. Crystallographic data for **2a**

formula	$\text{C}_{27}\text{H}_{24}\text{O}_3\text{FeP}_2\text{F}_6$
mol wt	628.27
cryst syst	triclinic
space group	$P\bar{1}$
$a$ (Å)	10.185(3)
$b$ (Å)	10.866(5)
$c$ (Å)	14.978(7)
$\alpha$ (deg)	74.39(4)
$\beta$ (deg)	104.12(3)
$\gamma$ (deg)	114.84(3)
$V$ (Å <sup>3</sup> )	1432.4(11)
$Z$	2
cryst size (mm)	0.20 × 0.20 × 0.25
monochromator	none
radiation wavelength (Å)	Mo K $\alpha$ (Zr filtered)
temp (°C)	ambient
$2\theta$ range (deg)	35
no. of rflns measd	1858
no. of rflns obsd	1310
linear abs coeff ( $\text{cm}^{-1}$ )	7.0
$R$	0.092
$R_w$	0.091

mL) for 21 h. The reaction mixture was added to a large excess of  $\text{Et}_2\text{O}$ , and the resultant precipitate was collected by vacuum filtration and dried in vacuo to give *E,E*-**12** as a yellow solid: 0.19 g, 77%; mp 156–158 °C; IR ( $\text{cm}^{-1}$ ,  $\text{CH}_2\text{Cl}_2$ ) 2048, 1981;  $^1\text{H}$  NMR (300 MHz,  $\text{CD}_3\text{NO}_2$ )  $\delta$  8.0–7.7 (m, 15H), 4.54 (d,  $J = 8.7$  Hz, 1H), 3.35 (dd,  $J = 10.2, 13.5$  Hz, 1H), 2.65 (m, 1H), 1.87 (s, 3H), 1.47 (d,  $J = 6.9$  Hz, 3H), 1.44 (s, 3H), 1.39 (m, 1H), 0.55 (ddd,  $J = 3.9, 8.7, 11.1$  Hz, 1H), 0.47 (d,  $J = 6.6$  Hz, 3H);  $^{31}\text{P}$  NMR (120 MHz,  $\text{CD}_3\text{NO}_2$ )  $\delta$  25.9. An analytically pure sample was prepared by precipitation from a concentrated  $\text{CH}_2\text{Cl}_2$  solution by slow addition of ether, followed by drying the yellow flakes in vacuo at 80 °C for 20 h. Anal. Calcd for  $\text{C}_{29}\text{H}_{32}\text{O}_3\text{FeP}_2\text{F}_6$ : C, 54.40; H, 4.71. Found: C, 54.21; H, 4.74.

**Tricarbonyl((2,6-dimethyl-4(Z),6(E)-octadien-3-yl)tris(p-methoxyphenyl)phosphonium)iron Hexafluorophosphate (*E,Z*-**14**).** To a solution of **11** (0.24 g, 0.57 mmol) in  $\text{CH}_2\text{Cl}_2$  (10 mL) was added  $\text{P}(\text{Anis})_3$  (0.21 g, 0.60 mmol). The reaction mixture was stirred for 21 h and then was added dropwise to excess hexanes (100 mL). The resultant precipitate was collected by vacuum filtration and dried in vacuo to afford *E,Z*-**14** as a yellow solid: 0.38 g, 86%. *E,Z*-**14**:  $^1\text{H}$  NMR (300 MHz,  $\text{CD}_3\text{NO}_2$ )  $\delta$  7.75 (dd,  $J = 9.0, 11.7$  Hz, 6H), 7.25 (m, 6H), 4.83 (d,  $J = 7.8$  Hz, 1H), 3.94 (s, 9H), 3.08 (t,  $J = 12.9$  Hz, 1H), 2.49 (d,  $J = 6.0$  Hz, 1H), 2.47 (m, 1H), 1.98 (m, 1H), 1.85 (s, 3H), 1.52 (d,  $J = 6.3$  Hz, 3H), 1.47 (d,  $J = 6.9$  Hz, 3H), 0.52 (d,  $J = 6.9$  Hz, 3H).

**Tricarbonyl((2(S),4(R)-dimethyl-2(Z),4-pentadien-1-yl)((S)-neomenthyl)diphenylphosphonium)iron Hexafluorophosphate (15a).** To a solution of **5** (0.19 g, 0.50 mmol) in  $\text{CH}_2\text{Cl}_2$  (10 mL) was added ((S)-neomenthyl)diphenylphosphine (0.16 g, 0.50 mmol). The reaction mixture was stirred for 22 h, the solvent was evaporated, the residue was dissolved in  $\text{CH}_2\text{Cl}_2$  (5 mL), this solution was added dropwise to excess  $\text{Et}_2\text{O}$  (100 mL), and the resultant precipitate was collected by vacuum filtration. The reprecipitation procedure was repeated a second time, and the product was dried in vacuo to afford **15a,b** as a yellow solid: 0.29 g, 82%. Slow diffusion-controlled recrystallization of the mixture (0.16 g) from  $\text{CH}_2\text{Cl}_2$ /ether gave a single diastereomer, **15a**: 0.13 g, 81% mass recovery. Over a period of 16 h in  $\text{CD}_3\text{CN}$  solution this isomerized to an equilibrium mixture of **15a** and **15b** (3:2). **15a**: mp 190–192 °C;  $[\alpha]_D^{25} = +119.1^\circ$  ( $\text{CH}_3\text{CN}$ ,  $t = 15$  min);  $^1\text{H}$  NMR (300 MHz,  $\text{CD}_3\text{CN}$ )  $\delta$  8.1–7.6 (m, 10H), 4.31 (br s, 1H), 3.87 (dd,  $J = 11.1, 15.6$  Hz, 1H), 3.49 (m, 1H), 2.31 (dd,  $J = 12.3, 15.6$  Hz, 1H), 2.26 (d,  $J = 4.8, 1H$ ), 1.84 (m), 1.72 (s, 3H), 1.63 (m), 1.50 (m), 1.38 (d,  $J = 2.1$  Hz, 3H), 1.25 (dd,  $J = 0.9, 4.8, 1H$ ), 0.97 (d,  $J = 6.3$  Hz, 3H), 0.91 (d,  $J = 6.9$  Hz, 3H), 0.46 (d,  $J = 6.6$  Hz, 3H);  $^{31}\text{P}$  NMR (120 MHz,  $\text{CDCl}_3$ )  $\delta$  32.2, –143.2. Anal. Calcd for  $\text{C}_{32}\text{H}_{40}\text{O}_3\text{P}_2\text{F}_6\text{Fe}$ : C, 54.55; H, 5.68. Found: C, 53.55; H, 5.63. **15b**:  $^1\text{H}$  NMR (300 MHz,  $\text{CD}_3\text{CN}$ , partial)  $\delta$  4.39 (br s,



**Table 3. Positional Parameters for the Two Molecules in the Unit Cell of 2a**

molecule I				molecule II			
atom	x	y	z	atom	x	y	z
Fe1	-0.17710(0)	1.16590(0)	-0.39640(0)	Fe2	0.2202(9)	0.1892(8)	0.3625(6)
P3	0.0005(13)	0.8191(11)	-0.2118(8)	P4	0.6101(13)	0.4803(11)	0.1833(8)
C1	-0.018(4)	0.990(4)	-0.248(2)	C31	0.440(4)	0.409(4)	0.224(3)
C2	-0.114(5)	0.992(5)	-0.346(4)	C32	0.426(4)	0.321(4)	0.321(3)
C3	-0.270(4)	0.969(4)	-0.356(2)	C33	0.402(5)	0.175(5)	0.347(3)
C4	-0.319(5)	1.031(4)	-0.306(3)	C34	0.280(5)	0.083(5)	0.314(3)
C5	-0.218(5)	1.132(5)	-0.263(3)	C35	0.189(5)	0.113(5)	0.242(3)
C6	-0.296(6)	1.220(5)	-0.231(4)	C36	0.045(5)	-0.010(5)	0.219(4)
C7	-0.287(6)	1.284(6)	-0.443(4)	C37	0.134(5)	0.308(5)	0.294(4)
C8	-0.000(5)	1.287(4)	-0.372(3)	C38	0.084(4)	0.058(4)	0.413(2)
C9	-0.188(6)	1.158(5)	-0.509(4)	C39	0.281(6)	0.253(5)	0.468(4)
O7	-0.333(4)	1.351(4)	-0.470(2)	O37	0.074(4)	0.374(4)	0.246(3)
O8	0.121(4)	1.370(3)	-0.362(2)	O38	-0.009(3)	-0.037(3)	0.4546(19)
O9	-0.183(4)	1.164(3)	-0.592(3)	O39	0.320(4)	0.292(4)	0.536(3)
C10	-0.175(2)	0.691(2)	-0.2354(19)	C40	0.748(3)	0.530(3)	0.2811(16)
C11	-0.272(2)	0.659(2)	-0.1732(19)	C41	0.732(3)	0.607(3)	0.3364(16)
C12	-0.419(2)	0.571(2)	-0.1930(19)	C42	0.844(3)	0.655(3)	0.4097(16)
C13	-0.468(2)	0.516(2)	-0.2750(19)	C43	0.970(3)	0.626(3)	0.4275(16)
C14	-0.370(2)	0.549(2)	-0.3373(19)	C44	0.985(3)	0.548(3)	0.3722(16)
C15	-0.224(2)	0.636(2)	-0.3174(19)	C45	0.874(3)	0.500(3)	0.2989(16)
C16	0.124(3)	0.814(3)	-0.2754(19)	C46	0.620(3)	0.632(2)	0.0962(16)
C17	0.142(3)	0.688(3)	-0.2489(19)	C47	0.493(3)	0.642(2)	0.0386(16)
C18	0.232(3)	0.664(3)	-0.2940(19)	C48	0.502(3)	0.759(2)	-0.0315(16)
C19	0.302(3)	0.765(3)	-0.3656(19)	C49	0.637(3)	0.866(2)	-0.0438(16)
C20	0.284(3)	0.891(3)	-0.3921(19)	C50	0.765(3)	0.856(2)	0.0139(16)
C21	0.194(3)	0.916(3)	-0.3470(19)	C51	0.756(3)	0.739(2)	0.0839(16)
C22	0.070(3)	0.793(3)	-0.0879(14)	C52	0.641(4)	0.363(3)	0.135(2)
C23	0.046(3)	0.659(3)	-0.0358(14)	C53	0.689(4)	0.400(3)	0.048(2)
C24	0.106(3)	0.640(3)	0.0591(14)	C54	0.717(4)	0.305(3)	0.015(2)
C25	0.190(3)	0.755(3)	0.1019(14)	C55	0.696(4)	0.174(3)	0.069(2)
C26	0.214(3)	0.888(3)	0.0497(14)	C56	0.648(4)	0.136(3)	0.156(2)
C27	0.154(3)	0.907(3)	-0.0452(14)	C57	0.620(4)	0.231(3)	0.189(2)
P1	0.4556(19)	0.7627(17)	0.3865(12)	P2	1.1450(18)	1.3011(17)	-0.0562(11)
F1	0.551(5)	0.841(5)	0.319(3)	F7	1.163(4)	1.253(4)	-0.140(2)
F2	0.356(6)	0.664(5)	0.460(4)	F8	1.139(3)	1.357(3)	0.030(2)
F3	0.598(5)	0.750(5)	0.448(3)	F9	1.264(4)	1.256(4)	0.005(3)
F4	0.333(5)	0.794(5)	0.327(3)	F10	1.035(4)	1.364(4)	-0.124(3)
F5	0.409(4)	0.638(4)	0.336(3)	F11	1.029(4)	1.161(4)	-0.031(2)
F6	0.499(4)	0.885(3)	0.436(2)	F12	1.263(4)	1.440(4)	-0.092(3)

1H), 3.74 (dd,  $J = 11.1, 15.6$  Hz, 1H), 1.71 (s, 3H), 1.30 (d,  $J = 2.4$  Hz, 3H), 0.99 (d,  $J = 6.3$  Hz, 3H), 0.72 (d,  $J = 6.6$  Hz, 3H), 0.49 (d,  $J = 6.9$  Hz, 3H);  $^{31}\text{P}$  NMR (120 MHz,  $\text{CDCl}_3$ )  $\delta$  27.6, -143.2.

**Crystallographic Analysis of Tricarbonyl((2(Z),4(E)-hexadien-1-yl)triphenylphosphonium)iron Hexafluorophosphate.** Golden yellow crystals of **2a** were grown from a concentrated  $\text{CH}_2\text{Cl}_2$  solution by slow addition of ether. The X-ray diffraction data were collected with a Picker diffractometer from a crystal of dimensions  $0.20 \times 0.20 \times 0.25$  mm<sup>3</sup>. The unit cell dimensions were determined from 12 reflections in the range  $4.83 \leq 2\theta \leq 9.77^\circ$ . Crystal data, data collection parameters, and results of the analysis are listed in Table 2. Data were globally sorted and collected using PCXTL,<sup>21</sup> and data handling, reduction, and analysis were performed using NRCVAX.<sup>22</sup> The structure was solved by direct methods using SHELXS-86.<sup>23</sup> All heavy atoms with the exception of iron were refined isotropically using SHELX-76.<sup>24</sup> Hydrogen atoms were

allowed to ride with the heavy atoms to which they were bonded. A single hydrogen isotropic thermal parameter was refined to a value of  $0.255 \text{ \AA}^2$ . Data for this structure were initially collected assuming a centrosymmetric structure with one molecule per asymmetric unit. The data set was limited to  $2\theta = 35^\circ$ . The structure could not be solved for several years. When the solution was finally obtained (by relaxing the centrosymmetric constraint), the reflection/parameter ratio was too low to allow for realistic anisotropic refinement. We no longer have the crystals for collection of a more complete data set. Final values are  $R = 0.092$  and  $R_w = 0.091$ . Atom positions are shown in Table 3.

**Acknowledgment.** Financial support for this work was provided by the National Institutes of Health (Grant No. GM-42641).

OM950523T

(21) Weinrach, J. B.; Bennett, D. W. *J. Appl. Crystallogr.* **1991**, *24*, 91.

(22) Gabe, E. J.; Le Page, Y.; Charland, P.-P.; Lee, F. L.; White, P. S. *J. Appl. Crystallogr.* **1989**, *22*, 384.

(23) Sheldrick, G. M. *Acta Crystallogr.* **1990**, *A46*, 467.

(24) Sheldrick, G. M. A Program for Crystal Structure Solution; Institute für Anorganische Chemie der Universität, Göttingen, FRG.

# Synthesis of a New Family of Metallafurans from (Oxapentadienyl)metal Precursors

John R. Bleeke,\* Pamela R. New, Jonathan M. B. Blanchard, Tesfamichael Haile, and Alicia M. Beatty

Department of Chemistry, Washington University, St. Louis, Missouri 63130-4899

Received June 26, 1995<sup>⊗</sup>

Treatment of ((1,2,5- $\eta$ )-4-methyl-5-oxapentadienyl)Ir(PMe<sub>3</sub>)<sub>3</sub> (**1**) with HBF<sub>4</sub>·OEt<sub>2</sub> leads to protonation at carbon C3 and production of [((1,2,5- $\eta$ )-4-methyl-5-oxapenta-1,4-diene)Ir(PMe<sub>3</sub>)<sub>3</sub>]<sup>+</sup>BF<sub>4</sub><sup>-</sup> (**4**). At room temperature, this species rearranges to the iridafuran complex [fac-CH<sub>3</sub>C<sup>+</sup>CH<sup>-</sup>C(CH<sub>3</sub>)<sup>-</sup>O<sup>-</sup>Ir(PMe<sub>3</sub>)<sub>3</sub>(H)]<sup>+</sup>BF<sub>4</sub><sup>-</sup> (**5**). Similar treatment of the five-membered iridacycle, *mer*-CH<sub>2</sub>=CCH=C(CH<sub>3</sub>)OIr(PMe<sub>3</sub>)<sub>3</sub>(H) (**3**) with HBF<sub>4</sub>·OEt<sub>2</sub> results in direct electrophilic attack at carbon C1 and production of the *mer* isomer of **5**, [*mer*-CH<sub>3</sub>C<sup>+</sup>CH<sup>-</sup>C(CH<sub>3</sub>)<sup>-</sup>O<sup>-</sup>Ir(PMe<sub>3</sub>)<sub>3</sub>(H)]<sup>+</sup>BF<sub>4</sub><sup>-</sup> (**6**). In the tris(PET<sub>3</sub>) reaction system, treatment of the six-membered ring compound, *mer*-CH=CHCH=C(CH<sub>3</sub>)OIr(PET<sub>3</sub>)<sub>3</sub>(H) (**7**), with HBF<sub>4</sub>·OEt<sub>2</sub> leads to protonation at C3 and production of [*mer*-CH=CHCH<sub>2</sub>C(CH<sub>3</sub>)=OIr(PET<sub>3</sub>)<sub>3</sub>(H)]<sup>+</sup>BF<sub>4</sub><sup>-</sup> (**9**). Upon heating in tetrahydrofuran at reflux, this species rearranges to the iridafuran complex, [*mer*-CH<sub>3</sub>C<sup>+</sup>CH<sup>-</sup>C(CH<sub>3</sub>)<sup>-</sup>O<sup>-</sup>Ir(PET<sub>3</sub>)<sub>3</sub>(H)]<sup>+</sup>BF<sub>4</sub><sup>-</sup> (**10**). Protonation of the five-membered-ring compound, *mer*-CH<sub>2</sub>=CCH=C(CH<sub>3</sub>)OIr(PET<sub>3</sub>)<sub>3</sub>(H) (**8**), with HBF<sub>4</sub>·OEt<sub>2</sub> also produces iridafuran **10** via direct electrophilic addition to C1. Excess I<sub>2</sub> reacts with compound **10** exclusively at the metal center to produce the neutral diiodide compound, *trans*-CH<sub>3</sub>C<sup>+</sup>CH<sup>-</sup>C(CH<sub>3</sub>)<sup>-</sup>O<sup>-</sup>Ir(PET<sub>3</sub>)<sub>2</sub>(I)<sub>2</sub> (**11**), while excess Br<sub>2</sub> reacts with **10** at both the iridium center and C3 of the ring to form the electrophilic aromatic substitution product, *trans*-CH<sub>3</sub>C<sup>+</sup>C(Br)<sup>-</sup>C(CH<sub>3</sub>)<sup>-</sup>O<sup>-</sup>Ir(PET<sub>3</sub>)<sub>2</sub>(Br)<sub>2</sub> (**12**). Molecular structures of [*mer*-CH<sub>3</sub>C<sup>+</sup>CH<sup>-</sup>C(CH<sub>3</sub>)<sup>-</sup>O<sup>-</sup>Ir(PET<sub>3</sub>)<sub>3</sub>(H)]<sup>+</sup>PF<sub>6</sub><sup>-</sup> (the PF<sub>6</sub><sup>-</sup> salt of **10**), *trans*-CH<sub>3</sub>C<sup>+</sup>CH<sup>-</sup>C(CH<sub>3</sub>)<sup>-</sup>O<sup>-</sup>Ir(PET<sub>3</sub>)<sub>2</sub>(I)<sub>2</sub> (**11**), and *trans*-CH<sub>3</sub>C<sup>+</sup>C(Br)<sup>-</sup>C(CH<sub>3</sub>)<sup>-</sup>O<sup>-</sup>Ir(PET<sub>3</sub>)<sub>2</sub>(Br)<sub>2</sub> (**12**) have been determined by single-crystal X-ray diffraction studies.

## Introduction

During the past several years, we have been developing a new synthetic route to unsaturated metallacycles, which utilizes pentadienide and heteropentadienide reagents as the source of ring carbons or heteroatoms and exploits C-H bond activation in the key ring-forming step. By using this approach, we have synthesized metallacyclohexadiene complexes<sup>1</sup> and a variety of unsaturated five- and six-membered thia-<sup>2</sup> and oxametallacycles.<sup>3</sup> Several of these species have been

subsequently converted to aromatic metallacycles, particularly metallabenzenes<sup>4</sup> and metallathiophenes.<sup>5</sup>

We now report the synthesis of a family of metallafurans.<sup>6</sup> These species are generated either by direct protonation of (oxapentadienyl)metal complexes or by protonation of the oxametallacycles produced from these complexes via C-H bond activation. X-ray crystal structures, NMR spectra, and chemical reactivity studies of the metallafurans fully support the characterization of these species as aromatic metallacycles. In these novel compounds, metal d orbitals participate with carbon and oxygen p orbitals in forming the  $\pi$  bonds of the aromatic rings.

## Results and Discussion

**A. Reaction of (Cl)Ir(PMe<sub>3</sub>)<sub>3</sub> with Potassium 4-Methyl-5-oxapentadienide.** As we reported earlier,<sup>3b</sup> treatment of (Cl)Ir(PMe<sub>3</sub>)<sub>3</sub> with potassium 4-methyl-5-oxapentadienide produces ((1,2,5- $\eta$ )-4-methyl-5-oxapen-

<sup>⊗</sup> Abstract published in *Advance ACS Abstracts*, October 15, 1995.

(1) (a) Bleeke, J. R.; Peng, W.-J. *Organometallics* 1987, 6, 1576. (b) Bleeke, J. R.; Peng, W.-J.; Xie, Y.-F.; Chiang, M. Y. *Organometallics* 1990, 9, 1113. (c) Bleeke, J. R.; Rohde, A. M.; Boorsma, D. W. *Organometallics* 1993, 12, 970.

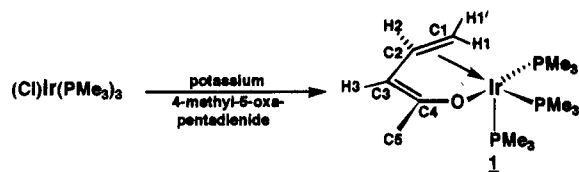
(2) (a) Bleeke, J. R.; Ortwerth, M. F.; Chiang, M. Y. *Organometallics* 1992, 11, 2740. (b) Bleeke, J. R.; Ortwerth, M. F.; Rohde, A. M. *Organometallics* 1995, 14, 2813.

(3) (a) Bleeke, J. R.; Haile, T.; Chiang, M. Y. *Organometallics* 1991, 10, 19. (b) Bleeke, J. R.; Haile, T.; New, P. R.; Chiang, M. Y. *Organometallics* 1993, 12, 517.

(4) (a) Bleeke, J. R.; Xie, Y.-F.; Peng, W.-J.; Chiang, M. Y. *J. Am. Chem. Soc.* 1989, 111, 4118. (b) Bleeke, J. R. *Acc. Chem. Res.* 1991, 24, 271.

(5) (a) Bleeke, J. R.; Ortwerth, M. F.; Chiang, M. Y. *Organometallics* 1993, 12, 985. (b) Bleeke, J. R.; Ortwerth, M. F.; Rohde, A. M. *Organometallics* 1995, 14, 2813.

Scheme 1



tadienyl)Ir(PMe<sub>3</sub>)<sub>3</sub> (**1**) (see Scheme 1). Compound **1** can be isolated and fully characterized, but upon stirring at room temperature in tetrahydrofuran, it slowly (over several days) equilibrates with the five-membered-ring

compound, *fac*-CH<sub>2</sub>=CCH=C(CH<sub>3</sub>)OIr(PMe<sub>3</sub>)<sub>3</sub>(H) (**2**) (see Scheme 2). The metallacycle is produced via intramolecular activation of C–H<sub>2</sub> in 16e intermediate **B** (Scheme 2) or the corresponding 18e agostic species.<sup>7</sup> This mixture then *even more slowly* (over several weeks at room temperature) converts to the thermodynamically preferred meridional isomer of the five-membered

(6) A sizable number of compounds containing the metallafuran structure have been reported, although the extent to which these species exhibit aromatic character varies widely. The largest classes of metallafurans are metal–carbonyl complexes of the group VI and VII metals. Key references include the following: (a) Green, M.; Nyathi, J. Z.; Scott, C.; Stone, F. G. A.; Welch, A. J.; Woodward, P. *J. Chem. Soc., Dalton Trans.* **1978**, 1067. (b) Allen, S. R.; Green, M.; Norman, N. C.; Paddick, K. E.; Orpen, A. G. *J. Chem. Soc., Dalton Trans.* **1983**, 1625. (c) Watson, P. L.; Bergman, R. G. *J. Am. Chem. Soc.* **1979**, 101, 2055. (d) Alt, H. G. *J. Organomet. Chem.* **1985**, 288, 149. (e) Alt, H. G.; Herrmann, G. S.; Engelhardt, H. E.; Rogers, R. D. *J. Organomet. Chem.* **1987**, 331, 329. (f) Burkhardt, E. R.; Doney, J. J.; Bergman, R. G.; Heathcock, C. H. *J. Am. Chem. Soc.* **1987**, 109, 2022. (g) Chaona, S.; Lalor, F. J.; Ferguson, G.; Hunt, M. M. *J. Chem. Soc., Chem. Commun.* **1988**, 1606. (h) Rusik, C. A.; Collins, M. A.; Gamble, A. S.; Tonker, T. L.; Templeton, J. L. *J. Am. Chem. Soc.* **1989**, 111, 2550. (i) Garrett, K. E.; Sheridan, J. B.; Pourreau, D. B.; Feng, W. C.; Geoffroy, G. L.; Staley, D. L.; Rheingold, A. L. *J. Am. Chem. Soc.* **1989**, 111, 8383. (j) Van der Zeijden, A. A. H.; Bosch, H. W.; Berke, H. *Organometallics* **1992**, 11, 563. (k) Carter, J. D.; Schoch, T. K.; McElwee-White, L. *Organometallics* **1992**, 11, 3571. (l) Masters, A. P.; Parvez, M.; Sorensen, T. S.; Sun, F. *Can. J. Chem.* **1993**, 71, 230. (m) Booth, B. L.; Hargreaves, R. G. *J. Chem. Soc. A* **1970**, 308. (n) Herrmann, W. A.; Ziegler, M. L.; Serhadli, O. *Organometallics* **1983**, 2, 958. (o) DeShong, P.; Sidler, D. R.; Rybczynski, P. J.; Slough, G. A.; Rheingold, A. L. *J. Am. Chem. Soc.* **1988**, 110, 2575. (p) DeShong, P.; Slough, G. A.; Sidler, D. R.; Rybczynski, P. J.; von Philipsborn, W.; Kuzn, R. W.; Bursten, B. E.; Clayton, T. W., Jr. *Organometallics* **1989**, 8, 1381. (q) Stack, J. G.; Simpson, R. D.; Hollander, F. J.; Bergman, R. G.; Heathcock, C. H. *J. Am. Chem. Soc.* **1990**, 112, 2716. (r) O'Connor, J. M.; Uhrhammer, R.; Rheingold, A. L.; Roddick, D. M. *J. Am. Chem. Soc.* **1991**, 113, 4530. (s) Adams, R. D.; Chen, G.; Chen, L.; Wu, W.; Yin, J. *J. Am. Chem. Soc.* **1991**, 113, 9406. (t) Adams, R. D.; Chen, L.; Wu, W. *Organometallics* **1992**, 11, 3505. (u) Padolik, L. L.; Gallucci, J. C.; Wojcicki, A. *J. Am. Chem. Soc.* **1993**, 115, 9986. A substantial number of Group VIII metallafurans have also been reported. Key references include the following: (v) Komiya, S.; Ito, T.; Cowie, M.; Yamamoto, A.; Ibers, J. A. *J. Am. Chem. Soc.* **1976**, 98, 3874. (w) Deeming, A. J.; Manning, P. J.; Rothwell, I. P.; Hursthouse, M. B.; Walker, N. P. C. *J. Chem. Soc., Dalton Trans.* **1984**, 2039. (x) Werner, H.; Weinand, R.; Otto, H. *J. Organomet. Chem.* **1986**, 307, 49. (y) Romero, A.; Vegas, A.; Dixneuf, P. H. *Angew. Chem., Int. Ed. Engl.* **1990**, 29, 215. (z) Akita, M.; Terada, M.; Oyama, S.; Sugimoto, S.; Moro-oka, Y. *Organometallics* **1991**, 10, 1561. (aa) Espuelas, J.; Esteruelas, M. A.; Lahoz, F. J.; Oro, L. A.; Valero, C. *Organometallics* **1993**, 12, 663. (bb) Werner, H.; Dirnberger, T.; Schulz, M. *Angew. Chem., Int. Ed. Engl.* **1988**, 27, 948. (cc) Sunley, G. J.; Menanteau, P. C.; Adams, H.; Bailey, N. A.; Maitlis, P. M. *J. Chem. Soc., Dalton Trans.* **1989**, 2415. (dd) Bianchini, C.; Innocenti, P.; Masi, D.; Meli, A.; Sabat, M. *Organometallics* **1986**, 5, 72. (ee) Carmona, E.; Gutierrez-Puebla, E.; Monge, A.; Marin, J. M.; Paneque, M.; Poveda, M. L. *Organometallics* **1989**, 8, 967. (ff) Allevi, C.; Garlaschelli, L.; Malatesta, M. C.; Ganazzoli, F. *Organometallics* **1990**, 9, 1383. One example of a metallafuran in which the oxygen atom resides beta to the metal center has been reported. See (gg) Shih, K.-Y.; Fanwick, P. E.; Walton, R. A. *J. Am. Chem. Soc.* **1993**, 115, 9319.

(7) A small quantity of the six-membered-ring compound *mer*-CH=CHCH=C(CH<sub>3</sub>)OIr(PMe<sub>3</sub>)<sub>3</sub>(H), produced via C–H1 bond activation, is also observed in the equilibrium mixture.

metallacycle, *mer*-CH<sub>2</sub>=CH=C(CH<sub>3</sub>)OIr(PMe<sub>3</sub>)<sub>3</sub>(H) (**3**).<sup>8</sup> Upon heating, this conversion occurs much more rapidly and is essentially complete in 20 h in refluxing tetrahydrofuran.

**B. Protonation of Compounds 1 and 3.** Treatment of compound **1** with HBF<sub>4</sub>·OEt<sub>2</sub> in diethyl ether at –30 °C results in electrophilic attack at carbon C3 and production of [(1,2,5-η)-4-methyl-5-oxapenta-1,4-diene]Ir(PMe<sub>3</sub>)<sub>3</sub><sup>+</sup>BF<sub>4</sub><sup>–</sup> (**4**) (see Scheme 3). Other acids, including HO<sub>3</sub>SCF<sub>3</sub>, HO<sub>2</sub>CCF<sub>3</sub>, and NH<sub>4</sub><sup>+</sup>PF<sub>6</sub><sup>–</sup>, yield the same cationic product.

In the <sup>1</sup>H NMR spectrum of **4**, H3 and H3' resonate at δ 3.55 and 3.27 and strongly couple to each other (*J*<sub>HH</sub> = 22.0 Hz!). The signal for H2 appears at δ 2.23, while H1 and H1' resonate at δ 0.52 and 1.48. In the <sup>13</sup>C-<sup>1</sup>H NMR spectrum of **4**, C3 resonates at δ 54.4, while C2 and C1 appear at δ 28.3 and 21.8, respectively. The C2 and C1 signals are doublets (*J* = 34.2 and 34.5 Hz), reflecting substantial coupling to the phosphorus nuclei of the PMe<sub>3</sub> ligands. C4 appears far downfield (δ 233.4), clearly indicating that it is not coordinated to the iridium center. The <sup>31</sup>P{<sup>1</sup>H} NMR spectrum shows the expected set of three doublet-of-doublet patterns, due to the three inequivalent PMe<sub>3</sub> ligands.

While **4** is relatively stable at –30 °C, it isomerizes to

the iridafuran complex [*fac*-CH<sub>3</sub>C<sup>–</sup>CH=C(CH<sub>3</sub>)<sup>–</sup>O<sup>–</sup>Ir(PMe<sub>3</sub>)<sub>3</sub>(H)]<sup>+</sup>BF<sub>4</sub><sup>–</sup> (**5**) at room temperature. Although the mechanistic details of this rearrangement have not been probed, a likely pathway is shown in Scheme 4. Dissociation of double bond C1–C2 from the iridium center, followed by C2–C3 bond rotation and C–H2 bond activation, generates the five-membered metallacycle **C**. Proton migration from C3 to C1 then produces iridafuran **5**.<sup>9</sup>

The <sup>1</sup>H NMR spectrum of **5** provides evidence for its aromatic character. The signal for ring proton H3 is shifted downfield, appearing as a doublet (*J*<sub>HP</sub> = 6.9 Hz)<sup>10</sup> at δ 7.00 in acetone-*d*<sub>6</sub>. By comparison, H3 in the nonaromatic five-membered-ring compound **2** resonates at δ 4.90 in acetone-*d*<sub>6</sub>.<sup>11</sup> A similar downfield shift is observed for the methyl protons on C5, which resonate at δ 2.42 in **5** vs δ 1.65 in **2** in acetone-*d*<sub>6</sub>. The methyl protons on C1 in **5** resonate at δ 2.83, while the metal hydride appears at δ –10.52 and is a doublet of triplets due to strong coupling to the *trans*-phosphine (*J*<sub>HP</sub> = 117.6 Hz) and weaker coupling to the two *cis*-phosphines (*J*<sub>HP</sub> = 19.7 Hz). In the <sup>13</sup>C{<sup>1</sup>H} NMR spectrum, ring carbons C2, C3, and C4 resonate at δ 231.0, 137.3, and 212.7, respectively, and the C2 signal is split into a widely spaced doublet of triplets due to strong coupling to the *trans*-PMe<sub>3</sub> ligand (*J*<sub>CP</sub> = 82.1 Hz) and weaker coupling to the two *cis*-PMe<sub>3</sub> ligands (*J*<sub>CP</sub> = 6.1 Hz). Methyl carbons C1 and C5 resonate at δ 37.0 and 23.9,

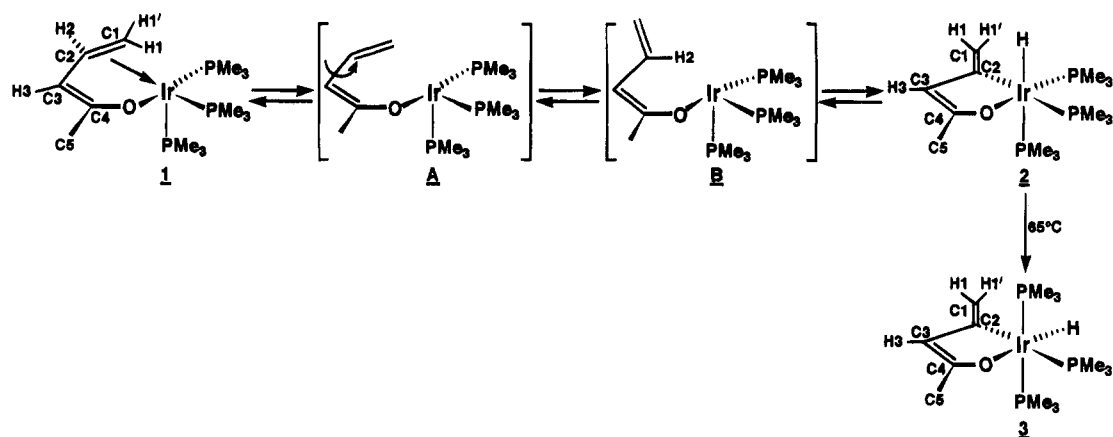
(8) Steric interactions between the phosphines are reduced in the *mer* isomer.

(9) It is possible that the proton transfer step precedes the C–H2 bond activation step. Support for the viability of this alternate sequence comes from the observation that treatment of (C1)Ir(PMe<sub>3</sub>)<sub>3</sub> with AgBF<sub>4</sub> in the presence of excess 3-penten-2-one produces **5** in about 50% yield. We thank one of the reviewers for suggesting this experiment.

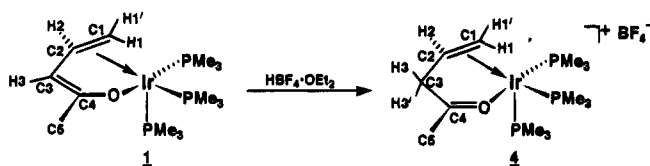
(10) Selective <sup>31</sup>P-decoupling experiments have established that this coupling is due to an equatorial (ring plane) phosphine ligand.

(11) The chemical shifts for the β proton in furan and the β proton in the nonaromatic analogue 4,5-dihydrofuran are δ 6.41 and 4.95, respectively. See Bird, C. W.; Cheeseman, G. W. H. *Comprehensive Heterocyclic Chemistry*; Pergamon Press: Oxford, 1984; Vol. 4.

Scheme 2



Scheme 3



respectively. The  $^{31}\text{P}\{^1\text{H}\}$  NMR spectrum consists of three doublet-of-doublet patterns for the three inequivalent  $\text{PMe}_3$  ligands.

When compound **5** is treated with lithium diisopropylamide (LDA), methyl group C1 is cleanly deprotonated, producing *fac*- $\text{CH}_2=\text{CCH}=\text{C}(\text{CH}_3)\text{OIr}(\text{PMe}_3)_3(\text{H})$  (**2**). Reprotonation of **2** occurs at C1, yielding **5** directly.<sup>12</sup> Compound **5** does not convert to its *mer* isomer, even upon heating in tetrahydrofuran at reflux for 2 weeks. However, this *mer* isomer can be cleanly synthesized by protonating *mer*- $\text{CH}_2=\text{CCH}=\text{C}(\text{CH}_3)\text{OIr}(\text{PMe}_3)_3(\text{H})$  (**3**).

Hence, as shown in Scheme 5, treatment of **3** with  $\text{HBF}_4\cdot\text{OEt}_2$  results in electrophilic attack at C1 and production of  $[\text{mer}-\text{CH}_3\text{C}^+\text{CH}=\text{C}(\text{CH}_3)\text{O}^-\text{Ir}(\text{PMe}_3)_3(\text{H})]^+\text{BF}_4^-$  (**6**).<sup>13</sup>

In the  $^1\text{H}$  NMR spectrum of **6**, ring proton H3 appears as a doublet ( $J_{\text{HP}} = 7.5$  Hz)<sup>10</sup> at  $\delta$  7.12 (as compared to  $\delta$  4.79 in precursor **3**),<sup>14</sup> while methyl groups C1 and C5 resonate at  $\delta$  2.82 and 2.41, respectively. The metal hydride, which resides *cis* to all three phosphine ligands, appears at  $\delta$  -24.54 and is split into a closely spaced triplet of doublets ( $J_{\text{HP}} = 17.5, 12.0$  Hz). The  $^{13}\text{C}\{^1\text{H}\}$  NMR spectrum strongly resembles that of **5**; ring carbons C2, C3, and C4 resonate at  $\delta$  229.4, 137.3, and 214.6, respectively, while methyl carbons C1 and C5 resonate at  $\delta$  36.7 and 25.4, respectively. C2 shows the expected strong coupling to the *trans*- $\text{PMe}_3$  ligand ( $J_{\text{CP}} = 77.6$  Hz) and weaker coupling to the two *cis*- $\text{PMe}_3$  ligands ( $J_{\text{CP}} = 10.2$  Hz). Compound **6** possesses mirror plane symmetry; hence, the *trans*-diaxial phosphines are equivalent and appear as a doublet in the  $^{31}\text{P}\{^1\text{H}\}$  NMR spectrum. The unique equatorial phosphine appears as a triplet.

**C. Reaction of  $(\text{Cl})\text{Ir}(\text{PET}_3)_3$  with Potassium 4-Methyl-5-oxapentadienide.** As we reported earlier,<sup>3b</sup>

(12) Low-temperature NMR monitoring of this reaction shows no evidence for initial protonation at C3.

(13) This reaction can be reversed by the addition of lithium diisopropylamide to the iridafuran.

(14) These chemical shifts are observed in acetone- $d_6$ .

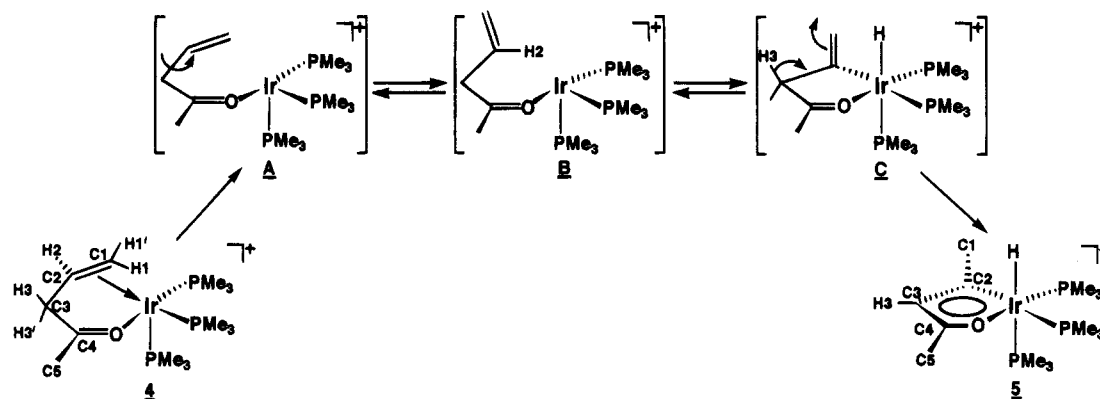
treatment of  $(\text{Cl})\text{Ir}(\text{PET}_3)_3$  with potassium 4-methyl-5-oxapentadienide results in the production of the six-membered-ring compound, *mer*- $\text{CH}=\text{CHCH}=\text{C}(\text{CH}_3)\text{OIr}(\text{PET}_3)_3(\text{H})$  (**7**) (see Scheme 6). This reaction proceeds through 16e compound  $(\eta^1\text{-4-methyl-5-oxapentadienyl})\text{-Ir}(\text{PET}_3)_3$  (**A**) (and perhaps through the related 18e agostic species), which undergoes intramolecular C-H1 bond activation. Unlike the  $\text{tris}(\text{PMe}_3)$  reaction system described earlier,  $((1,2,5\text{-}\eta)\text{-4-methyl-5-oxapentadienyl})\text{-Ir}(\text{PET}_3)_3$  cannot be isolated or even observed *in situ* by NMR monitoring.<sup>15</sup>

Upon heating in refluxing tetrahydrofuran for 2 h, compound **7** isomerizes to the thermodynamically favored five-membered-ring compound, *mer*- $\text{CH}_2=\text{CCH}=\text{C}(\text{CH}_3)\text{OIr}(\text{PET}_3)_3(\text{H})$  (**8**). The *fac* isomer of **8** is not observed. The X-ray crystal structure of **8**, which we reported earlier,<sup>3b</sup> shows the expected localized bonding around the metallacycle. Ring bond distances and angles are summarized in Table 1.

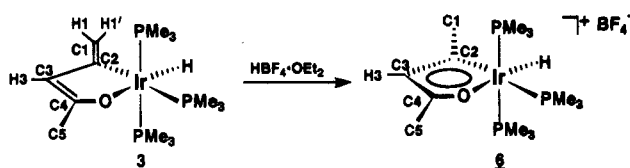
**D. Protonation of Compounds **7** and **8**.** Like compound **1**, *mer*- $\text{CH}=\text{CHCH}=\text{C}(\text{CH}_3)\text{OIr}(\text{PET}_3)_3(\text{H})$  (**7**) undergoes electrophilic addition at C3 when treated with  $\text{HBF}_4\cdot\text{OEt}_2$ , producing  $[\text{mer}-\text{CH}=\text{CHCH}_2\text{C}(\text{CH}_3)=\text{OIr}(\text{PET}_3)_3(\text{H})]^+\text{BF}_4^-$  (**9**) (see Scheme 7). Other acids, including  $\text{HO}_3\text{SCF}_3$ ,  $\text{HO}_2\text{CCF}_3$ , and  $\text{NH}_4^+\text{PF}_6^-$ , yield the identical cationic product. Because **9** possesses mirror plane symmetry, the two protons on C3 are equivalent and appear as a broad singlet at  $\delta$  4.27. The olefinic ring protons H1 and H2 resonate at  $\delta$  7.22 and 5.99, respectively, while the metal hydride signal appears at  $\delta$  -27.60 and is split into a closely spaced triplet of doublets ( $J = 16.5, 11.5$  Hz) as a result of phosphorus coupling. In the  $^{13}\text{C}\{^1\text{H}\}$  NMR spectrum, saturated carbon C3 appears at  $\delta$  47.1, while olefinic carbons C1 and C2 resonate at  $\delta$  134.0 and 117.3, respectively. Carbonyl carbon C4 appears far downfield at  $\delta$  215.7. As expected, the C1 signal is split into a widely spaced doublet of triplets ( $J = 71.8, 14.0$  Hz) due to phosphorus coupling. The  $^{31}\text{P}\{^1\text{H}\}$  NMR spectrum consists of a doublet/triplet pattern, characteristic of planar metallacycles with a *mer* arrangement of phosphine ligands.

(15) The 1,2,5- $\eta$  bonding mode is apparently destabilized by the steric bulk of the  $\text{tris}(\text{PET}_3)$  ligand set.

Scheme 4



Scheme 5



Although stable at room temperature, **9** isomerizes to the iridafuran compound [*mer*-

$\text{CH}_3\text{C}=\text{CH}=\text{C}(\text{CH}_3)\text{O}=\text{Ir}(\text{PEt}_3)_3(\text{H})\text{]}^+\text{BF}_4^-$  (**10**) upon heating in tetrahydrofuran at reflux.<sup>16</sup> The probable mechanism for this rearrangement, outlined in Scheme 8, involves migration of the hydride ligand back to C1, rotation about C2–C3, activation of C–H2, and proton transfer from C3 to C1. Iridafuran **10** is also produced

upon protonation of *mer*- $\text{CH}_2=\text{CCH}=\text{C}(\text{CH}_3)\text{OIr}(\text{PEt}_3)_3(\text{H})$  (**8**) (Scheme 9). In this case, electrophilic attack occurs directly on exocyclic carbon C1.<sup>13</sup>

The NMR spectra for **10** closely resemble those described earlier for the tris(PMe<sub>3</sub>) analogue **6**. In particular, ring proton H3 is shifted downfield to  $\delta$  7.15 (from  $\delta$  4.80 in precursor **8**),<sup>14</sup> which is consistent with the presence of an aromatic ring current. Ring methyl groups C1 and C5 resonate at  $\delta$  2.91 and 2.42, respectively. The metal hydride signal appears at  $\delta$  –24.68 and is split into a closely spaced triplet of doublets ( $J_{\text{HP}} = 15.5, 12.0$  Hz). In the  $^{13}\text{C}\{^1\text{H}\}$  NMR spectrum, ring carbons C2, C3, and C4 resonate at  $\delta$  228.3, 138.5, and 214.2, respectively, while methyl carbons C1 and C5 appear at  $\delta$  37.2 and 25.2, respectively. C2 strongly couples to the *trans*-PEt<sub>3</sub> ligand ( $J_{\text{CP}} = 75.1$  Hz) and weakly couples to the two *cis*-PEt<sub>3</sub> ligands ( $J_{\text{CP}} = 9.7$  Hz). The  $^{31}\text{P}\{^1\text{H}\}$  NMR spectrum consists of the expected doublet/triplet pattern.

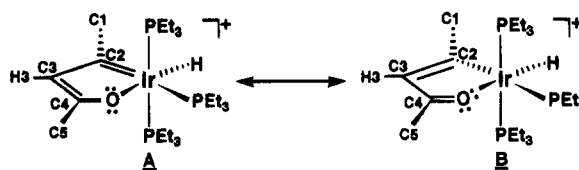
The X-ray crystal structure of the PF<sub>6</sub><sup>–</sup> salt of **10** (see Figure 1, Tables 2 and 3) provides additional evidence for the presence of an aromatic ring. Unlike precursor **8**, in which the bonding around the ring is localized,

(16) NMR monitoring of the reaction solution also shows the presence of a small quantity of the *fac* isomer of **10**, [*fac*-

$\text{CH}_3\text{C}=\text{CH}=\text{C}(\text{CH}_3)\text{O}=\text{Ir}(\text{PEt}_3)_3(\text{H})\text{]}^+\text{BF}_4^-$ , but this ultimately converts to the thermodynamically preferred *mer* geometry. Selected NMR data for the *facial* isomer of **10** are summarized here.  $^1\text{H}$  NMR (acetone-*d*<sub>6</sub>, 22 °C):  $\delta$  6.97 (d,  $J_{\text{HP}} = 6.9$  Hz, 1, H3), 2.84 (d,  $J_{\text{HP}} = 4.2$  Hz, 3, H1's), 2.35 (s, 3, H5's), –12.26 (d of t,  $J_{\text{HP}} = 114.6, 20.4$  Hz, 1, IrH).  $^{31}\text{P}\{^1\text{H}\}$  NMR (acetone-*d*<sub>6</sub>, 22 °C):  $\delta$  –20.2 (dd,  $J_{\text{PP}} = 11.0, 10.0$  Hz, 1, PEt<sub>3</sub>), –22.0 (dd,  $J_{\text{PP}} = 21.0, 11.0$  Hz, 1, PEt<sub>3</sub>), –22.7 (dd,  $J_{\text{PP}} = 21.0, 10.0$  Hz, 1, PEt<sub>3</sub>).

compound **10** exhibits delocalized  $\pi$  bonding. Ring bonds Ir–C2 [2.029(6) Å] and C4–O [1.258(8) Å] have shortened significantly with respect to their distances in **8** (see Table 1) to values intermediate between those of normal single and double bonds.<sup>17</sup> Similarly, the C–C distances within the ring have moved toward equalization, with C2–C3 shortening to 1.348(9) Å and C3–C4 lengthening to 1.408(10) Å. Overall, the circumference of the five-membered ring in **10** has shrunk by 0.169 Å from its value in **8** (8.249 Å in **10** vs 8.418 Å in **8**). The five internal angles within the ring range from 77.0(2)° (for C2–Ir–O) to 119.7(6)° (for C3–C4–O), but their sum of 539.7° falls very close to the theoretical value of 540° for planar five-membered rings.<sup>18</sup>

The spectroscopic and structural data described earlier suggest that several resonance structures contribute to the overall bonding picture in **10**. Structure A is supported by the short Ir–C2 distance and the downfield “carbene-like” chemical shift position of C2. Resonance form B, on the other hand, accounts for the short C4–O bond distance. The aromatic character of **10** can be explained qualitatively by noting that both resonance structures A and B possess a closed loop of six  $\pi$  electrons. In A, a lone pair on oxygen contributes two  $\pi$  electrons, while in B, a pair of metal-based d electrons completes the Hückel sextet.



### E. Reactions of Compound 10 with Halogens.

Ring halogenation is one of the characteristic reactions of aromatic compounds. Therefore, we have explored the reactivity of iridafuran **10** toward I<sub>2</sub> and Br<sub>2</sub>. As shown in Scheme 10, excess I<sub>2</sub> reacts exclusively at the metal center to produce the neutral dihalide compound,

(17) (a) Orpen, A. G.; Brammer, L.; Allen, F. H.; Kennard, O.; Watson, D. G.; Taylor, R. *J. Chem. Soc., Dalton Trans.* **1989**, S1. (b) Huheey, J. E. *Inorganic Chemistry*, 3rd ed.; Harper and Row: New York, 1983; Appendix E and references cited therein.

(18) In furan, the bond distances (Å) and angles (deg) are as follows: O–C $\alpha$  = 1.362, C $\alpha$ –C $\beta$  = 1.361, C $\beta$ –C $\beta$  = 1.430, C $\alpha$ –O–C $\alpha$  = 106.5, O–C $\alpha$ –C $\beta$  = 110.65, C $\alpha$ –C $\beta$ –C $\beta$  = 106.07. See Bird, C. W.; Cheeseman, G. W. H. *Comprehensive Heterocyclic Chemistry*; Pergamon Press: Oxford, 1984; Vol. 4.

(19) The structural parameters reported for compound **11** in Table 1 and in the text are averages of the bond distances and angles observed in the two independent molecules in the unit cell.

Scheme 6

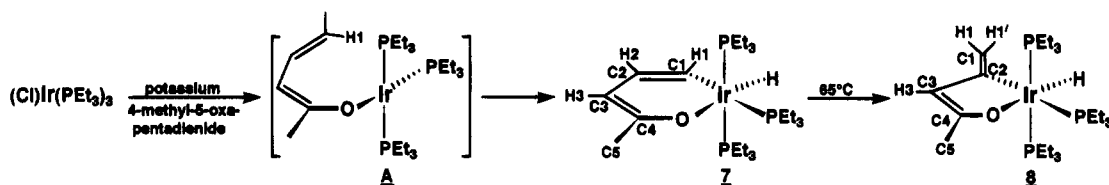


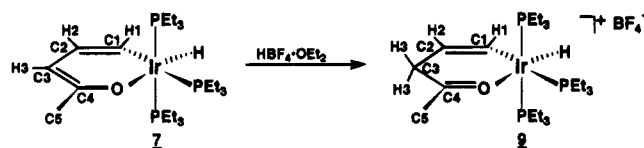
**Table 1. Comparison of Key Bond Distances (Å) and Bond Angles (deg) with Estimated Standard Deviations for *mer*-CH<sub>2</sub>=CCH=C(CH<sub>3</sub>)OIr(PEt<sub>3</sub>)<sub>3</sub>H**

(8), [*mer*-CH<sub>3</sub>C<sup>+</sup>CH=C(CH<sub>3</sub>)=O<sup>-</sup>Ir(PEt<sub>3</sub>)<sub>3</sub>(H)]<sup>+</sup>PF<sub>6</sub><sup>-</sup> (PF<sub>6</sub><sup>-</sup> Salt of 10), [*trans*-CH<sub>3</sub>C<sup>+</sup>CH=C(CH<sub>3</sub>)=O<sup>-</sup>Ir(PEt<sub>3</sub>)<sub>2</sub>(I)<sub>2</sub> (11), and *trans*-CH<sub>3</sub>C<sup>+</sup>CH=C(Br)<sup>-</sup>C(CH<sub>3</sub>)=O<sup>-</sup>Ir(PEt<sub>3</sub>)<sub>2</sub>(Br)<sub>2</sub> (12)

	compound			
	8 <sup>a</sup>	10 <sup>b</sup>	11 <sup>b,c</sup>	12 <sup>b</sup>
Bond Distances				
Ir-C2	2.107(5)	2.029(6)	1.996(12)	1.971(13)
C2-C3	1.484(6)	1.348(9)	1.349(18)	1.371(16)
C3-C4	1.338(6)	1.408(10)	1.406(21)	1.415(18)
C4-O	1.322(6)	1.258(8)	1.265(17)	1.283(17)
O-Ir	2.167(2)	2.206(4)	2.078(8)	2.054(7)
C1-C2	1.326(7)	1.516(9)	1.518(22)	1.498(17)
C4-C5	1.503(6)	1.505(12)	1.484(19)	1.481(15)
Bond Angles				
O-Ir-C2	80.1(1)	77.0(2)	79.3(5)	80.8(4)
Ir-C2-C3	108.0(3)	115.3(4)	113.0(10)	111.4(9)
C2-C3-C4	119.7(5)	116.6(6)	117.1(12)	118.8(13)
C3-C4-O	120.6(4)	119.7(6)	117.3(11)	114.7(10)
C4-O-Ir	111.5(2)	111.1(4)	113.4(9)	114.3(7)
Ir-C2-C1	132.6(4)	126.4(5)	128.3(9)	128.1(9)
C1-C2-C3	119.4(5)	118.3(6)	118.8(12)	120.5(12)
O-C4-C5	114.4(4)	118.6(6)	116.9(14)	117.9(12)
C3-C4-C5	124.9(5)	121.7(6)	125.9(13)	127.5(13)

<sup>a</sup> Reference 3b. <sup>b</sup> This work. <sup>c</sup> Average of two independent molecules.

Scheme 7



*trans*-CH<sub>3</sub>C<sup>+</sup>CH=C(CH<sub>3</sub>)=O<sup>-</sup>Ir(PEt<sub>3</sub>)<sub>2</sub>(I)<sub>2</sub> (11). This reaction involves formal loss of PEt<sub>3</sub> and H<sup>+</sup> from the Ir center, but its detailed mechanism has not been explored.

The <sup>1</sup>H NMR spectrum of 11 shows the presence of a downfield signal at δ 6.82,<sup>14</sup> indicating that ring proton H3 has not been replaced by halogen and that the aromatic ring remains intact. Unlike the H3 signal for 10, which is a doublet due to equatorial phosphine coupling, the H3 signal for 11 is a sharp singlet, because iodide ligands now occupy the equatorial positions. Ring methyl groups C1 and C5 in 11 resonate at δ 2.99 and 2.48, respectively.<sup>14</sup> No signals are observed in the upfield "hydride" region of the <sup>1</sup>H NMR spectrum. In the <sup>13</sup>C{<sup>1</sup>H} NMR spectrum, ring carbons C2, C3, and C4 resonate at δ 223.5, 134.1, and 212.4, respectively, while methyl carbons C1 and C5 resonate at δ 35.4 and 21.6, respectively. C2 resides *cis* to the two PEt<sub>3</sub> ligands and, hence, couples to them weakly (*J*<sub>CP</sub> = 5.4 Hz). The

<sup>31</sup>P{<sup>1</sup>H} NMR spectrum of 11 consists of a singlet, consistent with the presence of equivalent *trans*-diaxial phosphines.

The structure of 11 has been confirmed by single-crystal X-ray diffraction (see Figure 2, Tables 4 and 5). A comparison of structural parameters in 11 with those in 8 and 10 is provided in Table 1.<sup>19</sup> As in 10, the ring bond distances in 11 exhibit the delocalization that is characteristic of aromatic systems. The two ring carbon-carbon bond distances [1.349(18) and 1.406(21) Å] and the carbon-oxygen bond distance [1.265(17) Å] are intermediate in length between those of normal single and double bonds.<sup>17</sup> The iridium-ring bond distances of 1.996(12) Å for Ir-C2 and 2.078(8) Å for Ir-O are quite short, indicating substantial participation by the metal-ligand moiety in ring π bonding. As a result of these strong π interactions, the circumference of the metallacycle in 11 is reduced to 8.094 Å (vs 8.249 Å in 10). The sum of the five internal angles in 11 is 539.9°, which is very close to the theoretical value of 540° for planar five-membered rings.

As shown in Scheme 10, excess Br<sub>2</sub> adds to compound 10 at the metal center and at C3 of the ring to form the electrophilic aromatic substitution product, *trans*-

CH<sub>3</sub>C<sup>+</sup>CH=C(Br)<sup>-</sup>C(CH<sub>3</sub>)=O<sup>-</sup>Ir(PEt<sub>3</sub>)<sub>2</sub>(Br)<sub>2</sub> (12).<sup>20</sup> The substitution at C3 is apparent from the <sup>1</sup>H NMR spectrum of 12, because the downfield H3 signal is absent. All other features of the <sup>1</sup>H, <sup>13</sup>C, and <sup>31</sup>P spectra of 12 closely resemble those of 11.

The structure of 12 has also been confirmed by single-crystal X-ray diffraction (see Figure 3, Tables 6 and 7). As can be seen from the comparison of structural parameters in Table 1, the bond distances in the ring of 12 closely parallel those in 11. The circumference of the metallacycle in 12 is 8.094 Å, identical to that in 11, while the sum of the five internal angles is exactly 540°, as required for a planar five-membered ring.

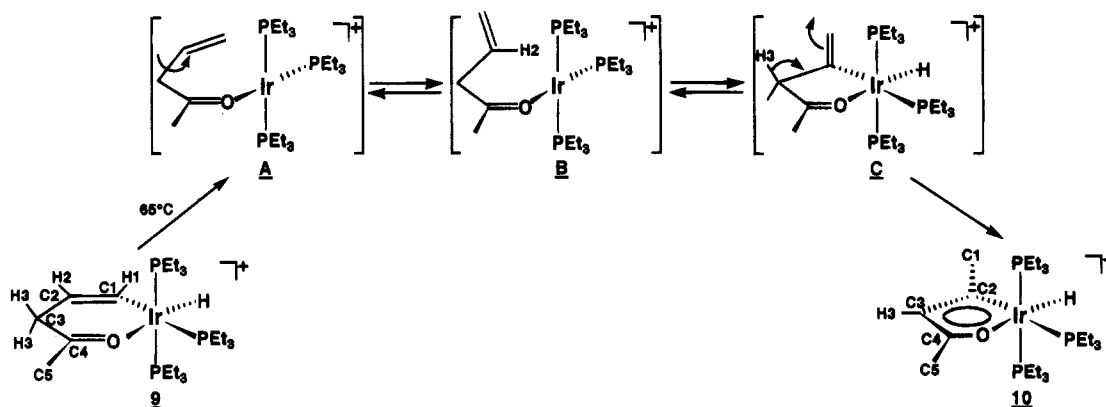
## Summary

A new family of metallafurans has been synthesized. These species are obtained either by direct protonation of (oxapentadienyl)metal complexes or by protonation of the oxametallacycles produced from these complexes via C-H bond activation. For example, treatment of ((1,2,5-η)-4-methyl-5-oxapentadienyl)Ir(PMe<sub>3</sub>)<sub>3</sub> (1) with HBF<sub>4</sub>·OEt<sub>2</sub> leads to initial protonation at C3 and formation of [(1,2,5-η)-4-methyl-5-oxapenta-1,4-diene]-Ir(PMe<sub>3</sub>)<sub>3</sub><sup>+</sup>BF<sub>4</sub><sup>-</sup> (4), but this species rearranges to the

iridafuran complex, [*fac*-CH<sub>3</sub>C<sup>+</sup>CH=C(CH<sub>3</sub>)=O<sup>-</sup>Ir(PMe<sub>3</sub>)<sub>3</sub>(H)]<sup>+</sup>BF<sub>4</sub><sup>-</sup> (5). Similarly, protonation of *mer*-CH<sub>2</sub>=CCH=C(CH<sub>3</sub>)OIr(PMe<sub>3</sub>)<sub>3</sub>(H) (3) (which is derived

(20) Analogous bromination of a related manganafuran system has been reported. See ref 6c.

Scheme 8



Scheme 9

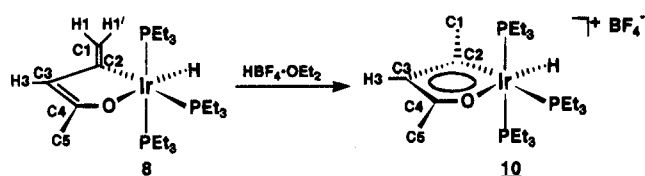


Table 2. Atomic Coordinates ( $\times 10^4$ ) and Equivalent Isotropic Displacement Coefficients ( $\text{\AA}^2 \times 10^3$ ) with Estimated Standard Deviations for Non-Hydrogen Atoms in  $\text{mer-CH}_3\text{C}\equiv\text{CH}\equiv\text{C}(\text{CH}_3)\equiv\text{O}\equiv\text{Ir}(\text{PEt}_3)_3(\text{H})^+\text{PF}_6^-$  ( $\text{PF}_6^-$  Salt of 10)

atom	x	y	z	U(eq)
Ir	2811(1)	5792(1)	7041(1)	26(1)
P1	2023(2)	4768(1)	7438(1)	37(1)
P2	5001(2)	5648(1)	7743(1)	36(1)
P3	3395(2)	6788(1)	6417(1)	36(1)
P4	7842(2)	7703(1)	5431(1)	45(1)
O	1927(4)	6345(2)	8037(2)	41(1)
C1	361(7)	5789(4)	5612(4)	53(2)
C2	935(6)	5974(3)	6503(4)	36(2)
C3	148(6)	6297(3)	6998(5)	41(2)
C4	749(7)	6511(3)	7792(4)	46(2)
C5	-3(9)	6909(5)	8382(6)	79(4)
C11	2022(8)	4616(4)	8574(5)	57(3)
C12	1055(9)	4993(5)	9030(5)	82(4)
C13	2872(8)	4041(4)	7069(5)	61(3)
C14	2900(11)	4006(5)	6120(6)	90(4)
C15	278(7)	4601(3)	7040(5)	55(3)
C16	-285(9)	3930(5)	7277(7)	92(4)
C21	5568(7)	4848(3)	8171(5)	52(2)
C22	6952(8)	4823(5)	8652(6)	80(4)
C23	6369(6)	5824(4)	7107(5)	49(2)
C24	6497(8)	5343(5)	6378(5)	72(3)
C25	5392(7)	6173(4)	8670(4)	50(2)
C26	4632(9)	5977(4)	9422(5)	69(3)
C31	1985(7)	7327(3)	6085(5)	53(3)
C32	2286(9)	7958(4)	5629(6)	83(4)
C33	4229(7)	6683(4)	5460(4)	54(3)
C34	3438(10)	6316(5)	4743(5)	80(4)
C35	4511(7)	7355(3)	7041(5)	52(2)
C36	3876(9)	7695(4)	7765(6)	80(4)
F1	8855(5)	7844(3)	6246(3)	81(2)
F2	8252(5)	8377(2)	5036(3)	75(2)
F3	8980(5)	7331(2)	5011(3)	78(2)
F4	7426(5)	7029(2)	5827(3)	84(2)
F5	6812(5)	7572(2)	4628(3)	87(2)
F6	6720(5)	8075(3)	5870(3)	81(2)
H	3344(66)	5504(33)	6326(40)	52(20)

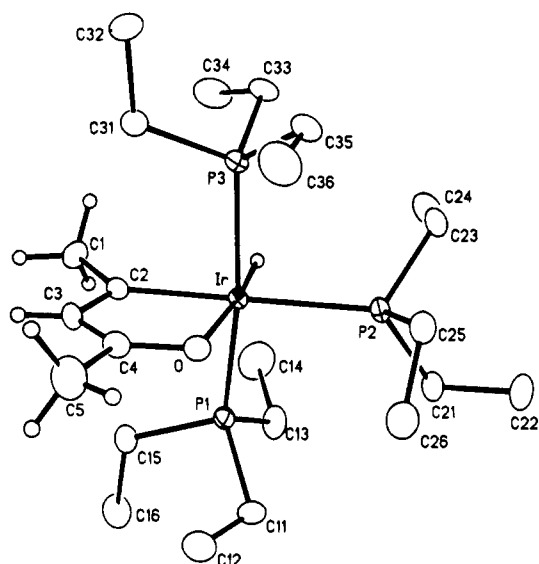


Figure 1. ORTEP drawing of  $[\text{mer-CH}_3\text{C}\equiv\text{CH}\equiv\text{C}(\text{CH}_3)\equiv\text{O}\equiv\text{Ir}(\text{PEt}_3)_3(\text{H})]^+\text{PF}_6^-$  ( $\text{PF}_6^-$  salt of 10).

from 1 via C–H2 bond activation) yields the *mer* isomer

of iridafuran 5,  $[\text{mer-CH}_3\text{C}\equiv\text{CH}\equiv\text{C}(\text{CH}_3)\equiv\text{O}\equiv\text{Ir}(\text{PMe}_3)_3(\text{H})]^+\text{BF}_4^-$  (6). In the tris( $\text{PEt}_3$ ) system, treatment of the six-membered-ring compound *mer*-

$\text{CH}=\text{CHCH}=\text{C}(\text{CH}_3)\text{OIr}(\text{PEt}_3)_3(\text{H})$  (7) with  $\text{HBF}_4\cdot\text{OEt}_2$  leads to initial protonation at C3 and formation of  $[\text{mer}$ -

$\text{CH}=\text{CHCH}_2\text{C}(\text{CH}_3)=\text{OIr}(\text{PEt}_3)_3(\text{H})]^+\text{BF}_4^-$  (9), but upon heating, this compound rearranges to the iridafuran

complex,  $[\text{mer-CH}_3\text{C}\equiv\text{CH}\equiv\text{C}(\text{CH}_3)\equiv\text{O}\equiv\text{Ir}(\text{PEt}_3)_3(\text{H})]^+\text{BF}_4^-$  (10). The identical iridafuran is obtained upon protonation of the five-membered-ring isomer of 7, *mer*-

$\text{CH}_2=\text{CCH}=\text{C}(\text{CH}_3)\text{OIr}(\text{PEt}_3)_3(\text{H})$  (8).

The aromatic character of iridafurans 5, 6, and 10 is supported by downfield  $^1\text{H}$  NMR chemical shifts for ring

proton H3. Furthermore, the X-ray crystal structure of 10 shows a planar metallacycle and delocalized  $\pi$  bonding around the ring. Treatment of compound 10 with excess  $\text{Br}_2$  leads to electrophilic substitution at C3

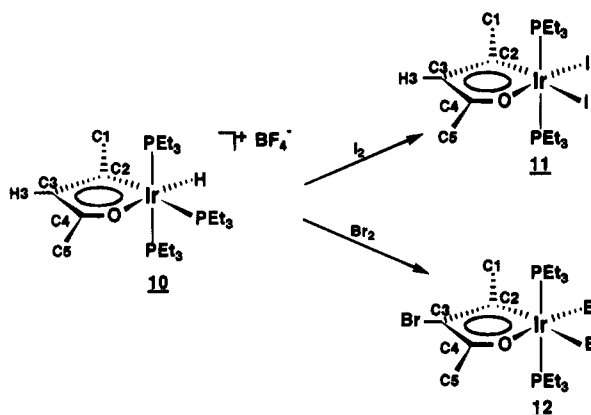
and production of *trans*- $\text{CH}_3\text{C}(\text{Br})\equiv\text{C}(\text{CH}_3)\equiv\text{O}\equiv\text{Ir}(\text{PEt}_3)_2(\text{Br})_2$  (12). The X-ray crystal structure of 12 shows a planar metallacycle whose circumference is smaller than that of 10 as a result of very strong  $\pi$  interactions within the ring.



**Table 3. Selected Bond Distances (Å) and Bond Angles (deg) with Estimated Standard Deviations**

for  $[\text{mer-CH}_3\text{C}\equiv\text{CH}\equiv\text{C}(\text{CH}_3)\equiv\text{O}\equiv\text{Ir}(\text{PEt}_3)_3(\text{H})]^+\text{PF}_6^-$   
( $\text{PF}_6^-$  Salt of 10)

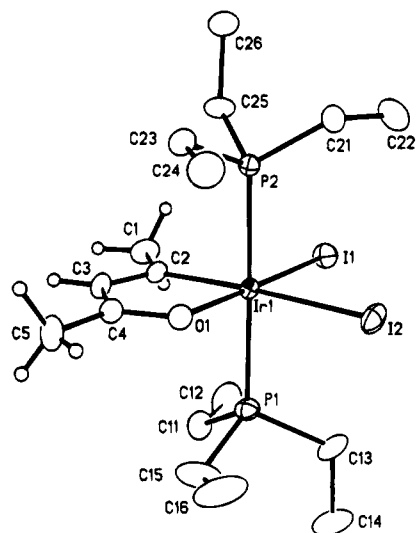
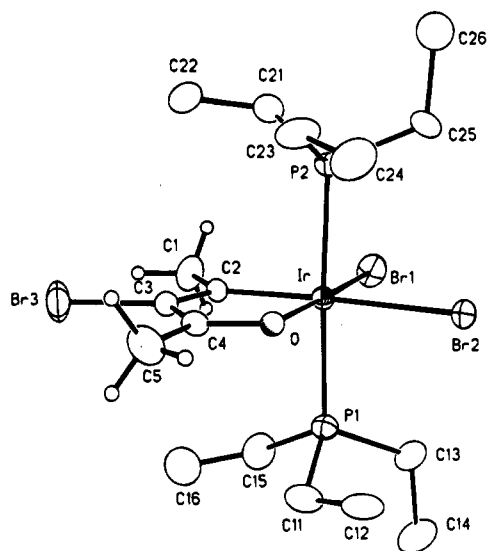
Bond Distances			
Ir-P1	2.347(2)	O-C4	1.258(8)
Ir-P2	2.387(2)	C1-C2	1.516(9)
Ir-P3	2.366(2)	C2-C3	1.348(9)
Ir-O	2.206(4)	C3-C4	1.408(10)
Ir-C2	2.029(6)	C4-C5	1.505(12)
Ir-H	1.431(67)		
Bond Angles			
P1-Ir-P2	95.1(1)	O-Ir-H	172.6(26)
P1-Ir-P3	170.3(1)	C2-Ir-H	99.0(26)
P2-Ir-P3	92.3(1)	O-Ir-C2	77.0(2)
P1-Ir-O	95.2(1)	Ir-O-C4	111.1(4)
P2-Ir-O	98.9(1)	Ir-C2-C1	126.4(5)
P3-Ir-O	89.8(1)	Ir-C2-C3	115.3(4)
P1-Ir-C2	87.0(2)	C1-C2-C3	118.3(6)
P2-Ir-C2	175.6(2)	C2-C3-C4	116.6(6)
P3-Ir-C2	86.0(2)	O-C4-C3	119.7(6)
P1-Ir-H	90.8(27)	O-C4-C5	118.6(6)
P2-Ir-H	84.8(26)	C3-C4-C5	121.7(6)
P3-Ir-H	83.7(26)		

**Scheme 10****Experimental Section**

**General Comments.** All manipulations were carried out under a nitrogen atmosphere, using either glovebox or double-manifold Schlenk techniques. Solvents were stored under nitrogen after being distilled from the appropriate drying agents. Deuterated NMR solvents were obtained from Cambridge Isotope Laboratories in 1 g sealed vials and used as received.

The following reagents were used as obtained from the supplier indicated: tetrafluoroboric acid (Aldrich), trifluoromethanesulfonic acid (Aldrich), trifluoroacetic acid (Aldrich), ammonium hexafluorophosphate (Aldrich), lithium diisopropylamide (Aldrich), iodine (Aldrich), bromine (Fisher), flash silica gel (Aldrich). ((1,2,5- $\eta$ )-4-Methyl-5-oxapentadienyl)Ir( $\text{PMe}_3$ )<sub>3</sub> (**1**), *mer*-CH<sub>2</sub>=CCH=C(CH<sub>3</sub>)OIr( $\text{PMe}_3$ )<sub>3</sub>(H) (**3**), *mer*-CH=CHCH=C(CH<sub>3</sub>)OIr( $\text{PEt}_3$ )<sub>3</sub>(H) (**7**), and *mer*-CH<sub>2</sub>=CCH=C(CH<sub>3</sub>)OIr( $\text{PEt}_3$ )<sub>3</sub>(H) (**8**) were prepared as previously described.<sup>3b</sup>

NMR experiments were performed on a Varian Unity-300 spectrometer (<sup>1</sup>H, 300 MHz; <sup>13</sup>C, 75 MHz; <sup>31</sup>P, 121 MHz), a Varian Unity-500 spectrometer (<sup>1</sup>H, 500 MHz; <sup>13</sup>C, 125 MHz; <sup>31</sup>P, 202 MHz), or a Varian VXR-600 spectrometer (<sup>1</sup>H, 600 MHz; <sup>13</sup>C, 150 MHz; <sup>31</sup>P, 242 MHz). <sup>1</sup>H and <sup>13</sup>C spectra were referenced to tetramethylsilane, while <sup>31</sup>P spectra were referenced to external H<sub>3</sub>PO<sub>4</sub>. In general, <sup>1</sup>H connectivities were determined from COSY (<sup>1</sup>H-<sup>1</sup>H correlation spectroscopy) data. APT (attached proton test), HETCOR (<sup>13</sup>C-<sup>1</sup>H heteronuclear

**Figure 2.** ORTEP drawing of *trans*-CH<sub>3</sub>-C≡CH≡C(CH<sub>3</sub>)≡O≡Ir(PEt<sub>3</sub>)<sub>2</sub>(I)<sub>2</sub> (**11**).**Figure 3.** ORTEP drawing of *trans*-CH<sub>3</sub>-C≡C(Br)≡C(CH<sub>3</sub>)≡O≡Ir(PEt<sub>3</sub>)<sub>2</sub>(Br)<sub>2</sub> (**12**).

correlation spectroscopy), and HMQC (<sup>1</sup>H-detected multiple quantum coherence) experiments aided in assigning some of the <sup>1</sup>H and <sup>13</sup>C peaks. The spectra of cationic compounds were recorded in acetone-*d*<sub>6</sub>, while those of neutral compounds were recorded in benzene-*d*<sub>6</sub>. In addition, <sup>1</sup>H NMR spectra of neutral compounds were obtained in acetone-*d*<sub>6</sub> to allow direct comparisons of <sup>1</sup>H NMR chemical shifts in related neutral and cationic compounds. Note: In all of the NMR spectra, carbon atoms and associated hydrogens in the oxapentadienyl group are numbered by starting at the end of the chain opposite oxygen.

Microanalyses were performed by Galbraith Laboratories, Inc. (Knoxville, TN).

**Synthesis of *fac*-CH<sub>2</sub>=CCH=C(CH<sub>3</sub>)OIr( $\text{PMe}_3$ )<sub>3</sub>(H) (**2**).** Note: Previously, we observed compound **2** in a complex mixture of isomers, including compounds **1** and **3**.<sup>3b</sup> The procedure described here produced **2** as a pure species, allowing full spectral characterization.

[*fac*-CH<sub>3</sub>C≡CH≡C(CH<sub>3</sub>)≡O≡Ir( $\text{PMe}_3$ )<sub>3</sub>(H)]<sup>+</sup>BF<sub>4</sub><sup>-</sup> (**5**) (0.38 g, 6.4 × 10<sup>-4</sup> mol) was dissolved in 100 mL of tetrahydrofuran (THF) and cooled to -30 °C. A cold (-30 °C) solution of

**Table 4. Atomic Coordinates ( $\times 10^4$ ) and Equivalent Isotropic Displacement Coefficients ( $\text{\AA}^2 \times 10^3$ ) with Estimated Standard Deviations for Non-Hydrogen Atoms in *trans*- $\text{CH}_3\text{C}\equiv\text{CH}\equiv\text{C}(\text{CH}_3)\equiv\text{O}\equiv\text{Ir}(\text{PEt}_3)_2(\text{I})_2$  (11)**

molecule 1					molecule 2				
atom	x	y	z	U(eq)	atom	x	y	z	U(eq)
Ir1	3971(1)	4054(1)	2376(1)	33(1)	Ir2	2444(1)	7335(1)	-1012(1)	33(1)
I1	5168(1)	4288(1)	2878(1)	55(1)	I3	2972(1)	7589(1)	164(1)	54(1)
I2	4004(1)	1198(1)	2835(1)	59(1)	I4	2920(1)	4482(1)	-978(1)	55(1)
P1	3993(2)	3011(4)	1509(2)	49(1)	P3	1582(2)	6261(5)	-964(2)	52(2)
P2	3927(2)	5125(4)	3223(1)	41(1)	P4	3294(2)	8410(4)	-1082(1)	42(1)
O1	3036(4)	3943(10)	1969(3)	48(4)	O2	1999(4)	7204(10)	-1929(3)	42(4)
C1	4211(8)	7259(16)	1988(7)	66(8)	C6	2059(7)	10583(15)	-786(6)	58(7)
C2	3791(6)	6083(14)	1990(5)	41(5)	C7	2036(5)	9297(12)	-1220(5)	37(5)
C3	3189(6)	6283(14)	1691(5)	45(6)	C8	1715(6)	9549(15)	-1802(6)	48(6)
C4	2795(7)	5139(17)	1674(6)	54(6)	C9	1715(6)	8345(17)	-2170(5)	46(5)
C5	2125(7)	5132(22)	1362(7)	79(8)	C10	1367(8)	8339(21)	-2820(6)	77(8)
C11	4202(8)	4244(19)	1034(7)	70(8)	C31	982(10)	5795(24)	-1692(10)	62(6)
C12	4822(10)	4702(21)	1234(9)	99(12)	C32	1171(13)	4509(32)	-1988(13)	87(8)
C13	4504(8)	1409(17)	1645(7)	68(8)	C33	1103(8)	7494(21)	-769(8)	86(9)
C14	4508(11)	658(22)	1094(9)	108(13)	C34	1307(10)	7970(24)	-157(9)	106(13)
C15	3250(9)	2465(28)	943(8)	109(12)	C35	1726(8)	4726(17)	-451(7)	73(9)
C16	2911(10)	1400(25)	1067(11)	128(16)	C36	1184(10)	3947(21)	-433(9)	105(13)
C21	4202(8)	4094(18)	3916(6)	74(8)	C41	3490(6)	10211(15)	-717(7)	57(6)
C22	4875(8)	3749(24)	4214(7)	98(10)	C42	4085(7)	10937(18)	-662(7)	70(7)
C23	3147(6)	5566(17)	3109(6)	57(6)	C43	3148(7)	8874(15)	-1857(6)	59(7)
C24	2770(7)	4211(19)	3093(7)	71(8)	C44	3139(9)	7486(17)	-2239(7)	74(9)
C25	4311(8)	6927(17)	3421(6)	62(7)	C45	4004(6)	7376(15)	-830(6)	51(6)
C26	4363(8)	7653(19)	3999(6)	75(8)	C46	4333(8)	7032(22)	-180(7)	84(9)

**Table 5. Selected Bond Distances ( $\text{\AA}$ ) and Angles (deg) with Estimated Standard Deviations for**

molecule 1		molecule 2	
Bond Distances			
Ir1-I1	2.665(1)	Ir2-I3	2.666(1)
Ir1-I2	2.787(1)	Ir2-I4	2.792(1)
Ir1-P1	2.375(4)	Ir2-P3	2.371(5)
Ir1-P2	2.364(4)	Ir2-P4	2.368(4)
Ir1-O1	2.079(8)	Ir2-O2	2.077(7)
Ir1-C2	2.013(12)	Ir2-C7	1.978(11)
O1-C4	1.291(17)	O2-C9	1.238(16)
C1-C2	1.473(23)	C6-C7	1.563(20)
C2-C3	1.353(18)	C7-C8	1.345(17)
C3-C4	1.396(22)	C8-C9	1.415(21)
C4-C5	1.491(20)	C9-C10	1.477(17)
Bond Angles			
I1-Ir1-I2	92.6(1)	I3-Ir2-I4	92.4(1)
I1-Ir1-P1	90.7(1)	I3-Ir2-P3	90.3(1)
I2-Ir1-P1	90.3(1)	I4-Ir2-P3	89.9(1)
I1-Ir1-P2	90.5(1)	I3-Ir2-P4	90.8(1)
I2-Ir1-P2	90.5(1)	I4-Ir2-P4	90.2(1)
P1-Ir1-P2	178.6(1)	P3-Ir2-P4	178.8(1)
I1-Ir1-O1	178.0(3)	I3-Ir2-O2	177.2(3)
I2-Ir1-O1	89.4(3)	I4-Ir2-O2	90.0(2)
P1-Ir1-O1	89.1(3)	P3-Ir2-O2	88.3(3)
P2-Ir1-O1	89.7(3)	P4-Ir2-O2	90.6(3)
I1-Ir1-C2	97.4(4)	I3-Ir2-C7	99.7(4)
I2-Ir1-C2	170.0(4)	I4-Ir2-C7	167.9(4)
P1-Ir1-C2	90.3(4)	P3-Ir2-C7	90.5(4)
P2-Ir1-C2	88.7(4)	P4-Ir2-C7	89.1(4)
O1-Ir1-C2	80.6(5)	O2-Ir2-C7	77.9(4)
Ir1-O1-C4	112.4(9)	Ir2-O2-C9	114.3(8)
Ir1-C2-C1	129.3(10)	Ir2-C7-C6	127.3(8)
Ir1-C2-C3	110.4(10)	Ir2-C7-C8	115.5(10)
C1-C2-C3	120.3(12)	C6-C7-C8	117.2(11)
C2-C3-C4	119.9(12)	C7-C8-C9	114.3(12)
O1-C4-C3	116.6(12)	O2-C9-C8	117.9(10)
O1-C4-C5	115.5(14)	O2-C9-C10	118.2(14)
C3-C4-C5	127.9(13)	C8-C9-C10	123.8(13)

lithium diisopropylamide (0.069 g,  $6.4 \times 10^{-4}$  mol) in 20 mL of THF was then added dropwise with vigorous stirring. Removal of the THF solvent *in vacuo* revealed an orange oil, which was extracted with benzene and filtered. The benzene was removed under vacuum, and the resulting residue was

**Table 6. Atomic Coordinates ( $\times 10^4$ ) and Equivalent Isotropic Displacement Coefficients ( $\text{\AA}^2 \times 10^3$ ) with Standard Deviations for Non-Hydrogen Atoms in**

<i>trans</i> - $\text{CH}_3\text{C}\equiv\text{C}(\text{Br})\equiv\text{C}(\text{CH}_3)\equiv\text{O}\equiv\text{Ir}(\text{PEt}_3)_2(\text{Br})_2$ (12)				
atom	x	y	z	U(eq)
Ir	7460(1)	541(1)	8437(1)	39(1)
Br1	8411(1)	173(2)	10143(1)	74(1)
Br2	6416(1)	1930(1)	8970(1)	61(1)
Br3	8232(1)	-1345(2)	6010(1)	102(1)
P1	6487(2)	-958(3)	8554(2)	50(1)
P2	8419(2)	2081(3)	8389(3)	58(2)
O	6710(5)	782(7)	7005(6)	48(3)
C1	8948(9)	-1185(13)	8327(10)	77(7)
C2	8133(7)	-470(11)	7834(8)	43(5)
C3	7765(8)	-464(12)	6843(9)	52(5)
C4	6987(10)	208(11)	6407(9)	52(6)
C5	6472(10)	312(12)	5360(8)	84(7)
C11	5464(9)	-1080(13)	7533(10)	83(7)
C12	4818(9)	-120(13)	7375(13)	94(8)
C13	6155(10)	-913(13)	9636(10)	76(7)
C14	5488(11)	-1799(15)	9734(11)	112(10)
C15	6979(12)	-2404(13)	8636(12)	92(9)
C16	6986(12)	-2957(13)	7732(14)	117(11)
C21	9596(9)	1706(14)	8547(11)	84(7)
C22	9804(9)	1346(13)	7632(11)	87(8)
C23	8058(10)	2865(13)	7251(12)	90(8)
C24	7183(11)	3500(14)	7026(14)	122(12)
C25	8546(11)	3084(15)	9420(15)	120(10)
C26	8988(20)	4295(27)	9192(24)	99(8)

washed repeatedly with pentane, producing a gummy yellow powder of **2**. Yield: 0.24 g, 75%. Anal. Calcd for  $\text{C}_{14}\text{H}_{34}\text{IrO}_3$ : C, 33.39; H, 6.82. Found: C, 33.08; H, 6.90.

$^1\text{H}$  NMR (acetone- $d_6$ , 23  $^\circ\text{C}$ ):  $\delta$  5.01 (br d,  $J_{\text{HP}} = 17.0$  Hz, 1, H1), 4.90 (d,  $J_{\text{HP}} = 5.7$  Hz, 1, H3), 3.97 (m, 1, H1'), 1.69 (d,  $J_{\text{HP}} = 9.3$  Hz, 9,  $\text{PMe}_3$ ), 1.65 (s, 3, H5's), 1.57 (d,  $J_{\text{HP}} = 8.1$  Hz, 9,  $\text{PMe}_3$ ), 1.31 (d,  $J_{\text{HP}} = 8.1$  Hz, 9,  $\text{PMe}_3$ ), -10.58 (d of t,  $J_{\text{HP}} = 156.6$ , 20.7 Hz, 1, IrH).

$^1\text{H}$  NMR (benzene- $d_6$ , 8  $^\circ\text{C}$ ):  $\delta$  5.90 (br d,  $J_{\text{HP}} = 17.0$  Hz, 1, H1), 5.70 (d,  $J_{\text{HP}} = 5.5$  Hz, 1, H3), 4.41 (m, 1, H1'), 2.18 (s, 3, H5's), 1.32 (d,  $J_{\text{HP}} = 9.3$  Hz, 9,  $\text{PMe}_3$ ), 1.25 (d,  $J_{\text{HP}} = 8.5$  Hz, 9,  $\text{PMe}_3$ ), 1.10 (d,  $J_{\text{HP}} = 7.5$  Hz, 9,  $\text{PMe}_3$ ), -10.02 (d of t,  $J_{\text{HP}} = 162.5$ , 20.5 Hz, 1, IrH).

$^{13}\text{C}\{^1\text{H}\}$  NMR (benzene- $d_6$ , 8  $^\circ\text{C}$ ):  $\delta$  170.4 (d,  $J_{\text{CP}} = 10.3$  Hz, C4) 160.0 (br d,  $J_{\text{CP}} = 86.1$  Hz, C2), 116.0 (s, C3), 100.9 (s,

**Table 7. Selected Bond Distances (Å) and Bond Angles (deg) with Estimated Standard Deviations**

for $\text{trans-CH}_3\text{C}\equiv\text{C}(\text{Br})\text{C}(\text{CH}_3)\text{O}=\text{Ir}(\text{PEt}_3)_2(\text{Br})_2$ (12)			
Bond Distances			
Ir-Br1	2.485(2)	O-C4	1.283(17)
Ir-Br2	2.596(2)	C1-C2	1.498(17)
Ir-P1	2.369(4)	C2-C3	1.371(16)
Ir-P2	2.365(4)	C3-C4	1.415(18)
Ir-O	2.054(7)	C3-Br3	1.910(14)
Ir-C2	1.971(13)	C4-C5	1.481(15)
Bond Angles			
Br1-Ir-Br2	92.3(1)	P1-Ir-C2	91.4(4)
Br1-Ir-P1	89.2(1)	P2-Ir-C2	91.1(4)
Br2-Ir-P1	88.4(1)	O-Ir-C2	80.8(4)
Br1-Ir-P2	89.2(1)	Ir-O-C4	114.3(7)
Br2-Ir-P2	89.3(1)	Ir-C2-C1	128.1(9)
P1-Ir-P2	177.1(1)	Ir-C2-C3	111.4(9)
Br1-Ir-O	177.1(2)	C1-C2-C3	120.5(12)
Br2-Ir-O	90.6(2)	Br3-C3-C2	123.5(9)
P1-Ir-O	90.5(2)	Br3-C3-C4	117.8(9)
P2-Ir-O	91.2(2)	C2-C3-C4	118.8(13)
Br1-Ir-C2	96.3(3)	O-C4-C3	114.7(10)
Br2-Ir-C2	171.4(3)	O-C4-C5	117.9(12)
		C3-C4-C5	127.5(13)

C1), 22.6 (d,  $J_{\text{CP}} = 37.3$  Hz,  $\text{PMe}_3$ ), 20.2 (d,  $J_{\text{CP}} = 26.5$  Hz,  $\text{PMe}_3$ ), 19.3 (s, C5), 14.9 (d,  $J_{\text{CP}} = 26.0$  Hz,  $\text{PMe}_3$ ).

$^{31}\text{P}\{^1\text{H}\}$  NMR (benzene- $d_6$ , 8 °C):  $\delta$  -46.5 (dd,  $J_{\text{PP}} = 15.0$ , 10.3 Hz, 1,  $\text{PMe}_3$ ), -47.5 (dd,  $J_{\text{PP}} = 10.3$ , 7.0 Hz, 1,  $\text{PMe}_3$ ), -47.8 (dd,  $J_{\text{PP}} = 15.0$ , 7.0 Hz, 1,  $\text{PMe}_3$ ).

**Synthesis of [(1,2,5- $\eta$ )-4-Methyl-5-oxapenta-1,4-diene- $\text{Ir}(\text{PMe}_3)_3(\text{H})\text{]}^+\text{BF}_4^-$  (4).** ((1,2,5- $\eta$ )-4-Methyl-5-oxapentadienyl) $\text{Ir}(\text{PMe}_3)_3$  (1) (0.35 g,  $7.0 \times 10^{-4}$  mol) was dissolved in 20 mL of diethyl ether and cooled to -30 °C. Cold (-30 °C)  $\text{HBF}_4 \cdot \text{OEt}_2$  (0.11 g,  $7.0 \times 10^{-4}$  mol) in 5 mL of diethyl ether was added dropwise with stirring, causing 4 to precipitate as a fluffy, white powder. The precipitate was collected and washed with diethyl ether and pentane. Yield: 0.38 g, 92%. Analogous products were obtained using the following acids:  $\text{HO}_3\text{SCF}_3$ ,  $\text{HO}_2\text{CCF}_3$ , and  $\text{NH}_4^+\text{PF}_6^-$ . Elemental analysis of 4 could not be obtained because of its thermal instability; however, analysis of isomeric compound 5 (to which 4 cleanly converts) was obtained.

$^1\text{H}$  NMR (acetone- $d_6$ , -30 °C):  $\delta$  3.55 (dd,  $J_{\text{HH}} = 22.0$  Hz,  $J_{\text{HP}} = 11.0$  Hz, 1, H3 or H3'), 3.27 (dd,  $J_{\text{HH}} = 22.0$ , 4.8 Hz, 1, H3' or H3), 2.40 (s, 3, H5's), 2.23 (m, 1, H2), 1.69 (d,  $J_{\text{HP}} = 8.4$  Hz, 9,  $\text{PMe}_3$ ), 1.54 (d,  $J_{\text{HP}} = 8.4$  Hz, 9,  $\text{PMe}_3$ ), 1.49 (d,  $J_{\text{HP}} = 10.8$  Hz, 9,  $\text{PMe}_3$ ), 1.48 (m, 1, H1' or H1), 0.52 (m, 1, H1 or H1').

$^{13}\text{C}\{^1\text{H}\}$  NMR (acetone- $d_6$ , -30 °C):  $\delta$  233.4 (d,  $J_{\text{CP}} = 9.9$  Hz, C4), 54.4 (s, C3), 28.5 (s, C5), 28.3 (dd,  $J_{\text{CP}} = 34.2$ , 7.3 Hz, C2), 21.8 (d,  $J_{\text{CP}} = 34.5$  Hz, C1), 20.2 (d,  $J_{\text{CP}} = 26.8$  Hz,  $\text{PMe}_3$ ), 19.5 (d,  $J_{\text{CP}} = 26.8$  Hz,  $\text{PMe}_3$ ), 18.3 (d,  $J_{\text{CP}} = 43.5$  Hz,  $\text{PMe}_3$ ).

$^{31}\text{P}\{^1\text{H}\}$  NMR (acetone- $d_6$ , -30 °C):  $\delta$  -38.5 (dd,  $J_{\text{PP}} = 18.9$ , 13.5 Hz, 1,  $\text{PMe}_3$ ), -42.0 (dd,  $J_{\text{PP}} = 35.8$ , 13.5 Hz, 1,  $\text{PMe}_3$ ), -45.8 (dd,  $J_{\text{PP}} = 35.8$ , 18.9 Hz, 1,  $\text{PMe}_3$ ).

**Synthesis of [fac- $\text{CH}_3\text{C}\equiv\text{C}(\text{CH}_3)\text{O}=\text{Ir}(\text{PMe}_3)_3(\text{H})\text{]}^+\text{BF}_4^-$  (5).** (((1,2,5- $\eta$ )-4-Methyl-5-oxapenta-1,4-diene) $\text{Ir}(\text{PMe}_3)_3(\text{H})\text{]}^+\text{BF}_4^-$  (4) (0.38 g,  $6.4 \times 10^{-4}$  mol) was dissolved in 20 mL of tetrahydrofuran and stirred at room temperature for 8 h. After the solvent was removed *in vacuo* and the light yellow residue was washed with pentane and diethyl ether, 5 was isolated as a light yellow powder. Yield: 0.37 g, 97%. Analogous products were obtained with the following anions:  $\text{O}_3\text{SCF}_3^-$ ,  $\text{O}_2\text{CCF}_3^-$ , and  $\text{PF}_6^-$ . Elemental analysis was obtained on the  $\text{PF}_6^-$  salt. Anal. Calcd for  $\text{C}_{14}\text{H}_{36}\text{F}_6\text{IrOP}_4$ : C, 25.88; H, 5.44. Found: C, 25.68; H, 5.34.

$^1\text{H}$  NMR (acetone- $d_6$ , 22 °C):  $\delta$  7.00 (d,  $J_{\text{HP}} = 6.9$  Hz, 1, H3), 2.83 (d,  $J_{\text{HP}} = 5.1$  Hz, 3, H1's), 2.42 (d,  $J_{\text{HP}} = 3.1$  Hz, 3, H5's), 1.90 (d,  $J_{\text{HP}} = 10.8$  Hz, 9,  $\text{PMe}_3$ ), 1.79 (d,  $J_{\text{HP}} = 9.3$  Hz, 9,

$\text{PMe}_3$ ), 1.43 (d,  $J_{\text{HP}} = 9.0$  Hz, 9,  $\text{PMe}_3$ ), -10.52 (d of t,  $J_{\text{HP}} = 117.6$ , 19.7 Hz, 1, IrH).

$^{13}\text{C}\{^1\text{H}\}$  NMR (acetone- $d_6$ , 22 °C):  $\delta$  231.0 (d of t,  $J_{\text{CP}} = 82.1$ , 6.1 Hz, C2), 212.7 (m, C4), 137.3 (s, C3), 37.0 (q,  $J_{\text{CP}} = 6.0$  Hz, C1), 23.9 (s, C5), 22.2 (d,  $J_{\text{CP}} = 43.0$  Hz,  $\text{PMe}_3$ ), 19.3 (d,  $J_{\text{CP}} = 32.0$  Hz,  $\text{PMe}_3$ ), 15.2 (d,  $J_{\text{CP}} = 30.3$  Hz,  $\text{PMe}_3$ ).

$^{31}\text{P}\{^1\text{H}\}$  NMR (acetone- $d_6$ , 22 °C):  $\delta$  -41.9 (dd,  $J_{\text{PP}} = 22.0$ , 13.4 Hz, 1,  $\text{PMe}_3$ ), -47.3 (dd,  $J_{\text{PP}} = 13.4$ , 12.2 Hz, 1,  $\text{PMe}_3$ ), -48.8 (dd,  $J_{\text{PP}} = 22.0$ , 12.2 Hz, 1,  $\text{PMe}_3$ ).

**Synthesis of [mer- $\text{CH}_3\text{C}\equiv\text{C}(\text{CH}_3)\text{O}=\text{Ir}(\text{PMe}_3)_3(\text{H})\text{]}^+\text{BF}_4^-$  (6).** A solution of mer- $\text{CH}_2=\text{C}(\text{CH}_3)\text{O}=\text{Ir}(\text{PMe}_3)_3(\text{H})$  (3) (0.086 g,  $1.7 \times 10^{-4}$  mmol) in 20 mL of diethyl ether was cooled to -30 °C.  $\text{HBF}_4 \cdot \text{OEt}_2$  (0.028 g,  $1.7 \times 10^{-4}$  mol) in 5 mL of diethyl ether was added dropwise to the cold solution, causing a fluffy, white powder (6) to precipitate out of solution. The powder was collected and washed with small portions of diethyl ether and pentane. Yield: 0.091 g, 90%. Analogous products were obtained using the following acids:  $\text{HO}_3\text{SCF}_3$ ,  $\text{HO}_2\text{CCF}_3$ , and  $\text{NH}_4^+\text{PF}_6^-$ . Elemental analysis was obtained on the  $\text{PF}_6^-$  salt. Anal. Calcd for  $\text{C}_{14}\text{H}_{35}\text{F}_6\text{IrOP}_4$ : C, 25.88; H, 5.44. Found: C, 25.49; H, 5.49.

$^1\text{H}$  NMR (acetone- $d_6$ , 22 °C):  $\delta$  7.12 (d,  $J_{\text{HP}} = 7.5$  Hz, 1, H3), 2.82 (d,  $J_{\text{HP}} = 5.0$  Hz, 3, H1's), 2.41 (m, 3, H5's), 1.76 (d,  $J_{\text{HP}} = 8.4$  Hz, 9,  $\text{PMe}_3$ ), 1.50 (m, 18,  $\text{PMe}_3$ 's), -24.54 (t of d,  $J_{\text{HP}} = 17.5$ , 12.0 Hz, IrH).

$^{13}\text{C}\{^1\text{H}\}$  NMR (acetone- $d_6$ , 22 °C):  $\delta$  229.4 (d of t,  $J_{\text{CP}} = 77.6$ , 10.2 Hz, C2), 214.6 (d,  $J_{\text{CP}} = 7.5$  Hz, C4), 137.3 (s, C3), 36.7 (d,  $J_{\text{CP}} = 5.4$  Hz, C1), 25.4 (s, C5), 19.0 (d,  $J_{\text{CP}} = 30.7$  Hz, equatorial  $\text{PMe}_3$ ), 17.2 (virtual t,  $J_{\text{CP}} = 38.9$  Hz, axial  $\text{PMe}_3$ 's).

$^{31}\text{P}\{^1\text{H}\}$  NMR (acetone- $d_6$ , 22 °C):  $\delta$  -39.2 (d,  $J_{\text{PP}} = 25.6$  Hz, 2, axial  $\text{PMe}_3$ 's), -50.9 (t,  $J_{\text{PP}} = 25.6$  Hz, 1, equatorial  $\text{PMe}_3$ ).

**Synthesis of [mer- $\text{CH}=\text{CHCH}_2\text{C}(\text{CH}_3)\text{O}=\text{Ir}(\text{PEt}_3)_3(\text{H})\text{]}^+\text{BF}_4^-$  (9).** mer- $\text{CH}=\text{CHCH}=\text{C}(\text{CH}_3)\text{O}=\text{Ir}(\text{PEt}_3)_3(\text{H})$  (7) (0.31 g,  $5.0 \times 10^{-4}$  mol) was dissolved in 20 mL of diethyl ether and cooled to -30 °C.  $\text{HBF}_4 \cdot \text{OEt}_2$  (0.081 g,  $5.0 \times 10^{-4}$  mol) in 5 mL of diethyl ether was added dropwise to the solution, causing 9 to precipitate as a fine, off-white powder. The diethyl ether was removed under vacuum, and the product was washed with pentane. Yield: 0.33 g, 92%. Analogous products were obtained using the following acids:  $\text{HO}_3\text{SCF}_3$ ,  $\text{HO}_2\text{CCF}_3$ , and  $\text{NH}_4^+\text{PF}_6^-$ . Elemental analysis was obtained on the  $\text{PF}_6^-$  salt. Anal. Calcd for  $\text{C}_{23}\text{H}_{53}\text{F}_6\text{IrOP}_4$ : C, 35.60; H, 6.90. Found: C, 35.40; H, 6.72.

$^1\text{H}$  NMR (acetone- $d_6$ , 22 °C):  $\delta$  7.22 (m, 1, H1), 5.99 (m, 1, H2), 4.27 (br s, 2, H3's), 2.33 (s, 3, H5's), 1.99, 1.90, 1.80 (m's, 18,  $\text{CH}_2$ 's of  $\text{PEt}_3$ 's), 1.11, 1.01 (m's, 27,  $\text{CH}_3$ 's of  $\text{PEt}_3$ 's), -27.60 (t of d,  $J_{\text{HP}} = 16.5$ , 11.5 Hz, 1, IrH).

$^{13}\text{C}\{^1\text{H}\}$  NMR (acetone- $d_6$ , 22 °C):  $\delta$  215.7 (s, C4), 134.0 (d of t,  $J_{\text{CP}} = 71.8$ , 14.0 Hz, C1), 117.3 (s, C2), 47.1 (s, C3), 30.7 (s, C5), 20.2 (d,  $J_{\text{CP}} = 25.5$  Hz,  $\text{CH}_2$ 's of equatorial  $\text{PEt}_3$ ), 17.0 (virtual t,  $J_{\text{CP}} = 34.0$  Hz,  $\text{CH}_2$ 's of axial  $\text{PEt}_3$ 's), 8.6 (s,  $\text{CH}_3$ 's of equatorial  $\text{PEt}_3$ ), 8.1 (s,  $\text{CH}_3$ 's of axial  $\text{PEt}_3$ 's).

$^{31}\text{P}\{^1\text{H}\}$  NMR (acetone- $d_6$ , 22 °C):  $\delta$  -6.9 (d,  $J_{\text{PP}} = 17.0$  Hz, 2, axial  $\text{PEt}_3$ 's), -19.1 (t,  $J_{\text{PP}} = 17.0$  Hz, 1, equatorial  $\text{PEt}_3$ ).

**Synthesis of [mer- $\text{CH}_3\text{C}\equiv\text{C}(\text{CH}_3)\text{O}=\text{Ir}(\text{PEt}_3)_3(\text{H})\text{]}^+\text{BF}_4^-$  (10).** Method 1: A solution of [mer- $\text{CH}=\text{CHCH}_2\text{C}(\text{CH}_3)\text{O}=\text{Ir}(\text{PEt}_3)_3(\text{H})\text{]}^+\text{BF}_4^-$  (9) (0.082 g,  $1.1 \times 10^{-4}$  mol) in 25 mL of tetrahydrofuran was heated at reflux for 10 h. After the solvent was removed *in vacuo* and the residue was washed with diethyl ether and pentane, 10 was isolated as a yellow powder. Yield: 0.057 g, 70%.

Method 2: A solution of mer- $\text{CH}_2=\text{C}(\text{CH}_3)\text{O}=\text{Ir}(\text{PEt}_3)_3(\text{H})$  (8) (0.31 g,  $5.0 \times 10^{-4}$  mol) in 15 mL of diethyl ether was cooled to -30 °C.  $\text{HBF}_4 \cdot \text{OEt}_2$  (0.081 g,  $5.0 \times 10^{-4}$  mol) in 5 mL of diethyl ether was added dropwise to the cold solution, causing compound 10 to precipitate as a yellow powder. The

Table 8. X-ray Diffraction Structure Summary

	compound		
	10	11	12
	Crystal Parameters and Data Collection Summary		
formula	C <sub>23</sub> H <sub>53</sub> F <sub>6</sub> IrOP <sub>4</sub>	C <sub>17</sub> H <sub>37</sub> I <sub>2</sub> IrOP <sub>2</sub>	C <sub>17</sub> H <sub>36</sub> Br <sub>3</sub> IrOP <sub>2</sub>
formula weight	775.7	762.9	750.3
crystal system	monoclinic	monoclinic	monoclinic
space group	P2 <sub>1</sub> /c	P2 <sub>1</sub> /n	P2 <sub>1</sub> /c
a (Å)	10.103(4)	24.527(8)	15.572(4)
b (Å)	20.435(7)	8.944(2)	11.786(4)
c (Å)	15.853(7)	24.940(7)	14.567(5)
α (deg)	90	90	90
β (deg)	96.12(3)	115.13(2)	108.86(2)
γ (deg)	90	90	90
V (Å <sup>3</sup> )	3254(2)	4953(2)	2530.0(13)
Z	4	8	4
crystal dimensions (mm)	0.68 × 0.70 × 0.56	0.10 × 0.50 × 0.22	0.22 × 0.40 × 0.20
crystal color and habit	yellow cube	dark orange plate	orange prism
density <sub>calcd</sub> (g/cm <sup>3</sup> )	1.583	2.046	1.970
radiation (Å)	Mo Kα (λ = 0.710 73)	Mo Kα (λ = 0.710 73)	Mo Kα (λ = 0.710 73)
scan type	θ-2θ	ω	θ-2θ
scan rate (deg/min in ω)	variable, 3.50-14.65	variable, 2.49-14.65	variable, 3.00-14.65
scan range (ω) (deg)	1.20 plus Kα separation	1.20 plus Kα separation	1.20 plus Kα separation
2θ range (deg)	3.0-55.0	3.0-50.0	3.0-50.0
data collected	h, 0 to 13 k, 0 to 26 l, -20 to +20	h, 0 to 29 k, 0 to 10 l, -29 to +26	h, -18 to +17 k, -14 to 0 l, 0 to 17
total decay	none detected	none detected	none detected
temperature	295	296	296
	Treatment of Intensity Data and Refinement Summary		
no. of data collected	8099	9507	4869
no. of unique data	7469	8662	4434
no. of data with I > 3σ(I)	5368	5231	2255
Mo Kα linear abs coeff (cm <sup>-1</sup> )	43.49	80.16	101.45
abs correction applied	semiempirical	semiempirical	semiempirical
data to parameter ratio	16.5:1	12.5:1	10.4:1
R <sup>a</sup>	0.0364	0.0367	0.0363
R <sub>w</sub> <sup>a</sup>	0.0419 <sup>b</sup>	0.0514 <sup>c</sup>	0.0375 <sup>d</sup>
GOF <sup>e</sup>	1.56	0.76	1.03

<sup>a</sup> R =  $\sum |F_o| - |F_c| / \sum |F_o|$ . <sup>b</sup> R<sub>w</sub> =  $[\sum w(|F_o| - |F_c|)^2 / \sum w|F_o|^2]^{1/2}$ . <sup>c</sup> w =  $[\sigma^2(F_o) + 0.0003(F_o)^2]^{-1}$ . <sup>d</sup> w =  $[\sigma^2(F_o) + 0.0031(F_o)^2]^{-1}$ . <sup>e</sup> GOF =  $[\sum w(|F_o| - |F_c|)^2 / (N_{\text{observations}} - N_{\text{variables}})]^{1/2}$ .

powder was collected and washed with small portions of diethyl ether. Yield: 0.30 g, 83%. Analogous products were obtained with the following anions: O<sub>3</sub>SCF<sub>3</sub><sup>-</sup>, O<sub>2</sub>CCF<sub>3</sub><sup>-</sup>, and PF<sub>6</sub><sup>-</sup>. Elemental analysis was obtained on the PF<sub>6</sub><sup>-</sup> salt. Anal. Calcd for C<sub>23</sub>H<sub>53</sub>F<sub>6</sub>IrOP<sub>4</sub>: C, 35.60; H, 6.90. Found: C, 35.71; H, 7.18.

<sup>1</sup>H NMR (acetone-*d*<sub>6</sub>, 22 °C): δ 7.15 (d, J<sub>HP</sub> = 8.0 Hz, 1, H3), 2.91 (d, J<sub>HP</sub> = 4.5 Hz, 3, H1's), 2.42 (m, 3, H5's), 2.04, 1.86 (m's, 18, CH<sub>2</sub>'s of PET<sub>3</sub>'), 1.19, 1.03 (m's, 27, CH<sub>3</sub>'s of PET<sub>3</sub>'), -24.68 (t of d, J<sub>HP</sub> = 15.5, 12.0 Hz, 1, IrH).

<sup>13</sup>C{<sup>1</sup>H} NMR (acetone-*d*<sub>6</sub>, 22 °C): δ 228.3 (d of t, J<sub>CP</sub> = 75.1, 9.7 Hz, C2), 214.2 (s, C4), 138.5 (s, C3), 37.2 (s, C1), 25.2 (s, C5), 18.8 (d, J<sub>CP</sub> = 26.6 Hz, CH<sub>2</sub>'s of equatorial PET<sub>3</sub>'s), 17.6 (virtual t, J<sub>CP</sub> = 33.3 Hz, CH<sub>2</sub>'s of axial PET<sub>3</sub>'), 7.9 (s, CH<sub>3</sub>'s of equatorial PET<sub>3</sub>'), 7.7 (s, CH<sub>3</sub>'s of axial PET<sub>3</sub>'s).

<sup>31</sup>P{<sup>1</sup>H} NMR (acetone-*d*<sub>6</sub>, 22 °C): δ -16.5 (d, J<sub>PP</sub> = 22.6 Hz, 2, axial PET<sub>3</sub>'s), -23.3 (t, J<sub>PP</sub> = 22.6 Hz, 1, equatorial PET<sub>3</sub>).

#### Synthesis of *trans*-CH<sub>3</sub>C≡C(CH<sub>3</sub>)<sub>2</sub>OIr(PET<sub>3</sub>)<sub>2</sub>(I)<sub>2</sub> (11).

A solution of [*mer*-CH<sub>3</sub>C≡C(CH<sub>3</sub>)<sub>2</sub>OIr(PET<sub>3</sub>)<sub>3</sub>(H)]<sup>+</sup>BF<sub>4</sub><sup>-</sup> (10) (0.10 g, 1.4 × 10<sup>-4</sup> mol) in 15 mL of tetrahydrofuran (THF) was cooled to -30 °C, and excess iodine (0.072 g, 2.8 × 10<sup>-4</sup> mol) in 15 mL of THF was added dropwise with stirring. After the resulting solution was warmed to room temperature and stirred for 27 h, the volatiles were removed under vacuum. The residue was extracted with benzene and filtered through Celite to yield an orange solution. After *in vacuo* concentration, the solution was placed onto a silica gel chromatography column and eluted with THF. The first orange band was collected. After removal of the solvent under

vacuum, the residue was redissolved in a minimal quantity of THF. Slow diffusion of diethyl ether into this THF solution at -30 °C caused 11 to crystallize as very dark orange plates. Yield: 0.045 g, 42%. Anal. Calcd for C<sub>17</sub>H<sub>37</sub>I<sub>2</sub>IrOP<sub>2</sub>: C, 26.67; H, 4.88. Found: C, 25.84; H, 4.84.

<sup>1</sup>H NMR (acetone-*d*<sub>6</sub>, 22 °C): δ 6.82 (s, 1, H3), 2.99 (s, 3, H1's), 2.48 (s, 3, H5's), 2.19, 1.87 (m's, 12, CH<sub>2</sub>'s of PET<sub>3</sub>'s), 1.11 (m, 18, CH<sub>3</sub>'s of PET<sub>3</sub>'s).

<sup>1</sup>H NMR (benzene-*d*<sub>6</sub>, 22 °C): δ 6.10 (s, 1, H3), 2.91 (s, 3, H1's), 2.06 (m, 6, CH<sub>2</sub>'s of PET<sub>3</sub>'s), 1.88 (s, 3, H5's), 1.78 (m, 6, CH<sub>2</sub>'s of PET<sub>3</sub>'s), 0.95 (m, 18, CH<sub>3</sub>'s of PET<sub>3</sub>'s).

<sup>13</sup>C{<sup>1</sup>H} NMR (benzene-*d*<sub>6</sub>, 22 °C): δ 223.5 (t, J<sub>CP</sub> = 5.4 Hz, C2), 212.4 (s, C4), 134.1 (s, C3), 35.4 (s, C1), 21.6 (s, C5), 15.8 (virtual t, J<sub>CP</sub> = 33.6 Hz, CH<sub>2</sub>'s of PET<sub>3</sub>'s), 9.0 (s, CH<sub>3</sub>'s of PET<sub>3</sub>'s).

<sup>31</sup>P{<sup>1</sup>H} NMR (benzene-*d*<sub>6</sub>, 22 °C): δ -35.2 (s, 2, equivalent axial PET<sub>3</sub>'s).

#### Synthesis of *trans*-CH<sub>3</sub>C≡C(Br)<sub>2</sub>OIr(PET<sub>3</sub>)<sub>2</sub>(Br)<sub>2</sub> (12).

A solution of [*mer*-CH<sub>3</sub>C≡C(CH<sub>3</sub>)<sub>2</sub>OIr(PET<sub>3</sub>)<sub>3</sub>(H)]<sup>+</sup>BF<sub>4</sub><sup>-</sup> (10) (0.18 g, 2.5 × 10<sup>-4</sup> mol) in 15 mL of tetrahydrofuran was cooled to -30 °C. Excess bromine (0.10 g, 6.0 × 10<sup>-4</sup> mol) was added to the solution dropwise, causing the color to change from yellow to orange. After the solution was warmed to room temperature, the volatiles were removed under vacuum. The residue was then extracted with pentane, filtered through Celite, and reduced in volume to 10 mL. Subsequent cooling of the solution to -30 °C caused 12 to crystallize as orange needles. Yield: 0.15 g,

80%. Anal. Calcd for  $C_{17}H_{36}IrBr_3P_2O$ : C, 27.21; H, 4.85. Found: C, 27.15; H, 4.78.

$^1H$  NMR (acetone- $d_6$ , 22 °C):  $\delta$  2.77 (s, 3, H1's), 2.67 (s, 3, H5's), 2.00, 1.74 (m's, 12,  $CH_2$ 's of  $PEt_3$ 's), 1.07 (m, 18,  $CH_3$ 's of  $PEt_3$ 's).

$^1H$  NMR (benzene- $d_6$ , 22 °C):  $\delta$  2.86 (s, 3, H1's), 2.20 (s, 3, H5's), 1.80, 1.60 (m's, 12,  $CH_2$ 's of  $PEt_3$ 's), 0.85 (m, 18,  $CH_3$ 's of  $PEt_3$ 's).

$^{13}C\{^1H\}$  NMR (benzene- $d_6$ , 22 °C):  $\delta$  214.8 (br s, C2), 208.5 (s, C4), 115.4 (s, C3), 33.6 (s, C1), 23.1 (s, C5), 13.5 (virtual t,  $J_{CP} = 30.4$  Hz,  $CH_2$ 's of  $PEt_3$ 's), 7.8 (s,  $CH_3$ 's of  $PEt_3$ 's).

$^{31}P\{^1H\}$  NMR (benzene- $d_6$ , 22 °C):  $\delta$  -25.3 (s, 2, equivalent axial  $PEt_3$ 's).

#### X-ray Diffraction Studies of [*mer*- $CH_3$ -

$C\equiv CH\equiv C(CH_3)\equiv O\equiv Ir(PEt_3)_3(H)]^+PF_6^-$  ( $PF_6^-$  salt of **10**),

*trans*- $CH_3C\equiv CH\equiv C(CH_3)\equiv O\equiv Ir(PEt_3)_2(I)_2$  (**11**), and

*trans*- $CH_3C\equiv C(Br)\equiv C(CH_3)\equiv O\equiv Ir(PEt_3)_2(Br)_2$  (**12**).

Single crystals of compounds **10**, **11**, and **12** were sealed in glass capillaries under an inert atmosphere. Data were collected at room temperature on a Siemens R3m/V diffractometer, using graphite-monochromated Mo  $K\alpha$  radiation. Standard reflections were measured every 100 events as check reflections for crystal deterioration and/or misalignment. All data reduction and refinement were done using the Siemens SHELXTL PLUS package on a VAX 3100 workstation.<sup>21</sup> Crystal data and details of data collection and structure analysis are listed in Table 8.

The iridium atom positions in **10**, **11**, and **12** were determined by direct methods. In each case, the remaining non-

hydrogen atoms were found by successive full-matrix least-squares refinement and difference Fourier map calculations. All non-hydrogen atoms were refined anisotropically, except for two carbon atoms in a disordered  $PEt_3$  ethyl group in **11** (C31/C31A and C32/C32A) and one carbon atom in a disordered  $PEt_3$  methyl group in **12** (C26/C26B); these disordered atoms were refined isotropically. The metal-bound hydrogen atom (H) and the hydrogen atom on C3 (H3) in **10** were refined isotropically, while all other hydrogens in **10**, **11**, and **12** (except those on disordered  $PEt_3$  carbons) were placed at idealized positions and assumed the riding model. In each case, a common isotropic  $U$  value for all hydrogens was refined.

**Acknowledgment.** We thank the National Science Foundation (Grants CHE-9003159 and CHE-9303516) and the donors of the Petroleum Research Fund, administered by the American Chemical Society, for support of this research. A loan of  $IrCl_3 \cdot 3H_2O$  from Johnson-Matthey Alfa/Aesar is gratefully acknowledged. Washington University's X-ray Crystallography Facility was funded by the National Science Foundation's Chemical Instrumentation Program (Grant CHE-8811456). The High Resolution NMR Service Facility was funded in part by National Institutes of Health Biomedical Support Instrument Grant 1 S10 RR02004 and by a gift from the Monsanto Company.

**Supporting Information Available:** Tables of structure determination summaries, final atomic coordinates, thermal parameters, bond lengths, and bond angles for compounds **10**–**12** (25 pages). Ordering information is given on any current masthead page.

OM950494M

(21) Atomic scattering factors were obtained from the following: *International Tables for X-Ray Crystallography*; Kynoch Press: Birmingham, England, 1974; Vol. IV.

**Synthesis of Heterobimetallaboranes and Related  
Species from [(PPh<sub>3</sub>)<sub>2</sub>(CO)OsB<sub>5</sub>H<sub>9</sub>]:  
*pileo*-[(PPh<sub>3</sub>)<sub>2</sub>(CO)OsB<sub>5</sub>H<sub>5</sub>IrH(PPh<sub>3</sub>)(CO)],  
*closo*-[(PPh<sub>3</sub>)<sub>2</sub>(CO)( $\mu$ -H)OsB<sub>4</sub>H<sub>5</sub>{ $\eta^5$ -(C<sub>5</sub>Me<sub>5</sub>)M}] (M = Rh,  
Ir), *nido*-[(PPh<sub>3</sub>)<sub>2</sub>(CO)Os( $\mu$ -H){ $\eta^5$ -(C<sub>5</sub>Me<sub>5</sub>)Ir}B<sub>3</sub>H<sub>6</sub>], and  
*nido*-[(PPh<sub>3</sub>)<sub>2</sub>(CO)OsB<sub>4</sub>H<sub>7</sub>(*n*-C<sub>4</sub>H<sub>9</sub>)]**

Jonathan Bould, Michael Pasieka, Janet Braddock-Wilking, Nigam P. Rath, and  
Lawrence Barton\*

*Department of Chemistry, University of Missouri—St. Louis, St. Louis, Missouri 63121*

Charles Gloeckner

*Analytical Sciences Center, Monsanto Company, 800 N Lindbergh Boulevard,  
St. Louis, Missouri 63167*

*Received June 26, 1995*<sup>⊗</sup>

A number of new heterobimetallaborane clusters have been synthesized from the addition of metal halide complexes to *nido*-[(PPh<sub>3</sub>)<sub>2</sub>(CO)OsB<sub>5</sub>H<sub>8</sub>][Li]. The compounds have been characterized fully by NMR, IR, mass spectroscopy, and single-crystal X-ray diffraction techniques as *pileo*-[1,1,1-H(PPh<sub>3</sub>)(CO)-2,2,2-(PPh<sub>3</sub>)<sub>2</sub>(CO)-1,2-IrOsB<sub>5</sub>H<sub>5</sub>] (**1**), *closo*-[1-(C<sub>5</sub>Me<sub>5</sub>)-2,2,2,-(CO)(PPh<sub>3</sub>)<sub>2</sub>-1,2-( $\mu$ H)-1,2-IrOsB<sub>4</sub>H<sub>5</sub>] (**2a**), and *nido*-[2-( $\eta^5$ -C<sub>5</sub>Me<sub>5</sub>)-3,3,3-(CO)(PPh<sub>3</sub>)<sub>2</sub>-2,3-( $\mu$ H)-2,3-IrOsB<sub>3</sub>H<sub>6</sub>] (**3**). A rhodium analogue of **2a** was also prepared and characterized by NMR spectroscopy as *closo*-[1-(C<sub>5</sub>Me<sub>5</sub>)-2,2,2,-(CO)(PPh<sub>3</sub>)<sub>2</sub>-1,2-( $\mu$ H)-1,2-RhOsB<sub>4</sub>H<sub>6</sub>] (**2b**). The complexes all contain seven cluster skeletal electron pairs within 7, 6, and 5 cluster vertices, thus attaining an interesting *pileo*–*closo*–*nido* sequence of structures. The alkyl substituted *nido*-osmapentaborane cluster *nido*-[2,2,2-(PPh<sub>3</sub>)<sub>2</sub>(CO)-2-OsB<sub>4</sub>H<sub>7</sub>(C<sub>4</sub>H<sub>9</sub>)] (**6**), identified by NMR, IR, and mass spectroscopy, is also described.

### Introduction

We are interested in the preparation of homo- and heteropolymetallaboranes based on borane templates containing five to seven vertices. These include systems derived both from the replacement of boron vertices by metal moieties or the addition of metal moieties to the cluster. Although there has been a resurgence of interest in such systems in recent years,<sup>1–3</sup> there are very few examples in the literature, especially for the heteropolymetallaboranes.<sup>4</sup> Most of the known systems contain more than one atom of the same element. Thus there are *nido*-pentaboranes including [Fe(CO)<sub>3</sub>]<sub>2</sub>-B<sub>3</sub>H<sub>7</sub>,<sup>5a</sup> PPN[Fe(CO)<sub>3</sub>]<sub>2</sub>B<sub>3</sub>H<sub>6</sub>,<sup>5b</sup> [H{Ru(CO)<sub>3</sub>]<sub>3</sub>B<sub>2</sub>H<sub>5</sub>,<sup>2a</sup>

[H{Ru<sub>3</sub>(CO)<sub>8</sub>PPh<sub>3</sub>]<sub>3</sub>B<sub>2</sub>H<sub>5</sub>,<sup>2b</sup> [1- $\{\eta^5$ -(C<sub>5</sub>Me<sub>5</sub>)Co}-2-( $\eta^4$ -C<sub>5</sub>-Me<sub>4</sub>H)CoB<sub>3</sub>H<sub>8</sub>],<sup>1b,c</sup> [2,4- $\{\eta^5$ -(C<sub>5</sub>Me<sub>5</sub>)Co<sub>2</sub>B<sub>3</sub>H<sub>7</sub>],<sup>1b,c</sup> the capped *nido*-system [2,3- $\{\text{Fe}(\text{PMe}_3)_2\}_2(\mu\text{-H})\text{B}_4\text{H}_9$ ],<sup>6</sup> the  $\sigma$ -bonded [B<sub>5</sub>H<sub>7</sub>-2,4- $\{\text{Fe}(\text{CO})_2\text{Cp}\}_2$ ],<sup>7</sup> and the *nido*-bico-baltaheptaborane [ $\{\eta^5$ -(C<sub>5</sub>Me<sub>5</sub>)Co<sub>2</sub>B<sub>5</sub>H<sub>9</sub>].<sup>8</sup> There are many examples of *closo*-polymetallaboranes including systems containing two boron atoms and many of them are quite novel. They include [ $\mu_3$ -H]<sub>2</sub>( $\eta^5$ -(C<sub>5</sub>H<sub>5</sub>)Co)<sub>4</sub>-B<sub>2</sub>H<sub>2</sub>,<sup>9</sup> with two triply bridging H atoms and the cobaltaphosphaborane [ $\{\eta^5$ -(C<sub>5</sub>H<sub>5</sub>)Co<sub>4</sub>(PPh)B<sub>2</sub>H<sub>2</sub>].<sup>10</sup> Systems containing three boron atoms include [ $\{\eta^5$ -(C<sub>5</sub>H<sub>5</sub>-Pr<sup>i</sup>)WH<sub>2</sub>]<sub>2</sub>B<sub>3</sub>H<sub>7</sub>,<sup>3</sup> [1,2,3- $\{\eta^5$ -(C<sub>5</sub>H<sub>5</sub>)Co<sub>3</sub>(CO)B<sub>3</sub>H<sub>3</sub>],<sup>11</sup> [1,2,3- $\{\eta^5$ -(C<sub>5</sub>H<sub>5</sub>)Co<sub>3</sub>B<sub>3</sub>H<sub>5</sub>],<sup>12</sup>,<sup>11a</sup> and the tetraboron examples include [1,2- $\{\eta^5$ -(C<sub>5</sub>H<sub>5</sub>)Co<sub>2</sub>B<sub>4</sub>H<sub>6</sub>],<sup>13</sup> [1,2- $\{\eta^5$ -(C<sub>5</sub>Me<sub>5</sub>)Co<sub>2</sub>-

<sup>⊗</sup> Abstract published in *Advance ACS Abstracts*, October 15, 1995.

(1) (a) Deck, K. J.; Fehlner, T. P.; Rheingold, A. L. *Inorg. Chem.* **1993**, *32*, 2794. (b) Nishihara, Y. N.; Deck, K. J.; Shang, M.; Fehlner, T. P.; Hagerty, B. S. *J. Am. Chem. Soc.* **1993**, *115*, 12224. (c) Nishihara, Y. N.; Deck, K. J.; Shang, M.; Fehlner, T. P.; Hagerty, B. S.; Rheingold, A. L. *Organometallics* **1994**, *13*, 4510.

(2) (a) Chipperfield, K.; Housecroft, C. E.; Matthews, D. M. *J. Organometal. Chem.* **1990**, *384*, C38. (b) Housecroft, C. E.; Matthews, D. M.; Rheingold, A. L. *J. Chem. Soc., Chem. Commun.* **1992**, 323.

(3) Bullick, H. J.; Grebenik, P. D.; Green, M. L. H.; Hughes, A. K.; Leach, J. B.; McGowan, P. C. *J. Chem. Soc., Dalton Trans.* **1995**, 67.

(4) (a) Kennedy, J. D. *Prog. Inorg. Chem.* **1984**, *32*, 519. (b) *Ibid.* **1986**, *36*, 211. (c) Gilbert, K. B.; Boccock, S. K.; Shore, S. G. in *Comprehensive Organometallic Chemistry*; Wilkinson, G., Abel, E. W., Stone, F. G. A., Eds.; Pergamon, New York, 1982; Part 6, Ch. 41, pp 879–945. (d) Barton, L.; Srivastava, D. K. *Comprehensive Organometallic Chemistry II*; Wilkinson, G., Abel, E. W., Stone, F. G. A., Eds.; Pergamon: New York, 1995; Vol. 1, Chapter 8, pp 275–373.

(5) (a) Andersen, E. L.; Haller, K. J.; Fehlner, T. P. *J. Am. Chem. Soc.* **1979**, *101*, 4390. (b) Haller, K. J.; Andersen, E. L.; Fehlner, T. P. *Inorg. Chem.* **1981**, *20*, 309.

(6) Grebenik, D.; Green, M. L. H.; Kelland, M. A.; Leach, J. B.; Mountford, P. *J. Chem. Soc., Chem. Commun.* **1990**, 1234.

(7) Greenwood, N. N.; Kennedy, J. D.; Savory, C. G.; Staves, J.; Trigwell, K. R. *J. Chem. Soc., Dalton Trans.* **1977**, 37.

(8) Venable, L.; Grimes, R. N. *Inorg. Chem.* **1982**, *21*, 887.

(9) Feilong, J.; Fehlner, T. P.; Rheingold, A. L. *J. Am. Chem. Soc.* **1987**, *109*, 1860.

(10) Feilong, J.; Fehlner, T. P.; Rheingold, A. L. *J. Chem. Soc., Chem. Commun.* **1987**, 1395.

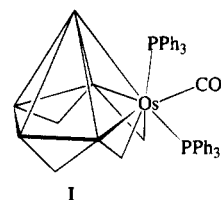
(11) (a) Zimmerman, G. J.; Hall, L. W.; Sneddon, L. G. *Inorg. Chem.* **1980**, *19*, 3642. (b) Gromek, J.; Donohue, J. *Cryst. Struct. Commun.* **1981**, *10*, 849.7

(12) Pipal, J. R.; Grimes, R. N. *Inorg. Chem.* **1977**, *16*, 3255.

(13) (a) Miller, V. R.; Grimes, R. N. *J. Am. Chem. Soc.* **1973**, *95*, 5078. (b) Pipal, J. R.; Grimes, R. N. *Inorg. Chem.* **1979**, *18*, 252.

$B_4H_6$ ],<sup>8,14</sup> [1,2,3- $\{\eta^5-(C_5H_5)Co\}_3B_4H_4$ ],<sup>14,15</sup> [1,2,3- $\{\eta^5-(C_5Me_5)Co\}_3B_4H_4$ ],<sup>8,16</sup> [(CO)<sub>3</sub>(PPh<sub>3</sub>)(Ph<sub>2</sub>PC<sub>6</sub>H<sub>4</sub>)<sub>2</sub>(Ir<sub>2</sub>B<sub>4</sub>H<sub>2</sub>)],<sup>17</sup> and the "rule breakers" [ $\{\eta^5-(C_5H_5)Co\}_4B_4H_4$ ] and [ $\{\eta^5-(C_5H_5)Ni\}_4B_4H_4$ ].<sup>18-20</sup> There are also examples of *closo*-bimetalloheptaborane containing five borons including [1,2,3- $\{\eta^5-(C_5H_5)Co\}_3B_5H_4R$ ],<sup>11a</sup> [1,2- $\{\eta^5-(C_5Me_5)Co\}_2B_5H_7$ ]<sup>8</sup> which contains two face-bridging H atoms, and the *pileo*-[1,2- $\{\eta^5-(C_5Me_5)Co\}_2B_5H_5$ ].<sup>8</sup> Very recent examples include the bicapped trigonal bipyramidal species [ $\{\eta^5-(C_5H_4Me)Mo\}_2B_5H_9$ ]<sup>3</sup> and our own *pileo*-system [ $\{\eta^5-(C_5Me_5)Ir\}_2B_5H_5$ ] (5).<sup>21</sup> There are many fewer examples of heteropolymetallaboranes.<sup>4</sup> The first *nido* species to be prepared was Cu[Ph<sub>3</sub>P]<sub>2</sub>B<sub>5</sub>H<sub>5</sub>Fe(CO)<sub>3</sub>,<sup>22</sup> a dimetallaborane in which the Fe is a true vertex and the Cu group may be considered as a "pseudo"-proton. The osmaplatinaheptaboranes [(CO)(PPh<sub>3</sub>)<sub>2</sub>( $\mu$ -H)Os(PMe<sub>2</sub>Ph)ClPtB<sub>5</sub>H<sub>7</sub>] and [(CO)(PPh<sub>3</sub>)(PPh<sub>2</sub>)Os(PPh<sub>3</sub>)PtB<sub>5</sub>H<sub>7</sub>Ph],<sup>23</sup> discovered a little later, and the recently reported isoelectronic *nido*-(PPh<sub>3</sub>)<sub>2</sub>CO( $\mu$ -H)Ir(PMe<sub>2</sub>Ph)ClPtB<sub>5</sub>H<sub>6</sub><sup>24</sup> may be considered to be true heterobimetallaboranes in that both metals are vertices. Finally there is [Cu(Ph<sub>3</sub>P)<sub>2</sub>B<sub>5</sub>H<sub>3</sub>Fe(CO)<sub>4</sub>],<sup>25</sup> in which both metals are "pseudo-protons" in that they occupy positions which may be replaced by protons. Grimes and co-workers described the first example of a *closo*-heteropolymetallaborane in this context, *closo*-[ $\{\eta^5-(C_5H_5)Co\}_2(CO)_4FeB_3H_3$ ],<sup>26</sup> which contains a trimetal triangle, and recently the novel species, *pileo*-[ $\{\eta^5-(C_5H_5)Fe\}(ML_3H)B_5H_7$ ], where M = Mo and L = PMe<sub>2</sub>Ph (4a) and M = W, L = PMe<sub>3</sub> (4b),<sup>27</sup> were reported from use of a similar synthetic approach to that we describe herein. We also reported the species *closo*-[(PPh<sub>3</sub>)<sub>2</sub>(CO)<sub>2</sub>IrB<sub>5</sub>H<sub>4</sub>(PPh<sub>3</sub>)Fe(CO)<sub>3</sub>], the first structurally characterized *closo*-heterobimetalloheptaborane.<sup>28</sup> Herein we extend the range of heterobimetalloheptaboranes by reporting the formation and complete characterization of *pileo*-[(PPh<sub>3</sub>)<sub>2</sub>(CO)OsB<sub>5</sub>H<sub>5</sub>IrH(PPh<sub>3</sub>)(CO)], *nido*-[(PPh<sub>3</sub>)<sub>2</sub>(CO)Os( $\mu$ -H) $\{\eta^5-(C_5Me_5)Ir\}B_3H_6$ ], and *closo*-[(PPh<sub>3</sub>)<sub>2</sub>(CO)OsB<sub>4</sub>H<sub>6</sub> $\{\eta^5-(C_5Me_5)Ir\}$ ], and we also provide spectroscopic and other evidence for *closo*-[(PPh<sub>3</sub>)<sub>2</sub>(CO)OsB<sub>4</sub>H<sub>6</sub> $\{\eta^5-(C_5Me_5)Rh\}$ ] and *nido*-[(PPh<sub>3</sub>)<sub>2</sub>(CO)OsB<sub>4</sub>H<sub>7</sub>(*n*-C<sub>4</sub>H<sub>9</sub>)] all derived from the osmahexabo-

rane [(PPh<sub>3</sub>)<sub>2</sub>(CO)OsB<sub>5</sub>H<sub>9</sub>]<sup>29</sup> (illustration I). A preliminary report of this work has been given previously.<sup>30</sup>



## Experimental Section

Reactions were carried out on a vacuum line using standard methods. Thin layer chromatography (TLC) of the products was performed in air using 20 × 20 cm glass plates coated with 0.1 cm of silica gel (Aldrich standard grade with gypsum binder and fluorescent indicator). Solvents used were reagent grade and were dried before use. [ $\{\eta^5-(C_5Me_5)Ir\}Cl_2$ ]<sub>2</sub> was prepared according to the literature method<sup>31</sup> as was Ir(CO)Cl(PPh<sub>3</sub>)<sub>2</sub><sup>32</sup> and [ $\{\eta^5-(C_5Me_5)Rh\}Cl_2$ ].<sup>33</sup> [(PPh<sub>3</sub>)<sub>2</sub>(CO)OsB<sub>5</sub>H<sub>9</sub>] was prepared essentially according to the literature method<sup>30</sup> although it was isolated *via* precipitation methods rather than chromatography giving more rapid routine yields of ca. 70%. NMR spectroscopy was carried out on a Bruker ARX 500 spectrometer operating at 500.1 MHz for proton and 160.5 MHz for boron-11 and on a Varian XL-300 MHz spectrometer for <sup>31</sup>P at 122 MHz. Chemical shifts are reported in ppm for CDCl<sub>3</sub> solutions unless otherwise stated to low field (high frequency) of Et<sub>2</sub>O·BF<sub>3</sub> for <sup>11</sup>B, of SiMe<sub>4</sub> for <sup>1</sup>H, and of 85% H<sub>3</sub>PO<sub>4</sub> for <sup>31</sup>P. Low resolution mass spectra were recorded at the Monsanto Co., St. Louis, on a Finnigan MAT 95 mass spectrometer in the FAB mode using a nitrobenzyl alcohol matrix. High resolution spectra were obtained by positive ion electrospray using electric sector scanning and standardized with PEG1000. Samples were run in MeOH/CHCl<sub>3</sub> (1:1) with 10 mmol of NH<sub>4</sub>OH. The masses reported are for the most abundant peak (100%) in the molecular ion envelope. Elemental analyses were carried out by Atlantic Microlabs Inc., Norcross, GA.

**Preparation of *pileo*-[(PPh<sub>3</sub>)<sub>2</sub>(CO)OsB<sub>5</sub>H<sub>5</sub>IrH(PPh<sub>3</sub>)(CO)] (1).** [(PPh<sub>3</sub>)<sub>2</sub>(CO)OsB<sub>5</sub>H<sub>9</sub>] (200 mg, 0.25 mmol) was placed in three-neck flask on the vacuum line and evacuated. One neck held a tipper tube containing [(PPh<sub>3</sub>)<sub>2</sub>(CO)IrCl] (200 mg, 0.25 mmol) and the other a rubber septum. The flask was evacuated, 15 mL of THF condensed in, and the mixture was stirred until a clear, pale yellow solution resulted. The solution was cooled to -35 °C, the flask filled with nitrogen, and MeLi syringed in (0.23 mL, 0.25 mmol of 1.1 M solution in ether) at which point the solution became clear lemon-yellow in color. After stirring for 15 m the iridium complex was added and stirring continued overnight with gradual warming to room temperature. A clear orange solution formed. The liquid was filtered in air giving 80 mg (40%) of unreacted [(PPh<sub>3</sub>)<sub>2</sub>(CO)IrCl]. The filtrate was reduced in volume and the residue applied to silica gel TLC plates using 60/40 CH<sub>2</sub>Cl<sub>2</sub>/pentane as eluent. Three bands were observed under UV light. The first band A, at R<sub>f</sub> 0.8, comprised a pale yellow band overlapping a UV active colorless band. The second band, B, R<sub>f</sub> 0.5, was identified as unreacted [(PPh<sub>3</sub>)<sub>2</sub>(CO)OsB<sub>5</sub>H<sub>9</sub>] (100 mg, 50%). A third faint band at R<sub>f</sub> 0.1 showed no presence of metallaborane products and was not further investigated. Band A was subjected to a second TLC separation using Et<sub>2</sub>O/

(14) Venable, T. L.; Brewer, C. T.; Grimes, R. N. *Inorg. Chem.* **1985**, *24*, 4751.

(15) (a) Miller, V. R.; Grimes, R. N. *J. Am. Chem. Soc.* **1976**, *98*, 1600. (b) Miller, V. R.; Weiss, R.; Grimes, R. N. *J. Am. Chem. Soc.* **1977**, *99*, 5646.

(16) Venable, L.; Sinn, E.; Grimes, R. N. *Inorg. Chem.* **1982**, *21*, 904.

(17) Crook, J. E.; Greenwood, N. N.; J. D. Kennedy, J. D.; McDonald, W. S. *J. Chem. Soc., Chem. Commun.* **1982**, 383.

(18) Pipal, J. R.; Grimes, R. N. *Inorg. Chem.* **1979**, *18*, 257.

(19) (a) Bowser, J. R.; Grimes, R. N. *J. Am. Chem. Soc.* **1978**, *100*, 4623. (b) Bowser, J. R.; Bonney, A.; Pipal, J. R.; Grimes, R. N. *J. Am. Chem. Soc.* **1979**, *101*, 6229.

(20) Cox, D. N.; Mingos, D. M. P.; Hoffman, R. J. *Chem. Soc., Dalton Trans.* **1981**, 1788.

(21) Bould, J.; Rath, N. P.; Barton, L. *Organometallics* **1995**, *14*, 2119.

(22) Mangion, M.; Ragaini, J. D.; Schmitkors, T. A.; Shore, S. G. *J. Am. Chem. Soc.* **1979**, *101*, 754.

(23) (a) Bould, J.; Crook, J. E.; Greenwood, N. N.; Kennedy, J. D. *J. Chem. Soc., Chem. Commun.* **1983**, 951. (b) Bould, J.; Crook, J. E.; Greenwood, N. N.; Kennedy, J. D. *J. Chem. Soc., Dalton Trans.* **1991**, 185. (c) Kennedy, J. D. *Main Group Metal Chem.* **1989**, *12*, 149.

(24) Bould, J.; Barton, L. *Abstracts, Fourth Boron-USA Workshop*, Syracuse, NY, July, 1994, No. 45.

(25) Barton, L.; Srivastava, D. K. *Organometallics* **1991**, *10*, 2982.

(26) Weiss, R.; Bowser, J. R.; Grimes, R. N. *Inorg. Chem.* **1978**, *17*, 1522.

(27) Bullick, H. J.; Grebenik, P. D.; Green, M. L. H.; Hughes, A. K.; Leach, J. B.; Mountford, P. *J. Chem. Soc., Dalton Trans.* **1994**, 3337.

(28) Bould, J.; Rath, N. P.; Barton, L. *Angew. Chem.* **1995**, *34*, 1641.

(29) Bould, J.; Greenwood, N. N.; Kennedy, J. D.; *J. Organomet. Chem.* **1983**, *249*, 11.

(30) Bould, J.; Rath, N. P.; Barton, L. *J. Chem. Soc., Chem Commun.* **1995**, 1285.

(31) Ball, R. G.; Graham, W. A. G.; Heineky, D. M.; Hoyars, J. K.; McMaster, A. D.; Mattson, B. M.; Michel, S. T. *Inorg. Chem.* **1990**, *29*, 2023.

(32) Collman, J. P.; Sears, C. T.; Kubota, M. *Inorg. Synth.* **1990**, *28*, 92.

(33) Kang, J. W.; Moseley, K.; Maitlis, P. M. *J. Am. Chem. Soc.* **1969**, *91*, 5970.



Table 1. Crystal Data and Structure Refinement for Compounds 1, 2a, and 3

compound no.	1	2a	3
empirical formula	C <sub>58</sub> H <sub>53</sub> B <sub>5</sub> Cl <sub>6</sub> IrO <sub>2</sub> OsP <sub>3</sub>	C <sub>53</sub> H <sub>56.8</sub> B <sub>4</sub> Cl <sub>0.2</sub> IrOOsP <sub>2</sub>	C <sub>53</sub> H <sub>58</sub> B <sub>3</sub> IrOOsP <sub>2</sub>
fw	1523.06	1204.45	1187.76
temp/K	295(2)	143(2)	126(5)
crystal system	monoclinic	triclinic	rhombohedral
space group	P2 <sub>1</sub> /c	P1	R3
a/Å	16.955(5)	11.112(3)	31.503(5)
b/Å	13.790(6)	12.765(4)	31.503(5)
c/Å	25.915(6)	18.323(5)	25.386(5)
α/deg	90	76.48(2)	90
β/deg	94.28(2)	72.71(2)	90
γ/deg	90	83.73(2)	120
V/Å <sup>-3</sup>	6042(4)	2410.6(12)	21819(6)
Z	4	2	18
D (calcd)/mg/m <sup>3</sup>	1.674	1.659	1.627
abs coeff/mm <sup>-1</sup>	4.687	5.506	5.463
cryst size/mm	0.50 × 0.40 × 0.30	0.30 × 0.30 × 0.30	0.3 × 0.3 × 0.25
F(000)	2964	1178	10476
θ range for data collcn/deg	1.58 to 28.57	1.64 to 29.06	1.69 to 26.58
index ranges	-22 ≤ h ≤ 22, -1 ≤ k ≤ 18, -34 ≤ l ≤ 34	0 ≤ h ≤ 14, -17 ≤ k ≤ 17, -23 ≤ l ≤ 25	-32 ≤ h ≤ 24, -14 ≤ k ≤ 37, -27 ≤ l ≤ 31
reflcns collcd	16701	13392	15602
independent reflcns	15076 (R <sub>int</sub> = 0.0860)	12758 (R <sub>int</sub> = 0.0359)	9370 (R <sub>int</sub> = 0.0701)
data/restraints/parameters	15073/0/778	12756/0/573	9171/0/504
goodness-of-fit on F <sup>2</sup>	1.017	1.063	1.033
final R indices [I > 2σ(I)]	R1 0.0992	0.0440	0.0694
	wR2 0.2444	0.1014	0.1469
largest diff peak and hole/e Å <sup>-3</sup>	1.841 and -1.938	3.057 and -2.071	6.254 and -3.018

pentane (50/50) as the mobile phase giving a broad undifferentiated band with two components. The band was divided in half, and NMR spectroscopy showed that the majority of the lower half comprised the title compound **1**. The two bands were repeatedly chromatographed until pure giving **1** as a pale yellow solid [53 mg, 0.041 mmol, 16.7% yield or 33% based on conversion, IR  $\nu_{\max}$  cm<sup>-1</sup> 2528(m) (B-H), 2000(s) (CO on iridium), 1941 (CO on osmium) 2093 (Os-H); low resolution FAB mass spectrum:  $m/e$ (100%) for C<sub>56</sub>H<sub>51</sub>B<sub>5</sub>O<sub>2</sub>P<sub>3</sub>IrOs<sub>1</sub> obsd: 1285, calcd: 1285.28]. The second UV active component was identified by NMR and IR spectroscopy as the known compound [(PPh<sub>3</sub>)<sub>2</sub>(CO)OsB<sub>4</sub>H<sub>6</sub>]<sup>28</sup> (ca. 13 mg). Crystals of **1** suitable for a single-crystal X-ray diffraction study were obtained by diffusion of pentane into a CH<sub>2</sub>Cl<sub>2</sub> solution of the compound which showed some decomposition during the crystallization period. After choosing a crystal for X-ray analysis the remaining crystals were dissolved in CDCl<sub>3</sub> and a boron-11 NMR spectrum taken resulting in a spectrum identical to the uncrystallized bulk solid. Due to the instability it was not possible to obtain a suitable amount of crystals for elemental analysis.

**Preparation of [(PPh<sub>3</sub>)<sub>2</sub>(CO)OsB<sub>4</sub>H<sub>6</sub>{ $\eta^5$ -(C<sub>5</sub>Me<sub>5</sub>)Ir}·CH<sub>2</sub>Cl<sub>2</sub>] (**2a**), [(PPh<sub>3</sub>)<sub>2</sub>(CO)OsB<sub>4</sub>H<sub>6</sub>{ $\eta^5$ -(C<sub>5</sub>Me<sub>5</sub>)Rh}] (**2b**), and [(PPh<sub>3</sub>)<sub>2</sub>(CO)Os( $\mu$ -H){ $\eta^5$ -(C<sub>5</sub>Me<sub>5</sub>)Ir}B<sub>3</sub>H<sub>6</sub>] (**3**). The experiment was carried out essentially as described above. [(PPh<sub>3</sub>)<sub>2</sub>(CO)OsB<sub>5</sub>H<sub>9</sub>] (200 mg, 0.25 mmol) was placed in the flask, stirred in THF until dissolved, and then deprotonated at -35 °C with *n*-BuLi (0.5 mmol). After stirring for 15 min, 0.114 g (0.125 mmol) of [{ $\eta^5$ -(C<sub>5</sub>Me<sub>5</sub>)Ir}Cl<sub>2</sub>]<sub>2</sub> was added *via* tipper tube, ca. 20 mL of CH<sub>2</sub>Cl<sub>2</sub> condensed in, and the mixture allowed to warm overnight to room temperature with stirring giving a clear red-brown solution. The reaction, including deprotonation, was also carried out at ambient temperature with similar results. The solution was reduced to dryness, redissolved in CH<sub>2</sub>Cl<sub>2</sub>, applied to TLC plates, and developed using 35/65 CH<sub>2</sub>Cl<sub>2</sub>/pentane as the mobile phase. Two strong bands at R<sub>f</sub> 0.1–0.4 (A) and 0.5–0.7 (B) were observed. Each was purified separately on TLC plates. Band A separated into three components, two of which have been identified as metallaborane products. One, at R<sub>f</sub> 0.5, was characterized, after crystallization, as [(PPh<sub>3</sub>)<sub>2</sub>(CO)Os( $\mu$ -H){ $\eta^5$ -(C<sub>5</sub>Me<sub>5</sub>)Ir}B<sub>3</sub>H<sub>6</sub>].0.9(C<sub>6</sub>H<sub>6</sub>) (**3**) (12.5 mg, 4.5% yield, IR  $\nu_{\max}$  cm<sup>-1</sup> 2500(m) (B-H), 1925(s) (CO); anal., C: calcd 53.33; H: 4.9; obsd C:53.11, H:5.0; low resolution FAB mass spectrum:  $m/e$  (100%) for C<sub>47</sub>H<sub>52</sub>B<sub>3</sub>O<sub>1</sub>P<sub>2</sub>IrOs<sub>1</sub> obsd: 1110.3, calcd: 1110.30),**

and it is described below. A second component of band A, at R<sub>f</sub> 0.3, was isolated as a yellow solid which on recrystallization from CH<sub>2</sub>Cl<sub>2</sub>/C<sub>5</sub>H<sub>12</sub> gave crystals which analyzed for [(PPh<sub>3</sub>)<sub>2</sub>(CO)OsB<sub>4</sub>H<sub>6</sub>{ $\eta^5$ -(C<sub>5</sub>Me<sub>5</sub>)Ir}]·CH<sub>2</sub>Cl<sub>2</sub> (**2a**) (1.9 mg, 6.8% yield, anal., calcd C: 47.87, H: 4.4, obsd C: 48.26, H: 4.4). Electrospray high resolution mass spectrum  $m/e$  (100%) for C<sub>47</sub>H<sub>51</sub>B<sub>4</sub>O<sub>1</sub>P<sub>2</sub>IrOs<sub>1</sub> obsd: 1120.295, calcd: 1120.305. IR  $\nu_{\max}$  cm<sup>-1</sup> for A 2497(m), 2425(sh) (B-H), 1950 (CO). In one experiment 58 mg (21% yield) of **2a** was isolated. The rhodium analogue of **2a** was prepared similarly using [{ $\eta^5$ -(C<sub>5</sub>Me<sub>5</sub>)Rh}Cl<sub>2</sub>]<sub>2</sub> to give [(PPh<sub>3</sub>)<sub>2</sub>(CO)OsB<sub>4</sub>H<sub>6</sub>{ $\eta^5$ -(C<sub>5</sub>Me<sub>5</sub>)Rh}] (**2b**) (10.4 mg, 4.1% yield). The CH<sub>2</sub>Cl<sub>2</sub>-solvated crystals of **2a** were found to lose solvent, and so crystals suitable for single-crystal X-ray structure determination were grown from diffusion of pentane into a benzene solution of the compound. Crystals of compound **3** were grown similarly. On repurification of band B using TLC, 43 mg (20%) of *nido*-[2,2,2-(PPh<sub>3</sub>)<sub>2</sub>(CO)OsB<sub>4</sub>H<sub>7</sub>(C<sub>4</sub>H<sub>9</sub>)] (**6**) [identified by NMR, IR, and high resolution mass spectroscopy:  $m/e$  (100%) C<sub>41</sub>H<sub>46</sub>B<sub>4</sub>O<sub>1</sub>P<sub>2</sub>Os<sub>1</sub>H<sub>1</sub> calcd 851.3109, obsd 851.3085; IR  $\nu_{\max}$  cm<sup>-1</sup> 2526 s (BH), 1949s (CO)], was obtained.

**X-ray Structure Determinations.** Crystals of the appropriate compound were obtained as described above and mounted on glass fibers in random orientations. Preliminary examination and data collection were performed using a Siemens R3 automated single-crystal X-ray diffractometer using a graphite monochromated Mo K $\alpha$  radiation ( $\lambda = 0.71073$  Å) at 295(5) K for **1**, 143 K for **2a**, and 126(5) K for **3**. Autoindexing of 10 centered reflections from the rotation photograph indicated a monoclinic lattice for **1**, a triclinic lattice for **2a**, and a rhombohedral lattice for **3**. Axial photographs were taken to confirm cell lengths. Final cell constants and orientation matrix for data collection were calculated by least squares refinement of the setting angles for 30 reflections (5° < 2 $\theta$  < 12°) **1**, (10° < 2 $\theta$  < 30°) **2a**, (8° < 2 $\theta$  < 33°) **3**. Intensity data were collected using  $\omega$ -2 $\theta$  scans with variable scan speed. Three representative reflections measured every 97 reflections showed <35% variation during data collection due to decay for **1**, <3% for **2a** and <15% for **3**. Crystal data and intensity data collection parameters are listed in Table 1. Data reduction and structure solutions were carried out using the SHELXTL-PLUS (VMS) software package.<sup>34</sup> Least-squares refinements were achieved using SHELXL-93.<sup>35</sup> Empirical absorption corrections were applied to the data using  $\psi$ -scan reflections. The structures were

**Table 2. Atomic Coordinates ( $\times 10^4$ ) and Equivalent Isotropic Displacement Parameters ( $\text{\AA}^2 \times 10^3$ ) for 1<sup>a</sup>**

	x	y	z	U(eq)
Os(2)	2544(1)	-6056(1)	6895(1)	36(1)
Ir(1)	2793(1)	-4565(1)	6197(1)	41(1)
P(1)	2076(3)	-7674(4)	6895(2)	44(1)
P(2)	2641(3)	-5749(4)	7815(2)	43(1)
P(3)	2625(3)	-3968(4)	5356(2)	46(1)
O(1)	4322(8)	-6434(12)	7007(7)	81(5)
O(2)	3612(10)	-2787(12)	6654(7)	88(6)
B(5)	1933(15)	-5785(17)	6129(8)	51(7)
B(4)	1337(12)	-5506(16)	6647(8)	40(5)
B(6)	1483(10)	-4577(17)	6242(7)	34(5)
B(7)	2929(13)	-6088(18)	6116(9)	48(6)
B(3)	2050(10)	-4547(14)	6856(7)	27(4)
C(1)	3656(14)	-6338(14)	6979(7)	51(5)
C(2)	3304(13)	-3449(16)	6460(9)	63(6)
C(3)	1487(9)	-7915(13)	6285(7)	40(5)
C(4)	671(9)	-7792(18)	6236(9)	70(7)
C(5)	230(14)	-7901(19)	5778(9)	80(8)
C(6)	575(15)	-8122(20)	5330(9)	83(8)
C(7)	1380(16)	-8242(17)	5383(9)	73(7)
C(8)	1850(13)	-8154(17)	5855(7)	61(6)
C(9)	2777(12)	-8666(15)	6920(8)	60(6)
C(10)	3477(11)	-8630(14)	7236(8)	58(6)
C(11)	3985(14)	-9389(19)	7271(12)	90(9)
C(12)	3787(18)	-10257(20)	7019(13)	98(10)
C(13)	3104(20)	-10315(20)	6739(12)	100(10)
C(14)	2606(16)	-9548(18)	6685(11)	94(9)
C(15)	1398(13)	-8046(14)	7364(7)	55(6)
C(16)	836(12)	-7405(17)	7529(8)	66(7)
C(17)	295(15)	-7642(25)	7864(9)	97(10)
C(18)	296(17)	-8606(26)	8072(8)	96(11)
C(19)	868(16)	-9228(22)	7923(9)	88(9)
C(20)	1391(12)	-8955(18)	7575(8)	66(6)
C(21)	3195(11)	-6690(15)	8190(7)	52(5)
C(22)	4000(10)	-6573(19)	8319(9)	72(7)
C(23)	4428(15)	-7366(21)	8545(12)	101(11)
C(24)	4100(19)	-8195(24)	8668(9)	103(10)
C(25)	3299(18)	-8279(19)	8569(10)	93(9)
C(26)	2857(14)	-7573(18)	8323(8)	67(7)
C(27)	1737(10)	-5596(14)	8172(7)	47(5)
C(28)	1096(11)	-5068(16)	7957(8)	60(6)
C(29)	461(13)	-4890(18)	8215(8)	74(8)
C(30)	423(11)	-5265(16)	8717(8)	54(6)
C(31)	1019(13)	-5726(16)	8917(8)	62(6)
C(32)	1679(13)	-5918(18)	8668(7)	69(7)
C(33)	3201(10)	-4656(15)	8045(6)	48(5)
C(34)	3687(13)	-4177(16)	7719(8)	67(7)
C(35)	4134(12)	-3426(18)	7893(9)	70(7)
C(36)	4138(14)	-3091(19)	8389(9)	74(7)
C(37)	3683(15)	-3587(20)	8709(10)	83(8)
C(38)	3200(13)	-4344(19)	8539(8)	74(8)
C(39)	2215(14)	-2748(16)	5283(8)	69(7)
C(40)	2217(14)	-2338(19)	4793(9)	81(8)
C(41)	1862(18)	-1448(24)	4726(13)	109(11)
C(42)	1536(14)	-969(19)	5141(14)	101(11)
C(43)	1539(14)	-1387(23)	5632(13)	100(10)
C(44)	1920(14)	-2282(20)	5690(11)	82(8)
C(45)	3518(14)	-3876(18)	5002(7)	71(7)
C(46)	3545(15)	-4187(19)	4493(8)	79(8)
C(47)	4233(20)	-4092(21)	4260(12)	106(11)
C(48)	4877(19)	-3696(24)	4490(13)	115(13)
C(49)	4881(14)	-3397(31)	4981(13)	146(17)
C(50)	4198(16)	-3550(29)	5244(11)	141(16)
C(51)	1912(13)	-4715(15)	4946(8)	59(6)
C(52)	2192(17)	-5620(17)	4811(10)	89(9)
C(53)	1664(23)	-6264(24)	4506(10)	102(11)
C(54)	909(29)	-5935(31)	4352(12)	140(19)
C(55)	699(17)	-5027(29)	4499(11)	110(12)
C(56)	1190(14)	-4413(22)	4782(8)	92(10)
C(57)	2115(23)	-12072(26)	7975(16)	151(16)
Cl(1)	1438(9)	-12299(14)	8337(7)	293(11)
Cl(2)	1738(8)	-11765(9)	7334(6)	208(6)
Cl(3)	2681(8)	-11073(11)	8152(6)	225(6)
C(58)	3692(44)	416(39)	5309(23)	296(41)
Cl(4)	4295(9)	1042(12)	5760(5)	241(8)
Cl(5)	3483(10)	957(19)	4808(6)	315(12)
Cl(6)	3956(11)	-784(16)	5324(7)	289(9)

<sup>a</sup> U(eq) is defined as one-third of the orthogonalized  $U_{ij}$  tensor.

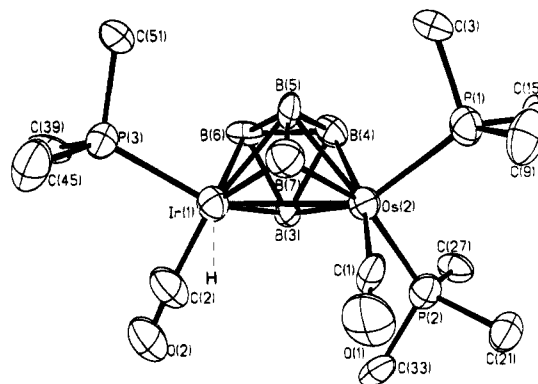


**Figure 1.** Molecular structure of *pileo*-[2,2,2-H(PPh<sub>3</sub>)(CO)-3,3,3-(PPh<sub>3</sub>)<sub>2</sub>(CO)-2,3-IrOsB<sub>5</sub>H<sub>5</sub>] (1), with phenyl rings with the exception of *ipso*-carbon atoms omitted for clarity. All heavy atoms were located from the X-ray data although the assignment of the relative positions of the metal atoms is made on the basis of other considerations as discussed in the text. Hydrogen atoms were not located although NMR data show a terminal hydrogen atom on each boron atom and a terminal metal hydride on a metal atom. The proposed position of the metal hydride is indicated by dashed lines.

solved by the Patterson Method and refined successfully in the space group as shown in Table 1. Full matrix least-squares refinement was carried out by minimizing  $\sum w(F_o^2 - F_c^2)^2$ .

For compound 1, *pileo*-[(PPh<sub>3</sub>)<sub>2</sub>(CO)OsB<sub>5</sub>H<sub>5</sub>IrH(PPh<sub>3</sub>)(CO)]·2CHCl<sub>3</sub>, the non-hydrogen atoms were refined anisotropically to convergence. Only three hydrogen atoms out of five connected to boron atoms were located from the difference Fourier synthesis, and these were included in the final refinement. The phenyl H atoms were calculated using a riding model (AFIX 43, SHELXL-93). The final residual values were:  $R(F) = 9.92$  for reflections  $I > 2\sigma(I)$ ,  $wR(F^2) = 24.44\%$ ,  $s = 1.017$ . Structure refinement parameters are listed in Table 1. The atomic coordinates for the non-hydrogen atoms and selected bond distances and angles are listed in Tables 2 and 7 respectively. A projection view of the molecule with non-hydrogen atoms represented by 25% probability ellipsoids for 1 is presented in Figure 1.

For compound 2a, [(PPh<sub>3</sub>)<sub>2</sub>(CO)OsB<sub>4</sub>H<sub>6</sub>{ $\eta^5$ -(C<sub>5</sub>Me<sub>5</sub>)Ir}]·C<sub>6</sub>H<sub>6</sub>, the non-hydrogen atoms were refined anisotropically to convergence except the disordered solvent C atoms. All hydrogen atoms connected to boron atoms were located from the difference Fourier synthesis, and the terminal H atoms were refined isotropically. Of the two bridging H atoms one was refined freely H(2,5) but the second, H(1,2), could not be refined. The phenyl H atoms were calculated using a riding model (AFIX 43, SHELXL-93) and the methyl H atoms were calculated using the appropriate riding model (AFIX 33). The SOF for the partial occupancy Cl/H was refined. The compound crystallizes with two 1/2 molecules of benzene as solvent; one is disordered and is centered around one of the (-) centers. The C atoms of the disordered solvent molecule were refined isotropically. Attempts to refine the disordered molecule as a rigid body or with geometrical restraints were not successful. The final residual values were:  $R(F) = 4.40$  for reflections  $I > 2\sigma(I)$ ,  $wR(F^2) = 10.14\%$ ,  $s = 1.063$ . Structure refinement parameters are listed in Table 1. The atomic coordinates for the non-hydrogen atoms and selected interatomic distances are listed in Tables 3 and 9, respectively. A projection view of the molecule with non-hydrogen atoms represented by 50% probability ellipsoids for 2a is shown in Figure 2.

(34) Sheldrick, G. M., Siemens Analytical X-Ray Division, Madison, WI, 1991.

(35) Sheldrick, G. M., 1993, SHELXL-93. Structure refinement package, Universität Göttingen, Germany.

**Table 3. Atomic Coordinates [ $\times 10^4$ ] and Equivalent Isotropic Displacement Parameters [ $\text{\AA}^2 \times 10^3$ ] for 2a**

	x	y	z	$U(\text{eq})^a$
Ir(1)	-95(1)	6997(1)	6466(1)	20(1)
Os(2)	-386(1)	7444(1)	7984(1)	17(1)
P(1)	-2199(1)	6464(1)	8846(1)	19(1)
P(2)	-1178(1)	9254(1)	8001(1)	19(1)
Cl	3237(13)	6758(11)	5949(8)	52(5)
B(3)	784(7)	8229(6)	6751(4)	25(1)
B(4)	1769(7)	7134(7)	6497(4)	31(2)
B(5)	928(7)	6218(6)	7301(4)	28(1)
B(6)	1663(7)	7433(6)	7322(5)	29(1)
O	770(4)	7575(4)	9259(3)	33(1)
C(1)	296(5)	7541(5)	8780(4)	24(1)
C(2)	-1652(6)	6834(5)	5904(4)	28(1)
C(3)	-756(7)	7552(5)	5352(4)	28(1)
C(4)	461(6)	6990(5)	5210(3)	27(1)
C(5)	276(7)	5888(5)	5667(3)	27(1)
C(6)	-1020(7)	5797(5)	6091(3)	28(1)
C(7)	-3036(7)	7060(6)	6164(4)	39(2)
C(8)	-997(7)	8684(5)	4928(4)	36(2)
C(9)	1626(7)	7433(6)	4624(4)	36(2)
C(10)	1259(7)	4995(5)	5643(4)	35(2)
C(11)	-1630(8)	4773(5)	6566(4)	38(2)
C(12)	-2240(6)	5105(5)	8681(3)	24(1)
C(13)	-3298(6)	4747(5)	8562(4)	30(1)
C(14)	-3324(7)	3678(5)	8499(4)	37(2)
C(15)	-2316(8)	2975(6)	8563(4)	42(2)
C(16)	-1262(8)	3316(5)	8681(5)	40(2)
C(17)	-1218(7)	4378(5)	8738(4)	33(1)
C(18)	-3758(5)	7038(4)	8798(3)	21(1)
C(19)	-3904(5)	7557(5)	8060(3)	23(1)
C(20)	-5072(6)	7996(5)	7988(4)	29(1)
C(21)	-6092(6)	7962(5)	8638(4)	31(1)
C(22)	-5955(6)	7460(5)	9372(4)	31(1)
C(23)	-4800(6)	6990(5)	9449(4)	25(1)
C(24)	-2352(6)	6137(5)	9898(3)	25(1)
C(25)	-2855(7)	5160(5)	10368(4)	35(2)
C(26)	-3026(8)	4944(7)	11172(4)	47(2)
C(27)	-2723(8)	5698(7)	11511(4)	44(2)
C(28)	-2226(7)	6670(7)	11058(4)	39(2)
C(29)	-2043(6)	6875(6)	10259(4)	30(1)
C(30)	-2363(5)	9884(4)	7494(3)	22(1)
C(31)	-3275(6)	10629(5)	7797(4)	28(1)
C(32)	-4157(7)	11115(5)	7410(4)	35(2)
C(33)	-4126(6)	10857(5)	6710(4)	33(1)
C(34)	-3217(6)	10136(5)	6401(4)	29(1)
C(35)	-2324(6)	9655(4)	6782(3)	23(1)
C(36)	-1920(5)	9492(5)	8991(3)	22(1)
C(37)	-3153(6)	9165(5)	9382(4)	29(1)
C(38)	-3711(6)	9270(5)	10144(4)	33(1)
C(39)	-3078(7)	9709(6)	10534(4)	36(2)
C(40)	-1874(7)	10055(6)	10152(4)	36(2)
C(41)	-1288(6)	9950(5)	9383(4)	26(1)
C(42)	37(6)	10269(5)	7642(3)	24(1)
C(43)	1256(6)	9975(5)	7719(4)	30(1)
C(44)	2164(7)	10750(6)	7498(4)	37(2)
C(45)	1881(7)	11808(6)	7188(5)	43(2)
C(46)	691(8)	12095(6)	7095(5)	47(2)
C(47)	-223(6)	11337(5)	7329(4)	30(1)
C(48)	3927(8)	9748(9)	5606(5)	56(3)
C(49)	4687(9)	8935(9)	5310(6)	59(3)
C(50)	5773(9)	9197(10)	4700(6)	61(3)
C(51)	5306(34)	5958(32)	4366(23)	258(16)
C(52)	5189(16)	5970(14)	3574(11)	116(5)
C(53)	4991(35)	4948(34)	4612(20)	239(15)

<sup>a</sup>  $U(\text{eq})$  is defined as one-third of the trace of the orthogonalized  $U_{ij}$  tensor.

The non-hydrogen atoms in compound **3**, *closo*-[( $\text{PPh}_3$ )<sub>2</sub>-(CO)Os( $\mu$ -H){ $\eta^5$ -(C<sub>5</sub>Me<sub>5</sub>)Ir}B<sub>5</sub>H<sub>5</sub>] $\cdot$ 0.9C<sub>6</sub>H<sub>6</sub>, were refined anisotropically to convergence except for those on the solvent C-atoms. All hydrogen atoms connected to boron atoms, except the H-bridging Ir-B(5), were located from the difference Fourier synthesis, and these were included in the final refinement. The phenyl H atoms were calculated using a riding model (AFIX 43, SHELXL-93), and the methyl H atoms

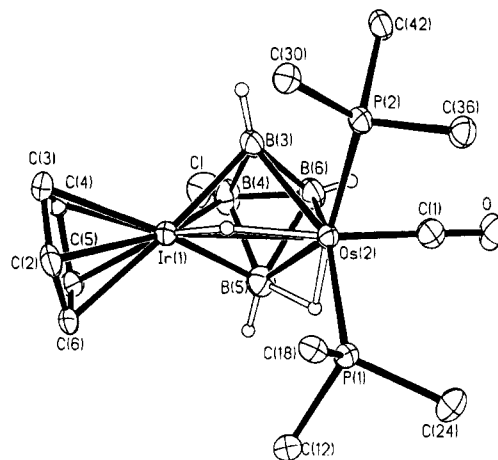


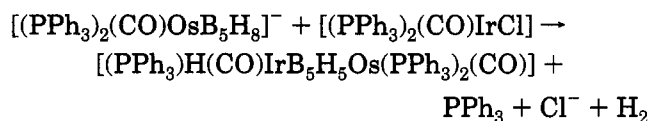
**Figure 2.** Molecular structure of *closo*-[1-(C<sub>5</sub>Me<sub>5</sub>)-2,2,2-(CO)(PPh<sub>3</sub>)<sub>2</sub>-1,2-( $\mu$ H)-1,2-IrOsB<sub>4</sub>H<sub>4</sub>Cl] (**2a**), with methyl groups on the C<sub>5</sub>Me<sub>5</sub> ring and the phenyl rings with the exception of *ipso*-carbon atoms omitted for clarity. All atoms were located from the X-ray data. The B(4) vertex holds disordered terminal Cl and H atoms with occupancy factors of 20% and 80%, respectively.

were calculated using the appropriate riding model. The SOF for the solvent molecule was refined and agrees well with the microanalytical data (91%). The final residual values were:  $R(F) = 6.94$  for reflections  $I > 2\sigma(I)$ ,  $wR(F^2) = 17.12\%$ ,  $s = 1.033$ . Structure refinement parameters are listed in Table 1. The atomic coordinates for the non-hydrogen atoms and selected bond distances and angles are listed in Tables 4 and 10, respectively. A projection view of the molecule with non-hydrogen atoms represented by 50% probability ellipsoids for **3** is presented in Figure 3.

A complete list of positional and isotropic displacement coefficients for hydrogen atoms and a list of anisotropic displacement coefficients for the non-hydrogen atoms are submitted as supporting information.

## Results and Discussion

Deprotonation of a tetrahydrofuran (THF) solution of *nido*-[(PPh<sub>3</sub>)<sub>2</sub>(CO)OsB<sub>5</sub>H<sub>5</sub>] with methylolithium at  $-35$  °C followed by addition of [*trans*-(PPh<sub>3</sub>)<sub>2</sub>(CO)IrCl] and slow warming to room temperature gave, after chromatographic separation, the heterobimetallaheptaborane *pileo*-[1,1,1-H(PPh<sub>3</sub>)(CO)-2,2,2-(PPh<sub>3</sub>)<sub>2</sub>(CO)-1,2-IrOsB<sub>5</sub>H<sub>5</sub>] (**1**) in up to 33% yield according to the following equation:



A small amount of the known osmapentaborane compound, *nido*-[2,2,2-(PPh<sub>3</sub>)<sub>2</sub>(CO)OsB<sub>4</sub>H<sub>5</sub>],<sup>29</sup> was also isolated from the reaction. If *n*-butyllithium is used as the deprotonating agent then a new, alkyl substituted analogue, *nido*-[2,2,2-(PPh<sub>3</sub>)<sub>2</sub>(CO)OsB<sub>4</sub>H<sub>7</sub>(*n*-Bu)] (**6**), is produced and it is described later. Compound **1** was identified by NMR spectroscopy (Table 5), IR and FAB mass spectroscopy, and a single-crystal X-ray diffraction study. All heavy atoms were located from the X-ray diffraction data although high ambient atmospheric humidity precluded a low-temperature structural determination and this resulted in significant decomposition of the crystal in the X-ray beam such that the structure is of a poorer quality than we would have

**Table 4. Atomic Coordinates [ $\times 10^4$ ] and Equivalent Isotropic Displacement Parameters [ $\text{\AA}^2 \times 10^3$ ] for 3**

	<i>x</i>	<i>y</i>	<i>z</i>	<i>U</i> (eq) <sup>a</sup>
Ir(2)	8791(1)	871(1)	3845(1)	29(1)
Os(3)	9427(1)	1675(1)	3139(1)	29(1)
P(1)	9964(1)	2499(1)	3000(1)	29(1)
P(2)	9326(1)	1356(1)	2264(1)	30(1)
O	10272(4)	1590(4)	3579(5)	57(3)
B(1)	9181(7)	1652(6)	3960(6)	42(4)
B(4)	8906(6)	1881(6)	3557(6)	34(4)
B(5)	8555(7)	1403(7)	3969(8)	48(5)
C(1)	9178(5)	611(5)	4390(6)	41(4)
C(2)	8764(6)	591(5)	4634(5)	38(3)
C(3)	8339(5)	248(5)	4347(5)	36(3)
C(4)	8491(5)	60(5)	3924(5)	32(3)
C(5)	9005(5)	288(5)	3948(5)	30(3)
C(6)	9693(6)	885(7)	4610(7)	68(6)
C(7)	8764(8)	849(6)	5138(6)	61(5)
C(8)	7805(6)	76(7)	4507(7)	59(5)
C(9)	8172(7)	-342(5)	3557(7)	60(5)
C(10)	9313(7)	173(7)	3590(7)	68(6)
C(11)	10449(5)	2669(5)	2501(5)	31(3)
C(12)	10636(5)	2360(5)	2406(7)	46(4)
C(13)	10976(6)	2452(6)	2010(8)	61(5)
C(14)	11139(5)	2874(6)	1717(7)	51(4)
C(15)	10969(6)	3195(6)	1799(6)	47(4)
C(16)	10629(5)	3094(5)	2191(6)	37(3)
C(17)	9719(5)	2895(5)	2801(5)	33(3)
C(18)	9322(5)	2707(5)	2465(5)	37(3)
C(19)	9160(6)	3032(6)	2269(6)	52(4)
C(20)	9378(7)	3512(6)	2438(7)	58(5)
C(21)	9772(6)	3693(6)	2772(6)	47(4)
C(22)	9941(6)	3394(5)	2956(6)	44(4)
C(23)	10325(5)	2817(4)	3591(6)	36(3)
C(24)	10819(5)	2973(5)	3626(6)	49(4)
C(25)	11073(7)	3194(6)	4093(7)	62(5)
C(26)	10845(7)	3274(5)	4499(7)	57(5)
C(27)	10361(7)	3128(5)	4462(6)	50(4)
C(28)	10092(6)	2892(5)	4004(6)	45(4)
C(29)	9256(5)	1682(5)	1704(5)	36(3)
C(30)	8821(6)	1542(8)	1470(8)	85(8)
C(31)	8796(7)	1793(10)	1033(10)	123(12)
C(32)	9183(7)	2198(9)	850(8)	87(8)
C(33)	9612(8)	2362(6)	1087(6)	60(5)
C(34)	9666(7)	2115(5)	1510(6)	54(5)
C(35)	9767(5)	1198(5)	2015(6)	34(3)
C(36)	9951(6)	967(6)	2365(7)	51(4)
C(37)	10236(6)	788(6)	2184(8)	60(5)
C(38)	10353(6)	817(7)	1673(9)	65(5)
C(39)	10209(8)	1046(8)	1328(8)	76(6)
C(40)	9911(6)	1239(6)	1495(6)	50(4)
C(41)	8755(5)	753(5)	2197(6)	36(3)
C(42)	8320(5)	669(6)	2433(6)	45(4)
C(43)	7909(6)	229(7)	2402(7)	64(5)
C(44)	7902(7)	-141(7)	2153(8)	64(5)
C(45)	8317(7)	-74(7)	1912(11)	92(8)
C(46)	8751(6)	385(6)	1928(8)	69(6)
C(47)	9940(6)	1623(5)	3396(6)	44(4)
C(48)	11170(16)	1939(21)	30(27)	305(20)
C(49)	11132(19)	2230(17)	417(19)	305(20)
C(50)	10722(27)	2287(14)	436(17)	305(20)
C(51)	10349(17)	2051(21)	67(26)	305(20)
C(52)	10388(19)	1760(17)	-320(18)	305(20)
C(53)	10798(27)	1704(14)	-339(18)	305(20)

<sup>a</sup> *U*(eq) is defined as one-third of the trace of the orthogonalized  $U_{ij}$  tensor.

desired. The structure is, however, fully in accord with the NMR, IR and mass spectrum data. A drawing of the molecule is shown in Figure 1. Table 6 lists selected interatomic dimensions for 1. The cluster contains a metal binuclear subunit with an approximate octahedral disposition of the phosphine and carbonyl moieties around the metal atoms incorporated into a  $\{\text{B}_5\text{H}_5\}$  subcluster such that one of the boron vertices is capping an  $\{\text{IrOsB}\}$  face, thus conforming to a *pileo* cluster

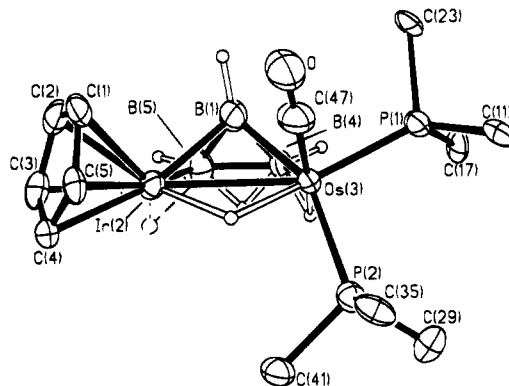


**Figure 3.** Molecular structure of *nido*-[2,2,2,-(CO)(PPh<sub>3</sub>)-3-(C<sub>5</sub>Me<sub>5</sub>)-2-( $\mu$ H)-2,3-IrOsB<sub>3</sub>H<sub>6</sub>](3), with methyl groups on the C<sub>5</sub>Me<sub>5</sub> ring and the phenyl rings with the exception of *ipso*-carbon atoms omitted for clarity. All atoms were located from the X-ray data with the exception of the hydrogen atom bridging Ir(2)–B(5) which is evident from NMR data. Its position is indicated by dashed lines.

description.<sup>36</sup> *Pileo* clusters, although well recognized in transition metal cluster chemistry,<sup>37</sup> are quite rare in metallaborane chemistry and this compound represents only the second  $2n$  skeletal electron *pileo*-metallaborane cluster, with a BH vertex capping an  $\text{M}_2\text{B}$  face, to be structurally characterized. We have recently published details on the isoelectronic isostructural analogue  $[\{(\eta^5\text{-C}_5\text{Me}_5)\text{Ir}\}_2\text{B}_5\text{H}_5]$  (5),<sup>21</sup> and the first row analogue  $[\{(\eta^5\text{-C}_5\text{Me}_5)\text{Co}\}_2\text{B}_5\text{H}_5]$ <sup>8</sup> was prepared some time ago and identified from NMR and mass spectroscopic data together with the trimetalla analogues  $[1,2,3\text{-}\{\eta^5\text{-C}_5\text{H}_5\}\text{Co}\}_3\text{B}_4\text{H}_4]$ ,<sup>12,15</sup> and  $[1,2,3\text{-}\{\eta^5\text{-C}_5\text{Me}_5\}\text{Co}\}_3\text{B}_4\text{H}_4]$ ,<sup>8,16</sup> in which the boron vertex caps the triangular  $[\{\eta^5\text{-C}_5\text{Me}_5\}\text{Co}\}_3]$  face. Recently *pileo* species have been characterized in which a BH<sub>2</sub> group caps an  $\text{M}_2\text{B}$  face in  $[1\text{-}\{\eta^5\text{-C}_5\text{Me}_5\}\text{Fe}\text{-}2\text{-Mo}(\text{PMe}_2\text{Ph})_3\text{B}_5\text{H}_7]$  (4).<sup>27</sup> Another system, a  $n + 1$  skeletal electron pair, bicapped molybdenadaborane species  $[\{(\eta^5\text{-C}_5\text{H}_4\text{Me})\text{Mo}\}_2\text{B}_5\text{H}_9]$ ,<sup>3</sup> in which the "capping" BH moieties are joined to the cluster *via* two bridging hydrogen atoms, thereby constituting what are essentially capping BH<sub>3</sub> groups, has been structurally characterized.<sup>3</sup>

Hydrogen atoms in 1 were not located from the X-ray data but, in addition to a terminal hydrogen atom on each boron vertex, the <sup>1</sup>H{<sup>11</sup>B} spectrum shows the presence of a terminal metal hydride. This is also supported by the IR spectrum which shows an absorption typical for an M–H bond [ $\nu(\text{MH})$  2093 cm<sup>-1</sup>]. The position of the terminal metal hydride may be deduced from a consideration of a number of factors. The hydride resonance is coupled to one *cis*-phosphorus nucleus (<sup>2</sup>*J* = 15.5 Hz) and shows no coupling to boron suggesting a terminal rather than a Ir–H–Os or M–H–B bridging position. The inclusion of the electron pair associated with the hydrogen atom into the cluster *via* a bridging interaction, along with the associated orbital, might be expected to result in a conventional *closo* structure rather than the observed *pileo* structure. The Ir(2)–Os(3) distance of 2.7916(13) Å is similar to the non-hydrogen-bridged value of 2.7079(10) Å for the

(36) For a definition of *pileo*, see ref 4a, p 523.

(37) For example see: (a) Albano, V. G.; Bellon, P. L.; Ciani, G. F. *J. Chem. Soc., D*, **1969**, 1024. (b) Eady, C. R.; Johnson, B. F. G.; Lewis, J. J. *Chem. Soc., Dalton Trans.* **1975**, 2606. (c) Mingos, D. M. P.; Wales, D. J. *Introduction to Cluster Chemistry*; Prentice Hall: New York, 1990.

**Table 5.**  $^{11}\text{B}$ ,  $^1\text{H}$ , and  $^{31}\text{P}$  NMR Data for  $[(\text{PPh}_3)_2(\text{CO})\text{HIrB}_5\text{H}_5\text{Os}(\text{CO})(\text{PPh}_3)_2]$  (**1**) with  $[\{\eta^5\text{-}(\text{C}_5\text{H}_5)\text{Fe}\}(\text{ML}_3\text{H})\text{B}_5\text{H}_7]$  (**4a**)<sup>27</sup> and  $[\{\eta^5\text{-}(\text{C}_5\text{Me}_5)\text{Ir}\}_2\text{B}_5\text{H}_5]$  (**5**)<sup>21</sup> for Comparison (Spectra Recorded at 25 °C, **1** and **5** in  $\text{CDCl}_3$ , **4a** in  $\text{C}_6\text{D}_6$ )

proposed assignment	compound <b>1</b>			compound <b>4a</b>		compound <b>5</b>	
	$\delta(^{11}\text{B})^b$	$\omega_{1/2}/\text{Hz}$	$\delta(^1\text{H})$	$\delta(^{11}\text{B})$	$\delta(^1\text{H})$	$\delta(^{11}\text{B})$	$\delta(^1\text{H})$
7	ca. +94	1200	+10.33	94.3	+9.22	+103.0	+11.28
4	$\left\{ \begin{array}{l} +77.2 \\ +71.5 \\ +56.8 \\ -7.5 \end{array} \right.$	500	+10.15 <sup>c</sup>	79.3	+9.15	$\left\{ \begin{array}{l} +52.6 \\ +52.6 \\ +52.3 \\ -17.3 \end{array} \right.$	+9.12
5		400	+10.59	15.5	+4.20		+6.75
6		400	+7.80	63.1	+6.30 <sup>f</sup>		+3.68
3		270	-4.03	-9.0	-0.91		+2.03
H <sub>Ir</sub>			-8.29 <sup>e</sup>				

<sup>a</sup>  $^{31}\text{P}$  NMR data in ppm:  $\text{P}_{(1/2)} + 7.86$  ( $^2J[^{31}\text{P}_{(1/2)} - ^{31}\text{P}_{(2/1)}] = 13$  Hz),  $\text{P}_{(3)} + 6.99$  ( $^2J[^{31}\text{P}_{(3)} - ^{31}\text{P}_{(2/1)}] = 24$  Hz),  $\text{P}_{(2/1)} + 0.96$  ( $^2J[^{31}\text{P}_{(2/1)} - ^{31}\text{P}_{(1/2)}] = 13$  Hz). <sup>b</sup> Resonances too broad to observe (B-H) coupling. <sup>c</sup> Doublet with coupling of undetermined origin:  $^nJ = 17.8$  Hz. <sup>d</sup> Doublet with coupling of undetermined origin:  $^nJ = 12.0$  Hz. <sup>e</sup> Doublet:  $^2J[^{31}\text{P}(3) - ^1\text{H}] = 15.5$  Hz. Collapses to singlet on irradiation of resonance at  $\delta(^{31}\text{P}) + 6.99$  ppm. <sup>f</sup> Doublet coupled to phosphorous,  $J = 17$  Hz.

**Table 6.** Selected Interatomic Distances [Å] and Angles [deg] for *pileo*- $[(\text{PPh}_3)_2(\text{CO})\text{OsB}_5\text{H}_5\text{IrH}(\text{PPh}_3)(\text{CO})]$  (**1**)

Os(2)-Ir(1)	2.7916(13)	Ir(1)-C(2)	1.87(2)
Os(2)-B(7)	2.17(2)	Ir(1)-B(7)	2.12(2)
Os(2)-B(5)	2.20(2)	Ir(1)-B(3)	2.20(2)
Os(2)-B(4)	2.23(2)	Ir(1)-B(5)	2.22(2)
Os(2)-B(3)	2.24(2)	Ir(1)-B(6)	2.23(2)
Os(2)-P(1)	2.369(5)	Ir(1)-P(3)	2.327(5)
Os(2)-P(2)	2.413(5)	O(1)-C(1)	1.13(2)
Os(2)-C(1)	1.92(2)	O(2)-C(2)	1.15(2)
B(5)-B(7)	1.74(3)	B(4)-B(6)	1.69(3)
B(5)-B(4)	1.78(3)	B(4)-B(3)	1.84(3)
B(5)-B(6)	1.87(3)	B(6)-B(3)	1.80(3)
C(1)-Os(2)-B(7)	74.9(8)	C(2)-Ir(1)-B(7)	143.0(9)
C(1)-Os(2)-B(5)	121.8(9)	C(2)-Ir(1)-B(3)	89.1(8)
B(7)-Os(2)-B(5)	47.0(9)	B(7)-Ir(1)-B(3)	99.3(8)
C(1)-Os(2)-B(4)	166.5(8)	C(2)-Ir(1)-B(5)	159.2(9)
B(7)-Os(2)-B(4)	94.1(8)	B(7)-Ir(1)-B(5)	47.2(9)
B(5)-Os(2)-B(4)	47.4(8)	B(3)-Ir(1)-B(5)	70.1(8)
C(1)-Os(2)-B(3)	123.6(7)	C(2)-Ir(1)-B(6)	115.0(9)
B(7)-Os(2)-B(3)	96.5(8)	B(7)-Ir(1)-B(6)	96.6(8)
B(5)-Os(2)-B(3)	69.6(8)	B(3)-Ir(1)-B(6)	47.8(7)
B(4)-Os(2)-B(3)	48.7(7)	B(5)-Ir(1)-B(6)	49.5(9)
C(1)-Os(2)-P(1)	97.7(6)	C(2)-Ir(1)-P(3)	94.0(7)
B(7)-Os(2)-P(1)	96.0(7)	B(7)-Ir(1)-P(3)	105.3(6)
B(5)-Os(2)-P(1)	91.4(6)	B(3)-Ir(1)-P(3)	133.4(5)
B(4)-Os(2)-P(1)	91.2(6)	B(5)-Ir(1)-P(3)	99.2(5)
B(3)-Os(2)-P(1)	138.6(5)	B(6)-Ir(1)-P(3)	89.9(5)
C(1)-Os(2)-P(2)	86.0(6)	C(2)-Ir(1)-Os(2)	117.3(7)
B(7)-Os(2)-P(2)	156.9(6)	B(7)-Ir(1)-Os(2)	50.1(6)
B(5)-Os(2)-P(2)	148.6(7)	B(3)-Ir(1)-Os(2)	51.8(5)
B(4)-Os(2)-P(2)	102.6(5)	B(5)-Ir(1)-Os(2)	50.6(5)
B(3)-Os(2)-P(2)	83.1(5)	B(6)-Ir(1)-Os(2)	76.2(6)
P(1)-Os(2)-P(2)	99.4(2)	P(3)-Ir(1)-Os(2)	148.66(14)
C(1)-Os(2)-Ir(1)	91.6(5)	B(6)-B(3)-B(4)	55.2(11)
B(7)-Os(2)-Ir(1)	48.8(6)	B(6)-B(3)-Ir(1)	67.1(8)
B(5)-Os(2)-Ir(1)	51.2(6)	B(4)-B(3)-Ir(1)	99.5(10)
B(4)-Os(2)-Ir(1)	75.1(5)	B(6)-B(3)-Os(2)	101.1(11)
B(3)-Os(2)-Ir(1)	50.3(4)	B(4)-B(3)-Os(2)	65.4(9)
P(1)-Os(2)-Ir(1)	139.47(13)	Ir(1)-B(3)-Os(2)	77.9(6)
P(2)-Os(2)-Ir(1)	120.59(13)	B(6)-B(4)-B(5)	65.0(12)
B(7)-B(5)-B(4)	132(2)	B(6)-B(4)-B(3)	61.0(11)
B(7)-B(5)-B(6)	129(2)	B(5)-B(4)-B(3)	88.9(13)
B(4)-B(5)-B(6)	55.0(12)	B(6)-B(4)-Os(2)	105.3(11)
B(7)-B(5)-Os(2)	65.5(11)	B(5)-B(4)-Os(2)	65.5(10)
B(4)-B(5)-Os(2)	67.2(10)	B(3)-B(4)-Os(2)	66.0(9)
B(6)-B(5)-Os(2)	100.4(11)	B(4)-B(6)-B(3)	63.9(12)
B(7)-B(5)-Ir(1)	63.4(11)	B(4)-B(6)-B(5)	60.0(12)
B(4)-B(5)-Ir(1)	100.5(12)	B(3)-B(6)-B(5)	87.8(13)
B(6)-B(5)-Ir(1)	65.5(9)	B(4)-B(6)-Ir(1)	103.3(12)
Os(2)-B(5)-Ir(1)	78.2(8)	B(3)-B(6)-Ir(1)	65.0(8)
B(5)-B(7)-Ir(1)	69.4(11)	B(5)-B(6)-Ir(1)	65.0(9)
B(5)-B(7)-Os(2)	67.5(10)	O(1)-C(1)-Os(2)	174(2)
Ir(1)-B(7)-Os(2)	81.1(8)	O(2)-C(2)-Ir(1)	175(2)

Ir-Ir distance in **5** and very close to that of 2.799(1) Å in *closo*- $[(\text{CO})_3(\text{PPh}_3)(\text{PPh}_2\text{C}_6\text{H}_4)_2\text{Ir}_2\text{B}_4\text{H}_4]$ <sup>38</sup> which has a very similar ligand environment about the metal atoms and the metal-metal distances in, for example,

osmium carbonyl clusters.<sup>39,40</sup> In comparison the two iridium-osmium compounds **2a** and **3** described below both clearly contain an Ir- $\mu\text{H}$ -Os moiety and feature metal separations of 2.888 and 2.927 Å respectively. The most likely position is as shown in Figure 1 in a vacant octahedral coordination site perpendicular to the C(2)-Ir(1)-P(3) plane and parallel to the carbonyl group on the osmium.

The assignment of the position of the metal atoms is less well defined, as X-ray methods are not suitable for distinguishing between osmium and iridium atoms. The main distinguishing feature is the NMR chemical shift of the metal hydride which, in this compound, is at  $\delta(^1\text{H}) - 8.29$  ppm. There is a tendency for the chemical shift of osmium bound hydrogen atoms to have values to lower field than their iridium analogues although there will be much overlap and iridaboranes with similar or lower chemical shift values are known.<sup>41</sup> Conversely, iridaborane clusters with triphenylphosphine ligands on the metal have shown a very marked tendency to exhibit phosphine loss from the metal or migration of the phosphine to the borane cluster,<sup>28,42,43</sup> in many reactions, in contrast to osmaborane clusters. This may however reflect the fact that iridaboranes have been studied to a greater extent than osmaborane compounds. Clearly, this evidence is not definitive and there remains a degree of ambiguity as to the assignment of the metal atom positions. While the identification of the metal atoms may affect the assignment of the electrolobal contribution of the individual cluster vertex atom to the cluster bonding, it does, however, not affect the description of the combined contribution of the binuclear metal fragment which may be regarded as the combination of two effectively octahedral 18-electron metal moieties. These latter  $\{(\text{PPh}_3)_2(\text{CO})\text{Os}\}$  and  $\{(\text{PPh}_3)\text{H}(\text{CO})\text{Ir}\}$  groups each provide a 2-skeletal electron and 3-orbital contribution to the cluster (thus

(38) Crook, J. E.; Greenwood, N. N.; Kennedy, J. D.; McDonald, W. S. *J. Chem. Soc., Chem. Commun.* **1982**, 383.

(39) Wei, C. Y.; Garlaschelli, L.; Bau, R.; Koetzle, T. F. *J. Organomet. Chem.* **1981**, 213, 63.

(40) Churchill, M. R.; Hollander, F. J. *Inorg. Chem.* **1980**, 19, 306.

(41) For example: (a) Nestor, K.; Fontaine, X. L. R.; Greenwood, N. N.; Kennedy, J. D.; Plešek, J.; Stibr, B.; Thornton-Pett, M. *Inorg. Chem.* **1989**, 28, 2219. (b) Stibr, B.; Kennedy, J. D.; Drdakova, E.; Thornton-Pett, M. *Coll. Czech. Chem. Commun.* **1992**, 57, 1262. (c) Stibr, B.; Kennedy, J. D.; Drdakova, E.; Thornton-Pett, M. *J. Chem. Soc. Dalton Trans.* **1994**, 229. (d) Alcock, N. W.; Taylor, J. G.; Wallbridge, M. G. H. *J. Chem. Soc., Chem. Commun.* **1983**, 1168.

(42) (a) Bould, J.; Crook, J. E.; Greenwood, N. N.; Kennedy, J. D.; Thornton-Pett, M. *J. Chem. Soc., Dalton Trans.* **1990**, 1441. (b) Bould, J.; Kennedy, J. D.; Thornton-Pett, M. *J. Chem. Soc., Dalton Trans.* **1992**, 563.

(43) Bould, J.; Rath, N. P.; Barton, L. Submitted for publication in *Inorg. Chem.*

**Table 7.**  $^{11}\text{B}$ ,  $^1\text{H}$ , and  $^{31}\text{P}$  NMR Data for  $[(\text{PPh}_3)_2(\text{CO})\text{OsB}_4\text{H}_5\{\eta^5\text{-}(\text{C}_5\text{Me}_5)\text{Ir}\}]$  (**2a**) and  $[(\text{PPh}_3)_2(\text{CO})\text{OsB}_4\text{H}_5\{\eta^5\text{-}(\text{C}_5\text{Me}_5)\text{Rh}\}]$  (**2b**) in  $\text{CD}_2\text{Cl}_2$  Solution

proposed assignt	compound <b>2a</b> <sup>b</sup>				compound <b>2b</b> <sup>b</sup>			
	$\delta(^{11}\text{B})$ 298 K	$\delta(^1\text{H})$ 298 K	$\delta(^{11}\text{B})$ 179 K	$\delta(^1\text{H})$ 179 K	$\delta(^{11}\text{B})$ 298 K	$\delta(^1\text{H})$ 298 K	$\delta(^{11}\text{B})$ 180 K	$\delta(^1\text{H})$ 180 K
4 }	+55.7	+9.18	+54.7	+9.20	+64.7	+8.72	+65.2	+8.50
6 }	+45.7	+10.03	+43.0	10.02	+47.4	+7.48	+46	+7.30
3 }	+23.9(2)	+3.98(2)	+35.4	+5.19	+34.3(2)	+4.51(2)	+46	+5.19
5 }			+6.7	+2.59			+23.4	+3.03
$\text{H}\mu_{2,5}$		-15.27(2)		-11.65 <sup>c</sup>		-13.6(2)		-11.12 <sup>c</sup>
$\text{H}\mu_{1,2}$				-19.20 <sup>d</sup>				-17.63 <sup>e</sup>
$\text{C}_5(\text{CH}_3)_5$		+1.74(15)		+1.65(15)		+1.65(15)		+1.54(15)

<sup>a</sup>  $^{31}\text{P}$  NMR data ( $\text{CDCl}_3$ , ppm): -6.24 (s, at 298 K), -5.53 (br s, at 182 K) for **2a** and +0.5 (s, 298 K), +0.5 (d), -0.48,  $^2J[^{31}\text{P}-^{31}\text{P}]$  17 Hz (180 K) for **2b**. <sup>b</sup> Intensities greater than unity in parentheses. <sup>c</sup> Sharpened on  $^1\text{H}-\{^{31}\text{P}\}$  irradiation. <sup>d</sup> Doublet structure,  $^2J[^{31}\text{P}-^1\text{H}]$  9 Hz. <sup>e</sup> Broad with apparent triplet structure,  $^2J[^{31}\text{P}-^1\text{H}]$  20 Hz,  $^2J[^{103}\text{Rh}-^1\text{H}]$  24 Hz.

subrogating two BH vertices) which, together with the 10-electron  $\{\text{B}_5\text{H}_5\}$  unit, results in 14 skeletal bonding electrons; correct for a 7-vertex *pileo* cluster.<sup>36,44</sup>

The  $^{11}\text{B}$  NMR spectrum of **1** reveals five broad resonances of which three are at very low field [ $\delta(^{11}\text{B})$  +71 to +94 ppm] and is broadly similar to the *pileo*-diiridaheptaborane  $[\{\eta^5\text{-}(\text{C}_5\text{Me}_5)\text{Ir}\}_2\text{B}_5\text{H}_5]$ ,<sup>8</sup> **5**, and remarkably similar to the ferramolybdaborane,  $[\{\eta^5\text{-}(\text{C}_5\text{H}_5)\text{Fe}\}(\text{Mo}(\text{PMe}_2\text{Ph})_3\text{H})\text{B}_5\text{H}_7]$ ,<sup>27</sup> **4a** (Table 5), with the exception of the resonance assigned to B(5) in **4a** which is *ca.* 60 ppm to high field of the equivalent resonance in **1**. It is not possible to correlate the boron and proton resonances in **1** directly to positions in the cluster, as the  $^{11}\text{B}$  resonances were too broad for ( $^{11}\text{B}-^{11}\text{B}$ ) COSY experiments although the resonances at  $\delta(^{11}\text{B})$  +94 and -7.5 ppm might reasonably be assigned to the capping boron atom B(7) and vertex B(3) on the basis of comparison with **5**, the cobalt analogue  $[\{\eta^5\text{-}(\text{C}_5\text{Me}_5)\text{Co}\}_2\text{B}_5\text{H}_5]$ ,<sup>8</sup> and **4a**. Other features of note are the presence of two terminal B-H resonances in the proton spectrum showing coupling to other nuclei ( $^nJ = 17.8, 12.0$  Hz) which we were unable to assign. The different couplings rule out a mutual ( $^1\text{H}-^{11}\text{B}_n-^1\text{H}$ ) pathway suggesting that the coupling may arise from the  $^{31}\text{P}$  nuclei on the phosphines. Similar couplings have been noted in the heterobimetalloboranes osmaplatinaheptaboranes  $[(\text{CO})(\text{PPh}_3)_2(\mu\text{-H})\text{Os}(\text{PMe}_2\text{Ph})\text{ClPtB}_5\text{H}_7]$ ,<sup>23</sup> *nido*-( $\text{PPh}_3$ )<sub>2</sub>CO( $\mu\text{-H}$ )Ir( $\text{PMe}_2\text{Ph}$ )ClPtB<sub>5</sub>H<sub>6</sub>,<sup>24</sup> and in [1-Fe( $\eta\text{-C}_5\text{H}_5$ )-2-Mo( $\text{PMe}_2\text{Ph}$ )<sub>3</sub>B<sub>5</sub>H<sub>7</sub>], **4**, where they were attributed to coupling to phosphorus.<sup>27</sup> A *transoid* coupling pathway from P(2) to B(4) and B(5) would be the most likely in the case of compound **1**.

All intracuster interatomic separations and angles for **1** are within normal ranges for metallaborane compounds<sup>4</sup> and there are no significant differences between the geometry around the osmium and iridium atoms. The distances and angles around the capping boron atom B(7) are not substantially different to those of the other boron atoms adjacent to the metal atoms although the B(7)-M(1/2) distances are slightly shorter [2.12(2) and 2.17(2) Å] than the other metal-boron distances [2.20(2)-2.24(2) Å]. In contrast, the Ir-B(7) distances in **5** [2.01(2) and 2.05(2) Å] are some of the shortest iridium-boron distances reported.<sup>21</sup> Much of this difference probably arises from the general reduction in iridium-boron separations in ( $\eta^5\text{-C}_5\text{Me}_5$ )-ligated

complexes compared to analogous triphenylphosphine ligated metallaboranes. This is also apparent in compounds **2a** and **3** described below. Although the only examples of *pileo* compounds so far contain two or three metal atoms in the capped face, the similarity of the cluster dimensions for the capping atom B(7) and the face capped atom B(5) to those for the other boron vertices suggests that, although the extended bonding capabilities of transition metals in the cluster must aid the strained  $\eta^3$  coordination of the capping vertex, *pileo* clusters with one metal atom vertex may be attainable. It is notable that the shortest B-B distance in compounds **1**, **4a**, and **5** is that for B(4)-B(6) which is opposite and parallel to the metal-metal vector, suggesting that longer intermetal distance causes a compression in this distance. This may also be noted for the *closo* compound **2a** described below.

In order to reduce the uncertainty with regard to metal atom identification, the ligands on the starting metal complex were changed. Attempts to use  $[(\text{PMe}_3)_2(\text{CO})\text{IrCl}]$  in the preparation of an analogue of **1** was unsuccessful, and we chose to use  $[\{\eta^5\text{-C}_5\text{Me}_5\}\text{Ir}\text{Cl}_2]_2$  which would also have the additional advantage of aiding crystallization due to the smaller ligand size. Deprotonation of the osmahexaborane with *n*-BuLi in THF solution at -35 °C, addition of  $[\{\eta^5\text{-C}_5\text{Me}_5\}\text{Ir}\text{Cl}_2]_2$ , and slow warming to room temperature followed by chromatographic separation of the products gave a number of compounds some of which have been characterized by NMR spectroscopy, mass spectrometry, and single-crystal X-ray diffraction studies. The first, isolated as a yellow, air stable, crystalline solid in variable yields of 7-21% was *closo*-[1-( $\eta^5\text{-C}_5\text{Me}_5$ )-2,2,2-(CO)(PPh<sub>3</sub>)<sub>2</sub>-1,2-( $\mu\text{H}$ )-1,2-IrOsB<sub>4</sub>H<sub>4</sub>Cl] (**2a**). The second, *nido*-[2-( $\eta^5\text{-C}_5\text{Me}_5$ )-3,3,3-(CO)(PPh<sub>3</sub>)<sub>2</sub>-2,3-( $\mu\text{H}$ )-2,3-IrOsB<sub>3</sub>H<sub>6</sub>] (**3**), was isolated in *ca.* 5% yield also as a yellow, air stable crystalline solid. NMR data for these compounds are listed in Tables 7 and 8, respectively. The molecular structures determined from single-crystal X-ray diffraction studies are shown in Figures 2 for compound **2a** and Figure 3 for compound **3**. Selected interatomic angles and separations for **2a** and **3** are given in Tables 8 and 9, respectively.

All atoms, including hydrogen atoms, were located and refined independently from the X-ray data for **2a** and agree with the other data. The unit cell for **2a** contains two disordered molecules one of which contains a chlorine atom on B(4) with an occupancy factor of 20%. This was not evident in the NMR spectra of **2a**, but a reexamination of the low resolution mass spectra of

(44) Mason, R.; Thomas, K. M.; Mingos, D. M. P. *J. Am. Chem. Soc.* **1973**, *95*, 3802. (b) Mingos, D. M. P.; Forsyth, M. I. *J. Chem. Soc., Dalton Trans.* **1977**, 610. (c) Johnson, R. L.; Mingos, D. M. P. *J. Chem. Soc., Dalton Trans.* **1987**, 1445.



**Table 8.**  $^{11}\text{B}$ ,  $^1\text{H}$ , and  $^{31}\text{P}$  NMR Data for  $[(\text{PPh}_3)_2(\text{CO})\text{Os}(\mu\text{-H})\{\eta^5\text{-}(\text{C}_5\text{Me}_5)\text{Ir}\}\text{B}_3\text{H}_6]$  (**3**) in  $\text{CDCl}_3$  Solution at 298 K

proposed assign	$\delta(^{11}\text{B})$ 298 K	$\delta(^1\text{H})^b$ 298 K	$^1\text{H}\text{-}^1\text{H}$ COSY correlns <sup>c</sup>
5	+19.8	+6.90	—
1 } or 4 }	+14.5	+6.78	—
	+14.5	+2.48	—
$\text{H}\mu_{4,5}$		-0.80	[(3,4), (2,5)]w
$\text{H}\mu_{3,4}$		-8.81	[2,5]w
$\text{H}\mu_{2,5}$		-16.20	[(2,3), (4,5), (3,4)]w
$\text{H}\mu_{2,3}$		-17.73 <sup>d</sup>	[2,5]w
$\text{C}_5(\text{CH}_3)_5$		+1.79(15)	

<sup>a</sup>  $^{31}\text{P}$  NMR data ( $\text{CDCl}_3$ , 298 K/ppm)  $\delta$ : +19.4( $\text{P}_A$ ), -1.4( $\text{P}_B$ ), ( $^2J[^{31}\text{P}\text{-}^{31}\text{P}] = 9.6$  Hz). <sup>b</sup> Intensities greater than unity in parentheses. <sup>c</sup> Broadband boron decoupling unavailable. <sup>d</sup> Doublet of doublets,  $^2J[^{31}\text{P}_A\text{-}^1\text{H}]_{\text{cis}} 19$  Hz,  $^2J[^{31}\text{P}_B\text{-}^1\text{H}]_{\text{trans}} 29$  Hz.

**Table 9.** Selected Interatomic Distances [Å] and Angles [deg] for  $\text{closo-}[(\text{PPh}_3)_2(\text{CO})\text{OsB}_4\text{H}_6\{\eta^5\text{-}(\text{C}_5\text{Me}_5)\text{Ir}\}]$  (**2a**)<sup>a</sup>

Ir(1)-B(4)	2.117(8)	Os(2)-C(1)	1.864(6)
Ir(1)-B(5)	2.168(8)	Os(2)-B(6)	2.239(8)
Ir(1)-B(3)	2.173(7)	Os(2)-B(3)	2.298(7)
Ir(1)-C(5)	2.190(6)	Os(2)-B(5)	2.341(7)
Ir(1)-C(4)	2.199(6)	Os(2)-P(2)	2.384(2)
Ir(1)-C(6)	2.266(6)	Os(2)-P(1)	2.419(2)
Ir(1)-C(3)	2.303(6)	Os(2)-H(25)	1.58(6)
Ir(1)-C(2)	2.309(6)	Os(2)-H(12)	2.0928(5)
Ir(1)-Os(2)	2.8882(8)	Cl-B(4)	1.726(14)
Ir(1)-H(12)	1.8295(6)	B(5)-B(6)	1.844(10)
B(3)-B(6)	1.724(11)	B(5)-H(5)	1.14(10)
B(3)-B(4)	1.742(11)	B(5)-H(25)	1.38(6)
B(3)-H(3)	1.03(8)	B(6)-H(6)	0.92(7)
B(4)-B(6)	1.613(11)	O-C(1)	1.161(7)
B(4)-B(5)	1.740(11)		
B(4)-Ir(1)-B(5)	47.9(3)	C(1)-Os(2)-B(6)	80.9(3)
B(4)-Ir(1)-B(3)	47.9(3)	C(1)-Os(2)-B(3)	114.2(2)
B(5)-Ir(1)-B(3)	71.5(3)	B(6)-Os(2)-B(3)	44.6(3)
B(4)-Ir(1)-Os(2)	75.4(2)	C(1)-Os(2)-B(5)	106.5(3)
B(5)-Ir(1)-Os(2)	52.9(2)	B(6)-Os(2)-B(5)	47.4(3)
B(3)-Ir(1)-Os(2)	51.7(2)	B(3)-Os(2)-B(5)	66.2(3)
C(5)-Ir(1)-Os(2)	151.7(2)	C(1)-Os(2)-P(2)	86.7(2)
C(4)-Ir(1)-Os(2)	165.5(2)	B(6)-Os(2)-P(2)	109.8(2)
C(6)-Ir(1)-Os(2)	131.5(2)	B(3)-Os(2)-P(2)	82.4(2)
C(3)-Ir(1)-Os(2)	143.2(2)	B(5)-Os(2)-P(2)	148.6(2)
C(2)-Ir(1)-Os(2)	128.2(2)	C(1)-Os(2)-P(1)	95.2(2)
B(6)-B(3)-B(4)	55.5(4)	B(6)-Os(2)-P(1)	149.1(2)
B(6)-B(3)-Ir(1)	100.5(4)	B(3)-Os(2)-P(1)	150.6(2)
B(4)-B(3)-Ir(1)	64.3(3)	B(5)-Os(2)-P(1)	106.3(2)
B(6)-B(3)-Os(2)	65.9(3)	P(2)-Os(2)-P(1)	100.45(5)
B(4)-B(3)-Os(2)	100.2(4)	C(1)-Os(2)-Ir(1)	150.5(2)
Ir(1)-B(3)-Os(2)	80.4(2)	B(6)-Os(2)-Ir(1)	70.6(2)
B(6)-B(4)-Cl	118.1(7)	B(3)-Os(2)-Ir(1)	47.9(2)
B(6)-B(4)-B(5)	66.6(5)	B(5)-Os(2)-Ir(1)	47.6(2)
Cl-B(4)-B(5)	120.0(7)	P(2)-Os(2)-Ir(1)	109.74(4)
B(6)-B(4)-B(3)	61.7(4)	P(1)-Os(2)-Ir(1)	105.18(4)
Cl-B(4)-B(3)	144.4(7)	H(25)-Os(2)-H(12)	95(2)
B(5)-B(4)-B(3)	93.4(5)	B(4)-B(5)-B(6)	53.4(4)
B(6)-B(4)-Ir(1)	106.8(4)	B(4)-B(5)-Ir(1)	64.5(4)
Cl-B(4)-Ir(1)	133.7(7)	B(6)-B(5)-Ir(1)	96.9(4)
B(5)-B(4)-Ir(1)	67.6(4)	B(4)-B(5)-Os(2)	98.7(4)
B(3)-B(4)-Ir(1)	67.8(3)	B(6)-B(5)-Os(2)	63.4(3)
B(3)-B(6)-B(5)	90.5(5)	Ir(1)-B(5)-Os(2)	79.6(2)
B(4)-B(6)-Os(2)	107.1(4)	B(5)-B(6)-Os(2)	69.2(3)
B(4)-B(6)-B(3)	62.8(5)	B(3)-B(6)-Os(2)	69.6(3)
B(4)-B(6)-B(5)	60.0(4)	O-C(1)-Os(2)	176.9(5)

<sup>a</sup> Symmetry transformations used to generate equivalent atoms: (1)  $-x + 1, -y + 2, -z + 1$ ; (2)  $-x + 1, -y + 1, -z + 1$ .

three samples of the compound showed a low intensity envelope at 1154 mass units corresponding to the Cl substituted species which was initially attributed to occasional higher mass species which may be present in FAB spectra. The chlorine substituent may arise

from reaction with the solvents or from the  $[(\eta^5\text{-C}_5\text{Me}_5)\text{IrCl}_2]_2$  reactant.

In addition to the terminal hydrogen atom on each boron vertex, as shown by the  $^1\text{H}\{^{11}\text{B}\}$  NMR spectrum, there are two bridging hydrogen atoms associated the Os(2)-B(5) and the Ir(1)-Os(2) edges. The low temperature proton spectrum shows resonances at  $\delta(^1\text{H})$  -19.20 and -11.65 ppm. The high-field chemical shift is reasonable for a hydride bridging between two metals.<sup>45</sup> The low field chemical shift is assigned to the Os-H-B bridging hydrogen atom and is in the range for other Os-H-B resonances in the literature<sup>29,23,46</sup> although the other examples are based on hydrogen atoms bridging the open-face edge of clusters rather than on the edge of a closed cluster as here. At 180 K coupling to  $^{31}\text{P}$  ( $^2J = 9$  Hz) is observed for  $\text{H}\mu_{1,2}$ , and  $\text{H}\mu_{2,5}$  shows an unresolved coupling with both peaks broadened due to the fluxional process described below. X-ray methods are, of course, an unreliable method for obtaining H atom positions, but one of the advantages of using metal complexes with two-electron ligands on the metal over those with  $\eta^5$ -cyclopentadienyl ligands is that directional information about the orbital interaction of the metal atom with the borane cluster may be deduced from an examination of the detailed dimensions of the interligand and ligand-cage angles which is not available in the  $\eta^5$ -cyclopentadienyl-ligated species. In particular, hydrogen atoms bridging the metal and the cage tend to take up a normal *pseudo*-octahedral position with respect to the other two-electron ligands on the metal. Thus in **2a** the C(1)-Os(2)-Ir(1) angle of 150.5(2)° is close to the P(2)-Os(3)-Ir(1) angle [150.01(9)°] in **3** in which there is a bridging hydrogen atom opposite the P(2)-Os(3) vector. Also, the angle that P(1) in **2a** makes with the boron cage [P(1)-Os(2)-B(5) 106.3(2)] is 24° greater than the non-hydrogen-bridged P(2)-Os(2)-B(3) [82.4(2)] angle, which is probably due to the steric effect of the bridging H atom. The final electron density map showed no significant residual electron density about the Os(2)-B(6)-B(3) or the Os(2)-B(5)-B(6) faces other than that we have attributed to  $\text{H}\mu_{2,5}$  and the H atom refined with a reasonable isotropic parameter leading us, together with the other evidence, to have a high degree of confidence in its position.

Other residual electron densities associated with the iridium atom were refined as hydrogen atoms resulting in the position assigned to  $\text{H}\mu_{1,2}$  being the only one to maintain a reasonable isotropic parameter after refinement and thus supporting the assignment of the position as given. This is also supported by the NMR data for the rhodium analogue of compound **2a**, *closo*-[1- $\{\eta^5\text{-}(\text{C}_5\text{Me}_5)\text{-}2,2,2\text{-}(\text{CO})(\text{PPh}_3)_2\text{-}1,2\text{-}(\mu\text{H})\text{-}1,2\text{-RhOsB}_4\text{H}_6\}$ ] (**2b**), which we prepared in order to confirm the metal-metal bridging character of  $\text{H}\mu_{1,2}$ . The low temperature proton NMR spectrum clearly shows coupling to  $^{103}\text{Rh}$  for  $\text{H}\mu_{1,2}$  in addition to coupling to one phosphorus atom on the osmium and no coupling to boron, suggesting that the hydrogen atom is also not in a face capping position. The  $^1\text{H}\{^{11}\text{B}\}$  spectrum with the  $^1\text{H}$  spectrum subtracted

(45) Humphries, A. P.; Kaesz, H. D.; Saillant, R. B. *Chem. Rev.* **1972**, *72*, 231.

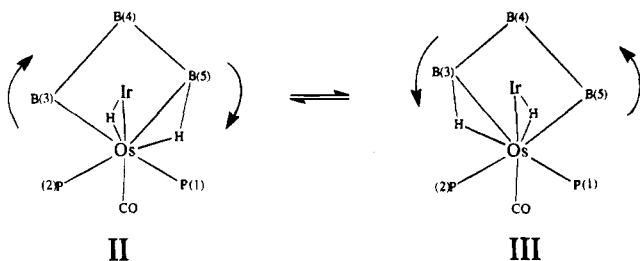
(46) (a) Beckett, M. A.; Greenwood, N. N.; Kennedy, J. D.; Thornton-Pett, M. J. *Chem. Soc., Dalton Trans.* **1986**, 795. (b) Bown, M.; Fontaine, X. L. R.; Greenwood, N. N.; Kennedy, J. D. *J. Organomet. Chem.* **1987**, *325*, 233. (c) Bown, M.; Fowkes, H.; Fontaine, X. L. R.; Greenwood, N. N.; Kennedy, J. D.; Mackinnon, P.; Nestor, K. J. *Chem. Soc., Dalton Trans.* **1988**, 2597.



features a larger residual resonance for  $H\mu_{2,5}$  than in **2a** due to stronger coupling to boron and no residual resonance for  $H\mu_{1,2}$ . The other NMR data are very similar to compound **2a**.

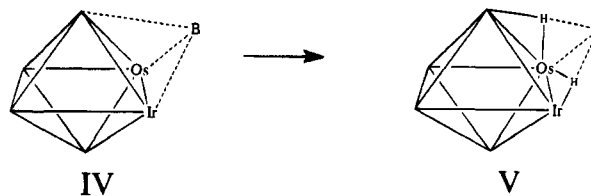
It is interesting to note that the two bridging H atoms occupy the face of the cluster that would hold the capping vertex in a *pileo* type cluster such as **1** and this too may be added to the evidence supporting the experimentally proposed positions. It may be noted that these locations contrast to those for the dicobalt analogue  $[\{\eta^5-(C_5Me_5)Co\}_2B_4H_4]^{13}$  in which face capping positions are proposed although the capping rather than edge-bridging positions are based largely on the refinement of X-ray structural data. Compounds **2a** and **2b** are examples of the unusual feature involving *closo* clusters which have been structurally identified as containing two edge bridging hydrogen atoms. An example containing one bridging H atom,  $[1,1-(PMe_2-Ph)_2-1,2-\mu-H-2,5-(OMe)_2-isocloso-1-RhB_{10}H_8]$ ,<sup>47</sup> exists, and the *pileo* systems described by Leach et al. and described above are related.<sup>3</sup> Of these latter,  $[\{\eta^5-(C_5H_4-Me)Mo\}_2B_5H_9]^{13}$  effectively contains a capping  $BH_3$  group with two bridging H atoms and *pileo*- $[\{\eta^5-(C_5H_5)Fe\}-(MoL_3H)B_5H_7]^{27}$  effectively contains a capping  $BH_2$  group with a bridging H atom.

Low temperature boron and proton NMR of **2a** and **2b** shows four inequivalent BH resonances whereas the cluster has an apparent *pseudo* plane of symmetry bisecting the Os(2)–Ir(1)–B(4)–B(6) plane. On raising the temperature the two boron resonances assigned to B(3) and B(5), their associated terminal proton resonances, and the bridging hydrogen atoms coalesce ( $\Delta G_{\pm 230 K} = 38 \text{ kJ mol}^{-1}$ ). The free energy barrier for the fluxional process is fairly low for a *pseudo*-rotational process involving, say, the rotation of the  $L_3Os$  moiety with respect to the borane cluster.<sup>48</sup> This may be rationalized by a mechanism (II, III) in which the Os–H–Ir bridging hydrogen atom moves to an Os–H–B(3) bridging position, and the Os–H–B(5) atom moves to a metal–metal bridging position. This would involve a concomitant increase in the P(2)–Os(2)–B(3) angle and a decrease in the P(1)–Os(2)–B(5) angle such that the B(3) and B(5) vertices would become equivalent in an effective rocking motion of the cluster with respect to the osmium vertex. These suggestions also apply to **2b** which has similar NMR spectra.

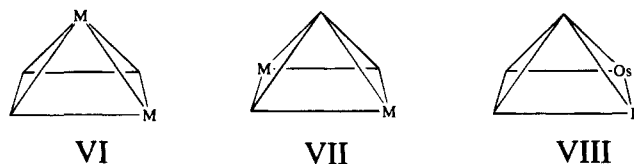


Compounds **2a/b** (illustration V) are related to the *pileo*-metallaheptaborane cluster **1** (illustration IV) by the simple removal of the capping boron vertex. The 2 skeletal bonding electrons lost by the removal of the vertex are formally replaced by the two bridging hydro-

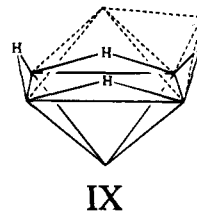
gen atoms, and thus the octahedral cluster conforms structurally to a *closo* system and has the requisite skeletal electron pair count of 7.<sup>49</sup>



The NMR spectra (Table 7), IR, analytical, and mass spectrum data for **3** suggested a *nido*-five vertex cluster analogous to that of *nido*- $B_5H_9$ <sup>50</sup> with the two metal atoms in adjacent basal positions. As such, the compound would fit into a series of structurally characterized bimetallopentaborane clusters in which two metal moieties subrogate BH vertices in various positions in a *nido*-pentaborane cluster although this compound is the first heterobimetallpentaborane species to be fully characterized. These are  $[1,2-\{Fe(CO)_3\}_2B_3H_7]$ ,<sup>5</sup>  $[1-\{\eta^5-(C_5Me_5)Co\}-2-(\eta^4-C_5Me_4H)CoB_3H_3]$ ,<sup>1b,c</sup>  $[2,4-\{\eta^5-(C_5Me_5)Co\}_2B_3H_7]$ ,<sup>1b,c</sup> the capped *nido*-system  $[2,3-\{Fe(PMe_3)_2\}_2-(\mu-H)B_4H_9]$ ,<sup>6</sup> and **3** (illustrations VI–VIII). To complete the series a single crystal X-ray structural study of **3** was carried out. Table 9 lists selected interatomic separations and angles for **3**. A drawing of the molecule is shown in Figure 3. All hydrogen atoms were located with the exception of the hydrogen atom bridging Ir(2)–B(5) the position of which is, however, is readily apparent from a consideration of the  $^1H\{^{11}B\}$  and  $(^1H-^1H)$  COSY spectra and is shown in Figure 3 with dotted lines.



It may be seen that the cluster is clearly based upon the *nido*-pentaborane cluster with the metal moieties subrogating two BH vertices, and that in addition to completing the above series VI–VIII, **3** is also related to the *closo* compound **2a** via loss of one B(H) vertex and to **1** via loss of two BH vertices as shown in illustration IX. The four face-bridging hydrogen atoms



may be regarded as pointing toward the two missing vertices of the *pileo* compound and effectively supplying

(49) (a) Williams, R. E. *Adv. Inorg. Chem. Radiochem.* **1971**, *18*, 67. (b) Wade, K. *Adv. Inorg. Chem. Radiochem.* **1971**, *18*, 1. (c) Rudolph, R. W. *Acc. Chem. Res.* **1976**, *9*, 446. (d) Mingos, D. M. P. *Acc. Chem. Res.* **1984**, *17*, 311.

(50) (a) Dulmage, W. J.; Lipscomb, W. N. *Acta Crystallogr.* **1952**, *5*, 260. (b) Hedberg, K.; Jones, M. E.; Schomaker, V. *Proc. Natl. Acad. Sci. U.S.A.* **1952**, *38*, 679. (c) Schwach, D.; Burg, A. B.; Beaudet, R. A. *Inorg. Chem.* **1977**, *16*, 3219. (d) Huffman, J. C. Dissertation, Indiana University, 1974, p 194.

(47) Fowkes, H.; Greenwood, N. N.; Kennedy, J. D.; Thornton-Pett, M. *J. Chem. Soc., Dalton Trans.* **1986**, 517.

(48) Bould, J.; Greenwood, N. N.; Kennedy, J. D. *J. Chem. Soc., Dalton Trans.* **1982**, 481, and references therein.

**Table 10. Selected Interatomic Distances [Å] and Angles [deg] for *nido*-[(PPh<sub>3</sub>)<sub>2</sub>(CO)Os(μ-H){η<sup>5</sup>-(C<sub>5</sub>Me<sub>5</sub>)Ir}B<sub>3</sub>H<sub>6</sub>] (3)**

Ir(2)–B(1)	2.15(2)	Os(3)–C(47)	1.83(2)
Ir(2)–B(5)	2.17(2)	Os(3)–B(1)	2.21(2)
Ir(2)–C(3)	2.171(3)	Os(3)–B(4)	2.30(2)
Ir(2)–C(2)	2.174(13)	Os(3)–P(1)	2.309(3)
Ir(2)–C(4)	2.248(12)	Os(3)–P(2)	2.393(4)
Ir(2)–C(1)	2.251(14)	O–C(47)	1.19(2)
Ir(2)–C(5)	2.268(12)	B(1)–B(4)	1.72(2)
Ir(2)–Os(3)	2.9269(8)	B(1)–B(5)	1.72(3)
P(1)–C(17)	1.835(14)	B(4)–B(5)	1.71(2)
P(1)–C(23)	1.847(13)	P(2)–C(35)	1.809(14)
P(1)–C(11)	1.847(14)	P(2)–C(29)	1.831(14)
		P(2)–C(41)	1.858(14)
O–C(47)–Os(3)	178.0(14)	B(4)–Os(3)–Ir(2)	71.7(4)
B(1)–Ir(2)–B(5)	46.9(7)	B(4)–B(1)–B(5)	59.7(10)
B(10)–Ir(2)–Os(3)	48.7(5)	B(4)–B(1)–Ir(2)	106.3(10)
B(5)–Ir(2)–Os(3)	76.7(5)	B(5)–B(1)–Ir(2)	67.1(8)
C(47)–Os(3)–B(1)	88.4(7)	B(4)–B(1)–Os(3)	70.5(8)
C(47)–Os(3)–B(4)	130.5(7)	B(5)–B(1)–Os(3)	109.2(10)
C(47)–Os(3)–P(2)	103.3(5)	Ir(2)–B(1)–Os(3)	84.3(6)
C(47)–Os(3)–Ir(2)	87.5(5)	B(5)–B(4)–B(1)	60.3(10)
C(47)–Os(3)–P(1)	88.4(5)	B(5)–B(4)–Os(3)	105.8(10)
B(10)–Os(3)–P(1)	103.2(4)	B(1)–B(4)–Os(3)	64.9(8)
B(94)–Os(3)–P(1)	88.8(4)	B(4)–B(5)–B(1)	60.1(10)
B(1)–Os(3)–B(4)	44.6(6)	B(4)–B(5)–Ir(2)	105.8(11)
B(1)–Os(3)–P(2)	152.9(5)	B(1)–B(5)–Ir(2)	66.0(8)
B(4)–Os(3)–P(2)	125.6(4)	P(1)–Os(3)–Ir(2)	150.01(9)
P(1)–Os(3)–P(2)	101.52(12)	P(2)–Os(3)–Ir(2)	108.33(9)
B(1)–Os(3)–Ir(2)	47.0(4)		

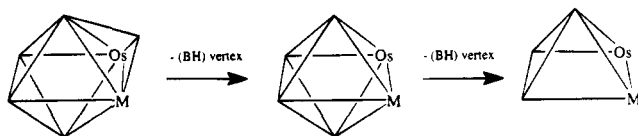
the four electrons and four orbitals of the “missing” {HB–BH} moiety, assuming that the B atoms are bonded, thus using two of the six available cluster orbitals.

One of the interesting features of borane and metallaborane chemistry is in the contrasting and comparison of borane and metallaborane fragments to isoelectronic and, possibly, isostructural carbon analogues.<sup>51</sup> For example, the cyclobutadienyl ligand [C<sub>4</sub>H<sub>4</sub>] is isoelectronic with [B<sub>4</sub>H<sub>6</sub>] for which metalla-derivatives exist such as *nido*-[1-{(CO)<sub>3</sub>Fe}B<sub>4</sub>H<sub>5</sub>]<sup>52a</sup> and *nido*-[1-{(η<sup>5</sup>-C<sub>5</sub>H<sub>5</sub>)Co}B<sub>4</sub>H<sub>5</sub>]<sup>52b</sup> and MB<sub>3</sub> compounds have been compared to MC<sub>3</sub>H<sub>5</sub> π-allyl complexes.<sup>53</sup> In this respect it may be noted that the coordination of the B<sub>3</sub> fragment in **3** to the binuclear metal fragment could also be viewed as the coordination of a [B<sub>3</sub>H<sub>6</sub>]<sup>3-</sup> moiety to a [(η<sup>5</sup>-C<sub>5</sub>Me<sub>5</sub>)Ir](μH)Os(CO)(PPh<sub>3</sub>)<sub>3</sub><sup>3+</sup> fragment. [B<sub>3</sub>H<sub>6</sub>]<sup>3-</sup> is formally isoelectronic with cyclopropane, C<sub>3</sub>H<sub>6</sub>, so the appropriate comparison would be with the coordination of cyclopropane to metals. The usefulness of this approach is somewhat limited, however, as the latter, in contrast to the cyclobutadiene and allyl analogues, is unlikely to exist. The related species [H{Ru(CO)<sub>3</sub>}<sub>3</sub>-B<sub>2</sub>H<sub>5</sub>]<sup>2a</sup> has been compared to a system in which the ethylene analogue [B<sub>2</sub>H<sub>5</sub>]<sup>-</sup> is coordinated to a trimetal Ru<sub>3</sub> face, analogous to the adsorption of alkenes on a metal surface. **3** is the reverse of this in that a bimetallic unit sits on the face of a tricarbon analogue. Thus **3** could be considered as comparable to a heterobimetallic complex adsorbed onto a triatom face of a carbon surface.

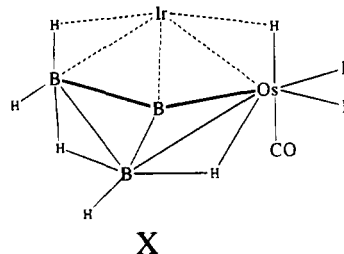
(51) Housecroft, C. E.; Fehlner, T. P. *Adv. Organomet. Chem.* **1982**, *21*, 57.

(52) (a) Greenwood, N. N.; Savory, G. C.; Grimes, R. N.; Sneddon, L. G.; Davison, A.; Wreford, S. S. *J. Chem. Soc., Chem. Commun.* **1974**, 718. (b) Venable, T. L.; Sinn, E.; Grimes, R. N. *J. Chem. Soc., Dalton Trans.* **1984**, 2275.

(53) (a) Housecroft, C. E.; Fehlner, T. P. *Inorg. Chem.* **1982**, *21*, 1739. (b) Kane, A. R.; Muetterties, E. L. *J. Am. Chem. Soc.* **1974**, *93*, 1041. (c) Haggerty, B. S.; Housecroft, C. E.; Rheingold, A. L.; Shaykh, A. M. *J. Chem. Soc., Dalton Trans.* **1991**, 2175. (d) Bould, J.; N. N.; Kennedy, J. D.; McDonald, W. S. *Inorg. Chim. Acta.* **1992**, *196*, 201.

**Scheme 1. Relationship between the Basic Clusters 1, 2, and 3**

Another way of viewing **3** is as a metalla-derivative of the known osmatetaborane *arachno*-[(PPh<sub>3</sub>)<sub>2</sub>(CO)-HOsB<sub>3</sub>H<sub>8</sub>]<sup>29</sup> (illustration X) in which two bridging hydrogens have been removed and replaced by the [(η<sup>5</sup>-C<sub>5</sub>H<sub>5</sub>)Ir] moiety. This suggested that it might be



possible to produce **3** directly from the reaction of [(η<sup>5</sup>-C<sub>5</sub>Me<sub>5</sub>)Ir]Cl<sub>2</sub> with [(PPh<sub>3</sub>)<sub>2</sub>(CO)HOsB<sub>3</sub>H<sub>8</sub>]. Although this would require a rearrangement of the ligands around the osmium and the incorporation of the osmium terminal metal hydride by the cluster, this is not unreasonable, as such an incorporation occurs in the reaction of B<sub>5</sub>H<sub>8</sub> and [(PPh<sub>3</sub>)<sub>3</sub>(CO)HClOs] to give [(PPh<sub>3</sub>)<sub>2</sub>(CO)OsB<sub>5</sub>H<sub>9</sub>]<sup>29</sup>. However, currently it has not been possible to produce larger amounts of **3** by this method.

The species 1–3 represent a novel series of heterobimetalloboranes essentially differing in the number of BH vertices (Scheme 1). They all conform to the polyhedral skeletal electron pair theory and may be considered as a unique series of homologous cluster types.<sup>49</sup> **1** conforms to the polyhedral skeletal electron pair theory (PSEPT) for a capped-closed octahedron containing 14 skeletal electrons and seven vertices.<sup>44</sup> As rationalized by the PSEPT and geometrical arguments,<sup>49</sup> formal removal of 1 BH vertex from **1** leads to the formation of the 14 skeletal electron *closo*-cluster, **2**, containing 6 vertices, and removal of a second BH vertex leads to the formation of the conventional 14 skeletal electron 5-vertex *nido*-cluster, **3**. As we noted above, in the case of both **2** and **3**, bridging H atoms sit on a face from which a vertex has been removed and point toward the missing vertex or vertices. Formation of **1** by insertion of the [(PPh<sub>3</sub>)<sub>2</sub>(CO)Ir]<sup>+</sup> moiety into the [OsB<sub>5</sub>]<sup>-</sup> cluster is clearly a complex process, not easily explained, but it is noteworthy that addition of a metal reagent to a *nido*-FeB<sub>5</sub>, described in reference 27, forms **4a** and **4b**, (*pileo*-[(η<sup>5</sup>-C<sub>5</sub>H<sub>5</sub>)Fe](ML<sub>3</sub>H)B<sub>5</sub>H<sub>7</sub>], where M = Mo and L = PMe<sub>2</sub>Ph (**4a**) and M = W and L = PMe<sub>3</sub>, **4b**), species which are also capped octahedral clusters. The evidence, so far, suggests that *pileo*-species may be the preferred closed structures in 7-vertex bimetalloborane clusters. Formation of **2** and **3** are also not easily explained, but it is known that MB<sub>5</sub> clusters tend to degrade to smaller clusters,<sup>54a</sup> an observation which is suggested by theory.<sup>54b</sup> Our results suggest that com-

(54) (a) Unpublished observations from our laboratory. (b) Mebel, A. M.; Morokuma, K.; Musaev, D. G. *J. Am. Chem. Soc.* **1994**, *116*, 3932.

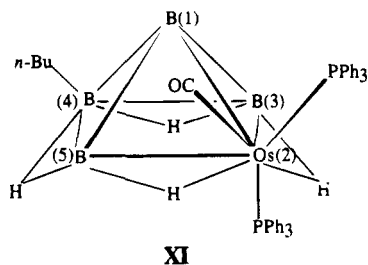
**Table 11.**  $^{11}\text{B}$ ,  $^1\text{H}$ , and  $^{31}\text{P}$  NMR Data for  $[(\text{PPh}_3)_2(\text{CO})\text{OsB}_4\text{H}_7(n\text{-Bu})]$  (**6**) in  $\text{CDCl}_3$  at  $25^\circ\text{C}$ 

proposed assignt	$\delta(^{11}\text{B})$	$\delta(^1\text{H})^b$	$[^1\text{H}-^1\text{H}]\text{COSY}^f$
4	+23.2	c	
3 }	-8.9	+3.10	
5 }	-15.3	+0.92	
1	-29.9	+0.41	
$\text{H}\mu_{4,5}$	-	-1.55	(2,5)s, (2,3)w, (3,4)m
$\text{H}\mu_{3,4}$	-	-1.91	(2,3)s, (2,3)w, (4,5)m
$\text{H}\mu_{2,5}$	-	-10.05 <sup>d</sup>	(4,5)s, (3,4)w, (2,3)m
$\text{H}\mu_{2,3}$	-	-10.46	(3,4)s, (4,5)w, (2,5)m
$\text{CH}_3$	-	ca. +0.87 (3) <sup>e</sup>	
$(\text{CH}_2)_3$	-	ca. +1.30 (6) <sup>e</sup>	

<sup>a</sup>  $^{31}\text{P}$  NMR data in  $\text{CDCl}_3$  solution at  $25^\circ\text{C}$  in ppm: +6.87, +14.36 ( $^2J[^{31}\text{P}-^{31}\text{P}] = 8.6\text{ Hz}$ ). <sup>b</sup> Intensities greater than one given in parentheses. <sup>c</sup> Site of *n*-Bu substituent. <sup>d</sup> Doublet structure  $^2J[^1\text{H}-^{31}\text{P}]$  42 Hz. <sup>e</sup> Complex multiplet. <sup>f</sup> Proton COSY correlations with broad-band boron decoupling could not be obtained due to machine problems, and therefore no terminal BH correlations are given.

pound **3** could possibly be formed from compound **2** so the idea of sequential loss of vertices in such series of clusters, as illustrated in Scheme 1, is not unreasonable.

Finally, a fourth compound, *nido*- $[(\text{PPh}_3)_2(\text{CO})\text{OsB}_4\text{H}_7(n\text{-Bu})]$  (compound **6**, illustration XI), was isolated in



yields of up to 20% when *n*-butyllithium was used as the deprotonating agent at room temperature or at

lower temperatures. The compound was identified from high resolution mass spectroscopy, infrared, and NMR data. The NMR data (Table 11) are very similar to the previously characterized osmapentaborane *nido*- $[(\text{PPh}_3)_2(\text{CO})\text{OsB}_4\text{H}_8]$ <sup>29</sup> with the exception of the *n*-butyl substituent which causes a downfield shift of the B(4) resonance of ca. 14 ppm. Amounts of the unsubstituted cluster were also detected, but when methyllithium was used as the deprotonating agent the unsubstituted cluster was the main byproduct although there were traces of what may have been the methyl substituted analogue.  $[(\text{PPh}_3)_2(\text{CO})\text{OsB}_5\text{H}_9]$  is known to degrade to  $[(\text{PPh}_3)_2(\text{CO})\text{OsB}_4\text{H}_8]$  on heating<sup>29</sup> in 40% yield as are many other metallapentaboranes.<sup>4a,54</sup> Thus it is possible that **2a/b** and **6** are formed *via* a *nido*-osmapentaborane intermediate although this has not been experimentally verified for this system.

**Acknowledgment.** We thank the Johnson Matthey Co. for a loan of  $\text{IrCl}_3 \cdot 3\text{H}_2\text{O}$ , and the National Science Foundation, the Missouri Research Board, and the University of Missouri—St. Louis for research grants which provided the financial support of this work. We also acknowledge the National Science Foundation and the UM—St. Louis Center for Molecular Electronics and DOE for funds to purchase the NMR spectrometers and the X-ray diffractometers. Finally, we acknowledge Dr. Fred Hileman of the Monsanto Co. for allowing the collaboration which led to the mass spectral data.

**Supporting Information Available:** Text giving experimental details, and tables of bond lengths and angles, fractional coordinates, and anisotropic thermal parameters for the structures of *pileo*- $[(\text{PPh}_3)_2(\text{CO})\text{OsB}_5\text{H}_5\text{IrH}(\text{PPh}_3)(\text{CO})]$ , *closo*- $[(\text{PPh}_3)_2(\text{CO})(\mu\text{-H})\text{OsB}_4\text{H}_5\{\eta^5\text{-}(\text{C}_5\text{Me}_5)\text{Ir}\}]$ , and *nido*- $[(\text{PPh}_3)_2(\text{CO})\text{Os}(\mu\text{-H})\{\eta^5\text{-}(\text{C}_5\text{Me}_5)\text{Ir}\}\text{B}_3\text{H}_6]$  (37 pages). Ordering information is given on any current masthead page.

OM9504922

**Fixation of CO<sub>2</sub> by a Series of Ethynyl-Bridged  
Polynuclear Aluminum–Magnesium Complexes.  
Synthesis, Characterization, and Crystal Structures of  
[Me<sub>2</sub>Al(μ-*i*-Pr<sub>2</sub>N)<sub>2</sub>Mg(μ-C≡CR)]<sub>2</sub> (R = C<sub>6</sub>H<sub>5</sub>, C<sub>6</sub>H<sub>4</sub>-*p*-CH<sub>3</sub>,  
*t*-Bu, SiMe<sub>3</sub>), [Me<sub>2</sub>Al(μ-Et<sub>2</sub>N)<sub>2</sub>Mg(μ-C≡CC<sub>6</sub>H<sub>5</sub>)]<sub>2</sub>,  
{(Me<sub>2</sub>Al)<sub>2</sub>[μ-OOC(*i*-Pr<sub>2</sub>N)]<sub>2</sub>}, and  
{(Me<sub>2</sub>Al)<sub>2</sub>[μ-OOC(*i*-Pr<sub>2</sub>N)]<sub>2</sub>Mg}**

Chung-Cheng Chang,\* Bhamidi Srinivas, Mung-Liang Wu, Wen-Ho Chiang,  
Michael Y. Chiang, and Chung-Sheng Hsiung

*Department of Chemistry, National Sun Yat-Sen University, Kaohsiung, Taiwan, ROC*

Received April 10, 1995<sup>®</sup>

A series of ethynyl-bridged polynuclear aluminum–magnesium complexes, [Me<sub>2</sub>Al(μ-R'N)<sub>2</sub>Mg(μ-C≡CR)]<sub>2</sub> (R = C<sub>6</sub>H<sub>5</sub> (1), C<sub>6</sub>H<sub>4</sub>-*p*-CH<sub>3</sub> (2), *t*-Bu (3), SiMe<sub>3</sub> (4), C<sub>6</sub>H<sub>5</sub> (5), C<sub>6</sub>H<sub>4</sub>-*p*-CH<sub>3</sub> (6); R' = *i*-Pr (1–4), Et for (5, 6)), were prepared by reaction of the aluminum–magnesium tetramer [Me<sub>2</sub>Al(μ-*i*-Pr<sub>2</sub>N)<sub>2</sub>Mg(μ-Me)]<sub>4</sub> (A) and the dimer [Me<sub>2</sub>Al(μ-Et<sub>2</sub>N)<sub>2</sub>Mg(μ-Me)]<sub>2</sub> (B) with various substituted acetylenes. Subsequent reaction of complexes 1 and 2 with CO<sub>2</sub> gives selective insertion products, viz. {[Me<sub>2</sub>Al(μ-*i*-Pr<sub>2</sub>N)<sub>2</sub>Mg(μ-OOC(C≡CR))] }<sub>2</sub> (R = C<sub>6</sub>H<sub>5</sub> (7), C<sub>6</sub>H<sub>4</sub>-*p*-CH<sub>3</sub> (8)), and the insertion occurs at the Mg–C bond. Reaction of compound A with CO<sub>2</sub> in diethyl ether gives two different insertion products, {(Me<sub>2</sub>Al)<sub>2</sub>[μ-OOC(*i*-Pr<sub>2</sub>N)]<sub>2</sub>} (9), a dialuminum carbamate complex, and {(Me<sub>2</sub>Al)<sub>2</sub>[μ-OOC(*i*-Pr<sub>2</sub>N)]<sub>2</sub>}-Mg (10), a mixed-metal aluminum–magnesium carbamate complex. Reaction of compound B with CO<sub>2</sub> gives {(Me<sub>2</sub>Al)<sub>2</sub>[μ-OOC(Et<sub>2</sub>N)]<sub>2</sub>Mg} (11), and sublimation of 11 gives compound 12, {(Me<sub>2</sub>Al)<sub>2</sub>[μ-OOC(Et<sub>2</sub>N)]<sub>2</sub>}. The crystal structures of 1–5, 9, and 10 were determined by single-crystal X-ray diffraction techniques. Complexes 1–5 all consist of three four-membered rings made of two tetrahedrally coordinated Al and Mg atoms with two bridging amido groups. The ethynyl bridging groups are almost perpendicular to the Mg–Mg vector. The pertinent bonding features (*d*(C<sub>α</sub>≡C<sub>β</sub>) = 1.183(6)–1.204(10) Å, ∠Mg–C<sub>α</sub>≡C<sub>β</sub> = 142.1(7)–165.9(6)°, ∠Mg\*–C<sub>α</sub>≡C<sub>β</sub> = 107.6(5)–131.8(7)°) indicate no substantial π-interaction between the magnesium and the ethynyl groups, yet a tendency toward such interactions is noticed. The dialuminum and aluminum–magnesium mixed-metal carbamate complexes 9 and 10 result from the insertion of CO<sub>2</sub> into the metal–N bond at the bridging amido ligands. Their syntheses and structures are discussed.

### Introduction

Activation of the inert carbon dioxide molecule is essential for its utilization. Several reactions of transition metals with CO<sub>2</sub> have opened a new area for catalytic CO<sub>2</sub> fixations.<sup>1</sup> However, only a few CO<sub>2</sub> insertion reactions on main-group elements such as aluminum<sup>2</sup> and magnesium<sup>3</sup> have been reported. Their intermediate carbamate complexes are often not isolated

either. We have recently reported the syntheses and crystal structures of an unusual cyclic tetrameric complex, [Me<sub>2</sub>Al(μ-*i*-Pr<sub>2</sub>N)<sub>2</sub>Mg(μ-Me)]<sub>4</sub>, containing tricoordinate magnesium atoms, and a linear dimer, [Me<sub>2</sub>Al(μ-Et<sub>2</sub>N)<sub>2</sub>Mg(μ-Me)]<sub>2</sub>, containing tetracoordinate magnesium atoms.<sup>4</sup> When treated with nucleophiles, these compounds undergo metathesis and insertion reactions.<sup>5</sup> Their reaction with CO<sub>2</sub> is facile and interesting. The CO<sub>2</sub>-inserted aluminum–magnesium complexes can provide useful information in understanding the mech-

<sup>®</sup> Abstract published in *Advance ACS Abstracts*, October 1, 1995.  
(1) (a) Palmer, D. A.; Eldik, R. V. *Chem. Rev.* **1983**, *83*, 651. (b) Behr, A. *Angew. Chem., Int. Ed. Engl.* **1988**, *27*, 661. (c) Braunstein, P.; Matt, D.; Nobel, D. *Chem. Rev.* **1988**, *88*, 747. (d) Kolomnikov, I. S.; Stepovska, G.; Tyrlík, S.; Vol'pin, M. E. *J. Gen. Chem. USSR (Engl. Transl.)* **1974**, *44*, 1710. (e) Darenbourg, D. J.; Kudarowski, R. A. The Activation of Carbon Dioxide by Metal Complexes. In *Advances in Organometallic Chemistry*; Stone, F. G. A., West, R., Eds.; Academic Press: New York, 1983; Vol. 22, p 129. (f) Kitajima, N.; Hikichi, S.; Tanaka, M.; Moro-oka, Y. *J. Am. Chem. Soc.* **1993**, *115*, 5496. (g) Kolomnikov, I. S.; Lobeeva, T. S.; Gorbachevskaya, V. V.; Aleksandrov, G. G.; Struchkov, Yu. T.; Vol'pin, M. E. *J. Chem. Soc. D* **1971**, 972. (h) Chetcuti, M. J.; Chisholm, M. H.; Foltling, K.; Haitko, D. A.; Huffman, J. C. *J. Am. Chem. Soc.* **1982**, *104*, 2138 and a number of references cited therein. (i) Gibson, D. H.; Ye, M.; Richardson, J. F. *J. Am. Chem. Soc.* **1992**, *114*, 9716. (j) Sakamoto, M.; Shimizu, I.; Yamamoto, A. *Organometallics* **1994**, *13*, 407 and references therein.

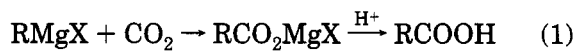
(2) Takeda, N.; Inoue, S. *Bull. Chem. Soc. Jpn.* **1978**, *51*, 3564. Kojima, F.; Aida, T.; Inoue, S. *J. Am. Chem. Soc.* **1986**, *108*, 391. Aida, T.; Inoue, S. *J. Am. Chem. Soc.* **1983**, *105*, 1304. Gilman, H.; Jones, R. G. *J. Am. Chem. Soc.* **1940**, *62*, 2353. Weidlein, J. *J. Organomet. Chem.* **1973**, *49*, 257.

(3) Weidlein, J. *Z. Anorg. Allg. Chem.* **1970**, *378*, 245. Han, R.; Parkin, G. *J. Am. Chem. Soc.* **1992**, *114*, 748.

(4) Her, T. Y.; Chang, C. C.; Liu, L. K. *Inorg. Chem.* **1992**, *31*, 2291.

(5) (a) Her, T. Y.; Chang, C. C.; Lee, G. H.; Peng, S. M.; Wang, Y. *Inorg. Chem.* **1994**, *33*, 99. (b) Chang, C. C.; Lee, W. H.; Her, T. Y.; Lee, G. H.; Peng, S. M.; Wang, Y. *J. Chem. Soc., Dalton Trans.* **1994**, 221. (c) Chang, C. C.; Her, T. Y.; Hsieh, F. Y.; Yang, C. Y.; Chiang, M. Y.; Lee, G. H.; Wang, Y.; Peng, S. M. *J. Chin. Chem. Soc. (Taipei)* **1994**, *41*, 783. (d) Chang, C. C.; Her, T. Y.; Li, M. D.; Williamson, R.; Lee, G. H.; Peng, S. M.; Wang, Y. *Inorg. Chem.* **1995**, *34*, 4296.

anism of the Grignard–CO<sub>2</sub> intermediate (eq 1). The



X = halide

complexes selected in the present study of CO<sub>2</sub> insertions, the aforementioned tetrameric and dimeric complexes of aluminum–magnesium, have a strong relevance to the Grignard intermediate, and their reactions with CO<sub>2</sub> may proceed through a similar intermediate.

In comparison to the well-known preparation of organic acids using Grignard reagent and CO<sub>2</sub>, the magnesium atom in these aluminum–magnesium complexes is more electropositive than that in the Grignard reagent.<sup>5d</sup> Therefore, it is more suitable for activation of inert molecules such as CO<sub>2</sub>.

In an attempt to investigate further the reactivity of these complexes, we have carried out the metathesis of the magnesium–alkyl bonds using substituted acetylenes. The polynuclear ethynyl-bridged aluminum–magnesium complexes obtained in the present study are valuable additions to the collection of the previously reported ethynyl-bridged complexes of aluminum,<sup>6</sup> beryllium,<sup>7</sup> gallium, and indium.<sup>8</sup> These complexes provide references for the study of possible  $\pi$ -interactions between the magnesium centers and ethynyl groups as well as reactivity toward CO<sub>2</sub> insertion reactions. In this paper, we describe the synthesis, characterization, and structural studies of the first ethynyl-bridged aluminum–magnesium complexes and their reaction with CO<sub>2</sub>.

## Results and Discussion

**Synthesis and Characterization of Ethynyl-Bridged Complexes.** The precursors [Me<sub>2</sub>Al( $\mu$ -*i*-Pr<sub>2</sub>N)<sub>2</sub>Mg( $\mu$ -Me)]<sub>4</sub> (**A**) and [Me<sub>2</sub>Al( $\mu$ -Et<sub>2</sub>N)<sub>2</sub>Mg( $\mu$ -Me)]<sub>2</sub> (**B**) could be obtained by reacting equimolar quantities of Mg(NR<sub>2</sub>)<sub>2</sub><sup>9</sup> (R = *i*-Pr for compound **A** and R = Et for compound **B**) with AlMe<sub>3</sub> as reported earlier.<sup>4</sup> The dimeric ethynyl-bridged complexes [Me<sub>2</sub>Al( $\mu$ -*i*-Pr<sub>2</sub>N)<sub>2</sub>Mg( $\mu$ -C≡C<sub>6</sub>H<sub>5</sub>)]<sub>2</sub> (**1**), [Me<sub>2</sub>Al( $\mu$ -*i*-Pr<sub>2</sub>N)<sub>2</sub>Mg( $\mu$ -C≡CC<sub>6</sub>H<sub>4</sub>-*p*-CH<sub>3</sub>)]<sub>2</sub> (**2**), [Me<sub>2</sub>Al( $\mu$ -*i*-Pr<sub>2</sub>N)<sub>2</sub>Mg( $\mu$ -C≡CCMe<sub>3</sub>)]<sub>2</sub> (**3**), and [Me<sub>2</sub>Al( $\mu$ -*i*-Pr<sub>2</sub>N)<sub>2</sub>Mg( $\mu$ -C≡CSiMe<sub>3</sub>)]<sub>2</sub> (**4**) were obtained by reacting HC≡CC<sub>6</sub>H<sub>5</sub>, HC≡CC<sub>6</sub>H<sub>4</sub>-*p*-CH<sub>3</sub>, HC≡CCMe<sub>3</sub>, and HC≡CSiMe<sub>3</sub>, respectively, with compound **A**. Reaction with equimolar quantities of the acetylenes thus yielded the polynuclear dimers [Me<sub>2</sub>Al( $\mu$ -*i*-Pr<sub>2</sub>N)<sub>2</sub>Mg( $\mu$ -C≡CR)]<sub>2</sub> from diethyl ether. Similarly, the polynuclear complexes **5** and **6** were obtained from

the reaction of equimolar quantities of HC≡CC<sub>6</sub>H<sub>5</sub> and HC≡CC<sub>6</sub>H<sub>4</sub>-*p*-CH<sub>3</sub>, respectively, with compound **B** (Scheme 1).

All of the complexes were fully characterized by <sup>1</sup>H, <sup>13</sup>C NMR, IR, and mass spectral studies. In the <sup>13</sup>C NMR spectra, for complex **1**, both acetylide carbon atoms show absorptions at a much lower field (C<sub>α</sub>,  $\delta$  123.15 ppm; C<sub>β</sub>,  $\delta$  111.37 ppm) than for the free substituted acetylenes HC≡C<sub>6</sub>H<sub>5</sub> (C<sub>α</sub>,  $\delta$  86.4; C<sub>β</sub>,  $\delta$  78.3) and HC≡C<sub>6</sub>H<sub>4</sub>-*p*-CH<sub>3</sub> (C<sub>α</sub>,  $\delta$  86.8; C<sub>β</sub>,  $\delta$  74.5). Similar chemical shifts for C<sub>β</sub> have been observed in other metal  $\sigma$ -alkynyl complexes, while C<sub>α</sub> shifts seem to cover a much wider range. For a comparison, refer to Cp<sub>2</sub>Zr( $\mu$ -C≡CCH<sub>3</sub>)<sub>2</sub> (C<sub>α</sub>,  $\delta$  131.6; C<sub>β</sub>,  $\delta$  120.0), Cp<sub>2</sub>Zr( $\mu$ -C≡CC<sub>6</sub>H<sub>5</sub>)<sub>2</sub> (C<sub>α</sub>,  $\delta$  141.7; C<sub>β</sub>,  $\delta$  124.8),<sup>10</sup> Me<sub>2</sub>Al(C≡CCH<sub>3</sub>) (C<sub>α</sub>,  $\delta$  90.3; C<sub>β</sub>,  $\delta$  132.92), Me<sub>2</sub>Ga(C≡CCH<sub>3</sub>) (C<sub>α</sub>,  $\delta$  89.8; C<sub>β</sub>,  $\delta$  122.4),<sup>8b</sup> Me<sub>2</sub>In(C≡CCH<sub>3</sub>) (C<sub>α</sub>,  $\delta$  90.9; C<sub>β</sub>,  $\delta$  122.4),<sup>8b</sup> (dppe)Pt(C≡CR) (C<sub>α</sub>,  $\delta$  107; C<sub>β</sub>,  $\delta$  111.8) (R = Ph) (C<sub>α</sub>,  $\delta$  91.2; C<sub>β</sub>,  $\delta$  105.3) (R = CH<sub>3</sub>),<sup>11</sup> and Cp(CO)<sub>2</sub>(PMe<sub>3</sub>)W(C≡CPh) (C<sub>α</sub>,  $\delta$  96.3; C<sub>β</sub>,  $\delta$  127.4).<sup>12</sup> For complex **2**, the chemical shifts of HC≡CC<sub>6</sub>H<sub>4</sub>-*p*-CH<sub>3</sub> were observed at  $\delta$  123.15 (C<sub>α</sub>) and  $\delta$  111.37 ppm (C<sub>β</sub>), for **3**, those of HC≡C(CH<sub>3</sub>)<sub>3</sub> at  $\delta$  137.97 (C<sub>α</sub>) and  $\delta$  97.84 (C<sub>β</sub>), for **4**, those of HC≡CSi(CH<sub>3</sub>)<sub>3</sub> at  $\delta$  140.95 (C<sub>α</sub>) and  $\delta$  136.55 (C<sub>β</sub>) for **5**, those of HC≡CC<sub>6</sub>H<sub>5</sub> at (C<sub>β</sub>),  $\delta$  122.45 (C<sub>α</sub>) and  $\delta$  105.87 (C<sub>β</sub>), and for **6**, those of HC≡CC<sub>6</sub>H<sub>4</sub>-*p*-CH<sub>3</sub> at  $\delta$  119.56 (C<sub>α</sub>) and  $\delta$  105.22 (C<sub>β</sub>).

It has been observed that the  $\pi$ -complexation to the additional metal center occurring in the dimerization of monozirconium acetylide complexes results in a downfield shift of ca. 100 ppm for these alkynyl resonances in comparison to the mononuclear complexes (typical examples are [Cp<sub>2</sub>Zr( $\mu$ -C≡CCH<sub>3</sub>)<sub>2</sub>]<sub>2</sub> and [(H<sub>3</sub>CCp)<sub>2</sub>Zr( $\mu$ -C≡CPh)]<sub>2</sub>,<sup>10</sup> exhibiting <sup>13</sup>C NMR absorptions of the  $\mu$ -C≡CR ligands at  $\delta$  204.2 (C<sub>α</sub>), 147.9 (C<sub>β</sub>) and  $\delta$  227.7 (C<sub>α</sub>), 155.4 (C<sub>β</sub>), respectively). Interestingly, in the case of the dimeric complex [Me<sub>2</sub>Al( $\mu$ -C≡CCH<sub>3</sub>)]<sub>2</sub>, such drastic deshielding signals were not observed for the acetylenic carbons, where the existence of  $\pi$ -complexation between aluminum and the acetylenic carbons was established.<sup>6c</sup> Similarly, in the IR spectrum, for the doubly ethynyl bridged zirconium complexes [Cp<sub>2</sub>Zr( $\mu$ -C≡CCH<sub>3</sub>)]<sub>2</sub> and [(H<sub>3</sub>CCp)<sub>2</sub>Zr( $\mu$ -C≡CPh)]<sub>2</sub><sup>10</sup> the absorptions due to  $\nu_{\text{C}=\text{C}}$  were observed at 1875 cm<sup>-1</sup>. In the present complexes these absorptions were observed at much higher frequencies (2025–2065 cm<sup>-1</sup>) similar to the corresponding value for the [Me<sub>2</sub>Al( $\mu$ -C≡CCH<sub>3</sub>)]<sub>2</sub> dimer. Therefore, it appears the chemical shifts of the acetylenic carbons and the IR stretching frequencies of **1–6** indicate that possible weak Mg–( $\pi$ -ethynyl) interactions exist in these complexes.

**X-ray Crystal Structures of Ethynyl-Bridged Complexes.** Although polynuclear aluminum–magnesium complexes have been studied extensively,<sup>13</sup> the

(6) For examples of ethynyl-bridged aluminum complexes, see: (a) Stucky, G. D.; McPherson, A. M.; Rhine, W. E.; Eisch, J. J.; Considine, J. L. *J. Am. Chem. Soc.* **1974**, *96*, 1941. (b) Albright, M. J.; Butler, W. M.; Anderson, T. J.; Glick, M. D.; Oliver, J. P. *J. Am. Chem. Soc.* **1976**, *98*, 3995. (c) Almendinger, A.; Fernholt, L.; Haaland, A. *J. Organomet. Chem.* **1978**, *155*, 245. (d) Mole, T.; Surtees, J. R. *Aust. J. Chem.* **1964**, *17*, 1229. (e) Jeffery, E. A.; Mole, T.; Saunders, J. K. *Aust. J. Chem.* **1968**, *21*, 137. (f) Eisch, J. J.; Kaska, W. C. *J. Organomet. Chem.* **1964**, *2*, 184.

(7) For examples of ethynyl-bridged beryllium complexes, see: (a) Morosin, B.; Howatson, J. *J. Organomet. Chem.* **1971**, *29*, 7. (b) Bell, N. A.; Nowell, I. W.; Shearer, H. M. *M. J. Chem. Soc., Chem. Commun.* **1982**, 147.

(8) For examples of ethynyl-bridged aluminum, gallium, and indium complexes, see: (a) Jeffery, E. A.; Mole, T. *J. Organomet. Chem.* **1968**, *11*, 393. (b) Fries, W.; Schwartz, W.; Hausen, H.-D.; Weidlein, J. *J. Organomet. Chem.* **1978**, *159*, 373. (c) Teclé, B.; Ilesley, H.; Oliver, J. P. *Inorg. Chem.* **1981**, *20*, 2335.

(9) Coates, G. E.; Ridley, D. *J. Chem. Soc. A* **1967**, 56.

(10) Erker, G.; Frömberg, W.; Benn, R.; Mynott, R.; Angermund, K.; Krüger, C. *Organometallics* **1989**, *8*, 911.

(11) Sebald, A.; Wrackmeyer, B. *Z. Naturforsch.* **1983**, *38B*, 1156.

(12) Kreissl, F. R.; Eberl, K.; Uedelhoven, W. *Angew. Chem.* **1978**, *90*, 908.

(13) Atwood, J. L.; Stucky, G. D. *J. Organomet. Chem.* **1968**, *3*, 53. Atwood, J. L.; Stucky, G. D. *J. Am. Chem. Soc.* **1969**, *91*, 2538. Ziegler, K.; Holzkamp, Z. *Justus Liebigs Ann. Chem.* **1957**, *605*, 93. Malpass, D. B.; Fannin, L. W. *J. Organomet. Chem.* **1975**, *93*, 1. Boncella, J. M.; Anderson, R. A. *Organometallics* **1985**, *4*, 205. Schaverien, C. J.; Orpen, A. G. *Inorg. Chem.* **1991**, *30*, 4968. McDade, C.; Gibson, V. C.; Santarsiero, B. D.; Bercaw, J. E. *Organometallics* **1988**, *7*, 1. Meese-Markscheffel, J. A.; Cramer, R. E.; Gilje, J. W. *Polyhedron* **1994**, *13*, 1045.



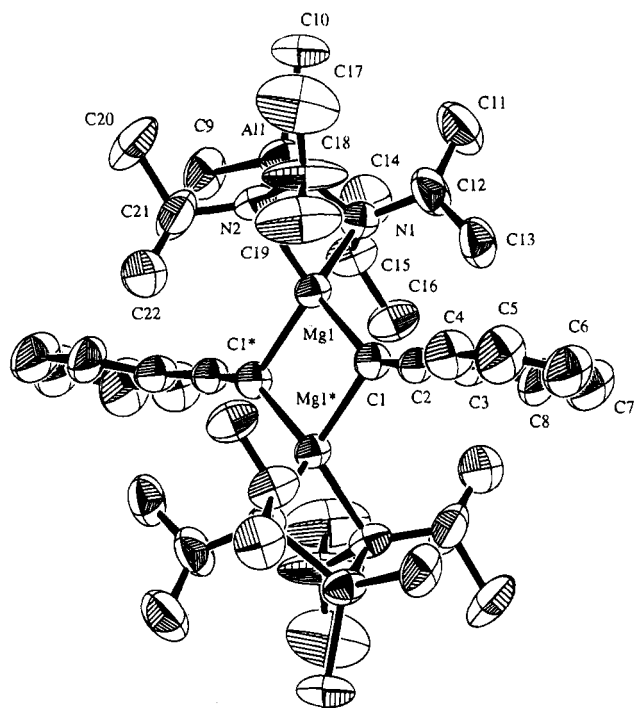


**Figure 1.** ORTEP view of the molecule  $[\text{Me}_2\text{Al}(\mu\text{-}i\text{-Pr}_2\text{N})_2\text{-Mg}(\mu\text{-C}\equiv\text{CC}_6\text{H}_5)]_2$  (**1**) using 30% probability ellipsoids.

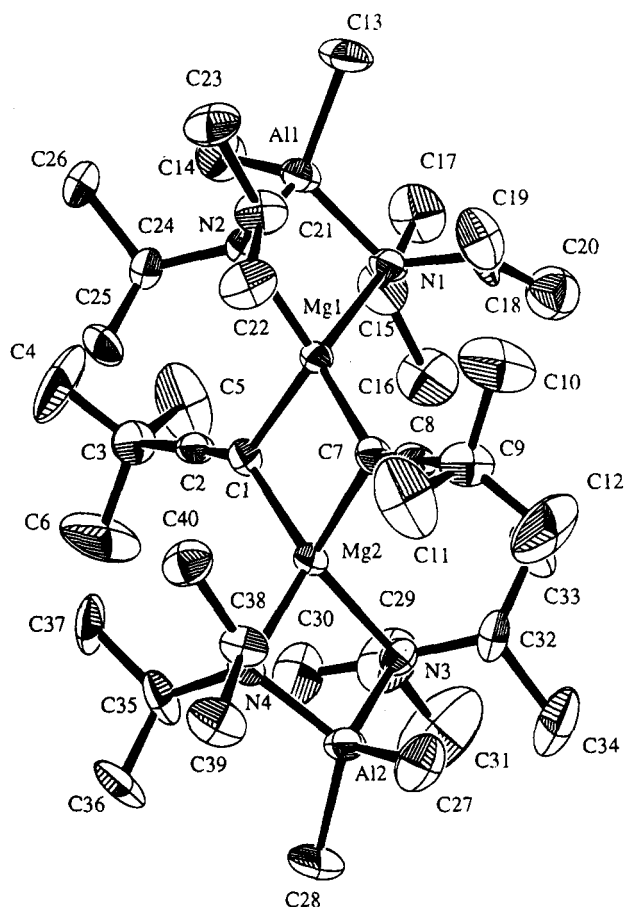


**Figure 3.** ORTEP view of the molecule  $[\text{Me}_2\text{Al}(\mu\text{-}i\text{-Pr}_2\text{N})_2\text{-Mg}(\mu\text{-C}\equiv\text{C-}t\text{-Bu})]_2$  (**3**) using 30% probability ellipsoids.

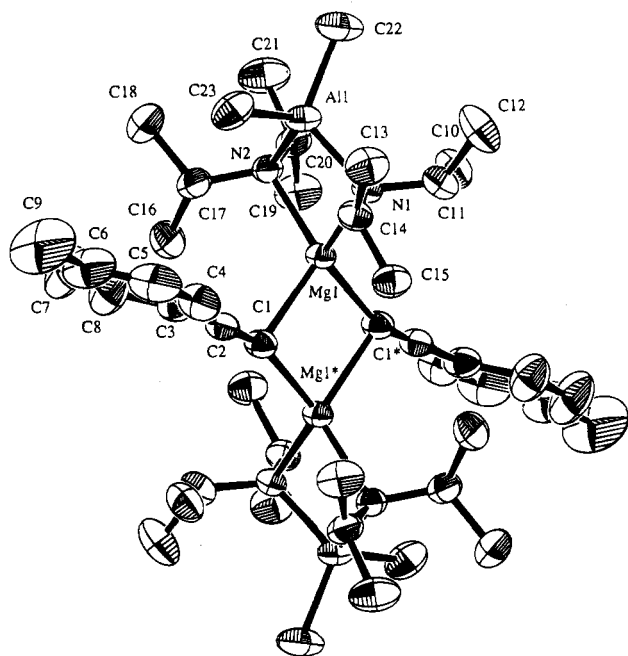


**Figure 2.** ORTEP view of the molecule  $[\text{Me}_2\text{Al}(\mu\text{-}i\text{-Pr}_2\text{N})_2\text{-Mg}(\mu\text{-C}\equiv\text{CC}_6\text{H}_4\text{-}p\text{-CH}_3)]_2$  (**2**) using 30% probability ellipsoids.

and 2.28 Å), and  $(\eta^5\text{-indenyl})_2\text{Mg}$  (2.26 Å)<sup>20c</sup> overlap with the typical  $\text{Mg}-(\sigma\text{-C})$  length (2.175–2.246 Å).<sup>15–17</sup>

One might think the  $\text{C}\equiv\text{C}$  bond length is a better criterion for  $\text{Mg}-(\pi\text{-C})$  interaction due to the bond weakening resulting from donation of  $\pi$ -electrons into an empty orbital on the Mg atom. As shown in Table 3, the  $\text{C}\equiv\text{C}$  distances in these  $\pi$ -complexes are either slightly longer than (maximum 1.26 Å) or sometimes equal to that observed in free acetylene (1.20 Å). This is in agreement with the observation of Oliver and co-workers<sup>8c</sup> suggesting that the  $\text{C}\equiv\text{C}$  length is not necessarily a good measure of  $\pi$ -interaction. The  $\text{C}\equiv\text{C}$  distances in the present set of complexes range from

1.181(6) to 1.204(10) Å. These values are very close to that for free acetylene. This seems to indicate that a  $\pi$ -interaction is not involved in these complexes.

Examination of the complexes with well-established  $\pi$ -character in the  $\text{Mg}$ -ethynyl bond revealed that other structural features (see below) may serve as better criteria for the existence of  $\pi$ -character. In those  $\pi$ -ethynyl–Mg complexes at least one of the following pronounced features exists: (1) a bent  $\text{C}\equiv\text{CR}$  group, (2) a short  $\text{Mg}-\text{C}_\alpha(\text{ethynyl})$  distance, (3) an acute  $\text{Mg}-\text{C}_\alpha\equiv\text{C}_\beta$  angle. The last two factors put the Mg atom close to the middle of the  $\text{C}\equiv\text{C}$  bond, thus constituting an orientation best suited for maximum  $\pi$ -interaction. In the case of  $\text{Ga}_2(\mu\text{-C}\equiv\text{CPh})_2\text{Me}_4$ <sup>8c</sup> no bending of the  $\text{C}\equiv\text{C}-\text{R}$  moiety was observed, yet a  $\text{Ga}-\pi$ -ethynyl interaction was concluded due to the proper orientation of gallium with respect to the ethynyl group.

The unequal  $\text{Mg}(1)-\text{C}_\alpha\equiv\text{C}_\beta$  and  $\text{Mg}(1^*)-\text{C}_\alpha\equiv\text{C}_\beta$  angles in complexes 1–5 led to the suspicion of a possible existence of  $\pi$ -interaction between magnesium and ethynyl groups. The difference of these two angles is smallest in complex 3, while it is the largest in complex 5. The orientation of the bridging ethynyl groups in complex 3 is almost perpendicular to the  $\text{Mg}-\text{Mg}$  vector, which is an orientation least suitable for any appreciable  $\pi$ -interaction. Complex 5, in contrast, has an orientation similar to the  $\pi$ -orientation in  $\text{Al}_2(\mu\text{-C}\equiv\text{CMe})_2\text{Me}_4$ .<sup>6c</sup> Complex 4 is structurally similar to complex 3. However, it has the most bent  $\text{C}\equiv\text{C}-\text{R}$  angle (172°), suggesting  $\pi$ -electron donation to Mg orbitals.

One may argue that packing effects (basically steric repulsion) may also be the cause of the distorted angles



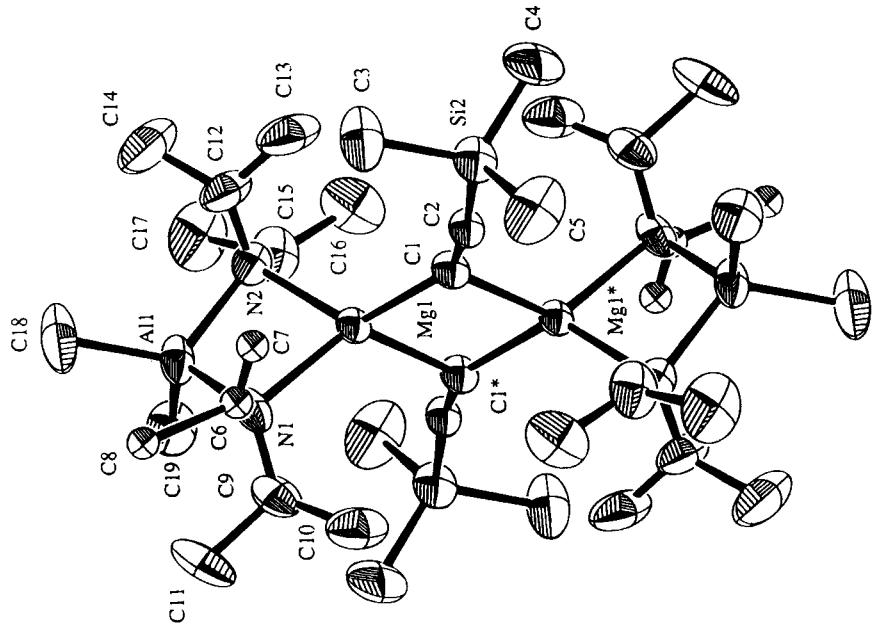


**Figure 4.** ORTEP view of the molecule  $[\text{Me}_2\text{Al}(\mu\text{-}i\text{-Pr}_2\text{N})_2]_2\text{Mg}(\mu\text{-C}\equiv\text{CSiMe}_3)_2$  (**4**) using 30% probability ellipsoids.

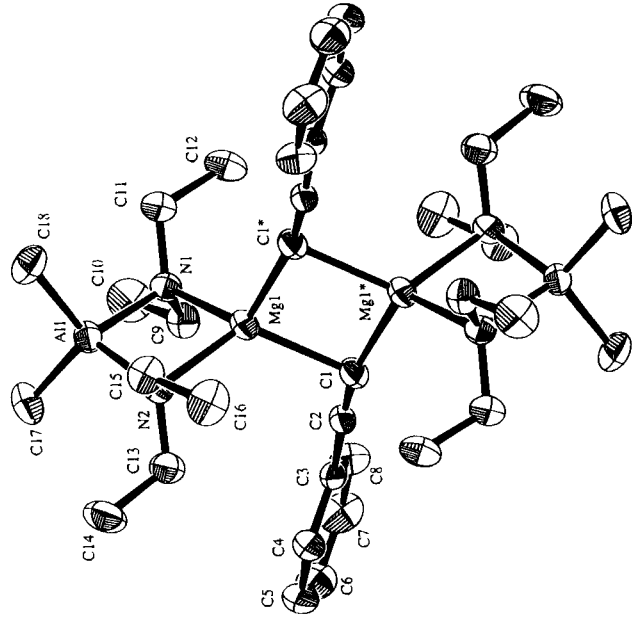


**Figure 5.** ORTEP view of the molecule  $[\text{Me}_2\text{Al}(\mu\text{-Et}_2\text{N})_2]_2\text{Mg}(\mu\text{-C}\equiv\text{CC}_6\text{H}_5)_2$  (**5**) using 30% probability ellipsoids.

mentioned above. Indeed, evidence found for complex **2** seems to support this idea. Complex **2** consists of two independent molecules in the asymmetric unit cell. Each molecule displays a unique set of  $\text{Mg}(1)-\text{C}_\alpha=\text{C}_\beta$  and  $\text{Mg}'-\text{C}_\alpha=\text{C}_\beta$  angles (see Table 3). Molecules of the same compound should have same structural parameters, except when distortion caused by packing occurs. This observation rules out a substantial  $\pi$ -bonding interaction between the ethynyl groups and the mag-

**Table 1.** Crystal and Intensity Collection Data for Complexes 1–5, 9, and 10

	1	2	3	4	5	9	10
formula	$\text{C}_{44}\text{H}_{78}\text{N}_4\text{Al}_2\text{Mg}_2$	$\text{C}_{23}\text{H}_{41}\text{N}_2\text{AlMg}$	$\text{C}_{40}\text{H}_{86}\text{N}_4\text{Al}_2\text{Mg}_2$	$\text{C}_{38}\text{H}_{86}\text{Al}_2\text{Mg}_2\text{N}_4\text{Si}_2$	$\text{C}_{36}\text{H}_{63}\text{Al}_2\text{N}_4\text{Mg}_2$	$\text{C}_{18}\text{H}_{40}\text{O}_4\text{N}_2\text{Al}_2$	$\text{C}_{32}\text{H}_{66}\text{O}_8\text{N}_4\text{Al}_2\text{Mg}$
molar mass/g	765.70	396.88	725.72	757.87	653.49	402.49	716.18
cryst syst	monoclinic	monoclinic	trigonal	trigonal	orthorhombic	monoclinic	monoclinic
diffractionmeter	Rigaku AFC6S	Rigaku AFC6S	Rigaku AFC7S	Rigaku AFC7S	Rigaku AFC6S	Rigaku AFC7S	Rigaku AFC6S
space group	$P2_1/n$ (No. 14)	$P1$ (No. 2)	$P2_1/c$ (No. 14)	$P1$ (No. 2)	$Pbc$ (No. 61)	$P2_1/n$ (No. 14)	$P2_1/n$ (No. 14)
$a/\text{\AA}$	10.655(3)	10.906(3)	16.817(5)	10.618(2)	20.215(2)	8.188(4)	12.826(2)
$b/\text{\AA}$	16.886(1)	14.129(2)	12.609(4)	13.010(1)	18.976(2)	15.044(6)	21.062(4)
$c/\text{\AA}$	13.851(2)	18.210(5)	22.905(5)	19.875(2)	10.922(2)	10.795(6)	17.555(2)
$\alpha/\text{deg}$	98.05(2)	78.12(2)	90.12(2)	81.772(8)		101.46(4)	103.76(1)
$\beta/\text{deg}$		73.89(2)		79.753(8)			
$\gamma/\text{deg}$	2467.6(6)	74.14(2)	4856(2)	71.898(8)	2556.7(6)	1303.2(10)	4606(1)
$Z$	2	4	8	2	4	2	4
$F(000)$	840.00	872.00	3232.00	840.00	2136.00	440.00	1560.00
$D^{\text{calc}}(\text{g}/\text{cm}^3)$	1.030	1.027	1.985	0.984	1.554	1.026	1.031
$\mu/\text{cm}^{-1}$	10.03	9.78	2.27	1.55	16.67	1.32	10.33
$2\theta(\text{max})/\text{deg}$	120.1	120.2	50.0	50.0	120.1	50.0	120.3
crystal dimens/mm	$0.48 \times 0.64 \times 0.96$	$0.38 \times 0.58 \times 0.63$	$0.80 \times 0.40 \times 0.40$	$0.33 \times 0.75 \times 1.00$	$0.33 \times 0.60 \times 0.90$	$0.16 \times 0.20 \times 0.30$	$0.48 \times 0.88 \times 0.27$
no. of meas rflns	4055	8005	9274	9443	3542	2552	7438
no. of unique rflns	3828	7646	8950	9012	3542	2382	7082
no. of obs rflns ( $I > 3.0\sigma(I)$ )	2622	4815	2952	4263	2002	931	2679
$R_f, R_w$	0.080; 0.073	0.057; 0.046	0.072; 0.084	0.104; 0.122	0.062; 0.074	0.050; 0.046	0.050; 0.051
radiation (graphite monoch)	Cu K $\alpha$	Cu K $\alpha$	Cu K $\alpha$	Cu K $\alpha$	Cu K $\alpha$	Cu K $\alpha$	Cu K $\alpha$
data collection temp/ $^\circ\text{C}$	23	23	24	24	23	22	23

Table 2. Selected Bond Distances (Å) and Angles (deg)

[Me <sub>2</sub> Al(μ- <i>i</i> -Pr <sub>2</sub> N) <sub>2</sub> Mg(μ-C≡CC <sub>6</sub> H <sub>5</sub> ) <sub>2</sub> ] (1)							
Al(1)–Mg(1)	2.825(2)	N(2)–C(21)	1.43(1)	N(1)–C(12)	1.501(7)	C(3)–C(4)	1.397(8)
Al(1)–N(2)	1.954(5)	N(1)–C(15)	1.511(7)	N(2)–C(18)	1.581(10)	Mg(1)–Mg(1*)	3.075(3)
Mg(1)–N(1)	2.152(4)	C(1)–C(2)	1.181(6)				
Mg(1)–C(1)–C(2)	145.7(5)	C(12)–N(1)–C(15)	113.4(5)	N(1)–Al(1)–C(10)	118.1(3)	N(1)–Mg(1)–N(2)	84.9(2)
C(2)–C(1)–Mg(1*)	126.4(5)	Al(1)–N(2)–C(18)	114.1(4)	Al(1)–Mg(1)–Mg(1*)	161.61(10)	Al(1)–N(2)–Mg(1)	87.6(2)
Mg(1)–Al(1)–C(9)	105.5(2)	Mg(1)–N(1)–C(15)	107.4(3)	Al(1)–Mg(1)–N(2)	43.7(1)	Mg(1*)–C(1)–C(2)	126.4(5)
Mg(1)–Al(1)–N(1)	49.5(1)	C(1)–C(2)–C(3)	178.4(6)	Al(1)–Mg(1)–C(1)	115.9(1)	C(1)–Mg(1)–C(1*)	92.2(2)
N(1)–Al(1)–N(2)	95.1(2)	Mg(1)–C(1)–Mg(1*)	87.8(2)	N(2)–Mg(1)–C(1)	123.9(2)	Al(1)–N(1)–C(12)	116.9(4)
[Me <sub>2</sub> Al(μ- <i>i</i> -Pr <sub>2</sub> N) <sub>2</sub> Mg(μ-C≡CC <sub>6</sub> H <sub>4</sub> - <i>p</i> -CH <sub>3</sub> ) <sub>2</sub> ] (2)							
Al(1)–Mg(1)	2.859(2)	C(1)–C(2)	1.197(5)	Mg(1)–C(1)	2.170(4)	N(1)–C(11)	1.497(5)
Al(1)–N(2)	1.971(3)	C(2)–C(3)	1.462(5)	Mg(1)–N(2)	2.149(3)	Mg(1)–Mg(1*)	3.130(2)
Mg(1)–Al(1)–N(1)	48.37(9)	Mg(1)–Mg(1*)–C(1)	46.6(1)	Al(1)–Mg(1)–N(1)	43.38(9)	Al(1)–N(2)–Mg(1)	87.8(1)
Mg(1)–Al(1)–C(22)	138.9(2)	N(1)–Mg(1)–N(2)	86.0(1)	Al(1)–Mg(1)–C(1)	146.5(1)	Mg(1)–C(1)–Mg(1*)	89.6(2)
Mg(1)–Al(1)–C(23)	112.1(1)	N(1)–Mg(1)–C(1*)	121.8(2)	Al(1)–Mg(1)–C(1*)	123.0(1)	Mg(1)–C(1)–C(2)	157.9(4)
N(1)–Al(1)–N(2)	96.0(1)	N(1)–Mg(1)–C(1)	117.9(1)	Mg(1*)–Mg(1)–N(1)	134.9(1)		
Al(1)–Mg(1)–Mg(1*)	166.73(8)	Al(1)–N(1)–Mg(1)	88.3(1)				
[Me <sub>2</sub> Al(μ- <i>i</i> -Pr <sub>2</sub> N) <sub>2</sub> Mg(μ-C≡C- <i>t</i> -Bu) <sub>2</sub> ] (3)							
Al(1)–N(1)	1.958(7)	N(2)–C(21)	1.49(1)	Mg(1)–N(1)	2.132(7)	C(1)–C(2)	1.204(10)
Al(2)–N(3)	1.977(8)	N(3)–C(29)	1.51(2)	Mg(1)–C(1)	2.225(8)	C(2)–C(3)	1.50(1)
Mg(2)–N(3)	2.129(7)	C(3)–C(4)	1.47(1)	Mg(2)–C(1)	2.210(9)	C(18)–C(20)	1.36(3)
N(1)–C(15)	1.49(1)						
N(1)–Al(1)–N(2)	96.2(3)	Mg(2)–N(4)–C(38)	106.1(5)	Al(1)–N(1)–C(18)	121.8(6)	Mg(2)–C(7)–C(8)	133.6(7)
N(3)–Al(2)–N(4)	96.1(3)	Mg(2)–N(4)–C(35)	114.2(6)	Mg(1)–N(1)–C(18)	111.1(6)	N(1)–C(18)–C(19)	109.0(9)
N(1)–Mg(1)–C(7)	124.8(3)	Mg(1)–C(1)–Mg(2)	86.2(3)	Al(1)–N(2)–Mg(1)	87.8(3)	N(4)–C(38)–C(39)	117.9(8)
N(3)–Mg(2)–N(4)	86.2(3)	Mg(2)–C(1)–C(2)	142.1(7)	Al(1)–N(2)–C(24)	113.2(5)	Mg(1)–C(1)–C(29)	108.3(7)
Al(1)–N(1)–Mg(1)	88.4(3)	C(2)–C(3)–C(4)	109.8(8)	Mg(1)–N(2)–C(21)	115.3(6)	Al(2)–N(4)–Mg(2)	87.9(3)
[Me <sub>2</sub> Al(μ- <i>i</i> -Pr <sub>2</sub> N) <sub>2</sub> Mg(μ-C≡CSiMe <sub>3</sub> ) <sub>2</sub> ] (4)							
Si(2)–C(2)	1.865(9)	Mg(1*)–C(1)	2.240(9)	Al(1)–N(2)	1.963(9)	C(1)–C(2)	1.20(1)
Si(2)–C(4)	1.81(1)	N(1)–C(6)	1.57(2)	Mg(1)–N(1)	2.138(8)	C(6)–C(7)	1.15(2)
Al(1)–N(1)	1.941(9)	N(2)–C(12)	1.49(1)	Mg(1)–C(1)	2.214(9)		
C(2)–Si(2)–C(5)	109.2(5)	Mg(1)–N(1)–C(9)	108.5(6)	N(1)–Mg(1)–C(1)	117.2(3)	C(1)–Mg(1)–C(1*)	92.0(3)
N(1)–Al(1)–N(2)	95.9(3)	Mg(1)–C(1)–Mg(1*)	88.0(3)	N(2)–Mg(1)–C(1)	116.8(3)	Al(1)–N(1)–C(6)	122.7(8)
N(2)–Al(1)–C(19)	109.8(5)	Mg(1)–C(1)–C(2)	122.3(7)	Al(1)–N(1)–Mg(1)	88.0(3)	Mg(1*)–C(1)–C(2)	149.6(8)
N(1)–Mg(1)–N(2)	85.3(3)	N(2)–C(12)–C(14)	116(1)	Al(1)–N(1)–C(9)	112.4(6)	Si(2)–C(2)–C(1)	172.1(8)
[Me <sub>2</sub> Al(μ-Et <sub>2</sub> N) <sub>2</sub> Mg(μ-C≡CC <sub>6</sub> H <sub>5</sub> ) <sub>2</sub> ] (5)							
Al(1)–Mg(1)	2.838(3)	N(1)–C(9)	1.490(7)	Mg(1)–N(2)	2.095(5)	C(2)–C(3)	1.457(8)
Al(1)–N(2)	1.946(5)	N(2)–C(13)	1.494(8)	Mg(1)–C(1)	2.240(7)	Mg(1)–Mg(1*)	3.002(4)
Mg(1)–N(1)	2.097(5)	C(1)–C(2)	1.198(8)	Mg(1)–C(1*)	2.157(7)		
Mg(1)–Al(1)–N(1)	47.6(2)	N(1)–Mg(1)–C(1)	123.5(2)	Al(1)–Mg(1)–Mg(1*)	170.5(1)	C(9)–N(1)–C(11)	112.4(5)
Mg(1)–Al(1)–C(17)	131.9(2)	N(2)–Mg(1)–C(1)	122.4(2)	Al(1)–Mg(1)–N(2)	43.3(1)	Mg(1)–C(1)–C(2)	107.6(5)
N(1)–Al(1)–N(2)	94.5(2)	C(1)–Mg(1)–C(1*)	93.9(2)	Al(1)–Mg(1)–C(1)	122.4(1)	C(1)–C(2)–C(3)	176.5(7)
N(1)–Al(1)–C(18)	110.1(3)	Al(1)–N(1)–C(9)	114.8(4)	Mg(1)–Mg(1*)–N(2)	136.3(2)	Mg(1)–Mg(1*)–C(1)	48.1(2)
{(Me <sub>2</sub> Al) <sub>2</sub> [μ-OOC( <i>i</i> -Pr <sub>2</sub> N) <sub>2</sub> ]} (9)							
Al(1)–O(1)	1.802(4)	O(2)–C(1)	1.287(5)	Al(1)–C(9)	1.937(5)	N(1)–C(5)	1.497(8)
Al(1)–O(2)	1.811(4)	N(1)–C(1)	1.328(6)	O(1)–C(1)	1.278(6)	C(2)–C(3)	1.500(9)
Al(1)–C(8)	1.936(6)	N(1)–C(2)	1.474(6)				
O(1)–Al(1)–O(2*)	106.2(2)	O(1)–C(1)–O(2)	118.5(5)	O(2*)–Al(1)–C(8)	108.1(2)	N(1)–C(5)–C(6)	113.3(6)
O(1)–Al(1)–C(8)	107.7(2)	N(1)–C(2)–C(4)	111.6(6)	Al(1)–O(1)–C(1)	135.6(4)	C(1)–N(1)–C(2)	120.7(5)
O(1)–Al(1)–C(9)	105.4(2)	C(3)–C(2)–C(4)	112.0(6)	Al(1)–O(2*)–C(1*)	129.7(4)	C(1)–N(1)–C(5)	120.9(5)
{(Me <sub>2</sub> Al) <sub>2</sub> [(μ-OOC( <i>i</i> -Pr <sub>2</sub> N) <sub>2</sub> ) <sub>2</sub> Mg]} (10)							
Al(1)–O(2)	1.782(5)	O(1)–C(1)	1.250(7)	Al(2)–O(7)	1.795(5)	N(2)–C(13)	1.494(8)
Al(1)–C(11)	1.937(7)	O(2)–C(1)	1.298(7)	Mg(1)–O(1)	1.903(5)	N(3)–C(3)	1.345(8)
Al(1)–O(3)	1.779(5)	O(5)–C(3)	1.247(7)	Mg(1)–O(5)	1.913(5)	N(3)–C(22)	1.482(8)
Al(2)–O(6)	1.776(5)	N(1)–C(1)	1.311(8)	Mg(1)–O(8)	1.875(4)		
O(2)–Al(1)–O(3)	105.7(2)	Al(1)–O(3)–C(2)	135.6(5)	O(1)–Mg(1)–O(4)	110.8(2)	C(3)–N(3)–C(19)	120.0(7)
O(2)–Al(1)–C(12)	105.2(3)	Al(2)–O(7)–C(4)	132.6(5)	O(1)–Mg(1)–O(8)	109.1(2)	C(19)–N(3)–C(22)	117.4(7)
O(6)–Al(2)–O(7)	106.9(2)	C(1)–N(1)–C(5)	116.0(7)	Mg(1)–O(1)–C(1)	146.7(5)	O(1)–C(1)–O(2)	121.4(8)
O(5)–Mg(1)–O(8)	112.0(2)	C(5)–N(1)–C(8)	124.1(7)	Mg(1)–O(4)–C(2)	151.2(5)	O(6)–C(3)–N(3)	117.2(7)

nesium centers. However, scattered structural features consistent with Mg– $\pi$ -ethynyl interactions are at least supportive of the tendency of these Mg–ethynyl moieties to acquire some  $\pi$ -character in their bonding scheme. The bonding mode of the bridging ethynyl group is best described principally as a two-electron–three-center bond, similarly observed in [MgR<sub>2</sub>]<sub>n</sub> (R = Me, Et).<sup>24</sup> However, some possible Mg– $\pi$ -ethynyl interaction is supported by the low-field shift in the <sup>13</sup>C

NMR signal as well as some scattered supporting structural features mentioned above.

**Formation of  $\mu$ -Carbamato Complexes by CO<sub>2</sub> Fixation.** The complexes [Me<sub>2</sub>Al(μ-*i*-Pr<sub>2</sub>N)<sub>2</sub>Mg(μ-C≡CR)<sub>2</sub>] (R = C<sub>6</sub>H<sub>5</sub> (1), C<sub>6</sub>H<sub>4</sub> *p*-CH<sub>3</sub> (2)) react readily with CO<sub>2</sub> in hydrocarbon solvents to give in quantitative yield the white crystalline [(Me<sub>2</sub>Al(μ-*i*-Pr<sub>2</sub>N)<sub>2</sub>Mg(μ-

**Table 3. Selected Interatomic Distances (Å) and Angles (deg) for the Ethynyl-Bridged Metal Derivatives**

compd	$d(\text{M}-\text{C}_\alpha)$	$d(\text{C}_\alpha\equiv\text{C}_\beta)$ (bridging)	$\angle\text{C}_\alpha\equiv\text{C}_\beta-\text{R}$	$\angle\text{M}-\text{C}_\alpha-\text{M}$ (bridge)	$\angle\text{M}-\text{C}_\alpha\equiv\text{C}_\beta$	$\angle\text{M}'-\text{C}_\alpha\equiv\text{C}_\beta$
$[(\text{MeCp})_2\text{Zr}(\mu-\text{C}\equiv\text{CPh})]_2^a$	2.188(2) 2.431(2)	1.261(2)	172.3(1)	99	172	74
$[\text{Cp}_2\text{Zr}(\mu-\text{C}\equiv\text{CSiMe}_3)]_2^b$	2.191(5) 2.420(5)	1.249(7)	141.4(3)	99.5(2)	172.7(4)	75.9(3)
$[(\text{Cp}_2\text{Zr}(\mu-\text{C}\equiv\text{C}-t\text{-Bu}))_2]^c$	2.29(1) 2.40(1)	1.22(2)	177.5(16)	96.0(6)	136.6(9)	127.4(9)
$[(\text{TMED})\text{Mg}(\mu_2-\eta^2-\text{C}\equiv\text{CPh})_2-$ $(\mu_3-\eta^1-\text{C}\equiv\text{CPh})\text{MgEt}]_2^d$	2.433 ( $\mu_3$ ) 2.541 2.231	1.202	178	88 87 94		
	2.258 ( $\mu_2$ ) 2.252	1.209	177	88	169	97
	2.252 ( $\mu_2$ ) 2.265	1.220	145	91	167	96
$(\eta^5-\text{C}_5\text{Me}_4\text{H})_2\text{Ti}(\mu_2-\eta^2-\text{C}\equiv\text{CSiMe}_3)_2\text{MgCl}(\text{THF})^e$	2.268 2.281	1.217 1.223	165 165	96 96		84 84
$\text{Al}_2(\mu-\text{C}\equiv\text{CMe})_2\text{Me}_4$ (gas phase) <sup>f</sup>	2.05(15)	1.229(4)	168(2)	92.0(1)	158(2)	110(1)
$\text{Ga}_2(\mu-\text{C}\equiv\text{CPh})_2\text{Me}_4^g$	2.004	1.183(6)	180(2)	86.7(3)	172.8(7)	93.8(5)
$[\text{Me}_2\text{Al}(\mu-i\text{-Pr}_2\text{N})_2\text{Mg}(\mu-\text{C}\equiv\text{CC}_6\text{H}_5)]_2^h$	2.203(5) 2.232(5)	1.181(6)	178.4(6)	87.8(2)	145.7(5)	126.4(5)
$[\text{Me}_2\text{Al}(\mu-i\text{-Pr}_2\text{N})_2\text{Mg}(\mu-\text{C}\equiv\text{CC}_6\text{H}_4-p\text{-Me})]_2^h$	2.170(4) 2.273(4)	1.197(5)	177.6(5)	89.6(2)	157.9(4)	112.1(3)
	2.192(5) 2.218(5)	1.199(5)	176.8(5)	88.2(2)	147.8(4)	122.3(4)
$[\text{Me}_2\text{Al}(\mu-i\text{-Pr}_2\text{N})_2\text{Mg}(\mu-\text{C}\equiv\text{C}-t\text{-Bu})]_2^h$	2.225(8) 2.201(9)	1.204(10)	177.0(9)	86.2(3)	142.1(7)	131.8(7)
$[\text{Me}_2\text{Al}(\mu-i\text{-Pr}_2\text{N})_2\text{Mg}(\mu-\text{C}\equiv\text{CSiMe}_3)]_2^h$	2.214(9) 2.240(9)	1.180(6)	172.1(8)	88.0(3)	149.6(8)	122.3(7)
$[\text{Me}_2\text{Al}(\mu\text{-Et}_2\text{N})_2\text{Mg}(\mu-\text{C}\equiv\text{CC}_6\text{H}_5)]_2^h$	2.240(7) 2.157(7)	1.198(8)	176.5(7)	86.1(2)	165.9(6)	107.6(5)
$\text{HC}\equiv\text{CH}^i$		1.204(2)				

<sup>a</sup> Reference 10. <sup>b</sup> Reference 21. <sup>c</sup> Reference 22. <sup>d</sup> Reference 19. <sup>e</sup> Reference 18. <sup>f</sup> Reference 6c. <sup>g</sup> Reference 8c. <sup>h</sup> This work. <sup>i</sup> Reference 23.

$\text{OOC}(\text{C}\equiv\text{CR})]_2$  ( $\text{R} = \text{C}_6\text{H}_5$  (**7**);  $\text{C}_6\text{H}_4-p\text{-CH}_3$  (**8**)), respectively. The products are fairly soluble in toluene. In their mass spectra, the molecular ion peak could not be detected but the  $^1\text{H}$ ,  $^{13}\text{C}$  NMR, IR, and elemental analysis data lead us to believe that the insertion takes place at the magnesium-carbon bond of ethynyl bridges rather than at the aluminum-nitrogen bond (Scheme 1). In the  $^{13}\text{C}$  NMR spectra, the absorption at  $\delta$  159 ppm was uniquely assigned to the OCO moiety. Infrared spectra of the carbamate complexes show strong absorptions in the 650 and 1560–1680  $\text{cm}^{-1}$  regions, assigned to the bending frequency and stretching frequency of the OCO unit.<sup>25,26</sup> Attempts to obtain crystal structure information failed due to decay of the sample.

**Reaction of  $\text{CO}_2$  with Compounds A and B.** The reaction of  $\text{CO}_2$  with compound **A** in diethyl ether yields two kinds of insertion products; one is the dialuminum carbamate complex **9** and the other is the aluminum-magnesium mixed-metal carbamate complex **10**. Similarly, reaction of  $\text{CO}_2$  with compound **B** gives the dialuminum- $\text{CO}_2$  insertion product **11** and subsequent sublimation of **11** gives compound **12**. In all IR spectra of the compounds **9–12**,  $\nu_{\text{str}}(\text{O}_2\text{CN})$  at 1558  $\text{cm}^{-1}$  is always observed. In order to understand the detailed structure features of these compounds, we carried out the crystal structure determination of these compounds.

The dialuminum- $\text{CO}_2$  insertion product  $\{(\text{Me}_2\text{Al})_2[\mu\text{-OOC}(i\text{-Pr}_2\text{N})]_2\}$  (**9**) possesses an inversion center. An ORTEP view of the molecular structure is shown in Figure 6. Selected bond distances and angles are given in Table 2.

The two Al centers are bridged by two  $\mu\text{-OOC}(i\text{-Pr}_2\text{N})$  groups. The bridging groups are formed during the  $\text{CO}_2$  incorporation process, as mentioned before. There is a pseudo-2-fold axis perpendicular to the Al-Al vector and passing through the two bridging units. The geometry of the aluminum centers is pseudotetrahedral. The bond lengths between the aluminum atom and two methyl carbons are both 1.936(6) Å, which are slightly shorter than those of the parent complex **A**.<sup>4</sup> The Al-O distances of 1.802(4) and 1.811(4) Å are equal to those (1.804(5), 1.817(5), 1.820(5), and 1.809(5) Å) found in  $[\text{Al}_2\text{O}(\text{C}_{10}\text{H}_8\text{NO})_4]$ .<sup>27</sup> The O(1)-C(1) and O(2)-C(1) distances of 1.278(6) and 1.287(5) Å, respectively, are slightly longer than the C=O distances in the usual aldehydes and ketones (1.23 Å). The C(1)-N(1) bond distance of 1.328(6) Å is considerably shorter than the N(1)-C(2) and N(1)-C(5) bond distances of 1.474(6) and 1.481(6) Å, indicating that the former is a double bond.

The less volatile fraction,  $\{(\text{Me}_2\text{Al})_2[\mu\text{-OOC}(i\text{-Pr}_2\text{N})]_2\text{-Mg}\}$  (**10**) was obtained as a second product during the sublimation process. The complex **10** possesses a linear Al-Mg-Al trinuclear unit in which the central Mg atom is surrounded by four  $\mu\text{-OOC}(i\text{-Pr}_2\text{N})$  units. A perspec-

(25) Chisholm, M. H.; Extine, M. W. *J. Am. Chem. Soc.* **1977**, *99*, 782.

(26) Nakamoto, K. *Infrared Spectra of Inorganic and Coordination Compounds*; Wiley-Interscience: New York, 1970.

(27) Kushi, Y.; Fernando, Q. *J. Am. Chem. Soc.* **1970**, *92*, 91.

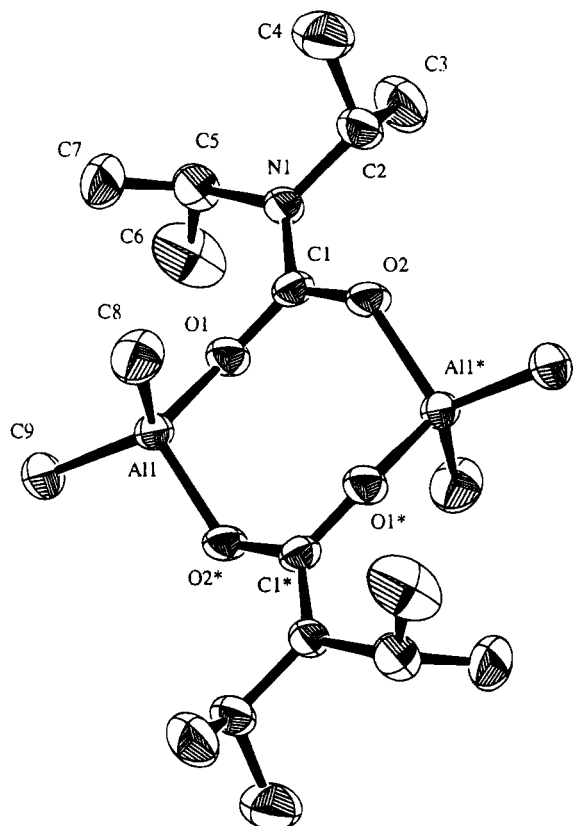


**Figure 6.** ORTEP view of the molecule  $\{(\text{Me}_2\text{Al})_2[\mu\text{-OOC}(i\text{-Pr}_2\text{N})]_2\}$  (**9**) using 30% probability ellipsoids.

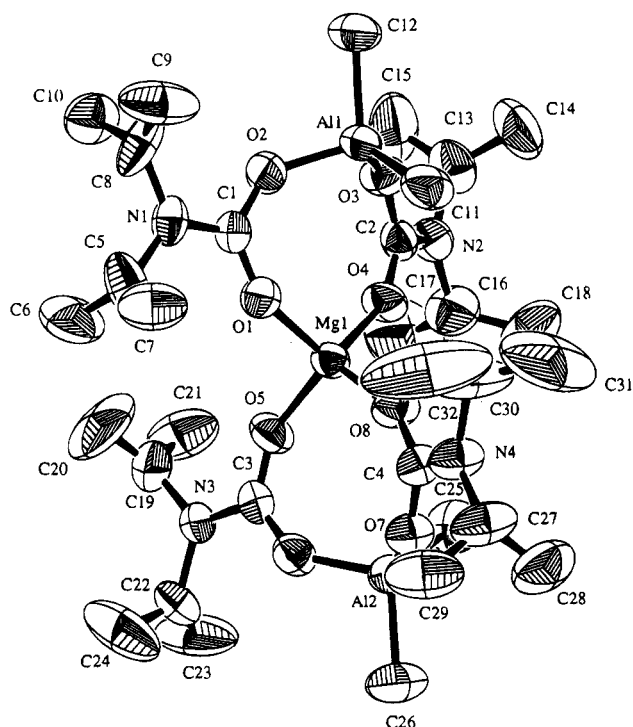


**Figure 7.** ORTEP view of the molecule  $\{(\text{Me}_2\text{Al})_2[\mu\text{-OOC}(i\text{-Pr}_2\text{N})]_2\text{Mg}\}$  (**10**) using 30% probability ellipsoids.

tive drawing of the molecule along with the atom-labeling scheme is shown in Figure 7. The selected bond lengths and angles are listed in Table 2. The geometries of the Al and Mg atoms are nearly tetrahedral. The two eight-membered chelate rings around the Mg atoms are approximately perpendicular to each other, as expected. The diisopropylamido groups sym-

metrically bridge the aluminum and magnesium atoms, while the bidentate carbamate ligands are bonded slightly asymmetrically. The two Al–O distances (1.782(5) and 1.779(5) Å) are similar to the corresponding values of the dialuminum carbamate complex **9**. In this complex also the N(1)–C(1) bond distance of 1.311(8) Å is considerably shorter than the N(1)–C(8) distance of 1.484(9) Å.

## Conclusions

We have demonstrated that the polynuclear ethyne-bridged aluminum–magnesium complexes could be synthesized in a facile manner by the metathesis reaction of the magnesium–alkyl bonds of the dimeric and tetrameric complexes with acetylenes. No substantial  $\pi$ -bonding interactions between the magnesium atom and the ethynyl carbons were noticed, but a close tendency toward such interactions is concluded. Reaction of compounds **A** and **B** with  $\text{CO}_2$  yields carbamate complexes of dialuminum and aluminum–magnesium mixed metals. The reaction of the polynuclear ethyne-bridged complexes with  $\text{CO}_2$  gives a single product, with insertion taking place at the Mg–C center with rupture at the magnesium–carbon bond rather than at the Al–N center. Future studies will focus on the activation of the Mg–halogen and Mg–alkoxide bonds of polynuclear aluminum–magnesium compounds.

## Experimental Section

All experiments were carried out in an  $\text{N}_2$ -flushed glovebag, in a drybox, or in vacuo using standard Schlenk techniques.<sup>28</sup> All solvents were distilled and degassed prior to use. Phenylacetylene, 4-ethynyltoluene, 3,3-dimethyl-1-butyne, and (trimethylsilyl)acetylene were purchased from Aldrich and were used as received. All  $^1\text{H}$ ,  $^{13}\text{C}$ , and  $^{27}\text{Al}$  NMR spectra were measured on a Varian VXR-300 spectrometer. Chemical shifts are referenced to either  $\text{SiMe}_4$  ( $^1\text{H}$ ) or  $\text{C}_6\text{D}_6$  ( $^1\text{H}$ ,  $\delta$  7.15;  $^{13}\text{C}\{^1\text{H}\}$ ,  $\delta$  128.00), while  $^{27}\text{Al}$  NMR spectra were referenced to  $[\text{Al}(\text{H}_2\text{O})_6]^{3+}$ . Mass spectral data were obtained on a VG-7025 GC/MS/MS spectrometer; IR spectra were obtained as Nujol mulls between KBr disks on a Bio-Rad FTS-40 FT-IR spectrometer. Elemental analyses (C, H, and N) were performed at the Analytische Laboratorien of H. Malissa and G. Reuter GmbH, Germany. Deviations in the results from calculated values are attributed to the extremely air-sensitive and hygroscopic nature of these compounds.

The starting materials  $[\text{Me}_2\text{Al}(\mu\text{-}i\text{-Pr}_2\text{N})_2\text{Mg}(\mu\text{-Me})_4]$  (**A**) and  $[\text{Me}_2\text{Al}(\mu\text{-Et}_2\text{N})_2\text{Mg}(\mu\text{-Me})_2]$  (**B**) were prepared as described elsewhere.<sup>4</sup>

**Synthesis of  $[\text{Me}_2\text{Al}(\mu\text{-}i\text{-Pr}_2\text{N})_2\text{Mg}(\mu\text{-C}\equiv\text{CC}_6\text{H}_5)]_2$  (**1**).** A solution of 0.9 g (8.4 mmol) of phenylacetylene in diethyl ether (20  $\text{cm}^3$ ) was added dropwise to a solution of compound **A** (2.5 g, 8.4 mmol) in diethyl ether under nitrogen. The resulting mixture was stirred for 2–3 h, and the solvent was removed partially. Recrystallization from diethyl ether yielded colorless crystals of **1**: mp 170–172 °C; yield 90%;  $^1\text{H}$  NMR ( $\text{C}_6\text{D}_6$ )  $\delta$  –0.324 (s, 6H,  $\text{Al}(\text{CH}_3)_2$ ), 1.40 (d, 12H,  $\text{N}(\text{CH}_3)_2$ ), 1.591 (d, 12H,  $\text{NCH}(\text{CH}_3)_2$ ), 3.82 (sep, 4H,  $\text{NCH}(\text{CH}_3)_2$ ), 6.99 (m, 1 *p*-H,  $\text{C}_6\text{H}_5$ ), 7.01 (m, 2 *m*-H,  $\text{C}_6\text{H}_5$ ), 7.50 (m, 2 *o*-H,  $\text{C}_6\text{H}_5$ );  $^{13}\text{C}$  NMR ( $\text{C}_6\text{D}_6$ )  $\delta$  –4.00 (broad,  $\text{Al}(\text{CH}_3)_2$ ), 27.40 ( $\text{NCH}(\text{CH}_3)_2$ ), 28.20 ( $\text{NCH}(\text{CH}_3)_2$ ), 48.84 ( $\text{NCH}(\text{CH}_3)_2$ ), 111.37 ( $\text{MgCCC}_6\text{H}_5$ ), 123.153 ( $\text{MgCCC}_6\text{H}_5$ ), 128.83 (*o*-C,  $\text{C}_6\text{H}_5$ ), 129.86 (ipso-C,  $\text{C}_6\text{H}_5$ ), 132.48 (*m*-C,  $\text{C}_6\text{H}_5$ );  $^{27}\text{Al}$  NMR ( $\text{C}_6\text{D}_6$ )  $\delta$  160 (broad); mass spectrum (EI, 70 eV) 10 most intense *m/e* peaks at 142, 86, 57, 44, 124, 281, 100, 43, 101, 209; IR 2982 m, 2926 m, 2856 s, 2064 s

(28) Shriver, D. F. *The Manipulation of Air-Sensitive Compounds*; McGraw-Hill: New York, 1969.

(C=C), 1475 s, 1388 s, 1370 s  $\text{cm}^{-1}$ . Anal. Calcd: C, 69.11; H, 10.21; N, 7.33. Found: C, 68.44; H, 10.22; N, 7.03.

**Synthesis of  $[\text{Me}_2\text{Al}(\mu\text{-}i\text{-Pr}_2\text{N})_2\text{Mg}(\mu\text{-C}\equiv\text{CC}_6\text{H}_4\text{-}p\text{-CH}_3)]_2$  (2).** A similar procedure was adopted, except for using 4-ethynyltoluene in place of phenylacetylene. Complex 2: mp 159–161 °C; yield 90%;  $^1\text{H}$  NMR ( $\text{C}_6\text{D}_6$ )  $\delta$  -0.30 (s, 6H,  $\text{Al}(\text{CH}_3)_2$ ), 1.45 (d, 12H,  $\text{NCH}(\text{CH}_3)_2$ ), 1.61 (d, 12H,  $\text{NCH}(\text{CH}_3)_2$ ), 1.93 (s, 3H,  $p\text{-C}_6\text{H}_4\text{CH}_3$ ), 3.82 (sep, 4H,  $\text{NCH}(\text{CH}_3)_2$ ), 6.89 (d, 2  $m\text{-H}$ ,  $\text{C}_6\text{H}_4$ ), 7.43 (m, 2  $o\text{-H}$ ,  $\text{C}_6\text{H}_4$ );  $^{13}\text{C}$  NMR ( $\text{C}_6\text{D}_6$ )  $\delta$  -3.70 (broad,  $\text{Al}(\text{CH}_3)_2$ ), 21.35 ( $p\text{-C}_6\text{H}_4\text{CH}_3$ ), 27.45 ( $\text{NCH}(\text{CH}_3)_2$ ), 28.32 ( $\text{NCH}(\text{CH}_3)_2$ ), 48.86 ( $\text{NCH}(\text{CH}_3)_2$ ), 110.64 ( $\text{MgCCC}_6\text{H}_4\text{CH}_3$ ), 120.31 ( $\text{MgCCC}_6\text{H}_4\text{CH}_3$ ), 129.64 ( $m\text{-C}$ ,  $\text{C}_6\text{H}_4$ ), 132.54 ( $o\text{-C}$ ,  $\text{C}_6\text{H}_4$ ), 140.24 ( $p\text{-C}$ ,  $\text{C}_6\text{H}_4$ );  $^{27}\text{Al}$  NMR ( $\text{C}_6\text{D}_6$ )  $\delta$  160 (broad); mass spectrum (EI, 70 eV) 10 most intense  $m/e$  peaks 44, 86, 142, 57, 124, 299, 281, 194, 214, 98; IR 2960 m, 2925 m, 2869 m, 2060 s (C=C), 1604 s, 1502 s, 1452 s, 1386 s, 1366 s  $\text{cm}^{-1}$ . Anal. Calcd: C, 69.61; H, 10.40; N, 7.06. Found: C, 69.44; H, 10.34; N, 7.01.

**Synthesis of  $[\text{Me}_2\text{Al}(\mu\text{-}i\text{-Pr}_2\text{N})_2\text{Mg}(\mu\text{-C}\equiv\text{CCMe}_3)]_2$  (3) and  $[\text{Me}_2\text{Al}(\mu\text{-}i\text{-Pr}_2\text{N})_2\text{Mg}(\mu\text{-C}\equiv\text{CSiMe}_3)]_2$  (4).** A procedure similar to that used for the complexes 1 and 2 was adopted, except for using 3,3-dimethyl-1-butyne or (trimethylsilyl)acetylene. Colorless crystals were obtained upon recrystallization from diethyl ether.

Complex 3: mp 169–171 °C; yield 90%;  $^1\text{H}$  NMR ( $\text{C}_6\text{D}_6$ )  $\delta$  -0.14 (s, 6H,  $\text{Al}(\text{CH}_3)_2$ ), 1.12 (s, 9H,  $\text{C}(\text{CH}_3)_3$ ), 1.41 (d, 12H,  $\text{NCH}(\text{CH}_3)_2$ ), 1.49 (d, 12H,  $\text{NCH}(\text{CH}_3)_2$ ), 3.78 (sep, 4H,  $\text{NCH}(\text{CH}_3)_2$ );  $^{13}\text{C}$  NMR ( $\text{C}_6\text{D}_6$ )  $\delta$  -3.20 (broad,  $\text{Al}(\text{CH}_3)_2$ ), 27.70 ( $\text{NCH}(\text{CH}_3)_2$ ), 29.01 ( $\text{NCH}(\text{CH}_3)_2$ ), 29.17 ( $\text{C}(\text{CH}_3)_3$ ), 30.23 ( $\text{C}(\text{CH}_3)_3$ ), 48.86 ( $\text{NCH}(\text{CH}_3)_2$ ), 97.85 ( $\text{MgCC}(\text{CH}_3)_3$ ), 137.98 ( $\text{MgCC}(\text{CH}_3)_3$ );  $^{27}\text{Al}$  NMR ( $\text{C}_6\text{D}_6$ )  $\delta$  155 (broad); mass spectrum (EI, 70 eV) 10 most intense  $m/e$  peaks at 44, 142, 86, 124, 67, 57, 262, 347, 281, 292; IR 2958 m, 2926 m, 2869 m, 2053 s (C=C), 1550 s, 1462 s, 1392 s, 1367 s  $\text{cm}^{-1}$ . Anal. Calcd: C, 66.21; H, 11.93; N, 7.72. Found: C, 65.93; H, 11.18; N, 6.87.

Complex 4: mp 125 °C; yield 90%;  $^1\text{H}$  NMR ( $\text{C}_6\text{D}_6$ )  $\delta$  -0.17 (s, 6H,  $\text{Al}(\text{CH}_3)_2$ ), 0.14 (s, 9H,  $\text{Si}(\text{CH}_3)_3$ ), 1.412 (d, 12H,  $\text{NCH}(\text{CH}_3)_2$ ), 1.47 (d, 12H,  $\text{NCH}(\text{CH}_3)_2$ ), 3.78 (sep, 4H,  $\text{NCH}(\text{CH}_3)_2$ );  $^{13}\text{C}$  NMR ( $\text{C}_6\text{D}_6$ )  $\delta$  -3.20 (broad,  $\text{Al}(\text{CH}_3)_2$ ), -0.51 ( $\text{Si}(\text{CH}_3)_3$ ), 27.56 ( $\text{NCH}(\text{CH}_3)_2$ ), 28.68 ( $\text{NCH}(\text{CH}_3)_2$ ), 48.77 ( $\text{NCH}(\text{CH}_3)_2$ ), 136.55 ( $\text{MgCCSi}(\text{CH}_3)_3$ ), 140.95 ( $\text{MgCCSi}(\text{CH}_3)_3$ );  $^{27}\text{Al}$  NMR ( $\text{C}_6\text{D}_6$ )  $\delta$  155 (broad); mass spectrum (EI, 70 eV) 10 most intense  $m/e$  peaks 124, 363, 298, 142, 43, 57, 83, 98, 264, 278; IR 2961 m, 2871 m, 2038 s (C=C), 1664 s, 1466 s, 1389 s  $\text{cm}^{-1}$ .

**Synthesis of  $[\text{Me}_2\text{Al}(\mu\text{-Et}_2\text{N})_2\text{Mg}(\mu\text{-C}\equiv\text{CC}_6\text{H}_5)]_2$  (5) and  $[\text{Me}_2\text{Al}(\mu\text{-Et}_2\text{N})_2\text{Mg}(\mu\text{-C}\equiv\text{CC}_6\text{H}_4\text{-}p\text{-CH}_3)]_2$  (6).** A solution of 0.9 g (8.4 mmol) of phenylacetylene or 0.9 g 4-ethynyltoluene in diethyl ether was added dropwise to a solution of compound B (2.0 g, 8 mmol) in ether under nitrogen. The mixture was stirred at room temperature for 1 h, and the crude product was recrystallized from diethyl ether.

Complex 5: mp 120–122 °C; yield 75%;  $^1\text{H}$  NMR ( $\text{C}_6\text{D}_6$ )  $\delta$  -0.42 (s, 6H,  $\text{Al}(\text{CH}_3)_2$ ), 1.15 (m, 12H,  $\text{N}(\text{CH}_2\text{CH}_3)_2$ ), 3.11 (m, 8H,  $\text{N}(\text{CH}_2\text{CH}_3)_2$ ), 6.96 (m, 1  $p\text{-H}$ ,  $\text{C}_6\text{H}_5$ ), 6.97 (m, 2  $m\text{-H}$ ,  $\text{C}_6\text{H}_5$ ), 7.53 (m, 2  $o\text{-H}$ ,  $\text{C}_6\text{H}_5$ );  $^{13}\text{C}$  NMR ( $\text{C}_6\text{D}_6$ )  $\delta$  -9.87 (broad,  $\text{Al}(\text{CH}_3)_2$ ), 13.69 ( $\text{N}(\text{CH}_2\text{CH}_3)_2$ ), 40.29 ( $\text{N}(\text{CH}_2\text{CH}_3)_2$ ), 105.87 ( $\text{MgCCC}_6\text{H}_5$ ), 122.45 ( $\text{MgCCC}_6\text{H}_5$ ), 125.80 (2  $o\text{-C}$ ,  $\text{C}_6\text{H}_5$ ), 129.77 (ipso-C,  $\text{C}_6\text{H}_5$ ), 132.48 ( $m\text{-C}$ ,  $\text{C}_6\text{H}_5$ );  $^{27}\text{Al}$  NMR ( $\text{C}_6\text{D}_6$ )  $\delta$  160 (broad); mass spectrum (EI, 70 eV) 10 most intense  $m/e$  peaks 44, 58, 73, 96, 102, 114, 196, 311, 451, 638; IR 2980 m, 2920 m, 2856 m, 2060 s (C=C), 1600 s, 1500 s, 1450 s, 1380 s, 1375 s  $\text{cm}^{-1}$ . Anal. Calcd: C, 66.15; H, 9.49; N, 8.57. Found: C, 66.04; H, 9.32; N, 8.45.

Complex 6: mp 132–134 °C; yield 75%;  $^1\text{H}$  NMR ( $\text{C}_6\text{D}_6$ )  $\delta$  -0.41 (s, 6H,  $\text{Al}(\text{CH}_3)_2$ ), 1.18 (m, 12H,  $\text{N}(\text{CH}_2\text{CH}_3)_2$ ), 1.93 (s, 3H,  $p\text{-C}_6\text{H}_4\text{CH}_3$ ), 3.140 (m, 8H,  $\text{N}(\text{CH}_2\text{CH}_3)_2$ ), 6.82 (d, 2  $m\text{-H}$ ,  $\text{C}_6\text{H}_4$ ), 7.47 (d, 2  $o\text{-H}$ ,  $\text{C}_6\text{H}_4$ );  $^{13}\text{C}$  NMR ( $\text{C}_6\text{D}_6$ )  $\delta$  -9.93 ( $\text{Al}(\text{CH}_3)_2$ ), 21.31 ( $p\text{-C}_6\text{H}_4\text{CH}_3$ ), 40.32 ( $\text{N}(\text{CH}_2\text{CH}_3)_2$ ), 13.72 ( $\text{N}(\text{CH}_2\text{CH}_3)_2$ ), 105.22 ( $\text{MgCCC}_6\text{H}_4\text{CH}_3$ ), 119.56 ( $\text{MgCCC}_6\text{H}_4\text{CH}_3$ ), 129.63 (2  $m\text{-C}$ ,  $\text{C}_6\text{H}_4$ ), 132.56 (2  $o\text{-C}$ ,  $\text{C}_6\text{H}_4$ ), 140.13 (2  $p\text{-C}$ ,  $\text{C}_6\text{H}_4$ );  $^{27}\text{Al}$  NMR ( $\text{C}_6\text{D}_6$ )  $\delta$  155 (broad); mass spectrum (EI, 70 eV) 10 most intense  $m/e$  peaks at 58, 73, 96, 115, 128, 210,

325, 479, 608, 666; IR 2970 m, 2920 m, 2850 m, 2025 s (C=C), 1470 s, 1390 s  $\text{cm}^{-1}$ . Anal. Calcd: C, 66.96; H, 9.69; N, 8.22. Found: C, 66.78; H, 9.52; N, 7.98.

**$\{[\text{Me}_2\text{Al}(\mu\text{-}i\text{-Pr}_2\text{N})_2\text{Mg}(\mu\text{-OOC}(\text{C}\equiv\text{CR}))_2]$  ( $\text{R} = \text{C}_6\text{H}_5$  (7),  $\text{C}_6\text{H}_4\text{-}p\text{-CH}_3$  (8)).** A solution of complex 1 or 2 in benzene was transferred to a three-necked Pyrex flask (100  $\text{cm}^3$ ) equipped with one inlet for  $\text{N}_2$  and another for bubbling dry  $\text{CO}_2$  gas. Dry  $\text{CO}_2$  is bubbled through the stirred solution for 20 min, and the resulting crude product upon removal of solvent was recrystallized from toluene to obtain transparent crystals. Compound 7: mp 160 °C dec; yield 70%;  $^1\text{H}$  NMR ( $\text{C}_6\text{D}_6$ )  $\delta$  -0.037 (s, 6H,  $\text{Al}(\text{CH}_3)_2$ ), 1.36 (d, 12H,  $\text{NCH}(\text{CH}_3)_2$ ), 1.40 (d, 12H,  $\text{NCH}(\text{CH}_3)_2$ ), 3.77 (sep, 4H,  $\text{NCH}(\text{CH}_3)_2$ ), 6.843 (m, 1  $p\text{-H}$ ,  $\text{C}_6\text{H}_5$ ), 6.88 (m, 2  $m\text{-H}$ ,  $\text{C}_6\text{H}_5$ ), 7.84 (m, 2  $o\text{-H}$ ,  $\text{C}_6\text{H}_5$ );  $^{13}\text{C}$  NMR ( $\text{C}_6\text{D}_6$ )  $\delta$  -4.15 (broad,  $\text{Al}(\text{CH}_3)_2$ ), 26.43 ( $\text{NCH}(\text{CH}_3)_2$ ), 26.72 ( $\text{NCH}(\text{CH}_3)_2$ ), 47.84 ( $\text{NCH}(\text{CH}_3)_2$ ), 84.23 ( $\text{MgCCC}_6\text{H}_5$ ), 85.38 ( $\text{MgCCC}_6\text{H}_5$ ), 119.92 (2  $o\text{-C}$ ,  $\text{C}_6\text{H}_5$ ), 130.29 (ipso-C,  $\text{C}_6\text{H}_5$ ), 133.04 (2  $m\text{-C}$ ,  $\text{C}_6\text{H}_5$ ), 159.36 (OCO);  $^{27}\text{Al}$  NMR ( $\text{C}_6\text{D}_6$ )  $\delta$  160 (broad); mass spectrum (EI, 70 eV) 10 most intense  $m/e$  peaks 44, 57, 71, 86, 91, 101, 129, 142, 214, 299; IR 2960 m, 2920 m, 2876 m, 2210 s (C=C), 1590 s, 1500 s, 1465 s, 1381 s  $\text{cm}^{-1}$ . Anal. Calcd: C, 64.75; H, 9.10; N, 6.56. Found: C, 64.47; H, 8.90; N, 6.31.

Complex 8: mp 125 °C dec; yield 75%;  $^1\text{H}$  NMR ( $\text{C}_6\text{D}_6$ )  $\delta$  -0.028 (s, 6H,  $\text{Al}(\text{CH}_3)_2$ ), 1.37 (d, 12H,  $\text{NCH}(\text{CH}_3)_2$ ), 1.42 (d, 12H,  $\text{NCH}(\text{CH}_3)_2$ ), 1.85 (s, 3H,  $p\text{-C}_6\text{H}_4\text{-CH}_3$ ), 3.79 (sep, 4H,  $\text{NCH}(\text{CH}_3)_2$ ), 6.70 (d, 2  $m\text{-H}$ ,  $\text{C}_6\text{H}_4$ ), 7.43 (m, 2  $o\text{-H}$ ,  $\text{C}_6\text{H}_4$ );  $^{13}\text{C}$  NMR ( $\text{C}_6\text{D}_6$ )  $\delta$  -3.79 (broad,  $\text{Al}(\text{CH}_3)_2$ ), 21.32 ( $p\text{-C}_6\text{H}_4\text{-CH}_3$ ), 26.80 ( $\text{NCH}(\text{CH}_3)_2$ ), 27.08 ( $\text{NCH}(\text{CH}_3)_2$ ), 48.18 ( $\text{NCH}(\text{CH}_3)_2$ ), 84.352 ( $\text{MgCCC}_6\text{H}_4\text{CH}_3$ ), 86.25 ( $\text{MgCCC}_6\text{H}_4\text{CH}_3$ ), 117.23 (ipso-C,  $\text{C}_6\text{H}_4$ ), 129.58 (2  $m\text{-C}$ ,  $\text{C}_6\text{H}_4$ ), 159.89 (OCO);  $^{27}\text{Al}$  NMR ( $\text{C}_6\text{D}_6$ )  $\delta$  160 (broad); mass spectrum (EI, 70 eV) 10 most intense  $m/e$  peaks 86, 44, 91, 101, 142, 115, 186, 228, 241, 298; IR 2967 m, 2925 m, 2874 m, 2210 s (C=C), 1590 s, 1508 s, 1463 s, 1381 s  $\text{cm}^{-1}$ . Anal. Calcd: C, 65.40; H, 9.30; N, 6.35. Found: C, 65.21; H, 9.39; N, 6.56.

**$\{[\text{Me}_2\text{Al}]_2[\mu\text{-OOC}(i\text{-Pr}_2\text{N})_2]$  (9) and  $\{[\text{Me}_2\text{Al}]_2[\mu\text{-OOC}(i\text{-Pr}_2\text{N})_2]\text{Mg}\}$  (10).** Compound A (2.5 g, 13 mmol) was dissolved in 75  $\text{cm}^3$  of diethyl ether.  $\text{CO}_2$  was bubbled through the solution for 40 min, and the solvent was removed under vacuum. Sublimation of the crude product gave two colorless crystals, complex 9 at 120 °C and another crystal at 135 °C (complex 10).

Complex 9:  $^1\text{H}$  NMR ( $\text{C}_6\text{D}_6$ )  $\delta$  -0.22 (s, 12H,  $\text{Al}(\text{CH}_3)_3$ ), 0.92 (d, 24H,  $\text{NCH}(\text{CH}_3)_2$ ), 3.61 (sep, 4H,  $\text{NCH}(\text{CH}_3)_2$ );  $^{13}\text{C}$  NMR ( $\text{C}_6\text{D}_6$ )  $\delta$  -10.73 (broad,  $\text{Al}(\text{CH}_3)_2$ ), 20.21 ( $\text{NCH}(\text{CH}_3)_2$ ), 47.19 ( $\text{NCH}(\text{CH}_3)_2$ ), 157.97 (OCO);  $^{27}\text{Al}$  NMR ( $\text{C}_6\text{D}_6$ )  $\delta$  140 (broad); mass spectrum (EI, 70 eV) 10 most intense  $m/e$  peaks 387, 371, 315, 244, 186, 144, 128, 102, 86, 43; IR 2921 (m), 1558 (s, br), 1496 (m), 1362 (s), 1214 (s), 1180 (s), 1157 (s), 1086 (s)  $\text{cm}^{-1}$ . Anal. Calcd: C, 53.72; H, 10.08; N, 6.96. Found: C, 53.12; H, 9.92; N, 7.47.

Complex 10: mp 133–135 °C;  $^1\text{H}$  NMR ( $\text{C}_6\text{D}_6$ )  $\delta$  -0.241 (s, 12H,  $\text{Al}(\text{CH}_3)_3$ ), 1.07 (d, 48H,  $\text{NCH}(\text{CH}_3)_2$ ), 2.80 (m, br, 8H,  $\text{NCH}(\text{CH}_3)_2$ );  $^{13}\text{C}$  NMR ( $\text{C}_6\text{D}_6$ )  $\delta$  -10.42 (broad,  $\text{Al}(\text{CH}_3)_2$ ), 20.65 ( $\text{NCH}(\text{CH}_3)_2$ ), 46.48 ( $\text{NCH}(\text{CH}_3)_2$ ), 159.41 (OCO);  $^{27}\text{Al}$  NMR  $\delta$  140 (broad); mass spectrum (EI, 70 eV), 10 most intense  $m/e$  peaks 685, 556, 498, 387, 315, 244, 186, 144, 102, 86; IR 2910 (m), 1550 (s, br), 1561 (s, br), 1480 (m), 1356 (s), 1217 (s), 1176 (s), 1070 (s)  $\text{cm}^{-1}$ . Anal. Calcd: C, 53.57; H, 9.58; N, 7.83. Found: C, 52.70; H, 9.25; N, 7.71.

**$\{[\text{Me}_2\text{Al}]_2[\mu\text{-OOC}(\text{Et}_2\text{N})_2]\text{Mg}\}$  (11) and  $\{[\text{Me}_2\text{Al}]_2[\mu\text{-OOC}(\text{Et}_2\text{N})_2]\}$  (12).**  $\text{CO}_2$  was bubbled through a solution of compound B dissolved in diethyl ether for 45 min. The precipitated magnesium salt was removed by filtration, and the filtrate was reduced under vacuum. The crude product was recrystallized from diethyl ether to give colorless needles of 11: mp 100–101 °C; yield 40%;  $^1\text{H}$  NMR ( $\text{C}_6\text{D}_6$ )  $\delta$  -0.24 (s, 12H,  $\text{Al}(\text{CH}_3)_2$ ), 0.88 (t, 24H,  $\text{NCH}_2\text{CH}_3$ ), 3.01 (m, 16H,  $\text{NCH}_2\text{CH}_3$ );  $^{13}\text{C}$  NMR ( $\text{C}_6\text{D}_6$ )  $\delta$  -10.58 ( $\text{Al}(\text{CH}_3)_2$ ), 13.47 ( $\text{NCH}_2\text{CH}_3$ ), 42.01 ( $\text{NCH}_2\text{CH}_3$ ), 159.83 (OCO);  $^{27}\text{Al}$  NMR ( $\text{C}_6\text{D}_6$ )  $\delta$  140 (broad); IR 2923 (m), 1572 (s, br), 1485 (m), 1358 (s), 1213 (s),

1182 (s), 1162 (s), 1075 (s). Anal. Calcd: C, 48.55; H, 9.25; N, 8.10. Found: C, 48.10; H, 9.12; N, 7.95.

The crude product **11**, upon sublimation, gave colorless crystals at 130 °C which were characterized to be  $\{(Me_2Al)_2[\mu-OOC(Et_2N)]_2\}$ : yield 20%;  $^1H$  NMR ( $C_6D_6$ )  $\delta$  -0.25 (s, 12H, Al(CH<sub>3</sub>)), -0.741 (t, 8H, CH<sub>2</sub>CH<sub>3</sub>), 2.81 (m, 12H, NCH<sub>2</sub>CH<sub>3</sub>);  $^{13}C$  NMR ( $C_6D_6$ )  $\delta$  -10.75 (broad, Al(CH<sub>3</sub>)<sub>2</sub>), 12.45 (NCH<sub>2</sub>CH<sub>3</sub>), 42.15 (NCH<sub>2</sub>CH<sub>3</sub>), 158.22 (OCO);  $^{27}Al$  NMR ( $C_6D_6$ ) 140 (broad); IR 2911 (m), 1571 (s, br), 1494 (s), 1357 (s), 1201 (s), 1152 (s). Anal. Calcd: C, 47.88; H, 8.56; N, 9.31. Found: C, 47.56; H, 8.42; N, 9.05.

**Structure Determination.** Crystals for X-ray measurements were sealed in glass capillaries. Preliminary examinations and intensity data collections were carried out with a Rigaku AFC6S or AFC7S diffractometer using graphite-monochromatized Cu K $\alpha$  ( $\lambda = 1.54178 \text{ \AA}$ ) or Mo K $\alpha$  ( $\lambda = 0.71069 \text{ \AA}$ ) radiation. Intensity data were collected using the  $\theta$ - $2\theta$  scan mode and corrected for absorption and decay. All structures were solved by SIR92<sup>29</sup> and refined with full-matrix least squares on  $F$ . In the final cycles all non-hydrogen atoms were refined anisotropically and all hydrogen atoms were fixed at idealized positions. All calculations were carried out with

a SGI R4000 computer using the teXsan program package.<sup>30</sup> A summary of the data collection and structure solution is given in Table 1, and final atomic coordinates are given in Table 2.

**Acknowledgment.** Financial assistance from the National Science Council, Taiwan, ROC, is gratefully acknowledged.

**Supporting Information Available:** Tables of crystal data, atomic coordinates and temperature factors, and intramolecular bond distances and angles of **1–5**, **9**, and **10** and figures giving additional views of **2** and **4** (111 pages). Ordering information is given on any current masthead page.

OM9502547

(29) SIR92: Altomare, A.; Burla, M. C.; Camalli, M.; Cascarano, M.; Giacovazzo, C.; Guagliardi, A.; Polidori, G. *J. Appl. Crystallogr.* **1994**, *27*, 1045.

(30) teXsan: Crystal Structure Analysis Package; Molecular Structure Corp.: College Station, TX, 1985, 1992.

# 1,3-Diphenylallyl Complexes of Palladium(II): NMR, X-ray, and Catalytic Studies

Pierluigi Barbaro,<sup>†</sup> Paul S. Pregosin,<sup>\*</sup> and Renzo Salzmann

Laboratorium für Anorganische Chemie, ETH Zentrum, 8092 Zürich, Switzerland

Alberto Albinati<sup>\*</sup>

Chemical Pharmacy, University of Milan, I-20131 Milan, Italy

Roland W. Kunz

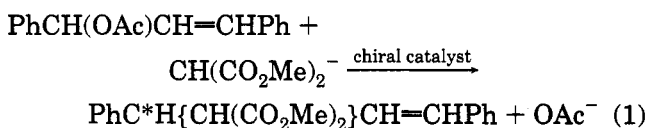
Laboratorium für Organische Chemie, Universität Zürich, 8057 Zürich, Switzerland

Received May 30, 1995<sup>⊗</sup>

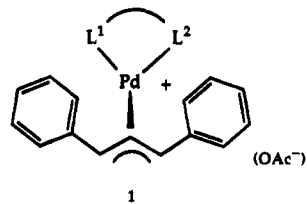
A series of 1,3-diphenylallyl complexes of Pd(II) containing achiral as well as new and commercially available chiral auxiliaries has been prepared, and their allyl <sup>13</sup>C-NMR characteristics have been recorded. Some results for the catalytic allylic alkylation reaction are given with the best new result, for (*R*)-BIPHEMP (BIPHEMP = 2,2'-bis(diphenylphosphino)-6,6'-dimethylbiphenyl), showing an enantiomeric excess of 90%. The solid-state structure for the complex [Pd(η<sup>3</sup>-PhCHCHCHPh)(TMEDA)]BF<sub>4</sub>, **2a**, has been determined by X-ray diffraction. Molecular mechanics methods have been used to understand some differences between the chiral pockets of selected chelating phosphine ligands. The selective allyl isomerization dynamics for the methoxy-BIPHEMP complex [Pd(η<sup>3</sup>-PhCHCHCHPh)-(2,2'-bis-diphenylphosphino)-6,6'-dimethoxybiphenyl]PF<sub>6</sub>, **2n**, and the ferrocene-based JOSIPHOS complex (JOSIPHOS = (*R*)-[1-[(*S*)-(diphenylphosphino)ferrocenyl]ethyl]dicyclohexylphosphine), [Pd(η<sup>3</sup>-PhCHCHCHPh){CpFe(C<sub>5</sub>H<sub>5</sub>(1-CH(CH<sub>3</sub>)PCy<sub>2</sub>)-2-PPh<sub>2</sub>)]CF<sub>3</sub>SO<sub>3</sub>, **9**, have been followed by 2-D exchange spectroscopy. The observed ee for **9** does not correlate with expectations based on <sup>13</sup>C data, together with a ground state population analysis; i.e., the reaction kinetics for different diastereomers may be important. The 1,3-diphenylallyl substrate is special in that its phenyl groups can stack with the phenyl groups of the chiral auxiliary.

## Introduction

The enantioselective allylic alkylation, reaction 1,



catalyzed by salts of Pd(II), is commonly<sup>1</sup> studied using a 1,3-diphenylallyl organic substrate. The chiral catalyst often contains a chelating diphosphine ligand;<sup>2–5</sup> however, in recent studies it has been shown that several ligand combinations afford excellent enantioselectivity; e.g., both bis(oxazoline)<sup>6a</sup> and bis(aziridine)<sup>6b</sup> compounds as well as a (diphenylphosphino)thiophene<sup>7</sup> are successful choices. There is a common mechanistic feature in that oxidative addition leads to an allyl intermediate of type **1**, where L<sup>1</sup> and L<sup>2</sup> are the donor atoms of the chiral chelating ligand in the Pd(II) complex.



Interestingly, there is relatively little known about the solid-state and solution characteristics of such 1,3-diphenylallyl–Pd complexes, but a great deal<sup>8</sup> has been reported on complexes of the η<sup>3</sup>-C<sub>3</sub>H<sub>5</sub> and η<sup>3</sup>-2-methylallyl ligands. In several recent studies<sup>9</sup> we have considered the β-pinene allyl, η<sup>3</sup>-C<sub>10</sub>H<sub>15</sub>, and shown that, since it

<sup>†</sup> Present address: ISSECC-CNR, Via J. Nardi 39, 50132 Firenze, Italy.

<sup>⊗</sup> Abstract published in *Advance ACS Abstracts*, September 15, 1995.  
(1) Noyori, R. *Asymmetric Catalysis in Organic Synthesis*; John Wiley and Sons, Inc.: New York, 1994. Consiglio, G.; Waymouth, R. M. *Chem. Rev.* **1989**, *89*, 257. Togni, A.; Venanzi, L. M. *Angew. Chem.* **1994**, *33*, 497.

(2) Hayashi, T. In *Catalytic Asymmetric Synthesis*; Ojima, I., Ed.; VCH Publishers, Inc.: New York, 1993; p 325.

(3) Trost, B. M.; Organ, M. G. *J. Am. Chem. Soc.* **1994**, *116*, 10320. Trost, B. M.; van Vranken, D. L.; Bingel, C. *J. Am. Chem. Soc.* **1992**, *114*, 9327. Trost, B. M.; Murphy, D. J. *Organometallics* **1985**, *4*, 1143.

(4) Hirasawa, K.; Kawamata, M.; Hiroi, K. *Yakugaku Zasshi* **1994**, *114* (2), 111. Yamaguchi, M.; Shima, T.; Hida, M. *Tetrahedron Lett.* **1990**, *31*, 5049. Yamaguchi, M.; Shima, T.; Yamagishi, T.; Hida, M. *Tetrahedron Asymmetry* **1991**, *2*, 663.

(5) Mackenzie, P. B.; Whelan, J.; Bosnich, B. *J. Am. Chem. Soc.* **1985**, *107*, 2046. Auburn, P. R.; Mackenzie, P. B.; Bosnich, B. *J. Am. Chem. Soc.* **1985**, *107*, 2033.

(6) (a) von Matt, P.; Lloyd-Jones, G. C.; Minidis, A. B. E.; Pfaltz, A.; Macko, L.; Neuburger, M.; Zehnder, M.; Rügger, H.; Pregosin, P. S. *Helv. Chim. Acta* **1995**, *78*, 265. (b) Andersson, P. G.; Harden, A.; Tanner, D.; Norrby, P. O. *Chem. Eur. J.* **1995**, *1*, 12.

(7) (a) Sprinz, J.; Kiefer, M.; Helmchen, G.; Reggelein, M.; Huttner, G.; Zsolnai, L. *Tetrahedron Lett.* **1994**, *35*, 1523. (b) Sprinz, J.; Helmchen, G.; *Tetrahedron Lett.* **1993**, 1769.



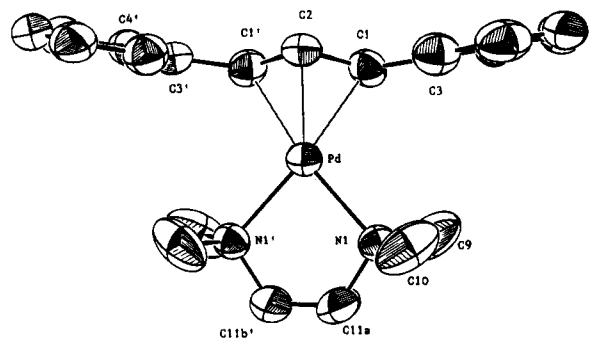


Figure 1. ORTEP plot for 2a.

Table 1. Selected Bond Lengths (Å) and Bond Angles (deg) for 2a

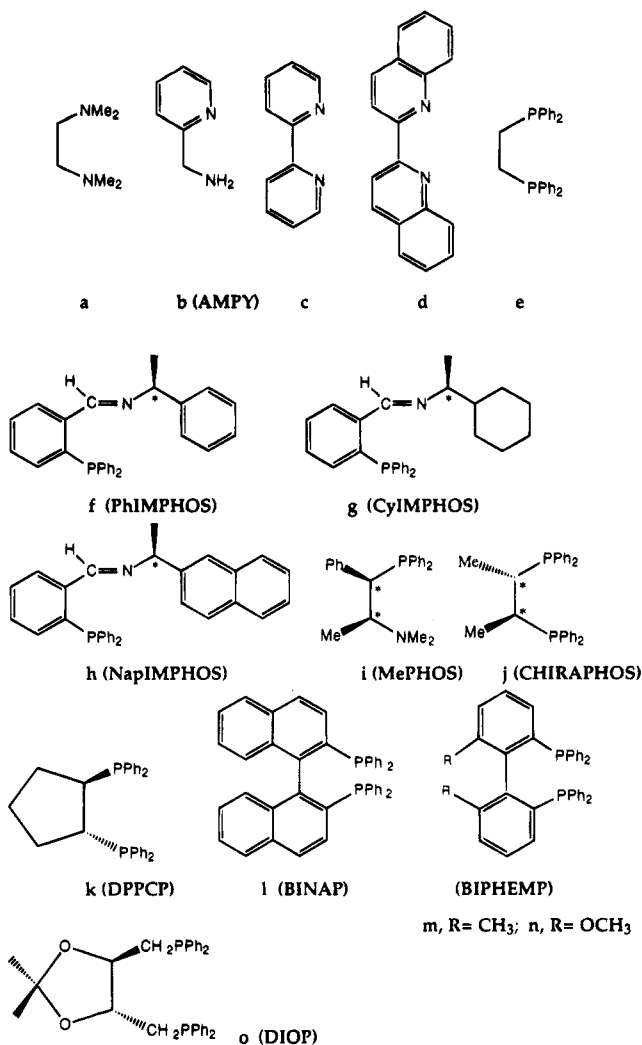
Pd–N	2.161(3)	N–Pd–N(1')	83.3(1)
Pd–C(1)	2.148(4)	N(1)–Pd–C(1')	170.0(1)
Pd–C(2)	2.111(6)	N(1)–Pd–C(1)	104.3(1)
C(1)–C(2)	1.392(5)	C(1)–Pd–C(1')	67.4(2)
C(1)–C(3)	1.489(6)	C(2)–C(1)–C(3)	123.5(4)

is larger than the two allyl ligands mentioned above, there are different interactions with the chelating ligand. Moreover, the dynamics of the allyl isomerization mechanism<sup>10,11</sup> need not be the same for an  $\eta^3$ -C<sub>3</sub>H<sub>5</sub> as it is for a coordinated 1,3-diphenylallyl ligand.<sup>12</sup> To continue developing our understanding of the structural and coordination chemistry of these and other Pd–allyl complexes, we have prepared and studied the complexes [Pd( $\eta^3$ -PhCHCHPh)(chelate)]X, **2**, with the various chelate ligands **a–o**, given in Scheme 1, and report here our results.

## Results and Discussion

**X-ray Diffraction Structure for [Pd( $\eta^3$ -PhCHCH-CHPh)(Me<sub>2</sub>NCH<sub>2</sub>CH<sub>2</sub>NMe<sub>2</sub>)](BF<sub>4</sub>), 2a.** As there are few solid-state results for the 1,3-diphenylallyl ligand, we have determined the structure for **2a**. This TMEDA complex was crystallized from CH<sub>2</sub>Cl<sub>2</sub>/ether/pentane, and an ORTEP plot of the cation is shown in Figure 1. Table 1 shows a selected list of bond lengths and bond

Scheme 1. Bidentate Ligands Used in Complexes 2



angles, Table 2 experimental parameters, and Table 3 positional and equivalent isotropic displacement parameters for this complex. The molecule lies on a crystallographic mirror plane containing the atoms C(2), Pd, and the midpoint of the C(11a) and C(11b) bond, so that only half of the molecule is crystallographically independent. The local coordination geometry is distorted square planar, with the two N atoms and the C atoms of the allyl ligand making up the ligand coordination sphere. The terminal allyl carbons are ca. 0.23 Å below the N–Pd–N plane, and the central allyl carbon, ca. 0.42 Å above this plane. The allyl plane makes an angle of ca. 112° with the N–Pd–N plane, with the central CH vector pointing away from the Pd atom. The allyl phenyl rings are not coplanar with the plane of the three allyl carbons, with the observed angle between these being ca. 29°. Taken together with the C(1)–C(3) bond length of 1.489(6) Å, it would appear as if there is no strong conjugation of the allyl and phenyl fragments. As expected, one of the two different N-methyl groups is closer to the phenyl  $\pi$ -cloud, see Figure 2, and this is reflected in very different methyl <sup>1</sup>H-chemical shifts for these spins,  $\delta$  = 1.75 and 2.53. We have found this type of anisotropic effect frequently in complexes of the 1,3-diphenylallyl ligand.<sup>13a</sup>

The terminal Pd–C(1) separation is 2.148(4) Å, the central Pd–C(2) distance is 2.111(6) Å, and the Pd–N bond length is 2.161(3) Å. In the TMEDA, 1-phenylallyl

(8) Hännson, S.; Norrby, P.; Sjöegren, M. P. T.; Åkermark, B.; Cucciolito M. E.; Giordano, F.; Vitagliano, A. *Organometallics* **1993**, *12*, 4940. Ozawa, F.; Son, T.; Ebina, S.; Osakada, K.; Yamamoto, A. *Organometallics* **1992**, *11*, 171. Knierzinger, A.; Scholzer, P. *Helv. Chim. Acta* **1992**, *75*, 1211. Cesarotti, E.; Grassi, M.; Prati, L.; Demartin, F. *J. Chem. Soc., Dalton Trans.* **1991**, 2073. Cesarotti, E.; Grassi, M.; Prati, L.; Demartin, F. *J. Organomet. Chem.* **1989**, *370*, 407. Facchin, G.; Bertani, R.; Calligaris, M.; Nardin, G.; Mari, M. *J. Chem. Soc., Dalton Trans.* **1987**, 1381. Gozum, J. E.; Pollina, D. M.; Jensen, J.; Girolami, G. S. *J. Am. Chem. Soc.* **1988**, *110*, 2688. Deeming, A. J.; Rothwell, I. P.; Hursthouse, M. B.; Malik, K. M. A. *J. Chem. Soc., Dalton Trans.* **1979**, 1899.

(9) (a) Pregosin, P. S.; Rüegger, H.; Salzmann, R.; Albinati, A.; Lianza, F.; Kunz, R. W. *Organometallics* **1994**, *13*, 83. (b) Pregosin, P. S.; Rüegger, H.; Salzmann, R.; Albinati, A.; Lianza, F.; Kunz, R. W. *Organometallics* **1994**, *13*, 5040. (c) Ammann, C. J.; Pregosin, P. S.; Rüegger, H.; Albinati, A.; Lianza, F.; Kunz, R. W. *J. Organomet. Chem.* **1992**, *423*, 415. (d) Rüegger, H.; Kunz, R. W.; Ammann, C. J.; Pregosin, P. S. *Magn. Reson. Chem.* **1992**, *29*, 197.

(10) Vrieze, K. In *Dynamic Nuclear Magnetic Resonance Spectroscopy*; Jackman, L. M.; Cotton, F. A., Eds.; Academic Press: New York, 1975. Vrieze, K.; Volger, H. C.; van Leeuwen, P. S. N. M. *Inorg. Chim. Acta Rev.* **1969**, 109.

(11) Faller, J. W. In *Determination of Organic Structures by Physical Methods*; Nachod, F. C.; Zuckerman, J. J., Eds.; Academic Press: New York, 1973; Vol. 5, p 75. Faller, J.; Thomsen, M. E. *J. Am. Chem. Soc.* **1969**, *91*, 6871. Faller, J.; Incorvia, M. J.; Thomsen, M. E. *J. Am. Chem. Soc.* **1969**, *91*, 518. Faller, J.; Incorvia, M. J. *J. Organomet. Chem.* **1969**, *19*, P13.

(12) (a) Breutel, C.; Pregosin, P. S.; Salzmann, R.; Togni, A. *J. Am. Chem. Soc.* **1994**, *116*, 4067. (b) Herrmann, J.; Pregosin, P. S.; Salzmann, R.; Albinati, A. *Organometallics* **1995**, *14*, 3311.

**Table 2. Experimental Data for the X-ray Diffraction Study of 2a**

formula	C <sub>21</sub> H <sub>29</sub> BF <sub>4</sub> N <sub>2</sub> Pd
mol wt	502.68
cryst dimens, mm	0.45 × 0.30 × 0.20
data coll T, °C	25
cryst syst	orthorhombic
space group	Pnma
a, Å	11.2126(32)
b, Å	17.4770(8)
c, Å	11.5284(26)
V, Å <sup>3</sup>	2259.1(9)
Z	4
ρ(calcd), g cm <sup>-3</sup>	1.478
radiation	Mo Kα (graphite monochromated λ = 0.710 69 Å)
μ, cm <sup>-1</sup>	8.497
transm coeff.	0.998 49–0.943 91
measd reflcns	+h,+k,+l
θ range, deg	2.5 < θ < 27.0
scan type	ω/2θ
scan width, deg	1.20 + 0.35 tan θ
max counting time, s	110
bkgd time, s	0.5 × scan time
max scan speed, deg min <sup>-1</sup>	7.1
prescan rejection lim	0.50 (2.0σ)
prescan acceptance lim	0.025 (40.0σ)
horiz receiving slit, mm	1.70 + tan θ
vert receiving slit, mm	4.0
no. indep data coll	2533
no. obs reflcns (n <sub>o</sub> )	1828 ( F <sub>o</sub>   <sup>2</sup> > 3.50σ( F <sup>2</sup>  ))
no. of params refined (n <sub>r</sub> )	138
fudge factor, f	0.060
max param shift Δp/σ (at convergence)	<0.15
R <sup>a</sup>	0.043
R <sub>w</sub> <sup>b</sup>	0.059
GOF <sup>c</sup>	1.686

<sup>a</sup>  $R = \sum(|F_o| - (1/k)|F_c|) / \sum|F_o|$ . <sup>b</sup>  $R_w = [\sum w(|F_o| - (1/k)|F_c|)^2] / \sum w|F_o|^2$ , where  $w = [\sigma^2(F_o)]^{-1}$ ;  $\sigma(F_o) = [\sigma^2(F_o^2) + f^2(F_o^2)]^{1/2} / 2F_o$ .  
<sup>c</sup>  $GOF = [\sum w(|F_o| - (1/k)|F_c|)^2 / (n_o - n_r)]^{1/2}$ .

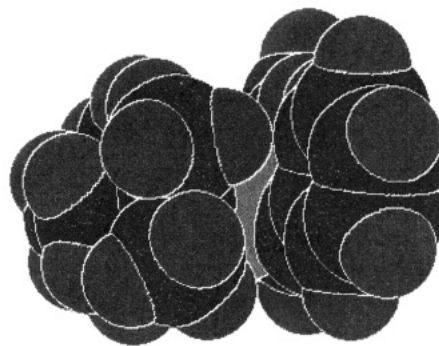
**Table 3. Final Positional and Isotropic Equivalent Displacement Parameters for 2a (Esd's in Parentheses)**

atom	x	y	z	B (Å <sup>2</sup> ) <sup>a</sup>
Pd	0.07077(4)	0.250	0.09943(4)	3.395(8)
N(1)	-0.0222(4)	0.3320(2)	-0.0076(3)	4.08(7)
C(1)	0.1569(4)	0.1817(3)	0.2301(4)	4.32(9)
C(2)	0.2182(6)	0.250	0.2128(5)	4.3(1)
C(3)	0.2080(4)	0.1050(3)	0.2046(4)	4.25(8)
C(4)	0.2979(5)	0.0937(3)	0.1255(4)	5.3(1)
C(5)	0.3445(6)	0.0217(4)	0.1081(5)	6.7(1)
C(6)	0.3042(5)	-0.0390(3)	0.1727(5)	6.7(1)
C(7)	0.2170(6)	-0.0300(3)	0.2510(5)	6.5(1)
C(8)	0.1675(5)	0.0420(3)	0.2684(4)	5.3(1)
C(9)	0.0594(6)	0.3741(5)	-0.0821(6)	8.2(2)
C(10)	-0.0899(6)	0.3849(5)	0.0639(7)	9.1(2)
C(11a)	-0.121(1)	0.2919(6)	-0.0644(9)	5.0(2)*
C(11b)	-0.0828(9)	0.2889(7)	-0.1034(9)	4.9(2)*
F(1)	0.094(1)	0.250	0.635(1)	15.0(4)
F(2)	-0.018(1)	0.250	0.4565(7)	13.5(3)
F(3)	-0.055(1)	0.3091(6)	0.6099(8)	23.4(4)
B	0.005(1)	0.250	0.565(1)	8.0(3)

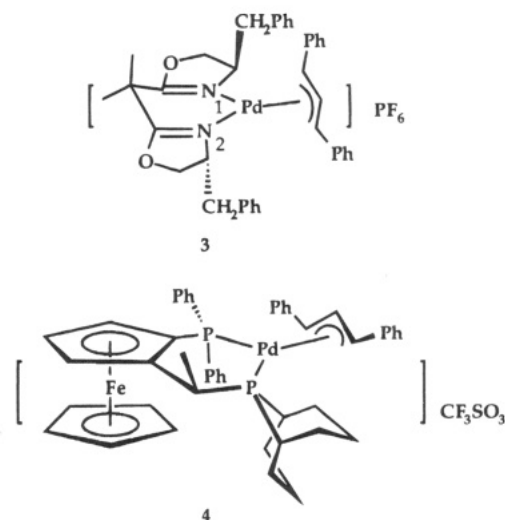
<sup>a</sup> Starred B values are for atoms the were refined isotropically. Anisotropically refined atoms are given in the form of the isotropic equivalent displacement parameter defined as  $(4/3)[a^2\beta(1,1) + b^2\beta(2,2) + c^2\beta(3,3) + ab(\cos \gamma)\beta(1,2) + ac(\cos \beta)\beta(1,3) + bc(\cos \alpha)\beta(2,3)]$ .

complex<sup>14</sup> [Pd(TMEDA)(PhCHCHCH<sub>2</sub>)]BF<sub>4</sub>, the Pd–C(allyl) separations are ca. 2.12–2.17 Å and the Pd–N

(13) (a) Abbenhuis, H. C. L.; Burckhardt, U.; Gramlich, V.; Koellner, C.; Pregosin, P. S.; Salzmann, R.; Togni, A. *Organometallics* **1995**, *14*, 759. (b) We have recently become aware of new structural results for 1,3-diphenylallyl complexes containing ligands of the JOSIPHOS family.

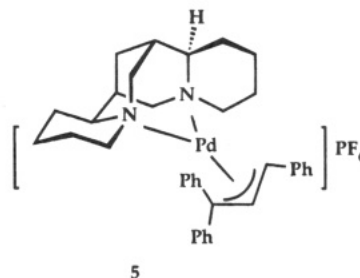
**Figure 2.** Space-filling model for **2a** showing that one of the methyl groups lies close to one of the phenyl rings of the 1,3-diphenylallyl ligand, thus leading to marked anisotropic effects in the solution spectra of such complexes.

distances 2.146(3) and 2.138(3) Å. We know<sup>13b</sup> of only two structural results for complexes of Pd(II) with the 1,3-diphenylallyl ligand, and these are **3** and **4**. In **3**,



reported by Pfaltz and co-workers,<sup>6a</sup> the two terminal allyl Pd–C distances are 2.169(3) and 2.118(3) Å so that our observed value for **2** is in good agreement with these. The two Pd–N separations in **3**, at 2.130(3) and 2.105(3) Å, are both significantly shorter than that found in our complex. As expected for **4** (a “phobiphos” complex<sup>13a</sup>) the Pd–C distances are >2.25 Å, in keeping with the difference in *trans* influence between nitrogen and phosphorus donors.<sup>15</sup> The C(1)–C(2) allyl distance for **2a**, 1.392(6) Å, is normal.

It is interesting that, in the 1,1',3-triphenylallyl cation **5**, which contains the nitrogen bidentate alkaloid



sparteine,<sup>16</sup> the Pd–N separations are 2.21(1) and 2.19-(1) Å, suggesting that the Pd–N distances for tertiary

(14) Murrall, N. W.; Welch, A. *J. Organomet. Chem.* **1986**, *301*, 109.

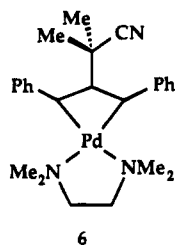
**Table 4.**  $^{13}\text{C}$  NMR  $\Delta\delta$  Data for the Terminal Allyl Carbons in the 1,3-Diphenylallyl-Pd(II) Complexes plus Optical Yields in the Allylic Alkylation

chelate	$\Delta\delta(^{13}\text{C})^a$	e.e., % <sup>b</sup>
(R)-BIPHEMP	17.4	90 (S)
	8.4	
(S)-MeO-BIPHEMP	18.6	87 (R)
(R)-DPPCP	2.2	85 (S)
(S)-BINAP	17.4	90 <sup>c</sup>
(S,S)-DIOP	2.7	6 (R)
(S,S)-CHIRAPHOS	1.9	22 <sup>c</sup>
(R)-(S)-JOSIPHOS	14.4	93 <sup>d</sup> (S)
(S)(R)-PHOBIPHOS	19.9	73 <sup>e</sup>
dibenzyl oxazoline	7	88 <sup>f</sup>
(S)-PhIMPHOS	35.0	10 (R)
	39.0	
(R)-CyIMPHOS	36.0	4 (R)
	36.7	
(S)-NapIMPHOS	33.0	17 (S)
	33.5	
(+)-MePHOS	24.6	10 (R)
	28.1	

<sup>a</sup>  $\text{CDCl}_3$ , 296 K. Difference between the two terminal  $^{13}\text{C}$ 's for the major isomer. <sup>b</sup> As described previously. Observed enantiomer in parentheses. <sup>c</sup> Auburn, P. R.; Mackenzie, P. B.; Bosnich, B. *J. Am. Chem. Soc.* **1985**, *107*, 2033–2046. <sup>d</sup> Togni, A.; Breutel, C.; Schnyder, A.; Spindler, F.; Landert, H.; Tijani, A. *J. Am. Chem. Soc.* **1994**, *116*, 4062. <sup>e</sup> See ref 13. <sup>f</sup> See ref 6. <sup>g</sup> See ref 4.

aliphatic amine donors may be slightly longer than for an  $\text{sp}^2$  nitrogen donor; however, we note that the experimental uncertainty is relatively large.

It is interesting that the solid-state structure of **6** has just been reported.<sup>17</sup> We note that the Pd–N separations in **6** are 2.230(4) and 2.233(4) Å, in keeping with what one might expect for carbon *trans* to nitrogen.



**Catalysis.** In previous studies<sup>9a</sup> we have carried out the catalytic allylic alkylation shown above, using a variety of known and new chiral ligands, in the hopes of correlating some of our NMR observations with reactivity. We have extended this work and show new data in Table 4. The results for the four chiral PN ligands plus those for the BIPHEMP and DPPCP ((R)-1,2-bis(diphenylphosphino)cyclopentane) ligands are new. The remaining catalytic results are taken from the literature. It is noteworthy that (a) the PN ligands were not especially successful with respect to their enantioselectivity and (b) the relatively small DPPCP is only slightly less effective, in terms of enantioselectivity, than the two relatively large BIPHEMP complexes, with ee's for these three in the range 85–90%. Although these ee's are good, other groups have done better.<sup>8,7,18</sup> Recently, the ligand DPPCP has been used successfully in the cross-coupling reaction with nickel.<sup>19</sup> All the ee's were determined using HPLC methods; however, for the

(15) Appleton, T.; Clark, H. C.; Manzer, L. *Coord. Chem. Rev.* **1973**, *10*, 335. Motoschi, H.; Pregosin, P. S.; Venanzi, L. M. *Helv. Chim. Acta* **1979**, *62*, 667.

**Table 5.** Mean Values for the Four Torsional Angles (deg) P–M–P–C<sub>ipso</sub><sup>a</sup>

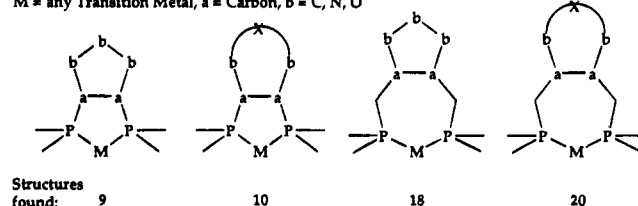
	A1	A2	B1	B2
R55	135(5)	98(5)	124(5)	107(4)
R5	143(8)	94(9)	129(6)	108(7)
R75	173(6)	63(10)	135(14)	105(14)
R7	164(7)	76(7)	151(9)	91(9)

<sup>a</sup> A and B refer to the fact that each P atom is associated with two angles.

DPPCP ligand both HPLC and NMR methods were employed and gave identical results within the experimental error of the NMR integration.

**Structure Analysis and MM2\*.** Given that several of the catalytic results were unexpected, and specifically that the larger BINAP and smaller DPPCP complexes were almost equally effective, we have considered the subject of the chiral pocket from a structural viewpoint, using MM2\*. As in our previous efforts<sup>9</sup> with such force-field calculations, we use a series of structures found via the Cambridge Crystallographic Structure Data Base (CCSDb) as a starting point. We restricted the search to 5- and 7-membered chelating phosphine rings of metal complexes

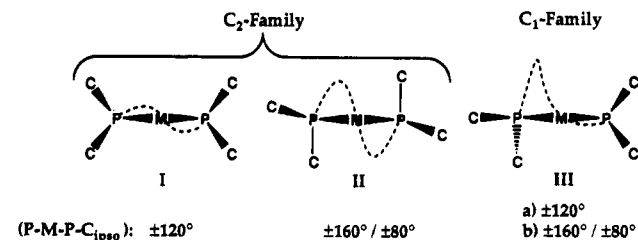
M = any Transition Metal, a = Carbon, b = C, N, O



and show below the structures the numbers of structures found (for which coordinates were deposited) for each of the four structural types, defined as R55, R5, R75, and R7 (R = ring; the second number indicates the second fused ring).

We now, arbitrarily, take the positions of the ipso-P–phenyl carbons as one measure of the chiral pocket. Further, we look at the four dihedral angles, P–M–P–C(ipso) and take these as a *description* of this aspect of the pocket and show these 16 angles in Table 5.

The values for these angles can be crudely rationalized by assigning them to two families of structures: one with an approximately  $C_2$  symmetry (containing I and II) and a second family, with  $C_1$  symmetry, which we



call III. Families R55, R5, and R7 belong to the  $C_2$  family. R55 and R5 are intermediate between I and II; R7 is very close to II, and R75 is of type III. Histograms

(16) Togni, A.; Rihs, G.; Pregosin, P. S.; Ammann, C. *Helv. Chim. Acta* **1990**, *73*, 723.

(17) Hoffmann, H. M. R.; Otte, A. R.; Wilde, A.; Menzer, S.; Williams, D. *J. Angew. Chem.* **1995**, *107*, 73.

(18) Togni, A.; Breutel, C.; Schnyder, A.; Spindler, F.; Landert, H.; Tijani, A. *J. Am. Chem. Soc.* **1994**, *116*, 4062.

(19) Indolese, A. F.; Consiglio, G. *Organometallics* **1994**, *13*, 2230.

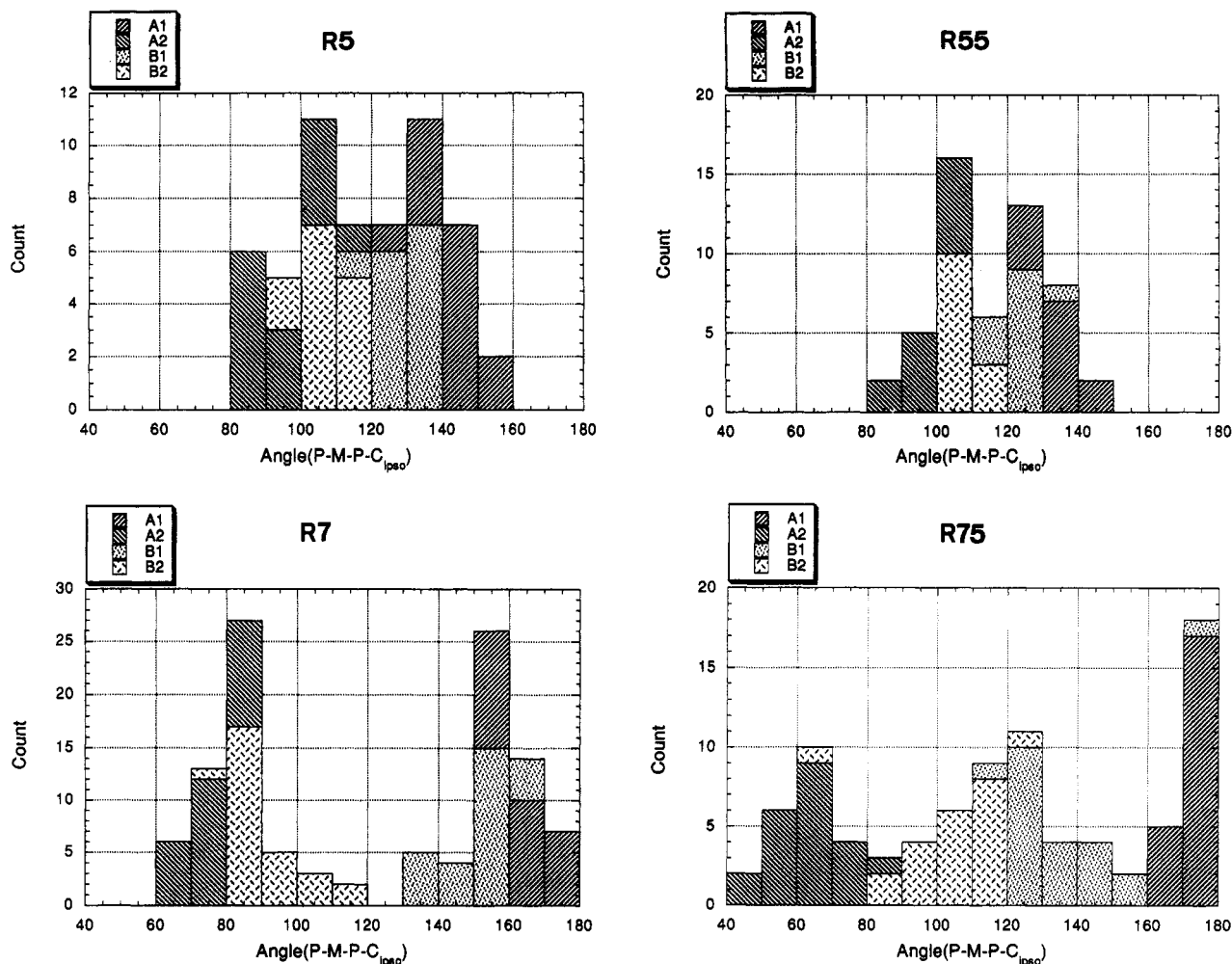
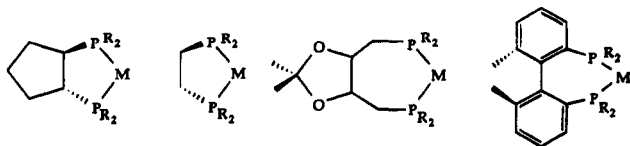


**Figure 3.** Four histograms showing the results of the P–M–P–C(ipso) angles found in the CCSDb search. The spread of angles is largest for the R75 (DIOP) type chelate. In the R7 and R55 histograms, the concentration of angles hints at a rigid pocket.

of these dihedral angles for the four types, are shown in Figure 3. It is sufficient to note that there is a large spread of angles for the R75 family and a much smaller distribution for R5 and R55 with R55 narrower than R5. The distribution for the R7 family is dimodal, with well-separated modes and a narrow distribution about each mode. This reflects the presence of a preferred conformation in the solid state.

Using an extension to the MM2\* force field found in MacroModel 4.5,<sup>20</sup> we now calculated all the ring conformations for the complexes PdCl<sub>2</sub>(chelate), where the chelate has been restricted to the following four types:



(These four are somewhat related to the types R55, R5, R75, and R7, respectively.) As we have used MM2\* for calculations involving allyl complexes of Pd(II), previously,<sup>9</sup> we decided to omit the allyl in these new

**Table 6.** Mean Values for the Four Torsional Angles (deg) P–M–P–C<sub>ipso</sub>

		A1	A2	B1	B2
R55	exptl	135(5)	98(5)	124(5)	107(4)
	MC calcd	133(9)	100(9)	122(8)	110(7)
R5	exptl	143(8)	94(9)	129(6)	108(7)
	MC calcd	140(11)	95(9)	127(5)	110(6)
R75	exptl	173(6)	63(10)	135(14)	105(14)
	MC calcd	167(15)	71(18)	143(16)	94(25)
R7	exptl	164(7)	76(7)	151(9)	91(9)
	MC calcd	173(9)	71(9)	156(13)	88(9)

calculations in order to concentrate on the chiral auxiliary. To validate the force field,<sup>21</sup> we calculated the conformations with the help of a Monte-Carlo scheme and show the mean values for the calculated dihedral angles, P–M–P–C(ipso), in Table 6, together with the angles from the search described above. There is good general agreement between the angles found in the CCSDb search and our calculations. Note that both the mean values and the relative sizes of the standard deviations are reproduced. This suggests that the calculations are finding legitimate angular distributions. From Figure 4, which shows comparisons for the R7 and R75 families, it is clear that the R7 family has a more

(20) Still, W. C. MacroModel Version 4.5, Columbia University, New York, 1994. Still, W. C.; Mohamadi, F.; Richards, N. G. J.; Guida, W. C.; Liskamp, R.; Lipton, M.; Caufield, C.; Chang, G.; Hendrickson, T. *J. Comput. Chem.* **1990**, *11*, 440.

(21) One usually tests the force field by using it on some known situation. We and others have done this previously (see ref 6 and: Norrby, P.; Åkermark, B.; Haefner, F.; Hansson, S.; Blomberg, M. *J. Am. Chem. Soc.* **1993**, *115*, 4859).

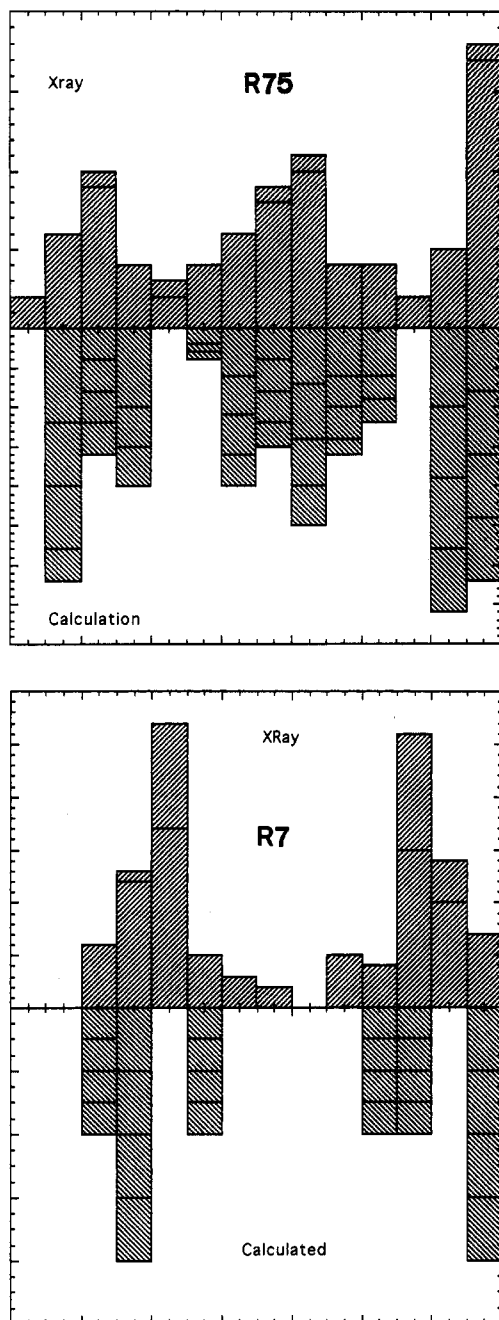


**Figure 4.** Histograms showing comparisons for the P–M–P–C angles observed (X-ray) and calculated (MM2\*), for the R7 and R75 classes of chelate.

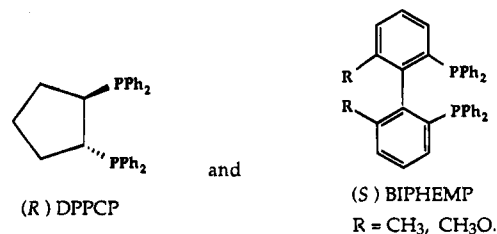
restricted set of angles, thus indicating a more rigid chiral pocket. Additional molecular dynamics calculations at various temperatures showed that for BIPHEMP (BINAP) and DPPCP type complexes, the chiral pocket remains stable. From both sources, the CCSDB and the calculations, one finds that BIPHEMP (BINAP) and the DPPCP angles are relatively limited, but quite different, so that a coordinated substrate can expect well-defined, relatively rigid, but different chiral pockets in both cases. This may be related to the catalytic observations; i.e., both BIPHEMP and DPPCP function reasonably well.

**$^{13}\text{C}$  NMR.** It has been suggested<sup>6a,22</sup> that the differences in the  $^{13}\text{C}$  chemical shifts of the terminal allyl

carbons are a measure of the differing electronic environments for these centers. The  $\Delta\delta$   $^{13}\text{C}$  data, also shown in Table 4, represent the differences in the chemical shifts of these two allyl carbons; the individual  $^{13}\text{C}$  chemical shifts are given in Table 7. For bidentate phosphine or bidentate nitrogen  $C_2$ -symmetrical chelates, the observed  $\Delta\delta$  arises from the selective steric interactions of the allyl phenyl groups with the chiral array offered by the chelate (e.g., the P-phenyl groups in a BIPHEMP but, for the bis(oxazoline), the two benzyl groups). For the chiral chelating ligands BIPHEMP, BINAP, DIOP, CHIRAPHOS and DPPCP, the  $\Delta\delta$  values range from ca. 1.9 to 18.6 ppm. We attribute the qualitative differences to the varying extents to which the chiral pocket extends "forward", toward the allyl ligand,<sup>9a,b</sup> leading to interligand steric interactions. These  $\Delta\delta$ 's are largest for the BINAP and BIPHEMP's and smallest for the CHIRAPHOS and DPPCP ligands. Since one can assign the two different terminal allyl  $^{13}\text{C}$  signals (*vide infra*), and further assuming that the carbon associated with the highest frequency (most olefin-like) will be attacked by the incoming nucleophile, then one can predict the chirality of the organic product.<sup>6a,22</sup> This  $^{13}\text{C}$  criterion has been used in the past and correctly predicts the chirality of the observed enantiomer for the new methoxy BIPHEMP and DPPCP complexes. We note that the size of the  $^{13}\text{C}$   $\Delta\delta$  does not seem to be important in that the magnitude of  $\Delta\delta$  does not correlate with observed enantiomeric excess.

The individual  $^{13}\text{C}$  allyl carbon data for the complexes **2a-o** are, to some extent, expected,<sup>23</sup> since different donor atoms possess substantial differences in their *trans* influences.<sup>15</sup> Consequently, there is nothing unusual about the >30 ppm difference found for the complexes containing chiral PN ligands. It is interesting that the relatively high-frequency terminal allyl chemical shift for the bis(oxazoline), **3**, is similar to the shift found in the relatively large biquinoline derivative, **2d**, thus reflecting the interaction of the bulky benzyl substituents of **3** with the allyl ligand. In order to have a reasonable  $^{13}\text{C}$  data base for the new 1,3-diphenylallyl complexes, we prepared a number of compounds containing standard ligands such as bis-1,2-(diphenylphosphino)ethane, biquinoline, and (*S*)-BINAP among others and show  $^{13}\text{C}$  data for these in Table 7 as well.

**DPPCP, MeO-BIPHEMP, and JOSIPHOS Complexes.** We have made detailed NMR studies for complexes, **2k** and **2n**, containing the following ligands:



These are interesting in that, although the  $\Delta\delta$   $^{13}\text{C}$  values, 2.2 and 18.6 ppm, respectively, are quite different, the two are almost equally effective in the catalysis. For the solution structures, and the allyl dynamics which follow, we have made extensive use of phase

(22) Pregosin, P. S.; Salzman, R.; Togni, A. *Organometallics* **1995**, *14*, 842.

(23) Åkermark, B.; Krakenberger, B.; Hansson S.; Vitagliano, A. *Organometallics* **1987**, *6*, 620.

Table 7.  $^{13}\text{C}$  NMR Data<sup>a</sup> for the 1,3-Diphenylallyl Complexes, 2 and 9

chelate	central allyl $^{13}\text{C}$		terminal allyl $^{13}\text{C}$	
( <i>R</i> )-BIPHEMP	110.1 [7.0], major	107.7 [7.0], minor	103.1 [22.0, 6.0]	85.7 [30.0, 7.0]
( <i>S</i> )-MeO-BIPHEMP	109.4 [7.5] major	ca. 107, minor	99.5 [25.0, 6.0]	91.2 [30.0, 7.0]
( <i>S</i> )-BINAP <sup>b</sup>	111.3 [7.0]		103.3 [21.5, 5.5]	84.8 [30.0, 7.0]
( <i>S,S</i> )-DIOP	112.1 (s, br)		98.2	90.7
( <i>S,S</i> )-CHIRAPHOS	112.5 [7.5]		104.6 [ 5.0]	87.2
(+)-DPPCP	112.4 [7.5]		95.5 [22.0]	92.9 [27.0]
DIPHOS	113.6 [7.4]		90.1 [24.2, 8.1]	88.1 [25.5, 9.6]
( <i>R</i> )( <i>S</i> )-JOSIPHOS <sup>c</sup>	110.9 [6.5], major	112.6 (s, br), minor	91.2 [21.5, 7.5]	89.0 [23.5, 8.5]
( <i>S</i> )( <i>R</i> )-PHOBIPHOS <sup>d</sup>	110.8		91.7 [16.0]	91.7 [16.0]
TMEDA <sup>b</sup>	108.9		96.4 [19.8, 3.1]	82.0 [29.0, 3.0]
bipy <sup>b</sup>	108.5		90.2 [ 6.1]	89.6 (s, br)
biquinoline <sup>b</sup>	112.1		100.7	80.8
AMPY <sup>b</sup>	108.4		78.9 (s)	78.9
<b>3</b> <sup>e</sup>	108.1		78.9 (s)	78.9
( <i>S</i> )-PhIMPHOS	111.9 (s, br)		83.2 (s)	83.2
( <i>R</i> )-CyIMPHOS	111.9 (s, br)		78.5 (s, br)	78.5 (br)
( <i>S</i> )-NapIMPHOS	111.9 (s, br)		74.2	81.8
(+)-MePHOS	111.25 [ 6.0]	110.2 [ 6.0]	105.9 [21.0]	66.9
			103.9 [21.0]	68.9
			104.5 [23.0]	67.9 (br)
			105.2 [23.0]	69.2 [5.9]
			103.0 [15.0]	70.0 [6.8]
			103.2 [14.0]	69.7 [6.8]
			95.9 [24.0]	71.4 [11.2]
			97.4 [23.0]	69.3 [10.8]

<sup>a</sup> CDCl<sub>3</sub>, 296 K, 125.8 MHz, P,C *J*-values in brackets. PF<sub>6</sub> salts, unless otherwise indicated. <sup>b</sup> BF<sub>4</sub> salts. <sup>c</sup> *Trans* to P. <sup>d</sup> 100.7, *trans* to P; see refs 12a and 13. <sup>e</sup> See ref 6.

Table 8. Allyl  $^1\text{H}$  NMR Data<sup>a</sup> for the 1,3-Diphenylallylic Cationic Pd Complexes

ligand	H1 $\delta$ ( <i>J</i> (P,H)), [ <i>J</i> (H,H)]	H3 $\delta$ ( <i>J</i> (P,H)), [ <i>J</i> (H,H)]	H2 (central) $\delta$ [ <i>J</i> (H,H)]
( <i>R</i> )-BIPHEMP	<i>g</i> 5.24 (7.8), [7.8]	4.19 (11.3), [11.3] 5.09 (13.4), [13.4]	<i>g</i> <i>g</i>
( <i>S</i> )-MeO-BIPHEMP	6.30 (9.1), [9.1] [2.8] 5.38 (8.1), [8.1]	4.21 (11.6), [11.6] 5.16 (13.2), [13.2]	<i>g</i> <i>g</i>
( <i>S</i> )-BINAP <sup>b</sup>	<i>g</i> 5.50 (8.1), [8.1]	4.51 (10.3), [10.3] 5.17 (13.6), [13.6]	<i>g</i> <i>g</i>
( <i>S,S</i> )-DIOP	5.46 (11.7), [11.7]	5.16 (11.6), [11.6]	6.27 [12.8]
( <i>S,S</i> )-CHIRAPHOS	5.03 (9.5), [3.0]	4.73 (9.8), [ 2.2]	6.48 [12.9]
(+)-DPPCP	5.29 (9.2), [3.5]	5.01 (8.0), [ 2.8]	6.46 [12.9]
DIPHOS	5.22 (6.5)	5.22 (6.5)	6.68 [13.0]
TMEDA <sup>b</sup>	4.70	4.70	6.46 [11.7]
bipy <sup>b</sup>	4.98	4.98	6.71 [11.7]
biquinoline <sup>b</sup>	5.31	5.31	6.01 [11.5]
AMPY <sup>b</sup>	4.92	4.92	6.55 [11.6]
( <i>S</i> )-PhIMPHOS	6.14 (10.3), [14.2] 6.06 (9.0), [14.0]	4.02 [9.4] 4.28 [10.5]	<i>g</i> <i>g</i>
( <i>R</i> )-CyIMPHOS	6.11 (8.8) 5.87 (9.7), [13.7]	4.18 4.46 [11.0]	6.68 [14.1], [10.5] <i>g</i>
( <i>S</i> )-NapIMPHOS	6.20 (9.5) 6.23 (10.0)	4.38 4.45	6.26 [13.9], [10.5] 6.35 [13.7], [10.8]
(+)-MePHOS	5.74 (9.5) 5.76 (9.2)	5.17 (3) 4.83	6.75 [12.8], [11.7] 6.61 [12.5], [11.8]

<sup>a</sup> CDCl<sub>3</sub>, 296 K, 500.1 MHz. Data refer to isomers listed in order of decreasing population. As PF<sub>6</sub> salts unless otherwise indicated. <sup>b</sup> BF<sub>4</sub> salts.

sensitive NOESY, plus  $^{31}\text{P}$ ,  $^1\text{H}$ - and  $^{13}\text{C}$ ,  $^1\text{H}$ -correlation measurements. These help to unequivocally assign key  $^1\text{H}$ ,  $^{13}\text{C}$ , and  $^{31}\text{P}$  signals and, via the NOESY, also provide  $^1\text{H}$ ,  $^1\text{H}$ -spatial relationships. We give the allyl proton data in Table 8.

For the DPPCP complex, **2k**, which has the allyl phenyls in syn positions relative to the central proton (syn/syn isomer), the terminal anti allyl protons do not show uniformly strong NOE's from the allyl ligand to the *ortho* "reporter"<sup>9</sup> protons of the P-phenyl groups. Indeed, most of these NOEs are quite weak and we find only one modest NOE, from the *ortho* protons of the pseudo-axial ring A, on P<sub>1</sub>, to the terminal anti allyl-H, as shown in Scheme 2.

There are normal, strong NOEs from the terminal allyl protons to their respective allyl *ortho*-phenyl

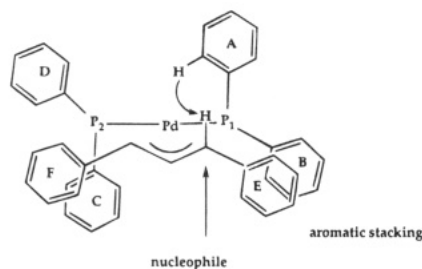
protons in rings E and F. The strongest interligand "ring-ring" NOE stems from the *ortho* protons of the pseudo-axial ring C to the *ortho* protons of the allyl phenyl ring F. We consider it important that the two rings B and E stack (little or no NOE between these two) and presumably move synchronously. Perhaps the allyl phenyl ring F finds more space between the C- and D-rings and/or the stacking causes the B- and E-rings to interact thus weakening the allyl carbon-Pd cis to P(1). For this DPPCP compound, when compared to other 1,3-diphenylallyl complexes, these NOE indications are rather subtle and, apart from the stacking, we would not have thought these, in themselves, to be indicative of a successful auxiliary.

For the (*S*)-MeO-BIPHEMP complex, **2n**, two isomers exist in solution in the ratio 4.3:1.0 (for the methyl



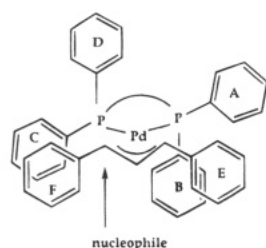
## Scheme 2

Fragment of the (*R*)-DPPCP complex **2k**. The site of attack (based on the organic product) and the ring-stacking are shown (five-membered chelate ring, charge and anion omitted for clarity).

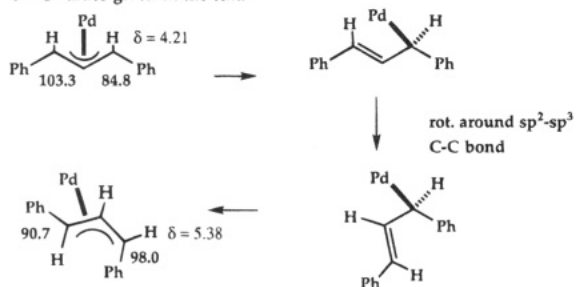


## Scheme 3

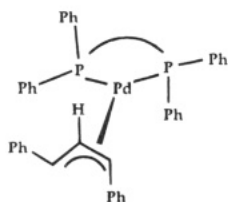
Fragment of the structure of the major isomer for **2n**, showing the site of the nucleophilic attack (five-membered chelate ring, charge and anion omitted for clarity).



Isomerization to the *syn/anti* isomer of **2n**. The bold numbers refer to the  $\delta^{13}\text{C}$  values given in the text.

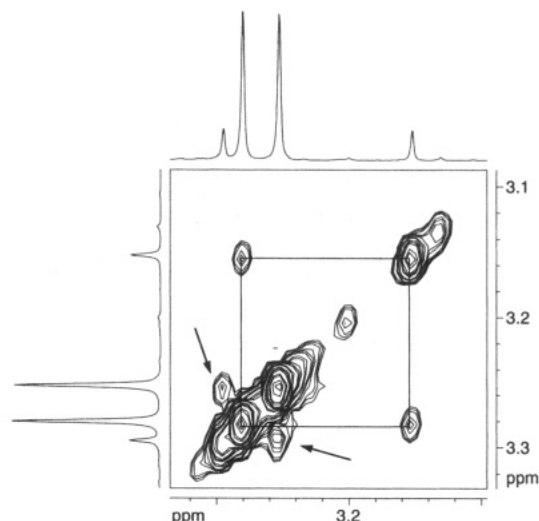


BIPHEMP this ratio is 3.8:1.0). Analysis of the allyl proton-proton coupling constants and the NOESY cross-peaks shows that the minor isomer has the *syn/anti* configuration of the allyl phenyls (see **7**). The allyl



**7** (abbreviated form of the *syn/anti* isomer of complex **2n**)

$^{13}\text{C}$  chemical shifts are quite different for these two isomers:  $\delta = 84.8$  and  $\delta 103.3$  (major) and  $\delta$  ca. 90.7 and ca. 98.2 (minor) with the allyl carbon with the anti phenyl group appearing at the higher frequency. The  $^{13}\text{C}$  values for the minor isomer can be found by using the  $^1\text{H}$ -exchange spectrum, to localize the allyl protons, followed by a  $^{13}\text{C}, ^1\text{H}$ -correlation. For the major isomer, we could assign the allyl  $^{13}\text{C}$  signal at 103.3 ppm to the carbon shown with the arrow in Scheme 3, i.e., immediately adjacent to ring F. Attack at this position

 $^1\text{H}$  Exchange Spectroscopy

**Figure 5.** Section of the phase-sensitive  $^1\text{H}$ -NOESY for **2n** revealing exchange cross-peaks between the BIPHEMP methoxy groups of the two isomers. The appropriate cross-peaks for the two exchanges are indicated by the square and by the arrows. One methoxy of the major isomer exchanges selectively with one methoxy of the minor isomer ( $\text{CDCl}_3$ , 500 MHz).

allows one to rationalize the observed enantiomer in the catalytic experiment.

The presence of exchange cross-peaks in the phase-sensitive  $^1\text{H}$ -NOESY shows that the two isomers are in equilibrium. Figure 5 demonstrates this for the methoxy methyl signals. The exchange is *selective* both in the allyl and methoxy regions, with one allyl proton of the major isomer in exchange with just one allyl proton in the minor isomer. The minor isomer can exist in two forms which differ with respect to the placement of the anti phenyl group relative to the BIPHEMP phenyl groups. The exchange and NOE data clearly point to **7** as the correct structure. For isomer **7**, the *syn* proton,  $\delta = 5.38$ , is in selective exchange with the low-frequency anti proton,  $\delta = 4.21$ , in the major isomer. For these terminal allyl protons, this exchange can be understood as shown in the lower half of Scheme 3.

A selective  $\eta^3$ - $\eta^1$  isomerization<sup>10-12</sup> is followed by a rotation around the  $\text{sp}^2$ - $\text{sp}^3$  bond. Re-formation of the allyl via an  $\eta^1$ - $\eta^3$  process gives the minor isomer and accounts for the observed selectivity. The allyl carbon attached to ring F opens. Presumably, it is this side of the allyl that is most affected by steric interactions from the phenyl groups of the chiral array. This is the third example of such  $\eta^3$ - $\eta^1$ - $\eta^3$  isomerization selectivity in a chiral chelate allyl complex of Pd(II).<sup>12</sup>

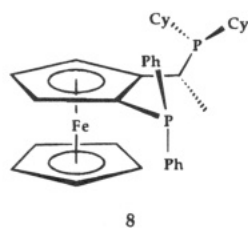
It is interesting that, although **2k,n** both have relatively rigid chiral pockets, as suggested by the calculations above, only **2n** shows significant quantities of a second diastereomer. Since we have no NMR data arising from *in situ* catalytic runs, we will not speculate on how the presence of this minor isomer affects the ee; however, in terms of the  $^{13}\text{C}$  parameters, we find that the observed enantiomer can be rationalized by assuming that the high-frequency terminal carbon is attacked preferentially in both isomers.

For the major isomer in **2n**, we note that there is only a very small NOE between the C and F rings (see Scheme 3), again suggesting ring stacking. This stack-

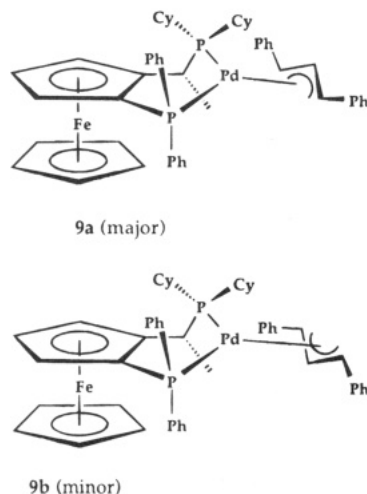


ing appears to be an important structural feature, and if so, it is specific for the 1,3-diphenylallyl ligand. Currently, we consider the ring-stacking as the compromise that the complex makes in order to accommodate two proximate phenyl groups. Its existence implies that "testing" new chiral auxiliaries using this allyl does not necessarily reflect on the general utility of the new auxiliary but rather how well it "tunes" to this particular allyl ligand.

The class of chiral bidentate ligands called JOSIPHOS has proven to contain useful auxiliaries.<sup>12a,18,24</sup> One of these, **8**, has been shown to afford a ca. 93% ee in the allylic alkylation of eq 1.<sup>13a,18</sup>



We have made the 1,3-diphenylallyl complex of **8**, as its triflate salt. This complex, **9**, exists in solution in two predominant forms which can be assigned, using NOESY methods, as the isomers **9a,b** in a ca. 2:1 ratio,



respectively.<sup>25</sup> However, **9a,b** are (a) each in equilibrium with two additional isomers, one at the 1–2% level, **9c**, and the other, **9d**, at a concentration too small to be accurately estimated, and (b) *not* in observable equilibrium with each other (see Figure 6). These selective equilibria are observable in *both* the <sup>31</sup>P, and <sup>1</sup>H 2-D exchange spectra. We believe that **9c,d** are *syn/anti* isomers and have shown this type of equilibrium for a phobane JOSIPHOS analog, previously.<sup>13</sup>

Complex **9** is important in connection with understanding the potential predictive value of the terminal allyl <sup>13</sup>C chemical shifts and, perhaps, the source of the enantioselection. The <sup>13</sup>C allyl chemical shifts for **9a** are 96.4 ppm (*trans* to PCy<sub>2</sub>) and 82.0 ppm (*trans* to

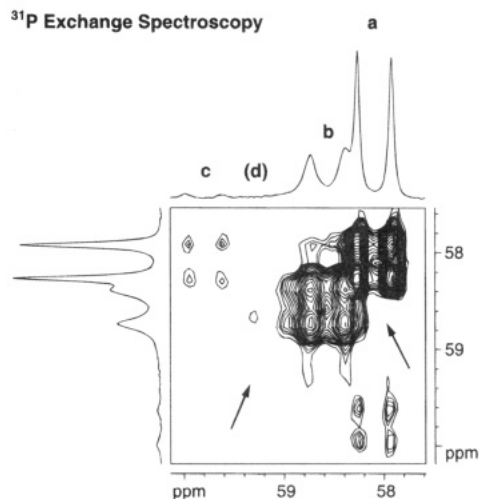


**Figure 6.** High-frequency section of the <sup>31</sup>P 2-D exchange spectrum for **9** (CDCl<sub>3</sub>, 200 MHz). The two major isomers are *not* in equilibrium. The arrow on the right indicates where the cross-peaks would be, if these two isomers were exchanging. There are readily visible cross-peaks between the major isomer, **9a**, and one of the minor isomers, **9c**. The <sup>31</sup>P signal for the second minor isomer, **9d**, is not visible (but suggested in parentheses); however, its exchange cross-peaks, with **9b**, are just barely visible, thereby allowing an estimation of the **9d** <sup>31</sup>P chemical shift (the arrow on the left). The **9b** ↔ **9d** exchange is readily observed in the much more complicated <sup>1</sup>H exchange spectrum.

PPh<sub>2</sub>) and, for **9b**, 89.6 ppm (*trans* to PCy<sub>2</sub>) and 90.2 ppm (*trans* to PPh<sub>2</sub>) (i.e., these last two are almost identical).

Assuming (a) the <sup>13</sup>C criterion reflects the site of attack, (b) the major isomer, **9a**, is attacked preferentially at the 96.4 ppm carbon (this gives the observed (*S*)-enantiomer), (c) for the minor isomer **9b**, these two termini are attacked almost equally (there seems to be no major electronic difference based on these δ(<sup>13</sup>C) values), and (d) the various isomers present react at about an equal rates, then one would expect a ca. 66% ee, and not the observed ee of 93%, since the two ends of **9b** will be attacked at ca. equal rates. The *syn/anti* isomers are only present at <2% level so that their populations are not significant contributors. Consequently, we conclude that, for **9**, the rates of nucleophilic attack at the various terminal allyl carbons of **9a,b** are *not* equal, e.g. **9a** > **9b**, and/or the <sup>13</sup>C criterion is suspect. Perhaps, for **9**, a minor isomer may react more rapidly (as is known in the rhodium-catalyzed enantioselective hydrogenation<sup>26,27</sup>) although we have no evidence for this. The <sup>13</sup>C allyl resonances for **9c,d** are much too weak to be observed.

## Conclusions

From all of our solution results we can conclude that the following: (a) The chiral auxiliary need not be extremely large to be effective; i.e., DPPCP functions reasonably well. (b) The molecular mechanics calculations can help us to visualize the chiral pockets of various chelating ligands. (c) A relatively large, intrusive auxiliary, e.g., BIPHEMP or BINAP (for which there are also two isomers in solution) can lead to

(24) Togni, A.; Breutel, C.; Soares, M.; Zanetti, N.; Gerfin, T.; Gramlich, V.; Spindler, F.; Rihs, G. *Inorg. Chim. Acta* **1994**, *222*, 213.

(25) A detailed analysis of the <sup>1</sup>H-NOESY results permits the assignment of these two isomers. Key NOEs involve that from the η<sup>5</sup>-Cp to the *ortho* protons of the "lower" P-phenyl ring and then NOEs from these *ortho* protons of the lower P-phenyl ring to either an anti allyl proton or the *ortho* protons of one allyl phenyl ring.

(26) Brown, J. M. *Chem. Brit.* **1989**, 276.

(27) Knowles, W. S. *Acc. Chem. Res.* **1983**, *16*, 106.

significant quantities of syn/anti isomers,<sup>28</sup> whose presence may or may not significantly affect the ee's, depending upon which carbon is attacked. (d) The observed ee for **9** does not correlate with expectations on the basis of a ground-state population analysis; i.e., the reaction kinetics for different diastereomers may be important. (e) The 1,3-diphenylallyl substrate is special in that its phenyl groups can stack with the phenyl groups of the chiral auxiliary, in solution as well as in the solid-state. (f) As in our previous work, phase sensitive <sup>1</sup>H-NOESY, which can provide both structural and dynamic information, is a potent tool in this chemistry.

### Experimental Section

**Materials and Methods.** The NMR spectra were recorded at RT (room temperature) on a Bruker AC 250 instrument operating at 250 MHz for <sup>1</sup>H, 101.3 MHz for <sup>31</sup>P, and 62.9 MHz for <sup>13</sup>C and on a Bruker AMX 500 instrument operating at 500.1 MHz for <sup>1</sup>H and 125.8 MHz for <sup>13</sup>C. The samples were prepared by dissolving 30 mg of complex in 0.5 mL of deuterated solvent (CDCl<sub>3</sub> or CD<sub>2</sub>Cl<sub>2</sub> depending on the solubility of the compounds). The shifts caused by solvent change do not significantly influence the data. Chemical shifts are given in ppm relative to TMS and external 85% H<sub>3</sub>PO<sub>4</sub>. The FID's were treated with an exponential factor (3 Hz line broadening) for <sup>31</sup>P and <sup>13</sup>C to obtain the final 1-D data set. In some cases resolution enhancement was used to resolve partially overlapping lines. <sup>13</sup>C-assignments were made with the help of literature values plus DEPT and 2-D correlation measurements. NOESY spectra were recorded using a 0.8 s mixing time. Elemental analysis were performed by the analytical service of the ETHZ, and these data are given in the Supporting Information.

**Crystallography.** Crystals of compound were obtained by crystallization from CH<sub>2</sub>Cl<sub>2</sub>/ether/pentane and are air stable. An Enraf-Nonius CAD4 diffractometer was used for the unit cell and space group determination and for the data collection. Unit cell dimensions were obtained by least squares fit of the 2θ values of 25 high-order reflections (9.4 < θ < 18.4°). Selected crystallographic and other relevant data are listed in Table 2.

Data were measured with variable scan speed to ensure constant statistical precision on the collected intensities. Three standard reflections were used to check the stability of the crystal and of the experimental conditions and measured every 1 h; no significant variation was detected. The orientation of the crystal was checked by measuring three reflections every 360 measurements.

Data were corrected for Lorentz and polarization factors and, empirically, for absorption<sup>29</sup> using azimuthal (ψ) scans of 6 reflections (χ > 86°, 11.2 < θ < 20.8°). The standard deviations on intensities were calculated in term of statistics alone, while those on F<sub>o</sub> were calculated as reported in Table 2.

The structure was solved by Patterson and Fourier methods and refined by full-matrix least squares. After some cycles of refinement, the high displacement parameter of carbon C(11) and the "flat" geometry of the diamine ligand clearly showed the presence of disorder, possibly due to the presence of two different conformations for the N-C-C-N-Pd ring. Thus atom C(11) was split into two sites (a and b with occupancy 0.5 each) thus allowing, through the crystallographic mirror symmetry, for the presence of the two ring conformations. The BF<sub>4</sub><sup>-</sup> counterion was found to be disordered across the mirror

### Chart 1. Cambridge Crystallographic Structure Data Base References Codes

	R 5 5	R 5	R 7 5	R 7
1	butwes	cuyyaw	bemgop	bnapr10
2	casdop	docpiu	bicloo	chpfmo
3	cozreo	dubtup	bicluu	datzon
4	hajkuy	kigtez	bicluu01	fuxsum
5	sachin	kigtid	buzbed	gahyap
6	sachot	ocpbrh	chdor01	gedyuj
7	sospev	sahneu	chdor01	gedzaq
8	vasxui	saztao	cipbni10	gefzas10
9	vudmai	saztes	diopfe	hajsoa
10	wapbyi	veljif	ficbic	hapbij
11			hoxlrh	japxaz
12			juzlev	jipcam
13			yajpii	jubvux
14			yajpoo	jubwae
15			yajpuu	jubwei
16			yajrac	koskuy
17			vofhon	legzom
18			vojbeb	vixzor
19			vojbeb10	viytus
20				viytus10

plane: as a result its geometry is imprecise. For the final cycles of refinement all atoms were refined anisotropically with the exception of the split carbon C(11) that was treated isotropically. The contribution of the hydrogen atoms in their idealized positions (C-H = 0.95 Å, B = 1.3B(carbon) Å<sup>2</sup>) was taken into account but not refined.

The function minimized was  $[\sum w(|F_o| - 1/k|F_c|)^2]$  with  $w = [\sigma^2(F_o)]^{-1}$ . No extinction correction was found to be necessary. The scattering factors used, corrected for the real and imaginary parts of the anomalous dispersion, were taken from the literature.<sup>30</sup> Upon convergence the final Fourier difference map showed no significant peaks. All calculations were carried out by using the Enraf-Nonius MOLEN crystallographic programs.<sup>31</sup> Final atomic coordinates and isotropic equivalent displacement parameters are given in Table 3.

**Cambridge Crystallographic Structure Data Base References Codes.** The codes used are listed in Chart 1.

**Calculations.** MM2\* parameters for the Pd(PR<sub>3</sub>)<sub>2</sub> fragment were taken from our previous studies.<sup>9</sup> The Cl-Pd-Cl fragment was assigned an angle of 90° and a Pd-Cl bond length of 2.3 Å. Parameter assignments within the coordination sphere should reflect the phosphonium-type character of the coordinated phosphine. Consequently, the partial charges +0.5, 0, and -0.5 were assigned to the P, Pd, and Cl atoms, respectively. The C-P-C bond angles within the phosphine moiety were given values between those found for uncoordinated (90°-100°) phosphines and 109°. The Pd-P-C(ipso) angles were assigned to 118°. All the parameters (charges, angles, force constants, etc.) were varied while testing. Observed changes within reasonable boundaries did not change the overall results. This is important in that MM results are more meaningful if the conclusions do not critically depend on the chosen parameters.

The Monte-Carlo (MC) simulation was an MCOMM-search as available within BatchMin 4.5. The search was global driving all bonds capable of rotation (including ring bonds) simultaneously. As carried out, the local minima should not depend on the height of the energy barrier separating them. In addition to the MC calculations, molecular dynamics (MD) simulations at various temperatures were performed, including energy barrier effects, to probe whether the minima shown by the MC simulations could be readily interconverted. The SHAKE protocol was applied to all bond lengths. The MD simulations were run to 500 ps in 1f steps using various temperatures up to 1000 K. A total of 5000 structure samples were taken from each run for subsequent minimization, and

(28) Åkermark and Hansson have found an increase in the anti/syn ratio in the presence of relatively large chelating nitrogen ligands: Åkermark, B.; Hansson S. *J. Am. Chem. Soc.* **1990**, *112*, 4587.

(29) North, A. C. T.; Phillips, D. C.; Mathews, F. S. *Acta Crystallogr., Sect. A* **1968**, *A24*, 351.

(30) *International Tables for X-ray Crystallography*; Kynoch: Birmingham, England, 1974; Vol. IV.

(31) MOLEN Enraf-Nonius Structure Determination Package; Enraf-Nonius, Delft, The Netherlands, 1990.

the data from these were compared with the MC results. These additional calculations showed, for BIPHEMP (BINAP) and DPPCP type complexes, that the chiral pocket remains stable whereas other ligand types, e.g. DIOP, easily interconvert the backbone geometries, thus affecting the chiral pocket.

**Synthesis.** All manipulations were performed under a nitrogen atmosphere. Diethyl ether, *n*-hexane, THF, CH<sub>2</sub>Cl<sub>2</sub>, and benzene were distilled over Na–benzophenone. All other chemicals were commercial products and were used as received without further purification.

The BIPHEMP and (*R*)-DPPCP ligands were generously provided by G. Consiglio, the chiral PN ligands, **f-i**, shown in Scheme 1, by Prof. C. Bianchini, CNRS, Florence, Italy, and the JOSIPHOS, by Prof. A. Togni, ETHZ.

**Bis-[( $\mu$ -chloro)(1,3-diphenylallyl)palladium(II)].** PdCl<sub>2</sub> (350 mg, 1.95 mmol) and LiCl (350 mg, 8.3 mmol) were stirred in H<sub>2</sub>O (2.3 mL) for 45 min. Ethanol (3.9 mL) and (*rac*)-(*E*)-3-acetoxy-1,3-diphenyl-1-propene (1 g, 3.97 mmol) in THF (11 mL) were then added, and the brown solution was cooled to 0 °C. After the addition of 1.2 mL of concentrated HCl, carbon monoxide was slowly bubbled through the solution for 15 min. Another 0.8 mL of concentrated HCl was added and CO bubbled for 1.5 h. The stream of CO was then stopped and the solution stirred under CO atmosphere for 7 h at room temperature. The yellow-orange suspension obtained was filtered over a G4 glass frit, washed with the mother liquors MeOH (100 mL) and diethyl ether (30 mL), and then dried under HV (high vacuum). Yield: 643 mg (98.4%). Anal. Calcd for C<sub>30</sub>H<sub>26</sub>Cl<sub>2</sub>Pd<sub>2</sub>: C, 53.76; H, 3.91. Found: C, 53.65; H, 4.09. <sup>1</sup>H NMR (CD<sub>2</sub>Cl<sub>2</sub>, 250 MHz):  $\delta$ (*H*<sub>anti</sub>) 4.64 (d, 4H, *J*<sub>HH</sub> = 11.21 Hz);  $\delta$ (*H*<sub>cent</sub>) 6.16 (t, 2H).

The preparation of chelating ligand–allyl complexes of Pd(II) has been reported on several occasions<sup>6,9,18,22</sup> so that we give only the general methods below. Yields after reaction were between 32% and 88% (70% for **2a**).

**Preparation of 2 with Phosphine Chelates.** The chelating ligand (0.22 mmol) was placed in a round bottomed flask with a gas inlet tube and then dissolved in 10–20 mL of acetone. Bis[( $\mu$ -chloro)(1,3-diphenylallyl)palladium(II)] (0.1 mmol) was added and the reaction mixture stirred until solution is obtained. Addition of TlPF<sub>6</sub> (0.2 mmol, 70 mg) affords immediate precipitation of TlCl. The solution was stirred for 10 min and then allowed to stand for ca. 1 h. The

TlCl was filtered out, and the solution was concentrated under a stream of nitrogen. Slow addition of ether induced precipitation of the complex, which was then filtered and recrystallized from acetone–ether. The crystals were washed with ether and dried under vacuum.

The diamino chelate ligands did not react under the above conditions so that the method of ref 16 was employed:

**Preparation of 2 with Nitrogen Chelates.** Bis[( $\mu$ -chloro)(1,3-diphenylallyl)palladium(II)] (0.1 mmol, 67 mg) was added to a solution of the nitrogen chelate (0.22 mmol) in ca. 20 mL of CH<sub>2</sub>Cl<sub>2</sub>, and this was stirred until a clear yellow solution was obtained. A solution of AgBF<sub>4</sub> (0.2 mmol, 39 mg) in a minimum volume of MeOH was added, and after 5 min of stirring, the mixture was allowed to stand for 1 h in the dark. The finely divided precipitate of AgCl was filtered off through a Celite plug and the filtrate concentrated under a stream of nitrogen. Slow addition of ether–pentane afforded precipitation of the product, which was recrystallized from CH<sub>2</sub>Cl<sub>2</sub>–ether–pentane, collected by filtration, and washed with ether–pentane and dried under vacuum.

**Enantioselective Allylic Alkylation Reactions.** The reactions were carried out under the conditions reported by Pfaltz.<sup>6</sup> A representative procedure is illustrated in ref 18.

**Acknowledgment.** P.S.P. thanks the Swiss National Science Foundation as well as the ETH for support and the Johnson-Matthey Research Foundation, Reading, England, for the loan of precious metals. A.A. thanks MURST for support. We also thank Dr. H. Rügger for helpful discussion and a C,H-correlation, Ariana Martelletti for experimental assistance, and Prof. A. Togni for the gift of the JOSIPHOS ligand.

**Supporting Information Available:** Calculated hydrogen positions and *B* values (Table S1), anisotropic displacement parameters for **2a** (Table S2), extended bond lengths and bond angles for **2a** (Table S3), microanalytical data for the complexes (Table S4), and force field parameters (Table S5) (7 pages). Ordering information is given on any current masthead page.

OM950399D

# Facile Oxidative Addition of Rhodium(I) to the Acyl-Oxygen Bond of 2-((Diphenylphosphino)methyl)quinolin-8-ol Acetate

Douglas B. Grotjahn\* and Camil Joubran

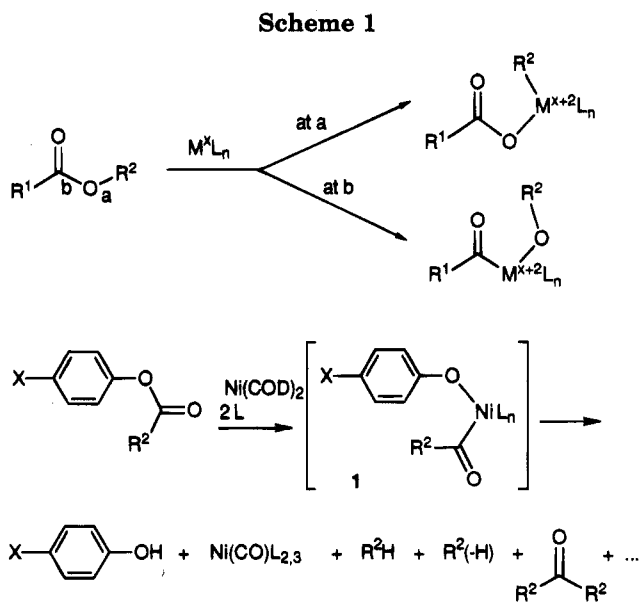
Department of Chemistry and Biochemistry, Box 871604, Arizona State University, Tempe, Arizona 85287-1604

Received May 31, 1995<sup>®</sup>

Conversion of 2-methylquinolin-8-ol to 2-((diphenylphosphino)methyl)quinolin-8-ol (**2**; 61% overall yield) by protection, lithiation, phosphinylation, and deprotection is described. The corresponding acetate **3** reacts with the dimer [(cyclooctene)<sub>2</sub>Rh(μ-Cl)]<sub>2</sub> (**4**) in a molar ratio of 4:1 within minutes at ambient temperatures. A single Rh bis(phosphine) acyl complex (**13a**) is obtained, whereas three diastereomers are possible. In **13a**, one molecule of **3** is a spectator ligand coordinated through P, whereas a second molecule of **3** has undergone unprecedentedly rapid oxidative addition to the acyl-oxygen bond, providing a COCH<sub>3</sub> ligand and the P,O,N-coordinated anion of **2**. The stereochemistry of **13a** (COCH<sub>3</sub> and Cl mutually trans) was determined by coupling information and 2D NMR experiments. The COCH<sub>3</sub> ligand of **13a** is unaffected by PhCH<sub>2</sub>NH<sub>2</sub> (room temperature, 6 h), and **13a** is essentially unchanged after 7 days at 120 °C in C<sub>6</sub>D<sub>6</sub>. Interactions of **2** and **4** or its Ir analog **5** in a molar ratio of 4:1 give metal hydride complexes as single diastereomers, from addition of the O-H bond to the metal.

## Introduction

The net oxidative addition of low-valent transition-metal centers to the alkyl-oxygen bond of carboxylic acid esters (bond a, Scheme 1) has been intensively studied<sup>1</sup> and forms the basis of a palette of organic transformations of esters of allylic alcohols.<sup>2</sup> The addition of metals at bond b, the acyl-oxygen bond, could lead to novel functionalizations of ester derivatives, yet few examples of additions to bond b are known.<sup>1</sup> That the control of such reactions may be problematic is illustrated by the pioneering studies of Yamamoto on the reaction of phenyl esters with Ni(0) species. The putative oxidative-addition product **1** was not isolated, but products which would be formed from **1** by alkyl migration and β-hydride elimination or disproportionation were obtained.<sup>3</sup> A special case is presented by addition of Ir(I) and Pt(II) complexes to the alkyl-oxygen bond of the strained ring of butyrolactone, in a reaction reminiscent of the attack of organic nucleophiles at the sp<sup>3</sup>-hybridized carbon.<sup>4</sup> Comparing these scattered reactions of esters with the much larger body of oxidative additions to more activated carboxylic acid derivatives such as anhydrides<sup>1,5</sup> and acid halides<sup>6</sup> reveals that much remains to be done with esters, which



because of their reduced water sensitivity can be easier to handle.

Thus, we wished to explore the controlled oxidative addition of metals to esters at bond b. To facilitate this process, we sought a polydentate ligand capable of binding a soft<sup>7</sup> low-valent metal center in the vicinity of a pendant ester carbonyl. Yamamoto's results with phenyl esters suggested esters of general form **3** (Scheme 2, from **2**) as initial synthetic targets, envisaged to lead to hexacoordinate **8** by way of complex **6** and initial addition product **7**. The coordination chemistry of

<sup>®</sup> Abstract published in *Advance ACS Abstracts*, October 1, 1995.  
 (1) Review: Yamamoto, A. *Adv. Organomet. Chem.* **1992**, *34*, 111-147.

(2) (a) Harrington, P. J. In *Comprehensive Organometallic Chemistry*; Abel, E. W., Stone, F. G. A., Wilkinson, G., Eds.; Pergamon: Oxford, U.K., 1995; Vol. 12. (b) Oppolzer, W. In ref 2a.

(3) Yamamoto, T.; Ishizu, J.; Kohara, T.; Komiya, S.; Yamamoto, A. *J. Am. Chem. Soc.* **1980**, *102*, 3758-3764.

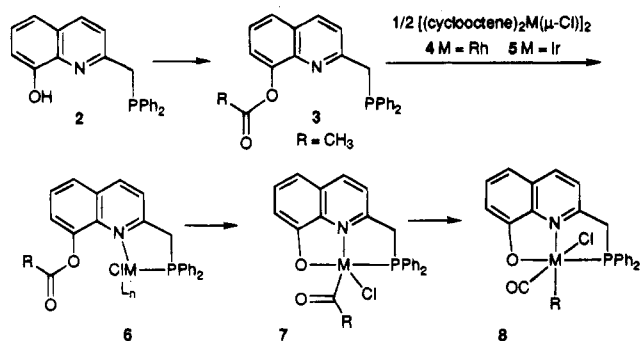
(4) Zlota, A. A.; Frolow, F.; Milstein, D. *Organometallics* **1990**, *9*, 1300-1302. Aye, K.-T.; Colpitts, D.; Ferguson, G.; Puddhepatt, R. J. *Organometallics* **1988**, *7*, 1454-1456.

(5) Castaño, A.; Echavarren, A. M. *Tetrahedron Lett.* **1990**, *31*, 4783-4786. Castaño, A.; Echavarren, A. M. *Tetrahedron Lett.* **1993**, *34*, 4361-4362.

(6) Reviews: Stille, J. K. *Angew. Chem., Int. Ed. Engl.* **1986**, *25*, 508-524. Mitchell, T. N. *Synthesis* **1992**, 803-815. Collman, J. P.; Hegedus, L. S.; Norton, J. R.; Finke, R. G. *Principles and Applications of Organotransition Metal Chemistry*; University Science Books: Mill Valley, CA, 1987; especially pp 363-365, 773-775.

(7) Ho, T.-L. *Tetrahedron* **1985**, *41*, 1-86.

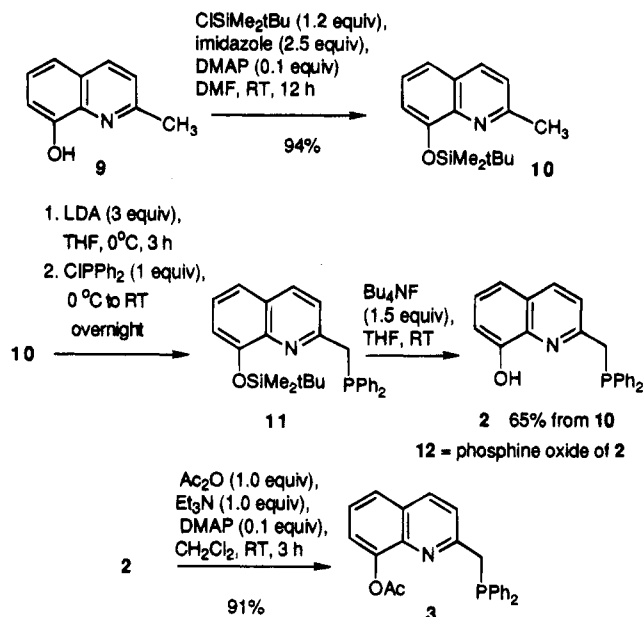
## Scheme 2



(deprotonated) quinolin-8-ol is well-established.<sup>8</sup> Quinolin-8-ols bearing a substituent at C-2 with a readily ionizable C–H bond furnish especially stable Pd  $\sigma$ -alkyl complexes with O,N,C-coordinated heterocycles.<sup>9</sup> Finally, the nitrogen atom in quinoline-8-carboxaldehyde<sup>10a,b</sup> and corresponding ketones<sup>10c</sup> has been shown to facilitate oxidative additions at the nearby carbonyl group, leading to relatively stable products. Because of the rich oxidative-addition chemistry of Rh(I) and Ir(I) complexes,<sup>11</sup> and the attractive stability of the anticipated Rh(III) and Ir(III) products, these metal derivatives were chosen for the studies described herein.

Furthermore, the synthesis and properties of alkoxides and amides of late transition metals are topics of increasing interest.<sup>12</sup> Such species may be involved in metal-catalyzed additions of O–H and N–H bonds to alkenes<sup>11d</sup> and other catalytic processes,<sup>12</sup> and the complexes themselves can show unusual bonding<sup>13</sup> or reactivity.<sup>14</sup> One route to alkoxy hydrides of late transition metals involves oxidative addition of an O–H bond to a low-valent metal. For these reasons and because phenol **2** would be available as a precursor to **3**, we also report here the interaction of **2** with Rh(I) and Ir(I) centers.

## Scheme 3



## Results and Discussion

**Synthesis of Ligands 2 and 3.** The previously reported deprotonation of the methyl group of 2-methylquinolines<sup>15</sup> and subsequent functionalizations encouraged us to attempt the introduction of a diphenylphosphino substituent on commercially available 2-methylquinolin-8-ol (**9**) following treatment with 2 mol of base. However, this strategy apparently failed to produce significant quantities of **2**, and it was unclear even if deprotonation at the methyl group had occurred. Thus, the hydroxy function was protected,<sup>16</sup> giving **10**. The conditions for lithiation of **10** were modeled after those optimized for the corresponding *O*-methyl ether, which involved the use of 3 equiv of LDA in  $Et_2O$ . After the red solution of lithiated **10** was quenched with  $ClPPh_2$ , the silyl ether **11** was normally not isolated but subjected to fluoride-mediated protodesilylation<sup>16</sup> to give multigram quantities of crystalline **2** in 61% overall yield from **9**. The position of the newly introduced diphenylphosphino group on **2** was indicated by the appearance of a two-proton singlet at  $\delta$  3.78 ppm and by a relatively sharp O–H stretch in the IR spectrum. Values for  $^2J_{PH}$  in benzylphosphines near 0 have been seen.<sup>17</sup> Acylation of **2**<sup>18</sup> provided **3** uneventfully.

The *O*-methyl ether of **9** could be lithiated and phosphinylated to give the *O*-methyl ether analog of **11**, but the methyl ether function could not be cleaved so as to produce **2**. Further, failure to use undeoxygenated solvents in the purification of **2** led to the isolation of the corresponding phosphine oxide **12**, as verified by  $^1H$  and  $^{31}P$  NMR spectra.<sup>17</sup>

**Oxidative-Addition Chemistry and Structure Elucidation of 13a.** Remarkably, between the time of addition of Rh dimer **4** to a  $C_6D_6$  solution of **3** (molar ratio 1:4) and acquisition of the first  $^1H$  and  $^{31}P\{^1H\}$  NMR spectra, cyclooctene and a single complex were

(15) Brandsma, L. *Preparative Polar Organometallic Chemistry*; Springer: Berlin, 1990; especially p 130.

(16) Corey, E. J.; Venkateswarlu, A. *J. Am. Chem. Soc.* **1972**, *94*, 6190–6191.

(17) Verstuyft, A. W.; Redfield, D. A.; Cary, L. W.; Nelson, J. H. *Inorg. Chem.* **1977**, *16*, 2776–2786.

(18) Höfle, G.; Steglich, W.; Vorbrüggen, H. *Angew. Chem., Int. Ed. Engl.* **1978**, *17*, 569–583.

(8) Phillips, J. P. *Chem. Rev.* **1956**, *56*, 271–297. Irving, H. M. N. H. In *Comprehensive Coordination Chemistry*; Wilkinson, G., Ed.; Pergamon: Oxford, U.K., 1987; Vol. 1, pp 521–563.

(9) Yoneda, Y.; Hakushi, T.; Newkome, G.; Fronczek, F. R. *Organometallics* **1994**, *13*, 4912–4918.

(10) (a) Koh, J. J.; Lee, W.-H.; Williard, P. G.; Risen, W. M., Jr. *J. Organomet. Chem.* **1985**, *284*, 409–419. (b) Suggs, J. W. *J. Am. Chem. Soc.* **1978**, *100*, 640–641. (c) Suggs, J. W.; Jun, C.-H. *J. Am. Chem. Soc.* **1984**, *106*, 3054–3056. Suggs, J. W.; Wovkulich, M. J.; Williard, P. G.; Lee, K. S. *J. Organomet. Chem.* **1987**, *307*, 71–82.

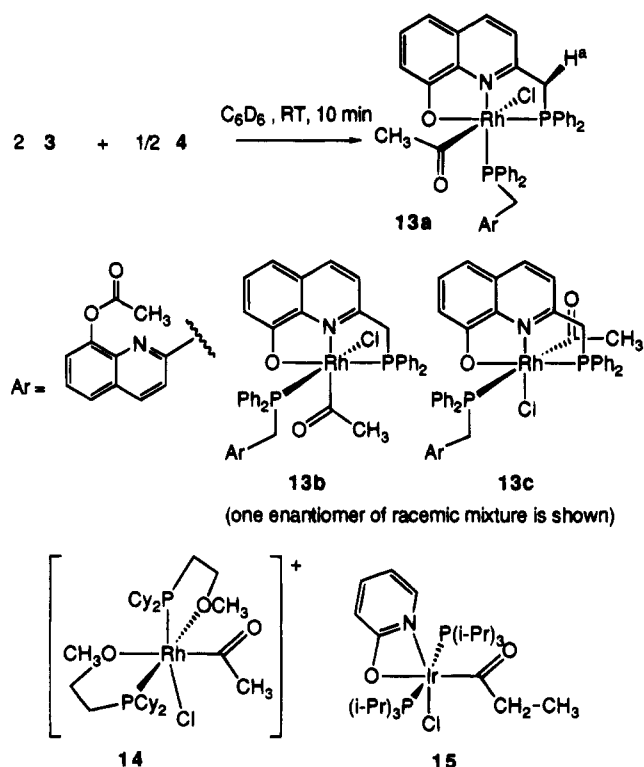
(11) Selected examples are as follows. (a) Chelate-driven additions of Rh(I) and Ir(I) to aldehydes: Reference 10b. Landvatter, E. F.; Rauchfuss, T. B. *Organometallics* **1982**, *1*, 506–513. (b) Cleavage of ketone C–C bonds directed by quinoline N: Reference 10c. (c) Chelate-driven oxidative additions to N–H bonds: Hedden, D.; Roundhill, D. M.; Fultz, W. C.; Rheingold, A. L. *J. Am. Chem. Soc.* **1984**, *106*, 5014–5016. Hedden, D.; Roundhill, D. M. *Inorg. Chem.* **1986**, *25*, 9–15. (d) Other additions to N–H bonds: Merola, J. S.; Ladipo, F. T. *Inorg. Chem.* **1990**, *29*, 4172–4173. Casalnuovo, A. L.; Calabrese, J. C.; Milstein, D. *J. Am. Chem. Soc.* **1988**, *110*, 6738–6744. (e) Additions to O–H bonds: Ladipo, F. T.; Kooti, M.; Merola, J. *Inorg. Chem.* **1993**, *32*, 1681–1688. Milstein, D.; Calabrese, J. C.; Williams, I. D. *J. Am. Chem. Soc.* **1986**, *108*, 6387–6389. (f) Additions to aldehydes: Milstein, D. *Acc. Chem. Res.* **1984**, *17*, 221–226. Milstein, D.; Fultz, W. C.; Calabrese, J. C. *J. Am. Chem. Soc.* **1986**, *108*, 1336–1338. (g) Additions to C–H bonds: Bergman, R. G. *J. Organomet. Chem.* **1990**, *400*, 273–282. Jones, W. D.; Feher, F. J. *Acc. Chem. Res.* **1989**, *22*, 91–100.

(12) Bryndza, H. E.; Tam, W. *Chem. Rev.* **1988**, *88*, 1163–1188. Fryzuk, M. D.; Montgomery, C. D. *Coord. Chem. Rev.* **1989**, *95*, 1–40.

(13) Hubbard, J. L.; McVicar, W. K. *Inorg. Chem.* **1992**, *31*, 910–913. Poulton, J. T.; Sigalas, M. P.; Foltling, K.; Streib, W. E.; Eisenstein, O.; Caulton, K. G. *Inorg. Chem.* **1994**, *33*, 1476–1485. Bickford, C. C.; Johnson, T. J.; Davidson, E. R.; Caulton, K. G. *Inorg. Chem.* **1994**, *33*, 1080–1086. Lunder, D. M.; Lobkovsky, E. B.; Streib, W. E.; Caulton, K. G. *J. Am. Chem. Soc.* **1991**, *113*, 1837–1838.

(14) Blum, O.; Milstein, D. *J. Am. Chem. Soc.* **1995**, *117*, 4582–4594 and references therein. Goldman, A. S.; Halpern, J. *J. Organomet. Chem.* **1990**, *382*, 237–253.

Scheme 4



formed in the mixture. The  $^{31}\text{P}\{^1\text{H}\}$  NMR spectrum of the new complex showed two doublets of doublets, each with a larger Rh–P coupling and a smaller, mutual P–P coupling, consistent with formation of a *cis*-diphosphine complex.<sup>19</sup> In the EI mass spectrum of the product, the highest molecular weight ions corresponded to a species composed of two molecules of **3** and one ClRh unit, but lacking HCl and  $\text{CH}_2=\text{C}=\text{O}$  (830 amu) or HCl,  $\text{CH}_2=\text{C}=\text{O}$ , and  $\text{CH}_3\text{CO}$  (787 amu). A larger scale reaction conducted in a flask provided the same product, ultimately identified as **13a** (*vide infra*), in 83% yield.

In the  $^1\text{H}$  NMR spectrum of the bis(phosphine) complex in  $\text{CDCl}_3$  at ambient probe temperatures, two three-proton singlets at  $\delta$  1.46 and 2.50 ppm were seen. Because the acetyl protons in **3** resonated at 2.30 ppm, it appeared likely that at least one molecule of **3** merely acted as a spectator ligand. To probe the bonding of the second phosphine, IR and  $^{13}\text{C}$  NMR data were inspected. One IR absorption at  $1765\text{ cm}^{-1}$  nearly coincided with that of the acetyl group of the uncomplexed phosphine **3** ( $1757\text{ cm}^{-1}$ ), whereas absorptions at  $1673$  and  $1656\text{ cm}^{-1}$  intimated the presence of an acyl ligand.<sup>20</sup> This was confirmed by observation of a downfield resonance in the  $^{13}\text{C}$  NMR spectrum at  $\delta$  229.27 ppm (ddd,  $J = 28, 8, 5\text{ Hz}$ ). Surprisingly little  $^{13}\text{C}$  NMR data for Rh or Ir acyls are available, but the structurally characterized complexes **14**<sup>21</sup> and **15**,<sup>22</sup> each featuring an acyl ligand *cis* to phosphines, exhibit  $^2J_{\text{PC}} = 5.5$  and  $5.0\text{ Hz}$ , respectively. Unfortunately, for **14**  $^1J_{\text{RhC}}$  was not reported,<sup>21</sup> but from various Rh(III)–alkyl, –vinyl, and –aryl complexes<sup>23</sup> it appeared that the 28 Hz splitting of the  $^{13}\text{C}$  NMR resonance for the  $\text{CH}_3\text{CO}-\text{Rh}$

moiety of **13** may be assigned as  $^1J_{\text{RhC}}$ , leaving the smaller couplings to those expected<sup>21,22</sup> between the acyl carbonyl carbon and two inequivalent  $^{31}\text{P}$  nuclei in *cis* positions. Of the three diastereomers (**13a–c**) theoretically possible, **13c** was deemed inconsistent with the data at hand.

In principle, **13a,b** might be distinguished by the position of the Rh–Cl stretching frequency;<sup>24</sup> however, the IR spectrum of the product in Nujol between polyethylene plates showed absorptions at 216, 239, 309, and  $356\text{ cm}^{-1}$ . Deeming and Shaw invoked solid-state splitting to explain the observation of unexpectedly high numbers of IR absorptions in Rh–Cl complexes,<sup>25</sup> but in this particular case a more straightforward explanation would be the superposition of the (unassigned) Rh–Cl absorption with several bands due to the quinoline system and other absorptions accompanying Rh–N or Rh–O stretching.<sup>26</sup>

Regardless of the origin of the confusing IR absorptions, we turned to NOE experiments.<sup>27</sup> It was thought that **13a** would be distinguished by mutual enhancements of the acetyl methyl protons and only the methylene proton  $\text{H}^a$  (Scheme 4), whereas this effect would be absent in **13b**. Unfortunately, enhancements in one-dimensional NOE experiments at both ambient probe temperatures and low temperatures were too small to be informative. Hence, we turned our attention to 2D NMR techniques such as NOESY and the rotating-frame ROESY experiments.<sup>28</sup> In order to further amplify NOE enhancements, the two-dimensional experiments were performed at  $-30\text{ }^\circ\text{C}$ , which increases the correlation time ( $\tau_c$ ) and reduces the spin–lattice relaxations.<sup>29</sup>

Both  $^1\text{H}$  and COSY NMR spectra<sup>30</sup> of the bis(phosphine) complex show four doublets of doublets in the region  $\delta$  4.3–5.1 ppm, ascribed to the four diastereotopic protons of the  $\text{CH}_2\text{PPh}_2$  units. On the basis of the mutual coupling revealed in the COSY spectrum, the four resonances can be separated into a downfield pair (4.8 and 5.1 ppm) and an upfield pair (4.3 and 4.6 ppm). Literature precedent would indicate that the upfield pair belongs to the methylene group of the metallacycle.<sup>31</sup> This assignment is corroborated by the  $^{13}\text{C}$  NMR chemical shifts of the corresponding benzylic carbons: as revealed by an GHMQC experiment conducted at  $-30\text{ }^\circ\text{C}$ , the upfield pair of protons are bound to the carbon resonating near 48 ppm, whereas the downfield pair of protons are associated with the carbon resonating at 37 ppm. In comparison, the signal for the

(23) Mann, B. E.; Taylor, B. F.  *$^{13}\text{C}$  NMR Data for Organometallic Complexes*; Academic: London, 1981. See also: Mann, B. E. In *Transition Metal Nuclear Magnetic Resonance*; Pregosin, P. S., Ed.; Elsevier: Amsterdam, 1991; p 208.

(24) Nakamoto, K. *Infrared and Raman Spectra of Inorganic and Coordination Compounds*, 4th ed.; Wiley: New York, 1986. Appleton, T. G.; Clark, H. C.; Manzer, L. E. *Coord. Chem. Rev.* **1973**, *10*, 335–422. Kubota, M.; Blake, D. M. *J. Am. Chem. Soc.* **1971**, *93*, 1368–1373.

(25) Deeming, A. J.; Shaw, B. L. *J. Chem. Soc. A* **1969**, 1128–1134.

(26) Ohkaku, N.; Nakamoto, K. *Inorg. Chem.* **1971**, *10*, 798–805.

(27) Neuhaus, D.; Williamson, M. *The Nuclear Overhauser Effect in Structural and Conformational Analyses*; VCH: New York, 1989; Chapter 7.

(28) Ernst, R. R.; Bodenhausen, G.; Wokaun, A. *Principles of Nuclear Magnetic Resonance in One and Two Dimensions*; Oxford University Press: New York, 1987.

(29) Juranic, N.; Likic, V.; Kostic, N. M.; Macura, S. *Inorg. Chem.* **1995**, *34*, 938–944. Giovanetti, J. S.; Kelly, C. M.; Landis, C. R. *J. Am. Chem. Soc.* **1993**, *115*, 4040–4057.

(30) See the Supporting Information.

(31) Deeming, A. J.; Rothwell, I. P.; Hursthouse, M. B.; Malik, K. M. A. *J. Chem. Soc., Dalton Trans.* **1980**, 1974–1982.

(19) Brown, T. H.; Green, P. J. *J. Am. Chem. Soc.* **1970**, *92*, 2359–2362.

(20) Suggs has reported the doubling of an acyl C=O absorption; see footnote 11 in ref 10b.

(21) Lindner, E.; Wang, Q.; Mayer, H. A.; Fawzi, R.; Steimann, M. *Organometallics* **1993**, *12*, 1865–1870.

(22) Grotjahn, D. B.; Lo, H. C.; Groy, T. L. *Acta Crystallogr., Sect. C*, in press.



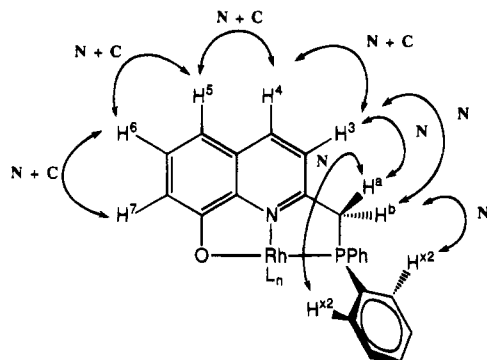


**Figure 1.** Proton notation and summary of cross-relaxations used in the structure elucidation of **13a**. "N" and "C" mean that NOESY/ROESY and COSY spectra were used in the assignments shown.

benzylic carbon of free ligand **3** appears at 38.6 ppm. Deeming and co-workers saw similar downfield  $^{13}\text{C}$  shifts only on chelation.<sup>31</sup>

In NOESY and ROESY spectra (Figures 2 and 3), the chelate methylene protons ( $\text{H}^a$  and  $\text{H}^b$ ) both show strong cross-peaks with signals at  $\delta$  7.31 (d, 1H) and 6.76 (dd, 2H) ppm. The former resonance is assigned to  $\text{H}^3$  of the quinoline ring, whereas the latter absorption is ascribed to the two *ortho* protons of one phenyl ring on P (for now arbitrarily labeled  $\text{H}^{x2}$  in Figure 1). Once the identity of  $\text{H}^3$  was established, the signals for the remaining protons  $\text{H}^4$ – $\text{H}^7$  on the quinoline ring were assigned on the basis of ROESY and COSY correlations (Figure 1).<sup>30</sup>

As indicated above, it was thought that only in **13a** would an NOE be detectable between the acyl methyl ( $\text{H}^c$ ) and the nearest methylene proton in the metallacycle ( $\text{H}^a$  or  $\text{H}^b$ ). Unfortunately, in neither NOESY nor ROESY experiments (not shown) were cross-peaks between the acyl methyl protons ( $\delta$  1.16 ppm) and  $\text{H}^a$  or  $\text{H}^b$  detectable; moreover, cross-peaks were not seen between either acyl methyl signal and any of the four  $\text{CH}_2\text{PPh}_2$  protons  $\text{H}^a$ ,  $\text{H}^a$ ,  $\text{H}^b$ , and  $\text{H}^b$ . Fortunately, other correlations serve to establish the stereochemistry about the metal. In the ROESY spectrum (Figure 4),

the acyl methyl protons  $\text{H}^c$  show two cross-peaks, one to the resonance at 6.76 ppm, identified above as belonging to  $\text{H}^{x2}$ . The other cross-peak involves a multiplet whose assignment remains incomplete because of the complication of several overlapping resonances. However, the *ortho* protons of the other, diastereotopic phenyl ring ( $\text{H}^{y2}$ , Figure 5) can be identified as follows: in the COSY spectrum,<sup>30</sup>  $\text{H}^{x2}$  shows a cross-peak with a multiplet near 7.0 ppm, whereas in the NOESY spectrum (Figure 2),  $\text{H}^{x2}$  exhibits cross-peaks not only with the multiplet near 7.0 ppm but also with  $\text{H}^a$ ,  $\text{H}^b$ , and a two-proton signal at 7.39 ppm. Thus, the (unresolved) resonance for  $\text{H}^{x3}$  must lie near 7.0 ppm, leaving the signal at 7.39 ppm to be attributed to  $\text{H}^{y2}$ . Significantly, in the ROESY spectrum (Figure 4), a cross-peak between  $\text{H}^{y2}$  and  $\text{H}^c$  is absent, which suggests that the acyl ligand is out of the plane defined by Rh and the O, N, and P atoms of the tridentate phosphine, as in **13a**.

Several other assignments are indicated in the figures. At  $-30$  °C, the signal at 7.66 ppm appears as a nearly featureless four-proton multiplet, but at ambient temperatures two sharp doublets of doublets are seen. The 2D spectra suggest that these four nuclei are the *ortho* protons  $\text{H}^{x2'}$  and  $\text{H}^{y2'}$  of the monodentate phosphine.

As monitored by  $^1\text{H}$  and  $^{31}\text{P}\{^1\text{H}\}$  NMR, attempts to form mono(phosphine) complexes **7** and **8** by using Rh dimer **4** and **3** (molar ratio 1:2) led to mixtures in which the only identifiable species were **13a** and **4**. However, once formed, complex **13a** showed exemplary stability: attempted thermolysis in  $\text{C}_6\text{D}_6$  at 120 °C for 1 week did not appreciably alter the NMR spectra of the solution, and exposure of **13a** to  $\text{PhCH}_2\text{NH}_2$  (room temperature, 6 h) left the acyl ligand untouched.

In contrast to the rapid and clean reaction producing **13a**, combination of iridium dimer **5** and **3** (molar ratio 1:4) in  $\text{C}_6\text{D}_6$  led to a complex mixture whose NMR spectrum most notably lacked recognizable multiplets in the region  $\delta$  3.0–5.0 ppm, even after more than 1 day.

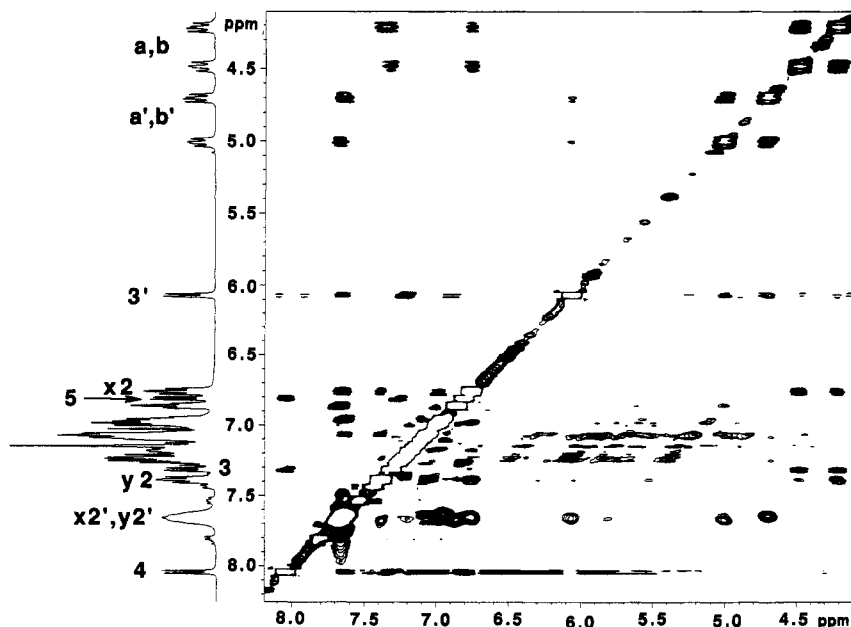


**Figure 2.** NOESY spectrum of **13a** in  $\text{CDCl}_3$  at  $-30$  °C in the region 4.1–8.2 ppm. The proton notation is given in Figures 1 and 5.



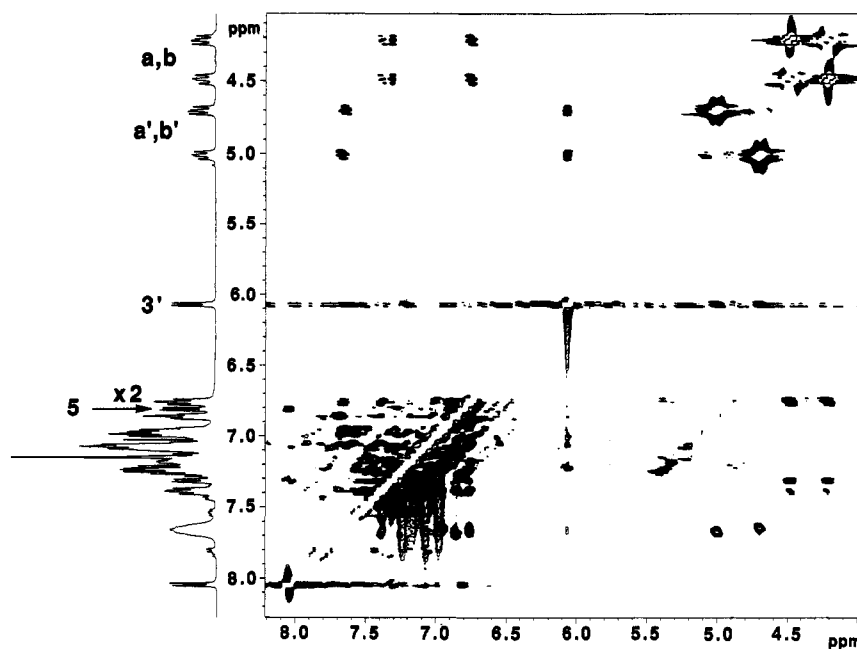


**Figure 3.** ROESY spectrum of **13a** in  $\text{CDCl}_3$  at  $-30\text{ }^\circ\text{C}$  in the region 4.1–8.2 ppm. The proton notation is given in Figures 1 and 5.

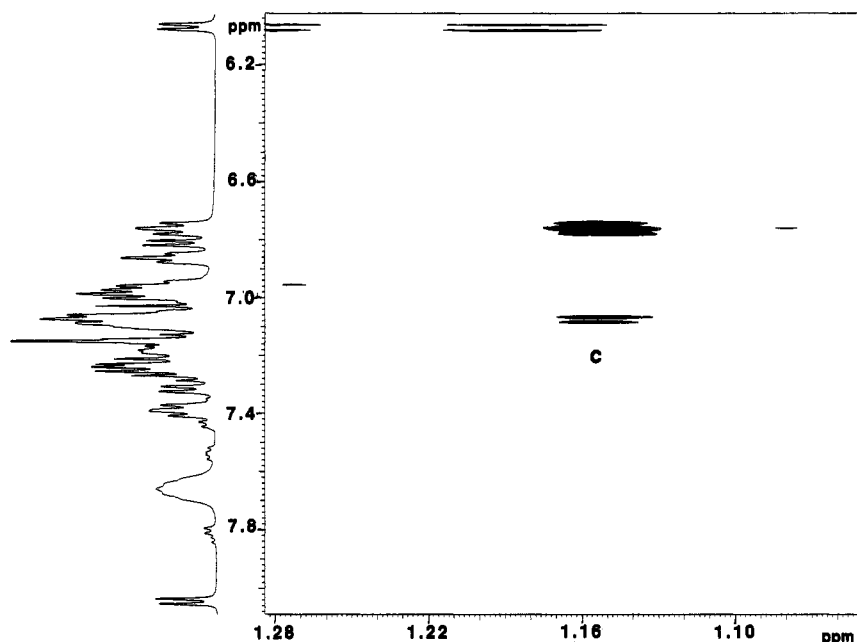


**Figure 4.** ROESY spectrum of **13a** in  $\text{CDCl}_3$  at  $-30\text{ }^\circ\text{C}$ , showing cross-peaks involving the acyl methyl resonance  $\text{H}^c$ . The proton notation is given in Figures 1 and 5.

As to the mechanism by which **13a** is formed, other workers have suggested that oxidative addition to an ester<sup>1,3</sup> C–O or ketone<sup>10c</sup> C–C bond is initiated by nucleophilic attack of an electron-rich metal center on the carbonyl carbon, to produce a tetrahedral intermediate. This should be possible in the case of the reaction of **3** and **5**. However, the explanation of the selective formation of **13a** as a single diastereomer by this mechanism (or others, such as direct oxidative addition) at this time appears impossible, in large part because of our ignorance of the precise bonding in putative intermediate **6**. Further work will be required to determine the origins of selectivity.

Finally, the potential of phenol **2** to produce phenoxy hydride complexes was examined.  $^1\text{H}$  NMR spectra of the reaction mixture of Rh dimer **4** and **2** showed a number of sharp resonances, most notably a single

upfield multiplet at  $\delta -13.93$  ppm (dt,  $J = 15.0$  and  $12.6$  Hz), ascribable to a hydride ligand coupled to Rh and two P nuclei, neither of which would be trans to the hydride.<sup>32</sup> However, in the region downfield of 1 ppm, several broad featureless peaks were seen. These did not change appreciably after 1 day and were not identified further, inasmuch as more promising results were obtained with the iridium dimer **5**. Reaction of **5** with **2** (molar ratio 1:4) gave cyclooctene and a single complex, as monitored by  $^1\text{H}$  and  $^{31}\text{P}\{^1\text{H}\}$  NMR. In the latter spectrum, two doublets of doublets were visible, each with couplings of 16.0 and 17.0 Hz, consistent with formation of a species with mutually cis phosphines. The additional coupling of the two  $^{31}\text{P}$  nuclei was to a

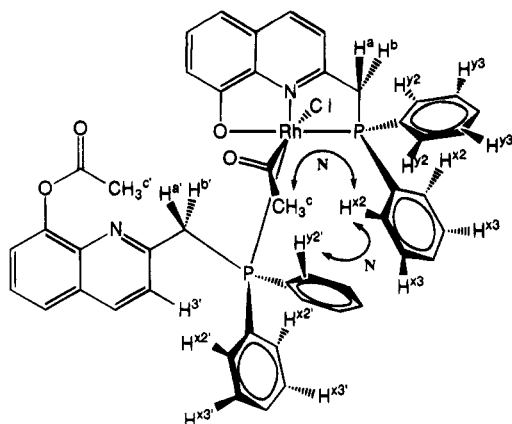
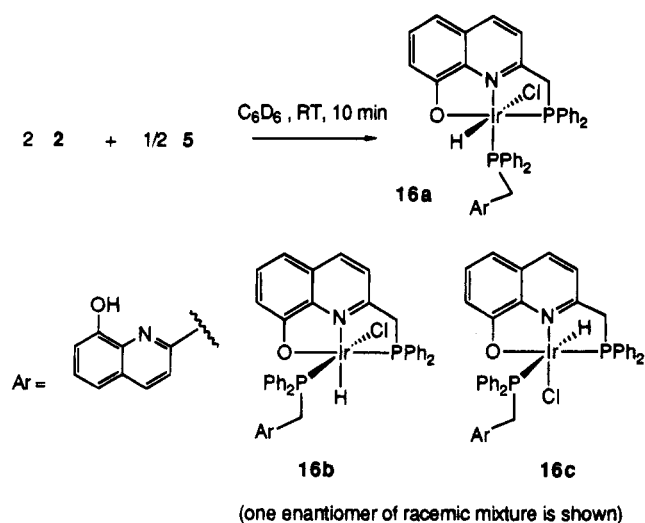


**Figure 5.** Additional proton notation and summary of cross-relaxations used in the structure elucidation of **13a**. "N" and "C" mean that NOESY/ROESY and COSY spectra were used in the assignments shown.

**Scheme 5**



hydric proton, which resonated at  $\delta -18.86$  ppm (t,  $J = 17.0$  Hz). The absence of a large coupling rules out structure **16c**. In the region  $\delta 3.6-5.1$  ppm four signals attributable to four diastereotopic methylene protons could be seen. On the basis of coupling constants alone, the four resonances could be divided into a downfield pair (4.58 and 5.09 ppm) and an upfield pair (3.69 and 4.18 ppm). As the discussion of **13a**, these pairs are assigned to the unchelated and chelated phosphines, respectively. The structure **16a** is preferred in analogy to the exclusive formation of **13a**.

### Conclusions

New quinolin-8-ol derivatives **2** and **3**, containing a (diphenylphosphino)methyl substituent at C-2, were prepared. Two moles of ester **3** combines with a chlororhodium(I) center within minutes at ambient temperature, cleaving the acyl-oxygen bond to give a thermally robust oxidative-addition product. Remarkably, the reaction gives one diastereomer of the three possible. Similarly, 2 mol of phenol **2** reacts at a chloroiridium(I) center to give a single phenoxy hydride. Although the origins of the complete stereoselectivity in these reactions are not understood, further studies in these laboratories are underway to control phosphine-metal stoichiometry and stereochemistry in oxidative additions to esters.

### Experimental Section

**General Considerations.** All reactions were carried out under an atmosphere of nitrogen using glovebox (M. Braun MBG 150G-II) and Schlenk techniques. The starting materials  $[\text{Rh}(\mu\text{-Cl})(\text{cyclooctene})_2]_2$  (**4**) and  $[\text{Ir}(\mu\text{-Cl})(\text{cyclooctene})_2]_2$  (**5**) were prepared as described in the literature.<sup>33</sup> 2-Methylquinol-8-ol, *t*-BuMe<sub>2</sub>SiCl, and tetrabutylammonium fluoride hydrate were purchased from Aldrich and were used without further purification. Diphenylphosphinous chloride was purchased from Strem and used without purification. TLC chromatography was performed on silica, in the glovebox for air-sensitive materials. All reaction solvents were dried and distilled under nitrogen prior to use. THF and diethyl ether were distilled from sodium/benzophenone ketyl. Radial chromatography was carried out using a Harrison Research Chromatotron under an atmosphere of N<sub>2</sub>. All chromatography solvents were deoxygenated by bubbling anhydrous nitrogen gas through them. IR spectra in the range 4000–600 cm<sup>-1</sup> were recorded using a Mattson FT-IR. Samples under scrutiny were pressed into a KBr pellet. NMR spectra were recorded at ambient probe temperature on a Varian Gemini-300, Varian UnityPlus-400, or Varian Unity-500, and all chemical shifts are reported on the  $\delta$  scale in ppm. <sup>1</sup>H NMR spectra were recorded on the Gemini at 300 MHz unless otherwise specified and are referenced to residual CHCl<sub>3</sub> in CDCl<sub>3</sub> or C<sub>6</sub>HD<sub>5</sub> in C<sub>6</sub>D<sub>6</sub> at 7.24 or 7.15 ppm, respectively. <sup>13</sup>C NMR spectra were observed using the Gemini at 75.5 MHz unless otherwise specified, the central peak of the CDCl<sub>3</sub> triplet being assigned a chemical shift of 77.0 ppm and that of C<sub>6</sub>D<sub>6</sub> a value of 128.0 ppm. <sup>31</sup>P spectra were referenced to external 85% H<sub>3</sub>PO<sub>4</sub>. Elemental analyses were performed in-house or by Atlantic Microlab, Norcross, GA.

#### 8-(*tert*-Butyldimethylsilyloxy)-2-methylquinoline (**10**).

A mixture of 2-methylquinol-8-ol (**9**; 5.0 g, 31.4 mmol), DMAP (0.384 g, 3.14 mmol), imidazole (5.34 g, 78.5 mmol), *tert*-butyldimethylsilyl chloride (5.68 g, 37.7 mmol), and DMF (150 mL) were placed in a 250 mL round-bottom flask, and the resulting mixture was stirred at room temperature for 3 h. The reaction was monitored by TLC. The reaction mixture was poured into 200 mL of distilled water. The resulting mixture was washed with diethyl ether (3 × 100 mL). The ether layers were combined, washed with water (100 mL) and saturated sodium chloride (100 mL), dried over magnesium sulfate, filtered, and concentrated in vacuo. The crude oil remaining was purified by column chromatography with a mixture of petroleum ether and ethyl acetate (5:1), yielding **10** as a light yellow oil (8.05 g, 94%). <sup>1</sup>H NMR (CDCl<sub>3</sub>):  $\delta$  0.27 (s, 6 H), 1.07 (s, 9 H), 2.72 (s, 3 H), 7.14 (dd,  $J = 6.6, 2.4$  Hz, 1 H), 7.24 (d,  $J = 8.4$  Hz, 1 H), 7.30–7.38 (m, 2 H), 7.98 (d,  $J = 8.4$  Hz, 1 H). <sup>13</sup>C{<sup>1</sup>H} NMR (CDCl<sub>3</sub>):  $\delta$  -4.28, 18.67, 24.74, 25.73, 118.19, 120.24, 122.06, 126.08, 128.01, 136.01, 141.63, 152.57, 157.38. Anal. Calcd for C<sub>16</sub>H<sub>23</sub>NOSi: C, 70.26; H, 8.49; N, 5.12. Found: C, 70.20; H, 8.61; N, 5.07.

**2-((Diphenylphosphino)methyl)quinolin-8-ol (**2**).** Diisopropylamine (5.49 g, 54.3 mmol) was added via syringe into a 100 mL Schlenk flask to dry THF (150 mL) under N<sub>2</sub>, and the flask was placed in an ice bath. *n*-BuLi (21.7 mL of 2.5 M in hexane, 54.3 mmol) was added to the flask in one portion via syringe, and the mixture was stirred for 15 min. A solution of **10** (4.949 g, 18.1 mmol) in dry THF (50 mL) was transferred to the LDA solution via cannula. The stirred mixture turned bright red. After 6 h at 0 °C, diphenylphosphinous chloride (3.99 g, 18.1 mmol) in THF (50 mL) was added via cannula and the reaction mixture was warmed to room temperature overnight. This mixture was then diluted with deoxygenated Et<sub>2</sub>O (50 mL) and extracted with three portions of deoxygenated 10% NaH<sub>2</sub>PO<sub>4</sub> in a Schlenk flask under N<sub>2</sub>. The organic layers were transferred into a flask fitted with a Schlenk filter, containing MgSO<sub>4</sub>, via cannula. After filtration, solvents were removed from the filtrate in vacuo. The crude red oil was

(33) van der Ent, A.; Onderdelinden, A. L. *Inorg. Synth.* **1973**, *14*, 92–95.

taken into the glovebox and dissolved in THF (100 mL). Tetrabutylammonium fluoride hydrate (4.393 g, 16.8 mmol) was added, and the mixture was stirred overnight. The reaction mixture was again worked up as above, and the solid residue was recrystallized from diethyl ether/hexanes, yielding **2** as a yellow solid (3.12 g, 65%). IR (KBr): 3397  $\text{cm}^{-1}$  (O-H).  $^1\text{H}$  NMR ( $\text{CDCl}_3$ ):  $\delta$  3.72 (s, 2 H), 7.01 (dd,  $J = 7.5$ , 1.4 Hz, 1 H), 7.14 (d,  $J = 8.1$  Hz, 1 H), 7.15 (d,  $J = 8.1$  Hz, 1 H), 7.25–7.44 (m, 11 H), 7.88 (d,  $J = 9.0$  Hz, 1 H), 7.82 (br s, 1 H).  $^1\text{H}$  NMR ( $\text{C}_6\text{D}_6$ ):  $\delta$  3.52 (s, 2 H), 6.83 (d,  $J = 8.5$  Hz, 1 H), 6.90 (dd,  $J = 8.1$ , 3.4 Hz, 1 H), 7.01 (m, 8 H), 7.37–7.43 (m, 5 H), 8.21 (br s, 1 H).  $^{13}\text{C}\{^1\text{H}\}$  NMR ( $\text{CDCl}_3$ , assignments were made from the results of 2D HMQC and HMQC experiments):  $\delta$  38.58 (d,  $J = 16.7$  Hz), 109.95, 117.63, 122.94 (d,  $J = 4.5$  Hz), 126.84, 127.07, 128.63 (d,  $J = 6.9$  Hz), 129.07, 133.10 (d,  $J = 19.5$  Hz), 136.43, 137.84, 138.13 (d,  $J = 13.7$  Hz), 152.00, 156.76 (d,  $J = 6.9$  Hz).  $^{31}\text{P}\{^1\text{H}\}$  NMR ( $\text{CDCl}_3$ , 202.3 MHz):  $\delta$  -11.21 ppm. Anal. Calcd for  $\text{C}_{22}\text{H}_{18}\text{NOP}$  ( $M_r = 343.38$ ): C, 76.96; H, 5.28; N, 4.08. Found: C, 76.11; H, 5.52; N, 3.94.

Workup of the mixture with undeoxygenated solvents led to the isolation of phosphine oxide **12** as a solid.  $^1\text{H}$  NMR ( $\text{CDCl}_3$ ):  $\delta$  4.10 (d,  $J = 14.2$  Hz, 2 H), 7.07 (d,  $J = 8.1$  Hz, 1 H), 7.25 (dd,  $J = 8.3$ , 1.1 Hz, 1 H), 7.36 (t,  $J = 7.9$  Hz, 1 H), 7.42–7.55 (m, 7 H), 7.79 (dd,  $J = 11.7$ , 4.9 Hz, 4 H), 8.04 (d,  $J = 8.5$  Hz, 1 H).  $^{31}\text{P}\{^1\text{H}\}$  NMR ( $\text{CDCl}_3$ , 202.3 MHz):  $\delta$  30.28.

**2-((Diphenylphosphino)methyl)quinolin-8-ol Acetate (3)**. In the glovebox, a 25 mL round-bottom flask was charged with **2** (0.020 g, 0.0583 mmol) and  $\text{CH}_2\text{Cl}_2$  (10 mL). Triethylamine (0.0590 g, 0.0583 mmol) and DMAP (0.0007 g, 0.00595 mmol) were added to the stirred mixture. Acetic anhydride (0.0595 g, 0.0593 mmol) was added dropwise. The solution was taken out of the glovebox after 3 h and worked up under standard Schlenk workup procedures. The crude product was further purified by elution from a short  $\text{Al}_2\text{O}_3$  column using  $\text{CH}_2\text{Cl}_2$ . Removal of solvents left **3** (0.0200 g, 91%) as a pale yellow solid. IR (KBr):  $\nu_{\text{CO}}$  1757  $\text{cm}^{-1}$ .  $^1\text{H}$  NMR ( $\text{CDCl}_3$ ):  $\delta$  2.30 (s, 3 H), 3.73 (s, 2 H), 7.21 (d,  $J = 8.5$  Hz, 1 H), 7.24–7.44 (m, 12 H), 7.56 (dd,  $J = 8.1$ , 1.5 Hz, 1 H), 7.93 (d,  $J = 8.5$  Hz, 1 H).  $^{13}\text{C}\{^1\text{H}\}$  NMR ( $\text{CDCl}_3$ ):  $\delta$  20.56, 39.88 (d,  $J = 16.7$  Hz), 121.42, 122.78 (d,  $J = 5.7$  Hz), 125.59, 128.02, 128.54 (d,  $J = 6.9$  Hz), 128.77, 133.02 (d,  $J = 19.5$  Hz), 136.22, 138.82 (d,  $J = 14.8$  Hz), 140.80, 147.46, 159.34 (d,  $J = 9.1$  Hz), 170.06.  $^{31}\text{P}\{^1\text{H}\}$  NMR ( $\text{C}_6\text{D}_6$ ):  $\delta$  -11.47. Anal. Calcd for  $\text{C}_{24}\text{H}_{20}\text{NO}_2\text{P}$  ( $M_r = 385.42$ ): C, 73.08; H, 5.38; N, 3.55. Found: C, 72.52; H, 5.31; N, 3.75.

**Formation of 13a from 4 and 3**. In the glovebox, **3** (0.0170 g, 0.0444 mmol) was dissolved in benzene (15 mL) in a 25 mL round-bottom flask. The rhodium dimer **4** (0.0080 g, 0.0111 mmol) was added, and the reaction mixture was stirred for 10 min. The solvent was removed in vacuo, yielding **13a** (0.0168 g, 83%) as a yellow solid. IR (KBr): 1765 (C=O, ester), 1673, 1656 (C=O, acyl)  $\text{cm}^{-1}$ .  $^1\text{H}$  NMR ( $\text{C}_6\text{D}_6$ , 500 MHz):  $\delta$  1.73 (s, 3 H), 2.15 (s, 3 H), 3.88 (dd,  $J = 17.0$ , 12.0 Hz, 1 H), 4.31 (dd,  $J = 17.0$ , 12.0 Hz, 1 H), 5.42 (dd,  $J = 14.9$ , 10.5 Hz, 1 H), 5.96 (dd,  $J = 14.9$ , 10.5 Hz, 1 H), 6.70 (d,  $J = 8.5$  Hz, 1 H), 6.78 (d,  $J = 8.5$  Hz, 1 H), 6.80–7.12 (m, 14 H), 7.19 (dd,  $J = 8.0$ , 1.5 Hz, 1 H), 7.35 (d,  $J = 8.5$  Hz, 1 H), 7.39 (t,  $J = 8.0$  Hz, 1 H), 7.46–7.49 (m, 4 H), 7.68 (d,  $J = 8.0$  Hz, 1 H), 7.78 (dd,  $J = 11.0$ , 3.5 Hz, 2 H), 8.11 (t,  $J = 9.5$  Hz, 2 H), 8.20 (dd,

$J = 7.5$ , 3.5 Hz, 2 H).  $^1\text{H}$  NMR ( $\text{CDCl}_3$ , 500 MHz):  $\delta$  1.46 (s, 3 H), 2.50 (s, 3 H), 4.42 (dd,  $J = 17.0$ , 11.0 Hz, 1 H), 4.65 (dd,  $J = 17.0$ , 11.0 Hz, 1 H), 4.98 (dd,  $J = 15.3$ , 10.0 Hz, 1 H), 5.30 (dd,  $J = 15.3$ , 10.0 Hz, 1 H), 6.53 (d,  $J = 9.0$  Hz, 1 H), 7.00–7.51 (m, 22 H), 7.66 (t,  $J = 8.5$ , 2 H), 7.86 (t,  $J = 9.5$  Hz, 2 H), 7.97 (t,  $J = 10.0$  Hz, 2 H), 8.23 (d,  $J = 8.5$  Hz, 1 H).  $^1\text{H}$  NMR ( $\text{CDCl}_3$ , 500 MHz,  $-30^\circ\text{C}$ ):  $\delta$  1.16 (s, 3 H,  $\text{RhCOCH}_3$ ), 2.34 (s, 3 H,  $\text{OCOCH}_3$ ), 4.21 (dd,  $J = 17.0$ , 11.9 Hz, 1 H,  $\text{H}^a$  or  $\text{H}^b$ ), 4.49 (dd,  $J = 17.0$ , 11.9 Hz, 1 H,  $\text{H}^b$  or  $\text{H}^a$ ), 4.70 (dd,  $J = 14.5$ , 10.5 Hz, 1 H,  $\text{H}^a$  or  $\text{H}^b$ ), 5.01 (dd,  $J = 14.5$ , 10.5 Hz, 1 H,  $\text{H}^b$  or  $\text{H}^a$ ), 6.07 (d,  $J = 8.5$  Hz, 1 H,  $\text{H}^3$ ), 6.76 (t,  $J = 8.0$  Hz, 2 H,  $\text{H}^{x2}$ ), 6.81 (d,  $J = 8.0$  Hz, 1 H,  $\text{H}^5$ ), 6.86 (t,  $J = 7.5$  Hz, 2 H,  $\text{H}^{x3}$ ), 6.94–7.00 (m, 4 H,  $\text{H}^{x3}$  + others), 7.05–7.10 (m, 4 H,  $\text{H}^7$  + other), 7.13–7.21 (m, 4 H,  $\text{H}^{x4}$  + other), 7.23–7.29 (m, 4 H,  $\text{H}^6$ ), 7.31 (d,  $J = 8.5$  Hz, 1 H,  $\text{H}^3$ ), 7.39 (t,  $J = 9.0$  Hz, 2 H,  $\text{H}^{y2}$ ), 7.60–7.74 (m, 4 H,  $\text{H}^{x2}$ ,  $\text{H}^{y2}$ ), 8.04 (d,  $J = 8.5$  Hz, 1 H,  $\text{H}^4$ ). Partial  $^{13}\text{C}\{^1\text{H}\}$  NMR ( $\text{CDCl}_3$ , 125.7 MHz):  $\delta$  21.16, 33.86, 37.64 (d,  $J = 19.9$  Hz), 48.87 (dd,  $J = 33.9$ , 2.2 Hz), 229.27 (ddd,  $J = 28$ , 8, 5 Hz).  $^{31}\text{P}\{^1\text{H}\}$  NMR ( $\text{CDCl}_3$ , 202.3 MHz):  $\delta$  27.49 (dd,  $J = 134.4$ , 27.3 Hz), 37.48 (dd,  $J = 146.7$ , 27.3 Hz). MS ( $m/z$  (relative intensity)): 830 ( $\text{M}^+ - \text{HCl} - \text{CH}_2=\text{C}=\text{O}$ ) (2%), 788 ( $\text{M}^+ - \text{HCl} - \text{CH}_2=\text{C}=\text{O} - \text{CH}_3\text{CO}$ ) (1%), 343 ( $\text{M}^+$ ,  $\text{C}_{22}\text{H}_{18}\text{NOP}^+ = 2^+$ ) (34%). Anal. Calcd for  $\text{C}_{48}\text{H}_{40}\text{N}_2\text{O}_4\text{P}_2\text{RhCl}$  ( $M_r = 909.20$ ): C, 63.41; H, 4.44; N, 3.08. Found: C, 64.79; H, 4.64; N, 3.26.

**Reaction of 2 and 5 To Give 16a**. In the glovebox, **2** (0.0306 g, 0.0892 mmol) was dissolved in benzene (15 mL) in a 25 mL round-bottom flask. The iridium dimer **5** (0.020 g, 0.0223 mmol) was added, and the mixture was stirred for 10 min. The solvent was removed in vacuo, leaving **16a** (0.0385 g, 94%) as a yellow solid. IR (KBr): 3300–3500 (O-H), 2258  $\text{cm}^{-1}$  (Ir-H).  $^1\text{H}$  NMR ( $\text{C}_6\text{D}_6$ , 500 MHz):  $\delta$  -18.86 (t,  $J = 17.0$  Hz, 1 H), 3.69 (dd,  $J = 17.8$ , 11.5 Hz, 1 H), 4.18 (dd,  $J = 17.8$ , 11.5 Hz, 1 H), 4.58 (dd,  $J = 15.0$ , 10.5 Hz, 1 H), 5.09 (dd,  $J = 15.0$ , 10.5 Hz, 1 H), 6.56 (d,  $J = 8.5$  Hz, 1 H), 6.67 (d,  $J = 8.5$  Hz, 1 H), 6.71 (d,  $J = 7.0$  Hz, 1 H), 6.76–7.49 (m, 24 H), 7.58 (dd,  $J = 12.0$ , 7.5 Hz, 1 H), 7.72–7.79 (m, 1 H), 7.83 (dd,  $J = 18.5$ , 7.5 Hz, 1 H), 8.00 (bs, 1 H).  $^{31}\text{P}\{^1\text{H}\}$  NMR ( $\text{C}_6\text{D}_6$ ):  $\delta$  2.14 (dd,  $J = 17.0$ , 16.0 Hz), -1.06 (dd,  $J = 17.0$ , 16.0 Hz). MS ( $m/z$  (relative intensity)): 878 ( $\text{M}^+ - 36$ , HCl) (29%), 343 ( $\text{M}^+ - 571$ ,  $\text{C}_{22}\text{H}_{18}\text{NOP}^+ = 2^+$ ) (100%). Anal. Calcd for  $\text{C}_{44}\text{H}_{36}\text{N}_2\text{O}_2\text{P}_2\text{IrCl}$  (914.49): C, 57.79; H, 3.98; N, 3.06. Found: C, 56.16; H, 3.76; N, 3.05.

**Acknowledgment.** We thank Johnson Matthey Aesar Alfa for a generous loan of iridium salts. Dr. Ron Nieman provided invaluable advice on NMR experiments, and the NSF (Grant Nos. CHE-88-13109, CHE-92-14799, and BBS 88-04992) and ASU provided funds for the necessary NMR instrumentation.

**Supporting Information Available:** Figures giving COSY NMR spectra for **13a** (3 pages). The material is contained in many libraries on microfiche, immediately follows this article in the microfilm version of this journal, can be ordered from the ACS, and can be downloaded from the Internet; see any current masthead page for ordering information and Internet access instructions.

OM950408I

# Selectivity in the Pentacarbonyliron-Promoted Cyclocarbonylation of Eneidyne

Anthony J. Pearson\* and Alvis Perosa

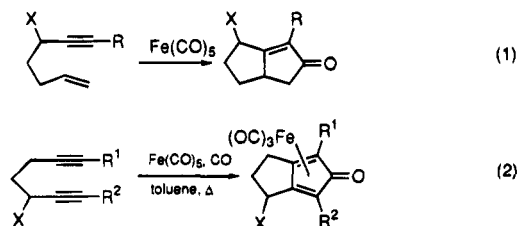
Department of Chemistry, Case Western Reserve University, Cleveland, Ohio 44106

Received June 19, 1995<sup>®</sup>

Cyclocarbonylation reactions of a series of eneidyne, promoted by pentacarbonyliron, proceed selectively on the diyne, resulting in the formation of cyclopentadienone–iron tricarbonyl complexes, without competing enyne cyclocarbonylation.

## Introduction

Previous papers from our laboratory have described the preparation and intramolecular cyclocarbonylation reactions of a number of different enynes and  $\alpha,\omega$ -diynes to give the corresponding cyclopentenones (Pauson–Khand type reaction) or the corresponding cyclopentadienone–Fe(CO)<sub>3</sub> complexes, exemplified by eqs 1 and 2.<sup>1–4</sup>



It was found that these reactions tolerate the presence of different functionalities. Hydroxy-substituted, electron-deficient acetylenes, as well as sterically crowded ones, undergo high-yielding intramolecular cyclocarbonylations. It was also shown that the hydroxy-substituted cyclopentadienone complexes can be oxidized to the corresponding ketones and that the products can be subjected to stereoselective nucleophilic addition. Demetalation was accomplished in some cases using trimethylamine *N*-oxide, and evidence of an unexpected mechanism for this reaction mechanism was obtained.<sup>1</sup>

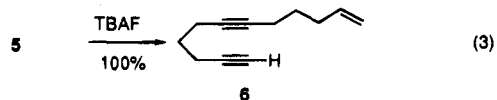
Further studies of this cyclocarbonylation reaction were needed if it is to be employed in organic synthesis. The construction of the bicyclo[3.3.0]octadienone skeleton is of interest for the synthesis of a number of natural polyquinanes, some of which have already been approached by similar and by more traditional chemistry, such as coriolin,<sup>5,6</sup> pentalene,<sup>7–9</sup> pentalenic acid,<sup>7,10</sup> crinipellin,<sup>11</sup> silphinene,<sup>7,12</sup> hirsutene,<sup>13</sup> and hirsutic acid.<sup>6</sup>

In the present work our first objective was to study the selectivity of these cyclocarbonylation reactions for substrates containing both acetylenic and olefinic functionalities. We will show how, under our conditions, the iron-promoted cyclocarbonylation reaction of eneidyne occurs specifically on the diyne moiety.

Next, demetalation of the cyclopentadienone–Fe(CO)<sub>3</sub> complexes had to be accomplished efficiently in order for the global scheme to be synthetically useful. Recently similar demetalation reactions have been reported from our laboratory<sup>1</sup> and from Knölker and co-workers,<sup>14,15</sup> by the use of Me<sub>3</sub>NO. We will describe the problems encountered and the applicability of such demetalation procedures to our cases.

## Results and Discussion

A series of eneidyne was prepared starting from 4-pentyn-1-ol (Scheme 1). In the presence of 2 equiv of lithium amide in liquid ammonia at –40 °C, 4-pentyn-1-ol reacted regioselectively with 5-bromo-1-pentene to give the kinetically preferred substitution product 1.<sup>16</sup> The resulting alcohol 1 was converted, via the methanesulfonate 2, to the corresponding iodide 3, which acts as a better leaving group in the subsequent acetylide addition.<sup>17</sup> It was then added to the appropriate acetylide to afford the desired eneidyne 4 and 5. Desilylation of 5 with TBAF gave 6 (eq 3).



Alcohol 1 was oxidized using the Swern<sup>18</sup> procedure to give the aldehyde 7, which was then treated with the appropriate acetylide to give the desired eneidyne alcohols 8 and 9 in good yields. This sequence can be easily performed on multigram scale, and rigorous purification of the intermediates is unnecessary.

Cyclocarbonylation of the eneidyne was then investigated. An interesting feature of this reaction is its

(12) Franck-Neumann, M.; Miesch, M.; Gross, L. *Tetrahedron Lett.* **1991**, *32*, 2135.

(13) Castro, J.; Sorensen, H.; Riera, A.; Morin, C.; Moyano, A.; Pericas, M. A.; Greene, A. E. *J. Am. Chem. Soc.* **1990**, *112*, 9388.

(14) Knölker, H.-J.; Heber, J.; Mahler, C. H. *Synlett* **1992**, 1002.

(15) Knölker, H.-J.; Heber, J. *Synlett* **1993**, *12*, 924.

(16) Brandsma, L. *Preparative Acetylenic Chemistry*, 2nd ed.; Elsevier: Amsterdam, 1988; Vol. 34.

(17) Ho, T. L. *Chem. Rev.* **1975**, *75*, 1.

(18) Swern, D.; Huang, S.-L.; Mancuso, A. J. *J. Org. Chem.* **1978**, *43*, 2480.

<sup>®</sup> Abstract published in *Advance ACS Abstracts*, October 15, 1995.

(1) Pearson, A. J.; Shively, R. J., Jr. *Organometallics* **1994**, *13*, 578.

(2) Pearson, A. J.; Shively, R. J., Jr.; Dubbert, R. A. *Organometallics* **1996**, *11*, 4096.

(3) Pearson, A. J.; Dubbert, R. A. *J. Chem. Soc., Chem. Commun.* **1991**, *91*, 202.

(4) Pearson, A. J.; Dubbert, R. A. *Organometallics* **1994**, *13*, 1656.

(5) Magnus, P.; Exon, C. *J. Am. Chem. Soc.* **1983**, *105*, 2477.

(6) Magnus, P.; Exon, C.; Albaugh-Robertson, G. J. *Tetrahedron* **1985**, *41*, 5861.

(7) Schore, N. E.; Rowley, E. G. *J. Org. Chem.* **1992**, *57*, 6853.

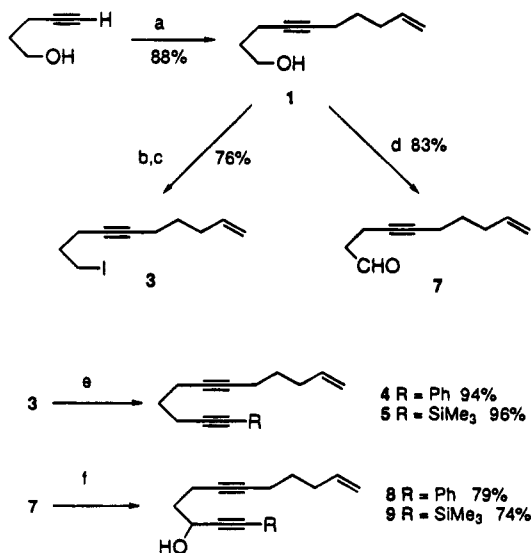
(8) Yamamura, S.; Shizuri, Y.; Maki, S.; Ohkubo, M. *Tetrahedron Lett.* **1990**, *31*, 7167.

(9) Burnell, D. J.; Zhu, Y.-Y.; Wu, Y.-J. *J. Org. Chem.* **1994**, *59*, 104.

(10) Schore, N. E.; Rowley, E. G. *J. Organomet. Chem.* **1991**, *413*, C5.

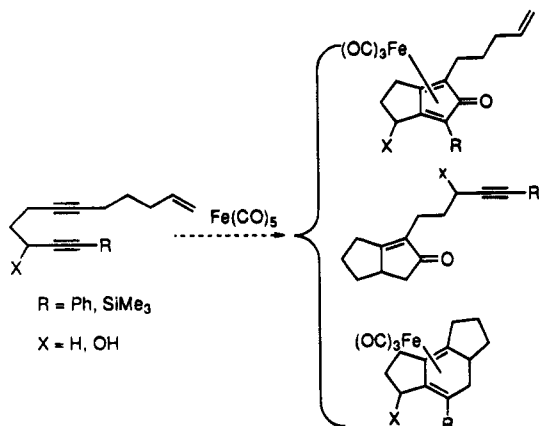
(11) Curran, D. P.; Schwartz, C. E. *J. Am. Chem. Soc.* **1990**, *112*, 9272.

Scheme 1

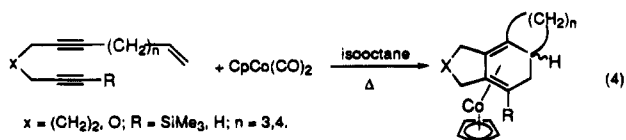
**Reagents:**

- a: 5-bromo-pent-1-ene, liq.  $\text{NH}_3$ , Li,  $\text{Fe}(\text{NO})_3$ , THF,  $-40^\circ\text{C}$  to RT, 12 h;  
 b:  $\text{NEt}_3$ ,  $\text{CH}_3\text{SO}_3\text{Cl}$ ,  $\text{CH}_2\text{Cl}_2$ , RT, 12 h;  
 c: NaI, acetone, reflux, 12 h;  
 d:  $(\text{ClCO})_2$ ,  $\text{Me}_2\text{SO}$ ,  $\text{NEt}_3$ ,  $\text{CH}_2\text{Cl}_2$ ,  $-60^\circ\text{C}$  to RT, 30 min;  
 e:  $\text{R}-\text{C}\equiv\text{C}-\text{H}$ ,  $n\text{-BuLi}$ , THF, reflux, 72 h;  
 f:  $\text{R}-\text{C}\equiv\text{C}-\text{H}$ ,  $n\text{-BuLi}$ , THF,  $-30^\circ\text{C}$  to RT, 30 min.

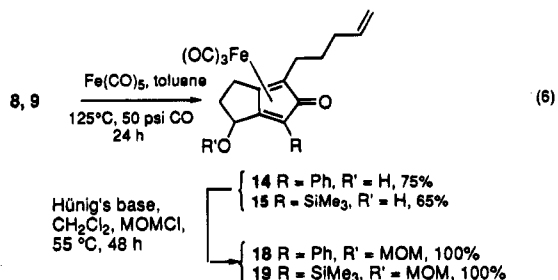
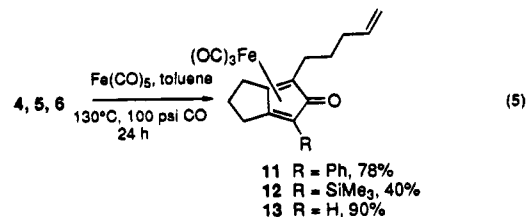
Scheme 2



possible chemoselectivity deriving from the presence of the diyne and enyne moieties. Iron pentacarbonyl has been shown to promote cyclocarbonylation of 1,6-enynes to the corresponding bicyclo[3.3.0]pentenones (eq 1),<sup>4</sup> and diynes react with iron pentacarbonyl under CO pressure to generate the tricarbonylironbicyclo[3.3.0]dienones;<sup>1-3</sup> a competing effect was thus possible, although we have observed that the enyne cyclocarbonylation is generally much slower than the diyne reaction. Vollhardt and co-workers have shown that acetylenic and olefinic functionalities present in the same molecule can participate in a cobalt-mediated annulation reaction to give a tricyclic complex (eq 4).<sup>19</sup> Thus, a mixture of products arising from multiple concurrent reaction pathways might have been expected (Scheme 2).

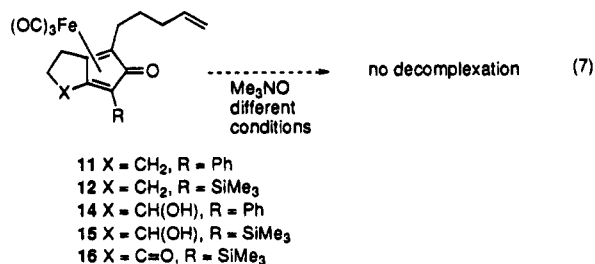


Very rewardingly it was found that the above enediynes, when subjected to the cyclocarbonylation conditions that have been previously described,<sup>1-3</sup> react cleanly to give solely the complexes arising from diyne cyclocarbonylation, as summarized in eqs 5 and 6.



Proton NMR spectra of the crude products from all the above reactions showed no evidence of any cyclopentenones arising from participation of the olefin in the reaction. In the cases of eq 6 a roughly equimolar mixture of the *syn* and *anti* diastereomers was obtained, which were usually not separated in view of the subsequent demetalation reaction which destroys the chirality of the organometallic.

At this point it seemed interesting to develop a general and efficient demetalation procedure for our complexes, which would hopefully lead to the corresponding bicyclo[3.3.0]octadienones. In our case an added curiosity derives from the possibility that the free olefin side chain might react in an intramolecular Diels-Alder fashion with the highly reactive cyclopentadienone upon decomplexation. The demetalation reactions of complexes 11, 12, and 14-16 proved quite difficult to accomplish (eq 7). Initial attempts using the



known procedures with  $\text{Me}_3\text{NO}$ <sup>4,15,20,21</sup> in acetone or benzene as solvents at various temperatures, and using ceric ammonium nitrate,<sup>22</sup> proved unsuccessful. It was thought that decreasing the electron density on the complexed cyclopentadienone ring might help in the demetalation. The hydroxy-substituted complex was

(19) Vollhardt, K. P. C.; Sternberg, E. D. *J. Am. Chem. Soc.* **1980**, *102*, 4839.

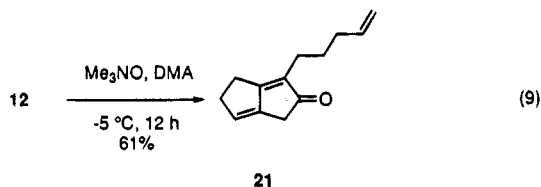
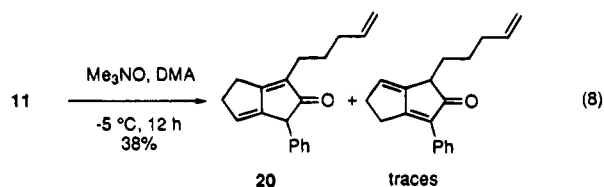
(20) Shvo, Y.; Hazum, E. *J. Chem. Soc., Chem. Commun.* **1974**, 74, 336.

(21) Hogeveen, H.; Eekhof, J. H.; Kellogg, R. M. *J. Chem. Soc., Chem. Commun.* **1976**, 76, 657.

(22) Vollhardt, K. P. C.; Gesing, E. R. F.; Tane, J. P. *Synlett* **1980**, 1002.

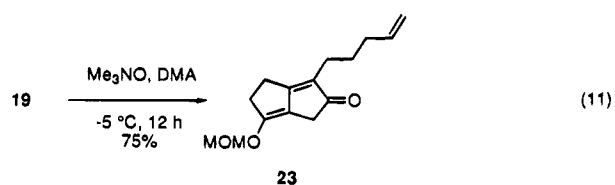
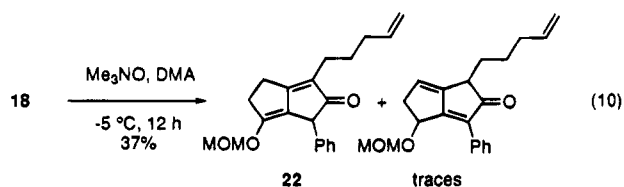
oxidized to the corresponding ketone **16** by standard treatment with PCC, but attempts to decomplex this compound by the usual methods also failed.

The importance of solvent is illustrated by the use of  $\text{Me}_3\text{NO}$  in *N,N*-dimethylacetamide (DMA), which led to successful demetalation at  $-5^\circ\text{C}$ .<sup>23</sup> The results are shown in eqs 8 and 9. As can be seen in each case, a



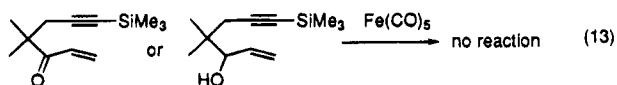
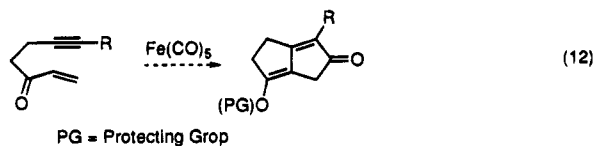
migration of one double bond occurs during this reaction, as has been observed previously by Knölker and co-workers.<sup>15</sup> We believe this is due to the increased basicity of  $\text{Me}_3\text{NO}$  in DMA that allows for an easy deprotonation at the  $\gamma$ -carbon followed by reprotonation at the  $\alpha$ -position, followed by desilylation. The trimethylsilyl group plays a very important role in controlling the site of deprotonation and accompanying deconjugation.

Surprisingly, decomplexation of the hydroxy complexes **14** and **15** did not occur under the preceding conditions. There appears to be some oxidation occurring at the hydroxyl oxygen, but the products were extremely unstable and were uncharacterizable. To overcome this, the hydroxy complex **15** was protected as the trimethylsilyl ether **17**. Although some TLC evidence of the demetalated product was obtained, it was not possible to isolate and characterize it. A second attempt was made by protecting **14** and **15** as their MOM ethers: **18** and **19**. Upon subjecting these compounds to our demetalation conditions, we were able to isolate the bicyclooctadienones **22** and **23** in moderate to good yields (eqs 10 and 11).



As in the preceding cases migration of a double bond and desilylation were observed. It should be noted that compounds **22** and **23** are each the protected and

masked enol form of an enedione, which can be considered as the products of a Pauson–Khand type reaction of an electron-deficient  $\alpha,\beta$ -unsaturated enyne such as that shown in eq 12. This is noteworthy since



electron-deficient alkenes are usually poor substrates for Pauson–Khand reactions,<sup>24,25</sup> there being only a few examples in the literature.<sup>26–28</sup> The pentacarbonyliron promoted Pauson–Khand type reaction on such electron-deficient alkenes also does not occur in the presence of pentacarbonyliron; unpublished attempts from our group to achieve the reaction shown in eq 13 proved unsuccessful. The scope of our pentacarbonyliron promoted cyclocarbonylation is thus extended to formally include intramolecular Pauson–Khand type cyclizations of electron deficient  $\alpha,\beta$ -unsaturated enynes.

## Experimental Section

**General Methods.** The syntheses were carried out under a purified nitrogen atmosphere. THF and  $\text{Et}_2\text{O}$  were distilled from  $\text{Na/benzophenone}$ ,  $\text{CH}_2\text{Cl}_2$  from  $\text{CaH}_2$ , and acetone from  $\text{CaSO}_4$ . All other solvents were used as purchased. All nonvolatile compounds were dried of residual solvents by exposure to high vacuum prior to analysis.

Infrared spectra were recorded on a Nicolet Impact FT-IR spectrometer in  $\text{NaCl}$  chambers.  $^1\text{H}$  ( $^{13}\text{C}$ ) NMR spectra were recorded at 300 (75) MHz on a Varian Gemini spectrometer, unless otherwise noted, and were referenced to the solvent or to TMS. NMR assignments for some complexes were made on separated pure diastereomers; in several other cases the assignments were made on the mixtures of diastereomers by comparison with the purified materials. Mass spectra were recorded on a Kratos MS25A instrument.

Gas chromatography was performed on an Hewlett Packard 5890 Series II instrument fitted with a HP-5 30 m  $\times$  0.32 mm capillary column coated with a 0.25 mm film of 5% PhMe Silicone, equipped with a flame ionization detector, using He as carrier gas. The temperature gradient program, in each case the same, was the following: start at  $120^\circ\text{C}$ , increase to  $150^\circ\text{C}$  at  $5^\circ\text{C}/\text{min}$ , and then to  $250^\circ\text{C}$  at  $10^\circ\text{C}/\text{min}$ , for 2 min.

**Deca-9-en-4-yne-1-ol (1).** To 300 mL of liquid ammonia at  $-78^\circ\text{C}$  is added enough lithium metal ( $\sim 30$  mg,  $\sim 4.3$  mmol) to turn the solution deep blue. After addition of a catalytic amount of ferric nitrate nonahydrate (5 mg, 0.02 mmol) the solution turns brownish, at which point the remaining lithium is added (200 mg, 28.8 mmol). The solution turns blue again, and as it is warmed to  $-40^\circ\text{C}$ , it becomes a whitish suspension ( $\text{LiNH}_2$ ). 4-Pentyn-1-ol (840 mg, 10 mmol) is added to the suspension at  $-40^\circ\text{C}$  over 20 min, followed by 1.49 g (10 mmol) of 5-bromopent-1-ene over 30 min. The solution is stirred at the boiling point of ammonia ( $-33^\circ\text{C}$ ) for 3 h after which 50 mL of THF is added; the ammonia is then left to evaporate overnight. The resulting THF solution is quenched with 100

(24) Pauson, P. L.; Khand, I. U. *J. Chem. Soc. Chem., Commun* **1974**, 379.

(25) Schore, N. E. *Org. React.* **1991**, *40*, 1.

(26) Veretenov, A. L.; Smit, W. A.; Vorontsova, L. G.; Kurella, M. G.; Caple, R.; Gybin, A. S. *Tetrahedron Lett.* **1991**, *32*, 2109.

(27) Costa, M.; Mor, A. *Tetrahedron Lett.* **1995**, *36*, 2867.

(28) Krafft, M. E.; Wright, C. *Tetrahedron Lett.* **1992**, *33*, 151.

(23) Bandara, B. M. R.; Birch, A. J.; Kelly, L. F. *J. Org. Chem.* **1984**, *49*, 2496.

mL of cold water, the aqueous layer is extracted three times with ethyl ether, and the combined organic layers are washed twice with brine. After drying over  $\text{MgSO}_4$  and removal of the solvent, the product is purified by flash chromatography ( $R_f = 0.40$  in 10% EtOAc/hexanes) and obtained as a yellow oil in 88% yield: GC Rt = 5.3 min; IR ( $\text{CCl}_4$ ) 3641, 3323, 3079, 2937  $\text{cm}^{-1}$ ;  $^1\text{H}$  NMR ( $\text{CDCl}_3$ )  $\delta$  5.84–5.60 (m, 1H), 5.02–4.92 (m, 2H), 3.73 (t, 2H,  $J = 6.1$  Hz), 2.25 (td, 2H,  $J = 4.3, 2.4$  Hz), 2.12 (m, 4H), 1.80–1.66 (m, 3H), 1.55 (p, 2H,  $J = 7.29$  Hz);  $^{13}\text{C}$  NMR ( $\text{CDCl}_3$ )  $\delta$  138, 115, 81, 80, 62, 33, 32, 28, 18, 15. HRMS: calcd for  $\text{C}_{10}\text{H}_{16}\text{O}$  ( $\text{M}^+$ ),  $m/e$  152.1201; found,  $m/e$  152.1191.

**1-((Methylsulfonyl)oxy)deca-9-en-4-yne (2).** To **1** (0.507 g, 3.3 mmol) in 25 mL of  $\text{CH}_2\text{Cl}_2$  are added 1 mL of  $\text{Et}_3\text{N}$  and, at  $-30$  °C, 0.25 mL (3.3 mmol) of methanesulfonyl chloride. The solution is stirred at room temperature overnight. The solvent is removed, and the solid mass is diluted with 30 mL of ethyl ether. Workup with 10%  $\text{NaHCO}_3$  and brine, followed by drying over magnesium sulfate and removal of the solvent, affords the product as a yellow oil ( $R_f = 0.74$  in 10% EtOAc/hexanes), in 86% yield: GC Rt = 12.1 min; IR ( $\text{CCl}_4$ ) 3161, 3085, 2945, 2262, 1807, 1645  $\text{cm}^{-1}$ ;  $^1\text{H}$  NMR ( $\text{CDCl}_3$ )  $\delta$  5.80–5.72 (m, 1H), 5.03–4.93 (m, 2H), 4.33 (t, 2H,  $J = 6.1$  Hz), 3.00 (s, 3H), 2.32–2.27 (m, 2H), 2.13 (m, 4H), 1.93–1.84 (m, 2H), 1.54 (p, 2H);  $^{13}\text{C}$  NMR ( $\text{CDCl}_3$ )  $\delta$  138, 115, 81, 77, 69, 37, 33, 28, 28, 18, 15. HRMS: calcd for  $\text{C}_{10}\text{H}_{15}\text{O}$  ( $\text{M}^+ - \text{SO}_2\text{CH}_3$ ),  $m/e$  151.1123; found,  $m/e$  151.1123.

**1-Iodo-deca-9-en-4-yne (3).** A solution of **2** in 25 mL of acetone (0.685 g, 2.85 mmol) was refluxed overnight with 0.500 g (3.2 mmol) of NaI. Removal of the acetone, dilution with ether, and aqueous workup, followed by drying over magnesium sulfate and removal of the solvent, affords the product as a yellow oil, which over time tends to darken (88% yield) ( $R_f = 0.61$  in 10% EtOAc/hexanes): GC Rt = 8.1 min; IR ( $\text{CCl}_4$ ) 3315, 3160, 2951, 2260  $\text{cm}^{-1}$ ;  $^1\text{H}$  NMR ( $\text{CDCl}_3$ )  $\delta$  5.82–5.72 (m, 1H), 5.04–4.94 (m, 2H), 3.28 (t, 2H,  $J = 6.7$  Hz), 2.30–2.24 (m, 2H), 2.13 (m, 4H), 1.98–1.89 (m, 2H), 1.55 (p, 2H);  $^{13}\text{C}$  NMR ( $\text{CDCl}_3$ )  $\delta$  138, 115, 81, 78, 33, 32, 28, 20, 18, 6. HRMS: calcd for  $\text{C}_{10}\text{H}_{15}\text{I}$  ( $\text{M}^+$ ),  $m/e$  262.0219; found,  $m/e$  262.0203.

**12-Phenyldodeca-6,11-diyne-1-ene (4) and 12-(Trimethylsilyl)dodeca-6,11-diyne-1-ene (5).** These products were prepared by following an identical procedure. The appropriate acetylene (3 mmol) dissolved in 10 mL of THF is treated at  $-78$  °C with 3 mmol of a 1.6 M solution of *n*-BuLi in hexanes. The solution is warmed to 0 °C to ensure complete deprotonation, 2 mmol of **3** is added, and the solution is brought to reflux. Small aliquots (1–2 mmol) of preformed acetylide are added via cannula until complete conversion of 10-iododec-6-yne-1-ene is observed by GC (1 to 2 days). The mixture is then worked up as usual and dried over  $\text{MgSO}_4$ . Removal of the solvent affords a clear yellow oil which is purified by flash chromatography. **4:** Yield 94%;  $R_f = 0.46$  (10% EtOAc in hexanes); IR ( $\text{CHCl}_3$ ) 2940, 2250  $\text{cm}^{-1}$ ;  $^1\text{H}$  NMR ( $\text{CDCl}_3$ )  $\delta$  7.38–7.35 (m, 2H), 7.27–7.22 (m, 3H), 5.82–5.73 (m, 1H), 2.50 (t, 2H), 2.31 (m, 2H), 2.14 (m, 4H), 1.76 (p, 2H), 1.56 (p, 2H);  $^{13}\text{C}$  NMR ( $\text{CDCl}_3$ )  $\delta$  138, 132, 128, 128, 124, 115, 89, 81, 80, 79, 33, 28, 28, 19, 18, 18. HRMS: calcd for  $\text{C}_{18}\text{H}_{20}$  ( $\text{M}^+$ ),  $m/e$  236.1565; found,  $m/e$  236.1567. **5:** Yield 96%;  $R_f = 0.75$  (10% EtOAc in hexanes); GC Rt = 10.7 min; IR 2945, 1649, 1248  $\text{cm}^{-1}$ ;  $^1\text{H}$  NMR ( $\text{CDCl}_3$ )  $\delta$  5.82–5.73 (m, 1H), 5.04–4.93 (m, 2H), 2.31 (t, 2H,  $J = 7.14$  Hz), 2.23 (m, 2H), 2.14 (m, 4H), 1.67 (p, 2H,  $J = 7.07$  Hz), 1.55 (p, 2H,  $J = 7.28$  Hz), 0.12 (s, 9H);  $^{13}\text{C}$  NMR ( $\text{CDCl}_3$ )  $\delta$  138, 115, 107, 85, 80, 79, 33, 28, 19, 18, 0. HRMS: calcd for  $\text{C}_{14}\text{H}_{21}\text{Si}$  ( $\text{M}^+ - \text{CH}_3$ ),  $m/e$  217.1412; found  $m/e$  217.1412.

**Dodeca-6,11-diyne-1-ene (6).** To **5** dissolved in THF is added 1.5 equiv of tetrabutylammonium fluoride (1.0 M in THF) at RT (room temperature) for 20 min. Usual workup affords a quantitative yield of the product ( $R_f = 0.56$  in 10% EtOAc/hexanes): IR ( $\text{CCl}_4$ ) 3308, 2934, 1552  $\text{cm}^{-1}$ ;  $^1\text{H}$  NMR ( $\text{CDCl}_3$ )  $\delta$  5.73–5.62 (m, 1H), 5.04–4.85 (m, 2H), 2.21 (qd, 2H,  $J_1 = 7.8$  Hz,  $J_2 = 2.9$  Hz), 2.09 (m, 4H), 1.88 (7, 1H,  $J = 2.9$

Hz), 1.64 (p, 2H,  $J = 8.0$  Hz), 1.51 (p, 2H,  $J = 7.8$  Hz);  $^{13}\text{C}$  NMR  $\delta$  138.0, 115.0, 83.8, 80.6, 79.1, 68.6, 32.8, 28.2, 28.0, 18.1, 17.8, 17.5. HRMS: calcd for  $\text{C}_{12}\text{H}_{16}$  ( $\text{M}^+$ ),  $m/e$  160.1252; found,  $m/e$  160.1251.

**Deca-9-en-4-yne-1-al (7).** Via the Swern procedure, to a solution of  $\text{CH}_2\text{Cl}_2$  (25 mL) and oxalyl chloride (13.7 mL, 15.1 mmol) is added, at  $-55$  °C,  $\text{Me}_2\text{SO}$  (23.3 mL, 30.2 mmol) dissolved in 5 mL of  $\text{CH}_2\text{Cl}_2$ . After the mixture is stirred for 2 min, 2.08 g (13.7 mmol) of **1** is added over 5 min, and the solution is stirred for an additional 15 min, after which triethylamine (9.6 mL, 68.5 mmol) is added. The reaction is then stirred below  $-50$  °C for 5 min and then allowed to warm to room temperature. Water (50 mL) is added, and the aqueous layer is reextracted with additional 50 mL of  $\text{CH}_2\text{Cl}_2$ . The combined organic layers are washed with saturated NaCl solution (100 mL), then with 1% HCl, water, and 5%  $\text{Na}_2\text{CO}_3$ , and finally with water. After drying over  $\text{MgSO}_4$  and removal of the solvent, the product is purified for analytical purposes by flash chromatography:  $R_f = 0.31$  in EtOAc in hexanes; yield 1.70 g (11.3 mmol), 83%; GC Rt = 4.5 min; IR ( $\text{CCl}_4$ ) 1729, 1546  $\text{cm}^{-1}$ ;  $^1\text{H}$  NMR ( $\text{CDCl}_3$ )  $\delta$  9.77 (t,  $J = 1.4$  Hz), 5.75 (ddt, 1H,  $J_{trans} = 17.0$  Hz,  $J_{cis} = 10.3$  Hz,  $J_1 = 6.6$  Hz), 4.99 (dd, 1H,  $J_{trans} = 17.0$  Hz,  $J_{gem} = 1.6$  Hz), 4.94 (dd, 1H,  $J_{cis} = 10.3$  Hz,  $J_{gem} = 1.6$  Hz), 2.60 (dt, 2H,  $J_1 = 7.1$  Hz,  $J_2 = 1.4$  Hz), 2.46 (m, 2H), 2.11 (m, 4H), 1.53 (p, 2H);  $^{13}\text{C}$  NMR ( $\text{CDCl}_3$ )  $\delta$  201.0, 137.9, 115.0, 81.1, 78.1, 43.0, 32.7, 28.0, 18.0, 12.1. HRMS: calcd for  $\text{C}_{10}\text{H}_{14}\text{O}$  ( $\text{M}^+$ ),  $m/e$  150.1045; found,  $m/e$  150.1041.

**3-Hydroxy-1-phenyldodeca-1,6-diyne-12-ene (8) and 3-Hydroxy-1-(trimethylsilyl)dodeca-1,6-diyne-12-ene (9).** These products were prepared following an identical procedure. The appropriate acetylene (3 mmol) dissolved in 10 mL of THF is treated at  $-78$  °C with 3 mmol of a 1.6 M solution of *n*-BuLi in hexanes. The solution is warmed to 0 °C to ensure complete deprotonation, it is cooled to between  $-50$  and  $-60$  °C, and dec-6-yne-10-ene-1-al (2.5 mmol) is added over 5–10 min. After the reaction mixture is allowed to warm to 0 °C, it is poured into a mixture of ice and 10%  $\text{NH}_4\text{Cl}$ , the aqueous layer is reextracted with ethyl ether, and the combined organic layers are dried over anhydrous  $\text{MgSO}_4$ ; after removal of the solvent the crude product is purified by flash chromatography. **8:** Yield = 79%;  $R_f = 0.19$  (10% EtOAc in hexanes); GC Rt = 16.6 min; IR ( $\text{CCl}_4$ ) 3679, 3605, 3035, 2943, 1224  $\text{cm}^{-1}$ ;  $^1\text{H}$  NMR ( $\text{CDCl}_3$ )  $\delta$  7.32 (m, 2H), 7.21 (m, 3H), 5.70 (ddt, 1H,  $J_{trans} = 17.0$  Hz,  $J_{cis} = 10.3$  Hz,  $J_1 = 6.6$  Hz), 4.94 (dd, 1H,  $J_{trans} = 17.0$  Hz,  $J_{gem} = 1.6$  Hz), 4.89 (dd, 1H,  $J_{cis} = 10.3$  Hz,  $J_{gem} = 1.6$  Hz), 4.66 (dt, 1H,  $J_a = J_b = 6.0$  Hz), 4.71 (s, 1H), 2.31 (m, 2H), 2.06 (m, 4H), 1.89 (td, 4H,  $J_a = J_b = 6.9$  Hz), 1.49 (q, 2H,  $J = 6.9$  Hz);  $^{13}\text{C}$  NMR ( $\text{CDCl}_3$ )  $\delta$  138, 132, 128, 128, 122, 115, 89, 85, 81, 79, 62, 37, 33, 28, 18, 15. HRMS: calcd for  $\text{C}_{18}\text{H}_{20}\text{O}$  ( $\text{M}^+$ ),  $m/e$  252.1514; found,  $m/e$  252.1509. **9:** Yield = 74%;  $R_f = 0.23$  (10% EtOAc in hexanes). IR ( $\text{CCl}_4$ ) 3600, 2936, 1547, 1245  $\text{cm}^{-1}$ ;  $^1\text{H}$  NMR ( $\text{CDCl}_3$ )  $\delta$  5.77 (ddt, 1H,  $J_{trans} = 17.0$  Hz,  $J_{cis} = 10.3$  Hz,  $J_1 = 6.6$  Hz), 5.01 (dd, 1H,  $J_{trans} = 17.0$  Hz,  $J_{gem} = 1.6$  Hz), 4.96 (dd, 1H,  $J_{cis} = 10.3$  Hz,  $J_{gem} = 1.6$  Hz), 4.49 (dt, 1H,  $J_a = J_b = 6.0$  Hz), 2.44–2.20 (m, 2H), 2.18–2.04 (m, 4H), 1.98 (d,  $J = 7.3$  Hz, 1H), 1.85 (dt,  $J_a = J_b = 6.7$  Hz, 2H), 1.55 (m, 2H);  $^{13}\text{C}$  NMR ( $\text{CDCl}_3$ )  $\delta$  138, 115, 106, 90, 81, 79, 62, 37, 33, 28, 18, 15, 0. HRMS: calcd for  $\text{C}_{15}\text{H}_{29}\text{OSi}$  ( $\text{M}^+ - 1$ ),  $m/e$  247.1518; found,  $m/e$  247.1516.

**3-((Trimethylsilyl)oxy)-1-(trimethylsilyl)dodec-1,6-diyne-12-ene (10).** To **9** (500 mg, 2.02 mmol) dissolved in 10 mL of THF are added 16 mmol of triethylamine and, after cooling to 0 °C, 6.1 mmol of trimethylsilyl chloride. The solution is stirred overnight and then worked up as usual to afford, after flash chromatography, the desired product: Yield = 82%;  $R_f = 0.73$  (10% EtOAc in hexanes); GC Rt = 11.3 min; IR ( $\text{CCl}_4$ ) 3320, 2965, 2184, 1259  $\text{cm}^{-1}$ ;  $^1\text{H}$  NMR ( $\text{CDCl}_3$ )  $\delta$  5.78 (ddt, 1H,  $J_{trans} = 17.0$  Hz,  $J_{cis} = 10.3$  Hz,  $J_1 = 6.6$  Hz), 5.01 (dd, 1H,  $J_{trans} = 17.0$  Hz,  $J_{gem} = 1.6$  Hz), 4.95 (dd, 1H,  $J_{cis} = 10.3$  Hz,  $J_{gem} = 1.6$  Hz), 2.23–2.20 (m, 2H), 2.18–2.06 (m, 4H), 1.88–1.74 (m, 2H), 1.54 (q, 2H,  $J = 7.5$  Hz);  $^{13}\text{C}$  NMR ( $\text{CDCl}_3$ )  $\delta$



138, 115, 107, 89, 80, 79, 62, 38, 33, 28, 18, 15, 0.1, -0.2. HRMS: calcd for  $C_{18}H_{32}OSi_2$  ( $M^+$ ),  $m/e$  320.1992; found,  $m/e$  320.1992.

**General Procedure for the Cyclocarbonylation Reactions.** To 2 mmol of the enediyne in 10 mL of toluene in a Fisher-Porter vessel is added 10 mmol of pentacarbonyliron filtered through a short pad of Celite. The reaction vessel is sealed and degassed by three freeze-pump-thaw cycles. During the last cycle it is charged with 100 psi of CO (50 psi for the hydroxy- and trimethylsilyloxy-substituted enediynes), and then it is heated at 125–130 °C for 22 hours. After cooling and release of the pressure, the reaction mixture is diluted with 10 mL of methylene chloride and filtered through a 30 mm Celite column to remove iron impurities; the solvent is evaporated and the dark residue chromatographed through a short column of silica gel to afford, after removal of the solvent, pure complex.

**Tricarbonyl{2-(pent-4-enyl)-4-phenylbicyclo[3.3.0]octa-1,4-dien-3-one}iron (11).** This was obtained from 4: Yield 78%;  $R_f$  = 0.35 (EtOAc); IR ( $CDCl_3$ ) 2063, 2011, 1979  $cm^{-1}$ ;  $^1H$  NMR ( $CDCl_3$ )  $\delta$  7.94–7.90 (m, 2H), 7.35–7.20 (m, 3H), 5.82 (ddt, 1H,  $J_{trans}$  = 17.0 Hz,  $J_{cis}$  = 10.3 Hz,  $J_1$  = 6.6 Hz), 5.01 (dd, 1H,  $J_{trans}$  = 17.0 Hz,  $J_{gem}$  = 1.6 Hz), 4.95 (dd, 1H,  $J_{cis}$  = 10.3 Hz,  $J_{gem}$  = 1.6 Hz), 2.99–2.86 (m, 2H), 2.64–2.57 (m, 2H), 2.57–2.37 (m, 2H), 2.18–1.98 (m, 4H), 1.75–1.58 (m, 2H);  $^{13}C$  NMR ( $CDCl_3$ )  $\delta$  208.9, 172.0, 138.0, 132.4, 128.6, 127.9, 127.6, 115.0, 108.5, 103.8, 82.2, 77.9, 33.8, 28.9, 28.4, 26.1, 25.8, 24.4. HRMS: calcd for  $C_{19}H_{24}O_4SiFe$  ( $M^+$ ), 0404.0711. Found: 404.0716.

**Tricarbonyl{2-(pent-4-enyl)-4-(trimethylsilyl)bicyclo[3.3.0]octa-1,4-dien-3-one}iron (12).** This was obtained from 5: Yield 58%;  $R_f$  = 0.08 (10% EtOAc in hexanes); IR ( $CDCl_3$ ) 2067, 2006, 2000  $cm^{-1}$ ;  $^1H$  NMR ( $CDCl_3$ )  $\delta$  5.79 (ddt, 1H,  $J_{trans}$  = 17.0 Hz,  $J_{cis}$  = 10.3 Hz,  $J_1$  = 6.6 Hz), 5.01 (dd, 1H,  $J_{trans}$  = 17.0 Hz,  $J_{gem}$  = 1.6 Hz), 4.95 (dd, 1H,  $J_{cis}$  = 10.3 Hz,  $J_{gem}$  = 1.6 Hz), 2.57–2.48 (m, 4H), 2.46–2.22 (m, 2H), 2.11 (dt, 2H,  $J_1 = J_2 = 7.2$  Hz), 2.03–1.80 (m, 2H), 1.79–1.53 (m, 2H), 0.25 (s, 9H);  $^{13}C$  NMR ( $CDCl_3$ )  $\delta$  209.0, 178.7, 138.1, 115.0, 112.3, 112.2, 85.1, 67.2, 33.9, 28.9, 27.4, 25.9, 25.8, 24.4, -0.7. HRMS: calcd for  $C_{19}H_{24}O_4SiFe$  ( $M^+$ ),  $m/e$  400.0793; found,  $m/e$  400.0832.

**Tricarbonyl{2-(pent-4-enyl)bicyclo[3.3.0]octa-1,4-dien-3-one}iron (13).** This was obtained from 6: Yield = 90%;  $R_f$  = 0.21 (30% EtOAc in hexanes); IR ( $CCl_4$ ) 2071, 2014, 1991, 1653  $cm^{-1}$ ;  $^1H$  NMR ( $CDCl_3$ )  $\delta$  5.77 (ddt, 1H,  $J_{trans}$  = 17.0 Hz,  $J_{cis}$  = 10.3 Hz,  $J_1$  = 6.6 Hz), 5.00 (dd, 1H,  $J_{trans}$  = 17.0 Hz,  $J_{gem}$  = 1.6 Hz), 4.93 (dd, 1H,  $J_{cis}$  = 10.3 Hz,  $J_{gem}$  = 1.6 Hz), 4.02 (s, 1H), 2.66–2.48 (m, 4H), 2.44–2.29 (m, 2H), 2.22–1.85 (m, 4H), 1.67–1.51 (m, 2H);  $^{13}C$  NMR ( $CDCl_3$ )  $\delta$  208.4, 174.1, 137.8, 115.0, 110.7, 105.7, 82.2, 84.7, 59.8, 33.7, 28.8, 26.7, 26.1, 26.0, 24.3. HRMS: calcd for  $C_{16}H_{16}O_4Fe$  ( $M^+$ ),  $m/e$  328.0398; found,  $m/e$  328.0390.

**Tricarbonyl{2-(pent-4-enyl)-4-phenyl-6-hydroxybicyclo[3.3.0]octa-1,4-dien-3-one}iron (14).** This was obtained from 8: Yield = 75% (mixture of diastereomers);  $R_f$  = 0.12–0.25 (30% EtOAc in hexanes); IR ( $CCl_4$ ) 2071, 2026, 2000  $cm^{-1}$ ;  $^1H$  NMR ( $CDCl_3$ )  $\delta$  8.14 (dd, 2H,  $J_1 = 8.2$  Hz,  $J_2 = 1.5$  Hz), 7.36–7.25 (m, 3H), 5.70 (ddt, 1H,  $J_{trans}$  = 17.0 Hz,  $J_{cis}$  = 10.3 Hz,  $J_1 = 6.6$  Hz), 5.38 (t, 1H), 5.02 (dd, 1H,  $J_{trans}$  = 17.0 Hz,  $J_{gem}$  = 1.6 Hz), 4.96 (dd, 1H,  $J_{cis}$  = 10.3 Hz,  $J_{gem}$  = 1.6 Hz), 4.06 (d, 1H), 3.04–2.90 (m, 1H), 2.51–2.25 (m, 3H), 2.12–1.93 (m, 3H), 1.91–1.56 (m, 2H), 1.40–1.23 (m, 1H);  $^{13}C$  NMR ( $CDCl_3$ )  $\delta$  (1st diastereomer) 208.2, 171.0, 137.9, 131.4, 129.1, 128.3, 127.8, 115.1, 110.1, 104.8, 81.9, 77.7, 71.2, 35.7, 33.7, 28.9, 24.1, 23.0,  $\delta$  (2nd diastereomer) 208.0, 172.4, 137.9, 131.8, 128.7, 128.2, 127.6, 114.9, 111.3, 98.9, 85.1, 75.2, 72.3, 36.8, 33.8, 29.3, 23.7, 23.6. HRMS: calcd for  $C_{22}H_{20}O_5Fe$  ( $M^+$ ),  $m/e$  420.0660; found,  $m/e$  420.0641.

**Tricarbonyl{2-(pent-4-enyl)-4-(trimethylsilyl)-6-hydroxybicyclo[3.3.0]octa-1,4-dien-3-one}iron (15).** This was obtained from 9: Yield = 65% (mixture of diastereomers);  $R_f$  = 0.09 (10% EtOAc in hexanes); IR ( $CCl_4$ ) 2069, 2016, 1989

$cm^{-1}$ ;  $^1H$  NMR ( $CDCl_3$ )  $\delta$  5.78 (ddt, 1H,  $J_{trans}$  = 17.0 Hz,  $J_{cis}$  = 10.3 Hz,  $J_1 = 6.6$  Hz), 5.13 (t, 1H,  $J = 9.7$  Hz), 4.99 (dd, 1H,  $J_{trans}$  = 17.0 Hz,  $J_{gem}$  = 1.6 Hz), 4.94 (dd, 1H,  $J_{cis}$  = 10.3 Hz,  $J_{gem}$  = 1.6 Hz), 3.11 (s, 1H), 3.00–1.51 (m, 10H), 0.23 (s, 9H);  $^{13}C$  NMR ( $CDCl_3$ )  $\delta$  209, (179, 178), 138, 115, (114, 112), (113, 109), (87, 85), (72, 71), (66, 65), (36, 35), 34, 29, (24, 23), 24, (-0.1, -0.8). HRMS: calcd for  $C_{19}H_{24}O_5SiFe$  ( $M^+$ ),  $m/e$  416.0742; found,  $m/e$  416.0590.

**Tricarbonyl{2-(pent-4-enyl)-4-(trimethylsilyl)-6-oxobicyclo[3.3.0]octa-1,4-dien-3-one}iron (16).** To 132 mg (0.32 mmol) of 15 in 5 mL of  $CH_2Cl_2$  is added 103 mg (0.48 mmol) of PCC, and the reaction is stirred at room temperature overnight. Aqueous workup, drying over  $MgSO_4$  and removal of the solvent afford the desired ketone: Yield = 90%;  $R_f$  = 0.40 (20% EtOAc in hexanes); IR ( $CCl_4$ ) 2081, 2027, 2001, 1723, 1653  $cm^{-1}$ ;  $^1H$  NMR ( $CDCl_3$ )  $\delta$  5.77 (ddt, 1H,  $J_{trans}$  = 17.0 Hz,  $J_{cis}$  = 10.3 Hz,  $J_1 = 6.6$  Hz), 5.01 (dd, 1H,  $J_{trans}$  = 17.0 Hz,  $J_{gem}$  = 1.6 Hz), 4.96 (dd, 1H,  $J_{cis}$  = 10.3 Hz,  $J_{syn} = 1.6$  Hz), 3.14–2.91 (m, 2H), 2.75 (t, 2H,  $J = 5.3$  Hz), 2.35–2.01 (m, 4H), 1.76–1.52 (m, 2H);  $^{13}C$  NMR ( $CDCl_3$ )  $\delta$  207, 179, 137, 123, 115, 93, 92, 65, 64, 37, 34, 29, 24, 22, -0.6. HRMS: calcd for  $C_{19}H_{22}O_5SiFe$  ( $M$ ),  $m/e$  414.0586; found,  $m/e$  414.0586.

**Tricarbonyl{2-(pent-4-enyl)-4-(trimethylsilyl)-6-((trimethylsilyloxy)bicyclo[3.3.0]octa-1,4-dien-3-one}iron (17).** This was obtained from 10: Yield = 81% (mixture of diastereomers);  $R_f$  = 0.46–0.56 (20% EtOAc in hexanes); IR ( $CCl_4$ ) 2963, 2070, 2014, 1990, 1641, 1257  $cm^{-1}$ ;  $^1H$  NMR ( $CDCl_3$ )  $\delta$  5.77 (ddt, 1H,  $J_{trans}$  = 17.0 Hz,  $J_{cis}$  = 10.3 Hz,  $J_1 = 6.6$  Hz), 5.09 (t, 1H,  $J = 7.5$  Hz), 4.98 (dd, 1H,  $J_{trans}$  = 17.0 Hz,  $J_{gem}$  = 1.6 Hz), 4.93 (dd, 1H,  $J_{cis}$  = 10.3 Hz,  $J_{gem}$  = 1.6 Hz), 2.92–1.50 (m, 10H), 0.25 (2s, 9H), 0.15 (2s, 9H);  $^{13}C$  NMR ( $CDCl_3$ )  $\delta$  209 (2), (179, 178), 138, 115, (115, 112), (114, 109), (87, 84), (73, 72), (66, 65), 36 (2), 34, 29 (2), (24, 23), 24, (0.7, 0.2), (0.1, -0.9). HRMS: calcd for  $C_{22}H_{32}O_5Si_2Fe$  ( $M^+$ ),  $m/e$  488.1138; found,  $m/e$  488.1151.

**Tricarbonyl{2-(pent-4-enyl)-4-phenyl-6-((methoxymethylene)oxy)bicyclo[3.3.0]octa-1,4-dien-3-one}iron (18).** The corresponding alcohol 14 (145 mg, 0.35 mmol) is dissolved in  $CH_2Cl_2$  with 2.8 mmol of Hünigs base, 1.7 mmol of methoxymethyl chloride is added at 0 °C, and the reaction is warmed to 55 °C for 48 h. Aqueous workup, followed by drying over  $MgSO_4$  and flash chromatography, affords the desired methoxymethyl ether as a 2:1 mixture of diastereomers: Yield = 100% (mixture of diastereomers);  $R_f$  = 0.30–0.40 (30% EtOAc in hexanes); IR ( $CCl_4$ ) 2945, 2069, 2018, 1990, 1645  $cm^{-1}$ ;  $^1H$  NMR (1st diastereomer,  $R_f$  = 0.4) ( $CDCl_3$ )  $\delta$  8.05 (d, 2H,  $J = 7.3$  Hz), 7.32 (m, 3H), 5.82 (ddt, 1H,  $J_{trans}$  = 17.0 Hz,  $J_{cis}$  = 10.3 Hz,  $J_1 = 6.6$  Hz), 5.37 (d, 1H,  $J = 4.7$  Hz), 5.03 (dd, 1H,  $J_{trans}$  = 17.0 Hz,  $J_{gem}$  = 1.6 Hz), 4.98 (dd, 1H,  $J_{cis}$  = 10.3 Hz,  $J_{gem}$  = 1.6 Hz), 4.74 (d, 1H,  $J_{gem}$  = 7.0 Hz), 4.64 (d, 1H,  $J_{gem}$  = 7.0 Hz), 3.31 (s, 3H), 3.00–1.60 (m, 10H), (2nd diastereomer,  $R_f$  = 0.3) ( $CDCl_3$ )  $\delta$  7.90 (d, 2H,  $J = 7.3$  Hz), 7.26 (m, 3H), 5.79 (ddt, 1H,  $J_{trans}$  = 17.0 Hz,  $J_{cis}$  = 10.3 Hz,  $J_1 = 6.6$  Hz), 5.21 (t, 1H,  $J = 7.4$  Hz), 5.03 (dd, 1H,  $J_{trans}$  = 17.0 Hz,  $J_{gem}$  = 1.6 Hz), 4.96 (dd, 1H,  $J_{cis}$  = 10.3 Hz,  $J_{gem}$  = 1.6 Hz), 4.74 (s, 2H), 3.37 (s, 3H), 2.85–1.55 (m, 10H);  $^{13}C$  NMR (1st diastereomer,  $R_f$  = 0.4) ( $CDCl_3$ )  $\delta$  208, 173, 138, 132, 129, 128, 128, 115, 110, 99, 95, 84, 77, 56, 34, 33, 29, 24, 24, (2nd diastereomer,  $R_f$  = 0.3) ( $CDCl_3$ )  $\delta$  208, 171, 138, 131, 129, 128, 127, 115, 109, 101, 96, 82, 78, 76, 56, 34, 33, 29, 24, 23. HRMS: calcd for  $C_{21}H_{28}O_6SiFe$  ( $M^+$ ),  $m/e$  464.0922; found,  $m/e$  464.0922.

**Tricarbonyl{2-(pent-4-enyl)-4-(trimethylsilyl)-6-((methoxymethylene)oxy)bicyclo[3.3.0]octa-1,4-dien-3-one}iron (19).** The corresponding alcohol 15 (80 mg, 0.19 mmol) is dissolved in  $CH_2Cl_2$  with 1.52 mmol of Hünigs base, 0.80 mmol of methoxymethyl chloride are added at 0 °C, and the reaction is warmed to 55 °C for 48 h. Aqueous workup, followed by drying over  $MgSO_4$  and flash chromatography, affords the desired methoxymethyl ether as a mixture of diastereomers: Yield = 100% (mixture of diastereomers);  $R_f$  = 0.68 (20% EtOAc in hexanes); IR ( $CCl_4$ ) 2956, 2066, 2013,

1990, 1641  $\text{cm}^{-1}$ ;  $^1\text{H}$  NMR ( $\text{CDCl}_3$ )  $\delta$  5.76 (ddt, 1H,  $J_{\text{trans}} = 17.0$  Hz,  $J_{\text{cis}} = 10.3$  Hz,  $J_1 = 6.6$  Hz), 4.98 (dd, 1H,  $J_{\text{trans}} = 17.0$  Hz,  $J_{\text{gem}} = 1.6$  Hz), 4.94 (dd, 1H,  $J_{\text{cis}} = 10.3$  Hz,  $J_{\text{gem}} = 1.6$  Hz), 4.84 (2t, 1H,  $J = 6.7$  Hz), 4.74 (d, 1H,  $J_{\text{gem}} = 7.0$  Hz), 4.68 (d, 1H,  $J_{\text{gem}} = 7.0$  Hz), 3.38 (s, 3H), 2.92–1.50 (m, 10H), 0.25 (s, 9H);  $^{13}\text{C}$  NMR ( $\text{CDCl}_3$ )  $\delta$  208, (179, 178), 138, 127, 125, 120, 115, 114, 113, 107, 98, 95, 87, 78, 77, 76, 57, 56, 33, 28, 24, 24, 23, -0.1, -1. HRMS: calcd for  $\text{C}_{21}\text{H}_{28}\text{O}_6\text{SiFe}$  ( $\text{M}^+$ ),  $m/e$  460.1004; found,  $m/e$  460.1003.

**Decomplexation Reactions.** The general procedure consists in dissolving the desired complex (0.2 mmol) in 5 mL of *N,N*-dimethylacetamide and cooling to  $-10$  °C under air, followed by addition of 0.8 mmol of trimethylamine *N*-oxide. The mixture is then stirred for 1 h after which time the temperature is raised to  $-5$  °C followed by additional 11 h of stirring. With care taken to maintain the product at around  $0$  °C, 10 mL of ethyl ether is added, and the solution is filtered through a short column of Celite, diluted with additional 10 mL of ether, and washed at least 6 times with 15 mL aliquots of cold half-saturated brine. The organic layer is dried over  $\text{MgSO}_4$  in an ice bath and the solvent removed by rotary evaporation without heating. In all cases the crude  $^1\text{H}$  NMR spectrum shows very few peaks due to impurities; the GC trace on the other hand shows a purity, relative to the crude mixture, of around 70%. After purification by HPLC the yield is somewhat lower due to losses in the chromatographic process. The three different yields are reported in each case.

**2-(Pent-4-enyl)-4-phenylbicyclo[3.3.0]octa-1,5-dien-3-one (20).** This was obtained from **11**: Yield, crude 65%, GC 38%, HPLC 10%;  $R_f = 0.28$  (30% EtOAc in hexanes); GC Rt = 18.6 min; IR ( $\text{CCl}_4$ ) 3558, 2939, 1716, 1634  $\text{cm}^{-1}$ ;  $^1\text{H}$  NMR (400 MHz,  $\text{CDCl}_3$ )  $\delta$  7.38–7.24 (m, 5H), 6.16 (t, 1H,  $J = 2.6$  Hz), 5.79 (ddt, 1H,  $J_{\text{trans}} = 17.0$  Hz,  $J_{\text{cis}} = 10.3$  Hz,  $J_1 = 6.6$  Hz), 4.99 (dd, 1H,  $J_{\text{trans}} = 17.0$  Hz,  $J_{\text{gem}} = 1.6$  Hz), 4.94 (dd, 1H,  $J_{\text{cis}} = 10.3$  Hz,  $J_{\text{gem}} = 1.6$  Hz), 2.93 (s, 2H), 2.90 (m, 2H), 2.84 (m, 2H), 2.33 (m, 2H), 2.06 (m, 2H), 1.62 (m, 2H);  $^{13}\text{C}$  NMR ( $\text{CDCl}_3$ )  $\delta$  208, 182, 151, 140, 138, 130, 130, 128, 127, 125, 115, 76, 36, 34, 27, 26, 24. HRMS: calcd for  $\text{C}_{19}\text{H}_{20}\text{O}$  ( $\text{M}^+$ ),  $m/e$  264.1514; found,  $m/e$  264.1512.

**2-(Pent-4-enyl)bicyclo[3.3.0]octa-1,5-dien-3-one (21).** This was obtained from **12**: Yield, crude 61%, GC 45%, HPLC 12%;  $R_f = 0.32$  (20% EtOAc in hexanes); IR ( $\text{CCl}_4$ ) 2951, 1717, 1634  $\text{cm}^{-1}$ ;  $^1\text{H}$  NMR (400 MHz,  $\text{CDCl}_3$ )  $\delta$  5.96 (t, 1H,  $J = 2.5$

Hz), 5.79 (ddt, 1H,  $J_{\text{trans}} = 17.0$  Hz,  $J_{\text{cis}} = 10.3$  Hz,  $J_1 = 6.6$  Hz), 4.99 (dd, 1H,  $J_{\text{trans}} = 17.0$  Hz,  $J_{\text{gem}} = 1.6$  Hz), 4.93 (dd, 1H,  $J_{\text{cis}} = 10.3$  Hz,  $J_{\text{gem}} = 1.6$  Hz), 2.85 (s, 2H), 2.83 (m, 2H), 2.72 (m, 2H), 2.25 (t, 2H,  $J = 7.7$  Hz), 2.03 (q, 2H,  $J = 7.7$  Hz), 1.62 (p, 2H,  $J = 7.7$  Hz);  $^{13}\text{C}$  NMR ( $\text{CD}_3\text{Cl}$ )  $\delta$  208, 182, 144, 138, 134, 129, 115, 36, 36, 34, 27, 25, 23. HRMS: calcd for  $\text{C}_{13}\text{H}_{16}\text{O}$  ( $\text{M}^+$ ),  $m/e$  188.1201; found,  $m/e$  188.1202.

**2-(Pent-4-enyl)-4-phenyl-6-(methoxymethylene)oxy-bicyclo[3.3.0]octa-1,5-dien-3-one (22).** This was obtained from **18**: Yield, crude 58%, GC 37%, HPLC 8%;  $R_f = 0.40$  (20% EtOAc in hexanes); IR ( $\text{CCl}_4$ ) 2986, 2940, 2866, 1697  $\text{cm}^{-1}$ ;  $^1\text{H}$  NMR ( $\text{CDCl}_3$ )  $\delta$  7.28–7.05 (m, 5H), 5.73 (ddt, 1H,  $J_{\text{trans}} = 17.0$  Hz,  $J_{\text{cis}} = 10.3$  Hz,  $J_1 = 6.6$  Hz), 4.92 (dd, 1H,  $J_{\text{trans}} = 17.0$  Hz,  $J_{\text{gem}} = 1.6$  Hz), 4.86 (dd, 1H,  $J_{\text{cis}} = 10.3$  Hz,  $J_{\text{gem}} = 1.6$  Hz), 4.82 (d, 1H,  $J = 6.2$  Hz), 4.54 (d, 1H,  $J = 6.2$  Hz), 3.96 (s, 1H), 3.24 (s, 3H), 2.98–2.80 (m, 4H), 2.16 (td, 2H,  $J_1 = 2.9$  Hz,  $J_2 = 7.5$  Hz), 1.96 (dt, 2H,  $J_1 = 6.6$  Hz,  $J_2 = 7.5$  Hz), 1.50 (p, 2H,  $J = 7.5$  Hz);  $^{13}\text{C}$  NMR ( $\text{CDCl}_3$ )  $\delta$  206, 183, 157, 139, 129, 128, 127, 127, 120, 115, 95, 57, 53, 34, 34, 27, 23, 23. HRMS: calcd for  $\text{C}_{21}\text{H}_{24}\text{O}_3$  ( $\text{M}^+$ ),  $m/e$  324.1725; found,  $m/e$  324.1721.

**2-(Pent-4-enyl)-6-((methoxymethylene)oxy)bicyclo[3.3.0]octa-1,5-dien-3-one (23).** This was obtained from **19**: Yield, crude 75%, GC 49%, HPLC 15%;  $R_f = 0.30$  (30% EtOAc in hexanes); IR ( $\text{CCl}_4$ ) 2933, 1694, 1669, 1620  $\text{cm}^{-1}$ ;  $^1\text{H}$  NMR ( $\text{CDCl}_3$ )  $\delta$  5.79 (ddt, 1H,  $J_{\text{trans}} = 17.0$  Hz,  $J_{\text{cis}} = 10.3$  Hz,  $J_1 = 6.6$  Hz), 5.05 (s, 2H), 4.98 (dd, 1H,  $J_{\text{trans}} = 17.0$  Hz,  $J_{\text{gem}} = 1.6$  Hz), 4.92 (dd, 1H,  $J_{\text{cis}} = 10.3$  Hz,  $J_{\text{gem}} = 1.6$  Hz), 3.43 (s, 3H), 2.98 (s, 2H), 2.84 (m, 2H), 2.75 (m, 2H), 2.19 (t, 2H,  $J = 7.6$  Hz), 2.03 (q, 2H,  $J = 7.6$  Hz), 1.54 (p, 2H,  $J = 7.6$  Hz);  $^{13}\text{C}$  NMR ( $\text{CDCl}_3$ )  $\delta$  207, 183, 156, 139, 129, 115, 114, 95, 57, 37, 35, 34, 27, 23, 23. HRMS: calcd for  $\text{C}_{15}\text{H}_{20}\text{O}_3$  ( $\text{M}^+$ ),  $m/e$  248.1412 found,  $m/e$  248.1413.

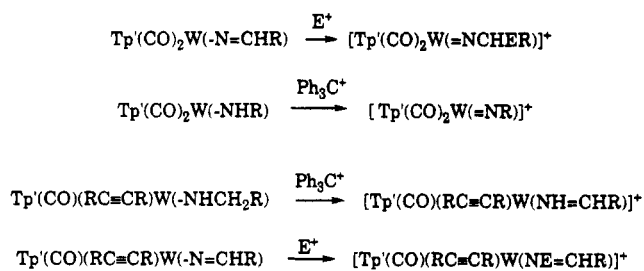
**Acknowledgment.** We are grateful to the National Science Foundation (Grant CHE 93-08105 to A.J.P.), the CNR (Italy; to A.P.) and the Fulbright Commission (to A.P.) for financial support of this research.

**Supporting Information Available:** Figures showing NMR spectra (49 pages). Ordering information is given on any current masthead page.

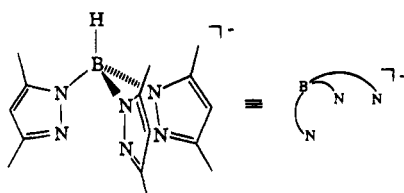
OM950465B



## Scheme 3



Tp = hydridotris(3,5-dimethylpyrazolyl)borate



$(CO)_2WNHR$  with trityl cation generates a nitrene ligand in  $[Tp'(CO)_2W=N(R)]^+$ , while hydride abstraction from  $Tp'(CO)(PhC\equiv CMe)WNHCH_2R$  with trityl cation generates an imine ligand in  $[Tp'(CO)(PhC\equiv CMe)W(NH=CHR)]^+$ .<sup>4</sup> Similarly, electrophilic addition to  $Tp'(CO)_2WN=CHR$  generates a nitrene ligand as  $[Tp'(CO)_2W=N(CHER)]^+$  forms,<sup>2,3</sup> while proton addition to  $Tp'(CO)(PhC\equiv CMe)WN=CHR$  converts a metalloimine ligand to an imine ligand in  $[Tp'(CO)(PhC\equiv CMe)W(NH=CHR)]^+$ <sup>5</sup> (Scheme 3). In the dicarbonyl system, it is the metal that acts as the electron reservoir and provides electrons as it is oxidized to W(IV), while with an alkyne in the coordination sphere it is the nitrogen that provides electrons and forms the dative bond.

Cationic metal carbonyl alkyne complexes are electrophilic at the carbonyl and alkyne carbons. Extended Huckel calculations indicate that both the carbonyl and alkyne carbons have substantial positive charge and contribute to the LUMO. Reaction of the cationic dicarbonyl alkyne complexes  $[Tp'(CO)_2W(RC_2R)]^+[BF_4]^-$  with nucleophiles has generated a variety of products:  $\eta^1$ -acyl complexes,<sup>6</sup>  $\eta^2$ -vinyl complexes,<sup>7</sup>  $\eta^3$ -allyl complexes (when an internal alkyne bearing  $\beta$ -hydrogens is the substrate),<sup>7</sup> and carbyne complex (via initial formation of an  $\eta^2$ -vinyl complex).<sup>8</sup> Similar reactivities were also observed in Green's  $CpL_2Mo^+$  system.<sup>9</sup>

This paper reports a study of the reactivity of cationic four-electron donor terminal alkyne complexes with amines as nucleophiles. We report here (1) the formation of amido complexes by amine addition across terminal alkyne ligands followed by rearrangement; (2) a crystal structure of a neutral amido complex,  $Tp'(CO)_2WN(CH_2Ph)(CH=CHPh)$ ; (3) formation of a cat-

ionic vinyl-nitrene ligand by oxidation of the amido ligand; (4) reduction of the vinyl nitrene ligand to a saturated nitrene by an  $H^-/H^+$  addition sequence.

## Experimental Section

**General Methods.** Manipulations involving air sensitive reagents were performed under a dry nitrogen atmosphere with standard Schlenk techniques. Solvents were purified as follows: methylene chloride was distilled from  $P_2O_5$ ;  $Et_2O$ , THF, and hexanes were distilled from potassium benzophenone ketyl. Other solvents were purged with  $N_2$  gas prior to use. Alkyne complexes of the type  $[Tp'(CO)_2W(RC\equiv CH)]^+[BF_4]^-$  were synthesized according to literature methods.<sup>10</sup> Other reagents were used as obtained from commercial sources.

Infrared spectra were recorded on a Mattson Polaris FT IR spectrometer. NMR spectra were recorded on a Varian XL-400 (400 MHz) spectrometer. Elemental analyses were performed by Oneida Research Services Inc., Whitesboro, NY.

Cyclic voltammograms were obtained on a Bioanalytical Systems CV-27 instrument; samples were dissolved in dry acetonitrile containing 0.1 M  $[NEt_4][PF_6]$  as supporting electrolyte. The voltammograms were obtained at scan rates of 5 and 10 mV/s, and  $E_{1/2}$  values were determined relative to ferrocene/ferrocenium as an internal standard. Scans were made from -100 mV to +750 mV. A three-electrode arrangement with a working electrode (graphite), auxiliary electrode (platinum), and reference electrode (Ag/AgCl) was used.

**Syntheses.**  $Tp'(CO)_2WN(Ph)(CH=CHPh)$  (**1a**). In a representative synthesis, aniline (0.40 mL, 4.4 mmol) in 10 mL of THF was added slowly, with stirring, to a solution of  $[Tp'(CO)_2W(PhC\equiv CH)]^+[BF_4]^-$  (1.00 g, 1.38 mmol) in 50 mL of THF. The solution color changed from green to brown as the solution was stirred for 6 h. Solvent removal left a dark brown tar which was chromatographed on alumina with toluene as eluent. The red band that eluted was collected, and the solvent was evaporated. Recrystallization from  $CH_2Cl_2$ /hexanes yielded red-brown crystals (0.71 g, 71%) of  $Tp'(CO)_2WN(Ph)(CH=CHPh)$  (**1a**): IR (KBr,  $cm^{-1}$ ),  $\nu_{BH} = 2549$ ;  $\nu_{CO} = 1911, 1793$ .  $^1H$  NMR ( $CD_2Cl_2$ ,  $\delta$ ): 7.36 (d,  $^3J_{HH} = 14.4$  Hz,  $CH=CHPh$ ), 7.43, 7.14, 7.04, 6.84 (m,  $2C_6H_5$ ), 6.05, 5.92 (1:2,  $Tp'CH$ ), 5.59 (d,  $^3J_{HH} = 14.4$  Hz,  $CH=CHPh$ ), 2.62, 2.42, 2.37, 2.04 (6:3:3:6,  $Tp'CCH_3$ ).  $^{13}C$  NMR ( $CD_2Cl_2$ ,  $\delta$ ): 253.5 ( $^1J_{WC} = 176$  Hz, CO), 153.5 (d,  $^1J_{HC} = 165$  Hz,  $CH=CHPh$ ), 164.3, 161.9, 151.7, 147.6, 145.6, 138.3 ( $2C_{ipso}$  and  $6Tp'CCH_3$ ), 129.0, 128.5, 126.9, 126.6, 125.6, 124.1 ( $Ph$ ), 111.3 (d,  $^1J_{HC} = 154$  Hz,  $CH=CHPh$ ), 109.3, 107.0 (1:2,  $Tp'CH$ ), 16.9, 16.5, 13.1, 12.7 (1:2:1:2,  $Tp'CCH_3$ ). Anal. Calcd for **1a**,  $WC_{31}H_{34}N_7O_2B$ : C, 50.91; H, 4.65; N, 13.41. Found: C, 50.53; H, 5.00; N, 13.66.

$Tp'(CO)_2WN(Bu^t)(CH=CHPh)$  (**1b**). This product was prepared according to the procedure described above for **1a** except *tert*-butylamine was added as the nucleophile (red-brown, 65%). IR (KBr,  $cm^{-1}$ ),  $\nu_{BH} = 2539$ ;  $\nu_{CO} = 1903, 1776$ .  $^1H$  NMR ( $CD_2Cl_2$ ,  $\delta$ ): 7.09, 6.73 (m,  $C_6H_5$ ), 6.44 (d,  $^3J_{HH} = 14.8$  Hz,  $CH=CHPh$ ), 5.93, 5.80 (1:2,  $Tp'CH$ ), 4.88 (d,  $^3J_{HH} = 14.8$  Hz,  $CH=CHPh$ ), 2.48, 2.42, 2.33, 1.93 (3:6:3:6,  $Tp'CCH_3$ ), 1.64 [ $C(CH_3)_3$ ].  $^{13}C$  NMR ( $CD_2Cl_2$ ,  $\delta$ ): 257.6 ( $^1J_{WC} = 176$  Hz, CO), 151.2 (d of d,  $^1J_{HC} = 162$  Hz,  $^2J_{HC} = 4$  Hz,  $CH=CHPh$ ), 160.5, 151.5, 146.5, 145.9 (2:1:2:1,  $Tp'CCH_3$ ), 138.8, 128.5, 126.1, 125.7 ( $Ph$ ), 116.3 (d of t,  $^1J_{HC} = 156$  Hz,  $^2J_{HC} = 4$  Hz,  $CH=CHPh$ ), 108.4, 106.9 (1:2,  $Tp'CH$ ), 77.3 [ $C(CH_3)_3$ ], 33.0 [ $C(CH_3)_3$ ], 16.4, 16.1, 13.1, 12.4 (2:1:1:2,  $Tp'CCH_3$ ). Anal. Calcd for **1b**,  $WC_{29}H_{28}N_7O_2B$ : C, 48.97; H, 5.35; N, 13.79. Found: C, 48.76; H, 5.32; N, 13.51.

$Tp'(CO)_2WN(CH_2Ph)(CH=CHPh)$  (**1c**). This product was prepared according to the procedure described above for **1a** except benzylamine was used as the amine reagent (red crystals, 75%). IR (KBr,  $cm^{-1}$ ),  $\nu_{BH} = 2544$ ;  $\nu_{CO} = 1898, 1778$ .  $^1H$  NMR ( $CD_2Cl_2$ ,  $\delta$ ): 7.20 (d,  $^3J_{HH} = 14.8$  Hz,  $CH=CHPh$ ),

- (4) Philipp, C. C.; Templeton, J. L. Unpublished results.  
 (5) (a) Feng, S. G.; Templeton, J. L. *Organometallics* **1992**, *11*, 1295. (b) Feng, S. G.; Templeton, J. L. *J. Am. Chem. Soc.* **1989**, *111*, 6477.  
 (6) Feng, S. G.; White, P. S.; Templeton, J. L. *Organometallics* **1993**, *12*, 2131.  
 (7) Feng, S. G.; Templeton, J. L. *Organometallics* **1992**, *11*, 2168.  
 (8) Feng, S. G.; Templeton, J. L. Unpublished results.  
 (9) (a) Green, M. J. *Organomet. Chem.* **1986**, *300*, 93. (b) Allen, S. R.; Beavor, R. G.; Green, M.; Norman, N. C.; Orpen, A. G.; Williams, I. D. *J. Chem. Soc., Dalton Trans.* **1985**, 435. (c) Allen, S. R.; Green, M.; Norman, N. C.; Paddick, K. E.; Orpen, A. G. *J. Chem. Soc., Dalton Trans.* **1983**, 1625. (d) Allen, S. R.; Baker, P. K.; Barnes, S. G.; Bottrill, M.; Green, M.; Orpen, A. G.; Williams, I. D.; Welch, A. J. *J. Chem. Soc., Dalton Trans.* **1983**, 1625.

- (10) Feng, S. G.; Philipp, C. C.; Gamble, A. S.; White, P. S.; Templeton, J. L. *Organometallics* **1991**, *10*, 3504.

7.64, 7.35, 7.33, 7.16, 7.07, 6.83 (m,  $2C_6H_5$ ), 6.65, 5.83 (1:2, Tp'CH), 6.00 (d,  $^3J_{HH} = 14.8$  Hz, CH=CHPh), 5.49 ( $CH_2Ph$ ), 2.60, 2.49, 2.43, 1.70 (6:3:3:6, Tp'CCH<sub>3</sub>). <sup>13</sup>C NMR ( $CD_2Cl_2$ ,  $\delta$ ): 256.2 ( $^1J_{WC} = 176$  Hz, CO), 151.1 (d,  $^1J_{HC} = 162$  Hz, CH=CHPh), 161.6, 151.7, 147.4, 145.5 (1:2:1:2, Tp'CCH<sub>3</sub>), 139.3, 138.8, 130.1, 129.0, 128.4, 127.6, 126.7, 126.2 (*Ph*), 110.3 (d,  $^1J_{HC} = 154$  Hz, CH=CHPh), 109.0, 106.8 (1:2, Tp'CH), 81.5 ( $CH_2Ph$ ), 16.8, 15.8, 13.1, 12.6 (1:2:1:2, Tp'CCH<sub>3</sub>). Anal. Calcd for **1c**,  $WC_{32}H_{36}N_7O_2B$ : C, 51.56; H, 4.83; N, 13.16. Found: C, 50.99; H, 4.90; N, 12.95.

**Tp'(CO)<sub>2</sub>WN(CH<sub>2</sub>CH<sub>2</sub>CH<sub>2</sub>CH<sub>3</sub>)(CH=CHPh) (1d)**. This product was prepared according to the procedure described above for **1a** except *n*-butylamine was the added amine (red-brown crystals, 70%). IR (KBr,  $cm^{-1}$ ),  $\nu_{BH} = 2549$ ;  $\nu_{CO} = 1908$ , 1709. <sup>1</sup>H NMR ( $CDCl_3$ ,  $\delta$ ): 7.00 (d,  $^3J_{HH} = 14.8$  Hz, CH=CHPh), 7.18, 7.08, 6.89 (m,  $C_6H_5$ ), 6.00 (d,  $^3J_{HH} = 14.8$  Hz, CH=CHPh), 5.98, 5.78 (1:2, Tp'CH), 4.42 (m,  $CH_2CH_2CH_2CH_3$ ), 2.56, 2.46, 2.39, 1.78 (6:3:3:6, Tp'CCH<sub>3</sub>), 1.94 (m,  $CH_2CH_2CH_2CH_3$ ), 1.50 (m,  $CH_2CH_2CH_2CH_3$ ), 1.05 (t,  $^3J_{HH} = 7.2$  Hz,  $CH_2CH_2CH_2CH_3$ ). <sup>13</sup>C NMR ( $CDCl_3$ ,  $\delta$ ): 255.9 ( $^1J_{WC} = 176$  Hz, CO), 149.9 (d,  $^1J_{HC} = 165$  Hz, CH=CHPh), 161.0, 151.0, 146.3, 144.3 (1:2:1:2, Tp'CCH<sub>3</sub>), 138.6, 128.7, 126.2, 126.1 (*Ph*), 105.9 (d,  $^1J_{HC} = 152$  Hz, CH=CHPh), 108.7, 106.6 (1:2, Tp'CH), 76.4 ( $CH_2CH_2CH_2CH_3$ ), 31.9 ( $CH_2CH_2CH_2CH_3$ ), 20.5 ( $CH_2CH_2CH_2CH_3$ ), 14.0 ( $CH_2CH_2CH_2CH_3$ ), 16.8, 15.7, 12.9, 12.4 (1:2:1:2, Tp'CCH<sub>3</sub>). Anal. Calcd for **1d**,  $WC_{25}H_{28}N_7O_2B$ : C, 48.97; H, 5.35; N, 13.79. Found: C, 48.42; H, 5.35; N, 13.08.

**Tp'(CO)<sub>2</sub>WN(CH<sub>2</sub>Ph)(CH=CHBu<sup>t</sup>) (1e)**. This product was prepared according to the procedure described above for **1a** except [ $Tp'(CO)_2W(Bu^tC=CH)$ ][BF<sub>4</sub>] was used as the metal reagent and benzylamine was the amine (yellow-brown crystals, 45%). IR (KBr,  $cm^{-1}$ ),  $\nu_{BH} = 2538$ ;  $\nu_{CO} = 1903$ , 1782. <sup>1</sup>H NMR ( $CD_2Cl_2$ ,  $\delta$ ): 7.08 (d,  $^3J_{HH} = 14.4$  Hz, CH=CHBu<sup>t</sup>), 7.11, 6.91 (m,  $C_6H_5$ ), 5.94, 5.79 (1:2, Tp'CH), 5.45 (d,  $^3J_{HH} = 14.4$  Hz, CH=CHBu<sup>t</sup>), 4.32 ( $CH_2Ph$ ), 2.58, 2.41, 2.36, 1.62 (6:3:3:6, Tp'CCH<sub>3</sub>), 1.12 [ $C(CH_3)_3$ ]. <sup>13</sup>C NMR ( $CD_2Cl_2$ ,  $\delta$ ): 255.5 ( $^1J_{WC} = 176$  Hz, CO), 157.3 (d,  $^1J_{HC} = 168$  Hz, CH=CHBu<sup>t</sup>), 160.4, 152.6, 146.8, 145.9 (2:1:2:1, Tp'CCH<sub>3</sub>), 136.7, 129.1, 127.8, 126.6 (*Ph*), 125.2 (d,  $^1J_{HC} = 149$  Hz, CH=CHBu<sup>t</sup>), 108.3, 106.9 (1:2, Tp'CH), 71.1 ( $CH_2Ph$ ), 32.6 [ $C(CH_3)_3$ ], 30.0 [ $C(CH_3)_3$ ], 16.7, 15.5, 13.0, 12.7 (1:2:1:2, Tp'CCH<sub>3</sub>). Anal. Calcd for **1e**,  $WC_{30}H_{40}N_7O_2B$ : C, 49.69; H, 5.52; N, 13.52. Found: C, 48.99; H, 5.49; N, 13.43.

**Tp'(CO)<sub>2</sub>WN(CH<sub>2</sub>Ph)(CH=CHBu<sup>n</sup>) (1f, 1f', and 1f'')**. This product was prepared according to the procedure described above for **1a** except [ $Tp'(CO)_2W(Bu^nC=CH)$ ][BF<sub>4</sub>] was used as the metal reagent and benzylamine was the amine (green-brown crystals, 60%). IR (KBr,  $cm^{-1}$ ),  $\nu_{BH} = 2543$ ;  $\nu_{CO} = 1908$ , 1786. NMR indicates that this green-brown product contains two isomers, **1f** and **1f'**, in a 4:1 ratio. <sup>1</sup>H NMR ( $CD_2Cl_2$ ,  $\delta$ ) for **1f**: 7.28 (d,  $^3J_{HH} = 14$  Hz, CH=CHBu<sup>n</sup>), 7.12, 6.94 (m,  $C_6H_5$ ), 5.95, 5.78 (1:2, Tp'CH), 5.46 (d of t,  $^3J_{HH} = 14$  Hz,  $^3J_{HH} = 7$  Hz, CH=CHBu<sup>n</sup>), 4.37 ( $CH_2Ph$ ), 2.58, 2.41, 2.36, 1.63 (6:3:3:6, Tp'CCH<sub>3</sub>), 1.88, 1.42, 1.36, 0.94 (*Bu<sup>n</sup>*). <sup>13</sup>C NMR ( $CD_2Cl_2$ ,  $\delta$ ) for **1f**: 255.7 ( $^1J_{WC} = 176$  Hz, CO), 161.2 (d,  $^1J_{HC} = 168$  Hz, CH=CHBu<sup>n</sup>), 160.4, 152.6, 146.7, 145.9 (1:2:1:2, Tp'CCH<sub>3</sub>), 136.7, 128.9, 127.9, 126.6 (*Ph*), 114.5 (d,  $^1J_{HC} = 150$  Hz, CH=CHBu<sup>n</sup>), 108.3, 106.9 (1:2, Tp'CH), 70.9 (t,  $^1J_{HC} = 140$  Hz,  $CH_2Ph$ ), 32.2, 30.5, 22.5, 14.1 (*Bu<sup>n</sup>*), 16.7, 15.6, 13.0, 12.7 (1:2:1:2, Tp'CCH<sub>3</sub>). <sup>1</sup>H NMR ( $CD_2Cl_2$ ,  $\delta$ ) for **1f'**: 7.57, 7.12 (m,  $C_6H_5$ ), 5.96, 5.84 (1:2, Tp'CH), 5.70 (d of t,  $^3J_{HH} = 10.4$  Hz,  $^4J_{HH} = 1.6$  Hz, CH=CHBu<sup>n</sup>), 5.55 ( $CH_2Ph$ ), 4.19 (d of t,  $^3J_{HH} = 10.4$  Hz,  $^3J_{HH} = 7.2$  Hz, CH=CHBu<sup>n</sup>), 2.55, 2.43, 2.36, 1.68 (6:3:3:6, Tp'CCH<sub>3</sub>), 1.97, 1.50–1.30, 0.89 (*Bu<sup>n</sup>*). <sup>13</sup>C NMR ( $CD_2Cl_2$ ,  $\delta$ ) for **1f'**: 256.2 ( $^1J_{WC} = 177$  Hz, CO), 150.6 (d,  $^1J_{HC} = 168$  Hz, CH=CHBu<sup>n</sup>), 160.9, 151.5, 146.8, 145.5 (1:2:1:2, Tp'CCH<sub>3</sub>), 139.8, 129.8, 128.2, 127.4 (*Ph*), 108.1 (d,  $^1J_{HC} = 151$  Hz, CH=CHBu<sup>n</sup>), 108.6, 106.8 (1:2, Tp'CH), 82.4 ( $CH_2Ph$ ), 32.7, 30.1, 22.9, 14.1 (*Bu<sup>n</sup>*), 16.6, 15.9, 13.0, 12.6 (1:2:1:2, Tp'CCH<sub>3</sub>). Stirring the green-brown crystalline solid in methanol for two days and then recrystallizing gives **1f** and another isomer **1f''**

(yellow-brown) in a 1:3 ratio. The isomer ratio changed to 2:3 over five days in the NMR sample (in  $CD_2Cl_2$ ). <sup>1</sup>H NMR ( $CD_2Cl_2$ ,  $\delta$ ) for **1f''**: 7.57, 7.32, 7.26 (m,  $C_6H_5$ ), 6.38 (d,  $^3J_{HH} = 14$  Hz, CH=CHBu<sup>n</sup>), 6.01, 5.84 (1:2, Tp'CH), 5.18 (d of t,  $^3J_{HH} = 14$  Hz,  $^3J_{HH} = 7.2$  Hz, CH=CHBu<sup>n</sup>), 5.28 ( $CH_2Ph$ ), 2.55, 2.50, 2.40, 1.73 (6:3:3:6, Tp'CCH<sub>3</sub>), 1.17, 1.03, 0.75 (*Bu<sup>n</sup>*). Anal. Calcd for  $WC_{30}H_{40}N_7O_2B$ : C, 48.97; H, 5.35; N, 13.79. Found: C, 48.76; H, 5.32; N, 13.51.

**[Tp'(CO)<sub>2</sub>W=N(CH=CHPh)][BF<sub>4</sub>] (2)**. To a cold ( $-40$  °C) solution of  $Tp'(CO)_2WN(CH_2Ph)(CH=CHPh)$  (0.60 g, 0.81 mmol) in 50 mL of  $CH_2Cl_2$  was added 1 equiv of [ $Ph_3C$ ][BF<sub>4</sub>] (0.27 g, 0.81 mmol) in 10 mL of  $CH_2Cl_2$ . The solution was allowed to warm to room temperature and then it was stirred for 10 h. The solvent volume was reduced to ca. 5 mL, and the solution was filtered into 30 mL of  $Et_2O$ . The solid was isolated by filtration and recrystallized from  $CH_2Cl_2/Et_2O$  to yield red-brown crystals of **2** (0.30 g, 47%). IR (KBr,  $cm^{-1}$ ),  $\nu_{BH} = 2563$ ;  $\nu_{CO} = 2079$ , 2002. <sup>1</sup>H NMR ( $CD_2Cl_2$ ,  $\delta$ ): 7.31, 7.18, 7.16 (m,  $C_6H_5$ ), 7.25 (d,  $^3J_{HH} = 14$  Hz, CH=CHPh), 6.92 (d,  $^3J_{HH} = 14$  Hz, CH=CHPh), 5.98, 5.80 (2:1, Tp'CH), 2.30, 2.29, 2.21, 2.19 (6:6:3:3, Tp'CCH<sub>3</sub>). <sup>13</sup>C NMR ( $CD_2Cl_2$ ,  $\delta$ ): 216.8 ( $^1J_{WC} = 155$  Hz, CO), 153.3, 152.9, 149.2, 147.6 (1:2:1:2, Tp'CCH<sub>3</sub>), 143.5 (d,  $^1J_{HC} = 178$  Hz,  $^2J_{WC} = 33$  Hz, CH=CHPh), 140.0 (d,  $^1J_{HC} = 156$  Hz, CH=CHPh), 132.4, 131.1, 129.3, 127.5 (*Ph*), 109.1, 108.5 (1:2, Tp'CH), 15.7, 15.4, 13.0, 12.4 (1:2:1:2, Tp'CCH<sub>3</sub>). Anal. Calcd for **2**,  $WC_{23}H_{31}N_7O_2B_2F_4$ : C, 40.40; H, 4.05; N, 13.09. Found: C, 40.11; H, 4.12; N, 13.17.

**Tp'(CO)<sub>2</sub>WN=CHCH<sub>2</sub>Ph (3)**. To a cold ( $-40$  °C) solution of **2** (0.46 g, 0.62 mmol) in 50 mL of acetonitrile was added LiBH<sub>4</sub> (0.10 g, 4.6 mmol) with stirring. As the solution was allowed to warm to room temperature, the color changed from red to green. Solvent removal left a green tar which was chromatographed on alumina with  $CH_2Cl_2$ /hexanes (1:3) as the eluent. The blue band that eluted was collected, and the solvent was evaporated. Recrystallization from  $CH_2Cl_2$ /hexanes yielded blue crystals (0.14 g, 34%). IR (KBr,  $cm^{-1}$ ),  $\nu_{BH} = 2542$ ;  $\nu_{CO} = 1928$ , 1813. <sup>1</sup>H NMR ( $CD_2Cl_2$ ,  $\delta$ ): 7.32, 7.24 (m,  $C_6H_5$ ), 5.94, 5.93 (2:1, Tp'CH), 4.21 (d,  $^3J_{HH} = 6$  Hz, N=CHCH<sub>2</sub>Ph), 3.23 (t,  $^3J_{HH} = 6$  Hz,  $^3J_{WH} = 5.6$  Hz, N=CHCH<sub>2</sub>Ph), 2.51, 2.48, 2.41, 2.31 (6:3:3:6, Tp'CCH<sub>3</sub>). <sup>13</sup>C NMR ( $CD_2Cl_2$ ,  $\delta$ ): 241.4 ( $^1J_{WC} = 171$  Hz,  $^2CO$ ), 151.7 (d of t,  $^1J_{HC} = 176$  Hz,  $^2J_{HC} = 7.6$  Hz,  $^2J_{WC} = 27$  Hz, N=CHCH<sub>2</sub>Ph), 157.5, 152.1, 146.6, 145.4 (1:2:1:2, Tp'CCH<sub>3</sub>), 140.2, 129.0, 126.9 (*Ph*), 107.9, 106.8 (1:2, Tp'CH), 32.2 (t,  $^1J_{HC} = 129$  Hz,  $CH_2Ph$ ), 16.5, 16.3, 12.9, 12.7 (2:1:1:2, Tp'CCH<sub>3</sub>). Anal. Calcd for **3**,  $WC_{25}H_{28}N_7O_2B$ : C, 45.80; H, 4.58; N, 14.96. Found: C, 45.66; H, 4.51; N, 14.95.

**[Tp'(CO)<sub>2</sub>W=NCH<sub>2</sub>CH<sub>2</sub>Ph][BF<sub>4</sub>] (4)**. To a cold (0 °C) solution of  $Tp'(CO)_2WN=CHCH_2Ph$  (**3**) (0.50 g, 0.76 mmol) in 20 mL of  $CH_2Cl_2$  was added 1 equiv of HBF<sub>4</sub> with stirring, resulting in a color change from blue to red-brown. The solution was allowed to warm to room temperature. The solvent volume was reduced to ca. 5 mL, and the solution was filtered into 30 mL of  $Et_2O$ . The red crystalline solid was isolated by filtration, washed with  $2 \times 5$  mL of  $Et_2O$ , and dried in vacuo (0.52 g, 92%). Recrystallization from  $CH_2Cl_2/Et_2O$  yielded red crystals of **4**. IR (KBr,  $cm^{-1}$ ),  $\nu_{BH} = 2577$ ;  $\nu_{CO} = 2076$ , 1996. <sup>1</sup>H NMR ( $CD_2Cl_2$ ,  $\delta$ ): 7.38–7.24 (m,  $C_6H_5$ ), 6.17, 5.97 (2:1, Tp'CH), 4.12 (t,  $^3J_{HH} = 6.8$  Hz,  $^3J_{WH} = 8.8$  Hz,  $CH_2CH_2Ph$ ), 3.16 (t,  $^3J_{HH} = 6.8$  Hz,  $CH_2CH_2Ph$ ), 2.48, 2.40, 2.36, 2.33 (6:6:3:3, Tp'CCH<sub>3</sub>). <sup>13</sup>C NMR ( $CD_2Cl_2$ ,  $\delta$ ): 216.9 ( $^1J_{WC} = 157$  Hz,  $^2CO$ ), 153.8, 153.1, 149.7, 148.2 (1:2:1:2, Tp'CCH<sub>3</sub>), 136.5, 129.3, 128.9, 127.8 ( $C_6H_5$ ), 109.1, 108.5 (1:2, Tp'CH), 68.1 (t,  $^1J_{HC} = 142$  Hz,  $^2J_{WC} = 26$  Hz,  $CH_2CH_2Ph$ ), 36.8 (t,  $^1J_{HC} = 130$  Hz,  $CH_2CH_2Ph$ ), 15.8, 15.7, 13.1, 12.5 (2:1:1:2, Tp'CCH<sub>3</sub>). Anal. Calcd for **4**,  $WC_{25}H_{31}N_7O_2B_2F_4$ : C, 40.38; H, 4.17; N, 13.19. Found: C, 40.26; H, 4.11; N, 13.18.

**Collection of Diffraction Data.** A red-brown cube of  $Tp'(CO)_2WN(CH_2Ph)(CH=CHPh)$  (**1c**) of dimensions  $0.30 \times 0.20 \times 0.15$  mm was selected and mounted on a glass wand coated with epoxy. Diffraction data were collected on a Rigaku automated diffractometer. Twenty-five centered reflections

**Table 1. Crystallographic Data Collection Parameters for  $Tp'(CO)_2W(N)(CH_2Ph)(CH=CHPh)$  (1c)**

molecular formula	$WC_{32}H_{36}N_7O_2B$
formula weight, g/mol	745.33
crystal dimensions, mm	$0.30 \times 0.20 \times 0.15$
space group	$P\bar{1}$
cell parameters	
$a$ , Å	12.497(5)
$b$ , Å	13.414(5)
$c$ , Å	10.992(5)
$\alpha$ , deg	111.94(3)
$\beta$ , deg	91.47(4)
$\gamma$ , deg	72.60(3)
vol, Å <sup>3</sup>	1623(1)
$Z$	2
density calcd, g/cm <sup>3</sup>	1.525
Collection and Refinement Parameters	
radiation (wavelength, Å)	Mo K $\alpha$ (0.70930)
monochromator	graphite
linear abs coeff, cm <sup>-1</sup>	36.7
scan type	$\theta/2\theta$
$2\theta$ limit	50°
quadrants collected	$\pm h, \pm k, \pm l$
total no. reflections	6005
data with $I \geq 2.5\sigma(I)$	4632
$R$	4.0%
$R_w$	4.5%
GOF	1.32
no. of parameters	389
largest parameter shift (shift/error ratio)	0.046

were found in the region  $23.0^\circ < 2\theta < 30.0^\circ$ , and when these were refined by least-squares calculations they indicated a triclinic cell. The cell parameters are listed in Table 1. Diffraction data were collected in the hemisphere  $\pm h, \pm k, \pm l$  under the conditions specified in Table 1. Only data with  $I > 2.5\sigma(I)$  were used in structure solution and refinement.<sup>11</sup> The data were corrected for Lorentz-polarization effects during the final stages of data reduction.

**Solution and Refinement of the Structure.** Space group  $P\bar{1}$  was confirmed, and the position of the tungsten was deduced from the three-dimensional Patterson function. The positions of the remaining non-hydrogen atoms were determined through subsequent Fourier and difference Fourier calculations.

The 43 non-hydrogen atoms were refined anisotropically. Hydrogen atom positions were calculated by using a C-H distance of 0.96 Å and an isotropic thermal parameter calculated from the anisotropic values for the atoms to which they were connected. The final residuals<sup>12</sup> for 389 variables refined against 4632 data with  $I > 2.5\sigma(I)$  were  $R = 4.0\%$  and  $R_w = 4.5\%$ .<sup>13</sup> The final difference Fourier map had no peak greater than 1.92 e/Å<sup>3</sup>.<sup>14</sup>

## Results and Discussion

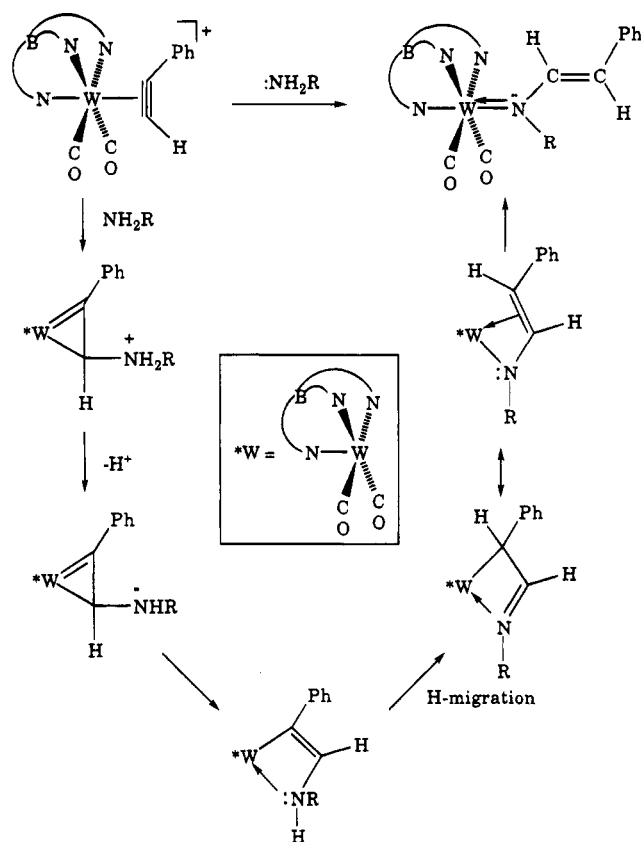
**Vinyl Amido Complexes.** Addition of primary amines ( $NH_2R'$ ) to a THF solution of  $[Tp'(CO)_2W(HC\equiv CR)]^+[BF_4]^-$  generates neutral vinyl amido complexes of the type  $Tp'(CO)_2W(N(R')CH=CHR)$  ( $R = Ph, R' = Ph$  (**1a**),  $Bu^t$  (**1b**),  $CH_2Ph$  (**1c**),  $Bu^n$  (**1d**);  $R = Bu^t, R' = CH_2Ph$  (**1e**);  $R = Bu^n, R' = CH_2Ph$  (**1f**, **1f'**))

(11) Programs used during solution and refinement were from the NRCVAX structure determination package. Gabe, E. J.; Le Page, Y.; Charland, J. P.; Lee, F. L.; White, P. S. *J. Appl. Chem.* **1989**, *22*, 384.

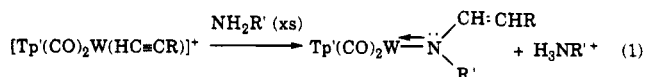
(12) The function minimized was  $\sum \omega(|F_o| - |F_c|)^2$ , where  $\omega$  is based on counter statistics.

(13)  $R_{unweighted} = \sum (|F_o| - |F_c|) / \sum |F_o|$  and  $R_{weighted} = [\sum \omega (|F_o| - |F_c|)^2 / \sum \omega F_o^2]^{1/2}$ .

(14) Scattering factors were taken from the following: Cromer, D. T.; Weber, J. T. *International Tables for X-Ray Crystallography*; Ibers, J. A., Hamilton, J. C., Eds.; Kynoch Press: Birmingham, England, 1974; Vol. IV, Table 2.2.

**Scheme 4**

(eq 1). These reactions are rapid at room temperature as the solution color quickly changes from green to brown. Chromatography followed by recrystallization from  $CH_2Cl_2$ /hexanes produced stable red-brown crystals in good yields.

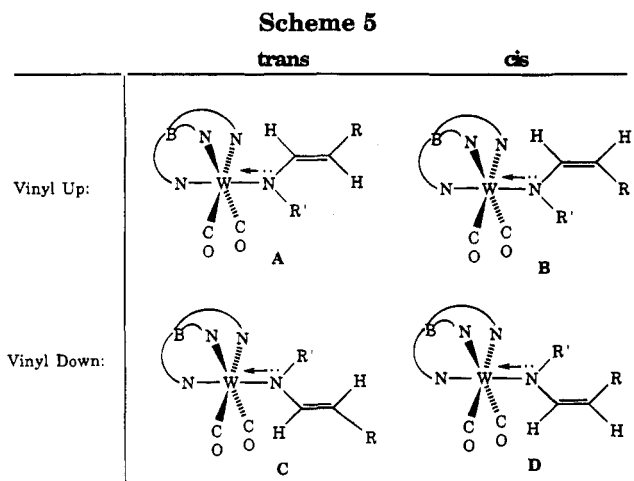


$R = Ph, R' = Ph$  (**1a**),  $Bu^t$  (**1b**),  $CH_2Ph$  (**1c**),  $Bu^n$  (**1d**);

$R = Bu^t, R' = CH_2Ph$  (**1e**);  $R = Bu^n, R' = CH_2Ph$  (**1f**);

Although we do not have mechanistic information in this system, nucleophilic addition to the terminal carbon of the alkyne ligand in  $[Tp'(CO)_2W(HC\equiv CR)]^+$  is known to be favored both sterically and electronically.<sup>7</sup> Addition of nucleophiles to the terminal carbon of the alkyne ligand in  $[Tp'(CO)_2W(CH\equiv CR)][BF_4]$  can form stable  $\eta^2$ -vinyl products.<sup>7</sup> By analogy, initial amine attack at the terminal alkyne carbon to create a  $R'NH_2CHCR$  linkage seems likely. Proton loss and proton migration from the nitrogen to the substituted carbon in this moiety would lead to an aza-allyl. Displacement of the chelating vinyl tail by donation from the lone pair on the nitrogen to the metal center would result in formation of the observed amido ligand with  $R'$  and vinyl substituents remaining on nitrogen (Scheme 4). An intermediate with low  $\nu_{CO}$  absorptions of 1884, 1774  $cm^{-1}$  was observed, possibly reflecting formation of a chelating nitrogen donor ligand.

Infrared spectra of **1a-e** display a medium intensity absorption for  $\nu_{BH}$  in the  $Tp'$  ligand (2538–2549  $cm^{-1}$ ) and strong  $\nu_{CO}$  absorptions for the cis-dicarbonyl ligands (around 1900, 1795  $cm^{-1}$ ). The relatively low  $\nu_{CO}$  frequencies are indicative of neutral complexes,<sup>2,3,7</sup>



and they are typical values for the  $\text{Tp}'(\text{CO})_2\text{W}$  fragment with an electron rich donor ligand in the remaining site. IR spectra exhibit cis-dicarbonyl absorptions around 1911 and 1793  $\text{cm}^{-1}$  for the phenyl derivative **1a** and at 1903 and 1776  $\text{cm}^{-1}$  for the butyl derivative **1b**; the alkyl group donates more electron density through the nitrogen to the metal than does the phenyl group. Amido complexes of the type  $\text{Tp}'(\text{CO})_2\text{W}(\text{NHR})$  also reflect strong electron donation from the lone pair on the nitrogen as evidenced by low infrared carbonyl stretching frequencies.<sup>2</sup> The carbonyl absorptions of the amido complexes here are lower than those of related azavinylidene complexes ( $\text{WN}=\text{CR}_2$ : 1925, 1815  $\text{cm}^{-1}$ ),<sup>3</sup> reflecting less electron-rich metal centers for the azavinylidene complexes. This trend was also observed in the alkyne monocarbonyl system<sup>5</sup> where net reduction from  $\text{Tp}'(\text{CO})(\text{RC}\equiv\text{CR})\text{WN}=\text{CHR}$  (1880  $\text{cm}^{-1}$ ) to the amido derivative,  $\text{Tp}'(\text{CO})(\text{RC}\equiv\text{CR})\text{WNHR}'$  (1855  $\text{cm}^{-1}$ ), caused a decrease of 25  $\text{cm}^{-1}$  in the carbonyl stretching frequency.

Note that donation of the lone pair on the amido nitrogen is required here for the metal to count eighteen electrons and optimally utilize all of the available metal orbitals. The vinyl amido ligand is the only  $\pi$ -donor in the coordination sphere, so unlike the case with an ancillary alkyne ligand there is no competition among  $\pi$  donor ligands here. The presence of both an alkyne and an amido ligand in  $\text{Tp}'(\text{CO})(\text{RC}\equiv\text{CR})\text{WNHR}'$  creates a 3-center-4-electron  $\pi$ -bonding scheme with an electron redundancy built in by simultaneous alkyne  $\pi_1$  donation and nitrogen lone pair donation.

Four isomers are possible for the vinyl substituted amido complexes due to restricted rotation around both the metal amido linkage (up and down) and the C=C bond (cis and trans) (Scheme 5). Only one isomer was detected by NMR for **1a–d** on the NMR time scale, suggesting either rapid rotation around the metal–nitrogen bond or that only a single isomer is populated. The rotational barrier about W–N bond could be relatively high and therefore rotation on the NMR time scale would be slow since the lone pair electrons on the nitrogen donate to the metal center to form a formal double bond. The rotational barrier measured for  $\text{Tp}'(\text{CO})_2\text{WNH}_2$  is 21 kcal/mol and that for  $\text{Tp}'(\text{CO})_2\text{WNHPh}$  is 24 kcal/mol.<sup>2</sup> The solid state structure of  $\text{Tp}'(\text{CO})_2\text{W}[\text{N}(\text{CH}_2\text{Ph})(\text{CH}=\text{CHPh})]$  (**1c**) shows that the planar vinyl fragment of the amido unit is proximal to the  $\text{Tp}'$  ligand and fits in between two pyrazoles of the

**Table 2. Selected  $^1\text{H}$  NMR Data<sup>a</sup> for Complexes **1a–f** and **2****

	CH=CHR	CH=CHR	Ph
<b>1a</b> (R = Ph, R' = Ph)	7.36 (14.4)	5.59	<b>7.14, 6.84</b> 7.43, 7.04
<b>1b</b> (R = Ph, R' = Bu <sup>t</sup> )	6.64 (14.8)	4.88	<b>7.09, 6.73</b>
<b>1c</b> (R = Ph, R' = Bz)	7.20 (14.8)	6.00	<b>7.16, 7.07, 6.83</b> 7.64, 7.35, 7.33
<b>1d</b> (R = Ph, R' = Bu <sup>n</sup> )	7.00 (14.8)	6.00	<b>7.18, 7.08, 6.89</b>
<b>1e</b> (R = Bu <sup>t</sup> , R' = Bz)	7.08 (14.4)	5.45	<b>7.11, 6.91</b>
<b>1f</b> (R = Bu <sup>n</sup> , R' = Bz)	7.28 (14)	5.46	<b>7.12, 6.94</b>
<b>1f'</b> (R = Bu <sup>n</sup> , R' = Bz)	6.38 (14)	5.18	7.57, 7.32, 7.26
<b>1f''</b> (R = Bu <sup>n</sup> , R' = Bz)	5.70 (10.4)	4.19	7.57, 7.30, 7.28
<b>2</b>	$[\text{Tp}'(\text{CO})_2\text{W}=\text{N}(\text{CH}=\text{CHPh})]^+$		
	7.25 (14)	6.92	7.31, 7.18, 7.16

<sup>a</sup> Reported in ppm ( $^3J_{\text{HH}}$  in Hz).

**Table 3. Selected  $^{13}\text{C}$  NMR Data<sup>a</sup> for Complexes **1a–f**, **2**, **3**, and **4****

	CH=CHR	CH=CHR	WCO
	$\text{Tp}'(\text{CO})_2\text{WN}(\text{R}')(\text{CH}=\text{CHR})$		
<b>1a</b> (R = Ph, R' = Ph)	153.5 (165)	111.3 (154)	253.5 (176)
<b>1b</b> (R = Ph, R' = Bu <sup>t</sup> )	151.2 (162)	116.3 (156)	257.6 (176)
<b>1c</b> (R = Ph, R' = Bz)	151.1 (162)	110.3 (154)	256.2 (176)
<b>1d</b> (R = Ph, R' = Bu <sup>n</sup> )	149.9 (165)	105.9 (152)	255.9 (176)
<b>1e</b> (R = Bu <sup>t</sup> , R' = Bz)	157.3 (168)	125.2 (149)	255.5 (176)
<b>1f</b> (R = Bu <sup>n</sup> , R' = Bz)	161.2 (168)	114.5 (150)	255.7 (176)
<b>1f'</b> (R = Bu <sup>n</sup> , R' = Bz)	150.6 (168)	108.1 (151)	256.2 (177)
<b>2</b>	$[\text{Tp}'(\text{CO})_2\text{W}=\text{N}(\text{CH}=\text{CHPh})]^+$		
	143.5 (178, 33)	140.0 (156)	216.8 (155)
	$\text{Tp}'(\text{CO})_2\text{W}(\text{N}=\text{CHCH}_2\text{Ph})$		
<b>3</b>	151.7 (176, 27)	32.2 (129)	241.4 (171)
	$[\text{Tp}'(\text{CO})_2\text{W}=\text{N}(\text{CH}_2\text{CH}_2\text{Ph})]^+$		
<b>4</b>	68.1 (142, 26)	36.8 (130)	216.9 (157)

<sup>a</sup> Reported in ppm ( $^1J_{\text{HC}}$  or  $^1$  or  $^2J_{\text{WC}}$  in Hz).

$\text{Tp}'$  ligand. This geometrical preference may be due to the fact that there are electronic interactions between the pyrazole rings and the planar phenyl ring of the vinyl group.<sup>3,6,7,10</sup>

NMR data support the formulation of **1a–e** as amido complexes. The presence of a molecular mirror plane is indicated by the two equivalent pyrazolyl rings evident in both  $^1\text{H}$  and  $^{13}\text{C}$  NMR spectra.  $C_s$  symmetry is consistent with a static orientation of the amido ligand in the mirror plane that bisects the two carbonyl ligands. Important NMR data that characterize the amido complexes are summarized in Tables 2 and 3. The two vinyl protons appear between 5.70–7.36 ppm ( $\text{NCH}=\text{CHR}$ ) and 4.19–6.00 ppm ( $\text{NCH}=\text{CHR}$ ) for **1a–f**.

$^1\text{H}$  NMR spectra are useful for recognizing and quantifying isomers. Previously we concluded that protons proximal to a  $\text{Tp}'$  pyrazole ring are shielded and resonate upfield to give high field  $^1\text{H}$  signals.<sup>6,7,10</sup> This empirical guideline allows us to determine the orientation of the amido substituents (up or down). In Table 2 the chemical shifts listed in bold print are for phenyl groups which are proximal to the  $\text{Tp}'$  ligand. The phenyl chemical shifts listed in plain numbers are further downfield and belong to phenyl groups distal to the  $\text{Tp}'$  ligand. The planar phenyl–vinyl fragment in **1a–d** is likely to be proximal to the  $\text{Tp}'$  ligand based on the observed chemical shifts. The bulky *tert*-butyl group in **1e** may be sterically restricted to the location away from the  $\text{Tp}'$  ligand. Three isomers (two trans and



one cis) were observed for **1f** (**1f**, **1f'**, and **1f''**), perhaps reflecting that the *n*-butyl group is non-planar and medium size. For **1a–e**, **1f**, and **1f'** the coupling between the two vinyl protons is larger than 14 Hz, suggesting a trans vinyl geometry. The smaller vicinal coupling of 10 Hz for **1f** is consistent with formation of a cis vinyl isomer.

As for the phenyl resonances, the chemical shifts for the vinyl protons in **1f** and **1f'** are located at substantially higher field than those in **1f** (which has the vinyl group distal to the  $Tp'$  ligand). The largest shielding effect was observed for the cis vinyl geometry in **1f**. In summary the  $^1H$  NMR data indicate that isomer **A** is dominant for **1a–d** and **1f'**, isomer **B** is present as **1f**, and isomer **C** is formed for **1e–f**; only isomer **D** was not observed.

$^{13}C$  NMR spectra revealed a single resonance for the two equivalent carbonyl ligands downfield at around 256 ppm with a large one-bond tungsten–carbon coupling of 176 Hz for **1a–f**. This lowfield chemical shift and large one-bond tungsten–carbon coupling suggests that the amido ligand is a good  $\pi$ -donor ligand, and the electron rich metal center provides substantial metal backbonding to the carbonyls. The  $sp^2$  hybridized vinyl carbons appear between 150–161 ppm ( $C_\alpha$ ,  $^1J_{HC} = \sim 165$  Hz) and 106–116 ppm ( $C_\beta$ ,  $^1J_{HC} = \sim 154$  Hz).

Metal complexes containing both amido ligands and terminal carbonyl ligands are rare. Amido complexes of the type  $Tp'(CO)_2WNHR$  have been prepared<sup>2</sup> from  $Tp'W(CO)_2I$  and  $NH_2R$ , and they exhibit similar spectral properties to those reported here. An unusual amido

complex,  $Tp'(CO)_2WN(C(=CH_2)N(Bu^t)C(=O))$ , was synthesized by treating  $[Tp'(CO)_3W(N=CMe)]^+$  with  $NH_2-Bu^t$ , and it has been structurally characterized.<sup>15</sup>

**Crystal Structure of  $Tp'(CO)_2WN(CH_2Ph)(CH=CHPh)$  (**1c**).** The coordination sphere of the tungsten atom adopts a pseudooctahedral geometry with a tridentate  $Tp'$  ligand occupying three facial coordination sites and two carbonyls and the amido ligand in the remaining coordination sites. Atomic positional parameters are listed in Table 4 and selected intramolecular bond distances and angles appear in Table 5. An ORTEP drawing of  $Tp'(CO)_2WN(CH_2Ph)(CH=CHPh)$  is shown with the atomic numbering defined in Figure 1.

Salient geometrical features of  $Tp'(CO)_2WN(CH_2Ph)(CH=CHPh)$  (**1c**) are consistent with those established by previous structures of tungsten(II) amido carbonyl complexes.<sup>2,15</sup> The carbonyl carbons lie in soft positions along the  $W-CO$  axes ( $W-C(1) = 1.943(7)$  Å and  $W-C(2) = 1.955(7)$  Å). The sum of the  $W-C$  and  $C-O$  distances for both carbonyl ligands is nearly constant (3.12 Å). The  $W-C-O$  angles are  $172.7(6)^\circ$  and  $172.9(6)^\circ$ . The amido  $W-N$  distance of  $1.997(5)$  Å is appropriate for a formal double bond and compares well with values in related  $W-NR_2$  complexes ( $\sim 2.00$  Å).<sup>2,15</sup> The  $Tp' W-N$  distance trans to the amido nitrogen is  $2.181(5)$  Å which is close to those trans to the carbonyls here ( $2.232(6)$  and  $2.244(5)$  Å), suggesting that the amido ligand is also a relatively strong trans influence ligand. The  $N(3)-C(4)$  and  $N(3)-C(5)$  distances are

**Table 4. Atomic Positional Parameters for  $Tp'(CO)_2WN(CH_2Ph)(CH=CHPh)$  (**1c**)**

	<i>x</i>	<i>y</i>	<i>z</i>	<i>B</i> <sub>iso</sub>
W1	0.184008(23)	0.193859(23)	0.01906(3)	3.111(11)
C1	0.0528(6)	0.2280(6)	-0.0746(7)	4.1(4)
O1	-0.0186(5)	0.2461(5)	-0.1428(6)	6.0(3)
C2	0.2386(6)	0.1237(6)	-0.1680(7)	4.3(4)
O2	0.2594(5)	0.0846(5)	-0.2819(5)	5.9(3)
N3	0.2036(4)	0.3436(4)	0.0500(5)	3.5(3)
C4	0.1768(6)	0.4076(6)	-0.0365(7)	4.2(4)
C5	0.2361(6)	0.4031(6)	0.1747(7)	4.1(4)
C6	0.2267(7)	0.5111(6)	0.2344(8)	5.0(4)
C11	0.2779(6)	0.4186(6)	-0.0960(7)	4.4(4)
C12	0.3487(8)	0.3311(8)	-0.1956(10)	7.1(6)
C13	0.4425(9)	0.3415(9)	-0.2495(11)	8.5(7)
C14	0.4644(9)	0.4425(12)	-0.1993(11)	9.0(8)
C15	0.3935(9)	0.5322(10)	-0.1025(10)	7.9(8)
C16	0.2983(8)	0.5230(8)	-0.0487(9)	5.9(5)
C21	0.2670(7)	0.5606(7)	0.3631(7)	5.2(4)
C22	0.2565(9)	0.6737(8)	0.4109(9)	7.1(6)
C23	0.2972(11)	0.7226(8)	0.5301(11)	9.9(7)
C24	0.3403(13)	0.6610(12)	0.6025(13)	11.7(10)
C25	0.3476(13)	0.5527(10)	0.5587(13)	11.6(10)
C26	0.3124(10)	0.5002(7)	0.4377(10)	7.6(6)
B1	0.2345(7)	0.0941(7)	0.2539(8)	3.9(4)
N31	0.0997(5)	0.2604(5)	0.2227(5)	3.7(3)
N32	0.1356(5)	0.2033(5)	0.3044(5)	3.7(3)
C33	0.0704(7)	0.2570(7)	0.4186(7)	4.7(4)
C34	-0.0078(7)	0.3522(7)	0.4134(7)	5.3(4)
C35	0.0122(6)	0.3518(6)	0.2897(7)	4.0(3)
C36	0.0866(10)	0.2166(9)	0.5298(9)	7.9(7)
C37	-0.0493(7)	0.4343(7)	0.2335(8)	5.2(4)
N41	0.3426(4)	0.1462(4)	0.1131(5)	3.7(3)
N42	0.3389(4)	0.1167(4)	0.2197(5)	3.5(3)
C43	0.4411(6)	0.1011(6)	0.2667(7)	4.3(4)
C44	0.5099(6)	0.1219(6)	0.1915(8)	4.5(4)
C45	0.4474(5)	0.1490(6)	0.0958(7)	3.9(4)
C46	0.4651(8)	0.0670(9)	0.3818(9)	6.8(6)
C47	0.4844(6)	0.1780(6)	-0.0093(8)	4.9(4)
N51	0.1710(4)	0.0367(4)	0.0235(5)	3.4(3)
N52	0.2057(5)	0.0077(4)	0.1289(6)	3.7(3)
C53	0.2064(6)	-0.0991(6)	0.1025(8)	4.4(4)
C54	0.1691(6)	-0.1376(6)	-0.0185(8)	4.7(4)
C55	0.1466(6)	-0.0536(6)	-0.0664(7)	4.1(3)
C56	0.2391(7)	-0.1542(7)	0.1981(10)	6.1(6)
C57	0.1007(7)	-0.0550(7)	-0.1919(8)	5.2(4)

**Table 5. Selected Bond Distances (Å) and Angles (deg) for  $Tp'(CO)_2W-N(CH=CHPh)(CH_2Ph)$  (**1c**)**

W-C(1)	1.943(7)	C(1)-O(1)	1.179(8)
W-C(2)	1.955(7)	C(2)-O(2)	1.164(9)
W-N(3)	1.997(5)	N(3)-C(4)	1.475(8)
W-N(31)	2.232(6)	N(3)-C(5)	1.425(9)
W-N(41)	2.244(5)	C(5)-C(6)	1.32(1)
W-N(51)	2.181(5)		
C(1)-W-C(2)	74.0(3)	N(31)-W-N(41)	84.4(2)
C(1)-W-N(3)	90.7(3)	N(31)-W-N(51)	80.8(2)
C(1)-W-N(31)	99.6(3)	N(41)-W-N(51)	81.9(2)
C(1)-W-N(41)	175.9(3)	W-C(1)-O(1)	172.7(6)
C(1)-W-N(51)	97.6(2)	W-C(2)-O(2)	172.9(6)
C(2)-W-N(3)	96.1(3)	W-N(3)-C(4)	127.6(4)
C(2)-W-N(31)	170.6(3)	W-N(3)-C(5)	117.9(4)
C(2)-W-N(41)	101.9(3)	C(4)-N(3)-C(5)	114.3(5)
C(2)-W-N(51)	93.0(2)	N(3)-C(4)-C(11)	114.6(5)
N(3)-W-N(31)	90.9(2)	N(3)-C(5)-C(6)	130.4(7)
N(3)-W-N(41)	90.3(2)	C(5)-C(6)-C(21)	124.4(7)
N(3)-W-N(51)	169.1(2)		

1.475(8) and 1.425(9) Å, respectively. The  $C(5)-C(6)$  distance of 1.32(1) Å is in the double bond range. The angles around the amido  $N(3)$  nitrogen are  $127.6(4)^\circ$  [ $W-N(3)-C(4)$ ],  $117.9(4)^\circ$  [ $W-N(3)-C(5)$ ] and  $114.3(5)^\circ$  [ $C(4)-N(3)-C(5)$ ], which sum to  $359.8^\circ$ , reflecting  $sp^2$  hybridization at the nitrogen. Furthermore  $C(5)$  and  $C(6)$  are also  $sp^2$  hybridized. The phenyl substituent on the vinyl group of the amido ligand lies in the vinyl

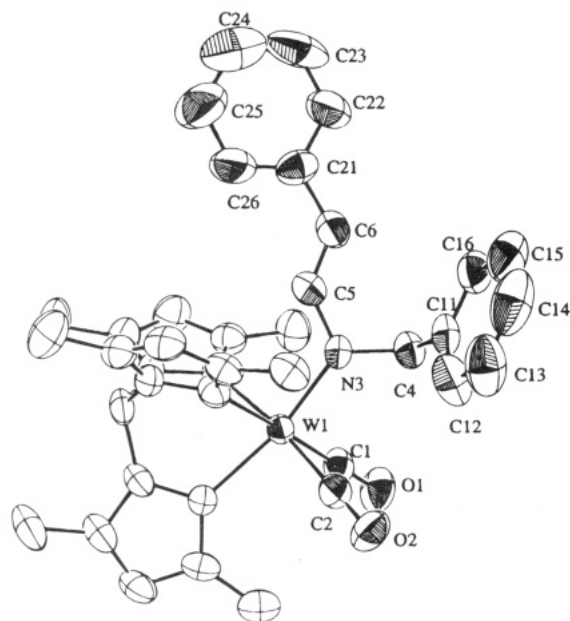


**Figure 1.** ORTEP drawing of  $\text{Tp}'(\text{CO})_2\text{WN}(\text{CH}_2\text{Ph})(\text{CH}=\text{CHPh})$  (**1c**).

**Table 6.** Cis Dicarbonyl Angles in  $[\text{Tp}'(\text{CO})_2\text{WL}]^{n+}$  Complexes with  $\pi$ -Donor Ligands

L	$\alpha(\text{OC}-\text{W}-\text{CO})$ , deg	ref
amido ( $\text{N}^-\text{Bz}(\text{CH}=\text{CHPh})$ , $n = 0$ )	74.0	this work
azavinylidene ( $\text{N}^-\text{CH}(\text{Bz})$ , $n = 0$ )	74.4	3
thiolate ( $\text{S}^-\text{Bz}$ , $n = 0$ )	73.6	19
alkyne ( $\text{PhC}\equiv\text{CMe}$ , $n = 1$ )	82.9	20

plane, and this entire  $\text{C}_3$  fragment is nearly planar and lies in the plane that bisects the two pyrazole rings and the two carbonyl ligands. Free rotation or even oscillation of the benzyl group would account for the molecular mirror symmetry observed by NMR in solution. The angle formed by the two carbonyls at the metal center is  $74.0(3)^\circ$ . Closure of this angle from the idealized  $90^\circ$  associated with an octahedron has been observed in other dicarbonyl complexes containing a single-faced  $\pi$ -donor ligand in related  $\text{W}(\text{II})$   $d^4$  systems (Table 6). This acute angle reflects preferential stabilization of the two filled  $d\pi$  orbitals by backbonding to the two  $\pi$ -acid carbonyl ligands as described below.

The coordinate system chosen to describe the  $\pi$ -bonding interactions places the  $\text{W}-\text{N}$  linkage along the  $z$  axis and places the two carbonyl ligands in the  $xy$  plane  $45^\circ$  off the  $x$  and  $y$  axes (Figure 2). Two electrons of this  $d^4$  configuration will occupy the  $d_{x^2-y^2}$  orbital since this orbital will be stabilized more than  $d_{xz}$  and  $d_{yz}$  because of effective orbital overlap between  $d_{x^2-y^2}$  and both  $\text{CO}$   $\pi^*$  orbitals in the  $xy$  plane. Closure of the carbonyl angle from  $90^\circ$  to the observed  $74^\circ$  will stabilize  $d_{yz}$  by increasing the overlap of the out-of-plane  $\text{CO}$   $\pi^*$  orbitals with  $d_{yz}$ . The second pair of metal  $d$  electrons will then occupy the  $d_{yz}$  orbital, and the  $d_{xz}$  orbital will be left vacant to provide the acceptor orbital for nitrogen lone pair donation. The  $\pi$ -donor ligand will be oriented so that the lone pair of electrons on the nitrogen can donate to the lone vacant metal  $d\pi$  orbital,  $d_{xz}$ . The bonding description for either an amido ( $\text{NR}_2$ ) or an azavinylidene ( $\text{N}=\text{CRR}'$ ) fragment is similar for the metal-nitrogen multiple bond, and the effect on ligand orientation is such that the planes of the two ligands will be

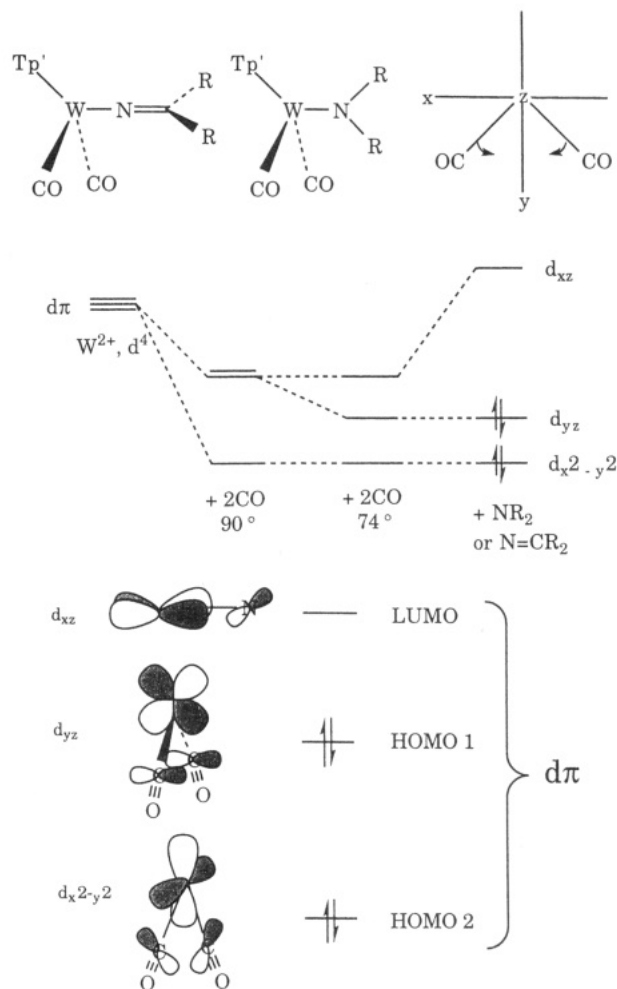


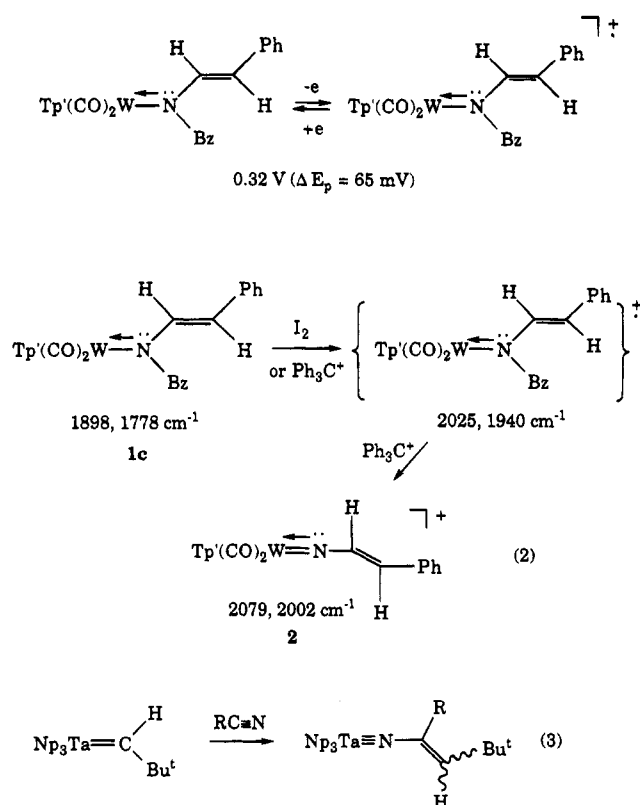
**Figure 2.** Qualitative bonding scheme for the  $d\pi$ -ligand interactions in  $\text{Tp}'(\text{CO})_2\text{WN}=\text{CR}_2$  and  $\text{Tp}'(\text{CO})_2\text{WNR}_2$ .

perpendicular to each other with the amido ligand in the molecular mirror plane. In other words, in order to have the lone pair of electrons on the nitrogen of an azavinylidene ligand donate into the same lone vacant metal  $d\pi$  orbital that the amido lone pair interacts with, the plane of the azavinylidene ligand will be approximately perpendicular to the plane of the amido ligand. In summary,  $d_{yz}$  is the HOMO stabilized by  $\text{CO}$  backbonding and  $d_{xz}$  is the LUMO as the  $\pi^*$  component of the  $\text{W}-\text{N}$  double bond in these systems.

**A Cationic Vinyl Nitrene Complex.** Electrochemical studies have been carried out on these amido complexes. The cyclic voltammogram for **1c** exhibits a reversible redox couple at  $E_{1/2} = +0.32$  V vs SCE ( $\Delta E_p = 65$  mV at 10 mV/s). The couple appears to be chemically reversible, suggesting that the electron rich tungsten amido complex **1c** is readily oxidized. This process is believed to involve a one electron oxidation to a radical cation as shown in Scheme 6. This interpretation is consistent with chemical reactions observed when **1c** was treated with oxidants such as iodine or  $[\text{Ph}_3\text{C}][\text{BF}_4]$  as described below.

Complex **2** was synthesized by oxidative removal of the benzyl group from the neutral amido complex **1c**. Reaction of **1c** with  $\text{I}_2$  or  $[\text{Ph}_3\text{C}][\text{BF}_4]$  produces an intermediate with  $\nu_{\text{BH}}$  at  $2562$   $\text{cm}^{-1}$  and  $\nu_{\text{CO}}$  at  $2025$  and  $1940$   $\text{cm}^{-1}$ . Attempts to isolate this species failed due to decomposition, but we speculate that this species

Scheme 6



may be a 17-electron radical cation (Scheme 6). Stirring the reaction mixture for 10 h converted this intermediate to the vinyl nitrene cation (eq 2). Crystalline products were isolated by filtering the concentrated methylene chloride solution into ether followed by recrystallization of the solid from  $CH_2Cl_2/Et_2O$ . A vinyl nitrene ligand has been prepared previously by insertion of a nitrile into a metal carbene bond (eq 3).<sup>16</sup>

Reaction of  $Tp'(CO)_2WNHR$  with  $[Ph_3C]^+$  generates nitrene complexes by oxidative removal of a hydride from the nitrogen.<sup>2</sup> This reaction was rapid in contrast to the benzyl group removal reported here, indicating that net removal of  $H^-$  is faster than net benzyl anion removal. Comparing the reactivity pattern observed here with the alkyne monocarbonyl system is informative. Reaction of  $Tp'(CO)(PhC\equiv CMe)WNHCH_2R$  with  $[Ph_3C]^+$  generated an imine complex,  $[Tp'(CO)(PhC\equiv CMe)W(NH=CHR)]^+$  by oxidative removal of a hydride from the carbon of the amido ligand.<sup>4</sup> In the  $Tp'(CO)_2WNRR'$  case the metal provides the electrons and is oxidized to W(IV) as an  $R^-$  group of the  $NRR'$  unit is removed by trityl cation. In contrast, the nitrogen lone pair in the alkyne system is redundant for the metal, and hence it is available to provide electrons to an incipient carbocation as the  $H^-$  of the  $NHCH_2R$  unit is removed by trityl cation. As a result

Table 7. Selected IR Data ( $cm^{-1}$ ) for Complexes 1a–f, 2, 3, and 4

	$\nu(B-H)$	$\nu(CO)$
$Tp'(CO)_2WN(R')(CH=CHR)$		
1a (R = Ph, R' = Ph)	2549	1911, 1793
1b (R = Ph, R' = Bu <sup>t</sup> )	2539	1903, 1776
1c (R = Ph, R' = Bz)	2544	1898, 1778
1d (R = Ph, R' = Bu <sup>n</sup> )	2549	1908, 1790
1e (R = Bu <sup>t</sup> , R' = Bz)	2538	1903, 1782
1f (R = Bu <sup>n</sup> , R' = Bz)	2543	1908, 1786
2	$[Tp'(CO)_2W=N(CH=CHPh)]^+$ 2563	2079, 2002
3	$Tp'(CO)_2W(N=CHCH_2Ph)$ 2542	1928, 1813
4	$[Tp'(CO)_2W=N(CH_2CH_2Ph)]^+$ 2577	2076, 1996

this converts the  $NHCH_2R$  ligand to an imine ligand,  $HN=CHR$ , and the metal center remains as W(II) with an 18-electron count. A similar change in regiochemistry dependent upon the auxiliary ligands was observed for electrophilic addition to azavinylidene ligands as  $Tp'(CO)_2W(N=CHR)$  was converted<sup>2,3</sup> to a nitrene complex,  $[Tp'(CO)_2W(=NCHRE)]^+$ , while  $Tp'(CO)(PhC\equiv CMe)WN=CHR$  was converted to an imine complex,  $[Tp'(CO)(PhC\equiv CMe)W(NE=CHR)]^+$ .<sup>5</sup>

Infrared spectra of complex **2** exhibit an absorption at 2563  $cm^{-1}$  ( $\nu BH$ ) which is 10–20  $cm^{-1}$  higher than comparable values for the  $Tp'$  ligand B–H stretches in neutral complexes (Table 7). The terminal carbonyl  $\nu CO$  absorptions appear at 2079 and 2002  $cm^{-1}$  for this cationic W(IV) nitrene complex. Those carbonyl stretching frequencies are about 200  $cm^{-1}$  higher than those of the amido precursor. Note that there is only one pair of d electrons for backdonation to the  $\pi$ -acid carbonyl ligands in the W(IV)  $d^2$  center as opposed to the  $d^4$  configuration of the amido W(II) complexes.

A 2:1 symmetry pattern for the  $Tp'$  ligand for **2** was evident in both  $^1H$  and  $^{13}C$  NMR spectra, indicating retention of mirror symmetry in the cationic product.  $^1H$  NMR assignments are straightforward. The vinyl protons ( $NCH=CHPh$ ) of the nitrene ligand in **2** resonates at 7.26 and 6.92 ppm, respectively, with a large three-bond vicinal coupling constant of 14 Hz which suggests retention of a trans geometry for the vinyl group. The terminal metal carbonyl carbons resonate at 217 ppm for **2** with a one-bond tungsten–carbon coupling of 155 Hz. These values are less than those of carbonyl ligands in the neutral amido complexes **1a–f** (256 ppm and 176 Hz), which reflects the fact that the cationic complex is more electron deficient than the neutral precursors. The nitrene carbon ( $W=NCH=CHPh$ ) appears at 143.5 ppm with a two-bond tungsten–carbon coupling of 33 Hz. The tungsten coupling to the nitrene carbon suggests a linear W–N–C linkage.<sup>2,3</sup>

**Reduction of the Cationic Vinyl Nitrene Complex to Azavinylidene and Saturated Nitrene Complexes.** Reduction of  $[Tp'(CO)_2W(=NCH=CHPh)]^+$  using  $LiBH_4$  in acetonitrile generated both vinyl amido and benzyl azavinylidene complexes (eq 4). An infrared spectrum showed a 6:1 ratio of the azavinylidene complex to the amido complex. So the reaction is not regioselective as the nucleophile has added to either the  $\alpha$  or the  $\gamma$  site, i.e. either to the vinyl tail or to the nitrogen. Recrystallization after column chromatogra-

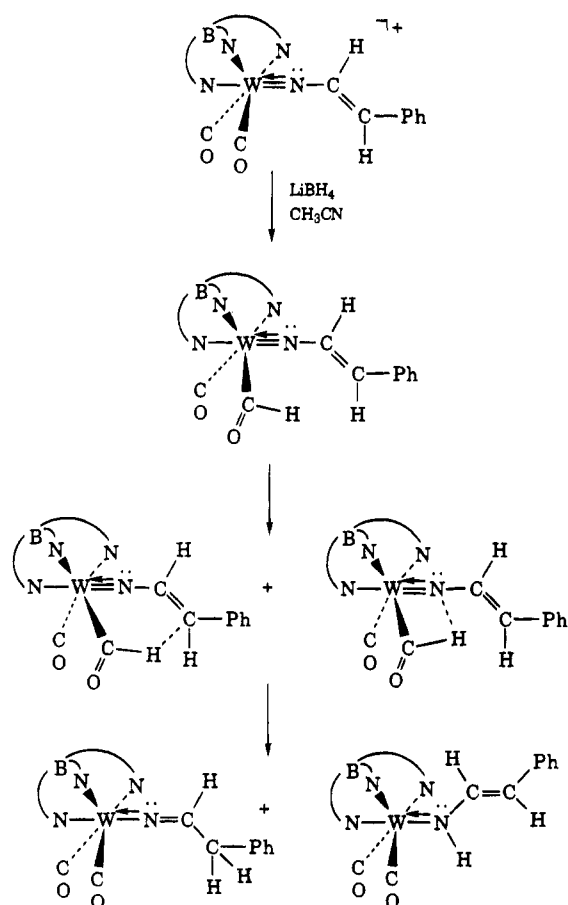
(16) (a) Schrock, R. R.; Fellmann, J. D. *J. Am. Chem. Soc.* **1978**, *100*, 3359. (b) Wood, C. D.; McLain, S. J.; Schrock, R. R. *J. Am. Chem. Soc.* **1979**, *101*, 3210.

(17) Luan, L.; Brookhart, M.; Templeton, J. L. Unpublished results. (18) Feng, S. G.; Luan, L.; White, P. S.; Brookhart, M.; Templeton, J. L.; Young, C. G. *Inorg. Chem.* **1991**, *30*, 2582.

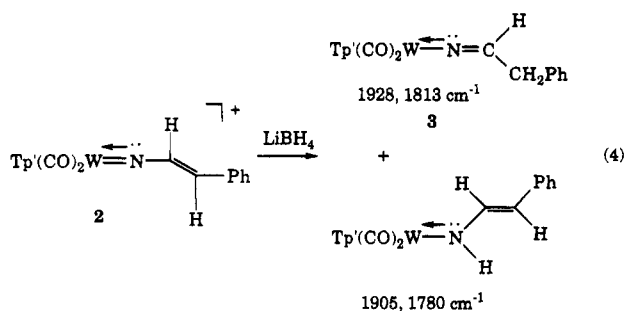
(19) Philipp, C. C.; Young, C. G.; White, P. S.; Templeton, J. L. *Inorg. Chem.* **1993**, *32*, 5437.

(20) Templeton, J. L.; Caldarelli, J. L.; Feng, S. G.; Philipp, C. C.; Wells, M. B.; Woodworth, B. E.; White, P. S. *J. Organomet. Chem.* **1994**, *478*, 103.

Scheme 7



phy gave pure azavinylidene complex, but in low yield (34%).

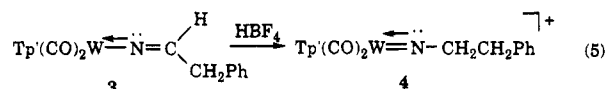


Reduction of a phenyl nitrene cation in a closely related system generated an amido complex by net hydride addition to the nitrene nitrogen.<sup>2</sup> This reaction was shown to pass through a formyl intermediate which underwent intramolecular hydride migration from carbon to nitrogen to form the amido product.

Formation of a formyl intermediate may be possible in this system, too. Intramolecular formyl bridging to form either a six- or a four-membered ring as the mechanism for hydride transfer could lead to the formation of the observed metalloimine and amido ligands. The ratio of the product distribution is consistent with the six-membered ring being favored compared to the strained four member ring (Scheme 7).

Formation of  $\text{Tp}'(\text{CO})_2\text{W}(\text{N}=\text{CHR})$  has been achieved by nucleophilic addition to the nitrile carbon in  $[\text{Tp}'(\text{CO})_3\text{W}(\text{N}=\text{CR})]^+$  and by insertion of nitriles into the  $\text{W}-\text{H}$  bond of  $\text{Tp}'(\text{CO})_3\text{WH}$ .<sup>2</sup> The benzyl azavinylidene derivative has been structurally characterized.

Reaction of azavinylidene complex **3** with electrophiles produced cationic saturated nitrene complexes (eq 5). The  $\beta$ -hydrogen of the nitrene ligand is acidic, and



therefore this reaction is reversible as the nitrene can be easily deprotonated. The terminal carbonyl ligands are sensitive to the electron-density on the metal center as reflected by their stretching frequencies in the infrared spectrum and their chemical shifts and one-bond  $\text{W}-\text{C}$  coupling constants in the C-13 NMR spectrum. Low CO stretching frequencies (due to back bonding from metal) and downfield carbon resonances with large one-bond  $\text{W}-\text{C}$  coupling are observed for metal carbonyls with an electron rich metal center. These trends are evident in Table 3 when comparing amido and azavinylidene ligands. Similar trends hold true for  $\text{Tp}'(\text{CO})(\text{PhC}=\text{CMe})\text{WNHCH}_2\text{Me}$  ( $1855\text{ cm}^{-1}$ , 239 ppm (168 Hz)) and  $\text{Tp}'(\text{CO})(\text{PhC}=\text{CMe})\text{WN}=\text{CHMe}$  ( $1880\text{ cm}^{-1}$ , 232 ppm (158 Hz)).<sup>5</sup>

**Summary.** Reaction of the terminal alkyne complexes with amines produces vinyl amido complexes, presumably by initial nucleophilic attack at the alkyne carbon. Addition of  $\text{HNHR}'$  across a terminal alkyne  $\pi$  bond to give an amido ligand is the result. Preferential stabilization of the two metal  $d\pi$  orbitals which are filled by backbonding to the two  $\pi$ -acid carbonyl ligands while allowing  $\pi$ -donation from the single-faced amido unit to the lone vacant metal  $d\pi$  orbital is reflected in an acute  $\text{OC}-\text{M}-\text{CO}$  angle in the dicarbonyl complexes containing a single-faced  $\pi$ -based amido ligand. This acute  $\text{OC}-\text{M}-\text{CO}$  angle will dictate that the amido fragment will reside in the molecular plane that bisects the two carbonyl ligands, while the orientation for an azavinylidene ligand will be perpendicular to the molecular plane.

The electron rich amido complexes can be oxidized to a nitrene cation by net removal of a benzyl group via an intermediate believed to be a radical cation. The regiochemistry in the oxidation reactions of  $\text{Tp}'(\text{CO})_2\text{WNR}_2$  and  $\text{Tp}'(\text{CO})(\text{RC}=\text{CR})\text{WNR}_2$  is noteworthy. The vinyl group of the nitrene ligand is activated for nucleophilic and electrophilic addition to give a saturated nitrene ligand.

**Acknowledgment.** We thank the Department of Energy, Office of Basic Energy Sciences (85ER 13430), and the Petroleum Research Foundation, administered by the American Chemical Society, for generous support of this research.

**Supporting Information Available:** Tables of anisotropic temperature factors and complete bond distances and angles (5 pages) for **1c**. Ordering information is given on any current masthead page.

OM950010M

# Synthesis and Structure of Even-Electron Paramagnetic Chromium(II) Complexes

Michael D. Fryzuk,\* Daniel B. Leznoff, and Steven J. Rettig†

Department of Chemistry, University of British Columbia, 2036 Main Mall,  
Vancouver, BC, Canada V6T 1Z1

Received April 12, 1995<sup>®</sup>

In an effort to develop the coordination chemistry of Cr(II), we have prepared the starting chloro-bridged dimer  $\{[(\text{Ph}_2\text{PCH}_2\text{SiMe}_2)_2\text{N}]\text{Cr}\}_2(\mu\text{-Cl})_2$  by reaction of the lithium salt  $\text{LiN}(\text{SiMe}_2\text{CH}_2\text{PPh}_2)_2$  with  $\text{CrCl}_2\cdot\text{THF}$ . Subsequent replacement of the remaining chloride leads to the formation of mononuclear organochromium complexes of the general formula  $\text{CrR}[\text{N}(\text{SiMe}_2\text{CH}_2\text{PPh}_2)_2]$  ( $\text{R} = \text{Me}, \text{CH}_2\text{Ph}, \text{C}_6\text{H}_5$ ). The methyl and benzyl complexes display nearly planar geometries around each Cr(II) and both show high-spin (spin-only)  $d^4$  configurations; the solid-state structure of the benzyl derivative shows that the benzyl ligand is bound in an  $\eta^2$  fashion. The cyclopentadienyl derivative is low spin (two unpaired electrons) and shows a geometry with the tridentate ligand in a distorted facial orientation and the cyclopentadienyl unit  $\eta^5$ -bound. Semiempirical ZINDO restricted open-shell Hartree-Fock studies confirm the stabilities of the various spin states of the isolated complexes.

## Introduction

Much of the progress made in our present understanding of the mechanisms of organometallic reactions has involved studies of diamagnetic compounds that contain metal-carbon bonds.<sup>1</sup> Less studied are the reactions of paramagnetic organometallic complexes, largely because solution characterization techniques can be difficult to interpret, ambiguous, or just unavailable for this class of derivatives. A good case in point involves complexes of chromium. Even though the coordination chemistry of this element encompasses oxidation states ranging from -II to +VI,<sup>2</sup> the most commonly studied derivatives are Werner-type complexes of Cr(II) and Cr(III) and most of these paramagnetic species display octahedral geometries. In contrast, the organometallic chemistry of chromium has concentrated on diamagnetic, formally Cr(0) carbonyl complexes, such as the Fischer carbenes and arene half-sandwich derivatives.<sup>3,4</sup> There is also the series of quadruply bonded Cr(II) dimers that has been well studied, but these too are essentially diamagnetic.<sup>2,5-7</sup> One notable exception is the reactivity of formally Cr(I) radicals such as  $\text{CpCr}(\text{CO})_3$  and  $\text{CpCr}(\text{NO})\text{X}(\text{L})$ .<sup>8-10</sup>

As already mentioned, most Cr(II) complexes display octahedral geometries; however, recently a number of studies have shown that paramagnetic square-planar derivatives are accessible. For example,  $\text{CrR}_2(\text{dippe})$  ( $\text{R} = \text{CH}_2\text{CMe}_3, \text{CH}_2\text{SiMe}_3, \text{C}_6\text{H}_2\text{Me}_3$ ; dippe = 1,2-bis(diisopropylphosphino)ethane),  $\text{Cr}(\text{C}_6\text{H}_2\text{Me}_3)_2(\text{PMe}_3)_2$ ,  $\text{Na}_2[\text{Cr}(\text{OR})_4]$ ,  $\text{Cr}[\text{N}(\text{SiMe}_3)_2]_2(\text{THF})_2$ ,  $\text{Cr}(\text{NR}_2)_2\text{L}_2$ , and  $\text{CrR}_2(\text{TMEDA})$  ( $\text{TMEDA} = N,N,N',N'$ -tetramethylethylenediamine) have been structurally characterized.<sup>11-15</sup> These studies typify the problems inherent in this chemistry, since these paramagnetic  $d^4$  complexes of Cr(II) are ESR silent and display broad, uninterpretable NMR spectra. In addition, as the above examples show, most of the paramagnetic organometallic derivatives seem to require bulky alkyl or aryl groups for isolation.

Our previous studies with group 10 metals incorporating the tridentate, uninegative ancillary ligand  $\text{N}(\text{SiMe}_2\text{CH}_2\text{PPh}_2)_2$  showed that, at least for  $d^8$  systems, square-planar geometries could be realized and small hydrocarbyl substituents such as methyl could be tolerated.<sup>16</sup> Given that four-coordinate  $d^4$  systems should also be square planar,<sup>11</sup> we undertook a study of the coordination chemistry of Cr(II) stabilized by the ancillary ligand  $\text{N}(\text{SiMe}_2\text{CH}_2\text{PPh}_2)_2$ .

## Results and Discussion

### Synthesis of $\text{CrR}[\text{N}(\text{SiMe}_2\text{CH}_2\text{PPh}_2)_2]$ Complexes.

The dimer  $\{[(\text{Ph}_2\text{PCH}_2\text{SiMe}_2)_2\text{N}]\text{Cr}\}_2(\mu\text{-Cl})_2$ , prepared from  $\text{LiN}(\text{SiMe}_2\text{CH}_2\text{PPh}_2)_2$ <sup>16</sup> and  $\text{CrCl}_2\cdot\text{THF}$ <sup>17</sup> as de-

\* Professional Officer: UBC Crystallographic Service.

<sup>®</sup> Abstract published in *Advance ACS Abstracts*, September 15, 1995.

(1) Collman, J. P.; Hegedus, L. S.; Norton, J. R.; Finke, R. G. *Principles and Applications of Organotransition Metal Chemistry*; University Science Books: Mill Valley, CA, 1987.

(2) Cotton, F. A.; Wilkinson, G. *Advanced Inorganic Chemistry*, 5th ed.; Wiley: New York, 1988; p 679.

(3) Davis, R.; Kane-Maguire, L. A. P. In *Comprehensive Organometallic Chemistry*; Wilkinson, G.; Stone, F. G. A., Eds.; Pergamon Press: New York, 1982; Vol. 3, Chapter 26.2.

(4) Kirtley, S. W. In *Comprehensive Organometallic Chemistry*; Wilkinson, G.; Stone, F. G. A., Eds.; Pergamon Press: New York, 1982; Vol. 3, Chapter 26.1.

(5) Cotton, F. A.; Chen, H.; Daniels, L. M.; Feng, X. *J. Am. Chem. Soc.* **1992**, *114*, 8980.

(6) Cotton, F. A.; Eglin, J. L.; Hong, B.; James, C. A. *J. Am. Chem. Soc.* **1992**, *114*, 4915.

(7) Edema, J. J. H.; Gambarotta, S. *Comments Inorg. Chem.* **1991**, *11*, 195.

(8) Baird, M. C. *Chem. Rev.* **1988**, *88*, 1217.

(9) Legzdins, P.; McNeil, W. S.; Shaw, M. J. *Organometallics* **1993**, *13*, 562.

(10) Legzdins, P.; McNeil, W. S.; Batchelor, R. J.; Einstein, F. W. *B. J. Am. Chem. Soc.* **1994**, *116*, 6021.

(11) Hermes, A. R.; Morris, R. J.; Girolami, G. S. *Organometallics* **1988**, *7*, 2372.

(12) Edema, J. J. H.; Gambarotta, S.; van Bolhuis, F.; Spek, A. L. *J. Am. Chem. Soc.* **1989**, *111*, 2142.

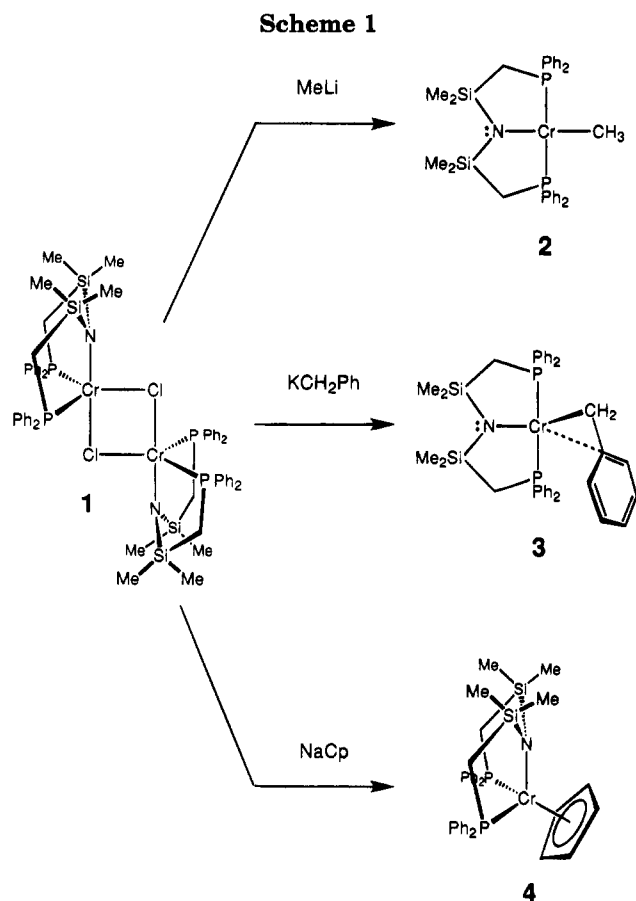
(13) Bradley, D. C.; Hursthouse, M. B.; Newing, C. W.; Welch, A. J. *J. Chem. Soc., Chem. Commun.* **1972**, 567.

(14) Edema, J. J. H.; Gambarotta, S.; Meetsma, A.; Spek, A. L.; Smeets, W. J. J.; Chiang, M. Y. *J. Chem. Soc., Dalton Trans.* **1993**, 789.

(15) Hao, S.; Song, J.-I.; Bierno, P.; Gambarotta, S. *Organometallics* **1994**, *13*, 1326.

(16) Fryzuk, M. D.; MacNeil, P. A.; Rettig, S. J.; Secco, A. S.; Trotter, J. *Organometallics* **1992**, *1*, 918.

(17) Kern, R. J. *J. Inorg. Nucl. Chem.* **1962**, *24*, 1105.



scribed previously,<sup>18</sup> reacts with lithium, sodium, or potassium alkyls or Grignard reagents in THF to yield monomeric chromium hydrocarbyl complexes (Scheme 1). Specifically, reaction with MeLi gives the high-spin, red-brown, 12-electron  $\text{CrCH}_3[\text{N}(\text{SiMe}_2\text{CH}_2\text{PPh}_2)_2]$  (**2**),<sup>18</sup> reaction with  $\text{KCH}_2\text{Ph}$  or  $\text{Mg}(\text{CH}_2\text{Ph})_2$  gives the high-spin, purple  $\text{CrCH}_2\text{Ph}[\text{N}(\text{SiMe}_2\text{CH}_2\text{PPh}_2)_2]$  (**3**), and reaction with NaCp-DME gives the low-spin, dark red, 16-electron  $\text{Cr}(\eta^5\text{-C}_5\text{H}_5)[\text{N}(\text{SiMe}_2\text{CH}_2\text{PPh}_2)_2]$  (**4**), with the formation of the alkali-metal halide salt as a byproduct in each case. The yields are generally very good and range from 80 to 90%.

The synthesis of a number of other alkyl and aryls was attempted. For example, the reaction of  $\text{LiCH}_2\text{-SiMe}_3$  with **1** does proceed to generate the expected compound  $\text{Cr}(\text{CH}_2\text{SiMe}_3)[\text{N}(\text{SiMe}_2\text{CH}_2\text{PPh}_2)_2]$  (**5**); however, it was not isolated as a solid but rather as a purple oil and thus was not characterized fully. The reaction of EtLi with the starting chloride **1** was examined in an attempt to generate the corresponding ethyl derivative  $\text{Cr}(\text{CH}_2\text{CH}_3)[\text{N}(\text{SiMe}_2\text{CH}_2\text{PPh}_2)_2]$ . Although it appears that the ethyl compound is generated, as evidenced by the formation of a deep brown-red solution similar to that observed for the methyl complex, attempts to work up the product led only to isolation in low yield of the hydride-bridged dimer<sup>18</sup>  $\{[\text{PPh}_2\text{PCH}_2\text{-SiMe}_2\text{N}]\text{Cr}\}_2(\mu\text{-H})_2$ , presumably by the loss of ethylene. The formation of other byproducts and the low yield of the hydride complicate analysis of this reaction. Similarly, attempts to form aryl derivatives by reaction with PhLi, for example, did not lead to tractable materials.

(18) Fryzuk, M. D.; Leznoff, D. B.; Rettig, S. J.; Thompson, R. *Inorg. Chem.* **1994**, *33*, 5528.

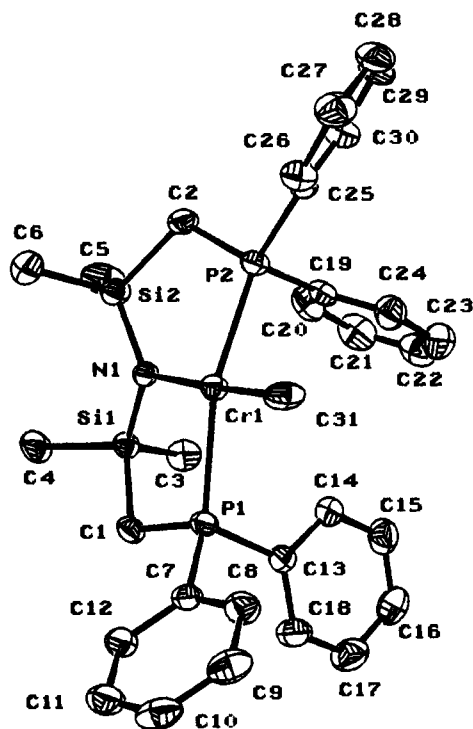


**Figure 1.** Molecular structure and numbering scheme for  $\text{CrMe}[\text{N}(\text{SiMe}_2\text{CH}_2\text{PPh}_2)_2]$  (**2**).

These air- and moisture-sensitive organometallic compounds of Cr(II) are all paramagnetic and hence show broadened <sup>1</sup>H NMR spectra that are generally unassignable. They are also ESR silent, both in solution and in frozen toluene glasses. As a result, X-ray crystallography (Table 1) in concert with magnetic studies were used to structurally characterize these  $\text{CrR}[\text{N}(\text{SiMe}_2\text{CH}_2\text{PPh}_2)_2]$  complexes.

**Structure of  $\text{CrMe}[\text{N}(\text{SiMe}_2\text{CH}_2\text{PPh}_2)_2]$ .** Solid-state Gouy and solution Evans method<sup>19</sup> magnetic susceptibility measurements of the methyl complex **2** were consistent with a high-spin  $d^4$  complex,<sup>20</sup> indicating a monomeric compound. This derivative is soluble in aromatic solvents and THF but only slightly soluble in hexanes. X-ray-quality crystals of **2** could be grown by cooling a saturated hexanes/toluene solution.

The structural analysis confirms that **2** is monomeric and square planar in the solid state (Figure 1), this being the preferred geometry for four-coordinate Cr(II).<sup>11</sup> What is particularly unique about this 12-electron species is that it contains the sterically undemanding methyl ligand; this is in stark contrast to other reported four-coordinate organochromium(II) complexes that contain bulky alkyl or aryl ligands such as  $\text{CH}_2\text{-CMe}_3$  or mesityl, respectively.<sup>11-15</sup> The methyl ligand can be used with Cr(II), for example, as has been found in the octahedral derivative  $\text{CrMe}_2(\text{dmpe})_2$ .<sup>21,22</sup>

In the methyl complex **2** the ancillary tridentate ligand  $\text{-N}(\text{SiMe}_2\text{CH}_2\text{PPh}_2)_2$  is meridionally bound. There is some distortion from pure square planar (Tables 3 and 4); the P(1)-Cr-P(2) and N-Cr-C(31) angles of 154.77(4) and 174.8(1)°, respectively (180° is ideal),

(19) Sur, S. K. *J. Magn. Reson.* **1989**, *82*, 169.

(20) Carlin, R. L. *Magnetochemistry*; Springer-Verlag: Heidelberg, Germany, 1986.

(21) Girolami, G. S.; Salt, J. E.; Wilkinson, G.; Thornton-Pett, M.; Hursthouse, M. B. *J. Am. Chem. Soc.* **1983**, *105*, 5954.

(22) Girolami, G. S.; Wilkinson, G.; Galas, A. M. R.; Thornton-Pett, M.; Hursthouse, M. B. *J. Chem. Soc., Dalton Trans.* **1985**, 1339.

Table 1. Crystallographic Data<sup>a</sup>

compd	CrMe[N(SiMe <sub>2</sub> CH <sub>2</sub> PPh <sub>2</sub> ) <sub>2</sub> ] (2) <sup>b</sup>	Cr(CH <sub>2</sub> Ph)[N(SiMe <sub>2</sub> CH <sub>2</sub> PPh <sub>2</sub> ) <sub>2</sub> ] (3) <sup>b</sup>	Cr( $\eta^5$ -C <sub>5</sub> H <sub>5</sub> )[N(SiMe <sub>2</sub> CH <sub>2</sub> PPh <sub>2</sub> ) <sub>2</sub> ] (4) <sup>c</sup>
formula	C <sub>31</sub> H <sub>39</sub> CrNP <sub>2</sub> Si <sub>2</sub>	C <sub>37</sub> H <sub>43</sub> CrNP <sub>2</sub> Si <sub>2</sub>	C <sub>35</sub> H <sub>41</sub> CrNP <sub>2</sub> Si <sub>2</sub>
fw	595.77	671.87	645.83
color and habit	brown prism	green needle	dark prism
cryst size, mm	0.08 × 0.25 × 0.35	0.25 × 0.35 × 0.40	0.40 × 0.50 × 0.50
cryst syst	triclinic	monoclinic	triclinic
space group	<i>P</i> $\bar{1}$	<i>P</i> 2 <sub>1</sub> / <i>c</i>	<i>P</i> $\bar{1}$
<i>a</i> , Å	11.274(1)	11.124(2)	10.942(2)
<i>b</i> , Å	15.557(2)	13.973(2)	11.257(2)
<i>c</i> , Å	9.8646(9)	23.691(2)	13.990(3)
$\alpha$ , deg	92.529(9)	90	89.31(3)
$\beta$ , deg	104.086(7)	95.24(1)	82.81(3)
$\gamma$ , deg	71.552(8)	90	89.93(3)
<i>V</i> , Å <sup>3</sup>	1590.8(3)	3666.9(9)	1709.5(6)
<i>Z</i>	2	4	2
<i>T</i> , °C	21	21	22
<i>D<sub>c</sub></i> , g/cm <sup>3</sup>	1.244	1.217	1.255
<i>F</i> (000)	644	1416	680
$\mu$ (Mo K $\alpha$ ), cm <sup>-1</sup>	5.43	4.90	5.23
transmission factors	0.92–1.00	0.96–1.00	0.82–1.00
scan type	$\omega$ -2 $\theta$	$\omega$ -2 $\theta$	$\omega$ -2 $\theta$
scan range in $\omega$ , deg	1.10 + 0.35 tan $\theta$	1.05 + 0.35 tan $\theta$	1.56 + 0.35 tan $\theta$
scan speed, deg/min	16 (up to 8 rescans)	16 (up to 8 rescans)	3–30
data collected	+ <i>h</i> , ± <i>k</i> , ± <i>l</i>	+ <i>h</i> , ± <i>k</i> , ± <i>l</i>	± <i>h</i> , ± <i>k</i> , <i>l</i>
2 $\theta$ <sub>max</sub> , deg	60	55	45
cryst decay, %	2.4	negligible	negligible
total no. of rflns	9712	9199	5187
no. of unique rflns	9266	8746	4378
<i>R</i> <sub>merge</sub>	0.043	0.030	0.046
no. with <i>I</i> ≥ <i>n</i> $\sigma$ ( <i>I</i> )	3915 ( <i>n</i> = 3)	4324 ( <i>n</i> = 3)	2250 ( <i>n</i> = 2.5)
no. of variables	335	396	370
<i>R</i>	0.040	0.033	0.064
<i>R<sub>w</sub></i>	0.035	0.030	0.045
GOF	1.82	1.80	1.83
max $\Delta/\sigma$ (final cycle)	0.02	0.02	0.004
residual density, e/Å <sup>3</sup>	-0.26, 0.25	-0.20, 0.20	-0.29, 0.32

<sup>a</sup> Conditions and definitions: Mo K $\alpha$  radiation,  $\lambda$  = 0.710 69 Å, graphite monochromator;  $\sigma^2(F^2)$  = [*S*<sup>2</sup>(*C* + 4*B*) + (*pF*<sup>2</sup>)<sup>2</sup>]/(*I*(*Lp*)<sup>2</sup>) (*S* = scan speed, *C* = scan count, *B* = normalized background count, *p* = 0.00 for **2** and **3**, 0.02 for **4**); function minimized  $\sum w(|F_o| - |F_c|)^2$ , where  $w = 4F_o^2/\sigma^2(F_o^2)$ ;  $R = \sum ||F_o| - |F_c||/\sum |F_o|$ ;  $R_w = (\sum w(|F_o| - |F_c|)^2/\sum w|F_o|^2)^{1/2}$ ; GOF = [ $\sum w(|F_o| - |F_c|)^2/(m - n)$ ]<sup>1/2</sup>. Values given for *R*, *R<sub>w</sub>*, and GOF are based on those reflections with *I* ≥ *n* $\sigma$ (*I*) (*n* = 3.0 for **2** and **3**, 2.5 for **4**). <sup>b</sup> Conditions: Rigaku AFC6S diffractometer; takeoff angle 6.0°; aperture 6.0 × 6.0 mm at a distance of 285 mm from the crystal; stationary background counts at each end of the scan (scan/background time ratio 2:1). <sup>c</sup> Conditions: Siemens P4 diffractometer; takeoff angle 2.8°; aperture (2.0–2.5) × 2.0 mm at a distance of 210 mm from the crystal; stationary background counts at each end of the scan (scan/background time ratio 2:1).

indicate the extent of the distortion. In addition, the dihedral angle between the planes defined by Cr–P(2)–C(31) and Cr–N–P(2) is 23.9°, and this represents the extent of the twist in what should ideally be a flat square-planar core. The Cr–P distances of 2.485(1) and 2.451(1) Å and the Cr–C distance of 2.151(3) Å are both comparable with known square-planar high-spin d<sup>4</sup> Cr(II) alkyls.<sup>11,23</sup> The Cr–N bond length of 2.117(3) Å is extremely long,<sup>13,14</sup> and this could indicate that there is very little, if any, amide lone pair–metal *p* $\pi$ –*d* $\pi$  interaction. Instead, the relatively short Si–N bonds of 1.699 Å indicate that there is some delocalization of the amide lone pair in these bonds.<sup>24</sup>

The electron density difference map revealed the Cr–methyl hydrogens to be 1:1 disordered, and in a normal geometry. In addition, there is no IR evidence for any Cr–C–H bond agostic interaction.<sup>25</sup> This lack of such an interaction, despite the coordinative and electronic unsaturation, has been previously noted as being due to conflicting symmetry requirements.<sup>11</sup>

**Structure of Cr(CH<sub>2</sub>Ph)[N(SiMe<sub>2</sub>CH<sub>2</sub>PPh<sub>2</sub>)<sub>2</sub>].** Reaction of the chloride starting complex **1** with KCH<sub>2</sub>Ph

or Mg(CH<sub>2</sub>Ph)<sub>2</sub>·2THF yields the purple compound **3** with a magnetic moment of 5.1  $\mu_B$ , consistent with a high-spin, monomeric complex.<sup>20</sup> Suitable crystals of **3** for X-ray analysis were grown by slow evaporation of a saturated hexanes solution.

The X-ray structure reveals the expected distorted-square-planar, monomeric **3** (Figure 2). The <sup>-</sup>N(SiMe<sub>2</sub>CH<sub>2</sub>PPh<sub>2</sub>)<sub>2</sub> ligand again is meridionally bound, but the distortion from square planar is more pronounced here than in **2** (Tables 3 and 4). The P(1)–Cr–P(2) and N–Cr–C(31) angles of 145.18(3) and 157.8(1)° show greater “bending-back” than in **2**. The dihedral angle between the Cr–P(1)–C(31) and Cr–P(2)–N planes is 38.7° (vs 23.9° in **2**), indicating again the increased twist in **3** from an ideal flat core compared to the twist in **2**. The Cr–P distances of 2.4758(9) and 2.4808(8) Å are similar to those in **2** and to those in other known square-planar Cr(II) alkyls.<sup>11</sup> The Cr–N bond of 2.067(2) Å, shorter than in **2**, coupled with comparatively slightly longer Si–N bonds of 1.707(2) and 1.706(2) Å suggests that the lone pair on nitrogen is interacting with the metal to a slightly greater extent than in the methyl complex **2**.

The increased distortion from ideal square-planar geometry could be due to the steric bulk of the benzyl moiety as compared to the methyl ligand. However, a more likely reason for the distortion could be the weak

(23) Hermes, A. R.; Girolami, G. S. *Inorg. Chem.* **1988**, *27*, 1775.

(24) Robiette, A. G.; Sheldrick, G. M.; Sheldrick, W. S.; Beagley, B.; Cruickshank, D. W. J.; Monaghan, J. J.; Aylett, B. J.; Ellis, I. A. *Chem. Commun.* **1968**, 909.

(25) Brookhart, M.; Green, M. L. H.; Wong, L.-L. *Prog. Inorg. Chem.* **1988**, *36*, 1.



**Table 2. Final Atomic Coordinates and  $B_{eq}$  Values ( $\text{\AA}^2$ )**

atom	x	y	z	$B_{eq}^a$	atom	x	y	z	$B_{eq}^a$
<b>CrMe[N(SiMe<sub>2</sub>CH<sub>2</sub>PPh<sub>2</sub>)<sub>2</sub>] (2)</b>									
Cr(1)	0.30658(5)	0.29666(4)	0.06770(6)	2.79(3)	C(14)	0.6072(4)	0.1210(3)	0.2357(4)	4.0(2)
P(1)	0.52798(9)	0.30498(6)	0.16157(10)	2.99(5)	C(15)	0.6953(4)	0.0375(3)	0.2830(4)	5.1(3)
P(2)	0.13098(9)	0.23252(6)	0.04941(9)	3.01(5)	C(16)	0.8233(4)	0.0264(3)	0.3129(4)	5.3(3)
Si(1)	0.38987(10)	0.34761(7)	0.39721(10)	3.13(5)	C(17)	0.8654(4)	0.0982(3)	0.2966(5)	5.7(3)
Si(2)	0.11360(10)	0.36656(7)	0.28087(11)	3.62(6)	C(18)	0.7785(4)	0.1819(3)	0.2505(4)	4.7(2)
N(1)	0.2669(2)	0.3410(2)	0.2626(3)	2.9(1)	C(19)	0.2290(3)	0.1241(2)	0.1372(4)	3.4(2)
C(1)	0.5192(3)	0.3667(2)	0.3205(3)	3.3(2)	C(20)	0.2538(4)	0.1064(3)	0.2795(4)	5.1(3)
C(2)	0.0290(3)	0.2938(2)	0.1619(4)	3.9(2)	C(21)	0.3428(5)	0.0241(4)	0.3411(5)	5.9(3)
C(3)	0.4637(4)	0.2448(3)	0.5158(4)	4.7(2)	C(22)	0.4037(4)	-0.0370(3)	0.2616(6)	5.8(3)
C(4)	0.3482(4)	0.4472(3)	0.5116(4)	5.1(3)	C(23)	0.3813(4)	-0.0229(3)	0.1209(5)	5.9(3)
C(5)	0.0959(4)	0.3454(3)	0.4595(4)	6.5(3)	C(24)	0.2948(4)	0.0575(3)	0.0602(4)	4.6(2)
C(6)	0.0184(4)	0.4870(3)	0.2309(5)	6.0(3)	C(25)	0.0255(3)	0.2001(2)	-0.1018(4)	3.2(2)
C(7)	0.6090(3)	0.3566(2)	0.0647(4)	3.2(2)	C(26)	0.0013(3)	0.2396(3)	-0.2320(4)	4.1(2)
C(8)	0.6307(4)	0.3198(3)	-0.0616(4)	4.3(2)	C(27)	-0.0829(4)	0.2180(3)	-0.3459(4)	5.1(3)
C(9)	0.6851(4)	0.3598(3)	-0.1415(4)	5.1(3)	C(28)	-0.1427(4)	0.1563(3)	-0.3286(5)	5.6(3)
C(10)	0.7179(4)	0.4365(3)	-0.0974(5)	5.2(3)	C(29)	-0.1209(4)	0.1169(3)	-0.2000(5)	5.5(3)
C(11)	0.6967(4)	0.4724(3)	0.0262(5)	4.8(3)	C(30)	-0.0366(4)	0.1380(3)	-0.0863(4)	4.4(2)
C(12)	0.6428(3)	0.4329(2)	0.1074(4)	3.8(2)	C(31)	0.3319(3)	0.2618(3)	-0.1391(3)	4.2(2)
C(13)	0.6467(3)	0.1948(2)	0.2189(3)	3.0(2)					
<b>Cr(<math>\eta^2</math>-CH<sub>2</sub>Ph)[N(SiMe<sub>2</sub>CH<sub>2</sub>PPh<sub>2</sub>)<sub>2</sub>] (3)</b>									
Cr(1)	0.81682(4)	0.36033(3)	0.35562(2)	3.466(10)	C(17)	1.2611(4)	0.2584(3)	0.2364(2)	8.5(1)
P(1)	0.97956(6)	0.24719(5)	0.33655(3)	3.71(2)	C(18)	1.1548(3)	0.2308(2)	0.2582(1)	5.90(9)
P(2)	0.70305(6)	0.43333(5)	0.43000(3)	3.70(2)	C(19)	0.7725(2)	0.4112(2)	0.5011(1)	3.89(7)
Si(1)	0.74153(7)	0.14412(6)	0.31928(3)	3.90(2)	C(20)	0.8963(3)	0.4037(2)	0.5104(1)	4.70(8)
Si(2)	0.60742(7)	0.23361(6)	0.40948(3)	4.08(2)	C(21)	0.9521(3)	0.3853(3)	0.5640(1)	6.39(10)
N(1)	0.7151(2)	0.2378(1)	0.36268(8)	3.59(5)	C(22)	0.8833(4)	0.3728(3)	0.6087(1)	7.0(1)
C(1)	0.8937(3)	0.1635(2)	0.2902(1)	4.36(7)	C(23)	0.7608(4)	0.3799(3)	0.6002(1)	7.1(1)
C(2)	0.5661(2)	0.3629(2)	0.4239(1)	4.30(7)	C(24)	0.7046(3)	0.3997(3)	0.5472(1)	5.92(9)
C(3)	0.7499(3)	0.0245(2)	0.3553(1)	5.67(8)	C(25)	0.6624(2)	0.5597(2)	0.4322(1)	4.04(7)
C(4)	0.6282(3)	0.1371(2)	0.2562(1)	5.58(8)	C(26)	0.7104(3)	0.6207(2)	0.4747(1)	5.43(9)
C(5)	0.6594(3)	0.1741(2)	0.4787(1)	5.64(9)	C(27)	0.6839(3)	0.7177(3)	0.4725(2)	6.7(1)
C(6)	0.4633(3)	0.1727(2)	0.3837(1)	5.97(9)	C(28)	0.6097(3)	0.7544(2)	0.4286(2)	6.6(1)
C(7)	1.0394(2)	0.1759(2)	0.3971(1)	3.79(7)	C(29)	0.5602(3)	0.6960(3)	0.3864(1)	5.83(10)
C(8)	0.9952(3)	0.1891(2)	0.4492(1)	4.81(8)	C(30)	0.5873(3)	0.5988(2)	0.3883(1)	4.95(8)
C(9)	1.0407(3)	0.1363(3)	0.4961(1)	6.16(10)	C(31)	0.8798(4)	0.5873(2)	0.3179(1)	4.62(9)
C(10)	1.1300(3)	0.0709(3)	0.4906(1)	6.23(10)	C(32)	0.8222(3)	0.4568(2)	0.2632(1)	4.14(7)
C(11)	1.1747(3)	0.0561(2)	0.4397(2)	6.09(9)	C(33)	0.6972(3)	0.4643(2)	0.2497(1)	6.07(10)
C(12)	1.1299(3)	0.1086(2)	0.3931(1)	5.06(8)	C(34)	0.6413(4)	0.4279(3)	0.1999(2)	8.3(1)
C(13)	1.1165(3)	0.2785(2)	0.3045(1)	4.25(7)	C(35)	0.7066(5)	0.3817(3)	0.1621(2)	8.8(2)
C(14)	1.1844(3)	0.3535(2)	0.3275(1)	5.33(8)	C(36)	0.8280(5)	0.3733(3)	0.1740(2)	7.6(1)
C(15)	1.2897(3)	0.3811(3)	0.3046(2)	7.4(1)	C(37)	0.8856(3)	0.4097(2)	0.2234(1)	5.41(9)
C(16)	1.3272(4)	0.3323(3)	0.2591(2)	8.6(1)					
<b>Cr(<math>\eta^5</math>-C<sub>5</sub>H<sub>5</sub>)[N(SiMe<sub>2</sub>CH<sub>2</sub>PPh<sub>2</sub>)<sub>2</sub>] (4)</b>									
Cr(1)	0.1229(1)	0.3108(1)	0.2731(1)	3.66(4)	C(16)	0.279(2)	-0.191(1)	0.1273(9)	7.7(5)
P(1)	0.0590(3)	0.1573(2)	0.1780(2)	3.68(7)	C(17)	0.153(1)	-0.196(1)	0.1425(9)	6.7(4)
P(2)	0.2636(3)	0.2170(2)	0.3650(2)	3.91(7)	C(18)	0.087(1)	-0.093(1)	0.1579(7)	5.5(3)
Si(1)	0.2196(3)	0.3261(3)	0.0500(2)	4.40(8)	C(19)	0.2706(10)	0.2784(9)	0.4833(7)	4.2(3)
Si(2)	0.3990(3)	0.3627(3)	0.2008(2)	5.02(9)	C(20)	0.202(1)	0.2288(9)	0.5633(9)	6.0(4)
N(1)	0.2638(6)	0.3309(6)	0.1612(5)	3.8(2)	C(21)	0.201(1)	0.281(1)	0.6538(9)	6.8(4)
C(1)	0.0790(9)	0.2240(8)	0.0588(6)	4.2(3)	C(22)	0.271(1)	0.384(1)	0.663(1)	7.8(5)
C(2)	0.4165(9)	0.2457(8)	0.2995(7)	4.5(3)	C(23)	0.336(2)	0.429(1)	0.582(1)	10.0(6)
C(3)	0.341(1)	0.269(1)	-0.0453(8)	6.8(4)	C(24)	0.335(1)	0.379(1)	0.4972(9)	7.4(4)
C(4)	0.175(1)	0.4741(9)	0.0020(7)	6.4(3)	C(25)	0.270(1)	0.0549(8)	0.3937(6)	3.6(3)
C(5)	0.5388(10)	0.343(1)	0.1101(8)	7.6(4)	C(26)	0.166(1)	-0.011(1)	0.3993(7)	5.1(3)
C(6)	0.413(1)	0.5174(10)	0.2474(8)	7.3(4)	C(27)	0.169(1)	-0.132(1)	0.4187(9)	7.1(4)
C(7)	-0.1005(9)	0.1047(8)	0.1982(7)	3.6(3)	C(28)	0.276(2)	-0.187(1)	0.4229(8)	6.5(4)
C(8)	-0.1512(10)	0.0718(9)	0.2875(8)	5.0(3)	C(29)	0.383(1)	-0.122(1)	0.4276(8)	6.6(4)
C(9)	-0.271(1)	0.024(1)	0.3066(8)	5.8(4)	C(30)	0.377(1)	-0.0004(10)	0.4115(7)	4.9(3)
C(10)	-0.338(1)	0.0152(10)	0.2284(10)	6.1(4)	C(31)	0.065(2)	0.495(1)	0.272(2)	8.8(5)
C(11)	-0.286(1)	0.0434(10)	0.1368(8)	5.5(4)	C(32)	-0.036(2)	0.422(2)	0.255(1)	9.4(6)
C(12)	-0.170(1)	0.0891(9)	0.1209(7)	5.1(3)	C(33)	-0.068(1)	0.356(1)	0.335(1)	6.6(4)
C(13)	0.1418(10)	0.0143(9)	0.1583(6)	3.7(3)	C(34)	0.005(2)	0.386(1)	0.4012(9)	6.9(4)
C(14)	0.272(1)	0.0189(9)	0.1421(7)	5.2(3)	C(35)	0.089(1)	0.460(1)	0.367(1)	6.9(4)
C(15)	0.340(1)	-0.085(1)	0.1270(9)	7.4(4)					

$$^a B_{eq} = \frac{1}{3}\pi^2(U_{11}(aa^*)^2 + U_{22}(bb^*)^2 + U_{33}(bb^*)^2 + 2U_{12}aa^*bb^* \cos \gamma + 2U_{13}aa^*cc^* \cos \beta + 2U_{23}bb^*cc^* \cos \alpha).$$

interaction of the benzyl ipso carbon with the metal center; this type of interaction has been represented in the literature<sup>26</sup> as an  $\eta^2$ -bound benzyl and is fundamentally distinct from either the  $\eta^1$ - $\sigma$ -bonded benzyl or an  $\eta^3$ -benzyl complex.

Several structural features have been highlighted as key in characterizing  $\eta^2$ -benzyls,<sup>26,27</sup> and these features have, for the most part, been recognized in **3**. First, the Cr-C<sub>ipso</sub> distance of 2.576(3) Å is short enough to consider as a metal-carbon single bond.<sup>2</sup> On the other

**Table 3. Selected Bond Lengths (Å) for the Complexes CrCH<sub>3</sub>[N(SiMe<sub>2</sub>CH<sub>2</sub>PPh<sub>2</sub>)<sub>2</sub>] (2), Cr(η<sup>2</sup>-CH<sub>2</sub>Ph)[N(SiMe<sub>2</sub>CH<sub>2</sub>PPh<sub>2</sub>)<sub>2</sub>] (3), and Cr(η<sup>5</sup>-C<sub>5</sub>H<sub>5</sub>)[N(SiMe<sub>2</sub>CH<sub>2</sub>PPh<sub>2</sub>)<sub>2</sub>] (4)**

	2	3	4
Cr-P(1)	2.485(1)	2.4758(9)	2.353(3)
Cr-P(2)	2.451(1)	2.4808(8)	2.366(3)
Cr-N	2.117(3)	2.067(2)	2.066(7)
Cr-C(31)	2.151(3)	2.132(3)	
Cr-Cp(centroid)			1.86
P(1)-C(1)	1.809(3)	1.815(3)	1.809(8)
P(1)-C(7)	1.830(3)	1.823(3)	1.831(9)
P(1)-C(13)	1.820(3)	1.817(3)	1.85(1)
P(2)-C(2)	1.815(3)	1.809(3)	1.832(9)
P(2)-C(19)	1.817(4)	1.814(3)	1.81(1)
P(2)-C(25)	1.829(3)	1.824(3)	1.867(10)
Si(1)-N	1.697(3)	1.707(2)	1.687(8)
Si(1)-C(1)	1.902(3)	1.904(3)	1.913(10)
Si(1)-C(3)	1.862(4)	1.875(3)	1.88(1)
Si(1)-C(4)	1.881(4)	1.868(3)	1.877(10)
Si(2)-N	1.699(3)	1.706(2)	1.684(8)
Si(2)-C(2)	1.894(4)	1.902(3)	1.924(9)
Si(2)-C(5)	1.875(4)	1.882(3)	1.88(1)
Si(2)-C(6)	1.859(4)	1.868(3)	1.88(1)
Cr-C(32)		2.576(3)	
C(31)-C(32)		1.456(4)	1.43(2)
C(31)-C(35)			1.43(2)
C(32)-C(33)		1.402(4)	1.35(2)
C(33)-C(34)		1.380(5)	1.34(2)
C(34)-C(35)		1.366(6)	1.28(2)
C(35)-C(36)		1.359(5)	
C(36)-C(37)		1.379(4)	
C(37)-C(32)		1.394(4)	
C(31)-H(37)		0.92(3)	
C(31)-H(38)		0.91(2)	

hand, the Cr-C<sub>ortho</sub> distances of 3.093(3) and 3.364(3) Å are clearly too long to consider any interaction as would exist in an η<sup>3</sup>-bonding mode. The Cr-CH<sub>2</sub>-C<sub>ipso</sub> angle of 89.7(2)° indicates the extent of the pull of the ipso carbon toward the metal, resulting in an angle much more acute than the expected tetrahedral 109°. The CH<sub>2</sub>-C<sub>ipso</sub> distance of 1.456(4) Å is comparable to the values found in other η<sup>2</sup>-benzyls;<sup>26,28</sup> this length is naturally shorter than in η<sup>1</sup>-benzyls. The C-C bonds in the phenyl ring of the benzyl ligand are all very similar in length (1.380(5), 1.366(6), 1.359(5), and 1.379(4) Å), indicating a delocalized system consistent with η<sup>2</sup> bonding; an η<sup>3</sup>-bound benzyl normally forces localization of the bonding in the phenyl ring, and this is not observed. Thus, one could almost consider this complex to be pentacoordinate. In terms of total electron count, **3** can be considered as a 14-electron system, if one takes into account the η<sup>2</sup>-benzyl formulation. One can discount the possibility of an agostic interaction between the benzyl CH<sub>2</sub> and the chromium center. The methylene hydrogens were located and refined, and the Cr-C(31)-H angles of 109(1) and 116(1)° clearly show no distortion characteristic of agostic interactions.<sup>25</sup>

The Cr-C bond length of 2.132(3) Å is shorter than that found in **2**. This length compares with other short Cr-C bonds recorded: 2.131(2) Å for Cr<sub>2</sub>(CH<sub>2</sub>SiMe<sub>3</sub>)<sub>4</sub>(PMe<sub>3</sub>)<sub>2</sub> and 2.128(4) Å for Cr(CH<sub>2</sub>SiMe<sub>3</sub>)<sub>2</sub>(dippe), for example.<sup>11,29</sup> Ideally it would be desirable to compare the structural features of the η<sup>2</sup>-benzyl in **3** with those of other chromium benzyls, but there is a paucity of such structures. Chromium benzyls are certainly

**Table 4. Selected Bond Angles (deg) for the Complexes CrCH<sub>3</sub>[N(SiMe<sub>2</sub>CH<sub>2</sub>PPh<sub>2</sub>)<sub>2</sub>] (2), Cr(η<sup>2</sup>-CH<sub>2</sub>Ph)[N(SiMe<sub>2</sub>CH<sub>2</sub>PPh<sub>2</sub>)<sub>2</sub>] (3), and Cr(η<sup>5</sup>-C<sub>5</sub>H<sub>5</sub>)[N(SiMe<sub>2</sub>CH<sub>2</sub>PPh<sub>2</sub>)<sub>2</sub>] (4)**

	2	3	4
P(1)-Cr-P(2)	154.77(4)	145.18(3)	103.9(1)
P(1)-Cr-N	88.13(7)	84.31(6)	83.9(2)
P(1)-Cr-C(31)	94.87(9)	100.4(1)	
P(2)-Cr-N	83.82(7)	87.96(6)	89.0(2)
P(2)-Cr-C(31)	95.1(1)	99.42(10)	
N-Cr-C(31)	174.8(1)	157.8(1)	
Cr-P(1)-C(1)	104.2(1)	99.72(9)	102.2(3)
Cr-P(1)-C(7)	123.6(1)	115.22(9)	119.8(3)
Cr-P(1)-C(13)	113.0(1)	125.28(9)	123.7(3)
C(1)-P(1)-C(7)	106.7(2)	105.0(1)	106.0(4)
C(1)-P(1)-C(13)	104.7(2)	108.5(1)	102.3(4)
C(7)-P(1)-C(13)	103.1(2)	101.6(1)	100.5(5)
Cr-P(2)-C(2)	108.7(1)	101.51(9)	105.6(3)
Cr-P(2)-C(19)	96.9(1)	112.80(9)	115.4(3)
Cr-P(2)-C(25)	131.6(1)	124.19(9)	126.3(3)
C(2)-P(2)-C(19)	107.3(2)	105.5(1)	104.4(5)
C(2)-P(2)-C(25)	106.7(2)	108.6(1)	102.5(5)
C(19)-P(2)-C(25)	102.8(2)	103.0(1)	100.3(4)
N-Si(1)-C(1)	108.0(1)	108.5(1)	106.7(4)
N-Si(1)-C(3)	114.1(2)	114.5(1)	114.3(5)
N-Si(1)-C(4)	115.0(2)	112.4(1)	114.2(5)
C(1)-Si(1)-C(3)	108.7(2)	106.4(1)	109.0(5)
C(1)-Si(1)-C(4)	103.9(4)	106.0(1)	108.0(5)
C(3)-Si(1)-C(4)	106.6(2)	108.6(1)	104.4(5)
N-Si(2)-C(2)	109.3(1)	106.2(1)	105.1(4)
N-Si(2)-C(5)	116.2(2)	113.8(1)	115.2(5)
N-Si(2)-C(6)	112.1(2)	115.8(1)	115.3(5)
C(2)-Si(2)-C(5)	104.9(2)	108.9(1)	104.7(4)
C(2)-Si(2)-C(6)	107.3(2)	106.1(1)	111.2(5)
C(5)-Si(2)-C(6)	106.6(2)	105.7(1)	105.0(5)
Cr-N-Si(1)	118.9(1)	117.4(1)	114.9(4)
Cr-N-Si(2)	119.1(1)	120.2(1)	112.1(4)
Si(1)-N-Si(2)	121.9(2)	122.3(1)	132.7(4)
P(1)-C(1)-Si(1)	110.0(2)	108.0(1)	107.8(5)
P(2)-C(2)-Si(2)	109.2(2)	108.4(1)	107.9(5)
P(1)-Cr-C(32)		96.04(7)	
P(2)-Cr-C(32)		116.19(7)	
N-Cr-C(32)		123.88(9)	
Cr-C(31)-C(32)		89.7(2)	
Cr-C(31)-H(37)		109(1)	
Cr-C(31)-H(38)		116(1)	
P(1)-Cr-Cp(centroid)			120.5
P(2)-Cr-Cp(centroid)			121.7

known as compounds, such as Cr(CH<sub>2</sub>Ph)Cl<sub>2</sub>(THF) (THF = tetrahydrofuran), Cr(CH<sub>2</sub>Ph)Cl<sub>2</sub>(py)<sub>3</sub> (py = pyridine), and [Cp\*Cr(CH<sub>2</sub>Ph)Cl]<sub>2</sub> illustrate.<sup>30-34</sup> Very recently the formation of the bis(benzyl) complex Cr-(CH<sub>2</sub>Ph)<sub>2</sub>(TMEDA) has been reported,<sup>15</sup> the solid-state structure clearly shows η<sup>1</sup>-benzyl type ligands with Cr-C bond lengths of 2.177(2) Å; in addition, the Cr-(II) benzyl complex Cp\*Cr(CH<sub>2</sub>Ph)bpy (bpy = bipyridine) also shows simple η<sup>1</sup> coordination.<sup>35</sup> Especially well studied are the [Cr(CH<sub>2</sub>Ph)(OH)<sub>2</sub>]<sub>5</sub><sup>2+</sup> cations,<sup>36</sup> but the only crystal structure of such a cation is that of [p-BrC<sub>6</sub>H<sub>4</sub>CH<sub>2</sub>CrL(H<sub>2</sub>O)](ClO<sub>4</sub>)<sub>2</sub> (L = [15]aneN<sub>4</sub>).<sup>37</sup> Here the sterically enlarged Cr-CH<sub>2</sub>-C<sub>ipso</sub> angle of 123°, slightly longer Cr-CH<sub>2</sub> bond length of 2.14(2) Å, and

(30) Glocking, F.; Sneed, R. P. A.; Zeiss, H. H. *J. Organomet. Chem.* **1964**, *2*, 109.

(31) Richeson, D. S.; Mitchell, J. F.; Theopold, K. H. *Organometallics* **1989**, *8*, 2570.

(32) Sneed, R. P. A.; Thronsen, H. P. *Chem. Commun.* **1965**, 509.

(33) Sneed, R. P. A.; Thronsen, H. P. *J. Organomet. Chem.* **1966**, *6*, 542.

(34) Sneed, R. P. A.; Thronsen, H. P. *J. Organomet. Chem.* **1966**, *6*, 542.

(35) Bhandari, G.; Kim, Y.; McFarland, J. M.; Rheingold, A. L.; Theopold, K. H. *Organometallics* **1995**, *14*, 738.

(36) Espenson, J. H. *Acc. Chem. Res.* **1992**, *25*, 222.

(37) Shi, S.; Espenson, J. H.; Bakac, A. *J. Am. Chem. Soc.* **1990**, *112*, 1841.

(28) Jordan, R. F.; LaPointe, R. E.; Baenziger, N.; Hinch, G. D. *Organometallics* **1990**, *9*, 1539.

(29) Hursthouse, M. B.; Malik, K. M. A.; Sales, K. D. *J. Chem. Soc., Dalton Trans.* **1978**, 1314.

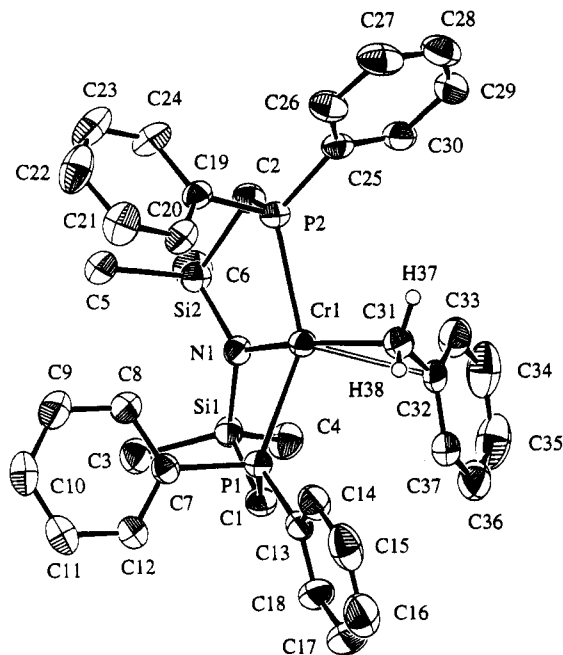


**Figure 2.** Molecular structure and numbering scheme for  $\text{Cr}(\eta^2\text{-CH}_2\text{Ph})[\text{N}(\text{SiMe}_2\text{CH}_2\text{PPh}_2)_2]$  (**3**).

longer  $\text{CH}_2\text{-C}_{\text{ipso}}$  bond length of 1.48(2) Å all are indicative of a standard  $\eta^1$ -benzyl. Comparison with known Mo, W, and Zr  $\eta^2$ -benzyls shows that the structural features are similar; however, a meaningful, quantitative comparison may be difficult to make.<sup>26,28,38</sup> To our knowledge, this is the first example of a paramagnetic  $\eta^2$ -benzyl complex and the first example of such a coordination mode for a chromium-based system.

**Structure of  $\text{Cr}(\eta^5\text{-C}_5\text{H}_5)[\text{N}(\text{SiMe}_2\text{CH}_2\text{PPh}_2)_2]$ .** The addition of  $\text{NaCp}\cdot\text{DME}$  to the chloride dimer **1** gives the cyclopentadienyl compound  $\text{Cr}(\eta^5\text{-C}_5\text{H}_5)[\text{N}(\text{SiMe}_2\text{CH}_2\text{PPh}_2)_2]$  (**4**), which was shown to have a magnetic moment of 2.7  $\mu_{\text{B}}$ , consistent with a low-spin configuration. The same compound can also be synthesized by reaction of the methyl complex **2** in toluene with freshly cracked cyclopentadiene, forming **4** with concomitant loss of  $\text{CH}_4$ . The magnetic moment of **4** is comparable to that of the similar compound  $\text{Cp}^*\text{CrMe}(\text{dmpe})$ , which has a reported magnetic moment of 2.79  $\mu_{\text{B}}$ .<sup>39</sup> Even in the absence of a crystal structure, the coordination of the Cp ligand was deduced to be  $\eta^5$ , as an  $\eta^1$ -Cp would be expected to be high-spin, as found for complexes **2** and **3**.

Dark red prismatic crystals of **4** were grown by slow evaporation of a saturated hexanes solution. The obtained crystal structure (Figure 3), showing a pseudooctahedral three-legged piano-stool-like monomeric  $\text{Cr}^{\text{II}}\text{-Cp}$  complex with  $C_s$  symmetry, confirms the spectroscopic observation of an  $\eta^5$ -Cp compound; selected bond lengths and bond angles are given in Tables 3 and 4.

The Cr–N bond of 2.066(7) Å is considerably shorter (0.05 Å) than in the methyl complex **2** but is comparable to that in **3**; this bond length is also very similar to that found in the chloride dimer **1** (2.078(8) Å). The N–Si

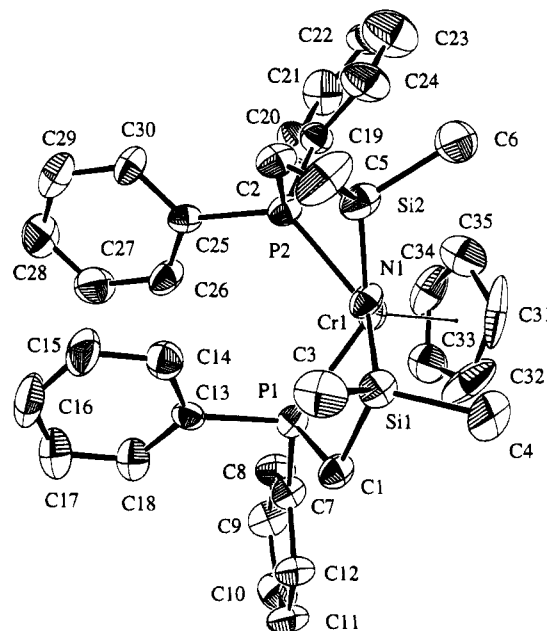


**Figure 3.** Molecular structure and numbering scheme for  $\text{Cr}(\eta^5\text{-C}_5\text{H}_5)[\text{N}(\text{SiMe}_2\text{CH}_2\text{PPh}_2)_2]$ .

bond lengths of 1.687(8) and 1.689(8) Å are comparable to those in  $\text{Cr}[\text{N}(\text{SiMe}_3)_2]_2(\text{THF})_2$  (1.674(17) Å).<sup>13</sup>

The Cr–P distances in **4** are 2.353(3) and 2.366(3) Å, much shorter than the analogous distances in **2** or **3**. This can easily be rationalized as being due to the low-spin nature of **4** as compared to the other, high-spin compounds. The sensitivity of the Cr–P distance to metal spin state and environment has been previously noted.<sup>11</sup> The octahedral, low-spin  $\text{Cr}(\text{II}) \text{CrX}_2(\text{dmpe})_2$  compounds ( $X = \text{Cl, Me, O}_2\text{CCF}_3$ ) have Cr–P distances ranging from 2.345 to 2.387 Å; compound **4** is well within this “typical” range.<sup>22,40–42</sup>

**Electronic Structure and Magnetism of  $\text{CrR}[\text{N}(\text{SiMe}_2\text{CH}_2\text{PPh}_2)_2]$ .** High-spin, four-coordinate  $\text{Cr}(\text{II})$  complexes have been shown to electronically prefer a square-planar environment, as the four lowest energy d orbitals are half-filled,<sup>11</sup> similar to that found for the fully occupied  $d^8$  systems such as  $\text{Rh}(\text{I})$  and  $\text{Pt}(\text{II})$ .<sup>2</sup>

The compounds presented in this work illustrate a wide variety of hapticity and total electron-donating ability. For the benzyl and cyclopentadienyl systems, each ligand donates the maximum number of electrons that can be used without invoking steric constraints, to stabilize the metal. Hence, the Cp ligand binds in an  $\eta^5$  fashion to enable donation of its full six electrons (using oxidation-state formalism). In addition, the benzyl ligand binds in an  $\eta^2$  fashion, formally acting as a four-electron donor as opposed to an  $\eta^1$ , two-electron donor. Steric constraints may restrict  $\eta^3$  or higher coordination of the benzyl ligand, but this seems unlikely, given the existence of the cyclopentadienyl complex **4** having the ancillary tridentate ligand bound in a facial manner. However, it could be that the high-spin-state  $\text{Cr}(\text{II})$  center cannot electronically bind the benzyl in a higher hapticity mode *without a change in*

(40) Barron, A. R.; Salt, J. E.; Wilkinson, G.; Motevalli, M.; Hursthouse, M. B. *J. Chem. Soc., Dalton Trans.* **1987**, 2947.

(41) Salt, J. E.; Wilkinson, G.; Motevalli, M.; Hursthouse, M. B. *J. Chem. Soc., Dalton Trans.* **1986**, 1141.

(42) Salt, J. E.; Girolami, G. S.; Wilkinson, G.; Motevalli, M.; Thronton-Pett, M.; Hursthouse, M. B. *J. Chem. Soc., Dalton Trans.* **1985**, 685.

(38) Davies, G. R.; Jarvis, J. A. J.; Kilbourn, B. T. *J. Chem. Soc. D* **1971**, 1511.

(39) Thomas, B. J.; Noh, S. K.; Schulte, G. K.; Sendlinger, S. C.; Theopold, K. H. *J. Am. Chem. Soc.* **1991**, *113*, 893.

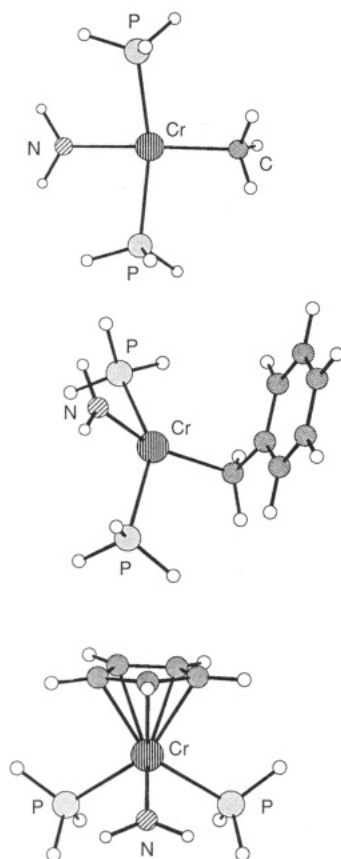


**Figure 4.** Simplified coordination sphere models for complexes 2–4 (top to bottom) used in ZINDO ROHF MO energy calculations.

**Table 5. ZINDO Relative Total Energy Calculations for the Simplified Complexes  $\text{CrR}(\text{NH}_2)(\text{PH}_3)_2$  in the Indicated Geometries (All Values in kcal/mol)**

spin state	$\text{CH}_3^a$	$\text{CH}_2\text{Ph}^a$	$\text{C}_5\text{H}_5^a$	$\text{CH}_3^b$	$\text{CH}_3^c$	$\text{C}_3\text{H}_5^d$	$\text{C}_3\text{H}_5^e$
singlet	74	66	32	66	52	43	25
triplet	49	46	0	45	40	13	4
quintet	0	0	15	0	0	0	0

<sup>a</sup> Simplified,  $C_s$ -symmetrized model based on the crystal structure. <sup>b</sup> Model identical with that in *a*, with Cr–P and Cr–N bond lengths altered to the low-spin values of 2.36 and 2.067 Å, respectively; taken from the crystal structure of **4**. <sup>c</sup> Mechanics (CACH version 3.6) minimized tetrahedral model structure,  $C_s$  symmetrized. <sup>d</sup> The two  $\text{PH}_3$  and one  $\text{NH}_2$  ligands are facially coordinated; high-spin Cr–phosphine and Cr–amide bond lengths used. <sup>e</sup> The two  $\text{PH}_3$  and one  $\text{NH}_2$  ligands are meridionally coordinated; bond distances are the same as found for *d*.

*spin state.* The fact that the benzyl derivative **3** remains a high-spin compound indicates that the  $\eta^2$  mode of coordination is insufficient to force spin pairing.

A ZINDO<sup>43,44</sup> restricted open-shell Hartree–Fock (ROHF) calculation confirms the stability of the experimentally observed spin states. Using a simplified coordination sphere as a calculation model (Figure 4), the total energy for each compound in a singlet, triplet, and quintet ground-state multiplicity was calculated (Table 5). The bond lengths of each model were taken from the relevant crystal structure and were fixed for each calculation; in this way a meaningful comparison

based on spin state could be made. The assumption of a fixed structure, while obviously not ideal (spin changes cause geometry changes in many cases), nevertheless suffices. To test this, the Cr–P bond lengths in the model compound *trans*- $\text{Cr}(\text{CH}_3)\text{NH}_2(\text{PH}_3)_2$  were fixed to both typical high-spin and typical low-spin values and the multiplicity calculations repeated. Although the absolute energy values were different, the stability of the quintet state relative to the triplet and singlet states did not change, nor did the approximate magnitude of the relative stability. In addition, the calculations were performed on a tetrahedral model of  $\text{Cr}(\text{CH}_3)\text{NH}_2(\text{PH}_3)_2$  without any change in the qualitative order of stability.

The graph in Figure 5 shows the energy differences between the three possible multiplicities for the hydrocarbyl compounds 2–4, where the most stable multiplicity is set at 0 kcal/mol and the energy difference between the most stable multiplicity and the others is plotted on the y axis. The results show that for methyl **2** and benzyl **3**, there are substantial stabilizations in the quintet state relative to the singlet of 74 and 66 kcal/mol, respectively. The stabilizations from the triplet state are still significant: 49 and 46 kcal/mol, respectively. Calculations on the cyclopentadienyl derivative **4**, however, show that the triplet state is the most preferred state, with stabilizations over the singlet and quintet states of 32 and 15 kcal/mol, respectively. As expected, for a high-spin square-planar  $d^4$  system, the unpaired electrons in **2** and **3** occupy the lower four *d* orbitals, leaving the  $d_{x^2-y^2}$  orbital empty. The ability of the ZINDO method to successfully describe the ground states of simple transition-metal complexes has been noted earlier,<sup>43–45</sup> our results show that the approach can be extended to slightly more complicated organometallic derivatives with good results.

This technique could be used to predict spin states of yet unsynthesized compounds. For example, the obviously missing  $\eta^3$ -allyl complex beckoned calculations on the model compound  $\text{Cr}(\eta^3\text{-C}_3\text{H}_5)\text{NH}_2(\text{PH}_3)_2$ . With the PNP ligand either facial or meridional, the results of the INDO study indicate that the quintet state should be stabilized by 4–13 kcal/mol (depending on the structure used), similar to that found for  $\text{Cr}(\eta^2\text{-CH}_2\text{Ph})\text{-}[\text{N}(\text{SiMe}_2\text{CH}_2\text{PPh}_2)_2]$ . Evidently, the benzyl moiety has nothing to gain by being  $\eta^3$ -bound; an  $\eta^3$ -allyl still prefers a high-spin, ground-state configuration, albeit by only a small energy difference.

In an attempt to put the theoretical prediction on firmer ground, we decided to try to synthesize the corresponding allyl complex  $\text{Cr}(\eta^3\text{-C}_3\text{H}_5)[\text{N}(\text{SiMe}_2\text{CH}_2\text{-PPh}_2)_2]$  to examine the structure and magnetism of a compound potentially intermediate between the high-spin  $\eta^2$ -benzyl and the low-spin  $\eta^5$ -Cp complexes. However, all of our efforts to prepare this derivative have so far met with failure, as only intractable materials could be obtained. It would appear that other factors are operative with this particular hydrocarbyl derivative.

With regard to the cyclopentadienyl compound **4**, the preference for a low-spin environment can be rationalized by invoking a comparison with  $\text{Cp}_2\text{Cr}$  (chromocene), which is also a 16-electron, low-spin  $d^4$  system. The tridentate ancillary ligand  $\text{N}(\text{SiMe}_2\text{CH}_2\text{PPh}_2)_2$ , for-

(43) Zerner, M. C.; Loew, G. H.; Kirchner, R. F.; Mueller-Westerhoff, U. T. *J. Am. Chem. Soc.* **1980**, *102*, 589.

(44) Anderson, W. P.; Edwards, W. D.; Zerner, M. C. *Inorg. Chem.* **1986**, *25*, 2728.

(45) Anderson, W. P.; Cundari, T. P.; Drago, R. S.; Zerner, M. C. *Inorg. Chem.* **1990**, *29*, 1.

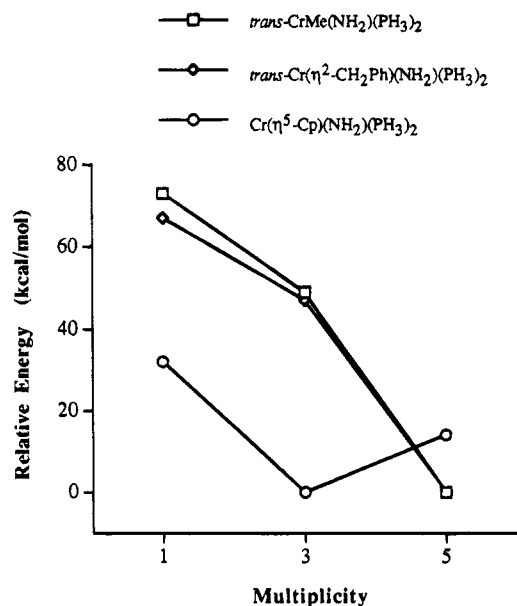
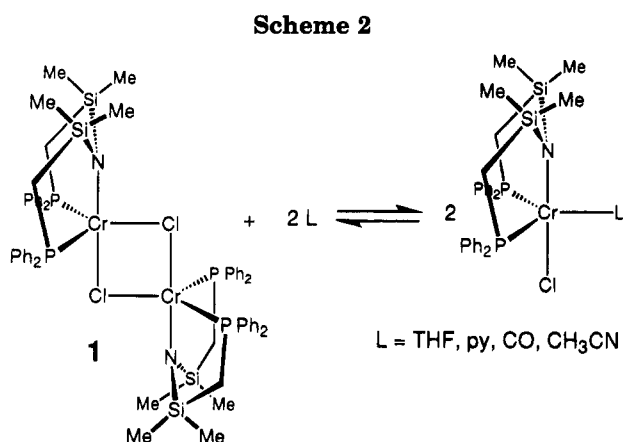


Figure 5. Graph of calculated relative energies vs spin multiplicity.



mally an anionic, six-electron donor, can qualitatively be considered as isoelectronic with a  $\text{C}_5\text{H}_5^-$  moiety. One could, therefore, envision the MO diagram for **4** to be similar to that for chromocene, with the appropriate removals of degeneracy for the reduction in symmetry. Thus, chromocene has an  $E_{2g}$ , doubly degenerate ground state with two unpaired electrons,<sup>46</sup> which for compound **4** translates as having a similar pair of SOMO's and from this the electronic structure and stability are derived.

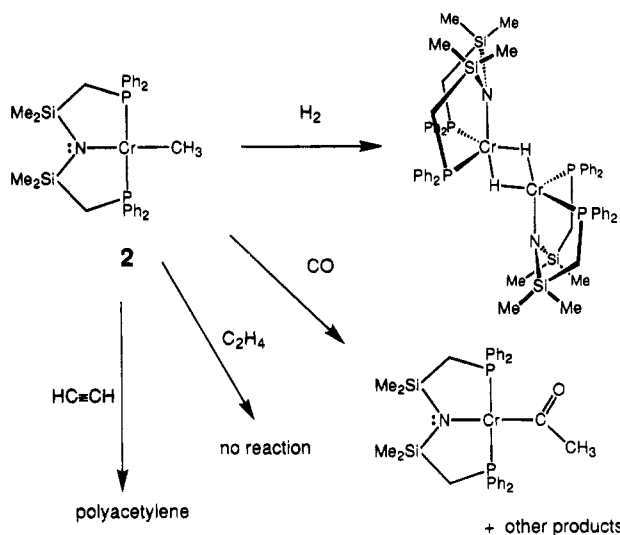
**Reactivity of  $\{[(\text{Ph}_2\text{PCH}_2\text{SiMe}_2)_2\text{N}]\text{Cr}\}_2(\mu\text{-Cl})_2$  with Donor Ligands.** The much higher solubility and color change of the chloride-bridged dimer **1** in THF, indicative of the formation of  $\text{CrCl}(\text{THF})[\text{N}(\text{SiMe}_2\text{CH}_2\text{PPh}_2)_2]$  in solution, suggested that other donor ligands had the potential to break up the dimer to form more soluble monomeric complexes; this reversible, general reaction is typified in Scheme 2.

The reaction with CO, for example, proceeds quickly, following the addition of CO gas to a blue toluene solution of **1** to yield a bright yellow solution, which quickly reverts to its original blue upon removal of CO. A solution IR measurement of the yellow solution shows one assignable CO stretch at  $\nu_{\text{CO}} = 1971\text{ cm}^{-1}$ , a value consistent with a simple, five-coordinate CO adduct.

Table 6. UV-vis Spectral Data, Equilibrium Constants (Scheme 2), and Solution Magnetic Moments for  $\{[(\text{Ph}_2\text{PCH}_2\text{SiMe}_2)_2\text{N}]\text{Cr}\}_2(\mu\text{-Cl})_2$  (**1**) and Its Adducts with Various Ligands

ligand	color	UV-vis (nm)	log <i>K</i>	$\mu_{\text{eff}}$ ( $\mu_{\text{B}}$ )
	purple	284, 342 (sh), 522 (w), 688 (w)		4.8
py	dark green	290, 352 (sh), 600 (w, broad)	$3.1 \pm 0.4$	4.7
CO	bright yellow	294, 390	$2.5 \pm 0.3$	2.7
THF	navy blue	304, 562 (w)	$1.0 \pm 0.1$	
MeCN	baby blue	296	$0.7 \pm 0.05$	4.7

**Scheme 3**



Similarly, the isolable pyridine adduct has an elemental analysis consistent with one bound pyridine;<sup>18</sup> hence, it is a five-coordinate monomer. The adducts all have substantially different colors, depending on the binding ligand, and hence equilibrium constants for ligand binding could be determined by spectrophotometric titration. All UV-vis titrations showed single isosbestic points, implying that the five-coordinate species was a final product; no six-coordinate monomer is formed. This is consistent with the fact that only one d orbital is available to accept a lone pair, the  $d_{x^2-y^2}$  orbital.

Table 6 shows the UV-vis data, equilibrium constants, and adduct solution magnetic moments (measured by the Evans method) for a series of ligands. The equilibrium constant data shows that strong  $\sigma$ -donors such as pyridine have a very high affinity, 2 orders of magnitude higher than the more weakly basic CH<sub>3</sub>CN and THF. Although there is an apparent lack of comparable data in the literature, a more in-depth study of this equilibrium was not attempted.

The magnetic moments observed are in concert with what could be predicted from following the ligand spectrochemical series: of the ligands tested, CO is the strongest field ligand and, thus, is able to force a low-spin configuration.

**Reactivity of  $\text{CrMe}[\text{N}(\text{SiMe}_2\text{CH}_2\text{PPh}_2)_2]$ .** The reactivity of **2**, in particular the Cr-Me bond, with a series of small molecules was examined; these reactions are outlined in Scheme 3.

While  $trans\text{-Cr}(\text{Mes})_2(\text{PMe}_3)_2$  did not react with dihydrogen,<sup>11</sup> reaction of **2** with H<sub>2</sub> yields a paramagnetic hydride dimer, the first such example for Cr(II).<sup>18</sup> Reaction with CO is less straightforward; a large number of IR bands in the region from 2058 to 1585

(46) Gordon, K. R.; Warren, K. D. *Inorg. Chem.* **1978**, *17*, 987.

cm<sup>-1</sup> indicate multiple products, which may include simple adducts, the acyl insertion product, rearranged reduced Cr(0) *N*-acylimidate species (as is observed in the NiMe[N(SiMe<sub>2</sub>CH<sub>2</sub>PPh<sub>2</sub>)<sub>2</sub>] system),<sup>47</sup> or a combination of all of these. Separation and identification were impossible. Reaction with 1 equiv of CO yields a difficult-to-purify compound with a single  $\nu_{\text{CO}} = 1842$  cm<sup>-1</sup>; likely this is the acylated product Cr(COCH<sub>3</sub>)-[N(SiMe<sub>2</sub>CH<sub>2</sub>PPh<sub>2</sub>)<sub>2</sub>]. In addition, solid **2** reacts with CO to yield a bright orange product with multiple CO stretches in the IR region.

The methyl complex **2** does not react with ethylene at 1 atm and at temperatures up to 80 °C. As has been shown by others, Cr(II) does not seem to be the active species in ethylene polymerization; hence, this lack of reactivity is not surprising.<sup>11,39,48</sup> However, although **2** does not react with ethylene, upon addition of acetylene, the rapid production of polyacetylene is observed. The mechanism is likely organic-radical-based, with the paramagnetic metal-based radical **2** merely initiating the polymerization. Even trace amounts of **2** can initiate polymerization. Using larger amounts of **2** results in the almost total recovery of unreacted methyl complex, strongly supportive of the notion that the compound itself is not directly interacting in the polymerization cycle. The methyl complex **2** also reacts with phenylacetylene quickly and diphenylacetylene more slowly, but the products in both cases could not be identified.

### Conclusions

The series of mononuclear, organochromium(II) complexes of the general formula CrR[N(SiMe<sub>2</sub>CH<sub>2</sub>PPh<sub>2</sub>)<sub>2</sub>] has been prepared and structurally characterized. The tridentate ancillary ligand supports both high-spin (four unpaired electrons) and low-spin (two unpaired electrons) d<sup>4</sup> configurations, the latter occurring with R =  $\eta^5$ -cyclopentadienyl. In the solid state, the benzyl ligand binds in a  $\eta^2$  fashion via the ipso carbon of the phenyl ring. Semiempirical MO studies using the ZINDO method support the stability of the quintet ground state for the methyl and benzyl derivatives and confirm that the triplet state for the cyclopentadienyl derivative is the most stable. Reactivity studies have been carried out with the methyl complex; however, the results have been capricious. The reaction with H<sub>2</sub> does proceed cleanly to form the binuclear hydride {[Ph<sub>2</sub>PCH<sub>2</sub>-SiMe<sub>2</sub>)<sub>2</sub>N]Cr}<sub>2</sub>( $\mu$ -H)<sub>2</sub>,<sup>18</sup> however, the reaction with CO led to a complicated mixture of products. Although starting materials were recovered essentially unchanged after the reaction with either ethylene or acetylene, the latter did produce polyacetylene.

### Experimental Section

**General Procedures.** Unless otherwise stated, all manipulations were performed under an atmosphere of dry, oxygen-free dinitrogen or argon by means of standard Schlenk or glovebox techniques. The glovebox used was a Vacuum Atmospheres HE-553-2 workstation equipped with a MO-40-2H purification system and a -40 °C freezer. <sup>1</sup>H NMR spectroscopy was performed on a Varian XL-300 or a Bruker

AC-200 instrument operating at 300 or 200 MHz, respectively. <sup>1</sup>H NMR spectra were referenced to internal C<sub>6</sub>D<sub>5</sub>H (7.15 ppm). Magnetic moments were measured by a modification of the Evans method (C<sub>6</sub>D<sub>5</sub>H as a reference peak) on the NMR spectrometers listed above and were also measured in the solid state using a Johnson-Matthey MSB-1 Gouy balance at room temperature. Infrared spectra were recorded on a BOMEM MB-100 spectrometer, UV-vis spectra were recorded on a HP-8452A diode array spectrophotometer. Microanalyses (C, H, N) were performed by Mr. P. Borda of this department.

**Materials.** The preparation of the lithium salt LiN(SiMe<sub>2</sub>CH<sub>2</sub>PPh<sub>2</sub>)<sub>2</sub><sup>16</sup> and complexes **1** and **2** have been previously described.<sup>18</sup> NaCp·DME was prepared by the reaction of Na with CpH in dry DME. KCH<sub>2</sub>Ph<sup>49</sup> and EtLi<sup>50</sup> were prepared by literature procedures. All other reagents were obtained from commercial sources and used as received.

Hexanes, toluene, and THF were heated to reflux over CaH<sub>2</sub> prior to a final distillation from either sodium metal or sodium benzophenone ketyl under an Ar atmosphere. Deuterated solvents were dried by activated 3-Å molecular sieves; oxygen was removed by trap-to-trap distillation and three freeze-pump-thaw cycles.

**Molecular Orbital Calculations.** All molecular orbital calculations were performed on the CAChe Worksystem, a product developed by Tektronix. The parameters (INDO/1) used in the ZINDO semiempirical molecular orbital calculations on all model compounds were taken from the literature.<sup>44,45</sup> The bond lengths for the models *trans*-CrR(NH<sub>2</sub>)(PH<sub>3</sub>)<sub>2</sub> (R = CH<sub>3</sub>,  $\eta^2$ -CH<sub>2</sub>Ph,  $\eta^5$ -C<sub>5</sub>H<sub>5</sub>) were taken from the X-ray crystal structure analyses of **2-4**, respectively, and the PH<sub>3</sub> groups were eclipsed to effect maximum symmetry. The model *trans*-Cr( $\eta^5$ -C<sub>5</sub>H<sub>5</sub>)(NH<sub>2</sub>)(PH<sub>3</sub>)<sub>2</sub> was constructed from the crystal structure of **4** with two Cp carbons removed. The Cartesian coordinates of the models can be found in the supporting information. For all models the following standard bond lengths were used: P-H, 1.380 Å; C-H, 1.090 Å; N-H, 1.070 Å.

**X-ray Crystallographic Analyses of CrMe[N(SiMe<sub>2</sub>CH<sub>2</sub>PPh<sub>2</sub>)<sub>2</sub>] (**2**), Cr( $\eta^2$ -CH<sub>2</sub>Ph)[N(SiMe<sub>2</sub>CH<sub>2</sub>PPh<sub>2</sub>)<sub>2</sub>] (**3**), and Cr( $\eta^5$ -C<sub>5</sub>H<sub>5</sub>)[N(SiMe<sub>2</sub>CH<sub>2</sub>PPh<sub>2</sub>)<sub>2</sub>] (**4**).** Crystallographic data appear in Table 1. All samples were sealed in Lindemann glass capillaries. The final unit-cell parameters were obtained by least squares on the setting angles for 25 reflections for **2** and 3 and 41 reflections for **4** with  $2\theta = 17.6-27.1, 27.4-33.0$ , and  $9.8-24.7^\circ$ , respectively, for **2-4**. The intensities of 3 standard reflections, measured every 200 reflections throughout the data collections, remained constant for **3** and **4** and decayed uniformly by 2.4% for **2**. The data were processed,<sup>51</sup> corrected for Lorentz and polarization effects, decay (for **2**), and absorption (empirical: based on azimuthal scans for three reflections for **2** and **3**, 6 reflections for **4**). Crystal quality for compound **4** was poor, with broad peaks and generally weak scattering. As a result, data for this sample could only collected to low resolution ( $2\theta = 45^\circ$ ) at room temperature.

The structure of **2** was solved by conventional heavy-atom methods, and those of **3** and **4** were solved by direct methods. The non-hydrogen atoms were refined with anisotropic thermal parameters. Hydrogen atoms were fixed in idealized positions (methyl groups, staggered or based on difference map positions, C-H = 0.98 Å,  $B_{\text{H}} = 1.2B_{\text{bonded atom}}$ ). A difference map indicated that the hydrogen atoms of the C(4) Si-Me and C(31) Cr-Me groups in **2** are 1:1 disordered over two orientations. This disorder was accounted for in the model. A correction for secondary extinction was applied for **2**, the final value of the extinction coefficient being  $[1.9(7)] \times 10^{-7}$ . Neutral atom

(49) Schlosser, M.; Ladenberger, V. *J. Organomet. Chem.* **1967**, *8*, 193.

(50) Bryce-Smith, D.; Turner, E. E. *J. Chem. Soc.* **1953**, 861.

(51) teXsan: Crystal Structure Analysis Package; Molecular Structure Corp., The Woodlands, TX, 1985, 1992.

(52) *International Tables for Crystallography*; Kluwer Academic: Boston, MA, 1992; Vol. C, pp 200-206, 219-222.

(47) Fryzuk, M. D.; MacNeil, P. A. *J. Am. Chem. Soc.* **1984**, *106*, 6993.

(48) Heintz, R. A.; Ostrander, R. L.; Rheingold, A. L.; Theopold, K. H. *J. Am. Chem. Soc.* **1994**, *116*, 11387.



scattering factors and anomalous dispersion corrections for all atoms were taken from ref 52. Final atomic coordinates and equivalent isotropic thermal parameters are given in Table 2 and selected bond lengths and angles in Tables 3 and 4, respectively. Complete tables of bond lengths and angles, hydrogen atom parameters, anisotropic thermal parameters, torsion angles, intermolecular contacts, and least-squares planes are included as supporting information.

**Synthesis of  $\text{Cr}(\eta^5\text{-C}_5\text{H}_5)[\text{N}(\text{SiMe}_2\text{CH}_2\text{PPh}_2)_2]$ . Method 1.** To a 15 mL THF solution of  $\{[(\text{Ph}_2\text{PCH}_2\text{SiMe}_2)_2\text{N}]\text{Cr}\}_2(\mu\text{-Cl})_2$  (0.20 g, 0.163 mmol) at  $-78^\circ\text{C}$  was added dropwise a 5 mL THF solution of  $\text{NaCp}\cdot\text{DME}$  (0.058 g, 0.325 mmol). The blue solution rapidly turned dark red and was warmed to room temperature. After the solution was stirred for 1 h, the THF was removed in vacuo and the residue extracted in hexanes and filtered through Celite. Red crystalline bars were obtained from a slow evaporation of a hexane solution; yield 0.18 g (86%).

**Method 2.** To a stirred solution of  $\text{CrCH}_3[\text{N}(\text{SiMe}_2\text{CH}_2\text{PPh}_2)_2]$  (0.115 g, 0.193 mmol) in 10 mL of toluene was added a 10-fold excess of  $\text{C}_5\text{H}_6$  by vacuum transfer. The light red solution turned a much darker red as soon as the transfer was complete. The reaction mixture was stirred overnight and then pumped to dryness. Extraction with a minimum amount of hexanes yielded a dark red solution, which yielded a dark red solid of  $\text{Cr}(\eta^5\text{-C}_5\text{H}_5)[\text{N}(\text{SiMe}_2\text{CH}_2\text{PPh}_2)_2]$  after 2 days of slow evaporation; yield 0.105 g (85%). Anal. Calcd for  $\text{C}_{35}\text{H}_{41}\text{CrNP}_2\text{Si}_2$ : C, 65.09; H, 6.40; N, 2.17. Found: C, 64.89; H, 6.54; N, 2.18.  $\mu = 2.7 \mu\text{B}$ . MS:  $m/e$  645 ( $\text{M}^+$ ), 580 ( $\text{M}^+ - \text{Cp}$ ).

**Synthesis of  $\text{Cr}(\eta^2\text{-CH}_2\text{Ph})[\text{N}(\text{SiMe}_2\text{CH}_2\text{PPh}_2)_2]$ .** To a 15 mL THF solution of  $\{[(\text{Ph}_2\text{PCH}_2\text{SiMe}_2)_2\text{N}]\text{Cr}\}_2(\mu\text{-Cl})_2$  (0.15 g, 0.122 mmol) was added a solution of  $\text{KCH}_2\text{Ph}$  (0.032 g, 0.246 mmol) in 5 mL of THF dropwise at  $-78^\circ\text{C}$ . The color turned from navy blue to dark purple. The solution was warmed to room temperature and the THF removed in vacuo. The residue was extracted in hexanes and filtered through Celite, yielding a purple solution from which large cubes formed after 5 h; yield 0.130 g (80%). Anal. Calcd for  $\text{C}_{37}\text{H}_{43}\text{CrNP}_2\text{Si}_2$ : C, 66.14; H, 6.45; N, 2.08. Found: C, 65.93; H, 6.46; N, 2.15.  $\mu = 5.1 \mu\text{B}$ . IR:  $1582 \text{ cm}^{-1}$  (Bz, C=C).

**Attempted Synthesis of  $\text{Cr}(\eta^3\text{-C}_3\text{H}_5)[\text{N}(\text{SiMe}_2\text{CH}_2\text{PPh}_2)_2]$ .** To a 10 mL THF solution of  $\{[(\text{Ph}_2\text{PCH}_2\text{SiMe}_2)_2\text{N}]\text{Cr}\}_2(\mu\text{-Cl})_2$  (0.22 g, 0.179 mmol) was added an ether solution of  $\text{C}_3\text{H}_5\text{MgBr}$  (0.36 mL, 0.360 mmol) dropwise at  $-78^\circ\text{C}$ . The color turned from navy blue to dark red-brown. The solution was warmed to room temperature and the THF removed in vacuo. The residue was extracted into toluene and filtered through Celite, yielding a brown solution from which only impure, intractable brown powders were isolated.

**Attempted Reaction of  $\text{CrCH}_3[\text{N}(\text{SiMe}_2\text{CH}_2\text{PPh}_2)_2]$  with  $\text{C}_2\text{H}_2$ .** A 0.05 g amount of **2** was dissolved in 15 mL of toluene in a bomb, which was then charged with 1 atm of ethylene. No immediate color change was observed, and upon heating to  $80^\circ\text{C}$  and stirring for 3 weeks, no reaction occurred and starting material was recovered.

**Reaction of  $\text{CrCH}_3[\text{N}(\text{SiMe}_2\text{CH}_2\text{PPh}_2)_2]$  with  $\text{C}_2\text{H}_2$ .** A solution of 20 mg of  $\text{CrCH}_3[\text{N}(\text{SiMe}_2\text{CH}_2\text{PPh}_2)_2]$  in 20 mL of toluene was placed under an atmosphere of acetylene. Rapid formation of a purple solid (polyacetylene) occurred, and the original 20 mg of the complex was mostly recovered.

**Attempted Synthesis of  $\text{Cr}(\text{CH}_2\text{CH}_3)[\text{N}(\text{SiMe}_2\text{CH}_2\text{PPh}_2)_2]$ .** To a stirred 10 mL THF solution of  $\text{CrCl}(\text{THF})[\text{N}(\text{SiMe}_2\text{CH}_2\text{PPh}_2)_2]$  (0.2 g, 0.325 mmol) was added  $\text{EtLi}$  (0.012 g, 0.333 mmol) in 2 mL of ether dropwise at  $-78^\circ\text{C}$ . The dark blue solution turned brown rapidly. After the solution was warmed to room temperature, the THF was removed in vacuo to yield a dark brown-green solid which was extracted with 2 mL of hexanes and filtered through Celite to give a brown solution. Brown crystals, along with some green crystals, formed overnight. The brown product was identified by IR as the  $\{-(\text{Ph}_2\text{PCH}_2\text{SiMe}_2)_2\text{N}\}\text{Cr}\}_2(\mu\text{-H})_2$  dimer. The green product was unidentifiable.

**Titration of  $\{[(\text{Ph}_2\text{PCH}_2\text{SiMe}_2)_2\text{N}]\text{Cr}\}_2(\mu\text{-Cl})_2$  with Donor Ligands.** Toluene solutions approximately  $10^{-3} \text{ M}$  in 1 in an airtight UV-vis quartz cell were titrated with  $\text{L} = \text{py}$ ,  $\text{CH}_3\text{CN}$ , THF, and CO. The pyridine titration used appropriately concentrated toluene stock solutions of the ligand, while the weak donors  $\text{CH}_3\text{CN}$  and THF were used neat. The CO titration was accomplished by injecting CO using a gastight syringe and calculating the  $[\text{CO}]$  in solution, given the CO solubility in toluene and the solution and head space volumes. Concentration data were collected at the following wavelengths with the given  $\Delta\text{OD}$  values (change in optical density): py, 400 nm ( $\Delta\text{OD} = 0.97$ );  $\text{CH}_3\text{CN}$ , 320 nm ( $\Delta\text{OD} = 0.57$ ); THF, 336 nm ( $\Delta\text{OD} = 0.45$ ); CO, 392 nm ( $\Delta\text{OD} = 1.40$ ). Equilibrium constants were calculated by the appropriate  $\log([\text{CrL}]/[\text{Cr}])$  vs  $\log[\text{L}]$  plot, where the intercept is  $\log K$ . Alternately, the midpoint of the titration yields  $K$  as  $K = 1/[\text{L}]$ .

**Note Added in Proof.** After this manuscript was accepted, an  $\eta^2$ -benzyl was reported for  $\text{Cr}(\text{VI})$ : Coles, M. P.; Dalby, C. I.; Gibson, V. C.; Clegg, W.; Elsegood, M. R. *J. Chem. Soc., Chem. Commun.* **1995**, 1709.

**Acknowledgment.** Financial support was provided by the NSERC of Canada in the form of operating grants (to M.D.F.) and a 1967 Science and Engineering Research Scholarship (to D.B.L.). We also thank Professor D. V. Stynes of York University for collecting data for and solving the structure of **4**.

**Supporting Information Available:** Tables giving Cartesian coordinates for molecular orbital calculation models and complete tables of bond lengths and bond angles, hydrogen atom parameters, anisotropic thermal parameters, torsion angles, intermolecular contacts, and least-squares planes for **2–4** (61 pages). Ordering information is given on any current masthead page.

OM950267K



# Unstable Species, CpW(CO)<sub>2</sub>Me and CpW(CO)<sub>3</sub>, Studied by Time-Resolved Infrared Spectroscopy

Ian G. Virrels, Michael W. George,\* Frank P. A. Johnson, James J. Turner,\* and Jeremy R. Westwell

Department of Chemistry, University of Nottingham, University Park, Nottingham NG7 2RD, U.K.

Received July 13, 1995<sup>⊙</sup>

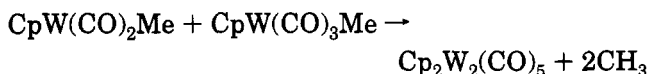
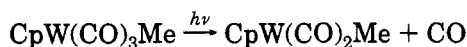
Photolysis of CpW(CO)<sub>3</sub>Me (**1**) in *n*-heptane generates mostly the solvated intermediate CpW(CO)<sub>2</sub>Me···*n*-heptane (**2**), detected by time-resolved infrared spectroscopy (TRIR). The reactions of **2** with CO, PPh<sub>3</sub>, and N<sub>2</sub> have been studied and appropriate second-order rate constants obtained. A small amount of the radical CpW(CO)<sub>3</sub><sup>•</sup> (**5**) is also generated on photolysis of **1** and can be characterized by the photolysis of [CpW(CO)<sub>3</sub>]<sub>2</sub> (**6**).

## Introduction

There has been considerable interest in the photochemistry of CpM(CO)<sub>3</sub>R complexes (Cp = η<sup>5</sup>-C<sub>5</sub>H<sub>5</sub>; M = Cr, Mo, W; R = H, alkyl).<sup>1–7</sup> It is generally agreed that the primary photochemical step is loss of CO. The subsequent chemistry, depending on the metal and R, can vary considerably; for example with R = ethyl there is very strong evidence that CO loss is followed by β-H migration. Fast time-resolved spectroscopy was very helpful in following the kinetics of this reaction.<sup>7</sup> CpCr(CO)<sub>3</sub>Me in a gas matrix at 10 K has been shown, upon photolysis, to form the α-elimination photoproduct CpCr(CO)<sub>2</sub>(CH<sub>2</sub>)H.<sup>4a</sup> However, the photochemistry of CpM(CO)<sub>3</sub>Me (M = Mo, W) is particularly intriguing, since at room temperature, in a wide range of solvents, irradiation leads to the stable dimer [CpM(CO)<sub>3</sub>]<sub>2</sub> and formation of CH<sub>4</sub>.



There have been a number of attempts to probe the mechanism of this reaction, with some particularly elegant experiments being carried out by Tyler.<sup>1</sup> The suggested mechanism for the photolysis of CpW(CO)<sub>3</sub>Me—and by implication for CpMo(CO)<sub>3</sub>Me—is



There was an early suggestion<sup>8</sup> that the primary

photochemical act in the dimerization of CpMo(CO)<sub>3</sub>Me involved mostly Mo–Me bond cleavage to give the radical CpMo(CO)<sub>3</sub><sup>•</sup>. The CO-loss species<sup>3</sup> CpM(CO)<sub>2</sub>Me (M = Mo, W) and the radicals<sup>4b</sup> CpM(CO)<sub>3</sub><sup>•</sup> (M = Mo, W) have been characterized by ν(CO) infrared spectroscopy in low-temperature matrices, and we recently showed how fast time-resolved infrared (TRIR) spectroscopy could both detect CpMo(CO)<sub>3</sub><sup>•</sup> and monitor its kinetics in room-temperature solution.<sup>9</sup> In this paper we show that TRIR can be used to probe the photochemistry of CpW(CO)<sub>3</sub>Me (**1**), to monitor the behavior of the solvated intermediate CpW(CO)<sub>2</sub>Me (**2**), and to suggest that the radical CpW(CO)<sub>3</sub><sup>•</sup> (**5**) plays only a minor role in the dimerization of CpW(CO)<sub>3</sub>Me to give [CpW(CO)<sub>3</sub>]<sub>2</sub>.

## Experimental Section

The Nottingham TRIR apparatus has been described elsewhere.<sup>10</sup> Briefly, it consists of a pulsed UV/vis source, a Nd:YAG laser (Quanta-Ray GCR-11; 355 or 532 nm, 7 ns pulse) to initiate photochemical reactions, and a cw IR diode laser (Mütek MDS 1100 fitted with a Mütek MDS 1200 monochromator) to monitor the transient IR absorptions. FTIR spectra were obtained with a Perkin-Elmer System 2000 FTIR spectrometer. CpW(CO)<sub>3</sub>Me was synthesized according to the literature method.<sup>11</sup> *n*-Heptane (Aldrich, HPLC grade) was distilled over CaH<sub>2</sub> prior to use, and PPh<sub>3</sub> (BDH), Ar (Air Products), and CO (BOC) were used as supplied.

## Results and Discussion

**(a) Identification and Reactivity of CpW(CO)<sub>2</sub>(Me) (**2**).** Figure 1a shows the ν(CO) FTIR spectrum of CpW(CO)<sub>3</sub>Me (**1**) in *n*-heptane. The two bands are assigned to the a<sub>1</sub> and e modes of the W(CO)<sub>3</sub> group with local C<sub>3v</sub> symmetry. Figure 1c shows the TRIR spectrum obtained 1 μs after photolysis (355 nm) of **1** in *n*-heptane solution in the presence of 2 bar of Ar. It is clear that on photolysis the parent absorptions at 2021

(8) Rausch, M. D.; Gismondi, T. E.; Alt, H. G.; Schwärzle, J. A. *Z. Naturforsch., B Anorg. Chem., Org. Chem.* **1977**, *32B*, 998–1000.

(9) Peters, J.; George, M. W.; Turner, J. J. *Organometallics* **1995**, *14*, 1503–1506.

(10) (a) Dixon, A. J.; Healy, M. A.; Hodges, P. M.; Moore, B. D.; Poliakoff, M.; Simpson, M. B.; Turner, J. J.; West, M. A. *J. Chem. Soc., Faraday Trans. 2* **1986**, *82*, 2083. (b) George, M. W.; Poliakoff, M.; Turner, J. J. *Analyst* **1994**, *119*, 551.

(11) Piper, T. S.; Wilkinson, G. *J. Inorg. Nucl. Chem.* **1956**, *3*, 104–124.

<sup>⊙</sup> Abstract published in *Advance ACS Abstracts*, October 1, 1995.

(1) Tyler, D. R. *Inorg. Chem.* **1981**, *20*, 2257–2261 and references therein.

(2) (a) Kazlauskas, R. J.; Wrighton, M. S. *J. Am. Chem. Soc.* **1980**, *102*, 1727–1730; (b) **1982**, *104*, 6005–6015.

(3) Mahmoud, K. A.; Narayanaswamy, R.; Rest, A. J. *J. Chem. Soc., Dalton Trans.* **1981**, 2199–2204.

(4) (a) Mahmoud, K. A.; Rest, A. J.; Alt, H. G. *J. Chem. Soc., Chem. Commun.* **1983**, 1011–1013; (b) *J. Organomet. Chem.* **1983**, *246*, C37–C41; (c) *J. Chem. Soc., Dalton Trans.* **1984**, 187–197.

(5) Hooker, R. H.; Rest, A. J. *J. Chem. Soc., Dalton Trans.* **1984**, 761–770.

(6) Yang, G. K.; Peters, K. S.; Vaida, V. *J. Am. Chem. Soc.* **1986**, *108*, 2511–2513.

(7) Johnson, F. P. A.; Gordon, C. M.; Hodges, P. M.; Poliakoff, M.; Turner, J. J. *J. Chem. Soc., Dalton Trans.* **1991**, 833–839.

**Table 1. Infrared Absorption Bands in the  $\nu(\text{CO})$  Region ( $\text{cm}^{-1}$ ) of Molybdenum and Tungsten Complexes**

	$\text{N}_2^a$	$\text{CO}^b$	PVC <sup>c</sup>	paraffin <sup>d</sup>	isooctane <sup>e</sup>	<i>n</i> -heptane <sup>f</sup>
$\text{CpW}(\text{CO})_3\text{Me}$			2012			2021
			{ 1919 <sup>g</sup> 1907 <sup>g</sup>			1932
$\text{CpW}(\text{CO})_2\text{Me}$			1939	1955		1959
$\text{CpW}(\text{CO})_2\text{Me}(\text{N}_2)$			1840	1865		1870
						1965
$\text{CpW}(\text{CO})_2\text{Me}(\text{PPh}_3)$					1936	1906
					1861	1939
$\text{CpW}(\text{CO})_3^*$		1999				1862
		{ 1900 <sup>g</sup> 1897 <sup>g</sup>				1999
						1902
$\text{CpMo}(\text{CO})_3\text{Me}$	2029		2015			
	1941		{ 1928 <sup>g</sup> 1918 <sup>g</sup>			
$\text{CpMo}(\text{CO})_2\text{Me}$	1973		1949			
	1884		1857			
$\text{CpMo}(\text{CO})_2\text{Me}(\text{N}_2)$	1970					
	1914					

<sup>a</sup> At 12 K. <sup>b</sup> At 12 K. <sup>c</sup> At 12 K. <sup>d</sup> At 77 K. <sup>e</sup> At 298 K. <sup>f</sup> At 298 K; this work. <sup>g</sup> Matrix-split bands.

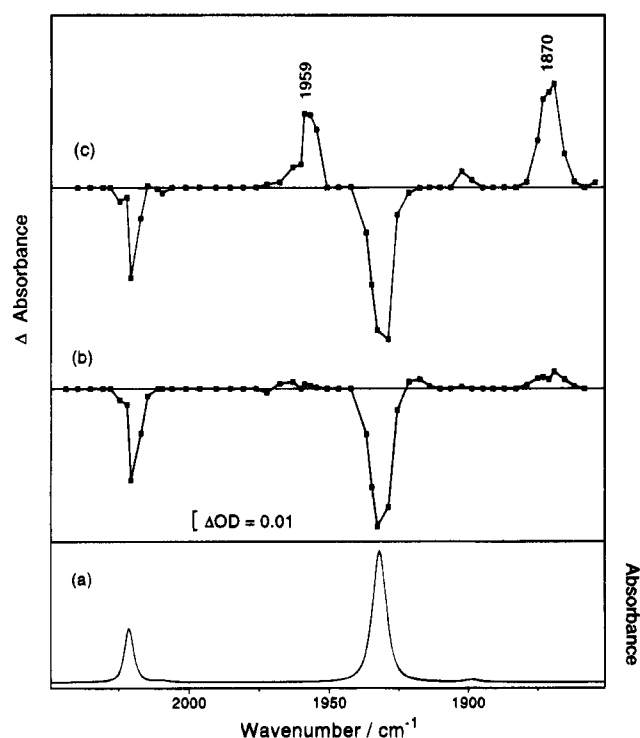


**Figure 1.** (a) FTIR spectrum of  $\text{CpW}(\text{CO})_3\text{Me}$  in *n*-heptane ( $5 \times 10^{-4}$  M). (b,c) Time-resolved IR spectra of  $\text{CpW}(\text{CO})_3\text{Me}$  in *n*-heptane ( $5 \times 10^{-4}$  M) in the presence of Ar (2 atm) obtained at (c) 1  $\mu\text{s}$  and (b) 40  $\mu\text{s}$  following excitation (355 nm). Data points plotted downward indicate loss of parent species, while those plotted upward indicate generation of a new species; the solid line simply joins up the data points.

and 1932  $\text{cm}^{-1}$  are bleached and two new absorptions are produced at 1959 and 1870  $\text{cm}^{-1}$  together with a small band at 1902  $\text{cm}^{-1}$ . The two new absorptions can be assigned to  $\text{CpW}(\text{CO})_2\text{Me}$  by comparison with results obtained by Wrighton and Kazlauskas<sup>2</sup> in a low-temperature paraffin matrix and by Rest and Hooker<sup>5</sup> in a poly(vinyl chloride) film at 12 K (see Table 1). With only one exception in the current literature,<sup>12</sup> photochemically generated 16-electron unsaturated transition-

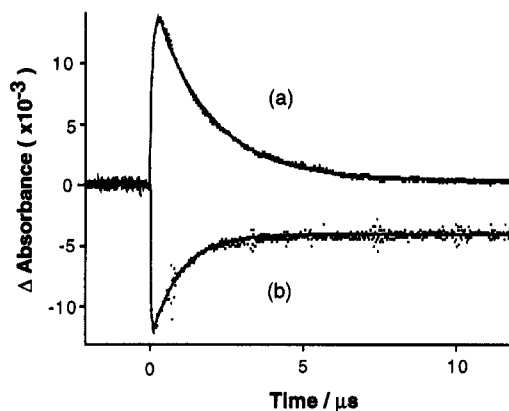
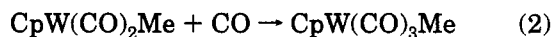


**Figure 2.** Time-resolved IR traces following excitation (355 nm) of  $\text{CpW}(\text{CO})_3\text{Me}$  in *n*-heptane ( $5 \times 10^{-4}$  M), in the presence of CO (2 atm) at (a) 1960  $\text{cm}^{-1}$  and (b) 1932  $\text{cm}^{-1}$ .

metal carbonyl intermediates interact with the solvent, which has been described as a "token" ligand.<sup>13</sup> The intermediate observed following photolysis of  $\text{CpW}(\text{CO})_3\text{Me}$  in *n*-heptane is best described as  $\text{CpW}(\text{CO})_2\text{Me} \cdots n\text{-heptane}$  (**2**), particularly since its rates of reaction with CO,  $\text{PPh}_3$ , and  $\text{N}_2$  (see later) are significantly slower than diffusion control. Figure 1b shows the TRIR spectrum 40  $\mu\text{s}$  after excitation; the bands due to **2** have fully decayed, while the intensities of the IR bands due to depleted **1** are unaltered. There is some evidence for the formation of other  $\nu(\text{CO})$  bands, but these are weak. There are several possible reasons for this behavior, and we return to a detailed consideration of the chemistry later. We first examine the behavior of the intermediate in the presence of potential ligands, and since we expect the reverse reaction



to be important, we consider it first.

**Reaction of  $\text{CpW}(\text{CO})_2\text{Me}$  (**2**) with CO.** Figure 2a shows the decay of **2**, recorded at 1960  $\text{cm}^{-1}$ , and Figure 2b shows the recovery of the parent at 1932  $\text{cm}^{-1}$ , following flash photolysis of **1** in the presence of 2 atm

(12) Recent work (Bengali, A. A.; Bergman, R. G.; Moore, C. B. *J. Am. Chem. Soc.* **1995**, *117*, 3879–3880) indicates that  $\text{CpCo}(\text{CO})$  may exist as a "naked" 16-electron complex in the presence of either noble-gas atoms or cyclohexane.

(13) Dobson, G. R.; Hodges, P. M.; Healy, M. A.; Poliakoff, M.; Turner, J. J.; Firth, S.; Asali, K. *J. Am. Chem. Soc.* **1987**, *109*, 4218–4224.

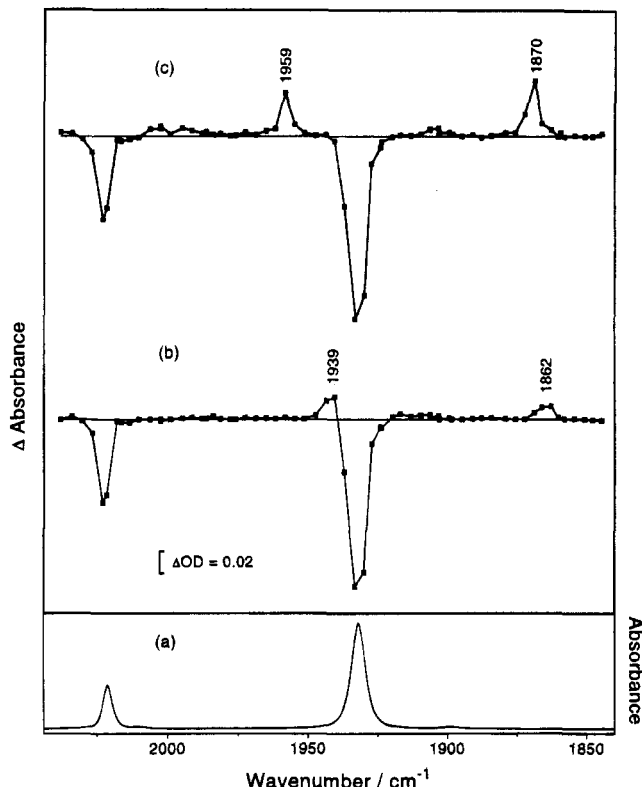


**Figure 3.** (a) FTIR spectrum of CpW(CO)<sub>3</sub>Me in *n*-heptane. (b,c) Time-resolved IR spectra of CpW(CO)<sub>3</sub>Me in *n*-heptane ( $5 \times 10^{-4}$  M) in the presence of PPh<sub>3</sub> ( $1 \times 10^{-3}$  M) obtained (c) 1  $\mu$ s and (b) 10  $\mu$ s following excitation (355 nm).

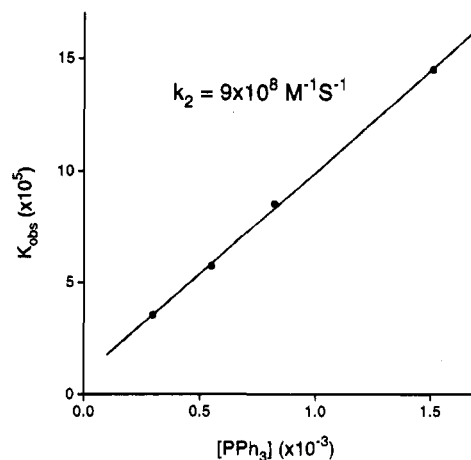
**Table 2. Rates of Reaction of Various Ligands with CpW(CO)<sub>2</sub>Me···*n*-Heptane (2)**

ligand	$k_{\text{obs}}$ (s <sup>-1</sup> )	$k_2$ (M <sup>-1</sup> s <sup>-1</sup> )
CO	$[4.5(\pm 0.5)] \times 10^5$	$[2(\pm 0.2)] \times 10^7$
PPh <sub>3</sub>	$[1.1(\pm 0.1)] \times 10^6$	$[1.1(\pm 0.1)] \times 10^9$
N <sub>2</sub>	$[9(\pm 1)] \times 10^4$	$[4.7(\pm 0.5)] \times 10^6$

of CO. Notice that even at this high concentration of CO the recovery of **1** is incomplete (~65%). This could be due to several reasons: reactions of **2** with other species, including impurities, or low solubility of **2**. At the highest concentration of CO ( $2.4 \times 10^{-2}$  mol dm<sup>-3</sup>)<sup>14</sup> the rate of loss of **2** fits a first-order decay with  $k_{\text{obs}} = [5.3(\pm 0.5)] \times 10^5$  s<sup>-1</sup>; the corresponding rate of recovery of **1** also fits a first-order plot with  $k_{\text{obs}} = [4.5(\pm 0.5)] \times 10^5$  s<sup>-1</sup>. These rates are similar, but we use the recovery of **1** to obtain the second-order rate constant for reaction 2:  $[2(\pm 0.2)] \times 10^7$  M<sup>-1</sup> s<sup>-1</sup> (see Table 2).

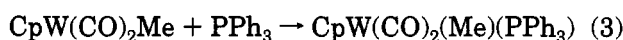
**Reaction of CpW(CO)<sub>2</sub>Me (2) with PPh<sub>3</sub>.** Photolysis of **1** in the presence of PPh<sub>3</sub> yields CpW(CO)<sub>2</sub>(Me)(PPh<sub>3</sub>) (**3**).<sup>2a</sup> We have monitored this process by TRIR.

Figure 3c shows the TRIR spectrum of CpW(CO)<sub>3</sub>Me with PPh<sub>3</sub> ( $1 \times 10^{-3}$  M) in *n*-heptane 1  $\mu$ s after UV irradiation (355 nm). The spectrum is essentially identical with that obtained in the absence of PPh<sub>3</sub> (Figure 1c), and the major absorptions are due to **2**. Figure 3b shows that after 10  $\mu$ s the absorptions due to **2** have decayed and two new absorptions are produced at 1939 and 1862 cm<sup>-1</sup>, which are assigned to the known compound **3** (see Table 1). The decay of **2** ( $k_{\text{obs}} =$



**Figure 4.** Plot of the observed rate of reaction (s<sup>-1</sup>) versus PPh<sub>3</sub> concentration, for the decay of CpW(CO)<sub>2</sub>Me···*n*-heptane.

$[1.1(\pm 0.1)] \times 10^6$  s<sup>-1</sup>) is very similar to the formation of **3** ( $k_{\text{obs}} = [1.1(\pm 0.1)] \times 10^6$  s<sup>-1</sup>); thus, under the conditions of this experiment PPh<sub>3</sub> appears to be swamping any competing reactions of **2**. The second-order rate constant for reaction 3 is  $[1.1(\pm 0.1)] \times 10^9$  M<sup>-1</sup> s<sup>-1</sup>, i.e.



50 times greater than the rate of reaction 2 (see Table 2). Similar observations have been reported<sup>15</sup> for the reactions of CpMn(CO)<sub>2</sub>···cyclohexane, where PPh<sub>3</sub> reacts ~20 times faster than CO. Figure 4 shows a plot of  $k_{\text{obs}}$  for reaction 3 against PPh<sub>3</sub> concentration; this is a straight line with a slope of  $9.1 \times 10^8$  M<sup>-1</sup> s<sup>-1</sup>. Obviously, at very low concentrations of PPh<sub>3</sub>, side reactions will become important, but nonetheless it is interesting that the slope gives a value, within experimental error, equal to that obtained from an experiment at high concentration of PPh<sub>3</sub>. The difference in the rates of reactions 2 and 3 suggests that the reaction does not proceed exclusively through a dissociative mechanism, since, in this case, the rates of (2) and (3) would be expected to be similar. We attempted quantitative measurements of the activation parameters of reactions 2 and 3 but were unsuccessful. However, we were able to show that, over the temperature range 20–50 °C, there was only a 50% increase in observed rate, which indicates an activation parameter of less than 3 kcal/mol. This is significantly lower than the W···*n*-heptane bond energy (of W(CO)<sub>5</sub>···*n*-heptane) of  $13.4(\pm 2.8)$  kcal/mol,<sup>16</sup> measured using photoacoustic calorimetry by Burkey and co-workers, and it is therefore likely that the pathway is not entirely dissociative. It is interesting to note that an interchange and not a dissociative mechanism was proposed<sup>17</sup> for the photochemical substitution reactions of ( $\eta^6$ -C<sub>6</sub>H<sub>6</sub>)Cr(CO)<sub>3</sub>.

**Reaction of CpW(CO)<sub>2</sub>Me (2) with N<sub>2</sub>.** Many organometallic fragments react with N<sub>2</sub> to form either stable or unstable complexes.<sup>19</sup> Photolysis of the Mo

(15) Creaven, B. S.; Dixon, A. J.; Kelly, J. M.; Long, C.; Poliakoff, M. *Organometallics* **1987**, *6*, 2600–2604.

(16) Morse, J. M., Jr.; Parker, G. H.; Burkey, T. J. *Organometallics* **1989**, *8*, 2471–2474.

(17) Creaven, B. S.; George, M. W.; Ginzburg, A. G.; Hughes, C.; Kelly, J. M.; Long, C.; McGrath, I. M.; Pryce, M. T. *Organometallics* **1993**, *12*, 3127–3131.

(18) Scott, S. L.; Espenson, J. H.; Zhu, Z. *J. Am. Chem. Soc.* **1993**, *115*, 1789–1797.

(14) Makranczy, J.; Megyery-Balog, K.; Ruzs, L.; Patyi, L. *Hung. J. Ind. Chem.* **1976**, *4*, 269–280.

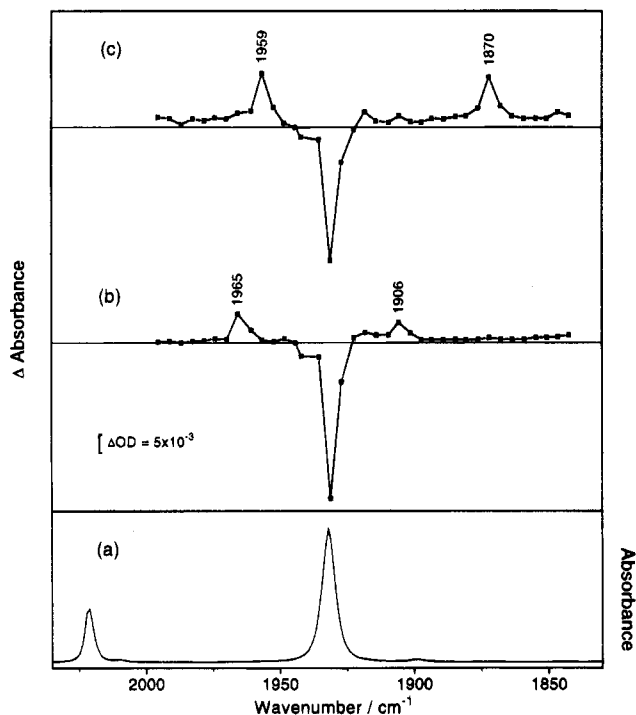
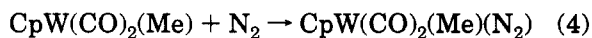


**Figure 5.** (a) FTIR spectrum of  $\text{CpW}(\text{CO})_3\text{Me}$  in *n*-heptane. (b,c) Time-resolved IR spectra of  $\text{CpW}(\text{CO})_3\text{Me}$  in *n*-heptane ( $5 \times 10^{-4}$  M) in the presence of  $\text{N}_2$  (2 atm) obtained at (c) 1  $\mu\text{s}$  and (b) 350  $\mu\text{s}$  following excitation (355 nm).

analogue of **1** in a low-temperature nitrogen matrix yields<sup>3</sup> the species  $\text{CpMo}(\text{CO})_2(\text{Me})(\text{N}_2)$ , in which the parent  $\nu(\text{CO})$  bands (2028.6 and 1941.4  $\text{cm}^{-1}$ ) are replaced by bands at 1969.7 and 1913.7  $\text{cm}^{-1}$  and a  $\nu(\text{NN})$  band appears at 2190.8  $\text{cm}^{-1}$  (see Table 1).

Figure 5c shows the TRIR spectrum of **1** in *n*-heptane under 2 bar of  $\text{N}_2$ , 1  $\mu\text{s}$  after UV irradiation (355 nm). Once more, the initial spectrum is essentially identical with that obtained in the absence of  $\text{N}_2$  and the observed bands are due to **2**. Figure 5b shows the TRIR spectrum after 350  $\mu\text{s}$ ; the absorptions due to **2** have decayed and two new absorptions, due to a new species **4**, have appeared at 1965 and 1906  $\text{cm}^{-1}$ . Noting that the 1932  $\text{cm}^{-1}$  band of **1** is doubly degenerate, this represents a mean shift to lower frequency from **1** to **4** of 26  $\text{cm}^{-1}$ ; comparing this with the shift in a  $\text{N}_2$  matrix from  $\text{CpMo}(\text{CO})_3(\text{Me})$  to  $\text{CpMo}(\text{CO})_2(\text{Me})(\text{N}_2)$  of 29  $\text{cm}^{-1}$ , we can readily assign the two bands of **4** to  $\text{CpW}(\text{CO})_2(\text{Me})(\text{N}_2)$  (see Table 1). Figure 6 shows that **4** is formed at the same rate as **2** decays ( $k_{\text{obs}} = [7(\pm 1)] \times 10^4$  and  $[9(\pm 1)] \times 10^4 \text{ s}^{-1}$ , respectively). With a  $\text{N}_2$  concentration of  $1.9 \times 10^{-2} \text{ mol dm}^{-3}$ ,<sup>14</sup> this gives a second order rate constant for



of  $[4.7(\pm 0.5)] \times 10^6 \text{ M}^{-1} \text{ s}^{-1}$ , which is 4 times slower

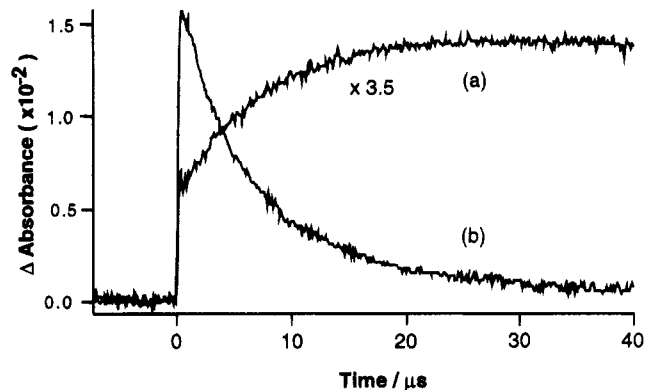


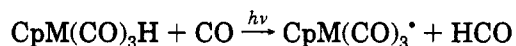
**Figure 6.** Time-resolved IR traces recorded at (a) 1966  $\text{cm}^{-1}$  and (b) 1959  $\text{cm}^{-1}$ , following excitation (355 nm) of  $\text{CpW}(\text{CO})_3\text{Me}$  in *n*-heptane ( $5 \times 10^{-4}$  M) in the presence of  $\text{N}_2$  (2 atm).

than the rate of reaction 2. In room-temperature *n*-heptane, **4** is not a stable complex, and in the presence of 2 bar of  $\text{N}_2$ , it decays within 20 ms after formation.

**(b) Photochemistry of  $\text{CpW}(\text{CO})_3\text{Me}$  (**1**) in the Absence of Other Ligands.** We have shown above that photolysis of **1** yields **2**, which is a reactive intermediate. We now return to the photobehavior of **1** in the absence of other ligands.

Although **2** is the major primary photoproduct (Figure 1c), there appears to be at least one other absorption (1902  $\text{cm}^{-1}$ ) produced in the terminal  $\nu(\text{CO})$  region. It is possible that this absorption is due to the radical  $\text{CpW}(\text{CO})_3^*$  (**5**), generated by photochemical cleavage of the W–Me bond. To investigate this possibility further, we have generated **5** by photolysis of  $[\text{CpW}(\text{CO})_3]_2$  (**6**) and studied its reactivity using TRIR.

**Identification of  $\text{CpW}(\text{CO})_3^*$  (**5**).** The radicals  $\text{CpM}(\text{CO})_3^*$  (M = Mo, W) were first characterized by  $\nu(\text{CO})$  IR spectroscopy following photolysis of  $\text{CpM}(\text{CO})_3\text{H}$  in solid CO matrices;<sup>4b</sup>



As mentioned above, we have been able<sup>9</sup> to detect the radical  $\text{CpMo}(\text{CO})_3^*$  by TRIR following photolysis of  $[\text{CpMo}(\text{CO})_3]_2$  in *n*-heptane solution and to monitor its reactivity. Visible photolysis (532 nm) of the dimer yields only the radical  $\text{CpMo}(\text{CO})_3^*$  with no production of the CO-loss species  $\text{Cp}_2\text{Mo}_2(\text{CO})_5$ , which is also produced on shorter wavelength photolysis. The W dimer is not very soluble in *n*-heptane; visible photolysis (532 nm) of **6** produced no detectable changes. We had to resort to 355 nm photolysis to produce a significant yield of photoproducts. Figure 7a shows the FTIR spectrum of **6** in *n*-heptane. Figure 7b shows the TRIR spectrum obtained 1  $\mu\text{s}$  after 355 nm excitation; there is loss of parent IR bands, and the most intense features in the product spectrum are two  $\nu(\text{CO})$  bands at 1999 and 1902  $\text{cm}^{-1}$ . The CO matrix bands of  $\text{CpW}(\text{CO})_3^*$  occur at 1999.3 and 1900.3/1896.5  $\text{cm}^{-1}$  ( $a_1$  and matrix-split  $e$  modes, respectively; see Table 1). Allowing for solvent shifts, the new intense  $\nu(\text{CO})$  bands in Figure 7b are assigned to the radical  $\text{CpW}(\text{CO})_3^*$  (**5**). By analogy with the experiments with  $[\text{CpMo}(\text{CO})_3]_2$ , the other features in Figure 7b are assigned to the CO-loss product  $\text{Cp}_2\text{W}_2(\text{CO})_5$ . The relative intensities of the two  $\nu(\text{CO})$  bands of  $\text{CpW}(\text{CO})_3^*$  allow an estimate of the bond

(19) Sellmann, D. *Angew. Chem., Int. Ed. Engl.* **1971**, *10*, 919. Rest, A. J. *J. Organomet. Chem.* **1972**, *40*, C76–78. Turner, J. J.; Simpson, M. B.; Poliakov, M.; Maier, W. B., II; Graham, M. A. *Inorg. Chem.* **1983**, *22*, 911–920. Turner, J. J.; Simpson, M. B.; Poliakov, M.; Maier, W. B., II; Graham, M. A. *J. Am. Chem. Soc.* **1983**, *105*, 3898–3904. Hitam, R. B.; Rest, A. J. *Organometallics* **1989**, *8*, 1598–1904. Howdle, S. M.; Grebenik, P.; Perutz, R. N.; Poliakov, M. *J. Chem. Soc., Chem. Commun.* **1989**, 1517–1519. George, M. W.; Haward, M. T.; Hamley, P. A.; Hughes, C.; Johnson, F. P. A.; Popov, V. K.; Poliakov, M. *J. Am. Chem. Soc.* **1993**, *115*, 2286–2299.

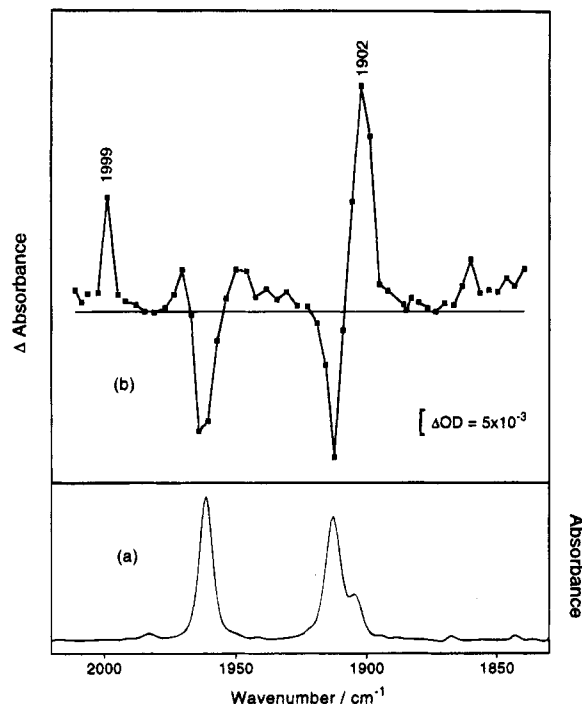


**Figure 7.** (a) FTIR spectrum of [CpW(CO)<sub>3</sub>]<sub>2</sub> in *n*-heptane. (b) Time-resolved IR spectrum of [CpW(CO)<sub>3</sub>]<sub>2</sub> in *n*-heptane ( $\sim 5 \times 10^{-4}$  M) in the presence of Ar (2 atm) obtained 1  $\mu$ s following excitation (355 nm).

angles in **5**:

$$[\text{intensity}(a_1)]/[\text{intensity}(e)] = \tan^2 \phi$$

where  $\phi$  is the angle of droop of the CO groups from the plane. From the relative intensities in Figure 7b we estimate  $\phi \sim 25^\circ$ . This can be compared with  $\phi \sim 30^\circ$  for the CpMo(CO)<sub>3</sub><sup>•</sup> radical generated at 12 K by photolysis of CpMo(CO)<sub>3</sub>H<sup>4b</sup> in a CO matrix. With the assignment of the  $\nu(\text{CO})$  bands of **5** in *n*-heptane, we can reexamine the TRIR spectrum following photolysis of **1** in *n*-heptane, either in the absence of other ligands or in the early stages of photolysis with other ligands. For example, close inspection of the decay curves and Figure 3c shows evidence for two low-intensity bands at  $\sim 2000$  and  $\sim 1900$  cm<sup>-1</sup>, which can now be assigned to **5**. Their low intensity is expected; W-Me bond homolysis of **1** is a minor pathway.

To obtain good kinetics for the recombination of the radical **5**, we have followed the photolysis of **6** in CH<sub>3</sub>CN, in which **6** is more soluble, and we have therefore been able to use visible light (532 nm) and suppress the formation of CO-loss species. Figure 8a shows the FTIR spectrum of **6** in CH<sub>3</sub>CN; it should be noted that in this more polar solvent there is considerably more of the *gauche* isomer, as is evident from the additional  $\nu(\text{CO})$  band at 2008 cm<sup>-1</sup>. Figure 8c shows the TRIR spectrum of **6** 1  $\mu$ s after the laser flash. This shows loss of parent and generation of the radical with the two  $\nu(\text{CO})$  bands at 1995 and 1882 cm<sup>-1</sup>; note that, as expected, there is no formation of CO-loss product. Figure 8b shows the TRIR spectrum at 80  $\mu$ s. There is loss of **5**, regeneration of some **6** (but this is complicated by the overlap of lower radical and parent bands), and some formation of the *gauche* isomer of **6**. The recombination of **5**

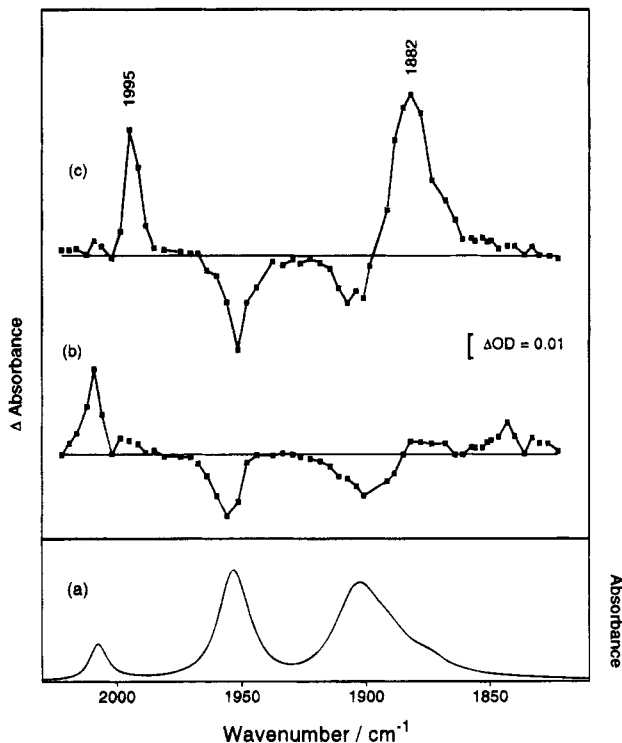


**Figure 8.** (a) FTIR spectrum of [CpW(CO)<sub>3</sub>]<sub>2</sub> in CH<sub>3</sub>CN ( $1 \times 10^{-3}$  M). (b,c) Time-resolved IR spectra of [CpW(CO)<sub>3</sub>]<sub>2</sub> in CH<sub>3</sub>CN ( $1 \times 10^{-3}$  M) in the presence of Ar (2 atm) obtained at (c) 1  $\mu$ s and (b) 80  $\mu$ s following excitation (532 nm).

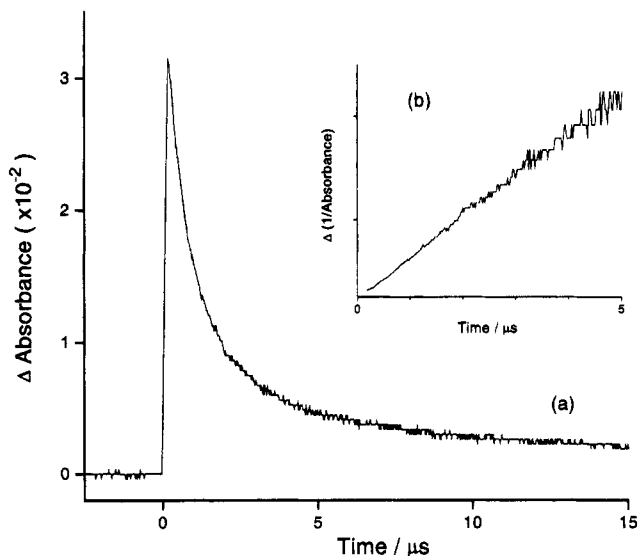
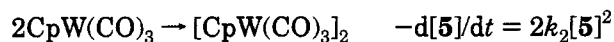


**Figure 9.** (a) Time-resolved IR decay trace of [CpW(CO)<sub>3</sub>]<sub>2</sub> ( $1 \times 10^{-3}$  M), recorded at 1995 cm<sup>-1</sup>, following excitation (532 nm) in CH<sub>3</sub>CN in the presence of Ar (2 atm). (b) Plot of  $1/\Delta A$  versus time for the decay trace shown in (a).



thus has been determined from the decay of the high-frequency band. Figure 9a shows the decay trace of the 1995 cm<sup>-1</sup> band of **5**; Figure 9b shows a plot of  $1/[\Delta(\text{absorbance})]$  versus time, which indicates that the loss of **5** follows second-order kinetics. This is further support for the two  $\nu(\text{CO})$  bands being due to the radical. To obtain the second-order rate constant, we need to know the relationship between the absorbance of **5** and the concentration of **5** ( $A = \epsilon cl$ ). In principle this is

easily determined. Since the IR extinction coefficient of **6** at a particular frequency is easily measured, the change in concentration of **6** is readily monitored from the change in absorbance of **6** at that frequency. If all of **6** is converted to **5**, then the concentration of **5** can be obtained. However, as in the case of  $[\text{CpMo}(\text{CO})_3]_2$ ,<sup>9</sup> it is possible that not all of the dimer is converted to monomer and there may be some photoinduced interconversion between the isomeric forms of **6**. If we ignore this problem, we can obtain an approximate value for the second-order recombination rate of **5**:  $1 \times 10^{10} \text{ M}^{-1} \text{ s}^{-1}$ . The diffusion-controlled limit in  $\text{CH}_3\text{CN}$  is  $2 \times 10^{10} \text{ M}^{-1} \text{ s}^{-1}$ ; for the recombination of two spin  $1/2$  radicals this will be  $0.25(2 \times 10^{10})$ .<sup>18</sup> Within experimental error, therefore, the radicals are combining at the diffusion-controlled limit.

**Reaction of  $\text{CpW}(\text{CO})_2\text{Me}$  (**2**) with  $\text{CpW}(\text{CO})_3\text{Me}$  (**1**).** If the mechanism of the conversion of **1** to **6** involves the reaction of **2** with **1**, then this should be observable by following the decay of **2** as a function of the concentration of **1**. Although it proved easy to demonstrate that the decay was faster as the concentration of **1** increased, it proved impossible to obtain meaningful kinetics, as the decay of **2** did not fit either first- or second-order decay. Peters<sup>6</sup> concluded like us that there was not such dependence on **1** but did not find evidence of dimer formation.

**Reaction of  $\text{CpW}(\text{CO})_3^*$  (**5**) with  $\text{CpW}(\text{CO})_3\text{Me}$  (**1**).** We have studied the kinetics to ascertain whether the formation of **6** involves the reaction of **5** with **1**. While the decay of **5** with no added **1** followed second-order kinetics (discussed earlier), with a large excess of **1** the kinetics were neither first nor second order. This suggests that the reaction of **5** with **1** may be significant, at least as a minor pathway.

### Conclusion

We have shown again that TRIR spectroscopy is an excellent probe for the mechanistic and kinetic study of organometallic photointermediates. The CO-loss species  $\text{CpW}(\text{CO})_2\text{Me} \cdots n$ -heptane is obtained on photolysis of  $\text{CpW}(\text{CO})_3\text{Me}$ ; its reaction rates with CO,  $\text{PPh}_3$ , and  $\text{N}_2$  have been measured. The radical  $\text{CpW}(\text{CO})_3^*$  has been identified as the primary photoproduct of photolysis of  $[\text{CpW}(\text{CO})_3]_2$ ; the radical probably plays little part in the photoreactions of  $\text{CpW}(\text{CO})_3\text{Me}$ .

**Acknowledgment.** We thank Prof. M. Poliakoff for helpful discussions. We also acknowledge support from the EPSRC (GR/H63296), the EC (Human Capital and Mobility), the Paul Instrument Fund of the Royal Society, Perkin-Elmer Ltd., and Müttek GmbH.  $[\text{CpW}(\text{CO})_3]_2$ .

OM950541A

# Deoxygenative Reduction of Dimolybdenum Carbonyl Complexes $\text{Mo}_2(\eta^5\text{-C}_5\text{H}_4\text{R}')_2(\text{CO})_4$ by Hydrosilane Giving Trinuclear $\mu_3$ -Methyldiyne and $\mu_3$ -Ethylidyne Complexes, $(\mu_3\text{-CR})[\text{Mo}(\eta^5\text{-C}_5\text{H}_4\text{R}')(\text{CO})_2]_3$ ( $\text{R}, \text{R}' = \text{H}, \text{CH}_3$ ), and Analysis of the Rotational Processes of the $\text{Mo}(\eta^5\text{-C}_5\text{H}_4\text{R}')(\text{CO})_2$ Moieties<sup>1</sup>

Munetaka Akita,\* Kazumi Noda, Yoshiaki Takahashi, and Yoshihiko Moro-oka\*

Research Laboratory of Resources Utilization, Tokyo Institute of Technology, 4259 Nagatsuta, Midori-ku, Yokohama 226, Japan

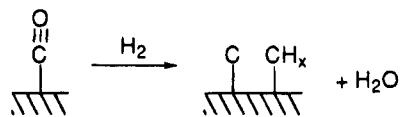
Received June 19, 1995\*

Photolysis of the dimolybdenum carbonyl complex  $(\eta^5\text{-C}_5\text{H}_4\text{R}')_2\text{Mo}_2(\text{CO})_4$  **1** (**a**-series:  $\text{R}' = \text{H}$ ; **b**-series:  $\text{R}' = \text{CH}_3$ ) in the presence of an excess amount of  $\text{HSiMe}_2\text{Ph}$  produces the trinuclear  $\mu_3$ -methyldiyne complex  $(\mu_3\text{-CH})[\text{Mo}(\eta^5\text{-C}_5\text{H}_4\text{R}')(\text{CO})_2]_3$  **2a,b** and the  $\mu_3$ -ethylidyne complex  $(\mu_3\text{-C-CH}_3)[\text{Mo}(\eta^5\text{-C}_5\text{H}_4\text{R}')(\text{CO})_2]_3$  **3a,b** along with siloxane  $\text{O}(\text{SiMe}_2\text{Ph})_2$  **4**. The structure with the tetrahedral  $\text{CMo}_3$  core and fluxional properties of **2** and **3** have been characterized by means of X-ray crystallography and NMR techniques. All of the three  $\eta^5\text{-C}_5\text{H}_4\text{R}'$  rings in the  $\mu_3$ -methyldiyne complexes **2a,b** project to the same side as does the  $\mu_3\text{-CH}$  ligand (conformer **A**), whereas one of the three  $\eta^5\text{-C}_5\text{H}_4\text{R}'$  rings in the  $\mu_3$ -ethylidyne complexes **3a,b** projects to the side distal from the  $\mu_3\text{-C-CH}_3$  (conformer **B**). The  $\text{C}_3$ -symmetrical structure (**A**) of **2** is supported by the three strong semibridging interactions of CO ligands with the adjacent Mo centers, but **3** with the unsymmetrical structure **B** contains less strong semibridging interactions. In solutions, **2** exists as an equilibrated mixture of two isomers **A** and **B** as revealed by variable temperature  $^1\text{H}$ - and  $^{13}\text{C}$ -NMR measurements. The complicated dynamic behavior of **2** can be analyzed as a combination of rotation of one of the three  $\text{Mo}(\eta^5\text{-C}_5\text{H}_4\text{R}')(\text{CO})_2$  units of **A** leading to **B** (local rotation) and concerted rotation of all the three metal fragments operating for **B** (gearlike rotation), which are associated with cleavage and regeneration processes of the semibridging interaction. The fluxional behavior of the  $\mu_3$ -ethylidyne complexes **3** can be explained by the gearlike rotation mechanism. Labeling experiments using  $1\text{-}^{13}\text{CO}$  and  $\text{DSiMe}_2\text{Ph}$  verify that all the hydrogen and carbon atoms of the  $\mu_3$ -alkyldiyne parts in **2** and **3** come from  $\text{HSiMe}_2\text{Ph}$  and CO in **1**, respectively. Therefore the present system can be viewed as a model system for a crucial step in Fischer–Tropsch mechanism, i.e. deoxygenative reduction of CO giving CH and  $\text{CCH}_3$  species. The deoxygenative reduction has been realized by using hydrosilane with high oxygenophilicity as an equivalent for  $\text{H}_2$ .

## Introduction

Deoxygenative reduction of carbon monoxide giving carbide or  $\text{CH}_x$  species on a heterogeneous catalyst surface has been recognized as a crucial step at an early stage of catalytic CO hydrogenation reactions (Scheme 1).<sup>2,3</sup> Although various types of model studies have been reported so far, we have been studying reduction of oxygen-containing species attached to a transition metal center by using hydrosilane as an equivalent for dihydrogen.<sup>4,5</sup> It has been well-established that the H–Si bond in hydrosilane shows reactivities quite similar to those of the H–H bond as typically exemplified by oxidative addition to a low valent metal center giving a hydride intermediate  $\text{M}(\text{H})(\text{X})$  ( $\text{X}: \text{H}, \text{SiR}_3$ ).<sup>6,7</sup> This

Scheme 1



reaction is involved as a key step of catalyzed addition reactions of  $\text{H-X}$  to unsaturated organic compounds, that is, catalytic hydrogenation and hydrosilylation. In addition to this feature, it is anticipated that the positively charged, highly electrophilic silyl moiety in  $\text{M}(\text{H})(\text{SiR}_3)$ <sup>6,7</sup> resulting from the oxidative addition (i) works as a Lewis acid (ii) so as to promote subsequent hydride transfer (iii) just like the acidic point on a heterogeneous catalyst surface (Scheme 2). Furthermore the oxygen atom may be removed as thermodynamically very stable siloxane (iv), that can be viewed as silylated water. Thus employment of hydrosilane as an equivalent for hydrogen would lead to a model system for the deoxygenative reduction of CO. In fact, we have found catalytic hydrosilylation of acyl metal complexes  $\text{MC}(=\text{O})\text{R}$  giving alkyl complexes  $\text{MCH}_2\text{R}^{\text{4a}}$

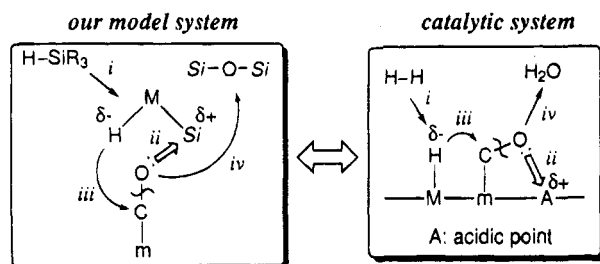
\* Abstract published in *Advance ACS Abstracts*, October 1, 1995.

(1) Abbreviations used in this paper: Cp: a general term for  $\eta^5\text{-C}_5\text{H}_4\text{R}'$  ligands; Cp:  $\eta^5\text{-C}_5\text{H}_5$ ; Cp':  $\eta^5\text{-C}_5\text{H}_4\text{CH}_3$ .

(2) (a) Fischer, F.; Tropsch, H. *Brennst. Chem.* **1926**, *7*, 97. (b) Brady, R. C.; Pettit, R. J. *Am. Chem. Soc.* **1980**, *102*, 6181. (c) Falbe, J. *New Synthesis with Carbon Monoxide*; Springer: Berlin, 1980. (d) Keim, W. *Catalysis in C1 Chemistry*; D. Reidel: Dordrecht, 1983. (e) Anderson, R. B. *The Fischer Tropsch Synthesis*; Academic Press: London, 1984.



Scheme 2

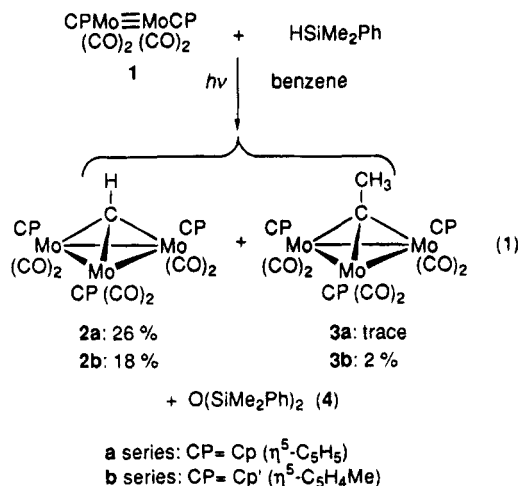


and transformation of a ruthenium carbonyl complex  $\text{Cp}_2\text{Ru}_2(\text{CO})_4$  into bridging methylene complexes  $\text{Cp}_2\text{Ru}_2(\mu\text{-CH}_2)_n(\mu\text{-CO})_{2-n}(\text{CO})_2$  ( $n = 1, 2$ ).<sup>4c</sup> This type of reduction is hardly realized by the action of hydrogen, because the hydride intermediate  $\text{M}(\text{H})_2$  shows quite low affinity toward polar substrates.

Herein we disclose the result of reduction of dimolybdenum carbonyl complexes  $(\eta^5\text{-C}_5\text{H}_4\text{R}')_2\text{Mo}_2(\text{CO})_4$  ( $\text{Mo}\equiv\text{Mo}$ ) **1** with hydrosilane affording the trimolybdenum  $\mu_3$ -alkylidyne complexes  $(\mu_3\text{-CR})[\text{Mo}(\eta^5\text{-C}_5\text{H}_4\text{R}')(\text{CO})_2]_3$  (**2**;  $\text{R}, \text{R}' = \text{H}, \text{CH}_3$ ). The molecular structure and complicated dynamic behavior of the resulting trinuclear complexes will also be discussed in detail. A preliminary communication of a part of this work already appeared.<sup>4e</sup>

## Results and Discussion

**Deoxygenative Reduction of  $(\eta^5\text{-C}_5\text{H}_4\text{R}')_2\text{Mo}_2(\text{CO})_4$  (**1**) Giving  $\mu_3$ -Methylidyne and  $\mu_3$ -Ethylydyne Complexes,  $(\mu_3\text{-CH})[\text{Mo}(\eta^5\text{-C}_5\text{H}_4\text{R}')(\text{CO})_2]_3$  (**2**) and  $(\mu_3\text{-CCH}_3)[\text{Mo}(\eta^5\text{-C}_5\text{H}_4\text{R}')(\text{CO})_2]_3$  (**3**).** Irradiation of a benzene solution of the dimolybdenum carbonyl complex  $\text{Cp}_2\text{Mo}_2(\text{CO})_4$  **1a** in the presence of an excess amount of  $\text{HSiMe}_2\text{Ph}$  afforded the trinuclear  $\mu_3$ -methylidyne complex  $(\mu_3\text{-CH})[\text{MoCp}(\text{CO})_2]_3$  **2a** in 26% yield (based on CO) along with the siloxane  $\text{O}(\text{SiMe}_2\text{Ph})_2$  **4** after chromatographic separation (eq 1). Although the  $\mu_3$ -ethylydyne



complex  $(\mu_3\text{-CCH}_3)[\text{MoCp}(\text{CO})_2]_3$  **3a** was detected by TLC and  $^1\text{H-NMR}$ , it could not be isolated from a reaction mixture because of the low yield. Yields determined by an NMR experiment carried out in  $\text{C}_6\text{D}_6$  in a sealed tube were 38% (**2a**; based on CO), trace (**3a**), and 115% (**4**; based on **1a**).

Photochemical reaction of the  $\eta^5$ -methylcyclopentadienyl analogue  $\text{Cp}'_2\text{Mo}_2(\text{CO})_4$  **1b** with  $\text{HSiMe}_2\text{Ph}$  also produced a mixture of the  $\mu_3$ -methylidyne  $(\mu_3\text{-CH})$

$[\text{MoCp}'(\text{CO})_2]_3$  (**2b**) and  $\mu_3$ -ethylydyne complexes  $(\mu_3\text{-CCH}_3)[\text{MoCp}'(\text{CO})_2]_3$  (**3b**). Compared to the Cp system, the yield of **2b** (18% based on CO) was lowered but a small amount of **3b** (2% based on CO) was isolated from a reaction mixture.

All the products **2** and **3** show complicated dynamic behavior as described below, but they are readily assigned to the  $\mu_3$ -alkylidyne complexes on the basis of the following NMR features (Table 1). As a typical example, the  $^1\text{H-NMR}$  spectrum of a  $^{13}\text{C}$ -enriched sample of  $(\mu_3\text{-}^* \text{CH})[\text{MoCp}'(\text{CO})_2]_3$  **2a- $^{13}\text{C}$**  ( $^*\text{C}$ : ca. 30%  $^{13}\text{C}$ -enriched) is reproduced in Figure 1. Although the presence of two isomers (**A** and **B**) is evident, the formulation is supported by the intensity ratio [1 ( $\text{CH}$ ): 15 ( $\eta^5\text{-C}_5\text{H}_5$ )<sub>3</sub>] and the highly deshielded signals appearing in the region characteristic of  $\mu_3\text{-CH}$  ligands ( $\delta_{\text{H}}$  11.85, 13.37;  $\delta_{\text{C}}$  245.6, 262.3).<sup>8,9</sup> As for the ethylydyne complex, **3a** is characterized by comparison of the  $^1\text{H-NMR}$  data with those of an authentic sample prepared by isolobal metal exchange reaction of the tricobalt  $\mu_3$ -ethylydyne complex  $(\mu_3\text{-CCH}_3)\text{Co}_3(\text{CO})_9$  with  $\text{Cp}_2\text{Mo}_2(\text{CO})_6$  reported by Vahrenkamp et al.<sup>10</sup> It is notable that both **2** and **3** contain several CO stretching vibrations in the range 2000–1800  $\text{cm}^{-1}$  indicating the presence of semibridging CO ligands. The structures of **2a, b** and **3b** have been determined unequivocally by X-ray crystallography (see below).

The present reaction also proceeds under thermal reaction conditions (120 °C), but the reproducibility is quite poor. In addition, the photochemical reaction is

(3) (a) Masters, C. *Adv. Organomet. Chem.* **1979**, *19*, 63. (b) Muettterties, E. L.; Rhodin, T. N.; Band, E.; Brucker, C. F.; Pretzer, W. R. *Chem. Rev.* **1979**, *79*, 79. (c) Roofer-DePoorter, C. K. *Chem. Rev.* **1981**, *81*, 447. (d) Herrmann, W. A. *Angew. Chem., Int. Ed. Engl.* **1982**, *21*, 117. For stepwise transformations: (e) Cutler, A. R.; Hanna, P. K.; Vites, J. C. *Chem. Rev.* **1988**, *88*, 1363 and references cited therein. For carbide complexes: (f) Tachikawa, M.; Muettterties, E. L. *Prog. Inorg. Chem.* **1981**, *28*, 203. (g) Bradley, J. S. *Adv. Organomet. Chem.* **1983**, *22*, 1. (h) Shriver, D. F.; Sailor, M. J. *Acc. Chem. Res.* **1988**, *21*, 374. (i) Beck, W.; Niemer, B.; Wieser, M. *Angew. Chem., Int. Ed. Engl.* **1993**, *32*, 923. (j) See also Neithamer, D. R.; LaPointe, R. E.; Wheeler, R. E.; Richeson, D. S.; Van Duyne, G. D.; Wolczanski, P. T. *J. Am. Chem. Soc.* **1989**, *111*, 9056.

(4) (a) Akita, M.; Mitani, O.; Sayama, M.; Moro-oka, Y. *Organometallics* **1991**, *10*, 1394. (b) Akita, M.; Oku, T.; Tanaka, M.; Moro-oka, Y. *Organometallics*, **1991**, *10*, 3080. (c) Akita, M.; Oku, T.; Moro-oka, Y. *J. Chem. Soc., Chem. Commun.* **1992**, 1031. (d) Akita, M.; Oku, T.; Hua, R.; Moro-oka, Y. *J. Chem. Soc., Chem. Commun.* **1993**, 1670. (e) Akita, M.; Noda, K.; Moro-oka, Y. *Organometallics* **1994**, *13*, 4145. (f) Akita, M.; Moro-oka, Y. *Stud. Surf. Sci. Cat.* **1995**, *92*, 137.

(5) Gregg, B. T.; Cutler, A. R. *Organometallics* **1992**, *11*, 4276 and references cited therein.

(6) Patai, S.; Rappoport, Z. *The chemistry of organic silicon compounds*; John-Wiley & Sons: Chichester, 1989.

(7) (a) Cundy, C. S.; Kingston, B. M.; Lappert, M. F. *Adv. Organomet. Chem.* **1973**, *11*, 253. (b) Aylett, B. J. *Adv. Inorg. Radiochem.* **1982**, *25*, 1.

(8) For reviews: (a) ( $\text{M} = \text{Co}$ ) Seyferth, D. *Adv. Organomet. Chem.* **1976**, *14*, 97. (b) Penfold, B. R.; Robinson, R. H. *Acc. Chem. Res.* **1973**, *6*, 73. (c) ( $\text{M} = \text{Ru}, \text{Os}$ ) Keister, J. B. *Polyhedron* **1988**, *26*, 1. (d) Deeming, A. J. *Adv. Organomet. Chem.* **1986**, *26*, 1.

(9)  $(\mu_3\text{-CH})\text{M}_3$  complexes: (a) ( $\text{M} = \text{Co}$ ) Seyferth, D.; Hallgren, J. E.; Hung, P. L. K. *J. Organomet. Chem.* **1973**, *50*, 265. (b) ( $\text{M} = \text{Ru}$ ) Kakigano, T.; Suzuki, H.; Igarashi, M.; Moro-oka, Y. *Organometallics* **1990**, *9*, 2192. (c) ( $\text{M} = \text{Os}$ ) Shapley, J. R.; Cree-Uchiyama, M. E.; St. George, G. M.; Churchill, M. R.; Bueno, C. J. *Am. Chem. Soc.* **1983**, *105*, 140. (d) ( $\text{M} = \text{Ru}$ ) Keister, J. B.; Horling, T. L. *Inorg. Chem.* **1980**, *19*, 2304. (e) ( $\text{M} = \text{Fe}$ ) Vites, J. C.; Jacobsen, G.; Dutta, T. K.; Fehlner, T. P. *J. Am. Chem. Soc.* **1985**, *107*, 5563. (f) Kolis, J. W.; Holt, E. M.; Shriver, D. F. *J. Am. Chem. Soc.* **1983**, *105*, 7307. (g) ( $\text{M} = \text{Os}$ ) Calvert, R. B.; Shapley, J. R. *J. Am. Chem. Soc.* **1977**, *99*, 5225. (h) ( $\text{M} = \text{Rh}$ ) Dimas, P. A.; Duesler, E. N.; Lawson, R. J.; Shapley, J. R. *J. Am. Chem. Soc.* **1980**, *102*, 7787. (i) Herrmann, W. A.; Plank, J.; Riedel, D.; Weidenhammer, K.; Guggolz, E.; Balbach, B. *J. Am. Chem. Soc.* **1981**, *103*, 63. (j) ( $\text{M}_3 = \text{Co}, \text{Cr}, \text{Mo}, \text{W}, \text{Ni}$ ) Duffy, D. N.; Kassir, M. M.; Rae, A. D. *J. Organomet. Chem.* **1993**, *460*, 97. (k) Schacht, H. T.; Vahrenkamp, H. *J. Organomet. Chem.* **1990**, *381*, 261.

(10) Blumhofer, R.; Fischer, K.; Vahrenkamp, H. *Chem. Ber.* **1986**, *119*, 194.

Table 1.  $^1\text{H}$ - and  $^{13}\text{C}$ -NMR data for **2a** and **3a**<sup>a</sup>

complex	solvent (A:B)	temp, °C	isomer	$^1\text{H}$ -NMR		$^{13}\text{C}$ -NMR		
				CR	Cp	CR	CO	Cp
<b>2a</b>	CD <sub>2</sub> Cl <sub>2</sub> (1:1)	rt	A	13.37 (1H)	5.22 (15H)	262.3 (156)	227.4, 231.2	92.5
			B	11.85 (1H)	5.16 (15H)	245.6 (162)	<i>b,c</i>	<i>b,c</i>
	(1:0.6)	-80	A	13.36 (1H)	5.28 (15H)	260.5	228.2, 231.2	92.5
			B	11.74 (1H)	5.11 (5H), 5.22 (10H)	243 <sup>c</sup>	229, <sup>c</sup> 232, <sup>c</sup> 234 <sup>c</sup>	<i>b,c</i>
	CDCl <sub>3</sub> (1:3)	rt	A	13.26 (1H)	5.14 (15H)	259.7 (156)	226.0, 230.9	92.0
			B	11.78	<i>b</i>	244.3 (162)	<i>b,c</i>	<i>b,c</i>
	-50	A	258.2	226.6, 230.85	91.9			
			B	242.4	228.2, 230.79, 233.9	93.7		
	C <sub>6</sub> D <sub>6</sub> (1:6)	rt	A	12.66 (1H)	4.73 (15H)	260.4 (154)	<i>b,c</i>	<i>b,c</i>
			B	11.39	<i>b</i>	246.1 (161)	231 <sup>c</sup>	92.0
<b>2a</b>	tol- <i>d</i> <sub>8</sub> <sup>d</sup> (1:6)	rt	A	12.65 (1H)	4.71 (15H)	<i>e</i>	<i>b,c</i>	<i>b,c</i>
			B	11.35	<i>b</i>	246.1 (162)	231.0	91.9
	(1:4)	-80	A	12.41 (1H)	4.56 (15H)	257.6	226.6, 230.9	<i>b,c</i>
			B	11.01 (1H)	4.54 (10H), 4.69 (5H)	244.1	229.6, 231.0, 233.2	90.8
<b>3a</b>	tol- <i>d</i> <sub>8</sub>	rt	B	3.73 <sup>f</sup> (3H)	4.73 (15H)	269.3 (5) <sup>g</sup>	226 <sup>c</sup>	91.6
			-80	B	3.57 (3H)	4.51 (10H), 4.60 (5H)		

<sup>a</sup> Observed at 400 MHz ( $^1\text{H}$ ) and 100 MHz ( $^{13}\text{C}$ ). Chemical shifts are reported in ppm down field from TMS unless otherwise stated. Values in parentheses are for  $^1J_{\text{C-H}}$  in Hz. <sup>b</sup> Overlapped or coalesced with the signals of the other isomer. <sup>c</sup> Broad. <sup>d</sup>  $\delta_{\text{H}}$  values are referenced to the residual solvent CHD<sub>2</sub> signal ( $\delta_{\text{H}}$  2.09). <sup>e</sup> Too broad to be located. <sup>f</sup>  $^2J_{\text{C-H}}$ . <sup>g</sup>  $\delta_{\text{C}}(\text{CH}_3) = 54.2$  (q,  $J = 128$  Hz).  $^1J_{\text{C-C}} = 32$  Hz.

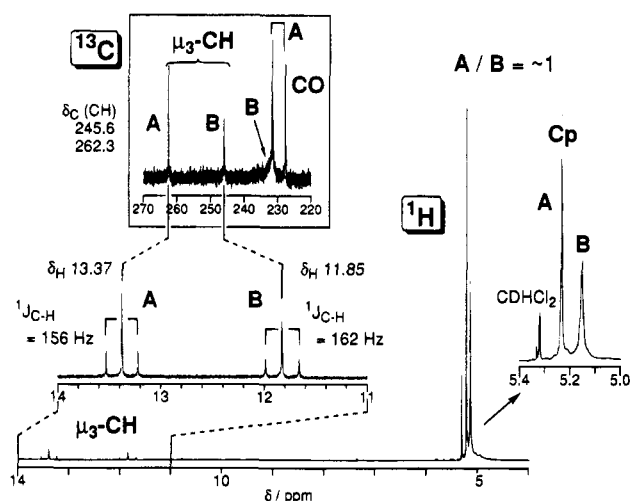


Figure 1.  $^1\text{H}$ (500 MHz)- and  $^{13}\text{C}$ -NMR spectra (125 MHz) of  $(\mu_3\text{-}^*\text{CH})[\text{MoCp}(\text{CO})_2]_3$  **2a**- $^{13}\text{C}$  (\*C: ca, 30%  $^{13}\text{C}$ -enriched) observed in CD<sub>2</sub>Cl<sub>2</sub> at room temperature.

specific to HSiMe<sub>2</sub>Ph. While sterically less demanding phenyl silanes such as HSiMePh<sub>2</sub> and H<sub>2</sub>SiPh<sub>2</sub> afforded **2** in low yields together with several byproducts,<sup>11</sup> the reaction of HSiEt<sub>3</sub>, H<sub>2</sub>SiEt<sub>2</sub>, and HSiPh<sub>3</sub> did not produce **2** and **3** at all but resulted in the formation of an intractable mixture of products. We also found that the HSiMe<sub>2</sub>Ph-reduction of Cp<sub>2</sub>Mo<sub>2</sub>(CO)<sub>6</sub>, Cp<sub>2</sub>W<sub>2</sub>(CO)<sub>4</sub>, and ( $\eta^5\text{-C}_5\text{Me}_5$ )<sub>2</sub>Mo<sub>2</sub>(CO)<sub>4</sub> under photochemical and thermal reaction conditions was sluggish. The reaction of Cp<sub>2</sub>Mo<sub>2</sub>(CO)<sub>6</sub> resulted in Mo–Mo bond cleavage<sup>7,12</sup> to give a mixture containing CpMo(H)(CO)<sub>3</sub> as detected by the hydride resonance ( $^1\text{H}$ -NMR). Although, in a reaction mixture of Cp<sub>2</sub>W<sub>2</sub>(CO)<sub>4</sub>, a couple of very weak deshielded  $^1\text{H}$ -NMR signals assignable to  $\mu\text{-CH}$  complexes were detected, none of them was isolable.

Compared to the well-established  $\mu_3$ -alkylidyne complexes of late transition metals (Co, Fe, Ru, Os, etc.),<sup>8</sup> the family of group 6 metal derivatives is small. Green et al. reported synthesis of a series of aryl derivatives ( $\mu_3\text{-CAr}$ )[MCp(CO)<sub>2</sub>]<sub>3</sub> **5** (M = Cr, Mo, W, mixed) via addition of dimetallic fragments to mononuclear  $\eta^1$ -

carbyne complexes Cp(CO)<sub>2</sub>W(=CAr).<sup>13</sup> Seppelt reported the fluoro-analogue of **2a**, ( $\mu_3\text{-CF}$ )[MoCp(CO)<sub>2</sub>]<sub>3</sub> **6**, which was formed via a curious reaction, i.e. photolysis of the difluoromalonyl dimolybdenum complex Cp(CO)<sub>3</sub>MoC(=O)CF<sub>2</sub>C(=O)MoCp(CO)<sub>3</sub>.<sup>14</sup> The CF complex **6** is the only structurally characterized compound of this family.

**Molecular Structures of 2a,b and 3b.** Before consideration on the behavior of the trimolybdenum  $\mu_3$ -alkylidyne complexes in solutions the molecular structures of **2a,b** and **3b** are investigated by X-ray crystallography. Because the isomer ratio (A:B) of **2a** in solutions depends on the solvent polarity, the crystals obtained from CH<sub>3</sub>CN–C<sub>6</sub>H<sub>6</sub>,<sup>15</sup> C<sub>6</sub>D<sub>6</sub>, and toluene<sup>16</sup> have been subjected to X-ray analysis. The crystallographic data and selected structural parameters are summarized in Tables 2 and 3, respectively, and the molecular structures of **2a**·CH<sub>3</sub>CN, **2b**, and **3b** are reproduced in Figures 2–4. An ORTEP view of **2a**·C<sub>6</sub>D<sub>6</sub> is included in the supporting information, because the structure is essentially the same as that of the CH<sub>3</sub>CN derivative. Although we also examined X-ray analysis of **3a**, the structure could not be refined well because of the low quality of the crystals. A sketch of its top view is reproduced in Figure 5.

The trimolybdenum  $\mu_3$ -alkylidyne complexes **2** and **3** contain the tetrahedral CM<sub>3</sub> core as usually observed for trimetallic  $\mu_3$ -alkylidyne complexes.<sup>8</sup> The Mo–Mo lengths of ca. 3.0 Å and the  $\mu_3\text{-C}$ –Mo distances of ca. 2.1 Å are essentially the same irrespective of the R and  $\eta^5\text{-C}_5\text{H}_4\text{R}'$  (CP) groups and are comparable to those found in the  $\mu_3\text{-CF}$  analogue **6**.<sup>14</sup>

The most characteristic feature of **2** and **3** is the orientation of the CPMo(CO)<sub>2</sub> moieties. In the meth-

(13) Green, M.; Porter, S. J.; Stone, F. G. A. *J. Chem. Soc., Dalton Trans.* **1983**, 513.

(14) Schulze, W.; Hartl, H.; Seppelt, K. *J. Organomet. Chem.* **1987**, *319*, 77.

(15) Because **2a** is insoluble in CH<sub>3</sub>CN, benzene was added.

(16) Because the molecular structure (A-type) as well as the crystal packing of **2a**·toluene is quite similar to those of **2a**·C<sub>6</sub>D<sub>6</sub>, the result is not included in this paper [C<sub>22</sub>H<sub>16</sub>O<sub>6</sub>Mo<sub>3</sub>·1/2(toluene),  $M = 710.3$ , orthorhombic space group *Pbca*,  $a = 17.295(5)$  Å,  $b = 17.449(5)$  Å,  $c = 16.270(3)$  Å,  $V = 4910(2)$  Å<sup>3</sup>,  $Z = 8$ ,  $d_{\text{calc}} = 1.92$  g cm<sup>-3</sup>,  $\mu = 15.5$  cm<sup>-1</sup>,  $R(R_w) = 0.048(0.049)$  for 2935 data with  $I > 3\sigma(I)$ ]. The toluene molecule sitting on a center of symmetry in a manner similar to C<sub>6</sub>D<sub>6</sub> is included in the space where C<sub>6</sub>D<sub>6</sub> occupies in **2a**·C<sub>6</sub>D<sub>6</sub>, although the methyl carbon atom of toluene could not be refined because of the completely disordered arrangement.

(11) This observation suggests a possibility that photoactivation of phenylsilane may also be involved as a key step of the transformation.

(12) Jetz, W.; Graham, W. A. G. *J. Am. Chem. Soc.* **1967**, *89*, 2773.

**Table 2. Crystallographic Data for 2a·CH<sub>3</sub>CN, 2a·C<sub>6</sub>D<sub>6</sub>, 2b, and 3b**

complexes	2a·CH <sub>3</sub> CN	2a·C <sub>6</sub> D <sub>6</sub>	2b	3b
formula	C <sub>22</sub> H <sub>16</sub> O <sub>6</sub> Mo <sub>3</sub> ·CH <sub>3</sub> CN (C <sub>24</sub> H <sub>19</sub> NO <sub>6</sub> Mo <sub>3</sub> )	C <sub>22</sub> H <sub>16</sub> O <sub>6</sub> Mo <sub>3</sub> ·1/2C <sub>6</sub> D <sub>6</sub> (C <sub>25</sub> H <sub>16</sub> D <sub>3</sub> O <sub>6</sub> Mo <sub>3</sub> )	C <sub>26</sub> H <sub>22</sub> O <sub>6</sub> Mo <sub>3</sub>	C <sub>26</sub> H <sub>24</sub> O <sub>6</sub> Mo <sub>3</sub>
formula weight	705.2	706.2	706.3	720.3
crystal system	orthorhombic	orthorhombic	cubic	monoclinic
space group	<i>Pbca</i>	<i>Pbca</i>	<i>Pa</i> $\bar{3}$	<i>P2</i> <sub>1</sub> / <i>a</i>
<i>a</i> /Å	18.205(6)	17.090(6)	16.872(5)	16.429(6)
<i>b</i> /Å	16.684(4)	17.426(5)	—	9.682(3)
<i>c</i> /Å	15.818(5)	16.111(5)	—	17.406(6)
$\beta$ /deg	—	—	—	117.80(2)
<i>V</i> /Å <sup>3</sup>	4804(4)	4798(2)	4807(2)	2449(1)
<i>Z</i>	8	8	8	4
<i>d</i> <sub>calcd</sub> /g cm <sup>-3</sup>	1.95	1.95	1.95	1.95
$\mu$ /cm <sup>-1</sup>	15.8	15.8	15.8	15.2
temp/°C	25	25	25	25
2 $\theta$ /deg	5–50	3–50	5–50	5–55
no. of data collected	4714	4697	4690	6152
no. of unique data with <i>I</i> > 3 $\sigma$ ( <i>I</i> )	3235	3399	821	3566
no. of variables	311	307	105	311
<i>R</i>	0.027	0.052	0.056	0.093
<i>R</i> <sub>w</sub>	0.021	0.049	0.040	0.075

ylidyne complexes **2a,b** all the CP rings project to the same side as does the  $\mu_3$ -CH ligand. The solid state structures of the **2a** part are essentially the same irrespective of the recrystallization solvents in contrast to the solution behavior (see below). In addition, one of the two CO ligands attached to each Mo center interacts with the adjacent Mo center with the Mo $\cdots$ CO distances ranging from 2.8 to 2.9 Å and the bent-back angles (Mo–C–O) of ca. 169°. The semibridging CO ligands are laid nearly coplanar to the Mo<sub>3</sub> plane, and the remaining terminal CO ligands project downward, almost perpendicular to the Mo<sub>3</sub> plane. The distances from the carbon atoms of  $\eta^1$ -CO ligands to the adjacent Mo centers (> 3.36 Å) are substantially longer than the semibridging interaction. As a result, the methylidyne complexes **2a,b** have a 3-fold symmetrical structure as can be seen from the top views. The semibridging Mo $\cdots$ CO interaction in group 6 metal carbonyl complexes has been usually observed for sterically congested multinuclear complexes as reported for dinuclear  $\mu$ -alkyne complexes ( $\mu$ - $\eta^2$ : $\eta^2$ -RC $\equiv$ CR)Mo<sub>2</sub>Cp<sub>2</sub>(CO)<sub>4</sub><sup>18</sup> and homo- and heterotrimetallic  $\mu_3$ -alkylidyne complexes<sup>19</sup> including **6**.

The ethylidyne complexes **3** adopt less symmetrical structure (Figures 4 and 5) in contrast to the methylidyne complexes **2**. The CP ring attached to Mo3 projects downward. In addition, the two CO ligands bonded to Mo3 do not interact with the adjacent metal centers, and instead three of the four CO ligands bonded to Mo1,2 work as semibridging ones. Although the Mo2 $\cdots$ C31 distance [3.14(2) Å] slightly longer than the Mo3 $\cdots$ C21 distance suggests a similar interaction, the small bent back angle [Mo3–C31–O31: 175(2)°] shows little bonding interaction between C31 and Mo2. When the top view of **3b** is compared with those of **2a,b**, the structure including the Mo1,2 moieties in **2** is retained to a considerable extent. But the removal of the

semibridging interaction with Mo2 resulting from the rotation of the Mo3 unit may induce additional semibridging interaction between Mo3 and C21. The semibridging interactions in **3** may be weaker than those in **2** as judged by the slight increase in the averaged Mo $\cdots$ CO distances from 2.88 Å (**2a**) and 2.84 Å (**2b**) to 2.94 Å (**3b**). In this paper the conformation found in **2** (all the CP rings projecting upward) and **3** and **6** (two CP rings projecting upward and the remaining one projecting downward) is denoted by **A** and **B**, respectively.

It is notable that the structures of the CCH<sub>3</sub> complexes **3a,b** and the CF complex **6** resemble each other as shown in Figures 4 and 5, although the semibridging interaction appears random at first glance. The overall geometry is quite similar to each other and the differences in the interatomic distances are less than 0.1 Å. This feature indicates that some rather strong semibridging interactions still remain in these complexes.

The orientation of the CPMo(CO)<sub>2</sub> fragments in the trimolybdenum  $\mu_3$ -alkylidyne complexes ( $\mu_3$ -C-R)[MoCP(CO)<sub>2</sub>]<sub>3</sub> may be correlated with the size of the substituent R. As can be seen from the space-filling models of **2a** and **2b** (Figure 6), little space is left above the shadowed methylidyne hydrogen atom. Therefore when a substituent bigger than hydrogen is introduced as R, one of the CPMo(CO)<sub>2</sub> fragments is forced to rotate so as to release the steric repulsion between the R group and the CP rings. In accord with this consideration, the CH<sub>3</sub> groups in the upward-projecting Cp' ligands in **3b** are oriented toward the direction distal from the C–CH<sub>3</sub> bridge, whereas those in **2** are located above the CH ligand.

In summary, (1) the **A**-type structure is the most stable conformer of ( $\mu_3$ -C-R)[MoCP(CO)<sub>2</sub>]<sub>3</sub> in the solid state, (2) a complex bearing a bigger R like **3** and **6** adopts a **B**-type structure owing to the steric repulsion between the R and CP groups, (3) both of the conformers **A** and **B** are stabilized by a combination of semibridging interaction of CO ligands, and (4) a structure with two inverted metal fragments has not been observed in our complexes and **6** at least in the solid state.

**Spectroscopic Characterization and Dynamic Behavior of the Trimolybdenum  $\mu_3$ -Alkylidyne Complexes 2 and 3.** In solutions, the  $\mu_3$ -alkylidyne complexes **2** and **3** exist as an equilibrated mixture of

(17) Estimation of the rate of process (d) may be difficult, because a spectrum where the fluxional processes are completely frozen out has not been obtained and probably the separation of the CO signals would be very small.

(18) Bailey, W. I., Jr.; Chisholm, M. H.; Cotton, F. A.; Rankel, L. A. *J. Am. Chem. Soc.* **1978**, *100*, 5764.

(19) (a) Chetcuti, M. J.; Chetcuti, P. A. M.; Jeffery, J. C.; Mills, R. M.; Mitrprachachon, P.; Pickering, S. J.; Stone, F. G. A.; Woodward, P. *J. Chem. Soc., Dalton Trans.* **1982**, 699. (b) Sutin, K. A.; Li, L.; Frampton, C. S.; Sayer, B. G.; McGlinchey, M. J. *Organometallics* **1991**, *10*, 2362.

**Table 3. Interatomic Distances (Å) and Bond Angles (deg) for 2a·CH<sub>3</sub>CN, 2a·C<sub>6</sub>D<sub>6</sub>, 2b, and 3b**

complexes	2a·CH <sub>3</sub> CN	2a·C <sub>6</sub> D <sub>6</sub>	2b	3b <sup>a</sup>	6 <sup>b,c</sup>
Interatomic Distances					
C1–Mo1	2.063(5)	2.077(8)	2.09(1)	2.13(1)	2.08(2)
C1–Mo2	2.081(4)	2.089(9)	—	2.11(1)	2.12(2)
C1–Mo3	2.079(4)	2.074(8)	—	2.13(1)	2.06
C1–C2	—	—	—	1.57(2)	1.39(2)
Mo1–Mo2	3.0624(9)	3.052(1)	3.049(1)	3.004(2)	3.02
Mo1–Mo3	3.046(1)	3.056(1)	—	2.985(2)	2.93
Mo2–Mo3	3.053(1)	3.054(1)	—	3.003(2)	3.00
Mo1–C11	1.978(5)	1.97(1)	2.05(1)	1.99(2)	1.99(2)
Mo1–C12	1.973(5)	1.94(1)	1.93(1)	2.01(2)	1.99(2)
Mo2–C21	1.970(5)	1.98(1)	—	1.95(2)	1.93(2)
Mo2–C22	1.966(5)	1.95(1)	—	1.95(2)	1.95(2)
Mo3–C31	1.960(5)	2.00(1)	—	1.98(2)	2.06
Mo3–C32	1.971(5)	1.96(1)	—	1.96(1)	1.97
C11–O11	1.157(5)	1.14(1)	1.12(1)	1.14(2)	1.14(3)
C12–O12	1.140(5)	1.18(1)	1.14(1)	1.12(2)	1.16(2)
C21–O21	1.167(5)	1.16(1)	—	1.15(2)	1.18(3)
C22–O22	1.150(5)	1.15(1)	—	1.15(2)	1.15(3)
C31–O31	1.158(5)	1.13(1)	—	1.13(2)	1.13
C32–O32	1.150(5)	1.15(1)	—	1.15(2)	1.14
Mo1–C13–17	2.324 <sup>d</sup>	2.334 <sup>d</sup>	2.33 <sup>d</sup>	2.33 <sup>d</sup>	2.33 <sup>d</sup>
Mo2–C23–27	2.329 <sup>d</sup>	2.34 <sup>d</sup>	—	2.35 <sup>d</sup>	2.34 <sup>d</sup>
Mo3–C33–37	2.229 <sup>d</sup>	2.32 <sup>d</sup>	—	2.34 <sup>d</sup>	2.32 <sup>d</sup>
Mo1–C21	2.895(5)	2.893(9)	2.84(1)	4.08(2)	4.10
Mo1–C22	3.826(5)	3.79(1)	3.72(1)	2.86(2)	2.90
Mo1–C32	3.447(5)	3.49(1)	3.43(1)	3.61(2)	3.57
Mo2–C12	3.441(5)	3.41(1)	—	4.54(2)	4.54
Mo2–C31	2.886(5)	2.92(1)	—	3.14(2)	3.18
Mo2–C32	3.805(5)	3.75(1)	—	4.35(2)	4.36
Mo3–C11	2.872(5)	2.91(1)	—	3.32(1)	3.31
Mo3–C12	3.736(5)	3.73(1)	—	2.93(2)	2.86
Mo3–C22	3.433(5)	3.36(1)	—	4.03(2)	4.05
Bond Angles					
Mo1–C1–Mo2	95.3(2)	94.2(3)	93.8(6)	90.4(6)	91.7(7)
Mo1–C1–Mo3	94.7(2)	94.8(3)	—	89.1(5)	92.0(5)
Mo2–C1–Mo3	94.4(2)	94.4(4)	—	90.2(5)	91.6(6)
Mo2–Mo1–Mo3	59.97(2)	60.01(3)	59.980(9)	60.19(5)	60.8
Mo1–Mo2–Mo3	59.75(2)	60.06(3)	—	59.60(5)	58.2
Mo1–Mo3–Mo2	60.28(1)	59.93(3)	—	60.21(5)	61.0
C1–Mo1–C11	103.5(2)	104.5(4)	102.1(4)	119.7(6)	116.0(7)
C1–Mo1–C12	119.6(2)	119.8(4)	120.7(6)	94.9(6)	95.7(7)
C1–Mo2–C21	104.0(2)	105.3(3)	—	117.2(6)	116.0(7)
C1–Mo2–C22	120.8(2)	119.1(4)	—	111.5(6)	111.1(7)
C1–Mo3–C31	104.4(2)	103.7(4)	—	80.2(6)	79.9(6)
C1–Mo3–C32	120.8(2)	121.4(3)	—	78.2(6)	76.3(6)
Mo1–C11–O11	168.5(4)	168.5(4)	164(1)	174(1)	174
Mo1–C12–O12	176.4(4)	177.4(9)	175(1)	171(1)	170
Mo2–C21–O21	168.9(4)	168.1(9)	—	169(1)	168
Mo2–C22–O22	175.5(5)	177.1(9)	—	167(2)	168
Mo3–C31–O31	169.6(5)	169.4(9)	—	175(2)	176
Mo3–C32–O32	174.8(5)	173.7(9)	—	175(1)	178

<sup>a</sup> Mo1–C31: 4.42(2) Å; Mo2–C11: 3.60(2) Å; Mo3–C21: 3.03(2) Å. <sup>b</sup> Parameters for one of the two independent molecules are listed. Because some of the important parameters were not reported in the original paper (ref 17), numbers without standard deviations are calculated by us. <sup>c</sup> Mo1–C31: 4.54 Å; Mo2–C11: 3.58 Å; Mo3–C21: 3.06 Å. <sup>d</sup> Averaged value.

isomers which are interconverted to each other at various rates.

### (i) Dynamic Behavior of the Methylidyne Complex 2a via a Combination of Gearlike Rotation and Local Rotation of the MoCp(CO)<sub>2</sub> Fragments.

Two isomers are detected for the methylidyne complex 2a by <sup>1</sup>H- and <sup>13</sup>C-NMR as shown in Figure 1. The μ<sub>3</sub>-CH signals at 11.85 and 13.37 ppm are correlated with the μ<sub>3</sub>-CH signals at 245.6 and 262.3 ppm, respectively, by means of a CH-HETCOR spectrum. The chemical shifts as well as the <sup>1</sup>J<sub>C-H</sub> values [156 (A) and 162 Hz (B)] are comparable to those for previously reported trinuclear μ<sub>3</sub>-methylidyne complexes: [Cp<sub>3</sub>Rh<sub>3</sub>(μ<sub>3</sub>-CH)(μ-CO)<sub>2</sub>]PF<sub>6</sub> δ<sub>H</sub> 16.2, δ<sub>C</sub> 303.6;<sup>9h,i</sup> [(η<sup>5</sup>-C<sub>5</sub>Me<sub>5</sub>)<sub>3</sub>Ru<sub>3</sub>(μ<sub>3</sub>-CH)(μ-Cl)<sub>2</sub>(μ-H)]BF<sub>4</sub> δ<sub>H</sub> 17.56, δ<sub>C</sub> 342.2, <sup>1</sup>J<sub>C-H</sub> = 164.6 Hz;<sup>9b</sup> Fe<sub>3</sub>(μ<sub>3</sub>-CH)(μ-H)<sub>3</sub>(CO)<sub>9</sub> δ<sub>H</sub> 11.5, δ<sub>C</sub> 232.0, <sup>1</sup>J<sub>C-H</sub> = 166 Hz;<sup>9e</sup> Ru<sub>3</sub>(μ<sub>3</sub>-CH)(μ-H)<sub>3</sub>(CO)<sub>9</sub> δ<sub>H</sub> 9.75,<sup>9d</sup> Os<sub>3</sub>(μ<sub>3</sub>-CH)-

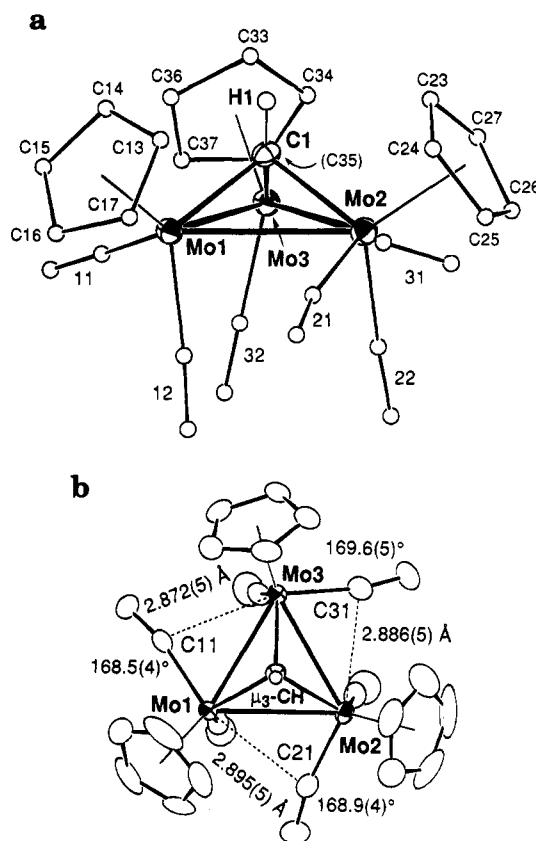


**Figure 2.** Molecular structure of 2a drawn at the 30% probability level. Numbers without atom names are for CO ligands. The MeCN molecule is omitted for clarity. (a) An overview. (b) A top view.

(μ-H)<sub>3</sub>(CO)<sub>9</sub> δ<sub>H</sub> 9.36, δ<sub>C</sub> 68.2, <sup>1</sup>J<sub>C-H</sub> = 171 Hz].<sup>9g</sup> The Cp (<sup>1</sup>H) and CO signals (<sup>13</sup>C) can be divided into the sharp signal set [δ<sub>H</sub> 5.22 (Cp); δ<sub>C</sub> 227.4, 231.2 (CO)] assignable to one isomer (A) and the rather broad signal set [δ<sub>H</sub> 5.16 (Cp); δ<sub>C</sub> ~230 (CO)] assignable to the other isomer (B). The grouping is further confirmed by comparison with the spectrum observed in tol-*d*<sub>8</sub> where B is present as the predominant species. The methylidyne complex 2a gives solvent- and temperature-dependent spectra, and data enough for consistent explanation of every aspect of the dynamic behavior is not available in a single solvent. Then variable temperature NMR measurements have been carried out in various solvents.

The two isomers are attributed to the two solid state structures A and B determined by X-ray crystallography on the basis of the following observations. First of all, comparison of a solution <sup>13</sup>C-NMR spectrum with a <sup>13</sup>C CP/MAS NMR spectrum of 2a-<sup>13</sup>C (recrystallized from toluene: A-type structure)<sup>16</sup> leads to the assignment of the sharp signal set to the 3-fold symmetrical structure A. This assignment is further confirmed by low temperature <sup>13</sup>C-NMR. The spectrum observed at -50 °C in CDCl<sub>3</sub> is reproduced in Figure 7, which can be explained by taking into account the structural formulae shown below the spectrum. The sharp shape of the signals of isomer A throughout the measured temperature range (rt to -80 °C) suggests that no dynamic process faster than the NMR line-broadening time scale is operating for this species. The separately observed two CO signals (a and b) and the simple spectral pattern containing only one Cp signal indicate that the semibridging interaction is considerably strong and, as

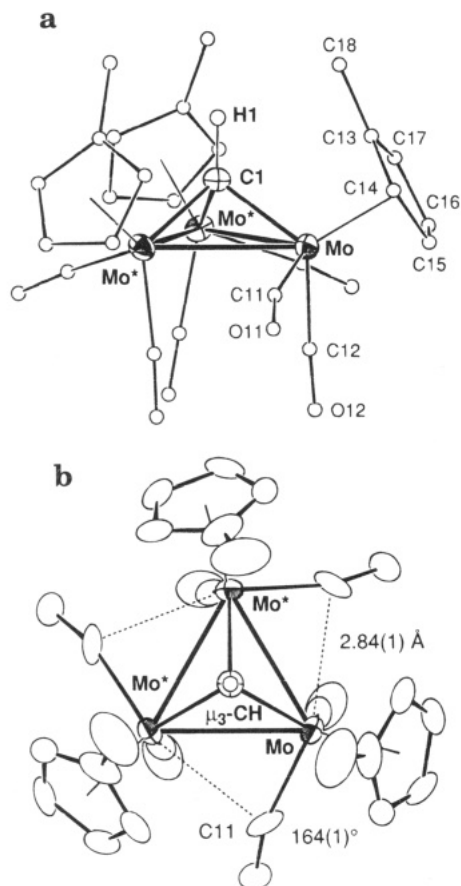


**Figure 3.** Molecular structure of **2b** drawn at the 30% probability level. Numbers without atom names are for CO ligands. (a) An overview. (b) A top view.

a result, the 3-fold symmetrical structure (**A**) is so rigid as to be retained even in a solution. The other isomer (**B**) is less symmetrical than isomer **A** as suggested by the increased number of the signals. The CO resonance observed as a very broad peak around 230 ppm at room temperature [Table 1; see also Figure 1 (in  $\text{CD}_2\text{Cl}_2$ )] splits into three signals at  $-50^\circ\text{C}$ , the central peak of which appears as a shoulder peak of one of the signals of **A** [Figure 8 (in  $\text{CDCl}_3$ )]. Furthermore the slightly broad  $^1\text{H-NMR}$  Cp signal in higher field ( $\delta_{\text{H}}$  5.16 in  $\text{CD}_2\text{Cl}_2$ ; Figure 1) also separates into two signals ( $\delta_{\text{H}}$  5.11, 5.22) in 1:2 ratio upon cooling down to  $-80^\circ\text{C}$  (Table 1). The number of the ancillary ligands' signals (2Cp, 3CO:  $^{13}\text{C}$ ) and the intensity ratio of the two Cp signals ( $^1\text{H}$ ) at low temperature suggest a structure with apparent  $C_s$  symmetry rather than the unsymmetrical structure (**B**) giving ten signals. The slightly broad signals of **B** indicate that still some dynamic process occurs, which can not be frozen out even at  $-80^\circ\text{C}$  in various solvents. The spectrum can be interpreted in terms of fast switching of the semibridging CO ligands ( $c_1$  and  $c_2$ ) attached to the Mo atoms bearing upward-projecting Cp rings (Figure 7). This motion ( $\mathbf{B} \rightleftharpoons \mathbf{B}'$  in Figure 7) gives a spectrum consistent with a  $C_s$  symmetrical structure with respect to the mirror plane passing through Mo3, CH and the midpoint of the Mo1–Mo2 bond [2Cp (2:1); Cp<sub>1</sub> = Cp<sub>2</sub>, Cp<sub>3</sub>; 3CO:  $a_1 = a_2$ ,  $b_1 = b_2$ ,  $c_1 = c_2$ ].

The ratio of the two species **A** and **B** present in solutions (**A/B**) is found to be dependent on the solvent as well as the temperature. As the solvent polarity decreases [ $\text{CD}_2\text{Cl}_2$  (1/1)  $\rightarrow$   $\text{CDCl}_3$  (1/4)  $\rightarrow$   $\text{C}_6\text{D}_6$  (1/6)  $\sim$   $\text{tol-}d_8$  (1/6)] and the temperature is raised [1/4 ( $-80^\circ\text{C}$

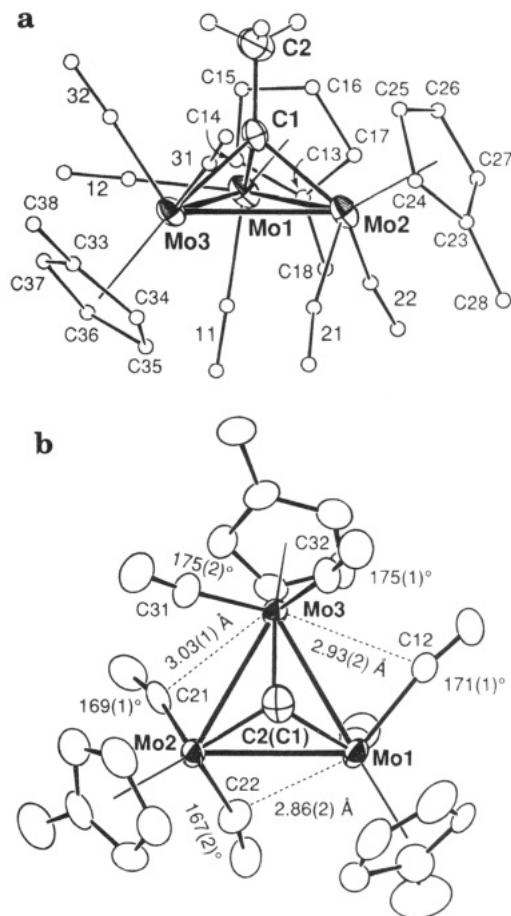


**Figure 4.** Molecular structure of **3b** drawn at the 30% probability level. Numbers without atom names are for CO ligands. (a) An overview. (b) A top view.

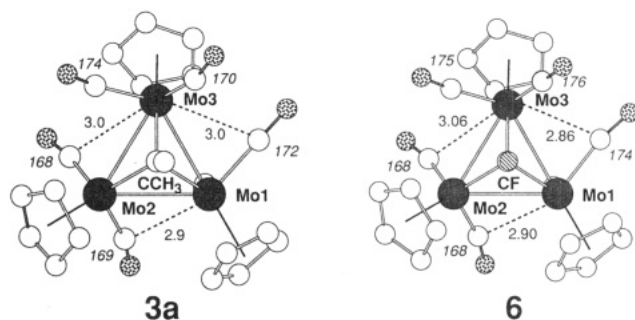


**Figure 5.** Top views of the molecular structures of ( $\mu_3\text{-CR}$ )[MoCp(CO)<sub>2</sub>]<sub>3</sub> [R = CH<sub>3</sub> (**3a**) and F (**6**)]. The roman and italicized numbers refer to the Mo $\cdots$ C distances ( $\text{\AA}$ ) and Mo–C–O angles (deg), respectively.

in  $\text{tol-}d_8$ )  $\rightarrow$  1/6 (rt)], the isomer **B** becomes dominant. In order to investigate the interconversion, attempts to get a coalesced spectrum were made. However, because the isomer **B** became the predominant species at higher temperature, it was impossible to differentiate coalescence of **A** and **B** from complete thermal isomerization of **A** to **B**. Then we carried out saturation transfer experiments (Figure 8). Irradiation of the  $\mu_3\text{-}^{12}\text{CH}$  signals of one isomer causes reduction of the intensity of the  $\mu_3\text{-}^{12}\text{CH}$  signals of the other isomer in a selective manner. Thus the two isomers are interconverted to each other at a rate slower than the  $^1\text{H-NMR}$  line-broadening time scale.

The dynamic processes operating for **2a** are summarized as follows: (i) The two isomers present in a solution are assigned to the structures **A** and **B** char-

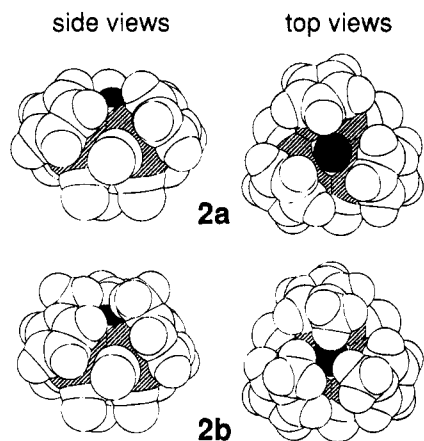


Figure 6. Space-filling models of **2a,b**.

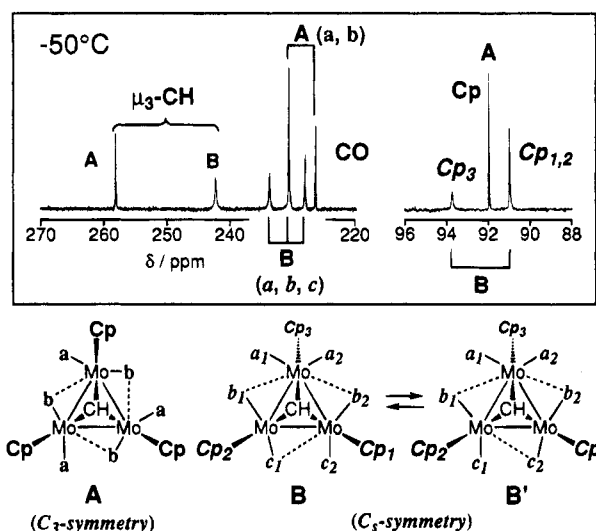


Figure 7. A low temperature  $^{13}\text{C}$ -NMR spectrum (at 100 MHz; in  $\text{CDCl}_3$ ; at  $-50\text{ }^\circ\text{C}$ ) of  $(\mu_3\text{-}^*\text{CH})[\text{MoCp}(\text{CO})_2]_3$  **2a**- $^{13}\text{C}$  ( $^*\text{C}$ : ca, 30%  $^{13}\text{C}$ -enriched).

acterized by X-ray crystallography; (ii) The two isomers are observed separately at room temperature, but they are interconverted to each other at a rate slower than the NMR line-broadening time scale; (iii) The spectra of isomer **A** containing only one Cp signal and sharp  $\eta^1$  and semibridging CO resonances are consistent with the  $C_3$ -symmetrical structure; (iv) Upon lowering temperature, spectra of isomer **B**, suggesting an apparent  $C_3$ -structure at room temperature, are changed to spectra consistent with an apparent  $C_s$ -structure where a CO-switching process is not frozen out.

The spectral features can be explained by a combination of a couple of rotational processes of the  $\text{MoCp}(\text{CO})_2$  units associated with cleavage and recombination of the semibridging interaction of CO ligands (Scheme 3). Rotation of one of the three  $\text{MoCp}(\text{CO})_2$  fragments in **A** gives structure **B** (b). The equivalent Cp rings of **B** at higher temperature (iv) can be explained in two ways. The first mechanism (c) involves a very fast concerted rotation of the three  $\text{MoCp}(\text{CO})_2$  fragments in the structure **B** (process c). As the  $\text{MoCp}(\text{CO})_2$  group projecting downward is flipped up, another  $\text{MoCp}(\text{CO})_2$  group rotates and projects downward. In this mechanism the three metal fragments rotate in a concerted manner just like a gear so as to relieve the steric repulsion around the site above the  $\mu_3\text{-C-R}$  bridge. If the rotation of the three metal fragments is faster than the NMR line-broadening time scale, all the Cp rings

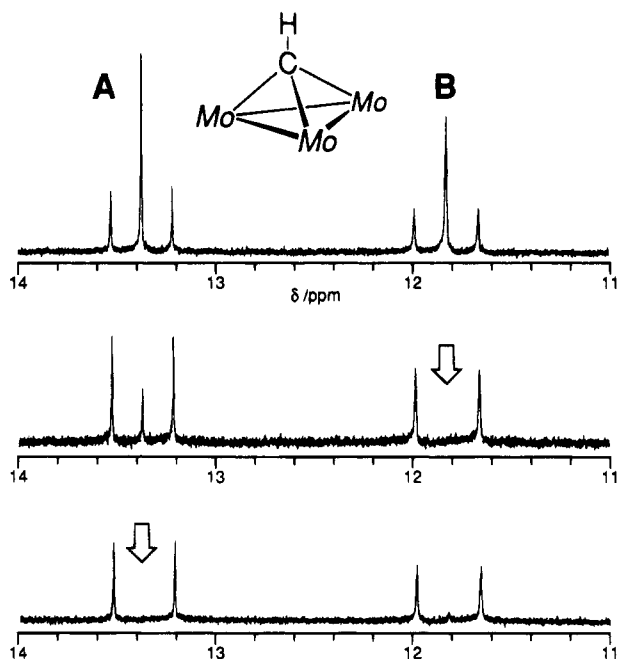


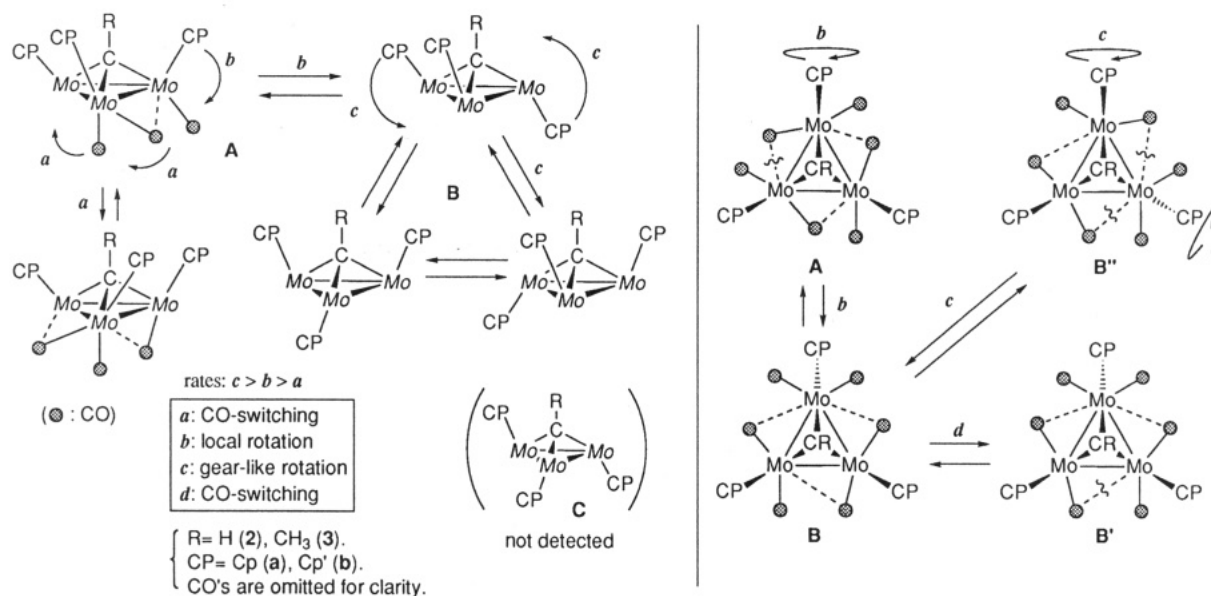
Figure 8.  $^1\text{H}$ -NMR saturation transfer experiments of  $(\mu_3\text{-}^*\text{CH})[\text{MoCp}(\text{CO})_2]_3$  **2a**- $^{13}\text{C}$  ( $\mu_3\text{-CH}$  region;  $^*\text{C}$ : ca, 30%  $^{13}\text{C}$ -enriched; at room temperature; at 500 MHz). Irradiated sites are indicated by arrows.

become equivalent. The second mechanism involves flipping back to **A** followed by local rotation of another metal fragment ( $\text{B} \rightarrow \text{A} \rightarrow \text{B}$ ). The latter mechanism can be eliminated on the basis of the change of the CO signals indicating that the interconversion between the two isomers **A** and **B** [via local rotation (b)] is slower than the averaging of the **B**'s signals [via gearlike rotation (c)]. Upon warming a sample from  $-50\text{ }^\circ\text{C}$  to rt (compare Figures 1 and 7; a similar  $^{13}\text{C}$ -NMR spectrum was obtained at rt in  $\text{CDCl}_3$ ), the CO signals of isomer **B** changes to a broad one without coalescence with those of isomer **A**, which remain rather sharp signals. Because the separation of the CO signals of the two isomers **A** and **B** at  $-50\text{ }^\circ\text{C}$  is comparable to each other, the coalescence temperature is roughly correlated with the activation energy of a rotational process. These observations lead to the above conclusion. The concerted gearlike rotation for **B** is frozen out at low temperature, but the spectrum suggesting a  $C_s$ -structure has been obtained. This result is explained by the fast switching of the semibridging CO ligands ( $\text{d: B} \rightleftharpoons \text{B}'$ ) as discussed above. In contrast to this process, switching of the CO ligands in **A** (a) is very slow as indicated by point iii. We also tried to observe coalescence of the two CO signals of **A**, but again our attempts were hindered by the complete thermal isomerization to **B** at higher temperature. Finally let us point out that a structure with two inverted metal units (**C**) has not been detected in the present system.

The coalescence temperatures of the CO signals lead to the estimation of the rates of the dynamic processes as follows:  $c > b > a$ .<sup>17</sup> The relative magnitude of the rates can be explained by taking into consideration the ease of cleavage of the semibridging  $\text{Mo}\cdots\text{CO}$  interactions (Scheme 3). Compared to process b where only one interaction is broken at first, the concerted switching (a) which requires breaking of three interactions should be a higher energy process. Therefore the local rotation (b) proceeds faster than the racemization of **A** (a). On the other hand, the CO switching of **B** ( $\text{B} \rightleftharpoons \text{B}'$ )



Scheme 3



**B'**) should be a low energy process, because the semibridging interaction with  $b_1$  and  $b_2$  (Figure 8) is retained throughout the process and the structural change can be attained via least motion of the ligands. As for local rotation (c:  $\mathbf{B} \rightleftharpoons \mathbf{B}''$ ), two interactions should be cleaved accompanied by rotation of two metal fragments. Because one of the interactions is a weak one (c) just mentioned and the semibridging interactions in **B** seem to be weaker than those in the highly symmetrical **A** as discussed before, the gearlike rotation (c) via cleavage of the rather weak interactions should proceed faster than the local rotation (b). Although we also have to consider rotational barrier of the metal units, we have no data to estimate it at present. The above discussion on the semibridging interaction apparently leads to a conclusion that isomer **A** should be more stable than **B**. Contrary to the expectation, **B** has proved to be the major isomer in solutions, though the ratio is dependent on the conditions. Also we don't have any data to explain the result. Some electrostatic interaction may be responsible for the ratio, because an apparent correlation between the isomer ratio and the solvent polarity has been observed. Isomer **A** with a larger dipole moment may be stable in a polar solvent.

Thus the complicated dynamic behavior of **2a** can be interpreted in terms of a combination of the rotation of the  $\text{MoCp}(\text{CO})_2$  units and switching of the semibridging CO ligands. The dynamic behavior of the dinuclear  $\mu$ -alkyne complexes  $(\mu\text{-}\eta^2\text{-}\eta^2\text{-RC}\equiv\text{CR})\text{Mo}_2\text{Cp}_2(\text{CO})_4$ <sup>18</sup> that are isolobal with **2** has also been explained by the switching of the semibridging interaction. In this case, however, complete rotation of the metal fragment has not been observed. As for the aryl derivatives (**5**)<sup>13</sup> of **2**, only one CO signal was observed at rt. Although some dynamic behavior which was frozen out at  $-30^\circ\text{C}$  was noted for a mixed metal complex ( $\text{M}_3 = \text{Mo}_2\text{W}$ ), further study was prevented by the low solubility. For the fluoride derivative **6**<sup>14</sup> only <sup>19</sup>F-NMR was recorded, and fluxional property was not mentioned at all. Recently, McGlinchey studied fluxional properties of mixed metal clusters  $(\eta^5\text{-C}_5\text{R}'_5)\text{MoCO}_2(\text{CO})_8(\mu_3\text{-CR})$  (M: Mo, W; R:  $\text{COOP}^i, \text{Ar}$ )<sup>20</sup> closely related to our system. The semibridging interaction of the Mo-CO ligands is also found in these complexes, and the dynamic behavior has

been interpreted successfully in terms of rotation of the  $\text{Mo}(\eta^5\text{-C}_5\text{R}'_5)(\text{CO})_2$  and  $\text{Co}(\text{CO})_3$  fragments as well as intermetallic CO transfer. Two rotamers corresponding to **A** and **B** are detected by low temperature <sup>13</sup>C-NMR, but the structure is still considerably mobile, because the semibridging interaction available for the complexes is not so effective for making the structure rigid on the NMR line-broadening time scale as that in **2** and **3**.

(ii) **Dynamic Behavior of  $(\mu_3\text{-CH})[\text{MoCp}'(\text{CO})_2]_3$  **2b**.** The spectra of **2b** are much more complicated than those of **2a**. As shown in Figure 9a, six  $\mu_3\text{-CH}$  signals are detected even at  $30^\circ\text{C}$ . Because all the signals coalesce into a broad one at  $110^\circ\text{C}$  (Figure 9b), the peaks arise from a single complex. On the other hand, lowering temperature to  $-90^\circ\text{C}$  results in appearance of nine signals (Figure 9c). The <sup>13</sup>C-NMR spectrum observed at  $30^\circ\text{C}$  (Figure 9d) contains three sharp signals (**AI**, **AII**, and **BIII**) in addition to a couple of very broad components. They are correlated with some of the <sup>1</sup>H-NMR signals by a CH-HETCOR spectrum as indicated in Figure 9. These data are consistent with the formulation of **2b** as an isomeric mixture of a  $\mu_3$ -methylidyne complex. Comparison of the  $\delta_{\text{H}}$ ,  $\delta_{\text{C}}$ , and  $^1J_{\text{C-H}}$  values with those of **2a** [ $\delta_{\text{H}}(\mathbf{A}) \sim 12.5 > \delta_{\text{H}}(\mathbf{B}) \sim 11.5$ ;  $\delta_{\text{C}}(\mathbf{A}) \sim 260 > \delta_{\text{C}}(\mathbf{B}) \sim 245$ ;  $^1J_{\text{C-H}}(\mathbf{A}) \sim 155 \text{ Hz}$ ;  $^1J_{\text{C-H}}(\mathbf{B}) \sim 160 \text{ Hz}$ ] leads to the tentative assignments of the peaks **AI**–**AIII** and **BI**–**BIII** to **A**- and **B**-type structures, respectively. The isomers may arise from hindered rotation of the Cp' rings (see, for example, **A** and **A'** in Scheme 4) or different modes of the semibridging interactions. The dynamic behavior of **2b** may be explained by Scheme 3. However, the spectra are too complicated to be analyzed sufficiently. To our surprise, saturation transfer experiments for the  $\mu_3\text{-CH}$  signals reveals that interconversion between **AI**  $\leftrightarrow$  **BI**, **AII**  $\leftrightarrow$  **BII**, and **AIII**  $\leftrightarrow$  **BIII** pairs takes place in a selective manner. For example, irradiation of the CH signal of **AII** results in disappearance of the CH signal of **BII** (Figure 9e). This means that interconversion between the two structure **A** and **B** via the local rotation (c) is

(20) (a) D'Agostino, M. F.; McGlinchey, M. J. *Polyhedron* **1988**, *7*, 807. (b) Sutin, K. A.; Kolis, J. W.; Mlekuz, M.; Bougeard, P.; Sayer, B. G.; Quilliam, M. A.; Faggiani, R.; Lock, C. J. L.; McGlinchey, M. J.; Jaouen, G. *Organometallics* **1987**, *6*, 439.



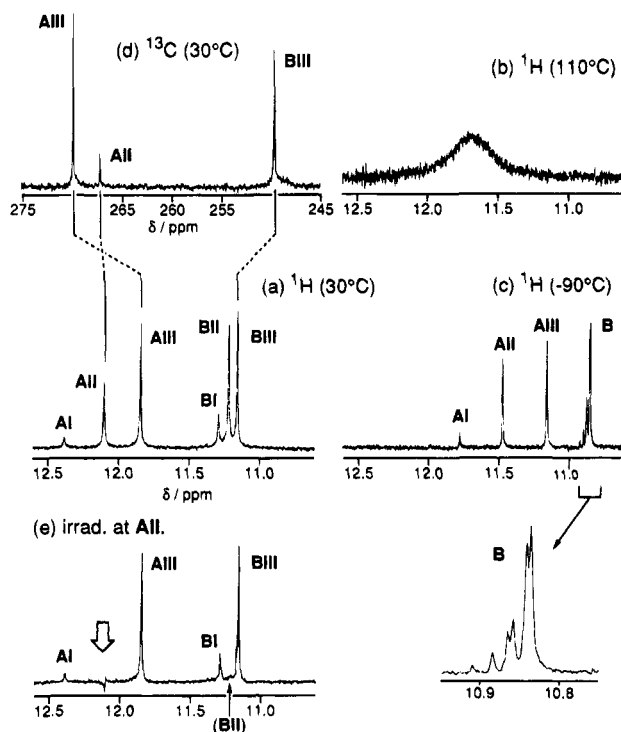
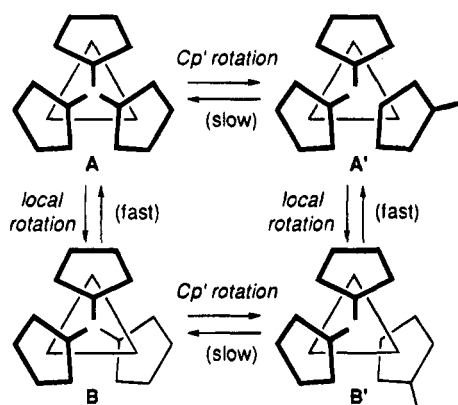


**Figure 9.** Variable temperature NMR spectra and saturation transfer experiment of  $(\mu_3\text{-CH})[\text{MoCp}'(\text{CO})_2]_3$  **2b** observed at 400 ( $^1\text{H}$ ) and 100 MHz ( $^{13}\text{C}$ ) in  $\text{tol-}d_3$ . (a) The  $\mu_3\text{-CH}$  region of  $^1\text{H}$ -NMR spectrum observed at 30 °C. (b) At 110 °C. (c) At -90 °C. (d) The  $\mu_3\text{-CH}$  region of  $^{13}\text{C}$ -NMR spectrum observed at 30 °C. (e) An example of saturation transfer experiment where the  $\mu_3\text{-CH}$  signal of **AII** being irradiated (at 30 °C).

**Scheme 4**



faster than the interconversion of **A** with another **A**-type structure (for example, **A'**) via simple rotation of a  $\text{Cp}'$  ring around the  $\text{Mo-Cp}'$  centroid axis (Scheme 4). Therefore in this case the local rotation (c) (Scheme 3) proceeds while keeping the different, relative configuration of the three  $\text{Cp}'$  rings. These phenomena should originate from the hindered rotation of the  $\text{Cp}'$  ring.

(iii) **Dynamic Behavior of  $(\mu_3\text{-CCH}_3)[\text{MoCp}'(\text{CO})_2]_3$  **3a** via Gearlike Rotation of the  $\text{MoCp}'(\text{CO})_2$  Fragments.** This complex has been characterized by comparison with an authentic sample<sup>10</sup> as described before, and its structure is further supported by the characteristic deshielded  $^{13}\text{C}$ -NMR signal ( $\delta_{\text{C}}$  269.3) as well as the preliminary X-ray result. The quaternary carbon signal coupled with both of the C and H atoms of the adjacent  $\text{CH}_3$  group clearly indicates the presence of an ethylidyne linkage  $\text{>CCH}_3$  [Table 1; see also the spectrum of **3b** (Figure 10)].

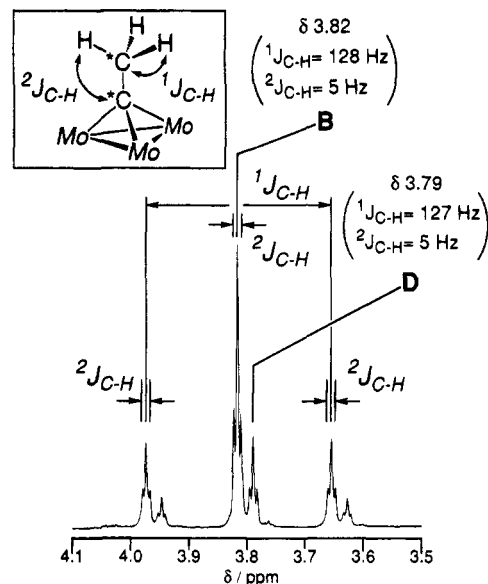


**Figure 10.** The  $\mu_3\text{-CCH}_3$  region of the  $^1\text{H}$ -NMR spectrum (400 MHz) of  $(\mu_3\text{-}^*\text{C}^*\text{CH}_3)[\text{MoCp}'(^*\text{CO})_2]_3$  **3b-}^{13}\text{C} ( $^*\text{C}$ : ca. 30%  $^{13}\text{C}$ -enriched) observed in  $\text{C}_6\text{D}_6$  at room temperature.**

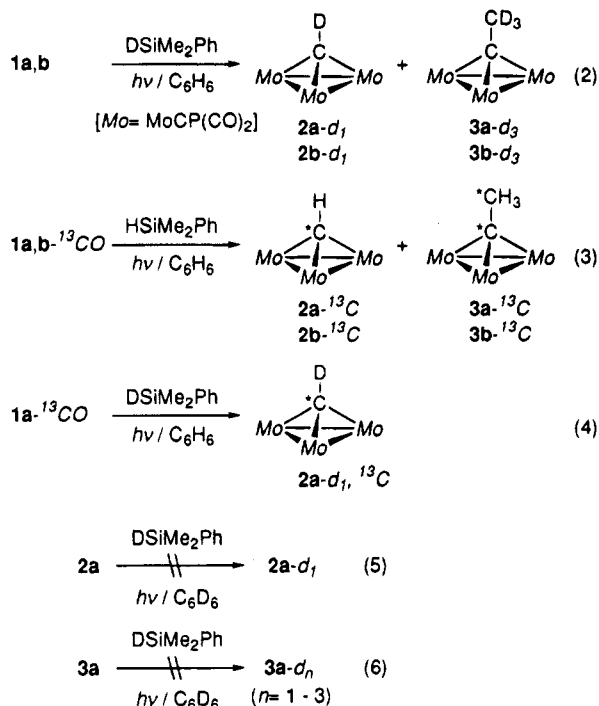
The  $^1\text{H}$ -NMR spectrum observed at room temperature contains a single  $\text{Cp}$  resonance, which splits into two singlets of 2 (10H):1 (5H) intensity ratio below -40 °C. The low temperature spectrum is consistent with the crystal structure (**B**), and further cooling down to -80 °C does not cause any notable change. Throughout the observed temperature range the  $\text{CCH}_3$  signal remains as a single peak and only one species has been detected by NMR analysis. The behavior of **3a** can be explained by the concerted gearlike rotation (c).<sup>21</sup>

(iv) **Dynamic Behavior of  $(\mu_3\text{-CCH}_3)[\text{MoCp}'(\text{CO})_2]_3$  **3b.**** A  $^1\text{H}$ -NMR spectrum of **3b** obtained from **1b-}^{13}\text{CO} (in  $\text{C}_6\text{D}_6$  at rt) contains two species **B** and **D** in 3:1 ratio (Figure 10). The major component **B** exhibits spectral features close to those of **3a**. Any notable change is not observed for the sharp  $\mu_3\text{-C-CH}_3$  signal in the range of rt to -80 °C, and the  $\eta^5\text{-C}_5\text{H}_4\text{CH}_3$  resonance splits into two signals of 1:2 ratio below -50 °C. Therefore the major species has been assigned to a **B**-type structure. The  $\mu_3\text{-CCH}_3$  signal of the minor component **D** does not show any notable change either, but analysis of the  $\eta^5\text{-C}_5\text{H}_4\text{CH}_3$  signals is hindered by broadening and overlap with the signals of **B** at low temperatures. Isomer **D** is tentatively assigned to an isomer of a **B**-structure with different  $\text{Cp}'$  orientation or different semibridging CO interactions. But the possibility of **D** being another structure **C** (Scheme 3) cannot be eliminated completely, because the situation around the  $\mu_3\text{-CCH}_3$  moiety is much more sterically congested than that of the  $\text{Cp}$  analogue **3a**.**

**Consideration on the Formation Mechanism of the  $\mu_3$ -Alkylidyne Complexes **2** and **3.**** At first, the source of the H and C atoms of the newly formed bridging hydrocarbyl groups ( $\mu_3\text{-CR}$ ) in **2** and **3** were investigated by labeling experiments (eqs 2-4). The reaction of **1a,b** with  $\text{DSiMe}_2\text{Ph}$  afforded the deuterated products **2a,b-}d\_1 and **3a,b-}d\_3** of more than 95% isotopic purity as estimated by  $^1\text{H}$ -NMR (eq 2). The blank experiments (eqs 5 and 6) showed that H-D exchange reactions of the resulting **2a** and **3a** with  $\text{DSiMe}_2\text{Ph}$  and**

(21) Because of the low yield of **3a** variable temperature  $^{13}\text{C}$ -NMR measurements could not be examined.

the deuterated solvent ( $C_6D_6$ ) did not take place at all. Next the reaction of  $1-^{13}CO$  (enriched with ca. 30%  $^{13}CO$ ) with  $HSiMe_2Ph$  gave a mixture of  $2-^{13}C$  and  $3-^{13}C$  (eq 3). As can be seen from the  $^1H$ -NMR spectrum of  $2a$ -



$^{13}C$  (Figure 1), the  $\mu_3$ -CH signals of the two isomers (A and B) which are accompanied by satellite peaks owing to the  $^1J_{C-H}$  coupling clearly indicate the origin of the  $\mu_3$ -CH atom to be CO in  $1a$ . As for the ethylidyne ligand, the  $\mu_3$ -CCH<sub>3</sub> region of the  $^1H$ -NMR spectrum of  $3b-^{13}C$  is reproduced in Figure 10. The triplet-of-tripletlike splitting pattern has been analyzed as a result of coupling with the two ethylidyne carbon atoms (B:  $^1J_{C-H} = 128$  Hz,  $^2J_{C-H} = 5$  Hz; D:  $^1J_{C-H} = 127$  Hz,  $^2J_{C-H} = 5$  Hz),<sup>22</sup> which reveals that both of the carbon atoms are enriched by  $^{13}C$  to an extent comparable to the starting compound  $1a-^{13}CO$ . The enrichment of the carbon atoms is also verified by the observation of the  $^1J_{C-C}$  coupling (32 Hz) of the C-CH<sub>3</sub> linkage. Similar spectra have been observed for  $2b$  and  $3a$ . Finally, the result of the double labeling experiment (eq 4) is consistent with the above experiments, and the  $^1J_{C-D}$  value for the  $\mu_3$ -CD ligand in  $2a-d_1$   $^{13}C$  has been determined to be 25 Hz. Thus the carbon atoms of the  $\mu_3$ -C-R bridge in  $2$  and  $3$  come from CO bonded to Mo in  $1$ , and all the hydrogen atoms are transferred from  $HSiMe_2Ph$  that is used as an equivalent for dihydrogen.

The formation of  $2$  from  $1$  should involve (1) Lewis acidic activation of CO, (2) hydride transfer to the CO carbon atom, (3) deoxygenation, and (4) formation of the trinuclear skeleton. The first function has been studied rather extensively for Co complexes. In 1973 MacDiarmid reported that thermolysis of  $Me_3SiCo(CO)_4$  afforded a mixture of a  $\mu_3$ -siloxyalkylidyne complex ( $\mu_3$ -COSiMe<sub>3</sub>)Co<sub>3</sub>(CO)<sub>9</sub> and a C-C coupling product ( $Me_3SiOC$ )<sub>4</sub>Co<sub>2</sub>(CO)<sub>4</sub>.<sup>23</sup> Recently, Do et al. reported formation

(22) Marshal, J. L. *Carbon-Carbon and Carbon-Proton Couplings*; Verlag Chemie International: Florida, 1983.

(23) (a) Ingle, W. M.; Preti, G.; MacDiarmid, A. G. *J. Chem. Soc., Chem. Commun.* **1973**, 497. (b) Baay, Y. L.; MacDiarmid, A. G. *Inorg. Chem.* **1969**, *8*, 986. Formation of ( $\mu_3$ -CSiMe<sub>3</sub>)Co<sub>3</sub>(CO)<sub>9</sub> was mentioned briefly but not at all in 25a.

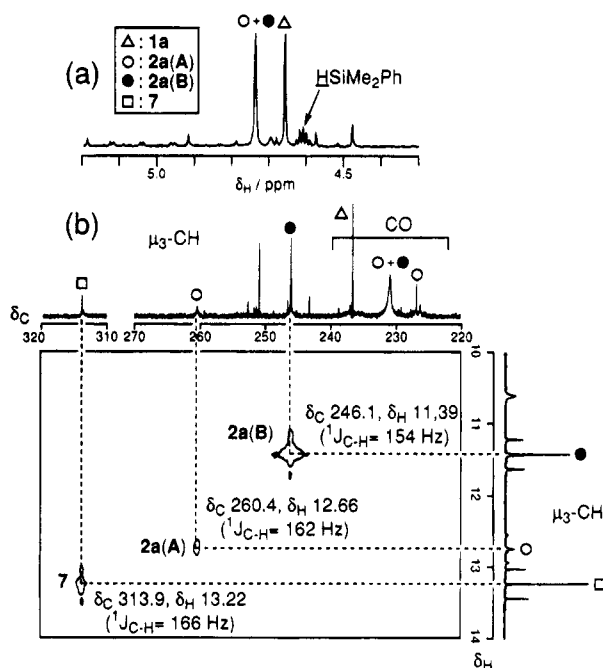


**Figure 11.** Spectra ( $^1H$ : 400 MHz;  $^{13}C$ : 100 MHz) of a reaction mixture of  $1a-^{13}CO$  with  $HSiMe_2Ph$  observed at room temperature in  $C_6D_6$ . (a)  $^1H$ -NMR (Cp region). (b) The low field region of a CH-HETCOR spectrum.

of a similar cluster compound through reaction of  $CO_2$  ( $CO$ )<sub>8</sub> with silatrane, where a Si-Co species was assumed as an intermediate.<sup>24</sup> The  $R_3Si$ -Co species is so oxygenophilic as to activate O-containing functional groups such as CO and  $>C=O$  groups as a Lewis acid and induce formal insertion of CO into the Si-Co bond giving a  $COSiR_3$  group. The unique properties of silyl-metal species are applied successfully to catalytic transformations using  $HSiR_3/CO/CO_2(CO)_8$  system developed by Murai and his co-workers.<sup>25</sup> But hydride transfer to the CO atom does not occur in previous systems.<sup>26</sup> In addition, to our knowledge, deoxygenation has never been observed for catalytic hydrosilylation of oxygenated compounds except for the reaction of acyl metal complexes reported by us.<sup>4a,26</sup> A rare example of stoichiometric deoxygenation of organic compounds was reported by Gladysz et al.<sup>27</sup> Treatment of ketone ( $R_2C=O$ ) with the 2,5-disila-1-ferracyclopentane ( $OC$ )<sub>4</sub>FeSiMe<sub>2</sub>(CH<sub>2</sub>)<sub>2</sub>SiMe<sub>2</sub> results in the formation of an iron-carbene intermediate ( $OC$ )<sub>4</sub>Fe=CR<sub>2</sub> and the cyclic disiloxane  $OSiMe_2(CH_2)_2SiMe_2$ .

In order to investigate unstable species which could not survive during the isolation procedures, a reaction mixture of  $1a-^{13}CO$  and  $HSiMe_2Ph$  was monitored by NMR (Figure 11). The reaction is considerably clean as can be seen from the Cp region of the  $^1H$ -NMR spectrum (Figure 11a), although deposition of a small amount of insoluble materials is evident. Only two major Cp peaks assignable to  $1a$  and  $2a$  are observed in this region. In the low field region (Figure 11b) a

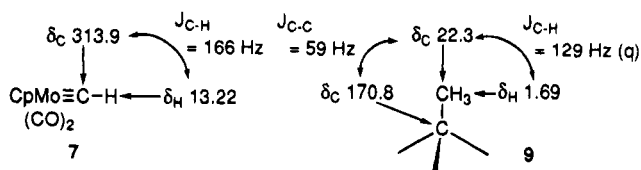
(24) Kim, M. W.; Uh, D. S.; Kim, S.; Do, Y. *Inorg. Chem.* **1993**, *32*, 5883 and references cited therein.

(25) Murai, S.; Seki, Y. *J. Mol. Cat.* **1987**, *41*, 197.

(26) Very recently, catalytic conversion of CO and  $HSiR_3$  into  $CH_3$ -( $CH_2$ )<sub>n</sub>-OSiR<sub>3</sub> and  $CH_3(CH_2)_nC(SiR_3)=CHOSiR_3$  was reported. Sisak, A.; Markó, L.; Angyalosy, Z.; Ungváry, F. *Inorg. Chim. Acta* **1994**, *222*, 131.

(27) (a) Nakazawa, H.; Johnson, D. L.; Gladysz, J. A. *Organometallics* **1983**, *2*, 1846. (b) Gladysz, J. A. *Acc. Chem. Res.* **1984**, *17*, 326.

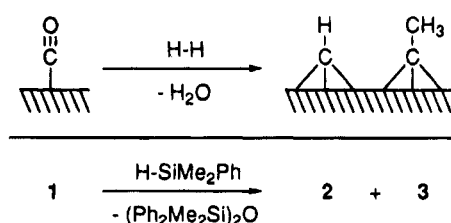
Chart 1



rather intense  $^1\text{H}$ -NMR signal ( $\delta_{\text{H}} 13.22$ ; **7**) is observed in addition to **2a(A,B)**.<sup>28</sup> The signal is found to be correlated with the  $^{13}\text{C}$ -NMR signal appearing in very low field ( $\delta_{\text{C}} 313.9$ ), and the coupling pattern (doublet,  $^1\text{J}_{\text{CH}} = 166$  Hz) leads to the assignment to a methylidyne (CH) group. On the basis of the  $\delta_{\text{C}}$  values close to those of mononuclear molybdenum carbyne complexes  $\text{Cp}(\text{CO})_2\text{Mo}(\equiv\text{CR})$  [ $\delta_{\text{C}}(\text{R}) 332.8$  ( $\text{CH}_2\text{Bu}^t$ ),<sup>29</sup>  $309.5$  ( $\text{C}_6\text{H}_4\text{Me}-2$ )],<sup>30</sup> **7** is attributed tentatively to the mononuclear  $\eta^1$ -methylidyne complex  $\text{Cp}(\text{CO})_2\text{Mo}(\equiv\text{CH})$  (Chart 1), although the  $^1\text{J}_{\text{CH}}$  value is larger than those of the previously reported methylidyne complexes [cf.  $\text{W}(\equiv\text{CH})\text{Cl}(\text{PMe}_3)_4$   $\delta_{\text{C}} 250$  ( $^1\text{J}_{\text{CH}} = 134$  Hz);<sup>31a</sup>  $(\text{Bu}^t\text{O})_3\text{W}(\equiv\text{CH})$   $\delta_{\text{C}} 252.4$  ( $^1\text{J}_{\text{CH}} = 150$  Hz);<sup>31b</sup>  $\text{HB}(3,5\text{-Me}_2\text{pz})_3(\text{CO})_2\text{W}(\equiv\text{CH})$   $\delta_{\text{C}} 280.6$  ( $^1\text{J}_{\text{CH}} = 142$  Hz)].<sup>31c</sup> Isolation of **7** has been unsuccessful despite several attempts. While another very weak CH signal is found at  $\delta_{\text{H}} 15.39$  (**8**), the corresponding  $^{13}\text{C}$ -NMR peak cannot be located owing to its low intensity. In higher field a signal set (**9**) assignable to an ethylidyne linkage is observed (Chart 1). The methyl signals are located at  $\delta_{\text{H}} 1.69$  and  $\delta_{\text{C}} 22.3$  ( $^1\text{J}_{\text{CH}} = 166$  Hz), and the latter signal is also correlated with the  $\delta_{\text{C}} 170.8$  signal on the basis of satellites due to  $^1\text{J}_{\text{CC}}$  coupling (59 Hz). The ratio of these species present in the mixture are estimated to be 0.2 (**2a-A**):1 (**2a-B**):0.4 (**7**):0.5 (**8**):0.1 (**9**). But unfortunately relationship between the isolated species **2** and **3** and the unstable species **7–9** cannot be established.

The detection of **7** in a reaction mixture suggests a reaction pathway involving initial deoxygenative reduction of **1** affording **7**. Subsequent addition of the dimetallic fragment **1** may give the trinuclear product **2**. The aryl derivatives **5** were actually prepared by this method starting from  $\text{Cp}(\text{CO})_2\text{M}(\equiv\text{CAr})$  as mentioned before.<sup>13</sup> As for the initial process, we assume that it should involve catalytic hydrosilylation as reported for acyl metal complexes (monometallaketones).<sup>4a</sup> The bridging and semibridging CO functional group in dinuclear complexes, which can be viewed formally as dimetallaketone, may be susceptible to catalytic hydrosilylation to give siloxymethylene group  $[\text{C}(\text{H})\text{OSiR}_3]$ . Although we don't have any evidence for the catalytic species (M in Scheme 2), the present system is a kind of self-catalyzed reaction effected by some unknown species present in a reaction mixture ( $\text{M} = \text{m} = \text{Mo}$ ; Scheme 2). The siloxymethylene species may be deoxygenated by the action of a silyl-metal species to form

Scheme 5



the CH ligand along with siloxane. A closely related system was reported by Fehlner et al.<sup>32</sup> Treatment of  $\text{Fe}(\text{CO})_5$  with a borane reagent produces a mixture of  $\mu_3$ -methylidyne and  $\mu_3$ -ethylidyne complexes,  $(\mu_3\text{-CH})\text{-Fe}_3(\mu\text{-H})_3(\text{CO})_9$  and  $(\mu_3\text{-CCH}_3)\text{Fe}_3(\mu\text{-H})_3(\text{CO})_9$ . Although the reaction mechanism has not been clarified so far, either, the Lewis acidic borane reagent should work as an efficient deoxygenative reducing agent in a manner similar to the hydrido-silyl-intermediate in Scheme 2. In both of our and Fehlner's systems the mechanism of carbon chain elongation leading to the ethylidyne complexes has remained to be solved.

Finally, let us point out that interaction of dinuclear carbonyl complexes with hydrosilane does not always result in the metal-metal bond cleavage giving H-M and/or Si-M species as established since 1960's.<sup>12</sup> Although the initial process may be photochemically or thermally induced CO dissociation,<sup>33</sup> the following step is dependent on several factors such as reaction conditions, metal, and structure of hydrosilane. In the present study, the reaction of the hexacarbonyl dimolybdenum complex  $\text{Cp}_2\text{Mo}_2(\text{CO})_6$  results in Mo-Mo bond cleavage, whereas that of the tetracarbonyl complex  $\text{Cp}_2\text{Mo}_2(\text{CO})_4$  **1** results in the deoxygenative reduction giving the alkylidyne complexes **2** and **3**. Similarly, the consequence of the interaction of  $\text{Cp}_2\text{Ru}_2(\text{CO})_4$  with monohydrosilane is Ru-Ru bond cleavage, but the reaction with di- and trihydrosilane is deoxygenative reduction leading to bridging methylene compounds.<sup>4c</sup>

## Conclusions

Photochemical reaction of the dimolybdenum carbonyl complex **1** with  $\text{HSiMe}_2\text{Ph}$  results in deoxygenative reduction of a CO ligand to give a mixture of the elemental hydrocarbyl complexes, i.e. the trinuclear  $\mu_3$ -methylidyne (**2**) and  $\mu_3$ -ethylidyne complexes (**3**). The present system serves as a good model system for formation of CH and  $\text{CCH}_3$  species via Fischer-Tropsch mechanism: Reduction of CO in **1** with  $\text{HSiMe}_2\text{Ph}$  (a  $\text{H}_2$ -equivalent) produces CH (**2**) and  $\text{CCH}_3$  species (**3**) with elimination of siloxane (**4**: silylated water) (Scheme 5). In the actual catalytic system  $\text{H}_2$  works as an reducing agent as well as a deoxygenating reagent. However, reduction of a model CO complex with  $\text{H}_2$  is not always successful, because the hydrido-metal intermediate shows little affinity toward polar substrates such as CO as mentioned in Introduction. The present

(28) The Cp signal of **7** may overlap with that of **2a** or **3a**. The  $^1\text{H}$ -NMR signal corresponding to the rather intense signal around  $\delta_{\text{C}} 250$  could not be located. It might be attributed to a bridging CO ligand or carbyne species. Isolation of this species was unsuccessful.

(29) Baker, P. K.; Baker, G. K.; Gill, D. S.; Green, M.; Orpen, A. G.; Welch, A. J. *J. Chem. Soc., Dalton Trans.* **1989**, 1321.

(30) Dossett, S. J.; Hill, A. F.; Jeffery, J. C.; Marker, F.; Sherwood, P.; Stone, F. G. A. *J. Chem. Soc., Dalton Trans.* **1988**, 2453.

(31) (a) Holms, S. J.; Clark, D. N.; Turner, H. W.; Schrock, R. R. *J. Am. Chem. Soc.* **1982**, *104*, 6322. (b) Chisolm, M. H.; Foltling, K.; Hoffman, D. M.; Huffman, J. C. *J. Am. Chem. Soc.* **1984**, *106*, 6794. (c) Jamison, G. M.; White, P. S.; Harris, D. L.; Templeton, J. L. in *Transition Metal Carbyne Complexes*; Kreissl, F. R., Ed.; Kluwer Academic: Dordrecht, 1993; p 201.

(32) (a) Wong, K. S.; Fehlner, T. P. *J. Am. Chem. Soc.* **1981**, *103*, 966. (b) Wong, K. S.; Haller, K. J.; Dutta, T. K.; Chipman, D. M.; Fehlner, T. P. *Inorg. Chem.* **1982**, *21*, 3197. (c) DeKock, R. L.; Wong, K. S.; Fehlner, T. P. *Inorg. Chem.* **1982**, *21*, 3203. (d) Vites, J. C.; Jacobsen, G.; Dutta, T. K.; Fehlner, T. P. *J. Am. Chem. Soc.* **1985**, *107*, 5563. (e) Dutta, T. K.; Vites, J. C.; Jacobsen, G. B.; Fehlner, T. P. *Organometallics* **1987**, *6*, 842.

(33) A pathway without CO dissociation may be possible. Alt et al. reported that reaction of  $(\eta^5\text{-C}_5\text{Me}_5)_2\text{Mo}_2(\text{CO})_4$  with  $\text{H}_2$  produced the addition product  $(\eta^5\text{-C}_5\text{Me}_5)_2\text{Mo}_2(\mu\text{-H})_2(\text{CO})_4$ . Alt, H.; Mahmoud, K. A.; Rest, A. *J. Angew. Chem., Int. Ed. Engl.* **1983**, *22*, 544.

transformation is realized by employment of HSiMe<sub>2</sub>-Ph with the high oxygenophilic Si moiety. As a deoxygenating agent, siloxane is superior to water, when the transformation is carried out in neutral organic media.

The dynamic behavior of **2** and **3** has been analyzed as a combination of the gearlike and local rotational processes of the metal fragments associated with switching of the semibridging Mo···CO interactions. The semibridging interaction is so rigid as to stabilize the intermediates of the rotational processes, two of which have been characterized by X-ray crystallography.

### Experimental Section

All manipulations were carried out under an argon atmosphere by using standard Schlenk tube techniques. Ether, THF, hexanes, benzene and toluene (Na–K alloy), and CH<sub>2</sub>Cl<sub>2</sub> and CH<sub>3</sub>CN (P<sub>2</sub>O<sub>5</sub>) were treated with appropriate drying agents, distilled, and stored under Ar. The dimolybdenum carbonyl complexes **1a** and **1b** were prepared according to the literature procedures.<sup>34</sup> The <sup>13</sup>CO-enriched isotopomers (ca. 30% enriched) were prepared by thermal decarbonylation of <sup>13</sup>CO-enriched Cp<sub>2</sub>Mo<sub>2</sub>(<sup>13</sup>CO)<sub>6</sub> and Cp'<sub>2</sub>Mo<sub>2</sub>(<sup>13</sup>CO)<sub>6</sub>, which were obtained by treatment of **1a** and **1b** with <sup>13</sup>CO (>90% <sup>13</sup>C-enriched; 2 atm) at room temperature in CH<sub>2</sub>Cl<sub>2</sub>, respectively. HSiMe<sub>2</sub>Ph was purchased from Aldrich, and DSiMe<sub>2</sub>Ph (~99% D-enriched) was prepared by reduction of ClSiMe<sub>2</sub>Ph by LiAlD<sub>4</sub>. An authentic sample of **4** was prepared by refluxing ClSiMe<sub>2</sub>Ph in ether/HCl aq. Column chromatography was performed on silica gel 60 [70–230 mesh ASTM (Merck Art. 7734)]. <sup>1</sup>H- and <sup>13</sup>C-NMR spectra were recorded on JEOL EX-400 (<sup>1</sup>H: 400 MHz; <sup>13</sup>C: 100 MHz) and GSX-500 spectrometers (<sup>1</sup>H: 500 MHz; <sup>13</sup>C: 125 MHz). Solvents for NMR measurements containing 1% TMS were dried over molecular sieves, degassed, and distilled under reduced pressure. IR and FDMS spectra were obtained on a JASCO FT/IR 5300 spectrometer and a Hitachi M-80 mass spectrometer, respectively. As a source of UV irradiation an Ushio UM-452 lamp was used.

**Deoxygenative Reduction of Cp<sub>2</sub>Mo<sub>2</sub>(CO)<sub>4</sub> Giving **2a** and **3a**.** A benzene solution (300 mL) of **1a** (3.34 g, 7.71 mmol) and HSiMe<sub>2</sub>Ph (4.0 mL, 26 mmol) in a Pyrex photoreaction vessel was irradiated by a high pressure mercury lamp while immersed in an ice–water bath. The irradiation was continued until most of Cp<sub>2</sub>Mo<sub>2</sub>(CO)<sub>4</sub> was consumed (43 h) as judged by TLC. Then the volatiles were removed under reduced pressure, and the resulting residue was subjected to column chromatography eluted by CH<sub>2</sub>Cl<sub>2</sub>–hexanes. The following bands were eluted in the order: (1) O(SiMe<sub>2</sub>Ph)<sub>2</sub>; (2) a mixture of Cp<sub>2</sub>Mo<sub>2</sub>(CO)<sub>4</sub> and Cp<sub>2</sub>Mo<sub>2</sub>(CO)<sub>6</sub>; (3) **2a** (green brown band, black purple crystals; 770 mg, 1.16 mmol, 26% yield based on CO). **2a** was recrystallized from CH<sub>2</sub>Cl<sub>2</sub>–hexanes. Although formation of **3a** was evident as detected by TLC, it could not be isolated from the reaction mixture (see text). An authentic sample of **3a** was prepared according to the reported method.<sup>10</sup> **2a**: NMR data (see Table 1); IR ν(C=O) (KBr) 1974, 1899, 1834; (CH<sub>2</sub>Cl<sub>2</sub>) 1989, 1939, 1927, 1871, 1852, 1810; (CHCl<sub>3</sub>) 1994, 1939, 1931, 1876, 1866; (CH<sub>3</sub>CN) 1983, 1908, 1847; (C<sub>6</sub>H<sub>6</sub>) 1992, 1938, 1928, 1873 cm<sup>-1</sup>; FDMS: *m/z* 670 (M<sup>+</sup> for the <sup>98</sup>Mo<sub>3</sub> isotopomer). Anal. Calcd for C<sub>22</sub>H<sub>16</sub>O<sub>6</sub>Mo<sub>3</sub>: C, 39.78; H, 2.43. Found: C, 39.76; H, 2.33.

Labeling experiments were carried out using appropriate isotopomers.

**Deoxygenative Reduction of Cp'<sub>2</sub>Mo<sub>2</sub>(CO)<sub>4</sub> Giving **2b** and **3b**.** A benzene solution (30 mL) of **1b** (1.92 g, 4.15 mmol) and HSiMe<sub>2</sub>Ph (2.3 mL, 15 mmol) was irradiated for 48 h. Separation as described above gave **2b** (green brown band, black purple crystals; 319 mg, 0.45 mmol, 18% yield based on CO) and **3b** (yellow green band, purple brown crystals; 37 mg, 0.55 mmol, 2% yield based on CO). **2b** and **3b** were recrystallized from CH<sub>2</sub>Cl<sub>2</sub>–hexanes. **2b**: <sup>1</sup>H-NMR (tol-*d*<sub>8</sub>: see Figure 9) δ 12.38 (**AI**), 12.10 (**AII**), 11.84 (**AIII**), 11.29 (**BI**), 11.21 (**BII**), 11.15 (**BIII**) (μ<sub>3</sub>-CH), 4.5–4.8 (η<sup>5</sup>-C<sub>5</sub>H<sub>4</sub>Me), 1.84, 1.83, 1.71, 1.68 (η<sup>5</sup>-C<sub>5</sub>H<sub>4</sub>Me); <sup>13</sup>C-NMR (tol-*d*<sub>8</sub>) δ 269.9 (<sup>1</sup>J<sub>C-H</sub> = 154

Hz; **AIII**), 267.1 (<sup>1</sup>J<sub>C-H</sub> = 154 Hz; **AII**), 249.7 (<sup>1</sup>J<sub>C-H</sub> = 161 Hz; **BII**) (μ<sub>3</sub>-CH), 4.5–4.8 (η<sup>5</sup>-C<sub>5</sub>H<sub>4</sub>Me), 232.2, 232.0, 231.8, 226.6 (CO), 108–90 (η<sup>5</sup>-C<sub>5</sub>H<sub>4</sub>Me), 14.1, 13.6 (η<sup>5</sup>-C<sub>5</sub>H<sub>4</sub>Me); IR ν(C=O) (KBr) 1975, 1909, 1846; (CH<sub>2</sub>Cl<sub>2</sub>) 1986, 1929, 1918, 1868, 1844; (CHCl<sub>3</sub>) 1990 (br), 1926 (br), 1859; (C<sub>6</sub>H<sub>6</sub>) 1991, 1933, 1924, 1868, 1846 cm<sup>-1</sup>. Anal. Calcd for C<sub>25</sub>H<sub>22</sub>O<sub>6</sub>Mo<sub>3</sub>: C, 42.51; H, 3.13. Found: C, 42.30; H, 2.93. **3b**: <sup>1</sup>H-NMR (tol-*d*<sub>8</sub>: see Figure 9) δ 4.5–4.8 (η<sup>5</sup>-C<sub>5</sub>H<sub>4</sub>Me), 3.82 (CH<sub>3</sub>; **B**), 3.79 (CH<sub>3</sub>; **D**), 1.89, 1.87, 1.86 (η<sup>5</sup>-C<sub>5</sub>H<sub>4</sub>Me); <sup>13</sup>C-NMR (tol-*d*<sub>8</sub>) δ 269.1 (<sup>1</sup>J<sub>C-C</sub> = 32 Hz; μ<sub>3</sub>-CCH<sub>3</sub>), 232.6 (CO), 108–90 (η<sup>5</sup>-C<sub>5</sub>H<sub>4</sub>Me), 54.0 (<sup>1</sup>J<sub>C-H</sub> = 127 Hz; μ<sub>3</sub>-CCH<sub>3</sub>; **D**), 53.8 (<sup>1</sup>J<sub>C-H</sub> = 127 Hz; μ<sub>3</sub>-CCH<sub>3</sub>; **B**), 13.5 (<sup>1</sup>J<sub>C-H</sub> = 127 Hz; η<sup>5</sup>-C<sub>5</sub>H<sub>4</sub>Me); IR ν(C=O) (KBr) 1982, 1942, 1914, 1864, 1841, 1783 cm<sup>-1</sup>. Anal. Calcd for C<sub>26</sub>H<sub>24</sub>O<sub>6</sub>Mo<sub>3</sub>: C, 43.35; H, 3.36. Found: C, 43.08; H, 3.22.

**Single Crystal X-ray Crystallography.** **2a**·CH<sub>3</sub>CN, **2a**·C<sub>6</sub>D<sub>6</sub>, **2b**, and **3b** were recrystallized from benzene–MeCN, benzene-*d*<sub>6</sub> from an NMR sample), hexanes–CH<sub>2</sub>Cl<sub>2</sub>, and THF–hexanes, respectively. Suitable crystals were mounted on glass fibers. Diffraction measurements were made on Rigaku AFC-5R (**2a**·CH<sub>3</sub>CN, **2a**·C<sub>6</sub>D<sub>6</sub>, and **3b**) and AFC5 (**2b**) automated four-circle diffractometers by using graphite-monochromated Mo Kα radiation (λ = 0.71058 Å). Unit cell was determined and refined by a least-squares method using 20 independent reflections. Data were collected with ω–2θ scan technique. If σ(*I*)/*I* was more than 0.1, a scan was repeated up to three times and the results were added to the first scan. Three standard reflections were monitored at every 150 (AFC5R) and 100 (AFC5) measurements. All data processing was performed on and Micro Vax II (AFC5R data collection), FACOM A-70 (AFC5 data collection) and IRIS Indigo computers (structure analysis) by using the teXsan structure solving program system obtained from the Rigaku Corp., Tokyo, Japan. Neutral scattering factors were obtained from the standard source.<sup>35</sup> In the reduction of data, Lorentz and polarization corrections were made. An empirical absorption corrections (Ψ scan) was made for **2a**·CH<sub>3</sub>CN, **2a**·C<sub>6</sub>D<sub>6</sub>, and **3b**. In the case of **2b**, an orthorhombic crystal system was established at first, and the diffraction data were collected under this condition. The refinement was converged to *R* = 0.066 (*R*<sub>w</sub> = 0.054), and examination of the positional parameters suggested a crystal system of higher symmetry. Then the structure was refined successfully according to a cubic system (*Pa* $\bar{3}$ ).

All the structures were solved by a combination of the direct method and Fourier synthesis (SAPI91 and DIRDIF). All the non-hydrogen atoms except for C13 of **3b** were refined anisotropically. The positions of H(1) of **2a**·CH<sub>3</sub>CN and **2b** were confirmed by using isotropic thermal parameters and the remaining Cp (Cp') and solvent H atoms were fixed at the calculated positions (C–H: 0.95 Å) and not refined.

Although we also attempted structure determination of **3a**, the refinement was unsuccessful because of the low quality of the crystals. However, the conformation of the CpMo(CO)<sub>2</sub> moieties similar to those in **3b** was confirmed by Fourier synthesis (Figure 4).

**Acknowledgment.** Financial support from the Ministry of Education, Science, Sports and Culture of the Japanese Government (Grants-in-Aids for Scientific Research on Priority Area, Nos. 04241105 and 05236103) is gratefully acknowledged. We wish to thank Drs. Yoshiyuki Nakamura and Masato Oshima for NMR measurements.

**Supporting Information Available:** Tables of positional and thermal parameters and bond lengths and angles for **2a**·CH<sub>3</sub>CN, **2a**·C<sub>6</sub>D<sub>6</sub>, **2b**, and **3b** and figures showing the numbering schemes for **2a**·CH<sub>3</sub>CN and **2a**·C<sub>6</sub>D<sub>6</sub> (19 pages). Ordering information is given on any current masthead page.

OM9504664

(34) Curtis, M. D.; Hay, M. S. *Inorg. Synth.* **1990**, *28*, 150.

(35) *International Tables for X-Ray Crystallography*; Kynoch Press: Birmingham, 1975; Vol. 4.

# Charge-Transfer Crystals of Octacarbonyldiferrate. Solid-State Structure and Oxidation–Reduction of an Iron–Iron-Bonded Electron Donor

T. M. Bockman, H.-C. Cho, and J. K. Kochi\*

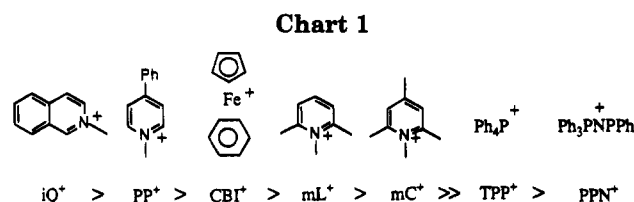
Department of Chemistry, University of Houston, Houston, Texas 77204-5641

Received May 31, 1995<sup>®</sup>

The dinuclear carbonylmetalate  $[\text{Fe}_2(\text{CO})_8]^{2-}$  forms deeply colored crystals  $\text{A}_2[\text{Fe}_2(\text{CO})_8]$  with various phosphonium and pyridinium cations ( $\text{A}^+$ ) by metathesis in aqueous solution. Diffuse reflectance absorption spectroscopy and X-ray crystallography establish the colors to derive from anion-to-cation charge-transfer (CT) within the triple ion  $[\text{A}^+, \text{Fe}_2(\text{CO})_8^{2-}, \text{A}^+]$  extant in the solid state. Partial electron transfer in the charge-transfer salts is established by the significant shortening of the iron–iron bond in the  $[\text{Fe}_2(\text{CO})_8]^{2-}$  moiety when it is ion paired with the *N*-methyllutidinium acceptor. In solution, the charge-transfer salts can undergo interionic electron transfer, and they lead to the dimeric  $\text{A}_2$  and a series of iron carbonyl products that are uniquely dependent on the solvent (water, ether, and acetonitrile).

## Introduction

Organometallic anions form brightly colored salts that can exhibit typical charge-transfer (CT) absorption bands.<sup>1–6</sup> Especially relevant are the simple carbonylmetalate anions:  $[\text{Co}(\text{CO})_4]^-$ ,  $[\text{Mn}(\text{CO})_5]^-$ ,  $[\text{V}(\text{CO})_6]^-$ , and  $[\text{Fe}(\text{CO})_4]^{2-}$  as electron donors in the formation of various types of charge-transfer salts.<sup>7</sup> Since polynuclear organometallic anions have enhanced degrees of electron richness associated with metal–metal bonds,<sup>8</sup> they are also highly desirable candidates for exploration as negatively charged donors. Among an extensive number of polynuclear iron carbonylates, hydrido car-



bonylates, and their derivatives,<sup>9</sup> the octacarbonyldiferrate dianion  $[\text{Fe}_2(\text{CO})_8]^{2-}$  is particularly noteworthy as the simplest member in which a pair of  $[\text{Fe}(\text{CO})_4]^-$  moieties are directly joined by a single unbridged iron–iron bond.<sup>10</sup> It is an excellent electron donor, owing to its very low oxidation potential ( $E_{\text{ox}}^0 = -1.43$  vs  $\text{Cp}_2\text{Fe}$ )<sup>11</sup> and facile reaction with various electrophilic reagents (e.g.  $\text{H}^+$ ,<sup>12</sup>  $\text{AuPPh}_3^+$ ,<sup>13</sup>  $\text{CH}_2\text{I}_2$ ,<sup>14</sup> etc.) to form complexes with a bridging group across the Fe–Fe bond. The latter are consistent with molecular orbital studies,<sup>15</sup> which show the HOMOs of  $[\text{Fe}_2(\text{CO})_8]^{2-}$  to be centered on the metal–metal bond. The donor properties of  $[\text{Fe}_2(\text{CO})_8]^{2-}$  are also qualitatively indicated by the contrasting (CT) colors of the sodium salt which is yellow<sup>16</sup> and the PPN salt which is orange.<sup>14,17</sup> In order to establish the charge-transfer characteristics of  $[\text{Fe}_2(\text{CO})_8]^{2-}$ , we now consider its interionic interaction with a graded series of cationic acceptors, shown in Chart 1. The relevant donor–acceptor property of the different crystalline charge-transfer salts of  $[\text{Fe}_2(\text{CO})_8]^{2-}$  is pinpointed in this study by X-ray diffraction and solid-state spectroscopic methods. In addition, the chemical

(10) Chin, H. B.; Smith, M. B.; Wilson, R. D.; Bau, R. J. *J. Am. Chem. Soc.* **1974**, *96*, 5285.

(11) Amatore, C.; Verpeaux, J.-N.; Krusic, P. J. *Organometallics* **1988**, *7*, 2426.

(12) (a) Hieber, W.; Brendel, G. Z. *Anorg. Allg. Chem.* **1957**, *289*, 324. (b) Collman, J. P.; Finke, R. G.; Matlock, P. L.; Wahren, R.; Kamoto, R. G.; Brauman, J. I. *J. Am. Chem. Soc.* **1978**, *100*, 1119.

(13) Rossell, O.; Seco, M.; Jones, P. G. *Inorg. Chem.* **1990**, *29*, 348.

(14) Sumner, C. E., Jr.; Collier, J. A.; Pettit, R. *Organometallics* **1982**, *1*, 1350.

(15) Dedieu, A.; Albright, T. A.; Hoffmann, R. *J. Am. Chem. Soc.* **1979**, *101*, 3141.

(16) Strong, H.; Krusic, P. J.; San Filippo, J., Jr. *Inorg. Synth.* **1990**, *28*, 203.

(17) PPN<sup>+</sup> = bis(triphenylphosphine)nitrogen(1+) cation.

<sup>®</sup> Abstract published in *Advance ACS Abstracts*, September 15, 1995.

(1) Schramm, C.; Zink, J. I. *J. Am. Chem. Soc.* **1979**, *101*, 4554.  
(2) (a) Calderazzo, F.; Pampaloni, G.; Lanfranchi, M.; Pelizzi, G. *J. Organomet. Chem.* **1986**, *296*, 1. (b) Calderazzo, F.; Pampaloni, G.; Pelizzi, G.; Vitali, F. *Organometallics* **1988**, *7*, 1083.

(3) (a) Bockman, T. M.; Kochi, J. K. *J. Am. Chem. Soc.* **1988**, *110*, 1294. (b) Bockman, T. M.; Kochi, J. K. *J. Am. Chem. Soc.* **1989**, *111*, 4669. (c) Lee, K. Y.; Kochi, J. K. *Inorg. Chem.* **1989**, *28*, 567. (d) Bockman, T. M.; Kochi, J. K. *New J. Chem.* **1992**, *16*, 39. (e) Wei, C.-H.; Bockman, T. M.; Kochi, J. K. *J. Organomet. Chem.* **1992**, *428*, 85. (f) Kochi, J. K.; Wei, C.-H. *J. Organomet. Chem.* **1993**, *451*, 111.

(4) (a) Vogler, A.; Kunkely, H. *Organometallics* **1988**, *7*, 1449. (b) Vogler, A.; Kunkely, H. *J. Organomet. Chem.* **1988**, *355*, 1. (c) Vogler, A.; Kunkely, H. *J. Organomet. Chem.* **1989**, *372*, C29. (d) Vogler, A.; Kunkely, H. Z. *Naturforsch.* **1989**, *44b*, 132. (e) Vogler, A.; Kunkely, H. *Top. Curr. Chem.* **1990**, *158*, 24.

(5) (a) Lahner, S.; Wakatsuki, Y.; Kisch, H. *Chem. Ber.* **1987**, *230*, 1011. (b) Nüsslein, F.; Peter, R.; Kisch, H. *Chem. Ber.* **1989**, *122*, 1023. (c) Kisch, H.; Dümmler, W.; Nüsslein, F.; Zenn, I.; Chiorboli, C.; Scandola, F.; Albrecht, W.; Meier, H. Z. *Phys. Chem.* **1991**, *170*, 117. (d) Kisch, H.; Dümmler, W.; Chiorboli, C.; Scandola, F.; Salbeck, J.; Daub, J. *J. Phys. Chem.* **1992**, *96*, 10232. (e) Nunn, I.; Eisen, B.; Benedix, R.; Kisch, H. *Inorg. Chem.* **1994**, *33*, 5079.

(6) (a) Hennig, H.; Rehorek, D.; Archer, R. D. *Coord. Chem. Revs.* **195**, *51*, 1. (b) Billing, R.; Rehorek, D.; Salvetter, J.; Hennig, H. Z. *Anorg. Allg. Chem.* **1988**, *557*, 234. (c) Billing, R.; Rehorek, D.; Hennig, H. *Top. Curr. Chem.* **1990**, *158*, 151. (d) Hennig, H.; Weber, L.; Rehorek, D. In *Photosensitive Metal–Organic Compounds*; Kutal, C., Serpone, N., Eds.; American Chemical Society: Washington, DC, 1993; p 351.

(7) Bockman, T. M.; Kochi, J. K. *Adv. Organomet. Chem.* **1991**, *33*, 52.

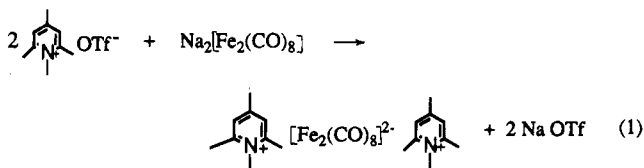
(8) (a) Chisholm, M. H. *Reactivity of Metal–Metal Bonds*; American Chemical Society: Washington, DC, 1981. (b) Geiger, W. E.; Connelly, N. G. *Adv. Organomet. Chem.* **1985**, *24*, 87.

(9) Shriver, D. F.; Whitmire, K. H. In *Comprehensive Organometallic Chemistry*; Wilkinson, G., Stone, F. G. A., Abel, E. W., Eds.; Pergamon: New York, 1982; Vol. 4, p 255 ff.

consequences of this interionic CT interaction is established by identifying the unique followup redox reactions of the charge-transfer salts in solution.

## Results

**I. Isolation of Crystalline Charge-Transfer Salts of Octacarbonyldiferrate.** Addition of *N*-methylcollidinium ( $mC^+$ ) triflate<sup>18</sup> to an aqueous solution of  $Na_2[Fe_2(CO)_8]$  resulted in the immediate precipitation of the methylcollidinium salt of the iron dianion in the form of a bright red powder. Recrystallization of the precipitate from acetonitrile afforded the 2:1 salt  $[mC]_2[Fe_2(CO)_8]$  as deep red crystals, i.e.



Similarly, the direct metathesis of  $Na_2[Fe_2(CO)_8]$  with the bis(triphenylphosphine)nitrogen(1+) (PPN<sup>+</sup>), tetraphenylphosphonium (Ph<sub>4</sub>P<sup>+</sup>), *N*-methyllutidinium (mL<sup>+</sup>), 4-phenyl-*N*-methylpyridinium (PP<sup>+</sup>), and *N*-methylisoquinolinium (iQ<sup>+</sup>) counterions in Chart 1 (as their halide or hexafluorophosphate salts) in aqueous solution yielded the corresponding 2:1 carbonylferrate salt. The colors of these salts ranged from yellow-orange (PPN<sup>+</sup> and Ph<sub>4</sub>P<sup>+</sup>) through deep red (mC<sup>+</sup> and mL<sup>+</sup>) to almost black (PP<sup>+</sup> and iQ<sup>+</sup>). The crystals lost color immediately upon dissolution in acetonitrile to uniformly produce a yellow-orange solution.<sup>19</sup> This qualitative observation was borne out by the identical visible spectrum of  $[Fe_2(CO)_8]^{2-}$  that was characterized by a low-energy tail extending from  $\lambda = 400$  to 800 nm<sup>16</sup> in all solutions irrespective of the counterion.

**II. Spectral Characterization of the Colored Charge-Transfer Salts.** Since the colors of the various salts  $[Fe_2(CO)_8]^{2-}$  could be observed only in the solid state, the interionic charge transfer was measured from the reflectance spectra of the crystalline salts as dispersions in KBr. Thus, the yellow disodium salt of  $[Fe_2(CO)_8]^{2-}$  was transparent at wavelengths  $\lambda > 500$  nm. On the other hand, the 2:1 salts of  $[Fe_2(CO)_8]^{2-}$  with the organic and organometallic anions absorbed over a broader spectral range of visible light owing to pronounced new absorptions at  $\lambda > 500$  nm (Figure 1). When the spectral position was assessed as the wavelength at which the absorbance reached a baseline value ( $\lambda_0$ ),<sup>20</sup> the bathochromic shift in  $\lambda_0$  proceeded in the following order: PPN<sup>+</sup>  $\approx$  Ph<sub>4</sub>P<sup>+</sup> ( $\lambda_0 \approx 600$  nm) < mL<sup>+</sup> ( $\lambda_0 \approx 700$  nm) < PP<sup>+</sup>  $\approx$  iQ<sup>+</sup> ( $\lambda_0 > 800$  nm). This trend was in qualitative accord with the electron affinities of the cationic acceptors, as evaluated by the values of their reduction potentials ( $E_{red}^0$  in Table 1). Accordingly, these colored octacarbonyldiferrates were identified as *charge-transfer salts*. As such, the new (visible) absorption band was readily assigned to the charge-transfer transition in eq 2, in which A<sup>+</sup> is the cationic

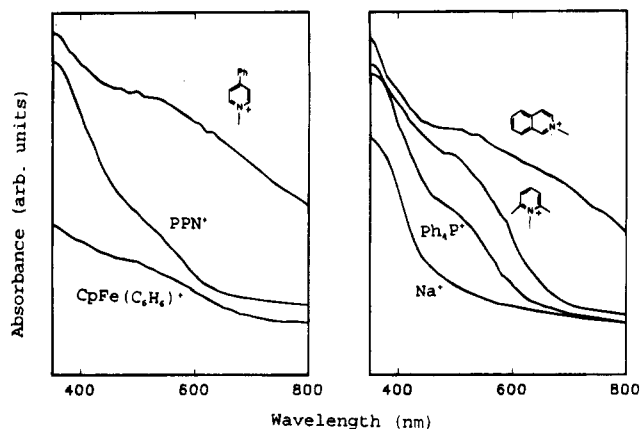


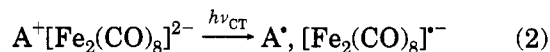
**Figure 1.** Diffuse reflectance (visible) spectra of the crystalline 2:1 charge-transfer salts of octacarbonyldiferrate with various acceptor cations, as 2% dispersions in KBr.

**Table 1. Charge-Transfer Absorption Bands of Octacarbonyldiferrate Salts,  $A_2[Fe_2(CO)_8]$**

acceptor, A <sup>+</sup>	$\lambda_{max}^a$ (nm)	$-E_p$ vs SCE <sup>b</sup> (V)	$-E_{red}^0$ vs Cp <sub>2</sub> Fe <sup>c</sup> (V)	$h\nu_{CT}^d$ (eV)
PPN <sup>+</sup>	430	2.13	2.60 (2.64) <sup>e</sup>	2.88
Ph <sub>4</sub> P <sup>+</sup>	440	1.91	2.40 <sup>f</sup>	2.82
mC <sup>+</sup> g	475	1.63	2.07	2.61
mL <sup>+</sup> h	500	1.45	1.92	2.48
[CpFe(C <sub>6</sub> H <sub>6</sub> ) <sup>+</sup>	510	1.39	1.64 <sup>i</sup>	2.43
PP <sup>+</sup> j	540	1.27	1.52 <sup>k</sup>	2.30
iQ <sup>+</sup> m	545	1.08	1.55	2.28

<sup>a</sup> Wavelength of maximum absorbance of the charge-transfer band, obtained by digital deconvolution of the diffuse reflectance spectra of the CT salts. <sup>b</sup> Irreversible CV peak potential for reduction of A<sup>+</sup>. <sup>c</sup> Reversible reduction potential of A<sup>+</sup>, obtained by correcting for dimerization of A in acetonitrile, except as noted. <sup>d</sup> Energy of the CT transition expressed as  $hc/\lambda_{max}$ . <sup>e</sup> Reversible  $E_{red}^0$  from ref 29. <sup>f</sup>  $E_{red}^0$  from ref 3c. <sup>g</sup> *N*-methylcollidinium. <sup>h</sup> *N*-methyllutidinium. <sup>i</sup>  $E_{red}^0$  from ref 68. <sup>j</sup> 4-Phenyl-*N*-methylpyridinium. <sup>k</sup>  $E_{red}^0$  from ref 69. <sup>m</sup> *N*-methylisoquinolinium.

acceptor and octacarbonyldiferrate is the electron donor, to accord with the Mulliken formulation of electron donor/acceptor interactions.<sup>21</sup>



The absence of low-energy absorption bands in the spectrum of  $Na_2[Fe_2(CO)_8]$  in Figure 1 was consistent with the weak electron affinity (high-energy LUMO) of the sodium cation,<sup>22</sup> and the absorption of  $Na_2[Fe_2(CO)_8]$  in the 400–500 nm region was readily assigned to the local transitions of the  $[Fe_2(CO)_8]^{2-}$  anion.<sup>23</sup> Digital subtraction of this spectral tail from the absorption of the charge-transfer salts yielded the difference spectra shown in Figure 2. The relatively well-defined maxima are listed in Table 1 as  $\lambda_{CT}$ , and they ranged from 430 nm for  $[PPN]_2[Fe_2(CO)_8]$  up to 545 nm for  $[iQ]_2[Fe_2(CO)_8]$ . The band maxima showed a consistent red shift as the reduction potential of the cationic acceptor became less negative. Indeed, the energy of the charge-transfer band ( $h\nu_{CT}$ ) could be expressed as a linear function of the reversible reduction potential  $E_{red}^0$  of the

(18) The trifluoromethanesulfonate anion,  $CF_3SO_3^-$ , is hereafter referred to as triflate.

(19) The charge-transfer salts  $A_2[Fe_2(CO)_8]$  were insoluble in non-polar media such as tetrahydrofuran, diethyl ether, or hydrocarbons, and they reacted with dichloromethane. Solution studies of contact ion pairing were thus precluded.

(20) Compare Nunn et al. in ref 5e.

(21) (a) Mulliken, R. S. *J. Am. Chem. Soc.* **1952**, *74*, 811. (b) Tamres, M.; Strong, R. L. In *Molecular Association*; Foster, R., Ed.; Wiley: New York, 1979; Vol. 2, p 332 ff. (c) Mataga, N.; Kubota, T. *Molecular Interactions and Electronic Spectra*; Marcel Dekker: New York, 1970.

(22) Cotton, F. A.; Wilkinson, G. *Advanced Inorganic Chemistry*, 4th ed.; Wiley: New York, 1980; p 253 ff.

(23) Hieber, W.; Beutner H. *Z. Naturforsch.* **1962**, *176*, 211.

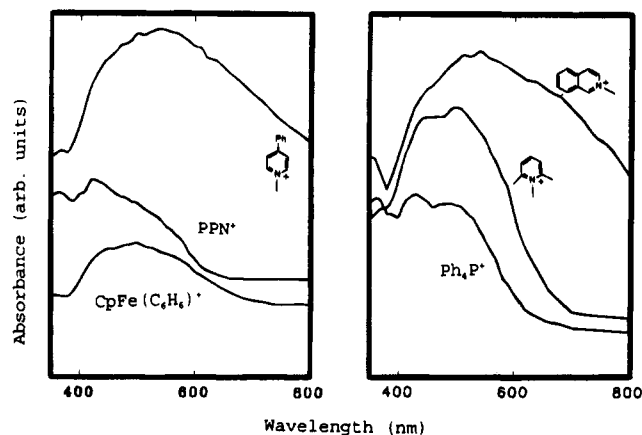


**Figure 2.** Visible absorption bands of the charge-transfer salts in Figure 1, after digital subtraction of the absorption due to the local transitions of  $[\text{Fe}_2(\text{CO})_8]^{2-}$ .

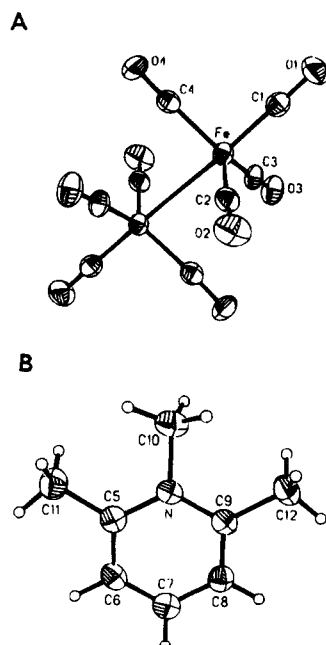


**Figure 3.** ORTEP diagram of (A) octacarbonyldiferrate  $[\text{Fe}_2(\text{CO})_8]^{2-}$  and (B) *N*-methyllutidinium ( $\text{mL}^+$ ) obtained by X-ray crystallography of the 2:1 salt  $[\text{mL}]_2[\text{Fe}_2(\text{CO})_8]$ .

cationic acceptor, *i.e.*

$$h\nu_{\text{CT}} = 0.55E^0_{\text{red}} + 1.57 \quad (3)$$

It is important to note that a similar correlation was previously observed in mononuclear carbonylmetalate salts of  $\text{A}^+$ .<sup>24</sup>

**III. Molecular Structure of the Charge-Transfer Salt of *N*-Methyllutidinium and Octacarbonyldiferrate.** The X-ray diffraction data of the ruby-red monoclinic crystals of the bis(*N*-methyllutidinium) octacarbonyldiferrate in the space group  $P2_1/n$  were collected at  $-50^\circ\text{C}$ , and final refinement yielded a residual value of 3.1%. The octacarbonyldiferrate dianion is located on a crystallographic inversion center and closely approximates  $D_{3d}$  symmetry. The ORTEP diagram in Figure 3A shows that the iron-iron bond is not bridged, and its length of 2.780(1) Å is short compared

(24) Bockman, T. M.; Kochi, J. K. In *Photosensitization and Photocatalysis Using Inorganic and Organometallic Compounds*; Kalyanasundaram, K., Graetzel, M., Eds.; Kluwer: Amsterdam, 1993; p 407.

(25) Cassidy, J. M.; Whitmire, K. H.; Long, G. J. *J. Organomet. Chem.* **1992**, *427*, 355.

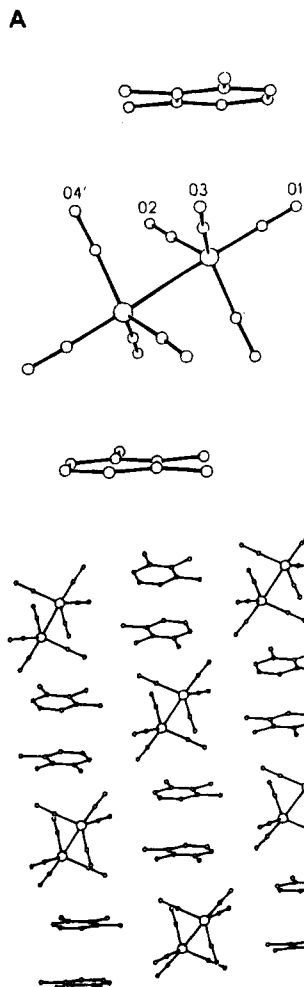


**Figure 4.** (A) Charge-transfer unit as the triple ion  $[\text{mL}^+, \text{Fe}_2(\text{CO})_8^{2-}, \text{mL}^+]$  in the unit cell of the 2:1 *N*-methyllutidinium/octacarbonyldiferrate salt showing the pairwise coordination of a lutidinium acceptor with three carbonyl groups of the ferrate donor. (B) View of the packing in the bis(*N*-methyllutidinium) octacarbonyldiferrate charge-transfer salt, showing the alignment of the triple ions along the 110 crystal axis.

to those of other  $[\text{Fe}_2(\text{CO})_8]^{2-}$  salts<sup>10,25,26</sup> (*vide infra*). The two sets of staggered equatorial carbonyls are slightly bent toward each other with an average  $\text{Fe}-\text{Fe}-\text{C}_{\text{eq}}$  angle of  $83.4^\circ$ . The aromatic ring of the *N*-methyllutidinium cation is planar (Figure 3B). Each cation is located within 2.9 Å of one of the carbonyl oxygens (O3), and it is oriented parallel to the plane formed by three of the carbonyl oxygens (O1, O2, and O3). Thus the overall repeating unit is the centrosymmetric triple ion  $[\text{mL}^+, \text{Fe}_2(\text{CO})_8^{2-}, \text{mL}^+]$  shown in Figure 4A. The individual triple ions are stacked along the 110 axis in the crystal, with each lutidinium cation in van der Waals contact ( $d = 3.45$  Å) with a cation in the adjacent unit cell (Figure 4B).

**IV. Infrared Spectra of the Octacarbonyldiferrate Charge-Transfer Salts.** The crystalline charge-transfer salts were uniformly dispersed in potassium bromide for infrared examination. The carbonyl IR spectrum of the bis-PPN<sup>+</sup> salt showed the expected

(26) Bhattacharya, N. K.; Coffy, T. J.; Quintana, W.; Salupo, T. A.; Bricker, J. C.; Shay, T. B.; Payne, M.; Shore, S. G. *Organometallics* **1990**, *9*, 2368.

(27) (a) Cotton, F. A. *Chemical Applications of Group Theory*, 2nd ed.; Wiley: New York, 1971. (b) Braterman, P. S. *Metal Carbonyl Spectra*; Academic: New York, 1975; p 19 ff.



**Table 2. Infrared Spectra ( $\nu_{\text{CO}}$ ) of the Charge-Transfer Salts of Octacarbonyldiferrate with Various Cations<sup>a</sup>**

assgnt <sup>b</sup>	CH <sub>3</sub> CN <sup>c</sup>	PPN <sup>+</sup>	Ph <sub>4</sub> P <sup>+</sup>	mL <sup>+</sup>	[CpFe-(C <sub>6</sub> H <sub>6</sub> )] <sup>+</sup>	PP <sup>+</sup>	iQ <sup>+</sup>
A <sub>2u</sub>	1914	1908	1908	1917	1904	1919	1920
				1910		1909	1912
A <sub>2u</sub>	1863	1850	1868 (sh) <sup>d</sup>	1867	1869	1846	1879 (sh) <sup>d</sup>
			1849	1845	1845	1840	1848
E <sub>u</sub>	1840	1833	1829	1832	1829	1831	1833

<sup>a</sup> As 2% dispersions in KBr, unless otherwise noted. Abbreviations for cations the same as in Table 1. <sup>b</sup> Assignment of bands in idealized  $D_{3d}$  symmetry. <sup>c</sup> Acetonitrile solution. <sup>d</sup> Shoulder.

**Table 3. Fractional Atomic Coordinates ( $\times 10^4$ ) and Equivalent Isotropic Thermal Parameters ( $\text{\AA}^2 \times 10^3$ ) for (*N*-Methyllutidinium)<sub>2</sub>[Fe<sub>2</sub>(CO)<sub>8</sub>]**

	<i>x</i>	<i>y</i>	<i>z</i>	<i>U</i> (eq) <sup>a</sup>
Fe	3931(1)	4923(1)	5561(1)	26(1)
O(1)	1686(2)	4952(3)	6727(2)	49(1)
O(2)	2326(2)	5982(3)	3743(2)	49(1)
O(3)	4605(2)	1890(2)	5715(2)	45(1)
O(4)	5494(2)	6962(3)	6872(2)	47(1)
N	1851(2)	837(3)	4489(2)	28(1)
C(1)	2597(3)	4908(3)	6267(2)	33(1)
C(2)	2990(3)	5551(3)	4442(2)	33(1)
C(3)	4351(3)	3081(3)	5646(2)	32(1)
C(5)	1096(3)	1991(3)	4182(2)	30(1)
C(6)	369(3)	2634(3)	4862(2)	34(1)
C(7)	398(3)	2135(3)	5826(2)	35(1)
C(8)	1165(3)	967(3)	6105(2)	34(1)
C(9)	1910(3)	318(3)	5442(2)	30(1)
C(10)	2645(3)	139(4)	3763(3)	43(1)
C(11)	1056(4)	2494(4)	3128(2)	44(1)
C(12)	2776(3)	-936(3)	5749(3)	41(1)

<sup>a</sup> Equivalent isotropic *U* defined as one-third of the trace of the orthogonalized  $U_{ij}$  tensor.

three allowed bands for  $D_{3d}$  symmetry<sup>27</sup> at  $\nu_{\text{CO}} = 1908$ , 1850, and 1833  $\text{cm}^{-1}$ , and they were assigned to vibrations of A<sub>2u</sub>, A<sub>2u</sub>, and E<sub>u</sub> symmetry, respectively, by comparison with the spectrum of the unbridged isomer of Co<sub>2</sub>(CO)<sub>8</sub>,<sup>28</sup> which is isostructural with [Fe<sub>2</sub>(CO)<sub>8</sub>]<sup>2-</sup>. The presence of exactly three strong bands was consistent with the minimal perturbation of the [Fe<sub>2</sub>(CO)<sub>8</sub>]<sup>2-</sup> framework by the large PPN<sup>+</sup> cations.<sup>29,30</sup> As the counterion was changed from PPN<sup>+</sup> to the pyridinium acceptors, the A<sub>2u</sub> bands were split (compare Table 2), but there was no overall shift to higher or lower energy. The splitting was reminiscent of similar changes in the IR spectra of other crystalline carbonylmetalate salts; it has been ascribed to the loss of symmetry induced by contact ion pairing in the crystal lattice.<sup>31</sup> Consistent with this formulation is the observation that the carbonyl infrared spectra of the various octacarbonyldiferrate salts dissolved in acetonitrile were independent of the counteranions, and they merely consisted of three strong bands ( $\nu_{\text{CO}} = 1914$ , 1865, and 1840  $\text{cm}^{-1}$ ) for the essentially unperturbed  $D_{3d}$  symmetry of the anion.

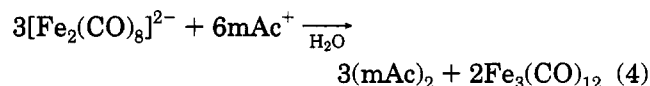
**V. Oxidation-Reduction Reactions of the Octacarbonyldiferrate Charge-Transfer Salts.** Yellow-orange solutions of Na<sub>2</sub>[Fe<sub>2</sub>(CO)<sub>8</sub>], [PPN]<sub>2</sub>[Fe<sub>2</sub>(CO)<sub>8</sub>] or [Ph<sub>4</sub>P]<sub>2</sub>[Fe<sub>2</sub>(CO)<sub>8</sub>] in acetonitrile showed no alteration in either color or infrared spectra, provided they were

**Table 4. Selected Bond Distances and Bond Angles for (*N*-methyllutidinium)<sub>2</sub>[Fe<sub>2</sub>(CO)<sub>8</sub>]**

Fe-Fe'	2.780(1)	Fe-C(1)	1.735(3)
Fe-C(2)	1.777(3)	Fe-C(3)	1.785(3)
Fe-C(4)	1.780(3)	O(1)-C(1)	1.168(4)
O(2)-C(2)	1.158(4)	O(3)-C(3)	1.150(4)
O(4)-C(4)	1.153(4)	N-C(5)	1.362(4)
N-C(9)	1.360(4)	N-C(10)	1.484(4)
C(5)-C(6)	1.376(5)	C(5)-C(11)	1.483(4)
C(6)-C(7)	1.370(5)	C(7)-C(8)	1.371(4)
C(8)-C(9)	1.374(4)	C(9)-C(12)	1.498(4)
C(1)-Fe-C(2)	95.1(1)	C(1)-Fe-C(3)	98.8(1)
C(2)-Fe-C(3)	118.4(1)	C(1)-Fe-C(4)	95.9(1)
C(2)-Fe-C(4)	118.7(1)	C(3)-Fe-C(4)	119.0(1)
C(1)-Fe-Fe'	177.5(1)	C(2)-Fe-Fe'	84.2(1)
C(3)-Fe-Fe'	83.7(1)	C(4)-Fe-Fe'	82.4(1)
C(5)-N-C(9)	122.0(3)	C(5)-N-C(10)	118.9(3)
C(9)-N-C(10)	119.2(2)	Fe-C(1)-O(1)	177.3(3)
Fe-C(2)-O(2)	176.4(3)	Fe-C(3)-O(3)	178.6(3)
Fe-C(4)-O(4)	176.6(3)	N-C(5)-C(6)	118.4(3)
N-C(5)-C(11)	119.5(3)	C(6)-C(5)-C(11)	122.1(3)
C(5)-C(6)-C(7)	121.2(3)	C(6)-C(7)-C(8)	118.7(3)
C(7)-C(8)-C(9)	121.1(3)	N-C(9)-C(8)	118.7(3)
N-C(9)-C(12)	120.0(3)	C(8)-C(9)-C(12)	121.4(3)

carefully protected from air and light. On the other hand, the charge-transfer salts of [Fe<sub>2</sub>(CO)<sub>8</sub>]<sup>2-</sup> with pyridinium counterions decomposed over a period of several hours to yield red-purple solutions in which the diagnostic carbonyl IR bands of [Fe<sub>2</sub>(CO)<sub>8</sub>]<sup>2-</sup> were absent. The same change occurred immediately upon addition of *N*-methylacridinium (mAc<sup>+</sup>) triflate to an acetonitrile solution of Na<sub>2</sub>[Fe<sub>2</sub>(CO)<sub>8</sub>]. This striking color change—from red-orange to deep purple—was accompanied by the spontaneous precipitation of the neutral dimeric reduction product of mAc<sup>+</sup>, namely, *N,N'*-dimethyl-9,9'-biacridanyl.<sup>32</sup> Since the ready isolation of this organic product provided unequivocal evidence for the 1-electron reduction of mAc<sup>+</sup>, the corresponding fate of the carbonylferrate donor was examined, and it was found to be highly dependent on the solvent in the following way.

**A. Oxidation of Octacarbonylferrate in Water or Ether.** Addition of 2 equiv of mAc<sup>+</sup>OTf<sup>-</sup> to an aqueous solution of Na<sub>2</sub>[Fe<sub>2</sub>(CO)<sub>8</sub>] resulted immediately in a green precipitate, and the orange-red (supernatant) solution became colorless. The green powder consisted of a mixture of (mAc)<sub>2</sub> and the trimeric iron carbonyl Fe<sub>3</sub>(CO)<sub>12</sub><sup>33</sup> in a 3:2 molar ratio. Quantification of the reaction products established the stoichiometry of the redox reaction as



Biacridanyl and the triiron cluster were isolated in 94 and 91% yields, respectively. The reaction took a similar course under quasi heterogeneous conditions in diethyl ether. Thus, a suspension of Na<sub>2</sub>[Fe<sub>2</sub>(CO)<sub>8</sub>] and 2 equiv of *N*-methylacridinium triflate gradually dissolved upon stirring for 36 h to yield a green solution of Fe<sub>3</sub>(CO)<sub>12</sub> and a colorless residue of dimethylbiacridanyl according to the stoichiometry in eq 4.

The course of the redox reactions in eq 4 was established by the exposure of [Fe<sub>2</sub>(CO)<sub>8</sub>]<sup>2-</sup> to a con-

(28) Noack, K. *Spectrochim. Acta* **1963**, *19*, 1925.

(29) Tilset, M.; Zlota, A. A.; Følting, K.; Caulton, K. G. *J. Am. Chem. Soc.* **1993**, *115*, 4113.

(30) (a) Darensbourg, M. Y. *Prog. Inorg. Chem.* **1985**, *33*, 221. (b) Compare Wei et al. in ref 3c.

(31) (a) Calderazzo, F.; Fachinetti, G.; Marchetti, F. *J. Chem. Soc., Chem. Commun.* **1981**, 181. (b) Teller, R. G.; Finke, R. G.; Collman, J. P.; Chin, H. B.; Bau, R. *J. Am. Chem. Soc.* **1977**, *99*, 1104.

(32) (a) Mader, F.; Zanker, V. *Chem. Ber.* **1964**, *97*, 2418. (b) Anne, A.; Hapiot, P.; Moiroux, J.; Neta, P.; Saveant, J.-M. *J. Am. Chem. Soc.* **1992**, *114*, 4694.

(33) The trinuclear cluster Fe<sub>3</sub>(CO)<sub>12</sub> was identified and quantified by its carbonyl infrared spectrum.<sup>34</sup>

(34) Kristoff, J. S.; Shriver, D. F. *Inorg. Chem.* **1974**, *13*, 499.



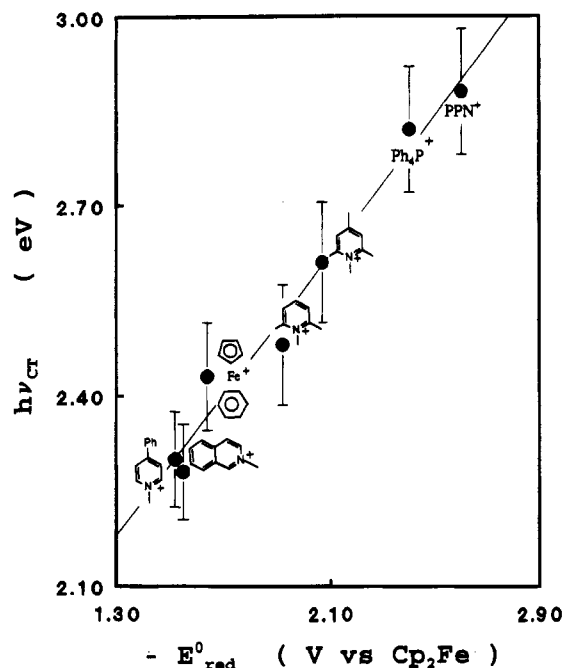


**Figure 5.** Variation of the energy of the charge-transfer transition ( $h\nu_{CT}$ ) in crystalline  $A_2[Fe_2(CO)_8]$  salts as a function of the reduction potential  $E^0_{red}$  of the cationic acceptor.

The various charge-transfer absorption bands, and their associated colors, vanish upon dissolution of the salts in polar solvents such as acetonitrile. Since such media act specifically to break up aggregates of ions,<sup>45</sup> the source of the colors of the crystalline salts must lie in the mutual interaction of the cations and anions extant in the solid state. The origin of these interionic interactions, in charge transfer, is underscored by the progressive bathochromic shift of the absorption bands in Figure 2 and Table 1 as the acceptor strength ( $E^0_{red}$ ) of the cation is increased in the following series:  $PPN^+ < Ph_4P^+ < mL^+ < iQ^+$ . Such a cation-dependent shift follows from the Mulliken theory of charge transfer, where the change in the energy of the CT bands ( $h\nu_{CT}$ ) is given by

$$h\nu_{CT} = IP(D) - EA(A) + \text{const} \quad (10)$$

in which  $IP(D)$  and  $EA(A)$  represent the ionization potential of the donor and electron affinity of the acceptor, respectively.<sup>21</sup> In the case of the cations and anions present in charge-transfer salts, for which values of  $EA$  and  $IP$  are not available, the Mulliken relation is alternatively expressed as<sup>7</sup>

$$h\nu_{CT} = a[E^0_{ox}(D) - E^0_{red}(A)] + \text{const} \quad (11)$$

in which  $E^0_{ox}(D)$  is the oxidation potential of the octacarbonyldiferrate donor,  $E^0_{red}(A)$  is the reduction potential of the various acceptor cations, and  $1.0 > a > 0$ . Thus the linear relationship observed in Figure 5 between the energy of the absorption band maxima ( $h\nu_{CT}$  in Table 1) and  $E^0_{red}$  follows from the theory of charge-transfer interactions.<sup>3,21</sup>

**Structural Consequences of the Interionic Charge-Transfer Interaction.** The molecular orbital

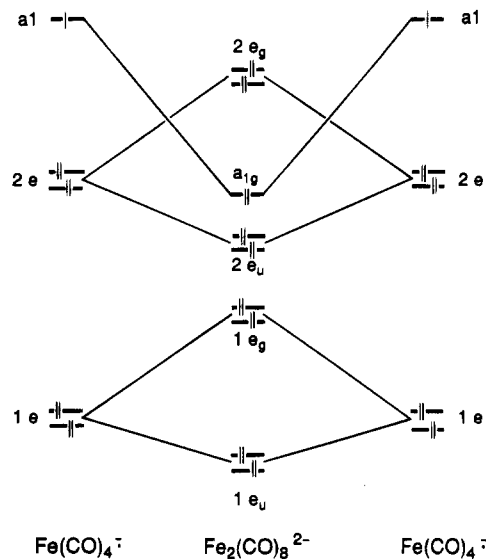


**Figure 6.** Energy levels of the occupied molecular orbitals of  $[Fe_2(CO)_8]^{2-}$  by the combination of two  $Fe(CO)_4^-$  fragments as adapted from Dedieu *et al.*<sup>15</sup>

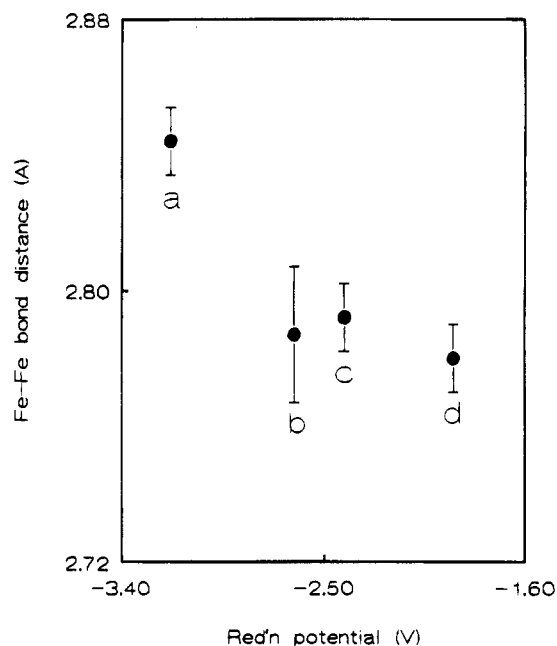


**Figure 7.** Variation of the iron-iron bond distances in crystalline salts of  $[Fe_2(CO)_8]^{2-}$  determined by X-ray crystallography plotted as a function of the reduction potential  $E^0_{red}$  of the counterions (a)  $Et_4N^+$ , (b)  $PPN^+$ , (c)  $Ph_4P^+$ , and (d) *N*-methyllutidinium. The error bars represent five times the reported standard deviation ( $5\sigma$ ).

scheme for  $[Fe_2(CO)_8]^{2-}$ , as previously developed,<sup>15</sup> assigns two degenerate orbitals ( $e_g$  in  $D_{3d}$  symmetry) to the HOMO of the dianion (Figure 6). Since these orbitals are Fe-Fe antibonding, the degree to which an electron is donated from  $[Fe_2(CO)_8]^{2-}$  to an acceptor should be represented by a corresponding increase in the intermetallic bond order, with concomitant shortening of the Fe-Fe bond. Put another way, electron donation from  $[Fe_2(CO)_8]^{2-}$  will reduce the electrostatic repulsion between the anionic iron centers.<sup>25</sup> Indeed, Figure 7 shows that the measured Fe-Fe bond distances in crystalline salts of  $[Fe_2(CO)_8]^{2-}$  decreases as a function of acceptor strength as measured by the reduction potential of the various monocationic acceptors, and it graphically illustrates the unmistakable trend of decreasing iron-iron distances  $d_{Fe-Fe}$  with

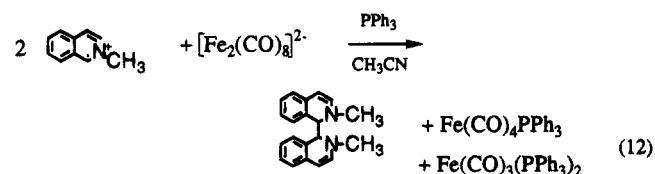
(45) (a) Edgell, W. F. In *Ion Pairs in Organic Reactions*; Szwarc, M., Ed.; Wiley: New York, 1972; Vol. 1, p 153 ff. (b) Masnovi, J. M.; Kochi, J. K. *J. Am. Chem. Soc.* **1985**, *107*, 7880. (c) Kosower, E. M.; Skorz, J. A. *J. Am. Chem. Soc.* **1960**, *82*, 2195.

increasing  $E_{\text{red}}^0(A^+)$  in the order  $\text{Et}_4\text{N}^+ > \text{PPN}^+ \approx \text{PPh}_4^+ > \text{mL}^+$ , that is consistent with the increasing interionic charge-transfer interactions in the crystalline salts.<sup>46</sup>

The logical limit for the comparison of the  $[\text{Fe}_2(\text{CO})_8]^{2-}$  salts with (partially) reduced electron density is the paramagnetic monoanion itself, that is  $[\text{Fe}_2(\text{CO})_8]^-$  which is independently produced by the 1-electron oxidation of  $[\text{Fe}_2(\text{CO})_8]^{2-}$ . Electron spin resonance studies have shown that the predominant isomer, which is stable at low temperatures, has an iron-iron bond bridged by two carbonyl groups.<sup>47</sup> The bridging carbonyls suggest considerable shortening of the Fe-Fe bond length, since  $d_{\text{Fe-Fe}}$  for doubly bridged iron carbonyls ranges from 2.33 to 2.60 Å, which is much shorter than that found in  $[\text{Fe}_2(\text{CO})_8]^{2-}$ .<sup>48</sup> Unfortunately, no further structural information concerning  $[\text{Fe}_2(\text{CO})_8]^-$  is available, and the quantitative estimation of the degree of charge transfer in crystalline  $\text{Fe}_2(\text{CO})_8^{2-}$  salts is not possible at this juncture.

The LUMO of pyridinium cations (such as  $\text{mL}^+$ ) is a  $\pi^*$  orbital centered on the pyridine ring.<sup>49</sup> Thus the charge-transfer interaction in  $[\text{mL}]_2[\text{Fe}_2(\text{CO})_8]$  can be identified as proceeding from the iron anion *via* the three coordinated carbonyls (see Figure 3A) on each iron atom to the delocalized  $\pi$  orbital on the lutidinium ring. The characteristic "tripod configuration" of three carbonyl groups coordinated to the aromatic acceptor is a common structural feature of pyridinium/carbonylmetallate CT salts. [In particular, compare the *N*-methylquinolinium  $[\text{Co}(\text{CO})_4]^-$ <sup>3b</sup> and 4-cyano-*N*-methylpyridinium  $[\text{TpMo}(\text{CO})_3]^-$ .<sup>3d</sup> Indeed, Figure 4 shows that, in  $[\text{mL}]_2[\text{Fe}_2(\text{CO})_8]$ , both iron centers are coordinated via three carbonyls to the  $\pi$ -face of the lutidinium cation, and the repeating unit consists of this triple ion.

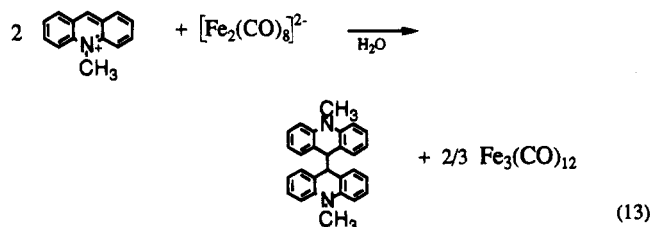
**Chemical Consequences of the Charge-Transfer Interaction Leading to Redox Reactions.** In contrast to the stable  $\text{PPN}^+$  and  $\text{Ph}_4\text{P}^+$  salts of  $[\text{Fe}_2(\text{CO})_8]^{2-}$ , the salts with pyridinium cations decompose when they are dissolved in acetonitrile. If the dissolutions are carried out in the presence of triphenylphosphine, the mononuclear Fe(0) substitution products  $\text{Fe}(\text{CO})_4\text{PPh}_3$  and  $\text{Fe}(\text{CO})_3(\text{PPh}_3)_2$  are obtained in 80–90% yield according to eq 7. The isoquinolinium salt also yields the characteristic one-electron reduction product  $(i\text{Q})_2$ <sup>44</sup> in 86% yield, i.e.



Since  $(i\text{Q})_2$  can also be obtained by the direct electrochemical reduction of *N*-methylisoquinolinium salts,<sup>44</sup> the overall process in eq 12 can be described as an interionic redox reaction. The critical nature of the

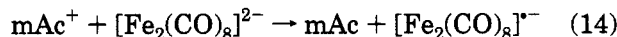
charge-transfer interaction in allowing this transformation is underscored by the unreactivity of  $\text{Na}_2[\text{Fe}_2(\text{CO})_8]$  when it is exposed to the phosphonium salts  $\text{TPP}^+$  and  $\text{PPN}^+$  in acetonitrile.<sup>50</sup>

The same oxidative transformation of  $[\text{Fe}_2(\text{CO})_8]^{2-}$  can be effected more rapidly by the use of a stronger acceptor, namely, *N*-methylacridinium cation ( $E_{\text{red}}^0 = -0.43$  V vs SCE), i.e.



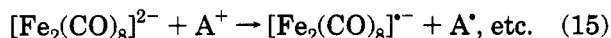
Consequently, all attempts to isolate the charge-transfer salt,  $(\text{mAc})_2[\text{Fe}_2(\text{CO})_8]$  *via* metathesis in aqueous medium are thwarted by the rapid redox reaction in eq 13.

The rapid oxidation of  $[\text{Fe}_2(\text{CO})_8]^{2-}$  by the acridinium cation in both water and acetonitrile as described in eqs 4 and 6, respectively, is clearly related to the exergonicity of the electron-transfer reaction, i.e.



with  $\Delta G_{\text{et}}^0 = -9.0$  kcal mol<sup>-1</sup>.<sup>51</sup> Contrastingly, the electron transfer from  $[\text{Fe}_2(\text{CO})_8]^{2-}$  to the pyridinium cations  $i\text{Q}^+$  and  $\text{mL}^+$ , as well as the other acceptor cations in Table 1, is endergonic,<sup>52</sup> a factor which indeed allows the isolation of the corresponding charge-transfer salts.

The metastable  $[\text{Fe}_2(\text{CO})_8]^-$  radical anion in eq 14 can be independently generated by 1-electron oxidation of  $[\text{Fe}_2(\text{CO})_8]^{2-}$  with 1 equiv of  $\text{AgBF}_4$ ,<sup>53</sup> and it is stable at  $-78$  °C. Importantly, the treatment of this radical anion with excess  $\text{PPh}_3$  in tetrahydrofuran at  $-78$  °C yields a mixture of  $\text{Fe}(\text{CO})_4\text{PPh}_3$  and  $\text{Fe}(\text{CO})_3(\text{PPh}_3)_2$ , and the dissolution of  $[\text{Fe}_2(\text{CO})_8]^-$  in water yields only  $\text{Fe}_3(\text{CO})_{12}$  (see the Experimental Section for details.) Since the same complexation of different iron carbonyl products is observed in the redox reactions described in eqs 7 and 4, respectively, the intermediacy of the radical anion  $[\text{Fe}_2(\text{CO})_8]^-$  is inferred in the redox process which always proceeds by way of an initial electron transfer from  $[\text{Fe}_2(\text{CO})_8]^{2-}$  to the acceptor anion,  $A^+$ , irrespective of the solvent, i.e.



As such, we attribute the various iron carbonyl products obtained in different solvents to the unique reactivity of this radical anion. Thus,  $[\text{Fe}_2(\text{CO})_8]^-$  is an odd-electron organometallic species<sup>54</sup> and expected to be

(51) The exergonicity was calculated from the relation:  $\Delta G_{\text{et}}^0 = -(RT/F) \{E_{\text{ox}}^0[\text{Fe}_2(\text{CO})_8^{2-}] + E_{\text{red}}^0[\text{mAc}^+]\}$  in which  $E_{\text{ox}}^0[\text{Fe}_2(\text{CO})_8^{2-}]$  and  $E_{\text{red}}^0$  are the reversible potentials for oxidation of  $[\text{Fe}_2(\text{CO})_8]^{2-}$  and for reduction of  $\text{mAc}^+$ ,<sup>32</sup> respectively.

(52) Owing to the substantially more negative  $E_{\text{red}}^0$  of  $-1.55$  V for  $i\text{Q}^+$ .

(53) Krusic, P. J.; Morton, J. R.; Preston, K. F.; Williams, A. J.; Lee, F. L. *Organometallics* **1990**, *9*, 697.

(54) For the enhanced reactivity of odd-electron organometallic species see: (a) Troglor, W. D., Ed. *Organometallic Radical Processes*; Elsevier: New York, 1990. (b) Baird, M. C. *Chem. Rev.* **1988**, *88*, 1217. (c) Astruc, D. *Chem. Rev.* **1988**, *88*, 1189.

(55) Compare: (a) Ohst, H. H.; Kochi, J. K. *J. Am. Chem. Soc.* **1986**, *108*, 2897. (b) Ragaini, F.; Song, J.-S.; Ramage, D. L.; Geoffrey G. L.; Yap, G. A. P.; Rheingold, A. L. *Organometallics* **1995**, *14*, 387.

(46) For  $d_{\text{Fe-Fe}}$  in the various  $[\text{Fe}_2(\text{CO})_8]^{2-}$  salts with  $\text{PPN}^+$ ,  $\text{Et}_4\text{N}^+$ , and  $\text{Ph}_4\text{P}^+$ , see refs 10, 25, and 26, respectively.

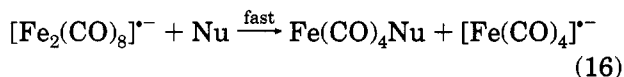
(47) Krusic, P. J.; San Filippo, J., Jr.; Hutchinson, B.; Hance, R. L.; Daniels, L. M. *J. Am. Chem. Soc.* **1981**, *103*, 2129.

(48) Fehlhammer, W. P. Stolzenberg, H. In *Comprehensive Organometallic Chemistry*; Wilkinson, G., Stone, F. G. A., Abel, E. W., Eds.; Pergamon: New York, 1982; Vol. 4, p 513 ff.

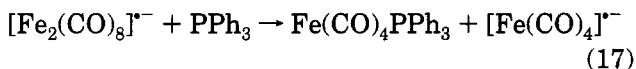
(49) (a) Grossi, L.; Minisci, F.; Pedulli, G. F. *J. Chem. Soc., Perkin Trans. 2* **1977**, 943. (b) Itoh, M.; Nagakura, S. *J. Am. Chem. Soc.* **1967**, *89*, 3959.

(50) Lin, C.-C.; Kong, G.; Cho, H.; Whittlesey, B. R. *Inorg. Chem.* **1993**, *32*, 2075.

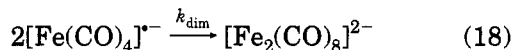
particularly labile to nucleophilic attack,<sup>55</sup> i.e.



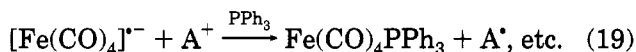
where Nu is a generic representation of any nucleophilic species present in the reaction medium, including the solvent itself. For example, when the nucleophile is an added phosphine, the electron-deficient  $[\text{Fe}_2(\text{CO})_8]^{2-}$  can undergo rapid cleavage to directly afford the mononuclear substitution products,<sup>56</sup> i.e.



Moreover, the 17-electron tetracarbonylferrate can dimerize,<sup>57</sup> i.e.

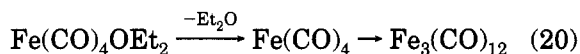


or it can be readily oxidized further<sup>58</sup>

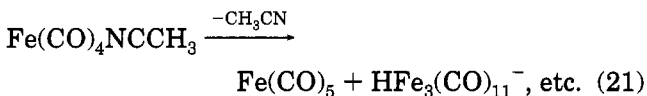


to account for all the products in eq 7 or 8.

The generic formulation in eq 16 also applies to the different iron carbonyl products obtained in water or ether (eq 4) compared to those obtained in acetonitrile (eq 6). Thus, *poor* nucleophiles such as  $\text{H}_2\text{O}$  or  $\text{Et}_2\text{O}$  react with  $[\text{Fe}_2(\text{CO})_8]^{2-}$  to generate  $\text{Fe}(\text{CO})_4\text{Nu}$ , which is unstable to ligand loss of water or ether, and the coordinatively unsaturated fragment  $\text{Fe}(\text{CO})_4$  rapidly associates to afford the stable trimeric carbonyl,<sup>59</sup> e.g.



On the other hand, *moderately* nucleophilic solvents such as acetonitrile or tetrahydrofuran generate  $\text{Fe}(\text{CO})_4\text{Nu}$  which does not trimerize but instead undergoes a complex set of reactions of the type that has previously been described in the base (nucleophile) induced disproportionation of polynuclear metal carbonyls,<sup>60</sup> e.g.



Indeed, such a behavior of  $\text{Fe}(\text{CO})_4\text{NCCH}_3$  is known from the dissolution of either  $\text{Fe}_3(\text{CO})_{12}$  or  $\text{Fe}_2(\text{CO})_9$  in acetonitrile,<sup>61</sup> and the decompositions ultimately lead

(56) Note that the further carbonyl substitution of  $\text{Fe}(\text{CO})_4\text{PPh}_3$  by  $\text{PPh}_3$  (present in excess) is rapid,<sup>41</sup> and it accounts for the relatively large amounts of  $\text{Fe}(\text{CO})_5(\text{PPh}_3)_2$  found. Indeed, the reaction of triphenylphosphine with various iron carbonyls under a variety of conditions (solvent and temperature) always yielded mixtures of  $\text{Fe}(\text{CO})_4\text{PPh}_3$  and  $\text{Fe}(\text{CO})_5(\text{PPh}_3)_2$ . See: Albers, M. O.; Singleton, E.; Coville, N. J. *Inorg. Synth.* **1990**, *28*, 168.

(57) The value of  $k_{\text{dim}}$  is  $5 \times 10^5 \text{ M}^{-1} \text{ s}^{-1}$ . See: Amatore, C. A.; Krusic, P. J.; Pedersen, S. U.; Verpeaux, J.-N. *Organometallics* **1995**, *14*, 640.

(58) See Amatore, et al. in refs 11 and 57.

(59) Poliakoff, M.; Turner, J. J. *J. Chem. Soc. A* **1971**, 2403.

(60) See: (a) Stiegman, A. E.; Tyler, D. R. *Inorg. Chem.* **1984**, *23*, 527. (b) Castellani, M. P.; Tyler, D. R. *Organometallics* **1988**, *8*, 2113. (c) Castellani, M. P.; Hesse, E. T.; Tyler, D. R. *Organometallics* **1994**, *13*, 399.

(61) (a) El-Murr, N.; Chaloyard, A. *Inorg. Chem.* **1982**, *21*, 2206. (b) Cotton, F. A.; Troup, J. N. *J. Am. Chem. Soc.* **1974**, *96*, 3438.

to the same mixture of mononuclear iron carbonyls that is identified in eq 21.

## Conclusion

The prototypical organometallic dinuclear anion  $[\text{Fe}_2(\text{CO})_8]^{2-}$  is identified as an electron donor in two ways: (i) Its interaction with cationic organic and organometallic acceptors  $\text{A}^+$  to form a series of 2:1 charge-transfer salts (in the solid state), the colors and structures of which indicate partial electron transfer from  $[\text{Fe}_2(\text{CO})_8]^{2-}$  to  $\text{A}^+$ ; (ii) its spontaneous electron transfer with strong cationic acceptors (in solution) yields products derived from the reduced pyridinium acceptor ( $\text{A}^{\cdot}$ ) and the oxidized diferrate donor  $[\text{Fe}_2(\text{CO})_8]^{-}$ .

The series of charge-transfer salts  $\text{A}_2[\text{Fe}_2(\text{CO})_8]$  encompass the weak interacting ion pairs of  $[\text{Fe}_2(\text{CO})_8]^{2-}$  with the redox-stable cations  $\text{PPN}^+$  and  $\text{TPP}^+$  at one extreme and the deeply colored salts of  $[\text{Fe}_2(\text{CO})_8]^{2-}$  with the pyridinium cations  $\text{mAc}^+$  and  $\text{iQ}^+$  at the other extreme. With the latter, the strong charge-transfer perturbation results in interionic electron transfer leading to the radical pair  $[\text{A}^{\cdot}, [\text{Fe}_2(\text{CO})_8]^{-}]$  which ultimately affords the dimeric  $\text{A}_2$  and various iron carbonyl products derived from nucleophilic (solvent) attack on the metastable  $[\text{Fe}_2(\text{CO})_8]^{-}$  as detailed in eq 16.

## Experimental Section

**Materials.**  $\text{Na}_2[\text{Fe}_2(\text{CO})_8]$ ,<sup>16</sup>  $[\text{Cp}_2\text{Fe}] \text{BF}_4$ ,<sup>62</sup>  $[\text{CpFe}(\eta^6\text{-C}_6\text{H}_6)]\text{PF}_6$ ,<sup>63</sup>  $\text{Fe}(\text{CO})_4\text{PPh}_3$ ,<sup>43</sup>  $\text{Fe}(\text{CO})_5(\text{PPh}_3)_2$ ,<sup>43</sup> and all pyridinium salts<sup>64</sup> were prepared according to literature methods. Silver(I) tetrafluoroborate ( $\text{AgBF}_4$ ) purchased from the Aldrich Chemical Co. was stored in the drybox. Triphenylphosphine (Strem) and  $(\text{PPN})\text{Cl}$ ,  $\text{PPh}_4\text{Br}$ ,  $(\text{TBA})\text{PF}_6$ , 2,4,6-collidine, 2,6-lutidine, isoquinoline, 4-phenylpyridine, and acridine (Aldrich) were used as received. All manipulations were carried out under an atmosphere of argon using standard Schlenk techniques or under nitrogen in a drybox. All glassware was dried in an oven at 135 °C and then evacuated prior to use. Infrared spectra were measured on a Nicolet 10DX FT-IR spectrometer. All measurements of liquid samples were made with 0.1 mm NaCl cells. The diffuse reflectance spectra were recorded on a Perkin-Elmer 330-A spectrometer equipped with a Hitachi H210-2101 integrating sphere accessory using an alumina disk as the reference, and all charge-transfer salts were prepared for spectroscopic measurement as 2% dispersions in dry KBr. Visible spectra of solutions were measured on a Hewlett-Packard 8450A diode-array spectrometer. Controlled potential electrolysis was performed using the Model-173 potentiostat/galvanostat provided by Princeton Applied Research in conjunction with the Model-178 electrometer probe. Elemental analyses were performed by Atlantic Microlab Inc. (Norcross, GA). Solvents were freshly distilled under an atmosphere of argon from sodium (hexane, toluene), sodium benzophenone ketyl (THF, diethyl ether), or calcium hydride ( $\text{CH}_2\text{Cl}_2$ ). Acetonitrile was refluxed over 0.1%  $\text{KMnO}_4$  for 1 h and distilled into another flask. The purified solvent was then redistilled serially from  $\text{P}_2\text{O}_5$  and  $\text{CaH}_2$ . Distilled water was boiled under an atmosphere of argon prior to use in order to remove dissolved oxygen.

**Preparation of Charge-Transfer Salts.**  $[\text{PPN}]_2[\text{Fe}_2(\text{CO})_8]$  was prepared by the literature method<sup>16</sup> in THF. It could also be prepared in aqueous solution as follows: A solution of  $\text{Na}_2$ -

(62) Hendrickson, D. N.; Sohn, Y. S.; Gray, H. B. *Inorg. Chem.* **1971**, *10*, 1559.

(63) King, R. B. *Organometallic Syntheses*; Academic: New York, 1965; p 138 ff.

(64) (a) Yoon, K. B.; Huh, T. J.; Corbin, D. R.; Kochi, J. K. *J. Phys. Chem.* **1993**, *97*, 6942. (b) Vogel, A. I. *Textbook of Practical Organic Chemistry*; Wiley: New York, 1956.

[Fe<sub>2</sub>(CO)<sub>8</sub>] (0.424 g, 1.113 mmol) in water (15 mL) was added to a suspension of (PPN)Cl (1.198 g, 2.09 mmol) in the same solvent (10 mL). An orange solid precipitated immediately, and the solution became colorless. The orange precipitate was filtered off and washed with THF. Infrared:  $\nu_{\text{CO}}$ , KBr, 1908 (s), 1850 (s), 1833 (s) cm<sup>-1</sup>;  $\nu_{\text{CO}}$ , MeCN, 1978 (w), 1943 (w), 1914 (m), 1862 (s), 1839 (sh, m) cm<sup>-1</sup>. Yield: 1.393 g (94%). [PPh<sub>4</sub>]<sub>2</sub>[Fe<sub>2</sub>(CO)<sub>8</sub>] was prepared by the literature method<sup>42</sup> in THF. However, this compound can also be prepared in an aqueous medium from Na<sub>2</sub>[Fe<sub>2</sub>(CO)<sub>8</sub>] (0.342 g, 0.896 mmol) and PPh<sub>4</sub>Br (0.749 g, 1.7888 mmol), as detailed for the PPN<sup>+</sup> salt. Infrared:  $\nu_{\text{CO}}$ , KBr, 1908 (m), 1849 (s), 1829 (s) cm<sup>-1</sup>;  $\nu_{\text{CO}}$ , MeCN, 1978 (w), 1946 (w), 1914 (m), 1862 (s), 1840 (sh, m) cm<sup>-1</sup>. Yield: 0.864 g (95%). [N-methylcollidinium]<sub>2</sub>[Fe<sub>2</sub>(CO)<sub>8</sub>]: A solution of N-methylcollidinium triflate (0.570 g, 2.001 mmol) in water (18 mL) was added with the aid of a hypodermic syringe to a solution of Na<sub>2</sub>[Fe<sub>2</sub>(CO)<sub>8</sub>] (0.382 g, 1.00 mmol) in water (10 mL) at room temperature. The immediate orange precipitate was filtered out, washed with water (10 mL × 2) and THF (10 mL), and then dried *in vacuo*. The orange powder was dissolved in MeCN (20 mL) to form a dark red solution, and the volume of the solution was reduced by about 10 mL. When the solution was cooled to -25 °C for 1 day, it afforded dark red crystals. Anal. Calcd for C<sub>28</sub>H<sub>28</sub>Fe<sub>2</sub>N<sub>2</sub>O<sub>8</sub>: C, 51.35; H, 4.64; N, 4.61. Found: C, 51.45; H, 4.56; N, 4.63. Infrared:  $\nu_{\text{CO}}$ , KBr, 1918 (sh, m), 1909 (m), 1877 (s), 1856 (s), 1833 (s) cm<sup>-1</sup>;  $\nu_{\text{CO}}$ , MeCN, 1978 (vw), 1942 (vw), 1915 (m), 1862 (s), 1838 (sh, m) cm<sup>-1</sup>. [N-methyllutidinium]<sub>2</sub>[Fe<sub>2</sub>(CO)<sub>8</sub>]: Disodium octacarbonyldiferrate (0.341 g, 0.892 mmol) was dissolved in THF (20 mL), and the solution was cooled to -78 °C with stirring. N-Methyllutidinium hexafluorophosphate (0.429 g, 1.607 mmol) was added to the mixture. A few min later, a dark red precipitate formed. The temperature was maintained at -78 °C for 5 h while the orange solution was stirred. The dark red precipitate was filtered off using a glass frit, washed with THF (10 mL × 3), and then dried *in vacuo*. Addition of MeCN (30 mL) yielded a dark red solution which was filtered from a trace of white precipitate. The volume of the dark red solution was reduced by evacuation, and dark-burgundy crystals formed upon cooling the solution to -25 °C. Yield: 0.336 g (72%). Anal. Calcd for C<sub>24</sub>H<sub>24</sub>Fe<sub>2</sub>N<sub>2</sub>O<sub>8</sub>: C, 49.69; H, 4.17; N, 4.83. Found: C, 49.63; H, 4.15; N, 4.86. Infrared:  $\nu_{\text{CO}}$ , KBr, 1917 (sh), 1910 (s), 1867 (sh), 1845 (s), 1832 (s) cm<sup>-1</sup>;  $\nu_{\text{CO}}$ , MeCN, 1979 (w), 1939 (w), 1914 (m), 1862 (s), 1840 (sh, m) cm<sup>-1</sup>. The alternative synthesis of [N-methyllutidinium]<sub>2</sub>[Fe<sub>2</sub>(CO)<sub>8</sub>] in aqueous solution followed that of [PPN]<sub>2</sub>[Fe<sub>2</sub>(CO)<sub>8</sub>], using 0.191 g (0.5 mmol) of Na<sub>2</sub>[Fe<sub>2</sub>(CO)<sub>8</sub>] and 0.267 g (1 mmol) of (N-methyllutidinium)PF<sub>6</sub>. Yield: 0.258 g (89%) of burgundy crystals. [CpFe(η<sup>6</sup>-C<sub>6</sub>H<sub>6</sub>)]<sub>2</sub>[Fe<sub>2</sub>(CO)<sub>8</sub>]: A solution of Na<sub>2</sub>[Fe<sub>2</sub>(CO)<sub>8</sub>] (0.250 g, 0.655 mmol) in water (15 mL) was added to a solution of [CpFe(η<sup>6</sup>-C<sub>6</sub>H<sub>6</sub>)] PF<sub>6</sub> (0.431 g, 1.254 mmol) in MeCN (4.5 mL) at room temperature. The red-brown precipitate was filtered off, washed with water (10 mL × 3), and dried *in vacuo*. The precipitate was dissolved in MeCN and cooled to -25 °C. A day later, dark red-brown hexagonal crystals were collected. Yield: 0.404 g (84%). Anal. Calcd for C<sub>30</sub>H<sub>22</sub>Fe<sub>4</sub>O<sub>8</sub>: C, 49.1; H, 3.02. Found: C, 48.82; H, 3.13. Infrared:  $\nu_{\text{CO}}$ , KBr, 1905 (s), 1867 (sh), 1845 (s), 1829 (s) cm<sup>-1</sup>;  $\nu_{\text{CO}}$ , MeCN, 1978 (w), 1939 (w), 1914 (m), 1862 (s), 1839 (sh, m) cm<sup>-1</sup>. [PP]<sub>2</sub>[Fe<sub>2</sub>(CO)<sub>8</sub>] was prepared from 0.191 g (0.5 mmol) of Na<sub>2</sub>[Fe<sub>2</sub>(CO)<sub>8</sub>] and 0.296 g (1.0 mmol) of 4-phenyl-N-methylpyridinium iodide by the procedure used for [PPN]<sub>2</sub>[Fe<sub>2</sub>(CO)<sub>8</sub>]. A dark brown precipitate of [PP]<sub>2</sub>[Fe<sub>2</sub>(CO)<sub>8</sub>] was obtained in 92% yield (0.258 g). Anal. Calcd for C<sub>32</sub>H<sub>24</sub>Fe<sub>2</sub>N<sub>2</sub>O<sub>8</sub>: C, 56.84; H, 3.58; N, 4.14. Found: C, 56.57; H, 3.55; N, 4.03. Infrared:  $\nu_{\text{CO}}$ , KBr, 1919 (sh), 1909 (s), 1867 (sh), 1846 (s), 1840 (s), 1832 (s) cm<sup>-1</sup>;  $\nu_{\text{CO}}$ , MeCN, 1979 (w), 1939 (w), 1914 (m), 1862 (s), 1840 (sh, m) cm<sup>-1</sup>. [iQ]<sub>2</sub>[Fe<sub>2</sub>(CO)<sub>8</sub>] was prepared in water and isolated by following the procedure described above for [PPN]<sub>2</sub>[Fe<sub>2</sub>(CO)<sub>8</sub>] using 0.224 g (0.568 mmol) of Na<sub>2</sub>[Fe<sub>2</sub>(CO)<sub>8</sub>] and 0.328 g (1.141 mmol) of (iQ)PF<sub>6</sub>. A yield of 0.319 g (89%) of [iQ]<sub>2</sub>[Fe<sub>2</sub>(CO)<sub>8</sub>] as red-black needles was obtained. Anal. Calcd for C<sub>28</sub>H<sub>20</sub>Fe<sub>2</sub>N<sub>2</sub>O<sub>8</sub>: C, 53.88; H,

3.23; N, 4.49. Found: C, 52.10; H, 3.31; N, 4.43. Infrared:  $\nu_{\text{CO}}$ , KBr, 1912 (s), 1879 (sh), 1848 (s), 1833 (s) cm<sup>-1</sup>;  $\nu_{\text{CO}}$ , MeCN, 1979 (w), 1939 (w), 1914 (m), 1862 (s), 1840 (sh, m) cm<sup>-1</sup>.

**Generation of Fe<sub>2</sub>(CO)<sub>8</sub><sup>-</sup> Anion Radical. (i) From Na<sub>2</sub>[Fe<sub>2</sub>(CO)<sub>8</sub>] and [Cp<sub>2</sub>Fe]BF<sub>4</sub>.** Ferrocenium tetrafluoroborate (0.136 g, 0.5 mmol) dissolved in MeCN (10 mL) was added with the aid of a hypodermic syringe to a solution of Na<sub>2</sub>[Fe<sub>2</sub>(CO)<sub>8</sub>] (0.191 g, 0.5 mmol) in MeCN (10 mL) at -40 °C. The solution immediately turned a dark brown, but no precipitate was observed. The infrared spectrum of the acetonitrile solution was recorded at -40 °C ( $\nu_{\text{CO}}$ , MeCN): 2024 (w), 1979 (s), 1946 (s), 1917 (sh), 1780 (vww), 1739 (w) cm<sup>-1</sup>.

**(ii) From Na<sub>2</sub>[Fe<sub>2</sub>(CO)<sub>8</sub>] and AgBF<sub>4</sub> in MeCN.** A solution of AgBF<sub>4</sub> (0.097 g, 0.5 mmol) in MeCN (10 mL) was added with the aid of a hypodermic syringe to a solution of Na<sub>2</sub>[Fe<sub>2</sub>(CO)<sub>8</sub>] (0.191 g, 0.5 mmol) in MeCN (10 mL) maintained at -40 °C. The solution turned dark brown and a silver mirror formed on the surface of the flask. The infrared spectrum was recorded at -40 °C ( $\nu_{\text{CO}}$ , MeCN): 2024 (w), 1979 (s), 1946 (s), 1917 (sh), 1780 (vww), 1737 (w) cm<sup>-1</sup>.

**(iii) From Na<sub>2</sub>[Fe<sub>2</sub>(CO)<sub>8</sub>] and mAcOTf in MeCN.** mAcOTf (0.172 g, 0.5 mmol) in MeCN (10 mL) was transferred with the aid of a hypodermic syringe to Na<sub>2</sub>[Fe<sub>2</sub>(CO)<sub>8</sub>] (0.191 g, 0.5 mmol) in MeCN (10 mL) at -40 °C. A white precipitate formed immediately. The infrared spectrum of the dark brown supernatant was recorded at -40 °C ( $\nu_{\text{CO}}$ , MeCN): 2024 (w), 1979 (s), 1951 (sh), 1943 (s), 1780 (vww), 1738 (w) cm<sup>-1</sup>.

**(iv) From Na<sub>2</sub>[Fe<sub>2</sub>(CO)<sub>8</sub>] and AgBF<sub>4</sub> in THF.** A solution of AgBF<sub>4</sub> (0.097 g, 0.5 mmol) in THF (10 mL) was added to a solution of Na<sub>2</sub>[Fe<sub>2</sub>(CO)<sub>8</sub>] (0.191 g, 0.5 mmol) in the same solvent (10 mL) maintained at -78 °C. The solution immediately turned dark brown, and a silver mirror formed. The infrared spectrum was recorded at -40 °C ( $\nu_{\text{CO}}$ , THF): 2030 (w), 2017 (s), 2001 (s), 1987 (s), 1965 (m), 1919 (w), 1820 (vw), 1787 (w) cm<sup>-1</sup>.

**Redox Reactions of Na<sub>2</sub>[Fe<sub>2</sub>(CO)<sub>8</sub>]. A. Reaction of mAc OTf with Na<sub>2</sub>[Fe<sub>2</sub>(CO)<sub>8</sub>] in water.** N-methylacridinium triflate (mAc OTf, 0.4030 g, 1.1749 mmol) was dissolved in degassed distilled water (10 mL), and the bright yellow solution was slowly transferred with the aid of a Teflon cannula to an orange solution of Na<sub>2</sub>[Fe<sub>2</sub>(CO)<sub>8</sub>] (0.2244 g, 0.588 mmol) in degassed distilled water (10 mL) at room temperature. Upon addition of the mAc OTf, the orange solution deposited a dark green precipitate and the aqueous solution became colorless. Stirring was continued for 1 h. The aqueous solution was decanted, and the green precipitate was dried *in vacuo* and then extracted with hexane (15 mL × 5) until the washings were colorless. The green solution contained Fe<sub>3</sub>(CO)<sub>12</sub><sup>48</sup> (yield: 0.180 g, 91%) as shown by its infrared spectrum ( $\nu_{\text{CO}}$ , hexane): 2046 (s), 2025 (m), 1868 (vww), 1839 (vww) cm<sup>-1</sup>. The white solid residue was identified as N,N'-dimethyl-9,9'-biacridanyl by its infrared spectrum. (yield: 0.214 g, 94%). IR (KBr): 3022 (w), 2905 (w), 2825 (w), 1594 (s), 1475 (vs), 1428 (w), 1344 (s), 1314 (m), 1281 (s), 1265 (s), 1132 (m), 1042 (m), 930 (w), 883 (m), 855 (w), 744 (vs), 635 (m), 587 (m), 557 (m), 482 (m) cm<sup>-1</sup>. Infrared spectrum of the authentic acridine dimer (KBr): 3022 (w), 2901 (w), 2825 (w), 1593 (s), 1476 (vs), 1425 (w), 1344 (s), 1312 (m), 1281 (s), 1263 (s), 1132 (m), 1044 (m), 930 (w), 885 (m), 855 (w), 743 (vs), 636 (m), 586 (m), 556 (m), 488 (m) cm<sup>-1</sup>.

**B. Reaction of 2 equiv of mAc OTf with 1 equiv Na<sub>2</sub>[Fe<sub>2</sub>(CO)<sub>8</sub>] in Acetonitrile.** A sample of Na<sub>2</sub>[Fe<sub>2</sub>(CO)<sub>8</sub>] (0.38 g, 0.98 mmol) was dissolved in 20 mL of acetonitrile. The solution was cooled to 0 °C, and N-methylacridinium triflate (0.68 g, 1.98 mmol) dissolved in acetonitrile (8 mL) was added in 1-mL portions. The orange solution of Na<sub>2</sub>[Fe<sub>2</sub>(CO)<sub>8</sub>] turned deep red. After being stirred for 5 h at 0 °C, the solution was filtered through a pad of Celite. The infrared spectrum of the filtered solution showed carbonyl bands at  $\nu_{\text{CO}}$  = 2024, 1995, and 1956 cm<sup>-1</sup>. Solvent and other volatile components of the solution were transferred *in vacuo* into a trap cooled to -78 °C. The contents of the trap were diluted to 100 mL, and the



yield of  $\text{Fe}(\text{CO})_5$  was determined by IR spectrophotometry using a cell calibrated with a solution of  $\text{Fe}(\text{CO})_5$  in MeCN at  $\nu_{\text{CO}} = 2025$  and at  $\nu_{\text{CO}} = 1998 \text{ cm}^{-1}$  (yield: 0.99 mmol, 50% based on Fe). The purple residue remaining after evaporation was redissolved in  $\text{CH}_3\text{CN}$ . IR ( $\nu_{\text{CO}}$ ): 2067 (vw), 2032, 1999, 1975, 1952, and 1732 (vw)  $\text{cm}^{-1}$ . An authentic sample of [PPN] [ $\text{HF}_3(\text{CO})_{11}$ ],<sup>43</sup> dissolved in acetonitrile, showed IR bands at 2067 (vw), 2001, 1976, 1947, and 1733  $\text{cm}^{-1}$ .

**C. Reaction of mAc OTf with  $\text{Na}_2[\text{Fe}_2(\text{CO})_8]$ .** (i) **In Diethyl Ether.** A suspension of mAc OTf (0.369 g, 1.076 mmol) in diethyl ether (10 mL) was slowly added with the aid of a Teflon cannula to a yellow suspension of  $\text{Na}_2[\text{Fe}_2(\text{CO})_8]$  (0.205 g, 0.538 mmol) in diethyl ether (20 mL) at room temperature. The yellow suspension slowly turned a beige-brown, and the supernatant solution became deep green. Stirring was continued for 36 h. The beige precipitate was removed by filtration, and the solvent was stripped from the green supernatant solution *in vacuo*. The portionwise addition of hexane (60 mL) resulted in a green solution which contained  $\text{Fe}_3(\text{CO})_{12}$ , as determined by its infrared spectrum (yield: 0.176 g, 97%). The white solid residue after washing with water was characterized as the acridine dimer by its infrared spectrum (yield: 0.203 g, 89% isolated).

(ii) **In Toluene.** mAc OTf (0.112 g, 0.327 mmol) was added to toluene (5 mL), and the resulting bright yellow suspension was transferred with the aid of a Teflon cannula to a yellow suspension of  $\text{Na}_2[\text{Fe}_2(\text{CO})_8]$  (0.062 g, 0.164 mmol) in toluene (5 mL) at room temperature. Stirring was continued for 36 h. The pale yellow solid residue was removed by filtration, and the deep-green supernatant solution was dried *in vacuo*. Extraction of the residual solids with portions of hexane (60 mL) yielded a green solution of  $\text{Fe}_3(\text{CO})_{12}$  (13%). The yellow residue from the initial filtration was colorless after washing with water. It was identified as *N,N'*-dimethyl-9,9'-biacridanyl by its infrared spectrum (yield: 0.0057 g, 9%).

**D. Reaction of  $\text{Na}_2[\text{Fe}_2(\text{CO})_8]$  with mAc OTf in the Presence of  $\text{PPh}_3$ .** Crystalline  $\text{Na}_2[\text{Fe}_2(\text{CO})_8]$  (0.114 g, 0.298 mmol) was dissolved in MeCN (10 mL). Triphenylphosphine (0.340 g, 1.30 mmol) was added to the solution of  $\text{Na}_2[\text{Fe}_2(\text{CO})_8]$ . A solution of mAc OTf (0.194 g, 0.567 mmol) in MeCN (30 mL) was transferred with the aid of a Teflon cannula into the mixture of  $\text{PPh}_3$  and  $\text{Na}_2[\text{Fe}_2(\text{CO})_8]$  which was held at room temperature. Initially, the solution was a dark red-brown and then gradually faded to yellowish-orange. After 24 h, the solution was light yellow and a white precipitate had formed. The solution was filtered, and the white precipitate was collected and dried. The infrared spectrum of the solution indicated the presence of  $\text{Fe}(\text{CO})_4\text{PPh}_3$ ,<sup>47</sup>  $\text{Fe}(\text{CO})_3(\text{PPh}_3)_2$ ,<sup>47</sup> and  $\text{Fe}(\text{CO})_5$ . Yield:  $\text{Fe}(\text{CO})_4\text{PPh}_3$  (54%). Infrared  $\nu(\text{CO})$ : 2049 (m), 1972 (m), 1941 (s)  $\text{cm}^{-1}$  in MeCN. Yield:  $\text{Fe}(\text{CO})_3(\text{PPh}_3)_2$  (17%). IR calibrated: 1889 (s)  $\text{cm}^{-1}$  in MeCN. The white precipitate was washed with water, dried, and identified as *N,N'*-dimethyl-9,9'-biacridanyl (yield: 0.0982 g, 89%).

**E. Reaction of  $\text{Na}[\text{Fe}_2(\text{CO})_8]$  with  $\text{PPh}_3$ .** Silver tetrafluoroborate (0.098 g, 0.5 mmol) in THF (10 mL) was added with the aid of a hypodermic syringe to the solution of  $\text{Na}_2[\text{Fe}_2(\text{CO})_8]$  (0.191 g, 0.5 mmol) to form the anion-radical salt  $\text{Na}[\text{Fe}_2(\text{CO})_8]$ . Triphenylphosphine (1.315 g, 5.02 mmol) was added, and the solution of  $\text{Na}[\text{Fe}_2(\text{CO})_8]$  was allowed to stir at  $-78^\circ\text{C}$  for 24 h. The infrared spectrum of the orange solution indicated the presence of  $\text{Fe}(\text{CO})_4\text{PPh}_3$  (2049, 1972, 1941  $\text{cm}^{-1}$ ) and  $\text{Fe}(\text{CO})_3(\text{PPh}_3)_2$  (1888  $\text{cm}^{-1}$ ). Yield:  $\text{Fe}(\text{CO})_4\text{PPh}_3$  (42%) and  $\text{Fe}(\text{CO})_3(\text{PPh}_3)_2$  (24%). The brown precipitate was transparent in the carbonyl region of the infrared spectrum. IR (KBr): 1637 (sh, w), 1525 (br, m), 1384 (br, m), 1123 (sh, m), 1082 (s), 1038 (sh, m), 856 (w), 803 (w), 748 (w), 698 (w), 533 (w), 522 (w)  $\text{cm}^{-1}$ .

**F. Reaction of  $\text{AgBF}_4$  with  $\text{Na}_2[\text{Fe}_2(\text{CO})_8]$  in THF.** A solution of  $\text{AgBF}_4$  (0.194 g, 1.0 mmol) in 10 mL of THF was added to a solution of  $\text{Na}_2[\text{Fe}_2(\text{CO})_8]$  (0.191 g, 0.5 mmol) in THF (10 mL) maintained at  $-78^\circ\text{C}$ . Immediately, a silver mirror formed and the solution became dark red. IR ( $\nu_{\text{CO}}$ , THF): 2048 (sh, vw), 2020 (m), 1996 (s), 1917 (w)  $\text{cm}^{-1}$ .

**G. Reaction of  $\text{AgBF}_4$  with  $\text{Na}_2[\text{Fe}_2(\text{CO})_8]$  in MeCN.** A solution of  $\text{AgBF}_4$  (0.194 g, 1.0 mmol) in MeCN (10 mL) was added to a solution of  $\text{Na}_2[\text{Fe}_2(\text{CO})_8]$  (0.191 g, 0.5 mmol) in MeCN cooled to  $-40^\circ\text{C}$  (10 mL). The solution became red-brown and silver precipitated. IR ( $\nu_{\text{CO}}$ , MeCN): 2024 (m), 2020 (m), 1996 (s), 1947 (w)  $\text{cm}^{-1}$ .

**H. Reaction of  $[\text{Cp}_2\text{Fe}] \text{BF}_4$  with  $\text{Na}_2[\text{Fe}_2(\text{CO})_8]$  in MeCN.** Ferrocenium tetrafluoroborate ( $[\text{Cp}_2\text{Fe}] \text{BF}_4$ , 0.136 g, 0.5 mmol) dissolved in MeCN (10 mL) was added to a solution of  $\text{Na}_2[\text{Fe}_2(\text{CO})_8]$  (0.095 g, 0.25 mmol) in MeCN (10 mL) previously cooled to  $-40^\circ\text{C}$ . Infrared spectrum of the dark red solution ( $\nu_{\text{CO}}$ , MeCN): 2024 (m), 1996 (s), 1947 (w)  $\text{cm}^{-1}$ .

**I. Reaction of  $\text{Na}_2[\text{Fe}_2(\text{CO})_8]$  with  $\text{AgBF}_4$  in Water.** The disodium salt,  $\text{Na}_2[\text{Fe}_2(\text{CO})_8]$  (0.191 g, 0.5 mmol), was dissolved in water (10 mL) and cooled to  $0^\circ\text{C}$ . A solution of  $\text{AgBF}_4$  (0.194 g, 1 mmol) in water (10 mL) was then added with the aid of a Teflon cannula. Immediately, a dark gray material precipitated, and the aqueous solution became colorless. The aqueous solution was removed, and the dark gray precipitate was dried *in vacuo*. Toluene (60 mL) was added to the dark gray precipitate. The infrared spectrum of the dark green solution showed only the carbonyl bands of  $\text{Fe}_3(\text{CO})_{12}$ . Yield: 93%, 0.156 g. In a separate experiment, a solution of  $\text{AgBF}_4$  (0.194 g, 1 mmol) dissolved in water (10 mL) was added to a solution of  $\text{Na}_2[\text{Fe}_2(\text{CO})_8]$  (0.382 g, 1 mmol) in water (20 mL) at room temperature. The solution immediately became dark greenish-gray, and a dark red precipitate formed. The precipitate was filtered off and extracted with hexane (60 mL). The green solution contained only  $\text{Fe}_3(\text{CO})_{12}$  (yield: 0.138 g, 41%).

**J. Reaction of  $\text{Na}_2[\text{Fe}_2(\text{CO})_8]$  with mAc OTf in Water.** A solution of mAc OTf (0.0879 g, 0.262 mmol) in 10 mL of water was added with the aid of a Teflon cannula to solid  $\text{Na}_2[\text{Fe}_2(\text{CO})_8]$  (0.1002 g, 0.262 mmol) at room temperature. A green precipitate was filtered off and dried. Extraction of the green solid with hexane (50 mL) yielded a green solution together with a white precipitate. The green solution contained  $\text{Fe}_3(\text{CO})_{12}$  as the only carbonyl product (yield: 0.0401 g, 46%). The white solid was identified as *N,N'*-dimethyl-9,9'-biacridanyl by its IR spectrum (yield: 0.0452 g, 90%).

**K. Reaction of  $\text{Na}[\text{Fe}_2(\text{CO})_8]$  with Water.** A solution of  $\text{Na}[\text{Fe}_2(\text{CO})_8]$  in THF (10 mL) was generated from  $\text{Na}_2[\text{Fe}_2(\text{CO})_8]$  (0.191 g, 0.5 mmol) and  $\text{AgBF}_4$  (0.097 g, 0.5 mmol) at  $-78^\circ\text{C}$  as detailed above. The solvent was removed *in vacuo* from the cold ( $-78^\circ\text{C}$ ) solution. Water (15 mL) was added to the solid, which had been allowed to warm to  $23^\circ\text{C}$ . A greenish-brown suspension formed. Water was removed by evacuation of the flask, and the suspension was extracted with hexane (30 mL  $\times$  2). The green supernatant solution was filtered and dried, and the solid residue was identified as  $\text{Fe}_3(\text{CO})_{12}$ . Yield: 0.076 g (45%). The hexane-insoluble residue, a dark red solid, was redissolved in MeCN to form a red solution. IR ( $\nu_{\text{CO}}$ , MeCN): 2067 (vvw), 2022 (vw), 1981 (s), 1968 (s), 1917 (sh), 1897 (m), 1888 (sh, m), 1834 (sh, vw), 1723 (vvw)  $\text{cm}^{-1}$ . Compare  $\text{HFe}_4(\text{CO})_{13}^-$  ( $\nu_{\text{CO}}$ : 2072 (w), 2031, 1984, 1961, 1936, 1916, 1723  $\text{cm}^{-1}$ ) and  $\text{HFe}(\text{CO})_4^-$  ( $\nu_{\text{CO}}$ : 1914 (m), 1880 (s)  $\text{cm}^{-1}$ ).

**L. Reaction of  $[\text{iQ}]_2[\text{Fe}_2(\text{CO})_8]$  with  $\text{PPh}_3$  in MeCN.** A solution of  $[\text{iQ}]_2[\text{Fe}_2(\text{CO})_8]$  (0.600 g, 0.96 mmol) in MeCN (15 mL) was added to a solution of  $\text{PPh}_3$  (2.277 g, 8.66 mmol) in 30 mL of the same solvent at  $23^\circ\text{C}$ . The color of the solution gradually changed from brown to orange, and the infrared spectrum of the solution indicated the presence of  $\text{Fe}(\text{CO})_4\text{PPh}_3$  and  $\text{Fe}(\text{CO})_3(\text{PPh}_3)_2$ . The reaction was complete in 2 h. The yields of  $\text{Fe}(\text{CO})_4\text{PPh}_3$  (63%) and  $\text{Fe}(\text{CO})_3(\text{PPh}_3)_2$  (23%) were determined by calibration of the infrared cell using the authentic samples.<sup>47</sup> The solvent was removed from the orange solution *in vacuo*, and the residue was extracted with hexane (20 mL  $\times$  4). The residual solid was dissolved in toluene (30 mL), and the solution was filtered through a column of silica gel. A pale-yellow eluant was the first fraction collected. The solvent was removed from this fraction and the yellow solid residue was identified as *N,N'*-dimethyl-1,1',2,2'-



tetrahydro-1,1-biisoquinolyl by comparison of its IR spectrum (KBr) with the authentic sample.<sup>44</sup> Yield: 0.338 g (86%).

**M. Reaction of [PP]<sub>2</sub>[Fe<sub>2</sub>(CO)<sub>8</sub>] with PPh<sub>3</sub> in MeCN.** A solution of [PP]<sub>2</sub>[Fe<sub>2</sub>(CO)<sub>8</sub>] (0.411 g, 0.608 mmol) in MeCN (10 mL) was added to 30 mL of an acetonitrile solution of PPh<sub>3</sub> (1.433 g, 5.472 mmol). The solution gradually turned from brown to orange. The infrared spectrum of the orange solution indicated that Fe(CO)<sub>4</sub>PPh<sub>3</sub> and Fe(CO)<sub>3</sub>(PPh<sub>3</sub>)<sub>2</sub> were formed. After 5 h, the reaction was complete. Infrared spectroscopy was used to quantify the products: Fe(CO)<sub>4</sub>PPh<sub>3</sub> (67%) and Fe(CO)<sub>3</sub>(PPh<sub>3</sub>)<sub>2</sub> (21%).

**N. Reactions of Carbonylferrate Charge-Transfer Salts in MeCN.** When a solution of [iQ]<sub>2</sub>[Fe<sub>2</sub>(CO)<sub>8</sub>] in MeCN was stirred at room temperature for several hours, the resulting red brown solution showed infrared bands ( $\nu_{\text{CO}}$ ) at 2024 (m), 1996 (s), and 1949 (w) cm<sup>-1</sup>. Similarly, the red-brown solution of [PP]<sub>2</sub>[Fe<sub>2</sub>(CO)<sub>8</sub>] in MeCN was stirred for several hours at room temperature. The carbonyl bands of [Fe<sub>2</sub>(CO)<sub>8</sub>]<sup>2-</sup> disappeared, and new infrared bands appeared at 2024 (m), 1994 (s), and 1952 (w) cm<sup>-1</sup> upon stirring at 23 °C for several hours. An identical infrared spectrum was obtained upon dissolution of [*N*-methyllutidinium]<sub>2</sub>[Fe<sub>2</sub>(CO)<sub>8</sub>] in MeCN at room temperature and stirring for several hours. IR ( $\nu_{\text{CO}}$ , MeCN): 2024 (m), 1994 (s), 1954 (w) cm<sup>-1</sup>.

**Electrochemistry of Cationic Acceptors and Octacarbonyldiferrate.** The electrochemistry of octacarbonyldiferrate and the cationic acceptors used in this study was performed in acetonitrile containing 0.1 M tetra-*n*-butylammonium hexafluorophosphate as the supporting electrolyte. Solutions of the analyte ( $5.0 \times 10^{-3}$  M for cations,  $2.5 \times 10^{-2}$  M for [Fe<sub>2</sub>(CO)<sub>8</sub>]<sup>2-</sup>) and supporting electrolyte, (TBA)PF<sub>6</sub> (0.1 M), were prepared in the cell by standard Schlenk techniques. Cyclic voltammetry was performed with the aid of a BAS 100A electrochemical analyzer, and potentials were referenced to an aqueous SCE connected to the analyte compartment via a cracked glass tip. Under these conditions the  $E^{\circ}$  and  $\Delta E_p$  for the oxidation of ferrocene was +0.40 (vs SCE) and 68 mV, respectively. For the cations, the irreversible cathodic peak potentials ( $E_p$ ) of *N*-methylcollidinium, *N*-methyllutidinium, and CpFe( $\eta^6$ -C<sub>6</sub>H<sub>6</sub>) cations were observed at -1.63, -1.45, and -1.39 V, respectively, at a sweep rate of 500 mV s<sup>-1</sup>. We found the first oxidation of [Fe<sub>2</sub>(CO)<sub>8</sub>]<sup>2-</sup> to be reversible on the CV time scale, as has been previously observed.<sup>11</sup> The large peak-to-peak separation ( $\Delta E_p = 300$  mV) was consistent with considerable structural reorganization upon electrooxidation of the dianion to [Fe<sub>2</sub>(CO)<sub>8</sub>]<sup>-</sup>. The value for the reversible oxidation potential in THF ( $E^{\circ}_{\text{ox}} = -1.41$  vs Cp<sub>2</sub>Fe) was in agreement with that previously reported.<sup>11</sup> The oxidation of the radical anion to the neutral fragment appeared as an irreversible anodic wave at  $E_p = -0.20$  V (vs Cp<sub>2</sub>Fe at 0.5 V s<sup>-1</sup>). Qualitatively, the same electrochemical behavior was observed in acetonitrile. The dianion was reversibly oxidized at  $E^{\circ}_{\text{ox}} = -1.20$  V vs Cp<sub>2</sub>Fe, and the radical anion was also irreversibly oxidized ( $E_p = -0.40$  V vs Cp<sub>2</sub>Fe at a sweep rate,  $v = 0.5$  V s<sup>-1</sup>).

The various acceptor cations, A<sup>+</sup>, were irreversibly reduced on the CV time scale at a scan rate of 0.5 V s<sup>-1</sup>. The reversible  $E^{\circ}_{\text{red}}$  values in Table 1 were obtained either from the literature or calculated by accounting for the kinetic potential shift<sup>65</sup> of  $E_p$  owing to follow up dimerization of the radicals, A<sup>•</sup>, according to the expression  $E^{\circ} = E_p + (RT/nF)0.905 - (RT/3nF) \ln\{^{2/3}k_{\text{dim}}C(RT/nFv)\}$ <sup>66</sup> where  $k_{\text{dim}}$  is the second-order rate constant for dimerization of the radicals,<sup>67</sup>  $C$  is the concentration of the cation ( $5 \times 10^{-3}$  M), and  $v$  is the scan rate of 0.5 V s<sup>-1</sup>.

**X-ray Crystallographic Structure Determination of [mL]<sub>2</sub>[Fe<sub>2</sub>(CO)<sub>8</sub>].** A ruby-red block having approximate dimensions 0.30 × 0.40 × 0.45 mm was mounted in a random orientation on a Nicolet R3m/V automatic diffractometer. Since the sample was potentially air-sensitive, all handling of the crystals was done under mineral oil. The sample was placed in a stream of dry nitrogen gas at -50 °C, and the radiation used was Mo K $\alpha$  monochromatized by a highly ordered graphite crystal. The Laue symmetry was determined to be 2/*m*, and from the systematic absences noted the space group was shown unambiguously to be *P*2<sub>1</sub>/*n*. Final cell constants, as well as other information pertinent to data collection and refinement, are listed as follows: space group *P*2<sub>1</sub>/*n* (monoclinic); cell constants  $a = 10.112(4)$  Å,  $b = 9.410(3)$  Å,  $c = 13.379(5)$  Å,  $\beta = 96.84(2)^{\circ}$ ;  $V = 1264$  Å<sup>3</sup>; formula (C<sub>8</sub>H<sub>12</sub>N<sup>+</sup>)<sub>2</sub>C<sub>8</sub>O<sub>8</sub>Fe<sub>2</sub><sup>2-</sup>; formula weight 580.20; formula units per cell,  $Z = 2$ ; density,  $\rho = 1.52$  g cm<sup>-3</sup>; absorption coefficient  $\mu = 11.95$  cm<sup>-1</sup>; radiation (Mo K $\alpha$ ),  $\lambda = 0.71073$  Å; collection range  $4^{\circ} \leq 2\theta \leq 50^{\circ}$ ; total data collected 2513; independent data,  $I > 3\sigma(I)$  1874; total variables, 173;  $R = 0.031$ ;  $R_w = 0.035$ . Intensities were measured using the  $\theta:2\theta$  scan technique, with the scan rate depending on the count obtained in rapid prescans of each reflection. Two standard reflections were monitored after every 2 h or every 100 data collected, and these showed no significant variation. During data reduction Lorentz and polarization corrections were applied, as well as a semi-empirical absorption correction based on  $\psi$  scans of 10 reflections having  $\chi$  values between 70 and 90°. The structure was solved by interpretation of the Patterson map, which revealed the position of the Fe atom in the asymmetric unit, consisting of one cation in a general position and one-half anion situated about an inversion center. Remaining atoms were located in subsequent difference Fourier syntheses. The usual sequence of isotropic and anisotropic refinement was followed, after which all hydrogens were entered in ideal calculated positions and constrained to riding motion, with a single variable isotropic temperature factor for all of them. The three methyl groups were treated as ideal rigid bodies and allowed to rotate independently. After all shift/esd ratios were less than 0.1, convergence was reached at the agreement factors listed above. No unusually high correlations were noted between any of the variables in the last cycle of full-matrix least squares refinement, and the final difference density map showed a maximum peak of about 0.4 e/Å<sup>3</sup>. All calculations were made using Nicolet's SHELXTL PLUS (1987) series of crystallographic programs.

**Acknowledgment.** We thank the National Science Foundation, the R. A. Welch Foundation, and the Texas Advanced Research Program for financial support.

**Supporting Information Available:** Crystallographic tables for *N*-methyllutidinium octacarbonyldiferrate including crystal and refinement data and thermal parameters (2 pages).

OM950403L

(66) Bard, A. J.; Faulkner, L. R. *Electrochemical Methods: Fundamentals and Applications*; Wiley: New York, 1980; p 451 ff.

(67) Taken as  $2 \times 10^{10}$  M<sup>-1</sup> s<sup>-1</sup> (diffusion control) except for *N*-methylcollidinium, with  $k_{\text{dim}} = 2.5 \times 10^6$ ; Pragst, F.; Koppel, H.; Walkhoff, E.; Boche, E. *J. Prakt. Chem.* **1987**, *329*, 645.

(68) Lacoste, M.; Astruc, D. *J. Chem. Soc., Chem. Commun.* **1987**, 667.

(69) Oturan, M. A.; Dostert, P.; Strolin Benedetti, M.; Morieux, J.; Anne, A.; Fleury, M. B. *J. Electroanal. Chem.* **1988**, *242*, 171.

(65) Tilset, M.; Parker, V. D. *J. Am. Chem. Soc.* **1989**, *111*, 6711.

## Diiron Aminoalkylidene Complexes

Valerio Zanotti,<sup>†</sup> Silvia Bordoni,<sup>†</sup> Luigi Busetto,<sup>\*,†</sup> Lucia Carlucci,<sup>†</sup>  
Antonio Palazzi,<sup>†</sup> Rossella Serra,<sup>†</sup> Vincenzo G. Albano,<sup>\*,‡</sup> Magda Monari,<sup>‡</sup>  
Fabio Prestopino,<sup>‡</sup> Franco Laschi,<sup>§</sup> and Piero Zanello<sup>§</sup>

Dipartimento di Chimica Fisica ed Inorganica, Università di Bologna, Viale Risorgimento 4,  
I-40136 Bologna, Italy, Dipartimento di Chimica "G. Ciamician", Università di Bologna,  
Via Selmi 2, I-40126 Bologna, Italy, and Dipartimento di Chimica, Università di Siena,  
Pian dei Mantellini 44, I-53100, Siena, Italy

Received May 17, 1995<sup>®</sup>

The reactions of the sulfonium salts  $[\text{Fe}_2(\text{CO})_2(\text{cp})_2(\mu\text{-CO})\{\mu\text{-C}(\text{X})\text{SMe}_2\}]\text{SO}_3\text{CF}_3$  [ $\text{X} = \text{CN}$  (**1a**),  $\text{H}$  (**1b**)] with a variety of amines are presented. **1a** yields ammonium cations  $[\text{Fe}_2(\text{CO})_2(\text{cp})_2(\mu\text{-CO})\{\mu\text{-C}(\text{CN})\text{NR}_3\}]$  [ $\text{R} = \text{Me}$  (**2**), Dabco (**3**) (Dabco = 1,4-diazabicyclo[2.2.2]-octane)], aminoalkylidene  $[\text{Fe}_2(\text{CO})_2(\text{cp})_2(\mu\text{-CO})\{\mu\text{-C}(\text{CN})\text{NR}_2\}]$  (**4**), isocyanide  $[\text{Fe}_2(\text{CO})_2(\text{cp})_2(\mu\text{-CO})(\mu\text{-CNR})]$  (**7**), or diaminoalkylidene  $[\text{Fe}_2\{\text{CN}(\text{H})(\text{CH}_2)_2\text{N}(\text{H})\}(\text{CO})(\text{cp})_2(\mu\text{-CO})_2]$  (**11**) complexes by reacting with tertiary amines, secondary amines, primary amines, or ethylenediamine, respectively. **1b** and secondary amines yield  $[\text{Fe}_2(\text{CO})\{\text{C}(\text{H})\text{NR}_2\}(\text{cp})_2(\mu\text{-CO})_2]$  (**6**). The formation of type **4** bridging and **6** terminal aminoalkylidene derivatives also *via*  $\mu\text{-C}$  addition of  $\text{CN}^-$  or  $\text{H}^-$  to aminoalkylidyne  $[\text{Fe}_2(\text{CO})_2(\text{cp})_2(\mu\text{-CO})(\mu\text{-CNR}_2)]^+$ , respectively, as well as the preparation of the terminal  $[\text{Fe}_2\{\text{C}(\text{CN})\text{NPr}^i_2\}(\text{CO})(\text{cp})_2(\mu\text{-CO})_2]$  (**5**) from **1a** and  $\text{NHPri}_2$ , allows to clarify the role of electronic and steric effects in determining the position of the aminoalkylidene ligands. The X-ray structure of **5** has been determined. The crystal contains two independent molecules of the *trans*-isomer. The terminally bonded aminoalkylidene ligand exhibits weaker  $\text{Fe}-\text{C}(\text{carbene})$  ( $\text{Fe}-\text{C}$  1.915(3) Å) and stronger  $\text{C}(\text{carbene})-\text{N}(\text{amine})$   $\pi$  bonds ( $\text{C}-\text{N}$  1.320(4) Å) with respect to the bridging coordination. Electrochemistry shows that **5** undergoes a chemically reversible one electron oxidation to the corresponding monocation  $[\mathbf{5}]^+$ , which has been characterized by X-band EPR spectroscopy. All the complexes have been spectroscopically characterized, and a variable-temperature NMR on  $[\text{Fe}_2(\text{CO})\{\text{C}(\text{H})\text{NMe}_2\}(\text{cp})_2(\mu\text{-CO})_2]$  (**6a**) indicates exchange of the aminoalkylidene ligand between the two Fe atoms.

### Introduction

Cationic binuclear  $\mu$ -alkylidyne complexes provide a very effective entry into the synthesis of bridging alkylidene derivatives, simply *via* nucleophilic addition at the  $\mu\text{-C}$  carbon.<sup>1</sup> However this method has been less successful in the preparation of heteroatom-substituted  $\mu$ -alkylidene complexes<sup>2</sup> which still represent a relatively unexplored class of compounds.<sup>3</sup>

In the last few years we have been developing an alternative approach to the synthesis of diiron  $\mu$ -alkylidene complexes, which consists of the  $\text{SMe}_2$  displacement from  $[\text{Fe}_2(\text{CO})_2(\text{cp})_2(\mu\text{-CO})\{\mu\text{-C}(\text{X})\text{SMe}_2\}]\text{SO}_3\text{CF}_3$  (**1a**,  $\text{X} = \text{CN}$ ;<sup>4</sup> **1b**,  $\text{X} = \text{H}^5$ ) with a variety of nucleo-

philes, including alcohols and phosphines.<sup>5-7</sup> Moreover, we have preliminarily communicated<sup>8</sup> that **1a**, like terminal carbene complexes, reacts with tertiary, secondary, or primary amines to form ammonium cations  $[\text{Fe}_2(\text{CO})_2(\text{cp})_2(\mu\text{-CO})\{\mu\text{-C}(\text{CN})\text{NR}_3\}]$ , aminoalkylidene  $[\text{Fe}_2(\text{CO})_2(\text{cp})_2(\mu\text{-CO})\{\mu\text{-C}(\text{CN})\text{NR}_2\}]$ , or isocyanide  $[\text{Fe}_2(\text{CO})_2(\text{cp})_2(\mu\text{-CO})(\mu\text{-CNR})]$  complexes, respectively.

We wish to report here on all the results obtained in this field, namely the reactions of **1a,b** with a variety of amines including diamines, focusing on the hitherto unexplored synthesis, spectroscopic properties, structure, and bonding of the bridging  $[\text{Fe}_2(\text{CO})_2(\text{cp})_2(\mu\text{-CO})\{\mu\text{-C}(\text{CN})\text{NR}_2\}]$  (**4**) and terminal  $[\text{Fe}_2(\text{CO})\{\text{C}(\text{H})\text{NRR}'\}(\text{cp})_2(\mu\text{-CO})_2]$  (**6**) aminoalkylidene complexes. In addition an alternative synthesis for these complexes will be described *via*  $\text{H}^-$  and  $\text{CN}^-$  nucleophilic addition at the  $\mu\text{-C}$  aminoalkylidyne  $[\text{Fe}_2(\text{CO})_2(\text{cp})_2(\mu\text{-CO})(\mu\text{-CNR}_2)]^+$ , and the role of electronic and steric factors in determining the bridging, as in type **4**, or the terminal, as in type **6**, coordination modes of the aminoalkylidene ligands will be pointed out. Finally for one of the latter complexes,  $[\text{Fe}_2\{\text{C}(\text{CN})\text{NPr}^i_2\}(\text{CO})(\text{cp})_2(\mu\text{-CO})_2]$  (**5**), the

<sup>†</sup> Dipartimento di Chimica Fisica ed Inorganica, Università di Bologna.

<sup>‡</sup> Dipartimento di Chimica "G. Ciamician", Università di Bologna.

<sup>§</sup> Dipartimento di Chimica, Università di Siena.

<sup>®</sup> Abstract published in *Advance ACS Abstracts*, October 1, 1995.  
(1) Jemmis, E. D.; Prasad, B. V. *Organometallics* **1992**, *11*, 2528 and references therein.

(2) Significant examples include: (a) Casey, C. P.; Crocker, M.; Vosejpk, P. C.; Fagan, P. J.; Marder, S. R.; Gohdes, M. A. *Organometallics* **1988**, *7*, 670. (b) Kao, S. C.; Lu, P. P. Y.; Pettit, R. *Organometallics* **1982**, *1*, 911. (c) Schroeder, N. C.; Funchess, R.; Jacobson, R. A.; Angelici, R. J. *Organometallics* **1989**, *8*, 521. (d) Howard, J. A. K.; Jeffery, J. C.; Laguna, M.; Navarro, R.; Stone, F. G. A. *J. Chem. Soc., Dalton Trans.* **1981**, 751.

(3) Adams, R. D. *Chem. Rev.* **1989**, *89*, 1703.

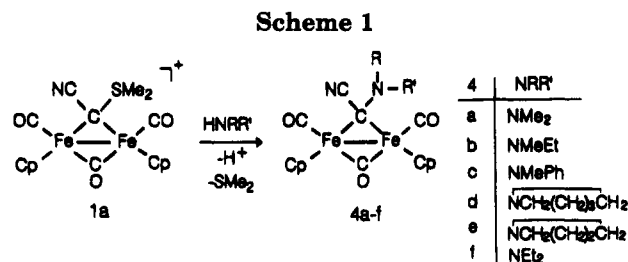
(4) Busetto, L.; Zanotti, V.; Bordoni, S.; Carlucci, L.; Albano, V. G.; Braga, D. *J. Chem. Soc., Dalton Trans.* **1992**, 1105.

(5) Bordoni, S.; Mazza, F.; Zanotti, V. *Inorg. Chim. Acta* **1994**, *223*, 31.

(6) Busetto, L.; Cassani, M. C.; Zanotti, V.; Albano, V. G.; Braga, D. *J. Organomet. Chem.* **1991**, *415*, 395.

(7) (a) Busetto, L.; Carlucci, L.; Zanotti, V.; Albano, V. G.; Monari, M. *Chem. Ber.* **1992**, *125*, 1125. (b) Bassi, M.; Carlucci, L.; Zanotti, V. *Inorg. Chim. Acta* **1993**, *204*, 171.

(8) (a) Albano, V. G.; Bordoni, S.; Braga, D.; Busetto, L.; Palazzi, A.; Zanotti, V. *Angew. Chem., Int. Ed. Engl.* **1991**, *30*, 847.



X-ray molecular structure together with the electrochemical properties are presented and discussed.

## Results

**Reactions with Amines.** The addition of a 5-fold excess of tertiary amines like NMe<sub>3</sub> or Dabco (Dabco = 1,4-diazabicyclo[2.2.2]octane) to a MeCN solution of [Fe<sub>2</sub>(CO)<sub>2</sub>(cp)<sub>2</sub>(μ-CO){μ-C(CN)SMe<sub>2</sub>}]SO<sub>3</sub>CF<sub>3</sub> (**1a**) causes the displacement of Me<sub>2</sub>S to form the corresponding ammonium complexes [Fe<sub>2</sub>(CO)<sub>2</sub>(cp)<sub>2</sub>(μ-CO){μ-C(CN)-NMe<sub>3</sub>}]SO<sub>3</sub>CF<sub>3</sub> (**2**) and [Fe<sub>2</sub>(CO)<sub>2</sub>(cp)<sub>2</sub>(μ-CO){μ-C(CN)-Dabco}]SO<sub>3</sub>CF<sub>3</sub> (**3**), respectively, which, owing to decomposition, have been characterized only by infrared spectroscopy in the reaction mixture. This result contrasts with the stability shown by the strictly related compound [Fe<sub>2</sub>(CO)<sub>2</sub>(cp)<sub>2</sub>(μ-CO){μ-C(H)NMe<sub>3</sub>}]SO<sub>3</sub>CF<sub>3</sub>, which has been analogously obtained by reacting NMe<sub>3</sub> with [Fe<sub>2</sub>(CO)<sub>2</sub>(cp)<sub>2</sub>(μ-CO){μ-C(H)SMe<sub>2</sub>}]SO<sub>3</sub>CF<sub>3</sub> (**1b**)<sup>5</sup> or, alternatively, by simple addition of NMe<sub>3</sub> to the cationic methylidyne complex [Fe<sub>2</sub>(CO)<sub>2</sub>(cp)<sub>2</sub>(μ-CO)(μ-CH)]<sup>+</sup>.<sup>2a</sup>

The room-temperature reactions of **1a**, in MeCN solution, with a large excess of anhydrous secondary amine (HNRR') readily form the corresponding bridging-aminoalkylidene complexes [Fe<sub>2</sub>(CO)<sub>2</sub>(cp)<sub>2</sub>(μ-CO){μ-C(CN)NRR'}] (**4a-f**) (Scheme 1), which could be isolated in variable yields (20–60%) as red air-stable crystalline solids. The bulky diphenylamine was found to be unreactive, under the same experimental conditions.

Compounds **4a-e** show, in their IR spectra, a weak ν(CN) absorption at about 2148 cm<sup>-1</sup> and a strong-weak-medium ν(CO) band pattern (e.g. for **4a** at 2004, 1970, and 1799 cm<sup>-1</sup>) (Figure 1a) common to all the analogous μ-cyanoalkylidene complexes [Fe<sub>2</sub>(CO)<sub>2</sub>(cp)<sub>2</sub>(μ-CO){μ-C(CN)X}] (X = SR,<sup>9</sup> OR,<sup>6</sup> PR<sub>2</sub>,<sup>7</sup> N(H)Ph<sup>8</sup>), which adopt a *cis* configuration (cp ligands on the same side of the Fe-Fe bond). Despite the possible presence of two *cis*-isomers, depending on the relative orientation of the CN and NRR' μ-C substituents with respect to the CO (or cp) ligands, only one isomer was observed in solution. In accordance, one single cp resonance in both the <sup>1</sup>H and <sup>13</sup>C NMR spectra of the **4a-e** complexes has been found (e.g. for **4d** at δ 4.76 and 91.2). Since the structurally characterized<sup>6-9</sup> μ-cyanoalkylidene complexes, including the precursor **1a**,<sup>4</sup> have been demonstrated to adopt the *cis* configuration with the CN group on the cp side, we assume that compounds **4a-e** also adopt this geometry. However, the <sup>13</sup>C NMR of **4a** shows, in addition to the usual cp resonances, two minor signals of equal intensity (at δ 87.5 and 87.2) which account for the presence of small amounts of the *trans* isomer. This is consistent with the fact that *trans*-isomers are observed only among the μ-cyanoalkylidene

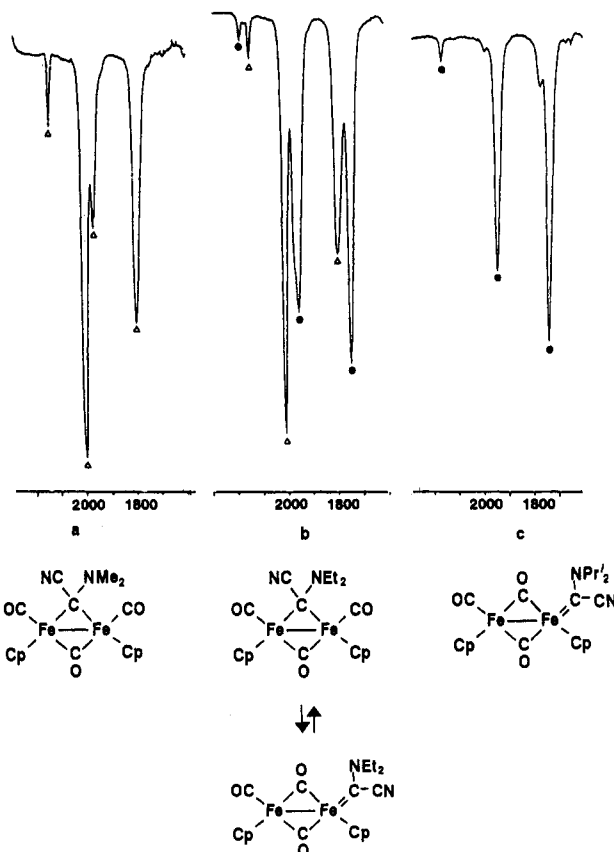


**Figure 1.** IR spectra (in CH<sub>2</sub>Cl<sub>2</sub> solution) of the complexes (a) **4a**, (b) **4b**, and (c) **5**. Absorptions attributable to the bridging-aminoalkylidene complexes are indicated with a Δ mark, and those due to the terminally bonded carbene isomer with a • dot.

complexes [Fe<sub>2</sub>(CO)<sub>2</sub>(cp)<sub>2</sub>(μ-CO){μ-C(CN)X}] bearing a less sterically demanding μ-C substituent (X = H,<sup>10</sup> CN,<sup>10</sup> OMe<sup>6</sup>).

In contrast to the IR absorptions of compounds **4a-e**, the product of the reaction of **1a** with diisopropylamine shows, in CH<sub>2</sub>Cl<sub>2</sub>, only two ν(CO) bands at 1949 (s) and 1742 (vs) cm<sup>-1</sup> (Figure 1c). This pattern is similar to that observed for [Fe<sub>2</sub>{CN(R)CH<sub>2</sub>CH<sub>2</sub>NR'}(CO)(cp)<sub>2</sub>(μ-CO)<sub>2</sub>] [R = H (see below), Me, Et<sup>11</sup>] and in agreement with the formulation of the complex as [Fe<sub>2</sub>{C(CN)NPr'<sub>2</sub>}(CO)(cp)<sub>2</sub>(μ-CO)<sub>2</sub>] (**5**) in which the cyanoaminoalkylidene ligand is terminally bonded to one of the iron atoms. Moreover, its <sup>13</sup>C NMR spectrum, recorded at -50 °C, shows two alkylidene carbon resonances (indicative of a *cis-trans* isomeric mixture) at δ 232.7 and 234.0, which are well within the range expected for terminal aminocarbene ligands<sup>12</sup> and about 60 ppm downfield with respect to the corresponding resonance in the bridging alkylidene complexes (e.g., for **4a** at δ 160 ppm). The proton resonances, at room temperature, appear as broad signals, presumably due to ligand exchange between bridging and terminal

(10) Aime, S.; Cordero, L.; Gobetto, R.; Bordoni, S.; Busetto, L.; Zanotti, V.; Albano, V. G.; Braga, D.; Grepioni, F.; *J. Chem. Soc., Dalton Trans.* **1992**, 2961.

(11) Lappert, M. F.; Pye, P. L. *J. Chem. Soc., Dalton Trans.* **1977**, 2172.

(12) Dotz, K. H.; Fischer, H.; Hoffman, P.; Kreissl, F. R.; Schubert, U.; Weiss, K., Eds. *Transition Metal Carbene Chemistry*; Verlag Chemie: Weinheim, West Germany, 1983.

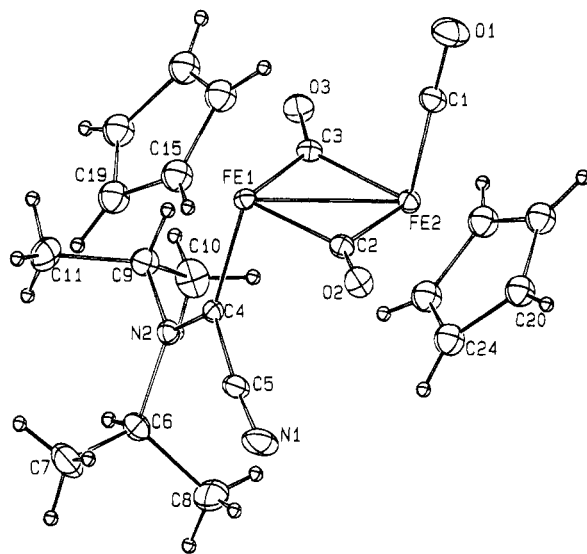
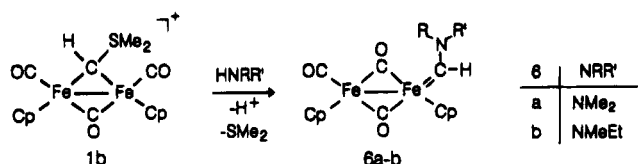


**Figure 2.** ORTEP drawing of  $[\text{Fe}_2\{\text{C}(\text{CN})\text{NPr}'_2\}(\text{CO})(\text{cp})_2(\mu\text{-CO})_2]$  (**5**) (molecule A).

### Scheme 2



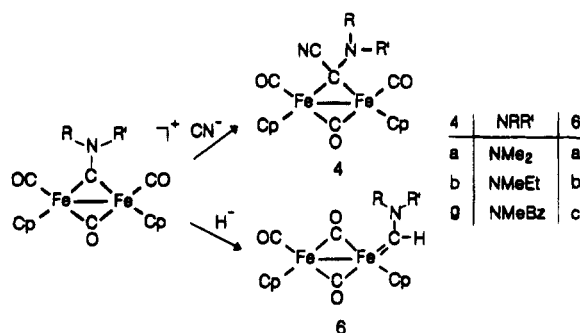
coordination positions.<sup>13</sup> The nature of compound **5** has been ascertained by an X-ray diffraction study, which has shown the terminal coordination of the aminoalkylidene ligand and the *trans*-configuration of the molecule (Figure 2). Stereochemical features are discussed in the structural section.

Finally complex **4f**, obtained by reacting **1a** with  $\text{HNEt}_2$ , shows in  $\text{CH}_2\text{Cl}_2$  solution IR  $\nu(\text{CO})$  absorptions at 2004 s, 1965 sh, 1949 s, 1796 m, and 1743 s  $\text{cm}^{-1}$ , (Figure 1b) which do not change with time and are the sum of the band patterns of type **4** and **5** complexes, indicating the presence, in solution, of an equilibrium mixture of the terminal and bridging isomers.

Likewise **1a**, the sulfonium  $[\text{Fe}_2(\text{CO})_2(\text{cp})_2(\mu\text{-CO})_2\{\mu\text{-C}(\text{H})(\text{SMe}_2)\}]\text{SO}_3\text{CF}_3$  (**1b**) readily reacts with the secondary amines  $\text{HNMe}_2$  or  $\text{HN}(\text{Me})\text{Et}$  to form the complexes  $[\text{Fe}_2(\text{CO})\{\text{C}(\text{H})(\text{NRR}')\}(\text{cp})_2(\mu\text{-CO})_2]$  (**6a,b**) (Scheme 2), whose spectroscopic properties are similar to those found for type **5** complexes. In fact the IR spectra of **6** consist of two  $\nu(\text{CO})$  absorptions at about 1933 and 1725  $\text{cm}^{-1}$ . In the  $^1\text{H}$  NMR spectra, at room temperature, the cyclopentadienyl ring protons give rise to a single very broad signal (e.g. for **6a** at  $\delta$  4.57) which becomes sharp by increasing the temperature (at about 40 °C) whereas, at lower temperature (-20 °C), two distinct sharp signals are originated (e.g. for **6a** at  $\delta$  4.69 and 4.49). These results are clearly indicative of a temperature dependent fluxional process involving the exchange of the aminoalkylidene ligand between the two Fe atoms. A very similar fluxional process has previously been observed in the alkoxy-alkylidene fulvalene complex  $[\text{FvMo}_2(\text{CO})_5(\text{=CO}(\text{CH}_2)_2\text{CH}_2)]$  (Fv = fulvalene)

(13) (a) Colborn, R. E.; Dyke, A. F.; Knox, S. A. R.; Mead, K. A.; Woodward, P. *J. Chem. Soc., Dalton Trans.* **1983**, 2099. (b) Drage, J. S.; Vollhardt, K. P. C. *Organometallics* **1986**, *5*, 280. (c) Farrugia, L. J.; Mustoo, L. *Organometallics* **1992**, *11*, 2941.

### Scheme 3



and likewise attributed to the movement of the alkylidene ligand about the Mo-Mo bond.<sup>13b</sup> We believe that a plausible mechanism of the exchange process involves the bridging alkylidene  $[\text{Fe}_2(\text{CO})_2(\text{cp})_2(\mu\text{-CO})_2\{\mu\text{-C}(\text{H})(\text{NMe}_2)\}]$  complex as intermediate. This idea is supported by the observation that terminal-bridging interconversion occurs in the related type **4** complexes. Moreover, whereas the cp protons exhibit a broadening at room temperature, the alkylidene ligand protons remain sharp indicating that the ligand remain intact while moving from one metal to the other. One more feature in the  $^1\text{H}$  NMR spectra of **6a** must be evidenced: the room-temperature, as well as the low-temperature, spectra show two singlets for the Me groups. Their expected inequivalence is the consequence of the hindered rotation around the C(carbene)-N bond, as usually found in aminocarbene complexes.<sup>12</sup> The rotational barrier for aminocarbene ranges about 25–30 kcal/mol. In fact the spectra of **6a** recorded at about 50 °C show a marked broadening of the Me signals which start to coalesce due to exchange occurring at that temperature.

It is worth mentioning that an alternative route to the synthesis of type **4** and **6** complexes is feasible. This consists in the room-temperature reaction of the cationic aminoalkylidene complexes  $[\text{Fe}_2(\text{CO})_2(\text{cp})_2(\mu\text{-CO})(\mu\text{-CNRR}')]^+$ <sup>14</sup> with  $\text{Bu}^n_4\text{NCN}$  or  $\text{NaBH}_4$ , respectively. Under these mild conditions, the bridging carbon selectively adds  $\text{CN}^-$  or  $\text{H}^-$  to give the corresponding cyano-aminoalkylidene complexes  $[\text{Fe}_2(\text{CO})_2(\text{cp})_2(\mu\text{-CO})\{\mu\text{-C}(\text{CN})(\text{NRR}')\}]$  (**4a,b,g**) and  $[\text{Fe}_2(\text{CO})\{\text{C}(\text{H})(\text{NRR}')\}(\text{cp})_2(\mu\text{-CO})_2]$  (**6a-c**) (Scheme 3).

Cyanide and hydride nucleophilic addition at the  $\mu\text{-C}$  of  $[\text{M}_2(\text{CO})_2(\text{cp})_2(\mu\text{-CO})(\mu\text{-CNRR}')]^+$  (M = Fe,<sup>15,16</sup> Ru<sup>17</sup>) has been previously reported. Formation of type **6** complexes also by this method confirms the tendency of the aminoalkylidene ligands  $=\text{C}(\text{H})\text{NRR}'$  to occupy a terminal coordination position. Therefore, on substituting  $\text{CN}$  with  $\text{H}$ , the formation of terminally bonded aminocarbene complexes **6** is observed even in the case of less sterically demanding amines which give the bridging complexes in the cyanide counterparts **4**.

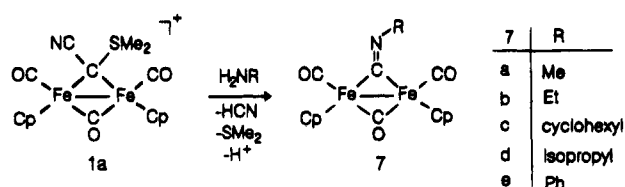
(14) (a) Cox, G.; Dowling, C.; Manning, A. R.; McArdle, P.; Cunningham, D. *J. Organomet. Chem.* **1992**, *438*, 143. (b) Willis, S.; Manning, A. R.; Stephens, F. S. *J. Chem. Soc., Dalton Trans.* **1980**, 186.

(15) Busetto, L.; Carlucci, L.; Zanotti, V.; Albano, V. G.; Braga, D. *J. Chem. Soc., Dalton Trans.* **1990**, 243.

(16) Albano, V. G.; Busetto, L.; Castellari, C.; Monari, M.; Palazzi, A.; Zanotti, V. *J. Chem. Soc., Dalton Trans.* **1993**, 3661.

(17) (a) Busetto, L.; Carlucci, L.; Zanotti, V.; Albano, V. G.; Monari, M. *J. Organomet. Chem.* **1993**, *447*, 271. (b) Albano, V. G.; Busetto, L.; Cassani, M. C.; Monari, M.; Zanotti, V. *J. Organomet. Chem.* **1995**, *488*, 133.

Scheme 4



Treatment of acetonitrile solutions of **1a** with a large excess of primary amine ( $\text{NH}_2\text{R}$ ) causes degradation of the  $\mu\text{-C}(\text{CN})\text{SMe}_2$  unit to form the corresponding isocyanide derivatives  $[\text{Fe}_2(\text{CO})_3(\text{cp})_2(\text{CNR})]$  (**7a-e**) (Scheme 4).

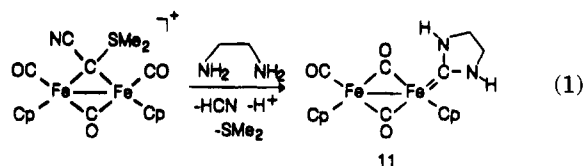
Complexes **7a-e** have been isolated (25–60% yield) by chromatography, purified by crystallization, and identified by comparison of their physical and spectroscopic properties with those reported in the literature.<sup>18</sup> Since formation of the isocyanides occurs very rapidly, possible intermediates containing the  $\mu\text{-C}(\text{CN})\text{N}(\text{H})\text{R}$  group are usually not detected. However, when the reactions described in Scheme 4 were performed by adding the stoichiometric amount of amines, it has been possible to detect by IR spectroscopy ( $\text{H}_2\text{NPr}^+$ ) and even to isolate ( $\text{H}_2\text{NPh}$ ) the intermediates  $[\text{Fe}_2(\text{CO})_2(\text{cp})_2(\mu\text{-CO})\{\mu\text{-C}(\text{CN})\text{N}(\text{H})\text{R}\}]$  (R = Ph, **8a**; R = Pr<sup>i</sup>, **8b**). Compound **8a**, which has been structurally characterized,<sup>8</sup> upon standing in  $\text{CH}_2\text{Cl}_2$  solution slowly converts into the  $\mu$ -phenyl isocyanide derivative **7e**.

The spectroscopic properties of **8a,b** are similar to those of the above described cyanoaminoalkylidene complexes **4a-e**. A comparison shows that in **8a,b** the IR  $\nu(\text{CN})$  absorptions are shifted (about  $20\text{ cm}^{-1}$ ) to higher wavenumbers, whereas the  $\nu(\text{CO})$  bands occur at somewhat lower wavenumbers compared to those of **4a-e**.

The reaction of **1a** with  $\text{NH}_3$  proceeds *via* the corresponding amino-alkylidene intermediate  $[\text{Fe}_2(\text{CO})_2(\text{cp})_2(\mu\text{-CO})\{\mu\text{-C}(\text{CN})\text{NH}_2\}]$  (**9**) which has been detected in solution by infrared spectroscopy. However, any attempt to isolate **9** has failed because of decomposition with formation of  $[\text{Fe}(\text{cp})(\text{CO})_2(\text{CN})]$  as the only recognizable product. Further evidence on the nature of **9** has been obtained by transforming the  $\text{NH}_2$  into a presumably more stable  $\text{NHC}(\text{O})\text{Me}$  group. Indeed, immediately after being generated, complex **9** reacts in a few minutes with acetyl chloride, in the presence of pyridine, to form in about 70% yield the expected complex  $[\text{Fe}_2(\text{CO})_2(\text{cp})_2(\mu\text{-CO})\{\mu\text{-C}(\text{CN})\text{NHC}(\text{O})\text{Me}\}]$  (**10**) which has been fully characterized. The presence of the amide group  $\text{NHC}(\text{O})\text{Me}$  is well evidenced in the <sup>13</sup>C NMR spectra by the occurrence of signals at  $\delta$  168.2 and 23.4 attributable to the carbonyl and methyl carbons, respectively, whereas the resonance due to the  $\mu$ -alkylidene carbon is observed at  $\delta$  130.7. Moreover the <sup>1</sup>H NMR spectra display a resonance at  $\delta$  6.79 assigned to the amidic proton, and the IR spectrum, in addition to the usual  $\nu(\text{CO})$  and  $\nu(\text{CN})$  bands, shows an absorption at  $1677\text{ cm}^{-1}$  attributable to the  $\nu(\text{C}=\text{O})$  of the  $\text{NHC}(\text{O})\text{Me}$  group.

**Reactions with Diamines.** The reaction of **1a** with ethylenediamine results in the cleavage of both the C–S and C–C bonds at the  $\mu$ -alkylidene carbon yielding  $[\text{Fe}_2$

$\{\text{CN}(\text{H})(\text{CH}_2)_2\text{N}(\text{H})\}(\text{CO})(\text{cp})_2(\mu\text{-CO})_2]$  (**11**) (eq 1). Analo-



gous formation of diaminocarbenes has been observed in the reactions of  $\text{H}_2\text{NCH}_2\text{CH}_2\text{NH}_2$  with the dithio- and dichlorocarbenes  $[(\text{cp})(\text{CO})\text{FeC}(\text{SMe}_2)_2]^+$ ,<sup>19c</sup>  $[(\text{CO})_5\text{WC}(\text{SMe}_2)_2]$ ,<sup>19d</sup> and  $[\text{RuCl}_2(\text{CCl}_2)(\text{PPh}_3)_2]$ .<sup>20</sup>

Formation of the terminally bonded diaminocarbene complex **11** presumably occurs *via* the bridging aminoalkylidene intermediate  $[\text{Fe}_2(\text{CO})_2(\text{cp})_2(\mu\text{-CO})\{\mu\text{-CN}(\text{H})(\text{CH}_2)_2\text{N}(\text{H})\}]$ . In fact, when the reaction is performed at  $-40\text{ }^\circ\text{C}$ , the infrared spectrum of the crude reaction mixture exhibits absorptions at 2169, 1981, 1948, and  $1791\text{ cm}^{-1}$  which are in accordance with the formation of the mentioned intermediate.

The infrared spectrum of **11** is similar to that of  $[\text{Fe}_2\{\text{C}(\text{CN})\text{NPr}^i_2\}(\text{CO})(\text{cp})_2(\mu\text{-CO})_2]$  (**5**), displaying two strong  $\nu(\text{CO})$  absorptions at  $1929$  and  $1716\text{ cm}^{-1}$ . The alkylidene carbon gives rise to a low-field <sup>13</sup>C NMR resonance at  $\delta$  222.6 which is comparable to the corresponding values in **5** (at about  $\delta$  230).

By analogy with the above described reactions of **1a** with primary amines, the *N,N*-dimethylethylenediamine converts the sulfonium alkylidene ligand into the isocyanide  $\text{CN}(\text{CH}_2)_2\text{NMe}_2$  affording  $[\text{Fe}_2(\text{CO})_3(\text{cp})_2\{\text{CN}(\text{CH}_2)_2\text{NMe}_2\}]$  (**12**). The latter compound is unstable, and it has been characterized only by infrared spectroscopy exhibiting the usual  $\nu(\text{CO})$  and  $\nu(\text{CN})$  band pattern. Likewise, the reaction of **1a** with *N,N*-dimethylethylenediamine affords one unstable product identified, on the basis of its IR spectrum, as  $[\text{Fe}_2(\text{CO})_2(\text{cp})_2(\mu\text{-CO})\{\mu\text{-C}(\text{CN})\text{N}(\text{Me})(\text{CH}_2)_2\text{NHMe}\}]$  (**13**). In fact its  $\nu(\text{CO})$  absorptions at  $2004$ ,  $1969$  and  $1801\text{ cm}^{-1}$  and  $\nu(\text{CN})$  band at  $2147\text{ cm}^{-1}$  are similar to the corresponding values of the  $\mu$ -aminoalkylidene complexes **4a-e**.

**Molecular Structure of *trans*- $[\text{Fe}_2\{\text{C}(\text{CN})\text{NPr}^i_2\}(\text{CO})(\text{cp})_2(\mu\text{-CO})_2]$  (**5**).** The crystals of the title compound contain two independent molecules based on the planar core  $\text{Fe}_2(\mu\text{-CO})_2$  to which two cp groups, a CO molecule, and the aminocarbene grouping  $=\text{C}(\text{CN})\text{NPr}^i_2$  are coordinated in a *trans* configuration (Figure 2). The two independent molecules are strictly equivalent in terms of the bond distances (Table 1). The orientation of the carbene ligand lowers the idealized molecular symmetry that, if the substituents at the carbene atom are ignored, is  $C_s$ . The actual molecular conformation is asymmetric, but the crystal is racemic.

The structural peculiarities of this compound with respect to the other carbene derivatives of the same family are the *trans* configuration of the ligands and,

(18) (a) Bellerby, J.; Boylan, M. J.; Ennis, M.; Manning, A. R. *J. Chem. Soc., Dalton Trans.* **1978**, 1185. (b) Howell, J. A. S.; Rowan, A. J. *J. Chem. Soc., Dalton Trans.* **1980**, 503.

(19) (a) Werner, H.; Fischer, E. O.; Heckl, B.; Kreiter, C. G. *J. Organomet. Chem.* **1971**, *28*, 367. (b) McCormick, F. B.; Angelici, R. *J. Inorg. Chem.* **1981**, *20*, 1118. (c) McCormick, F. B.; Angelici, R. *J. Inorg. Chem.* **1979**, *18*, 1231. (d) Steinmetz, A. L.; Hershberger, S. A.; Angelici, R. *J. Organometallics* **1984**, *3*, 461.

(20) Roper, W. R.; Wright, A. H. *J. Organomet. Chem.* **1982**, *233*, C59.

**Table 1. Selected Bond Lengths (Å) and Angles (deg) for [Fe<sub>2</sub>{C(CN)NPr<sup>i</sup><sub>2</sub>}(CO)(Cp)<sub>2</sub>(μ-CO)<sub>2</sub>]**

	molecule A	molecule B
Fe(1)–Fe(2)	2.536(1)	2.538(1)
Fe(1)–C(3)	1.909(3)	1.887(4)
Fe(2)–C(3)	1.932(3)	1.944(4)
Fe(1)–C(2)	1.891(3)	1.915(4)
Fe(2)–C(2)	1.944(3)	1.918(3)
C(2)–O(2)	1.184(4)	1.173(4)
C(3)–O(3)	1.181(4)	1.185(4)
Fe(1)–C(4)	1.919(3)	1.910(3)
C(4)–C(5)	1.450(4)	1.454(5)
C(4)–N(2)	1.317(4)	1.324(4)
C(5)–N(1)	1.159(5)	1.143(5)
N(2)–C(9)	1.484(4)	1.495(4)
C(9)–C(10)	1.522(6)	1.539(5)
C(9)–C(11)	1.515(6)	1.520(5)
Fe(2)–C(1)	1.745(4)	1.738(4)
C(1)–O(1)	1.146(4)	1.158(5)
N(2)–C(6)	1.504(4)	1.510(4)
C(6)–C(7)	1.522(6)	1.517(5)
C(6)–C(8)	1.510(6)	1.527(6)
Fe(1)–C(cp) <sub>av</sub>	2.169	2.160
Fe(2)–C(cp) <sub>av</sub>	2.137	2.122
Fe(1)–C(2)–O(2)	141.3(3)	140.6(3)
Fe(2)–C(2)–O(2)	135.9(3)	136.4(3)
Fe(1)–C(3)–O(3)	140.9(3)	141.5(3)
Fe(2)–C(3)–O(3)	136.5(3)	135.4(3)
Fe(2)–C(1)–O(1)	178.5(4)	177.2(4)
Fe(1)–C(4)–C(5)	110.7(2)	111.7(2)
Fe(1)–C(4)–N(2)	133.5(2)	133.6(2)
C(4)–C(5)–N(1)	173.0(4)	173.1(4)
C(4)–N(2)–C(6)	125.7(3)	125.5(3)
C(4)–N(2)–C(9)	119.8(3)	119.6(3)
C(6)–N(2)–C(9)	114.5(3)	114.9(3)
C(10)–C(9)–C(11)	112.9(3)	112.7(3)
C(7)–C(6)–C(8)	113.5(4)	114.9(4)
C(5)–C(4)–N(2)	115.3(3)	114.3(3)
C(8)–C(6)–N(2)	113.7(3)	110.1(3)
C(7)–C(6)–N(2)	111.0(3)	112.9(3)
C(10)–C(9)–N(2)	110.5(3)	110.9(3)
C(11)–C(9)–N(2)	111.0(3)	110.2(3)

more importantly, the terminal mode of bonding of the carbene function.

Being that the Fe<sub>2</sub>(μ-CO)<sub>2</sub> moiety is unchanged with respect to the unsubstituted molecules *cis*- and *trans*-[Fe<sub>2</sub>(μ-CO)<sub>2</sub>(CO)<sub>2</sub>(cp)<sub>2</sub>], the Fe–Fe distance [2.536(1) Å] is also strictly equivalent [2.531(2), 2.534(2) Å, respectively].<sup>21</sup> The chemical nonequivalence of the iron atoms gives rise to some asymmetry of the bridging CO ligands that exhibit slightly shorter distances from Fe(1), to which the carbene group is coordinated. The cp ligands show slightly different Fe–C(cp) average distances as well, with longer distances (0.035 Å) from Fe(1).

The Fe–C(carbene) distance [1.915(3)<sub>av</sub> Å] has to be compared with what found in other terminal aminocarbene species, e.g. 1.97(1) Å in [Fe<sub>2</sub>(μ-SPh)<sub>2</sub>(CO)<sub>5</sub>{C(NMe)<sub>2</sub>-Ph}],<sup>22</sup> 1.95(1) Å in [Fe(CO)<sub>3</sub>(PETe<sub>3</sub>){CN(Me)(CH<sub>2</sub>)<sub>2</sub>N(Me)}],<sup>23</sup> and 1.927(4) Å in [Fe(CO)(cp)C<sub>4</sub>H<sub>6</sub>N(C<sub>3</sub>H<sub>7</sub>)<sub>2</sub>].<sup>24</sup> These values are a bit longer than the present one but are in line with the observed variations of bond lengths around a metal center caused by the different nature and stereogeometry of the ligands. The strength of this interaction can be assessed if compared to the Fe–CO

bond in the same molecule and chemical environment. The Fe–C(carbene) value is 0.17 Å longer than the Fe–C(carbonyl) one. The difference is large and clearly indicates a weaker Fe–C(carbene) π interaction. That happens not only because the carbonyl ligand sets up a double π interaction but also because the unique carbene π orbital is in competition with the orbitals of suitable symmetry on the CN and NPr<sup>i</sup><sub>2</sub> substituents. The experimental evidence tells of substantial double bond localization between C(carbene) and N(amine) [C(4)–N(2) 1.320(4)<sub>av</sub> Å]. This value is in strict agreement with what was found in the just mentioned aminocarbenes.<sup>22,23</sup> In spite of the above observation the π component of the Fe–C(carbene) interaction is not canceled, as shown by the significantly longer values (0.14 Å on average) found for the Fe–C(sp<sup>3</sup>) distances, e.g. 2.060(6) Å in [Fe{C(CF<sub>3</sub>)<sub>2</sub>(OH)}(CO)<sub>2</sub>(cp)]<sup>25</sup> and 2.045(3) Å in [(OC)(cp)FeC{CN}(SMe)}SC{Fe(cp)-(CO)<sub>2</sub>}S].<sup>26</sup> A stronger iron–carbon bond is surely present when this ligand is in bridging geometry, as in *cis*-[Fe<sub>2</sub>(CO)<sub>2</sub>(cp)<sub>2</sub>(μ-CO){μ-C(CN)N(Me)C(O)SMe}] [Fe–C(carbene) 1.99<sub>av</sub>, C(carbene)–N(amine) 1.492(4) Å]<sup>15</sup> and *cis*-[Fe<sub>2</sub>(CO)<sub>2</sub>(cp)<sub>2</sub>(μ-CO){μ-C(CN)N(H)Ph}] [Fe–C(carbene) 2.016<sub>av</sub>, C(carbene)–N(amine) 1.429(3) Å].<sup>8</sup> In fact a C(carbene)–N(amine) double bond is absent in the former species, because the π orbitals on the two atoms are in orthogonal orientation, and is weak in the latter, because the implied orbitals are significantly twisted. Therefore the Fe atoms do not have competitors for π-donation to the carbene carbon.

In the light of these considerations the terminal coordination of the carbene group seems motivated by steric factors, but one should not forget that the loss in iron–carbon π bond is, at least in part, compensated by a gain in the C(carbene)–N(amine) double bond in the terminal coordination.

**Electrochemistry of [Fe<sub>2</sub>{C(CN)NPr<sup>i</sup><sub>2</sub>}(CO)(cp)<sub>2</sub>(μ-CO)<sub>2</sub>] (5) and EPR Spectra of [5]<sup>+</sup>.** Previously reported electrochemical studies on a series of μ-cyanoalkylidene complexes [Fe<sub>2</sub>(CO)<sub>2</sub>(cp)<sub>2</sub>(μ-CO){μ-C(CN)-(X)}], including **4d** (X = NCH<sub>2</sub>(CH<sub>2</sub>)<sub>3</sub>CH<sub>2</sub>), have shown that these complexes undergo a one-electron reduction complicated by relatively slow degradation of the corresponding monoanions to further electroreducible byproducts.<sup>27</sup> The redox behavior of complex **5** is quite different. As illustrated in Figure 3, it exhibits an irreversible cathodic step at very negative potential values (*E*<sub>p</sub> = –1.64 V) as well as two consecutive anodic processes (at *E*<sup>o'</sup> = +0.26 V and *E*<sub>p</sub> = +1.04 V, respectively), the first of which only shows preliminary features of chemical reversibility.

Controlled potential coulometry in correspondence to the first anodic step (*E*<sub>w</sub> = +0.5 V) shows the consumption of one electron/molecule. Cyclic voltammetric tests on the resulting solution exhibit a voltammetric profile quite complementary to that shown in Figure 3, thus confirming the chemical reversibility of the [5]/[5]<sup>+</sup> redox change also in the long times of macroelectrolysis.

(21) Bryan, R. F.; Greene, P. T. *J. Chem. Soc. A* **1970**, 3064.(22) Dillen, J. L. M.; van Dyk, M. M.; Lotz, S. *J. Chem. Soc., Dalton Trans.* **1989**, 2199.(23) Hitchcock, P. B.; Lappert, M. F.; Thomas, S. A.; Thorne, A. J.; Carty, A. J.; Taylor, N. J. *J. Organomet. Chem.* **1986**, 315, 27.(24) Stenström, Y.; Koziol, A. E.; Palenik, G. J.; Jones, W. M. *Organometallics* **1987**, 6, 2079.(25) Bruce, M. I.; Duffy, D. N.; Snow, M. R.; Tiekink, E. R. T. *J. Organomet. Chem.* **1986**, 310, C33.(26) Busetto, L.; Zanotti, V.; Albano, V. G.; Braga, D.; Monari, M.; *J. Chem. Soc., Dalton Trans.* **1988**, 1067.(27) Bordini, S.; Busetto, L.; Calderoni, F.; Carlucci, L.; Laschi, F.; Zanollo, P.; Zanotti, V. *J. Organomet. Chem.* **1995**, 488, 133.

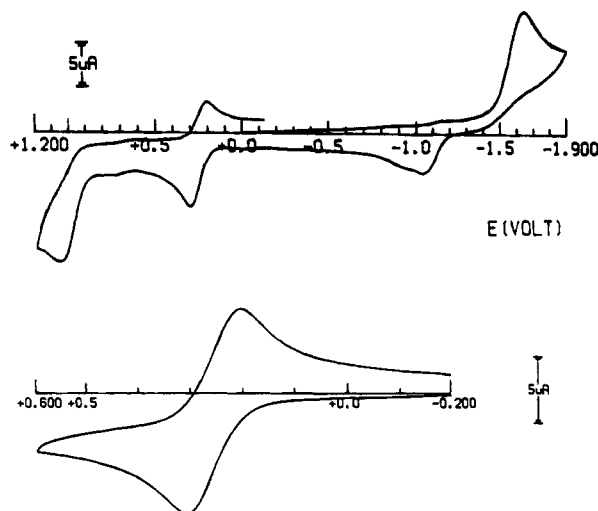


**Figure 3.** Cyclic voltammograms recorded on a platinum electrode on a THF solution containing **5** ( $1.7 \times 10^{-3}$  mol  $\text{dm}^{-3}$ ) and  $[\text{NBu}_4][\text{ClO}_4]$  ( $0.2$  mol  $\text{dm}^{-3}$ ). Scan rate =  $0.2$  V  $\text{s}^{-1}$ .

Analysis<sup>28</sup> of the cyclic voltammograms relevant to this reversible one-electron removal with scan rate varying from  $0.02$  to  $5.12$  V  $\text{s}^{-1}$  shows that: the  $i_{\text{pc}}/i_{\text{pa}}$  ratio is constantly equal to 1; the  $i_{\text{pa}} \times v^{-1/2}$  parameter remains substantially constant; the peak-to-peak separation progressively increases from  $71$  to  $410$  mV. In view of the fact that, under the same experimental conditions, the ferrocene/ferrocenium oxidation process ( $E^{\circ} = +0.55$  V) exhibits a quite similar significant departure from the constant value of  $59$  mV expected for a reversible one-electron transfer, we attribute it to uncompensated solution resistances of the low conductive THF medium. In this connection the fact that the  $5/[5]^+$  anodic oxidation is chemically as well as electrochemically reversible allows to think that  $[5]^+$  maintains a geometric structure substantially similar to that of its neutral parent **5**.<sup>29</sup>

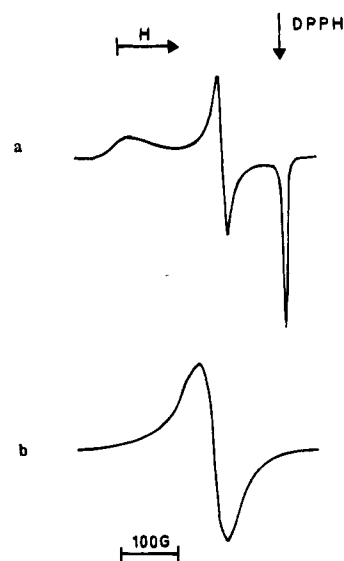
Because of the framework-destroying nature of the most anodic and cathodic steps, respectively, we discarded any further investigation on them.

Figure 4 illustrates the X-band EPR spectra of  $[5]^+$  electrogenerated at  $253$  K. The line shape recorded at liquid nitrogen temperature ( $100$  K), Figure 4a, can be suitably interpreted in terms of a  $S = 1/2$  spin Hamiltonian. It shows a well-recognizable rhombic structure, with a significant line-broadening effect at low field. The relevant anisotropic parameters are consistent with the presence of a paramagnetic metal-centered system:

$$g_1 = 2.176 \pm 0.005 \quad g_m = 2.067 \pm 0.005 \\ g_h = 1.999 \pm 0.005$$

$$\langle g \rangle = (1/3)(g_1 + g_m + g_h) = 2.081 \pm 0.005$$

The second derivative analysis and simulation procedures<sup>30</sup> point out the noticeable orbital contribution of the  $[5]^+$  monocation paramagnetism reflecting the overall unsymmetrical framework experienced by the



**Figure 4.** X-Band EPR spectra recorded on a THF solution of  $[5]^+$ , electrogenerated at  $253$  K: (a)  $100$  K; (b)  $200$  K.

unpaired electron. On the other hand, the line shape does not evidence any hyperfine interaction with nuclei external to the diiron core, thus suggesting that a very minor delocalization, if any, of the  $S = 1/2$  electron on the ligands occurs.

Comparison of the EPR features of  $[5]^+$  with those previously reported for  $[4d]^-$ , which exhibits an axial absorption pattern,<sup>27</sup> makes evident that the unsymmetrical position of the cyanoaminoalkylidene fragment significantly affects the EPR response, allowing us to assume that in  $[5]^+$  the unpaired electron should be mainly localized on the carbene-substituted iron atom.

At the glassy-fluid transition ( $200$  K) the rhombic line shape evolves toward a single isotropic signal, centered at  $g_{\text{iso}} = 2.081 \pm 0.005$  and with a relatively broad line width ( $\Delta H_{\text{iso}} = 55 \pm 5$  G), Figure 4. When the temperature is increased, the intensity slightly decreases, but the isotropic parameters remain unaltered and well-fitting the glassy ones; upon refreezing, the original rhombic pattern is restored. These data suggest that  $[5]^+$  maintains its geometry under very different thermal conditions.

## Discussion

The results described in the previous sections indicate that the sulfonium complexes **1a,b** undergo the well-documented aminolysis,<sup>12,19</sup> transforming the  $\text{C(X)SMe}_2$  into the  $\text{C(X)NRR}'$  or  $\text{CNR}$  ligand by reacting with secondary or primary amines, respectively. These reactions share several features with the aminolysis of the dithiocarbene complexes  $[(\text{cp})(\text{CO})\text{FeC}(\text{SMe})_2]^+$ <sup>19c</sup> or  $[(\text{CO})_5\text{WC}(\text{SMe})_2]$ .<sup>19d</sup> Similarly, the reactions with secondary amines show a marked dependence on the steric hindrance of the amine. Only small amines (like dimethylamines or heterocyclic amines) react promptly and give satisfactory yields. Further analogies come from the reactions with diamines, but these will be discussed later. These similarities strongly support the idea that the mechanism involved might closely resemble that proposed for the aminolysis of  $[(\text{OC})_5\text{WC}(\text{SMe})_2]$  which has been studied in detail.<sup>19d</sup> Therefore the reaction of **1a** with amines may proceed via  $\text{SMe}_2$  displacement to form the ammonium intermediate

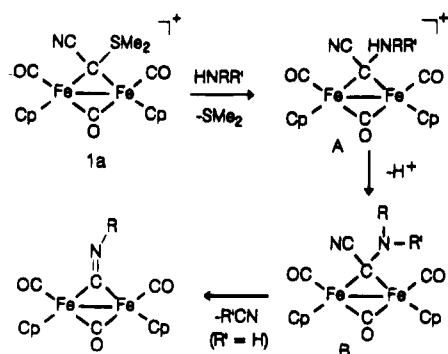
(28) Brown, E. R.; Sandifer, J. R. In *Physical Methods of Chemistry. Electrochemical Methods*; Rossiter, B. W., Hamilton, J. F., Eds.; Wiley: New York, 1986; Vol. 2, Chapter 4.

(29) Zanello, P. *Struct. Bonding* (Berlin) **1992**, *79*, 101.

(30) Lozos, G. P.; Hoffman, B. M.; Franz, C. G. *QCPE* **1974**, *11*, 265.



Scheme 5



(A), which is deprotonated by the excess of amine affording type (B) complexes. Finally, in the case of primary amines the aminothiocarbene intermediate is converted into the isocyanide product by elimination of HCN (Scheme 5).

Despite the mentioned instability of type A ammonium complexes  $[\text{Fe}_2(\text{CO})_2(\text{cp})_2(\mu\text{-CO})\{\mu\text{-C}(\text{NMe}_3)(\text{CN})\}]\text{SO}_3\text{CF}_3$  (**2**) and  $[\text{Fe}_2(\text{CO})_2(\text{cp})_2(\mu\text{-CO})\{\mu\text{-C}(\text{Dabco})(\text{CN})\}]\text{SO}_3\text{CF}_3$  (**3**), stable type B derivatives (compounds **4a-f**) are formed upon reaction with secondary amines. The analogous  $[\text{Fe}_2(\text{CO})_2(\text{cp})_2(\mu\text{-CO})\{\mu\text{-C}(\text{NHR})(\text{CN})\}]$  has been isolated in the reaction of **1a** with aniline. The  $[\text{Fe}_2(\text{CO})_2(\text{cp})_2(\mu\text{-CO})\{\mu\text{-C}(\text{CN})\text{N}(\text{H})\text{Ph}\}]$  (**8a**) complex, which is the unique type B intermediate isolated in the reaction with primary amines, slowly decomposes to the isocyanide derivative **7e**, in  $\text{CH}_2\text{Cl}_2$  solution. The **8a**  $\rightarrow$  **7e** transformation is faster in the presence of an excess of aniline suggesting that HCN elimination is probably favored by basic media. It is worth noting that cyanide elimination from several type 4 cyanoaminoalkylidene complexes  $[\text{Fe}_2(\text{CO})_2(\text{cp})_2(\mu\text{-CO})\{\mu\text{-C}(\text{CN})(\text{NRR}')\}]$  has also been observed to occur under acidic conditions to give the aminoalkylidene products  $[\text{Fe}_2(\text{CO})_2(\text{cp})_2(\mu\text{-CO})\{\mu\text{-CNRR}'\}]$ .<sup>16</sup>

In our opinion, the most important result of the present study is the isolation of type **4a-e** derivatives which are among the first stable bridging aminoalkylidene complexes so far reported.<sup>2a,11,15,17,31</sup> The lack of this class of complexes is generally believed to be a consequence of the destabilization caused by a competition of the nitrogen and iron  $\pi$ -electrons for the occupation of the empty p-orbital on the carbon atom.<sup>13,32</sup> This idea is supported by the observation that, in most of the  $\mu$ -aminoalkylidene complexes so far reported, the N atom exhibits  $\pi$ -donor character reduced by the presence of adjacent electron-withdrawing functional groups. Examples include the complexes  $[\text{Fe}_2(\text{CO})_2(\text{cp})_2(\mu\text{-CO})\{\mu\text{-C}(\text{CN})\text{N}(\text{Me})\text{C}(\text{O})\text{SR}\}]$ ,<sup>15</sup>  $[\text{Fe}_2(\text{CO})_2(\text{cp})_2(\mu\text{-CO})\{\mu\text{-C}(\text{H})\text{N}(\text{CPh}_2)\}]$ ,<sup>2a</sup>  $[\text{Co}_2(\text{CO})_3(\mu\text{-CO})\{\mu\text{-C}(\text{Ph})\text{N}(\text{Ph})\text{C}(\text{Ph})=\text{N}(\text{Ph})\}]$ ,<sup>31a</sup> and  $[\text{Fe}_2(\text{CO})_5\{\mu\text{-C}(\text{H})\text{NHC}(\text{O})\text{Me}\}]$ .<sup>31c</sup> In other cases, for instance in  $[\text{WPt}(\text{PR}_3)_3(\text{CO})_2\{\mu\text{-C}(\text{H})\text{NEt}_2\}]$ ,<sup>31b</sup>  $\pi$ -interaction between N and the  $\mu$ -alkylidene carbon is prevented by direct donation from N to the metal.

These considerations, together with the observation that strong  $\pi$ -acid ligands preferably adopt the bridging

over the terminal position in polynuclear complexes, may clearly explain the importance of the electron-withdrawing CN substituent in stabilizing the bridging coordination adopted by the carbene ligand in type **4** complexes. Further clues on the pivotal role assumed by the cyano group come from the coordination mode of the  $\text{C}(\text{H})\text{NR}_2$  group. A comparison between  $[\text{Fe}_2\{\text{C}(\text{H})(\text{NMe}_2)\}(\text{CO})(\text{cp})_2(\mu\text{-CO})_2]$  (**6a**) and  $[\text{Fe}_2(\text{CO})_2(\text{cp})_2(\mu\text{-CO})\{\mu\text{-C}(\text{CN})(\text{NMe}_2)\}]$  (**4a**) is particularly significant. The H for CN substitution dramatically affects the coordination mode: bridging in the cyanoaminoalkylidene **4a** and terminal in **6a**. Finally as found in the reaction of **1a** with ethylenediamine, the expected bridging is converted to terminal coordination mode in order to allow stronger  $\pi$ -interaction of the two N-atoms with the carbene carbon of the  $\text{=CN}(\text{H})\text{CH}_2\text{CH}_2\text{N}(\text{H})$  ligand.

These findings justify the complete absence of poly- and dinuclear complexes bearing the diamino carbene in bridging position.

Having shown the effects of the electronic factors on the coordination mode, one should also notice the formation of the terminally bonded cyanoaminoalkylidene ligand in the *trans*- $[\text{Fe}_2\{\text{C}(\text{CN})\text{NPr}^i_2\}(\text{CO})(\text{cp})_2(\mu\text{-CO})_2]$  complex (**5**) (see structural section) and the spectroscopic evidence of an equilibrium between bridging and terminal coordination in  $[\text{Fe}_2(\text{CO})_2(\text{cp})_2(\mu\text{-CO})\{\mu\text{-C}(\text{CN})\text{NEt}_2\}]$  (**5f**) (Figure 1), which clearly indicate that steric effects play an important role as well.

*The bridging coordination is favored by increasing the  $\pi$ -acid properties of the  $\mu\text{-C}$  and/or by decreasing the bulkiness of the  $\text{NR}_2$  substituent in the cyanoalkylidene ligand.*

The reaction of **1a** with *N,N*-dimethylethylenediamine offers a chance to compare its reactivity with primary and tertiary amines, both functional groups being present in the diamine reagent. Formation of the isocyanide product  $[\text{Fe}_2(\text{CO})_3(\text{cp})_2\{\text{CN}(\text{CH}_2)_2\text{NMe}_2\}]$  (**10**) shows that the  $\text{NH}_2$  group is, as expected, more reactive and that the synthetic method *via* the sulfonium **1a** can be of some interest for the preparation of functionalized isocyanide complexes.

In light of the reactivity of **1a** with primary amines, the reaction with anhydrous ammonia would be expected to give the hydrogen isocyanide (HCN)<sup>33</sup> complex  $[\text{Fe}_2(\text{CO})_3(\text{cp})_2(\text{CNH})]$ . The latter has been previously obtained, as an unstable intermediate, in the protonation reaction of the cyanide complex  $[\text{Fe}_2(\text{CO})_3(\text{cp})_2(\text{CN})]^-$ , which ultimately gives the aminoalkylidene  $[\text{Fe}_2(\text{cp})_2(\text{CO})_2(\mu\text{-CO})(\mu\text{-CNH}_2)]^+$  and  $[\text{Fe}_2(\text{CO})_3(\text{cp})_2(\text{CN})]^-$ , in a sort of acid/base disproportionation.<sup>34</sup> None of these species have been detected in the reaction mixture of **1a** with  $\text{NH}_3$ ; in contrast, IR data support formation of the cyanoalkylidene intermediate  $[\text{Fe}_2(\text{cp})_2(\text{CO})_2(\mu\text{-CO})\{\mu\text{-C}(\text{CN})(\text{NH}_2)\}]$  (**9**). It is worth mentioning that in the analogous reaction of **1a** with  $\text{PH}_3$  the phosphonium  $[\text{Fe}_2(\text{cp})_2(\text{CO})_2(\mu\text{-CO})\{\mu\text{-C}(\text{CN})(\text{PH}_3)\}]\text{SO}_3\text{CF}_3$  and the phosphinoalkylidene  $[\text{Fe}_2(\text{cp})_2(\text{CO})_2(\mu\text{-CO})\{\mu\text{-C}(\text{CN})(\text{PH}_2)\}]$  have been obtained, that, on the contrary, are very stable.<sup>7b</sup>

(31) (a) Adams, R. D.; Chodosh, D. F. *J. Organomet. Chem.* **1977**, *139*, C39. (b) Davis, J. H., Jr.; Lukehart, C. M.; Sacksteder, L. A. *Organometallics* **1987**, *6*, 50. (c) Sumner, C. E., Jr.; Collier, J. A.; Pettit, R. *Organometallics* **1982**, *1*, 1350.

(32) Mataschek, J. R.; Angelici, R. *J. Inorg. Chem.* **1986**, *25*, 2877.

(33) Fehlhammer, W. P.; Fritz, M. *Chem. Rev.* **1993**, *93*, 1243.

(34) Fehlhammer, W. P.; Schoder, F.; Beck, G.; Schrollkamp, S. Z. *Angew. Allg. Chem.* **1993**, *619*, 1171.

## Experimental Section

**General Procedures.** All reactions were routinely carried out under nitrogen by standard Schlenk techniques. Solvents were distilled immediately before use under nitrogen from appropriate drying agents. Instruments employed: IR, Perkin-Elmer 983-G; NMR, Varian Gemini 200. Elemental analyses were by Pascher Microanalytical Laboratory (Remagen, Germany). The compounds  $[\text{Fe}_2(\text{CO})_2(\text{cp})_2(\mu\text{-CO})\{\mu\text{-C}(\text{SMe}_2)(\text{CN})\}]\text{SO}_3\text{CF}_3$  (**1a**),<sup>4</sup>  $[\text{Fe}_2(\text{CO})_2(\text{cp})_2(\mu\text{-CO})\{\mu\text{-C}(\text{SMe}_2)(\text{H})\}]\text{SO}_3\text{CF}_3$  (**1b**),<sup>5</sup> and  $[\text{Fe}_2(\text{CO})_2(\text{cp})_2(\mu\text{-CO})\{\mu\text{-CN}(\text{Me})\text{R}\}]\text{SO}_3\text{CF}_3$  (R = Me, Et)<sup>14</sup> (R = Bz)<sup>35</sup> were prepared according to published methods. The syntheses and characterization of the complexes  $[\text{Fe}_2(\text{CO})_2(\text{cp})_2(\mu\text{-CO})\{\mu\text{-C}(\text{CN})(\text{NMe}_2)\}]$  (**4a**)<sup>8</sup> and  $[\text{Fe}_2(\text{CO})_2(\text{cp})_2(\mu\text{-CO})\{\mu\text{-C}(\text{CN})(\text{NCH}_2(\text{CH}_2)_3\text{CH}_2)\}]$  (**4d**)<sup>16</sup> have been previously reported. Materials and apparatus for electrochemistry and coupled EPR measurements have been described elsewhere.<sup>36</sup> Unless otherwise specified, all potential values refer to the saturated calomel electrode (SCE).

**Reaction of 1a with NMe<sub>3</sub>.** Trimethylamine was bubbled into a MeCN solution (10 mL) of **1a** (75 mg, 0.13 mmol) for 5 min. IR inspection of the crude reaction mixture evidenced the absorptions  $\nu(\text{CO})$  2003 s, 1980 w, 1821 m and  $\nu(\text{CN})$  2165 w  $\text{cm}^{-1}$ , which have been attributed to the formation of  $[\text{Fe}_2(\text{CO})_2(\text{cp})_2(\mu\text{-CO})\{\mu\text{-C}(\text{NMe}_3)(\text{CN})\}]\text{SO}_3\text{CF}_3$  (**2**). Attempts to isolate complex **2** have been unsuccessful.

**Reaction of 1a with Dabco.** Addition of a large excess of Dabco to a MeCN solution (10 mL) of **1a** (75 mg, 0.13 mmol), as described above, gave  $[\text{Fe}_2(\text{CO})_2(\text{cp})_2(\mu\text{-CO})\{\mu\text{-C}(\text{Dabco})(\text{CN})\}]\text{SO}_3\text{CF}_3$  (**3**) as detected from infrared spectra of the reaction mixture. IR (MeCN) ( $\text{cm}^{-1}$ ):  $\nu(\text{CO})$  2003 s, 1971 w, 1824 m;  $\nu(\text{CN})$  2165 w.

**Synthesis of  $[\text{Fe}_2(\text{CO})_2(\text{cp})_2(\mu\text{-CO})\{\mu\text{-C}(\text{CN})(\text{NMe}_2)\}]$  (**4a**).** **Method a.** The synthesis of **4a** has been previously briefly described.<sup>8</sup> Gaseous dimethylamine was bubbled into a MeCN solution (10 mL) of **1a** (91 mg, 0.16 mmol); the color of the solution turned immediately bright red, and the mixture was dried under vacuum. The residue was dissolved in  $\text{CH}_2\text{Cl}_2$  and filtered on an alumina pad (3 × 5 cm). The red filtered solution was evaporated to dryness under reduced pressure and the residue crystallized from  $\text{CH}_2\text{Cl}_2$  layered with *n*-pentane at  $-20^\circ\text{C}$  to yield 45 mg (69%) of **4a**, mp 132–133 °C dec. Anal. Calcd for  $\text{C}_{17}\text{H}_{16}\text{Fe}_2\text{N}_2\text{O}_3$ : C, 50.04; H, 3.95. Found: C, 50.12; H, 3.92. IR ( $\text{CH}_2\text{Cl}_2$ ) ( $\text{cm}^{-1}$ ):  $\nu(\text{CO})$  2004 s, 1970 mw, 1799 m;  $\nu(\text{CN})$  2148 w. <sup>1</sup>H NMR ( $\text{CDCl}_3$ ;  $\delta$ ): 4.79 (s, 10 H, cp), 2.84 (s, 6 H, Me). <sup>13</sup>C NMR ( $\text{CD}_2\text{Cl}_2$ ;  $\delta$ ): 267.6 ( $\mu\text{-CO}$ ), 211.0 (CO), 161.6 ( $\mu\text{-C}$ ), 127.5 (CN), 91.0 (Cp), 49.6 (Me).

**Method b.** To a stirred solution of  $[\text{Fe}_2(\text{CO})_2(\text{cp})_2(\mu\text{-CO})(\mu\text{-CNMe}_2)]\text{SO}_3\text{CF}_3$  (290 mg, 0.55 mmol) in  $\text{CH}_2\text{Cl}_2$  (25 mL) was added  $\text{Bu}^n\text{NCN}$  (150 mg, 0.55 mmol). After 60 min the mixture was filtered on an alumina pad. The red solution was evaporated to dryness under reduced pressure and the residue crystallized from  $\text{CH}_2\text{Cl}_2$  layered with *n*-pentane at  $-20^\circ\text{C}$ . Yield: 96 mg (43%).

**Synthesis of Compounds 4b–f.** The compounds **4b–f** were all synthesized according to the procedure for the synthesis of **4a** (method a) outlined above. The liquid amines were syringed into MeCN solutions of **1a**. A detailed description of the preparation of **4d** has been previously reported.<sup>16</sup> The complex **4b** has been prepared either from **1a** with  $\text{NHMeEt}$  (method a, 16% yield) and by reacting  $[\text{Fe}_2(\text{CO})_2(\text{cp})_2(\mu\text{-CO})\{\mu\text{-CN}(\text{Me})\text{Et}\}]\text{SO}_3\text{CF}_3$  with  $\text{Bu}^n\text{NCN}$  (method b, 38% yield).

$[\text{Fe}_2(\text{CO})_2(\text{cp})_2(\mu\text{-CO})\{\mu\text{-C}(\text{CN})\text{N}(\text{Me})\text{Et}\}]$  (**4b**): mp 112–113 °C dec. Anal. Calcd for  $\text{C}_{18}\text{H}_{18}\text{Fe}_2\text{N}_2\text{O}_3$ : C, 51.23; H, 4.30. Found: C, 50.12; H, 3.92. IR ( $\text{CH}_2\text{Cl}_2$ ) ( $\text{cm}^{-1}$ ):  $\nu(\text{CO})$  2005 s,

Table 2. Crystal Data and Experimental Details for  $[\text{Fe}_2\{\text{C}(\text{CN})\text{NPr}^i_2\}(\text{CO})(\text{Cp})_2(\mu\text{-CO})_2]$ 

chem formula	$\text{C}_{21}\text{H}_{24}\text{Fe}_2\text{N}_2\text{O}_3$
fw	464.13
system	monoclinic
space group	$P2_1/c$ (No. 14)
<i>a</i> , Å	15.791(3)
<i>b</i> , Å	13.741(2)
<i>c</i> , Å	18.937(6)
$\beta$ , deg	90.75(2)
<i>V</i> , Å <sup>3</sup>	4108.8
<i>Z</i>	8
<i>d</i> <sub>calcd</sub> , g cm <sup>-3</sup>	1.50
$\mu(\text{Mo K}\alpha)$ , cm <sup>-1</sup>	13.6
<i>F</i> (000)	1920
cryst dimens, mm	0.15 × 0.25 × 0.40
2 $\theta$ max, deg	54
octants of reciprocal space explored	± <i>h</i> , + <i>k</i> , + <i>l</i>
scan type	$\omega$
$\omega$ scan width, deg	0.9 + 0.35 tan $\theta$
reflens colled	8094
unique obsd reflens [ <i>F</i> <sub>o</sub> > 4 $\sigma$ ( <i>F</i> <sub>o</sub> )]	6140
<i>R</i> ( <i>F</i> ), w <i>R</i> ( <i>F</i> )	0.0394, 0.0446
GO <i>F</i>	1.84

1971 mw, 1799 m;  $\nu(\text{CN})$  2146 w. <sup>1</sup>H NMR ( $\text{CDCl}_3$ ;  $\delta$ ): 4.79 (s, 10 H, cp), 3.17 (q, 2 H,  $\text{NCH}_2\text{CH}_3$ ), 2.82 (s, 3 H, NMe), 1.10 (t, 3 H,  $\text{NCH}_2\text{CH}_3$ ).

$[\text{Fe}_2(\text{CO})_2(\text{cp})_2(\mu\text{-CO})\{\mu\text{-C}(\text{CN})\text{N}(\text{Me})\text{Ph}\}]$  (**4c**): yield 17%; mp 134–136 °C dec. Anal. Calcd for  $\text{C}_{22}\text{H}_{18}\text{Fe}_2\text{N}_2\text{O}_3$ : C, 56.17; H, 3.86. Found: C, 56.33; H, 3.90. IR ( $\text{CH}_2\text{Cl}_2$ ) ( $\text{cm}^{-1}$ ):  $\nu(\text{CO})$  2000 s, 1963 mw, 1799 m;  $\nu(\text{CN})$  2146 w. <sup>1</sup>H NMR ( $\text{CDCl}_3$ ;  $\delta$ ): 7.39–6.90 (m, 5 H, Ph), 4.84 (s, 10 H, cp), 3.51 (s, 3 H, Me).

$[\text{Fe}_2(\text{CO})_2(\text{cp})_2(\mu\text{-CO})\{\mu\text{-C}(\text{CN})(\text{NCH}_2(\text{CH}_2)_3\text{CH}_2)\}]$  (**4d**): yield 56%; mp 140–142 °C dec. Anal. Calcd for  $\text{C}_{20}\text{H}_{20}\text{Fe}_2\text{N}_2\text{O}_3$ : C, 53.61; H, 4.50. Found: C, 53.35; H, 4.60. IR ( $\text{CH}_2\text{Cl}_2$ ) ( $\text{cm}^{-1}$ ):  $\nu(\text{CO})$  2005 s, 1971 mw, 1798 m;  $\nu(\text{CN})$  2147 w. <sup>1</sup>H NMR ( $\text{CD}_2\text{Cl}_2$ ;  $\delta$ ): 4.76 (s, 10 H, cp), 3.15 (m, 4 H,  $\text{NCH}_2(\text{CH}_2)_3\text{CH}_2$ ), 1.52 (m, 6 H,  $\text{NCH}_2(\text{CH}_2)_3\text{CH}_2$ ). <sup>13</sup>C NMR ( $\text{CD}_2\text{Cl}_2$ ;  $\delta$ ): 268.9 ( $\mu\text{-CO}$ ), 211.2 (CO), 162.4 ( $\mu\text{-C}$ ), 128.3 (CN), 91.2 (cp), 60.1, 27.2, 25.2 ( $\text{NC}_5\text{H}_{10}$ ).

$[\text{Fe}_2(\text{CO})_2(\text{cp})_2(\mu\text{-CO})\{\mu\text{-C}(\text{CN})(\text{NCH}_2(\text{CH}_2)_2\text{CH}_2)\}]$  (**4e**): yield 43%. Anal. Calcd for  $\text{C}_{19}\text{H}_{18}\text{Fe}_2\text{N}_2\text{O}_3$ : C, 52.58; H, 4.18. Found: C, 52.60; H, 4.24. IR ( $\text{CH}_2\text{Cl}_2$ ) ( $\text{cm}^{-1}$ ):  $\nu(\text{CO})$  2004 s, 1965 mw, 1792 m;  $\nu(\text{CN})$  2147 w. <sup>1</sup>H NMR ( $\text{CDCl}_3$ ;  $\delta$ ): 4.74 (s, 10 H, cp), 3.19 (m, 4 H,  $\text{NCH}_2(\text{CH}_2)_2\text{CH}_2$ ), 1.88 (m, 4 H,  $\text{NCH}_2(\text{CH}_2)_2\text{CH}_2$ ).

$[\text{Fe}_2(\text{CO})_2(\text{cp})_2(\mu\text{-CO})\{\mu\text{-C}(\text{CN})(\text{NET}_2)\}]$  (**4f**): yield 52%; mp 98–100 °C dec. Anal. Calcd for  $\text{C}_{19}\text{H}_{20}\text{Fe}_2\text{N}_2\text{O}_3$ : C, 52.33; H, 4.62. Found: C, 52.31; H, 4.60. IR ( $\text{CH}_2\text{Cl}_2$ ) ( $\text{cm}^{-1}$ ):  $\nu(\text{CO})$  2004 s, 1965 sh, 1949 s, 1796 m, 1743 s;  $\nu(\text{CN})$  2183 w, 2145 w. IR (KBr) ( $\text{cm}^{-1}$ ):  $\nu(\text{CO})$  1999 s, 1964 mw, 1789 m;  $\nu(\text{CN})$  2143 w. <sup>1</sup>H NMR ( $\text{CDCl}_3$ ;  $\delta$ ): 4.70 (s, 10 H, cp), 3.6 (m, br, 4 H,  $\text{NCH}_2\text{CH}_3$ ), 1.25 (t, 6 H,  $\text{NCH}_2\text{CH}_3$ ).

$[\text{Fe}_2(\text{CO})_2(\text{cp})_2(\mu\text{-CO})\{\mu\text{-C}(\text{CN})\text{N}(\text{Me})\text{Bz}\}]$  (**4g**). A solution of  $[\text{Fe}_2(\text{CO})_2(\text{cp})_2(\mu\text{-CO})\{\mu\text{-CN}(\text{Me})\text{Bz}\}]\text{SO}_3\text{CF}_3$  (300 mg, 0.52 mmol) was treated with  $\text{Bu}^n\text{NCN}$  (150 mg, 0.55 mmol) in  $\text{CH}_2\text{Cl}_2$  (25 mL). After 30 min the mixture was filtered on an alumina pad. The red solution was evaporated to dryness under reduced pressure and the residue crystallized from  $\text{CH}_2\text{Cl}_2$  layered with *n*-pentane at  $-20^\circ\text{C}$ . Yield: 182 mg (73%). Anal. Calcd for  $\text{C}_{23}\text{H}_{20}\text{Fe}_2\text{N}_2\text{O}_3$ : C, 57.06; H, 4.16. Found: C, 56.98; H, 4.10. IR ( $\text{CH}_2\text{Cl}_2$ ) ( $\text{cm}^{-1}$ ):  $\nu(\text{CO})$  2004 s, 1969 mw, 1800 m;  $\nu(\text{CN})$  2147 w. <sup>1</sup>H NMR ( $\text{CD}_2\text{Cl}_2$ ;  $\delta$ ): 7.25 (m, 5 H, Ph), 4.86 (s, 10 H, cp), 4.32 (s, 2 H,  $\text{NCH}_2\text{Ph}$ ), 2.70 (s, 3 H, NMe). <sup>13</sup>C NMR ( $\text{CDCl}_3$ ;  $\delta$ ): 267.1 ( $\mu\text{-CO}$ ); 210.0 (CO); 160.5 ( $\mu\text{-C}$ ); 128.3 (CN); 139.8, 128.8, 127.4 (Ph); 90.9 (cp), 66.4 ( $\text{NCH}_2\text{Ph}$ ); 46.1 (NMe).

**Synthesis of  $[\text{Fe}_2\{\text{C}(\text{CN})\text{NPr}^i_2\}(\text{CO})(\text{cp})_2(\mu\text{-CO})_2]$  (**5**).** The synthesis of **5** has been previously briefly described:<sup>8</sup> compound **1a** (108 mg, 0.16 mmol) in MeCN (10 mL) was treated with  $\text{NHPr}^i_2$  (40 mg, 0.4 mmol). The reaction mixture

(35) Busetto, L.; Zanotti, V. Albano, V. G.; Monari, M.; Castellari, C. *Gazz. Chim. Ital.* **1993**, *123*, 703.

(36) Barbaro, P.; Bianchini, C.; Laschi, F.; Midollini, S.; Moneti, S.; Scapacci, G.; Zanella, P. *Inorg. Chem.* **1994**, *33*, 1622.

Table 3. Atomic Coordinates for  $[\text{Fe}_2\{\text{C}(\text{CN})\text{NPr}_2\}_2(\text{CO})(\text{Cp})_2(\mu\text{-CO})_2]$ 

atom	x	y	z	atom	x	y	z
Molecule A							
Fe(1A)	0.44175(3)	0.23439(3)	-0.00547(2)	C(16A)	0.5446(3)	0.1733(3)	0.0575(2)
Fe(2A)	0.30262(3)	0.18392(3)	0.04901(2)	C(17A)	0.5406(3)	0.1238(3)	-0.0082(2)
N(1A)	0.3726(3)	0.4894(2)	0.0065(2)	C(18A)	0.5547(3)	0.1929(3)	-0.0626(2)
N(2A)	0.3891(2)	0.3386(2)	-0.1370(1)	C(19A)	0.5675(3)	0.2852(3)	-0.0303(2)
C(1A)	0.3464(2)	0.0957(3)	0.1048(2)	C(20A)	0.1964(4)	0.2519(5)	0.0998(2)
O(1A)	0.3734(2)	0.0370(2)	0.1417(2)	C(21A)	0.1785(4)	0.1534(5)	0.0825(2)
C(2A)	0.3862(2)	0.2816(2)	0.0755(2)	C(22A)	0.1836(4)	0.1434(5)	0.0080(2)
O(2A)	0.3949(2)	0.3382(2)	0.1222(1)	C(23A)	0.2045(4)	0.2357(5)	-0.0206(2)
C(3A)	0.3633(2)	0.1344(2)	-0.0313(2)	C(24A)	0.2125(4)	0.3027(5)	0.0361(2)
O(3A)	0.3541(2)	0.0709(2)	-0.0727(1)	C(151)	0.5468(4)	0.2196(5)	0.0678(2)
C(4A)	0.3990(2)	0.3332(2)	-0.0680(2)	C(161)	0.5345(4)	0.1303(5)	0.0313(2)
C(5A)	0.3845(2)	0.4232(2)	-0.0300(2)	C(171)	0.5436(4)	0.1485(5)	-0.0420(2)
C(6A)	0.3681(2)	0.4292(3)	-0.1782(2)	C(181)	0.5616(4)	0.2490(5)	-0.0509(2)
C(7A)	0.4403(3)	0.5024(3)	-0.1738(3)	C(191)	0.5635(4)	0.2930(5)	0.0170(2)
C(8A)	0.2829(3)	0.4723(4)	-0.1606(3)	C(201)	0.1928(4)	0.2170(6)	0.1051(2)
C(9A)	0.3990(2)	0.2499(3)	-0.1809(2)	C(211)	0.1773(4)	0.1358(6)	0.0604(2)
C(10A)	0.3151(3)	0.2244(4)	-0.2159(2)	C(221)	0.1869(4)	0.1668(6)	-0.0105(2)
C(11A)	0.4700(3)	0.2623(3)	-0.2332(2)	C(231)	0.2083(4)	0.2672(6)	-0.0097(2)
C(15A)	0.5612(3)	0.2731(3)	0.0439(2)	C(241)	0.2119(4)	0.2982(6)	0.0618(2)
Molecule B							
Fe(1B)	0.06037(3)	0.66677(4)	0.19322(2)	C(16B)	-0.0381(4)	0.6179(2)	0.2642(4)
Fe(2B)	0.20068(3)	0.61221(4)	0.24684(3)	C(17B)	-0.0475(4)	0.7185(2)	0.2488(4)
N(1B)	0.1451(3)	0.9146(3)	0.1728(2)	C(18B)	-0.0618(4)	0.7283(2)	0.1750(4)
N(2B)	0.1086(2)	0.7371(2)	0.0504(1)	C(19B)	-0.0612(4)	0.6337(2)	0.1447(4)
C(1B)	0.1561(3)	0.5328(3)	0.3074(2)	C(20B)	0.3141(4)	0.5705(5)	0.1937(4)
O(1B)	0.1280(2)	0.4768(3)	0.3463(2)	C(21B)	0.3251(4)	0.5637(5)	0.2681(4)
C(2B)	0.1300(2)	0.5558(3)	0.1746(2)	C(22B)	0.3126(4)	0.6578(5)	0.2971(4)
O(2B)	0.1311(2)	0.4855(2)	0.1395(1)	C(23B)	0.2938(4)	0.7227(5)	0.2407(4)
C(3B)	0.1252(2)	0.7196(3)	0.2683(2)	C(24B)	0.2947(4)	0.6687(5)	0.1768(4)
O(3B)	0.1234(2)	0.7818(2)	0.3117(1)	C(152)	-0.0553(4)	0.6055(5)	0.1555(3)
C(4B)	0.1035(2)	0.7472(2)	0.1197(2)	C(162)	-0.0380(4)	0.5729(5)	0.2254(3)
C(5B)	0.1270(2)	0.8431(3)	0.1457(2)	C(172)	-0.0366(4)	0.6555(5)	0.2704(3)
C(6B)	0.1318(2)	0.8166(3)	-0.0009(2)	C(182)	-0.0530(4)	0.7392(5)	0.2284(3)
C(7B)	0.2220(2)	0.8524(3)	0.0091(2)	C(192)	-0.0646(4)	0.7083(5)	0.1574(3)
C(8B)	0.0644(3)	0.8963(3)	-0.0009(3)	C(202)	0.3178(4)	0.5522(3)	0.2166(4)
C(9B)	0.0866(2)	0.6416(3)	0.0171(2)	C(212)	0.3244(4)	0.5899(3)	0.2863(4)
C(10B)	0.0105(2)	0.6521(3)	-0.0339(2)	C(222)	0.3106(4)	0.6919(3)	0.2830(4)
C(11B)	0.1639(3)	0.5983(3)	-0.0182(2)	C(232)	0.2953(4)	0.7172(3)	0.2112(4)
C(15B)	-0.0465(4)	0.5655(2)	0.1999(4)	C(242)	0.2998(4)	0.6309(3)	0.1702(4)

was stirred for 15 min and the solvent removed under vacuum. After the residue was dissolved in  $\text{CH}_2\text{Cl}_2$ , the solution was chromatographed on an alumina column (15 × 3 cm) by using  $\text{CH}_2\text{Cl}_2$ /petroleum ether (1/2, v/v) as eluent. After elution of the first fraction containing  $[\text{Fe}_2(\text{cp})_2(\text{CO})_4]$ , the second red-violet fraction was collected and the solvent evaporated to dryness. Crystallization from  $\text{CH}_2\text{Cl}_2$  layered with *n*-hexane at  $-20^\circ\text{C}$  afforded 56 mg (64%) of **5**, mp 123–125 °C dec. Anal. Calcd for  $\text{C}_{21}\text{H}_{24}\text{Fe}_2\text{N}_2\text{O}_3$ : C, 54.35; H, 5.21. Found: C, 54.45; H, 5.32. IR ( $\text{CH}_2\text{Cl}_2$ ) ( $\text{cm}^{-1}$ ):  $\nu(\text{CO})$  1949 s, 1742 s;  $\nu(\text{CN})$  2177 w.  $^1\text{H}$  NMR ( $\text{CDCl}_3$ ;  $\delta$ ): 4.4 (s, br, 10 H, cp), 3.9 (m, br, 2 H,  $\text{CHMe}_2$ ), 1.5 (s, br, 12 H, Me).  $^{13}\text{C}$  NMR ( $\text{CD}_2\text{Cl}_2$ ,  $-50^\circ\text{C}$ ; *cis* + *trans* isomers;  $\delta$ ): 286.0, 282.0 ( $\mu\text{-CO}$ ), 232.7, 234.0 ( $\mu\text{-C}$ ), 212.3, 213.0 (CO), 113.3, 113.6 (CN), 88.4, 88.0 (cp), 62.3 ( $\text{CHMe}_2$ ), 21.1, 20.7, 20.1 ( $\text{CHMe}_2$ ).

#### Synthesis of $[\text{Fe}_2(\text{CO})\{\text{C}(\text{H})\text{NMe}_2\}(\text{cp})_2(\mu\text{-CO})_2]$ (**6a**).

**Method a.** Through a stirred solution of **1b** (0.19 g, 0.35 mmol) in MeCN (15 mL),  $\text{HNMe}_2$  was slowly bubbled for about 10 min. The mixture, which turned green-brown, was stirred for 30 min, and then the volatile material was removed *in vacuo*. The residue was redissolved in  $\text{CH}_2\text{Cl}_2$ -hexanes (1/2, v/v) and chromatographed on an alumina column, eluting with the same solvents mixture. A first yellow fraction containing unidentified mononuclear complexes and a second fraction containing some  $[\text{Fe}_2(\text{CO})_4(\text{cp})_2]$  were discharged. A green fraction was collected and evaporated to dryness under reduced pressure. The residue was crystallized from  $\text{CH}_2\text{Cl}_2$  layered with *n*-pentane at  $-20^\circ\text{C}$ . Yield: 56 mg (42%). Anal. Calcd for  $\text{C}_{16}\text{H}_{17}\text{Fe}_2\text{NO}_3$ : C, 50.18; H, 4.47. Found: C, 50.10; H, 4.46. IR ( $\text{CH}_2\text{Cl}_2$ ) ( $\text{cm}^{-1}$ ):  $\nu(\text{CO})$  1933 s, 1735 s.  $^1\text{H}$  NMR ( $\text{CD}_2\text{Cl}_2$ ;  $\delta$ ): 9.30 (s, br, 1 H,  $\text{CHNMe}_2$ ), 4.43 (s, br, 10 H, cp), 3.57 (s, br, 3 H, Me), 2.95 (s, br, 3 H, Me); ( $\text{CDCl}_3$ ;  $-20^\circ\text{C}$ ,  $\delta$ ) 9.49 (s,

br, 1 H,  $\text{CHNMe}_2$ ), 4.69 (s, 5 H, cp), 4.49 (s, 5 H, cp), 3.70 (s, 3 H, Me), 3.09 (s, 3 H, Me).  $^{13}\text{C}$  NMR ( $\text{CDCl}_3$ ,  $-20^\circ\text{C}$ ,  $\delta$ ): 286.9 ( $\mu\text{-CO}$ ); 260.4 ( $\text{CHNMe}_2$ ), 212.9 (CO), 86.0 (cp), 53.0, 44.1 (NMe).

**Method b.** To a stirred solution of  $[\text{Fe}_2(\text{CO})_2(\text{cp})_2(\mu\text{-CO})(\mu\text{-CNMe}_2)]\text{SO}_3\text{CF}_3$  (200 mg, 0.38 mmol) in MeCN (25 mL) was added  $\text{NaBH}_4$  (17 mg, 0.45 mmol). After 60 min the mixture was filtered on an alumina pad. The green-brownish solution was evaporated to dryness under reduced pressure and the residue crystallized from  $\text{CH}_2\text{Cl}_2$  layered with *n*-pentane at  $-20^\circ\text{C}$ . Yield: 77 mg (53%).

**Syntheses of the complexes **6b,c**.** The complex **6b** was prepared according to the procedures for the synthesis of **6a**; both methods (method a, from **1b** and  $\text{NHMeEt}$ , 36% yield; method b, from  $[\text{Fe}_2(\text{CO})_2(\text{cp})_2(\mu\text{-CO})\{\mu\text{-CN}(\text{Me})\text{Et}\}]\text{SO}_3\text{CF}_3$  and  $\text{NaBH}_4$ , 49% yield) have been used. The compound **6c** was obtained in 47% yield, reacting  $[\text{Fe}_2(\text{CO})_2(\text{cp})_2(\mu\text{-CO})\{\mu\text{-CN}(\text{Me})\text{Bz}\}]\text{SO}_3\text{CF}_3$  with  $\text{NaBH}_4$  according to the procedure described for the synthesis of **6a** (method b).

$[\text{Fe}_2(\text{CO})\{\text{C}(\text{H})\text{N}(\text{Me})\text{Et}\}(\text{cp})_2(\mu\text{-CO})_2]$  (**6b**): Anal. Calcd for  $\text{C}_{17}\text{H}_{19}\text{Fe}_2\text{NO}_3$ : C, 51.43; H, 4.82. Found: C, 51.45; H, 5.00. IR ( $\text{CH}_2\text{Cl}_2$ ) ( $\text{cm}^{-1}$ ):  $\nu(\text{CO})$  1934 s, 1723 s.  $^1\text{H}$  NMR ( $\text{CDCl}_3$ ;  $\delta$ ): 9.50 (s, br, 1 H,  $\text{CHNMeEt}$ ), 4.53 (s, br, 10 H, cp), 3.65 (s, br, 3 H, Me), 3.20 (m, br, 2 H,  $\text{CH}_2\text{CH}_3$ ), 0.97 (m, br, 3 H,  $\text{CH}_2\text{CH}_3$ ).

$[\text{Fe}_2(\text{CO})\{\text{C}(\text{H})\text{N}(\text{Me})\text{Bz}\}(\text{cp})_2(\mu\text{-CO})_2]$  (**6c**): Anal. Calcd for  $\text{C}_{22}\text{H}_{21}\text{Fe}_2\text{NO}_3$ : C, 57.56; H, 4.61. Found: C, 57.45; H, 4.82. IR ( $\text{CH}_2\text{Cl}_2$ ) ( $\text{cm}^{-1}$ ):  $\nu(\text{CO})$  1933 s, 1726 s.  $^1\text{H}$  NMR ( $\text{CDCl}_3$ ;  $\delta$ ): 9.77 (s, br, 1 H,  $\text{CHNMeBz}$ ), 7.43–6.94 (m, 5 H, Ph), 4.60 (s, br, 10 H, cp), 3.55 (s, br, 3 H, Me), 2.87 (s, br, 2 H,  $\text{CH}_2\text{Ph}$ ).  $^1\text{H}$  NMR ( $\text{CDCl}_3$ ;  $\delta$ ,  $-30^\circ\text{C}$ ): 9.54 (s, br, 1 H,  $\text{CHNMeBz}$ ),

7.35–6.90 (m, 5 H, Ph), 4.74, 4.52 (s, br, 10 H, cp), 3.53 (s, br, 3 H, Me), 2.87 (s, br, 2 H, CH<sub>2</sub>Ph).

**Synthesis of [Fe<sub>2</sub>(CO)<sub>3</sub>(cp)<sub>2</sub>(CNMe)] (7a).** Gaseous NH<sub>2</sub>-Me was bubbled into a stirred MeCN solution (10 mL) of **1a** (0.15 g, 0.26 mmol), for 10 min, and then the volatile material was removed under reduced pressure and the residue, redissolved in CH<sub>2</sub>Cl<sub>2</sub>, was filtered on an alumina column. Crystallization from a CH<sub>2</sub>Cl<sub>2</sub>-hexane mixture gave **7a** (34 mg, 37%), which was identified by comparison of its spectroscopic properties with those reported in the literature.<sup>18</sup>

**Synthesis of 7b–e.** The compounds **7b–e** were all synthesized by a procedure similar to that for **7a**, adding the corresponding primary amines dropwise, by a syringe, to MeCN solutions of **1a**. The complexes **7b–e** were obtained with the following yields: **7b**, 41%; **7c**, 20%; **7d**, 35%; **7e**, 46%. They were identified by comparison of their spectroscopic properties with those reported in the literature.<sup>18</sup>

**[Fe<sub>2</sub>(CO)<sub>2</sub>(cp)<sub>2</sub>(μ-CO){μ-C(CN)N(H)Ph}] (8a).** The synthesis of **8a** has been previously briefly described:<sup>8</sup> compound **1a** (160 mg, 0.28 mmol) in MeCN (10 mL) was treated with aniline (0.54 mmol). After 10 min the mixture was dried under vacuum and the residue, redissolved in CH<sub>2</sub>Cl<sub>2</sub>, was filtered on an alumina pad (3 × 5 cm). The red filtered solution was evaporated to dryness under reduced pressure and the residue crystallized from CH<sub>2</sub>Cl<sub>2</sub> layered with *n*-pentane at –20 °C to yield 40 mg (32%) of **8a**; mp 147–149 °C dec. Anal. Calcd for C<sub>21</sub>H<sub>16</sub>Fe<sub>2</sub>N<sub>2</sub>O<sub>3</sub>: C, 55.31; H, 3.54. Found: C, 55.33; H, 3.90. IR (CH<sub>2</sub>Cl<sub>2</sub>) (cm<sup>-1</sup>): ν(CO) 1992 s, 1954 mw, 1798 m; ν(CN) 2166 w. <sup>1</sup>H NMR (CDCl<sub>3</sub>; δ): 7.3–6.9 (m, 5 H, Ph), 5.4 (s, 1 H, NH), 4.9 (s, 10 H, cp); <sup>13</sup>C NMR (CD<sub>2</sub>Cl<sub>2</sub>; δ): 267.0 (μ-CO); 211.8 (CO); 147.0, 117.1, 130.3, 121.0, 124.9 (Ph); 91.8 (cp).

**Synthesis of [Fe<sub>2</sub>(CO)<sub>2</sub>(cp)<sub>2</sub>(μ-CO){μ-C(CN)N(H)Pr<sup>i</sup>}] (8b).** The reaction of **1a** with H<sub>2</sub>NPr<sup>i</sup> following the same procedure above described for the preparation of **8a** has allowed us to detect, but not to isolate, the compound **8b**. IR (CH<sub>2</sub>Cl<sub>2</sub>) (cm<sup>-1</sup>): ν(CO) 1977 s, 1943 mw, 1786 m; ν(CN) 2167 w.

**Reaction of 1a with NH<sub>3</sub>.** Gaseous ammonia was slowly bubbled into a MeCN solution (10 mL) of **1a** (0.52 g, 0.90 mmol) for 15 min. An IR inspection of the mixture showed ν(CO) absorptions at 1983 s, 1949 w, and 1792 m and ν(CN) at 2173 w cm<sup>-1</sup> which are in agreement with the formation of [Fe<sub>2</sub>(CO)<sub>2</sub>(cp)<sub>2</sub>(μ-CO){μ-C(CN)NH<sub>2</sub>}] (**9**). Any effort to isolate the compound failed because of extensive decomposition to [Fe(CO)<sub>2</sub>(cp)(CN)].

**Synthesis of [Fe<sub>2</sub>(CO)<sub>2</sub>(cp)<sub>2</sub>(μ-CO){μ-C(CN)N(H)C(O)Me}] (10).** A solution of **1a** (0.52 g, 0.90 mmol) was treated with NH<sub>3</sub> as above described. The mixture was then treated with CH<sub>3</sub>COCl (71 mg, 0.90 mmol) and pyridine (72 mg, 0.90 mmol) and stirred for 10 min. The solvent was then removed *in vacuo*, and the residue, redissolved in CH<sub>2</sub>Cl<sub>2</sub>, was chromatographed on an alumina column. A first green fraction containing traces of an unidentified product was discharged; a second red fraction was eluted with CH<sub>3</sub>CN, collected, and evaporated to dryness. Crystallization from CH<sub>2</sub>Cl<sub>2</sub> layered with *n*-pentane at –20 °C afforded 0.28 g (73%) of **10**, mp 159–160 °C dec. Anal. Calcd for C<sub>17</sub>H<sub>14</sub>Fe<sub>2</sub>N<sub>2</sub>O<sub>3</sub>: C, 48.39; H, 3.34. Found: C, 48.42; H, 3.30. IR (CH<sub>2</sub>Cl<sub>2</sub>) (cm<sup>-1</sup>): ν(CO) 1998 s, 1959 w, 1808 m, 1678 mw; ν(CN) 2170 w. <sup>1</sup>H NMR (CDCl<sub>3</sub>; δ): 6.79 (s, 1 H, NH), 4.95 (s, 10 H, cp), 1.92 (s, 3 H, Me). <sup>13</sup>C NMR (CD<sub>2</sub>Cl<sub>2</sub>; δ): 264.9 (μ-CO), 211.5 (CO), 168.2 (NCOMe), 131.5 (CN), 130.7 (μ-C), 91.9 (Cp), 23.4 (Me).

**Synthesis of [Fe<sub>2</sub>{CN(H)(CH<sub>2</sub>)<sub>2</sub>N(H)}(CO)(cp)<sub>2</sub>(μ-CO)<sub>2</sub>] (11).** Ethylenediamine (0.10 mL, 1.50 mmol) was added to a solution of **1a** (0.24 g, 0.42 mmol) in MeCN (10 mL), and the mixture was stirred for 15 min. Then the solvent was removed under vacuum and the residue, redissolved in CH<sub>2</sub>Cl<sub>2</sub>, was filtered on an alumina pad. Evaporation of the solvent to minimum volume and addition of Et<sub>2</sub>O gave, upon standing at –20 °C, red crystals of **11** (70 mg, 43%), mp 189–190 °C dec. Anal. Calcd for C<sub>16</sub>H<sub>16</sub>Fe<sub>2</sub>N<sub>2</sub>O<sub>3</sub>: C, 48.53; H, 4.07.

Found: C, 48.52; H, 4.10. IR (CH<sub>2</sub>Cl<sub>2</sub>) (cm<sup>-1</sup>): ν(CO) 1929 s, 1716 s. <sup>1</sup>H NMR (CDCl<sub>3</sub>; δ): 4.62, 4.38 (s, 10 H, cp), 3.25 (s, 4 H, NCH<sub>2</sub>), 6.24 (s, 2 H, NH). <sup>13</sup>C NMR (CD<sub>2</sub>Cl<sub>2</sub>; δ): 290.8 (μ-CO), 215.0 (CO), 222.6 (μ-C), 86.7, 86.5 (Cp), 45.9 (CH<sub>2</sub>).

**Reaction of 1a with N,N-Dimethylethylenediamine.** A solution of **1a** (0.11 g, 0.185 mmol) in MeCN (10 mL) was treated with N,N-dimethylethylenediamine (0.3 mL, 2.73 mmol). After 10 min the mixture was worked up as described for the preparation of type **7** complexes. Attempts to crystallize the product [Fe<sub>2</sub>(CO)<sub>3</sub>(cp)<sub>2</sub>{CN(CH<sub>2</sub>)<sub>2</sub>NMe<sub>2</sub>}] (**12**) have been unsuccessful. IR (CH<sub>2</sub>Cl<sub>2</sub>) (cm<sup>-1</sup>): ν(CO) 1989 w, 1948 s; ν(CN) 2138 w, 1748 s.

**Reaction of 1a with N,N'-Dimethylethylenediamine.** N,N'-Dimethylethylenediamine (0.3 mL, 2.73 mmol) was added to a solution of **1a** (98 mg, 0.17 mmol) in MeCN (10 mL) and the mixture was stirred for 10 min. Then the solvent was removed under vacuum yielding the complex [Fe<sub>2</sub>(CO)<sub>2</sub>(cp)<sub>2</sub>(μ-CO){μ-C(CN)N(Me)(CH<sub>2</sub>)<sub>2</sub>NHMe}] (**13**) as a red oily residue. IR (CH<sub>2</sub>Cl<sub>2</sub>) (cm<sup>-1</sup>): ν(CO) 2004 s, 1969 w, 1801 m; ν(CN) 2147 w.

**X-ray Structure Determination of trans-[Fe<sub>2</sub>{C(CN)NPr<sup>i</sup>}<sub>2</sub>(CO)(cp)<sub>2</sub>(μ-CO)<sub>2</sub>] (5).** Crystal data and details of the data collection for **5** are given in Table 2. The diffraction experiments were carried out at room temperature on a fully automated Enraf-Nonius CAD-4 diffractometer using graphite-monochromated Mo Kα radiation. The unit cell parameters were determined by a least-squares fitting procedure using 25 reflections. Data were corrected for Lorentz and polarization effects. No decay correction was necessary. The asymmetric unit was found to contain two independent molecules. The positions of the metal atoms were found by direct methods using the SHELXS 86 program<sup>37</sup> and all the non-hydrogen atoms located from difference Fourier syntheses. An empirical absorption was applied by using the azimuthal scan method.<sup>38</sup> The cyclopentadienyl rings were treated as rigid groups (C–C 1.42, C–H 0.96 Å) and presented positional disorder in both molecule A and B. They were disordered ca. 53 and 47% (C(15A)–C(19A) and C(151)–C(191)), 51 and 49% (C(20A)–C(24A) and C(201)–C(241)), 52 and 48% (C(15B)–C(19B) and C(152)–C(192)), and 50 and 50% (C(20B)–C(24B) and C(202)–C(242)). The hydrogen atoms of the diisopropyl amino ligand were located from difference-Fourier maps, and their positional parameters were allowed to refine. The refinement proceeded by full-matrix least-squares calculations (SHELXL 76)<sup>39</sup> using anisotropic thermal parameters for all the non-hydrogen atoms except the cyclopentadienyl C atoms. The H atoms of the amino group were assigned fixed isotropic thermal parameters 1.3 times U<sub>eq</sub> of the carbon atoms to which they were attached. The cyclopentadienyl H atoms were assigned a fixed isotropic thermal parameter (0.08 Å<sup>2</sup>). The final difference Fourier map showed peaks not exceeding 0.54 e Å<sup>-3</sup>. The final positional and equivalent isotropic thermal parameters with their esd's are given in Table 3.

**Acknowledgment.** This work was supported by the MURST (Ministero dell'Università e della Ricerca Scientifica) and the CNR (Consiglio Nazionale delle Ricerche).

**Supporting Information Available:** Tables of H coordinates, anisotropic thermal parameters, and bond lengths and angles and ORTEP diagrams (12 pages). Ordering information is given on any current masthead page.

OM950356X

(37) Sheldrick G. M. SHELXS 86, Program for Crystal Structure Solution, Göttingen, 1986.

(38) North, A. C.; Philips, D. C.; Mathews, F. S. *Acta Crystallogr.* **1968**, *A24*, 351.

(39) Sheldrick G. M. SHELXL 76, Program for Crystal Structure Determination, University of Cambridge, 1976.

# Nucleophilic Reactions of Chiral Heterobimetallic Cobalt–Molybdenum Propargylium Complexes, Involving the First Example of Phosphine Migration. X-ray Crystal Structures of

## $[(\mu\text{-}\eta^2\text{-}\eta^3\text{-HC}\equiv\text{CCH}(\text{CH}_3))\text{CoMoCp}(\text{CO})_5][\text{BF}_4]$ and $[(\mu\text{-}\eta^2\text{-}\eta^3\text{-HC}\equiv\text{CCH}(\text{CH}_3))\text{CoMoCp}(\text{CO})_4(\text{PPh}_3)][\text{BF}_4]$

Michel Gruselle,<sup>\*,†</sup> Mikhael A. Kondratenko,<sup>†,‡</sup> Hani El Amouri,<sup>†</sup> and Jacqueline Vaissermann<sup>§</sup>

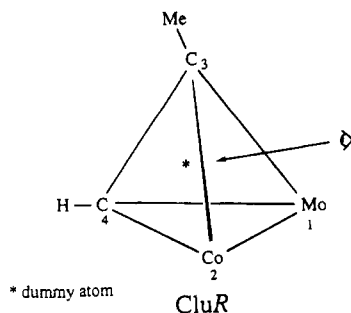
*Ecole Nationale Supérieure de Chimie de Paris, URA-CNRS 403, 11 rue Pierre et Marie Curie, 75231 Paris Cédex 05, France, Laboratoire de Chimie des Métaux de Transition, URA-CNRS 419, Université Pierre et Marie Curie, 4 place Jussieu, Bât F, 75252 Paris Cédex 05, France, and INEOS, Académie des Sciences de Russie, 28 rue Vavilov, 117813 Moscow, Russia*

Received April 12, 1995<sup>®</sup>

Chiral complexes of the type  $[(\mu\text{-}\eta^2\text{-}\eta^3\text{-R}_1\text{C}\equiv\text{C}^2\text{C}^3\text{H}(\text{R}_3))\text{CoMoCp}(\text{CO})_5][\text{BF}_4]$  [ $\text{R}_1 = \text{R}_3 = \text{H}$  (**2**);  $\text{R}_1 = \text{H}$ ,  $\text{R}_3 = \text{CH}_3$  (**4a,b**);  $\text{R}_1 = \text{CH}_3$ ,  $\text{R}_3 = \text{H}$  (**6**)] have been synthesized and characterized. These carbenium ions were obtained via the protonation of the corresponding alcohol or ether complexes  $[(\mu\text{-}\eta^2\text{-}\eta^2\text{-R}_1\text{C}\equiv\text{C}^2\text{C}^3\text{H}(\text{R}_3)(\text{OH}))\text{CoMoCp}(\text{CO})_5]$  [ $\text{R}_1 = \text{R}_3 = \text{H}$  (**1**);  $\text{R}_1 = \text{R}_3 = \text{CH}_3$  (**3a,b**)] or  $[(\mu\text{-}\eta^2\text{-}\eta^2\text{-R}_1\text{C}\equiv\text{C}^2\text{C}^3\text{H}(\text{R}_3)(\text{OCH}_3))\text{CoMoCp}(\text{CO})_5]$  [ $\text{R}_1 = \text{CH}_3$ ,  $\text{R}_3 = \text{H}$  (**5**)]. The diastereomeric alcohols **3a,b** give the same mixture of cations  $[(\mu\text{-}\eta^2\text{-}\eta^3\text{-HC}\equiv\text{CCH}(\text{CH}_3))\text{CoMoCp}(\text{CO})_5][\text{BF}_4]$  (**4a,b**) with a moderate diastereoselectivity (85/15). These cations react with sodium methanethiolate to give a mixture of thioethers  $[(\mu\text{-}\eta^2\text{-}\eta^2\text{-HC}\equiv\text{CCH}(\text{CH}_3)\text{SCH}_3)\text{CoMoCp}(\text{CO})_5]$  (**9a,b**), in the same diastereoselective ratio relative to the starting material. The reaction with triphenylphosphine leads to the expected phosphonium derivative  $[(\mu\text{-}\eta^2\text{-}\eta^3\text{-H}_3\text{CC}\equiv\text{CCH}_2(\text{PPh}_3))\text{CoMoCp}(\text{CO})_5][\text{BF}_4]$  (**10**) in the case of the primary cation. With the secondary cation (**4a**) the initially formed phosphonium ion  $[(\mu\text{-}\eta^2\text{-}\eta^3\text{-HC}\equiv\text{CCH}(\text{CH}_3)(\text{PPh}_3))\text{Co}(\text{CO})_3\text{MoCp}(\text{CO})_2][\text{BF}_4]$  (**11a,b**) is readily transformed to a cobalt-bonded triphenylphosphine, involving a phosphine migration from the carbenium center to the cobalt center,  $[(\mu\text{-}\eta^2\text{-}\eta^3\text{-HC}\equiv\text{CCH}(\text{CH}_3))\text{Co}(\text{CO})_2(\text{PPh}_3)\text{MoCp}(\text{CO})_2][\text{BF}_4]$  (**12a,b**). Structural and mechanistic models are proposed to explain the diastereoselectivity observed in the formation of the phosphinated carbenium ions (**12a,b**). The X-ray crystal structure of  $(3R^*, \text{cluster } R^*)\text{-}(\mathbf{4a})$  has been determined. It is the first described structure for a secondary carbenium center possessing a chiral cluster in the  $\alpha$ -position. The X-ray structure of  $(3R^*, \text{cluster } R^*)\text{-}(\mathbf{12a})$  was also determined and provides evidence that the phosphine ligand is bonded to the cobalt metallic center.

### Introduction

Propargylic bimetallic clusters are found to contain pseudotetrahedral  $\text{M}_2\text{C}_2$  "dimetallatetrahedrane cores".<sup>1</sup> The absolute configuration of a chiral tetrahedral  $\text{M}_2\text{C}_2$  cluster can be conveniently designated by assigning an *R* or *S* to a dummy atom placed at the center of the dimetallatetrahedrane core.



The presence of different substituents on the carbe-

nium center and the substitution of one of the metal vertices by another due to the isolobal analogy ( $\text{CpMo}(\text{CO})_2 = \text{Co}(\text{CO})_3$ )<sup>2</sup> render the metal cluster stereogenic.

This tool can be elegantly employed in the field of stereocontrolled syntheses using these kinds of binuclear metallic complexes as stereogenic centers, in particular in some asymmetric Khand reactions.<sup>3</sup> In several cases the resolution of the chirality was achieved using optically active ligands.<sup>2f,4,5</sup>

The use of stabilized  $-\text{Co}_2(\text{CO})_6$  or  $-\text{Cp}_2\text{Mo}_2(\text{CO})_4$  propargylium complexes in organic synthesis has been widely developed by several authors.<sup>6</sup> The stereo- and regiochemical courses of the reactions in the case of homobimetallic  $-\text{Co}_2(\text{CO})_6$  propargylium stabilized ions

(1) (a) Bailey, W. I.; Chisholm, F. A.; Cotton, F. A.; Rankel, J. J. *Amer. Chem. Soc.* **1978**, *100*, 5764. (b) McGlinchey, M. J.; Mlekuz, M.; Bougeard, P.; Sayer, B. G.; Marinetti, A.; Saillard, J. Y. *Can. J. Chem.* **1983**, *61*, 1319.

(2) (a) Manning, P. J.; Peterson, L. K. *Inorg. Chim. Acta* **1984**, *88*, L5. (b) Jensen, S. D.; Robinson, B. H.; Simpson, J. *Organometallics* **1986**, *5*, 1690. (c) Hart, I. J.; Jardin, A. E.; Jeffery, J. C.; Stone, F. G. A. *J. Organomet. Chem.* **1988**, *341*, 391. (d) Wido, T. M.; Young, G. H.; Wojcicki, A.; Calligaris, M.; Nardin, G. *Organometallics* **1988**, *7*, 452. (e) Chetcuti, M. J.; Grant, B. E.; Fanwick, P. E. *J. Amer. Chem. Soc.* **1989**, *111*, 2743. (f) D'Agostino, M. F.; Frampton, C. S.; McGlinchey, M. J. *Organometallics* **1990**, *9*, 2972.

<sup>†</sup> URA-CNRS 403.

<sup>‡</sup> INEOS.

<sup>§</sup> URA-CNRS 419.

<sup>®</sup> Abstract published in *Advance ACS Abstracts*, August 15, 1995.





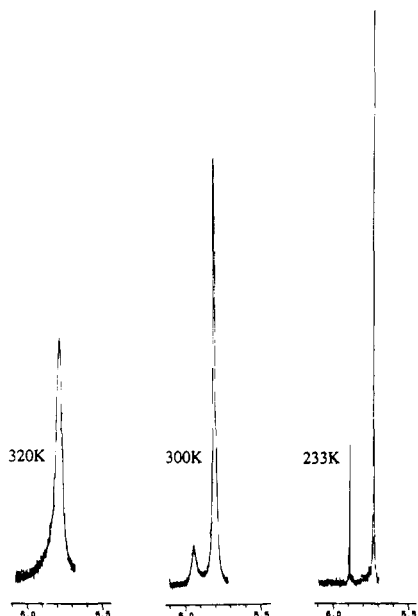


**Figure 1.** Evolution of the  $^1\text{H}$  cyclopentadienyl signal for **4** in  $\text{CD}_2\text{Cl}_2$  solution.

40 ratio. These products were separated by chromatography on silica plates. Starting from either **3a** or **3b** and action of  $\text{HBF}_4/\text{Et}_2\text{O}$  in ether leads to the same mixture of diastereomeric carbenium ions **4a,b** in a 85/15 ratio (determined by integration of the  $^1\text{H}$  NMR signals) (Scheme 2). These complexes were characterized by spectroscopic methods; in addition the X-ray structure of **4a** was resolved (vide infra).

**Fluxional and Solution Behavior of 4a,b.** Variable temperature  $^1\text{H}$  NMR studies were performed on a sample solution of **4a,b** in  $\text{CD}_2\text{Cl}_2$ . At 320 K, the  $^1\text{H}$  NMR spectrum shows broad signals. We note that the cyclopentadienyl unit appears as a broad peak at 5.79 ppm. We could not record the spectrum at higher temperature due to the instability of the cation species **4a,b** in solution. Cooling the sample solution results, however, in the appearance of two sets of signals indicating the presence of two species. For instance at 233 K the cyclopentadienyl groups appear as two sharp lines respectively at 5.88 and 5.72 ppm in the ratio 85/15 (Figure 1).

As demonstrated previously in the case of heterobimetallic stabilized propargylium ion, a simple rotation about the  $\text{C}^+$ -cluster bond is responsible of the observed exchange phenomenon.<sup>14</sup> After a long time at room temperature the relative ratio between the two diastereomers **4a** and **4b** remains unchanged. The activation energy for the rotation about the  $\text{C}^+$ -cluster bond can be calculated as 16 kcal.mol<sup>-1</sup> at 320 K, higher than that obtained for the secondary  $[\text{Mo}-\text{Co}]$  stabilized carbenium ions possessing a ferrocenyl or cymantrenyl substituent<sup>14</sup> for which activation energies are found as  $\Delta G^{\ddagger}_{253\text{K}} = 11.2$  kcal.mol<sup>-1</sup> and  $\Delta G^{\ddagger}_{283\text{K}} = 12.5$  kcal.mol<sup>-1</sup> respectively (Figure 2).

**X-ray Molecular Structure of  $[(\mu-\eta^2-\eta^3\text{-HC}\equiv\text{CCH}(\text{CH}_3))\text{-CoMoCp}(\text{CO})_5][\text{BF}_4]$  (**4a**).** Suitable crystals of  $[(\mu-\eta^2-\eta^3\text{-HC}\equiv\text{CCH}(\text{CH}_3))\text{CoMoCp}(\text{CO})_5][\text{BF}_4]$  (**4a**) for an X-ray study were obtained by slow evaporation of a  $\text{CH}_2\text{Cl}_2/\text{Et}_2\text{O}$  solution of (**4a,b**). The chiral heterobimetallic species crystallizes in the orthorhombic space group  $Pc2_1n$ . A view of the molecule with atomic numbering

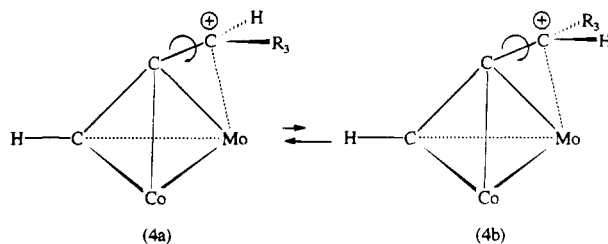


**Figure 2.** Activation energy associated with the rotation process around the  $\text{C}^+$ -cluster bond:  $\text{R}_3 = \text{Fc}$ ,  $\Delta G^{\ddagger}_{253\text{K}} = 11.2$  kcal mol<sup>-1</sup>;  $\text{R}_3 = \text{Cm}$ ,  $\Delta G^{\ddagger}_{283\text{K}} = 12.5$  kcal mol<sup>-1</sup>;  $\text{R}_3 = \text{CH}_3$ ,  $\Delta G^{\ddagger}_{320\text{K}} = 16.0$  kcal mol<sup>-1</sup>.

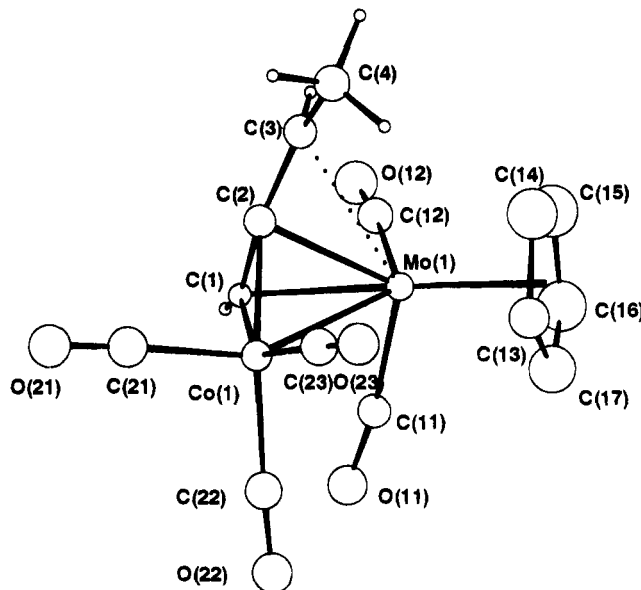


**Figure 3.** Cameron view for **4a**.

is shown on Figure 3. Crystallographic data collection parameters and selected bond lengths and angles are listed in Tables 1 through 3.

The cationic chiral species  $[(\mu-\eta^2-\eta^3\text{-HC}\equiv\text{CCH}(\text{CH}_3))\text{-CoMoCp}(\text{CO})_5]^+$  possesses a tetrahedron "MoCoC<sub>2</sub>" core with the acetylenic unit  $-\text{C}\equiv\text{C}-$  asymmetrically bridging the two metallic centers "closer to the cobalt center" and perpendicular to the metal-metal bond Mo-Co. An important feature depicted by the solid structure of the *anti* diastereomer (**4a**) is the relative configuration of the cluster core ( $R^*$ ) and that of the carbenium center ( $R^*$ ). A similar arrangement for the  $\eta^2,\eta^3$ -hydrocarbyl ligand relative to the cluster core was observed for the homobimetallic secondary carbenium ion  $[(\mu-\eta^2-\eta^3\text{-HC}\equiv\text{CCH}(\text{CH}_3))\text{Mo}_2\text{Cp}_2(\text{CO})_4]^+$ . Overlapped views of  $[\text{Mo}_2\text{Cp}_2(\text{CO})_4(\text{HC}\equiv\text{CCH}(\text{CH}_3))^+]$  (**4a**) and  $[(\text{Mo}-\text{Co})\text{Cp}(\text{CO})_5(\text{HC}\equiv\text{CCH}(\text{CH}_3))^+]$  were reported in Figure 4. The Mo-C<sup>+</sup> bond is 2.64 Å, similar to that reported for the analogous dimolybdenum derivative  $[(\mu-\eta^2-\eta^3\text{-HC}\equiv\text{CCH}(\text{CH}_3))\text{Mo}_2\text{Cp}_2(\text{CO})_4]^+$  with  $d(\text{Mo}-\text{C}^+) = 2.613$ .<sup>15</sup> The Mo-Co bond distance in **4a** is 2.719 (4) Å, typical of the molybdenum cobalt bond found in the heterobimetallic series of  $[\text{Co}-\text{Mo}]$  acetylenic complexes.<sup>5</sup>

**Reactivity of (4a,b) with Various Nucleophiles.** The carbenium ion complexes **4a,b** react with various nucleophilic reagents. With sodium thiolate, the reaction proceeds quickly leading to a mixture of two diastereomeric sulfides **9a,b** in the same ratio as the starting material (85/15), indicating kinetic control of the reaction. With water, in methylene chloride we



**Table 1. Crystal Data for [C<sub>14</sub>H<sub>10</sub>O<sub>5</sub>CoMo](BF<sub>4</sub>) (4a)**

fw	499.9
a (Å)	8.203(1)
b (Å)	13.158(2)
c (Å)	16.056(3)
α (deg)	90
β (deg)	90
γ (deg)	90
V (Å <sup>3</sup> )	1732.9(5)
Z	4
space group	Pc2 <sub>1</sub> n
linear abs coeff μ (cm <sup>-1</sup> )	17.23
density ρ (g cm <sup>-3</sup> )	1.92
diffractometer	CAD4 Enraf-Nonius
radiation	Mo Kα (λ = 0.710 69 Å)
scan type	ω/2θ
scan range (deg)	0.8 + 0.345 tan θ
θ limits (deg)	1–23
temp of measmt	room temp
octants colld	0.9; 14; 0.17
no. of unique data colld	1257
no. of unique data used for refinement	719, (F <sub>o</sub> ) <sup>2</sup> > 3σ(F <sub>o</sub> ) <sup>2</sup>
R = Σ  F <sub>o</sub>   -  F <sub>c</sub>   /Σ F <sub>o</sub>	0.0534
R <sub>w</sub> = Σw( F <sub>o</sub>   -  F <sub>c</sub>  ) <sup>2</sup> /ΣwF <sub>o</sub> <sup>2</sup>	0.0586, w = 1.0
abs corr	DIFABS (min = 0.805, max = 1.096)
extinction param (×10 <sup>-6</sup> )	no
goodness of fit s	1.99
no. of variables	105
ΔQ <sub>min</sub> (e/Å <sup>3</sup> )	-0.63
ΔQ <sub>max</sub> (e/Å <sup>3</sup> )	1.13

**Table 2. Fractional Parameters and U Values for [C<sub>14</sub>H<sub>10</sub>O<sub>5</sub>CoMo](BF<sub>4</sub>)**

atom	x/a	y/b	z/c	U(iso) (Å <sup>2</sup> )
Mo(1)	0.1949(3)	0.0988(3)	0.1495(1)	0.0348(5)
Co(1)	0.4149(4)	-0.0113(4)	0.0606(2)	0.0417(9)
O(11)	0.472(3)	0.265(2)	0.146(1)	0.068(6)
O(12)	0.213(3)	0.137(1)	0.342(1)	0.080(7)
O(21)	0.665(3)	-0.167(2)	0.061(1)	0.078(7)
O(22)	0.600(3)	0.160(1)	-0.012(1)	0.071(6)
O(23)	0.218(3)	-0.082(2)	-0.081(1)	0.075(7)
C(1)	0.416(3)	0.020(2)	0.176(1)	0.023(6)
C(2)	0.306(4)	-0.056(2)	0.162(2)	0.047(7)
C(3)	0.169(4)	-0.095(2)	0.190(2)	0.048(7)
C(4)	0.059(4)	-0.165(2)	0.145(2)	0.057(8)
C(11)	0.361(3)	0.2109(2)	0.150(2)	0.048(8)
C(12)	0.197(4)	0.121(2)	0.272(2)	0.055(8)
C(13)	0.022(4)	0.121(3)	0.038(2)	0.07(1)
C(14)	-0.069(6)	0.074(3)	0.103(3)	0.11(1)
C(15)	-0.073(6)	0.142(4)	0.166(3)	0.12(2)
C(16)	0.007(5)	0.223(3)	0.139(3)	0.11(1)
C(17)	0.056(5)	0.211(3)	0.062(3)	0.10(1)
C(21)	0.568(4)	-0.110(3)	0.061(2)	0.07(1)
C(22)	0.532(3)	0.090(3)	0.012(2)	0.061(8)
C(23)	0.293(4)	-0.055(2)	-0.025(2)	0.060(8)
B(1)	0.254(4)	0.483(3)	0.162(2)	0.051(9)
F(1)	0.214(2)	0.418(1)	0.223(1)	0.074(5)
F(2)	0.197(2)	0.450(1)	0.086(1)	0.089(6)
F(3)	0.413(2)	0.499(2)	0.156(1)	0.092(6)
F(4)	0.169(3)	0.575(2)	0.178(1)	0.097(7)

recover the same mixture of starting alcohols (85/15), while in acetone the ratio **3a**:**3b** was about 50/50. This result is consistent with a thermodynamically controlled reaction. Primary carbenium ion **2** or **6** reacts in the same way as **4a,b**.

Furthermore we investigated the reduction of cation **2** by sodium borohydride or, following the procedure described by Nicholas,<sup>16</sup> using zinc in methylene chloride solution. In both cases we obtain the corresponding [Co-Mo] propyne-1 complex (**7**). We believe that the reduction product is the result of abstraction of one hydrogen atom from the solvent. It is worth mentioning that other authors using similar conditions reported, in

**Table 3. Selected Interatomic Distances (Å) and Bond Angles (deg) for [C<sub>14</sub>H<sub>10</sub>O<sub>5</sub>CoMo](BF<sub>4</sub>)**

Mo(1)–Co(1)	2.719(4)	Mo(1)–C(2)	2.24(3)
Mo(1)–C(1)	2.14(2)	O(11)–C(11)	1.179(3)
Mo(1)–C(11)	2.00(3)	O(12)–C(12)	1.15(3)
Mo(1)–C(12)	1.99(2)	Mo(1)–C(14)	2.31(5)
Mo(1)–C(13)	2.30(3)	Mo(1)–C(16)	2.25(4)
Mo(1)–C(15)	2.28(5)		
Mo(1)–C(17)	2.34(4)		
Co(1)–C(1)	1.90(2)	Co(1)–C(2)	1.94(3)
Co(1)–C(21)	1.81(4)	O(21)–C(21)	1.09(4)
Co(1)–C(22)	1.82(4)	O(22)–C(22)	1.15(4)
Co(1)–C(23)	1.79(3)	O(23)–C(23)	1.14(3)
C(1)–C(2)	1.36(3)	C(2)–C(3)	1.31(4)
C(3)–C(4)	1.48(4)	C(13)–C(14)	1.42(5)
C(13)–C(17)	1.28(5)	C(14)–C(15)	1.35(5)
C(15)–C(16)	1.32(6)	C(16)–C(17)	1.31(5)
C(11)–Mo(1)–C(12)	83.6(12)	Mo(1)–C(11)–O(11)	170.8(26)
C(21)–Co(1)–C(22)	99.4(14)	Co(1)–C(21)–O(21)	176.9(32)
C(21)–Co(1)–C(23)	99.3(14)	Co(1)–C(22)–O(22)	173.1(28)
C(22)–Co(1)–C(23)	101.9(13)	Co(1)–C(23)–O(23)	177.9(27)
Mo(1)–C(1)–Co(1)	84.6(9)	Mo(1)–C(1)–C(2)	75.9(15)
Co(1)–C(1)–C(2)	71.0(15)	Mo(1)–C(2)–Co(1)	80.9(10)
Mo(1)–C(20)–C(1)	67.9(15)	Co(1)–C(2)–C(1)	67.4(16)
Mo(1)–C(2)–C(3)	92.3(19)	Co(1)–C(2)–C(3)	143.1(23)
C(1)–C(2)–C(3)	142.5(26)	C(2)–C(3)–C(4)	126.2(26)

addition to alkyl adducts, the formation of dimers obtained from coupling of the radical intermediates.<sup>16,17</sup>

The cation **6** was found to react with diethyl ether in methylene chloride solution leading to propargyl ether complex **14**.

A difference in reactivity with triphenylphosphine was observed between the primary cation **6** and the secondary ones **4a,b**. The primary cation **6** gave the corresponding phosphonium derivative **10** as previously reported for homobimetallic [Co<sub>2</sub>] and [Mo<sub>2</sub>] propargylium ion complexes.<sup>18</sup> Compound **10** is stable and can be stored under argon for a long time without any change. The reaction of the secondary carbenium ions **4a,b** leads primarily to the expected phosphonium ion **11** as demonstrated by its <sup>1</sup>H NMR and infrared spectra. However, in acetone solution the cation is regenerated and gives two diastereomeric secondary carbenium ion complexes **12a,b** in a 85:15 ratio. These new compounds possess a triphenylphosphine group bonded at the cobalt atom as demonstrated by their <sup>1</sup>H NMR spectra, (Scheme 3).

At this stage, a brief comment is required. As mentioned previously,<sup>19</sup> nucleophilic attack occurs usually at the propargylic carbon C<sup>3</sup>. This result is consistent with the proposed electronic structure of the complex, in which the metallic group [CpMo(CO)<sub>2</sub>] alleviates the electron deficiency at the carbenium center. Clearly the nucleophilic attack displaces the [C–Mo]<sup>+</sup> bond and affords the substituted alkyne adducts. EHMO analysis performed on monometallic systems has shown that nucleophilic attack on π-allyl complexes is frontier orbital controlled. In these cases attacks occur at the terminal carbon of the π-allyl.<sup>20</sup> Recently McClain et al.<sup>21</sup> demonstrated by EHMO calculations

(15) Le Berre-Cosquer, N.; Kergoat, R.; L'Hazidon, P. *Organometallics* **1992**, *11*, 721.

(16) Melikyan, G. G.; Combs, R. C.; Lamirand, J.; Khan, M.; Nicholas, K. M. *Tetrahedron Lett.* **1994**, *35*, 363.

(17) Capon, J. F.; Cornen, S.; Le Berre-Cosquer, N.; Pichon, R.; Kergoat, R.; L'hazidon, P. *J. Organomet. Chem.* **1994**, *470*, 137.

(18) El Amouri, H.; Gruselle, M.; Jaouen, G.; Daran, J. C.; Vaissermann, J. *Inorg. Chem.* **1990**, *29*, 3238.

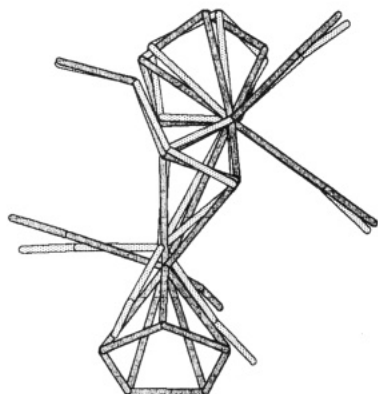
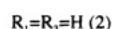
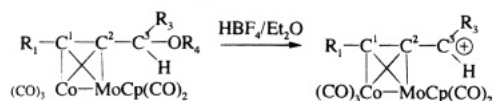
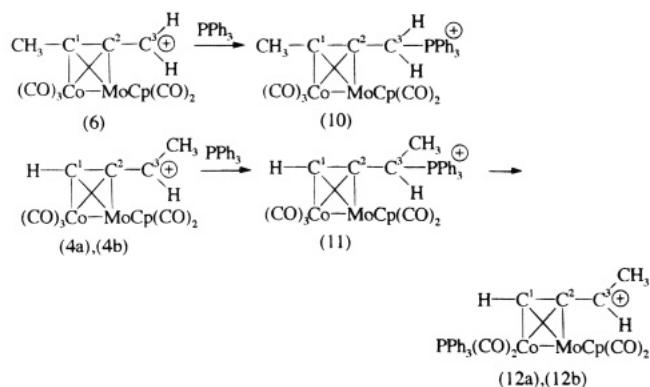


**Figure 4.** Overlapped view of  $(\text{Mo}_2\text{Cp}_2(\text{CO})_4)[\text{HCCCH}(\text{CH}_3)]^+$  and  $(\text{MoCoCp}(\text{CO})_5)[\text{HCCCH}(\text{CH}_3)]^+$  (**4a**).

**Scheme 2. Formation of the Primary and Secondary Carbenium Ions**

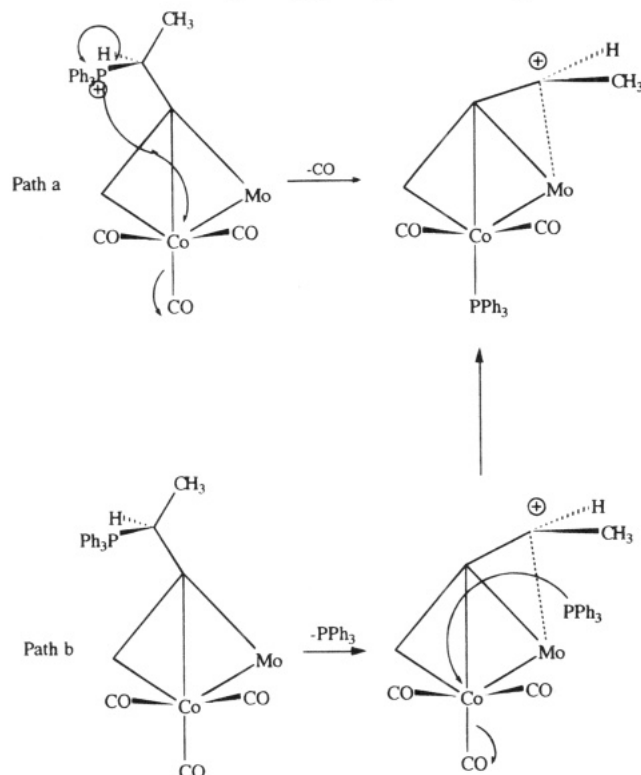


**Scheme 3. Reaction of Carbenium Ions 6 and 4a,b with PPh<sub>3</sub>**



that in the cationic allenyl complex the positive charge is transferred to the metal cluster. Such a result is not different from those obtained by our group<sup>22</sup> on the propargyl carbenium ion  $[(\text{HC}\equiv\text{CCH}_2)(\text{Mo}_2(\text{Cp}_2)(\text{CO})_4)]^+$ . Thus EHMO calculations on the latter system showed an important electronic transfer from the metallic group to the carbenium center. From these considerations we believe that nucleophilic attack including triphenylphosphine occurs on the carbocation. Curtis<sup>19</sup> pointed out that the regioselectivity, in such nucleophilic reactions, is determined not only by the preference for an attack on the carbocation but also on the stability of the obtained  $\mu$ -alkyne adducts. In conjunction with the previous suggestion we feel that the observed migration

**Scheme 4. Postulated Pathways for the Migration of the Triphenylphosphine Group**



of phosphine could be related to the relative thermodynamic stability of the phosphonium derivative **11a,b** and the phosphinated carbenium ion **12a,b**.

The migration process, however can proceed via two pathways: (a) One pathway is an intramolecular way in which the phosphine group migrates via a 1,3 shift and displaces the loosely bound carbonyl ligand from the cobalt center. Intramolecular phosphine migration was recently reported by Both, Richmond, et al. for the dinuclear cobalt complex  $[\text{Co}_2(\text{CO})_4(\mu\text{-PhC}\equiv\text{CH})]$ , containing a chelating phosphine (bma = 2,3-bis(diphenylphosphino)maleic anhydride).<sup>23</sup> (b) The second pathway is an intermolecular process, in which dissociation of the phosphine group occurs first followed by a subsequent attack of the cobalt center (Scheme 4).

Our results do not allow us to determine the mechanism of this phosphine group migration. It should be mentioned, however, that during this process, the relative configurations of the carbenium ion and the cluster remains unchanged when going from **4a** to the phosphinated carbenium ion **12a** (Figure 5).

**Variable-Temperature <sup>1</sup>H-NMR Study for  $[(\mu\text{-}\eta^2\eta^3\text{-HC}\equiv\text{CCH}(\text{CH}_3))\text{CoMoCp}(\text{CO})_4\text{PPh}_3][\text{BF}_4]$  (**12a,b**).** The <sup>1</sup>H NMR spectra recorded in the 293–253 K range for the phosphinated carbenium ions **12a,b** showed no changes or any line broadening. These results indicate that the isomerization process for such carbenium ions is higher in energy when compared to their analogous homo- or heterobimetallic  $[\text{Mo-Mo}]$  or  $[\text{Co-Mo}]$  complexes.

**X-ray Structure of  $[(\mu\text{-}\eta^2\eta^3\text{-HC}\equiv\text{CCH}(\text{CH}_3))\text{CoMoCp}(\text{CO})_4\text{PPh}_3][\text{BF}_4]$  (**12a**).** Suitable crystals for

(19) (a) Meyer, A.; McCabe, D. J.; Curtis, D. *Organometallics* **1987**, *6*, 191. (b) Galakhov, M. V.; Bakhmutov, V. I.; Barinov, I. V.; Reutov, O. A. *J. Organomet. Chem.* **1991**, *421*, 65. (c) Cordier, C.; Gruselle, M.; Jaouen, G.; Bakhmutov, V. I.; Galakhov, M. V.; Troitskaya, L. L.; Sokolov, V. I. *Organometallics* **1991**, *10*, 2303. (d) Cordier, C.; Gruselle, M.; Troitskaya, L. L.; Bakhmutov, V. I.; Sokolov, V. I.; Jaouen, G. *Organometallics* **1992**, *11*, 3825.

(20) Curtis, M. D.; Eisenstein, O. *Organometallics* **1984**, *3*, 887.

(21) McClain, M. D.; Hay, M. S.; Curtis, M. D.; Kampf, J. W. *Organometallics* **1994**, *13*, 4377.

(22) Cordier, C. Thesis, University P. M. Curie, Paris, 1991.

(23) Yang, K.; Bott, S. G.; Richmond, M. G. *Organometallics*, **1994**, *13*, 3788. Yang, K.; Bott, S. G.; Richmond, M. G. *Organometallics*, **1994**, *13*, 3767.

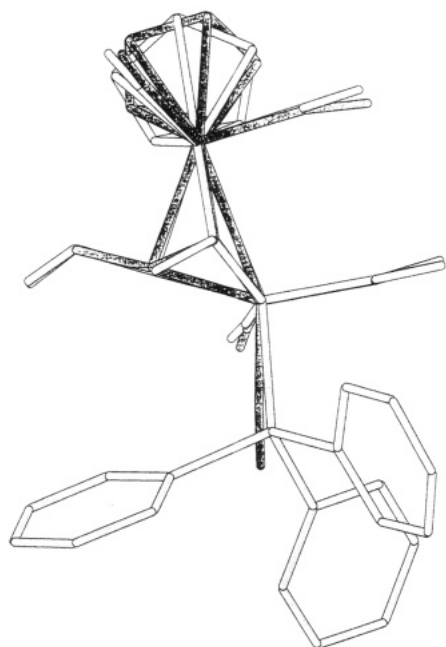


**Figure 5.** Overlapped view of  $[(\text{MoCoCp}(\text{CO})_5)(\text{HCCCH}(\text{CH}_3))^+]$  (**4a**) and  $[(\text{MoCoCp}(\text{PPh}_3)(\text{CO})_4)(\text{HCCCH}(\text{CH}_3))^+]$  (**12a**).

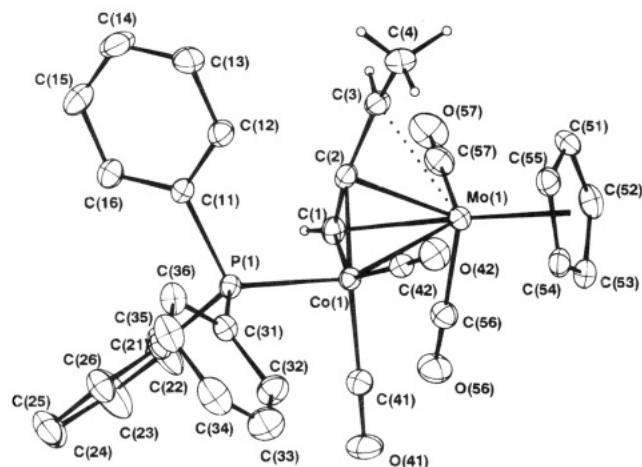


**Figure 6.** Cameron view for **12a**.

an X-ray study were obtained by slow diffusion of diethyl ether into a saturated acetone solution of **12a,b**. Complex **12a** crystallizes in the triclinic  $P\bar{1}$  space group. A view of the molecule with atomic numbering is shown in Figure 6. Crystallographic data, collection parameters, and selected bond lengths and angles are listed in Tables 4–6. The cationic species possesses a tetrahedral cluster core  $[\text{Mo}-\text{CoC}_2]$  with the acetylenic unit  $-\text{C}\equiv\text{C}-$  asymmetrically bridging the metal centers and perpendicular to the Co–Mo metal–metal bond. The relative configurations of the cluster core ( $R^*$ ) and that of the carbocation  $\text{C}^+$  ( $R^*$ ) are completely superimposable with those observed for the starting material  $[(\mu-\eta^2-\eta^3\text{-HC}\equiv\text{CCH}(\text{CH}_3))\text{CoMoCp}(\text{CO})_5]^+$  (**4a**). The structure also shows the  $-\text{PPh}_3$  ligand bonded to the cobalt center and trans to the Mo–Co metal–metal bond. This appears to be the preferred position. Similar results were obtained by Nicholas et al. where several X-ray structures of phosphinated alkyne adducts of formula  $[(\text{RC}\equiv\text{CR})\text{Co}_2(\text{CO})_5(\text{PPh}_3)]$  were reported and showed that the phosphine group is bonded to the cobalt center and trans to the Co–Co metal–metal bond.<sup>11a</sup> The Mo–

**Table 4. Crystal Data for  $[\text{C}_{31}\text{H}_{25}\text{O}_4\text{PCoMo}](\text{BF}_4)\cdot(\text{CH}_3)_2\text{CO}$  (**12a**)**

fw	786.2
$a$ (Å)	10.677(1)
$b$ (Å)	13.057(6)
$c$ (Å)	13.082(1)
$\alpha$ (deg)	98.06(1)
$\beta$ (deg)	101.29(1)
$\gamma$ (deg)	98.39(1)
$V$ (Å <sup>3</sup> )	1742
$Z$	2
space group	$P\bar{1}$
linear abs coeff $\mu$ (cm <sup>-1</sup> )	9.27
density $\rho$ (g cm <sup>-3</sup> )	1.50
diffractometer	Philips PW1100
radiation	Mo K $\alpha$ ( $\lambda = 0.71069$ Å)
scan type	$\omega/2\theta$
scan range	$0.8 + 0.345 \tan \theta$
$\theta$ limits (deg)	2–25
temp of measmt	room temp
octants colld	–12 to 12; –15 to 15; 0 to 15
no. of unique data colld	6129
no. of unique data used for refinement	5098, $(F_o)^2 > 3\sigma(F_o)^2$
$R = \sum  F_o  -  F_c  /\sum F_o $	0.0316
$R_w = \sum w( F_o  -  F_c )^2/\sum wF_o^2$	0.0334, $w = 1.0$
abs corr	DIFABS (min = 0.97, max = 1.02)
extinction param ( $\times 10^{-6}$ )	76
goodness of fit s	0.76
no. of variables	501
$\Delta\rho_{\text{min}}$ (e/Å <sup>3</sup> )	–0.41
$\Delta\rho_{\text{max}}$ (e/Å <sup>3</sup> )	0.51

$-\text{C}^+$  bond distance in **12a** is 2.58 Å, shorter than that found for **4a** with  $d(\text{Mo}-\text{C}^+) = 2.64$  Å. This result could be rationalized if we consider that the  $\text{PPh}_3$  increases the electron density on the cluster core and hence reinforces the Mo– $\text{C}^+$  interaction. Finally the Mo–Co bond distance in  $[(\mu-\eta^2-\eta^3\text{-HC}\equiv\text{CCH}(\text{CH}_3))\text{CoMoCp}(\text{PPh}_3)(\text{CO})_4]^+$  (**12a**) is 2.712 Å typically of a single bond but slightly shorter than that found in **4a** with  $d(\text{Mo}-\text{Co}) = 2.719$  Å.

## Discussion

The problem of the diastereoselectivity observed in the formation of this type of carbenium ions was previously discussed by Nicholas, who has concluded that this phenomenon is kinetically stereocontrolled, and has proposed two mechanisms for each starting diastereomeric alcohol leading with considerable selectivity to the anti carbenium ion. The syn/anti ratio depends on the nature of the substituents  $R_3$  and  $R'_3$ .

For  $R'_3 = \text{H}$  and relatively small substituents like  $R_3 = -\text{CH}_3$  or  $-\text{C}_6\text{H}_5$  the initially formed mixture of carbenium ions isomerizes, with the final ratio approaching values of nearly 1 at equilibrium. For bulky substituents, such as isopropyl or *tert*-butyl, isomerization is not observed. In our case the major isomer formed during the ionization process of any diastereomeric alcohols (**3a,b** is also the anti isomer **4a** and the anti/syn ratio = 6 is very close to those found by Nicholas. Nevertheless, in our case the ratio of initially formed carbenium ions remains unchanged.

As calculated according to the <sup>1</sup>H NMR results, the activation energy of the isomerization process for the carbenium center was found as 16 kcal·mol<sup>-1</sup> at 320 K. By comparison, the value grounded for the corresponding homobimetallic  $[\text{Co}-\text{CoPPh}_3]$  stabilized carbenium ion was found as 19.4 kcal·mol<sup>-1</sup>.<sup>11a</sup>

**Table 5. Fractional Atomic Coordinates and *U* Values for 12a**

atom	<i>x/a</i>	<i>y/b</i>	<i>z/c</i>	<i>U</i> (eq)
Mo(1)	0.25835(3)	0.12707(2)	0.90442(2)	0.0388
Co(1)	0.41797(4)	0.24175(3)	0.80817(3)	0.0356
P(1)	0.45719(8)	0.33784(7)	0.68726(7)	0.0365
O(41)	0.5920(3)	0.0955(2)	0.7625(3)	0.0697
O(42)	0.5619(3)	0.3911(2)	0.9966(2)	0.0614
O(56)	0.3271(3)	-0.0720(2)	0.7775(3)	0.0723
O(57)	-0.0279(3)	0.0114(3)	0.8038(3)	0.0794
C(1)	0.2448(3)	0.1618(3)	0.7458(3)	0.0439
C(2)	0.2427(3)	0.2551(3)	0.8069(3)	0.0410
C(3)	0.1619(4)	0.2914(3)	0.8666(3)	0.0486
C(4)	0.1910(5)	0.3898(4)	0.9449(4)	0.0614
C(11)	0.3408(3)	0.4259(3)	0.6607(3)	0.0408
C(12)	0.3234(4)	0.4935(3)	0.7460(3)	0.0558
C(13)	0.2363(5)	0.5616(4)	0.7315(4)	0.0679
C(14)	0.1667(5)	0.5611(4)	0.6318(5)	0.0739
C(15)	0.1835(5)	0.4962(4)	0.5475(4)	0.0718
C(16)	0.2709(4)	0.4276(3)	0.5609(3)	0.0560
C(21)	0.4583(3)	0.2670(3)	0.5570(3)	0.0431
C(22)	0.3797(6)	0.1708(4)	0.5182(4)	0.0722
C(23)	0.3751(7)	0.1182(5)	0.4182(5)	0.0861
C(24)	0.4468(5)	0.1576(4)	0.3553(4)	0.0677
C(25)	0.5288(5)	0.2509(4)	0.3937(4)	0.0691
C(26)	0.5344(5)	0.3051(3)	0.4934(3)	0.0595
C(31)	0.6141(3)	0.4265(3)	0.7236(3)	0.0433
C(32)	0.7226(4)	0.3927(4)	0.7751(4)	0.0627
C(33)	0.8425(4)	0.4579(5)	0.7980(5)	0.0756
C(34)	0.8566(5)	0.5562(5)	0.7728(4)	0.0675
C(35)	0.7500(5)	0.5911(4)	0.7245(4)	0.0617
C(36)	0.6285(4)	0.5273(3)	0.6991(3)	0.0528
C(41)	0.5277(4)	0.1534(3)	0.7818(3)	0.0482
C(42)	0.5090(3)	0.3324(3)	0.9231(3)	0.0440
C(51)	0.2135(4)	0.1602(4)	1.0691(3)	0.0561
C(52)	0.2311(5)	0.0548(4)	1.0522(3)	0.0593
C(53)	0.3536(4)	0.0549(4)	1.0450(3)	0.0564
C(54)	0.4237(4)	0.1585(3)	1.0594(3)	0.0509
C(55)	0.3339(4)	0.2241(3)	1.0735(3)	0.0522
C(56)	0.3031(4)	-0.0005(3)	0.8236(3)	0.0525
C(57)	0.0747(4)	0.0549(3)	0.8403(3)	0.0575
O(100)	0.8483(7)	0.0381(5)	0.4623(6)	0.1957
C(100)	0.898(1)	0.1298(6)	0.4919(9)	0.1288
C(101)	0.994(1)	0.1750(7)	0.4334(9)	0.1768
C(102)	0.874(1)	0.1940(9)	0.5816(8)	0.2012
B(1)	-0.1530(5)	0.237(4)	1.0289(5)	0.0623
F(1)	-0.1138(4)	0.1998(3)	0.9426(4)	0.1422
F(2)	-0.2798(2)	0.1976(2)	1.0185(3)	0.0873
F(3)	-0.1297(3)	0.3435(2)	1.0425(3)	0.1066
F(4)	-0.0830(4)	0.2067(4)	1.1101(5)	0.1442

The ionization process is probably stereocontrolled by steric factors for both systems i.e. [Mo-Co] and [Co-CoPPh<sub>3</sub>] as proposed by Nicholas<sup>11a</sup> for the [Co-CoPPh<sub>3</sub>] system (Figure 7). We have suggested a possible variant of this mechanism.<sup>13</sup> (This variant does not invalidate the main hypothesis of Nicholas about the role of steric factors.) In the Nicholas systems, the *anti* isomer clearly minimizes steric interactions with the phosphine, whereas in **12a,12b** it is not at all clear which isomer minimizes steric interaction with the phosphine. The preference for the *anti* isomer **12a** may well be due to steric interactions with the closer of the two molybdenum-bound carbonyl ligands.

The second problem is the regio- and stereochemical course of the nucleophilic attack. In all cases (NaSCH<sub>3</sub>, NaBH<sub>4</sub>, PPh<sub>3</sub>, H<sub>2</sub>O) the reaction occurs at the carbenium center. When the reaction is rapid, the stereochemistry is controlled by the *anti*/*syn* equilibrium ratio of the starting carbenium ions. When triphenylphosphine is used as a nucleophile, the reaction occurs first at the carbenium center. The resulting phosphonium salt evolves slowly leading to a new carbenium ion possessing a phosphine ligand bonded to the cobalt

**Table 6. Selected Interatomic Distances (Å) and Bond Angles (deg) for [C<sub>31</sub>H<sub>25</sub>O<sub>4</sub>PMoCo]BF<sub>4</sub>·(CH<sub>3</sub>)<sub>2</sub>CO**

Mo(1)-Co(1)	2.7122(5)		
Mo(1)-C(1)	2.167(4)	Mo(1)-C(2)	2.246(3)
Mo(1)-C(51)	2.293(4)	Mo(1)-C(52)	2.316(4)
Mo(1)-C(53)	2.329(4)	Mo(1)-C(54)	2.355(4)
Mo(1)C(55)	2.315(4)		
Mo(1)-C(56)	2.014(4)	O(56)-C(56)	1.128(4)
Mo(1)-C(57)	2.008(4)	O(57)-C(57)	1.135(5)
Co(1)-P(1)	2.2167(9)	P(1)-C(11)	1.830(3)
P(1)-C(21)	1.824(3)	P(1)-C(31)	1.828(3)
Co(1)-C(1)	1.944(4)	Co(1)-C(2)	1.902(3)
Co(1)-C(41)	1.807(4)	O(41)-C(41)	1.127(4)
Co(1)-C(42)	1.789(4)	O(42)-C(42)	1.133(4)
C(51)-C(52)	1.409(6)	C(51)-C(55)	1.413(6)
C(52)-C(53)	1.382(6)	C(53)-C(54)	1.397(6)
C(54)-C(55)	1.396(6)		
C(56)-Mo(1)-C(57)	83.7(2)	Mo(1)-C(56)-O(56)	179.3(4)
		Mo(1)-C(57)-O(57)	178.1(4)
P(1)-Co(1)-C(41)	95.1(1)	P(1)-Co(1)-C(42)	98.1(1)
C(41)-Co(1)-C(42)	103.7(2)	Co(1)-C(41)-O(41)	177.1(4)
		Co(1)-C(42)-O(42)	177.1(3)
Mo(1)-C(1)-Co(1)	82.4(1)	Mo(1)-C(1)-C(2)	75.2(2)
Co(10)-C(1)-C(2)	67.5(2)	Mo(1)-C(2)-Co(1)	81.2(1)
Mo(1)-C(2)-C(1)	68.9(2)	Co(1)-C(2)-C(1)	70.9(2)
Mo(1)-C(2)-C(3)	87.7(2)	Co(1)-C(2)-C(3)	144.1(3)
C(1)-C(2)-C(3)	135.5(4)	C(2)-C(3)-C(4)	126.5(4)

atom. This unexpected result is a consequence of a phosphine migration from the carbon cation to the cobalt center and loss of one carbonyl ligand. Evidently the phosphinated carbenium ion **12a** is more stable than the secondary carbenium ion **4a**, since the phosphine ligand at the cobalt center increases the electron density on the cluster core and eventually the molybdenum carbenium interaction will be strengthened. We note that *d*(Mo-C<sup>+</sup>) in **12a** is 2.58 Å and shorter than that found in **4a** *d*(Mo-C<sup>+</sup>) = 2.64 Å.

## Conclusions

In this paper we have described the synthesis and structure of chiral heterobimetallic carbenium ions of -CoMoCp(CO)<sub>5</sub>. These species are obtained with moderate diastereoselectivity (85/15) by protonation of their corresponding propargyl alcohol complexes. The X-ray structure of the secondary carbenium ion [(μ-η<sup>2</sup>-η<sup>3</sup>-HC≡CCHCH<sub>3</sub>)CoMoCp(CO)<sub>5</sub>][BF<sub>4</sub>] (**4a**) was determined and showed that the molybdenum center and not the cobalt is stabilizing the carbocation. Moreover the substituents on the carbenium center adopt the *anti*-configuration. We also note that the *syn*/*anti* ratio remains unchanged in solution, unlike that reported for the -Co<sub>2</sub>(CO)<sub>5</sub>PPh<sub>3</sub> analogues. The latter effect is manifested by the reactivity of these chiral carbenium ions. In this respect, when the cation complexes were treated with nucleophiles, we obtained the same mixture of diastereomers as that of the starting material. On the other hand when the secondary carbenium ion [(μ-η<sup>2</sup>-η<sup>3</sup>-HC≡CCH(CH<sub>3</sub>))CoMoCp(CO)<sub>5</sub>][BF<sub>4</sub>] was treated with PPh<sub>3</sub>, the initially formed phosphonium derivative is transformed to the stable phosphinated-carbenium ion [(μ-η<sup>2</sup>-η<sup>3</sup>-HC≡CCH(CH<sub>3</sub>))CoMoCp(PPh<sub>3</sub>)(CO)<sub>4</sub>][BF<sub>4</sub>] (**12a**) via phosphine migration from the carbocation to the cobalt center with CO decoordination. The X-ray structure of **12a** was determined and showed that the *anti*-configuration is also the more stable in the solid state. Our future objectives are directed toward the

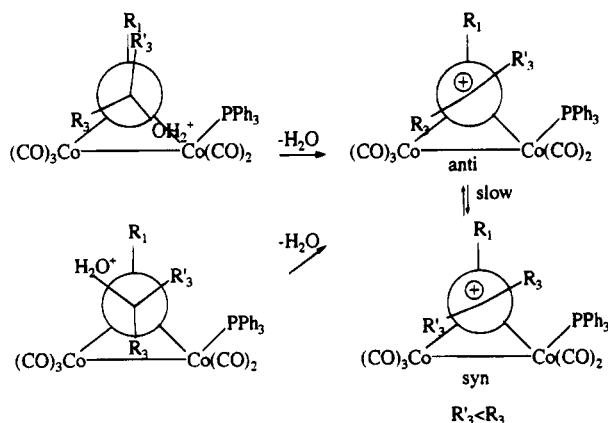


**Figure 7.** Mechanism proposed by Nicholas to explain the formation of anti/syn isomers.

preparation of a second generation of heterobimetallic carbenium ions but possessing chiral phosphines at the cobalt centers. As mentioned before, these heterobimetallic complexes possess stable [CoMo] cluster cores, i.e. cluster cores stable toward "epimerization". Hence the reactivity of these chiral species with optically active nucleophiles would no doubt induce high diastereoselectivity.

## Experimental Section

**General Methods.** All reactions were carried out under argon, using standard Schlenk techniques. Solvents were purified and dried before use by conventional distillation techniques under argon. HBF<sub>4</sub>/Et<sub>2</sub>O, Co<sub>2</sub>(CO)<sub>8</sub>, Mo<sub>2</sub>Cp<sub>2</sub>(CO)<sub>6</sub>, and deuterated solvents were used as purchased. NMR spectra were recorded on a Bruker AM-250 instrument. Infrared spectra were recorded on an FT Bomem Michelson 100 instrument. The adsorbent used for column and thin layer chromatography was silica gel 60GF<sub>254</sub>. Elemental analyses were performed by the "Centre de Microanalyse de l'Université Pierre et Marie Curie".

**NMR Experiments.** All NMR solution spectra were recorded on a Bruker AM 250 Spectrometer using methylene-d<sub>2</sub> chloride as solvent. Chemical shifts are reported in parts per millions (ppm) relative to TMS from the central peak of CD<sub>2</sub>Cl<sub>2</sub> (5.3 ppm). The proton spectra were obtained at 250.13 MHz in 32 scans in 32 K data points over a 2.5 kHz spectral width. Temperatures mentioned in Figure 4 have been determined with an accuracy of 2 K.

**X-Ray Studies of 4a and 12a.** Intensity data were collected at room temperature on an Enraf Nonius CAD4 diffractometer for compound **4a** and on a Philips PW 1100 diffractometer for compound **12a** using Mo K $\alpha$  radiation. Accurate cell dimensions and orientation matrices were obtained from least-squares refinements of the setting angles of 25 well-defined reflections. No decay in the intensities of two standard reflections was observed during the course of data collections. Complete crystal data, collection parameters, and other significant details are listed in Tables 1–3 for **4a** and Tables 4–6 for **12a**. The usual corrections for Lorentz and polarization effects were applied. Computations were performed by using the PC version of CRYSTALS.<sup>24</sup> Scattering factors and corrections for anomalous dispersion were taken from ref 25. Both structures were resolved by direct methods SHELXS 86<sup>26</sup> and refined by least squares. For compounds

**12a**, all non-hydrogen atoms were refined with anisotropic thermal parameters; hydrogen atoms were located on a Fourier difference map, and their coordinates were refined with an overall refinable isotropic thermal parameter. For compound **4a**, all atoms were left isotropic; hydrogen atoms were introduced as fixed contributors in theoretical positions, and their coordinates were recalculated after each refinement. The structure was refined to  $R = 0.0316$  with the use of 5098 reflections for 501 least-squares parameters for compound **12a** and to  $R = 0.0534$  with the use of 719 reflections for 105 least-squares parameters for compound **4a**.

**[( $\mu$ - $\eta^2$ - $\eta^2$ -HC=CCH<sub>2</sub>OH)CoMoCp(CO)<sub>5</sub>] (1).** Co<sub>2</sub>(CO)<sub>8</sub> (0.5 g, 1.46 mmol) in ether (20 mL) was added under argon to propargylic alcohol (0.08 g, 1.46 mmol) in THF (5 mL) at room temperature. The solution turned red and was stirred for 1 h. Under an atmosphere of argon [(CpMo(CO)<sub>3</sub>)<sub>2</sub>] (0.72 g, 1.46 mmol) in dry THF (10 mL) was treated with sodium amalgam (Hg, 7.0 g; Na, 0.07 g, 2.92 mmol), and the initially red solution became yellow-green as anion formation progressed. After filtration, the anion was added to the propargylic alcohol [Co<sub>2</sub>(CO)<sub>6</sub>] complex solution. The reaction was monitored by TLC on silica gel, using a 4.5/1 petroleum ether/ether mixture as eluent. After 1.5 h, the reaction was allowed to cool at room temperature, the solvent was removed, and the residue was extracted by ether. The product was chromatographed on silica plates using a 4.5/1 petroleum ether/ether mixture as eluent to yield 0.37 g (62%) of **1**.

<sup>1</sup>H NMR (CDCl<sub>3</sub>): 5.69 (1H, s, CH), 5.46 (5H, s, Cp), 4.90 (1H, dd,  $J = 13.8$ –2.5 Hz, CH<sub>2</sub>), 4.68 (1H, dd,  $J = 13.8$ –2.5 Hz, CH<sub>2</sub>), 1.56 (1H, s broad, OH). IR (CH<sub>2</sub>Cl<sub>2</sub>) (cm<sup>-1</sup>): 1886, 1943, 1980, 2001, 2050, 2063.

**[( $\mu$ - $\eta^2$ - $\eta^3$ -HC=CCH<sub>2</sub>-CoMoCp(CO)<sub>5</sub>][BF<sub>4</sub>] (2).** To a stirred solution of **1**, (0.19 g, 0.24 mmol) in ether (6 mL) was added 0.25 mL of HBF<sub>4</sub>/Et<sub>2</sub>O complex at room temperature. An ether-insoluble red brown oil was obtained which, after stirring 20 min, was washed five times with ether to give **2** as an orange powder. **2** was dried and crystallized by diffusion technique using CH<sub>2</sub>Cl<sub>2</sub> and ether. A 0.9 g amount of pale red crystals of **2** was obtained.

<sup>1</sup>H NMR (CD<sub>2</sub>Cl<sub>2</sub>): 6.39 (1H, s, CH), 5.94 (5H, s, Cp), 5.45 (1H, s, CH<sub>2</sub>), 5.07 (1H, s, CH<sub>2</sub>). IR (CH<sub>2</sub>Cl<sub>2</sub>) (cm<sup>-1</sup>): 1941, 1980, 2002, 2049, 2068, 2101. Anal. Calcd for C<sub>13</sub>H<sub>8</sub>O<sub>5</sub>BF<sub>4</sub>CoMo: C, 32.10; H, 1.65. Found: C, 32.12; H, 1.74.

**[( $\mu$ - $\eta^2$ - $\eta^2$ -HC=CCH(CH<sub>3</sub>)(OH)CoMoCp(CO)<sub>5</sub>] (3a,b).** The dicobalt alcohol complex was obtained and isolated, in 84.5% yield as described previously. A 0.35 g, (1 mmol) amount of this complex was treated with MoCp(CO)<sub>3</sub>Na, obtained from 0.49 g, (1 mmol) of Mo<sub>2</sub>Cp<sub>2</sub>(CO)<sub>6</sub>. After 1 h, the reaction was completed. After the solvent was removed, the crude mixture was chromatographed on silica plates using pentane/ether (4/1) as eluent. Two products were recovered as red oils, 0.28 g (65% yield), and were identified as diastereomers **3a** and **3b** in a 40/60 ratio.

**3a.** <sup>1</sup>H NMR (CD<sub>2</sub>Cl<sub>2</sub>): 5.80 (1H, s, CH), 5.52 (5H, s, Cp), 4.98 (1H, qui,  $J = 6.2$  Hz, CHCH<sub>3</sub>), 1.72 (1H, d,  $J = 3.5$  Hz, OH), 1.26 (3H, d,  $J = 6.2$  Hz, CH<sub>3</sub>). <sup>13</sup>C NMR (CDCl<sub>3</sub>): 202.0 (CO), 93.16 (CH– or C–C), 90.06 (Cp), 78.55 (CH–C or C–C), 74.44 (CHCH<sub>3</sub>), 25.31 (CH<sub>3</sub>). IR (CH<sub>2</sub>Cl<sub>2</sub>) (cm<sup>-1</sup>): 1888, 1942, 1980, 2000, 2050. Anal. Calcd for C<sub>14</sub>H<sub>11</sub>O<sub>6</sub>CoMo: C, 39.07; H, 2.56. Found: C, 39.62; H, 2.62.

**3b.** <sup>1</sup>H NMR (CD<sub>2</sub>Cl<sub>2</sub>): 5.74 (1H, s, CH), 5.48 (5H, s, Cp), 4.76 (1H, qui,  $J = 6.2$  Hz, CHCH<sub>3</sub>), 1.61 (1H, d,  $J = 5.7$  Hz, OH), 1.38 (3H, d,  $J = 6.15$  Hz, CH<sub>3</sub>). <sup>13</sup>C NMR (CDCl<sub>3</sub>): 202.0 (CO), 93.16 (CH= or C=C), 90.06 (Cp), 78.55 (CH= or C=C), 74.44 (CHCH<sub>3</sub>), 26.76 (CH<sub>3</sub>). IR (CH<sub>2</sub>Cl<sub>2</sub>) (cm<sup>-1</sup>): 1888, 1943, 1979, 2001, 2049. Anal. Calcd for C<sub>14</sub>H<sub>11</sub>O<sub>6</sub>CoMo: C, 39.07; H, 2.56. Found: C, 39.62; H, 2.62.

**[( $\mu$ - $\eta^2$ - $\eta^3$ -HC=CH(CH<sub>3</sub>)CoMoCp(CO)<sub>5</sub>][BF<sub>4</sub>] (4a,b).** **4a,b** were prepared in the same way as described for **2**. Starting from 0.08 g (0.18 mmol) of **3a** or **3b**, we obtained 0.07 g (75% yield) of a mixture of **4a** and **4b** in a 85/15 ratio. **4a** was obtained as a pure diastereomer after recrystallization, using

(24) Watkin, D. J.; Carruthers, J. R.; Betteridge, P. W. *Crystals User Guide*; Chemical Crystallography Laboratory: University of Oxford, Oxford, U.K., 1988.

(25) *International Tables for X-ray Crystallography*; Kynoch Press: Birmingham, U.K., 1974; Vol. IV.

(26) Sheldrick, G. M. SHELXS-86, Program for Crystal Structure Solution, University of Gottingen, 1986.



the diffusion technique of ether into a saturated solution of **4a,b** in CH<sub>2</sub>Cl<sub>2</sub>.

**4a.** <sup>1</sup>H NMR (CD<sub>2</sub>Cl<sub>2</sub>): 7.24 (1H, m, CHCH<sub>3</sub>), 6.27 (1H, s, CH), 5.74 (5H, s, Cp), 1.95 (3H, d, *J* = 7.2 Hz, CH<sub>3</sub>). <sup>1</sup>H NMR (acetone-*d*<sub>6</sub>): 7.42 (1H, m, CHCH<sub>3</sub>), 6.93 (1H, s, CH), 6.13 (5H, s, Cp), 2.04 (3H, d, *J* = 6.4 Hz, CH<sub>3</sub>). IR (CH<sub>2</sub>Cl<sub>2</sub>) (cm<sup>-1</sup>): 1941, 1982, 2000, 2034, 2048, 2068, 2098. Anal. Calcd for C<sub>14</sub>H<sub>10</sub>O<sub>5</sub>BF<sub>4</sub>CoMo: C, 33.60; H, 2.00. Found: C, 33.59; H, 2.09.

**4b.** <sup>1</sup>H NMR (CD<sub>2</sub>Cl<sub>2</sub>): 6.49 (1H, m, CHCH<sub>3</sub>), 5.89 (5H, s, Cp), 2.26 (3H, d, *J* = 7.8 Hz, CH<sub>3</sub>). <sup>1</sup>H NMR (acetone-*d*<sub>6</sub>): 7.22 (1H, m, CHCH<sub>3</sub>), 6.60 (1H, s, CH), 6.30 (5H, s, Cp), 2.32 (3H, d, *J* = 6.6 Hz, CH<sub>3</sub>). IR (CH<sub>2</sub>Cl<sub>2</sub>) (cm<sup>-1</sup>): 1941, 1982, 2000, 2034, 2048, 2068, 2098. Anal. Calcd for C<sub>14</sub>H<sub>10</sub>O<sub>5</sub>BF<sub>4</sub>CoMo: C, 33.60; H, 2.00. Found: C, 33.59; H, 2.09.

[(*μ*-η<sup>2</sup>-η<sup>2</sup>-CH<sub>3</sub>C≡CCH<sub>2</sub>OCH<sub>3</sub>)CoMoCp(CO)<sub>5</sub>]**(5)**. **5** was prepared in 81% yield according to the method described for **1**.

<sup>1</sup>H NMR (CDCl<sub>3</sub>): 5.40 (5H, s, Cp), 4.54 (2H, dd, *J* = 16.0–8.0 Hz, CH), 3.42 (3H, s, CH<sub>3</sub>O), 2.67 (3H, s, CH<sub>3</sub>≡C). <sup>13</sup>C NMR (CDCl<sub>3</sub>): 202.3 (CO), 95.3–88.7 (C≡C), 90.3 (Cp), 76.1 (CH<sub>2</sub>), 58.7 (CH<sub>3</sub>O), 20.5 (CH<sub>3</sub>). IR (CH<sub>2</sub>Cl<sub>2</sub>) (cm<sup>-1</sup>): 1932, 1977, 1994, 2046. Anal. Calcd for C<sub>15</sub>H<sub>13</sub>O<sub>6</sub>CoMo: C, 40.54; H, 2.93. Found: C, 40.43; H, 2.91.

[(*μ*-η<sup>2</sup>-η<sup>2</sup>-CH<sub>3</sub>C≡CCH<sub>2</sub>)CoMoCp(CO)<sub>5</sub>][BF<sub>4</sub>]**(6)**. **6** was prepared in 83% yield starting from **5**, according to the method described for **2**.

<sup>1</sup>H NMR (CD<sub>2</sub>Cl<sub>2</sub>): 5.93 (1H, m, CH<sub>2</sub>), 5.91 (5H, s, Cp), 5.04 (1H, m, CH<sub>2</sub>), 2.89 (3H, s, CH<sub>3</sub>). <sup>13</sup>C NMR (CD<sub>2</sub>Cl<sub>2</sub>): 218.3 (CO–Mo), 210.5 (CO–Mo), 199.2 (CO–Co), 135.2 (CH<sub>2</sub>), 101.9–95.1 (C≡C), 21.5 (CH<sub>3</sub>). IR (CH<sub>2</sub>Cl<sub>2</sub>) (cm<sup>-1</sup>): 1933, 1978, 1994, 2041, 2062, 2095. Anal. Calcd for C<sub>14</sub>H<sub>10</sub>O<sub>5</sub>BF<sub>4</sub>CoMo: C, 33.60; H, 2.00. Found: C, 33.12; H, 2.06.

[(*μ*-η<sup>2</sup>-η<sup>2</sup>-HC≡CCH<sub>3</sub>)CoMoCp(CO)<sub>5</sub>]**(7)**. **Method A.** To a solution of **2** (0.02 g, 0.041 mmol) in 5 mL of CH<sub>2</sub>Cl<sub>2</sub> was added at 0 °C, under argon, 0.20 g, (5.63 mmol) of NaBH<sub>4</sub>. After the addition was complete, 15 mL of ether was added to extract complex **(7)**. The ethereal layer was washed by water, dried under MgSO<sub>4</sub>, and evaporated leading to 0.015 g (100% yield) of a red oil identified as **7**.

**Method B.** To a solution of **2** (0.097 g, 0.20 mmol) in 7 mL of CH<sub>2</sub>Cl<sub>2</sub> was added 0.013 g, (0.20 mmol) of zinc powder at room temperature, and the mixture was stirred 3 h. After filtration, the solvent was removed and the residue chromatographed on silica plates (eluent 3/1 petroleum ether/ether) leading to 0.02 g, (20% yield) of a red oil.

<sup>1</sup>H NMR (CDCl<sub>3</sub>): 5.55 (1H, d, *J* = 1 Hz, CH), 5.39 (5H, s, Cp), 2.67 (3H, d, *J* = 1 Hz, CH<sub>3</sub>). IR (CH<sub>2</sub>Cl<sub>2</sub>) (cm<sup>-1</sup>): 1882, 1936, 1977, 1995, 2047, 2059. Anal. Calcd for C<sub>13</sub>H<sub>9</sub>O<sub>5</sub>CoMo: C, 39.00; H, 2.25. Found: C, 39.08; H, 2.30.

[(*μ*-η<sup>2</sup>-η<sup>2</sup>-HC≡CCH<sub>2</sub>SCH<sub>3</sub>)CoMoCp(CO)<sub>5</sub>]**(8)**. To 0.049 g (0.1 mmol) of **2** in CH<sub>2</sub>Cl<sub>2</sub> (10 mL) was added NaSCH<sub>3</sub> (0.07 g, 0.1 mmol). After 15 min the mixture was chromatographed on silica plates (eluent 4/1 pentane/ether) leading to 0.038 g of a red oil identified as **8**.

<sup>1</sup>H NMR (CDCl<sub>3</sub>): 5.88 (1H, s, CH), 5.43 (5H, s, Cp), 4.01 (1H, d, *J* = 14 Hz, CH<sub>2</sub>), 3.83 (1H, d, *J* = 14 Hz, CH<sub>2</sub>), 2.18 (3H, s, CH<sub>3</sub>). IR (CH<sub>2</sub>Cl<sub>2</sub>) (cm<sup>-1</sup>): 1885, 1941, 1980, 2000, 2049, 2063. Anal. Calcd for C<sub>14</sub>H<sub>11</sub>O<sub>5</sub>SCoMo: C, 37.67; H, 2.47. Found: C, 38.08; H, 2.59.

[(*μ*-η<sup>2</sup>-η<sup>2</sup>-HC≡CCH(CH<sub>3</sub>)(SCH<sub>3</sub>)CoMoCp(CO)<sub>5</sub>]**(9a,b)**. Starting from the 85/15 mixture of **4a,b**, we obtained the thiols **9a,b** in 85% yield in the same proportions.

**9a.** <sup>1</sup>H NMR (CDCl<sub>3</sub>): 5.94 (1H, s, CH), 5.47 (5H, s, Cp), 3.94 (1H, qua, *J* = 6.8 Hz, CH), 2.16 (3H, s, CH<sub>3</sub>S), 1.97 (3H, d, *J* = 6.8 Hz, CH<sub>3</sub>). <sup>13</sup>C NMR (CDCl<sub>3</sub>): 203.0 (CO), 90.29 (Cp), 80.99–79.30 (C≡C), 47.36 (CH), 24.05 (CH<sub>3</sub>S), 15.07 (CH<sub>3</sub>). IR (CH<sub>2</sub>Cl<sub>2</sub>) (cm<sup>-1</sup>): 1885, 1941, 1979, 2000, 2049, 2063. Anal. Calcd for C<sub>15</sub>H<sub>13</sub>O<sub>5</sub>CoMoS: C, 39.13; H, 2.83. Found: C, 40.55; H, 3.01.

**9b.** <sup>1</sup>H NMR (CDCl<sub>3</sub>): 5.86 (1H, s, CH), 5.45 (5H, s, Cp), 3.88 (1H, qua, *J* = 7.2 Hz, CH), 2.15 (3H, s, CH<sub>3</sub>S), 1.52 (3H,

d, *J* = 7.2 Hz, CH<sub>3</sub>). <sup>13</sup>C NMR (CDCl<sub>3</sub>): 203.0 (CO), 90.61 (Cp), 80.99–79.30 (C≡C), 47.23 (CH), 24.24 (CH<sub>3</sub>S), 14.77 (CH<sub>3</sub>). IR (CH<sub>2</sub>Cl<sub>2</sub>) (cm<sup>-1</sup>): 1884, 1940, 1979, 2000, 2048, 2064. Anal. Calcd for C<sub>15</sub>H<sub>13</sub>O<sub>5</sub>CoMoS: C, 39.13; H, 2.83. Found: C, 40.55; H, 3.01.

[(*μ*-η<sup>2</sup>-η<sup>3</sup>-H<sub>3</sub>CC≡CCH<sub>2</sub>PPh<sub>3</sub>)CoMoCp(CO)<sub>5</sub>][BF<sub>4</sub>]**(10)**. To a solution of **11** (0.15 g, 0.30 mmol) in CH<sub>2</sub>Cl<sub>2</sub> (20 mL) was added triphenylphosphine (0.086 g, 0.33 mmol). The mixture was stirred 1 h at room temperature. The solvent was then removed, and the residue was dissolved in acetone and precipitated with a 1:1 mixture of ether and pentane. The residue was washed three times with ether and pentane. The product was dried under vacuum for 2 h.

<sup>1</sup>H NMR (acetone-*d*<sub>6</sub>): 8.13–7.80 (15H, m, PPh<sub>3</sub>), 5.71 (5H, s, Cp), 5.52 (2H, dd, *J* = 4–13 Hz), 2.13 (3H, s, H<sub>4</sub>). <sup>13</sup>C NMR (acetone-*d*<sub>6</sub>): 133.0 (C<sub>para</sub>, d, *J* = 5 Hz), 134.7 (C<sub>ortho</sub>, d, *J* = 10 Hz), 131.2 (C<sub>meta</sub>, d, *J* = 15 Hz), 129.6 (C<sub>ipso</sub>, d, *J* = 107 Hz), 120.1 (C<sub>1</sub>, d, *J* = 85 Hz), 97.0–72.5 (C<sub>2</sub>–C<sub>3</sub>), 21.4 (C<sub>4</sub>, d, *J* = 12.5 Hz). IR (CH<sub>2</sub>Cl<sub>2</sub>) (cm<sup>-1</sup>): 1941.7, 1981.2, 1999.8, 2049.1. Anal. Calcd for C<sub>32</sub>H<sub>25</sub>O<sub>5</sub>BF<sub>4</sub>PCoMo: C, 50.43; H, 3.28. Found: C, 49.31; H, 3.41.

[(*μ*-η<sup>2</sup>-η<sup>3</sup>-HC≡CCH(CH<sub>3</sub>)Co(CO)<sub>2</sub>PPh<sub>3</sub>MoCp(CO)<sub>2</sub>][BF<sub>4</sub>]**(12a,b)**. To a solution of [(*μ*-η<sup>2</sup>-η<sup>3</sup>-HC≡CCH(CH<sub>3</sub>)-CoMoCp(CO)<sub>5</sub>][BF<sub>4</sub>]**(4)** (0.10 g, 0.2 mmol) in CH<sub>2</sub>Cl<sub>2</sub> (4 mL) was added 0.052 g (0.2 mmol) of triphenylphosphine in 2 mL of CH<sub>2</sub>Cl<sub>2</sub>. The mixture was stirred until all the solid material dissolved. After 4 h 30 mL of diethyl ether was added resulting in the precipitation of an orange-red microcrystalline material. The <sup>1</sup>H NMR spectrum recorded in acetone-*d*<sub>6</sub>, which is time dependent, showed the evolution of initially formed phosphonium ion **11** to the phosphinated carbenium ion **12**. The final product **12** was recrystallized from CH<sub>2</sub>Cl<sub>2</sub>/diethyl ether.

<sup>1</sup>H NMR (acetone-*d*<sub>6</sub>) (**11a,b**): 8.14–7.60 (15H, m, PPh<sub>3</sub>), 6.00 (1H, d, *J* = 2 Hz, CH), 5.80 (s, 5H, Cp), 5.78 (s, Cp minor), 5.56 (1H, sext, *J* = 14 Hz, 8 Hz, CHCH<sub>3</sub>), 1.84 (3H, qua, *J* = 15 Hz, 8 Hz, CH<sub>3</sub>), 1.78 (qua, *J* = 15 Hz, 8 Hz, minor). <sup>1</sup>H NMR (acetone-*d*<sub>6</sub>) (**12a,b**): 7.60 (15H, m, PPh<sub>3</sub>), 6.79 (1H, qua, *J* = 6.2 Hz, CHCH<sub>3</sub>), 6.44 (qua, *J* = 6.2 Hz, CHCH<sub>3</sub>, minor), 6.06 (1H, dd, *J* = 6.0–1.2, CH), 5.98 (5H, s, Cp), 6.12 (s, Cp, minor), 1.81 (3H, d, *J* = 6.0 Hz, CH<sub>3</sub>), 1.96 (dd, *J* = 6.0–1.2 Hz, CH<sub>3</sub>, minor). IR (CH<sub>2</sub>Cl<sub>2</sub>) (cm<sup>-1</sup>) (**12**): 2058, 2027, 2006, 1991. Anal. Calcd for C<sub>31</sub>H<sub>25</sub>O<sub>4</sub>BF<sub>4</sub>PCoMo: C, 52.96; H, 3.55. Found: C, 51.79; H, 3.65.

[(*μ*-η<sup>2</sup>-η<sup>2</sup>-H<sub>3</sub>CC≡CCH<sub>2</sub>SCH<sub>3</sub>)CoMoCp(CO)<sub>5</sub>]**(13)**. <sup>1</sup>H NMR (CDCl<sub>3</sub>): 5.39 (5H, s, Cp), 3.95 (2H, qua, *J* = 8 Hz, CH<sub>2</sub>), 2.72 (3H, s, CH<sub>3</sub>), 2.21 (3H, s, SCH<sub>3</sub>).

[(*μ*-η<sup>2</sup>-η<sup>2</sup>-H<sub>3</sub>CC≡CCH<sub>2</sub>OCH<sub>2</sub>CH<sub>3</sub>)CoMoCp(CO)<sub>5</sub>]**(14)**. <sup>1</sup>H NMR (CDCl<sub>3</sub>): 5.41 (5H, s, Cp), 4.65 (1H, d, *J* = 12 Hz, CH<sub>2</sub>), 4.50 (1H, d, *J* = 12 Hz), 3.57 (2H, m, OC<sub>2</sub>H<sub>5</sub>), 2.67 (3H, s, CH<sub>3</sub>), 1.22 (3H, t, *J* = 7.2 Hz).

[(*μ*-η<sup>2</sup>-η<sup>2</sup>-H<sub>3</sub>CC≡CCH<sub>2</sub>OH)CoMoCp(CO)<sub>5</sub>]**(15)**. <sup>1</sup>H NMR (CDCl<sub>3</sub>): 5.43 (5H, s, Cp), 4.90 (1H, d, *J* = 12 Hz, CH<sub>2</sub>), 4.63 (1H, d, *J* = 12 Hz), 2.67 (3H, s, CH<sub>3</sub>), 1.69 (1H, s broad, OH).

**Acknowledgment.** We thank the CNRS and the "Ministère de l'Education Nationale" (France) for financial support and the reviewers for their perceptive comments.

**Supporting Information Available:** Tables of thermal parameters, bond lengths, and bond angles for **4a** and **12a** (7 pages). Ordering information is given on any current masthead page.

# Matrix Photochemistry of *trans*-[Cp\*Fe(CO)]<sub>2</sub>(μ-CO)(μ-CH<sub>2</sub>): Generation of the Cis Isomer and of a Double-CO-Loss Photoproduct

Yvonne H. Spooner, Ellen M. Mitchell, and Bruce E. Bursten\*

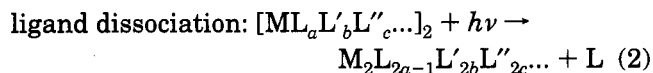
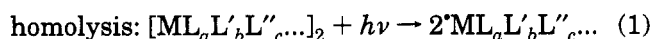
Department of Chemistry, The Ohio State University, Columbus, Ohio 43210

Received June 28, 1995<sup>⊙</sup>

The photochemistry of [Cp\*Fe(CO)]<sub>2</sub>(μ-CO)(μ-CH<sub>2</sub>) (**7\***; Cp\* = η<sup>5</sup>-C<sub>5</sub>Me<sub>5</sub>) has been investigated in a matrix of 3-methylpentane at low temperatures. Compound **7\*** undergoes CO loss to form the triply bridged product [Cp\*Fe]<sub>2</sub>(μ-CO)<sub>2</sub>(μ-CH<sub>2</sub>) (**8\***), a species similar to the CO-loss product from [CpFe(CO)]<sub>2</sub>(μ-CO)<sub>2</sub> (**1**). Compound **8\*** undergoes a subsequent photochemical CO loss to generate the double-CO-loss product Cp\*<sub>2</sub>Fe<sub>2</sub>(μ-η<sup>1</sup>:η<sup>2</sup>-CO)(μ-CH<sub>2</sub>) (**9\***), which contains a semibridging CO ligand. Because of the preference for CH<sub>2</sub> to serve as a bridging ligand, **9\*** is very different from the double-CO-loss product from **1**, i.e. [CpFe(CO)]<sub>2</sub> (**3**), which has terminal CO ligands. Compound **9\*** thermally reacts with CO to reform **8\***. Thermal ramping experiments demonstrate that **8\*** thermally reacts with CO to re-form **7\***, with a preference for the formation of the thermodynamically unfavored cis isomer. The cis isomer of **7\*** converts to the trans isomer via a first-order process that is considerably slower than cis/trans isomerization for **1** or [Cp\*Fe(CO)]<sub>2</sub>(μ-CO)<sub>2</sub> (**1\***). A scheme is proposed to explain the formation of *cis*-**7\*** in preference to *trans*-**7\***. The photochemistry of the Cp-containing, alkylidene-bridged compounds [CpFe(CO)]<sub>2</sub>(μ-CO)(μ-CH<sub>2</sub>) (**7**) and [CpFe(CO)]<sub>2</sub>(μ-CO)(μ-CHCH<sub>3</sub>) (**7'**) is not as straightforward as that of **7\***, owing to multiple isomers and low solubility.

## Introduction

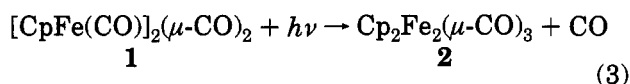
The photochemistry of dinuclear organometallic complexes has been and continues to be an area of intense interest.<sup>1</sup> Most of the dinuclear complexes that have been studied photochemically are *symmetric* complexes [ML<sub>a</sub>L'<sub>b</sub>L''<sub>c</sub>...]<sub>2</sub>; these complexes can be considered dimers of two identical mononuclear fragments, either with an unsupported metal–metal bond, such as the M<sub>2</sub>(CO)<sub>10</sub> (M = Mn, Re) systems, or with an even number of bridging ligands, such as in [CpFe(CO)]<sub>2</sub>(μ-CO)<sub>2</sub> (**1**; Cp = η<sup>5</sup>-C<sub>5</sub>H<sub>5</sub>) and [Cp\*Fe(CO)]<sub>2</sub>(μ-CO)<sub>2</sub> (**1\***; Cp\* = η<sup>5</sup>-C<sub>5</sub>Me<sub>5</sub>). A major reason for the interest in these symmetric systems is that they exhibit two very different photochemical reactions, namely photochemical homolysis into two identical mononuclear radical fragments (eq 1) and photochemical ligand dissociation (eq 2). The



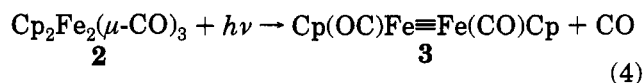
factors that govern which of the above processes occurs, and to what extent, are still poorly understood.

Frozen-matrix photochemistry has been an extremely useful technique for detecting ligand dissociation in symmetric complexes (eq 2), especially those with easily probed ligands such as CO. For example, symmetric complex **1** undergoes CO loss to yield the dinuclear complex Cp<sub>2</sub>Fe<sub>2</sub>(μ-CO)<sub>3</sub> (**2**),<sup>2</sup> a paramagnetic compound that contains three bridging CO ligands and a formal

Fe–Fe double bond (eq 3).<sup>3</sup> We have recently demon-



strated that complex **2** undergoes a second CO loss to yield the highly reactive double-CO-loss product [CpFe(CO)]<sub>2</sub> (**3**), a remarkable product inasmuch as both CO ligands are terminal (eq 4).<sup>4</sup> Complex **3** thus apparently



possesses an unsupported Fe–Fe triple bond. We have also recently reported double-CO loss from the symmetric dimer Mn<sub>2</sub>(CO)<sub>10</sub> (**4**).<sup>5</sup> Photolysis of **4** leads initially to the formation of Mn<sub>2</sub>(CO)<sub>9</sub> (**5**), which has a semibridging CO ligand.<sup>6</sup> Continued photolysis leads to additional CO loss and the formation of Mn<sub>2</sub>(CO)<sub>8</sub> (**6**), a species that, like **3**, contains only terminal CO ligands.

The above studies on the symmetric complexes **1** and **4** demonstrate the remarkable ease with which CO can change its bonding mode, from terminal to semibridging

(2) (a) Caspar, J. V.; Meyer, T. J. *J. Am. Chem. Soc.* **1980**, *102*, 7794–7795. (b) Hooker, R. H.; Mahmoud, K. A.; Rest, A. J. *J. Chem. Soc., Chem. Commun.* **1983**, 1022–1024. (c) Hepp, A. F.; Blaha, J. P.; Lewis, C.; Wrighton, M. S. *Organometallics* **1984**, *3*, 174–177.

(3) Blaha, J. P.; Bursten, B. E.; Dewan, J. C.; Frankel, R. B.; Randolph, C. L.; Wilson, B. A.; Wrighton, M. S. *J. Am. Chem. Soc.* **1985**, *107*, 4561–4562.

(4) Kvietok, F. A.; Bursten, B. E. *J. Am. Chem. Soc.* **1994**, *116*, 9807–9808.

(5) Kvietok, F. A.; Bursten, B. E. *Organometallics* **1995**, *14*, 2395–2399.

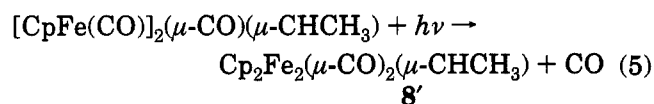
(6) (a) Hepp, A. F.; Wrighton, M. S. *J. Am. Chem. Soc.* **1983**, *105*, 5934–5935. (b) Dunkin, I. R.; Härter, P.; Shields, C. J. *J. Am. Chem. Soc.* **1984**, *106*, 7248–7249. (c) Zhang, H.-T.; Brown, T. L. *J. Am. Chem. Soc.* **1993**, *115*, 107–117.

\* Abstract published in *Advance ACS Abstracts*, September 15, 1995.  
(1) (a) Geoffroy, G. L.; Wrighton, M. S. *Organometallic Photochemistry*; Academic Press: New York, 1979. (b) Meyer, T. J.; Caspar, J. V. *Chem. Rev.* **1985**, *85*, 187–218.



to bridging. In these cases, the double-CO-loss products **3** and **6** apparently contain no bridging or semibridging CO ligands, results that are surprising and nonintuitive. We were therefore curious as to how this double-CO-loss chemistry would be altered in the case of a dinuclear complex that contained a ligand which strongly preferred a bridging rather than terminal bonding mode. A simple way of achieving this goal is to replace a bridging CO ligand in one of the symmetric complexes with a bridging CH<sub>2</sub> ligand, to yield one of the well-known methylene-bridged dinuclear complexes [M<sub>2</sub>L<sub>a</sub>-L'<sub>b</sub>L''<sub>c</sub>...](μ-CH<sub>2</sub>), where, in this instance, *a*, *b*, and *c* are not necessarily even integers.<sup>7</sup> Alkylidene ligands in low-valent complexes show a strong preference for bridging coordination; we therefore thought that any single- or multiple-CO-loss products would retain a methylene bridge and that the remaining CO ligands could be forced into a different coordination environment than in the symmetric complexes.

The present study will address in detail the photochemistry of one of the series of methylene-bridged analogs of the Fp<sub>2</sub> systems (**1**), namely the [(η<sup>5</sup>-C<sub>5</sub>R<sub>5</sub>)-Fe(CO)]<sub>2</sub>(μ-CO)(μ-CHR') systems (**7**, R = R' = H; **7\***, R = CH<sub>3</sub>, R' = H; **7'**, R = H, R' = CH<sub>3</sub>).<sup>8</sup> These particular systems are natural extensions of our studies on the symmetric complexes, for they are easily synthesized (especially given the methodology developed by Wright and Nelson<sup>9</sup>) and analyzed, and iron hydrocarbyl systems are becoming increasingly important in organic synthesis.<sup>10</sup> Further, we have previously investigated the photochemistry of **7'** with respect to the generation of CO-loss and radical photoproducts and to the kinetics of photosubstitution.<sup>11</sup> Two conclusions of this earlier study are particularly relevant to the present one: (1) the CHCH<sub>3</sub> bridge deactivates the homolysis process for **7'** and (2) compound **7'** undergoes CO loss to generate Cp<sub>2</sub>Fe<sub>2</sub>(μ-CO)<sub>2</sub>(μ-CHCH<sub>3</sub>) (**8'**), an analog of **2**, albeit with lower symmetry (eq 5).



For reasons that will be discussed below, we shall focus on the photochemistry of the Cp\* derivative **7\***, which is more amenable to study than **7** and **7'**. We shall demonstrate that complex **7\*** definitively undergoes double-CO loss, like that exhibited by the symmetric dimers. Further, we shall see that the methylene bridge, because of its unwillingness to adopt a terminal configuration, confers a very different structure on the double-CO-loss product, namely one in which the remaining CO ligand occupies a semibridging position. These studies will thus demonstrate another marked difference in the photochemistry of the methylene-

bridged systems relative to their symmetric, carbonyl-containing congeners.

## Experimental Section

**Materials.** Standard solvent and reagent purification techniques were used.<sup>12</sup> Tetrahydrofuran was dried and distilled over potassium/benzophenone. Hexanes (Mallinckrodt Analytical Reagent) were washed with concentrated sulfuric acid and distilled water, predried with MgSO<sub>4</sub>, and distilled over potassium metal. Methylcyclohexane and 3-methylpentane were purchased from Aldrich, dried over Na/K alloy, and vacuum-transferred to Kontes-sealed flasks for storage in an inert-atmosphere drybox. Chloromethyl pivalate and K(sec-C<sub>4</sub>H<sub>9</sub>)<sub>3</sub>BH (as K-Selectride) were purchased from Aldrich and used as received. Pentamethylcyclopentadienyliron dicarbonyl dimer (**1\***) was purchased from Strem and used without further purification. Cyclopentadienyliron dicarbonyl dimer (**1**) was synthesized according to the standard literature preparation.<sup>13</sup> The methylene-bridged compounds (η<sup>5</sup>-C<sub>5</sub>R<sub>5</sub>)<sub>2</sub>-Fe<sub>2</sub>(CO)<sub>2</sub>(μ-CO)(μ-CH<sub>2</sub>) (R = H, CH<sub>3</sub>) were prepared via literature methods<sup>9</sup> and purified on a refluxing column with hot hexanes,<sup>14</sup> and the ethylidene-bridged compound [(η<sup>5</sup>-C<sub>5</sub>H<sub>5</sub>)<sub>2</sub>Fe<sub>2</sub>(CO)<sub>2</sub>(μ-CO)(μ-CHCH<sub>3</sub>)] was prepared by literature methods.<sup>8</sup>

All synthetic manipulations were performed under an atmosphere of dry argon using standard Schlenk techniques. Argon was purified by passage through consecutive columns of activated Rydox catalyst and Drierite.<sup>12</sup> Alumina used for column separations was heated under vacuum until fully activated and converted to grade III via the addition of 6%, by weight, deionized water.<sup>12</sup>

**Instrumentation.** The following instrumentation was utilized: Bruker WM FT <sup>1</sup>H (250 MHz) NMR spectrometer; Nicolet Magna 550 FT-IR spectrometer; Cary-17 UV/vis spectrometer, upgraded by Olis. The matrix isolation studies employed a SPECAC Model 21500 variable-temperature system equipped with CaF<sub>2</sub> jacket windows. The present studies used a cell of CaF<sub>2</sub> windows with lead spacers and a path length of 1 mm. The irradiation source was a 200 W broad-spectrum, medium-pressure Hg-vapor UV/vis lamp (Oriel) equipped with an IR filter.

**Matrix Isolation Experiments.** Matrices were prepared by cooling solutions of the samples below the glass-transition temperature. The concentration of the photoactive species was between 0.5 and 2.0 mM. Fresh solutions were prepared for each matrix run. The matrix cell was placed 29–34 cm from the exit filter of the irradiation source. Most of the matrix experiments were performed at 93 K using liquid-nitrogen cooling and a thermocouple temperature controller monitored at the cell jacket. During portions of this study, the matrix was warmed to a specified temperature by removing liquid nitrogen from the Dewar, warming the matrix to the desired temperature, and then immediately recooling the matrix to 93 K. This procedure took between 5 and 35 min for warming (depending on final temperature) and approximately 10 min for the full recooling process, including allowances for reequilibrating at the lower temperature. All spectra were recorded at 93 K, except as noted. Because of differences in heat capacity, the measured jacket temperature is an upper bound to the actual temperature of the matrix, and we estimate the potential uncertainty in the actual matrix temperature during these warmup procedures to be as large as 10 K, dependent

(7) See, for example: (a) Herrmann, W. A. *Adv. Organomet. Chem.* **1982**, *20*, 159–263. (b) Herrmann, W. A. *J. Organomet. Chem.* **1983**, *250*, 319–343. (c) Holton, J.; Lappert, M. F.; Pearce, R.; Yarrow, P. I. *W. Chem. Rev.* **1983**, *83*, 135–201.

(8) Kao, S. C.; Lu, P. P. Y.; Pettit, R. *Organometallics* **1982**, *1*, 911–918.

(9) Wright, M. E.; Nelson, G. O. *J. Organomet. Chem.* **1984**, *263*, 371–373.

(10) See, for example: Fatiadi, A. J. *J. Res. Natl. Inst. Stand. Technol.* **1991**, *96*, 1–113.

(11) McKee, S. D.; Bursten, B. E. *J. Am. Chem. Soc.* **1991**, *113*, 1210–1217.

(12) (a) Gordon, A. J.; Ford, R. A. *The Chemist's Companion*; Wiley: New York, 1972. (b) Shriver, D. F. *The Manipulation of Air-Sensitive Compounds*; Krieger: Malabar, FL, 1969. (c) Perrin, D. D.; Armarego, W. L. F.; Perrin, D. R. *Purification of Laboratory Chemicals*; Pergamon: Oxford, U.K., 1988.

(13) King, R. B. *Organometallic Syntheses*; Academic Press: New York, 1965; Vol. 1.

(14) Casey, C. P.; Fagan, P. J.; Miles, W. H. *J. Am. Chem. Soc.* **1982**, *104*, 1134–1136 (supplementary materials).

on the final temperature. Because of these temperature uncertainties, multiple runs were performed to demonstrate the reproducibility of the results presented here.

During the matrix experiments, the times required to obtain IR and UV/vis spectra were approximately 3–5 min for IR (32 scans,  $2\text{ cm}^{-1}$  resolution) and 14–28 min for UV/vis (16 and 32 scans per data point, respectively). The IR window of interest was  $2400$  to  $1600\text{ cm}^{-1}$ , but only the region from  $2200$ – $1700\text{ cm}^{-1}$  is reported because this is the smallest window containing all the peaks of interest. The UV/vis observation window was from  $800$  to  $200\text{ nm}$ .

## Results and Discussion

As was the case in our earlier studies of double-CO-loss photoproducts, our main probe of the photochemical processes that occur in the frozen matrices is infrared spectroscopy of the CO-stretching region. The use of IR spectroscopy as our principal probe is one of the reasons that we have focused on the  $Cp^*$  complex  $[Cp^*Fe(CO)]_2(\mu-CO)(\mu-CH_2)$  (**7\***). As was the case in complex **1\***, the steric bulk of the  $Cp^*$  ligands forces **7\*** to adopt an essentially *trans*-only equilibrium conformation; in contrast, complexes **1**, **7**, and **7'** exist as *cis/trans* mixtures in solution.<sup>14,15,16</sup> Thus, the IR spectra of **7\*** and its photoproducts are much easier to interpret than those of **7** and **7'**. As with our other studies,<sup>4,5</sup> we have carried out the matrix experiments in neat 3-methylpentane (3-MP), which provides a softer matrix than do other common hydrocarbon matrix materials.<sup>17</sup>

**Matrix Photochemistry of 7\***. The methylene-bridged derivative **7\*** is an analog of the "Fp<sub>2</sub>" system **1\***, in which a bridging carbonyl ligand has been replaced by a bridging methylene ligand. Because *trans*-**1\*** has centrosymmetric  $C_{2h}$  point symmetry, it exhibits a very simple two-band IR spectrum, with one band each in the terminal and bridging CO-stretching regions. The replacement of a bridging CO by a bridging  $CH_2$  ligand to form *trans*-**7\*** reduces the molecular symmetry to a maximum of  $C_2$ , and the IR spectrum of *trans*-**7\*** could, in principle, show three CO-stretching bands. However, the *transoid* arrangement of the terminal CO ligands is expected to render the symmetric stretch of these ligands to be very weak. Figure 1a shows the IR spectrum of *trans*-**1\*** as a frozen solution (1 mM) in neat 3-MP at 93 K. As expected, two prominent bands are observed, at  $1915$  and  $1765\text{ cm}^{-1}$ . These absorptions correspond roughly to the antisymmetric stretch of the terminal CO ligands and to the stretch of the bridging CO, respectively. The simplicity of this starting spectrum greatly assists in the elucidation of subsequent photochemical changes.

Irradiation of the frozen matrix of *trans*-**7\*** produces significant spectral changes. After 6 min of broad-

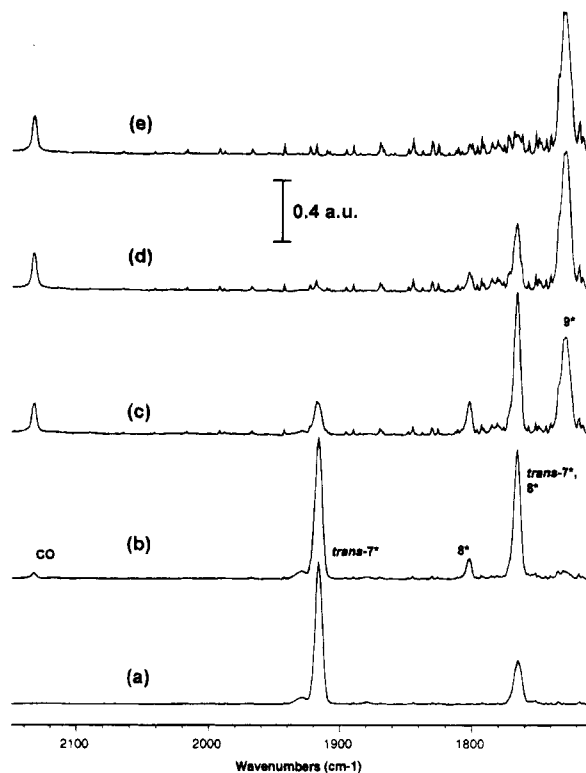


**Figure 1.** Progressive IR spectra during the irradiation of  $[Cp^*Fe(CO)]_2(\mu-CO)(\mu-CH_2)$  (**7\***) in 3-methylpentane at 93 K: (a) spectrum prior to irradiation; (b) spectrum after 6 min of irradiation; (c) spectrum after 40 min of irradiation; (d) spectrum after 80 min of irradiation; (e) spectrum after 180 min of irradiation. The peak labels in spectra b and c refer to the compound numbers in Scheme 1.

spectrum UV irradiation, the peak at  $1915\text{ cm}^{-1}$  shows a decrease in intensity, while the one at  $1765\text{ cm}^{-1}$  increases in intensity. In addition, new well-defined bands appear at  $1802$  and  $2132\text{ cm}^{-1}$  (Figure 1b). These changes are consistent with the photochemical formation of a CO-loss product that has CO-stretching modes at  $1802$  and  $1765\text{ cm}^{-1}$  (coincident with *trans*-**7\***). This species is readily identified as the  $C_{2v}$  triply bridged complex  $Cp^*_2Fe_2(\mu-CO)_2(\mu-CH_2)$  (**8\***; Scheme 1), a complex analogous to  $Cp_2Fe_2(\mu-CO)_2(\mu-CHMe)$  (**8'**), which we have observed in the solution and matrix photochemistry of **7'**.<sup>11,18</sup> The presence of two bridging-CO stretching modes in **8\*** suggests that its structure is analogous to the structurally characterized molecule  $Cp^*_2Fe_2(\mu-CO)_3$  (**2\***), the CO-loss product from **1\***.<sup>3</sup> The  $1802$  and  $1765\text{ cm}^{-1}$  bands are assigned to the symmetric ( $A_1$ ) and antisymmetric ( $B_1$  or  $B_2$ ) CO-stretching modes of **8\***, respectively; the symmetric stretch is expected to be at higher energy than the antisymmetric stretch,<sup>19</sup> and, because the angle between the CO ligands is expected to be  $\sim 120^\circ$ , the antisymmetric stretch should have the greater intensity. A comparison of the UV/vis spectra of **7\*** and **8\*** shows a marked shift in the position of the prominent visible band in each spectrum (Figure 2), and the matrix noticeably changes color from purple to orange. Complex **8\*** exhibits a well-defined electronic absorption at  $482\text{ nm}$ , consistent with

(15) (a) Cotton, F. A.; Yagupsky, G. *Inorg. Chem.* **1967**, *6*, 15–20. (b) Fischer, R. D.; Vogler, A.; Noack, K. *J. Organomet. Chem.* **1967**, *7*, 135. (c) Noack, K. *J. Organomet. Chem.* **1967**, *7*, 151. (d) Manning, A. R. *J. Chem. Soc. A* **1968**, 1319–1324. (e) Bullitt, J. G.; Cotton, F. A.; Marks, T. J. *J. Am. Chem. Soc.* **1970**, *92*, 2155–2156. (f) McArdle, P.; Manning, A. R. *J. Chem. Soc. A* **1970**, 2133–2136. (g) Bullitt, J. G.; Cotton, F. A.; Marks, T. J. *Inorg. Chem.* **1972**, *11*, 671–676. (h) Gansow, O. A.; Burke, A. R.; Vernon, W. D. *J. Am. Chem. Soc.* **1972**, *94*, 2550–2552. (i) Adams, R. D.; Cotton, F. A. *Inorg. Chim. Acta* **1973**, *7*, 153–156. (j) Kirchner, R. M.; Marks, T. J.; Kristoff, J. S.; Ibers, J. A. *J. Am. Chem. Soc.* **1973**, *95*, 6602–6613.

(16) The *cis* isomer of **7'** has additional isomers owing to the possibility of *exo* and *endo* orientations of the ethylidene methyl group relative to the  $Cp$  ligands. These additional isomers can make NMR analysis of reactions of **7'** more complex than that of either **7** or **7\***.

(17) Ling, A. C.; Willard, J. E. *J. Phys. Chem.* **1968**, *72*, 1918–1923.

(18) McKee, S. D. Ph.D. Dissertation, The Ohio State University, 1990.

(19) Cotton, F. A.; and Kraihanzel, C. S. *J. Am. Chem. Soc.* **1962**, *84*, 4432.

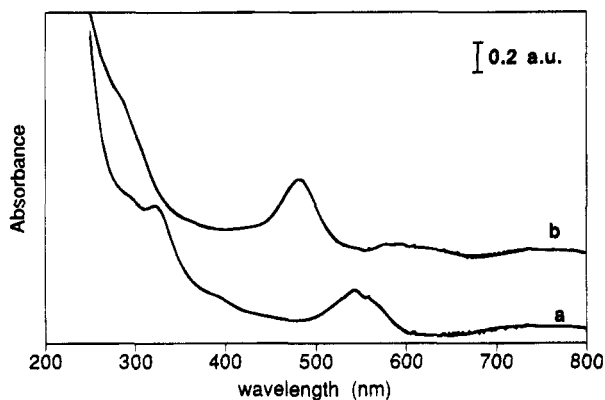
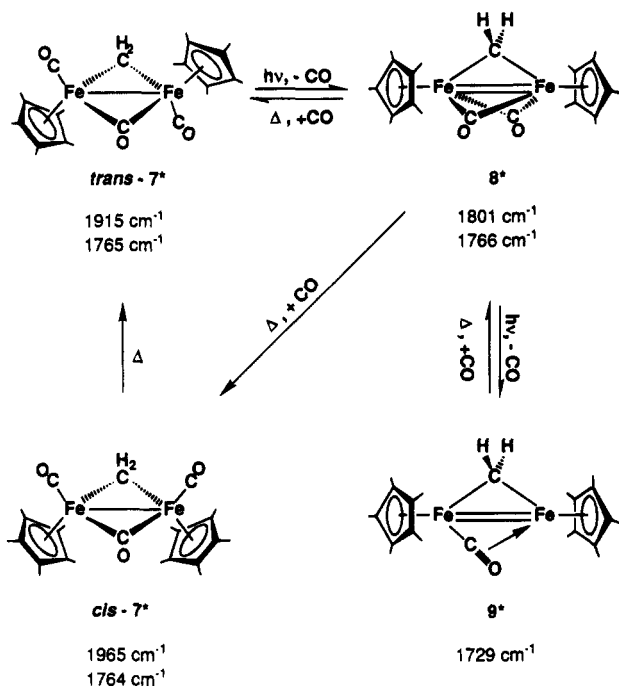


**Figure 2.** UV/vis spectra in 3-methylpentane at 93 K: (a) spectrum of **7\*** prior to irradiation; (b) spectrum obtained after irradiation and back-reaction of **9\*** to **8\***. After this procedure, the predominant species present in the matrix (by IR spectroscopy) is **8\***.

**Scheme 1. Photochemical CO-Loss Processes and Thermal Back-Reactions Exhibited by *trans*-**7\*** upon Irradiation in a Matrix of Frozen 3-Methylpentane**



the visible transitions we have observed in **8\*** (485 nm)<sup>11</sup> and **2\*** (515 nm).<sup>20</sup>

Further irradiation of the matrix leads to near-disappearance of the IR bands due to **7\*** and **8\*** and the appearance of an absorption at 1729 cm<sup>-1</sup>, which is attributed to the new photoproduct **9\*** (Figure 1c–e). The formation of **9\*** occurs only after **8\*** has been made, and **8\*** can be nearly completely converted to **9\*** at 93 K. During this subsequent irradiation, the matrix changes color from orange to pale green. Figure 3 shows plots of IR band intensity (measured as integrated peak areas) vs time for isolated bands of **7\***, **8\***, **9\***, and free CO. These plots demonstrate the facile formation of **8\*** from **7\*** and the equally facile conversion of **8\*** to **9\***. The intensity of the 2132 cm<sup>-1</sup> band for free CO appears to be increasing throughout these conversions, evidence

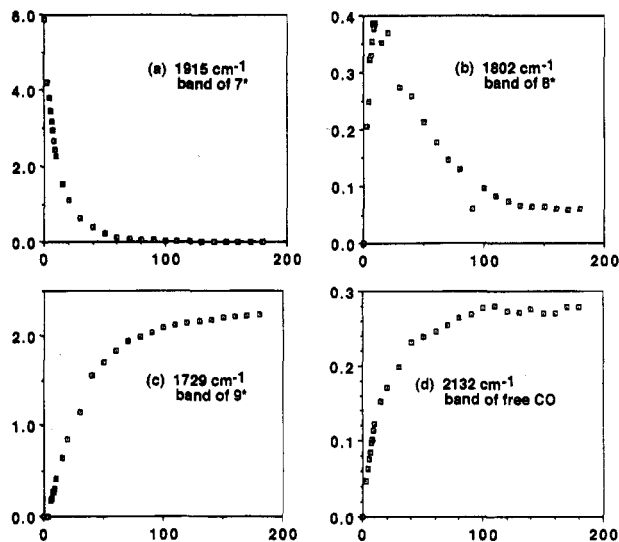


**Figure 3.** Temporal behavior of relevant IR bands during the irradiation of **7\*** in 3-MP at 93 K: (a) the 1915 cm<sup>-1</sup> band of **7\***; (b) the 1802 cm<sup>-1</sup> band of **8\***; (c) the 1729 cm<sup>-1</sup> band of **9\***; (d) the 2132 cm<sup>-1</sup> band of free CO. Abscissas are in minutes; ordinates are integrated intensities in units of absorbance units per centimeter.

that the process **8\*** → **9\*** involves additional CO evolution. However, the small intensity of the 2132 cm<sup>-1</sup> absorption makes it difficult to arrive at definite conclusions concerning the **8\*** → **9\*** conversion. In order to explore this conversion further, and to arrive at a more convincing conclusion as to the identity of **9\***, we have used the observation that **9\*** thermally converts back to **8\*** at 93 K.

**Thermal Back-Reaction of **9\*** to **8\***.** The thermal back-reaction of **9\*** to **8\*** is readily apparent in the difference spectrum shown in Figure 4. The matrix was irradiated for 180 min at 93 K, which leads to the spectrum in Figure 1e. The matrix was then allowed to react in the dark at 93 K for an additional 90 min. The spectrum in Figure 4 was obtained by subtracting the spectrum after 180 min irradiation from the spectrum obtained after 180 min irradiation plus 90 min thermal reaction. The negative peak at 1729 indicates that **9\*** is consumed during the dark reaction period, and the positive peaks at 1765 cm<sup>-1</sup> and 1802 cm<sup>-1</sup> show the conversion back to **8\***. No conversion to **7\*** is evident, probably because there is insufficient thermal energy at 93 K to effect the **8\*** → **7\*** conversion. The negative peak at 2132 cm<sup>-1</sup> shows conclusively that CO is consumed in the conversion of **9\*** to **8\***. We therefore conclude that **9\*** is a double-CO-loss product from **7\*** that has the formula Cp<sup>\*</sup><sub>2</sub>Fe<sub>2</sub>(CO)(CH<sub>2</sub>).

The 1729 cm<sup>-1</sup> absorption of the CO in **9\*** seems most consistent with a linear semibridging  $\mu\text{-}\eta^1\text{:}\eta^2\text{-CO}$ .<sup>21</sup> Thus, the likely structure for **9\*** is two Cp<sup>\*</sup>Fe fragments linked by a semibridging CO and, we assume, an intact methylene bridge (Scheme 1). The comparison of this structure to the double-CO-loss product from **1** (or **1\***) is quite striking. As noted above, we have proposed that double-CO loss from **1** leads to the species **3** with only terminal CO's and a formal Fe–Fe triple bond.<sup>4</sup> In contrast, the apparent instability of CH<sub>2</sub> in a terminal conformation forces **9\*** to adopt multiple bridging ligands

(20) Bursten, B. E.; McKee, S. D.; Platz, M. S. *J. Am. Chem. Soc.* **1989**, *111*, 3428–3429.

(21) (a) Crabtree, R. H.; Lavin, M. *Inorg. Chem.* **1986**, *25*, 805–812. (b) Zhang, S.; Brown, T. L. *J. Am. Chem. Soc.* **1993**, *115*, 1779–1789.

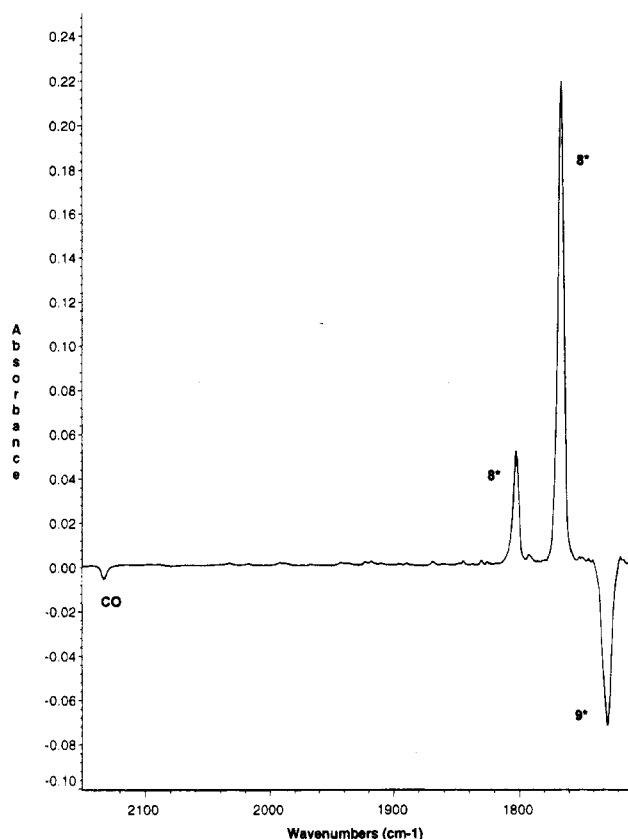


**Figure 4.** Difference IR spectrum from the irradiation and thermal back-reaction of **7\*** in 3-methylpentane at 93 K. The spectrum shown is the difference A – B, where A and B are defined as follows: (A) spectrum obtained after irradiation of the matrix for 180 min followed by 90 min of thermal (dark) reaction at 93 K; (B) spectrum obtained immediately after irradiation of the matrix for 180 min. As shown, the predominant species after the initial irradiation is **9\***. During the thermal reaction, **9\*** and CO are consumed (negative peaks) while **8\*** is produced (positive peaks).

and a formal Fe–Fe double bond. We will be comparing the bonding and electronic structures of these double-CO-loss diiron products in a later publication.

The progressive conversions **7\*** → **8\*** → **9\*** under photolytic conditions are reproducible and nearly complete at 93 K. The ease of the conversions does not depend upon the starting concentration of **7\*** in the matrix, which provides evidence for the reasonable expectation that all the CO-loss processes are unimolecular. It is notable that 3-MP is a relatively “soft” (low-viscosity) matrix material for these studies; if we use a more viscous matrix material, such as methylcyclohexane (MCH), the same photochemical conversion of **7\*** to **9\*** occurs, albeit not nearly as readily.

**Variable-Temperature Studies of the Thermal Back-Reactions: Formation of *cis*-7\*.** As noted earlier, at 93 K there is sufficient thermal energy for the back-reaction **9\*** + CO → **8\*** to occur quite readily. However, the reaction of **8\*** with CO to produce starting material **7\*** does not occur at 93 K to any significant extent over a period of 2 h. These observations are consistent with the notion that **9\*** is more coordinatively unsaturated than **8\*** and that, therefore, **9\*** should react with CO more easily than does **8\***.

Interestingly, when the matrix was warmed in the dark by only 5–10 K, the back-reaction **8\*** + CO → **7\***

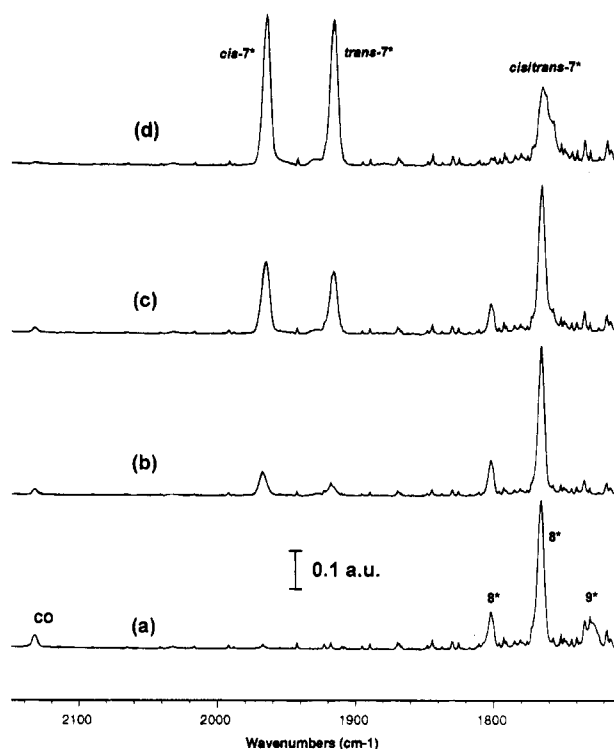


**Figure 5.** Progressive IR spectra following the irradiation of **7\*** for 6 min in 3-MP at 93 K: (a) spectrum at 93 K, prior to thermal ramping; (b) spectrum after ramping the matrix to 123 K; (c) spectrum after ramping the matrix to 138 K; (d) spectrum after ramping the matrix to 148 K. The peak labels in spectra a and d refer to the compound numbers in Scheme 1. The temperature of the matrix was ramped to a final temperature; the matrix was then cooled to 93 K and reequilibrated prior to collecting the spectra.

could be detected readily after only 30 min. This observation suggested to us that controlled warming of the matrix could be revealing. Figure 5 shows a series of IR spectra obtained by ramping the temperature of the matrix cell in the dark to successively higher temperatures, at a nominal warming speed of 2–3 K/min, followed by thermal quenching to 93 K to record each spectrum. Several observations are notable. First, as indicated by the disappearance of the peak at 1729 cm<sup>-1</sup>, the back-reaction **9\*** + CO → **8\*** is essentially complete by the time the matrix is warmed to 123 K. Second, as expected, the peak for free CO disappears as the back-reactions occur. Third, the appearance of the terminal-CO peak for *trans*-**7\*** (1915 cm<sup>-1</sup>) is accompanied by the concurrent appearance of another terminal-CO band of comparable intensity at 1967 cm<sup>-1</sup>, which is due to a new species. At the same time, the peak in the bridging-CO region at 1765 cm<sup>-1</sup> broadens significantly, suggesting that the new species may also have a peak in that region. When the matrix is melted and allowed to equilibrate at room temperature, the new species converts entirely to *trans*-**7\***, with no consumption or evolution of CO. These observations are consistent with the identification of the new species as *cis*-**7\***, which is thermodynamically unstable with respect to the *trans* isomer. The peak at 1967 cm<sup>-1</sup> is likely the symmetric stretching mode of *cis*-**7\***, which is expected to be at higher energy than the observed antisymmetric stretch of *trans*-**7\***. The antisymmetric terminal-CO-stretching mode of *cis*-**7\*** is expected to be allowed but to be very weak. We cannot provide a

definitive assignment of its position, although it may be nearly coincident with the strong antisymmetric stretching mode of *trans-7\**, as is the case for the corresponding bands of *cis-* and *trans-1*.<sup>15</sup> Likewise, the bridging-CO modes in the two isomers are expected to be at nearly the same energy, as are the antisymmetric bridging-CO-stretch modes in *cis-* and *trans-1*.<sup>15</sup>

Several aspects of the formation of *cis-7\** and its isomerization to *trans-7\** are of interest. First, the conversion *cis-7\** → *trans-7\** follows first-order kinetics, which is consistent with an intramolecular process. The process is slow: at room temperature, the first-order rate constant is on the order of 10<sup>-3</sup> s<sup>-1</sup>.<sup>22</sup> This rate constant is similar to that obtained by Casey et al. for the *cis/trans* equilibration of *trans*-enriched **7**, a process for which they report a half-life of 10 min at 36 °C,<sup>14</sup> and by Altbach et al. for the *cis/trans* isomerization of **7** in various solvents.<sup>23</sup> The *cis/trans* isomerization of **7** is much slower than that for **1**,<sup>24</sup> and we see the same phenomenon in the Cp\*-containing systems. Moore, Poliakov, and Turner have reported the first-order rate constant for the conversion of photochemically generated *cis-1\** to *trans-1\** in cyclohexane.<sup>25</sup> They find a rate constant of ca. 50 s<sup>-1</sup> at 24 °C, roughly 5 orders of magnitude greater than that for the isomerization of **7\***.

Several mechanisms have been proposed for the *cis/trans* isomerization of methylene-bridged (and related) complexes, most of which involve an unbridged isomer with a terminal CH<sub>2</sub> ligand.<sup>14,23,26</sup> It is generally accepted that the *cis/trans* isomerization is expected to be slower for **7** and **7\*** than for **1** and **1\*** because the latter can readily utilize an unbridged isomer to facilitate the isomerization; if **7** and **7\*** isomerize via the same mechanism, the unbridged intermediate that contains a terminal alkylidene is presumed to be significantly higher in energy than the unbridged isomers of **1** and **1\***.<sup>27</sup> Regardless of the true nature of the intermediate in the *cis/trans* isomerization of **7\***, the present studies reinforce the notion that it is a higher energy process than that in the parent carbonyl systems.

(22) Because of the limitations of our matrix cell upon warming to room temperature, it was not possible to maintain a constant temperature while monitoring the decay of *cis-7\** to *trans-7\**. The kinetic data were obtained over a temperature range of 18–26 °C. Six data points were obtained by measuring the integrated intensity *I* of the 1967 cm<sup>-1</sup> band of *cis-7\** over a 55 min interval, after which the band was too small to be integrated. A plot of -ln(*I*) vs time was linear (*R* = 0.99). The first-order rate constant obtained from this plot is 7 × 10<sup>-4</sup> s<sup>-1</sup>, which corresponds to a half-life of ca. 16 min.

(23) Altbach, M. I.; Muedas, C. A.; Korswagen, R. P.; Ziegler, M. L. *J. Organomet. Chem.* **1986**, *306*, 375–383.

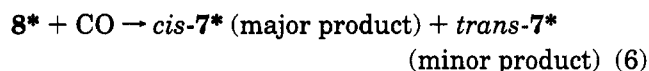
(24) Adams, R. D.; Cotton, F. A. *J. Am. Chem. Soc.* **1973**, *95*, 6589–6594.

(25) Moore, B. D.; Poliakov, M.; Turner, J. J. *J. Am. Chem. Soc.* **1986**, *108*, 1819–1822.

(26) (a) Adams, R. D.; Brice, M. D.; Cotton, F. A. *Inorg. Chem.* **1974**, *13*, 1080–1085. (b) Dyke, A. F.; Knox, S. A. R.; Mead, K. A.; Woodward, P. J. *Chem. Soc., Chem. Commun.* **1981**, 861–862. (c) Dyke, A. F.; Knox, S. A. R.; Morris, M. J.; Naish, P. J. *J. Chem. Soc., Dalton Trans.* **1983**, 1417–1426. (d) Colborn, R. E.; Dyke, A. F.; Knox, S. A. R.; Mead, K. A.; Woodward, P. J. *Chem. Soc., Dalton Trans.* **1983**, 2099–2108. (e) Theopold, K. H.; Bergman, R. G. *J. Am. Chem. Soc.* **1983**, *105*, 464–475. (f) Casey, C. P.; Gable, K. P.; Roddick, D. M. *Organometallics* **1990**, *9*, 221–226. (g) Ueno, K.; Hamashima, N.; Ogino, H. *Organometallics* **1992**, *11*, 1435–1437. (h) Fong, R. H.; Lin, C.-H.; Idmoumaz, H.; Hersh, W. H. *Organometallics* **1993**, *12*, 503–516.

(27) Moore et al.<sup>25</sup> derived activation parameters for the conversion of *cis-1\** to *trans-1\**. If we assume the same preexponential factor that they obtained (which presupposes a nearly identical mechanism, similar electronic rearrangement during isomerization, and negligible solvent effects), we find that the activation energy for *cis-7\** → *trans-7\** is about 100 kJ mol<sup>-1</sup>, ca. 30 kJ mol<sup>-1</sup> greater than the activation energy for *cis-1\** → *trans-1\**.

A second interesting aspect of the formation of *cis-7\** concerns the relative amounts of *cis-* and *trans-7\** produced during the reaction of **8\*** with CO. It is apparent in Figure 5 that the 1967 cm<sup>-1</sup> band for *cis-7\** is larger than the band at 1915 cm<sup>-1</sup>, which is exclusively or predominantly due to *trans-7\**. Previous results on **1** would lead us to expect that the 1967 cm<sup>-1</sup> band is intrinsically more intense than the 1915 cm<sup>-1</sup> band. Cotton et al. have estimated the relative intensities of the corresponding bands in **1**, namely the symmetric (A<sub>1</sub>) mode of *cis-1* at 1998 cm<sup>-1</sup> and the antisymmetric (B<sub>u</sub>) mode of *trans-1* at 1954 cm<sup>-1</sup>.<sup>15g</sup> They found an intensity ratio A<sub>1</sub>:B<sub>u</sub> = 3.80:3.04 = 1.25. If we assume this intensity ratio for the bands of *cis-* and *trans-7\**, the data presented in Figure 5 indicate that the reaction of **8\*** with CO leads to initial preferential formation of the *cis* isomer over the *trans* isomer (eq 6). For example, the ratio of the integrated intensi-

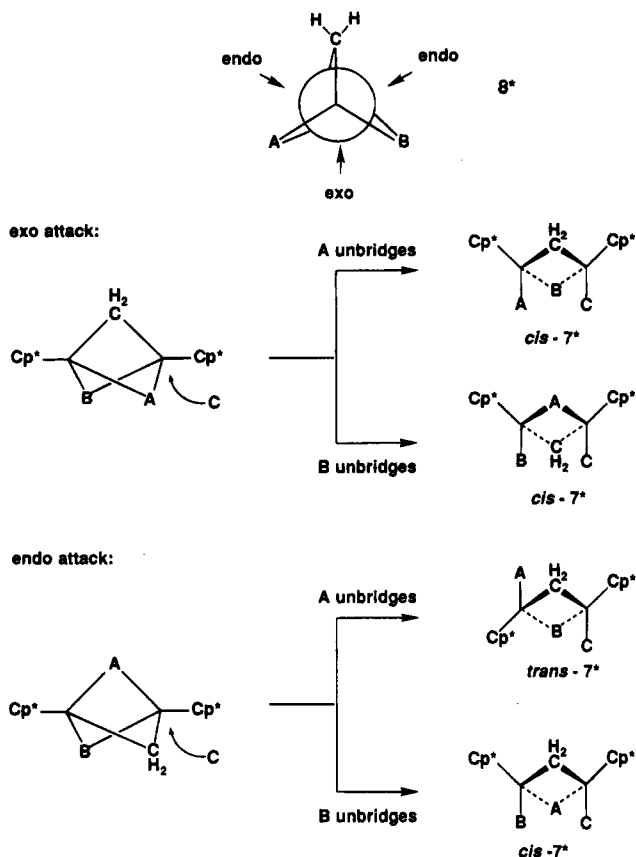


ties of the 1967 and 1915 cm<sup>-1</sup> bands in Figure 5b is 1.6, which, using the assumed ratio of absolute intensities, implies that ca. 55–60% of the product is the *cis* isomer.<sup>28</sup> At the warmer temperatures for Figure 5c,d, at which *cis/trans* isomerization may begin to occur at a significant rate, the percentage of *cis* isomer decreases to ca. 50% and 45%, respectively.

The detailed mechanism for the addition of CO to **8\*** is not known. Nevertheless, we can propose a simple scheme that rationalizes the apparent preferential formation of *cis-7\** (Scheme 2). We shall assume the following. (i) CO adds directly to an Fe atom of **8\*** along the bisectors of the dihedral angles formed by the three bridging ligands in **8\***. Under this assumption, there are two exo (one for each Fe atom) and four endo sites of attack with respect to the μ-CH<sub>2</sub> ligand. (ii) The incoming CO (denoted C in Scheme 2) ultimately becomes one of the terminal CO ligands of **7\***. One of the bridging CO ligands of **8\*** (denoted A or B) becomes the other terminal CO ligand of **7\***, while the other one remains bridging. (iii) The “unbridging” of CO A or B in **8\*** occurs via a “least-motion” rearrangement in which the unbridged CO ultimately ends up on the side of the plane defined by the other two bridging ligands that requires the lesser atomic motion. Under these assumptions, exo attack by carbonyl C leads exclusively to the formation of *cis-7\**; this direction of attack preserves the mirror symmetry of the system, and thus it makes no difference whether carbonyl A or B undergoes bridging-to-terminal conversion. If carbonyl C attacks along an endo direction, the mirror symmetry of the system is broken, and we predict that different isomers will be formed, depending on which of the bridging carbonyls moves to a terminal position. If the bridging CO that is nearer to the incoming ligand C is the one that unbridges, *cis-7\** will be formed, whereas unbridging of the other bridging CO will lead to formation of *trans-7\**. If the site of attack (exo or endo) and

(28) Because *cis-7\** isomerizes to *trans-7\**, in principle it is possible that the *trans-7\** observed in Figure 5b is due to isomerization rather than the direct reaction of **8\*** with CO. However, because the isomerization process is slow even at room temperature (*vide supra*), it is more likely that both *cis-* and *trans-7\** are formed directly according to eq 6.

**Scheme 2. Simplified Scheme for the Addition of CO to 8\* To Form a Mixture of *cis*- and *trans*-7\* (See Text)<sup>a</sup>**



<sup>a</sup> The labels A–C denote carbonyl ligands. It is assumed that attack of carbonyl C causes either A or B to undergo bridge-to-terminal conversion and that this conversion is a least-motion process. According to the scheme, attack exo to the μ-CH<sub>2</sub> ligand produces only *cis*-7\*, whereas attack in one of the *endo* positions will lead to an equal mixture of *cis*- and *trans*-7\*. Because there are twice as many *endo* sites as *exo* sites, the scheme predicts a 2:1 ratio of *cis*-7\*:*trans*-7\* produced.

the choice of which CO undergoes bridging-to-terminal conversion (A or B) are both statistical, the scheme predicts that the product ratio will be *cis*-7\*:*trans*-7\* = 2:1. Obviously, this simplified scheme neglects any energetic differences between different sites of attack, nor does it account for the relative rates of addition of CO to 8\* and *cis*/*trans* isomerization of 7\*, but the statistical treatment does lead to preferential formation of *cis*-7\*, as observed.

Our proposal of the kinetic formation of a thermodynamically unfavorable *cis* isomer is similar to the situation observed in the fast solution photochemistry of *trans*-1\* by Moore, Poliakoff, and Turner.<sup>25</sup> These authors found that photogenerated \*FeCp\*(CO)<sub>2</sub> radicals could recombine to form *cis*-1\* as well as *trans*-1\*, with the *cis* isomer rapidly reverting to the *trans* isomer in room-temperature solution. It is interesting to note that, if the scheme outlined in Scheme 2 is valid, the addition of CO to 2\* to form 1\* would lead to 2:1 preferential formation of *cis*-1\* over *trans*-1\*. Thus, it strikes us that some of the *cis*-1\* observed by these authors might result from CO addition to 2\*, in addition to that formed by radical recombination.

**Matrix Photochemistry of 7 and 7'.** Given the photochemistry exhibited by the Cp\* derivative 7\*, we

chose to try the same experiments with the Cp analogs 7 and 7'. Two factors contributed to making these additional studies less successful than we had hoped. First, as noted earlier, the presence of multiple stereoisomers in 7 and 7' greatly complicates the IR spectra of the starting materials and the photoproducts. Second, the Cp derivatives are markedly less soluble in the matrix solvents than is the Cp\* derivative. Because of this lower solubility, we were not able to achieve the same concentrations of starting materials in the frozen matrix without significant spectral broadening, possibly due to aggregation or precipitation at low temperatures.

Irradiation of the matrix of 7 for 10 min leads to the evolution of free CO (detected in the IR spectrum at 2132 cm<sup>-1</sup>) and new IR peaks at 1837 and 1800 cm<sup>-1</sup>. These latter bands are consistent with the formation of the CO-loss photoproduct Cp<sub>2</sub>Fe<sub>2</sub>(μ-CO)<sub>2</sub>(μ-CH<sub>2</sub>) (8); the approximately 35 cm<sup>-1</sup> blue shift in the bridging-CO IR bands of 8 relative to those of 8\* is reasonable upon the replacement of electron-rich Cp\* ligands with Cp ligands.<sup>25,29</sup> Additional bands at 1990 and 1734 cm<sup>-1</sup> are also observed, and these appear simultaneously at rates similar to those due to 8. These bands, which are not necessarily from the same product, do not correlate with any of those observed in the photochemistry of 7\*. Continued irradiation of the matrix of 7 leads to the appearance of multiple complex peaks, and we have been unable to assign any of these definitively to the Cp-containing analog of 9.

The matrix photochemistry of the ethylidene-bridged complex 7' in frozen 3-MP is similar to that of 7 and is similar to previous matrix studies of 7' in a 90% MCH, 10% 3-MP matrix.<sup>18</sup> The spectrum of the frozen matrix shows severe broadening and shifting relative to the room-temperature spectrum. Upon irradiation, free CO is produced, as is the triply bridged CO-loss product Cp<sub>2</sub>Fe<sub>2</sub>(μ-CO)<sub>2</sub>(μ-CHMe) (8'), which exhibits CO-stretching modes at 1833 and 1795 cm<sup>-1</sup>. As was the case for 7, we were unable to find definitive evidence for the formation of a double-CO-loss product analogous to 9.

## Conclusion

Each of the unsymmetric methylene-bridged diiron complexes 7, 7', and 7\* exhibits photochemical CO loss in frozen 3-MP to form a triply bridged intermediate (8, 8', or 8\*) that is analogous to the CO-loss photoproducts from the Fp<sub>2</sub> and Fp\*<sub>2</sub> systems 1 and 1\*. The Cp\* derivative 7\* exhibits loss of a second CO to generate a double-CO-loss product that we propose has the identity Cp\*<sub>2</sub>Fe<sub>2</sub>(μ-η<sup>1</sup>:η<sup>2</sup>-CO)(μ-CH<sub>2</sub>) (9\*). The strong bridging preference of the methylene bridge in 7\* has therefore led to a double-CO-loss photoproduct that is decidedly different from that obtained from 1 or 1\*. These studies of photochemical response to structural modification are ongoing.

**Acknowledgment.** We gratefully acknowledge the National Science Foundation (Grant CHE-9208703) for support of this research. We also thank Dr. Frank Kvietok for assistance and helpful discussions.

OM9505064

# $^1\text{H}$ NMR Exchange Reactions in Tellurium(IV) Derivatives with Cleavage of Te–N Bonds

Michael R. Detty,<sup>\*,†</sup> Antony J. Williams,<sup>‡</sup> J. Michael Hewitt,<sup>‡</sup> and Martin McMillan<sup>‡</sup>

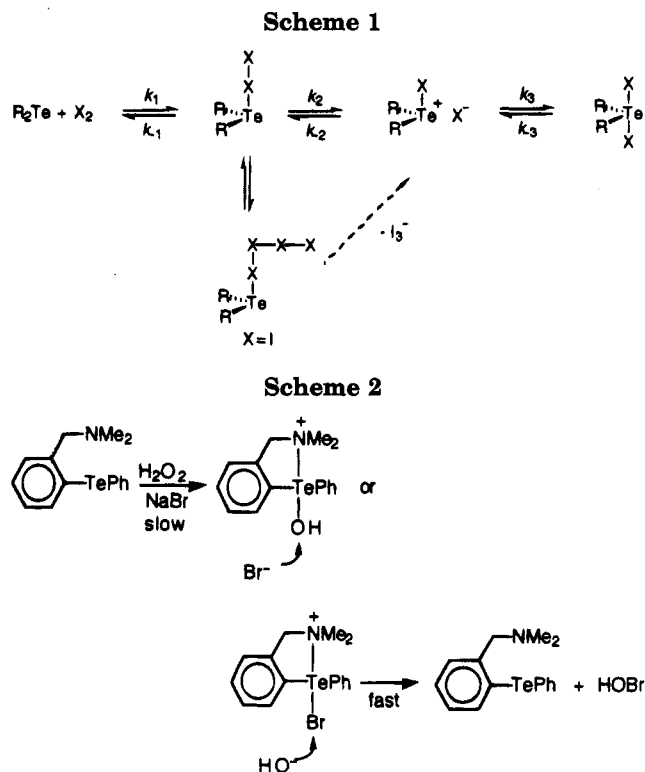
Office Imaging Research and Technical Development, Eastman Kodak Company, Rochester, New York 14560, Analytical Technology Division, Eastman Kodak Company, Rochester, New York 14652-3712, and Department of Medicinal Chemistry, State University of New York at Buffalo, Amherst, New York 14260

Received February 6, 1995<sup>⊗</sup>

Additions of iodine and bromine to phenyl *N,N*-dimethyl-2-(aminomethyl)phenyl telluride give Te(IV) derivatives **1** and **2**, respectively, bearing a formal positive charge. The X-ray structure of **1** as its 2:1  $\text{CCl}_4$  solvate ( $\text{C}_{15}\text{H}_{17}\text{I}_2\text{NTe}\cdot\frac{1}{2}\text{CCl}_4$ ) is consistent with an ionic structure. Both **1** and **2** have prochiral tellurium centers. The exchange of equivalent sites can be monitored by variable-temperature  $^1\text{H}$  NMR spectroscopy. The exchange rates are independent of concentration, which suggests a first-order process involving cleavage of the Te–N bond. Arrhenius and Eyring activation parameters were calculated to be  $E_a = 12.5 \pm 0.3 \text{ kcal mol}^{-1}$ ,  $\ln A = 26.5$ ,  $\Delta H^\ddagger = 12.0 \pm 0.3 \text{ kcal mol}^{-1}$ ,  $\Delta S^\ddagger = -8 \pm 4 \text{ cal mol}^{-1} \text{ K}^{-1}$ , and  $\Delta G_{298}^\ddagger = 14.4 \text{ kcal mol}^{-1}$  for **1** and  $E_a = 15.0 \pm 0.4 \text{ kcal mol}^{-1}$ ,  $\ln A = 29.3$ ,  $\Delta H^\ddagger = 14.4 \pm 0.4 \text{ kcal mol}^{-1}$ ,  $\Delta S^\ddagger = -2 \pm 5 \text{ cal mol}^{-1} \text{ K}^{-1}$ , and  $\Delta G_{298}^\ddagger = 15.0 \text{ kcal mol}^{-1}$  for **2**.

The kinetics of the oxidative addition reactions of bromine and iodine to organotellurium compounds<sup>1,2</sup> as well as the reductive-elimination reactions of chlorine and bromine from tellurium(IV) dihalides<sup>3,4</sup> have been studied. In solution, all steps are correctly written as an equilibrium.<sup>1–3</sup> Although the reaction sequence favors the products of oxidative addition with all halogens, the reductive elimination reactions can be driven to completion if the halogen is eliminated from the system as it is produced. For these reactions with chlorine and bromine, the reaction sequence can be written as shown in Scheme 1. In reactions with iodine, two-to-one complexes of iodine with diorgano tellurides may form and the resulting  $\text{R}_2\text{Te}-\text{I}_4$  complex may dissociate to the telluronium salt  $\text{R}_2\text{Te}-\text{I}^+$  and triiodide in addition to the path described by  $k_2$ .<sup>2</sup>

One relatively unexplored reaction of tellurium(IV) dihalides, the  $\eta^1$ -association complexes of halogen, or the halotelluronium intermediates of Scheme 1 is the transfer of halogen from Te(IV) to an appropriate substrate leading to Te(II) and electrophilic halogenation of the substrate. One of us has recently described the chlorination and bromination of organic substrates from the reaction of sodium halide and hydrogen peroxide with catalytic quantities of diorgano tellurides.<sup>5</sup> A particularly efficient catalyst in this process was phenyl *N,N*-dimethyl-2-(aminomethyl)phenyl telluride, which presumably is activated by intramolecular chelation as shown in Scheme 2 to give a cationic complex upon oxidation by peroxide.



Similar cationic complexes **1**<sup>2</sup> and **2**<sup>1</sup> have been described for the addition of iodine and bromine, respectively, to phenyl *N,N*-dimethyl-2-(aminomethyl)phenyl telluride. In these reactions, oxidation with halogen is the fast step.<sup>1,2</sup> The X-ray structure of **2** shows a prochiral environment for the tellurium center and suggests that, for halogenation reactions, the prochiral tellurium centers of **1** and **2** offer interesting potential for the design of chiral halogenating agents. The conformational rigidity at this center (which one might expect to influence selectivity) will be determined by the strength of the Te–N bond of which little is known. In this manuscript, we describe the X-ray

<sup>\*</sup> Office Imaging Research and Technical Development, Eastman Kodak Co., and SUNY at Buffalo (current address).

<sup>†</sup> Analytical Technology Division, Eastman Kodak Co.

<sup>‡</sup> Abstract published in *Advance ACS Abstracts*, October 1, 1995.

(1) Detty, M. R.; Friedman, A. E.; McMillan, M. *Organometallics* **1994**, *13*, 3338.

(2) Detty, M. R.; Friedman, A. E.; McMillan, M. *Organometallics* **1995**, *14*, 1442.

(3) Detty, M. R.; Frade, T. M. *Organometallics* **1993**, *12*, 2496.

(4) Detty, M. R.; Fleming, J. A. *Adv. Mater.* **1994**, *6*, 48.

(5) Detty, M. R.; Zhou, F. *J. Am. Chem. Soc.*, submitted for publication.



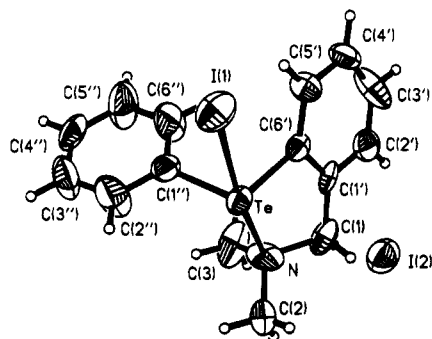
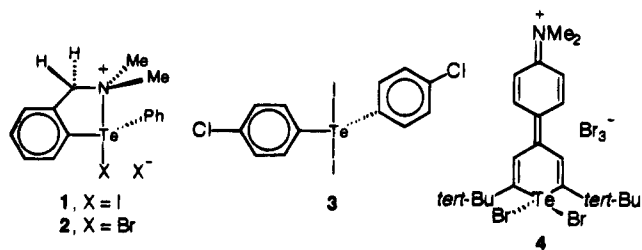


**Figure 1.** ORTEP drawing with thermal ellipsoids shown at the 50% probability level and numbering scheme for the crystal structure of **1**.

structure of **1** to confirm the similarity in structure to **2** and the kinetics of exchange of the prochiral centers of tellurium(IV) species **1** and **2** as measured by variable-temperature  $^1\text{H}$  NMR and DNMR $^{36}$  studies, which delineate the strength of the Te–N bonds in the two systems.



## Results and Discussion

**X-ray Crystal Structure of 1.** The addition of iodine to a carbon tetrachloride solution of phenyl *N,N*-dimethyl-2-(aminomethyl)phenyl telluride gave dark maroon crystals of **1** as the 2:1  $\text{CCl}_4$  solvate suitable for X-ray crystallographic analysis. The refined structure was indicative of the ionic structure **1** and is quite similar to the structure reported for bromide **2**.<sup>1</sup> An ORTEP drawing of **1** showing thermal ellipsoids at the 50% probability level and the numbering scheme for the molecule are presented in Figure 1. Crystal data are given in Table 1, bond lengths and angles are given in Table 2, and atomic coordinates and equivalent isotropic displacement parameters are given in Table 3. Anisotropic displacement parameters, and hydrogen coordinates with isotropic displacement parameters are found in Tables 4 and 5, respectively, in the Supporting Information.

The geometry about the Te atom in **1** is a distorted octahedron with I(1), I(2), C(1''), C(6'), N, and a stereochemically active lone pair of electrons occupying the octahedral sites. The C(1'')–Te–C(6') angle is  $94.7^\circ$ , and the N–Te–I(1) angle is  $172.3^\circ$ . In the latter angle, the distortion from linearity is due in part to the constraint of the five-membered ring, which is formed upon chelation by the dimethylamino nitrogen, and in part to Te lone-pair stereochemical activity. The I(1)–Te–I(2), I(1)–Te–C(1''), and I(1)–Te–C(6') angles are all nearly right angles as are the N–Te–C(1''), N–Te–C(6'), and N–Te–I(2) angles (Table 2). To complete the octahedron, the C(1'')–Te–I(2) angle is nearly linear at  $176.4^\circ$ . This geometry

**Table 1.** Crystal Data and Structure Refinement for Iodo 2-((Dimethylamino)methyl)phenyl Phenyl Telluronium Iodide (**1**)

identification code	TeI
empirical formula	$\text{C}_{15}\text{H}_{17}\text{I}_2\text{N}\text{Te}^{-1/2}\text{CCl}_4$
fw	669.60
temp	293(2) K
wavelength	0.710 73 Å
cryst system	monoclinic
space group	$C2/c$
unit cell dimens	$a = 25.913(5)$ Å, $\alpha = 90^\circ$ $b = 10.077(2)$ Å, $\beta = 115.71(3)^\circ$ $c = 17.594(4)$ Å, $\gamma = 90^\circ$
$V$	$4139(2)$ Å <sup>3</sup>
$Z$	8
$D(\text{calcd})$	2.149 g/cm <sup>3</sup>
abs coeff	$4.674 \text{ mm}^{-1}$
$F(000)$	2472
cryst size	$0.2 \times 0.4 \times 0.4$ mm
$\theta$ range for data collcn	$1.74\text{--}21.95^\circ$
index ranges	$-32 \leq h \leq 28, 0 \leq k \leq 12, 0 \leq l \leq 21$
independent reflns	2532
refinement method	full-matrix least-squares on $F^2$
data/restraints/params	2170/3/186
goodness-of-fit on $F^2$	1.042
final $R$ indices [ $I > 2\sigma(I)$ ]	$R_1 = 0.0701, wR_2 = 0.1889$
$R$ indices (all data)	$R_1 = 0.1207, wR_2 = 0.2359$
extinction coeff	0.0010(2)
largest diff peak and hole	1.666 and $-1.352 \text{ e}^{-\text{Å}^{-3}}$

**Table 2.** Bond Lengths (Å) and Angles (deg) for **1**

Te–C(6')	2.08(2)	C(4')–C(5')	1.43(3)
Te–C(1'')	2.120(10)	C(5')–C(6')	1.39(3)
Te–N	2.44(2)	C(1'')–C(2'')	1.39
Te–I(1)	2.824(2)	C(1'')–C(6'')	1.39
Te–I(2)	3.614(2)	C(2'')–C(3'')	1.39
C(1)–C(1')	1.48(3)	C(3'')–C(4'')	1.39
C(1)–N	1.49(3)	C(4'')–C(5'')	1.39
C(2)–N	1.46(3)	C(5'')–C(6'')	1.39
C(3)–N	1.46(3)	C–Cl(2)(#1)	1.7694(11)
C(1')–C(6')	1.38(3)	C–Cl(2)	1.7694(11)
C(1')–C(2')	1.45(3)	C–Cl(1)(#1)	1.7694(11)
C(2')–C(3')	1.36(4)	C–Cl(1)	1.7696(11)
C(3')–C(4')	1.36(3)		
Cl(2)(#1)–C–Cl(2)	113(2)	C(3)–N–C(1)	110(2)
Cl(2)#1–C–Cl(1)(#1)	109.51(9)	C(2)–N–C(1)	111(2)
Cl(2)–C–Cl(1)(#1)	107.9(9)	C(3)–N–Te	115(2)
Cl(2)(#1)–C–Cl(1)	107.9(9)	C(2)–N–Te	109(2)
Cl(2)–C–Cl(1)	109.50(9)	C(1)–N–Te	100.1(12)
Cl(1)(#1)–C–Cl(1)	109.2(11)	C(6')–C(1'')–C(1)	122(2)
C(2'')–C(3'')–C(4'')	120.0	C(6')–C(1'')–C(2')	118(2)
C(5'')–C(4'')–C(3'')	120.0	C(1)–C(1'')–C(2')	120(2)
C(5'')–C(6'')–C(1'')	120.0	C(3')–C(2'')–C(1')	119(3)
C(6')–Te–C(1'')	94.7(7)	C(4')–C(3'')–C(2')	123(3)
C(6')–Te–N	77.2(7)	C(3')–C(4')–C(5')	118(2)
C(1'')–Te–N	90.5(7)	C(6')–C(5')–C(4')	121(2)
C(6')–Te–I(1)	95.1(5)	C(5')–C(6')–C(1')	121(2)
C(1'')–Te–I(1)	89.8(5)	C(5')–C(6')–Te	125(2)
N–Te–I(1)	172.3(5)	C(1'')–C(6'')–Te	114.2(14)
C(6')–Te–I(2)	81.8(5)	C(2'')–C(1'')–C(6'')	120.0
C(1'')–Te–I(2)	176.4(4)	C(2'')–C(1'')–Te	116.5(8)
N–Te–I(2)	87.9(5)	C(6'')–C(1'')–Te	123.5(8)
I(1)–Te–I(2)	91.29(5)	C(3'')–C(2'')–C(1'')	120.0
C(1')–C(1)–N	110(2)	C(5'')–C(4'')–C(3'')	120.0
C(3)–N–C(2)	112(2)	C(4'')–C(5'')–C(6'')	120.0

can be contrasted with the geometry about the Te atom of **3**, which is trigonal bipyramidal.<sup>7</sup>

The Te–I(1) bond length of 2.824 Å is similar to the "hypervalent" Te–I bonds of 2.922–2.947 Å found in **3**.<sup>7</sup> This situation is similar to that observed in **2** with a Te–Br bond length of 2.632 Å, which is just under the Te–Br bond lengths of 2.682 Å observed for **4**.<sup>8</sup> However, the Te–I(2) distance is much longer at 3.614 Å, just

(6) Klein, D. A.; Bensch, G. *J. Magn. Reson.* **1970**, *3*, 146.

(7) Chao, G. Y.; McCullough, J. D. *Acta Crystallogr.* **1962**, *15*, 887.

(8) Detty, M. R.; Luss, H. R. *Organometallics* **1986**, *5*, 2250.

**Table 3. Atomic Coordinates and Equivalent Isotropic Displacement Parameters ( $\text{\AA}^2$ ) for 1**

	x	y	z	$U_{eq}^a$
Te	0.3335(1)	0.02074(1)	0.9577(1)	0.039(1)
I(1)	0.3301(1)	-0.0714(2)	0.9713(1)	0.066(1)
I(2)	0.1797(1)	0.2219(2)	0.8384(1)	0.055(1)
C(1)	0.3010(10)	0.4428(21)	0.8342(15)	0.056(6)
C(2)	0.3081(12)	0.5175(30)	0.9700(15)	0.078(8)
C(3)	0.3933(10)	0.4956(26)	0.9475(18)	0.078(8)
N	0.3364(9)	0.4431(16)	0.9275(13)	0.060(5)
C(1')	0.3150(8)	0.3259(20)	0.7956(12)	0.039(5)
C(2')	0.3129(9)	0.3348(26)	0.7119(15)	0.061(7)
C(3')	0.3232(12)	0.2246(31)	0.6760(16)	0.077(9)
C(4')	0.3377(10)	0.1053(23)	0.7157(14)	0.053(6)
C(5')	0.3394(9)	0.0950(21)	0.7976(14)	0.049(6)
C(6')	0.3299(8)	0.2057(17)	0.8371(13)	0.038(5)
C(1'')	0.4242(4)	0.2016(17)	1.0205(9)	0.047(5)
C(2'')	0.4488(6)	0.2176(23)	1.1076(9)	0.110(14)
C(3'')	0.5080(6)	0.2134(24)	1.1535(7)	0.107(13)
C(4'')	0.5426(4)	0.1930(18)	1.1124(10)	0.064(7)
C(5'')	0.5180(6)	0.1770(20)	1.0253(10)	0.102(11)
C(6'')	0.4588(6)	0.1813(20)	0.9794(7)	0.089(10)
C	0.5000	0.3694(16)	0.7500	0.124(19)
Cl(1)	0.4400(5)	0.4711(14)	0.7310(12)	0.210(8)
Cl(2)	0.5161(9)	0.2722(23)	0.8413(10)	0.368(19)

<sup>a</sup>  $U_{eq}$  is defined as one-third of the trace of the orthogonalized  $U_{ij}$  tensor.

under the sum of van der Waals radii for the two atoms (4.04  $\text{\AA}$ ).<sup>9</sup> While the  $I^-$  is located near the Te atom, the bonding interaction is quite weak and is mostly ionic. The two iodine atoms are found in a *cis*-geometry around the Te atom, which has not been observed in other Te(IV) diorgano diiodo derivatives. The Te–N bond length of 2.442  $\text{\AA}$  is longer than the 2.02–2.11- $\text{\AA}$  Te–N bond lengths found in several 1,2-tellurazoles<sup>10</sup> and 1,2,5-telluradiazoles<sup>11</sup> but is similar to the 2.389- $\text{\AA}$  bond length observed in **2**.<sup>1</sup> The observed Te–N bond length is much less than the sum of van der Waals radii for the two atoms (3.61  $\text{\AA}$ ).<sup>9</sup>

**<sup>1</sup>H NMR Exchange of Equivalent Sites.** The structures of both **1** and **2** show a prochiral center at tellurium, which should lead to nonequivalent methylene and methyl protons in the <sup>1</sup>H NMR spectra of **1** and **2**. At 298 K, the <sup>1</sup>H NMR spectra of both **1** and **2** are broadened by some exchange process. As shown in Figure 2 for **1**, the <sup>1</sup>H NMR spectrum of a  $3.4 \times 10^{-3}$  M solution of **1** in  $ClCD_2CD_2Cl$  is characterized by broadened signals at 298 K for all protons. At 253 K, the exchange process has slowed such that the two methyl groups are characterized by nonequivalent singlets and the methylene group is characterized by a well-resolved AB quartet.

**Effect of Reactant Concentrations.** The order of the exchange process was probed via variation of the concentration of exchanging species. The rate of the exchange process was not affected by the concentration of **1** over the range  $1.0 \times 10^{-3}$  to  $5.0 \times 10^{-3}$  M, which is indicative of a first-order reaction in the cationic complex unaffected by iodide concentration. The rate of exchange was not affected by the addition of  $1.0 \times 10^{-3}$  M iodine to  $1.0 \times 10^{-3}$  M **1**, which is indicative that free iodine, iodide, and triiodide are not involved in the exchange process. Compound **2** displayed similar be-

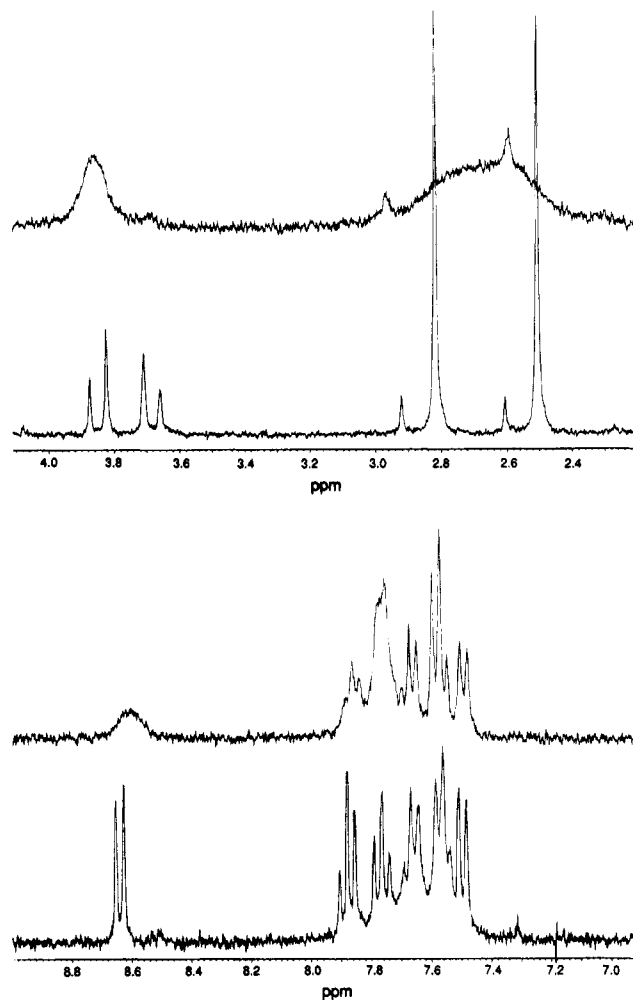


**Figure 2.** <sup>1</sup>H NMR spectra at 300 MHz for (a, top) the aliphatic region and (b, bottom) the aromatic region of **1** at 296 K (upper trace) and 253 K (lower trace).

havior. Neither the concentration of **2** over the range  $1.0 \times 10^{-3}$  to  $5.0 \times 10^{-3}$  M in  $ClCD_2CD_2Cl$  nor the addition of  $1.0 \times 10^{-3}$  M bromine to  $1.0 \times 10^{-3}$  M **2** affected the rate of exchange.

**DNMR3 Studies of the Rates of Exchange.** In the 300-MHz <sup>1</sup>H NMR spectrum of **1** at 233 K, the two methyl groups appear at 846 ( $\delta$  2.82) and 750 Hz ( $\delta$  2.50), which coalesce to a singlet at 798 Hz at higher temperatures. For **2**, the two methyl groups appear as two singlets at 840 ( $\delta$  2.80) and 753 Hz ( $\delta$  2.51) at 233 K, which coalesce to a singlet at 791 Hz at higher temperatures. These parameters were utilized for simulating spectra with the program DNMR3.<sup>6</sup> For iodo complex **1** and bromo complex **2**, rates of exchange were calculated by fitting sample spectra measured to simulated spectra (see Supporting Information for experimental and simulated spectra). Rates of exchange calculated in this manner are compiled in Table 6. As a check of the simulations, approximations of the exchange rates were made with the following equations:<sup>12</sup>  $k_{ex} = 0.5\pi(\Delta\nu)^2/\nu_{1/2}$  for coalesced peaks at fast exchange, where  $\nu_{1/2}$  is the width in Hz at half-height of the coalesced peak and  $\Delta\nu$  is the peak separation in Hz at slow exchange,  $k_{ex} = \pi\Delta\nu/\sqrt{2}$  at coalescence, where  $\Delta\nu$  is the peak separation in Hz at slow exchange, and

(9) Bondi, A. J. *Phys. Chem.* **1964**, *68*, 441.

(10) (a) DeMunno, G.; Lucchesini, F. *Acta Crystallogr., Sect. C: Cryst. Struct. Commun.* **1992**, *C48*, 1437. (b) Campsteyn, H.; Dupont, L.; Lamotte-Brasseur, J.; Vermeire, M. J. *Heterocycl. Chem.* **1978**, *15*, 745.

(11) Bertini, V.; Dapporto, P.; Lucchesini, F.; Sega, A.; DeMunno, A. *Acta Crystallogr., Sect. C: Cryst. Struct. Commun.* **1984**, *40C*, 653.

(12) Martin, M. L.; Delpuech, J.-J.; Martin, G. J. *Practical NMR Spectroscopy*; Heyden: Philadelphia, PA, 1980.

**Table 6. Rates of Exchange for 1 and 2 as Determined by Line Shape Analysis with DNMR3<sup>a</sup> and Estimation from Experimental Line Widths and Chemical Shifts**

compd	T, K	k(DNMR3), s <sup>-1</sup>	k(estimate), s <sup>-1</sup>
1	313.0	5.7 × 10 <sup>2</sup>	5.7 × 10 <sup>2</sup>
	303.0	3.05 × 10 <sup>2</sup>	2.8 × 10 <sup>2</sup>
	293.0	1.5 × 10 <sup>2</sup>	1.8 × 10 <sup>2</sup>
	282.3	6.5 × 10 <sup>1</sup>	7.6 × 10 <sup>1</sup>
	273.0	3.0 × 10 <sup>1</sup>	3.8 × 10 <sup>1</sup>
2	328.0	5.0 × 10 <sup>2</sup>	5.5 × 10 <sup>2</sup>
	323.0	3.7 × 10 <sup>2</sup>	3.7 × 10 <sup>2</sup>
	318.0	2.6 × 10 <sup>2</sup>	2.6 × 10 <sup>2</sup>
	313.0	1.7 × 10 <sup>2</sup>	2.1 × 10 <sup>2</sup>
	308.2	8.5 × 10 <sup>1</sup>	1.4 × 10 <sup>2</sup>
	303.0	7.5 × 10 <sup>1</sup>	8.3 × 10 <sup>1</sup>
	273.0	5.0 × 10 <sup>0</sup>	1.2 × 10 <sup>1</sup>

<sup>a</sup> Reference 6.

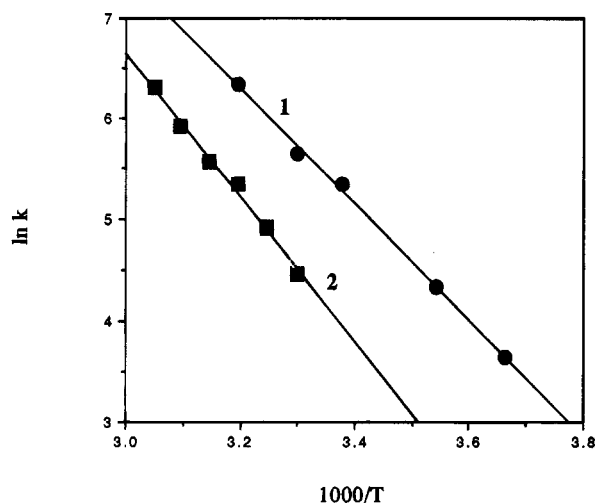
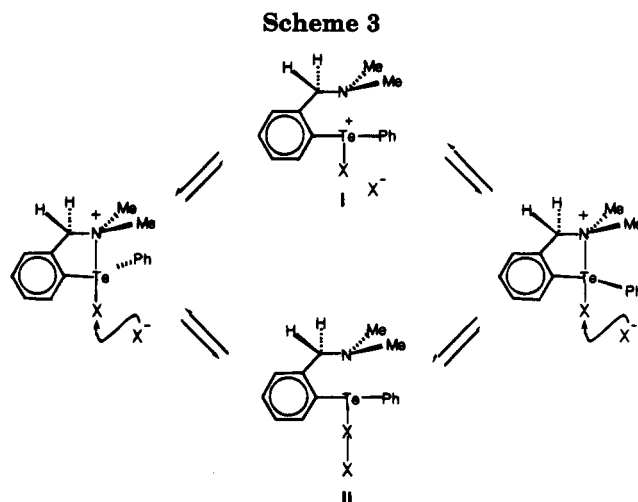


**Figure 3.** Arrhenius plot of the kinetic data generated by DNMR3 from variable-temperature <sup>1</sup>H NMR spectra of **1** and **2**. For **1**,  $m = -6.315$ ,  $b = 26.54$ , and  $R^2 = 1.000$ . For **2**,  $m = -7.566$ ,  $b = 29.27$ , and  $R^2 = 0.994$ .

$k_{\text{ex}} = \pi\nu_{1/2}$  for line-broadened, separated peaks at slower exchange rates, where  $\nu_{1/2}$  is the width in Hz at half-height.

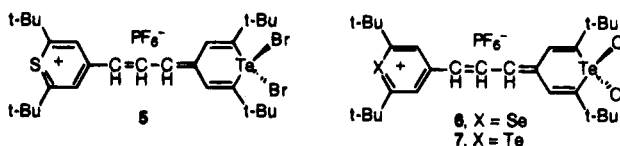
The exchange rates at various temperatures were used to calculate the Arrhenius and Eyring activation parameters for compounds **1** and **2**. From first-order exchange rates, the Arrhenius plot of  $\ln k$  vs  $1000/T$  is shown in Figure 3. Values of the Arrhenius and Eyring activation parameters for **1** were calculated to be  $E_a = 12.5 \pm 0.3$  kcal mol<sup>-1</sup>,  $\ln A = 26.5$ ,  $\Delta H^\ddagger = 12.0 \pm 0.3$  kcal mol<sup>-1</sup>,  $\Delta S^\ddagger = -8 \pm 4$  cal mol<sup>-1</sup> K<sup>-1</sup>, and  $\Delta G_{298}^\ddagger = 14.4$  kcal mol<sup>-1</sup>. Values of the Arrhenius and Eyring activation parameters for **2** were calculated to be  $E_a = 15.0 \pm 0.4$  kcal mol<sup>-1</sup>,  $\ln A = 29.3$ ,  $\Delta H^\ddagger = 14.4 \pm 0.4$  kcal mol<sup>-1</sup>,  $\Delta S^\ddagger = -2 \pm 5$  cal mol<sup>-1</sup> K<sup>-1</sup>, and  $\Delta G_{298}^\ddagger = 15.0$  kcal mol<sup>-1</sup>.

**Mechanistic Considerations.** The Te–N bond must be broken in the exchange process. Two of the possible exchange mechanisms are illustrated in Scheme 3. In the upper path, breaking the Te–N bond would lead to telluronium intermediate **I**, which could collapse to either enantiomer. In the lower path, iodide participation would generate the  $\eta^1$ -iodine association complex **II**, which could collapse to either enantiomer via ionic dissociation of the  $\eta^1$ -complex. The rate of exchange was constant over a 5-fold change in concentration for both **1** and **2**, which suggests that a second-order process



involving iodide in the rate-determining step is not involved. The absence of a concentration dependence suggests a first-order pathway, which is represented by the upper path of Scheme 3.

The strength of the hypervalent bonds to tellurium is in part a function of the electronegativity of the ligands to tellurium.<sup>13</sup> Nitrogen and bromine have nearly identical Pauling electronegativities (3.0) while iodine is somewhat more electropositive (2.7).<sup>14</sup> Consequently, the Te–N hypervalent bond should be stronger opposite a Te–Br bond relative to a Te–I bond. This is observed both in comparisons of X-ray structures of **1** (Te–N bond length of 2.442 Å) and **2** (Te–N bond length of 2.389 Å) and in the activation energies for <sup>1</sup>H NMR exchange of **1** ( $E_a = 12.5$  kcal mol<sup>-1</sup>) and **2** ( $E_a = 15.0$  kcal mol<sup>-1</sup>). The thermal cleavage of the Te–N bond in **1** and **2** requires much less energy than for the thermal cleavage of a Te–X bond in **5–7** where bond cleavage requires separation of charge. For **5–7**, values of  $E_a$  are in the 21.3–24.1 kcal mol<sup>-1</sup> range for reductive elimination of halogen.<sup>3,4</sup>



## Experimental Section

**Preparation of Materials.** Compound **2** was prepared as described in ref 2. Compound **1** was prepared by the addition of iodine (0.13 g, 0.51 mmol) to a solution of phenyl *N,N*-dimethyl-2-(aminomethyl)phenyl telluride (0.17 g, 0.50 mmol) in 10 mL of CCl<sub>4</sub>. After standing 15 h at ambient temperature, the chunky red crystals were collected by filtration and air-dried to give 0.215 g (73%) of **1**, mp 177–179 °C (lit.<sup>1</sup> mp 178–179 °C). The crystals of **1** as its CCl<sub>4</sub> solvate prepared in this manner were marginally suitable for X-ray crystallographic analysis.

**<sup>1</sup>H NMR Spectra.** <sup>1</sup>H NMR spectra were recorded on a Varian VXR-300S instrument equipped with a four-nucleus 5-mm probe operating at a resonance frequency of 299.956 MHz. Samples were dissolved in ClCD<sub>2</sub>CD<sub>2</sub>Cl (CIL) at a concentration of 1–5 mM. Sample spectra obtained at various temperatures are compiled in the Supporting Information.

(13) Detty, M. R.; Murray, B. J.; Smith, D. L.; Zumbulyadis, N. J. *Am. Chem. Soc.* **1983**, *105*, 875 and references cited therein.

(14) Pauling, L. *The Nature of the Chemical Bond*, 3rd ed.; Cornell University Press: Ithaca, NY, 1960.

**Calculation of Activation Parameters.** Arrhenius parameters were obtained by plotting  $\ln k_{ex}$  against  $1/T$ , with a slope equal to the negative of the energy of activation divided by the gas constant,  $-E_a/R$ , and an intercept equal to the pre-exponential factor,  $\ln A$ . Eyring activation parameters were determined using transition-state theory. A plot of  $R \ln(k_{ex}/T) + R \ln(Nh/R)$  versus  $1000/T$  gives a linear slope equal to  $-\Delta H^\ddagger$  and an intercept of  $\Delta S^\ddagger$ , where  $N$  is Avogadro's number,  $h$  is Planck's constant,  $\Delta H^\ddagger$  is the enthalpy of activation, and  $\Delta S^\ddagger$  is the entropy of activation.

**Crystal-Structure Data for 1.** The data were collected on an Enraf Nonius CAD-4 diffractometer in the  $\omega$ - $2\theta$  scan mode to a resolution of 0.93 Å using graphite-monochromated Mo K $\alpha$  radiation. The cell was determined on the diffractometer from the least-squares fitting of the angular settings of 25 reflections well distributed in reciprocal space. Three reference reflections were collected periodically for intensity and orientation control. The Bragg peak profiles were processed using the DREADD data reduction package<sup>15-17</sup> to give the intensity and variance for each reflection. An absorption correction was made by taking a number of  $\psi$  scans near  $\chi = 90^\circ$  and applying a least-squares procedure for modeling an empirical transmission surface by fitting coefficients of an expansion in real spherical harmonics to the multiple  $\psi$ -scanned reflections.<sup>18</sup> After the appropriate scaling and merg-

ing of data, the data were subjected to a Bayesian statistical treatment<sup>19</sup> in order to get a better estimate of the intensities and standard deviations of the weak and unobserved reflections. The structure was solved by direct methods using the SHELXTL package [SHELXTL version 4.1, Siemens Analytical X-Ray Instruments, Inc., Madison, WI, 1990, and ref 20] and then refined on  $F^2$  using SHELXL93.<sup>18</sup>

**Acknowledgment.** We acknowledge the assistance of Frank Michaels and David McClaughlin (Eastman Kodak Co.) in allowing access to and setting up DNMR3 (QCPE Program No. 466).

**Supporting Information Available:** Tables 4 and 5, listing anisotropic displacement parameters and hydrogen coordinates with isotropic displacement parameters for **1**, and figures showing sample <sup>1</sup>H NMR spectra at various temperatures for **1** and **2** and DNMR3 simulations (39 pages). This material is contained in libraries on microfiche, immediately follows the article in the microfilm version of the journal, and can be ordered from the ACS; see any current masthead page for ordering information.

OM950091M

(15) Blessing, R. H. *Crystallogr. Rev.* **1986**, *1*, 3.

(16) Blessing, R. H. *J. Appl. Crystallogr.* **1986**, *19*, 412.

(17) Blessing, R. H. *J. Appl. Crystallogr.* **1989**, *22*, 396.

(18) Sheldrick, G. M. *J. Appl. Crystallogr.*, submitted for publication.

(19) Wilson, K.; French, S. *Acta Crystallogr. A* **1978**, *34A*, 517.

(20) Sheldrick, G. M. *Acta Crystallogr. A* **1990**, *46A*, 467.

# Metallacumulenes: Activation of Dienes and Formation of New Allenylideneruthenium Complexes. Crystal Structures of *trans*-[(Ph<sub>2</sub>PCH<sub>2</sub>PPh<sub>2</sub>)<sub>2</sub>(Cl)Ru=C=C=CR<sup>1</sup>R<sup>2</sup>]<sup>+</sup> and *trans*-[(Ph<sub>2</sub>PCH<sub>2</sub>PPh<sub>2</sub>)<sub>2</sub>Ru(=C=C=C(OMe)CH=CPh<sub>2</sub>)<sub>2</sub>]<sup>2+</sup> Derivatives

Daniel Touchard,<sup>\*,†</sup> Nadine Pirio,<sup>†</sup> Loïc Toupet,<sup>‡</sup> Mohammed Fettouhi,<sup>§</sup> Lahcène Ouahab,<sup>§</sup> and Pierre H. Dixneuf<sup>\*,†</sup>

Laboratoire de Chimie de Coordination Organique, URA CNRS 415, Groupe Matière Condensée et Matériaux, URA CNRS 804, and Laboratoire de Cristallographie, URA CNRS 1495, Campus de Beaulieu, Université de Rennes 1, 35042 Rennes, France

Received June 19, 1995<sup>®</sup>

*cis*-RuCl<sub>2</sub>(Ph<sub>2</sub>PCH<sub>2</sub>PPh<sub>2</sub>)<sub>2</sub> (**1**) reacts with pentadiynes XC≡CC≡CCPh<sub>2</sub>(OSiMe<sub>3</sub>) [**2** (X = H) and **3** (X = Bu<sub>3</sub>Sn)], but in the presence of NaPF<sub>6</sub>, to afford *trans*-(Ph<sub>2</sub>PCH<sub>2</sub>PPh<sub>2</sub>)<sub>2</sub>(Cl)-RuC≡CC≡CCPh<sub>2</sub>(OSiMe<sub>3</sub>) (**4**). On protonation with HBF<sub>4</sub> complex **4** in methanol leads to allenylidene *trans*-[(Ph<sub>2</sub>PCH<sub>2</sub>PPh<sub>2</sub>)<sub>2</sub>(Cl)Ru=C=C=C(OMe)CH=CPh<sub>2</sub>]<sub>2</sub>X (**5a**) (a: X = BF<sub>4</sub>) and in dichloromethane to *trans*-[(Ph<sub>2</sub>PCH<sub>2</sub>PPh<sub>2</sub>)<sub>2</sub>(Cl)Ru=C=C=CCH=C(Ph)(*o*-C<sub>6</sub>H<sub>4</sub>)]<sub>2</sub>X (**6a**) via electrophilic *ortho*-substitution within the metallacumulene intermediate LnRu=C=C=C=C=CPh<sub>2</sub>X (**A**). Alternatively, complex **1** and diyne **2** with NaPF<sub>6</sub> afford in one step allenylidenes **5b** (b: X = PF<sub>6</sub>) in methanol and **6b** in dichloromethane. Bis(diyne) derivative *trans*-(Ph<sub>2</sub>PCH<sub>2</sub>PPh<sub>2</sub>)<sub>2</sub>Ru[(C≡CC≡CC(OMe)Ph<sub>2</sub>)]<sub>2</sub> (**7**), obtained by reaction of **2** with **1** and HN<sup>1</sup>Pr<sub>2</sub>, on protonation with HBF<sub>4</sub> in methanol offered a direct route to the first bis(allenylidene) complex *trans*-[(Ph<sub>2</sub>PCH<sub>2</sub>PPh<sub>2</sub>)<sub>2</sub>Ru(=C=C=C(OMe)CH=CPh<sub>2</sub>)<sub>2</sub>](BF<sub>4</sub>)<sub>2</sub> (**8**). The X-ray diffraction studies of two allenylidene complexes **6b** and **8** are reported. The structure of **6b** consists of two different allenylidene cations. That of **8** shows coplanar allenylidene ligands with a strong contribution of a ynyl resonance structure.

## Introduction

Metallacumulenes M=(C=)<sub>n</sub>CR<sub>2</sub> constitute a new class of organometallics containing a carbon-rich unsaturated chain with a M=C linkage. As unsaturated molecules they have potential for the access to metal containing copolymers<sup>1</sup> or for their materials properties.<sup>2</sup> Their M=C bond offers useful applications for both organometallic and organic syntheses, as expected from the richness and versatility of metal-carbene chemistry.<sup>3</sup> This interest provides impetus to the search for a general method of preparation of metallacumu-

lenes containing functionalities. After metal-vinylidene M=C=CR<sub>2</sub> complexes,<sup>4,5</sup> metal-allenylidene M=C=C=CR<sub>2</sub> species are the simplest metallacumulenes. They have initially been obtained by (C<sub>1</sub>)OR group elimina-

(3) (a) Cosset, C.; Del Rio I.; Le Bozec, H. *Organometallics* **1995**, *14*, 1938. (b) Dötz, K. H.; Schäfer, T.; Kröll, F.; Harms, K. *Angew. Chem., Int. Ed. Engl.* **1992**, *31*, 1236. (c) Wulff, W. D.; Bauta, W. E.; Kaesler, R. W.; Lankford, P. J.; Miller, R. A.; Murray, C. K.; Yang, D. C. *J. Am. Chem. Soc.* **1990**, *112*, 3642. (d) Anderson, B. A.; Wulff, W. D.; Powers, T. S.; Tribitt, S.; Rheingold, A. L. *J. Am. Chem. Soc.* **1992**, *114*, 10784.

(4) (a) King, R. B.; Saran, M. S. *Chem. Commun.* **1972**, 1052; *J. Am. Chem. Soc.* **1972**, *95*, 1817. (b) Bruce, M. I.; Swincer, A. G. *Adv. Organomet. Chem.* **1983**, *22*, 59. (c) Bruce, M. I. *Chem. Rev.* **1991**, *91*, 197. (d) Antonova, A. B.; Johansson, A. A. *Russ. Chem. Rev.* **1989**, *58*, 693.

(5) (a) Bruce, M. I.; Wallis, R. C. *J. Organomet. Chem.* **1978**, *161*, C1. (b) Bruce, M. I.; Wallis, R. C. *Aust. J. Chem.* **1979**, *32*, 1471. (c) Bruce, M. I.; Swincer, A. G.; Wallis, R. C. *J. Organomet. Chem.* **1979**, *171*, C5. (d) Bruce, M. I.; Koutsantonis, G. A. *Aust. J. Chem.* **1991**, *44*, 207. (e) Bullock, R. M. *J. Chem. Soc., Chem. Commun.* **1989**, 3, 165. (f) Lomphey, J. R.; Selegue, J. P. *J. Am. Chem. Soc.* **1992**, *114*, 5518. (g) Consiglio, G.; Morandini, F. *Inorg. Chim. Acta* **1987**, *127*, 79. (h) Consiglio, G.; Morandini, F.; Ciani, G. F.; Sironi, A. *Organometallics* **1986**, *5*, 1976. (i) Morandini, F.; Consiglio, G.; Sironi, A.; Moret, M. *J. Organomet. Chem.* **1988**, *356*, C79. (j) Werner, H.; Stark, A.; Shulz, M.; Wolf, J. *Organometallics* **1992**, *11*, 1126. (k) Gamasa, M. P.; Gimeno, J.; Martin-vaca, B. M.; Borge, J.; Garcia-Granda, S.; Perez-Carreño, E. *Organometallics* **1994**, *13*, 4045. (l) Touchard, D.; Haquette, P.; Pirio, N.; Toupet, L.; Dixneuf, P. H. *Organometallics* **1993**, *12*, 3132. (m) Le Lagadec, R.; Roman, E.; Toupet, L.; Müller, U.; Dixneuf, P. H. *Organometallics* **1994**, *13*, 5030.

(6) Fischer, E. O.; Kalder, H.-J.; Franck, A.; Köhler, F. H.; Huttner, G. *Angew. Chem., Int. Ed. Engl.* **1976**, *15*, 623.

(7) (a) Duetsch, M.; Stein, F.; Lackmann, R.; Pohl, E.; Herbst-Irmer, R.; de Meijere, A. *Chem. Ber.* **1992**, *125*, 2051. (b) Stein, F.; Duetsch, M.; Noltemeyer, M.; de Meijere, A. *Synlett* **1993**, 486. (c) Stein, F.; Duetsch, M.; Pohl, E.; Herbst-Irmer, R.; de Meijere, A. *K. Organometallics* **1993**, *12*, 2556. (d) Aumann, R. *Chem. Ber.* **1992**, *125*, 2773.

<sup>†</sup> URA CNRS 415.

<sup>‡</sup> URA CNRS 804.

<sup>§</sup> URA CNRS 1495.

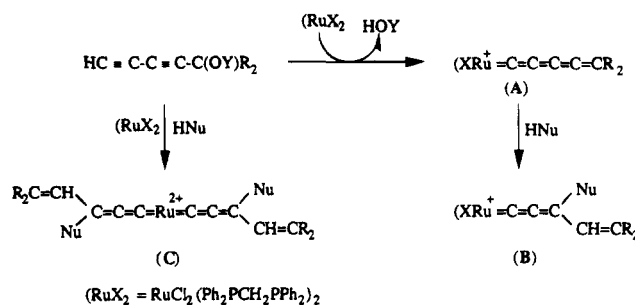
<sup>®</sup> Abstract published in *Advance ACS Abstracts*, October 1, 1995.

(1) (a) Lavastre, O.; Dixneuf, P. H.; Pacreau, A.; Vairon, J. P. *Organometallics* **1994**, *13*, 2500. (b) Carraher, J. E., Jr.; Pittman, C. E., Jr. *Metal-Containing Polymeric Systems*; Plenum: New York, 1985. (c) Hagihara, N.; Sonogashira, K.; Takashi, K. *Adv. Polym. Sci.* **1980**, *41*, 150. (d) Takahashi, S.; Morimoto, H.; Murata, F.; Kataoabe, S.; Sonogashira, K.; Hagihara, N. *J. Polym. Sci., Polym. Chem. Ed.* **1982**, *20*, 562. (e) Brefort, J. L.; Corriu, R. J.; Gerbier, P.K.; Guérin, C.; Henner, B. J. L.; Jean, A.; Kuhlmann, Th. *Organometallics* **1992**, *11*, 2500. (f) Davies, S. J.; Johnson, B. F. G.; Khan, M. S.; Lewis, J. J. *Chem. Soc., Chem. Commun.* **1991**, 187. (g) Takahashi, S.; Takai, Y.; Morimoto, H.; Sonogashira, K. *J. Chem. Soc., Chem. Commun.* **1984**, 3.

(2) (a) Dhenault, C.; Ledoux, I.; Samuel, I. D. W.; Zyss, J.; Bourgault, M.; Le Bozec, H. *Nature* **1995**, *374*, 339. (b) Yuan, Z.; Stringer, G.; Jobe, I. R.; Kreller, D.; Scott, K.; Koch, L.; Marder, T. B. *J. Organomet. Chem.* **1993**, *452*, 115. (c) Nalwa, H. S. *Appl. Organomet. Chem.* **1991**, *5*, 349. (d) Marder, S. R. In *Inorganic Materials*; Bruce, D. W., O'Hare, D., Eds.; Wiley: Chichester, U.K., 1992. (e) Giroud-Godquin, A. M.; Maitlis, P. M. *Angew. Chem., Int. Ed. Engl.* **1991**, *30*, 375.

tion of alkenyl<sup>6</sup> and alkynyl<sup>7</sup> carbene derivatives of group 6 metal carbonyls or by addition of a (C)<sub>3</sub> skeleton dianion, either [C≡CCR<sub>2</sub>O]<sup>2-</sup> to metal carbonyls<sup>8</sup> or Li<sub>2</sub>C<sub>3</sub>Ph<sub>2</sub> to Cp<sub>2</sub>TiCl<sub>2</sub>.<sup>9</sup> The most general method for the access to allenylidene metal compounds has appeared to consist, since the first evidence given by Selegue,<sup>10</sup> in the activation of propargyl alcohol derivatives which takes place with spontaneous dehydration, essentially by ruthenium(II) complexes.<sup>11-16</sup> Reactive allenylidene ruthenium intermediates have also been proposed to arise from prop-2-yn-1-ols to explain dimerization reactions<sup>15</sup> or access to alkenylcarbenes,<sup>16</sup> and they are now classical intermediates in the synthesis of unsaturated carbenes<sup>17</sup> and involved in catalysis.<sup>18</sup> Few examples of allenylidene derivatives of group 6<sup>3a,19</sup> and 7<sup>20</sup> metal, iron,<sup>21</sup> and rhodium<sup>22</sup> complexes have also been obtained from propargyl alcohol derivatives, but these usually require an external reagent or catalyst to promote the dehydration of the 3-hydroxyprop-1-enylidene intermediate. Alternatively, allenylidenes can be produced under mild conditions by activation of conjugated enynes, usually resulting from previous dehydration of propargyl alcohol derivatives, by 1,4 migration of the terminal alkyne hydrogen with RuCl<sub>2</sub>(L)(arene) complexes (L = PR<sub>3</sub>,<sup>23</sup> C≡NR,<sup>24</sup> or carbene<sup>24</sup>)

Scheme 1



or RuCl<sub>2</sub>(Ph<sub>2</sub>PCH<sub>2</sub>PPh<sub>2</sub>)<sub>2</sub>.<sup>11d</sup> Recently, new types of bimetallic systems containing a metallacumulene moiety of type M≡(C)<sub>n</sub>M (ReC<sub>3</sub>Mn,<sup>25</sup> ReC<sub>4</sub>Re<sup>26</sup>) and M=(C=)<sub>n</sub>M (ReC<sub>3</sub>Mn,<sup>27</sup> ReC<sub>4</sub>Re,<sup>25,28</sup> ReC<sub>5</sub>Mn,<sup>29</sup> Fe=C<sub>2</sub>C<sub>6</sub>H<sub>4</sub>C<sub>2</sub>=Fe<sup>30</sup>) have been produced either by oxidation of M-(C)<sub>n</sub>-M complexes or by methoxide elimination of a M-(C≡C)<sub>n</sub>-C(OMe)-M bridge.<sup>31</sup>

Preliminary study on the activation of a pentadiyne having a leaving group at the C(5) carbon atom, HC≡CC≡C-CR<sub>2</sub>(OY)<sup>32</sup> or Me<sub>3</sub>SiC≡C-C≡CCR<sub>2</sub>(OY),<sup>33</sup> by the electrophilic complexes RuCl<sub>2</sub>(PR<sub>3</sub>)(arene) suggested the formation of a metallacumulene intermediate of type Ru=C=C=C=C-CR<sub>2</sub> as a source of new functional allenylidene ruthenium complexes. By contrast to the chemistry of electrophilic RuCl<sub>2</sub>(PR<sub>3</sub>)(arene) complexes<sup>16,32,34</sup> the electron-rich ruthenium complex RuCl<sub>2</sub>(Ph<sub>2</sub>PCH<sub>2</sub>Ph<sub>2</sub>)<sub>2</sub> (**1**) is able to activate terminal alkynes and propargyl alcohol compounds to give very stable vinylidenes<sup>51</sup> and allenylidenes.<sup>11c,d</sup> Thus, we have attempted to activate the diyne XC≡CC≡CCPh<sub>2</sub>(OSiMe<sub>3</sub>) with **1** in order to directly generate the metallacumulene Ru=C=C=C=C-CR<sub>2</sub> intermediate (**A**) toward the formation of functional allenylidene ruthenium complexes of type **B** (Scheme 1). Moreover, the presence of two labile chloride groups on the ruthenium atom of **1** could be used for the access to bis(allenylidene) complexes of type **C**. This objective has just been strengthened by the isolation of the first penta-1,2,3,4-tetraenylidene complex [(Ph<sub>2</sub>PCH<sub>2</sub>CH<sub>2</sub>PPh<sub>2</sub>)<sub>2</sub>(Cl)Ru=C=C=C=C-CPh<sub>2</sub>]-PF<sub>6</sub> from a diynylruthenium derivative LnRu≡CC≡CC(OY)Ph<sub>2</sub>.<sup>35</sup>

We report here the full details of the activation of the diynes HC≡CC≡CCR<sub>2</sub>(OSiMe<sub>3</sub>) and Bu<sub>3</sub>Sn-C≡CC≡CCPh<sub>2</sub>(OSiMe<sub>3</sub>) by RuCl<sub>2</sub>(Ph<sub>2</sub>PCH<sub>2</sub>PPh<sub>2</sub>)<sub>2</sub> (**1**) following

(8) (a) Berke, H. *Angew. Chem., Int. Ed. Engl.* **1976**, *15*, 624. (b) Berke, H. *Chem. Ber.* **1980**, *113*, 1370. (c) Berke, H.; Härter, P.; Huttner, G.; Seyler, J. v. *J. Organomet. Chem.* **1981**, *219*, 317. (d) Berke, H.; Härter, P.; Huttner, G.; Zsolnai, L. *Z. Naturforsch.* **1981**, *36 b*, 929. (e) Berke, H.; Härter, P.; Huttner, G.; Zsolnai, L. *Chem. Ber.* **1982**, *115*, 695. (f) Berke, H.; Grössmann, U.; Huttner, G.; Zsolnai, L. *Chem. Ber.* **1984**, *117*, 3432. (g) Berke, H.; Härter, P.; Huttner, G.; Zsolnai, L. *Chem. Ber.* **1984**, *117*, 3423. (h) Berke, H.; Härter, P. *Angew. Chem., Int. Ed. Engl.* **1980**, *19*, 225. (i) Berke, H.; Huttner, G.; Seyler, J. v. *Z. Naturforsch.* **1981**, *36b*, 1277. (j) Fischer, H.; Reindl, D.; Roth, G. *Z. Naturforsch.* **1994**, *49b*, 1207.

(9) Binger, P.; Müller, P.; Wenz, R.; Mynott, R. *Angew. Chem., Int. Ed. Engl.* **1990**, *29*, 1037.

(10) Selegue, J. P. *Organometallics* **1982**, *1*, 217.

(11) (a) Wolinska, A.; Touchard, D.; Dixneuf, P. H.; Romero, A. J. *Organomet. Chem.* **1991**, *420*, 217. (b) Pirio, N.; Touchard, D.; Toupet, L.; Dixneuf, P. H. *J. Chem. Soc., Chem. Commun.* **1991**, 980. (c) Pirio, N.; Touchard, D.; Dixneuf, P. H. *J. Organomet. Chem.* **1993**, *462*, C18. (d) Touchard, D.; Pirio, N.; Dixneuf, P. H., *Organometallics*, in press.

(12) (a) Cadierno, V.; Gamasa, M. P.; Gimeno, J.; Lastra, E.; Borge, J.; Garcia-Granda, S. *Organometallics* **1994**, *13*, 745. (b) Cadierno, V.; Gamasa, M. P.; Gimeno, J.; Lastra, E. *J. Organomet. Chem.* **1994**, *474*, C27.

(13) (a) Matsuzaka, H.; Koizumi, H.; Takagi, Y.; Nishio, M.; Hidai, M. *J. Am. Chem. Soc.* **1993**, *115*, 10396. (b) Matsuzaka, H.; Takagi, Y.; Hidai, M. *Organometallics* **1994**, *13*, 13.

(14) (a) Braun, T.; Steinert, P.; Werner, H. *J. Organomet. Chem.* **1995**, *488*, 169. (b) Werner, H.; Stark, A.; Steinert, P.; Grünwald, C.; Wolf, J. *Chem. Ber.* **1995**, *128*, 49.

(15) (a) Selegue, J. P.; Young, B. A.; Logan, S. L. *Organometallics* **1991**, *10*, 1972. (b) Selegue, J. P. *J. Am. Chem. Soc.* **1983**, *105*, 5921. (c) Davies, S. G.; McNally, J. P.; Smallridge, A. J. *Adv. Organomet. Chem.* **1990**, *30*, 1.

(16) (a) Le Bozec, H.; Ouzzine, K.; Dixneuf, P. H. *J. Chem. Soc., Chem. Commun.* **1989**, 219. (b) Le Bozec, H.; Pilette, D.; Dixneuf, P. H. *New J. Chem.* **1990**, *14*, 793. (c) Pilette, D.; Ouzzine, K.; Le Bozec, H.; Dixneuf, P. H.; Rickard, C. E. F.; Roper, W. R. *Organometallics* **1992**, *11*, 809.

(17) Ruiz, N.; Péron, D.; Dixneuf, P. H. *Organometallics* **1995**, *14*, 1095.

(18) Trost, B. M.; Flygare, J. A. *J. Am. Chem. Soc.* **1992**, *114*, 5476.

(19) (a) Fischer, H.; Roth, G.; Reindl, D.; Troll, C. *J. Organomet. Chem.* **1993**, *454*, 133. (b) Capon, J. F.; Le Berre-Cosquer, N.; Bernier, S.; Pichon, R.; Kergoat, R.; L'Haridon, P. *J. Organomet. Chem.* **1995**, *487*, 201.

(20) (a) Kolobova, N. E.; Ivanov, L.; Zhvanko, O. S. *Izv. Akad. Nauk SSSR, Ser. Khim.* **1980**, 2646. (b) Kolobova, N. E.; Ivanov, L.; Zhvanko, O. S.; Derunov, U. V.; Chechulina, I. N. *Izv. Akad. Nauk SSSR, Ser. Khim.* **1982**, *11*, 2632.

(21) Nakanishi, S.; Goda, K.-I.; Uchiyama, S.-I.; Otsuji, Y. *Bull. Chim. Soc. Jpn.* **1992**, *65*, 2560.

(22) (a) Werner, H.; Rappert, T. *Chem. Ber.* **1993**, *126*, 669. (b) Werner, H.; Rappert, T.; Wiedemann, R.; Wolf, J.; Mahr, N. *Organometallics* **1994**, *13*, 2721. (c) Baum, M.; Mahr, N.; Werner, H. *Chem. Ber.* **1994**, *127*, 1877.

(23) Devanne, D.; Dixneuf, P. H. *J. Chem. Soc., Chem. Commun.* **1990**, 641.

(24) Dussel, R.; Pilette, D.; Dixneuf, P. H.; Fehlhammer, W. P. *Organometallics* **1991**, *10*, 3287.

(25) Weng, W.; Arif, A. N.; Gladysz, J. A. *Angew. Chem., Int. Ed. Engl.* **1993**, *32*, 891.

(26) Seyler, J. W.; Weng, W.; Zhou, Y.; Gladysz, J. A. *Organometallics* **1993**, *12*, 3802.

(27) Weng, W.; Ramsden, J. A.; Arif, A. N.; Gladysz, J. A. *J. Am. Chem. Soc.* **1993**, *115*, 3824.

(28) Zhou, Y.; Seyler, J. W.; Weng, W.; Arif, A. M.; Gladysz, J. A. *J. Am. Chem. Soc.* **1993**, *115*, 8509.

(29) Weng, W.; Bartik, T.; Gladysz, J. A. *Angew. Chem., Int. Ed. Engl.* **1994**, *33*, 2199.

(30) Le Narvor, N.; Lapinte, C. *Organometallics* **1995**, *14*, 634.

(31) For a review see: Lang, H. *Angew. Chem., Int. Ed. Engl.* **1994**, *33*, 547.

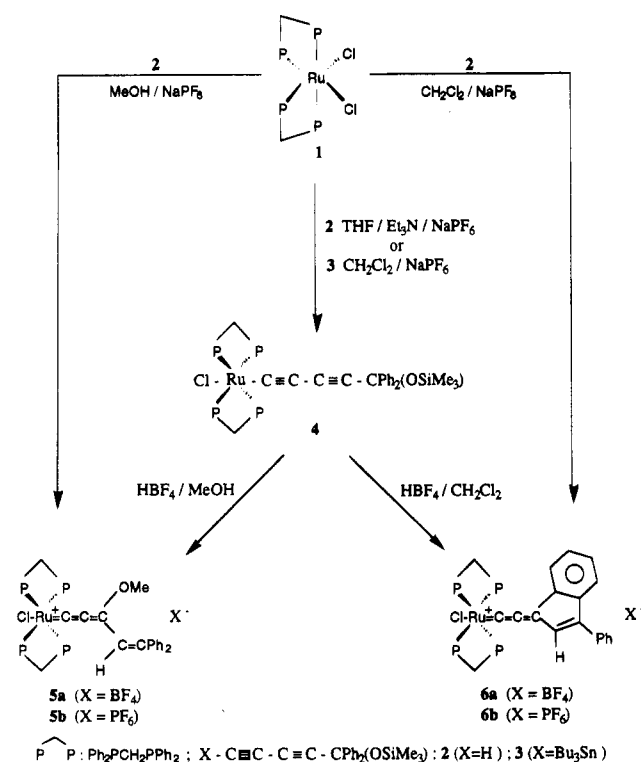
(32) Péron, D.; Romero, A.; Dixneuf, P. H. *Organometallics* **1995**, *14*, 3319.

(33) Péron, D.; Romero, A.; Dixneuf, P. H. *Gazz. Chim. Ital.* **1994**, *124*, 497.

(34) Le Bozec, H.; Ouzzine, K.; Dixneuf, P. H. *Organometallics* **1991**, *10*, 2768.

(35) Touchard, D.; Haquette, P.; Daridor, A.; Toupet, L.; Dixneuf, P. H. *J. Am. Chem. Soc.* **1994**, *116*, 11157.

Scheme 2



our initial works<sup>11b,36</sup> and the synthesis of mono-(alkenylallenylidene) and bis(alkenylallenylidene)ruthenium complexes. The present study is based on the X-ray diffraction structural determination of two complexes of types B and C.

## Results and Discussion

**1. Synthesis of Allenylideneruthenium Complexes 5a,b.** The orange diynylruthenium derivative **4** has first been obtained by two different ways starting from *cis*-RuCl<sub>2</sub>(dppm)<sub>2</sub> (**1**)<sup>37</sup> (dppm: Ph<sub>2</sub>PCH<sub>2</sub>PPh<sub>2</sub>). The first route is based on the Bu<sub>3</sub>SnCl elimination by reaction of **1** with Bu<sub>3</sub>SnC≡CC≡CC(OSiMe<sub>3</sub>)Ph<sub>2</sub> (**3**) in dichloromethane, but it requires the presence of NaPF<sub>6</sub>. After 16 h at room temperature complex **4** was thus obtained in 30% yield (Scheme 2). The second route is based on the formation of a vinylidene intermediate and its deprotonation, as previously established by the reaction of simple terminal alkyne with RuCl<sub>2</sub>(diphosphine)<sub>2</sub> complexes to produce mono- or bis(alkynyl)ruthenium derivatives.<sup>38,51</sup> The vinylidene is generated by displacement of one halide ligand of **1**, in a polar solvent and in the presence of NaPF<sub>6</sub>, and by reaction with HC≡CC≡CC(OSiMe<sub>3</sub>)Ph<sub>2</sub> (**2**). Its *in situ* deprotonation by NEt<sub>3</sub> lead to 40% yield of **4**.

The diynylruthenium complex **4** offers the possibility to remove the Me<sub>3</sub>SiO leaving group from carbon C(5) and generate the reactive metallacumulene **A**. Complex **4** in methanol was first treated with an excess of HBF<sub>4</sub>·OEt<sub>2</sub>, and a violet salt was isolated and identified as the allenylidene **5a** containing a methoxy group and

**Table 1.** <sup>13</sup>C NMR Data for (Ph<sub>2</sub>PCH<sub>2</sub>PPh<sub>2</sub>)<sub>2</sub>Ru[=C<sub>1</sub>=C<sub>2</sub>=C<sub>3</sub>R<sub>1</sub>R<sub>2</sub>] Complexes **5**, **6**, and **8** and (Ph<sub>2</sub>PCH<sub>2</sub>PPh<sub>2</sub>)<sub>2</sub>Ru[C<sub>1</sub>=C<sub>2</sub>C<sub>3</sub>=C<sub>4</sub>CPh<sub>2</sub>(OSiMe<sub>3</sub>)] Derivatives **4** and **7**

complex	δ, ppm		
	C1 ( <sup>2</sup> J <sub>PC</sub> , Hz)	C2 ( <sup>3</sup> J <sub>PC</sub> , Hz)	C3 ( <sup>4</sup> J <sub>PC</sub> , Hz)
<b>1</b> <sup>a</sup>	306.72 (14.4)	208.95 (2.5)	161.87 (s)
<b>5b</b>	252.76 (13.5)	150.18 (2.2)	155.71 (s)
<b>6b</b>	316.13 (14.6)	234.07 (3.3)	158.82 (2.2)
<b>8</b>	233.68 (14.3)	138.93 (1.6)	164.96 (s)
<b>4</b>	125.97 (15.1)	93.48 (s)	80.24 (s)
<b>7</b>	131.18 (15.2)	96.42 (s)	80.27 (s)

<sup>a</sup> **1** = [Ru=C=CPh<sub>2</sub>(Cl)(Ph<sub>2</sub>PCH<sub>2</sub>PPh<sub>2</sub>)<sub>2</sub>]PF<sub>6</sub>.<sup>11d</sup>

an alkenyl substituent at the C(3) carbon. The formation of the allenylidene **5a** can be easily explained by the initial generation of intermediate **A** followed by addition of methanol at the most accessible and electrophilic carbon C(3). We have shown previously in the structure of the *trans*-[Cl(Ph<sub>2</sub>PCH<sub>2</sub>PPh<sub>2</sub>)<sub>2</sub>Ru=C=CH<sub>2</sub>]<sup>+</sup> cation,<sup>51</sup> which is expected to be related to that of the intermediate **A**, that the (Ph<sub>2</sub>PCH<sub>2</sub>PPh<sub>2</sub>)<sub>2</sub>Ru displays on each side of the plane containing the four phosphorus and the ruthenium atoms four phenyl groups protecting by steric hindrance the C(1) carbon. Thus the addition of methanol at this carbon should be disfavored.

As complex **1** promotes the activation of propargyl alcohols HC≡CCAr<sub>2</sub>OH in the presence of NaPF<sub>6</sub>, to generate the stable allenylidene *trans*-[Cl(dppm)<sub>2</sub>Ru=C=C=CAr<sub>2</sub>]PF<sub>6</sub><sup>11d</sup> which does not add methanol, the direct formation of the cumulene intermediate **A** was attempted. Complex **1** was reacted with the diyne **2** in methanol and in the presence of NaPF<sub>6</sub>. After 24 h at room temperature the violet salt **5b** analogous to **5a** was obtained in 65% yield. The nature of **5b** suggests its initial formation *via* the vinylidene intermediate<sup>51</sup> [Cl(dppm)<sub>2</sub>Ru=C=CH-C≡C-CPh<sub>2</sub>(OSiMe<sub>3</sub>)]<sup>+</sup>, the precursor of the diynyl derivative **4** on deprotonation. This intermediate on H<sup>+</sup>/Me<sub>3</sub>SiO<sup>-</sup> elimination is expected to release the cumulene intermediate **A**, as in the formation of [(C<sub>5</sub>H<sub>5</sub>)(PMe<sub>3</sub>)<sub>2</sub>Ru=C=C=CR<sub>2</sub>]<sup>+</sup> from HC≡CC(OH)Ph<sub>2</sub> *via* the [Ru=C=CHC(OH)Ph<sub>2</sub>]<sup>+</sup> intermediate.<sup>10</sup> Addition of methanol would give **5b** as in the formation of **5a**.

Complexes **5** show a strong absorption ν(C=C=C) at ~1950 cm<sup>-1</sup> in the infrared. The equivalency of the <sup>31</sup>P nuclei demonstrates the *trans*-position of the chloride and allenylidene ligands. It is noteworthy that in the <sup>13</sup>C NMR spectrum the resonance for the three carbon nuclei of the allenylidene ligand appears at a much lower field as compared to those of **4** [**5b** (δ, ppm): 252.76 (quint, Ru=C(1), <sup>2</sup>J<sub>PC</sub> = 13.5 Hz), 150.18 (quint, Ru=C=C(2), <sup>3</sup>J<sub>PC</sub> = 2.2 Hz), and 155.71 (s, Ru=C=C=C(3)OMe)]. The low-field signal for the C(1) carbon nucleus is typical of a Ru=C= carbon nucleus involved in an allenylidene ligand but takes place at much higher field than that of *trans*-[Cl(dppm)<sub>2</sub>Ru=C=C=CPh<sub>2</sub>]PF<sub>6</sub><sup>11d</sup> [δ = 306.72 ppm, <sup>2</sup>J<sub>PC</sub> = 14.4 Hz]. This is likely due to the presence of the electron-donating OMe group at the C(3) carbon atom (Table 1).

**2. Synthesis of Allenylidenes 6a,b.** The formation of complexes **5** was first performed in methanol, but the electrophilic intermediate **A** was too reactive toward methanol to be isolated. Thus, a similar reaction was performed in an inert solvent as an attempt to isolate

(36) Pirio, N.; Touchard, D.; Dixneuf, P. H.; Fettouhi, M.; Ouahab, L. *Angew. Chem., Int. Ed. Engl.* **1992**, *31*, 651.

(37) Chaudret, B.; Commenges, G.; Poilblanc, R. *J. Chem. Soc., Dalton Trans.* **1984**, 1635.

(38) Touchard, D.; Morice, C.; Cadierno, V.; Haquette, P.; Toupet, L.; Dixneuf, P. H. *J. Chem. Soc., Chem. Commun.* **1994**, 859.



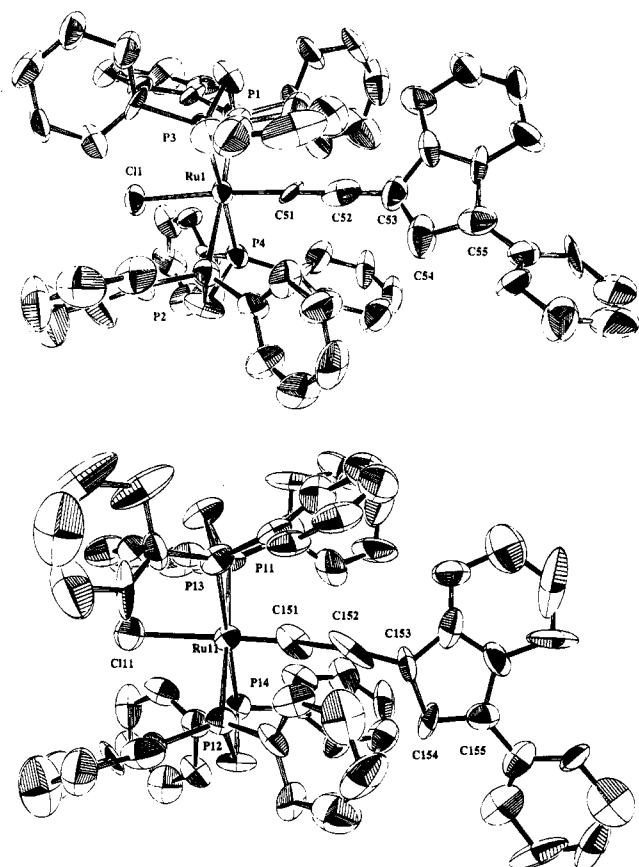
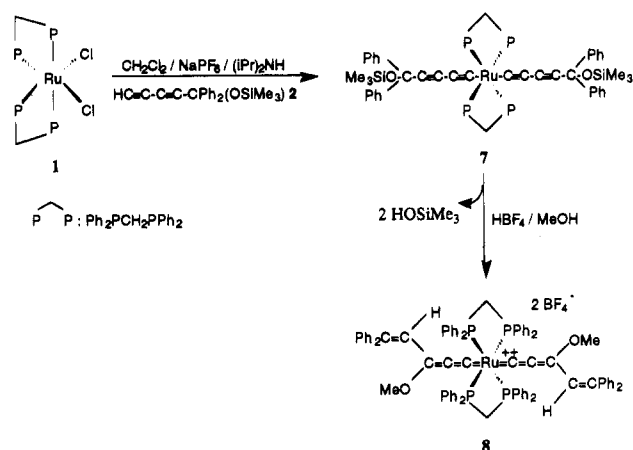


**Figure 1.** ORTEP diagram for *trans*-[(dppm)<sub>2</sub>(Cl)Ru=C=C=C(*o*-C<sub>6</sub>H<sub>4</sub>)-CPh=CH]PF<sub>6</sub> (**6b** (top), **6b** (bottom)).

**A.** Complex **4** was dissolved in dichloromethane and protonated with HBF<sub>4</sub>·OEt<sub>2</sub>. The violet complex **6a** was isolated in 30% yield. The analogous derivative **6b** was prepared in better yield (64%) by direct reaction at room temperature (28 h) of **1** with **2** in dichloromethane but in the presence of 1 equiv of NaPF<sub>6</sub>. The <sup>13</sup>C NMR of complexes **6** suggested the presence of an allenylidene P<sub>4</sub>Ru=C=C=C(R<sup>1</sup>)(R<sup>2</sup>) arrangement. However, the structure of **6b** was solved by an X-ray diffraction study (Figure 1). The <sup>13</sup>C NMR spectrum of **6b** showed for each allenylidene carbon a quintet signal due to the coupling with four identical <sup>31</sup>P nuclei [ $\delta$ , ppm: 316.13 (quint, Ru=C(1), <sup>2</sup>J<sub>PC</sub> = 14.6 Hz), 234.07 (quint, Ru=C=C(2), <sup>3</sup>J<sub>PC</sub> = 3.3 Hz), 158.82 (broad quint, Ru=C=C=C(3), <sup>4</sup>J<sub>PC</sub> = 2.2 Hz)]. The uncoupled <sup>13</sup>C NMR spectrum of **6b** shows the presence of a proton linked to the C(4) carbon nucleus [ $\delta$ , ppm: 130.27 (s, <sup>1</sup>J<sub>CH</sub> = 175.6 Hz)].

The unexpected formation of complex **6** can be understood in terms of the generation of the cumulene intermediate **A**, either indirectly by protonation of **4** or directly by reaction of **1** and **2** with "HOSiMe<sub>3</sub>" elimination. The electrophilicity of carbon C(3) was already demonstrated by the selective addition at carbon C(3) of methanol to give complexes **5**. The formation of the metallacumulene **A** is supported by the observation that a diynylruthenium complex analogous to **4** on treatment with Ph<sub>3</sub>C<sup>+</sup>PF<sub>6</sub><sup>-</sup> led to the isolable and characterized cumulene [(Ph<sub>2</sub>PCH<sub>2</sub>CH<sub>2</sub>PPh<sub>2</sub>)<sub>2</sub>(Cl)Ru=C=C=C=C=CPh<sub>2</sub>]PF<sub>6</sub> that reacts similarly as the intermediate **A**.<sup>35</sup> The stability of the latter with respect to **A** shows the subtle influence of the dppe with respect to the dppm ligand.

### Scheme 3



Thus the nature of **6** indicates that C(3) undergoes an electrophilic substitution at the *ortho* position of one phenyl group, with proton transfer from *ortho* phenyl carbon to carbon C(4). Such a reaction is analogous to the intramolecular electrophilic substitution at an *ortho*-phenyl carbon by a ketene intermediate in the Dötz reaction. It leads to a phenol by proton transfer from the newly C-C-bonded *ortho* carbon to the ketone oxygen.<sup>39</sup>

**3. Preparation of the First Bis(allenylidene)-ruthenium Complex 8.** The direct access to diynylruthenium derivative **4** from **1** and its selective transformation on protonation into **6a** via the expected cumulenyliene intermediate **A** led us to consider the possibility to generate the first bis(allenylidene) derivative from a *trans*-bis(diynyl)ruthenium derivative. Indeed a method has been established from precursors *cis*-RuCl<sub>2</sub>(Ph<sub>2</sub>P(CH<sub>2</sub>)<sub>n</sub>PPh<sub>2</sub>)<sub>2</sub> (*n* = 1 (**1**)<sup>51</sup> or 2<sup>38</sup>) to selectively generate mono(alkynyl) or bis(alkynyl)ruthenium derivatives directly from terminal alkynes, via their vinylidene intermediates on deprotonation. Thus complex **1** (0.5 mmol) and an excess of HC≡C≡CCPh<sub>2</sub>(OSiMe<sub>3</sub>) (**2**) (2 mmol) were reacted in dichloromethane in the presence of NaPF<sub>6</sub> with diisopropylamine (3 mmol). After 4 h at room temperature the yellow *trans*-bis(diynyl)ruthenium derivative **7** was isolated in 24% yield (Scheme 3).

The bis(diynyl) derivative **7** was further reacted in methanol with an excess of HBF<sub>4</sub>·OEt<sub>2</sub>, and a violet complex was immediately formed which was isolated in 76% yield and identified as the *trans*-bis(allenylidene) complex **8** (Scheme 3). The NMR spectra of **8** showed the symmetry of the cation as one line was observed for the four <sup>31</sup>P nuclei, and both proton nuclei of each (Ph<sub>2</sub>P)<sub>2</sub>CH<sub>2</sub> group were equivalent as in **7**. In addition both allenylidene groups appeared equivalent in <sup>13</sup>C NMR [ $\delta$ , ppm: one quintet at 233.68 for both Ru=C(1) (<sup>2</sup>J<sub>PC</sub> = 14.3 Hz), one broad quintet at 138.93 for Ru=C=C(2) (<sup>3</sup>J<sub>PC</sub> = 1.6 Hz), and one singlet for both Ru=C=C=C(3) at 164.96] (Table 1). The structure of **8** was established by an X-ray diffraction study (Figure 3).

**4. X-ray Diffraction Studies of the Mono(allenylidene) Complex 6b.** The molecular structure of **6b** is shown in Figure 1. Experimental crystallographic

(39) Fischer, H.; Mühlemeier, J.; Märkl, R.; Dötz, K. H. *Chem. Ber.* **1982**, *115*, 1355.

**Table 2. Experimental Crystallographic Data for 6b**

formula	$C_{67}H_{54}ClF_6P_5Ru^{+1/2}(CH_2Cl_2) \cdot \frac{1}{2}(C_5H_{12})$
fw	1342.1
cryst	triclinic
space group	$P\bar{1}$
a, Å	13.682(6)
b, Å	22.513(9)
c, Å	23.249(7)
$\alpha$ , deg	112.91(3)
$\beta$ , deg	96.18(3)
$\gamma$ , deg	94.43(4)
V, Å <sup>3</sup>	6500(2)
Z	4
$d_{calc}$ , Mg m <sup>-3</sup>	1.27
cryst size, mm	0.12 × 0.18 × 0.25
$2\theta_{max}$ , mm	50
diffractometer	CAD-4
$\Lambda$ (Mo K $\alpha$ radiation), Å	0.710 69
T, K	293
F(000)	2748
abs coeff $\mu$ , cm <sup>-1</sup>	4.96
scan type	$\omega/2\theta$
no. of rflns read	12 809
no. of unique rflns	4393 ( $I > 5\sigma(I)$ )
R, R <sub>w</sub>	0.076, 0.073

**Table 3. Selected Bond Distances (Å) for 6b and 6b**

6b		6b	
Ru(1)–Cl(1)	2.439(6)	Ru(11)–Cl(11)	2.421(5)
Ru(1)–P(1)	2.351(8)	Ru(11)–P(11)	2.407(7)
Ru(1)–P(2)	2.361(8)	Ru(11)–P(12)	2.381(6)
Ru(1)–P(3)	2.376(6)	Ru(11)–P(13)	2.379(7)
Ru(1)–P(4)	2.385(6)	Ru(11)–P(14)	2.363(7)
Ru(1)–C(51)	1.85(2)	Ru(11)–C(551)	1.67(2)
C(51)–C(52)	1.29(3)	C(151)–C(152)	1.43(3)
C(52)–C(53)	1.39(3)	C(152)–C(153)	1.42(3)
C(53)–C(54)	1.43(4)	C(153)–C(154)	1.50(3)
C(54)–C(55)	1.41(3)	C(154)–C(155)	1.34(3)

**Table 4. Selected Bond Angles (deg) for 6b and 6b**

6b		6b	
Cl(1)–Ru(1)–P(1)	94.1(2)	Cl(11)–Ru(11)–P(11)	85.8(2)
Cl(1)–Ru(1)–P(2)	84.0(2)	Cl(11)–Ru(11)–P(12)	91.5(2)
Cl(1)–Ru(1)–P(3)	94.7(2)	Cl(11)–Ru(11)–P(13)	86.3(2)
Cl(1)–Ru(1)–P(4)	83.5(2)	Cl(11)–Ru(11)–P(14)	94.5(2)
Cl(1)–Ru(1)–C(51)	175.6(6)	Cl(11)–Ru(11)–C(151)	176.2(7)
P(1)–Ru(1)–C(51)	88.3(8)	P(11)–Ru(11)–C(151)	96.9(6)
P(2)–Ru(1)–C(51)	93.6(8)	P(12)–Ru(11)–C(151)	85.8(5)
P(3)–Ru(1)–C(51)	90.2(4)	P(13)–Ru(11)–C(151)	92.2(6)
P(4)–Ru(1)–C(51)	91.5(5)	P(14)–Ru(11)–C(151)	87.2(7)
Ru(1)–C(51)–C(52)	179(2)	Ru(11)–C(151)–C(152)	175(1)
C(51)–C(52)–C(53)	177(2)	C(151)–C(152)–C(153)	172(2)
C(52)–C(53)–C(54)	124(2)	C(152)–C(153)–C(154)	126(2)
C(53)–C(54)–C(55)	107(2)	C(153)–C(154)–C(155)	105(2)

data, selected bond distances, bond angles, and positional parameters are given in Tables 2–5, respectively.

The ORTEP plot establishes the presence of an indenylidene group bonded to the end of a metallacumulene and demonstrates the cyclization involving the C(3) and an *ortho* carbon of one phenyl group. This structure shows the steric protection of the C(1) and C(2) carbon atoms by four phenyl groups of the dppm ligand. This protection accounts for the absence of addition of methanol at carbon C(1). The whole structure consists of two allenylideneruthenium complexes **6b** and **6b** with one molecule of dichloromethane and one of pentane. It shows disordered PF<sub>6</sub> anions. The two allenylideneruthenium cations are not similar and correspond to two different conformers. The main difference

between **6b** and **6b** appears in the orientation of the indenyl plane with respect to the linear P(1)–Ru–P(2) arrangement (Figure 2). The approximative angle of the P(1)–Ru–C plane with respect to the indenyl plane is 10° in **6b** [P(1)–Ru–C(51) and C(57)–C(53)–C(52)] and 28° in **6b** [P(11)–Ru–C(151) and C(157)–C(153)–C(152)]. In addition, differences in bond distances can be observed; however, it must be noticed that owing to restriction in the programs, it was not possible to include the hydrogen atoms in the calculation and to refine the whole structure in the same set.

**5. X-ray Diffraction Study of the Bis(allynylidene) Complex 8.** The molecular structure of **8** is shown in Figure 3. Experimental crystallographic data and selected bond distances, bond angles, and positional parameters are given in Tables 6–9, respectively.

Structural characterization of the dication **8** revealed the *trans* positions of two analogous allenylidene groups that are roughly in the same plane and perpendicular to the P<sub>4</sub>Ru plane (Figure 3). The C(3')–C(2')–C(1')–Ru–C(1)–C(2)–C(3) arrangement is almost linear, and the molecule is centrosymmetric. The Ru–C(1), C(1)–C(2), and C(2)–C(3) bond lengths in the bis(allynylidene)ruthenium **8** [1.997(7), 1.22(1), 1.39(1) Å] can be compared to those of structurally characterized allenylideneruthenium complexes [(C<sub>5</sub>H<sub>5</sub>)(PMe<sub>3</sub>)<sub>2</sub>Ru=C=C=CPh<sub>2</sub>][PF<sub>6</sub>]<sup>10</sup> (1.884(5), 1.255(8), and 1.329(9) Å), [N(CH<sub>2</sub>CH<sub>2</sub>PPh<sub>2</sub>)<sub>3</sub>(Cl)Ru=C=C=C(OMe)CH=CPh<sub>2</sub>][PF<sub>6</sub>]<sup>11a</sup> (1.921(5), 1.254(7) and 1.369(7) Å), [(C<sub>5</sub>Me<sub>5</sub>)<sub>2</sub>( $\mu$ -SiPr)<sub>2</sub>(Cl)Ru<sub>2</sub>=C=C=C(tolyl)<sub>2</sub>][OTf]<sup>3b</sup> (1.94(2), 1.24(2), 1.36(2) Å), and [( $\eta^5$ C<sub>9</sub>H<sub>7</sub>)(Ph<sub>3</sub>P)<sub>2</sub>Ru=C=C=C(R<sup>1</sup>)(R<sup>2</sup>)]PF<sub>6</sub><sup>12a</sup> (1.889(5), 1.256(7), 1.339(7) Å) and the neutral (<sup>i</sup>Pr<sub>2</sub>PCH<sub>2</sub>CO<sub>2</sub>CH<sub>3</sub>)<sub>2</sub>Cl<sub>2</sub>Ru=C=C=CPh<sub>2</sub><sup>14a</sup> (1.84(1), 1.27(2), 1.34(2) Å). Thus the Ru–C(1) bond of **8** appears very long whereas the C(1)–C(2) bond is short and the C(2)–C(3) long. This observation shows that the C(1)–C(2) bond in **8** has partial triple bond character, possibly due to conjugation with the electron-donating methoxy group at C(3), which is indicated by a short C(3)–O bond (1.292(9) Å). The structural parameters indicate a substantial contribution of the alkynyl mesomeric **B** and **C** forms as shown in Scheme 4 with the positive charge delocalized on C(3) or oxygen atoms.

The formation of the cumulene **8** can be explained by the generation of highly unsaturated "batonnet" type cations **I**–**III** by successive HOSiMe<sub>3</sub> elimination and methanol addition (Scheme 5). These intermediates are likely very reactive, but the recent isolation of a Ru=(C=)<sub>4</sub>CR<sub>2</sub> complex with stabilizing diphosphines<sup>35</sup> suggests that such carbon-rich molecules should be isolated in the near future.

## Experimental Section

**General Data.** All reactions were performed under an argon or nitrogen atmosphere with use of Schlenk techniques. The solvents were deoxygenated and dried by standard methods. Tetrahydrofuran and diethyl ether were distilled over benzophenone ketyl, pentane and hexane over calcium hydride, dichloromethane first over phosphorous pentoxide and then over calcium hydride, and methanol over magnesium. Infrared spectra were recorded on a Nicolet 205 FT-IR spectrometer. <sup>1</sup>H (300.134 MHz), <sup>31</sup>P (121.50 MHz), and <sup>13</sup>C (75.469 MHz) NMR spectra were recorded on a Bruker AC 300 P spectrometer at 297 K and referenced to TMS for <sup>1</sup>H and <sup>13</sup>C and to 85% H<sub>3</sub>PO<sub>4</sub> for <sup>31</sup>P. Elemental analysis were

**Table 5. Positional Parameters and Their Estimated Standard Deviations for 6b and 6'b**

atom	<i>x</i>	<i>y</i>	<i>z</i>	<i>B</i> , Å <sup>2</sup>	atom	<i>x</i>	<i>y</i>	<i>z</i>	<i>B</i> , Å <sup>2</sup>
Ru(1)	0.8389(1)	0.23561(9)	0.92836(8)	3.31(5)	P(13)	0.6483(5)	0.2327(3)	0.3590(3)	4.4(2)
Cl(1)	1.0113(4)	0.2298(3)	0.9113(3)	4.6(2)	P(14)	0.5974(4)	0.2164(3)	0.5511(3)	3.6(2)
P(1)	0.8171(4)	0.3140(3)	0.8863(3)	4.1(2)	C(101)	0.761(2)	0.187(1)	0.3500(9)	5.4(7)
P(2)	0.8650(4)	0.1550(3)	0.9676(3)	3.9(2)	C(102)	0.470(1)	0.244(1)	0.5535(8)	3.9(5)
P(3)	0.7726(4)	0.1809(3)	0.8195(3)	3.9(2)	C(103)	0.819(2)	0.122(1)	0.431(1)	4.7(6)
P(4)	0.9103(4)	0.2874(3)	1.0370(3)	3.7(2)	C(104)	0.889(2)	0.125(1)	0.484(1)	7.0(8)
C(1)	0.746(2)	0.253(1)	0.809(1)	4.7(7)	C(105)	0.914(2)	0.062(1)	0.485(1)	8.9(9)
C(2)	0.950(2)	0.2109(9)	1.041(1)	5.2(7)	C(106)	0.865(2)	0.002(1)	0.442(1)	9(1)
C(3)	0.743(2)	0.380(1)	0.918(1)	5.0(7)	C(107)	0.799(2)	0.001(1)	0.389(1)	7.8(9)
C(4)	0.741(2)	0.403(1)	0.985(1)	8.7(9)	C(108)	0.744(2)	0.059(1)	0.386(1)	5.7(7)
C(5)	0.686(2)	0.457(2)	1.012(2)	13(1)	C(109)	0.890(2)	0.253(1)	0.469(1)	7.2(8)
C(6)	0.626(2)	0.477(2)	0.972(1)	10(1)	C(110)	0.983(2)	0.247(1)	0.439(1)	8.8(9)
C(7)	0.622(2)	0.451(1)	0.907(1)	7.0(8)	C(111)	1.064(2)	0.298(2)	0.479(2)	11(1)
C(8)	0.677(2)	0.397(1)	0.876(1)	6.9(8)	C(112)	1.062(3)	0.345(1)	0.534(1)	12(1)
C(9)	0.915(2)	0.354(1)	0.8690(9)	4.0(6)	C(113)	0.975(2)	0.347(2)	0.561(1)	9(1)
C(10)	0.980(2)	0.315(1)	0.8256(9)	4.3(6)	C(114)	0.891(2)	0.303(1)	0.529(1)	7.0(9)
C(11)	1.063(2)	0.342(1)	0.812(1)	6.0(8)	C(115)	0.423(2)	0.325(1)	0.4892(9)	4.4(6)
C(12)	1.095(2)	0.410(1)	0.842(1)	8.2(9)	C(116)	0.451(2)	0.356(1)	0.453(1)	4.8(6)
C(13)	1.035(2)	0.448(1)	0.885(1)	8(1)	C(117)	0.422(2)	0.422(1)	0.466(1)	7.8(8)
C(14)	0.944(2)	0.419(1)	0.897(1)	5.1(7)	C(118)	0.365(2)	0.448(1)	0.513(1)	10(1)
C(15)	0.770(2)	0.1179(9)	0.991(1)	4.4(6)	C(119)	0.339(2)	0.410(1)	0.546(1)	9(1)
C(16)	0.778(2)	0.101(1)	1.043(1)	6.1(8)	C(120)	0.358(2)	0.350(1)	0.539(1)	5.7(7)
C(17)	0.717(2)	0.072(1)	1.061(1)	7.5(8)	C(121)	0.347(2)	0.192(1)	0.4298(9)	4.0(6)
C(18)	0.617(2)	0.049(1)	1.022(1)	7.9(9)	C(122)	0.282(2)	0.210(1)	0.392(1)	6.3(8)
C(19)	0.606(2)	0.064(1)	0.970(1)	7.2(8)	C(123)	0.199(2)	0.161(1)	0.351(1)	7.5(9)
C(20)	0.673(2)	0.097(1)	0.955(1)	5.6(7)	C(124)	0.185(2)	0.105(1)	0.357(2)	10(1)
C(21)	0.933(2)	0.086(1)	0.925(1)	5.4(7)	C(125)	0.256(2)	0.088(1)	0.394(2)	9(1)
C(22)	0.876(2)	0.030(1)	0.877(1)	6.9(9)	C(126)	0.336(2)	0.132(1)	0.433(1)	6.4(8)
C(23)	0.929(3)	-0.023(1)	0.845(1)	9(1)	C(127)	0.682(2)	0.307(1)	0.3556(9)	3.9(6)
C(24)	1.031(2)	-0.016(2)	0.857(2)	11(1)	C(128)	0.617(2)	0.344(1)	0.3408(9)	5.1(6)
C(25)	1.083(3)	0.037(2)	0.906(2)	14(2)	C(129)	0.644(2)	0.401(1)	0.335(1)	6.3(7)
C(26)	1.037(2)	0.092(1)	0.939(2)	11(1)	C(130)	0.742(2)	0.430(1)	0.354(1)	7.1(8)
C(27)	0.842(2)	0.140(1)	0.7580(9)	4.2(6)	C(131)	0.816(2)	0.398(1)	0.370(1)	7.0(8)
C(28)	0.812(2)	0.136(1)	0.6978(9)	5.6(7)	C(132)	0.786(2)	0.339(1)	0.373(1)	6.6(8)
C(29)	0.858(2)	0.098(1)	0.646(1)	6.9(9)	C(133)	0.561(2)	0.190(1)	0.288(1)	5.0(7)
C(30)	0.937(2)	0.065(1)	0.658(1)	6.4(8)	C(134)	0.602(3)	0.184(2)	0.227(1)	11(1)
C(31)	0.964(2)	0.068(1)	0.718(1)	6.7(8)	C(135)	0.522(3)	0.141(2)	0.169(1)	14(1)
C(32)	0.921(2)	0.107(1)	0.770(1)	5.2(7)	C(136)	0.434(2)	0.138(2)	0.176(2)	13(1)
C(33)	0.663(2)	0.124(1)	0.7955(9)	3.7(6)	C(137)	0.400(3)	0.141(1)	0.231(2)	12(1)
C(34)	0.567(2)	0.146(2)	0.810(1)	8(1)	C(138)	0.472(2)	0.173(1)	0.283(1)	7.6(8)
C(35)	0.484(2)	0.100(1)	0.797(1)	7.7(9)	C(139)	0.677(1)	0.272(1)	0.6192(9)	3.6(6)
C(36)	0.498(2)	0.033(1)	0.767(1)	8.9(9)	C(140)	0.650(2)	0.330(1)	0.663(1)	5.7(8)
C(37)	0.587(2)	0.013(1)	0.749(1)	7.7(9)	C(141)	0.721(2)	0.375(1)	0.711(1)	6.7(8)
C(38)	0.664(2)	0.059(1)	0.768(1)	4.8(7)	C(142)	0.816(3)	0.360(1)	0.719(1)	8(1)
C(39)	0.830(2)	0.320(1)	1.0945(8)	4.5(6)	C(143)	0.841(2)	0.300(1)	0.680(1)	7.2(8)
C(40)	0.831(2)	0.389(1)	1.122(1)	7.1(9)	C(144)	0.773(2)	0.254(1)	0.630(1)	6.3(8)
C(41)	0.767(2)	0.417(1)	1.166(1)	7.6(9)	C(145)	0.588(2)	0.147(1)	0.564(1)	4.7(7)
C(42)	0.705(2)	0.378(1)	1.180(1)	7.0(9)	C(146)	0.629(2)	0.091(1)	0.531(1)	5.3(7)
C(43)	0.705(2)	0.311(1)	1.156(1)	7.8(9)	C(147)	0.619(2)	0.031(1)	0.542(1)	6.9(8)
C(44)	0.777(2)	0.286(1)	1.113(1)	7.2(9)	C(148)	0.573(2)	0.029(1)	0.5894(9)	6.4(7)
C(45)	1.024(1)	0.347(1)	1.0653(9)	4.0(6)	C(149)	0.530(2)	0.088(1)	0.627(1)	7.1(8)
C(46)	1.074(2)	0.356(1)	1.124(1)	7.0(9)	C(150)	0.538(2)	0.1426(9)	0.6131(9)	4.5(6)
C(47)	1.159(2)	0.400(1)	1.151(1)	7.4(8)	C(151)	0.655(1)	0.3035(8)	0.4967(7)	3.2(4)
C(48)	1.196(2)	0.433(1)	1.116(1)	6.9(9)	C(152)	0.676(2)	0.372(1)	0.5336(9)	6.3(6)
C(49)	1.148(2)	0.423(1)	1.056(1)	6.7(9)	C(153)	0.691(2)	0.438(1)	0.577(1)	5.0(7)
C(50)	1.055(2)	0.376(1)	1.0311(9)	4.0(6)	C(154)	0.631(2)	0.468(1)	0.629(1)	5.1(7)
C(51)	0.712(1)	0.242(1)	0.9488(8)	4.0(6)	C(155)	0.672(2)	0.530(1)	0.659(1)	4.7(7)
C(52)	0.624(2)	0.246(1)	0.9638(9)	5.4(7)	C(156)	0.756(2)	0.541(1)	0.628(1)	5.7(7)
C(53)	0.528(1)	0.247(1)	0.9780(9)	4.9(6)	C(157)	0.768(2)	0.484(1)	0.579(1)	5.7(8)
C(54)	0.486(1)	0.210(1)	1.0091(9)	5.9(7)	C(158)	0.839(2)	0.480(1)	0.541(1)	6.7(8)
C(55)	0.386(2)	0.220(1)	1.011(1)	6.3(8)	C(159)	0.906(3)	0.541(1)	0.556(1)	10(1)
C(56)	0.369(1)	0.265(1)	0.977(1)	4.5(7)	C(160)	0.897(4)	0.598(2)	0.613(2)	17(2)
C(57)	0.453(1)	0.282(1)	0.955(1)	4.9(7)	C(161)	0.823(2)	0.604(1)	0.652(1)	9.6(9)
C(58)	0.461(2)	0.320(1)	0.921(1)	6.9(7)	C(162)	0.641(2)	0.577(1)	0.712(1)	5.3(7)
C(59)	0.365(2)	0.342(1)	0.911(1)	7.7(9)	C(163)	0.649(2)	0.645(1)	0.723(1)	5.6(8)
C(60)	0.282(2)	0.327(1)	0.935(1)	7.4(9)	C(164)	0.610(3)	0.691(2)	0.772(1)	13(1)
C(61)	0.278(2)	0.286(1)	0.969(1)	7.7(8)	C(165)	0.570(2)	0.672(1)	0.811(2)	10(1)
C(62)	0.312(2)	0.192(1)	1.039(1)	5.5(7)	C(166)	0.593(2)	0.557(1)	0.752(1)	8(1)
C(63)	0.312(2)	0.125(1)	1.024(1)	6.5(7)	C(167)	0.551(2)	0.605(2)	0.807(1)	11(1)
C(64)	0.243(2)	0.095(2)	1.050(1)	9(1)	P(20)	0.9789(6)	0.2186(4)	0.2383(3)	6.3(2)
C65	0.180(2)	0.134(2)	1.090(1)	10(1)	P(21)	0.6297(8)	0.6024(6)	0.2638(5)	11.3(4)
C(66)	0.191(1)	0.201(1)	1.1034(9)	8.0(8)	F(1)	0.998(2)	0.273(1)	0.216(1)	14.6(8)*
C(67)	0.251(1)	0.229(1)	1.077(1)	8.5(9)	F(1')	1.077(3)	0.186(2)	0.231(2)	12(1)*
Ru(11)	0.6194(1)	0.22424(9)	0.45478(8)	3.34(4)	F(2)	0.975(2)	0.171(1)	0.167(1)	13.0(7)*
CL(11)	0.5589(5)	0.1110(3)	0.3904(3)	5.0(2)	F(2')	1.090(2)	0.244(1)	0.256(1)	8.1(8)*
P(11)	0.7810(4)	0.1951(3)	0.4323(3)	4.3(2)	F(3)	0.972(1)	0.1638(9)	0.2617(9)	11.4(6)*
P(12)	0.4569(4)	0.2476(3)	0.4756(3)	3.7(2)	F(4)	1.010(3)	0.263(2)	0.313(2)	9.3(9)*

Table 5. (Continued)

atom	<i>x</i>	<i>y</i>	<i>z</i>	<i>B</i> , Å <sup>2</sup>	atom	<i>x</i>	<i>y</i>	<i>z</i>	<i>B</i> , Å <sup>2</sup>
F(5)	0.863(3)	0.205(2)	0.220(2)	9.2(9)*	F(12)	0.587(4)	0.650(3)	0.238(3)	18(2)*
F(6)	0.942(2)	0.268(2)	0.297(1)	8.5(9)*	CL(2)	0.932(1)	0.8001(7)	0.3570(7)	7.3(4)*
F(7)	0.707(3)	0.634(2)	0.239(2)	9.3(9)*	CL(3)	0.805(2)	0.810(1)	0.4429(9)	11.4(6)*
F(7')	0.642(4)	0.555(2)	0.202(2)	15(1)*	C(200)	0.867(5)	0.769(3)	0.380(3)	10(2)*
F(8)	0.642(3)	0.536(2)	0.269(2)	12(1)*	C(201)	0.781(2)	0.875(1)	0.178(1)	3.9(7)*
F(8')	0.526(3)	0.586(2)	0.239(2)	13(1)*	C(202)	0.786(3)	0.837(2)	0.208(2)	8(1)*
F(9)	0.553(3)	0.590(2)	0.305(2)	10(1)*	C(203)	0.743(4)	0.810(2)	0.241(2)	10(1)*
F(10)	0.629(3)	0.668(2)	0.319(2)	11(1)*	C(204)	0.780(4)	0.934(3)	0.198(3)	8(2)*
F(11)	0.723(4)	0.606(3)	0.298(3)	19(2)*	C(205)	0.683(6)	0.820(4)	0.265(4)	13(3)*

\* Starred *B* values are for atoms that were refined isotropically. Anisotropically refined atoms are given in the form of the isotropic equivalent displacement parameter defined as  $(4/3)[a^2B(1,1) + b^2B(2,2) + c^2B(3,3) + ab(\cos \gamma)B(1,2) + ac(\cos \beta)B(1,3) + bc(\cos \alpha)B(2,3)]$ .

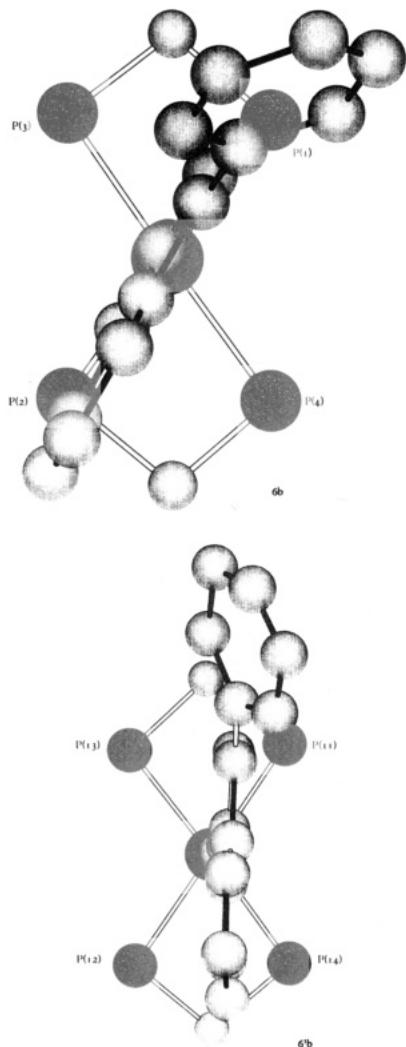


**Figure 2.** Views of cations **6b** and **6'b** in the C(3)–C(2)–C(1)–Ru axis. The Ph<sub>2</sub>P phenyl groups have been omitted. (a) Cation **6b**: approximate angle of the [P(1)–Ru–C(51)] and [C(57)–C(53)–C(52)] planes is 10°. (b) Cation **6'b**: approximate angle of the [P(11)–Ru–C(151)] and [C(157)–C(153)–C(152)] planes is 28°.

performed by the "Service Central de Microanalyse" of CNRS at Vernaison, France. The complex *cis*-RuCl<sub>2</sub>(Ph<sub>2</sub>PCH<sub>2</sub>PPh<sub>2</sub>)<sub>2</sub> (**1**, RuCl<sub>2</sub>(dppm)<sub>2</sub>) was prepared by the literature method.<sup>37</sup> The pentadiyne derivatives HC≡CC≡CCPh<sub>2</sub>(OSiMe<sub>3</sub>) (**2**) and Bu<sub>3</sub>SnC≡CC≡CCPh<sub>2</sub>(OSiMe<sub>3</sub>) (**3**) were prepared from butadiyne<sup>40</sup> according to literature.<sup>41</sup>

**Synthesis of *trans*-(dppm)<sub>2</sub>(Cl)Ru–C≡CC≡CCPh<sub>2</sub>(OSiMe<sub>3</sub>) (**4**). Method A: From Diyne **3**.** A solution of 1.19 g of

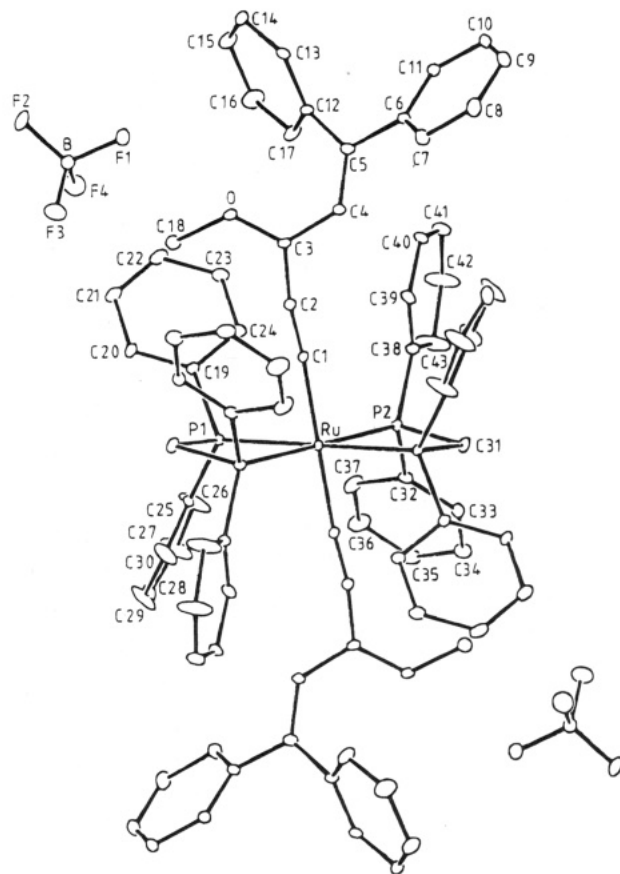


**Figure 3.** ORTEP diagram for *trans*-[(dppm)<sub>2</sub>Ru(=C=C=C(OMe)–CH=CPh<sub>2</sub>)](BF<sub>4</sub>)<sub>2</sub> (**8**).

Bu<sub>3</sub>SnC≡CC≡CCPh<sub>2</sub>(OSiMe<sub>3</sub>) (**3**) (2.0 mmol) in 60 mL of dichloromethane was added to 470 mg of **1** (0.5 mmol) and 168 mg of NaPF<sub>6</sub> (1.0 mmol). The reaction mixture was stirred at room temperature for 16 h. After filtration through a filter-paper-tipped cannula, the solvent was removed under vacuum and the precipitate was washed with pentane. The crude product was filtered on an alumina chromatography column and eluted with diethyl ether. Recrystallization from THF/pentane (10/50) afforded 180 mg of orange crystals of **4** (30%). Anal. Calcd for C<sub>70</sub>H<sub>63</sub>ClO<sub>4</sub>SiRu: C, 69.56; H, 5.25; Cl, 2.93. Found: C, 69.74; H, 5.28; Cl, 3.01. IR (cm<sup>-1</sup>, KBr): 2176, 2024 (s, ν<sub>C=C</sub>). <sup>1</sup>H NMR (300.13 MHz, CD<sub>2</sub>Cl<sub>2</sub>, δ ppm): 7.49–7.12 (m, 50 H, Ph), 4.95, 4.89 (ABX<sub>2</sub>X', 4 H, PCH<sub>2</sub>P, <sup>2</sup>J<sub>HAHB</sub> = 14.6 Hz, [<sup>2</sup>J<sub>PHA</sub> + <sup>4</sup>J<sub>PHA</sub>] = 8.6 Hz, [<sup>2</sup>J<sub>PHB</sub> + <sup>4</sup>J<sub>PHB</sub>] = 8.8 Hz), 0.01 (s, 9 H, OSiMe<sub>3</sub>). <sup>13</sup>C{<sup>1</sup>H} NMR (75.47 MHz, CD<sub>2</sub>Cl<sub>2</sub>, δ ppm): 149.12 (s, (Ph)Ci–C<sub>5</sub>), 134.82 (quint, (Ph)Ci–P, [<sup>1</sup>J<sub>PC</sub> + <sup>3</sup>J<sub>PC</sub>] = 21.5 Hz), 134.63 (quint, (Ph)Ci–P, [<sup>1</sup>J<sub>PC</sub> + <sup>3</sup>J<sub>PC</sub>] = 21.6 Hz), 134.01–126.53 (Ph), 125.97 (quint, RuC≡C, <sup>2</sup>J<sub>PC</sub> = 15.1 Hz), 93.48 (s, RuC≡C), 80.24, 63.79 (s, RuC=CC=C), 76.51 (s, RuC=CC=C), 50.11 (quint, PCH<sub>2</sub>P, [<sup>1</sup>J<sub>PC</sub> + <sup>3</sup>J<sub>PC</sub>] = 20.6 Hz), 2.03 (s, OSiMe<sub>3</sub>). <sup>13</sup>C NMR (75.47 MHz, CD<sub>2</sub>Cl<sub>2</sub>, δ ppm): 149.13 (t, (Ph)Ci–C<sub>5</sub>), <sup>3</sup>J<sub>CH</sub> = 7.2 Hz), 50.11 (t quint, PCH<sub>2</sub>P,

(40) Brandsma, L. *Preparative Acetylenic Chemistry* 2nd ed.; Elsevier: Amsterdam, 1988; p 179.

(41) Midland, S. M. M. *J. Org. Chem.* **1975**, *40*, 2250.

Table 6. Experimental Crystallographic Data for 8

formula	C <sub>86</sub> H <sub>72</sub> B <sub>2</sub> F <sub>8</sub> O <sub>2</sub> P <sub>4</sub> Ru
fw	1536.11
cryst	monoclinic
space group	P2 <sub>1</sub> /c
a, Å	16.076(4)
b, Å	11.514(5)
c, Å	20.778(6)
β, deg	103.53(2)
V, Å <sup>3</sup>	3739.1
Z	2
d <sub>calc</sub> , Mg m <sup>-3</sup>	1.364
cryst size, mm	0.62 × 0.50 × 0.12
2θ <sub>max</sub> , mm	50
diffractometer	CAD-4
λ (Mo Kα radiation), Å	0.710 73
T, K	293
abs coeff μ, cm <sup>-1</sup>	5.90
scan type	ω/2θ
no. of rflns read	6686
no. of unique rflns	2719 (I > 3σ(I))
R, R <sub>w</sub>	0.058, 0.073

Table 7. Selected Bond Distances (Å) for 8

Ru-P(1)	2.357(2)	C(1)-C(2)	1.22(1)
Ru-P(2)	2.378(2)	C(2)-C(3)	1.39(1)
Ru-C(1)	1.997(7)	C(3)-C(4)	1.45(1)
O-C(3)	1.292(9)	C(4)-C(5)	1.36(1)
O-C(18)	1.46(1)		

Table 8. Selected Bond Angles (deg) for 8

P(1)-Ru-P(2)	71.95(8)	C(1)-C(2)-C(3)	171.4(9)
P(1)-Ru-C(1)	93.3(2)	O-C(3)-C(2)	122.1(9)
P(2)-Ru-C(1)	98.1(2)	O-C(3)-C(4)	117.8(7)
C(3)-O-C(18)	121.3(8)	C(2)-C(3)-C(4)	120.1(7)
Ru-C(1)-C(2)	175.0(7)	C(3)-C(4)-C(5)	123.2(8)

$\omega_{\text{CH}} = 135.8$  Hz,  ${}^1J_{\text{PC}} + {}^3J_{\text{PC}} = 20.8$  Hz), 2.03 (q, OSiMe<sub>3</sub>,  $\omega_{\text{CH}} = 118.6$  Hz).  ${}^{31}\text{P}\{^1\text{H}\}$  NMR (121.50 MHz, CD<sub>2</sub>Cl<sub>2</sub>, δ ppm): -6.47 (s, PPh<sub>2</sub>).

**Method B: From Diyne 2.** A solution of 0.71 g of HC≡CC≡CCPh<sub>2</sub>(OSiMe<sub>3</sub>) (2) (2.0 mmol) and 0.56 mL of Et<sub>3</sub>N (4.0 mmol) in 25 mL of tetrahydrofuran was added to 940 mg of 1 (1.0 mmol) and 336 mg of NaPF<sub>6</sub> (2.0 mmol). The reaction mixture was stirred at room temperature for 3 h, and the product was extracted as above. Recrystallization from CH<sub>2</sub>-Cl<sub>2</sub>/hexane mixture afforded 470 mg of orange crystals of 4 (40%). Anal. Calcd for C<sub>70</sub>H<sub>63</sub>ClO<sub>4</sub>SiRu: C, 69.56; H, 5.25. Found: C, 69.23; H, 5.15. IR (cm<sup>-1</sup>, KBr): 2176, 2024 (s, ν<sub>C=C</sub>).  ${}^{31}\text{P}\{^1\text{H}\}$  NMR (121.50 MHz, CD<sub>2</sub>Cl<sub>2</sub>, δ ppm): -6.47 (s, PPh<sub>2</sub>).

**Synthesis of trans-[(dppm)<sub>2</sub>(Cl)Ru=C=C=C(OMe)-CH=CPh<sub>2</sub>]<sub>2</sub>X (X = BF<sub>4</sub> (5a), PF<sub>6</sub> (5b)). (a) Synthesis of 5a from 4.** To a solution of 121 mg of 4 (0.1 mmol) in 20 mL methanol was added 5 equiv of HBF<sub>4</sub>·Et<sub>2</sub>O. After 2 h of stirring at room temperature, the solvent was removed under vacuum. The precipitate was washed with diethyl ether and dissolved in 20 mL of dichloromethane. After filtration through a filter-paper-tipped cannula, the precipitation with 60 mL of hexane afforded 50 mg of 5a (39%) as a red microcrystalline powder. Anal. Calcd for C<sub>68</sub>H<sub>58</sub>BClF<sub>4</sub>OP<sub>4</sub>Ru: C, 65.95; H, 4.72. Found: C, 66.27; H, 4.55. IR (cm<sup>-1</sup>, KBr): 1955 (s, ν<sub>C=C</sub>).  ${}^{31}\text{P}\{^1\text{H}\}$  NMR (121.50 MHz, CD<sub>2</sub>Cl<sub>2</sub>, δ ppm): -11.71 (s, PPh<sub>2</sub>).

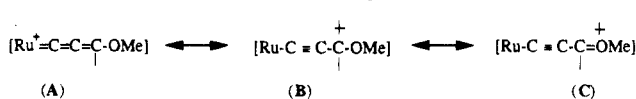
**(b) Direct Synthesis of 5b from 1.** A solution of 706 mg of HC≡CC≡CCPh<sub>2</sub>(OSiMe<sub>3</sub>) (2) (2.0 mmol) in 60 mL of methanol was added to 470 mg of 1 (0.5 mmol) and 336 mg of NaPF<sub>6</sub> (2.0 mmol). After 24 h of stirring at room temperature and filtration through a filter-paper-tipped cannula, the solvent was removed under vacuum. The precipitate was washed with diethyl ether and dissolved in 20 mL of dichloromethane. After filtration through a filter-paper-tipped cannula, the precipitation with 70 mL of hexane afforded 420 mg of 5b (65%) as a red microcrystalline powder. Anal. Calcd for C<sub>68</sub>H<sub>58</sub>ClF<sub>6</sub>OP<sub>5</sub>Ru: C, 62.99; H, 4.51; Cl, 2.73. Found: C,

Table 9. Positional Parameters and Their Estimated Standard Deviations for 8

atom	x	y	z	B, Å <sup>2</sup>
Ru	0	0	0	2.88(2)
P(1)	-0.0264(1)	0.0811(2)	-0.1070(1)	3.47(5)
P(2)	-0.0539(1)	-0.1494(2)	-0.0776(1)	3.79(5)
O	0.3472(3)	-0.0556(6)	0.0635(3)	5.7(2)
C(1)	0.1243(5)	-0.0231(7)	0.0049(4)	3.2(2)
C(2)	0.2016(5)	-0.0320(7)	0.0123(4)	3.6(2)
C(3)	0.2873(5)	-0.0426(8)	0.0104(5)	4.1(2)
C(4)	0.3119(5)	-0.0371(9)	-0.0522(4)	4.7(2)
C(5)	0.3763(5)	-0.1016(9)	-0.0659(5)	5.1(2)
C(6)	0.4017(5)	-0.076(1)	-0.1302(4)	5.2(2)
C(7)	0.4007(7)	0.034(1)	-0.1526(5)	6.5(3)
C(8)	0.4259(7)	0.056(1)	-0.2116(5)	8.6(4)
C(9)	0.4512(7)	-0.039(2)	-0.2446(5)	10.3(5)
C(10)	0.4511(7)	-0.147(2)	-0.2226(5)	10.7(4)
C(11)	0.4269(6)	-0.170(1)	-0.1635(5)	7.1(3)
C(12)	0.4176(5)	-0.2004(9)	-0.0235(5)	5.0(2)
C(13)	0.5055(6)	-0.207(1)	-0.0057(5)	6.2(3)
C(14)	0.5446(7)	-0.297(1)	0.0370(5)	7.2(3)
C(15)	0.4957(9)	-0.375(1)	0.058(7)	9.3(4)
C(16)	0.4034(9)	-0.370(1)	0.0395(8)	10.4(5)
C(17)	0.3679(7)	-0.280(1)	-0.0015(6)	7.4(3)
C(18)	0.3274(7)	-0.074(1)	0.1279(5)	7.8(3)
C(19)	-0.1014(5)	0.2005(8)	-0.1304(4)	4.2(2)
C(20)	-0.1504(6)	0.213(1)	-0.1932(5)	5.9(3)
C(21)	-0.2085(7)	0.304(1)	-0.2084(6)	8.3(4)
C(22)	-0.2167(7)	0.385(1)	-0.1597(6)	8.3(3)
C(23)	-0.1681(7)	0.372(1)	-0.0973(6)	6.9(3)
C(24)	-0.1101(6)	0.2791(9)	-0.0807(5)	5.1(2)
C(25)	0.0577(5)	0.1157(8)	-0.1487(4)	3.7(2)
C(26)	0.0930(8)	0.213(1)	-0.1476(8)	16.2(4)
C(27)	0.1604(9)	0.242(1)	-0.1743(8)	17.3(5)
C(28)	0.1924(7)	0.180(1)	-0.2061(5)	8.1(3)
C(29)	0.1643(9)	0.075(2)	-0.2078(7)	17.2(6)
C(30)	0.0982(9)	0.034(1)	-0.1764(7)	12.8(4)
C(31)	-0.0808(6)	-0.0518(8)	-0.1498(5)	4.5(2)
C(32)	-0.1540(5)	-0.2226(8)	-0.0759(5)	4.5(2)
C(33)	-0.2241(6)	-0.2190(9)	-0.1260(5)	5.4(3)
C(34)	-0.3008(6)	-0.273(1)	-0.1226(6)	7.5(3)
C(35)	-0.3045(6)	-0.329(1)	-0.0653(6)	7.3(3)
C(36)	-0.2345(8)	-0.339(1)	-0.0156(7)	10.6(4)
C(37)	-0.1579(7)	-0.279(1)	-0.0176(6)	8.9(3)
C(38)	0.0119(5)	-0.2639(9)	-0.0992(4)	4.8(2)
C(39)	0.0922(6)	-0.247(1)	-0.1024(5)	7.0(3)
C(40)	0.1430(6)	-0.334(1)	-0.1198(5)	9.7(4)
C(41)	0.1136(8)	0.561(1)	-0.1371(7)	10.9(4)
C(42)	0.034(1)	0.540(1)	-0.130(1)	17.9(7)
C(43)	-0.022(1)	-0.370(1)	-0.116(1)	17.1(6)
B	0.6776(8)	-0.030(2)	-0.3019(6)	7.5(4)
F1	0.6930(4)	-0.0417(8)	-0.3634(3)	10.3(2)
F2	0.7520(5)	-0.0150(9)	-0.2587(3)	11.6(3)
F3	0.6437(5)	-0.1344(8)	-0.2872(4)	12.3(3)
F4	0.6170(5)	0.0472(7)	-0.3026(4)	11.9(3)

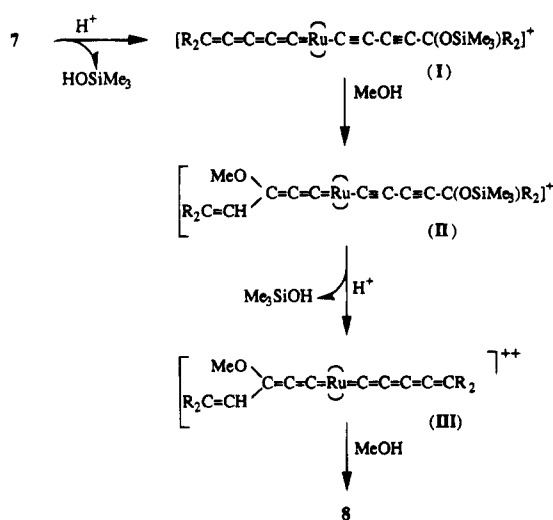
<sup>a</sup> Anisotropically refined atoms are given in the form of the isotropic equivalent displacement parameter defined as (4/3)[a<sup>2</sup>B(1,1) + b<sup>2</sup>B(2,2) + c<sup>2</sup>B(3,3) + ab(cos γ)B(1,2) + ac(cos β)B(1,3) + bc(cos α)B(2,3)].

Scheme 4



62.89; H, 4.71; Cl, 2.42. IR (cm<sup>-1</sup>, KBr): 1952 (s, ν<sub>C=C</sub>), 838 (s, ν<sub>PF</sub>).  ${}^1\text{H}$  NMR (300.13 MHz, CD<sub>2</sub>Cl<sub>2</sub>, δ ppm): 7.64–6.83 (m, 50 H, Ph), 5.26, 5.09 (ABX<sub>2</sub>X'<sub>2</sub>, 4 H, PCH<sub>2</sub>P,  ${}^2J_{\text{HAHB}} = 15.4$  Hz,  ${}^2J_{\text{PHA}} + {}^4J_{\text{PHB}} = 8$  Hz,  ${}^2J_{\text{PHB}} + {}^4J_{\text{PHB}} = 9$  Hz), 4.83 (s, 1 H, CH=), 2.35 (s, 3 H, OMe).  ${}^1\text{H}\{^{31}\text{P}\}$  NMR (300.134 MHz, CD<sub>2</sub>Cl<sub>2</sub>, δ ppm): 5.27, 5.09 (AB, 4H, PCH<sub>2</sub>P,  ${}^2J_{\text{HAHB}} = 15.5$  Hz).  ${}^{13}\text{C}\{^1\text{H}\}$  NMR (75.47 MHz, CD<sub>2</sub>Cl<sub>2</sub>, δ ppm): 252.76 (quint, Ru=C,  ${}^2J_{\text{PC}} = 13.5$  Hz), 155.71 (broad s, Ru=C=C=C), 154.0 (s, CH=CPh<sub>2</sub>), 150.18 (broad quint, Ru=C=C,  ${}^3J_{\text{PC}} = 2.2$  Hz), 141.43 (s, Ph), 139.66 (s, Ph), 133.68–128.36 (Ph), 124.43 (s, CH=CPh<sub>2</sub>), 58.73 (s, OMe), 46.92 (quint, PCH<sub>2</sub>P,  ${}^1J_{\text{PC}} + {}^3J_{\text{PC}} = 23.2$  Hz).  ${}^{13}\text{C}$  NMR (75.47 MHz, CD<sub>2</sub>Cl<sub>2</sub>, δ ppm): 124.43

Scheme 5



(d, CH=CPh<sub>2</sub>, <sup>1</sup>J<sub>CH</sub> = 163.8 Hz), 58.73 (q, OMe, <sup>1</sup>J<sub>CH</sub> = 148.3 Hz), 46.92 (t quint, PCH<sub>2</sub>P, <sup>1</sup>J<sub>CH</sub> = 136.3 Hz, <sup>1</sup>J<sub>PC</sub> + <sup>3</sup>J<sub>PC</sub> = 23.4 Hz). <sup>31</sup>P{<sup>1</sup>H} NMR (121.50 MHz, CD<sub>2</sub>Cl<sub>2</sub>, δ ppm): -11.28 (s, PPh<sub>2</sub>), -143.34 (sept, PF<sub>6</sub>, <sup>1</sup>J<sub>PF</sub> = 710.9 Hz).

**Synthesis of *trans*-[(dppm)<sub>2</sub>(Cl)Ru=C=C=C(*o*-C<sub>6</sub>H<sub>4</sub>)-CPh=CH]X (X = BF<sub>4</sub> (6a), PF<sub>6</sub> (6b)). (a) **Synthesis of 6a from 4.** To a solution of 121 mg of 4 (0.1 mmol) in 20 mL of dichloromethane was added 5 equiv of HBF<sub>4</sub>·Et<sub>2</sub>O. After 24 h of stirring at 28 °C, the solvent was removed under vacuum. The precipitate was washed with diethyl ether and dissolved in 20 mL of dichloromethane. After filtration through a filter-paper-tipped cannula, the precipitation with 60 mL of pentane afforded 40 mg of 6a (30%) as a violet microcrystalline powder. Anal. Calcd for C<sub>67</sub>H<sub>54</sub>BClF<sub>4</sub>Ru·1.5CH<sub>2</sub>Cl<sub>2</sub>: C, 61.68; H, 4.31. Found: C, 61.26; H, 4.27. IR (cm<sup>-1</sup>; KBr): 1934 (s, ν<sub>C-C</sub>). <sup>31</sup>P{<sup>1</sup>H} NMR (121.50 MHz, CD<sub>2</sub>Cl<sub>2</sub>, δ ppm): -16.62 (s, PPh<sub>2</sub>).**

(b) **Direct Synthesis of 6b from 1.** A solution of 1.06 g of HC≡CC≡CCPh<sub>2</sub>(OSiMe<sub>3</sub>) (2) (3.0 mmol) in 60 mL of dichloromethane was added to 470 mg of 1 (0.5 mmol) and 504 mg of NaPF<sub>6</sub> (3.0 mmol). After 28 h of stirring at 28 °C and filtration through a filter-paper-tipped cannula, the solvent was removed under vacuum. The precipitate was washed with diethyl ether and dissolved in 30 mL of dichloromethane. After filtration through a filter-paper-tipped cannula, the precipitation with 70 mL of pentane afforded 430 mg of 6b (64%) as a violet microcrystalline powder. Anal. Calcd for C<sub>67</sub>H<sub>54</sub>ClF<sub>6</sub>P<sub>2</sub>Ru·0.5CH<sub>2</sub>Cl<sub>2</sub>·0.5C<sub>5</sub>H<sub>12</sub>: C, 62.60; H, 4.58. Found: C, 62.22; H, 4.40. IR (cm<sup>-1</sup>; KBr): 1934 (s, ν<sub>C-C</sub>), 838 (s, ν<sub>PF</sub>). <sup>1</sup>H NMR (300.13 MHz, CD<sub>2</sub>Cl<sub>2</sub>, δ ppm): 7.72–6.87 (m, 48 H, Ph), 5.44 (d, 1 H, C<sub>6</sub>H<sub>4</sub>, <sup>3</sup>J<sub>HH</sub> = 7.3 Hz), 5.39, 5.27 (ABX<sub>2</sub>X<sub>2</sub>, 4H, PCH<sub>2</sub>P, <sup>2</sup>J<sub>HAHB</sub> = 15.7 Hz, <sup>2</sup>J<sub>PHA</sub> + <sup>4</sup>J<sub>PHB</sub> = 7.8 Hz, <sup>2</sup>J<sub>PHB</sub> + <sup>4</sup>J<sub>PHB</sub> = 10.2 Hz), 4.52 (s, 1 H, CH=). <sup>1</sup>H{<sup>31</sup>P} NMR (300.134 MHz, CD<sub>2</sub>Cl<sub>2</sub>, δ ppm): 5.40, 5.26 (AB, 4 H, PCH<sub>2</sub>P, <sup>2</sup>J<sub>HAHB</sub> = 15.7 Hz). <sup>13</sup>C{<sup>1</sup>H} NMR (75.47 MHz, CD<sub>2</sub>Cl<sub>2</sub>, δ ppm): 316.13 (quint, Ru=C, <sup>2</sup>J<sub>PC</sub> = 14.6 Hz), 234.07 (broad quint, Ru=C=C, <sup>3</sup>J<sub>PC</sub> = 3.3 Hz), 162.17 (s, CH=CPh), 158.82 (broad quint, Ru=C=C=C, <sup>4</sup>J<sub>PC</sub> = 2.2 Hz), 145.50 (s, Ph), 137.78 (s, Ph); 135.35 (s, Ph), 133.56–126.90 (Ph), 122.69, 122.65 (s, Ph), CH=CPh masked by signals of phenyl carbon nuclei, 45.98 (quint, PCH<sub>2</sub>P, <sup>1</sup>J<sub>PC</sub> + <sup>3</sup>J<sub>PC</sub> = 23.6 Hz). <sup>13</sup>C NMR with selective decoupling at 4.52 ppm (75.469 MHz, CD<sub>2</sub>Cl<sub>2</sub>, δ ppm): 130.27 (s, CH=). <sup>13</sup>C NMR (75.47 MHz, CD<sub>2</sub>Cl<sub>2</sub>, δ ppm): 130.26 (d, CH=CPh, <sup>1</sup>J<sub>CH</sub> = 175.6 Hz), 46.00 (t quint, PCH<sub>2</sub>P, <sup>1</sup>J<sub>CH</sub> = 136.5 Hz, <sup>1</sup>J<sub>PC</sub> + <sup>3</sup>J<sub>PC</sub> = 24.0 Hz). <sup>31</sup>P{<sup>1</sup>H} NMR (121.50 MHz, CD<sub>2</sub>Cl<sub>2</sub>, δ ppm): -16.16 (s, PPh<sub>2</sub>), -143.37 (sept, PF<sub>6</sub>, <sup>1</sup>J<sub>PF</sub> = 710.9 Hz).

**Synthesis of *trans*-(dppm)<sub>2</sub>Ru(C≡CC≡CCPh<sub>2</sub>(OSiMe<sub>3</sub>))<sub>2</sub> (7).** A solution of 0.71 g of HC≡CC≡CCPh<sub>2</sub>(OSiMe<sub>3</sub>) (2) (2.0 mmol) and 420 μL of <sup>i</sup>Pr<sub>2</sub>NH (3.0 mmol) in 60 mL of dichloromethane was added to 470 mg of 1 (0.5 mmol) and 336 mg

of NaPF<sub>6</sub> (2.0 mmol). The reaction mixture was stirred at room temperature for 4 h. After filtration through a filter-paper-tipped cannula, the solvent was removed under vacuum and the precipitate was washed with *n*-pentane. The crude product was filtered with diethyl ether through alumina using a chromatography column. Recrystallization from THF/*n*-pentane afforded 180 mg of yellow crystals of 7 (24%). Anal. Calcd for C<sub>90</sub>H<sub>82</sub>O<sub>2</sub>P<sub>4</sub>Si<sub>2</sub>Ru: C, 73.20; H, 5.60; P, 8.39. Found: C, 73.54; H, 5.45; P, 8.46. IR (cm<sup>-1</sup>; KBr): 2175, 2020 (s, ν<sub>C=C</sub>). <sup>1</sup>H NMR (300.13 MHz, CD<sub>2</sub>Cl<sub>2</sub>, δ ppm): 7.43–7.09 (60 H, Ph), 4.82 (quint, 4 H, PCH<sub>2</sub>P, <sup>2</sup>J<sub>PH</sub> + <sup>4</sup>J<sub>PH</sub> = 8.4 Hz), 0.01 (s, 18H, OSiMe<sub>3</sub>). <sup>1</sup>H{<sup>31</sup>P} NMR (300.13 MHz, CD<sub>2</sub>Cl<sub>2</sub>, δ ppm): 4.82 (s, 4H, PCH<sub>2</sub>P). <sup>13</sup>C{<sup>1</sup>H} NMR (75.47 MHz, CD<sub>2</sub>Cl<sub>2</sub>, δ ppm): 149.06 (s, Ph); 135.27 (quint, Ph, <sup>2</sup>J<sub>PC</sub> + <sup>3</sup>J<sub>PC</sub> = 22.4 Hz), 133.85–126.50 (Ph), 131.18 (quint, Ru=C=C, <sup>2</sup>J<sub>PC</sub> = 15.2 Hz), 96.42 (s, Ru=C=C), 80.27, 64.96 (s, RuC=CC=C), 76.60 (s, RuC=C-C=C-C), 52.05 (quint, PCH<sub>2</sub>P, <sup>1</sup>J<sub>PC</sub> + <sup>3</sup>J<sub>PC</sub> = 21.8 Hz), 2.08 (s, OSiMe<sub>3</sub>). <sup>13</sup>C NMR (75.47 MHz, CD<sub>2</sub>Cl<sub>2</sub>, δ ppm): 149.06 (t, Ph, <sup>3</sup>J<sub>CH</sub> = 7.2 Hz), 52.06 (t quint, PCH<sub>2</sub>P, <sup>1</sup>J<sub>CH</sub> = 135.0 Hz, <sup>1</sup>J<sub>PC</sub> + <sup>3</sup>J<sub>PC</sub> = 21.8 Hz), 2.08 (q, OSiMe<sub>3</sub>, <sup>1</sup>J<sub>CH</sub> = 118.6 Hz). <sup>31</sup>P{<sup>1</sup>H} NMR (121.50 MHz, CD<sub>2</sub>Cl<sub>2</sub>, δ ppm): -4.21 (s, PPh<sub>2</sub>).

**Synthesis of *trans*-(dppm)<sub>2</sub>Ru(=C=C=C(OMe)CH=CPh)<sub>2</sub>(BF<sub>4</sub>)<sub>2</sub> (8).** To a solution of 90 mg of 7 (0.06 mmol) in 20 mL of methanol was added 10 equiv of HBF<sub>4</sub>·Et<sub>2</sub>O. After 2 h of stirring at room temperature, the solution was filtered through a filter-paper-tipped cannula, the solvent was removed under vacuum, and the precipitate was washed with diethyl ether. Recrystallization from CH<sub>2</sub>Cl<sub>2</sub>/hexane afforded 70 mg of violet crystals of 8 (76%). Anal. Calcd for C<sub>68</sub>H<sub>72</sub>B<sub>2</sub>F<sub>8</sub>O<sub>2</sub>P<sub>4</sub>Ru: C, 67.24; H, 4.72; P, 8.06. Found: C, 67.37; H, 4.72; P, 7.55. IR (cm<sup>-1</sup>; KBr): 1958 (s, ν<sub>C=C</sub>). <sup>1</sup>H NMR (300.13 MHz, CD<sub>2</sub>Cl<sub>2</sub>, δ ppm): 7.62–7.18 (60 H, Ph), 7.08 (d, m, H, Ph, <sup>3</sup>J<sub>HH</sub> = 8.4 Hz), 6.85 (d, m, H, Ph, <sup>3</sup>J<sub>HH</sub> = 8.2 Hz), CH= masked by signal of PCH<sub>2</sub>P, 5.26 (quint, 4H, PCH<sub>2</sub>P, <sup>2</sup>J<sub>PH</sub> + <sup>4</sup>J<sub>PH</sub> = 8.8 Hz), 2.72 (s, 3H, OMe). <sup>1</sup>H{<sup>31</sup>P} NMR (300.13 MHz, CD<sub>2</sub>Cl<sub>2</sub>, δ ppm): CH= masked by signal of PCH<sub>2</sub>P, 5.27 (s, 4H, PCH<sub>2</sub>P). <sup>13</sup>C{<sup>1</sup>H} NMR (75.47 MHz, CD<sub>2</sub>Cl<sub>2</sub>, δ ppm): 233.68 (quint, Ru=C, <sup>2</sup>J<sub>PC</sub> = 14.3 Hz), 165.58 (s, CH=CPh<sub>2</sub>), 164.96 (broad s, Ru=C=C=C), 140.20 (s, Ph), 138.93 (broad quint, Ru=C=C, <sup>3</sup>J<sub>PC</sub> = 1.6 Hz), 138.50 (s, Ph), 133.31–128.72 (Ph), 122.01 (s, CH=CPh<sub>2</sub>), 61.31 (s, OMe), 48.87 (quint, PCH<sub>2</sub>P, <sup>1</sup>J<sub>PC</sub> + <sup>3</sup>J<sub>PC</sub> = 26.2 Hz). <sup>13</sup>C NMR (75.47 MHz, CD<sub>2</sub>Cl<sub>2</sub>, δ ppm): 140.20 (pseudo q, Ph), 138.50 (pseudo q, Ph), 122.01 (d, CH=CPh<sub>2</sub>, <sup>1</sup>J<sub>CH</sub> = 150.4 Hz), 61.31 (q, OMe, <sup>1</sup>J<sub>CH</sub> = 150.4 Hz), 48.87 (t quint, PCH<sub>2</sub>P, <sup>1</sup>J<sub>CH</sub> = 136.9 Hz, <sup>1</sup>J<sub>PC</sub> + <sup>3</sup>J<sub>PC</sub> = 26.2 Hz). <sup>31</sup>P{<sup>1</sup>H} NMR (121.50 MHz, CD<sub>2</sub>Cl<sub>2</sub>, δ ppm): -9.14 (s, PPh<sub>2</sub>).

**Crystal Structure Analysis of 6b.** The sample (prism 0.12 × 0.18 × 0.25 mm) was studied on an automatic diffractometer (CAD-4 Enraf-Nonius) with graphite-monochromatized Mo Kα radiation. The cell parameters were obtained by fitting a set of 25 high-θ reflections. The data collection (2θ<sub>max</sub> = 50°, scan ω/2θ = 1, t<sub>max</sub> = 60 s, range *hkl* *h* 0 to 13, *k* -21 to 21, *l* -22 to 22, intensity controls without appreciable decay (0.3%)) gave 12 809 reflections from which 4393 were independent (*R*<sub>int</sub> = 0.021) with *I* > 5 σ(*I*) (Table 2).

After Lorenz and polarization corrections, the structure was solved with a Patterson map which revealed the two Ru atoms. The remaining non-hydrogen atoms of the structure were found after successive scale factor refinements and Fourier differences. After isotropic refinement (*R* = 0.12), solvent molecules of pentane and methylene chloride were found, and an absorption correction was made with Difabs.<sup>42</sup> The anions PF<sub>6</sub><sup>-</sup> appeared as disordered. The whole structure was refined by the full-matrix least-square techniques (use of *F* magnitude; *x*, *y*, *z*, β<sub>*ij*</sub> for Ru, P, Cl, and C atoms; *x*, *y*, *z*, β<sub>iso</sub> for F atoms; *x*, *y*, *z*, fixed for H atoms; 629 variables and 4393 observations; *w* = 1/σ(*F*<sub>o</sub>)<sup>2</sup> = [σ<sup>2</sup>(*I*) + (0.04*F*<sub>o</sub><sup>2</sup>)<sup>2</sup>]<sup>-1/2</sup>) with the resulting *R* = 0.076, *R*<sub>w</sub> = 0.073, and *S*<sub>w</sub> = 4.42 (residual Δρ ≤ 0.84 e Å<sup>-3</sup>).

Atomic scattering factors were from ref 43. All the calculations were performed on a Digital PDP 11/60 computer with the SDP package.<sup>44</sup>

**X-ray Structure Determination of 8.** Crystal data of **8**, together with details of the X-ray diffraction experiment and subsequent crystallographic calculations, are reported in Table 6. Cell parameters were obtained by least-square refinement of the setting angles for 25 reflections ( $2\theta \leq 25^\circ$ ) on an Enraf-Nonius CAD4 diffractometer. The intensities were corrected for the Lorentz and polarization effects. The structure was solved by direct methods and successive Fourier difference synthesis. Neutral atom scattering factors with anomalous scattering contributions were employed.<sup>43</sup> The pertinent

crystallographic parameters for **8** are summarized in Table 6. Tables in the Supporting Information give the H atom coordinates and *B* values, and bond lengths, bond angles, and anisotropic thermal parameters. All calculations were performed on a MicroVax 3100 using SDP programs.<sup>44</sup>

**Acknowledgment.** We thank the "Ministère de l'enseignement Supérieur et de la Recherche" for the award of a thesis grant to N.P., the European Union (HCM Programme CHRX-CT94-0501) for financial support, and Alain Daridor for technical assistance.

**Supporting Information Available:** Tables of bond lengths, bond angles, hydrogen atomic fractional coordinates and *B* values, and thermal parameters for **6b** and **8** (22 pages). Ordering information is given on any current masthead page.

OM950467W

(43) *International Tables for X-Ray Crystallography*; Birmingham, Kynoch Press: Birmingham, U.K., 1974; Vol. IV. Present Distributor: D. Reidel.

(44) B. A. Frenz, and Associates Inc. SDP: Structure Determination Package. College Station, TX, and Enraf-Nonius, Delft, The Netherlands, 1985.



# Organometallics as Potential Protein Labels: Pirylium and Pyridinium Salts Bearing $(C_6H_5)Cr(CO)_3$ , $(C_5H_4)Mn(CO)_3$ , and Ferrocenyl Substituents

Krisztina L. Malisza,<sup>†</sup> Siden Top,<sup>\*,†</sup> Jacqueline Vaissermann,<sup>‡</sup> Bertrand Caro,<sup>§</sup> Marie-Claude Sénéchal-Tocquer,<sup>§</sup> Denis Sénéchal,<sup>§</sup> Jean-Yves Saillard,<sup>||</sup> Smail Triki,<sup>||</sup> Samia Kahlal,<sup>||</sup> James F. Britten,<sup>⊥</sup> Michael J. McGlinchey,<sup>⊥</sup> and Gérard Jaouen<sup>\*,†</sup>

*Ecole Nationale Supérieure de Chimie (URA 403, CNRS), 11, rue Pierre et Marie Curie, 75231 Paris Cédex 05, France, Laboratoire de Chimie de Métaux de Transition (URA 419, CNRS), Université Pierre et Marie Curie, 4 Place Jussieu, 75005 Paris, France, Laboratoire de Chimie des Organométalliques et Biologie, associé au CNRS, IUT de Lannion, 22302 Lannion Cédex, France, Laboratoire de Chimie du Solide et Inorganique Moléculaire (URA 254, CNRS), Université de Rennes I, 35042 Rennes Cédex, France, and Department of Chemistry, McMaster University, Hamilton, Ontario L8S 4M1, Canada*

Received May 26, 1995<sup>®</sup>

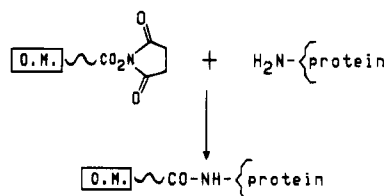
A series of 2,6-dimethyl- or 2,6-diphenylpyrylium cations,  $[R'-C_5H_2R''_2O]^+$ , which bear organometallic substituents at the 4-position, have been synthesized. The molecules in which  $R' = (C_6H_5)Cr(CO)_3$ ,  $R'' = Me$ , **1**,  $R' = (C_5H_4)Mn(CO)_3$ ,  $R'' = Ph$ , **8**,  $R' = (C_5H_4)Fe(C_5H_5)$ ,  $R'' = Me$ , **9**, and  $R' = (C_5H_4)Re(CO)_3$ ,  $R'' = Ph$ , **10**, have been identified spectroscopically, and the complexes **1** and **8** have also been characterized by X-ray crystallography as  $CrC_{16}H_{13}O_4^+ PF_6^-$  and  $MnC_{25}H_{16}O_4^+ BF_4^-$ , respectively. The  $\pi$ -complexed ring bearing either a  $Cr(CO)_3$  or a  $Mn(CO)_3$  moiety is almost coplanar with the pyrylium ring, as are the phenyl rings in **8**. The structural and spectroscopic data indicate that the delocalization of the positive charge on the pyrylium ring onto the metal is rather minimal. These pyrylium salts react readily with benzylamine, or with  $\beta$ -alanine ethyl ester, to form the corresponding pyridinium salts. In particular, the ferrocenyl derivative, **9**, yields a crystalline pyridinium salt, **15**, with the ethyl ester of  $\beta$ -alanine.

## Introduction

The organometallic chemistry of proteins is still a relatively undeveloped field.<sup>1</sup> Even at this early stage, however, certain potentially viable approaches to a variety of different applications can be foreseen. For example, it is possible to envisage the use of organometallic reagents for the specific cleavage of peptide chains.<sup>2</sup> The protein under study can also be coupled to organometallic moieties that play the role of specific markers; these complexes can then be used in the characterization of active sites,<sup>3</sup> for structural determinations by X-ray and NMR methods,<sup>4</sup> in immunological analyses,<sup>5</sup> and even as radiopharmaceuticals.<sup>6</sup>

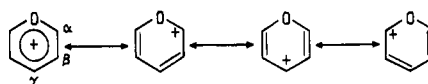
It is noteworthy that, of the organometallic conjugates with proteins that have been reported so far, the majority have been based on a single strategy, namely the coupling of neutral organometallic esters, activated

## Scheme 1. Labeling of Proteins with Organometallics



by a succinimidyl group, with lysine entities, as shown in Scheme 1. This approach is in fact too restrictive and has a number of limitations; for example, there are solubility problems, the global charge of the protein can become modified, and some of the free amino groups can become protonated and therefore unable to react with the organometallic label. Further progress in this area requires the synthesis of new organometallic reagents, preferably charged species, which can couple with specific residues in the protein. It is in this context that we have adopted a novel chemical strategy using organometallic pyrylium salts, and we here present the first results.

As shown as follows, pyrylium salts are heterocycles which possess carbocationic character at the  $\alpha$  and  $\gamma$  positions.



<sup>†</sup> URA 403, CNRS.

<sup>‡</sup> URA 419, CNRS.

<sup>§</sup> Laboratoire de Chimie des Organométalliques et Biologie.

<sup>||</sup> URA 254, CNRS.

<sup>⊥</sup> McMaster University.

<sup>®</sup> Abstract published in *Advance ACS Abstracts*, October 1, 1995.

(1) Jaouen, G.; Vessières, A.; Butler, I. S. *Acc. Chem. Res.* **1993**, *26*, 361 and references therein.

(2) Zhu, L.; Kostic, N. M. *J. Am. Chem. Soc.* **1993**, *115*, 4566.

(3) Vessières, A.; Top, S.; Vaillant, C.; Osella, D.; Mornon, J. P.; Jaouen, G. *Angew. Chem., Int. Ed. Engl.* **1992**, *31*, 753.

(4) Gorfti, A.; Salmain, M.; Jaouen, G. *J. Chem. Soc., Chem. Commun.* **1994**, 433.

(5) Varenne, A.; Salmain, M.; Brisson, C.; Jaouen, G. *Bioconjugate Chem.* **1992**, *3*, 471.

(6) Salmain, M.; Gunn, M.; Gorfti, S.; Top, S.; Jaouen, G. *Bioconjugate Chem.* **1993**, *4*, 425.

This property not only confers on them a key role in heterocyclic chemistry but also has led to the development of a variety of practical applications, notably in photography and reprography.<sup>7</sup>

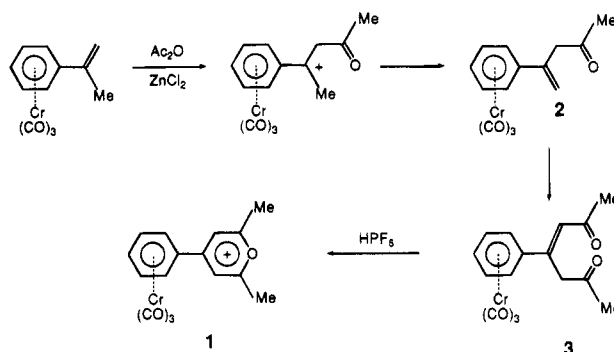
One of the most interesting general reactions of pyrylium salts involves the ready exchange of oxygen for nitrogen in the pyrylium ring to form the corresponding pyridinium salt; indeed, reactions with primary amines proceed under mild conditions and give excellent yields.<sup>8</sup> Surprisingly perhaps, a study of the reaction of pyrylium salts with amino acids or their derivatives was not an immediate undertaking; however, this was an obvious extension to the chemistry and has since been investigated in numerous laboratories.<sup>9</sup> Normally, 2,6-disubstituted or 2,4,6-trisubstituted pyrylium cations are not soluble in water and so make reactions with amino acids difficult. However, this problem has been overcome by synthesizing pyrylium salts containing two or three carboxylic or sulfonic acid groups; by this means, reactions with primary amines, and amino acids such as lysine, have been facilitated.<sup>10</sup>

The first reaction of pyrylium salts with proteins to form the analogous pyridinium salts was accomplished with  $\alpha$ -chymotrypsin, a protein of known amino acid composition. In this exchange process, it was noted that a 2,6-disubstituted pyrylium cation only reacts with a fraction of the available amino groups, presumably those which are particularly exposed.<sup>11</sup>

Despite their inherent interest, the metallocene chemistry of pyrylium ions appears to have been little developed. The only salts to have been isolated are those substituted at the  $\alpha$  or  $\gamma$  position by a ferrocenyl or (cyclopentadienyl)Mn(CO)<sub>3</sub> group.<sup>12,13</sup> We are unaware of any reports of organometallic complexes of pyrylium salts with amino acids, peptides, or proteins.

We here present the syntheses and complete characterizations of a series of pyrylium salts bearing organometallic substituents. In particular, the preparation and first crystallographic characterization of a pyrylium cation substituted by a (phenyl)Cr(CO)<sub>3</sub> group is described and, in the context of the problem of the stabilization of  $\alpha$ -carbocations by such moieties, we discuss the electronic influence of the Cr(CO)<sub>3</sub> tripod vis-à-vis the heterocyclic ring.<sup>14</sup> In particular, it is important for our purposes that the charge on the

## Scheme 2. Synthesis of 1 by Acetylation of (2-phenylpropene)Cr(CO)<sub>3</sub>



pyrylium ring not be too greatly delocalized onto the metal center since one must retain the ability to react readily with amines to yield pyridinium salts. We also describe the reactions of these complexes with benzylamine and with the ethyl ester of  $\beta$ -alanine and discuss the relevance of these observations to the use of organometallic probes to assay biomolecules and also to aid in the crystallization of proteins.

## Results and Discussion

**Synthetic Aspects.** One could envisage two general synthetic approaches to organometallic derivatives of pyrylium salts: the first involves building the heterocyclic ring onto an organometallic complex, while the second route requires incorporation of the organometallic fragment into an existing pyrylium framework. The novel synthesis of [(2,6-dimethyl-4-phenylpyrylium)Cr(CO)<sub>3</sub>]<sup>+</sup>, **1**, by the reaction of (2-phenylpropene)Cr(CO)<sub>3</sub> with acetic anhydride and zinc chloride is an example of the first type. As shown in Scheme 2, the acetyl cation can attack the methylene site in (2-phenylpropene)Cr(CO)<sub>3</sub> to generate a chromium-stabilized benzyl cation which suffers elimination to give the mono(acetyl) derivative, **2**. A second acetylation and subsequent cyclization leads to [(2,6-dimethyl-4-phenylpyrylium)Cr(CO)<sub>3</sub>]<sup>+</sup>, **1**, in 30% yield. In support of this proposed mechanism, we note that the mono- and bis(acetyl) derivatives, **2** and **3**, are isolable in yields of 11% and 12%, respectively.<sup>14,15</sup> The generality of this procedure is demonstrated by the analogous reaction of acetic anhydride and zinc chloride with (1-methyl-3,4-dihydronaphthalene)Cr(CO)<sub>3</sub>, **4**, which forms the first organometallic complex of a condensed ring pyrylium salt, **5**. However, under the same conditions, (1-meth-

(7) Balaban, A. T.; Dinculescu, A.; Dorofeenko, G. N.; Fischer, G. W.; Koblik, A. V.; Mezheritskii, V. V.; Schroth, W. *Pyrylium Salts: Synthesis, Reactions and Physical Properties. Advances in Heterocyclic Chemistry, Suppl. II*; Katritzky, A. R., Ed.; Academic Press: New York, 1982.

(8) Baeyer, A.; Piccard, J. *Justus Liebigs Ann. Chem.* **1911**, *384*, 208.

(9) (a) Toma, C.; Balaban, A. T. *Tetrahedron Suppl.* **1966**, *7*, 27. (b) Katritzky, A. R.; Grzeskowiak, N. E.; Eweiss, N. F.; Elsherbini, E. A. *J. Chem. Soc., Perkin Trans. 1*, **1983**, 497 and references therein.

(10) (a) Katritzky, A. R.; Yang, Y.-K.; Gabrielsen, B.; Marquet, J. *J. Chem. Soc., Perkin Trans. 2*, **1984**, 857. (b) Katritzky, A. R.; Mokrosz, J. L.; Lopez-Rodriguez, M. L. *J. Chem. Soc., Perkin Trans. 2*, **1984**, 875.

(11) O'Leary, M. H.; Samberg, G. A. *J. Am. Chem. Soc.* **1971**, *93*, 3530.

(12) (a) Dorofeenko, G. N.; Krasnikov, V. V.; Pyshchev, A. I. *Khim. Geterotsikl. Soedin.* **1977**, 599 [*Chem. Abs.* **1977**, *87*, 85121]. (b) Ukhin, L. Yu.; Pyshchev, A. I.; Krasnikov, V. V.; Orlova, Zh. I.; Dorofeenko, G. N. *Dokl. Akad. Nauk SSSR* **1977**, *234*, 1351 [*Chem. Abs.* **1977**, *87*, 168162]. (c) Krasnikov, V. V.; Andreichikov, Yu. P.; Kholodova, N. V.; Dorofeenko, G. N. *Zh. Org. Khim.* **1977**, *13*, 1566 [*Chem. Abs.* **1977**, *87*, 152357].

(13) (a) Krasnikov, V. V.; Dorofeenko, G. N. *Khim. Geterotsikl. Soedin.* **1979**, 21 [*Chem. Abs.* **1979**, *90*, 168702]. (b) Dorofeenko, G. N.; Krasnikov, V. V. *Zh. Org. Khim.* **1972**, *8*, 2620 [*Chem. Abs.* **1973**, *78*, 97785]. (c) Milaev, A. G.; Okhlobystin, O. Yu. *Khim. Geterotsikl. Soedin.* **1985**, 593 [*Chem. Abs.* **1986**, *104*, 68978].

(14) A preliminary communication has appeared: Caro, B.; Sénéchal-Tocquer, M.-C.; Sénéchal, D.; Marrec, P.; Saillard, J.-Y.; Triki, S.; Kahlal, S. *Tetrahedron Lett.* **1993**, *34*, 7259.

(15) It is noteworthy that treatment of either (2-phenylpropene)Cr(CO)<sub>3</sub> or (1-methyl-3,4-dihydronaphthalene)Cr(CO)<sub>3</sub>, **4**, with the Perrier complex, *i.e.* AlCl<sub>3</sub>-CH<sub>3</sub>COCl, leads only to the mono-acetylation product: Sénéchal-Tocquer, M.-C.; Le Bihan, J.-Y.; Gentric, D.; Sénéchal, D.; Caro, B. *J. Organomet. Chem.* **1988**, *356*, C5.

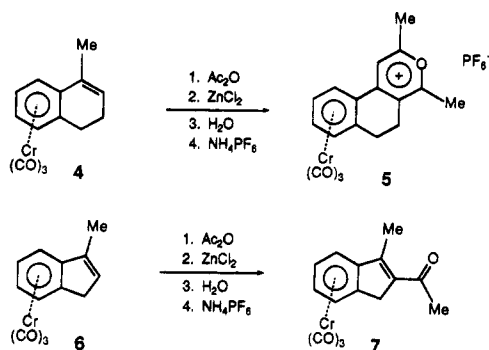
(16) (a) Prall, P. F. G.; Whitear, A. L. *J. Chem. Soc.* **1961**, 3573. (b) Dorofeenko, G. N.; Zhdanov, Yu. A.; Etmetchenko, L. N. *Khim. Geterotsikl. Soedin.* **1969**, 781 [*Chem. Abs.* **1970**, *72*, 111223].

(17) Elschenbroich, Ch.; Salzer, A. *Organometallics—A Concise Introduction*, 2nd ed.; VCH Publishers: Weinheim, Germany, 1992; pp 295–308.

(18) Holmes, J. D.; Jones, D. A. K.; Pettit, R. *J. Organomet. Chem.* **1965**, *4*, 324.

(19) (a) Seyferth, D.; Merola, J. S.; Eschbach, C. S. *J. Am. Chem. Soc.* **1978**, *100*, 4124. (b) Campora, M. A.; Ceccon, A.; Dal Farra, M.; Giacometti, G.; Rigetti, G. *J. Chem. Soc., Perkin 2*, **1977**, 483.

ylindene)Cr(CO)<sub>3</sub>, **6**, yields only the mono(acetyl) derivative **7**.<sup>14</sup>



At present, it is not clear just how much these cyclizations are dependent on the presence of an organometallic fragment to stabilize the intermediate cations. For example, analogous treatment of uncomplexed 2-phenylpropene yields the free pyrylium salt in 50% yield; moreover, attempts to extend this methodology by use of 2-ferrocenylbis(acetyl)propene were unsuccessful.

The second general approach to organometallic derivatives of pyrylium cations is exemplified by the syntheses of the (cyclopentadienyl)Mn(CO)<sub>3</sub> and ferrocenyl complexes **8** and **9**, respectively. In these cases, the appropriate organometallic anion is allowed to react with the preformed heterocycle, which can be either a pyrylium salt or a  $\gamma$ -pyrone.<sup>13</sup> In the former case, one can remove a hydride by means of trityl cation; in the latter, pyrylium formation is induced by protonation and subsequent dehydration (Scheme 3). (Analogously to the synthesis of the manganese complex **8**, [4-(C<sub>5</sub>H<sub>4</sub>)-Re(CO)<sub>3</sub>-2,6-diphenylpyrylium]<sup>+</sup>BF<sub>4</sub><sup>-</sup>, **10**, was also prepared, but discussion of the chemistry of **10** is deferred to a subsequent paper.)

**NMR Spectra of Pyrylium Cations.** It is interesting to compare the <sup>1</sup>H and <sup>13</sup>C NMR spectra of the pyrylium-Cr(CO)<sub>3</sub> complex, **1**, with those of the corresponding noncomplexed molecule, *i.e.* the 2,6-dimethyl-4-phenylpyrylium cation. As is normal, coordination of the Cr(CO)<sub>3</sub> fragment brings about a marked shift to low frequency (high field) of the <sup>1</sup>H and <sup>13</sup>C nuclei in the phenyl ring.<sup>17</sup> What is noticeable, however, is the shielding observed within the pyrylium ring of **1** in both the <sup>1</sup>H and <sup>13</sup>C regimes. The free (*complexed*) chemical shifts of  $\delta$  8.57 (8.34) for H <sub>$\beta$</sub> , and of 179.74 (178.59) for

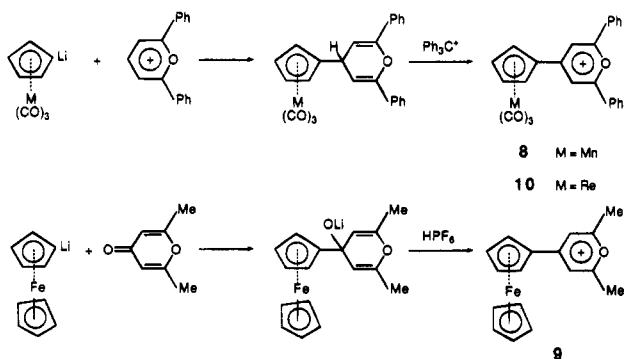
C <sub>$\alpha$</sub> , 119.32 (116.80) for C <sub>$\beta$</sub> , and 167.28 (165.39) for C <sub>$\gamma$</sub> , all indicate a small enhancement of the electron transfer from the phenyl group to the pyrylium ring upon complexation by the Cr(CO)<sub>3</sub> moiety. This metal carbonyl-mediated reinforcement of the phenyl substituent's capacity to delocalize the formal positive charge within the heterocyclic ring is also evident in the infrared spectrum of **1**, which exhibits rather high  $\nu_{CO}$  values of 1993 and 1932 cm<sup>-1</sup> in CH<sub>2</sub>Cl<sub>2</sub> solution.

The ability of a Cr(CO)<sub>3</sub> fragment to stabilize positive charge in the benzylic position has been extensively investigated,<sup>18,19</sup> and it has been demonstrated that one may correlate the barrier to tripodal rotation with the degree of anchimeric assistance provided by the electron-rich metal to the carbocationic center.<sup>20,21</sup> That is, the measured activation energy for rotation of the Cr(CO)<sub>3</sub> group is a sensitive probe for the strength of the direct interaction between the electron-deficient center and the metal atom. To this end, the variable-temperature <sup>13</sup>C NMR spectra of [(4-phenyl-2,6-dimethylpyrylium)Cr(CO)<sub>3</sub>]<sup>+</sup>PF<sub>6</sub><sup>-</sup>, **1**(PF<sub>6</sub>), were recorded down to -100 °C. However, the <sup>13</sup>CO signal remained as a sharp singlet, indicating that the barrier to tripodal rotation in **1** is very low, and consequently that the direct interaction between C <sub>$\gamma$</sub>  and the chromium atom is rather minimal.

**Extended Hückel Molecular Orbital Calculations.** EHMO calculations have revealed that benzyl cations, *e.g.* [(C<sub>6</sub>H<sub>5</sub>CH<sub>2</sub>)Cr(CO)<sub>3</sub>]<sup>+</sup>, or fulvene cations, such as [(C<sub>5</sub>H<sub>4</sub>CH<sub>2</sub>)Fe(C<sub>5</sub>H<sub>5</sub>)]<sup>+</sup>, are stabilized by direct interaction of the electron-deficient benzylic center by the metal atom.<sup>20,22</sup> The sp<sup>2</sup>-hybridized carbon must lean toward the chromium or iron so as to optimize the overlap between the vacant p orbital on carbon with a filled d orbital on the metal.<sup>23</sup> The calculations also suggest that the positive charge is delocalized onto the *ortho* and *para* phenyl carbons; this makes the *ipso* and *meta* sites better donors to the metal atom. Since the chromium maintains its preferred octahedral geometry, this translates into a strong preference for the tripod to adopt an orientation such that the three carbonyl ligands eclipse the *ortho* and *para* carbons of the phenyl ring.<sup>24</sup> For a simple [C<sub>6</sub>H<sub>5</sub>CH<sub>2</sub>]<sup>+</sup> group, the bend angle toward the Cr(CO)<sub>3</sub> is calculated to be approximately 20°. <sup>20,22</sup> There are no crystallographically established structures of [(benzyl)Cr(CO)<sub>3</sub>]<sup>+</sup> cations, but an ( $\eta^7$ -benzyl)zirconium cationic complex was recently reported in which the phenyl ring adopts a shallow boat conformation and the exocyclic methylene fragment bends toward the metal such that the Zr...C <sub>$\alpha$</sub>  distance is only 2.65 Å.<sup>25</sup>

EHMO calculations on [(4-phenyl-2,6-dimethylpyrylium)Cr(CO)<sub>3</sub>]<sup>+</sup>, **1**, show not only that the tripod should be oriented in the eclipsed manner indicated previously but also that the most energetically favored structure

### Scheme 3. Route to Pyrylium Salts by Reaction of Lithiated Organometallics with Preformed Heterocycles



(20) Downton, P. A.; Sayer, B. G.; McGlinchey, M. J. *Organometallics* **1992**, *11*, 3281.

(21) Malisza, K. L.; Chao, L. C. F.; Britten, J. F.; Sayer, B. G.; Jaouen, G.; Top, S.; Decken, A.; McGlinchey, M. J. *Organometallics* **1993**, *12*, 2462.

(22) Albright, T. A.; Hoffmann, R.; Hofmann, P. *Chem. Ber.* **1978**, *111*, 1591.

(23) (a) Lupon, S.; Kapon, M.; Cais, M.; Herstein, F. H. *Angew. Chem., Int. Ed. Engl.* **1972**, *11*, 1025. (b) Behrens, U. *J. Organomet. Chem.* **1979**, *182*, 89.

(24) (a) Carter, O. L.; McPhail, A. T.; Sim, G. A. *J. Chem. Soc. A* **1966**, 822. (b) *Ibid.* **1971**, 1619. (c) Albright, T. A.; Hoffmann, P. *R. J. Am. Chem. Soc.* **1977**, *99*, 7546.

(25) Pellecchia, C.; Immirzi, A.; Pappalardo, D.; Peluso, A. *Organometallics* **1994**, *13*, 3773.

Table 1. Structure Determination Summary

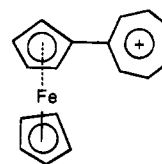
	1(PF <sub>6</sub> )	8(BF <sub>4</sub> )	15(PF <sub>6</sub> )
empirical formula	CrC <sub>16</sub> H <sub>13</sub> O <sub>4</sub> PF <sub>6</sub>	MnC <sub>25</sub> H <sub>16</sub> O <sub>4</sub> BF <sub>4</sub>	FeC <sub>22</sub> H <sub>26</sub> NO <sub>2</sub> BF <sub>4</sub>
fw	466.24	522.14	537.26
dimens, mm	0.4 × 0.15 × 0.15	0.32 × 0.34 × 0.50	0.25 × 0.08 × 0.01
cryst syst	monoclinic	monoclinic	monoclinic
space group	<i>P</i> 2 <sub>1</sub> / <i>n</i>	<i>P</i> 2 <sub>1</sub> / <i>n</i>	<i>P</i> 2 <sub>1</sub>
<i>a</i> , Å	10.739(6)	9.285(2)	7.8320(10)
<i>b</i> , Å	11.404(5)	13.668(2)	10.651(2)
<i>c</i> , Å	16.306(9)	17.894(8)	14.053(3)
<i>b</i> , deg	109.06(4)	94.95(3)	91.24(1)
<i>V</i> , Å <sup>3</sup>	1887.5	2262(5)	1172.0(4)
<i>F</i> (000)	936	1056	552
<i>Z</i>	4	4	2
$\rho_{\text{calc}}$ , g·cm <sup>-3</sup>	1.641	1.53	1.522
radiation ( $\lambda$ , Å)	Mo K $\alpha$ (0.710 73)	Mo K $\alpha$	Mo K $\alpha$
monochromator	graphite	graphite	graphite
temp, K	293	293	293
$\mu$ (Mo K $\alpha$ ), cm <sup>-1</sup>	7.484	6.21	7.79
scan method	$\theta$ -2 $\theta$	$\theta$ -2 $\theta$	$\theta$ -2 $\theta$
2 $\theta$ range, deg	2-50	2-56	5-60
index ranges	0 ≤ <i>h</i> ≤ 12, 0 ≤ <i>k</i> ≤ 13, -19 ≤ <i>l</i> ≤ 19	-12 ≤ <i>h</i> ≤ 12, 0 ≤ <i>k</i> ≤ 18, 0 ≤ <i>l</i> ≤ 23	-1 ≤ <i>h</i> ≤ 9, -12 ≤ <i>k</i> ≤ 12, -16 ≤ <i>l</i> ≤ 16
no. of measd rflns	3520	5607	4803
no. of unique rflns	3341	5443	4365
no. of obsd rflns	1697 ( <i>I</i> ≥ 6 $\sigma$ ( <i>I</i> ))	2834 ( <i>I</i> ≥ 3 $\sigma$ ( <i>I</i> ))	2643 ( <i>I</i> ≥ 2 $\sigma$ ( <i>I</i> ))
no. of variables	254	366	285
<i>R</i> <sup>*</sup>	0.062	0.047	0.1001
<i>R</i> <sub>w</sub>	0.081	0.046	0.2340
GOF	2.057	2.66	1.029
weighting scheme	4 <i>F</i> <sub>o</sub> <sup>2</sup> /[ $\sigma^2(I)^2 + (0.07 F_o ^2)^2$ ]	unit weights	<i>a</i>
largest diff peak, e Å <sup>-3</sup>	0.670	0.56	0.886
largest diff hole, e Å <sup>-3</sup>	-0.361	-0.49	-0.844

$$^a \omega = [\sigma^2 F_o^2 + (0.1360p)^2 + (3.63p)]^{-1}, \text{ where } p = [\max(F_o^2, 0) + 2F_c^2]/3.$$

maintains the coplanar nature of the phenyl and pyrylium rings. There is no tendency for the pyrylium ring to lean toward the Cr(CO)<sub>3</sub> moiety. Furthermore, to the extent that we choose to believe the EHMO-derived charge distribution, the pyrylium ring in the free ligand, [4-phenyl-2,6-dimethylpyrylium]<sup>+</sup>, carries 90% of the positive charge, but this is reduced to 88% in the chromium complex **1**. That is, in agreement with the NMR data, the calculations support the idea of somewhat enhanced delocalization of the positive charge from the pyrylium ring onto the (C<sub>6</sub>H<sub>5</sub>)Cr(CO)<sub>3</sub> fragment. However, it is clear that such a process cannot occur via direct interaction of the  $\gamma$ -carbon of the pyrylium ring with the chromium but rather via overlap between the filled  $\pi$ -manifold of the phenyl ring with vacant  $\pi^*$  levels of the heterocycle. The HOMO in **1** is primarily a d<sub>z<sup>2</sup></sub> orbital on chromium while the LUMO has  $\pi^*$  character distributed over both rings. The noncomplexed cations are colorless, their electronic absorption spectra have been interpreted by analogy to the analogous benzenes and pyridines, and the lowest energy absorption has been assigned as a  $\pi \rightarrow \pi^*$  transition.<sup>26</sup> However, the organometallic pyrylium salts **1**, **8**, **9**, and **10** are intensely colored (blue, red, or green) perhaps attributable to metal  $\rightarrow$  ligand charge transfer. Overall, the net result of incorporating a  $\pi$ -Cr(CO)<sub>3</sub> moiety is to reduce the HOMO-LUMO gap and so move the lowest energy transitions into the visible region.

In summary, as originally noted by Trahanovsky,<sup>27</sup> it appears as though the organometallic fragment has the capacity and electronic flexibility to respond appropriately to the demands of a neighboring benzylic

cation. Thus, in contrast to a CH<sub>2</sub><sup>+</sup> substituent, which requires considerable anchimeric assistance, a stable cationic system, such as a pyrylium ring, is almost unaffected by the organometallic moiety. This result is reminiscent of the ferrocenyl-substituted tropylium system, **11**, in which the aromatic C<sub>7</sub> ring has no need



11

for electronic assistance from the metal.<sup>28</sup> Overall therefore, the presence of the ferrocenyl or metal carbonyl moieties does not materially change the chemistry of these pyrylium salts; in particular, they retain their propensity to react with primary amines to yield pyridinium salts.

**X-ray Crystal Structures of 1 and 8.** Blue-purple crystals of [(4-phenyl-2,6-dimethylpyrylium)Cr(CO)<sub>3</sub>]<sup>+</sup>PF<sub>6</sub><sup>-</sup>, **1**(PF<sub>6</sub>), and red cubes of [(4-cyclopentadienyl-2,6-diphenylpyrylium)Mn(CO)<sub>3</sub>]<sup>+</sup>BF<sub>4</sub><sup>-</sup>, **8**(BF<sub>4</sub>), were selected for X-ray diffraction studies. The crystallographic data collection parameters appear in Table 1, and the atomic positional parameters for molecules **1**(PF<sub>6</sub>) and **8**(BF<sub>4</sub>) are collected in Tables 2 and 3, respectively. Views of the pyrylium cations **1** and **8** appear as Figures 1 and 2.

In the chromium complex, **1**, the pyrylium and phenyl rings are nearly coplanar; they exhibit a dihedral angle of 14° between the ring planes. The C <sub>$\gamma$</sub> -C<sub>ipso</sub> distance

(26) Wilt, J. R.; Reynolds, G. A.; Van Allen, J. A. *Tetrahedron* **1973**, *29*, 1488

(27) Trahanovsky, W. S.; Wells, D. K. *J. Am. Chem. Soc.* **1968**, *91*, 5870.

(28) Brownstein, S. K.; Gabe, E. J.; Hynes, R. C. *Can. J. Chem.* **1992**, *70*, 1011.

**Table 2. Atomic Coordinates ( $\times 10^4$ ) and Equivalent Isotropic Displacement Parameters ( $\text{\AA}^2 \times 10^3$ ) for 1(PF<sub>6</sub>)**

	<i>x</i>	<i>y</i>	<i>z</i>	<i>U</i> <sub>eq</sub> <sup>a</sup>
Cr	2365(1)	1969.5(9)	-0367.8(6)	42(4)
O(1)	-1002(4)	3702(4)	1566(3)	63(3)
C(1)	0210(6)	3358(5)	0334(4)	44(3)
C(2)	0828(6)	3936(6)	1108(4)	52(3)
C(3)	0240(6)	4091(6)	1709(4)	56(4)
C(4)	-1631(7)	3151(6)	0831(5)	59(4)
C(5)	-1084(6)	2964(6)	0204(4)	52(3)
C(6)	0784(8)	4681(7)	2562(5)	77(5)
C(7)	-2995(8)	2758(9)	0783(6)	96(6)
C(11)	0816(6)	3222(5)	-0346(4)	40(3)
C(12)	1997(6)	3826(5)	-0296(4)	48(3)
C(13)	2596(7)	3677(6)	-0936(4)	57(4)
C(14)	2074(8)	2870(6)	-1610(4)	66(5)
C(15)	0909(7)	2270(6)	-1665(4)	57(4)
C(16)	0302(6)	2407(6)	-1045(4)	50(3)
C(21)	1798(7)	0633(6)	0047(5)	64(4)
C(22)	3635(7)	2102(6)	0695(4)	51(3)
C(23)	3500(8)	1011(8)	-0702(5)	85(5)
O(21)	1524(7)	-0213(5)	0333(5)	114(5)
O(22)	4423(6)	2180(6)	1355(4)	88(4)
O(23)	4184(7)	0431(6)	-0928(4)	158(5)
P	4396(2)	5925(2)	2045(1)	62(1)
F(1)	4203(9)	5441(7)	1131(4)	224(9)
F(2)	2984(6)	6309(7)	1682(6)	215(9)
F(3)	3883(5)	4760(4)	2345(4)	101(4)
F(4)	458(1)	6412(7)	2922(4)	260(9)
F(5)	5777(6)	5404(6)	2274(5)	196(9)
F(6)	4910(6)	7073(4)	1733(4)	123(9)

<sup>a</sup> *U*<sub>eq</sub> is defined as one-third of the trace of the orthogonalized *U*<sub>ij</sub> tensor.

of 1.47 Å suggests that there is considerable conjugation between the two rings. These data may be compared with structural data for the noncomplexed 2,4,6-triphenylpyrylium cation in which the  $\gamma$ -phenyl ring is rotated by 18° and the  $\alpha$ -phenyls are rotated by 10.4 and 2.3° relative to the pyrylium ring.<sup>29</sup> The Cr(CO)<sub>3</sub> fragment in **1** is symmetrically bonded with respect to the carbons of the phenyl ring and adopts an anti-eclipsed conformation which is typical for aromatic complexes bearing strongly electron-withdrawing substituents;<sup>24</sup> that is, the carbonyl ligands lie directly beneath the *ortho* and *para* carbons of the phenyl ring, as anticipated from the EHMO calculations. Similarly, in the manganese system **8**, the pyrylium and cyclopentadienyl rings make an interplanar dihedral angle of only 6°. The phenyl substituents in **8** exhibit small dihedral angles (+4 and -8°) with the plane of the pyrylium ring, and they are displaced *exo* with respect to the metal by  $\approx 8^\circ$ ; thus, conjugation throughout the molecule is optimized. As in **1**, the Mn(CO)<sub>3</sub> tripod in **8** is oriented such that one carbonyl ligand lies in the (approximate) molecular mirror plane. It is especially noticeable that in both **1** and **8** there is no tendency for the  $\gamma$ -carbon of the pyrylium ring to lean toward the metal atom. Clearly, the pyrylium ring has no need for anchimeric assistance from the electron-rich metal center! This observation parallels the situation found in the ferrocenyl-substituted tropylium system, **11**, in which the C<sub>5</sub> and C<sub>7</sub> rings were essentially coplanar, at least in the solid state.<sup>28</sup>

**Bioassays and Pyridinium Salts.** The use of metal carbonyls as convenient, non-radioactive labels for bio-

**Table 3. Atomic Coordinates ( $\times 10^4$ ) and Equivalent Isotropic Displacement Parameters ( $\text{\AA}^2 \times 10^3$ ) for 8(BF<sub>4</sub>)**

	<i>x</i>	<i>y</i>	<i>z</i>	<i>U</i> <sub>eq</sub> <sup>a</sup>
Mn	2228.2(7)	9133.9(5)	9371.6(4)	44(3)
O(1)	1987(3)	4988(2)	9679(2)	46(2)
C(1)	2801(4)	6852(3)	9335(2)	41(2)
C(2)	3425(4)	6361(3)	9979(2)	44(2)
C(3)	3023(4)	5437(3)	10134(2)	43(2)
C(4)	1344(4)	5425(3)	9059(2)	44(2)
C(5)	1739(5)	6347(3)	8886(2)	46(3)
C(11)	3289(4)	7818(3)	9128(2)	43(2)
C(12)	4287(5)	8441(3)	9547(2)	48(3)
C(13)	4457(5)	9289(3)	9140(3)	50(3)
C(14)	3564(5)	9212(4)	8455(2)	52(3)
C(15)	2870(5)	8322(3)	8446(2)	48(3)
C(21)	1976(5)	9105(4)	10352(3)	58(3)
C(22)	1837(6)	10424(4)	9358(3)	67(4)
C(23)	0384(6)	8825(4)	9110(3)	68(4)
O(21)	1811(4)	9095(3)	10975(2)	84(3)
O(22)	1599(5)	11242(3)	9375(3)	93(4)
O(23)	-0781(4)	8591(4)	8936(3)	98(4)
C(31)	3594(4)	4811(3)	10752(2)	46(2)
C(32)	4605(5)	5174(4)	11294(3)	58(3)
C(33)	5142(6)	4593(4)	11882(3)	65(3)
C(34)	4686(6)	3645(4)	11937(3)	66(4)
C(35)	3691(6)	3281(4)	11404(3)	66(4)
C(36)	3150(5)	3846(3)	10810(3)	56(3)
C(41)	0268(5)	4807(3)	8645(2)	47(3)
C(42)	-0611(5)	5192(4)	8054(3)	53(3)
C(43)	-1638(5)	4609(4)	7667(3)	60(3)
C(44)	-1802(6)	3656(4)	7867(3)	66(4)
C(45)	-0937(7)	3270(4)	8445(3)	76(5)
C(46)	0099(6)	3832(4)	8832(3)	66(4)
B(1)	5863(7)	7875(5)	11748(3)	61(4)
F(10)	5146(3)	7425(3)	12288(2)	83(3)
F(92)	6953(4)	8423(3)	12076(2)	86(3)
F(3)	4960(5)	8484(4)	11350(2)	129(3)
F(4)	6328(5)	7229(3)	11260(3)	124(5)

<sup>a</sup> *U*<sub>eq</sub> is defined as one-third of the trace of the orthogonalized *U*<sub>ij</sub> tensor.

assays is now a viable and versatile technique.<sup>30</sup> The Carbonyl Metallo Immuno Assay (CMIA) method takes advantage of the very intense metal carbonyl infrared vibrations in the spectral window  $\approx 2100$ – $1900$  cm<sup>-1</sup> in which absorption by proteins or other biomolecules is minimal. The power of modern Fourier transform infrared spectrometers permits the ready detection of these  $\nu_{CO}$  resonances, even at picomolar levels, and so avoids the inconveniences and environmental problems associated with the disposal of radioactive materials. This approach has been extensively investigated for hormonal steroid receptor sites, and some progress has also been made toward labeling proteins by using Bolton–Hunter reagents (*N*-succinimidyl esters) bearing an (alkyne)Co<sub>2</sub>(CO)<sub>6</sub> moiety.<sup>5,31</sup> Another technique sufficiently sensitive for detecting organometallic labels in very low concentrations depends on the electrochemical properties of the ferrocenyl unit. Candidate molecules must satisfy several criteria for potential use in bio-organometallic assay procedures. Neutral reagents are generally insoluble in the same medium as the protein; moreover, organometallic cations such as co-

(29) Tamamura, T.; Yamare, T.; Yasuoka, N.; Kasai, N. *Bull. Chem. Soc. Jpn.* **1974**, *47*, 832.

(30) (a) Jaouen, G.; Vessières, A.; Top, S.; Ismail, A. A.; Butler, I. S. *J. Am. Chem. Soc.* **1985**, *107*, 4778. (b) Top, S.; Jaouen, G.; Vessières, A.; Abjean, J.-P.; Davoust, D.; Rodger, C. A.; Sayer, B. G.; McGlinchey, M. J. *Organometallics* **1985**, *4*, 2143. (c) Vessières, A.; Jaouen, G.; Gruselle, M.; Rossignol, J. L.; Savignac, M.; Top, S.; Greenfield, S. J. *Steroid Biochem.* **1988**, *30*, 301. (d) Gruselle, M.; Deprez, P.; Vessières, A.; Greenfield, S.; Jaouen, G.; Larue, J. C.; Thouvenot, D. *J. Organomet. Chem.* **1989**, *359*, C53.

(31) Bolton, A. E.; Hunter, W. M. *Biochem. J.* **1973**, *133*, 529.

**Table 4. Atomic Coordinates ( $\times 10^4$ ) and Equivalent Isotropic Displacement Parameters ( $\text{\AA}^2 \times 10^3$ ) for  $15(\text{PF}_6)$**

	<i>x</i>	<i>y</i>	<i>z</i>	<i>U</i> (eq) <sup>a</sup>
Fe	2624(2)	8637(2)	9372(1)	46(1)
C(11)	4776(13)	8369(11)	8615(8)	44(3)
C(12)	3658(16)	7336(10)	8516(9)	49(3)
C(13)	3363(20)	6793(13)	9401(11)	68(4)
C(14)	4285(15)	7468(12)	10089(9)	52(3)
C(15)	5165(13)	8446(12)	9633(8)	48(3)
C(21)	843(28)	9612(21)	8579(14)	47(6)
C(22)	20(24)	8767(20)	9166(17)	53(5)
C(23)	475(30)	9049(23)	10102(18)	58(7)
C(24)	1579(34)	10069(27)	10094(16)	66(8)
C(25)	1806(29)	10417(21)	9153(19)	61(9)
C(1)	5308(12)	9249(10)	7898(7)	35(2)
C(2)	4623(14)	9247(11)	6986(8)	45(3)
C(3)	5175(13)	10100(10)	6306(7)	39(2)
C(4)	7098(14)	10989(10)	7421(8)	41(2)
C(5)	6561(13)	10175(10)	8108(7)	39(2)
C(31)	4309(17)	10114(13)	5342(7)	57(3)
C(41)	8356(16)	11980(11)	7678(9)	55(3)
N(1)	6432(11)	10917(8)	6535(6)	37(2)
C(6)	7149(15)	11731(12)	5783(8)	50(3)
C(7)	8650(15)	11078(12)	5341(9)	49(3)
C(8)	9318(16)	11836(12)	4509(9)	53(3)
O(1)	8586(13)	12715(10)	4152(7)	80(3)
O(2)	10758(12)	11365(10)	4188(7)	72(3)
C(9)	11578(30)	12021(22)	3450(17)	69(6)
C(10)	12459(37)	11137(26)	2829(19)	151(10)
P(1)	2905(4)	13614(5)	7011(3)	76(1)
F(1)	3246(20)	15048(12)	6790(12)	81(2)
F(2)	2469(20)	12098(12)	7027(11)	81(2)
F(3)	3605(35)	13243(18)	5917(13)	84(3)
F(4)	4702(21)	13402(20)	7405(18)	84(3)
F(5)	1971(35)	13837(22)	7924(15)	84(3)
F(6)	1049(29)	13709(23)	6391(23)	84(3)

<sup>a</sup> *U*(eq) is defined as one-third of the trace of the orthogonalized  $U_{ij}$  tensor.

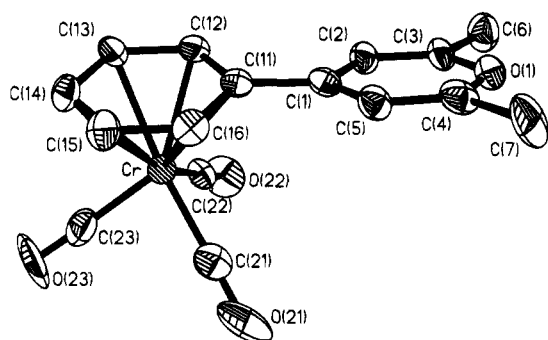


**Figure 1.** View of the chromium cation **1**, showing the atomic numbering scheme. *Salient bond lengths (Å) and angles (deg):* C(1)–C(11) 1.47(1), C(1)–C(2) 1.386(8), C(2)–C(3) 1.34(1), C(3)–O(1) 1.352(8), O(1)–C(4) 1.326(8), C(4)–C(5) 1.35(1), C(5)–C(1) 1.409(9), plane C(1)–C(5)/plane C(11)–C(16) 14°.

baltocenium merely interact in an ionic fashion with the protein.<sup>32</sup> What is needed is a strong covalent attachment which avoids significantly altering the electronic and structural characteristics of the protein. These criteria are well matched by pyrylium salts bearing organometallic substituents; the reactions of these oxygenated heterocycles with exposed amino acids, *e.g.* lysine, should lead to formation of pyridinium salts such that each accessible lysine is now tagged with an organometallic label.

To establish the viability of this approach, it is necessary to allow the organometallic-pyrylium cations

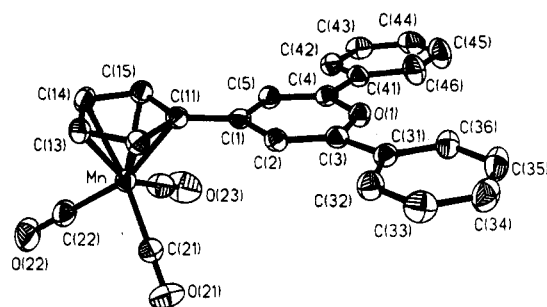


**Figure 2.** View of the manganese cation **8**, showing the atomic numbering scheme. *Salient bond lengths (Å) and angles (deg):* C(1)–C(11) 1.454(6), C(1)–C(2) 1.413(6), C(2)–C(3) 1.353(6), C(3)–O(1) 1.352(5), O(1)–C(4) 1.353(5), C(4)–C(5) 1.356(6), C(5)–C(1) 1.399(6), plane C(1)–C(5)/plane C(11)–C(15) 6°.

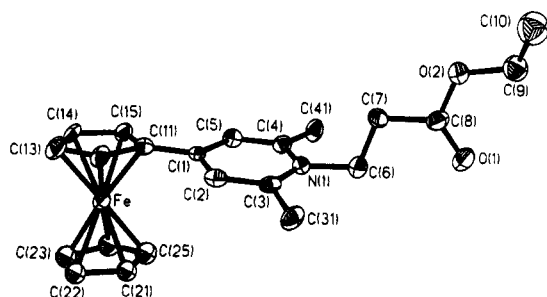
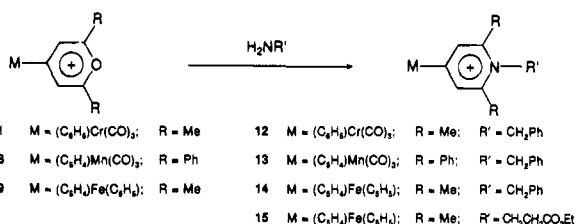


**Figure 3.** View of the ferrocenyl cation **15**, showing the atomic numbering scheme. *Salient bond lengths (Å) and angles (deg):* C(1)–C(11) 1.45(2), C(1)–C(2) 1.38(2), C(2)–C(3) 1.39(2), C(3)–N(1) 1.347(13), N(1)–C(4) 1.342(14), C(4)–C(5) 1.37(2), C(5)–C(1) 1.42(2), N(1)–C(6) 1.487(14), C(6)–C(7) 1.51(2), C(7)–C(8) 1.52(2), C(8)–O(1) 1.202(14), C(8)–O(2) 1.322(14), O(2)–C(9) 1.42(2), C(9)–C(10) 1.47(3), plane C(1)–C(5)/plane C(11)–C(15) 10°.

#### Scheme 4. Reactions of Pyrylium Salts with Amines To Generate Pyridinium Salts



to react with a variety of primary amines and amino acids, and to confirm the identity of the pyridinium salts formed. To this end, the chromium-, manganese-, and iron-containing pyrylium cations, **1**, **8**, and **9**, respectively, were treated with benzylamine and the ethyl ester of  $\beta$ -alanine (Scheme 4). The pyridinium salts produced were identified by their NMR spectra. Furthermore, the product arising from the reaction of the ferrocenylpyrylium cation, **9**, and the ethyl ester of  $\beta$ -alanine yielded crystals suitable for X-ray diffraction studies.

Blue crystals of  $[N-(\beta\text{-alaninyl ethyl ester})\text{-}4\text{-ferrocenyl-}2,6\text{-dimethylpyridinium}]^+ [\text{PF}_6]^-$ , **15**( $\text{PF}_6$ ), were obtained by recrystallization from dichloromethane/pentane. The X-ray crystal structure confirmed that the pyrylium cation had been transformed into a pyridinium salt, as shown in Figure 3. It is immediately apparent that the pyridinium ring follows the trend observed already with the pyrylium salts **1** and **8**; that is, the heterocycle is aligned almost coplanar with the  $\pi$ -com-

(32) Salmain, M. Unpublished results from these laboratories.

plexed cyclopentadienyl ring. The Fe...C $\gamma$  distance is 3.05 Å, too long for a viable direct interaction. Although there is no crystallographically imposed mirror plane, the molecular symmetry of the cation is close to C<sub>s</sub>. The alkyl chain adopts an almost planar conformation and is oriented almost orthogonal to the pyridinium ring.

These reactions to produce pyridinium salts are, of course, the basis for the modification of amino groups in proteins, especially lysine residues located at the surface. We note also that the incorporation of organometallic fragments, e.g. (C<sub>5</sub>Me<sub>5</sub>)Rh, into nucleobases has greatly facilitated crystallization of the modified biomolecule.<sup>33</sup> The extension of these concepts to proteins, in particular  $\alpha$ -chymotrypsin and also bovine serum albumin, is currently under investigation in these laboratories.<sup>34</sup>

## Experimental Section

All preparations involving organometallic pyrylium complexes were carried out under an atmosphere of dry nitrogen utilizing conventional benchtop techniques. Solvents were dried and distilled according to standard procedures.<sup>35</sup> <sup>1</sup>H and <sup>13</sup>C NMR spectra were recorded in acetone-*d*<sub>6</sub> on Bruker AM 200 or Bruker AM 250 spectrometers. Infrared spectra were recorded on a Bomem-Michelson 100 FT-IR spectrophotometer using NaCl plates. Microanalytical data are from Université Pierre et Marie Curie, Service Régional de Microanalyse, Paris, France.

[(2,6-dimethyl-4-phenylpyrylium)Cr(CO)<sub>3</sub>]<sup>+</sup>PF<sub>6</sub><sup>-</sup>, **1**(PF<sub>6</sub><sup>-</sup>). 2-Phenylpropanol (4.0 g, 29.4 mmol) and Cr(CO)<sub>3</sub> (7.0 g, 31.8 mmol) in dry THF (20 mL) and di-*n*-butyl ether (100 mL) were heated under reflux for 2 days. After cooling, the product was filtered to recover Cr(CO)<sub>3</sub> (1.3 g, 5.9 mmol) and the solvent was removed under vacuum. The mixture was chromatographed on a silica plate, and elution with ether: pentane (30:70) yielded yellow needles of (2-phenylpropanol)-Cr(CO)<sub>3</sub> (5.2 g, 19.1 mmol; 65%). The complexed alcohol (1.5 g, 5.5 mmol) was dissolved in CH<sub>2</sub>Cl<sub>2</sub> (30 mL), amberlyst acid catalyst (Fluka) was added, and the mixture was allowed to stir for 5 h at ambient temperature. The product was filtered, and the solvent removed under vacuum, to yield an orange solid. The mixture was chromatographed on a silica plate and elution with ether:pentane (35:65) to yield orange crystals of (2-phenylpropene)Cr(CO)<sub>3</sub> (1.04 g, 4.1 mmol; 74%).

(2-phenylpropene)Cr(CO)<sub>3</sub> (1.0 g, 3.9 mmol) was treated with acetic anhydride (130 mL) and a large excess of ZnCl<sub>2</sub> (12.0 g, 88 mmol). (Care must be taken to add the ZnCl<sub>2</sub> slowly so that the reaction temperature does not exceed room temperature.) The mixture was allowed to stir for 90 min and then poured onto crushed ice. After ether extraction, the aqueous layer was separated and treated with NH<sub>4</sub>PF<sub>6</sub> (3 g). The product was filtered and washed with ether to yield purple crystals of [(2,6-dimethyl-4-phenylpyrylium)Cr(CO)<sub>3</sub>]<sup>+</sup>PF<sub>6</sub><sup>-</sup>, **1**(PF<sub>6</sub><sup>-</sup>), (0.60 g, 1.29 mmol; 32%). IR (CH<sub>2</sub>Cl<sub>2</sub>):  $\nu_{\text{CO}}$  at 1993 and 1932 cm<sup>-1</sup>. <sup>1</sup>H NMR (200 MHz, acetone-*d*<sub>6</sub>):  $\delta$  8.35 (s, 2H, H<sub>3,5</sub>), 6.83 (d, 2H, H<sub>2,6</sub>), 6.39 (t, 1H, H<sub>4</sub>), 5.87 (t, 2H, H<sub>3,5</sub>), 2.96 (s, 6H, Me's).

[(2,6-dimethyl-3,4-dihydronaphtho[2',1':3,4]pyrylium)-Cr(CO)<sub>3</sub>]<sup>+</sup>PF<sub>6</sub><sup>-</sup>, **5**(PF<sub>6</sub><sup>-</sup>). The same protocol applied to (1-methyl-3,4-dihydronaphthalene)Cr(CO)<sub>3</sub>, **4** (0.66 g, 2.36 mmol), yielded blue crystals of **5**(PF<sub>6</sub><sup>-</sup>) (0.70 g, 1.42 mmol; 60%). IR (KBr):  $\nu_{\text{CO}}$  at 1985, 1950, and 1925 cm<sup>-1</sup>. <sup>1</sup>H NMR (300 MHz,

acetone-*d*<sub>6</sub>):  $\delta$  8.41 (s, 1H), 6.66 (d, 1H), 6.38 (t, 1H), 5.89 (t, 1H), 3.35–3.01 (m, 4H), 2.99 (s, 3H), 2.98 (s, 3H).

[(4-cyclopentadienyl-2,6-diphenylpyrylium)Mn(CO)<sub>3</sub>]<sup>+</sup>BF<sub>4</sub><sup>-</sup>, **8**(BF<sub>4</sub><sup>-</sup>). Following the method of Milaev,<sup>13c</sup> *n*-butyllithium (1.88 mL of 1.6 M solution in hexane, 3 mmol) was added dropwise, with rapid stirring, to (C<sub>5</sub>H<sub>5</sub>)Mn(CO)<sub>3</sub> (0.67 g, 3.27 mmol) in dry THF (10 mL) at -60 °C. After the mixture was stirred rapidly at -60 °C for 1 h, (2,6-diphenylpyrylium)<sup>+</sup>PF<sub>6</sub><sup>-</sup> (1.13 g, 3 mmol) in THF/ether was added slowly via a dropping funnel to the reaction mixture at -60 °C and the solution turned dark red. The mixture was slowly allowed to warm to 0 °C, and a solution of ammonium chloride was added. After extraction with ether, and drying over MgSO<sub>4</sub>, the product was subjected to flash column chromatography on Al<sub>2</sub>O<sub>3</sub> and eluted with pentane to yield a beige solid (0.315 g, 0.72 mmol; 24%). To this manganese complex was added acetonitrile (10 mL) and Ph<sub>3</sub>C<sup>+</sup>BF<sub>4</sub><sup>-</sup> (238 mg, 0.72 mmol). After being stirred for 30 min, the mixture was diluted with ether (50 mL) and filtered to give **8**(BF<sub>4</sub><sup>-</sup>) as dark red-brown crystals (0.335 g, 0.64 mmol; 89%). IR (CH<sub>2</sub>Cl<sub>2</sub>):  $\nu_{\text{CO}}$  at 2035 and 1962 cm<sup>-1</sup>. <sup>1</sup>H NMR (200 MHz, acetone-*d*<sub>6</sub>):  $\delta$  8.84 (s, 2H, H<sub>3,5</sub>), 8.55–7.7 (m, 10H, phenyl-H's), 6.78 (t, 2H, Cp-H's), 5.66 (t, 2H, Cp-H's). Anal. Calcd for C<sub>25</sub>H<sub>16</sub>O<sub>4</sub>MnBF<sub>4</sub>: C, 57.52; H, 3.07. Found: C, 57.47; H, 3.14.

(4-ferrocenyl-2,6-dimethylpyrylium)<sup>+</sup>PF<sub>6</sub><sup>-</sup>, **9**(PF<sub>6</sub><sup>-</sup>). Following the method of Dorofeenko,<sup>13b</sup> 2,6-dimethyl- $\gamma$ -pyrone (1.0 g, 8 mmol) in dry THF was added dropwise to ferrocenyllithium at -30 °C under argon. The stirred mixture was allowed to warm to room temperature slowly overnight, and the resulting material was treated with an excess of HPF<sub>6</sub> (1.8 mL, 20 mmol). The product was dissolved in CH<sub>2</sub>Cl<sub>2</sub>, washed with water, and treated with pentane to precipitate the salt. The product was filtered out and washed several times with ether to yield blue crystals of **9**(PF<sub>6</sub><sup>-</sup>) (0.95 g, 2.2 mmol; 27%). <sup>1</sup>H NMR (200 MHz, acetone-*d*<sub>6</sub>):  $\delta$  7.86 (s, 2H, H<sub>3,5</sub>), 5.47 (t, 2H, Cp-H's), 5.34 (t, 2H, Cp-H's), 4.37 (s, 5H, Cp), 2.70 (s, 6H, Me's).

[(4-cyclopentadienyl-2,6-diphenylpyrylium)Re(CO)<sub>3</sub>]<sup>+</sup>BF<sub>4</sub><sup>-</sup>, **10**(BF<sub>4</sub><sup>-</sup>). *n*-Butyllithium (1.15 mL of 1.6 M solution in hexane, 1.84 mmol) was added dropwise, with rapid stirring, to (C<sub>5</sub>H<sub>5</sub>)Re(CO)<sub>3</sub> (0.620 g, 1.85 mmol) in dry THF (20 mL) at -70 °C. After the mixture was stirred rapidly at -70 °C for 30 min, (2,6-diphenylpyrylium)<sup>+</sup>PF<sub>6</sub><sup>-</sup> (576 mg, 1.84 mmol) in THF/ether was added slowly via a dropping funnel to the reaction mixture at -70 °C. The mixture was allowed to warm to 0 °C over a 2 h period, and a solution of ammonium chloride was added. After extraction with ether, and drying over MgSO<sub>4</sub>, the residue was dissolved in acetonitrile (10 mL) and treated with Ph<sub>3</sub>C<sup>+</sup>BF<sub>4</sub><sup>-</sup> (590 mg, 1.8 mmol). After being stirred for 45 min, the mixture was diluted with ether (35 mL) and filtered to give **10** as a green-brown solid (0.770 g, 1.36 mmol; 72%). Recrystallization from CH<sub>2</sub>Cl<sub>2</sub>:ether gave dark green crystals. IR (CH<sub>2</sub>Cl<sub>2</sub>):  $\nu_{\text{CO}}$  at 2036 and 1952 cm<sup>-1</sup>. <sup>1</sup>H NMR (200 MHz, acetone-*d*<sub>6</sub>):  $\delta$  8.90 (s, 2H, H<sub>3,5</sub>), 8.6–7.7 (m, 10H, phenyl-H's), 7.34 (t, 2H, Cp-H's), 6.16 (t, 2H, Cp-H's).

[(*N*-benzyl-2,6-dimethyl-4-phenylpyridinium)Cr(CO)<sub>3</sub>]<sup>+</sup>PF<sub>6</sub><sup>-</sup>, **12**(PF<sub>6</sub><sup>-</sup>). [(2,6-dimethyl-4-phenylpyrylium)Cr(CO)<sub>3</sub>]<sup>+</sup>PF<sub>6</sub><sup>-</sup>, **1**(PF<sub>6</sub><sup>-</sup>), (213 mg, 0.46 mmol), benzylamine (0.05 mL, 0.457 mmol), and triethylamine (0.06 mL, 0.457 mmol) were stirred in dichloromethane at ambient temperature for 5 min. Acetic acid (0.05 mL, 0.914 mmol) was added and the mixture stirred for an additional 15 min. Addition of ether precipitates the pyridinium salt, **12**(PF<sub>6</sub><sup>-</sup>), as dark red crystals in (235 mg, 0.423 mmol; 93%). IR (CH<sub>2</sub>Cl<sub>2</sub>):  $\nu_{\text{CO}}$  at 1982 and 1914 cm<sup>-1</sup>. <sup>1</sup>H NMR (200 MHz, acetone-*d*<sub>6</sub>):  $\delta$  8.38 (s, 2H, H<sub>3,5</sub>), 7.50–7.15 (m, 5H, phenyl-H's), 6.56 (d, 2H, H<sub>2,6</sub>), 6.10 (s, 2H, CH<sub>2</sub>), 6.05 (t, 1H, H<sub>4</sub>), 5.90 (t, 2H, H<sub>3,5</sub>), 2.96 (s, 6H, Me's).

[(*N*-benzyl-4-cyclopentadienyl-2,6-diphenylpyridinium)-Mn(CO)<sub>3</sub>]<sup>+</sup>BF<sub>4</sub><sup>-</sup>, **13**(BF<sub>4</sub><sup>-</sup>). In an analogous manner to the synthesis of **12**, reaction of benzylamine with **8**(BF<sub>4</sub><sup>-</sup>) gave **13**(BF<sub>4</sub><sup>-</sup>) as yellow crystals in 99% yield. IR (CH<sub>2</sub>Cl<sub>2</sub>):  $\nu_{\text{CO}}$  at

(33) Smith, D. P.; Baralt, E.; Morales, B.; Olmstead, M. M.; Maestre, M. F.; Fish, R. H. *J. Am. Chem. Soc.* **1992**, *114*, 10647.

(34) Salmain, M.; Malisza, K. L.; Top, S.; Jaouen, G.; Sénéchal-Tocquer, M. C.; Sénéchal, D.; Caro, B. *Bioconjugate Chem.* **1994**, *5*, 655.

(35) Perrin, D. D.; Armarego, W. L. F.; Perrin, D. R. *Purification of Laboratory Chemicals*; Pergamon Press: New York, 1980.



2030 and 1951  $\text{cm}^{-1}$ .  $^1\text{H}$  NMR (250 MHz, acetone- $d_6$ ):  $\delta$  8.33 (s, 2H,  $\text{H}_{3,5}$ ), 7.67–6.62 (m, 15H, phenyl-H's), 6.44 (t, 2H, Cp-H's), 5.41 (t, 2H, Cp-H's), 5.84 (s, 2H,  $\text{CH}_2$ ).  $^{13}\text{C}$  NMR (62.5 MHz, acetone- $d_6$ ):  $\delta$  224.3 (CO), 158.2 ( $\text{C}_{3,5}$ ), 154.2 ( $\text{C}_4$ ), 135.1–125.7 (phenyl CH's), 90.5 (cyclopentadienyl C), 87.6, 86.8 (cyclopentadienyl CH's), 59.1 ( $\text{CH}_2$ ).

**(*N*-benzyl-4-ferrocenyl-2,6-dimethylpyridinium) $^+$ 14-( $\text{PF}_6^-$ ).** In an analogous manner to the syntheses of 12( $\text{PF}_6^-$ ) and 13( $\text{BF}_4^-$ ) reaction of benzylamine with 9( $\text{PF}_6^-$ ) gave 14( $\text{PF}_6^-$ ) as a dark red powder in 25% yield.  $^1\text{H}$  NMR (200 MHz, acetone- $d_6$ ):  $\delta$  8.70 (s, 2H,  $\text{H}_{3,5}$ ), 7.50–7.05 (m, 5H, phenyl-H's), 5.25 (t, 2H, Cp-H's), 4.85 (t, 2H, Cp-H's), 4.42 (s, 5H, Cp), 2.80 (s, 6H, Me's).

**[*N*-( $\beta$ -Alanyl ethyl ester)-4-ferrocenyl-2,6-dimethylpyridinium] $^+$ 15( $\text{PF}_6^-$ ).** The 4-ferrocenyl-2,6-dimethylpyridinium salt, 9 (400 mg, 0.914 mmol), was dissolved in acetone, and  $\beta$ -alanine ethyl ester (80 mg, 0.914 mmol) was added. The solution was stirred for 3 h to yield a blue oil which was purified on silica plates by eluting with THF. Recrystallization from  $\text{CH}_2\text{Cl}_2$ /pentane yielded blue needles of 15( $\text{PF}_6^-$ ) (226 mg, 0.42 mmol; 46%).  $^1\text{H}$  NMR (200 MHz, acetone- $d_6$ ):  $\delta$  7.97 (s, 2H,  $\text{H}_{3,5}$ ), 5.22 (t, 2H, Cp-H's), 5.20 (t, 2H,  $\text{CH}_2$ ), 4.81 (t, 2H, Cp-H's), 4.18 (s, 5H, Cp), 4.17 (q, 2H, ethyl- $\text{CH}_2$ ), 3.14 (dd, 2H,  $\text{CH}_2$ ), 2.94 (s, 6H, Me's), 1.23 (t, 3H, ethyl- $\text{CH}_3$ ). Anal. Calcd for  $\text{C}_{22}\text{H}_{26}\text{NO}_2\text{FePF}_6$ : C, 49.15; H, 4.88. Found: C, 49.31; H, 4.61.

**X-ray Crystallography.** Data collection parameters for the salts of 1, 8, and 15 are listed in Table 1. The structures were solved by using the Patterson method with the aid of the programs MULTAN84<sup>36</sup> for the Cr salt, 1, CRYSTALS<sup>37</sup>

for the Mn complex, 8, and SHELXTL-Plus<sup>38</sup> for 15. Scattering factors and corrections were taken from ref 39. An absorption correction was performed by using DIFABS.<sup>40</sup> For the salt of 15, the best fit of the data required two equally populated cyclopentadienyl sites, two ethyl sites, and three orientations of the  $\text{PF}_6^-$  counterion. The molecular disorder is illustrated by Figure S1 in the Supporting Information.

**Molecular Orbital Calculations.** These were performed via the extended Hückel method using weighted  $H_{ij}$ 's,<sup>41</sup> by use of the program CACAO.<sup>42</sup>

**Acknowledgment.** We thank the CNRS (France) and NSERC (Canada) for financial support. K.L.M. was the recipient of a Chateaubriand postdoctoral scholarship awarded by the Government of France.

**Supporting Information Available:** An ORTEP structure (Figure S1) and tables of complete positional parameters and thermal parameters and bond lengths and angles for the salts of 1, 8, and 15 (14 pages). Ordering information is given on any current masthead page.

OM950392W

(37) Watkin, D. J.; Carruthers, J. R.; Betteridge, P. W. *CRYSTALS User Guide*, Chemical Crystallography Laboratory, University of Oxford, Oxford, England, 1986.

(38) Sheldrick, G. M. *SHELXTLPC*, Release 4.1; Siemens Crystallographic Research System: Madison, WI, 1990.

(39) *International Tables for X-ray Crystallography*; Kynoch Press: Birmingham, England, 1974; Vol. IV.

(40) Walker, N.; Stuart, D. *Acta Crystallogr.* **1983**, *A39*, 159.

(41) (a) Hoffmann, R. *J. Chem. Phys.* **1963**, *39*, 1397. (b) Hoffmann, R.; Lipscomb, W. N. *J. Chem. Phys.* **1962**, *36*, 2179, 3489. (c) Ammeter, J. H.; Bürgi, H.-B.; Thibeault, J. C.; Hoffmann, R. *J. Am. Chem. Soc.* **1978**, *100*, 3686.

(42) Mealli, C.; Proserpio, D. M. *J. Chem. Educ.* **1990**, *67*, 3399.

(36) Main, P.; Fiske, S. J.; Hull, S. E.; Lessinger, L.; Germain, G.; Declercq, J. P.; Woolfson, M. M. *MULTAN 84*; Universities of York (England) and Louvain (Belgium), 1984.

# Diastereomeric Square-Planar Platinum(II) and Palladium(II) Complexes Due to Restricted Rotation about the Chelated M–N Heteroaryl Bond

Peter J. Stang,\* Bogdan Olenyuk, and Atta M. Arif

Department of Chemistry, The University of Utah, Salt Lake City, Utah 84112

Received June 14, 1995<sup>⊙</sup>

The reaction of 3-bromopyridine, quinoline, or isoquinoline with *cis*-M(L)<sub>2</sub>(OTf)<sub>2</sub> (M = Pd, Pt; L = triethylphosphine, <sup>1</sup>/<sub>2</sub> 1,3-bis(diphenylphosphino)propane (dppp) or <sup>1</sup>/<sub>2</sub> (R)-(+)-2,2'-bis(diphenylphosphino)-1,1'-binaphthyl ((R)-(+)-BINAP)) results in the formation of diastereomeric, square-planar, cationic complexes, which exhibit restricted rotation about the metal–nitrogen heteroaryl bond. All complexes were characterized by routine physical and spectroscopic methods, of which <sup>31</sup>P{<sup>1</sup>H} NMR spectroscopy was most valuable. Only the complexes [Pd(dppp)(isoquinoline)<sub>2</sub>][OTf]<sub>2</sub> (**14**), [Pt(dppp)(isoquinoline)<sub>2</sub>][OTf]<sub>2</sub> (**15**), and [Pd((R)-(+)-BINAP)(isoquinoline)<sub>2</sub>][OTf]<sub>2</sub> (**22**) were found to be dynamic at ambient temperature on the NMR time scale. Variable-temperature studies of the <sup>31</sup>P{<sup>1</sup>H} NMR spectra of these compounds were performed. The X-ray crystal structure of [Pt(dppp)(quinoline)<sub>2</sub>][OTf]<sub>2</sub> (**19**) in one of its stereoisomeric (*syn*) forms is reported. [Pd((R)-(+)-BINAP)(isoquinoline)<sub>2</sub>][OTf]<sub>2</sub> (**22**) and [Pt((R)-(+)-BINAP)(isoquinoline)<sub>2</sub>][OTf]<sub>2</sub> (**23**) exhibit three distinct rotamers at –20 °C and ambient temperature, respectively. The role of asymmetric induction of the chiral bis-phosphine ligand on the stereoisomeric ratio of the rotamers of **22** and **23** is discussed.

## Introduction

The square-planar, tetracoordinated complexes of divalent palladium and platinum are a most diverse group of organometallic compounds whose unique properties have found a vast number of applications, from natural product synthesis to chemotherapy. This includes catalytic hydroformylation,<sup>1</sup> carbonylation,<sup>2</sup> the Heck reaction,<sup>3</sup> transition-metal-mediated coupling,<sup>4</sup> and C–H bond activation.<sup>5</sup> One of the most recent applications is the self-assembly of the various metal-lamacrocycles<sup>6</sup> and metallacalixarenes.<sup>7</sup> Although many of these reactions involve the interaction between reactive metal bis-phosphines and different heteroaryls, studies of the stereochemistry of cationic Pd(II) and Pt(II) bis-phosphine complexes, implementing unsymmetrically substituted heterocycles, have not yet been made to date.

The effect of restricted rotation in covalent complexes of Pd, Pt, and Ni has been the subject of several investigations, which shed some light on this interesting phenomenon.<sup>8</sup> The growing interest in this area is manifested by the recent development of several chiral bis-phosphine Pd and Pt complexes with covalently

bound iodo aryls and bis-aryls (**1–5**; Chart 1) as well as their potential applications.<sup>9</sup>

Considering all these facts, our objectives were (1) to investigate the stereochemistry of noncovalent, cationic complexes of Pd and Pt, where the chelating M–N bond is considerably weaker as compared to the corresponding covalent systems, (2) to find the influence of nonchelating ligands in the *cis* arrangement on the impedance of free rotation, and (3) to determine the factors which influence both the isomeric ratio and the possibility of preferential formation of one of the diastereomers, especially with the chiral metal system. Also, the degree of rotational freedom for different types of heterocycles was of interest.

## Results and Discussion

**Synthesis of Cationic Complexes of Heteroaryls with Pt(II) and Pd(II) Bis-Phosphines.** Among a variety of the reactive complexes of metal bis-phosphines, the triflates are probably the most versatile group, because triflate ligands have long been recognized as labile leaving groups which can be utilized for many organometallic transformations.<sup>10</sup> The precursors, achiral *cis*-M(L)<sub>2</sub>(OTf)<sub>2</sub> (**6–9**; M = Pd, Pt; L = triethylphosphine, <sup>1</sup>/<sub>2</sub> 1,3-bis(diphenylphosphino)propane (dppp); Scheme 1) were prepared from the corre-

<sup>⊙</sup> Abstract published in *Advance ACS Abstracts*, September 15, 1995.

(1) (a) Doyle, M. M.; Jackson, W. R.; Perlmutter, P. *Tetrahedron Lett.* **1989**, *30*, 5357. (b) Kollar, L.; Sandor, P.; Szalontai, G. *J. Mol. Catal.* **1991**, *67*, 191.

(2) Huser, M.; Youinou, M.-T.; Osborn, J. A. *Angew. Chem., Int. Ed. Engl.* **1989**, *28*, 1386.

(3) Heck, R. F. *Org. React.* **1982**, *27*, 345.

(4) For a review, see: Mitchell, T. N. *Synthesis* **1992**, 803.

(5) For recent reviews see: Davies, J. A.; Watson, P. L.; Liebman, J. F.; Greenberg, A. *Selective Hydrocarbon Activation*; VCH: New York, 1990. Hill, C. L. *Activation and Functionalization of Alkanes*; Wiley: New York, 1989.

(6) Stang, P. J.; Cao, D. H. *J. Am. Chem. Soc.* **1994**, *116*, 4981.

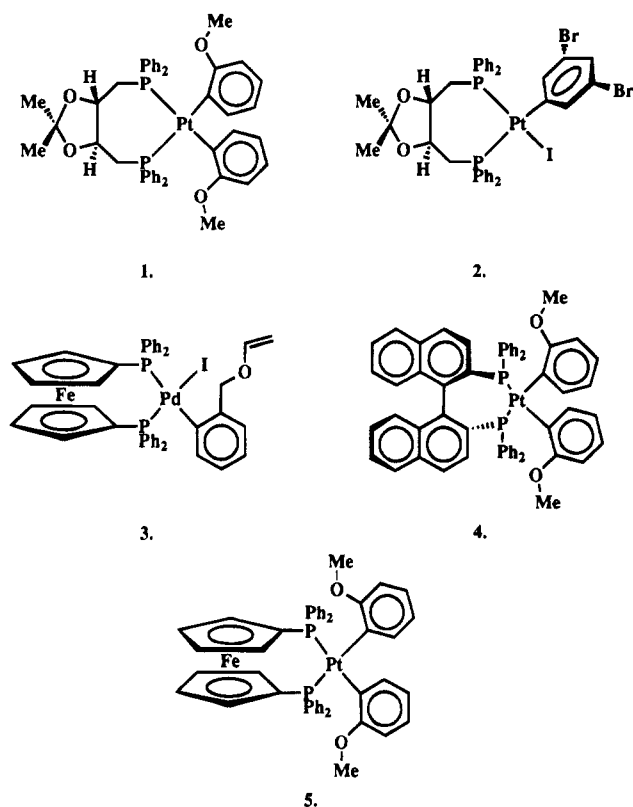
(7) Rauter, H.; Hillgeris, E. C.; Erxleben, A.; Lippert, B. *J. Am. Chem. Soc.* **1994**, *116*, 616.

(8) For examples of restricted rotation about Pd–aryl, Pt–aryl, or Ni–aryl bonds, see: (a) Wada, M.; Sameshima, K. *J. Chem. Soc., Dalton Trans.* **1981**, 240. (b) Griffiths, D. B.; Young, G. B. *Organometallics* **1986**, *5*, 1744. (c) Baumgärtner, R.; Brune, H. A. *J. Organomet. Chem.* **1988**, *350*, 115. (d) Anderson, G. K.; Cross, R. J.; Manojlovic-Muir, L.; Muir, K. W.; Rocamora, M. *Organometallics* **1988**, *7*, 1520. (e) Alster, P. L.; Boersma, J.; Smeets, W. J. J.; Spek, A. L.; van Koten, G. *Organometallics* **1993**, *12*, 1639.

(9) Alcock, N. W.; Brown, J. M.; Pérez-Torrente, J. J. *Tetrahedron Lett.* **1992**, *33*, 389. Brown, J. M.; Pérez-Torrente, J. J.; Alcock, N. W. *Organometallics* **1995**, *14*, 1195.

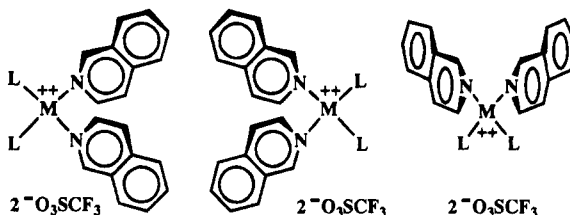
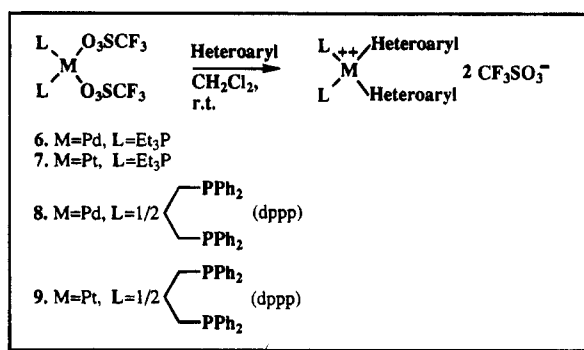
(10) Lawrance, G. A. *Chem. Rev.* **1986**, *86*, 17.

Chart 1

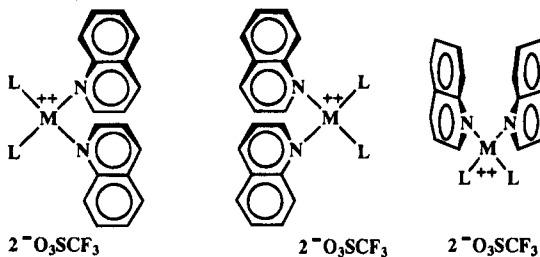


sponding *cis*-M(L)<sub>2</sub>Cl<sub>2</sub> by halide abstraction with AgO-Tf.<sup>11</sup> The chiral (*R*)-(+)-2,2'-bis(diphenylphosphino)-1,1'-binaphthyl ((*R*)-(+)-BINAP)<sup>12</sup> metal triflates **10** and **11** were prepared by employing a similar procedure (Scheme 2); however, their stable monohydrates were elaborated, as an alternative to highly hygroscopic anhydrous triflates.<sup>13</sup> Three heterocycles were chosen: quinoline, where the ortho influence of the annelated benzene ring is most effective in terms of impedance of free rotation, isoquinoline, where the influence of this ring is less significant, and 3-bromopyridine, where the remotely located bromine can only cause a minimal effect on the rotational freedom of the heterocycle ring, and so the interactions of its  $\alpha$ -hydrogens with the phosphine group may play the major role in the possible restriction of free rotation. The achiral complexes **12**–**21** were prepared by the reaction of the appropriate heterocycle with the metal bis-phosphine triflates (Scheme 1) or with their monoqua complexes (**22** and **23**; Scheme 2) in dichloromethane at ambient temperature. These products are air-stable, albeit hygroscopic, microcrystalline solids, with one or two water molecules often retained in the crystals. For the metal complexes of dppp and (*R*)-(+)-BINAP, the decomposition points are very high,

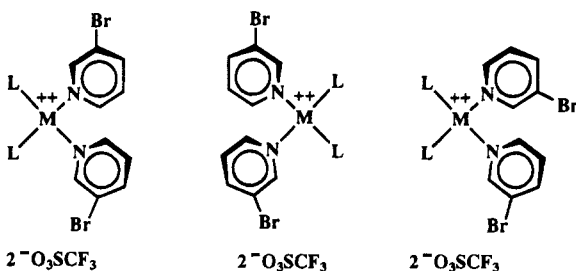
Scheme 1



12. M=Pd, L=Et<sub>3</sub>P, 3 h, 88%  
 13. M=Pt, L=Et<sub>3</sub>P, 5 h, 89%  
 14. M=Pd, L=1/2 dppp, 3 h, 89%  
 15. M=Pt, L=1/2 dppp, 5 h, 84%



16. M=Pd, L=Et<sub>3</sub>P, 3 h, 84%  
 17. M=Pt, L=Et<sub>3</sub>P, 3 h, 79%  
 18. M=Pd, L=1/2 dppp, 5 h, 83%  
 19. M=Pt, L=1/2 dppp, 5 h, 89%



20. M=Pt, L=Et<sub>3</sub>P, 3 h, 81%  
 21. M=Pt, L=1/2 dppp, 5 h, 91%

whereas the nonchelated bis-phosphine compounds with *cis*-Et<sub>3</sub>P ligands generally melt without decomposition at a relatively low temperature.

**NMR Studies of the Complexes.** <sup>31</sup>P NMR spectroscopy is an excellent tool for the observations of these interesting compounds. At room temperature, achiral bis-phosphine complexes **12**, **13** and **16**–**21** show two sharp distinct peaks in the phosphine region, indicating the presence of the one syn (*meso*) and two undistinguishable anti isomers (*dl* pair), and a barrier to rotation of at least 70 kJ mol<sup>-1</sup>. Except for complex **12**, which has a coalescence temperature slightly above ambient

(11) Stang, P. J.; Cao, D. H.; Saito, S.; Arif, A. M. *J. Am. Chem. Soc.* **1995**, *117*, 6273.

(12) (a) Miyashita, A.; Yasuda, A.; Takaya, H.; Torimi, K.; Ito, T.; Souchi, T.; Noyori, R. *J. Am. Chem. Soc.* **1980**, *102*, 7932. (b) Takaya, H.; Mashima, K.; Koyano, K.; Yagi, M.; Kumobayashi, H.; Taketomi, T.; Akutagawa, S.; Noyori, R. *J. Org. Chem.* **1986**, *51*, 629.

(13) Hydrogen bonding is important in the stabilization of the solid-state structure of aqua-transition-metal complexes: (a) Rochon, F. D.; Melanson, R. *Inorg. Chem.* **1987**, *26*, 989. (b) Britten, J. F.; Lippert, B.; Lock, C. J.; Pilon, P. *Inorg. Chem.* **1982**, *21*, 1936. (c) Hollis, L. S.; Lippard, S. J. *Inorg. Chem.* **1983**, *22*, 2605. (d) Brown, I. D. *Structure and Bonding in Crystals*; Academic Press: New York, 1981; Vol. II. (e) Braga, D.; Grepioni, F. *Acc. Chem. Res.* **1994**, *27*, 51. (f) Braga, D.; Grepioni, F.; Sabatino, P.; Desiraju, G. R. *Organometallics* **1994**, *13*, 3532.

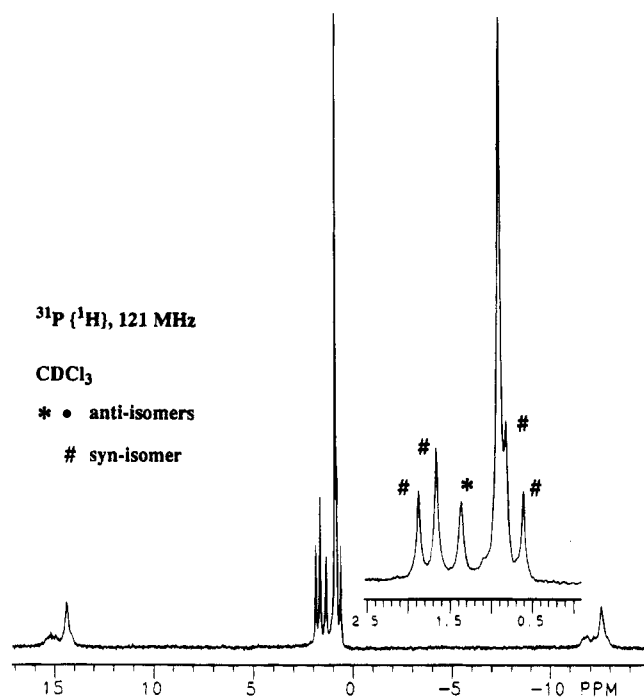
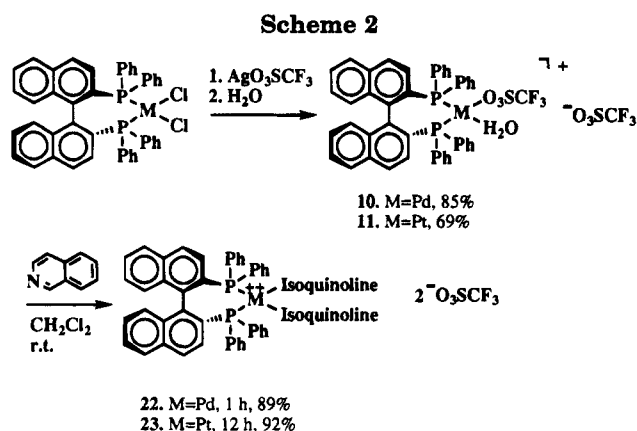


Figure 1.  $^{31}\text{P}$  NMR spectrum of compound **23**.



and a broadened proton spectrum, the  $^1\text{H}$  spectra of the others also exhibit two distinct groups of multiplets. Models indicate a low relative free energy for each rotamer but a high barrier to their interconversion. In the course of the synthetic studies it was apparent that the stoichiometric ratio of products of these isomers depends on the type of solvent used to perform the reaction. For example, if the preparation of complex **19** was carried out in  $\text{CH}_2\text{Cl}_2$ , the  $^{31}\text{P}$  spectrum of the product shows two peaks for the respective anti and syn isomers in an approximate 0.90:1 ratio. When a  $\text{CHCl}_3$ - $\text{CH}_2\text{Cl}_2$  (1:1) mixture was employed, this isomer ratio changed to approximately 1:3. Complexes **14**, **15**, and **22** have a single peak in the  $^{31}\text{P}$  spectrum at ambient temperature and significantly broadened lines in the  $^1\text{H}$  NMR spectra, thereby indicating lower coalescence barriers. The  $^{31}\text{P}$  spectrum of complex **23** contains two singlets and an AB-type doublet of doublets, thereby manifesting the presence of one unsymmetrical (syn) and two  $C_2$ -symmetrical (anti) diastereomers (*dl* pair) (Figure 1). The same observation was made for complex **22** at temperatures below  $-20^\circ\text{C}$ . The ratio of these isomers indicates a significant preference of one stereoisomeric anti form over the others. This interesting effect, analogous to the observed enantiomeric prefer-

ence in the neutral covalent bis-aryl complexes of Pt with chiral BINAP and DIOP ligands,<sup>9</sup> is the first such observation for the cationic complexes of Pd(II) and Pt(II).

Variable-temperature  $^{31}\text{P}$  NMR studies of **14**, **15**, and **22** were performed, and examples are presented in Figure 2. Above the coalescence temperatures, which are about  $0^\circ\text{C}$  for **14** and  $20^\circ\text{C}$  for **22**, sharp peaks appeared in the spectrum. The  $^{31}\text{P}$  spectrum of **15** is analogous to that of complex **14** except for the higher coalescence barrier. Interestingly, the palladium complexes are found to interconvert more readily than their platinum analogs. This can be demonstrated clearly with the chiral complexes **22** (Pd) and **23** (Pt). The Pd complex coalesces at about  $0^\circ\text{C}$ , whereas the Pt complex is above coalescence and its  $^{31}\text{P}$  spectrum exhibits signals of all three stereoisomeric forms at room temperature.

**X-ray Structure of  $[\text{Pt}(\text{dppf})(\text{quinoline})_2][\text{OTf}]_2$  (**19**).** Slow crystallization by the vapor diffusion of diethyl ether into a chloroform solution of the mixture of isomers **19** at room temperature provided X-ray-quality crystals, which were used for the structure determination. A summary of significant features of the structure is presented in Figure 3. The quinoline rings are in the syn configuration, positioned approximately perpendicular to the Pt coordination plane. This result is not unexpected, because our earlier X-ray observations of several pyrazine complexes<sup>6,11</sup> as well as published X-ray structures of pyridine complexes of Pd<sup>14</sup> show that a nitrogen-coordinated heteroaryl ligand possesses an electronic and steric preference for orthogonality to the coordination plane of the transition metal. Both Pt-P bonds are virtually of identical length, as are both Pt-N bonds (Table 1), which suggests the presence of an apparent plane of symmetry that crosses the molecule perpendicularly to the Pt coordination plane. The  $^{31}\text{P}$  NMR spectrum of analytically pure **19** shows two peaks at  $-15.7$  and  $-13.8$  ppm and, according to  $^1\text{H}$  NMR, a ratio of diastereomers of approximately 1:3. After recrystallization, the ratio in the recrystallized material changed to about 1:7, thereby indicating the absence of equilibration in solution. Hence, it can be implied, although not proven, that the X-ray structure represents the major isomer, which interestingly is the syn form. This syn stereochemistry is opposite to that of other known structures of covalent platinum bis-aryl complexes, where crystallographic analysis shows the anti form in the solid state.<sup>15</sup>

## Conclusion

The reaction of selected (achiral chelated, achiral nonchelated, and chiral chelated) Pd(II) or Pt(II) triflates with 3-bromopyridine, quinoline, or isoquinoline complexes results in the formation of diastereomeric, square-planar, cationic complexes. Restricted rotation about the chelated metal-nitrogen heteroaryl bond in these complexes was detected and investigated by

(14) For recent examples of Pd-pyridine complexes see: (a) Chakladar, S.; Paul, P.; Venkatasubramanian, K.; Nag, K. *J. Chem. Soc., Dalton Trans.* **1991**, 2669. (b) Kometzy, A.; Bailey, P. M.; Maikos, P. M. *J. Chem. Soc., Chem. Commun.* **1975**, 78. (c) Vicente, J.; Chicote, M.-J.; Saura-Licmos, I.; Lopez-Munoz, M.-J.; Jones, P. G. *J. Chem. Soc., Dalton Trans.* **1990**, 3683.

(15) Bebaerdemaker, T.; Weisemann, C.; Brune, H. A. *Acta Crystallogr., Sect. C* **1987**, *43*, 1253.

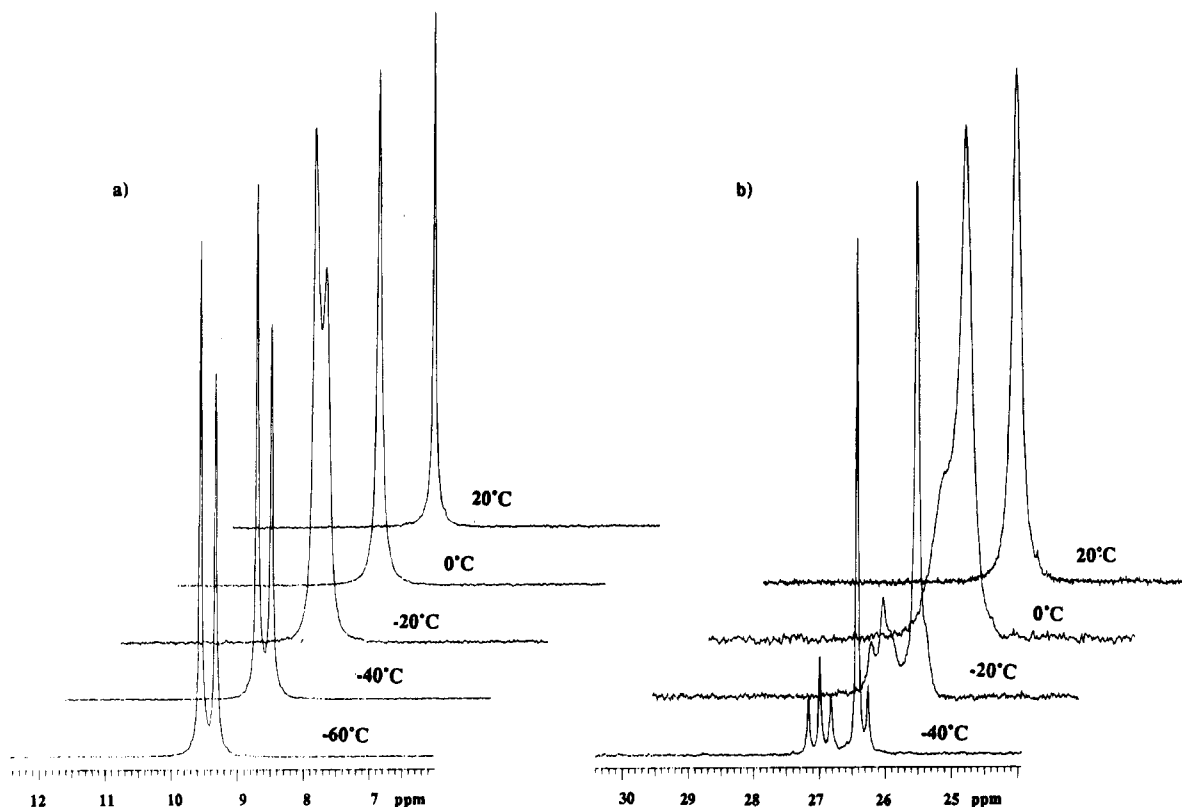


**Figure 2.** Variable-temperature  $^{31}\text{P}$  NMR spectra of compounds 14 (a) and 22 (b).

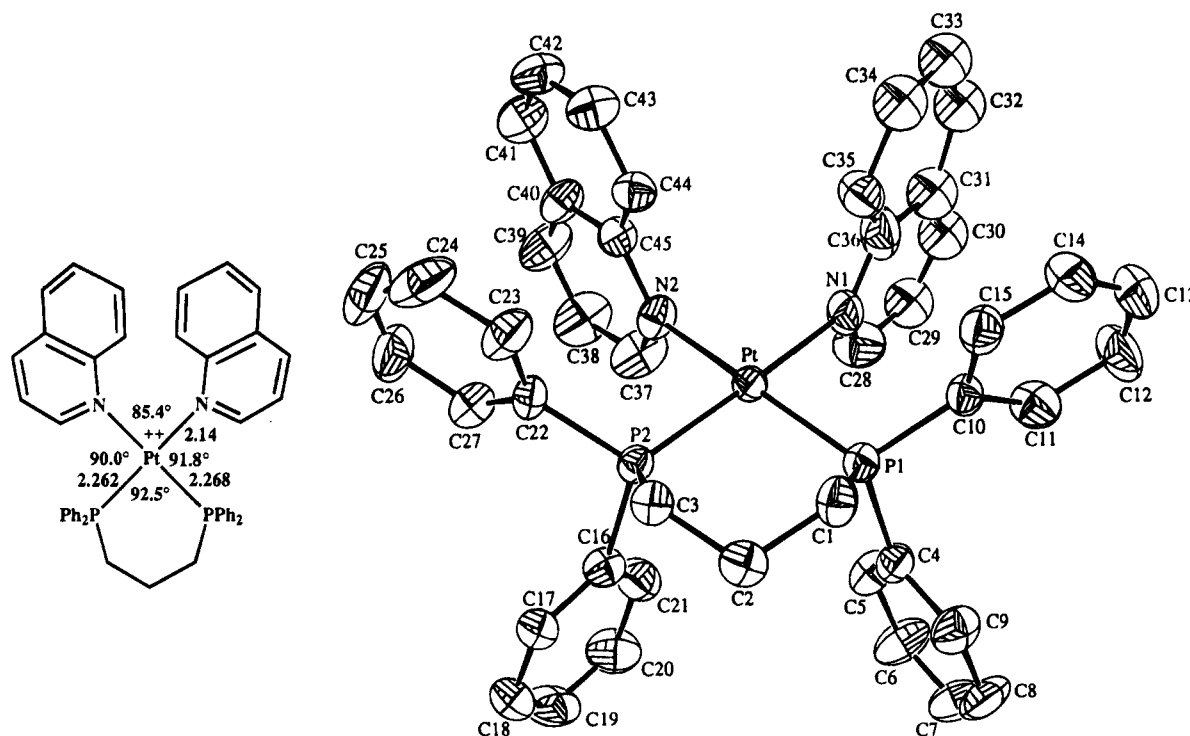


**Figure 3.** ORTEP diagram and selected bond lengths and bond angles of the cationic part of complex 19.

different physical and spectroscopic means. The complexes  $[\text{Pd}(\text{dppp})(\text{isoquinoline})_2][\text{OTf}]_2$  (14),  $[\text{Pt}(\text{dppp})(\text{isoquinoline})_2][\text{OTf}]_2$  (15), and  $[\text{Pd}((R)\text{-}(+)\text{-BINAP})(\text{isoquinoline})_2][\text{OTf}]_2$  (22) were found to be dynamic on the NMR time scale, whereas others exhibited multiple signals indicative of isomers in the  $^{31}\text{P}\{^1\text{H}\}$  spectra at ambient temperature. The hindrance to free rotation was found to be most effective for the *cis*-triethylphosphine complexes. Among the heteroaryls, as expected,

the quinoline complexes were found to undergo the slowest interconversion. The observation of restricted rotation in the complexes of 3-bromopyridine with achiral platinum bis-phosphines shows that the presence of an  $\alpha$ -substituent in the heteroaryl group or an annulated ring is not a necessary condition for the free rotation restriction. On the basis of the X-ray crystal structure of  $[\text{Pt}(\text{dppp})(\text{quinoline})_2][\text{OTf}]_2$  (19) and the analysis of its NMR data it can be implied that the

**Table 1. Important Bond Angles (deg) and Bond Distances (Å) for *syn*-[Pt(dppp)(quinoline)<sub>2</sub>][OTf]<sub>2</sub> (19)**

atom 1	atom 2	atom 3	angle <sup>a</sup>	atom 1	atom 2	distance <sup>a</sup>
P1	Pt	P2	92.5(1)	Pt	P1	2.268(3)
P1	Pt	N1	91.8(3)	Pt	P2	2.262(3)
P1	Pt	N2	175.5(3)	Pt	N1	2.14(1)
P2	Pt	N1	174.7(4)	Pt	N2	2.14(1)
P2	Pt	N2	90.0(3)	P1	C1	1.81(1)
N1	Pt	N2	85.4(5)	P2	C3	1.83(1)

<sup>a</sup> Numbers in parentheses are estimated standard deviations in the least significant digits.

major components of the Pd(II) and Pt(II) complexes **18** and **19** are in the *syn* configuration. In contrast, the spectroscopic data of chiral Pd(II) and Pt(II) complexes of (*R*)-(+)-BINAP strongly suggest that the major isomers are one of the C<sub>2</sub>-symmetric anti forms. The latter indicates the critical role of asymmetric induction by the chiral bis-phosphine ligand on the formation of these complexes.

### Experimental Section

**General Methods.** All reactions were conducted under a dry nitrogen atmosphere using Schlenk techniques even though the products can be handled in air. IR spectra were recorded on a Mattson Polaris FT-IR spectrophotometer. NMR spectra were recorded on a Varian XL-300 or Unity-300 spectrometer. <sup>1</sup>H NMR spectra were recorded at 300 MHz, and all chemical shifts (δ) are reported in ppm relative to tetramethylsilane (Me<sub>4</sub>Si) as an internal standard (0.0 ppm) or the proton resonance resulting from incomplete deuteration of the NMR solvent: CD<sub>2</sub>Cl<sub>2</sub> (5.32 ppm) or CD<sub>3</sub>OD (3.31 ppm). <sup>13</sup>C NMR spectra were recorded at 75 MHz, and all chemical shifts (δ) are reported in ppm relative to the carbon resonance of the deuterated NMR solvent: CD<sub>3</sub>OD (49.0 ppm) or CD<sub>2</sub>Cl<sub>2</sub> (53.8 ppm). <sup>31</sup>P NMR spectra were recorded at 121 MHz, and all chemical shifts (δ) are reported in ppm relative to external 85% H<sub>3</sub>PO<sub>4</sub> at 0.00 ppm. <sup>19</sup>F NMR spectra were recorded at 282 MHz, and all chemical shifts are reported relative to external CFCl<sub>3</sub> at 0.00 ppm. The water signals in <sup>1</sup>H NMR were omitted, except for the compound **10**. All *J* values are reported in Hz. Microanalyses were performed by Atlantic Microlab Inc., Norcross, GA. Melting points were obtained with a Mel-Temp capillary melting point apparatus and were not corrected. Abbreviations: br m, broad multiplet; br s, broad singlet, isoq, isoquinoline; quin, quinoline, 3-Br-py, 3-bromopyridine; dppp, 1,3-bis(diphenylphosphino)propane; H<sub>o</sub>, ortho proton; H<sub>m</sub>, meta proton; H<sub>p</sub>, para proton; C<sub>i</sub>, ipso carbons; C<sub>o</sub>, ortho carbons; C<sub>m</sub>, meta carbons; C<sub>p</sub>, para carbons. Isomer A denotes the diastereomer or NMR-equivalent enantiomeric pair, which is present in the greater amount, whereas isomer B refers to the diastereomer or NMR-equivalent enantiomeric pair, which is present in the lower amount, as indicated by the peak ratios in the <sup>1</sup>H and <sup>31</sup>P NMR. Isomer C indicates an asymmetrical *syn* isomer in chiral bis-phosphine complexes **22** and **23**.

**Materials.** Solvents were purified as follows: CH<sub>2</sub>Cl<sub>2</sub> and CHCl<sub>3</sub> were purified by literature procedures<sup>16</sup> and distilled over CaH<sub>2</sub>; Et<sub>2</sub>O was purified by literature procedures<sup>16</sup> and distilled over Na/benzophenone; CD<sub>2</sub>Cl<sub>2</sub> was vacuum-transferred from CaH<sub>2</sub>. All solvents were freeze-thaw-pump-degassed twice before use.

All commercial reagents were ACS reagent grade. 3-Bromopyridine, isoquinoline, quinoline, silver triflate, (*R*)-(+)-2,2'-bis(diphenylphosphino)-1,1'-binaphthyl ((*R*)-(+)-BINAP), and [Pd((*R*)-(+)-BINAP)](Cl)<sub>2</sub> were obtained from Aldrich and were

all used as received. The precursors **6** and **7**, along with **8** and **9**, were prepared according to literature methods;<sup>11</sup> [Pt-((*R*)-(+)-BINAP)](Cl)<sub>2</sub> was prepared by a modified literature procedure.<sup>17</sup>

**[Pd((*R*)-(+)-BINAP)(H<sub>2</sub>O)](OTf)<sub>2</sub> (**10**).** The orange powder [Pd((*R*)-(+)-BINAP)](Cl)<sub>2</sub> (0.300 g, 0.375 mmol) was placed into a 50-mL Schlenk flask equipped with a stirbar and dissolved in CH<sub>2</sub>Cl<sub>2</sub> (25 mL). Then, 0.240 g (0.938 mmol) of AgOTf was added, and the resulting solution was stirred under nitrogen for 20 h at room temperature. The precipitate was filtered, and the filtrate was transferred into a 50 mL flask and reduced in volume to 5 mL in vacuo. Then, 0.007 g (0.390 mmol) of distilled water was added, followed by the addition of diethyl ether. The yellow precipitate was collected and washed with ether. The filtrate was reduced in volume to 5 mL, and additional material was collected as above. Combined solids were dissolved in 10 mL of CH<sub>2</sub>Cl<sub>2</sub>, and the solution was evaporated to dryness in vacuo at 35–40 °C. The solid was collected and further dried in vacuo: yield of **10** 0.338 g (85%); mp 190–193 °C dec. <sup>1</sup>H NMR (CD<sub>2</sub>Cl<sub>2</sub>): 7.90 (dd, 4H, *J* = 7.6, 12.2), 7.75–7.56 (m, 14H), 7.49 (dd, 4H, *J* = 8.3, 15.0), 7.14 (t, 2H, *J* = 7.4), 6.98 (t, 2H, *J* = 7.4), 6.85 (br m, 4H), 6.63 (d, 2H, *J* = 8.7) (BINAP), 4.65 (br s, 2H) (H<sub>2</sub>O). <sup>31</sup>P{<sup>1</sup>H} NMR (CD<sub>2</sub>Cl<sub>2</sub>): 36.53 (s). <sup>19</sup>F NMR (CD<sub>2</sub>Cl<sub>2</sub>): -76.6 (s, 2 CF<sub>3</sub>-SO<sub>3</sub>). IR (neat, cm<sup>-1</sup>): 1294, 1162, 1104, 1026 (all OTf). Anal. Calcd for C<sub>46</sub>H<sub>34</sub>P<sub>2</sub>S<sub>2</sub>F<sub>6</sub>O<sub>7</sub>Pd: C, 52.9; H, 3.28; S, 6.13. Found: C, 53.2; H, 3.42; S, 5.96.

**[Pt((*R*)-(+)-BINAP)(H<sub>2</sub>O)](OTf)<sub>2</sub> (**11**).** A 100-mL Schlenk flask equipped with a stirbar was charged with 0.350 g (0.390 mmol) of [Pt((*R*)-(+)-BINAP)](Cl)<sub>2</sub> and 50 mL of CH<sub>2</sub>Cl<sub>2</sub>. To this colorless solution was added 0.709 g (2.76 mmol) of AgOTf, and the resulting mixture was stirred under nitrogen for 4 days at room temperature. The white precipitate was filtered, and the filtrate was transferred into a 50-mL flask and reduced in volume to 10 mL. Then, 0.007 g (0.390 mmol) of distilled water was added, followed by the addition of diethyl ether. The white precipitate was collected, washed with ether, and dried in vacuo: yield of **11** 0.315 g (69%); mp 232–234 °C dec. <sup>1</sup>H NMR (CD<sub>2</sub>Cl<sub>2</sub>): 7.81–7.58 (m, 18H), 7.50 (dd, 4H, *J* = 7.8, 14.1), 7.20 (t, 2H, *J* = 7.2), 7.02 (t, 2H, *J* = 7.2), 6.85 (br m, 4H), 6.71 (d, 2H, *J* = 8.0) (BINAP). <sup>31</sup>P{<sup>1</sup>H} NMR (CD<sub>2</sub>Cl<sub>2</sub>): 4.40 (s, <sup>195</sup>Pt satellites, <sup>1</sup>J<sub>P-Pt</sub> = 4023 Hz). <sup>19</sup>F NMR (CD<sub>2</sub>Cl<sub>2</sub>): -76.6 (s, 2 CF<sub>3</sub>SO<sub>3</sub>). IR (neat, cm<sup>-1</sup>): 1288, 1170, 1096, 1027 (all OTf). Anal. Calcd for C<sub>46</sub>H<sub>34</sub>P<sub>2</sub>S<sub>2</sub>F<sub>6</sub>O<sub>7</sub>Pt: C, 48.7; H, 3.02; S, 5.65. Found: C, 48.7; H, 3.12; S, 5.58.

***cis*-[Pd(Et<sub>3</sub>P)<sub>2</sub>(isoquinoline)<sub>2</sub>](OTf)<sub>2</sub> (**12**).** A 50-mL Schlenk flask equipped with a stirbar was charged with 0.116 g (0.898 mmol) of isoquinoline and CH<sub>2</sub>Cl<sub>2</sub> (10 mL). *cis*-Pd-(Et<sub>3</sub>P)<sub>2</sub>(OTf)<sub>2</sub> (0.128 g, 0.200 mmol) was added, and the resulting colorless mixture was stirred under nitrogen for 3 h at ambient temperature. The solution was transferred *via* syringe into a 50-mL flask and reduced in volume to ca. 2 mL. Diethyl ether was then added, resulting in the formation of a white precipitate, which was collected, washed with diethyl ether (10 mL), and dried in vacuo: yield of **12** 0.158 g (88%); mp 79–81 °C. <sup>1</sup>H NMR (CD<sub>2</sub>Cl<sub>2</sub>): 10.21 (br s, 4H, isoq H-1, isomers A and B), 9.03 (br s, 4H, isoq H-3, isomers A and B), 8.35 (br s, 4H, isoq H-8, isomers A and B), 7.72 (br s, 12H, overlap of isoq H-5, H-6, and H-4, isomers A and B), 7.69 (br s, 4H, isoq H-7, isomers A and B), 1.82 (m, 24H, PCH<sub>2</sub>CH<sub>3</sub>, isomers A and B), 1.32 (m, 36H, PCH<sub>2</sub>CH<sub>3</sub>, isomers A and B). <sup>13</sup>C{<sup>1</sup>H} NMR (CD<sub>2</sub>Cl<sub>2</sub>): 155.5 (s, isoq C-1, isomers A and B), 141.8 (s, isoq C-3, isomers A and B), 136.2 (s, isoq C-10, isomers A and B), 134.0 (s, isoq C-6, isomers A and B), 129.5 (overlap of s, isoq C-9, C-8, and C-7, isomers A and B), 126.6 (s, isoq C-5, isomers A and B), 124.8 (s, isoq C-4, isomers A and B), 121.3 (q, OTf, *J*<sub>C-F</sub> = 319 Hz, isomers A and B), 16.6 (t, PCH<sub>2</sub>CH<sub>3</sub>, *J*<sub>C-P</sub> = 28 Hz, isomers A and B), 8.2 (s, PCH<sub>2</sub>CH<sub>3</sub>, isomers

(17) The reaction between Pt(cod)Cl<sub>2</sub> (cod = cyclooctadiene) and (*R*)-(+)-BINAP in CH<sub>2</sub>Cl<sub>2</sub> for 30 min at room temperature provided Pt-((*R*)-(+)-BINAP)Cl<sub>2</sub> in 93% yield. Also, see ref 1b for the recent synthesis of this complex.

(16) Perrin, D. D.; Armarego, W. L. F. *Purification of Laboratory Chemicals*; Pergamon Press: Oxford, U.K., 1988.

A and B).  $^{31}\text{P}\{^1\text{H}\}$  NMR ( $\text{CD}_2\text{Cl}_2$ ): 26.38 (s, isomer A), 26.10 (s, isomer B).  $^{19}\text{F}$  NMR ( $\text{CD}_2\text{Cl}_2$ ):  $-76.3$  (s, 2  $\text{CF}_3\text{SO}_3$ ). IR (neat,  $\text{cm}^{-1}$ ): 1260, 1150, 1030 (all OTf). Anal. Calcd for  $\text{C}_{32}\text{H}_{44}\text{N}_2\text{P}_2\text{S}_2\text{F}_6\text{O}_6\text{Pd}$ : C, 42.7; H, 4.93; N, 3.12; S, 7.13. Found: C, 43.1; H, 5.18; N, 2.95; S, 6.68.

**cis-[Pt( $\text{Et}_3\text{P}$ ) $_2$ (isoquinoline) $_2$ ][OTf] $_2$  (13).** A 50-mL Schlenk flask equipped with a stirbar was charged with 0.058 g (0.45 mmol) of isoquinoline and  $\text{CH}_2\text{Cl}_2$  (15 mL). *cis*-Pt( $\text{Et}_3\text{P}$ ) $_2$ (OTf) $_2$  (0.131 g, 0.180 mmol) was then added. The resulting mixture was stirred under nitrogen for 5 h at ambient temperature. The solution was transferred *via* syringe into a 50-mL flask and reduced in volume to 5 mL in vacuo. Diethyl ether was added, resulting in the formation of a white precipitate, which was collected and washed with diethyl ether (ca. 10 mL) and dried in vacuo: yield 0.159 g of **13** (89%); mp 88–89 °C.  $^1\text{H}$  NMR ( $\text{CD}_2\text{Cl}_2$ ): 10.24 (s, 2H, isoq H-1, isomer A), 10.18 (s, 2H, isoq H-1, isomer B), 9.13 (d, 2H,  $J = 5.7$ , isoq H-3, isomer A), 9.02 (d, 2H,  $J = 5.4$ , isoq H-3, isomer B), 8.44 (d, 2H,  $J = 9.0$ , isoq H-8, isomer A), 8.40 (d, 2H,  $J = 11.0$ , isoq H-8, isomer B), 7.90 (d, 2H,  $J = 6.6$ , isoq H-5, isomer A), 7.87 (d, 2H,  $J = 9.9$ , isoq H-5, isomer B), 7.82 (m, 8H, overlap of isoq H-6 and H-4, isomers A and B), 7.74 (t, 4H,  $J = 6.0$ , isoq H-7, isomers A and B), 1.79 (m, 24H,  $\text{PCH}_2\text{CH}_3$ , isomers A and B), 1.31 (m, 36H,  $\text{PCH}_2\text{CH}_3$ , isomers A and B).  $^{13}\text{C}\{^1\text{H}\}$  NMR ( $\text{CD}_2\text{Cl}_2$ ): 155.83 (s, isoq C-1, isomer A), 155.75 (s, isoq C-1, isomer B), 142.02 (s, isoq C-3, isomer A), 141.95 (s, isoq C-3, isomer B), 136.67 (s, isoq C-10, isomer A), 136.63 (s, isoq C-10, isomer B), 134.84 (s, isoq C-6, isomer A), 134.79 (s, isoq C-6, isomer B), 130.32 (s, isoq C-9, isomer A), 130.29 (s, isoq C-9, isomer B), 130.27 (s, isoq C-8, isomer A), 130.24 (s, isoq C-8, isomer B), 130.08 (s, isoq C-7, isomer A), 130.05 (s, isoq C-7, isomer B), 126.87 (s, isoq C-5, isomers A and B), 125.86 (s, isoq C-4, isomer A), 125.76 (s, isoq C-4, isomer B), 121.3 (q, OTf,  $J_{\text{C-F}} = 319$  Hz, isomers A and B), 15.75 (t,  $\text{PCH}_2\text{CH}_3$ ,  $J_{\text{C-P}} = 32$  Hz, isomers A and B), 8.13 (s,  $\text{PCH}_2\text{CH}_3$ , isomers A and B).  $^{31}\text{P}\{^1\text{H}\}$  NMR ( $\text{CD}_2\text{Cl}_2$ ): 0.47 (s,  $^{195}\text{Pt}$  satellites,  $^1J_{\text{P-Pt}} = 3089$  Hz, isomer A), 0.21 (s,  $^{195}\text{Pt}$  satellites,  $^1J_{\text{P-Pt}} = 3089$  Hz, isomer B).  $^{19}\text{F}$  NMR ( $\text{CD}_2\text{Cl}_2$ ):  $-77.7$  (s, 2  $\text{CF}_3\text{SO}_3$ ). IR (neat,  $\text{cm}^{-1}$ ): 1257, 1149, 1029 (all OTf). Anal. Calcd for  $\text{C}_{32}\text{H}_{44}\text{N}_2\text{P}_2\text{S}_2\text{F}_6\text{O}_6\text{Pt}\cdot\text{H}_2\text{O}$ : C, 38.2; H, 4.61; N, 2.79; S, 6.37. Found: C, 38.4; H, 4.59; N, 2.84; S, 6.45.

**[Pd(dppp)(isoquinoline) $_2$ ][OTf] $_2$  (14).** A 50-mL Schlenk flask equipped with a stirbar was charged with 0.116 g (0.898 mmol) of isoquinoline and  $\text{CH}_2\text{Cl}_2$  (5 mL). Then, 0.331 g (0.405 mmol) of Pd(dppp)(OTf) $_2$  was added, and the resulting colorless mixture was stirred under nitrogen for 3 h at ambient temperature. To this solution was added pentane, resulting in the formation of a white precipitate, which was collected and washed with 5 mL of pentane and dried in vacuo: yield of **14** 0.389 g (89%); mp 276 °C dec.  $^1\text{H}$  NMR ( $\text{CD}_2\text{Cl}_2$ ): broadened lines, due to rapid interconversion between A and B): 9.63 (br s, 4H, isoq H-1, isomers A and B), 9.01 (br m, 4H, isoq H-3, isomers A and B), 7.88 (br m, 8H, isoq H-8 and H-5, isomers A and B), 7.65 (t, 4H,  $J = 7.0$ , isoq H-6 isomers A and B), 7.52 (d, 4H, isoq H-4 isomers A and B), 7.40 (br m, 40H, dppp Ph, isomers A and B), 7.10 (br m, 4H, isoq H-7 isomers A and B), 3.22 (br m, 8H, dppp  $\text{PCH}_2\text{CH}_2$ , isomers A and B), 2.28 (br m, 4H, dppp  $\text{PCH}_2\text{CH}_2$ , isomers A and B).  $^{13}\text{C}\{^1\text{H}\}$  NMR ( $\text{CD}_2\text{Cl}_2$ ): 155.3 (s, isoq C-1, isomers A and B), 141.5 (s, isoq C-3, isomers A and B), 135.5 (s, isoq C-10, isomers A and B), 133.4 (s, isoq C-6, isomers A and B), 132.3 (m, dppp Ph, isomers A and B), 132.2 (m, dppp Ph + isoq C-9, isomers A and B), 129.5 (br s, dppp Ph  $\text{C}_p$ , isomers A and B), 129.1 (s, isoq C-8, isomers A and B), 128.6 (s, isoq C-7, isomers A and B), 126.2 (s, isoq C-5, isomers A and B), 125.8 (br s, dppp  $\text{C}_i$ , isomers A and B), 123.7 (s, isoq C-4, isomers A and B), 121.3 (q, OTf,  $J_{\text{C-F}} = 319$  Hz, isomers A and B), 22.8 (t, dppp  $\text{PCH}_2\text{CH}_2$ ,  $J_{\text{C-P}} = 32$  Hz, isomers A and B), 18.0 (s, dppp  $\text{PCH}_2\text{CH}_2$ , isomers A and B).  $^{31}\text{P}\{^1\text{H}\}$  NMR ( $\text{CD}_2\text{Cl}_2$ ): 9.53 (s).  $^{19}\text{F}$  NMR ( $\text{CD}_2\text{Cl}_2$ ):  $-77.5$  (s, 2  $\text{CF}_3\text{SO}_3$ ). IR (neat,  $\text{cm}^{-1}$ ): 1252, 1158, 1104, 1030 (all OTf). Anal. Calcd for  $\text{C}_{47}\text{H}_{40}\text{N}_2\text{P}_2\text{S}_2\text{F}_6\text{O}_6$

$\text{Pd}\cdot\text{H}_2\text{O}$ : C, 51.6; H, 3.87; N, 2.56; S, 5.86. Found: C, 51.6; H, 3.86; N, 2.61; S, 5.85.

**[Pt(dppp)(isoquinoline) $_2$ ][OTf] $_2$  (15).** A 50-mL Schlenk flask equipped with a stirbar was charged with 0.116 g (0.898 mmol) of isoquinoline and 5 mL of  $\text{CH}_2\text{Cl}_2$ . A solution of 0.163 g (0.180 mmol) of Pt(dppp)(OTf) $_2$  in 20 mL of  $\text{CH}_2\text{Cl}_2$  was added *via* syringe, and the resulting mixture was stirred under nitrogen for 5 h at ambient temperature. The solution was transferred *via* syringe into a 50-mL flask and reduced in volume to ca. 1 mL on a rotary evaporator. A diethyl ether–pentane mixture (1:10) was added, resulting in the formation of a white precipitate, which was collected and washed with pentane. The filtrate was reduced in volume to 5 mL, and the additional product was isolated as above. The precipitates were combined, dissolved in  $\text{CH}_2\text{Cl}_2$ , and evaporated to dryness in vacuo at 35–40 °C. The white microcrystalline product was further dried in vacuo: yield of **15** 0.175 g (84%); mp 270–272 °C dec.  $^1\text{H}$  NMR ( $\text{CD}_2\text{Cl}_2$ ): broadened lines, due to rapid interconversion between isomers A and B): 9.70 (br s, 4H, isoq H-1, isomers A and B), 8.95 (br m, 4H, isoq H-3, isomers A and B), 7.95 (br m, 8H, isoq H-8 and H-5, isomers A and B), 7.75 (t, 4H,  $J = 11.0$ , isoq H-6 isomers A and B), 7.55 (d, 4H,  $J = 6.8$ , isoq H-4 isomers A and B), 7.35 (br m, 40H, dppp Ph, isomers A and B), 7.05 (br m, 4H, isoq H-7 isomers A and B), 3.35 (br m, 8H, dppp  $\text{PCH}_2\text{CH}_2$ , isomers A and B), 2.20 (br t, 4H, dppp  $\text{PCH}_2\text{CH}_2$ , isomers A and B).  $^{13}\text{C}\{^1\text{H}\}$  NMR ( $\text{CD}_2\text{Cl}_2$ ): 155.5 (s, isoq C-1, isomers A and B), 141.6 (s, isoq C-3, isomers A and B), 135.7 (s, isoq C-10, isomers A and B), 133.9 (s, isoq C-6, isomers A and B), 133.3 (m, dppp Ph, isomers A and B), 132.2 (m, dppp Ph + isoq C-9, isomers A and B), 129.4 (s, isoq C-8, isomers A and B), 129.36 (br s, dppp Ph  $\text{C}_p$ , isomers A and B), 128.9 (s, isoq C-7, isomers A and B), 126.3 (s, isoq C-5, isomers A and B), 124.5 (s, isoq C-4, isomers A and B), 124.4 (t, dppp  $\text{C}_i$ , isomers A and B), 121.3 (q, OTf,  $J_{\text{C-F}} = 319$  Hz, isomers A and B), 21.88 (t, dppp  $\text{PCH}_2\text{CH}_2$ ,  $J_{\text{C-P}} = 36$  Hz, isomers A and B), 18.0 (s, dppp  $\text{PCH}_2\text{CH}_2$ , isomers A and B).  $^{31}\text{P}\{^1\text{H}\}$  NMR ( $\text{CD}_2\text{Cl}_2$ ):  $-11.86$  (s,  $^{195}\text{Pt}$  satellites,  $^1J_{\text{P-Pt}} = 3032$  Hz).  $^{19}\text{F}$  NMR ( $\text{CD}_2\text{Cl}_2$ ):  $-76.6$  (s, 2  $\text{CF}_3\text{SO}_3$ ). IR (neat,  $\text{cm}^{-1}$ ): 1250, 1155, 1101, 1027 (all OTf). Anal. Calcd for  $\text{C}_{47}\text{H}_{40}\text{N}_2\text{P}_2\text{S}_2\text{F}_6\text{O}_6\text{Pt}\cdot\text{H}_2\text{O}$ : C, 47.8; H, 3.58; N, 2.37; S, 5.42. Found: C, 47.7; H, 3.63; N, 2.34; S, 5.47.

**cis-[Pd( $\text{Et}_3\text{P}$ ) $_2$ (quinoline) $_2$ ][OTf] $_2$  (16).** A 25-mL Schlenk flask equipped with a stirbar was charged with 0.116 g (0.898 mmol) of quinoline and  $\text{CH}_2\text{Cl}_2$  (10 mL). To this was added 0.128 g (0.200 mmol) of *cis*-Pd( $\text{Et}_3\text{P}$ ) $_2$ (OTf) $_2$ , and the resulting colorless solution was stirred under nitrogen for 3 h at ambient temperature. The solution was transferred *via* syringe into a 50-mL flask and reduced in volume to ca. 2 mL in vacuo. Diethyl ether was added, and the white precipitate was collected and washed with diethyl ether and dried in vacuo: yield 0.146 g of **16** (84%); mp 50–52 °C.  $^1\text{H}$  NMR ( $\text{CD}_2\text{Cl}_2$ ): 9.79 (br s, 2H, quin H-2, isomer B), 9.51 (br s, 2H, quin H-2, isomer A), 9.12 (br s, 2H, quin H-4, isomer A), 8.87 (br s, 2H, quin H-4, isomer B), 8.32–8.05 (br m, 4H, quin H-7 and H-5, isomer A), 7.85–7.70 (br m, 4H, quin H-7 and H-5, isomer B), 7.50–7.30 (br m, 8H, quin H-6, H-3, isomers A and B), 1.83 (m, 24H,  $\text{PCH}_2\text{CH}_3$ , isomers A and B), 1.28 (m, 36H,  $\text{PCH}_2\text{CH}_3$ , isomers A and B).  $^{13}\text{C}\{^1\text{H}\}$  NMR ( $\text{CD}_2\text{Cl}_2$ ): 154.9 (s, quin C-2, isomer A), 154.4 (s, quin C-2, isomer B), 145.1 (s, quin C-9, isomer B), 144.9 (s, quin C-9, isomer A), 141.3 (s, quin C-4, isomers A and B), 134.4 (s, quin C-8, isomer A), 133.7 (s, quin C-8, isomer B), 129.9 (s, quin C-10, isomers A and B), 129.7 (s, quin C-7, isomers A and B), 129.4 (s, quin C-5, isomers A and B), 127.7 (s, quin C-6, isomer B), 127.1 (s, quin C-6, isomer A), 123.6 (s, quin C-3, isomer B), 123.1 (s, quin C-3, isomer A), 121.3 (q, OTf,  $J_{\text{C-F}} = 319$  Hz, isomers A and B), 16.8 (t,  $\text{PCH}_2\text{CH}_3$ ,  $J_{\text{C-P}} = 28$  Hz, isomers A and B), 8.6 (s,  $\text{PCH}_2\text{CH}_3$ , isomers A and B).  $^{31}\text{P}\{^1\text{H}\}$  NMR ( $\text{CD}_2\text{Cl}_2$ ): 27.71 (s, isomer A), 27.51 (s, isomer B).  $^{19}\text{F}$  NMR ( $\text{CD}_2\text{Cl}_2$ ):  $-76.4$  (s, 2  $\text{CF}_3\text{SO}_3$ ). IR (neat,  $\text{cm}^{-1}$ ): 1281, 1143, 1031 (all OTf). Anal. Calcd for  $\text{C}_{32}\text{H}_{44}\text{N}_2\text{P}_2\text{S}_2\text{F}_6\text{O}_6\text{Pd}$ : C, 42.7; H, 4.93; N, 3.12; S, 7.13. Found: C, 42.4; H, 5.14; N, 3.10; S, 7.02.



**cis-[Pt(Et<sub>3</sub>P)<sub>2</sub>(quinoline)<sub>2</sub>][OTf]<sub>2</sub> (17).** A 50-mL Schlenk flask equipped with a stirbar was charged with 0.116 g (0.898 mmol) of quinoline and CH<sub>2</sub>Cl<sub>2</sub> (15 mL). *cis*-Pt(Et<sub>3</sub>P)<sub>2</sub>(OTf)<sub>2</sub> (0.131 g, 0.180 mmol) was added, and the resulting mixture was stirred under nitrogen for 3 h at ambient temperature. The solution was transferred *via* syringe into a 50-mL flask and reduced in volume to ca. 2 mL on a rotary evaporator. Diethyl ether was added, and the solution was stored for 1 h at -20 °C. The white precipitate was collected and washed with diethyl ether (ca. 10 mL) and dried in vacuo: yield of 17 0.141 g (79%); mp 142–144 °C. <sup>1</sup>H NMR (CD<sub>2</sub>Cl<sub>2</sub>): 9.89 (s, 2H, quin H-2), isomer B), 9.64 (s, 2H, quin H-2, isomer A), 9.34 (d, 2H, *J* = 8.8, quin H-4, isomer A), 9.10 (d, 2H, *J* = 8.5, quin H-4, isomer B), 8.38 (t, 2H, *J* = 8.0, quin H-7, isomer A), 8.31 (d, 2H, *J* = 8.1, quin H-5, isomer A), 8.19 (t, 2H, *J* = 7.2, quin H-7, isomer B), 7.94 (d, 2H, *J* = 8.1, quin H-5, isomer B), 7.84 (t, 2H, *J* = 8.0, quin H-6, isomer A), 7.79 (dd, 2H, *J* = 10.1, 4.0, quin H-3, isomer A), 7.66 (t, 2H, *J* = 7.2, quin H-6, isomer B), 7.58 (dd, 2H, *J* = 8.4, 5.6, quin H-3, isomer B), 1.86 (m, 24H, PCH<sub>2</sub>CH<sub>3</sub>, isomers A and B), 1.28 (m, 36H, PCH<sub>2</sub>CH<sub>3</sub>, isomers A and B). <sup>13</sup>C{<sup>1</sup>H} NMR (CD<sub>2</sub>Cl<sub>2</sub>): 155.2 (s, quin C-2, isomer A), 154.5 (s, quin C-2, isomer B), 145.0 (s, quin C-9, isomer B), 144.9 (s, quin C-9, isomer A), 141.9 (s, quin C-4, isomers A and B), 134.8 (s, quin C-8, isomer A), 133.9 (s, quin C-8, isomer B), 130.4 (s, quin C-10, isomer A), 130.3 (s, quin C-10, isomer B), 130.0 (s, quin C-7, isomer B), 129.7 (s, quin C-7, isomer A), 129.6 (s, quin C-5, isomer A), 129.5 (s, quin C-5, isomer B), 127.0 (s, quin C-6, isomer B), 126.3 (s, quin C-6, isomer A), 124.0 (s, quin C-3, isomer B), 123.4 (s, quin C-3, isomer A), 121.3 (q, OTf, *J*<sub>C-F</sub> = 319 Hz, isomers A and B), 15.98 (t, PCH<sub>2</sub>CH<sub>3</sub>, *J*<sub>C-P</sub> = 30 Hz, isomers A and B), 8.25 (s, PCH<sub>2</sub>CH<sub>3</sub>, isomers A and B). <sup>31</sup>P{<sup>1</sup>H} NMR (CD<sub>2</sub>Cl<sub>2</sub>): -0.28 (s, <sup>195</sup>Pt satellites, <sup>1</sup>*J*<sub>P-Pt</sub> = 3099 Hz, isomer A), -0.75 (s, <sup>195</sup>Pt satellites, <sup>1</sup>*J*<sub>P-Pt</sub> = 3099 Hz, isomer B). <sup>19</sup>F NMR (CD<sub>2</sub>Cl<sub>2</sub>): -77.8 (s, 2 CF<sub>3</sub>SO<sub>3</sub>). IR (neat, cm<sup>-1</sup>): 1258, 1148, 1030 (all OTf). Anal. Calcd for C<sub>32</sub>H<sub>44</sub>N<sub>2</sub>P<sub>2</sub>S<sub>2</sub>F<sub>6</sub>O<sub>6</sub>Pt·H<sub>2</sub>O: C, 38.2; H, 4.61; N, 2.79; S, 6.37. Found: C, 38.2; H, 4.56; N, 2.83; S, 6.44.

**[Pd(dppp)(quinoline)<sub>2</sub>][OTf]<sub>2</sub> (18).** A 25-mL Schlenk flask equipped with a stirbar was charged with 0.116 g (0.898 mmol) of quinoline and 10 mL of CH<sub>2</sub>Cl<sub>2</sub>. Pd(dppp)(OTf)<sub>2</sub> (0.147 g, 0.180 mmol) was then added, and the resulting colorless solution was stirred under nitrogen for 5 h at room temperature. The solution was transferred *via* syringe into a 50-mL flask and reduced in volume to ca. 2 mL in vacuo. Diethyl ether was added to the residue, resulting in the formation of a white precipitate, which was collected and washed with diethyl ether. The product was dried in vacuo: yield of 18 0.161 g (83%); mp 296–298 °C dec. <sup>1</sup>H NMR (CD<sub>2</sub>Cl<sub>2</sub>): 10.20 (m, 2H, quin H-2, isomer A), 9.86 (m, 2H, quin H-2, isomer B), 9.35 (d, 2H, *J* = 8.1, quin H-8, isomer B), 9.21 (d, 2H, *J* = 8.1, quin H-8, isomer A), 8.26 (m, 2H, quin H-7, isomer B), 8.07 (br m, 6H, overlap of quin H-4 and dppp, isomer A), 7.95 (m, 6H, quin H-7 and dppp, isomer A), 7.83 (d, 2H, *J* = 8.1, quin H-4, isomer B), 7.65–7.48 (m, 18H, quin H-5 and H-3, isomer A, H-6, isomer B, dppp, isomer B), 7.40 (m, 4H, quin H-6, isomer A, dppp, isomer A), 7.30–7.20 (m, 4H, quin H-5 and H-3, isomer B), 7.09 (m, 8H, dppp, isomer B), 7.02 (m, 4H, dppp, isomer A), 6.70 (t, 2H, *J* = 7.5, dppp, isomer A), 6.59 (t, 4H, *J* = 7.5, dppp, isomer A), 4.09 (m, 2H, dppp PCH<sub>2</sub>, isomer A), 3.39 (m, 4H, dppp PCH<sub>2</sub>, isomer B), 2.84 (m, 3H, dppp PCH<sub>2</sub> and dppp PCH<sub>2</sub>CHH, isomer A), 2.36 (m, 2H, dppp PCH<sub>2</sub>CH<sub>2</sub>, isomer B), 1.91 (m, 1H, dppp PCH<sub>2</sub>CHH, isomer A). <sup>13</sup>C{<sup>1</sup>H} NMR (CD<sub>2</sub>Cl<sub>2</sub>): 155.0, 153.3, 144.6, 144.1, 140.2, 139.9 (all singlets, quin, isomers A and B), 134.5 (m), 133.6 (s), 133.4 (s), 133.0 (m), 132.7 (s), 132.6 (s), 132.2 (s), 131.3 (t, *J* = 10), 131.0 (s), 130.3 (t, *J* = 10), 129.8 (s), 129.7 (t, *J* = 10), 129.3 (s), 129.2 (t, *J* = 10), 129.0 (s), 128.7 (s), 128.6 (s), 128.5 (s), 128.2 (t, *J* = 10), 128.1 (dppp and quin, isomers A and B), 126.7 (t, *J* = 25, dppp C<sub>i</sub>, isomer A), 126.1 (t, *J* = 25, dppp C<sub>i</sub>, isomer B), 123.2, 122.5 (both singlets, quinoline, isomers A and B), 121.3 (q, OTf, *J*<sub>C-F</sub> = 319 Hz, isomers A and B), 21.7 (t, *J*

**Table 2. Crystallographic Data for *syn*-[Pt(dppp)(quinoline)<sub>2</sub>][OTf]<sub>2</sub> (19)**

molecular formula	C <sub>47</sub> H <sub>40</sub> N <sub>2</sub> P <sub>2</sub> S <sub>2</sub> F <sub>6</sub> O <sub>6</sub> Pt
fw	1164.009
space group	<i>P</i> 2 <sub>1</sub> / <i>a</i>
space group no.	14
cryst syst	monoclinic
<i>a</i> , Å	17.615(3)
<i>b</i> , Å	16.111(3)
<i>c</i> , Å	18.979(3)
$\beta$ , deg	103.71(2)
cell vol, Å <sup>3</sup>	5232.75
<i>Z</i>	4
calcd density, g cm <sup>-3</sup>	1.477
cryst size, mm	0.35 × 0.29 × 0.17
abs coeff, cm <sup>-1</sup>	29.094
radiation	Mo, 0.710 73 Å
no. of rflns measured	8825
no. of unique rflns	8184
no. of observns	5073 ( <i>I</i> < 3.00σ( <i>I</i> ))
2θ range, deg	4.0–48.0
scan technique	θ–2θ scan
scan width, deg	0.8000 + 0.3400 tan θ
<i>R</i> factor	0.0529
weighted <i>R</i> factor	0.0607

= 20, dppp PCH<sub>2</sub>CH<sub>2</sub>, isomer B), 20.8 (t, *J* = 20, dppp PCH<sub>2</sub>CH<sub>2</sub>, isomer A), 17.8 (s, dppp PCH<sub>2</sub>CH<sub>2</sub>, isomers A and B). <sup>31</sup>P{<sup>1</sup>H} NMR (CD<sub>2</sub>Cl<sub>2</sub>): 6.88 (s, isomer A), 8.38 (s, isomer B). <sup>19</sup>F NMR (CD<sub>2</sub>Cl<sub>2</sub>): -77.5 (s, 2 CF<sub>3</sub>SO<sub>3</sub>). IR (neat, cm<sup>-1</sup>): 1249, 1154, 1028 (all OTf). Anal. Calcd for C<sub>47</sub>H<sub>40</sub>N<sub>2</sub>P<sub>2</sub>S<sub>2</sub>F<sub>6</sub>O<sub>6</sub>·Pd·H<sub>2</sub>O: C, 51.6; H, 3.87; N, 2.56; S, 5.86. Found: C, 51.5; H, 3.85; N, 2.61; S, 5.93.

**[Pt(dppp)(quinoline)<sub>2</sub>][OTf]<sub>2</sub> (19).** A 50-mL Schlenk flask equipped with a stirbar was charged with 0.140 g (1.084 mmol) of quinoline, 5 mL of CHCl<sub>3</sub>, and 10 mL of CH<sub>2</sub>Cl<sub>2</sub>. To this solution was added 0.163 g (0.180 mmol) of Pt(dppp)(OTf)<sub>2</sub>, and the resulting mixture was stirred under nitrogen for 10 h at ambient temperature. The solution was transferred *via* syringe into a 50-mL flask and reduced in volume to 5 mL on a rotary evaporator. Diethyl ether was then added, and the white precipitate was collected and washed with diethyl ether and dried in vacuo: yield 0.185 g of 19 (89%). Crystallization from CH<sub>2</sub>Cl<sub>2</sub>–ether solution afforded analytically pure product: mp 322 °C dec. <sup>1</sup>H NMR (CD<sub>2</sub>Cl<sub>2</sub>): 10.24 (m, 2H, quin H-2, isomer A), 9.85 (m, 2H, quin H-2, isomer B), 9.56 (d, 2H, *J* = 8.0, quin H-8, isomer B), 9.37 (d, 2H, *J* = 8.0, quin H-8, isomer A), 8.36 (m, 2H, quin H-7, isomer B), 8.10 (br m, 6H, overlap of quin H-4 and dppp, isomer A), 8.02 (m, 6H, quin H-7 and dppp, isomer A), 7.87 (d, 2H, *J* = 8.0, quin H-4, isomer B), 7.68–7.62 (m, 8H, quin H-5, isomer A, dppp, isomer B), 7.56–7.48 (m, 12H, quin H-3, isomer A, quin H-6, isomer B, dppp, isomer B), 7.45 (m, 4H, quin H-6, isomer A, dppp, isomer A), 7.29 (m, 4H, quin H-5 and H-3, isomer B), 7.05 (m, 8H, dppp, isomer B), 6.98 (m, 4H, dppp, isomer A), 6.69 (t, 2H, *J* = 7.5, dppp, isomer A), 6.57 (t, 4H, *J* = 7.5, dppp, isomer A), 4.18 (m, 2H, dppp PCH<sub>2</sub>, isomer A), 3.47 (m, 4H, dppp PCH<sub>2</sub>, isomer B), 3.20–2.70 (m, 3H, dppp PCH<sub>2</sub> and dppp PCH<sub>2</sub>CHH, isomer A), 2.40 (m, 2H, dppp PCH<sub>2</sub>CH<sub>2</sub>, isomer B), 1.98–1.80 (m, 1H, dppp PCH<sub>2</sub>CHH, isomer A). <sup>13</sup>C{<sup>1</sup>H} NMR (CD<sub>2</sub>Cl<sub>2</sub>): 155.2, 153.4, 144.8, 144.0, 140.7, 140.5 (s, quinoline, isomers A and B), 134.5 (m), 134.1 (s), 133.3 (s), 133.1 (s), 133.0 (m), 132.5 (s), 132.1 (s), 131.2 (t, *J* = 12), 131.1 (s), 130.1 (t, *J* = 12), 129.6 (t, *J* = 12), 129.5 (s), 129.0 (s), 128.9 (t, *J* = 12), 128.8 (s), 128.4 (s), 128.0 (t, *J* = 25), 127.5 (dppp and quin, isomers A and B), 125.5 (t, *J* = 25, dppp C<sub>i</sub>, isomer A), 125.0 (t, *J* = 25, dppp C<sub>i</sub>, isomer B), 123.5, 122.7 (both singlets, quinoline, isomers A and B), 121.3 (q, OTf, *J*<sub>C-F</sub> = 319 Hz, isomers A and B), 20.8 (t, *J* = 20, dppp PCH<sub>2</sub>CH<sub>2</sub>, isomer B), 20.5 (t, *J* = 20, dppp PCH<sub>2</sub>CH<sub>2</sub>, isomer A), 17.8 (s, dppp PCH<sub>2</sub>CH<sub>2</sub>, isomers A and B). <sup>31</sup>P{<sup>1</sup>H} NMR (CD<sub>2</sub>Cl<sub>2</sub>): -15.71 (s, <sup>195</sup>Pt satellites, <sup>1</sup>*J*<sub>P-Pt</sub> = 3032 Hz, isomer A), -13.80 (s, <sup>195</sup>Pt satellites, <sup>1</sup>*J*<sub>P-Pt</sub> = 3032 Hz, isomer B). <sup>19</sup>F NMR (CD<sub>2</sub>Cl<sub>2</sub>): -77.4 (s, 2 CF<sub>3</sub>SO<sub>3</sub>). IR (neat, cm<sup>-1</sup>): 1252, 1155, 1101, 1030

Table 3. Positional Parameters and Isotropic Thermal Factors ( $\text{\AA}^2$ ) for Compound 19

atom	x	y	z	$B^a$	atom	x	y	z	$B^a$
Pt	0.25026(3)	-0.00857(3)	0.21767(3)	3.717(8)	C31	0.255(1)	0.262(1)	0.266(1)	8.1(4)*
S1	0.7642(3)	0.0425(5)	0.4984(3)	10.6(2)	C32	0.281(1)	0.329(2)	0.227(1)	11.8(7)*
S2	0.2926(3)	0.0650(4)	0.9804(3)	9.8(1)	C33	0.304(2)	0.325(2)	0.169(1)	13.1(8)*
P1	0.1258(2)	-0.0065(2)	0.1494(2)	4.15(7)	C34	0.298(1)	0.251(1)	0.132(1)	10.5(6)*
P2	0.2688(2)	-0.1411(2)	0.1863(2)	3.82(7)	C35	0.2770(9)	0.1749(9)	0.1609(8)	6.4(4)
N1	0.2394(7)	0.1141(7)	0.2571(7)	6.3(3)	C36	0.257(1)	0.1842(9)	0.227(1)	7.9(5)
N2	0.3641(5)	-0.0078(7)	0.2891(5)	5.2(2)	C37	0.3707(9)	-0.030(1)	0.3568(7)	7.3(4)
C1	0.1076(8)	-0.0668(9)	0.0668(7)	5.3(3)	C38	0.443(1)	-0.033(1)	0.4082(8)	8.9(6)
C2	0.1310(8)	-0.1582(8)	0.0768(7)	5.0(3)	C39	0.5064(8)	-0.010(1)	0.3870(9)	8.1(5)
C3	0.2184(7)	-0.1721(8)	0.0943(6)	4.3(3)	C40	0.5024(7)	0.017(1)	0.3191(7)	5.5(3)
C4	0.0558(7)	-0.0393(8)	0.1985(7)	4.5(3)	C41	0.5695(9)	0.042(1)	0.2961(8)	7.0(4)
C5	0.0736(8)	-0.045(1)	0.2723(8)	6.2(4)	C42	0.5637(9)	0.065(1)	0.231(1)	8.0(5)
C6	0.0164(9)	-0.064(1)	0.3104(8)	7.6(5)	C43	0.4929(9)	0.063(1)	0.1788(9)	6.9(4)
C7	-0.0566(9)	-0.077(1)	0.2744(9)	8.1(5)	C44	0.4261(8)	0.0395(8)	0.1981(7)	5.2(3)
C8	-0.0777(8)	-0.071(1)	0.201(1)	7.9(5)	C45	0.4312(7)	0.0167(8)	0.2685(7)	5.2(3)
C9	-0.0226(9)	-0.053(1)	0.1637(8)	6.5(4)	C46	0.844(2)	0.015(2)	0.465(2)	6.6(7)*
C10	0.0943(7)	0.0942(8)	0.1167(7)	4.5(3)	C47	0.352(2)	0.015(2)	0.583(1)	5.8(6)*
C11	0.0497(9)	0.144(1)	0.1513(8)	6.6(4)	F1	0.823(1)	0.014(1)	0.394(1)	9.3(5)*
C12	0.023(1)	0.2246(9)	0.124(1)	8.5(5)	F2	0.898(3)	-0.026(3)	0.503(2)	13(1)*
C13	0.039(1)	0.2523(9)	0.064(1)	7.6(5)	F3	0.881(2)	0.082(2)	0.473(2)	14.2(9)*
C14	0.082(1)	0.207(1)	0.0301(9)	7.4(4)	F4	0.420(1)	-0.008(2)	0.985(1)	11.3(6)*
C15	0.1102(8)	0.1258(9)	0.0536(8)	5.9(4)	F5	0.333(2)	-0.072(2)	0.935(2)	13.6(8)*
C16	0.2422(7)	-0.2188(8)	0.2452(6)	4.5(3)	F6	0.369(1)	0.045(1)	0.883(1)	8.5(5)*
C17	0.2453(8)	-0.3017(8)	0.2303(8)	5.3(3)	O1	0.707(1)	-0.031(2)	0.483(1)	9.3(7)*
C18	0.2294(9)	-0.3599(9)	0.2763(9)	6.8(4)	O2	0.7869(7)	0.0481(8)	0.5727(7)	9.1(3)*
C19	0.212(1)	-0.336(1)	0.3399(9)	8.6(5)	O3	0.768(2)	0.139(3)	0.472(2)	13(1)*
C20	0.208(1)	-0.256(1)	0.3565(9)	7.5(5)	O4	0.2826(7)	0.0208(8)	1.0404(6)	8.8(3)*
C21	0.2257(9)	-0.1962(9)	0.3082(9)	6.3(4)	O5	0.262(2)	0.138(2)	0.957(2)	10.9(8)*
C22	0.3695(7)	-0.1626(8)	0.1899(7)	4.3(3)	O6	0.216(3)	0.014(3)	0.930(2)	11(1)*
C23	0.4011(8)	-0.147(1)	0.1326(9)	6.9(4)	F1'	0.916(2)	0.029(2)	0.497(1)	12.6(7)*
C24	0.4795(9)	-0.164(1)	0.137(1)	9.6(5)	F2'	0.852(2)	-0.062(2)	0.472(2)	13.6(8)*
C25	0.5268(9)	-0.195(1)	0.201(1)	10.6(5)	F4'	0.410(3)	0.065(3)	0.986(2)	13(1)*
C26	0.4962(9)	-0.209(1)	0.257(1)	8.8(6)	F5'	0.381(2)	-0.045(2)	0.950(1)	12.4(7)*
C27	0.4164(9)	-0.194(1)	0.2499(9)	7.1(4)	F6'	0.313(2)	0.000(3)	0.870(2)	12(1)*
C28	0.223(1)	0.121(1)	0.3232(9)	7.8(5)	O1'	0.710(2)	0.033(2)	0.453(2)	11.6(8)*
C29	0.222(1)	0.199(1)	0.361(1)	11.0(6)*	O4'	0.233(1)	0.106(1)	0.932(1)	8.3(6)*
C30	0.235(1)	0.263(1)	0.327(1)	10.0(6)*	O5'	0.362(2)	0.133(2)	1.014(2)	11.7(9)

<sup>a</sup> Starred values denote atoms refined isotropically. Anisotropically refined atoms are given in the form of the isotropic equivalent displacement parameter defined as:  $\frac{1}{3}[a^2B(1,1) + b^2B(2,2) + c^2B(3,3) + ab(\cos \gamma)B(1,2) + ac(\cos \beta)B(1,3) + bc(\cos \alpha)B(2,3)]$ .

(all OTf). Anal. Calcd for  $C_{47}H_{40}N_2P_2S_2F_6O_6Pt \cdot H_2O$ : C, 47.8; H, 3.58; N, 2.37; S, 5.42. Found: C, 47.5; H, 3.47; N, 2.35; S, 5.36.

**cis-[Pt(Et<sub>3</sub>P)<sub>2</sub>(3-bromopyridine)<sub>2</sub>][OTf]<sub>2</sub> (20).** A 25-mL Schlenk flask equipped with a stirbar was charged with 0.071 g (0.446 mmol) of 3-bromopyridine and CH<sub>2</sub>Cl<sub>2</sub> (5 mL). Then, 0.148 g (0.203 mmol) of *cis*-Pt(Et<sub>3</sub>P)<sub>2</sub>(OTf)<sub>2</sub> was added, and the resulting solution was stirred under nitrogen for 3 h at ambient temperature. The mixture was transferred *via* syringe into a 25-mL flask and reduced in volume to 2 mL on a rotary evaporator. Pentane was added, and the mixture was stored at -20 °C for 30 min. The white precipitate was collected and washed with pentane. Drying *in vacuo* afforded 0.173 g of **20** (81%). The compound melted at 168–170 °C. <sup>1</sup>H NMR (CD<sub>2</sub>Cl<sub>2</sub>): 9.52 (s, 2H, 3-Br-py H-2, isomer B), 9.45 (d, *J* = 6.5, 2H, 3-Br-py H-6, isomer B), 9.42 (s, 2H, 3-Br-py H-2, isomer A), 9.34 (d, *J* = 5.3, 2H, 3-Br-py H-6, isomer A), 8.05 (d, *J* = 8.4, 4H, 3-Br-py H-4, isomers A and B), 7.55 (dd, *J* = 11.3, 8.8, 4H, 3-Br-py H-5, isomers A and B), 1.77 (m, 24H, PCH<sub>2</sub>CH<sub>3</sub>, isomers A and B), 1.27 (m, 36H, PCH<sub>2</sub>CH<sub>3</sub>, isomers A and B). <sup>13</sup>C{<sup>1</sup>H} NMR (CD<sub>2</sub>Cl<sub>2</sub>): 152.2 (s, 3-Br-py C-2, isomer B), 151.9 (s, 3-Br-py C-2, isomer A), 150.6 (s, 3-Br-py C-6, isomer B), 150.4 (s, 3-Br-py C-6, isomer A), 144.2 (s, 3-Br-py C-4, isomers A and B), 129.0 (s, 3-Br-py C-5, isomers A and B), 124.2 (s, 3-Br-py C-3, isomers A and B), 121.3 (q, OTf, *J*<sub>C-F</sub> = 319 Hz, isomers A and B), 15.9 (t, PCH<sub>2</sub>CH<sub>3</sub>, *J*<sub>C-P</sub> = 39 Hz, isomers A and B), 8.0 (s, PCH<sub>2</sub>CH<sub>3</sub>, isomers A and B). <sup>31</sup>P{<sup>1</sup>H} NMR (CD<sub>2</sub>Cl<sub>2</sub>): -1.24 (s, <sup>195</sup>Pt satellites, <sup>1</sup>*J*<sub>P-Pt</sub> = 3160 Hz, isomer A), -1.38 (s, <sup>195</sup>Pt satellites, <sup>1</sup>*J*<sub>P-Pt</sub> = 3160 Hz, isomer B). <sup>19</sup>F NMR (CD<sub>2</sub>Cl<sub>2</sub>): -77.8 (s, 2 CF<sub>3</sub>SO<sub>3</sub>, isomers A and B). IR (neat, cm<sup>-1</sup>): 1270, 1158, 1102, 1031 (all OTf). Anal. Calcd for C<sub>24</sub>H<sub>38</sub>P<sub>2</sub>S<sub>2</sub>N<sub>2</sub>F<sub>6</sub>O<sub>6</sub>Pt: C, 27.6; H, 3.66; N, 2.68; S, 6.13. Found: C, 27.9; H, 3.85; N, 2.58; S, 5.83.

**[Pt(dppp)(3-bromopyridine)<sub>2</sub>][OTf]<sub>2</sub> (21).** A 50-mL Schlenk flask equipped with a stirbar was charged with 0.142 g (0.899 mmol) of 3-bromopyridine and CH<sub>2</sub>Cl<sub>2</sub> (25 mL). Then, 0.163 g (0.180 mmol) of Pt(dppp)(OTf)<sub>2</sub> in 20 mL of CH<sub>2</sub>Cl<sub>2</sub> was added, resulting in the formation of a white heterogeneous mixture, which was stirred under nitrogen for 5 h at ambient temperature. The mixture was filtered, the precipitate was collected, and a colorless filtrate was transferred *via* syringe into a 50-mL flask and reduced in volume to 5 mL *in vacuo*. Diethyl ether was added, resulting in the formation of a white precipitate, which was collected. Both precipitates were combined and washed with diethyl ether (ca. 10 mL). The product was dried *in vacuo*: yield of **21** 0.201 g (91%); mp 308–310 °C dec. <sup>1</sup>H NMR (CD<sub>3</sub>OD): 9.02 (br s, 2H, 3-Br-py H-2, isomers A and B), 8.78 (br m, 2H, 3-Br-py H-6, isomers A and B), 7.89 (d, 2H, *J* = 5.1, 3-Br-py H-4, isomer A), 7.82 (d, 2H, *J* = 5.0, 3-Br-py H-4, isomer B), 7.66 (br m, 16H, dppp Ph H<sub>o</sub>, isomers A and B), 7.46 (br m, 24H, dppp H<sub>m</sub>+H<sub>p</sub>, isomers A and B), 7.35 (t, 2H, *J* = 6.2, 3-Br-py H-5, isomer B), 7.27 (t, 2H, *J* = 6.5, 3-Br-py H-5, isomer A), 3.35 (br m, 8H, dppp PCH<sub>2</sub>CH<sub>2</sub>, isomers A and B), 2.25 (br m, 4H, dppp PCH<sub>2</sub>CH<sub>2</sub>, isomers A and B). <sup>13</sup>C{<sup>1</sup>H} NMR (CD<sub>3</sub>OD): 152.8 (s, 3-Br-py C-2, isomer A), 151.7 (s, 3-Br-py C-2, isomer B), 149.9 (s, 3-Br-py C-6, isomer A), 148.4 (s, 3-Br-py C-6, isomer B), 144.9 (s, 3-Br-py C-4, isomer A), 142.3 (s, 3-Br-py C-4, isomer B), 134.1 (br m, dppp Ph C<sub>o</sub>+C<sub>p</sub>, isomers A and B), 130.9 (br s, dppp Ph C<sub>m</sub>, isomers A and B), 129.4 (s, 3-Br-py C-5, isomer A), 129.0 (s, 3-Br-py C-5, isomer B), 126.6 (t, dppp C<sub>i</sub>, isomers A and B), 124.5 (s, 3-Br-py C-3, isomers A and B), 121.3 (q, OTf, *J*<sub>C-F</sub> = 319 Hz, isomers A and B), 22.5 (t, dppp PCH<sub>2</sub>CH<sub>2</sub>, isomers

A and B), 18.8 (s,  $\text{PCH}_2\text{CH}_2$ , isomers A and B).  $^{31}\text{P}\{^1\text{H}\}$  NMR ( $\text{CD}_3\text{OD}$ ): -11.24 (s,  $^{195}\text{Pt}$  satellites,  $^1J_{\text{P-Pt}} = 3036$  Hz, isomer B), -11.44 (s,  $^{195}\text{Pt}$  satellites,  $^1J_{\text{P-Pt}} = 3036$  Hz, isomer A).  $^{19}\text{F}$  NMR ( $\text{CD}_3\text{OD}$ ): -77.4 (s, 2  $\text{CF}_3\text{SO}_3$ ). IR (neat,  $\text{cm}^{-1}$ ): 1254, 1158, 1104, 1028 (all OTf). Anal. Calcd for  $\text{C}_{39}\text{H}_{34}\text{P}_2\text{N}_2\text{Br}_2\text{S}_2\text{O}_6\text{F}_6\text{Pt}\cdot\text{H}_2\text{O}$ : C, 37.8; H, 2.93; N, 2.26; S, 5.17. Found: C, 37.9; H, 2.89; N, 2.20; S, 5.19.

**[Pd(*R*)-(+)-BINAP(isoquinoline) $_2$ ][OTf] $_2$  (22).** A 10-mL Schlenk flask equipped with a stirbar was charged with 0.040 g (0.038 mmol) of Pd(*R*)-(+)-BINAP(OTf) $_2$  and 1 mL of  $\text{CH}_2\text{Cl}_2$ . A solution of 0.014 g (0.108 mmol) of isoquinoline in 1 mL of  $\text{CH}_2\text{Cl}_2$  was added, and the yellow solution was stirred under nitrogen for 1 h at ambient temperature. Slow addition of a diethyl ether-pentane (1:10) mixture afforded the product as a yellow precipitate, which was collected and washed with a minimum of diethyl ether-pentane: yield of **22** 0.044 g (89%); mp 282 °C dec.  $^1\text{H}$  NMR ( $\text{CD}_2\text{Cl}_2$ ): 9.51 (s, 2H), 8.72 (br s, 4H) (isoq), 8.07 (m, 4H), 7.90 (m, 4H), 7.80 (m, 4H), 7.73 (d, 2H,  $J = 7.8$ ), 7.64 (t, 2H,  $J = 7.3$ ), 7.53 (d, 4H,  $J = 7.8$ ), 7.46 (t, 2H,  $J = 7.8$ ) (BINAP and isoq), 7.29 (br m, 4H), 7.06 (br d, 8H,  $J = 7.2$ ), 6.87 (br m, 4H), 6.42 (d, 2H,  $J = 7.8$ ) (BINAP).  $^{13}\text{C}\{^1\text{H}\}$  NMR ( $\text{CD}_2\text{Cl}_2$ ): 156.5, 142.2, 140.3 (isoq), 135.5, 135.0, 133.4, 131.8, 131.4, 130.3, 129.6, 129.3, 128.9, 128.7, 128.6, 127.6, 127.3, 127.2, 126.1, 125.1 (BINAP and isoq), 124.6 ( $\text{C}_i$ , BINAP), 124.1 (BINAP), 123.5 (isoq), 121.3 (q, OTf,  $J_{\text{C-F}} = 319$  Hz), 120.0, 119.2 (BINAP).  $^{31}\text{P}\{^1\text{H}\}$  NMR ( $\text{CD}_2\text{Cl}_2$ ): 25.70 (s).  $^{19}\text{F}$  NMR ( $\text{CD}_2\text{Cl}_2$ ): -76.2 (s, 2  $\text{CF}_3\text{SO}_3$ ). IR (neat,  $\text{cm}^{-1}$ ): 1252, 1152, 1091, 1029 (all OTf). Anal. Calcd for  $\text{C}_{64}\text{H}_{46}\text{N}_2\text{P}_2\text{S}_2\text{F}_6\text{O}_6\text{Pd}\cdot 3\text{H}_2\text{O}$ : C, 57.4; H, 3.91; N, 2.09; S, 4.79. Found: C, 57.6; H, 3.70; N, 2.17; S, 4.88.

**[Pt(*R*)-(+)-BINAP(isoquinoline) $_2$ ][OTf] $_2$  (23).** A 10-mL Schlenk flask equipped with a stirbar was charged with 0.050 g (0.044 mmol) of Pt(*R*)-(+)-BINAP(OTf) $_2$  and  $\text{CH}_2\text{Cl}_2$  (1 mL). A solution of 0.028 g (0.217 mmol) of isoquinoline in 1 mL of  $\text{CH}_2\text{Cl}_2$  was added, and the combined solution was stirred under nitrogen for 12 h at room temperature. A diethyl ether-pentane mixture was added, and the product was collected and washed with diethyl ether-pentane and dried in vacuo: yield of **23** 0.057 g (92%); mp 368–370 °C dec.  $^1\text{H}$  NMR ( $\text{CD}_2\text{Cl}_2$ ): 9.59 (br s, 2H), 8.78 (br m, 2H), 8.51 (br m, 2H) (all isoq), 8.09–7.82 (m, 8H), 7.80–7.64 (m, 8H) (both BINAP), 7.56 (m, 4H), 7.41 (t, 2H,  $J = 7.0$ ), 7.33 (d, 2H,  $J = 6.3$ ) (isoq), 7.04 (m, 10H), 6.77 (t, 2H,  $J = 7.6$ ) (BINAP), 6.44 (d, 2H,  $J = 8.7$ ), 6.38 (d, 2H,  $J = 8.7$ ) (BINAP, isomers A and B).  $^{13}\text{C}\{^1\text{H}\}$  NMR ( $\text{CD}_2\text{Cl}_2$ ): 156.8, 156.5, 142.6, 142.3 (all isoq), 135.6, 135.1, 134.9, 134.8, 134.0, 133.4, 131.7, 131.4, 130.3, 129.8, 129.4, 129.2, 129.1, 128.8, 128.6, 127.6, 127.4, 127.2, 126.1 (BINAP and isoq), 124.5, 124.4 (isoq), 124.2, 123.9 ( $\text{C}_i$ , BINAP), 121.3 (q, OTf,  $J_{\text{C-F}} = 319$  Hz), 119.6, 119.3 (BINAP).  $^{31}\text{P}\{^1\text{H}\}$  NMR ( $\text{CDCl}_3$ ): 1.38 (s,  $^{195}\text{Pt}$  satellites,  $^1J_{\text{P-Pt}} = 4095$  Hz, isomer C), 1.24 (dd,  $J = 129$  Hz, 26 Hz,  $^{195}\text{Pt}$  satellites,  $^1J_{\text{P-Pt}} = 4095$  Hz, isomer B), 0.90 (s,  $^{195}\text{Pt}$  satellites,  $^1J_{\text{P-Pt}} = 4095$  Hz, isomer A).  $^{19}\text{F}$  NMR ( $\text{CD}_2\text{Cl}_2$ ): -77.0 (s, 2  $\text{CF}_3\text{SO}_3$ ). IR (neat,  $\text{cm}^{-1}$ ):

1256, 1152, 1100, 1029 (all OTf). Anal. Calcd for  $\text{C}_{64}\text{H}_{46}\text{N}_2\text{P}_2\text{S}_2\text{F}_6\text{O}_6\text{Pt}\cdot 2\text{H}_2\text{O}$ : C, 54.5; H, 3.57; N, 1.99; S, 4.55. Found: C, 54.55; H, 3.65; N, 1.77; S, 4.18.

**X-ray Crystallographic Analysis of 19.** X-ray-quality crystals were grown by the slow vapor diffusion of  $\text{Et}_2\text{O}$  into a  $\text{CHCl}_3$  solution of **19** at ambient temperature. A colorless plate,  $0.35 \times 0.29 \times 0.17$  mm, was glued onto a glass fiber and mounted for data collection on an Enraf-Nonius CAD4 diffractometer. The crystal and data collection information is presented in Table 2. The unit cell parameters were obtained by a least-squares refinement of 25 centered reflections in the range  $2\theta < 28^\circ$ . The space group was determined from systematic absences ( $h0l$ ,  $h+l = 2n$ ;  $0k0$ ,  $k = 2n$ ) and subsequent least-squares refinement. The data were collected by the  $\theta$ - $2\theta$  scan technique, with variable scanning rate, using monochromatic Mo ( $0.71073 \text{ \AA}$ ) radiation. A total of 8184 unique reflections were measured in the range  $4.0 < 2\theta < 48.0^\circ$ , of which 5073 were considered observed. Standard reflections showed no decay for the crystal during data collection. Lorentz and polarization corrections, and an empirical absorption correction based upon a series of  $\psi$  scans, were applied to the data. Intensities of equivalent reflections were averaged.

The structure was solved by the standard heavy-atom technique with the MolEN/VAX package. Non-hydrogen atoms were refined with anisotropic thermal parameters. Data were weighted using a non-Poisson scheme. All hydrogen atoms were calculated and added to the structure factor calculations. Scattering factors, and  $\Delta f'$  and  $\Delta f''$  values, were taken from the literature.<sup>18</sup> Positional parameters and isotropic thermal factors for non-hydrogen atoms are presented in Table 3. There is a disordered water molecule in the lattice and some disorder exhibited by one of the triflate anions.

**Acknowledgment.** We thank the National Science Foundation (Grant No. CHE-9101767) for financial support.

**Supporting Information Available:** Crystal structure data for **19**, including a table of calculated positional parameters for the hydrogen atoms, extended lists of bond lengths and bond angles, and a table of general displacement parameter expressions (8 pages). This material is contained in many libraries on microfiche, immediately follows this article in the microfilm version of the journal, can be ordered from the ACS, and can be downloaded from the Internet; see any current masthead page for ordering information and Internet access instructions.

OM950455A

(18) Chroemer, D. T.; Waber, J. T. In *International Tables for X-ray Crystallography*; Ibers, J. A., Hamilton, W. C., Eds.; Kynoch Press: Birmingham, U.K., 1974.

# Enthalpies of Reaction of Cp'Ru(COD)Cl (Cp' = C<sub>5</sub>H<sub>5</sub>, C<sub>5</sub>Me<sub>5</sub>; COD = Cyclooctadiene) with P(*p*-XC<sub>6</sub>H<sub>4</sub>)<sub>3</sub> (X = Cl, F, H, CH<sub>3</sub>, CF<sub>3</sub>, OCH<sub>3</sub>) Ligands: Ligand Steric vs Electronic Contributions to the Enthalpy of Reaction

Scaffold A. Serron, Lubin Luo, Chunbang Li, Michèle E. Cucullu, Edwin D. Stevens, and Steven P. Nolan\*

Department of Chemistry, University of New Orleans, New Orleans, Louisiana 70148

Received June 20, 1995<sup>®</sup>

The enthalpies of reaction of Cp'Ru(COD)Cl (1; Cp' =  $\eta^5$ -C<sub>5</sub>H<sub>5</sub>,  $\eta^5$ -C<sub>5</sub>Me<sub>5</sub>; COD = cyclooctadiene) with a series of para-substituted monodentate tertiary phosphine ligands, leading to the formation of Cp'Ru(PR<sub>3</sub>)<sub>2</sub>Cl, have been measured by anaerobic solution calorimetry in THF at 30.0 °C. These reactions are rapid and quantitative. Structural calorimetry have been carried out on three complexes in this series. The relative importance of phosphine steric vs electronic ligand parameters is more closely examined in terms of the presented quantitative thermochemical and structural information. Comparisons with enthalpy data in this and related organometallic systems are also presented.

## Introduction

A fundamental question addressed by a number of recent kinetic and thermodynamic studies deals with the relative importance of ligand steric vs electronic effects.<sup>1-3</sup> One such class of ligands which researchers have attempted to characterize in this fashion is tertiary phosphines. This class of ligand, of fundamental importance in organometallic chemistry and catalysis, has been employed to fine-tune reactivity and selectivity.<sup>4-6</sup> A better understanding of the exact nature of ligand effects can help direct synthetic and catalytic research efforts. Our solution calorimetric investigations of organo-group 8 complexes, focusing on ligand substitution reactions, have contributed to a clarification of the exact partitioning of steric and electronic ligand contributions present in tertiary phosphine based systems.<sup>7,8</sup>

Thermochemical studies performed on organometallic systems have gained recognition as an area of research that can provide important insights into reactivity and bonding patterns.<sup>9-12</sup> Our recent contribution on the thermochemistry of ligand substitution in the (L)<sub>2</sub>Fe(CO)<sub>3</sub> (L = PR<sub>3</sub>) system, where isosteric para-substituted triphenylphosphine ligands were employed as a diagnostic tool in the determination of the relative importance of ligand stereoelectronic factors, has clearly shown the importance of electronic contributions in this iron-based system.<sup>8c</sup>

(7) For organoruthenium systems see: (a) Nolan, S. P.; Martin, K. L.; Stevens, E. D.; Fagan, P. J. *Organometallics* **1992**, *11*, 3947-3953. (b) Luo, L.; Fagan, P. J.; Nolan, S. P. *Organometallics* **1993**, *12*, 3405-3411. (c) Luo, L.; Zhu, N.; Zhu, N.-J.; Stevens, E. D.; Nolan, S. P.; Fagan, P. J. *Organometallics* **1994**, *13*, 669-675. (d) Li, C.; Cucullu, M. E.; McIntyre, R. A.; Stevens, E. D.; Nolan, S. P. *Organometallics* **1994**, *13*, 3621-3627. (e) Cucullu, M. E.; Luo, L.; Nolan, S. P.; Fagan, P. J.; Jones, N. L.; Calabrese, J. C. *Organometallics* **1995**, *14*, 289-296. (f) Luo, L.; Li, C.; Cucullu, M. E.; Nolan, S. P. *Organometallics* **1995**, *14*, 1333-1338. (g) Serron, S. A.; Nolan, S. P. *Organometallics*, in press.

(8) For organoiron system see: (a) Luo, L.; Nolan, S. P. *Organometallics* **1992**, *11*, 3483-3486. (b) Luo, L.; Nolan, S. P. *Inorg. Chem.* **1993**, *32*, 2410-2415. (c) Li, C.; Nolan, S. P. *Organometallics* **1995**, *14*, 1327-1332. (d) Li, C.; Stevens, E. D.; Nolan, S. P. *Organometallics* **1995**, *14*, 3791-3797.

(9) For leading references in this area, see: (a) Nolan, S. P. *Bonding Energetics of Organometallic Compounds*. In *Encyclopedia of Inorganic Chemistry*; Wiley: New York, 1994. (b) Hoff, C. D. *Prog. Inorg. Chem.* **1992**, *40*, 503-561. (c) Martinho Simões, J. A.; Beauchamp, J. L. *Chem. Rev.* **1990**, *90*, 629-688. (d) Marks, T. J., Ed. *Bonding Energetics in Organometallic Compounds*; ACS Symposium Series 428; American Chemical Society: Washington, DC, 1990. (e) Marks, T. J., Ed. *Metal-Ligand Bonding Energetics in Organotransition Metal Compounds*; Polyhedron Symposium-in-Print 7; Elsevier: Oxford, U.K., 1988.

(10) See for example: (a) Nolan, S. P.; Hoff, C. D.; Stoutland, P. O.; Newman, L. J.; Buchanan, J. M.; Bergman, R. G.; Yang, G. K.; Peters, K. G. *J. Am. Chem. Soc.* **1987**, *109*, 3143-3145 and references therein. (b) Nolan, S. P.; Lopez de la Vega, R.; Hoff, C. D. *Organometallics* **1986**, *5*, 2529-2537.

(11) (a) Nolan, S. P.; Porchia, M.; Marks, T. J. *Organometallics* **1991**, *10*, 1450-1457. (b) Nolan, S. P.; Stern, D.; Marks, T. J. *J. Am. Chem. Soc.* **1989**, *111*, 7844-7854.

(12) (a) Nolan, S. P.; Stern, D.; Hedden, D.; Marks, T. J. In ref 1d, pp 159-174. (b) Nolan, S. P.; Lopez de la Vega, R.; Mukerjee, S. L.; Gonzalez, A. A.; Hoff, C. D. In ref 1e, pp 1491-1498. (c) Marks, T. J.; Gagné, M. R.; Nolan, S. P.; Schock, L. E.; Seyam, A. M.; Stern, D. L. *Pure Appl. Chem.* **1989**, *61*, 1665-1672. (d) Schock, L. E.; Marks, T. J. *J. Am. Chem. Soc.* **1988**, *110*, 7701-7715.

(13) Perrin, D. D.; Armarego, W. L. F. *Purification of Laboratory Chemicals*, 3rd ed.; Pergamon Press: New York, 1988.

<sup>®</sup> Abstract published in *Advance ACS Abstracts*, October 15, 1995.

(1) (a) Rahman, M. M.; Liu, H.-Y.; Eriks, K.; Prock, A.; Giering, W. P. *Organometallics* **1989**, *8*, 1-7. (b) Liu, H.-Y.; Eriks, K.; Prock, A.; Giering, W. P. *Inorg. Chem.* **1989**, *28*, 1759-1763. (c) Poe, A. J. *Pure Appl. Chem.* **1988**, *60*, 1209-1216 and references cited therein. (d) Gao, Y.-C.; Shi, Q.-Z.; Kersher, D. L.; Basolo, F. *Inorg. Chem.* **1988**, *27*, 188-191. (e) Baker, R. T.; Calabrese, J. C.; Krusic, P. J.; Therien, M. J.; Trogler, W. C. *J. Am. Chem. Soc.* **1988**, *110*, 8392-8412. (f) Rahman, M. M.; Liu, H.-Y.; Prock, A.; Giering, W. P. *Organometallics* **1987**, *6*, 650-658.

(2) (a) Huynh, M. H. V.; Bessel, C. A.; Takeuchi, K. J. *Abstracts of Papers*; 208th Annual Meeting of the American Chemical Society, Washington, DC, Aug 1994; American Chemical Society: Washington, DC, 1994; INOR 165. (b) Perez, W. J.; Bessel, C. A.; See, R. F.; Lake, C. H.; Churchill, M. R.; Takeuchi, K. J. In ref 2a, INOR 166. (c) Ching, S.; Shriver, D. F. *J. Am. Chem. Soc.* **1989**, *111*, 3238-3243. (d) Lee, K.-W.; Brown, T. L. *Inorg. Chem.* **1987**, *26*, 1852-1856. (e) Brown, T. L.; Lee, K. J. *Coord. Chem. Rev.* **1993**, *128*, 89-116.

(3) Lorsbach, B. A.; Prock, A.; Giering, W. P. *Organometallics* **1995**, *14*, 1694-1699 and references cited therein.

(4) (a) Collman, J. P.; Hegedus, L. S.; Norton, J. R.; Finke, R. G. *Principles and Applications of Organotransition Metal Chemistry*, 2nd ed.; University Science: Mill Valley, CA, 1987. (b) Bennett, M. A.; Matheson, T. W. In *Comprehensive Organometallic Chemistry*; Wilkinson, G.; Stone, F. G. A.; Abel, E. W., Eds.; Pergamon Press: Oxford, England, 1982; Chapter 32.9.

(5) (a) Tolman, C. A. *Chem. Rev.* **1977**, *77*, 313-348. (b) Pignolet, L. H., Ed.; *Homogeneous Catalysis with Metal Phosphine Complexes*; Plenum: New York, 1983.

(6) Noyori, R. *Asymmetric Catalysis in Organic Synthesis*; Wiley: New York, 1994 and references cited therein.

In the present study, we report on the application of this approach in determining the relative importance of such ligand effects in two related organoruthenium systems. Furthermore, structural investigations were carried out on three complexes in the present series, allowing for a wider sampling of bond length variation with change in ancillary ligation.

## Experimental Section

**General Considerations.** All manipulations involving organoruthenium complexes were performed under inert atmospheres of argon or nitrogen using standard high vacuum or Schlenk tube techniques or in a Vacuum/Atmospheres glovebox containing less than 1 ppm of oxygen and water. Ligands were purchased from Strem Chemicals or Aldrich and used as received. Solvents were dried and distilled under dinitrogen before use by employing standard drying agents.<sup>13</sup> Only materials of high purity, as indicated by IR and NMR spectroscopy were used in the calorimetric experiments. NMR spectra were recorded using a Varian Gemini 300 MHz spectrometer. Calorimetric measurements were performed using a Calvet calorimeter (Setaram C-80) which was periodically calibrated using the TRIS reaction<sup>14</sup> or the enthalpy of solution of KCl in water.<sup>15</sup> The experimental enthalpies for these two standard reactions compare very closely to literature values. This calorimeter has been previously described,<sup>16</sup> and typical procedures are described below. Experimental enthalpy data are reported with 95% confidence limits. Elemental analyses were performed by Oneida Research Services, Whitesboro, NY.

**Synthesis.** The compounds CpRu(COD)Cl<sup>17</sup> and Cp\*Ru(COD)Cl<sup>18</sup> were synthesized according to literature procedures. The identities of the organoruthenium products Cp\*Ru(PPh<sub>3</sub>)<sub>2</sub>Cl,<sup>7b</sup> CpRu(PPh<sub>3</sub>)<sub>2</sub>Cl,<sup>19</sup> CpRu(P(*p*-FC<sub>6</sub>H<sub>4</sub>)<sub>3</sub>)<sub>2</sub>Cl,<sup>20</sup> CpRu(P(*p*-CH<sub>3</sub>C<sub>6</sub>H<sub>4</sub>)<sub>3</sub>)<sub>2</sub>Cl,<sup>21</sup> and CpRu(P(*p*-CH<sub>3</sub>OC<sub>6</sub>H<sub>4</sub>)<sub>3</sub>)<sub>2</sub>Cl<sup>22</sup> were ascertained by comparison with literature NMR spectroscopic data. Experimental synthetic procedures, leading to isolation of crystalline materials, for previously unreported complexes are described below.

**CpRu(P(*p*-CF<sub>3</sub>C<sub>6</sub>H<sub>4</sub>)<sub>3</sub>)<sub>2</sub>Cl.** A 25 mL flask was charged with 108 mg (0.35 mmol) of CpRu(COD)Cl, 10 mL of dried THF, and 328 mg (0.70 mmol) of P(*p*-CF<sub>3</sub>C<sub>6</sub>H<sub>4</sub>)<sub>3</sub>. After it was stirred overnight, the solution was placed under vacuum to remove volatiles. Five milliliters of hexane was then added to the solid residue, and the mixture was stirred for about 20 min. The suspension was then filtered, and the remaining microcrystalline solid was washed with a small amount of hexanes. Solvent was removed, and the yellow/orange powder was dried under vacuum, giving a 340 mg (86%) yield. <sup>1</sup>H NMR (300 MHz, THF-*d*<sub>8</sub>, 25 °C): δ 4.34 (s, 5 H, Cp), 7.50 (d, 12H, Ph), 7.69 (m, 12 H, Ph). Anal. Calcd for RuClP<sub>2</sub>F<sub>18</sub>C<sub>47</sub>H<sub>24</sub>: C, 49.73; H, 2.58. Found: C, 49.70; H, 2.55.

(14) Ojelund, G.; Wadsö, I. *Acta Chem. Scand.* **1968**, *22*, 1691–1699.  
(15) Kilday, M. V. *J. Res. Natl. Bur. Stand. (U.S.)* **1980**, *85*, 467–481.

(16) (a) Nolan, S. P.; Hoff, C. D.; Landrum, J. T. *J. Organomet. Chem.* **1985**, *282*, 357–362. (b) Nolan, S. P.; Lopez de la Vega, R.; Hoff, C. D. *Inorg. Chem.* **1986**, *25*, 4446–4448.

(17) Albers, M. O.; Robinson, D. J.; Shaver, A.; Singleton, E. *Organometallics* **1986**, *5*, 2199–2205.

(18) (a) Fagan, P. J.; Ward, M. D.; Caspar, J. V.; Calabrese, J. C.; Krusic, P. J. *J. Am. Chem. Soc.* **1988**, *110*, 2981–2983. (b) Fagan, P. J.; Ward, M. D.; Calabrese, J. C. *J. Am. Chem. Soc.* **1989**, *111*, 1698–1719 and references therein. (c) Fagan, P. J.; Mahoney, W. S.; Calabrese, J. C.; Williams, I. D. *Organometallics* **1990**, *9*, 1843–1852.

(19) Bruce, M. I.; Hameister, C.; Swincer, A. G.; Wallis, R. C. *Inorg. Synth.* **1982**, *21*, 78–84.

(20) Hartwig, J. F.; Bhandari, S.; Rablen, P. R. *J. Am. Chem. Soc.* **1994**, *116*, 1839–1844.

(21) Bruce, M. I.; Windsor, N. J. *Aust. J. Chem.* **1977**, *30*, 1601–1604.

(22) Fiedler, P.; Braden, R.; Buding, H. Ger. Offen. DE 3 337 294, 1985.

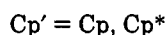
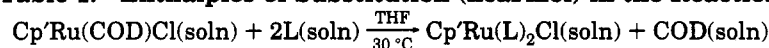
**CpRu(P(*p*-ClC<sub>6</sub>H<sub>4</sub>)<sub>3</sub>)<sub>2</sub>Cl.** A 25 mL flask was charged with 100 mg (0.32 mmol) of CpRu(COD)Cl and 236 mg (0.64 mmol) of P(*p*-ClC<sub>6</sub>H<sub>4</sub>)<sub>3</sub>. Then, 30 mL of dry THF was vacuum-transferred into this flask and the solution was stirred overnight. The solution was filtered, and the solvent was removed under vacuum until dryness. A 30 mL portion of hexane was then vacuum-transferred onto the residue and the mixture stirred for 20 min, after which time the suspension was filtered and the remaining orange solid was washed with a small amount (ca. 2 mL) of hexane. The solvent was removed and the powder was dried under vacuum, giving a 230 mg (77%) yield. <sup>1</sup>H NMR (300 MHz, THF-*d*<sub>8</sub>, 25 °C): δ 4.19 (s, 5 H, Cp), 7.18–7.41 (m, 24 H, Ph). Anal. Calcd for RuCl<sub>7</sub>P<sub>2</sub>C<sub>41</sub>H<sub>29</sub>: C, 52.79; H, 3.13. Found: C, 52.69; H, 3.10.

**Cp\*Ru(P(*p*-CF<sub>3</sub>C<sub>6</sub>H<sub>4</sub>)<sub>3</sub>)<sub>2</sub>Cl.** A 25 mL flask was charged with 90 mg (0.24 mmol) of Cp\*Ru(COD)Cl, 10 mL of dried THF, and 220 mg (0.48 mmol) of P(*p*-CF<sub>3</sub>C<sub>6</sub>H<sub>4</sub>)<sub>3</sub>. After it was stirred overnight, the solution was placed under vacuum to remove volatiles. Five milliliters of hexane was then added to the solid residue, and the mixture was stirred for about 20 min. The suspension was then filtered, and the remaining microcrystalline solid was washed with a small amount of hexanes. Solvent was removed, and the yellow powder was dried under vacuum, giving a 260 mg (90%) yield. <sup>1</sup>H NMR (300 MHz, THF-*d*<sub>8</sub>, 25 °C): δ 1.08 (s, 15 H, Cp\*), 7.46, 7.69 (br, 24 H, Ph). Anal. Calcd for RuClP<sub>2</sub>F<sub>18</sub>C<sub>52</sub>H<sub>39</sub>: C, 51.86; H, 3.26. Found: C, 51.57; H, 2.95.

**Cp\*Ru(P(*p*-ClC<sub>6</sub>H<sub>4</sub>)<sub>3</sub>)<sub>2</sub>Cl.** A 25 mL flask was charged with 200 mg (0.53 mmol) of Cp\*Ru(COD)Cl and 423 mg (1.06 mmol) of P(*p*-ClC<sub>6</sub>H<sub>4</sub>)<sub>3</sub>. Then, 20 mL of dry THF was vacuum-transferred into this flask and it was stirred overnight. The solution was filtered, and solvent was removed under vacuum until dryness. About 16 mL of a solvent mixture of hexane and THF (3:1) was vacuum-transferred into the cooled (–78 °C) flask containing the residue. This mixture was warmed to room temperature with stirring. After filtration, the solution was slowly cooled to –78 °C and kept at this temperature overnight. Cold filtration afforded orange-red crystals, which were washed with a small amount of hexane and dried under vacuum, giving a 451 mg (85%) yield. <sup>1</sup>H NMR (300 MHz, THF-*d*<sub>8</sub>, 25 °C): δ 1.06 (s, 15 H, Cp\*), 7.15, 7.42 (br, 24 H, Ph). Anal. Calcd for RuCl<sub>7</sub>P<sub>2</sub>C<sub>46</sub>H<sub>39</sub>: C, 55.09; H, 3.92. Found: C, 54.80; H, 4.17.

**Cp\*Ru(P(*p*-CH<sub>3</sub>OC<sub>6</sub>H<sub>4</sub>)<sub>3</sub>)<sub>2</sub>Cl.** A 25 mL flask was charged with 100 mg (0.26 mmol) of Cp\*Ru(COD)Cl, 20 mL of dried THF, and 183 mg (0.52 mmol) of P(*p*-CH<sub>3</sub>OC<sub>6</sub>H<sub>4</sub>)<sub>3</sub>. After it was stirred overnight, the solution was put under vacuum to remove volatiles. A 5 mL solvent mixture of THF and hexane (1:4) was then added to the solid, and the mixture was stirred for about 20 min. The suspension was then filtered, and the remaining solid was washed with a small amount of hexane. Solvent was removed, and the yellow powder was dried under vacuum, giving a 220 mg (87%) yield. <sup>1</sup>H NMR (300 MHz, THF-*d*<sub>8</sub>, 25 °C): δ 1.05 (s, 15 H, Cp\*), 3.73 (s, 18 H, CH<sub>3</sub>), 7.46, 7.69 (br, 24 H, Ph). Anal. Calcd for RuClP<sub>2</sub>O<sub>6</sub>C<sub>52</sub>H<sub>57</sub>: C, 63.96; H, 5.88. Found: C, 63.78; H, 5.68.

**Cp\*Ru(P(*p*-FC<sub>6</sub>H<sub>4</sub>)<sub>3</sub>)<sub>2</sub>Cl.** A 25 mL flask was charged with 200 mg (0.53 mmol) of Cp\*Ru(COD)Cl and 350 mg (1.06 mmol) of P(*p*-FC<sub>6</sub>H<sub>4</sub>)<sub>3</sub>. Then, 20 mL of dried THF was vacuum-transferred into this flask and the solution was stirred overnight. The solution was filtered and solvent was removed under vacuum until dry. About 16 mL of a solvent mixture of hexane and THF (3:1) was vacuum-transferred to the cooled (–78 °C) residue. This mixture was warmed to room temperature and stirred. After filtration, the solution was slowly cooled to –78 °C and kept at this temperature overnight. Cold filtration afforded orange-red crystals which were washed with a small amount of hexane and dried under vacuum, giving a 380 mg (80%) yield. <sup>1</sup>H NMR (300 MHz, THF-*d*<sub>8</sub>, 25 °C): δ 1.05 (s, 15 H, Cp\*), 6.87, 7.48 (br, 24 H, Ph). Anal. Calcd for RuClP<sub>2</sub>F<sub>6</sub>C<sub>46</sub>H<sub>39</sub>: C, 61.10; H, 4.35. Found: C, 61.37; H, 4.41.

**Table 1. Enthalpies of Substitution (kcal/mol) in the Reaction**

L	complex	$-\Delta H_{\text{reacn}}(\text{Cp}^*)^a$	$-\Delta H_{\text{reacn}}(\text{Cp})^a$
(C <sub>6</sub> H <sub>5</sub> ) <sub>3</sub> P	Cp <sup>*</sup> Ru[P(C <sub>6</sub> H <sub>5</sub> ) <sub>3</sub> ] <sub>2</sub> Cl	18.1 (0.2)	22.9 (0.3)
( <i>p</i> -CH <sub>3</sub> C <sub>6</sub> H <sub>4</sub> ) <sub>3</sub> P	Cp <sup>*</sup> Ru[P( <i>p</i> -CH <sub>3</sub> C <sub>6</sub> H <sub>4</sub> ) <sub>3</sub> ] <sub>2</sub> Cl		23.7 (0.3)
( <i>p</i> -CF <sub>3</sub> C <sub>6</sub> H <sub>4</sub> ) <sub>3</sub> P	Cp <sup>*</sup> Ru[[ <i>p</i> -CF <sub>3</sub> C <sub>6</sub> H <sub>4</sub> ] <sub>3</sub> ] <sub>2</sub> Cl	20.7 (0.3)	24.4 (0.2)
( <i>p</i> -CH <sub>3</sub> OC <sub>6</sub> H <sub>4</sub> ) <sub>3</sub> P	Cp <sup>*</sup> Ru[P( <i>p</i> -CH <sub>3</sub> OC <sub>6</sub> H <sub>4</sub> ) <sub>3</sub> ] <sub>2</sub> Cl	21.8 (0.4)	24.6 (0.3)
( <i>p</i> -ClC <sub>6</sub> H <sub>4</sub> ) <sub>3</sub> P	Cp <sup>*</sup> Ru[P( <i>p</i> -ClC <sub>6</sub> H <sub>4</sub> ) <sub>3</sub> ] <sub>2</sub> Cl	21.7 (0.4)	24.0 (0.2)
( <i>p</i> -FC <sub>6</sub> H <sub>4</sub> ) <sub>3</sub> P	Cp <sup>*</sup> Ru[P( <i>p</i> -FC <sub>6</sub> H <sub>4</sub> ) <sub>3</sub> ] <sub>2</sub> Cl	22.0 (0.5)	24.2 (0.2)

<sup>a</sup> Enthalpy values are reported with 95% confidence limits.

**Table 2. Summary of Crystallographic Data for Cp<sup>\*</sup>Ru(C<sub>8</sub>H<sub>12</sub>)Cl (1)**

empirical formula	C <sub>18</sub> H <sub>27</sub> ClRu
space group	Pbca
unit cell dimens	
<i>a</i> , Å	14.222(3)
<i>b</i> , Å	13.876(3)
<i>c</i> , Å	16.473(3)
α, deg	90
β, deg	90
γ, deg	90
<i>V</i> , Å <sup>3</sup>	3251 (2)
Z, molecule/cell	8
density (calcd), g/cm <sup>3</sup>	1.552
μ(Mo), cm <sup>-1</sup>	11.01
wavelength, Å	0.710 73
monochromator	highly ordered graphite crystal
temp, K	100(2)
abs cor	empirical ( $\psi$ -scan method)
diffractometer	Enraf-Nonius CAD 4
scan type	$\theta$ - $2\theta$
data collected	$0 \leq h \leq 16, 0 \leq k \leq 16,$ $0 \leq l \leq 18$
$2\theta$ range, deg	4.0–50.0
no. of collected rflns	2824
no. of obsd rflns	1903
$R_F$ (obsd data), %	3.2
$R_{wF}$ , %	4.8
goodness of fit	1.76
no. of variables	279
residual density, e/Å <sup>3</sup>	
max	0.56(5)
min	-0.86(5)

**<sup>1</sup>H NMR Titrations.** Prior to every set of calorimetric experiments involving a new ligand, an accurately weighed amount ( $\pm 0.1$  mg) of the organoruthenium complex was placed in a Wilmad screw-capped NMR tube fitted with a septum, and THF-*d*<sub>6</sub> was subsequently added. The solution was titrated with a solution of the ligand of interest by injecting the latter in aliquots through the septum with a microsyringe, followed by vigorous shaking. The reactions were monitored by <sup>1</sup>H NMR spectroscopy, and the reactions were found to be rapid, clean, and quantitative under experimental calorimetric (temperature and concentration), conditions necessary for accurate and meaningful calorimetric results. These conditions were satisfied for all organoruthenium reactions investigated.

**Solution Calorimetry. Calorimetric Measurement of Reaction between CpRu(COD)Cl (1) and P(*p*-MeOC<sub>6</sub>H<sub>4</sub>)<sub>3</sub>.** The mixing vessels of the Setaram C-80 were cleaned, dried in an oven maintained at 120 °C, and then taken into the glovebox. A 30–40 mg sample of recrystallized CpRu(COD)Cl was accurately weighed into the lower vessel, which was closed and sealed with 1.5 mL of mercury. Four milliliters of a stock solution of P(*p*-MeOC<sub>6</sub>H<sub>4</sub>)<sub>3</sub> (1 g of P(*p*-MeOC<sub>6</sub>H<sub>4</sub>)<sub>3</sub> in 25 mL of THF) was added, and the remainder of the cell was assembled, removed from the glovebox, and inserted in the calorimeter. The reference vessel was loaded in an identical fashion, with the exception that no organoruthenium complex was added to the lower vessel. After the calorimeter had

**Table 3. Selected Bond Distances (Å) and Bond Angles (deg) for Cp<sup>\*</sup>Ru(C<sub>8</sub>H<sub>12</sub>)Cl (1)**

Bond Lengths <sup>a</sup>			
Ru–Cl(1)	2.472(2)	Ru(1)–C(15)	2.225(4)
Ru–C(1)	2.235(4)	Ru–C(16)	2.236(5)
Ru–C(2)	2.247(5)	C(11)–C(12)	1.385(7)
Ru–C(3)	2.242(4)	C(11)–C(18)	1.495(8)
Ru–C(4)	2.209(4)	C(15)–C(16)	1.391(8)
Ru–C(5)	2.274(4)	C(14)–C(15)	1.507(7)
Ru–C(11)	2.200(4)	Ru–C(12)	2.190(4)
Ru–Cp(cen)	1.885(2)	Ru–C(Cp av)	2.241(2)
Bond Angles <sup>a</sup>			
Cl–Ru–C(1)	86.3(1)	C(11)–Ru–C(12)	36.8(2)
Cl–Ru–C(2)	84.3(2)	C(11)–Ru–C(15)	92.5(2)
Cl–Ru–C(3)	116.2(1)	C(11)–Ru–C(16)	79.7(2)
Cl–Ru–C(4)	145.4(2)	C(12)–Ru–C(15)	78.2(2)
Cl–Ru–C(5)	119.6(2)	C(12)–Ru–C(16)	88.0(2)
Cl–Ru–C(11)	80.5(1)	C(15)–Ru–C(16)	36.3(2)
Cl–Ru–C(12)	117.4(1)	C(11)–Ru–Cp(cen)	137.4(2)
Cl–Ru–C(15)	113.9(1)	C(12)–Ru–Cp(cen)	115.6(2)
Cl–Ru–C(16)	78.3(1)	C(15)–Ru–Cp(cen)	115.7(2)
Cl–Ru–Cp(cen)	112.2(1)	C(16)–Ru–Cp(cen)	141.5(2)

<sup>a</sup> Numbers in parentheses are the estimated standard deviations.

reached thermal equilibrium at 30.0 °C (about 2 h), the calorimeter was inverted, thereby allowing the reactants to mix. After the reaction had reached completion and the calorimeter had once again reached thermal equilibrium (ca. 2 h), the vessels were removed from the calorimeter. Conversion to CpRu(P(*p*-MeOC<sub>6</sub>H<sub>4</sub>)<sub>3</sub>)<sub>2</sub>Cl was found to be quantitative under these reaction conditions. Control reactions with Hg and no phosphine show no reaction. The enthalpy of reaction,  $-20.7 \pm 0.2$  kcal/mol, represents the average of five individual calorimetric determinations. The final enthalpy value listed in Table 1 ( $-24.6 \pm 0.3$  kcal/mol) represents the enthalpy of ligand substitution with all species in solution. The enthalpy of solution of 1 ( $3.9 \pm 0.1$  kcal/mol) has therefore been subtracted from the  $-20.7$  kcal/mol value. This methodology represents a typical procedure involving all organometallic compounds and all reactions investigated in the present study.

**Structure Determination of Cp<sup>\*</sup>Ru(COD)Cl (1).** An orange needle, grown from a saturated THF solution, having approximate dimensions 0.22 × 0.25 × 0.40 mm was selected and mounted on the end of a glass fiber in a random orientation. This selected crystal was mounted on an Enraf-Nonius CAD4 diffractometer, and data were collected using Mo K $\alpha$  radiation at 100 K under a stream of cold nitrogen gas. Cell dimensions were determined by least-squares refinement of the measured setting angles of 25 reflections with  $30^\circ < 2\theta < 46^\circ$ . The structure was solved using direct methods (MULTAN80) and refined by full-matrix least-squares techniques. Crystal data for 1 are summarized in Table 2, and selected bond distances and angles are listed in Table 3. Positional and equivalent isotropic thermal parameters are presented in Table 4. Figure 1 gives an ORTEP drawing of this molecule.

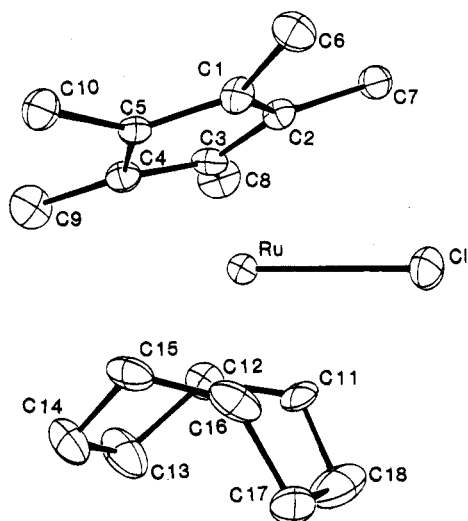
**Structure Determination of Cp<sup>\*</sup>Ru(P(*p*-CF<sub>3</sub>C<sub>6</sub>H<sub>4</sub>)<sub>2</sub>)Cl (2).** An orange needle, grown from slow evaporation of a saturated solution of anhydrous ethanol, having approximate



**Table 4. Fractional Coordinates ( $\times 10^4$ ) and Isotropic Thermal Parameters for  $\text{Cp}^*\text{Ru}(\text{C}_8\text{H}_{12})\text{Cl}$  (1)<sup>a</sup>**

atom	<i>x</i>	<i>y</i>	<i>z</i>	<i>B</i> (Å <sup>2</sup> )
Ru	0.88416(3)	0.17875(3)	0.70944(2)	1.140(7)
C(1)	0.8995(1)	0.00138(9)	0.71441(8)	2.15(3)
C(1)	0.9551(4)	0.1700(4)	0.5887(3)	1.5(1)
C(2)	0.8550(4)	0.1548(4)	0.5769(3)	1.5(1)
C(3)	0.8069(4)	0.2391(4)	0.6023(3)	1.7(1)
C(4)	0.8769(4)	0.3065(3)	0.6297(3)	1.6(1)
C(5)	0.9671(4)	0.2640(3)	0.6158(3)	1.23(9)
C(6)	1.0306(4)	0.1002(4)	0.5656(3)	1.9(1)
C(7)	0.8106(4)	0.0666(4)	0.5405(3)	2.0(1)
C(8)	0.7039(4)	0.2586(5)	0.5922(4)	2.4(1)
C(9)	0.8608(4)	0.4097(4)	0.6492(4)	2.5(1)
C(10)	1.0599(4)	0.3155(4)	0.6230(3)	1.8(1)
C(11)	0.7730(4)	0.1459(4)	0.7980(3)	2.1(1)
C(12)	0.7759(4)	0.2447(4)	0.7860(3)	2.0(1)
C(13)	0.8120(5)	0.3149(5)	0.8493(4)	3.5(1)
C(14)	0.9161(5)	0.3311(4)	0.8479(4)	2.7(1)
C(15)	0.9703(4)	0.2556(5)	0.8017(3)	2.0(1)
C(16)	0.9706(4)	0.1581(4)	0.8215(3)	2.4(1)
C(17)	0.9120(5)	0.1179(5)	0.8920(4)	3.3(1)
C(18)	0.8101(5)	0.0974(5)	0.8724(4)	3.9(2)

<sup>a</sup> Numbers in parentheses are the estimated standard deviations.

**Figure 1.** ORTEP of  $\text{Cp}^*\text{Ru}(\text{C}_8\text{H}_{12})\text{Cl}$  (1) with ellipsoids drawn in at the 50% probability level.

dimensions  $0.06 \times 0.06 \times 0.44$  mm was selected and mounted on the end of a glass fiber in a random orientation. This selected crystal was mounted on an Enraf-Nonius CAD4 diffractometer, and data were collected using Mo  $K\alpha$  radiation at 100 K under a stream of cold nitrogen gas. Cell dimensions were determined by least-squares refinement of the measured setting angles of 25 reflections with  $25^\circ < 2\theta < 38^\circ$ . The structure was solved by using the heavy-atom method and refined by full-matrix least-squares techniques. Crystal data for **2** are summarized in Table 5, and selected bond distances and angles are listed in Table 6. Positional and equivalent isotropic thermal parameters are presented in Table 7. Figure 2 gives an ORTEP drawing of this molecule.

**Structure Determination of  $\text{CpRu}(\text{p}\text{-CF}_3\text{C}_6\text{H}_4)_2\text{Cl}$  (3).** A rectangular orange plate, grown by slow evaporation of a saturated THF solution, having approximate dimensions  $0.46 \times 0.40 \times 0.22$  mm was selected and mounted on the end of a glass fiber in a random orientation. This selected crystal was mounted on an Enraf-Nonius CAD4 diffractometer, and data were collected using Mo  $K\alpha$  radiation at 100 K under a stream of cold nitrogen gas. Cell dimensions were determined by least-squares refinement of the measured setting angles of 25 reflections with  $42^\circ < 2\theta < 55^\circ$ . The structure was solved using direct methods (MULTAN80) and refined by full-matrix

**Table 5. Summary of Crystallographic Data for  $\text{Cp}^*\text{Ru}(\text{P}(\text{p}\text{-CF}_3\text{C}_6\text{H}_4)_2\text{Cl})\cdot 0.5\text{C}_2\text{H}_5\text{OH}$  (2)**

empirical formula	$\text{C}_{52}\text{H}_{39}\text{ClF}_{18}\text{P}_2\text{Ru}\cdot 0.5\text{C}_2\text{H}_5\text{OH}$
space group	I4
unit cell dimens	
<i>a</i> , Å	26.333(14)
<i>c</i> , Å	17.337(9)
<i>V</i> , Å <sup>3</sup>	12022 (18)
<i>Z</i> , molecule/cell	8
density (calcd), g/cm <sup>3</sup>	1.360
$\mu(\text{Mo})$ , cm <sup>-1</sup>	4.38
wavelength, Å	0.710 73
monochromator	highly ordered graphite crystal
temp, K	100(2)
abs cor	empirical ( $\psi$ -scan method)
diffractometer	Enraf-Nonius CAD 4
scan type	$\theta$ - $2\theta$
data collected	$0 \leq h \leq 25, 0 \leq k \leq 25,$ $0 \leq l \leq 16$
$2\theta$ range, deg	4.0–40.0
no. of collected rflns	3097
no. of obsd rflns	3074
$R_F$ (obsd data), %	7.9
$R_{wF}$ , %	10.2
goodness of fit	3.25
no. of variables	650
residual density, e/Å <sup>3</sup>	
max	1.01(5)
min	-1.20(5)

**Table 6. Selected Bond Distances (Å) and Bond Angles (deg) for  $\text{Cp}^*\text{Ru}(\text{P}(\text{p}\text{-CF}_3\text{C}_6\text{H}_4)_2\text{Cl})$  (2)**

Bond Lengths <sup>a</sup>			
Ru–Cl	2.439(5)	Ru–C(4)	2.20(2)
Ru–P(1)	2.315(6)	Ru–C(5)	2.17(2)
Ru–P(2)	2.334(5)	P(1)–C(11)	1.82(2)
Ru–C(1)	2.21(2)	P(1)–C(17)	1.86(2)
Ru–C(2)	2.19(3)	P(1)–C(23)	1.79(2)
Ru–C(3)	2.27(2)	P(2)–C(29)	1.83(2)
Ru–Cp(cen)	1.890(11)	P(2)–C(35)	1.80(2)
Cp C–C(av)	1.35 (2)	P(2)–C(41)	1.70(2)
Bond Angles <sup>a</sup>			
Cl–Ru–P(1)	92.3(2)	P(2)–Ru–C(2)	112.6(7)
Cl–Ru–P(2)	91.3(2)	P(2)–Ru–C(3)	144.9(6)
Cl–Ru–C(1)	127.9(11)	P(2)–Ru–C(4)	150.6(5)
Cl–Ru–C(2)	148.1(6)	P(2)–Ru–C(5)	111.5(5)
Cl–Ru–C(3)	120.7(6)	C(11)–P(1)–C(23)	93.9(9)
Cl–Ru–C(4)	88.8(5)	C(11)–P(1)–C(17)	105.8(9)
Cl–Ru–C(5)	90.7(5)	C(23)–P(1)–C(17)	102.6(9)
P(1)–Ru–P(2)	93.8(2)	C(29)–P(2)–C(35)	102.7(10)
P(1)–Ru–C(1)	138.0(12)	C(29)–P(2)–C(41)	101.9(10)
P(1)–Ru–C(2)	106.3(5)	C(35)–P(2)–C(41)	96.7(9)
P(1)–Ru–C(3)	98.5(5)	Cl–Ru–Cp(cen)	117.5(3)
P(1)–Ru–C(4)	115.6(5)	P(1)–Ru–Cp(cen)	125.6(3)
P(1)–Ru–C(5)	115.6(5)	P(2)–Ru–Cp(cen)	125.8(3)
P(2)–Ru–C(1)	96.7(7)		

<sup>a</sup> Numbers in parentheses are the estimated standard deviations.

least-squares techniques. Crystal data for **3** are summarized in Table 8, and selected bond distances and angles are listed in Table 9. Positional and equivalent isotropic thermal parameters are presented in Table 10. Figure 3 gives an ORTEP drawing of this molecule.

## Results

A facile entryway into the thermochemistry of  $\text{CpRu}(\text{PR}_3)_2\text{Cl}$  complexes is made possible by the rapid and quantitative reaction of  $\text{CpRu}(\text{COD})\text{Cl}$  (1) with a variety of phosphine ligands.<sup>7e</sup>

This type of phosphine binding reaction appears to be general and was found to be rapid and quantitative for all ligands calorimetrically investigated at 30.0 °C in tetrahydrofuran. A similar trend has previously been



**Table 7. Fractional Coordinates ( $\times 10^4$ ) and Isotropic Thermal Parameters for  $\text{Cp}^*\text{Ru}(\text{P}(p\text{-CF}_3\text{C}_6\text{H}_4)_3)_2\text{Cl}$  (2)<sup>a</sup>**

atom	<i>x</i>	<i>y</i>	<i>z</i>	<i>B</i> (Å <sup>2</sup> )	atom	<i>x</i>	<i>y</i>	<i>z</i>	<i>B</i> (Å <sup>2</sup> )
Ru	0.33946(9)	0.29444(8)	0.2206(1)	1.80(4)	C(18)	0.3326(9)	0.4499(8)	0.259(2)	2.2(7)
Cl	0.2850(3)	0.2355(3)	0.1503(4)	2.8(2)	C(19)	0.338(1)	0.485(1)	0.316(2)	3.9(8)
P(1)	0.2850(3)	0.3618(3)	0.1982(4)	2.5(2)	C(20)	0.303(1)	0.489(1)	0.376(2)	4.7(8)
P(2)	0.3012(3)	0.2726(3)	0.3374(4)	1.9(2)	C(21)	0.263(1)	0.457(1)	0.378(2)	2.5(7)
F(1)	0.3464(9)	0.4570(8)	-0.152(1)	8.0(6)	C(22)	0.2575(9)	0.4222(9)	0.324(2)	1.7(6)
F(2)	0.2915(9)	0.4057(6)	-0.1855(9)	5.8(5)	C(23)	0.2172(9)	0.358(1)	0.190(1)	1.8(6)
F(3)	0.273(1)	0.4744(9)	-0.149(1)	11.0(9)	C(24)	0.187(1)	0.314(1)	0.180(2)	3.4(8)
F(4)	0.2946(9)	0.5786(8)	0.408(2)	9.2(7)	C(25)	0.135(1)	0.318(1)	0.171(1)	2.7(7)
F(5)	0.361(1)	0.5396(8)	0.458(1)	10.9(7)	C(26)	0.1075(8)	0.362(1)	0.171(2)	4.3(8)
F(6)	0.284(1)	0.5258(9)	0.494(1)	15.1(9)	C(27)	0.138(1)	0.410(1)	0.180(2)	4.5(8)
F(7)	0.0344(8)	0.406(1)	0.141(2)	12(1)	C(28)	0.187(1)	0.404(1)	0.187(2)	3.9(8)
F(8)	0.0309(8)	0.359(1)	0.226(2)	16(1)	C(29)	0.3131(9)	0.3124(8)	0.421(2)	2.9(7)
F(9)	0.0377(8)	0.333(1)	0.114(2)	14(1)	C(30)	0.2888(9)	0.304(1)	0.496(2)	1.5(6)
F(10)	0.378(1)	0.4502(8)	0.594(1)	8.7(7)	C(31)	0.295(1)	0.334(1)	0.554(2)	4.0(8)
F(11)	0.3036(9)	0.4312(9)	0.638(1)	9.7(7)	C(32)	0.332(1)	0.373(1)	0.545(2)	4.9(8)
F(12)	0.3658(9)	0.3872(7)	0.669(1)	7.5(6)	C(33)	0.356(1)	0.386(1)	0.475(2)	5.4(8)
F(13)	0.402(1)	0.0564(7)	0.485(2)	11.0(8)	C(34)	0.344(1)	0.350(1)	0.413(2)	4.0(8)
F(14)	0.370(1)	0.0231(8)	0.385(1)	9.7(7)	C(35)	0.318(1)	0.2104(9)	0.371(1)	2.5(6)
F(15)	0.332(1)	0.0335(9)	0.477(2)	13.1(9)	C(36)	0.319(1)	0.1687(9)	0.319(2)	1.9(6)
F(16)	0.0579(6)	0.2008(7)	0.374(1)	5.9(5)	C(37)	0.334(1)	0.121(1)	0.337(2)	2.7(7)
F(17)	0.0511(6)	0.2427(9)	0.274(1)	7.9(6)	C(38)	0.349(1)	0.111(1)	0.414(2)	3.6(8)
F(18)	0.0462(8)	0.278(1)	0.381(1)	8.5(7)	C(39)	0.347(1)	0.159(2)	0.462(2)	9(1)
C(1)	0.4188(9)	0.283(2)	0.258(1)	7(1)	C(40)	0.331(1)	0.200(1)	0.434(2)	5.3(9)
C(2)	0.415(1)	0.3274(9)	0.236(1)	3.4(7)	C(41)	0.237(1)	0.2644(9)	0.342(2)	3.0(7)
C(3)	0.410(1)	0.3270(9)	0.165(2)	2.4(6)	C(42)	0.210(1)	0.224(1)	0.307(2)	3.9(8)
C(4)	0.398(1)	0.2825(8)	0.133(2)	2.1(7)	C(43)	0.157(1)	0.220(1)	0.305(1)	2.5(6)
C(5)	0.405(1)	0.247(1)	0.197(1)	2.8(7)	C(44)	0.1287(8)	0.252(1)	0.341(1)	2.9(7)
C(6)	0.434(1)	0.257(1)	0.323(2)	9.9(9)	C(45)	0.151(1)	0.2942(9)	0.376(1)	3.3(8)
C(7)	0.443(1)	0.366(1)	0.284(2)	4.5(7)	C(46)	0.203(1)	0.301(1)	0.371(2)	3.5(8)
C(8)	0.413(1)	0.378(1)	0.108(2)	4.9(9)	C(47)	0.301(1)	0.436(1)	-0.131(2)	3.7(8)
C(9)	0.391(1)	0.269(1)	0.050(3)	10(1)	C(48)	0.308(2)	0.537(1)	0.433(3)	7(1)
C(10)	0.406(1)	0.189(1)	0.187(2)	3.9(8)	C(49)	0.061(2)	0.367(2)	0.171(3)	7(1)
C(11)	0.293(1)	0.387(1)	0.101(1)	2.1(6)	C(50)	0.343(1)	0.410(1)	0.607(2)	3.1(7)
C(12)	0.287(1)	0.3514(9)	0.042(1)	1.7(6)	C(51)	0.362(1)	0.054(1)	0.436(2)	4.9(9)
C(13)	0.292(1)	0.371(1)	-0.032(2)	3.1(7)	C(52)	0.083(2)	0.248(2)	0.342(3)	10(2)
C(14)	0.298(1)	0.423(1)	-0.052(2)	3.2(7)	C(201)	0.137(3)	0.418(3)	0.458(4)	9(2)*
C(15)	0.302(1)	0.4535(9)	0.005(2)	2.8(7)	C(202)	0.158(1)	0.410(1)	0.509(2)	1.7(8)*
C(16)	0.298(1)	0.4401(9)	0.086(2)	2.3(7)	C(203)	0.1426	0.4262	0.5747	4(1)
C(17)	0.294(1)	0.417(1)	0.265(2)	3.0(7)					

<sup>a</sup> Numbers in parentheses are the estimated standard deviations. <sup>b</sup> Starred values denote atoms refined isotropically.

observed for the  $\text{Cp}^*\text{Ru}(\text{COD})\text{Cl}$  complex.<sup>7b</sup> A compilation of phosphine ligands with their respective enthalpies of reaction where all species are in solution is presented in Table 1.

Single-crystal structural studies were carried out on the three new complexes  $\text{Cp}^*\text{Ru}(\text{COD})\text{Cl}$  (1),  $\text{Cp}^*\text{Ru}(\text{P}(p\text{-CF}_3\text{C}_6\text{H}_4)_2\text{Cl}$  (2), and  $\text{Cp}^*\text{Ru}(\text{P}(p\text{-CF}_3\text{C}_6\text{H}_4)_3)_2\text{Cl}$  (3). Tables 2–10 give crystallographic data and important bond distances and angles as well as positional parameters. ORTEP drawings of the three complexes are presented in Figures 1–3.

## Discussion

The relative importance of steric vs electronic ligand effects has been the subject of numerous studies, and it has not been until fairly recently that clear stereoelectronic pictures have emerged from organometallic studies. We have taken the approach of gauging the relative importance of such effects based on ligand properties and metal–ligand reaction enthalpies. We judged this approach useful in view of a “common sense” understanding that strong metal–ligand interactions will result from strong electron donation from the ligand and minimal steric interaction (repulsion) with metal–ancillary ligation. This approach has been used in an iron-based system to clearly illustrate the overwhelming importance of electronic ligand effects. Enthalpies of

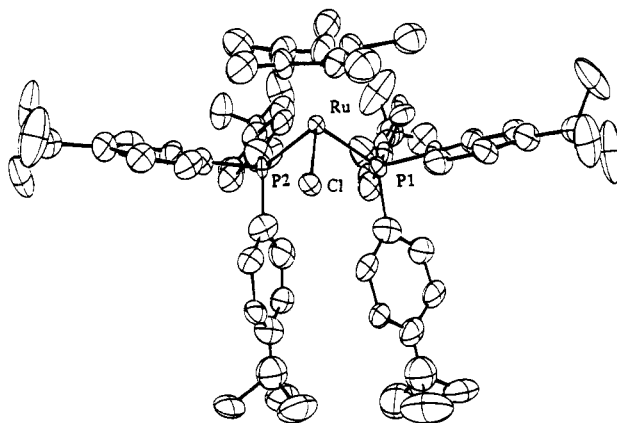


**Figure 2.** ORTEP of  $\text{Cp}^*\text{Ru}(\text{P}(p\text{-CF}_3\text{C}_6\text{H}_4)_3)_2\text{Cl}$  (2) with ellipsoids drawn in at the 50% probability level.

reaction span some 8 kcal/mol in the iron system and correlate very well with electronic parameter variation.<sup>8c</sup>

The present study clearly indicates an important lack of sensitivity associated with the enthalpies of ligand substitution reactions as a function of electronic variation (note here that the experimental approach and ligand selection maintain the phosphine cone angle constant at 145°). The measured enthalpies of reaction listed in Table 1 are fairly constant; some are the same within experimental error. This trend is valid for both systems ( $\text{Cp}' = \text{Cp}$  and  $\text{Cp}^*$ ) investigated. We take

**Table 8. Summary of Crystallographic Data for CpRu(P(*p*-CF<sub>3</sub>C<sub>6</sub>H<sub>4</sub>)<sub>3</sub>)<sub>2</sub>Cl·0.5THF (3)**

empirical formula	C <sub>47</sub> H <sub>29</sub> F <sub>18</sub> P <sub>2</sub> ClRu·0.5 C <sub>4</sub> H <sub>8</sub> O
space group	<i>P</i> 2 <sub>1</sub> / <i>n</i>
unit cell dimens	
<i>a</i> , Å	13.613(2)
<i>b</i> , Å	16.895(4)
<i>c</i> , Å	21.997(2)
α, deg	90
β, deg	101.96 (2)
γ, deg	90
<i>V</i> , Å <sup>3</sup>	4949 (3)
<i>Z</i> , molecule/cell	4
density (calcd), g/cm <sup>3</sup>	1.570
<i>μ</i> (Mo), cm <sup>-1</sup>	5.281
wavelength, Å	0.710 73
monochromator	highly ordered graphite cryst
temp, K	100(2)
abs cor	empirical ( <i>ψ</i> -scan method)
diffractometer	Enraf-Nonius CAD 4
scan type	<i>θ</i> -2 <i>θ</i>
data collected	0 ≤ <i>h</i> ≤ 16, 0 ≤ <i>k</i> ≤ 20, -26 ≤ <i>l</i> ≤ 25
2 <i>θ</i> range, deg	4.0–50.0
no. of collected rflns	9041
no. of obsd rflns	7376
<i>R</i> <sub>F</sub> (obsd data), %	5.8
<i>R</i> <sub>wF</sub> , %	9.4
goodness of fit	3.84
no. of variables	642
residual density, e/Å <sup>3</sup>	
max	0.52(5)
min	-0.99(5)

these similar trends to indicate that electronic ligand effects only play a minor role in dictating the magnitude of the reaction enthalpy.<sup>23</sup> We have previously explained relative stability trends for monodentate and bidentate ligands in both these systems as being primarily directed by ligand steric effects. The present study and observed trends clearly demonstrate that steric factors must be the overwhelming component influencing the magnitude of the reaction enthalpy. If a relationship is established between phosphine cone angle (steric factor) and enthalpy of reaction, good linear correlations are established for both systems investigated (Figures 4 and 5).

These relationships are surprisingly good, considering that they only account for the influence of one of the two ligand factors. Similar correlation can be established, with poorer correlation coefficients (*R* = 0.95 for Cp\* data and *R* = 0.90 for Cp data; treatment included all phosphine ligands but excluded phosphites), between enthalpy of reaction data and Brown's steric *E<sub>R</sub>* parameter values.<sup>2e</sup> Brown points out that these *E<sub>R</sub>* values are system-dependent and this might account for the poor fit of the ruthenium data to the corresponding steric parameters.<sup>2e</sup>

Enthalpy data within a system (Table 1) are essentially constant. When the Cp and Cp\* values are now compared, a variation in reaction enthalpy favoring the Cp-based system is observed. This has also been observed in our previous studies, and a graphical representation is given in Figure 6, which includes all ligands investigated thus far.

The only notable variation in Table 1 is observed in the PPh<sub>3</sub> cases, where the enthalpies of reaction indicate

**Table 9. Selected Bond Distances (Å) and Bond Angles (deg) for CpRu(P(*p*-CF<sub>3</sub>C<sub>6</sub>H<sub>4</sub>)<sub>3</sub>)<sub>2</sub>Cl (3)**

Bond Lengths <sup>a</sup>			
Ru–Cl	2.4294(6)	P(1)–C(15)	1.844(3)
Ru–P(1)	2.3087(7)	P(2)–C(21)	1.847(3)
Ru–P(2)	2.3102(6)	P(2)–C(23)	1.840(3)
P(2)–C(25)	1.845(6)	C(11)–C(12)	1.524(6)
C(13)–C(14)	1.529(4)	C(15)–C(16)	1.515(5)
C(21)–C(22)	1.515(5)	P(1)–C(11)	1.848(4)
C(23)–C(24)	1.524(5)	P(1)–C(13)	1.839(3)
C(25)–C(26)	1.522(5)	Ru–Cp(cen)	1.890(2)
Bond Angles <sup>a</sup>			
Cl–Ru–P(1)	90.43(3)	P(2)–Ru–C(4)	128.4(1)
Cl–Ru–P(2)	90.50(3)	P(2)–Ru–C(5)	158.6(1)
P(1)–Ru–P(2)	94.71(3)	Ru–P(1)–C(11)	120.5(1)
Ru–P(1)–C(13)	117.6(1)	Ru–P(1)–C(15)	111.8(1)
Ru–P(2)–C(21)	120.9(1)	Ru–P(2)–C(23)	118.1(1)
Ru–P(2)–C(25)	112.2(1)	C(11)–P(1)–C(13)	100.8(2)
C(11)–P(1)–C(15)	100.3(2)	P(1)–C(11)–C(12)	116.5(3)
C(13)–P(1)–C(15)	103.2(2)	P(1)–C(13)–C(14)	117.6(2)
C(21)–P(2)–C(23)	100.9(2)	P(1)–C(15)–C(16)	115.4(3)
C(21)–P(2)–C(25)	99.5(2)	P(2)–C(21)–C(22)	115.5(3)
C(23)–P(2)–C(25)	102.2(2)	P(2)–C(23)–C(24)	117.3(3)
P(2)–C(25)–C(26)	114.6(2)	P(1)–Ru–Cp(cen)	125.00(5)
P(2)–Ru–Cp(cen)	124.59(5)	Cl–Ru–Cp(cen)	115.98(5)

<sup>a</sup> Numbers in parentheses are the estimated standard deviations.

a weaker Ru–PPh<sub>3</sub> bond energy. These measurements have been repeated a number of times, and the reported enthalpy data represent a real difference from the isosteric relatives. The exact reason for this lower Ru–PR<sub>3</sub> BDE for PPh<sub>3</sub> is currently under investigation. Since Cp is less electron donating than Cp\*,<sup>4a</sup> the Cp system will be able to accommodate greater electron density from the incoming two-electron donor (higher electrophilicity), therefore leading to more exothermic enthalpies of ligand substitution.

A difference between enthalpies of reaction between the two reactions (2.3 ± 0.3 kcal/mol) is reminiscent of our earlier work comparing these two systems.<sup>7e</sup> This difference in electronic properties at the metal center gauges a change in metal basicity. Sowa and Angelici have investigated a series of iridium complexes and have observed a difference in enthalpies of protonation of 5.7 kcal/mol between CpIr(COD) and Cp\*Ir(COD) complexes.<sup>24</sup> In these experiments, H<sup>+</sup> proved to be more strongly bound to M–Cp\* by ca. 5 kcal/mol. This is in view of the increased electron density imparted by the better Cp\* donor. In the present ruthenium systems electron-donating phosphine groups are more strongly bound in the CpRu system. Both sets of experiments, although using different approaches, relate information concerning the same fundamental characteristics, namely metal basicity. Hoff and co-workers have first demonstrated this difference in metal basicity between Cp and Cp\* in their thermochemical investigations of organomolybdenum complexes.<sup>16</sup>

The enthalpy difference between ligand substitution reactions, –2.3 kcal/mol, reflects the difference in metal basicity accompanying a change of the ancillary ligation. This difference is of the same order of magnitude as Angelici's enthalpies of protonation and the average difference in enthalpy of ligand substitution in the Cp versus Cp\* organoruthenium systems.

A single-crystal diffraction study was carried out on the synthetic precursor to the Cp\*Ru(PR<sub>3</sub>)<sub>2</sub>Cl complexes.

(23) Another possible explanation, which cannot be discounted at this point, is the involvement of phosphine *π*-acid character, which could also explain for the lack of enthalpy variation associated with electronic variations observed to be significant in the L<sub>2</sub>Fe(CO)<sub>3</sub> system.<sup>8c</sup>

(24) (a) Sowa, J. R., Jr.; Angelici, R. J. *J. Am. Chem. Soc.* **1991**, *113*, 2537–2544. (b) Rottink, M. K.; Angelici, R. J. *J. Am. Chem. Soc.* **1993**, *115*, 7267–7274.

**Table 10. Fractional Coordinates ( $\times 10^4$ ) and Isotropic Thermal Parameters for  $\text{CpRu}(\text{P}(p\text{-CF}_3\text{C}_6\text{H}_4)_2\text{Cl})$  (**3**)<sup>a</sup>**

atom	x	y	z	B ( $\text{\AA}^2$ )	atom	x	y	z	B ( $\text{\AA}^2$ )
Ru	0.93656(3)	0.36846(2)	0.30539(2)	1.784(7)	C(15)	1.0534(4)	0.0298(3)	0.2718(3)	3.2(1)
Cl	0.77860(8)	0.43950(7)	0.29374(5)	2.50(2)	C(16)	1.0958(4)	0.1031(3)	0.2873(3)	3.0(1)
P(1)	0.94966(9)	0.38086(7)	0.20285(5)	2.04(2)	C(17)	1.0360(3)	0.1678(3)	0.2923(2)	2.34(9)
P(2)	0.85659(8)	0.24714(6)	0.29306(5)	1.74(2)	C(18)	0.8053(3)	0.2174(3)	0.3608(2)	2.12(8)
F(1)	0.4594(3)	0.1496(2)	0.0662(2)	4.64(8)	C(19)	0.8072(4)	0.1399(3)	0.3827(3)	3.8(1)
F(2)	0.5132(3)	0.2520(3)	0.0265(2)	6.8(1)	C(20)	0.7614(5)	0.1206(3)	0.4314(3)	4.2(1)
F(3)	0.4111(3)	0.2636(2)	0.0881(2)	6.6(1)	C(21)	0.7132(4)	0.1754(3)	0.4593(2)	3.0(1)
F(4)	1.2094(3)	-0.0273(2)	0.2701(4)	11.6(2)	C(22)	0.7121(5)	0.2538(3)	0.4393(2)	3.7(1)
F(5)	1.1128(4)	-0.0933(3)	0.3111(3)	11.7(2)	C(23)	0.7588(4)	0.2734(3)	0.3909(2)	3.2(1)
F(6)	1.0858(4)	-0.0847(3)	0.2194(3)	14.3(2)	C(24)	1.0373(4)	0.3088(3)	0.1813(2)	2.55(9)
F(7)	0.6012(3)	0.0912(3)	0.4951(2)	7.5(1)	C(25)	1.0031(4)	0.2415(3)	0.1477(3)	3.3(1)
F(8)	0.7269(4)	0.1298(3)	0.5610(2)	7.8(1)	C(26)	1.0706(5)	0.1836(3)	0.1372(3)	4.1(1)
F(9)	0.6084(3)	0.2085(3)	0.5284(2)	7.2(1)	C(27)	1.1731(4)	0.1938(3)	0.1609(3)	4.6(1)
F(10)	1.3362(4)	0.1405(3)	0.1788(2)	10.1(1)	C(28)	1.2070(4)	0.2594(3)	0.1942(3)	4.0(1)
F(11)	1.2500(3)	0.1298(3)	0.0880(2)	7.1(1)	C(29)	1.1396(4)	0.3166(3)	0.2041(3)	3.3(1)
F(12)	1.2123(4)	0.0592(3)	0.1554(3)	16.2(2)	C(30)	0.8451(4)	0.3814(3)	0.1341(2)	2.34(9)
F(13)	0.6074(6)	0.3524(3)	-0.0665(2)	11.6(2)	C(31)	0.7477(4)	0.3978(3)	0.1406(2)	2.6(1)
F(14)	0.6267(5)	0.4765(3)	-0.0576(2)	10.1(1)	C(32)	0.6706(5)	0.4080(3)	0.0890(3)	3.7(1)
F(15)	0.5191(4)	0.4182(3)	-0.0154(2)	10.6(1)	C(33)	0.6907(6)	0.4001(3)	0.0307(3)	4.7(1)
F(16)	1.0538(4)	0.7650(2)	0.1644(3)	10.7(1)	C(34)	0.7876(7)	0.3822(4)	0.0228(3)	5.8(2)
F(17)	1.0671(5)	0.7224(2)	0.0800(2)	10.4(2)	C(35)	0.8655(5)	0.3752(4)	0.0747(3)	4.4(1)
F(18)	1.1880(3)	0.7180(2)	0.1524(3)	9.7(2)	C(36)	1.0005(3)	0.4779(3)	0.1857(2)	2.39(9)
O(1)	0.3518(5)	0.3900(4)	0.5669(3)	3.0(1)*	C(37)	0.9618(4)	0.5449(3)	0.2074(2)	2.7(1)
C(1)	1.0773(4)	0.4381(3)	0.3407(3)	3.5(1)	C(38)	0.9907(4)	0.6200(3)	0.1921(2)	2.9(1)
C(2)	1.0961(4)	0.3561(3)	0.3516(3)	3.4(1)	C(39)	1.0589(4)	0.6271(3)	0.1550(3)	3.4(1)
C(3)	1.0351(4)	0.3319(3)	0.3934(3)	3.5(1)	C(40)	1.0998(4)	0.5618(3)	0.1336(3)	4.9(1)
C(4)	0.9758(5)	0.3968(4)	0.4052(2)	3.8(1)	C(41)	1.0690(4)	0.4869(3)	0.1469(3)	3.8(1)
C(5)	1.0028(5)	0.4625(3)	0.3721(3)	3.8(1)	C(42)	0.4902(4)	0.2241(3)	0.0791(3)	3.9(1)
C(6)	0.7438(3)	0.2352(2)	0.2304(2)	1.90(8)	C(43)	1.1164(5)	-0.0423(3)	0.2658(4)	6.0(2)
C(7)	0.6531(3)	0.2671(3)	0.2361(2)	2.19(9)	C(44)	0.6631(5)	0.1512(4)	0.5100(2)	4.1(1)
C(8)	0.5708(3)	0.2647(3)	0.1885(2)	2.6(1)	C(45)	1.2437(6)	0.1292(4)	0.1467(4)	6.7(2)
C(9)	0.5784(4)	0.2281(3)	0.1327(2)	2.8(1)	C(46)	0.6108(8)	0.4118(4)	-0.0268(3)	8.3(2)
C(10)	0.6693(4)	0.1953(3)	0.1262(2)	2.9(1)	C(47)	1.0925(5)	0.7077(3)	0.1392(3)	4.3(1)
C(11)	0.7501(4)	0.1997(3)	0.1751(2)	2.7(1)	C(48)	0.338(1)	0.3768(9)	0.5059(7)	5.5(3)*
C(12)	0.9320(3)	0.1599(3)	0.2816(2)	2.08(8)	C(49)	0.294(2)	0.441(2)	0.486(1)	14.7(11)*
C(13)	0.8885(4)	0.0868(3)	0.2651(3)	2.8(1)	C(50)	0.276(2)	0.492(2)	0.526(1)	11.3(7)*
C(14)	0.9494(4)	0.0217(3)	0.2596(3)	3.4(1)	C(51)	0.338(1)	0.4711(9)	0.5731(6)	5.1(3)*

<sup>a</sup> Numbers in parentheses are the estimated standard deviations. <sup>b</sup> Starred values denote atoms refined isotropically.

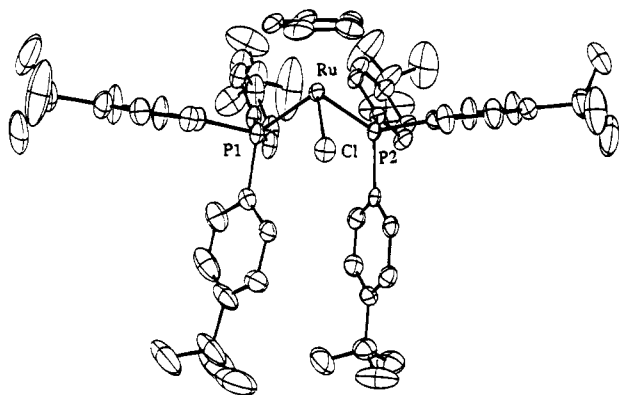


**Figure 3.** ORTEP of  $\text{CpRu}(\text{P}(p\text{-CF}_3\text{C}_6\text{H}_4)_2\text{Cl})$  (**3**) with ellipsoids drawn in at the 50% probability level.

The ORTEP of complex **1** (Figure 1) shows  $\text{Cp}^*\text{Ru}(\text{COD})\text{Cl}$  to have the cyclooctadiene ligand in a boat conformation, characteristic of other metal-COD complexes.<sup>4</sup> Important bond distances in **1** are listed in Table 3 and include  $\text{Ru}-\text{Cp}^*(\text{centroid}) = 2.241(2) \text{ \AA}$  and  $\text{Ru}-\text{Cl} = 2.472(2) \text{ \AA}$ .

In an effort to structurally compare the Cp and  $\text{Cp}^*$  systems, single crystals of two complexes bearing the same phosphine ligands were grown. Complexes **2** and **3** were investigated by single-crystal diffraction studies, results of which are presented in Tables 5–10. Complexes **2** and **3** have the same  $\text{Ru}-\text{Cp}(\text{centroid})$  bond distance ( $1.890 \text{ \AA}$ ), and their respective  $\text{Ru}-\text{Cl}$  bond distances are  $2.439(5)$  and  $2.4294(9) \text{ \AA}$ , a difference of

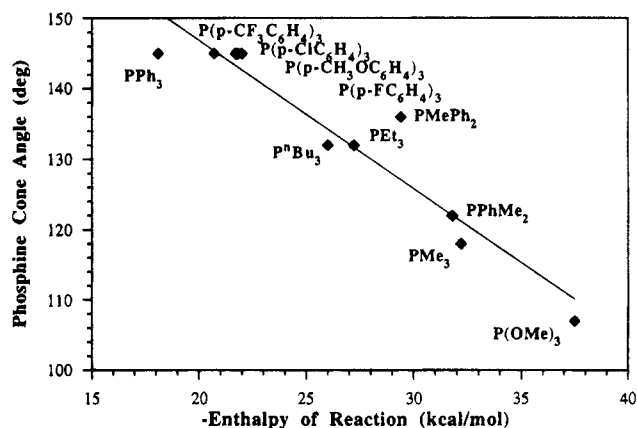


**Figure 4.** Phosphine cone angle vs enthalpy of reaction for a series of tertiary phosphine ligands in the  $\text{Cp}^*\text{Ru}(\text{PR}_3)_2\text{Cl}$  system (slope  $-2.11$ ;  $R = 0.96$ ).

$0.01 \text{ \AA}$ . The most important difference between the two structures resides in the  $\text{Ru}-\text{P}$  bond distances; for **2**,  $\text{Ru}-\text{P}$  distances are  $2.315(6)$  and  $2.334(5) \text{ \AA}$ , respectively. These values can be compared to the  $\text{Ru}-\text{P}$  distances in **3**,  $2.3087(7)$  and  $2.3102(6) \text{ \AA}$ . The average  $\text{Ru}-\text{P}$  distance is  $0.015 \text{ \AA}$  shorter in **2** than in **3**. The observed shortening of bonds in structure **2** supports the previously mentioned assumption that stronger bonds should exist in the  $\text{CpRu}(\text{PR}_3)_2\text{Cl}$  system in comparison to those in their  $\text{Cp}^*$  analogs.<sup>7e</sup>

Furthermore, a single-crystal diffraction study of **3** was undertaken in order to add to the number of known

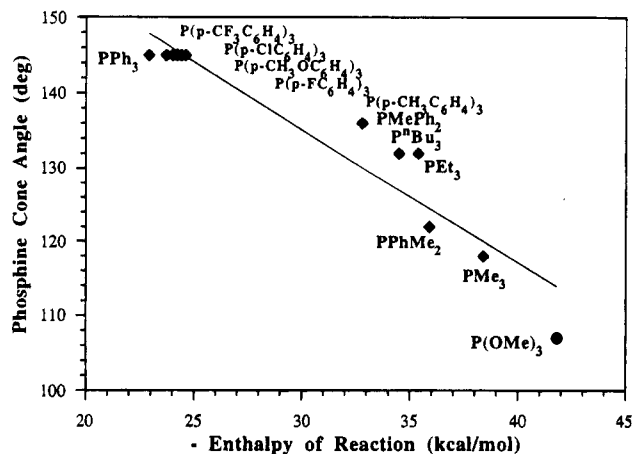


**Figure 5.** Phosphine cone angle vs enthalpy of reaction for a series of tertiary phosphine ligands in the  $\text{CpRu}(\text{PR}_3)_2\text{Cl}$  system (slope  $-1.80$ ;  $R = 0.95$ ).

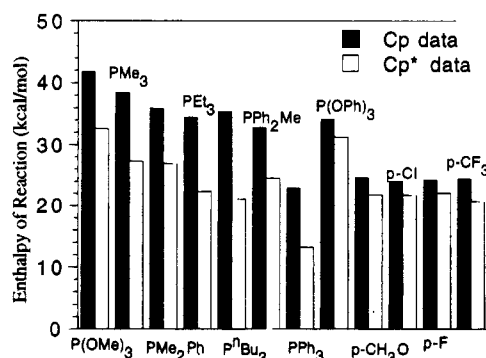


**Figure 6.** Enthalpies of reaction for  $\text{CpRu}(\text{PR}_3)_2\text{Cl}$  and  $\text{Cp}^*\text{Ru}(\text{PR}_3)_2\text{Cl}$  systems as a function of phosphine ligand.

Cp-based metal–ligand bond distances. These fundamental data enable us to examine whether there in fact exists a bond strength/bond length relationship in this system. Five other  $\text{CpRu}(\text{ER}_3)_2\text{Cl}$  ( $\text{ER}_3 = \text{AsEt}_3, \text{PET}_3, \text{PMe}_3, \text{P}(\text{OMe})_3$  and  $\text{PPh}_3$ ) complexes have previously been structurally characterized.<sup>25,26</sup> A comparison involving all six complexes in terms of bond distances (Table 11) suggests a linear relationship between bond enthalpy data and ruthenium–phosphine–arsine bond length information.<sup>27</sup> A graphic representation of the relationship is presented in Figure 7 and shows a good correlation ( $R = 0.89$ ) to exist in this system.

Further structural studies are in progress in order to examine to what extent this relationship remains valid within these ruthenium systems.<sup>28</sup>

### Conclusion

The labile nature of the COD ligand in  $\text{CpRu}(\text{COD})\text{Cl}$  and  $\text{Cp}^*\text{Ru}(\text{COD})\text{Cl}$  was used to gain access into the

(25) (a) Treichel, P. M.; Komar, D. A. *Synth. React. Inorg. Met.-Org. Chem.* **1980**, *10*, 205–210. (b) Bruce, M. I.; Wong, F. S.; Skelton, B. W.; White, A. H. *J. Chem. Soc., Dalton Trans.* **1981**, 1398–1405. (c) Bruce, M. I.; Wong, F. S.; Skelton, B. W.; White, A. H. *J. Chem. Soc., Dalton Trans.* **1982**, 2203–2207.

(26) (a) Treichel, P. M.; Komar, D. A. *Synth. React. Inorg. Met.-Org. Chem.* **1984**, *14*, 383–400. (b) Bruce, M. I.; Cifuentes, M. P.; Snow, M. R.; Tiekink, R. T. *J. Organomet. Chem.* **1989**, 379–399.

(27) Such a correlation is expected if no important variation in  $\text{Ru}-\text{L}_n$  ( $\text{L}_n = \text{ancillary ligand}$ ) bond distance or  $\text{L}_n-\text{Ru}-\text{L}_n$  bond angle is present in these complexes. Studies aimed at probing the extent and reasons for such a correlation to exist in the present system are currently underway.<sup>28</sup>

(28) Luo, L.; Li, C.; Cucullu, M. E.; Mahler, C. H.; Fagan, P. J.; Jones, N.; Calabrese, J. C.; Nolan, S. P. Manuscript in preparation.

**Table 11. Selected Bond Distances (Å) and Enthalpies of Ligand Substitution (kcal/mol) for  $\text{CpRu}(\text{ER}_3)_2\text{Cl}$  Complexes**

$\text{ER}_3$	$\text{M}-\text{ER}_3$	$-\Delta H$
$\text{P}(\text{OMe})_3^a$	2.217(3)	41.8(0.2)
$\text{PMe}_3^{b,c}$	2.28(1)	38.4(0.4)
$\text{PET}_3^d$	2.304(1)	34.5(0.2)
$\text{P}(p\text{-CF}_3\text{C}_6\text{H}_4)_3^e$	2.309(1)	24.4(0.2)
$\text{PPh}_3^b$	2.336(1)	22.9(0.4)
$\text{AsEt}_3^d$	2.414(1)	19.4(0.2)

<sup>a</sup> See ref 25b. <sup>b</sup> See ref 24c. <sup>c</sup> Two independent molecules are found in this unit cell. <sup>d</sup> See ref 7e. <sup>e</sup> This work.

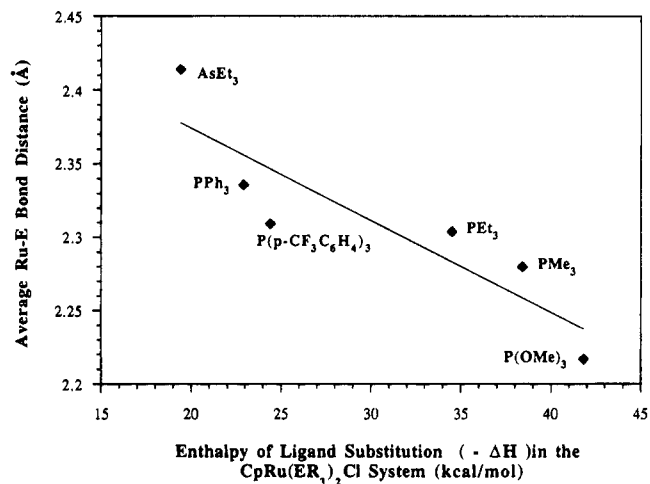


**Figure 7.** Average Ru–E bond distance vs enthalpy of ligand substitution reaction in the  $\text{CpRu}(\text{PR}_3)_2\text{Cl}$  complexes ( $\text{E} = \text{As}, \text{P}$ ) (slope  $-0.006$ ;  $R = 0.89$ ).

thermochemistry of ligand substitution for para-substituted triphenylphosphine ligands. The enthalpy trend can be explained in terms of overwhelming steric contribution to the enthalpy of reaction. The increased exothermicity displayed by the  $\text{CpRu}(\text{PR}_3)_2\text{Cl}$  system over its  $\text{Cp}^*$  parent is taken as a gauge of the increased metal basicity on going from  $\text{Cp}$  to  $\text{Cp}^*$ . A quantitative relationship is established between structural and thermodynamic parameters and displays a good correlation. Three structural determinations have been carried out and show interesting metal–ligand bond length modulations with respect to ancillary ligand variation. Further thermochemical, kinetic, mechanistic, and catalytic investigations focusing on this and related systems are presently underway.

**Acknowledgment.** The Board of Regents of the Louisiana Education Quality Support Fund (Grant No. LEQSF(RF/1993–96)-RD-A-47) and the National Science Foundation (Grant No. CHE-9305492) are gratefully acknowledged for support of this research. M.E.C. acknowledges Du Pont for partial support through an Educational Aid Grant. We are also indebted to Aesar/Johnson-Matthey for the generous loan of ruthenium salts.

**Supporting Information Available:** Tables of hydrogen atomic coordinates, selected bond distances and angles, and anisotropic thermal displacement parameters for 1–3 (42 pages). This material is contained in many libraries on microfiche, immediately follows this article in the microfilm version of the journal, and can be ordered from the ACS; see any current masthead page for ordering information.

# New Lipophilic Air-Stable Silanetriols: First Example of an X-ray Crystal Structure of a Silanetriol with Si-N Bonds

Ramaswamy Murugavel, Vadapalli Chandrasekhar,<sup>†</sup> Andreas Voigt, Herbert W. Roesky,\* Hans-Georg Schmidt, and Mathias Noltemeyer

Institut für Anorganische Chemie der Universität Göttingen,  
Tammannstrasse 4, D-37077 Göttingen, FRG

Received May 30, 1995<sup>®</sup>

By using hindered primary aromatic amines, the four silanetriols RN(SiMe<sub>3</sub>)(Si(OH)<sub>3</sub>) (R = 2,6-Me<sub>2</sub>C<sub>6</sub>H<sub>3</sub> (**2b**), 2,4,6-Me<sub>3</sub>C<sub>6</sub>H<sub>2</sub> (**2c**), 2-*i*-Pr-6-MeC<sub>6</sub>H<sub>3</sub> (**2d**), 2,6-*i*-Pr<sub>2</sub>C<sub>6</sub>H<sub>3</sub> (**2e**)) have been synthesized. These N-bonded silanetriols, apart from being air-stable, are also highly lipophilic, being soluble in a variety of organic solvents. The crystal structure of **2c** has been determined and represents a new structural form for silanetriols.

## Introduction

We have recently shown that the silanetriols RSi(OH)<sub>3</sub> can be used as versatile building blocks for the generation of discrete three-dimensional structures incorporating silicon and a transition metal.<sup>1,2</sup> We were also successful in assembling novel soluble aluminosilicates with ring and cage structures.<sup>3</sup> Previously described metallocsiloxanes with a lower metal to silicon ratio involved the corner-capping reactions of silsesquioxanes with three pendant OH groups and not a genuine silanetriol.<sup>4</sup> Since discrete silanetriols are better synthons for the assembly of three-dimensional structures with a higher metal to silicon ratio, we were interested in preparing new stable silanetriols with good solubility properties.<sup>2</sup>

Silanetriols containing a Si-C,<sup>1,5-8</sup> Si-O,<sup>2</sup> or Si-Si<sup>6</sup> bond have been described previously. These suffer from disadvantages such as poor solubility and/or sensitivity to self-condensation during their preparation and further reactions. Earlier, we described in a preliminary communication<sup>2</sup> the synthesis of a novel N-bonded silanetriol that obviates the disadvantages described above. Using this approach, we have now prepared three new air-stable silanetriols that are highly soluble in organic solvents. The characteristic feature of these silanetriols is the presence of a NSiMe<sub>3</sub> unit linking the

triole to an aromatic moiety with *ortho* substituents. We also describe the single-crystal X-ray structure of one of the triols, representing the first example of a silanetriol containing Si-N bonds.

## Results and Discussion

**Synthesis and Spectra.** Controlled hydrolysis of the N-substituted silicon trichlorides affords the new silanetriols in good yields. The silicon trichlorides **1a-e** were synthesized in a four-step sequence as shown in Scheme 1. Scheme 2 depicts the synthesis of the silanetriols **2b-e**. The syntheses of **1e** and **2e** have been described previously in a preliminary communication.<sup>2</sup>

The silicon trichlorides were distilled under vacuum and are stable for a long time in the absence of moisture. The silanetriols were isolated as white powders and are perfectly air-stable in the solid state over a long period of time. These silanetriols are highly soluble in common organic solvents such as aliphatic and aromatic hydrocarbons, ethers, chloro solvents, alcohols, and acetonitrile. This high solubility is attributable to the presence of the SiMe<sub>3</sub> group and the alkyl-substituted aryl group (*vide infra*). These favorable solubility properties are also advantageous in their use as building blocks for metallocsiloxanes with cage structures. In contrast to the rather high melting points reported for other silanetriols known in the literature,<sup>4-8</sup> the new silanetriols have sharp and low melting points. However, the melting is accompanied by small amounts of decomposition and the molten triols do not solidify on cooling.

The new silicon trichlorides and the silanetriols have been characterized by elemental analysis, IR, multinuclear NMR, and mass spectroscopy. All the compounds yielded good analytical data. The parent ions are clearly seen in the electron impact mass spectra. The infrared spectra of the silanetriols are characterized by the presence of a strong absorption centered around 3400 cm<sup>-1</sup>. While the <sup>29</sup>Si NMR resonance of -SiMe<sub>3</sub> is invariant in the trichlorides and the triols, the chemical shifts of -SiCl<sub>3</sub> move upfield upon hydrolysis (*vide infra*).

In contrast to the excellent yields of the silanetriols **1b-d**, our attempts to synthesize a stable silanetriol with the unsubstituted aniline as starting material have

<sup>†</sup> On sabbatical from the Department of Chemistry, IIT, Kanpur 208016, India.

<sup>®</sup> Abstract published in *Advance ACS Abstracts*, October 1, 1995.

(1) Winkhofer, N.; Roesky, H. W.; Noltemeyer, M.; Robinson, W. T. *Angew. Chem.* **1992**, *104*, 670; *Angew. Chem., Int. Ed. Engl.* **1992**, *31*, 599.

(2) Winkhofer, N.; Voigt, A.; Dorn, H.; Roesky, H. W.; Steiner, A.; Stalke, D.; Reller, A. *Angew. Chem.* **1994**, *106*, 1414; *Angew. Chem., Int. Ed. Engl.* **1994**, *33*, 1352.

(3) (a) Montero, M. L.; Usón, I.; Roesky, H. W. *Angew. Chem.* **1994**, *106*, 2198; *Angew. Chem., Int. Ed. Engl.* **1994**, *33*, 2103. (b) Chandrasekhar, V.; Murugavel, R.; Voigt, A.; Roesky, H. W.; Schmidt, H. G.; Noltemeyer, M. Manuscript under preparation.

(4) Feher, F. J.; Newman, D. A.; Walzer, J. F. *J. Am. Chem. Soc.* **1989**, *111*, 1741. (b) Feher, F. J.; Weller, K. J. *Organometallics* **1990**, *9*, 2638.

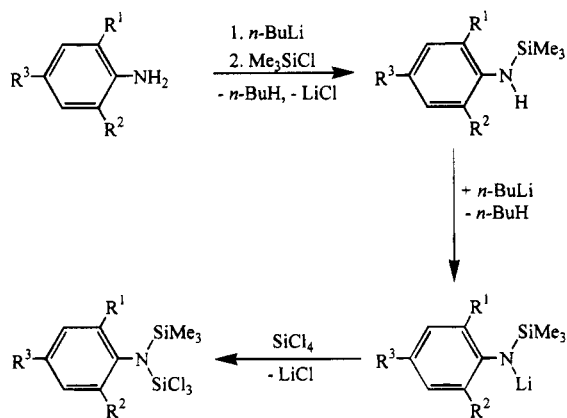
(5) Takiguchi, T. *J. Am. Chem. Soc.* **1959**, *81*, 2359.

(6) Al-Juaid, S. S.; Buttrus, N. H.; Damja, R. I.; Derouiche, Y.; Eaborn, C.; Hitchcock, P. B.; Lickiss, P. D. *J. Organomet. Chem.* **1989**, *371*, 287.

(7) Ishida, H.; Koenig, J. L.; Gardner, K. C. *J. Chem. Phys.* **1982**, *77*, 5748.

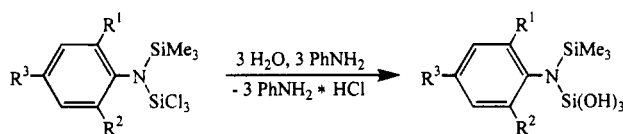
(8) Seyferth, D.; Rudie, C. N.; Nestle, M. O. *J. Organomet. Chem.* **1979**, *178*, 227.

Scheme 1



- 1a:  $R^1 = R^2 = R^3 = H$   
 1b:  $R^1 = R^2 = Me, R^3 = H$   
 1c:  $R^1 = R^2 = R^3 = Me$   
 1d:  $R^1 = i\text{-Pr}, R^2 = Me, R^3 = H$   
 1e:  $R^1 = R^2 = i\text{-Pr}, R^3 = H$

Scheme 2



- 2b:  $R^1 = R^2 = Me, R^3 = H$   
 2c:  $R^1 = R^2 = R^3 = Me$   
 2d:  $R^1 = i\text{-Pr}, R^2 = Me, R^3 = H$   
 2e:  $R^1 = R^2 = i\text{-Pr}, R^3 = H$

resulted in the isolation of noncharacterizable products. This observation underscores the importance of the *ortho* substituent such as methyl or isopropyl on the aromatic ring in stabilizing discrete silanetriols.

**X-ray Crystal Structure of 2c.** The molecule crystallizes in the centrosymmetric triclinic space group with two molecules in the asymmetric unit (Figure 1). The aryl ring is almost perpendicular with reference to the  $Si_2N$  unit. The dihedral angles between the  $Si-N-Si$  plane and the plane of the aromatic moiety in the two crystallographically independent molecules are  $91.9^\circ$  and  $87.1^\circ$ , respectively. The other selected structural parameters are summarized in Table 1.

The crystal structure of **2c** represents the first example of a silanetriol with  $Si-N$  bonds. Earlier reports have described the structures of silanetriols containing  $Si-C$  or  $Si-Si$  bonds.<sup>1,6,7</sup> In **2c**, there are two types of  $Si-N$  bonds, with the shorter bond length ( $1.710(2) \text{ \AA}$ ) being associated with the silicon atom bearing three oxygen atoms. The other  $Si-N$  bond length is substantially longer ( $1.762(2) \text{ \AA}$ ). This observation is consistent with multiple bonding effects found in group 14 and 15 elements that are bonded to electron-withdrawing substituents.<sup>9</sup> The average  $Si-O$  bond length ( $1.634(2) \text{ \AA}$ ) is comparable with that observed for the other silanetriols. The observed  $O-Si-O$  bond angles in the two molecules are  $108.2(1)$ ,  $113.3(1)$ ,  $103.5(1)$ ,  $105.9(1)$ ,  $111.6(1)$ , and  $106.1(1)^\circ$ . These values are comparable to those found in  $t\text{-BuSi(OH)}_3^1$  and  $(SiMe_3)_3SiSi(OH)_3$ .<sup>6</sup>

(9) Reed, A. E.; Schleyer, P. v. R. *J. Am. Chem. Soc.* **1990**, *112*, 1434.  
 (b) Murugavel, R.; Krishnamurthy, S. S.; Chandrasekhar, J.; Nethaji, M. *Inorg. Chem.* **1993**, *32*, 5447.

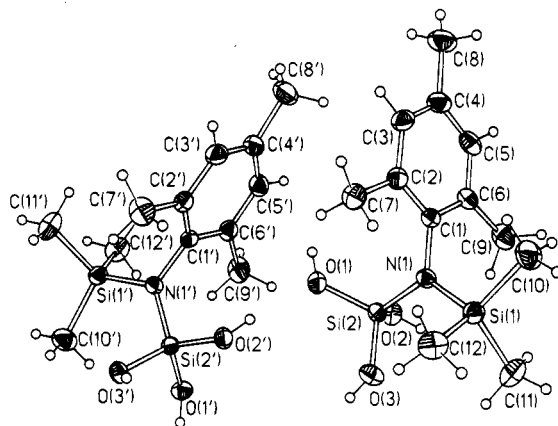


Figure 1. Molecular structure of the two crystallographically independent molecules of **2c** (thermal ellipsoids shown at 50% probability level).

Table 1. Selected Structural Parameters for **2c**

Bond Distances ( $\text{\AA}$ )			
Si(1)-N(1)	1.762(2)	Si(1')-N(1')	1.760(2)
Si(2)-N(1)	1.710(2)	Si(2')-N(1')	1.716(2)
Si(2)-O(1)	1.640(2)	Si(2')-O(1')	1.641(2)
Si(2)-O(2)	1.644(2)	Si(2')-O(2')	1.630(2)
Si(2)-O(3)	1.612(2)	Si(2')-O(3')	1.636(2)
Bond Angles (deg)			
Si(1)-N(1)-Si(2)	124.2(1)	Si(1')-N(1')-Si(2')	125.2(1)
C(1)-N(1)-Si(1)	119.4(2)	C(1')-N(1')-Si(1')	116.3(2)
C(1)-N(1)-Si(2)	116.4(2)	C(1')-N(1')-Si(2')	118.4(2)
O(1)-Si(2)-O(2)	103.5(1)	O(1')-Si(2')-O(2')	111.6(1)
O(1)-Si(2)-O(3)	108.2(1)	O(1')-Si(2')-O(3')	106.1(1)
O(2)-Si(2)-O(3)	113.3(1)	O(2')-Si(2')-O(3')	105.9(1)
Hydrogen Bonds ( $\text{\AA}$ )			
O(2)···O(3') <sup>a</sup>	2.739	O(2)···O(1') <sup>b</sup>	2.809
O(3)···O(3') <sup>c</sup>	2.778	O(1')···O(2') <sup>c</sup>	2.819
O(3')···O(2) <sup>d</sup>	2.739	O(1)···O(2)	2.579
O(1)···O(3)	2.633	O(2)···O(3)	2.720
O(1')···O(2')	2.705	O(1')···O(3')	2.618
O(2')···O(3')	2.606		

<sup>a</sup>  $1 + x, y, z$ . <sup>b</sup>  $1 - x, -y, -z$ . <sup>c</sup>  $2 - x, -y, -z$ . <sup>d</sup>  $x - 1, y, z$ .

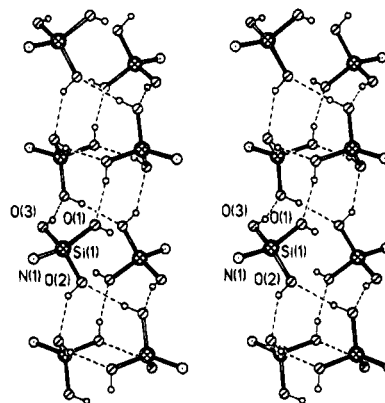
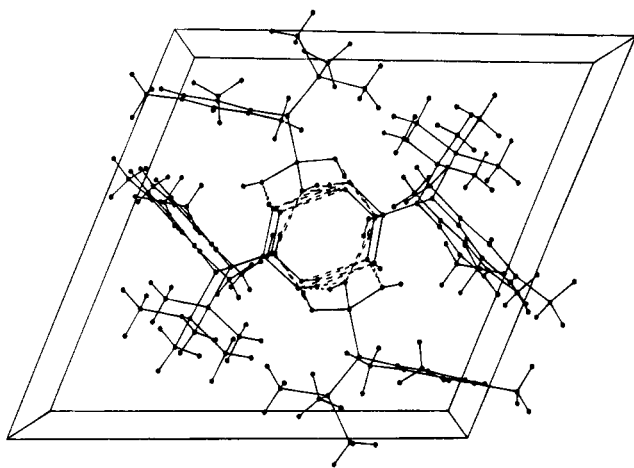


Figure 2. Stereo plot of the packing of the  $-NSi(OH)_3$  unit of **2c** in the crystal viewed perpendicular to the  $a$  axis (intramolecular hydrogen bonds are not shown).

The geometry about the nitrogen atom is perfectly planar, with the angles around nitrogen adding to  $360^\circ$ .

The silanetriol **2c** is involved in an extensive intra- and intermolecular hydrogen bonding through the hydroxyl groups, leading to a one-dimensional columnar polymeric network (Figure 2 and Table 1). Earlier known structures fall into two structural types: (a) a double-sheet structure, observed for  $C_6H_{11}Si(OH)_3$ <sup>7</sup> and  $t\text{-BuSi(OH)}_3$ ,<sup>1</sup> where the molecules arrange in a head-



**Figure 3.** Crystal packing of **2c** down the *a* axis clearly showing the *hydrophilic interior* and *hydrophobic exterior* of the *tubes* (see text).

to-head and tail-to-tail fashion with the alkyl groups and OH groups forming hydrophobic and hydrophilic alternating double sheets, respectively, and (b) a discrete hexameric cage structure with hydrogen-bonded silanetriols, as observed in  $(\text{SiMe}_3)_3\text{CSi}(\text{OH})_3$  and  $(\text{SiMe}_3)_3\text{-SiSi}(\text{OH})_3$ .<sup>6</sup>

**2c** does not belong to either of the two structural types described above. Instead, the molecules in **2c** arrange themselves in a tubular form which is made up of four linear columns. Another interesting aspect of this arrangement is the relative displacement of these four columns with respect to each other. It is clearly seen from the stereoview shown in Figure 2 that there is a 90° rotational relationship between these columns. A perpendicular view showing the hydrogen-bonding effects between these columns is shown in Figure 3. The net result is the formation of *tubes* of silanetriols in the crystal structure, which themselves are made up of a *hydrophilic interior* and a *hydrophobic exterior*. Figure 3 also shows the presence of a channel running through the hydrophilic interior. Thus, the structure of **2c** represents a new structural form for silanetriols.

### Conclusions

It has been shown that stable discrete silanetriols containing Si–N bonds are obtainable by a new synthetic strategy involving hindered aromatic primary amines. These compounds, apart from being air-stable, are also soluble in a variety of organic solvents, thus making them extremely useful as synthons for the construction of new silicon-containing rings, cages, and supramolecules. We are currently investigating these aspects.

### Experimental Section

**General Data.** All reactions were carried out using standard Schlenk procedures. Solvents were purified and dried according to standard methods. 2,4,6-Trimethylaniline and 2,6-dimethylaniline (Acros Chimica) and 2-isopropyl-6-methylaniline, trimethylsilyl chloride, silicon tetrachloride, and *n*-butyllithium (1.6 M solution in hexane) (Aldrich) were used as received. Aniline (Aldrich) was refluxed and distilled over  $\text{CaH}_2$ . NMR spectra were recorded on a Bruker AM 200 or a Bruker AS 400 instrument. The chemical shifts are reported in ppm with reference to  $\text{SiMe}_4$ . IR spectra were

recorded on a Bio-Rad Digilab FTS7 spectrometer (only strong absorption values are given; *vide infra*). Mass spectra were obtained on a Finnigan MAT System 8230 and a Varian MAT CH5 mass spectrometer. Melting points were obtained on a HWS-SG 3000 apparatus and are uncorrected. Elemental analyses were performed by the Analytical Laboratory of the Institute of Inorganic Chemistry at Göttingen.

All the trichlorides and the respective triols were prepared by following a similar procedure.

**Synthesis of the Trichlorides  $[\text{RN}(\text{SiMe}_3)(\text{SiCl}_3)]$ .** To a solution of  $\text{RNH}_2$  (0.2 mol) in ether (200 mL) was added *n*-BuLi (0.2 mol) dropwise at  $-78^\circ\text{C}$  with constant stirring. After the addition was complete, the reaction mixture was kept at this temperature for 4 h before allowing it to come to room temperature. It was again cooled to  $-78^\circ\text{C}$ , and a solution of  $\text{Me}_3\text{SiCl}$  (0.2 mol) in  $\text{Et}_2\text{O}$  (100 mL) was added dropwise. The reaction mixture was warmed to room temperature. The precipitated LiCl was filtered off, and the filtrate was reacted further with *n*-BuLi (0.2 mol) at room temperature. The reaction mixture was subsequently heated under reflux for 4 h. This solution was transferred to a dropping funnel and added dropwise to a solution of  $\text{SiCl}_4$  (0.2 mol) in  $\text{Et}_2\text{O}$  (100 mL) at  $0^\circ\text{C}$ . The reaction mixture was stirred overnight and filtered. The volatiles were stripped off from the filtrate, and the remaining viscous oil was distilled under vacuum to afford pure  $\text{RN}(\text{SiMe}_3)(\text{SiCl}_3)$ .

**( $\text{C}_6\text{H}_5$ )( $\text{SiMe}_3$ ) $\text{N}(\text{SiCl}_3)$  (**1a**).** Yield: 47.8 g (80%). Bp:  $99^\circ\text{C}/12\text{ mmHg}$ . Anal. Calcd for  $\text{C}_9\text{H}_{14}\text{Cl}_3\text{NSi}_2$ : C, 36.2; H, 4.7; Cl, 35.6; N, 4.7. Found: C, 36.7; H, 4.9; Cl, 32.8; N, 5.4. Mass spectrum (EI, 70 eV): *m/e* 297 ( $\text{M}^+$ , 20%, 3 Cl isotope pattern). IR (neat): 3020, 2599, 1564, 1495, 1260, 1075, 843, 800, 744, 682  $\text{cm}^{-1}$ .  $^1\text{H}$  NMR (200 MHz,  $\text{CDCl}_3$ ): 0.26 (s, 9H,  $\text{SiMe}_3$ ), 7.10 (m, 2H, aromatic), 7.30 (m, 3H, aromatic).  $^{13}\text{C}$  NMR (62.9 MHz,  $\text{CDCl}_3$ ): 1.4 ( $\text{SiMe}_3$ ), 126.1, 129.2, 129.8, 142.3 (aromatic).  $^{29}\text{Si}$  NMR (49.7 MHz,  $\text{CDCl}_3$ ):  $-28.2$  ( $\text{SiCl}_3$ ), 12.8 ( $\text{SiMe}_3$ ).

**(2,6- $\text{Me}_2\text{C}_6\text{H}_3$ ) $\text{N}(\text{SiMe}_3)(\text{SiCl}_3)$  (**1b**).** Yield: 42.5 g (65%). Bp:  $67^\circ\text{C}/0.07\text{ mmHg}$ . Anal. Calcd for  $\text{C}_{11}\text{H}_{18}\text{Cl}_3\text{NSi}_2$ : C, 40.4; H, 5.6; Cl, 32.5; N, 4.3. Found: C, 39.1; H, 5.4; Cl, 33.1; N, 4.4. Mass spectrum (EI, 70 eV): *m/e* 325 ( $\text{M}^+$ , 30%, 3 Cl isotope pattern). IR (neat): 2959, 1467, 1267, 1178, 1100, 990, 984, 879, 843, 769, 745, 722, 690, 598, 570, 552, 539, 494  $\text{cm}^{-1}$ .  $^1\text{H}$  NMR (200 MHz,  $\text{CDCl}_3$ ): 0.33 (s, 9H,  $\text{SiMe}_3$ ), 2.40 (s, 9H, Me), 7.10 (m, 3H, aromatic).  $^{13}\text{C}$  NMR (62.9 MHz,  $\text{CDCl}_3$ ): 1.6 ( $\text{SiMe}_3$ ), 20.0 ( $\text{CH}_3$ ), 125.6, 128.6, 136.8, 140.7 (aromatic).  $^{29}\text{Si}$  NMR (49.7 MHz,  $\text{CDCl}_3$ ):  $-28.2$  ( $\text{SiCl}_3$ ), 12.5 ( $\text{SiMe}_3$ ).

**(2,4,6- $\text{Me}_3\text{C}_6\text{H}_2$ ) $\text{N}(\text{SiMe}_3)(\text{SiCl}_3)$  (**1c**).** Yield: 54.5 g (80%). Bp:  $83^\circ\text{C}/0.07\text{ mmHg}$ . Anal. Calcd for  $\text{C}_{12}\text{H}_{20}\text{Cl}_3\text{NSi}_2$ : C, 42.3; H, 5.9; Cl, 31.2; N, 4.1. Found: C, 42.7; H, 6.0; Cl, 31.2; N, 4.6. Mass spectrum (EI, 70 eV): *m/e* 341 ( $\text{M}^+$ , 30%, 3 Cl isotope pattern). IR (neat): 2957, 2922, 1447, 1407, 1377, 1256, 1200, 1145, 1084, 986, 954, 865, 843, 759, 730, 647, 601, 583, 563, 485  $\text{cm}^{-1}$ .  $^1\text{H}$  NMR (200 MHz,  $\text{CDCl}_3$ ): 0.32 (s, 9H,  $\text{SiMe}_3$ ), 2.31 (s, 3H, Me), 2.36 (s, 6H, Me), 6.93 (s, 2H, aromatic).  $^{13}\text{C}$  NMR (62.9 MHz,  $\text{CDCl}_3$ ): 1.8 ( $\text{SiMe}_3$ ), 20.1, 20.2 ( $\text{CH}_3$ ), 129.5, 135.6, 136.6, 138.1 (aromatic).  $^{29}\text{Si}$  NMR (49.7 MHz,  $\text{CDCl}_3$ ):  $-28.3$  ( $\text{SiCl}_3$ ), 12.3 ( $\text{SiMe}_3$ ).

**(2-*i*-Pr-6- $\text{MeC}_6\text{H}_3$ ) $\text{N}(\text{SiMe}_3)(\text{SiCl}_3)$  (**1d**).** Yield: 56.8 g (80%). Bp:  $120^\circ\text{C}/0.01\text{ mmHg}$ . Anal. Calcd for  $\text{C}_{13}\text{H}_{22}\text{Cl}_3\text{NSi}_2$ : C, 44.0; H, 6.3; Cl, 30.0; N, 3.9. Found: C, 43.0; H, 6.1; Cl, 29.4; N, 3.7. Mass spectrum (EI, 70 eV): *m/e* 355 ( $\text{M}^+$ , 35%, 3 Cl isotope pattern). IR (Nujol): 1329, 1267, 1171, 1108, 1047, 983, 964, 926, 878, 847, 785, 759, 720, 690, 644, 610, 590, 574, 549, 523, 491  $\text{cm}^{-1}$ .  $^1\text{H}$  NMR (200 MHz,  $\text{CDCl}_3$ ): 0.22 (s, 9H,  $\text{SiMe}_3$ ), 1.21 (dd, 6H,  $\text{Me}_2$ ), 2.30 (s, 3H, Me), 3.30 (m, 1H, CH), 7.10 (m, 3H, aromatic).  $^{13}\text{C}$  NMR (62.9 MHz,  $\text{CDCl}_3$ ): 1.7 ( $\text{SiMe}_3$ ), 20.7, 24.4, 25.2 (Me), 27.9 (CH), 124.5, 126.1, 128.3, 136.7, 139.6, 147.5 (aromatic).  $^{29}\text{Si}$  NMR (49.7 MHz,  $\text{CDCl}_3$ ):  $-27.9$  ( $\text{SiCl}_3$ ), 12.2 ( $\text{SiMe}_3$ ).

**Synthesis of the Silanetriols  $[\text{RN}(\text{SiMe}_3)(\text{Si}(\text{OH})_3)]$ .** To a suspension of  $\text{H}_2\text{O}$  (0.3 mol) and  $\text{PhNH}_2$  (0.3 mol) in distilled ether (1000 mL) was added a solution of  $\text{RN}(\text{SiMe}_3)(\text{SiCl}_3)$  (0.1



**Table 2. Crystal Data and Structure Refinement Details for 2c**

empirical formula	C <sub>12</sub> H <sub>23</sub> NO <sub>3</sub> Si <sub>2</sub>
fw	285.49
temp	153(2) K
wavelength	0.710 73 Å
cryst syst	triclinic
space group	P1
unit cell dimensions	<i>a</i> = 8.104(1) Å <i>b</i> = 14.127(2) Å <i>c</i> = 14.979(2) Å $\alpha$ = 111.65(1)° $\beta$ = 93.93(2)° $\gamma$ = 92.00(1)°
V	1586.8(4) Å <sup>3</sup>
Z	4
density (calcd)	1.195 Mg/m <sup>3</sup>
abs coeff	0.224 mm <sup>-1</sup>
F(000)	616
cryst size	0.70 × 0.60 × 0.30 mm
$\theta$ range for data collection	3.64–24.95°
index ranges	–9 ≤ <i>h</i> ≤ 9, –16 ≤ <i>k</i> ≤ 15, –16 ≤ <i>l</i> ≤ 17
no. of rflns collected	7207
no. of indep rflns	5548 ( <i>R</i> <sub>int</sub> = 0.048)
refinement method	full-matrix least squares on <i>F</i> <sup>2</sup>
data/restraints/params	5527/6/356
goodness of fit on <i>F</i> <sup>2</sup>	1.058
final <i>R</i> indices ( <i>I</i> > 2σ( <i>I</i> ))	<i>R</i> 1 = 0.047, w <i>R</i> 2 = 0.118
<i>R</i> indices (all data)	<i>R</i> 1 = 0.060, w <i>R</i> 2 = 0.137
largest diff peak and hole	0.509 and –0.297 e/Å <sup>3</sup>

mol) in Et<sub>2</sub>O (100 mL) dropwise over a period of 1 h at 0 °C with vigorous stirring. The reaction mixture was stirred for 18 h, allowing it to come to room temperature. The precipitated PhNH<sub>3</sub>Cl was filtered off, and the solvent was removed from the filtrate *in vacuo*, affording RN(SiMe<sub>3</sub>)<sub>3</sub>(Si(OH)<sub>3</sub>) as an off-white solid which was purified by washing with pentane (2 × 50 mL).

**(2,6-Me<sub>2</sub>C<sub>6</sub>H<sub>3</sub>)N(SiMe<sub>3</sub>)<sub>3</sub>(Si(OH)<sub>3</sub>) (2b).** Yield: 20.4 g (75%). Mp: 131 °C. Anal. Calcd for C<sub>11</sub>H<sub>21</sub>NO<sub>3</sub>Si<sub>2</sub>: C, 48.7; H, 7.8; N, 5.2. Found: C, 48.7; H, 7.7; N, 5.2. Mass spectrum (EI, 70 eV): *m/e* 271 (M<sup>+</sup>, 30%). IR (Nujol): 3339, 1261, 1197, 1100, 1083, 978, 967, 936, 898, 840, 805, 762, 723, 687, 638, 563, 544, 494, 458, 423 cm<sup>-1</sup>. <sup>1</sup>H NMR (200 MHz, CDCl<sub>3</sub>): 0.02 (s, 9H, SiMe<sub>3</sub>), 2.17 (s, 6H, Me), 5.32 (s, 3H, OH), 6.85 (m, 3H, aromatic). <sup>13</sup>C NMR (62.9 MHz, CDCl<sub>3</sub>): 1.5 (SiMe<sub>3</sub>), 19.7 (Me), 124.1, 128.1, 137.5, 142.3 (aromatic). <sup>29</sup>Si NMR (49.7 MHz, CDCl<sub>3</sub>): –66.2 (Si(OH)<sub>3</sub>), 7.7 (SiMe<sub>3</sub>).

**(2,4,6-Me<sub>3</sub>C<sub>6</sub>H<sub>2</sub>)N(SiMe<sub>3</sub>)<sub>3</sub>(Si(OH)<sub>3</sub>) (2c).** Yield: 22.8 g (80%). Mp: 123–124 °C. Anal. Calcd for C<sub>12</sub>H<sub>23</sub>NO<sub>3</sub>Si<sub>2</sub>: C, 50.5; H, 8.1; N, 4.9. Found: C, 50.9; H, 8.1; N, 5.0. Mass spectrum (EI, 70 eV): *m/e* 325 (M<sup>+</sup>, 40%). IR (Nujol): 3400, 1476, 1376, 1303, 1249, 1213, 1154, 989, 967, 930, 889, 859, 836, 805, 757, 734, 687, 640, 572, 502, 441 cm<sup>-1</sup>. <sup>1</sup>H NMR (400 MHz, CDCl<sub>3</sub>): 0.03 (s, 9H, SiMe<sub>3</sub>), 2.15 (s, 6H, Me), 2.20 (s, 3H, Me), 4.80 (s, 3H, OH), 6.72 (s, 2H, aromatic). <sup>13</sup>C NMR (100.6 MHz, CDCl<sub>3</sub>): 1.4 (SiMe<sub>3</sub>), 19.7 (Me), 20.7 (Me), 128.9, 133.2, 137.1, 135.9 (aromatic). <sup>29</sup>Si NMR (49.7 MHz, CDCl<sub>3</sub>): –65.8 (Si(OH)<sub>3</sub>), 7.3 (SiMe<sub>3</sub>).

**(2-*i*-Pr-6-MeC<sub>6</sub>H<sub>3</sub>)N(SiMe<sub>3</sub>)<sub>3</sub>(Si(OH)<sub>3</sub>) (2d).** Yield: 20.9 g (70%). Mp: 85 °C. Anal. Calcd for C<sub>13</sub>H<sub>25</sub>NO<sub>3</sub>Si<sub>2</sub>: C, 52.2; H, 8.4; N, 4.7. Found: C, 51.6; H, 8.1; N, 4.8. Mass spectrum (EI, 70 eV): *m/e* 299 (M<sup>+</sup>, 40%). IR (Nujol): 3367, 1605, 1498, 1405, 1323, 1253, 1190, 1174, 1110, 1046, 973, 956, 912, 895, 837, 805, 791, 758, 692 cm<sup>-1</sup>. <sup>1</sup>H NMR (200 MHz, CDCl<sub>3</sub>): 0.03 (s, 9H, SiMe<sub>3</sub>), 1.10 (dd, 6H, Me<sub>2</sub>), 2.20 (s, 3H, Me), 3.40 (m, 1H, CH), 4.30 (s, 3H, OH), 6.90 (m, 3H, aromatic). <sup>13</sup>C NMR (62.9 MHz, CDCl<sub>3</sub>): 1.3 (SiMe<sub>3</sub>), 20.2, 24.5, 24.8 (Me), 115.5, 119.0, 124.2, 124.7, 127.7, 129.3, 137.1, 140.5, 145.7, 147.9 (aromatic). <sup>29</sup>Si NMR (49.7 MHz, CDCl<sub>3</sub>): –65.3 (Si(OH)<sub>3</sub>), 7.5 (SiMe<sub>3</sub>).

**Table 3. Atomic Coordinates (×10<sup>4</sup>) and Equivalent Isotropic Displacement Parameters (Å<sup>2</sup> × 10<sup>3</sup>) for 2c<sup>a</sup>**

	<i>x</i>	<i>y</i>	<i>z</i>	<i>U</i> (eq) <sup>a</sup>
Si(1)	4566(1)	781(1)	3361(1)	27(1)
Si(2)	4907(1)	3054(1)	3677(1)	21(1)
N(1)	4257(3)	1816(2)	2994(2)	22(1)
C(1)	3399(3)	1632(2)	2054(2)	22(1)
C(2)	4309(3)	1440(2)	1243(2)	26(1)
C(3)	3452(4)	1260(2)	350(2)	31(1)
C(4)	1743(4)	1274(2)	232(2)	33(1)
C(5)	875(3)	1454(2)	1039(2)	32(1)
C(6)	1661(3)	1622(2)	1947(2)	26(1)
C(7)	6170(3)	1412(2)	1310(2)	33(1)
C(8)	847(5)	1108(3)	–744(2)	48(1)
C(9)	624(3)	1772(2)	2783(2)	37(1)
C(10)	3484(5)	–384(2)	2414(2)	46(1)
C(11)	3692(4)	1026(3)	4541(2)	42(1)
C(12)	6803(4)	555(2)	3484(2)	37(1)
O(1)	5935(2)	3618(2)	3085(1)	28(1)
O(2)	3382(2)	3798(1)	4059(1)	28(1)
O(3)	6146(2)	2991(1)	4539(1)	29(1)
Si(1')	9870(1)	7058(1)	2875(1)	25(1)
Si(2')	9883(1)	5507(1)	3883(1)	20(1)
N(1')	9174(3)	5919(2)	2991(2)	21(1)
C(1')	7945(3)	5269(2)	2245(2)	21(1)
C(2')	8432(3)	4490(2)	1427(2)	27(1)
C(3')	7225(4)	3925(2)	693(2)	33(1)
C(4')	5551(4)	4100(2)	748(2)	32(1)
C(5')	5089(3)	4831(2)	1589(2)	31(1)
C(6')	6247(3)	5421(2)	2342(2)	26(1)
C(7')	10218(4)	4218(2)	1330(2)	39(1)
C(8')	4272(4)	3530(3)	–81(2)	45(1)
C(9')	5645(4)	6158(2)	3259(2)	38(1)
C(10')	11241(4)	7835(2)	3970(2)	44(1)
C(11')	11019(4)	6787(2)	1777(2)	41(1)
C(12')	8107(4)	7826(2)	2741(2)	38(1)
O(1')	9356(2)	6304(2)	4920(1)	26(1)
O(2')	9163(2)	4344(1)	3663(1)	25(1)
O(3')	11902(2)	5490(1)	4001(1)	23(1)

<sup>a</sup> *U*(eq) is defined as one-third of the trace of the orthogonalized *U*<sub>*ij*</sub> tensor.

**X-ray Structure Determination of 2c.** Colorless crystals of **2c** suitable for X-ray diffraction were grown from CH<sub>2</sub>Cl<sub>2</sub>/hexane solution (1:5) at room temperature by slow evaporation. A crystal of the dimensions 0.7 × 0.6 × 0.3 mm was mounted on a Siemens STOE AED2 four-circle diffractometer. The unit cell parameters were derived and refined by using 26 reflections randomly selected in the 2θ range 20–25°. The other details pertaining to data collection and refinement are listed in Table 2. The structure was solved by direct methods<sup>10a</sup> and refined by using SHELXL-93.<sup>10b</sup> Hydrogen atoms attached to oxygen atoms were located from the difference maps, and their positions were refined. The other hydrogen atoms attached to carbon atoms were refined using a riding model.<sup>10b</sup> The final fractional atomic coordinates are listed in Table 3.

**Acknowledgment.** R.M. and V.C. thank the AvH Foundation, Bonn, Germany, for research fellowships. This work was supported by the Deutsche Forschungsgemeinschaft.

**Supporting Information Available:** Tables giving complete bond distances and angles, final fractional coordinates for H atoms, and thermal parameters for **2c** (5 pages). Ordering information is given on any current masthead page.

OM950398L

(10) Sheldrick, G. M. *Acta Crystallogr., Sect. A* **1990**, *46*, 467. (b) Sheldrick, G. M. SHELXL-93, Program for Crystal Structure Refinement; University of Göttingen, Göttingen, Germany, 1993.

# Cationic Methallylnickel Complexes with Chelating Ligands: A New Dynamic Complex Isomerization Equilibrium<sup>†</sup>

Axel Ecke and Wilhelm Keim\*

*Institut für Technische Chemie und Petrolchemie, Templergraben 55,  
D-52056 Aachen, Germany*

Michel C. Bonnet and Igor Tkatchenko\*

*Institut de Recherches sur la Catalyse du CNRS, lié par Convention à l'Université Claude  
Bernard, 2, Avenue Albert Einstein, 69626 Villeurbanne Cedex, France*

Françoise Dahan

*Laboratoire de Chimie de Coordination du CNRS, 205 Route de Narbonne,  
31077 Toulouse Cedex, France*

Received April 6, 1995<sup>®</sup>

The synthesis of the cationic complexes [methyl 2-(diphenylphosphino)benzoate- $\kappa^2P,O$ ]( $\eta^3$ -methallyl)nickel(II) tetrafluoroborate (**1**), [methyl 2-(diphenylphosphino)nicotinate- $\kappa^2P,N$ ]( $\eta^3$ -methallyl)nickel(II) tetrafluoroborate (**2**), and bis[ $\mu$ -2-(diphenylphosphino)pyridine- $\kappa^2P,N$ ]bis( $\eta^3$ -methallyl)nickel(II) bis(tetrafluoroborate)·CH<sub>2</sub>Cl<sub>2</sub> (**3**) are reported. The crystal structures of **1** and **2** have been disclosed in a preliminary previous paper. The molecular structure of the cation of **2** in the crystal shows that the ligand forms a strained 4-membered ring with a  $\kappa^2P,N$  coordination. In solution a new dynamic complex isomerization was found, indicating an equilibrium between **2** and **4**, the latter with a 6-membered ring and a  $\kappa^2P,O$  coordination of the ligand methyl 2-(diphenylphosphino)nicotinate (**5**).

## Introduction

Hemilability of organometallic complexes with chelating ligands are of interest in catalytic processes.<sup>2</sup> We are studying the catalytic behavior of neutral and cationic methallylnickel complexes with chelating ligands in the ethene oligomerization.<sup>1</sup> Cationic organometallic nickel complexes with monodentate phosphines have already been thoroughly studied in the alkene oligomerization, but only very scarce results have been published for bidentate or multidentate ligands.<sup>3,4</sup> Since the knowledge about the structure of these cationic complexes in the solid state and in solution is also limited, we wanted first to investigate them in detail.

Two cationic ( $\eta^3$ -methallyl)nickel complexes have been synthesized, namely [methyl 2-(diphenylphosphino)benzoate- $\kappa^2P,O$ ]( $\eta^3$ -methallyl)nickel(II) tetrafluoroborate (**1**) and [methyl 2-(diphenylphosphino)nicotinate- $\kappa^2P,N$ ]( $\eta^3$ -methallyl)nickel(II) tetrafluoroborate (**2**), and their crystal structures have been determined, which are schematically presented in Figure 1.

<sup>†</sup> Dedicated to Prof. Dr. H.-D. Scharf on the occasion of his 65th birthday.

<sup>®</sup> Abstract published in *Advance ACS Abstracts*, October 1, 1995.

(1) (a) Bonnet, M. C.; Dahan, F.; Ecke, A.; Keim, W.; Schulz, R. P.; Tkatchenko, I. *J. Chem. Soc., Chem. Commun.* **1994**, 615. (b) Keim, W.; Schulz, R. P. *J. Mol. Catal.* **1994**, 92, 21.

(2) (a) Jeffrey, J. C.; Rauchfuss, T. B. *Inorg. Chem.* **1979**, 18, 2658. (b) Bader, A.; Lindner, E. *Coord. Chem. Rev.* **1991**, 108, 27. (c) Britovsek, G. J. P.; Keim, W.; Mecking, S.; Sainz, D.; Wagner, T. *J. Chem. Soc., Chem. Commun.* **1993**, 1632.

(3) (a) Pardy, R. B.; Tkatchenko, I. *J. Chem. Soc., Chem. Commun.* **1981**, 49. (b) Ascenso, J. R.; De C. T. Carrondo, M. A. A. F.; Dias, A. R.; Gomes, P. T.; Piedade, M. F. M.; Romão, C. C.; Revillon, A.; Tkatchenko, I. *Polyhedron* **1989**, 8, 2449. (c) Ceder, R.; Muller, G.; Sales, J.; Vidal, J.; Neibecker, D.; Tkatchenko, I. *J. Mol. Catal.* **1991**, 68, 23.

(4) Matt, D.; Huhn, M.; Fischer, J.; De Cian, A.; Kläui, W.; Tkatchenko, I.; Bonnet, M. C. *J. Chem. Soc., Dalton Trans.* **1993**, 1173.

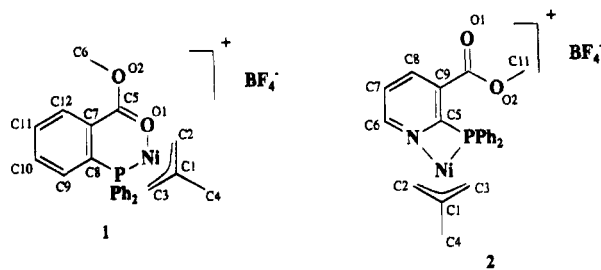


**Figure 1.** Schematic molecular structure of the cations of **1** and **2** in the solid state.

The cation moiety of **1** has a  $\kappa^2P,O$  and **2** a  $\kappa^2P,N$  coordination of the ligands. It is surprising that methyl 2-(diphenylphosphino)nicotinate (**5**) forms a strained 4-membered ring with the methallylnickel fragment and not the more common 6-membered ring like observed for methyl 2-(diphenylphosphino)benzoate (**6**) in complex **1**.

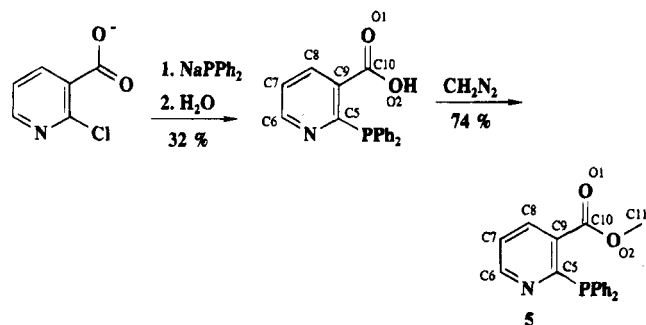
In this paper we present the details for the synthesis of **1**, **2**, and bis[ $\mu$ -2-(diphenylphosphino)pyridine- $\kappa^2P,N$ ]bis( $\eta^3$ -methallyl)nickel(II) bis(tetrafluoroborate) (**3**) and the crystal structure of **3** and discuss their structures in the solid state and in solution.

## Results and Discussion

**Synthesis of the Ligands.** The bidentate ligand methyl 2-(diphenylphosphino)benzoate (**6**) was obtained by known procedures.<sup>5</sup> By the adaptation of these methods (Scheme 1), the new 2-(diphenylphosphino)nicotinic acid was obtained with 32% and its pale yellow methyl ester **5** with 74% yield.

(5) (a) Hoots, J. E.; Rauchfuss, T. B.; Wroblewski, D. A. *Inorg. Synth.* **1982**, 21, 175. (b) Rauchfuss, T. B.; Wroblewski, D. A.; Rheingold, A. L.; Lewis, K. A. *Inorg. Chem.* **1984**, 23, 3124.

Scheme 1

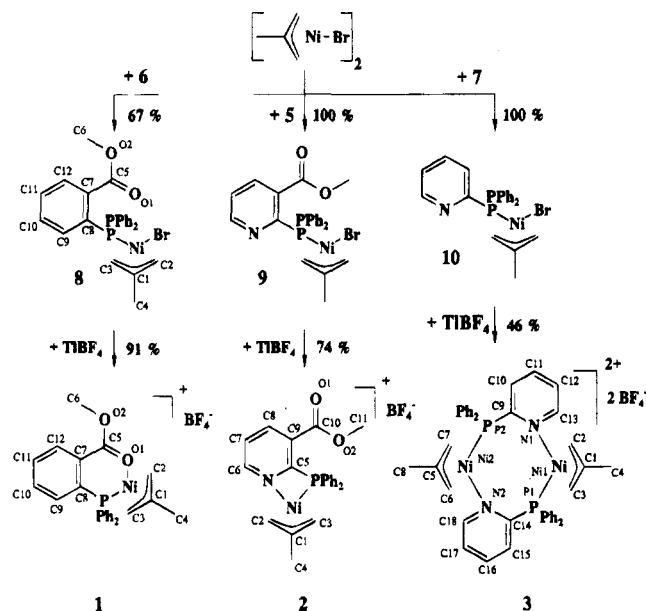


The ligand **5** offers compared to **6** three possible coordination sites: the phosphorus, the nitrogen, and the ester function can act as Lewis bases. The rigid aromatic ring makes the simultaneous coordination of all three donors in a mononuclear complex difficult.

The bidentate 2-(diphenylphosphino)pyridine (**7**) was synthesized according to the literature.<sup>6</sup>

**Synthesis of the Complexes.** Opening the dimeric structure of bis(bromomethallylnickel) in the presence of the phosphorus donor function of the ligands **6**, **5**, and **7** gives rise to the neutral precursors **8**, **9**, and **10**, which have been isolated and characterized. The bromo ligand can be abstracted by a metathetical exchange with tetrafluoroborate by adding TIBF<sub>4</sub>, and the liberated coordination site is occupied by the second donor function of the ligands, thus providing the red cationic complexes **1–3** (Scheme 2).

Scheme 2



The three structures **1–3** depicted for the cationic complexes reflect the structures present in the crystals.

**Crystal Structures.** The crystal and molecular structures of the mononuclear complexes **1** and **2** have already been published, but their syntheses are reported here.<sup>1</sup> The structure of **3** has also been determined by X-ray diffraction. Figure 2 shows a drawing of the binuclear cation. Selected bonds and angles are listed

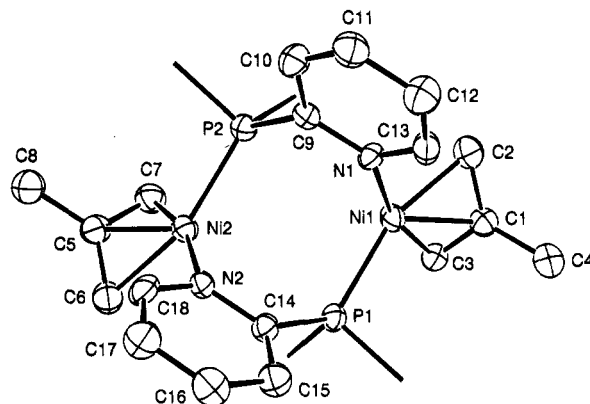


**Figure 2.** ORTEP plot of the cation of complex **3**. (The phenyl rings and hydrogen atoms have been omitted for clarity.)

**Table 1.** Selected Bond Lengths and Distances (Å) and Angles (deg) for the Cation of Complex **3**

Ni(1)–P(1)	2.201(1)	N(1)–C(9)	1.350(6)
Ni(1)–N(1)	1.953(4)	C(9)–P(2)	1.835(5)
Ni(1)–C(1)	2.022(6)	C(1)–C(2)	1.408(7)
Ni(1)–C(2)	2.064(6)	C(1)–C(3)	1.377(8)
Ni(1)–C(3)	2.028(6)	Ni(1), Ni(2)	3.932(1)
P(1)–Ni(1)–N(1)	102.2(1)	N(1)–C(9)–P(2)	117.1(4)
C(2)–Ni(1)–C(3)	70.4(2)	Ni(1)–P(1)–C(14)	120.1(1)
Ni(1)–N(1)–C(9)	123.3(3)		

in Table 1. The bond distances for **3**, as noticed for complexes **1** and **2**, are in the expected range.<sup>4,7</sup>

In complex **1** the P<sup>+</sup>O ligand **6** is  $\kappa^2P,O$  coordinated and forms a 6-membered ring. The ligand **5** offers the possibility to act as a P<sup>+</sup>O or a P<sup>+</sup>N chelating ligand in a mononuclear complex. The formation of a P<sup>+</sup>O chelated structure analog to **1** is expected to be preferred to a P<sup>+</sup>N coordination which implies a strained 4-membered ring. However the X-ray diffraction of **2** proves the formation of a 4-membered ring. The coordination of the nitrogen instead of the oxygen seems to counterbalance the ring strain. Accordingly, the ligand **7** should also form the strained 4-membered ring, but a dimeric structure was actually found, in which **7** acts as a bridging ligand. Such a bridged structure is known for homo- as well as heterobinuclear transition-metal complexes.<sup>8</sup> The chelating behavior of **7** is also known for Pt complexes.<sup>9</sup> In nickel chemistry only  $\kappa P$  coordination has been proven by X-ray diffraction.<sup>10</sup> The distance between the nickel centers Ni(1) and Ni(2) in **3** is out of the range 2.3–2.8 Å for which a Ni–Ni interaction is considered.<sup>7</sup>

To demonstrate the unusual 4-membered ring coordination for **2**, the distances between the coordinated non-carbon atoms of the ligands in the complexes and the angles in the rings are summarized in Table 2.

The angles in the 6-membered ring of **1** reflect a low ring tension. The P–Ni–O(1) angle of 92.6° nearly corresponds with the ideal value of 90° for the square-planar coordination sphere. The Ni–P–C(8) angle of 108.1° is close to the angle expected for a tetrahedron. The angles around sp<sup>2</sup> carbons C(8) and

(7) Jolly, P. W.; Wilke, G. *The Organic Chemistry of Nickel*; Academic Press: New York and London, 1974; Vols. I and II.

(8) Newkome, G. R. *Chem. Rev.* **1993**, *93*, 2067.

(9) Jain, V. K.; Jakkal, V. S.; Bohra, R. *J. Organomet. Chem.* **1990**, *389*, 417.

(10) (a) Honggen, W.; Ruji, W.; Zhongzhi, Z.; Xukun, W.; Weijun, Z.; Limei, Y. *J. Chin. Univ.* **1989**, *10*, 809. (b) Xinxin, G.; Weijun, Z.; Shuji, Z.; Yangquan, F.; Dengmin, Y.; Yangquan, L. *J. Mol. Catal. (China)* **1992**, *6*, 303.

(6) (a) Maisonnat, A.; Farr, J. P.; Balch, A. L.; Olmstead, M. M.; Hunt, C. T. *Inorg. Chem.* **1982**, *21*, 3965. (b) Zhao, W.-J.; Guan, X.-X.; Zhang, S.-J.; Fang, Y.-Q.; Wang, H.-G.; Wang, R.-J. *Acta Chim. Sinica* **1992**, *50* 300.

**Table 2. Selected Distances (Å), Angles (deg), and a Dihedral Angle (deg) in the Cationic Moieties of 1–3**

1		2		3	
P, O(1)	2.929(3)	P, N	2.482(5)	P(1), N(1)	3.236(4)
				P(1), N(2)	2.736(4)
		Distances			
		Ring Angles			
O(1)–Ni–P	92.6(1)	N–Ni–P	73.9(1)	N(1)–Ni(1)–P(1)	102.2(1)
Ni–P–C(8)	108.1(1)	Ni–P–C(5)	80.5(2)	Ni(1)–P(1)–C(14)	120.1(1)
P–C(8)–C(7)	125.5(3)	P–C(5)–N	100.2(4)	P(1)–C(14)–N(2)	115.2(4)
C(5)–C(7)–C(8)	120.0(4)	C(5)–N–Ni	105.0(3)	C(14)–N(2)–Ni(2)	124.9(3)
		Torsion Angles			
C(7)–C(8)–P–Ni	29.5(4)	P–C(5)–N–Ni	6.4(3)		
		Dihedral Angle <sup>a</sup>			
				P(1),N(1),M(12),M(13)	} 48.4(2)
				P(2),N(2),M(56),M(57)	

<sup>a</sup> Least-squares planes with M(12), M(13), M(56), and M(57) midpoints of C(1)–C(2), C(1)–C(3), C(5)–C(6), and C(5)–C(7), respectively.

C(7) have values of approximately 120°, whereas the angles in **2** and **3** exhibit neat differences. Compared to the ideal value of 90°, the P–Ni–N angle is decreased in the 4-membered ring and increased in the binuclear complex. The angles at the phosphorus and the nitrogen show similar behavior. The angle in the ligand between the phosphorus and the nitrogen is in the 4-membered ring of **2** smaller and in **3** bigger than in the noncoordinated ligand **7** with 111.9°. <sup>11</sup>

The planarity of the hetero rings containing the Ni atom of the two cations **1** and **2** can be shown *via* the torsion angles in the rings. In the 6-membered ring in **1**, the selected torsion angle C(7)–C(8)–P–Ni (29.5°) reflects the lack of planarity. For the 4-membered ring in **2**, P–C(5)–N–Ni is equal to 6.4°, which is a sufficient indication for a close to planar structure. The 8-membered hetero ring in the binuclear complex **3** is not planar which is demonstrated *via* the dihedral angle between the coordination planes P(1),N(1),M(12),M(13) and P(2),N(2),M(56),M(57) of 48.4°.

To demonstrate the influence of the different ring sizes on the coordination spheres, comparisons of the distances between the N-donor and the P-donor bonds to the nickel center in the complexes **2** and **3** are useful. The complexes both have a P,N coordination mode with the similar ligands **5** and **7**. The distances amount to 2.48 and 3.23 Å for the P–N ligand in **2** and in **3**, respectively. In comparison to the free ligand **7** with a P–N distance of 2.65 Å, <sup>11</sup> the distance is shorter in the 4-membered ring in **2** and longer in the binuclear complex **3**. In the latter the two donors do not belong to the same ligand. The difference between the N–P distances is approximately 0.8 Å for the complexes **2** and **3**.

**Structures in Solutions.** The X-ray crystal structures for **1–3** present a variety of different coordination modes for the three ligands **6**, **5**, and **7**. The three cationic complexes show the ability of nickel to form a 4-membered ring with  $\kappa^2P,N$  coordination a 6-membered ring with  $\kappa^2P,O$  coordination, and a binuclear complex with a bridging ligand in the solid state. The question arises whether these results are observable also in solution. Especially the tridentate P–O–N ligand **5** offers sites for a possible intramolecular, dynamic behavior. The complexes were studied by IR and NMR spectroscopy.

The IR spectroscopy is especially well adapted for the examination of the coordination of the ester function, since a downfield shift of the CO stretching band

**Table 3.  $\nu(\text{CO})$  ( $\text{cm}^{-1}$ ) of the Complexes **1** and **2** and the Ligands **6** and **5****

	medium		$\Delta\nu(\text{CH}_2\text{Cl}_2)^a$
	$\text{CH}_2\text{Cl}_2$	KBr	
	Ligands		
6	1717		
5	1723		
	Complexes		
1	1638		-79
2	1737, 1647	1729 <sup>b</sup>	+14, -76

<sup>a</sup> Difference of  $\nu(\text{C}=\text{O})$  between the complex and the free ligand.

<sup>b</sup> Crystals of **2** were used to prepare the KBr pellet.

indicates its coordination. The results are summarized in Table 3.

The carbonyl function of the free ligands absorbs in the expected region around 1720  $\text{cm}^{-1}$ . The cationic complex **1** shows a shift of  $\Delta\nu = -79 \text{ cm}^{-1}$  which indicates the coordination of the ester moiety of **6**. The complex **2** generates two absorption bands in solution: the first one located at 1737  $\text{cm}^{-1}$  is close to the free ligand **5** and corresponds to a noncoordinated ester function. The same result is observed in the IR spectrum of **2** crystals in KBr pellets, which show only one absorption at 1729  $\text{cm}^{-1}$ . The second band has a shift of  $-76 \text{ cm}^{-1}$ , which can be assigned, as in **1**, to the coordinated ester. These results indicate that there are two different species in solution for **2**.

<sup>31</sup>P NMR is a powerful tool to answer the question about the coordination of the phosphorus and the ring size by examining the contribution of the ring formation  $\Delta_R\delta$  to the chemical shift  $\delta$  of the phosphorus nucleus. Generally, the formation of 4- and 6-membered rings induces a highfield shift, but the 4-membered ring produces a more negative value for  $\Delta_R\delta$ . Five-membered rings are reflected in a positive  $\Delta_R\delta$ . In rings with a larger size, there is no ring contribution to the chemical shift.<sup>12</sup> There are also examples for nickel complexes.<sup>13</sup> The NMR experiments were carried out at different temperatures. The results are presented in Table 4.

The influence of the temperature on the chemical shift is low. For example a decrease of 52 K changes the chemical shifts for the compounds **5** and **9** by less than 1 ppm. The  $\kappa P$  coordination of the ligands in the neutral precursor complexes **8–10** is reflected in the  $\Delta\delta$  value of approximately 30 ppm. The complexes **1** and **3** form in solution only one species. The negative  $\Delta_R\delta$  for **1**

(12) Garrou, P. E. *Chem. Rev.* **1981**, *81*, 229.

(13) Del Zotto, A.; Mezzetti, A.; Novelli, V.; Rigo, P. *J. Chem. Soc., Dalton Trans.* **1990**, 1035.

(11) Charland, J.-P. *Acta Crystallogr.* **1989**, *C45*, 680.

**Table 4.**  $^{31}\text{P}\{^1\text{H}\}$  NMR ( $\text{CDCl}_3$ , ppm) Data for 1–10

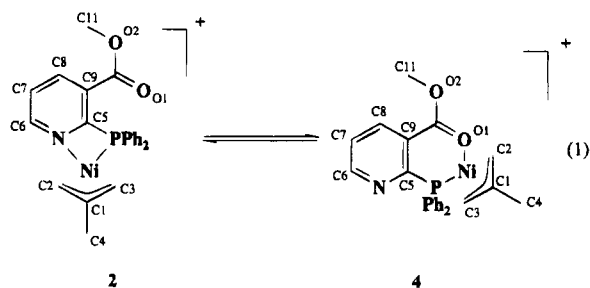
compd	$\delta$		coord effect		
	295 K	243 K	type	295 K	243 K
Ligands					
6	-4.1				
5	4.4	4.0			
7	-3.7				
Precursors					
8	29.2		$\Delta\delta^a$	33.3	
9	34.5	35.0		30.1	31.0
10	25.4			29.1	
Complexes					
1	19.7		$\Delta\text{R}\delta^b$	-9.5	
2, 4	10 (v br)	5.3 (2)		-25	-29.7 (2)
		20.5 (4) <sup>c</sup>			-14.5 (4)
3	26.0			0.4	

<sup>a</sup> Difference between free ligand and precursor. <sup>b</sup> Difference between precursor and complex, ring contribution. <sup>c</sup> Equilibrium constant  $K = (\text{integral of 4})/(\text{integral of 2}) = 0.41$ .

indicates the formation of a 6-membered ring in solution, as observed in the crystalline state. The  $\kappa^2\text{P},\text{O}$  coordination is also confirmed by the IR-spectroscopic results. The cationic complex **3** has a ring contribution value close to 0 ppm. Its  $\Delta\text{R}\delta$  is suited to the 8-membered ring of the binuclear complex. Thus, the same structures can be assumed for the crystal and the solution. It should be noticed that the  $\Delta\text{R}\delta$  values include two factors: the formation of the rings and the change of the complex charge from the neutral precursors to the cationic complexes. The latter has only a minor influence so that it can be omitted in the discussion.<sup>4</sup>

The situation for the complex **2** is more complicated, since its spectrum exhibits at room temperature a very broad signal, which indicates a fast exchange in the coordination sphere of the nickel center at the NMR time scale. The signal splits up at 243 K into two sharp peaks with  $\Delta\text{R}\delta = -29.7$  ppm and  $\Delta\text{R}\delta = -14.5$  ppm. The exchange is slowed down, and the two species can be distinguished. The negative  $\Delta\text{R}\delta$  values at low temperature mark the existence of 4- and 6-membered rings. The more negative value must be attributed to a 4-membered ring with a  $\kappa^2\text{P},\text{N}$  coordination of the ligand **5** like in the crystal **2**. The less negative  $\Delta\text{R}\delta$  value for the second peak implies that the phosphorus atom (**4**) is a member of a 6-membered ring like in **1** whereas the ligand has  $\kappa^2\text{P},\text{O}$  coordination. These two coordination modes of the ester group in **2** were confirmed by the IR spectra, in which the coordinated and the noncoordinated ester moiety could be identified at room temperature. The equilibrium constant of **2** and **4** is determined by the integration of the  $^{31}\text{P}$  NMR:  $K = (\text{integral of 4})/(\text{integral of 2}) = 0.41$ . The  $\kappa^2\text{P},\text{N}$  structure of **2**, which was isolated as crystals, dominates in solution.

The IR and  $^{31}\text{P}$  NMR spectra carried out in solution and the crystal structure of **2** are in agreement with an equilibrium for **2** in solution, as shown in eq 1.



The intramolecular substitution of the nitrogen donor by the oxygen donor and vice versa leads to a dynamic behavior. The equilibrium can also be confirmed by  $^{13}\text{C}$  NMR. At low temperature (243 K), different signals can also be identified for the carbons related to **2** and **4**.

### Concluding Remarks

The structures of three new cationic methallyl complexes in the solid state and in solution are described. Our results show that methallylnickel fragment forms with the  $\text{P}^{\text{O}}$  ligand **6** a cationic complex **1** with a 6-membered ring, in which the ligand is  $\kappa^2\text{P},\text{O}$  coordinated, in solution as well as in the crystal structure. Using the  $\text{N}^{\text{P}}\text{O}$  ligand **5**, two competitive coordination modes, a strained 4-membered ring with a  $\kappa^2\text{P},\text{N}$  coordination (**2**) and the 6-membered ring (**4**) as in **1**, are observed. A dynamic complex isomerization equilibrium between these two coordination forms exists in solution. In the crystal only 2 coordination occurs. As a chelating ligand in a monomeric complex the  $\text{P}^{\text{N}}$  ligand **7** would have the possibility to form a 4-membered-ring analogue to **2**. But in the crystal and in solution the dimeric structure **3**, in which **7** acts as a bridging ligand, is observed.

The results show that the determination of the crystal structure can give only hints to the structure of a complex in solution.

### Experimental Section

**General Comments.** All manipulations were performed under an argon atmosphere using standard Schlenk tube techniques, if not otherwise indicated. Reagents and solvents were purified, dried, and handled under argon with standard laboratory methods. Methyl 2-(diphenylphosphino)benzoate (**6**) was prepared according to the literature procedure.<sup>4</sup> NMR spectra were performed on a Bruker AM250 spectrometer at temperatures listed. The chemical shifts  $\delta$  are given in ppm, and the coupling constants  $J$ , in Hz. The numbers appearing in Figure 1, Schemes 1 and 2, and eq 1 for the carbon atoms in the ligands and complexes give convenient help to identify the atoms in the NMR spectra.

**2-(Diphenylphosphino)nicotinic Acid.** A 4.41 g (192 mmol) amount of sodium was dissolved in approximately 430  $\text{cm}^3$  of liquid ammonia. A 25.22 g (96 mmol) amount of triphenylphosphine was slowly added, and the mixture was stirred for 2.5 h at  $-40$   $^\circ\text{C}$ . The resulting orange solution was cooled down to  $-78$   $^\circ\text{C}$ , and 15.13 g (96 mmol) of 2-chloronicotinic acid was added. After the addition of 150  $\text{cm}^3$  of THF *via* a syringe, the reaction mixture was slowly warmed to room temperature overnight. The yellow suspension was dissolved in 400  $\text{cm}^3$  water and worked up under air by extraction with 115  $\text{cm}^3$  of  $\text{Et}_2\text{O}$ . The aqueous phase was acidified to pH 4 with concentrated HCl and extracted with three 60- $\text{cm}^3$  portions of  $\text{CH}_2\text{Cl}_2$ . The organic phase was dried over  $\text{CaSO}_4$  and evaporated, and the resulting solid was recrystallized twice from hot MeOH under an argon atmosphere. A 9.53 g (31 mmol, yield 32%) amount of the pale yellow product were isolated. Solvent traces could not be removed by recrystallization from chloroform. Anal. Calcd for  $\text{C}_{16}\text{H}_{14}\text{NO}_2 + \text{CH}_2\text{Cl}_2$ : C, 63.17; H, 4.46; N, 3.88. Found: C, 65.65; H, 4.64; N, 4.04. Melting point: 165  $^\circ\text{C}$ . IR (Nujol):  $\nu(\text{C}=\text{O})$  1699  $\text{cm}^{-1}$ .  $^1\text{H}$  NMR (250 MHz,  $[\text{D}_6]\text{acetone}$ ):  $\delta = 8.63$  {d ( $^3J(\text{H},\text{H}) = 4.8$ ), d ( $^4J(\text{H},\text{H}) = 1.8$ ), 1H,  $\text{H}^{\text{C}6}$ }, 8.29 {d ( $^3J(\text{H},\text{H}) = 7.9$ ), d ( $^4J(\text{H},\text{H}) = 1.8$ ), d ( $^4J(\text{H},\text{P}) = 4.3$ ), 1H,  $\text{H}^{\text{C}8}$ }, 7.40 {d ( $^3J(\text{H},\text{H}) = 7.9$ ), d ( $^3J(\text{H},\text{H}) = 4.8$ ), 1H,  $\text{H}^{\text{C}7}$ }, 7.4–7.2 {m, 10H,  $\text{H}^{\text{arom}}$ }.  $^{31}\text{P}\{^1\text{H}\}$  NMR (81 MHz,  $\text{CDCl}_3$ ):  $\delta = 4.5$ .  $^{13}\text{C}$  NMR (63 MHz,  $[\text{D}_6]\text{acetone}$ ):  $\delta = 166.6$  {s, C10}; 165.0 {d ( $^1J(\text{C},\text{P}) = 20$ ), C5}; 152.1 {d ( $^1J(\text{C},\text{H}) = 181$ ), C6}; 139–128 {m,  $\text{C}^{\text{arom}}$ }; 122.3 {d ( $^1J(\text{C},\text{H}) = 167$ ), C7}.

**Methyl 2-(diphenylphosphino)nicotinate (5).** At 0 °C under air, a 50-cm<sup>3</sup> of Et<sub>2</sub>O solution of approximately 16.6 mmol of diazomethane<sup>14</sup> was slowly added to a stirred suspension of 4.58 g (14.9 mmol) of 2-(diphenylphosphino)nicotinic acid in 300 cm<sup>3</sup> of Et<sub>2</sub>O. The precipitated product was dissolved by adding MeOH to the reaction mixture at room temperature. After addition of a small amount of acetic acid, the solvents were evaporated till the first crystals were formed. The solid was redissolved by heating to reflux under argon. A 3.52 g (11.0 mmol; yield 74%) amount of the pale yellow product was isolated by cooling to 4 °C. Anal. Calcd for C<sub>19</sub>H<sub>16</sub>NO<sub>2</sub>: C, 71.02; H, 5.02; N, 4.36. Found: C, 70.59; H, 5.20; N, 4.13. Melting point: 94 °C. IR (Nujol):  $\nu(\text{C}=\text{O})$  1717 cm<sup>-1</sup>. IR (CH<sub>2</sub>Cl<sub>2</sub>):  $\nu(\text{C}=\text{O})$  1723 cm<sup>-1</sup>. <sup>1</sup>H NMR (200 MHz, CDCl<sub>3</sub>):  $\delta$  = 8.69 {d (<sup>3</sup>J(H,H) = 4.7), d (<sup>4</sup>J(H,H) = 1.8), 1H, H<sup>C6</sup>}, 8.16 {d (<sup>4</sup>J(H,H) = 1.8), d (<sup>4</sup>J(H,P) = 4.2), d (<sup>3</sup>J(H,H) = 7.8), 1H, H<sup>C8</sup>}, 7.8–7.2 {m, 11H, H<sup>arom</sup>}, 3.69 {s, 3H, H<sup>C11</sup>} ppm. <sup>31</sup>P{<sup>1</sup>H} NMR (81 MHz, CDCl<sub>3</sub>):  $\delta$  = 4.4 ppm. <sup>31</sup>P{<sup>1</sup>H} NMR (101 MHz, CDCl<sub>3</sub>, T = 243 K):  $\delta$  = 4.0 ppm. <sup>13</sup>C NMR (63 MHz, CDCl<sub>3</sub>):  $\delta$  = 166.5 {s, C10}, 164.6 {d (<sup>1</sup>J(C,P) = 19), m, C5}, 152.0 {d (<sup>1</sup>J(C,H) = 178), m, C6}, 137–127 {m, C<sup>arom</sup>}, 121.5 {d (<sup>1</sup>J(C,H) = 166), m, C7}, 52.0 {q (<sup>1</sup>J(C,H) = 147), C11}.

**Bromo[methyl 2-(diphenylphosphino)benzoate- $\kappa$ P]( $\eta^3$ -methallyl)nickel(II) (8).** To a solution of 1.12 g (2.89 mmol) of bis[bromo( $\eta^3$ -methallyl)nickel] in 5 cm<sup>3</sup> of THF, 1.83 g (5.71 mmol) of **6** in 9 cm<sup>3</sup> of THF was slowly added at approximately -20 °C. The solution was warmed overnight to room temperature. The red precipitate was filtered out, washed with small amounts of THF, and dried under vacuum. A 1.96 g (3.81 mmol; yield 67%) amount of **8** was isolated. IR (Nujol):  $\nu(\text{C}=\text{O})$  = 1710 cm<sup>-1</sup>. <sup>1</sup>H NMR (200 MHz, CDCl<sub>3</sub>):  $\delta$  = 8.15 {m, 1H, H<sup>C12</sup>}, 7.7–6.9 {m, 14H, H<sup>arom</sup>}, 3.90 {s, 3H, H<sup>C6</sup>}, 3.26 {s, 2H, H<sup>C2+3, syn</sup>}, 2.42 {s, 2H, H<sup>C2+3, anti</sup>}, 1.99 {s, 3H, H<sup>C4</sup>} ppm. <sup>31</sup>P{<sup>1</sup>H} NMR (81 MHz, CDCl<sub>3</sub>):  $\delta$  = 29.2. <sup>13</sup>C NMR (50 MHz, [D<sub>2</sub>]THF):  $\delta$  = 167.7 {s, C5}, 136–128 {m, C<sup>arom</sup>}, 121.3 {s, C1}, 52.4 {q (<sup>1</sup>J(C,H) = 147), C6}, 22.6 {q (<sup>1</sup>J(C,H) = 128), C4}.

**Bromo[methyl 2-(diphenylphosphino)nicotinate- $\kappa$ P]( $\eta^3$ -methallyl)nickel(II) (9).** To a solution of 0.63 g (1.63 mmol) of bis[bromo( $\eta^3$ -methallyl)nickel] in 5 cm<sup>3</sup> of THF, 1.05 g (3.27 mmol) of **5** in 5 cm<sup>3</sup> of THF was slowly added at approximately -35 °C. The solution was warmed overnight to room temperature, and the solvent was evaporated under vacuum. A 1.68 g (3.27 mmol; yield 100%) amount of the red crude product was isolated. IR (CH<sub>2</sub>Cl<sub>2</sub>):  $\nu(\text{C}=\text{O})$  1713 cm<sup>-1</sup>. <sup>31</sup>P{<sup>1</sup>H} NMR (32 MHz, CDCl<sub>3</sub>):  $\delta$  = 34.5. <sup>31</sup>P{<sup>1</sup>H} NMR (101 MHz, CDCl<sub>3</sub>, T = 243 K):  $\delta$  = 35.0.

**Bromo[2-(diphenylphosphino)pyridine- $\kappa$ P]methallyl nickel(II) (10).** To a solution of 2.21 g (5.70 mmol) of bis[bromo( $\eta^3$ -methallyl)nickel] in 15 cm<sup>3</sup> of THF, 3.01 g (11.43 mmol) of **5** in 14 cm<sup>3</sup> of THF was slowly added at approximately -25 °C. The solution was warmed overnight to room temperature and the solvent was evaporated under vacuum. A 5.22 g (11.40 mmol; yield 100%) amount of the red crude product was isolated. <sup>31</sup>P{<sup>1</sup>H} NMR (101 MHz, CDCl<sub>3</sub>):  $\delta$  = 25.4.

**[Methyl 2-(diphenylphosphino)benzoate- $\kappa^2$ P,O]( $\eta^3$ -methallyl)nickel(II) Tetrafluoroborate (1).** To a solution of 1.16 g (2.26 mmol) of **8** in 30 cm<sup>3</sup> of THF, 0.66 g (2.27 mmol) of TlBF<sub>4</sub> was added at 0 °C and stirred for 2 h. The suspension was reduced to a solid, which was dissolved in a small amount of CH<sub>2</sub>Cl<sub>2</sub> and filtrated over Celite to remove the thallium bromide formed. By careful addition of 20 cm<sup>3</sup> of Et<sub>2</sub>O on the red solution (approximately 5 cm<sup>3</sup>) red crystals were grown at 4 °C overnight. By cooling down of the sample to -20 °C for 1 h, the crystallization was completed. The solution was removed, and the crystals were washed with Et<sub>2</sub>O. After drying under vacuum, 1.10 g (2.11 mmol, yield = 93%) of **1** was obtained. Anal. Calcd for C<sub>24</sub>H<sub>24</sub>BF<sub>4</sub>NiO<sub>2</sub>P: C, 55.34; H, 4.64. Found: C, 54.49; H, 4.55. IR (Nujol):  $\nu(\text{C}=\text{O})$  1635 cm<sup>-1</sup>. IR (CH<sub>2</sub>Cl<sub>2</sub>): 1638 cm<sup>-1</sup>. <sup>1</sup>H NMR (250 MHz, CDCl<sub>3</sub>, T = 213

**Table 5. Crystal Data and Experimental Details for Compound 3**

formula	C <sub>43</sub> H <sub>44</sub> B <sub>2</sub> Cl <sub>2</sub> F <sub>8</sub> N <sub>2</sub> Ni <sub>2</sub> P <sub>2</sub>
mol wt	1012.7
color and habit	orange, parallelepiped
cryst size, mm	0.40 × 0.30 × 0.15
cryst syst	monoclinic
space group	P2 <sub>1</sub> /c (No. 14)
a, Å	13.880(1)
b, Å	18.457(2)
c, Å	17.986(2)
$\beta$ , deg	103.86(1)
V, Å <sup>3</sup>	4473.6(9)
Z	4
D(calcd), g cm <sup>-3</sup>	1.504
diffractometer	Enraf-Nonius CAD4
$\Lambda$ (Mo K $\alpha$ ), Å	0.710 73
$\mu$ , mm <sup>-1</sup>	1.10
transm factor, max-min	1.000–0.967
temp, K	295
no. of colld data	7849, all unique
no. of obsd. data	3919 (I > 3 $\sigma$ (I))
no. of params refined	406
R, R <sub>w</sub> <sup>a</sup>	0.036, 0.038

$$^a R = \sum |F_o| - |F_c| / \sum |F_o|; R_w = [\sum w(|F_o| - |F_c|)^2 / \sum w |F_o|^2]^{1/2}.$$

K):  $\delta$  = 8.36 {s (br), 1H, H<sup>C12</sup>}, 7.7–7.1 {m(br), 13H, H<sup>arom</sup>}, 4.33 {s (br), 1H, H<sup>allyl</sup>}, 4.02 {s (br), 3H, H<sup>C6</sup>}, 3.70 {s (br), 1H, H<sup>allyl</sup>}, 2.36 {s (br), 1H, H<sup>allyl</sup>}, 2.23 {s (br), 3H, H<sup>C4</sup>}, 2.08 {s (br), 1H, H<sup>allyl</sup>}. <sup>31</sup>P{<sup>1</sup>H} NMR (36 MHz, CDCl<sub>3</sub>):  $\delta$  = 19.7. <sup>13</sup>C NMR (63 MHz, CDCl<sub>3</sub>, T = 213 K):  $\delta$  = 171.1 {d (<sup>3</sup>J(C,P) = 4), C5}, 135–126 {m, C<sup>arom</sup> + C1}, 78.1 {tr (<sup>1</sup>J(C,H) = 160), d (<sup>2</sup>J(C,P) = 19), C2}, 56.1 {q (<sup>1</sup>J(C,H) = 150), C6}, 48.5 {tr (<sup>1</sup>J(C,H) = 161), C3}, 23.5 {q (<sup>1</sup>J(C,H) = 127), C4}. Molar conductivity:  $\Lambda_m^0$  = 61 S·cm<sup>2</sup>·mol<sup>-1</sup>.

**[Methyl 2-(diphenylphosphino)nicotinate- $\kappa^2$ P,N]( $\eta^3$ -methallyl)nickel(II) Tetrafluoroborate (2) and [Methyl 2-(diphenylphosphino)nicotinate- $\kappa^2$ P,O]( $\eta^3$ -methallyl)nickel(II) Tetrafluoroborate (4).** In a solvent mixture of 45 cm<sup>3</sup> of THF and 30 cm<sup>3</sup> of CH<sub>2</sub>Cl<sub>2</sub>, 1.59 g (3.09 mmol) of **9** was kept in suspension and 0.92 g (3.16 mmol) of TlBF<sub>4</sub> added at 0 °C. The solution was warmed overnight to room temperature and the solvent evaporated under vacuum. The solid was extracted with small amounts of CH<sub>2</sub>Cl<sub>2</sub> and the resulting suspension filtered over Celite. By careful addition of 50 cm<sup>3</sup> of Et<sub>2</sub>O on the red solution (approximately 10 cm<sup>3</sup>), a red solid precipitated. The solution was removed and the solid washed 4 times with 2 cm<sup>3</sup> of Et<sub>2</sub>O. After drying under vacuum, 1.22 g (2.34 mmol, yield = 76%) of **2** was obtained. Anal. Calcd for C<sub>24</sub>H<sub>24</sub>BF<sub>4</sub>NiO<sub>2</sub>P: C, 52.93; H, 4.44; N, 2.68. Found: C, 52.28; H, 4.42; N, 2.54. IR (Nujol):  $\nu(\text{C}=\text{O})$  1731 cm<sup>-1</sup>. IR (KBr, crystals of **2**): 1729 cm<sup>-1</sup>. IR (CH<sub>2</sub>Cl<sub>2</sub>): 1737 + 1647 cm<sup>-1</sup>. <sup>1</sup>H NMR (250 MHz, CDCl<sub>3</sub>, T = 243 K):  $\delta$  = 8.88 {s, 1H, H<sup>C6</sup>}, 8.62 {d, 1H, H<sup>C7</sup>}, 8.0–7.5 {m, 11H, H<sup>arom</sup>}, 4.50 {s (br), H<sup>allyl</sup>}, 4.10 {s (br), H<sup>allyl</sup>}, 3.68 {s (br), H<sup>allyl</sup>}, 3.19 {s (br), H<sup>allyl</sup>}, 2.17 {s (br), H<sup>C4</sup>}. <sup>31</sup>P{<sup>1</sup>H} NMR (101 MHz, CDCl<sub>3</sub>):  $\delta$  = 10 {s (v br)}. <sup>31</sup>P{<sup>1</sup>H} NMR (101 MHz, CDCl<sub>3</sub>; T = 243 K):  $\delta$  = 20.5 (s, **4**, integration 41%); 5.3 {s, **2**, integration 100%}. In the following <sup>13</sup>C NMR the proposed assignments are marked with an asterisk. <sup>13</sup>C{<sup>1</sup>H} NMR (63 MHz, CDCl<sub>3</sub>):  $\delta$  = 155.8 {s, C6}, 141.1\* {s, C7}, 134–129 {m, C<sup>arom</sup> + C1}, 69 {s (v br), C2}, 53.7 {s (br), C11}, 51 {s (v br), C3}, 23.4 {s, C4}. <sup>13</sup>C NMR (63 MHz, CDCl<sub>3</sub>, T = 243 K):  $\delta$  = 171.4 {s, C10, **4**}, 166.6\* {d (<sup>1</sup>J(C,P) = 39), C5}, 161.7\* {s, C10, **2**}, 156.4 {d (<sup>1</sup>J(C,H) = 202), d (<sup>3</sup>J(C,P) = 19), C6, **2**}, 154.3 {d (<sup>1</sup>J(C,H) = 187), C6, **4**}, 142.9\* {d (<sup>1</sup>J(C,H) = 173), C8, **2**}, 141.4\* {d (<sup>1</sup>J(C,H) = 173), C8, **4**}, 134–122 {m, C<sup>arom</sup> + C1}, 78.9 {tr (<sup>1</sup>J(C,H) = 151), C2, **4**}, 68.4 {tr (<sup>1</sup>J(C,H) = 163), d (<sup>2</sup>J(C,P) = 17), C2, **2**}, 56.2\* {q (<sup>1</sup>J(C,H) = 148), C11, **4**}, 53.1\* {q (<sup>1</sup>J(C,H) = 148), C11, **2**}, 51.5\* {tr (<sup>1</sup>J(C,H) = 163), C3, **2**}, 48.1\* {tr (<sup>1</sup>J(C,H) = 154), C3, **4**}, 23.7 {q (<sup>1</sup>J(C,H) = 132), C4}. Molar conductivity:  $\Lambda_m^0$  = 50 S·cm<sup>2</sup>·mol<sup>-1</sup>.

**[Bis[ $\mu$ -2-(diphenylphosphino)pyridine- $\kappa^2$ P,N]bis( $\eta^3$ -methallyl)nickel(II)] Bis(tetrafluoroborate) (3).** To a solution of 4.20 g (9.19 mmol) of **10** in THF/CH<sub>2</sub>Cl<sub>2</sub> (120 cm<sup>3</sup>/

(14) Technical Information Bulletin; Aldrich: Milwaukee, WI, 1982; No. AL-121.

**Table 6. Fractional Atomic Coordinates and Isotropic or Equivalent Isotropic Temperature Factors ( $10^2 \text{ \AA}^2$ )<sup>a</sup> for Compound 3**

atom	<i>x/a</i>	<i>y/b</i>	<i>z/c</i>	<i>U</i> <sub>eq</sub> / <i>U</i> <sub>iso</sub>	atom	<i>x/a</i>	<i>y/b</i>	<i>z/c</i>	<i>U</i> <sub>eq</sub> / <i>U</i> <sub>iso</sub>
Ni(1)	0.19958(4)	0.61029(4)	0.28395(4)	3.76(4)	C(26)	-0.0459(3)	0.5144(2)	0.2399(2)	4.8(1)*
Ni(2)	0.17591(5)	0.39807(4)	0.28581(4)	3.82(4)	C(27)	-0.1395(3)	0.4847(2)	0.2352(2)	5.7(2)*
C(1)	0.1560(4)	0.7129(3)	0.2979(3)	4.4(3)	C(28)	-0.1849(3)	0.4426(2)	0.1722(2)	5.8(2)*
C(2)	0.2367(4)	0.6958(3)	0.3593(3)	5.2(4)	C(29)	-0.1366(3)	0.4302(2)	0.1137(2)	5.4(2)*
C(3)	0.0757(4)	0.6670(3)	0.2876(3)	4.4(3)	C(30)	-0.0430(3)	0.4599(2)	0.1183(2)	5.3(2)*
C(4)	0.1633(4)	0.7703(3)	0.2370(3)	5.6(4)	C(31)	0.2557(2)	0.5186(2)	0.4391(2)	3.8(1)*
C(5)	0.1187(4)	0.3049(3)	0.3176(3)	4.9(4)	C(32)	0.1569(2)	0.5236(2)	0.4435(2)	5.1(2)*
C(6)	0.0758(4)	0.3170(3)	0.2402(3)	5.2(4)	C(33)	0.1319(2)	0.5650(2)	0.5010(2)	5.3(2)*
C(7)	0.1098(5)	0.3607(3)	0.3673(4)	5.3(4)	C(34)	0.2058(2)	0.6014(2)	0.5542(2)	5.5(2)*
C(8)	0.1886(5)	0.2404(3)	0.3434(4)	5.8(4)	C(35)	0.3046(2)	0.5963(2)	0.5499(2)	5.5(2)*
P(1)	0.12084(9)	0.54618(7)	0.18474(8)	3.55(7)	C(36)	0.3295(2)	0.5549(2)	0.4923(2)	4.7(1)*
P(2)	0.2884(1)	0.45984(7)	0.36795(8)	3.59(7)	C(37)	0.3663(3)	0.3883(2)	0.4196(2)	3.7(1)*
N(1)	0.3370(3)	0.5794(2)	0.2954(2)	3.3(2)	C(38)	0.3708(3)	0.3747(2)	0.4966(2)	5.4(2)*
C(9)	0.3741(4)	0.5175(3)	0.3310(3)	3.4(3)	C(39)	0.4242(3)	0.3153(2)	0.5330(2)	5.4(2)*
C(10)	0.4747(4)	0.5029(3)	0.3408(3)	4.4(3)	C(40)	0.4731(3)	0.2696(2)	0.4924(2)	6.0(2)*
C(11)	0.5354(4)	0.5490(3)	0.3131(3)	4.8(3)	C(41)	0.4686(3)	0.2832(2)	0.4153(2)	5.8(2)*
C(12)	0.4961(4)	0.6116(3)	0.2779(3)	5.4(4)	C(42)	0.4152(3)	0.3425(2)	0.3789(2)	4.9(1)*
C(13)	0.3967(4)	0.6245(3)	0.2704(3)	4.2(3)	B(1)	0.4514(2)	0.6652(2)	0.7849(2)	9.5(8)
N(2)	0.2136(3)	0.4148(2)	0.1906(2)	3.3(2)	F(1)	0.4088(3)	0.6675(2)	0.8461(2)	11.4(4)
C(14)	0.1875(4)	0.4742(3)	0.1449(3)	3.5(3)	F(2)	0.5018(3)	0.6013(2)	0.7857(3)	13.2(5)
C(15)	0.2083(4)	0.4793(3)	0.0744(3)	4.6(3)	F(3)	0.5162(3)	0.7220(2)	0.7893(3)	15.1(6)
C(16)	0.2576(4)	0.4212(3)	0.0501(4)	5.4(4)	F(4)	0.3790(3)	0.6702(3)	0.7183(2)	13.2(5)
C(17)	0.2844(4)	0.3627(3)	0.0944(3)	5.3(4)	B(2)	0.1842(2)	0.1482(2)	0.1230(2)	8.6(7)
C(18)	0.2607(4)	0.3618(3)	0.1641(3)	4.2(3)	F(5)	0.2270(3)	0.0820(2)	0.1181(3)	14.7(5)
C(19)	0.0968(2)	0.6128(2)	0.1079(2)	4.5(1)*	F(6)	0.1730(3)	0.1842(2)	0.0549(2)	12.7(4)
C(20)	0.0006(2)	0.6327(2)	0.0699(2)	4.7(1)*	F(7)	0.0932(3)	0.1387(3)	0.1387(3)	15.6(5)
C(21)	-0.0144(2)	0.6893(2)	0.0170(2)	5.6(2)*	F(8)	0.2438(4)	0.1879(3)	0.1804(2)	15.9(6)
C(22)	0.0668(2)	0.7261(2)	0.0021(2)	5.9(2)*	C(43)	0.5135(7)	0.9713(5)	0.6040(6)	12.2(8)
C(23)	0.1630(2)	0.7062(2)	0.0402(2)	5.6(2)*	Cl(1)	0.6254(2)	0.9182(2)	0.6311(2)	12.3(2)
C(24)	0.1779(2)	0.6496(2)	0.0931(2)	5.4(2)*	Cl(2)	0.4185(2)	0.9177(1)	0.5489(2)	11.7(2)
C(25)	0.0024(3)	0.5020(2)	0.1814(2)	4.1(1)*					

<sup>a</sup>  $U_{eq} = 1/3[U_{11} + U_{22} + U_{33}]$ ; an asterisk denote an isotropic *U*.

40 cm<sup>3</sup> 2.90 g (9.96 mmol) of TlBF<sub>4</sub> was added at 0 °C. The solution was warmed overnight to room temperature and the solvent evaporated under vacuum. The solid was extracted with small amounts of CH<sub>2</sub>Cl<sub>2</sub> and the obtained suspension filtered over Celite. By careful addition of 75 cm<sup>3</sup> of Et<sub>2</sub>O on the red solution (approximately 15 cm<sup>3</sup>), red crystals precipitated. The solution was removed and the solid washed with Et<sub>2</sub>O. After drying under vacuum 1.94 g (2.09 mmol; yield = 45%) of **3** was obtained. Anal. Calcd for C<sub>42</sub>H<sub>49</sub>B<sub>2</sub>F<sub>8</sub>N<sub>2</sub>Ni<sub>2</sub>P<sub>2</sub> + CH<sub>2</sub>Cl<sub>2</sub>: C, 51.00; H, 4.38; N, 2.77. Found: C, 52.25; H, 4.37; N, 2.63. <sup>1</sup>H NMR (250 MHz, CD<sub>2</sub>Cl<sub>2</sub>): δ = 9.20 {d (<sup>3</sup>J(H,H) = 4.8), 2H, H<sup>C13+C18</sup>}, 7.9–7.3 {m, 26H, H<sup>arom</sup>}, 3.40 {s, 2H, H<sup>allyl</sup>}, 2.80 {d (<sup>3</sup>J(H,P) = 4.7), 2H, H<sup>allyl</sup>}, 2.40 {s, 2H, H<sup>allyl</sup>}, 1.41 {s, 6H, H<sup>C4+C8</sup>}, 1.17 {d (<sup>2</sup>J(H,P) = 7.0), 2H, H<sup>allyl</sup>}. <sup>31</sup>P{<sup>1</sup>H} NMR (81 MHz, CDCl<sub>3</sub>): δ = 26.0. <sup>31</sup>P{<sup>1</sup>H} NMR (101 MHz, CD<sub>2</sub>Cl<sub>2</sub>): δ = 26.1. <sup>13</sup>C NMR (63 MHz, CDCl<sub>3</sub>, T = 213 K): δ = 158.3 {d (<sup>1</sup>J(C,P) = 52), C9 + C14}, 154.6 {d (<sup>1</sup>J(C,H) = 184), C13 + C18}, 139–125 {m, C<sup>arom</sup> + C1 + C5}, 78.7 {tr (<sup>1</sup>J(C,H) = 155), C2 + C6}, 56.3 {tr (<sup>1</sup>J(C,H) = 158), C3 + C7}, 22.2 {q (<sup>1</sup>J(C,H) = 130), C4 + C8}. Molar conductivity (CH<sub>2</sub>Cl<sub>2</sub>): Λ<sub>m</sub><sup>0</sup> = 39 S·cm<sup>2</sup>·mol<sup>-1</sup>.

**X-ray Structure Determination for 3. Data Collection and Processing.** Crystal data are gathered in Table 5. Diffraction measurements were made on an Enraf-Nonius CAD4 diffractometer, with graphite-monochromated Mo Kα radiation (λ = 0.710 73 Å). The unit-cell parameters were obtained from a least-squares fit of 25 reflections (with θ between 11.0 and 16.0°). Data were collected with the ω–2θ scan technique (scan width (0.80 + 0.35 tan θ)°, 2θ max = 50°, +h, +k, ±l) and a variable scan rate with a maximum scan time of 60 s per reflection. Three reflections measured every 2 h showed a slight linear decay of standard intensity (–4.1%). Corrections for the Lorentz and the polarization effects and the decay were applied using the MolEN package.<sup>15</sup> Empirical absorption corrections<sup>16</sup> from ψ scans were applied. The 7849 collected reflections were unique.

(15) Fair, C. K. MolEN. Structure Solution Procedures, Enraf-Nonius, Delft, Holland, 1990.

(16) North, A. C. T.; Philips, D. C.; Mathews, F. S. *Acta Crystallogr., Sect. A* **1968**, *A21*, 351.

**Structure Solution and Refinement.** The structure was solved by direct methods (SHELXS-86<sup>17</sup>) and refined by full-matrix least squares (SHELX-76<sup>18</sup>). A solvent molecule (i.e. dichloromethane) was found. The non-hydrogen atoms were refined anisotropically, except those of phenyl rings which were refined as isotropic rigid groups. The hydrogen atoms were included in calculated positions, riding on the atom to which they are bonded, except the methylenic hydrogens were allowed to vary. H isotropic thermal parameters, first refined, were then kept fixed. The final refinement cycle was based on 3919 observed reflections ( $F_o^2 > 3\sigma(F_o^2)$ ) and 406 variable parameters and converged to  $R = 0.036$  and  $R_w = 0.038$  with unit weights and goodness of fit 1.336 (largest shift-to-error ratio 0.003). The final Fourier difference map was featureless.

Neutral atom scattering factors, including anomalous dispersion effects, were taken from the standard compilation.<sup>19</sup> All calculations were performed on a MicroVax 3400 computer. Atomic coordinates are listed in Table 6.

**Acknowledgment.** A.E. thanks the DAAD (“Deutscher Akademischer Austauschdienst”) for the financial support of the research at the Laboratoire de Chimie de Coordination, Centre National de la Recherche Scientifique, of Toulouse, France.

**Supporting Information Available:** Tables of hydrogen coordinates and *U* values, anisotropic thermal parameters, complete bond lengths and angles, least-squares planes equations and deviations therefrom, and dihedral and torsion angles and a figure showing the molecule with phenyl rings (7 pages). Ordering information is given on any current masthead page.

OM9502471

(17) Sheldrick, G. M. *SHELXS-86. Program for Crystal Structure Solution*; Univ. of Göttingen: Göttingen, FRG, 1986.

(18) Sheldrick, G. M. *SHELX-76. Program for Crystal Structure Determination*; Univ. of Cambridge: Cambridge, England, 1976.

(19) *International Tables for X-Ray Crystallography*; The Kynoch Press: Birmingham, England, 1974; Vol. IV.



# Si<sub>2</sub>H<sub>2</sub> and CSiH<sub>2</sub> Isomers as Ligands in High-Valent Transition Metal Complexes<sup>1</sup>

Ralf Stegmann and Gernot Frenking\*

Fachbereich Chemie, Philipps-Universität Marburg, Hans-Meerwein-Strasse,  
D-35032 Marburg, Germany

Received April 14, 1995<sup>®</sup>

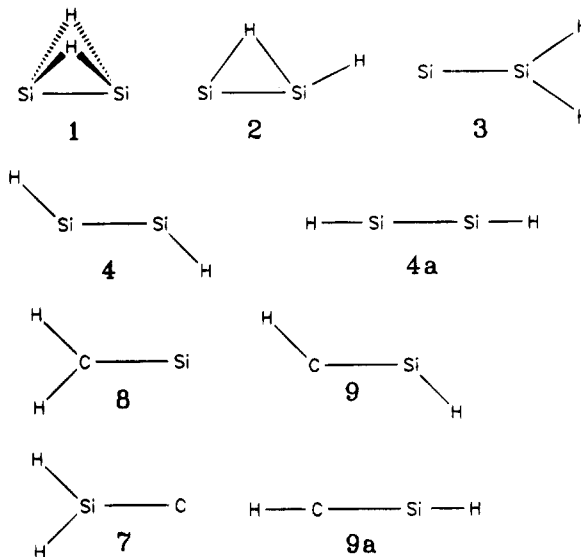
Quantum mechanical ab initio calculations using relativistic effective core potentials for tungsten are reported for isomers of WF<sub>4</sub>(Si<sub>2</sub>H<sub>2</sub>) and WF<sub>4</sub>(CSiH<sub>2</sub>). The geometries are optimized at the Hartree-Fock level, and the metal–ligand bond energies are calculated at MP2 and CCSD(T) using valence basis sets of DZP quality. Four energy minimum structures are predicted for WF<sub>4</sub>(Si<sub>2</sub>H<sub>2</sub>). The energetically lowest lying isomer is the disilaacetylene complex **C4**. Structure **C4** is 10.1 kcal/mol lower in energy than **C1a**, which has the most stable doubly bridged Si<sub>2</sub>H<sub>2</sub> form as a side-on bonded ligand. Two other isomeric forms **C1b** and **C2** are clearly higher in energy. Three energy minimum structures are predicted for the WF<sub>4</sub>(CSiH<sub>2</sub>) complex. The global energy minimum is the silavinylidene complex **C7**, which has a very short and strong W–C double bond. The silaacetylene complex **C9** is 9.9 kcal/mol higher in energy. The third isomer is the silylidene complex **C8**, which is 33.2 kcal/mol less stable than **C7**. The electronic structure of the complexes is analyzed using the NBO partitioning scheme and the topological analysis of the electron density distribution. The results show that the polarization of the W–Si bonds can be quite different among different molecules and that it is very different from related complexes with W–C bonds. The W–Si bonds are more polarized toward the tungsten atom.

## Introduction

The stunning results of theoretical<sup>2</sup> and experimental<sup>3</sup> research of the silicon analogues of acetylene have demonstrated that standard models of chemical structures are not good guidelines for predicting the most stable isomers of Si<sub>2</sub>H<sub>2</sub> and CSiH<sub>2</sub> compounds.<sup>4</sup> At the same time the power of modern quantum mechanical ab initio methods was once more documented by the correct prediction<sup>2a</sup> of the structures of the Si<sub>2</sub>H<sub>2</sub> global energy minimum form **1** and the next higher-lying isomer **2**, which was later confirmed by experimental studies.<sup>3</sup> The calculated geometries of **1** and **2** (Chart 1) are in excellent agreement with experimental results.<sup>2a,3</sup> Two other low-lying singlet isomers of Si<sub>2</sub>H<sub>2</sub> (**3** and **4**), which have not been observed yet, are calculated within 20 kcal/mol of the global energy minimum form **1**. The linear form HSiSiH (**4a**) is not a minimum on the potential energy surface.<sup>2</sup>

Theory has recently also made accurate predictions about the structures and relative energies of CSiH<sub>2</sub> isomers in the singlet state.<sup>5</sup> Three energy minimum forms were calculated at high levels of theory (CCSD(T)/

Chart 1 Relevant Si<sub>2</sub>H<sub>2</sub> and CSiH<sub>2</sub> Structures



TZ2P). The global energy minimum structure is the silylidene species **8**, which is predicted to be 34 kcal/mol lower in energy than trans-bent silaacetylene (**9**). The energetically high-lying vinylidene isomer **7** is calculated to be 84 kcal/mol less stable than **8**.<sup>5</sup> The linear form of HCSiH (**9a**) is a higher-order saddle point on the potential energy surface.<sup>5,6</sup> A molecule with the formula CSiH<sub>2</sub>, which is probably the most stable isomer

<sup>®</sup> Abstract published in *Advance ACS Abstracts*, October 1, 1995.

(1) Theoretical Studies of Organometallic Compounds. 15. Part 14: Antes, I.; Frenking, G. *Organometallics* **1995**, *14*, 4263.

(2) (a) Grev, R. S.; Schaefer, H. F., III. *J. Chem. Phys.* **1992**, *97*, 7990. (b) Colegrove, B. T.; Schaefer, H. F., III. *J. Phys. Chem.* **1990**, *94*, 5593. (c) Hühn, M. M.; Amos, R. D.; Kobayashi, R.; Handy, N. C. *J. Chem. Phys.* **1993**, *98*, 7107. (d) Curtiss, L. A.; Raghavachari, K.; Deutsch, P. W.; Pople, J. A. *J. Chem. Phys.* **1991**, *95*, 2433.

(3) (a) Bogey, M.; Bolvin, H.; Cordonnier, M.; Demuyneck, C.; Destombes, J. L.; Császár, A. G. *J. Chem. Phys.* **1994**, *100*, 8614. (b) Cordonnier, M.; Bogey, M.; Demuyneck, C.; Destombes, J. L. *Ibid.* **1992**, *97*, 7984. (c) Bogey, M.; Bolvin, H.; Demuyneck, C.; Destombes, J. L. *Phys. Rev. Lett.* **1991**, *66*, 413.

(4) Reviews: (a) Apeloig, Y. *The chemistry of functional groups: The chemistry of silicon compounds*; Patai, S., Rappoport, Z., Eds.; Wiley: New York, 1989; Chapter 2. (b) Schaefer, H. F., III. *Acc. Chem. Res.* **1982**, *15*, 283. (c) Grev, R. S. *Adv. Organomet. Chem.* **1993**, *33*, 125.

(5) Stegmann, R.; Frenking, G. *J. Comput. Chem.*, in press.

(6) (a) Gordon, M. S.; Pople, J. A. *J. Am. Chem. Soc.* **1981**, *103*, 2945. (b) Hoffmann, M. R.; Yoshioka, Y.; Schaefer, H. F., III. *J. Am. Chem. Soc.* **1983**, *105*, 1084. (c) Hopkinson, A. C.; Lien, M. H.; Csizmadia, I. G. *Chem. Phys. Lett.* **1983**, *95*, 232. (d) Luke, B. T.; Pople, J. A.; Krogh-Jespersen, M.-B.; Apeloig, Y.; Karni, M.; Chandrasekhar, J. *J. Am. Chem. Soc.* **1986**, *108*, 270.

8, has recently been observed in gas-phase experiments.<sup>7</sup> There are no other experimental studies of CSiH<sub>2</sub> species known to us.

Unstable molecules or energetically high-lying isomeric isomers can be studied in the gas phase or in low-temperature matrices. Another way to stabilize transient species is by complexing them as ligands in transition metal complexes. The metal–ligand interactions may be sufficiently strong to make it possible to isolate the complex even under room temperature. Of course, the resulting transition metal complex is only formally a stabilized form of the ligand. The metal–ligand interactions yield a new bond, and the electronic structure of the ligand may change considerably upon complexation. Nevertheless, the geometrical form of the ligand is frequently retained and the structure of the ligand resembles in many cases the isolated species. Examples of transient species stabilized in transition metal complexes are carbenes. Except for the Arduengo-type species,<sup>8</sup> isolated carbenes are only intermediates in chemical reactions. While classical carbenes can only be studied in the gas phase or in low-temperature matrices, transition metal carbene complexes in high and low oxidation states have become a very important class of organometallic compounds.<sup>9,10</sup>

Another class of very reactive compounds which can be stabilized as ligands in transition metal complexes are silenes and disilenes. Much progress has been made in recent years in the synthesis and characterization of silene<sup>11</sup> and disilene<sup>12</sup> complexes. Theoretical studies have been very helpful in the understanding of the bonding situation in these compounds.<sup>13</sup> The theoretical studies of silene and disilene complexes have been *a posteriori*; i.e., the theoretical studies were performed *after* the complexes were synthesized and the experimental geometries were known. *A priori* calculations of molecular structures are common for molecules of first- and second-row elements but not yet for transition metal compounds. It is still common saga that accurate quantum mechanical calculations of heavy-atom molecules are not feasible. Systematic theoretical studies using density functional methods<sup>14</sup> and effective core potentials (ECP)<sup>15</sup> have shown that this is not true. Electronically saturated transition metal compounds can be calculated with an accuracy comparable to that for main group compounds.

In this paper we predict theoretically the equilibrium structures and the relative energies of transition metal

complexes containing Si<sub>2</sub>H<sub>2</sub> and CSiH<sub>2</sub> isomers as ligands. To the best of our knowledge, no experimental evidence for silaacetylene or silavinylidene complexes or substituted analogues has been reported yet. There is also no theoretical study of the molecules known to us. We were interested in the changes of the structures and the relative energies of the Si<sub>2</sub>H<sub>2</sub> and CSiH<sub>2</sub> isomers when they are complexed as ligands. We have chosen WF<sub>4</sub> as a complex fragment, because previous studies have shown that the calculated geometries of acetylene and vinylidene complexes WF<sub>4</sub>(C<sub>2</sub>H<sub>2</sub>), WCl<sub>4</sub>(C<sub>2</sub>H<sub>2</sub>), MoF<sub>4</sub>(C<sub>2</sub>H<sub>2</sub>), and MoCl<sub>4</sub>(C<sub>2</sub>H<sub>2</sub>) are in excellent agreement with experimental results.<sup>16</sup> Although these complexes are usually dimers with two metal–halogen bridges, the structure of the metal–C<sub>2</sub>H<sub>2</sub> unit seems to be little disturbed by the dimerization. Also the corresponding monomeric molecules WF<sub>5</sub>(C<sub>2</sub>H<sub>2</sub>)<sup>−</sup> and WCl<sub>5</sub>(C<sub>2</sub>H<sub>2</sub>)<sup>−</sup> have metal–C<sub>2</sub>H<sub>2</sub> geometries very similar to those of the neutral dimers.<sup>16</sup> It seems therefore reasonable to chose WF<sub>2</sub>(Si<sub>2</sub>H<sub>2</sub>) and WF<sub>4</sub>(CSiH<sub>2</sub>) as model compounds to study the geometries and energies of silaacetylene and silavinylidene complexes. We present also an analysis of the metal–ligand interactions using the NBO partitioning scheme<sup>17</sup> and the topological analysis of the electron density distribution.<sup>18</sup>

## Methods

The geometries of the molecules have been optimized at the Hartree–Fock (HF) level of theory using a relativistic effective core potential (ECP) for tungsten, which replaces 60 core electrons.<sup>19</sup> The outermost of 5s and 5p electrons are treated explicitly, and they are not included in the core. The (5s/5p/3) valence basis set for the 5s<sup>2</sup>5p<sup>6</sup>6s<sup>2</sup>5d<sup>4</sup> electrons of tungsten is contracted to [441/2111/21]. This valence basis set has double- $\zeta$  plus p polarization functions quality. An all-electron basis set of 6-31G(d,p) quality has been used for C, Si, F, and H. The d-type polarization functions consist of a set of five spherical primitives. This basis set combination is our standard basis set II.<sup>15</sup> The stationary points on the potential energy surface were characterized by calculating the vibrational frequencies at HF/II using numerical second derivatives of the energy. Improved total energies have been calculated at the MP2 level (Møller–Plesset perturbation theory terminated at second order)<sup>20</sup> and using coupled cluster theory<sup>21</sup> with singles and doubles and a noniterative estimate of the triples CCSD(T)<sup>22</sup> in conjunction with the standard basis set III.<sup>15</sup> The latter basis set is basis set II with an additional set of f-type polarization functions at tungsten (exponent  $\alpha_f = 0.823$ ).<sup>23</sup> The correlation energy was calculated with the frozen-core approximation. Unless otherwise noted, energies are discussed at the CCSD(T)/III level using HF/II optimized geometries.

The geometries have been optimized using the program Turbomole.<sup>24</sup> The energy calculations at the correlated levels were calculated using the program ACES II.<sup>25</sup> For the

(7) Srinivas, R.; Sülzle, D.; Schwarz, H. *J. Am. Chem. Soc.* **1991**, *113*, 52.

(8) Arduengo, A. J.; Harlow, R. L.; Kline, M. *J. Am. Chem. Soc.* **1991**, *113*, 361.

(9) Dötz, K. H.; Fischer, H.; Hofmann, P.; Kreissl, F. R.; Schubert, U.; Weiss, K. *Transition Metal Carbene Complexes*; Verlag Chemie: Weinheim, Germany, 1983.

(10) Nugent, W. A.; Mayer, J. M. *Metal-Ligand Multiple Bonds*; Wiley: New York, 1988.

(11) (a) Campion, B. K.; Heyn, R. H.; Tilley, T. D. *J. Am. Chem. Soc.* **1988**, *110*, 7558. (b) Campion, B. K.; Heyn, R. H.; Tilley, T. D. *J. Am. Chem. Soc.* **1990**, *112*, 4079.

(12) (a) Pham, E. K.; West, R. *J. Am. Chem. Soc.* **1989**, *111*, 7667.

(b) Pham, E. K.; West, R. *Organometallics* **1990**, *9*, 1517. (c) Berry, D. H.; Chey, J.; Zipin, H. S.; Carroll, P. *J. Polyhedron* **1991**, *10*, 1189.

(13) (a) Anderson, A. B.; Shiller, P.; Zarate, E. A.; Tessier-Youngs, C. A.; Youngs, W. *J. Organometallics* **1989**, *8*, 2320. (b) Sakaki, S.; Ieki, M. *Inorg. Chem.* **1991**, *30*, 4218.

(14) Ziegler, T. *Chem. Rev.* **1991**, *91*, 651.

(15) Frenking, G.; Antes, I.; Böhme, M.; Dapprich, S.; Ehlers, A. W.; Jonas, V.; Neuhaus, A.; Otto, M.; Stegmann, R.; Veldkamp, A.; Vyboishchikov, S. F. *Reviews in Computational Chemistry*; Lipkowitz, K. B., Boyd, D. B., Eds.; VCH: New York, 1995; Vol. 7, in press.

(16) Stegmann, R.; Neuhaus, A.; Frenking, G. *J. Am. Chem. Soc.* **1993**, *115*, 11930.

(17) Reed, A. E.; Curtiss, L. A.; Weinhold, F. *Chem. Rev.* **1988**, *88*, 899.

(18) Bader, R. F. W. *Atoms in Molecules: A Quantum Theory*; Oxford University Press: Oxford, U.K., 1990.

(19) Hay, P. J.; Wadt, W. R. *J. Chem. Phys.* **1985**, *82*, 299.

(20) (a) Møller, C.; Plesset, M. S. *Phys. Rev.* **1934**, *46*, 618. (b) Binkley, J. S.; Pople, J. A. *Intern. J. Quantum Chem.* **1975**, *9S*, 229.

(21) Cizek, J. *J. Chem. Phys.* **1966**, *45*, 4256.

(22) (a) Raghavachari, K.; Trucks, G. W.; Pople, J. A.; Head-Gordon, M. *Chem. Phys. Lett.* **1989**, *157*, 479. (b) Bartlett, R. J.; Watts, J. D.; Kucharski, S. A.; Noga, J. *Ibid.* **1990**, *165*, 513.

(23) Ehlers, A. W.; Böhme, M.; Dapprich, S.; Gobbi, A.; Höllwarth, A.; Jonas, V.; Köhler, K. F.; Stegmann, R.; Veldkamp, A.; Frenking, G. *Chem. Phys. Lett.* **1993**, *208*, 111.

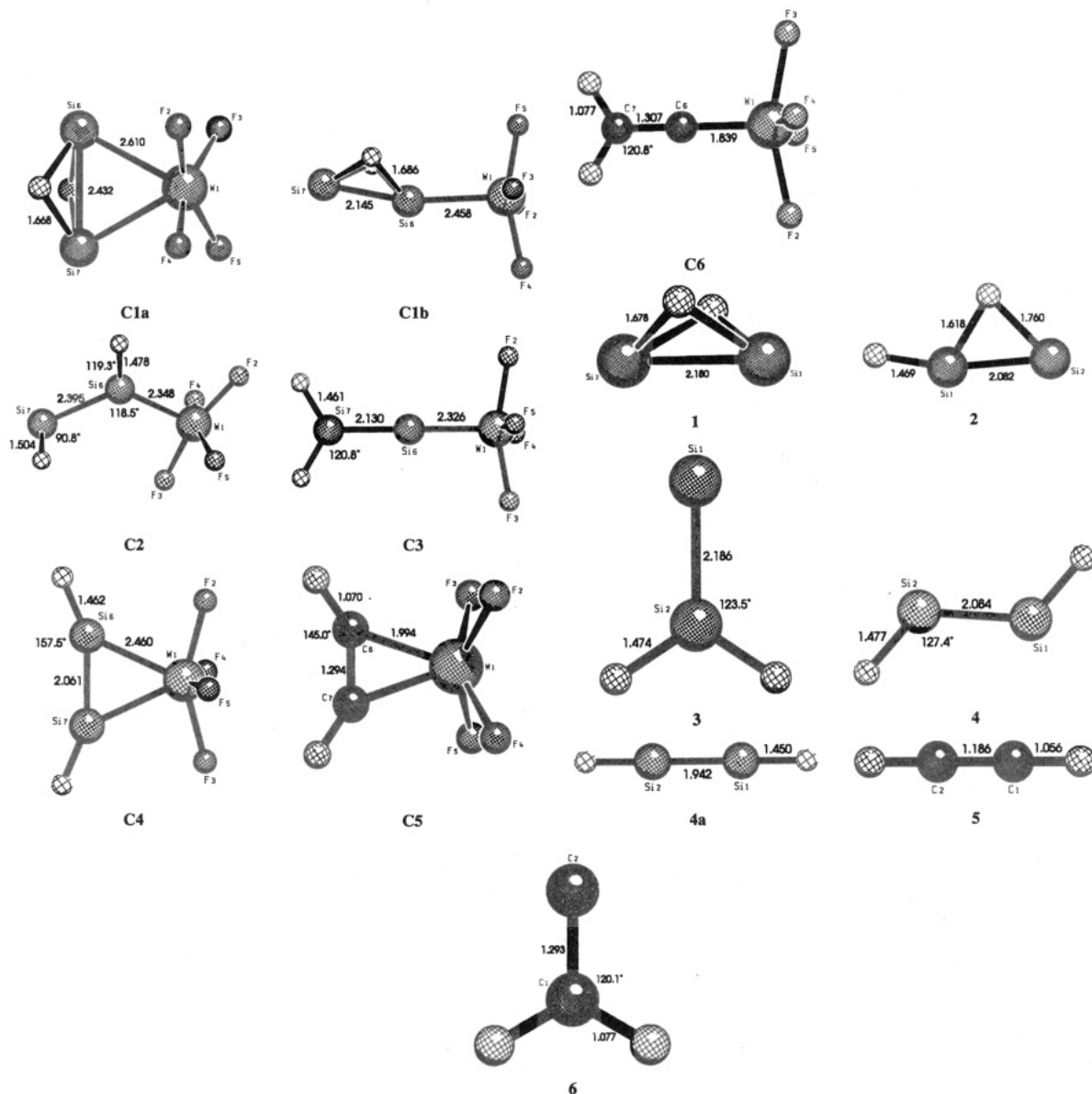


**Figure 1.** Optimized geometries (HF/II) of  $WF_4(Si_2H_2)$  complexes **C1a–C4**,  $WF_4(C_2H_2)$  complexes **C5** and **C6**,  $Si_2H_2$  isomers **1–4a**, and  $C_2H_2$  isomers **5** and **6**. The calculated bond distances are given in Å, and bond angles, in deg. The geometry of **9** was optimized at MP2/II.

calculation of the electron density distribution  $\rho(\mathbf{r})$ , the gradient vector field  $\nabla\rho(\mathbf{r})$ , and its associated Laplacian  $\nabla^2\rho(\mathbf{r})$  the programs EXTREME, GRID, and GRDVEC were used.<sup>26</sup> The NBO analysis<sup>17</sup> was carried out with the subroutine available in Gaussian 92.<sup>27</sup>

### $WF_4(Si_2H_2)$ Complexes

Figure 1 shows the optimized structures and the most

(24) (a) Häser, M.; Ahlrichs, R. *J. Comput. Chem.* **1989**, *10*, 104. (b) Ahlrichs, R.; Bär, M.; Häser, M.; Horn, H.; Kölmel, C. *Chem. Phys. Lett.* **1989**, *162*, 165. (c) Horn, H.; Weiss, H.; Häser, M.; Ehrig, M.; Ahlrichs, R. *J. Comput. Chem.* **1991**, *12*, 1058. (d) Häser, M.; Almlöf, J.; Feyereisen, M. W. *Theor. Chim. Acta* **1991**, *79*, 115.

(25) ACES II, an ab initio program system written by J. F. Stanton, J. Gauss, J. D. Watts, W. J. Lauderdale, and R. J. Bartlett, University of Florida, Gainesville, FL, 1991.

(26) Biegler-König, F. W.; Bader, R. F. W.; Ting-Hua, T. *J. Comput. Chem.* **1982**, *3*, 317.

(27) Gaussian 92, Revision C. Frisch, M. J.; Trucks, G. W.; Head-Gordon, M.; Gill, P. M. W.; Wong, M. W.; Foresman, J. B.; Johnson, B. G.; Schlegel, H. B.; Robb, M. A.; Replogle, E. S.; Gomperts, R.; Andres, J. L.; Raghavachari, K.; Binkley, J. S.; Gonzalez, C.; Martin, R. L.; Fox, D. J.; Defrees, D. J.; Baker, J.; Stewart, J. J. P.; Pople, J. A. Gaussian, Inc., Pittsburgh, PA, 1992.

important bond lengths of the  $WF_4(Si_2H_2)$  complexes **C1a–C4** predicted at HF/II. Previous theoretical studies have shown that the geometries of transition metal complexes in high oxidation states optimized at HF/II are in very good agreement with experimental values.<sup>15,16,28</sup> The HF/II optimized structure of the acetylene complex  $WF_4(HCCH)$  (**C5**) is also shown in Figure 1. The predicted W–C bond length (1.994 Å) is in very good agreement with experimental values of W(VI)–alkyne complexes, which are typically 1.98–2.04 Å.<sup>16,29</sup>

The theoretical geometries of the  $Si_2H_2$  structures **1–4a** optimized at HF/II are also shown in Figure 1. A comparison of the calculated Si–Si bond lengths with previously reported<sup>2b</sup> CISD/TZ2P values shows that the HF/II values are slightly ( $\sim 0.02$ – $0.03$  Å) shorter than

(28) (a) Jonas, V.; Frenking, G.; Reetz, M. T. *Organometallics* **1993**, *12*, 2111. (b) Veldkamp, A.; Frenking, G. *J. Am. Chem. Soc.* **1994**, *116*, 4937. (c) Neuhaus, A.; Veldkamp, A.; Frenking, G. *Inorg. Chem.* **1994**, *33*, 5278.

(29) (a) Kersting, M.; El-Kohli, A.; Müller, U.; Dehnicke, K. *Chem. Ber.* **1989**, *122*, 279. (b) Pauls, I.; Dehnicke, K.; Fenske, D. *Chem. Ber.* **1989**, *122*, 481. (c) Pauls, I. Dissertation, Universität Marburg, 1990.

**Table 1.** Calculated Total Energies  $E_{\text{tot}}$  (au) Relative Energies  $E_{\text{rel}}$  (kcal mol<sup>-1</sup>), Zero-Point Vibrational Energies ZPE (kcal mol<sup>-1</sup>), and Number of Imaginary Frequencies  $i$ 

molecule	no.	sym	HF/II				MP2/III		CCSD(T)/III	
			$E_{\text{tot}}$	$E_{\text{rel}}$	$i$	ZPE	$E_{\text{tot}}$	$E_{\text{rel}}$	$E_{\text{tot}}$	$E_{\text{rel}}^a$
WF <sub>4</sub> SiH <sub>2</sub> Si (side-on)	<b>C1a</b>	C <sub>2v</sub>	-1043.919 59	2.1	0	17.9	-1045.164 70	23.3	-1045.224 43	10.1 (9.8)
WF <sub>4</sub> SiH <sub>2</sub> Si (end-on)	<b>C1b</b>	C <sub>s</sub>	-1043.893 84	18.3	0	16.5	-1045.108 47	58.5	-1045.179 30	38.5 (36.8)
WF <sub>4</sub> SiHSiH	<b>C2</b>	C <sub>1</sub>	-1043.913 46	6.0	0	16.4	-1045.140 59	38.5	n.c. <sup>b</sup>	
WF <sub>4</sub> Si <sub>2</sub> H <sub>2</sub>	<b>C3</b>	C <sub>2v</sub>	-1043.902 16	13.1	1	17.6	-1045.148 50	33.5	-1045.220 26	12.8 (12.2)
WF <sub>4</sub> HSiSiH	<b>C4</b>	C <sub>2v</sub>	-1043.922 98	0.0	0	18.2	-1045.201 89	0.0	-1045.240 60	0.0 (0.0)
WF <sub>4</sub> HCCH	<b>C5</b>	C <sub>2v</sub>	-541.885 50	0.0	0	26.6	-543.239 13	0.0	-543.270 36	0.0 (0.0)
WF <sub>4</sub> CCH <sub>2</sub>	<b>C6</b>	C <sub>2v</sub>	-541.865 33	12.7	0	26.0	-543.213 71	16.0	-543.254 60	9.9 (9.3)
WF <sub>4</sub> CSiH <sub>2</sub>	<b>C7</b>	C <sub>2v</sub>	-792.904 57	0.0	0	20.6	-794.228 23	0.0	-794.255 08	0.0 (0.0)
WF <sub>4</sub> SiCH <sub>2</sub>	<b>C8</b>	C <sub>2v</sub>	-792.860 95	27.4	0	22.5	-794.135 67	58.1	-794.202 25	33.2 (35.1)
WF <sub>4</sub> HCSiH	<b>C9</b>	C <sub>s</sub>	-792.881 23	14.6	0	22.1	-794.206 73	13.5	-794.239 35	9.9 (11.4)
SiH <sub>2</sub> Si (butterfly)	<b>1</b>	C <sub>2v</sub>	-578.889 75	0.0	0	10.2	-579.061 52	0.0	-579.103 39	0.0 (0.0)
HSiHSi	<b>2</b>	C <sub>s</sub>	-578.868 92	13.1	0	9.0	-579.045 94	9.8	-579.087 38	10.0 (8.8)
SiSiH <sub>2</sub>	<b>3</b>	C <sub>2v</sub>	-578.883 61	3.9	0	10.1	-579.042 86	11.7	-579.088 37	9.4 (9.3)
HSiSiH (trans)	<b>4</b>	C <sub>s</sub>	-578.851 36	24.1	0	8.5	-579.036 88	15.5	-579.080 80	14.2 (12.5)
HSiSiH (linear)	<b>4a</b>	D <sub>∞h</sub>	-578.825 15	40.5	2	9.1	-579.002 61	37.0	-579.041 76	38.7 (37.6)
HCCH	<b>5</b>	D <sub>∞h</sub>	-76.821 70	0.0	0	18.4	-77.076 74	0.0	-77.104 44	0.0 (0.0)
CCH <sub>2</sub>	<b>6</b>	C <sub>2v</sub>	-76.767 02	34.3	0	16.3	-76.997 33	49.8	-77.036 62	42.6 (40.5)
CSiH <sub>2</sub>	<b>7</b>	C <sub>2v</sub>	-327.723 63	84.7	0	11.0	-327.912 67	98.2	-327.961 87	90.6 (86.7)
SiCH <sub>2</sub>	<b>8</b>	C <sub>2v</sub>	-327.858 67	0.0	0	14.9	-328.069 16	0.0	-328.106 32	0.0 (0.0)
CSiH (trans)	<b>9</b>	C <sub>s</sub>			0 <sup>c</sup>	12.8 <sup>c</sup>	-328.009 80 <sup>c</sup>	37.2	-328.045 27 <sup>c</sup>	38.3 (36.2)
HCSiH	<b>9a</b>	C <sub>∞</sub>	-327.769 36	56.0	2	12.9	-328.003 13	41.4	-328.033 88	45.5 (43.5)

<sup>a</sup> Values in parentheses include ZPE corrections. <sup>b</sup> Not calculated for technical reasons (single file size > 2GB). <sup>c</sup> Optimized at MP2/II.

the bond lengths predicted at the correlated level. These differences are probably not very important, because the relative stabilities of the Si<sub>2</sub>H<sub>2</sub> isomers calculated at CCSD(T)/III using the HF/II optimized geometries are nearly the same as those which are calculated at CISD/TZ2P//CISD/TZ2P.<sup>2b</sup> The calculated energies of **1–4a** and the complexes **C1a–C4** are shown in Table 1.

The doubly-bridged Si<sub>2</sub>H<sub>2</sub> global energy minimum **1** forms with WF<sub>4</sub> the side-on WF<sub>4</sub>(Si<sub>2</sub>H<sub>2</sub>) complex **C1a** and the end-on complex **C1b**. Both structures are minima on the potential energy surface at HF/II ( $i = 0$ ). The end-on isomer **C1b** is clearly higher in energy than **C1a**. Isomer **C1a** is calculated at CCSD(T)/III to be 28.4 kcal/mol more stable than **C1b**. The Si–Si bond of **C1a** is significantly longer (2.432 Å) than in the separated ligand **1** (2.180 Å), while it is even slightly shorter in **C1b** (2.145 Å) than in **1** (Figure 1). This is because different orbitals of the Si<sub>2</sub>H<sub>2</sub> ligands are involved in the formation of the tungsten–silicon bonds of **C1a** and **C1b**. The nature of the metal–ligand bonds in the complexes is discussed below.

Geometry optimizations of a side-on bonded WF<sub>4</sub>-(Si<sub>2</sub>H<sub>2</sub>) complex of next higher lying Si<sub>2</sub>H<sub>2</sub> isomer **2** did not lead to an energy minimum structure. A geometry optimization of end-on bonded **2** gave the molecule **C2** shown in Figure 1. However, the structure of the Si<sub>2</sub>H<sub>2</sub> ligand of **C2** does not correspond to **2**. Rather, it has a twisted form which indicates a disilylene structure. Such a structure is an energy minimum form of Si<sub>2</sub>H<sub>2</sub> only at a low level of theory.<sup>2b,30</sup> At higher levels of theory the C<sub>2</sub>-symmetric twisted form collapses to the dibridged global minimum **1**. It is not uncommon that species which are not a minimum on the energy hypersurface may become stable molecules upon complexation by a transition metal. A recent example is cyclopropyne.

Singlet cyclopropyne is a transition state,<sup>31</sup> but it forms stable complexes such as WF<sub>4</sub>(c-C<sub>3</sub>H<sub>2</sub>).<sup>32</sup>

The structure of **C2** is interesting because it is an example of a silylene complex, the silicon analogue of a carbene complex. Transition metal silylene complexes have been discussed for a long time,<sup>33</sup> but only recently have the first stable silylene complexes been isolated.<sup>34</sup> There is no experimental geometry of a tungsten silylene complex known to us. The calculated W–Si distance of **C2** (2.348 Å) is slightly shorter than experimental values for typical W–Si single bonds. The W–Si bond of a W(IV) trimethylsilyl complex has been reported with a bond length  $r_{\text{W-Si}} = 2.388$  Å.<sup>35a</sup> The W–Si bond length of a W(0) complex is longer (2.53–2.56 Å).<sup>35b</sup> A recent study of transition metal carbene and carbyne complexes in high and low oxidation states has shown that the calculated metal–carbon distances are in excellent agreement with experimental values.<sup>36</sup> The same can be assumed for the calculated and silylene complexes. The complex **C2** has a second silylene center. It is conceivable that a second WF<sub>4</sub> fragment can bind to silicon and that a bis(silylene) complex is formed.

The geometry optimization of the end-on complex of disilavinylidene (**3**) with WF<sub>4</sub> gave the structure **C3** shown in Figure 1. However, **C3** is not a minimum at HF/II on the potential energy surface ( $i = 1$ ). Also

(31) (a) Fitzgerald, G.; Schaefer, H. F., III. *J. Chem. Phys.* **1983**, *78*, 3239. (b) Saxe, P.; Schaefer, H. F., III. *J. Am. Chem. Soc.* **1980**, *102*, 3239.

(32) Stegmann, R.; Frenking, G. Manuscript in preparation. (33) (a) Tilley, T. D. *Comments Inorg. Chem.* **1990**, *10*, 37. (b) Zybilla, C. *Top. Curr. Chem.* **1992**, *160*, 1.

(34) (a) Zybilla, C.; Müller, G. *Angew. Chem., Int. Ed. Engl.* **1987**, *26*, 669. (b) Straus, D. A.; Tilley, T. D.; Rheingold, A. L.; Geib, S. J. *J. Am. Chem. Soc.* **1987**, *109*, 5872. (c) Straus, D. A.; Grumbine, S. D.; Tilley, T. D. *J. Am. Chem. Soc.* **1990**, *112*, 7801. (d) Grumbine, S. D.; Tilley, T. D.; Arnold, F. P.; Rheingold, A. L. *J. Am. Chem. Soc.* **1993**, *115*, 7884. (e) Grumbine, S. D.; Tilley, T. D.; Arnold, F. P.; Rheingold, A. L. *J. Am. Chem. Soc.* **1994**, *116*, 5495.

(35) (a) Barron, A. R.; Wilkinson, G.; Motevalli, M.; Hursthouse, M. B. *J. Chem. Soc., Dalton Trans.* **1987**, 837. (b) Schmitzer, S.; Weis, U.; Kab, H.; Buchner, W.; Malisch, W.; Polzer, T.; Posset, U.; Kiefer, W. *Inorg. Chem.* **1993**, *32*, 303.

(36) Vyboishchikov, S. F.; Frenking, G. Manuscript in preparation.

(30) (a) Lischka, H.; Köhler, H. *J. Am. Chem. Soc.* **1983**, *105*, 6646. (b) Binkley, J. S. *J. Am. Chem. Soc.* **1984**, *106*, 603. (c) Luke, B. T.; Pople, J. A.; Krogh-Jespersen, M.-B.; Apeloig, Y.; Karni, M.; Chandrasekhar, J.; Schleyer, P. v. R. *J. Am. Chem. Soc.* **1986**, *108*, 270.

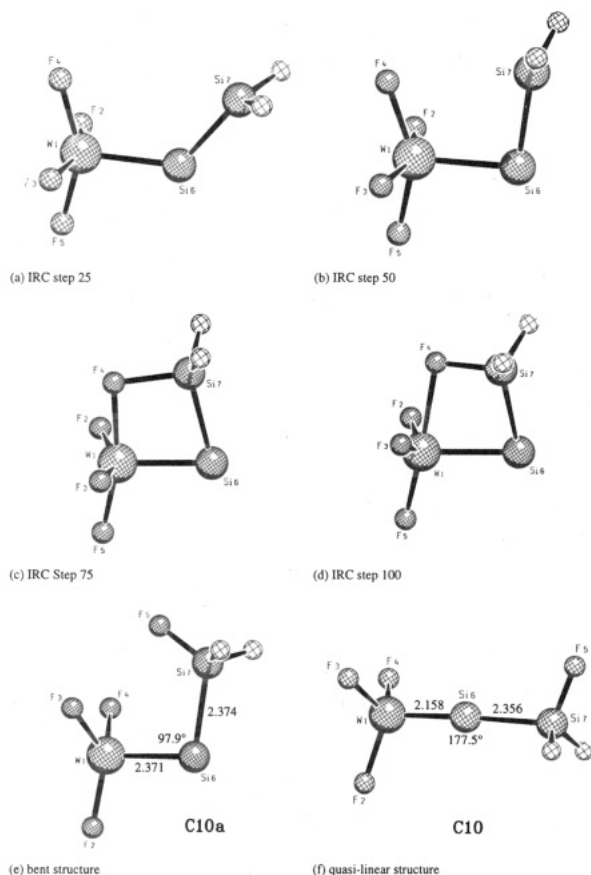


**Figure 2.** Calculated structures at HF/II along the intrinsic reaction coordinate (IRC) leading from the transition state **C3** to the silyne complex **C10**: (a) after 25 IRC steps; (b) after 50 IRC steps; (c) after 75 IRC steps; (d) after 100 IRC steps; (e) bent structure **C10a** (minimum at HF/II); (f) HF/II optimized structure **C10**.

geometry optimizations of a  $WF_4$  complex with side-on bonded **3** did not give an energy minimum structure. We searched for the stationary points to which the transition state **C3** is connected to. This was done by calculating the intrinsic reaction coordinate (IRC)<sup>37</sup> starting from **C3**. The results are very interesting. Figure 2 shows the structures along the reaction coordinate calculated after 25, 50, 75, and 100 steps using default values for the IRC calculations as used in Gaussian 92.<sup>27</sup> The reaction is a 1,3 fluorine rearrangement from tungsten to the terminal silicon atom, leading to the tungsten silyne complex **C10** (Figure 2). The W-Si bond of **C10**, which is formally a tungsten-silicon triple bond, is very short (2.158 Å). The W-Si-Si angle is nearly linear (177.5°). To the best of our knowledge there are no silyne complexes known. The structures and bond energies of transition metal silene and silyne complexes are subjects of a present study by us. The structure **C10** is 20.0 kcal/mol (MP2/III) lower in energy than **C4**. There is also a bent tungsten silyne complex **C10a** predicted as an energy minimum structure at HF/II (Figure 2). This may be an artifact of the HF calculations. The bent form **C10a** is 25.0 kcal/mol (MP2/III) higher in energy than **C10**.

The energetically lowest lying  $WF_4(Si_2H_2)$  complex calculated in our study is the structure **C4** (Figure 1). This is remarkable, because the corresponding structure

**Table 2.** Calculated Reaction Energies (kcal mol<sup>-1</sup>) at CCSD(T)/III/HF/II<sup>b</sup>

complex	ligand	$\Delta E_R(1)^a$	$\Delta E_R(2)^a$
<b>C1a</b>	<b>1</b>	-28.2 (-27.7)	-60.8 (-58.8)
<b>C1b</b>	<b>1</b>	-56.5 (-54.6)	-89.2 (-85.8)
<b>C2</b>	<b>1</b>	-52.3 (-50.3)	-86.2 (-82.7)
<b>C4</b>	<b>4</b>	-3.8 (-5.3)	-36.5 (-36.5)
<b>C7</b>	<b>7</b>	79.9 (78.5)	42.2 (42.3)
<b>C8</b>	<b>8</b>	-43.9 (-43.3)	-76.6 (-74.5)
<b>C9</b>	<b>9</b>	17.7 (16.6)	-15.0 (-14.6)

<sup>a</sup> Values in parentheses include ZPE corrections. <sup>b</sup> MP2/III/HF/II for **C2**.

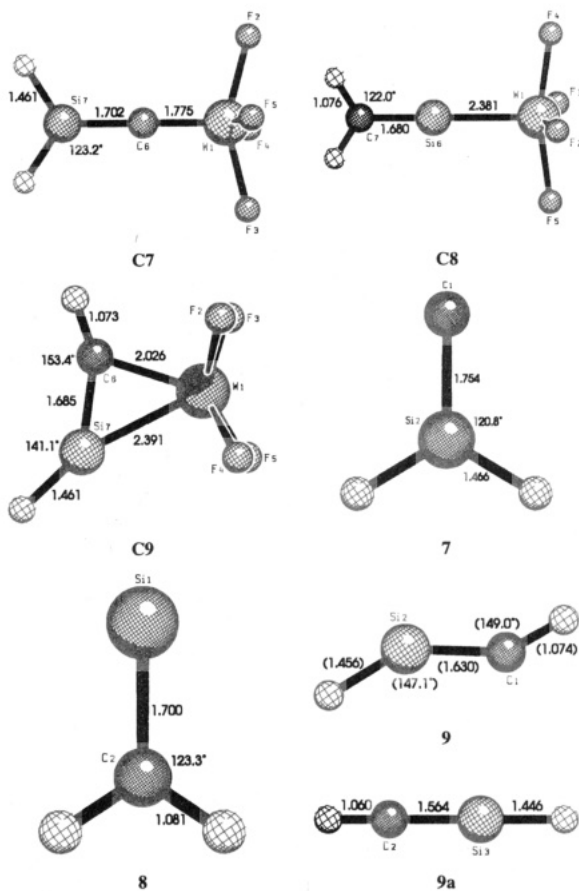


**Figure 3.** Optimized geometries (HF/II) of  $WF_4(CSiH_2)$  complexes **C7**–**C9** and  $CSiH_2$  isomers **7**–**9a**. The calculated bond distances are given in Å, and bond angles, in deg.

of the  $Si_2H_2$  ligand (**4**) is the least stable isomer investigated here. The complex **C4** is predicted to be 10.1 kcal/mol lower in energy than **C1a** (Table 1). The geometry of the  $Si_2H_2$  ligand of **C4** is very similar to a classical acetylene complex (see structure **C5** in Figure 1). The structure and bonding properties of **C5** have been reported in a previous paper.<sup>16</sup> The isolated  $Si_2H_2$  ligand with the connectivity  $HSiSiH$  has a trans-bent geometry as shown in Figure 1 (structure **4**). The Si-Si bond of the complex **C4** is slightly shorter (2.061 Å) than in **4** (2.084 Å). Also the bending angle Si-Si-H of **C4** is larger (147.5°) than in **4** (127.4°). The W-Si bonds of **C4** are clearly shorter (2.460 Å) than those of **C1a**. This indicates the electronically less stable nature of **4** compare with **1**, which is the reason why the silicon atoms of the former isomer have shorter and stronger W-Si bonds in **C4** than the latter isomer in the complex **C1a**.

(37) (a) Fukui, K. *Acc. Chem. Res.* **1981**, *14*, 363. (b) Gonzalez, C.; Schlegel, H. B. *J. Chem. Phys.* **1991**, *95*, 5853.

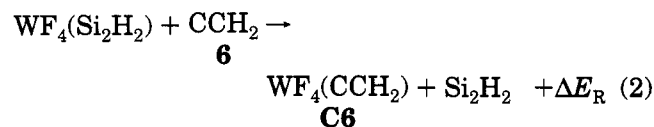
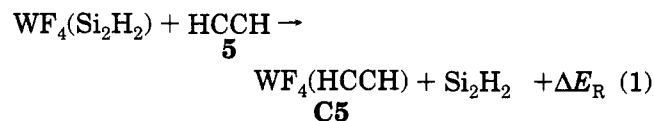
Table 3. Results of the NBO Analysis<sup>a</sup>

complex	q(W)	q(Si)	q(C)	bond	% W	% 6s(W)	% 6p(W)	% 5d(W)	% s(C/Si)	% p(C/Si)	BO
<b>C1a</b>	2.14	0.53		σ W-Si <sub>6</sub>	64.6	12.5	3.8	83.6	7.5	90.7	0.73
				σ W-Si <sub>7</sub>	64.6	12.5	3.8	83.6	7.5	90.7	0.73
<b>C1b</b>	2.30	0.40		σ W-Si	28.2	22.5	1.4	76.1	46.1	53.8	0.91
<b>C2</b>	2.21	0.30		σ W-Si	47.4	22.8	17.0	60.2	24.4	74.4	1.42
				π W-Si	65.7	10.2	20.0	69.9	10.8	87.5	
<b>C4</b>	2.12	0.32		σ W-Si <sub>6</sub>	50.7	13.5	3.4	83.2	28.1	70.7	1.13
				σ W-Si <sub>7</sub>	50.7	13.5	3.4	83.2	28.1	70.7	1.13
<b>C5</b>	2.83		-0.42	σ W-C <sub>2</sub>	36.0	12.6	0.3	87.1	24.7	75.1	0.97
				σ W-C <sub>3</sub>	36.0	12.6	0.3	87.1	24.7	75.1	0.97
<b>C6</b>	2.75		-0.45	σ W-C	26.8	21.0	0.1	79.0	50.3	49.7	1.67
				π W-C	60.6	0.0	0.6	99.4	0.0	99.8	
<b>C7</b>	2.80	1.51	-1.37	σ W-C	30.4	29.6	0.0	70.4	46.9	53.1	2.06
				π W-C	34.1	0.0	25.7	74.3	0.0	99.9	
<b>C8</b>	2.25	1.01	-1.21	σ W-Si	29.4	41.7	1.2	57.1	48.5	51.4	1.16
				π W-Si	85.6	0.0	33.6	66.4	0.0	96.7	
<b>C9</b>	2.52	0.98	-1.13	σ W-Si	46.2	16.1	2.1	81.8	33.3	66.0	1.01
				σ W-C	32.6	12.7	0.3	87.0	25.8	74.1	1.21
				π W-C	27.7	0.0	1.6	98.4	0.0	99.7	

<sup>a</sup> Partial atomic charges *q* and analysis of the W-Si/W-C bonds. Polarity given by % W, hybridization of W and C/Si, Wiberg bond index in NAO basis BO.

We tried to find other minima for complexes of WF<sub>4</sub> with Si<sub>2</sub>H<sub>2</sub>. None was found. Although we cannot exclude that other structures may exist, we believe that the structures **C1a**–**C4** are probably the most stable WF<sub>4</sub>(Si<sub>2</sub>H<sub>2</sub>) isomers.

In order to estimate the F<sub>4</sub>W-Si<sub>2</sub>H<sub>2</sub> bond strengths in **C1a**–**C4** we calculated the energies of the isostructural reactions 1 and 2.



The calculated reaction energies of reactions 1 and 2 for the energy minimum complexes **C1a**–**C4** are shown in Table 2. All calculated reaction energies are negative. This means that the respective Si<sub>2</sub>H<sub>2</sub> isomer is more weakly bound to WF<sub>4</sub> than acetylene in **C5** and vinylidene in **C6**. The WF<sub>4</sub>-Si<sub>2</sub>H<sub>2</sub> bond strength of the most stable Si<sub>2</sub>H<sub>2</sub> complex **C4**, however, is nearly as large as the tungsten-acetylene bonding in **C5**. The reaction energy is only slightly exothermic by -3.8 kcal/mol (-5.3 kcal/mol after ZPE corrections, Table 2).

### WF<sub>4</sub>(CSiH<sub>2</sub>) Complexes

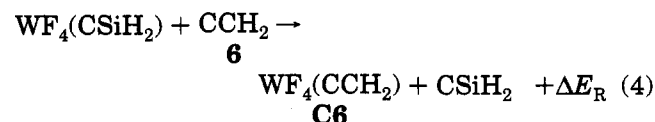
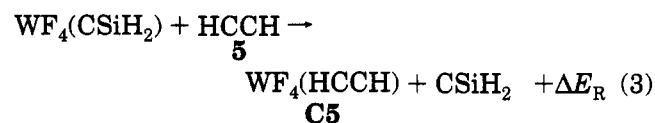
Figure 3 shows the optimized geometries of the WF<sub>4</sub>-(CSiH<sub>2</sub>) complexes **C7**–**C9** and the corresponding CSiH<sub>2</sub> isomers **7**–**9**. The calculated energies are shown in Table 1.

The energetically lowest-lying complex is the silavinylidene structure **C7** (Figure 3). The complex **C7** is 33.2 kcal/mol lower in energy than the silylidene complex **C8** (Table 1). The energy ordering of the CSiH<sub>2</sub> complexes **C7** and **C8** is a dramatic reversal of the stabilities of the separate CSiH<sub>2</sub> ligands. The silavinylidene isomer **7** is 90.6 kcal/mol (!) higher in energy than **8** (Table 1). The carbon atom of **7** is much more reactive than the silicon atom of **8**. The electronically unsatu-

rated state of the carbon atom of **8** is the reason for the very short W-C bond of **C7** (1.775 Å). The W-C bond of **C7** is significantly shorter than the W-C bond of the vinylidene complex **C6** (1.839 Å), which is shown in Figure 1. It is interesting to note that the C-Si bond of the free CSiH<sub>2</sub> ligand **7** is longer (1.754 Å) than in the complex (1.702 Å). The same holds true for the Si-C bond of SiCH<sub>2</sub>. The Si-C bond length of the complex **C8** is shorter (1.680 Å) than that of the free ligand **8** (1.700 Å). The silylidene complex **C8** is a minimum on the potential energy surface, unlike the disilavinylidene complex **C3** which is a transition state.

The CSiH<sub>2</sub> ligand with the connectivity HCSiH gives the complex **C9** (Figure 3). This complex is 9.9 kcal/mol higher in energy than **C7** (Table 1). The HCSiH ligand has a cis-bent geometry in **C9**. The separated HCSiH ligand **9** has a trans-bent geometry (Figure 3). Structure **9** can only be calculated at a correlated level of theory; at the Hartree-Fock level it is not a minimum on the potential energy surface.<sup>38</sup> Geometry optimization of **9** at CCSD(T)/TZ2P gives a shallow minimum with an energy barrier of 5.1 kcal/mol for rearrangement to **7**.<sup>5</sup> The sila-acetylene form **9** is 52.3 kcal/mol more stable than **7**, but the complex **C9** is 9.9 kcal/mol less stable than **C7**. It should be noted that the W-Si bond of **C9** is clearly shorter (2.391 Å) than the W-Si bond at **C4**, while the W-C bond is slightly longer (2.026 Å) than the W-C bond of **C5** (1.994 Å).

We calculated the energies of the isostructural reactions 3 and 4 for the different complexes **C7**–**C9**. The results are shown in Table 2.



The CSiH<sub>2</sub> ligand is much stronger bound in **C7** than acetylene or vinylidene in **C5** and **C6**, respectively. The calculations predict that the W-C bond of the sila-



**Table 4. Results of the Topological Analysis of the Electron Density Distribution: Values of the W-C and W-Si Bonds<sup>a</sup>**

complex	bond	$\rho_b$	$\nabla^2\rho_b$	$H_b$	$r_b$
<b>C1a</b>	W-Si <sub>6</sub>	0.38	-0.42	-0.31	1.55
	W-Si <sub>7</sub>	0.38	-0.42	-0.31	1.55
<b>C1b</b>	W-Si	0.56	1.53	-0.20	1.19
	W-Si	0.74	-2.13	-0.40	1.25
<b>C4</b>	W-Si <sub>6</sub>	0.66	-2.41	-0.33	1.34
	W-Si <sub>7</sub>	0.66	-2.41	-0.33	1.34
<b>C5</b>	W-C <sub>2</sub>	1.05	1.77	-0.56	1.07
	W-C <sub>3</sub>	1.05	1.77	-0.56	1.07
<b>C6</b>	W-C	1.32	8.63	-0.85	0.97
<b>C7</b>	W-C	1.55	4.72	-1.19	0.97
<b>C8</b>	W-Si	0.63	1.09	-0.26	1.18
<b>C9</b>	W-Si	0.64	-1.49	-0.31	1.29
	W-C	1.06	1.22	-0.56	1.07

<sup>a</sup> Charge density at the bond critical point  $\rho_b$  ( $e/\text{\AA}^3$ ); Laplacian at the bond critical point  $\nabla^2\rho_b$  ( $e/\text{\AA}^5$ ); energy density at the bond critical point  $H_b$  (hartree/ $\text{\AA}^3$ ); location of the bond critical point  $r_b$  given by the distance from the tungsten atom ( $\text{\AA}$ ).

vinylidene complex **C7** is 42.2 kcal/mol stronger than the W-C bond of the vinylidene complex **C6** (Table 2). This is in agreement with the very short tungsten-carbon bond of **C7**. The silylidene complex **C8**, however, has a significantly weaker metal ligand (W-Si) bond than the acetylene and vinylidene complexes **C5** and **C6**. The silaacetylene ligand of the complex **C9** is rather strongly bound; it is 17.7 kcal/mol stronger bound than the acetylene ligand in **C5** (Table 2).

### Electronic Structure Analysis

In order to investigate the metal-ligand bonding in the complexes we analyzed the electronic structure of **C1a-C9** using the natural bond orbital (NBO) partitioning scheme<sup>17</sup> and the topological analysis of the electron density distribution.<sup>18</sup> The results of the NBO analysis are shown in Table 3. The results of the topological analysis are shown in Table 4. The contour line diagrams of the Laplacian distribution of **C1a-C9** are shown in Figure 4.

The NBO analysis shows that the W-Si bonds of **C1a** are polarized toward the tungsten end. A 64.6% amount of the W-Si bond orbital belongs to tungsten (Table 3). The hybridization at W has mainly d character (83.6%), while the W-Si bond at Si has mainly p character (90.7%). The Wiberg bond order for the W-Si bond of **C1a** is only 0.73. The polarization of the W-Si bond toward tungsten is also obvious from the topological analysis. The ring critical point  $r_b$  is 1.55 Å away from the tungsten atom, which is more than half of the W-Si bond length (Table 4). This means that a larger part of the W-Si bond belongs to the tungsten atom than to silicon.

The W-Si bond of the end-on complex **C1b** is clearly different from **C1a**. The NBO analysis shows that the W-Si bond is strongly polarized toward the silicon atom; only 28.2% of the bond is at tungsten (Table 3).

(38) One reviewer pointed out that the failure of the HF method to predict **9** as an energy minimum structure could indicate that the present approach is not sufficient for calculating the geometries of the complexes. This might be true for those isomers of  $\text{WF}_4(\text{Si}_2\text{H}_2)$  and  $\text{WF}_4(\text{CSiH}_2)$  which are shallow minima on the potential energy hypersurface. We think, however, that the structures discussed here are the most important isomers of the  $\text{WF}_4$  complexes with the ligands  $\text{Si}_2\text{H}_2$  and  $\text{CSiH}_2$ .

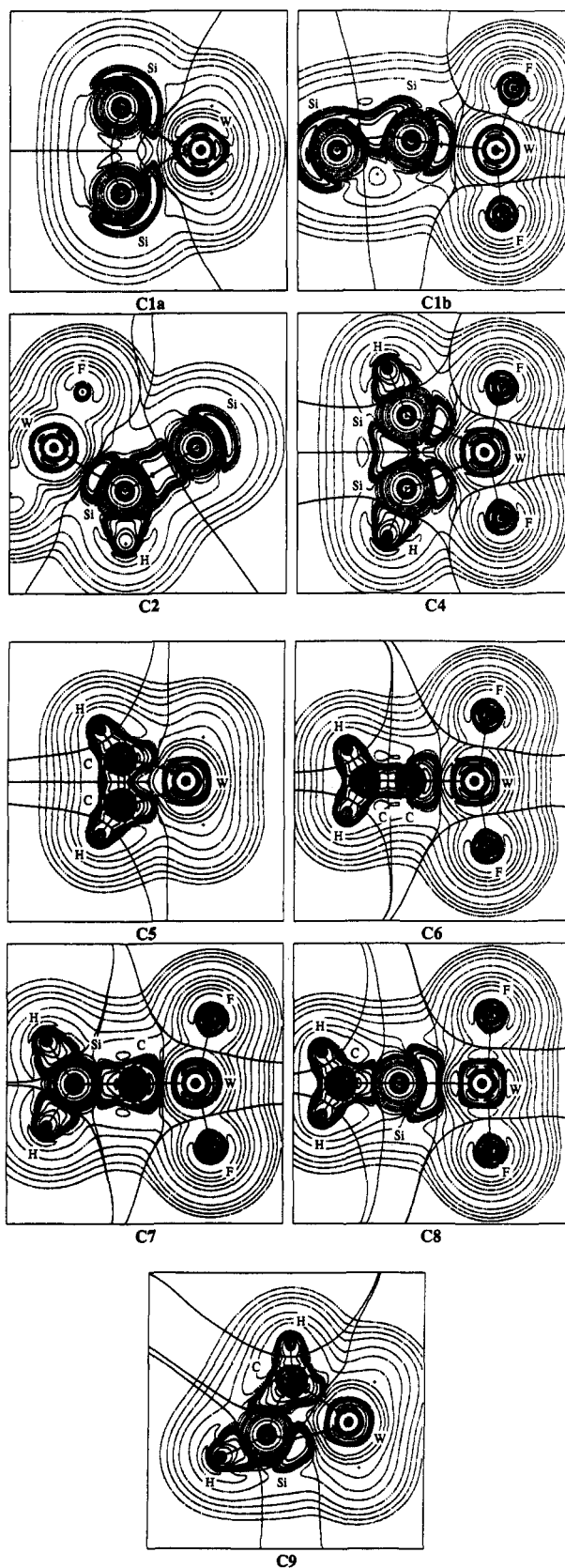


**Figure 4.** Contour line diagrams of the Laplacian distribution  $\nabla^2\rho(\mathbf{r})$  of the complexes **C1a-C9**. Dashed lines indicate charge depletion ( $\nabla^2\rho(\mathbf{r}) > 0$ ), and solid lines indicate charge concentration ( $\nabla^2\rho(\mathbf{r}) < 0$ ). The solid lines connecting the atomic nuclei are the bond paths, and the solid lines separating the atomic nuclei indicate the zero-flux surface in the plane. The crossing points of the bond paths and zero-flux surfaces are the bond critical points  $r_b$ .



The hybridization at Si has 46.1% s character, which means that it is sp hybridized. The Laplacian distribution (Figure 4) and the position of the bond critical point  $r_b$ , which is closer to the Si end, demonstrate also that the W–Si bond of **C1b** is significantly different from the W–Si bonds of **C1a**. The bond order of the former is slightly higher (0.91) than the bond order of the latter bonds (0.73).

The NBO analysis indicates a W–Si double bond for the silylene complex **C2**. Because the complex has C<sub>1</sub> symmetry, there are no clear  $\sigma$  and  $\pi$  bonds. One bond is nearly unpolar, while the other is polarized toward tungsten (65.7% at W). The accumulated bond order for the double bond is 1.42. The NBOs for the two W–Si bonds of **C4** are less polarized than those of **C1a** (Table 3). The NBO analysis indicates that the bonds are nearly unpolar (50.7% at W). The hybridization at Si is approximately sp<sup>3</sup>. The main difference compared to the W–C bonds of the related acetylene complex **C5** is the polarization. The W–Si bonds are clearly less polarized than the W–C bonds. The W–C bonds of **C5** have a 36% contribution from the tungsten atom; the W–Si bonds of **C4** have 50.7%.

The bonding situation of the WF<sub>4</sub>(CSiH<sub>2</sub>) complexes is very interesting. The NBO method gives two metal–ligand bonds, a  $\sigma$  and a  $\pi$  bond for the silavinylidene complex **C7** and the silylidene complex **C8**. The  $\sigma$  and the  $\pi$  W–C bonds of **C7** are polarized toward the carbon end (30.4 and 34.1% at W, respectively). A comparison with the vinylidene complex **C6** shows that the  $\pi$  bond of the latter is much more polarized toward the tungsten end. This is an important result for the reactivity of the two complexes. An electrophilic attack upon the W–C  $\pi$  bond of **C6** should occur at the tungsten end, while nucleophilic attack should be preferred at the carbon end. The opposite regioselectivity should be expected for the W–C bond of **C7**.

The W–Si  $\sigma$  bond of **C8** has nearly the same polarity as the W–C  $\sigma$  bond of **C7** (29.4 and 30.4%, Table 3). The  $\pi$  components of the two bonds are very different,

however. The W–Si  $\pi$  bond of **C8** is strongly polarized toward tungsten (85.6% at W), while the W–C  $\pi$  bond of **C7** is polarized toward the carbon end (34.1% at W). The NBO analysis gives three metal–ligand bonds for the silaacetylene complex **C9**. The W–C bond has  $\sigma$  and  $\pi$  components, which are both clearly polarized toward carbon (Table 3). This means that **C9** can be considered as an alkylidene complex with an additional W–Si bond. The calculated charge distribution predicted by the NBO scheme indicates that the tungsten atom carries always a positive charge between +2 and +3.

### Summary

The energetically lowest lying WF<sub>4</sub>(Si<sub>2</sub>H<sub>2</sub>) complex is the disilaacetylene complex **C4**. The compound **C4** is 10.1 kcal/mol lower in energy than the isomeric form **C1a**, which has the most stable doubly bridged Si<sub>2</sub>H<sub>2</sub> form as a ligand. Two other isomeric forms **C1b** and **C2** are clearly higher in energy. Three energy minimum structures are predicted for the WF<sub>4</sub>(CSiH<sub>2</sub>) complex. The global energy minimum is the silavinylidene complex **C7**, which has a very short and strong W–C double bond. The silaacetylene complex **C9** is 9.9 kcal/mol higher in energy. The third isomer is the silylidene complex **C8**, which is 33.2 kcal/mol less stable than **C7**. The analysis of the electronic structure of the complexes shows that the polarization of the W–Si bonds is clearly different compared to related complexes with W–C bonds. The W–Si bonds are more polarized toward the tungsten atom.

**Acknowledgment.** This work has been supported by the Deutsche Forschungsgemeinschaft (Grant SFB 260-D19) and the Fonds der Chemischen Industrie. We acknowledge generous support and excellent service by the computer centers HRZ Marburg, HHLRZ Darmstadt, and HLRZ Jülich.

OM950273G

# Mechanism of the Chelation Controlled Addition of $\text{CH}_3\text{TiCl}_3$ to $\alpha$ -Alkoxy Carbonyl Compounds. A Theoretical Study<sup>1</sup>

Volker Jonas,<sup>†,‡</sup> Gernot Frenking,<sup>\*,†</sup> and Manfred T. Reetz<sup>§</sup>

Fachbereich Chemie, Philipps-Universität Marburg, Hans-Meerwein-Strasse, D-35032 Marburg, Germany, and Max-Planck-Institut für Kohlenforschung, Kaiser-Wilhelm-Platz 1, D-45470 Mülheim an der Ruhr, Germany

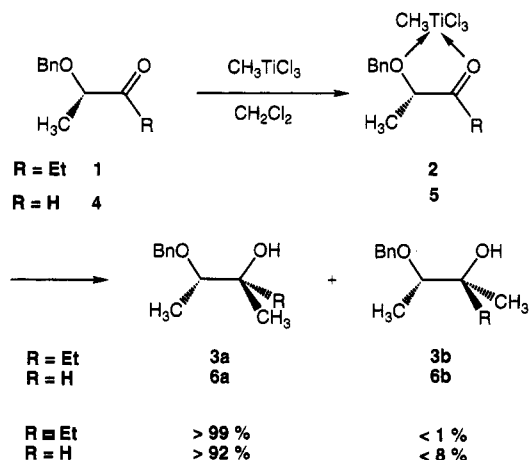
Received May 9, 1995<sup>®</sup>

The mechanism of the chelation controlled addition of  $\text{CH}_3\text{TiCl}_3$  to  $\alpha$ -alkoxy aldehydes has been studied using quantum chemical ab initio methods. The geometries of the  $\text{CH}_3\text{-TiCl}_3$  complexes of  $\alpha$ -alkoxy aldehydes have been optimized at the MP2 level of theory employing effective core potentials with valence double- $\zeta$  basis sets at titanium and polarized double- $\zeta$  all electron basis sets at the ligands. IGLO-calculations of the  $^{13}\text{C}$  chemical shifts have been carried out at the MP2 optimized geometries with large all electron basis sets. The calculations indicate that the rearrangement between the isomeric octahedral  $\text{CH}_3\text{-TiCl}_3$ -complexes occurs via a dissociation–association mechanism with pentacoordinated intermediates. The barrier for the methyl shift from titanium to the carbonyl group of the complexed aldehyde is calculated to be ca. 19 kcal/mol at the MP2 level of theory. The calculations also give a possible explanation for the different mechanism of the analogous reaction of  $\text{CH}_3\text{TiCl}_3$  with  $\alpha$ -alkoxy ketones.

## 1. Introduction

Octahedral chelate complexes of  $\text{TiCl}_4$  and  $\text{CH}_3\text{TiCl}_3$  are important species in stereoselective reactions, because the formation of chelates as intermediates may strongly influence the stereoselectivity of carbonyl addition reactions.<sup>2</sup> For example,  $\text{CH}_3\text{TiCl}_3$  reacts with chiral  $\alpha$ -alkoxy carbonyl compounds **1** and **4** with high diastereoselectivity to form the chelation controlled products **3a** and **6a**, respectively (Scheme 1).<sup>2,3</sup> Octahedral chelate complexes **2** and **5** as intermediates have been suggested to account for the observed diastereoselectivity, which is opposite to what is predicted by the Felkin-Anh model.<sup>4</sup> Later, these Cram-type chelates were observed directly by  $^1\text{H}$  and  $^{13}\text{C}$  NMR spectroscopy.<sup>5,6</sup> Since the ligands are not symmetrical, four diastereomeric octahedral chelates **2a–d** (and **5a–d**, respectively; Figure 1) are possible, but only two are observed. It was proposed that the two observed complexes have the methyl groups at titanium trans to the chelating donor ligand.<sup>5</sup>

## Scheme 1



In a previous theoretical study we have predicted on the basis of ab initio methods that the octahedral model complexes **8a** and **8c** are 1.2 and 0.6 kcal/mol higher in energy than **8b**, respectively (Figure 1).<sup>7</sup> The same trend was calculated for the related  $\text{CH}_3\text{TiCl}_3$  complexes of glycol and ethylenediamine.<sup>7</sup> Glycol ether and diamine adducts of  $\text{CH}_3\text{TiCl}_3$  have the methyl group in the "equatorial" position, as shown by  $^1\text{H-NMR}$  spectroscopy.<sup>8</sup> In this context, we use the terms "axial" and "equatorial" for ligands which are above (axial) or in the plane (equatorial) of the chelate ring. Green has published the results of an X-ray structural analysis of a diphosphine adduct of  $\text{CH}_3\text{TiCl}_3$ , which also shows the methyl group in the equatorial position.<sup>9</sup> To our knowl-

(7) Jonas, V.; Frenking, G.; Reetz, M. T. *Organometallics* 1993, 12, 2111.

(8) (a) Clark, R. J. H.; McAlees, A. J. *J. Chem. Soc. A* 1970, 2026. (b) Clark, R. J. H.; McAlees, A. J. *Inorg. Chem.* 1972, 11, 342.

(9) Dawoodi, Z.; Green, M. L. H.; Mtetwa, V. S. B.; Prout, K.; Schultz, A. J.; Williams, J. M.; Koetzle, T. F. *J. Chem. Soc. Dalton Trans.* 1986, 1629.

<sup>†</sup> Philipps-Universität Marburg.

<sup>‡</sup> Present address: Bayer, AG, MD-IM-FA, Q18, D-51368 Leverkusen.

<sup>§</sup> Max-Planck-Institut für Kohlenforschung, Mülheim.

<sup>®</sup> Abstract published in *Advance ACS Abstracts*, October 15, 1995.

(1) Theoretical Studies of Organometallic Compounds. 16. Part 15: Stegmann, R.; Frenking, G. *Organometallics* 1995, 14, 5308.

(2) (a) Reetz, M. T. *Angew. Chem.* 1984, 96, 542. *Angew. Chem., Int. Ed. Engl.* 1984, 23, 556. (b) Reetz, M. T. *Organotitanium Reagents in Organic Synthesis*; Springer: Berlin, 1986.

(3) Reetz, M. T.; Hüllmann, M. *J. Chem. Soc., Chem. Commun.* 1986, 1600.

(4) (a) Chérest, M.; Felkin, H.; Prudent, N. *Tetrahedron Lett.* 1968, 2201, 2205. (b) Anh, N. T.; Eisenstein, O. *Nouv. J. Chim.* 1977, 1, 61. (c) Anh, N. T. *Top. Curr. Chem.* 1980, 68, 145.

(5) (a) Reetz, M. T.; Hüllmann, M.; Seitz, T. *Angew. Chem.* 1987, 99, 478. *Angew. Chem., Int. Ed. Engl.* 1987, 26, 477. (b) Seitz, T.; Dissertation, Marburg, 1987. (c) Hüllmann, M.; Dissertation, Marburg, 1986.

(6) Reetz, M. T.; Raguse, B.; Seitz, T. *Tetrahedron* 1993, 49, 8561.

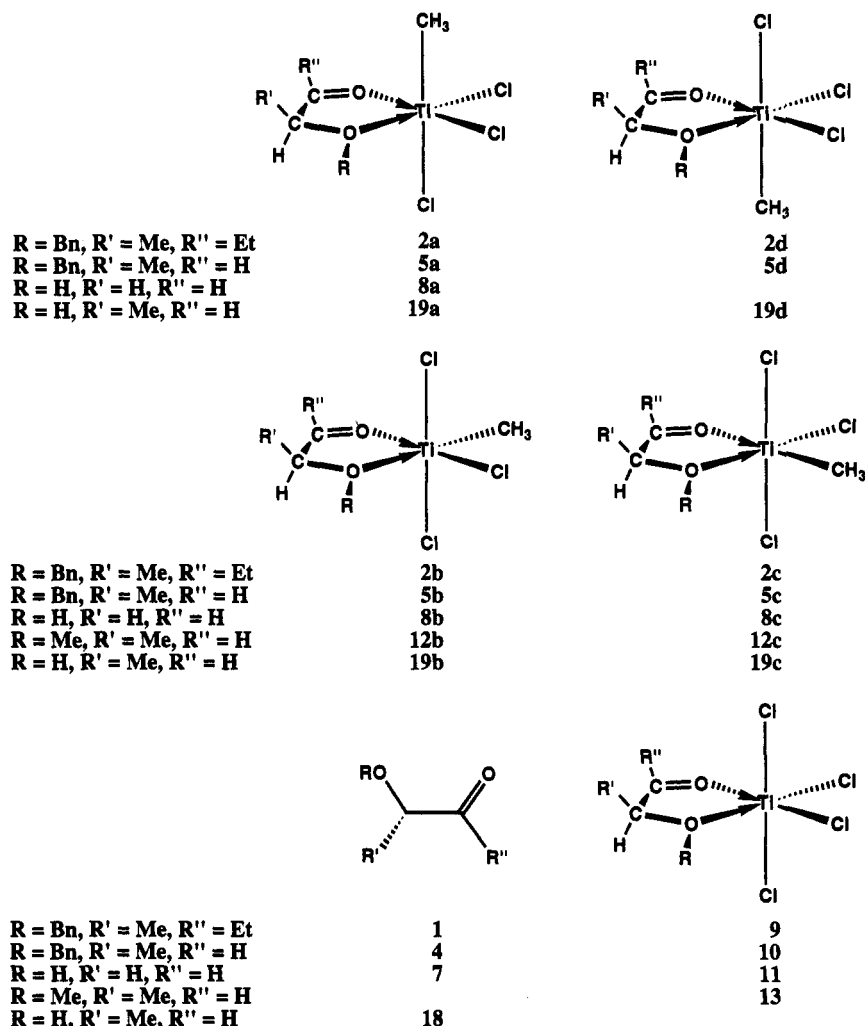


**Figure 1.** Experimental complexes of ketone **1** and aldehyde **4** with  $\text{CH}_3\text{TiCl}_3$  and  $\text{TiCl}_4$ . Model aldehydes and complexes with  $\text{CH}_3\text{TiCl}_3$  and  $\text{TiCl}_4$ .

edge, this is the only complex of  $\text{CH}_3\text{TiCl}_3$  for which the experimental structure is known. Our calculations suggest that the different deformation energies of  $\text{CH}_3\text{-TiCl}_3$  when forming the isomeric octahedral complexes determine the relative energies.<sup>7</sup> However, the calculated energies did not provide any insight into the reaction mechanism of the actual chelation controlled C–C bond formation.

Complexes **2** are the first and so far only Cram-type chelates which have been characterized directly by NMR spectroscopy,<sup>5</sup> whereas attempts to observe magnesium Cram-type chelates failed due to the high rate of C–C bond formation.<sup>10</sup> At  $-80\text{ }^\circ\text{C}$  **1** and  $\text{CH}_3\text{TiCl}_3$  form an octahedral chelate complex **2** which gives a discrete set of signals in the  $^{13}\text{C}$ -NMR spectrum.<sup>5c</sup> When warming the solution up to  $-60\text{ }^\circ\text{C}$  a second set of signals appears. The ratio of the two carbonyl signals is then 85:15; the new carbonyl signal is shifted 0.8 ppm to lower field. At  $-45\text{ }^\circ\text{C}$  the observed ratio is 60:40. At this temperature the actual C–C bond formation begins, the complex with the carbonyl signal at higher field reacting faster. From this observation it can be concluded that at  $-80\text{ }^\circ\text{C}$  one of the complexes **2b/2c** is formed in a kinetically controlled reaction. Structures **2b** and **2c** begin to equilibrate at higher temperatures.

Equilibrium is not reached because the nucleophilic reaction takes place.<sup>5</sup> The question how the methyl group reaches the carbonyl C atom could not be answered unambiguously. The ketone chelates **2b/2c** do not afford **3a** with first-order kinetics, which would indicate an intramolecular 1,3 methyl shift. Rather, the data obtained at  $-15\text{ }^\circ\text{C}$  is more in line with second order kinetics, although an ideal fit (perfect straight line for the plot of  $(1/c - 1/c_0)$  against time) was not observed.<sup>5</sup> Thus, a complicated mechanism seems to be operating for this synthetically clean reaction.

In the analogous reaction of aldehyde **4**, the complex formation with  $\text{CH}_3\text{TiCl}_3$  at low temperatures is very similar to that of ketone **1**. At  $-60\text{ }^\circ\text{C}$  **4** forms two octahedral chelate complexes **5b/5c** which result in two sets of  $^{13}\text{C}$ -NMR signals. The ratio of the two carbonyl signals is 93:7. In analogy to complexes **2**, the carbonyl signal of the major diastereomer is at higher field.<sup>6</sup> Warming the solution changes the ratio of signals to 70:30. As for **2b/2c**, the ratio of 93:7 for **5b/5c** is kinetically controlled and thermodynamic equilibration is not reached due to the nucleophilic addition reaction.<sup>5,6</sup> In the kinetic study, data were obtained at  $-20\text{ }^\circ\text{C}$ , which are in line with clean first-order kinetics, i.e. a plot of  $-\ln c/c_0$  against time results in a straight line. This indicates an intramolecular 1,3 methyl shift, probably via the higher energy species **5a**, which is

(10) Chen, X.; Hortelano, E. R.; Eliel, E. L.; Frye, S. V. *J. Am. Chem. Soc.* 1992, 114, 1778.

**Table 1. Basis Set Combinations Used in This Study<sup>a</sup>**

	Ti	Cl	C,O,H
II	(441/2111/41) <sup>b</sup>	6-31G(d) <sup>c</sup>	6-31G(d) <sup>c</sup>
III	(441/2111/41/1) <sup>c</sup>	6-31G(d)	6-31G(d)
IV	(53321/52111/311) <sup>d</sup>	6-31G(d)	6-31G(d)
V	(53321/52111/311/1) <sup>e</sup>	6-31G(d)	6-31G(d)
VI	(62111111/5111111/3111) <sup>f</sup>	TZ2P <sup>h</sup>	TZP <sup>h</sup>

<sup>a</sup> 5d and 7f functions are used throughout. <sup>b</sup> ECP basis set, refs 16, 17. <sup>c</sup> ECP basis set with one set of f functions (exponent 1.506), ref 18. <sup>d</sup> All electron basis set, refs 19, 20. <sup>e</sup> All electron basis set with one set of f functions (exponent 1.506). <sup>f</sup> References 21, 22, see also ref 27. <sup>g</sup> Reference 23. <sup>h</sup> Triple- $\zeta$  type basis sets, see ref 27.

expected to be in equilibrium with **5b/5c**. Crossover experiments turned out to be inconclusive.<sup>6</sup> The difference in behavior between **2b/2c** and **5b/5c** is presently unclear and will be discussed in this study.

The mechanistic aspects of the reactions of ketone **1** and aldehyde **4** with CH<sub>3</sub>TiCl<sub>3</sub> are investigated theoretically in this paper. The structural, mechanistic, and theoretical aspects of chelation controlled carbonyl addition reactions have recently been reviewed.<sup>11</sup> Here we will focus on further aspects concerning the details of the reaction mechanism, including the C–C bond-forming step.

## 2. Theoretical Methods

The calculations were performed using the program packages Gaussian92<sup>12</sup> and Turbomole.<sup>13</sup> The geometries were optimized at the Hartree–Fock (HF) and MP2 (Møller–Plesset perturbation theory<sup>14</sup> terminated at second order) levels of theory.<sup>15</sup> The basis sets used in this study are listed in Table 1. From our systematic basis set studies for the Hay/Wadt ECP valence basis sets we have derived “standard combinations”.<sup>17</sup> In this nomenclature, basis set I is a (441/41/41) valence basis set at the transition metal in combination with a 3-21G basis set at the ligands. This basis set is not used in this study. Therefore, Table 1 begins with basis set II.

For the optimization of the energy minimum structures the pseudopotential basis sets II and III were used. For the transition states and the corresponding reactants and products the all electron basis sets IV and V were used because the Gaussian92 program does not offer analytical second derivatives in combination with ECP wavefunctions. Harmonic vibrational frequencies were calculated at the HF/II or HF/IV level, respec-

tively.<sup>24,25</sup> The calculated zero point energies (ZPE) were scaled by a factor of 0.89 to correct for the overestimation of vibrational frequencies at this level of theory.<sup>26</sup> All complexes were verified as minima on the potential energy hypersurface by only positive eigenvalues of the Hessian matrix. The transition states were verified by one negative eigenvalue of the Hessian matrix.

The calculations of the <sup>13</sup>C-NMR chemical shifts  $\delta$  were done with the IGLO method<sup>27</sup> with basis set VI at MP2/II optimized geometries.

## 3. Results and Discussion

**General Remarks.** For our calculations, the alkyl and benzyl groups of the experimental complexes **2a–d** and **5a–d** have been replaced by methyl groups and hydrogens, respectively, as shown in Figure 1. The geometries around the titanium atom and relative energies of isomeric complexes should not be affected very much by variations of the alkyl groups of the chelating ligand. Therefore, our first calculations were done with the model complexes **8a–c**, which contain only hydrogens at the chelating ligand. For the calculations of the <sup>13</sup>C-chemical shifts, the experimental chemical shifts of the ether carbons turned out to be particularly interesting. Therefore, we also used the model complexes **12b,c** and **13** for the calculation of the <sup>13</sup>C-chemical shifts. The chiral model complexes **19a–d** have been used for the calculation of the two transition states which lead to the major and minor product within the methyl group migration.

**Structures and Energies.** The theoretically predicted energy minimum structures of the model complexes **8a–c** are shown in Figure 2. The calculated bond lengths are given in Table 2, the calculated complex formation energies are listed in Table 3. The geometries were optimized at the HF and MP2 levels of theory. It has been shown recently that for a related diphosphine complex of CH<sub>3</sub>TiCl<sub>3</sub> the agreement between the calculated and experimental geometries is much better at the MP2 level than at the HF level.<sup>28</sup> At the HF level, the

(18) Ehlers, A. W.; Böhme, M.; Dapprich, S.; Gobbi, A.; Höllwarth, A.; Jonas, V.; Köhler, K. F.; Stegmann, R.; Veldkamp, A.; Frenking, G. *Chem. Phys. Lett.* **1993**, *208*, 111.

(19) Andzelm, J.; Huzinaga, S.; Klobukowski, M.; Radzio, E.; Sakai, Y.; Tatewaki, H. *Gaussian Basis Sets For Molecular Calculations*; Elsevier: Amsterdam, 1984.

(20) Barandiaran, Z.; Seijo, L.; Huzinaga, S.; Klobukowski, M. *Int. J. Quantum Chem.* **1986**, *29*, 1047.

(21) Wachters, A. J. H. *J. Chem. Phys.* **1970**, *52*, 1033.

(22) Hay, P. J. *J. Chem. Phys.* **1977**, *66*, 4377.

(23) (a) Ditchfield, R.; Hehre, W. J.; Pople, J. A. *J. Chem. Phys.* **1971**, *54*, 724. (b) Hehre, W. J.; Ditchfield, R.; Pople, J. A. *J. Chem. Phys.* **1972**, *56*, 2257. (c) Hariharan, P. C.; Pople, J. A. *Theoret. Chim. Acta.* **1973**, *28*, 213. (d) Francl, M. M.; Pietro, W. J.; Hehre, W. J.; Binkley, J. S.; Gordon, M. S.; Defrees, D. J.; Pople, J. A. *J. Chem. Phys.* **1982**, *77*, 3654.

(24) Pople, J. A.; Krishnan, R.; Schlegel, H. B.; Binkley, J. S. *Int. J. Quantum Chem. Symp.* **1979**, *13*, 225.

(25) Breidung, J.; Thiel, W.; Komornicki, A. *Chem. Phys. Lett.* **1988**, *153*, 76.

(26) Hout, R. F.; Levi, B. A.; Hehre, W. J. *J. Comput. Chem.* **1982**, *2*, 234.

(27) (a) Kutzelnigg, W. *Isr. J. Chem.* **1980**, *19*, 193. (b) Kutzelnigg, W.; Fleischer, U.; Schindler, M. *NMR Basic Principles and Progress*; Springer: New York, 1990; Vol. 23, p 165. For Ti, an all electron [14s9p5d]/(8s5p3d) basis set from Wachters<sup>21</sup> was chosen, augmented by two additional 4p functions as recommended by Wachters and a diffuse d function.<sup>22</sup> This gives a [14s11p6d]/(8s7p4d) basis set for Ti. For the ligand atoms the IGLO-basis set II is used which is a [11s7p2d]/(7s6p2d) basis set for Si and Cl, [9s5p1d]/(5s4p1d) for C, and [5s1p]/(3s1p) for H.

(11) Reetz, M. T. *Acc. Chem. Res.* **1993**, *26*, 462.

(12) Gaussian92, Revision C: Frisch, M. J.; Trucks, G. W.; Head-Gordon, M.; Gill, P. M. W.; Wong, M. W.; Foresman, J. B.; Johnson, B. G.; Schlegel, H. B.; Robb, M. A.; Replogle, E. S.; Gomperts, R.; Andres, J. L.; Raghavachari, K.; Binkley, J. S.; Gonzalez, C.; Martin, R. L.; Fox, D. J.; Defrees, D. J.; Baker, J.; Stewart, J. J. P.; Pople, J. A.; Gaussian, Inc., Pittsburgh PA, 1992.

(13) Turbomole: (a) Häser, M.; Ahlrichs, R. *J. Comput. Chem.* **1989**, *10*, 104. (b) Ahlrichs, R.; Bär, M.; Häser, M.; Horn, H.; Kölmel, C. *Chem. Phys. Lett.* **1989**, *162*, 165. (c) Horn, H.; Weiss, H.; Häser, M.; Ehrig, M.; Ahlrichs, R. *J. Comput. Chem.* **1991**, *12*, 1058. (d) Häser, M.; Almlöf, J.; Feyereisen, M. W. *Theoret. Chim. Acta* **1991**, *79*, 115. (e) Häser, M.; Ahlrichs, R.; Baron, H. P.; Weis, P.; Horn, H. *Theoret. Chim. Acta* **1992**, *83*, 455. (f) Haase, F.; Ahlrichs, R. *J. Comput. Chem.* **1993**, *14*, 907.

(14) (a) Møller, C.; Plesset, M. S. *Phys. Rev.* **1934**, *46*, 618. (b) Binkley, J. S.; Pople, J. A. *Int. J. Quantum Chem.* **1975**, *9*, 229.

(15) Hehre, W. J.; Radom, L.; Schleyer, P. v. R.; Pople, J. A. *Ab Initio Molecular Orbital Theory*; Wiley: New York, 1986.

(16) Hay, P. J.; Wadt, W. R. *J. Chem. Phys.* **1985**, *82*, 299.

(17) Jonas, V.; Frenking, G.; Reetz, M. T. *J. Comput. Chem.* **1992**, *13*, 919.

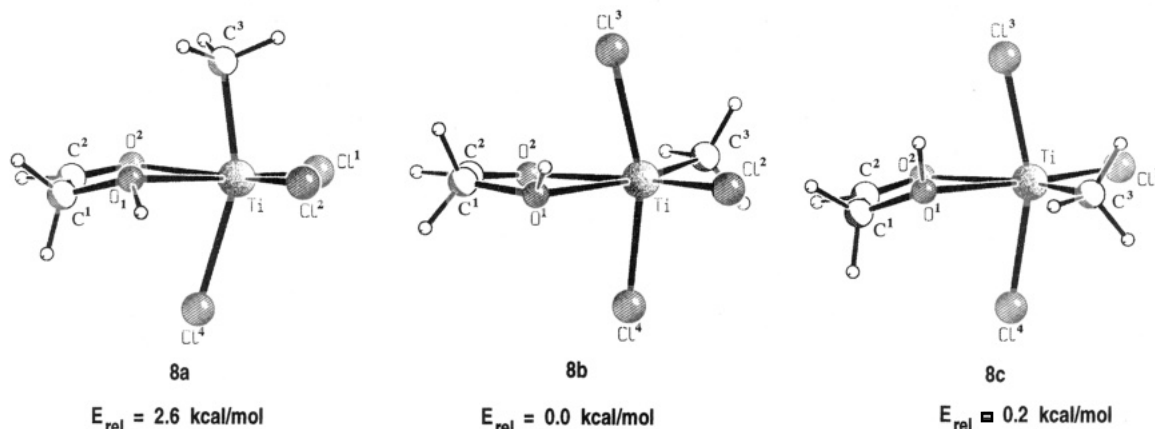


**Figure 2.** Calculated structures of **8a–c** at MP2/II. The respective bond lengths are given in Table 2. Relative energies are given in kcal/mol at MP2/III//MP2/II + ZPE(HF/II).

**Table 2.** Calculated Bond Lengths (Å) for **8a–c**, **11–13**, and **14a,b**<sup>a</sup>

	8a	8b	8c	11	12b	12c	13	14a	14b
Ti–Cl <sup>1</sup>	2.171		2.165	2.170		2.175	2.172	2.221	2.190
Ti–Cl <sup>2</sup>	2.194	2.170		2.176	2.187		2.195		
Ti–Cl <sup>3</sup>		2.302	2.311	2.317	2.274	2.282	2.284	2.188	2.239
Ti–Cl <sup>4</sup>	2.335	2.259	2.259	2.267	2.283	2.283	2.289	2.188	2.204
Ti–C <sup>3</sup>	2.131	2.070	2.076		2.074	2.094		2.079	2.080
Ti–O <sup>1</sup>	2.314	2.309	2.307	2.287	2.300	2.318	2.283	2.286	2.217
Ti–O <sup>2</sup>	2.223	2.352	2.337	2.298	2.267	2.250	2.241		
C <sup>1</sup> –O <sup>1</sup>	1.431	1.431	1.430	1.431	1.429	1.432	1.432	1.440	1.445
C <sup>2</sup> –O <sup>2</sup>	1.230	1.229	1.230	1.230	1.229	1.230	1.229		

<sup>a</sup> Calculated at MP2/II.

**Table 3.** Calculated Complex Formation Energies (kcal/mol) for **8a–c** and **14a,b**

method	8a	8b	8c	14a	14b
MP2/II + ZPE(HF/II)	-17.0	-19.4	-19.2	-16.8	-16.8
MP2/III//MP2/II + ZPE	-15.6	-18.2	-18.0	-15.9	-15.9

deviations for the metal–ligand bond lengths are  $-0.03$  Å (Ti–Cl<sup>1</sup>),  $+0.04$  Å (Ti–Cl<sup>3</sup>),  $+0.06$  Å (Ti–Cl<sup>4</sup>),  $-0.06$  Å (Ti–C),  $+0.11$  Å (Ti–P<sup>1</sup>), and  $+0.19$  Å (Ti–P<sup>2</sup>) between the experimental  $\text{Me}_2\text{PCH}_2\text{CH}_2\text{PMe}_2\text{-CH}_3\text{-TiCl}_3$  complex and the calculated  $\text{H}_2\text{PCH}_2\text{CH}_2\text{PH}_2\text{-CH}_3\text{-TiCl}_3$  complex. Especially the Ti–P bond trans to the Ti–C bond is calculated much too long. At the MP2 level, the corresponding deviations are  $-0.04$  Å,  $+0.02$  Å, and  $+0.03$  Å for Ti–Cl,  $-0.01$  Å for Ti–C, and  $+0.02$  Å and  $+0.05$  Å for Ti–P.<sup>28</sup>

Very recently, it has been shown that for binary transition metal carbonyl complexes the *relative* bond dissociation energies calculated at the MP2 level show the same trend as at the CCSD(T)-level.<sup>29</sup> As we expect that the theoretical description of a titanium complex with  $d^0$  electron configuration is easier than that of a transition metal carbonyl complex with  $d^n$  electron configuration, we think that the relative MP2 energies calculated in this study are quite reliable. For these reasons, we will only discuss the MP2 optimized geometries and MP2 energies of the titanium chelate complexes in this paper.

The optimized structures have a distorted octahedral geometry around titanium with the axial ligands tilted toward the bidentate ligand. Structure **8a** is calculated as clearly higher in energy than **8c** at all levels of

theory. The difference between **8b** and **8c** is much smaller. At the highest level of theory (MP2/III//MP2/II + ZPE) structure **8b** is only 0.2 kcal/mol lower in energy than **8c**. Thus, the calculations support the interpretation of the <sup>13</sup>C-NMR spectra of **2** and **5**, which are observed in the reactions of  $\text{CH}_3\text{TiCl}_3$  with  $\alpha$ -alkoxy carbonyl compounds (Scheme 1).<sup>5,6</sup> In these reactions, only the isomers with the methyl group in an equatorial position are formed.

**<sup>13</sup>C-NMR Chemical Shifts.** The small energy differences calculated for **8a–c** do not allow a definitive answer as to which complex (**8b** or **8c**) is thermodynamically more stable (Figure 2). In order to find out which of the two “equatorial” isomers of **2** and **5** is the major diastereomer, we have also calculated the <sup>13</sup>C-NMR chemical shifts of the model complexes **8b/8c** and **12b/12c** and the respective  $\text{TiCl}_4$ -complexes **11** and **13** with the IGLO method.<sup>27</sup> IGLO-calculations for  $\text{Ti}(\text{CH}_3)_n\text{Cl}_{4-n}$  ( $n = 1-4$ ) show that the agreement with experimental data for the <sup>13</sup>C-NMR signals is very good for MP2 optimized geometries.<sup>30</sup> Figure 3 shows the optimized structures for **11**, **12b/12c**, and **13**. Figure 4 summarizes the assignment of the experimental <sup>13</sup>C signals<sup>5,6,31</sup> for the complexes of **1** and **4** with  $\text{CH}_3\text{TiCl}_3$  and  $\text{TiCl}_4$  (**2b**, **2c**, **5b**, **5c**, **9**, and **10**). Figure 5 contains the calculated <sup>13</sup>C-NMR shifts for the respective model complexes **8b**, **8c**, **11**, **12b**, **12c**, and **13**.

The calculated <sup>13</sup>C-NMR chemical shifts for the ether carbon atoms of **8b/8c** and **12b/12c** support the assignment that **2b/5b** are the “kinetic” isomers and **2c/5c** are the “thermodynamic” isomers. The experimental <sup>13</sup>C-NMR signals of the ether carbon atoms of **2b** and **2c** differ by 6.1 and 6.6 ppm, respectively. For **5b** and **5c**, the differences are 5.9 and 6.2 ppm. Because of the trans-influence of the methyl group at titanium the signals of the ether carbon atoms are at lower field in **2c/5c** than in **2b/5b**. The experimental <sup>13</sup>C-NMR chemical shifts of the ether carbon atoms of **9** and **10** are very close to the values of **2c** and **5c**, respectively. In both cases a chlorine ligand occupies the position trans to the ether group.

The calculated shifts for the ether carbon atoms of **8b/8c** and **12b/12c** show the same trend as the experi-

(28) Weiss, H.; Haase, F.; Ahlrichs, R. *Chem. Phys. Lett.* **1992**, *194*, 492.

(29) Dapprich, S.; Pidun, U.; Ehlers, A. W.; Frenking, G. *Chem. Phys. Lett.* **1995**, *242*, 521.

(30) Berger, S.; Bock, W.; Frenking, G.; Jonas, V.; Müller, F. *J. Am. Chem. Soc.* **1995**, *117*, 3820.

(31) In contrast to reference 5c we assign the signals at 84.8 and 89.4 ppm to the ether carbons of **11**.

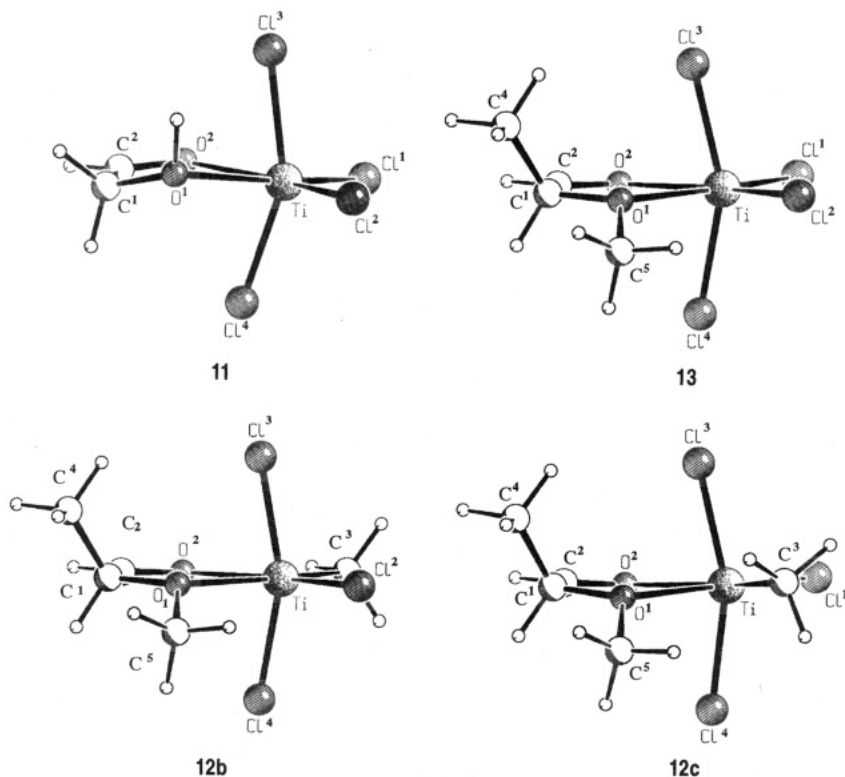


Figure 3. Calculated structures of **11**, **12b/c**, and **13** at MP2/II. The respective bond lengths are given in Table 2.

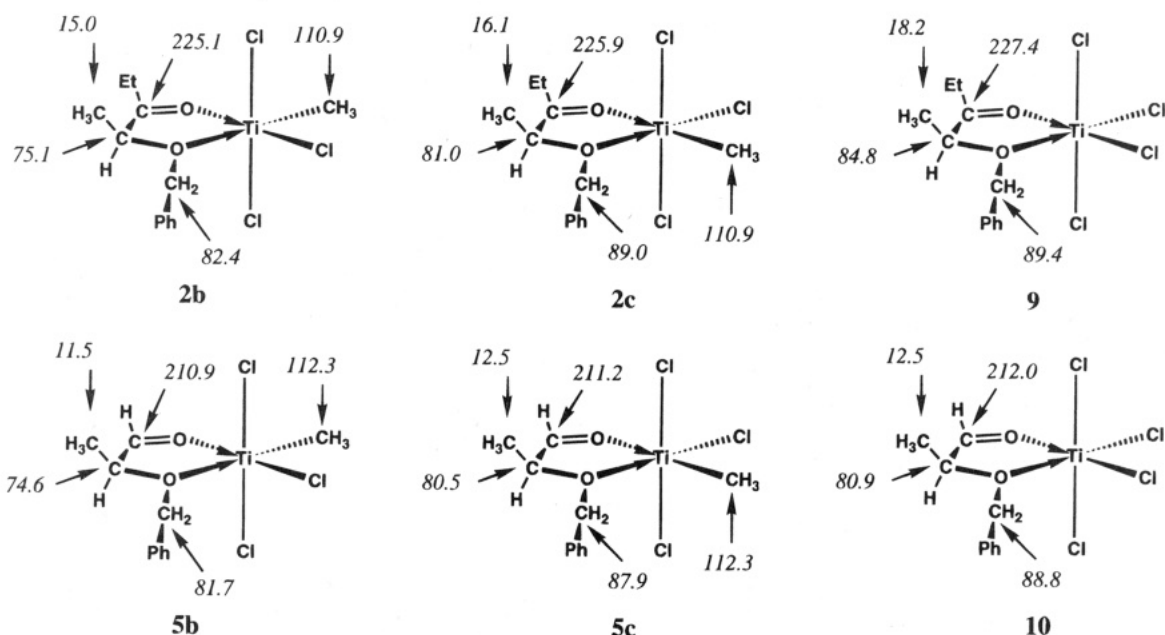
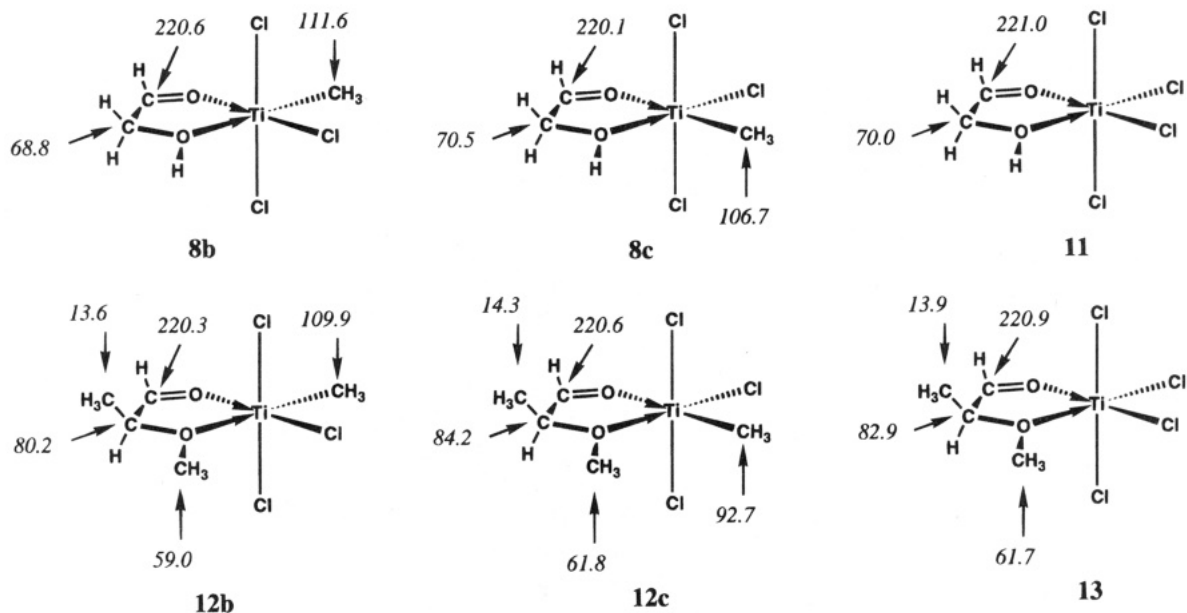


Figure 4. Experimental  $^{13}\text{C}$  chemical shifts (ppm) for **2b/c**, **5b/c**, **9**, and **10**.

mental  $^{13}\text{C}$ -NMR values of the ether carbon atoms of **2b** versus **2c** and **5b** versus **5c**. As the alkyl substitution at the chelating ligand is different, the absolute chemical shifts of **8b/8c** and **12b/12c** are different from the experimental values of **2b/2c** and **5b/5c**, but the trend is the same. For **8b/8c**, the calculated difference is 1.7 ppm at HF/VI/MP2/II. The calculated differences for the ether carbon atoms of **12b/12c** are 4.0 and 2.8 ppm, respectively. As for the experimental structures **2c/9** and **5c/10**, the values for the ether carbon atoms of **11** and **13** are close to the values of **8c** and **12c**. The very small differences of the  $^{13}\text{C}$ -NMR chemical shifts of the carbonyl carbon atoms (<1 ppm) found by theory and experiment are too small to be conclusive.

The experimental spectra of **2b/2c** and **5b/5c** show only one signal for the methyl carbon atoms bonded to titanium, which is broadened relative to the spectrum at lower temperatures. Our calculations for the model complexes **8b/8c** and **12b/12c** result in two clearly different chemical shifts. At this point we do not have an explanation for the two calculated  $^{13}\text{C}$ -NMR chemical shifts of the methyl groups bonded to titanium. Nevertheless, the calculated  $^{13}\text{C}$ -NMR chemical shifts of the ether carbons which are two bonds away from the metal center should be quite reliable. They support the conclusion that in those isomers which are formed at low temperatures in a kinetically controlled reaction, i.e. **2b** and **5b**, the methyl group at titanium occupies





**Figure 5.** Calculated  $^{13}\text{C}$  chemical shifts (ppm) at HF/VI/MP2/II for the model complexes **8b/c**, **11**, **12b/c**, and **13**. The calculated bond lengths of **8b/c**, **11**, **12b/c**, and **13** are given in Table 2.

the position trans to the ether group. Isomers **2c/5c** are thermodynamically more stable and are formed in the equilibrium with **2b/5b**, respectively, when warming up the solutions.

**Reaction Kinetics.** Since the rearrangement of **5b/5c** occurs according to a first order rate law,<sup>6</sup> the rate-determining step should be the intramolecular methyl shift from titanium to the carbonyl group via complex **5a**. For this, **5a** must be formed besides **5b** and **5c**. Theoretically, there are two mechanisms for the rearrangement among the isomers: One mechanism involves a rotation of one face of the octahedron with respect to the opposite face as viewed along a three-fold axis of a regular octahedron. The other mechanism is a dissociation–association mechanism with pentacoordinated intermediates in which one of the original donor–acceptor bonds has been broken.

The two mechanisms were investigated theoretically starting from the model complexes **8a–c** involving hydroxyacetaldehyde and  $\text{CH}_3\text{TiCl}_3$ . For the search of a transition state for rotation about a face of the octahedron the six ligands were oriented in a trigonal prismatic arrangement (**8a** to **8b**, **8b** to **8c**, and **8a** to **8c**). In the first step, the metal–ligand bond lengths and one torsion angle  $\text{Cl–Ti–Cl–O}$  were kept frozen to fix the trigonal prismatic arrangement. After some optimization cycles, the calculation was continued without frozen variables. Then, in each of the three cases dissociation of the carbonyl group from titanium occurred leading to pentacoordinated complexes. The dissociation–association mechanism should therefore be favored for the equilibrium between **8a–c**.

To simulate the formation of **8a–c** in a kinetically controlled reaction we calculated the model complexes of  $\text{CH}_3\text{OH}$  with  $\text{CH}_3\text{TiCl}_3$ . In this case,  $\text{CH}_3\text{OH}$  serves as model for **7** because it is assumed that within the complex formation of **7** with  $\text{CH}_3\text{TiCl}_3$  under kinetically controlled conditions the two donor–acceptor bonds are formed separately. Since the donor strength of the OH-group is higher than that of the carbonyl group,<sup>32</sup> the first bond should be formed by the OH group. The

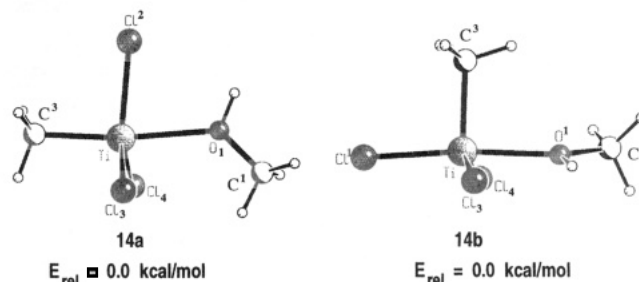


**Figure 6.** Calculated structures of **14a,b**. The respective bond lengths are given in Table 2. Relative energies are given in kcal/mol at MP2/III/MP2/II + ZPE(HF/II).

optimization of complexes of  $\text{CH}_3\text{OH}$  with  $\text{CH}_3\text{TiCl}_3$  leads to two minimum structures **14a** and **14b** (Figure 6). The geometries of **14a** and **14b** are given in Table 2; the calculated complex formation energies are listed in Table 3.

Isomers **14a** and **14b** are energetically degenerate at the highest level of theory used in this study (Table 3). Because it can be assumed that the relative energies of **15a** and **15b** (Figure 7) are very similar to those of **14a** and **14b**, the energy calculations cannot be used to predict which isomer is initially formed in the first step of the chelation process. However, the IGLO-calculations of the  $^{13}\text{C}$ -NMR-chemical shifts suggest that **15a** is the first step of complex formation in the kinetically controlled reaction of **7**. As the bonding angles in tetrahedral  $\text{CH}_3\text{TiCl}_3$  are  $104.9^\circ$  for  $\text{C–Ti–Cl}$  and  $113.6^\circ$  for  $\text{Cl–Ti–Cl}$  (MP2/II values),<sup>30</sup> the attack of an electron donor trans to the methyl group of  $\text{CH}_3\text{TiCl}_3$  is probably favored for steric reasons between two chlorine ligands rather than between the methyl group and one chlorine ligand.

To calculate the energy barrier between **14a** and **14b** we fixed the angle  $\text{C–O–Ti}$  in small steps from  $90^\circ$  (in **14b**) to  $187^\circ$  (in **14a**) and optimized the rest of the

(32) Jonas, V.; Frenking, G.; Reetz, M. T. *J. Am. Chem. Soc.* **1994**, *116*, 8741.



**Table 4.** Calculated Bond Lengths (Å) for **8a**, **16**, **17**, and **19a–21b**<sup>a</sup>

	<b>8a</b>	<b>16</b>	<b>17</b>	<b>19a</b>	<b>19b</b>	<b>19c</b>	<b>19d</b>	<b>20a</b>	<b>20b</b>	<b>21a</b>	<b>21b</b>
Ti–Cl <sup>1</sup>	2.181	2.186	2.209	2.231		2.233	2.230	2.224	2.223	2.231	2.232
Ti–Cl <sup>2</sup>	2.197	2.211	2.217	2.264	2.250		2.257	2.273	2.270	2.242	2.239
Ti–Cl <sup>3</sup>					2.368	2.368	2.442		2.303		2.268
Ti–Cl <sup>4</sup>	2.365	2.297	2.261	2.440	2.322	2.331		2.304		2.268	
Ti–C <sup>3</sup>	2.148	2.281		2.078	2.024	2.039	2.080	2.304	2.313		
Ti–O <sup>1</sup>	2.302	2.279	2.348	2.334	2.419	2.338	2.348	2.317	2.312	2.276	2.269
Ti–O <sup>2</sup>	2.243	2.155	1.760	2.213	2.240	2.322	2.211	1.994	1.996	1.749	1.750
C <sup>1</sup> –O <sup>1</sup>	1.429	1.436	1.442	1.412	1.408	1.412	1.410	1.417	1.417	1.432	1.431
C <sup>2</sup> –O <sup>2</sup>	1.229	1.255	1.443	1.198	1.197	1.195	1.197	1.253	1.254	1.414	1.412
C <sup>2</sup> –C <sup>3</sup>	3.227	2.394	1.516	3.486			3.401	2.254	2.234	1.521	1.520

<sup>a</sup> MP2/IV geometries for **8a**, **16**, and **17**. HF/IV geometries for **19a–21b**.

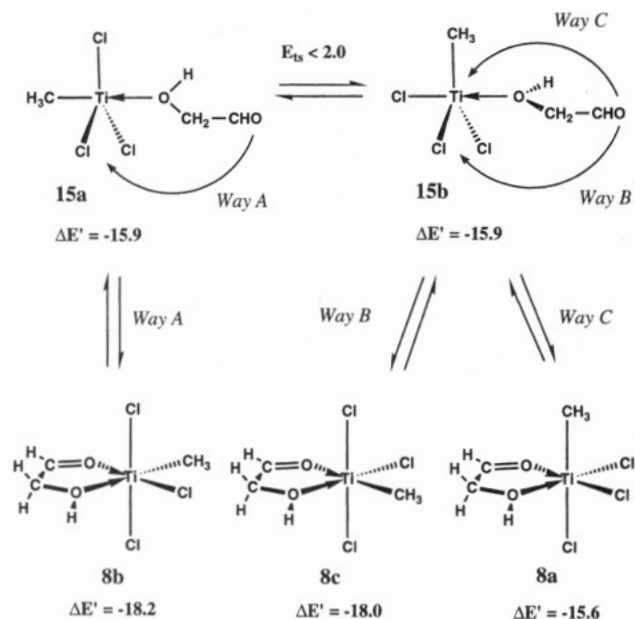


**Figure 7.** Illustration of the equilibrium between **8a–c** and **15a,b**. Energies are given in kcal/mol at MP2/III//MP2/II +  $\Delta ZPE$ .

structures. The calculated energies show that the potential energy hypersurface between **14a/14b** is very flat. From the data calculated for **14a/14b** we estimate the barrier between **15a** and **15b** to be smaller than 2 kcal/mol.

The suggested mechanism of complex formation and the equilibrium processes is summarized in Figure 7. Complex formation between **7** and  $\text{CH}_3\text{TiCl}_3$  under kinetically controlled conditions first leads to **15a** (major) and **15b** (minor). In both complexes the position of the methyl group at titanium is already adjusted with respect to the chelate ligand: the attack of the uncoordinated CHO-group in **15a** (way A in Figure 7) leads to **8b**. The additional complex formation energy of the second donor–acceptor bond in **8b** is very small. This is an important result because carbonyl compounds normally have a significant donor–acceptor interaction energy with titanium or other Lewis acids.<sup>32,33</sup> It can be concluded that there is a considerable amount of strain energy in the five-membered ring of the octahedral isomers and that the carbonyl–titanium bond can easily dissociate. The attack of the uncoordinated CHO-group in **15b** is possible in two ways (way B and C in Figure 7) and leads to **8c** and **8a**. The calculations suggest that the energy barriers between **8a**, **8b**, and

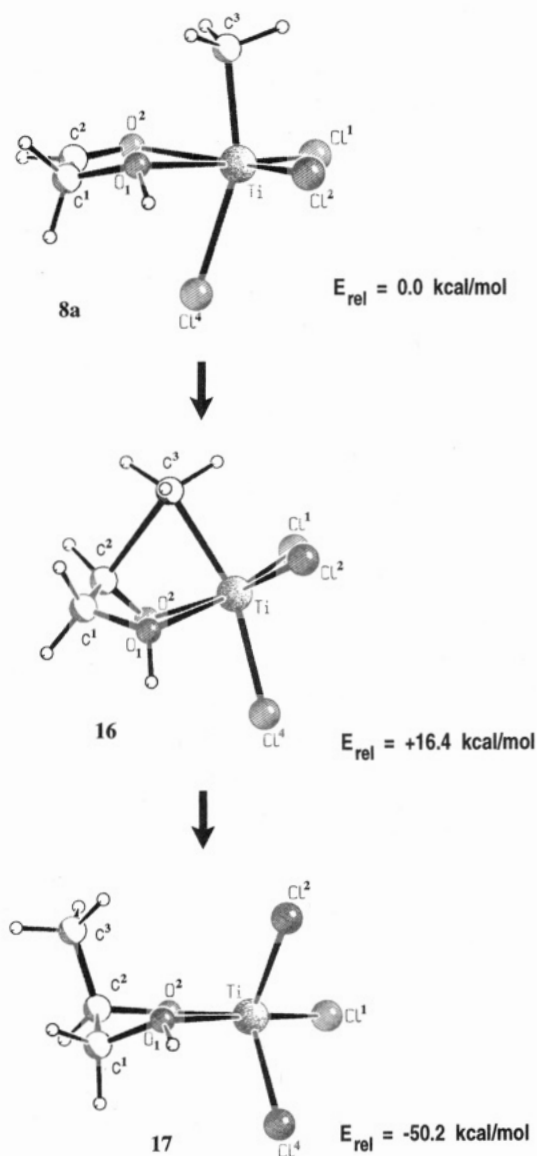


**Figure 8.** Methyl group migration from **8a** to the product **17** via the transition state **16**. The respective bond lengths are given in Table 4. Relative energies are given in kcal/mol at MP2/V//MP2/IV + ZPE(HF/IV).

**8c** are very small. The chelation controlled nucleophilic addition may occur from **8a** by methyl group migration from titanium to the carbonyl group.

From the calculated data, a possible explanation for the rather complicated kinetics of the ketone **1** may also be given. The binding energy of this ketone to a Lewis acid is higher than that of aldehyde **4**.<sup>32</sup> Thus, cleavage of the carbonyl–donor–acceptor bond of complexes **2b/**

(33) Branchadell, V.; Oliva, A. *J. Am. Chem. Soc.* **1992**, *114*, 4357.

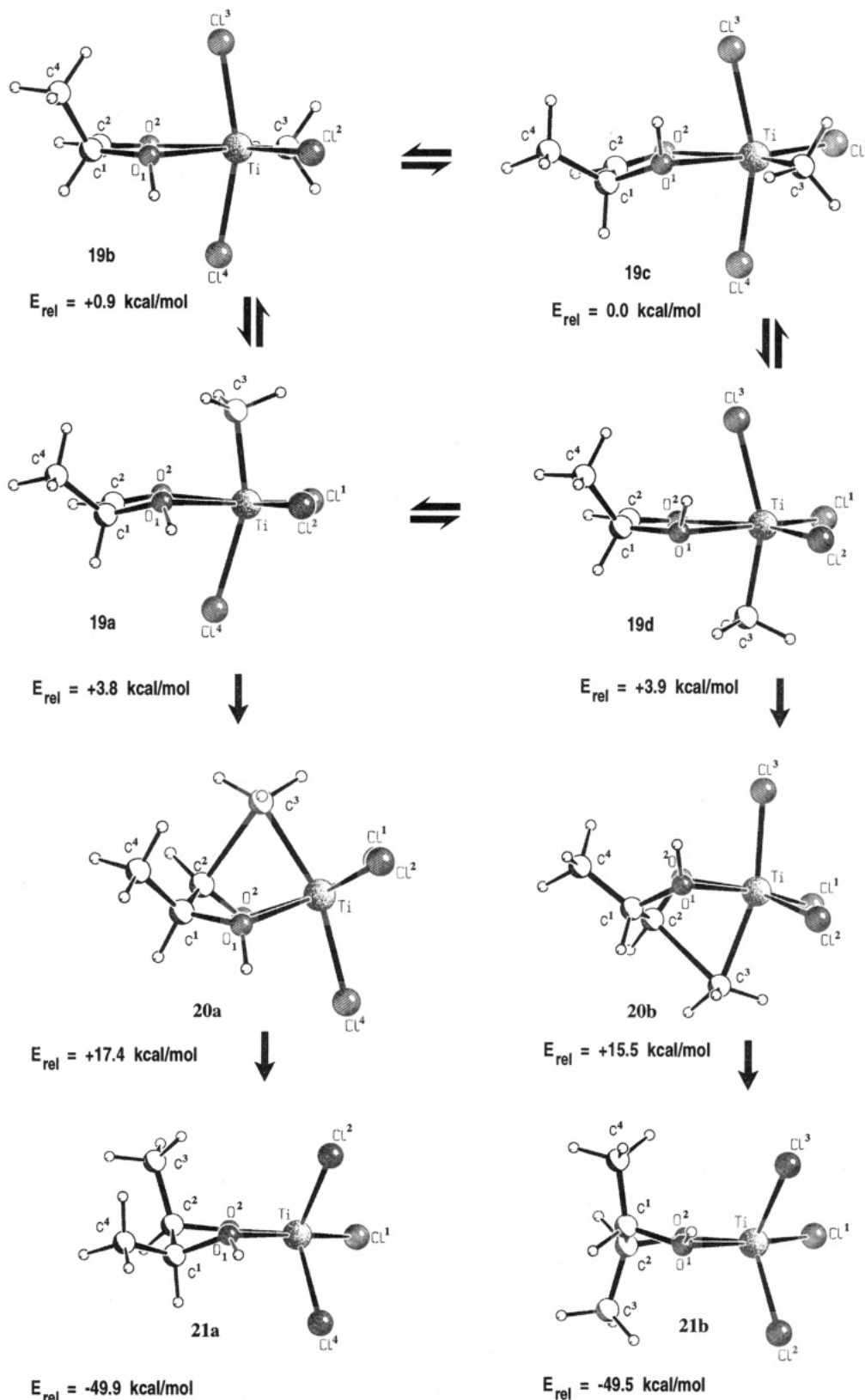


**Figure 9.** Calculated complexes **19a–d** and methyl group migration from **19a/d** to the products **21a** (minor) and **21b** (major) via the transition states **20a** and **20b**. The respective bond lengths are given in Table 4. Relative energies are given in kcal/mol at MP2/V//HF/IV + ZPE(HF/IV).

**2c** has a higher barrier as is indicated by the reduced reactivity of **1** relative to **4**. A higher barrier for the intramolecular rearrangement means that the bimolecular Grignard-type reaction between two molecules **2b/2c** becomes a higher weight in the overall reaction. The addition reaction of ketone **1** would then be a

superposition of a first order and second order reaction which makes the reaction kinetics more complicated. We want to point out that this is only a speculation, which is, however, supported by the calculated energies.

**Transition States of the Nucleophilic Addition Reaction.** The methyl group migration of the model

process **8a** → **16** → **17** has been calculated at the MP2/IV level of theory. Figure 8 shows the optimized structures and calculated relative energies for **8a**, **16**, and **17**. The calculated geometries are given in Table 4.

The calculated energy difference between **8a** and **16** is 16.4 kcal/mol at MP2/V//MP2/IV. Thus, the total activation barrier starting from **8c** (Table 3) is 18.8 kcal/mol at the MP2 level of theory.

We have also optimized the analogous transition states **20a/20b** starting from the chiral model complexes **19a–d** (Figure 1) at the HF/IV level of theory. The optimized geometries and relative energies for **19a–d** and the methyl group migrations from **19a** and **19d** to **21a** (minor product) and **21b** (major product) are shown in Figure 9. We found that the relative energies at MP2/V//MP2/IV for **8a**, **16**, and **17** are very similar to those at MP2/V//HF/IV. Thus, we believe that for complexes **19a–21b** the accuracy of the calculated relative MP2 energies does not depend very much on the underlying geometries (HF or MP2).

The energy difference between the transition states **20b** (major) and **20a** (minor) is calculated to be 1.9 kcal/mol at MP2/V//HF/IV. From a Boltzmann distribution at 253 K (temperature of the kinetic investigation), the calculated energy difference of 1.9 kcal/mol results in a distribution factor of 0.022 which corresponds to a ratio of 98:2. This difference is in line with the experimentally derived product ratio of 92:8 for **6a/6b**.

#### 4. Summary

The mechanism of the chelation controlled addition of  $\text{CH}_3\text{TiCl}_3$  to  $\alpha$ -alkoxy aldehydes has been studied using quantum chemical ab initio methods at the MP2 level of theory. The calculated relative energies and  $^{13}\text{C}$ -NMR chemical shifts of the isomeric  $\text{CH}_3\text{TiCl}_3$  complexes indicate that only the complexes with the methyl group at titanium in the equatorial position are formed in the reaction of  $\text{CH}_3\text{TiCl}_3$  with  $\alpha$ -alkoxy aldehydes. The investigation of pentacoordinated complexes of  $\text{CH}_3\text{-TiCl}_3$  in which one donor–acceptor bond is broken suggests a barrier smaller than 2 kcal/mol for the intramolecular rearrangement between the octahedral chelate complexes via a dissociation–association mechanism. For the intramolecular methyl shift from titanium to the complexed carbonyl group, the calculations give a barrier of ca. 19 kcal/mol. For the chiral ligand **17**, the difference between the major transition state **20b** and minor transition state **20a** is calculated as 1.9 kcal/mol which agrees well with the experimental diastereoselectivity of 92:8.

**Acknowledgment.** This study was supported by the Deutsche Forschungsgemeinschaft (SFB 260 and Leibniz program) and the Fonds der Chemischen Industrie. We thank the HLRZ Jülich and the TH Darmstadt for additional computer time at the CRAY Y-MP 864 and the Fujitsu S400/40 supercomputers.

OM950332Q

# Complexes of Transition Metals in High and Low Oxidation States with Side-On-Bonded $\pi$ -Ligands<sup>1</sup>

Ulrich Pidun and Gernot Frenking\*

Fachbereich Chemie, Philipps-Universität Marburg, Hans-Meerwein-Strasse,  
D-35032 Marburg, Germany

Received August 7, 1995<sup>⊗</sup>

The equilibrium geometries of the transition metal compounds  $WCl_4L$  and  $W(CO)_5L$  ( $L = HCCH, C_2H_4, CO_2, CS_2, CH_2O$ ) have been calculated at the HF and MP2 levels of theory by using a relativistic effective core potential for tungsten and valence shell basis sets of DZ+P quality. The W–L bond dissociation energies are predicted at CCSD(T). The calculations show that the inclusion of correlation energy is essential for the accurate description of transition metal donor–acceptor complexes. The theoretically determined geometries at the MP2 level are in very good agreement with experimental results. The calculated  $(CO)_5W-CO_2$  bond strength ( $D_0 = 10.2 \text{ kcal mol}^{-1}$ ) is in accord with the experimental estimate ( $D_0 = 8.2 \pm 1.0 \text{ kcal mol}^{-1}$ ). The calculations predict that the metal–ligand bond strength has the order for  $W(CO)_5L$  of  $L = C_2H_4 > HCCH > CH_2O > CS_2 > CO_2$ . For the  $WCl_4L$  complexes, the order is  $L = HCCH > CH_2O > C_2H_4 > CS_2 > CO_2$ . The different sequences of W–L bond strengths are explained by the nature of the metal–ligand interactions in the two sets of compounds. The W–L bonds of  $WCl_4L$  are covalent bonds, while the  $W(CO)_5L$  complexes have donor–acceptor bonds. Ethylene is a better donor than acetylene and formaldehyde and, therefore, forms a stronger bond in the  $W(CO)_5L$  complexes. The  $WCl_4L$  compounds with  $L = HCCH, C_2H_4, CH_2O$  should be considered as metallacycles. Since the carbon atoms of the metallacycloprenes are approximately  $sp^2$  hybridized, while the carbon atoms of the metallacycloprenes are  $sp^3$  hybridized, the former W–L bonds are stronger than the latter. In general, the W–L bond dissociation energies are clearly smaller for the  $WCl_4L$  complexes than for  $W(CO)_5L$ , although the metal–ligand bonds are much shorter in the former compounds. This puzzling result can easily be explained by the high excitation energy that is necessary to promote the ligand into the triplet state prior to formation of the strong covalent bond. The classification of the  $WCl_4L$  compounds as covalently bonded molecules and the  $W(CO)_5L$  complexes as donor–acceptor species is supported by the examination of the electronic structure using topological analysis of the electron density distribution, covalent bond orders, and charge decomposition analysis (CDA). The CDA method is found to be particularly useful for the analysis of the metal–ligand interactions. For the  $W(CO)_5L$  complexes, reasonable values are calculated for the  $L \rightarrow W$  donation, the  $W \rightarrow L$  back-donation, and the  $W \leftrightarrow L$  repulsive polarization by using closed-shell fragments  $W(CO)_5$  and  $L$ . The CDA results for  $WCl_4L$  using closed-shell fragments  $WCl_4$  and  $L$  are physically unreasonable, which indicates that the Dewar–Chatt–Duncanson model for these compounds is not appropriate.

## 1. Introduction

The bonding in transition metal complexes with side-on-coordinated  $\pi$ -ligands is usually described by the Dewar–Chatt–Duncanson model.<sup>2,3</sup> The model considers the bonding to arise from two interdependent components. In the first part, electron donation from a filled  $\pi$ -orbital of the ligand into a suitably directed vacant metal orbital forms the electron pair donor bond. This bond has  $\sigma$ -symmetry with regard to the metal–ligand axis. The bonding is reinforced by the second component, which derives from the  $\pi$ -symmetrical overlap of a filled metal d-orbital with the vacant antibonding  $\pi^*$ -orbital of the ligand (Figure 1). Due to the

flexible interplay of these two components, the Dewar–Chatt–Duncanson (DCD) model allows one to explain a number of experimental observations; in particular, the theory convincingly interprets the orientation of the  $\pi$ -ligand with respect to the remaining fragment and the observed lengthening of the intraligand bond length. However, the DCD model is not suited to quantify the distortion of the ligand in the complex or to predict details of the different bonding properties of different ligands. Also, the model does not distinguish between a  $\pi$ -bonded complex and a metallacycle as an alternative description of the three-membered cyclic structure. The latter bonding model appears to be more appropriate for high-valent transition metal complexes.

The Dewar–Chatt–Duncanson model has been supported by a number of semiempirical molecular orbital studies in the framework of extended Hückel theory.<sup>4</sup> The aims of the present work are to investigate the

<sup>⊗</sup> Abstract published in *Advance ACS Abstracts*, October 15, 1995.

(1) Theoretical Studies of Organometallic Compounds. 17. Part 16: Jones, V.; Frenking, G.; Reetz, M. T. *Organometallics* 1995, 14, 5316.

(2) Dewar, M. J. S. *Bull. Soc. Chim. Fr.* 1951, 18, C71.

(3) Chatt, J.; Duncanson, L. A. *J. Chem. Soc.* 1953, 2939.

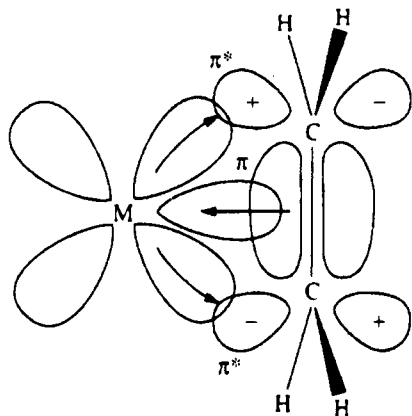


**Figure 1.** Dewar-Chat-Duncanson model of the bonding between a transition metal and a side-on-bonded  $\pi$ -ligand. Note that the ligand  $\pi$ -orbital has  $\sigma$ -symmetry in the complex.

bonding in transition metal complexes with side-on-coordinated  $\pi$ -ligands by using modern ab initio quantum chemical methods and to check the validity of the DCD model. We focus particularly on the different bonding situations of complexes where the transition metal is in a high or low oxidation state. For that purpose, calculations on two series of compounds were performed:  $WCl_4L$  and  $W(CO)_5L$ , with  $L = HCCH$ ,  $C_2H_4$ ,  $CO_2$ ,  $CS_2$ ,  $CH_2O$ . The investigation thus considers the cases of a metal in a formally high and in a formally low oxidation state and a number of different  $\pi$ -bonded ligands. The geometries of the complexes were optimized at the Hartree-Fock and MP2 levels of theory, using basis sets of double-zeta + polarization quality and effective core potentials for the heavier elements. The bond dissociation energies were calculated at the HF, MP2, and CCSD(T) levels. To gain insight into the metal-ligand bonding, we analyzed the wave function by using modern methods for the investigation of the electronic structure, including the topological analysis of the electron density of Bader,<sup>5,6</sup> the covalent bond orders of Cioslowski and Mixon,<sup>7</sup> and the charge decomposition analysis of Dapprich and Frenking.<sup>8,9</sup>

The compounds investigated are of interest, not only from a theoretical point of view. Transition metal complexes of acetylene and ethylene play a dominant role as intermediates in a number of homogeneously catalyzed organometallic processes, such as alkene metathesis, oligomerization and polymerization of alkynes and alkenes, hydration and oxidation of olefins, and the hydroformylation process. A deeper understanding of the nature of the bonding in the reactive intermediates of these processes should lead to better insight into the mechanisms of the catalytic reactions. This knowledge might help to improve the present catalysts and to extend the processes to a wider range of systems. Transition metal complexes of  $CO_2$  are a

subject of current interest in the endeavor to fix the  $CO_2$  in air and to use it as a chemical  $C_1$  source.<sup>10</sup> In this context,  $CS_2$  complexes are often used as model compounds, and it must still be explained why  $CS_2$  complexes are usually so much easier to prepare than their  $CO_2$  analogues.<sup>11</sup> Finally,  $\pi$ -complexes of formaldehyde are postulated as intermediates in homogeneously catalyzed Fischer-Tropsch processes. In view of the decreasing resources of mineral oil, the mechanistical investigation of these traditional  $C_1$  processes becomes more and more important.

There are only a few experimental studies concerned with the complexes investigated by us.  $W(CO)_5(HCCH)$  and  $W(CO)_5(C_2H_4)$  were synthesized by Stolz, Dobson, and Sheline through ultraviolet irradiation of  $W(CO)_6$  in the presence of acetylene and ethylene, respectively.<sup>12</sup> The compounds are rather unstable, and their isolation was difficult because of a tendency toward reversal of the reaction once irradiation was stopped. The third experimentally observed complex is  $W(CO)_5(CO_2)$ . It was prepared in 1985 by Almond, Downs, and Perutz<sup>13</sup> through photolysis of  $W(CO)_6$  in the presence of  $CO_2$  and was characterized by IR, Raman, and UV spectroscopies in solid argon matrices at 20 K. From the changes in the signals of the  $W(CO)_5$  fragment compared with  $W(CO)_6$  and  $W(CO)_5(NCCH_3)$ , the authors inferred an  $\eta^1$  end-on coordination of the  $CO_2$  molecule. In 1993, Zheng, Wang, Lin, She, and Fu observed  $W(CO)_5(CO_2)$  in the gas phase by time-resolved infrared spectroscopy.<sup>14</sup> They found the complex to be in equilibrium with its precursor  $W(CO)_5$  at room temperature and estimated the bond energy for binding of  $CO_2$  to  $W(CO)_5$  to be  $8.2 \pm 1.0$  kcal mol<sup>-1</sup>.

For the remaining complexes investigated in this work, no experimental results are available. However, a considerable number of related compounds are known, which allows an indirect comparison at least. A whole series of  $WCl_4L$  complexes with substituted acetylenes [monophenylacetylene,<sup>15</sup> diphenylacetylene,<sup>16</sup> bis(trimethylsilyl)acetylene<sup>17</sup>] as ligand  $L$  has been prepared by Dehnicke and co-workers. The crystal structure analyses showed C-C bond lengths on the order of 1.34 Å and relatively short W-C bonds of about 2.00 Å. Most of the crystal structure analyses of transition metal  $CO_2$  complexes found in the literature show the  $CO_2$  ligand in the side-on  $\eta^2$ -coordination. Prominent examples are  $Nb(\eta^5-C_5H_4Me)_2(CH_2SiMe_3)(CO_2)$ ,<sup>18</sup>  $Mo(\eta^5-C_5H_5)_2(CO_2)$ ,<sup>19</sup> and *trans,mer*- $Mo(CN-i-Pr)(PMe_3)_3(CO_2)_2$ .<sup>20</sup> Typical C-O bond lengths are on the order of 1.26–1.30 Å for the

(10) (a) Braunstein, P.; Matt, D.; Nobel, D. *Chem. Rev.* **1988**, *88*, 747. (b) Behr, A. *Angew. Chem.* **1988**, *100*, 681; *Angew. Chem., Int. Ed. Engl.* **1988**, *27*, 661.

(11) (a) Ibers, J. A. *Chem. Soc. Rev.* **1982**, *11*, 57. (b) Butler, I. S.; Fenster, A. E. *J. Organomet. Chem.* **1974**, *66*, 161.

(12) Stolz, I. W.; Dobson, G. R.; Sheline, R. K. *Inorg. Chem.* **1963**, *2*, 1264.

(13) Almond, M. J.; Downs, A. J.; Perutz, R. N. *Inorg. Chem.* **1985**, *24*, 275.

(14) Zheng, Y.; Wong, W.; Lin, J.; She, Y.; Fu, K. *Chem. Phys. Lett.* **1993**, *202*, 148.

(15) Pauls, I. Dissertation, Universität Marburg, Marburg, Germany, 1990.

(16) Hey, E.; Weller, F.; Dehnicke, K. *Naturwissenschaften* **1983**, *70*, 41.

(17) Hey, E.; Weller, F.; Dehnicke, K. *Z. Anorg. Chem.* **1984**, *514*, 18.

(18) Bristow, G. S.; Hitchcock, P. B.; Lappert, M. F. *J. Chem. Soc., Chem. Commun.* **1981**, 1145.

(19) Gambarotta, S.; Floriani, C.; Chiesi-Villa, A.; Guastini, C. *J. Am. Chem. Soc.* **1985**, *107*, 2985.

(4) (a) Hoffmann, R.; Chen, M. M. L.; Thorn, D. L. *Inorg. Chem.* **1977**, *16*, 503. (b) Schilling, B. E. R.; Hoffmann, R. *J. Am. Chem. Soc.* **1979**, *101*, 3456. (c) Mingos, D. M. P. In *Comprehensive Organometallic Chemistry*; Wilkinson, G., Stone, F. G. A., Abel, E. W., Eds.; Pergamon Press: New York, 1982.

(5) Bader, R. F. W. *Atoms in Molecules*; Clarendon Press: Oxford, 1990.

(6) Bader, R. F. W. *Chem. Rev.* **1991**, *91*, 893.

(7) Cioslowski, J.; Mixon, S. T. *J. Am. Chem. Soc.* **1991**, *113*, 4142.

(8) Dapprich, S.; Frenking, G. *J. Phys. Chem.* **1995**, *99*, 9352.

(9) Dapprich, S.; Frenking, G. CDA 2.1.; Philipps-Universität Marburg, Marburg, Germany.

coordinated bond and on the order of 1.20–1.22 Å for the non-coordinated bond. The O–C–O angle usually amounts to 132–135°. Transition metal complexes with CO<sub>2</sub> end-on coordinated via an oxygen lone pair have not yet been confirmed by X-ray crystal structure analysis, but this coordination is postulated for W(CO)<sub>5</sub>(CO<sub>2</sub>) on the basis of spectroscopic data.<sup>13,14</sup> The situation for CS<sub>2</sub> is rather similar to that of CO<sub>2</sub>: all crystal structure analyses of transition metal complexes of CS<sub>2</sub> found in the literature show the ligand in the side-on  $\pi$ -bonded coordination. Important examples are Pt-(PPh<sub>3</sub>)<sub>2</sub>(CS<sub>2</sub>),<sup>21</sup> Nb( $\eta^5$ -C<sub>5</sub>H<sub>5</sub>)<sub>2</sub>( $\sigma$ -C<sub>3</sub>H<sub>5</sub>)(CS<sub>2</sub>),<sup>22</sup> Co( $\eta^5$ -C<sub>5</sub>H<sub>5</sub>)(PMe<sub>3</sub>)(CS<sub>2</sub>),<sup>23</sup> and V( $\eta^5$ -C<sub>5</sub>H<sub>5</sub>)<sub>2</sub>(CS<sub>2</sub>).<sup>24</sup> For these compounds, typical C–S bond lengths are on the order of 1.67–1.72 Å for the coordinated bond and 1.54–1.62 Å for the non-coordinated bond; S–C–S bond angles lie between 134° and 141°. In spite of their supposedly high importance as intermediates in the reduction of carbon monoxide in the Fischer–Tropsch process, there are only a small number of transition metal complexes of formaldehyde that could be characterized experimentally. All compounds found in the literature have the CH<sub>2</sub>O ligand  $\eta^2$ -coordinated. They can be understood to be the product of the addition of a carbene-type metal fragment to the C–O double bond of the formaldehyde: Os(CO)<sub>2</sub>(PPh<sub>3</sub>)<sub>2</sub>(CH<sub>2</sub>O),<sup>25</sup> Fe(CO)<sub>2</sub>(P(OMe)<sub>3</sub>)<sub>2</sub>(CH<sub>2</sub>O),<sup>26</sup> V( $\eta^5$ -C<sub>5</sub>H<sub>5</sub>)<sub>2</sub>(CH<sub>2</sub>O),<sup>27</sup> and Mo( $\eta^5$ -C<sub>5</sub>H<sub>5</sub>)<sub>2</sub>(CH<sub>2</sub>O)<sup>28</sup> are prominent examples.

A number of theoretical studies of transition metal complexes with side-on-bonded  $\pi$ -ligands have been found in the literature. Schwerdtfeger and co-workers investigated the anionic complex [WCl<sub>5</sub>(HCCH)]<sup>-</sup> at the Hartree–Fock and MS-X $\alpha$  levels.<sup>29</sup> Ziegler and Rauk studied ethylene complexes of Cu<sup>+</sup>, Ag<sup>+</sup>, Au<sup>+</sup>, Pt<sup>0</sup>, and Pt<sup>2+</sup> at the Hartree–Fock–Slater level.<sup>30</sup> By using the transition state method to analyze the bonding properties, they found support for the Dewar–Chatt–Duncanson model. Kitaura, Sakaki, and Morokuma investigated Ni(PH<sub>3</sub>)<sub>2</sub>(HCCH) and Ni(PH<sub>3</sub>)<sub>2</sub>(C<sub>2</sub>H<sub>4</sub>)<sup>31</sup> in a comparative Hartree–Fock study. The acetylene complex was calculated to be more stable than the ethylene complex, but according to an energy decomposition analysis, the nature of the bond is very similar in these two complexes. The same authors also studied the bonding between carbon dioxide and transition metals.<sup>32</sup> Hartree–Fock calculations of the model complexes Ni-(PH<sub>3</sub>)<sub>2</sub>(CO<sub>2</sub>) and [Cu(PH<sub>3</sub>)<sub>2</sub>(CO<sub>2</sub>)]<sup>+</sup> yielded a remarkable

result: while the Ni(0) complex shows the expected side-on coordination of the CO<sub>2</sub> ligand, in the Cu(I) complex the most stable structure has CO<sub>2</sub> in an end-on-coordinated mode. The authors explained their results on the basis of an energy decomposition analysis by the more favorable electrostatic interaction between positively charged Cu<sup>+</sup> and the oxygen lone pair of CO<sub>2</sub>.

To our knowledge, there are no further ab initio studies on transition metal complexes with side-on-bonded  $\pi$ -ligands. Here we present a systematic investigation of the two series of compounds WCl<sub>4</sub>L and W(CO)<sub>5</sub>L (L = HCCH, C<sub>2</sub>H<sub>4</sub>, CO<sub>2</sub>, CS<sub>2</sub>, CH<sub>2</sub>O), including geometry optimizations, bond energy calculations, and analyses of the electronic structure. It is the first theoretical study of these molecules at a correlated level, and we will show that the inclusion of correlation effects is essential for a proper description of these compounds.

## 2. Computational Details

The geometries of the compounds have been optimized at the Hartree–Fock (HF) and MP2 (Møller–Plesset perturbation theory terminated at second order)<sup>33</sup> levels of theory. The symmetries were restricted to C<sub>2v</sub> for the HCCH and C<sub>2</sub>H<sub>4</sub> complexes and to C<sub>s</sub> for the CO<sub>2</sub>, CS<sub>2</sub>, and CH<sub>2</sub>O complexes. The characterization of the stationary points was effected by evaluating the second energy derivative matrix at the Hartree–Fock level of theory. Bond dissociation energies have been calculated at the HF and MP2 levels. For the WCl<sub>4</sub>L complexes, improved bond energies were predicted at the CCSD(T) level (coupled-cluster method<sup>34</sup> with single and double excitations and a perturbative estimate of the triple excitations<sup>35</sup>) by using the MP2-optimized structures. CCSD(T) calculations were technically not accessible for the W(CO)<sub>5</sub>L complexes (single file size limit), but an estimate of the CCSD(T) bond dissociation energies by using isostructural reactions<sup>33</sup> is given. The harmonic vibrational frequencies and zero-point energies were calculated at the HF level; all frequencies are unscaled.

For the heavier elements W, Cl, and S, effective core potentials were used. The quasirelativistic pseudopotential for tungsten was developed by Hay and Wadt (HW3).<sup>36</sup> The 5s, 5p, and 5d, and 6s electrons are treated explicitly. The corresponding valence basis set is of double-zeta quality with a contraction (441/2111/21).<sup>36</sup> The pseudopotentials for the elements Cl and S have been developed by Stoll, Preuss, and co-workers and are of the MEFIT type.<sup>37</sup> The valence basis sets are contracted as (31/31/1). Thus, they are also of double-zeta quality, with an additional d-polarization function (exponent: 0.65). For the lighter elements C, O, and H, the all-electron 6-31G(d) standard basis sets<sup>38</sup> were used. The basis sets and pseudopotentials (denoted as basis set II) have proven to be very appropriate for the description of transition

(20) Alvarez, R.; Carmona, E.; Marin, J. H.; Poveda, M. L.; Gutiérrez-Puebla, E.; Monge, A. *J. Am. Chem. Soc.* **1986**, *108*, 2286.

(21) Baird, M.; Hartwell, G.; Mason, R.; Rae, A. I. M.; Wilkinson, G. *Chem. Commun.* **1967**, 92.

(22) Drew, M. G. B.; Pu, L. S. *Acta Crystallogr.* **1977**, *833*, 1207.

(23) Werner, H.; Leonhard, K.; Burschka, C. *J. Organomet. Chem.* **1978**, *160*, 291.

(24) Fachinetti, G.; Floriani, C.; Chiesi-Villa, A.; Guastini, C. *J. Chem. Soc., Dalton Trans.* **1979**, 1612.

(25) Brown, K. L.; Clark, G. R.; Headford, C. E. L.; Marsden, K.; Raper, W. R. *J. Am. Chem. Soc.* **1979**, *101*, 503.

(26) (a) Berke, H.; Huttner, G.; Weiter, G.; Zsolnai, L. *J. Organomet. Chem.* **1981**, *219*, 353. (b) Berke, H.; Bankhardt, W.; Huttner, G.; v. Seyerl, J.; Zsolnai, L. *Chem. Ber.* **1981**, *114*, 2754.

(27) Gambarotta, S.; Floriani, C.; Chiesi-Villa, A.; Guastini, C. *J. Am. Chem. Soc.* **1982**, *104*, 2019.

(28) Gambarotta, S.; Floriani, C.; Chiesi-Villa, A.; Guastini, C. *J. Am. Chem. Soc.* **1985**, *107*, 2985.

(29) Nielson, A. J.; Bayd, P. D. W.; Clark, G. R.; Hunt, T. A.; Melson, J. B.; Rickard, C. E. F.; Schwerdtfeger, P. *Polyhedron* **1992**, *11*, 1419.

(30) Ziegler, T.; Rauk, A. *Inorg. Chem.* **1979**, *18*, 1558.

(31) Kitaura, K.; Sakaki, S.; Morokuma, K. *Inorg. Chem.* **1981**, *20*, 2292.

(32) Sakaki, S.; Kitaura, K.; Morokuma, K. *Inorg. Chem.* **1982**, *21*, 760.

(33) (a) Møller, C.; Plesset, M. S. *Phys. Rev.* **1934**, *46*, 618. (b) Binkley, J. S.; Pople, J. A. *Int. J. Quantum Chem.* **1975**, *9*, 229.

(34) Cizek, J. *J. Chem. Phys.* **1966**, *45*, 4256.

(35) (a) Pople, J. A.; Krishnan, R.; Schlegel, H. B.; Binkley, J. S. *Int. J. Quantum Chem.* **1978**, *14*, 545. (b) Bartlett, R. J.; Purvis, G. D. *Int. J. Quantum Chem.* **1978**, *14*, 561. (c) Purvis, G. D.; Bartlett, R. J. *J. Chem. Phys.* **1982**, *76*, 1910. (d) Raghavachari, K.; Trucks, G. W.; Pople, J. A.; Head-Gordon, M. *Chem. Phys. Lett.* **1989**, *157*, 479. (e) Bartlett, R. J.; Watts, J. D.; Kucharski, S. A.; Noga, J. *Chem. Phys. Lett.* **1990**, *165*, 513.

(36) Hay, P. J.; Wadt, W. R. *J. Chem. Phys.* **1985**, *82*, 299.

(37) (a) Dolg, M.; Wedig, U.; Stoll, H.; Preuss, H. *J. Chem. Phys.* **1987**, *86*, 866. (b) Andrae, D.; Häussermann, U.; Dolg, M.; Stoll, H.; Preuss, H. *Theor. Chim. Acta* **1990**, *77*, 123. (c) Bergner, A.; Dolg, M.; Küchle, W.; Stoll, H.; Preuss, H. *Mol. Phys.* **1993**, *80* (6), 1431.

(38) (a) Ditchfield, R.; Hehre, W. J.; Pople, J. A. *J. Chem. Phys.* **1971**, *54*, 724. (b) Hehre, W. J.; Ditchfield, R.; Pople, J. A. *J. Chem. Phys.* **1972**, *56*, 2257. (c) Francl, M. M.; Pietro, W. J.; Hehre, W. J.; Binkley, J. S.; Gordon, M. S.; Defrees, D. J.; Pople, J. A. *J. Chem. Phys.* **1982**, *77*, 3654.

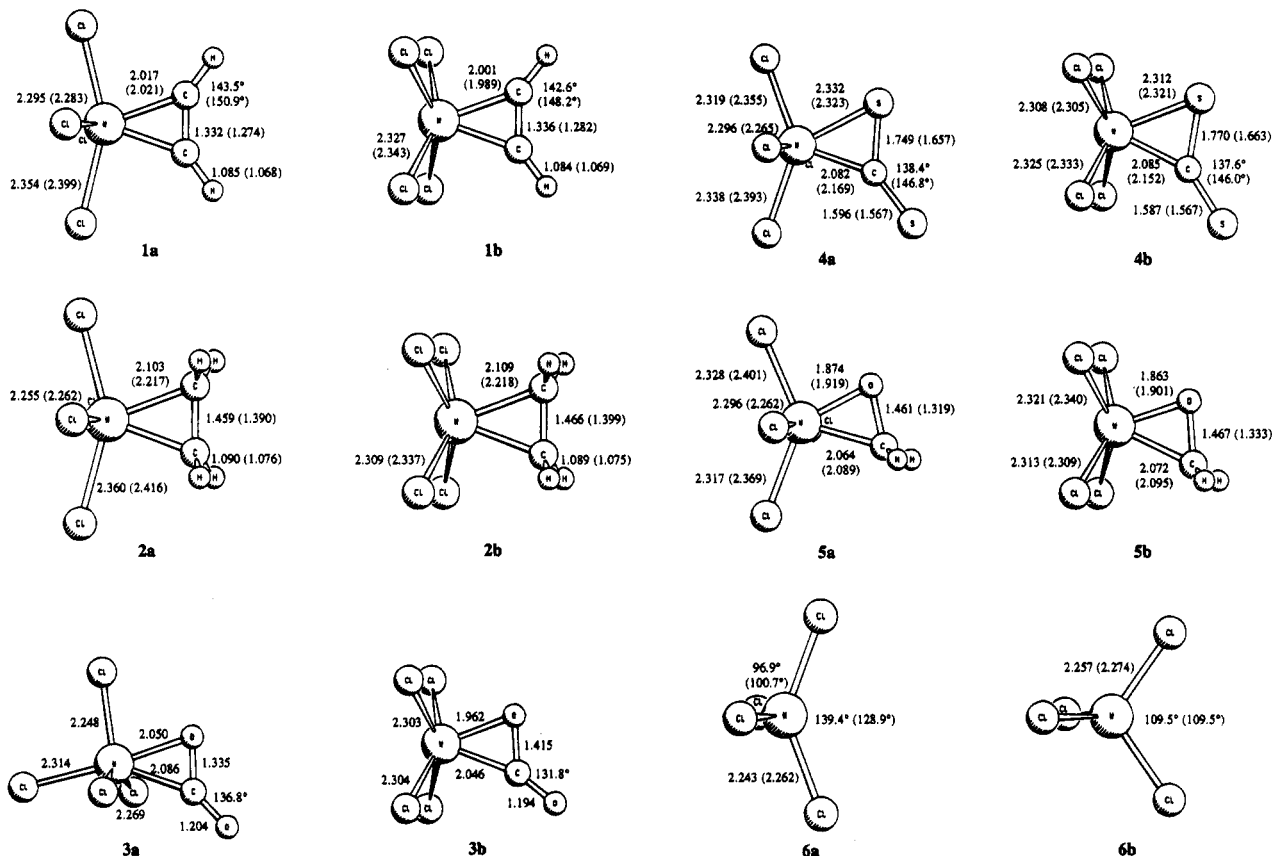


**Figure 2.** Optimized geometries at MP2/II of the  $WCl_4L$  complexes. Values at HF/II are given in parentheses.

metal complexes.<sup>39</sup> The calculations have been carried out basis set W Cl, S C, O, H II [ECP] 441/2111/21 [ECP] 31/31/1 6-31G(d)

using the program packages GAUSSIAN 92,<sup>40</sup> TURBOMOLE,<sup>41</sup> and ACES II.<sup>42</sup> For the topological analysis of the electron density, the programs SADDLE, GRID, CONTOUR, GRDVEC, and VECAIM<sup>43</sup> were used, and for the calculation of the covalent bond orders, the programs MAKAMP2 and BONDERMP2<sup>44</sup> were used. The charge decomposition analysis was carried out with the program CDA 2.1.<sup>8,9</sup>

### 3. Results and Discussion

In this section, we will first present the results of the geometry optimizations and bond energy calculations

(39) Frenking, G.; Antes, I.; Boehme, M.; Dapprich, S.; Ehlers, A. W.; Jonas, V.; Neuhaus, A.; Otto, M.; Stegmann, R.; Veldkamp, A.; Vyboishchikov, S. F. *Reviews in Computational Chemistry*; VCH Publishers: New York, in press, Vol. 7.

(40) Frisch, M. J.; Trucks, G. W.; Head-Gordon, M.; Gill, P. M. W.; Wong, M. W.; Foresman, J. B.; Johnson, B. G.; Schlegel, H. B.; Robb, M. A.; Replogle, E. S.; Gomperts, R.; Andres, J. L.; Raghavachari, K.; Binkley, J. S.; Gonzalez, C.; Martin, R. L.; Fox, D. J.; Defrees, D. J.; Baker, J.; Stewart, J. J. P.; Pople, J. A. GAUSSIAN 92, Revision C; Gaussian Inc.: Pittsburgh, PA, 1992.

(41) TURBOMOLE: (a) Häser, M.; Ahlrichs, R. *J. Comput. Chem.* **1989**, *10*, 104. (b) Ahlrichs, R.; Bär, M.; Häser, M.; Horn, H.; Kölmel, M. C. *Chem. Phys. Lett.* **1989**, *162*, 165. (c) Horn, H.; Weiss, H.; Häser, M.; Ehring, M.; Ahlrichs, R. *J. Comput. Chem.* **1991**, *12*, 1058. (d) Häser, M.; Almlöf, J.; Feyereisen, M. W. *Theor. Chim. Acta* **1991**, *79*, 115. (e) Schäfer, A.; Horn, H.; Ahlrichs, R. *J. Chem. Phys.* **1992**, *97*, 2571. (f) Häser, M.; Ahlrichs, R.; Baron, H. P.; Weiss, P.; Horn, H. *Theor. Chim. Acta* **1992**, *83*, 455.

(42) ACES II, an ab initio program written by J. F. Stanton, J. Gauss, J. D. Watts, W. J. Lauderdale, and R. J. Bartlett, University of Florida, Gainesville, FL, 1991.

(43) Biegler-König, F. W.; Bader, R. F. W.; Ting-Hua, T. *J. Comput. Chem.* **1982**, *3*, 317.

(44) Cioslowski, J. BONDER; Florida State University, Tallahassee, FL, 1990.

for the  $WCl_4L$  and  $W(CO)_5L$  complexes. Subsequently, the most important conclusions from the electronic structure analyses are described, and in the end the comparison of the  $WCl_4L$  and  $W(CO)_5L$  complexes is summarized.

#### 3.1. Structures and Bond Dissociation Energies.

**3.1.1.  $WCl_4L$  Complexes.** Figure 2 shows the optimized structures (MP2/II) of the complexes  $WCl_4$ -(HCCH) (**1a** eclipsed, **1b** staggered),  $WCl_4$ -( $C_2H_4$ ) (**2a** eclipsed, **2b** staggered),  $WCl_4$ -( $CO_2$ ) (**3a** eclipsed, **3b** staggered),  $WCl_4$ -( $CS_2$ ) (**4a** eclipsed, **4b** staggered), and  $WCl_4$ -( $CH_2O$ ) (**5a** eclipsed, **5b** staggered) and of  $WCl_4$  (**6a** singlet, **6b** triplet). The results of the Hartree-Fock optimizations are given in parentheses. The corresponding total energies, relative energies of the two conformers, and zero-point energies (HF/II) are given in Table 1. With the exception of the acetylene complex, the eclipsed conformations are more stable than the staggered ones at all theoretical levels. For the HF structures the more stable conformer was verified as a true minimum on the potential energy surface by only positive eigenvalues of the Hessian matrix. In the same way, the other conformer could be characterized as a transition state of first order (one negative eigenvalue of the Hessian matrix). The only exception is the  $WCl_4$ -( $CO_2$ ) complex, which dissociates during optimization at the Hartree-Fock level so that no HF frequencies could be determined.

The calculated structures of the acetylene complexes **1a** and **1b** are in very good agreement with experimental data for  $WCl_4$  complexes of substituted acetylenes. The theoretical W-C and C-C bond lengths of the more stable conformer **1b** at the MP2 level (2.001 and 1.336 Å) are identical to the experimental values (2.00 and



**Table 1.** Calculated Total Energies  $E_{\text{tot}}$  (au), Relative Energies of the Two Conformations  $E_{\text{rel}}$  (kcal mol<sup>-1</sup>), Zero-Point Energies ZPE (kcal mol<sup>-1</sup>), and Number of Imaginary Frequencies  $i$  of the WCl<sub>4</sub>L Complexes

molecule	HF/II/HF/II				MP2/II/MP2/II		CCSD(T)/II/MP2/II	
	$E_{\text{tot}}$	$E_{\text{rel}}$	ZPE	$i$	$E_{\text{tot}}$	$E_{\text{rel}}$	$E_{\text{tot}}$	$E_{\text{rel}}$
<b>1a</b>	-203.185 45	0.0	23.7	1	-204.253 03	0.0		
<b>1b</b>	-203.188 42	-1.9	23.8	0	-204.256 94	-2.5	-204.314 75	
<b>2a</b>	-204.370 39	0.0	40.0	0	-205.427 90	0.0	-205.504 40	
<b>2b</b>	-204.363 40	+4.3	39.8	1	-205.422 56	+3.4		
<b>3a</b>					-315.206 09	0.0	-315.252 72	0.0
<b>3b</b>					-315.197 77	+5.2	-315.239 77	+8.1
<b>4a</b>	-184.122 97	0.0	8.6	0	-185.342 39	0.0	-185.410 37	
<b>4b</b>	-184.121 06	+1.2	8.5	1	-185.340 33	+1.3		
<b>5a</b>	-240.184 79	0.0	24.2	0	-241.329 75	0.0	-241.381 99	
<b>5b</b>	-240.180 78	+2.5	24.1	1	-241.323 61	+3.9		
<b>6a</b>	-126.335 44	0.0	3.1	0	-127.069 26	0.0	-127.132 12	0.0
<b>6b</b>	-126.394 04	-36.8	3.0	0	-127.105 27	-22.6	-127.165 68	-21.1

1.34 Å).<sup>15-17</sup> It should be noted that the W-C bond lengths of **1a** and **1b** calculated at the HF and MP2 levels are very similar, while the C-C distances clearly are different. This is because the C-C bond length of free acetylene is calculated to be much shorter at HF/6-31G(d) (1.185 Å) than at MP2/6-31G(d) (1.218 Å). At both theoretical levels HF/II and MP2/II it is predicted that the C-C bond length of the complex **1** is significantly longer than that in free acetylene. The calculated C-C bond length at MP2/II of **1b** is exactly the same as that in free ethylene (1.336 Å), which suggests that **1b** should be considered as a metallacyclopentene.

In the case of WCl<sub>4</sub>(C<sub>2</sub>H<sub>4</sub>), the eclipsed conformer **2a** is more stable than the staggered one (**2b**), and the consideration of correlation effects is more important than for **1**: on going from the HF to the MP2 level, the W-C bond length decreases by about 0.11 Å, while the C-C bond is lengthened by 0.07 Å to a value of 1.459 Å. Thus, due to the neglect of correlation effects, the Hartree-Fock method severely underestimates the bonding interactions between the ethylene ligand and the WCl<sub>4</sub> fragment, and it is only at the MP2 level that the C-C bond in the complex approaches the order of a typical C-C single bond (1.54 Å), according to a description of WCl<sub>4</sub>(C<sub>2</sub>H<sub>4</sub>) as a metallacyclopentane.

For the WCl<sub>4</sub>(CO<sub>2</sub>) complex, the differences between the results at HF/II and MP2/II are even more dramatic: at the Hartree-Fock level, no stable adduct between WCl<sub>4</sub> and CO<sub>2</sub> could be found. The complex dissociates during the optimization. The MP2 optimizations yield two conformations with significantly different structural features. The eclipsed conformer **3a** was calculated to be 5 kcal mol<sup>-1</sup> (8 kcal mol<sup>-1</sup> at CCSD(T)/II) more stable than the staggered one (**3b**). In **3a** the CO<sub>2</sub> ligand occupies an axial position in the trigonal-bipyramidal coordination sphere of the tungsten, and the W-C and W-O bonds are rather long (2.086 and 2.050 Å, respectively), while the coordinated C-O bond length remains quite short (1.335 compared to 1.204 Å for the non-coordinated bond). These calculated structural parameters compare favorably with the experimental data available:<sup>18-20</sup> typical C-O distances of 1.26-1.30 Å for the coordinated C-O bond and 1.20-1.22 Å for the exocyclic C-O bond and a O-C-O angle of 132-135° are reproduced reasonably well. Surprisingly, in the energetically less stable staggered conformer **3b**, the interaction between the CO<sub>2</sub> ligand and the metal seems to be stronger. The W-C and W-O bonds are considerably shorter (2.046 and 1.962 Å), and the coordinated C-O bond is lengthened to 1.415 Å, which is on the order of magnitude of a typical C-O

single bond (1.43 Å). These structural results indicate that there might be a fundamental difference in the nature of the bonding in the two conformations of WCl<sub>4</sub>(CO<sub>2</sub>). While the eclipsed conformer seems to correspond to a typical donor-acceptor complex, which can be described by the Dewar-Chart-Duncanson model, the staggered conformer approaches a metallacycle with polar covalent bonds.

In the case of WCl<sub>4</sub>(CS<sub>2</sub>), the two conformations calculated at the HF and MP2 levels of theory are very similar; the eclipsed conformation **4a** is more stable by 1.2 and 1.3 kcal mol<sup>-1</sup>, respectively. The W-C distance is significantly shorter (0.07-0.09 Å) and the coordinated C-S bond is longer (0.09-0.11 Å) at the MP2 level. The calculated MP2 energy minimum structure **4a** compares well (C-S bond lengths of 1.749 and 1.596 Å; S-C-S angle of 138.4°) with crystal structure analysis data of experimentally found CS<sub>2</sub> complexes<sup>21-24</sup> (C-S bond lengths of 1.67-1.72 and 1.54-1.62 Å; S-C-S angles between 134 and 141°). The optimized geometries of **3** and **4** can also be interpreted as snapshots of the formation of oxo-carbonyl and sulfido-thiocarbonyl complexes, respectively. In fact, side-on- $\eta^2$ -bonded CS<sub>2</sub> complexes are known as intermediates in the formation of thiocarbonyl complexes.<sup>45</sup>

The MP2 geometry optimizations of WCl<sub>4</sub>(CH<sub>2</sub>O) yielded the structures **5a** and **5b**. Again, the structural differences between the two conformations are not very significant, and the eclipsed conformation **5a** is slightly more stable than **5b**. The most striking feature of the MP2-optimized conformations is the very long C-O bond in the complex (1.461 Å for **5a**), which is even longer than a typical C-O single bond (1.43 Å). On the other hand, the W-O bond is very short (1.874 Å for **5a**) and should be compared with W-O double bonds in WCl<sub>4</sub> (1.684 Å)<sup>46</sup> and WOF<sub>4</sub> (1.666 Å).<sup>47</sup> Figure 2 clearly indicates that the tungsten atom and the methylene group of **5a** and **5b** lie almost in one plane (dihedral angle: 19.5°). Thus, the theoretically determined geometry of WCl<sub>4</sub>(CH<sub>2</sub>O) shows some indications for a transformation of the  $\eta^2$ -formaldehyde complex into an oxo-carbene complex. Such a reaction has actually been observed experimentally: the formation of the oxo-carbene complex W(O)(=C<sub>5</sub>H<sub>9</sub>)Cl<sub>2</sub>(PMePh<sub>2</sub>)<sub>2</sub> by reacting WCl<sub>2</sub>(PMePh<sub>2</sub>)<sub>4</sub> with cyclopentanone was reported by Bryan and Mayer.<sup>48</sup> Structure **5a** may be

(45) Broadhurst, P. V. *Polyhedron* **1985**, *4*, 1801.(46) Robiette, A. G.; Hedberg, K.; Hedberg, L. *J. Mol. Struct.* **1977**, *37*, 105.(47) Iijima, K.; Shibata, S. *Chem. Lett.* **1972**, 1033.(48) Bryan, J. C.; Mayer, J. M. *J. Am. Chem. Soc.* **1987**, *109*, 7213.

**Table 2.** Calculated Bond Dissociation Energies  $D_0$  (kcal mol<sup>-1</sup>) for the WCl<sub>4</sub>L Complexes Relative to Singlet WCl<sub>4</sub> (S) and Triplet WCl<sub>4</sub> (T)<sup>a</sup>

molecule	HF/II/HF/II		MP2/II/MP2/II		CCSD(T)/II/MP2/II	
	S	T	S	T	S	T
<b>1b</b>	22.4	-14.4	74.7	52.1	57.7 (55.4)	36.6 (34.4)
<b>2a</b>	2.3	-34.5	45.0	22.4	33.2 (30.6)	12.1 (9.6)
<b>3a</b>			18.8	-3.8	3.8	-17.7
<b>4a</b>	-34.3	-71.1	36.5	13.9	17.9 (16.9)	-3.2 (-4.1)
<b>5a</b>	-10.3	-47.1	58.2	35.6	39.8 (37.0)	18.7 (16.0)

<sup>a</sup> ZPE-corrected values  $D_0$  (kcal mol<sup>-1</sup>) are given in parentheses.

considered as a snapshot along the reaction coordinate of the formation of the oxo-carbene complex. Experimental studies of formaldehyde complexes have shown that the CH<sub>2</sub>O ligand is always  $\eta^2$ -coordinated to the metal and that the metal-oxygen distance is 0.03–0.15 Å shorter than the metal-carbon distance.<sup>25–28</sup> However, the calculated C–O distance of **5a** is much longer than the observed values for low-valent transition metal formaldehyde complexes.<sup>25–28</sup>

The theoretically determined bond dissociation energies for the MP2-optimized energy minimum structures of the WCl<sub>4</sub>L complexes are given in Table 2. The bond energies were calculated with respect to the singlet (**6a**) and triplet forms (**6b**) of WCl<sub>4</sub>. The MP2-optimized geometries of the WCl<sub>4</sub> fragment are displayed in Figure 2. In the triplet case, the calculation yielded a tetrahedral ( $T_d$ ) geometry, while the singlet structure shows a tetragonal distortion toward  $D_{2d}$  symmetry, as expected for a d<sup>2</sup>-transition metal (Jahn-Teller effect). The triplet state of WCl<sub>4</sub> is lower in energy than the singlet state. Since we are mainly concerned with the relative bond strengths of the ligands L in the WCl<sub>4</sub>L complexes, the calculated absolute bond energies are less important. As mentioned earlier, no stable HF structure could be found for the WCl<sub>4</sub>(CO<sub>2</sub>) complex, and consequently no ZPE correction can be provided.

The calculations for the Cl<sub>4</sub>W–L bond strength show the order HCCH > CH<sub>2</sub>O > C<sub>2</sub>H<sub>4</sub> > CS<sub>2</sub> > CO<sub>2</sub>. This trend is predicted at all levels of theory. The calculated bond energies at MP2/II are much higher than those at HF/II. The predicted bond dissociation energies at CCSD(T)/II are somewhat lower than those at MP2/II. Previous theoretical studies have shown that bond energies calculated at CCSD(T)/II are in good agreement with experimental results, while the HF/II values are much too low and the MP2/II values are too high.<sup>39,49</sup>

No experimental data for the Cl<sub>4</sub>W–L bond energies are available, but the predicted trend is in agreement with experimental observations. Numerous acetylene complexes of WCl<sub>4</sub> are known, which are usually found as dimers in the solid state.<sup>15–17</sup> Olefin complexes of transition metals are a well-characterized class of compounds, but there is no olefin complex of WCl<sub>4</sub> known to us. The acetylene complex **1b** is calculated to be significantly more stable than the ethylene complex **2a** (Table 2). This can be explained if both complexes are considered as metallacyclic compounds. The carbon atoms of **1b** are approximately sp<sup>2</sup> hybridized, while the carbon atoms of **2a** are sp<sup>3</sup> hybridized. The former carbon atoms should have stronger bonds to the metal than the latter carbon atoms. Yet the calculations indicate that olefin complexes such as **2a**

might be stable enough to be synthesized under appropriate conditions. The calculated metal–ligand bond energies also show that CS<sub>2</sub> is much more strongly bound than CO<sub>2</sub>. This is in agreement with the considerably larger number of CS<sub>2</sub> complexes than CO<sub>2</sub> complexes, which are usually rather unstable.

**3.1.2. W(CO)<sub>5</sub>L Complexes.** The optimized structures (MP2/II) of the complexes W(CO)<sub>5</sub>(HCCH) (**7a** eclipsed, **7b** staggered), W(CO)<sub>5</sub>(C<sub>2</sub>H<sub>4</sub>) (**8a** eclipsed, **8b** staggered), W(CO)<sub>5</sub>(CO<sub>2</sub>) (**9a** eclipsed, **9b** staggered), W(CO)<sub>5</sub>(CS<sub>2</sub>) (**10a** eclipsed, **10b** staggered), W(CO)<sub>5</sub>(CH<sub>2</sub>O) (**11a** eclipsed, **11b** staggered), and W(CO)<sub>5</sub> (**12**) are shown in Figure 3, with the geometrical parameters of the HF optimizations given in parentheses. The corresponding total energies, relative energies of the two conformers, and zero-point energies (HF/II) are given in Table 3. For all complexes, the eclipsed conformations are slightly more stable than the staggered ones. For the HF structures, the eclipsed conformers could be verified as true minima on the potential energy surface by only positive eigenvalues of the Hessian matrix.

There are significant differences between the HF- and MP2-optimized conformations of the acetylene complexes **7a** and **7b**. At the MP2 level, the tungsten-carbonyl bonds clearly are shorter, while the carbonyl C–O bonds are longer. The acetylene ligand is bonded more strongly at the correlated level: the W–C bond length decreases (by 0.12 Å for **7a**), the C–C bond length increases (by about 0.05 Å), and the H–C–C angle becomes markedly smaller. Thus, the neglect of correlation effects leads to a severe underestimation of the bonding interactions between the W(CO)<sub>5</sub> fragment and the acetylene ligand. In agreement with previous studies, the investigations clearly indicate that correlated methods are essential for a proper description of transition metal complexes in low oxidation states.<sup>39</sup> The differences in the structures between W(CO)<sub>5</sub>(HCCH) (**7a**) and WCl<sub>4</sub>(HCCH) (**1b**) are remarkable. In **7a** the C–C distance is shorter than that in **1b** by about 0.07 Å. The C–C bond length of **7a** (1.262 Å) is intermediate between the C–C distance in free acetylene (1.205 Å) and that in free ethylene (1.330 Å). The W–C bond length is significantly larger in **7a** (by 0.33 Å) and the H–C–C angle is expanded by about 10°. It follows that the HCCH ligand keeps its acetylene character to a larger extent in the W(CO)<sub>5</sub> complex than in **1b**. While WCl<sub>4</sub>(HCCH) is best described as a metallacyclopentene, W(CO)<sub>5</sub>(HCCH) seems to be a genuine donor-acceptor complex, with the acetylene ligand occupying just one coordination site at tungsten. The examination of the electronic structure will show that these conclusions based on geometrical results can be confirmed by the bonding analysis.

The situation for W(CO)<sub>5</sub>(C<sub>2</sub>H<sub>4</sub>) (**8a** and **8b**) is similar to the case of W(CO)<sub>5</sub>(HCCH). Again, the structural differences between the two conformations are only small and the eclipsed conformer is slightly more stable. The consideration of correlation effects at the MP2 level leads to the typical changes: the W–carbonyl and W–ethylene distances decrease, while the C–O and C–C bonds become longer. As compared to WCl<sub>4</sub>(C<sub>2</sub>H<sub>4</sub>), the C–C bond length in W(CO)<sub>5</sub>(C<sub>2</sub>H<sub>4</sub>) is shorter by 0.06 Å, and with a value of 1.402 Å it is more similar to a typical double bond (1.33 Å) than to a typical single bond

(49) Ehlers, A. W.; Frenking, G. *J. Am. Chem. Soc.* **1994**, *116*, 1514.

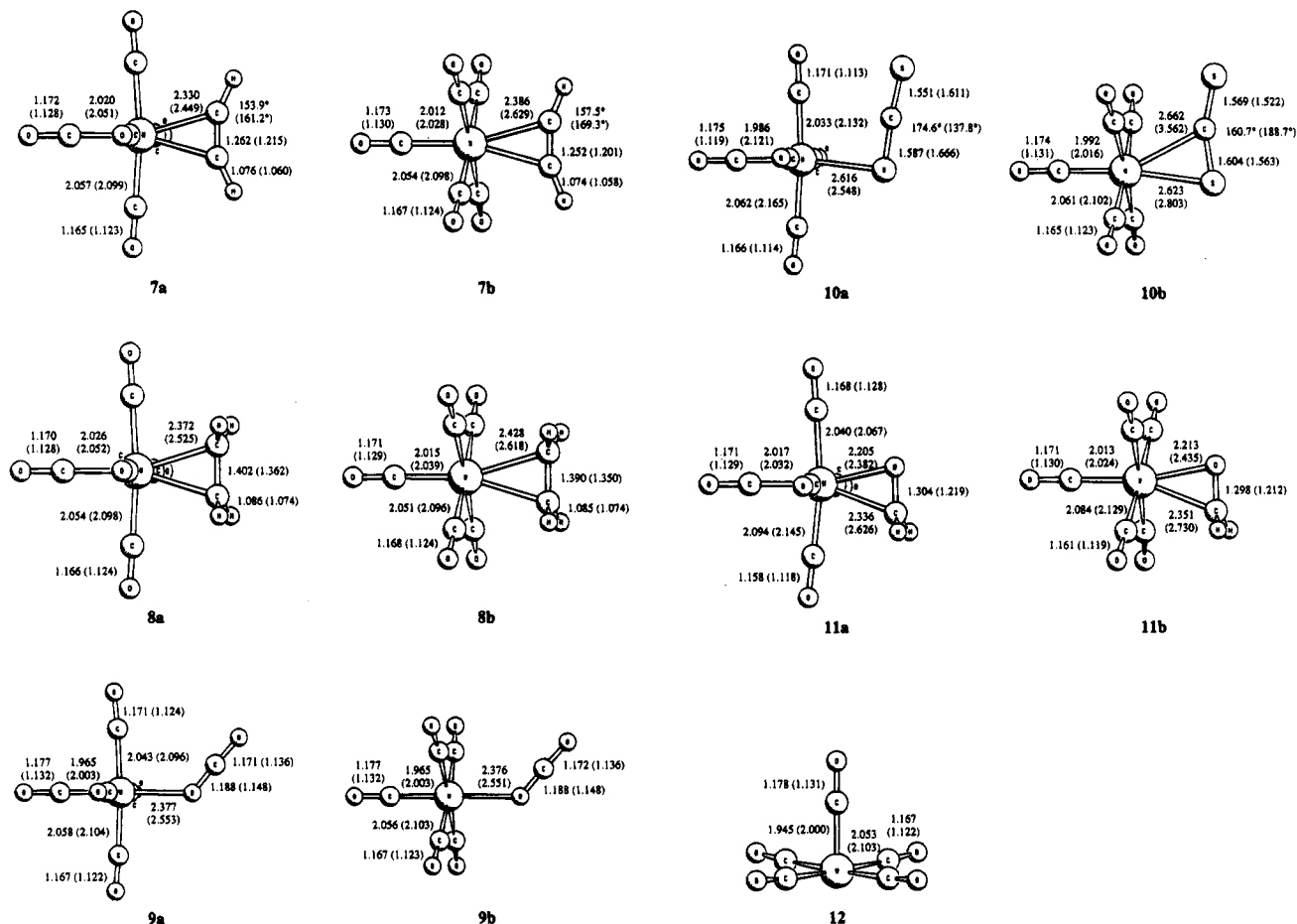


Figure 3. Optimized geometries at MP2/II of the  $W(CO)_5L$  complexes. Values at HF/II are given in parentheses.

Table 3. Calculated Total Energies  $E_{tot}$  (au), Relative Energies of the Two Conformations  $E_{rel}$  (kcal mol<sup>-1</sup>), Zero-Point Energies ZPE (kcal mol<sup>-1</sup>), and Number of Imaginary Frequencies  $i$  of the  $W(CO)_5L$  Complexes

molecule	HF/II/HF/II				MP2/II/MP2/II	
	$E_{tot}$	$E_{rel}$	ZPE	$i$	$E_{tot}$	$E_{rel}$
7a	-707.720 44	0.0	47.2	0	-709.759 73	0.0
7b	-707.717 14	+2.1	47.1	1	-709.754 83	+3.1
8a	-708.939 94	0.0	64.3	0	-710.987 94	0.0
8b	-708.937 19	+1.7	64.4	2	-710.982 28	+3.6
9a	-818.520 85	0.0	36.3	0	-820.758 96	0.0
9b	-818.520 85	±0.0	36.3	0	-820.758 97	±0.0
10a	-688.723 97	0.0	32.9	0	-690.889 11	0.0
10b	-688.731 53	-4.7	32.9	1	-690.888 22	+0.5
11a	-744.760 09	0.0	47.8	0	-746.845 95	0.0
11b	-744.759 83	+0.2	47.7	1	-746.844 53	+0.9
12	-630.876 30		27.7	0	-632.623 96	

(1.54 Å). Accordingly, the W–C distance is longer by 0.17 Å in the  $W(CO)_5$  complex. Thus, the  $C_2H_4$  ligand still has some ethylene character in  $W(CO)_5(C_2H_4)$ , and a description as a donor–acceptor complex seems appropriate.

A compilation of experimentally determined W–C bond distances<sup>50</sup> for hexacoordinated W(0) complexes with side-on-bonded substituted alkenes ( $L = CH_2CHR$ ) yields an average value of 2.386 Å, which is in excellent agreement with the calculated W–C distance for **8a** (2.372 Å, Figure 3). As mentioned in the Introduction,  $W(CO)_5(HCCH)$  and  $W(CO)_5(C_2H_4)$  could be detected

experimentally by IR spectroscopy as unstable species.<sup>12</sup> Stolz, Dobson, and Sheline observed that the decrease in the C–O stretching frequency of the *trans*-carbonyl group is significantly larger for  $W(CO)_5(HCCH)$  than for  $W(CO)_5(C_2H_4)$ . This experimental result is in accord with our calculations: the *trans* W–C distance is shorter in the acetylene complex (2.026 compared to 2.026 Å), while the corresponding C–O distance is slightly longer in the case of acetylene (1.172 compared to 1.170 Å).

IR spectroscopic studies suggest for  $W(CO)_5(CO_2)$  an end-on coordination of the  $CO_2$  ligand,<sup>13,14</sup> but a crystal structure analysis could not be provided for this unstable species. Our calculations strongly support the experimental conjecture: as can be seen from Figure 3, the geometry optimizations at MP2 as well as HF yielded structures with end-on-coordinated carbon dioxide (**9a** and **9b**). At both theoretical levels, the bond lengths and relative energies of the two conformations are virtually the same, as can be anticipated from the locally  $\sigma$ -symmetrical coordination of the ligand. The calculated W–O distance is rather large (2.377 Å), and the two C–O bond lengths of the bonded  $CO_2$  differ by only 0.017 Å. A strong *trans* effect is predicted by the calculations: the W–C(O) bond *trans* to the  $CO_2$  ligand is more than 0.08 Å shorter than the *cis* W–carbonyl bonds, and the *trans* C–O bond is longer by about 0.01 Å than the *cis* C–O bonds. The strong *trans* effect can be traced back to the end-on-coordinated  $CO_2$  being a strong  $\sigma$ -donor without  $\pi$ -acceptor properties.

The geometry optimization of the eclipsed and staggered conformations of  $W(CO)_5(CS_2)$  at the HF and MP2

(50) Orpen, A. G.; Brammer, L.; Allen, F. H.; Kennard, O.; Watson, D. G.; Taylor, R. *J. Chem. Soc., Dalton Trans.* **1989**, S1.

**Table 4. Calculated Bond Dissociation Energies  $D_e$  (kcal mol<sup>-1</sup>) for the W(CO)<sub>5</sub>L Complexes<sup>a</sup>**

molecule	HF/II/HF/II	MP2/II/MP2/II	CCSD(T)/II/MP2/II (estimated)
<b>7a</b>	16.8	42.2	35.3 (34.3)
<b>8a</b>	20.3	48.3	41.4 (39.1)
<b>9a</b>	6.9	17.6	10.7 (10.2)
<b>10a</b>	3.4	31.5	24.6 (24.1)
<b>11a</b>	11.4	34.1	27.2 (25.4)

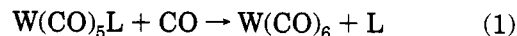
<sup>a</sup> ZPE-corrected values  $D_0$  (kcal mol<sup>-1</sup>) are given in parentheses.

levels led to stationary points on the potential energy surface that are quite different (Figure 3, **10a** and **10b**). At the HF level the eclipsed conformation **10a**, with side-on-coordinated CS<sub>2</sub>, is found as energy minimum structure.<sup>51</sup> At the MP2 level, the energetically favored form **10a** has an end-on-coordinated CS<sub>2</sub>. The W–S distance of **10a** is rather large (2.616 Å), the two C–S bond lengths differ by only 0.036 Å, and the CS<sub>2</sub> ligand is approximately linear (174.6°). A significant trans effect is observed for **10a**: the W–CO trans bond is much shorter (1.986 Å) than the W–CO cis bond (2.062 Å). The MP2-optimized staggered conformer **10b** is higher in energy by only 0.5 kcal mol<sup>-1</sup>. Its structure lies between a side-on and an end-on coordination of the CS<sub>2</sub> ligand: on the one hand, the W–C distance (2.662 Å) is longer than the W–S distance (2.623 Å), the two C–S bond lengths are rather similar (difference only 0.035 Å), and a marked trans effect occurs. On the other hand, the CS<sub>2</sub> molecule is significantly bent (160.7°) and the W–C distance is too short to exclude an interaction. On the whole, the results at the MP2 level suggest that an end-on coordination of the CS<sub>2</sub> ligand is likely for W(CO)<sub>5</sub>(CS<sub>2</sub>), as was postulated on the basis of IR spectroscopic studies for the related complex Fe(CO)<sub>4</sub>(CS<sub>2</sub>).<sup>52</sup>

The geometry optimizations of W(CO)<sub>5</sub>(CH<sub>2</sub>O) (**11a** and **11b**) yielded structures with side-on-coordinated formaldehyde. The HF and MP2 geometries differ significantly; the W–C and W–O distances particularly are much shorter at the MP2 level than at the HF level (0.29–0.38 and 0.18–0.22 Å, respectively). Figure 3 shows that the CH<sub>2</sub>O ligand occupies just one coordination site at tungsten. As compared to WCl<sub>4</sub>(CH<sub>2</sub>O), the W–C(H<sub>2</sub>O) and the W–O(CH<sub>2</sub>) bonds of **11a** are 0.33 Å longer, while the C–O bond of the formaldehyde ligand is 0.16 Å shorter. The small departure of the coordinated formaldehyde molecule from planarity (dihedral angle: 25.9°) also supports the description of W(CO)<sub>5</sub>(CH<sub>2</sub>O) as a typical donor–acceptor complex, rather than a metallacycle with polar covalent bonds. The calculated formaldehyde C–O bond length (1.304 Å) favorably compares with the measured C–O distances (1.32–1.35 Å) of experimentally known transition metal–formaldehyde complexes.<sup>25–28</sup>

The calculated bond dissociation energies of the MP2 energy minimum structures of the W(CO)<sub>5</sub>L complexes are given in Table 4. The optimized geometry of the

W(CO)<sub>5</sub> fragment (**12**) is shown in Figure 3; it has a quadratic-pyramidal geometry (C<sub>4v</sub> symmetry). The bond dissociation energies were determined at the Hartree–Fock and MP2 levels by using the respective optimized structures. CCSD(T) bond energies were not feasible for the W(CO)<sub>5</sub>L complexes for technical reasons (single file size limit), but the CCSD(T) bond energies could be estimated by calculating the reaction energy of the isostructural reaction:<sup>53</sup>



The energy of reaction 1 gives the *difference* of the metal–ligand bond energy between L and CO. Since the reactant and the product are both octahedral complexes, the reaction energy predicted at the MP2 level is quite accurate. By adding the MP2 value for the reaction energy of reaction 1 to the CCSD(T) value for the first CO dissociation energy of W(CO)<sub>6</sub> ( $D_0 = 45.7$  kcal mol<sup>-1</sup>, experimental value =  $46.0 \pm 2.0$  kcal mol<sup>-1</sup>),<sup>54</sup> one obtains an estimated CCSD(T) value for the (CO)<sub>5</sub>W–L dissociation energy. It has been shown that calculated energies of isostructural reactions yield rather accurate bond dissociation energies.<sup>53</sup>

Table 4 shows that the (CO)<sub>5</sub>W–L bond energies calculated at HF/II are very low and that they clearly are higher at MP2/II. The estimated CCSD(T)/II values are somewhat lower than the MP2/II results. The theoretical results give a relative order of bond strengths for the ligands L = C<sub>2</sub>H<sub>4</sub> > HCCH > CH<sub>2</sub>O > CS<sub>2</sub> > CO<sub>2</sub>. A comparison with the trend predicted for the WCl<sub>4</sub>L complexes shows that ethylene becomes relatively more strongly bound in W(CO)<sub>5</sub>L than in WCl<sub>4</sub>L. This is readily explained by the higher donor strength of ethylene over acetylene, which appears to be the dominant factor for the metal–ligand interactions in the donor–acceptor complexes W(CO)<sub>5</sub>L.

Experimentally, the complexes W(CO)<sub>5</sub>(HCCH), W(CO)<sub>5</sub>(C<sub>2</sub>H<sub>4</sub>), and W(CO)<sub>5</sub>(CO<sub>2</sub>) could be detected, although as rather unstable species.<sup>12–14</sup> However, the calculated bond energies suggest that the corresponding CS<sub>2</sub> and CH<sub>2</sub>O complexes should also be worthwhile as synthetic targets, at least from a thermodynamic point of view. For W(CO)<sub>5</sub>(CO<sub>2</sub>) an experimental bond dissociation energy of  $8.2 \pm 1.0$  kcal mol<sup>-1</sup> has been determined on the basis of time-resolved IR spectroscopy.<sup>14</sup> This value is in good agreement with our estimated CCSD(T) bond energy of 10.2 kcal mol<sup>-1</sup>.

**3.2. Analysis of the Electronic Structure.** To gain deeper insight into the nature of the metal–ligand bonds in the complexes, we analyzed the electronic structure of the molecules. To this end, we carried out a topological analysis of the electron density distributions<sup>5,6</sup> and determined atomic charges and covalent bond orders according to the definition of Cioslowski and Mixon.<sup>7</sup> In addition, we used the newly developed charge decomposition analysis (CDA)<sup>8,9</sup> to estimate the relative importance of charge donation and back-donation between the metal and the ligand.

Figure 4 shows the contour line diagrams of the Laplacian distribution  $\nabla^2\rho(\mathbf{r})$  of the complexes **1b**, **2a**, **3a**, **4a**, **5a**, **7a**, **8a**, **9a**, **10a**, and **11a** in the respective

(53) Dapprich, S.; Pidun, U.; Ehlers, A. W.; Frenking, G. *Chem. Phys. Lett.* **1995**, *242*, 521.

(54) Ehlers, A. W. Dissertation, Universität Marburg, Marburg, Germany, 1994.

(51) Optimization of the staggered conformation **10b** yielded a structure with end-on-coordinated CS<sub>2</sub> which is 4.7 kcal mol<sup>-1</sup> more stable than **10a**. However, the frequency analysis showed that **10b** is a transition state of first order with respect to the rotation of the CS<sub>2</sub> molecule out of the plane of symmetry. It can be anticipated that on the HF potential energy surface there exists another minimum of lower symmetry with end-on-coordinated CS<sub>2</sub>.

(52) Baird, M. C.; Hartwell, G.; Wilkinson, G. *J. Chem. Soc. A* **1967**, 2037.

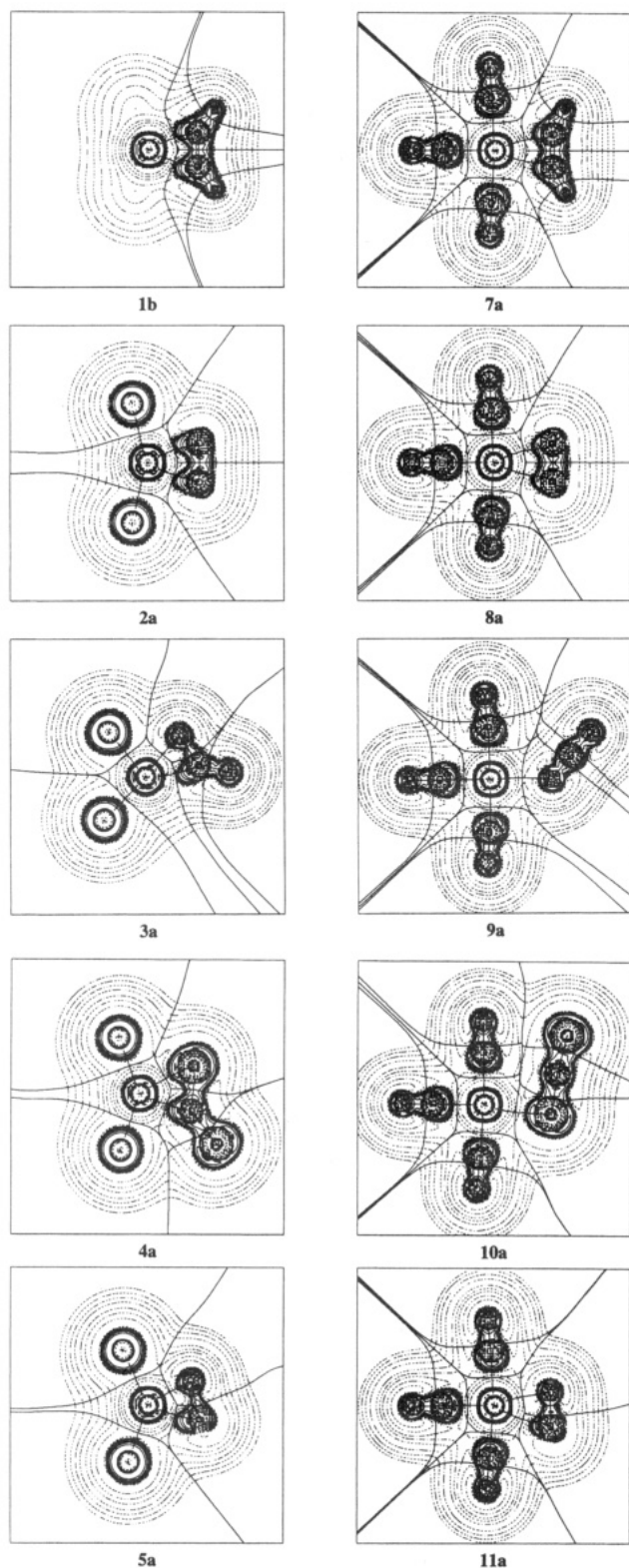


**Figure 4.** Contour line diagrams of the Laplacian distribution  $\nabla^2\rho(\mathbf{r})$  at MP2/II of the complexes in their respective plane of symmetry. Dashed lines indicate charge depletion [ $\nabla^2\rho(\mathbf{r}) > 0$ ], and solid lines indicate charge concentration [ $\nabla^2\rho(\mathbf{r}) < 0$ ]. The solid lines connecting the atomic nuclei are the bond paths, and the solid lines separating the atomic nuclei indicate the zero-flux surfaces in the plane. The crossing points of the bond paths and the zero-flux surfaces are the bond critical points  $\mathbf{r}_b$ .

plane of symmetry of the molecule. For each ligand, the  $\text{WCl}_4\text{L}$  and  $\text{W}(\text{CO})_5\text{L}$  complexes in their lower

energy conformations are compared.<sup>55</sup> The most striking feature of the contour line diagrams in Figure 4 is that for all complexes investigated with side-on-coordinated ligands a cyclic structure of the tungsten–ligand fragment is found, with two metal–ligand bonds and a ring critical point. Thus, even for the  $\text{W}(\text{CO})_5\text{L}$  complexes, whose structural properties indicate a donor–acceptor type of bonding, cyclic structures are predicted for the WL moiety. However, the topological definition of a cyclic structure may be quite different from the chemical interpretation. For example, the  $\text{W}(\text{H}_2)$  unit of the dihydrogen complex  $\text{W}(\text{CO})_5\text{H}_2$  is suggested by the topological analysis of the electron density distribution to have a cyclic structure.<sup>56</sup> Other criteria such as a strong distortion of the Laplacian distribution of the ligand L should be used as a measure for the nature of the ML moiety.

Indeed, there are significant differences in the Laplacian distributions between the  $\text{WCl}_4\text{L}$  and  $\text{W}(\text{CO})_5\text{L}$  series of compounds. For each ligand L, the Laplacian distribution shows a markedly stronger distortion toward the metal in the  $\text{WCl}_4\text{L}$  complexes than in the  $\text{W}(\text{CO})_5\text{L}$  complexes. This indicates a higher degree of covalent W–L bonding for the  $\text{WCl}_4\text{L}$  complexes, as was already inferred from the structural data. In particular, the end-on-coordinated complex  $\text{W}(\text{CO})_5(\text{CO}_2)$  (**9a**) has a Laplacian distribution typical for a pure closed-shell interaction. There is virtually no distortion of the  $\text{CO}_2$  Laplacian distribution in **9a**. Generally, the carbon atoms of the ligands respond more strongly to the perturbation caused by the metal than the oxygen atoms, in accordance with the smaller difference in electronegativity between W and C compared to W and O. The carbon atom is softer than the oxygen atom.

The visual impression of the Laplacian distributions shown in Figure 4 is supported by the calculated results of the topological analysis (Table 5). The energy density at the bond critical point  $H_b$  of the W–L bonds of the  $\text{WCl}_4\text{L}$  complexes clearly is more negative than those for the respective  $\text{W}(\text{CO})_5\text{L}$  complexes. It has been shown that a negative value for  $H_b$  indicates covalent character for the bond, while  $H_b \approx 0$  indicates closed-shell interactions.<sup>57</sup> Another indicator for a more covalent W–L bond in the  $\text{WCl}_4\text{L}$  complexes is the covalent bond order. The calculated BO values for the W–L bonds are much higher for the  $\text{WCl}_4\text{L}$  complexes than for  $\text{W}(\text{CO})_5\text{L}$  (Table 5). Also, the difference of the intraligand bond order between the free ligand L (Table 5, values in parentheses) and the coordinated ligand L is much higher for the  $\text{WCl}_4\text{L}$  complexes than for  $\text{W}(\text{CO})_5\text{L}$ .

In the case of the acetylene and ethylene complexes, the results of the electronic analyses fully support the conclusions from the geometry calculations. The tungsten–carbon bond orders are higher for  $\text{WCl}_4(\text{HCCH})$  (**1b**) than for  $\text{WCl}_4(\text{C}_2\text{H}_4)$  (**2a**) (1.09 compared to 0.91), in accordance with the markedly shorter W–C bond lengths for **1b** (2.001 Å) than for **2a** (2.103 Å). This observation can easily be explained in the framework

(55) Note that for computational reasons the Laplacian distributions of the  $\text{CS}_2$  complexes **4a** and **10a** have been calculated without using effective core potentials for sulfur.

(56) Dapprich, S.; Frenking, G. *Angew. Chem.* **1995**, *107*, 383; *Angew. Chem., Int. Ed. Engl.* **1995**, *34*, 354.

(57) Cremer, D.; Kraka, E. *Angew. Chem.* **1984**, *96*, 612; *Angew. Chem., Int. Ed. Engl.* **1984**, *23*, 627.



**Table 5. Calculated Bond Orders BO, Energy Densities at the Bond Critical Point  $H_b$  (hartrees/ $\text{\AA}^3$ ), Atomic Charges  $q(A)$  and  $q(B)$ , and Charges of the Ligands  $q(L)$  in the Complexes<sup>a</sup>**

molecule	bond (A-B)	BO	$H_b$	$q(A)$	$q(B)$	$q(L)$
<b>1b</b>	W-C	1.09	-0.486	+2.34	-0.35	-0.34
	C-C	1.64 (2.76)	-2.605	-0.35	-0.35	
<b>7a</b>	W-C	0.40	-0.088	+1.76	-0.30	-0.22
	C-C	2.46 (2.76)	-3.273	-0.30	-0.30	
<b>2a</b>	W-C	0.91	-0.391	+2.28	-0.38	-0.36
	C-C	1.11 (1.89)	-1.694	-0.38	-0.38	
<b>8a</b>	W-C	0.39	-0.094	+1.73	-0.24	-0.15
	C-C	1.61 (1.89)	-2.078	-0.24	-0.24	
<b>3a</b>	W-O <sub>b</sub>	0.80	-0.128	+2.35	-1.02	-0.73
	W-C	0.84	-0.412	+2.35	+1.40	
	C-O <sub>b</sub>	0.96 (1.35)	-3.354	+1.40	-1.02	
	C-O <sub>nb</sub>	1.32 (1.35)	-4.548	+1.40	-1.11	
<b>9a</b>	W-O <sub>b</sub>	0.24	-0.034	+1.73	-1.21	±0.00
	C-O <sub>b</sub>	1.25 (1.35)	-4.785	+2.31	-1.21	
<b>4a</b>	C-O <sub>nb</sub>	1.39 (1.35)	-4.940	+2.31	-1.10	
	W-S <sub>b</sub>	1.16	-0.202	+2.22	±0.00	-0.42
<b>10a</b>	W-C	0.92	-0.409	+2.22	-0.96	
	C-S <sub>b</sub>	1.30 (2.32)	-1.034	-0.96	±0.00	
	C-S <sub>nb</sub>	2.02 (2.32)	-1.902	-0.96	+0.53	
	W-S <sub>b</sub>		-0.049			
<b>5a</b>	C-S <sub>b</sub>		-1.912			
	C-S <sub>nb</sub>		-1.949			
	W-O	1.19	-0.432	+2.49	-0.85	-0.64
	W-C	0.82	-0.405	+2.49	-0.01	
<b>11a</b>	C-O	0.89 (1.45)	-2.038	-0.01	-0.85	
	W-O	0.46	-0.027	+1.77	-1.11	-0.40
	W-C	0.46	-0.101	+1.77	+0.57	
	C-O	1.13 (1.45)	-3.664	+0.57	-1.11	

<sup>a</sup> The bond orders of the free ligands are given in parentheses.

of a covalent bonding picture by the  $sp^2$  hybridization of the acetylene C-atom being more favorable than the  $sp^3$  hybridization of the ethylene carbon in the complex. The C-C bond orders in the  $WCl_4L$  complexes (1.64 for **1b**, 1.11 for **2a**) are significantly smaller in comparison with the free ligand, and they are on the order of a typical double bond (1.89 in ethylene) and a typical single bond (1.02 in ethane), respectively, as expected for a substituted metallacyclopentene or metallacyclopentane. In contrast, the C-C bond orders in the  $W(CO)_5L$  complexes **7a** and **8a** are only slightly smaller than those in the free ligand, in accordance with the Dewar-Chatto-Duncanson description of the bonding: donation and back-donation weaken the C-C multiple bond, but they do not lead to a significant reduction of the bond order. The W-C bond orders of **7a** and **8a** are rather low.

As mentioned earlier, the very short W-O and very long C-O bonds of **5a** provide some indications for a transformation of the  $\eta^2$ -formaldehyde complex into an oxo-carbene complex. This conclusion is supported by the electronic structure analysis. Table 5 shows a large bond order of 1.19 for the W-O bond, which suggests some double-bond character. The C-O bond order clearly is reduced in the complex, and the charge distribution in the coordinated ligand indicates an important change in the bonding situation: the formaldehyde ligand is negatively charged in the complex (-0.64), but the oxygen atom loses electronic charge upon coordination (-0.85 compared to -1.10 in free  $CH_2O$ ), while the carbon atom gains about 1 unit of negative charge and is virtually neutral in the complex. Apparently, the C-O bond is weakened to such an extent that the electron-attracting influence of the oxygen atom on the carbon has decreased markedly.

**Table 6. MP2 Charge Decomposition Analysis of the Complexes in Their MP2 Geometries<sup>a</sup>**

molecule	$d$	$b$	$r$
<b>7a</b>	0.297	0.165	-0.391
<b>8a</b>	0.225	0.148	-0.422
<b>11a</b>	0.241	0.163	-0.350
<b>9a</b>	0.126	-0.011	-0.100
<b>10a</b>	0.322	0.033	-0.275
$W(CO)_6$	0.315	0.233	-0.278
<b>3a</b>	0.265	0.168	-0.569

<sup>a</sup>  $d$ , donation;  $b$ , back-donation;  $r$ , repulsive part.

The calculated charge distribution shows that the ligand L always has a higher formal charge in  $WCl_4L$  than in  $W(CO)_5L$ . It is noteworthy that the ethylene ligand is more negatively charged in **2a** than the acetylene ligand in **1b**, while the opposite trend is found for **7a** and **8a** (Table 5). Taken together, the topological analyses of the electron density distribution indicate that the W-L bonds of the  $W(CO)_5L$  complexes have more donor-acceptor character than the  $WCl_4L$  complexes. The electronic structure of the ligands L is much more distorted in the  $WCl_4L$  complexes than in  $W(CO)_5L$ .

Further insight into the bonding situation of the complexes is given by the results of the CDA<sup>8,9</sup> calculations. The CDA method considers the bonding in a complex in terms of (fragment) molecular orbital interactions between two closed-shell fragments. In the present case, the fragments are  $W(CO)_5$  and L for the  $W(CO)_5L$  complexes and  $WCl_4$  and L for the  $WCl_4L$  complexes. The mixing of the occupied orbitals of L and the unoccupied orbitals of  $W(CO)_5$  or  $WCl_4$  gives the electron donation  $d$ . The mixing of the unoccupied orbitals of L and the occupied orbitals of  $W(CO)_5$  or  $WCl_4$  gives the back-donation  $b$ . The mixing of the occupied orbitals of the two fragments gives the repulsive polarization  $r$ . The CDA method can be used as a quantitative expression of the familiar Dewar-Chatto-Duncanson model.<sup>2,3</sup> Previous studies of  $M(CO)_5L$  ( $M = Cr, Mo, W$ ) and  $M(CO)_3L$  complexes ( $M = Ni, Pd, Pt$ ) with various ligands L have shown that the results of the CDA method are in agreement with qualitative bonding models of transition metal complexes.<sup>58,59</sup>

Table 6 shows the CDA results for  $W(CO)_5L$ . The amount of  $L \rightarrow M$  charge donation is always higher than the  $M \rightarrow L$  back-donation, even for  $W(CO)_6$ . This should not be taken as evidence that the ligand  $\rightarrow$  metal charge donation is the dominant contribution to the bond energy. It is now generally agreed that the metal  $\rightarrow$  ligand back-donation from the filled metal d-orbitals into the  $\pi^*$ -orbitals of CO ( $t_{2g}$  in octahedral symmetry) contributes more to the bond energy in  $Cr(CO)_6$  than the  $OC \rightarrow Cr$   $\sigma$ -donation.<sup>60</sup> There are also repulsive interactions between the occupied orbitals of the two fragments, which lead to negative values for the repulsive polarization  $r$  (Table 6). Negative values indicate that electronic charge is depleted from the overlapping

(58) Ehlers, A. W.; Dapprich, S.; Vyboishchikov, S. F.; Frenking, G. *Organometallics*, in press.

(59) Frenking, G.; Dapprich, S.; Ehlers, A. W.; Otto, M.; Vyboishchikov, S. F. In *Metal-Ligand Interactions: Structure and Reactivity*; Russo, N., Salahub, D., Eds.; Proceedings of the NATO Advanced Study Institute, Cetraro, Italy, 1994, in press.

(60) (a) Li, J.; Schreckenbach, G.; Ziegler, T. *J. Am. Chem. Soc.* **1995**, *117*, 486. (b) Blomberg, M. R. A.; Siegbahn, P. E. M.; Lee, T. L.; Rendell, A. P.; Rice, J. E. *J. Chem. Phys.* **1991**, *95*, 5898. (c) Davidson, E. R.; Kunze, K. L.; Machado, F. B. C.; Chakravorty, S. *J. Acc. Chem. Res.* **1993**, *26*, 628 (and references cited therein).

area of the occupied orbitals. A detailed CDA study of  $W(CO)_6$  has shown that most of the repulsive term  $r$  arises from the interactions between the occupied lone pair  $\sigma$ -orbital of CO and the respective filled orbitals of tungsten.<sup>58</sup> Consequently, the net effect of  $OC \rightarrow M$  donation upon the metal–ligand interactions is less stabilizing than the  $M \rightarrow CO$  back-donation, although the CDA shows a larger amount of  $OC \rightarrow M$  charge donation. However, this does not necessarily hold for other ligands L.

For the  $CO_2$  and  $CS_2$  complexes (**9a** and **10a**), the CDA shows that there is virtually only donation of electron density from the ligand to the metal and no back-donation  $M \rightarrow L$ , as can be expected for an end-on coordination of the ligand. Besides, the value of  $d$  is significantly larger for the  $CS_2$  complex than for the  $CO_2$  complex (0.322 versus 0.126), in accordance with the higher bond dissociation energy for **10a** than for **9a**. The clearly larger donation  $d$  and repulsive polarization  $r$  of **10a** than **9a** is also in agreement with the Laplacian distribution of the complexes, which shows that the deformation of the electronic structure of the  $CO_2$  ligand in the latter complex is much lower than that for  $CS_2$  in **10a** (Figure 4).

In  $W(CO)_5(HCCH)$  (**7a**) and  $W(CO)_5(C_2H_4)$  (**8a**), significant values are found for the donation (0.297 and 0.225, respectively) as well as for the back-donation (0.165 and 0.148). In both cases the donation from the ligand to the metal is markedly larger than the back-donation. This result seems to be in opposition to the results of the topological analysis, which yielded negative charges for the ligands in the complexes. However, the repulsive term  $r$  also has an effect upon the charge distribution. The direction of this effect is not obvious from the calculated data. The data for  $W(CO)_5(CH_2O)$  (**11a**) are intermediate between those of the acetylene and ethylene complexes. Apparently, the bonding situation is very similar in these three compounds.

The comparison of the CDA results for the complexes **7a**, **8a**, and **11a** with the results for  $W(CO)_6$  clearly indicates that the carbonyl ligand is a better donor, as well as a better acceptor, than the ligands HCCH,  $C_2H_4$ , and  $CH_2O$ . Thus, the structurally observed small trans effect in these complexes (Figure 3) can be traced back to the poorer  $\pi$ -acceptor capacity of the ligands, rather than to their better  $\sigma$ -donor ability.

On the whole, the end-on-coordinated  $W(CO)_5L$  complexes **9a** and **10a** are clearly distinguished from the side-on-coordinated complexes by the charge decomposition analysis. On the other hand, the results for the side-on-coordinated compounds **7a**, **8a**, and **11a** are quite similar to each other. The donation from the ligand to the metal is larger than the back-donation in each case.

The CDA results for the  $WCl_4L$  complexes using closed-shell  $WCl_4$  and L as interacting fragments are very interesting. The values for the donation and back-donation are nearly always negative, while the repulsive polarization has positive values. This would indicate that electronic charge is removed from the occupied/unoccupied area and concentrated in the occupied/occupied area. Obviously, this is a physically absurd result. The conclusion is that the electronic structure of  $WCl_4L$  cannot reasonably be explained by the Dewar–Chatt–Duncanson model. Closed-shell fragments  $WCl_4$

and L are not proper reference systems for the metal–ligand bonds in these complexes. This is in agreement with the information gained by the optimized geometries and the topological analysis of the electron density distribution. The bonding in  $WCl_4L$  should not be considered as donor–acceptor-type bonding. Rather, it is a normal covalent bond between open-shell fragments.  $WCl_4$  has a triplet ground state. The ligands L have a singlet ground state and a rather high excitation energy to the first open-shell electronic state. Because of the high excitation energy of the ligands L from the closed-shell ground state to the open-shell valence state, the net bonding of the complexes is rather low (Table 2).

**3.3. Comparison of  $WCl_4L$  and  $W(CO)_5L$  Complexes.** The assessment of the interaction between a metal and its ligand as covalent or as of the donor–acceptor type is an often-used method for the classification of transition metal compounds, which is very useful for an understanding of the reactivity of the molecules. However, this classification is not canonical, and it is necessary to formulate criteria for the presence of donor–acceptor or covalent bonds. These criteria might be structural in nature: in the case of a donor–acceptor interaction, the metal–ligand distance should be longer than in the covalent case, and the structure of the ligand should be changed less markedly compared to the nonbonded state. The theoretical investigation may provide some further electronic criteria: the characteristic values of the critical points in the gradient field of the electron density [Laplacian  $\nabla^2\rho(\mathbf{r}_b)$ , energy density  $H(\mathbf{r}_b)$ , and electron density  $\rho(\mathbf{r}_b)$ ] make possible the classification of the metal–ligand bond as a closed shell or as a shared interaction. In the same way, the comparison of the characteristic values of the critical points of the intraligand bonds with the values of the free ligand informs on the electronic changes within the ligand upon coordination. Covalent bond orders may also help for a classification: the bond orders in donor–acceptor interactions can be expected to be significantly smaller than those in covalent bonds.

The results of our calculations clearly indicate that the  $WCl_4L$  complexes should be classified as covalent, while the  $W(CO)_5L$  complexes are of the donor–acceptor type. This follows from all criteria cited in this paper. However, we want to point out that for the donor–acceptor complexes covalent contributions to the bonds are also found, as given by cyclic structures in the gradient field of the electron density (ring critical points) and by finite covalent metal–ligand bond orders. The CDA method appears to be very useful to classify a transition metal compound as a donor–acceptor complex or as a covalent compound. The CDA results for a complex using properly chosen closed-shell fragments give positive (or nearly zero) values for the charge donation and back-donation and negative values for the repulsive polarization. The CDA results of a covalent compound show positive values for the repulsive polarization, which is a physically unreasonable result.

A principal structural difference between  $WCl_4L$  and  $W(CO)_5L$  complexes can be observed for the ligands  $CO_2$  and  $CS_2$ . In the  $WCl_4L$  complexes the ligands are side-on- $\pi$ -coordinated, but for the  $W(CO)_5L$  complexes an end-on coordination via an oxygen or sulfur lone pair is found. Presumably, this result can be traced back to the different number of coordination sites available at



the two metal fragments. However, there might also be electronic reasons: the side-on coordination is better suited for the development of covalent bonds, while the end-on coordination is more favorable for a donation of electron density to the electron-deficient metal center.

The different types of metal–ligand bonding in  $WCl_4L$  and  $W(CO)_5L$  explain the puzzling result that the bond dissociation energies relative to the fragments in their electronic ground states are much lower for  $Cl_4W-L$  than for  $(CO)_5W-L$  (Tables 2 and 4; for  $L = \text{acetylene}$  the  $D_e$  values are similar), although the  $Cl_4W-L$  bond lengths are much shorter than the  $(CO)_5W-L$  distances (Figures 2 and 3). The covalent  $Cl_4W-L$  bonds are formally formed from the triplet states of  $WCl_4$  and  $L$ . The triplet states of  $L$  are much higher in energy than the singlet ground states. For example, the lowest lying ( $^3B_2$ ) triplet state of acetylene, which has a cis-bent geometry, is calculated (CISDT/TZ2P//CISD/TZ2P) to be 82.6 kcal mol $^{-1}$  higher in energy than the ( $^1\Sigma_g^-$ ) singlet ground state.<sup>61</sup> By using this value and the calculated  $Cl_4W-(\text{HCCH})$  bond dissociation energy (34.4 kcal mol $^{-1}$ , Table 2), the theoretically predicted tungsten–ethylene bond strength amounts to 117.0 kcal mol $^{-1}$ . This large value correlates with the short  $W-C$  bond length of **1b** (Figure 2). Thus, the metal–ligand bonds in the  $WCl_4L$  complexes clearly are stronger than those in the  $W(CO)_5L$  complexes, but the corresponding bond dissociation energies relative to the fragments in their electronic ground states are rather low because the ligand  $L$  must first be excited into the triplet state in order to form the short covalent  $Cl_4W-L$  bonds.

#### 4. Summary

The equilibrium geometries and metal–ligand bond energies of the  $WCl_4L$  and  $W(CO)_5L$  complexes predicted at the CCSD(T)/II/MP2/II level of theory are in very good agreement with available experimental data. The results show that the inclusion of correlation energy is

(61) Yamaguchi, Y.; Vacek, G.; Schaefer, H. F., III *Theor. Chim. Acta* **1993**, *86*, 97.

essential for the accurate description of transition metal donor–acceptor complexes. The calculations predict that the order of the metal–ligand bond strengths for  $W(CO)_5L$  is  $L = C_2H_4 > HCCH > CH_2O > CS_2 > CO_2$ . For the  $WCl_4L$  complexes the order is  $L = HCCH > CH_2O > C_2H_4 > CS_2 > CO_2$ . The different orders of the bond strengths are explained by the nature of the metal–ligand interactions. The  $W-L$  bonds of the  $WCl_4L$  compounds are covalent bonds, and the molecules with  $L = HCCH, C_2H_4, CH_2O$  should be considered as metallacycles. Since the carbon atoms of the metallacyclopropene are approximately  $sp^2$  hybridized, while the carbon atoms of the metallacyclopropane are  $sp^3$  hybridized, the former  $W-L$  bonds are stronger than the latter. The  $W-L$  bonds of the respective  $W(CO)_5L$  complexes are donor–acceptor bonds. Since ethylene is a better donor than acetylene, the  $(CO)_5W-C_2H_4$  bonds are stronger than the  $(CO)_5W-HCCH$  bonds. For  $CO_2$  and  $CS_2$ , the calculations predict a side-on-coordinated mode for the  $WCl_4L$  complexes and an end-on-coordinated mode for the  $W(CO)_5L$  complexes. The  $C-O$  bond of the formaldehyde ligand is significantly lengthened in the  $WCl_4(CH_2O)$  complex, which can be considered as a snapshot along the formation of an oxo–carbene complex.

The analysis of the electronic structure supports the classification of the  $WCl_4L$  compounds as covalently bonded molecules and the  $W(CO)_5L$  complexes as donor–acceptor-type structures. In particular, the CDA results are qualitatively different for the two types of compounds.

**Acknowledgment.** This work has been supported by the Deutsche Forschungsgemeinschaft (SFB 260 and Graduiertenkolleg Metallorganische Chemie) and the Fonds der Chemischen Industrie. We acknowledge generous support and excellent service by the computer centers HRZ Marburg, HHLRZ Darmstadt, and HLRZ Jülich. U.P. thanks the Studienstiftung des deutschen Volkes for a scholarship.

OM950610L

# Molecular Structures of the Bimetallic Sulfido Clusters $\text{Cp}'_2\text{Mo}_2\text{Co}_2\text{S}_4(\text{CO})_2$ , $\text{Cp}'_2\text{Mo}_2\text{Co}_2\text{S}_3(\mu_3\text{-PPh})(\text{CO})_2$ , $\text{Cp}'_3\text{Mo}_3\text{CoS}_4(\text{CO})$ , and $\text{Cp}'_3\text{Mo}_3\text{FeS}_4(\text{SH})$

M. David Curtis,\* Umar Riaz, Owen J. Curnow, and Jeff W. Kampf

Department of Chemistry, The Willard H. Dow Laboratory, The University of Michigan,  
 Ann Arbor, Michigan 48109-1055

Arnold L. Rheingold and Brian S. Haggerty

Department of Chemistry, University of Delaware, Newark, Delaware 19716

Received June 12, 1995<sup>®</sup>

The preparation and molecular structures of the clusters  $\text{Cp}'_3\text{Mo}_3\text{CoS}_4(\text{CO})$ ,  $\text{Cp}'_3\text{Mo}_3\text{-FeS}_4(\text{SH})$ , and  $\text{Cp}'_2\text{Mo}_2\text{Co}_2\text{S}_3(\text{PPh})(\text{CO})$  are reported along with the structure of the previously known cluster  $\text{Cp}'_2\text{Mo}_2\text{Co}_2\text{S}_4(\text{CO})_2$ . All these compounds have a tetrahedron of metal atoms at distances corresponding to metal–metal single bonds with  $\mu_3\text{-S}$  ligands capping the triangular metal faces of the tetrahedron to give an overall cubanelike geometry to the clusters. In  $\text{Cp}'_2\text{Mo}_2\text{Co}_2\text{S}_3(\text{PPh})(\text{CO})$ , there is one  $\mu_3\text{-PPh}$  ligand in addition to three  $\mu_3\text{-S}$  ligands.

## Introduction

Hydrodesulfurization (HDS) is a major catalytic process used to remove sulfur from organosulfur compounds contained in fossil fuels. The usual catalyst consists of a complex mixture of molybdenum and cobalt sulfides (and oxides?) impregnated on a high surface-area alumina support.<sup>1</sup> Elegant studies by Topsøe and others have led to a model of the catalytically active site in which cobalt atoms are bound to the edges of the basal planes of an "MoS<sub>2</sub>-like" phase on the surface.<sup>2</sup> These extensive studies, while providing a rather detailed picture of the physical and chemical nature of the catalyst surface, have yet to provide a widely accepted mechanism for C–S bond activation,<sup>3</sup> adsorption modes of the organosulfur substrates, etc.

The difficulty of developing a detailed model for the HDS catalysis has been due, at least in part, to a lack of good model systems for these complex, sulfided surfaces; until recently, little was known concerning the reactivity of thiophenes and other organosulfur compounds with transition metal complexes. Over the last several years, the latter situation has changed dramatically with the work of Angelici, Jones, Rauchfuss, and others.<sup>4–7</sup> These studies have demonstrated C–S and C–H bond activation by oxidative addition reactions at the metal center and by electrophilic or nucleophilic attack on the coordinated sulfur-containing ligands.

Adams et al. have published an extensive series of papers in which the interactions of thiols and cyclic sulfides with triosmium clusters led to new insights on the mechanism of C–S and C–H bond cleavage reactions.<sup>8</sup> We have been addressing the problem of modeling the Co/Mo/S HDS catalyst by studying the reactions of bimetallic sulfido clusters with organic sulfides and related compounds.<sup>9,10</sup> The cluster  $\text{Cp}'_2\text{Mo}_2\text{Co}_2\text{S}_3(\text{CO})_4$  (**1**) (Scheme 1) is a precursor to an HDS catalyst when supported on Al<sub>2</sub>O<sub>3</sub>.<sup>11</sup> In solution, cluster **1** desulfurizes a variety of organic sulfur compounds under relatively mild conditions and is quantitatively converted to the cubane cluster  $\text{Cp}'_2\text{Mo}_2\text{Co}_2\text{S}_4(\text{CO})_2$  (**2**) (Scheme 1).

In this paper we report the structures of several cubanelike clusters that have been prepared during the course of our studies on the reactions of bimetallic clusters with organosulfur compounds and with organophosphines, as well as the structure of the previously

(5) (a) Jones, W. D.; Chin, R. M. *Organometallics* **1992**, *11*, 2698. (b) Rosini, C. P.; Jones, W. D. *J. Am. Chem. Soc.* **1992**, *114*, 10767. (c) Dong, L.; Duckett, S. B.; Ohman, K. F.; Jones, W. D. *J. Am. Chem. Soc.* **1992**, *114*, 151. (d) Jones, W. D.; Chin, R. M. *J. Am. Chem. Soc.* **1992**, *114*, 9851. (e) Jones, W. D.; Dong, L. *J. Am. Chem. Soc.* **1991**, *113*, 559.

(6) (a) Rauchfuss, T. B. *Prog. Inorg. Chem.* **1991**, *39*, 260. (b) Giolando, D. M.; Rauchfuss, T. B.; Reingold, A. L.; Wilson, S. R. *Organometallics* **1987**, *6*, 667. (c) Bolinger, C. M.; Rauchfuss, T. B.; Reingold, A. L. *J. Am. Chem. Soc.* **1983**, *105*, 6321. (d) Ogilvy, A. E.; Draganjac, M.; Rauchfuss, T. M.; Wilson, S. R. *Organometallics* **1988**, *7*, 1171. (e) Luo, S.; Ogilvy, A. E.; Rauchfuss, T. M.; Reingold, A. L.; Wilson, S. R. *Organometallics* **1991**, *10*, 1002. (f) Luo, S.; Rauchfuss, T. B.; Gan, Z. *J. Am. Chem. Soc.* **1993**, *115*, 4943. (g) Krautscheid, H.; Feng, Q.; Rauchfuss, T. B. *Organometallics* **1993**, *12*, 3273. (h) Krautscheid, H.; Feng, Q.; Rauchfuss, T. B. *Organometallics* **1993**, *12*, 3273. (i) Luo, S.; Rauchfuss, T. B.; Gan, Z. *J. Am. Chem. Soc.* **1993**, *115*, 4943. (j) Skaugset, A. E.; Rauchfuss, T. B.; Wilson, S. R. *J. Am. Chem. Soc.* **1992**, *114*, 8521.

(7) (a) Boorman, P. M.; Gao, X.; Fait, J. F.; Parvez, M. *Inorg. Chem.* **1991**, *30*, 3886. (b) Gabay, J.; Dietz, S.; Bernatis, P.; Rakowski DuBois, M. *Organometallics* **1993**, *12*, 3630.

(8) (a) Review: Adams, R. D. *Polyhedron* **1985**, *4*, 2003. (b) Adams, R. D.; Pompeo, M. P.; Wu, W.; Yamamoto, J. H. *J. Am. Chem. Soc.* **1993**, *115*, 8207 and references therein.

(9) Curtis, M. D. *Appl. Organomet. Chem.* **1992**, *6*, 429.

(10) Riaz, U.; Curnow, O. J.; Curtis, M. D. *J. Am. Chem. Soc.* **1994**, *116*, 4357.

(11) Curtis, M. D.; Penner-Hahn, J. E.; Schwank, J.; Baralt, O.; McCabe, D. J.; Thompson, L.; Waldo, G. *Polyhedron* **1988**, *7*, 2411.

<sup>®</sup> Abstract published in *Advance ACS Abstracts*, October 1, 1995.

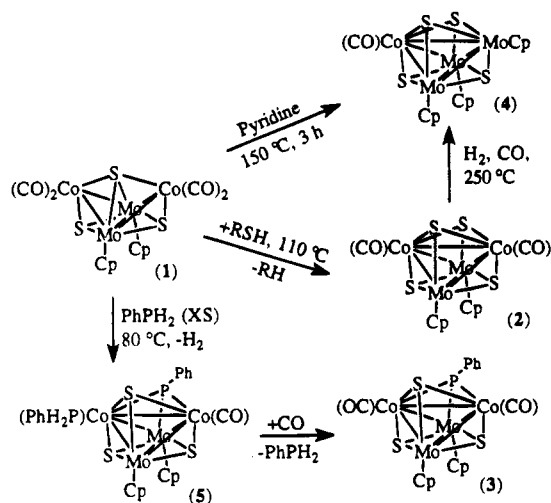
(1) Prins, R.; de Beer, V. H. J.; Somorjai, G. A. *Catal. Rev.-Sci. Eng.* **1989**, *31*, 1.

(2) Topsøe, H.; Clausen, B. S. *Catal. Rev.-Sci. Eng.* **1984**, *26*, 395.

(3) Review: Chianelli, R. R.; Daage, M.; Ledoux, M. *J. Adv. Catal.* **1994**, *40*, 177–232.

(4) (a) Review: Angelici, R. J. *Acc. Chem. Res.* **1988**, *21*, 387. (b) Spies, G. H.; Angelici, R. J. *J. Am. Chem. Soc.* **1988**, *110*, 5569. (c) Lesch, D. A.; Richardson, J. W., Jr.; Jacobson, R. A.; Angelici, R. J. *J. Am. Chem. Soc.* **1984**, *106*, 2901. (d) Hachgenei, J. W.; Angelici, R. J. *J. Organomet. Chem.* **1988**, *355*, 359. (e) Chen, J.; Angelici, R. J. *Organometallics* **1990**, *9*, 879, 849. (f) Hachgenei, J.; Angelici, R. J. *Organometallics* **1989**, *8*, 14. (g) Benson, J. W.; Angelici, R. J. *Organometallics* **1993**, *12*, 680. (h) Benson, J. W.; Angelici, R. J. *Organometallics* **1992**, *11*, 922. (i) Choi, M.-G.; Angelici, R. J. *Inorg. Chem.* **1991**, *30*, 1417.

Scheme 1



synthesized cluster 2. The structure of the phosphinidene cluster  $\text{Cp}'_2\text{Mo}_2\text{Co}_2\text{S}_3(\mu_3\text{-PPh})(\text{CO})_2$  (3) was communicated in a preliminary report.<sup>12</sup>

### Experimental Section

**General Considerations.** All manipulations and reactions were carried out under a nitrogen atmosphere by use of standard Schlenk line techniques or by use of a glovebag. All high-pressure, high-temperature reactions were carried out in a glass-lined, stainless steel Parr high-pressure reactor. Reagent grade solvents were dried and distilled prior to use: toluene, diethyl ether and tetrahydrofuran from Na/benzophenone; dichloromethane and hexane from  $\text{CaH}_2$ .  $\text{Cp}'_2\text{Mo}_2\text{Co}_2\text{S}_3(\text{CO})_4$ <sup>13</sup> (1),  $\text{Cp}'_2\text{Mo}_2\text{Fe}_2\text{S}_2(\text{CO})_8$ ,<sup>13</sup> and  $\text{Cp}'_2\text{Mo}_2\text{Co}_2\text{S}_4(\text{CO})_2$ <sup>14</sup> (2) were prepared by published procedures. All other reagents were purchased from Aldrich Chemical Co.  $^1\text{H}$  and  $^{13}\text{C}$  NMR data were collected on a Bruker AM-300 or Bruker WM-360 spectrometer.  $^{31}\text{P}$  NMR data were collected on a General Electric GN-500 NB spectrometer. IR spectra were obtained on a Nicolet 5-DXB spectrometer. GC-MS spectra were collected on a Finnegan 4021 quadrupole mass spectrometer. Mass spectra were obtained on a VG-70-250-S high-resolution mass spectrometer. Elemental analyses were done by Galbraith Laboratories Inc., Spang Microanalytical Laboratory, or the Microanalysis Laboratory, University of Michigan.

**Preparation of  $\text{Cp}'_2\text{Mo}_2\text{Co}_2\text{S}_3(\mu_3\text{-PPh})(\text{CO})_2$  (3).**  $\text{Cp}'_2\text{Mo}_2\text{Co}_2\text{S}_3(\text{CO})_4$  (0.295 g, 0.436 mmol) was dissolved in 50 mL of benzene. In a glovebag,  $\text{PhPH}_2$  (0.3 mL, 2.7 mmol) was added. The solution was then refluxed for 5 h under a slow stream of  $\text{N}_2$ . The solution IR showed peaks due to  $\text{Cp}'_2\text{Mo}_2\text{Co}_2\text{S}_3(\mu_3\text{-PPh})(\text{CO})(\text{PhPH}_2)$  (5), so the solvent and excess  $\text{PhPH}_2$  were removed in vacuo. The brown solid was then redissolved in benzene and the solution stirred under a CO atmosphere for 2 h. Removal of solvent and flash chromatography down 1 in. of alumina with 1:1  $\text{CH}_2\text{Cl}_2$ /hexane produced 0.15 g of dark green crystals (47% yield) after recrystallization from  $\text{CH}_2\text{Cl}_2$ /hexane.  $^1\text{H-NMR}$  ( $\text{C}_6\text{D}_6$ ):  $\delta$  7.52 (m, 2H, PhH), 6.95 (m, 3H, PhH), 5.25 (t,  $J = 2.3$  Hz, 2H), 5.02 (t,  $J = 2.3$  Hz, 2H), 5.00 (t,  $J = 2.3$  Hz, 2H), 4.84 (t,  $J = 2.3$  Hz, 2H) ( $2\text{A}_2\text{B}_2$  pattern for CpH), 1.79 (s, 3H, CpCH<sub>3</sub>), 1.60 (s, 3H, CpCH<sub>3</sub>).  $^{31}\text{P-NMR}$  ( $\text{C}_6\text{D}_6$ ):  $\delta$  451.5 ppm. IR (benzene):  $\nu(\text{CO})$  1968 (ms), 1952 (s)  $\text{cm}^{-1}$ . Anal. Calcd for  $\text{C}_{20}\text{H}_{19}\text{Co}_2\text{Mo}_2\text{O}_2\text{PS}_3$ : C, 33.01; H, 2.63. Found: C, 33.12; H, 2.55.

**Preparation of  $\text{Cp}'_2\text{Mo}_2\text{Co}_2\text{S}_3(\mu_3\text{-PPh})(\text{CO})(\text{PhPH}_2)$  (5).**  $\text{Cp}'_2\text{Mo}_2\text{Co}_2\text{S}_3(\text{CO})_4$  (0.22 g, 0.33 mmol) and  $\text{PhPH}_2$  (6.0 mL of

0.332 M, 2.0 mmol) were dissolved in 30 mL of benzene and refluxed under a slow stream of  $\text{N}_2$  for 12 h. Chromatography down a  $20 \times 2$  in. column of alumina with 1:1  $\text{CH}_2\text{Cl}_2$ /hexane eluted a small amount of 3 followed by  $\text{Cp}'_2\text{Mo}_2\text{Co}_2\text{S}_3(\mu_3\text{-PPh})(\text{CO})(\text{PhPH}_2)$  (0.10 g, 38% yield) after recrystallization from  $\text{CH}_2\text{Cl}_2$ /hexane.  $^1\text{H-NMR}$  ( $\text{C}_6\text{D}_6$ ):  $\delta$  7.53 (m, 4H, PhH), 7.00 (m, 6H, PhH), 6.30 (m,  $J_{\text{PH}} \sim 315$  Hz, 2H, PH<sub>2</sub>), 5.41 (m, 2H), 5.16 (m, 2H), 5.12 (m, 2H), 5.02 (m, 2H) (2ABCD pattern for CpH), 1.93 (s, 3H, CpCH<sub>3</sub>), 1.79 (s, 3H, CpCH<sub>3</sub>). IR (toluene):  $\nu(\text{CO})$  1947 (s)  $\text{cm}^{-1}$ . Anal. Calcd for  $\text{C}_{25}\text{H}_{21}\text{Co}_2\text{Mo}_2\text{OP}_2\text{S}_3$ : C, 37.05; H, 3.23. Found: C, 32.90; H, 2.94. The thermal instability of this compound with respect to loss of phosphine prevented a good microanalysis.

**Formation of  $\text{Cp}'_3\text{Mo}_3\text{Co}(\text{CO})\text{S}_4$  (4).** (a) **From the Reaction of 2 with  $\text{H}_2$  and CO.** Toluene (40 mL) and 100 mg of 2 were placed in a reactor. The reactor was charged with 200 psi of  $\text{H}_2$  and 50 psi of CO as above and heated to  $150^\circ\text{C}$  for 3 h. The reaction mixture was worked up as described above. Cluster 2 was recovered unreacted. The reaction was repeated as described, except that the temperature was raised to  $250^\circ\text{C}$ . An NMR spectrum of the product in  $\text{C}_6\text{D}_6$  showed the absence of both 1 and 2 and the appearance of a new product. The reaction mixture was transferred to a  $30 \times 3$  cm column of alumina. Elution with a 1:1 mixture of  $\text{CH}_2\text{Cl}_2$ /hexane yielded a green band. Elution with pure dichloromethane did not yield any new products, but some black material remained irreversibly adsorbed to the alumina. The solvent was removed from the green fraction, and a dark, crystalline solid identified as  $\text{Cp}'_3\text{Mo}_3\text{Co}(\text{CO})\text{S}_4$  (4) was obtained. Yield: 15–30%. Data for 4: IR (KBr)  $1903\text{ cm}^{-1}$  ( $\nu_{\text{CO}}$ );  $^1\text{H NMR}$  ( $\text{C}_6\text{D}_6$ ) 5.04 (m, 2H), 4.92 (m, 2H), 1.79 (s, 3H); MS (EI)  $m/z$  740 ( $\text{P}^+$ ), 712 ( $\text{P}^+ - \text{CO}$ ). Anal. Calcd for  $\text{C}_{19}\text{H}_{21}\text{Mo}_3\text{CoOS}_4$ : C, 30.82; H, 2.86. Found: C, 31.64; H, 3.77.

(b) **From Reaction of 1 with Pyridine.** Compound 4 was also formed in ca. 15% yield when cluster 1 (100 mg) was allowed to react with pyridine (5 mL in 40 mL of toluene) at  $150^\circ\text{C}$  for 3 h. An NMR spectrum of the reaction mixture indicated the presence of a complex mixture of products. The cluster was isolated by column chromatography as a green band with hexane/ $\text{CH}_2\text{Cl}_2$  as eluant. A dark band remained at the top of the column and would not elute.

**Formation of  $\text{Cp}'_3\text{Mo}_3\text{Fe}_3\text{S}_4(\text{SH})$  (6) from the Reaction of  $\text{Cp}'_2\text{Mo}_2\text{Fe}_2(\text{CO})_8\text{S}_2$  with Thiophene.** Thiophene (40 mL) and 100 mg of 4 were placed in the Parr pressure reactor. The reactor was heated to  $150^\circ\text{C}$  for 4 h. After the reactor had cooled to room temperature, the head gases were vented through a liquid nitrogen trap to collect the condensables that were subsequently analyzed by GC (FID). With this technique, the identity of the product gases could be established, but a quantitative analysis was not possible. The solution remaining in the reactor was decanted into a Schlenk flask and the thiophene evaporated in vacuo to give a solid residue. This material did not elute from a column of alumina or silica. Fractional crystallization of the reaction solids yielded a mixture of crystalline products, but no pure compounds could be obtained due to the similar solubilities of the components. One particularly well-formed crystal was selected by hand from the mixture and shown by X-ray crystallography to be  $\text{Cp}'_3\text{Mo}_3\text{Fe}_3\text{S}_4(\text{SH})$ , 6. However, the IR spectrum of the crystalline mixture still showed strong CO bands, so compound 6 is not representative of the entire sample.

**X-ray Data Collection.** A black crystal of 2 (ground to a spherical shape) and dark brown crystals of 4 and of 6 were cemented on glass fibers with epoxy, whereas the dark crystal of 3 was sealed in a capillary. These crystals were mounted on a Siemens R3m/v diffractometer (2–4) or on a Nicolet R3m (6). The unit cell parameters were obtained from the least squares fit of 25 reflections ( $20^\circ < 2\theta < 25^\circ$  (2, 4, and 6) or  $20^\circ < 2\theta < 34^\circ$  (3)). Preliminary photographic characterization showed  $2/m$  symmetry; systematic absences in the diffraction data ( $0k0$ ,  $k = 2n + 1$ ;  $h0l$ ,  $h + l = 2n + 1$ ) uniquely established the space group  $P2_1/n$  for 2, 4, and 6. The orthorhombic,

(12) Curnow, O. J.; Kampf, J. W.; Curtis, M. D. *Organometallics* **1991**, *10*, 2546.

(13) Curtis, M. D.; Williams, P. D.; Butler, W. M. *Inorg. Chem.* **1988**, *27*, 2853.

(14) Brunner, H.; Wachter, J. *J. Organomet. Chem.* **1982**, *240*, C41.

Table 1. Summary of Selected Crystallographic Data

	Cp <sub>2</sub> 'Mo <sub>2</sub> Co <sub>2</sub> S <sub>4</sub> (CO) <sub>2</sub> (2)	Cp <sub>2</sub> 'Mo <sub>2</sub> Co <sub>2</sub> S <sub>4</sub> (PPh)(CO) (3)	Cp <sub>3</sub> 'Mo <sub>3</sub> CoS <sub>4</sub> (CO) (4)	Cp <sub>3</sub> 'Mo <sub>3</sub> FeS <sub>4</sub> (SH) (6)
color	dark brown	black	dark brown	black
chem formula	C <sub>14</sub> H <sub>14</sub> Co <sub>2</sub> Mo <sub>2</sub> O <sub>2</sub> S <sub>4</sub>	C <sub>20</sub> H <sub>19</sub> Co <sub>2</sub> Mo <sub>2</sub> OPS	C <sub>19</sub> H <sub>21</sub> CoMo <sub>3</sub> OS <sub>4</sub>	C <sub>18</sub> H <sub>22</sub> FeMo <sub>3</sub> OS <sub>5</sub>
mol wt	652.3	728.3	740.37	758.37
space group	P <sub>2</sub> <sub>1</sub> /n (No. 14)	Pc <sub>2</sub> <sub>1</sub> /n (alt of Pna <sub>2</sub> <sub>1</sub> , No. 33)	P <sub>2</sub> <sub>1</sub> /n (No. 14)	P <sub>2</sub> <sub>1</sub> /n (No. 14)
cryst system	monoclinic	orthorhombic	monoclinic	monoclinic
a (Å)	9.6749(1)	10.210(2)	8.139(5)	8.264(1)
b (Å)	20.491(4)	12.767(3)	17.86(1)	17.942(4)
c (Å)	9.771(1)	18.097(4)	15.231(7)	15.298(3)
β (deg)	99.595(9)	90	91.43	92.79(1)
V (Å <sup>3</sup> )	1905.0(4)	2358.8(7)	2213(2)	2265.7(8)
Z	4	4	4	4
ρ(calcd) (g/cm <sup>-3</sup> )	2.27	2.05	2.22	2.22
R(F), R(wF)	0.0290, 0.0309	0.0584, 0.0493	0.0935, 0.0908	0.0539, 0.0626

noncentrosymmetric space group *Pc*<sub>2</sub><sub>1</sub>*n* (alternate setting of *Pna*<sub>2</sub><sub>1</sub>, No. 33) was chosen as the correct space group for **3** after refinement in the symmetric alternative, *Pcmn* (alternate setting of *Pnma*, No. 62), yielded a highly disordered model with *R* = 0.0881, *R*<sub>w</sub> = 0.1188, and GOF = 1.61 for 1995 reflections and 230 parameters. Three standard reflections, monitored every 197 data points for **6** and after every 97 data points for **2–4**, showed insignificant variation (<2%). Empirical corrections for absorption were applied to the data sets (*ψ*-scan reflections, pseudoellipsoid model) for **2**, **3**, and **6**, whereas an analytical correction was applied to the data for **4**. Additional crystallographic information is contained in the Supporting Information. Table 1 gives a brief summary of unit cell dimensions, etc.

The cluster Cp<sub>2</sub>'Mo<sub>2</sub>Co<sub>2</sub>S<sub>4</sub>(CO)<sub>2</sub> was found to crystallize in two forms, the one reported in Table 1 and a monoclinic form, *a* = 18.0629(5) Å, *b* = 8.163(2) Å, *c* = 40.921(10) Å, space group *C*<sub>2</sub>/*c*, and *Z* = 12. This polymorph had one molecule in a general position and one lying on a 2-fold axis. Their structures differed only in the rotational orientation of the Cp' rings, and the core geometries were essentially identical to that reported here.

**Structure Solution and Refinement.** All the structures were solved by direct methods to locate the metal atoms, and the remaining non-hydrogen atoms were located through subsequent difference Fourier syntheses. All non-hydrogen atoms were refined with anisotropic thermal parameters, and all hydrogen atoms were included as idealized isotropic contributions (*d*<sub>C-H</sub> = 0.96 Å; *U* = 1.2*U* of attached C for **2** and **6**; *U* = 0.07 for **4**, and for **3** the isotropic value refined to *U* = 0.084(4)).

## Results and Discussion

**Synthesis. (a) Mo/Co/S Clusters.** Scheme 1 summarizes the transformations of the Mo/Co/S clusters described in this work. The cluster Cp<sub>2</sub>'Mo<sub>2</sub>Co<sub>2</sub>S<sub>4</sub>(CO)<sub>2</sub> (**2**) was originally synthesized from the reaction of Cp<sub>2</sub>'Mo<sub>2</sub>S<sub>4</sub> and Co<sub>2</sub>(CO)<sub>8</sub>.<sup>14</sup> We have obtained this cluster as the organometallic product resulting from the desulfurization of organic sulfur compounds by cluster **1**. Cluster **1** also reacts with PhPH<sub>2</sub> to give as the initial product the CO-substituted complex, Cp<sub>2</sub>'Mo<sub>2</sub>Co<sub>2</sub>S<sub>3</sub>(CO)<sub>3</sub>(PPhH<sub>2</sub>).<sup>15</sup> Further reaction in the presence of excess phosphine leads to the "abstraction" of the phenyl phosphinidene (PhP) group from the phenylphosphine and the to the formation of phosphine-substituted cubane cluster, **5**.<sup>12</sup> The PhP group is isoelectronic and isolobal to the sulfur atom as far as its ligating properties, so the phosphinidene group abstraction shown in Scheme 1 is analogous to the sulfur atom abstraction. The coordinated phosphine ligand in compound **5** is

easily displaced by 1 atm of CO to give the parent phosphinidene cluster, **3**. These transformations can be driven to completion in either direction and are easily followed by monitoring the IR spectrum of the reaction mixture.

The cluster Cp<sub>2</sub>'Mo<sub>2</sub>Co<sub>2</sub>S<sub>3</sub>(μ<sub>3</sub>-PPh)(CO)(PhPH<sub>2</sub>) (**5**) belongs to the C<sub>1</sub> point group, and thus should exhibit two sets of ABCD multiplets for the Cp' ring protons. The anisotropic effect of the phosphine ligand is small in this case, and only four multiplets are observed (δ 5.41–5.02) rather than the expected eight if all were resolved. The two singlets for the Cp' methyl protons appear at 1.93 and 1.79 ppm. The phosphine protons are also diastereotopic and thus give overlapping multiplets due to H–H coupling and coupling to two different P atoms. Because of the complexity, and some overlap with the phenyl proton region, spin-simulation to determine the parameters was not attempted. The average chemical shift is 6.30 ppm with an average coupling constant to the phosphine P atom of ~315 Hz.

Cp<sub>2</sub>'Mo<sub>2</sub>Co<sub>2</sub>S<sub>3</sub>(μ<sub>3</sub>-PPh)(CO)<sub>2</sub> (**3**) belongs to the C<sub>s</sub> point group, with the mirror plane going through the Cp' ligands. The Cp' groups are therefore chemically distinct and show two A<sub>2</sub>B<sub>2</sub> patterns for the ring protons (δ 5.24–4.84) and two singlets for the methyl protons (δ 1.79 and 1.60). The ν(CO) absorptions (1968 and 1952 cm<sup>-1</sup>) are shifted to lower wavenumbers than those in **2** (1984 and 1965 cm<sup>-1</sup>). These values suggest that the μ<sub>3</sub>-sulfur ligand is a better π-acceptor or a poorer σ-donor than the μ<sub>3</sub>-PPh ligand. A <sup>31</sup>P-NMR spectrum showed a chemical shift for the μ<sub>3</sub>-P atom of 451.5 ppm. This is in the expected range for a phosphorus atom bridging two 3d transition metals and a 4d transition metal.<sup>16</sup>

The trimolybdenum cluster Cp<sub>3</sub>'Mo<sub>3</sub>CoS<sub>4</sub>(CO) (**4**) appears to be a thermodynamic sink for the decomposition of clusters **1** or **2**. If **2** is heated to over 200 °C in toluene solution, cluster decomposition occurs and the NMR spectrum of the crude product shows the presence of more than one product. Column chromatography of the mixture gave a 30% yield of **4**. This cluster is also formed apparently in the thermal decomposition of clusters **1** or **2** on the direct insert probe of a mass spectrometer, since major peaks ascribable to cluster **4** were observed in the electron impact MS of **1** or **2**. In the FAB mass spectra of the same clusters, no peaks due to **4** were detected. Although we have not performed experiments to verify this impression, it seems that the presence of hard ligands facilitates the forma-

(16) Verkade, J. G. In *Phosphorus-31 NMR Spectroscopy in Stereochemical Analysis*; Quin, L. D., Ed.; VCH Publishers Inc.: Deerfield Beach, FL, 1987.

(15) Curnow, O. J.; Kampf, J. W.; Curtis, M. D.; Shen, J.-K.; Basolo, F. *J. Am. Chem. Soc.* **1994**, *116*, 224.

Table 2. Bond Distances Involving the Core Atoms<sup>a</sup>

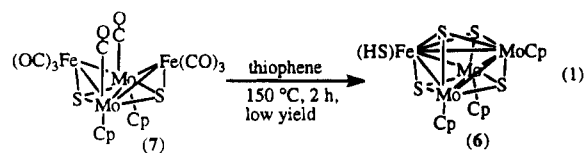
Cp <sub>2</sub> Mo <sub>2</sub> Co <sub>2</sub> S <sub>4</sub> (CO) <sub>2</sub> (2)		Cp <sub>2</sub> Mo <sub>2</sub> Co <sub>2</sub> S <sub>3</sub> (PPh)(CO) (3)		Cp <sub>3</sub> Mo <sub>3</sub> CoS <sub>4</sub> (CO) (4)		Cp <sub>3</sub> Mo <sub>3</sub> FeS <sub>4</sub> (SH) (6)	
atoms	dist (Å)	atoms	dist (Å)	atoms	dist (Å)	atoms	dist (Å)
Mo2-S4	2.324(1)	Mo(2)-S(3)	2.288(5)	Mo3-S4	2.322(06)	Mo3-S4	2.354(3)
Mo2-S3	2.328(1)	Mo(2)-S(2)	2.297(4)	Mo3-S3	2.343(06)	Mo3-S3	2.343(3)
Mo2-S1	2.319(1)	Mo(2)-S(1)	2.334(4)	Mo3-S2	2.310(07)	Mo3-S2	2.324(3)
Mo2-Co2	2.7040(7)	Mo(2)-Co(2)	2.720(2)	Mo3-Co1	2.757(04)	Mo3-Fe1	2.807(2)
Mo2-Co1	2.6939(7)	Mo(2)-Co(1)	2.712(2)	Mo2-S4	2.317(07)	Mo2-S3	2.342(3)
Mo1-S3	2.323(1)	Mo(1)-S(2)	2.362(4)	Mo2-S2	2.323(06)	Mo2-S2	2.326(2)
Mo1-S2	2.326(1)	Mo(1)-S(1)	2.334(4)	Mo2-S1	2.334(06)	Mo2-S1	2.355(2)
Mo1-S1	2.324(1)	Mo(1)-P(1)	2.338(5)	Mo2-Mo3	2.825(03)	Mo2-Mo3	2.835(1)
Mo1-Mo2	2.8313(5)	Mo(1)-Mo(2)	2.822(1)	Mo2-Co1	2.742(04)	Mo2-Fe1	2.796(2)
Mo1-Co2	2.7053(8)	Mo(1)-Co(2)	2.740(3)	Mo1-S3	2.328(07)	Mo1-S4	2.344(3)
Mo1-Co1	2.6990(7)	Mo(1)-Co(1)	2.746(3)	Mo1-S2	2.324(06)	Mo1-S2	2.336(2)
Co2-S4	2.205(1)	Co(2)-S(3)	2.215(5)	Mo1-S1	2.330(06)	Mo1-S1	2.344(2)
Co2-S3	2.177(1)	Co(2)-S(2)	2.190(3)	Mo1-Mo3	2.846(03)	Mo1-Mo3	2.869(1)
Co2-S2	2.217(1)	Co(2)-P(1)	2.158(5)	Mo1-Mo2	2.843(02)	Mo1-Mo2	2.869(1)
Co1-S4	2.215(1)	Co(1)-S(3)	2.213(5)	Mo1-Co1	2.735(03)	Mo1-Fe1	2.772(1)
Co1-S2	2.217(1)	Co(1)-S(1)	2.188(3)	Co1-S4	2.188(06)	Fe1-S5	2.242(4)
Co1-S1	2.173(1)	Co(1)-P(1)	2.152(5)	Co1-S3	2.156(06)	Fe1-S4	2.240(3)
Co1-Co2	2.5816(9)	Co(1)-Co(2)	2.560(2)	Co1-S1	2.189(07)	Fe1-S3	2.268(3)
						Fe1-S1	2.244(3)
av Mo-S	2.324(0.003)		2.323(0.030)		2.327(0.010)		2.341(0.011)
av Co(Fe)-S	2.201(0.020)		2.202(0.014)		2.178(0.019)		2.249(0.013)
av Mo-Mo					2.838(0.011)		2.858(0.020)
av Mo-Co(Fe)	2.701(0.005)		2.730(0.016)		2.745(0.011)		2.792(0.018)

<sup>a</sup> Standard deviations are in parentheses. The standard deviations of the averages are calculated with the  $n - 1$  formula.

tion of **4** from **1** in these decomposition reactions, since appreciable quantities of **4** were formed in the reactions of **1** with aniline, pyridine, and other nitrogen bases. In these reactions, neither substitution products nor denitrogenation of the substrates was observed. Perhaps the weakly bound, hard ligands stabilize fragments until they can recombine to form the stable cluster **4**.

The clusters **2** and **4**, with Cp<sub>4</sub>Mo<sub>4</sub>S<sub>4</sub>, form an iso-electronic series, and all three adopt the cubane type structure. The missing members of this series, CpMoCo<sub>3</sub>S<sub>4</sub>(CO)<sub>3</sub> and Co<sub>4</sub>S<sub>4</sub>(CO)<sub>4</sub>, are presently unknown. Attempts to synthesize the former by using an excess of Co<sub>2</sub>(CO)<sub>8</sub> in a reaction with Cp<sub>2</sub>Mo<sub>2</sub>S<sub>4</sub> were not successful, although a Co-rich cluster, Cp<sub>2</sub>Mo<sub>2</sub>Co<sub>3</sub>S<sub>2</sub>(CO)<sub>7</sub>, has been made by a related route and characterized.<sup>17</sup> The greater stability of Mo-Mo bonds relative to Co-Co bonds<sup>18</sup> probably accounts for preference of forming Mo-rich clusters when Mo-S complexes are reacted with Co<sub>2</sub>(CO)<sub>8</sub>. Two paramagnetic trichromium clusters Cp<sub>4</sub>Cr<sub>3</sub>MS<sub>4</sub>, M = V and Nb, analogous to **4** have been synthesized but not structurally characterized,<sup>19</sup> and the electronic structures of these types of clusters have been investigated.<sup>20-22</sup>

(b) **Mo/Fe/S Cluster.** The iron-containing cluster Cp<sub>3</sub>Mo<sub>3</sub>FeS<sub>4</sub>(SH) (**6**) was obtained from the reaction of Cp<sub>2</sub>Mo<sub>2</sub>Fe<sub>2</sub>S<sub>2</sub>(CO)<sub>8</sub> (**7**) with thiophene at 150 °C for 2 h (eq 1). This reaction produced a brown solution that



exhibited weak  $\nu(\text{CO})$  bands in the IR spectrum, and

the NMR spectrum of the crude reaction product gave broad peaks whose positions did not correspond with those expected for diamagnetic products, indicating that paramagnetic species were present although no room-temperature ESR spectrum was observed. The brown solid could not be chromatographed due to extensive decomposition on the chromatography column, and fractional crystallization did not yield a pure product. However, some large, well-formed crystals were present in the mixture. A few of these were separated by hand, and a structure determination showed them to be Cp<sub>3</sub>Mo<sub>3</sub>FeS<sub>4</sub>(SH), **6**. Since the IR spectrum of the solid mixture still showed some  $\nu(\text{CO})$  bands but none due to  $\nu(\text{SH})$  stretches, it was concluded that the compound **6** was not representative of the reaction mixture. However, continued efforts to further characterize the mixture were unsuccessful.

When the reaction of Cp<sub>2</sub>Mo<sub>2</sub>Fe<sub>2</sub>S<sub>2</sub>(CO)<sub>8</sub> (**7**) with thiophene was carried out under 200 psi of H<sub>2</sub> at 150 °C, a mixture of hydrocarbons was observed and analyzed by GC. The mixture contained saturated hydrocarbons only, mainly ethane, propane, isobutane, and butane. The brown, intractable residue appeared to be the same as that obtained in the absence of hydrogen (see above). In comparison, the reaction of thiophene with cluster **1** under these conditions produced more unsaturated hydrocarbons and gave a single organometallic product, cluster **2**.<sup>10</sup>

**Structures.** (a) Cp<sub>2</sub>Mo<sub>2</sub>Co<sub>2</sub>(CO)<sub>2</sub>S<sub>4</sub>, **2**. Bond distances for **2** are tabulated in Table 2, and the bond angles are in Table 3. Figure 1 shows the ORTEP drawing of the structure. The asymmetric unit for **2** consists of one molecule on a general position so there is no crystallographically constrained symmetry. The structure of **2** consists of an array of the four metal atoms at the corners of a tetrahedron with the four sulfur atoms capping each face of the tetrahedron, thus

(17) Li, P.; Curtis, M. D. *Inorg. Chem.* **1990**, *29*, 1242.

(18) Harris, S. *Inorg. Chem.* **1987**, *26*, 4278.

(19) Pasyankii, A. A.; Eremenko, I. L.; Orazsakhmatov, B.; Kalinnikov, V. T.; Aleksandrov, G. G.; Struchkov, Yu. T. *J. Organomet. Chem.* **1981**, *216*, 211.

(20) Williams, P. D.; Curtis, M. D. *Inorg. Chem.* **1986**, *25*, 4562.

(21) Davies, C. E.; Green, J. C.; Kaltsoyannis, N.; MacDonald, M. A.; Qin, J.; Rauchfuss, T. B.; Redfern, C. M.; Stringer, G. H.; Woolhouse, M. G. *Inorg. Chem.* **1992**, *31*, 3779.

(22) Harris, S. *Polyhedron* **1989**, *8*, 2843.

Table 3. Average Bond Angles (deg) in the Cluster Cores for Clusters 2–4 and 6<sup>a,b</sup>

	M' = Co			M' = Fe	global av
	cluster 2	cluster 3	cluster 4	cluster 6	
Mo–M'–S	55.54(0.15)	54.7(0.88)	55.05(0.39)	54.99(1.7)	55.07(0.35)
	105.25(0.15)	104.68(0.39)	105.07(0.21)	103.4(0.29)	104.60(0.83)
Mo–Mo–S	52.46(0.10)	52.78(0.86)	52.37(0.22)	52.48(0.47)	52.52(0.18)
	98.37(0.04)	100.00(0.10)	98.23(0.21)	99.03(0.35)	98.91(0.81)
M'–Mo–S	51.11(0.54)	50.89(0.66)	50.00(0.15)	51.06(0.36)	50.76(0.52)
	96.83(0.08)	96.20(1.01)	98.37(0.15)	98.66(0.34)	97.5(1.2)
Mo–S–Mo	75.08(0.11)	74.47(0.12)	75.28(0.28)	75.34(0.57)	75.04(0.21)
Mo–S–M'	73.21(0.39)	74.18(0.47)	74.97(0.42)	74.73(0.37)	74.27(0.04)
S–Mo–S	101(2)	103(3)	103.60(0.22)	102(2)	103(1)
S–M'–S	107(2)	106(1)	107.20(0.44)	105.9(9)	106.6(7)
Mo–Mo–Mo			60.03(0.38)	60.00(0.68)	60.02(0.22)
Mo–Mo–M'	58.39(0.10)	59.07(0.48)	58.87(0.34)	59.22(0.56)	58.88(0.20)
Mo–M'–Mo	63.23(0.16)	62.26(0.01)	62.23(0.38)	61.57(0.68)	62.32(0.29)
Co–Co–Mo	61.61(0.03)	62.03(0.24)			61.82(0.30)
Co–Mo–Co	57.11(0.05)	55.94(0.42)			56.53(0.83)
Co–Co–S	54.33(0.16)	54.33(0.07)			54.33(0.12)
	104.39(0.26)	105.08(0.18)			104.74(0.49)
Co–S–Co	71.34(0.02)	70.70(0.01)			71.02(0.01)
Mo–P–Co		75.15(0.21)			
Co–P–Co		72.90(0.02)			
Co–Mo–P		49.40(0.14)			
Co–Co–P		53.55(0.21)			
Mo–Co–P		55.45(0.07)			
		104.10(0.28)			
Mo–Mo–P		96.30(0.01)			
S–Mo–P		97.75(0.49)			
S–Co–P		107(2)			

<sup>a</sup> Standard deviations are in parentheses. <sup>b</sup> Some bond angles occur in two sets, obtuse and acute. Averages are given separately for these sets.

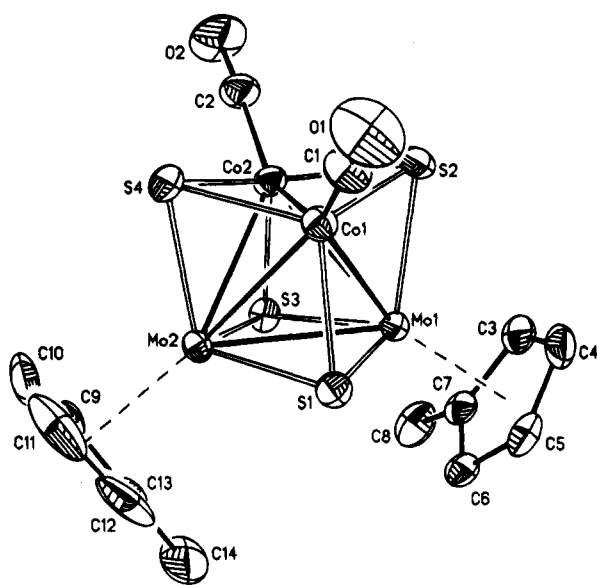


Figure 1. ORTEP plot of the molecule Cp'<sub>2</sub>Mo<sub>2</sub>Co<sub>2</sub>S<sub>4</sub>(CO)<sub>2</sub> (2). In this and the other figures, the thermal ellipsoids are plotted at the 50% level.

giving an overall cubane structure. The coordination sphere of the Mo atoms is completed by Cp' ligands, and each Co atom has a terminally bonded CO ligand. The metal–metal distances, 2.8313(5) Å (Mo–Mo), 2.701 ± 0.005 Å (Mo–Co), and 2.5816(9) Å (Co–Co), are all consistent with single bonds between the metal atoms as expected for a cluster with 60 VSE (valence shell electrons); i.e., the metal atoms in the cluster obey the 18 electron rule with 6 M–M bonds.

Within experimental error, all six of the Mo–S bond lengths are equal at 2.324 ± 0.003 Å. The Co–S bond lengths show a systematic variation, however. The four Co–S bonds to the sulfur atoms that cap a Co<sub>2</sub>Mo face ( $\mu_3$ -Co<sub>2</sub>Mo) have an average distance of 2.214 ± 0.006

Å, whereas the two Co–S distances to the sulfur atoms that cap a CoMo<sub>2</sub> face ( $\mu_3$ -CoMo<sub>2</sub>) average 2.175 ± 0.002 Å. It is interesting to note that the same distance is found for the  $\mu_3$ -CoMo<sub>2</sub> S atoms in the Mo<sub>3</sub>CoS<sub>4</sub> cluster, 4, where the average Co–S distance is 2.18 ± 0.02 Å.

A related Mo–Co thiocubane, Co<sub>2</sub>Mo<sub>2</sub>(S<sub>2</sub>CN<sub>2</sub>Et<sub>2</sub>)<sub>2</sub>(CH<sub>3</sub>CN)<sub>2</sub>(CO)<sub>2</sub>, has been synthesized and structurally characterized.<sup>23</sup> The structural parameters of this cluster and 2 are very similar, although the M–M bond lengths seem to be contracted by about 0.04 Å in 2 relative to those in the dithiocarbamate cluster. Another feature of these cubanes, previously noticed,<sup>23</sup> is that the structures of the "parent" R<sub>2</sub>Mo<sub>2</sub>S<sub>4</sub> (R = S<sub>2</sub>CN<sub>2</sub>Et<sub>2</sub> or Cp<sup>24</sup>) precursors remain essentially intact in the clusters; apparently there is a strong structural preference in the Mo<sub>2</sub>S<sub>4</sub> "core".

(b) Cp'<sub>2</sub>Mo<sub>2</sub>Co<sub>2</sub>S<sub>3</sub>( $\mu_3$ -PPh)(CO)<sub>2</sub> (3). Bond distances and bond angles are collected in Tables 2 and 3, respectively, and Figure 2 is an ORTEP drawing of the molecular structure. The structure of 3 is essentially the same as that of 2 but with one  $\mu_3$ -sulfur atom replaced by a  $\mu_3$ -phosphinidene (PhP) ligand. The S and PPh ligands are isolobal and supply four electrons to the cluster framework when counted as neutral  $\mu_3$ -ligands. Hence, clusters 2 and 3 are isoelectronic with 60 VSE.

The most notable difference in the structural parameters between these two clusters are the relatively short Co–P bonds, 2.155 ± 0.003 Å, compared to 2.20 ± 0.01 Å for the corresponding Co–S bonds. The covalent radius of P is 0.06 Å larger than that of S, so that a Co–P bond length of ca. 2.27 Å is anticipated. Indeed, the Mo2–S3 distance, 2.288(5) Å, is 0.05 Å shorter than the Mo1–P1 distance, as expected. The remaining

(23) Halbert, T. R.; Cohen, S. A.; Stiefel, E. I. *Organometallics* 1985, 4, 1689.

(24) DuBois, M. R.; DuBois, D. L.; Van DerVeer, M. C.; Haltiwanger, R. C. *Inorg. Chem.* 1981, 20, 3064.

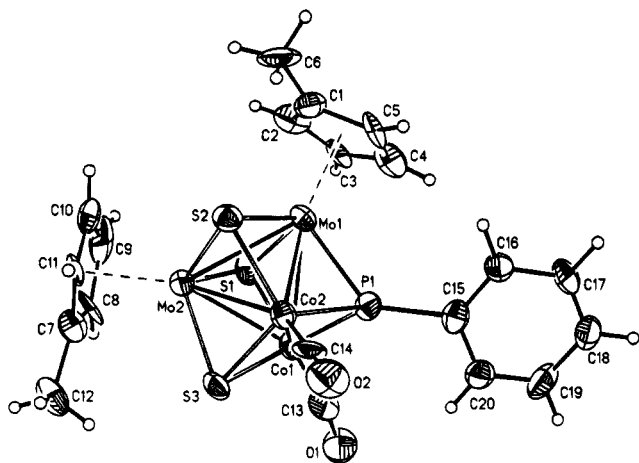


**Figure 2.** ORTEP plot of the molecule  $\text{Cp}'_2\text{Mo}_2\text{Co}_2\text{S}_4(\text{PPh})(\text{CO})$  (**3**).

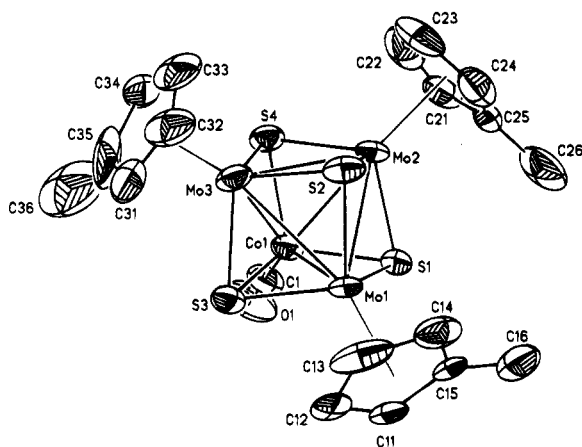


**Figure 3.** ORTEP plot of the molecule  $\text{Cp}'_3\text{Mo}_3\text{CoS}_4(\text{CO})$  (**4**).

Mo–S distances have an average value of  $2.33 \pm 0.03$  Å. The observed shortening of the Co–P bond may be related to the relative  $\sigma$ -donor/ $\pi$ -acid synergism at a given metal center as this effect is also present in a related cluster.<sup>25</sup> As noted above, the  $\nu(\text{CO})$  frequencies in **3** are lower than those in **2**, so the short Co–P bonds may be a consequence of a better  $\sigma$ -donor interaction of the P atom with the relatively electron-poor Co(CO) vertex.

The Mo1–Co bonds are slightly longer (ca.  $0.02$  Å) than the Mo2–Co bonds, possibly as a result of the slightly larger radius of the PPh capping group. The average Mo–Co distance in **3**,  $2.730 \pm 0.016$  Å, is also about  $0.03$  Å longer than that in **2**,  $2.701 \pm 0.005$  Å.

(c)  $\text{Cp}'_3\text{Mo}_3\text{Co}(\text{CO})\text{S}_4$ , **4**. Listings of bond distances and bond angles for **4** are given in Tables 2 and 3, respectively. An ORTEP plot of the molecule is shown in Figure 3. The structure of **4** is similar to the structure for **2**, with an isoelectronic CpMo unit replacing a Co(CO) vertex. The four metals form a tetrahedron with the four sulfur atoms triply bridging the four faces. Relative to **2**, the Mo–Mo bond lengths are essentially unchanged, but the Mo–Co bond distances are lengthened by ca.  $0.04$  Å:  $2.74 \pm 0.01$  in **4** vs  $2.701 \pm 0.004$  Å in **2**. The Mo–Mo bond distance decreases by  $0.05$  Å on going from  $\text{Cp}_4\text{Mo}_4\text{S}_4$ <sup>20</sup> to  $\text{Cp}_3\text{Mo}_3\text{Co}(\text{CO})$ -

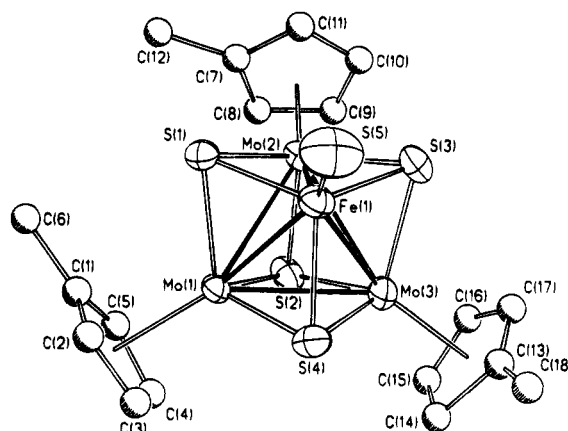


**Figure 4.** ORTEP plot of the molecule  $\text{Cp}'_3\text{Mo}_3\text{FeS}_4(\text{SH})$  (**6**).

$\text{S}_4$  so that there is a trend of decreasing Mo–Mo bond length with increasing substitution of Co(CO) for MoCp vertices. This decrease in the Mo–Mo distance with increasing Co substitution may be explained simply by noting that the Co atoms are bridging the Mo–Mo bonds in the mixed-metal clusters, and it is well-known that smaller bridging atoms usually shrink the bridged bond.

(d)  $\text{Cp}'_3\text{Mo}_3\text{FeS}_4\text{SH}$ , **6**. Bond distances and bond angles for **6** are tabulated in Tables 2 and 3, respectively. An ORTEP of the structure is shown in Figure 4. The basic structure of **6** is also the cubane type similar to **4** with the 11-electron, Co(CO) vertex replaced by a 9-electron, FeSH vertex. The average Mo–Mo bond distance is  $2.86 \pm 0.02$  Å, and the average Mo–Fe distance is  $2.79 \pm 0.02$  Å. The Mo–Mo distances in **6** are barely longer than those in clusters **2–4**, but the Mo–Fe average distance in **6** is about  $0.07$  Å longer than the global average of the Mo–Co distances,  $2.72 \pm 0.02$  Å, in clusters **2–4**. The latter increase is just what is expected on the basis of the slightly larger covalent radius of Fe as compared to Co, and the average Fe–S distance,  $2.25 \pm 0.01$  Å, is in fact  $0.05$  Å longer than the average Co–S distance,  $2.20 \pm 0.02$  Å, in these clusters. Hence, all the core distances in cluster **6** seem “normal” for a completely metal–metal-bonded, heterocubane cluster.

This behavior is unexpected in a 58 VSE cluster since there is an insufficient number of electrons to form 6 M–M bonds in the usual bonding schemes.<sup>20–22</sup> In fact, we have recently synthesized a series of 58 VSE cubanes of the type  $\text{Cp}^*_2\text{Mo}_2\text{Co}_2\text{S}_4\text{X}_2$  (X = Cl, Br, I, SPh).<sup>26</sup> These clusters show a marked increase in the  $\text{Co}\cdots\text{Co}$  distance, to  $2.936(1)$  Å (X = I). The latter distance is about the maximum nonbonded M–M length that the  $\text{M}_2\text{M}'_2\text{S}_4$  cubane geometry can accommodate and is found in several 62 VSE clusters with five M–M bonds, e.g.  $\text{Cp}_2\text{Mo}_2\text{Ni}_2\text{S}_4(\text{CO})_2$ <sup>13</sup> and  $\text{Cp}_2\text{Mo}_2\text{Fe}_2\text{S}_4(\text{NO})_2$ .<sup>27</sup> The lack of a similar effect in cluster **6** or in the oxidized clusters  $\text{Cp}_4\text{Mo}_4\text{S}_4^{n+}$  ( $n = 1, 2$ )<sup>21</sup> suggests that the HOMOs in the tri- and tetramolybdenum clusters are more delocalized and nonbonding than the HOMO in **2** and related  $\text{Mo}_2\text{M}'_2$  clusters. Structural results suggest that the character of the HOMO in the latter is primarily  $\text{M}'\text{–M}'$  bonding.<sup>26</sup>

(26) Mansour, M. A.; Curtis, M. D.; Kampf, J. W. Submitted for publication.

(27) Mansour, M. A.; Curtis, M. D.; Kampf, J. W. Unpublished results.

(25) Müller, M.; Schacht, H.-T.; Fischer, K.; Enslin, J.; Gütlich, P.; Vahrenkamp, H. *Inorg. Chem.* **1986**, *25*, 4032.



In both clusters **4** and **6**, the ligand environments around the Co and Fe are nearly tetrahedral as shown by the S–M'–S (M' = Co, Fe) and S–Co–CO and S–Fe–SH angles. In **4**, the average of the S–Co–S angles is 107.2° and the average of the S–Co–CO angles is 112°. In **6**, the S–Fe–S average value is 106° and the S–Fe–SH average is 113°. In both clusters, the overall average of the angles around the Co or Fe atom is 109.4°. It is rather surprising that the angles subtended by the  $\mu_3$ -sulfido ligands are almost the same as those involving the terminal ligands, especially in **4** where the terminal ligand is CO.

The cluster **6** is probably paramagnetic (no NMR or ESR signal was observed at room temperature), which implies that it is at least a spin = 1 system. The clusters Cp\*<sub>2</sub>Mo<sub>2</sub>Co<sub>2</sub>S<sub>4</sub>X<sub>2</sub> (X = Cl, Br, I, SPh) exhibit complex spin equilibria with S = 1, 2, and 3 states thermally accessible for the iodide.<sup>27</sup> All the metal atoms in **6** can be assigned a formal oxidation state of +3. Although the Fe is then a 16e<sup>-</sup> center, the cluster is air stable (the structure was determined after the crystals had been exposed to air for over 1 month).

Clusters with terminal –SH groups are very rare, presumably because the SH group is readily deprotonated to give a  $\mu$ -sulfido ligand that is more stable.<sup>28</sup> One surprising exception to this generalization is the cluster [Fe<sub>4</sub>S<sub>4</sub>(SH)<sub>4</sub>]<sup>2-</sup>, synthesized from CpFe(CO)<sub>2</sub>I and H<sub>2</sub>S in air.<sup>29</sup> The structure of this cluster consists of a Fe<sub>4</sub>S<sub>4</sub> core with the thiocubane structure and terminal SH groups on each Fe. The Fe–S<sub>t</sub> distance in this cluster is 2.269 Å, which is slightly longer than the Fe–S<sub>i</sub> distance in **6**, 2.242(4) Å. The Fe–S distances in the cluster core for Fe<sub>4</sub>S<sub>4</sub>(SH)<sub>4</sub><sup>2-</sup> range from 2.256 to 2.290 Å, which are slightly longer than similar distances in **6**, 2.24–2.27 Å, average 2.25 ± 0.01 Å. These distances support the formulation of the cluster with an FeSH vertex rather than an Fe=S vertex.

**Comparisons to Idealized Cubane Structure.** In the idealized cubane cluster formed by the interpenetration of two equally sized M<sub>4</sub> and S<sub>4</sub> tetrahedra, all M–S–M and all S–M–S angles are 90°, and the M–M–S angles are divided into two sets: 45° for the angles to the S atom that bridges the M–M bond (face 1) and 90° for the angles to the S atoms that bridge the

M'–M' bond in the opposite face. In all the cluster structures reported here, the M–S–M angles are much more acute, 75°, and the S–M–S angles more obtuse, 103–107°, than the ideal values. This is a consequence of the fact that the M<sub>4</sub> tetrahedron is smaller than the S<sub>4</sub> tetrahedron as a result of the strong metal–metal bonds in the clusters. The contraction of the M<sub>4</sub> tetrahedron spreads the S–M–S angles and contracts the M–S–M angles. The M–M–S angles also show the effects of this distortion: instead of 45 and 90° sets, the observed angles are ca. 55 and 105°. Structurally speaking, these clusters appear more as face-capped tetrahedra than “cubanes”.

All M–M–M angles in a regular tetrahedron are 60°, and the observed angles are very close to this ideal value. The deviations are a consequence of the shorter Mo–M' (M' = Co or Fe) and Co–Co distances relative to the Mo–Mo distance. Thus, in the Mo<sub>3</sub>M' clusters, **4** and **6**, the Mo–Mo–Mo angles are very close to 60° while the Mo–Mo–M' angles are compressed to 59° and the Mo–M'–Mo angles are spread to 62°; i.e. the M' atom is pulled toward the Mo<sub>3</sub> basal plane because of the shorter Mo–M' bond distance. In the Mo<sub>2</sub>Co<sub>2</sub> clusters, **2** and **3**, the order of increasing bond distances is Co–Co < Co–Mo < Mo–Mo, so the Co–Co edge of the tetrahedron is pulled toward the Mo–Mo edge. The Mo–Co–Mo angles, 62.5°, and the Co–Co–Mo angles, 62°, are therefore greater than 60°, and Mo–Mo–Co (59°) and Co–Mo–Co (56.5°) are contracted.

**Conclusions.** One of the more striking features of this series of structures is the constancy of the basic structural motif that is little affected by substitution of heterometals or external ligands. Most surprising is the lack of structural changes in the 58 VSE cluster **6** *vis-à-vis* the 60 VSE clusters. This suggests that the HOMO of **6** is similar to that of the Mo<sub>4</sub> cluster, Cp<sub>4</sub>Mo<sub>4</sub>S<sub>4</sub>, for which EHMO calculations and PES spectra have indicated the HOMO to be a nonbonding, triply degenerate MO delocalized over the M<sub>4</sub> skeleton.<sup>20,21</sup> Although the symmetry of **6** precludes a triply degenerate level, a weakly metal–metal-bonded, delocalized MO is indicated.

**Acknowledgment.** The authors are grateful for the support furnished by the National Science Foundation, Grants CHE-8619864 and CHE-9205018.

**Supporting Information Available:** Text and tables of crystallographic data and data collection statistics, tables of fractional atomic coordinates, anisotropic thermal parameters, and hydrogen atom fractional coordinates, and complete tables of bond lengths and bond angles (31 pages). Ordering information is given on any current masthead page.

OM950447U

(28) (a) Ozawa, Y.; Vazquez de Miguel, A.; Isobe, K. *J. Organomet. Chem.* **1992**, *433*, 183. (b) Secheresee, F.; Manoli, J. M.; Potvin, C. *Inorg. Chem.* **1986**, *25*, 3967. (c) Osakada, K.; Yamamoto, T.; Yamamoto, A.; Takenaka, A.; Sasada, Y. *Inorg. Chim. Acta* **1985**, *105*, L9. (d) Ghilardi, C. A.; Midollini, S.; Orlandini, A.; Battistoni, C.; Mattogno, G. *J. Chem. Soc., Dalton Trans.* **1984**, 939. (e) Bottomley, F.; Day, R. W. *Can. J. Chem.* **1992**, *70*, 1250. (f) Cragel, J.; Pett, V. B., Jr.; Glick, M. D.; DeSimone, R. E. *Inorg. Chem.* **1978**, *17*, 2885.

(29) Muller, A.; Schladerbeck, N. H.; Bogue, H. *J. Chem. Soc., Chem. Comm.* **1987**, 35.

# Using Zirconium Half-Sandwich Complexes as Building Blocks in a New Class of Zr–M Heterobimetallics Containing Unsupported Zr–M Bonds (M = Fe, Ru, Co)<sup>†</sup>

Stefan Friedrich and Lutz H. Gade\*

*Institut für Anorganische Chemie, Universität Würzburg, Am Hubland,  
D-97074 Würzburg, Germany*

Ian J. Scowen and Mary McPartlin

*School of Chemistry, University of North London, Holloway Road, London N7 8DB, U.K.*

Received July 24, 1995<sup>®</sup>

A new class of Zr–M heterobimetallic complexes (M = Fe, Ru, Co) containing the {CH<sub>2</sub>(CH<sub>2</sub>–NSiMe<sub>3</sub>)<sub>2</sub>(Cp)Zr} fragment as a building block has been synthesized by salt metathesis of CH<sub>2</sub>(CH<sub>2</sub>NSiMe<sub>3</sub>)<sub>2</sub>(Cp)ZrCl (**5**) with K[CpM'(CO)<sub>2</sub>] (M' = Fe, Ru) and Na[Co(CO)<sub>3</sub>(PR<sub>3</sub>)] (R = Ph, Tol). The zirconium half-sandwich complex **5** was obtained in four reaction steps from ZrCl<sub>4</sub> via the spirocyclic complex [CH<sub>2</sub>(CH<sub>2</sub>NSiMe<sub>3</sub>)<sub>2</sub>]<sub>2</sub>Zr (**1**), the (diamido)dichlorozirconium complex CH<sub>2</sub>(CH<sub>2</sub>NSiMe<sub>3</sub>)<sub>2</sub>ZrCl<sub>2</sub> (**2**), and its soluble THF-adduct CH<sub>2</sub>(CH<sub>2</sub>NSiMe<sub>3</sub>)<sub>2</sub>ZrCl<sub>2</sub>(THF)<sub>2</sub> (**3**). The latter was converted to **5** in good yield by reaction with LiCp. The Zr–Fe heterodinuclear complex CH<sub>2</sub>(CH<sub>2</sub>NSiMe<sub>3</sub>)<sub>2</sub>(Cp)Zr–Fe(CO)<sub>2</sub>Cp (**6**) has been characterized by X-ray crystal structure analysis which has established the presence of an unsupported Zr–Fe bond. The ν(CO) infrared bands of the CpM'(CO)<sub>2</sub> moieties in the Zr–M' complexes (M' = Fe, Ru) indicate a significant ionic contribution to the Zr–M' bonding.

## Introduction

Ever since the first successful syntheses of Zr–Fe and Zr–Ru heterobimetallic complexes in Casey's group a decade ago<sup>1,2</sup> there have been several efforts to prepare stable complexes containing unsupported Zr–M' bonds (M' = late transition metal) (type A, Figure 1).<sup>3</sup> These are thought to generate two reactive fragments upon cleavage of the metal–metal bond which, as a consequence of their different electronic properties, could then react regioselectively with (and thus activate) functionalized unsaturated hydrocarbons. Whereas the Zr–Ru species studied by Casey and co-workers were sufficiently stable to study their reactivity toward various substrates,<sup>4</sup> all other Zr–M' compounds prepared to date proved to be too labile to either fully characterize them or even investigate their chemical behavior.

We have recently prepared a series of stable M–M' heterobimetallics (M = Fe, Ru, Co; M' = Ti, Zr, Hf) with unsupported M–M' bonds in which the early transition metal is stabilized by a tripodal triamido ligand (type B in Figure 1).<sup>5,6</sup> This has in fact proved to be the key to stabilization of a whole range of such species which has opened up the possibility of systematic comparative studies. Remarkably, the metal–metal bond in the

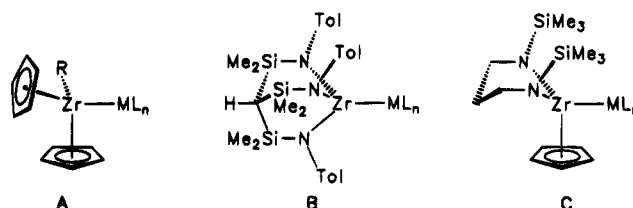


Figure 1. Zr–M heterobimetallics of types A–C.

amido–zirconium–iron and amido–zirconium–ruthenium complexes appears to be significantly less ionic than in Casey's compounds, a situation which is reflected in the infrared ν(CO) spectra. This situation may be interpreted as being a consequence of the greater Lewis acidity of the amido–zirconium fragments in comparison to the Cp<sub>2</sub>Zr fragments in the complexes of type A. The M–M' bonding electron pair in type B complexes is thus probably more evenly distributed between the two metal centers.

In our quest for new types of Zr–M' complexes and in order to probe the influence of the set of ligands at the Zr center, we have now attempted the combination of Casey's approach using CpZr complex fragments as building blocks while simultaneously utilizing the stabilizing effect that a chelating amido ligand has in such systems. To this end we have synthesized a new type of Zr half-sandwich complex which may be used in metathetical condensation reactions with transition metal carbonylates (type C).<sup>7</sup> Here we report the synthesis of such "early–late heterobimetallics" and the structural characterization of a Zr–Fe-bonded complex.

(5) (a) Friedrich, S.; Memmler, H.; Gade, L. H.; Li, W.-S.; McPartlin, M. *Angew. Chem., Int. Ed. Engl.* **1994**, *33*, 676. (b) Friedrich, S.; Memmler, H.; Gade, L. H.; Li, W.-S.; Scowen, I.; McPartlin, M.; Housecroft, C. E. Submitted for publication in *Inorg. Chem.*  
(6) Findeis, B.; Schubart, M.; Platzek, C.; Gade, L. H.; Scowen, I.; McPartlin, M. Submitted for publication.

<sup>†</sup> We dedicate this paper to Professor Max Schmidt on the occasion of his 70th birthday.

<sup>®</sup> Abstract published in *Advance ACS Abstracts*, November 1, 1995.  
(1) (a) Casey, C. P.; Jordan, R. F.; Rheingold, A. L. *J. Am. Chem. Soc.* **1983**, *105*, 665. (b) Casey, C. P.; Jordan, R. F.; Rheingold, A. L. *Organometallics* **1984**, *3*, 504. (c) Casey, C. P. *J. Organomet. Chem.* **1990**, *400*, 205.

(2) Review: Stephan, D. W. *Coord. Chem. Rev.* **1989**, *95*, 41.  
(3) (a) Thiele, K.-H.; Krüger, C.; Sorkau, A.; Ötvös, I.; Bartik, T.; Palyi, G. *Organometallics* **1987**, *6*, 2290. (b) Bartik, T.; Windisch, H.; Sorkau, A.; Thiele, K.-H.; Kriebel, C.; Herfurth, A.; Thoerner, C. M.; Zucchi, C.; Palyi, G. *Inorg. Chim. Acta* **1994**, *227*, 201 and references cited therein.

(4) (a) Casey, C. P.; Palermo, R. E.; Jordan, R. F. *J. Am. Chem. Soc.* **1985**, *107*, 4597. (b) Casey, C. P.; Palermo, R. E. *J. Am. Chem. Soc.* **1986**, *108*, 549.

## Experimental Section

All manipulations were performed under an inert gas atmosphere of dried argon in standard (Schlenk) glassware which was flame dried with a Bunsen burner prior to use. Solvents were dried according to standard procedures and saturated with Ar. The deuterated solvents used for the NMR spectroscopic measurements were degassed by three successive "freeze–pump–thaw" cycles and dried over 4-Å molecular sieves.

The  $^1\text{H}$ -,  $^{13}\text{C}$ -,  $^{29}\text{Si}$ -, and  $^{31}\text{P}$ -NMR spectra were recorded on a Bruker AC 200 spectrometer equipped with a B-VT-2000 variable-temperature unit (at 200.13, 50.32, 39.76, and 81.03 MHz, respectively) with tetramethylsilane and  $\text{H}_3\text{PO}_4$  (85%, ext.) as references. Infrared spectra were recorded on Perkin-Elmer 1420 and Bruker IRS 25 FT-spectrometers.

Elemental analyses were carried out in the microanalytical laboratory of the chemistry department at Würzburg. The amine  $\text{CH}_2(\text{CH}_2\text{NHSiMe}_3)_2$  was prepared from the commercially available  $\text{CH}_2(\text{CH}_2\text{NH}_2)_2$  as reported in the literature.<sup>8</sup> The salts of the transition metal carbonylates  $[\text{CpFe}(\text{CO})_2]$ ,  $[\text{CpRu}(\text{CO})_2]$ ,  $[\text{Na}[\text{Co}(\text{CO})_3(\text{PPh}_3)]]$ , and  $[\text{Na}[\text{Co}(\text{CO})_3(\text{PTol}_3)]]$  (Tol = 4- $\text{CH}_3\text{C}_6\text{H}_4$ ) were synthesized by literature methods.<sup>9</sup> All other chemicals used as starting materials were obtained commercially and used without further purification.

**(1) Preparation of  $[\text{CH}_2(\text{CH}_2\text{NSiMe}_3)_2]_2\text{Zr}$  (1).** To a stirred solution of  $\text{CH}_2(\text{CH}_2\text{NHSiMe}_3)_2$  (3.03 g = 13.87 mmol) in 15 mL of toluene, which was cooled at  $-40^\circ\text{C}$ , was slowly added 27.75 mmol of *n*BuLi (11.10 mL of a 2.5 M solution in hexanes). The reaction mixture was warmed to room temperature and, after the butane evolution had subsided, heated under reflux for a short period of time. After the solution of the lithiated amine had been stirred at room temperature for another 30 min, it was cooled to  $-50^\circ\text{C}$ . Solid  $\text{ZrCl}_4$  (1.56 g = 6.69 mmol) was added, the reaction mixture was warmed to room temperature over a period of 15 h, and the solvent was evaporated in vacuo. The residue was extracted with pentane (50 mL), the extract filtered, and the volume of the solution reduced to ca. 15 mL. Storage at  $-35^\circ\text{C}$  yielded  $[\text{CH}_2(\text{CH}_2\text{NSiMe}_3)_2]_2\text{Zr}$  (1) as a colorless crystalline solid: yield 3.21 g (88%); mp  $85^\circ\text{C}$  dec; IR (KBr) 2950 vs, 2890 vs, 2880 vs, 2830 vs, 2780 m, 2635 w, 1915 vw, 1860 vw, 1590 w, 1425 m, 1395 m, 1365 m, 1352 m, 1285 s, 1245 vs, 1090 s, 1052 vs, 955 s, 890 vs, 835 vs, 780 s, 742 s, 675 s  $\text{cm}^{-1}$ ;  $^1\text{H}$  NMR ( $\text{C}_6\text{D}_6$ , 200 MHz)  $\delta$  0.24 [s,  $\text{Si}(\text{CH}_3)_3$ ], 1.90 (m,  $\text{CH}_2$ ), 3.33 (m,  $\text{CH}_2\text{N}$ );  $^{13}\text{C}$  NMR ( $\text{C}_6\text{D}_6$ , 50.3 MHz)  $\delta$  0.5 [ $\text{Si}(\text{CH}_3)_3$ ], 39.8 ( $\text{CH}_2$ ), 51.5 ( $\text{CH}_2\text{N}$ );  $^{29}\text{Si}$  NMR ( $\text{C}_6\text{D}_6$ , 39.8 MHz)  $\delta$  -2.6. Anal. Calcd for  $\text{C}_{18}\text{H}_{48}\text{N}_4\text{Si}_4\text{Zr}$ : C, 41.25; H, 9.23; N, 10.69. Found: C, 41.57; H, 9.12; N, 10.54.

**(2) Preparation of  $\text{CH}_2(\text{CH}_2\text{NSiMe}_3)_2\text{ZrCl}_2$  (2).** A suspension of 2.02 g (3.85 mmol) of  $[\text{CH}_2(\text{CH}_2\text{NSiMe}_3)_2]_2\text{Zr}$  (1) and 0.89 g (3.82 mmol) of  $\text{ZrCl}_4$  in 15 mL of toluene was heated at  $60^\circ\text{C}$  for 3 d. After evaporation of the solvent in vacuo, the residue was washed with 15 mL of pentane and the colorless solid dried in vacuo: yield 2.23 g (77%); mp  $74^\circ\text{C}$  dec; IR (KBr) 2955 vs, 2900 s, 2865 s, 2000 vw, 1925 vw, 1870 vw, 1635 w, 1598 w, 1568 w, 1465 m, 1442m, 1408 m, 1350 m, 1312 w, 1248 vs, 1223 m, 1188 vw, 1082 s, 1040 vs, 935 vs, 845 vs br, 752 s, 718 vs, 682 s  $\text{cm}^{-1}$ ;  $^1\text{H}$  NMR ( $\text{C}_6\text{D}_6$ , 200 MHz)  $\delta$  0.29 [s,  $\text{Si}(\text{CH}_3)_3$ ], 1.74 (m,  $\text{CH}_2$ ), 3.31 (m,  $\text{CH}_2\text{N}$ );  $^{13}\text{C}$  NMR ( $\text{C}_6\text{D}_6$ , 50.3 MHz)  $\delta$  -0.3 [ $\text{Si}(\text{CH}_3)_3$ ], 39.3 ( $\text{CH}_2$ ), 52.9 ( $\text{CH}_2\text{N}$ );  $^{29}\text{Si}$  NMR ( $\text{C}_6\text{D}_6$ , 39.8 MHz)  $\delta$  0.8. Anal. Calcd for  $\text{C}_9\text{H}_{24}\text{Cl}_2\text{N}_2\text{Si}_2\text{Zr}$ : C, 28.55; H, 6.39; N, 7.40. Found: C, 28.37; H, 6.21; N, 7.21.

**(3) Preparation of  $\text{CH}_2(\text{CH}_2\text{NSiMe}_3)_2\text{ZrCl}_2(\text{THF})_2$  (3).** A solution of 1.03 g (2.72 mmol) of  $\text{CH}_2(\text{CH}_2\text{NSiMe}_3)_2\text{ZrCl}_2$  (2)

in 5 mL of THF was stored at  $-35^\circ\text{C}$  to yield  $\text{CH}_2(\text{CH}_2\text{NSiMe}_3)_2\text{ZrCl}_2(\text{THF})_2$  (3) as colorless crystals: yield 1.08 g (76%); mp  $98^\circ\text{C}$  dec; IR (KBr) 2940 vs, 2880 vs, 2850 vs, 2820 s, 2690 m, 1995 vw, 1918 vw, 1865 vw, 1685 w, 1458 m, 1415 m, 1402 m, 1365 m, 1348 m, 1285 m, 1245 vs, 1190 w, 1175 w, 1095 s, 1030 vs, 1010 s, 940 vs, 895 vs, 845 vs br, 755 s, 720 s, 680  $\text{cm}^{-1}$ ;  $^1\text{H}$  NMR ( $\text{C}_6\text{D}_6$ , 200 MHz)  $\delta$  0.32 [s,  $\text{Si}(\text{CH}_3)_3$ ], 1.35 (m,  $\text{CH}_2\text{CH}_2\text{O}$ ), 1.71 (m,  $\text{CH}_2$ ), 3.37 (m,  $\text{CH}_2\text{N}$ ), 3.71 (m,  $\text{CH}_2\text{CH}_2\text{O}$ );  $^{13}\text{C}$  NMR ( $\text{C}_6\text{D}_6$ , 50.3 MHz)  $\delta$  0.3 [ $\text{Si}(\text{CH}_3)_3$ ], 25.6 ( $\text{CH}_2\text{CH}_2\text{O}$ ), 37.8 ( $\text{CH}_2$ ), 51.3 ( $\text{CH}_2\text{N}$ ), 70.3 ( $\text{CH}_2\text{CH}_2\text{O}$ );  $^{29}\text{Si}$  NMR ( $\text{C}_6\text{D}_6$ , 39.8 MHz)  $\delta$  0.7. Anal. Calcd for  $\text{C}_{17}\text{H}_{40}\text{Cl}_2\text{N}_2\text{O}_2\text{Si}_2\text{Zr}$ : C, 39.06; H, 7.71; N, 5.36. Found: C, 38.78; H, 7.81; N, 5.43.

**(4) Preparation of  $\text{CH}_2(\text{CH}_2\text{NSiMe}_3)_2\text{ZrCl}_2(\text{C}_5\text{H}_5\text{N})_2$  (4).** To a stirred suspension of 1.74 g (4.60 mmol) of  $\text{CH}_2(\text{CH}_2\text{NSiMe}_3)_2\text{ZrCl}_2$  (2) in 20 mL of toluene was added 5 mL (4.90 g, 61.95 mmol) of pyridine. After the solution was stirred for 1 h, the solvent was evaporated in vacuo. The residue was washed twice with 10 mL of pentane and dried in vacuo: yield 1.65 g (67%); mp  $113^\circ\text{C}$  dec; IR (KBr) 3060 m, 2950 vs, 2890 s, 2860 s, 1995 vw, 1935 vw, 1865 vw, 1638 w, 1602 vs, 1572 w, 1485 m, 1468 m, 1442 vs, 1408 w, 1348 w, 1325 vw, 1305 vw, 1245 vs, 1220 s, 1152 w, 1068 s, 1040 vs, 1010 s, 938 vs, 865 vs, 835 vs br, 808 s, 755 s, 715 s, 702 s, 678 s  $\text{cm}^{-1}$ ;  $^1\text{H}$  NMR ( $\text{C}_6\text{D}_6$ , 200 MHz)  $\delta$  0.07 [s  $\text{Si}(\text{CH}_3)_3$ ], 1.67 [quint,  $^3J(\text{HH}) = 5.8$  Hz,  $\text{CH}_2$ ], 4.19 (t,  $\text{CH}_2\text{N}$ ), 6.51 (m, *meta*-H of  $\text{NC}_5\text{H}_5$ ), 6.87 (m, *para*-H of  $\text{NC}_5\text{H}_5$ ), 9.06 (m, *ortho*-H of  $\text{NC}_5\text{H}_5$ );  $^{13}\text{C}$  NMR ( $\text{C}_6\text{D}_6$ , 50.3 MHz)  $\delta$  0.9 [ $\text{Si}(\text{CH}_3)_3$ ], 29.7 ( $\text{CH}_2$ ), 45.3 ( $\text{CH}_2\text{N}$ ), 123.8 (*meta*-C of  $\text{NC}_5\text{H}_5$ ), 138.5 (*para*-C of  $\text{NC}_5\text{H}_5$ ), 152.1 (*ortho*-C of  $\text{NC}_5\text{H}_5$ );  $^{29}\text{Si}$  NMR ( $\text{C}_6\text{D}_6$ , 39.8 MHz)  $\delta$  1.0. Anal. Calcd for  $\text{C}_{19}\text{H}_{34}\text{Cl}_2\text{N}_4\text{Si}_2\text{Zr}$ : C, 42.51; H, 6.38; N, 10.44. Found: C, 42.48; H, 6.31; N, 10.42.

**(5) Preparation of  $\text{CH}_2(\text{CH}_2\text{NSiMe}_3)_2\text{Zr}(\text{Cp})\text{Cl}$  (5).** To a stirred solution of 2.51 g (4.80 mmol) of  $\text{CH}_2(\text{CH}_2\text{NSiMe}_3)_2\text{ZrCl}_2(\text{THF})_2$  (3) in 50 mL of toluene was slowly added a solution of 347 mg (4.82 mmol) of LiCp in 30 mL of THF. After the solution was stirred for 16 h, the solvent was evaporated in vacuo. The residue was extracted with 50 mL of pentane, the extract filtered, and the volume of the solution reduced to ca. 5 mL. Storage at  $-78^\circ\text{C}$  yielded  $\text{CH}_2(\text{CH}_2\text{NSiMe}_3)_2\text{Zr}(\text{Cp})\text{Cl}$  (5) as a colorless crystalline solid: yield 1.49 g (76%);  $^1\text{H}$  NMR ( $\text{C}_6\text{D}_6$ , 200 MHz)  $\delta$  0.08 [s,  $\text{Si}(\text{CH}_3)_3$ ], 1.20–1.51 (m,  $\text{H}^{\text{c/c'}}$  of  $\text{CH}_2$ ), 3.00 [ddd,  $^2J(\text{H}^{\text{a}}\text{H}^{\text{b}}) = 14.8$  Hz,  $^3J(\text{H}^{\text{a}}\text{H}^{\text{c/c'}}) = 7.7$  Hz,  $^3J(\text{H}^{\text{a}}\text{H}^{\text{c/c'}}) = 4.0$  Hz,  $\text{H}^{\text{a}}$  of  $\text{CHHN}$ ], 3.48 [ddd,  $^3J(\text{H}^{\text{b}}\text{H}^{\text{c/c'}}) = 5.8$  Hz,  $^3J(\text{H}^{\text{b}}\text{H}^{\text{c/c'}}) = 4.5$  Hz,  $\text{H}^{\text{b}}$  of  $\text{CHHN}$ ], 6.21 (s,  $\text{C}_5\text{H}_5$ );  $^{13}\text{C}$  NMR ( $\text{C}_6\text{D}_6$ , 50.3 MHz)  $\delta$  1.0 [ $\text{Si}(\text{CH}_3)_3$ ], 33.6 ( $\text{CH}_2$ ), 46.8 ( $\text{CH}_2\text{N}$ ), 112.1 ( $\text{C}_5\text{H}_5$ );  $^{29}\text{Si}$  NMR ( $\text{C}_6\text{D}_6$ , 39.8 MHz)  $\delta$  1.5. Anal. Calcd for  $\text{C}_{14}\text{H}_{28}\text{ClN}_2\text{Si}_2\text{Zr}$ : C, 41.19; H, 7.16; N, 6.86. Found: C, 41.16; H, 7.23; N, 6.91.

**(6) Preparation of  $\text{CH}_2(\text{CH}_2\text{NSiMe}_3)_2(\text{Cp})\text{Zr}-\text{Fe}(\text{CO})_2\text{Cp}$  (6).** To a solid mixture of 197 mg (0.48 mmol) of  $\text{CH}_2(\text{CH}_2\text{NSiMe}_3)_2\text{Zr}(\text{Cp})\text{Cl}$  (5) and 130 mg (0.62 mmol) of  $[\text{CpFe}(\text{CO})_2]$  was slowly added 15 mL of toluene and 2 mL of THF. After the mixture was stirred for 1 h, ca. 50 mg of Na powder was added and the reaction mixture stirred for another 2 h. After evaporation of the solvent in vacuo, the residue was extracted with 20 mL of pentane, the extract filtered, and the solvent removed in vacuo. The residue was dissolved in 1.5 mL of diethyl ether and the solution stored at  $-78^\circ\text{C}$ . Compound  $\text{CH}_2(\text{CH}_2\text{NSiMe}_3)_2(\text{Cp})\text{Zr}-\text{Fe}(\text{CO})_2\text{Cp}$  (6) precipitated as a yellow highly crystalline solid which was dried in vacuo: yield 108 mg (41%); IR (pentane) 2017 m, 1947 vs, 1895 vs  $\text{cm}^{-1}$ ;  $^1\text{H}$  NMR ( $\text{C}_6\text{D}_6$ , 200 MHz)  $\delta$  0.13 [s,  $\text{Si}(\text{CH}_3)_3$ ], 1.31 (m,  $\text{H}^{\text{a}}$  of  $\text{CHH}$ ), 1.46 (m,  $\text{H}^{\text{c}}$  of  $\text{CHH}$ ), 3.14 [ddd,  $^2J(\text{H}^{\text{a}}\text{H}^{\text{b}}) = 15.7$  Hz,  $^3J(\text{H}^{\text{a}}\text{H}^{\text{c/c'}}) = 5.7$  Hz,  $^3J(\text{H}^{\text{a}}\text{H}^{\text{c/c'}}) = 5.6$  Hz,  $\text{H}^{\text{a}}$  of  $\text{CHHN}$ ], 4.12 [s, ( $\text{C}_5\text{H}_5$ )Fe], 4.20 [ddd,  $^3J(\text{H}^{\text{b}}\text{H}^{\text{c/c'}}) = 6.2$  Hz,  $^3J(\text{H}^{\text{b}}\text{H}^{\text{c/c'}}) = 4.9$  Hz,  $\text{H}^{\text{b}}$  of  $\text{CHHN}$ ], 6.30 [s, ( $\text{C}_5\text{H}_5$ )Zr];  $^{13}\text{C}$  NMR ( $\text{C}_6\text{D}_6$ , 50.3 MHz)  $\delta$  1.4 [ $\text{Si}(\text{CH}_3)_3$ ], 30.6 ( $\text{CH}_2$ ), 42.8 ( $\text{CH}_2\text{N}$ ), 81.4 [( $\text{C}_5\text{H}_5$ )Fe], 110.9 [( $\text{C}_5\text{H}_5$ )Zr], 218.6 (CO);  $^{29}\text{Si}$  NMR ( $\text{C}_6\text{D}_6$ , 39.8 MHz)  $\delta$  = 2.7. Anal. Calcd for  $\text{C}_{21}\text{H}_{34}\text{FeN}_2\text{O}_2\text{Si}_2\text{Zr}$ : C, 45.88; H, 6.23; N, 5.10. Found: C, 45.90; H, 6.25; N, 5.11.

**(7) Preparation of  $\text{CH}_2(\text{CH}_2\text{NSiMe}_3)_2(\text{Cp})\text{Zr}-\text{Ru}(\text{CO})_2\text{Cp}$  (7).** To a solid mixture of 423 mg (1.04 mmol) of  $\text{CH}_2(\text{CH}_2\text{NSiMe}_3)_2\text{Zr}(\text{Cp})\text{Cl}$  (5) and 130 mg (0.62 mmol) of  $[\text{CpRu}(\text{CO})_2]$  was slowly added 15 mL of toluene and 2 mL of THF. After the mixture was stirred for 1 h, ca. 50 mg of Na powder was added and the reaction mixture stirred for another 2 h. After evaporation of the solvent in vacuo, the residue was extracted with 20 mL of pentane, the extract filtered, and the solvent removed in vacuo. The residue was dissolved in 1.5 mL of diethyl ether and the solution stored at  $-78^\circ\text{C}$ . Compound  $\text{CH}_2(\text{CH}_2\text{NSiMe}_3)_2(\text{Cp})\text{Zr}-\text{Ru}(\text{CO})_2\text{Cp}$  (7) precipitated as a yellow highly crystalline solid which was dried in vacuo: yield 108 mg (41%); IR (pentane) 2017 m, 1947 vs, 1895 vs  $\text{cm}^{-1}$ ;  $^1\text{H}$  NMR ( $\text{C}_6\text{D}_6$ , 200 MHz)  $\delta$  0.13 [s,  $\text{Si}(\text{CH}_3)_3$ ], 1.31 (m,  $\text{H}^{\text{a}}$  of  $\text{CHH}$ ), 1.46 (m,  $\text{H}^{\text{c}}$  of  $\text{CHH}$ ), 3.14 [ddd,  $^2J(\text{H}^{\text{a}}\text{H}^{\text{b}}) = 15.7$  Hz,  $^3J(\text{H}^{\text{a}}\text{H}^{\text{c/c'}}) = 5.7$  Hz,  $^3J(\text{H}^{\text{a}}\text{H}^{\text{c/c'}}) = 5.6$  Hz,  $\text{H}^{\text{a}}$  of  $\text{CHHN}$ ], 4.12 [s, ( $\text{C}_5\text{H}_5$ )Fe], 4.20 [ddd,  $^3J(\text{H}^{\text{b}}\text{H}^{\text{c/c'}}) = 6.2$  Hz,  $^3J(\text{H}^{\text{b}}\text{H}^{\text{c/c'}}) = 4.9$  Hz,  $\text{H}^{\text{b}}$  of  $\text{CHHN}$ ], 6.30 [s, ( $\text{C}_5\text{H}_5$ )Zr];  $^{13}\text{C}$  NMR ( $\text{C}_6\text{D}_6$ , 50.3 MHz)  $\delta$  1.4 [ $\text{Si}(\text{CH}_3)_3$ ], 30.6 ( $\text{CH}_2$ ), 42.8 ( $\text{CH}_2\text{N}$ ), 81.4 [( $\text{C}_5\text{H}_5$ )Fe], 110.9 [( $\text{C}_5\text{H}_5$ )Zr], 218.6 (CO);  $^{29}\text{Si}$  NMR ( $\text{C}_6\text{D}_6$ , 39.8 MHz)  $\delta$  = 2.7. Anal. Calcd for  $\text{C}_{21}\text{H}_{34}\text{FeN}_2\text{O}_2\text{Si}_2\text{Zr}$ : C, 45.88; H, 6.23; N, 5.10. Found: C, 45.90; H, 6.25; N, 5.11.

(7) Very recently, the use of  $\{\text{Cp}^*(\text{NMe}_2)_2\text{Ti}\}$  as a building block in a Ti–Ru heterobimetallic compound has been reported: Galakhov, M.; Martin, A.; Mena, M.; Yelamos, C. *J. Organomet. Chem.* **1995**, *496*, 217.

(8) Dämmgen, U.; Bürger, H. *Z. Anorg. Allg. Chem.* **1977**, *429*, 173.  
(9) Brookhart, M.; Studabaker, W. B.; Husk, R. *Organometallics* **1987**, *6*, 1141.

$\text{NSiMe}_3)_2\text{Zr}(\text{Cp})\text{Cl}$  (**5**) and 290 mg (1.10 mmol) of  $\text{K}[\text{CpRu}(\text{CO})_2]$ , which was cooled to  $-25^\circ\text{C}$ , were slowly added 20 mL of cold toluene and 1 mL of THF. The reaction mixture was warmed to room temperature over a period of 16 h. After evaporation of the solvent in vacuo, the residue was extracted with 20 mL of pentane, the extract filtered, and the solvent removed in vacuo. The residue was redissolved in 2 mL of diethyl ether and the solution stored at  $-78^\circ\text{C}$ . Compound  $\text{CH}_2(\text{CH}_2\text{NSiMe}_3)_2(\text{Cp})\text{Zr}-\text{Ru}(\text{CO})_2\text{Cp}$  (**7**) precipitated as a yellow highly crystalline solid which was dried in vacuo: yield 445 mg (72%); IR (toluene) 2880 vs, 2850 vs, 2015 m, 1957 vs, 1895 vs, 1362 w, 1288 m, 1248 s, 1190 m, 1170 m, 1066 vs, 912 vs, 865 s, 840 s, 800 s  $\text{cm}^{-1}$ ;  $^1\text{H}$  NMR ( $\text{C}_6\text{D}_6$ , 200 MHz)  $\delta$  0.13 [s,  $\text{Si}(\text{CH}_3)_3$ ], 1.32 (m,  $\text{H}^c$  of  $\text{CHH}$ ), 1.41 (m,  $\text{H}^c$  of  $\text{CHH}$ ), 3.11 [ddd,  $^2J(\text{H}^a\text{H}^b) = 15.7$  Hz,  $^3J(\text{H}^a\text{H}^{c'}) = 6.3$  Hz,  $^2J(\text{H}^a\text{H}^{c'}) = 4.9$  Hz,  $\text{H}^a$  of  $\text{CHHN}$ ], 4.18 [ddd,  $^3J(\text{H}^b\text{H}^{c'}) = 5.7$  Hz,  $^2J(\text{H}^b\text{H}^{c'}) = 5.7$  Hz,  $\text{H}^b$  of  $\text{CHHN}$ ], 4.64 [s,  $(\text{C}_5\text{H}_5)\text{Ru}$ ], 6.34 [s,  $(\text{C}_5\text{H}_5)\text{Zr}$ ];  $^{13}\text{C}$  NMR ( $\text{C}_6\text{D}_6$ , 50.3 MHz)  $\delta$  1.5 [ $\text{Si}(\text{CH}_3)_3$ ], 30.8 ( $\text{CH}_2$ ), 42.6 ( $\text{CH}_2\text{N}$ ), 84.7 [( $\text{C}_5\text{H}_5$ )Ru], 110.7 [( $\text{C}_5\text{H}_5$ )Zr], 207.1 (CO);  $^{29}\text{Si}$  NMR ( $\text{C}_6\text{D}_6$ , 39.8 MHz)  $\delta$  2.8. Anal. Calcd for  $\text{C}_{21}\text{H}_{34}\text{N}_2\text{O}_2\text{RuSi}_2\text{Zr}$ : C, 42.39; H, 5.76; N, 4.71. Found: C, 42.28; H, 5.65; N, 4.63.

(8) Preparation of  $\text{CH}_2(\text{CH}_2\text{NSiMe}_3)_2(\text{Cp})\text{Zr}-\text{Co}(\text{CO})_3(\text{PPh}_3)$  (**8**). To a solid mixture of 314 mg (0.77 mmol) of  $\text{CH}_2(\text{CH}_2\text{NSiMe}_3)_2\text{Zr}(\text{Cp})\text{Cl}$  (**5**) and 468 mg (0.82 mmol) of  $\text{Na}[\text{Co}(\text{CO})_3(\text{PPh}_3)](\text{THF})_2$ , which was cooled to  $-20^\circ\text{C}$ , was slowly added 20 mL of cold toluene. The reaction mixture was warmed to room temperature over a period of 2 h and stirred for another 20 min. After removal of the solvent in vacuo, the residue was extracted with 30 mL of pentane, the extract filtered, and the volume of the solution reduced to ca. 5 mL. Storage at  $-60^\circ\text{C}$  yielded  $\text{CH}_2(\text{CH}_2\text{NSiMe}_3)_2(\text{Cp})\text{Zr}-\text{Co}(\text{CO})_3(\text{PPh}_3)$  (**8**) as a yellow solid: yield 210 mg (35%); IR (toluene) 1902 vs, 1887 vs  $\text{cm}^{-1}$ ;  $^1\text{H}$  NMR ( $\text{C}_6\text{D}_6$ , 200 MHz)  $\delta$  0.19 [s,  $\text{Si}(\text{CH}_3)_3$ ], 1.39 (m,  $\text{H}^c$  of  $\text{CHH}$ ), 1.62 (m,  $\text{H}^c$  of  $\text{CHH}$ ), 3.37 [ddd,  $^2J(\text{H}^a\text{H}^b) = 16.1$  Hz,  $^3J(\text{H}^a\text{H}^{c'}) = 5.7$  Hz,  $^3J(\text{H}^a\text{H}^{c'}) = 5.5$  Hz,  $\text{H}^a$  of  $\text{CHHN}$ ], 4.33 [ddd,  $^3J(\text{H}^b\text{H}^{c'}) = 5.7$  Hz,  $^3J(\text{H}^b\text{H}^{c'}) = 5.7$  Hz,  $\text{H}^b$  of  $\text{CHHN}$ ], 6.52 (s,  $\text{C}_5\text{H}_5$ ), 6.93–7.04, 7.51–7.59 [m,  $\text{P}(\text{C}_6\text{H}_5)_3$ ];  $^{13}\text{C}$  NMR ( $\text{C}_6\text{D}_6$ , 50.3 MHz)  $\delta$  1.3 [ $\text{Si}(\text{CH}_3)_3$ ], 29.9 ( $\text{CH}_2$ ), 43.2 ( $\text{CH}_2\text{N}$ ), 111.8 ( $\text{C}_5\text{H}_5$ ), 128.6 [d,  $^3J(\text{PC}) = 10.3$  Hz, *meta*-C of  $\text{C}_6\text{H}_5$ ], 129.9 (s, *para*-C of  $\text{C}_6\text{H}_5$ ), 133.4 [d,  $^2J(\text{PC}) = 11.9$  Hz, *ortho*-C of  $\text{C}_6\text{H}_5$ ], 136.6 [d,  $^1J(\text{PC}) = 39.9$  Hz, *ipso*-C of  $\text{C}_6\text{H}_5$ ], 207.2 [br, CO,  $^2J(\text{PC})$  not resolved];  $^{29}\text{Si}$  NMR ( $\text{C}_6\text{D}_6$ , 39.8 MHz)  $\delta$  3.7;  $^{31}\text{P}$  NMR ( $\text{C}_6\text{D}_6$ , 81.0 MHz)  $\delta$  62.0. Anal. Calcd for  $\text{C}_{35}\text{H}_{44}\text{CoN}_2\text{O}_3\text{PSi}_2\text{Zr}$ : C, 54.03; H, 5.70; N, 3.60. Found: C, 54.28; H, 5.58; N, 3.53.

(9) Preparation of  $\text{CH}_2(\text{CH}_2\text{NSiMe}_3)_2(\text{Cp})\text{Zr}-\text{Co}(\text{CO})_3(\text{PpTol}_3)$  (**9**). To a solid mixture of 260 mg (0.64 mmol) of  $\text{CH}_2(\text{CH}_2\text{NSiMe}_3)_2\text{Zr}(\text{Cp})\text{Cl}$  (**5**) and 400 mg (0.65 mmol) of  $\text{Na}[\text{Co}(\text{CO})_3(\text{PpTol}_3)](\text{THF})_2$ , which was cooled to  $-20^\circ\text{C}$ , was slowly added 20 mL of cold toluene. The reaction mixture was slowly warmed to room temperature and stirred for another 20 min. After removal of the solvent in vacuo, the residue was extracted with 30 mL of pentane, the extract filtered, and the volume of the solution reduced to ca. 5 mL. Storage at  $-60^\circ\text{C}$  yielded  $\text{CH}_2(\text{CH}_2\text{NSiMe}_3)_2(\text{Cp})\text{Zr}-\text{Co}(\text{CO})_3(\text{PpTol}_3)$  (**9**) as a yellow solid: yield 168 mg (32%); IR (toluene) 1900 vs, 1885 vs  $\text{cm}^{-1}$ ;  $^1\text{H}$  NMR ( $\text{C}_6\text{D}_6$ , 200 MHz)  $\delta$  0.22 [s,  $\text{Si}(\text{CH}_3)_3$ ], 1.37 (m,  $\text{H}^c$  of  $\text{CHH}$ ), 1.58 (m,  $\text{H}^c$  of  $\text{CHH}$ ), 1.94 (s,  $\text{CH}_3\text{C}_6\text{H}_4$ ), 3.41 [ddd,  $^2J(\text{H}^a\text{H}^b) = 15.7$  Hz,  $^3J(\text{H}^a\text{H}^{c'}) = 6.1$  Hz,  $^3J(\text{H}^a\text{H}^{c'}) = 5.0$  Hz,  $\text{H}^a$  of  $\text{CHHN}$ ], 4.38 [ddd,  $^3J(\text{H}^b\text{H}^{c'}) = 5.7$  Hz,  $^3J(\text{H}^b\text{H}^{c'}) = 5.7$  Hz,  $\text{H}^b$  of  $\text{CHHN}$ ], 6.57 (s,  $\text{C}_5\text{H}_5$ ), 6.92 [dd,  $^3J(\text{H}^{\text{ortho}}\text{H}^{\text{meta}}) = 7.9$  Hz,  $^4J(\text{HP}) = 1.8$  Hz, *meta*-H of  $\text{C}_6\text{H}_4\text{CH}_3$ ], 7.66 [dd,  $^3J(\text{HP}) = 10.7$  Hz, *ortho*-H of  $\text{C}_6\text{H}_4\text{CH}_3$ ];  $^{13}\text{C}$  NMR ( $\text{C}_6\text{D}_6$ , 50.3 MHz)  $\delta$  1.4 [ $\text{Si}(\text{CH}_3)_3$ ], 21.1 ( $\text{CH}_3\text{C}_6\text{H}_4$ ), 29.9 ( $\text{CH}_2$ ), 43.2 ( $\text{CH}_2\text{N}$ ), 111.7 ( $\text{C}_5\text{H}_5$ ), 129.4 [d,  $^3J(\text{PC}) = 9.9$  Hz, *meta*-C of  $\text{C}_6\text{H}_4\text{CH}_3$ ], 133.5 [d,  $^2J(\text{PC}) = 11.9$  Hz, *ortho*-C of  $\text{C}_6\text{H}_4\text{CH}_3$ ], 136.8 [d,  $^1J(\text{PC}) = 42.0$  Hz, *ipso*-C of  $\text{C}_6\text{H}_4\text{CH}_3$ ], 139.8 [s, *para*-C of  $\text{C}_6\text{H}_4\text{CH}_3$ ], 207.7 [br, CO,  $^2J(\text{PC})$  not resolved];  $^{29}\text{Si}$  NMR ( $\text{C}_6\text{D}_6$ , 39.8 MHz)  $\delta$  3.6;  $^{31}\text{P}$  NMR ( $\text{C}_6\text{D}_6$ , 81.0 MHz)  $\delta$  59.2. Anal. Calcd for  $\text{C}_{38}\text{H}_{50}\text{CoN}_2\text{O}_3\text{PSi}_2\text{Zr}$ : C, 55.65; H, 6.15; N, 3.42. Found: C, 55.28; H, 6.28; N, 3.53.

**X-ray Crystallographic Study of  $\text{CH}_2(\text{CH}_2\text{NSiMe}_3)_2(\text{Cp})\text{Zr}-\text{Fe}(\text{CO})_2\text{Cp}$  (**6**).** A yellow block-shaped crystals of **6** was mounted under argon in a Lindemann capillary. The X-ray diffraction data were collected by using a Philips PW 1100 diffractometer with graphite-monochromated Mo K $\alpha$  radiation. Unit cell parameters were determined by a least-squares analysis of 25 automatically centered reflections in the range of  $10^\circ < \theta < 15^\circ$ . Data were collected at 295 K in the range of  $\theta = 3\text{--}25^\circ$  with a scan width of  $0.80^\circ$  by using a technique described previously.<sup>10</sup>

Crystal data for **6**:  $\text{C}_{21}\text{H}_{34}\text{N}_2\text{O}_2\text{Si}_2\text{FeZr}$ , monoclinic, space group  $P2_1/c$ ,  $M = 549.75$ ,  $Z = 4$ ,  $a = 10.446(3)$  Å,  $b = 26.504(5)$  Å,  $c = 10.446(3)$  Å,  $\beta = 112.71(4)^\circ$ ,  $V = 2574.39$  Å<sup>3</sup>,  $\rho_{\text{calc}} = 1.418$  g  $\text{cm}^{-3}$ ,  $F(000) = 1136$ ,  $\mu(\text{Mo K}\alpha) = 10.2$   $\text{cm}^{-1}$ .

The structure solution and refinement were carried out with the programs of the SHELX 76 software package. The coordinates of the metal atoms were deduced from a Patterson synthesis. The remaining atoms were located from subsequent difference Fourier syntheses and the hydrogen atoms were included in the structure factor calculations with thermal factors of  $0.08$  Å<sup>2</sup>, but their parameters not refined. Empirical absorption corrections, using the program DIFABS<sup>11</sup> were applied to all data, after initial refinement with isotropic thermal parameters for all atoms. In the final cycles the full-matrix least-squares refinement anisotropic thermal parameters were assigned to all non-hydrogen atoms with weights of  $1/\sigma^2(F)$  for individual reflections. Refinement converged at  $R = 0.046$  and  $R_w = 0.045$  for 3253 data with  $I/\sigma(I) > 3$  and 265 parameters.

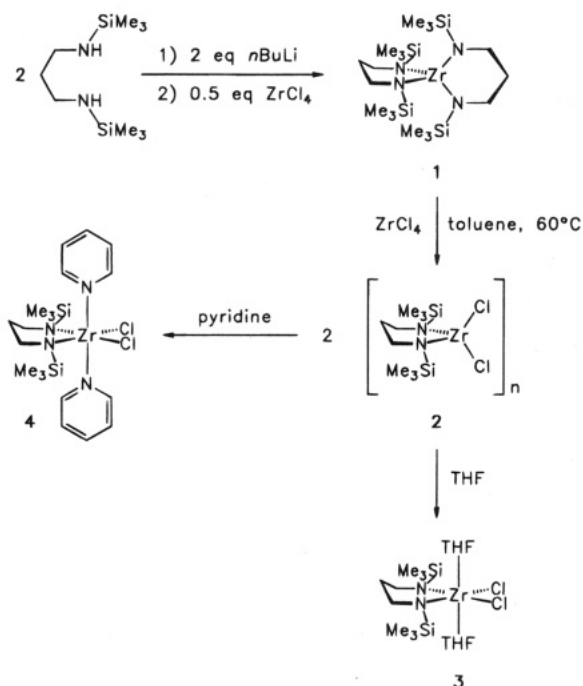
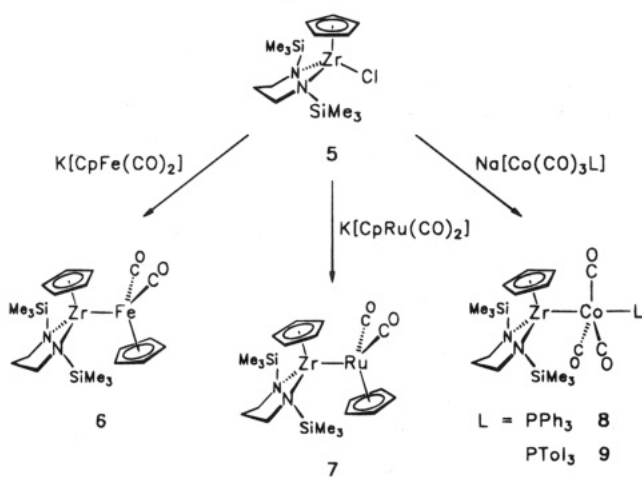
## Results and Discussion

**Synthesis of Chelate-(Diamido)dichlorozirconium Complexes and the Half-Sandwich Compound  $\text{CH}_2(\text{CH}_2\text{NSiMe}_3)_2\text{Zr}(\text{Cp})\text{Cl}$  (**5**).** The most versatile synthetic strategy for the synthesis of Cp-(RNNR)<sub>2</sub>-half-sandwich complexes is based upon an initial introduction of the amido ligand at the metal center and the subsequent substitution of a halide ligand by LiCp. The "difunctional" (diamido)dichlorozirconium complex  $\text{CH}_2(\text{CH}_2\text{NSiMe}_3)_2\text{ZrCl}_2$  (**2**), a key intermediate in the synthesis of the type of half-sandwich complex mentioned above, is most conveniently prepared by a ligand redistribution upon reaction of the symmetrical species  $[\text{CH}_2(\text{CH}_2\text{NSiMe}_3)_2]_2\text{Zr}$  (**1**) with  $\text{ZrCl}_4$  in toluene at  $60^\circ\text{C}$  (Scheme 1). The route via the spirocyclic system **1** was chosen in view of the low solubility of the probably oligomeric complex **2** in aromatic hydrocarbons which prohibited the separation of LiCl generated in the direct synthesis based upon a 1:1 stoichiometric reaction of the lithiated amine  $[\text{CH}_2\text{-}\{\text{CH}_2\text{N}(\text{Li})\text{SiMe}_3\}_2]_n$  with  $\text{ZrCl}_4$ . The method employing the ligand redistribution was first reported by Bürger and co-workers in their synthesis of several chelating amido-zirconium halides.<sup>12</sup> In the presence of the donor solvents THF and pyridine, **2** is converted to the hexacoordinate solvent adducts  $\text{CH}_2(\text{CH}_2\text{NSiMe}_3)_2\text{-ZrCl}_2(\text{THF})_2$  (**3**) and  $\text{CH}_2(\text{CH}_2\text{NSiMe}_3)_2\text{-ZrCl}_2(\text{NC}_5\text{H}_5)_2$  (**4**), respectively, which are soluble in benzene or toluene and may therefore be conveniently employed in further transformations. The THF-adduct **3**, in particular, was found to be a useful reagent since it spontaneously loses

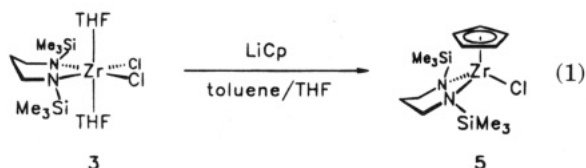
(10) Cooper, M. K.; Guernsey, P. J.; McPartlin, M. *J. Chem. Soc., Dalton Trans.* **1982**, 757.

(11) Walker, N.; Stuart, D. *Acta Crystallogr., Sect. A* **1983**, *39*, 158.

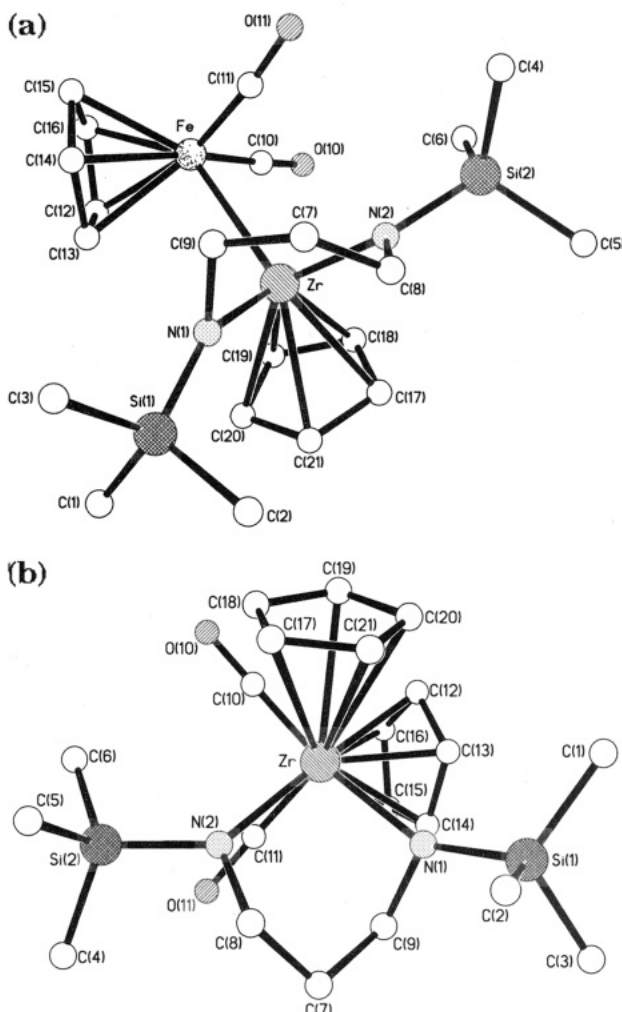
(12) (a) Bürger, H.; Beiersdorf, D. *Z. Allg. Anorg. Chem.* **1979**, *459*, 111. (b) Wiegel, K.; Bürger, H. *Ibid.* **1976**, *426*, 301. (c) Brauer, D. J.; Bürger, H.; Essig, E.; Gschwandtner, W. *J. Organomet. Chem.* **1980**, *190*, 343. (d) Bürger, H.; Gschwandtner, W.; Liewald, G. R. *Ibid.* **1983**, *259*, 145.

**Scheme 1. Synthesis of  $\text{CH}_2(\text{CH}_2\text{NSiMe}_3)_2\text{ZrCl}_2(\text{L})_2$   
(L = THF (3), Pyridine 4))**

**Scheme 2. Synthesis of the Zr–M Heterodinuclear Complexes 6–9**


its solvent ligands upon substitution of the halide by a bulkier anionic ligand. Reaction of **3** with 1 molar equiv of LiCp smoothly yielded the half-sandwich complex  $\text{CH}_2(\text{CH}_2\text{NSiMe}_3)_2\text{Zr}(\text{Cp})\text{Cl}$  (**5**) in 76% yield (eq 1).



**Synthesis of the Zr–M Heterobimetallic Complexes (M = Fe, Ru, Co).** Reaction of **5** with the metal carbonylates  $\text{K}[\text{Cp}(\text{CO})_2\text{Fe}]$ ,  $\text{K}[\text{Cp}(\text{CO})_2\text{Ru}]$ ,  $\text{Na}[\text{Co}(\text{CO})_3(\text{PPh}_3)]$ , and  $\text{Na}[\text{Co}(\text{CO})_3(\text{PTol}_3)]$  yielded the corresponding heterobimetallic complexes **6–9** (Scheme 2). Due some degree of single electron transfer from the carbonylate to the Zr complex as a reaction competing with the metathetical condensation in the formation of the



**Figure 2.** Molecular structure of **6** in the crystal: (a) View perpendicular to the Fe–Zr axis; (b) view along the Zr–Fe axis showing the *gauche* conformation of the Cp rings in the two molecular halves.

Zr–Co complexes, these species were only obtained in a yield of 35% (**8**) and 32% (**9**). The effective  $C_s$  symmetry of **6** and **7** reflected in the  $^1\text{H}$ -,  $^{13}\text{C}$ -, and  $^{29}\text{Si}$ -NMR spectra indicates either free rotation around the metal–metal bond or a libration around this bond generating the apparent  $C_s$  symmetry. This rotation (or libration) could not be frozen out at 180 K although exchange broadening is observed below 210 K. The shift of the  $\nu(\text{CO})$  bands to higher wavenumbers relative to those of the alkali metal salts of the anions is an indirect indication of the formation metal–metal bonds. Electron density is thus transferred to the Lewis acidic early transition metal center. The shift of the asymmetric  $^{12}\text{C}$ –O stretching frequency, in particular, may be viewed as a measure of the acceptor strength of the Lewis acidic metal fragment relative to the base  $[\text{Cp}(\text{CO})_2\text{M}]^-$ .<sup>13</sup>

It is particularly interesting to compare the position of the  $\nu(\text{CO})$  bands in the complexes of type A (Casey), type B (tripodamido–zirconium) and, as first described here, type C (Cp/diamido–Zr) (Table 1). As is readily apparent, less electron density is withdrawn from the carbonyl metal fragment by the 16-electron fragment  $[\text{Cp}_2\text{ZrX}]^+$  than by the 14-electron fragment  $[\text{Cp}$

(13) See for example: Fischer, R. A.; Priemeier, T. *Organometallics* **1994**, *13*, 4306 and references cited therein.

Table 1. Carbonyl Infrared Bands in Complexes of Types A–C

compd	type	$\nu(\text{CO})$ ( $\nu_{\text{sym}}, \nu_{\text{as}}$ )		ref
		Zr–Fe ( $\text{cm}^{-1}$ )	Zr–Ru ( $\text{cm}^{-1}$ )	
MeSi{SiMe <sub>2</sub> N(4-CH <sub>3</sub> C <sub>6</sub> H <sub>4</sub> ) <sub>3</sub> Zr–M(CO) <sub>2</sub> Cp	B	1961, 1910	1986, 1932	6
CH <sub>2</sub> (CH <sub>2</sub> NSiMe <sub>3</sub> ) <sub>2</sub> (Cp)Zr–M(CO) <sub>2</sub> Cp	C	1947, 1895	1957, 1895	a
Cp <sub>2</sub> (Cl)Zr–M(CO) <sub>2</sub> Cp	A		1953, 1886	1a
Cp <sub>2</sub> (Me)Zr–M(CO) <sub>2</sub> Cp	A	1937, 1872	1950, 1880	1a
Cp <sub>2</sub> ( <sup>t</sup> BuO)Zr–M(CO) <sub>2</sub> Cp	A	1939, 1874	1958, 1884	1a

<sup>a</sup> This work (recorded in toluene).

Table 2. Selected Bond Lengths (Å) and Bond Angles (deg) for **6**

Zr–Fe	2.745(1)	Zr–N(1)	2.039(4)
Zr–C(9)	2.632(5)	Zr–N(2)	2.047(5)
Zr–C(17)	2.529(5)	Zr–C(18)	2.541(5)
Zr–C(19)	2.579(5)	Zr–C(20)	2.572(5)
Zr–C(21)	2.523(5)	Fe–C(10)	1.733(7)
Fe–C(11)	1.689(6)	Fe–C(12)	2.077(7)
Fe–C(13)	2.108(6)	Fe–C(14)	2.101(6)
Fe–C(15)	2.116(6)	Fe–C(16)	2.104(6)
Si(1)–C(1)	1.848(7)	Si(1)–C(2)	1.866(6)
Si(1)–C(3)	1.865(6)	Si(1)–N(1)	1.748(4)
Si(2)–C(4)	1.867(8)	Si(2)–C(5)	1.849(8)
Si(2)–C(6)	1.858(7)	Si(2)–N(2)	1.741(5)
C(10)–O(10)	1.163(7)	C(11)–O(11)	1.198(6)
N(1)–Zr–Fe	108.1(1)	C(9)–Zr–Fe	91.8(1)
C(9)–Zr–N(1)	34.0(2)	N(2)–Zr–Fe	111.9(1)
N(2)–Zr–N(1)	94.6(2)	N(2)–Zr–C(9)	73.1(2)
C(17)–Zr–Fe	133.3(1)	C(17)–Zr–N(1)	112.6(2)
C(17)–Zr–C(9)	134.9(2)	C(17)–Zr–N(2)	86.8(2)
C(18)–Zr–Fe	101.3(1)	C(18)–Zr–N(1)	138.8(2)
C(18)–Zr–C(9)	166.8(2)	C(18)–Zr–N(2)	100.5(2)
C(18)–Zr–C(17)	32.0(2)	C(19)–Zr–Fe	87.4(1)
C(19)–Zr–N(1)	121.3(2)	C(19)–Zr–C(9)	152.6(2)
C(19)–Zr–N(2)	132.1(2)	C(19)–Zr–C(17)	52.2(2)
C(19)–Zr–C(18)	31.6(2)	C(20)–Zr–Fe	105.9(1)
C(20)–Zr–N(1)	91.0(2)	C(20)–Zr–C(9)	124.6(2)
C(20)–Zr–N(2)	137.7(2)	C(20)–Zr–C(17)	52.7(2)
C(20)–Zr–C(18)	52.8(2)	C(20)–Zr–C(19)	31.5(2)
C(21)–Zr–Fe	137.3(1)	C(21)–Zr–N(1)	85.8(2)
C(21)–Zr–C(9)	116.8(2)	C(21)–Zr–N(2)	106.7(2)
C(21)–Zr–C(17)	32.1(2)	C(21)–Zr–C(18)	53.2(2)
C(21)–Zr–C(19)	52.4(2)	C(21)–Zr–C(20)	32.0(2)
C(10)–Fe–Zr	87.7(2)	C(11)–Fe–Zr	84.5(2)
C(11)–Fe–C(10)	94.6(3)	C(12)–Fe–Zr	106.7(2)
C(12)–Fe–C(10)	96.8(3)	C(12)–Fe–C(11)	164.2(3)
C(13)–Fe–Zr	82.0(2)	C(13)–Fe–C(10)	127.1(3)
C(13)–Fe–C(11)	135.1(3)	C(13)–Fe–C(12)	39.8(2)
C(14)–Fe–Zr	99.0(2)	C(14)–Fe–C(10)	162.2(3)
C(14)–Fe–C(11)	102.4(3)	C(14)–Fe–C(12)	65.5(3)
C(14)–Fe–C(13)	39.1(2)	C(15)–Fe–Zr	137.9(2)
C(15)–Fe–C(10)	133.1(3)	C(15)–Fe–C(11)	99.3(3)
C(15)–Fe–C(12)	65.0(3)	C(15)–Fe–C(13)	65.8(2)
C(15)–Fe–C(14)	39.1(3)	C(16)–Fe–Zr	145.0(2)
C(16)–Fe–C(10)	100.3(3)	C(16)–Fe–C(11)	128.0(3)
C(16)–Fe–C(12)	38.8(2)	C(16)–Fe–C(13)	65.9(2)
C(16)–Fe–C(14)	65.0(3)	C(16)–Fe–C(15)	38.3(3)

(amide)<sub>2</sub>Zr]<sup>+</sup>. The Lewis acidity at the Zr is in turn markedly further increased on going to the 12-electron fragment [(tripodtriamide)Zr]<sup>+</sup>.

Infrared absorptions attributable to bridging carbonyl or isocarbonyl ligands were not observed in the spectra recorded for **6**–**9** which supports the structural arrangements depicted in Scheme 2.

**Crystal Structure of CH<sub>2</sub>(CH<sub>2</sub>NSiMe<sub>3</sub>)<sub>2</sub>(Cp)Zr–Fe(CO)<sub>2</sub>Cp (**6**).** We have recently carried out the first structural characterization of a compound with an unsupported Zr–Fe bond, MeSi{SiMe<sub>2</sub>N(4-CH<sub>3</sub>C<sub>6</sub>H<sub>4</sub>)<sub>3</sub>Zr–Fe(CO)<sub>2</sub>Cp (**10**),<sup>6</sup> which was found to have a Zr–Fe bond length of 2.605(2) Å. In view of this result, the effect that the ligand shell at the early transition metal has upon the metal–metal bond was of particular

Table 3. Fractional Atomic Coordinates for **6**

atom	x	y	z
Zr	0.34383(5)	0.13727(2)	0.08922(5)
Fe	0.37448(8)	0.06510(3)	0.29456(8)
Si(1)	0.0836(2)	0.1135(1)	–0.2682(2)
C(1)	–0.0712(7)	0.1342(3)	–0.2367(7)
C(2)	0.1195(7)	0.1589(3)	–0.3912(6)
C(3)	0.0400(7)	0.0512(2)	–0.3608(7)
Si(2)	0.6901(2)	0.1626(1)	0.1461(2)
C(4)	0.8141(7)	0.1151(3)	0.1272(8)
C(5)	0.7319(9)	0.2243(3)	0.0873(10)
C(6)	0.7203(7)	0.1667(3)	0.3399(7)
N(1)	0.2278(4)	0.1072(2)	–0.1066(4)
C(9)	0.3304(6)	0.0684(2)	–0.1038(6)
C(7)	0.4379(7)	0.0866(3)	–0.1652(7)
C(8)	0.4927(6)	0.1385(3)	–0.1106(6)
N(2)	0.5192(4)	0.1448(2)	0.0466(4)
C(10)	0.4453(7)	0.1116(3)	0.4231(6)
O(10)	0.4928(6)	0.1408(2)	0.5152(5)
C(11)	0.5251(6)	0.0520(2)	0.2764(6)
O(11)	0.6323(4)	0.0388(1)	0.2700(5)
C(12)	0.1851(7)	0.0598(3)	0.3162(8)
C(13)	0.1626(6)	0.0531(2)	0.1685(7)
C(14)	0.2398(7)	0.0101(3)	0.1637(8)
C(15)	0.3055(7)	–0.0094(2)	0.3043(8)
C(16)	0.2708(7)	0.0214(3)	0.3964(7)
C(17)	0.3338(6)	0.2326(2)	0.0902(7)
C(18)	0.3552(6)	0.2178(2)	0.2303(6)
C(19)	0.2338(7)	0.1941(2)	0.2243(6)
C(20)	0.1391(6)	0.1927(2)	0.0816(6)
C(21)	0.2025(6)	0.2163(2)	–0.0019(6)

interest. Single crystals of **6** could be readily obtained from diethyl ether and were used to carry out a single-crystal X-ray structure analysis of the compound. The molecular structure of **6** is depicted in Figure 2, the principal bond lengths and interbond angles are given in Table 2, and the positional parameters are listed in Table 3.

The crystal structure analysis unambiguously establishes the presence of an unsupported metal–metal bond linking the two complex fragments. Although the two carbonyl ligands are slightly tilted toward the Zr center [ $\angle(\text{C}(10)\text{–Fe–Zr}) = 87.7(2)^\circ$ ,  $\angle(\text{C}(11)\text{–Fe–Zr}) = 84.5(2)^\circ$ ,  $\angle(\text{C}(10)\text{–Fe–C}(11)) = 94.6(3)^\circ$ ], the Zr···C distances of  $d(\text{Zr–C}(10)) = 3.19$  Å and  $d(\text{Zr–C}(11)) = 3.08$  Å preclude any semibridging interaction of the CO ligands in the molecule. The Zr–Fe distance of 2.745(1) Å is significantly greater than the value found in the structure of **10**. Although this situation may be due to steric repulsion of the two ligand shells, the dynamic behavior of the two molecular units observed in the NMR spectra recorded in solution at low temperature (*vide supra*) appears to indicate that any repulsive interaction may not be severe. This raises the question of the role that the different electronic structure of the early transition metal complex fragment in **6** in comparison to that in **10** may play in determining the structural characteristics of the metal–metal bond.



Comparative theoretical studies related to this question are currently underway and will be published elsewhere.

The view along the axis of the metal–metal bond given in Figure 2b shows a *gauche* conformation of the two molecular fragments with the Cp ring at the Fe center occupying a staggered position between the Me<sub>3</sub>SiN(1) and Cp groups in the Zr complex fragment while the two carbonyl ligands are arranged almost eclipsed relative to the ligands at the zirconium center. That an initially expected *anti* conformation of the two Cp ligands is not observed is probably due to the steric demand of the folded propylene chain in the chelate-amido ligand which shields the Zr atom.

### Conclusions

This study has established a new type of Zr–M heterobimetallic complex in which the early transition metal is shielded by both a bidentate amido ligand and a cyclopentadienyl ring. The  $\nu(\text{CO})$  infrared bands indicate a higher degree of electron density remaining at the late transition metal center upon metal–metal bond formation than observed for the previously characterized binuclear Zr–M systems. In the latter the high Lewis acidity of the zirconium complex fragment

apparently leads to a greater degree of redistribution of electron density to the early transition metal. In this respect the compound discussed in this paper bridges the gap between the (tripod-amido)zirconium species and the Cp<sub>2</sub>Zr(R)–MCp(CO)<sub>2</sub> complexes reported previously by Casey and co-workers.

We are currently studying the reactivity of the Zr–M bonds toward polar unsaturated hydrocarbon derivatives.

**Acknowledgment.** We thank the Deutsche Forschungsgemeinschaft, the Fonds der Chemischen Industrie, the DAAD, and the British Council (ARC 313 grant to L.H.G and M.McP.) for financial support and Degussa AG as well as Wacker Chemie AG for generous gifts of basic chemicals. Thanks is also due to Professor H. Werner (Würzburg, Germany) for his continued interest and support of this work.

**Supporting Information Available:** Text detailing the structure determination and tables of crystallographic data, including positional and thermal parameters and interatomic distances and angles for **6** (14 pages). Ordering information is given on any current masthead page.

OM950568U



# Intramolecular and Intermolecular Bonding in Crystalline Clusters of the Type $(\text{Cp}^{\text{R}})_3\text{M}_3(\text{CO})_3$ [ $\text{M} = \text{Co}, \text{Rh}, \text{Ir}; \text{Cp}^{\text{R}} = \text{C}_5\text{H}_5, \text{C}_5\text{Me}_5, \text{C}_5\text{H}_4\text{Me}$ ]

Dario Braga\* and Fabrizia Grepioni

*Dipartimento di Chimica G. Ciamician, Università di Bologna, Via Selmi 2, 40126 Bologna, Italy*

Hubert Wadepohl\* and Stefan Gebert

*Anorganisch-Chemisches Institut der Universität, 69120 Heidelberg 1, Germany*

Maria José Calhorda\*

*Instituto de Tecnologia Química e Biológica, R. da Quinta Grande 6, 2780 Oeiras, and Instituto Superior Técnico, Lisboa, Portugal*

Luis F. Veiros

*Centro de Química Estrutural, Instituto Superior Técnico, 1096 Lisboa Codex, Portugal*

Received June 1, 1995<sup>®</sup>

The relationship between molecular and crystal structures of  $(\text{Cp}^{\text{R}})_3\text{M}_3(\text{CO})_3$  clusters [ $\text{M} = \text{Co}, \text{Rh}, \text{Ir}; \text{Cp}^{\text{R}} = \text{C}_5\text{H}_5, \text{C}_5\text{Me}_5, \text{C}_5\text{H}_4\text{Me}$ ] has been investigated by a combined use of extended Hückel molecular orbital calculations, empirical atom-atom pairwise packing potential energy calculations, and computer graphics. The indenyl derivative  $(\text{Ind})_3\text{Ir}_3(\mu_2\text{-CO})_3$  has also been investigated. The molecules present several isomers of similar energies, and the number of bridging carbonyl groups decreases along the family cobalt, rhodium, iridium, as the metal-metal antibonding character of the orbitals populated in consequence of their formation increases. Hydrogen-bonding networks of the C-H...O type involving the carbonyl oxygen atoms have been detected in all of these crystalline complexes. Facial and edge bridging CO's are observed to form preferential interactions with respect to terminal ligands. The intermolecular and intramolecular interactions in each case are discussed and compared in crystal isomers and polymorphs.

## Introduction

The molecular structure features of *flexible* organometallic molecules in the solid state depend on the subtle interplay between intramolecular interactions (the bonding between atoms and the steric interaction between nonbonded atoms within the molecule) and intermolecular interactions (the "bonding" between molecules responsible for crystal structure stability and cohesion).<sup>1</sup> It is often difficult to grasp how the process of *global energy* minimization, which leads to the ultimate isolation of a molecule in its crystalline form(s), determines the molecular and crystal structure features. When the molecule is structurally nonrigid,<sup>2</sup> *viz.* when some geometric or bonding features at the molecular level can vary along a smooth potential energy hypersurface,<sup>3</sup> there can be several *alternative* ways to attain comparable crystal cohesion with the same molecule in one or more of its isomeric forms. This is the basic idea behind the existence of conformational polymorphs of a given organic molecule, a field widely

investigated by J. Bernstein and others.<sup>4</sup> The possibility of structural reorganization, as a manifestation of structural nonrigidity, directly in the solid state should also be considered.<sup>5</sup>

Systematic studies of systems in which the very same organometallic molecule is present in different crystal forms are very rare. Few examples are known and were mainly reported by some of us.<sup>6</sup> The practical reason for this paucity is mainly due to the difficulty of handling organometallic systems in different crystal-

(4) (a) Bernstein, J. In *Organic Solid State Chemistry*; Desiraju, G. R., Ed.; Elsevier: Amsterdam, 1987; pp 471. (b) Bernstein, J.; Hagler, A. T. *J. Am. Chem. Soc.* **1978**, *100*, 673. (c) Destro, R.; Gavezzotti, A. J. In *Structure and Properties of Molecular Crystals*; Pierrot, M., Ed.; Elsevier: Amsterdam, 1990; pp 161-210.

(5) Braga, D. *Chem. Rev.* **1992**, *92*, 633.

(6) (a) Braga, D.; Grepioni, F. *Acta Crystallogr.* **1989**, *B45*, 378. (b) Braga, D.; Grepioni, F.; Johnson, B. F. G.; Dyson, P.; Frediani, P.; Bianchi, M.; Piacenti, F.; Lewis, J. J. *Chem. Soc., Dalton Trans.* **1992**, 2565. (c) Hong, F. E.; Coffy, T. J.; McCarthy, D. A.; Shore, S. G. *Inorg. Chem.* **1989**, *17*, 3284. (d) Draper, S. M.; Housecroft, C. E.; Keep, A. K.; Matthews, D. M.; Song, X.; Rheingold, A. L. *J. Organomet. Chem.* **1992**, *423*, 241. (e) Adams, R. D.; Babin, J. E.; Tasi, M. *Organometallics* **1988**, *7*, 503. (f) Braga, D.; Grepioni, F. *J. Chem. Soc., Dalton Trans.* **1993**, 1223. (g) Della Pergola, R.; Garlaschelli, L.; Martinengo, S.; DeMartin, F.; Manassero, M.; Sansoni, M. *Gazz. Chim. Ital.* **1987**, *117*, 245. (h) Brown, M. P.; Burns, D.; Harding, M. M.; Maginn, S.; Smith, A. K. *Inorg. Chim. Acta* **1989**, *162*, 287. (i) Braga, D.; Grepioni, F.; Sabatino, P.; Dyson, P. J.; Johnson, B. F. G.; Lewis, J.; Bailey, P. J.; Raithby, P. R.; Stalke, D. *J. Chem. Soc., Dalton Trans.* **1993**, 985. (j) Dyson, P. J.; Johnson, B. F. G.; Lewis, J.; Martinelli, M.; Braga, D.; Grepioni, F. *J. Am. Chem. Soc.* **1993**, *115*, 9062.

<sup>®</sup> Abstract published in *Advance ACS Abstracts*, September 1, 1995.

(1) Braga, D.; Grepioni, F. *Acc. Chem. Res.* **1994**, *27*, 51.

(2) (a) Cotton, F. A.; Hanson, B. E. *Rearrangements in Ground and Excited States*; De Mayo, P., Ed.; Academic Press: New York, 1980; p 379. (b) Faller, J. W. *Adv. Organomet. Chem.* **1978**, *16*, 211. (c) Band, E.; Muettterties, E. L. *Chem. Rev.* **1978**, *78*, 639.

(3) (a) Crabtree, R. H.; Lavin, M. *Inorg. Chem.* **1986**, *25*, 805.

**Table 1. Molecular and Crystal Structure Parameters for Cluster Species of the Type  $(Cp^R)_3M_3(C_5R_5)_3(CO)_3$  [ $M = Co, Rh, Ir$ ;  $Cp^R = C_5H_5, C_5Me_5, C_5H_4Me$ ]**

formula	CO type	ref code	space group	$V_{mol}$ ( $\text{\AA}^3$ )	pc	ppe	ref
$Cp_3Co_3(\mu_3-CO)(\mu_2-CO)_2$	FE <sub>2</sub>	CPTCCO10	$P\bar{1}$	291.8	0.73	-60.32	13
$Cp_3Rh_3(\mu_2-CO)_3$	E <sub>3</sub>	CPNCRH10	$P2_1/m$	311.3	0.76	-64.73	14
$Cp_3Rh_3(\mu_2-CO)_3 \cdot 0.24(\text{acetone})^a$	E <sub>3</sub>	CABBEM	$p3m1$	313.6	0.64	-52.64	15
$Cp_3Rh_3(\mu_2-CO)_2(CO)$	TE <sub>2</sub>	CPRHCT01	$P2_12_12_1$	315.5	0.74	-68.08	16
$Cp_3Ir_3(CO)_3$	T <sub>3</sub>	BEZMAU	$P\bar{1}$	324.9	0.76	-70.00	17
$Cp'_3Co_3(\mu_3-CO)(\mu_2-CO)_2$	FE <sub>2</sub>	BIKBAY	$P2_1$	344.1	0.73	-65.16	13
$Cp^*_2Cp^*Co_3(\mu_3-CO)(\mu_2-CO)_2$	FE <sub>2</sub>	CMNCOD	$P2_1/n$	417.9	0.71	-69.91	18
$Cp^*_3Rh_3(\mu_3-CO)(\mu_2-CO)_2$	FE <sub>2</sub>	VENPEJ	$P2_1/c$	560.4	0.71	-77.20	19
$Cp_2Cp^*Co_2Ir(\mu_2-CO)_3$	E <sub>3</sub>	FOHFOX	$P2_1$	384.6	0.72	-64.11	20

<sup>a</sup> No coordinates of acetone given.

lization conditions. One way around this difficulty it is to make use of the large body of structural information deposited in the Cambridge Structural Database,<sup>7</sup> (CSD). Many organometallic systems belong to fairly populated families or classes of compounds. The differences and analogies in chemical and structural behavior of complexes and clusters in which, for instance, the metal atom changes along a group of the periodic table, can be used to correlate molecular and crystal structure features with the idea in mind that the *electronic* characteristics, as well as the crystal environment, can be changed by modifying the nature of the metal atoms and/or with the bonding mode of the ligand(s). Some of us have previously investigated the relationship between molecular and crystal structures of ruthenium clusters carrying benzene bound in terminal- or facial-bonding mode,<sup>8a</sup> as well as the relationship between the presence of intermolecular hydrogen bonds and the bending of C-H bonds in bisarene complexes of the type  $[(\text{arene})_2Ru_2Cl_3]^+$  (arene = benzene, toluene).<sup>8b</sup> The problem of the existence of different isomeric forms for  $M_4$  clusters ( $M = Co, Rh, and Ir$ ) and their derivatives with a variety of ligands<sup>9a</sup> as well as the intramolecular and intermolecular bonding in  $Ru_5(CO)_{12}$  and its derivatives with facial ligands, have also been addressed.<sup>9b</sup>

The relationship between intramolecular and intermolecular bonding can be conveniently tackled with the aid of two complementary tools, namely, molecular orbital calculations of the extended Hückel type<sup>10</sup> (to address specific bonding problems) and packing potential energy calculations<sup>11</sup> and packing analysis (to study the intermolecular bonding).

In this paper, we report on the family of compounds of general formula  $(Cp^R)_3M_3(CO)_3$ , where  $M = Co, Rh, and Ir$  and  $Cp^R = C_5H_5$  (Cp),  $C_5H_4Me$ , (Cp'),  $C_5Me_5$  (Cp\*). Several compounds of this type have been characterized mostly over the past decade, and the molecular structures and the chemistry of these and related cluster complexes have recently been reviewed.<sup>12</sup> Formulae, crystallographic information, and references<sup>13-20</sup> are grouped in Table 1. The CSD<sup>7</sup> was used to extract the atomic coordinates. Sketches of all the molecules under investigation are grouped in Figure 1.

The main features of the molecular structures can be described as follows:

(i) CO ligands are present in all three main bonding modes: terminal (hereafter mode T), edge-bridging ( $\mu_2$ -coordination, hereafter mode E), and face-bridging ( $\mu_3$ -coordination, hereafter mode F).

(ii) Three terminal ligands (T<sub>3</sub>) are shown only by the Ir complex  $Cp_3Ir_3(CO)_3$  [BEZMAU].

(iii) Only edge-bridges (E<sub>3</sub>) are present in two forms of  $Cp_3Rh_3(\mu_2-CO)_3$  [CPNCRH10 and CABBEM], in the mixed-metal species  $Cp_2Cp^*Co_2Ir(\mu_2-CO)_3$  [FOHFOX], and in the indenyl derivative of Ir (see below).

(iv) One facial  $\mu_3$ -bridge is present in  $Cp_3Co_3(\mu_3-CO)(\mu_2-CO)_2$  [CPTCCO10], in  $Cp'_3Co_3(\mu_3-CO)(\mu_2-CO)_2$  [BIKBAY], and in  $Cp^*_2Cp^*Co_3(\mu_3-CO)(\mu_2-CO)_2$  [CMNCOD]; the other two CO's are  $\mu_2$ -bridging in all three complexes.

(v) The fourth type of CO-ligand distribution is characterized by the presence of one terminally bound CO and by two bridges; such is the arrangement in  $Cp_3Rh_3(\mu_2-CO)_2(CO)$  [CPRHCT01].

If the labels T, E, and F are used, these CO-ligand distributions can be called T<sub>3</sub>, TE<sub>2</sub>, E<sub>3</sub>, and FE<sub>2</sub>, respectively.

The trend toward a decreasing importance of bridging ligands on descending through the group from Co to Ir, which is observed in the family of  $M_4(CO)_{12}$  clusters and of their derivatives,<sup>10a</sup> is also clear in the  $Cp_3M_3(CO)_3$  systems. Cobalt is preferentially involved in  $\mu_3$  or  $\mu_2$  bridges, whereas iridium atoms prefer to carry terminal CO's. The indenyl derivative  $(\text{ind})_3Ir_3(\mu_2-CO)_3$  is exceptional in this respect because the cluster bears three

(7) (a) Allen, F. H.; Bellard, S.; Brice, M. D.; Cartwright, C. A.; Doubleday, A.; Higgs, H.; Hummelink, T.; Hummelink-Peters, B. J.; Kennard, O.; Motherwell, W. D. S.; Rodgers, J. R.; Watson, D. G. *Acta Crystallogr.* **1979**, B35, 2331. (b) Allen, F. H.; Davies, J. E.; Galloy, J. J.; Johnson, O.; Kennard, O.; Macrae, C. F.; Watson, D. G. *J. Chem. Inf. Comput. Sci.* **1991**, 31, 204.

(8) (a) Braga, D.; Dyson, P. J.; Grepioni, F.; Johnson, B. F. G.; Calhorda, M. J. *Inorg. Chem.* **1994**, 33, 3218. (b) Grepioni, F.; Braga, D.; Dyson, P.; Johnson, B. F. G.; Sanderson, F. M.; Calhorda, M. J.; Veiros, L. *Organometallics* **1995**, 14, 121.

(9) (a) Braga, D.; Byrne, J. J.; Calhorda, M. J.; Grepioni, F. Submitted for publication. (b) Braga, D.; Grepioni, F.; Calhorda, M. J.; Veiros, L. *Organometallics* **1995**, 14, 1992.

(10) (a) Hoffmann, R. *J. Chem. Phys.* **1963**, 39, 1397. (b) Hoffmann, R.; Lipscomb, W. N. *J. Chem. Phys.* **1962**, 36, 2179, 3489. (c) Thorn, D. L.; Hoffmann, R. *Inorg. Chem.* **1978**, 17, 126. (d) Albright, T. A.; Whangbo, M.-H.; Burdett, J. K. *Orbital Interactions in Chemistry*; John Wiley & Sons: New York, 1985.

(11) (a) Kitaigorodskii, A. I. *Molecular Crystals and Molecules*; Academic Press: New York, 1973. (b) Pertsin, A. J.; Kitaigorodskii, A. I. *The Atom-Atom Potential Method*; Springer-Verlag: Berlin, 1987. (c) Gavezzotti, A.; Simonetta, M. *Chem. Rev.* **1982**, 82, 1.

(12) Wadepohl, H.; Gebert, S. *Coord. Chem. Rev.*, in press.

(13) Bailey Junior, W. I.; Cotton, F. A.; Jamerson, J. D.; Kolthammer, B. W. S.; *Inorg. Chem.* **1982**, 21, 3131.

(14) Mills, O. S.; Paulus, E. F. *J. Organomet. Chem.* **1967**, 10, 331.

(15) Faraone, F.; Lo Schiavo, S.; Bruno, G.; Piraino, P.; Bombieri, G. *J. Chem. Soc., Dalton Trans.* **1983**, 1813.

(16) Paulus, E. F. *Acta Crystallogr., Sect. B* **1969**, 25, 2206.

(17) Shapley, J. R.; Adair, P. C.; Lawson, R. J.; Pierpont, C. G. *Inorg. Chem.* **1982**, 21, 1701.

(18) Cirjak, L. M.; Huang, J.-S.; Zhu, Z.-H.; Dahl, L. F. *J. Am. Chem. Soc.* **1980**, 102, 6623.

(19) Brunner, H.; Janietz, N.; Wachter, J.; Neumann, H.-P.; Nuber, B.; Ziegler, M. L. *J. Organomet. Chem.* **1990**, 388, 203.

(20) Horlein, R.; Herrmann, W. A.; Barnes, C. E.; Weber, C.; Kruger, C.; Ziegler, M. L.; Zahn, T. *J. Organomet. Chem.* **1987**, 321, 257.

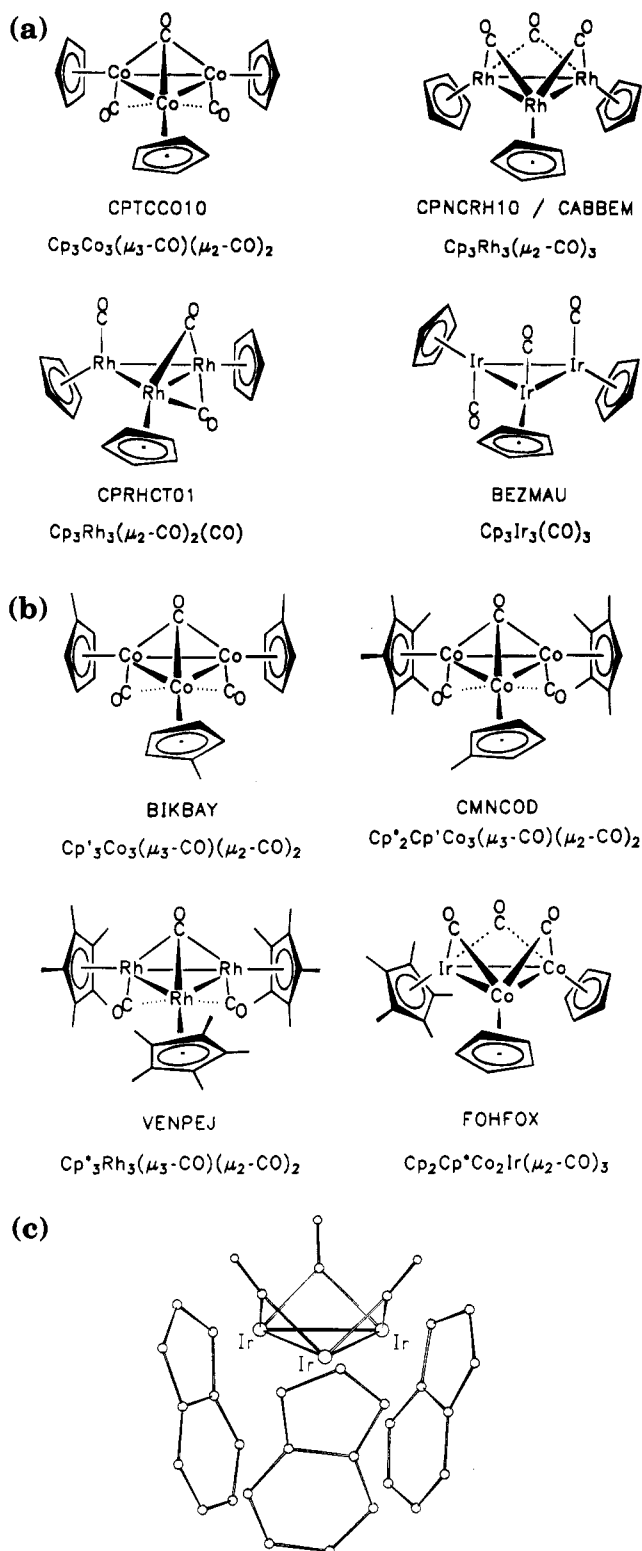


**Figure 1.** Sketches of the molecular structures of  $(\text{Cp}^{\text{R}})_3\text{M}_3(\text{CO})_3$  clusters (a,b) and of the indenyl derivative  $(\text{ind})_3\text{Ir}_3(\text{CO})_3$  (c) as determined in the solid state.

edge-bridging ligands (see Figure 1c). This will be discussed in detail below. With  $\text{C}_5\text{H}_5$  ligands, however, all four types of CO-ligand distributions ( $\text{FE}_2$ ,  $\text{E}_3$ ,  $\text{TE}_2$ ,  $\text{T}_3$ ) are found.

The  $\text{Rh}_3$  system shows the greatest structural variability, presenting systems with the combination  $\text{TE}_2$ ,  $\text{E}_3$ , and  $\text{FE}_2$  depending (apparently) on the size of the  $\text{Cp}^{\text{R}}$  ligand. The increase in the steric bulk of the  $\text{Cp}^{\text{R}}$

ligands is perhaps responsible for the "switch" from  $\text{E}_3$  to  $\text{FE}_2$  when  $\text{M} = \text{rhodium}$ .

The reasons for these differences will be explored by extended Hückel calculations. Introduction of methyl groups does not significantly alter the structures: although the series is far from complete, the same structure is observed for Cp with cobalt and for  $\text{Cp}^*$  with rhodium ( $\text{TE}_2$ ). Interestingly, when the substituent is an indenyl, the  $\text{E}_3$  structure is observed for the first time in an  $\text{Ir}_3$  cluster.<sup>21</sup> Indenyl leads to specific steric hindrance problems, but there are electronic factors responsible for reverting the normal trend and for forcing the formation of bridges along metal-metal bonds involving the heaviest element of the cobalt group.

The second objective of this study is the investigation of how the molecular arrangements of these complexes in the solid state compare with those of other carbonyl clusters in terms of efficiency of volume occupation and packing patterns.<sup>22</sup> The molecules selected for this study also form a particularly well suited sample for the investigation of hydrogen-bonding interactions of the C-H...O type<sup>23,24</sup> because the only acceptors are the CO ligands in their different coordination modes and because the only H atoms are those present on the Cp ligands or on the methyl substituents. In previous studies<sup>25</sup> it was shown that edge-bridging CO's tend to form shorter C-H...O linkages than terminal ones in keeping with the different basicity of the oxygen atom in the two bonding modes.<sup>26</sup> The simultaneous presence of CO ligands in the three most frequent bonding fashions (*viz.* terminal, doubly, and triply bridging bonding modes) can be used to study the different strength of the intermolecular (and intramolecular) C-H...OC hydrogen-bonding interactions. Although the sample is formed by a limited number of compounds, it is homogeneous and should permit an appreciation of the subtle differences in CO oxygen atom basicity as the coordination mode varies. This all will be put in the light of the choice exerted on the type of CO coordination by the characteristics of the metals.

**Molecular Structures.** The family of clusters represented in Figure 1 is formed of trinuclear  $\text{M}_3$  clusters typically possessing 48 electrons.<sup>27</sup> It is not surprising, therefore, that these species will in some ways behave like the related  $\text{M}_3(\text{CO})_{12}$  species ( $\text{M} = \text{Fe}, \text{Ru}, \text{Os}$ ),<sup>28</sup> assuming a  $[\text{Cp}^{\text{R}}]^-$  ring to replace there carbonyls and

(21) Comstock, M. C.; Wilson, S. R.; Shapley, J. R. *Organometallics* **1994**, *13*, 3805.

(22) (a) Braga, D.; Grepioni, F. *Organometallics* **1991**, *10*, 2563. (b) Braga, D.; Grepioni, F. *Organometallics* **1992**, *11*, 711. (c) Braga, D.; Grepioni, F.; Sabatino, P.; Gavezzotti, A. *J. Chem. Soc., Dalton Trans.* **1992**, 1185.

(23) (a) Green, R. D. *Hydrogen Bonding by C-H Groups*; Wiley: New York, 1974. (b) Taylor, R.; Kennard, O. *J. Am. Chem. Soc.* **1982**, *104*, 5063.

(24) Desiraju, G. R. *Acc. Chem. Res.* **1991**, *24*, 290.

(25) (a) Braga, D.; Grepioni, F.; Sabatino, P.; Desiraju, G. R. *Organometallics* **1994**, *13*, 3532. (b) Braga, D.; Biradha, K.; Grepioni, F.; Pedireddi, V. R.; Desiraju, G. R. *J. Am. Chem. Soc.* **1995**, *117*, 3156.

(26) Horwitz, C. P.; Shriver, D. F. *Adv. Organomet. Chem.* **1984**, *23*, 218.

(27) (a) Lauher, J. W. *J. Am. Chem. Soc.* **1978**, *100*, 5305. (b) Kharas, K. C. C.; Dahl, L. F. *Advances in Chemical Physics*; John Wiley & Sons: New York, 1988; Vol. 70. (c) Evans, D. G.; Mingos, D. M. P. *Organometallics* **1983**, *2*, 435. (d) Mingos, D. M. P. *Inorganic Chemistry*; Plenum Press: New York, 1992; p 179.

**Table 2. Relative Energies (eV) of Four Possible Isomers of  $Cp_3M_3(CO)_3$  ( $M = Co, Rh, Ir$ )**

structural type	cobalt	rhodium	iridium
FE <sub>2</sub>	0	0	0
E <sub>3</sub>	0.528	0.588	0.275
TE <sub>2</sub>	0.635	0.883	0.509
T <sub>3</sub>	0.962	1.266	0.520

noting the same metal electron count ( $d^8$ ).<sup>29a</sup> From this point of view, the all-terminal structure  $Cp_3Ir_3(CO)_3$  [BEZMAU] is the analogue of the "all-terminal"  $Os_3(CO)_{12}$ , while the structure exhibited by  $Fe_3(CO)_{12}$  is observed in  $Cp_3Rh_3(\mu_2-CO)_2(CO)$  [CPRHCT01], containing an  $Rh_3$  unit. Symmetry is also different: for instance, while  $Os_3(CO)_{12}$  has idealized  $D_{3h}$  symmetry,  $Cp_3Ir_3(CO)_3$  is only  $C_s$ , not even the expected  $C_{3v}$ . Some of these aspects, especially those dealing with the existence of bridges, have been addressed theoretically.<sup>29b</sup>

We can also point out that, while  $Ru_3(CO)_{12}$  presents no bridging carbonyls, no such structure is observed for the rhodium derivatives addressed here. The rhodium species exhibit three different structures, all carrying bridging carbonyls arranged in different ways. The cobalt clusters, on the contrary, depict the same  $(\mu_2-CO)_2(\mu_3-CO)Co_3$  motif, whichever the coligand is: Cp, Cp', or Cp\*. Moving down toward iridium, the terminal carbonyls become dominant. However, the simultaneous presence of three indenyl ligands forces the E<sub>3</sub> structure in the cluster  $(ind)_3Ir_3(\mu_2-CO)_3$ .

Having these results in mind, we started by carrying out calculations on rhodium clusters, as three out of the four known types of CO arrangements are actually observed here. These calculations were then repeated for cobalt and iridium, and the comparative analysis is based on these two extremes. All the model structures were of the  $Cp_3M_3(CO)_3$  type and based on the experimental ones; angles were optimized using rhodium (details are given in the Methodology section). The indenyl case will be discussed later on its own. It is worth mentioning at this stage that clusters apparently similar but with different electron counts, such as  $Cp_2-Rh_3(CO)_4$ , have been studied.<sup>30</sup>

The relative energies of the model clusters (0 for the most stable form, positive values for all the others) are given in Table 2.

In analyzing these data, one should keep in mind that extended Hückel calculations tend to favor energetically bridging carbonyls over terminal ones, and all values are therefore biased toward structures containing bridging CO's. FE<sub>2</sub> is always the most stable, followed by E<sub>3</sub>, etc. These values have to be taken in a very qualitative way, as indicative of trends. For example, T<sub>3</sub> is comparatively more stable for iridium than for Rh and Co, and TE<sub>2</sub> keeps the same trend. Conversely, for

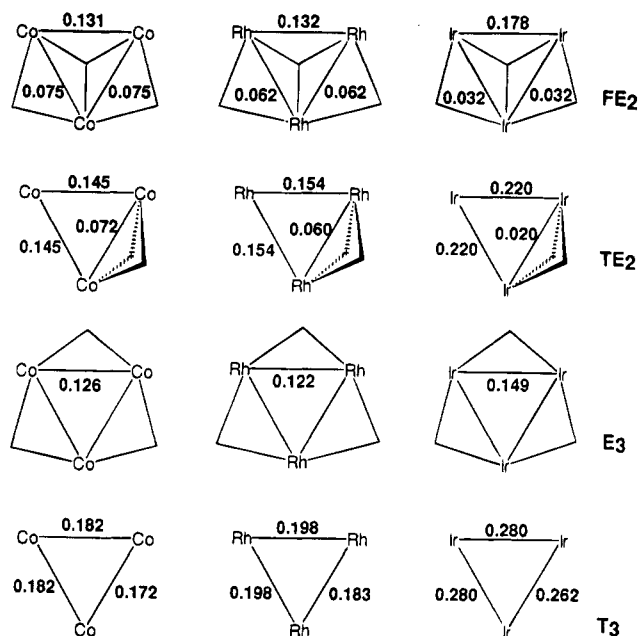


**Figure 2.** Metal-metal overlap populations in four cluster isomers of  $Cp_3M_3(CO)_3$ . Note the nonequivalence of the three M-M bonds for the terminal structure of  $C_{2v}$  symmetry.

cobalt, there is a larger energy gap between FE<sub>2</sub> and T<sub>3</sub>, suggesting that FE<sub>2</sub> should be the most favorable. This goes well with the available structural evidence. The energies for rhodium clusters parallel them, suggesting the actual difficulty in obtaining T<sub>3</sub>. These values cannot be taken literally and are affected by the use of models having fixed bond lengths and only partial optimization. Steric constraints are different for the four structures, and are particularly important for TE<sub>2</sub>.

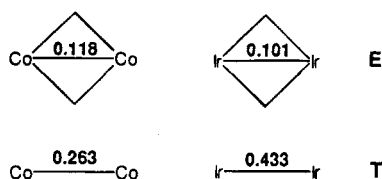
The overlap populations are more helpful in understanding the trends. All M-M overlap populations are shown in Figure 2, where the fame of the cluster is also represented.

Starting from the all-terminal T<sub>3</sub> structure, the metal-metal bonds are strong and they weaken as bridging carbonyls are added; not only do the bonds spanned by the carbonyls weaken, but also the unsupported bonds, though not to such extent. For iridium, the drop in overlap population (in percentage) is much larger than for cobalt and rhodium. Only structures maintaining an appreciable amount of metal-metal bonding will be favored: this is achieved with terminal CO's for iridium, while the presence of bridging CO's in cobalt complexes does not prevent the formation of relatively strong metal-metal bonds.

There are electronic reasons, which will now be examined, behind the preferences for bridged structures in cobalt and for terminal ones in iridium. Rhodium is in between and does not have well-defined preferences. For the sake of simplification and having taken care that all the reasoning kept its validity, a simpler model, containing only two metals with geometry and environment similar to that in the triangular cluster, will be used here. Two bridging of two terminal carbonyls coordinate to the fragment  $M_2Cp_2$  ( $M = Co$  or  $Ir$ ). The two cyclopentadienyl rings are staggered, so that the overall idealized symmetry is  $C_{2h}$ . This type of model has also been used with success in the study of the

(28) (a) Hoffmann, R. *Angew. Chem., Int. Ed. Engl.* **1982**, *21*, 711. (b) Schilling, B. E. R.; Hoffmann, R. *J. Am. Chem. Soc.* **1979**, *101*, 3456. (c) Delley, B.; Manning, M. C.; Ellis, D. E.; Berkowitz, J.; Troglor, W. C. *Inorg. Chem.* **1982**, *21*, 2247. (d) Minot, C.; Criado-Sancho, M. *Nouv. J. Chim.* **1984**, *8*, 537. (e) Rosa, A.; Baerends, E. *J. New J. Chem.* **1991**, *15*, 815. (f) Li, J.; Jug, K. *Inorg. Chim. Acta* **1992**, *196*, 89. (29) (a) Low, A. A.; Kunze, K. L.; MacDougall, P. J.; Hall, M. B. *Inorg. Chem.* **1991**, *30*, 1079. (b) Thorn, D. L.; Hoffmann, R. *Inorg. Chem.* **1978**, *17*, 126. (c) Shaik, S.; Hoffmann, R. *J. Am. Chem. Soc.* **1980**, *102*, 1194. (d) Jemmis, E. D.; Pinhas, A. R.; Hoffmann, R. *J. Am. Chem. Soc.* **1980**, *102*, 2576. (e) Sironi, A. *Inorg. Chem.* **1992**, *31*, 2467. (f) Crabtree, R. H.; Lavin, M. *Inorg. Chem.* **1986**, *25*, 805. (g) Evans, D. G. *J. Chem. Soc., Chem. Commun.* **1983**, 675. (30) Pinhas, A. R.; Allbright, T. A.; Hoffmann, P.; Hoffmann, R. *Helv. Chim. Acta* **1980**, *63*, 29.

Chart 1



metallic ring puckering.<sup>31a</sup> For cobalt this model is a known compound containing, as expected, two bridging carbonyl ligands.<sup>31b</sup> Chart 1 indicates the metal-metal overlap populations and the skeleton of the model dimer.

The basic feature is still there: a more pronounced drop in overlap population for the iridium species when the metals are connected through bridges. This can be traced to a particular interaction in the interaction diagram, depicted in Figure 3 (cobalt on the left side; iridium on the right side) for the structure with CO bridges.

Following the typical bonding mode, there are two donation components from the carbonyl lone pairs ( $a_g$  and  $b_u$ ) to appropriate orbitals of the metallic fragment (an empty M-M  $\sigma_{sp}$  orbital of  $a_g$  symmetry; and the HOMO,  $b_u$ , which is the in-phase combination of  $xy$ , strongly metal-metal bonding). The antibonding orbital of  $2b_u$  symmetry is highly destabilized and therefore empty; there is also mixing in a bonding way of a very high energy level (not shown in the diagram) of the  $Ir_2Cp_2$  fragment. We can anticipate that loss of electrons from this orbital will weaken the bond between metals (its occupation drops from 2.00 to 0.723 in Ir and to 0.716 in Co).

Back-donation involves, in principle, occupied orbitals of the metal and empty  $\pi^*$  on the carbonyls. These give rise to four combinations of  $b_g$ ,  $a_g$ ,  $a_u$ , and  $b_u$  symmetry to which low-energy  $Cp_2M_2$  orbitals of symmetry  $b_g$ ,  $a_u$ , and  $b_u$  donate their electrons (only the stronger interactions,  $a_g$  and  $a_u$ , are represented in Figure 3, for clarity purposes). The interaction of  $a_g$  symmetry is more interesting, because there is no available occupied metal orbital of the same symmetry. The best one would be the LUMO of  $Cp_2M_2$ , an out of phase combination of  $xy$  orbitals. The overlap integral is so large that the resulting bonding molecular orbital is much stabilized and becomes an occupied MO of the final species. This can be clearly seen happening for both metals and is expected to contribute also to the weakening of the metal-metal bond, as an initially empty M-M antibonding orbital becomes partially occupied (1.107 in the Ir complex, 1.368 in the Co complex). The acceptor CO  $a_g$  orbital receives, respectively, 0.875 and 0.621 electrons for Ir and Co. Though this interaction is qualitatively similar for the two metals, the quantitative consequences are different. The iridium orbital has a higher energy, which will be reflected in the higher energy of the resulting bonding  $2a_g$  orbitals, owing to its larger antibonding character.

In order to check this interpretation, we calculated metal-metal overlap populations for the dicationic species, obtained by taking two electrons out of the model dimers. For iridium, it rises from 0.101 to 0.159. The bond becomes stronger because the electrons leave

an antibonding orbital. The same calculation for the cobalt compound results in a weakening of the Co-Co bond (OP varies from 0.118 to 0.086), because the HOMO is a Co-Co-bonding  $a_u$  orbital. It is possible to force occupation of  $a_u$ , leaving  $a_g$  empty. The new Co-Co overlap population is now 0.156. This shows the metal-metal antibonding character of this previously empty orbital, which is even larger for iridium than for cobalt. Its depopulation increases the M-M OP by 57% for Ir, but only by 32% for Co. Thus, although Co can afford CO's bridging M-M bonds, Ir, being the heaviest of the group, has more diffuse orbitals and would create highly destabilizing M-M antibonding interactions in doing so.

This explanation holds for the trinuclear clusters as well, but the greater number of atoms and orbitals obscures the picture. Although the numbers will not be same, the trends are the same. Having rationalized the situation in the Cp derivatives we can now proceed to address the problem of the existence of the iridium  $E_3$  structure when Cp is substituted by indenyl.

In  $(ind)_3Ir_3(CO)_3$ , the structure is of the  $E_3$  type and, at least at first sight, seemingly belongs to the family of the compounds discussed above. A closer look at the structure, however, reveals that, as it happens in most indenyl derivatives, the benzenic ring is planar and forms an angle, the folding angle, [average  $10.1^\circ$  in  $(ind)_3Ir_3(CO)_3$ ], with the plane of the other atoms in the ligand. This value is relatively large compared to other indenyl derivatives and much larger than the negligible folding angles observed in  $Cp^R$  compounds. Such distortions of the indenyl rings have been largely ignored.<sup>32a</sup> Each metal is slipped relative to the center of the attached five-membered ring by 0.27 Å, so that the coordinated indenyl is behaving more as an allyl than as a cyclopentadienyl ligand. The ease of indenyl slipping from  $\eta^5$  to  $\eta^3$  coordination is well-known and responsible for the different chemistry indenyl derivatives exhibit when compared with Cp analogues.<sup>32b</sup> The Ir-C distances are significantly shorter for three of the carbon atoms in each ring (*ca.* 2.20–2.50 Å). For these reasons an allyl group was used in the modeling of the cluster instead of the indenyl. Though the steric requirements of the indenyl and allyl groups are very different, the electronic aspects will be similar.

Calculations on the model  $(allyl)_3Ir_3(CO)_3$ , having structures of types  $E_3$  and  $T_3$ , showed the bridging structure to be more stable by 1.9 eV. By comparison with the relative energies of Table 2, it is clear that the form with three bridges is decidedly preferred, and the origin of this preference should arise from the presence of the allylic ligands. To clarify the picture, a simpler model was used, for which the same trends (energies, overlap populations, and charges) were obtained. It contains two iridium atoms, two Cp or allyl rings, and one bridging or terminal carbonyl and has  $C_{2v}$  symmetry. As the CO ligand becomes a bridge, the Ir-Ir overlap population drops from 0.591 to 0.147 in the case of Cp ligands, but only from 0.384 to 0.205 in the allyl case. A more pronounced decrease of the total energy is observed for the allyl model. The diagram in Figure 4 shows how a bridging CO group interacts with an  $(allyl)_2Ir_2$  (left side) or a  $Cp_2Ir_2$  fragment (right side).

(31) (a) Pinhas, A. R.; Hoffmann, R. *Inorg. Chem.* **1979**, *18*, 654.  
(b) Bailey, W. I., Jr.; Collins, D. M.; Cotton, F. A.; Baldwin, J. C.; Kaska, W. C. *J. Organomet. Chem.* **1979**, *165*, 373.

(32) (a) Szajek, L. P.; Shapley, J. R. *Organometallics* **1994**, *13*, 1395.  
(b) Faller, J. W.; Crabtree, R. H.; Habib, A. *Organometallics* **1985**, *4*, 929.



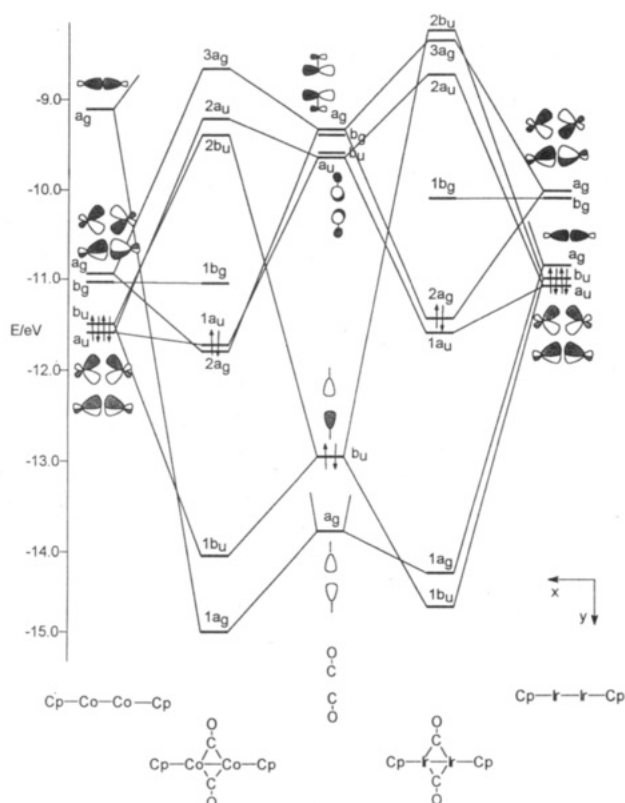


**Figure 3.** The interaction diagram between a binuclear  $M_2Cp_2$  fragment and two bridging carbonyls for  $M = Co$  (left) and  $Ir$  (right). Only the more relevant orbitals are drawn.

The right hand side of the diagram is very similar to the right hand side of Figure 3, though only the interactions which are determining for the outcome are shown, with special emphasis on the one which stabilizes the metal-metal antibonding orbital  $b_1$ . In Figure 3, the corresponding  $a_g$  orbital ended as the HOMO for the iridium species, and as a very close second HOMO for cobalt. Here, the geometry is slightly different and the orbital is the second HOMO, of  $b_1$  symmetry.

The orbitals of the final allylic species are very different and we can trace the influence on the Ir-Ir overlap populations of the features of the  $b_1$  back-donation component. In the  $(allyl)_2Ir_2$  fragment, the  $b_1$  orbital is an occupied Ir-Ir antibonding orbital, without allyl participation. Loss of electrons toward an empty CO  $\pi^*$  will decrease the antibonding character of this orbital, so that the metal-metal bond does not weaken. Notice that in the Cp situation, the comparable  $b_1$  orbital of the  $Cp_2Ir_2$  fragment was pushed up by interaction with one of the Cp  $\pi e_1$  set (the allyl has no such  $\pi$  orbital at suitable energy), going from empty to partially occupied when the CO bridges the M-M bond. This difference accounts for the fact that the Ir-Ir bond is not so much weakened by the allyl ligand but rather by other interactions, not shown in Figure 4, which are still at work (loss of electrons from Ir-Ir bonding orbitals).

This type of effect holds for the indenyl situation. Though the Cp and indenyl clusters look similar, they belong to different groups, owing to the indenyl behaving like an allyl. The cluster is less electron rich, and it is not surprising that other structures may be preferred. On the indenyl side, the choice is between a coordinated allyl plus a "free" aromatic benzene and a

coordinated Cp plus a butadiene. The first is energetically more favorable.<sup>32a</sup>

To conclude this section, we would like to briefly address one question raised in ref 21, as the authors discussed the nature of the HOMO and LUMO of the  $(ind)_3Ir_3(CO)_3$  cluster in the light of spectroscopic studies. Our calculations show, as proposed, that the HOMO is a metal-metal bonding orbital and the LUMO an antibonding one, as it is shown in Figure 5.

**Crystal Structures.** General information on the crystal structures discussed below are also reported in Table 1. The reader is addressed to previous papers<sup>22</sup> on the use of packing coefficients (pc) and packing potential energy calculations to evaluate cohesion and intermolecular arrangements in crystalline organic and organometallic systems. A brief description of the computational procedures are given in the Methodology section below.

With respect to the data collected in Table 1 the following general considerations can be made:

(i)  $(Cp^R)_3M_3(CO)_3$  clusters crystallize in the space groups typical of most organic and organometallic molecules. The only violations are represented by CPNCRH10 which crystallizes in  $P2_1/m$  (crystallographically imposed  $m$ -symmetry is quite rare) and by CABBEM which crystallizes as acetone solvate in the highly symmetric  $P\bar{3}m$  space group.

(ii) Molecular volumes, calculated with the integration method,<sup>33</sup> show a small but significant variation along the series formed by  $Cp_3Co_3(CO)_3$  [ $291.8 \text{ \AA}^3$ ], the three clusters of formula  $Cp_3Rh_3(CO)_3$  [ $311.3, 313.6, \text{ and } 315.5 \text{ \AA}^3$  in the forms  $E_3, E_3, \text{ and } TE_2$ , respectively], and by  $Cp_3Ir_3(CO)_3$  [ $324.9 \text{ \AA}^3$ ]. The volume increases *ca.*  $33 \text{ \AA}^3$  on going from Co to Ir. These differences very likely depend both on the increase in size of the inner metal framework [M-M distances vary from 2.47 Å for M = Co to 2.68 Å for M = Ir] and on the fact the bridging CO's are more "embedded" than terminal ligands in the metal atom van der Waals spheres because of the different bonding modes.

(iii) When substituted Cp's take the place of Cp, the volume increase follows the increase in size of the Cp substituents, *viz.* the largest volume is that of  $Cp_3^*Rh_3(\mu_3-CO)(\mu_2-CO)_2$  [VENPEJ,  $560.4 \text{ \AA}^3$ ].

(iv) Packing coefficients (pc) fall in a narrow range (0.71–0.76), and the pc values for CABBEM is not reliable because the solvent coordinates are not reported in the original study; without the solvent the pc value is 0.64 which shows how the crystal must have, in comparison with the other species, voids in which acetone molecules can be accommodated.

(v) The pc value appears to be slightly higher for Cp clusters (0.73–0.76) than for clusters carrying Cp', and Cp\* (0.71–0.73).

(vi) Packing potential energy values (although based on several far from trivial approximations)<sup>34</sup> reflect the increased molecular complexity on going from Cp to Cp' and finally to Cp\*.

The patterns of intermolecular and intramolecular hydrogen bonds will now be examined. As mentioned

(33) Gavezzotti, A. *J. Am. Chem. Soc.* **1983**, *105*, 5220.

(34) Intermolecular hydrogen bonds of the C-H...O type give rise to repulsions in the partitioning of the packing energy among the atom pairs. These repulsions are, in the crystal, compensated by electrostatic terms that cannot be easily modeled. This is an additional reason to take the ppe values with great caution.

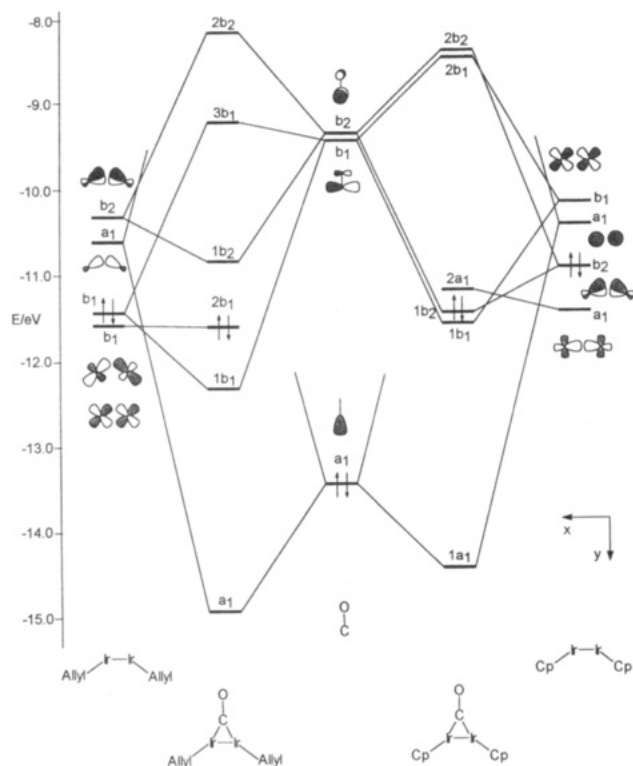


**Figure 4.** Diagram showing the relevant interactions between one bridging carbonyl and an  $(\text{allyl})_2\text{Ir}_2$  (left) or  $\text{Cp}_2\text{Ir}_2$  (right) fragment.

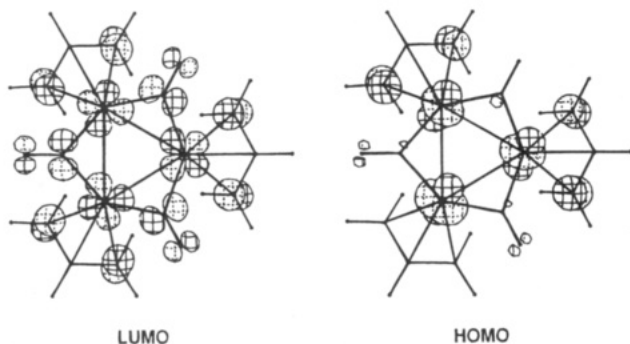


**Figure 5.** Three-dimensional representation of the HOMO (left) and the LUMO (right) of the  $(\text{ind})_3\text{Ir}_3(\text{CO})_3$  cluster.

in the Introduction, the crystal structures under examination constitute a homogeneous sample to study the effect of the change in coordination mode of the CO ligands on the C-H...O interactions. The H atoms belong either to the Cp ligand itself or to methyl substituents whereas the only acceptor groups are the carbonyl ligands. Details of the C-H...O hydrogen-bonding geometries for all the species discussed herein are listed in Table 3. In particular, donor-acceptor distances as well as H...OC distances are reported; the angles at the hydrogen atoms and at the oxygen atoms (C-H...O, and H...O-C) are also reported. The H...O-C angles should carry information on the location of the lone pair(s) on the oxygen atoms. These values can be compared with the values obtained previously from the statistical survey of intermolecular C-H...OC interactions in crystal structures present in the CSD.<sup>7</sup> In this previous study, it was shown that bridging CO ligands have a clear tendency to form shorter and more linear hydrogen bonds than do the terminal CO ligands, reflecting their higher basicity.

C-H...O bonds are also quite directional with both terminal and bridging CO's. There is a definite tendency for the CO...H angle to be around 120°, hinting that there is oxygen lone-pair density in these ketonic directions. In a number of cases, the presence of several C-H groups pointing toward a single O atom was detected.

With respect to the data listed in Table 3, the following general considerations (with the exclusion of the indenyl derivative that will be discussed later) can be made:

(i) The shortest intermolecular C-H...O separation is present in CPTCCO10, and involves the unique F ligand in the structure [C13-H13...O3, 2.30 Å; C-H-O, 177.3°; C-O...H, 133.4°]. Similarly in BIKBAY, the F ligands (there are two independent molecules in the asymmetric unit) form the shortest bonds in the whole set (C34-H34...O1, 2.43 Å, 163.8°, 149.7°; C53-H53...O4, 2.43 Å, 154.7°, 139.0°; C62-H62...O4, 2.49 Å, 174.5°, 117.9°).

(ii) IN CMNCOD and VENPEJ, which also carry F type ligands, intermolecular interactions are prevented by the intramolecular crowding around the ligand (see below).

(iii) E type CO ligands are also involved in C-H...O bonds, the shortest being observed in crystalline CPN-CRH10 (C6H5...O2, 2.38 Å; C6-C5...O2, 161.0°; H5...O2-C2, 136.0°) and FOHFOX (H14...O1, 2.36 Å; C141-H14...O1, 168.3°; H14...O1-C1, 139.9°).

(iv) The shortest interactions involving terminal ligands are observed in crystalline BEZMAU (for example: C21-H21...O(1), 2.40 Å; C13-H13...O3, 2.47 Å), which is the only species where only terminal ligands are present.

(v) Generally, the shortest intermolecular interactions involve the hydrogen atoms belonging to the C<sub>5</sub>H<sub>5</sub> ligands; it is difficult to say, however, if this is due to the difference in polarity between methyl and Cp hydrogens or to the fact the CO ligands are screened from the neighboring molecules when Cp\* or Cp' are substituted for Cp.

C-H...O hydrogen bonds are also present in the indenyl derivative  $(\text{ind})_3\text{Ir}_3(\mu_2\text{-CO})_3$ . All three bridging CO's are involved, although with some difference: O1 participates in only one interaction which is, however, the shortest in the crystal (C16-H6...O1, 2.295 Å), O2 forms two bonds of similar length (2.434 and 2.430 Å), while O3 participates in a trifurcated interaction with one short, one intermediate, and one long separation (H33...O3, 2.34, H26...O3, 2.48; H11...O3, 2.54 Å).

We will now proceed by discussing the individual crystal structures with particular attention on the relationship between complexes of the same typology.

In the crystalline complex  $\text{Cp}_3\text{Co}_3(\mu_3\text{-CO})(\mu_2\text{CO})_2$  [CPTCCO10] there are two main linkages related by the centers of inversion in the space group  $P\bar{1}$ . As shown in Figure 6, centrosymmetric pairs are formed via interactions between H(Cp) atoms and CO(F) ligands and between the H(Cp) and the CO(E) ligands. These are the shortest C-H...O bonds in CPTCCO10 and link together molecules generating a pile in the crystal structure. The third bond (which is longer) branches the packing on either sides of these molecular piles.

The rhodium complexes  $\text{Cp}_3\text{Rh}_3(\mu_2\text{-CO})_3$  (CPNCRH10),  $\text{Cp}_3\text{Rh}_3(\mu_2\text{-CO})_3\text{acetone}$  (CABBEM), and  $\text{Cp}_3\text{Rh}_3(\mu_2\text{-CO})_3$



**Table 3. Geometric Characteristics of the C-H...O Hydrogen Bond Patterns for Terminal (T), Edge-Bridging (E), and Face-Bridging (F) CO-Ligands**

formula ref code	C-H...O	C...O (Å)	H...O (Å)	C-H...O (deg)	C-O...H (deg)	
Cp <sub>3</sub> Co <sub>3</sub> (μ <sub>3</sub> -CO)(μ <sub>2</sub> -CO) <sub>2</sub> CPTCCO10	C(12)-H(12)...O(1) E	3.51	2.53	150.4	149.6	
	C(31)-H(31)...O(2) E	3.41	2.43	149.7	152.8	
	C(13)-H(13)...O(3) F	3.38	2.30	177.3	133.4	
Cp <sub>3</sub> Rh <sub>3</sub> (μ <sub>2</sub> -CO) <sub>3</sub> CPNCRH10	C(5)-H(4)...O(1) E	3.55	2.50	166.6	123.4	
	C(6)-H(5)...O(2) E	3.42	2.38	161.0	136.3	
	C(7)-H(6)...O(2) E	3.40	2.46	144.8	112.9	
	C(3)-H(3)...O(2) E	3.54	2.60	145.1	109.3	
	C(1)-H(1)...O(2) E	3.66	2.65	154.5	137.2	
Cp <sub>3</sub> Rh <sub>3</sub> (μ <sub>2</sub> -CO) <sub>3</sub> ·0.24(acetone) CABBEM	C(3)-H(3)...O(1) E	3.46	2.41	165.6	128.9	
	C(2)-H(2)...O(1) E	3.43	2.44	152.1	114.0	
Cp <sub>3</sub> Rh <sub>3</sub> (μ <sub>2</sub> -CO) <sub>2</sub> (CO) CPRHCT01	C(13)-H(1)...O(1) E	3.49	2.42	167.3	80.0	
	C(10)-H(7)...O(1) E	3.47	2.51	147.9	115.7	
	C(7)-H(4)...O(1) E	3.24	2.58	119.1	121.7	
	C(17)-H(11)...O(2) E	3.47	2.48	152.2	122.0	
	C(5)-H(2)...O(2) E	3.60	2.56	162.2	136.9	
Cp <sub>3</sub> Ir <sub>3</sub> (CO) <sub>3</sub> <sup>a</sup> BEZMAU	C(7)-H(4)...O(3) T	3.68	2.62	167.4	119.7	
	C(21)-H(21)...O(1) T	3.47	2.40	171.2	129.2	
	C(53)-H(53)...O(2) T	3.50	2.47	158.7	88.3	
	C(13)-H(13)...O(3) T	3.54	2.48	165.7	150.4	
	C(41)-H(41)...O(3) T	3.43	2.52	140.9	151.7	
intra	C(22)-H(22)...O(1)	3.26	2.48	128.3	90.1	
Cp' <sub>3</sub> Co <sub>3</sub> (μ <sub>3</sub> -CO)(μ <sub>2</sub> -CO) <sub>2</sub> <sup>a,b</sup> BIKBAY	C(34)-H(34)...O(1) F	3.48	2.43	163.8	149.7	
	C(14)-H(14)...O(1) F	3.44	2.61	132.4	134.8	
	C(15)-H(15)...O(2) E	3.22	2.58	116.9	126.7	
	C(13)-H(13)...O(3) E	3.50	2.56	144.4	98.7	
	C(23)-H(23)...O(3) E	3.59	2.61	151.2	161.1	
	1:2	C(46)-H(46)...O(2) E	3.64	2.60	161.6	100.7
	2	C(53)-H(53)...O(4) F	3.43	2.43	154.7	139.0
		C(62)-H(62)...O(4) F	3.56	2.49	174.5	117.9
		C(44)-H(44)...O(4) F	3.69	2.61	174.7	146.2
		C(43)-H(43)...O(6) E	3.57	2.51	169.4	170.6
2:1	C(26)-H(26)...O(5) E	3.47	2.54	144.6	138.6	
intra	C(36)-H(36B)...O(1)	3.01	2.40	114.1	110.2	
intra	C(16)-H(16B)...O(1)	3.27	2.52	126.2	106.5	
Cp* <sub>2</sub> Cp'Co <sub>3</sub> (μ <sub>3</sub> -CO)(μ <sub>2</sub> -CO) <sub>2</sub> CMNCOD	C(10)-H(102)...O(2) E	3.54	2.49	165.4	120.5	
	intra	C(10)-H(103)...O(1)	3.21	2.19	155.3	97.2
	intra	C(17)-H(172)...O(1)	3.19	2.38	130.4	106.6
	intra	C(6)-H(62)...O(1)	3.21	2.44	126.5	104.9
	intra	C(8)-H(83)...O(2)	3.33	2.40	142.6	99.2
	intra	C(19)-H(192)...O(2)	3.03	2.50	109.1	102.3
	intra	C(9)-H(91)...O(2)	3.22	2.53	120.9	96.8
	intra	C(7)-H(73)...O(3)	3.34	2.76	113.5	88.5
	intra	C(13)-H(13B)...O(3)	3.23	2.55	120.8	110.9
	intra					
	Cp <sub>2</sub> Cp*Co <sub>2</sub> Ir(μ <sub>2</sub> -CO) <sub>3</sub> FOHFOX	C(141)-H(14)...O(1) E	3.42	2.36	168.3	139.9
C(8)-H(83)...O(2) E		3.23	2.54	120.9	115.4	
C(11)-H(1)...O(3) E		3.56	2.50	165.8	120.1	
(indenyl) <sub>3</sub> Ir(μ <sub>2</sub> -CO) <sub>3</sub> <sup>c</sup>	C(16)-H(16)...O(1) E	3.29	2.30	151.9	110.9	
	C(25)-H(25)...O(2) E	3.43	2.43	153.4	132.5	
	C(36)-H(36)...O(2) E	3.26	2.43	132.5	146.5	
	C(33)-H(33)...O(3) E	3.40	2.34	166.5	118.2	
	C(26)-H(26)...O(3) E	3.55	2.48	174.0	121.8	
	C(11)-H(11)...O(3) E	3.60	2.54	167.8	117.5	

<sup>a</sup> Hydrogens added in calculated positions. <sup>b</sup> Two independent molecules (1,2). <sup>c</sup> Not yet in CSD.

CO)<sub>2</sub>(CO) (CPRHCT01) will now be discussed. The key packing pattern for the two isostructural species (CP-

NCRH10 and CABBEM) is identical in the two crystals: the molecules pile along the shortest cell axis,

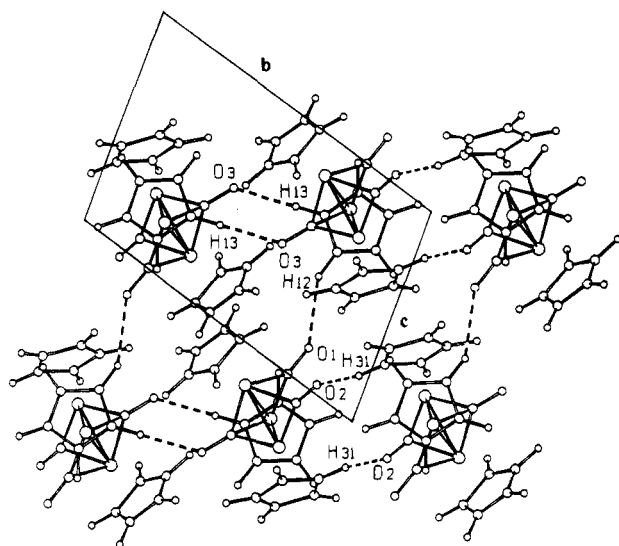


**Figure 6.** The C-H...O interactions in crystalline  $\text{Cp}_3\text{Co}_3(\mu_3\text{-CO})(\mu_2\text{-CO})_2$  [CPTCCO10]: centrosymmetric pairs are formed *via* interactions between H(Cp) atoms and CO(F) ligands and between the H(Cp) and the CO(E) ligands.

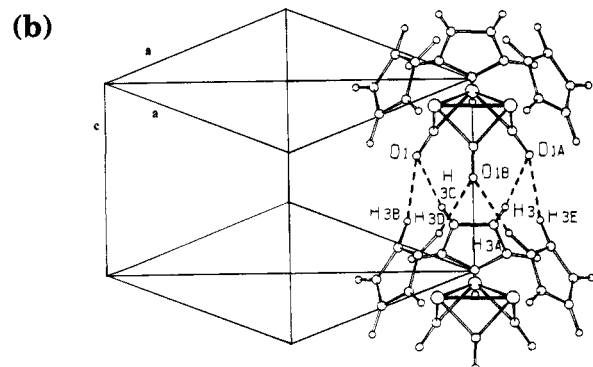
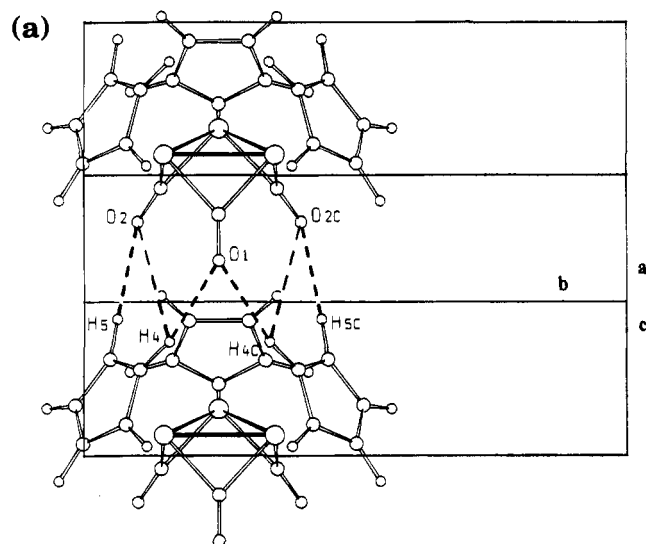


**Figure 7.** Packing with cell axes for CPNCRH10 (a) and for CABBEM (b): the molecules pile along the shortest cell axis (*c* axis) and are linked by bifurcated C-H...O(CO) interactions.

linked by bifurcated C-H...O(CO) interactions as shown in Figure 7a,b. Note that the two species present a different number of independent hydrogen bonds; this is due to the different site symmetries (a mirror plane

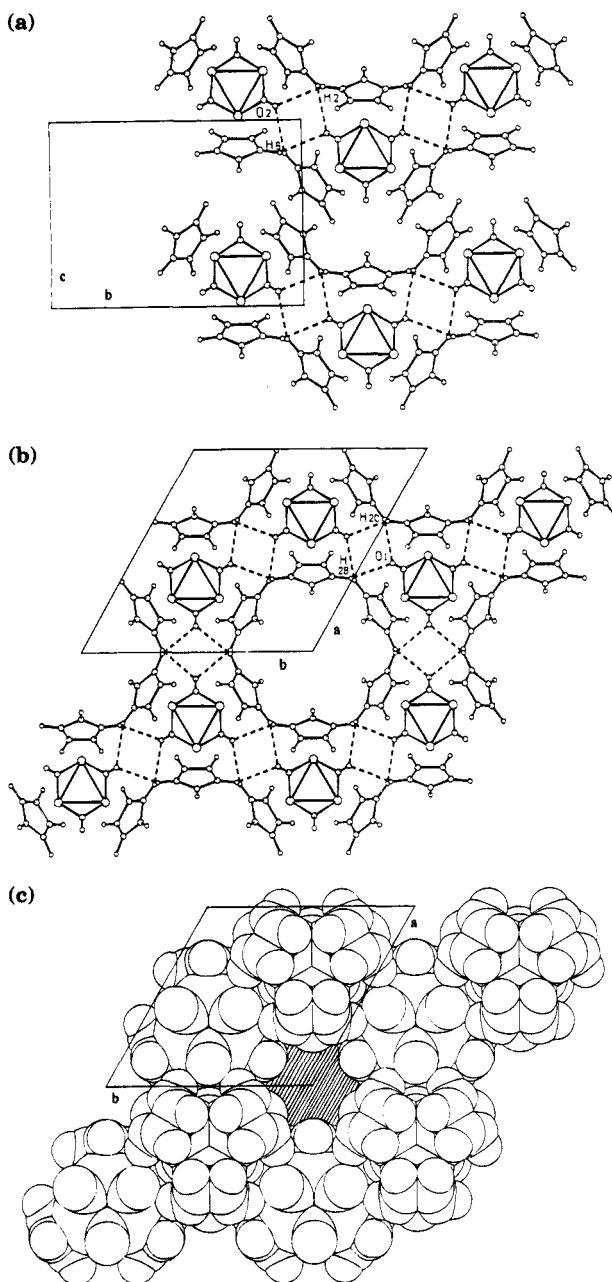


**Figure 8.** Packing arrangement along the *c* axis in CPNCRH10 (a) and in CABBEM (b): in both these crystals the molecular piles shown in Figure 7 are linked *via* CH...O bonds; (c) space-filling representation of CABBEM showing the van der Waals width of the channel occupied by the disordered acetone molecules.

for CPNCRH10 and a 3-fold axis for CABBEM). In both these crystals there are additional pile-to-pile links so that the two crystals can be described as formed by rods of molecules interacting in van der Waals fashion, with additional stabilization arising from CH...O bonds. Projections of the packing arrangements are shown in Figure 8a-c. Interestingly, the *same molecule*  $[(\text{Cp})_3\text{Rh}_3(\text{CO})_3]$  achieves a 12% less efficient volume occupation in CABBEM than in CPNCRH10. The voids in CABBEM are partially filled by disordered acetone molecules. These molecules are very likely trapped in the crystal structure of CABBEM at nucleation stage *via* the same type of weak C-H...O interactions that stabilize the crystal structures discussed thus far. In considering crystallization processes, however, a word

of caution is in order. One should always keep in mind that the formation of a crystal is a process of free energy minimization; therefore entropy terms take part in the process. Kinetic aspects arising from the different type of crystallization conditions must also be considered. The interplay between thermodynamics and kinetics is (as usual) difficult to assess.

As discussed above, the rhodium complex is known in the solid in two isomeric forms:  $\text{Cp}_3\text{Rh}_3(\mu_2\text{-CO})_3$  (CPNCRH10) and  $\text{Cp}_3\text{Rh}_3(\mu_2\text{-CO})_2(\text{CO})$  (CPRHCT01). The few examples of flexible cluster molecules known to crystallize in different isomeric forms were discussed in the Introduction. In all those cases the energy difference between the isomers is sufficiently small to the point that less stable isomers can be isolated in crystalline forms because crystal packing interactions afford the necessary additional stabilization. Interestingly, the comparative analysis of the data grouped in Tables 1 and 2 for these two species shows that the difference in stability between the two molecular isomers is related to the difference in cohesion between the two crystal isomers. The  $E_3$  isomer (CPNCRH10), which is more stable in terms of molecular structure than the  $E_2T$  isomer (CPRHCT01) [0.588 eV (13.56 kcal mol<sup>-1</sup>) versus 0.883 eV (20.36 kcal mol<sup>-1</sup>) over the reference  $\text{FE}_2$  isomer] forms a less cohesive crystal structure than this latter isomer (-64.7 versus -68.1 kcal mol<sup>-1</sup>). The energy differences between the isolated molecules and the respective crystals are much more trustworthy than the actual values, thus indicating that CPNCRH10 and CPRHCT01 may well represent a case in which crystal cohesion compensates for the loss of *internal* energy. For reasons given above CABEM cannot be compared with CPNCRH10 and CPRHCT01.

The second isomeric form of  $\text{Cp}_3\text{Rh}_3(\mu_2\text{-CO})_2(\text{CO})$  (CPRHCT01) contains two edge-bridging and one terminal ligand. The edge-bridging ligands are involved in an intricate network of H bonds, with both O1 and O2 (see Table 3) forming interactions as short as 2.42 Å, whereas the terminal ligand forms a longer interaction (2.62 Å). Both O1 and O2 are involved in bifurcated interactions. At this stage one may object that, on comparing the crystal stability of CPRHCT01 and CPNCRH10, C-H...O interactions are neglected. While this is correct, the contribution to cohesion of these interactions is likely to be small (against a difference of ca. 10% in van der Waals energy).

In crystalline  $\text{Cp}_3\text{Ir}_3(\text{CO})_3$  (BEZMAU) only T type CO ligands are present, the three CO's participate in the network shown in Figure 9. The H...O distances fall toward the lower limits between 2.40 and 2.52 Å, with the oxygen atom O3 involved in a bifurcated interaction toward two different Cp's of the same molecule.

The molecular arrangement in crystalline  $\text{Cp}'_3\text{Co}_3(\mu_3\text{-CO})(\mu_2\text{-CO})_2$  (BIKBAY) is complicated by the presence of two independent molecules in the asymmetric unit. Both molecules carry F and E type CO ligands. As discussed above the shortest interactions involve the facial CO's. The methyl group present on one Cp ligand participates in intramolecular interactions. From the data collected in Table 3 it is apparent that both F ligands form trifurcated interactions: O1 forms two inter- and one intramolecular interactions, whereas O4 forms only intermolecular bonds. We will see in the

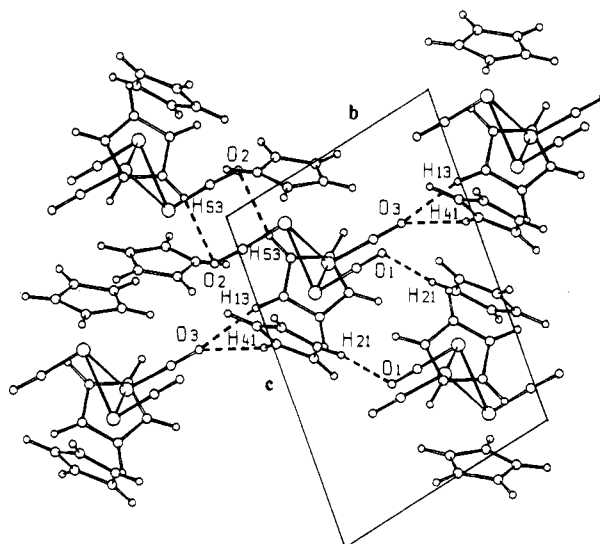


**Figure 9.** The network of C-H...O interactions formed by the terminal ligands in crystalline  $\text{Cp}_3\text{Ir}_3(\text{CO})_3$  (BEZMAU).

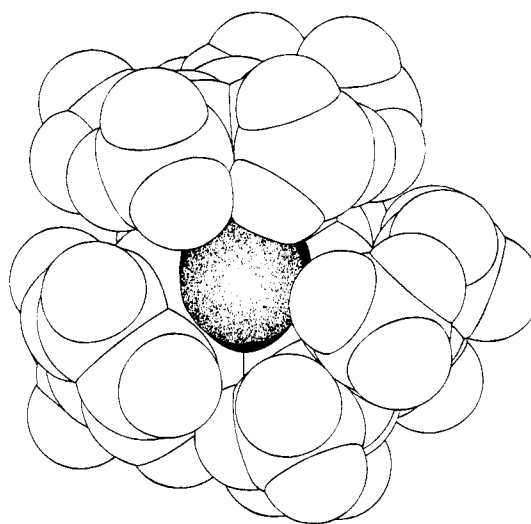


**Figure 10.** The environment around the unique F type CO ligand in  $\text{Cp}^*_2\text{Cp}'\text{Co}_3(\mu_3\text{-CO})(\mu_2\text{-CO})_2$  (CMNCOD). Note how the CO ligand is screened from the surroundings and cannot participate in intermolecular H bonding.

following that, as the complexity of the Cp ligand increases on increasing the number of substituents, the intermolecular H bonding will progressively give way to intramolecular interactions.

Steric crowding is observed in crystalline  $\text{Cp}^*_2\text{Cp}'\text{Co}_3(\mu_3\text{-CO})(\mu_2\text{-CO})_2$  (CMNCOD) and  $\text{Cp}^*_3\text{Rh}_3(\mu_3\text{-CO})(\mu_2\text{-CO})_2$  (VENPEJ), which carry two Cp\* and one Cp', and three Cp\* ligands, respectively. As a matter of fact, no intermolecular CH...O interactions are present in the latter crystal, while only one hydrogen bond is observed in the former (C10-H102...O2, 2.49 Å). In both systems, on the other hand, many short intramolecular H...O separations are seen (Table 3). We have analyzed the steric effect by drawing space-filling representations of these molecules. Figure 10 shows the environment of the unique F type CO ligand in CMNCOD. It can be easily appreciated how the CO ligand is completely embedded in a sheath of methyl groups and cannot protrude from the surface of the complex. A similar situation is observed in crystalline VENPEJ.

The participation of methyl H atoms to intermolecular hydrogen bonds is seen in crystalline  $\text{Cp}_2\text{Cp}^*\text{Co}_2\text{Ir}(\mu_2\text{-CO})_3$  (FOHFOX), which contains only E type CO ligands bound to the heterometallic  $\text{Co}_2\text{Ir}$  cluster. The two shortest interactions (C14-H14...O1 and C11-H1...O3, 2.36 and 2.50 Å) involve H atoms belonging to Cp ligands, while the interaction C8...H83...O2 (2.54 Å) involves a methyl atom. It should be kept in mind, however, that, contrary to  $\text{sp}^2$  atoms, the geometric positioning of methyl hydrogens is not unambiguous so that the C-H...O may be shorter than actually observed.

### Conclusions

In this paper we have focused our attention on the molecular and crystal isomers formed by carbonyl-cyclopentadienyl clusters of the type  $\text{Cp}_3\text{M}_3(\text{CO})_3$ . The isomeric forms differ at the molecular level mainly for the number and type of CO bridges in the structure. Only iridium favors the all-terminal structure. We have shown, using appropriate simple models, that there is a type of interaction responsible for the fact that bridging ligands are avoided in the iridium case. The metal to carbonyl back-donation component of the bonding involves an initially empty metal-metal antibonding orbital. Its partial occupancy leads to such a weakening of the Ir-Ir bond that other structures become more favored. For lighter metals, having more contracted orbitals, this effect is less important and bridges prevail.

The indenyl iridium derivative belongs to a different cluster type, and its bonding follows another pattern. The previously referred repulsive interaction is absent, and the structure with bridges is the one observed.

In terms of intermolecular interactions and crystal packing the systems investigated in this work have the following characteristics:

(i) The molecules are neutral and form van der Waals type crystals in which high-volume occupation is generally achieved, as well as high cohesion.

(ii) Exceptional to this behavior is crystalline CABBEM which possesses a low packing coefficient with the molecules occupying a 3-fold symmetry site, and solvent molecules are trapped in the crystal structure to fill in the voids and raise the energy of cohesion.

(iii) CABBEM and CPNCRH10 represent *pseudopolymorphs* of the same material ("pseudo" because of the solvent trapped in the crystal edifice), whereas CPRHCT-01 represents an isomeric modification of CABBEM and CPNCRH10, and its crystal represents a case of crystal isomer.

(iv) The difference in stability between the two isomers  $\text{Cp}_3\text{Rh}_3(\mu_2\text{-CO})_3$  (CPNCRH10) and  $\text{Cp}_3\text{Rh}_3(\mu_2\text{-CO})_2(\text{CO})$  (CPRHCT01) is related to the difference in cohesion between the respective crystal structures. Although the actual ppe values and relative molecular energies have to be taken with great caution, because of the approximation inherent to the application of extended Hückel and packing energy calculations to complex organometallic systems, it is encouraging that there is consistency between molecular and crystal relative stability, *viz.* the least stable isomer crystallizes in the most stable crystal form and vice versa.

(v) CO ligands form intramolecular and intermolecular hydrogen bonds of the C-H...O type, these are clearly detected from the H...O distances.

(vi) The length of the C-H...O interactions follows roughly the trend F type CO > E type CO > T type CO, which is the well-known trend of decreasing basicity of the CO ligand.

(vii) The indenyl derivative is exceptional, in this respect, since the C-H...O distance is very short (2.30 Å) and comparable to the distances attained by F ligands.

(ix) If large  $\text{Cp}^*$  ligands are substituted for the smaller Cp ligands, the CO ligands bound to the metal atoms become segregated within the organic sheath and can no longer form intermolecular H bonds.

(x) In these cases, however, the CO ligands establish intramolecular interactions with the surrounding methyl groups.

These results represent, in our opinion, a (small) step ahead in the understanding of the relationship between the structure of the isolated (gas-phase) molecule and that of an ensemble of such molecules. The information on the interplay between size of the cyclopentadienyl ligand, type of coordination of the CO ligands, and the network of intermolecular and intramolecular interactions that can be established in the solid state are useful in the engineering of molecules which are able to participate in predictable intermolecular assemblies.<sup>35</sup> Apart from this general outcome, we have provided further evidence, based on a small, though consistent, set of molecular systems of the participation of CO ligands in intermolecular hydrogen bonds. These bonds become particularly important in organometallic cluster systems because of the large number of CO ligands and of the large number of hydrogen atoms present on the organic ligands.

### Methodology

All the molecular orbital calculations were done using the extended Hückel method<sup>11</sup> with modified  $H_{ij}$ 's.<sup>36</sup> The basis set for the metal atoms consisted of  $ns$ ,  $np$  and  $(n-1)d$  orbitals. The  $s$  and  $p$  orbitals were described by single Slater type wave functions, and the  $d$  orbitals were taken as contracted linear combinations of two Slater type wave functions. Standard parameters were used for C, O, and H, while those for the metals were as follows ( $H_{ij}/\text{eV}$ ,  $\zeta$ ): Co, 4s, -5.29, 2.1; 4p, -5.29, 2.1; 3d, -13.18, 5.55, 2.1 ( $\zeta_2$ ), 0.5679 ( $c_1$ ), 0.6059 ( $c_2$ ). Rh, 5s, -8.09, 2.135; 5p, -4.57, 2.1; 4d, -12.50, 5.542, 2.39 ( $\zeta_2$ ), 0.5823 ( $c_1$ ), 0.6405 ( $c_2$ ). Ir, 6s, -11.3, 2.504; 6p, -4.5, 2.2; 5d, -12.1, 5.796, 2.557 ( $\zeta_2$ ), 0.6351 ( $c_1$ ), 0.5556 ( $c_2$ ). Three-dimensional representations of orbitals were drawn using the program CACAO.<sup>37</sup>

In all calculations idealized models were used, based on the experimentally observed structures. The following distances (Å) were used: Co-Co, 2.45, Rh-Rh and Ir-Ir, 2.65, M-C(bridging carbonyl), 2.0, M-C(terminal carbonyl), 1.8 (M = Co, Rh, Ir), Co-Cp(centroid), 1.75, M'-Cp(centroid), 2.0 (M' = Rh, Ir), C-O (bridging carbonyl), 1.18, C-O (terminal carbonyl), 1.15, Ir-C(allyl), 2.2, C-C, 1.4, and C-H, 1.08 Å. The bond angles of the ligands relative to the  $M_3$  plane were optimized. The definitions are pictured in Chart 2. Thus,  $\alpha$  is the angle between the bridging CO bond and the  $M_3$  plane,  $\beta$  is the angle between the normal to the Cp ring and the  $M_3$  plane, and  $\gamma$  measures the "sideways" deviation of each M-Cp

(35) (a) Desiraju, G. R. *Crystal Engineering, The Design of Organic Solids*; Elsevier: Amsterdam, 1989; p 47. (b) *Inorganic Materials*; Bruce, D. W., O'Hare, D., Eds.; John Wiley & Sons: Chichester. U.K., 1992.

(36) Ammeter, J. H.; Bürgi, H.-B.; Thibault, J. C.; Hoffmann, R. *J. Am. Chem. Soc.* **1978**, *100*, 3686.

(37) Mealli, C.; Proserpio, D. M. *J. Chem. Ed.* **1990**, *67*, 39.

Chart 2

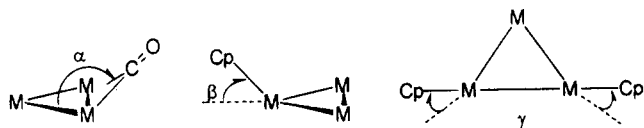


Table 4

	structures					
	$\text{Cp}_3\text{M}_3(\text{CO})_3$				$(\text{allyl})_3\text{Ir}_3(\text{CO})_3$	
	$\text{FE}_2$	$\text{TE}_2$	$\text{E}_3$	$\text{T}_3$	$\text{E}_3$	$\text{T}_3$
$\alpha/\text{deg}$	121.0	103.0	126.0	90.0	132.0	90.0
$\beta/\text{deg}$	15.0	42.0	30.0	36.0	56.0	62.0
$\gamma/\text{deg}$	15.0	21.0	0.0	0.0	0.0	0.0

bond around the symmetry unequivalent bond of the  $\text{M}_3$  triangle. The optimized values are compiled in Table 4.

Crystal structure analysis was carried out with the aid of the computer program OPEC,<sup>38</sup> which allows, within the atom-atom potential energy method, the calculation of packing potential energies as well as molecular volumes and packing coefficients. The molecular volumes were estimated by the integration method. The light atoms were attributed van der Waals radii available in the literature, while the cobalt, rhodium, and iridium atoms were attributed radii of 2.15, 2.35, and 2.35 Å, respectively.<sup>39</sup> The values of the molecular volumes were in turn used to calculate the packing

(38) (a) Gavezzotti, A. *OPEC: Organic Packing Potential Energy Calculations*; University of Milano: Milan, Italy.

coefficients by means of the expression  $pc = V_{\text{mol}}Z/V_{\text{cell}}$ . A Buckingham type potential energy function was used to estimate the cohesive energy of the crystalline species under investigation. The C, O, and H atoms were given the generalized potential parameters put forward by Gavezzotti and Filippini, while the Co, Rh, and Ir atoms were treated as Kr and Ar atoms.<sup>40</sup> The geometric features of the intermolecular and intramolecular hydrogen-bonding networks were investigated by using the graphic program SCHAKAL92<sup>41a</sup> and the suite of programs PLATON.<sup>41b</sup> Atomic coordinates and crystal data were obtained from the Cambridge Structural Database. The available coordinates for the hydrogen atoms were normalized by extending the C-H distances along the C-H vectors to the typical neutron-derived value of 1.08 Å.<sup>42</sup>

**Acknowledgment.** D.B., F.G., M.J.C., and L.F.V. acknowledge the CNR (Italy) and the JNICT (Portugal) for joint financial support; D.B., F.G., H.W., and S.G. thank the Deutscher Akademischer Austauschdienst, Bonn, Germany, and the Conferenza Nazionale dei Rettori, Roma, Italy, for a scientific exchange grant within the Programme Vigoni.

OM9504112

(39) (a) Bondi, A. *J. Phys. Chem.* **1964**, *68*, 441. (b) Gavezzotti, A. *Nouv. J. Chim.* **1982**, *6*, 443.

(40) Gavezzotti, A.; Filippini, G. *Acta Crystallogr., Sect. B* **1993**, *49*, 868.

(41) (a) Keller, E. *SCHAKAL92*; University of Freiburg: Freiburg, Germany, 1992. (b) Spek, A. L. *PLATON; Acta Crystallogr., Sect. A* **1990**, *46*, C31.

(42) Murray-Rust, P.; Glusker, J. P. *J. Am. Chem. Soc.* **1984**, *106*, 1018.

# Preparation of Carbosilane Dendrimers with Peripheral Acetylenedicobalt Hexacarbonyl Substituents<sup>†</sup>

Dietmar Seyferth\* and Tsuyoshi Kugita

Department of Chemistry, Massachusetts Institute of Technology,  
Cambridge, Massachusetts 02139

Arnold L. Rheingold and Glenn P. A. Yap

Department of Chemistry, University of Delaware, Newark, Delaware 19716

Received August 25, 1995<sup>®</sup>

The carbosilane dendrimers  $\text{Si}[\text{CH}_2\text{CH}_2\text{SiMe}_2\text{C}\equiv\text{CH}]_4$ , **1**,  $\text{Si}[\text{CH}_2\text{CH}_2\text{SiMe}(\text{C}\equiv\text{CH})_2]_4$ , **2**, and  $\text{Si}[\text{CH}_2\text{CH}_2\text{Si}(\text{CH}_2\text{CH}_2\text{SiMe}_2\text{C}\equiv\text{CH})_3]_4$ , **5**, have been prepared. Reaction of  $\text{Co}_2(\text{CO})_8$  with all the  $\text{C}\equiv\text{CH}$  groups in **1** and **5** gave the corresponding acetylenedicobalt hexacarbonyl complexes. The structure of  $\text{Si}[\text{CH}_2\text{CH}_2\text{SiMe}_2\text{-C}_2\text{HC}_2\text{O}_2(\text{CO})_6]_4$  was determined in an X-ray diffraction study.

## Introduction

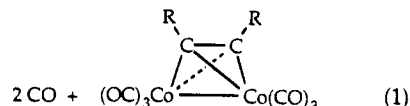
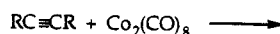
The availability of carbosilane dendrimers that have reactive peripheral groups such as  $\text{Si}-\text{Cl}$ ,  $\text{Si}-\text{H}$ ,  $\text{Si}-\text{CH}=\text{CH}_2$  and  $\text{Si}-\text{CH}_2\text{CH}=\text{CH}_2$ <sup>1</sup> offers the opportunity of introducing, through appropriate chemistry, many other interesting and potentially useful inorganic, organic, and organometallic substituents.<sup>2</sup> In a continuation of our work in this area, we have prepared small (first- and second-generation) dendrimers that contain peripheral ethynyl groups. In view of the high reactivity of the  $\text{C}\equiv\text{CH}$  group, these new dendrimers offer many different opportunities for further functionalization of the periphery. We report here the reactions of these new dendrimers with  $\text{Co}_2(\text{CO})_8$ .

## Results and Discussion

The preparative methodology used in the present carbosilane dendrimer syntheses followed that described in our previous report<sup>1a</sup> (Scheme 1). Starting with tetravinylsilane as the initiator core molecule, hydrosilylation with  $\text{Me}_2\text{SiHCl}$ , followed by treatment of the resulting adduct with  $\text{HC}\equiv\text{CMgBr}$  gave the first generation product **1**. Alternatively, hydrosilylation with  $\text{MeSiHCl}_2$  followed by reaction with  $\text{HC}\equiv\text{CMgBr}$  gave **2**, which contains eight ethynyl groups. To obtain a second-generation dendrimer containing 12 ethynyl groups, **5**, the growth sequence tetravinylsilane, hydrosilylation with  $\text{HSiCl}_3$ , vinylation with  $\text{CH}_2=\text{CHMgBr}$ ,

hydrosilylation with  $\text{Me}_2\text{SiHCl}$  and ethynylation with  $\text{HC}\equiv\text{CMgBr}$  was used. Dendrimers **1**, **2**, and **5** were purified by column chromatography and were isolated as analytically pure, white solids in moderate yield. Their IR and <sup>1</sup>H and <sup>13</sup>C NMR spectra showed the  $\text{C}\equiv\text{CH}$  groups to be present.

Among the many conversions of the  $\text{C}\equiv\text{C}$  bond is its reaction with dicobalt octacarbonyl to form a  $\text{C}_2\text{Co}_2$  tetrahedrane cluster, the acetylenedicobalt hexacarbonyl complex (eq 1).<sup>3</sup> In view of reactions that such



complexes are known to undergo,<sup>3</sup> dendrimers containing such substituents at the end of each arm seemed a worthwhile goal.

The reactions of the carbosilane dendrimers that contain ethynyl groups at the periphery with  $\text{Co}_2(\text{CO})_8$  proceed readily and completely, provided that the terminal silicon atom on each arm is substituted with only one ethynyl group (Scheme 2). Thus, 1 molar equiv of dendrimer **1** reacted with 4 molar equiv of  $\text{Co}_2(\text{CO})_8$  in petroleum ether (bp 40–69 °C) during 24 h at room temperature to give, after filtration through Celite and removal of solvent, a dark red solid. Purification of the latter by column chromatography (silica gel/hexane) gave dendrimer **5** (84% yield) as dark red crystals. Crystals suitable for study by X-ray diffraction were obtained. The structure is shown in Figure 1; it clearly shows the presence of four acetylenedicobalt hexacarbonyl units in the molecule. The observed  $\text{C}_2\text{Co}_2$  cluster bond distances ( $d_{\text{av}}(\text{Co}-\text{Co}) = 2.485(3) \text{ \AA}$ ;  $d_{\text{av}}(\text{C}-\text{C}) = 1.32(2) \text{ \AA}$ ;  $d_{\text{av}}(\text{C}-\text{Co})$  (within one of the clusters) =  $1.95(2) \text{ \AA}$ ) fall within the limits reported for other acetylenedicobalt hexacarbonyl complexes.<sup>3b</sup>

(3) (a) Hübel, W. In *Organic Syntheses via Metal Carbonyls*; Wender, I., Pino, P., Eds.; Interscience: New York, 1968; Vol. 1, pp 299–304. (b) Dickson, R. S.; Fraser, P. J. *Adv. Organomet. Chem.* **1974**, *12*, 323. (c) Nicholas, K. M.; Nestle, M. O.; Seyferth, D. In *Transition Metal Organometallics in Organic Synthesis*; Alper, H., Ed.; Academic: New York, 1978; Vol. 2, pp 2–63.

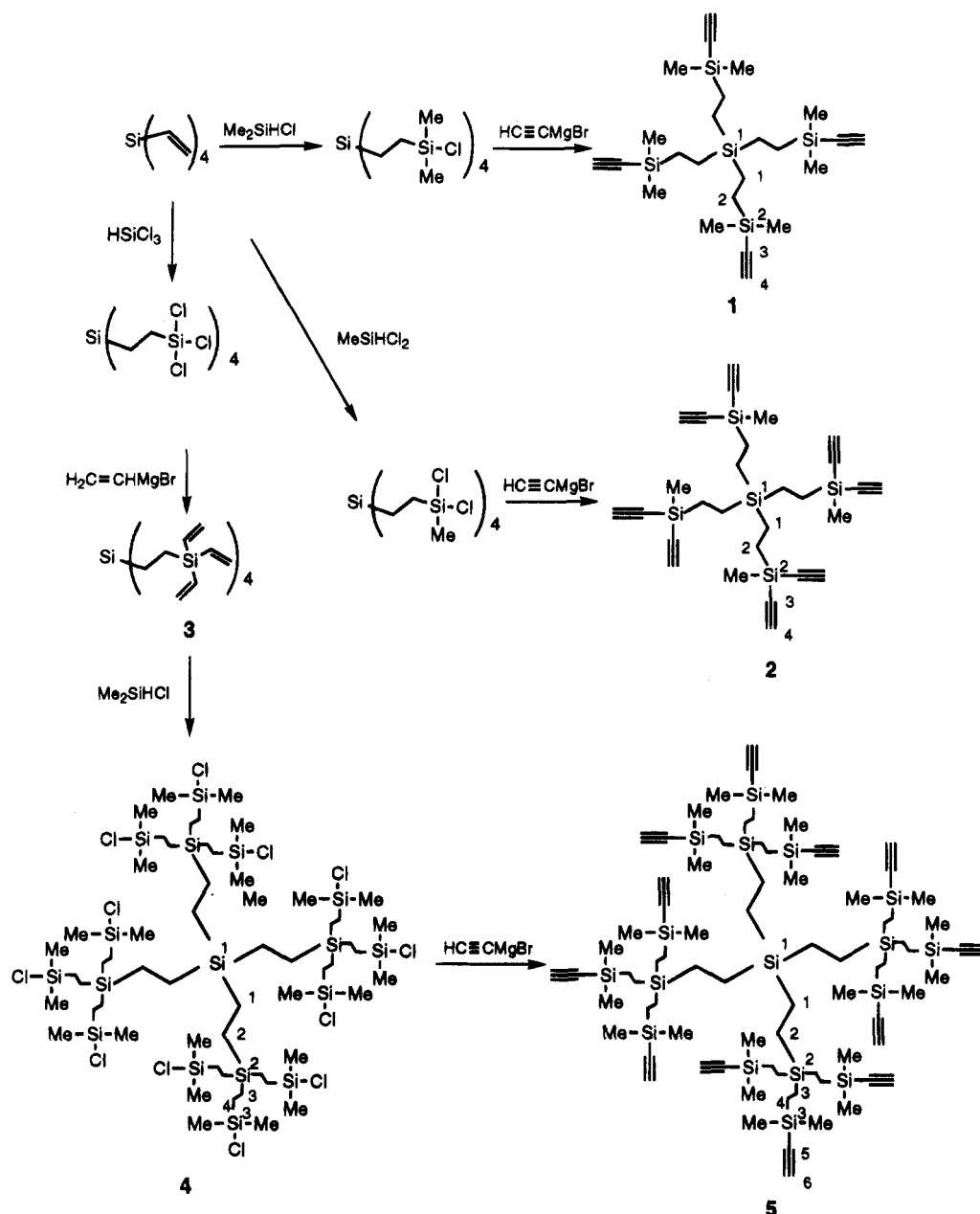
<sup>†</sup> Dedicated to Professor Herbert Schumann on the occasion of his 60th birthday.

<sup>®</sup> Abstract published in *Advance ACS Abstracts*, October 15, 1995.

(1) (a) Seyferth, D.; Son, D. Y.; Rheingold, A. L.; Ostrander, R. L. *Organometallics* **1994**, *13*, 2682. (b) van der Made, A. W.; van Leeuwen, P. W. N. M. *J. Chem. Soc., Chem. Commun.* **1992**, 1400. (c) Roovers, J.; Toporowski, P. M.; Zhou, L.-L. *Polym. Prepr. (Am. Chem. Soc., Div. Polym. Chem.)* **1992**, *33*, 182. (d) Zhou, L.-L.; Roovers, J. *Macromolecules*, **1993**, *26*, 963. (e) Roovers, J.; Zhou, L.-L.; Toporowski, P. M.; van der Zwan, M.; Iatrou, H.; Hadjichristidis, N. *Macromolecules* **1993**, *26*, 4324. (f) van der Made, A. W.; van Leeuwen, P. W. N. M. de Wilde, J. C.; Brandes, R. A. C. *Adv. Mater.* **1993**, *5*, 466. (g) Hadjichristidis, N.; Guyot, A.; L. Fetters, J. *Macromolecules* **1978**, *11*, 668.

(2) (a) Knapen, J. W. L.; van der Made, A. W.; de Wilde, J. C.; van Leeuwen, P. W. N. M.; Wijkens, R.; Grove, D. M.; van Koten, G. *Nature* **1994**, *372*, 659. (b) Alonso, B.; Cuadrado, I.; Morán, M.; Losada, J. *J. Chem. Soc., Chem. Commun.* **1994**, 2575. (c) Lorenz, K.; Mülhaupt, R.; Frey, H.; Rapp, U.; Mayer-Posner, F. *J. Macromolecules* **1995**, *28*, 6657.

Scheme 1



A similar reaction of 1 molar equiv of dendrimer 4 with 12 molar equiv of  $\text{Co}_2(\text{CO})_8$  using the same workup gave dendrimer 6 as a dark red solid, mp (decomp) ca.  $50^\circ\text{C}$ , in 98% yield. An analytical sample was obtained by recrystallization from pentane.

The reaction of  $\text{Co}_2(\text{CO})_8$  with carbosilane dendrimer 2, with two ethynyl substituents on each peripheral silicon atom, was accompanied by vigorous gas evolution and apparent decomposition. An organocobalt product could not be isolated. Very likely, the formation of two acetylenedicobalt hexacarbonyl substituents on a silicon atom is prevented by steric factors and the reaction takes another course.

When one considers the many reactions that the  $\text{C}\equiv\text{CH}$  (and substituted  $\text{C}\equiv\text{CR}$ ) groups can undergo,<sup>4</sup> it is clear that carbosilane dendrimers 1, 2, and 4, as well as later  $\text{Si}-\text{C}\equiv\text{CH}$ - and  $\text{Si}-\text{C}\equiv\text{CR}$ -terminated

generations, offer many opportunities for the functionalization of the periphery of carbosilane dendrimers. Our efforts in this direction are continuing.

### Experimental Section

**General Comments.** All reactions were carried out under an atmosphere of argon or prepurified nitrogen. Solvents were purified by standard procedures. NMR spectra were measured using samples in  $\text{CDCl}_3$  solution:  $^1\text{H}$  NMR spectra at 299.937 MHz,  $^{13}\text{C}$  NMR spectra at 75.427 MHz, and  $^{29}\text{Si}$  NMR spectra at 59.590 MHz. The Karstedt platinum catalyst was purchased from Hüls America as a 5% solution in xylene. Dicobalt octacarbonyl was purchased from Strem Chemical Company,  $\text{HC}\equiv\text{CMgBr}$  as a 0.5 M solution in THF from Aldrich Chemical Co. Elemental analyses were performed by the Scandinavian Microanalytical Laboratory, Herlev, Denmark.

**Crystallographic Studies.** Crystal, data collection, and refinement parameters are given in Table 1. A suitable crystal for single-crystal X-ray diffraction was selected and mounted within a nitrogen-flushed glass capillary. The unit-cell pa-

(4) Jäger, V.; Viehe, H. G. In *Houben-Weyl Methoden der Organischen Chemie*, 4th ed.; Müller, E., Ed.; Georg Thieme Verlag: Stuttgart, 1977; Vol. 5, Part 2a, pp 677-912.



Table 1. Crystallographic Data for 1

(a) Crystal Parameters			
formula	C <sub>46</sub> H <sub>44</sub> Co <sub>8</sub> O <sub>24</sub> Si <sub>5</sub>	$\gamma$ , deg	84.237(4)
fw	1616.72	$V$ , Å <sup>3</sup>	3458(4)
cryst syst	triclinic	$Z$	2
space group	$P\bar{1}$	cryst dimens, mm <sup>3</sup>	0.40 × 0.10 × 0.23
$a$ , Å	9.427(6)	cryst color	red
$b$ , Å	14.462(7)	$D$ (calcd), g cm <sup>-3</sup>	1.553
$c$ , Å	25.85(2)	$\mu$ (Mo K $\alpha$ ), cm <sup>-1</sup>	20.24
$\alpha$ , deg	89.97(6)	temp, K	296
$\beta$ , deg	80.49(5)	$T$ (max)/ $T$ (min)	1.98
(b) Data Collection			
diffractometer	Siemens P4	no. of reflns colld	7697
monochromator	graphite	no. of indpt reflns	7494
radiation	Mo K $\alpha$ ( $\lambda$ = 0.710 73 Å)	no. of indpt obsd	3992
$2\theta$ scan range, deg	4.0–42.0	reflns $F_o \geq 4\sigma(F_o)$	
(c) Refinement <sup>a</sup>			
$R(F)$ , %	8.31	$\Delta(\rho)$ , e Å <sup>-3</sup>	0.7
$R(wF^2)$ , %	22.18	$N_o/N_v$	9.8
$\Delta/\sigma$ (max)	0.0	GOF	1.08

<sup>a</sup> Quantity minimized =  $\sum[w(F_o^2 - F_c^2)^2]/\sum[(wF_o^2)^2]^{1/2}$ ;  $R = \sum|\Delta|/\sum(F_o)$ ;  $R(w) = \sum\Delta w^{1/2}/\sum(F_o w^{1/2})$ ,  $\Delta = |F_o - F_c|$ .

Scheme 2

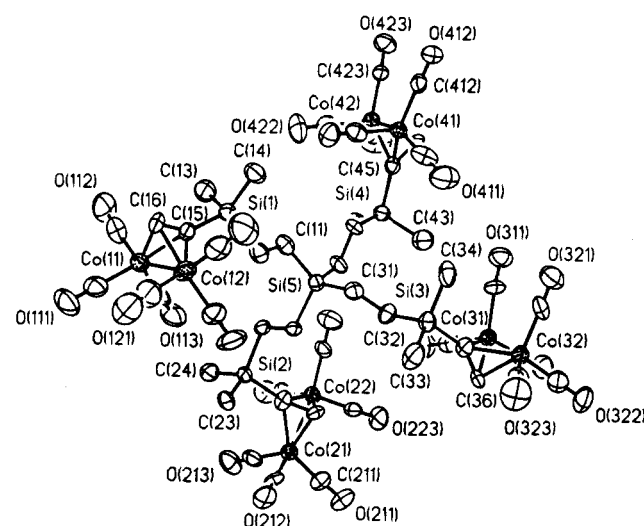
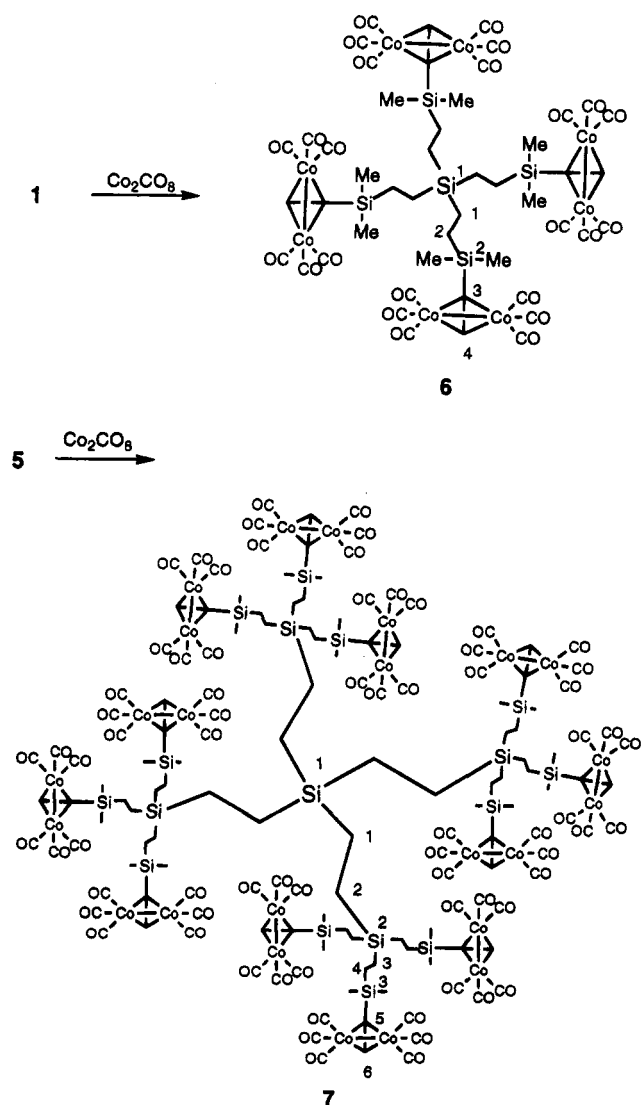


Figure 1. ORTEP diagram of dendrimer 6 showing 40% probability ellipsoids.

ally reasonable results of refinement. Semiempirical ellipsoid absorption corrections were applied to the data set. The structure was solved by direct methods, completed by subsequent difference Fourier syntheses, and refined by full-matrix least-squares procedures. All non-hydrogen atoms were refined with anisotropic displacement parameters. Hydrogen atoms were treated as idealized contributions. Atomic coordinates are given in Table 2.

All software and sources of the scattering factors are contained in the SHELXTL (5.1) program libraries (G. Sheldrick, Siemens XRD, Madison, WI).

**Preparation of Dendrimer 1.** A 50 mL round-bottomed flask equipped with a magnetic stir bar and a rubber septum was charged with 2.0 g (14.7 mmol) of  $(\text{CH}_2=\text{CH})_4\text{Si}$ , 8.8 g (93 mmol) of  $\text{Me}_2\text{SiHCl}$ , 20 mL of THF, and 3 drops of the Karstedt catalyst solution. The reaction mixture was stirred and heated slowly to reflux. Heating was stopped when reflux was observed, and the mixture was stirred for 30 min at room temperature and, subsequently, for 4 h at 50 °C. Volatile components were removed at reduced pressure, leaving 7 g (93%) of  $\text{Si}(\text{CH}_2\text{CH}_2\text{SiMe}_2\text{Cl})_4$ . <sup>1</sup>H NMR:  $\delta$  0.39 (s, 24 H,  $\text{CH}_3$ -Si), 0.61 (m, 16 H,  $\text{CH}_2\text{CH}_2$ ). <sup>13</sup>C NMR:  $\delta$  0.80 ( $\text{CH}_3$ ), 1.81 ( $\text{coreSiCH}_2\text{CH}_2\text{Si}$ ), 11.00 ( $\text{coreSiCH}_2\text{CH}_2\text{Si}$ ). <sup>29</sup>Si NMR:  $\delta$  31.82 (SiCl), 9.15 (core Si).

A 250 mL three-necked, round-bottomed flask equipped with a pressure-equalizing addition funnel, a reflux condenser, and a rubber septum was charged with 46 mL of a 0.5 M solution

rameters were obtained by the least-squares refinement of the angular settings of 24 reflections ( $20 \leq 2\theta \leq 25^\circ$ ).

No evidence of symmetry higher than triclinic was observed in either the photographic or diffraction data.  $E$ -statistics suggested a centrosymmetric space group, and  $P\bar{1}$  was chosen. The space group choice was subsequently verified by chemi-

**Table 2. Atomic Coordinates ( $\times 10^4$ ) and Equivalent Isotropic Displacement Parameters ( $\text{\AA}^2 \times 10^3$ ) for 1**

atom	x	y	z	$U(\text{eq})^a$	atom	x	y	z	$U(\text{eq})^a$
Co(11)	8088(3)	6838(2)	6391.4(9)	76(1)	C(111)	7167(23)	5809(16)	6522(7)	100(6)
Co(12)	5958(3)	8011(2)	6624.2(9)	66(1)	C(112)	9505(24)	6360(14)	5906(10)	104(7)
Co(21)	12115(2)	8749(2)	9720(8)	66(1)	C(113)	9078(25)	6973(13)	6909(9)	106(7)
Co(22)	13735(2)	9627(1)	9086.3(8)	63(1)	C(121)	4519(32)	7256(18)	6746(10)	144(10)
Co(31)	10010(2)	14523(1)	8800.5(8)	60(1)	C(122)	4932(22)	8958(18)	6433(9)	109(7)
Co(32)	7433(2)	15146(1)	9022.1(8)	67(1)	C(123)	6285(21)	8371(15)	7269(9)	102(7)
Co(41)	12752(2)	13542(2)	5637.9(8)	65(1)	O(211)	12271(12)	9799(10)	10673(5)	103(4)
Co(42)	15328(2)	12909(2)	5404.1(8)	67(1)	O(212)	9298(15)	8080(11)	10065(6)	117(5)
Si(1)	9046(5)	9063(3)	6065(2)	63(1)	O(213)	14008(15)	7007(11)	9744(7)	125(6)
Si(2)	11788(4)	8182(3)	8414(2)	56(1)	O(221)	14510(17)	10558(12)	8103(6)	132(6)
Si(3)	7775(5)	13140(3)	8232(2)	68(1)	O(222)	16234(15)	8238(12)	8969(6)	122(5)
Si(4)	13972(5)	12586(3)	6754(3)	65(1)	O(223)	14184(15)	11167(10)	9756(6)	109(5)
Si(5)	10572(5)	10641(3)	7377(2)	60(1)	C(211)	12210(17)	9369(13)	10287(8)	83(5)
C(11)	10381(18)	10121(11)	6737(7)	79(5)	C(212)	10369(27)	8334(14)	9932(7)	101(7)
C(12)	9195(17)	9522(12)	6715(7)	81(5)	C(213)	13286(23)	7660(15)	9729(7)	92(6)
C(13)	10800(20)	8555(13)	5718(7)	102(6)	C(221)	14167(21)	10198(12)	8485(8)	82(5)
C(14)	8289(21)	9984(12)	5662(7)	97(6)	C(222)	15310(21)	8747(14)	9011(8)	86(6)
C(15)	7782(19)	8138(10)	6160(6)	70(5)	C(223)	14026(18)	10562(13)	9499(6)	69(4)
C(16)	6979(16)	7594(10)	5943(6)	66(4)	O(311)	10765(15)	15301(10)	7762(6)	119(5)
C(21)	10543(15)	9791(10)	7920(5)	56(4)	O(313)	11117(15)	15743(10)	9507(6)	113(5)
C(22)	11747(16)	8946(10)	7820(5)	59(4)	O(312)	12155(15)	12893(11)	8763(6)	118(5)
C(23)	9991(17)	7729(11)	8611(6)	77(5)	O(321)	7191(17)	16311(11)	8097(6)	127(5)
C(24)	13235(19)	7204(12)	8299(7)	92(6)	O(322)	7580(16)	16431(10)	9891(6)	120(5)
C(25)	12053(14)	8945(11)	8951(6)	64(4)	O(323)	4377(16)	14760(13)	9319(8)	158(7)
C(26)	11614(17)	9716(12)	9241(5)	67(4)	C(311)	10485(21)	14988(14)	8149(7)	86(6)
C(31)	9016(17)	11558(11)	7590(6)	71(5)	C(312)	11342(22)	13533(16)	8787(7)	89(6)
C(32)	9263(17)	12201(11)	8035(6)	75(5)	C(313)	10671(21)	15267(13)	9243(7)	84(5)
C(33)	6051(22)	12635(15)	8544(8)	126(8)	C(321)	7252(20)	15897(12)	8463(9)	87(6)
C(34)	7492(23)	13873(12)	7663(8)	110(8)	C(322)	7549(21)	15907(15)	9540(9)	102(6)
C(35)	8220(16)	13878(11)	8742(7)	68(4)	C(323)	5547(30)	14918(15)	9215(9)	125(8)
C(36)	8426(17)	14004(9)	9237(7)	66(4)	O(411)	10453(21)	14383(14)	6444(7)	172(8)
C(41)	12281(17)	11219(11)	7265(6)	73(5)	O(412)	12569(16)	14817(10)	4747(5)	105(4)
C(42)	12443(17)	11846(10)	6807(6)	71(5)	O(413)	11463(15)	11839(10)	5443(6)	109(5)
C(43)	13495(22)	13482(14)	7287(7)	109(7)	O(421)	18197(17)	12842(16)	5716(8)	172(8)
C(44)	15654(20)	11829(13)	6810(7)	101(6)	O(422)	14970(20)	10972(11)	5225(8)	152(7)
C(45)	14192(16)	13168(11)	6120(6)	63(4)	O(423)	15983(16)	13721(10)	4371(6)	118(5)
C(46)	14498(17)	13912(12)	5869(5)	71(5)	C(411)	11418(24)	14035(17)	6084(9)	115(8)
O(111)	6551(21)	5154(12)	6604(7)	156(7)	C(412)	12616(18)	14326(12)	5084(8)	74(5)
O(112)	10400(19)	6118(11)	5565(8)	146(7)	C(413)	11980(21)	12493(15)	5518(8)	89(6)
O(113)	9732(18)	7087(11)	7242(6)	133(6)	C(421)	17169(23)	12824(13)	5604(8)	94(6)
O(121)	3609(19)	6805(15)	6835(7)	170(8)	C(422)	15116(21)	11721(16)	5289(8)	94(6)
O(122)	4343(22)	9655(14)	6281(8)	170(8)	C(423)	15667(20)	13416(12)	4772(7)	77(5)
O(123)	6476(21)	8569(14)	7676(6)	162(8)					

<sup>a</sup>  $U(\text{eq})$  is defined as one-third of the trace of the orthogonalized  $U_{ij}$  tensor.

of  $\text{HC}\equiv\text{CMgBr}$  in THF (23.0 mmol). A solution of 2.0 g (3.9 mmol) of  $\text{Si}(\text{CH}_2\text{CH}_2\text{SiMe}_2\text{Cl})_4$  in 20 mL of THF was added dropwise with stirring. A slight exotherm was observed. After the addition had been completed, the mixture was stirred and heated at 50 °C for 15 h. Subsequently, it was cooled to room temperature and poured into a saturated aqueous solution of  $\text{NH}_4\text{Cl}$ . The aqueous layer was extracted with diethyl ether, and the combined organic layers were washed with 2 portions of water and 1 portion of saturated aqueous  $\text{NaCl}$  and were dried over anhydrous  $\text{MgSO}_4$ . Rotary evaporation of volatiles left 1.7 g of a dark brown semisolid, which was dissolved in a minimum volume of hexane and subjected to column chromatography (silica gel). The first band, eluted with 3:500 v/v EtOAc/hexane, contained the product which was isolated as a white, crystalline solid (0.85 g, 46% crude yield). Recrystallization ( $\text{MeOH}/\text{H}_2\text{O}$ ) gave 0.76 g (41%) of **1**, mp 56–57.5 °C. Anal. Calcd for  $\text{C}_{24}\text{H}_{44}\text{Si}_5$ : C, 60.94; H, 9.38. Found: C, 61.08; H, 9.39. IR (KBr,  $\text{cm}^{-1}$ ):  $\nu(\equiv\text{CH})$  3281, 3266,  $\nu(\text{C}=\text{C})$  2032,  $\nu(\text{Me}_2\text{Si})$  1248.  $^1\text{H}$  NMR:  $\delta$  0.16 (s, 24 H,  $\text{CH}_3$ -Si), 0.51 (m, 16 H,  $\text{CH}_2\text{CH}_2$ ), 2.36 (s, 4 H,  $\equiv\text{CH}$ ).  $^{13}\text{C}$  NMR:  $\delta_{\text{C}}$  -2.54 ( $\text{CH}_3$ ), 2.63 ( $\text{C}^1$ ), 8.07 ( $\text{C}^2$ ), 89.38 ( $\text{C}^3$ ), 93.42 ( $\text{C}^4$ ).  $^{29}\text{Si}$  NMR:  $\delta_{\text{Si}}$  -13.67 ( $^2\text{Si}$ ), 9.51 (core Si).

**Preparation of Dendrimer 2.** Essentially the same procedure was used in the reaction of 4.0 g (29.4 mmol) of  $(\text{CH}_2=\text{CH})_4\text{Si}$  and 20.0 g (0.174 mol) of  $\text{MeSiHCl}_2$  in the presence of 3 drops of Karstedt catalyst solution in 40 mL of THF. Workup as above gave 16.7 g (28 mmol) of  $\text{Si}(\text{CH}_2\text{CH}_2\text{SiMe}_2\text{Cl})_4$ .  $^1\text{H}$  NMR:  $\delta$  0.77 (s, 12 H,  $\text{CH}_3$ -Si), 0.68–1.52 and 0.92–1.00 (m, 16 H,  $\text{CH}_2\text{CH}_2$ ).  $^{13}\text{C}$  NMR:  $\delta_{\text{C}}$  1.68 ( $\text{CH}_3$ -Si),

4.33 (core  $\text{SiCH}_2\text{CH}_2\text{Si}$ ), 14.02 (core  $\text{SiCH}_2\text{CH}_2\text{Si}$ ).  $^{29}\text{Si}$  NMR:  $\delta_{\text{Si}}$  32.16 (SiCl), 10.03 (core Si).

Ethynylation of 4.7 g (7.88 mmol) of this compound with 190 mL of 0.5 M  $\text{HC}\equiv\text{CMgBr}$  in THF (95 mmol) using the procedure and workup as described for **1** gave 3.7 g of a yellow oil. Chromatography (silica gel, 3:500 v/v EtOAc/hexane) gave as a first fraction a white powder. Recrystallization from hexane yielded 2.0 g (49%) of white needles, mp 69–70 °C. Anal. Calcd for  $\text{C}_{28}\text{H}_{36}\text{Si}_5$ : C, 65.55; H, 7.07. Found: C, 65.48; H, 7.13. IR (KBr,  $\text{cm}^{-1}$ ): 3276, 3264 (s,  $\equiv\text{CH}$ ), 2040 (s,  $\text{C}=\text{C}$ ), 1258 (s,  $\text{Me}_2\text{Si}$ ).  $^1\text{H}$  NMR:  $\delta$  0.34 (s, 12 H,  $\text{CH}_3$ -Si), 0.66 (m, 16 H,  $\text{CH}_2\text{CH}_2$ ), 2.47 (s, 8 H,  $\equiv\text{CH}$ ).  $^{13}\text{C}$  NMR:  $\delta_{\text{C}}$  -2.16 ( $\text{CH}_3$ ), 2.41 ( $\text{C}^1$ ), 7.88 ( $\text{C}^2$ ), 85.32 ( $\text{C}^3$ ), 94.94 ( $\text{C}^4$ ).  $^{29}\text{Si}$  NMR:  $\delta_{\text{Si}}$  -35.14 ( $\text{Si}^2$ ), 10.28 (core Si).

**Preparation of Dendrimer 5.** The compound **3**,  $\text{Si}(\text{CH}_2\text{CH}_2\text{Si}(\text{CH}=\text{CH}_2)_3)_4$ , was prepared as described in ref 1. Using the procedure described above, reaction was carried out between 2.5 g (4.3 mmol) of **3** and 7.4 g (78.3 mmol) of  $\text{Me}_2\text{SiHCl}$  in the presence of 3 drops of the Karstedt catalyst solution in 20 mL of THF (15 h at 50 °C). Evaporation of volatiles left 7.4 g (100%) of **4**, as a white, oily solid.  $^1\text{H}$  NMR:  $\delta$  0.39 (s, 72 H,  $\text{CH}_3$ -Si), 0.42 (m, 16 H,  $\text{C}^1\text{H}_2\text{C}^2\text{H}_2$ ), 0.62 (m, 48 H,  $\text{C}^3\text{H}_2\text{C}^4\text{H}_2$ ).  $^{13}\text{C}$  NMR:  $\delta_{\text{C}}$  0.99 ( $\text{CH}_3$ ), 2.31 ( $\text{C}^1$ ), 2.81 ( $\text{C}^2$ ), 1.99 ( $\text{C}^3$ ), 11.46 ( $\text{C}^4$ ).  $^{29}\text{Si}$  NMR:  $\delta_{\text{Si}}$  32.26 ( $\text{Si}^3$ ), 9.73 ( $\text{Si}^2$ ) 9.14 (core Si).

The usual procedure was used to carry out the reaction of chlorosilane dendrimer **4** (7.4 g, 4.3 mmol) with 130 mL of 0.5 M  $\text{HC}\equiv\text{CMgBr}$  in THF (75.0 mmol). The usual workup left 4 g of a yellow oil, which was purified by column chromatography

(silica gel, 5:200 v/v EtOAc/hexane) to give a white powder (2.9 g, 42% crude yield). Recrystallization of the latter from MeOH gave 2.5 g (37%) of white needles, mp 125–131 °C. Anal. Calcd for  $C_{80}H_{148}Si_{17}$ : C, 60.05; H, 9.40. Found: C, 60.37; H, 9.37. IR (KBr,  $cm^{-1}$ ): 3289 (m,  $\equiv CH$ ), 2034 (s,  $C\equiv C$ ), 1253 (s,  $Me_2Si$ ).  $^1H$  NMR:  $\delta$  0.15 (s, 72 H,  $CH_3-Si$ ), 0.37 (m, 16 H,  $C^1H_2C^2H_2$ ), 0.50 (m, 48 H,  $C^3H_2C^4H_2$ ), 2.35 (s, 12 H,  $\equiv CH$ ).  $^{13}C$  NMR:  $\delta_C$  1.23 ( $CH_3$ ), 2.26 ( $C^1$ ), 2.86 ( $C^2$ ), 2.48 ( $C^3$ ), 8.24 ( $C^4$ ), 89.31 ( $C^5$ ), 93.66 ( $C^6$ ).  $^{29}Si$  NMR:  $\delta_{Si}$  -13.88 ( $Si^3$ ), 9.51 ( $Si^2$ ), 9.17 (core Si).

#### Reaction of Dendrimer 1 with Dicobalt Octacarbonyl.

A 50 mL round-bottomed flask equipped with a reflux condenser, a stir bar, and a septum was charged with 1.50 g (4.39 mmol) of  $Co_2(CO)_8$ , 20 mL of 40–60 °C petroleum ether and a solution of 0.50 g (1.06 mmol) of dendrimer 1 in 10 mL of petroleum ether. The reaction, which was accompanied by an initial evolution of CO, was carried out at room temperature for 1 day. The reaction mixture was filtered through a bed of Celite and evaporated at reduced pressure. The dark red solid residue was dissolved in a minimum volume of hexane and purified by column chromatography on silica gel. Hexane eluted a dark red band from which 1.50 g (84%) of dendrimer 6 was isolated. Recrystallization from acetone gave dark red crystals, mp 64–65 °C. Anal. Calcd for  $C_{48}H_{44}O_{24}Si_5Co_8$ : C, 35.63; H, 2.74. Found: C, 35.77; H, 2.94. IR (KBr,  $cm^{-1}$ ): 2962 (w), 2880 (w), 2091 (s, CO), 2049 (s, CO), 2024 (s, CO), 1250 (m,  $CH_3Si$ ), 1136 (m).  $^1H$  NMR:  $\delta$  0.23 (s, 24 H,  $CH_3-Si$ ), 0.55 (m, 16 H,  $CH_2CH_2$ ), 6.35 (s, 4 H,  $\equiv CH$ ).  $^{13}C$  NMR:

$\delta_C$  -1.62 ( $CH_3$ ), 3.14 ( $C^1$ ), 9.62 ( $C^2$ ), 75.88 ( $C^3$ ), 85.15 ( $C^4$ ), 200.34 (CO).  $^{29}Si$  NMR:  $\delta_{Si}$  3.07 ( $Si^2$ ), 8.90 (core Si).

#### Reaction of Dendrimer 5 with Dicobalt Octacarbonyl.

The same procedure was used in the reaction of 1.32 g (3.89 mmol) of  $Co_2(CO)_8$  and 0.50 g (0.31 mmol) of dendrimer 5 in 30 mL of petroleum ether for 1 day at room temperature. Column chromatography (silica gel) using 100:1 v/v hexane/EtOAc first removed unreacted  $Co_2(CO)_8$  and then 1.51 g (98%) of dendrimer 7. Recrystallization from pentane gave red crystals, mp 50 °C. Anal. Calcd for  $C_{152}H_{148}O_{72}Si_{17}Co_{24}$ : C, 36.34; H, 2.97. Found: C, 36.42; H, 3.17. IR (KBr,  $cm^{-1}$ ): 2960 (w) 2903 (w), 2787 (w), 2091 (s, CO), 2048 (s, CO), 2021 (s, CO), 1249 (m,  $CH_3Si$ ), 1129 (m), 1052 (m).  $^1H$  NMR:  $\delta$  0.24 (s, 72 H,  $CH_3-Si$ ), 0.32 (s, 16 H,  $C^1H_2C^2H_2$ ), 0.56 (m, 48 H,  $C^3H_2C^4H_2$ ), 6.33 (s, 12 H,  $\equiv CH$ ).  $^{13}C$  NMR:  $\delta_C$  1.43 ( $CH_3$ ), 2.62 ( $C^1$ ), 3.54 ( $C^2$ ), 3.08 ( $C^3$ ), 9.69 ( $C^4$ ), 75.50 ( $C^5$ ), 85.44 ( $C^6$ ), 200.30 (CO).  $^{29}Si$  NMR:  $\delta_{Si}$  5.67 ( $Si^3$ ), 11.57 ( $Si^2$ ), 11.02 (core Si).

**Acknowledgment.** The authors are grateful to the National Science Foundation for support of this work. T.K. thanks Nishi-Tokyo University for granting a sabbatical leave of absence.

**Supporting Information Available:** Tables of bond lengths and angles, of anisotropic displacement coefficients and of H atom coordinates (7 pages). Ordering information is given on any current masthead page.

OM950665N

**Preparation of Trinuclear Ruthenium Clusters with Capped Sulfide Ligand, [(Cp\*Ru)<sub>3</sub>(μ<sub>3</sub>-S)(μ<sub>3</sub>-Cl)], [(Cp\*Ru)<sub>3</sub>(μ<sub>3</sub>-S)(μ<sub>3</sub>-S<sup>i</sup>Pr)], and [(Cp\*Ru)<sub>3</sub>(μ<sub>3</sub>-S)<sub>2</sub>(μ<sub>2</sub>-H)] (Cp\* = η<sup>5</sup>-C<sub>5</sub>Me<sub>5</sub>), and Reactivities of [(Cp\*Ru)<sub>3</sub>(μ<sub>3</sub>-S)(μ<sub>3</sub>-Cl)] toward CO and Alkynes**

Kohjiro Hashizume, Yasushi Mizobe, and Masanobu Hidai\*

*Department of Chemistry and Biotechnology, Graduate School of Engineering,  
The University of Tokyo, Hongo, Bunkyo-ku, Tokyo 113, Japan*

Received May 5, 1995<sup>⊗</sup>

Treatment of [(Cp\*Ru)<sub>4</sub>(μ<sub>3</sub>-Cl)<sub>4</sub>] (**1**; Cp\* = η<sup>5</sup>-C<sub>5</sub>Me<sub>5</sub>) with either Li<sub>2</sub>S alone or a mixture of Li<sub>2</sub>S and NaS<sup>i</sup>Pr in THF at 50 °C afforded trinuclear clusters with an equilateral triangular core [(Cp\*Ru)<sub>3</sub>(μ<sub>3</sub>-S)(μ<sub>3</sub>-Cl)] (**2**) and [(Cp\*Ru)<sub>3</sub>(μ<sub>3</sub>-S)(μ<sub>3</sub>-S<sup>i</sup>Pr)] (**3**), respectively, while an analogous reaction of **1** with (Me<sub>3</sub>Si)<sub>2</sub>S resulted in the formation of a mixture of **2** and [(Cp\*Ru)<sub>3</sub>(μ<sub>3</sub>-S)<sub>2</sub>(μ<sub>2</sub>-H)] (**4**). Cluster **2** dissolved in THF reacted with CO at 50 °C to give trinuclear carbonyl clusters [(Cp\*Ru)<sub>3</sub>(μ<sub>3</sub>-S)(μ<sub>2</sub>-CO)<sub>2</sub>(μ<sub>2</sub>-Cl)] (**5**) and [(Cp\*Ru)<sub>3</sub>(μ<sub>3</sub>-S)(μ<sub>2</sub>-CO)<sub>3</sub>]-Cl (**8**). In **5**, two Ru–Ru bonds are each bridged by a CO ligand, and one Ru–Ru edge without direct bonding interaction is bridged by the Cl atom, whereas **8** has an equilateral Ru<sub>3</sub> core with three CO ligands bridging each Ru–Ru bond. It has also been demonstrated that reaction of **2** with excess HC≡CCOOMe in THF at 50 °C results in the almost quantitative formation of cyclic trimers of the alkyne C<sub>6</sub>H<sub>3</sub>(COOMe)<sub>3</sub> in a 1,3,5- and 1,2,4-isomers ratio of 42:58. In contrast, from a reaction mixture of **2** with MeC≡CCOOMe under the similar conditions a dinuclear complex [Cp\*Ru{μ<sub>2</sub>-SCMeC(COOMe)CMeC(COOMe)}RuCp\*] (**10**) was isolated. Detailed structures of **2**–**5**, **8**, and **10** have been determined by X-ray crystallography.

### Introduction

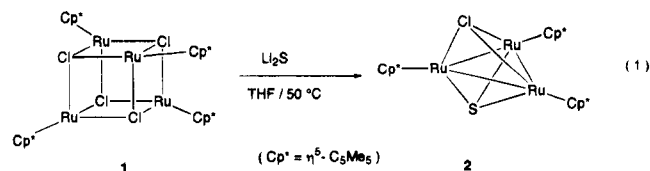
Our current interest has been centered on the exploitation of novel chemical transformations catalyzed by dinuclear and polynuclear complexes. Significant emphasis has been placed upon the studies on the synthesis and reactivities of sulfur-bridged multimetallic compounds, since these are expected to provide a relatively robust metal framework facilitating the substrate transformation accessible only at the multimetallic reaction site with retention of its high nuclearity.<sup>1</sup>

Recently we have reported that the reactions of dimeric or tetrameric Ru complexes with Cp\* ligand [Cp\*RuCl(μ<sub>2</sub>-Cl)<sub>2</sub>RuCp\*Cl], [(Cp\*Ru)<sub>4</sub>(μ<sub>3</sub>-Cl)<sub>4</sub>] (**1**), and [Cp\*Ru(μ<sub>2</sub>-OMe)<sub>2</sub>RuCp\*] (Cp\* = η<sup>5</sup>-C<sub>5</sub>Me<sub>5</sub>) with various thiolate sources afford a series of diruthenium complexes with two or three bridging thiolate ligands. The bimetallic sites in these complexes have proved to exhibit numerous intriguing reactivities toward the substrates including alkynes, CO, isocyanide, H<sub>2</sub>, and alkyl halides.<sup>2</sup> Interestingly, it has also been demonstrated that the reaction of **1** with Li<sub>2</sub>S instead of thiolate compounds results in the formation of a triangular cluster with a capped sulfide ligand, [(Cp\*Ru)<sub>3</sub>(μ<sub>3</sub>-S)(μ<sub>3</sub>-Cl)] (**2**). Furthermore, treatment of **1** with a thiolate compound NaS<sup>i</sup>Pr in the presence of Li<sub>2</sub>S has also led to the formation of a related triruthenium

cluster [(Cp\*Ru)<sub>3</sub>(μ<sub>3</sub>-S)(μ<sub>3</sub>-S<sup>i</sup>Pr)] (**3**).<sup>3</sup> In this paper, we wish to report the details of **2** and **3** along with the another triruthenium cluster [(Cp\*Ru)<sub>3</sub>(μ<sub>3</sub>-S)<sub>2</sub>(μ<sub>2</sub>-H)] (**4**) isolated from the reaction of **1** with (Me<sub>3</sub>Si)<sub>2</sub>S. Reactivities of **2** toward CO and alkynes are also described.

### Results and Discussion

**Reactions of 1 with Li<sub>2</sub>S Alone or a Mixture of Li<sub>2</sub>S and NaS<sup>i</sup>Pr.** Previously we have reported that treatment of **1** with excess NaSR in THF at room temperature gives dinuclear Ru(II) complexes with two thiolate bridges [Cp\*Ru(μ<sub>2</sub>-SR)<sub>2</sub>RuCp\*] (R = <sup>i</sup>Pr, <sup>t</sup>Bu, 2,6-Me<sub>2</sub>C<sub>6</sub>H<sub>3</sub>).<sup>4</sup> Now we have found that treatment of **1** with Li<sub>2</sub>S instead of the thiolates as a sulfur source results in the formation of a trinuclear Ru(II) cluster **2**. Thus, when **1** was reacted with Li<sub>2</sub>S in THF at 50 °C in a Ru:S atomic ratio of 2:1, **2** was isolated from the reaction mixture as dark brown crystals in 50% yield based on Ru atom (eq 1). Reactions with excess Li<sub>2</sub>S also afforded **2** as the only isolable Ru-containing product.



<sup>⊗</sup> Abstract published in *Advance ACS Abstracts*, October 1, 1995.

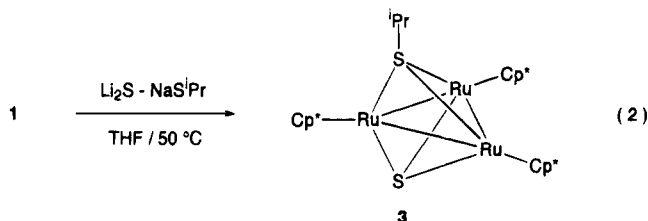
(1) (a) Rakowski DuBois, M. *Chem. Rev.* **1989**, *89*, 1. (b) Adams, R. D. *Polyhedron* **1985**, *4*, 2003.

(2) (a) Hidai, M.; Mizobe, Y.; Matsuzaka, H. *J. Organomet. Chem.* **1994**, *473*, 1 and references therein. (b) Hörnig, A.; Rietmann, Chr.; Englert, U.; Wagner, T.; Koelle, U. *Chem. Ber.* **1993**, *126*, 2609.

(3) Mizobe, Y.; Hashizume, K.; Murai, T.; Hidai, M. *J. Chem. Soc., Chem. Commun.* **1994**, 1051.

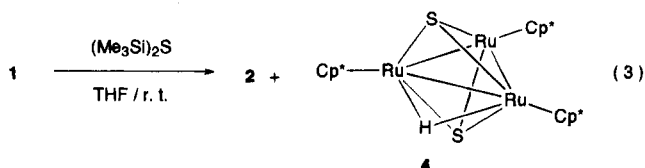
(4) Takahashi, A.; Mizobe, Y.; Matsuzaka, H.; Dev, S.; Hidai, M. *J. Organomet. Chem.* **1993**, *456*, 243.

On the other hand, when the reaction of **1** with  $\text{Li}_2\text{S}$  was performed in the presence of  $\text{NaS}^i\text{Pr}$ , a trinuclear sulfido-thiolato Ru(II) cluster **3** was obtained as dark brown crystals (eq 2). Although the reaction of these three substrates in a stoichiometric  $\text{Ru}:\text{S}^{2-}:\text{S}^i\text{Pr}^-$  ratio of 3:1:1 afforded a mixture of **2** and **3**, change in the ratio to 3:1:2 gave **3** exclusively, which was isolated in 63% yield. Preparation of a SPh analogue of **3** from the reaction of **1** with a  $\text{Li}_2\text{S}$ - $\text{NaSPh}$  mixture was unsuccessful under these conditions. It should be noted that treatment of **2** with excess  $\text{NaS}^i\text{Pr}$  in THF at 50 °C resulted in the almost quantitative recovery of **2**, which may suggest that the formation of **3** from **1** does not proceed via **2** as an intermediate stage.



The  $^1\text{H}$  NMR spectrum of **2** shows a singlet at 1.83 ppm assignable to the  $\text{Cp}^*$  methyl protons, while that of **3** recorded at 40 °C exhibits a singlet at 1.92 ppm due to the  $\text{Cp}^*$  methyl protons as well as one septet and one doublet at 4.06 and 1.97 ppm which are ascribed to the methine and methyl protons of the  $\text{S}^i\text{Pr}$  group, respectively. These data are indicative of the equivalent nature of three  $\text{Cp}^*\text{Ru}$  units in both **2** and **3** in solutions.

**Reaction of 1 with  $(\text{Me}_3\text{Si})_2\text{S}$ .** When **1** was treated with  $(\text{Me}_3\text{Si})_2\text{S}$  in place of  $\text{Li}_2\text{S}$  under the similar conditions, a mixture of **2** and another triruthenium cluster **4** having two capped sulfide and one hydride ligands was obtained. The  $^1\text{H}$  NMR spectrum of the evaporated reaction mixture residue dissolved in  $\text{C}_6\text{D}_6$  indicates the formation of these two products in ca. 1:2 ratio (eq 3), which was almost reproducible in the repeated runs. The hydrogen source of **4** seems to be the adventitious moisture present in THF, since the reaction of **1** and  $(\text{Me}_3\text{Si})_2\text{S}$  in the presence of  $\text{H}_2\text{O}$  gave **4**, while that using  $\text{D}_2\text{O}$  in place of  $\text{H}_2\text{O}$  resulted in the formation of a deuteride analogue of **4**.<sup>5</sup> Clusters **2** and **4** were inseparable by either fractional crystallization or chromatography. However, by treatment with CO in THF the mixture of **2** and **4** was converted into a mixture of a carbonyl cluster  $[(\text{Cp}^*\text{Ru})_3(\mu_3\text{-S})(\mu_2\text{-CO})_2(\mu_2\text{-Cl})]$  (**5**) derived from **2** (vide infra) and unreacted **4** in solution,<sup>6</sup> from which pure **4** was able to be isolated in 14% yield by fractional crystallization because of its much higher solubility into THF than **5**.



In the  $^1\text{H}$  NMR spectrum of **4**, the  $\text{Cp}^*$  methyl protons appear as two singlets at 1.92 and 2.07 ppm in a 2:1

(5) The reaction of **1** with  $(\text{Me}_3\text{Si})_2\text{S}$  in the presence of  $\text{H}_2\text{O}$  did not give **2**. The  $^1\text{H}$  NMR spectrum of the reaction mixture revealed the formation of other product(s) in addition to **4**, one of which has been characterized to be  $[(\text{Cp}^*\text{Ru})_2(\mu\text{-SH})_2]$  by the preliminary X-ray results. Details will be reported subsequently.

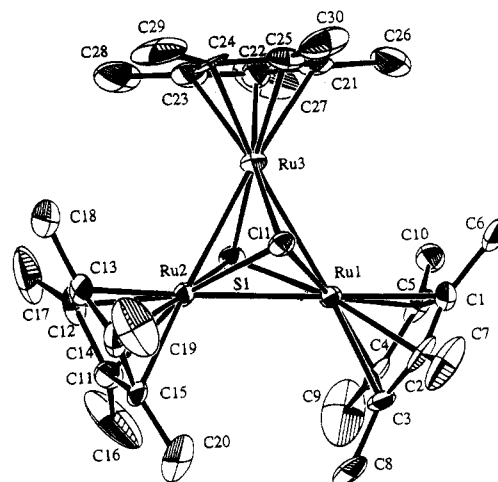


**Figure 1.** Molecular structure of **2** with atom numbering scheme.

intensity ratio, and the hydride resonance is observed at  $-22.3$  ppm as a singlet. This spectral feature is consistent with the structure containing a  $\mu_2\text{-H}$  ligand determined by the X-ray analysis (vide infra).

The related reactions giving ruthenium sulfide clusters include formation of a triangular Ru(II) cluster  $[(p\text{-cymene})\text{Ru}]_3(\mu_3\text{-S})_2]^{2+}$  (**6**) by treatment of a Ru(II) dimer  $[(p\text{-cymene})\text{RuCl}_2]_2$  with either  $(\text{Me}_3\text{Si})_2\text{S}$ , methanolic  $\text{NaSH}$ , or aqueous  $\text{Na}_2\text{S}$ <sup>7</sup> and synthesis of a cubane-type Ru(III) cluster  $[(\text{Cp}^*\text{Ru})_4(\mu_3\text{-S})_4]$  from **1** and  $\text{NaSH}$ .<sup>8</sup>

It is not clear how the trinuclear cores in **2-4** are produced from the tetra-ruthenium cluster **1**. Formation of a closed triangular Ru cluster from **1** has recently been observed in the reaction with  $\text{Me}_2\text{C}=\text{CHCHO}$ , yielding a  $\mu_3$ -cyclopentenyl complex  $[(\text{Cp}^*\text{Ru})_3(\mu_3\text{-CO})(\mu_3\text{-MeCCHCH})]$  together with a mononuclear complex  $[\text{Cp}^*\text{Ru}(\text{CO})(\eta^3\text{-CH}_2\text{CMeCH}_2)]$ .<sup>9</sup> In the above reactions to give **2-4**, however, mononuclear Ru species are not detectable in the reaction mixtures. Assembly of a triangular  $(\text{Cp}^*\text{Ru})_3$  cluster from dinuclear complexes is also precedented; these examples are preparation of  $[(\text{Cp}^*\text{Ru})_3(\mu_3\text{-OMe})_2][\text{PF}_6]$  from reaction of  $[(\text{Cp}^*\text{Ru})(\mu_2\text{-OMe})_2\text{RuCp}^*]$  with  $\text{NH}_4\text{PF}_6$  in  $\text{MeOH}$ <sup>10</sup> and synthesis of  $[(\text{Cp}^*\text{Ru})_3(\mu_3\text{-O})(\mu_3\text{-OR})]$  ( $\text{R} = ^i\text{Pr}, ^t\text{Bu}$ ) by treatment of  $[(\text{Cp}^*\text{Ru})(\mu_2\text{-H})_2(\mu_2\text{-OCOCF}_3)_2\text{RuCp}^*]$  with  $\text{NaO}^i\text{Pr}$  in  $\text{HO}^i\text{Pr}/\text{THF}$  or  $\text{KO}^t\text{Bu}$  in THF.<sup>11</sup>

**X-ray Structures of 2-4.** To clarify the detailed structures of the new sulfide clusters, X-ray analyses have been carried out using single crystals of **2-4**. ORTEP drawings of these clusters are shown in Figures 1-3, while important bond distances and angles are listed in Table 1. As suggested by the  $^1\text{H}$  NMR spectrum, **2** consists of an essentially equilateral triangular  $\text{Ru}_3$  core capped by both the  $\mu_3\text{-S}$  and  $\mu_3\text{-Cl}$  ligands. The Ru-Ru distances in the range of 2.874(2)-2.901-

(6) A small amount of the tricarbonyl cluster **8** (vide infra) was also formed, which was almost insoluble in THF.

(7) Lockemeyer, J. R.; Rauchfuss, T. B.; Rheingold, A. L. *J. Am. Chem. Soc.* **1989**, *111*, 5733.

(8) Houser, E. J.; Dev, S.; Ogilvy, A. E.; Rauchfuss, T. B.; Wilson, S. R. *Organometallics* **1993**, *12*, 4678.

(9) Trakarnpruk, W.; Arif, A. M.; Ernst, R. D. *Organometallics* **1994**, *13*, 2423.

(10) Keolle, U.; Kassakowski, J.; Boese, R. *J. Organomet. Chem.* **1989**, *378*, 449.

(11) Suzuki, H.; Kakigano, T.; Igarashi, M.; Usui, A.; Noda, K.; Oshima, M.; Tanaka, M.; Moro-oka, Y. *Chem. Lett.* **1993**, 1707.

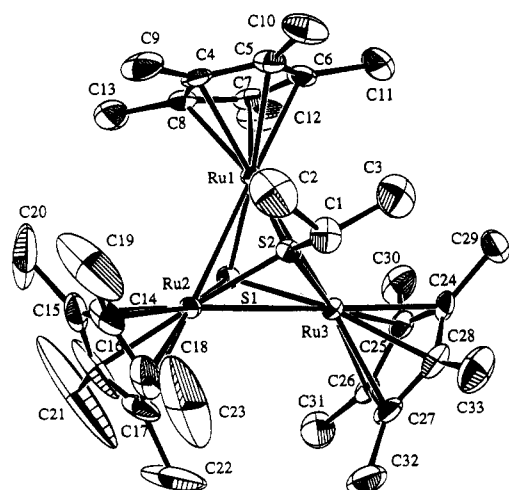


Figure 2. Molecular structure of **3** with atom numbering scheme.

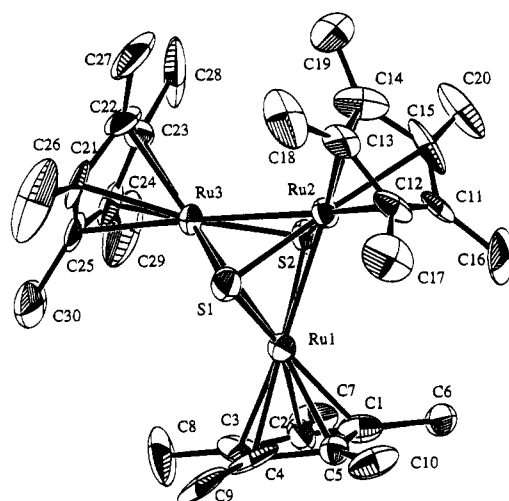


Figure 3. Molecular structure of **4** with atom numbering scheme.

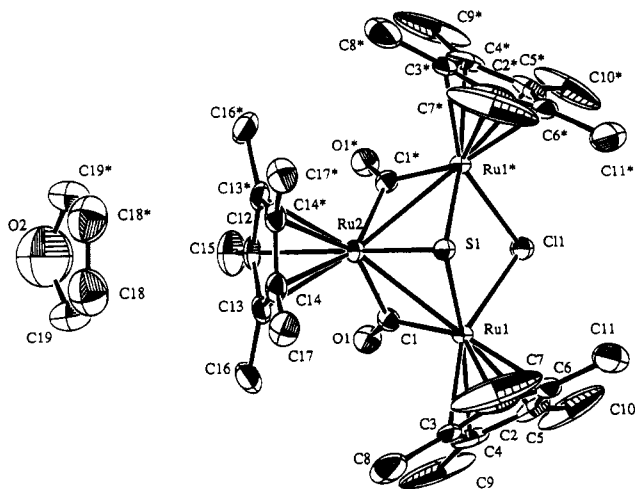


Figure 4. Molecular structure of **5**·THF with atom numbering scheme.

(2) Å are indicative of the presence of the Ru–Ru single bonds. The Cp\* ligands coordinate to Ru atoms perpendicularly to the Ru<sub>3</sub> plane, the dihedral angles of which vary from 84° to 88°. Two atoms capping the Ru<sub>3</sub> basal plane almost symmetrically could not be assigned unambiguously due to the small difference in electron densities between the S and Cl atoms. However, the

Table 1. Selected Bond Distances (Å) and Angles (deg) in **2–4**

Compound 2			
Bond Distances			
Ru(1)–Ru(2)	2.877(2)	Ru(1)–Ru(3)	2.901(2)
Ru(2)–Ru(3)	2.874(2)		
Ru(1)–Cl(1)	2.359(5)	Ru(1)–S(1)	2.300(5)
Ru(2)–Cl(1)	2.358(5)	Ru(2)–S(1)	2.287(5)
Ru(3)–Cl(1)	2.370(4)	Ru(3)–S(1)	2.288(5)
Bond Angles			
Ru(1)–Ru(2)–Ru(3)	60.59(5)	Ru(1)–Ru(3)–Ru(2)	59.75(5)
Ru(2)–Ru(1)–Ru(3)	59.66(5)	Cl(1)–Ru(1)–S(1)	88.5(2)
Cl(1)–Ru(2)–S(1)	88.8(2)	Cl(1)–Ru(3)–S(1)	88.5(2)
Ru(1)–Cl(1)–Ru(2)	75.2(2)	Ru(1)–Cl(1)–Ru(3)	75.7(1)
Ru(2)–Cl(1)–Ru(3)	74.9(1)	Ru(1)–S(1)–Ru(2)	77.7(2)
Ru(1)–S(1)–Ru(3)	78.4(2)	Ru(2)–S(1)–Ru(3)	77.8(2)
Compound 3			
Bond Distances			
Ru(1)–Ru(2)	2.9449(8)	Ru(1)–Ru(3)	2.9599(9)
Ru(2)–Ru(3)	2.944(1)		
Ru(1)–S(1)	2.281(2)	Ru(1)–S(2)	2.249(2)
Ru(2)–S(1)	2.287(2)	Ru(2)–S(2)	2.240(2)
Ru(3)–S(1)	2.280(2)	Ru(3)–S(2)	2.247(2)
S(2)–C(1)	1.818(8)		
Bond Angles			
Ru(1)–Ru(2)–Ru(3)	60.34(2)	Ru(1)–Ru(3)–Ru(2)	59.84(2)
Ru(2)–Ru(1)–Ru(3)	59.82(2)	S(1)–Ru(1)–S(2)	82.37(7)
S(1)–Ru(2)–S(2)	82.46(7)	S(1)–Ru(3)–S(2)	82.43(7)
Ru(1)–S(1)–Ru(2)	80.29(6)	Ru(1)–S(1)–Ru(3)	80.92(6)
Ru(2)–S(1)–Ru(3)	80.29(6)	Ru(1)–S(2)–Ru(2)	82.00(6)
Ru(1)–S(2)–Ru(3)	82.33(6)	Ru(2)–S(2)–Ru(3)	82.02(6)
Ru(1)–S(2)–C(1)	131.2(3)	Ru(2)–S(2)–C(1)	130.6(3)
Ru(3)–S(2)–C(1)	130.2(3)		
Compound 4			
Bond Distances			
Ru(1)–Ru(2)	2.806(3)	Ru(1)–Ru(3)	2.851(3)
Ru(2)–Ru(3)	2.798(2)		
Ru(1)–S(1)	2.291(5)	Ru(1)–S(2)	2.289(5)
Ru(2)–S(1)	2.278(6)	Ru(2)–S(2)	2.286(6)
Ru(3)–S(1)	2.285(6)	Ru(3)–S(2)	2.302(6)
Bond Angles			
Ru(1)–Ru(2)–Ru(3)	61.16(8)	Ru(1)–Ru(3)–Ru(2)	59.57(8)
Ru(2)–Ru(1)–Ru(3)	59.27(6)	S(1)–Ru(1)–S(2)	89.3(2)
S(1)–Ru(2)–S(2)	89.7(2)	S(1)–Ru(3)–S(2)	89.1(2)
Ru(1)–S(1)–Ru(2)	75.8(2)	Ru(1)–S(1)–Ru(3)	77.1(2)
Ru(2)–S(1)–Ru(3)	75.6(2)	Ru(1)–S(2)–Ru(2)	75.7(2)
Ru(1)–S(2)–Ru(3)	76.8(2)	Ru(2)–S(2)–Ru(3)	75.2(2)

distances between these two atoms and the Ru atoms differ significantly, and the atom having the shorter bonds with the Ru atoms has been assigned as S, while the other has been characterized to be Cl. Indeed, the Ru–S distances at 2.287(5)–2.300(5) Å in **2** are in good agreement with the Ru–S(sulfide) lengths in **3** (vide infra). Analogous assignment of the μ<sub>3</sub>-S and μ<sub>3</sub>-Cl ligands based on the differences between the M–S and M–Cl bond distances has been done, for example, for [Mo<sub>3</sub>Ni<sub>2</sub>S<sub>4</sub>Cl<sub>4</sub>(PET<sub>3</sub>)<sub>5</sub>].<sup>12</sup> It is to be noted that the Ru–S bonds in **2** are slightly shorter than those in the lower valent Ru<sub>3</sub> cluster [{Ru(CO)<sub>3</sub>]<sub>3</sub>(μ<sub>3</sub>-CO)(μ<sub>3</sub>-S)] (2.334(2)–2.361(2) Å)<sup>13</sup> but are slightly longer than those in the Ru(II) triangular cluster **6** (2.263(2)–2.272(1) Å).<sup>7</sup> The Ru–Cl distances in **2** fall in the range of 2.358(5)–2.370(4) Å, which are much shorter than those previously reported for the μ<sub>3</sub>-Cl ligands in the complexes without

(12) Saito, T.; Kajitani, Y.; Yamagata, T.; Imoto, H. *Inorg. Chem.* **1990**, *29*, 2951.

(13) Adams, R. D.; Babin, J. E.; Tasi, M. *Organometallics* **1988**, *7*, 219.

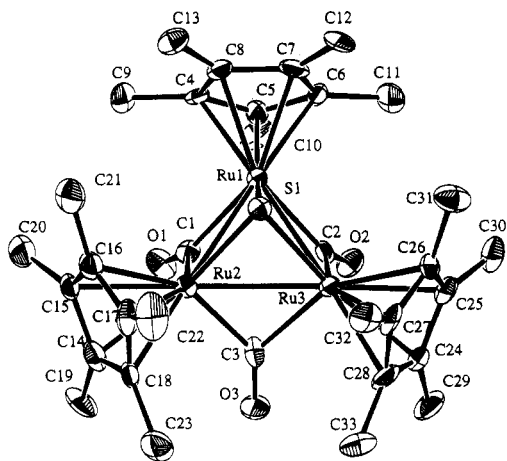


**Figure 5.** Structure of the cation in **8**. The Cl anion and the solvating  $\text{CH}_2\text{Cl}_2$  molecule are omitted for clarity.

Ru–Ru interactions such as **1** (2.513(3)–2.537(3) Å)<sup>14</sup> and  $[\text{Cp}^*_3\text{Ru}_3(\mu_3\text{-Cl})(\mu_2\text{-Cl})_2(\eta^2\text{-}\mu_2\text{-HCCSiMe}_3)]$  (**7**; 2.559–(2) Å (mean)).<sup>15</sup> The Ru–S–Ru and Ru–Cl–Ru angles in **2** are in the ranges of 77.7(2)–78.4(2)° and 74.9(1)–75.7(1)°, respectively.

Cluster **3** also contains an equilateral  $\text{Ru}_3$  triangle with the Ru–Ru bond distances at 2.944(1)–2.960(1) Å, which are slightly longer than those in **2**. The  $\text{Cp}^*$  and  $\text{Ru}_3$  planes are almost perpendicular with the dihedral angles of 81–85°. Both S atoms coordinate to the  $\text{Ru}_3$  plane symmetrically and the Ru–S(sulfide) distances (2.280(2)–2.287(2) Å) are comparable to those in **2**. Interestingly, the Ru–S(thiolate) bonds at 2.240(2)–2.249(2) Å are slightly shorter than the Ru–S(sulfide) bonds. This contrasts to the feature observed in the related oxo–alkoxo complex  $[(\text{Cp}^*\text{Ru})_3(\mu_3\text{-O})(\mu_3\text{-O}^i\text{Pr})]$ , which consists of the Ru–O(alkoxide) bonds (2.14(1)–2.16(1) Å) longer than the Ru–O(oxide) bonds (2.03(1)–2.09(1) Å).<sup>11</sup> The thiolate ligand coordinated to a  $\text{Ru}_3$  face was observed previously in *e.g.*  $[(\mu_3\text{-}\eta^7\text{-C}_7\text{H}_7\text{-Ru}_3(\text{CO})_6(\mu_3\text{-S}^t\text{Bu}))]$ ,<sup>16</sup> which has the Ru–S bonds at 2.272(1)–2.274(1) Å. The  $\mu_2$ -thiolate ligands bound to a Ru–Ru single bond in a  $\text{Ru}_3$  triangular array are more unprecedented, *e.g.*  $[\text{Ru}_3(\mu_2\text{-H})(\mu_2\text{-SCH}_2\text{COOH})(\text{CO})_{10}]$ ,<sup>17</sup>  $[\text{Ru}_3(\mu_2\text{-H})(\mu_2\text{-SPh})(\text{CO})_8(\text{Ph}_2\text{PCH}_2\text{PPh}_2)]$ ,<sup>18</sup> and  $[(\text{Cp}\text{-Ru})_3(\mu_2\text{-S}^n\text{Pr})_3]$  ( $\text{Cp} = \eta^5\text{-C}_5\text{H}_5$ ),<sup>19</sup> which contain slightly or substantially longer Ru–S bonds of 2.387(6) and 2.388(3) Å, 2.395(1) and 2.387(1) Å, and 2.286(1)–2.304(1) Å, respectively, than **3**. The Ru–S(sulfide)–Ru and Ru–S(thiolate)–Ru angles are 80.29(6)–80.92(6)° and 82.00(6)–82.33(6)°, respectively. The S–C bond in the  $\text{S}^i\text{Pr}$  ligand is almost perpendicular to the basal plane (Ru–S–C angles: 130.2(3)–131.2(3)°) and two methyl groups are oriented toward the directions so that the C(2)–C(1)–S(2) and C(3)–C(1)–S(2) planes bisect the Ru–Ru vectors. Appearance of the all  $\text{Cp}^*$  methyl protons as one singlet in  $^1\text{H}$  NMR spectrum suggests

(14) Fagan, P. J.; Mahoney, W. S.; Calabrese, J. C.; Williams, I. D. *Organometallics* **1990**, *9*, 1843.

(15) Campion, B. K.; Heyn, R. H.; Tilley, T. D. *Organometallics* **1990**, *9*, 1106.

(16) Howard, J. A. K.; Kennedy, F. G.; Knox, S. A. R. *J. Chem. Soc., Chem. Commun.* **1979**, 839.

(17) Jeannin, S.; Jeannin, Y.; Lavigne, G. *Inorg. Chem.* **1978**, *17*, 2103.

(18) Fompeyrine, P.; Lavigne, G.; Bonnet, J.-J. *J. Chem. Soc., Dalton Trans.* **1987**, 91.

(19) Shaver, A.; Plouffe, P.-Y.; Liles, D. C.; Singleton, E. *Inorg. Chem.* **1992**, *31*, 997.

**Table 2.** Selected Bond Distances (Å) and Angles (deg) in **5** and **8**

Compound <b>5</b>			
Bond Distances			
Ru(1)–Ru(2)	2.7973(7)	Ru(1)–Cl(1)	2.480(1)
Ru(1)–S(1)	2.311(1)	Ru(2)–S(1)	2.285(2)
Ru(1)–C(1)	2.010(5)	Ru(2)–C(1)	2.089(5)
C(1)–O(1)	1.179(5)		
Bond Angles			
Ru(1)–Ru(2)–Ru(1)*	76.80(2)	Ru(2)–Ru(1)–Cl(1)	88.31(4)
Ru(2)–Ru(1)–S(1)	52.08(4)	Ru(1)–Ru(2)–S(1)	52.94(3)
Ru(1)–Ru(2)–C(1)	45.8(1)	Ru(2)–Ru(1)–C(1)	48.2(1)
Cl(1)–Ru(1)–S(1)	83.16(5)	Cl(1)–Ru(1)–C(1)	85.6(1)
S(1)–Ru(1)–C(1)	99.5(1)	S(1)–Ru(2)–C(1)	98.0(1)
Ru(1)–Cl(1)–Ru(1)*	88.97(6)	Ru(1)–S(1)–Ru(1)*	97.48(7)
Ru(1)–S(1)–Ru(2)	74.97(5)	Ru(1)–C(1)–Ru(2)	86.1(2)
Ru(1)–C(1)–O(1)	140.4(4)	Ru(2)–C(1)–O(1)	133.4(4)
Compound <b>8</b>			
Bond Distances			
Ru(1)–Ru(2)	2.769(1)	Ru(1)–Ru(3)	2.769(1)
Ru(2)–Ru(3)	2.771(1)	Ru(1)–S(1)	2.287(3)
Ru(2)–S(1)	2.276(3)	Ru(3)–S(1)	2.285(3)
Ru(1)–C(1)	2.056(10)	Ru(1)–C(2)	2.066(9)
Ru(2)–C(1)	2.03(1)	Ru(2)–C(3)	2.01(1)
Ru(3)–C(2)	2.02(1)	Ru(3)–C(3)	2.047(10)
C(1)–O(1)	1.18(1)	C(2)–O(2)	1.18(1)
C(3)–O(3)	1.21(1)		
Bond Angles			
Ru(1)–Ru(2)–Ru(3)	59.99(3)	Ru(1)–Ru(3)–Ru(2)	59.96(3)
Ru(2)–Ru(1)–Ru(3)	60.04(3)		
S(1)–Ru(1)–C(1)	99.3(3)	S(1)–Ru(1)–C(2)	99.3(3)
S(1)–Ru(2)–C(1)	100.6(3)	S(1)–Ru(2)–C(3)	100.2(3)
S(1)–Ru(3)–C(2)	100.8(3)	S(1)–Ru(3)–C(3)	98.6(3)
Ru(1)–S(1)–Ru(2)	74.70(8)	Ru(1)–S(1)–Ru(3)	74.56(9)
Ru(2)–S(1)–Ru(3)	74.81(8)	Ru(1)–C(1)–Ru(2)	85.4(4)
Ru(1)–C(2)–Ru(3)	85.4(4)	Ru(2)–C(3)–Ru(3)	86.3(4)
Ru(1)–C(1)–O(1)	135.4(9)	Ru(2)–C(1)–O(1)	139.1(9)
Ru(1)–C(2)–O(2)	135.2(9)	Ru(3)–C(2)–O(2)	139.3(8)
Ru(2)–C(3)–O(3)	138.8(8)	Ru(3)–C(3)–O(3)	134.8(8)

the rapid rotation of the  $^i\text{Pr}$  group around the S–C bond in a solution state.

In **4**, there exists a triangular  $\text{Ru}_3$  core capped by two  $\mu_3\text{-S}$  ligands from both sides. The Ru–S distances fall in the range of 2.278(6)–2.302(6) Å. For the  $\text{Ru}_3$  core in **4**, all three Ru–Ru distances are diagnostic of the Ru–Ru single bond interaction, and the coordination geometry around the Ru atoms is analogous for the three Ru atoms. However, the Ru(1)–Ru(3) bond at 2.851(3) Å is significantly longer than the other two Ru–Ru bonds (2.806(3) and 2.798(2) Å), which is indicative of the presence of the hydride as a  $\mu_2$ -bridge between the Ru(1) and Ru(3) atoms, although the position of the hydride could not be found in the final Fourier map. The hydride-bridged Ru–Ru single bonds longer than the unsupported Ru–Ru single bonds in a triangular  $\text{Ru}_3$  cores have been demonstrated previously for the clusters such as  $[(\mu_2\text{-H})_2\{\text{Ru}(\text{CO})_3\}_3(\mu_3\text{-S})]$  (2.879(1) and 2.882(1) Å vs 2.760(1) Å),<sup>20</sup>  $[(\mu_2\text{-H})\{\text{Ru}(\text{CO})_3\}_3(\mu_4\text{-S})\text{Mn}(\text{CO})_3(\text{MeCN})_2]$  (2.848(1) Å vs 2.784(1) and 2.770(1) Å),<sup>21</sup> and  $[(\mu_2\text{-H})\{\text{Ru}(\text{CO})_3\}_3(\mu_4\text{-S})\text{Ru}(\text{CO})_3(\eta^2\text{-CH}_2\text{CMe}_2\text{NHCNH}^t\text{Bu})]$  (2.8935(6) Å vs 2.750(1) and 2.757(1) Å).<sup>22</sup> Three  $\text{Cp}^*$  planes are almost perpendicular to the  $\text{Ru}_3$  basal plane with the dihedral angles of 88.5–90.0°.

#### Reactivities of Sulfide Capped Trinuclear Clusters. Reactivities on the trimetallic sites surrounded

(20) Adams, R. D.; Katahira, D. A. *Organometallics* **1982**, *1*, 53.

(21) Voss, E. J.; Stern, C. L.; Shriver, D. F. *Inorg. Chem.* **1994**, *33*, 1087.

(22) Bodensieck, U.; Stoeckli-Evans, H.; Süss-Fink, G. *J. Chem. Soc., Chem. Commun.* **1990**, 267.



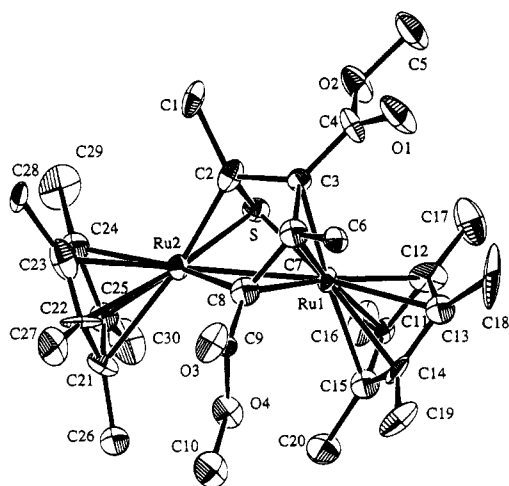
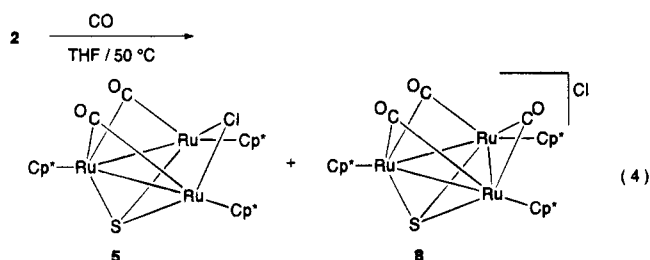


Figure 6. Molecular structure of **10** with atom numbering scheme.

by cyclopentadienyl ligands in **2-4** is of particular interest. It should be noted that the unique C–C bond cleavage of cyclopentadiene facilitated on a Ru<sub>3</sub> site provided by [(Cp\**Ru*)<sub>3</sub>(μ<sub>2</sub>-H)<sub>3</sub>(μ<sub>3</sub>-H)<sub>2</sub>] has been reported recently.<sup>23</sup> Coordination of certain π-acceptor molecules to a trimetallic site capped by a μ<sub>3</sub>-S ligand has been demonstrated most extensively for Co clusters [(CpCo)<sub>3</sub>(μ<sub>3</sub>-S)(μ<sub>3</sub>-L)], where L = CO,<sup>24</sup> CS,<sup>25</sup> and CNR.<sup>26</sup> Reactions of CO, isocyanides, and alkynes with the Ru<sub>3</sub> clusters obtained here have therefore been investigated. Among three clusters **2-4**, cluster **2** may exhibit higher reactivity than **3** and **4** toward these molecules, since the former has the Cl ligand which is probably more labile than the S<sup>i</sup>Pr and S ligands. Indeed, **2** has proved to react with CO at 50 °C to give carbonyl clusters, while neither **3** nor **4** reacts with CO under the same conditions. Reactivities of **2** with π-acceptor molecules have therefore been studied in detail, which are described below.

**Reactions of 2 with CO and Isocyanides.** Cluster **2** dissolved in THF reacted with CO gas at 50 °C to give a dicarbonyl cluster **5** as the major product. A small amount of the cationic tricarbonyl cluster [(Cp\**Ru*)<sub>3</sub>(μ<sub>3</sub>-S)(μ<sub>2</sub>-CO)<sub>3</sub>]Cl (**8**) was also formed as byproduct, which was easily separated from the reaction mixture by filtration because of its low solubility into THF (eq 4).



As expected, treatment of the isolated **5** with CO at 50

Table 3. Selected Bond Distances (Å) and Angles (deg) in **10**

Bond Distances			
Ru(1)–Ru(2)	2.786(3)		
Ru(1)–S	2.341(6)	Ru(2)–S	2.245(6)
Ru(1)–C(3)	2.14(2)	Ru(1)–C(7)	2.14(2)
Ru(1)–C(8)	2.11(2)	Ru(2)–C(2)	1.98(2)
Ru(2)–C(8)	2.05(2)	C(2)–C(3)	1.52(2)
C(3)–C(7)	1.39(2)	C(7)–C(8)	1.46(2)
Bond Angles			
Ru(1)–S–Ru(2)	74.8(2)	Ru(1)–Ru(2)–S	54.2(1)
Ru(2)–Ru(1)–S	51.0(1)	Ru(2)–Ru(1)–C(3)	72.6(5)
Ru(2)–Ru(1)–C(7)	73.0(5)	Ru(2)–Ru(1)–C(8)	47.2(4)
S–Ru(1)–C(3)	68.2(5)	S–Ru(1)–C(7)	97.8(5)
S–Ru(1)–C(8)	94.3(4)	Ru(1)–Ru(2)–C(2)	64.7(6)
Ru(1)–Ru(2)–C(8)	48.8(7)	S–Ru(2)–C(2)	46.4(5)
S–Ru(2)–C(8)	98.7(6)	C(2)–Ru(2)–C(8)	79.7(7)
Ru(2)–C(2)–C(3)	114(1)	C(2)–C(3)–C(4)	125(1)
C(2)–C(3)–C(7)	110(1)	C(4)–C(3)–C(7)	121(2)
C(3)–C(7)–C(6)	128(1)	C(3)–C(7)–C(8)	113(1)
Ru(2)–C(8)–C(7)	114(1)	Ru(2)–C(8)–C(9)	121(1)
C(7)–C(8)–C(9)	118(1)		

°C resulted in the formation of **8**, although uptake of the third CO molecule proceeded only slowly under these conditions and most of **5** was recovered unreacted after 15 h. However, **8** once formed is considerably stable and **8** dissolved in polar solvents under N<sub>2</sub> or in vacuo did not regenerate **5**. For clusters **3** and **4**, no reactions took place with CO under these conditions. In **5**, coordination of two CO ligands to the Ru<sub>3</sub> core resulted in the cleavage of one Ru–Ru single bond forming an open cluster core, along with the change in the coordination mode of the Cl ligand from a six-electron-donating μ<sub>3</sub> type to a four-electron donating μ<sub>2</sub> one, while **8** consists of a cation containing three μ<sub>2</sub>-CO ligands coordinated to a closed Ru<sub>3</sub> core together with a discrete Cl anion (vide infra). The IR spectra exhibit intense ν(CO) bands at 1777 cm<sup>-1</sup> for **5** and at 1778 and 1823 cm<sup>-1</sup> for **8**, respectively. In the <sup>1</sup>H NMR spectra, the Cp\* methyl protons of **5** dissolved in C<sub>6</sub>D<sub>6</sub> appear as two singlets at 1.65 and 1.87 ppm in a 2:1 intensity ratio, while those of **8** in CDCl<sub>3</sub> were observed as one singlet at 1.92 ppm.

Reactions of **2** with an excess amount of isocyanides such as <sup>t</sup>BuNC and 2,4,6-Me<sub>3</sub>C<sub>6</sub>H<sub>2</sub>NC have also been attempted. However, the products could not be characterized satisfactorily. <sup>1</sup>H NMR spectra of the crude products suggest that degradation of the Ru<sub>3</sub> core to give mononuclear complexes may be taking place in both reactions. On the other hand, treatment of **2** with various alkenes such as ethylene, isoprene, and CH<sub>2</sub>=CHCOOR at 50–80 °C in THF or toluene resulted in the quantitative recovery of **2**.

**X-ray Structures of 5 and 8.** To clarify the detailed structures of these two clusters, X-ray analysis has been performed by using the single crystals of **5**·THF and **8**·CH<sub>2</sub>Cl<sub>2</sub>. ORTEP drawings of **5** and **8** are shown in Figures 4 and 5, respectively, while important bonding parameters in these clusters are summarized in Table 2.

Cluster **5**·THF crystallized in monoclinic space group *P*2<sub>1</sub>/*m* with two molecules in the unit cell and the molecule consists of a crystallographically imposed mirror plane defined by the Ru(2), S(1), and Cl(1) atoms. The Ru<sub>3</sub> core in **5** has only two Ru–Ru bonds and the nonbonding Ru–Ru vector is bisected by this mirror plane. A sulfide ligand coordinates to all three Ru atoms as a μ<sub>3</sub> bridge and each Ru–Ru bond at 2.7973–

(23) Suzuki, H.; Takaya, Y.; Takemori, T. *J. Am. Chem. Soc.* **1994**, *116*, 10779.

(24) (a) Otsuka, S.; Nakamura, A.; Yoshida, T. *Ann. Chem.* **1968**, *719*, 54. (b) Frisch, P. D.; Dahl, L. F. *J. Am. Chem. Soc.* **1972**, *94*, 5082.

(25) (a) Werner, H.; Leonhard, K. *Angew. Chem.* **1979**, *91*, 663. (b) Werner, H.; Leonhard, K.; Kolb, O.; Rottinger, E.; Vahrenkamp, H. *Chem. Ber.* **1980**, *113*, 1654.

(26) (a) Fortune, J.; Manning, A. R.; Stephens, F. S. *J. Chem. Soc., Chem. Commun.* **1983**, 1071. (b) Manning, A. R.; O'Dwyer, L.; McArdle, P. A.; Cunningham, D. *J. Organomet. Chem.* **1995**, *474*, 173.

Table 4. X-ray Crystallographic Data for 2, 3, 4, 5·THF, 8·CH<sub>2</sub>Cl<sub>2</sub>, and 10

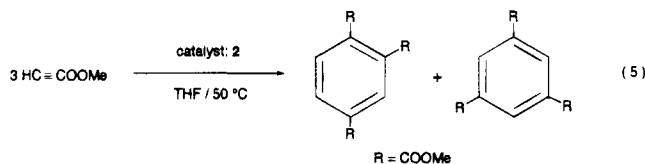
	2	3	4	5·THF	8·CH <sub>2</sub> Cl <sub>2</sub>	10
(a) Crystal Data						
formula	C <sub>30</sub> H <sub>45</sub> SClRu <sub>3</sub>	C <sub>33</sub> H <sub>52</sub> S <sub>2</sub> Ru <sub>3</sub>	C <sub>30</sub> H <sub>46</sub> S <sub>2</sub> Ru <sub>3</sub>	C <sub>36</sub> H <sub>53</sub> O <sub>3</sub> SClRu <sub>3</sub>	C <sub>34</sub> H <sub>47</sub> O <sub>3</sub> SCl <sub>3</sub> Ru <sub>3</sub>	C <sub>30</sub> H <sub>42</sub> O <sub>4</sub> SRu <sub>2</sub>
fw	776.4	816.1	774.0	904.5	945.4	700.9
cryst system	monoclinic	triclinic	orthorhombic	monoclinic	orthorhombic	triclinic
space group	<i>P</i> 2 <sub>1</sub> / <i>n</i> (No. 14)	<i>P</i> $\bar{1}$ (No. 2)	<i>P</i> bca (No. 61)	<i>P</i> 2 <sub>1</sub> / <i>m</i> (No. 11)	<i>P</i> 2 <sub>1</sub> 2 <sub>1</sub> 2 <sub>1</sub> (No. 19)	<i>P</i> $\bar{1}$ (No. 2)
cryst color	dark brown	dark brown	dark brown	dark red	dark purple	dark green
cryst dimens, mm	0.3 × 0.5 × 0.6	0.3 × 0.5 × 0.7	0.1 × 0.1 × 0.3	0.2 × 0.3 × 0.7	0.2 × 0.3 × 0.7	0.2 × 0.2 × 0.3
<i>a</i> , Å	11.588(2)	11.149(3)	18.576(7)	8.788(2)	17.611(2)	11.094(4)
<i>b</i> , Å	22.517(4)	17.795(4)	22.277(4)	18.518(2)	19.977(2)	16.128(7)
<i>c</i> , Å	12.443(2)	9.041(1)	15.392(9)	11.317(1)	10.682(3)	8.774(5)
$\alpha$ , deg	90.00	90.05(2)	90.00	90.00	90.00	91.16(4)
$\beta$ , deg	101.90(2)	102.09(2)	90.00	90.42(1)	90.00	106.87(4)
$\gamma$ , deg	90.00	89.33(2)	90.00	90.00	90.00	101.20(3)
<i>V</i> , Å <sup>3</sup>	3176(1)	1754.0(6)	6369(4)	1841.6(5)	3758.0(10)	1468(1)
<i>Z</i>	4	2	8	2	4	2
<i>D</i> <sub>calc</sub> , g cm <sup>-3</sup>	1.623	1.545	1.614	1.631	1.671	1.585
<i>F</i> (000), electrons	1560	828	3120	916	1896	716
$\mu$ (Mo K $\alpha$ ), cm <sup>-1</sup>	15.75	14.14	15.53	13.77	14.91	11.32
(b) Data Collection						
diffractometer	Rigaku AFC7R					
monochromator	graphite					
radiation ( $\lambda$ , Å)	Mo K $\alpha$ (0.7107)					
temperature	room temperature					
2 $\theta$ <sub>max</sub> , deg	55					
scan type	$\omega$ -2 $\theta$					
scan rate, deg min <sup>-1</sup>	16					
reflectns measured	+ <i>h</i> , + <i>k</i> , $\pm$ <i>l</i>	+ <i>h</i> , $\pm$ <i>k</i> , $\pm$ <i>l</i>	+ <i>h</i> , + <i>k</i> , + <i>l</i>	+ <i>h</i> , + <i>k</i> , $\pm$ <i>l</i>	+ <i>h</i> , + <i>k</i> , + <i>l</i>	+ <i>h</i> , $\pm$ <i>k</i> , $\pm$ <i>l</i>
no. of unique reflectns	7483	8055	7996	4385	4832	6747
absorption correctns	$\psi$ -scans					
transmission factors	0.545–1.00	0.789–1.00	0.655–1.00	0.861–1.00	0.912–1.00	0.699–1.00
(c) Solution and Refinement						
data used ( <i>I</i> > 3 $\sigma$ ( <i>I</i> ))	3750	4964	2700	3365	3206	2791 ( <i>I</i> > 4 $\sigma$ ( <i>I</i> ))
no. of variables	316	343	316	208	397	334
<i>R</i>	0.077	0.044	0.079	0.038	0.043	0.092
<i>R</i> <sub>w</sub>	0.110	0.045	0.050	0.032	0.028	0.064
max residual, e Å <sup>-3</sup>	1.7	1.5	1.8	0.66	1.0	2.3

(7) Å is further bridged by a  $\mu_2$ -CO ligand. On the other hand, the Ru(1) and Ru(1)\* atoms separated by 3.48 Å are connected by a  $\mu_2$ -Cl ligand. The Ru(2)–S(1) bond length at 2.285(2) Å, being slightly shorter than the Ru(1)–S(1) distance of 2.311(1) Å, is comparable to the Ru–S(sulfide) bond lengths in 2–4. It is to be noted that the  $\mu_3$ -S ligand in the previously reported Ru<sub>3</sub> clusters with only two Ru–Ru bonds such as [(*p*-cymene)Ru]<sub>3</sub>( $\mu_3$ -S)<sub>2</sub>]<sup>7</sup> and [Ru<sub>3</sub>(CO)<sub>8</sub>( $\mu_3$ -S)( $\mu_2$ -H)<sub>2</sub>( $\mu_2$ -Cl)(SnCl<sub>3</sub>)] (9)<sup>20</sup> has the longer Ru–S bonds in the range of 2.328(2)–2.351(2) Å and 2.361(2)–2.411(2) Å, respectively. As for the  $\mu_2$ -Cl ligand bridging the nonbonded Ru atoms, the Ru–Cl distance at 2.480(1) Å is comparable to those in the analogous  $\mu_2$ -Cl ligands in 7 (2.445(2)–2.496(2) Å) and 9 (2.443(2)–2.469(2) Å). However, it is considerably longer than the Ru–Cl lengths for the Cl ligands bridging the Ru–Ru single bond in [(Cp\*Ru)<sub>3</sub>( $\mu_2$ -Cl)<sub>2</sub>( $\mu_2$ -H)( $\mu_3$ -CH)] [BF<sub>4</sub>]<sup>-</sup> (2.416(1) and 2.363(1) Å)<sup>27</sup> as well as that capping the Ru<sub>3</sub> core with three Ru–Ru single bonds in 2, and is shorter than those for the  $\mu_3$ -Cl ligands bound to nonbonded Ru<sub>3</sub> cores in 1 and 7 (vide supra). The Ru–Ru–C(1) and Ru–Ru–Cl planes are not coplanar with the Ru<sub>3</sub> basal plane and folded to the direction opposite to the  $\mu_3$ -S ligand.

The cationic part of cluster 8 contains a triangular core of three mutually bonded Ru atoms with the Ru–Ru distances at 2.769(1)–2.771(1) Å, which is capped by a  $\mu_3$ -S ligand. The Ru–S bond lengths varying from 2.276(3) to 2.287(3) Å are not different from those in the other clusters reported here. Each Ru–Ru bond is

bridged by a  $\mu_2$ -CO ligand almost symmetrically and the C(1)–, C(2)–, and C(3)–Ru–Ru planes are bent from the Ru<sub>3</sub> basal plane by the angles of 117.8°, 118.4°, and 119.5°, respectively, toward the other side of the capped S ligand. These three planes are almost coplanar with the corresponding Ru–Ru–S(1) planes; dihedral angles around the Ru(1)–Ru(2), Ru(1)–Ru(3), and Ru(2)–Ru(3) bonds are 178.3°, 178.0°, and 176.5°, respectively. Three Cp\* ligands bind to the Ru<sub>3</sub> plane almost perpendicularly by the angles of 82.0–82.9°.

**Reactions of 2 with HC≡CCOOMe and MeOCO-C≡CCOOMe To Give Cyclic Alkyne Trimers.** It has been demonstrated that 2 readily reacts with excess HC≡CCOOMe in THF at 50 °C to give the alkyne trimers in high yield (eq 5). Thus, in the reaction using



180 equiv of the alkyne per mole of 2, all the alkyne charged has been consumed, and the <sup>1</sup>H NMR study has disclosed that the reaction mixture after 15 h contains 1,3,5- and 1,2,4-C<sub>6</sub>H<sub>3</sub>(COOMe)<sub>3</sub> along with 2 as the sole organic and organometallic species detectable by <sup>1</sup>H NMR criteria. The alkyne trimers were isolated in 95% combined yield, and the 1,3,5- and 1,2,4-isomers ratio has been determined to be 42:58 by the <sup>1</sup>H NMR and GLC studies. Reaction of MeOCOC≡CCOOMe with 2 proceeded analogously to give C<sub>6</sub>(COOMe)<sub>6</sub> exclusively,

(27) Kakigano, T.; Suzuki, H.; Igarashi, M.; Moro-oka, Y. *Organometallics* 1990, 9, 2192.

Table 5. Coordinates of Non-Hydrogen Atoms in 2

atom	x	y	z
Ru(1)	0.1538(1)	0.09130(7)	-0.2055(1)
Ru(2)	0.2853(1)	0.09841(7)	-0.3775(1)
Ru(3)	0.0886(1)	0.17679(7)	-0.3820(1)
Cl(1)	0.0856(4)	0.0717(2)	-0.3941(4)
S(1)	0.2602(4)	0.1696(2)	-0.2533(4)
C(1)	0.028(2)	0.068(1)	-0.107(2)
C(2)	0.090(2)	0.018(1)	-0.125(2)
C(3)	0.209(2)	0.0238(10)	-0.080(2)
C(4)	0.228(2)	0.0790(8)	-0.036(2)
C(5)	0.114(2)	0.1094(6)	-0.048(2)
C(6)	-0.102(2)	0.081(1)	-0.132(2)
C(7)	0.025(3)	-0.037(1)	-0.178(2)
C(8)	0.305(3)	-0.020(1)	-0.075(3)
C(9)	0.344(3)	0.099(2)	0.029(3)
C(10)	0.094(3)	0.174(1)	-0.002(3)
C(11)	0.467(2)	0.0844(10)	-0.353(2)
C(12)	0.432(2)	0.1306(9)	-0.434(2)
C(13)	0.360(2)	0.095(1)	-0.520(2)
C(14)	0.349(2)	0.038(1)	-0.494(2)
C(15)	0.412(2)	0.028(1)	-0.387(2)
C(16)	0.553(3)	0.098(2)	-0.244(3)
C(17)	0.481(3)	0.186(2)	-0.446(4)
C(18)	0.304(3)	0.125(2)	-0.634(3)
C(19)	0.266(3)	-0.006(2)	-0.568(3)
C(20)	0.421(4)	-0.031(1)	-0.329(3)
C(21)	-0.065(2)	0.2329(9)	-0.375(2)
C(22)	0.040(2)	0.2690(8)	-0.368(2)
C(23)	0.087(2)	0.2572(10)	-0.470(2)
C(24)	0.006(2)	0.2184(9)	-0.534(2)
C(25)	-0.083(2)	0.204(1)	-0.477(2)
C(26)	-0.139(3)	0.231(2)	-0.294(3)
C(27)	0.086(3)	0.311(2)	-0.272(3)
C(28)	0.189(3)	0.291(1)	-0.495(4)
C(29)	0.012(3)	0.203(2)	-0.649(2)
C(30)	-0.183(3)	0.168(1)	-0.523(3)

but that of *p*-MeC<sub>6</sub>H<sub>4</sub>C≡CH resulted in the complete recovery of the alkyne under the similar conditions. Our recent studies on the reactions of various terminal alkynes HC≡CR with the dinuclear Ru(II) complex [Cp\*<sub>2</sub>Ru(μ<sub>2</sub>-Si<sup>i</sup>Pr)<sub>2</sub>RuCp\*] have disclosed the formation of either ruthenacyclic compounds (R = COOMe, *p*-MeC<sub>6</sub>H<sub>4</sub>, cyclohexenyl) or a π-alkyne complex (R = Me<sub>3</sub>Si) in which two or three alkyne molecules are coupled and incorporated at the diruthenium centers.<sup>28</sup> However, cyclotrimerization of the alkynes does not proceed in none of these systems.

Transition metal-catalyzed cyclotrimerization of alkynes to give benzene derivatives has been studied extensively, and numerous catalyst systems promoting this reaction have been reported.<sup>29</sup> However, reactions catalyzed by Ru species have been relatively poorly studied.<sup>30</sup> Moreover, most of the systems reported to date involve mono- and dinuclear complexes and those using metal clusters as catalysts or catalyst precursors are still limited,<sup>31</sup> e.g. [Fe<sub>3</sub>(CO)<sub>12</sub>] and [Co<sub>4</sub>(CO)<sub>10</sub>-(PhCCPh)] for PhC≡CPh,<sup>32</sup> [Ni<sub>4</sub>(CN<sup>t</sup>Bu)<sub>7</sub>] for HC≡CH

(28) (a) Matsuzaka, H.; Mizobe, Y.; Nishio, M.; Hidai, M. *J. Chem. Soc., Chem. Commun.* **1991**, 1101. (b) Nishio, M.; Matsuzaka, H.; Mizobe, Y.; Hidai, M. *Ibid.* **1993**, 375. (c) Nishio, M.; Matsuzaka, H.; Mizobe, Y.; Tanase, T.; Hidai, M. *Organometallics* **1994**, *13*, 4214. (d) Koelle, U.; Rietmann, Chr.; Tjoe, J.; Wagner, T.; Englert, U. *Ibid.* **1995**, *14*, 703.

(29) (a) Schore, N. E. *Chem. Rev.* **1988**, *88*, 1081. (b) Winter, M. J. In *The Chemistry of Metal-Carbon Bond*; Hartley, F. R., Patai, S., Eds.; John Wiley & Sons: Chichester, 1985; Vol. 3, p 259.

(30) Formation of arene complexes from coupling of three alkyne molecules in the coordination sphere of Ru was previously observed. See, for example: (a) Lucherini, A.; Porri, L. *J. Organomet. Chem.* **1978**, *155*, C45. (b) Burt, R.; Cooke, M.; Green, M. *J. Chem. Soc. (A)* **1970**, 2981. (c) Reference 15.

(31) Süss-Fink, G.; Meister, G. *Adv. Organomet. Chem.* **1993**, *35*, 41.

Table 6. Coordinates of Non-Hydrogen Atoms in 3

atom	x	y	z
Ru(1)	0.26648(5)	-0.15937(3)	-0.18462(7)
Ru(2)	0.32250(5)	-0.32166(3)	-0.17183(7)
Ru(3)	0.06525(5)	-0.26954(3)	-0.23066(7)
S(1)	0.2208(2)	-0.24969(10)	-0.0269(2)
S(2)	0.2148(2)	-0.25037(10)	-0.3584(2)
C(1)	0.2098(9)	-0.2514(5)	-0.5606(9)
C(2)	0.337(1)	-0.2346(7)	-0.586(1)
C(3)	0.116(1)	-0.1916(6)	-0.634(1)
C(4)	0.4172(7)	-0.0835(4)	-0.181(1)
C(5)	0.3144(8)	-0.0510(4)	-0.285(1)
C(6)	0.2218(8)	-0.0380(4)	-0.201(1)
C(7)	0.2669(7)	-0.0596(4)	-0.0490(10)
C(8)	0.3913(7)	-0.0887(4)	-0.036(1)
C(9)	0.5384(8)	-0.1023(5)	-0.222(2)
C(10)	0.309(1)	-0.0280(6)	-0.444(1)
C(11)	0.0992(8)	-0.0017(5)	-0.262(1)
C(12)	0.1994(10)	-0.0494(5)	0.078(1)
C(13)	0.4779(10)	-0.1113(5)	0.104(1)
C(14)	0.488(1)	-0.3742(7)	-0.209(2)
C(15)	0.504(1)	-0.3574(6)	-0.059(2)
C(16)	0.423(2)	-0.397(1)	-0.002(2)
C(17)	0.354(1)	-0.4378(7)	-0.120(3)
C(18)	0.396(1)	-0.4246(7)	-0.244(2)
C(19)	0.572(2)	-0.346(1)	-0.308(3)
C(20)	0.602(2)	-0.3084(8)	0.024(3)
C(21)	0.402(3)	-0.404(2)	0.152(2)
C(22)	0.256(1)	-0.4943(8)	-0.109(4)
C(23)	0.354(2)	-0.458(1)	-0.396(2)
C(24)	-0.1228(6)	-0.2305(5)	-0.311(1)
C(25)	-0.0979(6)	-0.2418(5)	-0.1503(10)
C(26)	-0.0707(6)	-0.3191(5)	-0.123(1)
C(27)	-0.0789(7)	-0.3555(5)	-0.264(1)
C(28)	-0.1110(7)	-0.3023(6)	-0.379(1)
C(29)	-0.1666(8)	-0.1600(6)	-0.393(1)
C(30)	-0.1083(8)	-0.1826(5)	-0.035(1)
C(31)	-0.0415(9)	-0.3566(6)	0.034(1)
C(32)	-0.0635(9)	-0.4392(5)	-0.284(2)
C(33)	-0.1437(10)	-0.3205(8)	-0.542(1)

and dialkylacetylenes,<sup>33</sup> and [Ru<sub>3</sub>(CO)<sub>12</sub>]/L (L = PPh<sub>3</sub>, P<sup>n</sup>Bu<sub>3</sub>, P(OPh)<sub>3</sub>, and PPh<sub>2</sub>Cl) for HC≡CCOOMe.<sup>34</sup> If compared with the latter [Ru<sub>3</sub>(CO)<sub>12</sub>] based system, the present reaction using **2** may be featured by the much higher yield of the cyclic trimers (95% vs 26–58%) and the lower reaction temperature for effective catalysis (50 °C vs 130 °C). Difference in the 1,2,4- and 1,3,5-isomer ratio between these systems is also noteworthy (**2**: 1.4; [Ru<sub>3</sub>(CO)<sub>12</sub>]/L: 1.7–3.4).

Although detailed studies on the mechanism of the cyclotrimerization of alkynes have appeared already, these are limited mostly to the reactions using mononuclear<sup>29,35</sup> or binuclear<sup>29,36</sup> catalysts, and few mechanistic studies are available associated with the trimerization facilitated at the trimetallic site.<sup>37,40</sup> In this

(32) Hübel, W.; Hoogzand, C. *Chem. Ber.* **1960**, *93*, 103.

(33) Thomas, M. G.; Pretzer, W. R.; Beier, B. F.; Hirsekorn, F. J.; Muetterties, E. L. *J. Am. Chem. Soc.* **1977**, *99*, 743.

(34) Ren, C. Y.; Cheng, W. C.; Chan, W. C.; Yeung, C. H.; Lau, C. P. *J. Mol. Catal.* **1990**, *59*, L1.

(35) See also, for example: (a) Bianchini, C.; Caulton, K. G.; Chardon, C.; Doublet, M.-L.; Eisenstein, O.; Jackson, S. A.; Johnson, T. J.; Meli, A.; Poruzzini, M.; Streib, W. E.; Vacca, A.; Vizza, F. *Organometallics* **1994**, *13*, 2010. (b) Smith, D. P.; Strickler, J. R.; Gray, S. D.; Bruck, M. A.; Holmes, R. S.; Wigley, D. E. *Ibid.* **1992**, *11*, 1275. (c) Wakatsuki, Y.; Nomura, O.; Kitaura, K.; Morokuma, K.; Yamazaki, H. *J. Am. Chem. Soc.* **1983**, *105*, 1907. (d) Maitlis, P. M. *Acc. Chem. Res.* **1976**, *9*, 93.

(36) (a) Dickson, R. S.; Fraser, P. J. *Adv. Organomet. Chem.* **1974**, *12*, 323. (b) Polyi, G.; Varadi, G.; Marko, L. In *Stereochemistry of Organometallic and Inorganic Compounds*; Bernal, I., Ed.; Elsevier: Amsterdam, 1986; p 358.

(37) Coordination of alkynes to the triangular Ru<sub>3</sub> core has been well defined previously, e.g. [Ru(CO)<sub>3</sub>]<sub>3</sub>(μ<sub>3</sub>-S)(μ<sub>3</sub>-HCCPh)<sup>38</sup> and [Pt<sub>3</sub>(CO)<sub>20</sub>(μ<sub>3</sub>-H)(μ<sub>2</sub>-H)(μ<sub>3</sub>-PhCCPh)]<sup>39</sup>. See also: Sappa, E.; Tiripicchio, A.; Braunstein, P. *Chem. Rev.* **1983**, *83*, 203.

**Table 7. Coordinates of Non-Hydrogen Atoms in 4**

atom	x	y	z
Ru(1)	0.2607(1)	0.06934(7)	0.1367(1)
Ru(2)	0.18407(8)	0.15005(9)	0.0316(2)
Ru(3)	0.33456(8)	0.15508(10)	0.0320(2)
S(1)	0.2627(3)	0.0775(2)	-0.0117(3)
S(2)	0.2575(3)	0.1718(2)	0.1465(3)
C(1)	0.214(2)	0.030(1)	0.252(2)
C(2)	0.289(2)	0.037(2)	0.271(2)
C(3)	0.328(2)	0.006(1)	0.213(2)
C(4)	0.285(2)	-0.023(2)	0.161(2)
C(5)	0.207(2)	-0.012(1)	0.185(2)
C(6)	0.154(1)	0.053(1)	0.309(2)
C(7)	0.314(1)	0.0777(9)	0.347(1)
C(8)	0.409(1)	0.003(2)	0.203(2)
C(9)	0.302(2)	-0.0698(10)	0.087(2)
C(10)	0.142(1)	-0.041(1)	0.146(2)
C(11)	0.068(1)	0.153(2)	0.049(2)
C(12)	0.081(1)	0.129(1)	-0.028(3)
C(13)	0.121(1)	0.171(2)	-0.087(2)
C(14)	0.131(2)	0.225(2)	-0.033(3)
C(15)	0.089(2)	0.209(2)	0.048(3)
C(16)	0.022(1)	0.127(2)	0.115(2)
C(17)	0.061(1)	0.069(1)	-0.064(2)
C(18)	0.143(2)	0.164(2)	-0.177(2)
C(19)	0.161(1)	0.283(2)	-0.063(2)
C(20)	0.088(1)	0.263(2)	0.110(2)
C(21)	0.416(2)	0.158(2)	-0.074(2)
C(22)	0.380(2)	0.216(2)	-0.065(3)
C(23)	0.403(2)	0.235(1)	0.024(3)
C(24)	0.440(1)	0.186(2)	0.060(2)
C(25)	0.450(1)	0.144(2)	0.007(3)
C(26)	0.421(2)	0.118(2)	-0.154(2)
C(27)	0.344(2)	0.250(2)	-0.139(2)
C(28)	0.383(2)	0.297(1)	0.042(3)
C(29)	0.468(2)	0.197(2)	0.153(2)
C(30)	0.492(1)	0.087(2)	0.019(3)

**Table 8. Coordinates of Non-Hydrogen Atoms in 5·THF**

atom	x	y	z
Ru(1)	0.13232(5)	0.15617(2)	0.21659(4)
Ru(2)	0.26607(6)	0.2500	0.38087(5)
Cl(1)	-0.0629(2)	0.2500	0.1774(2)
S(1)	0.2992(2)	0.2500	0.1808(2)
O(1)	0.0133(4)	0.1526(2)	0.4655(3)
O(2)	0.604(2)	0.2500	0.879(1)
C(1)	0.0900(5)	0.1744(3)	0.3883(4)
C(2)	0.2401(8)	0.0790(3)	0.0995(8)
C(3)	0.226(1)	0.0463(4)	0.2062(8)
C(4)	0.068(1)	0.0404(4)	0.2321(6)
C(5)	-0.0103(6)	0.0716(3)	0.1365(7)
C(6)	0.1004(8)	0.0947(3)	0.0558(5)
C(7)	0.389(1)	0.0913(5)	0.038(1)
C(8)	0.358(2)	0.0095(5)	0.271(1)
C(9)	0.003(2)	0.0027(5)	0.3346(8)
C(10)	-0.1774(8)	0.0756(5)	0.120(1)
C(11)	0.067(1)	0.1281(4)	-0.0616(6)
C(12)	0.3121(9)	0.2500	0.5745(6)
C(13)	0.3818(6)	0.1879(3)	0.5265(5)
C(14)	0.4937(5)	0.2118(3)	0.4468(4)
C(15)	0.196(1)	0.2500	0.6686(8)
C(16)	0.3547(8)	0.1116(4)	0.5664(5)
C(17)	0.6084(6)	0.1651(4)	0.3837(5)
C(18)	0.7449(9)	0.2104(5)	0.7248(7)
C(19)	0.638(1)	0.1877(4)	0.8107(9)

respect, the present reaction using **2** is of particular interest. However, all attempts to isolate or detect the

(38) Adams, R. D.; Babin, J. E.; Tasi, M.; Wolfe, T. A. *Organometallics* **1987**, *6*, 2228.

(39) Adams, R. D.; Li, Z.; Swepston, P.; Wu, W.; Yamamoto, J. J. *Am. Chem. Soc.* **1992**, *114*, 10657.

(40) Transformation of HC≡CPh into 1,3,5-Ph<sub>3</sub>C<sub>6</sub>H<sub>3</sub> using a cluster [Cp<sub>2</sub>Mo<sub>2</sub>Ru(μ<sub>3</sub>-S)(CO)<sub>7</sub>] has been shown to proceed through an intermediate [Cp<sub>2</sub>Mo<sub>2</sub>Ru(μ<sub>3</sub>-S)(CO)<sub>5</sub>(μ<sub>3</sub>-η<sup>6</sup>-CHCPhCHCPhCHCPh)]: Adams, R. D.; Babin, J. E.; Tasi, J. E.; Wang, J.-G. *Organometallics* **1988**, *7*, 755.

**Table 9. Coordinates of Non-Hydrogen Atoms in 8·CH<sub>2</sub>Cl<sub>2</sub>**

atom	x	y	z
Ru(1)	0.05001(4)	0.14773(4)	0.05648(8)
Ru(2)	0.10345(5)	0.05150(4)	-0.10793(8)
Ru(3)	-0.02126(4)	0.02440(4)	0.04186(9)
Cl(1)	0.7420(2)	0.1955(2)	0.2902(4)
Cl(2)	0.7636(3)	0.1207(3)	0.6527(6)
Cl(3)	0.8769(4)	0.2192(3)	0.6424(6)
S(1)	-0.0117(1)	0.1032(1)	-0.1125(3)
O(1)	0.2100(4)	0.0985(4)	0.0951(7)
O(2)	0.0447(4)	0.0638(4)	0.2912(6)
O(3)	0.1154(4)	-0.0660(3)	0.0691(7)
C(1)	0.1514(6)	0.0973(5)	0.042(1)
C(2)	0.0324(5)	0.0715(5)	0.1838(9)
C(3)	0.0841(5)	-0.0179(6)	0.0239(9)
C(4)	0.1141(6)	0.2437(4)	0.0780(9)
C(5)	0.0879(6)	0.2224(5)	0.196(1)
C(6)	0.0058(6)	0.2222(5)	0.195(1)
C(7)	-0.0181(6)	0.2424(5)	0.076(1)
C(8)	0.0488(6)	0.2558(5)	0.0022(10)
C(9)	0.1950(5)	0.2599(5)	0.041(1)
C(10)	0.1370(7)	0.2115(6)	0.307(1)
C(11)	-0.0418(7)	0.2091(5)	0.309(1)
C(12)	-0.1008(6)	0.2517(6)	0.030(1)
C(13)	0.0492(7)	0.2843(5)	-0.131(1)
C(14)	0.2102(6)	0.0052(6)	-0.176(1)
C(15)	0.2089(7)	0.0738(5)	-0.218(1)
C(16)	0.1458(7)	0.0806(5)	-0.296(1)
C(17)	0.1072(7)	0.0203(7)	-0.308(1)
C(18)	0.1468(6)	-0.0279(6)	-0.236(1)
C(19)	0.2703(6)	-0.0276(6)	-0.097(1)
C(20)	0.2713(7)	0.1232(6)	-0.190(1)
C(21)	0.1268(7)	0.1450(6)	-0.366(1)
C(22)	0.0425(6)	0.0063(6)	-0.3938(10)
C(23)	0.1330(7)	-0.1030(5)	-0.231(1)
C(24)	-0.0698(6)	-0.0582(6)	0.159(1)
C(25)	-0.1153(6)	0.0004(5)	0.175(1)
C(26)	-0.1469(5)	0.0165(5)	0.058(1)
C(27)	-0.1209(6)	-0.0309(6)	-0.034(1)
C(28)	-0.0739(6)	-0.0778(5)	0.031(1)
C(29)	-0.0321(7)	-0.0958(6)	0.259(1)
C(30)	-0.1353(6)	0.0328(6)	0.298(1)
C(31)	-0.2036(6)	0.0716(6)	0.030(1)
C(32)	-0.1428(6)	-0.0348(6)	-0.171(1)
C(33)	-0.0448(7)	-0.1394(5)	-0.028(1)
C(34)	0.824(1)	0.163(1)	0.565(1)

intermediate stages were unsuccessful.<sup>41</sup> The <sup>1</sup>H NMR spectra of the mixtures at the various stages of the reaction demonstrated only the presence of **2** as the Cp\*-containing Ru species, and **2** was actually recovered almost quantitatively after catalysis. However, the rate of the trimerization did not increase linearly with increase in the concentration of **2**.<sup>42</sup> Thus, the trimerization might be catalyzed by a small amount of mono- or dinuclear Ru species generated in situ during the reaction.<sup>43</sup> It should also be noted that reactions of HC≡CCOOMe and MeOCOC≡CCOOMe with the dicarbonyl cluster **5** under N<sub>2</sub> also proceeded analogously to that with **2**, giving cyclic trimers selectively, and after catalysis **5** was recovered quantitatively with both CO ligands intact.

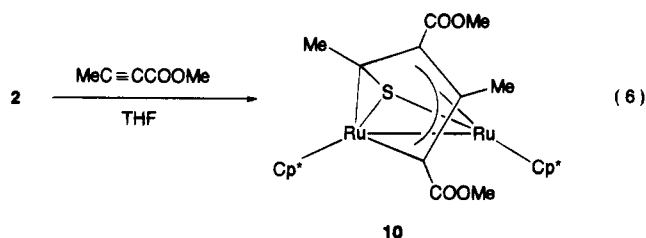
**Reaction of 2 with MeC≡CCOOMe.** To isolate or detect the intermediate stages involved in the cyclotri-

(41) The NMR studies of the reaction mixtures under various conditions (changing the reaction time, temperature, and substrate/cluster ratio) revealed only the presence of either the cyclic trimers and **2** or these together with the unreacted alkyne.

(42) The rates of the formation of the trimers observed in the three independent runs with the cluster concentration of 5.0, 10.8, and 13.4 mM are 0.42, 0.60, and 0.51 mmol min<sup>-1</sup>, respectively. The initial concentration of HC≡CCOOMe in these runs is about 0.39 M.

(43) Even if a monometallic Ru complex [Cp\*Ru(PMePh<sub>2</sub>)<sub>2</sub>Cl] was used, the trimerization of HC≡CCOOMe occurred under these conditions, although the yield and selectivity of the cyclic trimers were poor.

merization, reactions of more diversified alkynes with **2** were attempted. This has led to the finding that treatment of **2** with excess MeC≡CCOOMe in THF at 50 °C results in degradation of the Ru<sub>3</sub> core, and diruthenium complex [Cp\*Ru{μ<sub>2</sub>-SCMeC(COOMe)CMeC(COOMe)}RuCp\*] (**10**) has been isolated from the reaction mixture in moderate yield (eq 6). Other fragmentation product(s) presumably containing a Cp\*RuCl moiety could not be isolated. The GC-MS study of the reaction mixture has shown that the alkyne trimers are produced also in this reaction but the yields are quite low. Reaction of this alkyne with **5** did not occur under the similar conditions.



The structure of **10** has been determined unambiguously by X-ray crystallography; ORTEP drawing is shown in Figure 6 and selected bond distances and angles are listed in Table 3. Complex **10** has two Cp\*Ru units connected by a Ru-Ru single bond (2.786(3) Å). Two Cp\* ligands are mutually cis, the dihedral angle between two Cp\* planes being 59.1°. In **10**, four C atoms of two alkynes linked in a head-to-tail manner comprise a five-membered ring together with one Ru atom, of which the three C atoms further coordinate to the other Ru atom in a π-allyl manner. The bonding parameters around the C(3), C(7), and C(8) atoms are consistent with this feature. Relating μ<sub>2</sub>-ruthenacyclopentenyl cores have been demonstrated recently for the products from the reactions of [Cp\*Ru(μ<sub>2</sub>-Si<sup>i</sup>Pr)<sub>2</sub>Ru(Cp\*)] with TolC≡CH, cyclohexenylacetylene,<sup>28b</sup> and HC≡C-COOMe.<sup>28c</sup> The sulfur atom bridging the two Ru atoms is further bound to the α-C atom involved in the five-membered ruthenacycle.

### Experimental Section

**General.** All manipulations were performed under an atmosphere of nitrogen using standard Schlenk techniques. Solvents were dried by common procedures and degassed before use. Compound **1** was prepared according to the literature method,<sup>44</sup> while NaS<sup>i</sup>Pr was obtained from the reaction of HS<sup>i</sup>Pr with NaH in THF. Lithium sulfide was used as received, while alkynes commercially obtained were degassed and stored over molecular sieve 4 Å. IR spectra were recorded on a Shimadzu FTIR-8100M spectrometer, and <sup>1</sup>H NMR spectra were obtained by a JEOL EX-270 spectrometer. GLC analysis was performed using a Shimadzu GC-14A gas chromatograph equipped with a HiCap-CBP10-M25-025 capillary column, while GC-MS study was carried out by the use of a Shimadzu GCMS-QP2000 spectrometer. Elemental analyses were done by a Perkin-Elmer 2400II CHN analyzer (for C, H, and N) or at the Elemental Analysis Laboratory, Department of Chemistry, Faculty of Science, The University of Tokyo (for Cl and S).

**Preparation of 2.** A suspension of **1** (104 mg, 0.096 mmol) and Li<sub>2</sub>S (10 mg, 0.21 mmol) in THF (5 mL) was stirred at 50 °C for 15 h. The resultant brown solution was filtered, and

**Table 10.** Coordinates of Non-Hydrogen Atoms in **10**

atom	x	y	z
Ru(1)	0.1989(2)	0.2336(1)	-0.1480(2)
Ru(2)	0.4334(2)	0.2791(1)	-0.2129(2)
S	0.3504(5)	0.3618(3)	-0.0792(6)
O(1)	-0.042(2)	0.336(1)	-0.447(2)
O(2)	0.096(1)	0.431(1)	-0.280(2)
O(3)	0.243(1)	0.0872(9)	-0.542(2)
O(4)	0.313(1)	0.0635(9)	-0.292(2)
C(1)	0.346(2)	0.438(1)	-0.367(2)
C(2)	0.315(2)	0.358(1)	-0.280(2)
C(3)	0.173(2)	0.316(1)	-0.337(3)
C(4)	0.069(2)	0.358(2)	-0.366(3)
C(5)	0.000(2)	0.478(2)	-0.287(3)
C(6)	0.033(2)	0.179(1)	-0.532(3)
C(7)	0.156(2)	0.234(1)	-0.402(2)
C(8)	0.266(2)	0.195(1)	-0.333(3)
C(9)	0.269(2)	0.113(1)	-0.409(2)
C(10)	0.321(2)	-0.016(1)	-0.344(3)
C(11)	0.195(2)	0.217(1)	0.095(2)
C(12)	0.090(2)	0.248(1)	0.010(3)
C(13)	0.026(2)	0.179(2)	-0.086(3)
C(14)	0.098(2)	0.116(1)	-0.089(3)
C(15)	0.206(2)	0.142(1)	0.040(2)
C(16)	0.288(2)	0.272(2)	0.242(2)
C(17)	0.031(2)	0.313(2)	0.046(3)
C(18)	-0.111(2)	0.169(2)	-0.218(3)
C(19)	0.059(2)	0.030(2)	-0.183(3)
C(20)	0.300(2)	0.091(1)	0.101(2)
C(21)	0.593(2)	0.205(1)	-0.130(3)
C(22)	0.572(2)	0.224(1)	-0.278(3)
C(23)	0.594(2)	0.300(2)	-0.304(3)
C(24)	0.634(1)	0.352(1)	-0.156(3)
C(25)	0.631(2)	0.287(2)	-0.038(2)
C(26)	0.599(2)	0.124(1)	-0.063(3)
C(27)	0.562(2)	0.163(1)	-0.428(3)
C(28)	0.612(2)	0.352(1)	-0.448(2)
C(29)	0.683(2)	0.446(1)	-0.093(3)
C(30)	0.659(2)	0.297(2)	0.139(3)

the filtrate was concentrated in vacuo. Dark brown crystals precipitated after storage at -20 °C were filtered off and dried (50 mg, 50% yield based on Ru atom). <sup>1</sup>H NMR (C<sub>6</sub>D<sub>6</sub>): δ 1.83 (s, Cp\*). Anal. Calcd for C<sub>30</sub>H<sub>45</sub>SClRu<sub>3</sub>: C, 46.41; H, 5.84; S, 4.13; Cl, 4.57. Found: C, 45.96; H, 5.84; S, 4.51; Cl, 5.14.

**Preparation of 3.** A suspension containing **1** (174 mg, 0.160 mmol), Li<sub>2</sub>S (10 mg, 0.21 mmol), and NaS<sup>i</sup>Pr (42 mg, 0.43 mmol) in THF (10 mL) was stirred at 50 °C for 15 h. The resultant brown solution was filtered, and the concentrated filtrate was kept at -20 °C. Dark brown crystals deposited were collected by filtration and dried in vacuo (116 mg, 68% yield based on Ru atom). <sup>1</sup>H NMR (C<sub>6</sub>D<sub>6</sub>): δ 1.92 (s, 45H, Cp\*), 1.97 (d, *J* = 6.8 Hz, 6H, SCHMe<sub>2</sub>), 4.06 (sep, *J* = 6.8 Hz, 1H, SCHMe<sub>2</sub>). Anal. Calcd for C<sub>33</sub>H<sub>52</sub>S<sub>2</sub>Ru<sub>3</sub>: C, 48.56; H, 6.42; S, 7.86. Found: C, 47.85; H, 6.38; S, 8.35.

**Preparation of 4.** Into a suspension of **1** (133 mg, 0.122 mmol) in THF (10 mL) was added (Me<sub>3</sub>Si)<sub>2</sub>S (218 μL, 1.23 mmol), and the mixture was stirred at room temperature for 15 h. Carbon monoxide gas was passed through the resultant yellow-brown solution for 2 min, and then the mixture was continuously stirred at 50 °C under CO atmosphere for 15 h. Red precipitate of **8** was removed by filtration, and the storage of the filtrate at -20 °C afforded additional amount of **5**. After separating the precipitate by filtration, the filtrate was concentrated and cooled to -20 °C, giving **4** as brown crystals (14 mg, 14%). <sup>1</sup>H NMR (C<sub>6</sub>D<sub>6</sub>): δ 1.92 (s, 30H, Cp\*), 2.07 (s, 15H, Cp\*), -22.3 (s, 1H, RuHRu). Anal. Calcd for C<sub>30</sub>H<sub>46</sub>S<sub>2</sub>Ru<sub>3</sub>: C, 46.55; H, 5.99; S, 8.28. Found: C, 46.28; H, 6.12; S, 7.81.

**Preparation of 5.** After dissolving **2** (32 mg, 0.041 mmol) in THF (12.5 mL), CO gas was bubbled through the solution for 2 min, and the mixture was stirred continuously under CO for 15 h at 50 °C. The initial brown solution changed in color to red-purple, and formation of a small amount of red solid

(44) Fagan, P. J.; Ward, M. D.; Calabrese, J. C. *J. Am. Chem. Soc.* **1989**, *111*, 1698.

was observed, which was characterized to be **8** by its IR spectrum. After removing the solid by filtration, the filtrate was concentrated in vacuo and stored at  $-20\text{ }^{\circ}\text{C}$ . Dark red crystals of **5**·THF were filtered off and dried (27 mg, 74%).  $^1\text{H}$  NMR ( $\text{C}_6\text{D}_6$ ):  $\delta$  1.65 (s, 30H, Cp\*), 1.87 (s, 15H, Cp\*), 1.45 and 3.60 (m, 4H each, THF). IR (KBr disk,  $\text{cm}^{-1}$ ): 1777s ( $\nu(\text{CO})$ ). Prolonged drying under high vacuum resulted in complete loss of the solvating THF, which was confirmed by the NMR spectrum of the residue. Anal. Calcd for  $\text{C}_{32}\text{H}_{45}\text{O}_2\text{ScRu}_3$ : C, 46.17; H, 5.45; S, 3.85; Cl, 4.26. Found: C, 46.40; H, 5.41; S, 3.62; Cl, 4.45.

**Preparation of 8.** Carbon monoxide gas was passed through the solution of **5**·THF (56 mg, 0.062 mmol) in THF (10 mL) for 2 min, and the mixture was stirred for 15 h at  $50\text{ }^{\circ}\text{C}$  under CO. A red solid precipitated was filtered off and crystallized from  $\text{CH}_2\text{Cl}_2$ -ether (5–10 mL), yielding dark purple crystals of **8**· $\text{CH}_2\text{Cl}_2$  (5.0 mg, 8.6%). Most of the unreacted **5** was recovered from the filtrate of the reaction mixture.  $^1\text{H}$  NMR ( $\text{CDCl}_3$ ):  $\delta$  1.92 (s, 45H, Cp\*), 5.30 (s, 2H,  $\text{CH}_2\text{Cl}_2$ ). IR (KBr disk,  $\text{cm}^{-1}$ ): 1823s and 1778s ( $\nu(\text{CO})$ ). Anal. Calcd for  $\text{C}_{34}\text{H}_{47}\text{O}_3\text{ScCl}_3\text{Ru}_3$ : C, 43.20; H, 5.01. Found: C, 42.57; H, 5.02.

**Reaction of  $\text{HC}\equiv\text{CCOOMe}$  with **2**.** To a solution of **2** (42 mg, 0.055 mmol) in THF (5 mL) was added  $\text{HC}\equiv\text{CCOOMe}$  (823 mg, 9.78 mmol), and the mixture was stirred at  $50\text{ }^{\circ}\text{C}$  for 15 h. The GLC analysis of the reaction mixture showed that the alkyne has been consumed completely during this period. The resultant solution was dried up in vacuo, and the residue was subjected to Kugelrohr distillation, giving a mixture of 1,3,5- and 1,2,4- $\text{C}_6\text{H}_3(\text{COOMe})_3$  (95%). The ratio of these isomers determined by GLC as well as  $^1\text{H}$  NMR spectrum was 42:58. The products were characterized by GC-MS, IR, and  $^1\text{H}$  NMR spectra. Reaction of **2** with  $\text{MeOCOC}\equiv\text{CCOOMe}$  and that of **5** with  $\text{HC}\equiv\text{CCOOMe}$  or  $\text{MeOCOC}\equiv\text{CCOOMe}$  were carried out similarly.

**Reaction of **2** with  $\text{MeC}\equiv\text{CCOOMe}$  Forming **10**.** A solution containing **2** (64 mg, 0.082 mmol) and  $\text{MeC}\equiv\text{CCOOMe}$  (61 mg, 0.62 mmol) in THF (5 mL) was stirred at  $50\text{ }^{\circ}\text{C}$  for 15 h. The resultant yellow-green solution was dried up and the residue was extracted with hexane (15 mL). Green crystals

precipitated from the concentrated extract were filtered off and dried (25 mg, 0.44 mol of **10**/mol of **2**).  $^1\text{H}$  NMR ( $\text{C}_6\text{D}_6$ ):  $\delta$  1.66 and 1.80 (s, 15H each, Cp\*), 3.60 and 3.71 (s, 3H each, COOMe), 1.43 and 2.48 (s, 3H each, CMe). IR (KBr disk,  $\text{cm}^{-1}$ ): 1689s ( $\nu(\text{CO})$ ). Anal. Calcd for  $\text{C}_{30}\text{H}_{42}\text{O}_4\text{SRu}_2$ : C, 51.41; H, 6.04. Found: C, 51.43; H, 6.26.

**X-ray Diffraction Studies.** Single crystals of the studied complexes prepared as described above were mounted in glass capillaries under  $\text{N}_2$  and transferred to a Rigaku AFC7R diffractometer. Diffraction studies were performed at room temperature by using graphite-monochromatized Mo K $\alpha$  radiation. Orientation matrices and unit cell parameters were determined by least squares treatment of 25 reflections with  $25 < 2\theta < 40^{\circ}$ . The intensities of three check reflections were monitored every 150 reflections during data collection, which revealed no significant decay for all crystals. Intensity data were corrected for Lorentz and polarization effects and for absorption ( $\psi$  scans). Details of crystal and data collection parameters are shown in Table 4.

Structure solution and refinements were carried out by using the teXsan program package.<sup>45</sup> The heavy atom positions were determined by Patterson methods program (DIRDIF-PATY),<sup>46</sup> and remaining non-hydrogen atoms were found by subsequent Fourier syntheses. All non-hydrogen atoms were refined anisotropically by full-matrix least-squares techniques, while hydrogen atoms were placed at calculated positions and included in the final stages of refinements with fixed parameters. Structure solution and refinements of **3** and **10** by selecting space group  $P1$  instead of  $P\bar{1}$  were unsuccessful. For **8**, refinements of the structure with an opposite polarity did not result in the lower  $R$  values. Coordinates of non-hydrogen atoms in **2**, **3**, **4**, **5**·THF, **8**· $\text{CH}_2\text{Cl}_2$ , and **10** are listed in Tables 5–10, respectively.

**Acknowledgment.** We are grateful to the Ministry of Education, Science, and Culture of Japan for financial support and to Ms Tohko Murai for experimental assistance.

**Supporting Information Available:** Tables containing hydrogen atom coordinates, anisotropic temperature factors of non-hydrogen atoms, and extensive bond distances and angles and figures showing the full views including hydrogen atoms for **2**, **3**, **4**, **5**·THF, **8**· $\text{CH}_2\text{Cl}_2$ , and **10** (65 pages). Ordering information is given on any current masthead page.

OM950328E

(45) teXsan: Crystal Structure Analysis Package, Molecular Structure Corp. (1985 and 1992).

(46) PATY: Beurskens, P. T.; Admiraal, G.; Beurskens, G.; Bosman, W. P.; Garcia-Granda, S.; Gould, R. O.; Smits, J. M. M.; Smykalla, C. (1992). The DIRDIF program system: Technical Report of the Crystallography Laboratory, University of Nijmegen, The Netherlands.

# Multiple Bonds between Main Group Elements and Transition Metals. 144.<sup>1</sup> Photoreactivity of Organorhenium(VII) Oxides

Wolfgang A. Herrmann,<sup>\*,†</sup> Fritz E. Kühn,<sup>†,‡</sup> Dirk A. Fiedler,<sup>†</sup> Mike R. Mattner,<sup>†,§</sup> Martin R. Geisberger,<sup>†</sup> Horst Kunkely,<sup>||</sup> Arnd Vogler,<sup>\*,||</sup> and Steen Steenken<sup>⊥</sup>

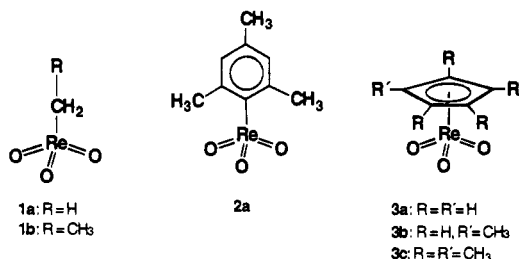
Anorganisch-chemisches Institut der Technischen Universität München, Lichtenbergstrasse 4, D-85747 Garching, Germany, Institut für Anorganische Chemie der Universität Regensburg, Universitätsstrasse 31, D-93040 Regensburg, Germany, and Max-Planck-Institut für Strahlenchemie, Stiftsstrasse 34-36, D-45470 Mülheim/Ruhr, Germany

Received November 21, 1994<sup>⊗</sup>

Ligand-to-metal charge transfer excitation of organorhenium(VII) oxides R–ReO<sub>3</sub> [R = CH<sub>3</sub>, C<sub>2</sub>H<sub>5</sub>, η<sup>1</sup>-mesityl, C<sub>6</sub>H<sub>5</sub>, η<sup>5</sup>-C<sub>5</sub>H<sub>5</sub>, η<sup>5</sup>-C<sub>5</sub>H<sub>4</sub>(CH<sub>3</sub>), and η<sup>5</sup>-C<sub>5</sub>(CH<sub>3</sub>)<sub>5</sub>] in acetonitrile or dichloromethane solution leads to photoredox decomposition. It is shown by EPR spectroscopy that radical pairs R<sup>•</sup>/ReO<sub>3</sub> are generated in the primary step. The overall efficiency is determined by the reactivity of the radicals R<sup>•</sup>, which decreases in the order CH<sub>3</sub> > C<sub>2</sub>H<sub>5</sub> > mesityl > C<sub>5</sub>H<sub>5</sub> > C<sub>5</sub>H<sub>4</sub>(CH<sub>3</sub>) > C<sub>5</sub>(CH<sub>3</sub>)<sub>5</sub>. The regeneration of R–ReO<sub>3</sub> is favored with increasing stability of R<sup>•</sup>. Accordingly the quantum yield varies with R.

## Introduction

Organometallic oxides containing transition metals in high oxidation states have been attracting much attention.<sup>2</sup> However, very little is known about their photoreactivity. Recently, we reported some qualitative observations regarding the light sensitivity of CH<sub>3</sub>ReO<sub>3</sub> (**1a**).<sup>3</sup> The present work is an extension of the previous



study, and it includes a variety of other complexes of the type R–ReO<sub>3</sub>,<sup>4</sup> with R = C<sub>2</sub>H<sub>5</sub> (**1b**), mesityl (**2a**), C<sub>6</sub>H<sub>5</sub> (**2b**), Cp (η<sup>5</sup>-C<sub>5</sub>H<sub>5</sub>) (**3a**), Cp\* [η<sup>5</sup>-C<sub>5</sub>H<sub>4</sub>(CH<sub>3</sub>)] (**3b**), and Cp\*\* [η<sup>5</sup>-C<sub>5</sub>(CH<sub>3</sub>)<sub>5</sub>] (**3c**).<sup>5–7</sup> In the case of **1a,b** and

**2a,b**, the ligands are coordinated to the metal *via* R–C σ-bonds, while complexes **3a–c** adopt “half-sandwich” structures. It is known that organorhenium(VII) oxides decompose more quickly in light than in the dark.<sup>4–8</sup> Since the formula R–ReO<sub>3</sub> implies heptavalent rhenium with a d<sup>0</sup> electron configuration, all low-energy electronic transitions must be of the ligand-to-metal charge transfer type (LMCT). The radical pair R<sup>•</sup>/ReO<sub>3</sub> (Re<sup>VI</sup>) is expected to be generated in the primary photochemical step.

## Results and Discussion

(1) **Electronic Spectra.** The absorption spectra of all hitherto examined complexes of formula R–ReO<sub>3</sub> (σ-type ligands R) exhibit characteristic intense bands. They differ in wavelength and intensity with the organic ligands R (Table 1). However, the absorption spectra of the (π-aryl)rhenium(VII) oxides **3a–c** in CH<sub>3</sub>CN and CH<sub>2</sub>Cl<sub>2</sub> are insensitive with respect to R. The UV/vis spectrum of **3c** is shown in Figure 1.

In contrast to the parent compound **1a**<sup>3</sup> other complexes R–ReO<sub>3</sub> do not show an emission in solution or in the solid state, neither at room temperature nor at 77 K.

In analogy to **1a**, the longest-wavelength absorption of **2a** at λ<sub>max</sub> = 334 nm is assigned to the LMCT transition which involves promotion of an electron from the Re–C σ-bond to empty d orbitals of Re (a<sub>1</sub> → e\* in

(6) (a) Kühn, F. E.; Herrmann, W. A.; Hahn, R.; Elison, M.; Blümel, J.; Herdtweck, E. *Organometallics* **1994**, *13*, 1601. (b) Herrmann, W. A.; Taillefer, M.; de Méric de Bellefon, C.; Behm, J. *Inorg. Chem.* **1991**, *30*, 3247. (c) Thiel, W. R.; Fischer, R. W.; Herrmann, W. A. *J. Organomet. Chem.* **1993**, *459*, C9. (d) Herrmann, W. A.; Serrano, R.; Bock, H. *Angew. Chem., Int. Ed. Engl.* **1984**, *23*, 383. (e) Klahn-Oliva, A. H.; Sutton, D. *Organometallics* **1984**, *3*, 1313.

(7) (a) de Méric de Bellefon, C.; Herrmann, W. A.; Kiprof, P.; Whitaker, C. *Organometallics* **1992**, *11*, 1072. (b) Herrmann, W. A.; Ladwig, M.; Kiprof, P.; Riede, J. *J. Organomet. Chem.* **1989**, *371*, C13.

(8) (a) Herrmann, W. A.; Kühn, F. E.; Fischer, R. W.; Thiel, W. R.; Romão, C. C. *Inorg. Chem.* **1992**, *31*, 4431. (b) Herrmann, W. A.; Kuchler, J. G.; Felixberger, J. K.; Herdtweck, E.; Wagner, W. *Angew. Chem., Int. Ed. Engl.* **1988**, *27*, 394. (c) Beattie, I. R.; Jones, P. J. *Inorg. Chem.* **1979**, *18*, 2318.

\* To whom correspondence should be addressed.

† Technische Universität München.

‡ Fellow of the Hermann Schlosser-Foundation, 1992–1994.

§ Fellow of the Fonds der Chemischen Industrie, 1994–1996.

|| Universität Regensburg.

⊥ MPI Mülheim.

⊗ Abstract published in *Advance ACS Abstracts*, September 15, 1995.

(1) Preceding paper of this series: Herrmann, W. A.; Kühn, F. E.; Romão, C. C. *J. Organomet. Chem.*, in press.

(2) Reviews on organometallic oxides in general: (a) Nugent, W. A.; Mayer, J. M. *Metal to Metal Multiple Bonds*; Wiley-Interscience: New York, 1988. (b) Bottomley, F.; Sutin, L. *Adv. Organomet. Chem.* **1988**, *28*, 339.

(3) Kunkely, H.; Türk, T.; Teixeira, C.; de Méric de Bellefon, C.; Herrmann, W. A.; Vogler, A. *Organometallics* **1991**, *10*, 2090.

(4) Comprehensive review articles: (a) Herrmann, W. A. *J. Organomet. Chem.* **1986**, *300*, 111. (b) Herrmann, W. A.; Herdtweck, E.; Flöel, M.; Kulpe, J.; Küsthardt, U.; Okuda, J. *Polyhedron* **1987**, *6*, 1165. (c) Herrmann, W. A. *Angew. Chem., Int. Ed. Engl.* **1988**, *27*, 1297. (d) Herrmann, W. A. *J. Organomet. Chem.* **1990**, *382*, 1.

(5) (a) Herrmann, W. A.; Kühn, F. E.; Romão, C. C.; Tran Huy, H.; Wang, M.; Fischer, R. W.; Kiprof, P.; Scherer, W. *Chem. Ber.* **1993**, *126*, 45. (b) Herrmann, W. A.; Romão, C. C.; Fischer, R. W.; Kiprof, P.; de Méric de Bellefon, C. *Angew. Chem., Int. Ed. Engl.* **1991**, *30*, 185.



**Table 1. Characteristic Maxima in the Absorption Spectra of Selected Organorhenium(VII) Oxides**

compd	no.	$\lambda_{\max}$ (nm)	$\epsilon$ ( $M^{-1} \text{ cm}^{-1}$ )	solvent
$\text{CH}_3\text{ReO}_3$	<b>1a</b>	205	1600	<i>n</i> -hexane <sup>b</sup>
		231	1500	
		260	1020	
$\text{C}_2\text{H}_5\text{ReO}_3$	<b>1b</b>	210	2300	$\text{CH}_3\text{CN}$
		240	1250	
		262	1040	
$[\eta^1\text{-C}_6\text{H}_2(\text{CH}_3)_3]\text{ReO}_3$	<b>2a</b>	334	8550	$\text{CH}_3\text{CN}$
	$[\eta^5\text{-C}_5\text{H}_5]\text{ReO}_3$	<b>3a</b>	212	6700
297		3700		
344 <sup>a</sup>		1200		
377 <sup>a</sup>		800		
$[\eta^5\text{-C}_5\text{H}_4(\text{CH}_3)]\text{ReO}_3$	<b>3b</b>	212	7600	$\text{CH}_3\text{CN}$
		296	4100	
		346 <sup>a</sup>	1040	
		380 <sup>a</sup>	670	
$[\eta^5\text{-C}_5(\text{CH}_3)_5]\text{ReO}_3$	<b>3c</b>	213	6500	$\text{CH}_3\text{CN}$
		300	3900	
		357 <sup>a</sup>	1050	
		402 <sup>a</sup>	750	

<sup>a</sup> Shoulder. <sup>b</sup> Taken from ref 3.

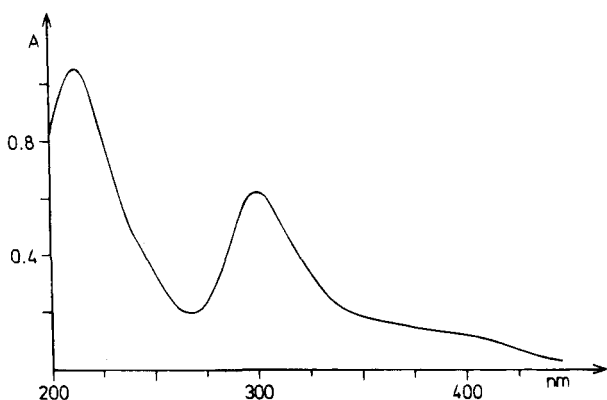
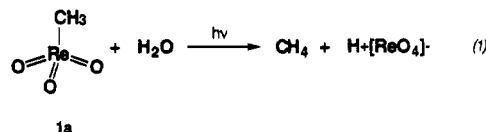


**Figure 1.** Electronic absorption spectrum of  $[\eta^5\text{-C}_5(\text{CH}_3)_5]\text{-ReO}_3$  (**3c**) in acetonitrile at room temperature (1 cm cell,  $c = 1.62 \times 10^{-4} \text{ M}$ ).

$\text{C}_{3v}$  symmetry). The assignments of the absorptions of **1b** correspond to that of **1a**.<sup>3</sup>

Band assignments are based on recent MO calculations<sup>9a</sup> in the case of the half-sandwich complexes **3a–c**. The HOMO is bonding and derived from the doubly degenerate  $e_1''$   $\pi$ -orbitals of the aromatic ligands. The precise nature of the LUMO is not clear, because two types of antibonding d-based MOs are close in energy.<sup>9</sup> One of them results from the  $\pi$ -interaction of the  $e^*$  orbitals ( $\text{ReO}_3$ ) with the aromatic ligand, while the other one is generated by the  $\sigma$ -type overlap of the aromatic ligand with the  $a_1^*$  orbital of the  $\text{ReO}_3$  moiety. The similarity of the absorption spectra of all three complexes suggests that the sequence of the  $e^*$  and  $a_1^*$  orbitals is invariant with R. According to the calculations, the two longest-wavelength absorptions of **3a–c** near 350 and 390 nm are assigned to the  $e_1'' \rightarrow e^*$  and  $e_1 \rightarrow a_1^*$  LMCT transitions from the  $\pi$ -orbitals of the aromatic ligands to the  $\text{ReO}_3$  group. The more intense band at shorter wavelength (*ca.* 300 nm) very likely arises from a LMCT process, too.

**(2) Photolysis Studies.** Solutions of **1a**<sup>3,8</sup> and **1b** are sensitive to short-wavelength light. On photolysis of **1a** with 254 nm light in aqueous solution (eq 1),



photochemical products observed are  $\text{CH}_4$  (by GC and NMR) and  $\text{C}_2\text{H}_6$  (by GC); see Figure 2. In the presence of small concentrations of  $\text{O}_2$ , the formation of  $\text{C}_2\text{H}_6$  is inhibited, while that of  $\text{CH}_4$  is only reduced (see Figure 3). From this it is concluded that  $\text{CH}_4$  is formed in a cage reaction, while  $\text{C}_2\text{H}_6$  is produced by dimerization of freely diffusing methyl radicals. Experiments with solutions of **1a** (*ca.*  $10^{-3} \text{ M}$ ) in  $\text{D}_2\text{O}$  (purity 99.3%) show the formation of  $\text{CH}_3\text{D}$  and  $\text{CH}_4$  (detected by  $^1\text{H-NMR}$ ). A mechanism suggested for the formation of  $\text{CH}_3\text{D}$  is  $\text{D}^{\bullet}$  abstraction from the solvent. Photolysis generates a radical pair inside a solvent cage. Coordination of  $\text{D}_2\text{O}$  to an electron deficient metal center may lower the bonding energy in the  $\text{D}_2\text{O}$  molecule and facilitate deuterium abstraction by methyl radicals, an otherwise thermodynamically not expected reaction. Concerning  $\text{CH}_4$ , it is probably the product of  $\text{H}^{\bullet}$  abstraction by  $\text{CH}_3^{\bullet}$  from **1a** or photolysis products.

The kinetics of the photolysis were studied by GC analysis. The rates are influenced by the nature of the atmosphere in which the experiments are conducted. If aqueous solutions of **1a** are saturated with oxygen—a typical radical scavenger—the formation of  $\text{C}_2\text{H}_6$  exhibits an induction period of 3–4 min (Figure 3). No inhibition effect is observed in argon atmosphere (Figure 2). Additionally in comparison to argon atmosphere the absolute concentrations of  $\text{CH}_4$  and  $\text{C}_2\text{H}_6$  are lower in the presence of oxygen. These results establish further evidence for the suggested radical mechanism.

The photochemical decomposition of **1b** is similar. Ethane and perrhenate are formed in the presence of traces of water (Figure 4). In concentrated, absolutely *dry* solutions in  $\text{CH}_3\text{CN}$  formation of ethane and low amounts of ethylene and *n*-butane is observed (GC) upon photolysis; a dark residue consisting mainly of  $\text{ReO}_3$  (IR, elemental analysis) is concomitantly formed. The quantum yield ( $\phi$ ) for the disappearance of **1b** was determined by measuring the change of extinction at 254 nm:  $\phi = 0.53 \pm 0.03$  at  $\lambda_{\text{irr}} = 254 \text{ nm}$ ; see Table 2.

Photolysis of the  $\sigma$ -mesityl complex **2a** in  $\text{CH}_3\text{CN}$  was accompanied by spectral changes (Figure 5) that are characterized by the occurrence of two new absorption bands attributed to mesitylene,  $\lambda_{\max} = 265$  and 272 nm. The mesitylene was also detected by GC/MS. The increase of the optical density was caused by light scattering of colloidal  $\text{ReO}_3$ , which is formed in analogy to the photolysis of **1b** (*vide supra*).

The quantum yield for the disappearance of **2a** was determined by measuring the change of extinction at 334 nm:  $\phi = 0.18 \pm 0.01$  at  $\lambda_{\text{irr}} = 333 \text{ nm}$ . When the photolysis was carried out in  $\text{CH}_2\text{Cl}_2$ , the spectral changes were similar to those observed in  $\text{CH}_3\text{CN}$  (Figure 5).

Solutions of the  $\pi$ -complexes **3a,b** in  $\text{CH}_3\text{CN}$  are also light-sensitive. The spectral changes occurring upon photolysis are similar in both cases (Figure 6). The same type of photoreaction should thus be involved.

EPR studies were performed to obtain evidence of free radicals  $\text{R}^{\bullet}$  occurring during photolysis. Solutions of **1a,b**, **2b**, and **3a** and nitrosodurene (ND) or 5,5-

(9) (a) Szyperski, T.; Schwerdtfeger, P. *Angew. Chem., Int. Ed. Engl.* **1989**, *28*, 1128. (b) Herrmann, W. A.; Rösch, N.; Bock, H.; Köstlmeier, S.; Kühn, F. E.; Solouki, B. Unpublished results, 1993/1994.

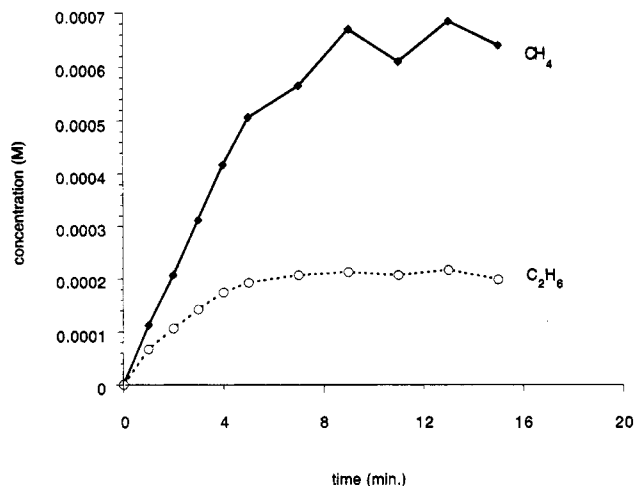


**Figure 2.** Photolytic formation of  $\text{CH}_4$  and  $\text{C}_2\text{H}_6$  in aqueous solution of **1a** ( $c = 1.64 \times 10^{-3}$  M, argon atmosphere).

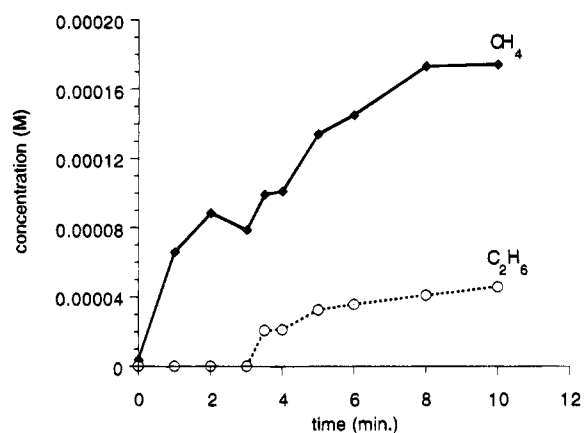


**Figure 3.** Photolytic formation of  $\text{CH}_4$  and  $\text{C}_2\text{H}_6$  in aqueous solution of **1a** ( $c = 1.64 \times 10^{-3}$  M, oxygen atmosphere).

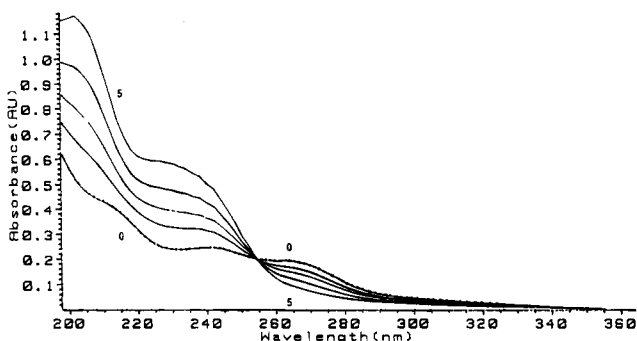


**Figure 4.** Spectral changes during photolysis of  $\text{C}_2\text{H}_5\text{ReO}_3$  (**1b**) in acetonitrile at (0) 0 min and (5) 5 min irradiation time with  $\lambda_{\text{irr}} = 254$  nm (1 cm cell,  $c = 1.97 \times 10^{-4}$  M).

dimethyl-1-pyrroline 1-oxide (DMPO) as radical scavengers were irradiated in the cavity of an EPR spectrometer. The hyperfine splitting constants and the  $g$ -values of simultaneously recorded EPR spectra are in excellent agreement with reported data (*cf.* Figure 7 and Table 3), especially if one considers a possible solvent effect on the hyperfine splitting constants.<sup>10</sup> A control

**Table 2. Quantum Yield  $\phi$  of Disappearance of Organorhenium(VII) Oxides during Irradiation**

compd	no.	$\lambda_{\text{irr}}$ (nm)	$\phi$ (%)	solvent
$\text{CH}_3\text{ReO}_3$	<b>1a</b>	254	0.58	$\text{H}_2\text{O}^a$
$\text{C}_2\text{H}_5\text{ReO}_3$	<b>1b</b>	254	0.53	$\text{CH}_3\text{CN}^b$
$[\eta^1\text{-C}_6\text{H}_2(\text{CH}_3)_3]\text{ReO}_3$	<b>2a</b>	333	0.18	$\text{CH}_3\text{CN}^b$
$(\eta^5\text{-C}_5\text{H}_5)\text{ReO}_3$	<b>3a</b>	313	0.028	$\text{CH}_3\text{CN}^b$
$[\eta^5\text{-C}_5\text{H}_4(\text{CH}_3)]\text{ReO}_3$	<b>3b</b>	313	0.013	$\text{CH}_3\text{CN}^b$
$[\eta^5\text{-C}_5(\text{CH}_3)_5]\text{ReO}_3$	<b>3c</b>	313	0.0001	$\text{CH}_3\text{CN}^b$

<sup>a</sup> Taken from ref 3. <sup>b</sup> Photolysis in  $\text{CH}_2\text{Cl}_2$  led to the same results.

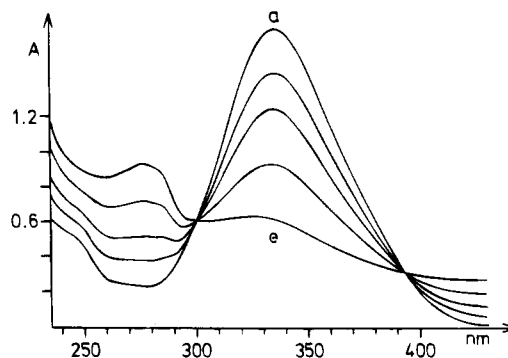


**Figure 5.** Spectral changes during photolysis of  $(\eta^1\text{-mesityl})\text{ReO}_3$  (**2a**) in acetonitrile at (a) 0 min and (e) 5 min irradiation time with  $\lambda_{\text{irr}} = 333$  nm (1 cm-cell,  $c = 1.76 \times 10^{-4}$  M).

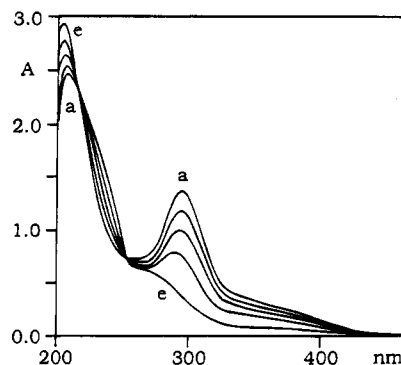


**Figure 6.** Spectral changes during the photolysis of  $(\eta^5\text{-C}_5\text{H}_4\text{CH}_3)\text{ReO}_3$  in acetonitrile at (a) 0 min and (e) 8 min irradiation time with  $\lambda_{\text{irr}} = 313$  nm (1 cm cell,  $c = 3.44 \times 10^{-4}$  M).

experiment with benzoyl peroxide as a source of phenyl radicals confirmed the generation of  $\text{C}_6\text{H}_5^{\cdot}$  upon irradiation of **2b** in solution.

Photolysis of **3a,b** yields dark-colored precipitates that mostly consist of  $\text{ReO}_3$  (IR, elemental analyses). Black precipitates of  $\text{Re}_2\text{S}_7$  (elemental analyses) are obtained upon dissolution in concentrated HCl and addition of  $\text{H}_2\text{S}$ .

The  $\pi$ -cyclopentadienyl complexes **3a,b** decomposed with quantum yields of  $\phi = 0.028 \pm 0.001$  and  $0.013 \pm 0.001\%$ , respectively, at  $\lambda_{\text{irr}} = 313$  nm. When the irradiation was carried out in  $\text{CH}_2\text{Cl}_2$ , the spectral changes were quite similar to those in  $\text{CH}_3\text{CN}$ . The fully methylated derivative **3c** was almost insensitive to light. Only slow photodecomposition took place with  $\phi = 10^{-4}$ . This very low quantum yield explains why radicals were not detectable by means of EPR spectroscopy. Irradiation causes (radical) reactions between ND and the solvent before a sufficient Cp\* radical concentration is established.

(10) (a) Janzen, E. G.; Coulter, G. A.; Oeler, U. M.; Bergsma, J. P. *Can. J. Chem.* **1982**, *60*, 2725. Reheorek, D. *Chem. Soc. Rev.* **1991**, *2*, 341. (b) Terabe, S.; Kuruma, K.; Konaka, R. *J. Chem. Soc., Perkin Trans. 2* **1973**, 1252. (c) Barker, P. J.; Stobart, S. R.; West, P. R. *J. Chem. Soc., Perkin Trans. 2* **1986**, 127.

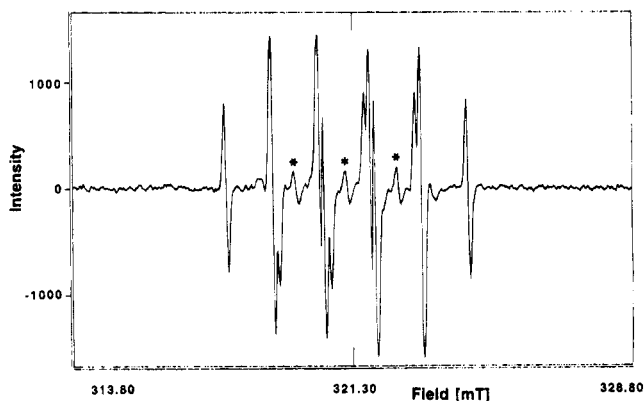


**Figure 7.** EPR spectrum of the  $\text{CH}_3\text{-ND}$  radical at 20 °C generated during irradiation at  $\lambda_{\text{irr}} = 254$  nm (1 mM  $\text{CH}_3\text{-ReO}_3$  and 10 mM ND in  $\text{CH}_2\text{Cl}_2$ ; ND = nitrosodurene; asterisks indicate solvent background signals).

According to the LMCT character of the low-energy excited states and as shown by EPR experiments, organorhenium(VII) oxides undergo a photoredox decomposition *via* generation of  $\text{R}^\bullet$  and  $\bullet\text{ReO}_3$  radicals. The photolytic efficiency depends on the competition of several processes. The  $\text{ReO}_3$  radicals aggregate mainly to bulk, insoluble  $\text{ReO}_3$ , which is a well-known compound.<sup>11</sup> The organic radicals  $\text{R}^\bullet$  can recombine with the (monomeric)  $\text{ReO}_3$  fragment, if not yet aggregated to regenerate  $\text{R-ReO}_3$ . They can also abstract (mostly) hydrogen from solvent molecules coordinated to the metal center or can dimerize to  $\text{R-R}$ .<sup>12</sup> The occurrence of the latter reactions has been shown by GC, GC/MS, and NMR techniques (see above). It is known that such processes also take place in the *thermal* decomposition of organorhenium(VII) oxides.<sup>4-7,13</sup>

The majority of carbon-based radicals are very reactive, readily abstracting hydrogen from various solvents including  $\text{CH}_3\text{CN}$  and  $\text{CH}_2\text{Cl}_2$ . Less reactive radicals facilitate recombination and dimerization. Although the latter process is generally rapid,<sup>12</sup> it is hampered by the low steady-state concentration of  $\text{R}^\bullet$  in a conventional stationary photolysis.

In analogy to phenyl radicals,<sup>12</sup> the mesityl radical undergoes facile hydrogen abstraction from the solvent (GC/MS and UV/vis detection of mesitylene) while the recombination with  $\text{ReO}_3$  and the dimerization are expected to be slow due to the steric situation of the mesityl radical. This is in accordance with the observation that the photolysis of **2a** yielding mesitylene is rather efficient ( $\phi = 0.18$ ).

The radicals Cp and Cp' generated in the photolysis of **3a,b** are so stable<sup>14-16</sup> that they dimerize in the absence of suitable scavengers (no  $\text{H}^\bullet$  abstraction from

solvent). The recombination of  $\text{R}^\bullet$  and  $\bullet\text{ReO}_3$  should thus determine the photoreactivity. As a matter of fact, the photochemical quantum yields are low. GC/MS analyses have shown that various isomers of dihydrofulvalene are formed during photolysis. They can participate in subsequent reactions including polymerization.<sup>15-17</sup> It is interesting to note that the formation of Cp radicals was also confirmed by EPR spectroscopy for the photolysis of  $(\text{Cp})_n\text{SnX}_{4-n}$  and  $\text{HgCp}_2$ .<sup>14</sup> The Sn(IV) and Hg(II) complexes, like the Re(VII) species **3a**, possess only LMCT states at low energies due to their  $s^0$  configuration.<sup>18</sup>

No radicals were detected during the (inefficient) photochemical decomposition of **3c**. By way of contrast, exposition of **3a,b** in any organic solvent to daylight effects darkening of the yellow colored solutions within *ca.* 30 min. **3c** does not show a significant color change within 1 day. It remains unclear whether this different behavior is due to an efficient radical recombination process or to the high photostability.

## Conclusion

The present study has revealed that organorhenium(VII) oxides of formula  $\text{R-ReO}_3$  undergo photolytic homolysis of the carbon-rhenium single bonds, thus resembling the thermal decomposition pathways.<sup>4-7</sup> Subsequent reactions of the radicals are listed in Scheme 1. Light in the range of  $\lambda = 200\text{--}400$  nm is most efficient for homolysis. Most of these compounds thus decompose slowly in daylight. Temperature sensitive organorhenium(VII) oxides show at room temperature both light- and temperature-induced decomposition. Decomposition by light is in most cases quicker than thermal degradation.<sup>4-7</sup> While thermal degradation takes weeks, complete photolysis can be achieved within minutes. Interestingly the thermally most stable compound  $\text{CH}_3\text{ReO}_3$  (dec > 250 °C) shows the highest quantum yield during irradiation and thus is the most light-sensitive of the examined compounds. The most light-stable derivatives of this class are the  $\pi$ -aromatic complexes of the cyclopentadienyl type.

## Experimental Section

**(1) Materials.** The organorhenium(VII) complexes **1-3** were prepared according to published procedures.<sup>4b,5b,6a,7a,8</sup> Acetonitrile,  $\text{CH}_2\text{Cl}_2$ , and  $\text{D}_2\text{O}$  were of at least spectrograde quality. The isotopic purity of  $\text{D}_2\text{O}$  was 99.3%. Water was triply distilled.

**(2) Photolytic Investigations.** Photolyses were carried out at room temperature in 1 cm spectrophotometer cells. The light source was a Hanovia Xe/Hg 977 B-1 (1000 W) lamp. Monochromatic light ( $\lambda_{\text{irr}} = 254, 313, 333, \text{ and } 436$  nm) was obtained by means of a Schoeffel GM 250-1 high-intensity monochromator. For quantum yield determinations, the concentrations were such that complete light absorption ( $A \geq 2$ ) was ensured. Absorbed light intensities were determined by a Polytec pyroelectric radiometer which was calibrated and equipped with an RkP-345 detector. The progress of photolysis was monitored by UV/vis spectral measurements with an Uvikon 860 double-beam spectrophotometer or a Hewlett Packard 8452A diode array spectrometer. All photolytic

(17) Moulton, R. D.; Farid, R.; Bard, A. *J. Electroanal. Chem.* **1988**, *256*, 309.

(18) (a) Vogler, A.; Paukner, A.; Kunkely, H. *Coord. Chem. Rev.* **1990**, *97*, 285. (b) Vogler, A.; Nikol, H. *Pure Appl. Chem.* **1992**, *64*, 1511.

(11) (a) Kiprof, P.; Herrmann, W. A.; Kühn, F. E.; Scherer, W.; Kleine, M.; Elison, M.; Rypdal, K.; Volden, H. V.; Gundersen, S.; Haaland, A. *Bull. Soc. Chim. Fr.* **1992**, *129*, 655. (b) Krebs, B.; Müller, A. *Z. Naturforsch.* **1968**, *23b*, 415. (c) Nechamkin, H.; Hiskey, C. F. *Inorg. Synth.* **1950**, *3*, 168.

(12) Monograph on organic radicals: Kochi, J. K., Ed. *Free Radicals*; CRC Press: Boca Raton, FL, 1989.

(13) Herrmann, W. A.; Kühn, F. E.; Romão, C. C.; Tran Huy, H. *J. Organomet. Chem.* **1994**, *481*, 227.

(14) (a) Barker, P. J.; Davies, A. G.; Fisher, J. D. *J. Chem. Soc., Chem. Commun.* **1979**, 587. (b) Barker, P. J.; Davies, A. G.; Tse, M. W. *J. Chem. Soc., Perkin Trans. 2* **1980**, 941.

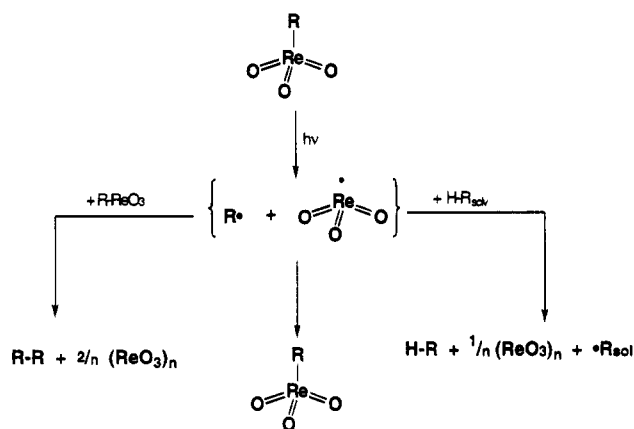
(15) Davies, A. G.; Giles, J. R.; Luszyk, J. *J. Chem. Soc., Perkin Trans. 2* **1981**, 747.

(16) Davies, A. G.; Luszyk, J. *J. Chem. Soc., Chem. Commun.* **1980**, 554.

**Table 3. Conditions, EPR Parameters, and Comparison with Known Data (in Parentheses)**

R	$\lambda$ (nm)	$a(N)$ (mT)	$a(\alpha-H)$ (mT)	$g$	ref
CH <sub>3</sub> <sup>a</sup>	254	1.37 (1.37)	1.24 (1.22)	2.0057 (2.0060)	10c
C <sub>2</sub> H <sub>5</sub> <sup>a</sup>	254	1.37 (1.37)	1.13 (1.10)	2.0057 (2.0061)	10c
C <sub>5</sub> H <sub>5</sub> <sup>a</sup>	300–340	1.33 (1.32–1.38)	0.50 (0.53–0.73)	2.0057 (2.0060–2.0072)	10d
C <sub>6</sub> H <sub>5</sub> <sup>b</sup>	300–340	1.42	2.05	2.0055	

<sup>a</sup> Spin trap: ND. Solvent: CH<sub>2</sub>Cl<sub>2</sub>. <sup>b</sup> Spin trap: DMPO. Solvent: CH<sub>3</sub>CN.

**Scheme 1**

studies, except for **1a**, were carried out in air-saturated solutions since deaeration of solvents gave identical results.

(3) **GC and GC/MS Analyses.** The composition of the gas phase was analyzed with a Hewlett Packard capillary gas-chromatograph (HP 5890) with a flame ionization detector and a HP 3394-A integrator. The liquid phase and the labeling experiments were analyzed with a HP 5890-A gas chromatograph coupled with a HP 5970 mass detector, using a HP, BP5, Scientific Glass Engineering GmbH column (95% methylpolysiloxane/5% phenylpolysiloxane;  $l = 25$  m,  $\phi = 0.22$  mm, thickness 25 mm).

(4) **EPR Studies.** EPR spectra were recorded on a Jeol RE2X spectrometer equipped with a TE<sub>011</sub> cylindrical cavity resonator and an Advantec frequency counter. The temperature was kept at 20 °C in all experiments. Test solutions containing 1–2.0 mM **1a,b**, **2b**, and **3a,b** and 5–20 mM 2,3,5,6-tetramethylnitrosobenzene (nitrosodurene, ND) or 10 mM 5,5-dimethyl-1-pyrroline 1-oxide (DMPO) were prepared using dichloromethane and acetonitrile, respectively. CH<sub>2</sub>Cl<sub>2</sub> (Merck, pa; saturated with argon) was purified by passing it through a column filled with basic activated alumina (Aldrich; activity grade I). CH<sub>3</sub>CN (Sigma-Aldrich, HPLC grade, satu-

rated with argon) was similarly purified using neutral alumina of equal activity. ND was prepared according to the method of Smith and Taylor.<sup>19</sup> A 0.18 mL volume of solution were transferred under argon into a cylindrical EPR tube (Jeol no. ES-LC $\phi$ 2) or a flat cell (Jeol no. ES-LCM). Spectra were then accumulated by means of the ESPRIT data acquisition and manipulation package (version 3.4) connected to the spectrometer in the fast-sweep mode. For simultaneous irradiation of the sample tube, either a Katadyn mercury low-pressure lamp (TiO<sub>2</sub>-doped quartz cylinder, 8 W nominal power) or a HBO 200 W/4 Xe lamp was used. The former only emits the 254 nm Hg line, whereas the latter required the use of an appropriate filter to prevent side reactions. In this work, a solution of 1.75 M NiSO<sub>4</sub>·6H<sub>2</sub>O + 0.50 M CoSO<sub>4</sub>·7H<sub>2</sub>O in water was positioned between the lamp and the sample tube as close to the cavity as possible in either a 1 cm wide quartz cuvette or a 2 cm wide Schlenk tube with flattened walls. Thus, irradiation could be carried out at 331 nm or 300–340 nm, respectively.  $g$ -values were calculated relative to the two central lines of a Mn<sup>2+</sup>-doped sample of MgO located in the same cavity during subsequent irradiation experiments.

(5) **NMR Studies.** The NMR spectra were obtained on a Bruker DPX 400 NMR spectrometer, using a 5-mm quartz tube.

**Acknowledgment.** Support of this research by the Deutsche Forschungsgemeinschaft and the Fonds der Chemischen Industrie (graduate fellowship for M.R.M.) is gratefully acknowledged. We thank the Hermann Schlosser-Foundation (graduate fellowship for F.E.K.), the DEGUSSA AG (Prof. Offermanns and Dr. Gerhartz) for a generous gift of Re<sub>2</sub>O<sub>7</sub>, and Prof. J. F. Endicott for valuable comments. Dr. I. Wurdack is thanked for providing DMPO.

OM940889Q

(19) (a) Smith, L. I.; Taylor, F. L. *J. Chem. Soc.* **1935**, 57, 2370. (b) Smith, L. I.; Taylor, F. L. *J. Chem. Soc.* **1935**, 57, 2460 and references cited therein.

# Protonation at the Aromatic Ring *vs* at the Carbonyl Group of Lanthanide–Diaryl Ketone Dianion Species by Aryl Alcohols. Formation, Structural Characterization, and Reactivity of Lanthanide Aryloxy, Mixed Aryloxy/Alkoxide, and Aryloxy/Enolate Complexes

Takashi Yoshimura, Zhaomin Hou,\* and Yasuo Wakatsuki\*

The Institute of Physical and Chemical Research (RIKEN),  
Hirosawa 2-1, Wako, Saitama 351-01, Japan

Received May 30, 1995\*

Reaction of the ytterbium–benzophenone dianion complex  $[\text{Yb}(\mu\text{-}\eta^1, \eta^2\text{-OCPh}_2)(\text{HMPA})_2]_2$  (**1**), which was formed by reaction of Yb metal with benzophenone in THF/HMPA, with 2,6-di-*tert*-butyl-4-methylphenol, yielded the ytterbium(II) aryloxy complex  $\text{Yb}(\text{OAr})_2(\text{HMPA})_2$  (**2**, Ar =  $\text{C}_6\text{H}_2\text{-}^t\text{Bu}_2\text{-}2,6\text{-Me-4}$ ) as a major product (80%) and the ytterbium(III) enolate complex  $\text{Yb}(\text{OC}(\text{=CCH=CHCH}_2\text{CH=CHPh})_2(\text{OAr})(\text{HMPA})_2$  (**3**, Ar =  $\text{C}_6\text{H}_2\text{-}^t\text{Bu}_2\text{-}2,6\text{-Me-4}$ ) as a minor one (ca. 5% yield). In contrast, the similar reaction of samarium benzophenone dianion species with ArOH (Ar =  $\text{C}_6\text{H}_2\text{-}^t\text{Bu}_2\text{-}2,6\text{-Me-4}$  or  $\text{C}_6\text{H}_3\text{-}^t\text{Bu}_2\text{-}2,6$ ) gave the samarium(III) enolate complex  $\text{Sm}(\text{OC}(\text{=CCH=CHCH}_2\text{CH=CHPh})_2(\text{OAr})(\text{HMPA})_2$  (**4a**, Ar =  $\text{C}_6\text{H}_2\text{-}^t\text{Bu}_2\text{-}2,6\text{-Me-4}$ , 60%; **4b**, Ar =  $\text{C}_6\text{H}_3\text{-}^t\text{Bu}_2\text{-}2,6$ , 56%) as a major product, while samarium(II) aryloxy analogous to **2** was not obtained. When ArOD (Ar =  $\text{C}_6\text{H}_2\text{-}^t\text{Bu}_2\text{-}2,6\text{-Me-4}$ ) was used instead of ArOH, the deuterated enolate  $\text{Sm}(\text{OC}(\text{=CCH=CHCHDCH=CHPh})_2(\text{OAr})(\text{HMPA})_2$  (**4c**, Ar =  $\text{C}_6\text{H}_2\text{-}^t\text{Bu}_2\text{-}2,6\text{-Me-4}$ ) was formed. In the reaction with 2,6-*t*-Bu<sub>2</sub>-4-Me-C<sub>6</sub>H<sub>2</sub>OH, a mixed aryloxy/alkoxide complex  $\text{Sm}(\text{OCHPh}_2)(\text{OAr})_2(\text{HMPA})_2$  (**5a**, Ar =  $\text{C}_6\text{H}_2\text{-}^t\text{Bu}_2\text{-}2,6\text{-Me-4}$ ) was also isolated in ca. 2% yield. When samarium fluorenone dianion species was allowed to react with 2,6-*t*-Bu<sub>2</sub>-C<sub>6</sub>H<sub>3</sub>OH, the fluorenoxy analogue of **5a**,  $\text{Sm}(\text{fluorenoxy})(\text{OAr})_2(\text{HMPA})_2$  (**6**, Ar =  $\text{C}_6\text{H}_3\text{-}^t\text{Bu}_2\text{-}2,6$ , 64%), was obtained as the only isolable product. Upon heating at 180 °C in toluene, **4a,b** isomerized into **7a,b**  $\text{Sm}(\text{OCHPh}_2)_2(\text{OAr})(\text{HMPA})_2$  (**7a**, Ar =  $\text{C}_6\text{H}_2\text{-}^t\text{Bu}_2\text{-}2,6\text{-Me-4}$ ; **7b**, Ar =  $\text{C}_6\text{H}_3\text{-}^t\text{Bu}_2\text{-}2,6$ ). Deuterium labeled experiments indicated that this isomerization was an intramolecular one step 1,5-hydrogen shift process. Reaction of **4a** and **7a** with 2,6-*t*-Bu<sub>2</sub>-C<sub>6</sub>H<sub>3</sub>OH yielded the aryloxy exchange products **4b** and **7b**, respectively, while the reaction of **7a** with 2,6-Me<sub>2</sub>-C<sub>6</sub>H<sub>3</sub>OH gave the diphenylmethoxy substitution product  $\text{Sm}(\text{OAr})(\text{OAr}'')_2(\text{HMPA})_2$  (**8**, Ar =  $\text{C}_6\text{H}_2\text{-}^t\text{Bu}_2\text{-}2,6\text{-Me-4}$ ; Ar'' =  $\text{C}_6\text{H}_3\text{-Me}_2\text{-}2,6$ ). The mechanisms of these reactions are discussed. X-ray crystallographic studies reveal that **3**, **4a**, and **7b** are isostructural, and so are **5a** and **6**. The central metal ions in these complexes are all five-coordinated in a trigonal bipyramid form (highly distorted in the case of **5a** and **6**) with two HMPA ligands at the apical and three anionic oxygen ligands at the equatorial positions.

## Introduction

The formation of ketone dianions *via* two electron-reduction of diaryl ketones by alkali metals was first reported in 1911.<sup>1</sup> It is now known that other reducing metals such as low-valent titanium species<sup>2</sup> and lanthanide metals<sup>3</sup> are also able to reduce diaryl ketones into the corresponding dianions. Since these dianionic

species are extremely sensitive to air and moisture, their isolation is difficult and they are usually used *in-situ* for next reactions. Their reactivities are therefore judged mainly based on the final hydrolysis products. Although the final products are dependent on the nature of the metals in some cases (*e.g.*, in the case of titanium, deoxygenation reaction often occurs), the results presented so far in the literature have shown that all these ketone dianion species show a similar reactivity: when

\* Abstract published in *Advance ACS Abstracts*, October 1, 1995.

(1) For the formation of alkali metal–diaryl ketone dianions and their use in organic synthesis, see: (a) Schlenk, W.; Weichel, T. *Ber.* **1911**, *44*, 1182. (b) Schlubach, H. *Ibid.* **1915**, *48*, 12. (c) Wooster, C. B. *J. Am. Chem. Soc.* **1928**, *50*, 1388. (d) Bachmann, W. E. *Ibid.* **1933**, *55*, 1179. (e) Hamrick, P. J., Jr.; Hauser, C. R. *Ibid.* **1959**, *81*, 493. (f) Selman, S.; Easthan, J. F. *J. Org. Chem.* **1965**, *30*, 3804. (g) Anderson, E. L.; Casey, J. E., Jr. *Ibid.* **1965**, *30*, 3959. (h) Murphy, W. S.; Buckley, D. J. *Tetrahedron Lett.* **1969**, 2975. (i) Huffman, J. W. in *Comprehensive Organic Synthesis*; Trost, B. M., Fleming, I., Eds; Pergamon: New York, 1991; Vol. 8, Chapter 1.4. (j) Robertson, G. M. *Ibid.* Trost, B. M., Fleming, I., Eds; Vol. 3, Chapter 2.6.

(2) (a) McMurry, J. E.; Krepiski, L. R. *J. Org. Chem.* **1976**, *41*, 3929. (b) McMurry, J. E.; Fleming, M. P.; Kees, K. L.; Krepiski, L. R. *J. Org. Chem.* **1978**, *43*, 3255. (c) Pons, J. M.; Santelli, M. *Tetrahedron Lett.* **1982**, *23*, 4937. (d) McMurry, J. E. *Acc. Chem. Res.* **1983**, *16*, 405. **1974**, *7*, 281. *Chem. Rev.* **1989**, *89*, 1513.

(3) (a) Hou, Z.; Takamine, K.; Fujiwara, Y.; Taniguchi, H. *Chem. Lett.* **1987**, 2061. (b) Hou, Z.; Takamine, K.; Aoki, O.; Shiraiishi, H.; Fujiwara, Y.; Taniguchi, H. *J. Chem. Soc., Chem. Commun.* **1988**, 668. *J. Org. Chem.* **1988**, *53*, 6077. (c) Olivier, H.; Chauvin, Y.; Saussine, L. *Tetrahedron* **1989**, *45*, 165.

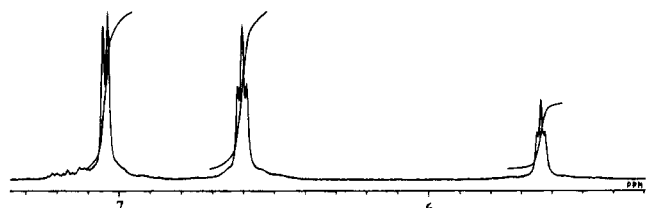
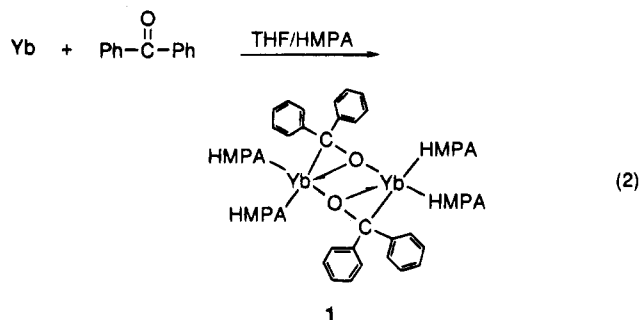
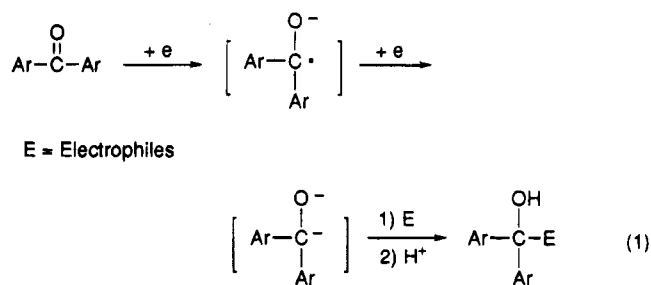
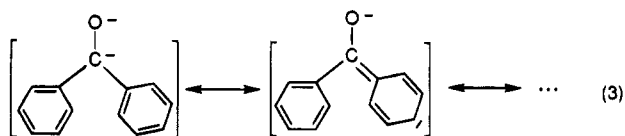


Figure 1. Phenyl part of the  $^1\text{H}$  NMR spectrum of **1**.

they are mixed with electrophiles, reactions always take place at the carbonyl carbon to give the corresponding cross-coupling products (eq 1).<sup>1-3</sup>



Our recent isolation of the ytterbium(II)-benzophenone dianion complex  $[\text{Yb}(\mu-\eta^1, \eta^2\text{-OCPh}_2)(\text{HMPA})_2]_2$  (**1**) from the reaction of Yb metal with benzophenone in THF/HMPA provided the first structurally characterizable metal-ketone dianion complex (eq 2).<sup>4</sup> An X-ray analysis has revealed that the anionic carbonyl carbon atom in **1** is still in a  $\text{sp}^2$ -hybrid state, which therefore allows a good conjugation of the negative charges with the phenyl rings. The  $^1\text{H}$  NMR spectrum of **1** in THF- $d_6$  shows that the signals for the phenyl protons are greatly upfield shifted to as high as  $\delta$  5.63–7.04 (Figure 1), demonstrating that the negative charges of this ketone dianion are highly delocalized into the phenyl rings, especially to the para-positions ( $\delta$  5.63) (eq 3).

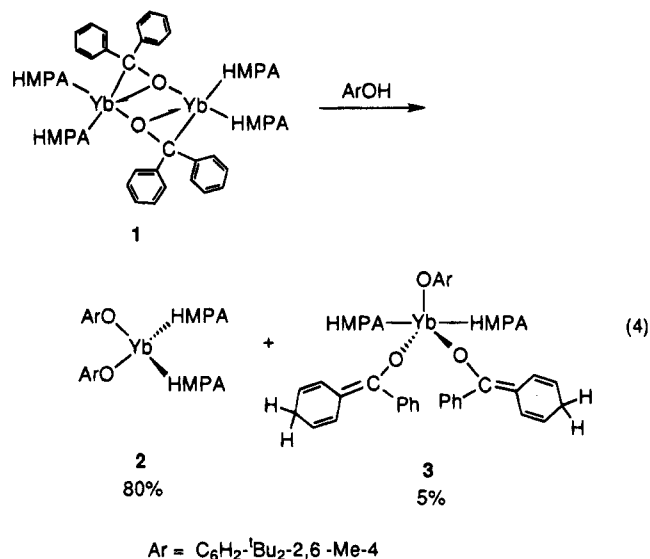


These data indicate that a new type of reaction, *i.e.*, the reaction at the aromatic ring, might also be achievable. In this paper we report a detailed study on the protonation reactions of samarium- and ytterbium-diaryl

ketone dianion species with 2,6-di-*tert*-butylphenols. We have found that these reactions take place not only at the carbonyl group but also at the aromatic ring, which leads to the formation of a new class of lanthanide aryloxide, mixed aryloxide/alkoxide, and aryloxide/enolate complexes, with the selectivity being dependent on the nature of both metals and ketones. The structures and reactivities of these newly formed lanthanide complexes are also described. A portion of this work has been previously communicated.<sup>4a,5</sup>

## Results and Discussion

**Reaction of the Ytterbium(II)-Benzophenone Dianion Complex  $[\text{Yb}(\mu-\eta^1, \eta^2\text{-OCPh}_2)(\text{HMPA})_2]_2$  (**1**) with 2,6-Di-*tert*-butyl-4-methylphenol.** Our investigation on the reaction of complex **1** with an alcohol was initially promoted by both the novel structural features of **1** and our interests in low-valent lanthanide alkoxide (aryloxide) complexes.<sup>6</sup> Since both an Yb–C bond and an Yb–O ionic bond are present for each Yb(II) ion in complex **1**, we thought that if the Yb–C bond could be selectively protonated during alcoholysis, formation of an ytterbium(II) complex bearing mixed alkoxide ligands might be possible. The reaction of **1** with 2 equiv of tertiary butyl alcohol was attempted first, but no isolable product was obtained. However, the use of a bulky aryl alcohol such as 2,6-di-*tert*-butyl-4-methylphenol (ArOH) enabled us to isolate a crystalline product. Addition of 2 equiv of ArOH in THF to a purple solution of **1** generated gradually a light brown solution in a few hours. Evaporation of THF and addition of diethyl ether precipitated fine orange crystals which after recrystallization from THF yielded orange-red blocks of **2** (eq 4). Contrary to our expecta-



tion,  $^1\text{H}$  NMR spectroscopic study suggested that **2** was the ytterbium(II) aryloxide  $\text{Yb}(\text{OAr})_2(\text{HMPA})_2$ , a product resulted from the alcoholysis of both the Yb–C bond and the Yb–O bond of **1**. This compound could be isolated

(4) (a) Hou, Z.; Yamazaki, H.; Kobayashi, K.; Fujiwara, Y.; Taniguchi, H. *J. Chem. Soc., Chem. Commun.* **1992**, 722. (b) Hou, Z.; Yamazaki, H.; Fujiwara, Y.; Taniguchi, H. *Organometallics* **1992**, *11*, 2711.

(5) Hou, Z.; Yoshimura, T.; Wakatsuki, Y. *J. Am. Chem. Soc.* **1994**, *116*, 11169.

(6) (a) Hou, Z.; Miyano, T.; Yamazaki, H.; Wakatsuki, Y. *J. Am. Chem. Soc.* **1995**, *117*, 4421. (b) Hou, Z.; Wakatsuki, Y. *Yuki Gosei Kagaku Kyokaiishi* **1995**, *53*, No.10, in press.

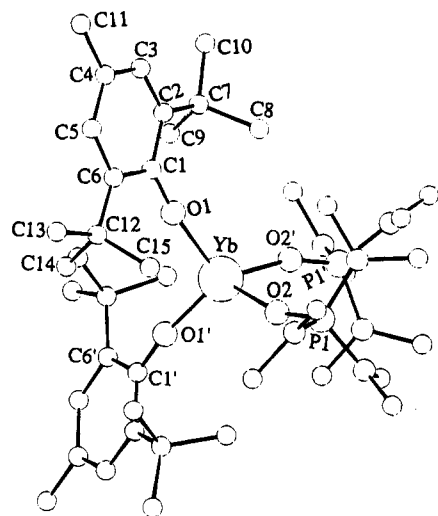


Figure 2. X-ray structure of 2.

Table 1. Selected Bond Lengths (Å) and Angles (deg) of 2

Yb-O(1)	2.179(8)	Yb-O2	2.299(7)
P(1)-O(2)	1.480(7)	O(1)-C(1)	1.30(2)
C(1)-C(2)	1.46(1)	C(1)-C(6)	1.46(2)
C(2)-C(3)	1.41(2)	C(2)-C(7)	1.52(2)
C(3)-C(4)	1.40(2)	C(4)-C(5)	1.39(2)
C(4)-C(11)	1.53(2)	C(5)-C(6)	1.37(2)
C(6)-C(12)	1.52(2)	C(7)-C(8)	1.54(3)
C(7)-C(9)	1.55(2)	C(7)-C(10)	1.56(2)
C(12)-C(13)	1.57(2)	C(12)-C(14)	1.55(2)
C(12)-C(15)	1.50(3)		
O(1)-Yb-O(2)	122.1(3)	O(1)-Yb-O(1')	110.3(3)
O(1)-Yb-O(2')	103.0(3)	O(2)-Yb-O(1')	103.0(3)
O(2)-Yb-O(2')	97.0(3)	O(1')-Yb-O(2')	122.1(5)
Yb-O(1)-C(1)	171.3(6)	Yb-O(2)-P(1)	163.9(7)

in 80% yield when 4 equiv of ArOH was used. Reflecting the diamagnetic property of the divalent ytterbium species, the  $^1\text{H}$  NMR spectrum of **2** in  $\text{C}_6\text{D}_6$  showed well-resolved signals at  $\delta$  7.33 (s,  $\text{C}_6\text{H}_2$ ), 2.53 (s, Me), and 1.85 (s,  $^t\text{Bu}$ ) for the ArO parts and  $\delta$  2.15 (d,  $J_{\text{P-H}} = 9.3$  Hz) for the HMPA ligands. An X-ray analysis reveals that the central Yb atom in **2** is sitting on a two-fold axis and is bonded by two ArO and two HMPA ligands in a distorted tetrahedral form (Figure 2 and Table 1). The Yb-O(HMPA) bond distance (2.298(7) Å) in **2** is comparable with those found in **1** (av 2.28(2) Å)<sup>4</sup> and is also comparable with those found in the six-coordinated Yb(II) complexes  $[\text{Yb}(\text{HMPA})_4(\text{THF})_2]\text{I}_2$  (av 2.357(6) Å)<sup>7</sup> and *cis*-Yb( $\mu, \eta^1$ -OCMo(CO)<sub>2</sub>Cp)<sub>2</sub>(HMPA)<sub>4</sub> (av 2.33(1) Å),<sup>8</sup> when the influence of coordination number is taken into account.<sup>9</sup> The Yb-OAr bonds (2.179(9) Å) in **2** are slightly longer than those found in another four-coordinated ytterbium(II) aryloxy complex (ArO)<sub>2</sub>Yb-(THF)<sub>2</sub> (Ar =  $\text{C}_6\text{H}_2$ - $^t\text{Bu}_2$ -2,6-Me-4) (av 2.137(10) Å),<sup>10</sup> probably due to the electronic and steric influence of the HMPA ligands.<sup>7,11</sup>

During the isolation of **2**, a few yellow needle-like crystals of **3** precipitated from the diethyl ether mother

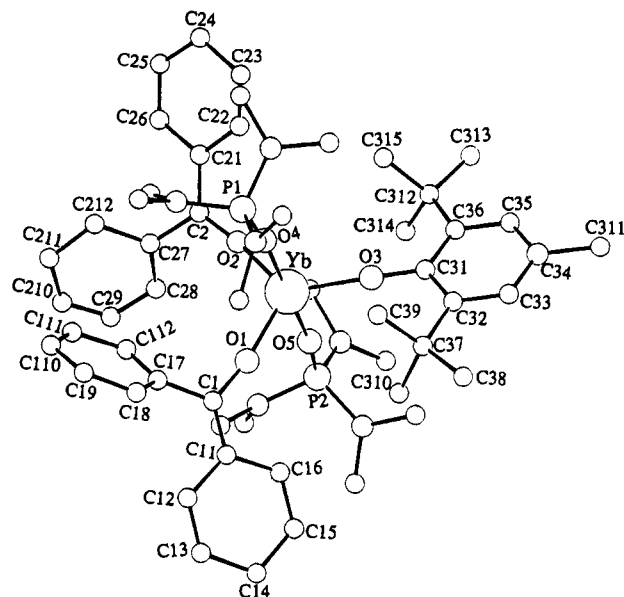


Figure 3. X-ray structure of 3.

liquor after a few weeks (eq 4). Its  $^1\text{H}$  NMR spectrum in  $\text{C}_6\text{D}_6$  showed unassignable complicated signals at the region of  $\delta$  -8.0 to 18.0, suggesting that this compound was a paramagnetic species. A single crystal suitable for diffraction studies was then selected for crystallographic study which revealed that **3** was a trivalent

ytterbium complex, Yb(OC(=CCH=CHCH<sub>2</sub>CH=CH)-Ph)<sub>2</sub>(OAr)(HMPA)<sub>2</sub>, in which the central Yb atom was five-coordinated by one ArO, two benzophenone-originated units, and two HMPA ligands in a trigonal bipyramidal form (Figure 3 and Table 2). Consistent with the trivalent feature of the central ytterbium ion,<sup>9</sup> the Yb-OAr bond (2.094(8) Å) and the Yb-O(HMPA) bonds (av 2.223(9) Å) in **3** are, respectively, 0.085 and 0.075 Å shorter than those found in the four-coordinated Yb(II) complex **2**. The bond distances between the Yb ion and the oxygen atoms of the benzophenone units (Yb-O(1): 2.091(11), Yb-O(2): 2.090(11) Å) are almost the same as that of the Yb-OAr bond (2.094(8) Å), and both are comparable with the Yb(III)-O(naphthoxy) bond (2.06(1) Å) found in Cp<sub>2</sub>Yb(naphthoxy)(THF).<sup>12</sup> The sum of the bond angles around the carbonyl carbon atom in each benzophenone unit is 360(1)° for C(1) and 359(2)° for C(2), showing that the C(1) and C(2) atoms are still in a sp<sup>2</sup>-hybrid state. The bond distances for the benzophenone units indicate that one of the two phenyl groups in each benzophenone unit possesses two different types of C-C bonds, which is significantly deviated from a normal phenyl ring. As shown in Table 2 and Figure 3, the C(1)-C(11), C(12)-C(13) and C(15)-C(16) bonds (av 1.37(2) Å) are significantly shorter than the C(11)-C(12), C(11)-C(16), C(13)-C(14), and C(14)-C(15) bonds (av 1.48(3) Å). Similarly, the C(2)-C(21), C(22)-C(23), and C(25)-C(26) bonds (av 1.35(3) Å) are shorter than the C(21)-C(22), C(21)-C(26), C(23)-C(24), and C(24)-C(25) bonds (av 1.47(3) Å). Both demonstrate a characteristic of a cyclohexadienylidene structure. Based on all these structural data and elemental analysis, complex **3** could be best described as an ytterbium(III) aryloxy/enolate complex, which

(7) Hou, Z.; Wakatsuki, Y. *J. Chem. Soc., Chem. Commun.* **1994**, 1205.

(8) Hou, Z.; Aida, K.; Takagi, Y.; Wakatsuki, Y. *J. Organomet. Chem.* **1994**, 473, 101.

(9) Shannon, R. D. *Acta Crystallogr., Sect. 32A* **1976**, 751.

(10) Deacon, G. B.; Hitchcock, P. B.; Holmes, S. A.; Lappert, M. F.; Mackinnon, P.; Newham, R. H. *J. Chem. Soc., Chem. Commun.* **1989**, 935.

(11) Hou, Z.; Kobayashi, K.; Yamazaki, H. *Chem. Lett.* **1991**, 265.

(12) Zhou, X.-G.; Wu, Z.-Z.; Jin, Z.-S. *J. Organomet. Chem.* **1992**, 431, 289.



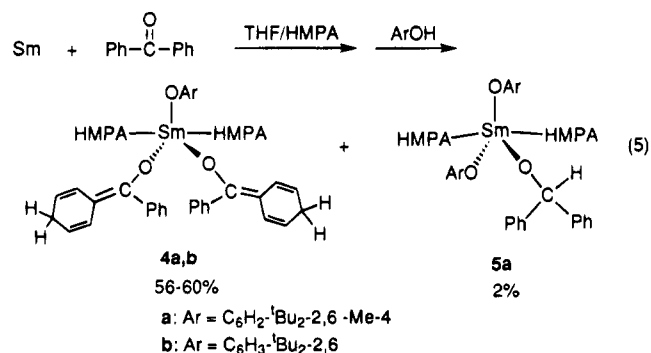
**Table 2. Selected Bond Lengths (Å) and Angles (deg) of 3**

Yb-O(1)	2.091(11)	Yb-O(2)	2.090(11)
Yb-O(3)	2.093(8)	Yb-O(4)	2.233(9)
Yb-O(5)	2.213(9)	P(1)-O(4)	1.495(10)
P(2)-O(5)	1.490(10)	O(1)-C(1)	1.34(2)
O(2)-C(2)	1.31(2)	O(3)-C(31)	1.34(1)
C(1)-C(11)	1.35(2)	C(1)-C(17)	1.50(2)
C(11)-C(12)	1.46(2)	C(11)-C(16)	1.46(2)
C(12)-C(13)	1.36(2)	C(13)-C(14)	1.49(3)
C(14)-C(15)	1.50(3)	C(15)-C(16)	1.39(3)
C(17)-C(18)	1.46(2)	C(17)-C(112)	1.40(2)
C(18)-C(19)	1.41(3)	C(19)-C(110)	1.42(3)
C(110)-C(111)	1.34(3)	C(111)-C(112)	1.45(2)
C(2)-C(21)	1.40(3)	C(2)-C(27)	1.50(2)
C(21)-C(22)	1.43(3)	C(21)-C(26)	1.45(3)
C(22)-C(23)	1.27(3)	C(23)-C(24)	1.56(3)
C(24)-C(25)	1.44(3)	C(25)-C(26)	1.37(3)
C(27)-C(28)	1.34(3)	C(27)-C(212)	1.48(3)
C(28)-C(29)	1.38(3)	C(29)-C(210)	1.26(3)
C(210)-C(211)	1.38(4)	C(211)-C(212)	1.49(3)
C(31)-C(32)	1.44(2)	C(31)-C(36)	1.42(2)
C(32)-C(33)	1.39(2)	C(32)-C(37)	1.57(2)
C(33)-C(34)	1.42(3)	C(34)-C(35)	1.40(3)
C(34)-C(311)	1.56(2)	C(35)-C(36)	1.38(2)
C(36)-C(312)	1.55(2)	C(37)-C(38)	1.58(3)
C(37)-C(39)	1.59(3)	C(37)-C(310)	1.55(3)
C(312)-C(313)	1.56(3)	C(312)-C(314)	1.55(3)
C(312)-C(315)	1.57(3)		
O(1)-Yb-O(2)	114.3(4)	O(1)-Yb-O(3)	121.0(5)
O(1)-Yb-O(4)	91.1(4)	O(1)-Yb-O(5)	89.8(4)
O(2)-Yb-O(3)	124.7(5)	O(2)-Yb-O(4)	90.1(4)
O(2)-Yb-O(5)	89.1(4)	O(3)-Yb-O(4)	90.3(4)
O(3)-Yb-O(5)	89.8(4)	O(4)-Yb-O(5)	178.9(4)
Yb-O(1)-C(1)	169(1)	Yb-O(2)-C(2)	170(1)
Yb-O(3)-C(31)	178(1)	Yb-O(4)-P(1)	173(1)
Yb-O(5)-P(2)	173(1)	O(1)-C(1)-C(11)	123(1)
O(1)-C(1)-C(17)	114(1)	C(11)-C(1)-C(17)	123(1)
O(2)-C(2)-C(21)	121(2)	O(2)-C(2)-C(27)	116(2)
C(21)-C(2)-C(27)	122(2)		

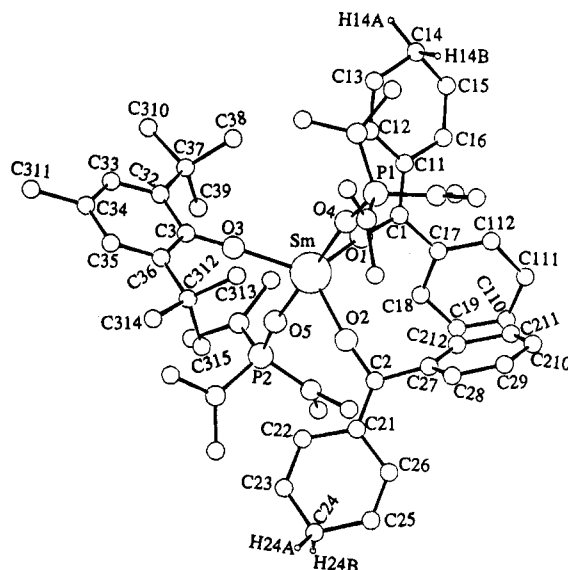
is formally formed *via* the protonation at the para-position of the phenyl ring in **1** by ArOH (*vide infra*).

**Reaction of Samarium-Benzophenone Dianion Species with 2,6-Di-*tert*-butylphenols.** Samarium-benzophenone dianion species was generated by the reaction of Sm metal with benzophenone in THF/HMPA. Its reaction with ArOH (Ar = C<sub>6</sub>H<sub>2</sub>-*t*Bu<sub>2</sub>-2,6-Me-4),

however, yielded the enolate complex Sm(OC(=CCH=CHCH<sub>2</sub>CH=CH)Ph)<sub>2</sub>(OAr)(HMPA)<sub>2</sub> (**4a**), which was the samarium analogue of **3**, as a major product (60% yield based on benzophenone, 30% based on Sm) (eq 5), while Sm(II) aryloxide analogous to **2** was not obtained. An



X-ray analysis revealed that complex **4a** was isostructural with **3** (Figure 4 and Table 3). The quality of the diffraction data for **4a** seemed to be higher than those obtained in the case of **3** and the cyclohexadienylidene

**Figure 4.** X-ray structure of **4a**.

features of the enolate parts in **4a** were more clear. The C-C double bonds (av 1.35(3) Å) of the enolate parts are obviously shorter than the C-C single ones (av 1.48(3) Å). Both hydrogen atoms in each CH<sub>2</sub> group can be easily located at the difference Fourier map and the C-C-C angles around the CH<sub>2</sub> units (C(14): 113(2)°, C(24): 114(2)°) are significantly deviated from 120°. The average bond distance of Sm-O(HMPA) (2.333(10) Å) in **4a** is about 0.17 Å shorter than that found in the divalent samarium complex Sm(HMPA)<sub>4</sub>I<sub>2</sub> (2.500(6) Å),<sup>7</sup> and the Sm-OAr bond (2.187(8) Å) is about 0.12–0.15 Å shorter than those of the Sm(II)-OAr bonds found in (ArO)<sub>2</sub>Sm(THF)<sub>3</sub> (av 2.304(8) Å)<sup>6a,13</sup> and [KSm(OAr)<sub>3</sub>(THF)]<sub>n</sub> (av 2.339(9) Å).<sup>14</sup> These data suggest that the central samarium ion in **4a** is in a trivalent state.<sup>9</sup> The bond distances of Sm-O(enolate) (av 2.180(12) Å) is comparable with that of the Sm-OAr bond, and both are close to but slightly longer than the terminal Sm-O bonds found in other samarium(III) aryloxides such as Sm<sub>2</sub>(OC<sub>6</sub>H<sub>3</sub>Me<sub>2</sub>-2,6)<sub>6</sub> (2.101(6) Å)<sup>15</sup> and (η<sup>5</sup>-C<sub>5</sub>Me<sub>5</sub>)<sub>2</sub>Sm(OC<sub>6</sub>HMe<sub>4</sub>-2,3,5,6) (2.13(1) Å).<sup>16</sup> Such bond lengthening was also previously observed in other HMPA-coordinated lanthanide complexes<sup>7,8</sup> and probably resulted from the unusually strong electron donating ability of the HMPA ligands.

The <sup>1</sup>H NMR spectrum of **4a** in C<sub>6</sub>D<sub>6</sub> was consistent with its X-ray structure. Well-resolved signals for the ArO (δ 7.75, 2.67, 1.35), HMPA (δ 2.11), and Ph (δ 7.90, 7.28, 7.21) groups could be easily assigned. The broad peaks for the enolate units at δ 6.94–5.28 (CH=CH) and δ 2.97 (CH<sub>2</sub>) were further confirmed by the DEPT and H,C-COSY experiments.

In order to confirm the source of the hydrogen atoms in the CH<sub>2</sub> units of the enolates **3** and **4a**, the reaction of the samarium-benzophenone dianion species with ArOD (Ar = C<sub>6</sub>H<sub>2</sub>-*t*Bu<sub>2</sub>-2,6-Me-4) was carried out. A

(13) Qi, G.-Z.; Shen, Q.; Lin, Y.-H. *Acta Crystallogr., Sect. C* **1994**, *50C*, 1456.

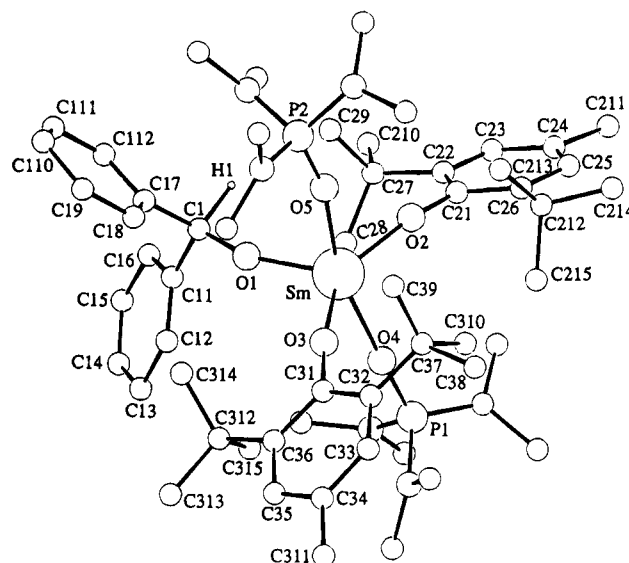
(14) Evans, W. J.; Anwender, R.; Ansari, M. A.; Ziller, J. W. *Inorg. Chem.* **1995**, *34*, 5.

(15) Barnhart, D. M.; Clark, D. L.; Gordon, J. C.; Huffman, J. C.; Vincent, R. L.; Watkin, J. G.; Zwick, B. D. *Inorg. Chem.* **1994**, *33*, 3487.

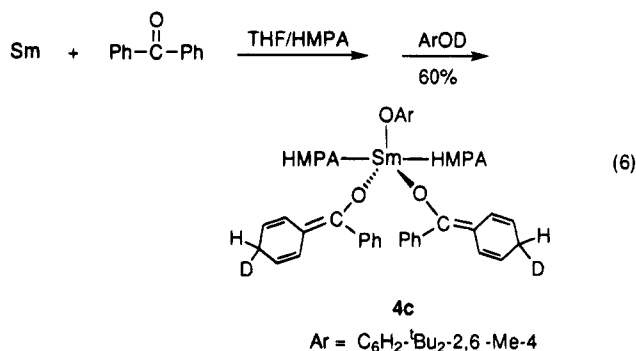
(16) Evans, W. J.; Hanusa, T. P.; Levan, K. R. *Inorg. Chim. Acta* **1985**, *110*, 191.

**Table 3. Selected Bond Lengths (Å) and Angles (deg) of 4a**

Sm-O(1)	2.189(13)	Sm-O(2)	2.170(11)
Sm-O(3)	2.187(8)	Sm-O(4)	2.331(10)
Sm-O(5)	2.335(10)	P(1)-O(4)	1.499(11)
P(2)-O(5)	1.480(11)	O(1)-C(1)	1.32(2)
O(2)-C(2)	1.34(2)	O(3)-C(31)	1.33(1)
C(1)-C(11)	1.36(2)	C(1)-C(17)	1.49(2)
C(11)-C(12)	1.46(3)	C(11)-C(16)	1.47(3)
C(12)-C(13)	1.31(3)	C(13)-C(14)	1.57(4)
C(14)-C(15)	1.45(4)	C(15)-C(16)	1.36(3)
C(17)-C(18)	1.41(3)	C(17)-C(112)	1.43(3)
C(18)-C(19)	1.40(3)	C(19)-C(110)	1.33(4)
C(110)-C(111)	1.41(4)	C(111)-C(112)	1.41(3)
C(2)-C(21)	1.36(2)	C(2)-C(27)	1.49(2)
C(21)-C(22)	1.47(2)	C(21)-C(26)	1.44(2)
C(22)-C(23)	1.38(3)	C(23)-C(24)	1.46(3)
C(24)-C(25)	1.51(3)	C(25)-C(26)	1.34(3)
C(27)-C(28)	1.45(2)	C(27)-C(212)	1.37(3)
C(28)-C(29)	1.42(2)	C(29)-C(210)	1.37(3)
C(210)-C(211)	1.39(3)	C(211)-C(212)	1.46(3)
C(31)-C(32)	1.43(3)	C(31)-C(36)	1.43(2)
C(32)-C(33)	1.39(2)	C(32)-C(37)	1.57(3)
C(33)-C(34)	1.40(3)	C(34)-C(35)	1.37(3)
C(34)-C(311)	1.54(2)	C(35)-C(36)	1.41(2)
C(36)-C(312)	1.56(3)	C(37)-C(38)	1.55(3)
C(37)-C(39)	1.54(3)	C(37)-C(310)	1.57(3)
C(312)-C(313)	1.59(3)	C(312)-C(314)	1.59(3)
C(312)-C(315)	1.56(3)		
O(1)-Sm-O(2)	111.5(4)	O(1)-Sm-O(3)	126.1(5)
O(1)-Sm-O(4)	89.5(4)	O(1)-Sm-O(5)	89.4(4)
O(2)-Sm-O(3)	122.5(4)	O(2)-Sm-O(4)	91.4(4)
O(2)-Sm-O(5)	90.0(4)	O(3)-Sm-O(4)	90.5(4)
O(3)-Sm-O(5)	89.4(4)	O(4)-Sm-O(5)	178.4(4)
Sm(1)-O(1)-C(1)	168(1)	Sm(1)-O(2)-C(2)	170(1)
Sm(1)-O(3)-C(31)	179(1)	Sm(1)-O(4)-P(1)	172(1)
Sm(1)-O(5)-P(2)	171(1)	O(1)-C(1)-C(11)	121(2)
O(1)-C(1)-C(17)	116(2)	C(11)-C(1)-C(17)	123(2)
C(1)-C(11)-C(12)	120(2)	C(1)-C(11)-C(16)	123(2)
C(12)-C(11)-C(16)	117(2)	C(11)-C(12)-C(13)	124(2)
C(12)-C(13)-C(14)	120(2)	C(13)-C(14)-C(15)	114(2)
C(14)-C(15)-C(16)	124(2)	C(11)-C(16)-C(15)	120(2)
C(1)-C(17)-C(18)	118(2)	C(1)-C(17)-C(112)	120(2)
C(18)-C(17)-C(112)	122(2)	C(17)-C(18)-C(19)	119(2)
C(18)-C(19)-C(110)	120(2)	C(19)-C(110)-C(111)	123(2)
C(110)-C(111)-C(112)	120(2)	C(17)-C(112)-C(111)	116(2)
O(2)-C(2)-C(21)	125(1)	O(2)-C(2)-C(27)	112(1)
C(21)-C(2)-C(27)	123(1)	C(2)-C(21)-C(22)	118(1)
C(2)-C(21)-C(26)	123(1)	C(22)-C(21)-C(26)	118(1)
C(21)-C(22)-C(23)	118(2)	C(22)-C(23)-C(24)	125(2)
C(23)-C(24)-C(25)	113(2)	C(24)-C(25)-C(26)	122(2)
C(21)-C(26)-C(25)	122(2)	C(2)-C(27)-C(28)	122(1)
C(2)-C(27)-C(212)	118(1)	C(28)-C(27)-C(212)	121(1)
C(27)-C(28)-C(29)	119(2)	C(28)-C(29)-C(210)	121(2)
C(29)-C(210)-C(211)	121(2)	C(210)-C(211)-C(212)	121(2)
C(27)-C(212)-C(211)	118(2)	O(3)-C(31)-C(32)	120(2)
O(3)-C(31)-C(36)	120(2)	C(32)-C(31)-C(36)	120(1)
C(31)-C(32)-C(33)	117(2)	C(31)-C(32)-C(37)	122(1)
C(33)-C(32)-C(37)	121(2)	C(32)-C(33)-C(34)	123(2)
C(33)-C(34)-C(35)	120(1)	C(33)-C(34)-C(311)	120(2)
C(35)-C(34)-C(311)	121(2)	C(34)-C(35)-C(36)	121(2)
C(31)-C(36)-C(35)	120(1)	C(31)-C(36)-C(312)	122(1)
C(35)-C(36)-C(312)	118(1)	C(32)-C(37)-C(38)	106(1)
C(32)-C(37)-C(39)	110(2)	C(32)-C(37)-C(310)	112(1)
C(38)-C(37)-C(39)	114(2)	C(38)-C(37)-C(310)	108(2)
C(39)-C(37)-C(310)	107(2)	C(36)-C(312)-C(313)	110(2)
C(36)-C(312)-C(314)	113(1)	C(36)-C(312)-C(315)	111(2)
C(313)-C(312)-C(314)	105(2)	C(313)-C(312)-C(315)	112(2)
C(314)-C(312)-C(315)	106(2)		

**Figure 5. X-ray structure of 5a.**

corresponding enolate  $\text{Sm}(\text{OC}(\text{=CCH}=\text{CHCH}_2\text{CH}=\text{CH})\text{Ph})_2(\text{OAr})(\text{HMPA})_2$  (**4b**, Ar =  $\text{C}_6\text{H}_3\text{-}^t\text{Bu}_2\text{-2,6}$ , 56% yield based on benzophenone) (eq 5).



In the course of the synthesis of **4a**, when leaving the diethyl ether mother liquor to stand at room temperature for a few months, several pale blocks of  $\text{Sm}(\text{OCHPh})_2(\text{OAr})_2(\text{HMPA})_2$  (**5a**, Ar =  $\text{C}_6\text{H}_2\text{-}^t\text{Bu}_2\text{-2,6-Me-4}$ ) precipitated (eq 5). These crystals rapidly lost their crystallinity upon removal of the mother liquor. Although a single crystal that was qualified for X-ray analysis was eventually sealed in a capillary, rapid decay occurred during the data collection and only the data with  $2\theta$  range of  $4\text{--}35^\circ$  were successfully collected. Luckily, however, these data were good enough for us to solve the structure after a decay correction. As shown in Figure 5 and Table 4, this complex **5a** possesses a highly distorted trigonal bipyramidal structure with one benzophenone unit and two ArOs at the equatorial, and two HMPA ligands at the apical vertices. In contrast to the enolates **3** and **4a**, the benzophenone unit in **5a** was proved to be a diphenylmethoxy ( $\text{OCHPh}_2$ ) group rather than an enolate one. The carbonyl carbon atom C(1) was clearly of a typical tetrahedral configuration (Table 4), and the hydrogen atom attached to it was easily found in the difference Fourier map. Since there are two bulky ArO groups in **5a** in contrast with only one in **3** or **4a**, the apical HMPA ligands in **5a** are more bent toward each other, forming an  $\text{O}(\text{HMPA})\text{-Sm-O}(\text{HMPA})$  angle of  $163.3(4)^\circ$ , which is much smaller than the  $\text{O}(\text{HMPA})\text{-Yb-O}(\text{HMPA})$  angle in **3** ( $178.9(4)^\circ$ ) and

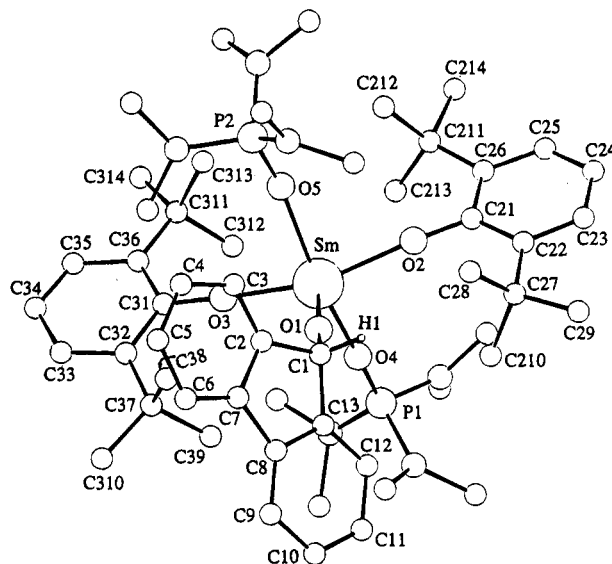
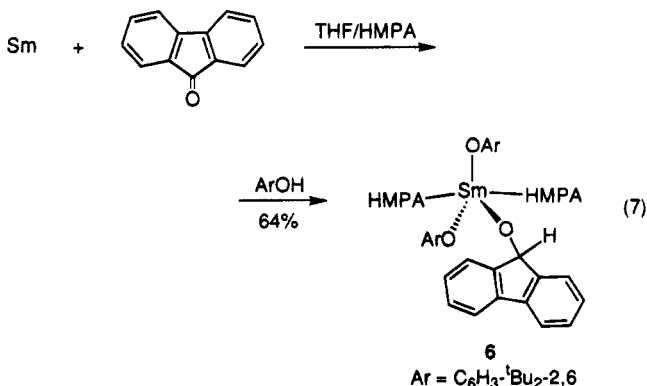
similar treatment yielded the deuterated enolate  $\text{Sm}(\text{OC}(\text{=CCH}=\text{CHCHDCH}=\text{CH})\text{Ph})_2(\text{OAr})(\text{HMPA})_2$  (**4c**) (eq 6), as identified by comparing its  $^1\text{H}$  NMR spectrum with that of **4a**. This result suggests that the formation of **3** and **4a** is *via* the direct protonation by ArOH. The similar reaction of the samarium-benzophenone dianion species with 2,6-di-*tert*-butylphenol afforded the

**Table 4. Selected Bond Lengths (Å) and Angles (deg) of 5a**

Sm–O(1)	2.15(1)	Sm–O(2)	2.21(1)
Sm–O(3)	2.22(1)	Sm–O(4)	2.34(1)
Sm–O(5)	2.37(1)	P(1)–O(4)	1.51(1)
O(1)–C(1)	1.41(2)	O(2)–C(21)	1.36(2)
O(3)–C(31)	1.36(2)	C(1)–C(11)	1.51(3)
C(1)–C(17)	1.53(3)	C(11)–C(12)	1.37(3)
C(11)–C(16)	1.46(3)	C(12)–C(13)	1.45(3)
C(13)–C(14)	1.46(3)	C(14)–C(15)	1.34(3)
C(15)–C(16)	1.41(4)	C(17)–C(18)	1.38(3)
C(17)–C(112)	1.42(3)	C(18)–C(19)	1.43(3)
C(19)–C(110)	1.44(3)	C(110)–C(111)	1.35(3)
C(111)–C(112)	1.41(3)		
O(1)–Sm–O(2)	107.8(4)	O(1)–Sm–O(3)	107.9(4)
O(1)–Sm–O(4)	104.5(4)	O(1)–Sm–O(5)	92.2(4)
O(2)–Sm–O(3)	144.4(4)	O(2)–Sm–O(4)	83.8(4)
O(2)–Sm–O(5)	90.1(4)	O(3)–Sm–O(4)	86.7(4)
O(3)–Sm–O(5)	89.3(3)	O(4)–Sm–O(5)	163.3(4)
Sm–O(1)–C(1)	161(1)	Sm–O(2)–C(21)	170(1)
Sm–O(3)–C(31)	170(1)	Sm–O(4)–P(1)	177.8(7)
Sm–O(5)–P(2)	165.9(7)	O(1)–C(1)–C(11)	112(1)
O(1)–C(1)–C(17)	111(2)	C(11)–C(1)–C(17)	109(2)

that in **4a** (178.4(4)°). Possibly reflecting this steric influence, the <sup>1</sup>H NMR signals for the <sup>t</sup>Bu (δ 1.45), HMPA (δ 1.86), and diphenylmethoxy (δ 7.70–6.90) groups in **5a** were rather broad, while those for the Me (δ 2.69) and the C<sub>6</sub>H<sub>2</sub> (δ 7.75) groups were relatively sharp.

**Reaction of Samarium–Fluorenone Dianion Species with 2,6-Di-*tert*-butylphenols.** Samarium–fluorenone dianion species was generated as in the case of benzophenone. A similar reaction with 2,6-di-*tert*-butyl-4-methylphenol did not give any isolable solid product. However, colorless crystals of **6** were isolated from the reaction with 2,6-di-*tert*-butylphenol (eq 7). <sup>1</sup>H NMR, X-ray crystallography, and elemental analysis confirmed that **6** was the fluorenoxy analogue of **5a**, Sm(fluorenoxy)-(OAr)<sub>2</sub>(HMPA)<sub>2</sub> (**6**, Ar = C<sub>6</sub>H<sub>3</sub>-<sup>t</sup>Bu<sub>2</sub>-2,6, 64% yield). The overall structure of **6** is identical to that of **5a** (Figure 6 and Table 5). The bond angles of O(aryloxy)–Sm–O(aryloxy) (148.1(2)°) and O(HMPA)–Sm–O(HMPA) (158.9(2)°) in **6** parallel well those found in **5a** (144.4(4) and 163.3(4)°, respectively). Reflecting the difference between an alkoxide and an aryloxy, the Sm–O(fluorenoxy) bond (2.111(5) Å) in **6** is shorter than the Sm–OAr bonds (av 2.236(6) Å), which is also similar to what was seen in **5a** (Sm–O(diphenylmethoxy): 2.154(11) Å, Sm–OAr: av 2.217(10) Å). Such difference in Sm–O bond distances between an alkoxide and an aryloxy was also observed in other Sm(III) complexes such as (η<sup>5</sup>-C<sub>5</sub>Me<sub>5</sub>)<sub>2</sub>Sm[O(CH<sub>2</sub>)<sub>4</sub>(C<sub>5</sub>Me<sub>5</sub>)](THF) (2.08(1) Å)<sup>17</sup> and (η<sup>5</sup>-C<sub>5</sub>Me<sub>5</sub>)<sub>2</sub>Sm(OC<sub>6</sub>HMe<sub>4</sub>-2,3,5,6) (2.13(1) Å)<sup>18</sup> and was apparently due to the conjugation of the aryloxy anion with its aromatic ring.

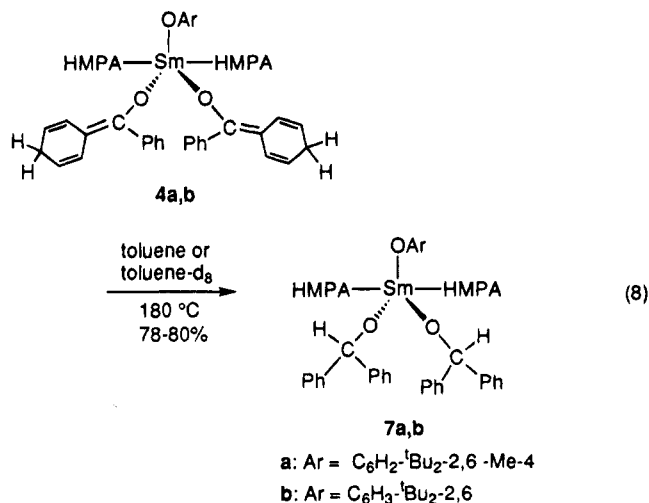
**Figure 6.** X-ray structure of **6**.**Table 5. Selected Bond Lengths (Å) and Angles (deg) of 6**

Sm–O(1)	2.111(5)	Sm–O(2)	2.229(6)
Sm–O(3)	2.243(5)	Sm–O(4)	2.383(4)
Sm–O(5)	2.399(4)	P(1)–O(4)	1.497(5)
O(1)–C(1)	1.404(8)	O(2)–C(21)	1.34(1)
O(3)–C(31)	1.33(1)	C(1)–C(2)	1.53(1)
C(1)–C(13)	1.51(1)		
O(1)–Sm–O(2)	103.9(2)	O(1)–Sm–O(3)	108.0(2)
O(1)–Sm–O(4)	106.7(2)	O(1)–Sm–O(5)	94.3(2)
O(2)–Sm–O(3)	148.1(2)	O(2)–Sm–O(4)	84.9(2)
O(2)–Sm–O(5)	87.9(2)	O(3)–Sm–O(4)	86.9(2)
O(3)–Sm–O(5)	88.8(2)	O(4)–Sm–O(5)	158.9(2)
Sm–O(1)–C(1)	174.0(5)	Sm–O(2)–C(21)	173.7(4)
Sm–O(3)–C(31)	172.4(4)	Sm–O(4)–P(1)	178.4(4)
Sm–O(5)–P(2)	163.6(3)	O(1)–C(1)–C(2)	115.6(6)
O(1)–C(1)–C(13)	113.8(5)	C(2)–C(1)–C(13)	101.3(7)

Similar to those of **5a**, the <sup>1</sup>H NMR signals of **6** for the C<sub>6</sub>H<sub>3</sub> parts (δ 7.90 (d), 7.31 (t)) of the ArO groups were well-resolved, while those for the <sup>t</sup>Bu units (δ 1.56), the fluorenyl (δ 7.51, 7.21, 7.04, 5.62), and the HMPAs (δ 1.86) were quite broad.

**Thermolysis of the Samarium Enolates 4a–c.** In the course of measuring the melting point of the enolate **4a** under nitrogen, a color change from yellow to blue and finally to colorless was observed at the temperature range of 150–180 °C. Thermolysis of **4a** was then carried out overnight in toluene at 180 °C in a flame-sealed ampoule. Evaporation of the solvent left a colorless crystalline product which after recrystallization from toluene/hexane yielded Sm(OCHPh)<sub>2</sub>(OAr)-(HMPA)<sub>2</sub> (**7a**, Ar = C<sub>6</sub>H<sub>2</sub>-<sup>t</sup>Bu<sub>2</sub>-2,6-Me-4, 80% yield) (eq 8), a product which is formally derived from the 1,5-hydrogen shift at the enolate groups of **4a**. The <sup>1</sup>H NMR spectrum of **7a** in C<sub>6</sub>D<sub>6</sub> was much clearer than that of its parent enolate **4a** and could be assigned very easily. Signals for the aromatic protons of the diphenylmethoxy groups appeared at δ 8.08 (d, ortho), 7.33 (t, meta), and 7.20 (t, para), while that for the CH appeared at δ 7.61 as a slightly broad singlet. The ArO unit showed sharp singlets at δ 7.77 (C<sub>6</sub>H<sub>2</sub>), 2.71 (Me) and 2.01 (<sup>t</sup>Bu). HMPAs gave a doublet at δ 1.62.

(17) Evans, W. J.; Ulibarri, T. A.; Chamberlain, L. R.; Ziller, J. W.; Alvarez, D., Jr. *Organometallics* **1990**, *9*, 2124.



The similar thermolysis of a toluene solution of **4b** at 180 °C resulted in the formation of Sm(OCHPh)<sub>2</sub>(OAr)-(HMPA)<sub>2</sub> (**7b**, Ar = C<sub>6</sub>H<sub>3</sub>-<sup>t</sup>Bu<sub>2</sub>-2,6, 78% yield) (eq 8). An X-ray analysis of **7b** shows that the geometry around the central Sm atom is very similar to that in **4a** (Figure 7). Reflecting the characteristic of an alkoxide, however, the average bond distance of the Sm-O(diphenylmethoxy) bond (2.143(5) Å) in **7b** is shorter than that of the Sm-O(enolate) bond (2.18(1) Å) in **4a**, while the Sm-OAr (2.202(4) Å) and Sm-O(HMPA) (2.364(4) Å) bonds are comparable with those (2.187(8) and 2.333-(10) Å, respectively) found in **4a**.

To understand the mechanism of the hydrogen shift process in the formation of **7a,b**, deuterium labeled experiments were performed. It was found that no deuterium was incorporated into the product **7a** when **4a** was thermolyzed in toluene-*d*<sub>8</sub>. Furthermore, thermolysis of the deuterated enolate **4c** in toluene afforded selectively **7c** (eq 9), as identified by comparing its <sup>1</sup>H NMR spectrum with that of **7a**. Scrambling of deuterium at the phenyl ring was not observed. These results suggest that the formation of **7a-c** from **4a-c** is an intramolecular one-step 1,5-hydrogen shift process. It is also noteworthy that although the complexes of type of **5a** and **6** are isolable, disproportionation (ligand redistribution) in either the starting aryloxide/enolate complexes **4a-c** or the aryloxide/alkoxide products **7a-c** was not observed under the present thermolysis conditions.

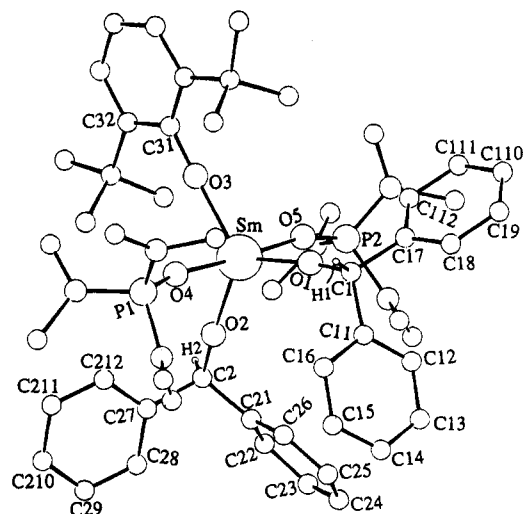
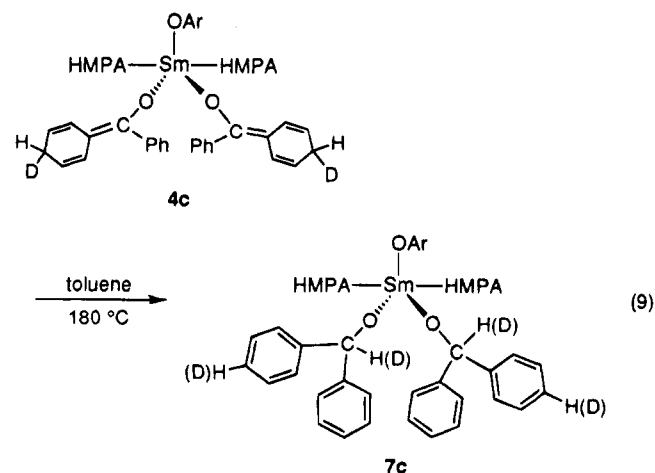


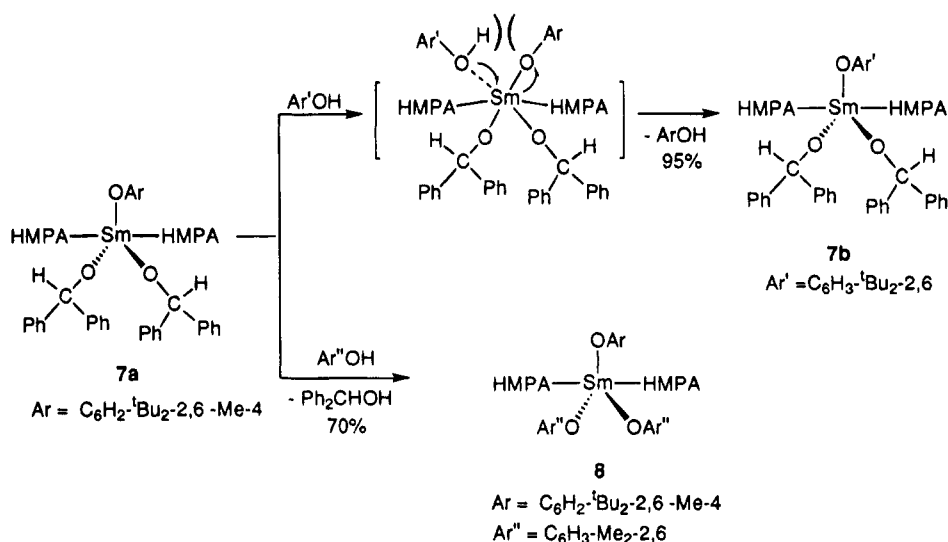
Figure 7. X-ray structure of **7b**.

Table 6. Selected Bond Lengths (Å) and Angles (deg) of **7b**

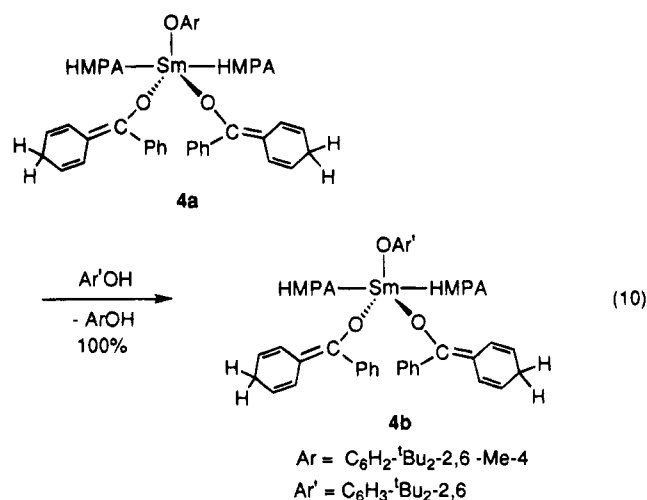
Sm-O(1)	2.145(5)	Sm-O(2)	2.141(5)
Sm-O(3)	2.202(4)	Sm-O(4)	2.359(4)
Sm-O(5)	2.368(5)	P(1)-O(4)	1.477(5)
O(1)-C(1)	1.388(8)	O(2)-C(2)	1.386(9)
O(3)-C(31)	1.335(7)	C(1)-C(11)	1.52(1)
C(1)-C(17)	1.53(1)	C(11)-C(12)	1.39(1)
C(11)-C(16)	1.39(1)	C(12)-C(13)	1.39(1)
C(13)-C(14)	1.35(2)	C(14)-C(15)	1.37(2)
C(15)-C(16)	1.40(2)	C(17)-C(18)	1.41(1)
C(17)-C(112)	1.387(9)	C(18)-C(19)	1.40(1)
C(19)-C(110)	1.36(1)	C(110)-C(111)	1.38(1)
C(111)-C(112)	1.41(1)	C(2)-C(21)	1.522(9)
C(2)-C(27)	1.546(9)	C(21)-C(22)	1.40(1)
C(21)-C(26)	1.382(9)	C(22)-C(23)	1.39(1)
C(24)-C(23)	1.37(1)	C(24)-C(25)	1.39(1)
C(25)-C(26)	1.39(1)	C(27)-C(28)	1.39(1)
C(27)-C(212)	1.37(1)	C(28)-C(29)	1.40(1)
C(29)-C(210)	1.37(1)	C(210)-C(211)	1.38(1)
C(211)-C(212)	1.41(1)		
O(1)-Sm-O(2)	117.7(2)	O(1)-Sm-O(3)	121.6(2)
O(1)-Sm-O(4)	90.6(2)	O(1)-Sm-O(5)	90.2(2)
O(2)-Sm-O(3)	120.7(2)	O(2)-Sm-O(4)	90.4(2)
O(2)-Sm-O(5)	91.4(2)	O(3)-Sm-O(4)	89.0(2)
O(3)-Sm-O(5)	88.5(2)	O(4)-Sm-O(5)	177.4(2)
Sm-O(1)-C(1)	171.2(4)	Sm-O(2)-C(2)	166.3(4)
Sm-O(3)-C(31)	179.1(4)	Sm-O(4)-P(1)	169.6(3)
Sm-O(5)-P(2)	165.6(3)	O(1)-C(1)-C(11)	110.3(6)
O(1)-C(1)-C(17)	112.3(5)	C(11)-C(1)-C(17)	112.6(6)
O(2)-C(2)-C(21)	112.1(5)	O(2)-C(2)-C(27)	111.4(5)
C(21)-C(2)-C(27)	111.0(5)		

**Reactions of Complexes 2, 4a, and 7a with Aryl Alcohols.** In the reactions of the lanthanide ketone dianion species with 2,6-di-*tert*-4-methylphenols, it seemed that the use of a further excess amount of the alcohols gave little influence on the distribution of the products. In order to gain more information on the stability of the products in the presence of an aryl alcohol and to have a better understanding about their formation, reactions of **2**, **4a**, and **7a** with aryl alcohols were investigated. In the reaction of **2** with ArOH (Ar = C<sub>6</sub>H<sub>2</sub>-<sup>t</sup>Bu<sub>2</sub>-2,6-Me-4), no change was observed as monitored overnight in C<sub>6</sub>D<sub>6</sub> by <sup>1</sup>H NMR spectroscopy, although oxidation of divalent ytterbium species by a proton was seen previously.<sup>8</sup> The reaction of **4a** with Ar'OH (Ar' = C<sub>6</sub>H<sub>3</sub>-<sup>t</sup>Bu<sub>2</sub>-2,6) in benzene yielded quan-

Scheme 1



tatively the aryloxy exchange product **4b** (eq 10). No



protonation occurred at either the carbon or oxygen atoms of the enolate parts, even when 2 equiv of  $Ar'OH$  was added. The similar reaction of **7a** with  $Ar'OH$  ( $Ar' = C_6H_3-tBu_{2,6}$ ) also afforded the corresponding aryloxy exchange product **7b** (Scheme 1), while the expected protonation at the more basic diphenylmethoxy anion to release benzhydrol was not observed. In contrast, however, when less bulky 2,6-dimethylphenol ( $Ar''OH$ ) was allowed to react with **7a**, the diphenylmethoxy substitution product  $Sm(OAr)(OAr'')_2(HMPA)_2$  (**8**,  $Ar'' = C_6H_3-Me_{2,2,6}$ , 70% yield) was isolated (Scheme 1). It is apparent from these results that steric influence plays an important role in the 2,6-di-*tert*-butylphenol-involved reactions. Electronically, attack of a proton on a more basic alkoxy anion should be favored over on a less basic aryloxy one. In the reaction of **7a** with  $Ar'OH$ , however, steric repulsion between the two bulky 2,6-di-*tert*-butylphenoxy groups probably forced the more bulky  $ArO$  group, rather than the diphenylmethoxy group, to leave the metal center by taking the proton from the incoming  $Ar'OH$  (Scheme 1). In the reaction of **7a** with the less bulky  $Ar''OH$ , the electronic factor (basic-

ity) became dominant, and the more basic diphenylmethoxy anions were protonated.<sup>18</sup>

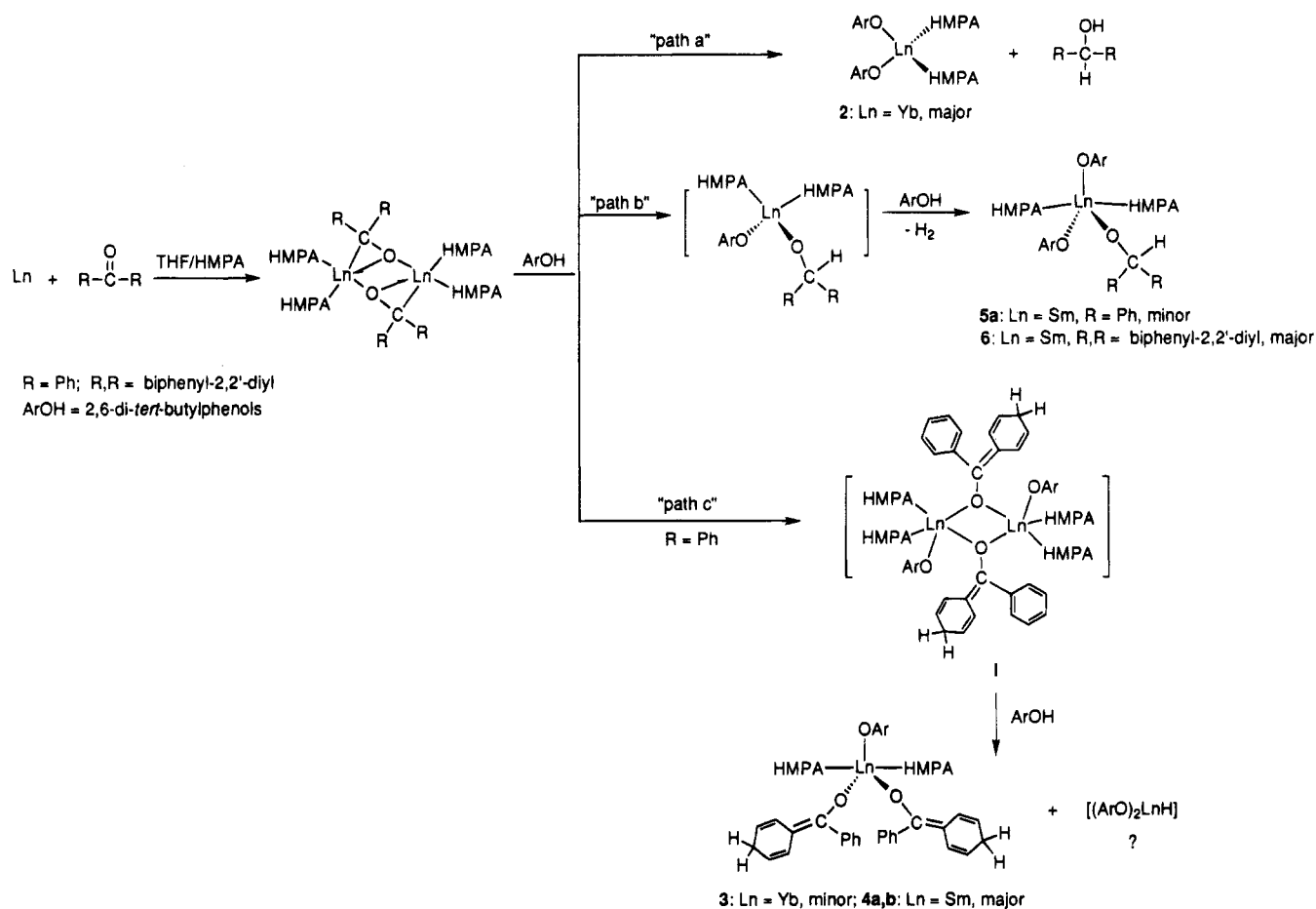
**Concluding Remarks.** The overall reactions of lanthanide ketone dianion species with aryl alcohols are summarized in Scheme 2.<sup>19</sup> These reactions can be classified into the following three types: (a) simultaneous protonation at both the carbon and the oxygen atoms of the carbonyl group, (b) protonation only at the carbonyl carbon, and (c) protonation at the para-position of the phenyl ring. The selectivity among these three types of reactions seems to be dependent on both the metals and the ketones. In the case of benzophenone ( $R = Ph$ ), when the metal is ytterbium, "path a" to yield **2** dominates the reaction, while when the metal is samarium, protonation at the phenyl ring ("path c") to give the enolates **4a,b** occurs selectively. This metal-dependent selectivity probably originates from the difference between the  $Sm(II)$  and  $Yb(II)$  ions. Since  $Sm(II)$  ion is bigger in radius and softer than  $Yb(II)$ , the negative charges in the  $Sm(II)$ -benzophenone dianion species must be more delocalized into its phenyl rings, which probably causes the protonation to occur more easily at the aromatic ring. Ketone dependence of the reactivity is also observed. The reaction of samarium fluorenone dianion species ( $R,R =$  biphenyl-2,2'-diyl) proceeds exclusively *via* "path b" to give **6**, while in the case of samarium benzophenone dianion this path leading to **5a** is a minor process. This reactivity difference between benzophenone and fluorenone suggests that the "localization" of the electron density at the para-position of the fluorenone dianion is not as high as in the case of benzophenone, which is probably caused by the planarity of the fluorenyl ring.

Reaction paths a and b, which proceed *via* protonation at the carbonyl group, are not difficult to understand, while path c to yield the dienolate complexes **3** and **4a,b** is not very clear. This process is probably mediated by

(18) The reaction of **4a** with 2,6-dimethylphenol was similar to its reaction with 2,6-di-*tert*-butylphenol and gave the aryloxy exchange product as monitored by <sup>1</sup>H NMR spectroscopy, which implies that the enolate anions in **4a** are less basic than the aryloxy one.

(19) Although the structure of the fluorenone dianion species is not yet known, for simplicity we choose the structure of the  $Yb(II)$ -benzophenone dianion (**1**) to represent all the lanthanide ketone dianion species in Scheme 2.

Scheme 2



a Ln(II) enolate intermediate like **I** which is formed by direct protonation at the para-position of the phenyl ring (Scheme 2). Further reaction of **I** with ArOH produces the monomeric Ln(III) enolates **3** and **4a,b**. The possible byproduct  $(\text{ArO})_2\text{LnH}$  or  $(\text{ArO})_3\text{Ln}$ , however, is yet to be identified. The selective formation of trivalent rather than divalent samarium complexes in the present reactions probably reflects the strong reducing power of HMPA-coordinated samarium(II) species.<sup>7,20</sup>

The formation of the enolates **3** and **4a,b** in the present reactions is closely related to the well-known Birch reductions of aromatic compounds bearing electron-withdrawing groups, in which metal enolate intermediates are believed to be formed *via* monoprotection of dianionic species but have never been well characterized.<sup>5,21</sup> As far as we are aware, complexes **3** and **4a** represent the first examples of structurally characterized metal enolate compounds which model the enolate intermediates formed in the Birch reductions.

The alcohol substitution reactions of the aryloxide/enolate **4a** and the aryloxide/alkoxide **7a** demonstrate that both electronic and steric factors play an important

role in determining the composition of the products. These reactions, combined with the thermolysis of the enolate complexes, could constitute a useful method for the synthesis of a variety of samarium complexes with mixed aryloxide/alkoxide ligands, a class of compounds which is difficult to access by conventional methods.<sup>6,22</sup>

## Experimental Section

**General Methods.** All manipulations were carried out under dry and oxygen-free argon atmosphere by using Schlenk techniques or under nitrogen atmosphere in an Mbraun glove box. The argon was purified by passing through a DRY-CLEAN column (4A molecular sieves, Nikka Seiko Co.) and a GASCLEAN GC-RX column (Nikka Seiko Co.). The nitrogen in the glove box was constantly circulated through a copper/molecular sieves (4A) catalyst unit. The oxygen and moisture concentrations in the glove box atmosphere were monitored by an  $\text{O}_2/\text{H}_2\text{O}$  COMBI-ANALYZER (Mbraun) to assure both were always below 1 ppm. Samples for NMR spectroscopic studies were prepared in the glove box. J. Young valve NMR tubes (Wilmad 528-JY) were used to maintain the inert atmosphere all the time during the measurements. Thermolysis study in toluene- $d_6$  was conducted in an NMR tube sealed under vacuum.  $^1\text{H}$  NMR spectra were recorded on a JNM-GSX 500 (FT, 500 MHz) or a JNM-EX 270 (FT, 270 MHz) spectrometer and are reported in ppm downfield from tetramethylsilane. Elemental analyses were performed by the chemical analysis laboratory of The Institute of Physical and

(20) Oxidation of a divalent ytterbium species by a proton was reported.<sup>8</sup>

(21) For reviews on Birch reductions, see: (a) Birch, A. J. *Q. Rev., Chem. Soc.* **1950**, *4*, 69. (b) Birch, A. J.; Smith, H. *ibid.* **1958**, *12*, 17. (c) Smith, H. *Organic Reactions in Liquid Ammonia*; Wiley: New York, 1963; Vol. 1, Part 2. (d) Harvey, R. G. *Synthesis* **1970**, 161. (e) House, H. O. in *Modern Synthetic Reactions*, 2nd ed.; W. A. Benjamin: Menlo Park, CA, 1972; Chapter 3. (f) Hook, J. M.; Mander, L. N. *Nat. Prod. Rep.* **1986**, *3*, 35. (g) Mander, L. N. in *Comprehensive Organic Synthesis*; Trost, B. M., Fleming, I., Eds; Pergamon: New York, 1991; Vol. 8, Chapter 3.4.

(22) For recent reviews on lanthanide alkoxides or aryloxides, see: (a) Mehrotra, R. C.; Singh, A.; Tripathi, U. M. *Chem. Rev.* **1991**, *91*, 1287. (b) Schaverien, C. J. In *Advances in Organometallic Chemistry*; Stone, F. G. A., West, R., Eds.; Academic Press: San Diego, 1994; Vol. 36, p 283.

Chemical Research (RIKEN). Tetrahydrofuran (THF), diethyl ether, toluene, benzene, and hexane were distilled from sodium/benzophenone ketyl, degassed by the freeze-thaw method (three times), and dried over fresh Na chips in the glove box. Hexamethylphosphoramide (HMPA) was distilled from Na under reduced pressure, degassed by the freeze-thaw method (three times), and dried over molecular sieves (4A). THF-*d*<sub>8</sub>, toluene-*d*<sub>8</sub>, and C<sub>6</sub>D<sub>6</sub> were commercial grade and were degassed by the freeze-thaw method (three times) and dried over fresh Na chips in the glove box. Diaryl ketones and aryl alcohols (Tokyo Kasei Co.) were the highest commercial grade and used as received. ArOD was prepared by deuteration of ArONa, which was generated by reaction of ArOH with Na, with CH<sub>3</sub>OD. Lanthanide metals (40 mesh) were obtained from Rare Metallic Co. and Aldrich.

#### Generation of Lanthanide Ketone Dianion Species.

The methods for generation of samarium and ytterbium ketone dianion species were similar and only a typical procedure is given below. The metal was first activated by stirring with 2% of ICH<sub>2</sub>CH<sub>2</sub>I in THF at room temperature for about 1 h. HMPA was then introduced. Addition of 1 equiv of a diaryl ketone in THF yielded the corresponding metal ketone dianion species in 30–60 min. Dramatic color changes were always observed, and the color of the metal ketone dianion species was dependent on both metals and ketones: Yb/benzophenone, purple; Yb/fluorenone, dark-green; Sm/benzophenone, red-brown; Sm/fluorenone, dark-brown.

**Yb(μ-η<sup>1</sup>,η<sup>2</sup>-OCPh<sub>2</sub>)(HMPA)<sub>2</sub>(1).** Complex **1** was isolated similarly as previously described.<sup>4</sup> A minor modification was made. Evaporation of the reaction mixture of Yb metal and benzophenone followed by addition of diethyl ether precipitated **1** as needlelike purple-black crystals in 65% yield. This reaction could be done on a 10 mmol scale.

**Yb(ArO)<sub>2</sub>(HMPA)<sub>2</sub> (Ar = C<sub>6</sub>H<sub>2</sub>-<sup>t</sup>Bu<sub>2</sub>-2,6-Me-4) (2).** To a purple THF (5 mL) solution of **1** (714 mg, 0.5 mmol) was added a THF (5 mL) solution of ArOH (Ar = C<sub>6</sub>H<sub>2</sub>-<sup>t</sup>Bu<sub>2</sub>-2,6-Me-4) (440 mg, 2 mmol). The resulting light brown solution was then stirred at room temperature for 3 h. Evaporation of THF and addition of diethyl ether precipitated an orange crystalline product which was separated by filtration. Recrystallization of the crystalline product from THF yielded (ArO)<sub>2</sub>Yb(HMPA)<sub>2</sub> (**2**) as orange-red blocks (775 mg, 80% yield). One-pot reaction of the Yb/benzophenone mixture with ArOH gave a similar result. The reaction of the Yb-fluorenone dianion species with ArOH also afforded **2** in 65% yield. <sup>1</sup>H NMR (C<sub>6</sub>D<sub>6</sub>, 22 °C): δ 7.33 (s, 4 H, C<sub>6</sub>H<sub>2</sub>), 2.53 (s, 6 H, Me), 2.15 (d, *J*<sub>P-H</sub> = 9.3 Hz, 36 H, NMe), 1.85 (s, 36 H, <sup>t</sup>Bu); (THF-*d*<sub>8</sub>, 22 °C) δ 6.64 (s, 4 H, C<sub>6</sub>H<sub>2</sub>), 2.61 (d, *J*<sub>P-H</sub> = 9.3 Hz, 36 H, NMe), 2.07 (s, 6 H, Me), 1.44 (s, 36 H, <sup>t</sup>Bu). Anal. Calcd for C<sub>42</sub>H<sub>82</sub>N<sub>6</sub>O<sub>4</sub>P<sub>2</sub>Yb: C, 52.00; H, 8.52; N, 8.66. Found: C, 51.85; H, 8.62; N, 8.46.

**Yb(OC(=CCH=CHCH<sub>2</sub>CH=CH)Ph)<sub>2</sub>(OAr)(HMPA)<sub>2</sub> (Ar = C<sub>6</sub>H<sub>2</sub>-<sup>t</sup>Bu<sub>2</sub>-2,6-Me-4) (3).** During the isolation of **2** (see above), when leaving the diethyl ether filtrate, from which **2** had been separated, to stand at room temperature for a few weeks, yellow needlelike crystals of Yb(OC(=CCH=CHCH<sub>2</sub>CH=CH)Ph)<sub>2</sub>(OAr)(HMPA)<sub>2</sub> (**3**) precipitated (ca. 30 mg, 5% yield based on benzophenone). Anal. Calcd for C<sub>53</sub>H<sub>81</sub>N<sub>6</sub>O<sub>5</sub>P<sub>2</sub>Yb: C, 56.98; H, 7.31; N, 7.52. Found: C, 56.35; H, 7.62; N, 7.46.

**Sm(OC(=CCH=CHCH<sub>2</sub>CH=CH)Ph)<sub>2</sub>(OAr)(HMPA)<sub>2</sub> (Ar = C<sub>6</sub>H<sub>2</sub>-<sup>t</sup>Bu<sub>2</sub>-2,6-Me-4) (4a).** To a red-brown reaction mixture of Sm (1.503g, 10 mmol) and benzophenone (1.822g, 10 mmol) in THF (20 mL) and HMPA (8 mL) was added ArOH (Ar = C<sub>6</sub>H<sub>2</sub>-<sup>t</sup>Bu<sub>2</sub>-2,6-Me-4) (4.408 g, 20 mmol) in THF (15 mL). The resulting light brown solution was then stirred at room temperature for 3 h. Evaporation of THF and addition of diethyl ether precipitated a yellow crystalline product which was further separated by filtration. Recrystallization of the crystalline compound from THF yielded Sm(OC(=CCH=

CHCH<sub>2</sub>CH=CH)Ph)<sub>2</sub>(OAr)(HMPA)<sub>2</sub> (**4a**) as yellow needlelike crystals (3.28 g, 60% yield based on benzophenone). The reaction with 1 equiv of ArOH also gave **4a** as the only isolable product. <sup>1</sup>H NMR (C<sub>6</sub>D<sub>6</sub>, 22 °C; assignment was confirmed by DEPT and H,C-COSY experiments): δ 7.90 (d, *J* = 7.3 Hz, 4 H, Ph), 7.75 (s, 2 H, C<sub>6</sub>H<sub>2</sub>), 7.28 (t, *J* = 7.3 Hz, 4 H, Ph), 7.21 (t, *J* = 7.3 Hz, 2 H, Ph), 6.94 (br d, *J* = 8.9 Hz, 2 H, CH), 6.76 (br d, *J* = 8.9 Hz, 2 H, CH), 5.55–5.65 (br m, 2 H, CH), 5.28–5.40 (br m, 2H, CH), 2.97 (br s, 4 H, CH<sub>2</sub>), 2.67 (s, 3 H, Me), 2.11 (d, *J* = 9.6 Hz, 36 H, NMe), 1.35 (s, 18 H, <sup>t</sup>Bu). Anal. Calcd for C<sub>53</sub>H<sub>81</sub>N<sub>6</sub>O<sub>5</sub>P<sub>2</sub>Sm: C, 58.16; H, 7.46; N, 7.68. Found: C, 59.45; H, 7.62; N, 7.86.

**Sm(OC(=CCH=CHCH<sub>2</sub>CH=CH)Ph)<sub>2</sub>(OAr)(HMPA)<sub>2</sub> (Ar = C<sub>6</sub>H<sub>3</sub>-<sup>t</sup>Bu<sub>2</sub>-2,6) (4b).** Complex **4b** was synthesized in 56% yield similarly as **4a** by the reaction of samarium benzophenone dianion species with 2,6-<sup>t</sup>Bu<sub>2</sub>-C<sub>6</sub>H<sub>3</sub>OH. It could also be obtained quantitatively by reaction of **4a** with 2 equiv of 2,6-<sup>t</sup>Bu<sub>2</sub>-C<sub>6</sub>H<sub>3</sub>OH in benzene. <sup>1</sup>H NMR (C<sub>6</sub>D<sub>6</sub>, 22 °C): δ 7.95–7.85 (m, 6 H, Ph, C<sub>6</sub>H<sub>3</sub>), 7.35–7.10 (m, 7 H, Ph, C<sub>6</sub>H<sub>3</sub>), 6.90 (br d, *J* = 10.6 Hz, 2 H, CH), 6.77 (br d, *J* = 10.2 Hz, 2 H, CH), 5.55–5.65 (br m, 2 H, CH), 5.30–5.40 (br m, 2H, CH), 2.96 (br s, 4 H, CH<sub>2</sub>), 2.10 (d, *J* = 9.3 Hz, 36 H, NMe), 1.33 (s, 18 H, <sup>t</sup>Bu). Anal. Calcd for C<sub>52</sub>H<sub>79</sub>N<sub>6</sub>O<sub>5</sub>P<sub>2</sub>Sm: C, 57.80; H, 7.37; N, 7.78. Found: C, 57.20; H, 7.46; N, 7.74.

**Sm(OC(=CCH=CHCHDCH=CH)Ph)<sub>2</sub>(OAr)(HMPA)<sub>2</sub> (Ar = C<sub>6</sub>H<sub>2</sub>-<sup>t</sup>Bu<sub>2</sub>-2,6-Me-4) (4c).** Complex **4c** was synthesized similarly as **4a** by the reaction of samarium benzophenone dianion species with ArOD (Ar = C<sub>6</sub>H<sub>2</sub>-<sup>t</sup>Bu<sub>2</sub>-2,6-Me-4). <sup>1</sup>H NMR (C<sub>6</sub>D<sub>6</sub>, 22 °C): δ 7.90 (d, *J* = 7.3 Hz, 4 H, Ph), 7.75 (s, 2 H, C<sub>6</sub>H<sub>2</sub>), 7.28 (t, *J* = 7.3 Hz, 4 H, Ph), 7.21 (t, *J* = 7.3 Hz, 2 H, Ph), 6.94 (br d, *J* = 8.9 Hz, 2 H, CH), 6.76 (br d, *J* = 8.9 Hz, 2 H, CH), 5.55–5.65 (br m, 2 H, CH), 5.28–5.40 (br m, 2H, CH), 2.97 (br s, 2 H, CHD), 2.67 (s, 3 H, Me), 2.11 (d, *J* = 9.6 Hz, 36 H, NMe), 1.35 (s, 18 H, <sup>t</sup>Bu).

**Sm(OCHPh<sub>2</sub>)(OAr)<sub>2</sub>(HMPA)<sub>2</sub> (Ar = C<sub>6</sub>H<sub>2</sub>-<sup>t</sup>Bu<sub>2</sub>-2,6-Me-4) (5a).** During the isolation of **4a**, when leaving the diethyl ether filtrate, from which **4a** had been separated, to stand at room temperature for a few months, a few pale blocks of Sm(OCHPh<sub>2</sub>)(OAr)<sub>2</sub>(HMPA)<sub>2</sub> (**5a**) precipitated (ca. 2% yield). <sup>1</sup>H NMR (C<sub>6</sub>D<sub>6</sub>, 22 °C): δ 7.75 (s, 4 H, C<sub>6</sub>H<sub>2</sub>), 7.70–6.90 (br m, 11 H, CH, Ph), 2.69 (s, 6 H, Me), 1.86 (br s, 36 H, NMe), 1.45 (br s, 36 H, <sup>t</sup>Bu). Anal. Calcd for C<sub>55</sub>H<sub>93</sub>N<sub>6</sub>O<sub>5</sub>P<sub>2</sub>Sm: C, 58.42; H, 8.29; N, 7.43. Found: C, 58.95; H, 8.47; N, 7.54.

**Sm(fluorenoxy)(OAr)<sub>2</sub>(HMPA)<sub>2</sub> (Ar = C<sub>6</sub>H<sub>3</sub>-<sup>t</sup>Bu<sub>2</sub>-2,6) (6).** To a dark brown reaction mixture of Sm (151 mg, 1 mmol) and fluorenone (180 mg, 1 mmol) in THF (5 mL) and HMPA (1 mL) was added a THF (5 mL) solution of ArOH (Ar = C<sub>6</sub>H<sub>3</sub>-<sup>t</sup>Bu<sub>2</sub>-2,6) (413 mg, 2 mmol). The resulting light brown solution was then stirred at room temperature for 3 h. Evaporation of THF and addition of ether precipitated a yellow crystalline product which after recrystallization from THF/ether gave Sm(fluorenoxy)(ArO)<sub>2</sub>(HMPA)<sub>2</sub> (**6**, Ar = C<sub>6</sub>H<sub>3</sub>-<sup>t</sup>Bu<sub>2</sub>-2,6) as colorless crystals (708 mg, 64% yield). Using 1 equiv of ArOH in this reaction also afforded **6** as the only isolated product. <sup>1</sup>H NMR (C<sub>6</sub>D<sub>6</sub>, 22 °C): δ 7.90 (d, *J* = 7.6 Hz, 4 H, C<sub>6</sub>H<sub>3</sub>), 7.51 (br m, 4 H, C<sub>12</sub>H<sub>8</sub>), 7.31 (t, *J* = 7.6 Hz, 2 H, C<sub>6</sub>H<sub>3</sub>), 7.21 (br m, 2 H, C<sub>12</sub>H<sub>8</sub>), 7.04 (br m, 2 H, C<sub>12</sub>H<sub>8</sub>), 5.62 (s, 1 H, CH), 1.86 (d, *J* = 8.9 Hz, 36 H, NMe), 1.56 (br s, 36 H, <sup>t</sup>Bu). Anal. Calcd for C<sub>63</sub>H<sub>87</sub>N<sub>6</sub>O<sub>5</sub>P<sub>2</sub>Sm: C, 57.84; H, 7.97; N, 7.64. Found: C, 58.40; H, 8.08; N, 7.80.

**Sm(OCHPh<sub>2</sub>)(OAr)<sub>2</sub>(HMPA)<sub>2</sub> (Ar = C<sub>6</sub>H<sub>2</sub>-<sup>t</sup>Bu<sub>2</sub>-2,6-Me-4) (7a).** In the glove box **4a** (415 mg, 0.38 mmol) was dissolved into 20 mL of toluene in a ampoule which was then connected to a vacuum line, cooled down to -196 °C and flame-sealed under vacuum. After being thawed at room temperature, the light yellow solution was heated at 180 °C overnight in an oven. The resultant colorless solution was cooled down to room temperature and then taken into the glove box where the reaction mixture was transferred into a Schlenk flask. Evaporation of the solvent yielded colorless fine crystals which after



Table 7. Summary of Crystal Data

	2	3	4a	5a	6	7b
formula	C <sub>42</sub> H <sub>82</sub> N <sub>6</sub> O <sub>4</sub> P <sub>2</sub> Yb	C <sub>53</sub> H <sub>81</sub> N <sub>6</sub> O <sub>5</sub> P <sub>2</sub> Yb	C <sub>53</sub> H <sub>81</sub> N <sub>6</sub> O <sub>5</sub> P <sub>2</sub> Sm	C <sub>55</sub> H <sub>93</sub> N <sub>6</sub> O <sub>5</sub> P <sub>2</sub> Sm	C <sub>53</sub> H <sub>87</sub> N <sub>6</sub> O <sub>5</sub> P <sub>2</sub> Sm	C <sub>52</sub> H <sub>79</sub> N <sub>6</sub> O <sub>5</sub> P <sub>2</sub> Sm
cryst syst	hexagonal	monoclinic	monoclinic	monoclinic	triclinic	triclinic
space group	P6 <sub>1</sub> 22 (No. 178)	P2 <sub>1</sub> /n (No. 14)	P2 <sub>1</sub> /n (No. 14)	P2 <sub>1</sub> /n (No. 14)	P $\bar{1}$ (No. 2)	P $\bar{1}$ (No. 2)
a (Å)	11.672(1)	10.631(5)	10.663(8)	15.496(3)	12.546(2)	10.637(2)
b (Å)	11.672(1)	33.666(3)	33.827(4)	20.686(3)	19.836(4)	15.721(2)
c (Å)	65.664(10)	16.022(1)	16.205(2)	18.992(4)	12.411(2)	17.102(3)
α (deg)					100.76(1)	89.88(1)
β (deg)		96.80(1)	96.61(2)	95.08(2)	105.32(1)	101.72(2)
γ (deg)					74.60(1)	95.40(2)
V (Å <sup>3</sup> )	7747.3	5694.0	5805.7	6064.0	2849.3	2787.5
Z	6	4	4	4	2	2
D <sub>calcd</sub> (g cm <sup>-3</sup> )	1.248	1.303	1.250	1.239	1.283	1.287
radiation, λ (Å)	Cu Kα, 1.54184	Mo Kα, 0.71073	Mo Kα, 0.71073	Mo Kα, 0.71073	Mo Kα, 0.71073	Mo Kα, 0.71073
data colld	+h, +k, +l	±h, +k, +l	±h, +k, +l	±h, +k, +l	±h, ±k, +l	±h, ±k, +l
scan speed (deg/min)	4	4	4	16	8	8
2θ range (deg)	4–136	4–55	4–55	4–35	4–55	4–55
μ (mm <sup>-1</sup> )	19.045	17.378	11.132	10.678	11.345	11.589
no. of reflns colld	2736	8560	9685	4065	12593	12154
no. of reflns with ( F <sub>o</sub>   > xσ( F <sub>o</sub>  ))	2161 (x = 4)	6923 (x = 4)	5679 (x = 5)	3420 (x = 3)	11344 (x = 5)	10355 (x = 5)
no. of variables	249	605	621	627	665	696
R (%)	5.12	7.14	7.81	6.60	5.67	4.68
R <sub>w</sub> (%)	6.14	8.75	8.92	7.43	7.26	5.80

recrystallization from toluene/hexane gave **7a** as colorless plates (332 mg, 80% yield). If the thermolysis was done at temperatures below 150 °C, a mixture of **4a** and **7a** was obtained. <sup>1</sup>H NMR (C<sub>6</sub>D<sub>6</sub>, 22 °C) δ 8.08 (d, *J* = 7.3 Hz, 8 H, Ph), 7.77 (s, 2 H, C<sub>6</sub>H<sub>2</sub>), 7.61 (br s, 2 H, CH), 7.33 (t, *J* = 7.3 Hz, 8 H, Ph), 7.20 (t, *J* = 7.3 Hz, 4 H, Ph), 2.71 (s, 3 H, Me), 2.01 (s, 18 H, <sup>t</sup>Bu), 1.62 (d, *J* = 9.6 Hz, 36 H, NMe). Anal. Calcd for C<sub>53</sub>H<sub>81</sub>N<sub>6</sub>O<sub>5</sub>P<sub>2</sub>Sm: C, 58.16; H, 7.46; N, 7.68. Found: C, 58.19; H, 7.46; N, 7.61.

**Sm(OCHPh)<sub>2</sub>(OAr)(HMPA)<sub>2</sub> (Ar = C<sub>6</sub>H<sub>3</sub>-<sup>t</sup>Bu<sub>2</sub>-2,6) (7b).** Colorless **7b** was obtained in 78% yield similarly as **7a** by thermolysis of **4b**. <sup>1</sup>H NMR (C<sub>6</sub>D<sub>6</sub>, 22 °C) δ 8.07 (d, *J* = 7.3 Hz, 8 H, Ph), 7.93 (d, *J* = 7.9 Hz, 2 H, C<sub>6</sub>H<sub>3</sub>), 7.59 (br s, 2 H, CH), 7.36–7.15 (m, 13 H, Ph, C<sub>6</sub>H<sub>3</sub>), 1.99 (s, 18 H, <sup>t</sup>Bu), 1.61 (d, *J* = 9.6 Hz, 36 H, NMe). Anal. Calcd for C<sub>52</sub>H<sub>79</sub>N<sub>6</sub>O<sub>5</sub>P<sub>2</sub>Sm: C, 57.80; H, 7.37; N, 7.78. Found: C, 57.73; H, 7.39; N, 7.70.

**Sm(OC<sub>13</sub>H<sub>10</sub>D)<sub>2</sub>(OAr)(HMPA)<sub>2</sub> (Ar = C<sub>6</sub>H<sub>2</sub>-<sup>t</sup>Bu<sub>2</sub>-2,6-Me-4) (7c).** Colorless **7c** was obtained in 80% yield similarly as **7a** by thermolysis of **4c**. <sup>1</sup>H NMR (C<sub>6</sub>D<sub>6</sub>, 22 °C) δ 8.08 (d, *J* = 7.3 Hz, 8 H, *o*-Ph), 7.77 (s, 2 H, C<sub>6</sub>H<sub>2</sub>), 7.61 (br s, *ca.* 1 H, CH(D)), 7.33 (t, *J* = 7.3 Hz, 8 H, *m*-Ph), 7.20 (t, *J* = 7.3 Hz, *ca.* 3 H, *p*-Ph), 2.71 (s, 3 H, Me), 2.01 (s, 18 H, <sup>t</sup>Bu), 1.62 (d, *J* = 9.6 Hz, 36 H, NMe).

**Sm(OAr)(OAr'')(HMPA)<sub>2</sub> (Ar = C<sub>6</sub>H<sub>2</sub>-<sup>t</sup>Bu<sub>2</sub>-2,6-Me-4, Ar'' = C<sub>6</sub>H<sub>3</sub>-Me<sub>2</sub>-2,6) (8).** To a THF solution (4 mL) of **7a** (58 mg, 0.053 mmol) was added 2,6-dimethylphenol (13 mg, 0.11 mmol) in THF (4 mL). After being stirred at room temperature overnight, the solvent was evaporated. The residue was washed with hexane and recrystallized from Et<sub>2</sub>O/hexane to give **8** as colorless fine crystals (36 mg, 70% yield). <sup>1</sup>H NMR (C<sub>6</sub>D<sub>6</sub>, 22 °C) δ 7.88 (s, 2 H, C<sub>6</sub>H<sub>2</sub>), 7.28 (d, *J* = 7.4 Hz, 4 H, C<sub>6</sub>H<sub>3</sub>), 6.92 (t, *J* = 7.4 Hz, 2 H, C<sub>6</sub>H<sub>3</sub>), 2.75 (s, 3 H, Me), 2.70 (s, 12 H, Me), 1.89 (d, *J* = 9.6 Hz, 36 H, NMe), 1.55 (s, 18 H, <sup>t</sup>Bu). Anal. Calcd for C<sub>43</sub>H<sub>77</sub>N<sub>6</sub>O<sub>5</sub>P<sub>2</sub>Sm: C, 53.22; H, 8.00; N, 8.66. Found: C, 53.33; H, 7.85; N, 8.70.

**X-ray Crystallographic Studies.** Crystals of X-ray quality were obtained as described in the preparations. The crystals were manipulated in the glove box under a microscope (Wild M3Z, Leica) mounted on the glove box window and were sealed in thin-walled glass capillaries. Data collections were performed at 20 °C on an Enraf-Nonius CAD4 diffractometer with a rotating anode (Cu Kα radiation, λ = 1.54184 Å, graphite monochromator, ω-scan) for **2** and an Enraf-Nonius CAD4 diffractometer with Mo Kα radiation (λ = 0.71069 Å, graphite monochromator, ω-scan) for **3**, **4a**, **5a**, **6**, and **7b**. Lattice constants and orientation matrices were obtained by

least-squares refinement of 25 reflections with 30° ≤ θ ≤ 35° for **2** and 10° ≤ θ ≤ 13° for **3**, **4a**, **5a**, **6**, and **7b**. Three reflections were monitored periodically as a check for crystal decomposition or movement. In the case of **5a**, a rapid decay was observed and only the data with 2θ range of 4–35° were successfully collected. All data were corrected for X-ray absorption effects and in the case of **5a** a decay correction was also made. The observed systematic absences were consistent with the space groups given in Table 7. In the case of **2**, anomalous dispersion effects were further used to distinguish P6<sub>1</sub>22 from P6<sub>5</sub>22. The structures were solved by MULTAN<sup>23</sup> to locate the metal atoms, and the remaining non-hydrogen atoms were found from subsequent difference Fourier syntheses. Important hydrogen atoms were also located from the difference Fourier maps, but attempts to find other hydrogen atoms were not made. Refinements were performed anisotropically for non-hydrogen atoms and isotropically for hydrogen atoms by the full-matrix least squares method for **2** and block-diagonal least squares method for **3**, **4a**, **5a**, **6**, and **7b**.<sup>24</sup> The function minimized in the least-squares refinements was Σ(|F<sub>o</sub>| - |F<sub>c</sub>|)<sup>2</sup>. Neutral atomic scattering factors were taken from the *International Tables for X-Ray Crystallography*.<sup>25</sup> The residual electron densities were of no chemical significance. Crystal data, data collection, and processing parameters are given in Table 7.

**Acknowledgment.** This work was partly supported by The Special Grant for Promotion of Research from The Institute of Physical and Chemical Research (RIKEN) and by grants from the Ministry of Education, Science and Culture of Japan.

**Supporting Information Available:** Listings of atomic coordinates, thermal parameters, and bond distances and angles for **2**, **3**, **4a**, **5a**, **6**, and **7b** (40 pages). This material is contained in many libraries on microfiche, immediately follows this article in the microfilm version of the journal, and can be ordered from the ACS; see any current masthead page for ordering information.

OM9503961

(23) Main, P.; Hull, S. E.; Lessinger, L.; Germain, G.; Decherq, J.-P.; Woolfson, M. M. *MULTAN 78*, University of York, York, 1978.

(24) Sakurai, T.; Kobayashi, K. *Rikagaku kenkyusho Hokoku* **1979**, 55, 69.

(25) Cromer, D. T.; Waber, J. T. In *International Tables for X-Ray Crystallography*; Kynoch: Birmingham, England, 1974; Vol. IV.

# X-ray Crystallographic Analysis of the Oxytellurium Compounds [10-Te-4(C3O)] and Solvent Effect on the Hypervalency

Soichi Sato,<sup>†</sup> Norihisa Kondo, and Naomichi Furukawa\*

Tsukuba Advanced Research Alliance Center, Department of Chemistry, University of Tsukuba, Tsukuba, Ibaraki 305, Japan

Received May 19, 1995<sup>⊗</sup>

2,2'-Biphenylene-2-biphenylphenoxytellurane derivatives ([10-Te-4(C3O)]) having an *o*- or *p*-substituted phenoxy group RPhO- (**2a**, R = Me; **2b**, R = H; **2c**, R = Cl; **2d**, R = MeOCO; **2e**, MeCO; **2f**, R = NO<sub>2</sub>; **2g**, R = 2,4,6-Cl<sub>3</sub>) were synthesized by the reaction of bis(2,2'-biphenylene)tellurane with the corresponding phenol derivatives. The compounds **2f,g** were subjected to X-ray crystallographic analysis which revealed that their structures are distorted trigonal bipyramids or typical telluronium salts. The hypervalency of the tellurium compounds in solution was estimated by correlating their <sup>125</sup>Te NMR chemical shifts and the Gutmann donor number, DN, employed in the experiments.

## Introduction

Tellurane is the most stable species among the hypervalent organic chalcogen compounds. A number of telluranes have been synthesized by many chemists, and especially, telluranes having electronegative ligands like oxygen and halogens have been isolated as stable compounds.<sup>1</sup> Although the oxytelluranes [10-Te-4(O4)] and [10-Te-4(C2O2)] having alkoxy or carboxyl group were reported by Denney et al.,<sup>2</sup> Martin et al.,<sup>3</sup> and others,<sup>4</sup> the preparation of monoxytellurane [10-Te-4(C3O)] species has never been reported. As examples of triorganooxytellurium compounds, triphenyltellurium alkoxy and diphenylmethyltellurium carboxylate have been reported by Wieber et al.<sup>5</sup> and McWhinnie et al.<sup>6</sup> However, they considered these compounds not to be hypervalent compounds but telluronium salts. The formation of stable monoalkoxyantimony(V) derivatives by reacting perarylated hypervalent main group element derivatives has been reported by Wittig et al.<sup>7</sup> Recently, we undertook the reaction of bis(2,2'-biphenylene)tellurane (**1**) prepared originally by Hell-

winkel<sup>8</sup> and phenol derivatives in order to investigate the reactivity of tellurane having only carbon ligands and succeeded in isolating 2,2'-biphenylene-2-biphenylphenoxytellurane (**2b**) as the stable compound [10-Te-4(C3O)]. The structure was determined by X-ray crystallographic analysis. The compound underwent ligand coupling reactions to give both *o*-phenoxybiphenyl and dibenzotellurophene in high yield on heating.<sup>9</sup> Similarly, various monoaryloxytelluranes can easily be obtained by modification of the procedures and, hence, facilitate the investigation of how the bond distance (Te-O) and the structure of unsymmetrical hypervalent species are influenced by changing systematically the electronegativity and steric hindrance of the substituents attached to the aryl oxygen ligand. Therefore, we studied the hypervalency of the compounds (**2**) obtained by the reaction of tellurane **1** with *o*- or *p*-substituted phenols in the solid or solution states. Here we describe the isolation of the compounds **2** having an *o*- or a *p*-substituted phenolate group, their structural determination by X-ray crystallographic analysis, and estimation of the hypervalency of the tellurium compounds by examining the chemical shifts of <sup>125</sup>Te NMR in several solvents.

## Experimental Section

**General Methods.** All NMR spectra were obtained with a JEOL LMN-EX-270 spectrometer. Mass spectra were taken with a Shimadzu QP-2000 and a JEOL JMX SX102 mass spectrometer. X-ray crystallographic analysis was performed on an Enraf-Nonius CAD4 automatic diffractometer. Preparative liquid chromatography was performed on Japan Analytical Industry Co., Ltd., Models LC-09 and LC-908. Elemental analyses were carried out by the Chemical Analytical Center at the University of Tsukuba. All melting points are uncorrected. Each chemical shift was determined by two-dimensional shift correlation (<sup>1</sup>H-<sup>1</sup>H- and <sup>13</sup>C-<sup>1</sup>H-COSY) spectra.

(8) The preparation of bis(2,2'-biphenylene)tellurane was reported by Hellwinkel et al., more than 25 years ago: (a) Hellwinkel, D.; Fahrbach, G. *Liebigs Ann. Chem.* **1968**, 712, 1. (b) Hellwinkel, D.; Fahrbach, G. *Liebigs Ann. Chem.* **1968**, 715, 68. (c) Hellwinkel, D.; Fahrbach, G. *Tetrahedron Lett.* **1965**, 1823. (d) Hellwinkel, D.; Fahrbach, G. *Chem. Ber.* **1968**, 101, 74.

(9) Sato, S.; Kondo, N.; Furukawa, N. *Organometallics* **1994**, 13 (9), 1193.

<sup>†</sup> Research Fellow of the Japan Society for the Promotion of Science.

<sup>⊗</sup> Abstract published in *Advance ACS Abstracts*, September 15, 1995.

(1) (a) Bergman, J.; Engman, L.; Siden, J. Tetra- and higher-valent (hypervalent) derivatives of selenium and tellurium. In *The chemistry of organic selenium and tellurium compounds*; Patai, S., Rappoport, Z., Eds.; John Wiley and Sons, Inc.: New York, 1986; Vol. 1, pp 517-558 (see also references therein). (b) Irgolic, K. J. *The Organic Chemistry of Tellurium*; Gordon and Breach, Inc.: New York, 1974; pp 234-241 (see also references therein).

(2) Denny, D. B.; Denny, D. Z.; Hammond, P. J.; Hsu, Y. F. *J. Am. Chem. Soc.* **1981**, 103, 2340.

(3) (a) Michalak, R. S.; Wilson, S. R.; Martin, J. C. *J. Am. Chem. Soc.* **1984**, 106, 7529. (b) Wieber, M.; Kaunzinger, E. *J. Organomet. Chem.* **1977**, 129, 339.

(4) (a) Pant, B. C.; McWhinnie, W. R.; Dance, N. S. *J. Organomet. Chem.* **1973**, 63, 305. (b) Petragnani, N.; Comassetto, J. V.; Varella, N. H. *J. Organomet. Chem.* **1976**, 120, 375. (c) Sadekov, J. D.; Rivkin, B. B. *Zh. Organ. Khim.* **1982**, 18, 227. (d) Pant, B. C. *J. Organomet. Chem.* **1974**, 65, 51. (e) Alkock, N. W.; Harrison, W. D.; Howes, C. J. *Chem. Soc., Dalton Trans.* **1984**, 1709. (f) Dance, N. S.; McWhinnie, W. R. *J. Organomet. Chem.* **1976**, 104, 317. (g) Tamagaki, S.; Hatanaka, I.; Kozuka, S. *Bull. Chem. Soc. Jpn.* **1977**, 50, 2501. (h) Takaguchi, Y.; Furukawa, N. *Heteroatom Chem.* **1995**, in press.

(5) Wieber, M.; Schmidt, E. Z. *Anorg. Allg. Chem.* **1988**, 556, 189.

(6) (a) Dance, N. S.; McWhinnie, W. R.; Mallaki, J.; Monze-Mirzai, Z. *J. Organomet. Chem.* **1980**, 198, 131. (b) McWhinnie, W. R.; Mallaki, J. *Polyhedron* **1982**, 1, 13.

(7) Wittig, G.; Hellwinkel, D. *Chem. Ber.* **1964**, 97, 789.

**Materials.** All solvents and reagents were dried and purified according to standard methods. Bis(2,2'-biphenylene)tellurane **1** was prepared according to ref 8.

**2,2'-Biphenylene-2-biphenyl-(4-methylphenoxy)-tellurane (2a).** To a solution of tellurane **1** (106 mg, 0.25 mmol) in dry benzene (20 mL) was added the purified 4-methylphenol (*p*-cresol) (28 mg, 0.26 mmol), and the solution was stirred for 3 h under argon at room temperature. After removal of the solvent, the residue was recrystallized from 3:1 dry benzene:*n*-hexane under argon to give pale yellow crystals (112 mg, 83%): mp 121–127 (dec); <sup>1</sup>H NMR (270 MHz, CDCl<sub>3</sub>, room temperature) δ 2.22 (s, 3H, Me), 6.54 (d, 2H, *J* = 11.4 Hz, 18-ArH), 6.95 (d, 2H, *J* = 11.4 Hz, 19-ArH), 7.12 (t, 1H, *J* = 8.0 Hz, 9-ArH), 7.28 (d, 1H, *J* = 8.0 Hz, 8-ArH), 7.33 (t, 1H, *J* = 8.0 Hz, 10-ArH), 7.34 (d, 1H, *J* = 8.0 Hz, 11-ArH), 7.34 (t, 2H, *J* = 9.0 Hz, 4-ArH), 7.50 (t, 2H, *J* = 9.0 Hz, 5-ArH), 7.50 (t, 1H, *J* = 8.7 Hz, 16-ArH), 7.53 (t, 2H, *J* = 8.7 Hz, 15-ArH), 7.58 (d, 2H, *J* = 8.7 Hz, 14-ArH), 7.71 (d, 2H, *J* = 9.0 Hz, 3-ArH), 7.86 (d, 2H, *J* = 9.0 Hz, 6-ArH); <sup>13</sup>C NMR (67.8 MHz, CDCl<sub>3</sub>, room temperature) δ 20.5, 119.4, 123.6, 125.4, 128.2, 128.8, 129.1, 129.2, 129.3, 129.7, 129.8, 130.1, 130.2, 130.7, 130.9, 133.7, 134.5, 141.9, 144.0, 145.2, 160.4; <sup>125</sup>Te NMR (85.2 MHz, CDCl<sub>3</sub>, room temperature) δ 721.0; MS (*m/z*) 542 (M<sup>+</sup>), 435 (M<sup>+</sup> - 107). Anal. Calcd for C<sub>31</sub>H<sub>24</sub>O<sub>2</sub>Te: C, 68.94; H, 4.48. Found: C, 68.98; H, 4.56.

**2,2'-Biphenylene-2-biphenylphenoxytellurane (2b).** The preparation of **2b** was performed by using tellurane **1** (104 mg, 0.24 mmol) and the purified phenol (23 mg, 0.24 mmol) in a similar manner to that described above. Recrystallization was carried out in dry ether under argon to give pale yellow crystals (59 mg, 47%): mp 179–183 °C (dec); <sup>1</sup>H NMR (270 MHz, CDCl<sub>3</sub>, -20 °C) δ 6.62 (d, *J* = 7.6 Hz, 1H, 9-ArH), 6.64 (t, *J* = 7.6 Hz, 1H, 10-ArH), 7.11 (t, *J* = 7.6 Hz, 1H, 11-ArH), 7.25 (d, *J* = 7.6 Hz, 1H, 12-ArH), 7.30 (t, *J* = 7.6 Hz, 1H, 15-ArH), 7.32 (d, *J* = 7.6 Hz, 2H, 14-ArH), 7.33 (t, *J* = 7.6 Hz, 1H, 20-ArH), 7.47 (t, *J* = 7.6 Hz, 2H, 5-ArH), 7.48 (t, *J* = 7.6 Hz, 2H, 4-ArH), 7.48 (t, *J* = 7.6 Hz, 2H, 19-ArH), 7.56 (t, *J* = 7.6 Hz, 1H, 16-ArH), 7.56 (d, *J* = 7.6 Hz, 2H, 6-ArH), 7.69 (bd, 2H, 3-ArH), 7.84 (d, *J* = 7.6 Hz, 2H, 18-ArH); <sup>13</sup>C NMR (68 MHz, CDCl<sub>3</sub>, -20 °C) δ 115.7, 120.8, 123.6, 128.8, 129.1, 129.1, 129.3, 129.8, 130.0, 130.1, 130.6, 130.9, 130.9, 133.9, 134.5, 141.8, 143.9, 145.1, 164.6; <sup>125</sup>Te NMR (85 MHz, CDCl<sub>3</sub>) δ 721.3; MS (*m/z*) 528 (M<sup>+</sup>), 435 (M<sup>+</sup> - 137). Anal. Calcd for C<sub>30</sub>H<sub>22</sub>O<sub>2</sub>Te: C, 68.49; H, 4.22. Found: C, 68.31; H, 4.35.

**2,2'-Biphenylene-2-biphenyl-(4-chlorophenoxy)tellurane (2c).** The preparation of **2c** was performed by using tellurane **1** (101 mg, 0.23 mmol) and the purified 4-chlorophenol (23 μL, 0.23 mmol) in a similar manner to that described above. Recrystallization was carried out in 3:1 dry benzene:*n*-hexane under argon to give pale yellow crystals (96 mg, 73%): mp 162–171 °C (dec); <sup>1</sup>H NMR (270 MHz, CDCl<sub>3</sub>, room temperature) δ 6.48 (d, 2H, *J* = 11.2 Hz, 18-ArH), 7.02 (d, 2H, *J* = 11.2 Hz, 19-ArH), 7.13 (t, 1H, *J* = 9.1 Hz, 9-ArH), 7.22 (d, 1H, *J* = 9.1 Hz, 11-ArH), 7.33 (t, 1H, *J* = 9.1 Hz, 10-ArH), 7.36 (d, 1H, *J* = 9.1 Hz, 8-ArH), 7.38 (t, 2H, *J* = 9.6 Hz, 5-ArH), 7.54 (t, 2H, *J* = 9.6 Hz, 4-ArH), 7.54 (d, 2H, *J* = 10.0 Hz, 14-ArH), 7.54 (t, 2H, *J* = 10.0 Hz, 15-ArH), 7.54 (t, 1H, *J* = 10.0 Hz, 16-ArH), 7.71 (d, 2H, *J* = 9.6 Hz, 3-ArH), 7.88 (d, 2H, *J* = 9.6 Hz, 6-ArH); <sup>13</sup>C NMR (67.8 MHz, CDCl<sub>3</sub>, room temperature) δ 120.5, 120.6, 123.9, 129.0, 129.1, 129.3, 129.4, 129.4, 129.7, 130.2, 130.6, 131.3, 132.9, 134.4, 136.2, 141.7, 144.2, 145.4, 161.9; <sup>125</sup>Te NMR (85.2 MHz, CDCl<sub>3</sub>, room temperature) δ 722.2; MS (*m/z*) 562 (M<sup>+</sup>), 435 (M<sup>+</sup> - 127). Anal. Calcd for C<sub>30</sub>H<sub>21</sub>ClO<sub>2</sub>Te: C, 64.27; H, 3.75. Found: C, 63.85; H, 3.76.

**2,2'-Biphenylene-2-biphenyl-(4-(methylcarbonyl)phenoxy)tellurane (2d).** The preparation of **2d** was performed by using tellurane **1** (138 mg, 0.32 mmol) and the purified 4-hydroxyacetophenone (44 mg, 0.32 mmol) in a similar manner to that described above. Recrystallization was carried out in 3:1 dry benzene:*n*-hexane under argon to give pale yellow crystals (100 mg, 55%): mp 176–178 °C (dec); <sup>1</sup>H

NMR (270 MHz, CDCl<sub>3</sub>, room temperature) δ 2.48 (s, 3H, Me), 6.48 (d, 2H, *J* = 9.3 Hz, 18-ArH), 7.17 (t, 1H, *J* = 8.8 Hz, 9-ArH), 7.22 (d, 1H, *J* = 8.8 Hz, 11-ArH), 7.37 (t, 1H, *J* = 8.8 Hz, 10-ArH), 7.37 (d, 1H, *J* = 8.8 Hz, 8-ArH), 7.38 (t, 2H, *J* = 8.6 Hz, 5-ArH), 7.53 (t, 1H, *J* = 9.8 Hz, 16-ArH), 7.53 (t, 2H, *J* = 9.8 Hz, 15-ArH), 7.55 (d, 2H, *J* = 9.8 Hz, 14-ArH), 7.56 (t, 2H, *J* = 8.6 Hz, 4-ArH), 7.72 (d, 2H, *J* = 8.6 Hz, 3-ArH), 7.78 (d, 2H, *J* = 9.3 Hz, 19-ArH), 7.90 (d, 2H, *J* = 8.6 Hz, 6-ArH); <sup>13</sup>C NMR (67.8 MHz, CDCl<sub>3</sub>, room temperature) δ 25.9, 119.6, 124.0, 124.8, 129.1, 129.3, 129.4, 129.5, 129.7, 130.3, 130.5, 130.6, 131.1, 131.4, 132.6, 134.4, 135.5, 141.5, 144.3, 145.5, 171.6, 196.5; <sup>125</sup>Te NMR (85.2 MHz, CDCl<sub>3</sub>, room temperature) δ 719.3; MS (*m/z*) 587 (M<sup>+</sup> + 17), 435 (M<sup>+</sup> - 135). Anal. Calcd for C<sub>32</sub>H<sub>24</sub>O<sub>3</sub>Te: C, 67.65; H, 4.26. Found: C, 67.46; H, 4.21.

**2,2'-Biphenylene-2-biphenyl-(4-(methoxycarbonyl)phenoxy)tellurane (2e).** The preparation of **2e** was performed by using tellurane **1** (105 mg, 0.24 mmol) and the purified methyl 4-hydroxybenzoate (38 mg, 0.25 mmol) in a similar manner to that described above. Recrystallization was carried out in 3:1 dry benzene:*n*-hexane under argon to give pale yellow crystals (76 mg, 54%): mp 16–163 °C (dec); <sup>1</sup>H NMR (270 MHz, CDCl<sub>3</sub>, room temperature) δ 3.81 (s, 3H, Me), 6.51 (d, 2H, *J* = 10.1 Hz, 18-ArH), 7.14 (t, 1H, *J* = 9.1 Hz, 9-ArH), 7.20 (d, 1H, *J* = 9.1 Hz, 11-ArH), 7.35 (t, 1H, *J* = 9.1 Hz, 10-ArH), 7.36 (d, 1H, *J* = 9.1 Hz, 8-ArH), 7.38 (t, 2H, *J* = 9.2 Hz, 5-ArH), 7.52 (t, 1H, *J* = 9.8 Hz, 15-ArH), 7.53 (t, 2H, *J* = 9.8 Hz, 16-ArH), 7.53 (d, 2H, *J* = 9.8 Hz, 14-ArH), 7.54 (t, 2H, *J* = 9.2 Hz, 4-ArH), 7.72 (d, 2H, *J* = 9.2 Hz, 3-ArH), 7.80 (d, 2H, *J* = 10.1 Hz, 19-ArH), 7.88 (d, 2H, *J* = 9.2 Hz, 6-ArH); <sup>13</sup>C NMR (67.8 MHz, CDCl<sub>3</sub>, room temperature) δ 51.2, 116.6, 119.2, 124.0, 129.1, 129.3, 129.4, 129.5, 129.7, 130.2, 130.5, 130.5, 131.4, 131.7, 132.5, 134.4, 135.5, 141.5, 144.3, 145.5, 167.8, 169.8; <sup>125</sup>Te NMR (85.2 MHz, CDCl<sub>3</sub>, room temperature) δ 720.7; MS (*m/z*) 586 (M<sup>+</sup>), 435 (M<sup>+</sup> - 151). Anal. Calcd for C<sub>32</sub>H<sub>24</sub>O<sub>2</sub>Te: C, 65.80; H, 4.14. Found: C, 65.59; H, 4.16.

**2,2'-Biphenylene-2-biphenyl-(4-nitrophenoxy)tellurane (2f).** The preparation of **2e** was performed by using tellurane **1** (58 mg, 0.13 mmol) and the purified *p*-nitrophenyl (16 mg, 0.12 mmol) in a similar manner to that described above. Recrystallization was carried out in dry ether under argon to give pale yellow crystals (48 mg, 65%): mp 201–205 °C (dec); <sup>1</sup>H NMR (270 MHz, CDCl<sub>3</sub>, room temperature) δ 6.31 (d, *J* = 9.2 Hz, 2H, 18-ArH), 7.17 (t, *J* = 7.6 Hz, 1H, 11-ArH), 7.18 (d, *J* = 7.6 Hz, 1H, 12-ArH), 7.38 (d, *J* = 7.6 Hz, 1H, 9-ArH), 7.39 (t, *J* = 7.6 Hz, 1H, 10-ArH), 7.40 (t, *J* = 7.6 Hz, 2H, 5-ArH), 7.53 (d, *J* = 7.6 Hz, 2H, 14-ArH), 7.54 (t, *J* = 7.6 Hz, 1H, 16-ArH), 7.55 (t, *J* = 7.6 Hz, 2H, 15-ArH), 7.60 (t, *J* = 7.6 Hz, 2H, 4-ArH), 7.74 (d, *J* = 7.6 Hz, 2H, 3-ArH), 7.92 (b, *J* = 7.6 Hz, 2H, 6-ArH), 8.00 (d, *J* = 9.2 Hz, 2H, 19-ArH); <sup>13</sup>C NMR (68 MHz, CDCl<sub>3</sub>, room temperature) δ 119.3, 124.3, 126.8, 129.3, 129.4, 129.5, 129.6, 129.7, 130.4, 130.5, 130.9, 131.9, 134.4, 134.4, 135.4, 141.3, 144.6, 145.8, 145.8, 174.6; <sup>125</sup>Te NMR (85 MHz, CDCl<sub>3</sub>) δ 718.0; MS (*m/z*) 586 (M<sup>+</sup> - 13), 473 (M<sup>+</sup>). Anal. Calcd for C<sub>30</sub>H<sub>21</sub>N<sub>2</sub>O<sub>3</sub>Te: C, 63.09; H, 3.71; N, 2.45. Found: C, 62.98; H, 3.55; N, 2.24.

**2,2'-Biphenylene-2-biphenyl-(2,4,6-trichlorophenoxy)tellurane (2g).** The preparation of **2e** was performed by using tellurane **1** (107 mg, 0.25 mmol) and the purified 2,4,6-trichlorophenol (49 mg, 0.25 mmol) in a similar manner to that described above. Recrystallization was carried out in 3:1 dry benzene:*n*-hexane under argon to give pale yellow crystals (105 mg, 67%): mp 209–210 °C (dec); <sup>1</sup>H NMR (270 MHz, CDCl<sub>3</sub>, room temperature) δ 7.18 (s, 2H, 19-ArH), 7.19 (d, 1H, *J* = 8.0 Hz, 8-ArH), 7.31 (d, 1H, *J* = 8.0 Hz, 11-ArH), 7.33 (t, 2H, *J* = 8.5 Hz, 4-ArH), 7.35 (t, 1H, *J* = 8.0 Hz, 9-ArH), 7.44 (t, 1H, *J* = 8.0 Hz, 10-ArH), 7.47 (d, 2H, *J* = 8.8 Hz, 14-ArH), 7.52 (t, 2H, *J* = 8.8 Hz, 15-ArH), 7.54 (t, 2H, *J* = 8.5 Hz, 5-ArH), 7.54 (t, 1H, *J* = 8.8 Hz, 16-ArH), 7.71 (d, 2H, *J* = 8.5 Hz, 3-ArH), 7.82 (d, 2H, *J* = 8.5 Hz, 6-ArH); <sup>13</sup>C NMR (67.8 MHz, CDCl<sub>3</sub>, room temperature) δ 120.3, 124.0, 124.4, 127.7, 128.3, 129.2, 129.3, 129.3, 129.5, 129.7, 130.2, 130.5, 131.5, 131.9, 132.0, 134.1, 135.1, 141.2, 144.0, 145.9, 152.6; <sup>125</sup>Te

**Table 1. Isolated Yields and Pyrolysis of Intermediates 2**

R	yield (2)/%	mp/°C (dec)	yield/%		
			3	4	5
4-MeC <sub>6</sub> H <sub>4</sub> (2a)	83	121–127	88	34	11
C <sub>6</sub> H <sub>5</sub> (2b)	47	179–183	80	68	19
4-ClC <sub>6</sub> H <sub>4</sub> (2c)	73	162–171	72	62	20
4-MeOCOC <sub>6</sub> H <sub>4</sub> (2d)	55	160–163	38	44	7
4-MeCOC <sub>6</sub> H <sub>4</sub> (2e)	54	176–178	70	62	23
4-NO <sub>2</sub> C <sub>6</sub> H <sub>4</sub> (2f)	65	201–205	84	74	11
2,4,6-Cl <sub>3</sub> C <sub>6</sub> H <sub>2</sub> (2g)	67	209–210	51	30	8

**Table 2. X-ray Crystallographic Data for Diffraction Studies of 2f,g**

compd	2f	2g
formula	C <sub>30</sub> H <sub>21</sub> NO <sub>3</sub> Te	C <sub>36</sub> H <sub>25</sub> Cl <sub>3</sub> OTe
fw	571.11	707.56
cryst syst	triclinic	triclinic
space group	P $\bar{1}$ (No. 2)	P $\bar{1}$ (No. 2)
a, Å	9.833(1)	10.082(3)
b, Å	10.149(1)	12.552(3)
c, Å	13.502(1)	14.178(4)
$\alpha$ , deg	99.05(1)	75.21(2)
$\beta$ , deg	109.81(1)	70.60(2)
$\gamma$ , deg	100.11(1)	66.18(2)
V, Å <sup>3</sup>	1219.5	1532.9
Z	2	2
D <sub>calcd</sub> , g cm <sup>-3</sup>	1.56	1.53
F(000)	568	704
temp, °C	23 ± 1	23 ± 1
radiation ( $\lambda$ , Å)	Mo K $\alpha$ (0.710 73)	Mo K $\alpha$ (0.710 73)
cryst dims, mm	0.20 × 0.20 × 0.20	0.10 × 0.60 × 0.70
$\mu$ , cm <sup>-1</sup>	12.5	12.6
scan type	$\omega$ -2 $\theta$	$\omega$ -2 $\theta$
scan rate	2–20 deg/min	2–20 deg/min
scan width, deg	0.7 + 0.460 tan $\theta$	0.7 + 0.550 tan $\theta$
max 2 $\theta$ , deg	50.0	50.0
tot no. of rflns	4538	5722
no. of unique rflns	4275	5389
no. of params refined	316	370
no. of rflns included	4134 with $F_o^2 > 3.0\sigma(F_o^2)$	5138 with $F_o^2 > 3.0\sigma(F_o^2)$
agreement factors <sup>a</sup>		
R	0.031	0.030
R <sub>w</sub>	0.038	0.033

$$^a R = \sum ||F_o| - |F_c|| / \sum |F_o|; R_w = [\sum w(|F_o| - |F_c|)^2 / \sum w F_o^2]^{1/2}.$$

NMR (85.2 MHz, CDCl<sub>3</sub>, room temperature)  $\delta$  725.3; MS (*m/z*) 629 (M<sup>+</sup>), 435 (M<sup>+</sup> - 194). Anal. Calcd for C<sub>30</sub>H<sub>19</sub>Cl<sub>3</sub>OTe: C, 57.25; H, 3.04. Found: C, 57.10; H, 2.89.

**Thermolysis of Intermediates 2a–g.** A crystal of 2a–g was heated at the melting point under argon. The residue was separated with HPLC to give the corresponding coupling products, dibenzotellurophene (3), 2-biphenyl phenyl ether derivatives (4), and 2-(2-phenoxy)biphenyl 2'-biphenyl telluride derivatives (5). The yields of 3–5 are summarized in Table 1.

**X-ray Crystallographic Analysis.** Diffraction measurements were made on an Enraf-Nonius CAD4 computer-controlled  $\kappa$  axis diffractometer by using graphite-monochromatized Mo K $\alpha$  radiation. The unit cell was determined and refined from 25 randomly selected reflections obtained by using the CAD4 automatic search, center, index, and least-squares routines. Crystal data collection parameters are listed in Table 2. Atom coordinates and selected bond lengths and angles for 2f and 2g are collected in Tables 3–6. All data processing was performed on a Micro VAX 3100 computer by using the MolEN structure-solving program obtained from Enraf Nonius Corp., Delft, The Netherlands. An empirical absorption correction based on a series of  $\psi$  scans was also applied to the data. The structure was refined in full-matrix least-squares where the function minimized was  $\sum w(|F_o| - |F_c|)^2$ , and the weight  $w$  is defined as 1.0 for all observed reflections. All hydrogen atoms were located, and their

**Table 3. Positional Parameters with Esd's for the Non-Hydrogen Atoms of 2f**

atom	x	y	z	B (Å <sup>2</sup> ) <sup>a</sup>
Te(1)	0.19750(3)	0.46200(3)	0.12470(2)	2.922(5)
O(1)	0.3974(3)	0.6354(3)	0.1146(2)	4.19(7)
O(2)	0.8941(5)	1.1094(5)	0.4672(4)	9.4(1)
O(3)	0.7256(5)	1.1033(5)	0.5328(3)	8.0(1)
N(1)	0.77(5)	1.0592(4)	0.4628(3)	5.1(1)
C(11)	-0.0279(4)	0.2143(4)	-0.0274(4)	4.3(1)
C(12)	0.0317(4)	0.2728(4)	0.0834(4)	4.0(1)
C(13)	-0.0171(5)	0.2183(5)	0.1582(5)	5.8(1)
C(14)	-0.1316(5)	0.0914(6)	0.1136(5)	7.1(2)
C(15)	-0.1890(6)	0.0327(6)	0.0038(6)	7.6(2)
C(16)	-0.1417(5)	0.0901(5)	-0.0697(6)	6.3(2)
C(21)	0.0280(4)	0.2879(4)	-0.0959(4)	3.7(1)
C(22)	0.1350(4)	0.4132(4)	-0.0443(3)	3.17(9)
C(23)	0.1874(5)	0.4976(5)	-0.1015(3)	3.8(1)
C(24)	0.1326(5)	0.4551(6)	-0.2152(4)	5.0(1)
C(25)	0.0300(5)	0.3302(6)	-0.2674(4)	5.4(1)
C(26)	-0.0220(5)	0.2462(5)	-0.2100(4)	4.9(1)
C(31)	0.4072(5)	0.3148(5)	0.2641(3)	4.0(1)
C(32)	0.3721(4)	0.3587(4)	0.1676(3)	3.22(9)
C(33)	0.4374(4)	0.3277(4)	0.0929(3)	3.7(1)
C(34)	0.5376(5)	0.2432(5)	0.1123(4)	4.6(1)
C(35)	0.5706(6)	0.1943(5)	0.2067(5)	5.7(1)
C(36)	0.5083(6)	0.2306(5)	0.2826(4)	5.4(1)
C(41)	0.3430(5)	0.3527(5)	0.3460(4)	4.8(1)
C(42)	0.3440(6)	0.4906(6)	0.3803(4)	5.6(1)
C(43)	0.2742(7)	0.5250(7)	0.4525(4)	7.9(2)
C(44)	0.2089(8)	0.4221(9)	0.4923(5)	9.8(2)
C(45)	0.2130(8)	0.2842(8)	0.4608(5)	9.2(2)
C(46)	0.2803(6)	0.2488(6)	0.3874(4)	6.9(1)
C(51)	0.4828(4)	0.7341(4)	0.1966(3)	3.22(9)
C(52)	0.6347(5)	0.7830(5)	0.2127(3)	4.0(1)
C(53)	0.7290(5)	0.8891(5)	0.2997(3)	4.0(1)
C(54)	0.6730(5)	0.9482(4)	0.3732(3)	3.48(9)
C(55)	0.5270(5)	0.9036(4)	0.3624(3)	3.9(1)
C(56)	0.4321(5)	0.7982(4)	0.2740(3)	3.9(1)

<sup>a</sup> Anisotropically refined atoms are given in the form of the isotropic equivalent displacement parameter defined as  $(4/3)[a^2B(1,1) + b^2B(2,2) + c^2B(3,3) + ab(\cos \gamma)B(1,2) + ac(\cos \beta)B(1,3) + bc(\cos \alpha)B(2,3)]$ .

**Table 4. Selected Bond Distances (Å) and Angles (deg) with Esd's in Parentheses for 2f<sup>a</sup>**

Te(1)–O(1)	2.461(3)	Te(1)–C(12)	2.150(4)
Te(1)–C(22)	2.102(4)	Te(1)–C(32)	2.136(4)
C(11)–C(12)	1.392(7)	C(11)–C(16)	1.421(6)
C(11)–C(21)	1.462(8)	C(12)–C(13)	1.403(8)
C(13)–C(14)	1.444(6)	C(14)–C(15)	1.38(1)
C(15)–C(16)	1.39(1)	C(21)–C(22)	1.404(5)
C(21)–C(26)	1.415(7)	C(22)–C(23)	1.386(7)
C(23)–C(24)	1.407(6)	C(24)–C(25)	1.384(7)
C(25)–C(26)	1.385(8)	O(1)–C(51)	1.289(4)
O(2)–N(1)	1.220(6)	O(3)–N(1)	1.226(7)
N(1)–C(54)	1.435(5)		
O(1)–Te(1)–C(12)	159.6(2)	O(1)–Te(1)–C(22)	82.2(1)
O(1)–Te(1)–C(32)	81.0(1)	C(12)–Te(1)–C(22)	80.2(2)
C(12)–Te(1)–C(32)	91.6(2)	C(22)–Te(1)–C(32)	99.1(2)
Te(1)–O(1)–C(51)	122.1(3)	Te(1)–C(12)–C(11)	112.1(4)
Te(1)–C(12)–C(13)	124.2(3)	Te(1)–C(22)–C(21)	113.3(3)
Te(1)–C(22)–C(23)	124.3(2)	Te(1)–C(32)–C(31)	119.0(4)
Te(1)–C(32)–C(33)	118.0(3)	O(2)–N(1)–O(3)	121.2(4)
O(2)–N(1)–C(54)	119.5(5)	O(3)–N(1)–C(54)	119.2(4)

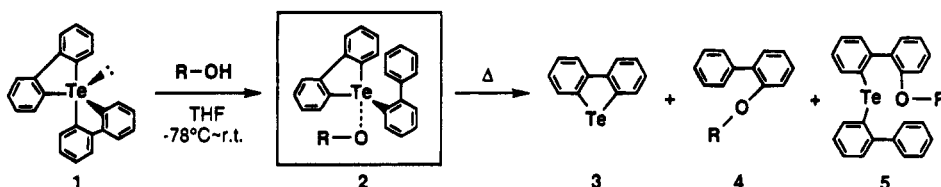
<sup>a</sup> Numbers in parentheses are estimated standard deviations in the least significant digits.

positions were refined in least-squares; their isotropic thermal parameters were held fixed at 4.0 Å.

## Results and Discussion

The tellurane 1 reacted with 1 equimolar equiv of *o*- or *p*-substituted phenol in dry THF at -78 °C to give the corresponding compounds (2a–g) each as stable light yellow crystals in 47–83% yields. The structures

Scheme 1

Table 5. Positional Parameters with Esd's for the Non-Hydrogen Atoms of **2g**

atom	x	y	z	B (Å <sup>2</sup> ) <sup>a</sup>
Te(1)	0.63672(2)	0.39199(2)	0.40562(2)	2.742(4)
Cl(1)	0.4264(1)	0.80632(8)	0.33564(7)	4.60(2)
Cl(2)	0.2265(1)	0.47238(9)	0.32093(9)	5.52(3)
Cl(3)	0.1486(1)	0.8659(1)	0.05130(8)	6.87(4)
O(1)	0.3721(2)	0.5803(2)	0.4033(2)	3.56(6)
C(11)	0.7512(4)	0.5629(3)	0.2526(3)	3.72(9)
C(12)	0.7241(4)	0.5294(3)	0.3573(3)	3.31(8)
C(13)	0.7528(4)	0.5831(3)	0.4184(3)	4.13(9)
C(14)	0.8095(4)	0.6734(3)	0.3737(3)	5.2(1)
C(15)	0.8368(5)	0.7077(3)	0.2713(4)	5.4(1)
C(16)	0.8091(5)	0.6538(3)	0.2111(3)	4.8(1)
C(21)	0.7116(4)	0.5031(3)	0.1954(3)	3.73(9)
C(22)	0.6572(4)	0.4129(3)	0.2489(2)	3.27(8)
C(23)	0.6117(4)	0.3540(3)	0.2019(3)	3.96(9)
C(24)	0.6247(5)	0.3849(4)	0.0991(3)	5.2(1)
C(25)	0.6776(6)	0.4734(4)	0.0453(3)	5.9(1)
C(26)	0.7224(5)	0.5325(4)	0.0917(3)	5.2(1)
C(31)	0.8887(3)	0.1461(3)	0.3750(3)	3.17(8)
C(32)	0.8522(3)	0.2545(3)	0.4048(2)	3.06(8)
C(33)	0.9526(4)	0.2791(3)	0.4351(3)	4.07(9)
C(34)	1.0951(4)	0.1961(4)	0.4322(3)	5.1(1)
C(35)	1.1355(4)	0.0899(4)	0.4009(3)	4.9(1)
C(36)	1.0346(4)	0.0645(3)	0.3729(3)	4.09(9)
C(41)	0.7836(4)	0.1121(3)	0.3465(3)	3.31(8)
C(42)	0.6400(4)	0.1244(3)	0.4090(3)	3.74(9)
C(43)	0.5429(4)	0.0915(4)	0.3811(3)	5.1(1)
C(44)	0.5891(5)	0.0465(3)	0.2919(3)	5.6(1)
C(45)	0.7301(5)	0.0335(3)	0.2308(3)	5.4(1)
C(46)	0.8277(4)	0.0651(3)	0.2573(3)	4.3(1)
C(51)	0.3246(4)	0.6425(3)	0.3253(3)	3.29(8)
C(52)	0.3375(4)	0.7534(3)	0.2815(3)	3.48(8)
C(53)	0.2863(4)	0.8223(3)	0.1984(3)	4.1(1)
C(54)	0.2186(4)	0.7800(4)	0.1546(3)	4.5(1)
C(55)	0.2022(4)	0.6723(3)	0.1905(3)	4.5(1)
C(56)	0.2528(4)	0.6067(3)	0.2744(3)	3.84(9)
C(61)	0.3159(7)	0.1352(5)	0.0265(5)	8.0(2)
C(62)	0.3787(6)	0.1767(5)	0.0753(5)	7.9(2)
C(63)	0.2902(6)	0.2536(5)	0.1413(4)	7.1(2)
C(64)	0.1399(6)	0.2940(5)	0.1571(4)	7.6(2)
C(65)	0.0761(5)	0.2520(5)	0.1107(5)	7.4(2)
C(66)	0.1612(5)	0.1735(4)	0.0466(4)	6.8(1)

<sup>a</sup> See footnote *a* of Table 3.

of **2a-g** were identified by <sup>1</sup>H, <sup>13</sup>C, and <sup>125</sup>Te NMR, mass spectroscopy, and elemental analysis. Each compound was decomposed on heating to give the corresponding coupling products, dibenzotellurophene (**3**), 2-biphenyl phenyl ether derivatives (**4**), and 2-(2-phenoxy)biphenyl 2'-biphenyl telluride derivatives (**5**) as shown in Scheme 1 and Table 1.

We also succeeded in determining by X-ray crystallographic analysis the structures of the products **2f,g** having *p*-nitrophenoxy and 2,4,6-trichlorophenoxy groups. The ORTEP drawings and atom-numbering schemes of **2f,g** are shown in Figures 1 and 2, and Tables 2-6 give the experimental data for the crystal structures of **2f,g**.

As shown in Table 4, the Te(1)-O(1) bond distance of **2f** is longer than that of compound **2b** (2.294 Å).<sup>9</sup> The bond angles O(1)-Te(1)-C(12) and C(22)-Te(1)-C(32) of **2f** are 159.6(2) and 99.1(2)°, respectively. The configuration of **2f** is similar to that of the compound **2b**,

Table 6. Selected Bond Distances (Å) and Angles (deg) with Esd's in Parentheses for **2g**<sup>a</sup>

Te(1)-O(1)	2.762(2)	Te(1)-O(1')	2.787(2)
Te(1)-C(12)	2.108(4)	Te(1)-C(22)	2.119(3)
Te(1)-C(32)	2.159(3)	C(11)-C(12)	1.399(5)
C(11)-C(16)	1.399(6)	C(11)-C(21)	1.467(7)
C(12)-C(13)	1.382(7)	C(13)-C(14)	1.389(6)
C(14)-C(15)	1.371(7)	C(15)-C(16)	1.368(8)
C(21)-C(22)	1.394(5)	C(21)-C(26)	1.400(6)
C(22)-C(23)	1.389(7)	C(23)-C(24)	1.384(5)
C(24)-C(25)	1.373(7)	C(25)-C(26)	1.377(9)
O(1)-C(51)	1.292(4)	Cl(1)-C(52)	1.742(5)
Cl(2)-C(56)	1.740(4)	Cl(3)-C(54)	1.753(4)
O(1)-Te(1)-O(1')	91.9(1)	Te(1)-O(1)-Te(1')	88.1(1)
O(1)-Te(1)-C(12)	81.1(1)	O(1)-Te(1)-C(22)	83.31(9)
O(1)-Te(1)-C(32)	175.6(1)	O(1')-Te(1)-C(12)	83.4(1)
O(1')-Te(1)-C(22)	164.6(1)	O(1')-Te(1)-C(32)	87.1(1)
C(12)-Te(1)-C(22)	81.3(2)	C(12)-Te(1)-C(32)	94.5(1)
C(22)-Te(1)-C(32)	96.5(1)	Te(1)-O(1)-C(51)	127.5(2)
Te(1)-C(12)-C(11)	111.9(3)	Te(1)-C(12)-C(13)	126.0(2)
Te(1)-C(22)-C(21)	111.8(3)	Te(1)-C(22)-C(23)	126.5(2)
Te(1)-C(32)-C(31)	121.7(3)	Te(1)-C(32)-C(33)	116.7(2)
O(1)-C(51)-C(52)	123.9(4)	O(1)-C(51)-C(56)	123.6(3)

<sup>a</sup> Numbers in parentheses are estimated standard deviations in the least significant digits.

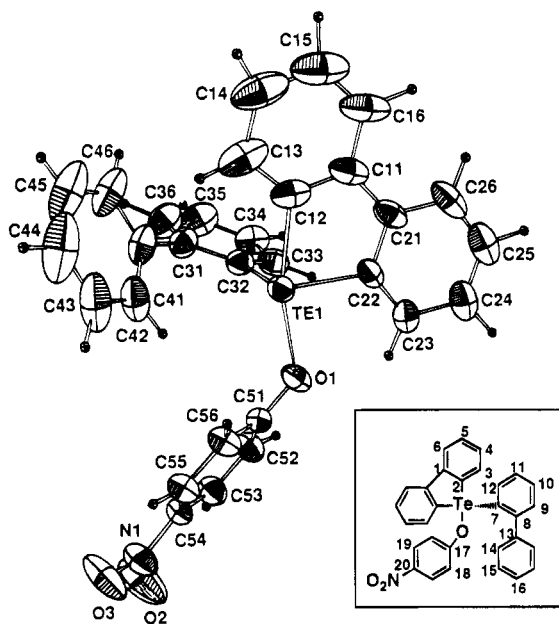
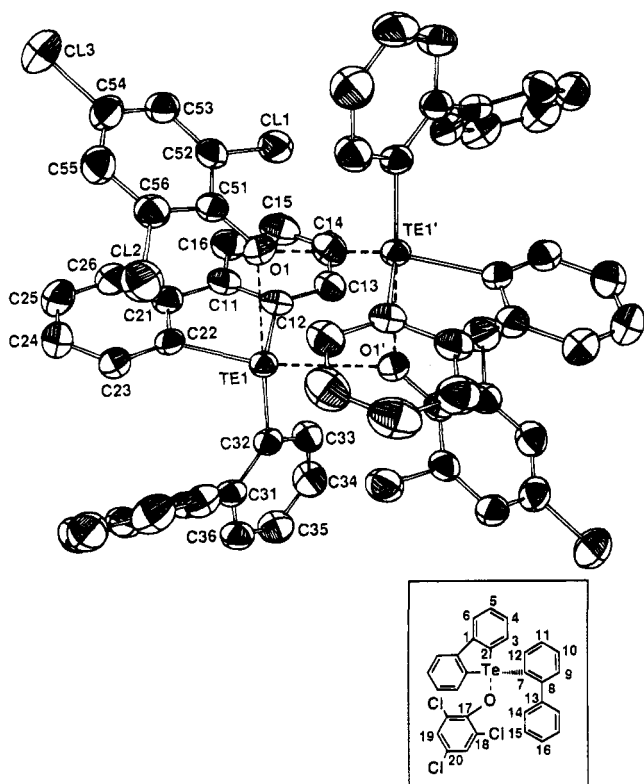


Figure 1. ORTEP drawing of **2f** showing the atom-numbering scheme.

and hence, the structure of **2f** obviously can be represented as a distorted tellurane [10-Te-4(C3O)] in which the phenolic oxygen and one Te-C bond of dibenzotellurophene compose the apical bond.

On the other hand, compound **2g** is a solvated centrosymmetric *O*-bridged dimer in the unit cell, and the configuration on the tellurium atom is different from that of **2g** as shown in Figure 2. Each tellurium atom is five-coordinate in a distorted square-pyramidal geometry. Two such square pyramids sharing a common



**Figure 2.** ORTEP drawing of **2g** showing the atom-numbering scheme.

basal edge through the bridging oxides of the 2,4,6-trichlorophenoxy group compose the dimer, and the axial Te–C vectors point in opposing directions. Te(1)–O(1) and Te(1)–O'(1) bond distances of compound **2g** are 2.762(2)–2.787(2) Å and are the almost intermediary values between the single bond distance (Te–O) of 2.101 Å<sup>10</sup> and the van der Waals distance of 3.60 Å,<sup>11</sup> while the bond angles O(1)–Te(1)–O'(1) and Te(1)–O(1)–Te'(1) are 91.9(1) and 88.1(1)°, respectively. Therefore, the two tellurium and oxygen atoms in the dimer are on the same plane because this structure has a crystallographic inversion center in the middle. The bond angles around the tellurium atom and the dimer's form have the same tendency as those of triaryltellurium salts, the structure of which have been already determined by X-ray crystallographic analysis.<sup>12</sup> The results demonstrate clearly that the Te–O distances of these species become longer and their structures change from the hypervalent structure to the onium salt by changing the electronegativity and steric hindrance of the substituents on the phenoxy group. The X-ray crystallographic data of the diffraction studies are listed in Table 2.

<sup>125</sup>Te NMR spectroscopy reflects the change of charge on the tellurium nucleus and characterization of the bonding in a molecule.<sup>13</sup> The <sup>125</sup>Te chemical shifts of each tellurium compound having a *p*-substituted phenoxy group were measured in various aprotic solvents (benzene, nitrobenzene, acetone, DMSO).<sup>14</sup> Interestingly, the observed chemical shifts shift downfield by

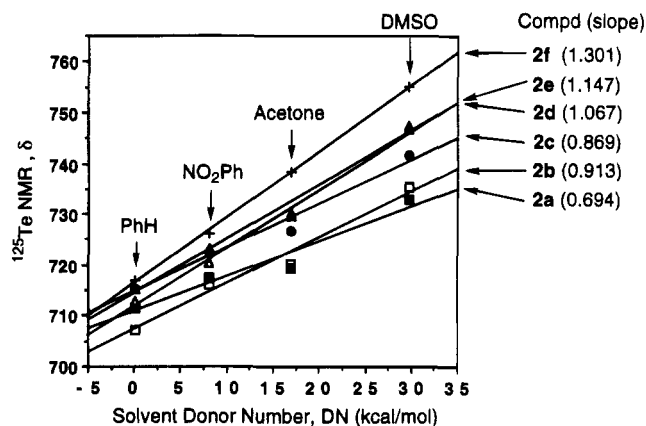


**Figure 3.** <sup>125</sup>Te NMR chemical shifts of intermediates versus donor number for **2a** (■), **2b** (□), **2c** (●), **2d** (▲), **2e** (△), and **2f** (+). Solvents and donor numbers are as follows: benzene, 0.1; nitrobenzene, 8.1; acetone, 17.0; dimethyl sulfoxide, 29.8.

intensifying, respectively, the polarity of the solvent employed in the measurement. This phenomenon revealed that the positive charge on the tellurium atom becomes larger so that the Te–O bond distance becomes longer as higher polar solvents are used, which solvate easily on the tellurium atom to diminish the positive charge of Te. The plots of the chemical shifts (ppm) versus the Gutmann donor number (DN)<sup>15</sup> of the solvents employed gave good straight lines ( $R = 0.971$ – $0.999$ ), and in the case of tellurium compounds having an electron-withdrawing substituent in the *p*-position of the phenoxy groups the ratio of change of each chemical shift, in other words, the given slope values (0.694–1.302), becomes large as shown in Figure 3.

A correlation between the chemical shifts of atoms having an electropositive charge and the donor number, which is a measure of solvent Lewis basicity, has often been found.<sup>16</sup> The solvent-induced chemical shifts can be viewed as a measure of the strength of the corresponding-atom/solvent interaction, with the solvent acting as a Lewis base and interacting electrostatically and covalently with the cation. Therefore, these results indicate that the tellurium compounds having an electron-withdrawing substituent in the *p*-position of the phenoxy groups tend to be more solvated as a large positive charge develops on the tellurium atom. Fur-

(13) (a) Luthra, N. P.; Odom, J. D. Nuclear magnetic resonance and electron spin resonance studies of organic selenium and tellurium compounds. In *The chemistry of organic selenium and tellurium compounds*; Patai, S., Rappoport, Z., Eds.; John Wiley and Sons, Inc.: New York, 1986; Vol. 1, pp 189–285 (see also references therein). (b) O'Brien, D. H.; Irgolic, K. J.; Huang, C.-K. *Proc. Int. Conf. Org. Chem. Selenium Tellurium* **1983**, *4*, 468. (c) Zumbulyadis, N.; Gysling, H. J. *J. Organomet. Chem.* **1980**, *192*, 183. (d) Schumann, H.; Magerstädt, M. *Ibid.* **1982**, *232*, 147. (e) Rodger, C.; Sheppard, N.; McFarlane, C.; McFarlane, W. Group VI-Oxygen Sulfur, Selenium and Tellurium. In *NMR and the Periodic Table*; Harris, R. K., Mann, B. E., Eds.; Academic Press: New York, 1978; pp 383–419.

(14) All <sup>125</sup>Te chemical shifts were measured by the same concentration (0.1 M) of intermediates in order to neglect the concentration dependence. In the case of using protic solvents, the correlation of <sup>125</sup>Te chemical shifts and solvent donor number was not observed.

(15) Solvent donor number  $DN = -\Delta H_{D-SbCl_5}$  (kcal/mol). (a) Gutmann, V. *The Donor-Acceptor Approach to Molecular Interactions*; Plenum Publ. Corp.: New York, 1978. (b) Maria, P.-C.; Gal, J.-F.; Franceschi, J.; Fargin, E. *J. Am. Chem. Soc.* **1987**, *109*, 483. (c) Reichardt, C. *Solvents and Solvent Effects in Organic Chemistry*; VCH Publ.: Weinheim, Germany, 1988.

(16) (a) Williams, E. A.; Cargioli, J.; Laroche, R. W. *J. Organomet. Chem.* **1978**, *108*, 153. (b) Qingyun, C.; Zhenyu, Y.; Yabo, H. *J. Fluorine Chem.* **1987**, *37* (2), 171–6.

(10) Glidewell, C. *Inorg. Chem. Acta* **1976**, *20*, 113.

(11) Bondi, A. J. *Phys. Chem.* **1964**, *68*, 441.

(12) (a) Ziolo, R. F.; Extine, M. *Inorg. Chem.* **1980**, *19*, 2964. (b) Lee, Jung-S.; Titus, D. D.; Extine, M. *Inorg. Chem.* **1977**, *10*, 2487. (c) Lee, Jung-S.; Titus, D. D. *J. Chem. Soc., Chem. Commun.* **1976**, 501. (d) Titus, D. D.; Lee, Jung-S.; Zioro, R. F. *J. Organomet. Chem.* **1976**, *120*, 381.



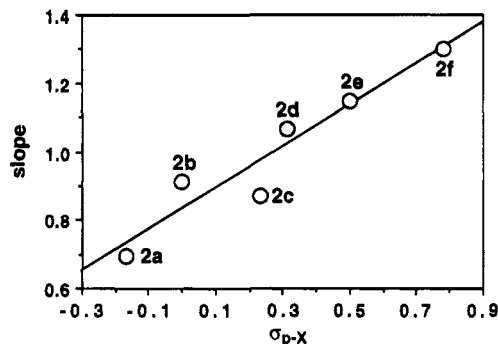


**Figure 4.** Correlation of the given slope values and the  $\sigma_p$  values of the *p*-substituted groups ( $R = 0.96$ ; slope = 0.61).

thermore, the given slope values were correlated with the  $\sigma_q$  values of these solvents except for the case of compound **2c** ( $R-O = p$ -chlorophenoxy) as shown in Figure 4.

The above  $^{125}\text{Te}$  NMR studies on the solvent effect of oxytellurium species gave information on the Te—O bond. Therefore, the hypervalency of the corresponding species in solution can be estimated by obtaining the value of the slope observed in each compound. The given values are in the range from that of 2,2'-biphe-

nylene-2-biphenyltelluronium chloride<sup>17</sup> of 1.493 to that of diphenyl telluride of  $-0.247$ . These results suggest that the structure of the corresponding species may also change continuously from the hypervalent type to onium salt type in solution. Moreover, it is hard to rule out that the structure of **2** in solution may differ from that in the solid state. Further studies on the characterization and application of oxytellurium compounds [10-Te-4(C3O)] to organic synthesis are in progress.

**Acknowledgment.** This work was supported by the Ministry of Education, Science, and Culture of Japan (Priority Area of Grant No. 05236205) and the TARA Project Fund (University of Tsukuba).

**Supporting Information Available:** A textual presentation of experimental data and tables of crystal data, positional parameters, thermal parameters, root mean-square amplitudes, and bond distances and angles (54 pages). Ordering information is given on any current masthead page.

OM950362T

(17) The preparation of 2,2'-biphenylene-2-biphenyltelluronium chloride has been reported by Hellwinkel.  $^{125}\text{Te}$  NMR (85 MHz,  $\text{CDCl}_3$ , room temperature):  $\delta$  690.6. See refs 5 and 6.



# Shapes and Thermodynamic Stabilities of $E(\text{CH}_3)_4$ Compounds ( $E = \text{S, Se, Te}$ )

Colin J. Marsden\*

Laboratoire de Physique Quantique, URA 505 du CNRS, Université Paul Sabatier,  
118 route de Narbonne, 31062 Toulouse Cedex, France

Bruce A. Smart

School of Chemistry, The University of Melbourne, Parkville, Victoria 3052, Australia

Received October 26, 1994<sup>†,‡</sup>

We report a systematic *ab initio* computational study, using a carefully graded range of basis sets with full geometry optimization at both SCF and MP2 levels of theory, of the structures, isomerism, binding energies and vibrational frequencies of  $E(\text{CH}_3)_4$  compounds ( $E = \text{S, Se, Te}$ ). Some higher-level calculations were also undertaken at MP2 geometries. The related dimethyl compounds have also been studied to indicate the accuracy which should be achieved in our calculations for the tetramethyl compounds, which are as yet unknown for  $E = \text{S}$  or  $\text{Se}$ . The equilibrium molecular structure of each tetramethyl compound is based on a trigonal bipyramid, with an equatorial lone pair ( $C_{2v}$  symmetry). Inter-methyl repulsions have significant structural effects for the S derivative, but these are progressively less important for the Se and Te species. All  $E(\text{CH}_3)_4$  compounds are fluxional, especially the Te system; barriers to Berry pseudorotation are estimated to be about 20, 15, and 3 kJ/mol for the S, Se, and Te tetramethyl. The low-frequency vibrational spectra for  $\text{Te}(\text{CH}_3)_4$  have been satisfactorily assigned and provide no evidence for the coexistence of  $C_{2v}$  and  $C_{4v}$  isomers. All  $E(\text{CH}_3)_4$  compounds are thermodynamically unstable with respect to  $(E(\text{CH}_3)_2 + \text{ethane})$ , but the instability decreases with the size of the central atom; estimated binding energies are about -350, -300, or -225 kJ/mol for  $E = \text{S, Se, or Te}$ . The influence which d-type orbitals on E have on the stability of the tetramethyls is discussed. As the Te compound has recently been prepared, the S and Se derivatives seem possible but difficult synthetic targets.

## Introduction

There has been substantial interest in "hypervalent" compounds (those which violate the octet rule) of group 16 (Group VI) elements for some time, since they pose intriguing questions about bonding.<sup>1</sup> Derivatives of S(IV) and S(VI) are, in general, stable only if highly electronegative substituents such as O or F are bonded to S. Thus  $\text{SF}_4$ ,  $\text{SF}_6$ ,  $\text{SO}_3$ , etc., are known compounds, but  $\text{SH}_4$ ,  $\text{S}(\text{CH}_3)_4$ , or  $\text{SH}_6$  are not. There has been extensive debate about the contribution made by d-type orbitals on S to the bonding in hypervalent compounds. While compounds of Se and Te in high oxidation states tend to be more stable than their S counterparts (for example,  $\text{TeCl}_4$  is thermally stable to at least 400 °C, whereas  $\text{SCl}_4$  decomposes above -30 °C<sup>2</sup>), the successful preparation of  $\text{Te}(\text{CH}_3)_4$ , by reduction of  $\text{TeCl}_4$  with methyllithium, has been achieved only relatively recently.<sup>3</sup> The compound was characterized by NMR and vibrational spectroscopies.

Compounds of the type  $\text{ER}_4$ , where E is an element of the chalcogen group such as S, Se, or Te, almost invariably have a structure derived from a slightly

distorted trigonal bipyramid, in which one equatorial position is occupied by a lone pair to give  $C_{2v}$  symmetry. This is the structure predicted by the VSEPR rules,<sup>4</sup> which have an impressive record of success in main-group structural chemistry. In the case of  $\text{Te}(\text{CH}_3)_4$ , however, the <sup>13</sup>C NMR spectra at room temperature displayed only a single peak,<sup>3</sup> which stays single down to -90 °C, presumably because the compound is fluxional, with equatorial and axial  $\text{CH}_3$  groups interchanging rapidly by the process known as Berry pseudorotation.<sup>5</sup> However, such a spectrum would also be compatible with a square-pyramidal structure of  $C_{4v}$  symmetry. The vibrational spectra of  $\text{Te}(\text{CH}_3)_4$  were not assigned in detail, but it was suggested that the large number of peaks in the low-frequency region could indicate that both square-pyramidal and trigonal-bipyramidal isomers coexist. A few years ago, such a suggestion would probably have been regarded as far-fetched, but the work of Seppelt has shown that five-coordinate bismuth systems adopt both square-pyramidal and trigonal-bipyramidal geometries.<sup>6</sup> In conjunction with the square-pyramidal structures found for  $\text{InCl}_5^-$ <sup>7</sup> and  $\text{Sb}(\text{C}_6\text{H}_5)_5$ ,<sup>8</sup> Seppelt's results imply that heavy elements favor the

<sup>†</sup> Delayed publication due to loss of revised manuscript in the mail.

<sup>‡</sup> Abstract published in *Advance ACS Abstracts*, October 1, 1995.

(1) See, for example: Magnusson, E. *J. Am. Chem. Soc.* **1993**, *115*, 1051 and references therein.

(2) See, for example: Cotton, F. A.; Wilkinson, G. *Advanced Inorganic Chemistry*; Wiley-Interscience: New York, 1988; p513.

(3) Gedridge, R. W., Jr.; Harris, D. C.; Higa, K. T.; Nissan, R. A. *Organometallics* **1989**, *8*, 2817.

(4) Gillespie, R. J.; Hargittai, I. *The VSEPR Model of Molecular Geometry*; Allyn and Bacon: Boston, MA, 1991.

(5) Berry, R. S. *J. Chem. Phys.* **1960**, *32*, 933.

(6) Schmuck, A.; Seppelt, K. *Chem. Ber.* **1989**, *122*, 803.

(7) Brown, D. S.; Einstein, F. W. B.; Tuck, D. G. *Inorg. Chem.* **1960**, *8*, 14.

(8) Wheatley, P. J. *J. Chem. Soc.* **1964**, 3718.

$C_{4v}$  structures more than do lighter ones. Gedridge's suggestion for  $\text{Te}(\text{CH}_3)_4$  must therefore be taken seriously.

Since experimental data had not been able to provide unequivocal results concerning the molecular structure of  $\text{Te}(\text{CH}_3)_4$ , we decided that a theoretical study would be worthwhile. The techniques of computational quantum chemistry are now sufficiently refined to be able to yield reliable data on the structures, vibrational frequencies, and binding energies of small molecules.<sup>9</sup> We decided that a parallel study of the related compounds  $\text{S}(\text{CH}_3)_4$  and  $\text{Se}(\text{CH}_3)_4$  would be valuable, even though these have not yet been prepared. The comparison of their binding energies with that calculated for  $\text{Te}(\text{CH}_3)_4$  would be of considerable interest. Moreover, as  $C_{4v}$  structures have been predicted for  $\text{SH}_4$ ,  $\text{SeH}_4$ , and  $\text{TeH}_4$ ,<sup>10</sup> it cannot be assumed with certainty that  $C_{2v}$  structures will be adopted by the tetramethyl derivatives. We are not aware of any theoretical study of these compounds published before the recent paper by Fowler and Schaefer, which appeared just after the submission of the original version of our own work.<sup>11</sup> They also examined the three  $\text{E}(\text{CH}_3)_4$  compounds ( $\text{E} = \text{S}, \text{Se}, \text{and Te}$ ) which are the subject of our own work, using computational methods. Their results, which are broadly similar to our own, will be compared with ours at appropriate places in the text.

We predict that all three tetramethyl derivatives adopt trigonal-bipyramidal structures of  $C_{2v}$  symmetry, that all are thermodynamically unstable with respect to  $(\text{E}(\text{CH}_3)_2 + \text{C}_2\text{H}_6)$ , by about 350, 280 and 200 kJ/mol for  $\text{E} = \text{S}, \text{Se}, \text{Te}$ , respectively, but that all are local minima on their potential energy surfaces. All three molecules are fluxional, but there are important differences in behavior between  $\text{Te}$  and the other group 16 elements. The barriers to pseudorotation are found to be about 20 or 15 kJ/mol for  $\text{E} = \text{S}$  or  $\text{Se}$  but as little as 3 kJ/mol for  $\text{Te}(\text{CH}_3)_4$ .

Independently of our work, two other groups of structural chemists also decided that the intriguing problems posed by tetramethyltellurium merited further attention. The compound has very recently been studied in the solid phase by X-ray diffraction and in the gas phase by electron diffraction; a preliminary account of these studies has already appeared.<sup>12</sup> The essential features of the results obtained by all three groups are closely similar, so there can now be no doubt that a  $C_{2v}$  structure is preferred for tetramethyltellurium.

### Theoretical Methods

We have employed a carefully graded range of both all-electron and pseudopotential basis sets in this work. Since the computational cost of performing SCF calculations rises roughly as the fourth power of the number of electrons, while the factor for the more reliable correlated calculations involves the fifth or even sixth power, it was not feasible for us to use

all-electron basis sets for the tellurium-containing molecules. We wished to show that our calculated results are not especially sensitive to the size of basis set and to establish that pseudopotential methods are reliable for this class of compound, by comparing all-electron and pseudopotential results for the  $\text{S}$  and  $\text{Se}$  derivatives, where both styles of calculation were feasible. The Gaussian series of programs<sup>13,14</sup> was used for all the calculations in this work, which were performed in Melbourne, Australia. Geometries were optimized using gradient methods and vibrational frequencies were calculated either from analytical second derivatives or numerically from first derivatives, at both SCF and MP2 levels of theory. A few calculations were undertaken using more elaborate correlation treatments (MP4SDQ, QCISD, and QCISD(T)) at MP2 geometries.

Calculations were performed on all of the molecules considered in this work using the pseudopotential basis sets of Hay and Wadt<sup>15</sup> (hereinafter referred to as PS). These bases were supplemented first with a single d-type function on the central atom with exponents of 0.6 for  $\text{S}$ , 0.38 for  $\text{Se}$  and 0.3 for  $\text{Te}$ , to give the PS(P) set, and then with a single d-type function on the carbon atoms (exponent 0.75) to give the PSP basis. The five spherical-harmonic components of d-type functions were adopted. No p-type functions were used on hydrogen with pseudopotential bases.

The sulfur compounds were investigated using several standard all-electron basis sets, ranging in size from 3-21G\*<sup>16,17</sup> through DZP<sup>18</sup> and DZP\* to valence triple- $\zeta$  (TZP); the latter comprised 6-311G\* or 6-311G bases for  $\text{C}$  or  $\text{H}^{19}$  and a 12s9p/6s5p set for  $\text{S}$ .<sup>20</sup> d-type polarization functions were added to  $\text{S}$  and  $\text{C}$  atoms in the DZP and TZP bases, with exponents of 0.532 and 0.75, respectively. In a few cases, a larger TZ(2)P basis was used, which differs from TZP in having two sets of d functions on  $\text{S}$ , whose exponents are 1.1 and 0.35. For the DZP\* basis we also added p-type functions to the hydrogen atoms (exponent 1.0).

All-electron calculations were performed on the selenium compounds using a DZ(P)-style set. The  $\text{Se}$  basis was of the form 14s11p6d/8s6p3d, as proposed by Dunning.<sup>21</sup> This contraction is a little more flexible than that used by Fowler and Schaefer, which was 7s5p3d,<sup>11</sup> and as a result our total energy of  $\text{Se}(\text{CH}_3)_4$  is lower than theirs by nearly 20 kJ/mol. An additional d-type function was added to allow for polarization effects, the exponent of 0.38 being adopted from the optimized value found with the pseudopotential basis. Standard double- $\zeta$  bases<sup>18</sup> were used for the carbon and hydrogen atoms.

### Results and Discussion

(a)  $\text{E}(\text{CH}_3)_2$ . In order to obtain binding energies for the tetramethyl molecules, we needed calculated energies for their dimethyl analogues. Since these species are well characterized, our results for these molecules

(9) See, for example: Hehre, W. J.; Radom, L.; Schleyer, P. v. R.; Pople, J. A. *Ab Initio Molecular Orbital Theory*; J. Wiley & Sons: New York, 1986.

(10) (a) Yoshioka, Y.; Goddard, J. D.; Schaeffer, H. F., III. *J. Chem. Phys.* **1981**, *74*, 1855. (b) Moc, J.; Dorigo, A. E.; Morokuma, K. *Chem. Phys. Lett.* **1993**, *204*, 65. (c) Marsden, C. J.; Smart, B. A. *Aust. J. Chem.* **1994**, *47*, 1431.

(11) Fowler, J. E.; Schaefer, H. F., III. *J. Am. Chem. Soc.* **1994**, *116*, 9596.

(12) Blake, A. J.; Pulham, C. R.; Greene, T. M.; Downs, A. J.; Haaland, A.; Verne, H. P.; Volden, H. V.; Marsden, C. J.; Smart, B. A. *J. Am. Chem. Soc.* **1994**, *116*, 6043.

(13) Gaussian 86. Frisch, M. J.; Binkley, J. S.; Schlegel, H. B.; Raghavachari, K.; Melius, C. F.; Martin, R. L.; Stewart, J. J. P.; Bobrowicz, F. W.; Rohlfing, C. M.; Khan, L. R.; Defrees, D. J.; Seeger, R.; Whiteside, R. A.; Fox, D. J.; Fleuder, E. M.; Pople, J. A. Carnegie-Mellon Quantum Chemistry Publishing Unit, Pittsburgh, PA, 1984.

(14) Gaussian 90, Revision F. Frisch, M. J.; Head-Gordon, M.; Trucks, G. W.; Foresman, J. B.; Schlegel, H. B.; Raghavachari, K.; Robb, M.; Binkley, J. S.; Gonzalez, C.; Defrees, D. J.; Fox, D. J.; Whiteside, R. A.; Seeger, R.; Melius, C. F.; Baker, J.; Martin, R. L.; Kahn, L. R.; Stewart, J. J. P.; Topiol, S.; Pople, J. A. Gaussian Inc., Pittsburgh, PA, 1990.

(15) Wadt, W. R.; Hay, P. J. *J. Chem. Phys.* **1985**, *82*, 284.

(16) Binkley, J. S.; Pople, J. A.; Hehre, W. J. *J. Am. Chem. Soc.* **1980**, *102*, 939.

(17) Pietro, W. J.; Francl, M. M.; Hehre, W. J.; Defrees, D. J.; Pople, J. A.; Binkley, J. S. *J. Am. Chem. Soc.* **1982**, *104*, 5039.

(18) Dunning, T. H., Jr.; Hay, P. J. *Modern Theoretical Chemistry*; Plenum: New York, 1976; pp 1-28.

(19) Krishnan, R.; Binkley, J. S.; Seeger, R.; Pople, J. A. *J. Chem. Phys.* **1980**, *72*, 650.

(20) McLean, A. D.; Chandler, G. S. *J. Chem. Phys.* **1980**, *72*, 5639.

(21) Dunning, T. H., Jr. *J. Chem. Phys.* **1977**, *66*, 1382.

**Table 1. Structural Parameters and Energies Calculated for S(CH<sub>3</sub>)<sub>2</sub><sup>a</sup>**

basis	theory	energy	r(S-C)	r(C-H)	∠(C-S-C)
3-21G*	SCF	-474.456 985	1.813	1.082	99.5
DZP	SCF	-476.739 063	1.812	1.083	99.8
	MP2	-477.222 489	1.814	1.097	98.3
TZP	SCF	-476.771 822	1.809	1.081	100.0
	MP2	-477.339 021	1.803	1.091	98.6
PS	SCF	-89.078 447 5	1.864	1.079	100.2
	MP2	-89.307 578	1.894	1.101	98.4
PS(P)	SCF	-89.112 733	1.809	1.082	100.1
	MP2	-89.410 713	1.827	1.103	98.8
PSP	SCF	-89.145 731	1.801	1.082	99.9
	MP2	-89.527 500	1.808	1.095	98.6
exptl <sup>b</sup>			1.802(2)	1.091(5)	98.9(2)

<sup>a</sup> Bond lengths in Å, bond angles in deg, energies in hartree.

<sup>b</sup> Reference 22, with uncertainties in parentheses.

serve to calibrate the accuracy which should be achieved for the structures and vibrational frequencies predicted for the tetramethyl systems. Fowler and Schaefer did not present results for these molecules.<sup>11</sup> Our results for the principal structural parameters of dimethyl sulfide are presented in Table 1, together with experimental data for comparison. *C*<sub>2v</sub> molecular symmetry was assumed. The molecular geometry of dimethyl sulfide was predicted with satisfying accuracy at both the SCF and MP2 levels of theory, with all bases except the simplest (PS, which lacked any polarization functions). The PSP basis predicted geometrical parameters to within 1.5% at both the SCF and MP2 levels. The S-C bond length was found to be 1.801 Å (SCF) or 1.808 Å (MP2) compared to the experimental value of 1.802-(2)Å.<sup>22</sup> The most pleasing results were obtained using the TZP basis at the MP2 level, where the two bond lengths were predicted to lie within the experimental uncertainties, while the C-S-C angle lay outside that uncertainty by only 0.1°. When making these comparisons, it should be appreciated that the experimental structural parameters are vibrational averages, while the computed results are equilibrium values, so exact agreement between the two sets should not be expected; we may anticipate that equilibrium bond lengths will be slightly shorter than thermal-average values, by a few thousandths of an Å, but that equilibrium bond angles should be very similar to vibrationally averaged quantities for the E(CH<sub>3</sub>)<sub>2</sub> molecules under consideration here.

The vibrational frequencies for S(CH<sub>3</sub>)<sub>2</sub> were also calculated. Many of the vibrational motions for E(CH<sub>3</sub>)<sub>2</sub> and E(CH<sub>3</sub>)<sub>4</sub> molecules are of course internal to the methyl groups and are thus of limited interest to the general reader. They may be obtained from either author on request. Our results for the skeletal modes are presented in Table 2, together with the torsional vibrations, since these are at low frequency and could conceivably be confused with bending motions in some cases. The experimental results obtained by Allkins and Hendra<sup>23</sup> and by Durig *et al.*<sup>24</sup> are also displayed in Table 2. We have attempted to correlate the experimentally observed Raman and infrared spectra with our calculated values, from reported infrared intensities and frequencies. It is difficult to classify bands in certain

crowded regions of the spectra, and we do not claim that our assignments are unequivocal. Most basis sets provided at least reasonably good estimates for each of the 21 vibrational modes, with the PS(P) basis set at the MP2 level of theory proving most accurate overall, while the DZP and TZP bases at the same level of theory are also very satisfactory. The nonpolarized PS basis was, however, significantly less reliable than the others. In general, frequencies were overestimated by between 3% and 4% using the better basis sets when second-order Møller-Plesset perturbation theory was used. SCF values were found to be overestimated by about 7% to 8%. Systematic errors of this magnitude are quite typical.<sup>9</sup> It may appear from Table 2 that the frequencies calculated for the torsional modes are less accurate than for the others, as they are apparently underestimated by as much as 60 cm<sup>-1</sup>, or 25% of the value reported. However, it should be noted that the experimental measurements were obtained from the solid phase,<sup>24</sup> and it seems quite possible for intermolecular interactions to provide an additional restriction on torsional motion in the solid, leading to a higher frequency than that which would be observed in the gas phase. It is also possible, as suggested by a reviewer, that the anharmonicity correction is positive, rather than negative as usually found, i.e. that the representation of the real torsional potential as a cosine function which is then approximated as a harmonic function is inadequate.

These structural and vibrational results for S(CH<sub>3</sub>)<sub>2</sub> show the following desirable features: the experimental results are well reproduced, provided that the basis contains polarization functions on the central atom; further improvement of the basis beyond PS(P) or DZ(P) quality has only marginal effects on the geometrical parameters or vibrational frequencies predicted; the performance of the pseudopotential and all-electron bases is almost equivalent; and the influence of electron correlation effects on the structural parameters is only slight. Other E(CH<sub>3</sub>)<sub>2</sub> molecules need not be analyzed in such detail, but the results for the S derivative are in no way exceptional.

The molecular geometry and vibrational frequencies for dimethyl selenide were calculated using a smaller number of basis sets than for the corresponding sulfur species, since there was so little variation in the results once the basis contained polarization functions on S. Our structural results are presented in Table 3. Once again the polarized bases give good structural results at both SCF and MP2 levels of theory, with the MP2 values being slightly better. An electron diffraction experiment performed by Goldish *et al.*<sup>25</sup> found the selenium-to-carbon bond distance to be 1.977(12) Å. The DZ(P) and PS(P) MP2 values of 1.971 and 1.977 Å both lie comfortably within the experimental uncertainty, while the PSP/MP2 result of 1.956 is just a little outside it. The study by Goldish *et al.* also determined the C-Se-C bond angle to be 98° but with a large uncertainty of 10°. Our results suggest that their quoted uncertainty is unnecessarily pessimistic, and we expect that the bond angle lies within the range 95.5-98.5°.

Our calculated skeletal and torsional vibrational frequencies for Se(CH<sub>3</sub>)<sub>2</sub> are reported in Supporting

(22) Pierce, L.; Hayashi, M. *J. Chem. Phys.* **1961**, *35*, 479.

(23) Allkins, J.; Hendra, P. J. *Spectrochim. Acta* **1966**, *22*, 2075.

(24) Durig, J. R.; Player, C. M., Jr.; Bragin, J.; Li, Y. S. *J. Chem. Phys.* **1971**, *55*, 2895.

(25) Goldish, E.; Hedberg, K.; Marsh, R. E.; Schomaker, V. *J. Am. Chem. Soc.* **1955**, *77*, 2948.

**Table 2. Skeletal and Torsional Vibrational Frequencies for S(CH<sub>3</sub>)<sub>2</sub><sup>a</sup>**

basis set	theory	skeletal motions			torsional motions	
		a <sub>1</sub>	a <sub>1</sub>	b <sub>1</sub>	a <sub>2</sub>	b <sub>1</sub>
3-21G*	SCF	727 (3.9)	288 (0.0)	1107 (9.0)	198 (0.0)	204 (1.3)
DZP	SCF	755 (5.4)	284 (0.1)	1086 (3.5)	191 (0.0)	197 (1.3)
	MP2	736 (3.2)	274 (0.1)	1028 (6.9)	160 (0.0)	191 (1.3)
TZP	SCF	744 (5.4)	285 (0.0)	1090 (11)	198 (0.0)	205 (1.1)
	MP2	736 (3.3)	273 (0.1)	1041 (18)	181 (0.0)	196 (1.1)
PS	SCF	692 (4.8)	269 (0.2)	1105 (10)	169 (0.0)	173 (1.6)
	MP2	645 (1.2)	251 (0.2)	1023 (12)	129 (0.0)	157 (1.1)
PS(P)	SCF	755 (4.2)	293 (0.1)	1103 (9.5)	188 (0.0)	200 (1.7)
	MP2	710 (3.3)	275 (0.2)	1037 (9.7)	147 (0.0)	183 (1.5)
exptl <sup>23,24</sup>		691	284	1027	210 <sup>b</sup>	247 <sup>b</sup>

<sup>a</sup> Frequencies in cm<sup>-1</sup>, infrared intensities in parentheses. <sup>b</sup> Solid-phase experimental data.

**Table 3. Structural Parameters and Energies Calculated for Se(CH<sub>3</sub>)<sub>2</sub><sup>a</sup>**

basis	theory	energy	r(Se-C)	r(C-H)	∠(C-Se-C)
DZ(P) <sup>b</sup>	SCF	-78.938 380	1.950	1.082	97.9
	MP2	-79.593 061	1.971	1.103	96.4
PS	SCF	-88.203 638	1.986	1.080	97.6
	MP2	-88.428 042	2.013	1.101	95.9
PS(P)	SCF	-88.226 459	1.955	1.082	97.5
	MP2	-88.516 017	1.977	1.103	96.1
PSP	SCF	-88.255 983	1.952	1.081	97.5
	MP2	-88.628 270	1.956	1.094	95.9
exptl <sup>25</sup>			1.977 (12)	1.094 (ass)	98 (10)

<sup>a</sup> Bond lengths in Å, bond angles in degrees, energies in hartree.

<sup>b</sup> Energy below -2400 E<sub>h</sub>.

**Table 4. Structural Parameters and Energies Calculated for Te(CH<sub>3</sub>)<sub>2</sub><sup>a</sup>**

basis	theory	energy	r(Te-C)	r(C-H)	∠(C-Te-C)
PS	SCF	-87.038 229	2.158	1.081	95.0
	MP2	-87.260 200	2.182	1.102	93.8
PS(P)	SCF	-87.051 168	2.143	1.083	95.3
	MP2	-87.326 746	2.168	1.103	93.7
PSP	SCF	-87.077 749	2.144	1.081	95.2
	MP2	-87.436 589	2.148	1.095	93.5
exptl <sup>26</sup>			2.142 (5)	1.07 (2)	94 (2)

<sup>a</sup> Bond lengths in Å, bond angles in deg, energies in hartree.

Information Table S1, in the interests of using less journal space, together with the experimental results.<sup>23,24</sup> Once again some of the frequencies predicted by the nonpolarized PS basis were underestimated, particularly at the MP2 level of theory. Other bases performed well, with frequencies typically being overestimated by up to 10% at the SCF level, while the errors were reduced to about 5% with the inclusion of second-order Møller-Plesset perturbation theory. The calculated frequencies for the torsional modes are again appreciably lower than those measured for the solid.<sup>24</sup>

Calculations on dimethyl tellurium were performed using pseudopotential basis sets only, and our principal geometrical results are shown in Table 4. An electron diffraction study by Blom *et al.* reported a Te-C bond length of 2.142(5) Å,<sup>26</sup> which is scarcely distinguishable from our best (PSP) results of 2.144 Å (SCF) or 2.148 Å (MP2). Addition of a set of d functions to the Te basis produces a shortening of the Te-C distance of only 0.015/0.014 Å at the SCF/MP2 level, which is noticeably smaller than the comparable changes found for the S-C (0.055/0.067 Å) and Se-C (0.031/0.036 Å) bonds. These differences are provocative, since the d functions are

expected to act almost wholly as "polarization" rather than "hybridization" functions for these E(CH<sub>3</sub>)<sub>2</sub> species, and one might expect the larger, less electronegative Te atom to be more polarizable than the smaller, more electronegative S atom. This comparison of the behaviors of different group 16 elements is considered in more detail below for the tetramethyls. The C-Te-C bond angle was observed to be 94(2)°,<sup>26</sup> which again compares very favorably with our PSP results of 95.2° (SCF) or 93.5° (MP2).

Vibrational frequencies were also calculated for Te(CH<sub>3</sub>)<sub>2</sub>, and our results for the skeletal and torsional modes may be found in Supporting Information Table S2. They are also available from the authors on request. As was found for the corresponding sulfur and selenium species, the PS basis yielded frequencies which were somewhat unreliable, but again when this basis is supplemented with a single d-function, reasonably accurate predictions of frequencies are obtained. At the SCF level the frequencies were characteristically overestimated by up to 10% compared to the values reported by Allkins and Hendra<sup>23</sup> and by Durig *et al.*,<sup>24</sup> but with the introduction of second-order Møller-Plesset perturbation theory these errors were reduced to about 5%, a value which seems to be characteristic of this type of compound at this level of theory. However, the frequencies calculated for the torsional modes once again are substantially lower than the single experimental observation made on the solid phase.

**E(CH<sub>3</sub>)<sub>4</sub>.** Two basic structural types can be envisaged for EL<sub>4</sub> compounds, where E is an element from group 16. The first has C<sub>2v</sub> symmetry and may be described as a distorted trigonal bipyramid in which the lone pair on E occupies an equatorial position. In the second structure, which has C<sub>4v</sub> symmetry, the four L groups occupy equivalent positions at the base of a square pyramid while the lone pair on E is in the apical position. However, where L is a methyl group, several different conformations are possible within the constraints of either C<sub>2v</sub> or C<sub>4v</sub> symmetries.

Four possible arrangements of the methyl groups were considered for S(CH<sub>3</sub>)<sub>4</sub> with C<sub>2v</sub> symmetry imposed. They are illustrated in Figure 1 as 1-4. In order of increasing energy, after full geometry optimization at the DZP/SCF level of theory, they are as follows.

(1) Both equatorial and axial methyl groups are staggered with respect to the lone pair: this conformer was found to be a true minimum with all real vibrational frequencies. (2) The equatorial groups are eclipsed but the axial groups staggered: this structure is 11.1 kJ/mol above (1) and has two imaginary vibrational

(26) Blom, R.; Haaland, A.; Seip, R. *Acta Chem. Scand.* **1983**, A37, 595.

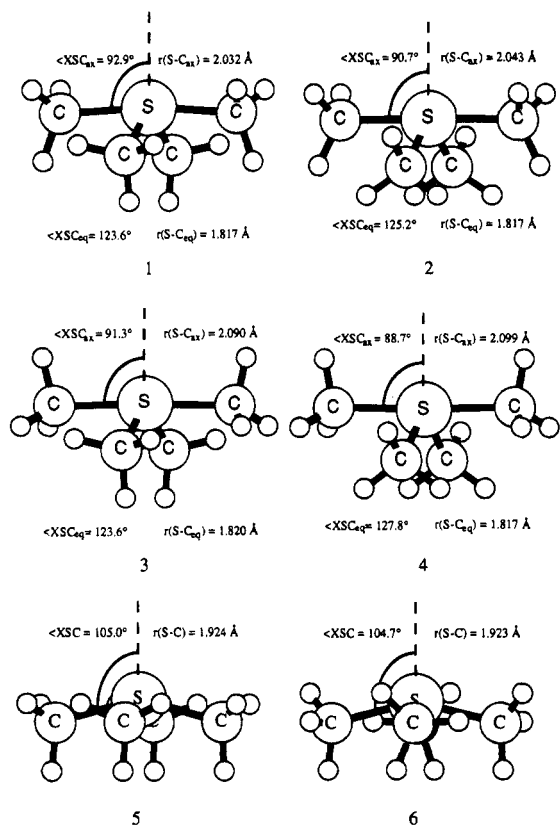


**Figure 1.** Different structural forms of S(CH<sub>3</sub>)<sub>4</sub> discussed in the text. The predicted equilibrium structure is **1**. Point-group symmetries are C<sub>2v</sub> for isomers **1**–**4**, C<sub>4v</sub> for **5**, and C<sub>4</sub> for **6**. Principal geometrical parameters are indicated.

frequencies. (3) The equatorial groups are staggered but the axial groups are eclipsed: this arrangement is 39.7 kJ/mol above (1) and has four imaginary vibrational frequencies. (4) Both equatorial and axial methyl groups are eclipsed with respect to the lone pair: this conformer is 39.9 kJ/mol above (1) and also has four imaginary vibrational frequencies.

There are two possible arrangements for the methyl groups for C<sub>4v</sub> symmetry S(CH<sub>3</sub>)<sub>4</sub>; either all methyl groups are staggered, or all are eclipsed, with respect to the lone pair. No stationary point could be located for the latter, as it reverted spontaneously to the staggered conformer by undergoing an inversion at S. The staggered conformer is illustrated in Figure 1 as **5**.

Isomers **1** and **5** of tetramethylsulfur were examined with the set of bases adopted for the dimethyl species. Structural results for the C<sub>2v</sub> isomer **1** are displayed in Table 5. The same symmetry and conformation were found by Fowler and Schaefer.<sup>11</sup> The two carbon-to-sulfur bond distances are quite different; the axial bonds are consistently longer than the equatorial bonds by a surprisingly large amount (0.228 Å at the highest level of theory used; Fowler and Schaefer report a difference of 0.241 Å using DZ(P)/CISD theory). In the isoelectronic compound SF<sub>4</sub>, the difference between axial and equatorial bond lengths is only 0.099 Å.<sup>27</sup> Comparison of the results in Tables 1 and 5 shows that the equatorial bonds in tetramethylsulfur are scarcely different in length from those in the analogous dimethyl derivative. It is likely that the very long axial bonds in S(CH<sub>3</sub>)<sub>4</sub> reflect the weakly bound nature of this com-

pound (see below). The C<sub>ax</sub>–S–C<sub>ax</sub> angle is consistently found to lie between 172 and 175°, scarcely different from the angle of 173° found in SF<sub>4</sub>. Although the C<sub>eq</sub>–S–C<sub>eq</sub> angle lies between 110 and 113°, with our highest-level prediction being 111.4° (111.6° in the work of Fowler and Schaefer) compared to 101.5° for SF<sub>4</sub>, a widening of the bond angle should not be unexpected; it is almost certainly due to the bulky nature of the methyl group as compared to fluorine. The closest H···H distance between equatorial methyl groups is about 2.39 Å with the optimum geometrical parameters but would be only about 2.05 Å if the equatorial angle were the same as in SF<sub>4</sub>. This latter value would result in substantial steric distress, as the sum of the van der Waals radii for two H atoms is usually taken to be 2.4 Å.<sup>28</sup>

The C<sub>4v</sub> isomer **5** of S(CH<sub>3</sub>)<sub>4</sub> was found to have a single imaginary vibrational frequency of b<sub>2</sub> symmetry at the 3-21G\*/SCF level of theory, indicating that this isomer is the transition state along the Berry pseudorotation pathway.<sup>5</sup> However, when the DZP basis set was used, a second imaginary frequency was found, of a<sub>2</sub> symmetry, corresponding to a spontaneous rotation of the four methyl groups about their local approximate 3-fold axes, to give a C<sub>4</sub> structure in which the methyl groups were twisted by 9° from the all-staggered C<sub>4v</sub> conformation. This C<sub>4</sub> isomer, illustrated in Figure 1 as **6**, was then found to have only a single imaginary vibrational frequency. The C<sub>4v</sub> structure was also found to have two imaginary frequencies with both PS(P) and PSP bases, at both SCF and MP2 levels of theory. The twist angle of the methyl groups increases from about 10° at the SCF level to about 17° when MP2 theory is used. Fowler and Schaefer also report that the pseudorotation transition state has C<sub>4</sub> rather than C<sub>4v</sub> symmetry, with methyl twist angles of 8.8° (SCF) or 15.6° (CISD theory).<sup>11</sup> This rotation is presumably caused by repulsions between hydrogen atoms on neighboring methyl groups; their separation is only 2.055 Å at the DZP/SCF level of theory for the C<sub>4v</sub> structure, which is substantially less than the sum of the van der Waals radii, but the concerted methyl twisting motion increases this distance slightly. Full details of the structural parameters found for isomer **6** of S(CH<sub>3</sub>)<sub>4</sub> are presented in Supporting Information Table S4. Here we note particularly that the S–C bonds are rather long, at 1.913 Å with our most reliable level of theory (1.922 Å in the work by Fowler and Schaefer); they are thus close to the average of the axial and equatorial values for the C<sub>2v</sub> geometry. In SF<sub>4</sub>, by way of contrast, the calculated bond length (SCF theory with a DZ(P) basis) in the C<sub>4v</sub> pseudorotation transition state is 1.609 Å,<sup>29</sup> which is only 0.06 Å longer than the equatorial bonds in the ground-state C<sub>2v</sub> structure, but again close to the average of the axial and equatorial bond lengths. The C–S–C bond angle in the C<sub>4</sub> structure of S(CH<sub>3</sub>)<sub>4</sub> is 87°, which corresponds to an angle of 104° between the lone pair and an S–C bond. In SF<sub>4</sub>, where the ligands are less bulky, more space is available to the lone pair; we find that the F–S–F angle is 83° in the C<sub>4v</sub> transition state structure for SF<sub>4</sub>, which corresponds to an angle of 110° between the lone pair and an S–F bond. These geometrical comparisons clearly indicate the significant

(28) Pauling, L. *Nature Of The Chemical Bond*; Cornell University Press: Ithaca, NY, 1960; p 260.

(29) Marsden, C. J.; Smart, B. A. Unpublished observations.

(27) Tolles, M. W.; Gwinn, W. D. *J. Chem. Phys.* **1962**, *36*, 1119.

**Table 5. Structural Parameters and Energies Calculated for S(CH<sub>3</sub>)<sub>4</sub> (C<sub>2v</sub>)<sup>a</sup>**

basis	theory	energy	r(C-S <sub>ax</sub> )	r(C-S <sub>eq</sub> )	∠(X-S-C <sub>ax</sub> ) <sup>b</sup>	∠(X-S-C <sub>eq</sub> ) <sup>c</sup>
3-21G*	SCF	-553.094 265	2.028	1.811	93.2	124.3
DZP	SCF	-555.808 432	2.032	1.817	92.9	123.6
	MP2	-556.615 211	2.060	1.818	93.4	124.6
TZP	SCF	-555.847 970	2.018	1.814	92.9	123.6
	MP2	-556.773 858	2.036	1.808	93.6	124.6
PS	SCF	-168.077 885	2.176	1.870	92.8	124.4
	MP2	-168.536 195	2.275	1.893	94.0	126.6
PS(P)	SCF	-168.157 290	2.025	1.810	92.5	123.7
	MP2	-168.667 435	2.083	1.830	92.9	124.7
PSP	SCF	-168.217 020	2.013	1.812	92.9	123.4
	MP2	-168.896 907	2.037	1.814	93.4	124.3

<sup>a</sup> Bond lengths in Å, bond angles in deg, energies in hartree. <sup>b</sup> Angle between C<sub>2</sub> axis and S-C<sub>ax</sub> bond. <sup>c</sup> Angle between C<sub>2</sub> axis and S-C<sub>eq</sub> bond.

**Table 6. Skeletal Vibrational Frequencies for S(CH<sub>3</sub>)<sub>4</sub> (C<sub>2v</sub>)<sup>a</sup>**

basis	theory	skeletal motions								
		a <sub>1</sub>	a <sub>1</sub>	a <sub>1</sub>	a <sub>1</sub>	a <sub>2</sub>	b <sub>1</sub>	b <sub>1</sub>	b <sub>2</sub>	b <sub>2</sub>
3-21G*	SCF	699 (1.3)	433 (0.6)	335 (0.1)	193 (2.7)	445 (0.0)	764 (18)	374 (3.0)	443 (0.6)	403 (480)
DZP	SCF	717 (1.7)	424 (0.3)	316 (0.1)	180 (3.2)	430 (0.0)	783 (4.4)	338 (670)	425 (1.5)	363 (4.2)
	MP2	689 (0.9)	391 (170)	293 (0.01)	177 (2.3)	408 (0.0)	740 (3.8)	345 (3.1)	409 (240)	383 (0.9)
TZP	SCF	706 (1.6)	429 (1.6)	325 (0.5)	184 (3.8)	438 (0.0)	774 (2.7)	371 (0.1)	431 (0.3)	377 (3.6)
PS	SCF	665 (3.8)	368 (14)	269 (920)	135 (5.3)	364 (0.0)	708 (7.3)	289 (0.3)	421 (0.3)	297 (36)
	MP2	623 (2.7)	313 (12)	246 (3.2)	158 (2.9)	310 (0.0)	654 (15)	251 (0.3)	401 (200)	305 (0.2)
PS(P)	SCF	726 (1.2)	374 (3.7)	331 (0.1)	187 (2.9)	441 (0.0)	797 (2.1)	425 (1.5)	436 (0.08)	351 (640)
	MP2	671 (0.7)	406 (130)	290 (0.01)	177 (2.2)	361 (0.0)	728 (2.80)	363 (0.8)	443 (2.6)	374 (240)

<sup>a</sup> Frequencies in cm<sup>-1</sup>, infrared intensities in parentheses.

structural influence of H···H interactions in S(CH<sub>3</sub>)<sub>4</sub>. Their thermodynamic consequences also appear to be significant, as discussed below.

The important skeletal vibrational frequencies calculated for isomer 1 of S(CH<sub>3</sub>)<sub>4</sub> are reported in Table 6. It is hoped that these results may be useful for future experiments designed to synthesize the compound. Frequencies for the modes which are essentially internal to the methyl groups are not reported, as they are unlikely to be particularly useful for the characterization of the compound, but they may be obtained from either author on request. As for the dimethyl derivative, we note that none of the calculated frequencies is particularly sensitive to the type of basis used, once polarization functions are included on the sulfur atom, and correlation effects do not appear to be especially important. By analogy with the results already obtained for S(CH<sub>3</sub>)<sub>2</sub>, we anticipate that the frequencies in Table 6 will be about 8–10% too high if calculated at the SCF level and perhaps 4–5% too high at the MP2 level. The IR intensities should be semiquantitatively useful, particularly for the MP2 results. The most easily identified IR bands for S(CH<sub>3</sub>)<sub>4</sub> appear to be the axial symmetric (a<sub>1</sub>) and antisymmetric (b<sub>2</sub>) stretching modes, both of which are intense and which both lie near 400 cm<sup>-1</sup>. The frequencies and intensities reported by Fowler and Schaefer were limited to DZ(P)/SCF results,<sup>11</sup> which agree very well with our DZP/SCF values; however, they used a different choice of axis system which interchanges the b<sub>1</sub> and b<sub>2</sub> symmetry labels compared with our work. Calculated torsional frequencies are presented in Supporting Information Table S5. These will not be easy to observe, as they lie at low frequencies and have zero or very low IR intensities.

We have calculated the thermodynamic stability of tetramethyl sulfur, or more precisely its electronic binding energy compared to (dimethyl sulfide + ethane), with a variety of basis sets, at both SCF and MP2 levels of theory, and with more sophisticated methods up to

**Table 7. Binding Energies<sup>a</sup> for E(CH<sub>3</sub>)<sub>4</sub> Relative to (E(CH<sub>3</sub>)<sub>2</sub> + C<sub>2</sub>H<sub>6</sub>)**

basis	theory	S(CH <sub>3</sub> ) <sub>4</sub>	Se(CH <sub>3</sub> ) <sub>4</sub>	Te(CH <sub>3</sub> ) <sub>4</sub>
3-21G*	SCF	-411		
DZP	SCF	-444	-374	
	MP2	-352	-300	
DZP*	SCF	-440		
	MP2	-340		
	MP3	-363		
	MP4SDQ	-364		
TZP	SCF	-438		
	MP2	-336		
TZ(2)P <sup>b</sup>	SCF	-427		
	MP2	-329		
	MP3	-353		
	MP4SDQ	-351		
PS	SCF	-542	-452	-322
	MP2	-410	-330	-226
PS(P)	SCF	-424	-360	-269
	MP2	-336	-287	-198
PSP	SCF	-439	-381	-295
	MP2	-328	-283	-207

<sup>a</sup> Binding energies are in kJ/mol. <sup>b</sup> Geometry taken from TZP/MP2 optimization.

fourth-order perturbation theory (MP4SDQ), as this is such an important indication of whether the compound can ever be prepared. Our results in Table 7 show that S(CH<sub>3</sub>)<sub>4</sub> is consistently unstable in a thermodynamic sense. There is some variation with the size of the basis used, with the compound becoming slightly less unstable as the basis is enlarged, and it is possible that even larger basis sets than those used here would lead to further reductions in the calculated thermodynamic instability. Correlation effects make the compound appreciably less unstable, by about 100 kJ/mol. But as the basis-set effects are relatively minor, and as the use of progressively more exact treatments of correlation (MP2 through MP3 to MP4SDQ) changes the predicted binding energy by only some 20 or 25 kJ/mol, we are confident that the thermodynamic instability of S(CH<sub>3</sub>)<sub>4</sub> is firmly established; our best estimate of the binding energy is -350 kJ/mol. Fowler and Schaefer did not



Table 8. Structural Parameters and Energies for Se(CH<sub>3</sub>)<sub>4</sub> (C<sub>2v</sub>)<sup>a</sup>

basis	theory	energy	r(C-Se <sub>ax</sub> )	r(C-Se <sub>eq</sub> )	∠(C <sub>ax</sub> -Se-C <sub>ax</sub> )	∠(C <sub>eq</sub> -Se-C <sub>eq</sub> )
DZ(P)	SCF	-2558.002 017	2.137	1.944	169.8	110.5
	MP2	-2558.863 386	2.181	1.968	168.4	109.0
PS	SCF	-167.237 640	2.201	1.978	168.8	110.5
	MP2	-167.687 030	2.248	2.007	166.4	107.5
PS(P)	SCF	-167.295 224	2.132	1.947	169.5	110.7
	MP2	-167.791 473	2.172	1.973	168.0	109.3
PSP	SCF	-167.347 355	2.128	1.947	168.9	111.2
	MP2	-167.997 949	2.141	1.954	167.4	109.9

<sup>a</sup> Bond lengths in Å, angles in deg, energies in hartree.

discuss the thermodynamic stability of the tetramethyl compounds.<sup>11</sup> Although S(CH<sub>3</sub>)<sub>4</sub> is thermodynamically unstable, its future preparation is of course not absolutely excluded by these results. Its possible kinetic stability would be determined by the barrier to dissociation to (S(CH<sub>3</sub>)<sub>2</sub> + ethane), but it was beyond the scope of this work to locate the corresponding transition state, which probably has only C<sub>1</sub> symmetry.<sup>10b</sup> As the barrier to dissociation is quite unknown at present, it is not very important to attempt to give uncertainty limits for the thermodynamic instability.

Interesting information concerning the importance of d orbitals for the bonding of the hypervalent tetramethyl compounds may be obtained from Table 7. By comparing the SCF results for the PS and PS(P) basis sets, we learn that d-type functions on S improve the binding energy of S(CH<sub>3</sub>)<sub>4</sub> by about 100 kJ/mol. This does not mean that the total energy of S(CH<sub>3</sub>)<sub>4</sub> is lowered only by that amount but rather that it is lowered by 100 kJ/mol more than the energy of S(CH<sub>3</sub>)<sub>2</sub>, a compound where S follows the octet rule. In fact the total energetic effect at the SCF level in S(CH<sub>3</sub>)<sub>4</sub> of d-type orbitals on S is just over 200 kJ/mol, as shown by the data in Table 5. Now 100 kJ/mol is not a trivial amount of energy when considering binding, but it is not sufficiently large to be taken as a dominant contribution, in general terms. We note that the correlation contribution to the binding energy is also of the order of 100 kJ/mol, while the total valence correlation energy obtained in our MP2 calculations is as large as 1785 kJ/mol. Correlation effects arise from the inadequacies of the one-electron or orbital model, the model which is used almost to the exclusion of all others by chemists who are not experts in electronic structure calculations. As the energetic consequences of d-type orbital contributions to the binding energy are similar in magnitude to those due to the failure of the orbital model itself, it does not seem reasonable to ascribe a primary importance to d-type bonding contributions. We believe that a more realistic approach is to consider the d-type orbitals as polarization functions, which are important in a quantitative sense for relatively "soft" (polarizable) atoms such as S. More detailed numerical analyses of many hypervalent compounds may be found in ref 1.

The barrier to Berry pseudorotation in S(CH<sub>3</sub>)<sub>4</sub>, *i.e.* the difference in energy between the C<sub>2v</sub> and C<sub>4</sub> isomers, is not large. Calculated values at the SCF level of theory are 32.5 (3-21G\* basis), 28.7 (DZP), 31.1 (PS(P)), or 26.2 (PSP) kJ/mol. These decrease to 21.3 (DZP), 24.9 (PS(P)), or 20.0 (PSP) kJ/mol when MP2 theory is used. Fowler and Schaefer obtained barriers with their DZ(P) basis of 32.6 (SCF) or 25.1 (CISD) kJ/mol,<sup>11</sup> which are quite consistent with our own results. They also located transition states on the methyl rotation surface, finding low barriers of 12.5 or 3.8 kJ/mol for axial or

equatorial rotation. There is some variation in these values for the pseudorotation barrier, but similar trends have been found in detailed studies of the isoelectronic species SF<sub>4</sub>, where energies were obtained for C<sub>2v</sub> and C<sub>4v</sub> isomers using MP4SDQ and QCISD levels of theory with bases ranging to TZ(2)P(f) in size at SCF geometries; enlargement of the basis reduces the barrier, as does inclusion of electron correlation effects.<sup>29</sup> It is clear that S(CH<sub>3</sub>)<sub>4</sub> is a fluxional molecule and more flexible than SF<sub>4</sub>, whose barrier is about 45 kJ/mol.

Tetramethylselenium was examined using the basis sets adopted for the dimethyl species, and isomers of C<sub>2v</sub>, C<sub>4v</sub>, and C<sub>4</sub> symmetry were investigated. As for S(CH<sub>3</sub>)<sub>4</sub>, a stationary point of C<sub>2v</sub> symmetry was located for Se(CH<sub>3</sub>)<sub>4</sub> in which both equatorial and axial methyl groups are staggered with respect to the equatorial lone pair; it proved to be a true minimum. The C<sub>4v</sub> isomer was found to have two imaginary frequencies, again like S(CH<sub>3</sub>)<sub>4</sub>, one corresponding to the collapse to the C<sub>2v</sub> species and the other giving the C<sub>4</sub> isomer by a concerted methyl group rotation. However, the methyl twist is only some 0.3°, or barely noticeable for Se(CH<sub>3</sub>)<sub>4</sub>. It seems clear that this reduced departure from idealized C<sub>4v</sub> symmetry is due to the longer bonds, and hence reduced steric hindrance, associated with the selenium species. The shortest H···H distance between methyl groups is 2.193 Å in C<sub>4v</sub> Se(CH<sub>3</sub>)<sub>4</sub> at the DZ(P)/SCF level of theory, compared to 2.055 Å for S(CH<sub>3</sub>)<sub>4</sub>.

Optimized geometrical parameters for the C<sub>2v</sub> isomer of Se(CH<sub>3</sub>)<sub>4</sub> are reported in Table 8. The main structural features, which are not sensitive to details of the basis set used and are not greatly influenced by correlation effects, are very similar to those already described for S(CH<sub>3</sub>)<sub>4</sub>. The equatorial C-Se bonds are of "normal" length, being almost exactly the same as those in Se(CH<sub>3</sub>)<sub>2</sub>, but the axial bonds are substantially longer, by about 0.20 Å. Although this difference is slightly less than that described for S(CH<sub>3</sub>)<sub>4</sub>, which is some 0.23 Å, it is much greater than that found in SeF<sub>4</sub> (0.089 Å).<sup>30</sup> The C<sub>ax</sub>-Se-C<sub>ax</sub> angle is close to 168°, scarcely different from the value of 169° in SeF<sub>4</sub>, while the C<sub>eq</sub>-Se-C<sub>eq</sub> angle is about 110°, compared to 100.6° for SeF<sub>4</sub>. An analogous widening of the equatorial bond angle was noted above for tetramethylsulfur. It is slightly less pronounced for the selenium compound, presumably due to the reduced H···H interactions between equatorial methyl groups, which result from the longer C-Se bonds compared to those between carbon and sulfur. Once again, the results obtained by Fowler and Schaefer are almost identical to our own where they overlap,<sup>11</sup> despite the different contraction schemes used in the two studies.

(30) Bowater, I. C.; Brown, R. D.; Burden, F. R. *J. Mol. Spectrosc.* 1968, 28, 454.



**Table 9. Skeletal Vibrational Frequencies for Se(CH<sub>3</sub>)<sub>4</sub> (C<sub>2v</sub>)<sup>a</sup>**

basis	theory	skeletal motions								
		a <sub>1</sub>	a <sub>1</sub>	a <sub>1</sub>	a <sub>1</sub>	a <sub>2</sub>	b <sub>1</sub>	b <sub>1</sub>	b <sub>2</sub>	b <sub>2</sub>
DZ(P)	SCF	631 (0.1)	425 (0.9)	257 (1.0)	159 (2.7)	369 (0.0)	664 (0.1)	289 (3.9)	395 (220)	327 (170)
PS	SCF	588 (0.2)	307 (6.3)	175 (1.8)	128 (1.6)	351 (0.0)	628 (0.03)	267 (10)	345 (25)	148 (230)
	MP2	547 (0.2)	347 (1.0)	217 (0.8)	141 (3.0)	313 (0.0)	580 (0.9)	236 (4.79)	361 (190)	298 (15)
PS(P)	SCF	612 (1.8)	443 (1.5)	221 (3.5)	110 (0.2)	372 (0.0)	594 (5.0)	286 (10)	385 (250)	333 (110)
	MP2	569 (0.3)	382 (0.9)	218 (0.2)	160 (1.9)	327 (0.0)	596 (1.0)	268 (3.6)	378 (210)	327 (15)

<sup>a</sup> Frequencies in cm<sup>-1</sup>, infrared intensities in parentheses.

**Table 10. Structural Parameters and Energies Calculated for Te(CH<sub>3</sub>)<sub>4</sub> (C<sub>2v</sub>)<sup>a</sup>**

basis	theory	energy	r(C <sub>ax</sub> -Te)	r(C <sub>eq</sub> -Te)	∠(C <sub>ax</sub> -Te-C <sub>ax</sub> )	∠(C <sub>eq</sub> -Te-C <sub>eq</sub> )
PS	SCF	-166.121 718	2.268	2.142	160.0	113.1
	MP2	-166.559 054	2.294	2.175	157.3	112.0
PS(P)	SCF	-166.154 790	2.251	2.128	161.5	111.8
	MP2	-166.636 088	2.277	2.161	158.9	112.2
PSP	SCF	-166.204 991	2.252	2.131	161.0	112.3
	MP2	-166.852 117	2.256	2.142	158.7	111.6
X-ray D <sup>b</sup>			2.275(17)	2.127(6)	162.2(4)	109.1(3)
electron D <sup>c</sup>			2.265(9)	2.140(8)	152(3)	123(5)

<sup>a</sup> Bond lengths in Å, bond angles in deg, energies in hartree. <sup>b</sup> X-ray diffraction results for solid, from ref 12; uncertainties in parentheses. <sup>c</sup> Electron diffraction results for gas, from ref 12; uncertainties in parentheses.

Predicted skeletal vibrational frequencies for the C<sub>2v</sub> isomer of Se(CH<sub>3</sub>)<sub>4</sub> are displayed in Table 9. The most reliable values are those calculated with the PS(P) basis. It is likely that the SCF results are too high by about 10%, while the error for the MP2 values is probably of the order of 5%. It is somewhat surprising that correlation effects have a pronounced influence on the IR intensities; MP2 theory predicts that there is only one intense band for Se(CH<sub>3</sub>)<sub>4</sub>, located a little below 400 cm<sup>-1</sup>, whereas there are two intense IR bands in that region for the sulfur compound, and two are predicted for Se(CH<sub>3</sub>)<sub>4</sub> at the SCF level of theory. This observation shows just how difficult it can be to make reliable estimates of vibrational spectra for even moderately complex molecules without assistance from quantitative calculations.

Calculated structural parameters for the C<sub>4</sub> isomer of Se(CH<sub>3</sub>)<sub>4</sub> are reported in Supporting Information Table S6. The C-Se bonds are long, at about 2.05 Å or very close to the average of the equatorial and axial bond lengths for the C<sub>2v</sub> isomer, while the C-Se-C angle of 85° is somewhat smaller than the comparable value of 87° in the C<sub>4</sub> isomer of S(CH<sub>3</sub>)<sub>4</sub>; as argued above, the angle in the sulfur compound is larger than would be expected, so the smaller value here is another indication of the reduced role of H···H repulsions in the Se-containing molecule. The barrier to Berry pseudorotation for tetramethylselenium is rather less than for tetramethylsulfur. Calculated values range from 24.7 (DZ(P)/SCF) to 14.2 (PSP/MP2) kJ/mol. Fowler and Schaefer also obtained 24.7 kJ/mol at the DZ(P)/SCF level of theory.<sup>11</sup> As for the sulfur system, the barrier decreases as the basis is enlarged and as correlation effects are considered. We believe that the true value will be close to 15 kJ/mol.

Tetramethylselenium is less thermodynamically unstable than its sulfur analogue. Calculated values of the binding energy, compared to (ethane and the dimethyl species), are presented in Table 7. Rather similar trends with basis size and theoretical method are found for both tetramethyls, though the selenium compound was studied in less detail than the sulfur species, as the variations with level of theory for the

sulfur compound were not large. Our final estimate for the binding energy of Se(CH<sub>3</sub>)<sub>4</sub>, obtained by applying a "correction" to the MP2 result based on the experience obtained from S(CH<sub>3</sub>)<sub>4</sub>, is about -300 kJ/mol, compared to about -350 kJ/mol for S(CH<sub>3</sub>)<sub>4</sub>.

C<sub>2v</sub> and C<sub>4v</sub> isomers of tetramethyltellurium were examined. The C<sub>2v</sub> isomer was found to be a true minimum, following the pattern established by the S and Se analogues. The all-staggered conformer similar to **1** in Figure 1 was again found to be the most stable, with the equatorial-eclipsed/axial-staggered, equatorial-staggered/axial eclipsed and all-eclipsed arrangements higher in energy by 10.0, 22.8 and 31.0 kJ/mol, respectively, at the PS(P)/SCF level of theory with full geometry optimization. However, only a single imaginary vibrational frequency was found for the C<sub>4v</sub> isomer, which is therefore a true transition state, in contrast to the selenium and sulfur systems described above for which the transition state has C<sub>4</sub> symmetry. Twisting of the methyl groups is not favored for the C<sub>4v</sub> isomer of Te(CH<sub>3</sub>)<sub>4</sub>, as due to the long Te-C bonds, the separation between H atoms in different groups has increased to 2.39 Å at the PS(P)/SCF level of theory, indicating insignificant steric repulsion since the sum of the van der Waals radii is 2.4 Å.<sup>28</sup>

Optimized structural parameters for the C<sub>2v</sub> isomer of Te(CH<sub>3</sub>)<sub>4</sub> are reported in Table 10. The calculated difference between the equatorial and axial bond lengths to carbon is rather small, at only 0.114 Å with the most sophisticated theory we used. This difference is much less than the values of 0.23 or 0.20 Å for the S or Se analogues. It is noticeable that the variation in axial bond length for Te(CH<sub>3</sub>)<sub>4</sub> with the size of basis is much less pronounced than found for the S or Se derivatives. When the basis is improved from PS to PSP, the Te-C<sub>ax</sub> bond shortens by only 0.038 Å at the MP2 level, compared to reductions of 0.238 Å for S-C<sub>ax</sub> and 0.107 Å for Se-C<sub>ax</sub>. There is a steady reduction in the C<sub>ax</sub>-E-C<sub>ax</sub> angles as the central atom increases in size; PSP/MP2 values are 173.2° for E = S, 167.4° for the Se compound, and 158.7° for Te(CH<sub>3</sub>)<sub>4</sub>. This trend appears to be yet another reflection of the decreasing importance of intermethyl H···H repulsions as the E-C bonds

Table 11. Skeletal Vibrational Frequencies for Te(CH<sub>3</sub>)<sub>4</sub> (C<sub>2v</sub>)<sup>a</sup>

basis	theory	skeletal motions									
		a <sub>1</sub>	a <sub>1</sub>	a <sub>1</sub>	a <sub>1</sub>	a <sub>2</sub>	b <sub>1</sub>	b <sub>1</sub>	b <sub>2</sub>	b <sub>2</sub>	
PS	SCF	543 (1.0)	429 (0.5)	211 (5.4)	100 (2.0)	313 (0.0)	569 (7.3)	239 (8.8)	430 (180)	281 (25)	
	MP2	507 (1.1)	419 (0.4)	193 (3.9)	82 (1.2)	291 (0.0)	523 (10)	221 (7.7)	437 (110)	260 (9.1)	
PS(P)	SCF	566 (1.4)	442 (0.3)	216 (3.8)	112 (1.5)	314 (0.0)	586 (9.0)	240 (5.9)	447 (190)	286 (22)	
	MP2	515 (1.0)	406 (0.3)	193 (2.3)	87 (0.9)	296 (0.0)	535 (8.6)	226 (5.8)	425 (120)	268 (11)	
PSP	SCF	550 (1.2)	439 (0.3)	209 (3.9)	108 (1.7)	310 (0.0)	581 (8.1)	240 (5.8)	445 (192)	281 (21)	
	exptl <sup>b</sup>	507	383				520	219	383 (?)	263	

<sup>a</sup> Frequencies in cm<sup>-1</sup>, infrared intensities in parentheses. <sup>b</sup> Experimental results from ref 3.

lengthen; following the VSEPR principles,<sup>4</sup> the lone pair is more sterically demanding than the bond pairs, but its desire to seek a large share of the coordination sphere about E is frustrated if E is relatively small by the consequent H · · · H nonbonded repulsions. Fowler and Schaefer<sup>11</sup> used an all-electron basis on Te rather than a pseudopotential of the type used in our work. They obtained nonnegligible differences for some of the structural parameters. In particular, the C<sub>eq</sub>-Te-C<sub>eq</sub> angle is 118.6° in their work, but our SCF values are close to 112°; for that parameter, the Te compound has an appreciably larger angle than the S or Se species in their work, whereas we found differences of no more than 1–2° from compound to compound. It is not clear to us why these differences should arise, but we note that the potential surface for Te(CH<sub>3</sub>)<sub>4</sub> is very flat for angular deformations (see below), so the values obtained for equilibrium structural parameters are likely to be unusually sensitive to details of the basis employed.

The comparison of our calculated structural results for Te(CH<sub>3</sub>)<sub>4</sub> with those available from the recent X-ray diffraction and electron diffraction (ED) experiments<sup>12</sup> is also presented in Table 10. It will be noted that the agreement with our PSP/MP2 values is very satisfactory for both axial and equatorial bond lengths, as our results are either within or just outside the experimental uncertainties. The situation regarding the bond angles is more complicated, but particularly interesting. As the ED experiments were performed in the gas phase, one might anticipate that the ED results would be in better agreement with our calculated values, which also refer to isolated molecules, than would the X-ray results which were obtained in the solid phase and which might perhaps be distorted by "packing effects" or by "secondary bonding" in the crystal. The latter are common for atoms as heavy as Te,<sup>31</sup> and one would probably anticipate non-negligible interactions with neighboring molecules for a system in which the formal Te coordination number is as low as 5. However, while the calculated equatorial bond angle agrees tolerably well with the X-ray value, with a difference of only some 2°, the ED result is about 12° larger. For the axial bond angle our calculated value is between the X-ray and ED results, though closer to the X-ray value. We believe that these angular discrepancies are a reflection of the extraordinary fluxional nature of tetramethyltellurium, which is discussed in detail below.

Skeletal vibrational frequencies calculated for the C<sub>2v</sub> isomer of Te(CH<sub>3</sub>)<sub>4</sub> are reported in Table 11. We have attempted to assign the experimental observations<sup>3</sup> where possible, but unfortunately many of the (3N – 6) fundamental vibrational frequencies for tetramethyltellurium have not yet been observed. Although we

do not have calculated frequencies at the PSP/MP2 level of theory, as those calculations would have been too time-consuming, we can obtain extrapolations by combining the PS(P)/SCF and /MP2 results with the PSP/SCF data. The resulting estimates are 504, 403, 186, and 83 cm<sup>-1</sup> for the a<sub>1</sub> block, 292 cm<sup>-1</sup> for the single a<sub>2</sub> mode, 530 and 226 cm<sup>-1</sup> for b<sub>1</sub> symmetry, and 423 and 263 cm<sup>-1</sup> for the b<sub>2</sub> block. The particularly low a<sub>1</sub> bending frequency of only some 83 cm<sup>-1</sup> implies immediately that the molecule is unusually flexible, as the skeletal bending frequency in dimethyl tellurium is 198 cm<sup>-1</sup>.<sup>23</sup> We expect the a<sub>1</sub> modes to be the most intense in the Raman spectrum and so assign the 507 and 383 cm<sup>-1</sup> peaks to the modes predicted near 504 and 403 cm<sup>-1</sup>. As no spectral features were detected below 200 cm<sup>-1</sup>, we cannot make assignments for the two remaining a<sub>1</sub> skeletal modes. An IR band at 520 cm<sup>-1</sup> is readily assigned to the skeletal stretching b<sub>1</sub> mode, while the Raman feature at 219 cm<sup>-1</sup> matches quite satisfactorily the b<sub>1</sub> bend expected near 226 cm<sup>-1</sup>. It is not clear whether the antisymmetric stretching motion of the Te–C axial bonds (b<sub>2</sub> symmetry) expected near 423 cm<sup>-1</sup> has been detected; unfortunately the IR spectrum could not be studied below 450 cm<sup>-1</sup>, and while there is a Raman peak at 383 cm<sup>-1</sup>, it is more natural to assign it to the a<sub>1</sub> axial stretching motion, in view of its high intensity and better match with our calculated frequencies. The remaining Raman band at 263 cm<sup>-1</sup> fits splendidly with the b<sub>2</sub> bending mode expected near 263 cm<sup>-1</sup>; such good agreement is pleasant but no doubt somewhat fortuitous. This discussion shows that all observed low-frequency bands in both infrared and Raman spectra can be assigned quite satisfactorily to the fundamental skeletal vibrations of C<sub>2v</sub> Te(CH<sub>3</sub>)<sub>4</sub>. In particular, we note that there is no need to invoke a possible co-existence of C<sub>2v</sub> and C<sub>4v</sub> isomers, in order to understand the substantial number of low-frequency bands.<sup>3</sup> The conclusions reached by Fowler and Schaefer about the vibrational frequencies are broadly similar to our own,<sup>11</sup> though they did not attempt such a detailed assignment of the observed data. In addition to the nine skeletal vibrations, there are four torsional vibrations for Te(CH<sub>3</sub>)<sub>4</sub>. All are at low frequency and all have low IR intensities, so their detection will be difficult. Our detailed calculated values appear in Supporting Information Table S7. Briefly, the expected frequencies are 169 (twice), 143, and 142 cm<sup>-1</sup>.

Calculated structural parameters for the C<sub>4v</sub>-symmetry transition-state isomer of Te(CH<sub>3</sub>)<sub>4</sub> are presented in Supporting Information Table S8. The predicted Te–C bond length is 2.20 Å; as already seen for the other C<sub>4</sub> or C<sub>4v</sub> tetramethyls described in this work, this value is very close to the average of the axial and equatorial bond distances in the C<sub>2v</sub> ground state.

(31) Alcock, N. R. *Adv. Inorg. Chem. Radiochem.* **1972**, *15*, 2.

**Table 12. Pseudorotation Barriers for Te(CH<sub>3</sub>)<sub>4</sub><sup>a</sup>**

basis	theory	<i>E</i> (C <sub>2v</sub> )	<i>E</i> (C <sub>4v</sub> )	Δ <i>E</i>
PS(P)	SCF	-166.154 79	-166.145 15	25.3
	MP2	-166.636 09	-166.626 64	24.8
PSP	SCF	-166.204 99	-166.201 88	8.4
	MP2	-166.852 12	-166.850 53	4.2
PSP(f) <sup>b</sup>	MP2	-166.886 25	-166.885 25	2.6
	MP3	-166.947 09	-166.946 00	2.9
	MP4DQ	-166.953 27	-166.952 07	3.1
	MP4SDQ	-166.958 06	-166.956 79	3.3
	QCISD	-166.960 70	-166.959 37	3.5
	QCISD(T)	-166.982 89	-166.981 83	2.8
	QCISD(T) + ZPV <sup>c</sup>			3.4

<sup>a</sup> Absolute energies *E* in hartree, energy differences Δ*E* in kJ/mol. <sup>b</sup> Results obtained at PSP/MP2 geometries. <sup>c</sup> Zero-point energies of vibration, unscaled, obtained at PSP/SCF level of theory.

Continuing another well-established trend in this series, the C–Te–C bond angle of 83° is smaller than those for Se(CH<sub>3</sub>)<sub>4</sub> (85°) or S(CH<sub>3</sub>)<sub>4</sub> (87°); we argue that the long Te–C bonds allow the lone pair to acquire its “natural” share of the coordination sphere about tellurium, without having to compromise to reduce H· · H repulsions. In this case the C–Te–C angle reported by Fowler and Schaefer agrees very well with our value, and the bond length differs by less than 1%.<sup>11</sup>

To our minds, the most interesting aspect of the potential energy surface for Te(CH<sub>3</sub>)<sub>4</sub> is its flatness; in other words, the molecule is extraordinarily fluxional and the barrier to pseudorotation remarkably low. Calculated values are reported in Table 12. It will be seen that the addition of d functions to the C atom basis produces a large reduction in the barrier, and in this respect Te(CH<sub>3</sub>)<sub>4</sub> behaves quite differently from the other tetramethyl compounds already discussed; for the Se derivative, for example, increasing the size of the basis from PS(P) to PSP changes the barrier by only 0.1 kJ/mol with MP2 theory. We have not discovered why the basis requirements for Te(CH<sub>3</sub>)<sub>4</sub> are more stringent than those for the other tetramethyl compounds, but the variational principle is quite clear; the addition of extra functions to a basis necessarily lowers the energy, even if only slightly, and if the extra functions make an appreciable change in the calculated value of some property, then the original basis without those functions was inadequate. We note that the all-electron basis used by Fowler and Schaefer gave a very small pseudorotation barrier of only 2.1 kJ/mol at the SCF level,<sup>11</sup> whereas our most directly comparable SCF result is 25.3 kJ/mol, obtained with the PS(P) basis. The origin of this discrepancy is not clear to us.

To test the adequacy of the PSP basis, we undertook further calculations using a still larger PSP(f) basis, which contained a set of f-type functions on Te only (exponent 0.35). These calculations were performed for both the C<sub>2v</sub> and C<sub>4v</sub> isomers of tetramethyltellurium at the geometries obtained at the PSP/MP2 level of theory. This further basis extension reduced the calculated barrier to pseudorotation from 4.2 to 2.6 kJ/mol using MP2 energies; in percentage terms, this is an appreciable change, though in practice its significance is probably limited, as we cannot claim accuracy to within 1 kJ/mol. The precise value of the barrier fluctuated somewhat as progressively more sophisticated correlation treatments were employed, rising to 3.5 kJ/mol with QCISD theory but then decreasing to 2.8 kJ/mol at the QCISD(T) level. When the zero-point

vibrational energies of the two isomers are considered, as computed at the PSP/SCF level of theory, the effective barrier increases by 0.6 kJ/mol to 3.4 kJ/mol. Fowler and Schaefer also noted that the zero-point energy calculated for the C<sub>4v</sub> transition state is, rather unusually, slightly larger than for the C<sub>2v</sub> true minimum.<sup>11</sup>

These results allow us to understand why the bond angles obtained by gas-phase electron diffraction at room temperature appear to be somewhat different from those calculated for the equilibrium geometry or obtained by X-ray diffraction for the solid phase at low temperatures (183 K) in the solid phase.<sup>12</sup> The average thermal energy available to molecules at 298 K is 2.5 kJ/mol, or about 75% of our most sophisticated calculated barrier to pseudorotation. Even if this calculated value is not exactly correct, it is clear that a nonnegligible number of gas-phase molecules will be in excited vibrational states which effectively lie above the barrier, and thus have 4-fold symmetry, while a substantial number of others will have energies close to the top of the barrier. Now the electron diffraction experiment samples all the molecules distributed over their various vibrational states and thus obtains average bond angles. While for normal, relatively rigid molecules there is little difference between average and equilibrium bond angles, appreciable differences can arise for highly fluxional molecules such as Te(CH<sub>3</sub>)<sub>4</sub>. The apparent bond angles observed by electron diffraction are thus the Boltzmann-weighted superposition of all geometries between the equilibrium C<sub>2v</sub> and transition-state C<sub>4v</sub> geometries. Thus the axial and equatorial angles obtained by electron diffraction are closer to each other (153 and 118°) than are the corresponding X-ray (109 and 162°) or calculated (113 and 161°) values, since all four adjacent C–Te–C angles in the C<sub>4v</sub> transition state are equal and intermediate between the axial and equatorial angles for the C<sub>2v</sub> ground state. The vibrational amplitudes found in the electron diffraction experiment are exceptionally large for the C· · C distances due to the flexible nature of the molecule. We note the particularly low vibrational frequency of only some 83 cm<sup>-1</sup> estimated for the equatorial bending motion. This large-amplitude vibrational motion causes a smearing-out of the C· · C distances, and thus leads to relatively large uncertainties in the bond angles measured by electron diffraction. The X-ray diffraction experiment does not suffer from these difficulties, since it was performed at lower temperatures and since the molecules are somewhat constrained in the crystal by contacts with their neighbors.

Although tetramethyltellurium is thermodynamically unstable, its formation from ethane and the dimethyl derivative is less unfavorable than for either its S or Se analogues. Calculated results are presented in Table 7. Our best estimate of the binding energy is -225 kJ/mol. Te(CH<sub>3</sub>)<sub>4</sub> is not stable in a practical sense above 100 °C and is light-sensitive.<sup>3</sup> There is a progressive increase in stability as the size of the central atom increases, presumably due at least in part to the reduction in H· · H steric repulsions, and the change from Se(CH<sub>3</sub>)<sub>4</sub> to Te(CH<sub>3</sub>)<sub>4</sub> is substantially greater than that between the S and Se compounds. It is interesting to note from Table 7 that d-type orbitals on Te have a smaller influence on the stability of Te(CH<sub>3</sub>)<sub>4</sub> (about 50

kJ/mol) than is the case for the corresponding S compound (about 100 kJ/mol). This observation implies that polarization effects are less important for Te than for S; although this may appear surprising, as Te is "softer" than S, the inhomogeneous electric fields about Te in molecular compounds may be expected to be less intense than about S, simply because Te is a larger atom. The orbital model appears to be comparably accurate for Te(CH<sub>3</sub>)<sub>4</sub> and S(CH<sub>3</sub>)<sub>4</sub>; the differences in binding energies calculated at SCF and MP2 levels of theory are about 110 and 90 kJ/mol, respectively, with the PSP basis.

### Conclusions

We have undertaken a systematic theoretical study of the tetramethyl derivatives of the chalcogens S, Se, and Te. All three compounds adopt a C<sub>2v</sub> geometry at equilibrium, based on a trigonal bipyramid with an equatorial lone pair. Steric repulsions due to CH<sub>3</sub> · · CH<sub>3</sub> interactions are pronounced for S(CH<sub>3</sub>)<sub>4</sub> but progressively less important as the size of the central atom increases. Calculated vibrational frequencies are reported. Barriers to Berry pseudorotation decrease from 20 kJ/mol for S(CH<sub>3</sub>)<sub>4</sub> through 15 for Se(CH<sub>3</sub>)<sub>4</sub> to only 3 kJ/mol for Te(CH<sub>3</sub>)<sub>4</sub>. The Te compound is thus exceptionally fluxional, and the concept of an equilibrium structure is perhaps misleading; the flexible nature of this species explains why previous room-temperature

electron diffraction and low-temperature X-ray diffraction experiments obtained rather different bond angles.<sup>12</sup>

All three tetramethyls are thermodynamically unstable with respect to the dimethyl plus ethane, though the instability decreases from about 350 kJ/mol for S(CH<sub>3</sub>)<sub>4</sub> to some 225 kJ/mol for Te(CH<sub>3</sub>)<sub>4</sub>. The contribution of d orbitals to the binding of the tetramethyl compounds is significant but not crucial; in keeping with a recent extensive analysis,<sup>1</sup> the d-type orbitals on S/Se/Te are best considered as polarization functions, whose importance decreases as the central atom becomes larger. Since Te(CH<sub>3</sub>)<sub>4</sub> has recently been prepared, the other tetramethyl chalcogen derivatives seem feasible but challenging synthetic targets.

**Acknowledgment.** We thank the Australian Research Council for financial support and both Melbourne University and Cray Research (Australia) for generous access to supercomputing facilities. B.A.S. thanks Melbourne University for a Melbourne University Postgraduate Award.

**Supporting Information Available:** Tables S1–S8, listing vibrational frequencies, energies, structural parameters, and geometries (5 pages). Ordering information is given on any current masthead page.

OM940821A

# Synthesis, Structural Characterization, and Reactions of [PdPhCl(2,9-dimethyl-1,10-phenanthroline)] with Olefins

Maria E. Cucciolito, Augusto De Renzi,\* Federico Giordano, and Francesco Ruffo

Dipartimento di Chimica, Università degli Studi di Napoli "Federico II",  
Via Mezzocannone 4, I-80134 Napoli, Italy

Received June 19, 1995<sup>®</sup>

Dichlorodiphenyllead(IV) acts, through an oxidative-addition process, as a phenylating reagent on [Pd(N,N-chelate)(olefin)] substrates. The previously unknown [PdPhCl(dmphen)] (dmphen = 2,9-dimethyl-1,10-phenanthroline) compound has been synthesized and characterized by an X-ray structural analysis. The reactions of this complex and of its related cationic species [PdPh(dmphen)(MeCN)]<sup>+</sup> with ethylene and propene have also been studied.

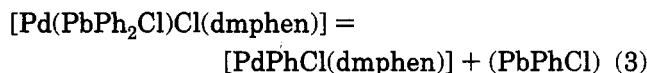
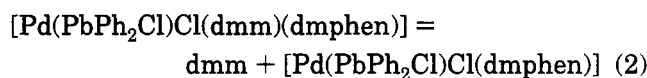
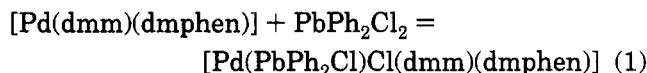
## Introduction

It is proposed<sup>1</sup> that the ability of the 2,9-dimethyl-1,10-phenanthroline (dmphen) to promote the formation of coordinatively saturated trigonal-bipyramidal (tbp) complexes of d<sup>8</sup> ions is related to steric constraints which strongly disfavor the presence of more than one ligand in the (dmphen)M plane. The expected counterpart of this statement is that destabilizing features should be evident in square-planar dmphen-containing complexes and their synthesis should be difficult compared to that of similar compounds with less encumbering N-N ligands. In fact, the X-ray structural analysis of the two square-planar complexes [PdMeCl(dmphen)]<sup>2</sup> and [PtCl<sub>2</sub>(dmphen)]<sup>3</sup> shows that the dmphen and the metal coordination planes are distorted from coplanarity, thus reducing the nitrogen-metal orbital overlap. In addition, in a recent paper<sup>4</sup> some of us have reported a lack of success in the synthesis of the [PdPhI(dmphen)] complex through ligand exchange from the readily available precursor [PdPhI(tmeda)] (tmeda = N,N,N',N'-tetramethyl-1,2-ethanediamine).<sup>5</sup> In contrast, this procedure works well when 1,10-phenanthroline (phen) or 2,2'-bipyridine (bpy) is used.<sup>4,6</sup>

Since Pd(II)-phenyl species are valuable substrates for mechanistic studies of the Heck reaction,<sup>7</sup> we have devised a different synthetic approach that couples the ability of a suitable three-coordinate dmphen-alkene-Pd(0) complex to undergo an oxidative addition<sup>8</sup> with the instability of the resulting five-coordinate species toward olefin release.<sup>9</sup>

## Results and Discussion

**Synthesis and Reactivity.** [Pd(dmm)(dmphen)] (dmm = dimethyl maleate) was selected as the substrate for use with the more simple class B oxidative-addition reagents, *i.e.* phenyl iodide<sup>5</sup> and phenylmercuric halides,<sup>10</sup> that effectively promote the formation of phenyl-metal bonds. Using these reagents, unsatisfactory results were obtained. [PdPhCl(dmphen)] has been successfully synthesized by using PbPh<sub>2</sub>Cl<sub>2</sub>, whose phenylating ability in the chemistry of platinum(II) is already known.<sup>11</sup> A possible reaction path is



Although the formation of the five-coordinate intermediate shown in step 1 is only speculative, it should be noted that the corresponding Pt(II) complex has been isolated and fully characterized.<sup>11</sup> The above procedure can be applied to other [Pd(dmm)(N-N)] compounds (*e.g.*, N-N = phen, bpy) with good results.

[PdPhCl(dmphen)] (A) has been characterized by the usual procedures, and an X-ray structural determination has been undertaken. As it is known<sup>9</sup> that the related [PdMeCl(dmphen)] complex forms five-coordinate olefin adducts whose stability is strongly affected by the presence of substituents on the double bond, attempts to synthesize the analogous phenyl species have been made by using the simple ethylene. Bubbling ethylene in a deuteriochloroform solution of [PdPhCl(dmphen)] at 223 K results in the quantitative formation of the five-coordinate complex [PdPhCl(C<sub>2</sub>H<sub>4</sub>)(dmphen)] (B), as suggested by the <sup>1</sup>H NMR spectrum. This species seems to be inert until 253 K. When the tem-

<sup>®</sup> Abstract published in *Advance ACS Abstracts*, September 15, 1995.

(1) Albano, V. G.; Natile, G.; Panunzi, A. *Coord. Chem. Rev.* **1994**, *133*, 67.

(2) De Felice, V.; Albano, V. G.; Castellari, C.; Cucciolito, M. E.; De Renzi, A. *J. Organomet. Chem.* **1991**, *403*, 269.

(3) Fanizzi, F. P.; Intini, F. P.; Maresca, L.; Natile, G.; Lanfranchi, M.; Tiripicchio, A. *J. Chem. Soc., Dalton Trans.* **1991**, 1007.

(4) De Felice, V.; Cucciolito, M. E.; De Renzi, A.; Ruffo, F.; Tesaro, D. *J. Organomet. Chem.* **1995**, *493*, 1.

(5) de Graaf, W.; van Wegen, J.; Boersma, J.; Spek, A. L.; van Koten, G. *Recl. Trav. Chim. Pays-Bas* **1989**, *108*, 275.

(6) Markies, B. A.; Cauty, A. J.; de Graaf, W.; Boersma, J.; Janssen, M. D.; Hogerheide, M. P.; Smeets, W. J. J.; Spek, A. L.; van Koten, G. *J. Organomet. Chem.* **1994**, *482*, 191.

(7) Brown, J. M.; Pérez-Torrente, J. J.; Alcock, N. W.; Clase, H. *J. Organomet. Chem.* **1995**, *14*, 207 and references therein.

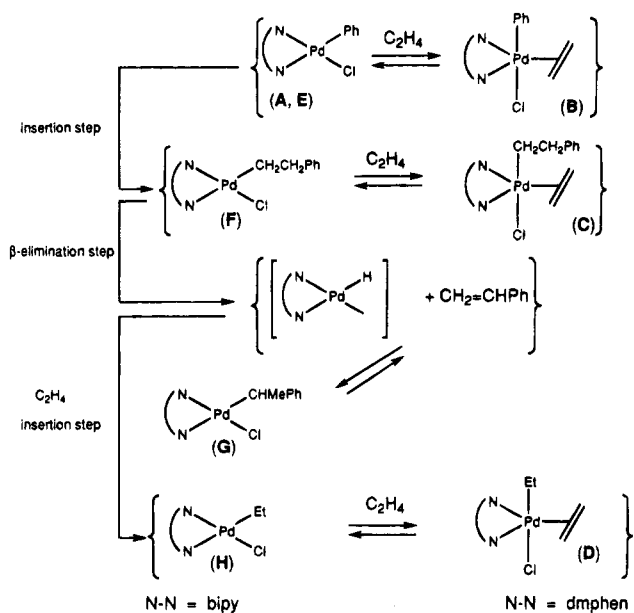
(8) Cucciolito, M. E.; De Felice, V.; Panunzi, A.; Ruffo, F. *Gazz. Chim. Ital.* **1990**, *119*, 461.

(9) Albano, V. G.; Castellari, C.; Cucciolito, M. E.; Panunzi, A.; Vitagliano, A. *Organometallics* **1990**, *9*, 1269.

(10) Sokolov, V. I.; Bashilov, V. V.; Reutov, O. A. *J. Organomet. Chem.* **1975**, *97*, 299.

(11) Albano, V. G.; Castellari, C.; Monari, M.; De Felice, V.; Ferrara, M. L.; Ruffo, F. *Organometallics*, in press.

Scheme 1



perature is raised, a moderately fast insertion process takes place and styrene is formed over time. Comparable amounts of a new five-coordinate complex, identified as  $[\text{PdEtCl}(\text{C}_2\text{H}_4)(\text{dmphen})]$  (**D**), are also observed. This is substantially the only complex present in solution after 1 h. No attempts to isolate **D** in the solid state have been performed, and the ultimate decomposition to palladium black, dmphen-HCl, and  $[\text{PdCl}_2(\text{dmphen})]^{3-}$  is observed on longer standing. This behavior and the inertness of **D** to undergo an insertion process is consistent with what has been reported<sup>4</sup> in the case of the known  $[\text{PdMeCl}(\text{C}_2\text{H}_4)(\text{dmphen})]$  compound. We note that, in the early stages of the reaction, signals attributable to the Pd-CH<sub>2</sub>CH<sub>2</sub>Ph fragment in a five-coordinate environment (**C**) have also been detected. A comprehensive reaction scheme, including a suggested hydrido intermediate, is depicted in Scheme 1.

On the left side of Scheme 1 there are reported for sake of comparison the compounds **F-H**, which are identified in solution when  $[\text{PdPhCl}(\text{bpy})]$  (**E**) is allowed to react with ethylene under the same experimental conditions adopted for **A**. In this case **E** disappears within a few minutes and **F** quantitatively forms. Subsequently **F** gradually decomposes, while increasing amounts of **G** and **H** are formed. The concentration of the former species reaches a maximum and then gradually decreases with time until **H** is the predominant species detected in solution. The whole process requires more than 24 h for completion.

When the behavior of **A** is compared with that of the corresponding bpy derivative **E**, three main differences should be noted:

(i) Only coordinatively unsaturated species (**F-H**) are detected as products from **E**, while only 18e compounds (**B-D**) are identified as products from **A**. This is easily explained on the grounds<sup>1</sup> of previous observations concerning the role of the "in plane" steric hindrance of the N-N chelate.

(ii) The time required for the reaction completion is longer (more than 24 vs 1 h) in the case where the starting substrate is **E**. More precisely, by inspection of the <sup>1</sup>H NMR spectra recorded with time, it appears

**Table 1. Composition (%) of the Mixture of the Organic Products from the Reaction between Propene and  $[\text{PdPh}(\text{N-N})(\text{L})]^{0/+}$  Complexes**

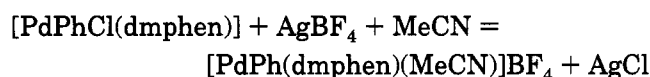
complex	CH <sub>2</sub> =CMePh	( <i>E</i> )-MeCH=CHPh
$[\text{PdPhCl}(\text{dmphen})]$	24	76
$[\text{PdPhCl}(\text{bpy})]$	50	50
$[\text{PdPh}(\text{dmphen})(\text{MeCN})]^{+}$	82	18
$[\text{PdPh}(\text{bpy})(\text{MeCN})]^{+}$ <sup>a</sup>	<5	>95

<sup>a</sup> See reference 4.

that insertion is the fastest step in the case of the bpy substrate, while in the case of the dmphen species the styrene release occurs more rapidly. The former observation should be related to the steric "in plane" constraints of dmphen, which moderately stabilize the five-coordinate ethylene adduct **B**, thus disfavoring the insertion, which requires a square-planar geometry.<sup>12</sup> As for the second observation, once the (dmphen)Pd-CH<sub>2</sub>CH<sub>2</sub>Ph fragment is formed, the same steric factors should favor its irreversible decomposition.

(iii) A bpy species (**G**), including a secondary carbon σ-bound to the metal, occurs in substantial amount, while a corresponding dmphen compound was not detected. In our opinion this result can be related to the above-noted difference in the insertion rate between the dmphen and bpy substrates. In the former case the ethylene substitutes the styrene before the α-olefin inserts and **D** is ultimately formed. In contrast, a relatively fast β-elimination/hydride insertion equilibrium should be involved in the case of the bpy ligand, allowing the formation of the Pd-CHMePh fragment, notwithstanding the presence of excess free ethylene. This β-phenethyl/α-phenethyl isomerization has already<sup>4</sup> been observed and attributed to a stabilizing η<sup>3</sup> transient interaction of Pd with the organic moiety.

The cationic species  $[\text{PdPh}(\text{dmphen})(\text{MeCN})]^{+}$  (**A**<sup>+</sup>) has been synthesized by chlorine abstraction with AgBF<sub>4</sub> from the parent neutral complex



and reacted with ethylene in CD<sub>3</sub>NO<sub>2</sub>. Styrene immediately forms, and a cationic Pd-Et compound is detected in solution. The fate of this latter species, involving the subsequent formation of (*E*)-2-butene, shows no differences with what was already reported<sup>4</sup> in the case of a similar reaction of the  $[\text{PdPh}(\text{bpy})(\text{MeCN})]^{+}$  complex.

Propene has also been reacted at room temperature with both  $[\text{PdPhCl}(\text{dmphen})]$  and  $[\text{PdPh}(\text{dmphen})(\text{MeCN})]^{+}$ . When the neutral substrate is used, the reaction goes to completion within 4 h and a nearly 4:1 mixture of (*E*)-β- and α-methylstyrene is obtained. A quite fast formation of these two organic products in the reverse ratio is instead observed by reacting the corresponding cationic complex. A comparison with the results obtained for the related Pd-Ph/bpy compounds is reported in Table 1.

A rationale of the results concerning the behavior of the neutral Pd substrates seems difficult. The low reaction rate, the presence in the reaction mixture of some unidentifiable Pd species, and the partial formation of palladium black give rise to the possibility of



**Table 2. Fractional Atomic Coordinates and Equivalent Isotropic Thermal Parameters ( $\text{\AA}^2$ ) of the Non-Hydrogen Atoms with their Esd's in Parentheses**

	<i>x</i>	<i>y</i>	<i>z</i>	$B_{\text{eq}}^a$
Pd(1)	0.85428(4)	0.05464(2)	0.37407(2)	3.02(1)
Cl(1)	1.0473(1)	0.0266(1)	0.3365(1)	4.95(3)
N(1)	0.6727(4)	0.0773(3)	0.4015(2)	3.24(9)
N(2)	0.8044(4)	-0.0527(2)	0.4163(2)	3.45(9)
C(1)	0.6119(5)	0.1407(3)	0.4086(2)	3.7(1)
C(2)	0.4775(6)	0.1433(4)	0.4076(3)	4.5(1)
C(3)	0.4056(5)	0.0813(4)	0.4021(3)	4.7(1)
C(4)	0.4672(5)	0.0123(4)	0.4020(3)	4.0(1)
C(5)	0.4012(6)	-0.0565(4)	0.4047(3)	4.9(1)
C(6)	0.4653(6)	-0.1201(4)	0.4117(3)	4.9(1)
C(7)	0.6049(6)	-0.1214(3)	0.4173(3)	4.2(1)
C(8)	0.6772(7)	-0.1863(4)	0.4310(4)	5.5(2)
C(9)	0.8090(8)	-0.1828(4)	0.4392(4)	5.8(2)
C(10)	0.8716(6)	-0.1147(3)	0.4320(3)	4.4(1)
C(11)	0.6729(5)	-0.0555(3)	0.4110(3)	3.5(1)
C(12)	0.6029(5)	0.0124(3)	0.4028(3)	3.4(1)
C(13)	0.6869(6)	0.2115(3)	0.4209(3)	4.5(1)
C(14)	1.0178(7)	-0.1122(4)	0.4435(4)	5.5(2)
C(15)	0.8681(5)	0.1493(3)	0.3241(3)	3.2(1)
C(16)	0.9673(5)	0.1996(3)	0.3463(3)	4.1(1)
C(17)	0.9706(6)	0.2665(4)	0.3115(4)	5.1(1)
C(18)	0.8753(7)	0.2854(4)	0.2543(4)	5.4(2)
C(19)	0.7777(6)	0.2353(4)	0.2312(3)	4.8(1)
C(20)	0.7732(5)	0.1675(3)	0.2662(3)	3.8(1)
Pd(1')	0.36351(3)	0.10710(2)	0.00118(2)	2.76(1)
Cl(1')	0.5540(1)	0.1625(1)	0.0547(1)	3.91(3)
N(1')	0.1830(4)	0.0693(2)	-0.0478(2)	2.85(8)
N(2')	0.2601(4)	0.1045(2)	0.0933(2)	3.06(8)
C(1')	0.1441(5)	0.0389(3)	-0.1119(3)	3.4(1)
C(2')	0.0118(6)	0.0397(3)	-0.1438(3)	4.3(1)
C(3')	-0.0787(6)	0.0698(3)	-0.1087(3)	4.2(1)
C(4')	-0.0417(5)	0.0971(3)	-0.0390(3)	3.7(1)
C(5')	-0.1319(5)	0.1262(3)	0.0028(3)	4.2(1)
C(6')	-0.0927(5)	0.1461(3)	0.0710(3)	4.5(1)
C(7')	0.0387(5)	0.1377(3)	0.1058(3)	3.6(1)
C(8')	0.0809(5)	0.1482(4)	0.1795(3)	4.4(1)
C(9')	0.2076(6)	0.1343(4)	0.2083(3)	4.4(1)
C(10')	0.2975(5)	0.1135(3)	0.1642(3)	3.8(1)
C(11')	0.1324(5)	0.1141(3)	0.0647(3)	3.0(1)
C(12')	0.0910(5)	0.0948(3)	-0.0091(3)	2.9(1)
C(13')	0.2390(6)	0.0005(3)	-0.1511(3)	4.5(1)
C(14')	0.4355(6)	0.1009(4)	0.1969(3)	5.3(2)
C(15')	0.4214(5)	0.1263(3)	-0.0914(3)	3.4(1)
C(16')	0.5261(5)	0.0920(4)	-0.1130(3)	4.5(1)
C(17')	0.5563(6)	0.1063(5)	-0.1810(3)	6.5(2)
C(18')	0.4823(7)	0.1543(5)	-0.2274(3)	7.6(2)
C(19')	0.3793(8)	0.1887(4)	-0.2064(4)	6.2(2)
C(20')	0.3478(6)	0.1756(3)	-0.1383(3)	4.3(1)

$$^a B_{\text{eq}} = \frac{1}{3} \sum_i \sum_j \beta_{ij} \mathbf{a}_i \cdot \mathbf{a}_j$$

different reaction paths with different reactive intermediates. Thus, the final organic product composition could be the result of several competing mechanisms.

The figures referring to the two cationic complexes indicate a substantial inversion of the regiochemical control on going from bpy to the more crowded dmphen. Conceivably, the reactive intermediate is a square-planar species of the type  $[\text{PdPh}(\text{MeCH}=\text{CH}_2)(\text{N}-\text{N})]^+$  with an equatorial double bond, propitious to the attainment of a four-center transition state.<sup>12</sup> Thus, the preferred phenyl addition on the unsubstituted carbon  $C_\alpha$  in the bpy species could be the consequence of unfavorable Me-Ph interactions and of the lack of steric hindrance toward the formation of a Pd-C $_\beta$  bond. The presence of the 2,9-substituents in dmphen acts, to some extent, in the opposite direction. Thus, a preference toward the formation of an intermediate containing a Pd-C bond with the less substituted carbon atom is observed. However, loss of regioselectivity is observed

**Table 3. Geometric Parameters with Their Esd's in Parentheses in the Coordination Sphere of Pd**

	unprimed molecule	primed molecule
Bond Lengths ( $\text{\AA}$ )		
Pd(1)-Cl(1)	2.306(1)	2.304(1)
Pd(1)-N(1)	2.092(4)	2.070(4)
Pd(1)-N(2)	2.200(5)	2.195(4)
Pd(1)-C(15)	1.976(5)	1.972(5)
Bond Angles (deg)		
Cl(1)-Pd(1)-N(1)	176.1(1)	173.4(1)
Cl(1)-Pd(1)-N(2)	100.9(1)	99.7(1)
Cl(1)-Pd(1)-C(15)	84.7(1)	86.4(2)
N(1)-Pd(1)-N(2)	78.7(2)	79.1(2)
N(1)-Pd(1)-C(15)	95.1(2)	93.4(2)
N(2)-Pd(1)-C(15)	169.5(2)	165.7(2)
Shortest Intramolecular Contacts ( $\text{\AA}$ )		
Cl(1)⋯C(14)	3.27(1)	3.33(1)
Cl(1)⋯C(15)	2.89(1)	2.94(1)
C(13)⋯C(15)	3.06(2)	3.06(2)
C(13)⋯C(16)	3.47(2)	3.40(2)
C(13)⋯C(20)	3.29(2)	3.37(2)
Distances ( $\text{\AA}$ ) from the N(1)-Pd(1)-N(2) Plane		
C(13)	-1.02(1)	-1.06(1)
C(14)	-0.79(1)	-0.84(1)
Cl	0.154(4)	0.261(4)
C(15)	0.29(1)	0.42(1)
C(18)	0.73(1)	1.09(1)
Interplanar Angles (deg)		
N(1)-Pd(1)-N(2)/ N(1)-C(12)-C(11)-N(2)	24.4(1)	29.8(1)
N(1)-Pd(1)-N(2)/phenyl	60.4(2)	60.7(2)

in the whole process. It should be noted that when  $[\text{PdMe}(\text{dmphen})(\text{MeCN})]^+$  has been reacted with styrene, only (*E*)- $\beta$ -methylstyrene has been detected as an organic product.<sup>4</sup> Therefore, a complex combination of electronic and steric factors are involved in determining the regiochemical control.

**X-ray Structure of  $[\text{PdPhCl}(\text{dmphen})]$ .** The asymmetric unit of the crystal contains two independent molecules whose final atomic coordinates are listed in Table 2. Corresponding values of bond lengths and angles in the two molecules fit very closely. The most relevant of them are presented in Table 3. The Pd-C(phenyl) distances agree well with those reported in the literature for comparable complexes,<sup>5,6,13</sup> while the patterns of Pd-N and Pd-Cl distances parallel closely that found in the structure of  $[\text{PdMeCl}(\text{dmphen})]$ .<sup>2</sup>

Both molecules display distortions in the square-planar coordination geometry, owing to the crowding in the coordination plane. The crucial van der Waals intramolecular contacts involve the two methyl groups of the dmphen ligand, the chlorine atom, and the coordination point of the phenyl group and are listed in Table 3. The distortions are of the same kind in both molecules, and the differences, which are significant, are an effect of the crystalline field. Figure 1 gives a perspective view of the primed molecule, where the repulsive van der Waals contacts are slightly less hard and the distortions slightly more marked.

The crowding is responsible for the following effects.

(i) The coordination plane is ill-definable, as Pd and the coordinated atoms poorly satisfy the planarity condition. In fact, in both molecules the values of  $\chi^2$  distribution are very large. We have taken the N-Pd-N plane as the coordination plane and reported in Table

(13) Canty, A. J.; Jin, H.; Roberts, A. S.; Traill, P. R.; Skelton, B. W.; White, A. H. *J. Organomet. Chem.* **1995**, *489*, 153.



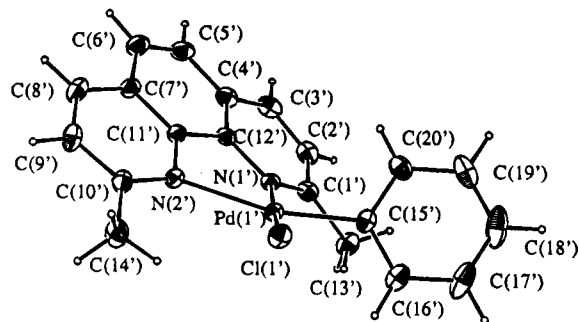


**Figure 1.** View of the molecular structure of [PdPhCl(dmphen)].

3 the main atomic distances from it. Their distribution indicates clearly the methyl groups, and mainly C(13), as the sources of the strain. Moreover, phenyl turns out to be the most stressed coordinated group. In fact, C(15) is displaced as much as 0.29(1) and 0.42(1) Å, in the unprimed and primed molecules, respectively, out of the plane on the side opposite the methyl groups. The C(15)–C(18) vector is inclined with respect to the N–Pd–N plane by 8.9(2) and 13.9(2)°, while the phenyl plane forms with the same plane dihedral angles of 60.4(2) and 60.7(2)° for the unprimed and primed molecules, respectively.

(ii) The dmphen ligand, under the action of contrasting forces, attractive on the N atoms and repulsive on the methyl groups, is forced to bend, so that it loses its intrinsic planarity and takes a slightly convex lens like conformation. The same effect was observed in other crowded coordination complexes of dmphen.<sup>2,3</sup>

Moreover, the dmphen ligand is remarkably rotated with respect to the coordination plane. In fact, the dihedral angles between the N–Pd–N plane and the chelating fragment N(1)–C(12)–C(11)–N(2) are 24.6(3) and 29.6(3)° for the unprimed and primed molecules, respectively. These values are comparable with those found (31.3(3) and 27.5(5)°)<sup>14</sup> in the structures of [Pd-MeCl(dmphen)]<sup>2</sup> and [PtCl<sub>2</sub>(dmphen)]<sup>3</sup> respectively.

(iii) The Cl–Pd–C(phenyl) and N(2)–Pd–C(phenyl) angles are narrowed from the theoretical values of 90 and 180° to 84.7(1) and 86.4(2)° in the first case, and to 169.5(2) and 165.7(2)° in the second case, for the unprimed and primed molecules, respectively.

## Experimental Section

<sup>1</sup>H NMR spectra have been recorded at 400, 270, or 200 MHz on a Bruker AM-400, a Bruker AC-270, or a Varian XL-200 spectrometer, respectively. Unless otherwise stated, the spectra have been recorded at 298 K. <sup>1</sup>H NMR chemical shifts are reported in δ (ppm) relative to the solvent (CHCl<sub>3</sub>, 7.26 ppm; CHD<sub>2</sub>NO<sub>2</sub>, 4.33 ppm). The following abbreviations are used in descriptions of NMR multiplicities: s, singlet; d, doublet; t, triplet; q, quartet; m, multiplet; app, apparent; br, broadened. [PdPh(bpy)(MeCN)]BF<sub>4</sub><sup>4</sup> and PbPh<sub>2</sub>Cl<sub>2</sub><sup>15</sup> have been prepared according to literature methods. Solvents and reagents were of AnalR grade and were

(14) In order to obtain a homogeneous comparison, the values refer to the dihedral angle between the N(1)–M–N(2) plane and the corresponding N(1)–C(12)–C(11)–N(2) plane. When a different choice was made,<sup>2</sup> the indicated figure was calculated from the proper atomic coordinates reported in the paper.

(15) Lieber, E.; Keane, F. M. *Inorg. Synth.* **1966**, *8*, 57.

used without further purification. All the isolated compounds gave satisfactory elemental analyses.

**Synthesis of [Pd(dmm)(N-N)] (N-N = dmphen, bpy, phen).** The title complexes have been synthesized in 60–65% yield by properly adapting the procedure described for related [Pd(N-N)(olefin)] species.<sup>8</sup> <sup>1</sup>H NMR (CDCl<sub>3</sub>) and analytical data are as follows.

[Pd(dmm)(dmphen)]: δ 8.22 (d, 2H, 4- and 7-H-dmphen), 7.74 (s, 2H, 5- and 6-H-dmphen), 7.64 (d, 2H, 3- and 8-H-dmphen), 3.65 (s, 6H, OMe), 3.52 (s, 2H, CH=CH), 3.08 (s, 6H, Me-dmphen) ppm. Anal. Calcd for C<sub>20</sub>H<sub>20</sub>N<sub>2</sub>O<sub>4</sub>Pd: C, 52.36; H, 4.39; N, 6.11. Found: C, 52.01; H, 4.46; N, 6.28.

[Pd(dmm)(bpy)]: 8.99 (d, 2H, 6- and 6'-H-bpy), 8.03 (d, 2H, 3- and 3'-H-bpy), 7.94 (t, 2H), 7.45 (t, 2H), 3.70 (s, 6H, OMe), 3.43 (s, 2H, CH=CH) ppm. Anal. Calcd for C<sub>16</sub>H<sub>16</sub>N<sub>2</sub>O<sub>4</sub>Pd: C, 47.25; H, 3.97; N, 6.89. Found: C, 47.18; H, 3.91; N, 6.78.

[Pd(dmm)(phen)]: 9.28 (dd, 2H, 2- and 9-H-phen), 8.39 (dd, 2H, 4- and 7-H-phen), 7.88 (s, 2H, 5- and 6-H-phen), 7.78 (dd, 2H, 3- and 8-H-phen), 3.73 (s, 6H, OMe), 3.55 (s, 2H, CH=CH) ppm. Anal. Calcd for C<sub>18</sub>H<sub>16</sub>N<sub>2</sub>O<sub>4</sub>Pd: C, 50.19; H, 3.74; N, 6.50. Found: C, 50.29; H, 3.76; N, 6.58.

**Synthesis of [PdPhCl(N-N)] (N-N = dmphen, bpy, phen).** A fresh solution of [Pd(dmm)(N-N)] (0.33 mmol) in 8 mL of chloroform (methylene chloride when N-N = phen) is rapidly added with stirring to solid PbPh<sub>2</sub>Cl<sub>2</sub> (0.14 g, 0.33 mmol). After 10 min the dark suspension is filtered through Celite and the residue extracted with chloroform (2 × 6 mL). The combined filtrates are dried under vacuum. The light brown residue is dissolved in chloroform, and the volume of the filtered yellow solution is reduced to ca. 1 mL under vacuum. Pale yellow crystals of the product are obtained by careful addition of diethyl ether (65–70% yield). <sup>1</sup>H NMR (CDCl<sub>3</sub>) and analytical data are as follows:

[PdPhCl(dmphen)]: 8.25 (d, 2H, 4- and 7-H-dmphen), 7.61 (s, 2H, 5- and 6-H-dmphen), 7.50 (br, 2H, 3- and 8-H-dmphen), 7.02 (m, 2H, Ph), 6.65 (m, 3H, Ph), 3.28 (br, 3H, Me), 2.07 (br, 3H, Me) ppm; at 223 K, 8.30 (d, 1H), 8.26 (d, 1H), 7.85 (AB q, 2H), 7.58 (d, 1H), 7.46 (d, 1H), 7.05 (m, 2H, Ph), 6.89 (m, 3H, Ph), 3.23 (s, 3H, Me), 2.00 (s, 3H, Me) ppm. Anal. Calcd for C<sub>20</sub>H<sub>17</sub>ClN<sub>2</sub>Pd: C, 56.23; H, 4.01; N, 6.56. Found: C, 56.21; H, 4.04; N, 6.61.

[PdPhCl(bpy)]: 9.26 (d, 1H), 8.15–7.92 (m, 5H), 7.55 (m, 1H), 7.42 (d, 2H, Ph), 7.31 (m, 1H), 7.13–6.92 (m, 3H, Ph) ppm. Anal. Calcd for C<sub>16</sub>H<sub>13</sub>ClN<sub>2</sub>Pd: C, 51.23; H, 3.49; N, 7.47. Found: C, 51.32; H, 3.46; N, 7.55.

[PdPhCl(phen)]: 9.54 (d, 1H), 8.50 (d, 1H), 8.47 (d, 1H), 8.35 (d, 1H), 7.97 (AB q, 2H), 7.90 (dd, 1H), 7.65 (dd, 1H), 7.52 (d, 2H, Ph), 7.13 (t, 2H, Ph), 7.03 (m, 1H, Ph) ppm. Anal. Calcd for C<sub>18</sub>H<sub>13</sub>ClN<sub>2</sub>Pd: C, 54.16; H, 3.28; N, 7.02. Found: C, 54.13; H, 3.24; N, 6.96.

**Synthesis of [PdPh(dmphen)(MeCN)]BF<sub>4</sub>.** A solution of AgBF<sub>4</sub> (0.045 g, 0.23 mmol) in 2 mL of acetonitrile is added at 273 K to [PdPhCl(dmphen)] (0.10 g, 0.23 mmol) dissolved in 5 mL of dichloromethane under nitrogen. After 10 min of stirring AgCl is removed by filtration and the solvent is removed under vacuum. The product is obtained as a yellow-orange glassy solid (0.11 g, 90% yield). <sup>1</sup>H NMR (CD<sub>3</sub>NO<sub>2</sub>) and analytical data: 8.58 (d, 2H, 4- and 7-H-dmphen), 8.07

(s, 2H, 5- and 6-H-dmphen), 7.77 (d, 2H, 3- and 8-H-dmphen), 7.04 (m, 5H, Ph), 2.60 (br, 6H, Me-dmphen), 2.43 (s, 3H, MeCN) ppm. Anal. Calcd for  $C_{22}H_{20}BF_4N_3$ -Pd: C, 50.85; H, 3.88; N, 8.09. Found: C, 50.74; H, 3.99; N, 8.00.

**Monitoring of the Reactions between [PdPhCl(N-N)] (N-N = dmphen (A), bpy (E)) or [PdPh(dmphen)(MeCN)]BF<sub>4</sub> (A<sup>+</sup>) and the Olefins through <sup>1</sup>H NMR Spectroscopy.** NMR samples are obtained by dissolving 0.015–0.020 g of the complexes in ca. 1 mL of deuterated solvent (CDCl<sub>3</sub> and CD<sub>3</sub>NO<sub>2</sub> for neutral and cationic substrates, respectively). An excess of the appropriate olefin is bubbled through the solution, and the NMR spectra of the reaction mixture are recorded until no more chemical changes are detected. The organic products (styrene and α- and β-methylstyrene) have been identified by comparing the <sup>1</sup>H NMR spectra of the reaction mixtures with spectra of authentic samples in the same solvent at a comparable concentration.

**[PdPhCl(dmphen)] and Ethylene.** <sup>1</sup>H NMR data are as follows.

[PdPhCl(dmphen)(C<sub>2</sub>H<sub>4</sub>)] (223 K) (B): 8.21 (d, 2H, 4- and 7-H-dmphen), 7.78 (d, 2 H, 3- and 8-H-dmphen), 7.65 (s, 2 H, 5- and 6-H-dmphen), 6.80 (m, 2H, Ph), 6.61 (m, 3H, Ph), 4.70 (app d, 2H, CHH=CHH), 3.78 (app d, 2H, CHH=CHH), 3.66 (s, 6H, Me) ppm.

[Pd(CH<sub>2</sub>CH<sub>2</sub>Ph)Cl(dmphen)(C<sub>2</sub>H<sub>4</sub>)] (223 K) (C): 4.45 (app d, CHH=CHH), 3.52 (app d, CHH=CHH), 1.88 (m, CH<sub>2</sub>CH<sub>2</sub>Ph), 1.42 (m, CH<sub>2</sub>CH<sub>2</sub>Ph) ppm.

[PdEtCl(dmphen)(C<sub>2</sub>H<sub>4</sub>)] (D): 8.26 (d, 2H, 4- and 7-H-dmphen), 7.79 (s, 2H, 5- and 6-H-dmphen), 7.69 (d, 2H, 3- and 8-H-dmphen), 4.39 (app d, 2H, CHH=CHH), 3.42 (app d, 2H, CHH=CHH), 3.37 (s, 6 H, Me-dmphen), 1.34 (q, 2H, CH<sub>2</sub>CH<sub>3</sub>), 0.13 (t, 3 H, CH<sub>2</sub>CH<sub>3</sub>) ppm.

**[PdPhCl(bpy)] and Ethylene.** <sup>1</sup>H NMR data are as follows.

[Pd(CH<sub>2</sub>CH<sub>2</sub>Ph)Cl(bpy)] (F): 9.22 (d, 1H), 8.52 (d, 1H), 8.15–7.90 (m, 4H), 7.60–7.10 (m, 7H), 2.85 (t, 2H, CH<sub>2</sub>CH<sub>2</sub>Ph), 2.24 (t, 2H, CH<sub>2</sub>CH<sub>2</sub>Ph) ppm.

[Pd(CHMePh)Cl(bpy)] (G): identified by comparison with literature data.<sup>4</sup>

[PdEtCl(bpy)] (H): 2.06 (q, CH<sub>2</sub>CH<sub>3</sub>); 0.92 (t, CH<sub>2</sub>CH<sub>3</sub>) ppm; see also the analogy with the spectrum of [PdEtI(bpy)].<sup>16</sup>

**X-ray Structure Determination of [PdPhCl(dmphen)].** Details of the structure analysis are listed in Table 4. The compound was recrystallized from a mixture of methylene chloride and *n*-pentane at 277 K. X-ray data were collected at room temperature on an Enraf-Nonius CAD4-F automatic diffractometer using Mo Kα graphite-monochromated radiation and operating in the ω/θ scan mode. The unit cell parameters were obtained by a least-squares fitting of the setting values of 25 strong reflections in the θ range 11 ≤ θ ≤ 14°. Three monitoring reflections, measured every 500 re-

**Table 4. Summary of Crystallographic Data**

cryst size/mm	0.20 × 0.30 × 0.40
formula	PdClN <sub>2</sub> C <sub>20</sub> H <sub>17</sub>
fw	427.2
cryst syst	monoclinic
space group	P2 <sub>1</sub> /c
a/Å	10.456(4)
b/Å	18.148(9)
c/Å	18.828(9)
β/deg	99.83(2)
V/Å <sup>3</sup>	3520(5)
Z	8 (2 molecules per asym unit)
F(000)	1712
D <sub>c</sub> /g cm <sup>-3</sup>	1.61
λ(Mo Kα)/Å	0.710 73
θ <sub>max</sub> /deg	26
μ/cm <sup>-1</sup>	12.0
no. of indep rflns	6883
no. of rflns above 3σ(I)	4817
no. of refined params	433
goodness of fit	1.038
R	0.037
R <sub>w</sub>	0.044

flections, showed insignificant intensity fluctuations. The structure was solved by routine application of the Patterson and Fourier techniques. The full-matrix least-squares refinement minimized the quantity  $\sum w(\Delta F)^2$ , with  $w^{-1} = \sigma^2(F_o) + (0.02F_o)^2 + 0.1$ , where  $\sigma$  is derived from counting statistics. All non-hydrogen atoms were refined anisotropically. The H atoms were added at their geometrically calculated positions with isotropic thermal parameters 1.2 times larger than the  $B_{eq}$  values of the carrier atoms and held fixed during the last refinement. A correction for absorption effects was applied according to Walker and Stuart,<sup>17</sup> by using the computer program DIFABS (maximum and minimum values of the absorption correction were 1.1 and 0.8). The final Fourier difference map was within ±0.59 e Å<sup>-3</sup>. Neutral atomic scattering factors were taken from the literature.<sup>18</sup> All calculations were performed with the Enraf-Nonius (SDP) set of programs.<sup>19</sup>

**Acknowledgment.** We thank the Consiglio Nazionale delle Ricerche and MURST for financial support and the Centro Interdipartimentale di Metodologie Chimico-Fisiche, Università di Napoli "Federico II", for X-ray and NMR facilities.

**Supporting Information Available:** Lists of bond distances and angles, hydrogen atom parameters, and anisotropic thermal parameters of the non-hydrogen atoms for [PdPhCl(dmphen)] (4 pages). Ordering information is given on any current masthead page.

OM9504720

(17) Walker, N.; Stuart, D. *Acta Crystallogr.* **1983**, A39, 158.

(18) *International Tables for X-ray Crystallography*; Kynoch Press: Birmingham, U.K., 1984; Vol. IV.

(19) B. A. Frenz & Associates, Inc., Structure Determination Package (SDP), College Station, TX, and Enraf-Nonius, Delft, The Netherlands, 1982.

(16) Byers, P. K.; Canty, A. J.; Traill, P. R.; Watson, A. A. *J. Organomet. Chem.* **1990**, 390, 399.

# Synthesis and Structure of Pyrazole-Containing Ferrocenyl Ligands for Asymmetric Catalysis

Urs Burckhardt, Lukas Hintermann, Anita Schnyder, and Antonio Togni\*

Laboratory of Inorganic Chemistry, Swiss Federal Institute of Technology, ETH-Zentrum, CH-8092 Zürich, Switzerland

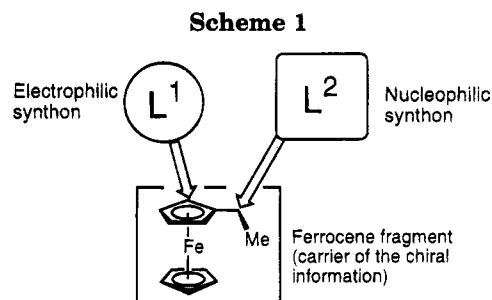
Received June 20, 1995<sup>®</sup>

A series of new chiral ferrocenyl chelating ligands containing a tertiary phosphine and a pyrazole moiety (**3**) have been obtained in moderate to good yields from the reaction of the corresponding phosphinoferochenyl amine derivatives **1a–k** with the 1*H*-pyrazoles **2a–w** in acetic acid at temperatures between 70 and 90 °C. For unsymmetrically substituted pyrazoles a remarkable site selectivity is observed, leading in most cases to only one regioisomer. Six compounds have been characterized by X-ray diffraction and were found to display very similar conformational features.

## Introduction

Progress in asymmetric catalysis relies on the design of new chiral ligands, an important aspect in this regard being the synthetic versatility of the system chosen. We have been interested in chelating ferrocenyl ligands,<sup>1</sup> because they offer the unique opportunity of varying the nature of the two ligating moieties attached to the same cp ring independently from one another.<sup>2</sup> As shown in Scheme 1, the assembly of these ligands requires two consecutive synthetic steps, the first utilizing an electrophilic and the second a nucleophilic ligand synthon.

In recent years important developments in asymmetric catalysis have been achieved by using nitrogen-containing ligands.<sup>3</sup> In particular, the combination of nitrogen and phosphorus donor atoms has led to highly selective palladium catalysts for allylic substitution reactions.<sup>4</sup> Moreover, the coordination chemistry of the pyrazolyl fragment, most often as imbedded in a tris-(pyrazolyl)hydroborate, has been thoroughly investigated over the past two decades.<sup>5</sup> However, reports on the incorporation of this heterocycle into chiral ligands



as well as applications to homogeneous catalysis are still quite rare.<sup>6</sup> This is somewhat surprising, since this kind of derivative is synthetically easily accessible, and the substitution pattern of the five-membered ring can be varied virtually with no restrictions.

We recently reported the successful application of some novel pyrazole-containing ferrocenylphosphines in the asymmetric rhodium-catalyzed hydroboration of styrene with catecholborane.<sup>2f</sup> Our new ligands have been shown to afford the highest known enantioselectivities for this particular reaction. Furthermore, they were found to exhibit a pronounced electronic effect on stereoselectivity, depending on the nature of the pyrazole substituents. In this paper we present full experimental details for the preparation, characterization, and structure of this new class of ligands.

## Results and Discussion

**Synthesis.** A series of pyrazole ligands has been obtained from the reaction of a dimethyl{1-[2-(phosphino)ferrocenyl]ethyl}amine (**1a–k**) and the corresponding 1*H*-pyrazole (**2a–w**), as illustrated in Scheme 2. This S<sub>N</sub>1-like substitution reaction is carried out in acetic acid at temperatures between 70 and 90 °C over 3–7 h and occurs (via a ferrocenyl carbocationic intermediate) with retention of configuration at the stereo-

(6) (a) Bovens, M.; Togni, A.; Venanzi, L. M. *J. Organomet. Chem.* **1993**, *451*, C28–C31. (b) Tokar, C. J.; Kettler, P. B.; Tolman, W. B. *Organometallics* **1992**, *11*, 2737–2739. (c) LeCloux, D. D.; Tolman, W. B. *J. Am. Chem. Soc.* **1993**, *115*, 1153–1154. (d) LeCloux, D. D.; Tokar, C. J.; Osawa, M.; Houser, R. P.; Keyes, M. C.; Tolman, W. B. *Organometallics* **1994**, *13*, 2855–2866. (e) Christenson, D. L.; Tokar, C. J.; Tolman, W. B. *Organometallics* **1995**, *14*, 2148–2150.

<sup>®</sup> Abstract published in *Advance ACS Abstracts*, October 1, 1995.

(1) For reviews, see: (a) Hayashi, T. In *Ferrocenes: Homogeneous Catalysis, Organic Synthesis, Materials Science*; Togni, A., Hayashi, T., Eds.; VCH: Weinheim, Germany, 1995; pp 105–142. (b) Sawamura, M.; Ito, Y. *Chem. Rev.* **1992**, *92*, 857–871. See also: (c) Hayashi, T.; Mise, T.; Fukushima, M.; Kagotani, M.; Nagashima, N.; Hamada, Y.; Matsumoto, A.; Kawakami, S.; Konishi, M.; Yamamoto, K.; Kumada, M. *Bull. Chem. Soc. Jpn.* **1980**, *53*, 1138–1151.

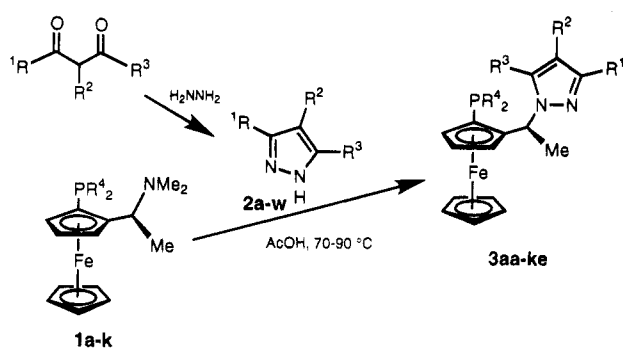
(2) (a) Togni, A.; Breutel, C.; Schnyder, A.; Spindler, F.; Landert, H.; Tijani, A. *J. Am. Chem. Soc.* **1994**, *116*, 4062–4066. (b) Breutel, C.; Pregosin, P. S.; Salzmänn, R.; Togni, A. *J. Am. Chem. Soc.* **1994**, *116*, 4067–4068. (c) Togni, A.; Breutel, C.; Soares, M. C.; Zanetti, N.; Gerfin, T.; Gramlich, V.; Spindler, F.; Rihs, G. *Inorg. Chim. Acta* **1994**, *222*, 213–224. (d) Abbenhuis, H. C. L.; Burckhardt, U.; Gramlich, V.; Togni, A.; Albinati, A.; Müller, B. *Organometallics* **1994**, *13*, 4481–4493. (e) Abbenhuis, H. C. L.; Burckhardt, U.; Gramlich, V.; Köllner, C.; Pregosin, P. S.; Salzmänn, R.; Togni, A. *Organometallics* **1995**, *14*, 759–766. (f) Schnyder, A.; Hintermann, L.; Togni, A. *Angew. Chem.* **1995**, *107*, 996–998; *Angew. Chem., Int. Ed. Engl.* **1995**, *34*, 931–933.

(3) For a recent review, see: Togni, A.; Venanzi, L. M. *Angew. Chem.* **1994**, *106*, 517–547; *Angew. Chem., Int. Ed. Engl.* **1994**, *33*, 497–526.

(4) For successful chiral P,N-ligands recently reported, see: (a) von Matt, P.; Pfaltz, A. *Angew. Chem.* **1993**, *105*, 614–615; *Angew. Chem., Int. Ed. Engl.* **1993**, *32*, 566–567. (b) von Matt, P.; Loiseleur, O.; Koch, G.; Pfaltz, A.; Lefeber, C.; Feucht, T.; Helmchen, G. *Tetrahedron: Asymmetry* **1994**, *5*, 573–584. (c) Sprinz, J.; Helmchen, G. *Tetrahedron Lett.* **1993**, *34*, 1769–1772. (d) Sprinz, J.; Kiefer, M.; Helmchen, G.; Reggelin, M.; Hüttner, G.; Walter, O.; Zsolnai, L. *Tetrahedron Lett.* **1994**, *35*, 1523–1526.

(5) See, e.g.: (a) Trofimenko, S. *Chem. Rev.* **1993**, *93*, 943–980. (b) Trofimenko, S. *Prog. Inorg. Chem.* **1986**, *34*, 115–210.

Scheme 2

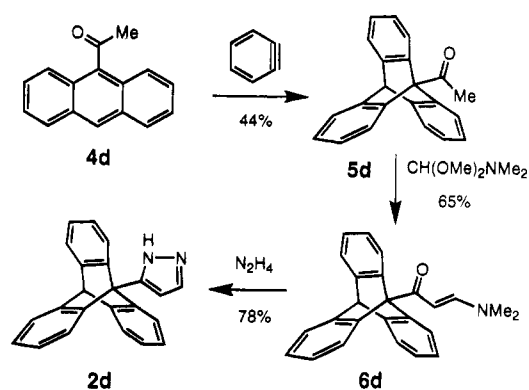


genic center.<sup>7</sup> As compared to the corresponding reaction with a secondary phosphine as a nucleophile,<sup>2a</sup> the transformation involving pyrazoles was found to be more sluggish. Besides the desired compounds, varying amounts of unidentified decomposition products were formed. Nevertheless, the ligands were isolated in pure form after chromatographic purification and/or recrystallization, generally in moderate yields (up to 78%). Table 1 collects all the derivatives prepared, along with some selected analytical data.

Several pyrazoles have been reported previously in the literature; some others are new. Since their preparation was achieved via conventional synthetic methods,<sup>8</sup> they will not be described in detail here, and only the triptycyl derivative **2d** is given as a representative example. Reaction of 1-acetyltriptycene<sup>9</sup> (**5d**) with *N,N*-dimethylformamide according to a reported procedure<sup>10</sup> afforded 3-(dimethylamino)-1-(9-triptycyl)-2-propen-1-one (**6d**) in 65% yield. The latter was converted to the desired 1*H*-pyrazole **2d** by treatment with hydrazine, as illustrated in Scheme 3.

In the case of a nonsymmetrical pyrazole 3,5-substitution pattern, a potential regioselectivity problem arises for the reaction with the ferrocene derivatives **1**, because the two pyrazole nitrogen atoms are not equivalent. However, besides the two cases described below, only one regioisomer was generally detected and isolated. The common observation is that the nitrogen adjacent to the less bulky and/or less electron-withdrawing group will behave as the nucleophilic center (becomes alkylated). Considering that the pyrazolyl fragment ends up at a sterically demanding secondary center, it is not surprising that the simple argument based on the different bulks of the substituents correctly predicts the regioselectivity. However, for sterically similar 3,5-substituents it is known that *N*-alkylation tends to give mixtures of the two regioisomers, the ratio of which is often dependent on the reaction conditions.<sup>11</sup>

Scheme 3



In such cases the position of the incoming alkyl substituent may or may not be related to the stabilization of one of the two possible tautomeric forms. It has been shown that a correlation exists between the sign of the Hammett parameter  $\sigma_m$  of the substituent and its position in the major tautomer at equilibrium.<sup>12</sup> Thus, electron-withdrawing groups (positive  $\sigma_m$ ) prefer position 3, whereas electron-donating substituents (negative  $\sigma_m$ ) are rather to be found at position 5. In the case of the 5-methyl-3-trifluoromethyl derivative **3af** this thermodynamic argument would predict the preferred formation of the regioisomer opposite to the one that was found (electrophilic attack at the doubly bonded nitrogen). This is taken as an indication that for this particular pyrazole *N*-alkylation is kinetically controlled. The 3-isopropyl-5-methyl ligand **3ag** was found to be accompanied by its regioisomer, whereby a ratio of 7:3 was determined by NMR of the crude mixture (the minor isomer could not be obtained in pure form). This is not too surprising, since both the electronic and steric differences between the two substituents are relatively small. Finally, the 9-anthryl derivative **3aq** does not fit this simple steric argument. In analogy to all other aryl-substituted pyrazoles, one would in fact expect the formation of only one regioisomer. A 5:1 mixture of the two possible products was found instead, the major isomer being the expected one (vide infra). A tentative explanation for the formation of the minor isomer is as follows. A charge-transfer (stacking) interaction between the 9-anthryl moiety and the ferrocenyl carbocationic intermediate could enable the approach of the nitrogen atom adjacent to the electrophilic center, as illustrated in Chart 1. Such an interaction would overcome part of the unfavorable steric repulsions resulting in the product.

**Structural Characteristics of the Ligands.** In order to define the conformational properties of the ligands, and to prove the structure of the single regioisomers obtained from the reactions with unsymmetrically substituted pyrazoles, X-ray crystallographic studies of several compounds have been carried out. Suitable single crystals were obtained for the ligands **3af**, **3ah**, **3aj**, **3aq'**, **3as**, and **3ec** by recrystallization from hexane (**3ah**, **3aj**) or from mixtures of  $\text{CH}_2\text{Cl}_2$  and hexane (all others). Because of the structural similarities existing between the six compounds, only a representative view of one molecule is shown in Figure 1 for the compound **3aq'** (ORTEP views for all other com-

(7) (a) Marquarding, D.; Klusacek, H.; Gokel, G.; Hoffmann, P.; Ugi, I. *J. Am. Chem. Soc.* **1970**, *92*, 5389–5393. (b) Gokel, G. W.; Marquarding, D.; Ugi, I. *K. J. Org. Chem.* **1972**, *94*, 3052–3058. (c) Gokel, G. W.; Ugi, I. *K. J. Chem. Educ.* **1972**, *49*, 294–296.

(8) (a) Kirschke, K. In *Methoden der Organischen Chemie (Houben-Weyl)*; Thieme: Stuttgart, Germany, 1994; Hetarene III/Teil 2 Vol. E8b, pp 399–763. (b) Fusco, R. In *Pyrazoles, Pyrazolines, Pyrazolidines, Indazoles, and Condensed Rings*; Wiley, R. H., Ed.; Interscience: New York, 1967; pp 1–176.

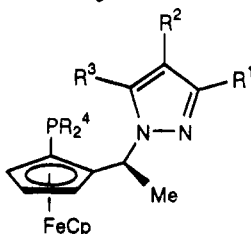
(9) 9-Acetyltriptycene was prepared from the commercially available 9-acetylanthracene by cycloaddition of benzyne, as reported for 9-bromotriptycene. See: (a) Jefford, C. W.; McCreadie, R.; Müller, P.; Siegfried, B. *J. Chem. Educ.* **1971**, *48*, 708–710. (b) Molle, G.; Bauer, P.; Dubois, J. E. *J. Org. Chem.* **1983**, *48*, 2975–2981.

(10) Brunner, H.; Scheck, T. *Chem. Ber.* **1992**, *125*, 701–709.

(11) Katritzky, A. R.; Lagowsky, J. M. In *Comprehensive Heterocyclic Chemistry*; Potts, K. T., Ed.; Pergamon: Oxford, U.K., 1984; pp 39–110.

(12) Elguero, J.; Marzin, C.; Katritzky, A. R.; Linda, P. *Adv. Heterocycl. Chem.* **1976**, Suppl. 1 (The Tautomerism of Heterocycles).

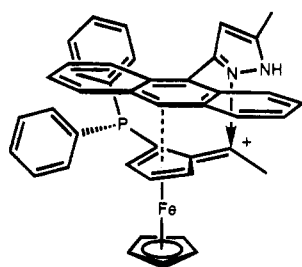
Table 1. Selected Properties of Pyrazole-Containing Ferrocenyl Ligands



entry no.	compd	R <sup>1</sup>	R <sup>2</sup>	R <sup>3</sup>	R <sup>4</sup>	conf	yield (%)	[α] <sub>D</sub> (deg)	mp (°C)	δ( <sup>31</sup> P) (ppm)	δ(C <sub>5</sub> H <sub>5</sub> ) (ppm)	δ(C <sup>6</sup> H) (ppm)	δ(C <sup>7</sup> H <sub>3</sub> ) (ppm)	δ(R <sup>2</sup> = H) (ppm)
1	<b>3aa</b>	H	H	H	Ph	(S)-(R)	64	363	131	-24.0	4.05	5.77	1.92	5.58
2	<b>3ab</b>	Ph	H	H	Ph	(S)-(R)	41	303	122	-25.3	4.11	5.86	1.99	5.92
3	<b>3ac</b>	2-Py	H	H	Ph	(S)-(R)	78	291	121	-25.2	4.08	5.84	1.96	6.29
4	<b>3ad</b>	9-triptycyl	H	H	Ph	(R)-(S)	74	-200	167	-26.0	4.09	6.01	2.10	6.12
5	<b>3ae</b>	Me	H	Me	Ph	(S)-(R)	55	329	127	-24.1	4.05	5.58	1.70	5.06
6	<b>3af</b>	CF <sub>3</sub>	H	Me	Ph	(S)-(R)	35	282	148	-24.7	4.08	5.72	1.84	5.52
7	<b>3ag</b>	iPr	H	Me	Ph	(S)-(R)	26	256	oil	-23.9	4.04	5.61	1.84	5.20
8	<b>3ah</b>	Cy	H	Me	Ph	(S)-(R)	26	297	94	-23.8	4.04	5.62	1.86	5.23
9	<b>3ai</b>	OEt	H	Me	Ph	(S)-(R)	24	293	116	-23.6	4.05	5.46	1.79	4.73
10	<b>3aj</b>	Ph	H	Me	Ph	(S)-(R)	55	338	171	-23.9	4.09	5.66	1.91	5.61
11	<b>3ak</b>	2-Py	H	Me	Ph	(S)-(R)	64	330	130	-24.1	4.06	5.69	1.87	6.01
12	<b>3al</b>	3-Py	H	Me	Ph	(S)-(R)	32	294	167	-23.9	4.08	5.70	1.88	5.61
13	<b>3am</b>	4-Py	H	Me	Ph	(S)-(R)	37	365	158	-24.5	4.10	5.72	1.88	5.66
14	<b>3an</b>	2,4(OMe) <sub>2</sub> Ph	H	Me	Ph	(S)-(R)	19	314	83	-23.9	4.09	5.65	1.91	5.83
15	<b>3ao</b>	1-naphthyl	H	Me	Ph	(S)-(R)	45	386	192	-23.9	4.12	5.75	1.98	5.69
16	<b>3ap</b>	2-naphthyl	H	Me	Ph	(S)-(R)	28	337	129	-23.9	4.14	5.75	1.96	5.76
17	<b>3aq</b>	9-anthryl	H	Me	Ph	(S)-(R)	37	338	202	-24.2	4.08	5.85	2.09	5.81
18	<b>3aq'</b>	Me	H	9-An	Ph	(S)-(R)	7	265	217	-24.0	3.82	5.10	1.68	6.01
19	<b>3ar</b>	ferrocenyl	H	Me	Ph	(R)-(S)	18	-283	163	-23.8	4.07	5.54	1.92	5.47
20	<b>3as</b>	Me	Me	Me	Ph	(S)-(R)	40	310	a	-24.2	4.08	5.63	1.80	
21	<b>3at</b>	Me	NO <sub>2</sub>	Me	Ph	(S)-(R)	63	296	163	-26.1	4.13	5.74	1.82	
22	<b>3au</b>	Me	Br	Me	Ph	(S)-(R)	62	284	150	-25.0	4.09	5.63	1.78	
23	<b>3av</b>	CF <sub>3</sub>	H	CF <sub>3</sub>	Ph	(S)-(R)	35	154	125	-25.5	4.15	5.97	1.94	6.26
24	<b>3aw</b>	iPr	H	iPr	Ph	(S)-(R)	43	265	130	-22.9	4.03	5.52	1.92	5.28
25	<b>3be</b>	Me	H	Me	4-F-Ph	(R)-(S)	67	-308	136	-26.6	4.06	5.57	1.78	5.07
26	<b>3ce</b>	Me	H	Me	4-Cl-Ph	(R)-(S)	59	-354	150	-26.0	4.07	5.57	1.77	5.09
27	<b>3de</b>	Me	H	Me	4-Me-Ph	(R)-(S)	25	-323	156	-24.9	4.04	5.57	1.80	5.05
28	<b>3ec</b>	2-Py	H	H	4-CF <sub>3</sub> -Ph	(R)-(S)	60	-323	201	-24.6	4.10	5.90	1.95	6.31
29	<b>3ee</b>	Me	H	Me	4-CF <sub>3</sub> -Ph	(R)-(S)	67	-263	112	-24.0	4.10	5.58	1.79	4.99
30	<b>3ej</b>	Ph	H	Me	4-CF <sub>3</sub> -Ph	(R)-(S)	59	-292	102	-23.6	4.15	5.71	1.91	5.57
31	<b>3ew</b>	CF <sub>3</sub>	H	CF <sub>3</sub>	4-CF <sub>3</sub> -Ph	(R)-(S)	51	-214	73	-25.3	4.16	5.91	1.91	6.23
32	<b>3fe</b>	Me	H	Me	4-NMe <sub>2</sub> -Ph	(R)-(S)	50	-366	177	-28.5	4.08	5.56	1.82	5.08
33	<b>3ge</b>	Me	H	Me	4-OMe-Ph	(R)-(S)	57	-324	167	-27.6	4.06	5.56	1.79	5.07
34	<b>3gj</b>	Ph	H	Me	4-OMe-Ph	(R)-(S)	20	-333	112	-27.7	4.13	5.66	1.89	5.60
35	<b>3gw</b>	CF <sub>3</sub>	H	CF <sub>3</sub>	4-OMe-Ph	(R)-(S)	28	-200	93	-29.1	4.13	5.91	1.89	6.25
36	<b>3he</b>	Me	H	Me	3,5-Me <sub>2</sub> -Ph	(R)-(S)	53	-289	182	-23.9	4.08	5.64	1.87	5.21
37	<b>3ie</b>	Me	H	Me	3,5-(CF <sub>3</sub> ) <sub>2</sub> -Ph	(R)-(S)	63	-251	122	-63.3	4.07	5.65	1.67	5.00
38	<b>3je</b>	Me	H	Me	Bu	(R)-(S)	26	-249	oil	-42.3	4.13	5.58	1.75	5.65
39	<b>3jj</b>	Ph	H	Me	Bu	(R)-(S)	14	-225	oil	-42.3	4.18	5.74	1.86	6.21
40	<b>3ke</b>	Me	H	Me	Cy	(R)-(S)	45	-128	100	-16.1	4.14	5.51	1.75	5.67

<sup>a</sup> Not determined.

Chart 1



pounds are provided as Supporting Information). The bond distances and angles turn out to be rather routine and fall in the expected ranges.<sup>13</sup> However, the six ligands examined show interesting common conforma-

tional aspects. A selection of important torsion angles is given in Table 2, and Figure 2 illustrates the conformational similarities between the six different compounds. Thus, one recognizes the following common features.

(1) The pyrazolyl ring and one of the two phosphino-phenyl groups lie in a pseudoaxial position, pointing away from the ferrocene core (exo-axial). The corresponding diagnostic torsion angles C(1)-C(2)-C(6)-N(1) and C(2)-C(1)-P(1)-C<sub>ipso</sub>(Ph<sub>ax</sub>) are in the ranges 63-84° and 90-104°, respectively. The second phenyl ring is therefore in an endo-equatorial position with the angle C(5)-C(1)-P(1)-C<sub>ipso</sub>(Ph<sub>eq</sub>) lying between 10 and 27°.

(2) In all but one derivative the planes defined by the pyrazolyl and the axial phenyl groups are nearly parallel, the angle between them varying from 12.1° (**3aj**) to 23.5° (**3af**). The proximity of these two rings is possibly responsible for this relative arrangement, thereby mini-

(13) (a) Orpen, A. G.; Brammer, L.; Allen, F. H.; Kennard, O.; Watson, D. G.; Taylor, R. *J. Chem. Soc., Dalton Trans.* **1989**, Supplement S1-S83. (b) Allen, F. H.; Kennard, O.; Watson, D. G.; Brammer, L.; Orpen, A. G.; Taylor, R. *J. Chem. Soc., Perkin Trans. 2* **1987**, Supplement S1-S19.

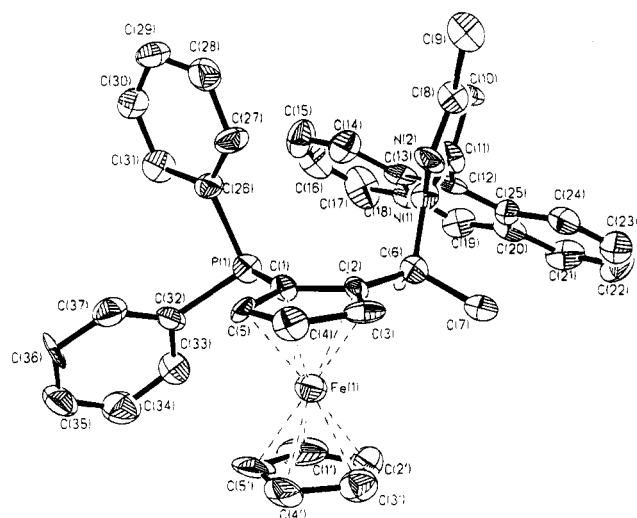


**Figure 1.** ORTEP view of one of the crystallographically independent molecules of the ligand **3aq'** (30% probability ellipsoids).

**Table 2.** Selected Torsion Angles (deg)<sup>a</sup> for **3af**, **3ah**, **3aj**, **3aq'**, **3as**, and **3ec**

torsion angle	<b>3af</b>	<b>3ah</b>	<b>3aj</b>	<b>3aq'</b> <sup>b</sup>	<b>3as</b>	<b>3ec</b>
C(1)–C(2)–C(6)–N(1) <sup>c</sup>	80	80	76	84	71	63
C(2)–C(1)–P(1)–C(Ph <sub>ax</sub> )	93	93	91	104	90	103
C(5)–C(1)–P(1)–C(Ph <sub>eq</sub> )	17	10	17	22	14	27
C(3)–C(2)–C(6)–C(7)	22	26	21	30	19	11
C(2)–C(6)–N(1)–N(2)	51	57	56	36	60	45
C(7)–C(6)–N(1)–N(2)	74	69	70	88	70	82
C(1)–P(1)–C <sub>ipso</sub> (Ph <sub>ax</sub> )–C <sub>ortho</sub> (Ph <sub>ax</sub> )	1	1	3	27	1	8

<sup>a</sup> Absolute values are given. <sup>b</sup> The figures given correspond to average values for the three independent molecules in the unit cell. <sup>c</sup> The numbering of relevant atoms for all compounds corresponds to that shown in Figure 1.

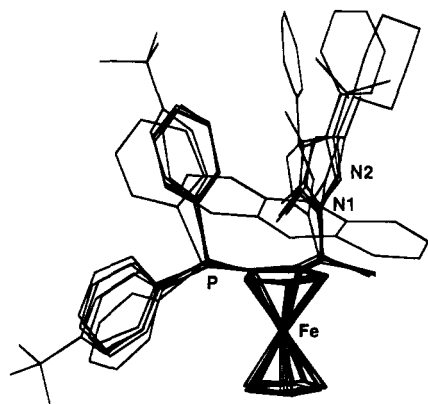


**Figure 2.** Superposition of the structures of the ligands **3af**, **3ah**, **3aj**, **3aq'**, **3as**, and **3ec**. The most significant deviation from the common conformation is shown by the 9-anthryl derivative **3aq'**. All ligands are shown in their (S)-R absolute configuration.

mizing steric interactions between the two groups. A significant deviation from the described geometry is found in the 9-anthryl derivative **3aq'** (minor isomer), where the latter interplanar angle (average value for the three independent molecules in the unit cell) is 69.4°. This is most likely due to the bulky 9-anthryl group, lying in an almost orthogonal orientation with respect to the pyrazolyl ring (the average interplanar angle being 81°), thus "reaching over" to the phosphino fragment. The consequence of this is a different relative

orientation of the axial phenyl ring, as reflected by the torsion angle C(1)–P(1)–C<sub>ipso</sub>(Ph)–C<sub>ortho</sub>(Ph) of 27°, describing the rotation around the P–Ph axis, as compared to angles of 1–8° for all other compounds.

(3) The nearly parallel arrangement of the axial phenyl and pyrazolyl rings may be considered as one of two possible low-energy relative conformations. For all ligands under study the observed one is such that the nitrogen atom N(2) is in an anti position with respect to the hydrogen atom attached to the stereogenic center C(6). This orientation is not expected to be well-suited for the ligands to coordinate in a chelating manner to a metal center, since the lone pairs of N(2) and of the phosphorus atom are pointing in roughly opposite directions. Therefore, in the coordinated form the pyrazolyl fragment is expected to be rotated by ca. 180° around the C(6)–N(1) axis, with respect to the free ligands. Such an arrangement would correspond to the second low-energy conformation having parallel pyrazolyl and phenyl rings.

## Conclusions

We have shown that a new class of chiral chelating ferrocenyl ligands incorporating a phosphine and a pyrazole is easily obtained by the unique substitution reaction occurring at the pseudo-benzylic stereogenic center of the ferrocenyl precursors **1**. This simple synthetic approach allows the preparation of a great variety of ligands, the electronic and steric properties of which can easily be modified. This still uncommon aspect offers the opportunity to tailor the ligands to a specific reaction and/or substrate. We have already demonstrated the effectiveness of our new P,N chelating ligands in the Rh-catalyzed hydroboration of styrenes.<sup>2f</sup> On the basis of these first very encouraging results, we are currently exploring further asymmetric transition-metal-catalyzed reactions. We will be reporting on developments in this area in due course.

## Experimental Section

**General Considerations.** All reactions with air- or moisture-sensitive materials were carried out under Ar using standard Schlenk techniques. Freshly distilled, dry, and oxygen-free solvents were used throughout. Routine <sup>1</sup>H (250.133 MHz), <sup>13</sup>C (62.90 MHz), <sup>19</sup>F (188.31 MHz), and <sup>31</sup>P NMR (101.26 MHz) spectra were recorded with a Bruker AM 250 spectrometer. Chemical shifts are given in ppm, and coupling constants (*J*) are given in Hz. Merck silica gel 60 (230–400 mesh) was used for column chromatography. Optical rotations were measured with a Perkin-Elmer 341 polarimeter using 10 cm cells. The IR spectra were recorded on a Perkin-Elmer Paragon 1000 FT-IR spectrophotometer. Melting points were obtained from samples in open capillary tubes with a Büchi SMP-20 apparatus and are uncorrected. Elemental analyses and EI/MS spectra were performed by the "Mikroelementar-analytisches Laboratorium der ETH". Dimethyl[(*R*)-1-ferrocenylethyl]amine, dimethyl[(*S*)-1-ferrocenylethyl]amine, and dimethyl[(*R*)-1-(*S*)-2-bis(3,5-bis(trifluoromethyl)phenyl)phosphino]ferrocenyl]ethyl]amine (**1i**) were obtained from Ciba Geigy AG. 1*H*-Pyrazole (**2a**), 3,5-dimethyl-1*H*-pyrazole (**2e**), and 4-bromo-3,5-dimethyl-1*H*-pyrazole (**2u**) were used as received from Fluka AG. Dimethyl[(*S*)-1-(*R*)-2-(diphenylphosphino)ferrocenyl]ethyl]amine<sup>1c</sup> (**1a**), dimethyl[(*R*)-1-(*S*)-2-(diphenylphosphino)ferrocenyl]ethyl]amine<sup>1c</sup> (**1a'**), dimethyl[(*R*)-1-(*S*)-2-(bis(4-fluorophenyl)phosphino)ferrocenyl]-

ethyl]amine<sup>14</sup> (**1b**), dimethyl[(*R*)-1-[(*S*)-2-(bis(4-(trifluoromethyl)phenyl)phosphino)ferrocenyl]ethyl]amine<sup>14</sup> (**1e**), dimethyl[(*R*)-1-[(*S*)-2-(bis(4-methoxyphenyl)phosphino)ferrocenyl]ethyl]amine<sup>14</sup> (**1g**), dimethyl[(*R*)-1-[(*S*)-2-(bis(3,5-dimethylphenyl)phosphino)ferrocenyl]ethyl]amine<sup>14</sup> (**1h**), 3-phenyl-1*H*-pyrazole<sup>15</sup> (**2b**), 3-(2-pyridyl)-1*H*-pyrazole<sup>10</sup> (**2c**), 3-(trifluoromethyl)-5-methyl-1*H*-pyrazole<sup>16</sup> (**2f**), 3-isopropyl-5-methyl-1*H*-pyrazole<sup>15</sup> (**2g**), 3-cyclohexyl-5-methyl-1*H*-pyrazole<sup>15</sup> (**2h**), 5-ethoxy-3-methyl-1*H*-pyrazole<sup>17</sup> (**2i**), 3-phenyl-5-methyl-1*H*-pyrazole<sup>15</sup> (**2j**), 3-(2-pyridyl)-5-methyl-1*H*-pyrazole<sup>15</sup> (**2k**), 3-(3-pyridyl)-5-methyl-1*H*-pyrazole<sup>15</sup> (**2l**), 3-(4-pyridyl)-5-methyl-1*H*-pyrazole<sup>15</sup> (**2m**), 3-(2,4-dimethoxyphenyl)-5-methyl-1*H*-pyrazole<sup>15</sup> (**2n**), 3-( $\alpha$ -naphthyl)-5-methyl-1*H*-pyrazole<sup>15</sup> (**2o**), 3-( $\beta$ -naphthyl)-5-methyl-1*H*-pyrazole<sup>15</sup> (**2p**), 3-(9-anthryl)-5-methyl-1*H*-pyrazole<sup>15</sup> (**2q**), 3-ferrocenyl-5-methyl-1*H*-pyrazole<sup>15</sup> (**2r**), 3,4,5-trimethyl-1*H*-pyrazole<sup>15</sup> (**2s**), 3,5-dimethyl-4-nitro-1*H*-pyrazole<sup>18</sup> (**2t**), 3,5-bis(trifluoromethyl)-1*H*-pyrazole<sup>19</sup> (**2v**), 3,5-diisopropyl-1*H*-pyrazole<sup>15</sup> (**2w**), and dicyclohexylchlorophosphine<sup>20</sup> were prepared by literature methods.

**General Method for the Synthesis of Chlorophosphines.** The Grignard mixture (prepared *in situ* from 2.2 equiv of magnesium and 2.2 equiv of alkyl or aryl bromide) was slowly added to a cooled solution of 1 equiv of PCl<sub>2</sub>(NEt<sub>2</sub>) in ether. The precipitate was filtered off, and 2.2 equiv of dry pyridine hydrochloride was added to the clear solution. The mixture was stirred overnight and filtered, the solvent removed, and the oily residue distilled *in vacuo*. Yield: 12–80%.

**General Method for the Synthesis of R\*PFA (1).** *sec*-Butyllithium in cyclohexane (1.2 equiv) was added to a solution of dimethyl[(*R*)-1-ferrocenylethyl]amine (1 equiv) in ether over a period of 20 min. The resulting red-brown solution was stirred at room temperature overnight, and then diaryl- or dialkylchlorophosphine (1.5–4 equiv) in 10 mL of ether was added. After 5 h reflux aqueous sodium hydrogencarbonate was slowly added with cooling in a ice bath. The resulting organic layer and the ether extracts from the aqueous layer were combined, washed with water, dried over anhydrous sodium sulfate, and concentrated *in vacuo* to afford a red oil. Purification by chromatography on silica, followed by recrystallization from hexane, gave pure **1** as orange crystals.

**Dimethyl[(*R*)-1-[(*S*)-2-(bis(4-chlorophenyl)phosphino)ferrocenyl]ethyl]amine (1c):** from 2 mL of dimethyl[(*R*)-1-ferrocenylethyl]amine (9.3 mmol, 1 equiv), 8.2 mL of 1.4 M *sec*-butyllithium in hexane (11.2 mmol, 1.2 equiv) and 6 g of bis(4-chlorophenyl)chlorophosphine (21 mmol, 2.2 equiv), according to the general method. Flash chromatography (FC) (silica, hexane/ethyl acetate 10/1): yield 1.744 g (37%). [ $\alpha$ ]<sub>D</sub><sup>25</sup> = –328 (*c* = 0.495, CHCl<sub>3</sub>). <sup>1</sup>H NMR (CDCl<sub>3</sub>):  $\delta$  7.55–7.10 (m, 8 ar H), 4.39 (m, cp H), 4.26 (m, cp H), 4.20 (dq, *J* = 2.5, *J* = 6.9, CHMeN), 3.99 (s, 5 cp H), 3.80 (m, cp H), 1.80 (s, 2 NMe), 1.25 (d, *J* = 6.9, CHMeN). <sup>13</sup>C{<sup>1</sup>H} NMR (CDCl<sub>3</sub>):  $\delta$  136–127 (8 ar CH), 71.4 (2 cp CH), 69.6 (5 cp CH), 68.3 (cp CH), 57.1 (CHMeN), 38.7 (2 NMe), 8.2 (CHMeN). <sup>31</sup>P{<sup>1</sup>H} NMR (CDCl<sub>3</sub>):  $\delta$  –25.0 (s). Anal. Calcd for C<sub>26</sub>H<sub>26</sub>Cl<sub>2</sub>FeNP: C, 61.21; H, 5.14; N, 2.75. Found: C, 61.36; H, 5.36; N, 2.65.

**Dimethyl[(*R*)-1-[(*S*)-2-(bis(4-methylphenyl)phosphino)ferrocenyl]ethyl]amine (1d):** from 3 mL of dimethyl[(*R*)-1-ferrocenylethyl]amine (14 mmol, 1 equiv), 10.5 mL of 1.4 M

*sec*-butyllithium in hexane (17 mmol, 1.2 equiv), and 3.5 mL of bis(4-methylphenyl)chlorophosphine (17 mmol, 1.2 equiv), according to the general method. FC (silica, hexane/ethyl acetate 10/1): yield 1.79 g (27%). [ $\alpha$ ]<sub>D</sub><sup>25</sup> = –305 (*c* = 0.40, CHCl<sub>3</sub>). <sup>1</sup>H NMR (CDCl<sub>3</sub>):  $\delta$  7.5–6.96 (m, 8 ar H), 4.36 (m, cp H), 4.23 (m, cp H), 4.15 (dq, *J* = 2.6, *J* = 6.9, CHMeN), 3.92 (s, 5 cp H), 3.88 (m, cp H), 2.36 (s, PhMe), 2.27 (s, PhMe), 1.79 (s, 2 NMe), 1.28 (d, *J* = 6.9, CHMeN). <sup>13</sup>C{<sup>1</sup>H} NMR (CDCl<sub>3</sub>):  $\delta$  138–128 (8 ar CH), 96.8 (C), 71.8 (cp CH), 69.7 (5 cp CH), 69.2 (cp CH), 68.2 (cp CH), 51.1 (CHMeN), 39.3 (2 NMe), 21.3 (2 PhMe), 10.1 (CHMeN). <sup>31</sup>P{<sup>1</sup>H} NMR (CDCl<sub>3</sub>):  $\delta$  –25.3 (s). Anal. Calcd for C<sub>28</sub>H<sub>33</sub>FeNP: C, 71.65; H, 6.87; N, 2.98. Found: C, 71.64; H, 6.85; N, 2.68.

**Dimethyl[(*R*)-1-[(*S*)-2-(bis(4-dimethylamino)phenyl)phosphino)ferrocenyl]ethyl]amine (1f):** from 2 mL of dimethyl[(*R*)-1-ferrocenylethyl]amine (9.3 mmol, 1 equiv), 8.2 mL of 1.4 M *sec*-butyllithium in cyclohexane (11.3 mmol, 1.2 equiv), and 6.77 g of bis(4-(dimethylamino)phenyl)chlorophosphine (22 mmol, 2.4 equiv), according to the general method. FC (silica, hexane/ethyl acetate 5/1): yield 1.32 g (27%). Mp: 182 °C dec. [ $\alpha$ ]<sub>D</sub><sup>25</sup> = –383 (*c* = 0.345, CHCl<sub>3</sub>). <sup>1</sup>H NMR (CDCl<sub>3</sub>):  $\delta$  7.51–6.55 (m, 8 ar H), 4.33 (m, cp H), 4.22 (m, cp H), 4.07 (dq, *J* = 2.6, *J* = 6.9, CHMeN), 4.06 (m, cp H), 3.94 (s, 5 cp H), 2.97 (s, 2 NMe), 2.89 (s, 2 NMe), 1.83 (s, 2 NMe), 1.34 (d, *J* = 6.9, CHMeN). <sup>13</sup>C{<sup>1</sup>H} NMR (CDCl<sub>3</sub>):  $\delta$  136–112 (8 ar CH), 71.6 (cp CH), 69.5 (5 cp CH), 68.8 (cp CH), 67.9 (cp CH), 57.0 (CHMeN), 40.4 (2 NMe), 40.3 (2 NMe), 39.7 (2 NMe), 11.8 (CHMeN). <sup>31</sup>P NMR (CDCl<sub>3</sub>):  $\delta$  –28.4 (s). Anal. Calcd for C<sub>30</sub>H<sub>36</sub>FeN<sub>3</sub>P: C, 68.31; H, 7.26; N, 7.97. Found: C, 68.49; H, 7.41; N, 7.86.

**Dimethyl[(*R*)-1-[(*S*)-2-(dibutylphosphino)ferrocenyl]ethyl]amine (1j):** from 3 mL of dimethyl[(*R*)-1-ferrocenylethyl]amine (14 mmol, 1 equiv), 10.5 mL of 1.6 M *n*-butyllithium in hexane (17 mmol, 1.2 equiv) and 5 g of dibutylchlorophosphine (28 mmol, 2 equiv), according to the general method. FC (silica, hexane/ethyl acetate 5/1): yield 3.19 g (57%). [ $\alpha$ ]<sub>D</sub><sup>25</sup> = –80 (*c* = 0.55, CHCl<sub>3</sub>). <sup>1</sup>H NMR (CDCl<sub>3</sub>):  $\delta$  4.23 (m, cp H), 4.17–4.11 (m, cp H), 4.09 (dq, *J* = 2.6, *J* = 6.9, CHMeN), 4.03 (s, 5 cp H), 4.01–3.91 (m, cp H), 2.06 (s, 2 NMe), 1.22 (d, *J* = 6.9, CHMeN), 1.94–0.76 (m, 6 Bu CH<sub>2</sub> and 2 Bu CH<sub>3</sub>). <sup>13</sup>C{<sup>1</sup>H} NMR (CDCl<sub>3</sub>):  $\delta$  96.7 (C), 69.4 (5 cp CH), 69.3 (cp CH), 68.7 (cp CH), 67.2 (cp CH), 56.6 (CHMeN), 39.2 (2 NMe), 29.6–24.3 (6 Bu CH<sub>2</sub>), 14.0 (Bu CH<sub>3</sub>), 13.8 (Bu CH<sub>3</sub>), 8.1 (CHMeN). <sup>31</sup>P{<sup>1</sup>H} NMR (CDCl<sub>3</sub>):  $\delta$  –39.8 (s). Anal. Calcd for C<sub>22</sub>H<sub>36</sub>FeNP: C, 65.83; H, 9.04; N, 3.49. Found: C, 66.26; H, 9.50; N, 3.23.

**Dimethyl[(*R*)-1-[(*S*)-2-(dicyclohexylphosphino)ferrocenyl]ethyl]amine (1k):** from 3.35 g of dimethyl[(*R*)-1-ferrocenylethyl]amine (13 mmol, 1 equiv), 9.8 mL of 1.6 M *n*-butyllithium in hexane (15.7 mmol, 1.2 equiv), and 3.8 g of dicyclohexylchlorophosphine (16.3 mmol, 1.25 equiv), according to the general method. FC (silica, hexane/ethyl acetate 5/1): yield 3.80 g (64%). [ $\alpha$ ]<sub>D</sub><sup>25</sup> = –30 (*c* = 0.39, CHCl<sub>3</sub>). <sup>1</sup>H NMR (CDCl<sub>3</sub>):  $\delta$  4.26 (m, cp H), 4.23 (m, cp H), 4.08 (m, cp H), 4.05 (s, 5 cp H), 4.00 (dq, *J* = 2.7, *J* = 6.8, CHMeN), 2.10 (s, 2 NMe), 1.27 (d, *J* = 6.8, CHMeN), 2.04–1.0 (m, 10 Cy CH<sub>2</sub> and 2 Cy CH). <sup>13</sup>C{<sup>1</sup>H} NMR (CDCl<sub>3</sub>):  $\delta$  69.7 (cp CH), 69.5 (5 cp CH), 68.2 (cp CH), 66.9 (cp CH), 56.2 (CHMeN), 39.0 (2 NMe), 36.3–26.2 (10 Cy CH<sub>2</sub> and 2 Cy CH), 8.3 (CHMeN). <sup>31</sup>P{<sup>1</sup>H} NMR (CDCl<sub>3</sub>):  $\delta$  –11.7 (s). Anal. Calcd for C<sub>26</sub>H<sub>40</sub>FeNP: C, 68.87; H, 8.89; N, 3.09. Found: C, 68.96; H, 8.91; N, 3.09.

**9-Acetyltriptycene (5d):** synthesis analogous to that of 9-bromotriptycene.<sup>9</sup> From 20 g (0.09 mol) of 9-acetylanthracene (**4d**) and benzyne, generated *in situ* with 30 g (0.22 mol) of anthranilic acid and 32 g (0.28 mol) of isopentyl nitrite (in two portions), the crude product was recrystallized two times from hot methanol to give 11.8 g (44%) of **5d** as an orange-brown powder, which was used without further purification for the synthesis of **6d**. Recrystallization from ethyl acetate/heptane of an analytical sample of **5d** afforded brownish yellow needles. Mp: 188 °C. <sup>1</sup>H NMR (CDCl<sub>3</sub>):  $\delta$  7.74 (m, 3 trp H), 7.43 (m, 3 trp H), 7.07 (m, 6 trp H), 5.39 (s, 1 H, trp

(15) General protocol for the preparation of 1*H*-pyrazoles (**2**): the corresponding 1,3-diketone (or the enamine analogon) was dissolved or suspended in ethanol (*ca.* 10%). From a syringe 2 equiv of hydrazine hydrate was added at room temperature. The mixture was stirred for 10 min and then heated at reflux temperature for 30 min, unless otherwise stated. After complete removal of the solvent, the crude product was dissolved in dichloromethane, washed twice with water to remove any unreacted hydrazine, dried, and purified as appropriate.<sup>9</sup>

(16) Nishiwaki, T. *J. Chem. Soc. B* **1967**, 885–888.

(17) Wolff, W. *Chem. Ber.* **1904**, 2827–2836.

(18) Morgan, G. T.; Ackerman, I. *J. Chem. Soc.* **1923**, 1308–1318.

(19) Claire, P. P. K.; Coe, P. L.; Jones, C. J.; McCleverty, J. A. *J. Fluorine Chem.* **1991**, *51*, 283–289.

(20) Voskuil, W.; Arens, J. F. *Recl. Trav. Chim. Pays-Bas* **1963**, *82*, 302–304.



H), 2.82 (s, COMe).  $^{13}\text{C}\{^1\text{H}\}$  NMR ( $\text{CDCl}_3$ ):  $\delta$  206.7 (COMe), 146.1, 142.8 (trp C), 125.3, 124.8, 123.5, 123.4 (trp CH), 54.4 (trp CH), 32.7 (COMe). IR ( $\text{cm}^{-1}$ ): 3067, 3016, 2962, 1713 (C=O), 1459, 1358, 1236, 1150, 750, 610, 582. Anal. Calcd for  $\text{C}_{22}\text{H}_{16}\text{O}$ : C, 89.16; H, 5.44. Found: C, 89.03; H, 5.58.

**3-(Dimethylamino)-1-(9-triptycyl)-2-propen-1-one (6d):** from 3 g (0.01 mol) of 9-acetyltriptycene (**5d**) and ca. 5 mL (0.03 mol) of *N,N*-dimethylformamide diethylacetal, analogously to the preparation of 3-(dimethylamino)-1-(2-pyridyl)-2-propen-1-one.<sup>10</sup> The crude product was washed thoroughly with cold ethanol to yield 2.3 g (65%) of **6d** as a fine cream-white solid. An analytical sample was recrystallized from hot acetone (white microcrystals). Mp: 297 °C.  $^1\text{H}$  NMR ( $\text{CDCl}_3$ ):  $\delta$  8.05 (m, 3 trp H), 7.40 (m, 3 trp H), 7.06–6.96 (m, 6 trp H and CHN), 5.50 (d,  $J = 12.5$ , COCH), 5.35 (s, trp H), 3.21, 2.77 (br s, 2 NMe, *cis/trans*).  $^{13}\text{C}\{^1\text{H}\}$  NMR ( $\text{CDCl}_3$ ):  $\delta$  194.1 (CO), 151.8 (CHN), 146.8, 145.2 (trp C), 125.7, 125.1, 124.8, 123.4 (trp CH), 100.4 (COCH), 55.1 (trp CH), 33.2 (NMe). IR ( $\text{cm}^{-1}$ ): 3056, 2915 (CH), 1712, 1655, 1563 (C=O, C=C), 1433, 1350, 1278, 1097, 1073, 891, 758, 640, 624. Anal. Calcd for  $\text{C}_{25}\text{H}_{21}\text{NO}$ : C, 85.44; H, 6.02; N, 3.99. Found: C, 85.73; H, 5.93; N, 3.87.

**3-(9-Triptycyl)-1H-pyrazole (2d):** from 2.0 g (5.7 mmol) of 3-(dimethylamino)-1-(9-triptycyl)-2-propen-1-one (**5d**), according to the general method (12 h reflux time).<sup>15</sup> Recrystallization from hot EtOH and then from ethyl acetate/heptane yielded 1.43 g (78%) of **2d** as white needles. Mp: 251 °C dec.  $^1\text{H}$  NMR ( $\text{CDCl}_3$ ):  $\delta$  11.4 (br s, NH), 7.58 (m, 3 trp H), 7.51 (d, 1 pz CH,  $J = 2.2$ ), 7.46 (m, 3 trp H), 7.07–6.94 (m, 6 trp H), 6.77 (d, 1 pz CH,  $J = 2.2$ ), 5.49 (s, 1 trp H).  $^{13}\text{C}\{^1\text{H}\}$  NMR ( $\text{CDCl}_3$ ):  $\delta$  146.0, 145.7 (trp C), 125.0–123.1 (4 trp CH), 124.8 (pz CH), 108.1 (pz CH), 54.5 (trp CH). IR ( $\text{cm}^{-1}$ ): 3168 (NH), 3054, 2952 (CH), 1531, 1449, 1353, 1213, 1062, 914, 749, 634. Anal. Calcd for  $\text{C}_{23}\text{H}_{16}\text{N}_2$ : C, 86.22; H, 5.03; N, 8.74. Found: C, 85.56; H, 5.12; N, 8.64.

**General Method for the Preparation of P,N Ligands (3).** A solution of an R\*PFA (**1**) and a 1H-pyrazole (**2**) (1–14 equiv) in 1–3 mL of glacial acetic acid was stirred at 70–80 °C for 3–9 h. The orange to red reaction mixture was quenched with excess saturated aqueous sodium bicarbonate and extracted three times with dichloromethane. The combined organic layers were washed with brine, dried over magnesium sulfate, and filtered. Solvent was removed by rotary evaporation, and the crude product thus obtained was purified by flash column chromatography as detailed below, filtered over alumina to remove phosphine oxides, recrystallized, and dried *in vacuo*.

**1-[(S)-1-[(R)-2-(Diphenylphosphino)ferrocenyl]ethyl]-1H-pyrazole (3aa):** from **1a** (441 mg, 1 mmol) and 3,5-diphenyl-1H-pyrazole (**2a**) (136 mg, 2 mmol, 2 equiv), according to the general method. FC (silica, hexane/ethyl acetate 1/1, 1%  $\text{NEt}_3$ ): yield 300 mg (64%). Mp: 131 °C dec.  $[\alpha]_D^{25} = +363$  ( $c = 0.50$ ,  $\text{CHCl}_3$ ).  $^1\text{H}$  NMR ( $\text{CDCl}_3$ ):  $\delta$  7.56–7.26 (m, 5 ar H), 7.15 (m, 2 pz CH), 7.06–6.95 (m, 5 ar H), 5.77 (dq,  $J = 2.6$ ,  $J = 6.9$ , CHMeN), 5.58 (m, pz CH), 4.78 (m, cp H), 4.40 (m, cp H), 4.05 (s, 5 cp H), 3.85 (m, cp H), 1.92 (d,  $J = 6.9$  Hz, CHMeN).  $^{13}\text{C}\{^1\text{H}\}$  NMR ( $\text{CDCl}_3$ ):  $\delta$  150–120 (10 ar CH), 113.1 (3 pz CH), 69.8 (2 cp CH), 69.6 (5 cp CH), 69.3 (cp CH), 55.5 (CHMeN), 21.0 (CHMeN).  $^{31}\text{P}\{^1\text{H}\}$  NMR ( $\text{CDCl}_3$ ):  $\delta$  -24.0 (s). MS ( $m/z$ ): 464 ( $\text{M}^+$ , 100%), 396 ( $\text{M}^+ - \text{Hpz}$ ), 331 (396 - cp), 276 (331 - Fe). Anal. Calcd for  $\text{C}_{27}\text{H}_{25}\text{FeN}_2\text{P}$ : C, 69.84; H, 5.43; N, 6.03. Found: C, 69.68; H, 5.36; N, 5.97.

**1-[(S)-1-[(R)-2-(Diphenylphosphino)ferrocenyl]ethyl]-3-phenyl-1H-pyrazole (3ab):** from **1a** (300 mg, 0.68 mmol) and 3-phenyl-1H-pyrazole (**2b**) (118 mg, 0.82 mmol, 1.2 equiv), according to the general method. FC (silica, hexane/ethyl acetate 5/1): yield 150 mg (41%). Mp: 122 °C.  $[\alpha]_D^{25} = +303$  ( $c = 0.50$ ,  $\text{CHCl}_3$ ).  $^1\text{H}$  NMR ( $\text{CDCl}_3$ ):  $\delta$  7.65–7.56 (m, 4 ar H), 7.41–7.23 (m, 6 ar H), 7.02 (d,  $J = 2.3$ , pz CH), 6.97–6.79 (m, 5 ar H), 5.92 (d,  $J = 2.3$ , pz CH), 5.86 (dq,  $J = 6.9$ ,  $J = 3.2$ , CHMeN), 4.80 (m, cp H), 4.43 (m, cp H), 3.90 (m, cp H), 4.11 (s, 5 cp H), 1.99 (d,  $J = 6.9$ , CHMeN).  $^{13}\text{C}\{^1\text{H}\}$  NMR ( $\text{CDCl}_3$ ):

$\delta$  150.5, 138.8–125.8 (ar CH, ar C), 101.9 (pz CH), 93.6 (cp C), 76.4 (cp C), 72.0 (cp CH), 70.0 (5 cp CH), 69.9 (cp CH), 69.8 (cp CH), 56.2 (CHMeN), 21.6 (CHMeN).  $^{31}\text{P}\{^1\text{H}\}$  NMR ( $\text{CDCl}_3$ ):  $\delta$  -25.3 (s). IR ( $\text{cm}^{-1}$ ): 1497, 1459, 1433, 1246, 1043, 1001, 816, 742, 694. MS ( $m/z$ ): 540 ( $\text{M}^+$ , 100%), 475 ( $\text{M}^+ - \text{cp}$ ), 396 ( $\text{M}^+ - \text{Hpz}$ ), 355, 331 (396 - cp), 276 (396 - Fe-cp), 253, 183, 144 (Hpz<sup>+</sup>). Anal. Calcd for  $\text{C}_{33}\text{H}_{25}\text{FeN}_2\text{P}$ : C, 73.34; H, 5.41; N, 5.18. Found: C, 73.14; H, 5.29; N, 5.00.

**1-[(S)-1-[(R)-2-(Diphenylphosphino)ferrocenyl]ethyl]-3-(2-pyridyl)-1H-pyrazole (3ac):** from **1a** (300 mg, 0.68 mmol) and 3-(2-pyridine)-1H-pyrazole (**2c**) (109 mg, 0.75 mmol, 1.1 equiv), according to the general method. FC (silica, hexane/ethyl acetate 2/1, 2%  $\text{NEt}_3$ ): yield 288 mg (78%). Mp: 121 °C.  $[\alpha]_D^{25} = +291$  ( $c = 0.46$ ,  $\text{CHCl}_3$ ).  $^1\text{H}$  NMR ( $\text{CDCl}_3$ ):  $\delta$  8.52 (m, py CH), 7.71 (m, 1 ar H), 7.62–7.50 (m, 3 ar H), 7.35 (m, 3 ar H), 7.09 (m, 1 ar H), 7.03 (m, pz CH), 6.88–6.73 (m, 5 ar H), 6.29 (m, pz CH), 5.84 (dq,  $J = 7.0$ ,  $J = 3.3$ , CHMeN), 4.74 (m, cp H), 4.40 (m, cp H), 4.08 (s, 5 cp H), 3.86 (m, cp H), 1.96 (d,  $J = 7.0$ , CHMeN).  $^{13}\text{C}\{^1\text{H}\}$  NMR ( $\text{CDCl}_3$ ):  $\delta$  150.1 (py C), 148.6 (py CH), 138.4, 137.2, 135.7–127.1 (ar CH, ar C), 121.3, 119.8 (py CH), 103.3 (pz CH), 71.7 (cp CH), 69.6 (5 cp CH), 69.3 (cp CH), 69.0 (cp CH), 56.1 (CHMeN), 21.1 (CHMeN).  $^{31}\text{P}\{^1\text{H}\}$  NMR ( $\text{CDCl}_3$ ):  $\delta$  -25.2 (s). IR ( $\text{cm}^{-1}$ ): 1592, 1566, 1490, 1458, 1434, 1405, 1245, 1217, 1106, 815, 768, 744, 700, 503, 484, 469. MS ( $m/z$ ): 541 ( $\text{M}^+$ ), 476 ( $\text{M}^+ - \text{cp}$ , 100%), 396 ( $\text{M}^+ - \text{Hpz}$ ), 331 (396 - cp), 291, 265, 200, 145 (Hpz<sup>+</sup>). Anal. Calcd for  $\text{C}_{32}\text{H}_{28}\text{N}_3\text{PFe}$ : C, 70.99; H, 5.21; N, 7.76. Found: C, 70.77; H, 5.46; N, 7.63.

**1-[(R)-1-[(S)-2-(Diphenylphosphino)ferrocenyl]ethyl]-3-(9-triptycyl)-1H-pyrazole (3ad):** from **1a'** (574 mg, 1.30 mmol) and 3-(9-triptycyl)-1H-pyrazole (**2d**) (500 mg, 1.56 mmol, 1.2 equiv), according to the general method. FC (silica, hexane/diethyl ether 4/1): yield 687 mg (74%). Mp: 167 °C.  $[\alpha]_D^{25} = -200$  ( $c = 0.18$ ,  $\text{CHCl}_3$ ).  $^1\text{H}$  NMR ( $\text{CDCl}_3$ ):  $\delta$  7.65–7.58 (m, 2 ar H), 7.44–7.33 (m, 10 ar H), 7.10–6.88 (m, 11 ar H), 6.12 (d,  $J = 2.2$ , pz CH), 6.01 (dq,  $J = 6.9$ ,  $J = 3.5$ , CHMeN), 5.38 (s, trp CH), 4.90 (m, cp H), 4.50 (m, cp H), 4.09 (s, 5 cp H), 4.00 (m, cp H), 2.10 (d,  $J = 6.9$ , CHMeN).  $^{13}\text{C}\{^1\text{H}\}$  NMR ( $\text{CDCl}_3$ ):  $\delta$  147.3, 146.3, 145.7 (ar C), 139.2–122.7 (ar C, ar CH), 107.1 (pz CH), 93.5 (cp C), 75.8 (cp C), 71.6 (cp CH), 70.1 (cp CH), 69.8 (cp CH), 69.6 (5 cp CH), 55.7 (CHMeN), 21.8 (CHMeN).  $^{31}\text{P}\{^1\text{H}\}$  NMR ( $\text{CDCl}_3$ ):  $\delta$  -26.0 (s). IR ( $\text{cm}^{-1}$ ): 1519, 1456, 1434, 1247, 1220, 1168, 1106, 1055, 916, 821, 749, 697, 631. MS ( $m/z$ ): 716 ( $\text{M}^+$ ), 651 ( $\text{M}^+ - \text{cp}$ ), 441, 397 ( $\text{M}^+ - \text{Hpz}$ ), 331 (397 - cp), 320 (Hpz<sup>+</sup>), 289, 252 (trp<sup>+</sup>), 212 ( $\text{M}^+ - \text{Hpz} - \text{PPh}_2$ , 100%), 183, 121 (Fe-cp<sup>+</sup>). Anal. Calcd for  $\text{C}_{47}\text{H}_{37}\text{FeN}_2\text{P} \cdot \text{CH}_2\text{Cl}_2$ : C, 71.92; H, 4.90; N, 3.49. Found: C, 71.95; H, 5.14; N, 3.46.

**1-[(S)-1-[(R)-2-(Diphenylphosphino)ferrocenyl]ethyl]-3,5-dimethyl-1H-pyrazole (3ae):** from **1a** (2.5 g, 5.6 mmol) and 3,5-dimethyl-1H-pyrazole (**2e**) (0.65 g, 6.8 mmol, 1.2 equiv), according to the general method. Yield: 1.52 g (55%). Mp: 127 °C dec.  $[\alpha]_D^{25} = +329$  ( $c = 0.42$ ,  $\text{CHCl}_3$ ).  $^1\text{H}$  NMR ( $\text{CDCl}_3$ ):  $\delta$  7.53–6.68 (m, 10 ar H), 5.58 (dq,  $J = 6.9$ ,  $J = 2.6$ , CHMeN), 5.06 (s, pz CH), 4.80 (m, cp H), 4.36 (m, cp H), 4.05 (s, 5 cp H), 3.73 (m, cp H), 2.13 (s, pzMe), 1.95 (s, pzMe), 1.70 (d,  $J = 6.9$ , CHMeN).  $^{13}\text{C}\{^1\text{H}\}$  NMR ( $\text{CDCl}_3$ ):  $\delta$  150–120 (10 ar CH), 103.9 (pz CH), 94.0 (cp C), 70.3 (2 cp CH), 69.5 (5 cp CH), 69.2 (cp CH), 51.5 (CHMeN), 20.3 (CHMeN), 13.4 (pzMe), 10.9 (pzMe).  $^{31}\text{P}\{^1\text{H}\}$  NMR ( $\text{CDCl}_3$ ):  $\delta$  -24.1 (s). MS ( $m/z$ ): 492 ( $\text{M}^+$ ), 396 ( $\text{M}^+ - \text{Hpz}$ ), 331 (396 - cp), 276 (331 - Fe), 56 (Fe, 100%). Anal. Calcd for  $\text{C}_{29}\text{H}_{25}\text{FeN}_2\text{P}$ : C, 70.72; H, 5.96; N, 5.69. Found: C, 70.74; H, 6.01; N, 5.59.

**1-[(S)-1-[(R)-2-(Diphenylphosphino)ferrocenyl]ethyl]-5-methyl-3-(trifluoromethyl)-1H-pyrazole (3af):** from **1a** (441 mg, 1 mmol) and 3-methyl-5-(trifluoromethyl)-1H-pyrazole (**2f**) (150 mg, 1 mmol), according to the general method. Yield: 188 mg (35%). Mp: 148 °C.  $[\alpha]_D^{25} = +282$  ( $c = 0.66$ ,  $\text{CHCl}_3$ ).  $^1\text{H}$  NMR ( $\text{CDCl}_3$ ):  $\delta$  7.53–6.61 (m, 10 ar H), 5.72 (dq,  $J = 6.9$ ,  $J = 2.6$ , CHMeN), 5.52 (s, pz CH), 4.82 (m, cp H), 4.38 (m, cp H), 4.08 (s, 5 cp H), 3.75 (m, cp H), 2.16 (s, pzMe), 1.84 (d,  $J = 6.9$ , CHMeN).  $^{13}\text{C}\{^1\text{H}\}$  NMR ( $\text{CDCl}_3$ ):  $\delta$  135–127

(10 ar CH), 102.8 (pz CH), 71.7 (cp CH), 70.9 (cp CH), 70.1 (cp CH), 69.9 (5 cp CH), 53.5 (CHMeN), 20.7 (CHMeN), 10.9 (pzMe).  $^{31}\text{P}\{^1\text{H}\}$  NMR ( $\text{CDCl}_3$ ):  $\delta$  -24.7 (s). MS ( $m/z$ ): 562 ( $\text{M}^+$ ), 396 ( $\text{M}^+ - \text{Hpz}$ ), 331 (396 - cp), 276 (331 - Fe, 100%). Anal. Calcd for  $\text{C}_{29}\text{H}_{26}\text{F}_3\text{FeN}_2\text{P}$ : C, 63.62; H, 5.03; N, 5.02. Found: C, 63.75; H, 4.80; N, 5.13.

**1-[(S)-1-[(R)-2-(Diphenylphosphino)ferrocenyl]ethyl]-5-methyl-3-isopropyl-1H-pyrazole (3ag):** from **1a** (662 mg, 1.50 mmol) and 3-methyl-5-isopropyl-1H-pyrazole (**2g**) (280 mg, 2.25 mmol, 1.5 equiv), according to the general method. FC (silica, hexane/ethyl acetate 4/1): yield 205 mg (red oil, 26%).  $[\alpha]_D^{25} = +256$  ( $c = 0.16$ ,  $\text{CHCl}_3$ ).  $^1\text{H}$  NMR ( $\text{CDCl}_3$ ):  $\delta$  7.80–6.60 (m, 10 ar H), 5.61 (dq,  $J = 6.9$ ,  $J = 2.6$ , CHMeN), 5.20 (s, pz CH), 4.78 (m, cp H), 4.34 (m, cp H), 4.04 (s, 5 cp H), 3.80 (m, cp H), 2.75 (st,  $J = 6.1$ ,  $^i\text{Pr}$  CH), 2.09 (s, pzMe), 1.84 (d,  $J = 6.9$ , CHMeN), 1.05 (d,  $J = 6.1$ ,  $2^i\text{Pr}$  CH<sub>3</sub>).  $^{13}\text{C}\{^1\text{H}\}$  NMR ( $\text{CDCl}_3$ ):  $\delta$  135–125 (10 ar CH), 100.4 (pz CH), 71.4 (cp CH), 70.4 (cp CH), 69.5 (5 cp CH), 69.2 (cp CH), 51.8 (CHMeN), 27.3 ( $^i\text{Pr}$  CH), 22.9 ( $2^i\text{Pr}$  CH<sub>3</sub>), 20.5 (CHMeN), 11.1 (pzMe).  $^{31}\text{P}\{^1\text{H}\}$  NMR ( $\text{CDCl}_3$ ):  $\delta$  -23.9 (s). MS ( $m/z$ ): 520 ( $\text{M}^+$ ), 396 ( $\text{M}^+ - \text{Hpz}$ ), 331 (396 - cp), 109 (pz - Me, 100%). No correct EA is obtained.

**1-[(S)-1-[(R)-2-(Diphenylphosphino)ferrocenyl]ethyl]-5-methyl-3-cyclohexyl-1H-pyrazole (3ah):** from **1a** (300 mg, 0.68 mmol) and 5-methyl-3-cyclohexyl-1H-pyrazole (**2h**) (134 mg, 0.82 mmol, 1.2 equiv), according to the general method. FC (silica, hexane/ethyl acetate 10/1, 2%  $\text{NEt}_3$ ): yield 100 mg (26%). Mp: 94 °C.  $[\alpha]_D^{25} = +297$  ( $c = 0.39$ ,  $\text{CHCl}_3$ ).  $^1\text{H}$  NMR ( $\text{CDCl}_3$ ):  $\delta$  7.54 (m, 2 ar H), 7.37 (m, 3 ar H), 7.10–6.95 (m, 3 ar H), 6.71 (m, 2 ar H), 5.62 (dq,  $J = 6.9$ ,  $J = 2.9$ , CHMeN), 5.23 (s, pz CH), 4.81 (m, cp H), 4.37 (m, cp H), 4.04 (s, 5 cp H), 3.79 (m, cp H), 2.47 (m, Cy CH), 2.10 (s, pzMe), 1.86 (d,  $J = 6.9$ , CHMeN), 1.83–1.62 (m, 4 Cy CH), 1.42–0.86 (m, 6 Cy CH).  $^{13}\text{C}\{^1\text{H}\}$  NMR ( $\text{CDCl}_3$ ):  $\delta$  156.7, 136.8–127.0, 117.6 (10 ar CH), 101.0 (pz CH), 94.7 (cp C), 78.0 (cp C), 71.4 (cp CH), 70.8 (cp CH), 69.8 (5 cp CH), 69.6 (cp CH), 52.0 (CHMeN), 37.4 (Cy CH), 33.6, 26.5, 26.3 (Cy CH), 20.9 (CHMeN), 11.5 (pzMe).  $^{31}\text{P}\{^1\text{H}\}$  NMR ( $\text{CDCl}_3$ ):  $\delta$  -23.8 (s). IR ( $\text{cm}^{-1}$ ): 1654, 1550, 1434, 1247, 1170, 1106, 1038, 818, 743, 696. MS ( $m/z$ ): 560 ( $\text{M}^+$ , 100%), 545 ( $\text{M}^+ - \text{CH}_3$ ), 495 ( $\text{M}^+ - \text{cp}$ ), 396 ( $\text{M}^+ - \text{Hpz}$ ), 360, 331 (396 - cp), 276 (396 - Fe-cp), 253, 212, 183, 164 ( $\text{Hpz}^+$ ). Anal. Calcd for  $\text{C}_{34}\text{H}_{37}\text{FeN}_2\text{P} \cdot 0.5\text{CH}_2\text{Cl}_2$ : C, 68.72; H, 6.35; N, 4.65. Found: C, 68.65; H, 6.29; N, 4.55.

**1-[(S)-1-[(R)-2-(Diphenylphosphino)ferrocenyl]ethyl]-5-methyl-3-ethoxy-1H-pyrazole (3ai):** from **1a** (441 mg, 1 mmol) and 3-methyl-5-ethoxy-1H-pyrazole (**2i**) (189 mg, 1.5 mmol, 1.5 equiv), according to the general method. FC (silica, hexane/ethyl acetate 5/1, 2%  $\text{NEt}_3$ ): yield 125 mg (24%). Mp: 116 °C.  $[\alpha]_D^{25} = +293$  ( $c = 0.195$ ,  $\text{CHCl}_3$ ).  $^1\text{H}$  NMR ( $\text{CDCl}_3$ ):  $\delta$  7.53–6.71 (m, 10 ar H), 5.46 (dq,  $J = 6.9$ ,  $J = 2.6$ , CHMeN), 4.77 (m, cp H), 4.73 (s, pz CH), 4.33 (m, cp H), 4.05 (s, 5 cp H), 3.84 (2 q,  $J = 6.9$ , diast Et CH<sub>2</sub>), 3.68 (m, cp H), 2.06 (s, pzMe), 1.79 (d,  $J = 6.9$ , CHMeN), 1.29 (t,  $J = 6.9$ , Et CH<sub>3</sub>).  $^{13}\text{C}\{^1\text{H}\}$  NMR ( $\text{CDCl}_3$ ):  $\delta$  138–127 (10 ar CH), 88.1 (pz CH), 71.0 (cp CH), 70.8 (cp CH), 69.6 (5 cp CH), 69.5 (cp CH), 64.3 (Et CH<sub>2</sub>), 51.5 (CHMeN), 20.6 (CHMeN), 14.9 (Et CH<sub>3</sub>), 10.8 (pzMe).  $^{31}\text{P}\{^1\text{H}\}$  NMR ( $\text{CDCl}_3$ ):  $\delta$  -23.6 (s). MS ( $m/z$ ): 522 ( $\text{M}^+$ , 100%), 493 ( $\text{M}^+ - \text{Et}$ ), 457 ( $\text{M}^+ - \text{cp}$ ), 396 ( $\text{M}^+ - \text{Hpz}$ ), 331 (396 - cp), 276 (331 - Fe). Anal. Calcd for  $\text{C}_{30}\text{H}_{31}\text{FeN}_2\text{OP}$ : C, 68.24; H, 5.91; N, 4.99. Found: C, 68.97; H, 5.98; N, 5.36.

**1-[(S)-1-[(R)-2-(Diphenylphosphino)ferrocenyl]ethyl]-5-methyl-3-phenyl-1H-pyrazole (3aj):** from **1a** (300 mg, 0.68 mmol) and 3-methyl-5-phenyl-1H-pyrazole (**2j**) (129 mg, 0.82 mmol, 1.2 equiv), according to the general method. FC (silica, hexane/ethyl acetate 5/1): yield 208 mg (55%). Mp: 171 °C dec.  $[\alpha]_D^{25} = +338$  ( $c = 0.45$ ,  $\text{CHCl}_3$ ).  $^1\text{H}$  NMR ( $\text{CDCl}_3$ ):  $\delta$  7.61–6.68 (m, 15 ar H), 5.66 (dq,  $J = 6.9$ ,  $J = 2.9$ , CHMeN), 5.61 (s, pz CH), 4.85 (m, cp H), 4.38 (m, cp H), 4.09 (s, 5 cp H), 3.74 (m, cp H), 2.15 (s, pzMe), 1.91 (d,  $J = 6.9$ , CHMeN).  $^{13}\text{C}\{^1\text{H}\}$  NMR ( $\text{CDCl}_3$ ):  $\delta$  149.3, 138.0, 137.6, 136.9 (ar C), 135.0–125.2 (ar CH), 101.6 (pz CH), 93.7 (cp C), 75.2 (cp C), 71.2 (cp

CH), 70.7 (cp CH), 69.5 (5 cp CH), 69.1 (cp CH), 52.1 (CHMeN), 20.7 (CHMeN), 11.0 (pzMe).  $^{31}\text{P}\{^1\text{H}\}$  NMR ( $\text{CDCl}_3$ ):  $\delta$  -23.9 (s). MS ( $m/z$ ): 554 ( $\text{M}^+$ , 100%), 489 ( $\text{M}^+ - \text{cp}$ ), 396 ( $\text{M}^+ - \text{Hpz}$ ), 331 (396 - cp), 276 (331 - Fe). Anal. Calcd for  $\text{C}_{34}\text{H}_{31}\text{FeN}_2\text{P}$ : C, 73.65; H, 5.64; N, 5.05. Found: C, 73.52; H, 5.85; N, 4.94.

**1-[(S)-1-[(R)-2-(Diphenylphosphino)ferrocenyl]ethyl]-5-methyl-3-(2-pyridyl)-1H-pyrazole (3ak):** from **1a** (300 mg, 0.68 mmol) and 5-methyl-3-(2-pyridyl)-1H-pyrazole (**2k**) (130 mg, 0.82 mmol, 1.2 equiv), according to the general method. FC (silica, hexane/ethyl acetate 2/1): yield 242 mg (64%). Mp: 130 °C.  $[\alpha]_D^{25} = +330$  ( $c = 0.74$ ,  $\text{CHCl}_3$ ).  $^1\text{H}$  NMR ( $\text{CDCl}_3$ ):  $\delta$  8.50 (m, py CH), 7.81 (m, py CH), 7.62–7.46 (m, 3 ar H), 7.30 (m, 3 ar H), 7.04–6.67 (m, 6 ar H), 6.01 (s, pz CH), 5.69 (dq,  $J = 6.9$ ,  $J = 2.9$ , CHMeN), 4.82 (m, cp H), 4.34 (m, cp H), 4.06 (s, 5 cp H), 3.73 (m, cp H), 2.15 (s, pzMe), 1.87 (d,  $J = 6.9$ , CHMeN).  $^{13}\text{C}\{^1\text{H}\}$  NMR ( $\text{CDCl}_3$ ):  $\delta$  152.9 (py C), 149.5 (ar C), 148.6 (py CH), 137.9–126.8 (ar C, ar CH), 121.2, 119.6 (py CH), 103.1 (pz CH), 93.4 (cp C), 75.4 (cp C), 71.2 (cp CH), 70.6 (cp CH), 69.5 (5 cp CH), 69.0 (cp CH), 52.4 (CHMeN), 20.7 (CHMeN), 11.0 (pzMe).  $^{31}\text{P}\{^1\text{H}\}$  NMR ( $\text{CDCl}_3$ ):  $\delta$  -24.1 (s). IR ( $\text{cm}^{-1}$ ): 1592, 1499, 1426, 1246, 1204, 1106, 824, 784, 744, 699. MS ( $m/z$ ): 555 ( $\text{M}^+$ ), 490 ( $\text{M}^+ - \text{cp}$ , 100%), 396 ( $\text{M}^+ - \text{Hpz}$ ), 331 (396 - cp), 305, 279, 214. Anal. Calcd for  $\text{C}_{33}\text{H}_{30}\text{FeN}_3\text{P} \cdot \text{CH}_2\text{Cl}_2$ : C, 63.77; H, 5.04; N, 6.56. Found: C, 64.35; H, 4.96; N, 6.60.

**1-[(S)-1-[(R)-2-(Diphenylphosphino)ferrocenyl]ethyl]-5-methyl-3-(3-pyridyl)-1H-pyrazole (3al):** from **1a** (300 mg, 0.68 mmol) and 5-methyl-3-(3-pyridyl)-1H-pyrazole (**2l**) (118 mg, 0.75 mmol, 1.1 equiv), according to the general method. FC (silica, hexane/ethyl acetate 2/1, 2%  $\text{NEt}_3$ ): yield 122 mg (32%). Mp: 167 °C.  $[\alpha]_D^{25} = +294$  ( $c = 0.56$ ,  $\text{CHCl}_3$ ).  $^1\text{H}$  NMR ( $\text{CDCl}_3$ ):  $\delta$  8.76, 8.44 (m, py CH), 7.87 (m, py CH), 7.48 (m, 2 ar H), 7.32 (m, 3 ar H), 7.20 (m, ar H), 6.90–6.65 (m, 5 ar H), 5.70 (dq,  $J = 6.9$ ,  $J = 2.9$ , CHMeN), 5.61 (s, pz CH), 4.83 (m, cp H), 4.37 (m, cp H), 4.08 (s, 5 cp H), 3.73 (m, cp H), 2.18 (s, pzMe), 1.88 (d,  $J = 6.9$ , CHMeN).  $^{13}\text{C}\{^1\text{H}\}$  NMR ( $\text{CDCl}_3$ ):  $\delta$  148.7 (ar C), 147.6, 146.8 (py CH), 146.2, 138.0, 135.0–126.7 (ar-C, ar CH), 122.9 (py CH), 101.7 (pz CH), 93.1 (cp C), 75.8 (cp C), 71.3 (cp CH), 70.6 (cp CH), 69.5 (5 cp CH), 69.2 (cp CH), 52.4 (CHMeN), 20.5 (CHMeN), 11.0 (pzMe).  $^{31}\text{P}\{^1\text{H}\}$  NMR ( $\text{CDCl}_3$ ):  $\delta$  -24.5 (s). IR ( $\text{cm}^{-1}$ ): 1547, 1475, 1432, 1371, 1312, 1248, 1182, 1170, 1127, 1105, 1043, 1027, 1002, 829, 772, 742, 696. MS ( $m/z$ ): 555 ( $\text{M}^+$ , 100%), 540 ( $\text{M}^+ - \text{CH}_3$ ), 490 ( $\text{M}^+ - \text{cp}$ ), 396 ( $\text{M}^+ - \text{Hpz}$ ), 370, 355, 331 (396 - cp), 276 (396 - Fe-cp), 183. Anal. Calcd for  $\text{C}_{33}\text{H}_{30}\text{FeN}_3\text{P}$ : C, 71.36; H, 5.44; N, 7.57. Found: C, 71.34; H, 5.16; N, 7.54.

**1-[(S)-1-[(R)-2-(Diphenylphosphino)ferrocenyl]ethyl]-5-methyl-3-(4-pyridyl)-1H-pyrazole (3am):** from **1a** (300 mg, 0.68 mmol) and 5-methyl-3-(4-pyridyl)-1H-pyrazole (**2m**) (130 mg, 0.82 mmol, 1.2 equiv), according to the general method. FC (silica, diethyl ether, 2%  $\text{NEt}_3$ ): yield 140 mg (37%) as orange crystals (from dichloromethane/hexane). Mp: 158 °C.  $[\alpha]_D^{25} = +365$  ( $\text{CHCl}_3$ ,  $c = 0.44$ ).  $^1\text{H}$  NMR ( $\text{CDCl}_3$ ):  $\delta$  8.51 (m, 2 py CH), 7.50–7.42 (m, 4 ar H), 7.35 (m, 3 ar H), 6.91–6.64 (m, 5 ar H), 5.72 (dq,  $J = 6.9$ ,  $J = 2.9$ , CHMeN), 5.66 (s, pz CH), 4.83 (m, cp H), 4.39 (m, cp H), 4.10 (s, 5 cp H), 3.74 (m, cp H), 2.19 (s, pzMe), 1.88 (d,  $J = 6.9$ , CHMeN).  $^{13}\text{C}\{^1\text{H}\}$  NMR ( $\text{CDCl}_3$ ):  $\delta$  149.5 (py CH), 146.5, 141.3, 138.2–126.9 (ar C, ar CH), 119.5 (py CH), 102.3 (pz CH), 93.1 (cp C), 75.5 (cp C), 71.3 (cp CH), 70.6 (cp CH), 69.5 (5 cp CH), 69.1 (cp CH), 52.6 (CHMeN), 20.5 (CHMeN), 11.0 (pzMe).  $^{31}\text{P}\{^1\text{H}\}$  NMR ( $\text{CDCl}_3$ ):  $\delta$  -24.5 (s). IR ( $\text{cm}^{-1}$ ): 1603, 1433, 1247, 1106, 747, 698. MS ( $m/z$ ): 555 ( $\text{M}^+$ , 100%), 490 ( $\text{M}^+ - \text{cp}$ ), 396 ( $\text{M}^+ - \text{Hpz}$ ), 370, 355, 331 (396 - cp), 276 (396 - Fe-cp), 253, 183. Anal. Calcd for  $\text{C}_{33}\text{H}_{30}\text{FeN}_3\text{P} \cdot \text{CH}_2\text{Cl}_2$ : C, 63.77; H, 5.04; N, 6.56. Found: C, 63.64; H, 5.02; N, 6.42.

**1-[(S)-1-[(R)-2-(Diphenylphosphino)ferrocenyl]ethyl]-3-(2,4-dimethoxyphenyl)-5-methyl-1H-pyrazole (3an):** from **1a** (300 mg, 0.68 mmol) and 3-(2,4-dimethoxyphenyl)-5-methyl-1H-pyrazole (**2n**) (178 mg, 0.82 mmol, 1.2 equiv), according to the general method. FC (silica, hexane/ethyl acetate 5/1):

yield 80 mg (19%). Mp: 83 °C.  $[\alpha]^{25}_D = +314$  ( $c = 0.54$ ,  $\text{CHCl}_3$ ).  $^1\text{H NMR}$  ( $\text{CDCl}_3$ ):  $\delta$  7.70 (d,  $J = 8.4$ , ar H), 7.54 (m, 2 ar H), 7.38 (m, 3 ar H), 6.95–6.80 (m, 3 ar H), 6.71 (m, 2 ar H), 6.51 (m, 2 ar H), 5.83 (s, pz CH), 5.65 (dq,  $J = 6.8$ ,  $J = 2.9$ ,  $\text{CHMeN}$ ), 4.87 (m, cp H), 4.39 (m, cp H), 4.09 (s, 5 cp H), 3.75 (m, cp H), 2.15 (s, pzMe), 1.91 (d,  $J = 6.8$ ,  $\text{CHMeN}$ ).  $^{13}\text{C}\{^1\text{H}\}$  NMR ( $\text{CDCl}_3$ ):  $\delta$  159.5, 157.3 (Ph-COMe), 146.1, 136.6–126.8 (ar C, ar CH), 116.5 (Ph C), 104.9, 104.5, 98.3 (2 Ph CH, pz CH), 94.1 (cp C), 74.9 (cp C), 71.1 (cp CH), 70.8 (cp CH), 69.4 (5 cp CH), 69.1 (cp CH), 55.1 ( $\text{CHMeN}$ ), 20.8 ( $\text{CHMeN}$ ), 11.0 (pzMe).  $^{31}\text{P}\{^1\text{H}\}$  NMR ( $\text{CDCl}_3$ ):  $\delta$  -23.9 (s). IR ( $\text{cm}^{-1}$ ): 1613, 1583, 1517, 1465, 1432, 1302, 1280, 1247, 1208, 1159, 1037, 822, 742, 697. MS ( $m/z$ ): 614 ( $\text{M}^+$ ), 549 ( $\text{M}^+ - \text{cp}$ ), 396 ( $\text{M}^+ - \text{Hpz}$ , 100%), 331 (396 - cp), 288, 252, 218 ( $\text{Hpz}^+$ ). Anal. Calcd for  $\text{C}_{36}\text{H}_{35}\text{FeN}_2\text{O}_2\text{P}$ : C, 70.36; H, 5.74; N, 4.56. Found: C, 70.63; H, 5.96; N, 4.28.

**1-[(S)-1-[(R)-2-(Diphenylphosphino)ferrocenyl]ethyl]-5-methyl-3-(1-naphthyl)-1H-pyrazole (3ao)**: from **1a** (300 mg, 0.68 mmol) and 5-methyl-3-( $\alpha$ -naphthyl)-1H-pyrazole (**2o**) (212 mg, 1.02 mmol, 1.5 equiv), according to the general method. FC (silica, hexane/ethyl acetate 6/1): yield 183 mg (45%). Mp: 192 °C dec.  $[\alpha]^{25}_D = +386$  ( $c = 0.45$ ,  $\text{CHCl}_3$ ).  $^1\text{H NMR}$  ( $\text{CDCl}_3$ ):  $\delta$  8.52 (m, ar H), 7.76 (m, ar H), 7.56–7.38 (m, 9 ar H), 6.94–6.79 (m, 5 ar H), 6.51 (m, 2 ar H), 5.75 (dq,  $J = 6.9$ ,  $J = 3.1$ ,  $\text{CHMeN}$ ), 5.69 (s, pz CH), 4.93 (m, cp H), 4.43 (m, cp H), 4.12 (s, 5 cp H), 3.80 (m, cp H), 2.25 (s, pzMe), 1.98 (d,  $J = 6.9$ ,  $\text{CHMeN}$ ).  $^{13}\text{C}\{^1\text{H}\}$  NMR ( $\text{CDCl}_3$ ):  $\delta$  149.2, 138.0–125.0 (ar C, ar CH), 116.5 (ar C), 104.9 (pz CH), 94.4 (cp C), 73.8 (cp C), 71.1 (cp CH), 70.8 (2 cp CH), 69.5 (5 cp CH), 51.9 ( $\text{CHMeN}$ ), 21.0 ( $\text{CHMeN}$ ), 11.0 (pzMe).  $^{31}\text{P}\{^1\text{H}\}$  NMR ( $\text{CDCl}_3$ ):  $\delta$  -23.9 (s). IR ( $\text{cm}^{-1}$ ): 1549, 1433, 1418, 1370, 1318, 1248, 1108, 1002, 822, 804, 792, 778, 743, 696. MS ( $m/z$ ): 604 ( $\text{M}^+$ , 100%), 589 ( $\text{M}^+ - \text{CH}_3$ ), 539 ( $\text{M}^+ - \text{cp}$ ), 396 ( $\text{M}^+ - \text{Hpz}$ ), 331 (396 - cp), 302, 276 (396 - Fe-cp), 208 ( $\text{Hpz}^+$ ). Anal. Calcd for  $\text{C}_{38}\text{H}_{33}\text{FeN}_2\text{P}$ : C, 75.50; H, 5.50; N, 4.63. Found: C, 75.52; H, 5.31; N, 4.60.

**1-[(S)-1-[(R)-2-(Diphenylphosphino)ferrocenyl]ethyl]-5-methyl-3-(2-naphthyl)-1H-pyrazole (3ap)**: from **1a** (300 mg, 0.68 mmol) and 5-methyl-3-( $\beta$ -naphthyl)-1H-pyrazole (**2p**) (212 mg, 1.02 mmol, 1.5 equiv), according to the general method. FC (silica, hexane/toluene or diethyl ether 5/1, 2%  $\text{NEt}_3$ ): yield 114 mg (28%). Mp: 129 °C.  $[\alpha]^{25}_D = +337$  ( $c = 0.34$ ,  $\text{CHCl}_3$ ).  $^1\text{H NMR}$  ( $\text{CDCl}_3$ ):  $\delta$  8.02 (d,  $J = 0.8$ , ar H), 7.88–7.82 (m, 4 ar H), 7.58–7.36 (m, 7 ar H), 6.90–6.73 (m, 5 ar H), 5.76 (s, pz CH), 5.75 (dq,  $J = 6.9$ ,  $J = 3.1$ ,  $\text{CHMeN}$ ), 4.93 (m, cp H), 4.43 (m, cp H), 4.14 (s, 5 cp H), 3.78 (m, cp H), 2.22 (s, pzMe), 1.96 (d,  $J = 6.9$ ,  $\text{CHMeN}$ ).  $^{13}\text{C}\{^1\text{H}\}$  NMR ( $\text{CDCl}_3$ ):  $\delta$  149.2, 138.0–123.2 (ar C, ar CH), 101.9 (pz CH), 93.6 (cp C), 75.4 (cp C), 71.3 (cp CH), 70.7 (cp CH), 69.5 (5 cp CH), 69.1 (cp CH), 52.3 ( $\text{CHMeN}$ ), 20.6 ( $\text{CHMeN}$ ), 11.1 (pzMe).  $^{31}\text{P}\{^1\text{H}\}$  NMR ( $\text{CDCl}_3$ ):  $\delta$  -23.9 (s). IR ( $\text{cm}^{-1}$ ): 1630, 1550, 1433, 1416, 1385, 1318, 1247, 1169, 1126, 1106, 1044, 1000, 858, 821, 779, 743, 697. MS ( $m/z$ ): 604 ( $\text{M}^+$ , 100%), 589 ( $\text{M}^+ - \text{CH}_3$ ), 539 ( $\text{M}^+ - \text{cp}$ ), 396 ( $\text{M}^+ - \text{Hpz}$ ), 331 (396 - cp), 302, 276 (396 - Fe-cp), 208 ( $\text{Hpz}^+$ ). Anal. Calcd for  $\text{C}_{38}\text{H}_{33}\text{FeN}_2\text{P}$ : C, 75.50; H, 5.50; N, 4.63. Found: C, 75.60; H, 5.34; N, 4.43.

**1-[(S)-1-[(R)-2-(Diphenylphosphino)ferrocenyl]ethyl]-3-(9-anthryl)-5-methyl-1H-pyrazole (3aq)**: from **1a** (513 mg, 1.16 mmol) and 3-(9-anthryl)-5-methyl-1H-pyrazole (**2q**) (360 mg, 1.39 mmol, 1.2 equiv), according to the general method, yielding a 5:1 mixture of the two regioisomers **3aq** and **3aq'** (see below). FC (silica, hexane/diethyl ether 5/1): yield 280 mg (37%). Mp: 202 °C dec.  $[\alpha]^{25}_D = +338$  ( $c = 0.24$ ,  $\text{CHCl}_3$ ).  $^1\text{H NMR}$  ( $\text{CDCl}_3$ ):  $\delta$  8.43 (s, ar H), 7.98 (d,  $J = 9.4$ , ar H), 7.67–7.60 (m, 2 ar H), 7.47–7.32 (m, 7 ar H), 7.10–6.94 (m, 5 ar H), 5.85 (dq,  $J = 6.9$ ,  $J = 3.3$ ,  $\text{CHMeN}$ ), 5.81 (s, pz CH), 4.93 (m, cp H), 4.42 (m, cp H), 4.08 (s, 5 cp H), 3.91 (m, cp H), 2.32 (s, pzMe), 2.09 (d,  $J = 6.9$ ,  $\text{CHMeN}$ ).  $^{13}\text{C}\{^1\text{H}\}$  NMR ( $\text{CDCl}_3$ ):  $\delta$  146.6, 139.4, 137.2, 135.4–124.6 (ar C, ar CH), 107.9 (pz CH), 94.6 (cp C), 74.6 (cp C), 71.0 (cp CH), 70.9 (cp CH), 69.8 (cp CH), 69.5 (5 cp CH), 51.9 ( $\text{CHMeN}$ ), 21.6 ( $\text{CHMeN}$ ), 11.2 (pzMe).  $^{31}\text{P}\{^1\text{H}\}$  NMR ( $\text{CDCl}_3$ ):  $\delta$  -24.2 (s).

IR ( $\text{cm}^{-1}$ ): 1546, 1434, 1416, 1318, 1247, 1168, 1106, 1013, 888, 823, 799, 734, 721, 695. MS ( $m/z$ ): 654 ( $\text{M}^+$ ), 639 ( $\text{M}^+ - \text{CH}_3$ ), 589 ( $\text{M}^+ - \text{cp}$ ), 396 ( $\text{M}^+ - \text{Hpz}$ ), 331 (396 - cp), 275 (396 - Fe-cp), 258 ( $\text{Hpz}^+$ , 100%). Anal. Calcd for  $\text{C}_{42}\text{H}_{35}\text{FeN}_2\text{P}$ : C, 77.07; H, 5.39; N, 4.28. Found: C, 77.20; H, 5.33; N, 4.22.

**1-[(S)-1-[(R)-2-(Diphenylphosphino)ferrocenyl]ethyl]-5-(9-anthryl)-3-methyl-1H-pyrazole (3aq')**: regioisomer of **3aq** (for synthesis see above). FC (silica, hexane/diethyl ether 5/1): yield 53 mg (7%). Mp: 217 °C.  $[\alpha]^{25}_D = +265$  ( $c = 0.36$ ,  $\text{CHCl}_3$ ).  $^1\text{H NMR}$  ( $\text{CDCl}_3$ ):  $\delta$  8.52 (s, ar H), 8.02 (m, ar H), 7.59 (d,  $J = 8.8$ , ar H), 7.51–7.27 (m, 10 ar H), 7.11–6.99 (m, 3 ar H), 6.90–6.84 (m, 2 ar H), 6.01 (s, pz CH), 5.10 (dq,  $J = 6.9$ ,  $J = 2.4$ ,  $\text{CHMeN}$ ), 4.12 (m, cp H), 4.00 (m, cp H), 3.82 (s, 5 cp H), 3.76 (m, cp H), 2.28 (s, pzMe), 1.68 (d,  $J = 6.9$ ,  $\text{CHMeN}$ ).  $^{13}\text{C}\{^1\text{H}\}$  NMR ( $\text{CDCl}_3$ ):  $\delta$  146.4, 140.1, 138.2, 137.9, 135.3–124.6 (ar C, ar CH), 108.7 (pz CH), 95.5 (cp C), 74.2 (cp C), 70.7 (cp CH), 69.5 (cp CH), 68.7 (cp CH), 69.3 (5 cp CH), 53.7 ( $\text{CHMeN}$ ), 21.8 ( $\text{CHMeN}$ ), 13.6 (pzMe).  $^{31}\text{P}\{^1\text{H}\}$  NMR ( $\text{CDCl}_3$ ):  $\delta$  -24.0 (s). IR ( $\text{cm}^{-1}$ ): 1625, 1540, 1432, 1367, 1164, 1108, 890, 822, 739, 699. MS ( $m/z$ ): 654 ( $\text{M}^+$ , 100%), 589 ( $\text{M}^+ - \text{cp}$ ), 454, 396 ( $\text{M}^+ - \text{Hpz}$ ), 378, 331 (396 - cp), 275 (396 - Fe-cp), 258 ( $\text{Hpz}^+$ ). Anal. Calcd for  $\text{C}_{42}\text{H}_{35}\text{FeN}_2\text{P} \cdot 0.5\text{H}_2\text{O}$ : C, 75.00; H, 5.54; N, 4.17. Found: C, 75.06; H, 5.47; N, 4.15.

**1-[(R)-1-[(S)-2-(Diphenylphosphino)ferrocenyl]ethyl]-3-ferrocenyl-5-methyl-1H-pyrazole (3ar)**: from **1a'** (300 mg, 0.68 mmol) and 3-ferrocenyl-5-methyl-1H-pyrazole (**2r**) (218 mg, 0.82 mmol, 1.2 equiv), according to the general method. FC (silica, hexane/toluene or diethyl ether 4/1, 2%  $\text{NEt}_3$ ): yield 80 mg (18%). Mp: 163 °C dec.  $[\alpha]^{25}_D = -283$  ( $c = 0.36$ ,  $\text{CHCl}_3$ ).  $^1\text{H NMR}$  ( $\text{CDCl}_3$ ):  $\delta$  7.56–7.48 (m, 2 ar H), 7.38 (m, 3 ar H), 7.12–6.92 (m, 3 ar H), 6.75 (m, 2 ar H), 5.54 (dq,  $J = 6.8$ ,  $J = 2.8$ ,  $\text{CHMeN}$ ), 5.47 (s, pz CH), 4.75 (m, cp H), 4.48 (m, 2 cp H), 4.34 (m, cp H), 4.15 (m, 2 cp H), 4.07 (s, 5 cp H), 3.98 (m, 5 cp H), 3.75 (m, cp H), 2.03 (s, pzMe), 1.92 (d,  $J = 6.8$ ,  $\text{CHMeN}$ ).  $^{13}\text{C}\{^1\text{H}\}$  NMR ( $\text{CDCl}_3$ ):  $\delta$  147.8, 138.7–126.9 (ar C, ar CH), 102.4 (pz CH), 94.4 (cp C), 74.8, 72.3 (cp C), 70.0 (cp CH), 69.5 (5 cp CH), 69.0 (5 cp CH), 67.4 (4 cp CH), 66.6 (4 cp CH), 51.8 ( $\text{CHMeN}$ ), 21.0 ( $\text{CHMeN}$ ), 10.9 (pzMe).  $^{31}\text{P}\{^1\text{H}\}$  NMR ( $\text{CDCl}_3$ ):  $\delta$  -23.8 (s). IR ( $\text{cm}^{-1}$ ): 1568, 1433, 1404, 1248, 1105, 1001, 821, 748, 821, 696. MS ( $m/z$ ): 662 ( $\text{M}^+$ ), 397 ( $\text{M}^+ - \text{Hpz}$ ), 347, 331 (397 - cp), 266 ( $\text{Hpz}^+$ ), 212 ( $\text{M}^+ - \text{Hpz} - \text{PPh}_2$ , 100%), 121 (Fe-cp $^+$ ). Anal. Calcd for  $\text{C}_{38}\text{H}_{35}\text{Fe}_2\text{N}_2\text{P}$ : C, 68.91; H, 5.33; N, 4.23. Found: C, 68.91; H, 5.44; N, 4.15.

**1-[(S)-1-[(R)-2-(Diphenylphosphino)ferrocenyl]ethyl]-3,4,5-trimethyl-1H-pyrazole (3as)**: from **1a** (441 mg, 1 mmol) and 3,4,5-trimethyl-1H-pyrazole (**2s**) (110 mg, 1 mmol), according to the general method. Yield: 205 mg (40%).  $[\alpha]^{25}_D = +310$  ( $c = 0.27$ ,  $\text{CHCl}_3$ ).  $^1\text{H NMR}$  ( $\text{CDCl}_3$ ):  $\delta$  7.50–6.73 (m, 10 ar H), 5.63 (dq,  $J = 6.8$ ,  $J = 2.5$ ,  $\text{CHMeN}$ ), 4.80 (m, cp H), 4.34 (m, cp H), 4.08 (s, 5 cp H), 3.67 (m, cp H), 2.01 (s, pzMe), 1.87 (s, pzMe), 1.80 (d,  $J = 6.8$ ,  $\text{CHMeN}$ ), 1.36 (s, pzMe).  $^{13}\text{C}\{^1\text{H}\}$  NMR ( $\text{CDCl}_3$ ):  $\delta$  140–127 (10 ar CH), 71.7 (cp CH), 70.6 (cp CH), 70.3 (cp C), 69.8 (5 cp CH), 69.2 (cp CH), 52.0 ( $\text{CHMeN}$ ), 20.4 ( $\text{CHMeN}$ ), 11.9 (pzMe), 9.7 (pzMe), 7.6 (pzMe).  $^{31}\text{P}\{^1\text{H}\}$  NMR ( $\text{CDCl}_3$ ):  $\delta$  -24.2 (s). MS ( $m/z$ ): 506 ( $\text{M}^+$ ), 396 ( $\text{M}^+ - \text{Hpz}$ ), 331 (396 - cp), 276 (331 - Fe), 149 (100%). Anal. Calcd for  $\text{C}_{30}\text{H}_{31}\text{FeN}_2\text{P}$ : C, 71.17; H, 6.17; N, 5.53. Found: C, 71.26; H, 6.30; N, 5.60.

**1-[(S)-1-[(R)-2-(Diphenylphosphino)ferrocenyl]ethyl]-3,5-dimethyl-4-nitro-1H-pyrazole (3at)**: from **1a** (157 mg, 0.35 mmol) and 3,5-dimethyl-4-nitro-1H-pyrazole (**2t**) (157 mg, 0.39 mmol, 1.1 equiv), according to the general method. FC (silica, hexane/ethyl acetate 3/1, 2%  $\text{NEt}_3$ ): yield 120 mg (63%). Mp: 163 °C.  $[\alpha]^{25}_D = +296$  ( $c = 0.175$ ,  $\text{CHCl}_3$ ).  $^1\text{H NMR}$  ( $\text{CDCl}_3$ ):  $\delta$  7.47–6.75 (m, 10 ar H), 5.74 (dq,  $J = 6.9$ ,  $J = 2.5$ ,  $\text{CHMeN}$ ), 4.78 (m, cp H), 4.40 (m, cp H), 4.13 (s, 5 cp H), 3.73 (m, cp H), 2.52 (s, pzMe), 2.19 (s, pzMe), 1.82 (d,  $J = 6.9$ ,  $\text{CHMeN}$ ).  $^{13}\text{C}\{^1\text{H}\}$  NMR ( $\text{CDCl}_3$ ):  $\delta$  140–127 (10 ar CH), 72.2 (cp CH), 70.2 (cp CH), 69.9 (5 cp CH), 69.6 (cp CH), 53.6

(CHMeN), 19.7 (CHMeN), 14.3 (pzMe), 11.6 (pzMe).  $^{31}\text{P}\{^1\text{H}\}$  NMR ( $\text{CDCl}_3$ ):  $\delta$  -26.1 (s). IR (KBr): 3068, 3049, 2977, 2932, 1560, 1489, 1458, 1433, 1360. MS ( $m/z$ ): 537 ( $\text{M}^+$ , 100%), 491 ( $\text{M}^+ - \text{NO}_2$ ), 396 ( $\text{M}^+ - \text{Hpz}$ ), 331 (396 - cp), 276 (331 - Fe). Anal. Calcd for  $\text{C}_{29}\text{H}_{28}\text{FeN}_3\text{O}_2\text{P}$ : C, 64.82; H, 5.25; N, 7.82. Found: C, 64.97; H, 5.40; N, 7.79.

**1-[(S)-1-[(R)-2-(Diphenylphosphino)ferrocenyl]ethyl]-4-bromo-3,5-dimethyl-1H-pyrazole (3au)**: from **1a** (441 mg, 1 mmol) and 4-bromo-3,5-dimethyl-1H-pyrazole (**2u**) (364 mg, 2 mmol, 2 equiv), according to the general method. Yield: 352 mg (62%). Mp: 150 °C dec. [ $\alpha\text{D}^{25}$ ] = +284 ( $c = 0.505$ ,  $\text{CHCl}_3$ ).  $^1\text{H}$  NMR ( $\text{CDCl}_3$ ):  $\delta$  7.53–6.61 (m, 10 ar H), 5.63 (dq,  $J = 6.9$ ,  $J = 2.5$ , CHMeN), 4.78 (m, cp H), 4.38 (m, cp H), 4.09 (s, 5 cp H), 3.73 (m, cp H), 2.10 (s, pzMe), 1.89 (s, pzMe), 1.78 (d,  $J = 6.9$ , CHMeN).  $^{13}\text{C}\{^1\text{H}\}$  NMR ( $\text{CDCl}_3$ ):  $\delta$  150–120 (10 ar CH), 71.6 (cp CH), 70.4 (cp CH), 69.6 (5 cp CH), 69.1 (cp CH), 53.3 (CHMeN), 20.0 (CHMeN), 12.0 (pzMe), 11.6 (pzMe).  $^{31}\text{P}\{^1\text{H}\}$  NMR ( $\text{CDCl}_3$ ):  $\delta$  -25.0 (s). MS ( $m/z$ ): 570 ( $\text{M}^+$ , 100%), 491 ( $\text{M}^+ - \text{Br}$ ), 396 ( $\text{M}^+ - \text{Hpz}$ ), 331 (396 - cp), 276 (331 - Fe), 183. Anal. Calcd for  $\text{C}_{29}\text{H}_{28}\text{BrFeN}_3\text{P}$ : C, 60.97; H, 4.94; N, 4.90. Found: C, 60.89; H, 4.89; N, 4.86.

**1-[(S)-1-[(R)-2-(Diphenylphosphino)ferrocenyl]ethyl]-3,5-bis(trifluoromethyl)-1H-pyrazole (3av)**: from **1a** (441 mg, 1 mmol) and 3,5-bis(trifluoromethyl)-1H-pyrazole (**2v**) (205 mg, 1 mmol), according to the general method. FC (silica, hexane/ethyl acetate 10/1, 2%  $\text{NEt}_3$ ): yield 210 mg (35%). Mp: 125 °C dec. [ $\alpha\text{D}^{25}$ ] = +154 ( $c = 0.465$ ,  $\text{CHCl}_3$ ).  $^1\text{H}$  NMR ( $\text{CDCl}_3$ ):  $\delta$  7.51–6.75 (m, 10 ar H), 6.26 (s, pz CH), 5.97 (dq,  $J = 6.9$ ,  $J = 2.5$ , CHMeN), 4.81 (m, cp H), 4.44 (m, cp H), 4.15 (s, 5 cp H), 3.73 (m, cp H), 1.94 (d,  $J = 6.9$ , CHMeN).  $^{13}\text{C}\{^1\text{H}\}$  NMR ( $\text{CDCl}_3$ ):  $\delta$  138–127 (10 ar CH), 104.9 (pz CH), 90.4 (cp CH), 71.8 (cp CH), 71.1 (cp CH), 69.7 (5 cp CH), 69.5 (cp CH), 56.7 (CHMeN), 22.5 (q,  $J = 549$ ,  $\text{pzCF}_3$ ), 21.2 (CHMeN).  $^{19}\text{F}\{^1\text{H}\}$  NMR ( $\text{CDCl}_3$ ):  $\delta$  -58.9 (d,  $J = 21$ ,  $\text{pzCF}_3$ ), -62.2 (s,  $\text{pzCF}_3$ ).  $^{31}\text{P}$  NMR ( $\text{CDCl}_3$ ):  $\delta$  -25.5 (q,  $J = 21$ ). MS ( $m/z$ ): 600 ( $\text{M}^+$ , 100%), 396 ( $\text{M}^+ - \text{Hpz}$ ), 276 (396 - Fe-cp), 183, 166, 121. Anal. Calcd for  $\text{C}_{29}\text{H}_{23}\text{F}_6\text{FeN}_3\text{P}$ : C, 58.02; H, 3.86; N, 4.67. Found: C, 56.44; H, 3.80; N, 4.50.

**1-[(S)-1-[(R)-2-(Diphenylphosphino)ferrocenyl]ethyl]-3,5-bis(isopropyl)-1H-pyrazole (3aw)**: from **1a** (574 mg, 1.3 mmol) and 3,5-isopropyl-1H-pyrazole (**2w**) (2.80 g, 18.4 mmol, 14 equiv), according to the general method. FC (silica, toluene/diethyl ether 9/1, 2%  $\text{NEt}_3$ ): yield 308 mg (43%). Mp: 130 °C dec. [ $\alpha\text{D}^{25}$ ] = +265 ( $c = 0.525$ ,  $\text{CHCl}_3$ ).  $^1\text{H}$  NMR ( $\text{CDCl}_3$ ):  $\delta$  7.60–6.65 (m, 10 ar H), 5.52 (dq,  $J = 6.9$ ,  $J = 2.5$ , CHMeN), 5.28 (s, pz CH), 4.80 (m, cp H), 4.36 (m, cp H), 4.03 (s, 5 cp H), 3.70 (m, cp H), 3.21 (st,  $J = 6.9$ ,  $^i\text{Pr}$  CH), 1.92 (d,  $J = 6.9$ , CHMeN), 1.11 (d,  $J = 6.9$ , 3  $^i\text{Pr}$   $\text{CH}_3$ ), 0.75 (d,  $J = 6.9$ ,  $^i\text{Pr}$   $\text{CH}_3$ ).  $^{13}\text{C}\{^1\text{H}\}$  NMR ( $\text{CDCl}_3$ ):  $\delta$  160–120 (10 ar CH), 103.9 (pz CH), 71.8 (cp CH), 70.8 (2 cp CH), 69.4 (6 cp CH), 50.7 (CHMeN), 21.2 (CHMeN), 27.5 ( $^i\text{Pr}$  CH), 24.8 ( $^i\text{Pr}$  CH), 23.8 ( $^i\text{Pr}$   $\text{CH}_3$ ), 22.7 ( $^i\text{Pr}$   $\text{CH}_3$ ), 21.5 ( $^i\text{Pr}$   $\text{CH}_3$ ), 21.1 (CHMeN), 0.7 ( $^i\text{Pr}$   $\text{CH}_3$ ).  $^{31}\text{P}\{^1\text{H}\}$  NMR ( $\text{CDCl}_3$ ):  $\delta$  -22.9 (s). MS ( $m/z$ ): 548 ( $\text{M}^+$ ), 396 ( $\text{M}^+ - \text{Hpz}$ , 100%), 331 (396 - cp), 212 (396 -  $\text{PPh}_2$ ). Anal. Calcd for  $\text{C}_{33}\text{H}_{37}\text{FeN}_3\text{P}$ : C, 72.26; H, 6.80; N, 5.11. Found: C, 72.33; H, 6.58; N, 5.03.

**1-[(R)-1-[(S)-2-(Bis(4-fluorophenyl)phosphino)ferrocenyl]ethyl]-3,5-dimethyl-1H-pyrazole (3be)**: from **1b** (400 mg, 0.83 mmol) and 3,5-dimethyl-1H-pyrazole (**2e**) (96 mg, 1 mmol, 1.2 equiv), according to the general method. FC (silica, hexane/ethyl acetate 1/1, 1%  $\text{NEt}_3$ ): yield 293 mg (67%). Mp: 136 °C. [ $\alpha\text{D}^{25}$ ] = -308 ( $c = 0.205$ ,  $\text{CHCl}_3$ ).  $^1\text{H}$  NMR ( $\text{CDCl}_3$ ):  $\delta$  7.48–6.66 (m, 8 ar H), 5.57 (dq,  $J = 6.9$ ,  $J = 2.5$ , CHMeN), 5.07 (s, pz CH), 4.82 (m, cp H), 4.38 (m, cp H), 4.06 (s, 5 cp H), 3.68 (m, cp H), 2.12 (s, pzMe), 1.93 (s, pzMe), 1.78 (d,  $J = 6.9$ , CHMeN).  $^{13}\text{C}\{^1\text{H}\}$  NMR ( $\text{CDCl}_3$ ):  $\delta$  165–120 (8 ar CH), 104.0 (pz CH), 71.5 (cp CH), 71.0 (cp CH), 69.9 (5 cp CH), 69.7 (cp CH), 52.1 (CHMeN), 20.5 (CHMeN), 13.7 (pzMe), 11.3 (pzMe).  $^{19}\text{F}\{^1\text{H}\}$  NMR ( $\text{CDCl}_3$ ):  $\delta$  -111.87 (d,  $J = 4$ , ar F), -114.87 (d,  $J = 5$ , ar F).  $^{31}\text{P}\{^1\text{H}\}$  NMR ( $\text{CDCl}_3$ ):  $\delta$  -26.6 (s). MS ( $m/z$ ): 528 ( $\text{M}^+$ , 100%), 463 ( $\text{M}^+ - \text{cp}$ ), 432 ( $\text{M}^+ - \text{Hpz}$ ), 367 (482 -

cp), 311 (367 - Fe). Anal. Calcd for  $\text{C}_{28}\text{H}_{27}\text{F}_2\text{FeN}_2\text{P}$ : C, 65.92; H, 5.15; N, 5.30. Found: C, 66.02; H, 5.22; N, 5.30.

**1-[(R)-1-[(S)-2-(Bis(4-chlorophenyl)phosphino)ferrocenyl]ethyl]-3,5-dimethyl-1H-pyrazole (3ce)**: from **1c** (340 mg, 0.67 mmol) and 3,5-dimethyl-1H-pyrazole (**2e**) (77 mg, 0.8 mmol, 1.2 equiv), according to the general method. FC (silica, hexane/ethyl acetate 2/1, 1%  $\text{NEt}_3$ ): yield 222 mg (59%). Mp: 150 °C. [ $\alpha\text{D}^{25}$ ] = -354 ( $c = 0.28$ ,  $\text{CHCl}_3$ ).  $^1\text{H}$  NMR ( $\text{CDCl}_3$ ):  $\delta$  7.40–6.61 (m, 8 ar H), 5.57 (dq,  $J = 6.9$ ,  $J = 2.5$ , CHMeN), 5.09 (s, pz CH), 4.82 (m, cp H), 4.38 (m, cp H), 4.07 (s, 5 cp H), 3.67 (m, cp H), 2.14 (s, pzMe), 1.94 (s, pzMe), 1.77 (d,  $J = 6.9$ , CHMeN).  $^{13}\text{C}\{^1\text{H}\}$  NMR ( $\text{CDCl}_3$ ):  $\delta$  147–127 (8 ar CH), 104.2 (pz CH), 71.3 (2 cp CH), 70.9 (cp CH), 69.8 (5 cp CH), 51.9 (CHMeN), 20.3 (CHMeN), 13.6 (pzMe), 11.4 (pzMe).  $^{31}\text{P}\{^1\text{H}\}$  NMR ( $\text{CDCl}_3$ ):  $\delta$  -26.0 (s). MS ( $m/z$ ): 560 ( $\text{M}^+$ ), 464 ( $\text{M}^+ - \text{Hpz}$ ), 398 (464 - cp), 343 (398 - Fe), 121 (Fe-cp, 100%). Anal. Calcd for  $\text{C}_{28}\text{H}_{27}\text{Cl}_2\text{FeN}_2\text{P}$ : C, 62.06; H, 4.85; N, 4.99. Found: C, 61.95; H, 5.08; N, 4.92.

**1-[(R)-1-[(S)-2-(Bis(4-methylphenyl)phosphino)ferrocenyl]ethyl]-3,5-dimethyl-1H-pyrazole (3de)**: from **1d** (354 mg, 0.75 mmol) and 3,5-dimethyl-1H-pyrazole (**2e**) (109 mg, 1.5 mmol, 2 equiv), according to the general method. FC (silica, hexane/ethyl acetate 5/1, 1%  $\text{NEt}_3$ ): yield 96 mg (25%). Mp: 156 °C. [ $\alpha\text{D}^{25}$ ] = -323 ( $c = 0.45$ ,  $\text{CHCl}_3$ ).  $^1\text{H}$  NMR ( $\text{CDCl}_3$ ):  $\delta$  7.41–6.56 (m, 8 ar H), 5.57 (dq,  $J = 6.9$ ,  $J = 2.6$ , CHMeN), 5.05 (s, pz CH), 4.78 (m, cp H), 4.33 (m, cp H), 4.04 (s, 5 cp H), 3.73 (m, cp H), 2.35 (s,  $\text{tolMe}$ ), 2.21 (s,  $\text{tolMe}$ ), 2.15 (s, pzMe), 1.95 (s, pzMe), 1.80 (d,  $J = 6.9$ , CHMeN).  $^{13}\text{C}\{^1\text{H}\}$  NMR ( $\text{CDCl}_3$ ):  $\delta$  135–128 (8 ar CH), 104.1 (pz CH), 94.2 (cp C), 71.7 (cp CH), 70.5 (cp CH), 69.8 (5 cp CH), 69.4 (cp CH), 51.8 (CHMeN), 21.4 (s,  $\text{tolMe}$ ), 21.2 (s,  $\text{tolMe}$ ), 20.7 (CHMeN), 13.7 (pzMe), 11.3 (pzMe).  $^{31}\text{P}\{^1\text{H}\}$  NMR ( $\text{CDCl}_3$ ):  $\delta$  -24.9 (s). MS ( $m/z$ ): 520 ( $\text{M}^+$ ), 424 ( $\text{M}^+ - \text{Hpz}$ , 100%), 359 (424 - cp). Anal. Calcd for  $\text{C}_{31}\text{H}_{33}\text{FeN}_2\text{P}$ : C, 71.55; H, 6.61; N, 5.30. Found: C, 71.54; H, 6.39; N, 5.38.

**1-[(R)-1-[(S)-2-(Bis(4-(trifluoromethyl)phenyl)phosphino)ferrocenyl]ethyl]-3-(2-pyridyl)-1H-pyrazole (3ec)**: from **1e** (200 mg, 0.35 mmol) and 3-(2-pyridine)-1H-pyrazole (**2c**) (60 mg, 0.42 mmol, 1.2 equiv), according to the general method. FC (silica, hexane/ethyl acetate 3/1, 1%  $\text{NEt}_3$ ): yield 140 mg (60%) of a 2:1 mixture of the two regioisomers, **3ec** and **3ec'**, respectively. **3ec** was isolated in analytically pure form by crystallization from dichloromethane/hexane in 25% yield. Mp: 201 °C dec. [ $\alpha\text{D}^{25}$ ] = -323 ( $c = 0.76$ ,  $\text{CHCl}_3$ ).  $^1\text{H}$  NMR ( $\text{CDCl}_3$ ):  $\delta$  8.51 (m, py H), 7.64–7.50 (m, 5 ar H, pz CH), 7.08 (m, 2 ar H), 7.01 (m, 2 ar H), 6.79 (m, 2 ar H), 6.31 (d, pz CH,  $J = 2.3$ ), 5.90 (dq,  $J = 6.9$ ,  $J = 3.1$ , CHMeN), 4.80 (m, cp H), 4.46 (m, cp H), 4.10 (s, 5 cp H), 3.78 (m, cp H), 1.95 (d,  $J = 6.9$ , CHMeN).  $^{13}\text{C}\{^1\text{H}\}$  NMR ( $\text{CDCl}_3$ ):  $\delta$  150.2 (ar C), 148.8 (py CH), 135.5 (py CH), 135.0, 131.6 (2 Ph CH), 127.4 (pz CH), 124.6, 123.9 (2 Ph CH), 121.5, 119.3 (2 py CH), 103.8 (pz CH), 93.3 (cp C), 73.9 (cp C), 71.7 (cp CH), 70.0 (cp CH), 69.9 (5 cp CH), 69.7 (cp CH), 56.1 (CHMeN), 20.8 (CHMeN).  $^{19}\text{F}\{^1\text{H}\}$  NMR ( $\text{CDCl}_3$ ):  $\delta$  -63.2 (s), -63.3 (s).  $^{31}\text{P}\{^1\text{H}\}$  NMR ( $\text{CDCl}_3$ ):  $\delta$  -24.6 (s) [**3ec'** -24.8 (s)]. IR ( $\text{cm}^{-1}$ ): 1607, 1594, 1489, 1397, 1324, 1246, 1168, 1128, 1106, 1060, 1016, 830, 766, 698. MS ( $m/z$ ): 677 ( $\text{M}^+$ ), 658 ( $\text{M}^+ - \text{F}$ ), 612 ( $\text{M}^+ - \text{cp}$ , 100%), 532 ( $\text{M}^+ - \text{Hpz}$ ), 518, 411, 291, 265 ( $\text{M}^+ - \text{Fe-cp} - (\text{PhCF}_3)_2$ ), 145 ( $\text{Hpz}^+$ ). Anal. Calcd for  $\text{C}_{34}\text{H}_{26}\text{F}_3\text{FeN}_3\text{P}$ : C, 60.29; H, 3.87; N, 6.20. Found: C, 60.31; H, 3.83; N, 6.09.

**1-[(R)-1-[(S)-2-(Bis(4-(trifluoromethyl)phenyl)phosphino)ferrocenyl]ethyl]-3,5-dimethyl-1H-pyrazole (3ee)**: from **1e** (300 mg, 0.52 mmol) and 3,5-dimethyl-1H-pyrazole (**2e**) (60 mg, 0.62 mmol, 1.2 equiv), according to the general method. FC (silica, hexane/ethyl acetate 10/1, 1%  $\text{NEt}_3$ ): yield 218 mg (67%). Mp: 112 °C. [ $\alpha\text{D}^{25}$ ] = -263 ( $c = 1.0$ ,  $\text{CHCl}_3$ ).  $^1\text{H}$  NMR ( $\text{CDCl}_3$ ):  $\delta$  7.64–7.53 (m, 4 Ph H), 7.25 (m, 2 Ph H), 6.84 (m, 2 Ph H), 5.58 (dq,  $J = 6.9$ ,  $J = 2.5$ , CHMeN), 4.99 (s, pz CH), 4.88 (m, cp H), 4.43 (m, cp H), 4.10 (s, 5 cp H), 3.66 (m, cp H), 2.15 (s, pzMe), 1.90 (s, pzMe), 1.79 (d,  $J = 6.9$ , CHMeN).  $^{13}\text{C}\{^1\text{H}\}$  NMR ( $\text{CDCl}_3$ ):  $\delta$  146.6, 141.8, 140.0, 136.6 (ar C), 135.0, 131.6 (2 Ph CH), 124.6, 123.9 (2 Ph CH), 104.0 (pz CH), 93.7



(cp C), 73.2 (cp C), 71.0 (cp CH), 70.9 (2 cp CH), 69.6 (5 cp CH), 51.8 (CHMeN), 19.9 (CHMeN), 13.1 (s, pzMe), 10.9 (s, pzMe).  $^{19}\text{F}\{^1\text{H}\}$  NMR ( $\text{CDCl}_3$ ):  $\delta$  -63.0 (s).  $^{31}\text{P}\{^1\text{H}\}$  NMR ( $\text{CDCl}_3$ ):  $\delta$  -24.0 (s). IR ( $\text{cm}^{-1}$ ): 1607, 1555, 1396, 1323, 1163, 1125, 1106, 1068, 1016, 829, 700. MS ( $m/z$ ): 628 ( $\text{M}^+$ ), 563 ( $\text{M}^+ - \text{cp}$ ), 532 ( $\text{M}^+ - \text{Hpz}$ ), 411 (532 - Fe-cp), 216 (Fe(cp) $_2$ P, 100%), 96 (Hpz $^+$ ). Anal. Calcd for  $\text{C}_{31}\text{H}_{27}\text{F}_6\text{FeN}_2\text{P}$ : C, 59.26; H, 4.33; N, 4.46. Found: C, 59.67; H, 4.78; N, 4.24.

**1-[(R)-1-[(S)-2-(Bis(4-(trifluoromethyl)phenyl)phosphino)ferrocenyl]ethyl]-5-methyl-3-phenyl-1H-pyrazole (3ej)**: from **1e** (300 mg, 0.52 mmol) and 5-methyl-3-phenyl-1H-pyrazole (**2j**) (100 mg, 0.62 mmol, 1.2 equiv), according to the general method. FC (silica, hexane/ethyl acetate 20/1, 1%  $\text{NEt}_3$ ): yield 210 mg (59%). Mp: 102 °C.  $[\alpha]_D^{25} = -292$  ( $c = 0.55$ ,  $\text{CHCl}_3$ ).  $^1\text{H}$  NMR ( $\text{CDCl}_3$ ):  $\delta$  7.70–7.57 (m, 6 Ph H), 7.37–7.22 (m, 3 Ph H), 7.05 (m, 2 Ph H), 6.83 (m, 2 Ph H), 5.71 (dq,  $J = 6.9$ ,  $J = 2.7$ , CHMeN), 5.57 (s, pz CH), 4.94 (m, cp H), 4.47 (m, cp H), 4.15 (s, 5 cp H), 3.70 (m, cp H), 2.19 (s, pzMe), 1.91 (d,  $J = 6.9$ , CHMeN).  $^{13}\text{C}\{^1\text{H}\}$  NMR ( $\text{CDCl}_3$ ):  $\delta$  149.7, 142.4, 141.6 (ar C), 137.7–124.4 (ar C, ar CH), 101.9 (pz CH), 93.9 (cp C), 73.5 (cp C), 71.5 (cp CH), 71.4 (cp CH), 69.9 (6 cp CH), 52.8 (CHMeN), 20.4 (CHMeN), 11.4 (s, pzMe).  $^{19}\text{F}\{^1\text{H}\}$  NMR ( $\text{CDCl}_3$ ):  $\delta$  -63.1 (s), -63.2 (s).  $^{31}\text{P}\{^1\text{H}\}$  NMR ( $\text{CDCl}_3$ ):  $\delta$  -23.6 (s). IR ( $\text{cm}^{-1}$ ): 1606, 1396, 1323, 1167, 1126, 1106, 1060, 1016, 830, 763, 696. MS ( $m/z$ ): 690 ( $\text{M}^+$ , 100%), 625 ( $\text{M}^+ - \text{cp}$ ), 532 ( $\text{M}^+ - \text{Hpz}$ ), 467 (532 - cp), 412 (532 - Fe-cp), 373, 345, 278, 217 ( $\text{M}^+ - \text{Fe-cp} - (\text{PhCF}_3)_2$ ), 158 (Hpz $^+$ ). Anal. Calcd for  $\text{C}_{36}\text{H}_{29}\text{F}_6\text{FeN}_2\text{P}$ : C, 62.63; H, 4.23; N, 4.06. Found: C, 62.83; H, 4.30; N, 3.81.

**1-[(R)-1-[(S)-2-(Bis(4-(trifluoromethyl)phenyl)phosphino)ferrocenyl]ethyl]-3,5-bis(trifluoromethyl)-1H-pyrazole (3ev)**: from **1e** (300 mg, 0.52 mmol) and 3,5-bis(trifluoromethyl)-1H-pyrazole (**2v**) (204 mg, 1.04 mmol, 2 equiv), according to the general method. FC (silica, hexane/ethyl acetate 10/1, 2%  $\text{NEt}_3$ ): yield 193 mg (51%). Mp: 73 °C.  $[\alpha]_D^{25} = -214$  ( $c = 0.45$ ,  $\text{CHCl}_3$ ).  $^1\text{H}$  NMR ( $\text{CDCl}_3$ ):  $\delta$  7.65–7.55 (m, 4 Ph H), 7.27 (m, 2 Ph H), 6.87 (m, 2 Ph H), 6.23 (s, pz CH), 5.91 (dq,  $J = 6.7$ ,  $J = 3.7$ , CHMeN), 4.88 (m, cp H), 4.51 (m, cp H), 4.16 (s, 5 cp H), 3.72 (m, cp H), 1.91 (d,  $J = 6.7$ , CHMeN).  $^{13}\text{C}\{^1\text{H}\}$  NMR ( $\text{CDCl}_3$ ):  $\delta$  141.8, 140.2 (ar C), 134.9, 131.9 (2 Ph CH), 124.7, 124.3 (2 Ph CH), 104.9 (pz CH), 90.5 (cp C), 73.9 (cp C), 71.8 (cp CH), 71.5 (cp CH), 70.1 (cp CH), 69.8 (5 cp CH), 56.7 (CHMeN), 21.1 (CHMeN).  $^{19}\text{F}\{^1\text{H}\}$  NMR ( $\text{CDCl}_3$ ):  $\delta$  -59.0 (d, pz  $\text{CF}_3$ ,  $J = 21.5$ ), -62.5 (s, pz  $\text{CF}_3$ ), -63.2, -63.5 (s, 2 Ph $\text{CF}_3$ ).  $^{31}\text{P}\{^1\text{H}\}$  NMR ( $\text{CDCl}_3$ ):  $\delta$  -25.3 ( $q$ ,  $J = 21.5$ ). IR ( $\text{cm}^{-1}$ ): 1608, 1561, 1396, 1324, 1270, 1208, 1169, 1129, 1107, 1061, 1017, 830, 700. MS ( $m/z$ ): 736 ( $\text{M}^+$ , 100%), 717, 615, 532 ( $\text{M}^+ - \text{Hpz}$ ), 412 (532 - Fe-cp), 321 (PR $_2^+$ ), 234, 121 (Fe-cp $^+$ ). Anal. Calcd for  $\text{C}_{31}\text{H}_{21}\text{F}_{12}\text{FeN}_2\text{P}$ : C, 50.57; H, 2.87; N, 3.80. Found: C, 50.72; H, 3.11; N, 3.62.

**1-[(R)-1-[(S)-2-(Bis(4-(dimethylamino)phenyl)phosphino)ferrocenyl]ethyl]-3,5-dimethyl-1H-pyrazole (3fe)**: from **1f** (100 mg, 0.19 mmol) and 3,5-dimethyl-1H-pyrazole (**2e**) (70 mg, 0.73 mmol, 3.8 equiv), according to the general method. FC (silica, hexane/ethyl acetate 10/1, 2%  $\text{NEt}_3$ ): yield 55 mg (50%). Mp: 177 °C.  $[\alpha]_D^{25} = -366$  ( $c = 0.13$ ,  $\text{CHCl}_3$ ).  $^1\text{H}$  NMR ( $\text{CDCl}_3$ ):  $\delta$  7.38–6.38 (m, 8 ar H), 5.56 (dq,  $J = 6.9$ ,  $J = 2.7$ , CHMeN), 5.08 (s, pz CH), 4.74 (m, cp H), 4.30 (m, cp H), 4.08 (s, 5 cp H), 3.75 (m, cp H), 2.97 (s, 2 NMe), 2.84 (s, 2 NMe), 2.05 (s, pzMe), 2.00 (s, pzMe), 1.82 (d,  $J = 6.9$ , CHMeN).  $^{13}\text{C}\{^1\text{H}\}$  NMR ( $\text{CDCl}_3$ ):  $\delta$  136–112 (8 ar CH), 104.0 (pz CH), 71.5 (cp CH), 70.3 (cp CH), 69.7 (5 cp CH), 68.9 (cp CH), 51.6 (CHMeN), 40.5 (s, 2 NMe), 40.5 (s, 2 NMe), 20.8 (CHMeN), 12.7 (pzMe), 11.5 (pzMe).  $^{31}\text{P}\{^1\text{H}\}$  NMR ( $\text{CDCl}_3$ ):  $\delta$  -28.5 (s). MS ( $m/z$ ): 578 ( $\text{M}^+$ , 100%), 513 ( $\text{M}^+ - \text{cp}$ ), 482 ( $\text{M}^+ - \text{Hpz}$ ), 417 (482 - cp), 362 (417 - Fe). Anal. Calcd for  $\text{C}_{33}\text{H}_{39}\text{FeN}_4\text{P}$ : C, 68.51; H, 6.79; N, 9.68. Found: C, 68.11; H, 7.13; N, 9.48.

**1-[(R)-1-[(S)-2-(Bis(4-methoxyphenyl)phosphino)ferrocenyl]ethyl]-3,5-dimethyl-1H-pyrazole (3ge)**: from **1g** (472 mg, 1 mmol) and 3,5-dimethyl-1H-pyrazole (**2e**) (144 mg, 1.5 mmol, 1.5 equiv), according to the general method. FC (silica,

hexane/ethyl acetate 5/1, 2%  $\text{NEt}_3$ ): yield 321 mg (57%). Mp: 167 °C.  $[\alpha]_D^{25} = -324$  ( $c = 0.38$ ,  $\text{CHCl}_3$ ).  $^1\text{H}$  NMR ( $\text{CDCl}_3$ ):  $\delta$  7.43–6.51 (m, 8 ar H), 5.56 (dq,  $J = 6.9$ ,  $J = 2.6$ , CHMeN), 5.07 (s, pz CH), 4.78 (m, cp H), 4.34 (m, cp H), 4.06 (s, 5 cp H), 3.81 (s, OMe), 3.72 (m, cp H), 3.71 (s, OMe), 2.12 (s, pzMe), 1.97 (s, pzMe), 1.79 (d,  $J = 6.9$ , CHMeN).  $^{13}\text{C}\{^1\text{H}\}$  NMR ( $\text{CDCl}_3$ ):  $\delta$  137–113 (8 ar CH), 104.0 (pz CH), 71.6 (cp CH), 70.5 (cp CH), 69.7 (5 cp CH), 69.2 (cp CH), 55.1 (s, OMe), 55.0 (s, OMe), 51.7 (CHMeN), 20.5 (CHMeN), 13.7 (pzMe), 11.3 (pzMe).  $^{31}\text{P}\{^1\text{H}\}$  NMR ( $\text{CDCl}_3$ ):  $\delta$  -27.6 (s). MS ( $m/z$ ): 552 ( $\text{M}^+$ , 100%), 537 ( $\text{M}^+ - \text{Me}$ ), 487 ( $\text{M}^+ - \text{cp}$ ), 456 ( $\text{M}^+ - \text{Hpz}$ ), 391 (456 - cp), 335 (391 - Fe). Anal. Calcd for  $\text{C}_{31}\text{H}_{33}\text{FeN}_2\text{O}_2\text{P}$ : C, 67.22; H, 5.90; N, 4.79. Found: C, 67.40; H, 6.02; N, 5.07.

**1-[(R)-1-[(S)-2-(Bis(4-methoxyphenyl)phosphino)ferrocenyl]ethyl]-5-methyl-3-phenyl-1H-pyrazole (3gj)**: from **1g** (275 mg, 0.55 mmol) and 5-methyl-3-phenyl-1H-pyrazole (**2j**) (130 mg, 0.82 mmol, 1.5 equiv), according to the general method. FC (silica, hexane/ethyl acetate 5/1, 2%  $\text{NEt}_3$ ): yield 66 mg (20%). Mp: 112 °C.  $[\alpha]_D^{25} = -333$  ( $c = 0.27$ ,  $\text{CHCl}_3$ ).  $^1\text{H}$  NMR ( $\text{CDCl}_3$ ):  $\delta$  7.61–7.15 (m, 6 Ph H), 6.99–6.62 (m, 5 Ph H), 6.34 (m, 2 Ph H), 5.66 (dq,  $J = 6.9$ ,  $J = 2.8$ , CHMeN), 5.60 (s, pz CH), 4.83 (m, cp H), 4.37 (m, cp H), 4.13 (s, 5 cp H), 3.81 (s, OMe), 3.72 (m, cp H), 3.38 (s, OMe), 2.19 (s, pzMe), 1.89 (d,  $J = 6.9$ , CHMeN).  $^{13}\text{C}\{^1\text{H}\}$  NMR ( $\text{CDCl}_3$ ):  $\delta$  160.1, 158.7 (Ph-COMe), 149.1, 137.5–125.1, 113.9 (ar C, ar CH), 113.3, 112.9 (2 Ph CH), 101.4 (pz CH), 93.0 (cp C), 76.6 (cp C), 71.2 (cp CH), 70.6 (cp CH), 69.5 (5 cp CH), 68.8 (cp CH), 54.9 (s, OMe), 54.3 (s, OMe), 52.1 (CHMeN), 20.5 (CHMeN), 11.1 (pzMe).  $^{31}\text{P}\{^1\text{H}\}$  NMR ( $\text{CDCl}_3$ ):  $\delta$  -27.7 (s). IR ( $\text{cm}^{-1}$ ): 1593, 1497, 1462, 1440, 1284, 1246, 1176, 1095, 1030, 823, 763. MS ( $m/z$ ): 614 ( $\text{M}^+$ ), 599 ( $\text{M}^+ - \text{CH}_3$ ), 549 ( $\text{M}^+ - \text{cp}$ ), 456 ( $\text{M}^+ - \text{Hpz}$ , 100%), 391 (456 - cp), 336 (456 - Fe-cp), 158 (Hpz $^+$ , 100%). Anal. Calcd for  $\text{C}_{36}\text{H}_{35}\text{FeN}_2\text{O}_2\text{P}$ : C, 70.36; H, 5.74; N, 4.56. Found: C, 70.73; H, 5.91; N, 4.09.

**1-[(R)-1-[(S)-2-(Bis(4-methoxyphenyl)phosphino)ferrocenyl]ethyl]-3,5-bis(trifluoromethyl)-1H-pyrazole (3gv)**: from **1g** (472 mg, 1 mmol) and 3,5-bis(trifluoromethyl)-1H-pyrazole (**2v**) (306 mg, 1.5 mmol, 1.5 equiv), according to the general method. FC (silica, hexane/ethyl acetate 3/1, 2%  $\text{NEt}_3$ ): yield 183 mg (28%). Mp: 93 °C dec.  $[\alpha]_D^{25} = -200$  ( $c = 0.21$ ,  $\text{CHCl}_3$ ).  $^1\text{H}$  NMR ( $\text{CDCl}_3$ ):  $\delta$  7.39–6.52 (m, 8 ar H), 6.25 (s, pz CH), 5.91 (dq,  $J = 6.9$ ,  $J = 2.8$ , CHMeN), 4.75 (m, cp H), 4.39 (m, cp H), 4.13 (s, 5 cp H), 3.81 (s, OMe), 3.73 (m, cp H), 3.68 (s, OMe), 1.89 (d,  $J = 6.9$ , CHMeN).  $^{13}\text{C}\{^1\text{H}\}$  NMR ( $\text{CDCl}_3$ ):  $\delta$  136–113 (8 ar CH), 105.1 (pz CH), 72.1 (cp CH), 71.3 (cp CH), 70.0 (5 cp CH), 69.4 (cp CH), 57.0 (s, OMe), 55.1 (s, OMe), 54.8 (CHMeN), 21.4 (CHMeN).  $^{19}\text{F}\{^1\text{H}\}$  NMR ( $\text{CDCl}_3$ ):  $\delta$  -58.85 (d,  $J = 21$ , pz $\text{CF}_3$ ), -62.18 (s, pz $\text{CF}_3$ ).  $^{31}\text{P}\{^1\text{H}\}$  NMR ( $\text{CDCl}_3$ ):  $\delta$  -29.1 (s). MS ( $m/z$ ): 660 ( $\text{M}^+$ , 100%), 539 ( $\text{M}^+ - \text{Fe-cp}$ ), 456 ( $\text{M}^+ - \text{Hpz}$ ), 391 (456 - cp), 336 (456 - Fe-cp). Anal. Calcd for  $\text{C}_{31}\text{H}_{27}\text{F}_6\text{FeN}_2\text{O}_2\text{P}$ : C, 56.01; H, 4.65; N, 3.51. Found: C, 56.38; H, 4.12; N, 4.24.

**1-[(R)-1-[(S)-2-(Bis(3,5-dimethylphenyl)phosphino)ferrocenyl]ethyl]-3,5-dimethyl-1H-pyrazole (3he)**: from **1h** (497 mg, 1 mmol) and 3,5-dimethyl-1H-pyrazole (**2e**) (306 mg, 3.2 mmol, 3.2 equiv), according to the general method. FC (silica, hexane/ethyl acetate 5/1, 2%  $\text{NEt}_3$ ): yield 290 mg (53%). Mp: 182 °C.  $[\alpha]_D^{25} = -289$  ( $c = 0.225$ ,  $\text{CHCl}_3$ ).  $^1\text{H}$  NMR ( $\text{CDCl}_3$ ):  $\delta$  7.29–6.35 (m, 6 ar H), 5.64 (dq,  $J = 6.9$ ,  $J = 2.7$ , CHMeN), 5.21 (s, pz CH), 4.82 (m, cp H), 4.38 (m, cp H), 4.08 (s, 5 cp H), 3.81 (m, cp H), 2.36 (s, 2 PhMe), 2.12 (s, pzMe and 2 PhMe), 2.03 (s, pzMe), 1.87 (d,  $J = 6.9$ , CHMeN).  $^{13}\text{C}\{^1\text{H}\}$  NMR ( $\text{CDCl}_3$ ):  $\delta$  133–129 (6 ar CH), 104.0 (pz CH), 71.6 (cp CH), 70.4 (cp CH), 69.7 (5 cp CH), 69.3 (cp CH), 51.8 (CHMeN), 21.3 (CHMeN and 2 PhMe), 13.7 (pzMe and 2 PhMe), 11.3 (pzMe).  $^{31}\text{P}\{^1\text{H}\}$  NMR ( $\text{CDCl}_3$ ):  $\delta$  -23.9 (s). MS ( $m/z$ ): 548 ( $\text{M}^+$ , 100%), 483 ( $\text{M}^+ - \text{cp}$ ), 452 ( $\text{M}^+ - \text{Hpz}$ ), 387 (452 - cp), 332 (387 - Fe), 226 (332 - xyl), 121 (Fe-cp), 96 (Hpz $^+$ ). Anal. Calcd for  $\text{C}_{33}\text{H}_{37}\text{FeN}_2\text{P}$ : C, 72.26; H, 6.80; N, 5.11. Found: C, 72.35; H, 6.95; N, 5.05.

**1-[(R)-1-[(S)-2-(Bis(3,5-bis(trifluoromethyl)phenyl)phosphino)ferrocenyl]ethyl]-3,5-dimethyl-1H-pyrazole (3ie):** from **1i** (100 mg, 0.14 mmol) and 3,5-dimethyl-1H-pyrazole (**2e**) (27 mg, 0.28 mmol, 2 equiv), according to the general method. FC (silica, hexane/ethyl acetate 10/1, 2% NEt<sub>3</sub>): yield 67 mg (63%). Mp: 122 °C. [ $\alpha$ ]<sub>D</sub><sup>25</sup> = -251 (*c* = 0.28, CHCl<sub>3</sub>). <sup>1</sup>H NMR (CDCl<sub>3</sub>):  $\delta$  7.85–7.21 (m, 6 ar H), 5.65 (dq, *J* = 6.9, *J* = 2.7, CHMeN), 5.00 (s, pz CH), 4.84 (m, cp H), 4.45 (m, cp H), 4.07 (s, 5 cp H), 3.56 (m, cp H), 2.05 (s, pzMe), 1.72 (d, *J* = 6.9, CHMeN), 1.67 (s, pzMe). <sup>13</sup>C{<sup>1</sup>H} NMR (CDCl<sub>3</sub>):  $\delta$  147–125 (6 ar CH), 105.1 (pz CH), 71.6 (cp CH), 71.4 (cp CH), 70.1 (6 cp CH), 53.6 (CHMeN), 19.5 (CHMeN), 12.9 (pzMe), 11.5 (pzMe). <sup>19</sup>F{<sup>1</sup>H} NMR (CDCl<sub>3</sub>):  $\delta$  -63.3 (s, 4 ar CF<sub>3</sub>). <sup>31</sup>P{<sup>1</sup>H} NMR (CDCl<sub>3</sub>):  $\delta$  -23.4 (s). MS (*m/z*): 764 (M<sup>+</sup>, 100%), 643 (M<sup>+</sup> - Fe-cp), 216 (Ph with 2 CF<sub>3</sub>), 121 (Fe-cp). Anal. Calcd for C<sub>33</sub>H<sub>25</sub>F<sub>12</sub>FeN<sub>2</sub>P: C, 51.86; H, 3.30; N, 3.66. Found: C, 51.59; H, 3.54; N, 3.64.

**1-[(R)-1-[(S)-2-(Dibutylphosphino)ferrocenyl]ethyl]-3,5-dimethyl-1H-pyrazole (3je):** from **1j** (401 mg, 1 mmol) and 3,5-dimethyl-1H-pyrazole (**2e**) (192 mg, 2 mmol, 2 equiv), according to the general method. FC (silica, hexane/ethyl acetate 4/1, 2% NEt<sub>3</sub>): yield 117 mg (26%, red oil). [ $\alpha$ ]<sub>D</sub><sup>25</sup> = -249 (*c* = 0.145, CHCl<sub>3</sub>). <sup>1</sup>H NMR (CDCl<sub>3</sub>):  $\delta$  5.65 (s, pz CH), 5.58 (dq, *J* = 6.9, *J* = 2.8, CHMeN), 4.67 (m, cp H), 4.32 (m, cp H), 4.13 (s, 5 cp H), 3.42 (m, cp H), 2.32 (s, pzMe), 2.08 (s, pzMe), 1.75 (d, *J* = 6.9, CHMeN), 1.72–0.6 (m, 6 Bu CH<sub>2</sub> and 2 Bu CH<sub>3</sub>). <sup>13</sup>C{<sup>1</sup>H} NMR (CDCl<sub>3</sub>):  $\delta$  104.7 (pz CH), 69.9 (cp CH), 69.8 (5 cp CH), 69.3 (cp CH), 68.6 (cp CH), 52.5 (CHMeN), 29.5–24.3 (6 Bu CH<sub>2</sub>), 20.4 (CHMeN), 13.9 (pzMe), 13.8 (2 Bu CH<sub>3</sub>), 11.6 (pzMe). <sup>31</sup>P{<sup>1</sup>H} NMR (CDCl<sub>3</sub>):  $\delta$  -42.3 (s). MS (*m/z*): 452 (M<sup>+</sup>), 395 (M<sup>+</sup> - Bu, 100%), 299 (395 - Hpz), 243 (299 - Bu), 121 (Fe-cp), 95 (Hpz<sup>+</sup>), 56 (Fe). Anal. Calcd for C<sub>25</sub>H<sub>37</sub>FeN<sub>2</sub>P: C, 66.37; H, 8.24; N, 6.19. Found: C, 67.10; H, 7.83; N, 5.85.

**1-[(R)-1-[(S)-2-(Dibutylphosphino)ferrocenyl]ethyl]-5-methyl-3-phenyl-1H-pyrazole (3jj):** from **1j** (300 mg, 0.75 mmol) and 5-methyl-3-phenyl-1H-pyrazole (**2j**) (142 mg, 0.90 mmol, 1.2 equiv), according to the general method. FC (silica, hexane/diethyl ether 10/1): yield 54 mg (14%, orange oil). [ $\alpha$ ]<sub>D</sub><sup>25</sup> = -225 (*c* = 0.14, CHCl<sub>3</sub>). <sup>1</sup>H NMR (CDCl<sub>3</sub>):  $\delta$  7.67 (m, 2 Ph H), 7.33–7.20 (m, 3 Ph H), 6.21 (s, pz CH), 5.74 (dq, *J* = 6.9, *J* = 2.8, CHMeN), 4.71 (m, cp H), 4.36 (m, cp H), 4.18 (s, 5 cp H), 4.09 (m, cp H), 2.39 (s, pzMe), 1.86 (d, *J* = 6.9, CHMeN), 1.82–0.5 (m, 6 Bu CH<sub>2</sub> and 2 Bu CH<sub>3</sub>). <sup>13</sup>C{<sup>1</sup>H} NMR (CDCl<sub>3</sub>):  $\delta$  149.2, 137.8, 134.0 (ar C), 127.9, 126.6, 125.2 (Ph CH), 102.2 (pz CH), 92.5 (cp C), 78.2 (cp C), 69.8 (cp CH), 69.3 (5 cp CH), 69.1 (cp CH), 68.2 (cp CH), 53.1 (CHMeN), 29.5–23.9 (6 Bu CH<sub>2</sub>), 20.2 (CHMeN), 13.7 (Bu CH<sub>3</sub>), 13.3 (Bu CH<sub>3</sub>), 11.5 (pzMe). <sup>31</sup>P{<sup>1</sup>H} NMR (CDCl<sub>3</sub>):  $\delta$  -42.3 (s). MS (*m/z*): 514 (M<sup>+</sup>), 457 (M<sup>+</sup> - Bu), 372, 356 (M<sup>+</sup> - Hpz), 327, 300 (356 - Bu), 272, 258, 243, 212, 158 (Hpz<sup>+</sup>, 100%), 121 (Fe-cp<sup>+</sup>).

Anal. Calcd for C<sub>30</sub>H<sub>38</sub>FeN<sub>2</sub>P: C, 70.04; H, 7.64; N, 5.45. Found: C, 70.05; H, 7.74; N, 5.27.

**1-[(R)-1-[(S)-2-(Dicyclohexylphosphino)ferrocenyl]ethyl]-3,5-dimethyl-1H-pyrazole (3ke):** from **1k** (1.13 g, 2.5 mmol) and 3,5-dimethyl-1H-pyrazole (**2e**) (365 mg, 3.75 mmol, 1.5 equiv), according to the general method. FC (silica, hexane/ethyl acetate 10/1, 2% NEt<sub>3</sub>): yield 588 mg (45%). Mp: 100 °C. [ $\alpha$ ]<sub>D</sub><sup>25</sup> = -128 (*c* = 0.405, CHCl<sub>3</sub>). <sup>1</sup>H NMR (CDCl<sub>3</sub>):  $\delta$  5.67 (s, pz CH), 5.51 (dq, *J* = 6.9, *J* = 2.6, CHMeN), 4.66 (m, cp H), 4.38 (m, cp H), 4.14 (s, 5 cp H), 4.11 (m, cp H), 2.35 (s, pzMe), 2.11 (s, pzMe), 1.75 (d, *J* = 6.9, CHMeN), 1.6–0.5 (m, 10 Cy CH<sub>2</sub> and 2 Cy CH). <sup>13</sup>C{<sup>1</sup>H} NMR (CDCl<sub>3</sub>):  $\delta$  104.9 (pz CH), 70.2 (cp CH), 70.0 (5 cp CH), 69.8 (cp CH), 68.8 (cp CH), 52.1 (CHMeN), 33.4–26.5 (10 Cy CH<sub>2</sub> and 2 Cy CH), 21.5 (CHMeN), 13.9 (pzMe), 11.7 (pzMe). <sup>31</sup>P{<sup>1</sup>H} NMR (CDCl<sub>3</sub>):  $\delta$  -16.1 (s). MS (*m/z*): 504 (M<sup>+</sup>), 421 (M<sup>+</sup> - Cy), 326 (421 - Hpz), 243 (326 - Cy, 100%). Anal. Calcd for C<sub>29</sub>H<sub>41</sub>FeN<sub>2</sub>P: C, 69.05; H, 8.19; N, 5.55. Found: C, 68.24; H, 8.20; N, 5.44.

**X-ray Crystallographic Studies of 3af, 3ah, 3aj, 3aq', 3as, and 3ec.** Data were measured with variable scan speeds to ensure constant statistical precision on the collected intensities. One standard reflection was measured every 120 reflections; no significant variation was detected.

The structures were solved either by direct (**3ah**, **3aj**, **3aq'**, and **3as**) or Patterson (**3af** and **3ec**) methods and refined by full-matrix least squares using anisotropic displacement parameters for all non-hydrogen atoms. The contributions of the hydrogen atoms in their idealized positions (Riding model with fixed isotropic *U* = 0.080 Å<sup>2</sup>) were taken into account but not refined. All calculations were carried out by using the Siemens SHELXTL PLUS system.

**Acknowledgment.** This research was in part supported by LONZA Ltd. (Ph.D. grant to U.B.). We are grateful to V. Gramlich for his valuable help with the X-ray structural analyses.

**Supporting Information Available:** Tables of crystal data and refinement details, atomic coordinates, all bond distances and angles, anisotropic displacement coefficients for non-carbon atoms, and coordinates of hydrogen atoms for **3af**, **3ah**, **3aj**, **3aq'**, **3as**, and **3ec**, ORTEP views of molecules A and B as well as of all three independent molecules in the unit cell for **3aq'** (Figures S1–S3), and ORTEP views of **3af**, **3ah**, **3aj**, **3as**, and **3ec** (Figures S4–S8) (78 pages). Ordering information is given on any current masthead page. Tables of calculated and observed structure factors for all six compounds (55 pages) may be obtained from the authors upon request.

OM950475C

# Mechanism of Reactivity of a Nickel Acylate Complex with Vinyl Halides†

James R. Hermanson,<sup>1a</sup> James W. Hershberger,<sup>\*,1b</sup> and Allan R. Pinhas<sup>\*,1a</sup>

Departments of Chemistry, University of Cincinnati, Cincinnati, Ohio 45221-0172, and Miami University, Oxford, Ohio 45056

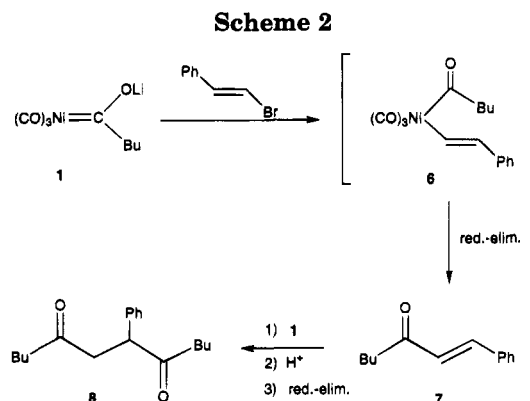
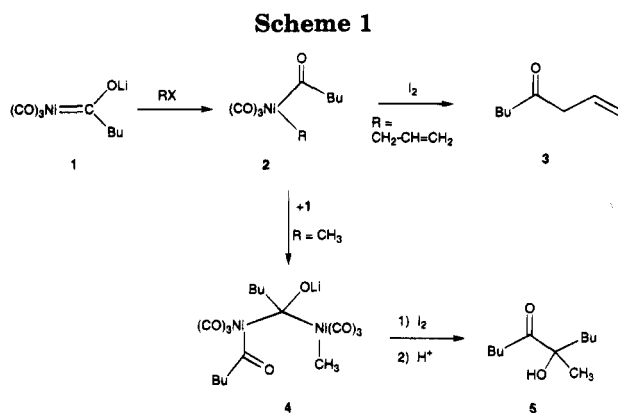
Received May 24, 1995<sup>®</sup>

The reaction of alkyl nickel acylate complex **1** with a variety of vinyl halides was investigated. Depending upon the leaving group and the reaction time, the reaction product can be a furan, an  $\alpha,\beta$ -unsaturated ketone, a 1,4-diketone, or a cyclopentenone. The mechanism for formation of each of these compounds is discussed. In all cases, it was found that the organic products are formed only after an oxidative workup, *i.e.*, all reaction intermediates are metal complexes.

Recently, we have been studying the reactivity of nickel acylate complex **1**, in THF, with a variety of electrophiles. Particularly relevant to this paper is our discovery that although acylate complex **1** is monomeric, products which contain a 1:1 ratio or a 2:1 ratio of acyl to electrophile can be generated depending upon the rate of the initial reaction (Scheme 1). Specifically, the reaction of **1** with allyl bromide, which has a  $t_{1/2}$  of about a minute at  $-78\text{ }^\circ\text{C}$ , gives only the 1:1 adduct,  $\beta,\gamma$ -unsaturated ketone **3**. In contrast, the reaction of **1** with methyl iodide, which has a  $t_{1/2}$  of a few hours at room temperature, generates only the 2:1 adduct, acyloin **5**.<sup>2</sup> The rate of the reaction affects which type of product is formed because in the allyl bromide reaction, due to the rapid rate of the first step, none of complex **1** is available to attack organonickel intermediate **2**; whereas in the methyl iodide reaction, due to the slow rate of the first step, there is a great deal of acylate complex **1** available to attack complex **2**.

Another fact that is important to this manuscript is our observation that the nickel intermediates are stable for days at room temperature, under an inert atmosphere, and can be spectroscopically characterized. They can be decomposed (*i.e.*, forced to undergo a reductive-elimination) to generate the observed organic products by reacting with an oxidant such as  $\text{I}_2$ . This result is consistent with theoretical studies which indicate that reductive-elimination of a  $d^8$  five-coordinate trigonal bipyramidal nickel(II) center is a forbidden reaction.<sup>3</sup>

In addition to reacting with allyl and alkyl halides, nickel acylate complexes react with vinyl halides (Scheme 2). When acylate complex **1** reacts with *trans*-2-bromostyrene in  $\text{Et}_2\text{O}$ , both the 1:1 and 2:1 adducts, **7** and **8**, are formed with compound **8** being the predominant product. Due to the known ability of acylate complexes to undergo conjugate addition to  $\alpha,\beta$ -unsaturated ke-



tones, a mechanism involving  $\alpha,\beta$ -unsaturated ketone **7** was proposed and nicely accounts for this chemistry.<sup>4-6</sup>

Because the conversion of **6** to **7** is a forbidden reaction<sup>3</sup> and because we have been looking for but have

(4) (a) Corey, E. J.; Hegedus, L. S. *J. Am. Chem. Soc.* **1969**, *91*, 1233, 4926. (b) Hegedus, L. S. Ph.D. Thesis; Harvard University: Cambridge, MA, 1970.

(5) For other reactions of acylate complexes, see: (a) Myeong, S. K.; Sawa, Y.; Ryang, M.; Tsutsumi, S. *Bull. Chem. Soc. Jpn.* **1965**, *38*, 330. (b) Ryang, M.; Myeong, S. K.; Sawa, Y.; Tsutsumi, S. *J. Organomet. Chem.* **1966**, *5*, 305. (c) Sawa, Y.; Hashimoto, I.; Ryang, M.; Tsutsumi, S. *J. Org. Chem.* **1968**, *33*, 2159. (d) Fukuoka, S.; Ryang, M.; Tsutsumi, S. *J. Org. Chem.* **1968**, *33*, 2973; **1970**, *35*, 3184; **1971**, *36*, 2721. (e) Sawa, Y.; Ryang, M.; Tsutsumi, S. *J. Org. Chem.* **1970**, *35*, 4183.

(6) Also see: (a) Hegedus, L. S.; Tamura, R. *Organometallics* **1982**, *1*, 1188. (b) Semmelhack, M. F.; Brickner, S. J. *J. Org. Chem.* **1981**, *46*, 1723. (c) Semmelhack, M. F.; Keller, L.; Sato, T.; Spiess, E. J.; Wulff, W. J. *J. Org. Chem.* **1985**, *50*, 5566. (d) Semmelhack, M. F.; Keller, L.; Sato, T.; Spiess, E. J. *J. Org. Chem.* **1982**, *47*, 4382.

† A.R.P. would like to dedicate this paper to Prof. Jerome A. Berson upon his 70th birthday and his retirement from Yale University.

<sup>®</sup> Abstract published in *Advance ACS Abstracts*, October 1, 1995.

(1) (a) University of Cincinnati. (b) Miami University.

(2) (a) Simunic, J. L.; Pinhas, A. R. *Organometallics* **1987**, *6*, 1358.

(b) Simunic, J. L.; Pinhas, A. R. *Inorg. Chem.* **1989**, *28*, 2400.

(3) (a) Grubbs, R. H.; Miyashita, A.; Liu, M.; Burk, P. *J. Am. Chem. Soc.* **1978**, *100*, 2418. (b) Tatsumi, K.; Hoffmann, R.; Yamamoto, A.; Stille, J. K. *Bull. Chem. Soc. Jpn.* **1981**, *54*, 1857. (c) McKinney, R. J.; Thorn, D. L.; Hoffmann, R.; Stockis, A. *J. Am. Chem. Soc.* **1981**, *103*, 2595. (d) Stockis, A.; Hoffmann, R. *J. Am. Chem. Soc.* **1980**, *102*, 2952.



never observed a spontaneous reductive-elimination from a five-coordinate nickel(II) complex, we decided to reinvestigate the reactivity of acylate complex **1** with vinyl halides. In this manuscript, we show that a reductive-elimination does not take place, but rather, all intermediates are metal complexes. In addition, we show that different types of products can be formed depending on the nature of the leaving group and the time of the reaction.

Before we begin, one point that must be mentioned is, we have shown spectroscopically that the structure of the acylate complex in Et<sub>2</sub>O at -50 °C or below is **1**; however, complex **1** dimerizes when the temperature is raised to about -20 °C.<sup>7</sup> In contrast, in THF, the acylate complex is stable upon warming to room temperature.<sup>2,7</sup> Thus, all the chemistry we will discuss in this manuscript has been performed in THF due to the much wider temperature range and much greater solubility of the nickel complexes which it affords.

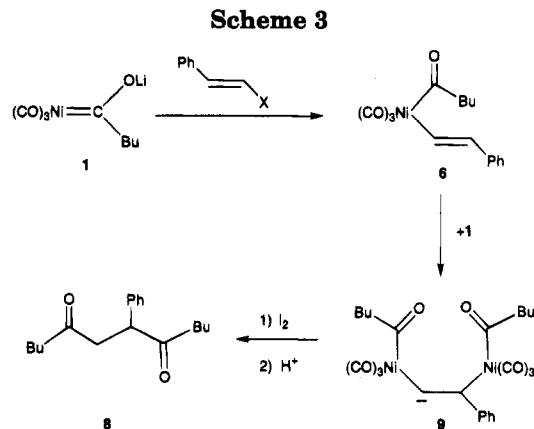
## Results and Discussion

**Reaction of Acylate Complex **1** with Bromostyrene.** Running the reaction of *trans*-2-bromostyrene with acylate complex **1** at -30 °C in THF using either a 1:1 or a 1:2 ratio of bromostyrene to **1** generates only the 2:1 adduct **8** (85% yield); none of the 1:1 adduct **7** was observed. In fact, if the reaction temperature is continually lowered in consecutive experiments, though the product yield does decrease, only **8** is obtained. This observation led us to suspect that compound **7** (Scheme 2) may not be an intermediate in this reaction, and hence, a simple Michael addition between **1** and **7** may not be part of the mechanism.

In contrast, when the reaction temperature is raised to -10 °C, both compounds **7** and **8** are formed but in very low yields, 5% and 7%, respectively. The mass balance is low because the majority of the starting material has been converted to (1) compounds which previously have been identified as resulting from oxidation of acylate complex **1**,<sup>2</sup> (2) coupling products of styrene radicals, and (3) unidentifiable, high molecular weight material.

To confirm the idea that oxidation is the dominant side reaction between bromostyrene and acylate complex **1**, two sets of reactions were performed. In the first, the reaction of bromostyrene and the analogous phenyl acylate complex, a compound which is harder to oxidize than its butyl analog,<sup>7</sup> was investigated. At -10 °C, analogs of both compounds **7** and **8** are formed, but now the yields are 30% and 24%, respectively. Qualitatively, it was found that the phenyl complex gives crude reaction mixtures which are significantly cleaner, as determined by thin layer and by gas chromatography, than the corresponding reactions with the butyl complex.

Secondly, when the reaction of a 1:1 mixture of **1** and bromostyrene was monitored by IR spectroscopy, at room temperature, we find little evidence for the presence of any nickel complexes. In contrast, when a 2:1 ratio of **1** to bromostyrene is used to insure that all the bromostyrene has reacted, peaks which indicate the



presence of a nickel complex can be observed for days, as long as the reaction mixture is kept under an inert atmosphere, *i.e.*, no spontaneous reductive-elimination has occurred. When this latter reaction mixture is exposed to air, an oxidant such as I<sub>2</sub> or ferrocenium, or to an additional 1 equiv of bromostyrene, the carbonyl peaks in the IR spectrum disappear, indicating decomposition of the intermediate complex.

Our next goal was to determine if we could observe the formation of compound **7** or any free organic compound during the reaction. To insure that all the bromostyrene is consumed so it cannot act as an oxidant, the reaction between **1** and bromostyrene was run at -20 °C for 3 h using a 2:1 ratio of reactants. When this reaction is taken to room temperature and monitored by IR spectroscopy, the peaks which are assigned to the carbonyls of a nickel complex are present for periods of up to 10 days; however, no peaks which are assigned to any organic compounds can be observed. These results again suggest that reductive-elimination of the intermediate nickel complexes is not taking place under the reaction conditions and led us to propose the mechanism shown in Scheme 3 (X = Br).

For the mechanism in Scheme 3 to be correct, complex **6** must be stable at room temperature and must undergo a Michael-type addition with acylate complex **1**. To test this, we needed a method to generate complex **6**. As discussed earlier,<sup>2</sup> the faster the reaction of acylate complex **1** with an electrophile the greater the yield of the 1:1 adduct, such as **7**. Unfortunately, we have just shown that to increase the reaction rate, the temperature cannot be raised nor can additional bromostyrene be added because both of these modifications lead to low yields and many side products. Therefore, we decided to use a better leaving group on the styrene. Initially we attempted to run the reaction of acylate complex **1** with iodostyrene. However, the reaction mixture turned very dark in color and a large variety of different products were obtained, probably due to a large number of redox processes.

Therefore, what was needed was a good leaving group that would not undergo redox reactions. As might be expected, the best match for both these criteria proved to be styrene triflate (Scheme 3, X = OTf). Unlike some of the published general procedures for the syntheses of enol-triflates from aldehydes, which require first generating the TMS-enol ether and then converting it to the triflate, we have found that here treatment of phenyl acetaldehyde with base and triflic anhydride

(7) (a) Pinhas, A. R.; Hershberger, J. W. *Organometallics* **1990**, *9*, 2840. (b) LaDuca, M. J. T.; Simunic, J. L.; Hershberger, J. W.; Pinhas, A. R. *Inorg. Chim. Acta* **1994**, *222*, 165.

forms styrene triflate easily and in high yield.<sup>8,9</sup> When KH is used as the base, the predominant styrene triflate is the trans isomer; whereas when 2,6-di-*tert*-butyl-4-methylpyridine is used as the base, the predominant isomer is cis.

The reaction of acylate complex **1** with the trans isomer of styrene triflate generates almost exclusively compound **7**, after the workup. When this reaction is monitored spectroscopically, it was found that complex **6** is stable for days at room temperature and that compound **7** is not formed until *after* the reaction mixture has been treated with an oxidant such as I<sub>2</sub> or exposed to air.

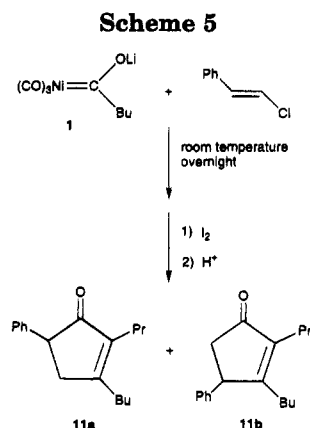
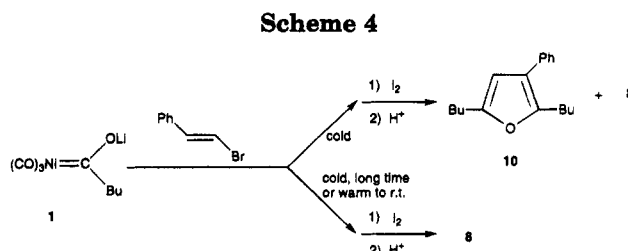
Surprisingly, the cis isomer of the styrene triflate reacts more slowly with acylate complex **1** than does the trans isomer. Given the slower rate of the reaction, as expected based on all our previous results, more of compound **8** is formed when the cis isomer is used. Another interesting point is that the only 1:1 adduct formed is compound **7**; none of the cis analog of **7** is observed.

Therefore, a reaction between the trans isomer of styrene triflate and acylate complex **1** (using a 1:1 ratio) was set up in the usual manner. Prior to the addition of the oxidant, an additional equiv of **1** was added to the reaction mixture and the course of the reaction was followed by IR spectroscopy. Again, none of the peaks associated with any organic compound were observed, only absorbances due to nickel complex were obtained. After workup, the final product of this reaction is the 2:1 adduct **8**.

To summarize what we know so far (Scheme 3): following initial attack of nickel acylate complex **1** on the bromostyrene, organometallic complex **6** is formed. This complex is stable under an inert atmosphere and in the absence of acylate complex **1**. Upon oxidation, complex **6** generates organic compound **7**. However, in the presence of additional (or large amounts of unconsumed) acylate complex **1**, complex **6** undergoes nucleophilic attack by **1** to give a second binuclear organometallic complex **9**. Oxidation of this reaction mixture causes reductive-elimination of the nickel centers to generate the 2:1 adduct **8**. Although this sequence of reactions does account for the continued presence of organonickel complexes, as will be seen shortly, it is not yet the complete picture.

It next was decided to monitor the entire period of the reaction between acylate complex **1** and bromostyrene. While the reaction was kept at -30 °C, a nickel complex with strong absorbances in the bridging carbonyl region of the IR spectrum appeared and then disappeared in about 15 min. When the reaction was worked-up while these peaks were at their maximum, in addition to compound **8**, furan derivative **10** was obtained (Scheme 4). However, when the reaction is worked-up after these bridging carbonyl peaks disappear, only compound **8** was obtained. These results strongly suggest that this transient intermediate is the precursor to furan **10**.

**Reaction of Acylate Complex 1 with Chlorostyrene.** In an effort to decrease the rate of the reaction,



and thus, make it easier to monitor, it was next decided to study the reaction of acylate complex **1** using chlorostyrene as the electrophile. In addition, because chlorostyrene is a poorer oxidizing agent than bromostyrene, it was hoped that this would clean-up the room temperature reactions.

As expected, the reaction of **1** with chlorostyrene was much slower, requiring overnight to obtain good yields of the product, and does give much cleaner reaction mixtures, as determined by TLC and GC, than the corresponding reaction with bromostyrene. However, **8** was found only as a minor product, instead two new compounds, **11a** and **11b**, were obtained (Scheme 5, approximately a 6:1 ratio, 65% combined yield). Attempts to isolate the likely alcohol precursor or the anionic organometallic precursor in this reaction were unsuccessful.

(Although it was clear, based on spectroscopic data, that both the major and minor cyclization products are cyclopentenone derivatives, an unambiguous assignment of the regiochemistry of the phenyl group could not be made. It was felt that this was needed in order to formulate a reasonable mechanism. In the Appendix of this manuscript, the unambiguous synthesis of analogs of each isomer and their use for the assignment of **11a** as the major isomer are described.)

**Cyclization.** Because the cyclic products **11a** and **11b** were observed only in the chlorostyrene reaction (Scheme 5) and not in the bromostyrene reaction (Scheme 3), our first goal was to determine what variables affect the amount of cyclization which occurs. In short, time is the only variable which causes an increase in the amount of cyclic product **11**. It was found that the oxidant (I<sub>2</sub> or Cp<sub>2</sub>Fe<sup>+</sup>), the rate at which the oxidation at the end of the reaction is performed, the addition of salts (LiCl, LiBr, or Bu<sub>4</sub>N<sup>+</sup> ClO<sub>4</sub><sup>-</sup>), or the addition of 12-crown-4 do change the ratio of **8**:**11** but not significantly, as long as the reaction is allowed to go for the same length of time. In addition, diluting the reaction by about a factor of 16 has no effect on the ratio of straight chain to cyclic product.

(8) Stang, P. J.; Hanack, M.; Subramanian, L. R. *Synthesis* 1982, 85.

(9) Stang, P. J.; Treptow, W. *Synthesis* 1980, 283.

**Table 1. Ratio of Products for the Long Term Study of the Reactions of Bromostyrene and Chlorostyrene**

bromostyrene <sup>a</sup>					chlorostyrene <sup>b</sup>				
time	st <sup>c</sup>	10	8	11	time	st <sup>c</sup>	10	8	11
15 min	17	50	33	0	15 min	100	0	0	0
30 min	0	0	100	0	30 min	66	8	26	0
1.5 h	0	0	88	12	1.5 h	25	6	68	1
2.5 h	0	0	33	67	2.5 h	9	0	76	15
4.5 h	0	0	3	97	4.5 h	0	0	40	60
6 h	0	0	0	100	6 h	0	0	2	98
2 days	0	0	0	100	2 days	0	0	1	99
3 days	0	0	0	100	3 days	0	0	0	100

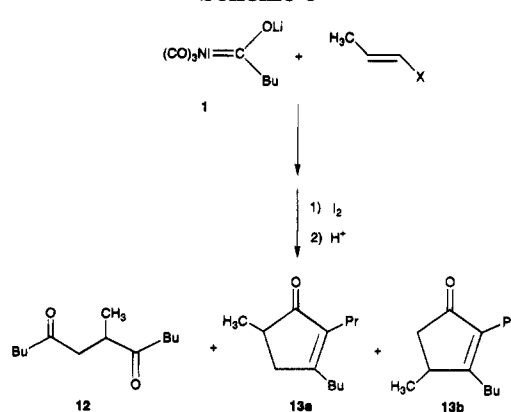
<sup>a</sup> The yield of 11 at the end of the reaction was 70%. <sup>b</sup> The yield of 11 at the end of the reaction was 80%. <sup>c</sup> st indicates the unreacted halostyrene.

In contrast, time does have a large effect on the product ratio. It must be remembered that initially the bromostyrene reactions were run at room temperature or below for about 1 h; whereas the chlorostyrene reactions were run at room temperature overnight. When the reaction of 1 with bromostyrene is given more time (at least 2 h at room temperature), the precursors to these cyclic products are generated.

In order to help determine the rate at which cyclization occurs, two identical reactions were set up at room temperature, one using chlorostyrene and the other using bromostyrene, both in a 1:halostyrene ratio of 2:1 in order to assure complete consumption of the halostyrene, and thus, avoid problems with oxidative side-reactions. At specific times, an aliquant was removed, an IR spectrum was obtained to insure the integrity of the reaction solution, the solution then was worked-up, and the product distribution was determined using gas chromatography (Table 1).

Several important points immediately became clear from the data in Table 1. Not surprisingly, chlorostyrene is much less reactive than bromostyrene. Secondly, both reactions produce the precursor to furan 10 only during the initial phase of the reaction, and they generate none of cyclic products 11 in less than 1 h after the reaction mixture has been warmed to room temperature. Finally, these data indicate that in both reactions, the organometallic precursor(s) to cyclic products 11 is(are) formed irreversibly and not in equilibrium with the nickel precursor to straight chain product 8. Thus, the chemistry for the chloro- and bromostyrene appears to be identical following initial attack of nickel acylate complex 1.

We were curious why this is the first reported observation of cyclopentenone products from the nickel acylate reactions.<sup>4-6</sup> Because most of the previously published chemistry with nickel acylate complexes used Et<sub>2</sub>O and we used THF as the solvent, the reaction of 1 with a halostyrene was repeated in Et<sub>2</sub>O. It was discovered that cyclopentenone derivatives 11 are generated in Et<sub>2</sub>O; however, the cyclization takes considerably longer. For example, using bromostyrene in Et<sub>2</sub>O, after 6 days at room temperature, about half the product is straight chain compound 8 and about half is cyclic products 11. After 16 days at room temperature, cyclization to 11 in Et<sub>2</sub>O is nearly complete, with only a small amount of compound 8 still present. In contrast, this same reaction in THF generated only the cyclic product in about 5 h.

**Scheme 6**

**Reaction of Acylate Complex 1 with 1-Halo-1-propene.** The reactions discussed above are not restricted to halostyrenes. Treatment of 1-bromo-1-propene with nickel acylate complex 1 and working-up the reaction after just 3 h readily generates 1,4-diketone 12 and only minute amounts of the two cyclic products 13a and 13b (Scheme 6). As expected, none of the 1:1 adduct analogous to compound 7 was observed because the initial attack on the electrophile is relatively slow and, as has been seen, this leads to generation of the 2:1 adduct as the sole product. In addition, none of the furan analogous to compound 10 was observed.

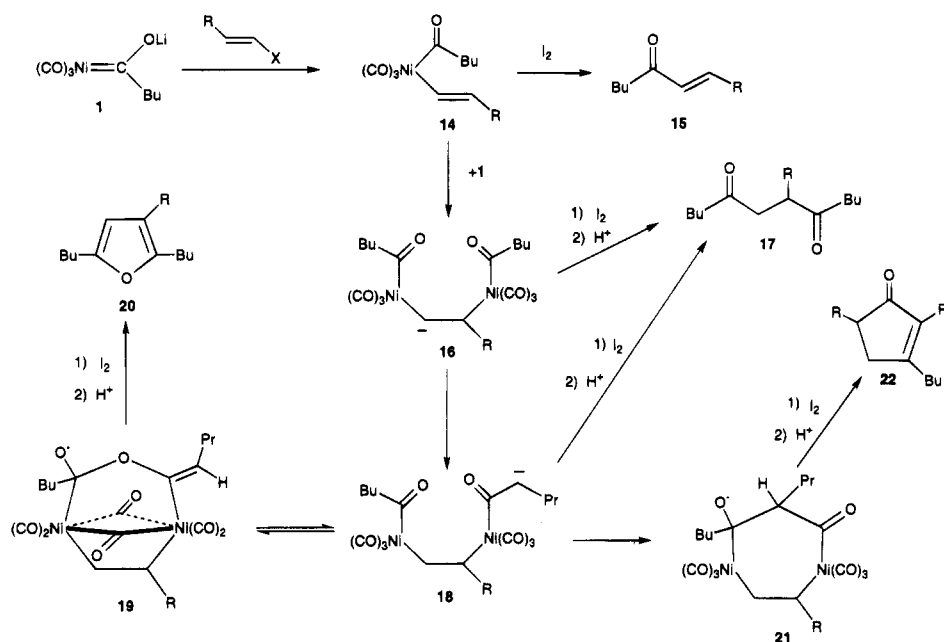
Running this reaction for seven days results in complete cyclization to give compounds 13 (58% combined yield, 3:1 ratio, respectively). Essentially, none of compound 12 remains. As in the styrene reactions, IR spectroscopic data indicate the presence of only metal complexes throughout the reaction, prior to the workup. (In the Appendix of this manuscript, the unambiguous synthesis of analogs of each isomer and their use for the unambiguous assignment of 13a as the major cyclic isomer is described.)

When the reaction was run using 1-chloro-1-propene and monitored by IR spectroscopy, it was observed that even after 2 days at room temperature a substantial amount of acylate complex 1 was still present, indicating that chloropropene undergoes the initial substitution slowly. Furthermore, upon workup the reaction mixture with I<sub>2</sub>, cyclic compounds 13a and 13b are the only products generated (again in about a 3:1 ratio) aside from typical oxidation products from the presence of unconsumed 1. Straight chain product 12 was present in only trace amounts as determined by gas chromatography. Most likely, the presence of only a trace amount of compound 12 is a result of the fact that chloropropene reacts with 1 much more slowly than bromopropene; however, the cyclization reactions proceed at similar rates because the halides are not directly involved in this step. Thus, at about the same rate as the precursor to 12 is being formed, it is cyclizing to give 13.

### Summary of Evidence and Overall Mechanism

1. IR spectroscopic monitoring of the reaction mixture indicates the presence of nickel complexes throughout the reaction. Thus, spontaneous reductive-elimination is not taking place, and all nickel complexes are stable under our reaction conditions at room temperature for extended periods of time in the absence of an oxidant.

Scheme 7



2. IR monitoring also reveals that initial absorbances associated with bridging carbonyls appear and then disappear. The amount of furan **10** that can be isolated is at a maximum when these absorbances are at their maximum.

3. For both chloro- and bromostyrene, the precursor to furan **10** must isomerize to an intermediate (or intermediates) which can generate products **8** and **11** upon workup.

4. Both the halostyrenes and the halopropenes, if allowed enough time, will generate only cyclic products **11** and **13**, respectively. This result suggests the irreversible generation of precursors to these cyclic products.

5. Diluting the reaction by a factor of 16 results in no change in the relative product ratios from the undiluted reaction, indicating the absence of a bimolecular step in or before the rate-determining step.

6. Adding a crown ether to the reaction of **1** with a halostyrene has a negligible effect on the reaction, thus eliminating  $\text{Li}^+$  bridging as an important effect.

7. Adding  $\text{Br}^-$  or  $\text{Cl}^-$  salts to the reaction of **1** with a halostyrene, qualitatively, increases the rate of the initial attack by acylate complex **1**, probably due to a change in solvent polarity; however, it does not have a large effect on the ratio of **8** to **11**.

8. Using  $\text{Et}_2\text{O}$  as the solvent for the reaction of **1** with bromostyrene causes cyclization to proceed at a much slower rate.

Our overall mechanism is shown in Scheme 7. In the first step of the reaction, acylate complex **1** reacts with the vinyl halide (or triflate) to generate vinyl(acyl)nickel complex **14**. This complex is stable under an inert atmosphere but in the presence of an oxidant it will undergo a reductive-elimination to generate **15**. In the presence of added or unreacted acylate complex **1**, a second equivalent will add to generate **16**. Oxidation of this complex will generate product **17**. (Because having the anion  $\alpha$  to the phenyl is more stable than in its present position, a proton transfer may take place; however, this does not affect the proposed mechanism.)<sup>10</sup>

An intramolecular proton transfer takes place to give complex **18**, which also upon oxidation can give product **17**. This complex must then establish a rapid equilibrium with a complex such as **19** which has bridging carbonyls. Upon an oxidative workup, complex **19** generates furan **20**. This product is observed only when  $\text{R} = \text{Ph}$  most likely because of the slow rate of formation of **18** when  $\text{R} = \text{CH}_3$ .

Complex **18** must then undergo an irreversible cyclization to give a complex such as **21** which upon an oxidative workup generates compound **22**. The other regioisomer of **22** can be obtained if the proton that is transferred in going from **16** to **18** is next to the other acyl carbonyl.

## Experimental Section

**General.** All reactions were carried out using glassware dried in a  $110^\circ\text{C}$  oven and cooled under an argon atmosphere or in a desiccator. All reactions were run under an inert atmosphere. Tetrahydrofuran was freshly distilled from potassium benzophenone ketyl. Nickel tetracarbonyl was transferred from a one pound lecture bottle into a 10 mL sidearm flask, maintaining a strong argon flow, and stored under argon until used. Transfers were made via syringe and excess  $\text{Ni}(\text{CO})_4$  was quenched in a bath of iodine/ $\text{CCl}_4$ . ( $\text{Ni}(\text{CO})_4$  is toxic and flammable when exposed to air. All work should be conducted in a well ventilated hood, maintaining an argon atmosphere during all transfers and using nonflammable solvents in the iodine bath to reduce the probability of fire.)

(10) We would like to thank a reviewer for suggesting an alternative mechanism in which complex **14** is deprotonated by acylate **1** to give a nickel acyl hydride complex, which then reacts with the enolate of **14** by an alkene insertion mechanism. We favor the mechanism in Scheme 7 because (1) protonation of acylate complex **1** occurs on the oxygen, and not on the nickel, to give initially a hydroxy carbene complex,<sup>2</sup> (2) at present, we have no evidence for an insertion reaction between a nickel acyl or acylate complex and an alkene, though this type of reaction is being actively pursued, and (3) we believe, as the reviewer also does, that the equilibrium for the acid/base reaction between **1** and **14** would greatly favor the starting materials and not the products (the  $\text{p}K_a$  of the conjugate acid of **1** = **16** and the  $\text{p}K_a$  of an alkyl ketone is about 22). However, we cannot definitively rule out the possibility that the hydroxy carbene complex derived from protonation of **1** reacts with the enolate of **14** to generate a complex which is isomeric to **18**.

**Instrumentation.** Gas chromatographic analyses were done using a Varian Model 3300 gas chromatograph with a flash vaporization injector at 225 °C, a flame ionization detector at 270 °C, and a 10 ft × 1/8 in 5% SP-2100 on 100/120 Supelcoport column. Temperature programming was used: 50 °C hold for 2 min, increase at 10 °C/min to 250 °C and then increase at 30 °C/min to 300 °C, and hold for 6.5 min. All infrared spectra were recorded on a Perkin-Elmer Model 1600 series FTIR spectrophotometer using KBr or CaF<sub>2</sub> cells. All NMR spectra were recorded on a Bruker 250 MHz spectrometer and referenced to tetramethylsilane at 0.00 ppm. The substitution pattern on each carbon was determined by the DEPT method. All mass spectra and GC/MS were obtained on a Hewlett-Packard Model 5995 spectrometer using a 0.25 mm × 15 m fused silica capillary SPB-1 column and temperature programming. High resolution mass spectra were done on a Kratos model mass spectrometer. Chromatotron separations were performed on a Harrison Research Model 7924T preparative centrifugally accelerated radial thin layer chromatotron. Samples were loaded onto a rotor packed with 2 mm × 7.5 cm of silica gel 60 PF<sub>254</sub> containing gypsum.

**Nickel Acylate Complex 1.** This was done in a similar manner to our published procedure.<sup>2</sup> To a three-neck round-bottom flask, under an inert atmosphere and equipped with a glass stopper, a rubber septum, a stir bar, and a gas inlet adapter, was added approximately 25 mL of degassed THF. The solvent was cooled to -78 °C, and 0.60 mL (5.0 mmol) of nickel tetracarbonyl was added. To this was added 3.1 mL of 1.6 M butyllithium (5.0 mmol) over a 15 min period. (It has been found that near the end of the addition there is a significant darkening of the color of the reaction mixture. Cleaner reactions result when the addition is stopped at this point and the remaining butyllithium is discarded.) The reaction was kept at -78 °C for an additional 15 min and then allowed to warm to room temperature for 1 h.

**General Procedure.** To a three-neck flask, equipped with a glass stopper, gas inlet adapter, and a rubber septum under an inert atmosphere, was added 5.0 mmol of the vinyl halide dissolved in 3 mL of degassed THF. The solution was cooled to -30 °C or to -10 °C. To this, over a 40 min period, was added 5.0 mmol of nickel acylate complex 1 dissolved in 25 mL THF. The reaction was allowed to stir cold for an additional period of time, and then 15 mL of a degassed saturated NH<sub>4</sub>Cl solution was added. The cold bath was removed, and the reaction mixture was allowed to stir for 2 h at room temperature. The solution was poured directly onto 1.90 g (7.54 mmol) of I<sub>2</sub> and allowed to react for 15 min. A 10% NaHSO<sub>3</sub> solution was added to remove excess I<sub>2</sub>, and the entire mixture was extracted with 75 mL of Et<sub>2</sub>O. The organic layer was washed with additional bisulfite until the water layer was colorless. The organic layer then was washed with water, followed by a saturated NaCl solution, and dried with MgSO<sub>4</sub>. The solvent was then removed under vacuum. All yields are as reported in Results and Discussion.

Because many of the reaction mixtures were analyzed by gas chromatography using an internal standard, it was necessary to insure the accuracy of the internal standard. Therefore, a reaction was run between nickel acylate complex 1 and styrene triflate. After the workup, a known amount of benzil was added as an internal standard and a 45% yield was determined using this method. The reaction mixture then was chromatographed using a Chromatotron, and a 44% isolated yield was obtained. The accuracy of this method for determining the yields of other compounds was confirmed in a similar manner.

**Vinyl Halides.** *trans*-2-bromostyrene (0.64 mL, 5.0 mmol); *trans*-2-chlorostyrene (0.69 mL, 5.0 mmol); *trans*-1-bromopropene (0.43 mL, 5.0 mmol); *trans*-1-chloropropene (0.42 mL, 5.0 mmol).

**6-Phenyl-5,8-dodecanedione (8).** To maximize the yield of compound 8 the following procedure was used: to a two-neck flask, equipped with a gas inlet adapter and a rubber

septum, under an inert atmosphere, was added 1.28 mL (10.0 mmol) of *trans*-2-bromostyrene dissolved in 5 mL of degassed THF. This solution was cooled to -30 °C, and over a 45 min period, 10.0 mmol of pentanoyl nickel acylate complex 1 dissolved in 35 mL of THF was added. Care was taken to drip the solution down the side of the cooled flask. The reaction was kept cold an additional 3 h. Next, 15 mL of a degassed, saturated NH<sub>4</sub>Cl solution was added. The cold bath was removed, and the reaction was allowed to warm to room temperature for 15 min. The mixture was poured directly onto 2.8 g (11.1 mmol) of solid I<sub>2</sub> and allowed to react 15 min. A 10% NaHSO<sub>3</sub> solution was added to remove excess I<sub>2</sub>, and the entire mixture was extracted with 75 mL of Et<sub>2</sub>O. The organic layer was washed with additional bisulfite until the water layer was clear. The organic layer then was washed with water, followed by a saturated NaCl solution, and dried with MgSO<sub>4</sub>. The solvent was removed under vacuum, and the resulting oil was chromatographed on a silica gel (32 g) column, eluting with 1:99 Et<sub>2</sub>O:petroleum ether to give 1.164 g (4.27 mmol, 85% yield) of 8. GC retention time 20.5 min. <sup>1</sup>H NMR (CDCl<sub>3</sub>) δ: 7.41–7.13 (m, 5H), 4.23 (dd, *J* = 3.9, 10.5 Hz, 1H), 3.41 (dd, *J* = 10.5, 18.0 Hz, 1H), 2.57–2.36 (m, 5H), 1.60–1.41 (m, 4H), 1.35–1.10 (m, 4H), [0.87 (t, *J* = 8.7 Hz), 0.79 (t, *J* = 8.7 Hz), 6H]; <sup>13</sup>C NMR (CDCl<sub>3</sub>) δ: 209.595 (C), 209.518 (C), 138.209 (C), 129.121 (CH), 128.299 (CH), 127.512 (CH), 53.313 (CH), 45.864 (CH<sub>2</sub>), 42.645 (CH<sub>2</sub>), 41.421 (CH<sub>2</sub>), 25.935 (CH<sub>2</sub>), 25.810 (CH<sub>2</sub>), 22.357 (CH<sub>2</sub>), 22.183 (CH<sub>2</sub>), 13.957 (CH<sub>3</sub>), 13.876 (CH<sub>3</sub>); IR (neat oil): 3060 (w), 3028 (w), 2958 (vs), 2935 (vs), 2865 (s), 1953 (vw), 1883 (vw), 1809 (vw), 1712 (vs), 1598 (w), 1493 (m), 1466 (m), 1451 (m), 1369 (m), 1123 (m), 1046 (m), 1030 (w) cm<sup>-1</sup>; MS (EI) *m/e*: 274 (5%), 232 (3%), 189 (4%), 148 (10%), 104 (8%), 91 (5%), 86 (5%), 85 (100%), 57 (70%), 41 (29%); HRMS: exp 274.1938, calculated for C<sub>18</sub>H<sub>26</sub>O<sub>2</sub> 274.1933.

**Phenyl Acylate Complex Reacting with Bromostyrene.** This was done in a similar manner to all the reactions with acylate complex 1 except here the acylate complex was generated using phenyllithium (2.8 mL of 1.8 M phenyllithium, 5.0 mmol) rather than butyllithium. GC retention time 26.2 min. <sup>1</sup>H NMR (CDCl<sub>3</sub>) δ: [8.04 (d, *J* = 7.4 Hz), 7.97 (d, *J* = 7.4 Hz), 4H], 7.56–7.21 (m, 11H), 5.33 (dd, *J* = 3.6, 9.9 Hz, 1H), 4.21 (dd, *J* = 9.8, 18.0 Hz, 1H), 3.29 (dd, *J* = 3.6, 18.3 Hz, 1H); <sup>13</sup>C NMR (CDCl<sub>3</sub>) δSPCLN 199.002 (C), 198.159 (C), 138.706 (C), 136.515 (C), 133.350 (CH), 133.014 (CH), 129.301 (CH), 129.004 (CH), 128.667 (CH), 128.586 (CH), 128.332 (CH), 128.244 (CH), 127.457 (CH), 48.759 (CH), 43.989 (CH<sub>2</sub>); IR (CCl<sub>4</sub>): 3088 (w), 3064 (w), 2099 (w), 1959 (vw), 1890 (vw), 1809 (vw), 1683 (vs), 1598 (m), 1582 (m), 1482 (m), 1448 (s), 1229 (m) cm<sup>-1</sup>; MS (EI) *m/e*: 315 (16%), 314 (52%), 297 (17%), 296 (58%), 210 (18%), 209 (69%), 192 (19%), 191 (19%), 106 (45%), 105 (100%), 104 (22%); HRMS: exp 314.1290, calculated for C<sub>22</sub>H<sub>18</sub>O<sub>2</sub> 314.1307.

**Bromostyrene Acting as an Oxidant.** To a solution of 10 mmol of acylate complex 1 dissolved in 35 mL of THF and cooled to -50 °C was added, over a 2 min period via syringe neat, 0.64 mL (5.0 mmol) of bromostyrene. The reaction was kept at -25 °C for 2.5 h and then allowed to slowly warm to room temperature. Aliquants were removed over the next 10 days and worked up by pouring directly onto approximately 1.2 equiv of solid I<sub>2</sub> and allowed to react 15 min after which a 10% saturated solution of NaHSO<sub>3</sub> was added to remove excess I<sub>2</sub>. The organic layer was washed with additional bisulfite until the water layer was clear and the entire mixture was extracted with 75 mL of Et<sub>2</sub>O. The organic layer was then washed with water, followed by a saturated NaCl solution and dried with MgSO<sub>4</sub>. IR spectroscopy was run on an additional sample taken at the time of each aliquant. After a period of 10 days at room temperature, an additional 5.0 mmol of bromostyrene was added via syringe to the solution at room temperature. Aliquants were removed immediately and over the next 24 h for IR analysis and workup as described above. For all aliquants taken, the solvent was removed under

vacuum and the product ratios were determined using GC analysis. Representative IR data (CO region of reaction solution): complex **1** + 1 equiv of bromostyrene, 3 h at room temperature: 2043 (vs), 1995 (vs), 1947 (s), 1821 (s), 1800 (s), 1703 (s), 1642 (m); complex **1** + 1 equiv of bromostyrene, 7 days at room temperature: 2042 (vs), 1995 (vs), 1954 (s), 1821 (s), 1801 (s), 1703 (s), 1641 (m); complex **1** + 2 equiv of bromostyrene, 30 min at room temperature: 2042 (vs), 2008 (s), 1991 (m), 1956 (vs), 1842 (m), 1827 (m), 1703 (s), 1643 (s); complex **1** + 2 equiv of bromostyrene, 17 h at room temperature: 2042 (s), 1990 (w), 1956 (vs), 1703 (m), 1645 (m); complex **1** + 1 equiv of chlorostyrene, 7 days at room temperature: 2042 (vs), 1995 (vs), 1948 (m), 1821 (m), 1801 (m), 1703 (m), 1641 (w); complex **1** + 2 equiv of chlorostyrene, 41 h at room temperature: 2042 (vs), 1995 (vs), 1948 (m), 1821 (m), 1801 (m), 1703 (m), 1641 (w); complex **1** + 2 equiv of chlorostyrene followed by 1 equiv of bromostyrene, 2 h at room temperature: 2042 (vs), 1960 (w), 1704 (m), 1643 (m), 1603 (m), 1578 (m).

**2-(Trifluoromethanesulfonyl)styrene.** Predominantly the trans isomer: This synthesis was adapted from a literature procedure.<sup>8</sup> Approximately 1.4 g of KH slurry (35% in mineral oil) was added to a tared, argon filled, three-neck flask equipped with a stir bar and two gas inlet adapters. The mineral oil was removed by four washings with dry petroleum ether (5 mL each), and the residual petroleum ether was removed under high vacuum until the KH was a free flowing powder (0.477 g, 11.9 mmol). To the dried KH was added 10 mL of dry DME, and the resulting slurry was cooled to  $-10$  °C. Distilled phenylacetaldehyde (1.3 g, 11 mmol) dissolved in 2 mL of dry DME was added to the KH via syringe over a 5 min period. The reaction was allowed to stir between  $-5$  °C and  $0$  °C for 15 min and then cooled to  $-40$  °C. The trifluoromethanesulfonic anhydride (2.0 mL, 12 mmol) was added neat via syringe over 45 min. The reaction was left in the cold bath overnight and allowed to reach room temperature slowly. The black reaction mixture was diluted with pentane and washed with 25 mL of a 20% NaHSO<sub>3</sub> solution. The aqueous layer was back-extracted with 30 mL of pentane. The combined pentane layers were dried with MgSO<sub>4</sub> and filtered through a short plug of silica (<200 mesh). The pentane was removed under vacuum, and the crude product was purified by Kugelrohr distillation (ca. 2 torr) collecting the fraction between 80–110 °C to yield 1.36 g (5.4 mmol, 50% based on the aldehyde) of the triflate in a 2:1 trans:cis ratio of isomers. The product also can be purified by silica gel column chromatography eluting with pure petroleum ether. GC retention times for the cis and trans isomers are 11.9 and 12.7 min. <sup>1</sup>H NMR (CDCl<sub>3</sub>) δ: 7.49–7.47 (m, 1.3H), 7.34–7.24 (m, 8.7H), 7.13 (d, *J* = 12.1 Hz, 1.4H), 6.69 (d, *J* = 6.6 Hz, 0.64H), 6.62 (d, *J* = 12.1 Hz, 1.3H), 5.94 (d, *J* = 6.4 Hz, 0.66H); <sup>13</sup>C NMR (CDCl<sub>3</sub>) δ: 136.531 (CH), 134.001 (CH), 131.083 (C), 129.403 (CH), 129.050 (CH), 128.949 (CH), 128.727 (CH), 126.786 (CH), 122.312 (CH), 118.622 (q, CF<sub>3</sub>, *J* = 321 Hz), 117.401 (CH); IR (CCl<sub>4</sub>): 3108 (w), 3091 (w), 3066 (w), 3030 (w), 1956 (w), 1876 (w), 1804 (w), 1653 (m), 1448 (m), 1425 (vs), 1246 (vs), 1213 (vs), 1141 (vs), 1076 (m), 1032 (s), 1020 (vs), 988 (s), 933 (s) cm<sup>-1</sup>; MS (EI) *m/e*: 253 (2%), 252 (19%), 119 (17%), 92 (7%), 91 (100%), 90 (9%), 89 (10%), 69 (29%), 65 (20%), 63 (11%), 51 (7%), 50 (5%); HRMS: exp 252.0066, calculated for C<sub>9</sub>H<sub>7</sub>O<sub>3</sub>SF<sub>3</sub> 252.0068.

Second method, predominantly the cis isomer: This method also is adapted from a literature procedure.<sup>9</sup> To a 250 mL three-neck flask equipped with a magnetic stir bar, a gas inlet adapter, reflux condenser, and rubber septum, under an argon atmosphere, were added 100 mL of 1,2-dichloroethane, 3.55 g (17.3 mmol) of 2,6-di-*tert*-butyl-4-methylpyridine, and 2.90 mL (17.3 mmol) of triflic anhydride. To this mixture was added 1.84 mL (15.7 mmol) of phenylacetaldehyde. The solution was allowed to reflux 13 h, the solution was allowed to cool, and the solvent removed under vacuum. Pentane (50 mL) was added to the resulting material, and the solution was filtered

using a Buchner funnel. The solid in the funnel, which is mainly the protonated hindered base, then was washed with an additional 75 mL of pentane. The solid was saved in order to reclaim the base. The collected pentane solution was washed twice with 50 mL portions of 1 M HCl and once with a 50 mL portion of water. The pentane solution then was dried over anhydrous K<sub>2</sub>CO<sub>3</sub>, and the solvent was removed under vacuum. The crude oil was redissolved in a minimal amount of pentane and filtered through a plug of silica gel (60.0 g placed in a fritted glass filter funnel) using 150 mL of pentane. Again, the solvent was removed, and the yellow oil was vacuum distilled to give 2.50 g (9.95 mmol, 64% yield) of the triflate in a 1:3 trans:cis ratio of isomers: <sup>1</sup>H NMR (CDCl<sub>3</sub>) δ: 7.51–7.29 (m, 7.5H), 7.15 (d, *J* = 12.1 Hz, 0.4H), 6.73–6.47 (m, 1.4H), 5.98 (d, *J* = 6.92 Hz, 1.0H); <sup>13</sup>C NMR (CDCl<sub>3</sub>) δ: 136.531 (CH), 134.001 (CH), 131.083 (C), 129.403 (CH), 129.050 (CH), 128.949 (CH), 128.727 (CH), 126.786 (CH), 122.312 (CH), 118.622 (q, CF<sub>3</sub>, *J* = 321 Hz), 117.401 (CH); IR (CCl<sub>4</sub>): 3108 (w), 3091 (w), 3066 (w), 3030 (w), 1956 (w), 1876 (w), 1804 (w), 1653 (m), 1448 (m), 1425 (vs), 1246 (vs), 1213 (vs), 1141 (vs), 1076 (m), 1032 (s), 1020 (vs), 988 (s), 933 (s) cm<sup>-1</sup>; MS (EI) *m/e*: 253 (2%), 252 (19%), 119 (17%), 92 (7%), 91 (100%), 90 (9%), 89 (10%), 69 (29%), 65 (20%), 63 (11%), 51 (7%), 50 (5%); HRMS: exp 252.0066, calculated for C<sub>9</sub>H<sub>7</sub>O<sub>3</sub>SF<sub>3</sub> 252.0068.

**Acylate Complex 1 Reacting with *trans*-Styrene Triflate.** To a two-neck flask, equipped with a gas inlet adapter and a rubber septum, under an inert atmosphere, was added 0.85 g (3.4 mmol) of styryl triflate (2:1 trans:cis ratio) dissolved in 10 mL of degassed THF. The solution was cooled to  $-40$  °C. To this, over a 45 min period, was added 1.0 mmol of acylate complex **1** dissolved in 20 mL of THF. Care was taken to drip the solution down the side of the cooled flask. Samples were removed about every 15 min for IR analysis. Upon completing the addition, the cold bath was removed and the reaction mixture was allowed to stir for an additional 15 min at room temperature. To this solution was added 0.48 g (1.9 mmol) of I<sub>2</sub>. The reaction then was washed with a saturated NaHSO<sub>3</sub> solution. The entire mixture was extracted with 75 mL of Et<sub>2</sub>O. The organic layer was washed with water, followed by a saturated NaCl solution, and dried with MgSO<sub>4</sub>.

As determined by GC, the trans to cis ratio of the recovered starting material changed from 2:1 to 1.6:1, indicating that the trans isomer is reacting more rapidly, and the ratio of **7** to **8** is 7:1. IR data of the solution after 15 min at room temperature but before workup (THF): 2042 (vs) 1968 (vs), 1851 (w), 1813 (vw), 1714 (vs), 1694 (w), 1696 (w) 1642 (s), 1613 (w), 1578 (s).

The solvent then was removed under vacuum. The resulting oil was loaded onto a silica gel column (25 g) and was eluted with 300 mL of 1:99 Et<sub>2</sub>O:petroleum ether, followed by 300 mL of 1:99 EtOAc:petroleum ether. The yield also can be determined using the internal standard method. A 49% yield of **7** was obtained. GC retention time 17.5 min. <sup>1</sup>H NMR (CDCl<sub>3</sub>) δ: [7.55 (d, *J* = 15.9 Hz), 7.57–7.53 (m), 7.40–7.38 (m), 6H], 6.74 (d, *J* = 16.8 Hz, 1H), 2.67 (t, *J* = 7.4 Hz, 2H), 1.67 (quintet, *J* = 7.4 Hz, 2H), 1.37 (sextet, *J* = 7.3 Hz, 2H), 0.95 (t, *J* = 7.3 Hz, 3H); <sup>13</sup>C NMR (CDCl<sub>3</sub>) δ: 200.707 (C), 142.315 (CH), 134.594 (C), 130.374 (CH), 128.939 (CH), 128.218 (CH), 126.236 (CH), 40.676 (CH<sub>2</sub>), 26.453 (CH<sub>2</sub>), 22.444 (CH<sub>2</sub>), 13.923 (CH<sub>3</sub>); IR (CCl<sub>4</sub>): 3084 (w), 3064 (w), 3029 (w), 2959 (s), 2932 (s), 2872 (m), 1948 (vw), 1878 (vw), 1800 (vw), 1692 (s), 1669 (s), 1612 (vs), 1576 (m), 1495 (m), 1449 (s), 1366 (w), 1330 (m), 1178 (m), 1059 (m), 975 (m) cm<sup>-1</sup>; MS (EI) *m/e*: 189 (3%), 188 (16%), 147 (8%), 146 (72%), 145 (12%), 132 (19%), 131 (100%), 104 (9%), 103 (62%), 102 (8%), 77 (22%); HRMS: exp 188.1222, calculated for C<sub>13</sub>H<sub>15</sub>O 188.1201.

**Acylate Complex 1 Reacting with *cis*-Styrene Triflate.** To a two-neck flask, equipped with a gas inlet adapter and a rubber septum, under an inert atmosphere, was added 0.62 g (2.5 mmol) of styryl triflate (1:3 trans:cis ratio) dissolved in 10 mL of degassed THF. The solution was cooled to  $-40$  °C.



To this, over a 45 min period, was added 1.0 mmol of acylate complex **1** dissolved in 20 mL of THF. Care was taken to drip the solution down the side of the cooled flask. Samples were removed about every 15 min for IR analysis. Upon completing the addition, the cold bath was removed and the reaction mixture was allowed to stir for an additional 15 min at room temperature. To this solution was added 0.48 g (1.9 mmol) of I<sub>2</sub>. The reaction then was washed with a saturated NaHSO<sub>3</sub> solution. The entire mixture was extracted with 75 mL of Et<sub>2</sub>O. The organic layer was washed with water, followed by a saturated NaCl solution, and dried with MgSO<sub>4</sub>.

As determined by GC, the trans to cis ratio of the recovered starting material changed from 1:8 to 1:11, again indicating the trans isomer is reacting more rapidly, and the ratio of **7** to **8** is 1.5:1 IR data of the solution after 15 min at room temperature but before workup (THF): 2042 (vs) 1968 (vs), 1880 (w), 1846 (vw), 1778 (vw), 1716 (vs), 1694 (w), 1655 (w), 1643 (s), 1613 (w), 1577 (s).

#### Synthesis of Authentic 1-Phenyl-1-hepten-3-one (**7**).

The synthesis of this compound was adapted from a literature preparation.<sup>11</sup> To a 100 mL three-neck flask equipped with a stir bar, rubber septa, and a gas inlet adapter under an inert atmosphere and charged with 35 mL of Et<sub>2</sub>O was added 0.81 g (5.5 mmol) of *trans*-cinnamic acid. The solution was cooled to 0 °C and to this, over a 75 min period, was added 6.2 mL (10 mmol) of 1.6 M BuLi. The ice bath was removed, and the reaction was allowed to go to room temperature. After 16 h, 50 mL of saturated NH<sub>4</sub>Cl (cooled to 0 °C) was added. The solution was allowed to react 15 min after which it was extracted with 100 mL of Et<sub>2</sub>O, washed three times with 20 mL saturated K<sub>2</sub>CO<sub>3</sub>, three times with 40 mL water, two times with 50 mL saturated NaCl, and dried with MgSO<sub>4</sub>. The product was dissolved in a minimal amount of hot MeOH and cooled in an 2-propanol-dry ice bath. Pure white crystals were separated by vacuum filtration. Spectroscopic data were identical to those obtained from crystals prepared earlier in our laboratory using **1** and styrene triflate.

**Reaction of Styrene Triflate with 1.** To a solution of 0.13 g (0.50 mmol) of styrene triflate dissolved in 2 mL of dry THF and cooled to -35 °C was added, over a 30 min period via a cannula, 0.50 mmol of pentanoyl nickel acylate complex **1** dissolved in 15 mL of THF also cooled to -35 °C. The solution was kept at -35 °C for an additional 15 min after which it was allowed to warm to room temperature and react overnight. An aliquant was removed for IR analysis, and the solution was again cooled to -35 °C. To the cooled solution was added, in the same manner as above, an additional 0.50 mmol **1**. Again, the reaction was kept at -35 °C for 15 min and then allowed to warm to room temperature and react overnight. An aliquant was removed for IR analysis, and the remaining solution was poured directly onto 0.40 g (1.6 mmol) of solid I<sub>2</sub>. A 10% saturated solution of NaHSO<sub>3</sub> was added to remove excess I<sub>2</sub>. The organic layer was washed with additional bisulfite until the water layer was clear, and the entire mixture was then extracted with 75 mL of Et<sub>2</sub>O. The organic layer was washed with water, followed by a saturated NaCl solution, and dried with MgSO<sub>4</sub>. For all aliquants taken and worked up, solvent was removed under vacuum and the product ratios were determined using GC analysis. IR (CO region of reaction solution): 1 equiv of **1** + 1 equiv of styrene triflate, room temperature, 24 h: 1995 (vs), 1972 (s), 1825 (m), 1714 (m), 1692 (w), 1669 (w), 1610 (m); 2 equiv of **1** + 1 equiv of styrene triflate, room temperature, 24 h: 2041 (vs), 2008 (vs), 1994 (vs), 1825 (m), 1714 (m), 1639 (w), 1601 (w).

**2,5-Dibutyl-3-phenylfuran (**10**).** To a solution of 10 mmol of nickel acylate complex **1** in 35 mL of THF and cooled to -50 °C was added over a 2 min period via syringe neat 0.64 mL (5.0 mmol) of bromostyrene. The reaction was kept at -50 °C while 5 mL aliquants were removed every 20 minutes over

the next 3 h and worked up by pouring directly onto approximately 1.2 equiv of solid I<sub>2</sub>. After 15 min, a 10% saturated solution of NaHSO<sub>3</sub> was added to remove excess I<sub>2</sub>. The organic layer was washed with additional bisulfite until the water layer was clear, and the entire mixture was extracted with 75 mL of Et<sub>2</sub>O. The organic layer was then washed with water, followed by a saturated NaCl solution and dried with MgSO<sub>4</sub>. NOTE: The yields are exceedingly variable since it is difficult to assess what conditions give the maximal results. A pure sample of **10** was obtained while separating **8** on a silica column and characterized spectroscopically. The compound was unstable at room temperature after about 7 days. GC ret time 20.50 min; <sup>1</sup>H NMR (CDCl<sub>3</sub>) δ: 7.37–7.21 (m, 5H), 6.01 (s, 1H), 2.73 (t, *J* = 2.6 Hz, 2H), 2.61 (t, *J* = 7.5 Hz, 2H), 1.73–1.61 (m, 4H), 1.45–1.32 (m, 4H), 0.97–0.88 (m, 6H); <sup>13</sup>C NMR (CDCl<sub>3</sub>) δ: 154.453 (C), 150.181 (C), 135.003 (C), 128.629 (CH), 127.778 (CH), 126.222 (CH), 121.204 (CH), 106.276 (CH), 31.079 (CH<sub>2</sub>), 30.371 (CH<sub>2</sub>), 27.884 (CH<sub>2</sub>), 26.930 (CH<sub>2</sub>), 22.692 (CH<sub>2</sub>), 22.523 (CH<sub>2</sub>), 14.090 (CH<sub>3</sub>); IR (neat oil both isomers): 3082 (w), 3054 (w), 3026 (w), 2958 (vs), 2930 (vs), 2873 (s), 2859 (s), 1943 (vw), 1870 (vw), 1803 (vw), 1624 (w), 1602 (m), 1575 (m), 1495 (m), 1466 (m), 1455 (m), 1446 (m), 1378 (w), 1225 (w), 1065 (w), 980 (m) cm<sup>-1</sup>; MS (EI) *m/e*: 257 (9%), 256 (45%), 214 (33%), 213 (100%), 141 (9%), 129 (10%), 128 (12%), 57 (8%).

**Synthesis of Authentic Cyclic Products 11.** Approximately 0.41 g of KH slurry (35% in mineral oil) was added to a tared, argon filled, three-neck flask equipped with a stir bar rubber septa and a gas inlet adapter. The mineral oil was removed by four washings with dry petroleum ether (5 mL each) and the residual petroleum ether was removed under high vacuum until the KH was a free flowing powder (0.17 g, 4.3 mmol). To the dried KH was added 30 mL of dry THF, and the resulting slurry was cooled to -78 °C. To this KH slurry was added, via syringe over a 5 min period, 1.16 g (4.23 mmol) of **8** dissolved in 5 mL of dry THF. The reaction was allowed to slowly warm to room temperature and reacted overnight after which 10 mL of saturated NH<sub>4</sub>Cl was added. The solution was allowed to react 1 h and then was extracted with 100 mL of diethyl ether and dried over MgSO<sub>4</sub>. The product was purified using 35 g of silica gel eluting with 2% THF:98% petroleum ether to yield 0.92 g (3.6 mmol, 86% yield both isomers) of **11a** and **11b**. **11a**: GC ret time 21.95 min; <sup>1</sup>H NMR (CDCl<sub>3</sub>) δ: 7.31–7.07 (m, 5H), 3.54 (dd, *J* = 2.3, 7.2 Hz, 1H), 3.05 (dd, *J* = 7.2, 18.4 Hz, 1H), [2.60 (br d, *J* = 18.6 Hz), 2.53–2.46 (m), 3H], 2.21 (t, *J* = 7.5 Hz, 2H), 1.59–1.36 (m, 6H), 1.00–0.85 (m, 6H); <sup>13</sup>C NMR (CDCl<sub>3</sub>) δ: 208.640 (C), 173.352 (C), 140.546 (C), 139.485 (C), 128.691 (CH), 127.469 (CH), 126.620 (CH), 50.936 (CH), 39.126 (CH<sub>2</sub>), 30.852 (CH<sub>2</sub>), 29.705 (CH<sub>2</sub>), 25.270 (CH<sub>2</sub>), 22.845 (CH<sub>2</sub>), 21.812 (CH<sub>2</sub>), 14.091 (CH<sub>3</sub>), 13.920 (CH<sub>3</sub>); IR (neat oil both isomers): 3086 (w), 3062 (w), 3026 (w), 2958 (vs), 2931 (vs), 2871 (s), 1943 (vw), 1874 (vw), 1802 (vw), 1700 (vs), 1692 (sh vs), 1637 (s), 1602 (m), 1494 (m), 1455 (s), 1377 (m), 1360 (m) cm<sup>-1</sup>; MS (EI) *m/e*: 257 (7%), 256 (37%), 228 (17%), 227 (100%), 199 (21%), 141 (8%), 129 (16%), 128 (15%), 115 (15%), 105 (18%), 104 (16%), 103 (10%), 91 (43%), 79 (12%), 78 (15%), 77 (18%), 67 (8%), 65 (12%), 55 (15%), 53 (13%); HRMS: exp 256.1826, calculated for C<sub>18</sub>H<sub>24</sub>O 256.1827.

**11b**: Isomer **11b** could not be obtained in a ratio to **11a** of greater than 1:1. Thus the spectroscopic data are the difference spectra for the 1:1 mixture of **11a** and **11b** and the pure **11a**. GC ret time 21.02 min; <sup>1</sup>H NMR (CDCl<sub>3</sub>) δ: 7.32–7.07 (m, 5H), 3.93 (br d, *J* = 6.6 Hz, 1H), 2.87 (dd, *J* = 7.1, 19.1 Hz, 1H), 2.62–2.45 (m, 3H), 2.36–2.17 (m, 2H), 1.59–1.20 (m, 6H), 0.99–0.82 (m, 6H); <sup>13</sup>C NMR (CDCl<sub>3</sub>) δ: 209.431 (C), 175.842 (C), 142.469 (C), 141.283 (C), 129.048 (CH), 127.615 (CH), 127.105 (CH), 46.462 (CH), 44.958 (CH<sub>2</sub>), 29.853 (CH<sub>2</sub>), 28.836 (CH<sub>2</sub>), 23.017 (CH<sub>2</sub>), 22.889 (CH<sub>2</sub>), 21.963 (CH<sub>2</sub>), 14.248 (CH<sub>3</sub>), 13.807 (CH<sub>3</sub>); MS (EI) *m/e*: 257 (7%), 256 (37%), 228 (17%), 227 (100%), 199 (13%), 171 (8%), 129 (13%), 128 (14%), 115 (12%), 105 (8%), 104 (7%), 91 (36%), 79 (9%), 78 (9%), 77

(11) House, H. O.; Respass, W. L.; Whitesides, G. M. *J. Am. Chem. Soc.* **1966**, *31*, 3128.



(17%), 55 (16%), 53 (9%); HRMS: exp 256.1819, calculated for  $C_{18}H_{24}O$  256.1827.

**Reactions of Chlorostyrene Using Added Salts and Crown Ether.** Note, all salts were obtained from previously unopened bottles stored in an inert atmosphere glove box. Furthermore, all reactions using added salts (LiBr, LiCl, LiOTf, KBr,  $R_4N^+ClO_4^-$ , crown ethers, and  $LiClO_4$ ) were performed as described below: To a solution of 2.00 mmol of acylate complex **1** in 10 mL of THF was added 2.00 mmol of one of the following dry salts LiBr, LiCl, LiOTf, KBr,  $R_4N^+ClO_4^-$ , or  $LiClO_4$ . After 30 min at room temperature, 0.26 g (2.00 mmol) of neat chlorostyrene were added via syringe over a 2 min period. The solution was allowed to react 4.5 h at room temperature, after which it was poured directly onto 0.80 g of  $I_2$  (3.2 mmol). A 10% saturated solution of  $NaHSO_3$  was added to remove excess  $I_2$ . The organic layer was washed with additional bisulfite until the water layer was clear and the entire mixture was extracted with 75 mL of  $Et_2O$ . The organic layer was then washed with water, followed by a saturated NaCl solution, and dried with  $MgSO_4$ . Solvent was removed under vacuum, and all product ratios were determined using GC analysis. The product ratio of **8:11** for each added salt: no salt, 2:3; LiCl, 1:1; LiBr, 1:1; LiBr (3 equiv), 1:1; KBr, 1:2;  $Bu_4N^+ClO_4^-$ , 1:2; 12-crown-4, 1:4.

**Slow Oxidation Using Ferrocenium Ion.** To a solution of 1 mmol of acylate complex **1** in 15 mL of THF and cooled to  $-40^\circ C$  was added 0.26 g (1.0 mmol) of neat chlorostyrene via syringe over a 2 min period. The solution was allowed to react 15 min at  $-40^\circ C$  and then taken to room temperature overnight. In the first experiment, the reaction mixture was cooled again to  $-78^\circ C$  and 1 equiv of ferrocenium<sup>7a</sup> was added rapidly. After the solution was reacted for 1 h at  $-78^\circ C$ , 10 mL of degassed saturated  $NH_4Cl$  was added and the solution was taken to room temperature for 2 h. The solution was poured directly onto 0.30 g (1.2 mmol) of solid  $I_2$  and worked up as described below. The second experiment was identical to the first except that after adding the ferrocenium ion, the reaction was taken to room temperature for 2 h and then worked up. The third experiment was identical to the second except that 2 equiv of the ferrocenium was added. All reactions were worked up after addition the of  $I_2$  as follows: A 10% saturated solution of  $NaHSO_3$  was added to remove excess  $I_2$ . The organic layer was washed with additional bisulfite until the water layer was clear, and the entire mixture was extracted with 75 mL of  $Et_2O$ . The organic layer was then washed with water, followed by a saturated NaCl solution, and dried with  $MgSO_4$ . Solvent was removed under vacuum, and all product ratios were determined using GC analysis.

**Slow Oxidation Using an  $I_2$ /THF Solution.** To a solution of 3.00 mmol of acylate complex **1** in 25 mL of THF and cooled to  $-10^\circ C$  was added 3.00 mmol of neat chlorostyrene via syringe over a 2 min period. The solution was allowed to react 15 min at  $-10^\circ C$  and then taken to room temperature overnight. A solution of 1.0 g (4.0 mmol) of  $I_2$  dissolved in 20 mL of THF was added slowly over a 2 h period until the solution color just remained brown. A 10% saturated solution of  $NaHSO_3$  was added to remove excess  $I_2$ . The organic layer was washed with additional bisulfite until the water layer was clear, and the entire mixture was extracted with 75 mL of  $Et_2O$ . The organic layer was then washed with water, followed by a saturated NaCl solution, and dried with  $MgSO_4$ . Solvent was removed under vacuum, and all product ratios were determined using GC analysis.

**Diluted Reaction of Bromostyrene with **1** with Long Term Monitoring.** To a solution of 2 mmol of acylate complex **1** in 10 mL of THF and cooled to  $-78^\circ C$  was added 0.13 mL (1.0 mmol) of neat bromostyrene via syringe over a 2 min period. The solution was allowed to react at  $-25^\circ C$  for 3.5 h after which 80 mL of dry degassed THF at room temperature was rapidly added. The reaction was allowed to react 7 days at room temperature while aliquants of 5 mL each were periodically removed and poured directly onto 0.8 g (3

mmol) of solid  $I_2$ . (Though the reaction is done in a matter of hours, this very long time period was used to determine if any changes would occur.) A 10% saturated solution of  $NaHSO_3$  was added to remove excess  $I_2$ , and the organic layer was washed with additional bisulfite until the water layer was clear. The entire mixture was extracted with 50 mL of  $Et_2O$ , and the organic layer was washed with water, followed by a saturated NaCl solution, and dried with  $MgSO_4$ . Solvent was removed under vacuum, and all product ratios were determined using GC analysis. In addition, at the time of each aliquant, a sample was removed for IR analysis. The ratio of **8:11** is 1:6 for both a 0.20 M and a 0.012 M reaction, both run for 3 h.

**Reaction of **1** with Bromostyrene in  $Et_2O$ .** To a solution of 10.0 mmol of nickel acylate complex **1** in 35 mL of  $Et_2O$  and cooled to  $-50^\circ C$  was added neat, over a 2 min period via syringe, 0.64 mL (5.0 mmol) of bromostyrene. The reaction was kept at  $-25^\circ C$  for 2.5 h and then allowed to slowly warm to room temperature. Aliquants were removed after 6 days and 16 days and worked up by pouring directly onto approximately 1.2 equiv of solid  $I_2$  and allowed to react 15 min after which a 10% saturated solution of  $NaHSO_3$  was added to remove excess  $I_2$ . The organic layer was washed with additional bisulfite until the water layer was clear, and the entire mixture was extracted with 75 mL of  $Et_2O$ . The organic layer was then washed with water, followed by a saturated NaCl solution and dried with  $MgSO_4$ . For all aliquants taken, solvent was removed under vacuum and the product ratios were determined using GC analysis.

**Acylate Complex **1** Reacting with 1-Bromo-1-propene.** This reaction was performed as in the general procedure. After the solvent was removed under vacuum, the resulting oil was chromatographed on a silica gel (21 g) column eluting first with 500 mL of 0.75:99.25  $EtOAc$ :petroleum ether, followed by 100 mL of 3:97  $EtOAc$ :petroleum ether, to give 0.41 g (1.9 mmol, 39% yield) of **12**. GC retention time 16.2 min.  $^1H$  NMR ( $CDCl_3$ )  $\delta$ : 3.12–2.90 (m, 2H), 2.55 (t,  $J = 7.3$  Hz, 2H), 2.43–2.30 (m, 3H), 1.62–1.48 (m, 4H), 1.38–1.22 (m, 4H), 1.80 (d,  $J = 7.1$  Hz, 3H), 0.94–0.86 (m, 6H);  $^{13}C$  NMR ( $CDCl_3$ )  $\delta$ : 213.902 (C), 209.978 (C), 45.722 ( $CH_2$ ), 42.685 ( $CH_2$ ), 41.210 ( $CH_2$ ), 41.085 (CH), 26.024 ( $CH_2$ ), 25.850 ( $CH_2$ ), 22.522 ( $CH_2$ ), 22.432 ( $CH_2$ ), 16.908 ( $CH_3$ ), 14.073 ( $CH_3$ ), 13.989 ( $CH_3$ ); IR (neat oil): 2960 (s), 2929 (s), 2875 (s), 1708 (vs), 1456 (s), 1406 (m), 1375 (m), 1123 (m), 1042 (m)  $cm^{-1}$ ; MS (EI)  $m/e$ : 212 (3%), 194 (18%), 170 (20%), 155 (32%), 152 (12%), 151 (10%), 149 (17%), 127 (18%), 109 (9%), 85 (37%), 57 (5%); HRMS: exp 212.1773, calculated for  $C_{13}H_{24}O_2$  212.1776.

**Reaction of Bromopropene with **1** with Long Term Monitoring.** To a solution of 10.0 mmol of acylate complex **1** in 35 mL of THF at room temperature was added neat 0.43 mL (5.0 mmol) of 1-bromo-1-propene via syringe over a 2 min period. The solution was allowed to react at room temperature for seven days. Aliquants of 1 mL each were periodically removed and poured directly onto 1.0 g (4.0 mmol) of solid  $I_2$ . A 10% saturated solution of  $NaHSO_3$  was added to remove excess  $I_2$ , and the organic layer was washed with additional bisulfite until the water layer was clear. The entire mixture was extracted with 50 mL of  $Et_2O$ , and the organic layer was washed with water, followed by a saturated NaCl solution, and dried with  $MgSO_4$ . Solvent was removed under vacuum, and all product ratios were determined using GC analysis. In addition, at the time of each aliquant, a sample was removed for IR analysis. Representative IR data (CO region of reaction solution): 6 h at room temperature: 2042 (s), 2008 (s), 1996 (s), 1838 (m), 1820 (m), 1802 (m), 1714 (m), 1702 (m), 1537 (s); seven days at room temperature: 2042 (vs), 2006 (vs), 1995 (vs), 1953 (s), 1822 (s), 1802 (s), 1701 (s).

**Acylate Complex **1** Reacting with 1-Chloro-1-propene.** To a solution of 3.0 mmol of acylate complex **1** in 25 mL of THF cooled to  $-40^\circ C$  was added neat, over a 2 min period via syringe, 0.26 mL (3.0 mmol) of 1-chloro-1-propene. The solution was allowed to react an additional 15 min at  $-40^\circ C$

after which it was taken to room temperature for 2 days. Samples were removed over the next 2 days and worked up as follows. A 3 mL aliquant was removed and poured directly onto 0.20 g (0.79 mmol) of solid  $I_2$ . A 10% saturated solution of  $NaHSO_3$  was added to remove excess  $I_2$ . The organic layer was washed with additional bisulfite until the water layer was clear, and the entire mixture was extracted with 75 mL of  $Et_2O$ . The organic layer was then washed with water, followed by a saturated  $NaCl$  solution, and dried with  $MgSO_4$ . The solvent was removed by vacuum and the product analyzed using GC. After 2 days, the remaining solution was poured directly onto 1.5 g (5.9 mmol) of solid  $I_2$  and worked up the same as above. The product was purified using 30 g of silica gel, eluting first with 500 mL of 0.75%  $EtOAc$ :99.25% petroleum ether followed by 100 mL of 2%  $EtOAc$ :98% petroleum ether and finally 100 mL of 3%  $EtOAc$ :97% petroleum ether to give a mixture of isomers of **13a** and **13b**. **13a**: GC ret time 15.31 min;  $^1H$  NMR ( $CDCl_3$ )  $\delta$ : 2.75 (dd,  $J = 6.8, 18.0$  Hz, 1H), 2.43–2.30 (m, 3H), 2.17–2.04 (m, 3H), 1.57–1.29 (m, 6H), 1.15 (d,  $J = 7.4$  Hz, 3H), 0.97–0.85 (m, 6H);  $^{13}C$  NMR ( $CDCl_3$ )  $\delta$ : 212.504 (C), 172.274 (C), 138.969 (C), 39.937 (CH), 38.211 ( $CH_2$ ), 30.841 ( $CH_2$ ), 29.779 ( $CH_2$ ), 25.221 ( $CH_2$ ), 22.899 ( $CH_2$ ), 21.931 ( $CH_2$ ), 16.852 ( $CH_3$ ), 14.165 ( $CH_3$ ), 13.997 ( $CH_3$ ); IR (neat oil): 2957 (vs), 2927 (vs), 2868 (vs), 1700 (vs), 1640 (vs), 1457 (s), 1435 (m), 1368 (s), 1342 (M), 1319 (m), 1170 (m), 1092 (m)  $cm^{-1}$ ; MS (EI)  $m/e$ : 195 (2%), 194 (18%), 166 (10%), 165 (100%), 137 (13%), 109 (11%), 95 (5%), 67 (9%), 55 (11%); HRMS: exp 194.1688, calculated for  $C_{13}H_{22}O$  194.1671.

**13b**:  $^1H$  NMR ( $CDCl_3$ )  $\delta$ : 2.86–2.81 (m, 1H), 2.59 (dd,  $J = 1.8, 18.6$  Hz, 1H), 2.53–2.45 (m, 1H), 2.36–2.25 (m, 1H), 2.19–2.09 (m, 2H), 1.94 (dd,  $J = 1.8, 18.5$  Hz, 1H), 1.60–1.29 (m, 6H), 1.16 (d,  $J = 6.7$  Hz, 3H), 0.97–0.85 (m, 6H);  $^{13}C$  NMR ( $CDCl_3$ )  $\delta$ : 209.128 (C), 178.039 (C), 139.820 (C), 43.160 ( $CH_2$ ), 34.597 (CH), 29.685 ( $CH_2$ ), 28.174 ( $CH_2$ ), 25.191 ( $CH_2$ ), 22.986 ( $CH_2$ ), 21.945 ( $CH_2$ ), 19.356 ( $CH_3$ ), 14.125 ( $CH_3$ ), 13.950 ( $CH_3$ ); IR (neat oil): 2956 (vs), 2932 (vs), 2873 (vs), 1701 (vs), 1638 (vs), 1464 (s), 1411 (m), 1378 (s), 1358 (s), 1340 (m), 1236 (w), 1168 (m), 1109 (m)  $cm^{-1}$ ; MS (EI)  $m/e$ : 195 (2%), 194 (22%), 166 (10%), 165 (100%), 137 (15%), 124 (7%), 109 (11%), 95 (11%), 81 (11%), 79 (11%), 67 (13%), 55 (15%); HRMS: exp 194.1678, calculated for  $C_{13}H_{22}O$  194.1671.

**4-Phenyl-2,5-nonadione (24)**. To a solution of 10 mmol of pentanoyl nickel acylate complex **1** dissolved in 35 mL of THF and cooled to  $-30^\circ C$  was added, over a 3 min period via syringe, 1.97 g (10.0 mmol) of **23** dissolved in 3 mL of dry THF. The reaction was kept at  $-30^\circ C$  for 15 min and then allowed to slowly warm to room temperature. After 1 h at room temperature, 10 mL of saturated  $NH_4Cl$  was added. The solution was allowed to react 15 min after which it was poured directly onto 2.90 g (11.5 mmol) of  $I_2$ . A 10% saturated solution of  $NaHSO_3$  was added to remove excess  $I_2$ . The organic layer was washed with additional bisulfite until the water layer was clear, and the entire mixture was extracted with 75 mL of  $Et_2O$ . The organic layer was then washed with water, followed by a saturated  $NaCl$  solution, and dried with  $MgSO_4$ . The product was purified using 43 g of silica gel-60, eluting first with 400 mL of 1%  $Et_2O$ :99% petroleum ether followed by 200 mL of 1% THF:99% petroleum ether and finally 400 mL of 2% THF:98% petroleum ether to give 1.76 g (7.58 mmol 76% yield) of **24**. GC ret time 18.29 min;  $^1H$  NMR ( $CDCl_3$ )  $\delta$ : 7.35–7.17 (m, 5H), 4.21 (dd,  $J = 3.6, 10.5$  Hz, 1H), 3.46 (dd,  $J = 10.6, 18.0$  Hz, 1H), 2.60–2.30 (m, 3H), 2.16 (s, 3H), 1.56–1.40 (m, 2H), 1.23–1.13 (m, 2H), 0.78 (t,  $J = 14.5$  Hz, 3H);  $^{13}C$  NMR ( $CDCl_3$ )  $\delta$ : 209.560 (C), 207.024 (C), 138.172 (C), 129.179 (CH), 128.335 (CH), 127.622 (CH), 53.445 (CH), 46.727 ( $CH_2$ ), 41.422 ( $CH_2$ ), 30.114 ( $CH_3$ ), 25.852 ( $CH_2$ ), 22.222 ( $CH_2$ ), 13.911 ( $CH_3$ ); IR (neat oil): 3081 (w), 3059 (w), 3029 (w), 2955 (s), 2933 (s), 2986 (m), 1955 (vw), 1885 (vw), 1811 (vw), 1711 (vs), 1596 (w), 1493 (m), 1452 (m), 1400 (m), 1363 (m), 1163 (m), 1126 (m), 1030 (m)  $cm^{-1}$ ; MS (EI)  $m/e$ : 232 (7%), 190 (13%), 171 (6%), 148 (28%), 147 (14%), 131 (24%), 119 (35%), 104 (34%), 85

(100%), 77 (8%), 69 (28%); HRMS: exp 232.1439, calculated for  $C_{15}H_{20}O_2$  232.1463.

**3-Methyl-5-phenyl-2-propyl-2-cyclopentenone (25a)**. Approximately 0.20 g (5.0 mmol) of powdered KH was prepared as before in the synthesis of **11**. To the dried KH was added 30 mL of dry THF, and the resulting slurry was cooled to  $-78^\circ C$ . To this KH slurry was added over a 5 min period via syringe 1.01 g (4.36 mmol) of **24** dissolved in 3 mL of dry degassed THF. The reaction was slowly warmed to room temperature and allowed to react 90 min after which 15 mL of saturated  $NH_4Cl$  was added. The solution was allowed to react an additional 15 min after which it was extracted with 100 mL of diethyl ether, washed with three 50 mL portions of water, followed by 50 mL of saturated  $NaCl$ , and dried using  $MgSO_4$ . The product required no additional purification, giving 0.93 g of (4.3 mmol, 99% yield) of **25a**, a light yellow oil. GC ret time 19.58 min;  $^1H$  NMR ( $CDCl_3$ )  $\delta$ : 7.30–7.08 (m, 5H), 3.51 (dd,  $J = 2.6, 7.2$  Hz, 1H), 3.00 (dd,  $J = 7.6, 18.0$  Hz, 1H), 2.55 (dd,  $J = 2.2, 18.8$  Hz, 1H), 2.21 (t,  $J = 7.3$  Hz, 2H), 2.08 (s, 3H), 1.45 (sextet,  $J = 7.4$  Hz, 2H), 0.89 (t,  $J = 7.4$  Hz, 3H);  $^{13}C$  NMR ( $CDCl_3$ )  $\delta$ : 208.172 (C), 169.151 (C), 140.336 (C), 139.517 (C), 136.531 (CH), 134.001 (CH), 131.083 (C), 129.403 (CH), 129.050 (CH), 128.558 (CH), 127.418 (CH), 126.516 (CH), 50.934 (CH), 41.433 (CH<sub>2</sub>), 25.021 (CH<sub>2</sub>), 21.471 (CH<sub>2</sub>), 17.046 (CH<sub>3</sub>), 13.882 (CH<sub>3</sub>); IR ( $CCl_4$ ): 3085 (w), 3062 (w), 3029 (m), 2961 (m), 2931 (m), 2872 (m), 2848 (m), 1945 (vw), 1869 (vw), 1801 (vw), 1701 (vs), 1697 (vs sh), 1647 (s), 496 (m), 1453 (m), 1385 (m), 1181 (m), 1061 (m)  $cm^{-1}$ ; MS (EI)  $m/e$ : 215 (18%), 214 (100%), 199 (57%), 186 (44%), 185 (24%), 172 (11%), 171 (53%), 157 (17%), 143 (38%), 142 (17%), 141 (19%), 131 (17%), 129 (38%), 128 (31%), 118 (19%), 115 (28%), 105 (17%), 104 (55%), 103 (28%), 95 (13%), 91 (50%), 79 (17%), 78 (28%), 77 (40%), 67 (14%), 65 (19%), 63 (14%), 55 (12%), 53 (23%), 51 (21%); HRMS: exp 214.1342, calculated for  $C_{15}H_{18}O$  214.1358.

**3-Phenyl-2,5-nonadione (27)**. To a solution of 4.27 mmol of methanoyl nickel acylate complex **26** in 25 mL of THF and cooled to  $-30^\circ C$  was added, over a 3 min period via syringe, 0.81 g (4.3 mmol) of **7** dissolved in 3 mL of dry THF. The reaction was kept at  $-30^\circ C$  for 15 min and then allowed to slowly warm to room temperature. After 30 min at room temperature, 10 mL of saturated  $NH_4Cl$  was added. The solution was allowed to react 15 min after which it was poured directly onto 1.75 g (6.90 mmol) of  $I_2$ . A 10% saturated solution of  $NaHSO_3$  was added to remove excess  $I_2$ . The organic layer was washed with additional bisulfite until the water layer was clear and the entire mixture was extracted with 75 mL of  $Et_2O$ . The organic layer was then washed with water, followed by a saturated  $NaCl$  solution, and dried with  $MgSO_4$ . The product was purified using 40 g of silica gel 60, eluting first with 400 mL of 1%  $Et_2O$ :99% petroleum ether followed by 200 mL of 1% THF:99% petroleum ether and finally 400 mL of 2% THF:98% petroleum ether to give 0.63 g (2.7 mmol 63% yield) of **27**. GC ret time 18.56 min;  $^1H$  NMR ( $CDCl_3$ )  $\delta$ : 7.36–7.18 (m, 5H), 4.23 (dd,  $J = 3.8, 10.2$  Hz, 1H), 3.41 (dd,  $J = 10.3, 17.8$  Hz, 1H), 2.54 (dd,  $J = 3.9, 17.8$  Hz, 1H), 2.48–2.37 (m, 2H), 2.12 (s, 3H), 1.55 (quintet,  $J = 7.7$  Hz, 2H), 1.29 (sextet,  $J = 7.4$  Hz, 2H), 0.89 (t,  $J = 7.3$  Hz, 3H);  $^{13}C$  NMR ( $CDCl_3$ )  $\delta$ : 209.472 (C), 207.360 (C), 138.041 (C), 128.221 (CH), 128.336 (CH), 127.661 (CH), 53.993 (CH), 45.770 ( $CH_2$ ), 42.647 ( $CH_2$ ), 29.143 ( $CH_3$ ), 25.942 ( $CH_2$ ), 22.393 ( $CH_2$ ), 13.958 ( $CH_3$ ); IR (neat oil): 3085 (vw), 3062 (w), 3028 (w), 2960 (s), 2934 (m), 2872 (m), 1957 (vw), 1890 (vw), 1813 (vw), 1718 (vs, sh), 1715 (vs), 1600 (w), 1494 (m), 1454 (m), 1356 (m), 1161 (m), 1126 (m)  $cm^{-1}$ ; MS (EI)  $m/e$ : 232 (10%), 233 (2%), 190 (12%), 148 (28%), 133 (20%), 130 (17%), 105 (47%), 104 (38%), 103 (21%), 91 (52%), 86 (18%), 85 (100%), 78 (20%), 77 (34%); HRMS: exp 232.1449, calculated for  $C_{15}H_{20}O_2$  232.1463.

**3-Butyl-5-phenyl-2-cyclopentenone (28a) and 3-Methyl-4-phenyl-2-propyl-2-cyclopentenone (28b)**. Approximately 0.11 g (2.7 mmol) of powdered KH was prepared as

before in the synthesis of **11**. To the dried KH was added 30 mL of dry THF, and the resulting slurry was cooled to  $-78$  °C. To this KH slurry over a 5 min period was added via syringe 0.52 g (2.3 mmol) of **27** dissolved in 3 mL of dry degassed THF. The reaction was slowly warmed to room temperature and allowed to react 90 min after which 15 mL of saturated  $\text{NH}_4\text{Cl}$  was added. The solution was allowed to react an additional 15 min after which it was extracted with 100 mL of diethyl ether, washed with three 50 mL portions of water, followed by 50 mL of saturated NaCl, and dried using  $\text{MgSO}_4$ . The product was separated using 31 g of silica gel, eluting first with 200 mL of 1%  $\text{Et}_2\text{O}$ :99% petroleum ether followed by 450 mL of 1% THF:99% petroleum ether giving 0.41 g (1.9 mmol, 85% yield) of **28b**, a light yellow oil. GC ret time 18.85 min;  $^1\text{H}$  NMR ( $\text{CDCl}_3$ )  $\delta$ : 7.34–7.07 (m, 5H), 3.82–3.78 (br d,  $J = 6.7$  Hz, 1H), 2.88 (dd,  $J = 6.83$ , 18.6 Hz, 1H), 2.35 (dd,  $J = 1.7$ , 18.5 Hz, 1H), 2.24 (t,  $J = 7.5$  Hz, 2H), 1.82 (s, 3H), 1.50 (sextet,  $J = 7.5$  Hz, 2H), 0.93 (t,  $J = 7.3$  Hz, 3H);  $^{13}\text{C}$  NMR ( $\text{CDCl}_3$ )  $\delta$ : 208.761 (C), 171.806 (C), 142.203 (C), 141.258 (C), 128.937 (CH), 127.291 (CH), 127.000 (CH), 49.073 (CH), 44.691 ( $\text{CH}_2$ ), 25.163 ( $\text{CH}_2$ ), 21.686 ( $\text{CH}_2$ ), 15.529 ( $\text{CH}_3$ ), 14.051 ( $\text{CH}_3$ ); IR (neat oil): 3083 (w), 3063 (w), 3027 (m), 2959 (s), 2929 (s), 2870 (m), 1951 (vw), 1875 (vw), 1806 (vw), 1702 (vs), 1647 (s), 1602 (m), 1494 (m), 1454 (m), 1383 (s), 1077 (m)  $\text{cm}^{-1}$ ; MS (EI)  $m/e$ : 214 (23%), 167 (29%), 150 (21%), 149 (100%), 117 (24%), 105 (50%), 91 (63%), 83 (40%), 71 (47%), 70 (45%), 69 (60%), 57 (59%); HRMS: exp 214.1375, calculated for  $\text{C}_{15}\text{H}_{18}\text{O}$  214.1358.

**28a**. GC ret time 20.71 min;  $^1\text{H}$  NMR ( $\text{CDCl}_3$ )  $\delta$ : 7.32–7.10 (m, 5H), 6.00 (s, 1H), 3.58 (dd,  $J = 2.7$ , 7.2 Hz, 1H), 3.09 (dd,  $J = 7.3$ , 18.9 Hz, 1H), 2.66 (br d,  $J = 18.8$  Hz, 1H), 2.46 (t,  $J = 7.6$  Hz, 2H), 1.61 (quintet,  $J = 7.5$  Hz, 2H), 1.40 (sextet,  $J = 7.3$  Hz, 2H), 0.95 (t,  $J = 7.3$  Hz, 3H);  $^{13}\text{C}$  NMR ( $\text{CDCl}_3$ )  $\delta$ : 208.936 (C), 182.385 (C), 139.865 (C), 128.727 (CH), 128.353 (CH), 127.510 (CH), 126.786 (CH), 52.161 (CH), 41.266 ( $\text{CH}_2$ ), 33.163 ( $\text{CH}_2$ ), 29.122 ( $\text{CH}_2$ ), 22.444 ( $\text{CH}_2$ ), 13.798 ( $\text{CH}_3$ ); IR (neat oil  $\text{CaF}_2$  plates): 3088 (w), 3066 (w), 3031 (m), 2960 (s), 2929 (s), 2872 (m), 1946 (vw), 1875 (vw), 1802 (vw), 170 (vs), 1616 (vs), 1496 (m), 1454 (m), 1381 (m), 1173 (s)  $\text{cm}^{-1}$ ; MS (EI)  $m/e$ : 215 (7%), 214 (41%), 158 (18%), 157 (100%), 143 (15%), 129 (87%), 128 (66%), 115 (35%), 105 (69%), 104 (43%), 91 (82%), 77 (48%), 69 (81%); HRMS: exp 214.1378, calculated for  $\text{C}_{15}\text{H}_{18}\text{O}$  214.1358.

**4-Methyl-2,5-nonadione**. To a solution of 10 mmol of nickel acylate complex **1** in 35 mL of THF and cooled to  $-50$  °C was added, over a 2 min period via syringe, 1.49 mL (10.0 mmol) of neat 3-penten-2-one (Note: 3-penten-2-one purchased from Aldrich was contaminated with mesityl oxide (35%), thus the amount of reagent is only an estimate). The reaction was kept at  $-50$  °C for 5 min and then allowed to slowly warm to room temperature. After 45 min at room temperature, 10 mL of saturated  $\text{NH}_4\text{Cl}$  was added. The solution was allowed to react 30 min after which it was poured directly onto 3.0 g (12.0 mmol) of  $\text{I}_2$ . A 10% saturated solution of  $\text{NaHSO}_3$  was added to remove excess  $\text{I}_2$ . The organic layer was washed with additional bisulfite until the water layer was clear, and the entire mixture was extracted with 75 mL of  $\text{Et}_2\text{O}$ . The organic layer was then washed with water, followed by a saturated NaCl solution, and dried with  $\text{MgSO}_4$ . The product was purified using 26 g of silica gel-60, eluting first with 500 mL of 0.75%  $\text{EtOAc}$ :99.25% petroleum ether followed by 200 mL of 5%  $\text{EtOAc}$ :95% petroleum ether to give 1.04 g (6.10 mmol, 61% yield). GC ret time 11.72 min;  $^1\text{H}$  NMR ( $\text{CDCl}_3$ )  $\delta$ : 7.35–7.17 (m, 5H), 4.21 (dd,  $J = 3.6$ , 10.5 Hz, 1H), 3.46 (dd,  $J = 10.6$ , 18.0 Hz, 1H), 2.60–2.30 (m, 3H), 2.16 (s, 3H), 1.56–1.40 (m, 2H), 1.23–1.13 (m, 2H), 0.78 (t,  $J = 14.5$  Hz, 3H);  $^{13}\text{C}$  NMR ( $\text{CDCl}_3$ )  $\delta$ : 213.521 (C), 207.191 (C), 46.357 ( $\text{CH}_2$ ), 40.956 (CH), 40.874 ( $\text{CH}_2$ ), 29.862 ( $\text{CH}_2$ ), 25.641 ( $\text{CH}_2$ ), 22.270 ( $\text{CH}_2$ ), 16.614 ( $\text{CH}_3$ ), 13.855 ( $\text{CH}_3$ ); IR (neat oil): 2958 (s), 2935 (s), 2875 (s), 1713 (vs), 1459 (m), 1400 (m), 1400 (m), 1376 (m), 1361 (s), 1172 (m), 1122 (w), 1043 (w)  $\text{cm}^{-1}$ ; MS (EI)  $m/e$ : 170 (3%),

129 (2%), 128 (25%); 113 (18%), 85 (98%), 71 (8%), 57 (100%); HRMS: exp 170.1308, calculated for  $\text{C}_{10}\text{H}_{18}\text{O}_2$  170.1307.

**3-Butyl-4-methyl-2-cyclopentenone and 3,5-Dimethyl-2-propyl-2-cyclopentenone**. Approximately 0.28 g (7.0 mmol) of powdered KH was prepared as before in the synthesis of **11**. To the dried KH was added 35 mL of dry THF, and the resulting slurry was cooled to  $-78$  °C. To this KH slurry over a 2 min period was added via syringe 1.02 g (6.00 mmol) of **12** dissolved in 4 mL of dry degassed THF. The reaction was allowed to go 15 min at  $-78$  °C after which the dry ice bath was removed. The reaction was warmed to room temperature and allowed to react overnight after which 20 mL of saturated  $\text{NH}_4\text{Cl}$  was added. The solution was allowed to react an additional 2 h after which it was first washed with three 25 mL portions of water extracted with 100 mL of diethyl ether, washed with three 50 mL portions of water, followed by 50 mL of saturated NaCl, and dried using  $\text{MgSO}_4$ . Solvent was removed under pressure to give 0.61 g of product (67% yield combined). The products were purified using 25 g of silica gel-60, eluting first with 600 mL of 1.0% THF:99% petroleum ether followed by 300 mL of 1.5% THF:97.5% petroleum ether. 3-Butyl-4-methyl-2-cyclopentenone: GC ret time 15.77 min;  $^1\text{H}$  NMR ( $\text{CDCl}_3$ )  $\delta$ : 5.90 (s, 1H), 2.88 (br quintet,  $J = 7.0$  Hz, 1H), 2.64 (dd,  $J = 6.5$ , 18.5 Hz, 1H), 2.53–2.40 (m, 1H), 2.35–2.23 (m, 1H), 2.00 (dd,  $J = 2.2$ , 18.5 Hz, 1H), 1.63–1.51 (m, 2H), 1.39 (sextet,  $J = 17.5$  Hz, 2H), 1.20 (d,  $J = 7.2$  Hz, 3H), 0.95 (t,  $J = 7.2$  Hz, 3H);  $^{13}\text{C}$  NMR ( $\text{CDCl}_3$ )  $\delta$ : 209.018 (C), 187.108 (C), 128.717 (CH), 44.086 ( $\text{CH}_2$ ), 37.793 (CH), 30.661 ( $\text{CH}_2$ ), 29.145 ( $\text{CH}_2$ ), 22.561 ( $\text{CH}_2$ ), 19.069 ( $\text{CH}_3$ ), 13.877 ( $\text{CH}_3$ ); IR (neat oil): 2959 (vs), 2931 (vs), 2871 (s), 1717 (vs), 1693 (vs), 1610 (s), 1466 (s), 1413 (m), 1379 (m), 1364 (m), 1268 (s), 1240 (s), 1172 (m)  $\text{cm}^{-1}$ ; MS (EI)  $m/e$ : 153 (4%), 152 (38%), 137 (30%), 110 (34%), 109 (10%), 96 (12%), 95 (70%), 82 (100%), 81 (26%), 79 (16%), 77 (12%), 68 (17%), 67 (71%), 55 (23%), 53 (27%); HRMS: exp 152.1211, calculated for  $\text{C}_{10}\text{H}_{16}\text{O}$  152.1201.

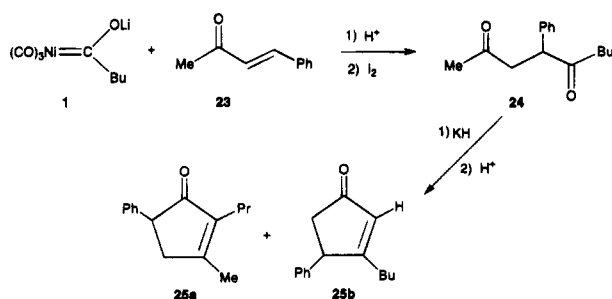
**3,5-Dimethyl-2-propyl-2-cyclopentenone**: GC ret time 13.75 min;  $^1\text{H}$  NMR ( $\text{CDCl}_3$ )  $\delta$ : 7.32–7.10 (m, 5H), 6.00 (s, 1H), 3.58 (dd,  $J = 2.7$ , 7.2 Hz, 1H), 3.09 (dd,  $J = 7.3$ , 18.9 Hz, 1H), 2.66 (br d,  $J = 18.8$  Hz, 1H), 2.46 (t,  $J = 7.6$  Hz, 2H), 1.61 (quintet,  $J = 7.5$  Hz, 2H), 1.40 (sextet,  $J = 7.3$  Hz, 2H), 0.95 (t,  $J = 7.3$  Hz, 3H);  $^{13}\text{C}$  NMR ( $\text{CDCl}_3$ )  $\delta$ : 212.337 (C), 168.507 (C), 139.382 (C), 40.870 ( $\text{CH}_2$ ), 39.727 (CH), 25.178 ( $\text{CH}_2$ ), 21.798 ( $\text{CH}_2$ ), 17.292 ( $\text{CH}_3$ ), 16.862 ( $\text{CH}_3$ ), 14.169 ( $\text{CH}_3$ ); IR (neat oil): 2960 (vs), 2932 (vs), 2872 (s), 1699 (vs), 1648 (s), 1613 (w), 1457 (m), 1436 (m), 1385 (s), 1354 (m), 1334 (m), 1176 (m)  $\text{cm}^{-1}$ ; MS (EI)  $m/e$ : 153 (7%), 152 (77%), 138 (10%), 137 (100%), 124 (58%), 123 (14%), 110 (9%), 109 (78%), 96 (27%), 95 (38%), 91 (10%), 81 (27%), 79 (21%), 77 (20%), 69 (9%), 67 (56%), 65 (12%), 55 (31%), 53 (27%); HRMS: exp 152.1209, calculated for  $\text{C}_{10}\text{H}_{16}\text{O}$  152.1201.

**Acknowledgment.** We wish to thank Drs. John Belletire, Michael Gunther, and Chad Hagedorn formally of the Department of Chemistry, University of Cincinnati, for many helpful discussions and some preliminary experiments. In addition, we wish to thank the donors of the Petroleum Research Fund, administered by the American Chemical Society (to J.W.H. and to A.R.P.), and the University of Cincinnati for an OBR Research Challenge Award (to A.R.P. and J.W.H.) for financial support of this work, and the Quantum Chemical Corp. for a fellowship (to J.R.H.). The 250 MHz NMR spectrometer used in this study was purchased with the aid of an Academic Challenge Award from the Ohio Board of Regents.

## Appendix

**Unambiguous Identification of 11a and 11b.** The cyclopentenone derivatives **11a** and **11b** can be independently synthesized by the reaction of 1,4-diketone **8**

Scheme 8



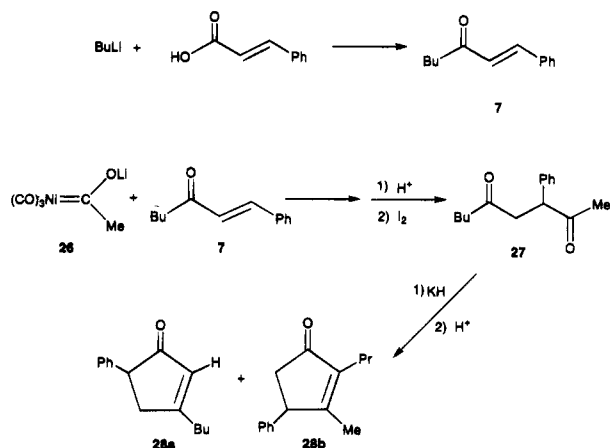
and  $\text{KH}$ . Products **11a** and **11b** were obtained in a 95% yield and in a clean reaction with a 9:1 ratio. None of the furan derivative **10** was generated, implying that a nickel complex is necessary to generate the furan product.

As mentioned earlier, the spectroscopic data for **11a** and **11b** did not permit unambiguous structural assignments. In particular, the regiochemistry of the phenyl group was unknown. Therefore, it was decided that the most direct method to determine the regiochemistry was to synthesize closely related and unambiguously assigned analogs in order to compare  $^1\text{H}$  NMR and  $^{13}\text{C}$  NMR spectra. Because cyclization can be accomplished almost quantitatively through deprotonation of **8** using  $\text{KH}$ , this proved an ideal method for synthesizing analogs of compounds **11**.

Synthesis of 1,4-diketone **24**, an analog of **8**, was accomplished by reacting pentanoyl nickel acylate **1** with commercially available  $\alpha,\beta$ -unsaturated ketone **23** in a Michael addition (79% yield) (Scheme 8). Reacting diketone **24** with  $\text{KH}$  generated almost quantitatively compound **25a** (90% yield) with none of isomer **25b** observed. These compounds are easily distinguishable due to vinyl methyl and vinyl proton in the  $^1\text{H}$  NMR spectrum. The only difference in structure between **25a** and **11a** is replacement of the butyl group on the vinyl carbon,  $\beta$  to the carbonyl, with a methyl group. The spectroscopic data for compound **25a** are nearly identical to those for the major isomer which can now be assigned as having structure **11a**.

To further verify the structural assignments, synthesis of  $\alpha,\beta$ -unsaturated ketone **7** was accomplished by reacting  $\text{BuLi}$  with *trans*-cinnamic acid (Scheme 9).<sup>11</sup> The resulting compound was identical to samples pre-

Scheme 9



pared and characterized earlier in our laboratory from the reaction of acylate complex **1** and styrene triflate. 1,4-Diketone **27** then was synthesized by the reaction of  $\alpha,\beta$ -unsaturated ketone **7** with nickel acylate complex **26**. Compound **27** subsequently was allowed to react with  $\text{KH}$  and then protonated to give **28a** and **28b** (**28b** is the major compound in a ratio of 3:1 and a combined yield of 79%).

Spectroscopic data for **28b** are almost identical to those for **11b**. As before, the difference between **11b** and **28b** is replacement of the butyl group on the vinyl carbon  $\beta$  to the carbonyl with a methyl group. Thus, the structure of the minor cyclic isomer was assigned as **11b**.

**Unambiguous Identification of 13a and 13b.** As in the styrene case, the major and minor isomers in the reaction of acylate complex **1** with bromo- or chloropropene (**13a** and **13b**) were positively identified through the synthesis of analogs and then a comparison of their NMR spectral data. Following the same reasoning found above, acylate complex **1** was reacted with 3-penten-2-one (methyl analog of **23**) to give 4-methyl-2,5-nonadione (methyl analog of **24**), which was subsequently cyclized with  $\text{KH}$  to cyclopentenone derivatives (methyl analogs of **25a** and **25b**). These results indicate that **13a** is the major product in the reaction with bromopropene.

OM950382V

## Notes

Nickel-Catalyzed Carbonylation of  $\alpha$ -Keto Alkynes under Phase Transfer Conditions

Henri Arzoumanian,\*<sup>†</sup> Magali Jean,<sup>†</sup> Didier Nuel,<sup>†</sup> Armando Cabrera,<sup>§</sup>  
Jose Luis Garcia Gutierrez,<sup>‡</sup> and Noe Rosas<sup>‡</sup>

*Ecole Nationale Supérieure de Synthèse, de Procédés et d'Ingénierie Chimiques d'Aix-Marseille, URA du 1410, Université d'Aix-Marseille III, 13397 Marseille, France, and Instituto de Quimica, Universidad Nacional Autonoma de Mexico, 04510 Mexico, D.F., Mexico*

Received June 9, 1995<sup>®</sup>

**Summary:**  $\alpha$ -Keto alkynes are carbonylated in the presence of  $Ni(CN)_2$  under phase transfer conditions (toluene, 5 N NaOH, tetrabutylammonium bromide) to give either unsaturated hydroxybutyrolactones or 2-alkylidene 3-keto carboxylic acids depending on the presence or absence of an  $\alpha$ -H on the carbon  $\alpha$  to the alkynyl group. This is rationalized, in the second case, by a rearrangement following abstraction of this  $\alpha$ -H by base. A rearrangement to an allenic intermediate prior to carbonylation is excluded.

## Introduction

Transition-metal-mediated carbonylation reactions have been of great interest in recent years, and they continue to arouse increasing interest.<sup>1</sup> Among the numerous metals used, nickel cyanide, under transfer conditions, has been shown to be a versatile catalytic system.<sup>2</sup> A large variety of substrates have been carbonylated either stoichiometrically or catalytically, and the synthesis of lactones or their hydrolysis products,  $\gamma$ -hydroxy or  $\gamma$ -keto carboxylic acids, has been one of the most studied areas.<sup>1</sup>

Five-membered lactones can thus be readily obtained by carbonylation of allylic alcohols, under oxygen, in the presence of catalytic quantities of Pd(II) and Cu(II)<sup>3</sup> or with a ruthenium catalyst.<sup>4</sup> They can also be prepared under pressure of CO/H<sub>2</sub> from allylic esters with Co<sub>2</sub>(CO)<sub>8</sub><sup>5</sup> or from alkynes and iodomethane in the presence of Mn(CO)<sub>5</sub>Br.<sup>6</sup> Unsaturated five- or six-membered lactones can also be obtained through various synthetic routes.  $\alpha$ -Methylene lactones are obtained by carbonylation of vinyl halides in the presence of stoichiometric quantities of Ni(PPh<sub>3</sub>)<sub>2</sub>(CO)<sub>2</sub><sup>7,8</sup> or from ethynyl alcohols by carbonylation either stoichiometrically with Ni(CO)<sub>4</sub><sup>9</sup>

or catalytically with PdCl<sub>2</sub>.<sup>10-12</sup> Ethynyl alcohols also give 2(5H)furanones upon carbonylation using Pd(CH<sub>3</sub>CN)<sub>2</sub>(PPh<sub>3</sub>)<sub>2</sub>(BF<sub>4</sub>)<sub>2</sub> as catalyst.<sup>13</sup> Recently, Pd(Cl)<sub>2</sub>(PPh<sub>3</sub>)<sub>2</sub>-catalyzed carbonylation of either an internal alkyne-organic halide mixture or (*Z*)- $\beta$ -iodo enones was reported to give the corresponding 2-butenolides or the (*Z*)-3-alkylidene-2-butenolides, depending on the substrate structure.<sup>14</sup> Another way to attain unsaturated lactones, although more specific to aromatic lactones, is carbonylating *o*-halobenzyl alcohols in the presence of Pd(II) and tertiary amines.<sup>15</sup>

Unsaturated hydroxybutyrolactones have been obtained through Co(CO)<sub>4</sub>-catalyzed carbonylation of alkynes in the presence of alkyl iodide<sup>16-18</sup> or by double carbonylation of styrene oxide.<sup>18</sup>

Finally, an unsaturated ketobutyrolactone was the result of a double carbonylation of halodienes catalyzed by Ni(CN)<sub>2</sub> under phase transfer conditions.<sup>19</sup>

In our pursuit of studying carbonylation reactions of substituted alkynes, we report the case of  $\alpha$ -keto alkynes which afford, in the presence of Ni(CN)<sub>2</sub> under phase transfer conditions, unsaturated hydroxybutyrolactones or 2-alkylidene 3-keto carboxylic acids, depending on the presence or absence of an  $\alpha$ -H on the group attached to the alkynyl function.

## Results and Discussion

Nickel-catalyzed carbonylations of alkynols<sup>20,21</sup> or alkynyl halides<sup>20-23</sup> have been reported to give mono- or dicarboxylated products. When they are performed

(10) Norton, J. R.; Shenton, K. E.; Schwartz, J. *Tetrahedron Lett.* **1975**, 51.

(11) Murray, T. F.; Norton, J. R. *J. Am. Chem. Soc.* **1979**, *101*, 4107.

(12) Murray, T. F.; Samsel, E. G.; Varma, V.; Norton, J. R. *J. Am. Chem. Soc.* **1981**, *103*, 7520.

(13) Matsushita, K.; Komori, T.; Oi, S.; Inoue, Y. *Tetrahedron Lett.* **1994**, *35*, 5889.

(14) Copéret, C.; Sugihara, T.; Wu, G.; Shimoyama, I.; Negishi, E.-I. *J. Am. Chem. Soc.* **1995**, *117*, 3422.

(15) Cowell, A.; Stille, J. K. *J. Am. Chem. Soc.* **1980**, *102*, 4193.

(16) Alper, H.; Currie, J. K.; Des Abbayes, H. *J. Chem. Soc., Chem. Commun.* **1978**, 311.

(17) Heck, R. F. *J. Am. Chem. Soc.* **1964**, *86*, 2819.

(18) Arzoumanian, H.; Petrigiani, J. F. *Tetrahedron Lett.* **1986**, *27*, 5979.

(19) Alper, H.; Vasapollo, G. *Tetrahedron Lett.* **1989**, *30*, 2617.

(20) Jones, E. R. H.; Whitham, G. H.; Whiting, M. C. *J. Chem. Soc.* **1957**, 4628.

(21) Satyanarayana, N.; Alper, H. *Organometallics* **1991**, *10*, 804.

(22) Arzoumanian, H.; Cochini, F.; Nuel, D.; Petrigiani, J. F.; Rosas, N. *Organometallics* **1992**, *11*, 493.

(23) Arzoumanian, H.; Cochini, F.; Nuel, D.; Rosas, N. *Organometallics* **1993**, *12*, 1871.

<sup>†</sup> Université d'Aix-Marseille III.

<sup>‡</sup> Universidad Nacional Autonoma de Mexico.

<sup>§</sup> Abstract published in *Advance ACS Abstracts*, October 1, 1995.

(1) Colquhoun, H. M.; Thompson, D. J.; Twigg, M. V. *Carbonylation: Direct Synthesis of Carbonyl Compounds*; Plenum: New York, 1991.

(2) Joó, F.; Alper, H. *Organometallics* **1985**, *4*, 1775.

(3) Alper, H.; Leonard, D. *Tetrahedron Lett.* **1985**, *26*, 5639.

(4) Kondo, T.; Kodoi, K.; Mitsudo, T.; Watanabe, Y. *J. Chem. Soc., Chem. Commun.* **1994**, 755.

(5) Falbe, J.; Huppel, N.; Korte, F. *Chem. Ber.* **1964**, *97*, 863.

(6) Wang, J.-X.; Alper, H. *J. Org. Chem.* **1986**, *51*, 273.

(7) Semmelhack, M. F.; Brickner, S. J. *J. Am. Chem. Soc.* **1981**, *103*, 3945.

(8) Semmelhack, M. F.; Brickner, S. J. *J. Org. Chem.* **1981**, *46*, 1723.

(9) Jones, E. R. H.; Shen, T. Y.; Whiting, M. C. *J. Chem. Soc.* **1950**, 230.

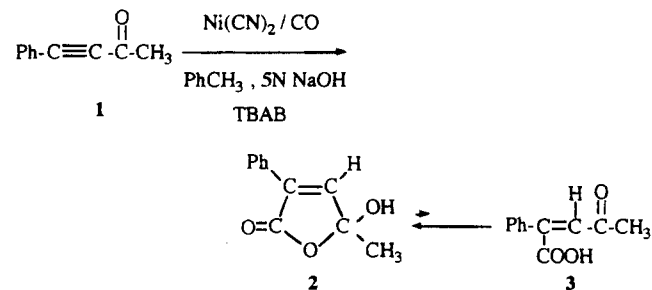
Table 1. Carbonylation of  $\alpha$ -Keto Alkynes<sup>a</sup>

entry no.	R-C $\equiv$ C-C(=O)R'		temp, °C	time, h	yield, <sup>b</sup> %	product distribn	
	R	R'				Furanone	acid
1	C <sub>6</sub> H <sub>5</sub>	CH <sub>3</sub> (1)	25	6	78	100 (2)	
2	C <sub>6</sub> H <sub>5</sub>	C(CH <sub>3</sub> ) <sub>3</sub> (5)	80	24	35 <sup>c</sup>	41 (6)	59 (7)
3	C <sub>4</sub> H <sub>9</sub>	CH <sub>3</sub> (8)	55	24	53		100 (9)
4	C <sub>4</sub> H <sub>9</sub>	C(CH <sub>3</sub> ) <sub>3</sub> (10)	80	15	67		100 (11)

<sup>a</sup> Reaction conditions: keto alkyne (10 mmol), toluene (25 mL), 5 N NaOH (25 mL), Ni(CN)<sub>2</sub>·4H<sub>2</sub>O (1.0 mmol), tetrabutylammonium bromide (0.3 mmol), CO (1 atm). <sup>b</sup> Isolated yields. <sup>c</sup> Based on 50% conversion.

in the presence of base under phase transfer conditions (PTC), a nucleophilic attack by the anionic nickel catalyst onto the alkyne is thought to be the initial step,<sup>24</sup> with the corresponding leaving group being either a nickelate or a halide ion. Considering an electron pair on a carbonyl group as being a "leaving" entity, carbonylation of  $\alpha$ -keto alkynes with the Ni(CN)<sub>2</sub>/PTC catalytic system should a priori result in a carboxylated product without loss of the oxygenated function.

Treatment of 4-phenyl-3-butyn-2-one (1) with carbon monoxide (1 atm) and catalytic quantities of Ni(CN)<sub>2</sub> under phase transfer conditions (toluene, 5 N NaOH, tetra-*n*-butylammonium bromide) afforded as the only product the unsaturated hydroxylactone (2) in 78% isolated yield.



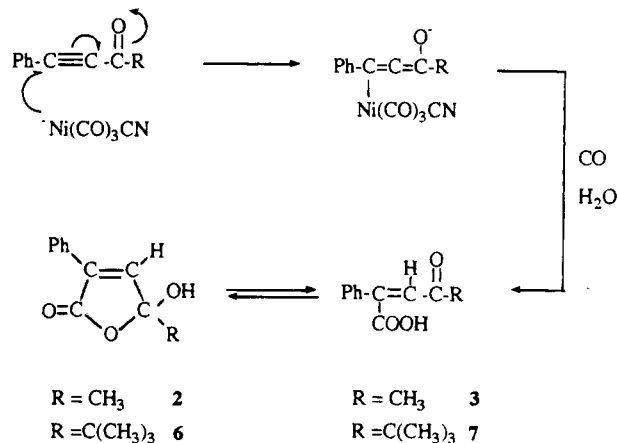
Hydroxylactones, either saturated or not, are well-known to undergo a rapid tautomeric equilibrium to the corresponding  $\gamma$ -keto acid; compound 3 could have thus plausibly been expected to be observed, but its presence was not detected under the experimental conditions. This is in agreement with the ring-chain tautomerism generally observed with such  $\gamma$ -keto acids.<sup>25-27</sup> Indeed, the absence of sterically demanding groups on the keto function leads almost exclusively to the cyclic tautomer.

Supporting evidence for this is given by replacing the methyl group in 1 by a bulkier *tert*-butyl group (5). This altered somewhat the lactonization step and yielded, as expected, both the hydroxylactone (6) and the corresponding open-chain keto acid (7)<sup>28</sup> (see Table 1).

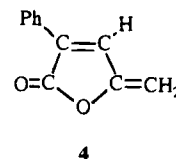
A plausible mechanism for the formation of 2, 6, and 7 is illustrated in Scheme 1.

One other product might have been found, the dehydrated hydroxylactone 4-phenyl-1-methylene-2-butenolide (4). Its presence, again, was not detected. This could be due to either the experimental conditions that

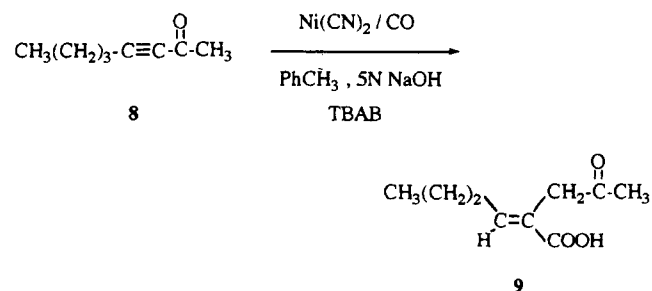
## Scheme 1. Formation of Hydroxylactone



render dehydration difficult or the lower stability expected for compound 4 compared to 2.



In striking contrast with substrates 1 and 5, replacing the phenyl group by an  $\alpha$ -H-containing alkyl group results in a carboxylated product in which the unsaturation has undergone a migration. Thus, the reaction of 3-octyn-2-one (8) with CO afforded as the only isolated product (53%) the unsaturated keto acid 9. None of the corresponding hydroxylactone was detected. The absence of cyclic tautomer in this case is expected, since saturated hydroxylactone rings are known to be less stable.<sup>25-27</sup>



Replacing the methyl group  $\alpha$  to the keto function by a *tert*-butyl group (10) had, as expected, no effect, and the reaction proceeded in an analogous manner to give the corresponding unsaturated keto acid 11 (see Table 1).

(24) Arzoumanian, H.; Choukrad, M.; Nuel, D. *J. Mol. Catal.* **1993**, *85*, 285.

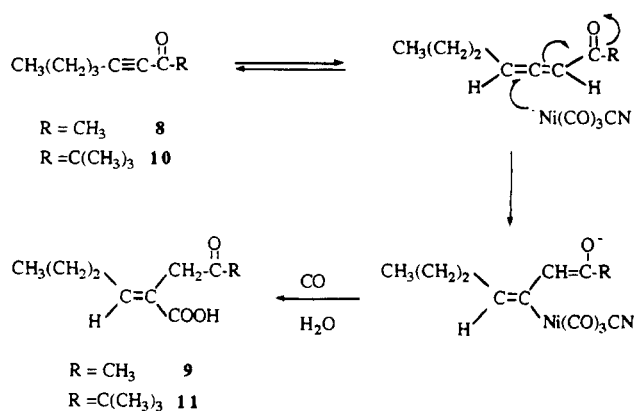
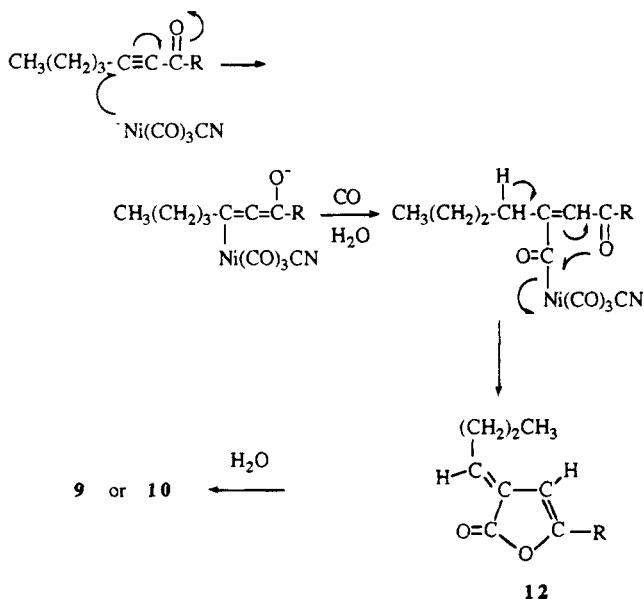
(25) Jones, P. R. *Chem. Rev.* **1963**, *63*, 461.

(26) Escale, R.; Verducci, J. *Bull. Soc. Chim. Fr.* **1974**, 1203.

(27) Valters, R. E.; Flitsch, W. *Ring-Chain Tautomerism*; Plenum Press: New York, 1985.

(28) Roussel, C.; Gallo, R.; Chanon, M.; Metzger, J. *Bull. Soc. Chim. Fr.* **1971**, 1902.



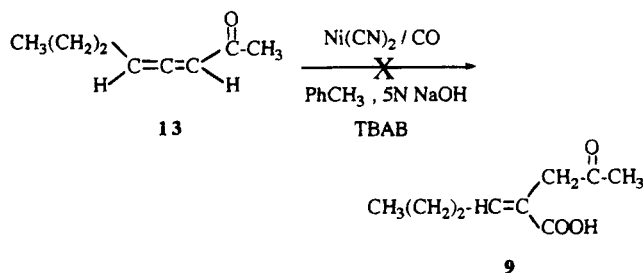
**Scheme 2. Formation of Keto Acid via Allene****Scheme 3. Formation of Keto Acid via  $\alpha$ -Hydrogen Abstraction**

Two possible paths can be envisaged to explain this striking difference in selectivity between **2**, **6** and **8**, **10**. The first one (Scheme 2) involves a prior rearrangement of the keto alkyne into a keto allene, followed by a carbonylation catalyzed by the nickel anion and hydrolysis.<sup>29</sup>

The second (Scheme 3) involves an initial nucleophilic attack by the nickel catalyst at the alkynyl carbon in a manner analogous to that for substrates **1** and **5**. The intermediate obtained, either before or after CO insertion into the carbon-nickel bond, undergoes a proton abstraction by base on the  $\alpha$ -carbon of the alkyl group followed by rearrangement and lactonization to give **12**. Hydrolysis of this latter species gives the observed product.

In order to differentiate between these two possibilities, the keto allene **13** was synthesized and allowed to react under the same reaction conditions. The reaction proceeded faster and afforded only polymeric tarry material, thus excluding the path shown in Scheme 2.

In summary,  $\alpha$ -keto alkynes, in the presence of catalytic amounts of  $\text{Ni(CN)}_2$ , are carboxylated under phase transfer conditions to give either unsaturated



hydroxylactones or unsaturated keto acids. The structure of the final product is dependent on the nature of the substituent of the alkynyl group.

**Experimental Section**

**General Comments.** Unless otherwise noted, all materials were obtained from commercial suppliers and used without further purification. NMR spectra were recorded on a Bruker AC100 or a Bruker AC200 spectrophotometer. The chemical shifts (ppm) were determined relative to  $(\text{CH}_3)_4\text{Si}$ . IR spectra were recorded on a Perkin-Elmer 1720X FTIR spectrometer. Thin-layer or column chromatography was performed on silica gel (Merck). Reactions were done in a 100 mL double-walled, thermostated reactor equipped with a magnetic stirrer and inlet tube for gas bubbling. The alkynyl ketones and octa-3,4-dien-2-one were prepared according to published methods.<sup>30</sup>

**General Procedure for the Nickel Cyanide and Phase Transfer Catalyzed Carbonylations.** Toluene (25 mL) and 5 N NaOH (25 mL) were degassed and saturated with CO under atmospheric pressure before  $\text{Ni(CN)}_2 \cdot 4\text{H}_2\text{O}$  (1.0 mmol) and tetrabutylammonium bromide (0.3 mmol) were introduced, and the mixture was kept at room temperature overnight with stirring while CO was slowly (2–3 mL/min) bubbled through the solution. To the yellow two-phase mixture was then added 10 mmol of substrate. Stirring and flow of CO were maintained for the desired time and at a given temperature. The treatment of the two phases was done as follows.

**With R = Bu or Et.** The aqueous phase is acidified (pH ~ 1) (*Caution!* HCN is formed). Extraction with ethyl acetate (2  $\times$  25 mL), drying ( $\text{MgSO}_4$ ) of the combined extracts, and rotary evaporation yielded the corresponding acids. The organic phase contained none of the acid or the corresponding lactonized hydroxyfuranone.

**With R = Ph and R' = Me.** The aqueous phase is acidified (pH ~ 1) (*Caution!* HCN is formed). Extraction with ethyl acetate (2  $\times$  25 mL), drying ( $\text{MgSO}_4$ ) of the combined extracts, and rotary evaporation yielded part (22%) of the hydroxyfuranone. The organic phase, upon evaporation, gave an orange oily residue, from which the hydroxyfuranone was isolated in 65% yield. It could be recrystallized from  $\text{CH}_2\text{Cl}_2/n$ -pentane (1/1).

**With R = Ph and R' = Bu.** The aqueous phase is acidified (pH ~ 1), (*Caution!* HCN is formed). Extraction with ethyl acetate (2  $\times$  25 mL), drying ( $\text{MgSO}_4$ ) of the combined extracts, and rotary evaporation yielded the acid **7**.

Evaporating the organic phase to dryness led to an orange residue, which was purified by liquid chromatography on silica (*n*-pentane/ethyl acetate, 85/15) to yield the hydroxyfuranone **6**.

**1-Phenylbut-1-yn-3-one (1):** colorless liquid; bp 70 °C (0.76 mmHg); IR selected  $\nu$  ( $\text{cm}^{-1}$ ) 2200 (C=C), 1670 (CO);  $^1\text{H}$  NMR (100 MHz,  $\text{CDCl}_3$ )  $\delta$  2.31 (s, 3H,  $\text{CH}_3$ ), 7.35 (m, 5H, Ph),  $^{13}\text{C}$ - $\{^1\text{H}\}$  NMR (25 MHz,  $\text{CDCl}_3$ )  $\delta$  32.8 ( $\text{CH}_3$ ), 88.3, 90.3 (C=C), 120.0 (C ipso), 128.7, 133.1, 130.8 (CH of Ph), 184.7 (CO).

(29) Allenic carboxylic acids have been reported to afford 2(5H)-furanones.<sup>13</sup>

(30) Brandsma, L. *Preparative Acetylenic Chemistry*; Elsevier: New York, 1988.



**3-Phenyl-5-methyl-5-hydroxy-2(5H)-furanone (2):** white solid; mp 145 °C; IR selected  $\nu$  ( $\text{cm}^{-1}$ ) 1697 (CO);  $^1\text{H}$  NMR (200 MHz,  $\text{CDCl}_3$ )  $\delta$  1.67 (s, 3H,  $\text{CH}_3$ ), 6.75 (s broad, 1H, OH), 6.97 (s, 1H,  $\text{HC}=\text{C}$ ), 7.33 (t, 3H, H ar m & p), 7.73–7.78 (m, 2H, H ar o);  $^{13}\text{C}\{^1\text{H}\}$  NMR (50 MHz,  $\text{CDCl}_3$ )  $\delta$  30.6 ( $\text{CH}_3$ ), 88.8 (C—OH), 132.3, 133.4, 132.5 (CH of Ph), 136.5, 137.8 (C ipso and C=CH), 151.0 (CH=C), 175.0 (CO).

**1-Phenyl-4,4-dimethylpent-1-yn-3-one (5):** colorless liquid; bp 80 °C (0.6 mmHg); IR selected  $\nu$  ( $\text{cm}^{-1}$ ) 2200 (C=C), 1664 (CO);  $^1\text{H}$  NMR (200 MHz,  $\text{CDCl}_3$ )  $\delta$  1.21 (s, 9H,  $(\text{CH}_3)_3\text{C}$ ), 7.35, 7.49 (m, 5H, Ph);  $^{13}\text{C}\{^1\text{H}\}$  NMR (50 MHz,  $\text{CDCl}_3$ )  $\delta$  26.1 ( $(\text{CH}_3)_3\text{C}$ ), 44.8 ( $(\text{CH}_3)_3\text{C}$ ), 85.9, 92.1 (C=C), 120.1 (C ipso), 128.6, 130.5, 132.9 (CH of Ph), 194.0 (CO).

**3-Phenyl-5-(1,1-dimethylethyl)-5-hydroxy-2(5H)-furanone (6):** white solid; IR selected  $\nu$  ( $\text{cm}^{-1}$ ) 1672 (CO);  $^1\text{H}$  NMR (200 MHz,  $\text{DMSO}-d_6$ )  $\delta$  0.98 (s, 9H,  $(\text{CH}_3)_3\text{C}$ ), 5.77 (s broad, 1H, OH), 7.33, 7.94 (m, 5H, Ph), 8.50 (broad s, 1H, CH);  $^{13}\text{C}\{^1\text{H}\}$  NMR (50 MHz,  $\text{DMSO}-d_6$ )  $\delta$  25.2 ( $(\text{CH}_3)_3\text{C}$ ), 37.3 ( $(\text{CH}_3)_3\text{C}$ ), 90.2 (COH), 127.2, 128.2 (CH or phenyl), 131.6 (C=CH), 134.0 (C ipso), 143.9 (CH=C), 170.7 (CO).

**5,5-Dimethyl-4-oxo-2-phenylhex-2-enoic acid (7):** white solid; mp 120 °C;  $^1\text{H}$  NMR (200 MHz,  $\text{CDCl}_3$ )  $\delta$  1.26 (s, 9H,  $(\text{CH}_3)_3\text{C}$ ), 7.45, 8.1 (m, 6H, Ph and  $\text{CH}=\text{C}$ );  $^{13}\text{C}\{^1\text{H}\}$  NMR (50 MHz,  $\text{CDCl}_3$ )  $\delta$  26.3 ( $(\text{CH}_3)_3\text{C}$ ), 38.6 ( $(\text{CH}_3)_3\text{C}$ ), 127.5, 130.2 (CH of phenyl), 133.8 (C=CH), 137.0 (C ipso), 145.0 (CH=C), 170.7 (COOH), 180.9 (CO).

**Oct-3-yn-2-one (8):** colorless liquid; bp 70 °C (7.5 mmHg); IR selected  $\nu$  ( $\text{cm}^{-1}$ ) 2212 (C=C), 1670 (CO);  $^1\text{H}$  NMR (200 MHz,  $\text{CDCl}_3$ )  $\delta$  0.90 (t, 3H,  $\text{CH}_3\text{CH}_2$ , 7.1 Hz), 1.39 (sext, 2H,  $\text{CH}_2\text{CH}_2\text{CH}_3$ , 7.4 Hz), 1.53 (quint, 2H,  $\text{CH}_2\text{CH}_2\text{CH}_2\text{CH}_3$ , 6.9 Hz), 2.29 (s, 3H,  $\text{CH}_3\text{CO}$ ), 2.34 (t, 2H,  $\text{CH}_2\text{C}=\text{C}$ , 6.9 Hz);  $^{13}\text{C}\{^1\text{H}\}$  NMR (50 MHz,  $\text{CDCl}_3$ )  $\delta$  13.4 ( $\text{CH}_3\text{CH}_2$ ), 18.5

( $\text{CH}_2\text{C}=\text{C}$ ), 21.8 ( $\text{CH}_3\text{CO}$ ), 29.6, 32.6 ( $\text{CH}_2$ ), 81.3 ( $\text{C}=\text{CCH}_2$ ), 93.9 (C=CCO), 184.8 (CO).

**2-(2-Oxopropyl)hex-2-enoic acid (9):** white solid; mp 77 °C;  $^1\text{H}$  NMR (200 MHz,  $\text{CDCl}_3$ )  $\delta$  0.94 (t, 3H,  $\text{CH}_3$ , 7.3 Hz), 1.44 (sext, 2H,  $\text{CH}_2\text{CH}_2\text{CH}_3$ , 7.3 Hz), 2.05–2.21 (q, 2H,  $\text{CH}_2\text{CH}=\text{C}$ , 7.3 Hz), 2.20 (s, 3H,  $\text{CH}_3\text{CO}$ ), 3.43 (s, 2H,  $\text{CH}_2\text{CO}$ ), 7.14 (t, 1H,  $\text{CH}=\text{C}$ , 7.3 Hz);  $^{13}\text{C}\{^1\text{H}\}$  NMR (50 MHz,  $\text{CDCl}_3$ )  $\delta$  13.8 ( $\text{CH}_3\text{CH}_2$ ), 21.6 ( $\text{CH}_2\text{CH}_3$ ), 29.6 ( $\text{CH}_3\text{CO}$ ), 31.1 ( $\text{CH}_2\text{CH}=\text{C}$ ), 41.1 ( $\text{CH}_2\text{CO}$ ), 125.4 (C=CH), 148.7 (CH=C), 172.3 (COOH), 205.5 (CO).

**1,1-Dimethylnon-4-yn-3-one (10):** colorless liquid; bp 80 °C (6 mmHg); IR selected  $\nu$  ( $\text{cm}^{-1}$ ) 2211 (C=C), 1672 (CO);  $^1\text{H}$  NMR (100 MHz,  $\text{CDCl}_3$ )  $\delta$  0.90 (t, 3H,  $\text{CH}_3\text{CH}_2$ , 6.7 Hz), 1.15 (s, 9H,  $(\text{CH}_3)_3\text{C}$ ), 1.3–1.8 (m, 4H,  $\text{CH}_2\text{CH}_2\text{CH}_3$ ), 2.35 (t, 2H,  $\text{CH}_2\text{C}=\text{C}$ , 6.6 Hz);  $^{13}\text{C}\{^1\text{H}\}$  NMR (25 MHz,  $\text{CDCl}_3$ )  $\delta$  13.5 ( $\text{CH}_3\text{CH}_2$ ), 18.7 ( $\text{CH}_2\text{C}=\text{C}$ ), 22.0, 29.8 ( $\text{CH}_2$ ), 26.1 ( $(\text{CH}_3)_3\text{C}$ ), 44.6 (C( $\text{CH}_3$ ) $_3$ ), 78.8 ( $\text{CH}_2\text{C}=\text{C}$ ), 95.7 (C=CCO), 194.5 (CO).

**2-(2-Oxo-3,3-dimethylbutyl)hex-2-enoic acid (11):** white solid;  $^1\text{H}$  NMR (200 MHz,  $\text{CDCl}_3$ )  $\delta$  0.92 (t, 3H,  $\text{CH}_3$ , 7.3 Hz), 1.23 (s, 9H, C( $\text{CH}_3$ ) $_3$ ), 1.48 (sext, 2H,  $\text{CH}_2\text{CH}_3$ , 7.3 Hz), 2.07 (q, 2H,  $\text{CH}_2\text{CH}_2\text{CH}_3$ , 7.3 Hz), 3.51 (s, 2H,  $\text{CH}_2$ ), 7.09 (t, 1H,  $\text{CH}=\text{C}$ , 7.3 Hz);  $^{13}\text{C}\{^1\text{H}\}$  NMR (50 MHz,  $\text{CDCl}_3$ )  $\delta$  13.9 ( $\text{CH}_3\text{CH}_2$ ), 21.7 ( $\text{CH}_3\text{CH}_2$ ), 26.5 (C( $\text{CH}_3$ ) $_3$ ), 31.2 ( $\text{CH}_3\text{CH}_2\text{CH}_2$ ), 34.4 ( $\text{CH}_2$ ), 44.4 (C( $\text{CH}_3$ ) $_3$ ), 126.0 (C=CH), 147.7 (C=CH), 172.4 (COOH), 212.0 (CO).

**Acknowledgment.** This work was done under the auspices of the program PCP Franco-Mexicain. Financial support by CONACYT is kindly acknowledged.

OM950443P

# Reactivity Studies of Tricyclohexylphosphine (PCy<sub>3</sub>) Square-Planar Iridium Complexes with Small Gaseous Molecules (O<sub>2</sub>, H<sub>2</sub>, Cl<sub>2</sub>, and SO<sub>2</sub>). Molecular and Crystal Structure of Ir(CO)[OS(O)OH](SO<sub>2</sub>)(PCy<sub>3</sub>)<sub>2</sub>·C<sub>6</sub>H<sub>6</sub>, the First Structurally Characterized Oxygen-Coordinated SO<sub>3</sub>H Complex Formed by Insertion of SO<sub>2</sub>(g) into an M-OH Bond

Cynthia A. Miller, Charles H. Lake, Melvyn Rowen Churchill,\* and Jim D. Atwood\*

Department of Chemistry, University at Buffalo, State University of New York, Buffalo, New York 14260-3000

Received June 1, 1995\*

**Summary:** Square-planar iridium complexes of the large but strongly donating PCy<sub>3</sub> (Cy = cyclohexyl) ligand, *trans*-Ir(CO)(Cl)(PCy<sub>3</sub>)<sub>2</sub> and *trans*-Ir(CO)(OH)(PCy<sub>3</sub>)<sub>2</sub>, have been reacted with the molecules O<sub>2</sub>, H<sub>2</sub>, Cl<sub>2</sub>, and SO<sub>2</sub>. In comparison to the analogous PPh<sub>3</sub> complexes, the presence of PCy<sub>3</sub> inhibits reactions with H<sub>2</sub> and O<sub>2</sub> but has little effect on reactions with Cl<sub>2</sub> and SO<sub>2</sub>. In the latter two reactions the greater electron density compensates for the larger size of the PCy<sub>3</sub> ligands. Reaction of SO<sub>2</sub> with *trans*-Ir(CO)(OH)(PCy<sub>3</sub>)<sub>2</sub> leads to an oxygen-coordinated hydrogen sulfite ligand, and the structure was determined. The molecules exist in the crystals as weakly bound dimers.

## Introduction

Addition reactions to square-planar iridium(I) complexes have been a useful source for mechanistic information.<sup>1,2</sup> Oxidative addition of molecules such as H<sub>2</sub> and CH<sub>3</sub>I<sup>3,4</sup> and binding studies of O<sub>2</sub><sup>5</sup> and alkenes<sup>2</sup> have proved very useful for understanding the role of steric and electronic factors in such reactions. Complexes of the type *trans*-Ir(CO)(Cl)L<sub>2</sub>, L = a phosphine ligand, have allowed variation of the electron density at the iridium. Such studies have shown that enhanced electron density at the iridium increases the rate of oxidative addition of CH<sub>3</sub>I,<sup>4</sup> has little effect on oxidative addition of H<sub>2</sub>,<sup>3</sup> and enhances binding of O<sub>2</sub> and SO<sub>2</sub> to the iridium center.<sup>5,6</sup>

Relatively few studies have examined the reactivity of square-planar complexes of the strongly donating but large PCy<sub>3</sub> ligand. A few complexes of nickel, palladium, and platinum have been reported, MXX'(PCy<sub>3</sub>)<sub>2</sub>.<sup>7-9</sup> A rhodium complex, RhCl(SO<sub>2</sub>)(PCy<sub>3</sub>)<sub>2</sub>,<sup>10</sup> and its reac-

tion with oxygen<sup>11</sup> were described. In this manuscript the reactions of *trans*-Ir(CO)(PCy<sub>3</sub>)<sub>2</sub>X (X = Cl or OH) with H<sub>2</sub>, Cl<sub>2</sub>, O<sub>2</sub>, and SO<sub>2</sub> are examined. Reaction of the hydroxo complex with SO<sub>2</sub> leads to an oxygen-coordinated hydrogen sulfite ligand. The hydrogen sulfite ion has been much discussed with regard to the site of the proton, HSO<sub>3</sub><sup>-</sup> or SO<sub>2</sub>OH<sup>-</sup>.<sup>12-19</sup> Observation of an S-H stretch demonstrated the presence of HSO<sub>3</sub><sup>-</sup>,<sup>12</sup> which has been corroborated with crystal structure determinations.<sup>13,14</sup> Evidence for SO<sub>2</sub>OH<sup>-</sup> in the presence of extra infrared modes in solution<sup>17</sup> and from calculations has been presented.<sup>18</sup> Oxygen-17 NMR was used to show an equilibrium between the two isomers in water and indicated the more abundant isomer to be that with protonation on the oxygen.<sup>19</sup> In the structure of Ir(CO)[OS(O)OH](SO<sub>2</sub>)(PCy<sub>3</sub>)<sub>2</sub> we provide the first structural evidence for protonation of hydrogen sulfite on the oxygen and the first example of a hydrogen sulfite ligand coordinated through an oxygen.

## Experimental Section

IrCl<sub>3</sub>·3H<sub>2</sub>O was purchased or borrowed from Johnson Matthey. Tricyclohexylphosphine was purchased from Strem Chemical Company. The gases, SO<sub>2</sub>, H<sub>2</sub>, 10% SO<sub>2</sub> in N<sub>2</sub>, and 1.1% SO<sub>2</sub> in N<sub>2</sub>, were purchased from Matheson. Solvents were dried and purified by standard methods.

All syntheses were accomplished under an argon or nitrogen atmosphere using an argon-filled glovebox or Schlenk or high-vacuum techniques. Square-planar iridium complexes *trans*-Ir(CO)(Cl)(PCy<sub>3</sub>)<sub>2</sub> and *trans*-Ir(CO)(OH)(PCy<sub>3</sub>)<sub>2</sub><sup>6</sup> were prepared as previously described.

<sup>1</sup>H and <sup>31</sup>P NMR spectra were recorded on a Varian VXR-400. References were set to residual solvent peaks in the <sup>1</sup>H

(10) van Gaal, H. L. M.; Verlaan, J. P. J. *J. Organomet. Chem.* **1977**, *133*, 93.

(11) Kubas, G. J. *Inorg. Chem.* **1979**, *18*, 182.

(12) Maylor, R.; Gill, J. B.; Goodall, D. C. *J. Chem. Soc., Dalton Trans.* **1972**, 2001.

(13) Johansson, L.-G.; Lindqvist, O.; Vannerberg, N.-G. *Acta Crystallogr.* **1980**, *B36*, 2523.

(14) Magnusson, A.; Johansson, L.-G.; Lindqvist, O. *Acta Crystallogr.* **1983**, *C39*, 819.

(15) Meyer, B.; Peter, L.; Spitzer, K. *Inorg. Chem.* **1977**, *16*, 27.

(16) Guthrie, J. P. *Acc. Chem. Res.* **1983**, *16*, 122.

(17) Connick, R. E.; Tam, T. M.; von Deuster, E. *Inorg. Chem.* **1982**, *21*, 103.

(18) Strömberg, A.; Gropen, O.; Wahlgren, U.; Lindqvist, O. *Inorg. Chem.* **1983**, *22*, 1129.

(19) Horner, D. A.; Connick, R. E. *Inorg. Chem.* **1986**, *25*, 2414.

\* Abstract published in *Advance ACS Abstracts*, October 15, 1995.

(1) Atwood, J. D. *Coord. Chem. Rev.* **1988**, *83*, 93.

(2) Vaska, L. *Acc. Chem. Res.* **1968**, *1*, 335.

(3) Chock, P. B.; Halpern, J. *J. Am. Chem. Soc.* **1966**, *88*, 3511.

(4) Ugo, R.; Pasini, A.; Fusi, A.; Cenini, S. *J. Am. Chem. Soc.* **1972**, *94*, 7364.

(5) Lawson, H. J.; Atwood, J. D. *J. Am. Chem. Soc.* **1989**, *111*, 6223.

(6) Miller, C. A.; Janik, T. S.; Lake, C. H.; Toomey, L. M.; Churchill, M. R.; Atwood, J. D. *Organometallics* **1994**, *13*, 5080.

(7) Seligson, A. L.; Cowan, R. L.; Trogler, W. C. *Inorg. Chem.* **1991**, *30*, 3371.

(8) Imoto, H.; Moriyama, H.; Saito, T.; Sasaki, Y. *J. Organomet. Chem.* **1976**, *126*, 453.

(9) Darensbourg, D. J.; Wiegraffe, P.; Riordan, C. G. *J. Am. Chem. Soc.* **1990**, *112*, 5759.

NMR spectra.  $^{31}\text{P}$  NMR spectra were referenced to an external sample of  $\text{H}_3\text{PO}_4$  at 0.0 ppm and are proton decoupled. All chemical shifts are reported in ppm and all coupling constants ( $J$ ) are reported in Hz. Infrared spectra were obtained using a Mattson Polaris Fourier Transform spectrometer with 0.5 mm NaCl solution cells or KBr disks. Elemental analysis was done at E & R Microanalytical.

**$\text{Ir}(\text{CO})[\text{OS}(\text{O})\text{OH}](\text{SO}_2)(\text{PCy}_3)_2$  Crystallization.**<sup>20</sup> A suspension of 0.210 g of *trans*- $\text{Ir}(\text{CO})(\text{OH})(\text{PCy}_3)_2$  in 15 mL of benzene was prepared in an argon atmosphere. The reaction vessel was sealed and transferred to a hood. The mixture was refluxed under a  $\text{N}_2$  atmosphere for 5 min, causing it to completely dissolve. The reaction mixture was then cooled to 0 °C, and  $\text{SO}_2$  was bubbled through it for 15 min, followed by stirring at 0 °C under an  $\text{SO}_2$  atmosphere for another 15 min. Next, the homogeneous mixture was layered with an  $\text{SO}_2$ -saturated heptane solution and placed in a refrigerator overnight. No crystals resulted, so the volume of the solution was reduced by the addition of  $\text{SO}_2$  while allowing it to warm to room temperature. After 24 h at room temperature yellow-green crystals resulted. IR (KBr):  $\nu_{\text{CO}} = 1939\text{ cm}^{-1}$ ,  $\nu_{\text{SO}} = 1078$  and  $940\text{ cm}^{-1}$  for the hydrogen sulfite, and the other S–O stretches are obscured by the cyclohexyl absorbances.  $^{31}\text{P}$  NMR ( $\text{CD}_2\text{Cl}_2$ ): 8.4 ppm. The crystals were suitable for X-ray crystallography. Anal. Calcd: C, 46.63; H, 7.25. Found: C, 47.98; H, 7.29.

**Reaction of  $\text{H}_2$  with  $\text{Ir}(\text{CO})[\text{OS}(\text{O})\text{OH}](\text{SO}_2)(\text{PCy}_3)_2$ .** In an argon atmosphere, a dilute solution of *trans*- $\text{Ir}(\text{CO})(\text{OH})(\text{PCy}_3)_2$  in toluene was prepared. The Schlenk flask was equipped with a gas adapter, sealed, and transferred to a hood. In the hood 1.1%  $\text{SO}_2$  in  $\text{N}_2$  was passed over the solution for 2 h. An IR spectrum of the bright yellow solution showed one absorbance,  $\nu_{\text{CO}} = 1935\text{ cm}^{-1}$ , attributed to  $\text{Ir}(\text{CO})[\text{OS}(\text{O})\text{OH}](\text{SO}_2)(\text{PCy}_3)_2$ . Hydrogen gas was passed over this solution for 2 h more, and another infrared spectrum was recorded, showing no evidence of  $\text{Ir}(\text{CO})[\text{OS}(\text{O})\text{OH}](\text{SO}_2)(\text{PCy}_3)_2$  or *trans*- $\text{Ir}(\text{CO})(\text{OH})(\text{PCy}_3)_2$ . The toluene was removed in vacuo, and the yellow powder was transferred to an argon atmosphere where it was dissolved in  $\text{CD}_2\text{Cl}_2$ . A  $^1\text{H}$  NMR spectrum was recorded showing resonances in the hydride region at  $-12.1$  ppm (td) [2H]  $J = 14.8, 5.6$ ;  $-12.8$  ppm (tt) [1H]  $J = 20, 5.6$ ;  $-9.9$  ppm (td) [1H]  $J = 16.4, 3.6$ ; and  $-18.4$  ppm (td) [1H]  $J = 16.4, 3.6$ . The resonances at  $-12.1$  and  $-12.8$  ppm are assigned to *mer*- $\text{H}_3\text{Ir}(\text{CO})(\text{PCy}_3)_2$ ,<sup>22</sup> and the  $-9.9$  and  $-18.4$  ppm resonances are assigned to  $\text{H}_2\text{Ir}(\text{CO})[\text{OS}(\text{O})\text{OH}](\text{PCy}_3)_2$  on the basis of NMR shifts, coupling patterns, and coupling constants.

**Collection of X-ray Diffraction Data for  $\text{Ir}(\text{CO})[\text{OS}(\text{O})\text{OH}](\text{SO}_2)(\text{PCy}_3)_2 \cdot \text{C}_6\text{H}_6$ .** A single yellow-green crystal (dimensions  $0.15 \times 0.15 \times 0.20\text{ mm}^3$ ) was inserted into a thin-walled glass capillary and aligned on an upgraded Syntex P21/Siemens R3 diffractometer. The crystal belongs to the monoclinic system. The systematic absences  $h0l$  for  $h + l = 2n + 1$  and  $0k0$  for  $k = 2n + 1$  uniquely define the centrosymmetric monoclinic space group  $P2_1/n$ . All data were corrected for Lorentz and polarization effects and for absorption. Crystal data:  $\text{C}_{37}\text{H}_{67}\text{IrO}_6\text{P}_2\text{S}_2 \cdot \text{C}_6\text{H}_6$ , monoclinic, space group  $P2_1/n$  (No. 14),  $a = 16.7164(27)\text{ \AA}$ ,  $b = 16.9954(25)\text{ \AA}$ ,  $c = 17.1373(28)\text{ \AA}$ ,  $\beta = 107.578(12)^\circ$ ,  $V = 4641.4(13)\text{ \AA}^3$ ,  $Z = 4$ ,  $fw = 1004.35$  ( $926.24 + 78.11$ ),  $D = 1.438\text{ g cm}^{-3}$ ,  $\mu = 3.079\text{ mm}^{-1}$ , 6103 reflections,  $3854 > 6\sigma(F)$ ,  $R = 3.61$  and  $wR = 3.83$  for  $6\sigma$  data, and  $R = 6.93$  and  $wR = 6.19$  for all data.

**Solution and Refinement of the Structure.** All crystallographic calculations were performed with use of the Siemens SHELXTL PLUS program set on a VAXstation 3100 computer system. Scattering factors for neutral atoms were corrected for both components ( $\Delta f'$  and  $i\Delta f''$ ) of anomalous dispersion. The structure was solved by a combination of Patterson and

**Table 1. Final Atomic Coordinates ( $\times 10^4$ ) and Isotropic Displacement Coefficients ( $\text{\AA}^2 \times 10^3$ ) for  $\text{Ir}(\text{CO})[\text{OS}(\text{O})\text{OH}](\text{SO}_2)(\text{PCy}_3)_2 \cdot \text{C}_6\text{H}_6$**

atom	x	y	z	$U(\text{eq})^a$
Ir(1)	4667(1)	758(1)	2452(1)	34(1)
S(1)	3391(2)	1607(2)	2086(2)	76(1)
S(2)	4003(2)	369(2)	427(2)	58(1)
P(1)	3951(2)	-441(1)	2585(1)	43(1)
P(2)	5704(1)	1703(1)	2383(1)	37(1)
O(1)	5009(5)	1043(5)	4232(4)	90(4)
O(2)	3406(6)	2109(6)	2706(6)	117(5)
O(3)	3193(9)	1724(8)	1298(6)	192(7)
O(4)	4638(4)	502(4)	1264(3)	51(2)
O(5)	4177(5)	-493(4)	234(4)	72(3)
O(6)	4339(6)	860(5)	-140(5)	81(4)
H(6)	4907(65)	875(54)	-60(56)	49(29)
C(1)	4867(6)	948(5)	3542(6)	49(4)
C(11)	3166(6)	-823(5)	1650(6)	45(3)
C(12)	3051(6)	-1702(6)	1565(7)	64(4)
C(13)	2488(6)	-1935(6)	716(7)	73(5)
C(14)	1638(7)	-1505(6)	510(7)	72(5)
C(15)	1768(7)	-618(6)	591(7)	68(4)
C(16)	2330(6)	-390(6)	1445(6)	56(4)
C(21)	4751(6)	-1227(5)	2885(6)	53(4)
C(22)	5238(7)	-1309(7)	2250(8)	83(6)
C(23)	5844(8)	-2006(8)	2453(11)	114(9)
C(24)	6432(9)	-1937(10)	3277(14)	152(12)
C(25)	5981(9)	-1844(8)	3937(11)	132(8)
C(26)	5384(8)	-1132(7)	3730(7)	89(6)
C(31)	3486(7)	-456(6)	3448(6)	61(4)
C(32)	2950(7)	253(7)	3489(7)	76(5)
C(33)	2734(8)	230(8)	4310(7)	89(6)
C(34)	2277(10)	-507(10)	4377(9)	113(8)
C(35)	2783(10)	-1226(10)	4331(8)	111(8)
C(36)	3053(7)	-1229(7)	3542(6)	70(5)
C(41)	6062(6)	2345(5)	3296(5)	47(4)
C(42)	6852(6)	2820(6)	3397(6)	54(4)
C(43)	7171(7)	3179(6)	4243(6)	72(5)
C(44)	6518(7)	3687(6)	4427(6)	70(5)
C(45)	5694(7)	3236(7)	4297(7)	86(6)
C(46)	5381(7)	2885(7)	3445(7)	73(5)
C(51)	6681(6)	1162(5)	2456(5)	46(4)
C(52)	7057(7)	729(6)	3262(6)	63(4)
C(53)	7910(8)	360(8)	3320(7)	88(6)
C(54)	7856(8)	-154(7)	2615(7)	78(5)
C(55)	7500(7)	265(8)	1817(7)	85(6)
C(56)	6614(7)	598(6)	1740(6)	65(5)
C(61)	5473(5)	2273(5)	1412(5)	43(3)
C(62)	6225(8)	2604(9)	1204(8)	110(7)
C(63)	5966(9)	2952(10)	336(8)	116(8)
C(64)	5273(9)	3531(9)	196(8)	103(7)
C(65)	4572(9)	3229(11)	443(10)	148(10)
C(66)	4828(10)	2888(9)	1300(9)	134(9)
C(1S)	3840(10)	6436(9)	2564(16)	114(9)
C(2S)	4081(15)	6239(15)	3355(17)	141(13)
C(3S)	4730(17)	5812(22)	3613(14)	199(18)
C(4S)	5127(15)	5491(17)	3151(24)	216(19)
C(5S)	4879(16)	5654(15)	2358(19)	168(16)
C(6S)	4233(12)	6155(15)	2068(9)	131(10)

<sup>a</sup> Equivalent isotropic  $U$  defined as one-third of the trace of the orthogonalized  $U_{ij}$  tensor.

difference-Fourier methods. All non-hydrogen atoms were located (as was H(6), the hydrogen atom of the  $-\text{OS}(\text{O})\text{OH}$  ligand, which was subsequently refined), and hydrogen atoms of the tricyclohexylphosphine ligands were included in calculated positions (their  $U$  values each being defined as equal to that of the  $U(\text{equiv})$  value of the carbon atom to which they were attached). Refinement converged ( $\Delta/\sigma_{\text{max}} = 0.004$  with  $R = 3.61$  for those 3854 reflections above  $6\sigma(F)$  and  $R = 6.93$  for all 6103 independent data. Final atomic coordinates are collected in Table 1.

## Results

**Reactions.** The  $\text{PCy}_3$  complexes show reduced reactivity in comparison with their  $\text{PPh}_3$  analogues,<sup>1,2</sup>

(20) This procedure follows closely that previously reported for crystallizing  $\text{Ir}(\text{CO})(\text{I})(\text{SO}_2)_2(\text{PPh}_3)_2$ .<sup>21</sup>

(21) Snow, M. R.; Ibers, J. A. *Inorg. Chem.* **1973**, *12*, 224.

(22) Harrod, J. F.; Yorke, W. J. *Inorg. Chem.* **1981**, *20*, 1156.

with no reaction observed between *trans*-Ir(CO)(Cl)-(PCy<sub>3</sub>)<sub>2</sub> and H<sub>2</sub> or O<sub>2</sub> after 1 and 4 days, respectively, at 25 °C in cyclohexane. However, the complex does retain reactivity toward Cl<sub>2</sub> and SO<sub>2</sub>, the reactions complete in under 10 min.<sup>23</sup>

Reactions of the hydroxy complex, *trans*-Ir(CO)(OH)-(PCy<sub>3</sub>)<sub>2</sub>, with H<sub>2</sub> and O<sub>2</sub> occur only to the extent of 5% after 1 and 4 days, respectively, forming Ir(CO)(H)<sub>3</sub>-(PCy<sub>3</sub>)<sub>2</sub> ( $\nu_{\text{CO}} = 1934 \text{ cm}^{-1}$ ,  $\nu_{\text{IrH}} = 2035, 1787 \text{ cm}^{-1}$ ) and Ir(CO)(O<sub>2</sub>)(OH)(PCy<sub>3</sub>)<sub>2</sub> ( $\nu_{\text{CO}} = 1930 \text{ cm}^{-1}$ ), respectively. In both cases the starting complex *trans*-Ir(CO)(OH)-(PCy<sub>3</sub>)<sub>2</sub> was present (~95%) after 4 days at room temperature. These products are those expected on the basis of reactions of the PPh<sub>3</sub> analogue<sup>25</sup> but are formed in much less quantity.

Reaction of SO<sub>2</sub> with *trans*-Ir(CO)(OH)(PCy<sub>3</sub>)<sub>2</sub> produces two products depending on the conditions employed. Reaction with 1 atm of SO<sub>2</sub> in toluene produces a product with a single  $\nu_{\text{CO}}$  at 1997 cm<sup>-1</sup> and a single <sup>31</sup>P resonance at 18 ppm. Neither free PCy<sub>3</sub> nor any evidence of an Ir-H was observed. Workup (as described in the Experimental Section) produced Ir(CO)-[OS(O)OH](SO<sub>2</sub>)(PCy<sub>3</sub>)<sub>2</sub> with a  $\nu_{\text{CO}}$  at 1939 cm<sup>-1</sup> and a <sup>31</sup>P resonance at 8.4 ppm. The complex Ir(CO)[OS(O)OH](SO<sub>2</sub>)(PCy<sub>3</sub>)<sub>2</sub> was formed as the sole product by reaction of Ir(CO)(OH)(PCy<sub>3</sub>)<sub>2</sub> with 1% SO<sub>2</sub> in an N<sub>2</sub> gas mixture. To assist in interpreting these products a crystal structure of Ir(CO)[OS(O)OH](SO<sub>2</sub>)(PCy<sub>3</sub>)<sub>2</sub> was determined.

**Crystal Structure of Ir(CO)[OS(O)OH](SO<sub>2</sub>)(PCy<sub>3</sub>)<sub>2</sub>·C<sub>6</sub>H<sub>6</sub>.** The crystal consists of ordered molecular units of Ir(CO)[OS(O)OH](SO<sub>2</sub>)(PCy<sub>3</sub>)<sub>2</sub> and benzene of solvation in a 1:1 ratio. The crystallographic asymmetric unit is shown in Figure 1. Selected interatomic distances and angles are collected in Table 2. The crystal packing is stabilized by hydrogen bonding between the OS(O)OH units of adjacent molecules. Thus, the defined molecule interacts with that related by inversion (about 1/2, 0, 0) such that H(6)···O(5a) = H(6a)···O(5) = 1.77(11) Å with O(6)···O(5a) = O(5)···O(6a) = 2.610(11) Å and  $\angle \text{O(6)···H(6)···O(5a)} = \angle \text{O(6a)-H(6a)···O(5)} = 151(8)^\circ$ . This is clearly shown in Figure 2.

The iridium complex is related to a previously studied species, Ir(CO)[OS(O)OMe](SO<sub>2</sub>)(PPh<sub>3</sub>)<sub>2</sub>·0.5 (toluene),<sup>24</sup> but now has the previously uncharacterized OS(O)OH ligand and PCy<sub>3</sub> ligands. The iridium(I) atom has a square-pyramidal coordination geometry with the SO<sub>2</sub> ligand in the apical site. The Ir(1)-S(1) bond length is 2.493(3) Å (cf. 2.451(2) Å in the OS(O)OMe/PPh<sub>3</sub> derivative cited above). The sulfur atom has a pyramidal geometry (with, presumably, a lone pair of electrons). Bond lengths are S(1)-O(2) = 1.356(11) and S(1)-O(3) = 1.305(11) Å, while interatomic angles are Ir(1)-S(1)-O(2) = 110.8(4)°, Ir(1)-S(1)-O(3) = 106.2(7)°, and O(2)-S(1)-O(3) = 130.8(8)°. We should note that dimensions in the SO<sub>2</sub> ligand vary significantly from those for the SO<sub>2</sub> ligand in the OS(O)OMe/PPh<sub>3</sub> derivative in which S-O = 1.435(7) and 1.437(4) Å and  $\angle \text{O-}$

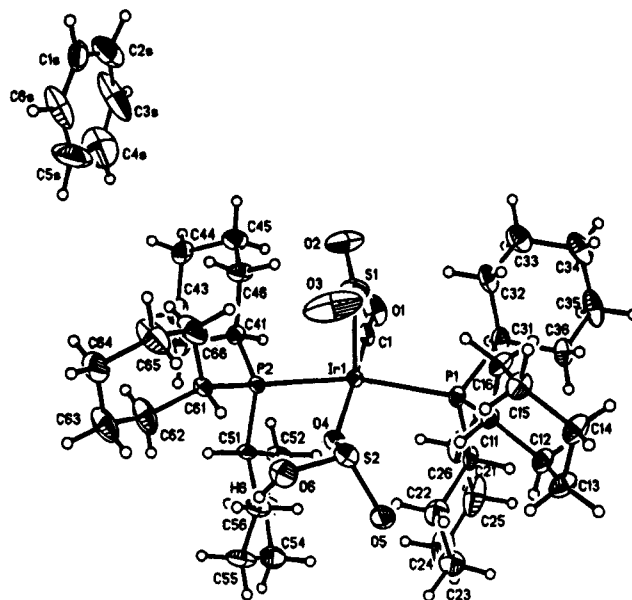


**Figure 1.** Atomic labeling for the basic asymmetric unit of Ir(CO)[OS(O)OH](SO<sub>2</sub>)(PCy<sub>3</sub>)<sub>2</sub>·C<sub>6</sub>H<sub>6</sub>. ORTEP2 diagram with 20% probability contours for non-hydrogen atoms and with hydrogen atoms artificially reduced.

**Table 2.** Selected Interatomic Distances (Å) and Angles (deg) for Ir(CO)[OS(O)OH](SO<sub>2</sub>)(PCy<sub>3</sub>)<sub>2</sub>·C<sub>6</sub>H<sub>6</sub>

Ir(1)-P(1)	2.408(3)	Ir-O(4)	2.068(6)
Ir(1)-P(2)	2.392(3)	Ir-C(1)	1.826(10)
Ir(1)-S(1)	2.493(3)	C(1)-O(1)	1.143(12)
S(1)-O(2)	1.356(11)	S(1)-O(3)	1.305(11)
S(2)-O(4)	1.521(6)	O(5a)···H(6)	1.77(11)
S(2)-O(5)	1.549(8)	O(5a)···O(6)	2.610(11)
S(2)-O(6)	1.511(10)	O(5)···O(6a)	2.610(11)
O(6)-H(6)	0.92(11)		
P(1)-Ir(1)-P(2)	163.9(1)	P(2)-Ir(1)-O(4)	84.0(2)
P(1)-Ir(1)-S(1)	95.8(1)	P(2)-Ir(1)-C(1)	91.2(3)
P(1)-Ir(1)-O(4)	92.9(2)	S(1)-Ir(1)-O(4)	96.3(3)
P(1)-Ir(1)-C(1)	89.7(3)	S(1)-Ir(1)-C(1)	91.9(3)
P(2)-Ir(1)-S(1)	100.2(1)	O(4)-Ir(1)-C(1)	171.1(4)
Ir(1)-S(1)-O(2)	110.8(4)	O(2)-S(1)-O(3)	130.8(8)
Ir(1)-S(1)-O(3)	106.2(7)	O(5)-S(2)-O(6)	104.7(5)
Ir(1)-O(4)-S(2)	139.6(4)	S(2)-O(6)-H(6)	119(6)
O(4)-S(2)-O(5)	102.7(4)	O(6)-H(6)···O(5a)	151(8)
O(4)-S(2)-O(6)	103.6(4)		

S-O = 113.8(3)°. It is possible that the shorter S-O distances in the present molecule are an artifact of the larger thermal motions of this group.

The -OS(O)OH ligand is associated with the following distances: O(4)-S(2) = 1.521(6), S(2)-O(5) = 1.549(8), S(2)-O(6) = 1.511(10), and O(6)-H(6) = 0.92(11) Å. It is surprising that the S(2)-O(5) distance (formally an S=O linkage) is indistinguishable from the S(2)-O(6) distance (an S-OH linkage). Either this is a result of intermolecular hydrogen bonding (see above) or there could be some disorder of S=O and S-OH linkages, concerning hydrogen bonding, which we have been unable to detect. Angles around the chiral pyramidal sulfur(IV) atom S(2) are O(4)-S(2)-O(5) = 102.7(4), O(4)-S(2)-O(6) = 103.6(4), and O(5)-S(2)-O(6) = 104.7(5)°.

Other features in the molecule are normal; the cyclohexyl rings in the PCy<sub>3</sub> ligands have a chair conformation, with the phosphorus atoms occupying equatorial sites on one of the four coplanar carbon atoms which define the "seat" of the chair.

Sulfur dioxide insertions into metal hydride,<sup>26</sup> metal

(23) The trichloro complex was characterized only by the shift in  $\nu_{\text{CO}}$  (1933 → 2033 cm<sup>-1</sup>) upon Cl<sub>2</sub> addition. This shift is very similar to the shift for the PPh<sub>3</sub> analogue upon reaction with Cl<sub>2</sub> (1955 → 2075 cm<sup>-1</sup>).<sup>2</sup> The SO<sub>2</sub> adduct was characterized by its  $\nu_{\text{CO}}$  (1991 cm<sup>-1</sup>) and its <sup>31</sup>P NMR resonance (14.9 ppm). Each is in the expected location based on the P(*p*-tolyl)<sub>3</sub> analogue.<sup>24</sup>

(24) Randall, S. L.; Miller, C. A.; See, R. F.; Churchill, M. R.; Atwood, J. D. *Organometallics* **1994**, *13*, 141.

(25) Thompson, J. S.; Randall, S. L.; Atwood, J. D. *Organometallics* **1991**, *10*, 3906.

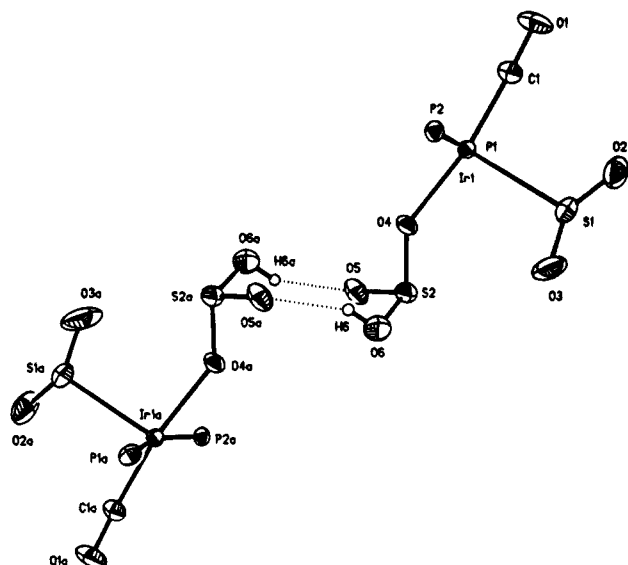


**Figure 2.** Hydrogen bonding between the defined unit and that with coordinates related by inversion about  $1/2, 0, 0$  (labeled with suffix "a"). This view also shows the square-pyramidal coordination geometry about iridium. Note that atom P(1) is hidden from view behind Ir(1).

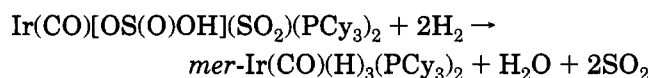
alkyl,<sup>27</sup> and metal alkoxide bonds<sup>6,24</sup> have been reported. Insertion into a hydride produced the  $\text{SO}_2\text{H}$  complex for  $\text{CpMo}(\text{CO})_3\text{H}$ ; reaction with  $\text{Cp}^*\text{Ru}(\text{CO})_2\text{H}$  produced a sulfur-coordinated  $\text{SO}_3\text{H}$  (hydrogen sulfite) ligand through a disproportionation reaction.<sup>26</sup> A sulfur-coordinated hydrogen sulfite ( $\text{CpFe}(\text{CO})_2\text{SO}_3\text{H}$ ) was also obtained by hydrolysis of  $\text{CpFe}(\text{CO})_2\text{SO}_3\text{Me}$ .<sup>27</sup>

Reaction of  $\text{SO}_2$  with *trans*- $\text{Ir}(\text{CO})(\text{OH})(\text{PCy}_3)_2$  provides the first example of insertion of  $\text{SO}_2$  into a metal hydroxide producing oxygen-coordinated hydrogen sulfite. It is likely that steric constraints prevent the rearrangement of the oxygen-coordinated to the presumably more stable sulfur-coordinated hydrogen sulfite ligand. The complex formed,  $\text{Ir}(\text{CO})[\text{OS}(\text{O})\text{OH}](\text{SO}_2)(\text{PCy}_3)_2$ , is quite similar to the kinetic product of the addition of  $\text{SO}_2$  to *trans*- $\text{Ir}(\text{CO})(\text{OR})(\text{P}(p\text{-tolyl})_3)_2$ .<sup>24</sup> Two aspects of the  $\text{OS}(\text{O})\text{OH}^-$  ligand are unique for hydrogen sulfite: (1) The proton is located on an oxygen instead of the sulfur. While infrared<sup>17</sup> and  $^{17}\text{O}$  NMR<sup>19</sup> evidence for the existence of the oxygen-protonated isomer of hydrogen sulfite has been presented,  $\text{Ir}(\text{CO})(\text{SO}_2)(\text{OS}(\text{O})\text{OH})(\text{PCy}_3)_2$  provides the first structural evidence. (2) In the two other examples in which hydrogen sulfite is a ligand in organometallic complexes, the ligand is coordinated through the sulfur to the metal. Thus, for the  $\text{OS}(\text{O})\text{OH}$  ligand reported herein the pair of electrons on sulfur is stereochemically active, but does not participate in bonding to the proton or to the iridium. Possibly the oxygen coordination to the iridium reduces the steric interactions, and the protonation on the oxygen allows extra stability from intermolecular hydrogen bonding

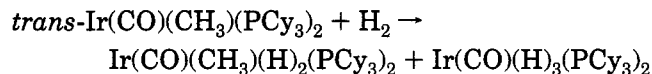
(Figure 2). Regardless of the rationale, the  $\text{OS}(\text{O})\text{OH}^-$  ligand is highly unusual.

When 10%  $\text{SO}_2$  in  $\text{N}_2$  or greater concentrations are used, an intermediate is formed that rearranges to  $\text{Ir}(\text{CO})[\text{OS}(\text{O})\text{OH}](\text{SO}_2)(\text{PCy}_3)_2$  upon workup. Two possibilities for this species ( $\nu_{\text{CO}} = 1997 \text{ cm}^{-1}$  and a  $^{31}\text{P}$  resonance at 18.0 ppm) cannot presently be discerned: (1) A species is formed containing either  $\text{SO}_2$  bound differently (coplanar instead of pyramidal, for instance) or hydrogen sulfite bound through sulfur. It is difficult to rationalize that, if the sulfur-coordinated  $\text{HSO}_3^-$  could form, the soft sulfur ligand would rearrange to the harder oxygen coordination for the sulfite. A change in coordination of the  $\text{SO}_2$  is quite possible, though how this could be affected by the concentration of  $\text{SO}_2$  is not readily apparent. (2) A third  $\text{SO}_2$  could coordinate, possibly reversibly inserting into the iridium–oxygen bond of the sulfite ligand or coordinating to the oxygen of the hydrogen sulfite ligand. The Ir–O bond of the coordinated sulfite ligand may not be very different from that of the Ir–O from the hydroxide. These reactions would be similar to the known reactions of  $\text{HSO}_3^-$  forming bisulfite  $\text{S}_2\text{O}_5^{2-}$ ; in this case,  $\text{HSO}_3^- + \text{SO}_2 \rightarrow \text{HS}_2\text{O}_5^-$ . On the basis of the positions of the  $^{31}\text{P}$  resonance and the infrared frequency and on the formation only at higher concentrations of  $\text{SO}_2$ , the second is more likely, but our inability to isolate this product precludes assigning a structure.

While *trans*- $\text{Ir}(\text{CO})(\text{OH})(\text{PCy}_3)_2$  does not react with  $\text{H}_2$ , the five-coordinate hydrogen sulfite complex reacts readily forming two iridium-containing products.



The ultimate product, *mer*- $\text{Ir}(\text{CO})(\text{H})_3(\text{PCy}_3)_2$ , has the characteristic triplet of doublets and triplet of triplets splitting with the appropriate coupling.<sup>25</sup> This is the product observed when many *trans*- $\text{Ir}(\text{CO})(\text{R})\text{L}_2$  complexes react with  $\text{H}_2$ .<sup>1,25</sup> The second product, formed at intermediate times and not isolated, has two triplets of doublets in a 1:1 ratio characteristic of iridium *cis* dihydride complexes. We assign this product as  $\text{Ir}(\text{CO})(\text{H})_2[\text{OS}(\text{O})\text{OH}](\text{PCy}_3)_2$ . That electronic effects and not just steric factors are important is further shown by the fact that  $\text{H}_2$  reacts with *trans*- $\text{Ir}(\text{CO})(\text{CH}_3)(\text{PCy}_3)_2$ .



The methyl complex is not significantly smaller than the chloro complex.

**Acknowledgment.** We are grateful to the National Science Foundation for funding the upgrade and purchase of our diffractometers (Grant 89-13733 from the Chemical Instrumentation Program).

**Supporting Information Available:** Complete tables of distances, angles, anisotropic thermal parameters, and calculated hydrogen atom positions for  $\text{Ir}(\text{CO})[\text{OS}(\text{O})\text{OH}](\text{SO}_2)(\text{PCy}_3)_2 \cdot \text{C}_6\text{H}_6$  (5 pages).

OM950410+

(26) (a) Kubat-Martin, K. A.; Kubas, G. J.; Ryan, R. R. *Organometallics* **1989**, *8*, 1910. (b) Kubas, G. J.; Wasserman, H. J.; Ryan, R. R. *Organometallics* **1985**, *4*, 2012.

(27) (a) Kroll, J. O.; Wojcicki, A. J. *Organomet. Chem.* **1974**, *66*, 95 and references therein. (b) Hartman, T. A.; Wojcicki, A. J. *Am. Chem. Soc.* **1966**, *88*, 844. (c) Poffenberger, C. A.; Wojcicki, A. *Inorg. Chem.* **1980**, *19*, 3795.

# *exo,exo*-Bis(isodicyclopentadienyl)titanium and -zirconium Dichlorides: Conformational Characterization of the Homogeneous Ziegler Catalyst Precursors in Solution

Cornelia Fritze, Markus Knickmeier, and Gerhard Erker\*

Organisch-Chemisches Institut der Universität Münster, Corrensstrasse 40,  
D-48149 Münster, Germany

Florence Zaegel, Bernard Gautheron, and Philippe Meunier

Université de Bourgogne, Laboratoire de Synthèse et d'Electrosynthèse Organométalliques,  
Faculté des Sciences "Gabriel", 6, Boulevard Gabriel, 21000-Dijon, France

Leo A. Paquette

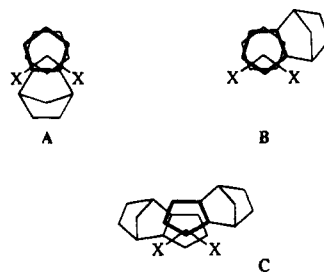
Evans Chemical Laboratories, The Ohio State University, 120 West 18th Avenue,  
Columbus, Ohio 43210-1173

Received February 8, 1995<sup>®</sup>

**Summary:** *exo,exo*-Bis(isodicyclopentadienyl)titanium dichloride (**1**) exhibits a chiral  $C_2$ -symmetric structure in solution that is characterized by a bis-lateral:anti orientation of the annulated bicyclo[2.2.1]heptene moieties at the bent-metallocene wedge. This was shown by dynamic NMR spectroscopy of complex **1** in  $[D_2]$ dichloromethane solution. The activation energy for the conformational inversion of complex **1** is  $\Delta G_{\text{rot}}^\ddagger(198 \text{ K}) = 9.8 \pm 0.4 \text{ kcal mol}^{-1}$ . The bent-metallocene rotational barrier of the analogous zirconium complex (**2**) is much lower ( $\sim 6 \text{ kcal mol}^{-1}$ ). Complexes **1** and **2** were both used to generate active homogeneous Ziegler catalyst systems for  $\alpha$ -olefin polymerization.

## Introduction

The group 4 metals can very selectively be coordinated to the *exo* or *endo* faces of the isodicyclopentadienyl ligand system, respectively, by carefully selecting the reaction conditions.<sup>1</sup> Several representative examples of such group 4 bent-metallocene complexes were characterized by X-ray diffraction.<sup>1,2</sup> For the (isodicyclopentadienyl) $M\text{CpX}_2$  complexes two rotamers were observed, one where the annulated bicyclo[2.2.1]heptene structural unit is oriented toward the open front part of the bent-metallocene wedge (A) and another where the annulated norbornene moiety occupies a lateral sector (B). Consequently, three conformations of the corresponding (isodicyclopentadienyl) $_2M\text{Cl}_2$  complexes can be envisaged, having the annulated bicyclic ring systems arranged in a  $C_2$ -symmetric bis-lateral:anti (C), a  $C_{2v}$ -symmetric bis-central:syn, or a lateral/central (symmetry group  $C_1$ ) arrangement.



Of the *exo,exo*-(isodicyclopentadienyl) $_2M\text{Cl}_2$  complexes **1** ( $M = \text{Ti}$ ) and **2** ( $M = \text{Zr}$ ) in the crystal state, the structures of the bis-lateral:anti bent-metallocene conformers were determined by X-ray diffraction.<sup>2</sup> For remotely related group 4 bent-metallocene complexes, examples of all three conformations have been found in the solid state and in solution.<sup>3,4</sup> It has also been shown that X-ray crystal structure analyses can only serve to identify possible structural types.<sup>5</sup> Which of these is present in solution (i.e. in the absence of crystal-packing forces) and might determine the chemistry of a particu-

(3) Krüger, C.; Nolte, M.; Erker, G.; Thiele, S. *Z. Naturforsch.* **1992**, *47B*, 995. See also: Benn, R.; Grondey, H.; Nolte, R.; Erker, G. *Organometallics* **1988**, *7*, 777. Erker, G.; Nolte, R.; Tainturier, G.; Rheingold, A. *Organometallics* **1989**, *8*, 454. Erker, G.; Nolte, R.; Krüger, C.; Schlund, R.; Benn, R.; Grondey, H.; Mynott, R. *J. Organomet. Chem.* **1989**, *364*, 119. Benn, R.; Grondey, H.; Erker, G.; Aul, R.; Nolte, R. *Organometallics* **1990**, *9*, 2493.

(4) For selected examples see: Petersen, J. L.; Dahl, L. F. *J. Am. Chem. Soc.* **1975**, *97*, 6422. Dusaosoy, Y.; Protas, J.; Renaut, P.; Gautheron, B.; Tainturier, G. *J. Organomet. Chem.* **1978**, *157*, 167. Luke, W. D.; Streitwieser, A. *J. Am. Chem. Soc.* **1981**, *103*, 3241 and references cited therein. Howie, R. A.; McQuillan, G. P.; Thompson, D. W. *J. Organomet. Chem.* **1984**, *268*, 149. Howie, R. A.; McQuillan, G. P.; Thompson, D. W.; Lock, G. A. *J. Organomet. Chem.* **1986**, *303*, 213. Antinolo, A.; Lappert, M. F.; Singh, A.; Winterborn, D. J. W.; Engelhardt, L. M.; Raston, C.; White, A. H.; Carty, A. J.; Taylor, N. J. *J. Chem. Soc., Dalton Trans.* **1987**, 1463. Okuda, J. *J. Organomet. Chem.* **1988**, *356*, C43. Broussier, R.; Da Rold, A.; Gautheron, B.; Dromzee, Y.; Jeannin, Y. *Inorg. Chem.* **1990**, *29*, 1817. Mallin, D. T.; Rausch, M. D.; Mintz, E. A.; Rheingold, A. L. *J. Organomet. Chem.* **1990**, *381*, 35. Winter, C. H.; Dobbs, D. A.; Zhou, X.-X. *J. Organomet. Chem.* **1991**, *403*, 145. See also: Janiak, C.; Schumann, H. *Adv. Organomet. Chem.* **1991**, *33*, 291. Okuda, J. *Top. Curr. Chem.* **1991**, *160*, 97 and references cited therein.

(5) Erker, G.; Aulbach, M.; Knickmeier, M.; Wingbermühle, D.; Krüger, C.; Nolte, M.; Werner, S. *J. Am. Chem. Soc.* **1993**, *115*, 4590. Krüger, C.; Lutz, F.; Nolte, M.; Erker, G.; Aulbach, M. *J. Organomet. Chem.* **1993**, *452*, 79.

<sup>®</sup> Abstract published in *Advance ACS Abstracts*, October 1, 1995.

(1) Paquette, L. A.; Moriarty, K. J.; Meunier, P.; Gautheron, B.; Crocq, V. *Organometallics* **1988**, *7*, 1873. Paquette, L. A.; Moriarty, K. J.; Meunier, P.; Gautheron, B.; Sornay, C.; Rogers, R. D.; Rheingold, A. L. *Organometallics* **1989**, *8*, 2159. Sornay, C.; Meunier, P.; Gautheron, B.; O'Doherty, G. A.; Paquette, L. A. *Organometallics* **1991**, *10*, 2082. Zaegel, F.; Gallucci, J. C.; Meunier, P.; Gautheron, B.; Sivik, M. R.; Paquette, L. A. *J. Am. Chem. Soc.* **1994**, *116*, 6466.

(2) Gallucci, J. C.; Gautheron, B.; Gugelchuk, M.; Meunier, P.; Paquette, L. A. *Organometallics* **1987**, *6*, 15. Zaegel, F.; Meunier, P.; Gautheron, B.; Gallucci, J. C.; Paquette, L. A. *Organometallics*, submitted for publication.

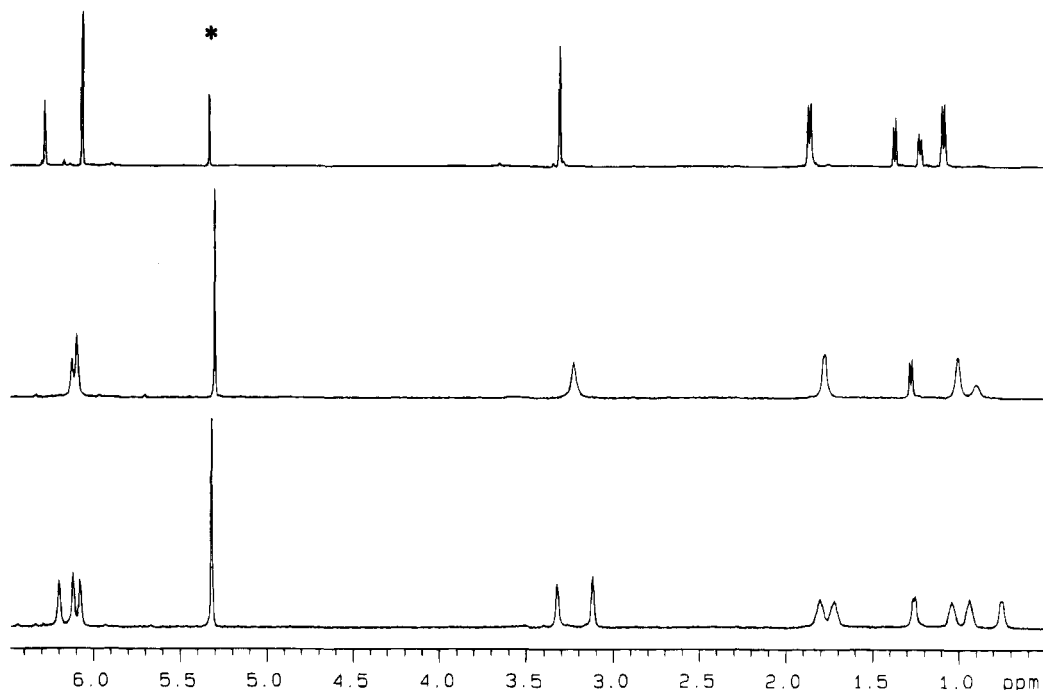
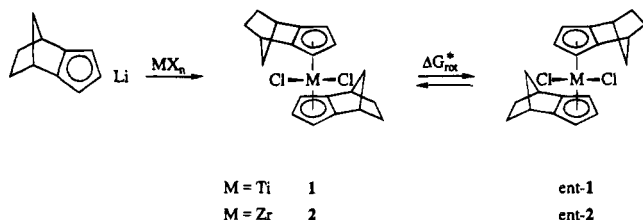


**Figure 1.** Dynamic  $^1\text{H}$  NMR spectra of **1** in  $[\text{D}_2]$ dichloromethane (600 MHz) at 300 K (top), 213 K (center), and 173 K (bottom) (the asterisk denotes residual solvent  $\text{CH}_2\text{Cl}_2$ ).

lar system cannot, however, be deduced from the solid-state structural analysis, since the crystallization process serves as a kinetic exit for the rapidly equilibrating metallocene conformers. In such an *open* system any information about the equilibrium situation of the bent-metalocene conformations is lost. We have recently shown that in such cases the conformational equilibration can be sometimes studied by dynamic NMR spectroscopy and that in selected cases it is even possible to obtain information about the properties of bent-metalocene catalysts by such studies.<sup>5</sup> Therefore, we have tried to learn about the solution structures and behavior of complexes **1** and **2** by using this method.

### Results and Discussion

Complexes **1** and **2** were prepared according to a literature procedure<sup>2</sup> by treating 2 molar equiv of (isodicyclopentadienyl)lithium with titanium trichloride (followed by oxidation) and zirconium tetrachloride, respectively, in tetrahydrofuran at high temperature. Under the conditions of thermodynamic control, only the *exo,exo*-(isodicyclopentadienyl)<sub>2</sub>MCl<sub>2</sub> products (M = Ti, Zr) are obtained.



The titanium complex **1** exhibits  $^1\text{H}$  and  $^{13}\text{C}$  NMR at ambient temperature that would be compatible with an overall  $C_{2v}$ -symmetric structure. The alleged presence of the two symmetry planes would result in a total of seven  $^1\text{H}$  NMR resonances, which are observed at  $\delta$  6.26, 6.05, 3.31, 1.87, 1.37, 1.23, and 1.09 ppm (600 MHz, 300

K in  $[\text{D}_2]$ dichloromethane) in a 1:2:2:2:1:1:2 ratio, and six  $^{13}\text{C}$  signals (150.8 MHz, 300 K, observed at  $\delta$  145.8, 129.1, 107.4, 48.0, 41.9, and 28.3 ppm). However, this spectral appearance does not reflect the actual molecular symmetry of **1** in solution, as it is in fact the result of an equilibration process of metallocene conformations which is fast on the NMR time scale. Complex **1** exhibits dynamic NMR spectra upon lowering the temperature. Below coalescence ( $T_c = 198$  K) 11  $^1\text{H}$  NMR resonances of equal intensity are observed (see Figure 1). This indicates that the molecular symmetry of **1** in solution is  $C_2$ . Complex **1** thus exhibits two symmetry-equivalent isodicyclopentadienyl ligands in an orientation that results in a chemical differentiation of the hydrogen atoms of the H-*exo*, H-*endo*, bridgehead-H, and Cp-H pairs, as is typically found in the bis-lateral: anti conformation (*C* type). As expected, the analogous splitting of the respective  $^{13}\text{C}$  NMR resonance (with the exception of the isochronous bridgehead carbon atom signals) is also observed at sufficiently low temperatures. At 200 K one observes  $^{13}\text{C}$  NMR resonances of the  $C_2$ -symmetric complex **1** at  $\delta$  152.6, 134.7, 129.1, 109.9, 104.6, 46.6, 40.7 (double intensity), 27.7, and 26.4 ppm. We thus conclude that, within the accuracy of the NMR measurement, complex **1** exhibits a single  $C_2$ -symmetric bent-metalocene conformation in solution that is detected when the rapid **1**  $\rightleftharpoons$  ent-1 equilibration becomes frozen on the NMR time scale. From the coalescence of the pair of bridgehead hydrogens (173 K,  $\delta$  3.32, 3.12 ppm;  $T_c = 198$  K) and independently of the pair of hydrogen signals at  $\delta$  1.04/1.25 ppm (173 K) an activation barrier of  $\Delta G_{\text{rot}}^\ddagger(198 \text{ K}) = 9.8 \pm 0.4 \text{ kcal mol}^{-1}$

(6) Binsch, G. In *Dynamic Nuclear Magnetic Resonance Spectroscopy*; Jackman, L. M., Cotton, F. A., Eds.; Academic Press: New York, 1975; p 45–81. Binsch, G.; Kessler, H. *Angew. Chem.* **1980**, *92*, 445; *Angew. Chem., Int. Ed. Engl.* **1980**, *19*, 411. Green, M. L. H.; Wong, L. L.; Sella, A. *Organometallics* **1992**, *11*, 2660 and references cited therein. Gutowsky, H. S. In *Dynamic Nuclear Magnetic Resonance Spectroscopy*; Jackman, L. M., Cotton, F. A., Eds.; Academic Press: New York, 1975; pp 1–21. See also: Günther, H. *NMR-Spectroscopy*; Thieme: Stuttgart, Germany, 1992; pp 303–350.



was estimated<sup>6</sup> for the equilibration ( $1 \rightleftharpoons ent-1$ ) of the enantiomeric conformations of the *exo,exo*-(isodicyclopentadienyl)<sub>2</sub>TiCl<sub>2</sub> complex **1** in solution at the coalescence temperature.

The analogous rotational barrier of the zirconium complex **2** is much lower. The rapid equilibration of conformations could not be frozen out on the <sup>1</sup>H NMR time scale. At all temperatures seven <sup>1</sup>H NMR resonances were observed ( $\delta$  6.28, 5.89, 3.30, 1.83, 1.45, 1.38, and 1.01 ppm at 253 K in [D<sub>2</sub>]dichloromethane solution); only at 173 K (600 MHz) was some line broadening monitored that was not due to viscosity effects. Even the chemical shift difference in the <sup>13</sup>C NMR spectrum at 14 T (150.8 MHz) was not sufficient to allow observation of the low-temperature limiting spectrum below the coalescence (six "high temperature" <sup>13</sup>C NMR signals of **2** are observed at 253 K:  $\delta$  142.3, 122.3, 103.3, 48.9, 40.9, and 28.2 ppm). Only the quarternary Cp resonance signal at  $\delta$  142.3 becomes broad below 213 K. If one assumes a separation of the resulting pair of the corresponding <sup>13</sup>C NMR signals in the static low-temperature spectrum for **2** similar to that observed for **1** ( $\Delta\delta \approx 20$  ppm, i.e.  $\Delta\nu \approx 3000$  Hz), this would lead to an estimate of the activation barrier of the  $2 \rightleftharpoons ent-2$  rearrangement of  $<7$  kcal mol<sup>-1</sup> (in [D<sub>2</sub>]dichloromethane solution).

Complexes **1** and **2** were activated with methylalumoxane<sup>7</sup> to give highly reactive homogeneous Ziegler-type propene polymerization catalysts. The **2**/MAO catalyst (Zr:Al  $\approx$  1400) produces atactic polypropylene in toluene solution (2 bar propene pressure, 0 °C, 4.65 kg of polymer (mmol of Zr)<sup>-1</sup> h<sup>-1</sup> bar<sup>-1</sup> obtained; -40 °C, 220 g of polymer (mmol of Zr)<sup>-1</sup> h<sup>-1</sup> bar<sup>-1</sup>; stereochemical analysis by <sup>13</sup>C NMR methyl pentad analysis;<sup>8</sup>  $\bar{M}_n = 13\,000$  (0 °C) and 150 000 (-40 °C), respectively).

The corresponding titanium Ziegler catalyst **1**/MAO is much less active. In the temperature range between -50 and +50 °C it exhibits a broad activity maximum at ca. -10 °C (**1**:MAO ratio of the individual experiments between 900 and 1200; activity (g of polymer (mmol of Ti)<sup>-1</sup> h<sup>-1</sup> bar<sup>-1</sup>): 0.7 (-50 °C), 7.6 (-29 °C), 21.8 (-11 °C), 10.9 (+12 °C), 3.2 (+30 °C), 2.3 (+50 °C)).  $\bar{M}_n$  decreased from  $\sim 120\,000$  to  $\sim 20\,000$  within this temperature range. Over the whole temperature range the stereochemistry is exclusively determined by chain end control,<sup>9</sup> similar to the behavior observed previously by Ewen using simple Cp<sub>2</sub>Ti-derived catalyst systems.<sup>8b</sup> At low temperature this stereocontrol is rather efficient; the isotactic polymer obtained at the **1**/MAO catalyst at -50 °C in toluene exhibits only three <sup>13</sup>C NMR methyl signals at  $\delta$  21.9, 21.6, and 20.8 ppm in a 82:11:7 intensity ratio, representing the *mmmm*, *mmmr*, and *mrmr* methyl pentad resonances, respectively. Statistical analysis of this spectrum leads to a prob-

ability of finding a polypropylene *m* pentad at the **1**/MAO catalyst under these conditions of  $\sigma = 0.95$ . Increasing the polymerization temperature results in a rapid decrease of the selectivity, although also at higher temperatures the stereochemistry exclusively is chain end controlled. At -29 °C the *mmmm* methyl pentad signal has dropped to 70% intensity ( $\sigma = 0.91$ ) (-11 °C, 32% *mmmm*,  $\sigma = 0.75$ ) and the atactic situation is reached at +12 °C (5% *mmmm*,  $\sigma = 0.48$ ). The remarkable feature of this series of polymerization reactions at the **1**/MAO catalyst is that the maximum nonselectivity does not represent the limiting high-temperature situation. Increasing the polymerization temperature leads to a further reduction of the *mmmm* <sup>13</sup>C NMR methyl resonance intensity (+30 °C,  $\sim 1\%$  *mmmm*,  $\sigma = 0.40$ ; +50 °C, no detectable *mmmm* intensity,  $\sigma = 0.35$ ). This means that the system has crossed the atactic borderline ( $\sigma = 0.5$ ) and entered into the syndiotactic polypropylene regime just from an increase in the polymerization temperature.<sup>10</sup> The overall stereocontrol has remained completely chain end controlled, even at +50 °C.

This study has shown that *exo,exo*-bis(isodicyclopentadienyl)titanium dichloride exhibits a single conformation in solution that is best described as of the bis-lateral:anti metallocene conformational type (**C**; see above). This chiral C<sub>2</sub>-symmetric structure in solution is probably very similar to the molecular geometry found of **1** in the solid state by X-ray crystallography.<sup>2</sup> The enantiomerization barrier of **1** is rather high at  $\Delta G^{\ddagger}_{rot} \approx 10$  kcal mol<sup>-1</sup>. The *exo,exo*-bis(isodicyclopentadienyl)-zirconium dichloride homolog (**2**) is probably also C<sub>2</sub>-symmetric, but it exhibits a much lower enantiomerization barrier. If the metallocene conformation in the active catalyst systems derived from **1** and **2** is also C<sub>2</sub>, this chirality information is not transferred onto the growing polypropylene chain, either from the titanium complex **1** or the zirconium system **2**. This may be due to an extreme lateral arrangement of the bulky annulated ring systems (similar to that found for **1** and **2** in the solid state<sup>2</sup>).

We find it remarkable how different the stereochemical behaviors of the **1**/MAO and **2**/MAO catalyst systems are during propene polymerization. Of course, this conformational study does not give any direct evidence or explanation as to why the zirconium catalyst (**2**/MAO) provides no stereocontrol at all whereas the titanium system (**1**/MAO) is able to exert a pronounced chain end stereocontrol in the investigated temperature interval, ranging from rather highly isotactic polypropylene block polymer<sup>8</sup> to slightly syndiotactic polypropylene formation. Chain end stereocontrol probably requires that the *re*- vs. *si*-face coordination of the incoming  $\alpha$ -olefin monomer is determined by the precise conformational arrangement of the adjacent chiral M-CH<sub>2</sub>CH(CH<sub>3</sub>)R (R = polymer chain)  $\sigma$ -ligand system. It may be that the rotational barrier of the M-CH<sub>2</sub> linkage in these catalyst systems also exhibits a pronounced dependence on the size of the central metal atom, similar to what is observed for the rotation around the M-Cp vector in **1** and **2**. Then it would be expected that the chain end chirality information associated with the zirconium

(7) Sinn, H.; Kaminsky, W. *Adv. Organomet. Chem.* **1980**, *18*, 99 and references cited therein.

(8) (a) Bovey, F. A.; Tiers, G. V. D. *J. Polym. Sci.* **1960**, *44*, 173. Sheldon, R. A.; Fueno, T.; Tsutsuga, R.; Kurukawa, J. *J. Polym. Sci., Part B; Polym. Lett.* **1965**, *3*, 23. Zambelli, A.; Locatelli, P.; Bajo, G.; Bovey, F. A. *Macromolecules* **1975**, *8*, 1565. Farina, M. *Top. Stereochem.* **1987**, *17*, 1. (b) Ewen, J. A. *J. Am. Chem. Soc.* **1984**, *106*, 6355. Ewen, J. A. *Stud. Surf. Sci. Catal.* **1986**, *25*, 271. Ewen, J. A.; Elder, M. J.; Jones, R. L.; Curtis, S.; Cheng, H. N. *Stud. Surf. Sci. Catal.* **1990**, *56*, 439.

(9) (a) Inoue, J.; Itabashi, Y.; Chujo, R.; Doi, Y. *Polymer* **1984**, *25*, 1640. (b) Erker, G.; Nolte, R.; Tsay, Y.-H.; Krüger, C. *Angew. Chem.* **1989**, *101*, 642; *Angew. Chem., Int. Ed. Engl.* **1989**, *28*, 628. (c) Erker, G.; Nolte, R.; Aul, R.; Wilker, S.; Krüger, C.; Noe, R. *J. Am. Chem. Soc.* **1991**, *113*, 7594.

(10) Erker, G.; Fritze, C. *Angew. Chem.* **1992**, *104*, 204; *Angew. Chem., Int. Ed. Engl.* **1992**, *31*, 199. See also: Resconi, L.; Abis, L.; Franciscano, G. *Macromolecules* **1992**, *25*, 6814.

catalyst system is much less persistent than that of the titanium catalyst, and consequently the zirconium-containing homogeneous Ziegler catalyst (here **2**/MAO) is expected to be much less stereoselective than the corresponding titanium system (**1**/MAO) even outside the enantiomorphic site control regime. A detailed investigation about the remarkable temperature dependence of the isotactic vs syndiotactic chain end controlled polypropylene formation at this and other titanocene/methylalumoxane catalyst systems is currently being carried out in our laboratory. The results of that study will be described in a forthcoming publication.

### Experimental Section

Complexes **1** and **2** were prepared as described in the literature.<sup>2</sup> The dynamic NMR spectra of complexes **1** and **2** were measured on a Bruker AC 200 P and a Varian Unity Plus 600 NMR spectrometer. The activation barriers were determined at the coalescence temperature of the respective pair of signals using the Gutowsky-Holm approximation.<sup>6</sup>

Propene polymerization reactions were carried out in a Büchi glass autoclave at 2 bar of propene pressure in toluene solvent, analogous to the procedure previously described in detail.<sup>5,9,10</sup> The molecular weights of the polymers were determined with an Ubbelohde viscosimeter (Schott AVS 440) in decalin solution at 135 °C. The <sup>13</sup>C NMR spectra of the polymers were recorded in 1,2,4-trichlorobenzene/[D<sub>6</sub>]benzene (4:1) solution at 350 K. The methyl pentad signals were integrated by a curve-fitting procedure as previously described and then subjected to a statistical treatment to determine the partition between enantiomorphic site control ( $\omega$ ) and chain end stereocontrol ( $1 - \omega$ ) as well as the isotacticity ( $\sigma$ ) and, respectively, syndiotacticity ( $1 - \sigma$ ) of the obtained polymer sample under chain end control. A detailed description of this procedure can be found in the literature.<sup>5,9c</sup>

**Acknowledgment.** This work was supported by the Fonds der Chemischen Industrie, the Alfried Krupp von Bohlen und Halbach-Stiftung, and Hoechst AG.

OM950102B

# Ligand-Dependent Relative Stability Order in Allyl Sulfide/Palladium(0) Species vs ( $\eta^3$ -Allyl)palladium(II) Thiolate Species

Yoshinori Miyauchi, Saisuke Watanabe, Hitoshi Kuniyasu, and Hideo Kurosawa\*

Department of Applied Chemistry, Faculty of Engineering, Osaka University, Suita, Osaka 565, Japan

Received July 13, 1995<sup>®</sup>

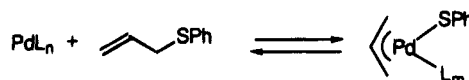
**Summary:** Oxidative additions of allyl phenyl sulfide and selenide to  $\text{Pd}_2(\text{dba})_3$  or  $\text{Pd}(\text{MA})(\text{COD})$  ( $\text{dba}$  = dibenzylideneacetone,  $\text{MA}$  = maleic anhydride,  $\text{COD}$  = cyclooctadiene) provided  $[\text{Pd}(\eta^3\text{-C}_3\text{H}_5)(\text{EPh})]_2$  ( $\text{E} = \text{S}, \text{Se}$ ) in good yields. Competitive reactions employing the sulfide and the selenide showed the higher reactivity of the selenide with regard to oxidative addition. The reaction of  $[\text{Pd}(\eta^3\text{-C}_3\text{H}_5)(\text{SPh})]_2$  with  $\text{PR}_3$  afforded different types of products, depending on the nature of  $\text{R}$  and the molar ratio of the reagents. The reaction with both 1 equiv and 2 equiv of  $\text{PCy}_3$  ( $\text{Cy}$  = cyclohexyl) gave  $\text{Pd}(\eta^3\text{-C}_3\text{H}_5)(\text{SPh})(\text{PCy}_3)$  as the sole product. In the reactions with  $\text{PPh}_3$  and  $\text{P}(\text{OMe})_3$ , comparable amounts of the  $\mu$ -allyl Pd–Pd complex  $\text{Pd}_2(\mu\text{-C}_3\text{H}_5)(\mu\text{-SPh})(\text{PR}_3)_2$  ( $\text{R} = \text{Ph}, \text{OMe}$ ) and allyl phenyl sulfide were obtained in the case of  $\text{PR}_3/\text{Pd} = 1$ , while the latter product predominated in the case of  $\text{PR}_3/\text{Pd} > 3$ . Analogous reactions employing  $\eta^3$ -5-(methoxycarbonyl)cyclohexenyl analogs and excess  $\text{PPh}_3$  indicated that the formation of allyl phenyl sulfides took place with inversion of stereochemistry at the allylic carbon, suggesting *exo* attack of the thiolate at the  $\eta^3$ -allyl group in  $[\text{Pd}(\eta^3\text{-allyl})(\text{PPh}_3)_2]^+$ .

## Introduction

Cleavage and formation of C–S bonds mediated by transition metal complexes are subjects of increasing synthetic and mechanistic interest.<sup>1</sup> Allylic sulfides and selenides reacted with Pd(0)–trialkylphosphine complexes to give dinuclear  $\mu$ -allylic complexes probably via oxidative addition to generate allylpalladium(II) thiolate and selenolate intermediates, followed by their reaction with the Pd(0) complex,<sup>2</sup> but definitive evidence for this

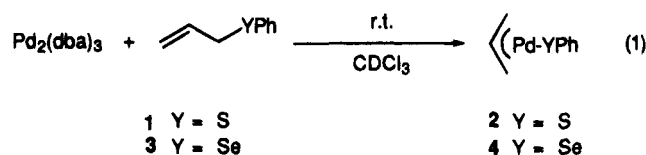
sequence was lacking. In contrast, it has been proposed in some catalytic transformations of allylic substrates<sup>3</sup> that similar ( $\eta^3$ -allyl)palladium(II) thiolate intermediates are rather prone to undergo reductive elimination to generate allylic sulfides and Pd(0) species. In order to shed more light on such apparently conflicting stability order of a Pd(0) complex plus allyl sulfide on one side and an allylpalladium(II) thiolate complex on the other (Scheme 1), we examined reactions of related ( $\eta^3$ -allyl)palladium(II) thiolate and selenolate complexes with some ligands. Reported herein are results of such experiments and a unified explanation for the previous findings.

Scheme 1



## Results and Discussion

When the reaction of allyl phenyl sulfide (**1**) and  $\text{Pd}_2(\text{dba})_3$  was carried out in  $\text{CDCl}_3$  solution at ambient temperature for 3 h, the formation of ( $\eta^3$ -allyl)palladium benzenethiolate,  $[\text{Pd}(\eta^3\text{-C}_3\text{H}_5)(\text{SPh})]_2$  (**2**),<sup>4</sup> in 78% yield was confirmed by the <sup>1</sup>H NMR spectrum (eq 1). A



similar treatment using allyl phenyl selenide **3** gave the corresponding selenolate complex **4**<sup>4</sup> in 88% yield. The oxidative addition also occurred in the reaction between  $\text{Pd}(\text{MA})(\text{COD})$  and **1** or **3**. When a 1:1 mixture of **1** and **3** was reacted with  $\text{Pd}_2(\text{dba})_3$ , formation of **4** predominated over that of **2**, suggesting much higher reactivity of the selenide. This trend is different from that in the corresponding reaction of  $\text{Pd}(\text{PCy}_3)_2$  with **1** and **3**, where the two substrates showed similar reactivities.<sup>2a</sup>

The facile oxidative addition of **1** and **3** to Pd(0)-olefin complexes can be compared with the known reactivity patterns between **1** and Pd(0)– $\text{PR}_3$  complexes,<sup>2a</sup> no reaction took place in the case of  $\text{R} = \text{Ph}$ , but apparent oxidative addition occurred in the case of  $\text{R} = \text{Cy}$ . Attempts were made to rationalize these results by examining reactions of **2** and **4** with various  $\text{PR}_3$  species.

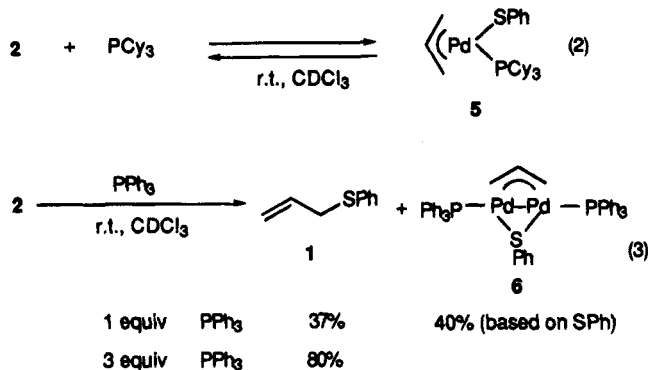
(3) (a) Auburn, P. R.; Whelan, J.; Bosnich, B. *J. Chem. Soc., Chem. Commun.* **1986**, 146. (b) Goux, C.; Lhoste, P.; Sinou, D. *Tetrahedron* **1994**, 50, 10321.

<sup>®</sup> Abstract published in *Advance ACS Abstracts*, November 1, 1995.

(1) (a) Petillon, F. Y.; Le Floch-Perennou, F.; Guerchais, J. E.; Sharp, D. W. A. *J. Organomet. Chem.* **1979**, 173, 89. (b) Osakada, K.; Maeda, M.; Nakamura, Y.; Yamamoto, T.; Yamamoto, A. *J. Chem. Soc., Chem. Commun.* **1986**, 442. (c) Kuniyasu, H.; Ogawa, A.; Miyazaki, S.; Ryu, I.; Kambe, N.; Sonoda, N. *J. Am. Chem. Soc.* **1991**, 113, 9796. (d) Kuniyasu, H.; Ogawa, A.; Sato, K.; Ryu, I.; Kambe, N.; Sonoda, N. *J. Am. Chem. Soc.* **1992**, 114, 5902. (e) Nishio, M.; Matsuzaka, H.; Mizobe, Y.; Hidai, M. *J. Chem. Soc., Chem. Commun.* **1993**, 375. (f) Garcia, J. J.; Maitlis, P. M. *J. Am. Chem. Soc.* **1993**, 115, 12200. (g) Wong, K.; Yuan, T.; Wang, M. C.; Tung, H.; Luh, T. *J. Am. Chem. Soc.* **1994**, 116, 8920. (h) Jones, W. D.; Chin, R. M. *J. Am. Chem. Soc.* **1994**, 116, 198. (i) Rondon, D.; Delbeau, J.; He, X.; Sabo-Etienne, S.; Chaudret, B. *J. Chem. Soc., Dalton Trans.* **1994**, 1895. (j) Martinez, A. G.; Barcina, J. O.; Cerezo, A. F.; Subramanian, L. R. *Synlett.* **1994**, 561. (k) Garcia, J. J.; Mann, B. E.; Adams, H.; Bailey, N. A.; Maitlis, P. M. *J. Am. Chem. Soc.* **1995**, 117, 2179. (l) Baranano, D.; Hartwig, J. F. *J. Am. Chem. Soc.* **1995**, 117, 2937.

(2) (a) Yamamoto, T.; Akimoto, M.; Saito, O.; Yamamoto, A. *Organometallics* **1986**, 5, 1559. (b) Osakada, K.; Chiba, T.; Nakamura, Y.; Yamamoto, T.; Yamamoto, A. *Organometallics* **1989**, 8, 2602. (c) Osakada, K.; Ozawa, Y.; Yamamoto, A. *J. Organomet. Chem.* **1990**, 399, 341.

The reaction of **2** with 1 equiv of  $\text{PCy}_3$  in  $\text{CH}_2\text{Cl}_2$  or  $\text{CDCl}_3$  at room temperature gave  $\text{Pd}(\eta^3\text{-C}_3\text{H}_5)(\text{SPh})(\text{PCy}_3)$  (**5**) in 61% yield (eq 2). Addition of another 1

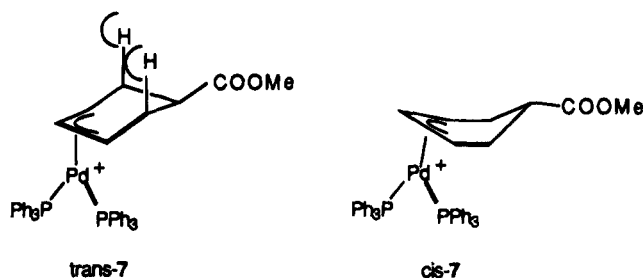


equiv of  $\text{PCy}_3$  into the solution led to the formation of a quantitative yield of **5**; however, no further transformation of **5** took place. On the other hand, the reaction of **2** with 1 equiv of  $\text{PPh}_3$  gave **1** in 37% yield together with the dinuclear palladium complex  $\text{Pd}_2(\mu\text{-C}_3\text{H}_5)(\mu\text{-SPh})(\text{PPh}_3)_2$  (**6**)<sup>5</sup> in 40% (based on SPh) yield, while the reaction using 3 equiv of  $\text{PPh}_3$  for 2 h gave **1** in 80% yield, with the yield of **6** being reduced to a very small amount (eq 3).

The reaction of **2** with  $\text{P}(\text{OMe})_3$  proceeded in a manner similar to that with  $\text{PPh}_3$ . Thus, by using 1 equiv of  $\text{P}(\text{OMe})_3$  the reaction gave the corresponding dinuclear complex  $\text{Pd}_2(\mu\text{-C}_3\text{H}_5)(\mu\text{-SPh})[\text{P}(\text{OMe})_3]_2$  (44%) together with **1** (39%), and that with 5 equiv of  $\text{P}(\text{OMe})_3$  gave a high yield of **1** (93%). Similarly, when the reaction of **4** with 1 equiv of  $\text{PPh}_3$  was carried out in  $\text{C}_6\text{D}_6$ , the formation of **3** (41%) and the dinuclear complex<sup>5</sup>  $\text{Pd}_2(\mu\text{-C}_3\text{H}_5)(\mu\text{-SePh})(\text{PPh}_3)_2$  (48%) was confirmed by a  $^1\text{H}$  NMR spectrum. The reaction using excess  $\text{PPh}_3$  (5 equiv) gave **3** in 80% yield.

To elucidate the stereochemistry of C–S bond formation induced by excess  $\text{PPh}_3$ , we attempted the reaction of the stereochemical probe complexes<sup>6</sup> *trans*-**7** and *cis*-**7** with  $\text{PPh}_3$  (eqs 4 and 5). These complexes gave the

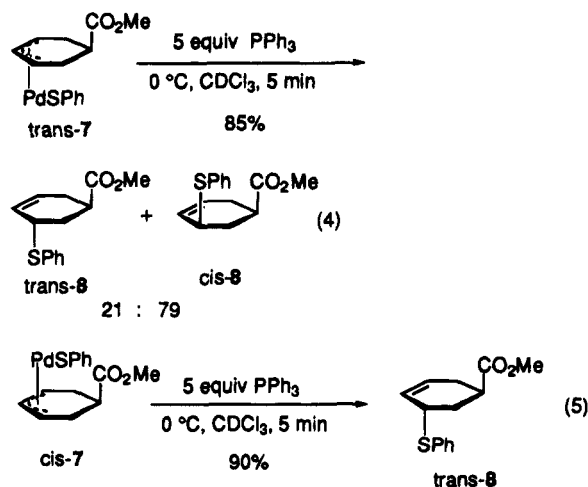
Chart 1



The difference in the degrees of stereospecificity in the reactions of *trans*-**7** and *cis*-**7** can be explained in terms of the different conformational preferences of these complexes established by X-ray crystallography.<sup>6</sup> In the pseudo-chair conformation of the cyclohexenyl ring of *trans*-**7**, two axial hydrogens at the carbons vicinal to the allyl terminals exert steric hindrance to the exo-attacking nucleophile (Chart 1). Then a facile stereochemical scrambling of the  $\eta^3$ -allyl complex via attack of a  $\text{Pd}(0)$  species,<sup>7</sup> which is produced in increasing amounts with continuation of the reaction, becomes competitive with the attack of  $\text{SPh}^-$ .<sup>8</sup> There is no such hindrance to the approach of  $\text{SPh}^-$  in the pseudo-boat conformation of *cis*-**7**, so that the attack of  $\text{SPh}^-$  proceeds with sufficient ease to result in high stereospecificity.

A reaction path of **2** with  $\text{PPh}_3$  can be envisaged as shown in Scheme 2. By the reaction of **2** with 1 equiv of  $\text{PPh}_3$ , the bridging by sulfur in **2** was split to form the phosphine-coordinated complex **9**. Although **9** was not detected spectroscopically, its 2-methylallyl analog  $\text{Pd}(\eta^3\text{-CH}_2\text{CMeCH}_2)(\text{SPh})(\text{PPh}_3)$  was unambiguously confirmed to exist transiently when  $[\text{Pd}(\eta^3\text{-CH}_2\text{CMeCH}_2)(\text{SPh})]_2$  was treated with 1 equiv of  $\text{PPh}_3$  in  $\text{CDCl}_3$  at room temperature for 10 min. This intermediate gradually disappeared to give a mixture of the dinuclear complex  $\text{Pd}_2(\mu\text{-CH}_2\text{CMeCH}_2)(\mu\text{-SPh})(\text{PPh}_3)_2$  and  $\text{CH}_2=\text{CMeCH}_2\text{SPh}$  almost quantitatively after 1 h. Presumably **9** and its 2-methylallyl analog are stable with respect to the C–S bond formation. However, they decompose readily via the ionic intermediates  $[\text{Pd}(\eta^3\text{-CH}_2\text{CR-CH}_2)(\text{PPh}_3)_2]^+\text{PhS}^-$  (**10**) when attacked by even a small amount of  $\text{PPh}_3$ , which exists due to incompleteness of the phosphine coordination equilibrium between **2** and **9** as well as their 2-methylallyl derivatives.

The collapse of the ionic intermediates gives allyl phenyl sulfides and  $\text{Pd}(\text{PPh}_3)_2$ . The latter  $\text{Pd}(0)$  complex would have reacted quite rapidly with  $[\text{Pd}(\eta^3\text{-CH}_2\text{-$



allylic sulfides **8** rapidly and stereospecifically. *trans*-**7** gave *cis*-**8** selectively, and *cis*-**7** provided *trans*-**8** exclusively. These results suggest that the  $\text{PPh}_3$ -induced C–S bond formation takes place via exo attack of the thiolate ion, released by coordination of  $\text{PPh}_3$  (see later), at the allyl carbon from the side opposite to Pd.

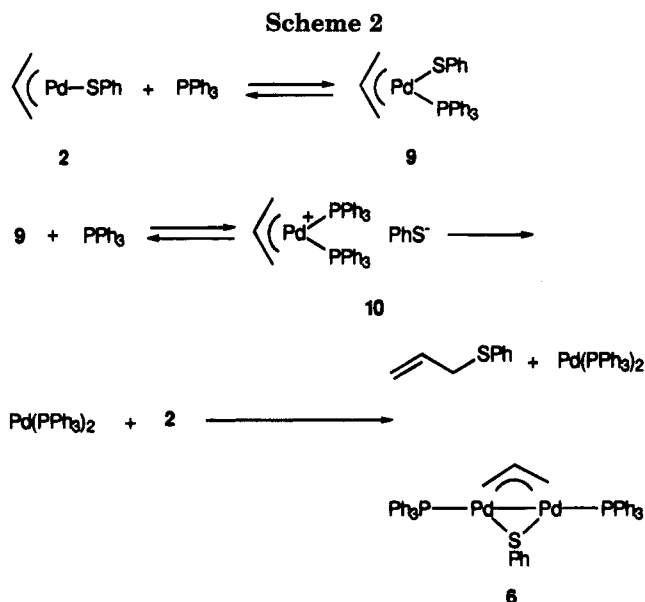
(4) (a) Singhal, A.; Jain, V. K. *J. Organomet. Chem.* **1995**, *494*, 75. (b) For the sake of simplicity, a monomeric form is shown in equations and schemes.

(5)  $^1\text{H}$  NMR spectra of these complexes showed the existence of two isomers possibly owing to two different dispositions of the two bridging ligands, allyl and benzenethiolate or -selenolate (see ref 2c for the X-ray structure of  $\text{Pd}_2(\mu\text{-C}_3\text{H}_5)(\mu\text{-SPh})(\text{PMe}_3)_2$ ).

(6) (a) Kurosawa, H.; Kajimaru, H.; Ogoshi, S.; Yoneda, H.; Miki, K.; Kasai, N.; Murai, S.; Ikeda, I. *J. Am. Chem. Soc.* **1992**, *114*, 8417. (b) Grennberg, H.; Langer, V.; Bäckvall, J. E. *J. Chem. Soc., Chem. Commun.* **1991**, 1190.

(7) (a) Kurosawa, H.; Ogoshi, S.; Chatani, N.; Kawasaki, Y.; Murai, S.; Ikeda, I. *Chem. Lett.* **1990**, 1745. (b) Granberg, K. L.; Bäckvall, J. E. *J. Am. Chem. Soc.* **1992**, *114*, 6858. (c) Ogoshi, S.; Kurosawa, H. *Organometallics* **1993**, *12*, 2869.

(8) Use of 2 equiv of  $\text{PPh}_3$ , instead of 5 equiv of  $\text{PPh}_3$ , resulted in the slower reaction of eq 4 where  $^1\text{H}$  NMR monitoring showed somewhat higher product selectivity (*trans*-**8**:*cis*-**8** = ca. 13:87) at the earlier stages of the reaction (yield 30–50%, 10–30 min at room temperature). This ratio gradually changed with further reaction up to the final value of *trans*-**8**/*cis*-**8** = 21/79.



CRCH<sub>2</sub>(SPh)]<sub>2</sub>, which must have remained unchanged in a half-amount in the case of PPh<sub>3</sub>/Pd = 1, forming the Pd–Pd-bonded product. Formation of  $\mu$ -allyl Pd–Pd complexes from Pd(0) and allyl–Pd(II) complexes is a well-established process.<sup>9</sup> We have separately confirmed that treatment of the Pd–Pd complex **6** with more than 4 equiv of PPh<sub>3</sub> leads to high-yield formation of **1** and the Pd(0) complex Pd(PPh<sub>3</sub>)<sub>n</sub> (*n* = 3, 4), explaining the results of the reaction of [Pd( $\eta^3$ -allyl)(SPh)]<sub>2</sub> with excess PPh<sub>3</sub>.

The relative stability of a combination of **1** and PdL<sub>n</sub> vs Pd( $\eta^3$ -C<sub>3</sub>H<sub>5</sub>)(SPh)L<sub>m</sub> (Scheme 1) must be highly ligand dependent. The stability is in favor of the Pd(0) side when L = PPh<sub>3</sub>, P(OMe)<sub>3</sub>. On the other hand, the Pd(II) side is more stable when L = PCy<sub>3</sub> (*m* = 1) and L = olefin (*m* = 0). Thus, it is now evident that the initial product of the reaction of Pd(PCy<sub>3</sub>)<sub>2</sub> with **1** is indeed a complex of the type **5**, which is followed by an extremely facile trapping of the ( $\eta^3$ -allyl)palladium(II) thiolate by a Pd(0) complex, as was proposed originally.<sup>2</sup>

Finally, the inversion of stereochemistry established here for the C–S bond-forming step in the ionic intermediate is consistent with the stereochemical results of palladium–phosphine complex catalyzed synthesis of allyl sulfides from either allyl carbonates with sulfur nucleophiles<sup>3b</sup> or allyl dithiocarbonates via decarboxylation;<sup>3a</sup> net retention of stereochemistry at the allylic carbon was observed as a result of oxidative addition (inversion) and subsequent C–S bond formation (inversion).

### Experimental Section

All manipulations were carried out under argon by the use of standard vacuum line techniques. Solvents were dried by standard methods and distilled prior to use. The following materials were prepared according to reported methods: [Pd( $\eta^3$ -C<sub>3</sub>H<sub>5</sub>)Cl]<sub>2</sub> and [Pd( $\eta^3$ -C<sub>4</sub>H<sub>7</sub>)Cl]<sub>2</sub>;<sup>10</sup> *trans*- and *cis*-[5-(methoxycarbonyl)-(1-3- $\eta$ -cyclohexenyl)]palladium chlorides;<sup>6</sup> Pd<sub>2</sub>(dba)<sub>3</sub>;<sup>11</sup> Pd(MA)-

(COD);<sup>12</sup> *trans*- and *cis*-3-chloro-5-(methoxycarbonyl)-1-cyclohexene.<sup>13</sup> Other reagents were of commercial grade.

<sup>1</sup>H and <sup>31</sup>P NMR spectra in CDCl<sub>3</sub> and C<sub>6</sub>D<sub>6</sub> solutions were recorded with JEOL JNM-GSX-270 (270 MHz), JEOL GSX-400 (400 MHz), and Bruker AM-600 (600 MHz) spectrometers. Chemical shifts in the <sup>1</sup>H and <sup>31</sup>P NMR spectra were determined relative to internal Me<sub>4</sub>-Si and external P(OMe)<sub>3</sub>, respectively.

**Synthesis of Authentic Samples of 2 and 4.** A flame-dried two-necked flask was charged with [Pd( $\eta^3$ -C<sub>3</sub>H<sub>5</sub>)Cl]<sub>2</sub> (175 mg, 0.95 mmol) in 10 mL of dry CH<sub>2</sub>Cl<sub>2</sub> and cooled to –78 °C in a dry ice/acetone bath. To the solution was added PhSTl (300 mg, 0.95 mmol), and the mixture was stirred for 3 h at 0 °C. The reaction mixture was filtered and evaporated in vacuo. **2** was recrystallized from a CH<sub>2</sub>Cl<sub>2</sub>/*n*-hexane solution: yield 158 mg (61%); mp 128–130 °C dec. <sup>1</sup>H NMR (C<sub>6</sub>D<sub>6</sub>):  $\delta$  2.59 (d, *J* = 12.6 Hz, 2H), 2.62 (d, *J* = 12.6 Hz, 2H), 3.32 (m, 4H), 4.67 (m, 1H), 4.83 (m, 1H). Anal. Calcd for C<sub>9</sub>H<sub>10</sub>PdS: C, 42.12; H, 3.93; S, 13.00. Found: C, 41.87; H, 3.88; S, 12.52. Complex **4** was prepared similarly from [Pd( $\eta^3$ -C<sub>3</sub>H<sub>5</sub>)Cl]<sub>2</sub> and PhSeNa in THF: yield 70%; mp 99–100 °C dec. <sup>1</sup>H NMR (C<sub>6</sub>D<sub>6</sub>):  $\delta$  2.66 (d, *J* = 12.5 Hz, 4H), 3.54 (d, *J* = 5.6 Hz, 4H), 4.65 (b, 1H), 4.78 (m, 1H). Anal. Calcd for C<sub>9</sub>H<sub>10</sub>PdSe: C, 35.61; H, 3.32. Found: C, 35.70; H, 3.56. [Pd( $\eta^3$ -CH<sub>2</sub>-CMeCH<sub>2</sub>)(SPh)]<sub>2</sub> was prepared similarly: yield 78%; mp 138–139 °C dec. <sup>1</sup>H NMR (CDCl<sub>3</sub>):  $\delta$  1.94 (s, 3H), 1.99 (s, 3H), 2.79 (s, 2H), 2.81 (s, 2H), 3.32 (s, 2H), 3.34 (s, 2H). Anal. Calcd for C<sub>10</sub>H<sub>12</sub>PdS: C, 44.37; H, 4.47; S, 11.84. Found: C, 44.25; H, 4.56; S, 11.99.

**Reaction of 2 with PCy<sub>3</sub>.** A flame-dried two-necked flask was charged with **2** (100 mg, 0.39 mmol) in 20 mL of dry CH<sub>2</sub>Cl<sub>2</sub> at ambient temperature under argon. To the solution was added PCy<sub>3</sub> (218 mg, 0.78 mmol). The reaction mixture was evaporated in vacuo. **5** was recrystallized from a CH<sub>2</sub>Cl<sub>2</sub>/*n*-hexane solution: yield 81.2 mg (39%), m.p., 129–130 °C. <sup>1</sup>H NMR (CDCl<sub>3</sub>):  $\delta$  2.54 (d, *J* = 12.4 Hz, 1H), 3.21 (dd, *J* = 13.7, 8.9 Hz, 1H), 3.60 (m, 2H), 5.28 (m, 1H). <sup>31</sup>P NMR (CDCl<sub>3</sub>):  $\delta$  –103.33. Anal. Calcd for C<sub>27</sub>H<sub>43</sub>PPdS: C, 60.38; H, 8.07; S, 5.97. Found: C, 60.52; H, 8.24; S, 6.16.

Also in an NMR tube were placed **2** (5.06 mg, 0.02 mmol), PCy<sub>3</sub> (5.40 mg, 0.02 mmol), and CDCl<sub>3</sub> (0.6 mL). <sup>1</sup>H NMR measurements showed the formation of **5** in 61% yield. When another 1 equiv of PCy<sub>3</sub> was added to the reaction mixture, **5** formed almost quantitatively.

**Reaction of 2 with PPh<sub>3</sub>.** **2** (500 mg, 1.95 mmol) was reacted with PPh<sub>3</sub> (511 mg, 1.95 mmol) in 50 mL of CH<sub>2</sub>Cl<sub>2</sub> solution. After 2 h at room temperature, the reaction mixture was evaporated in vacuo. **6** was recrystallized from CH<sub>2</sub>Cl<sub>2</sub>/*n*-hexane solution: yield 798 mg (46%); mp 100–102 °C dec. <sup>1</sup>H NMR (toluene-*d*<sub>8</sub>):  $\delta$  1.63 (d, *J* = 7.2 Hz, 2H), 3.02 (m, 1H), 3.14 (d, *J* = 7.6 Hz, 2H). The signal at  $\delta$  1.63 split into two broad signals ( $\delta$  1.55 and 1.85) at –80 °C. <sup>31</sup>P NMR (CDCl<sub>3</sub>):  $\delta$  –113.17. Anal. Calcd for C<sub>45</sub>H<sub>40</sub>P<sub>2</sub>Pd<sub>2</sub>S: C, 60.89; H, 4.54. Found: C, 60.66; H, 4.64.

Alternatively, in an NMR tube were placed **2** (9.8 mg, 0.038 mmol), PPh<sub>3</sub> (10.0 mg, 0.038 mol), and CDCl<sub>3</sub> (0.6 mL). Measurements of <sup>1</sup>H NMR spectra showed the

(9) Werner, H. *Adv. Organomet. Chem.* **1981**, *19*, 155.

(10) Tatsuno, Y.; Yoshida, T.; Otsuka, S. *Inorg. Synth.* **1979**, *19*, 220.

(11) Moseley, K.; Maitlis, P. M. *J. Chem. Soc., Dalton Trans.* **1974**, 169.

(12) Itoh, K.; Ueda, F.; Hirai, K.; Ishii, Y. *Chem. Lett.* **1977**, 877.

(13) Sheffy, F. K.; Godschalx, J. P.; Stille, J. K. *J. Am. Chem. Soc.* **1984**, *106*, 4833.

formation of allyl phenyl sulfide **1** in 37% yield and binuclear palladium complex **6** in 40% yield (80% based on Pd). When the reaction was carried out in the presence of 3 equiv of PPh<sub>3</sub> (30 mg, 0.11 mmol), **1** was formed in 80% yield.

**Reaction of 4 with PPh<sub>3</sub>.** This was carried out similarly to that described above for **2** with PPh<sub>3</sub>: yield of Pd<sub>2</sub>(μ-C<sub>3</sub>H<sub>5</sub>)(μ-SePh)(PPh<sub>3</sub>)<sub>2</sub> 47%; mp 150–152 °C dec. <sup>1</sup>H NMR (C<sub>6</sub>D<sub>6</sub>): δ 1.70 (br, 2H), 1.85 (br, 2H), 3.0 (vbr, 1H), 3.15 (vbr, 1H), 3.27 (br, 4H). The signals at δ 1.70 and 1.85 as well as those at δ 3.0 and 3.15 coalesced at ca. 40 °C. <sup>31</sup>P NMR (C<sub>6</sub>D<sub>6</sub>): δ -109.75, -110.92. Anal. Calcd for C<sub>45</sub>H<sub>40</sub>P<sub>2</sub>Pd<sub>2</sub>Se·½CH<sub>2</sub>Cl<sub>2</sub>: C, 55.94; H, 4.23. Found: C, 56.34; H, 4.14.

Alternatively, in an NMR tube were placed **4** (10.0 mg, 0.033 mmol), PPh<sub>3</sub> (8.6 mg, 0.033 mmol), and C<sub>6</sub>D<sub>6</sub> (0.6 mL) under argon. After 5 h at 25 °C, <sup>1</sup>H NMR measurements showed the formation of **3** (41%) and the corresponding dinuclear complex (48%). When the reaction was carried out in the presence of 5 equiv of PPh<sub>3</sub> (43.2 mg, 0.165 mmol), **3** was formed in 80% yield.

**Reaction of 2 with P(OMe)<sub>3</sub>.** A flame-dried two-necked flask was charged with complex **2** (300 mg, 1.17 mmol) in 10 mL of dry THF under argon. The reaction vessel was cooled to 0 °C. To the solution was added P(OMe)<sub>3</sub> (145 mg, 1.17 mmol) with a syringe. The reaction mixture was stirred for 4 h and was evaporated in vacuo. The dinuclear complex Pd<sub>2</sub>(μ-C<sub>3</sub>H<sub>5</sub>)(μ-SPh)-[P(OMe)<sub>3</sub>]<sub>2</sub> was recrystallized from CH<sub>2</sub>Cl<sub>2</sub>/*n*-hexane solution: yield 194 mg (27%); mp 75–77 °C. <sup>1</sup>H NMR (C<sub>6</sub>D<sub>6</sub>): δ 1.84 (d, *J* = 13.2 Hz, 2H), 2.56 (m, 1H), 3.94 (d of virtual triplet, *J*<sub>H</sub> = 7.6 Hz, *J*<sub>P</sub> = 7.6 Hz, 2H), 3.43 (virtual t, *J*<sub>P</sub> = 6.4 Hz, 18H). <sup>31</sup>P NMR (C<sub>6</sub>D<sub>6</sub>): δ 44.18. Anal. Calcd for C<sub>15</sub>H<sub>28</sub>O<sub>6</sub>P<sub>2</sub>Pd<sub>2</sub>S: C, 29.48; H, 4.62; S, 5.25. Found: C, 29.23; H, 4.58; S, 5.25.

The analogous reaction in an NMR tube in CDCl<sub>3</sub> solution afforded 44% of the μ-allylic dipalladium complex and 39% of **1** in the case of P(OMe)<sub>3</sub>/Pd = 1 and 93% of **1** in the case of P(OMe)<sub>3</sub>/Pd = 5.

**Reaction of [Pd(η<sup>3</sup>-CH<sub>2</sub>CMeCH<sub>2</sub>)(SPh)]<sub>2</sub> with PPh<sub>3</sub>.** In an NMR tube were placed [Pd(η<sup>3</sup>-CH<sub>2</sub>-CMeCH<sub>2</sub>)(SPh)]<sub>2</sub> (10.6 mg, 0.039 mmol), PPh<sub>3</sub> (10.1 mg, 0.039 mmol), and CDCl<sub>3</sub> (0.6 mL). <sup>1</sup>H NMR measurements at 10 min after mixing showed the formation of the phosphine-coordinated palladium complex Pd(η<sup>3</sup>-CH<sub>2</sub>CMeCH<sub>2</sub>)(SPh)(PPh<sub>3</sub>) in 58% yield. <sup>1</sup>H NMR (CDCl<sub>3</sub>): δ 1.85 (s, 3H), 2.64 (s, 1H), 3.15 (s, 1H), 3.32 (d, *J*<sub>P</sub> = 9.2 Hz, 1H), 3.41 (s, 1H). The assignment of this complex was made by comparison with the spectrum of **5**. Attempts to isolate pure forms of the PPh<sub>3</sub> adduct failed, because of the rapid formation of 2-methylallyl phenyl sulfide and the binuclear palladium complex Pd<sub>2</sub>(μ-CH<sub>2</sub>CMeCH<sub>2</sub>)(μ-SPh)(PPh<sub>3</sub>)<sub>2</sub>: <sup>1</sup>H NMR (CDCl<sub>3</sub>) δ 1.13 (s, 3H), 1.60 (s, 2H), 3.08 (br s, 2H).

**Synthesis of an Authentic Sample of cis-8.** A 100 mL dried round-bottom flask was charged with Na (177 mg, 7.70 mmol) and 30 mL of dry methanol under argon at 0 °C. To the solution was added benzenethiol (880 mg, 8.0 mmol) with a syringe and the mixture was stirred for 10 min at ambient temperature. To the solution was added *trans*-3-chloro-5-(methoxycarbonyl)-1-cyclohexene (900 mg, 5.1 mmol). After 15 h at ambient temperature, the reaction mixture was separated with 100 mL of Et<sub>2</sub>O and 50 mL of H<sub>2</sub>O. The organic layers were combined, washed with 10% aqueous NaOH, dried over MgSO<sub>4</sub>, and evaporated in vacuo. The residue was distilled to give the colorless liquid *cis*-**8** (867 mg, 3.50 mmol, 69%); bp 160 °C/1.5 mmHg. <sup>1</sup>H NMR (CDCl<sub>3</sub>): δ 1.73 (dt, *J* = 12.7, 10.8 Hz, 1H), 2.25 (m, 2H), 2.40 (m, 1H), 2.63 (m, 1H), 3.68 (s, 3H), 3.84 (m, 1H), 5.74 (d, *J* = 10.1 Hz, 1H), 5.79 (m, 1H). Mass: 248 (M<sup>+</sup>, 24), 217 (6), 189 (4), 139 (95), 109 (46), 77 (100), 59 (45). HR mass: calcd for C<sub>14</sub>H<sub>16</sub>O<sub>2</sub>S 248.0871, found 248.0874.

**Synthesis of an Authentic Sample of trans-8.** The synthesis was carried out by the same method as that described for *cis*-**8**, but the corresponding chloride was replaced with the *cis* isomer: *cis*-3-chloro-5-(methoxycarbonyl)-1-cyclohexene (3.0 g, 17.1 mmol), Na (395 mg, 17.1 mmol), PhSH (1.89 g, 17.1 mol), yield 2.56 g (60%) (*trans*:*cis* = 3:1). <sup>1</sup>H NMR (CDCl<sub>3</sub>): δ 1.95 (ddd, *J* = 13.6, 11.9, 4.6 Hz, 1H), 2.17 (d, *J* = 13.6 Hz, 1H), 2.25 (m, 1H), 2.37 (dt, *J* = 17.8, 4.6 Hz, 1H), 3.03 (m, 1H), 3.69 (s, 3H), 3.93 (b, 1H), 5.84 (m, 2H). HR mass: calcd for C<sub>14</sub>H<sub>16</sub>O<sub>2</sub>S 248.0871, found 248.0878.

**Reaction of 7 with PPh<sub>3</sub>.** In an NMR tube was placed *trans*-[5-(methoxycarbonyl)-(1-3-η)-cyclohexenyl]-palladium chloride (10.0 mg, 0.036 mmol), TlSPH (11.3 mg, 0.036 mmol), and CDCl<sub>3</sub> (0.6 mL) at 0 °C under an Ar atmosphere. After 5 min at the same temperature, 5 equiv of PPh<sub>3</sub> (47.2 mg, 0.18 mmol) was added. <sup>1</sup>H NMR measurements showed the formation of allyl sulfides *trans*-**8** and *cis*-**8** in 85% yield in the ratio of 21:79. A similar experiment using 2 equiv of PPh<sub>3</sub> was also carried out. In a similar manner, the *cis* isomer of **7** was generated and reacted with PPh<sub>3</sub> to show the formation of only *trans*-**8** in 90% yield.

**Acknowledgment.** Thanks are due to the Analytical Center, Faculty of Engineering, Osaka University, for the use of NMR facilities. Financial support of this work through a Grant-in-Aid for Scientific Research, the Ministry of Education, and Nagase Research Foundation is also acknowledged.

OM950539J

# Additions and Corrections

1995, Volume 14

**Matti Haukka, Jari Kiviaho, Markku Ahlgrén, and Tapani A. Pakkanen\***: Studies on Catalytically Active Ruthenium Carbonyl Bipyridine Systems. Synthesis and Structural Characterization of [Ru(bpy)(CO)<sub>2</sub>Cl<sub>2</sub>], [Ru(bpy)(CO)<sub>2</sub>Cl(C(O)OCH<sub>3</sub>)], [Ru(bpy)(CO)<sub>2</sub>Cl]<sub>2</sub>, and [Ru(bpy)(CO)<sub>2</sub>ClH] (bpy = 2,2'-Bipyridine).

Page 832. Entries in Tables 7 and 8 were placed in the wrong columns. The correct versions of these tables appear below.

**Table 7. Selected Bond Lengths (Å) for *cis*-(CO),*cis*-(Cl)-[Ru(bpy)(CO)<sub>2</sub>Cl<sub>2</sub>] (1a), *cis*-(CO),*trans*-(Cl)-[Ru(bpy)(CO)<sub>2</sub>Cl<sub>2</sub>]-CH<sub>2</sub>Cl<sub>2</sub> (1b), [Ru(bpy)(CO)<sub>2</sub>Cl(COOCH<sub>3</sub>)] (2), [Ru(bpy)(CO)<sub>2</sub>Cl]<sub>2</sub> (3), and [Ru(bpy)(CO)<sub>2</sub>ClH] (4)**

	1a	1b	2	3	4
Ru-Cl(1)	2.439(3)	2.391(5)	2.496(3)	2.512(1)	2.524(2)
Ru-Cl(2) <sup>a</sup>	2.411(4)	2.390(5)			
Ru-N(1)	2.117(8)	2.112(12)	2.117(8)	2.040(6)	2.118(4)
Ru-N(2)	2.090(8)	2.102(9)		2.179(7)	2.120(5)
Ru-C(11)	1.899(11)	1.835(17)	1.859(13)	1.953(8)	1.874(6)
Ru-C(12)		1.841(16)		1.817(8)	1.860(8)
Ru-C(31)	1.938(10)		2.041(12)		
C(11)-O(11)	1.115(14)	1.133(22)	1.161(16)	1.148(10)	1.142(8)
C(12)-O(12)		1.123(20)		1.159(11)	1.130(10)
C(31)-O(31)	1.012(15)		1.175(18)		
C(31)-O(32)			1.299(20)		
O(32)-C(32)			1.397(17)		
Ru-Ru				2.860(1)	

<sup>a</sup> Cl(2) = Cl(3) for 1b.

**Table 8. Selected Bond Angles (deg) for *cis*-(CO),*cis*-(Cl)-[Ru(bpy)(CO)<sub>2</sub>Cl<sub>2</sub>] (1a), *cis*-(CO),*trans*-(Cl)-[Ru(bpy)(CO)<sub>2</sub>Cl<sub>2</sub>]-CH<sub>2</sub>Cl<sub>2</sub> (1b), [Ru(bpy)(CO)<sub>2</sub>Cl(COOCH<sub>3</sub>)] (2), [Ru(bpy)(CO)<sub>2</sub>Cl]<sub>2</sub> (3), and [Ru(bpy)(CO)<sub>2</sub>ClH] (4)**

	1a	1b	2	3	4
Cl(1)-Ru-Cl(2) <sup>b</sup>	92.1(1)	176.3(1)			
Cl(1)-Ru-N(1)	86.5(2)	89.4(4)	86.1(2)	86.0(1)	86.6(1)
Cl(1)-Ru-N(2)	89.1(2)	87.3(3)		84.6(1)	87.3(1)
Cl(1)-Ru-C(11)	88.5(3)	91.0(6)	94.0(3)	94.8(2)	97.9(2)
Cl(1)-Ru-C(12)				95.0(2)	98.4(2)
Cl(1)-Ru-C(31)	178.8(3)		175.2(5)		
N(1)-Ru-Cl(2) <sup>b</sup>	96.0(2)	88.9(4)			
N(1)-Ru-N(2) <sup>a</sup>	77.6(3)	77.2(4)	76.6(5)	78.2(2)	77.0(2)
N(1)-Ru-C(11)	174.1(4)	174.8(6)	174.3(5)	172.3(3)	172.5(2)
N(1)-Ru-C(12) <sup>a</sup>		95.0(6)	97.7(5)	101.9(3)	97.5(2)
N(1)-Ru-C(31)	94.0(4)		90.1(4)		
N(2)-Ru-Cl(2) <sup>b</sup>	89.1(2)	89.2(3)			
N(2)-Ru-C(11)	99.3(4)	97.6(6)		94.3(3)	97.2(3)
N(2)-Ru-C(12)		172.1(6)		179.6(2)	171.9(2)
N(2)-Ru-C(31)	92.1(4)				
C(11)-Ru-Cl(2) <sup>b</sup>	88.5(3)				
C(11)-Ru-C(12) <sup>a</sup>		90.2(7)	88.0(8)	85.6(3)	87.8(3)
C(11)-Ru-C(31)	91.0(5)		89.5(4)		
Ru-C(11)-O(11)	174.5(10)	178.6(15)	179.7(8)	179.6(8)	176.7(7)
Ru-C(12)-O(12)		177.9(13)		177.0(6)	176.7(7)
Ru-C(31)-O(31)	171.1(11)		129.8(11)		
Ru-C(31)-O(32)			113.2(10)		
C(31)-O(32)-C(32)			117.0(11)		
Ru-Ru(A)-Cl(1)				177.0(1)	

<sup>a</sup> N(2) = N(1a) and C(12) = C(11a) for 2. <sup>b</sup> Cl(2) = Cl(3) for 1b.